東京帝國大學

地震研究所彙報

第13號

昭和10年

BULLETIN
OF THE
EARTHQUAKE RESEARCH INSTITUTE
TOKYO IMPERIAL UNIVERSITY

Vol. XIII.

1935

目次

第13號

第1冊（昭和10年3月）

頁
1. 深さのある震源から發生するラブ波（英文）…………… 妹澤克惟 1
2. L位相M位相の振動週期及振幅（英文）…………… 妹澤克惟・金井清 18
3. 地球の核の蔭に於ける波（獨文）…………… 松澤武雄 39
4. 灣口に於ける水位變化に伴ふ灣內海水の運動（共の2）（邦文）…………… 西村源六郎・高山威雄・金井清 46
5. 日本に適合する回轉楕圓體の近似的計算（英文）…………… 川畑幸夫 54
6. 地殼運動の分類（英文）…………… 今村學郎 80
7. 山崩れの研究（英文）…………… 宮部直巳 85
8. 地殼の上層內に震源を有する地震の初動分布と不連續層の厚さ（佛文）…………… 水上武 114
9. 地震動の表面層內における擴散（佛文）…………… 石本巳四雄 130
10. 地震動の變位，速度及加速度の比較（英文）…………… 萩原尊禮 138
11. 水平動地震計によつて觀測された週期4秒の脈動（英文）…………… 岸上冬彥 146
12. 伊東地震群に關する統計（英文）…………… 宮部直巳 155
13. 昭和8年3月3日の地震（共の1）震央（獨文）…………… 松澤武雄 171
14. 人工地震の實驗（英文）…………… 井上宇胤・木村隼 194
15. 物質の粘彈性性質に關する實驗（I）（英文）…………… 飯田汲事 198
16. 岩手縣北部新第三系下部門の澤統と四ツ役統との北海道幌內統に對する層位學的關係及び日本中新世前半の海進（英文）…………… 大塚彌之助 213
17. 能登半島南部邑知地溝（1）（英文）…………… 大塚彌之助 218

第 2 冊（昭和 10 年 6 月）

18. レーレー波の分散曲線に於ける不連續性（英文）……… 妹澤克惟・金井清 237
19. 太平洋及大陸を通過するレーレー波及ラブ波（英文）… 妹澤克惟 245
20. 地表層の震動減衰恒數（英文）……… 妹澤克惟・金井清 251
21. 大正 12 年 9 月 1 日の地震の際土地隆起に伴つて生じた東京灣の靜振（英文）……… 鈴木武夫 266
22. 地殼の地塊的構造に就て（英文）……… 宮部直巳 280
23. 岩手，宮城縣下に於ける地殼の變形（英文）……… 宮部直巳 286
24. "地塊とその運動" 第 1 報の訂正（英文）……… 宮部直巳 307
25. 博多灣沿岸水準高低測量（邦文）……… 鈴木清太郎・長澤武雄・中原孫吉 310
26. 淺間火山中央火口丘の相對的上昇と火口底の昇降變化（邦文）……… 水上武 318
27. 昭和 8 年 3 月 3 日の地震（其 2）カリフォーニアで觀測された表面波（獨文）……… 松澤武雄 328
28. 昭和 2 年丹後大地震の餘震の震原立體分布に關する研究補遺（英文）……… 那須信治 335
29. 伊豆半島に於ける最近の地震活動に就いて（第 2 報）（英文）……… 那須信治 400
30. 昭和 9 年 1 月 15 日の印度大地震に就いて（英文）……… 那須信治 417
31. 物質の粘彈性性質に關する實驗（II）（英文）……… 飯田汲事 433
32. 西南日本中央構造線と長崎三角地域とに關する二三の考察（邦文）……… 大塚彌之助 457
33. 室戸岬附近の水準再測成果（邦文）……… 469

第 3 冊（昭和 10 年 9 月）

34. M_2 地震波（英文）……… 妹澤克惟・金井清 471
35. 陸棚に於けるセイシの成長及老衰（英文）……… 妹澤克惟 476
36. 不均一彈性又は密度の地表層の震動減衰の割合（英文）… 妹澤克惟・金井清 484
37. 歪の潜勢力によつて起される彈性波（英文）……… 河角廣・吉山良一 496
38. 地表面に作用する風力その他によつて起される脈動（英文）……… 飯田汲事 504

39. 不連續面が彈性波の傳播に及ぼす影響（共の6）（邦文）… 西村源六郎 金井清 519
40. 不連續面が彈性波の傳播に及ぼす影響（共の7）（邦文）… 西村源六郎 540
41. 日本の重力に最もよく適合する式（英文）…………… 坪井忠二 淵田隆門 555
42. 三鷹基線菱形の最近の面積變化（英文）…………… 坪井忠二 558
43. コロイドと地震學（英文）…………… 寺田寅彦 562
44. 地震と雨雪量，氣壓，及氣溫との關係（英文）…………… 山口生知 569
45. 溫泉及鑛泉の分布と地殼運動（英文）…………… 寺田寅彦 宮部直巳 576
46. 驗潮記錄より知られたる深川に於ける地盤の沈降（英文）…………… 宮部直巳 587
47. 東京横濱市內 10 個所における地震動加速度觀測（2）（邦文）…………… 石本巳四雄 592
48 週期4秒の脈動（共の2）（英文）…………… 岸上冬彥 608
49. 南伊豆，蓮臺寺溫泉に就て（英文）…………… 福富孝治 中田正一 616
50. 1935 年の淺間火山の活動（共の1）（英文）…………… 水上武 629
51. 富士火山の數種の熔岩に就いて（英文）…………… 津屋弘逵 645
52. エゾタマキガヒの化石介殼內に於ける微結晶の配列（英文）…………… 坪井忠二 平田森三 660
53. シリカの剛性率及び固體粘度の溫度による變化（英文）… 飯田汲事 665
54. 勢力の地下逸散の爲に生ずる高層構造物の震動減衰（英文）…………… 妹澤克惟 金井清 681
55. 架構構造物の震動に於ける勢力逸散（英文）…………… 妹澤克惟 金井清 698
56. 瀨田川鐵橋に於ける車輛顚覆の振動的原因（英文）…… 妹澤克惟 715
57. 岡山一鳥取，鳥取一米子，及び岡山一米子間水準再測成果（邦文）…………… 723

第 4 册（昭和 10 年 12 月）

58. 局所的脈動の性質（英文）…………… 妹澤克惟 金井清 729
59. 靜力學的力を加へ又は除く爲に生ずる彈性波（英文）… 妹澤克惟 740
60. 不連續面の銳さが彈性波の透過反射に及ぼす影響（英文）…………… 妹澤克惟 金井清 750
61. 偏心物體の廻轉に依つて起された地表面の波に就いて（邦文）…………… 井上宇胤 757
62. 江東地域に於ける地盤の沈下（英文）…………… 宮部直巳 763

63. 地震發生機巧に關する一つの模型實驗（英文）………… 山口生知 772
64. 空氣制振器に就て（英文）………… 萩原尊禮 783
65. 1935 年の淺間火山の活動（其の2）（英文）………… 水上武 790
66. 淺間山小爆發の二例に就て（邦文）………… 寺田寅彦 801
67. 能登半島南部邑知地溝（II）（英文）………… 大塚彌之助 806
68. 能登半島南部邑知地溝（III）（英文）………… 大塚彌之助 846
69. 面河酸性岩類に就いて（英文）………… 津屋弘逵 910
70. 三菱仲13號舘，仲12號舘6號，東7號舘別舘の震動に於ける勢力逸散性（英文）………… 妹澤克惟 金井清 925
71. 靜岡强震に就て（邦文）………… 那須信治 保田柱二 942
72. 昭和10年7月11日の靜岡地震に就て（邦文）………… 萩原尊禮 951
73. 昭和10年7月11日靜岡地震震害調査報告（邦文）………… 金原壽郎 竹村千幹 966
74. 昭和10年7月11日靜岡地震に就て（邦文）………… 齊田時太郎 985
75. 清水港岸壁の震害と之に對する安定計算（英文）………… 松尾春雄 999
76. 昭和10年7月11日靜岡地震後に於ける水準測量結果報告（邦文）………… 福富孝治 1010

Contents

Vol. XIII.

Part 1.—March, 1935.

Page

1. K. SEZAWA, Love-waves Generated from a Source of a certain Depth. (in English) 1
2. K. SEZAWA and K. KANAI, Periods and Amplitudes of Oscillations in L- and M-phases. (in English) 18
3. T. MATUZAWA, Über Schattenwellen und Kernwellen. (in deutsch) 39
4. G. NISHIMURA, T. TAKAYAMA and K. KANAI, On the Long Waves in a Bay of Variable Section Generated by the Changes in the Elevation at the Mouth of It. (in Japanese) ... 46
5. Y. KAWABATA, Approximate Determination of the Spheroid most nearly Representing the Surface of Japan. (in English) .. 54
6. G. IMAMURA, Classification of Crustal Movements. (in English) 80
7. N. MIYABE, A Study of Landslides. (in English) 85
8. T. MINAKAMI, Distribution des mouvements initiaux d'un séisme dont le foyer se trouve dans la couche superficielle et détermination de l'épaisseur de cette couche. (en français) . 114
9. M. ISHIMOTO, La diffusion des secousses sismiques dans la couche superficielle du terrain. (en français) 130
10. T. HAGIWARA, A Comparison of the Displacement, the Velocity, and the Acceleration Seismograms. (in English) 138
11. F. KISHINOUYE, Microseisms of Four Second Period observed with Horizontal Seismographs. (in English) 146

12. N. **MIYABE**, A Statistical Study of the Itô Earthquake Swarms. (in English) 155
13. T. **MATUZAWA**, Seismometrische Untersuchungen des Erdbebens vom 2. März 1933. (1) Bestimmung des Herdes. (in deutsch) 171
14. W. **INOUYE** and H. **KIMURA**, Experiments on Artificial Earthquakes. (in English) 194
15. K. **IIDA**, Experiments on the Visco-elastic Properties of Pitch-like Materials. (I). (in English) 198
16. Y. **OTUKA**, The Stratigraphic Relation of the Lower Kadonosawa and the Yotuyaku Series of Iwate to the Poronai Series in Hokkaidô, and the Marine Transgression of the Early Miocene, in Japan. (in English) 213
17. Y. **OTUKA**, The Oti Graben in Southern Noto Peninsula, Japan. (Part I). (in English) 218

Part 2.—June, 1935.

18. K. **SEZAWA** and K. **KANAI**, Discontinuity in the Dispersion Curves of Rayleigh Waves. (in English) 237
19. K. **SEZAWA**, Rayleigh- and Love-waves transmitted through the Pacific Ocean and the Continents. (in English) 245
20. K. **SEZAWA** and K. **KANAI**, Decay Constants of Seismic Vibrations of a Surface Layer. (in English) 251
21. T. **SUZUKI**, Seiche in the Tôkyô Bay Caused by the Land Upheaval on the Occasion of the Great Earthquake of September 1, 1923. (in English) 266
22. N. **MIYABE**, Notes on the Block Structure of the Earth's Crust. (in English) 280
23. N. **MIYABE**, Deformation of the Earth's Crust in the Iwate and Miyagi prefectures. (in English) 286
24. N. **MIYABE**, Correction to my paper entitled "Blocks in the Earth's Crust and Their Movements, Part I". (in English) ... 307

25. S. SUZUKI, T. NAGAZAWA and M. NAKAHARA, The Revision of Precise Levelling along the Coast of the Hakata Bay. (in Japanese) 310
26. T. MINAKAMI, Changements relatifs de l'hauteur du cône central du volcan d'Asamà et la profondeur de lave dans son cratère. (en Japonais) 318
27. T. MATUZAWA, Seismometrische Untersuchungen des Erdbebens vom 2. März 1933. 2. Analyse der in Californien beobachteten Obelflächenwellen. (in deutsch) 328
28. N. NASU, Supplementary Study on the Stereometrical Distribution of the After-shocks of the Great Tango Earthquake of 1927. (in English) 335
29. N. NASU, Recent Seismic Activities in the Idu Peninsula. (Part 2). (in English) 400
30. N. NASU, The Great Indian Earthquake of January 15, 1934. (in English) 417
31. K. IIDA, Experiments on the Visco-elastic Properties of Pitch-like Materials. (II). (in English) 433
32. Y. OTUKA, Median Dislocation Line of Southwest Japan and the Nagasaki "Dreiecke". (in Japanese) 457
33. Precise Levellings in the Neighbourhood of the Muroto Promontory. (in Japanese) 469

Part 3.—September, 1935.

34. K. SEZAWA and K. KANAI, The M_2 Seismic Waves. (in English) 471
35. K. SEZAWA, Growth and Decay of Seiches in an Epicontinental Sea. (in English) 476
36. K. SEZAWA and K. KANAI, The Rate of Damping in Seismic Vibrations of a Surface Layer of Varying Density of Elasticity. (in English) 484
37. H. KAWASUMI and R. YOSIYAMA, On an Elastic Wave Ani-

mated by the Potential Energy of Initial Strain. (in English) 496

38. K. IIDA, Pulsatory Oscillations of the Earth's Crust due to Surface Force. (in English) 504

39. G. NISHIMURA and K. KANAI, On the Effect of Discontinuity Surfaces on the Propagation of Elastic Waves. (VI). (in Japanese) 519

40. G. NISHIMURA, On the Effect of Discontinuity Surfaces on the Propagation of Elastic Waves. (VII). (in Japanese) ... 540

41. C. TSUBOI and T. FUCHIDA, Supplementary Notes on the Most Suitable Formula for the Japanese Gravity Values. (in English) 555

42. C. TSUBOI, Recent Changes in Area of the Base Line Rhombus at Mitaka. (in English) 558

43. T. TERADA, Colloids and Seismology. (in English) 562

44. S. YAMAGUTI, Relations between the Earthquakes and Precipitation, Barometric Pressure, and Temperature. (in English) 569

45. T. TERADA and N. MIYABE, Geographical Distribution of Hot and Mineral Springs and Deformation of Earth's Crust. (in English) 576

46. N. MIYABE, Sinking of the Earth's Crust in Hukagawa, Tokyo, as Deduced from Mareogram Data. (in English) 587

47. M. ISHIMOTO, Observations accélérométriques des secousses sismiques dans les villes de Tôkyô et Yokohama (2me rapport). (en Japonais) 592

48. F. KISHINOUYE, On Microseisms of Four Second Period. (The Second Paper). (in English) 608

49. T. FUKUTOMI and M. NAKADA, On the Rendaizi Thermal Spring in Southern Idu Peninsula. (in English) 616

50. T. MINAKAMI, The Explosive Activities of Volcano Asama in 1935. (Part 1.). (in English) 629

51. H. TSUYA, On Some Lavas of Volcano Huzi (Fuji). (in Eng-

lish) 645

52. C. **Tsuboi** and M. **Hirata**, Arrangement of Micro-Crystals of Calcium Carbonate in Some Fossil Shells, *Glycymeris yessoensis* Sowerby. (in English) 660

53. K. **Iida**, Changes in Rigidity and Internal Friction of Amorphous Silica with Temperature. (in English) 665

54. K. **Sezawa** and K. **Kanai**, Decay in the Seismic Vibrations of a Simple or Tall Structure by Dissipation of their Energy into the Ground. (in English) 681

55. K. **Sezawa** and K. **Kanai**, Energy Dissipation in Seismic Vibrations of a Framed Structure. (in English) 698

56. K. **Sezawa**, Vibrational Causes of the Overturning of Railway Carriages on the Setagawa Bridge in the Typhoon of Sept. 21, 1934. (in English) 715

57. Results of Recent Precise Levellings along the lines Okayama—Tottori, Tottori—Yonago and Okayama—Yonago. (in Japanese) 723

Part 4.—December, 1935.

58. K. **Sezawa** and K. **Kanai**, The Nature of Microseisms of Local Type. (in English) 729

59. K. **Sezawa**, Elastic Waves Produced by Applying Statical Force to a Body or by Releasing it from a Body. (in English) 740

60. K. **Sezawa** and K. **Kanai**, The Effect of Sharpness of Discontinuities on the Transmission and Reflection of Elastic Waves. (in English) 750

61. W. **Inouye**, Some Experiments on the Waves generated by the Rotation of Some Eccentric Masses. (in Japanese) 757

62. N. **Miyabe**, On the Sinking of the Earth's Crust in the Eastern Part of the City of Tokyo. (in English) 763

63. S. **Yamaguti**, A Model Experiment on the Mechanism of

Occurrence of Earthquake. (in English) 772

64. T. **HAGIWARA**, The Air Damper. (in English) 783

65. T. **MINAKAMI**, The Explosive Activities of Volcano Asama in 1935. (Part 2). (in English) 790

66. T. **TERADA**, On Two Cases of Minor Eruption of Mt. Asama. (in Japanese) 801

67. Y. **OTUKA**, The Oti Graben in Southern Noto Peninsula, Japan. (Part 2). (in English) 806

68. Y. **OTUKA**, The Oti Graben in Southern Noto Peninsula, Japan. (Part 3). (in English) 846

69. H. **TSUYA**, On the Omogo Acidic Rocks. (in English) 910

70. K. **SEZAWA** and K. **KANAI**, Energy Dissipation in Seismic Vibration of Actual Buildings. (in English) 925

71. N. **NASU** and C. **YASUDA**, The Siduoka Earthquake of July 11, 1935. (in Japanese) 942

72. T. **HAGIWARA**, The Sizuoka Earthquake of July 11, 1935. (in Japanese) 951

73. T. **KINBARA** and C. **TAKEMURA**, Reports on the Siduoka Earthquake of July 11, 1935. (in Japanese) 966

74. T. **SAITA**, The Shizuoka Earthquake of July 11th, 1935. (in Japanese) 985

75. H. **MATUO**, Damages to the Quay Walls of Simizu Harbour due to the Earthguake on July 11, 1935, and the Seismic Stability of the Quay Walls. (in English) 999

76. T. **FUKUTOMI**, On the Result of Precise Levellings in the Strongly Shaken Area of the Siduoka Earthquake of July 11th, 1935. (in Japanese) 1010

1. Love-waves Generated from a Source of a certain Depth.

By Katsutada SEZAWA,

Earthquake Research Institute.

(Read Oct. 16, 1934.—Received Dec. 20, 1934.)

1. The problem of the generation of Love-waves from a seismic origin has attracted very little attention of investigators until recently and it appears that my previous paper[1] was the first attempt at finding the relation between the depth of the origin and the amplitudes of Love-waves which are generated therefrom. Even though that paper was correct in its result, the method of analysis used in it was not accurate from physical conception in lieu of the fact that I postulated in that paper stationary oscillations in the layer harmonizing with the excitation of shocks from the seismic origin. The present paper has been written with view to establish a theory of the generation of Love-waves which is free from such physical difficulty that was involved in the method in the previous paper and therefore adaptable to practical use with greater certainty.

In the present paper the effect of the free surface as well as the boundary between two media specializing the behaviour of waves in their multiple reflection and refraction at these boundaries was accurately taken into consideration. The present investigation, however, has given rise to results which are very like those of my previous calculation.[2] Among results which came out from my previous calculation the fact that Love-waves may be produced even from a source in the subjacent medium did not convince me in the light of geometrical consideration.[3] But, even from the present calculation it was found that the results of the problem are not much different for both cases at least in relation to the point in question.

2. In the first place the case where a point source lying within the stratum generates distortional waves with amplitudes oriented horizontally in the direction perpendicular to the incident plane will be dealt with, the problem being two-dimensional. Let the thickness of

---

1) 2) K. SEZAWA, "Propagation of Love-waves on a Spherical Surface and Allied Problems", *Bull. Earthq. Res. Inst.*, 7 (1929), 437∼455.

3) K. SEZAWA, *Publication du Bureau Central Séismologique International*, No. 10 (1934), 115.

the stratum and the depth of the seismic origin from the free surface be η and $\eta-\xi$ respectively and the densities and rigidities of the stratum and those of the subjacent medium ρ, μ, ρ', μ', the axes of x, y being taken as shown in the figure.

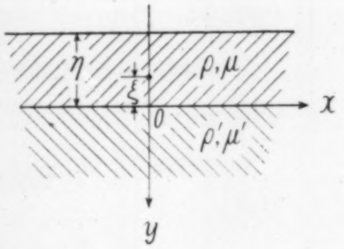

Fig. 1.

The displacement of waves generated from the origin is denoted by

$$v_0=e^{-ipt}H_0^{(1)}(kr), \tag{1}$$

where $r^2=x^2+(y+\xi)^2$ and $k^2=\rho p^2/\mu$. Now, it is possible to write

$$\left.\begin{aligned} H_0^{(1)}(kr)&=\frac{1}{\pi}\int_{-\infty}^{\infty}\frac{e^{\alpha(y+\xi)+ifx}}{\alpha}df, && [y<-\xi] \\ H_0^{(1)}(kr)&=\frac{1}{\pi}\int_{-\infty}^{\infty}\frac{e^{-\alpha(y+\xi)+ifx}}{\alpha}df, && [y>-\xi] \end{aligned}\right\} \tag{2}$$

provided $\alpha=\sqrt{f^2-k^2}$. From (1) and (2) we have

$$v_0=\frac{e^{-ipt}}{\pi}\int_{-\infty}^{\infty}\frac{e^{ifx+\alpha(y+\xi)}}{\alpha}df, \qquad [y<-\xi] \tag{3}$$

$$v_0=\frac{e^{-ipt}}{\pi}\int_{-\infty}^{\infty}\frac{e^{ifx-\alpha(y+\xi)}}{\alpha}df. \qquad [y>-\xi] \tag{4}$$

The expression (3) gives the displacement of primary waves propagated upwards and (4) that of waves transmitted downwards. It will be shown that, if waves of the type:

$$V_0=\phi(ifx+\alpha y-ipt) \tag{5}$$

are transmitted in the stratum and incident on the free surface, the reflected waves are written in the form:

$$V=\phi[ifx-\alpha(y+2\eta)-ipt], \tag{6}$$

and, if the waves of the type:

$$V_{01}=\phi_1(ifx-\alpha y-ipt) \tag{7}$$

are transmitted in the stratum and incident on the lower boundary of that stratum, the reflected waves V_1 as well as refracted waves V_1' are expressed by

$$\left.\begin{aligned} V_1&=q\phi_1(ifx+\alpha y-ipt), \\ V_1'&=\tau\phi_1(ifx-\beta y-ipt), \end{aligned}\right\} \tag{8}$$

where

$$q=\frac{\mu\alpha-\mu'\beta}{\mu\alpha+\mu'\beta}, \qquad \tau=\frac{2\mu\alpha}{\mu\alpha+\mu'\beta}, \tag{9}$$

in which $\beta=\sqrt{f^2-k'^2}$, $k'^2=\rho' p^2/\mu'^2$. Thus, taking account of all kinds of waves successively reflected at two boundaries, we obtain the displacement of the stratum due to primary waves (3) as follows:

$$v=\frac{e^{-ipt}}{\pi}\int_{-\infty}^{\infty} e^{ifx+\alpha\xi}\left\{e^{\alpha y}+e^{-\alpha(y+2\eta)}\right\}\left\{1+qe^{-2\alpha\eta}+q^2e^{-4\alpha\eta}+\cdots\cdot\right\}\frac{df}{\alpha},$$

$$[y+\xi<0] \qquad (10)$$

$$v=\frac{e^{-ipt}}{\pi}\int_{-\infty}^{\infty} e^{ifx+\alpha\xi}\left\{qe^{\alpha(y-2\eta)}+e^{-\alpha(y+2\eta)}\right\}\left\{1+qe^{-2\alpha\eta}+q^2e^{-4\alpha\eta}+\cdots\cdot\right\}\frac{df}{\alpha}.$$

$$[y+\xi>0] \qquad (10')$$

Similarly, the displacement of the stratum due to primary waves (4) is expressed by

$$v=\frac{e^{-ipt}}{\pi}\int_{-\infty}^{\infty} e^{ifx-\alpha\xi}\,q\left\{e^{\alpha\eta}+e^{-\alpha(y+2\eta)}\right\}\left\{1+qe^{-2\alpha\eta}+q^2e^{-4\alpha\eta}+\cdots\cdot\right\}\frac{df}{\alpha},$$

$$[y+\xi<0] \qquad (11)$$

$$v=\frac{e^{-ipt}}{\pi}\int_{-\infty}^{\infty} e^{ifx-\alpha\xi}\left\{e^{-\alpha y}+qe^{\alpha y}\right\}\left\{1+qe^{-2\alpha\eta}+q^2e^{-4\alpha\eta}+\cdots\cdot\right\}\frac{df}{\alpha}.$$

$$[y+\xi>0] \qquad (11')$$

Summing up (10) and (11) and simplifying the resulting expression we have

$$v=\frac{e^{-ipt}}{\pi}\int_{-\infty}^{\infty}\frac{e^{ifx}\{(\mu\alpha+\mu'\beta)e^{\alpha\xi}+(\mu\alpha-\mu'\beta)^{-\alpha\xi}\}}{\alpha\{(\mu\alpha+\mu'\beta)e^{\alpha\eta}-(\mu\alpha-\mu'\beta)e^{-\alpha\eta}\}}\{e^{\alpha(\eta+y)}+e^{-\alpha(\eta+y)}\}\,df,$$

$$[y+\xi<0] \qquad (12)$$

$$v=\frac{e^{-ipt}}{\pi}\int_{\infty}^{\infty}\frac{e^{ifx}\{(\mu\alpha+\mu'\beta)e^{-\alpha y}+(\mu\alpha-\mu'\beta)^{\alpha y}\}}{\alpha\{(\mu\alpha+\mu'\beta)e^{\alpha\eta}-(\mu\alpha-\mu'\beta)^{-\alpha\eta}\}}\{e^{\alpha(\eta-\xi)}+e^{-\alpha(\eta-\xi)}\}\,df.$$

$$[y+\xi>0] \qquad (12')$$

The resulting refracted waves in the subjacent material are expressed by

$$v'=\frac{e^{-ipt}}{\pi}\int_{-\infty}^{\infty}\frac{2\mu\, e^{ifx-\beta y}\{e^{\alpha(\eta-\xi)}+e^{-\alpha(\eta-\xi)}\}}{(\mu\alpha+\mu'\beta)e^{\alpha\eta}-(\mu\alpha-\mu'\beta)e^{-\alpha\eta}}\,df. \quad [y>0] \qquad (13)$$

If we put $y=-\xi$, we find that v for $y+\xi<0$ is equal to v for $y+\xi>0$. If we put $y=0$, it follows that $v'=v$ for $y+\xi>0$.

If we put $y=-\eta$ in the expression of (12), we get the displacement at the free surface as follows:

$$v=\frac{2e^{-ipt}}{\pi}\int_{-\infty}^{\infty}\frac{e^{ifx}\{(\mu\alpha+\mu'\beta)e^{\alpha\xi}+(\mu\alpha-\mu'\beta)e^{-\alpha\xi}\}}{\alpha\{(\mu\alpha+\mu'\beta)e^{\alpha\eta}-(\mu\alpha-\mu'\beta)e^{-\alpha\eta}\}}\,df. \qquad (14)$$

This integral may be transformed to:

$$v=\frac{2e^{-ipt}}{\pi}\int_{0}^{\infty}\frac{(e^{ifx}+e^{-ifx})\{(\mu\alpha+\mu'\beta)e^{\alpha\xi}+(\mu\alpha-\mu'\beta)e^{-\alpha\xi}\}}{(\mu\alpha+\mu'\beta)e^{\alpha\eta}-(\mu\alpha-\mu'\beta)e^{-\alpha\eta}}\frac{df}{\alpha}. \qquad (14')$$

To evaluate this expression we consider two integrals:

$$\int_c \frac{e^{iZx}\chi(Z)}{F(Z)}\frac{dZ}{\sqrt{Z^2-k^2}}=0, \qquad (15)$$

$$\int_c \frac{e^{-iZx}\chi(Z)}{F(Z)}\frac{dZ}{\sqrt{Z^2-k^2}}=0, \tag{16}$$

in which

$$\chi(Z)=(\mu\sqrt{Z^2-k^2}+\mu'\sqrt{Z^2-k'^2})e^{\sqrt{Z^2-k^2}\xi} \\ +(\mu\sqrt{Z^2-k^2}-\mu'\sqrt{Z^2-k'^2})e^{-\sqrt{Z^2-k^2}\xi}, \tag{17}$$

$$F(Z)=(\mu\sqrt{Z^2-k^2}+\mu'\sqrt{Z^2-k'^2})e^{\sqrt{Z^2-k^2}\eta} \\ -(\mu\sqrt{Z^2-k^2}-\mu'\sqrt{Z^2-k'^2})e^{-\sqrt{Z^2-k^2}\eta}, \tag{18}$$

taken round contours in the first and fourth quadrants respectively. The integral (15) has branch points at $Z=k$ and $Z=k'$, and poles at $Z=\kappa_1, \kappa_2, \ldots.$, where $\kappa_1, \kappa_2, \ldots.$ are roots of $F(Z)=0$. $F(\kappa_n)=0$ is the characteristic equation of Love-waves and gives the velocity of that kind of waves. The integral (16) has no branch point nor pole. The reason why these singular points reside in the first quadrant but not in the fourth comes from the assumption that there are temporarily small frictional terms in the original equations of motion as follows:

$$\left.\begin{aligned}\frac{\partial^2 v}{\partial x^2}+\frac{\partial^2 v}{\partial y^2}&=\frac{\rho}{\mu}\left(\frac{\partial^2 v}{\partial t^2}+c\ \frac{\partial v}{\partial t}\right),\\ \frac{\partial^2 v'}{\partial x^2}+\frac{\partial^2 v'}{\partial y^2}&=\frac{\rho'}{\mu'}\left(\frac{\partial^2 v'}{\partial t^2}+c'\ \frac{\partial v'}{\partial t}\right),\end{aligned}\right\} \tag{19}$$

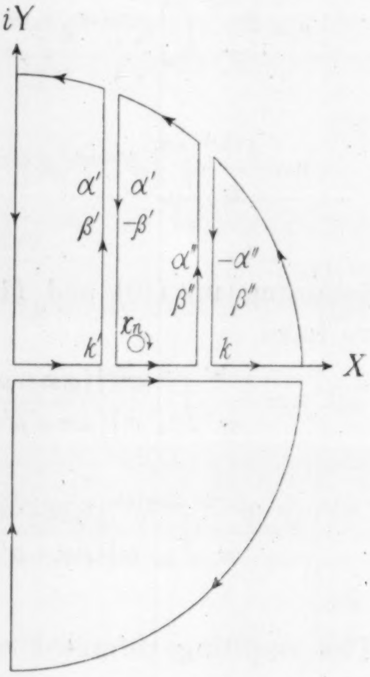

Fig. 2,

where c, c' are very small quantities and may be made zero finally. If the solutions of these equations be expressed by the types:

$$v=e^{-ipt+ifx\pm\alpha y}, \quad v'=e^{-ipt+ifx\pm\beta y}, \qquad [x>0]$$

we have

$$\alpha=\sqrt{f^2-k^2(1+ik_1/k^2)}, \quad \beta=\sqrt{f^2-k^2(1+ik'_1/k'^2)}, \tag{20}$$

where $k^2=\rho p^2/\mu^2$, $k'^2=\rho' p^2/\mu'^2$, $k_1=cp$, $k'_1=c'p$. It follows therefore that branch points come into the first quadrant. It is possible to prove that poles $\kappa_1, \kappa_2, \ldots.$ are in the same quadrant.

Now, the integral (15) may be expressed by

$$\int_0^\infty \frac{e^{ifx}\{(\mu\alpha+\mu'\beta)e^{\alpha\xi}+(\mu\alpha-\mu'\beta)e^{-\alpha\xi}\}}{(\mu\alpha+\mu'\beta)e^{\alpha\eta}-(\mu\alpha-\mu'\beta)e^{-\alpha\eta}}\frac{df}{\alpha}$$

$$+\int_\infty^0 \frac{e^{-Yx}\{(\mu\sqrt{Y^2+k^2}+\mu'\sqrt{Y^2+k'^2})e^{i\sqrt{Y^2+k^2}\xi}}{\{(\mu\sqrt{Y^2+k^2}+\mu'\sqrt{Y^2+k'^2})e^{i\sqrt{Y^2+k^2}\eta}}$$

$$\frac{+(\mu\sqrt{Y^2+k^2}-\mu'\sqrt{Y^2+k'^2})e^{-i\sqrt{Y^2+k^2}\xi}\}}{-(\mu\sqrt{Y^2+k^2}-\mu'\sqrt{Y^2+k'^2})e^{-i\sqrt{Y^2+k^2}\eta}\}}\frac{dY}{\sqrt{Y^2+k^2}}$$

$$-2\pi i\sum_n e^{i\kappa_n x}\frac{\{(\mu\alpha_1+\mu'\beta_1)e^{\alpha_1\xi}+(\mu\alpha_1-\mu'\beta_1)e^{-\alpha_1\xi}\}}{\alpha_1F'(\kappa_n)}$$

$$+e^{ik'x}\int_0^\infty\left[\frac{\mu\alpha'\cosh\alpha'\xi+\mu'\beta'\sinh\alpha'\xi}{\mu\alpha'\sinh\alpha'\eta+\mu'\beta'\cosh\alpha'\eta}\right.$$

$$\left.-\frac{\mu\alpha'\cosh\alpha'\xi-\mu'\beta'\sinh\alpha'\xi}{\mu\alpha'\sinh\alpha'\eta-\mu'\beta'\cosh\alpha'\eta}\right]e^{-xY}\frac{idY}{\alpha'}=0, \tag{21}$$

in which κ_n are roots of $F(Z)=0$ and $\alpha_1=\sqrt{\kappa_n^2-k^2}$, $\beta_1=\sqrt{\kappa_n^2-k'^2}$, while $\alpha'=\sqrt{(k'+iY)^2-k^2}$, $\beta'=\sqrt{(k'+iY)^2-k'^2}$. The integral along the circumference of a circular arc of infinite radius R vanishes in virtue of the factor $\exp.(ixR\cos\theta-xR\sin\theta)$ and of the relation $\eta>\xi$.

The integral (16) is written by

$$\int_0^\infty\frac{e^{ifx}\{(\mu\alpha+\mu'\beta)e^{\alpha\xi}+(\mu\alpha-\mu'\beta)e^{-\alpha\xi}\}}{(\mu\alpha+\mu'\beta)e^{\alpha\eta}-(\mu\alpha-\mu'\beta)e^{-\alpha\eta}}\frac{df}{\alpha}$$

$$-\int_\infty^0\frac{e^{-Yx}\{(\mu\sqrt{Y^2+k^2}+\mu'\sqrt{Y^2+k'^2})e^{i\sqrt{Y^2+k^2}\xi}}{\{(\mu\sqrt{Y^2+k^2}+\mu'\sqrt{Y^2+k'^2})e^{i\sqrt{Y^2+k^2}\eta}}$$

$$\frac{+(\mu\sqrt{Y^2+k^2}-\mu'\sqrt{Y^2+k'^2})e^{-i\sqrt{Y^2+k^2}\xi}\}}{-(\mu\sqrt{Y^2+k^2}-\mu'\sqrt{Y^2+k'^2})e^{-i\sqrt{Y^2+k^2}\eta}\}}\frac{dY}{\sqrt{Y^2+k^2}}=0. \tag{22}$$

The integral along the circumference of a circular arc of infinite radius vanishes in virtue of the factor $\exp.(ixR\cos\theta+xR\sin\theta)$ and of the relation $\eta>\xi$.

Adding (21) and (22) and substituting the resulting expression in (14′), we arrive at

$$v=\sum_n 8ie^{i(\kappa_n x-pt)}\frac{\{\mu\sqrt{k^2-\kappa_n^2}\cos\sqrt{k^2-\kappa_n^2}\xi+\mu'\sqrt{\kappa_n^2-k'^2}\sin\sqrt{k^2-\kappa_n^2}\xi\}}{\sqrt{k^2-\kappa_n^2}F'(\kappa_n)}$$

$$-\frac{2ie^{i(k'x-pt)}}{\pi}\int_0^\infty\frac{\mu\mu'\beta'\cosh\alpha'(\eta-\xi)}{(\mu'\beta')^2\cosh^2\alpha'\eta-(\mu\alpha')^2\sinh^2\alpha'\eta}e^{-xY}dY. \tag{23}$$

The important part of the integral term of the above expression is in the vicinity of small Y, so that we may put

$$\alpha'=i\sqrt{k^2-k'^2},\qquad \beta'=\sqrt{2k'Y}\,e^{\frac{i\pi}{4}}, \tag{24}$$

and therefore the integral in question becomes approximately

$$i^{\frac{1}{2}}\int_0^\infty\frac{\mu\mu'\cos\sqrt{k^2-k'^2}(\eta-\xi)}{i\mu'^2 2k'Y\cos^2\sqrt{k^2-k'^2}\eta-\mu^2(k^2-k'^2)\sin^2\sqrt{k^2-k'^2}\eta}e^{-xY}\sqrt{2k'Y}\,dY. \tag{25}$$

It is well known that

$$\int_0^\infty Y^{\frac{1}{2}}\psi(Y)e^{-Yx}dY=\frac{\Pi(1/2)}{x^{3/2}}\psi(0)+\frac{\Pi(3/2)}{x^{5/2}}\frac{\psi'(0)}{1!}+\frac{\Pi(5/2)}{x^{7/2}}\frac{\psi''(0)}{2!}+\cdots, \tag{26}$$

so that (25) reduces to

$$-i^{\frac{1}{2}}\sqrt{\frac{\pi k'}{2}}\frac{\mu'}{\mu}\frac{\cos\sqrt{k^2-k'^2}(\eta-\xi)}{(k^2-k'^2)\sin^2\sqrt{k^2-k'^2}\,\eta}\frac{1}{x^{3/2}}+\cdots. \tag{25'}$$

Substituting (25′) in (23), we arrive at

$$v=\sum_n 8e^{i\left(\kappa_n x-pt+\frac{\pi}{2}\right)}\frac{\{\mu\sqrt{k^2-\kappa_n^2}\cos\sqrt{k^2-\kappa_n^2}\,\xi+\mu'\sqrt{\kappa_n^2-k'^2}\sin\sqrt{k^2-\kappa_n^2}\,\xi\}}{\sqrt{k^2-\kappa_n^2}\,F'(\kappa_n)}$$

$$-\sqrt{\frac{2k'}{\pi}}e^{i\left(k'x-pt-\frac{\pi}{4}\right)}\frac{\mu'}{\mu}\frac{\cos\sqrt{k^2-k'^2}(\eta-\xi)}{(k^2-k'^2)\sin^2\sqrt{k^2-k'^2}\,\eta}\frac{1}{x^{3/2}}+\cdots. \quad [x>0] \tag{27}$$

The first term of the right-hand side of this equation represents waves transmitted with the velocity of Love-waves, while the second one gives distortional waves propagated with the velocity of transverse waves proper to the subjacent medium. The amplitudes of Love-waves thus formed is not strikingly different whether the seismic origin is deep or not. The amplitudes of pure distortional waves vary inversely as 3/2 th power of the epicentral distance. This is similar to the result of Lamb's problem[4] on Rayleigh-waves in which the amplitudes of dilatational or distortional waves accompanying Rayleigh-waves vary inversely as 3/2 th power of the epicentral distance in a two-dimensional problem and inversely as the square of the same distance in a three-dimensional one. Although similar results were given by a few authors[5] and also involved in some part of our paper[6], it is not certain that the fact is dynamically possible. Such law of decrease of amplitudes in accordance with epicentral distance is the mere result of the treatment of the integral of the type shown in (26) or analogous formulae with the condition that x is large. The true nature may be ascertained by investigating the distribution of displacements within the layer and the subjacent medium.

The distribution of displacements in the stratum is obtained as follows. Taking the expressions (12) and (12′) and considering the contour integrals (15) and (16) with the modification that

$$2\chi(Z)=(\mu\sqrt{Z^2-k^2}+\mu'\sqrt{Z^2-k'^2})\{e^{\sqrt{Z^2-k^2}(\xi+y+\eta)}+e^{\sqrt{Z^2-k^2}(\xi-y-\eta)}\}$$

---

4) H. LAMB, *Phil. Trans. Roy. Soc., London*, **203** (1904), 1~42.

5) H. NAKANO, *Geophys. Mag.*, **2** (1930), 189~348; T. SAKAI, *Proc. Phys.-Math. Soc., Japan*, [iii], **15** (1933), 291~327; *Geophys. Mag.*, **3** (1934), 1~72.

6) K. SEZAWA and G. NISHIMURA, "Movement of the Ground due to Atmospheric Disturbance in a Sea Region," *Bull. Earthq. Res. Inst.*, **9** (1931), 291~309.

$$+(\mu\sqrt{Z^2-k^2}-\mu'\sqrt{Z^2-k'^2})\{e^{-\sqrt{Z^2-k^2}(\xi-y-\eta)}+e^{-\sqrt{Z^2-k^2}(\xi+y+\eta)}\},$$

$$[y+\xi<0] \qquad (28)$$

$$2\chi(Z)=(\mu\sqrt{Z^2-k^2}+\mu'\sqrt{Z^2-k'^2})\}e^{-\sqrt{Z^2-k^2}(y-\eta+\xi)}+e^{-\sqrt{Z^2-k^2}(y+\eta-\xi)}\}$$

$$+(\mu\sqrt{Z^2-k^2}-\mu'\sqrt{Z^2-k'^2})\}e^{\sqrt{Z^2-k^2}(y+\eta-\xi)}+e^{\sqrt{Z^2-k^2}(y-\eta+\xi)}\},$$

$$[y+\xi>0] \qquad (28')$$

and proceeding in the same manner of treatment as in the preceding calculation, we arrive at finally

$$v=\sum_n 8e^{i\left(\kappa_n x-pt+\frac{\pi}{2}\right)}.$$

$$\cdot\frac{\{\mu\sqrt{k^2-\kappa_n^2}\cos\sqrt{k^2-\kappa_n^2}\xi+\mu'\sqrt{\kappa_n^2-k'^2}\sin\sqrt{k^2-\kappa_n^2}\xi\}\cos\sqrt{k^2-\kappa_n^2}(\eta+y)}{\sqrt{k^2-\kappa_n^2}\,F'(\kappa_n)}$$

$$-\sqrt{\frac{2k'}{\pi}}\,e^{i\left(k'x-pt-\frac{\pi}{4}\right)}\,\frac{\mu'}{\mu}\,\frac{\cos\sqrt{k^2-\kappa'^2}(\eta-\xi)\cos\sqrt{k^2-k'^2}(\eta+y)}{(k^2-k'^2)\sin^2\sqrt{k^2-k'^2}\,\eta}\,\frac{1}{x^{3/2}}+\cdots,$$

$$[x>0,\ y+\xi<0] \qquad (29)$$

$$v=\sum_n 8e^{i\left(\kappa n x-pt+\frac{\pi}{2}\right)}$$

$$\cdot\frac{\{\mu\sqrt{k^2-\kappa_n^2}\cos\sqrt{k^2-\kappa_n^2}\,y-\mu'\sqrt{\kappa_n^2-k'^2}\sin\sqrt{k^2-\kappa_n^2}\,y\}\cos\sqrt{k^2-\kappa_n^2}(\eta-\xi)}{\sqrt{k^2-\kappa_n^2}\,F'(\kappa_n)}$$

$$-\sqrt{\frac{2k'}{\pi}}\,e^{i\left(k'x-pt-\frac{\pi}{4}\right)}\,\frac{\mu'}{\mu}\,\frac{\cos\sqrt{k^2-k'^2}(\eta-\xi)\cos\sqrt{k^2-k'^2}(\eta+y)}{(k^2-k'^2)\sin^2\sqrt{k^2-k'^2}\,\eta}\,\frac{1}{x^{3/2}}+\cdots.$$

$$[x>0,\ y+\xi>0] \qquad (29')$$

The distribution of displacements in the subjacent medium will be considered. The integral (13) is transformed to

$$v'=\frac{2\mu e^{-ipt}}{\pi}\int_0^\infty\frac{(e^{ifx}+e^{-ifx})e^{-\beta y}\{e^{\alpha(\eta-\xi)}+e^{-\alpha(\eta-\xi)}\}}{(\mu\alpha+\mu'\beta)e^{\alpha\eta}-(\mu\alpha-\mu'\beta)e^{-\alpha\eta}}\,df. \qquad (30)$$

To evaluate this expression we consider two integrals of the types (15), (16), where

$$\chi(Z)=\{e^{\sqrt{Z^2-k^2}(\eta-\xi)}+e^{-\sqrt{Z^2-k^2}(\eta-\xi)}\}e^{-\sqrt{Z^2-k'^2}y} \qquad (31)$$

in the present case, taken round two contours shown in Fig. 2. The integral of the type (15) may be expressed by

$$\int_0^\infty\frac{e^{ifx}\{e^{\alpha(\eta-\xi)}+e^{-\alpha(\eta-\xi)}\}e^{-\beta y}}{(\mu\alpha+\mu'\beta)e^{\alpha\eta}-(\mu\alpha-\mu'\beta)e^{-\alpha\eta}}\,df$$

$$+\int_\infty^0\frac{e^{-Yx}\{e^{i\sqrt{Y^2+k^2}(\eta-\xi)}+e^{-i\sqrt{Y^2+k^2}(\eta-\xi)}\}e^{-i\sqrt{Y^2+k'^2}y}\,dY}{(\mu\sqrt{Y^2+x^2}+\mu'\sqrt{Y^2+k'^2})e^{i\sqrt{Y^2+k^2}(\eta-\xi)}-(\mu\sqrt{Y^2+k^2}+\mu'\sqrt{Y^2+k'^2})e^{-i\sqrt{Y^2+k^2}(\eta-\xi)}}$$

$$-2\pi i\sum_n \frac{e^{i\kappa_n x}\{e^{\alpha_1(\eta-\xi)}+e^{-\alpha_1(\eta-\xi)}\}e^{-\beta_1 y}}{F'(\kappa_n)}$$
$$+e^{ik'x}\int_0^\infty\left[\frac{\cosh\alpha'(\eta-\xi)e^{-\beta' y}}{\mu\alpha'\sinh\alpha'\eta+\mu'\beta'\cosh\alpha'\eta}-\frac{\cosh\alpha'(\eta-\xi)e^{\beta' y}}{\mu\alpha'\sinh\alpha'\eta-\mu'\beta'\cosh\alpha'\eta}\right]e^{-xY}i\,dY=0, \tag{32}$$

in which κ_n, α_1, β_1, α', β' have the same meanings as those in (21). The integral of the type (16) becomes

$$\int_0^\infty \frac{e^{-ifx}\{e^{\alpha(\eta-\xi)}+e^{-\alpha(\eta-\xi)}\}e^{-\beta y}}{(\mu\alpha+\mu'\beta)e^{\alpha\eta}-(\mu\alpha-\mu'\beta)e^{-\alpha\eta}}\,df$$
$$-\int_{-\infty}^0 \frac{e^{-Yx}\{e^{i\sqrt{Y^2+k^2}(\eta-\xi)}+e^{-i\sqrt{Y^2+k^2}(\eta-\xi)}\}e^{-i\sqrt{Y^2+k'^2}y}\,dY}{(\mu\sqrt{Y^2+k^2}+\mu'\sqrt{Y^2+k'^2})e^{i\sqrt{Y^2+k^2}(\eta-\xi)}-(\mu\sqrt{Y^2+k^2}+\mu'\sqrt{Y^2+k'^2})e^{-i\sqrt{Y^2+k^2}(\eta-\xi)}}=0. \tag{33}$$

Adding (32) and (33) and remembering (30), we get

$$v'=\sum_n 8\mu i e^{i(\kappa_n x-pt)}\frac{\cos\sqrt{k^2-\kappa_n^2}(\eta-\xi)e^{-\sqrt{\kappa_n^2-k'^2}\,y}}{F'(\kappa_n)}$$
$$-\frac{2\mu i e^{i(k'x-pt)}}{\pi}\int_0^\infty \frac{\{\mu\alpha'\sinh\alpha'\eta\sinh\beta'\eta+\mu'\beta'\cosh\alpha'\eta\cosh\beta' y\}\cosh\alpha'(\eta-\xi)}{(\mu'\beta')^2\cosh^2\alpha'\eta-(\mu\alpha')^2\sinh^2\alpha'\eta}\,e^{-xY}dY. \tag{34}$$

To get the approximate integral of the second term of this expression we use the relation (24) under the condition that x is large and y is small. Then the integral reduces to

$$i^{\frac{1}{2}}\int_0^\infty \frac{(\mu'\cos\sqrt{k^2-k'^2}\eta-\mu\sqrt{k^2-k'^2}y\sin\sqrt{k^2-k'^2}\eta)\cos\sqrt{k^2-k'^2}(\eta-\xi)}{i\mu'^2 2k'Y\cos^2\sqrt{k^2-k'^2}\eta-\mu^2(k^2-k'^2)\sin^2\sqrt{k^2-k'^2}\eta}\,e^{-xY}\sqrt{2k'Y}\,dY. \tag{35}$$

This becomes in virtue of (26)

$$i^{\frac{1}{2}}\sqrt{\frac{\pi k'}{2}}\,\frac{(\mu'\cos\sqrt{k^2-k'^2}\eta-\mu\sqrt{k^2-k'^2}y\sin\sqrt{k^2-k'^2}\eta)\cos\sqrt{k^2-k'^2}\eta}{-\mu^2(k^2-k'^2)\sin^2\sqrt{k^2-k'^2}\eta}\,\frac{1}{x^{3/2}}+\cdots\cdots. \tag{35'}$$

Substituting (35′) in (34) we arrive at

$$v'=\sum_n 8e^{i\left(\kappa_n x-pt+\frac{\pi}{2}\right)}\frac{\mu\cos\sqrt{k^2-\kappa_n^2}(\eta-\xi)e^{-\sqrt{\kappa_n^2-k'^2}\,y}}{F'(\kappa_n)}$$
$$-\sqrt{\frac{2k'}{\pi}}\,e^{i\left(k'x-pt-\frac{\pi}{4}\right)}$$

$$\cdot\frac{(\mu'\cos\sqrt{k^2-k'^2}\eta-\mu\sqrt{k^2-k'^2}y\sin\sqrt{k^2-k'^2}\eta)\cos\sqrt{k^2-k'^2}(\eta-\xi)}{\mu(k^2-k'^2)\sin^2\sqrt{k^2-k'^2}\eta}\frac{1}{x^{3/2}}+\cdots\cdots.$$

$$[x>0] \qquad (36)$$

It is a suitable occasion to compare the expression (27), (29), (29′), (36) giving displacements v at the surface, v for $y+\xi<0$, v for $y+\xi>0$, and v' in some particular cases of coordinates. Let us denote v at the surface by $v_{0l}+v_{0s}$, v at $y+\xi<0$ by $v_{1l}+v_{1s}$, v at $y+\xi>0$ by $v_{2l}+v_{2s}$, where v_{0l}, v_{1l}, v_{2l} correspond to displacements of Love-waves and v_{0s}, v_{1s}, v_{2s} those of pure distortional waves. Similarly, v_l' and v_s' are to be displacements of Love-waves and pure distortional waves at $y>0$. The comparison between these displacements gives us

$$y=-\eta\,; \quad v_{0l}=v_{1l}, \quad v_{0s}=v_{1s}, \quad \frac{\partial v_{0l}}{\partial y}=\frac{\partial v_{1l}}{\partial y}, \quad \frac{\partial v_{0s}}{\partial y}=\frac{\partial v_{1s}}{\partial y}\,;$$

$$y=-\xi\,; \quad v_{1l}=v_{2l}, \quad v_{1s}=v_{2s}, \quad \frac{\partial v_{1l}}{\partial y}=\frac{\partial v_{2l}}{\partial y}, \quad \frac{\partial v_{1s}}{\partial y}=\frac{\partial v_{2s}}{\partial y}\,;$$

$$y=0\,; \quad v_{2l}=v_l', \quad v_{2s}=v_s', \quad \mu\frac{\partial v_{2l}}{\partial y}=\mu'\frac{\partial v_l'}{\partial y}, \quad \mu\frac{\partial v_{2s}}{\partial y}=\mu'\frac{\partial v_s'}{\partial y}.$$

It should be borne in mind that the condition, $y=-\xi\,;\ \partial v_{1l}/\partial y=\partial v_{2l}/\partial y$, is obtained by the relation that

$$\frac{\mu'\sqrt{\kappa_n^2-k'^2}}{\mu\sqrt{k^2-\kappa_n^2}}=\frac{\sin\sqrt{k^2-\kappa_n^2}\eta}{\cos\sqrt{k^2-\kappa_n^2}\eta},$$

which is the characteristic equation of Love-waves to determine κ_n.

It will be confirmed from each first term of the expressions (29), (29′), (36) that the displacements of the motion with the velocity of transmission of pure distortional waves are not of the type of bodily waves but resembles superficial waves with amplitude which is maximum at the free surface and decreases in the interior of the body at least within the stratum. This is apparently curious in the case of bodily waves. It is still impossible to explain the fact that the amplitudes of the same waves decrease inversely as 3/2 th power of the epicentral distance even at a range where the energy of transmission of Love-waves becomes stationary. The equation (36) indicates that the bodily waves of v' having the velocity of distortional waves does not satisfy the equation of motion, so that it is not certain that the waves in question exist even from mathematical point of view. The similar uncertainty seems to exist in bodily waves accompanying Rayleigh-waves.[7]

---

[7] H. LAMB, H. NAKANO, T. SAKAI, K. SEZAWA, G. NISHIMURA, *loc. cit.* in foot-notes 4), 5), 6).

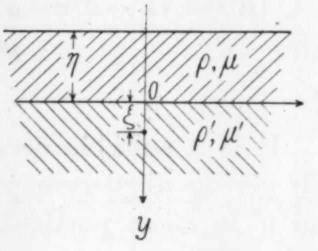

Fig. 3.

3. The case where a point source generating distortional waves lies within the subjacent medium will now be studied. Let the depth of the seismic origin from the free surface be $\eta+\xi$. The displacement of the waves generated from the origin is expressed by

$$v_0=e^{-ipt}H_0^{(1)}(k'r), \tag{37}$$

where $r^2=x^2+(y-\xi)^2$ and $k'^2=\rho'p^2/\mu'$. It is possible to write

$$\left.\begin{aligned} H_0^{(1)}(k'r)&=\frac{1}{\pi}\int_{-\infty}^{\infty}\frac{e^{\beta(y-\xi)+ifx}}{\beta}\,df, \qquad [y<\xi] \\ H_0^{(1)}(k'r)&=\frac{1}{\pi}\int_{-\infty}^{\infty}\frac{e^{-\beta(y-\xi)+ifx}}{\beta}\,df, \qquad [y>\xi] \end{aligned}\right\} \tag{38}$$

provided $\beta=\sqrt{f^2-k'^2}$. From (1) and (2) we find

$$v_0=\frac{e^{-ipt}}{\pi}\int_{-\infty}^{\infty}\frac{e^{ifx+\beta(y-\xi)}}{\beta}\,df, \qquad [y<\xi] \tag{39}$$

$$v_0=\frac{e^{-ipt}}{\pi}\int_{-\infty}^{\infty}\frac{e^{ifx+\beta(y-\xi)}}{\beta}\,df. \qquad [y>\xi] \tag{40}$$

The expression (39) gives the displacement of primary wave propagated upwards and (40) that of waves transmitted downwards. It is shown that, if waves of the type:

$$V_0=\phi(ifx+\beta y-ipt) \tag{41}$$

are transmitted in the lower medium and incident on the boundary surface between the lower medium and the stratum, the reflected waves V from this surface and the refracted waves V_1 in the stratum are expressed by

$$\left.\begin{aligned} V&=q'\phi(ifx-\beta y-ipt), \\ V_1&=\tau'\phi(ify+\alpha y-ipt), \end{aligned}\right\} \tag{42}$$

where

$$q'=\frac{\mu'\beta-\mu\alpha}{\mu'\beta+\mu\alpha}, \qquad \tau'=\frac{2\mu'\beta}{\mu'\beta+\mu\alpha}, \tag{43}$$

in which $\alpha=\sqrt{f^2-k^2}$, $k^2=\rho p^2/\mu$. The refracted waves in the stratum make multiple reflection and refraction at two boundaries of the stratum in the similar manner as those in the preceding section. Thus, the resulting displacement of the stratum becomes

$$v=\frac{e^{-ipt}}{\pi}\int_{-\infty}^{\infty}\frac{\tau'}{\beta}\,e^{ifx-\beta\xi}\{e^{\alpha y}+e^{-\alpha(y+2\eta)}\}\{1+qe^{-2\alpha\eta}+q^2e^{-4\alpha\eta}+\cdots\}\,df, \tag{44}$$

where $q=(\mu\alpha-\mu'\beta)/(\mu\alpha+\mu'\beta)$. Rewriting this we have

$$v=\frac{e^{-ipt}}{\pi}\int_{-\infty}^{\infty}\frac{2\mu' e^{ifx-\beta\xi}\{e^{\alpha(\eta+y)}+e^{-\alpha(\eta+y)}\}}{(\mu\alpha+\mu'\beta)e^{\alpha\eta}-(\mu\alpha-\mu'\beta)e^{-\alpha\eta}}\,df. \tag{45}$$

Similarly the displacement in the lower medium is expressed by

$$\begin{aligned} v'=\frac{e^{-ipt}}{\pi}\int_{-\infty}^{\infty}\frac{e^{ifx-\beta\xi}}{\beta}\Bigg[&\frac{(\mu\alpha+\mu'\beta)\{e^{\alpha\eta+\beta y}+e^{-(\alpha\eta+\beta y)}\}}{(\mu\alpha+\mu'\beta)e^{\alpha\eta}} \\ &\frac{-(\mu\alpha-\mu'\beta)\{e^{\alpha\eta-\beta y}+e^{-(\alpha\eta-\beta y)}\}}{-(\mu\alpha-\mu'\beta)e^{-\alpha\eta}}\Bigg]df, \quad [y<\xi] \end{aligned} \tag{46}$$

$$\begin{aligned} v'=\frac{e^{-ipt}}{\pi}\int_{-\infty}^{\infty}\frac{e^{ifx-\beta y}}{\beta}\Bigg[&\frac{(\mu\alpha+\mu'\beta)\{e^{\alpha\eta+\beta\xi}+e^{-(\alpha\eta+\beta\xi)}\}}{(\mu\alpha+\mu'\beta)e^{\alpha\eta}} \\ &\frac{-(\mu\alpha-\mu'\beta)\{e^{\alpha\eta-\beta\xi}+e^{-(\alpha\eta-\beta\xi)}\}}{-(\mu\alpha-\mu'\beta)e^{-\alpha\eta}}\Bigg]df. \quad [y>\xi] \end{aligned} \tag{46'}$$

The expression (45) has a form similar to that of (13), so that the integral of (45) is readly written by

$$\begin{aligned} v=&\sum_n 8e^{i\left(\kappa_n x-pt+\frac{\pi}{2}\right)}\frac{\mu'\cos\sqrt{k^2-\kappa_n^2}(\eta-y)e^{-\sqrt{\kappa_n^2-k'^2}\xi}}{F'(\kappa_n)} \\ &-\sqrt{\frac{2k'}{\pi}}\,e^{i\left(k'x-pt-\frac{\pi}{4}\right)}\frac{\mu'}{\mu}\cdot \\ &\cdot\frac{(\mu'\cos\sqrt{k^2-k'^2}\eta-\mu\sqrt{k^2-k'^2}\sin\sqrt{k^2-k'^2}\eta)\cos\sqrt{k^2-k'^2}(\eta+y)}{\mu(k^2-k'^2)\sin^2\sqrt{k^2-k'^2}\eta}\frac{1}{x^{3/2}}+\cdots\cdots. \\ &\qquad [x>0] \end{aligned} \tag{47}$$

When we put $y=-\eta$ in this expression, we get the displacement at the surface as follows:

$$\begin{aligned} v=&\sum_n 8e^{i\left(\kappa_n x-pt+\frac{\pi}{2}\right)}\frac{\mu' e^{-\sqrt{\kappa_n^2-k'^2}\xi}}{F'(\kappa_n)} \\ &-\sqrt{\frac{2k'}{\pi}}\,e^{i\left(k'x-pt-\frac{\pi}{4}\right)}\frac{\mu'}{\mu}\frac{(\mu'\cos\sqrt{k^2-k'^2}\eta-\mu\sqrt{k^2-k'^2}\xi\sin\sqrt{k^2-k'^2}\eta)}{\mu(k^2-k'^2)\sin^2\sqrt{k^3-k'^2}\eta}\frac{1}{x^{3/2}}+\cdots\cdots. \\ &\qquad [x>0] \end{aligned} \tag{48}$$

The expression (46) may be transformed to

$$\begin{aligned} v'=\frac{e^{-ipt}}{\pi}\int_{-\infty}^{\infty}e^{ifx-\beta\xi}\Bigg[&\frac{\mu\alpha}{\beta}\frac{\{e^{\alpha\eta+\beta y}+e^{-(\alpha\eta+\beta y)}-e^{\alpha\eta-\beta y}-e^{-(\alpha\eta-\beta y)}\}}{(\mu\alpha+\mu'\beta)e^{\alpha\eta}-(\mu\alpha-\mu'\beta)e^{-\alpha\eta}} \\ &+\frac{\mu'\{e^{\alpha\eta+\beta y}+e^{-(\alpha\eta+\beta y)}+e^{\alpha\eta-\beta y}+e^{-(\alpha\eta-\beta y)}\}}{(\mu\alpha+\mu'\beta)e^{\alpha\eta}-(\mu\alpha-\mu'\beta)e^{-\alpha\eta}}\Bigg]df. \quad [y<\xi] \end{aligned} \tag{49}$$

To evaluate this expression we consider two integrals (15) and (16), where

$$\begin{aligned} \chi(Z)=2\mu e^{-\sqrt{Z^2-k'^2}}\frac{\sqrt{Z^2-k^2}}{\sqrt{Z^2-k'^2}}\{&\cosh(\sqrt{Z^2-k^2}\eta+\sqrt{Z^2-k'^2}y) \\ &-\cosh(\sqrt{Z^2-k^2}\eta-\sqrt{Z^2-k'^2}y)\} \end{aligned}$$

$$+2\mu' e^{-\sqrt{Z^2-k'^2}}\{\cosh(\sqrt{Z^2-k^2}\eta+\sqrt{Z^2-k'^2}y)$$
$$+\cosh(\sqrt{Z^2-k^2}\eta-\sqrt{Z^2-k'^2}y)\}, \tag{50}$$

taken round contours in Fig. 2. Proceeding in the same manner as in preceding cases, we find

$$v'=\sum_n 8e^{i\left(\kappa_n x-pt+\frac{\pi}{2}\right)}\frac{\mu'\cos\sqrt{k^2-\kappa_n^2}\eta\,(\cos\sqrt{\kappa_n^2-k'^2}y-\sin\sqrt{\kappa_n^2-k'^2}y)e^{-\sqrt{\kappa_n^2-k'^2}\xi}}{F'(\kappa_n)}$$
$$-\sqrt{\frac{2k'}{\pi}}\,e^{i\left(k'x-pt-\frac{\pi}{4}\right)}\cdot$$
$$\cdot\left\{\frac{\mu'}{\mu}\frac{(\mu'\cos\sqrt{k^2-k'^2}\eta-\mu\sqrt{k^2-k'^2}\xi\sin\sqrt{k^2-k'^2}\eta)\cos\sqrt{k^2-k'^2}\eta}{\mu(k^2-k'^2)\sin^2\sqrt{k^2-k'^2}\eta}\right.$$
$$\left.-\frac{\mu'\cos\sqrt{k^2-k'^2}\eta-\mu\sqrt{k^2-k'^2}\xi\sin\sqrt{k^2-k'^2}\eta}{\mu\sqrt{k^2-k'^2}\sin\sqrt{k^2-k'^2}\eta}\,y\right\}\frac{1}{x^{3/2}}+\cdots\cdot$$
$$[x>0,\ y<\xi] \tag{51}$$

In the same manner of mathematical treatment we obtain the displacement for $y>\xi$ as follows:

$$v'=\sum_n 8e^{i\left(\kappa_n x-pt+\frac{\pi}{2}\right)}\frac{\mu'\cos\sqrt{k^2-\kappa_n^2}\eta\,(\cos\sqrt{\kappa_n^2-k'^2}\xi-\sin\sqrt{\kappa_n^2-k'^2}\xi)e^{-\sqrt{\kappa_n^2-k'^2}\eta}}{F'(\kappa_n)}$$
$$-\sqrt{\frac{2k'}{\pi}}\,e^{i\left(k'x-pt-\frac{\pi}{4}\right)}\left\{\frac{\mu'}{\mu}\frac{(\mu'\cos\sqrt{k^2-k'^2}\eta-\mu\sqrt{k^2-k'^2}y\sin\sqrt{k_2-k'^2}\eta)\cos\sqrt{k^2-k'^2}\eta}{\mu(k^2-k'^2)\sin^2\sqrt{k^2-k'^2}\eta}\right.$$
$$\left.-\frac{\mu'\cos\sqrt{k^2-k'^2}\eta-\mu\sqrt{k^2-k'^2}y\sin\sqrt{k^2-k'^2}\eta}{\mu\sqrt{k^2-k'^2}\sin\sqrt{k^2-k'^2}\eta}\,\xi\right\}\frac{1}{x^{3/2}}+\cdots\cdot$$
$$[x>0,\ y>\xi] \tag{51'}$$

Comparison between (47), (51), (51′) indicates the existence of the relations:

$$y=-\eta;\quad \frac{\partial v_{0l}}{\partial y}=0,\quad \frac{\partial v_{0s}}{\partial y}=0;$$
$$y=0;\quad v_l=v_{1l}',\quad v_s=v_{1s}',\quad \mu\frac{\partial v_l}{\partial y}=\mu'\frac{\partial v_{1l}'}{\partial y},\quad \mu\frac{\partial v_s}{\partial y}=\mu'\frac{\partial v_{1s}'}{\partial y},$$
$$y=\xi;\quad v_{1l}'=v_{2l}',\ v_{1s}'=v_{2s}',\quad \frac{\partial v_{1l}'}{\partial y}=\frac{\partial v_{2l}'}{\partial y},\quad \frac{\partial v_{1s}'}{\partial y}=\frac{\partial v_{2s}'}{\partial y},$$

where v_{1l}', v_{2l}', v_{1s}', v_{2s}' denote displacements due to Love-waves and pure bodily waves for $y<\xi$ and $y>\xi$ respectively.

4. When the seismic origin comes to a point on the boundary surface between the stratum and the subjacent medium, it is able to put $\xi=0$. Then, from (29), (29′), (36) we get

$$v=\sum_n 8e^{i\left(\kappa_n x-pt+\frac{\pi}{2}\right)}\frac{\mu\cos\sqrt{k^2-\kappa_n^2}(\eta+y)}{F'(\kappa_n)}$$

$$-\sqrt{\frac{2k'}{\pi}}\,e^{i\left(k'x-pt-\frac{\pi}{4}\right)}\,\frac{\mu'}{\mu}\,\frac{\cos\sqrt{k^2-k'^2}\,\eta\,\cos\sqrt{k^2-k'^2}\,(\eta+y)}{(k^2-k'^2)\sin^2\sqrt{k^2-k'^2}\,\eta}\,\frac{1}{x^{3/2}}+\cdots,$$

$$[x>0,\ y<0] \qquad (52)$$

$$v'=\sum_n 8e^{i\left(\kappa_n x-pt+\frac{\pi}{2}\right)}\,\frac{\mu\cos\sqrt{k^2-k'^2}\,\eta\;e^{-\sqrt{\kappa_n{}^2-\kappa'^2}\,y}}{F'(\kappa_n)}$$

$$-\sqrt{\frac{2k'}{\pi}}\,e^{i\left(k'x-pt+\frac{\pi}{4}\right)}\,.$$

$$\cdot\frac{(\mu'\cos\sqrt{k^2-k'^2}\,\eta-\mu\sqrt{k^2-k'^2}\,y\,\sin\sqrt{k^2-k'^2}\,\eta)\cos\sqrt{k^2-k'^2}\,\eta}{\mu(k^2-k'^2)\sin^2\sqrt{k^2-k'^2}\,\eta}\,\frac{1}{x^{3/2}}+\cdots.$$

$$[x>0,\ y>0] \qquad (53)$$

From (47), (51), (51′) we find

$$v=\frac{\mu'}{\mu}\sum_n 8e^{i\left(\kappa_n x-pt+\frac{\pi}{2}\right)}\,\frac{\mu\cos\sqrt{k^2-\kappa_n^2}\,(\eta+y)}{F'(\kappa_n)}$$

$$-\frac{\mu'}{\mu}\sqrt{\frac{2k'}{\pi}}\,e^{i\left(\kappa'x-pt-\frac{\pi}{4}\right)}\,\frac{\mu'}{\mu}\,\frac{\cos\sqrt{k^2-k'^2}\,\eta\,\cos\sqrt{k^2-k'^2}\,(\eta+y)}{(k^2-k'^2)\sin^2\sqrt{k^2-k'^2}\,\eta}\,\frac{1}{x^{3/2}}+\cdots,$$

$$[x>0,\ y<0] \qquad (54)$$

$$v'=\frac{\mu'}{\mu}\sum_n 8e^{i\left(\kappa_n x-pt+\frac{\pi}{2}\right)}\,\frac{\mu\cos\sqrt{k^2-\kappa_n^2}\,\eta\;e^{-\sqrt{\kappa_n{}^2-k'^2}\,y}}{F'(\kappa_n)}$$

$$-\frac{\mu'}{\mu}\sqrt{\frac{2k'}{\pi}}\,e^{i\left(k'x-pt-\frac{\pi}{4}\right)}\,.$$

$$\cdot\frac{(\mu'\cos\sqrt{k^2-k'^2}\,\eta-\mu\sqrt{k^2-k'^2}\,y\,\sin\sqrt{k^2-k'^2}\,\eta)\cos\sqrt{k^2-k'^2}\,\eta}{\mu(k^2-k'^2)\sin^2\sqrt{k^2-k'^2}\,\eta}\,\frac{1}{x^{3/2}}+\cdots.$$

$$[x>0,\ y>0] \qquad (55)$$

It will be seen from (52), (53), (54), (55) that v, v' due to seismic disturbance from the source in the subjacent medium are μ'/μ times those due to the one from the origin in the stratum. As the movements at the origin have been assumed equal for both cases, the stresses due to the disturbance of the former case should be μ'/μ times those due to the one of the latter case.

5. We are now to solve a three-dimensional problem where a point source lying within the stratum generates distortional waves with amplitudes oriented horizontally perpendicular to the direction of propagation. Let the axes of r, z be taken as shown in the sketch. The displacement of waves generated from the origin is written by

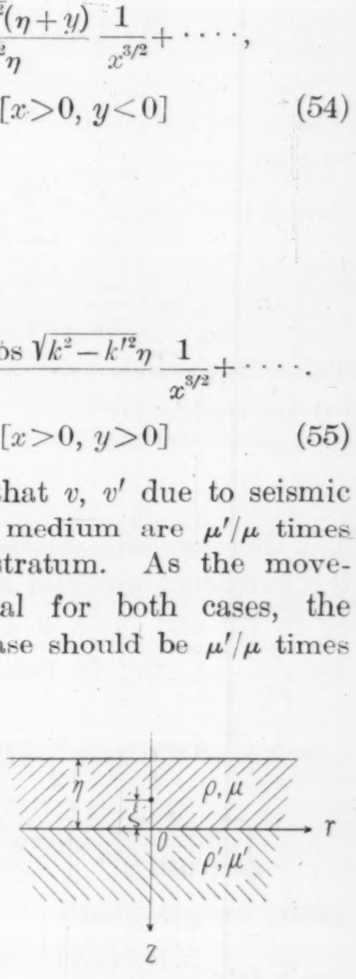

Fig. 4.

$$v_0=e^{-ipt}\frac{\partial}{\partial r}\frac{e^{ikR}}{R}, \tag{56}$$

where $R^2=r^2+(z+\xi)^2$ and $k^2=\rho p^2/\mu$. It is possible to write

$$\left.\begin{aligned}\frac{e^{ikR}}{R}&=\int_0^\infty\frac{e^{\alpha(z+\xi)}}{\alpha}J_0(fr)f\,df, \qquad [z<-\xi]\\ \frac{e^{ikR}}{R}&=\int_0^\infty\frac{e^{-\alpha(z+\xi)}}{\alpha}J_0(fr)f\,df, \qquad [z>-\xi]\end{aligned}\right\} \tag{57}$$

provided $\alpha=\sqrt{f^2-k^2}$. From (56) and (57) we obtain

$$v_0=e^{-ipt}\int_0^\infty\frac{e^{\alpha(z+\xi)}}{\alpha}\frac{\partial J_0(fr)}{\partial r}f\,df, \qquad [z<-\xi] \tag{58}$$

$$v_0=e^{-ipt}\int_0^\infty\frac{e^{-\alpha(z+\xi)}}{\alpha}\frac{\partial J_0(fr)}{\partial r}f\,df. \qquad [z>-\xi] \tag{59}$$

Now, we know that

$$\begin{aligned}J_0(fr)&=\frac{2}{\pi}\int_0^\infty\sin(fr\cosh j)\,dj\\ &=\frac{1}{i\pi}\int_0^\infty e^{ifr\cosh j}dj-\frac{1}{i\pi}\int_0^\infty e^{-ifr\cosh j}\,dj,\end{aligned} \tag{60}$$

so that

$$v_0=\frac{\partial}{\partial r}\frac{e^{-ipt}}{\pi i}\int_0^\infty dj\int_{-\infty}^\infty\frac{e^{\alpha(z+\xi)}}{\alpha}e^{ifr\cosh j}f\,df, \qquad [z<-\xi] \tag{61}$$

$$v_0=\frac{\partial}{\partial r}\frac{e^{-ipt}}{\pi i}\int_0^\infty dj\int_{-\infty}^\infty\frac{e^{-\alpha(z+\xi)}}{\alpha}e^{ifr\cosh j}f\,df. \qquad [z>-\xi] \tag{62}$$

These equations are equal to the respective products of (3) as well as (4) by the factor

$$\frac{\partial}{\partial r}\frac{1}{i}\int_0^\infty dj\cdot f, \tag{63}$$

and therefore the solutions of all waves propagated in the stratum and the subjacent medium are readily obtained by putting $f\cdot df$ in place of df in (3) and (4) and afterwards by multiplying the resulting solutions by $\frac{\partial}{\partial r}\frac{1}{i}\int_0^\infty dj$. In the evaluation of integral use has been made of

$$\left.\begin{aligned}&\frac{1}{i}\int_0^\infty e^{i\xi\cosh j}\,dj=\frac{\pi}{2}H_0^{(1)}(\xi),\\ &\frac{1}{i}\int_0^\infty\frac{e^{i\xi\cosh j}}{(\cosh j)^{3/2}}\,dj=e^{-i\left(\xi+\frac{3\pi}{2}\right)}\sqrt{\frac{\pi}{2\xi}}\left(1+\frac{7}{4}\,i\,\frac{1}{2\xi}-\frac{15}{8}\frac{1.3}{4\xi^2}+\cdots\right).\end{aligned}\right\} \tag{64}$$

Thus, we get finally

$$v=\sum_n 4\pi\kappa_n\frac{\partial H_0^{(1)}(\kappa_n r)}{\partial r}e^{-i\left(pt-\frac{\pi}{2}\right)}.$$

$$\cdot\frac{\{\mu\sqrt{k^2-\kappa_n^2}\cos\sqrt{k^2-\kappa_n^2}\xi+\mu'\sqrt{\kappa_n^2-k^2}\sin\sqrt{k^2-\kappa_n^2}\xi\}\cos\sqrt{k^2-\kappa_n^2}(\eta+z)}{\sqrt{k^2-\kappa_n^2}\,F'(\kappa_n)}$$

$$+k'^2e^{i\left(k'r-pt+\frac{\pi}{2}\right)}\frac{\mu'}{\mu}\frac{\cos\sqrt{k^2-k'^2}(\eta-\xi)\cos\sqrt{k^2-k'^2}(\eta+z)}{(k^2-k'^2)\sin^2\sqrt{k^2-k'^2}\eta}\frac{1}{r^2}+\cdots,$$

$$[y+z<0] \qquad (65)$$

$$v=\sum_n 4\pi\kappa_n\frac{\partial H_0^{(1)}(\kappa_n r)}{\partial r}e^{-i\left(pt-\frac{\pi}{2}\right)}.$$

$$\cdot\frac{\{\mu\sqrt{k^2-\kappa_n^2}\cos\sqrt{k^2-\kappa_n^2}z-\mu'\sqrt{\kappa_n^2-k'^2}\sin\sqrt{k^2-\kappa_n^2}z\}\cos\sqrt{k^2-\kappa_n^2}(\eta-\xi)}{\sqrt{k^2-\kappa_n^2}\,F'(\kappa_n)}$$

$$+k'^2e^{i\left(k'r-pt+\frac{\pi}{2}\right)}\frac{\mu'}{\mu}\frac{\cos\sqrt{k^2-k'^2}(\eta-\xi)\cos\sqrt{k^2-k'^2}(\eta+z)}{(k^2-k'^2)\sin^2\sqrt{k^2-k'^2}\eta}\frac{1}{r^2}+\cdots,$$

$$[y+z>0] \qquad (65')$$

$$v'=\sum_n 4\pi\kappa_n\frac{\partial H_0^{(1)}(\kappa_n r)}{\partial r}e^{-i\left(pt-\frac{\pi}{2}\right)}\frac{\mu\sqrt{k^2-\kappa_n^2}\cos\sqrt{k^2-\kappa_n^2}(\eta-\xi)\,e^{-\sqrt{\kappa_n{}^2-k'^2}z}}{\sqrt{k^2-\kappa_n^2}\,F'(\kappa_n)}$$

$$+k'^2e^{i\left(k'r-pt+\frac{\pi}{2}\right)}\frac{(\mu'\cos\sqrt{k^2-k'^2}\eta-\mu\sqrt{k^2-k'^2}z\sin\sqrt{k^2-k'^2}\eta)\cos\sqrt{k^2-k'^2}(\eta-\xi)}{\mu(k^2-k'^2)\sin^2\sqrt{k^2-k'^2}\eta}\frac{1}{r^2}$$

$$+\cdots. \qquad (66)$$

The first term of the right-hand side of each expression of (65), (65′), (66) represents Love-waves, while the second one gives pure distortional waves transmitted with the velocity proper to the subjacent medium. The amplitudes of Love-waves vary inversely as the square root of the epicentral distance, while those of bodily waves as the inverse square of the same distance.

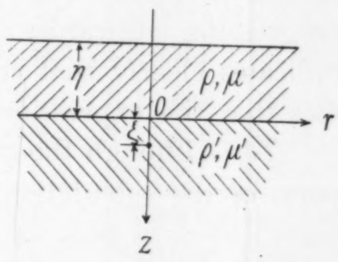

Fig. 5.

6. In a similar manner it is possible to determine the three-dimensional problem of wave motion due to a seismic origin residing in the lower medium. Thus, we obtain

$$v=\sum_n 4\pi\kappa_n\frac{\partial H_0^{(1)}(\kappa_n r)}{\partial r}e^{-i\left(pt-\frac{\pi}{2}\right)}\frac{\mu'\cos\sqrt{k^2-\kappa_n^2}(\eta+z)e^{-\sqrt{\kappa_n{}^2-k'^2}\xi}}{F'(\kappa_n)}$$

$$+k'^2e^{-i\left(k'r-pt+\frac{\pi}{2}\right)}\frac{\mu'}{\mu}.$$

$$\cdot\frac{(\mu'\cos\sqrt{k^2-k'^2}\eta-\mu\sqrt{k^2-k'^2}\xi\sin\sqrt{k^2-k'^2}\eta)\cos\sqrt{k^2-k'^2}(\eta+z)}{\mu(k^2-k'^2)\sin^2\sqrt{k^2-k'^2}\eta}\frac{1}{r^2}$$

$$+\cdots, \qquad (67)$$

$$v'=\sum_n 4\pi\kappa_n\frac{\partial H_0^{(1)}(\kappa_n r)}{\partial r}e^{-i\left(pt-\frac{\pi}{2}\right)}.$$

$$\cdot\frac{\mu'\cos\sqrt{k^2-\kappa_n^2}\eta\,(\cos\sqrt{\kappa_n^2-k'^2}z-\sin\sqrt{\kappa_n^2-k'^2}z)e^{-\sqrt{\kappa_n^2-k'^2}\xi}}{F'(\kappa_n)}$$

$$+k'^2e^{i\left(k'r-pt+\frac{\pi}{2}\right)}\left\{\frac{\mu'}{\mu}\frac{(\mu'\cos\sqrt{k^2-k'^2}\eta-\mu\sqrt{k^2-k'^2}\xi\sin\sqrt{k^2-k'^2}\eta)\cos\sqrt{k^2-k'^2}\eta}{\mu(k^2-k'^2)\sin^2\sqrt{k^2-k'^2}\eta}\right.$$

$$\left.-\frac{\mu'\cos\sqrt{k^2-k'^2}\eta-\mu\sqrt{k^2-k'^2}\xi\sin\sqrt{k^2-k'^2}\eta}{\mu\sqrt{k^2-k'^2}\sin\sqrt{k^2-k'^2}\eta}z\right\}\frac{1}{r^2}+\cdots,$$

$$[z<\xi] \qquad (68)$$

$$v'=\sum_n 4\pi\kappa_n\frac{\partial H_0^{(1)}(\kappa_n r)}{\partial r}e^{-i\left(pt-\frac{\pi}{2}\right)}.$$

$$\cdot\frac{\mu'\cos\sqrt{k^2-\kappa_n^2}\eta(\cos\sqrt{\kappa_n^2-k'^2}\xi-\sin\sqrt{\kappa_n^2-k'^2}\xi)e^{-\sqrt{\kappa_n^2-k'^2}z}}{F'(\kappa_n)}$$

$$+k'^2e^{i\left(k'r-pt+\frac{\pi}{2}\right)}\left\{\frac{\mu'}{\mu}\frac{(\mu'\cos\sqrt{k^2-k'^2}\eta-\mu\sqrt{k^2-k'^2}z\sin\sqrt{k^2-k'^2}\eta)\cos\sqrt{k^2-k'^2}\eta}{\mu(k^2-k'^2)\sin^2\sqrt{k^2-k'^2}\eta}\right.$$

$$\left.-\frac{\mu'\cos\sqrt{k^2-k'^2}\eta-\mu\sqrt{k^2-k'^2}z\sin\sqrt{k^2-k'^2}\eta}{\mu\sqrt{k^2-k'^2}\sin\sqrt{k^2-k'^2}\eta}\xi\right\}\frac{1}{r^2}+\cdots.$$

$$[z>\xi] \qquad (68')$$

The nature of the problem is the same as that of the two-dimensional one. It is a very difficult question why the energy of bodily waves involved in an annular area decreases with epicentral distance in spite of the existence of the conservation of energy of Love-waves which are progressing outwards. The part of v' corresponding to bodily waves indicates clearly that such waves are not possible to exist owing to the fact that the expression does not satisfy the equation of motion.

7. Although the general results were too well explained in respective parts of the calculation to warrant summarizing here, it is not without significance to pick up some important ones.

As already mentioned, there are two kinds of waves that are generated from a seismic origin having horizontal displacements. One of them corresponds to Love-type waves and the other pure distortional waves having the proper velocity peculiar to the lower medium. The displacement of Love-type waves varies as a certain negative exponential function of the depth when the origin is in the lower medium, but it varies as some harmonic function of the depth when the origin resides in the stratum. The distribution of displacements of pure distortional waves in the body is somewhat similar to that of surface waves, but the variation of amplitudes according to the depth of the origin is different; even when the depth of the seismic origin is very large, the diminution of displacement at the surface is not remarkable. The law of decrease of displacements of this type of waves with the increase of the epicentral distance is the same as that of bodily waves accompanying Rayleigh-waves; the displacement decreases inversely as 3/2th power of the epicentral distance in the two-dimensional problem and as the square of the same distance in the three-dimensional one, but this encounters contradiction with the principle of the conservation of energy of waves owing to the fact that the energy of surface waves is not changed in progressing outwards and also that the distribution of amplitudes of bodily waves for different depth is the same at any epicentral distance. Moreover, the expressions of displacements corresponding to these bodily waves do not satisfy the equations of motion. If this be the case, we are not yet now in position to explain the smallness of amplitudes of bodily waves from the basis of the present result; another paper8) appears to confirm the true nature of the amplitudes of this kind of waves.

1. 深さのある震源から發生するラブ波

地震研究所 **妹 澤 克 惟**

表層がある半無限固體中に水平變位だけの震動原點があるとき，それによつて生ずる横波及びラブ波の性質をしらべてみた．波動は波の反射及び屈折を正確に考へて算出したものである．原點が表面層中にあるときは勿論ラブ波を發生するけれども，原點が下層の中にある場合でも僅かであるがラブ波の出ることがわかつた．このラブ波に伴つて遠い震央距離に現れる横波は計算上では震央距離の二乘に反比例して振幅が小さくなることになる．これは常識でわかるやうに距離の一乘に反比例することと矛盾してゐるやうに思はれたので，固體中のすべての深さに於ける振幅の解を出して見たところがその解は彈性體の振動方程式を滿足しないことがわかつた．これは恐らく計算中に現れる函數論の分岐點の應用に不充分な所があつた爲と思はれる．果してそうであるとするとラムがその中年に出したレーレー波に伴ふ固體波の問題にも多少の疑がないとはいはれない．固體波の振幅の問題は次に現れる論文のやうな行方で出るものと思ふ．固體波の問題にはこのやうな疑があるけれどもラブ波については何等の問題はないと思ふ．筆者は數年前に同じ問題を別の解法で出したことがあるが，その結果は只今の結果とよく一致してゐるのである．

---

8) K. SEZAWA and K. KANAI, "Periods and Amplitudes of Oscillations in L- and M-phases," *Bull. Earthq. Res. Inst.*, 13 (1935), 18.

2. *Periods and Amplitudes of Oscillations in L- and M-phases.*

7

By Katsutada SEZAWA and Kiyoshi KANAI,

Earthquake Research Institute.

(Read Oct. 16 & Dec. 18, 1934.—Received Dec. 20, 1934.)

1. It is a well known fact that in L-phase of seismic waves oscillations of longer periods and of relatively smaller amplitudes are predominant, while in M-phase the periods become rather smaller and the amplitudes are frequently very large. It appears recognized that L- and M-phases are equivalent in the majority of cases to those of oscillations due to Love- and Rayleigh-waves respectively. For this purpose we have calculated the displacement distribution of Love-waves in the media, through which they are transmitted, and compared the result with the similar data obtained in our preceding paper[1] concerning Rayleigh-waves, and also with the known nature of bodily waves.

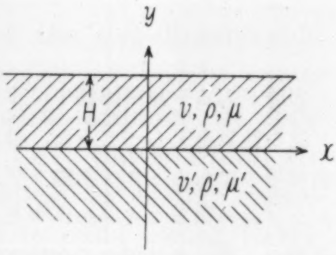

Fig. 1.

2. The method of finding solutions of Love-waves is too well established to explain here. In the case of a one-stratified body the characteristic equation[2] to determine the velocity of transmisson is expressed by

$$\tan\sqrt{k^2-f^2}\,H=\frac{\mu'\sqrt{f^2-k'^2}}{\mu\sqrt{k^2-f^2}},\tag{1}$$

where $k^2=\rho p^2/\mu$, $k'^2=\rho' p^2/\mu'$, $2\pi/f=L=$wave length, $2\pi/p=T=$period, $H=$thickness of the stratum, $\rho, \rho', \mu, \mu'=$densities and rigidities of the stratum and the subjacent medium. The equations of displacement are expressed by

$$\left.\begin{aligned} v&=\frac{A\cos\{\sqrt{k^2-f^2}(H-y)\}\cos(pt-fx)}{\cos\sqrt{k^2-f^2}H},\\ v'&=Ae^{\sqrt{f^2-k'^2}y}\cos(pt-fx), \end{aligned}\right\}\tag{2}$$

where v, v' are displacements in the stratum and in the subjacent medium respectively. The relation between L/H and the velocity p/f for

---

[1] K. SEZAWA and K. KANAI, "Amplitudes of Dispersive Rayleigh-waves at Different Depths of a Body," *Bull. Earthq. Res. Inst.*, 12 (1934), 641.

[2] A. E. H. LOVE, *Some Problems of Geodynamics*, (Cambridge, 1911), 162.

$\mu'/\mu=\infty$, 5, 3, 2, 1·1 are indicated in Fig. 2. The ratios of displacements at depths $\frac{1}{4}H$, $\frac{1}{2}H$, $\frac{3}{4}H$, H from the surface to the one at that surface for $\mu'/\mu=\infty$, 5, 3, 2, 1·1 are plotted in Figs. 3, 4, 5, 6, 7.

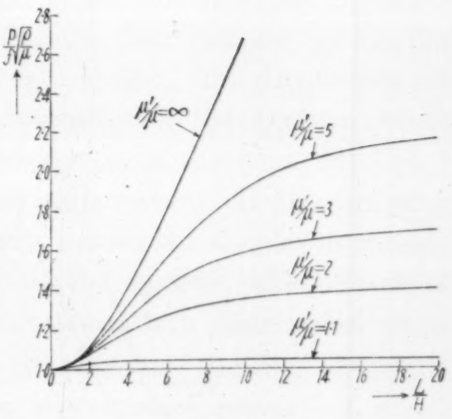

Fig. 2

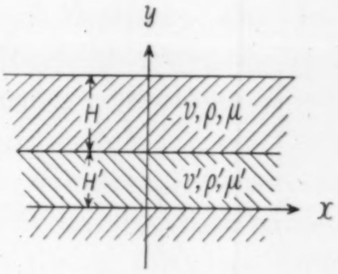

Fig. 8.

3. The case, where there are two superficial layers, was studied independently by Matuzawa[3] and Stoneley[4] and their solutions are not difficult to deduce here. But, in the present case we consider a simplest problem in which the lowest medium is infinitely rigid, so that the boundary conditions are simply denoted by $y=0$, $v'=0$; $y=H'$, $v'=v$, $\mu'\partial v'/\partial y=\mu\partial v/\partial y$; $y=H+H'$, $\partial v/\partial y=0$. We, thus, find the characteristic equation to determine the velocity of transmission as follows:

$$\tanh\sqrt{f^2-k'^2}H'\tan\sqrt{k^2-f^2}H=\frac{\mu'\sqrt{f^2-k'^2}}{\mu\sqrt{k^2-f^2}}, \tag{3}$$

where H, H' are thicknesses of the upper and the second strata respectively. The displacements v, v' are expressed by

$$\left.\begin{aligned} v&=\frac{A\cos\{\sqrt{k^2-f^2}(H+H'-y)\}}{\cos\sqrt{k^2-f^2}(H+H')}\cos(pt-fx),\\ v'&=\frac{A\cos\sqrt{k^2-f^2}H\sinh\sqrt{f^2-k'^2}y}{\cos\sqrt{k^2-f^2}(H+H')\sinh\sqrt{f^2-k'^2}H'}\cos(pt-fx). \end{aligned}\right\} \tag{4}$$

The dispersion curves for $H/H'=\infty$, 10, 1, 1/10, when $\mu'/\mu=5$, are plotted in Fig. 9 and similar curves, when $\mu'/\mu=2$, in Fig. 10. The ratios of displacements at various depths to the one at the surface for different H/H' of the case $\mu'/\mu=5$ are plotted in Figs. 12, 13, 14; the similar ratios of the case $\mu'/\mu=2$ in Figs. 15, 16, 17.

4. The ratios of displacements for various depths in the case of Rayleigh-waves were obtained in our preceding paper[5], so that it is not necessary now to show the result. Nevertheless, we shall reproduce one of the results, namely the case $\mu'/\mu=2$. The ratios of horizontal

---

[3] T. Matuzawa, "Propagation of Love Waves along Trebly Stratified Body," *Proc. Phys.-Math. Soc., Japan*, [iii], 10 (1928), 25~33.

[4] R. Stoneley and E. Tillotson, "The Effect of a Double Surface Layer on Love Waves," *M. N. R. A. S., Geophys. Suppl.*, 1 (1928), 521~527.

[5] K. Sezawa and K. Kanai, *loc. cit.*

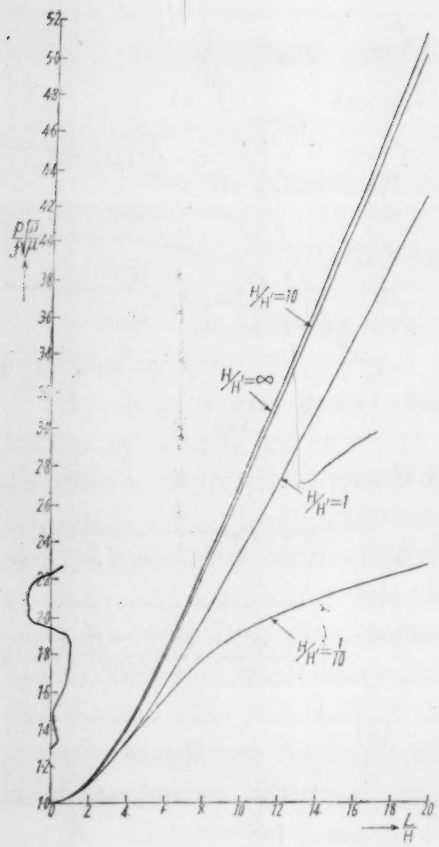

Fig. 9. $\mu'/\mu=5$.

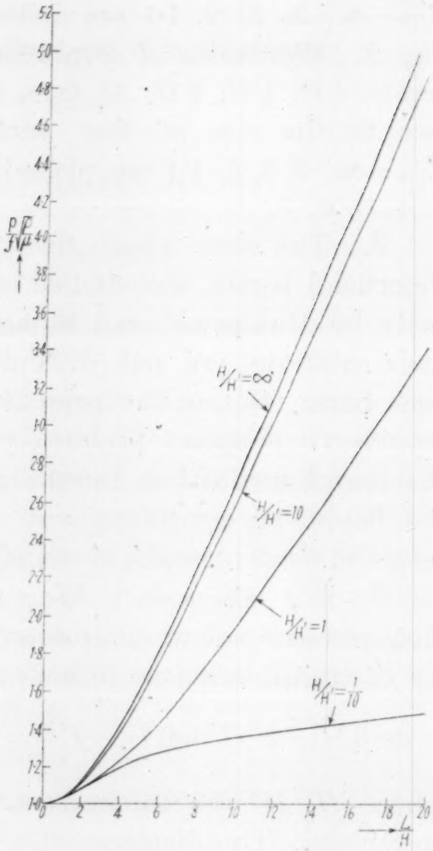

Fig. 10. $\mu'/\mu=2$.

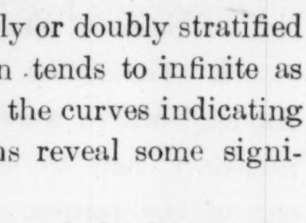

Fig. 18.

components, $u_{H/2}/u_0$, u_H/u_0, and those of vertical ones, $v_{H/2}/v_0$, v_H/v_0, are plotted in Fig. 19.

5. It is impossible to find features in dispersion curves of Love-waves that are special to that kind of waves as there are nearly similar characters in relation to the connection between the velocity of transmission and the ratio of L/H for Love-waves as well as for Rayleigh-waves. It is a common fact that, if the rigidity of the lowest medium in a singly or doubly stratified body is infinitely large, the velocity of transmission tends to infinite as L/H becomes very large. It seems, however, that the curves indicating the distribution of dispalcements at different depths reveal some significant qualities.

It is certain that, if the rigidities of the strata and the lowest medium are not much different, displacements are approximately constant at any depth for relatively longer wave length in both cases of Love-waves and Rayleigh-waves, tending to take the types of bodily waves having velocities of distortional- and Rayleigh-waves peculiar to the lowest medium in respective cases. In the same condition of rigidities of both media the displacements take different distributions when the wave length is not large. For smaller wave length, the displacements of Rayleigh-waves are concentrated more intensely on the surface, while the accumulation of displacements of Love-waves in the superficial part of the body is not so intense as that of Rayleigh-waves. In the limiting case, where the wave length is exceedingly small, the displacements of Rayleigh-waves are found practically only at the surface, while those of Love-waves are not accumulated at the surface but distributed in a sinusoidal type in the uppermost stratum. In this case the displacements of all lower strata are exactly zero. This is a special feature of short Love-waves, which plays an important part on the fundamental nature of L-phase and is extremely differing from that of M-phase. The difference between short Love-waves and short Rayleigh-waves is also directly connected with two kinds of high-frequency vibrations of an elastic plate.[6]

If the rigidity of the lower medium of a one-stratified body is very large compared with that of the superficial layer, the distribution of displacements of Love-waves in the layer takes always the same type for any wave length. This type is precisely equivalent to that of displacements of the critical case of Love-waves for any ratio of μ'/μ when the wave length is exceedingly small. The distribution of displacements of Rayleigh-waves in such condition of rigidities takes different types according to wave lengths. If there are two or more superficial strata on a very rigid medium, the distribution of displacements of Love-waves in the strata depends upon the wave lengths over a range, but beyond a certain wave length the distribution tends to take the same type, the type conforming with the ratio of thicknesses as well as that of rigidities of respective media. If there are two superficial strata and the upper stratum is much thicker than the second one, the distribution tends to the asymptotic type at a smaller ratio of L/H, while, if the upper stratum is much thinner than the second one, the approach to the asymptotic type takes place at a larger ratio of L/H. The effect of rigidities of both media is remarkable when the upper medium is much thinner than the second one, and in this case the waves tend to take asymptotic type at a smaller ratio of L/H when the difference of the rigidities is not large.

Generally speaking, the distribution of displacements of Love-waves in a one-stratified body tends to take asymptotic type, namely the type of waves of an infinite length, at smaller wave length if the difference of rigidities of the layer and the subjacent medium becomes smaller and smaller. Thus, when the rigidities of both media differ very little, the displacements of extremely short waves in the stratum are distributed in a sinusoidal form of $\frac{1}{4}$ period and those in the subjacent medium are zero, while the displacements of waves, which are longer than the above, are distributed approximately uniformly in the stratum as well as in the subjacent medium. But, if the medium is uniform at all depths, the displacements are distributed uniformly for any wave length.

---

[6] K. SEZAWA, "On the Accumulation of Energy of High-frequency Vibrations of an Elastic Plate on Its Surfaces," *Proc. 3-int. Congr. f. Appl. Mech., Stockholm, 1930*, **3**, 167~172.

6. The explanation, which we wish to suggest here as to the reason why periods of oscillations of L-phase are relatively longer than those of M-phase in spite of the smaller amplitudes of the former phase, comes directly from the above result with respect to the distribution of displacements. It is, however, necessary to assume that the law of equipartition of energy holds: in other words, that the transmitted disturbance consists of an aggregate of trains of harmonic waves of different periods and the energy involved in each train of waves is constant when there is no any damping force. This criterion may be in contradiction with the recent conception of energy partition. Such conception will, of course, modify our result to a certain extent, yet the character due our result will still remain as a certain element of the problem. Let the surface values of displacements of Rayleigh-waves, Love-waves and bodily distortional waves be

$$v_1 = A_1 e^{-b_1 l/H} \cos\frac{2\pi V_1 t}{l}, \quad v_2 = A_2 e^{-b_2 l/H} \cos\frac{2\pi V_2 t}{l}, \quad v_3 = A_3 \cos\frac{2\pi v_3 t}{l} \tag{5}$$

respectively, where H is effective thickness of the layer, l wave length, V_1, V_2, V_3 velocities of transmission of Rayleigh-waves, Love-waves, and bodily waves, A_1, A_2, A_3, b_1, b_2 constants depending upon the distribution of displacements of respective kinds of waves under the preceding assumption of energy partition.

In the first place, we take the case in which there is little damping due to solid viscosities, etc.. It is certain that, the more the energy of waves is accumulated in the vicinity of the surface, the larger becomes the surface values of the displacements. Similarly, the variation of the distribution of displacements in accordance with the length of waves determines the law of variation of surface displacements. This criterion and the results of the preceding section show that

$$A_1 \gg A_2 \gg A_3, \quad b_1 \gg b_2, \tag{6}$$

from which it follows:

$$v_1 > v_2 > v_3 \tag{7}$$

for small wave lengths. Thus, the amplitudes of M-phase are greater than those of L-phase, and the amplitudes of L-phase are greater than those of S-phase at least for smaller wave lengths. For longer waves we have merely

$$v_1 > v_3, \quad v_2 > v_3 \tag{8}$$

in virtue of (6). Let us suppose that the wave length, at which the amplitude becomes a certain fraction of that at zero wave length, is used as a criterion of comparison of effective wave length. Then, if l_1, l_2 are respective criterion wave lengths of Rayleigh-waves and Love-waves, we find

$$b_1 l_1 = b_2 l_2,$$

so that, from $b_1 \gg b_2$, we get

$$l_1 \ll l_2. \tag{9}$$

It appears therefore that the effective period of L-phase is less than that of M-phase.

Secondly, we consider the case that the damping due to the visco-elastic nature of the media is influential on the transmission of waves. We know that the damping factor[7] of waves is of the type *exp.*$(-ct/l^2)$, where t is time and c a constant depending on the type of waves. Thus, we write

$$\left.\begin{aligned} v_1 &= A_1 e^{-\left(\frac{c_1 r}{V_2 l^2} + b_1 \frac{l}{H}\right)} \cos \frac{2\pi V_1 t}{l}, \\ v_2 &= A_2 e^{-\left(\frac{c_2 r}{V_2 l^2} + b_2 \frac{l}{H}\right)} \cos \frac{2\pi V_2 t}{l}, \\ v_3 &= A_3 e^{-\frac{c_3 r}{V_3 l^2}} \cos \frac{2\pi V_3 t}{l}, \end{aligned}\right\} \tag{10}$$

where r is epicentral distance. Maxima of v_1, v_2 take place at

$$l_1 = \left(\frac{2c_1 r}{V_1} H\right)^{\frac{1}{3}} \Big/ b_1^{\frac{1}{3}}, \quad l_2 = \left(\frac{2c_2 r}{V_2} H\right)^{\frac{1}{3}} \Big/ b_2^{\frac{1}{3}} \tag{11}$$

respectively. As it may be assumed that $c_1 \approx c_2$, $V_1 \approx V_2$ in comparison with the inequality $b_1 \gg b_2$, it follows that

$$l_1 < l_2. \tag{12}$$

Thus, it is probable that the periods of maximum amplitudes of M-phase are less than those of L-phase. Substituting (11) in (10) we find the respective maxima of the forms:

---

[7] K. Sezawa, "On the Decay of Waves in Visco-elastic Solid Bodies," *Bull Earthq. Res. Inst.*, 3 (1927), 43; "On the Diffusion of Tremors on the Surface of a Semi-infinite Body," *ditto*, 5 (1928), 85.

$$\left.\begin{aligned} v_1 &= A_1 e^{-\frac{3}{2} b_1 l_1/H}, \\ v_2 &= A_2 e^{-\frac{3}{2} b_2 l_2/H}. \end{aligned}\right\} \tag{13}$$

Rewriting these we get the maxima :

$$\left.\begin{aligned} v_1 &= A\, e^{-\frac{3}{2} C_1 b_1^{2/3}/H}, \\ v_2 &= A_2 e^{-\frac{3}{2} C_2 b_2^{2/3}/H}, \end{aligned}\right\} \tag{13'}$$

provided $C_1=\left(\frac{2c_1 r}{V_1}H\right)^{\frac{1}{3}}$, $C_2=\left(\frac{2c_2 r}{V_2}H\right)^{\frac{1}{3}}$. Although $b_1 \gg b_2$ exists, c_1 and c_2 are actually very small, and therefore the exponential factors do not take an important part in comparison with A_1 and A_2 in (13′) within a range of a certain epicentral distance d. Thus, we have

$$v_1 > v_2, \quad l_1 < l_2. \quad (r < d) \tag{14}$$

Beyond the epicentral distance, d, the exponential factors become important and

$$v_1 < v_2, \quad l_1 < l_2 \quad (r > d) \tag{14'}$$

exist. In these both cases $l_1 < l_2$ holds with the condition that the absolute values of l_1 and l_2 increase as $r^{3/2}$.

7. In order to confirm the validity of our present conclusion we have analysed the records of earthquakes of various epicentral distances which were principally observed at Tôkyô (two special ones were observed at Osaka) and determined the approximate ratio of v_1/v_2 as well as that of T_1/T_2 together with the value of T_1, where v_1, v_2, T_1, T_2 are the effective values of the amplitudes and the periods of oscillations in M- and L-phases, the result being tabulated in Table I and the seismic records used being shown in Figs. 20∼44. In this table EW-component of two cases, III and XV, are the results of observation in Osaka. The values of v_1/v_2 and T_1 are plotted in Figs. 45 and 46.

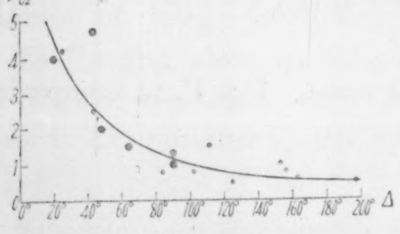

Fig. 45. {⊙ Trans-Pacific, ◎ Trans-continental.

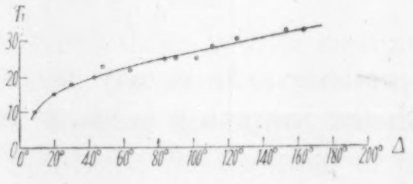

Fig. 46.

Even though there are special features of wave forms according to the paths of transmission of waves as already mentioned by Matuzawa[8],

---

[8] T. Matuzawa, *Bull. Earthq. Res. Inst.*, **6** (1929), 211.

Table I.[9][10]

	Δ	Epicentre	Date	T_1/T_2	v_1/v_2	T_1 (sec.)
I	8°38′	Sakurazima	1914 I 12	1·0	15	10
II	20°	Taiwan	1919 XII 20	0·6	4·0	15
III	25°	Aleutian	1906 VIII 17	0·7	4·2	18
IV	43°	Mandate	1913 X 11	0·7	2·5	20
V	43°	Tibet	1924 VII 3	0·7	4·7	20
VI	48°	India	1934 I 15	0·8	2·0	23
VII	64°	Baluchistan	1931 VIII 27	0·7	1·5	22
VIII	84°	New Zealand	1931 II 2	0·7	0·8	25
IX	90°	Calabria	1905 IX 8	0·7	1·0	25
X	90°	Messina	1908 XII 28	0·7	1·3	25
XI	102°	Mexico	1932 VI 3	0·7	0·8	25
XII	111°	Mexico	1931 I 15	0·7	1·5	25
XIII	125°	South Pacific	1920 III 20	0·6	0·5	28
XIV	153°	Atacama	1922 IX 11	0·6	1·0	30
XV	156°	Valparaiso	1906 VIII 17	0·6	0·8	32
XVI	163°	South Atlantic	1929 VI 27	0·7	0·6	32
XVII	197°	......(Major arc)	....	0·7	0·5	?

yet the existence of the characteristics due to our conclusion in (12), (14), (14′) can be recognized with certainty as far as for the seismic records we have taken up. It seems that the distance d, at which v_1 becomes v_2, is roughly $\Delta = 100°$.

Now, from Table I it is possible to put $T_1/T_2 = 0{\cdot}7$. If we assume that $V_1 = 3{\cdot}6$ km./sec. and $V_2 = 4{\cdot}2$ km./sec., it follows:

$$\frac{l_1}{l_2} = \frac{T_1 V_1}{T_2 V_2} = 0{\cdot}6. \tag{15}$$

From (11) and (15) we get $b_2 c_1 / b_1 c_2 = 0{\cdot}185$. Again, we may take for simplicity that $c_1 = c_2 = c$, then we obtain $b_2 = 0{\cdot}185\, b_1$. From the first equation of (11) and the curve in Fig. 46 we have

$$\frac{cH}{b_1} = 144 \text{ km}^3\text{./sec..} \tag{16}$$

---

9) Records of I, III, IX, X, XV are copied from Omori's papers, *Bull. Earthq. Inv. Comm.*, **1**, **8**; those of XVI, XVII from Imamura's paper, *Proc. Imp. Acad.*, **8** (1932), 354; XIII and XIV from the original records cited in Matuzawa's paper, *Bull. Earthq. Res. Inst.*, **6** (1929), 215; and VI and VIII from *Seism. Rep. Earthq. Res. Inst.*, 1931 and 1934.

10) In determining initial phases of L- and M-waves we used Oxford Summary, Macelwane's table and etc.. But, some corrections were necessary to get times of arrival of waves through Pacific Ocean and through East China Sea.

From (13), (15), and (16) we find

$$\frac{v_1}{v_2}=\frac{A_1}{A_2}e^{-4\cdot31\frac{b_1}{H}r^{\frac{1}{3}}}. \tag{17}$$

Comparing this equation with the curve in Fig. 45 it follows:

$$\frac{A_1}{A_2}=6\cdot82,\quad \frac{b_1}{H}=0\cdot041\,\text{km}^{-1}., \tag{18}$$

and accordingly $c=5\cdot90\,\text{km.}^2/\text{sec.}$. Hence we find the following expression in place of (13):

$$\left.\begin{aligned} v_1&=Ae^{-\left(\frac{5\cdot90\,r}{3\cdot6\,l^2}+0\cdot041\,l\right)}\cos\frac{7\cdot2\pi t}{l},\\ v_2&=\frac{A}{6\cdot82}e^{-\left(\frac{5\cdot90\,r}{4\cdot2\,l^2}+0\cdot00759\,l\right)}\cos\frac{8\cdot4\,\pi t}{l},\end{aligned}\right\} \tag{19}$$

where r is epicentral distance (km.), and l wave length (km.). With view to get damping coefficients of the earth crust the following equation is assumed to exist:

$$\frac{\mu'}{2\rho}=\frac{c}{4\pi^2}, \tag{20}$$

from which we find

$$\frac{\mu'}{\rho}=0\cdot3 \quad \text{in C. G. S. units.}$$

This value is exceedingly small in comparison with those observed experimentally by means of small test pieces. This tells the fact that the effect of the material damping on long seismic waves, especially when the length of waves is so large as 100 km., is negligibly small.

In conclusion our sincerest thanks are due to Professor Imamura and Dr. Nasu who gave us many important knowledges on seismic analysis, to Drs. Kishinouye, Suzuki, and Yasuda who supplied us a good deal of seismic records, and also to Mr. Hirano who assisted us in copying some records.

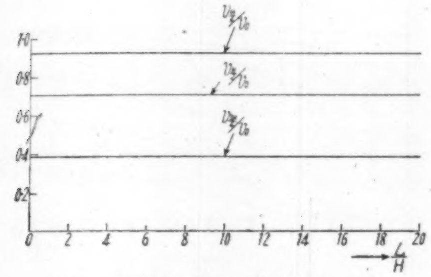

Fig. 3. $\mu'/\mu=\infty$.

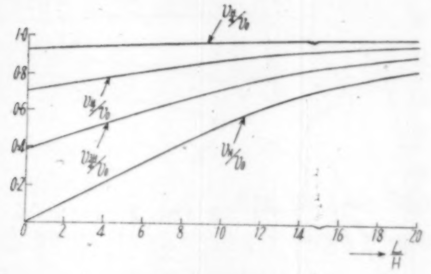

Fig. 4. $\mu'/\mu=5$.

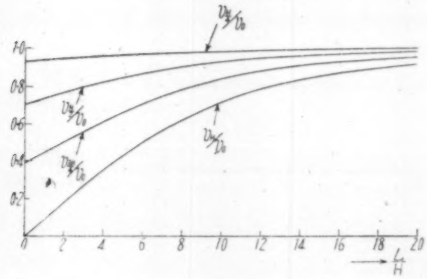

Fig. 5. $\mu'/\mu=3$.

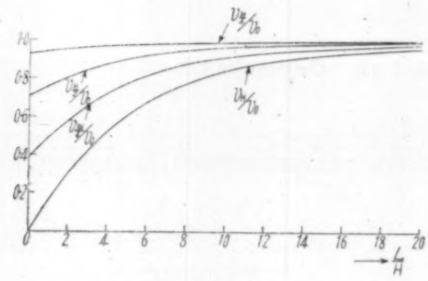

Fig. 6. $\mu'/\mu=2$.

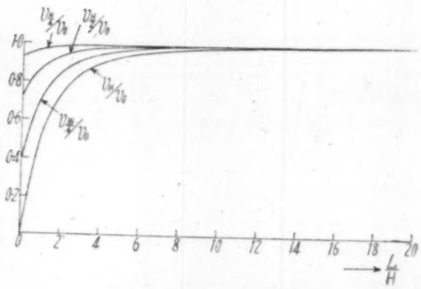

Fig. 7. $\mu'/\mu=1.1$.

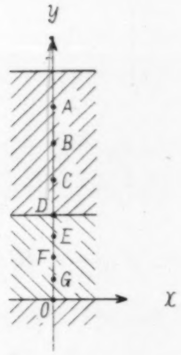

Fig. 11.

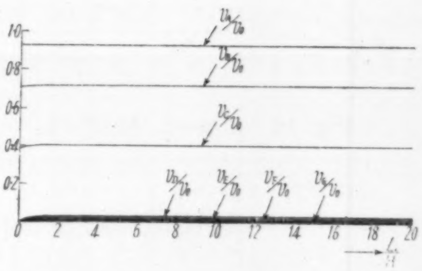

Fig. 12. $\mu'/\mu=5,\ H/H'=10$.

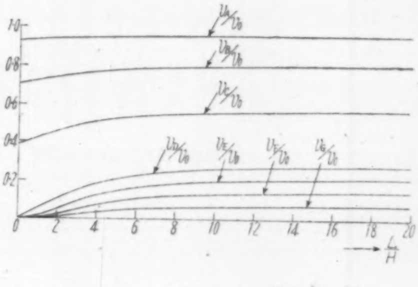

Fig. 13. $\mu'/\mu=5,\ H/H'=1$.

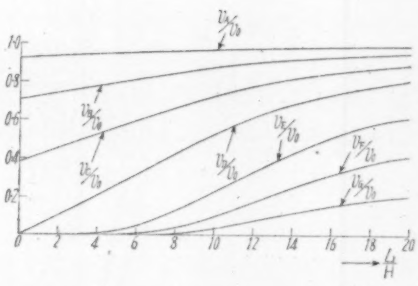

Fig. 14. $\mu'/\mu=5,\ H/H'=1/10$.

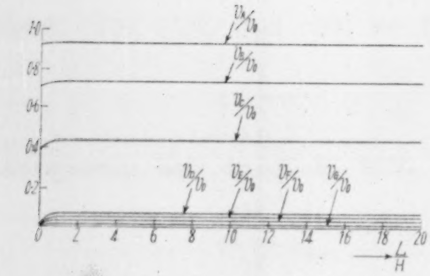

Fig. 15. $\mu'/\mu=2$, $H/H'=10$.

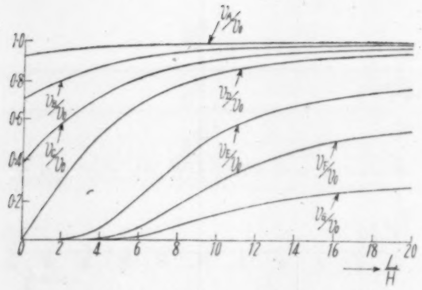

Fig. 17. $\mu'/\mu=2$, $H/H'=1/10$.

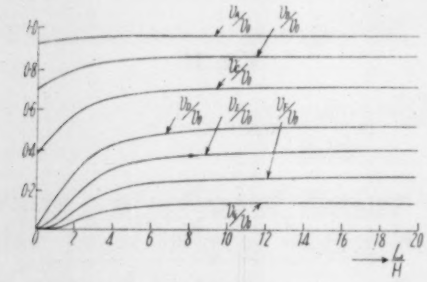

Fig. 16. $\mu'/\mu=2$, $H/H'=1$.

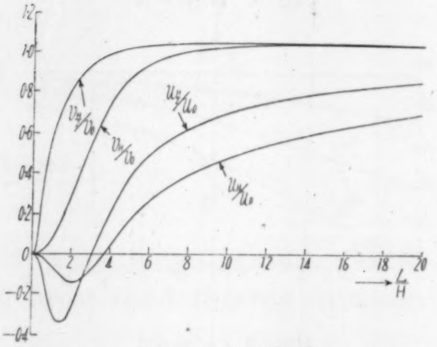

Fig. 19. $\mu'/\mu=2$. (Rayleigh-waves)

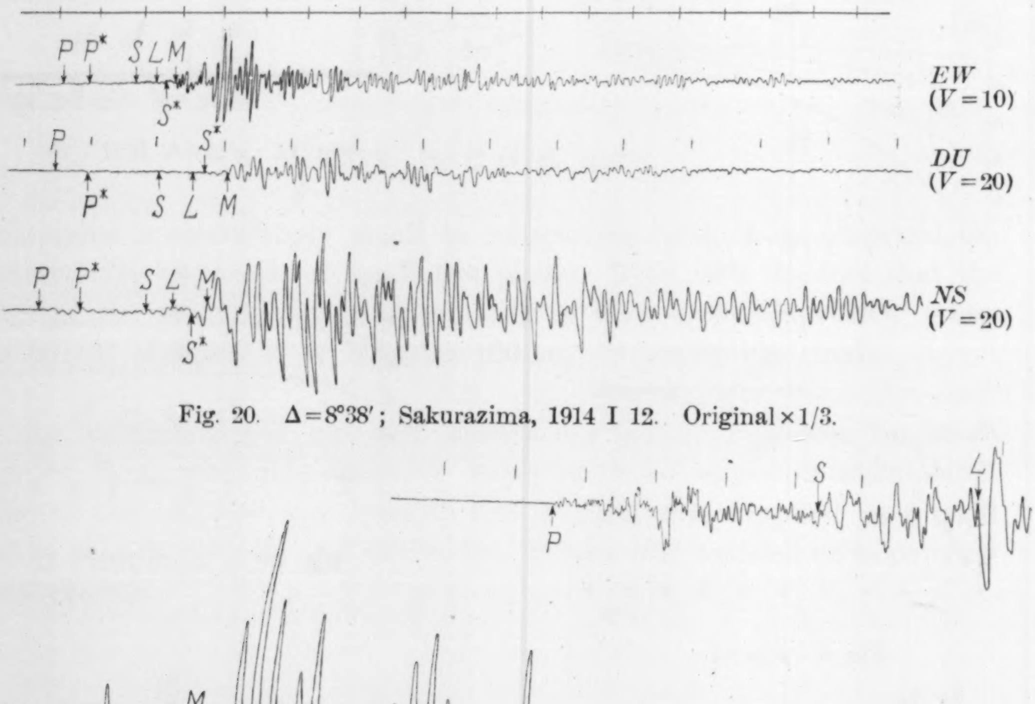

Fig. 20. Δ=8°38′; Sakurazima, 1914 I 12. Original×1/3.

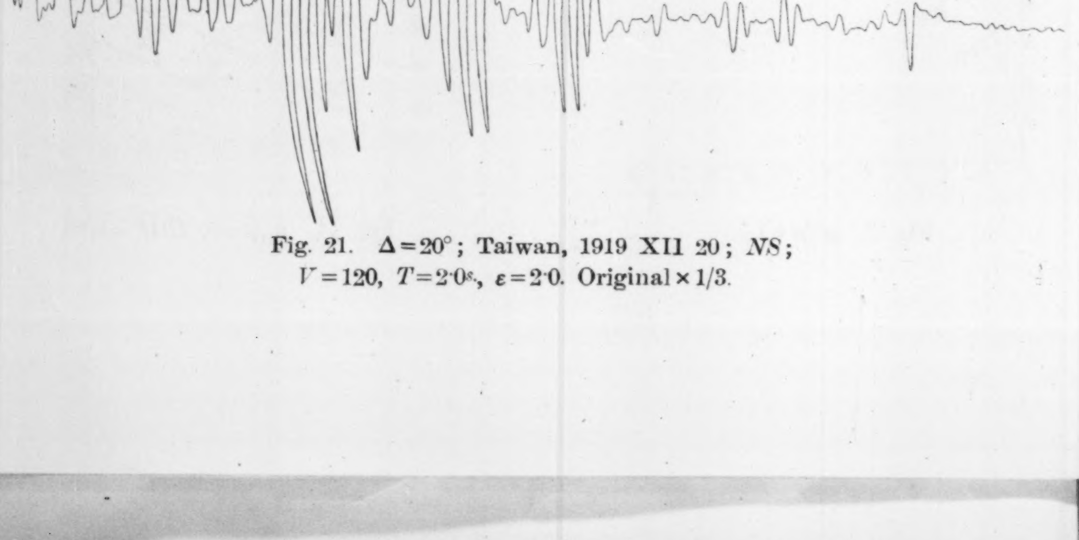

Fig. 21. Δ=20°; Taiwan, 1919 XII 20; *NS*;
$V=120$, $T=2{\cdot}0^{s}$, $\varepsilon=2{\cdot}0$. Original×1/3.

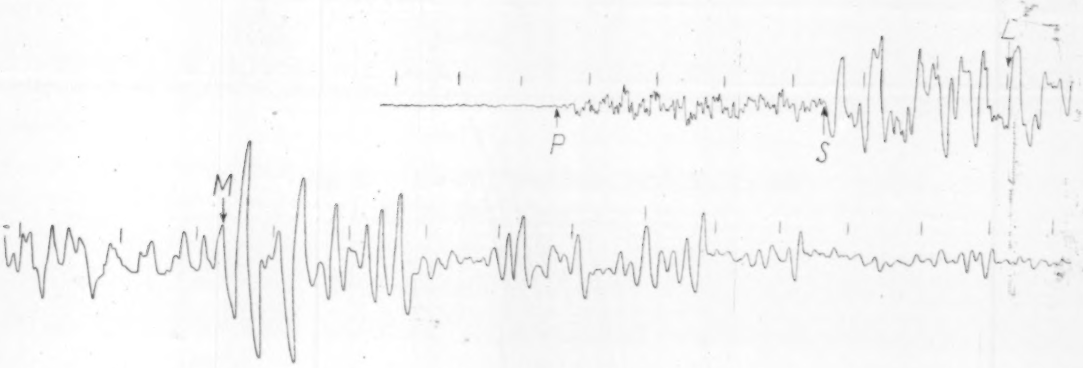

Fig. 22. $\Delta = 20°$; Taiwan, 1919 XII 20; *EW*; $V = 120$, $T = 20^s$, $\varepsilon = 2{\cdot}0$. Original × 1/3.

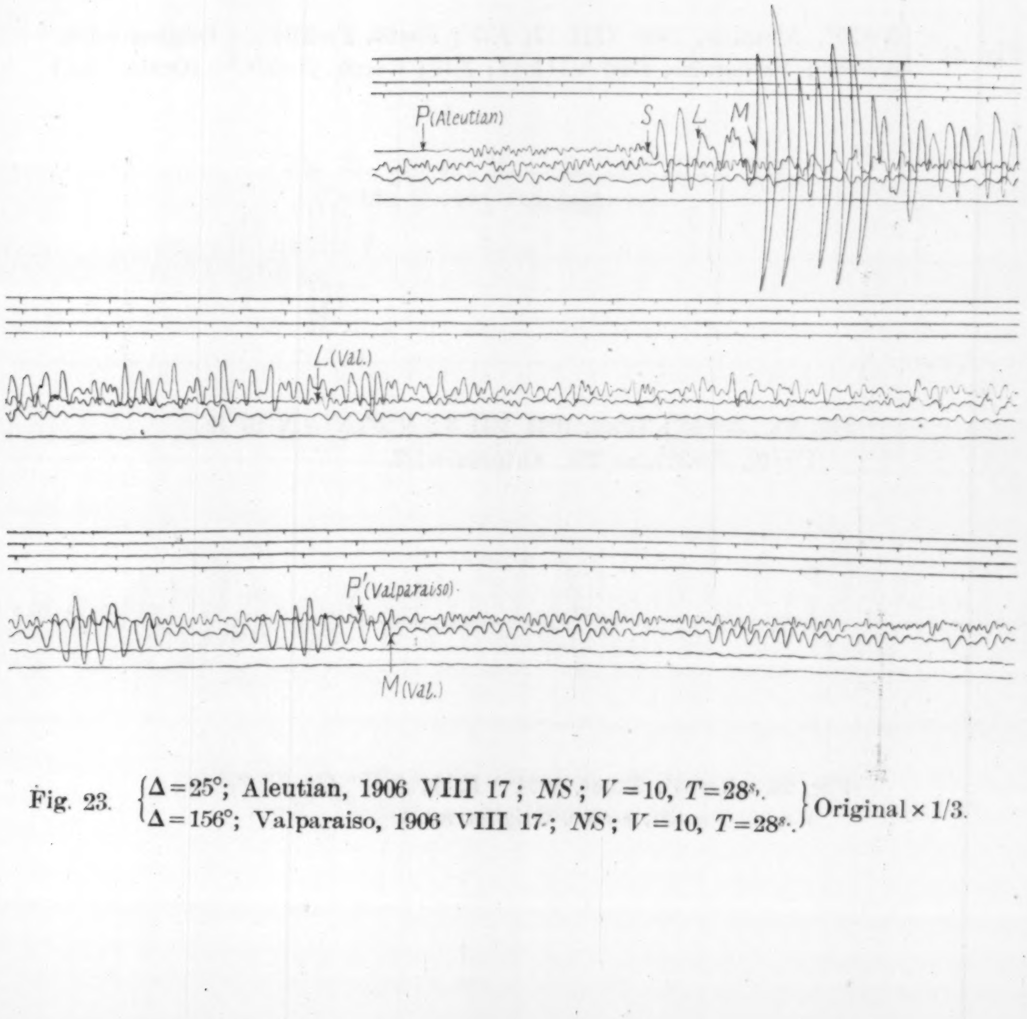

Fig. 23. $\left\{\begin{array}{l}\Delta = 25°\text{; Aleutian, 1906 VIII 17; } NS\text{; } V = 10,\ T = 28^s. \\ \Delta = 156°\text{; Valparaiso, 1906 VIII 17; } NS\text{; } V = 10,\ T = 28^s.\end{array}\right\}$ Original × 1/3.

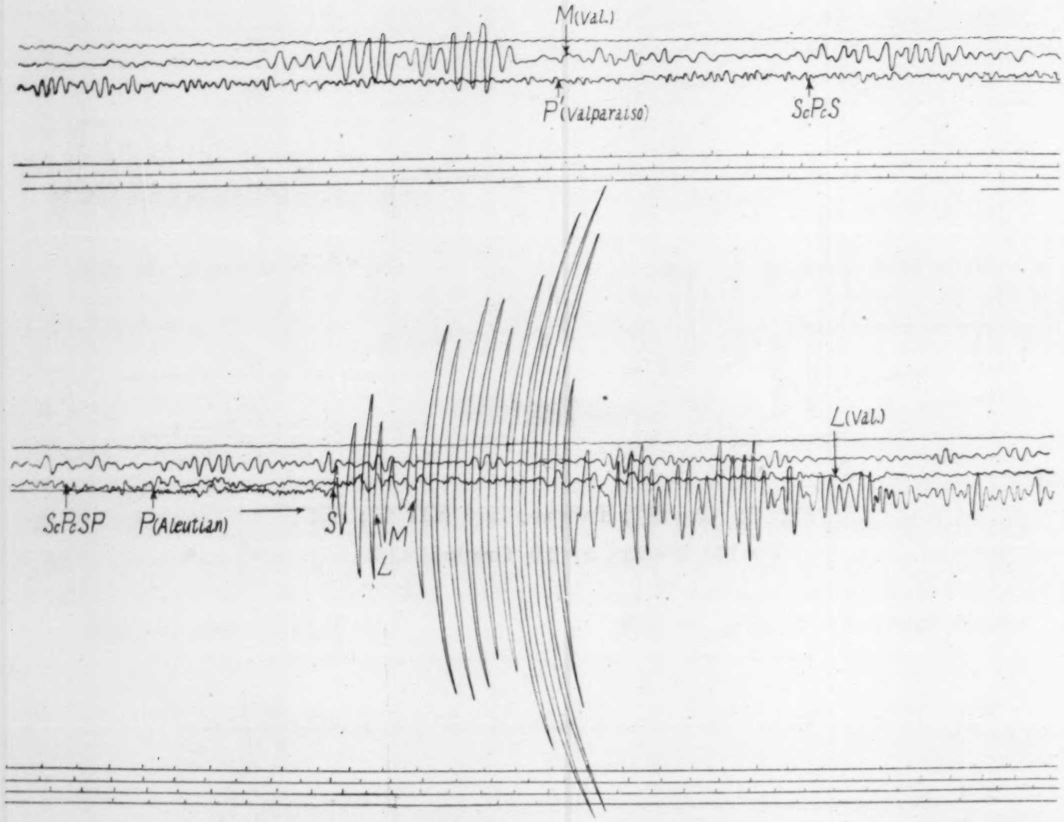

Fig. 24. {Δ=25°; Aleutian, 1906 VIII 17; *EW*; $V=20$, $T=27^s$. } Original × 1/3.
{Δ=156°; Valparaiso, 1906 VIII 17; *EW*; $V=20$, $T=27^s$. } (Osaka obs.)

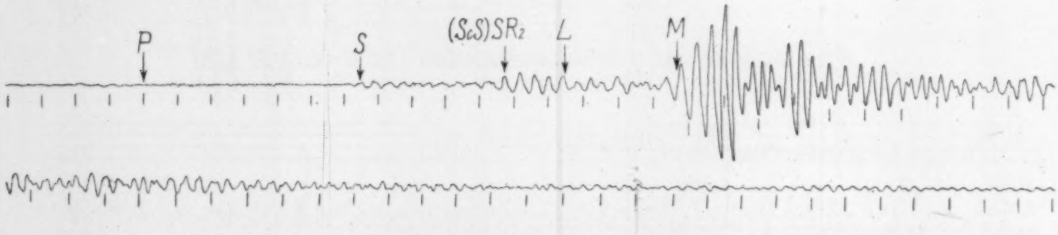

Fig. 25. Δ=43°; Tibet, 1924 VII 3; $N'S'(N'=N\ 13°\ W)$; $V=10$, $T=30^s$, $\varepsilon=2{\cdot}0$. Original × 1/3.

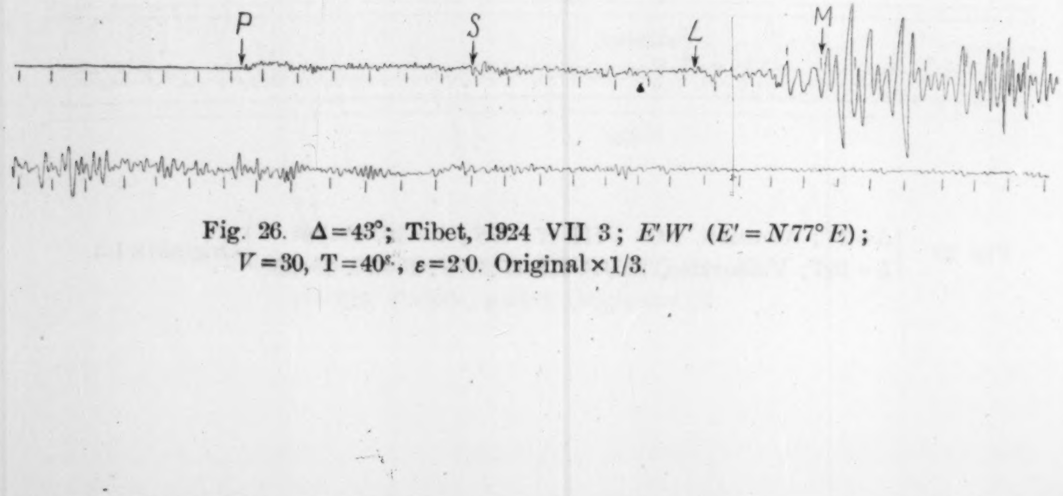

Fig. 26. Δ=43°; Tibet, 1924 VII 3; $E'W'$ $(E'=N77°E)$; $V=30$, $T=40^s$, $\varepsilon=2{\cdot}0$. Original × 1/3.

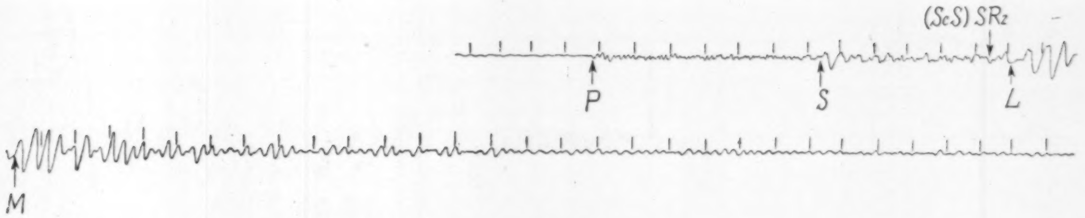

Fig. 27. $\Delta=43^\circ$; **Mandate, 1913 X 11;** *NS*;
$V=20$, $T=59^{s}$. **Original × 1/3.**

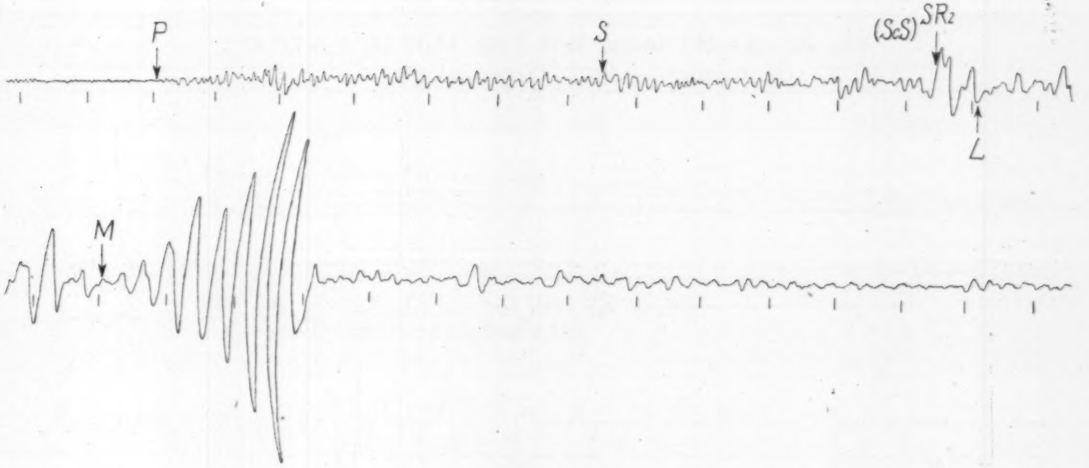

Fig. 28. $\Delta=43^\circ$; **Mandate, 1913 X 11;** *EW*;
$V=120$, $T=20^{s}$. **Original × 1/3.**

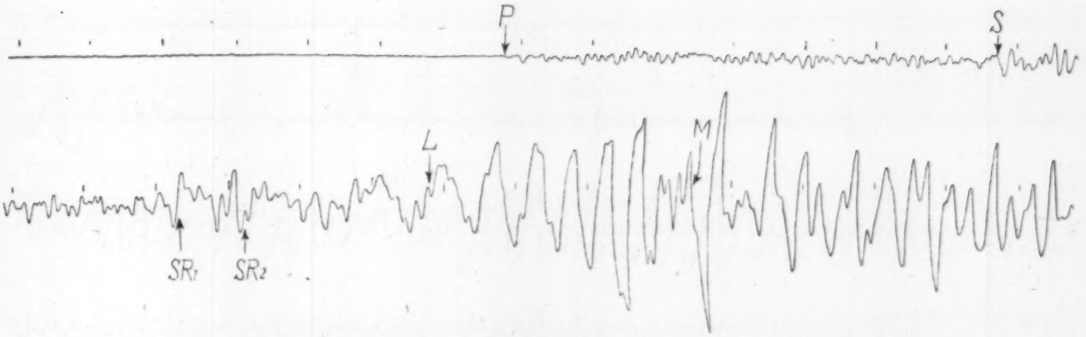

Fig. 29. $\Delta=48^\circ$; **India, 1934 I 15;** $N'S'$ ($N'=N\ 13^\circ\ W$);
$V=10$, $T=33{\cdot}2^{s}$, $\varepsilon=2{\cdot}2$. **Original × 1/3.**

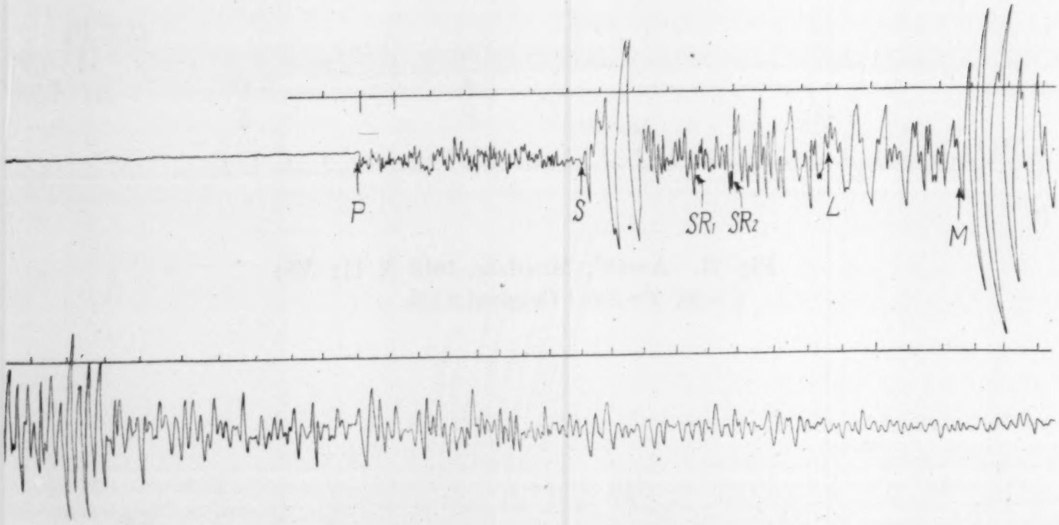

Fig. 30. $\Delta=48^\circ$; India, 1934 I 15; $E'W'$ (E' $N\,77^\circ E$);
$V=15$, $T=40{\cdot}9^{s}$, $\varepsilon=2{\cdot}7$. Original × 1/3.

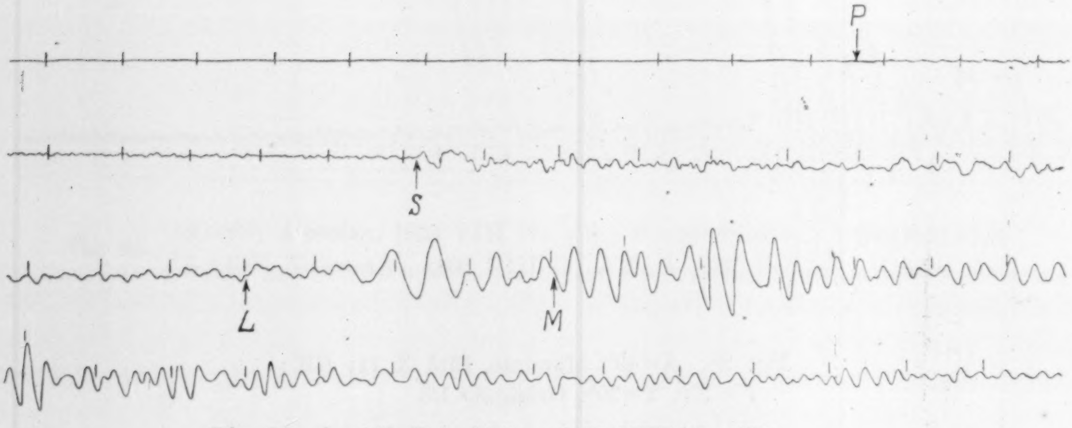

Fig. 31. $\Delta=64^\circ$; Baluchistan, 1931 VIII 27; NS;
$V=20$, $T=55^{s}$, $\varepsilon=1{\cdot}9$. Original × 1/3.

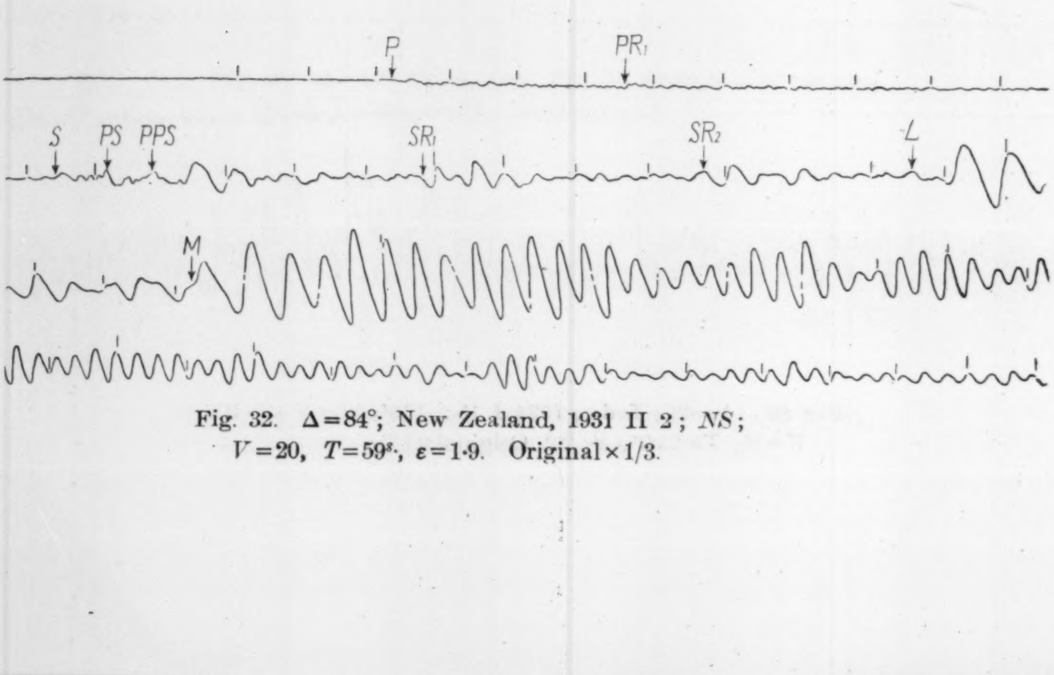

Fig. 32. $\Delta=84^\circ$; New Zealand, 1931 II 2; NS;
$V=20$, $T=59^{s}$, $\varepsilon=1{\cdot}9$. Original × 1/3.

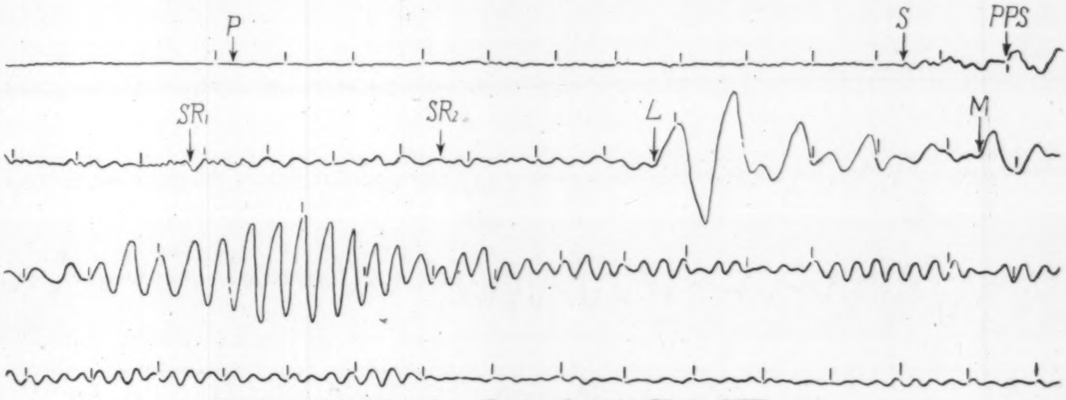

Fig. 33. $\Delta=84^\circ$; New Zealand, 1931 II 2; *EW*;
$V=15$, $T=71^s$., $\varepsilon=1{\cdot}9$. Original × 1/3.

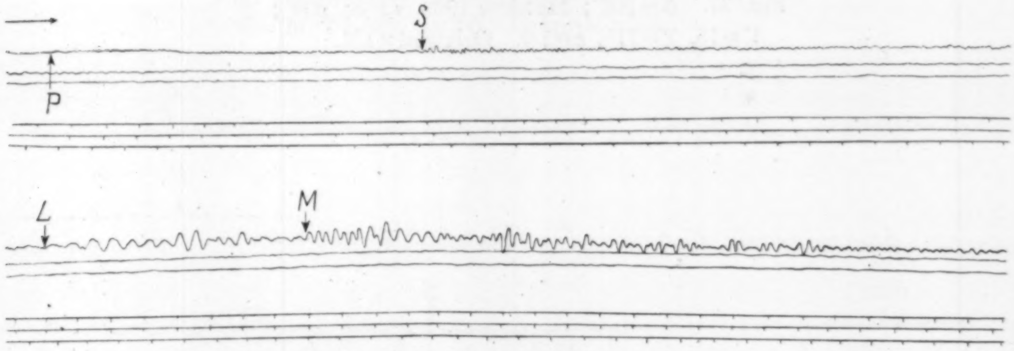

Fig. 34. $\Delta=90^\circ$; Calabria, 1905 IX 8; *NS*;
$V=20$, $T=48{\cdot}5^s$. Original × 1/3.

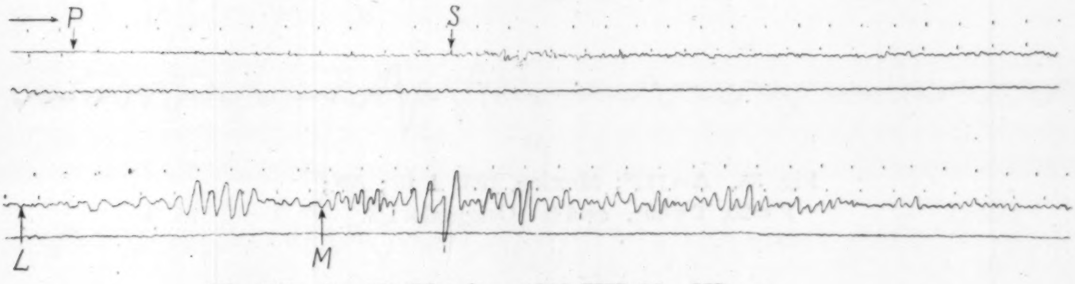

Fig. 35. $\Delta=90^\circ$; Messina, 1908 XII 28; *NS*;
$V=20$, $T=48{\cdot}5^s$. Original × 1/3.

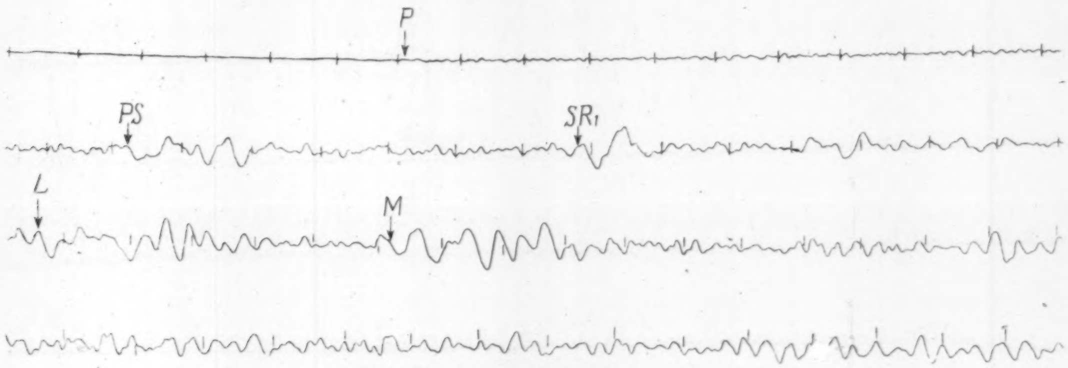

Fig. 36. $\Delta=102^\circ$; Mexico, 1932 VI 3; *NS*;
$V=20$, $T=59^s$., $\varepsilon=1{\cdot}9$. Original × 1/3.

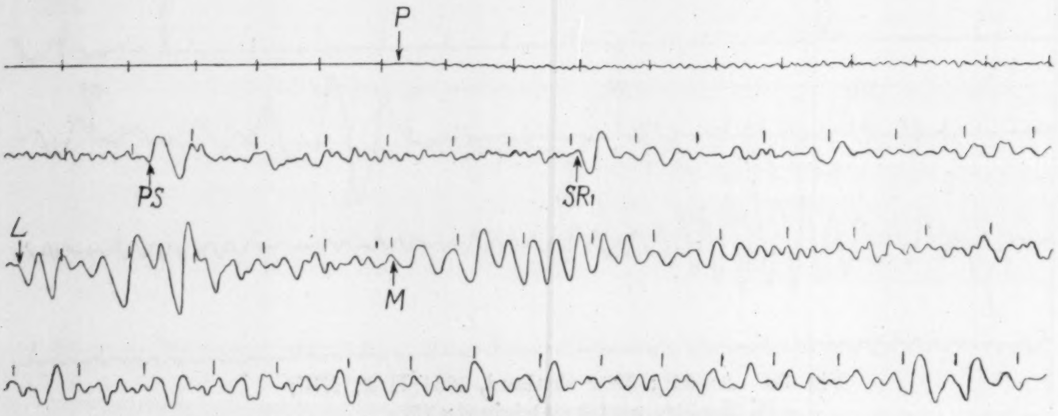

Fig. 37. Δ=102°; Mexico, 1932 VI 3; *EW*;
$V=15$, $T=71^{s}$, $\varepsilon=1{\cdot}9$. Original × 1/3.

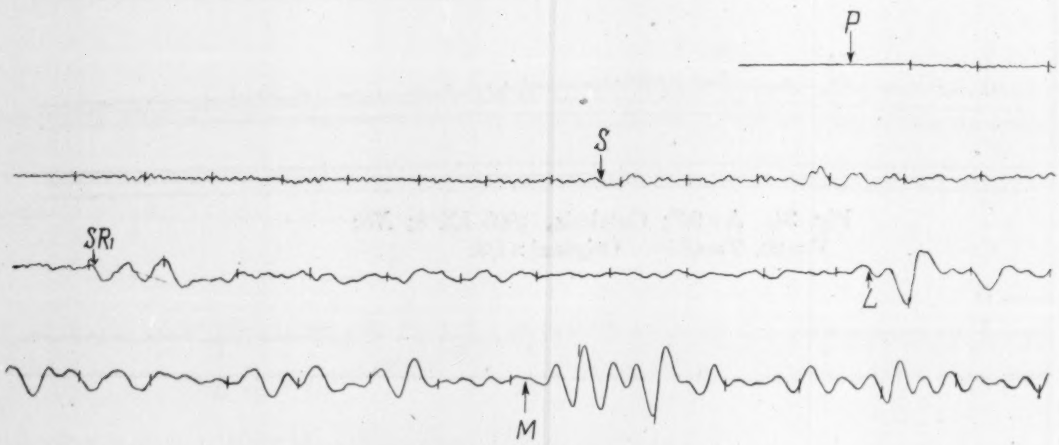

Fig. 38. Δ=111°; Mexico, 1931 I 15; *NS*;
$V=20$, $T=59^{s}$, $\varepsilon=1{\cdot}9$. Original × 1/3.

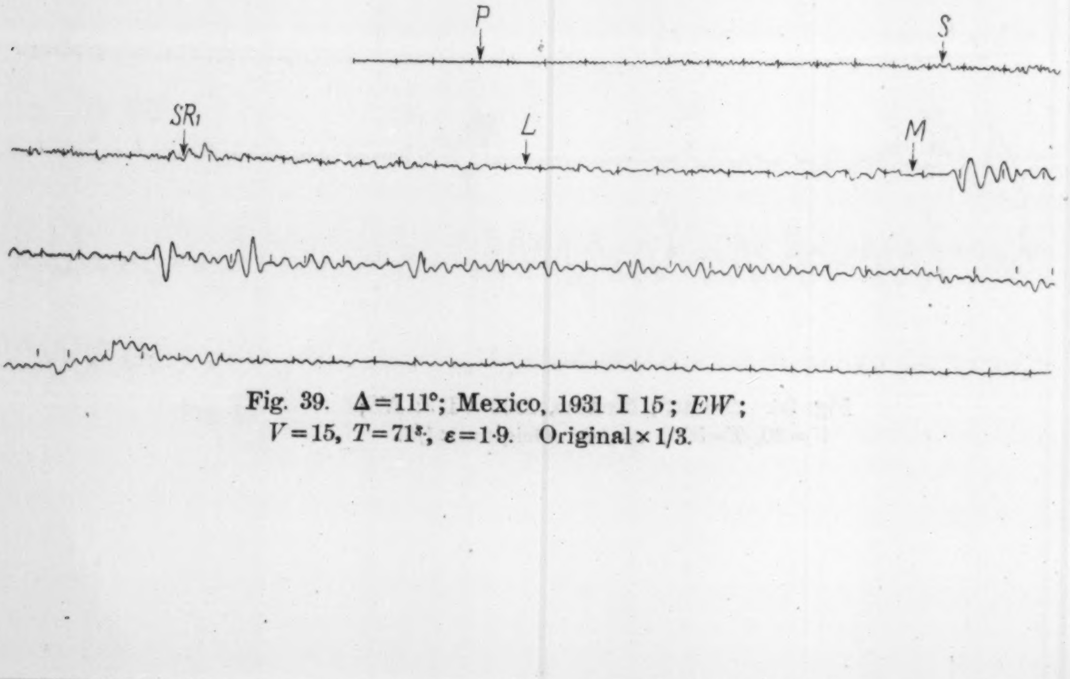

Fig. 39. Δ=111°; Mexico, 1931 I 15; *EW*;
$V=15$, $T=71^{s}$, $\varepsilon=1{\cdot}9$. Original × 1/3.

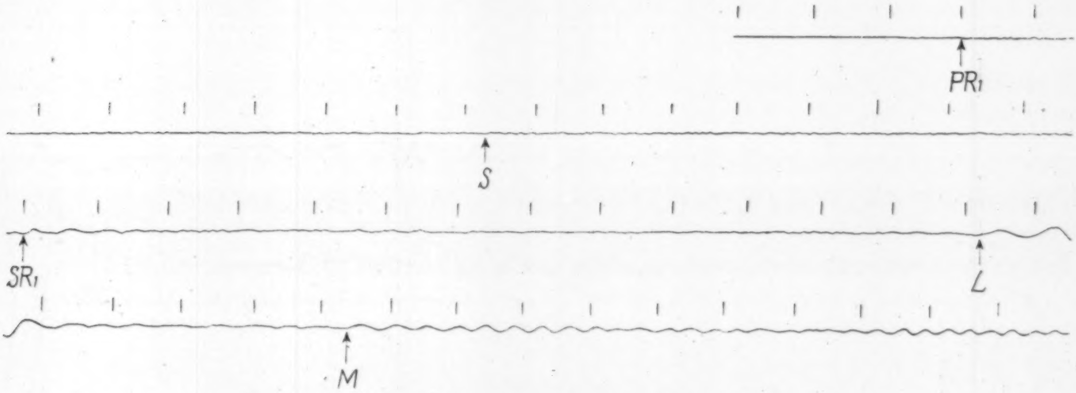

Fig. 40. $\Delta=125°$; **South Pacific, 1920 III 20;** ***NS*****;**
$V=20$, $T=50^{s}$, $\varepsilon=2{\cdot}0$. **Original × 1/3.**

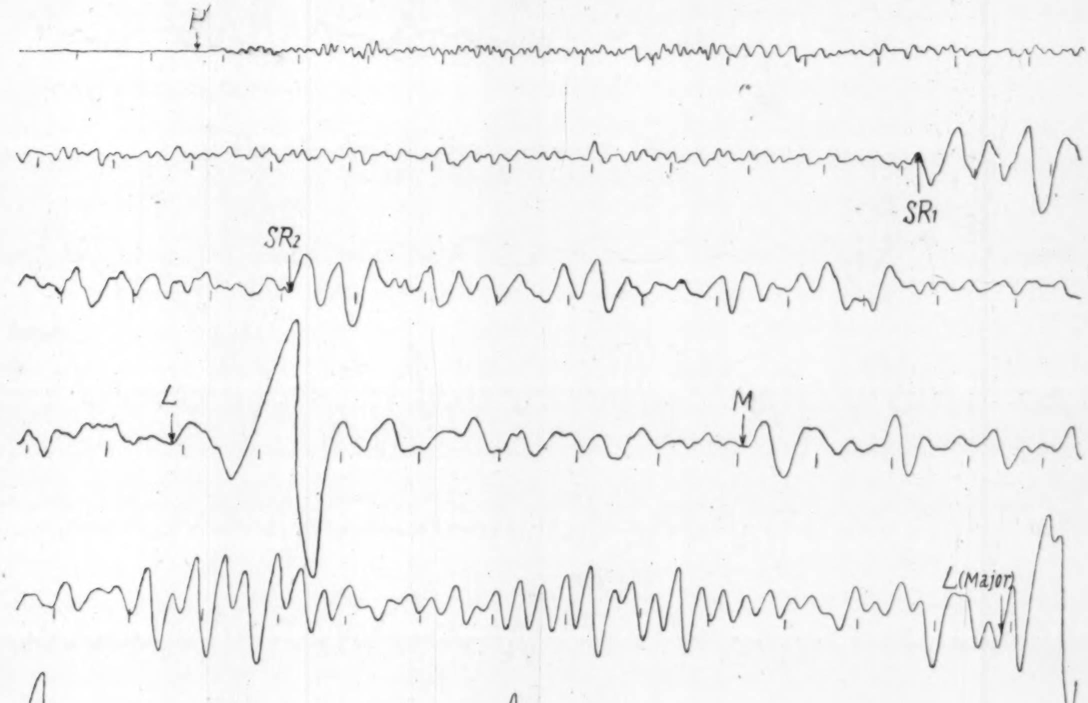

Fig. 41. $\Delta=153°$; **Atacama, 1922 XI 11;** ***NS*****;**
$V=20$, $T=50^{s}$, $\varepsilon=2{\cdot}0$. **Original × 1/3.**

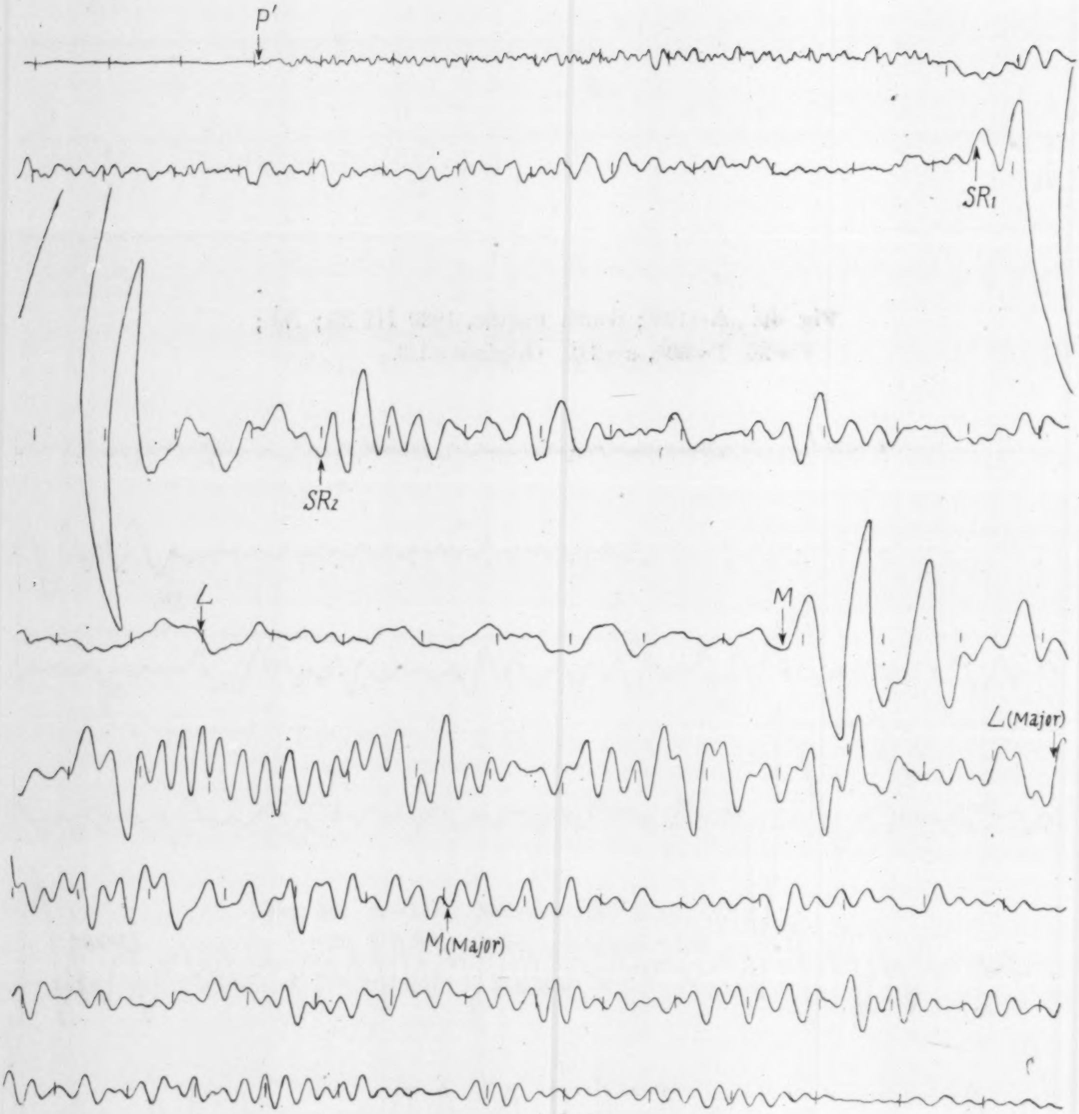

Fig. 42. Δ=153°; Atacama, 1922 XI 11; *EW*; $V=15$, $T=60^s$., $\varepsilon=3{\cdot}2$. Original × 1/3.

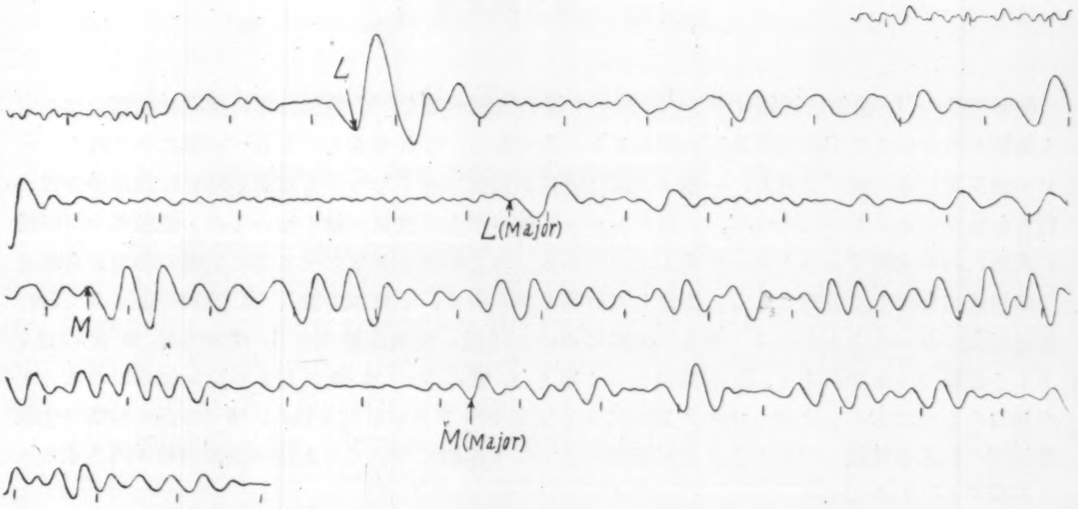

Fig. 43. $\Delta=163°$; South Atlantic, 1929 VI 27; *NS*;
$V=20$, $T=49^s$, $\varepsilon=1{\cdot}56$. Original × 1/3.

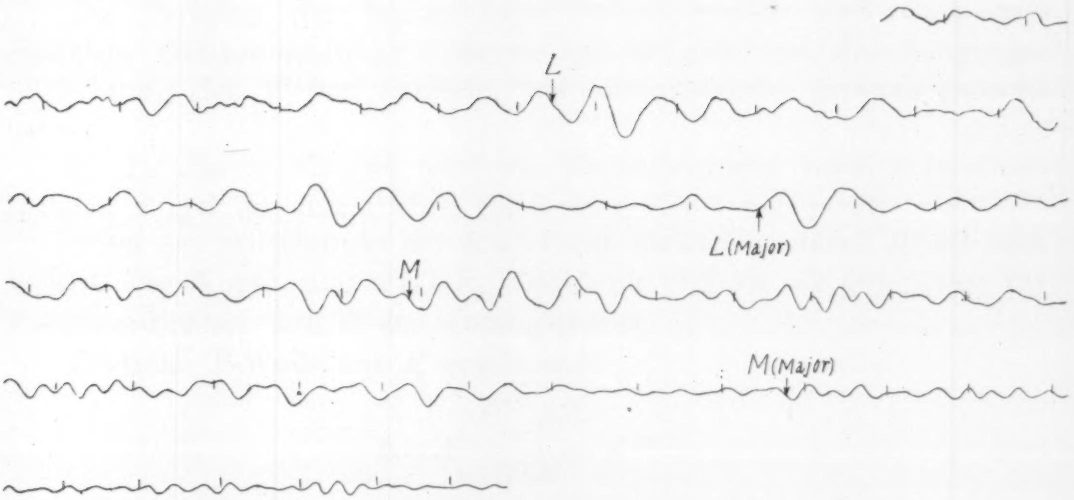

Fig. 44. $\Delta=163°$; South Atlantic, 1929 VI 27; *EW*;
$V=15$, $T=53^s$, $\varepsilon=1{\cdot}96$. Originial × 1/3.

2. L位相M位相の振動週期及振幅

地震研究所 ｛妹澤克惟
金井清

地震記象の L 位相は振幅は小さいけれども振動週期が長く，M 位相は逆に週期は稍短いけれども振幅が大きいことが普通認められてゐるところである．これを委しくしらべる爲にラブ波とレーレー波を更に考へ直して見た．一體ラブ波は波長が如何に短くなつても其振動部分は表面層全體に行きわたつてゐるものであつて，これをレーレー波のやうに波長の極く短いものゝ振動部分が固體の表面にのみ蓄積するのと大いに違ふものである．さて問題を簡單にする爲に震動の勢力が各波長の調和波に各等しく分配されると假定して計算を試みると，L 位相の波は M 位相の波よりも常に振動週期が長いことがわかる．然るに振幅については近い震央距離では L 波の方が M 波の方よりも小振幅であるけれども，遠距離になると寧ろ L 波の方が M 波の方よりも大振幅になることが知られるのである．之等の結果が實際にあてはまるかどうかを見る爲に，種々の震央距離の遠距離地震の記象を比較して見たところが週期についても振幅についても上述の議論が略々成立することが確められたのである．

3. *Über Schattenwellen und Kernwellen.*

Von Takeo MATUZAWA,

Institut für Erdbebenforschung.

(Vorgelegt 18. Dez. 1934.—Eingegangen 20. Dez. 1934.)

1. Es ist schon fast bestätigte Tatsache, dass wir so wie P-Welle im sogenannten Schattengebiet des Erdkerns als auch P-Wellen ausserhalb der durch den Erdkern erzeugten Brennzone deutlich beobachten können, was von der Anschauung der geometrischen Optik unmöglich zu erklären sein soll, wenn die Kerngrenze ganz unstetig ist.

Unstetigkeit der Grenze für Wellenfortpflanzung hängt von der Wellenlänge und der örtlichen Veränderung der elastischen Konstanten ab. Die Elastizitätstheorie im heterogenen Mittel zeigt uns, dass eine Unstetigkeit einerseits für sehr lange Welle andererseits dagegen für sehr kurze Welle manchmal als stetig angesehen werden könne.

Deutliche Entstehung mancher gebrochenen Wellen und reflektierten Wellen an der Kerngrenze zeigt uns, dass man für Erdbebenwellen von gewöhnlicher Periode, nämlich etwa über einige Sekunden, die Kerngrenze als unstetig ansehen kann.

Die Perioden der beobachteten Schattenwellen sind auch von derselben Grössenordnung. Darum soll es sich um die Beugungserscheinung der Wellen handeln, wie schon manche Autoren gedacht haben.

2. In diesem Kapitel wird die Wellenbeugung durch eine eingebetteten Kugel im unendlichen elastischen Mittel behandelt.

O sei der Mittelpunkt der Kugel mit Radius a. Herd H sei ausserhalb der Kugel, und $OH=b$. Die Linie OH sei die Polarachse für Polarkoordinaten, und O der Anfangspunkt.

Einfache P-Welle aus H ergibt sich

$$\Delta = A' \frac{H^{(1)}_{\frac{1}{2}}(hR)}{\sqrt{hR}} e^{-ipt},$$

wo

$$h^2 = \frac{\rho p^2}{\lambda+2\mu}, \quad R^2 = r^2+b^2-2br\cos\theta,$$

und

$$\Delta = \frac{1}{R^2}\frac{\partial(R^2U)}{\partial R}.$$

U ist die radiale Verschiebung in der Richtung von H. In Bezug auf O ergibt sich, für $r \leqq b$,

$$\frac{H_{\frac{1}{2}}^{(1)}(hR)}{\sqrt{hR}}=\sqrt{2\pi}\sum_{n=0}^{\infty}\left(n+\frac{1}{2}\right)\frac{H_{n+\frac{1}{2}}^{(1)}(hb)}{\sqrt{hb}}\,\frac{J_{n+\frac{1}{2}}(hr)}{\sqrt{hr}}\,P_n(\cos\theta),$$

$$u_0=-\frac{A'\sqrt{2\pi}}{h^{\frac{5}{2}}}\sum_{n=0}^{\infty}\left(n+\frac{1}{2}\right)\left\{\frac{d}{dr}\,\frac{J_{n+\frac{1}{2}}(hr)}{\sqrt{r}}\right\}\frac{H_{n+\frac{1}{2}}^{(1)}(hb)}{\sqrt{hb}}\,P_n(\cos\theta)e^{-ipt},$$

$$v_0=-\frac{A'\sqrt{2\pi}}{h^{\frac{5}{2}}}\sum_{n=0}^{\infty}\left(n+\frac{1}{2}\right)\frac{J_{n+\frac{1}{2}}(hr)}{r^{\frac{3}{2}}}\,\frac{H_{n+\frac{1}{2}}^{(1)}(hb)}{\sqrt{hb}}\,\frac{dP_n(\cos\theta)}{d\theta}\,e^{-ipt}.$$

Für $r\geqq b$ sollte man Konvergenz halber H und J in der rechten Seite miteinander austauschen, wovon in der folgenden Berechnung unnötig die Rede ist.

Die am Kern reflextierte Dilatationwelle[1] ergibt sich,

$$\Delta'=\sum_{n=0}^{\infty}\frac{B_n}{\sqrt{hr}}\,H_{n+\frac{1}{2}}^{(1)}(hr)\,P_n(\cos\theta)\,e^{-ipt},$$

$$u_1=-\sum_{n=0}^{\infty}\frac{B_n}{h^{\frac{5}{2}}}\,\frac{d}{dr}\,\frac{H_{n+\frac{1}{2}}^{(1)}(hr)}{\sqrt{r}}\,P_n(\cos\theta)\,e^{-ipt},$$

$$v_1=-\sum_{n=0}^{\infty}\frac{B_n}{h^{\frac{5}{2}}r^{\frac{3}{2}}}\,H_{n+\frac{1}{2}}^{(1)}(hr)\,\frac{d\,P_n(\cos\theta)}{d\theta}\,e^{-ipt},$$

wo
$$\Delta'=\frac{\partial u_1}{\partial r}+2\,\frac{u_1}{r}+\frac{1}{r}\,\frac{\partial v_1}{\partial\theta}+\frac{v_1}{r}\cot\theta.$$

Die am Kern reflextierte S-Welle lautet,

$$2\varpi'=\sum_{n=1}^{\infty}\frac{C_n}{\sqrt{kr}}\,H_{n+\frac{1}{2}}^{(1)}(kr)\,\frac{d\,P_n(\cos\theta)}{d\theta}\,e^{-ipt},$$

$$u_2=-\sum_{n=1}^{\infty}\frac{C_n\,n(n+1)}{k^{\frac{5}{2}}\,r^{\frac{3}{2}}}\,H_{n+\frac{1}{2}}^{(1)}(kr)\,P_n(\cos\theta)\,e^{-ipt},$$

$$v_2=-\sum_{n=1}^{\infty}\frac{C_n}{k^{\frac{5}{2}}r}\,\frac{d}{dr}\left\{\sqrt{r}\;H_{n+\frac{1}{2}}^{1)}(kr)\right\}\frac{d\,P_n(\cos\theta)}{d\theta}\,e^{-ipt},$$

wo
$$k^2=\frac{\rho p^2}{\mu},$$

$$2\varpi'=\frac{\partial v_2}{\partial r}+\frac{v_2}{r}-\frac{1}{r}\,\frac{\partial u_2}{\partial\theta}.$$

P- und S-Wellen innerhalb des Kerns lauten, mit Kennziffer „1" für elastische Konstanten,

$$\Delta''=\sum_{n=0}^{\infty}\frac{D_n}{\sqrt{h_1\,r}}\,J_{n+\frac{1}{2}}(h_1\,r)\,P_n(\cos\theta)\,e^{-ipt},$$

---

[1] K. SEZAWA, *Bull. Earthq. Res. Inst.*, 2 (1927), 13~20.

$$u_3 = -\sum_{n=0}^{\infty} \frac{D_n}{h_1^{\frac{5}{2}}} \frac{d}{dr} \frac{J_{n+\frac{1}{2}}(h_1 r)}{\sqrt{r}} P_n(\cos\theta)\, e^{-ipt},$$

$$v_3 = -\sum_{n=0}^{\infty} \frac{D_n}{h_1^{\frac{5}{2}} r^{\frac{3}{2}}} J_{n+\frac{1}{2}}(h_1 r) \frac{d\, P_n(\cos\theta)}{d\theta} e^{-ipt},$$

$$2\varpi'' = \sum_{n=1}^{\infty} \frac{E_n}{\sqrt{k_1 r}} J_{n+\frac{1}{2}}(k_1 r) \frac{d\, P_n(\cos\theta)}{d\theta} e^{-ipt},$$

$$u_4 = -\sum_{n=1}^{\infty} \frac{E_n n(n+1)}{k_1^{\frac{5}{2}}\, r^{\frac{3}{2}}} J_{n+\frac{1}{2}}(k_1 r)\, P_n(\cos\theta)\, e^{-ipt},$$

$$v_4 = -\sum_{n=1}^{\infty} \frac{E_n}{k_1^{\frac{5}{2}} r} \frac{d}{dr}\left\{\sqrt{r}\, J_{n+\frac{1}{2}}(k_1 r)\right\} \frac{d\, P_n(\cos\theta)}{d\theta} e^{-ipt}.$$

Hier soll die Zylinderfunktion die Bessel'sche J-funktion sein, sonst konvergiert die Reihe nicht, was nach der Bestimmung der Koeffizienten klar wird.

Die Grenzbedingungen lauten, am $r=a$,

$$\left\{\begin{array}{l} \lambda(\Delta+\Delta') + 2\mu \dfrac{\partial}{\partial r}(u_0 + u_1 + u_2) = \lambda_1 \Delta'' + 2\mu_1 \dfrac{\partial}{\partial r}(u_3 + u_4), \\[2ex] \mu\left\{\dfrac{\partial}{\partial r}(v_0 + v_1 + v_2) - \dfrac{1}{r}(v_0 + v_1 + v_2) + \dfrac{1}{r}\dfrac{\partial}{\partial\theta}(u_0 + u_1 + u_2)\right\} \\[2ex] \qquad\qquad = \mu_1\left\{\dfrac{\partial}{\partial r}(v_3 + v_4) - \dfrac{v_3 + v_4}{r} + \dfrac{1}{r}\dfrac{\partial}{\partial\theta}(u_3 + u_4)\right\}, \\[2ex] u_0 + u_1 + u_2 = u_3 + u_4, \\ \text{und} \\ v_0 + v_1 + v_2 = v_3 + v_4. \end{array}\right.$$

Nach Erledigung der Rechnung bekommen wir die folgenden vier Gleichungen mit vier Unbekannten.

$$\begin{aligned} \beta_{n1} B_n + \gamma_{n1} C_n + \delta_{n1} D_n + \varepsilon_{n1} E_n &= \alpha_{n1} A, \\ \beta_{n2} B_n + \gamma_{n2} C_n + \delta_{n2} D_n + \varepsilon_{n2} E_n &= \alpha_{n2} A, \\ \beta_{n3} B_n + \gamma_{n3} C_n + \delta_{n3} D_n + \varepsilon_{n3} E_n &= \alpha_{n3} A, \\ \beta_{n4} B_n + \gamma_{n4} C_n + \delta_{n4} D_n + \varepsilon_{n4} E_n &= \alpha_{n4} A, \end{aligned}$$

wo,

$$\left\{\begin{array}{l} \alpha_{n1} = -\left(n+\dfrac{1}{2}\right) \dfrac{H^{(1)}_{n+\frac{1}{2}}(\zeta)}{\sqrt{\zeta}} \dfrac{1}{\sqrt{\xi}} \left[\left\{(\lambda+2\mu) - 2\mu \dfrac{(n+1)(n+2)}{\xi^2}\right\} J_{n+\frac{1}{2}}(\zeta) \right. \\[2ex] \qquad\qquad\qquad\qquad\qquad\qquad \left. + \dfrac{4\mu}{\xi} J_{n-\frac{1}{2}}(\xi)\right], \\[2ex] \beta_{n1} = \dfrac{1}{\sqrt{\xi}} \left[\left\{(\lambda+2\mu) - 2\mu \dfrac{(n+1)(n+2)}{\xi^2}\right\} H^{(1)}_{n+\frac{1}{2}}(\xi) + \dfrac{4\mu}{\xi} H^{(1)}_{n-\frac{1}{2}}(\xi)\right], \end{array}\right.$$

$$\left\{\begin{aligned}
\gamma_{n1}&=-2\mu n(n+1)\frac{1}{\sqrt{\eta^3}}\left\{-\frac{n+2}{\eta}H^{(1)}_{n+\frac{1}{2}}(\eta)+H^{(1)}_{n-\frac{1}{2}}(\eta)\right\},\\
\delta_{n1}&=-\frac{1}{\sqrt{\xi_1}}\left[\left\{(\lambda_1+2\mu_1)-2\mu_1\frac{(n+1)(n+2)}{\xi_1}\right\}J_{n+\frac{1}{2}}(\xi_1)+\frac{4\mu_1}{\xi_1}J_{n-\frac{1}{2}}(\xi_1)\right],\\
\varepsilon_{n1}&=2\mu_1 n(n+1)\frac{1}{\sqrt{\eta^3}}\left\{-\frac{n+2}{\eta_1}J_{n+\frac{1}{2}}(\eta_1)+J_{n-\frac{1}{2}}(\eta_1)\right\},
\end{aligned}\right.$$

$$\left\{\begin{aligned}
\alpha_{n2}&=-2\mu\frac{n+\frac{1}{2}}{\sqrt{\xi^3}}\frac{H^{(1)}_{n+\frac{1}{2}}(\zeta)}{\sqrt{\zeta}}\left\{\frac{n+2}{\xi}J_{n+\frac{1}{2}}(\xi)-J_{n-\frac{1}{2}}(\xi)\right\},\\
\beta_{n2}&=2\mu\frac{1}{\sqrt{\xi^3}}\left\{\frac{n+2}{\xi}H^{(1)}_{n+\frac{1}{2}}(\xi)-H^{(1)}_{n-\frac{1}{2}}(\xi)\right\},\\
\gamma_{n2}&=\frac{\mu}{\sqrt{\eta}}\left[\left(1-\frac{2n(n+2)}{\eta^2}\right)H^{(1)}_{n+\frac{1}{2}}(\eta)+2\frac{H^{(1)}_{n-\frac{1}{2}}(\eta)}{\eta}\right],\\
\delta_{n2}&=-2\frac{\mu_1}{\sqrt{\xi_1^3}}\left\{\frac{n+2}{\xi_1}J_{n+\frac{1}{2}}(\xi_1)-J_{n-\frac{1}{2}}(\xi_1)\right\},\\
\varepsilon_{n2}&=-\frac{\mu_1}{\sqrt{\eta_1}}\left[\left(1-\frac{2n(n+2)}{\eta_1^{\,2}}\right)J_{n+\frac{1}{2}}(\eta_1)+\frac{2}{\eta_1}J_{n-\frac{1}{2}}(\eta_1)\right],
\end{aligned}\right.$$

$$\left\{\begin{aligned}
\alpha_{n3}&=-\frac{n+\frac{1}{2}}{h}\frac{H^{(1)}_{n+\frac{1}{2}}(\zeta)}{\sqrt{\zeta}}\frac{1}{\sqrt{\xi}}\left\{-\frac{n+1}{\xi}J_{n+\frac{1}{2}}(\xi)+J_{n-\frac{1}{2}}(\xi)\right\},\\
\beta_{n3}&=\frac{1}{h}\frac{1}{\sqrt{\xi}}\left\{-\frac{n+1}{\xi}H^{(1)}_{n+1}(\xi)+H^{(1)}_{-\frac{1}{2}}(\xi)\right\},\\
\gamma_{n3}&=\frac{n(n+1)}{k}\frac{H^{(1)}_{n+\frac{1}{2}}(\eta)}{\sqrt{\xi^3}},\\
\delta_{n3}&=-\frac{1}{h_1}\frac{1}{\sqrt{\xi_1}}\left\{-\frac{n+1}{\xi_1}J_{n+\frac{1}{2}}(\xi_1)+J_{n-\frac{1}{2}}(\xi_1)\right\},\\
\varepsilon_{n3}&=-\frac{n(n+1)}{k_1}\frac{J_{n+\frac{1}{2}}(\eta_1)}{\sqrt{\eta_1^{\,3}}},
\end{aligned}\right.$$

$$\left\{\begin{aligned}
\alpha_{n4}&=-\frac{n+\frac{1}{2}}{h}\frac{H^{(1)}_{n+\frac{1}{2}}(\zeta)}{\sqrt{\zeta}}\frac{J_{n+\frac{1}{2}}(\xi)}{\sqrt{\xi^3}},\\
\beta_{n4}&=\frac{1}{h}\frac{H^{(1)}_{n+\frac{1}{2}}(\xi)}{\sqrt{\xi^3}},\\
\gamma_{n4}&=\frac{1}{k}\frac{1}{\sqrt{\eta}}\left\{-\frac{n}{\eta}H^{(1)}_{n+\frac{1}{2}}(\eta)+H^{(1)}_{n-\frac{1}{2}}(\eta)\right\},
\end{aligned}\right.$$

$$\left\{\begin{aligned} \delta_{n4} &= -\frac{1}{h_1}\frac{J_{n+\frac{1}{2}}(\xi_1)}{\sqrt{\xi_1^3}}, \\ \varepsilon_{n4} &= -\frac{1}{k_1}\frac{1}{\sqrt{\eta_1}}\left\{-\frac{n}{\eta_1}J_{n+\frac{1}{2}}(\eta_1)+J_{n-\frac{1}{2}}(\eta_1)\right\}, \end{aligned}\right.$$

$A=\sqrt{2\pi}A'$, $\xi=ha$, $\xi_1=h_1a$, $\eta=ka$, $\eta_1=k_1a$ and $\zeta=hb$.

Aus diesen Gleichungen können wir die Koeffizienten B_n, C_n, D_n, und E_n bestimmen. Wir können ohne Schwierigkeiten beweisen, dass die allen so erhaltenen Reihen konvergieren. Je grösser die Argmenten der Zylinderfunktionen, nämlich ξ, η, ζ, ξ_1 und η_1 sind, desto schlechter wird die Konvergenz der Reihen, das heisst, für kürzere Wellen sind immer mehr Gliedern nötig, um zugeschriebene Genauigkeit zu bekommen.

3. Wenn der Erdkern flüssig sein sollte, dann kommt S-Welle im Kern nicht vor. In solchem Fall muss die Grenzbedingung lauten,

$$\left\{\begin{aligned} &\lambda(\Delta+\Delta')+2\mu\frac{\partial}{\partial r}(u_0+u_1+u_2)=\lambda_1\Delta'', \\ &\frac{\partial}{\partial r}(v_0+v_1+v_2)-\frac{1}{r}(v_0+v_1+v_2)+\frac{1}{r}\frac{\partial}{\partial\theta}(u_0+u_1+u_2)=0, \\ &u_0+u_1+u_2=u_3+u_4. \end{aligned}\right.$$

Nach Einsetzung der Lösung für Verschiebungen bekommt man,

$$\left\{\begin{aligned} \beta_{n1}B_n+\gamma_{n1}C_n+\delta_{n1}D_n&=\alpha_{n1}A, \\ \beta_{n2}B_n+\gamma_{n2}C_n+\delta_{n2}D_n&=\alpha_{n2}A, \\ \beta_{n3}B_n+\gamma_{n3}C_n+\delta_{n3}D_n&=\alpha_{n3}A, \end{aligned}\right.$$

wo,

$$\left\{\begin{aligned} \alpha_{n1} &= -\left(n+\frac{1}{2}\right)\frac{H^{(1)}_{n+\frac{1}{2}}(\zeta)}{\sqrt{\zeta}}\frac{1}{\sqrt{\xi}}\left[\left\{(\lambda+2\mu)-2\mu\frac{(n+1)(n+2)}{\xi^2}\right\}J_{n+\frac{1}{2}}(\xi)\right. \\ &\qquad\left.+\frac{4\mu}{\xi}J_{n-\frac{1}{2}}(\xi)\right], \\ \beta_{n1} &= \frac{1}{\sqrt{\xi}}\left[\left\{(\lambda+2\mu)-2\mu\frac{(n+1)(n+2)}{\xi^2}\right\}H^{(1)}_{n+\frac{1}{2}}(\xi)+\frac{4\mu}{\xi}H^{(1)}_{n-\frac{1}{2}}(\xi)\right], \\ \gamma_{n1} &= -n(n+1)\frac{2\mu}{\sqrt{\eta^3}}\left\{-\frac{n+2}{\eta}H^{(1)}_{n+\frac{1}{2}}(\eta)+H^{(1)}_{n-\frac{1}{2}}(\eta)\right\}, \\ \delta_{n1} &= -\frac{\lambda_1}{\sqrt{\xi_1}}J_{n+\frac{1}{2}}(\xi_1), \end{aligned}\right.$$

$$\left\{\begin{aligned}
\alpha_{n2}&=-2\,\frac{n+\frac{1}{2}}{\sqrt{\xi}^{3}}\,\frac{H^{(1)}_{n+\frac{1}{2}}(\zeta)}{\sqrt{\zeta}}\left\{\frac{n+2}{\xi}\,J_{n+\frac{1}{2}}(\xi)-J_{n-\frac{1}{2}}(\xi)\right\},\\
\beta_{n2}&=\frac{2}{\sqrt{\xi}^{3}}\left\{\frac{n+2}{\xi}\,H^{(1)}_{n+\frac{1}{2}}(\xi)-H^{(1)}_{n-\frac{1}{2}}(\xi)\right\},\\
\gamma_{n2}&=\frac{1}{\sqrt{\eta}}\left[\left(1-\frac{2n(n+2)}{\eta^{2}}\right)H^{(1)}_{n+\frac{1}{2}}(\eta)+2\,\frac{H^{(1)}_{n-\frac{1}{2}}(\eta)}{\eta}\right],\\
\delta_{n2}&=0,
\end{aligned}\right.$$

$$\left\{\begin{aligned}
\alpha_{n3}&=-\,\frac{n+\frac{1}{2}}{h}\,\frac{H^{(1)}_{n+\frac{1}{2}}(\zeta)}{\sqrt{\zeta}}\,\frac{1}{\sqrt{\xi}}\left(-\frac{n+1}{\xi}\,J_{n+\frac{1}{2}}(\xi)+J_{n-\frac{1}{2}}(\xi)\right),\\
\beta_{n3}&=\frac{1}{h\sqrt{\xi}}\left\{-\frac{n+1}{\xi}\,H^{(1)}_{n+\frac{1}{2}}(\xi)+H^{(1)}_{n-\frac{1}{2}}(\xi)\right\},\\
\gamma_{n2}&=\frac{n(n+1)}{k}\,\frac{H^{(1)}_{n+\frac{1}{2}}(\eta)}{\sqrt{\eta}^{3}},\\
\delta_{n3}&=-\frac{1}{h_1}\,\frac{1}{\sqrt{\xi_1}}\left\{-\frac{n+1}{\xi_1}\,J_{n+\frac{1}{2}}(\xi_1)+J_{n-\frac{1}{2}}(\xi_1)\right\}.
\end{aligned}\right.$$

Bemerkung zu der Konvergenz der Reihen ist dasselbe wie im elastischen Kern..

Zum Beispiel, für $\xi=6{\cdot}81$, $\eta=12{\cdot}19$, $\zeta=12{\cdot}44$ und $\xi_1=10{\cdot}53$, was der Wellenlänge von P, $\lambda_p=3232$ Km. und der von S, $\lambda_s=1800$ Km. in demselben Mittel wie die Erde in der Nähe vom Kern entsprechen, muss man etwa über 16 Gliedern berechnen, um die Genauigkeit zu ein Prozent zu erzielen, was aber sehr zeitraubende und umständliche Arbeit sein soll.

Physikalisch kann man leicht vermuten, dass die Störung immer weniger werden soll, wenn die eingebettete Kugel immer kleiner ist im Vergleich mit der Wellenlänge. Mathematischer Beweis davon ist auch nicht schwer. Im Grenzübergang zu $\xi=\eta=\xi_1=\eta_1=\zeta=0$ verschwinden und zwar gliedweise alle Verschiebungen ausser u_0 und v_0. Wenn man die Beugung durch sehr kleine eingebettete Kugel behandeln will, darf man gewöhnlich den allgemeinen Fall der Kugelwelle durch den der Ebenewelle ersetzen, wie schon K. Sezawa[2] einmal getan hat.

Im Gegensatz mathematisch ist nicht leicht einzusehen, wie die Erscheinung vorkommt, wenn die Wellenlänge im Vergleich mit der Kugel sehr klein ist. Aber physikalisch könne man ruhig vermuten, dass die Schattenerscheinung immer ausgeprägter eintreten soll und sich

---

2) K. SEZAWA, *Bull. Earthq. Res. Inst.*, 3 (1927), 32~34.

zum Falle des Huygens'schen Prinzips annähern wird.

Die ausgeprägte Periode der Schattenwellen, welche beim Japanbeben[3] vom 2. März 1933 in La Paz, Huancayo oder San Juan beobachtet wurde, war im Durchschnitt etwa 8 Sekunden.

Die Wellenlänge sollte also in der Nähe vom Kern ungefähr 104 Km. sein, vorausgesetzt dass die Fortpflanzungsgeschwindigkeit der Welle 13 Km./Sek. sei. Diese Länge ist sehr klein im Vergleich mit der Kerngrösse. Darum sollte näherungsweise das Huygens'sche Prinzip gelten. Tatsächlich ist die Laufzeitkurve im Schattengebiet praktisch geradlinig.

Unter ähnlicher Betrachtung ist Eintritt der Kernwelle ausserhalb der Brennzone auch verständlich.

Bei dieser Betrachtung ist die Wellenbeugung wegen des Erdkerns fast von derselben Deutung wie die Wellenstreuung wegen des Kerns.

3. 地球の核の蔭に於ける波

地震研究所　松　澤　武　雄

P 波の走時曲線は地球の核の蔭の部分迄續けてひく事が出來るし，又核の中を通過した波に就いては反對に焦點の内側迄引き延ばす事が出來る.

此の現象を彈性論から說明を試みた.

---

[3] T. MATUZAWA, *Bull. Earthq. Res. Inst.*, **13** (1935), Pl. VI, Fig. 5a, 5b; Pl. VII, Fig. 6: Fig. 7.

4. 灣口に於ける水位變化に伴ふ灣内海水の運動(其の2)

地震研究所 西村源六郎
高山威雄
金井清

(昭和 9 年 10 月 15 日發表——昭和 9 年 12 月 20 日受理)

緒言

曩にストークスの解析方法を利用して灣口に於ける水位變化に伴ふ灣内海水の運動を一般的に研究し，そして深さの一定な長方形の灣内に於ける海水の運動を圖をもつて研究した.[1] 本論文，第 1 章では海水内に運動抵抗があつて，海水の水平方向の速さに比例した反力が作用してゐる場合の一般解を求め，第 2 章では深さ一定な梯形の灣に就て，そこに起される波動の週期，位相を研究してある.

第 1 章 灣口に於ける水位變化に伴ふ灣内海水の運動

第 1 圖を參照してオイラーの海水運動方程式は，$u\dfrac{\partial u}{\partial x}$ 等の量，及び垂直方向即ち重力方向の海水の加速度を考へなければ，次の様になる.

$$\frac{\partial u}{\partial t}+2f\frac{\partial \xi}{\partial t}=-g\frac{\partial \eta}{\partial x}. \tag{1}$$

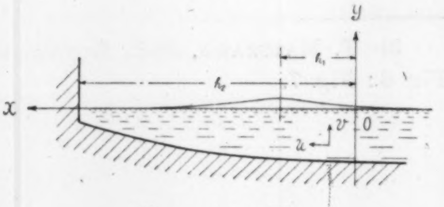

第 1 圖

勿論 u は海水分子の水平方向の速度，η は海水の表面の靜止面 $y=0$ よりの上昇量，ξ は海水分子の水平變位量，g 及び t は夫々重力による加速度及び時間を表はしてゐる. 尙 f は海水運動に伴ふ水平方向の速度に比例した抵抗の抵抗係數である. 海水運動の連續方程式

$$\eta b(x)=-\frac{\partial}{\partial x}\{\xi b(x)h(x)\} \tag{2}$$

によつて，(1) は次式 (3) に書き改める事が出來る. 尙 (2) に於て，$b(x)$，$h(x)$ は夫々港灣の幅，深さを表はし，これ等の量は，水平軸 x のみの函數と考へる.

---

[1] 西村源六郎，金井清 地震研究所彙報別册 1 (1930), 182.

$$\frac{\partial^2\eta}{\partial t^2}=\frac{g}{b(x)}\frac{\partial}{\partial x}\left\{b(x)\,h(x)\frac{\partial\eta}{\partial x}\right\}-2f\frac{\partial\eta}{\partial t}. \tag{3}$$

さて (3) なる運動方程式を海水運動の始めの條件，及び灣口 $x=h_1$，灣頭 $x=h_2$ に於ける境界條件

$$t=0\;;\quad \eta=0,\quad \frac{\partial\eta}{\partial t}=0,\quad \frac{\partial^2\eta}{\partial t^2}=0, \tag{4}$$

$$x=h_1\;;\quad \eta=\varphi(t), \tag{5}$$

$$x=h_2\;;\quad \frac{\partial\eta}{\partial x}=k\eta \tag{6}$$

によつて解く事は全く前論文と同じ．前論文を參照して

$$\frac{1}{b(x)}\frac{d}{dx}\left\{b(x)h(x)\frac{d\chi_s(x)}{dx}\right\}+\frac{\lambda_s^2}{h_1}\chi_s(x)=0 \tag{7}$$

なる方程式の積分値 $\chi_s(x)$ は

$$\left.\begin{aligned}&\chi_s(h_1)=0,\\&\frac{d\chi_s(h_2)}{dh_2}=k\chi_s(h_2)\end{aligned}\right\} \tag{8}$$

を滿足する時は直交函數である事を知つてゐる．この $\chi_s(x)$ を利用して式 (3) に於ける各項を $\chi_s(x)$ を項とする級數に展開する時は，

$$\eta(x,\,t)=\sum_{s=1}^{\infty}A_s\chi_s(x), \tag{9}$$

$$\frac{\partial\eta}{\partial t}=\sum_{s=1}^{\infty}\frac{dA_s}{dt}\chi_s(x), \tag{10}$$

$$\frac{\partial^2\eta}{\partial t^2}=\sum_{s=1}^{\infty}\frac{d^2A_s}{dt^2}\chi_s(x), \tag{11}$$

$$\frac{1}{b(x)}\frac{\partial}{\partial x}\left\{b(x)\,h(x)\frac{\partial\eta}{\partial x}\right\}=\sum_{s=1}^{\infty}\chi_s(x)\frac{b(h_1)h(h_1)\dfrac{d\chi_s(h_1)}{dh_1}\varphi(t)-\dfrac{\lambda_s^2}{h_1}A_s\displaystyle\int_{h_1}^{h_2}b(x)\chi_s^2(x)dx}{\displaystyle\int_{h_1}^{h_2}b(x)\chi_s^2(x)dx} \tag{12}$$

を得．勿論此れ等の展開式を得るには (5), (6), (7), (8) の關係は利用してゐる．然る時 式 (3) より

$$\frac{d^2A_s}{dt^2}+2f\frac{dA_s}{dt}+g\frac{\lambda_s^2}{h_1}A_s=\frac{gb(h_1)h(h_1)\dfrac{d\chi_s(h_1)}{dh_1}}{\displaystyle\int_{h_1}^{h_2}b(x)\chi_s^2(x)dx}\varphi(t). \tag{13}$$

(13) を解くには, (4) より $t=0$ の場合

$$\left.\begin{aligned} A_s&=0,\\ \frac{dA_s}{dt}&=0,\\ \frac{d^2A_s}{dt^2}&=0 \end{aligned}\right\} \tag{14}$$

なる條件によつて式 (13) の積分を求むればよい事がわかる. (14) の最後の條件 $\frac{d^2A_s}{dt^2}=0$ 即ち $\frac{\partial^2\eta}{\partial t^2}=0$ は, $\varphi(t)$ のなかに含めておけばよいから, 式 (13) を解くには (14) の初めの 2 條件のみに着眼しておればよい. 然る時

$$A_s=\frac{gb(h_1)h(h_1)\dfrac{d\chi_s(h_1)}{dh_1}e^{-ft}}{\sqrt{\left(\dfrac{g}{h_1}\lambda_s^2-f^2\right)}\displaystyle\int_{h_1}^{h_2}b(x)\chi_s^2(x)dx}\int_0^t e^{f\alpha}\sin\left\{\sqrt{\frac{g}{h_1}\lambda_s^2-f^2}(t-\alpha)\right\}\varphi(\alpha)d\alpha. \tag{15}$$

故に求むる灣内海水の運動は次式によつて解決する事が出來る.

$$\eta=gb(h_1)h(h_1)\sum_{s=1}^{\infty}\frac{\dfrac{d\chi_s(h_1)}{dh_1}\chi_s(x)e^{-ft}}{\sqrt{\left(\dfrac{g}{h_1}\lambda_s^2-f^2\right)}\displaystyle\int_{h_1}^{h_2}b(x)\chi_s^2(x)dx}$$

$$\cdot\int_0^t e^{f\alpha}\sin\left\{\sqrt{\frac{g}{h_1}\lambda_s^2-f^2}(t-\alpha)\right\}\varphi(\alpha)d\alpha. \tag{16}$$

勿論式 (16) に於ける $\varphi(t)$ は $\frac{d^2\varphi(t)}{dt^2}$ が $t=0$ の場合零になる様な形である事が必要である.

第 2 章 水深一様な梯形灣内に於ける海水の運動問題

第1章の一般解を利用して深さ一定, 灣口が $2A$, 灣頭が $2B$, 奥行 H なる梯形灣内の海水運動を解く. 第2圖を參照して,

$$\left.\begin{aligned} b(x)&=\gamma+\delta x,\\ h(x)&=D. \end{aligned}\right\} \tag{17}$$

但し

$$\left.\begin{aligned} \gamma&=\frac{Ah_2-Bh_1}{H},\\ \delta&=\frac{B-A}{H} \end{aligned}\right\} \tag{18}$$

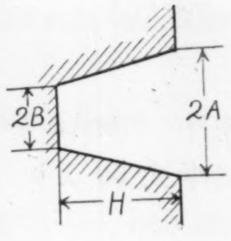

第 2 圖

である．求むべき直交函數 $\chi_s(x)$ の滿足すべき方程式は (7) より，

$$\frac{d^2\chi_s(x)}{dx^2}+\frac{\delta}{\gamma+\delta x}\frac{d\chi_s(x)}{dx}+\frac{\lambda_s^2}{h_1D}\chi_s(x)=0. \tag{19}$$

(8) なる條件に於て $k=0$[2] とせる場合，即ち

$$\left.\begin{aligned}&\chi_s(h_1)=0,\\&\frac{d\chi_s(h_2)}{dh_2}=0\end{aligned}\right\} \tag{20}$$

を滿足する $\chi_s(x)$ は

$$\chi_s(x)=Y_0\left\{\frac{\lambda_s(\gamma+\delta h_1)}{\delta\sqrt{h_1D}}\right\}J_0\left\{\frac{\lambda_s(\gamma+\delta x)}{\delta\sqrt{h_1D}}\right\}-J_0\left\{\frac{\lambda_s(\gamma+\delta h_1)}{\delta\sqrt{h_1D}}\right\}Y_0\left\{\frac{\lambda_s(\gamma+\delta x)}{\delta\sqrt{h_1D}}\right\} \tag{21}$$

であり，λ_s は次式の第 s 番目の根である．s は 1, 2‥‥ 等の正の整數を意味す．

$$Y_0\left\{\frac{\lambda_s(\gamma+\delta h_1)}{\delta\sqrt{h_1D}}\right\}J_1\left\{\frac{\lambda_s(\gamma+\delta h_2)}{\delta\sqrt{h_1D}}\right\}-J_0\left\{\frac{\lambda_s(\gamma+\delta h_1)}{\delta\sqrt{h_1D}}\right\}Y_1\left\{\frac{\lambda_s(\gamma+\delta h_2)}{\delta\sqrt{h_1D}}\right\}=0. \tag{22}$$

式 (22) によつて，この灣內に起される海水運動週期は決定される．

さて

$$\begin{aligned}U_0\left\{\frac{\lambda_s(\gamma+\delta x)}{\delta\sqrt{h_1D}}\right\}=&Y_0\left\{\frac{\lambda_s(\gamma+\delta h_1)}{\delta\sqrt{h_1D}}\right\}J_0\left\{\frac{\lambda_s(\gamma+\delta x)}{\delta\sqrt{h_1D}}\right\}\\&-J_0\left\{\frac{\lambda_s(\gamma+\delta h_1)}{\delta\sqrt{h_1D}}\right\}Y_0\left\{\frac{\lambda_s(\gamma+\delta x)}{\delta\sqrt{h_1D}}\right\}\end{aligned} \tag{23}$$

とおく時[3]，

---

[2] $\frac{d\chi_s(h_2)}{dh_2}=k\chi_s(h_2)$ に應ずる解は (21) である事は全く同じであるが，たゞ λ_s が

$$Y_0\left\{\frac{\lambda_s(\gamma+\delta h_1)}{\delta\sqrt{h_1D}}\right\}J_1\left\{\frac{\lambda_s(\gamma+\delta h_2)}{\delta\sqrt{h_1D}}\right\}-J_0\left\{\frac{\lambda_s(\gamma+\delta h_1)}{\delta\sqrt{h_1D}}\right\}Y_1\left\{\frac{\lambda_s(\gamma+\delta h_2)}{\delta\sqrt{h^1D}}\right\}$$

$$=-\frac{k\sqrt{h_1D}}{\lambda_s}\left[Y_0\left\{\frac{\lambda_s(\gamma+\delta h_1)}{\delta\sqrt{h_1D}}\right\}J_0\left\{\frac{\lambda_s(\gamma+\delta h_2)}{\delta\sqrt{h_1D}}\right\}-J_0\left\{\frac{\lambda_s(\gamma+\delta h_1)}{\delta\sqrt{h_1D}}\right\}Y_0\left\{\frac{\lambda_s(\gamma+\delta h_2)}{\delta\sqrt{h_1D}}\right\}\right]$$

を滿足する方程式の根となる．從つて灣內に起される海水の自由運動週期も k の値によつて色々異つて來るが，今は單に $k=0$ の場合のみを取扱ふ事にする．

[3] (24) を求めるには

$$U_0\left\{\frac{\lambda_s(\gamma+\delta h_1)}{\delta\sqrt{h_1D}}\right\}=0,$$

$$U_1\left\{\frac{\lambda_s(\gamma+\delta h_2)}{\delta\sqrt{h_1D}}\right\}=0$$

及び圓壔函數に關するロンメルの公式を利用してゐる．

$$I=\int_{h_1}^{h_2} b(x)\chi_s^2(x)\,dx=\int_{h_1}^{h_2}(\gamma+\delta x)\,U_0^2\left\{\frac{\lambda_s(\gamma+\delta x)}{\delta\sqrt{h_1D}}\right\}dx$$

$$=\frac{(\gamma+\delta h_2)^2}{2\delta}\,U_0^2\left\{\frac{\lambda_s(\gamma+\delta h_2)}{\delta\sqrt{h_1D}}\right\}-\frac{2}{\pi^2}\,\frac{\delta h_1D}{\lambda_s^2} \tag{24}$$

を得. 故に求むる海水の運動は

$$\eta=\frac{2\delta gD}{\pi}\sum_{s=1}^{\infty}\frac{U_0\left\{\dfrac{\lambda_s(\gamma+\delta x)}{\delta\sqrt{h_1D}}\right\}e^{-ft}}{\sqrt{\left(\dfrac{g}{h_1}\lambda_s^2-f^2\right)}\left\{\dfrac{2}{\pi^2}\,\dfrac{\delta h_1D}{\lambda_s^2}-\dfrac{(\gamma+\delta h_2)^2}{2\delta}\,U_0^2\left\{\dfrac{\lambda_s(\gamma+\delta h_2)}{\delta\sqrt{h_1D}}\right\}\right\}}$$

$$\cdot\int_0^t e^{f\alpha}\varphi(\alpha)\sin\sqrt{\left(\frac{g}{h_1}\lambda_s^2-f^2\right)}(t-\alpha)\,d\alpha \tag{25}$$

によつて表される. 勿論 λ_s は (22) の根である.

(25) より $B>A$, $B<A$ 及び $A=B$ なる場合を求めてみる.

$B>A$ なる場合

$$\eta=\frac{2(B-A)gD}{\pi H}$$

$$\cdot\sum_{s=1}^{\infty}\frac{U_0\left\{\dfrac{\lambda_s\{(Ah_2-Bh_1)-(A-B)x\}}{(B-A)\sqrt{h_1D}}\right\}e^{-ft}}{\sqrt{\left(\dfrac{g}{h_1}\lambda_s^2-f^2\right)}\left\{\dfrac{2}{\pi^2}\,\dfrac{(B-A)}{H}\,\dfrac{h_1D}{\lambda_s^2}-\dfrac{B^2H}{2(B-A)}\,U_0^2\left(\dfrac{\lambda_sBH}{(B-A)\sqrt{h_1D}}\right)\right\}}$$

$$\cdot\int_0^t e^{f\alpha}\varphi(\alpha)\sin\sqrt{\left(\frac{g}{h_1}\lambda_s^2-f^2\right)}(t-d)\,d\alpha. \tag{26}$$

但し λ_s[4] は

$$Y_0\left\{\frac{\lambda_sAH}{(B-A)\sqrt{h_1D}}\right\}J_1\left\{\frac{\lambda_sBH}{(B-A)\sqrt{h_1D}}\right\}-J_0\left\{\frac{\lambda_sAH}{(B-A)\sqrt{h_1D}}\right\}Y_1\left\{\frac{\lambda_sBH}{(B-A)\sqrt{h_1D}}\right\}=0 \tag{27}$$

の根である.

---

[4] (27) の圓壔函數のアーギュメントが大になればこの函數の漸近展開を利用して, λ_s は

$$\sin\left\{\frac{\lambda_sH}{\sqrt{h_1D}}-\frac{\pi}{2}\right\}=0$$

の根となり, λ_s は A 及び B に無關係となる.

$B<A$ なる場合

$$\eta=\frac{2(A-B)gD}{\pi H}$$

$$\cdot\sum_{s=1}^{\infty}\frac{U_0\left\{\frac{\lambda_s\{(Ah_2-Bh_1)-(A-B)x\}}{(A-B)\sqrt{h_1D}}\right\}e^{-ft}}{\sqrt{\left(\frac{g}{h_1}\lambda_s^2-f^2\right)}\left\{\frac{2}{\pi^2}\frac{(A-B)}{H}\frac{h_1D}{\lambda_s^2}-\frac{B^2H}{2(A-B)}U_0^2\left(\frac{\lambda_sBH}{(A-B)\sqrt{h_1D}}\right)\right\}}$$

$$\cdot\int_0^t e^{f\alpha}\varphi(\alpha)\sin\sqrt{\left(\frac{g}{h_1}\lambda_s^2-f^2\right)}(t-\alpha)\,d\alpha. \tag{28}$$

但し λ_s5) は次式の根である.

$$Y_0\left\{\frac{\lambda_sAH}{(A-B)\sqrt{h_1D}}\right\}J_1\left\{\frac{\lambda_sAH}{(A-B)\sqrt{h_1D}}\right\}-J_0\left\{\frac{\lambda_sAH}{(A-B)\sqrt{h_1D}}\right\}Y_1\left\{\frac{\lambda_sBH}{(A-B)\sqrt{h_1D}}\right\}=0 \tag{29}$$

$A=B$ なる場合

この時は

$$\eta=\frac{4\sqrt{g}}{\pi\sqrt{h_1}}\sum_{s=1}^{\infty}\frac{\lambda_s\sin\left\{\frac{\lambda_s(x-h_1)}{\sqrt{h_1D}}\right\}e^{-ft}}{\sqrt{\left(\frac{g}{h_1}\lambda_s^2-f^2\right)}\left\{\frac{2\lambda_s}{\sqrt{h_1D}}-\sin\left(\frac{2\lambda_sH}{\sqrt{h_1D}}\right)\right\}}$$

$$\cdot\int_0^t e^{f\alpha}\varphi(\alpha)\sin\sqrt{\left(\frac{g}{h_1}\lambda_s^2-f^2\right)}(t-\alpha)\,d\alpha \tag{30}$$

となり, λ_s は

$$\lambda_s=\left(s-\frac{1}{2}\right)\frac{\pi\sqrt{h_1D}}{H}. \tag{31}$$

今 (27), (29) 及び (31) を用ひて, $\frac{A}{B}$ の色々の値に應じて灣内に起される海水の自由運動週期を求めると次表を得. これは $s=1$, $s=2$, $s=3$ 及 $s=4$ の場合に就て夫々圖示計算法によつて求めたのである. 勿論本計算結果は $\frac{A}{B}$ が 1 より餘り小さくとも又大きくとも適用し難いものであるが, $\frac{A}{B}$ の値による週期の變化狀態を定性的に知るには不都合がない故第 I 表を求めておいた. これを圖示すると第 3 圖を得. $s=1$ の場合卽ち灣内に節のない時以外は, 週期は殆んど灣の形卽 $\frac{A}{B}$ には無關係にな

---

5) (27) と同じく漸近展開が用ひ得る範圍となれば, (29) の代りに λ_s は

$$\sin\left\{\frac{\lambda_sH}{\sqrt{h_1D}}+\frac{\pi}{2}\right\}=0$$

の根となり, A, B に無關係になる事は前と同じ.

る. $s=1$ の場合には週期は $\frac{A}{B}$ が大になる程小となる傾向がある. 勿論灣の長さ H には比例し, 深さ D に就ては $D^{1/2}$ に逆比例して變化する事は明かである. 尙 $s=2$ 以上では $\frac{B}{A}$ の値に無關係に週期 T は

$$T \fallingdotseq \frac{2H}{\sqrt{gD}}\left(s-\frac{1}{2}\right)^{-1} \tag{32}$$

で表される.

第 I 表 灣内海水の自由運動週期 $\left(\text{單位}=\frac{\sqrt{gD}}{H}\right)$

A/B \ s	0·20	0·40	0·60	0·80	1·00	1·20	1·50	2·00	2·50
1	5·61	4·87	4·41	4·19	4·00	3·855	3·70	3·50	3·38
2	1·38	1·359			1·333		1·32	1·31	1·30
3	0·800	0·80	0·80	0·80	0·80	0·80	0·80	0·80	0·80
4	0·572	0·572	0·572	0·572	0·572	0·572	0·572	0·572	0·572

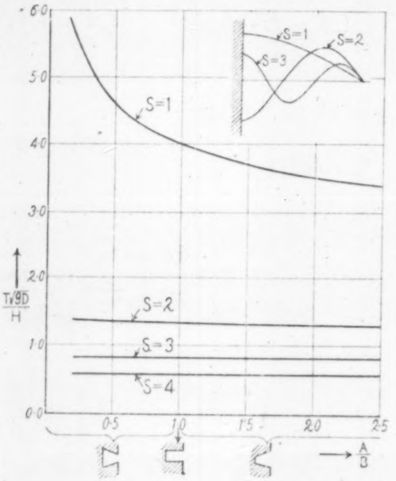

第 3 圖

灣口 $x=h_1$ に於て水位が次式で示される様な變化をする時, 即ち

$$\varphi(t)=\eta_0\left(\frac{\sqrt{gD}}{H}t\right)^3 e^{-\beta\frac{\sqrt{gD}}{H}t} \tag{33}$$

の時は,

$$\int_0^t \xi^3 e^{-a\xi}\sin b(t-\xi)\,d\zeta$$

$$=\left[\frac{bt^3e^{-at}}{(a^2+b^2)}+\frac{babt^2e^{-at}}{(a^2+b^2)^2}+\frac{b(3a^2-b^2)bte^{-at}}{(a^2+b^2)^3}+\frac{24ab(a^2-b^2)\,e^{-at}}{(a^2+b^2)^4}\right.$$
$$\left.+\frac{6(a^4-6a^2b^2+b^4)}{(a^2+b^2)^4}\sin bt-\frac{24ab(a^2-b^2)}{(a^2+b^2)^4}\cos lt\right] \tag{34}$$

なる關係を用ひて, (25) 或は (26), (28), (30) によつて夫々の灣内での海水運動を研究する事が出來る. 即ちかくする事によつて, (4) なる加速度までも $t=0$ の時零にする條件も完全に滿足さす事が出來る. 具體的な海水面變化の研究は次の機會に讓つておく.

4. *On the Long Waves in a Bay of Variable Section Generated by the Changes in the Elevation at the Mouth of It.*

By Genrokuro NISHIMURA, Takeo TAKAYAMA
and Kiyoshi KANAI,

Earthquake Research Institute.

Taking into account water friction proportional to the horizontal velocity of water particle, we obtained a general expression for the surface elevation of water in a bay of variable section due to changes in the elevation at the mouth of it. As in the previous paper, we ignore the decay of wave motion in the bay that occurs from the fact that a part of the energy of the reflected wave in the bay is propagated in the open sea as circular wave of diverging type.

Using the general expression of the water elevation thus obtained, we studied the case of a trapezoidal bay of rectangular section and with horizontal bed.

5. *Approximate Determination of the Spheroid most nearly Representing the Surface of Japan.*[*]

By Yukio KAWABATA,

The Japanese Land Survey.

(Read Nov. 20, 1934.—Received Dec. 20, 1934.)

I. Theory, observation and measurement agree in showing that the figure of the earth is very closely represented by an ellipsoid of revolution about the axis of the earth. Strictly speaking, however, that is not so; the visible irregularities of the physical surface, variations of density of the materials composing the crust, irregular perturbative forces arising from the motion of the planets, etc., all these superinduce on the ellipsoidal form undulations that cannot be expressed by any mathematical formulae. The result of both extensive geodetical operations and astronomical observations enable us however to determine a spheroid to which the mathematical surfaces of the earth may be very conveniently referred, the deviations from which are very small. We shall call this ellipsoid of reference R, and the actual mathematical surface of the earth M. Our problem is to determine the surfaces R and M which satisfy the condition that surface R shall most closely represent the surface M of Japan.

As will be seen from Table I, a number of astronomical observations have been made by the officials of the Japanese Geodetic Commission, the Land Survey Department, the Hydrographic Department, and others. The accuracy of these observations generally differs according to the purposes of their observations: the Geodetic Commission to find the deviation of the plumb line, the Land Survey Department to compute the new base line in the course of their geodetic work, the Hydrographic Department in their cartographic views.

The deviations of the plumb line are expressed by the well known formulae

$$\xi = B_g - B_a, \tag{1}$$

$$\eta = (L_g - L_a) \cos B_g, \tag{2}$$

$$\eta = (A_g - A_a) \cot B_g, \tag{3}$$

where B, L and A are latitude, longitude and azimuth, respectively, reckoned in the usual manner; a and g the respective astronomical and geodetic indices. These quantities are computed in the last column of Table I.

---

[*] Communicated by T. TERADA.

Although the deviation of the plumb line at any given station is affected by local attractions of the surrounding mass, as is evident from conditions in the neighbourhood of Tanzawayama and Mt. Aso, they are still too large and too systematic to be interpreted as arising solely from these local topographic deflections. They occurred in all probability from errors with respect to the situation, shape, and dimension of the reference ellipsoid we have taken in the geodetic work in Japan.

A short time ago, Mr. K. Atumi,[1] after examining the deviations of plumb lines at 68 astronomical stations, determined what he considered the most suitable reference ellipsoid and geoid undulations in Japan. Although, to simplify the calculation of the coefficients in his equations of condition, he assumed the earth to be a sphere, those coefficients differ more and more from the values exactly based on the ellipsoid of revolution with increase of distance. In particular, it will be apparent from the later part of this paper that the coefficients of da and de^2, the corrections that must be applied to the semi-major axis and the eccentricity of the meridian ellipse, increase in proportion to the distance, with the result that these coefficients differ widely. For this reason his computations should be regarded as determinations from these erroneous values alone. Since, moreover, he has assigned an equal weight to all the observations, not taking into account their accuracy, the results of his computations do not appear to be very accurate.

In the following, in the first place I have computed the coefficients exactly on the ellipsoid of rotation, and in the second place I took into consideration the different weights in making out the conditional equations, although roughly, taking into account Laplace's condition which must exist in the components of the deviation of the plumb line as deduced from the longitudinal and azimuthal observations.

II. Geodetic Data.

Before entering into details it is necessary to explain how the geodetic data in this report were obtained.

Geodetic work in Japan, since 1870, has been done by the Land Survey Department. The instrument used in measuring the horizontal angles of the primary triangulation is the theodolite made by Carl Bamberg, the diameter of the horizontal circle of which is 27 cm, the circle being divided into five minutes and read by two microscopes. The instrument rests on a pedestal provided with three levelling screws. One

---

[1] Captaine du génie K. Atumi, "La déviation de la varticale au Japon," *Jap. Jour. Astr. Geophys.*, **10** (1933), 305.

Table I

No.	Station	Height	*Ba*, *La*, *Aa*	*Bg* *Lg* *Ag*	Epoch	Observer	Direction of azimuth
1	Handasawa		49°59′60″·28±0″·17 142 46 — —	50″·89 16·18 —	1930	Author	—
2	Higasiyama		49 59 46·90±0·18 143 7 57·30±0·68 269 11 4·29	44·61 78·79 13·96	1930	Author	Aimidake
3	Syana		45 13 46·1 147 52 30·0±0·33 —	28·88 55·84 —	1904	Hydro. Depart.	—
4	Abasiri		44 1 10·7 144 16 26·3 —	9·70 35·77 —	1905	„	—
5	Nemuro		43 20 23·41±0·038 145 34 52·0 ±0·225 —	28·22 54·15 —	1911	„	—
6	Sapporo	m 15·0	43 4 34·4 141 21 — 349 53 58·2±0·85	20·9 26·67 54·7	1900	Land survey	Northern point of Sapporo base
7	Urakawa		42 9 15·0 142 46 29·0 —	36·2 49·5 —	?	Hokkaidotyo	—
8	Hakodate		41 45 67·0 140 43 16·6 —	57·21 35·15 —	1884	Hydro-Depart.	—
9	Aomori		40 49 63·86±0·059 140 46 17·52±0·135 —	43·58 40·61 —	1914	„	—
10	Turukotai	43·1	40 42 76·8 141 9 — 244 15 11·5	59·3 26·8 8·3	1898	M. Sugiyama.	Western point of Turukotai base
11	Sionohara	221·7	38 49 61·1 140 21 — 266 18 16·2	50·8 47·7 28·7	1894	M. Yazima	Western point of Sionohara base
12	Matugasaki	26·4	37 56 70·57±0·249 139 8 19·89±0·75 —	54·17 45·45 —	1923	T. Nakasima	—
13	Toriyayama	580·6	37 34 66·09±0·127 139 33 — —	53·24 43· —	1923	„	—
14	Keizyô	—	37 33 43·48 126 58 29·94 —	32·7 43·2 —	1907	M. Yamada	—
15	Wazima	—	37 23 67·12 136 53 25·46 —	51·09 49·80 —	1888	Hydro. Depart.	—
16	Sakatoyama	633·9	37 3 46·21±0·211 138 53 36·20±3·600 149 22 59·20±0·90	21·56 65·73 22·00	1923	T. Nakasima	—

Instruments	Method of observation	*Ba−Bg*	*La−Lg*	*Aa−Ag*
Bamberg's transit	15 pairs in 3 nights by Talcott's method. Resistering micrometer in 2 nights.	+ 9″·39	+16″·37	—
Bamberg's transit 27 cm theodolite	21 pairs in 3 nights by Talcott's method. Resistering micrometer in 3 nights. 24 times by circumpolar stars.	+ 2·29	– 21·49	– 9″·67
	Zinger's method in 10 nights.	+ 17·22	– 25″84	—
		+ 1″00	– 9·47	—
	Talcott's method in 5 nights.	– 4″81	– 2·15	—
Bamberg's transit	54 pairs in 7 nights by Talcott's method (Time ; equal altitude of sun) 6 times in 3 nights by any hour angle of polaris.	+ 13·5	—	+ 3·5
		– 21·2	– 20·5	—
		+ 9·79	– 18·55	—
	Talcott's method	+ 20·28	—	– 23·09
Universal theodolite	Altitude of Polaris in 4 nights (Time: equal altitude of sun by sextant) Elongation of polaris or 51 Cephei in 4 nights.	+ 17·5	-	+ 3·2
21 cm. universal theodolite	Altitude of polaris in any time or meridian altitude of any stars (Time: equal altitude of sun) 6 times in elongation of polaris.	+ 10·3	—	– 12·5
Bamberg's transit	17 pairs in 4 nights by Talcott's method. Chronograph and Key in 4 nights.	+ 16·40	– 25·56	—
„	15 pairs in 3 nights by Talcott's method.	+ 12·75	—	—
13·5 cm theodolite	Talcott's and sing. altitude of polaris. Equal altitude	+ 10·78	– 13·26	—
—	—	+ 16·03	– 24·34	—
Bamberg's transit 13·5 cm theodolite	18 pairs in 5 nights by Talcott's method. Chronograph and key in 3 nights. Any hour angle of polaris.	+ 24·56	– 29·53	– 22·80

(*to be continued.*)

Table I.

No.	Station	Height	*Ba*, *La*, *Aa*,	*Bg* *Lg* *Ag*	Epoch	Observer	Direction of azimuth
17	Nanao	m —	37°2′58″·0 — 136 57 31·6 —	39″·52 47·94 —	1887	Hydro. Depart.	—
18	Suzaka	353·3	36 40 37·0 138 18 — 102 44 15·3±0·70	17·8 29·2 29·5	1896	Land Survey	Eastern point of the Suzaka base
19	Takasuzuyama	623·7	36 37 3·53±0·098 140 35 — —	4·22 28·2 —		N. Itinoe	—
20	Utunomiya	58·7	36 34 9·0 139 53 24·0 —	0·7 25·9 —		Land Survey	—
21	Akagi	1673·9	36 32 17·57±0·054 139 10 —	16·37 50·0 —	1903	N. Itinoe K. Sôtome	—
22	Teruisiyama	419·1	36 21 26·71±0·091 139 40 — —	25·63 43·0 —	1907	N. Itinoe	—
23	Kariyado	1096·3	36 21 21·04±0·072 138 33 44·1±0·260 —	13·76 55·3 —	1921	T. Matukuma S. Kanda	—
24	Tukubasan	709·0	36 13 22·0 140 5 55·0 —	22·3 67·2 —	1902	K. Sotome S. Tasiro R. Ootani	—
25	Kirigamine	1021·1	36 2 49·00±0·093 138 2 40·6 ±1·01 —	30·61 56·8 —	1921	T. Matukuma S. Kanda	—
26	Dôhirayama	857·8	36 0 21·08±0·053 139 11 — —	9·26 35·73 —	1903	N. Itinoe K. Sotome	—
27	Takagamimura	73·6	35 42 5·96±0·071 140 51 — —	11·03 24·4 —	1907	N. Itinoe	—
28	Ako	685·4	35 42 16·97±0·056 137 55 49· 5±0·38 —	5·38 60·4 —	1921	T. Matukuma S. Kanda	—
29	Siozakimura	349·6	35 40 25·55 138 30 22·5 —	21·54 26·3 —	1921	T. Matukuma S. Kanda	—
30	Mitaka	58·0	35 40 21·0 139 32 31·5 —	20·6 24·1 —		Astronomical Observatory	—
31	Turuga	—	35 39 14, 136 4 15, —	7· 28·8 —	1890	Hydro. Depart.	—
32	Sakae	—	35 32 49·70±0 037 133 14 31·77±0·330 —	39 77 41·96 —	1920	Hydro. Depart.	—

(conitnued.)

Instruments	Method of observation	$Ba-Bg$	$La-Lg$	$Aa-Ag$
		+18″·48	−16″·34	—
21 cm universal theodolite	86 pairs in 3 nights by Talcott's method (Time; meridian transit by theodolite or eqal altitude of sun by sextant). 17 times in 4 nights by elongation of circumpolar stars.	+ 19·2	—	− 14·2
—	29 pairs in 5 nights by Talcott's method.	− 0·69	—	—
—		+ 8·3	− 1·9	—
Bamberg's transit	60 pairs in 6 nights by Talcott's method.	+ 1·2	—	—
Bamberg's transit	40 pairs in 4 nights by Talcott's method.	+ 1·08	—	—
Bamberg's transit	34 pairs in 3 nights by Talcott's method. Chronograph and key in 3 nights.	+ 7·28	− 11·2	—
—		− 0·3	− 12·2	—
Bamberg's transit	31 pairs in 4 nights by Talcott's method. Chronograph and key in 2 nights.	+ 18·39	−16·20	—
Bamberg's transit	39 pairs in 6 nights by Talcott's method.	+ 11·82	—	—
Bamberg's transit	34 pairs in 5 nights by Talcott's method.	− 5·07	—	—
Bamberg's transit	39 pairs in 4 nights by Talcott's method. Chronograph and key in 4 nights.	+ 11·59	− 10·9	—
Bamberg's transit	26 pairs in 3 nights by Talcott's method.	+ 4·01	− 3·8	—
Bamberg's transit	Numerous pairs in 3 years. Resistering micrometer.	+ 0·4	+ 7·4	—
		+ 7·	− 13·8	—
	Talcott's method. Transit observation (Zinger ?)	+ 9·93	− 10·19	—

(to be continued.)

Table I.

No.	Station	Height	*Ba La Aa*	*Bg* *Lg* *Ag*	Epoch	Observer	Direction of azimuth
33	Tobio-yama	m 234·8	35°30′10″·44±0″·280 139 19 61·38±0·375 183 11 14·79±0·790	4″42 40·47 3·26	1927	T. Tiba N. Saito	Sengenyama
34	Maiduru	—	35 28 39·43±0·035 135 23 3·54±0·135 —	20·86 14·15 —	1918	Hydro. Depart.	—
35	Tanzawa-yama	1567·4	35 28 20·48±0·111 139 9 74·72±0·600 178 34 65·59±0·18	15·75 57·07 56·7	1926	M. Kaga-wa	Togadake
36	Rokudizô	173·2	35 26 47·19±0·035 140 12 — —	39·72 31·0 —	1903	N. Itinoe K. Soto-me	—
37	Tenzinno	52·2	35 24 73·1 133 47 — 214 32 35·1	51·5 48·8 37·1	1883	Land Survey	Yakebayasi-mura
38	Kenasi-yama	1954·4	35 24 41·45±0·087 138 32 17·04±0·252 17 1 2·15±0·57	38·59 28·99 7·76	1926	M. Kaga-wa	Kokusidake
39	Aibano	233·7	35 23 26·9 135 59 — 273 43 4,7	2·6 48·0 4·0	1888	M. Yazi-ma	Western point of Aibano base.
40	Kanda-mura	138·5	35 21 35·68 136 17 16·41 —	28·89 31·10 —	1922	T. Naka-sima M. Tyo	—
41	Sengen-yama	181·3	35 19 9·67±137 139 18 — —	7·93 55·9 —	1907	N. Itinoe	—
42	Kanôzan	353·3	35 15 25·09±0·038 139 57 — —	6·10 32·3 —	1903	K. Sotome	—
43	Sanomura	—	39 9 20·85 138 55 20·25 156 7 59·38	17·35 33·32 55·77	1931	D. Saida	Daibamura
44	Daiba-mura	—	35 6 27·79 138 56 57·45 336 8 55·98	21·45 68·04 50·28	1931	D. Saida	Sanomura
45	Kwasan	221·3	34 59 36· 135 47 33·4 —	25· 48· —	1930	Kwasan Obser-vatory	—
46	Bôdaisan	—	34 57 58·78±0·075 139 46 — —	39·14 51·4 —	1907	N. Itinoe	—
47	Mera	—	34 54 46·97±0·038 139 49 59·64 —	28·91 56·34 —	1916	Hydro. Depart.	—
48	Hamada	—	34 53 53·2±0·04 132 54 4·4±0·38 —	36·39 12·71 —	1920	Hydro. Depart.	—

(continued.)

Instruments	Method of observation	*Ba − Bg*	*La − Lg*	*Aa − Ag*
Bamberg's transit 21 cm theodolite	10 pairs in 3 nights by Talcott's method. Chronograph and key in 3 nights. Any hour angle of polaris in 2 nights.	+ 6″·02	+ 20·91	+ 11·54
	Talcott's method. Transit Observation.	+ 18·57	− 10·61	—
Bamberg's transit 27·5 cm theodolite	35 pairs in 5 nights by Talcott's method. Chronograph and key in 3 nights. Any hour angle of polaris in 2 nights.	+ 4·74	+ 17·65	+ 8·89
Bamberg's transit	53 pairs in 3 nights by Talcott's method.	+ 7·47	—	—
	17 pairs by Talcott's method. 14 times by any hour angle of circumpolar stars.	+ 21·6	—	− 2·0
Bamberg's transit 27·5 cm theodolite	38 pairs in 6 nights by Talcott's method. Chronograph and key in 3 nights. Any hour angle of polaris in 3 nights.	+ 2·86	− 11·95	− 5·61
	Altitude in meridian of any stars in 1 night. Greatest elongation of polaris in 1 night.	+ 24·3	—	+ 0·7
		+ 6·79	− 14·69	—
Bamberg's transit	30 pairs in 4 nights by Talcott's method.	+ 1·74	—	—
Bamberg's transit	67 pairs in 5 nights by Talcott's method.	+ 18·99	—	—
		+ 3.50	− 13·07	+ 3·61
		+ 6·34	− 10·59	+ 5·70
		+ 11·[illegible]	− 14·6	—
Bamberg's transit	51 pairs in 5 nights by Talcott's method.	+ 19·64	—	—
	Talcott's method. Transit observatien.	+ 18·06	+ 3·3	—
	Talcott's method. Transit observation (Zinger ?).	+ 16·81	− 8·31	—

(to be continued.)

Table I.

No.	Station	Height	*Ba* *La* *Aa*	*Bg* *Lg* *Ag*	Epoch	Observer	Direction of azimuth
49	Rokkôzan	m 932·1	34°46′40″·19±0″·29 135 15 51·40±1·25 224 24 39· 3±0·53	28″·83 59·49 43·7	1928	M. Takasaki T. Matui	Kumogaiwa
50	Sakabe	151·1	34 45 62.52±0·121 138 12 15·49±0·292 318 51 19·53±0·494	57·86 22·52 21·74	1931	T. Urano K. Kirihara	Hakkozan
51	Oosaka-zyô	44·2	34 41 21·0 135 31 28·0 —	3·37 42·71 —		Land Survey	—
52	Mikomotozima	—	34 34 27·2 138 56 31·05 —	19·2 46·72 —	1928	Hydro. Depart.	—
53	Kasaoka	—	34 29 61·5 133 30 12·2 —	52·30 32·19 —	1893	Hydro. Depart.	—
54	Edazima	—	34 14 37·0 132 28 27·6 —	31·20 39·86 —	1888	Hydro. Depart.	—
55	Nisibayasi	37·0	34 4 31·3 134 11 — 97 33 33·0±0·77	9·3 41·0 31·7	1890	Land Survey	Eastern point of Nisibayasi base.
56	Simonoseki	—	33 57 22·6±0·04 130 56 16·2±0·08 —	8·89 26·72 —	1917	Hydro. Depart.	—
57	Saeki	—	32 54 10·11±0·048 131 57 51·42±0·320 —	3·10 46·51 —	1920	Hydro. Depart.	—
58	Nagasaki	—	32 43 58· 129 52 10·5 —	42·2 21·2 —	1917	Hydro. Depart.	—
59	Miyazaki	4·4	31 54 62·67±0·048 131 25 37·96±0·315 —	53·75 22·56 —	1920	Hydro. Depart.	—
60	Kagosima	—	31 35 41·9 130 33 33·0 —	41·7 29·1 —		Hydro. Depart.	—
61	Kasanohara	106·3	31 23 15·6 130 51 — 38 29 26·1	3·9 54·4 30·2	1892	M. Yazima	Northern point of Kasanohara base

revolution of the micrometer, when in perfect adjustment, is equal to 2′. As the micrometer head has 60 divisions, it can be read to 2″, but by taking the mean of two micrometers *A* and *B*, it can be read down to 1″, and by mentally dividing the space down to one-tenth of a second.

One angle was measured twenty-four times by the angle method, not by that of direction. To eliminate collimation errors, one-half of

(*continued.*)

Instrument	Method of observation	*Ba*−*Bg*	*La*−*Lg*	*Aa*−*Ag*
Bamberg's transit Universal theodolite	18 pairs in 5 nights by Talcott's method. Chronograph and key in 3 nights. Any hour angle of polaris in 1 night.	+11″·36	− 8″·09	− 4″·4
Bamberg's transit 27·5 cm theodolite	52 pair in 8 nights by Talcott's method. Resistering micrometer in 7 nights. Any hour angle of polaris in 3 nights.	+ 4·66	− 7·03	− 2·21
		+ 17·63	− 14·71	—
		+ 8·0	− 15·67	—
		+ 9·20	− 19·99	—
		+ 5·8	− 12·26	—
12 cm universal theodolite	25 pairs in 2 nights by Talcott's method. 5 times in 2 nights by elongation of polaris.	+ 22·0	—	+ 1·3
		+ 13·71	− 10·52	—
	Zinger's method.	+ 7·01	+ 4·91	—
		+ 5·8	− 10·7	—
	Talcott's method. Transit observation.	+ 8·92	+ 15·40	—
		+ 0·2	+ 3·9	—
21 cm universal theodolite	4 times by altitude at any hour angle of polaris or meridian altitude of circumpolar stars (Time: equal altitude of sun by sextant). 24 times at greatest elongation of polaris.	+ 11·7	—	− 4·1

these twenty-four observations was made in one position of the telescope and the remaining half in the reversed position. At each of these twenty-four observations, the position of the circle was systematically altered according to the law of O. Schreiber, to eliminate errors arising from the eccentricity and graduation of the circle. Since the run of the microscope is apt to get out of order in transporting the instrument from mountain to mountain, it was always accurately adjusted upon arrival of the observer at any station, and rechecked after completion of the observation at that station.

As the distances separating the primary triangulation points in Japan generally exceed 30 kilometers, and as the zenith distance makes nearly a right angle, the error that arises from the axes is considered very small when the axes are almost fully adjusted. For this reason the error that arises from the axes, or the correction for errors that arise from the height of the observing stations owing the disagreement of the vertical sections of the rotation ellipsoid, may generally be neglected, so long as the instrument is adjusted frequently during observations. The value of one division of the striding level used in these adjustment is generally $3'' \sim 4''$.

The triangulation net of the whole country, except Taiwan and Tyôsen, therefore was divided into twenty-four individual nets as shown in the map appended. With a few exceptions, each of them has generally one base line.

The base line, the length of which is usually several kilometers, was measured with a 5-meter Guillaume apparatus, or a 4-meter Hilgard contact slide apparatus; instruments similar to those used in previous surveys. Recently, 25-meter Jäderin wires, the length of which was determined just before and after field survey work by comparing it with comparison base line at Mitaka Astronomical Observatory, was used. It was ascertained when re-measuring the Aibano and Tenzinno base lines, that previous measurements of them were almost as accurate as those made much later. These base lines were projected on the mean sea level of Tôkyô Bay by means of precise levellings.

Were the observed angles of a triangulation free from error, calculation of the distance between pairs of points would present no difficulty, but the errors with which every observed angle is vitiated lead to conflicting results. These contradictions in the measured angles however were removed and a consistent figure was obtained after adjusting the net so as to satisfy the following two conditions:—

(I) Station adjustment:—Those arising at a station from the relation of the angles to one another at that station.

(II) General adjustment:—Those due to the geometrical relations needed to form a closed figure.

The general adjustment is based on two conditions:—

(a) Angle equation:—That the sum of the angles of each triangle in the figure should be equal to 180° plus spherical excess of the triangle.

(b) Side equation:—Even if the angle equations be satisfied, the figure does not close, so that the length of any side as computed from the known base line or the side, should be the same whatever the route chosen.

The trigonometrical nets were adjusted step by step as geodetic work proceeded in accordance with the conditions laid down as just mentioned. It should be mentioned here that, in expanding the net, observations at the station on the boundary of two nets were made with utmost care in order to eliminate errors in connection with the orientation of the new net, a way of observing that differed somewhat from those at other stations. The above mentioned twenty-four observations were divided into two groups, one-half of them being measurements from one known point and the remaining half from the other known point. The result was that we obtained a consistent figure.

After Bessel's spheroid

$$a = 6377397{\cdot}15 \text{ meters},$$

$$b = 6356078{\cdot}96 \text{ meters},$$

$$\alpha = 1 : 299{\cdot}152813,$$

had been adopted as the reference ellipsoid and all the angles and lengths had been completely fixed, it was still necessary, before the calculation of latitudes, longitudes, and azimuths could be made, to adopt a standard latitude and longitude for a special station and a standard azimuth of a line from that station. For convenience of reference, the adopted standard position of a given station, together with the adopted standard azimuth of a line from that station, is called the geodetic datum.

One geodetic datum in our survey was the center of the meridian circle at Azabu Astronomical Observatory, Tôkyô, and the other the astronomical azimuth to the primary triangulation point, Kanôzan, from that station.

$$B = 35°39'17''{\cdot}5148,$$

$$L = 139°44'40''{\cdot}5020,$$

$$A = 156°25'30''{\cdot}156.$$

The site, which is shown in Fig. 1, served as the basis for all the geodetic values in this report.

Using these values and results of the adjustment, we calculated the latitude, longitude, and azimuth of all the stations according to O. Schreiber's[2] formulae, which is exact up to $0''{\cdot}0001$ for latitude and longitude and up to $0''{\cdot}001$ for azimuth applied to a point, the distance

---

2) O. SCHREIBER, "Formeln und Tafeln zur Berechnung der geographischen Koordinaten aus den Richtungen und Längen der Dreiecks seiten," Berlin (1878).

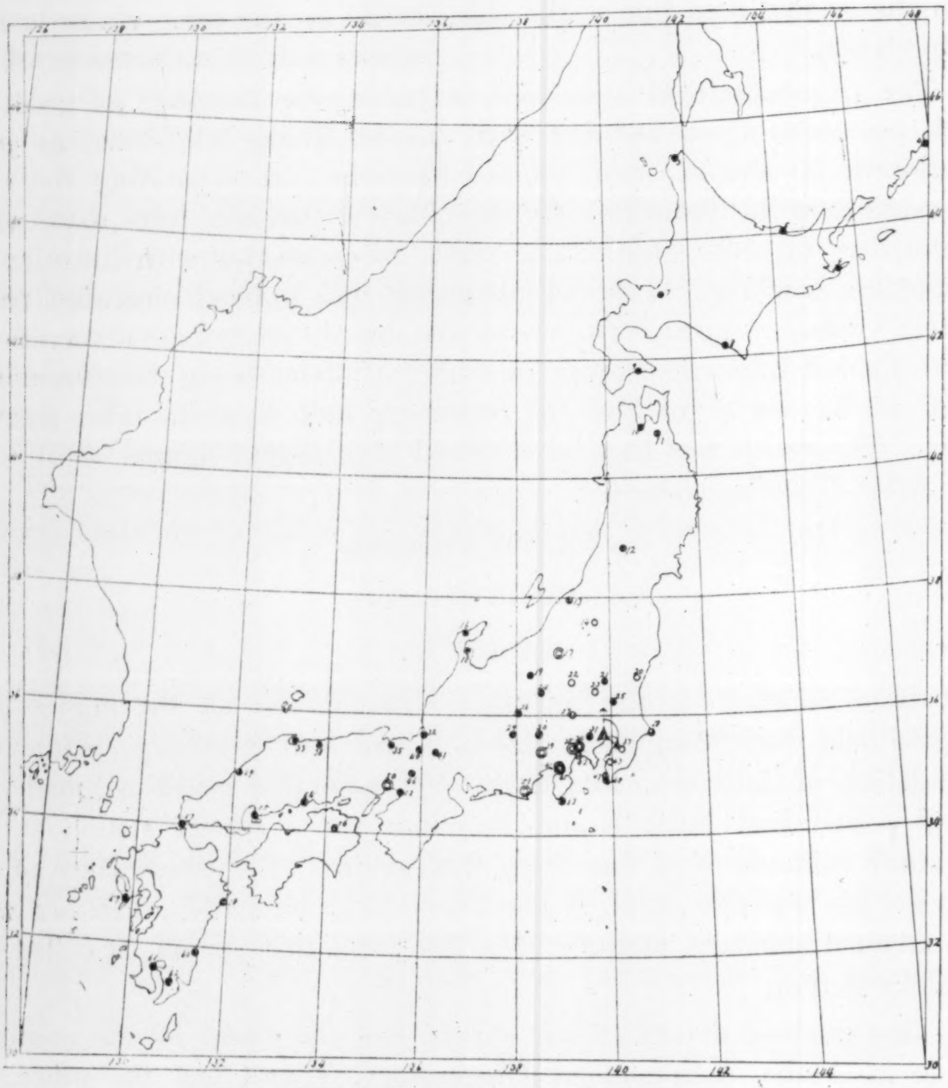

Fig. 1. Distribution of astronomical stations.

▲ : Standard datum.

◎ : Latitude, longitude and azimuth.

● : Latitude and one of longitude or azimuth.

○ : Latitude only.

of which is 120 km. These quantities were always calculated from two directions and controlled.

III. Determination of the Surface *R*.

Since measured base lines are reduced to the surface of the mean sea level of Tôkyô Bay, and since the angles measured by the theodolite are the same as were measured on that surface, it follows that the trigonometrical operations may be considered as having been virtually conducted on the surface *M*. But, since the angles measured on *M* are not identical with the angles measured on *R*, the former must be reduced to the surface *R*. Meanwhile, for purposes of reduction, it is necessary that the form of the geoid shall be known before beginning the geodetic work, and even if that were known, it is almost impossible to calculate the triangulation on a surface so complexed. Fortunately, however, since in the case of a distant object observed in a trigonometrical survey, the angles of elevation of the signal are generally small, and since in ordinary cases, ξ's and η's are very small angles, we may infer that the angle observed on M is not sensibly different from the corresponding angle on R. It may therefore be concluded that the larger part of ξ's and η's arises from absolute deviations of the plumb line at the geodetic datum ξ_0 and η_0, and from the differences of magnitude and shape da and de^2 of the ellipsoid, adopted as reference and assumed to represent most closely the surface of M of Japan. In consideration of the foregoing we can now state that, at every point from which the astronomical observations were made, the ξ_i and η_i belonging to that point can be expressed in terms of $\xi_0\,\eta_0$, da and de^2.

The equation of condition thus obtained are

$$a_i\xi_0+b_i\eta_0+c_i\frac{da}{a}+d_i\frac{1}{2}\frac{de^2}{1-e^2}-\xi_i=0, \tag{4}$$

$$a_i'\xi_0+b_i'\eta_0+c_i'\frac{da}{a}+d_i'\frac{1}{2}\frac{de^2}{1-e^2}-\eta_i=0, \tag{5}$$

$$a_i''\xi_0+b_i''\eta_0+c_i''\frac{da}{a}+d_i''\frac{1}{2}\frac{de^2}{1-e^2}-\eta_i=0, \tag{6}$$

of which (4), (5), (6) were deduced from the observations of latitude, longitude, and azimuth respectively. When longitude is measured eastward and the azimuth reckoned from the south, the value of the coefficient[3] may be expressed as follows:

$$\left.\begin{aligned}
a_i&=\frac{W_i^3}{W_0^3}\left\{\cos\Delta\alpha+\left[1-\left(\frac{dm}{ds}\right)_{i0}\right]\sin\alpha_{0i}\sin\alpha_{i0}\right\},\\
b_i&=-\frac{m}{a}\frac{W_i^3}{1-e^2}\tan B_0\sin\alpha_{i0},\\
c_i&=-\rho''\frac{S_{i0}}{a}\frac{W_i^3}{1-e^2}\cos\alpha_{i0},\\
d_i&=\rho''\frac{W_i^3}{1-e^2}\left(\frac{D}{a}\cos\alpha_{i0}+\frac{E}{a}\sin\alpha_{i0}\right),\\
a_i'&=\frac{(1-e^2)W_i}{W_0^3}\left\{\sin\Delta\alpha-\left[1-\left(\frac{dm}{ds}\right)_{i0}\right]\sin\alpha_{0i}\cos\alpha_{i0}\right\},\\
b_i'&=\left\{1+\frac{m}{a}W_i\sin B_0\sec B_i\cos\alpha_{i0}\right\}\sec B_0\cos B_i,\\
c_i'&=-\rho''\frac{S_{i0}}{a}W_i\sin\alpha_{i0},
\end{aligned}\right\} \tag{7}$$

---

[3] F. R. Helmert, "Theorien der Höheren Geodasie," I Teil.

$$\left.\begin{aligned}
d_i' &= \rho'' W_i\left(\frac{D}{a}\sin\alpha_{i0} - \frac{E}{a}\cos\alpha_{i0}\right),\\
a_i'' &= -\frac{a}{m}\frac{1-c^2}{W_0^3}\left\{\left[1-\left(\frac{dm}{ds}\right)_{0i} + 1-\left(\frac{dm}{ds}\right)_{i0}\right]\cos\Delta\alpha\sin\alpha_{i0} - \frac{\sin^2\Delta\alpha}{\sin\alpha_{0i}}\right.\\
&\qquad \left. + \left[1-\left(\frac{dm}{ds}\right)_{0i}\right]\left[1-\left(\frac{dm}{ds}\right)_{i0}\right]\sin^2\alpha_{i0}\sin\alpha_{0i}\right\}\cot B_i,\\
b_i'' &= \left\{\left(\frac{dm}{ds}\right)_{0i} + \frac{m}{a}W_i\tan B_i\cos\alpha_{i0}\right\}\tan B_0\cot B_i,\\
c_i'' &= -\rho''\frac{S_{i0}}{a}W_i\sin\alpha_{i0},\\
d_i'' &= \rho'' W_i\left(\frac{D}{a}\sin\alpha_{i0} - \frac{E}{a}\cos\alpha_{i0} + \frac{F}{W_i}\right),
\end{aligned}\right\}$$

$$\left.\begin{aligned}
&\text{where} \qquad W=\sqrt{1-e^2\sin^2 B}, \quad B=\frac{1}{2}(B_0+B_i),\\
&m: \ \text{reduced length of the geodesic line}\\
&\quad = s\left(1-\frac{S^2}{6a^2}K+\ldots\ldots\right),\\
&K=\frac{a^2}{\rho_m\rho_n}, \ \rho_m, \rho_n: \ \text{radii of curvature in meridian and parallel},\\
&D=\frac{S}{W^2}\left(2\cos^2 B\cos^2\frac{\alpha_{i0}+\alpha_{0i}-180^\circ}{2} - [1-e^2]\sin^2 B + \ldots\ldots\right),\\
&E=S\left\{\frac{1}{W_0^2}\cos^2 B_0\cos\alpha_{0i}\sin\alpha_{0i}\left[1-\frac{1}{6}\frac{S^2}{a^2}\right]\right.\\
&\qquad\qquad\qquad \left. + \frac{1}{W_i^2}\cos^2 B_i\cos\alpha_{i0}\sin\alpha_{i0} + \ldots\right\},\\
&F=\frac{S}{2a^2}B - \frac{S^3}{6a^3}\sin B_0\cos B_0\sin\alpha_{0i} + \ldots\ldots
\end{aligned}\right\} \tag{8}$$

The first step in the work is the calculation of the azimuth, the backazimuth, and the distance to the astronomical stations. After slight modification of the spheroidal formulae given by Jordan,[4] we have

$$\left.\begin{aligned}
\log S\sin\alpha &= \log\frac{(L_i''-L_0'')\cos B}{[2]}\\
&\qquad -[3](L_i''-L_0'')^2\sin^2 B + [4] \quad (B_i''-B_0'')^2\\
\log S\cos\alpha &= \log\frac{B_i''-B_0''}{[1]} - [5](L_i''-L_0'')^2\cos^2 B - [6] \quad (B_i''-B_0'')^2,\\
\log\Delta\alpha &= \log(L_i''-L_0'')\sin B + [7](L_i''-L_0'')^2\cos^2 B + [8](B_i''-B_0'')^2,
\end{aligned}\right\} \tag{9}$$

From these we have

---

[4] JORDAN-EGGERT, "Handbuch der Vermessungskunde," Band III.

$$\left.\begin{aligned}\alpha_{i0}&=\alpha+\frac{\Delta\alpha}{2},\\ \alpha_{0i}&=\alpha-\frac{\Delta\alpha}{2}-180^\circ.\end{aligned}\right\}\qquad(10)$$

In the above

$$\left.\begin{aligned}&[1]=\frac{\rho}{N}V^2,\quad[2]=\frac{\rho}{N^{t}},\quad[3]=\frac{\mu}{24\rho^2},\quad[4]=\frac{\mu}{24\rho^2}\frac{1+\eta^2-9\eta^2t^2}{V^4},\\ &[5]=\frac{\mu}{24\rho^2}(2+3t^2+2\eta^2),\quad[6]=\frac{\mu}{8\rho^2}\eta^2\frac{t^2-1-\eta^2-4\eta^2t^2}{V^4},\quad[7]=\frac{\mu}{12\rho^2}V^2,\\ &[8]=\frac{\mu}{24\rho^2}\frac{3+8\eta^2+5\eta^4}{V^4},\\ &V=\sqrt{1+\frac{e^2}{1-e^2}\cos^2B},\quad N=\frac{a}{W},\quad\rho=\frac{1}{\sin1''},\\ &\qquad\qquad\mu=\text{modulus of natural logarithm},\\ &\eta^2=\frac{e^2}{1-e^2}\cos^2B,\quad t=\tan B.\end{aligned}\right\}\qquad(11)$$

(Argument of all quantities are $B=\frac{1}{2}(B_0+B_{.})$)

The following Table II contains an abstract from the result of the computation, together with the reduced length of the geodetic lines.

There is no general principle by means of which we can assign to the equations derived from longitude and azimuth their values relative to the equations derived from the observed latitude. Since the probable errors in the astronomical observations of longitude or azimuth are considerably greater than in the case of latitude, in view of the nature of such observations, the longitudinal and azimuthal equations are entitled to much less weight than the latitude equations, although what the exact ratios are cannot generally be determined. In addition to these difficulties, the azimuth equations in particular are directly affected by cumulative errors in the observed angles of triangulation or by errors arising from observations of the geodetic datum. But we now lack the necessary means of examining the error of the azimuth in the geodetic datum owing to changes brought about as the result of the great Kwantô Earthquake of 1923, making it very difficult to estimate how much these errors accumulate at each station. But, with respect to the errors that arise in the observations of the intervening trigonometrical stations, they could be inferred to a certain extent from the mean value of the closing errors of the intervening triangles, or of the closing error of sides between the two base lines, although it would be a question to what extent the weights obtained in this manner can be trusted. On the other hand, η's that were deduced from the longitudinal and the azimuthal observations must, in the existence of the two observations, be equal. So that in making out the error equations, the mean of the two equations were taken and also given the same weight unity as that given to the latitude equations, and to the remaining equations of the half weight.

Table II.

No.	Station	$\log S$ in meters	$\log m$ in meters	α_{oi}	α_{io}
1	Handasawa	6·2073440	5·99772	187° 49′ 32″	9° 54′ 9″
2	Higasiyama	6·2085437	5·99742	188 43 43	11 3 1
3	Syana	6·1022009	5·98519	210 24 45	35 42 36
4	Abasiri	6·0025528	5·93232	201 13 52	24 8 29
5	Nemuro	5·9136407	5·86829	215 56 54	39 40 22
6	Sapporo	5·9222801	5·87498	189 31 2	10 32 32
7	Urakawa	5·6302909	5·61845	217 4 9	38 58 33
8	Hakodate	5·8347983	5·80373	187 50 13	7 26 56
9	Aomori	5·7643472	5·74212	188 35 2	9 13 14
10	Turukotai	5·7598381	5·73808	191 59 32	12 52 0
11	Sionohara	5·5522737	5·54403	188 39 54	9 2 23
12	Matugasaki	5·4152475	5·41088	168 11 36	347 49 50
13	Toriyayama	5.3314592	5·32850	175 17 44	355 10 37
14	Keizyô	6·0633378	5·96761	104 17 12	276 39 1
15	Wazima	5·5057784	5·49914	127 57 4	306 15 7
16	Sakatoyama	5·23859	5·23854	154 5 8	333 34 52
17	Nanao	5·4679065	5·46234	122 28 44	300 49 40
18	Suzaka	5·23424	5·23419	131 31 28	310 40 36
19	Takasuzuyama	5·11804	5·11801	215 14 49	35 44 45
20	Utunomiya	5·00873	5·00871	187 20 10	7 25 18
21	Akagi	5·04275	5·04273	152 46 10	332 26 14
22	Teruisiyama	4·89286	4·89285	175 39 49	355 37 29
23	Kariyado	5·11992	5·11989	126 23 13	305 41 31
24	Tukubasan	4·84907	4·84906	206 45 57	26 58 25
25	Kirigamine	5·20259	5·20255	106 7 2	285 7 18
26	Dôhirayama	4·79925	4·79924	127 55 40	307 36 20
27	Takagamimura	5·00354	5·00352	266 38 7	87 17 3
28	Ako	5·21562	5·21557	92 20 0	271 16 30
29	Siozakimura	5·04962	5·04960	90 38 51	270 38 51

(*to be continued.*)

Table II. (*continued.*)

No.	Station	log S in meters	log m in meters	α_{0i}	α_{i0}
30	Mitaka	4·26568	4·26568	96° 6′ 42″	275° 59′ 39″
31	Turuga	5·5219365	5·51478	91 7 36	268 59 6
32	Sakae	5·7702356	5·74734	90 42 11	266 54 55
33	Tobioyama	4·61225	4·61225	65 31 23	245 17 3
34	Maiduru	55974241	5·58725	88 20 21	265 48 8
35	Tanzawayama	4·74722	4·74722	68 45 40	248 25 38
36	Rokudizô	4·68240	4·68240	298 53 40	119 9 52
37	Tenzinno	5·7323292	5·71320	88 53 56	265 26 24
38	Kenasiyama	5·05192	5·05192	76 26 42	255 44 38
39	Aibano	5·5330280	5·52549	86 2 25	263 51 41
40	Kandamura	5·4986779	5·49225	85 0 38	263 0 9
41	Sengenyama	4·73309	4·73309	46 33 42	226 18 38
42	Kanôzan	4·68824	4·68824	336 25 9	156 32 37
43	Sanomura	4·96861	4·96859	53 37 58	233 9 22
44	Daibamura	4·97539	4·97537	50 6 28	229 38 50
45	Kwasan	5·5642584	5·55554	79 32 54	257 15 46
46	Bôdaisan	4·88683	4·88682	357 30 42	177 31 58
47	Mera	4·92034	4·92033	354 25 3	174 28 7
48	Hamada	5·8471207	5·81412	85 19 49	260 53 33
49	Rokkôzan	4·68240	4·68240	298 53 40	119 9 52
50	Sakabe	5·23414	5·23413	55 20 29	234 27 13
51	Oosakazyô	5·6011358	5·59079	75 34 30	253 8 36
52	Mikomotozima	5·14811	5·14808	31 34 15	211 6 33
53	Kasaoka	5·7659060	5·74349	79 5 56	255 30 35
54	Edazima	5·8338318	5·80287	78 49 40	254 39 28
55	Nisibayasi	5·7299492	5·71103	72 28 54	249 18 26
56	Simonoseki	5·9341555	5·88394	72 8 47	249 6 42
57	Saeki	5·8912259	5·85044	69 8 0	244 44 44
58	Nagasaki	5·9848552	5·92041	73 11 57	247 38 19
59	Miyazaki	5·9417458	5·88960	64 2 38	237 24 39
60	Kagosima	5·9837233	5·91958	64 45 15	239 39 25
61	Kasanohara	5·9779584	5·91563	62 38 53	237 44 4

Table III. Equation of condition derived from observed latitudes (Square root of the remarked weight were already multiplied)

No.	Station			[10000 ×]	[10000 ×]	− [illegible]	Weight
1	Handasawa	+0·996 ξ_0	−0·019 η_0	−5·130 $\frac{da}{a}$	+3·199½ $\frac{de^2}{1-e^2}$	″ + 9·39 = ξ_1	1
2	Higasiyama	+0·987 〃	−0·021 〃	−5·129 〃	+3·192 〃	+ 2·29 = ξ_2	1
3	Syana	+0·988 〃	−0·064 〃	−3·329 〃	+2·583 〃	+17·22 = ξ_3	1
4	Abasiri	+0·996 〃	−0·039 〃	−2·974 〃	+2·128 〃	+ 1·00 = ξ_4	1
5	Nemuro	+0·994 〃	−0·053 〃	−2·045 〃	+1·674 〃	− 4·81 = ξ_5	1
6	Sapporo	+0·998 〃	−0·015 〃	−2·665 〃	+2·129 〃	+13·50 = ξ_6	1
7	Urakawa	+0·997 〃	−0·029 〃	−1·076 〃	+0·909 〃	−21·20 = ξ_7	1
8	Hakodate	+0·999 〃	−0·009 〃	−2·197 〃	+1·821 〃	+ 9·79 = ξ_8	1
9	Aomori	+0·999 〃	−0·010 〃	−1·860 〃	+1·530 〃	+20·28 = ξ_9	1
10	Turukotai	+0·999 〃	−0·014 〃	−1·818 〃	+1·551 〃	+17·50 = ξ_{10}	1
11	Sionohara	+1·000 〃	−0·006 〃	−1·142 〃	+1·055 〃	+10·30 = ξ_{11}	1
12	Matugasaki	+1·000 〃	+0·006 〃	−0·825 〃	+0·393 〃	+16·40 = ξ_{12}	1
13	Toriyayama	+1·000 〃	+0·002 〃	−0·693 〃	+0·641 〃	+12·75 = ξ_{13}	1
14	Keizyô	+0·975 〃	+0·104 〃	−0·435 〃	−0·290 〃	+10·78 = ξ_{14}	1
15	Wazima	+0·999 〃	+0·029 〃	−0·615 〃	+0·600 〃	+16·03 = ξ_{15}	1
16	Sakatoyama	+1·000 〃	+0·009 〃	−0·503 〃	+0·480 〃	+24·56 = ξ_{16}	1
17	Nanao	+0·999 〃	+0·028 〃	+1·588 〃	+0·496 〃	+18·48 = ξ_{17}	1
18	Suzaka	+1·000 〃	+0·015 〃	−0·363 〃	+0·352 〃	+19·20 = ξ_{18}	1
19	Takasuzuyama	+1·000 〃	−0·009 〃	−0·346 〃	+0·333 〃	− 0·69 = ξ_{19}	1
20	Utunomiya	+1·000 〃	−0·001 〃	−0·328 〃	+0·314 〃	+ 8.30 = ξ_{20}	1
21	Akagi	+1·000 〃	+0·006 〃	−0·317 〃	+0·306 〃	+ 1·20 = ξ_{21}	1
22	Teruisiyama	+1·000 〃	+0·001 〃	−0·253 〃	+0·252 〃	+ 1·08 = ξ_{22}	1
23	Kariyado	+0·999 〃	+0·012 〃	−0·249 〃	+0·244 〃	+ 7·28 = ξ_{23}	1
24	Tukuba	+1·000 〃	−0·004 〃	−0·204 〃	+0·199 〃	− 0·30 = ξ_{24}	1
25	Kirigamine	+0·999 〃	+0·017 〃	−0·136 〃	+0·137 〃	+18·39 = ξ_{25}	1
26	Dôhirayama	+1·000 〃	+0·006 〃	−0·125 〃	+0·122 〃	+11·82 = ξ_{26}	1
27	Takagamimura	+1·000 〃	−0·011 〃	−0·016 〃	+0·019 〃	− 5·07 = ξ_{27}	1
28	Ako	+0·999 〃	+0·019 〃	−0·012 〃	+0·019 〃	+11·59 = ξ_{28}	1
29	Siozakimura	+1·000 〃	+0·013 〃	+0·004 〃	+0·000 〃	+ 4·01 = ξ_{29}	1
30	Mitaka	+1·000 〃	+0·002 〃	−0·006 〃	+0·006 〃	+ 0·40 = ξ_{30}	1
31	Turuga	+0·998 〃	+0·037 〃	+2·094 〃	+0·062 〃	+ 7·00 = ξ_{31}	1
32	Sakae	+0·994 〃	+0·063 〃	+3·704 〃	−0·021 〃	+ 9·93 = ξ_{32}	1
33	Tobioyama	+1·000 〃	+0·004 〃	+0·056 〃	−0·005 〃	+ 6·02 = ξ_{33}	1
34	Maiduru	+0·997 〃	+0·044 〃	+2·485 〃	−0·041 〃	+18·57 = ξ_{34}	1
35	Tanzawayama	+1·000 〃	+0·006 〃	+0·067 〃	−0·066 〃	+ 4·73 = ξ_{35}	1
36	Rokudizô	+1·000 〃	−0·005 〃	+0·076 〃	−0·074 〃	+ 7·47 = ξ_{36}	1

(*to be continued.*)

Table III. (*continued.*)

No.	Station			[10000 ×]	[10000 ×]	$-\xi_i$	Weight
37	Tenzinno	$+0{\cdot}994\,\xi_0$	$+0{\cdot}058\,\eta_0$	$+3{\cdot}388\,\frac{da}{a}$	$-0{\cdot}083\tfrac{1}{2}\,\frac{de^2}{1-e^2}$	$+21''{\cdot}60=\xi_{37}$	1
38	Kenasiyama	+1·000 ″	+0·012 ″	+0·090 ″	−0·087 ″	$+\ 2{\cdot}86=\xi_{38}$	1
39	Aibano	+0·998 ″	+0·038 ″	+2·136 ″	−0·083 ″	$+24{\cdot}30=\xi_{39}$	1
40	Kandamura	+0·991 ″	+0·035 ″	+1·971 ″	−0·103 ″	$+\ 6{\cdot}79=\xi_{40}$	1
41	Sengenyama	+1·000 ″	+0·004 ″	+0·121 ″	−0·163 ″	$+\ 1{\cdot}74=\xi_{41}$	1
42	Kanôzan	+1·000 ″	−0·002 ″	+0·145 ″	−0·145 ″	$+18{\cdot}99=\xi_{42}$	1
43	Sanomura	+1·000 ″	+0·008 ″	+0·181 ″	−0·178 ″	$+\ 3{\cdot}50=\xi_{43}$	1
44	Daibamura	+1·000 ″	+0·008 ″	+0·199 ″	−0·168 ″	$+\ 6{\cdot}34=\xi_{44}$	1
45	Kwasan	+0·998 ″	+0·040 ″	+0·262 ″	+0·393 ″	$+11{\cdot}00=\xi_{45}$	1
46	Bôdaizan	+0·999 ″	−0·000 ″	+0·250 ″	−0·250 ″	$+19{\cdot}64=\xi_{46}$	1
47	Mera	+1·000 ″	+0·001 ″	+0·269 ″	−0·267 ″	$+18{\cdot}06=\xi_{47}$	1
48	Hamada	+0·991 ″	+0·073 ″	+4·372 ″	−0·248 ″	$+16{\cdot}81=\xi_{48}$	1
49	Rokkôzan	+0·999 ″	+0·045 ″	+0·346 ″	−0·331 ″	$+11{\cdot}36=\xi_{49}$	1
50	Sakabe	+1·000 ″	+0·016 ″	+0·321 ″	−0·480 ″	$+\ 4{\cdot}66=\xi_{50}$	1
51	Oosakazyô	+0·997 ″	+0·042 ″	+2·405 ″	−0·352 ″	$+17{\cdot}63=\xi_{51}$	1
52	Mikomotozima	+1·000 ″	+0·008 ″	+0·391 ″	−0·391 ″	$+\ 8{\cdot}00=\xi_{52}$	1
53	Kasaoka	+0·994 ″	+0·061 ″	+3·556 ″	+0·704 ″	$+\ 9{\cdot}20=\xi_{53}$	1
54	Edazima	+0·992 ″	+0·069 ″	+4·141 ″	−0·497 ″	$+\ 5{\cdot}80=\xi_{54}$	1
55	Nisibayasi	+0·996 ″	+0·054 ″	+3·162 ″	−0·580 ″	+22·[illegible]0 = ξ_{55}	1
56	Simonoseki	+0·998 ″	+0·080 ″	+4·987 ″	−0·952 ″	$+13{\cdot}71=\xi_{56}$	1
57	Saeki	+0·991 ″	+0·072 ″	+4·434 ″	−0·994 ″	$+\ 7{\cdot}01=\xi_{57}$	1
58	Nagasaki	+0·986 ″	+0·087 ″	+5·626 ″	−1·506 ″	$+\ 5{\cdot}80=\xi_{58}$	1
59	Miyazaki	+0·990 ″	+0·075 ″	+4·740 ″	−0·828 ″	$+\ 8{\cdot}92=\xi_{59}$	1
60	Kagosima	+0·988 ″	+0·081 ″	+5·235 ″	−0·467 ″	$+\ 0{\cdot}20=\eta_{60}$	1
61	Kasanohara	+0·989 ″	+0·079 ″	+5·063 ″	−0·932 ″	$+11{\cdot}70=\xi_{61}$	1

Equation of condition derived from observed longitudes and azimuths
Table IV. (Square root of the remarked weight were already multiplied.)

No.	Station			[10000 ×]	[10000 ×]	$-\eta_i$	Weight
62	Handazawa	—	—	—	—	—	—
63	Higasiyama	$-0{\cdot}284\,\xi_0$	$+0{\cdot}710\,\eta_0$	$-1{\cdot}950\,\frac{da}{a}$	$+1{\cdot}503\tfrac{1}{2}\,\frac{de^2}{1-e^2}$	$-10''{\cdot}96=\eta_{63}$	1
64	Syana	+0·071 ″	+0·675 ″	−3·287 ″	+1·893 ″	$-12{\cdot}88=\eta_{64}$	$\frac{1}{2}$
65	Abasiri	+0·038 ″	+0·688 ″	−1·831 ″	+1·421 ″	$-\ 4{\cdot}95=\eta_{65}$	$\frac{1}{2}$
66	Nemuro	+0·048 ″	+0·677 ″	−2·328 ″	+1·237 ″	$-\ 1{\cdot}10=\eta_{66}$	$\frac{1}{2}$
67	Sapporo	−0·022 ″	+0·648 ″	−0·142 ″	+0·697 ″	$+\ 2{\cdot}52=\eta_{67}$	$\frac{1}{2}$
68	Urakawa	+0·024 ″	+0·671 ″	−1·195 ″	+0·670 ″	$-10{\cdot}74=\eta_{68}$	$\frac{1}{2}$

(*to be continued.*)

Table IV. (*continued.*)

No.	Station			[10000 ×]	[10000 ×]	$-\eta_i$	Weight
						″	
69	Hakodate	$+0·008\ \xi_0$	$+0·699\ \eta_0$	$-0·395\ \frac{da}{a}$	$+0.407\frac{1}{2}\ \frac{de^2}{1-e^2}$	$-\ 9·79=\eta_{69}$	$\frac{1}{2}$
70	Aomori	+0·008 〃	+0·702 〃	−0·414 〃	+0·161 〃	$-12·35=\eta_{70}$	$\frac{1}{2}$
71	Turukotai	−0·019 〃	+0·686 〃	−0·620 〃	+0·618 〃	$+\ 2·12=\eta_{71}$	$\frac{1}{2}$
72	Sionohara	−0·009 〃	+0·715 〃	−0·272 〃	+0·301 〃	$-\ 7·75=\eta_{72}$	$\frac{1}{2}$
73	Matugasaki	+0·004 〃	+0·706 〃	+0·244 〃	−0·204 〃	$-14·37=\eta_{73}$	$\frac{1}{2}$
74	Toriyayama	—	—	—	—	—	—
75	Keizyô	+0·092 〃	+0·698 〃	+5·117 〃	−0·889 〃	$-\ 7·43=\eta_{75}$	$\frac{1}{2}$
76	Wazima	+0·021 〃	+0·706 〃	+1·150 〃	−0·336 〃	$-13·69=\eta_{76}$	$\frac{1}{2}$
77	Sakatoyama	+0·008 〃	+1·162 〃	+0·789 〃	+0·084 〃	$-26·88=\eta_{77}$	1
78	Nanao	−0·021 〃	+0·706 〃	+1·123 〃	−0·233 〃	$-\ 9·23=\eta_{78}$	$\frac{1}{2}$
79	Suzaka	+0·030 〃	+0·960 〃	+0·579 〃	+0·032 〃	$-13·48=\eta_{79}$	$\frac{1}{2}$
80	Takasuzuyama	—	—	—	—	—	—
81	Utunomiya	+0·001 〃	+0·707 〃	−0·059 〃	−0·010 〃	$-\ 1·08=\eta_{81}$	$\frac{1}{2}$
82	Akagi	—	—	—	—	—	—
83	Teruisiyama	—	—	—	—	—	—
84	Kariyado	−0·008 〃	+0·707 〃	+0·477 〃	+0·083 〃	$-\ 6·38=\eta_{84}$	$\frac{1}{2}$
85	Tukuba	+0·003 〃	+0·707 〃	−0·143 〃	−0·025 〃	$-\ 6·95=\eta_{85}$	$\frac{1}{2}$
86	Kirigamine	−0·012 〃	+0·707 〃	+0·684 〃	+0·119 〃	$-\ 9·35=\eta_{86}$	$\frac{1}{2}$
87	Dôhirayama	—	—	—	—	—	—
88	Takagamimura	—	—	—	—	—	—
89	Ako	−0·013 〃	+0·707 〃	+0·731 〃	+0·160 〃	$-\ 6·25=\eta_{89}$	$\frac{1}{2}$
90	Siozakimura	−0·009 〃	+0·707 〃	+0·499 〃	+0·169 〃	$-\ 2·19=\eta_{90}$	$\frac{1}{2}$
91	Mitaka	−0·001 〃	+0·707 〃	+0·081 〃	+0·014 〃	$+\ 4·25=\eta_{91}$	$\frac{1}{2}$
92	Turuga	−0·028 〃	+0·769 〃	+1·613 〃	+2·809 〃	$-\ 8·63=\eta_{92}$	$\frac{1}{2}$
93	Sakae	−0·050 〃	+0·768 〃	+2·852 〃	+0·492 〃	$-\ 5·86=\eta_{93}$	$\frac{1}{2}$
94	Tobioyama	+0·004 〃	+1·002 〃	+0·234 〃	+0·040 〃	$+16·59=\eta_{94}$	1
95	Maiduru	−0·034 〃	+0·769 〃	+1·914 〃	+0·333 〃	$-\ 6·67=\eta_{95}$	$\frac{1}{2}$
96	Tanzawayama	+0·006 〃	+1·002 〃	+0·327 〃	+0·057 〃	$+13·42=\eta_{96}$	1
97	Rokudizô	—	—	—	—	—	—
98	Tenzinno	+0·143 〃	+0·770 〃	+2·606 〃	+0·444 〃	$-\ 1·09=\eta_{98}$	$\frac{1}{2}$
99	Kenasiyama	+0·012 〃	+1·003 〃	+0·688 〃	+0·120 〃	$-\ 8·82=\eta_{99}$	1
100	Aibano	+0·088 〃	+0·773 〃	+1·642 〃	+0·254 〃	$+\ 0·38=\eta_{100}$	$\frac{1}{2}$
101	Kandamura	−0·027 〃	+0·770 〃	+1·518 〃	+0·238 〃	$-\ 9·22=\eta_{101}$	$\frac{1}{2}$
102	Sengenyama	—	—	—	—	—	—
103	Kanôzan	—	—	—	—	—	—
104	Sanomura	+0·008 〃	+1·210 〃	+0·469 〃	+0·080 〃	$-\ 2·78=\eta_{104}$	1
105	Daibamura	+0·008 〃	+1·212 〃	+0·453 〃	−0·381 〃	$-\ 0·28=\eta_{105}$	1

(*to be continued.*)

Table IV. (*continued.*)

No.	Station			[10000 ×]	[10000 ×]	$-\eta_i$	Weight
						″	
106	Kwasan	+0·028 ξ_0	+0·707 η_0	+1592 $\frac{da}{a}$	+0·190 $\frac{1}{2}\frac{de^2}{1-e^2}$	− 8·45 = η_{106}	$\frac{1}{2}$
107	Bôdaisan	—	—	—	—	—	—
108	Mera	+0·001 ″	+0·707 ″	−0·036 ″	−0·006 ″	+ 1·92 = η_{108}	$\frac{1}{2}$
109	Hamada	−0·059 ″	+0·769 ″	+3·367 ″	+0·492 ″	− 5·25 = η_{109}	$\frac{1}{2}$
110	Rokkôzan	+0·075 ″	+1·010 ″	+2·552 ″	+0·247 ″	− 6·49 = η_{110}	1
111	Sakabe	+0·016 ″	+1·220 ″	+0·878 ″	−0·065 ″	− 4·48 = η_{111}	1
112	Oosakazyô	−0·032 ″	+0·769 ″	+1·852 ″	+0·111 ″	− 9·32 = η_{112}	$\frac{1}{2}$
113	Mikomotozima	−0·006 ″	+0·707 ″	+0·324 ″	+0·054 ″	− 9·12 = η_{113}	$\frac{1}{2}$
114	Kasaoka	−0·047 ″	+0·769 ″	+2·738 ″	+3·601 ″	−12·68 − η_{114}	$\frac{1}{2}$
115	Edazima	−0·055 ″	+0·769 ″	+3·189 ″	+0·270 ″	− 7·80 = η_{115}	$\frac{1}{2}$
116	Nisibayasi	+0·133 ″	+0·797 ″	+2·440 ″	+0·032 ″	+ 0·52 = η_{116}	$\frac{1}{2}$
117	Simonoseki	−0·065 ″	+0·760 ″	+3·840 ″	−0·048 ″	− 6·72 = η_{117}	$\frac{1}{2}$
118	Saeki	−0·056 ″	+0·769 ″	+3·415 ″	−0·222 ″	− 3·17 = η_{118}	$\frac{1}{2}$
119	Nagasaki	−0·056 ″	+0·770 ″	+4·333 ″	−0·048 ″	− 6·95 = η_{119}	$\frac{1}{2}$
120	Miyazaki	−0·059 ″	+0·770 ″	+3·650 ″	−0·635 ″	+10·05 = η_{120}	$\frac{1}{2}$
121	Kagosima	−0·059 ″	+0·771 ″	+4·031 ″	−0·127 ″	+ 2·57 = η_{121}	$\frac{1}{2}$
122	Kasaoka	+0·300 ″	+0·859 ″	+3·900 ″	−0·842 ″	− 2·00 = η_{122}	$\frac{1}{2}$

The solution of the normal equation :—

[10000 ×] [10000 ×]

$$60{\cdot}8651\,\xi_0+1{\cdot}2973\,\eta_0+34{\cdot}7293\,\frac{da}{a}+16{\cdot}9588\,\frac{1}{2}\,\frac{de^2}{1-e^2}=-582{\cdot}5337,$$

$$1{\cdot}2973\,\xi_0+3{\cdot}27452\,\eta_0+49{\cdot}9064\,\frac{da}{a}+9{\cdot}9784\,\frac{1}{2}\,\frac{de^2}{1-e^2}=+181{\cdot}6181,$$

$$34{\cdot}7293\,\xi_0+4{\cdot}99064\,\eta_0+587{\cdot}1374\,\frac{da}{a}-107{\cdot}2847\,\frac{1}{2}\,\frac{de^2}{1-e^2}=-359{\cdot}4006,$$

$$16{\cdot}9588\,\xi_0+9{\cdot}9784\,\eta_0-107{\cdot}2847\,\frac{da}{a}+93{\cdot}9366\,\frac{1}{2}\,\frac{de^2}{1-e^2}=-2{\cdot}9009$$

gives

$$\xi_0=-9''363,$$

$$\eta_0=+6''665,$$

$$10000\,\frac{da}{a}=-0{\cdot}5552,$$

$$10000\,\frac{1}{2}\,\frac{de^2}{1-e^2}=+0{\cdot}3664.$$

From these we have

$$da=-354\text{ meter},$$

$$\frac{a-b}{a}=\frac{1}{296}.$$

IV. Determination of Geoid.

By substituting these in the equations of condition we get the following residuals:—

Table V.

No.	Station	ξ	η	No.	Station	ξ	η
1	Handasawa	+ 3″·8	—	32	Sakae	– 1″·2	– 1″·7
2	Higasiyama	– 3·2	– 1″·8	33	Tobioyama	– 3·5	+23·1
3	Syana	+10·2	– 6·5	34	Maiduru	– 7·9	– 2·2
4	Abasiri	– 6·3	+ 0·8	35	Tanzawayama	– 4·8	+19·9
5	Nemuro	–12·9	+ 4·7	36	Rokudizô	– 2·2	—
6	Sapporo	+ 6·2	+ 7·7	37	Tenzinno	+10.6	+ 1·4
7	Urakawa	–30·0	– 5·6	38	Kenasi	– 6·6	– 4·6
8	Hakodate	+ 2·1	– 4·8	39	Aibano	+13·6	+ 3·9
9	Aomori	+12·3	– 7·4	40	Kandamura	– 3·6	– 4·6
10	Turukotai	+ 9·5	+ 7·5	41	Sengenyama	– 7·9	—
11	Sionohara	+ 1·8	– 2·6	42	Kanôzan	+ 9·3	—
12	Matugasaki	+ 7·5	– 9·9	43	Sanomura	– 6·1	+ 5·0
13	Toriyayama	+ 3·8	—	44	Daibamura	– 3·3	+ 7·3
14	Keizyô	+ 3·3	– 6·9	45	Kwasan	+ 1·7	– 4·8
15	Wazima	+ 7·3	– 9·9	46	Bôdaizan	+ 9·9	—
16	Sakatoyama	+15·6	–19·6	47	Mera	+ 8·3	+ 6·6
17	Nanao	+ 8·4	– 5·0	48	Hamada	+ 5·3	– 1·3
18	Suzaka	+10·1	– 7·7	49	Rokkôzan	+ 1·7	– 1·8
19	Takasuzuyama	–10·0	—	50	Sakabe	– 5·1	+ 3·0
20	Utunomiya	– 0·9	+ 3·7	51	Oosakazyô	+ 6·9	– 4·9
21	Akagi	– 8·0	—	52	Mikomotozima	– 1·8	– 4·5
22	Teruisiyama	– 8·2	—	53	Kasaoka	– 1·6	– 7·3
23	Kariyado	– 1·9	– 1·8	54	Edazima	– 3·6	– 3·9
24	Tukubasan	– 9·7	– 2·2	55	Nisibayasi	+10·6	+ 3·2
25	Kirigamine	+ 9·1	– 4·9	56	Simonoseki	+ 2·0	– 3·2
26	Dôhirayama	+ 2·4	—	57	Saeki	– 4·1	+ 6·8
27	Takagami	–14·6	—	58	Nagasaki	– 6·8	– 3·8
28	Ako	+ 2·2	– 1·8	59	Miyazaki	– 3·0	+13·4
29	Siozakimura	– 5·4	+ 2·4	60	Kagosima	–11·8	+ 5·9
30	Mitaka	– 9·1	+ 8·9	61	Kasanohara	– 0·4	– 1·6
31	Turuga	– 3·4	– 3·3				

The quantities in this table have the property that the sum of their squares is less than that of any other system that can be obtained in connection with any spheroidal surface whatsoever. These are therefore to be understood as the actual inclinations of the surface to that of the spheroid we have above determined. Assuming then that the distance between geoid and reference ellipsoid is uniformly increasing or decreasing between two successive stations, it is possible to trace the profile in the meridian from ξ_s and the profile in the parallel from η_s, as shown in Fig. 3.

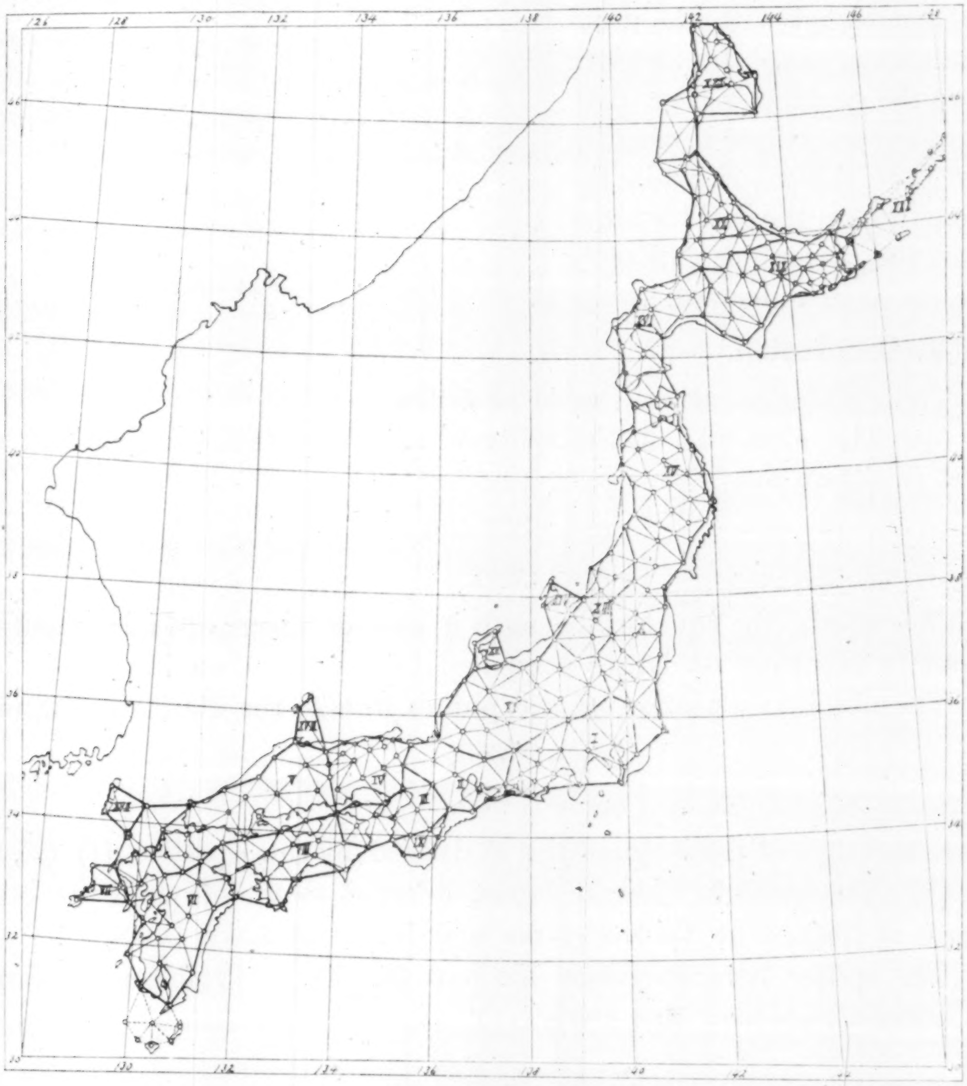

Fig. 2. Triangulation in Japan.

As shown in Fig. 1, the small number of astronomical stations in the intervening regions between the Kwantô and the Kwansai renders it doubtful if the linearity above assumed does actually hold throughout such a long distance. The errors of observation are particularly large in η, which was extensively used in determining the relative height of the geoid in Kwantô and Kwansai, and this makes the obtained height of Kwansai somewhat questionable. As however there are a number of astronomical stations in the vicinity of both Kwantô and Kwansai, the contours drawn for the vicinities of these two regions should be fairly correct.

It is interesting to note that the vertical displacements of bench marks that were detected after the great Kwantô earthquake in 1923, seem to be somewhat correlated with the geoid undulations, ie., the regions where the geoid is higher than the reference ellipsoid seem to have been depressed, while the regions where the geoid is lower than the reference ellipsoid seem to have upheaved.

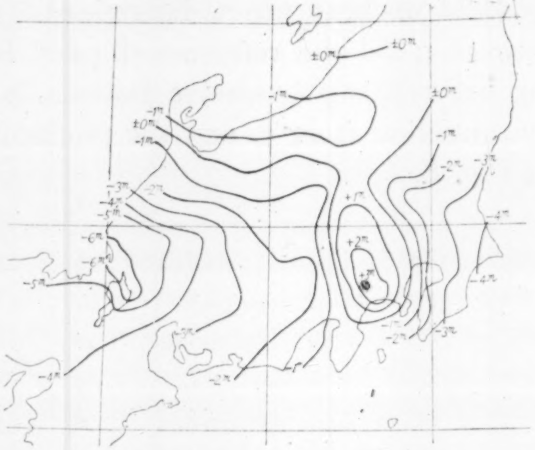

Fig. 3. Geoid in Central Japan.

V. Conclusion.

The conclusion arrived at is as follows:—

(a) The elements of the spheroid that most closely represent the geoid in Japan are

$$da = -354 \text{ meter},$$

$$\alpha = 1:296.$$

In other words, the equatorial length is shorter about 354 meter and the ellipticity is somewhat larger compared to the Bessel's ellipsoid.

The absolute deviation of the plumb line at the standard datum is

$$\xi_0 = -9''363,$$

$$\eta_0 = +6''665,$$

where the sign of these quantities is defined by the equation (1), (2), (3).

(b) The geoid in Central Japan, referred to the ellipsoid just determined, is highest at Tanzawayama and lowest at Lake Biwa.

The writer here expresses his best thanks to Professor T. Terada for interest shown in this study.

5. 日本に適合する回轉楕圓體の近似的計算

陸地測量部 川畑幸夫

日本に於ける垂直線偏倚の量は可成り大きい.

これを測地的計算に採用した準據楕圓體が不適當であつたために起つたものと考へて問題を解いて見る. 即ち原點に於ける垂直線偏倚の成分 ξ_0, η_0 及び準據楕圓體の赤道半經及び偏率の修正量 da 及び $d\alpha$ を未知數として最小二乘法にかける. その際これらの未知數にかゝる係數は地球を回轉楕圓體と見做した場合と簡單に球と見做した場合とではかなり相違しその相違は原點を遠ざかれば遠ざかる程著しくなるから係數を出來る丈け嚴密に算定する必要がある. 又天體觀測による經度及び方位角の觀測は緯度の觀測に比べて極めて困難を伴ふからこれらを同一重量と考へないで緯度を一樣に 1 とし他を $\frac{1}{2}$ とする. 但し經度及方位角の觀測が同時に存在する樣な點では兩方から求めた η が同じでなければならないから之を平均して緯度と同一重量と見做す. 一方測地的座標は原點に於ける觀測誤差途中に蓄積された觀測の誤差或は geoid が回轉楕圓體でないために起る水平角觀測の誤差など色々な量を含むから大體原點からの距離に逆比例する樣な重量を想定する必要があるがそれらは個人的の研究としては困難である. 斯くして方程式を解いて見ると原點に於ける垂直線偏倚は $\xi_0=-9''36$, $\eta_0=+6''67$ (但し符號は本文方程式 (1) (2), (3) を參照せられたい) となり赤道半經は Bessel の値より 354 m. 短くなり偏率は 1/296 となる.

これらの値を各方程式に入れてその剩餘を求めて見ると, それは今算定した準據楕圓體に對する垂直線偏倚をあらはすから之から geoid を概略畫いて見ると第 3 圖の樣になつて丹澤山で一番高くビワ湖附近で一番低いと言ふ結果が得られる.

6. *Classification of Crustal Movements.**

By Gakurô IMAMURA,

Geographical Institute, College of Literature and Science, Tokyo.

(Read June 19, 1934.—Received Nov. 22, 1934.)

Orogenic and epeirogenic crustal movements, as well as those caused by isostatic adjustments, are familiar expressions in geomorphology, geology, and geophysics. The following is merely a suggestion for their classification from the quantitative point of view.

The author examined their gradients with relation to (1) sea level, (2) rivers (chiefly antecedent rivers) as local base-levels, (3) erosion surfaces, and (4) deposition surfaces. In the cases of depositional and erosional surfaces, the increases in the gradient, instead of the gradient itself were calculated. The results are arranged in the following tables.

Table I. Orogenic Zones.

Locality	after	10^{-1}	10^{-2}	10^{-3}	10^{-4}
WITH RELATION TO SEA LEVEL:					
Yuzaki, Kii, Japan:					
outer part of Sandan Kabé	G. Imamura[1]		2·6		
inner part of Sandan Kabé	〃	0·77			
average gradient of Sandan Kabé	〃	0·63			
outer part of abandoned mine	〃		2·7		
inner part of abandoned mine	〃	1·6			
average gradient of abandoned mine	〃	0·62			
average gradient of the whole region	〃		5·4		
Eastern coast of Kitakami, Japan	R. Tayama[2]			3·7(?)	
Yaku Island, Japan	G. Imamura[3]		2·0		
Okusiri Island, Hokkaidô, Japan:					
III terrace	A. Watanabé[4]			1·3	
IV 〃	〃			1·2	
V 〃	〃			1·7	
VI 〃	〃				4·7

(*to be continued.*)

---

* Communicated by C. Tsuboi.

[1] *Proc. Imp. Acad.*, 10 (1934), 483∼485.

[2] *Tirigaku Hyôron*, 7 (1931), 337∼362.

[3] *Tirigaku Hyôron*, 4 (1928), 237∼247.

[4] *Tirigaku Hyôron*, 4 (1928), 298∼309.

Table I. (*continued.*)

Locality	after	10^{-1}	10^{-2}	10^{-3}	10^{-4}
Riviera:					
Milazzien	Depéret[5], Caziot,[6] Maury[7], Boule[8], Denizot[9], etc.		1·8(?)		
Tyrrhénien, locality 1			1·0(?)		
〃 〃 2			1·7(?)		
WITH RELATION TO RIVER, AS LOCAL BASE-LEVEL:					
Hidi Kawa, Japan:					
K niveau, upper course	G. Imamura		2·5		
〃 lower course	& Y. Mino[10]		1·6		
S niveau, upper course	〃		2·4		
〃 lower course	〃		2·4		
WITH RELATION TO EROSIONAL AND DEPOSITIONAL SURFACES:					
Western Sikoku, Japan	G. Imamura & Y. Mino[10]		4·3		
Eisernes Tor, Donau:					
locality 1	J. Cvijic[11]	0·57			
〃 2	〃		2·5		
〃 3	〃		4·9		
〃 4	〃		3·5		
〃 5	〃		2·2		
Elevated fans, Toyama plain, Japan:					
Kurobé Gawa, older fan	A. Watanabé[12]		4·0		
〃 younger fan (right bank)	〃		2·4		
〃 〃 (left bank)	〃		3·1		
Katakai Gawa, older fan	〃		1·1		
〃 younger fan (right bank)	〃		2·0		
〃 〃 (left bank)	〃		1·0		
Hayatuki Gawa, older fan	〃		0·77		
〃 younger fan (right bank)	〃		3·1		
〃 〃 (left bank)	〃		1·1		
Kamiiti Gawa, older fan	〃		2·0		
〃 younger fan	〃		2·0		
Jôganji Gawa	〃		0·74		

---

5) *Bull. Soc. Géol. France*, 4 t.6 (1906), 207∼230.

6) 7) *Bull. Soc. Géol. France*, 4 t.4 (1904), 420∼431; t.5 (1905), 581∼592; t.11 (1911), 177∼189.

8) *Bull. Soc. Géol. France*, 4 t.4 (1904), 10∼13.

9) *CR somm. Soc. Géol. France*, **17** (1924), 181∼182.

10) *Tirigaku Nenpô*, **1** (1933), 25∼50.

11) *Pet. Mit.* (Erg.), Nr. 160 (1908).

12) *Tirigaku Hyôron*, **5** (1929), 1∼15.

Table II. Neo-Paläiden.

Locality	after	10^{-1}	10^{-2}	10^{-3}	10^{-4}
WITH RELATION TO SEA LEVEL:					
L'Esterel, Monastérien	Lutaux[13]		0·64(?)		
WITH RELATION TO RIVER, AS LOCAL BASE-LEVEL:					
Mosel, antecedent course	Oestreich[14]			1·7	
Rhein, antecedent course:					
locality 1	〃			2·3	
〃 2	〃			1·3	
〃 3	〃				
Basin de la Ourthe:					
Meuse	Fourmarier[15]			0·69	
Ourthe	〃			0·78	
Amblève	〃			0·86	
WITH RELATION TO DEPOSITIONAL SURFACE:					
Le Crau	Baulig[16]			1·3	

Table III. Regions of Isostatic Compensation.

Locality	after	10^{-1}	10^{-2}	10^{-3}	10^{-4}
WITH RELATION TO SEA LEVEL:					
Greenland, e-line:					
Southeast Greenland	Vogt[17]				1·2
Julianehaab	〃				0·76
Disco region	〃				0·93
West Scandinavia, tapes line:					
Oslo-Southland	Tanner[18]				2·1
Westland	〃				2·6
Northland	〃				2·7
Troms	〃				2·5
West Finnmark	〃				2·1
East Fenno-Scandinavia, tapes line:					
East Finnmark	〃				1·8
Kola	〃				1·3

(to be continued.)

---

13) *Rev. Géogra.*, t.12, f.1 (1924).
14) *Zeits. Geomorph.*, **2** (1926), 135~159.
15) *CR Cong. int. Géogra. Paris*, t.2 (1933), f.1, 90~108.
16) *Ann. Géogra.*, **36** (1927), 499~508.
17) 18) *Skr. Sval. Ishav.*, Nr. 60 (1933).

Table III. (*continued.*)

Locality	after	10^{-1}	10^{-2}	10^{-3}	10^{-4}
Carelia	Tanner				1·4
Baltic	〃				1·6
West Sweden	〃				2·0
Olonsay and Colonsay	Wright[19]			0·60(?)	
Islay	〃				1·5(?)

Table IV. Epirogenic Regions.

Locality	after	10^{-1}	10^{-2}	10^{-3}	10^{-4}
WITH RELATION TO SEA LEVEL:					
Atlantic coast of U.S.A., submerged shoreline	D. W. Johnson[20]				0·70(?)

In constructing these tables, attention was directed (1) to measuring the maximum gradient, and (2) to choosing such examples as occurred during approximately the same lapse of time; at any rate, the *order* of the length of time was made to be the same (say, 10^5 years). In these tables, such examples as in which the direction of the maximum gradient is uncertain, are indicated by question marks.

The above table and the accompanying frequency diagram show that the gradients are in the order of 10^{-2} in the so-called orogenic zones, 10^{-3} in the regions of "Neo-Paläiden," 10^{-4} in regions where isostatic adjustment is now going on. For epeirogenic movements, meagreness of data precludes me from coming to any conclusion.

If the total gradients during the supposed epoch are considered, and those examples covering longer periods are rejected, we shall then have a frequency curve for the orogenic zones as drawn with a dotted line in the accompanying figure. For other groups of crustal movements the curves remain unchanged.

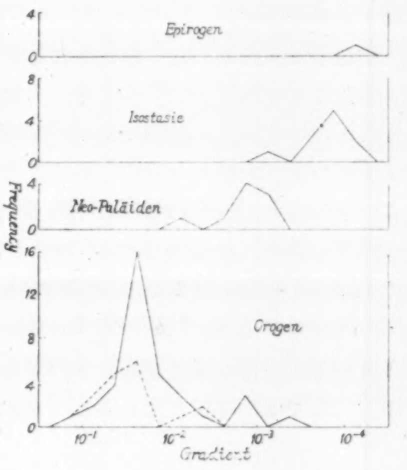

Fig. 1.

These results show us that shorelines, once formed in almost horizontal situation, were afterwards so strongly deformed by crustal movement that some of them attained a gradient of 10^{-1}. The author cannot accept Y. Ôtuka's opinion[21] that shorelines were *originally* made with such a strong gradient.

---

[19] *Geol. Mag.*, 8 (1911), 97.

[20] The New England-Acadian Shoreline (1925), 299.

Along the coast of Kii Peninsula, the author[22] found a recent crustal movement with an average gradient of $5{\cdot}4\times10^{-2}$. This agrees well with the result obtained above, and suggests the existence of a kind of "Flexurküste" in the region in question.

In Japan, where crustal movements in the order of 10^{-2} prevail, it is rather difficult, not to say impossible, to find any indisputable geomorphological traces of *eustatic* changes of level.

6. 地殼運動の分類

東京文理科大學
地理學教室　今村學郎

海岸段丘, 河岸段丘(特に先行性流路に於けるもの), 堆積面, 及び侵蝕面等の變位から地殼運動を求め, その gradient を定めた. これらの材料の内, 海岸段丘は最も正しく地殼運動を示すものであり, その他のものは多少より不正確な結果を與へるものである. かくて 61 の觀測値を得てこれを頻度曲線にして見ると, 造山帶は 10^{-2}, Neo-Paläiden 帶は 10^{-3}, アイソスタシーの地方は 10^{-4} の gradient を示すことが判る.

これらの測定値は 1) その最大傾斜の方向に測ることが必要であり 2) その運動した時間を知ることが大切である. 幸にして傾斜方向は多くの場合に於て明かであり, 二三疑はしいものは (?) を附けて區別した. 時間は大略 10^5 年としてよいと思ふが, これよりも長いものは除外し, 又この間に數回の運動をしたものはその傾斜の總和を出すことにして見ると, 第1圖の頻度曲線の形は造山帶のものゝみが點線で書いたやうに變るが, その他のものは不變である. 即ち上の結論はこれを變更する必要はない.

汀線は元來水平に近く形成されるものであるから, 上述の gradient は形成後の地殼運動によると考へるを至當とする. かく考へれば各々の群に於て一つづゝ order が違ふことも無理なく說明されるけれども, 大塚彌之助氏が昭和 9 年の 6 月及び 7 月の地震研究所談話會で述べたやうに, 汀線そのものが始から 10^{-2} のやうな大きな gradient で作られるとすれば, 造山帶はそのまゝでよいとしても, Neo-Paläiden 帶, アイソスタシーの地方及び造陸帶では, その後一樣に gradient の減少が起り, 然も一つづゝ order が違ふやうに減少しなくてはならないといふ事になり, 甚しく不合理な結果となることは明瞭である.

本邦に於ては 10^{-2} が一般であるから, この樣な地方では汀線變化 eustatic changes of level の地形學的證據は求め難い. 又世界各地で獨立に出した結果の order が合つて來ることは, 地形學的方法で地殼運動を定めることが相當合理的であるといふことを示すものと思はれる.

---

21) An opinion expressed at the meetings of the Earthquake Research Institute, June 19 and July 3, 1934.

22) G. Imamura, "Crustal Movements as indicated by an Elevated Shoreline near Yuzaki, Kii Peninsula, Japan," *Proc. Imp. Acad.*, **10** (1934), 483~485.

7. *A Study of Landslides.*

By Naomi MIYABE,

Earthquake Research Institute.

(Read June 19, 1934.—Received Dec. 20, 1934.)

1. Introduction. Landslides frequently accompany destructive earthquakes. One of the most conspicuous examples in Japan associated with a destructive earthquake is that which occurred at the time of the Zenkôzi earthquake of 1847, at Iwakurayama (Kokuzôyama), Nagano prefecture. Enormous quantities of earth slid down and filled the valley of the Saigawa (river), damming up the river water with consequent flooding in its upper course, a recent example, although on a greatly reduced scale, being the Tôge landslide of 1932.

When as in the case of the Iwakurayama landslide, the damm was broken at last after 20 days, during last several days of which it was rainy, the water flooded the Zenkôzi plain, a number of houses in the plain being swept away and destroyed.

The destructive earthquakes of Akita in 1914 and of North Idu in 1930 were also accompanied by a number of landslides. People were killed and houses demolished.

Not all landslides however are associated with earthquakes. In many parts of the earth's surface, land is now sliding or creeping, although very slowly. Landslides belonging in this cathegory seem as a rule to be related in some way to precipitations, except for such cases as when the landslide is attributed to the caving in of old mines, as at Ube, in Yamaguti prefecture[1].

Whatever the cause, landslides damage or destroy property and take toll of human lives, so that it is important to study its phenomena scientifically, as so little has yet been done in the matter.

The other names for "landslide" sometimes used are "mud flow", "solifluction", "rockslides"[2], according to their apparent types. Prof. A. Heim[3] tried to distinguish more than 20 different types of landslides. It seems to the author, however, that several of the types distinguished by Heim may be the same phenomena observed under different conditions.

---

[1] Landslide of Ube occurred on Sept. 23, 1933.

[2] VANDERWILDT, *Journ. Geol.*, 42 (1934), 163.

[3] A. HEIM, "*Bergsturze und Menschenleben*", (Berlin 1932).

It may be somewhat interesting in this connection to note that, in Japan, such words as "Kue", "Nuke", "Boke ", etc., forming parts of the names of certain villages, mean " landslide " or " cave-in ". In several region, we notice also in the names of villgaes, "——kubo ", " Rondi ", " Ronda ", etc.,[4] which may indicate some reference to landslides.

2. Landslides on topographical maps. To investigate the geographical distribution of landslides we use topographical maps of 1/50000 scale. It is however not easy to find traces of landslides on these maps. Some form of indication is needed. In this connection, Mr. H. Honma[5] pointed out that the configuration of the contour lines have certain characteristics in regions of landslides, as shown in Figs. 1a, 1b. Profiles of landslides are generally characterized by a cliff with a gentle but irregular slope, as in the case pointed out in our previous report.[6] But such characteristics in the configurations of contour lines due to landslides may not always be noticeable in 1/50000 topographical maps. Areas that have been disturbed by landslides are rarely so large that their irregular contour lines can be noticed in 1/50000 topographical maps. In maps of this scale a characteristic in the configurations of the contour lines is noticeable only if the horizontal dimensions of the area of the landslide exceed half a kilometre, with considerable vertical displacement.

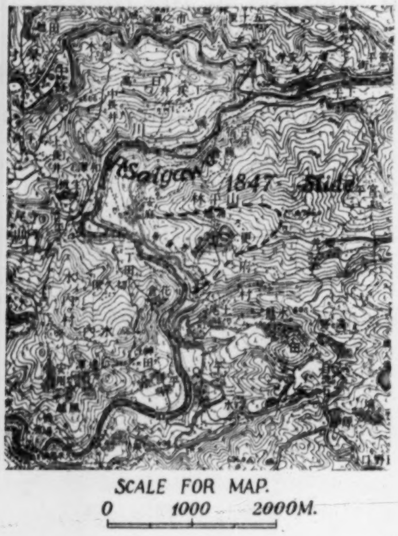

Fig. 1a. Characteristic feature of contour lines in the area of landslide.

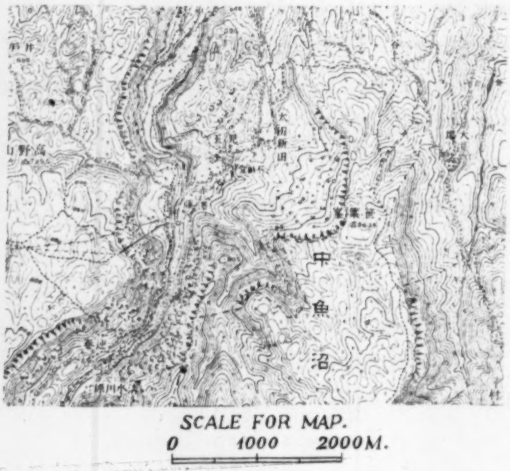

Fig. 1b. Characteristic feature of the contour lines in the area of the landslide.

---

4) K. NAKAMURA, *Tirigaku-Hyôron*, 8 (1932), 848, (in Japanese).
T. TERADA and N. MIYABE, *Bull. Earthq. Res. Inst.*, 10 (1932), 192, (in Japanese).

5) H. HONMA, *Tuti-to-Midu Iinkwai Hôkoku*, No. 4 (1930), 13~21, (in Japanese).

6) T. TERADA and N. MIYABE, *loc. cit.*

We also notice in topographical maps that marks, as shown in Fig. 2, represent cliffs. Some of these cliffs are undoubtedly landslides, but, others may have been formed by washing away of the superficial covering by precipitations, exposing the steep base rock.

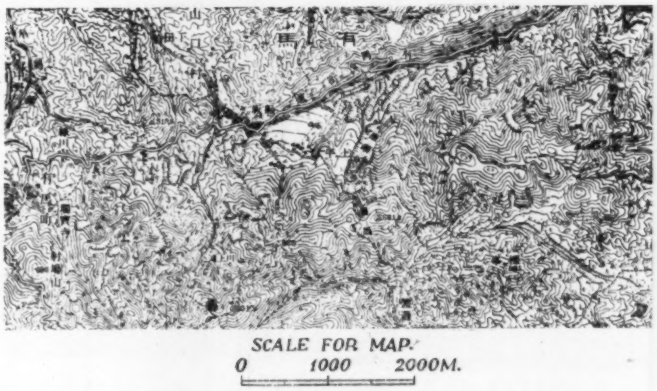
SCALE FOR MAP.
0 1000 2000M.

Fig. 2. Marks of cliffs, representing landslides.

The actual areas of landslides therefore cannot be determined from map study alone. To measure the areas of landslides, nothing surpasses actual field observation, but their large number renders it impossible to observe them all in the field. In the present investigation, therefore, the distribution of landslides is studied by means of the marks (see Fig. 2) in 1/50000 topographical maps.

3. Geographical distribution of traces of landslides.

Several examples of the distribution of cliffs, typical of which will be found in Fig. 2, are shown in Figs. 3, 4.

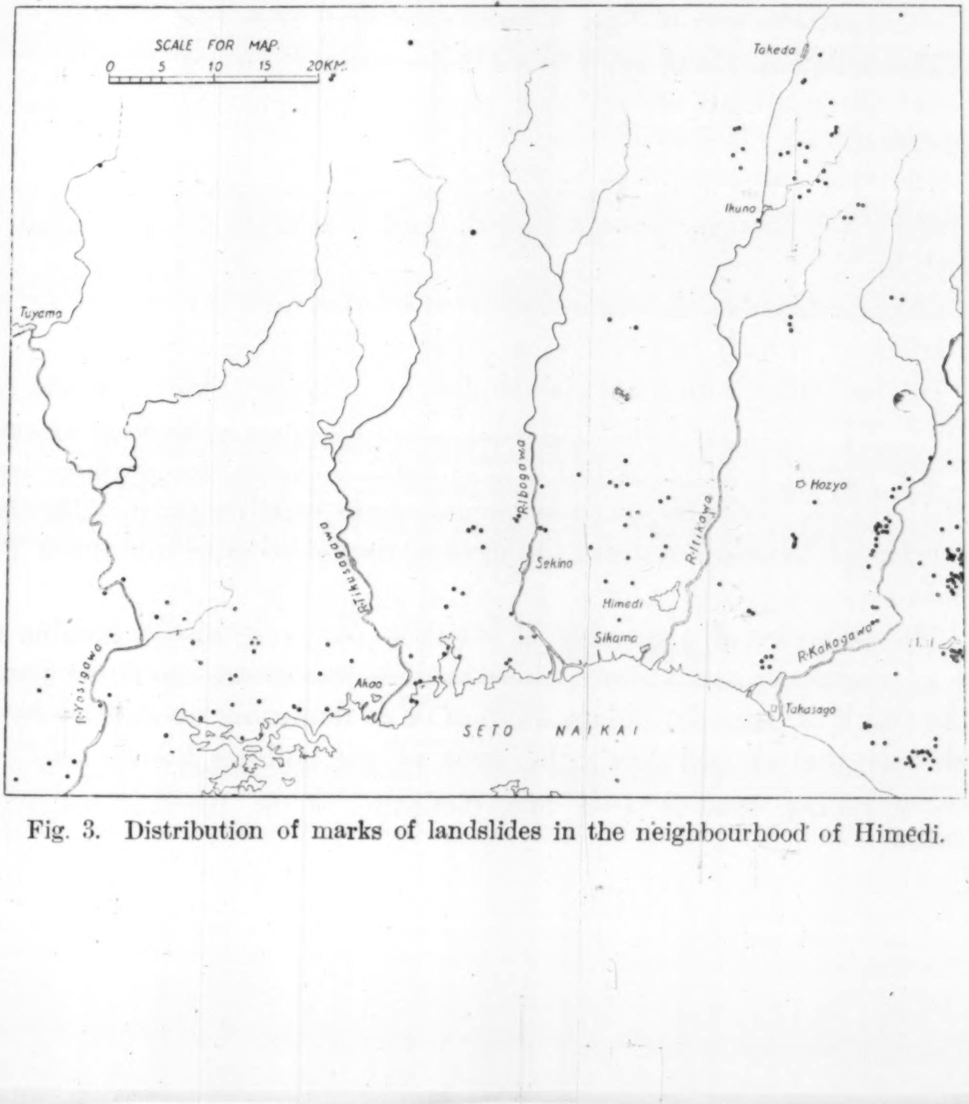
SCALE FOR MAP.
0 5 10 15 20KM.
Takeda
Ikuno
Tuyama
R.Ibogawa
R.Tikusagawa
R.Itikawa
Hozyo
Sekino
Himedi
Sikama
R.Kakogawa
R.Yosigawa
Akao
Takasago
SETO NAIKAI

Fig. 3. Distribution of marks of landslides in the neighbourhood of Himedi.

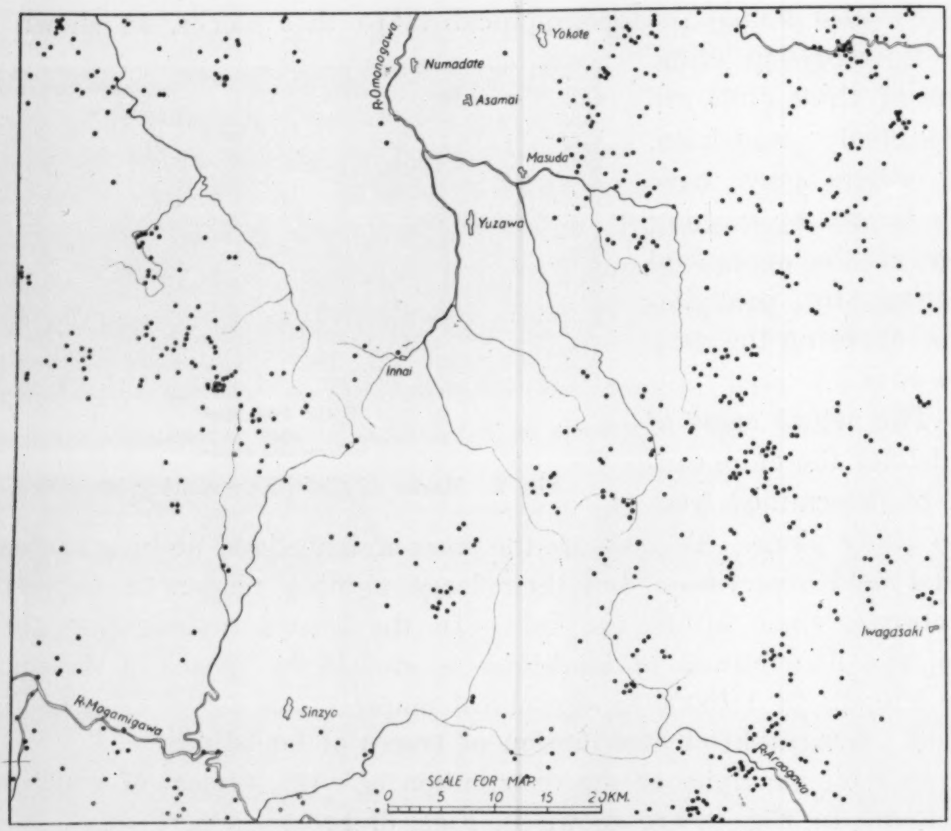

Fig. 4. Distribution of marks of landslides in the neighbourhood of boundaries of Akita, Yamagata and Iwate prefectures.

The following facts are elicited from these figures:

(i) Geographical distribution points to certain regions or zones of landslides.

(ii) Not all landslides occur in regions of steepest slope.

(iii) Not always are geological faults associated with zones of landslides.

(iv) Landslides sometimes seem to be restricted to regions of particular rocks, which however may differ with the locality.

In the distribution of landslides in Sikoku, Prof. Terada has pointed out[7] that landslides depend not only on meteorological causes and the mechanical properties of the rocks forming the surface layers of the regions, but also on movements of the earth's crust. The facts just referred to (elicited from the figures) do not seem to contradict Prof. Terada's statements.

The presence of a number of shallow ponds is also a notable feature of regions of landslides. These shallow ponds were no doubt formed as the result of irregular deformation of or of damming up streams by the earth mass that slipped down, the same as the hollows known as "——

---

[7] T. TERADA, Read at April, 1930, Colloquium of the Institute, but not yet published.

kubo", referred to in a previous paper[8]. Examples of these ponds are found in regions of landslides in the neighbourhood of Hirosima, Gozyô

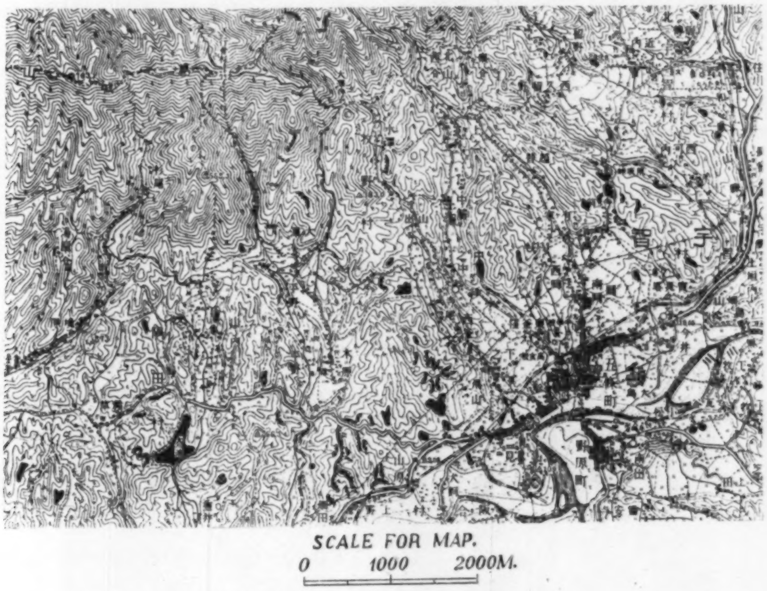
SCALE FOR MAP.
0 1000 2000M.

Fig. 5. Distribution of small ponds in association with landslides.

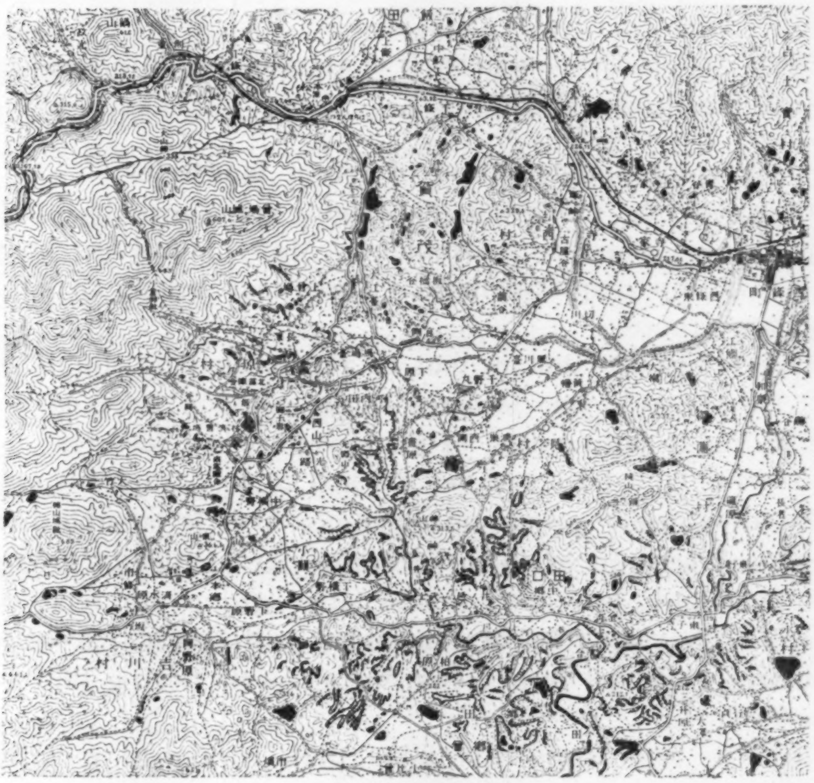
SCALE FOR MAP.
0 1000 2000M.

Fig. 6. Distribution of small ponds in association with landslides.

---

[8] T. TERADA and N. MIYABE, *loc. cit.*

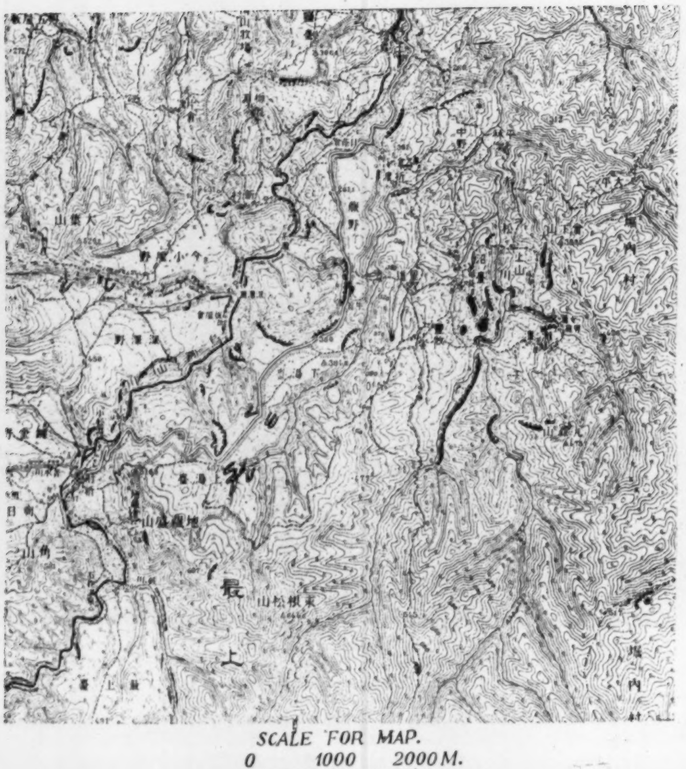

Fig. 7. Distribution of small ponds in association with the landslides.

(Wakayama Pref.), etc. (Figs. 5~7).

4. Geographical distribution of recent landslides.

In the preceding paragraph, landslides not shown by marks denoting cliffs in the maps were excluded. Many landslides however are not marked in topographical maps. These may belong in either of the following two groups:

i) Old landslides that cannot be represented by simple marks, or in which the characteristic features of the contour lines cannot be recognized owing to obliteration of all topographical features.

ii) Recent landslides not yet marked in topographical maps.

As to the former group no reference to it is possible here in the absence of any account of them excepting the studies of geologists.

The landslides belonging in the latter group are reported in the newspapers. The localities of landslides with areas exceeding 10000 square metres, collected from newspapers reports during 1931~1933, are given in Table I.

It will be seen from this table that, so far as reported, recent landslides have been most frequent in the prefectures of Nagano and Niigata.

In Fig. 8, the geographical distribution of these recent landslides is shown, together with those of marks of landslides referred

Table I.

No.	Locality Prefecture, County, Village	Date	Extent
1	Niigata, Higasi-Kubiki, Hisisato, Busuno	1931 Apr. 5	5×10^4 m²
2	〃 , 〃 , 〃	〃 8	9·9
3	〃 , 〃 , 〃 , Kamibuna	〃 〃	5
4	〃 , 〃 , Osima, Syôbu	〃 〃	2·6
5	〃 , 〃 , Hisisato, Maogi	〃 11	2
6	〃 , , Koide-mati	〃 16	—
	Siduoka, ———, Kobutano-yama	〃 21	—
	Toyama, Higasi-Tonami, Higasi-Yamami	〃 25	1
	Siduoka, Takata, Itô	〃 24	3
7	Niigata, Higasi-Kubiki, Matudai, Aizawa	〃 16	1
8	〃 , 〃 , Urata, Kurokura	May 1	5
	Siduoka, Iwata, Kômyô, Huneaki	〃 2	—
	Tiba, ———, Kiyosumi-yama	〃 3	1
9	Niigata, Nisi-Kubiki, Nôdani, Maseguti	June 4	5
	Toyama. , Yamakadumi, Tôhukuzino	〃 9	1
	Saga, Kisima, Yamaguti, Nisi-ku	〃 20	10
10	Niigata, Higasi-Kubiki, Matudai, Aizawa	July 11	—
11	Nagano, Kami-Minuti, Odagiri, Yamada	〃 23	1·5
12	〃 , 〃 , Nisi-Mamabe	〃 23	9·5
13	〃 , Tiisagata, Kanau, Kamamurata	〃 24	(300 m. in length)
	Hyôgo, Akasi, Tarumi, Nadami	〃 29	1
15	Nagano, Kita-Azumi, Nakatuti	Aug. 4	2
14	Niigata, Nisi-Kubiki. Kanaya, Nakanomata	〃 3	—
	Osaka, Minami-Kôti, Kokubu	Oct. 12	1
	Saitama, Titibu, Otaki, Otigawa	〃 4	4
	Osaka, Naka-Kôti, Katagami, Tôge	Oct. —	100
	Isikawa, Suzu, Saikai, Sasanami	Dec. 20	5
16	Nagano, Kita-Azumi, Nakatuti	1933 Mar. 17	12
	Yamagata, Mogami, Araki, Osawa	Apr. 11	2
17	Niigata, Naka-Onuma, Tazawa, Togura	〃 9	50
18	〃 , Higasi-Kubiki, Yamahira	〃 14	5
	Wakayama, Nisi-Muro, Inaki	〃 24	(60 m. depress. 1000 m. upheaval)
19	Niigata, Naka-Kubiki, Miduhara, Ozawa	〃 29	22
	Nagano, Sarasina, Akesina	June 9	—
	Hukusima, Iwaki, Ono, Yagyû	July 5	(1400 m. depress.)

(to be continued.)

Table I. (*continued.*)

No.	Locality Prefecture, County, Village	Date	Extent
20	Niigata, Higasi-Kubiki, Osima, Syôbu	July 9	$1{\cdot}1\times10^4$ m^2
22	Nagano, ———, Simosuwa, Tomibe	〃 11	(100 m.)
21	Nagano, Higasi-Sarasina, Nobusato, Yamabuse	〃 10	5
	Ibaraki, Nisi-Ibaraki, Minami-Yamaguti	〃 16	2·1
	Toyama, ———, Kurobe valley	〃 19	20
	Nagano, Higasi-Sarasina, Kôhu	Oct. 2	0·5
23	Niigata, Nisi-Kubiki, Kinoura	Nov. 19	10
24	〃 , 〃 , 〃	〃 21	4
	Isikawa, Kasima, Kita-Otani	〃 24	2
		Dec. 2	
26	Niigata, Nisi-Kubiki, Saikai, Maki	〃 17	3
27	Nagano, Kita-Azumi, Nakatuti	1933 Jan. 14	3
	Kyôto, ———, on the Miyadu-wan	Feb. 2	(90 m. crack)
	Nara, Yosino, Totugawa	Mar. 18	1·8
28	Niigata, Higasi-Kubiki, Oguro	Apr. 4	(150 m. crack)
29	Nagano, Kita-Azumi, Aizome	〃 6	3
30	Niigata, Naka-Kubiki, Miduhara	〃 9	10
31	〃 , Higasi-Kubiki, Yasuduka	〃 9	0·3
	Isikawa Toyama , ———, Ameda pass.	〃 10	1
	Tottori, Iwami, Gamô, Arai	〃 20	50
32	Nagano, Kita-Azumi, Kita-Koya	〃 14	1
	Toyama, Simo-Sinkawa, Higasi-Huse	〃 18	5
33	Niigata, Higasi-Kubiki, Hisisato	May 4	8
	Nara, ———, Nara Park	July 21	(100 m. crack)
	Toyama, Simo-Sinkawa, Katakaiya	Aug. 1	6
	〃 , Higasi-Tonami, Riga	〃 20	5
	Nagano, Tikuma, Hadamura	〃 6	—
	Yamaguti, ———, Ube, Hudiyama	Sept. 23	100
34	Nagano, Kita-Azumi, Nakatuti	Dec. 30	1·1

to in the preceding paragraph, and from which it is interesting to note that the zones of recent landslides differ considerably from those of the old, the reason for which is not apparent; all that we can do being to speculate that the zones of active landslides may have migrateed.

The frequency of landslides in Nagano and Niigata prefectures

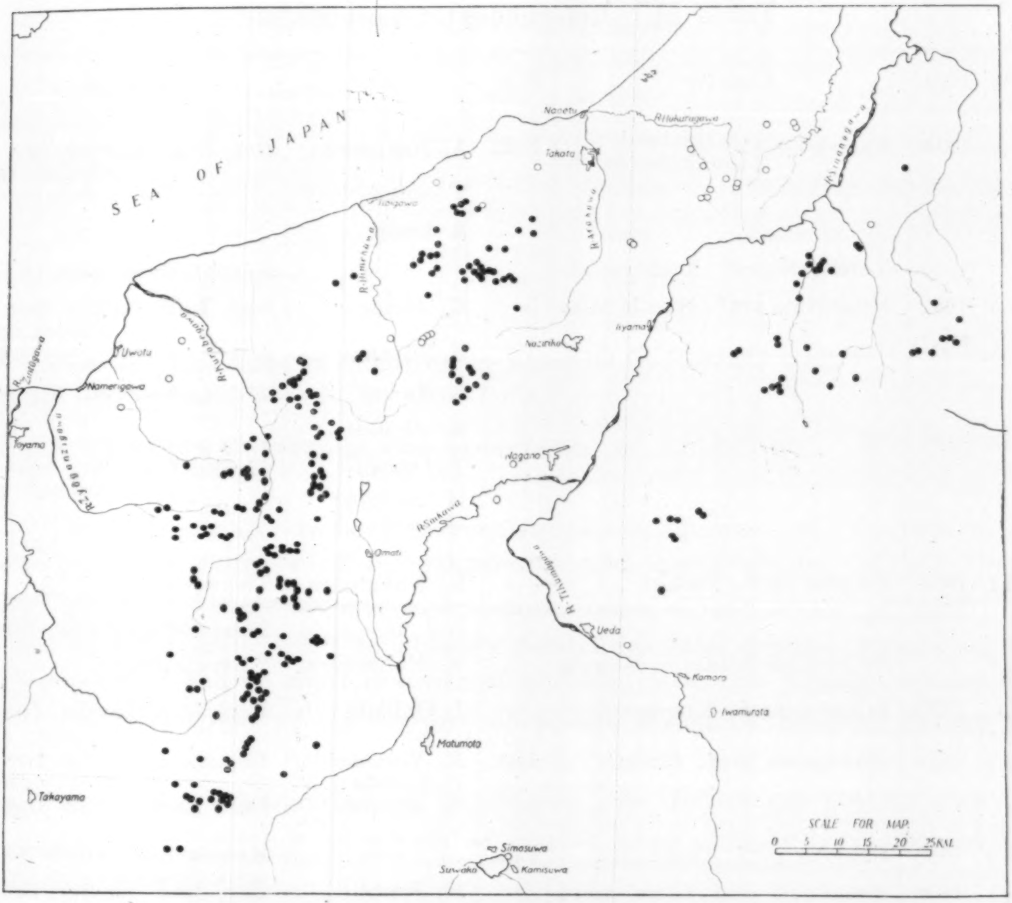
SEA OF JAPAN
Naoetu
R.Hokurugawa
Takata
R.Arakawa
R.Sinanogawa
Itoigawa
R.Himekawa
Iiyama
Nozirikō
Uwotu
Namerigawa
R.Kurobegawa
R.Zintûgawa
Toyama
R.Zyôganzigawa
Nagano
R.Saikawa
Omati
R.Tikumagawa
Ueda
Komoro
Iwamurata
Matumoto
Takayama
Simosuwa
Suwako
Kamisuwa
SCALE FOR MAP
0 5 10 15 20 25KM.

Fig. 8. Distribution of recent landslides (denoted by ○) and that of the marks of cliffs in the prefectures of Niigata, Nagano and Toyama.

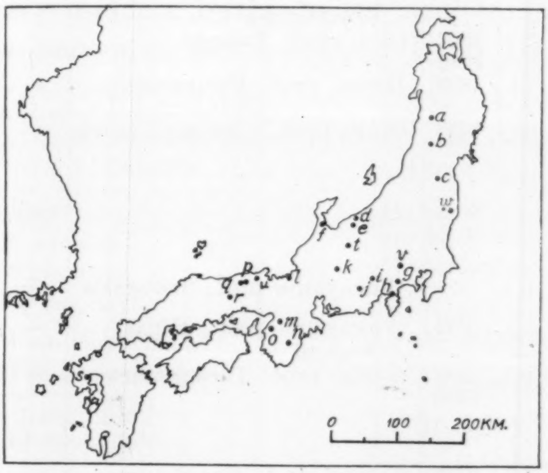
a
b
c
w
d
e
f
t
k
v
l
g
j
m
o
0 100 200KM.

Fig. 9. Distribution of the landslides reported by the geologists.

seem to be related to some way to the geological structure of these districts, which are said to be in the zone of compression[9]. In the zone of tension, that is, in the Kwantô districts and those along the northern Pacific, earthquakes are frequent.

As already stated, a number of geologists have studied the phenomena of landslides, the localities of which are shown in Fig. 9, and the literatures given in Table II.[10]

---

[9] T. Tokuda, *Tiriguku-Hyôron*, 1 (1925), 341, (in Japanese).

[10] Much of these literatures are collected in the resume :—"Abstracts of literatures on landslides", N. Miyabe, (Tokyo 1932), (in Japanese).

Table II. References of Landslides.

No.	Date	Locality	N.B.	Author.	Reference.
a.)	1914	Akita pref., (on the bank of the Omonogawa)	Eqk.	A. Imamura	Rep. Imp. Earthq. Inv. Comm., 82
				Y. Aomi	〃
		—		R. Ohasi	〃
		Yamagata pref., Araki-mura		——	Kisyô-Yôran, 1932, IV.
b.)	1932	Hukusima pref., Handa Mine	—	K. Jimbo	Rep. Imp. Earthq. Inv. Comm., 49
c.)	1987-		—	E. Tamura	〃 38
				K. Inoue	Tisitugaku-Zassi, No. 89
				K. Jimbo	〃 10
				T. Ogawa	Tigaku-Zassi, No. 159
				H. Inouye D. Satô	〃 〃 〃
				〃	〃 〃 No. 160
d.)	1918 1933	Niigata pref., Tutuisi	—	K. Nakamura	Tisitugaku-Zassi, 36
				I. J. R.	Tetsudô Saigai Kizi (1918)
e.)	—	Several landslides in Niigata pref.		K. Nakamura	"Yamakudure"
f.)	1892-	Isikawa pref., Kue-mura	—	J. Ohikata	Rep. Imp. Earthq. Inv. Comm.. 49
g.)	1923	Kanagawa pref., Hatano	Eqk.	N. Yamasaki	Rep. Imp. Earthq. Inv. Comm., 100
				T. Terada N. Miyabe	Bull. Earthq. Res. Inst. 10
h.)	1930	Siduoka pref., Omi-mura	Eqk.	——	Kensin-Zihô, Vol. 5. No. 1
i.)	1898	Yamanasi pref., Gokai-mura	—	K. Jimbo	Rep. Imp. Earthq. Inv. Comm., 38
		Siduoka pref., Kanaya tunnel	—	〃	〃 〃
j.)	1912	Siduoka pref., along the Tenryûgawa	—	T. Wakamidu	Tigaku-Zassi, 24
k.)	1904 1932	Gihu pref., Tozawa	—	T. Kamiya	Tikyû, 19
l.)	1898	Hukui pref., Utiura-mura	—	T. Iki	Rep. Imp. Earthq. Inv. Comm., 21
m.)	1932	Osaka pref., Katagami-mura	—	M. Matuyama	Tikyû, 17
				A. Takata	Doboku Sikenzyo Hôkoku
				K. Nasu	Bull. Earthq. Res. Inst. 10
				N. Miyabe	〃 〃
n.)		Wakayama pref., Totugawa	—	Cf. T. Wakimidu	Tigaku-Zassi 24
o.)	1932	Wakayama pref., Higasi Nogami	—	F. Kishinouye	Bull. Earthq, Res. Inst. 11
p.)	1897 1922	Hyôgo pref., Teragi-mura	—	H. Okada	Rep. Imp. Earthq. Inv. Comm., 38
				K. Tanahasi	Umi to Sora
				M. Matuyama	Tikyû, 17
q.)	1933	Tottori pref., Gamô-mura	—	M. Katuya	Sinrin-Tisui Kisyô Ihô, 14
r.)	1907	Okayama pref., Nariho-mati	—	T. Tyûsa	Tisitugaku-Zassi, 40
s.)	1913- 193	Nagasaki pref.,	—	——	Bull. Geotech. Comm., Vol. 2.

(to be continued.)

Table II. (*continued.*)

No.	Date	Locality	N.B.	Author	Reference.
t.)	1912	Nagano pref., Hiyeda-yama	—	M. Yokoyama	Tigaku-Zassi, 24
u.)	1903	Hyôgo pref., Okusatu-mura	—	J. Ohikata	Rep. Imp. Earthq. Inv. Comm., 47
v.)	1970	Tokyo pref., Hibara-mura	—	Y. Otuki	Tigaku-Zassi, 19
w.)	1921	Hukusima pref., Taira Colliery	—	S. Tokunaga	Tisitugaku-Zassi, 28

There are two cases of landslides in Karahuto (Sagharene) reported by H. Saitô, though they are not shown in the map of Fig. 9.

5. Factors governing the occurrence of landslides: Descriptions of landslides.

There are many factors governing the occurrence of landslides, as revealed by a number of investigations and observations. From these data we can distinguish several common characteristic in the phenomena. Some authors have tried to classify landslides into groups, according to types as exhibited in their manner of sliding, or to the physical character of the earth's crust of the region, or to the direct or indirect causes of the landslide, etc.[11]

As to the phenomena of landslides, the following points may be enumerated, a number of which of course have already been noticed by earlier investigators:

(a) While some landslides move with great velocity others do so very slowly. Attempts have been made to classify them according to these velocities, which however is very difficult, owing to the wide range through which their speeds vary as shown in the following Table III.

Table III. Velocities of Landslides.

Locality	Velocity	Observer
Karahuto, Kurasi (West coast)	10 m./day.	H. Saitô
Karahuto, Siritori (East coast)	40~25 cm./day.	H. Saitô
Hyôgo pref., Teragi-mura	27~25 cm./year.	M. Matuyama
Kagosima pref. Yosimatu	300~10 cm./day.	I. G. R.
Osaka pref. Katagami-mura	3 cm./day. (max.)	N. Nasu M. Matuyama
Isikawa pref. Kue-mura	30 m./hour. (max.)	(Rep. by J. Ohikata)
Kirchenstock, Switzerland (I)	3~1 cm./month.	A. Heim
(II)	100~10 cm./month.	

---

[11] A. Heim, *loc. cit.*
T. Wakimidu. *Tigaku-Zassi*, **24** (1912), 379, 379, (in Japanese).
K. Jimbo, *Rep. Imp. Earthq. Inv. Comm.*, **98** (1902), (in Japanese).
K. Watanabe, "*Doboku-Tisitugaku*", (Tokyo 1928).
K. Nakamura, "*Yamakudure*", (Tokyo 1934).

It may also be noticed that, as in the case of the Tôge landslide in Osaka[12], the velocities of sliding fluctuate with the quantity of precipitation.

(b) As already stated, the character of the rocks composing the surface of the earth seem to be related to landslides. Investigations so far show that the rocks in regions of frequent landslides are chiefly shales, especially sandy shales, agglomerates, and andesites, as will be seen from the following Table IV.

Table IV. Rocks Composing the Surface Layers in the Region where the Landslides occurred.

No.	Locality	Rock	N.B.
a)	Akita pref. Senpoku	Sandy Shales.	W.
c)	Hukusima pref. Hand Mine.	Agglomerate, Shale, Sandstone etc.	
d)	Niigata pref. Tutuisi	Shale.	W.
f)	Isikwaa pref. Kue	Mudstone, Sandstone (Tertiary). Fragments of Schists and Granite.	W.
i)	Yamanasi pref. Gokai-mura	Agglomerates, Shales.	
	Siduoka pref. Kanaya tunnel	Shale Sandstone	
j)	Siduoka pref. along the Tenryûgawa	Clay Slate, Slate. Black Mudstone.	
k)	Gihu pref. Tozawa	Sand, Gravel, Clay,	W.
l)	Hukui pref. Utiura-mura	Sandstone, Mudslate etc. Andesite, Gabbro, Conglomerate etc.	
m)	Osaka pref. Katagami-mura.	Andesites	W.
p)	Hyôgo pref. Teragi-mura	(Diluvium)	
r)	Okayama pref. Nariha	(Triasic) Shale	W.
t)	Nagano pref. Hiyeda-yama	Andesites etc.	W.
u)	Hyôgo pref. Okusatu-mura	Andesites.	
v)	Tôkyô pref. Hibara-mura	Mudstone.	
—	Several landslides in Karahuto.	Sandy Shale, (Tertiary) Sandstone, Shale.	

The mark "W" in the column of "N.B." denotes that the rocks are decomposed by weatherings.

(c) Although the classification of landslides according to their apparent types is, as already stated, not so easy as according to differences in their velocities, it is possible to distinguish several different types of landslides in extreme cases. These types are

---

[12] A. TAKATA, *Doboku-Sikenzyo Hôkoku*, No. 23 (1932), (in Japanese).
N. NASU, *Bull. Earthq. Res. Inst.*, **10** (1932), 694, (in Japanese).
M. MATUYAMA, *Tikyû*, **17** (1932), 323, (in Japanese).

(i) Slides of superficial layers of the earth's crust.

(ii) Streams or flows of masses of earth or rock fragments.

(iii) Relatively slow movements of fairly large masses of earth, generally bounded by zones of cracks.

(iv) Fall of great masses of rock fragments.

Of these types of landslides, the last three seem to show the same mechanism in their movements, and Type (ii) is generally associated with Type (iii). The landslide at Tôzaki, near Tutuisi, Niigata prefecture, is a typical example of Type (iii), while that at Tyausuyama, near Nagano, exemplifies Type (iii) associated with Type (ii).

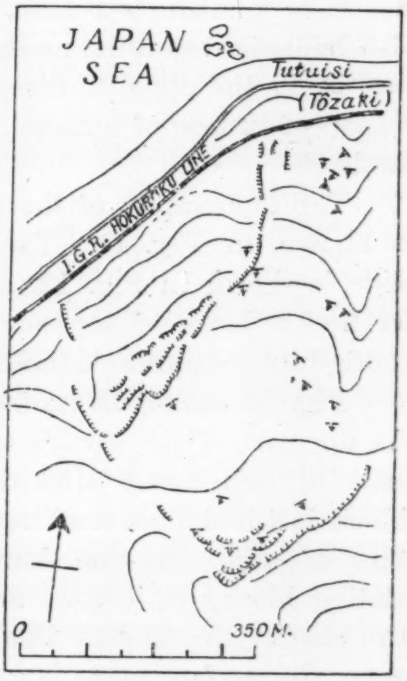
JAPAN SEA
Tutuisi
(Tôzaki)
I.G.R. HOKURIKU LINE
0
350M.

Fig. 10. Distribution of cracks in the Tôsaki landslide (reproduced from Nakamura's book.)

In the case of the Tôzaki landslide, cracks were formed as shown in Fig. 10, reproduced from Nakamura's book[13]. It will be seen that there is a

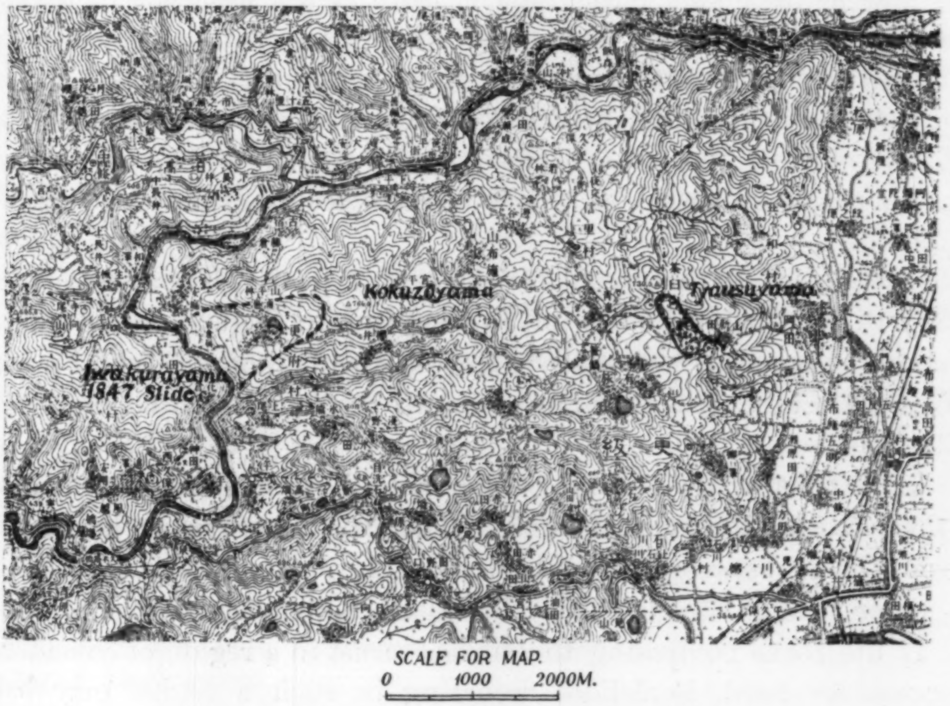
Kokuzoyama
Tyausuyama
Iwakurayama
1847 Slide
SCALE FOR MAP.
0
1000
2000M.

Fig. 11. Map showing the topographical features in the neighbourhood of the Tyausuyama lendslide.

---

13) K. Nakamura, *loc. cit.* "Yamakudure",

relatively undisturbed area, surrounded by zones of cracks. It may also be noticed that the undisturbed area is on the whole tilted southward, that is, in the opposite direction to that of sliding. A similar configuration of zones of cracks was also witnessed in the case of Tôge landslide[14].

The topography of the neighbourhood of the Tyausuyama landslide is shown in Fig. 11. The mud flow in the lower part of this landslide is shown in Fig. 12. In the upper part of the landslide, however, we find a block of the surface crust tilted, with zones of cracks of configurations similar to those mentioned above in connection with Type (ii).

Fig. 13 shows the profile of the Tyausuyama landslide schematically. As the part of the earth's surface that is represented by the hachured area in this figure slips down, a cliff is formed at A, and the sliding block is tilted backward against the direction of slip. At the lower end of the sliding block, B, cracks are formed as in the case of the Tôzaki landslide. In this zone, the surface crust is greatly deformed, in consequence of which fragments of rocks and small earth masses are formed, the whole sliding down the slope either as a mud flow or as a rock flow. The velocity of the mud flow or rock flow thus formed may be increased, should considerable quantities of water be mixed as the result of precipitations, since the water added to the mud flow may diminish the friction between the mud particles. In landslide of such type, the surface of slip seems to be, as shown in Fig. 13, nearly spherical, as would be expected from the theory of soil mechanics[15].

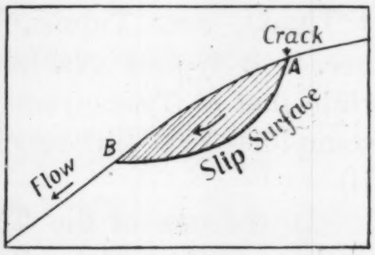

Fig. 13. Schematical profile of the landslide.

Landslides of this type are those of Tôge in Osaka prefecture, of Tôzaki in Niigata prefecture, of Tyausuyama in Nagano prefecture; and although I have not personally observed them, those of Teragi-mura in Hyôgo prefecture, Kue-mura in Isikawa prefecture, the Gamô-mura in Tottori prefecture, etc.

Landslides of type (i) may differ slightly from those just mentioned in their mechanism of occurrence. The cause here may be loosening of connection between the thin surface layer and the bed rock, since the water held in the boundary layers on the surface.

If the rocks composing the surface crust in a region of considerable steepness are hard, landslides occurring in such a region may belong to Type (iv). The harder rocks composing the region may first be broken into small pieces by fissures and joints developing in the rock mass. When such a region is exposed to heavy rain or earthquake, or suffers from some other triggar action, the internal friction is diminished, so that it cannot retain the original form of the slope, resulting in pieces of rock falling down in flows with considerable velocity, forming a cliff at the top of the disturbed area. The mud flow of Nebukawa at the time of the Kwantô earthquake of 1923[16], the Totugawa landslide[17] and several landslides in the Alps[18], may belong to this Type, iv.

---

[14] A. TAKATA, *loc. cit.*, etc.

[15] REDLICH, TERZAGHI, KAMPE. "Ingeniur Geologie", (Berlin 1932),. S. 430

Often in landslide of types ii) and iv), mud and rock flows damup valleys, forming ponds or small lakes. Examples are the Hatano landslide[19] associated with the Kwantô earthquake, and several others associated with the Akita earthquake of 1914.

In landslides of type iii), the block of earth that slips along the slip surface deforms considerably, loosening the earth and exposing a larger surface to erosion. The irregular contours and, sometimes, shallow ponds in regions of landslides are formed in this way.

(d) Landslides are closely related to the amount of precipitation, as will be discussed in detail later.

(e) In the case of some landslides, explosive shocks are felt and loud noises heard in the neighbourhood.

In the rockslide at Durango, Colorado, U.S.A., explosive shocks are reported to have been felt in the neighbourhood[20]. Similar noises were also reported to have been heard at the time of the Hiedayama landslide of 1905[21]. Such noises or shocks are supposed to have been produced by the crushing of rocks under the ground, In the case of Kue landslide[22], crunching, grinding noises were heard as the earth mass slid down, believed to have been caused by the crushing of the rock and the earth mass.

It may also be worthy of note that the topographical feature of the northern part of Bandaisan volcano which lost the northern half of its cone as the result of the 1888 explosion, closely resembles that of a landslide. The cones of several volcanoes exhibit features similar to that formed by landslides.

(f) In several landslides the odour of sulfur has been noticed as also flashes of light. The sulfur odour may in most cases be a psychological illusion or it may be due to pulverization of sulfides.[23]

---

[16] T. Matuzawa, *Rep. Imp. Earthq. Inv. Comm.*, **100** B (1925), (in Japanese).

[17] Cf. T. Wakimidu, *Tigaku-Zassi*, **24** (1912), 379, (in Japanese).

[18] A. Heim, *loc. cit.*

[19] T. Terada and N. Miyabe, *loc. cit.*

[20] Vanderwildt, *loc. cit.*

[21] M. Yokoyama, *Tigaku-Zassi*, **24** (1912), 609, (in Japanese).

[22] J. Ohikata, *Rep. Imp. Earthq. Inv. Comm.*, **49** (1904), (in Japauese).

The origin of light flashes seen at times of landslides is not yet understood. Many geologists[24] think it is due to frictional electricity as the rocks grind against each other when they flow down. Lights in association with landslides were reported to have been observed at the time of the North Idu earthquake of 1930[25].

6. Correlation between landslides and precipitations. As already stated, a number of landslides occurred in Niigata prefecture in the years, 1930~1933. We shall now compare the frequencies of these landslides with the quantity of precipitation for the corresponding period, the result being quite similar to those already obtained by K. Nakamura[26].

The annual distribution of the frequency of these landslides during 1930~1933, which is given in Fig. 14, shows that in Nagano and Niigata prefectures landslides occur most frequently in April, while there is another maximum of frequency in July. Upon comparison with the curve showing the annual variation in precipitations in Fig. 15, the second maximum landslide frequency in July suggests some relation to the heavy summer rains.

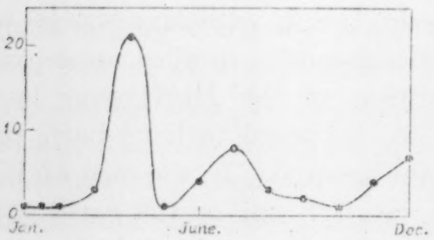

Fig. 14. Annual variation in frequency of landslides (1931-1933).

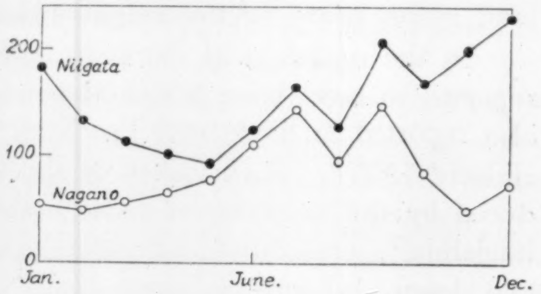

Fig. 15. Annual variation in monthly mean precipitations at Nagano and Niigata.

In Fig. 16, are shown the daily values of precipitation during January 1931~December 1933, together with marks denoting the occurrence of landslides. Fig. 16 shows several cases of landslides having been preceded by heavy rains. It must, of course, be remarked that the values of the precipitation are those observed in the cities of Nagano, Takata, and Niigata, so that they may not represent the actual amounts of precipitation in the regions where the landslides occurred, although these stations lie very close to them. Of landslides accompanying heavy rains, those that occurred in Higasi-Kubiki Gun, etc, that is, the

---

23) VANDERWILDT, *loc. cit.*

24) A. HEIM, *loc. cit.*

25) K. MUSYA, "*Luminous phenomena accompanying the destructive earthquakes*," (Tokyo 1931).

26) K. NAKAMURA, "*Yamakudure*", *loc. cit.*

eastern region of the district under consideration, are generally associated with precipitation maxima at Niigata and Takata or Niigata, Takata, and Nagano, while those that occurred in Nisi-Kubiki Gun, in Niigata prefecture and Nagano prefecture, that is, in the western region, are associated with the precipitation maxima at Takata and Nagano or Nagano alone.

Landslides that occurred in March April and May are generally not connected with the heavy rains. These landslides may be, as mentioned already, caused by the melting of the snow accumulated during the preceding winter.

Landslides have also occurred some time after the atmospheric temperature rose several degrees above freezing point[27].

If the heat that melts the snow is supplied by conduction alone, the quantity of snow melted in unit time per unite area will is estimated roughly by

$$s\rho v=\lambda(\theta-\theta_0),$$

$$\text{or}\quad \rho v=\frac{\lambda}{s}(\theta-\theta_0),$$

where $(\theta-\theta_0)$ is the temperature difference between the snow and the surroundings, λ the conductivity, s the specific heat of the melted snow and pv the melted mass of the snow. Should radiation be an important factor in the supply of heat, another term, which is a function of T, should be added. The quantity of the melted snow during t_2-t_1 is therefore nearly

$$\int_{t_1}^{t_2}\frac{\lambda}{s}(\theta-\theta_0)dt \fallingdotseq \frac{\lambda}{s}(\theta-\theta_0)(t_2-t_1).$$

Taking $0{\cdot}5\times10^{-3}$ and 80 cal. for the numerical values of λ and s respectively, the quantity of melted snow for a temperature difference of 10 degrees and a duration of 1000 hours is estimated to be 2200 g., which corresponds to a precipitation of 22000 mm. approximately.

7. Physical considerations on the factors connected with landslides. From the preceding paragraphs, we can select the following factors as being the most effective in activating or initiating landslides.

(i) Destructive earthquakes,

(ii) Water, rain and melted snow.

The physical properties of the rocks composing the surface layers of the earth may also conduce to the occurrence of landslides, as is suggested by the fact that landslides frequently occur in regions of shales and andesites.

In landslide of type (iii), cited in the preceding paragraph, resistance to slip is given by

---

[27] K. Nakamura, *Tisitugaku-Zassi*, **37** (1930), 411, (in Japanese).

$$\mu N+K,$$[28]

where μ is the coefficient of friction, N the normal component of the weight of the slipping mass, K the cohesion along the slip surface. No landslide can occur when the pull of gravity does not exceed the resistance by the above expression.

The distribution of stress under the action of gravity, in the surface layer of earth may not be uniform, owing to irregularities in its surface features. The mode of stress distribution determines the slip surface, or, as a two-dimensional problem, the slip line, the differential equation of which is given by

$$\frac{dy}{dx}=-\frac{2\tau}{\sigma_x-\sigma_y}\left\{1\pm\sqrt{1+\frac{(\sigma_x-\sigma_y)^2}{4\tau^2}}\right\},$$[29]

where σ_x, σ_y, τ are the stress components given as functions of the coordinates x and y.

Since the pull causing the landslide may be gravity, the factors, enumerated above as responsible for the landslides, may act to reduce the resistance, that is, to reduce the values of μ and K.

We first consider the effect of earthquakes. The effect of earthquake waves on the earth's crust may consist of two components; the one in which earthquake vibration may reduce the effective value of μ along the slip surface, the other in which earthquake waves may exert stresses on the surface layer of the earth and break it. The stresses exerted by earthquake waves causing landslides may act in two different ways; one of which is due to variation in direction of the effective gravitational force by a small angle θ, which is connected with the intensity of the earthquake K by the relation

$$\theta=\tan^{-1}K.$$[30]

In this case, the resisting force to breaking is reduced to

$$(1-k_v)$$

times that in the case of statical state. If this reduction in resisting force were sufficient, the pull due to gravity will cause a landslide.

On the other hand, earthquake waves may as they are propagated in the earth's interior, exert stresses on the surface layer of its crust. As to deep focus earthquake, Mr. H. Kawasumi[31] calculated the stress due to earthquake waves in the neighbourhood of the origin to be of the order of 10^9 c. g. s., which exceeds the order of magnitude of the breaking stress of the rocks composing the earth's crust, which is

---

28) A. Krey, "*Erddruck, Erdwiderstand etc.*", (Berlin 1928).

29) C.f. Z. Anzô, *Mem. Kyûsyû Imp. Univ.*, **7** (1933), 89.

30) N. Mononobe, "*Doboku Taisin-Gaku,*" (Tokyo 1930), etc.

31) H. Kawasumi, *Disin*, **4** (1932), 693, (in Japanese).

assumed to be of the order of $10^7 \sim 10^8$ c.g.s. In the surface layer however the breaking stress may be smaller in order of magnitude compared with that of the interior of the earth's crust. Hence stresses of smaller magnitude are sufficient to break the surface layers.

It may be remarked that in addition to stresses due to earthquake waves, are chronic deformations of the earth's crust, as were found in association with the Kwantô and other earthquakes, and which may cause breaking of the surface layers.

Let the components of displacments of a point be u, v and w as found by precise geodetic method. Then the components of stress are given in the form

$$\widehat{xx}=\lambda\left(\frac{\partial u}{\partial x}+\frac{\partial v}{\partial y}+\frac{\partial w}{\partial z}\right)+2\mu\frac{\partial u}{\partial x}, \quad \text{etc.},$$

$$\widehat{yz}=\mu\left(\frac{\partial u}{\partial y}+\frac{\partial v}{\partial x}\right), \quad \text{etc.},$$

where λ and μ are elastic constants of the earth's crust. Of these components of displacement gradients, we have data measured at the surface for several districts, except for those of $\frac{\partial w}{\partial x}, \frac{\partial w}{\partial y}, \frac{\partial w}{\partial z}$. For values of $\frac{\partial u}{\partial x}, \frac{\partial v}{\partial x}$, etc., of the surface of the earth, we obtained magnitudes of the order of 10^{-5}[32] from analyses of horizontal displacements of triangulation points. Assuming the elastic constants of the surface layers to be of the order of 10^{10} and, substituting the above mentioned values of the displacement gradients, we have for $\widehat{xx}$ and $\widehat{yz}$, values of the order of 10^5. Since however the surface layers of the earth will be deformed permanently, and since the horizontal displacements of the triangulation points measured contain component accumulated in the course of several tens of years, only a part of the above mentioned value may exert stress on the surface layer, although, under certain conditions, it may be enough to activate landslides.

In association with the North Idu earthquake, landslides occurred at many places, of which the Zyô landslide,[33] together with several others, were found to lie on a zone of virtually active fault, that is, the zone where the earth's crust was deformed conspicuously. A landslide similar in type to the Zyô landslide occurred on the southern bank of the Omonogawa in association with the Akita earthquake of 1914,[34] in which earthquake, the landslide slipped along the boundary surfaces of layers of different geological series. These landslides might have been activated by the triggar action of earthquake vibration, stress exerted by earthquake waves, or by the slow crustal deformation associated with earthquakes which, it is difficult to say.

---

[32] C. Tsuboi, *Jap. Journ. Astr. Geophys.*, **9** (1933), 95.
N. Miyabe, *Bull. Earthq. Res. Inst.*, **11** (1933), 639.

[33] *Kensin-Zihô*, **4** (1930~1931), (in Japanese).

[34] A. Imamura, *Rep. Imp. Earthq. Inv. Comm.*, *loc. cit.*
Y. Aomi, *ibid.*
R. Ohasi, *ibid.*

We shall next deal with the effect of precipitation which, as already stated, is an important factor in the activation of landslides. There can be no doubt that penetration of water into the rock, layers causes conditions favourable to the occurrence of landslides, although its precise mechanism is as yet unknown. The following experiments may however be throw some light on the question of mechanism.

Small blocks of rock from landslides in the prefectures of Nagano and Niigata were exposed to water penetration, with the result that, as shown in Fig. 17, the hair cracks that were in the rocks prior to the experiment generally widened, while in severel cases the rock disintegrated. The widening and formation of these cracks in the rock may be the result of partial contraction in the rock mass due to complete penetration of water.

Further experiments were made with respect to the contraction of sand mass by water penetration. The water was first allowed to permeate a column of sand loosely piled in a glass cylinder of 3 cm. diameter and 30 cm. length, with a permeable membrane at the base. The cylinder into which the sand was piled was sunk into a bath of water, and the height of the penetrated water and the displacements of the surface of the sand measured with respect to various water levels. The result is shown in Fig. 18, in which the contraction of the sand column is plotted against the heights of the water that had penetrated. In Fig. 18, we notice that, within a certain range, the contraction of the sand column is approximately proportional to the height of the water in the sand.

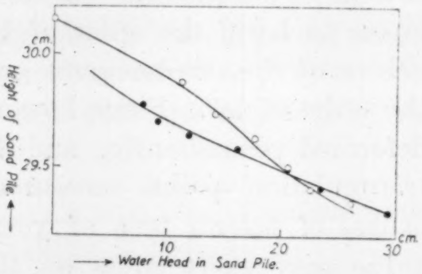

Fig. 18. Contraction of sand pile due to penetration of water.

The sand was then piled in a meter glass, to which water was added, after which the upper part of the sand mass that was found to have risen considerably had separated into a block, as shown in Fig. 19. The intermediate part between the upper and lower ends of the sand mass was filled with the air that had been forced out of the interstices in the sand mass by penetration of the water.

We shall consider two plates standing side by side in a vessel of water with a very small distance h separating them. When the space

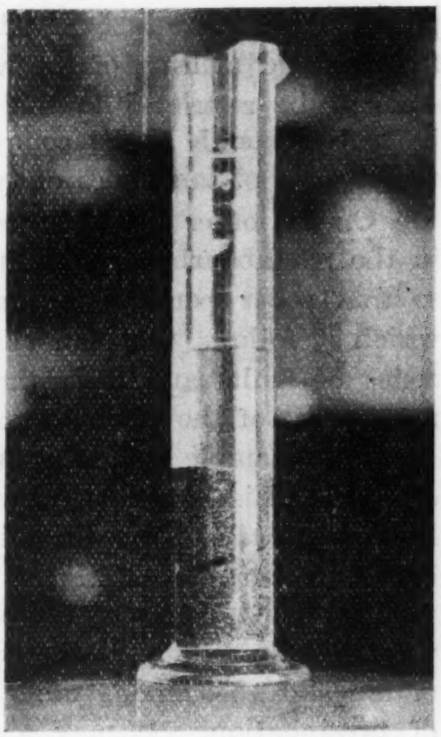

Fig. 19. Cracks in the sand piles.

between these two places is filled with water they will be pulled towards each other by the force of capillary attraction, which is a function of h, (neglecting the gravity component) of the form

$$P=-\frac{s\alpha^{2}}{h},$$ [35]

where s is the area of the plates and α^2 is the surface tension of the water. We shall imagine many such plates standing side by side, the distances between the plates being unequal. If water fills every space, then stress is exerted on the mass of these plates, owing to inequality in the values of h. that is

$$\frac{\partial P}{\partial x}=\frac{\partial P}{\partial h}\,\frac{\partial h}{\partial x}=+\frac{s\alpha^{2}}{h^{2}}\,\frac{\partial h}{\partial x}.$$

If the above expression be applicable to the case of the surface layers of the earth in estimating the stress exerted on the interior of it by penetration of water, we shall then obtain as the stress the value of 2×10^5 dyne/cm^2, or 1 kg/cm^2, on the assumption that $h=10^{-3}$ cm. $=10$ micron, $s=1=$ unit area, $\alpha^2=80$ dyne/cm., and $\frac{\partial h}{\partial x}=1$. The value of $\frac{\partial h}{\partial x}$ may be large for smaller values of x. The value for the stress thus estimated is comparable with the tensile strength of clay, which if several kilograms per square centimetre[36], as given in Table V.

Table V. Tensile Strength of Clay.

	Strength kg./cm.^{2}
Wet clay	0·17
Dry 〃	4·50

If, in an actual case, the stress due to the force of capilarity overcomes the strength of the rocks composing the surface layers of the earth, either fresh cracks will be formed or old ones widened, in consequence of which the friction and cohesion on the slip plane will be reduced considerably. It may therefore be concluded that the cracks are developed in the rock mass composing the surface layer of the earth through complete penetration of water accompanying heavy precipitations.

As to cracks forming in the rocks, periodic variations in atmos-

---

35) NEUMANN, *Theorie der Kapilarität.*

36) Cf. K. TANAHASI, *Umi to Sora*, **12** (1932), 221, (in Japanese).

pheric temperature is believed to be an important factor[37]. The periodic freezing and melting of the water contained in rocks or clays however seem to be restricted to the superficial layer, which however may not be thick enough to be comparable with that of the layer that moves at the time of landslides of type (iii).

On the other hand, it may be worthy of note that the crustal layers in the neighbourhood of faults and folds are comparatively disturbed, so that water penetration may be much easier to such regions, from which it follows that landslides are sometimes found associated with zones of faults and folds that have been much disturbed by chronic movements of the earth's crust.

The example of a landslides pointed out by Terzaghi[38] is also worthy of note. This landslide, which occurred on the bank of river, might have been caused by breakdown of underground sand layers loosened by the penetration of water.

8. Crustal movements and landslides. It may be suggested from what has been stated in the preceding paragraphs that the phenomenon of landslides is, among other things, intimately related to the quantity of precipitation. It may also be suggested that the part played by precipitation in causing landslides may be more pronounced in the case of earth mass or rocks that are subjected to greater prevailing chronic crustal movements than others.

Before we deal with the relation between chronic crustal movements and landslides, it should be remarked that disturbance of the earth's crust is conspicuous not only in regions of landslides, but also in Alluvial plains in regions close to epicentres of destructive earthquakes. For this reason a number of the examples cited in the present paragraph to show that chronic crustal movements seem to be related in some way to the occurrence of landslide, may serve also as data for future investigations that may be made of the relation between the two. The examples are as follows:

(i) Higasi-Kubiki Gun, Niigata prefecture, situated between two nearly parallel lines of precise levels from Naoetu to Nagaoka and from Nagaoka to Nagano, as shown in Fig. 20, is a region of frequent landslides. The vertical displacements of bench-marks along these level lines (Fig. 21) do not show conspicuous disturbance in the earth's crust which might have been associated with landslides, except the small fluctuations in the neighbourhood of Iiyama. This may of course be to due on the one hand to the widely separated bench-marks, whose changes

---

37) G. WATANABE, *Tuti-to-Midu Iinkwai Hôkoku*, No. 4 (1930), 29~43, (in Japanese).
38) C. TERZAGHI, *Ingeniur Geologie*, S. 436, *loc. cit.*

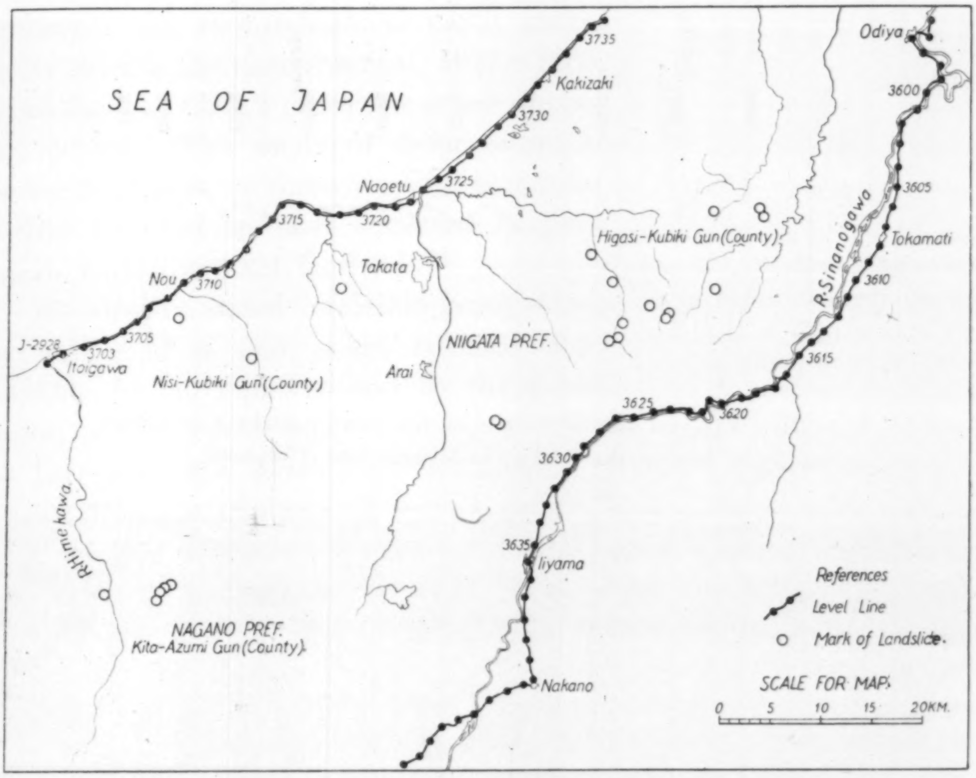
SEA OF JAPAN
3735
Kakizaki
3730
Naoetu
3725
3720
3715
Takata
Nou
3710
J-2928
3703
3705
Itoigawa
Nisi-Kubiki Gun(County)
Arai
NIIGATA PREF.
Higasi-Kubiki Gun(County)
Odiya
3600
3605
Tokamati
R.Sinanogawa
3610
3615
3620
3625
3630
3635
Iiyama
Nakano
Rhime kawa
NAGANO PREF.
Kita-Azumi Gun(County)
References
Level Line
Mark of Landslide.
SCALE FOR MAP.
0
5
10
15
20KM.

Fig. 20. Lines of levels and distribution of recent landslides in Higasi-Kubiki Gun (county), Niigata Pref.

in heights are measured, and on the other hand to the fact that the region under considerations forms part of a block different from those traversed by the level lines.

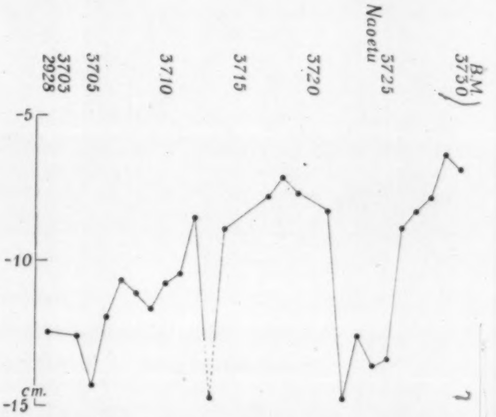

Fig. 21a. Vertical displacements of the bench-marks along the line from the Itoigawa to Kakizaki via Naoetu.

(ii) The landslide in 1922 at Teragi-mura, Hyogo prefecture, was studied in detail by Prof. M. Matuyama[39]. Recently another landslide occurred at Gamo-mura, Tottori prefecture, ten or more kilometres west of Teragi-mura landslide[40]. Topographical feature of the neighbourhood of these landslides are shown in Fig. 22. From the vertical displacements shown in Fig. 23 of bench-marks along the level lines in Fig. 22, it will be seen that the regions where the landslides occurred are situated close to the tilted blocks.

---

[39] M. Matuyama, *Tikyû, loc. cit.*

[40] M. Katuya, *Sinrin-Tisui Kisyô Ihô*, No. 14 (1934), (in Japanese).

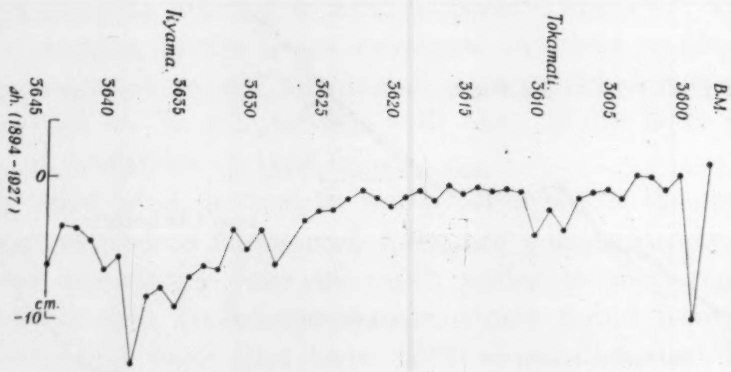

Fig. 21b. Vertical displacements of the bench-marks along the line from Nagano to Odiya via Iiyama and Tôkamati.

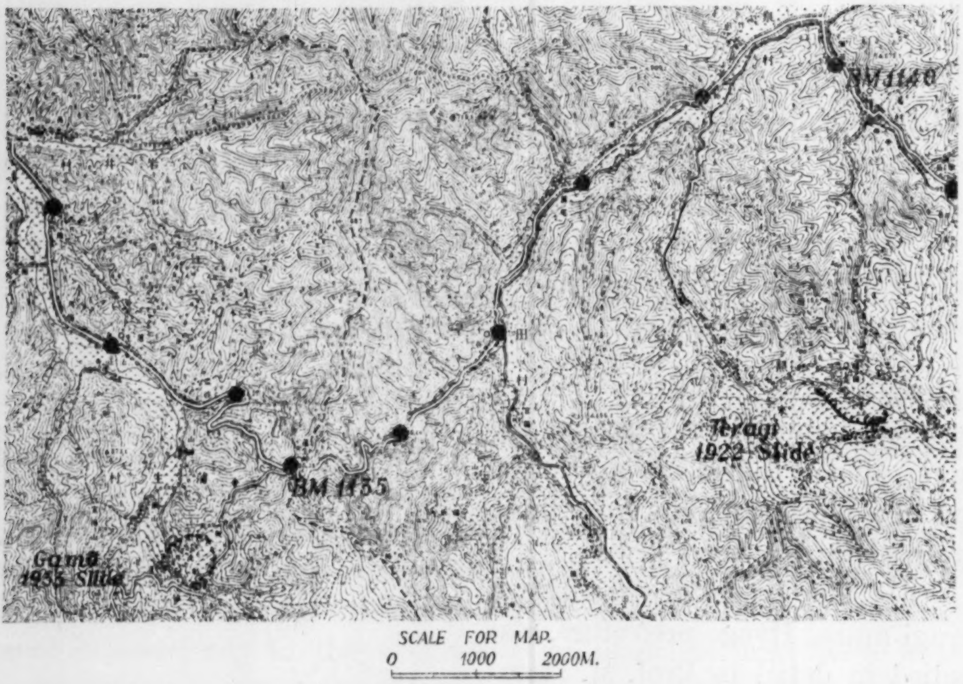

Fig. 22. Map showing the distribution of bench-marks in the neighbourhood of Teragi-mura and Gamô-mura landslides.

(iii) At the neck of the Noto peninsula is a mountain range extending NE-SW. Landslides have occurred on the northern and southern slopes of this mountain range, the localities of which are shown in Fig. 24, together with the topographical features. Of these landslides, those that occurred in 1904 and 1932 were studied by several authors[41]. On the other hand, the vertical displacements of bench-marks along the level lines that cross this mountain range have been measured a number of times as shown in Fig. 25. Of these curves representing the recent vertical displacements (Fig. 25), the one that represents the recent vertical earth movements during the time interval, 1927~1933, shows that the earth's crust upwarped during that period. The mode of deformation of the earth's crust in these regions is similar to that believed to have occurred in association with the 1904 landslide[42].

---

[41] J. Ohikata, *loc. cit.*; H. Honda, *Kensin-Zihô*, 4 (1930~1931), 403.

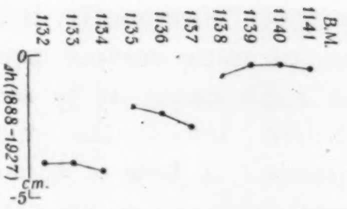

Fig. 23. Vertical displacements of the bench-marks in the neighbourhood of the Gamô-mura and the Teragi-mura landslides.

As already stated landslide occur when the values of K and μ are reduced considerably by earthquakes and by the penetration of the water into the layers of the earth. Crustal deformations may of course contribute in some measure to increase the pull by one of the components of the gravitational force, which however may not be sensibly large. The crustal disturbance just mentioned may also assist in causing the water to penetrate into the surface layers of the earth and the rocks.

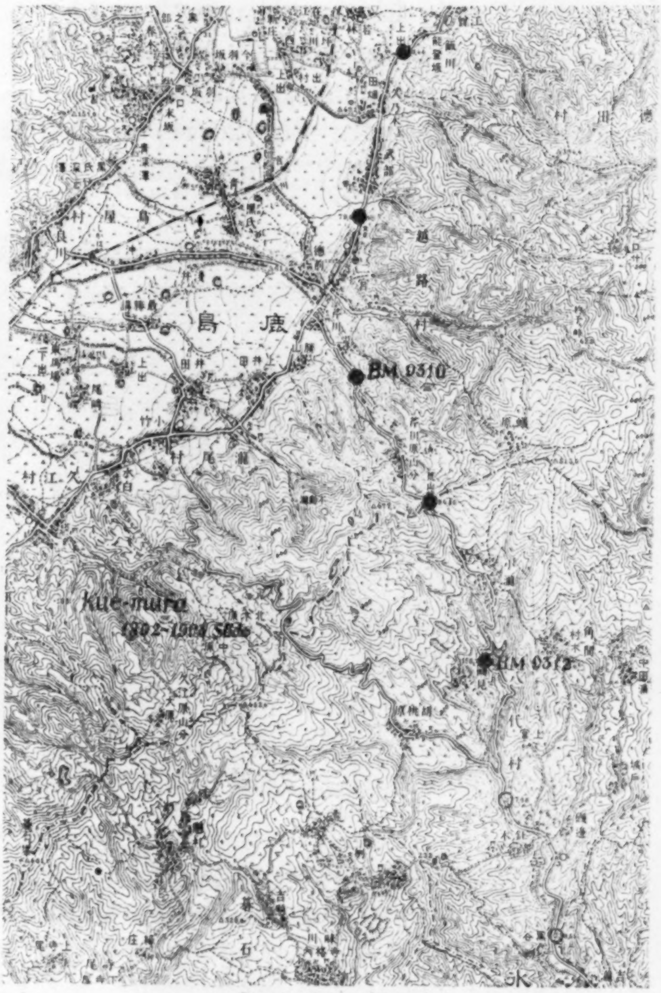

Fig. 24. Map showing the distribution of bench-marks in the neighbourhood of the boundary of prefectures of Toyama and Isikawa.

9. Mud flows. The reader's attention may now be drawn to the phenomena of mud flows. As already stated, several landslides, have been accompanied by either mud flows or rock flows. These flows sometimes sweep away farms and houses and do much damage.

The flows are generally initiated at the rear of landslides of type (iii). The velocity of the flow varies within wide

---

[42] J. OHIKATA, *loc. cit.*

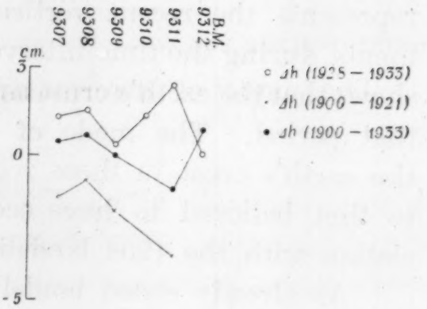

Fig. 25. Vertical displacements of the bench-marks situated in the neighbourhood of the boundary of the prefectures of Toyama and Isikawa.

ranges. Frequently it is as much as ten or more metres per second, while, in some cases, it is so small that we cannot notice the movements at a glance. A flow of considerable mass of earth or rocks moving with considerable velocity is sometimes called "Yama-tunami" (mountain-tunami). Several of the Alpine landslides[43], the landslides associated with the Kwantô eartnquake[44] and the North Idu earthquake[45], and the Hieda-yama landslide[46] (a map of the neighbourhood of the Hieda-yama landslide is shown in Fig. 26 reproduced from Yokoyama's paper), are what may be called "Yama-tunami", while the mud flow associated with the Tyausuyama landslide is a typical example of the mud flow that moves very slowly.

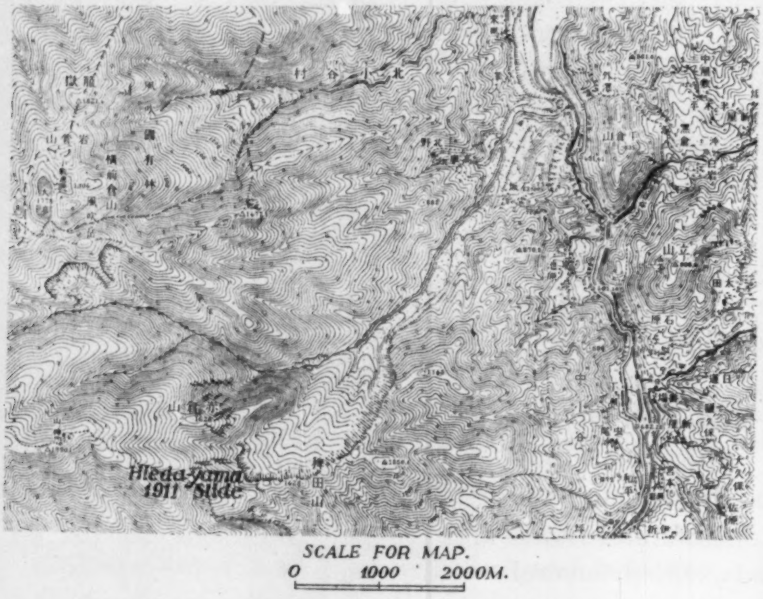

Fig. 26. The map in the neighbourhood of the Hieda-yama landslide.

When, however, the velocity of flow is considerable, the mode of flow seems to differ somewhat from that of a viscous liquid, the analogy being applicable to mud flows with small velocity.

---

[43] The cases are shown in A. HEIM'S book, *loc. cit.*

[44] The Nebukawa landslide reported by T. MATUZAWA, *loc. cit.*

[45] The Kadiyama landslide etc. reported in *Kensin-Zihô*, *loc. cit.*

[46] Report by M. YOKOYAMA, *loc. cit.*

To investigate the mode of mud flows in greater detail, an experiment was made with dry sand. The velocities of the sand flow on slopes of various inclinations are shown in Fig. 27.[47]

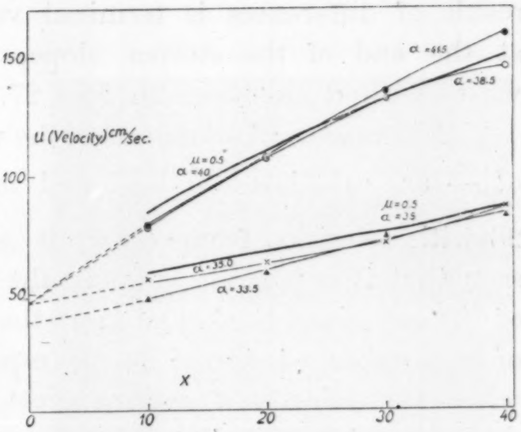

Fig. 27. Relation between the terminal velocity of sand flow and the distance which has been flown by sand.
(The thick lines shows the theoretical relation represented by $u=\sqrt{2g(\cos\alpha-\mu\sin\alpha)x}$.)

This figure seems to suggest that the dissipation of energy as the sand flows along the slope may be due mainly to friction of the boundary surface. According to our experiments, equivalent viscosity does not seem to sensibly reduce the velocity. This may be due mainly to thinness of the layer of flowing sand.

In such cases therefore we can calculate the velocity, as did Heim, by a simple formula

$$\frac{du}{dt}=g(\sin\alpha-\mu\cos\alpha),$$

where α is the inclination of the slope and μ the coefficient of friction. The calculates values of u on the assumption, that $\mu=0{\cdot}5$ and $u_0=45$ cm./sec., agree very well with those observed, as shown in Fig. 27.

Further experiments were carried out with respect to the flow of sand along a slope, using two slopes of different inclinations, namely, a steep slope followed by a gentler one. In this case, the distances traversed by the sand over the gentler slope was measured relative to various combinations of inclinations of the two slopes.

In Fig. 28, the values of x_1/x_0, that is, the ratios of the distances traversed by the sand over the gentler slope to these over the steeper are plotted against inclinations of the gentler slope, from which we see that the ratios become larger as the inclinations of the gentler slope increase, that is, the greater the inclination the larger the rate of increase, and that the ratios suddenly increase when the inclimation of the steeper slope exceeds 35°.

Of the receipts just mentioned, the former may be due mainly to frictional resistance of the gentler slope, while the latter may be the

---

47) The detail of the results of the experiments will be reported in due course.

48) A. Heim, *Bergsturze und Menschenleben, loc. cit.*

result of differences is terminal velocity at the end of the steeper slope, which varies with α as shown in Fig. 27.

Taking several actual cases, the values of $\frac{x_1}{x_0}$ are calculated and plotted in Fig. 28 with asterisks, from which it will be seen that it is possible to apply the result of the experiments of sand flows the study of a number of actual cases, especially when the velocity of flow is great. The deviation of the actual values of x_1/x_0 may be considered as due to the following causes:

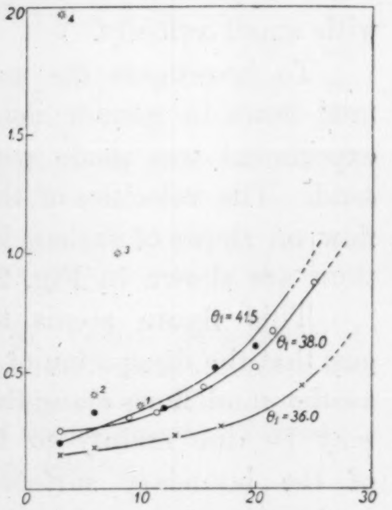

Fig. 28. Relation between x_1/x_0 and θ_2.

The values of x_1/x_0 for actual cases of

1. Val Bedretto landslide 1898 (48).
2. Schächental landslide 1887 (43).
3. Aegerti landslide 1897 (45).
4. Elm landslide 1881 (41).

are plotted by *.

(i) The frictional resistance at the bottom of the flow may be reduced considerably if the flowing earth mass contains water.

(ii) In the flow of a water-bearing earth masses, the dissipation of energy in the course of its flow may also be reduced.

(iii) In certain cases the inertia mass of the flowing earth may play an important rôle, when the value of x_1 will be larger than these estimated by considering the dissipation due to frictional resistance only.

10. Summary and conclusion. In the present paper, the writer described the modes of a number of landslides and discussed the relationship between several probable factors and landslides. The most important factors are

(i) Stresses exerted by earthquakes on the layers of the earth, the effect of the vibration reducing the effective value of friction along the slip surface.

(ii) The water that has penetrated into the layers of the earth, exerts local stress within the mass of earth or rocks to widen the cracks or form new ones, in consequence of which the effective values of μ and k are reduced considerably.

(iii) The relation between chronic crustal deformation and landslides is not yet understood.

In the last paragraph, the modes of mud flows are described in comparison with experimental sand flows.

To avoid dangers from landslides, the next best way to avoiding

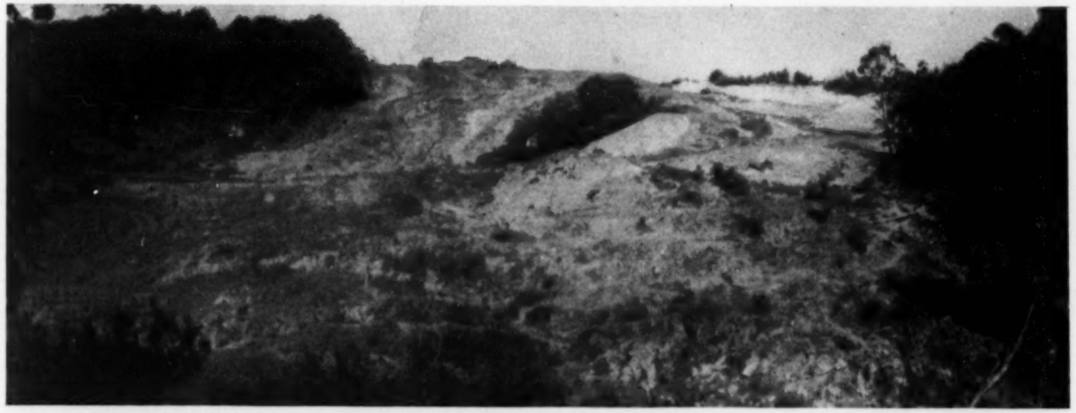

Fig. 12. Mud flow of the Tyausuyama landslide.

（震研彙報 第十三號 圖版 宮部）

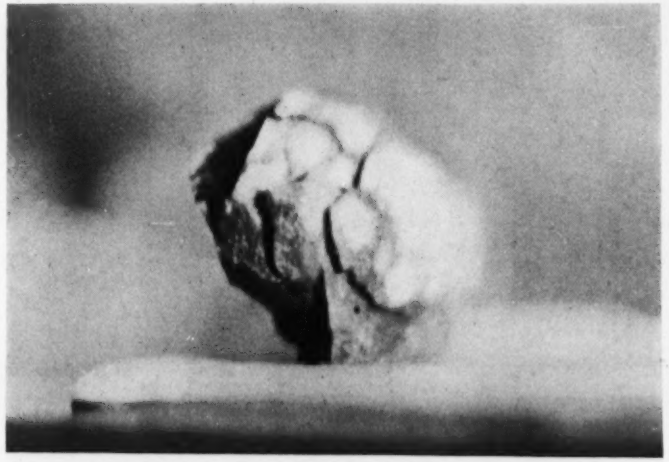

Fig. 17. Cracks in the rock produced by the water penetrated.

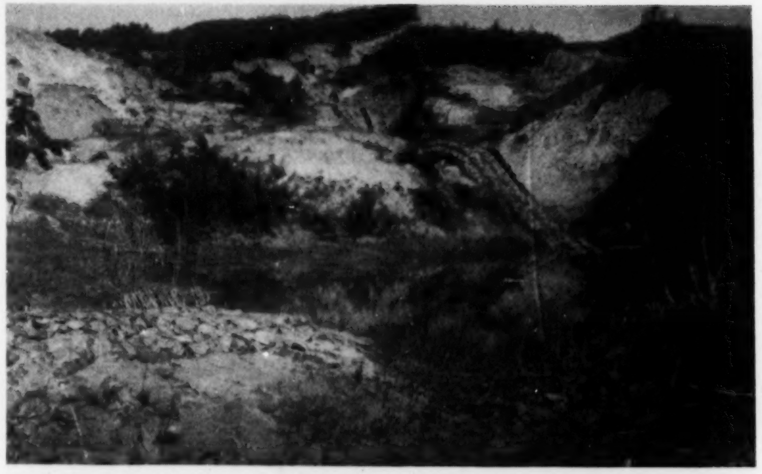

Fig. 29. The deformation of the surface layer of the earth in the Tyausuyama landslide.

[N. MIYABE.]

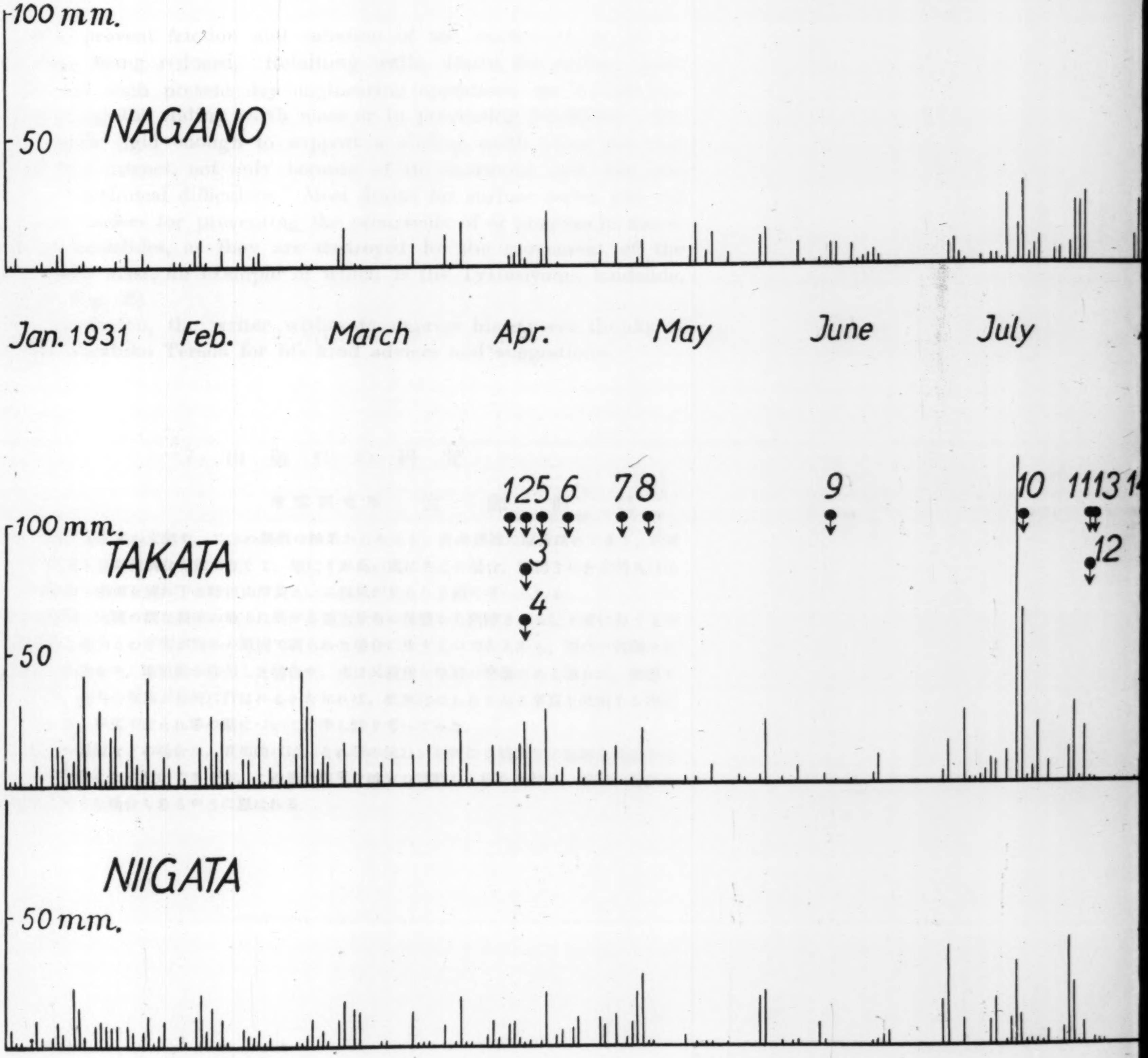

（震研彙報 第十三號 圖版 宮部）

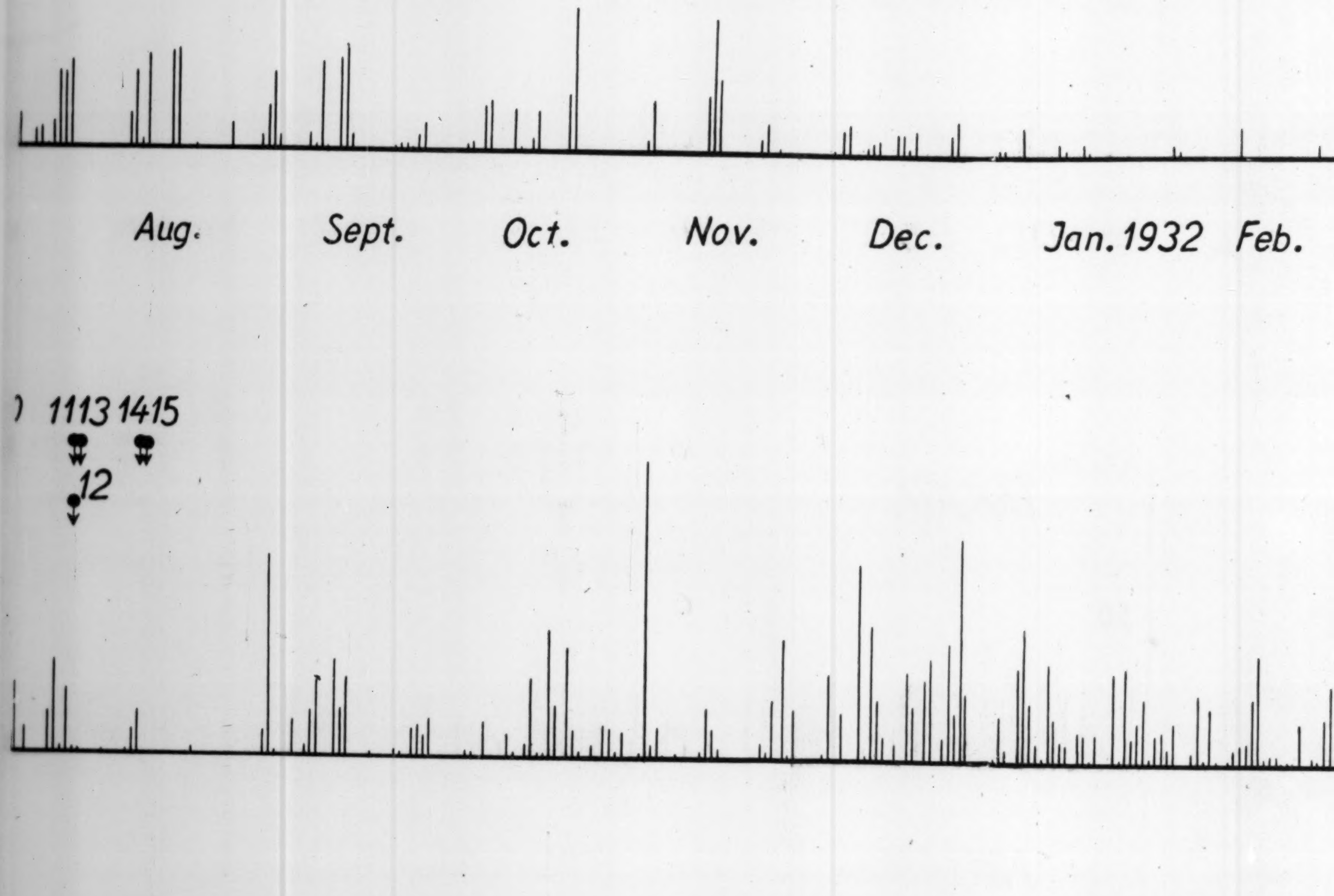

Aug.
Sept.
Oct.
Nov.
Dec.
Jan. 1932
Feb.
) 11 13 14 15
12

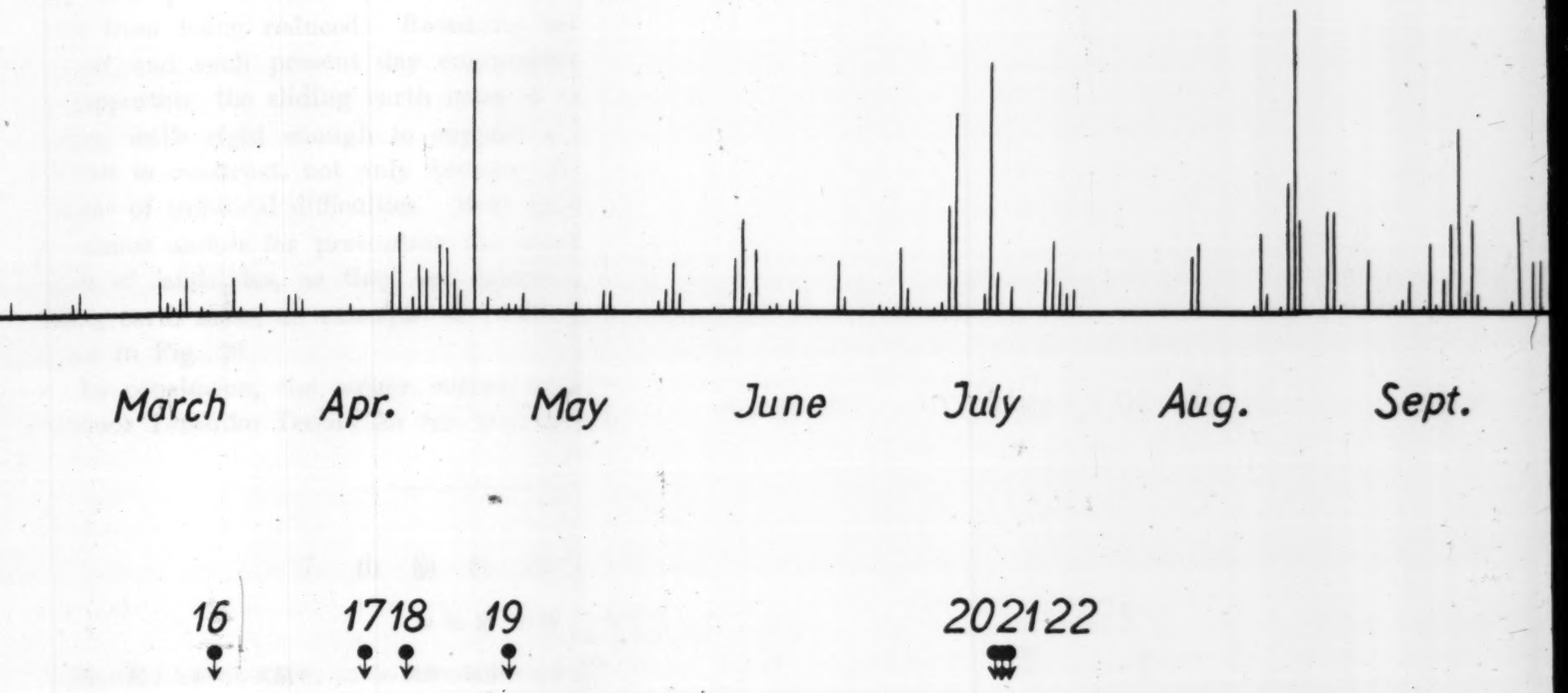

Fig. 16. Precipitations at Nagano, Takata and Niigata and occurrences of landslides

The numbers against the marks of landslides designate these in the first column of Table I.

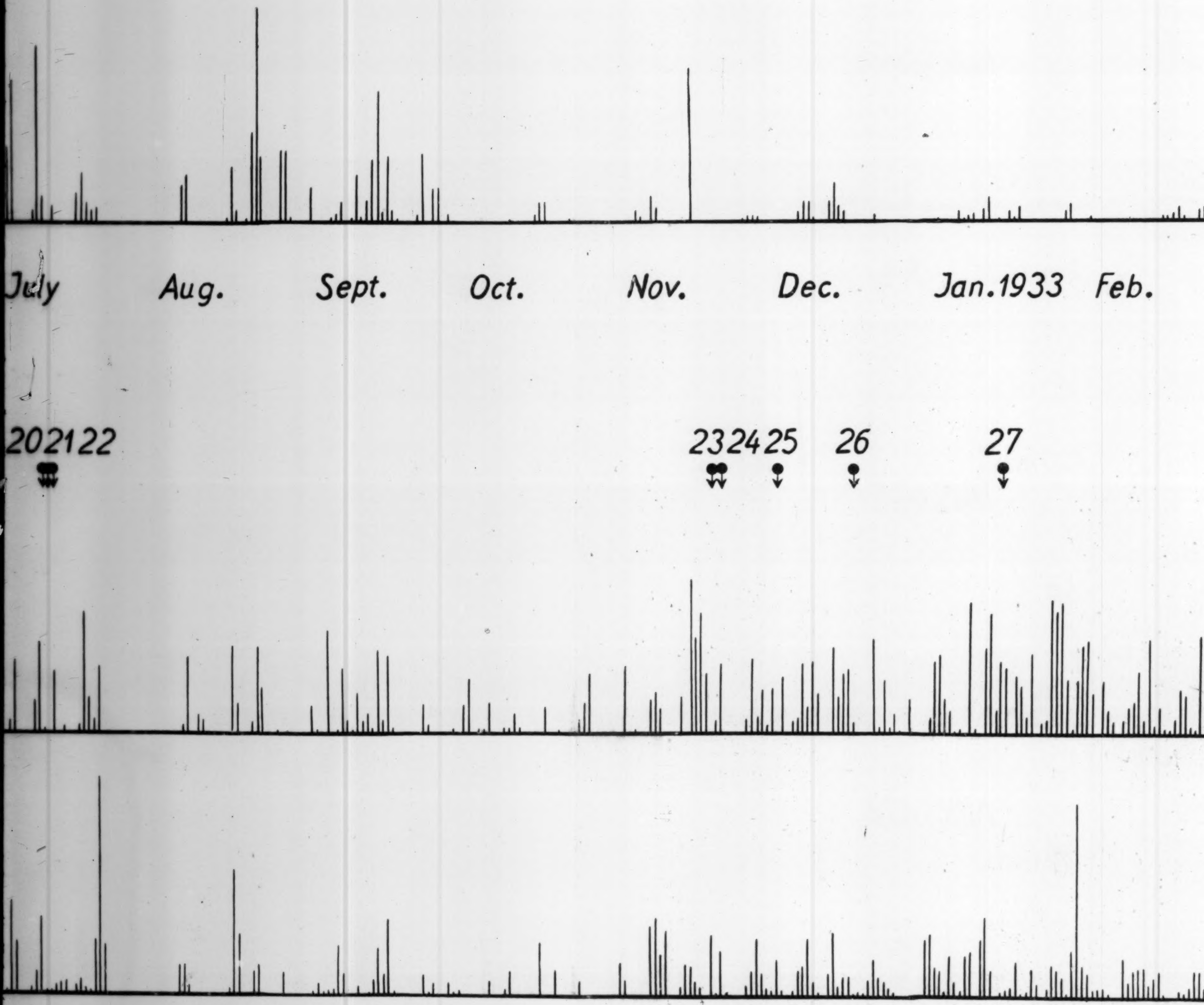

ta and Niigata and occurrences of landslides
designate these in the first column of Table I.

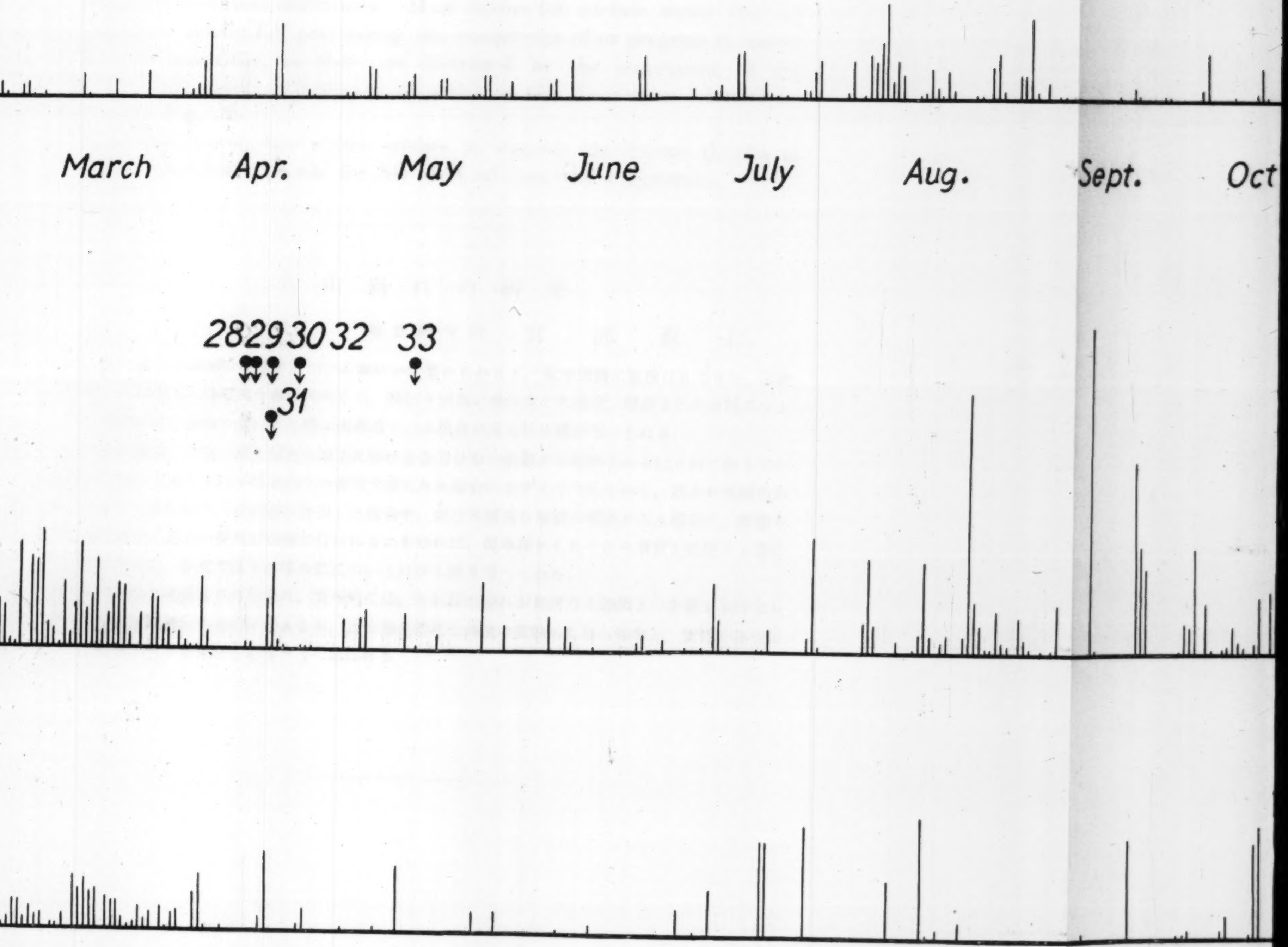
March
Apr.
May
June
July
Aug.
Sept.
Oct
28
29
30
32
33
31

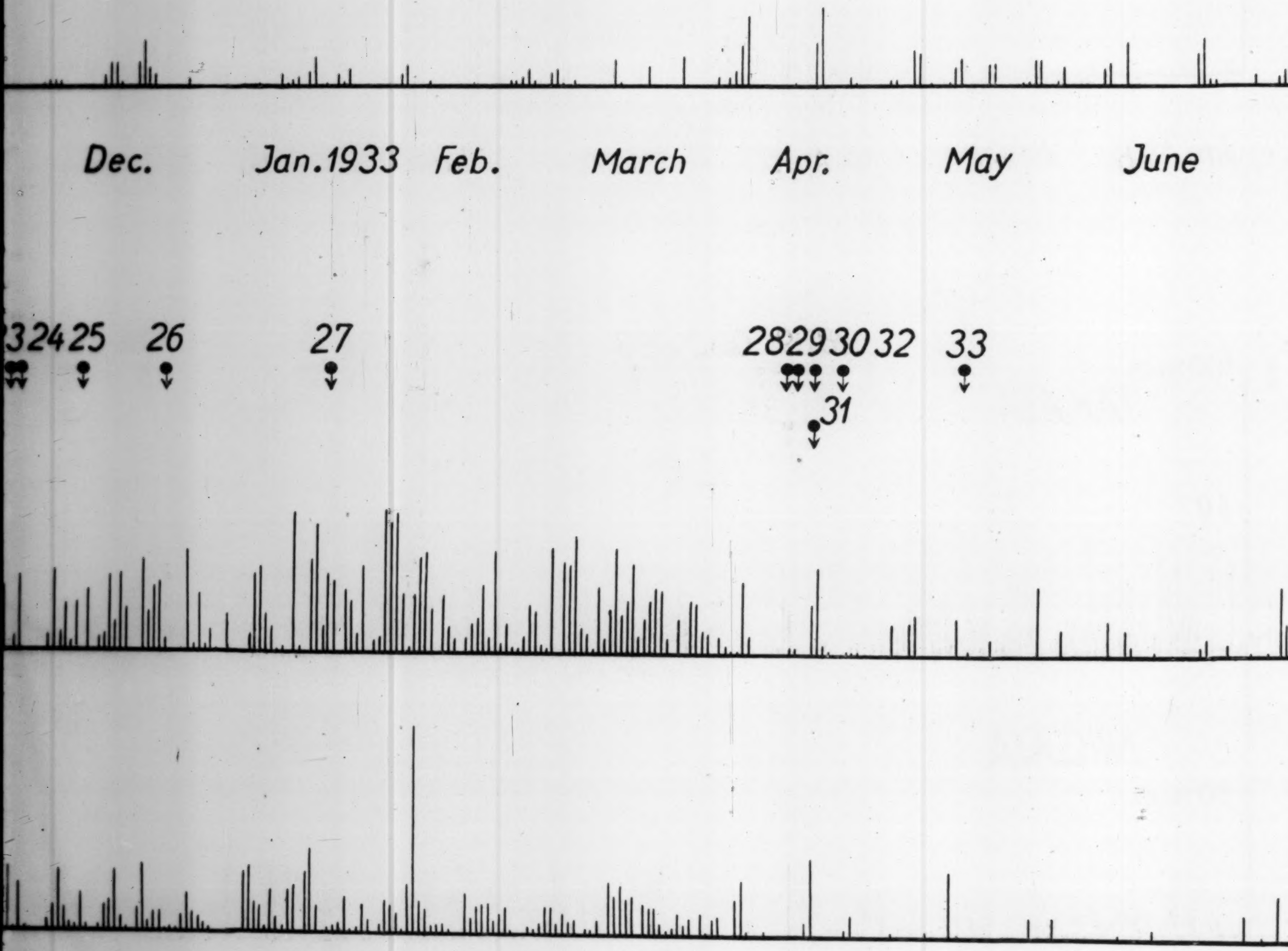
Dec.
Jan. 1933
Feb.
March
Apr.
May
June
23
24
25
26
27
28
29
30
31
32
33

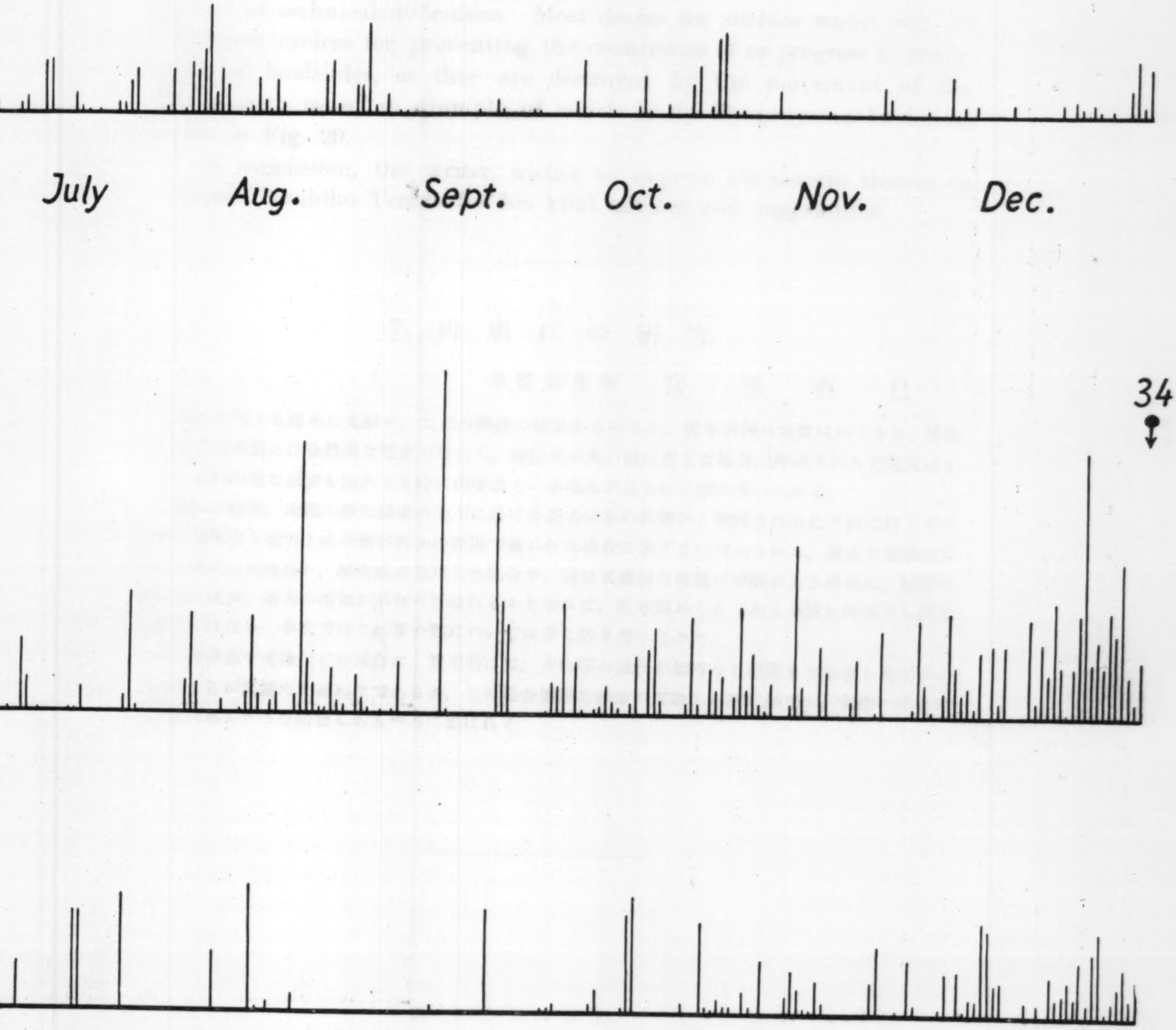
July
Aug.
Sept.
Oct.
Nov.
Dec.
34

7

them is to prevent friction and cohesion of the surface layers of the earth from being reduced. Retaining walls, drains for surface water run off, and such present day engineering operations are in effective in supporting the sliding earth mass or in preventing landslides. Retaining walls rigid enough to support a sliding earth mass are very difficult to construct, not only because of its enormous cost, but also because of technical difficulties. Most drams for surface water run off are almost useless for preventing the occurrence of or progress in movements of landslides, as they are destroyed by the movement of the sliding earth mass, an example of which is the Tyausuyama landslide, shown in Fig. 29.

In conclusion, the writer wishes to express his sincere thanks to Professor Torahiko Terada for his kind advices and suggestions.

---

7. 山崩れの研究

地震研究所　宮部直巳

山崩れに關する從來の文献や，二三の觀察の結果からみると，從來別種に取扱はれてきた，所謂地辷りと山津浪とは全然別な現象でなくて，地辷りが高い處に生じた場合，押出された岩塊又は土塊が，比較的急な斜面を流れ下る時に山津浪といふ現象が見られる樣に考へられる.

山崩れは結局，山腹の樣な斜面の地下に於ける歪力分布の狀態から期待される辷り面に沿うての摩擦や凝集力と歪力との平衡が何かの原因で破られた場合に生ずるのであるから，雨水や雪融水が地下に透入した場合や，地震動が作用した場合や，或は又緩慢な地殼の變動がある場合に，摩擦や凝集力の減少，歪力の增加が如何に行はれるかを知れば，從來認められてゐる事實を說明する幾分の助けにはなる. 本文ではそれ等の點については少し許り考へてみた.

又. 山津浪や泥流などの場合に，實用的には，それ等の流れが如何なる範圍まで影響を及ぼすかといふことが問題になるわけであるが，この場合簡單な砂流の實驗から得た結果が，實際の場合にも延用出來るやうな場合もあるやうに思はれる.

---

8. *Distribution des mouvements initiaux d'un séisme dont le foyer se trouve dans la couche superficielle et détermination de l'épaisseur de cette couche*

par Takeshi MINAKAMI,

Institut de Recherches sur les Tremblements de terre.

(Lu le 20 février 1934, reçu le 20 décembre 1934.)

1. Introduction.

On sait que le regretté Prof. Omori[1] a été le premier à étudier le mouvement initial des secousses d'un séisme et a constaté qu'il se fait dans la direction épicentrale. Après sa découverte, des sismologues japonais se sont intéressés à ce problème particulièrement pour déterminer la position épicentrale. En fait les mouvements initiaux des séismes se dirigent tantôt dans la direction épicentrale, tantôt dans la direction opposée : on distingue deux sortes d'ondes correspondant aux deux cas ; c'est-à-dire l'onde tirante (l'onde de dilatation) pour la première, l'onde poussante (l'onde de compression) pour la dernière.

D'un autre côté, le Prof. Sida[2] a remarqué, à l'occasion du séisme du 18 mai 1917, auprès du fleuve Tenryû, que ces deux sortes d'ondes se distribuent dans les quadrants. Sa découverte a fourri certainement une clef aux sismologues japonais pour élucider le mécanisme de la production des ondes sismiques à l'hypocentre. Evidemment, depuis ce jour, les études sur le mécanisme de l'hypocentre ont progressé peu à peu grâce aux efforts des investigateurs. Parmi eux nous remarquons le Prof. Nakamura[3] qui a constaté, juste après le séisme de Miyosi ainsi qu'après le séisme de Simabara, en 1922, que les lignes nodales, partageant les deux sortes d'ondes, coïncident avec les lignes téctoniques, c'est-à-dire les failles. Il a étudié aussi la distribution des mouvements initiaux du séisme d'Ômati de mai 1918, mais cette fois-ci il a constaté que leur distribution n'a pas été la même que celle des mouvements des séismes déjà étudiés et il a laissé ce séisme dans un état insoluble.

---

[1] F. OMORI, *Pub. Earthq. Inv. Comm.*, **21** (1905), 58.

[2] Il en a parlé, en 1917 à la séance anuelle de la Société japonaise de physique mathématique.

[3] S. NAKAMURA, *Kisyô Shûsi* **12** (1918); **2** (1919); **12** (1919); **1** (1923).

D'un autre côté, le Prof. Ishimoto[4] a proposé, en 1932, une idée nouvelle sur le mécanisme de la production des ondes au foyer ; il a appliqué son idée aux distributions régionales des mouvements initiaux des séismes du 2 juin 1931 ainsi que du 3 juin 1929 etc. dont les foyers étaient placés profondément dans la croûte terrestre.

Les mouvements initiaux d'un séisme de grande profondeur sont toujours enregistrés par les sismographes, distribués partout au Japon, tandis que ceux d'un séisme de petite profondeur ne sont généralement enregistrés que par certaines stations qui se trouvent autour de son épicentre.

Par conséquent, la plupart des études déjà faites sont généralement sur les séismes de grande profondeur. Bien que les faits quantitatifs sur les mouvements initiaux des secousses sismiques soient assez exacts, nous ne pouvons pas nous fier aux explications concernant le mécanisme du foyer, surtout pour les séismes de petite profondeur, parce que la portion surperficielle du terrain possède des propriétés bien compliquées.

D'autre part, nous constatons l'existence d'une surface discontinue (Surface discontinue de Mohorovičič.) au sein de la croûte terrestre d'après les études sur la propagation des ondes sismiques ; mais, du fait que l'on ne peut pas distinguer généralement les intervalles d'une seconde dans les enregistrements sismographiques, il nous semble que nous n'avons pas les éléments nécessaires pour pousser notre étude sur la détermination de la profondeur de cette surface discontinue.

Pour constater du moins l'existence de cette surface discontinue nous remarquerons les distributions des mouvements initiaux des séismes de petite profondeur. Depuis 1927, il y a eu presque 200 séismes qui ont rempli les conditions nécessaires. Nous avons utilisé les données des " Kisyô-Yôran ", publié par l'Observatoire Central de Météorologie, ainsi que celles de " Seismological Report " publié par notre Institut. En tout cas, nous n'avons pas osé nous-même examiner à nouveau les mouvements initiaux de secousses enregistrées. Car, nous ne voulons pas y introduire une idée préconçue que nous pourrait conduire peut-être à une conclusion personnelle.

Or, dans les études sur la distribution des mouvements initiaux des secousses sismiques, nous pouvons distinguer deux sortes de mécanisme de la production des ondes sismiques au foyer. L'un est le mécanisme proposé par le Prof. Ishimoto[5] qui met une source quadruple au foyer et qui définit l'amplitude des ondes initiales par $P_2(\cos\theta)-\frac{1}{4}P_0(\cos\theta)$.

---

[4] M. ISHIMOTO, *Bull. Earthq. Res. Inst.*, **10** (1932), 449; *Proc. Imp. Acad., Japan.* **8** (1932), 36.

[5] M. ISHIMOTO, *loc. cit.*

L'autre est le mécanisme proposé par le Prof. S. Nakamura[6] et adopté par MM. Kunitomi[7] et Honda[8] etc., qui expliquent la production des ondes au foyer avec le déplacement brusque de la faille.

Ce dernier système explique la distribution régionale des mouvements initiaux des secousses sismiques avec le glissement relatif de deux parties de la croûte trerrestre; il nous semble qu'il attache trop d'importance à l'apparition d'une faille à la surface terrestre, au moment d'un grand tremblement de terre.

2. Distribution régionale des mouvements initiaux d'un séisme dont le foyer est placé au dessus de la surface discontinue.

Il nous semble que M. Suda[9] a, pour la première fois, remarqué l' influence de la surface discontinue pour expliquer la distribution irrégulière des mouvements initiaux des secousses sismiques produites par le séisme du 1er septembre 1923.

A l'occasion de son étude sur le séisme de Tazima, de mai 1925, M. Wadati[10] a aussi introduit la théorie de la surface discontinue de Mohorovičič et tracé un *cercle d'inversion* où les deux sortes ondes changent leur propriété entre elles. Cette fois-ci, il a déterminé la profondeur de la surface discontinue à 42km d'après l'étude sur l'hodographe sismique. Le Prof. Ishimoto[11] a discuté la propriété de la croûte terrestre d' après son mécanisme de la production des ondes sismiques au foyer. Il a étudié les séismes[12] du 27 juillet 1929 ainsi que du 1er septembre 1923; qui ont leur foyer au dessus de la surface discontinue. D'un autre côté, M. Kawasumi[12] a étudié aussi ces séismes et tracé plusieurs modèles de distribution suivant les deux types de mécanismes déjà définis. Enfin M. Kawasumi est arrivé à la conclusion que la distribution des mouvements initiaux du 27 juillet 1929 n'est plus expliquée par le mécanisme avec une production de faille.

D'après les propositions du Prof. Ishimoto et de M. Kawasumi, nous avons réexaminé les distributions régionales des mouvements initiaux surtout de ceux des séismes peu profonds. Nous avons constaté, d'une

---

6) S. NAKAMURA, *loc. cit.*

7) S. KUNITOMI, *Geophs. Mag.*, **1** (1927), 89; **2** (1930), 65; **3** (1931), 149; **4** (1931), 73. *Kisyô-Syûsi*, **6** (1928), 59. etc.

8) K. HONDA, *Geophs Mag.*, **4** (1931), 185; **5** (1932), 301. *Kisyô-Syûsi*, **9** (1931), 682 etc.

9) K. SUDA, *Umi to Sora*, **5** (1925), 80; 182; 202.

10) K. WADATI, *Geophs. Mag.*, **1** (1927) 89.

11) M. ISHIMOTO. *Bull. Earthq. Res. Inst.*, **11** (1933), Il en a parlé (le 18 oct. 1933) à la séance d' Institut sismologique.

12) K. HAYATA, *Kensin Zihô*, **4** (1930), 17.

13) H. KAWASUMI, *Disin*, **6** (1934), 32; *Bull. Earthq. Res. Inst.*, **12** (1934), 660.

part, qu'il y a des séismes qui sont expliqués par le mécanisme de la source quadruple aussi que par l'autre mécanisme : d'autre part, qu'il y a des séismes qui ne peurent pas être expliqués par le deuxième mécanisme.

Les fig. 1, 2, 3, et 4 représentent plusieurs modèles de distribution des mouvements initiaux avec le mécanisme de la source quadruple affectées par l'existence d'une surface discontinue de la croûte terrestre. Cette fois-ci nous avons fixé l'angle du cône à 45°. Naturellement, les ondes poussantes se trouvent toujours dans les courbes représentées par les sections côniques, mais l'effet de la surface discontinue dans la croûte produit encore une région d'ondes poussantes représentée par un secteur terminé par un arc circulaire. Pour avoir un traitement simple, nous donnons le nom de type-X aux fig. 1 et 2, de type-Y aux fig. 3 et de type-Z aux fig. 4.

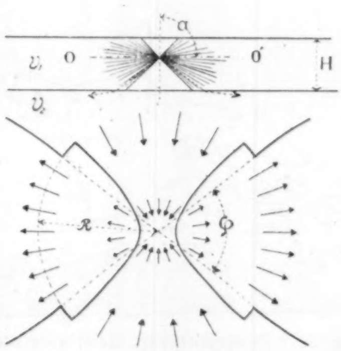

Fig. 1. le type-X

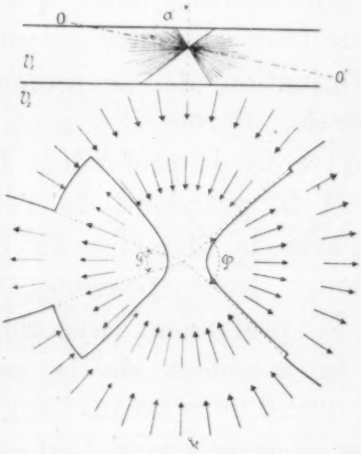

Fig. 2. le type-X

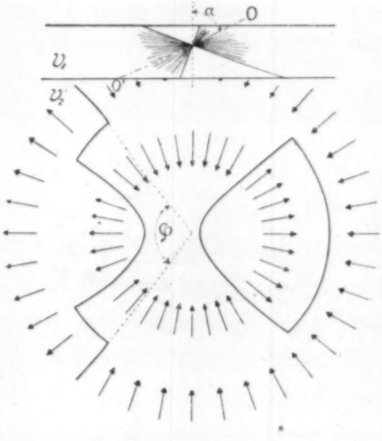

Fig. 3. le type-Y

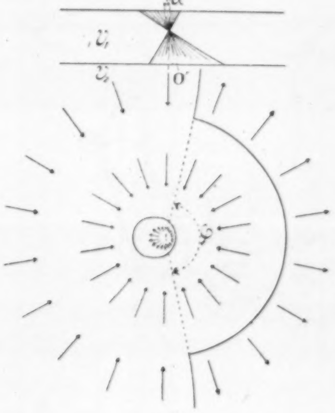

Fig. 4. le type-Z

Modèles de distribution des mouvements initiaux avec le mécanisme de la source quadruple affectée par l'existence d'une surface discontinue de la croûte terrestre.

D'un autre côté, généralement les ondes sismiques dans la croûte ne se propagent pas en ligne droite, à cause du fait que la croûte ne possède pas des propriétés homogènes et isotropes. Mais, comme nous ne discutons que les distributions des mouvements initiaux des secousses des séismes voisins, nous adoptons simplement v_1 et v_2 pour les vitesses moyennes des ondes longitudinales respectivement au dessus et au dessous de la surface discontinue. Le fait que nous adoptons des deux vitesses moyennes correspondant aux deux milieux, n'apportera aucun changement aux caractéristiques de la propagation des ondes sismiques.

Les distributions régionales des mouvements initiaux, représentées par les fig. 5, 6, 7, 8, 9, 10, 11, 12 et 13, seront comprises facilement dans le type-Z. Il n'y aura aucune nécessité de donner une interprétation particulière pour chaque séisme. Nous voulons cependant ajouter quelques mots pour faire connaître le procédé de détermination de la profondeur hypocentrale. Certes, il y a un rapport étroit entre la profondeur hypocentrale et la grandeur de l'ellipse ainsi qu'avec le diamètre du cercle d'inversion. Nous pouvons, donc, trouver la profondeur hypocentrale d'après la grandeur de la section cônique, quand nous savons l'angle du cône : par exemple quand il est du 45°.

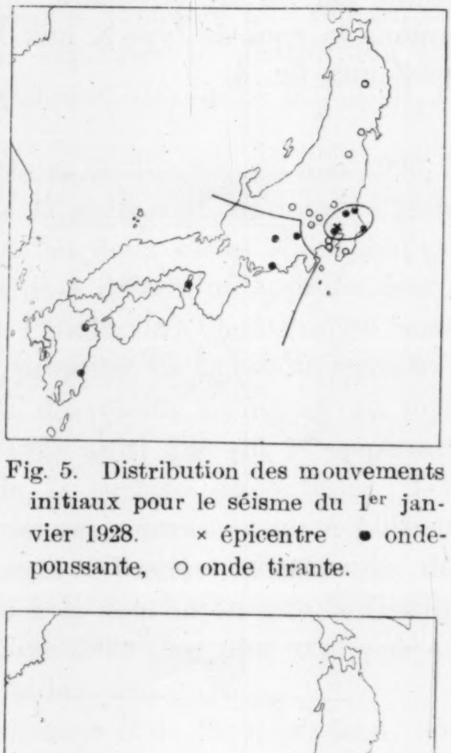

Fig. 5. Distribution des mouvements initiaux pour le séisme du 1er janvier 1928. × épicentre ● onde-poussante, ○ onde tirante.

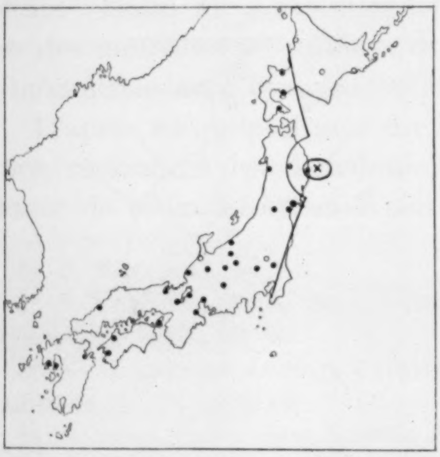

Fig. 6. Distribution des mouvements initiaux pour le séisme du 27 mai 1928. × épicentre, ● onde poussante, ○ onde tirante.

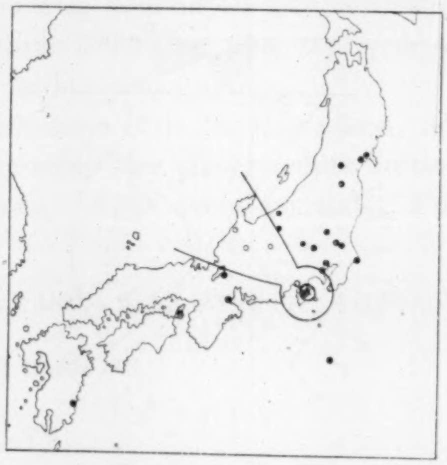

Fig. 7. Distribution des mouvements initiaux pour le Ito séisme du 22 mars 1930. × épicentre, ● onde poussante, ○ onde tirante.

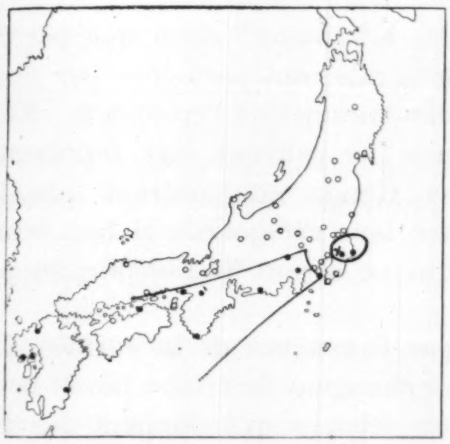

Fig. 8. Distribution des mouvements initiaux pour le séisme du 1er juin 1930. × épicentre, ● onde poussante, ○ onde tirante.

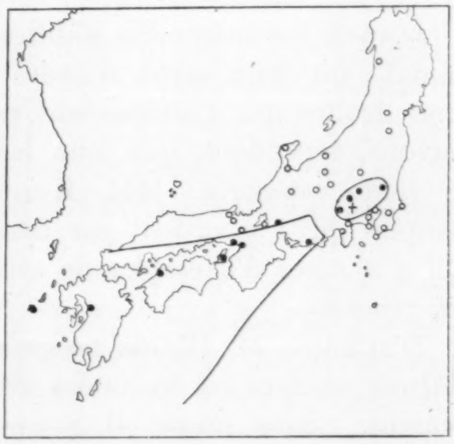

Fig. 9. Distribution des mouvements initiaux pour le séisme du 17 juin 1931. × épicentre, ● onde poussante. ○ onde tirante.

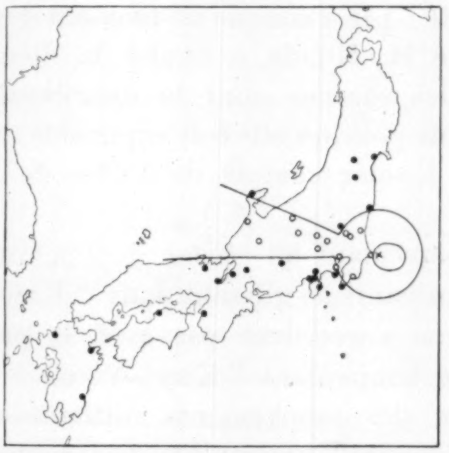

Fig. 10. Distribution des mouvements initiaux pour le séisme du 22 juin 1932. × épicentre, ● onde poussante, ○ onde tirante.

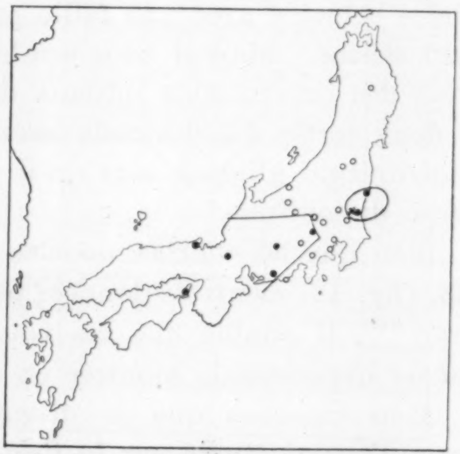

Fig. 11. Distribution des mouvements initiaux pour le séisme du 2 décembre 1932. × épicentre, ● onde poussante, ○ onde tirante.

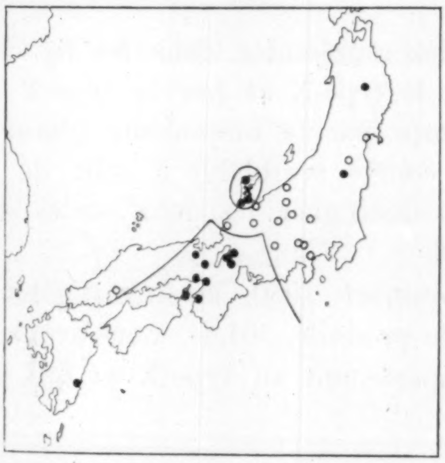

Fig. 12. Distribution des mouvements initiaux pour le séisme du 21 septembre 1933. × épicentre, ● onde poussante, ○ onde tirante.

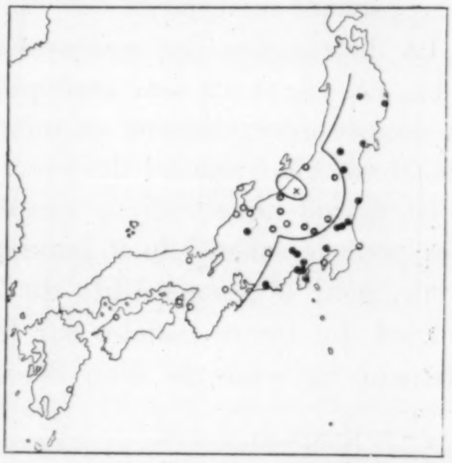

Fig. 13. Distribution des mouvements initiaux pour le séisme du 4 octobre 1933. × épicentre, ● onde poussante, ○ onde tirante.

D'après les mémoires publiés par M. Kunitomi[14] ainsi que par M. Honda[15], les deux sortes d'ondes sont généralement partagées par deux lignes droites qui s'intersectent perpendiculairement à l'épicentre. Nous trouvons, cependant, que tous les séismes ne peuvent être représentés une seule catégorie. MM. Kunitomi et Honda ne montrent que des exemples qui s'accordent par hasard avec leur catégorie. Il faut savoir qu'il y a assez d'exemples de séismes qui ne seront pas expliqués par leur procédé.

D'ailleurs, M. Honda ne constate pas l'existence de la surface discontinue, surface où les ondes sismiques changent de vitesse plutôt brusquement. Sans doute, il y a quelques séismes qui donnent des distributions régionales des mouvements initiaux que peut expliquer le mécanisme glissant sans qu'on y introduise aucun effet de la surface discontinue. Nous savons qu'il y a certains séismes dont une des lignes nodales coïncide avec une faille produite : par exemple au moment d'un grand séisme. Mais il nous semble que M. Honda a étudié la distribution des mouvements initiaux dans les séismes dont la distribution des deux sortes d'ondes reste assez simple pour qu'elle soit explicable par le mécanisme glissant sans qu'il y ait à tenir compte de l'effet de la surface discontinue.

Bien que les courbes nodales correspondant au séisme du 4 octobre 1933, (fig. 13) aient été données par le mécanisme glissant dans " Kisyô-Yôran "[16], il semble que ces courbes ne s'accordent pas avec la profondeur hypocentrale montrée en même temps dans " Kisyô-Yôran ".

Nous trouvons que la distribution des mouvements initiaux du séisme d'Ômati étudié par le Prof. Nakamura[17], ressemble beaucoup à celle des mouvements du séisme du 4 octobre 1933. Nous pouvons, en effet, expliquer facilement la façon de distribution des deux sortes ondes : elle appartient au type-Z.

La distribution des secousses initiales représentée dans les fig. 14, 15, 16, 17, 18, et 19 sera expliquée par le type-X et par le type-Y et sera donnée généralement en même temps par le mécanisme glissant. Mais, il est bien naturel de tracer une courbe semblable à celle de la fig. 18, quand nous voulons simplement distinguer les deux sortes des ondes pour le séisme du 9 janvier 1934.

Or, pour le séisme d'Idu du 26 novembre 1930, les investigateurs ont tracé des lignes nodales sur la faille produite. Mais, nous avons là seulement un exemple d'un séisme appartenant au type-X et qui est

---

[14] S. KUNITOMI, *loc. cit.*
[15] K. HONDA, *loc. cit.*
[16] *Kisyô-Yôran*, publié en octobre 1934.
[17] S. NAKAMURA, *loc. cit.*

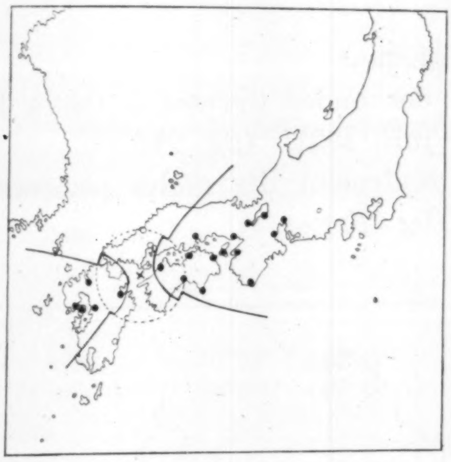

Fig. 14. Distribution des mouvements initiaux pour le séisme du 25 septembre 1928. × épicentre, ● onde poussante, ○ onde tirante.

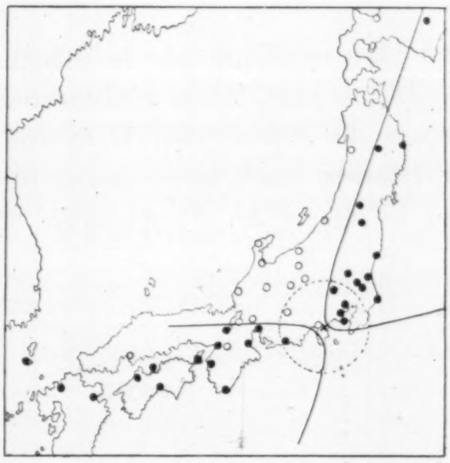

Fig. 15. Distribution des mouvements initiaux pour le séisme du 26 novembre 1930. × épicentre, ● onde poussante ○ onde tirante.

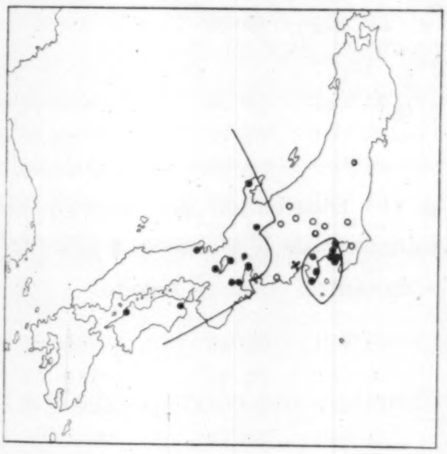

Fig. 16. Distribution des mouvements initiaux pour le séisme du 10 août 1931. × épicentre, ● onde poussante, ○ onde tirante.

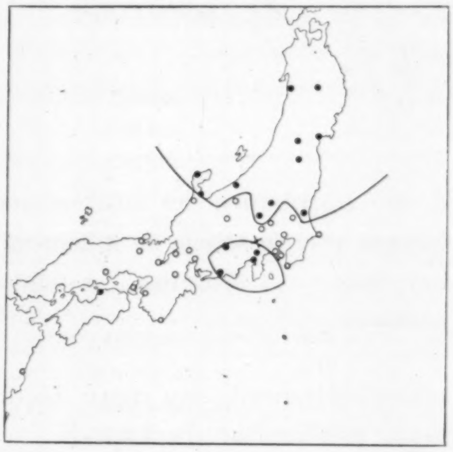

Fig. 17. Distribution des mouvements initiaux pour le séisme du 16 septembre 1928. × épicentre, ● onde poussante, ○ onde tirante.

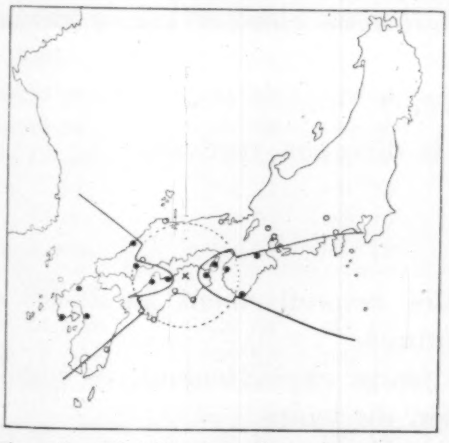

Fig. 18. Distribution des mouvements initiaux pour le séisme du 9 janvier 1934. × épicentre, ● onde poussante, ○ onde tirante.

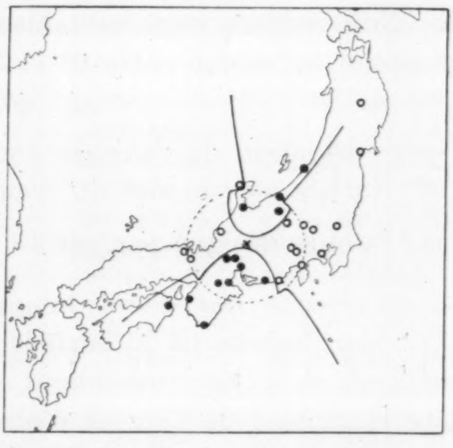

Fig. 19. Distribution des mouvements initiaux pour le séisme du 18 août 1934. × épicentre. ● onde poussante, ○ onde tirante.

aussi bien expliqué par le mécanisme glissant.

D'une part, nous n'observons que des ondes tirantes à toutes les stations du Japon pour le séisme du 9 juin 1931. (fig. 21.)

D'autre part, nous avons observé seulement des ondes poussantes pour le séisme du 3 septembre 1932. (fig. 20.)

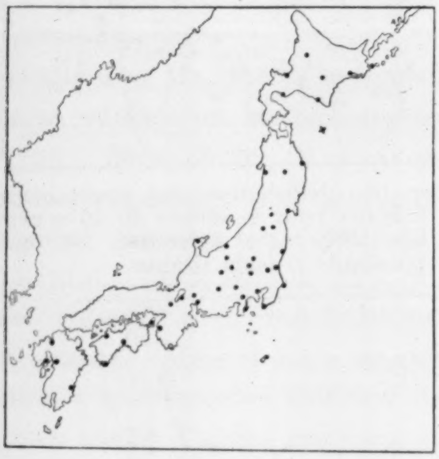

Fig. 20 Distribution des mouvements initiaux pour le séisme du 3 septembre 1932. × épicentre, ● onde poussante

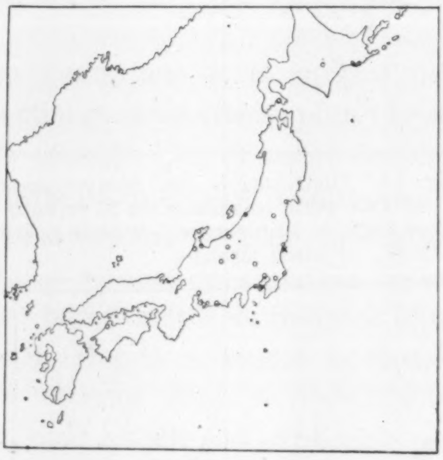

Fig. 21. Distribution des mouvements initiaux pour le séisme du 9 juin 1931. × épicentre, ○ onde tirante.

Naturellement, ces deux façons de distributions correspondent à un exemple particulier du type-Z.

Le tableau I montre les distributions des mouvements initiaux pour les séismes remarquables de petite profondeur : où $2R$ est le diamètre du cercle d'inversion et φ est l'angle représenté dans les fig. 1, 2, 3, et 4. Nous voyons dans ce tableau que R reste entre 80 km et 200 km et φ prend sa valeur entre 0° et 360°.

$$\text{où} \quad \varphi = f(\alpha, \theta, i)$$

où α ; déviation de l'axe du cône de la direction verticale.

θ ; angle au sommet du cône.

i ; angle désigné par, $\sin i = \frac{v_1}{v_2}$.

v_1, v_2 ; vélocité des ondes longitudinales respectivement au dessus et au dessous de la surface discontinue.

Comme R et φ ne contiennent pas le temps explicitement, ils restent indépendamment de l'erreur d'observation du temps.

Tableau I. (a)

Séismes de petite profondeur dans la région de Kantô.

Date	épicentre		profondeur hypocentrale h	rayon du cercle d'inversion. R	angle du secteur φ	type
	φ_N	λ_E				
1927			km			
le 5 sept.	36° 23′	140° 42′		140 km	135°	Y
le 11 oct.	36° 29′	140° 58′		150 km	143°	Y
1928						
le 1er jan.	36° 03′	139° 49′	35 km	140 km	80°	Z
le 21 mai	35° 30′	140° 00′		100 km	125°	Y
le 19 mai	36° 21′	141° 05′	30 km	130∼150 km	100°	Z
le 27 août	36° 18′	140° 57′	30 km	130∼150 km		Y
le 5 oct.	36° 01′	139° 25′	47 km	130∼140 km	70 et 90°	X
1929						
le 16 avril	36° 21′	140° 56′	20 km	130 km		Z
le 18 avril	36° 35′	140° 55′		130 km		Z
le 23 avril	36° 04′	139° 53′	43 km	120 km		Y
le 27 juin	36° 00′	141° 15′		130∼140 km	85°	Y
le 27 juil.	35° 35′	139° 35′	23 km	100∼120 km	135°	Z
le 16 août.	36° 23′	139° 23′				Z
1930						
le 9 mars	34° 55′	139° 10′		130 km	320°	Z
le 22 mars	34° 55′	139° 10′	10 km	80∼100 km	310°	Z
le 1er mai	35° 36′	140° 51′		120 km	25°	Z
le 1er mai	35° 53′	140° 47′	30 km	120 km	95°	Z
le 17 mai	34° 55′	139° 15′	20 km	150 km	125°	Y
le 1er juin	36° 00′	140° 23′	30∼40 km	130 km	80°	Z
le 17 août	35° 21′	140° 02′		100 km	80° et 100°	X
le 19 août	36° 23′	141° 21′		150 km		Y
le 26 nov.	34° 55′	139° 10′	10 km	80∼100 km	75° et 75°	X
1931						
le 17 juin	35° 36′	139° 24′	30∼40 km		35°	Z
le 19 juil.	37° 19′	140° 25′		110 km		Y
le 18 août	36° 15′	141° 00′		120∼130 km	30°	Z
le 9 sept.	36° 42′	141° 26′		130 km	120°	Y
le 21 sept.	36° 00′	139° 12′	20 km	100∼120 km	80° et 80°	X
le 3 oct.	35° 55′	139° 12′	24 km	130∼150 km	35°	Y
1932						
le 22 juin	35° 58′	141° 00′	30∼40 km	130 km	330°	Z
le 2 déc.	36° 28′	140° 17′	30∼40 km	100 km	30 et 35°	X
1933						
le 23 avril	36° 10′	140° 00′		180 km	100° et 100°	X
1934						
le 11 fév.	37° 04′	142° 00′		160 km	90° et 130°	X

Tableau I. (b)

Séismes de petite profondeur dans la région de Tyûbu.

date	épicentre		profondeur hypocentrale h	rayon du cercle d'inversion R	angle du secteur φ	type
	φ_N	λ_E				
1930						
le 17 oct.	36° 35′	136° 30′	20 km	120~150 km	72°	Y
le 17 oct.	36° 35′	136° 30′	20 km	150 km	75°	Y
1931						
le 10 août	35° 09′	138° 18′		170~180 km	120°	Y
le 16 sept.	35° 33′	138° 49′	20~30 km	130 km	120°	Y
1933						
le 21 sept.	37° 04′	136° 57′	5~10 km	150 km	60°	Z
le 4 oct.	37° 12′	138° 48′	35 km	130 km	195°	Z
1934						
le 18 août	35° 43′	137° 02′		170 km	45° et 95°	X

Tableau I. (c)

Séisme de petite profondeur dans la région de Kinki et de Kyûsyû.

date	épicentre		profondeur hypocentrale h	rayon du cercle d'inversion R	angle du secteur φ	type
	φ_N	λ_E				
1927						
le 7 mars	35° 40′	135° 14′	10~20 km	80~100 km	78° et 76°	X
le 1 avril	35° 40′	135° 14′	10~20 km	90 km	85° et 85°	X
1928						
le 25 sept.	33° 40′	132° 05′		100 km	60° et 50°	X
1929						
le 22 mai	31° 40′	131° 50′		150 km	105°	Y
le 4 juil.	34° 10′	135° 40′	10 km	100 km	95° et 70°	X
le 20 nov.	34° 10′	135° 24′		120~150 km	80°	Y
1930						
le 6 déc.	34° 30′	134° 40′		150 km	120°	Y
le 20 déc.	35° 00′	132° 40′		100 km	115°	Y
le 21 déc.	35° 00′	132° 40′		100 km	113°	Y
1931						
le 2 nov.	32° 24′	131° 54′		120~150 km	115°	Y
le 2 nov.	32° 24′	132° 06′		150 km	130°	Y
le 21 déc.	32° 24′	130° 24′		130 km	95°	Y
le 22 déc.	32° 24′	130° 30′		120 km	130°	Y
1932						
le 3 mai	31° 24′	131° 06′		130 km	110°	Y
1933						
le 18 fév.	35° 00′	134° 30′		130~150 km	150°	Y
le 23 avril	36° 10′	140° 00′		180~200 km	105°	Z
le 29 juil.	34° 00′	135° 00′	5~10 km	100 km	130°	Z
1934						
le 9 jan.	34° 00′	133° 54′		180 km	40° et 80°	X

Tableau I. (d)

Séismes de petite profondeur dans la région de Tôhoku.

date	épicentre		profondeur hypocentrale h	rayon du cercle d'inversion R	angle du secteur φ	type
	φ_N	λ_E				
1927						
le 18 jan.	38° 15′	141° 58′		140～150 km	120°	Y
1928						
le 27 mai	39° 40′	142° 45′		150～160 km	135°	Y
le 29 mai	39° 45′	142° 50′		180 km	110°	Y
le 1 juin	39° 35′	143° 10′		150 km	135°	Y
le 23 oct.	38° 35′	141° 40′		170～180 km	25° et 20°	X
1932						
le 3 juin	38° 12′	141° 42′		130～150 km		Z
le 4 juin	41° 00′	143° 36′		150 km	80° et 85°	X
le 10 juil.	39° 36′	145° 00′			115°	Z
le 3 sept.	41° 05′	142° 49′			235°	Z
le 26 nov.	42° 21′	142° 16′		170～180 km	125°	Y
1933						
le 3 mars	38° 30′	140° 00′			100°	Z

3. La distribution des mouvements initiaux d'un séisme voisin.

M. Hukutomi[18] a révélé le fait que des séismes dans un endroit donnent la même distribution des mouvements initiaux, surtout pour les séismes qui se produisent aux environs de Tôkyô.

D'après l'étude de M. Honda[19] sur la façon de distribution des mouvements initiaux des répliques du séisme de Titibu (le 21 septembre 1931.), était toujours la même. Nous constatons le même rapport dans ces deux sortes de séismes comme représentés dans le tableau II.

Tableau II.

le séisme fort date	sa réplique date	leur épicentre	
		φ	λ
le 7 mars 1927	le 1er avril 1927	35° 40′	135° 14′
le 20 décembre 1930	le 21 décembre 1930	35° 00′	132° 40′
le 2 novembre 1931	le 2 novembre 1931	32° 24′	131° 54′
le 17 octobre 1930	le 17 octobre 1930	36° 35′	136° 30′
le 1er mai 1930	le 1er mai 1930	35° 36′	140° 51′
le 9 mars 1930	le 22 mars 1930	34° 55′	139° 10′

---

[18] K. FUKUTOMI, *Bull. Earthq. Res. Inst.*, **11** (1933), 510; *Disin*, **3** (1931), 592.
F. KISHINOUYE, *Disin*, **4** (1932), 18.

[19] K. HONDA, *Geophs. Mag.*, **5** (1932), 69.

Les positions des courbes nodales données par les deux séismes du 1er octobre 1919 et du 20 décembre 1930, dont les épicentres se trouvaient aussi près de Miyosi, coïncidaient exactement. Pourtant, les deux sortes d'ondes changeaient leurs places dans les deux cas.

Nous avons déjà fait remarquer que la distribution régionale des deux sortes d'ondes du séisme du 4 octóber 1933, coïncidait avec celle de mai 1918; ce dernier a été étudié par le Prof. Nakamura.

Nous avons constaté sur les séismes apparus au large du Sanriku que les ondes poussantes prédominaient dans le Honsyû, île principale du Japon; par exemple, sur le séisme du 3 septembre 1932 (fig. 20.), sur le séisme du 3 mars 1933, lequel a provoqué le raz de marée sur la côte de Sanriku. Nous avons trouvé de plus la même sorte de distribution des mouvements initiaux dans le séisme du 1er juin 1928, ainsi que dans

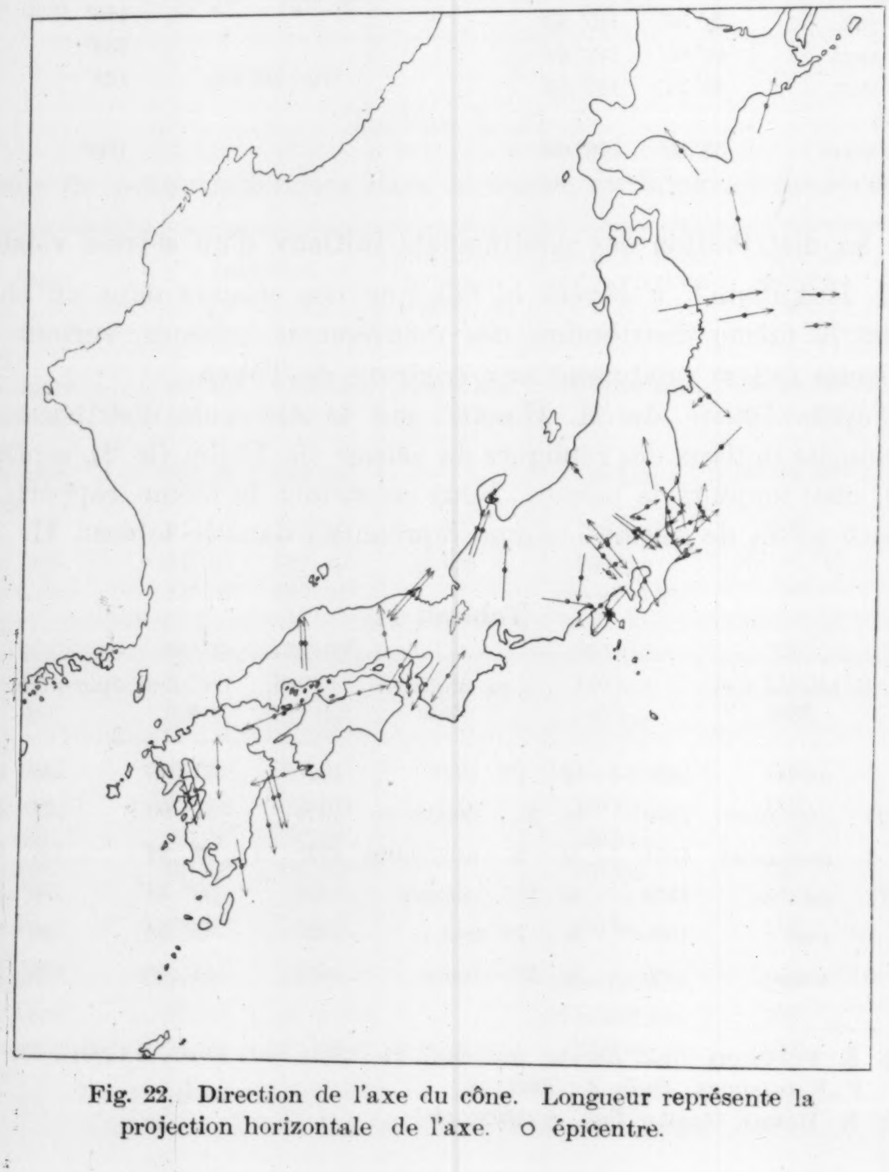

Fig. 22. Direction de l'axe du cône. Longueur représente la projection horizontale de l'axe. ○ épicentre.

le séisme du 29 mai 1928. La fig. 22 montre la direction de l'axe du cône correspondant à chaque séisme distribué partout au Japon. La flèche indique le sens de l'axe par en haut et la longueur représente la projection horizontale de l'axe. D'après cette figure, nous constatons d'une part que la plupart des axes, dans les régions de Kyûsyû et de Tyûgoku, se dirigent vers le nord-sud, d'autre part, qu'il y a beaucoup de séismes du type-Z dans la région de Kantô.

4. La profondeur de la surface discontinue.

En considérant l'effet de la surface discontinue, nous avons réussi à tracer des lignes nodales qui partagent les deux sortes d'ondes données par les séismes dont les foyers se placent au dessus de cette surface.

D'un autre côté, nous pouvons constater aussi l'existence de la surface discontinue d'après l'étude de la propagation des ondes sismiques. En conséquence, nous croyons, donc, l'existence de la surface discontinue dans la croûte.

Nous pouvons donc déterminer la profondeur (H) de cette surface d'après la formule suivante :

$$R=(2H-h)\tan i+2\sec i\sqrt{H(H-h)} \qquad (1)$$

R ; rayon du cercle d'inversion.
h ; profondeur hypocentrale.
H ; profondeur de la surface discontinue.

$$\sin i=\frac{v_1}{v_2}$$

Appliquons, alors, la formule (1) pour plusieurs séismes, en prenant 5·5 km/sec. pour v_1 et 7·5 km/sec. pour v_2.

Nous avons, enfin, diverses valeurs de l'épaisseur de la couche superficielle représentées dans le tableau III.

Tableau III.

séismes date				h profondeur hypocentrale	R rayon du cercle d'inversion	H épaisseur de la couche	
le	1er	janvier	1928	35 km	102 km	41·6 km	(fig. 5)
le	4	octobre	1933	30 km	130 km	43·1 km	(fig. 13)
le	16	septembre	1928	30 km	138 km	44·4 km	(fig. 17)
le	22	juin	1932	40 km	136 km	50·8 km	(fig. 10)

D'un autre côté, nous avons 200 km de rayon maximum pour le cercle d'inversion pour un séisme du 23 avril 1931, dont la profondeur hypocentrale se place probablement près de la surface terrestre. Nous obtenons ainsi 43 km. d'épaisseur avec les données de ce séisme.

Il est probable que la profondeur de la surface discontinue ne reste pas la même selon les diverses régions.

Les diverses valeurs de la profondeur moyenne, obtenues d'après des études sur l'hodographe sismique, sont données dans le tableau suivant.

Tableau IV.

date.	profondeur hypocentral	épaisseur de la couche	déterminateur
le 23 mai 1925	33 km	42 km	Wadati
le 3 août 1926	40 km	42 km	Sagisaka
le 7 mars 1927	14 km	45 km	Kunitomi
le 27 octobre 1927	18 km	34 km	Kunitomi
le 1er septembre 1923	28 km	39 km	Kunitomi
le 27 juillet 1928	23·3 km	44·5 km	Hayata
	moyenne	41·1 km	

La valeur moyenne coïncide bien avec celle d'obtenue par notre procédé. En tout cas, il nous semble que la profondeur de cette surface discontinue se place entre 40 km et 50 km.

5. Conclusion.

En jetant un coup d'oeil sur la distribution des mouvements initiaux des secousses sismiques, nous pouvons distinguer les séismes dont le foyer se place au dessus ou ceux dont le foyer est au dessous de la surface discontinue. Car la façon de distribution régionale des deux sortes d'ondes ne reste pas la même dans les deux sortes de séismes.

Ce fait nous démontre l'existence d'une surface discontinue dans la croûte terrestre. Nous avons pu déterminer la profondeur de cette surface, avec le diamètre du cercle d'inversion, dans l'intervalle de 40 km à 50 km.

R et φ que nous avons introduits permettent d'étudier certaines propriétés de la croûte terrestre.

Le Prof. Ishimoto a constaté, d'ailleurs, que la distribution régionale des mouvements initiaux des secousses sismiques coïncide bien avec la déformation de la croûte produite par un grand séisme, la déformation produite surtout dans la région épicentrale. Il a ainsi déduit la déformation produite au fond de la mer à l'occasion du séisme du 3 mars 1933, lequel

a déterminé un tunami (raz de marée) sur les côtes du Pacifique du Japon, et y causé des sinistres considérables.

Nous nous proposons d'étudier aussi à l'avenir, la déformation de la croûte terrestre produite par les séismes qui ont un rapport étroit avec la distribution des mouvements initiaux des secousses sismiques.

En terminant nous voulons exprimer nos vifs remerciements au Professeur Ishimoto et au Docteur Kawasumi pour leurs conseils et leurs encouragements au cours de cette étude.

---

8. 地殼の上層内に震源を有する地震の初動分布と不連續層の厚さ

地震研究所 水上 武

1. 現在，發震機巧の説明に大體二つの型が認められる．一つは中村（左）博士，國富，本多學士等に依つて主張される斷層の横辷りを以つて説明するものであり，他の一つは石本博士の提唱に依る四重源の假定と岩漿運動を以つて説明するものである．

地殼內に不連續層の存在する事は P^* 波，P 波或は $\bar{P}$ 波の觀測からも認められて居る．須田氏は初めて地震の初動の方向分布の問題に不連續層の影響を考慮された．石本博士及び，河角學士は淺い地震の初動の分布は不連續層の存在すると假定する事に依つて說明される事を示し，更に昭和4年7月27日の地震はその初動分布から，斷層の機巧では說明されない事を明かにされた．

2. 地殼內に不連續層が存在すると假定して昭和2年から昭和9年迄に起つた數百の淺い地震の初動分布を調べ直して見た．その結果約半數の地震は上記何れの機巧でも說明されるが，斷層の機巧では說明されない可成多くの地震の存在する事を確めた．

3. 或る地震とその餘震の初動の「押し」「引き」が同じ分布をなす事は本多，福富學士等に依つて既に指摘されたが，この研究に依つても同樣の結果を得た．又三陸沖に起る地震の初動は本州では殆ど常に押波のみ觀測される事を知つた．この說明に就て色々想像されるけれども，確な事は今後の研究に待たねばならぬ．

4. 不連續層の存在するために現れる轉向圓の半徑を用ひて，この層の厚さを求めて見ると40km～50kmの間にあると云ふ結果を得た．この値は和達博士等が走時から求められたものと略一致する．

9. La diffusion des secousses sismiques dans la couche superficielle du terrain

par Mishio ISHIMOTO,

Institut de Recherches sur les Tremblements de terre.

(Lu le 3 juillet 1934, reçu le 20 décembre 1934)

1.

Dernièrement nous avons publié un mémoire[1] constatant l'analogie des secousses sismiques avec les mouvements de l'eau dans un bassin et cette expérience nous a conduit à étudier la diffusion des secousses sismiques dans la couche superficielle du terrain. Maintenant nous voulons discuter particulièrement ce suject, afin d'élucider les caractéristiques des secousses sismiques enregistrées par le sismographe accélérométrique de la composante horizontale.

Quand on étudie la propagation des ondes sismiques dans la croûte terrestre, on a l'habitude de considérer la reflexion des ondes au contact de la surface terrestre comme celle de la lumière sur la surface d'un miroir qui n'y produit aucune perturbation. Cette considération n'est naturellement juste que lorsqu'on considère seulement les phases, c'est-à-dire les changements brusques de l'amplitude des secousses. Mais, dans le cas où l'on fait attention à toutes les ondes qui constituent la plus part des enregistrements accélérométriques des séismes voisins, on est obligé de traiter des secousses comme des oscillations produites dans la couche superficielle du terrain dont l'épaisseur se limite plusieurs dixaines de mètre.

Quand nous remarquons la composante horizontale des secousses sismiques observées à un endroit couvert par une couche superficielle, il y a, d'une part, une portion que nous appelerons les "*secousses préliminaires*" qui conserve son intensité toujours constante; d'autre part, un changement brusque d'intensité au commencement de ce que nous appelerons les "*secousses principales*", dont l'amplitude diminue progressivement. D'un autre côté, les secousses observées à un endroit qui ne possède pas de couche superficielle, ne manifestent pas généralement cette particularité: nous en avons un exemple dans les secousses de petit séisme de Tukuba représentées dans la Fig. 1.[2] Nous allons étudier seulement les secousses produites dans une région couverte par une couche superficielle.

---

[1] M. ISHIMOTO, Ce *Bulletin* 12 (1934), 706.

[2] W. INOUÉ, Ce *Bulletin* 11 (1933), 69

Nous pouvons expliquer ces caractéristiques des secousses par la simple hypothèse que toutes les secousses, enregistrées par le sismographe, sont celles qui sont produites secondairement dans la couche superficielle. Lorsque les ondes sismiques arrivent à la surface, elles produisent les oscillations dans la couche et leur diffusion apparaît en suite à l'intérieur. L'intensité initiale distribuée dans chaque région autour d'un épicentre, ainsi que la manière de sa diffusion ne resteront pas les mêmes, selon les deux sortes de secousses.

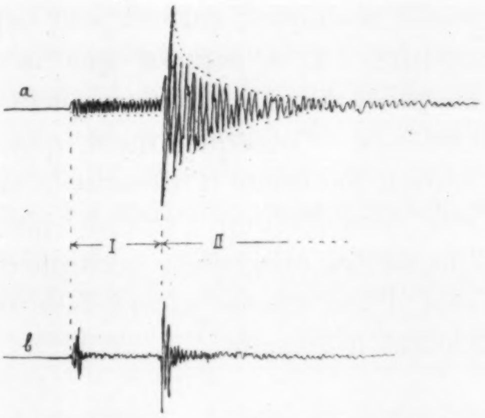

Fig. 1. Exemples de secousses sismiques enregistrées par le sismographe accélérométrique : a) à un endroit couvert par une couche superficielle, b) à un endroit (Tukuba) qui ne posséde pas de couche
I.... Secousses préliminaires.
II... Secousses principales.

Nous constatons d'une autre côté que la diminution de l'intensité dans les secousses principales varie avec la distance épicentrale ainsi qu'avec la distance hypocentrale : l'intensité des secousses dure comparativement plus longtemps pour un séisme lointain (Fig. 2)[3]. Pour expliquer cette caractéristique des secousses, nous devrons considérer aussi leur diffusion dans la couche superficielle.

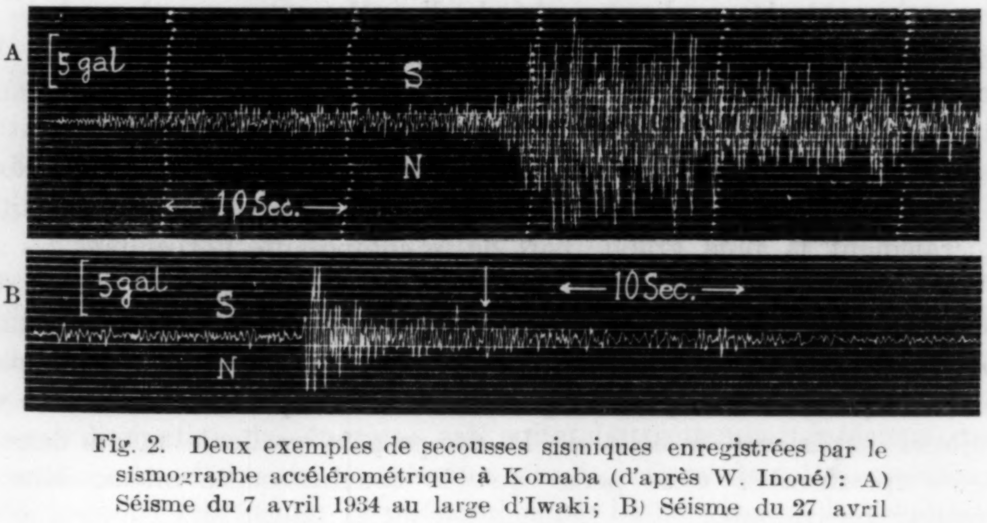

Fig. 2. Deux exemples de secousses sismiques enregistrées par le sismographe accélérométrique à Komaba (d'après W. Inoué) : A) Séisme du 7 avril 1934 au large d'Iwaki; B) Séisme du 27 avril 1934 au sud de la péninsule de Bôsô.

---

[3] W. Inoué, *ibid.*, 12 (1934), 712.

Le Prof. T. Terada⁴⁾ a déjà proposé une considération sur les secousses sismiques, surtout pour expliquer la distribution anormale de leur intensité. Il a supposé que la surface terrestre est constituée par un groupe de blocs liés dynamiquement : c'est-à-dire formant des couplages entre eux. Conséquemment, quand les blocs oscillent, il y a une distribution anormale d'intensité à cause de l'échange d'énergie entre eux. Cette considération s'accorde plus ou moins avec la nôtre. Au lieu d'introduire un système multiple d'oscillations, nous adoptons simplement l'idée d'une couche superficielle où les oscillations sont produites et se difusent à la suite.

2.

Le phénomène de propagation des ondes sismiques dans la croûte terrestre est comparé à celle de la lumière dans un milieu ; cependant il nous semble qu'il s'agit d'un milieu non transparent : mais plutôt brumeux. Bien que la vitesse de propagation des ondes ne varie pas beaucoup, leurs propriétés deviennent assez compliquées pendant leur propagation. Même une onde unique à l'origine, arrivera à la surface comme une série d'ondes. Il est probable que la portion superficielle du terrain possédra une condition des plus compliquées.

Pour avoir un traité simple, nous commençons notre considération à partir de la production des secousses dans la couche superficielle. Nous savons que la plus part des secousses sont constituées par l'oscillation propre de la couche; sa période d'oscillation propre depend de la rigidité (μ) et la densité (ρ) du sol, ainsi que de son épaisseur (l). Le mode d'oscillation du sol enregistrée par le sismographe de la composante horizontale correspond à celui d'une oscillation cisaillante du sol dont la période d'oscillation fondamentale sera représentée par $T=4l\sqrt{\mu/\rho}$. Nous ne considérons que l'oscillation fondamentale, parce qu'elle constitue généralement la plus grande part de la composante horizontale des secousses sismiques. Naturellement, nous supposons que l'intensité des oscillations produites est toujours proportionelle à celle de la composante horizontale des ondes originales. D'après ces considérations, nous pouvons accepter le fait que l'amplitude de la composante horizontale est toujours supérieure à celle de la composante verticale même dans la région épicentrale : c'est parce que la couche oscille mieux dans la direction horizontale.

Il nous semble qu'il y a des personnes qui supposent que les secousses préliminaires sont constituées par des ondes longitudinales et que les secousses principales sont constituées par des ondes transverselles.

---

[4] T. Terada, *Revues géographiques*, 1 (1925), 841.

Pour nous, cependant, ces deux distinctions n'existent plus dans la propriété des secousses observées. Cela vient de ce que nous observons toujours la composante horizontale des secousses produites l'une après l'autre dans la couche superficielle par les deux sortes d'ondes originales. Il est certain, cependant, qu'il y a aussi une oscillation de la couche dans la direction verticale, mais elle ne peut être constatée que par le sismographe de la composante verticale. En tout cas, notre observation porte toujours sur la composante horizontale d'oscillation propre produite dans la couche superficielle. Partant de cette idée, nous voudrions traiter les caractéristiques des secousses sismiques d'une façon analogue à celles de la chaleur se diffusant dans un milieu. Dans ce cas la température correspond à l'intensité des secousses. Quant au coefficient de conductivité de la chaleur, nous n'avons pas encore trouvé son correspondance dans les secousses, mais il aura certainement un rapport étroit avec la vitesse des ondes superficielle dans la couche.

Or, supposons que $4\pi I$ de l'énergie rayonne du foyer qui est placé à la profondeur H au sein de la croûte terrestre. Quand les ondes arrivent à la surface, elles produient des oscillations cisaillantes dans la couche superficielle, oscillations dont l'intensité est proportionnelle à l'énergie de la composante horizontale des ondes originales. Donc, l'intensité horizontale des oscillations produites dans la couche sera donnée proportionnellement par les formules suivantes:

$\frac{I_p}{R^2}\cos^2\theta\cdot\sin\theta$ pour les secousses préliminaires,

$\frac{I_s}{R^2}\cos^3\theta$ pour les secousses principales,

où R est la distance entre la station d'observation et le foyer et θ est l'angle entre H et R (voir la Fig. 3).

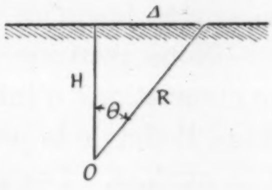

Fig. 3.

Quand la vitesse de diffusion des secousses dans la couche reste comparativement plus lente que celle de la propagation des ondes sismiques dans la croûte, il sera permis de supposer que les intensités initiales definies ci-desus seront données instantanément à la couche et que la diffusion commencera à la suite. Naturellement, nous ne considérons aucune dissipation des énergies par suite du frottement intérieur dans le milieu afin d'obtenir un résultat simple. Dans de telles conditions, nous pouvons représenter ce phénomène par l'analogie avec la conduction de la chaleur dans un milieu étendu à deux dimensions.

Désignons, alors, par v la température, par r le rayon et par t le temps: nous aurons[5]

---

[5] voir Carslow, Conduction of Heat, 152~153.

$$\frac{\partial v}{\partial t}=k^2\left(\frac{\partial^2 v}{\partial r^2}+\frac{1}{r}\,\frac{\partial v}{\partial r}\right), \tag{1}$$

où k est le coefficient de conductivité. La solution de cette formule sera

$$v=A_1e^{-k_1^2v^2t}J_0(\mu_1 r)+A_2e^{-k_2^2v^2t}J_0(\mu_2 r)+A_3e^{-k_3^2v^2t}J_0(\mu_3 r)+\cdots\cdots. \tag{2}$$

Considérons ainsi deux cas distincts : 1° pour une source linéaire perpendiculairement au plan

$$v=\frac{Q}{4\pi kt}\,e^{-\frac{r^2}{4kt}}, \tag{3}$$

et 2° pour une source de surface cylindrique

$$v=\frac{Q}{4\pi kt}\,e^{-\frac{r_0^2+r^2}{4kt}}\,J_0\left[\frac{ir_0r}{2kt}\right]. \tag{4}$$

Les équations (3) et (4) seront appliquées respectivement aux secousses préliminaires ainsi qu'aux secousses principales.

3.

D'après le calcul obtenu de l'équation (4), nous comprenons aisément que l'intensité des secousses ne varie pas beaucoup pendant une certaine durée de temps, surtout dans la région épicentrale. Ce résultat correspond avec le fait que les secousses préliminaires commencent à zéro et arrivent ensuite à une certaine valeur d'amplitude, laquelle reste constante jusqu'au commencement des secousses principales.

Nous pouvons faire correspondre le calcul obtenu de l'équation (3) aux variations d'intensité des secousses principales. Considérons, d'ailleurs, l'effet de la profondeur pour la distribition de l'intensité de l'énergie à la surface. Désignons par H la profondeur hypocentrale et cherchons une relation entre H et t. Quand la distribution directionelle de l'énergie sera représentée par

$$I \infty \cos^5\theta \tag{5}$$

nous obtiendrons une condition convenable pour resoudre la question. Cette supposition ne sera pas rigoureusement exacte dans tous les cas, mais elle sera admissible tant que nous considérerons au moins la propriété qualitative du phénomène de la diffusion. Nous aurons ainsi l'intensité des secousses représentée par

$$E \infty \cos^8\theta/R^2. \tag{6}$$

D'après cette relation, nous pouvons tracer une série de courbes correspondant aux différentes profondeurs du foyer. Elles sont représentées par la Fig. 4a. D'un autre côté nous traçons une autre série du courbes d'après l'équation (3) qui sont représentées par la Fig. 4b ; cette fois-ci nous prenons kt comme le paramètre. En comparant ces deux

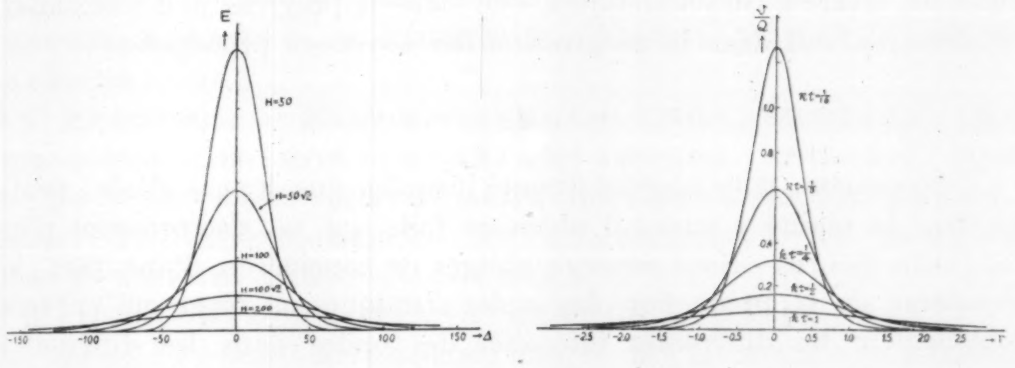

a b

Fig. 4. a) Intensités initiales de secousses produites par les séismes de différentes profondeurs; b) progression de la diffusion de charleur.

séries de courbes nous pouvons conclure que la profondeur hypocentrale peut être remplacée par kt et représentée par

$$H = 200\sqrt{kt}. \tag{7}$$

Naturellement il est nécessaire *d'* introduire aussi une certaine relation entre $\varDelta$ et r.

Nous n'avons, donc, aucune nécessité de considérer la profondeur hypocentrale. La distribution initiale d'intensité des secousses provoquées par un séisme d'une profondeur H sera donnée par une courbe dans la série de la Fig. 4b, dont le paramètre est $t = H^2/40000k$. La Fig. 5 représente la diminution d'intensité à la station d'observation correspondant au passage du temps. Quand la station est placée près de l'épicentre, l'intensité arrive au maximum tout de suite et diminue assez vite. Quand elle est placée assez loin de l'épicentre, les circonstances deviennent contraires. De plus, dans le cas où le foyer est profond, les secousses commencent à une certaine époque déterminée par la relation (7). Ce sont les caractéristiques dans le passage des secousses principales et on a pu distinguer vaguement la distance du foyer ainsi que celle de l'épicentre. En tout cas, notre considération part du fait que la plus grande part des secousses sismiques sont constituées par des oscillations cisaillantes de la couche superficielle produites par l'arrivée des ondes originales. Les oscillations se diffusent dans la couche à la suite comme la chaleur se diffuse dans un milieu. D'après cette idée, nous croyons avoir ex-

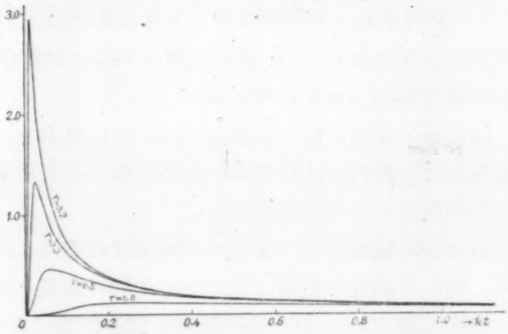

Fig. 5. Progression de la diffusion de charleur aux diverses distances épicentrale.

pliqué les diverses caractéristiques, soit dans la progression des secousses préliminaires, soit dans la progression des secousses principales.

4.

Evidemment, nous n'avons discuté jusqu'ici que les cas idéals ; peut-être dans la réalité y aura-t-il plusieurs faits qui ne s'accorderont plus avec notre théorie. Nous sommes obligés de concidérer, d'une part, le mécanisme de la production des ondes sismiques au foyer qui enverra probablement les différentes intensités des ondes dans les différentes directions ; d'autre part, l'inégalité régionale des propriétés de la couche, soit sa rigidité, soit son épaisseur ; nous savons que leurs propriétés ne restent pas les mêmes, même dans la ville de Tôkyô.[6] Cette variation des propriétés de la couche produit naturellement différentes périodes dans l'oscillation propre ; dans ce cas nous ne pouvons pas appliquer directement notre théorie. Nous avons besoin d'introduire certaines modificications pour étudier et expliquer certains faits réels de la nature.

9. 地震動の表面層内における擴散

地震研究所 石本巳四雄

1. 最近著者は水槽内における水の振動様式が加速度地震計を以て記錄した東京地方の地震動に酷似する事を示したが，其の現象の中には振動の擴散する事實のある事を述べた．本論文は特に此の問題を取扱つたものである．

地震波の傳播に關する研究においては地表を一鏡面と考へ，波動は其の儘反射されるとなすが，近地地震の記象内には數十米の厚さを有する表面層内に誘起される定常性振動の認められる事から，光學的類似のみでは充分でない．

吾々は地震動の中，多く水平動成分に着目し，其の震動の中に初期微動と主要動との區別を認める．而して前者の振幅は大でないが時の經過に從つて減衰は少く，後者は急激に大振幅から初まるが減衰も著しい．但し特に後者は震源距離によつて狀況に變化ある事は申迄もない．

此等の事實は全く地震動を表面層内に惹起された層の一次振動となし，其の振幅は層内における振動の擴散する現象を以て說明し得るのであつて，固體粘度の影響は全く無視し得るのである．

2. 以上の考察に從ふと，吾々は地震動の水平成分を見て居る限り，表面層に惹起された自己振動の振幅を見て居る事となり．若し震源において發せられた縱波，横波の勢力を夫れ夫れ $4\pi I_p$, $4\pi I_s$ となし，其の勢力が地表に到達して表面層の振動を誘發するならば，其の強さは夫々

$$\frac{I_p}{R^2}\cos^2\theta\cdot\sin\theta, \qquad \frac{I_s}{R^2}\cos^3\theta$$

に比例する量と考へて差支へない．而して若し擴散速度が地震波の速度に比較して充分小であるならば，以上の強さが瞬間的に附與され，其れに續いて擴散が行はれると考へて宜敷い． 從つて此の

---

[6] M. ISHIMOTO, Ce *Bulletin* **10** (1932), 171; **12** (1934), 234.

問題は最初條件の與へられた熱の平面媒質内に擴散する現象として解く事が出來る. 但し此の場合溫度は振動の强さに相當する. 而して初期微動に對しては圓筒源を, 主要動に對しては線源を當嵌める事が出來るのである.

3. 數式を解く事によつて圓筒源の場合は震源附近において擴散による强度變化は著しく無く, 實際の初期微動が比較的一定の强さを保つ事實を說明する事か出來る. 又線源の場合は, 實際震源から發せられる勢力が $\cos^5\theta$ に比例すると云ふ特別の場合を採用するならば事柄は簡單となり, 震源の深さの影響は設定時間後の擴散狀況から出發すると云ふ結果を得るのである. 此の假定は質的現象を論ずる限りにおいては差支へないものと思はれる.

第 4 圖は以上の假定から震源の深さの及ぼす震動配置狀況, 及び線源の擴散狀況を示すものである. 兩者の間に充分の類似を認める事が出來るであらう. 第 5 圖は第 4 圖 b から各震央距離に從つて其の場所における地震動の强さが, 時の經過に從つて如何に變化するかを示すもので, 近い地震, 遠い地震或ひは震源の深い地震に從つて各々の特徵ある事を圖示したものである.

4. 以上は全く理想的の場合を考へて居るが, 實際は層の性質が各地で不同である事, 震源より放射される波動勢力が各方向一樣でない事等が影響する結果は, なほ進んだ議論を行ふに際しては數式の取扱を多少複雜にする事を餘儀なくされるのであらう.

10. *A Comparison of the Displacement, the Velocity, and the Acceleration Seismograms.*

By Takahiro HAGIWARA,

Earthquake Research Institute.

(Read Nov. 20, 1934.—Received Dec. 20, 1934.)

1. Introduction. In his previous paper[1], the author described the construction of a velocity seismograph that registrates mechanically the velocity of the earthquake motion by means of an over damped pendulum. This instrument renders possible the mechanical registration of the three different amplitudes of the earth movement, namely, displacement, velocity, and acceleration. As the result, a displacement seismograph, a velocity seismograph, and an acceleration seismograph have been installed in the same room at Hongô, Tôkyô, and observations begun since the end of August, 1934. During the past four months a number of sensible earthquakes were recorded by these instruments.

Usually in studying on a seismograph, whether in theory or in experiment, we assume the earth movement to be of the form of a simple mathematical expression, such as a pure sine. But, as is well known, the actual earthquake motion is much more complicated, so that it is of more than usual interest to examine if a actual seismogram gives the true earth movement or not. This paper describes the comparisons that were made of each of the three kinds of seismograms above mentioned with curves obtained by differentiating and integrating the curves of the respective kinds of seismograms.

2. Instruments. The seismographs used in the comparisons were N-S component instruments. The *displacement* seismograph used was a portable seismograph[2] designed and constructed by the author, a photograph and the elevation diagrams of which are shown in Figs. 2 and 1 respectively. The bob (M) of the pendulum is supported by the aluminium pillar (E) and inverted by two flat springs (F). The air damper is of piston type, the bob of the pendulum itself acting as piston. Since the sectional size of the bob that is cut off by the vertical plane involving the axis of the damper is fan-shaped, the center of arc

---

[1] T. HAGIWARA, "A Velocity Seismograph," *Bull. Earthq. Res. Inst.*, **12** (1934), 776.

[2] T. HAGIWARA, "A new portable seismograph," *Disin*, **6** (1934), 654, (in Japanese).

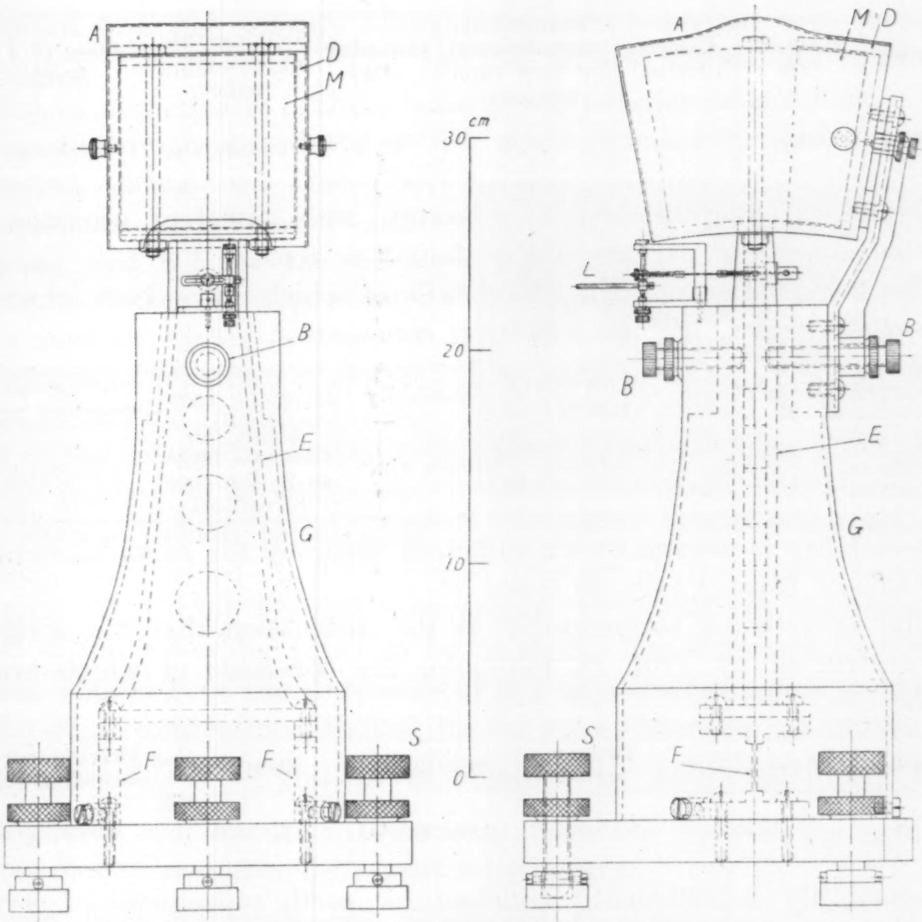

Fig. 1. Elevation of the displacement seismograph.
A cover, *M* bob of the pendulum, *D* air damper, *C* cock for adjusting the damping force, *B* cramp, *L* lever for magnification, *E* aluminium pillar, *G* cylindrical wall, *F* flat spring, *S* level screw.

of which lies on the axis of rotation of the pendulum, the clearance of the piston (about 0·4 mm.) is unchanged when the bob moves, describing the arc. Magnification is obtained by means of a lever (*L*). The connection between the pendulum and the minor arm of the lever is made by a steel rod of 1 mm. diameter, both ends of which being pivotted, compress the agate cups affixed to the lever and the pendulum with the aid of weak helical springs. The constants of the instrument are as follows.

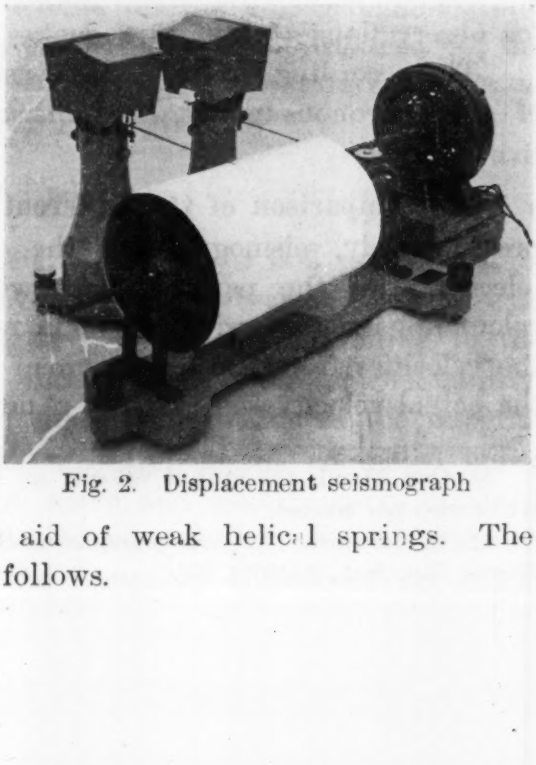

Fig. 2. Displacement seismograph

Component	Mass of bob	Proper period	Dynamical magnification for very rapid vibration	Damping ratio	Driving rate of recording paper	Term of solid friction
N-S	6 kg.	5 sec.	26·8	10 : 1	1·05 mm/sec.	0·015 cm

The dynamical magnification is constant, with sufficient accuracy for earth movements of periods of less than 5 or 6 sec.

The *velocity* seismogram, the details of which have been given in the previous paper, has the following constants.

Component	Mass of bob	Proper period	Sensibility	Damping force	Driving rate of recording paper
N-S	15 kg.	1·0 sec.	1·18 cm/kine[3]	About ten times as large as in the case of critical	1·05 mm/sec.

The sensibility is constant with sufficient accuracy for earth movements of periods of from 0·2 sec. to 5 sec.

The *acceleration* seismograph[4] is the instrument that was designed and constructed by Prof. M. Ishimoto, the constants of which are as follows:

Component	Mass of bob	Proper period	Sensibility	Damping	Driving rate of recording paper
N-S	15 kg.	0·15 sec.	1·0 mm/gal.	Critical	0·95 mm/sec.

The sensibility is sufficiently constant for earth movements of periods longer than 0·1 sec.

The earthquake motions observed at Hongô had in general periods ranging from 0·1 sec. to 5 or 6 sec., provided the epicentral distances are not far, so that the seismographs just mentioned should be adequate for observations of near earthquakes.

The recording drum in each seismograph was revolved by means of a synchronous motor, time marks being given automatically every five seconds.

3. Comparison of the Different Kinds of Seismograms. For our present study, seismograms of the earthquake of Sept. 1st, 1934, were selected. On the parts marked with a white line in Fig. 3, the calculations were carried out for a range of 30 sec. We first computed the velocities from the displacement seismogram and compared it with the actual velocity seismogram. And in the same manner, accelerations computed from the velocity seismogram were compared with the actual acceleration seismogram. The problem was to obtain the differential coefficient numerically. The process of computation is as follows. First, enlarged photographs of the actual seismograms were made, the magnification being 6·7 for the displacement and velocity seismogram and 8·2 for the acceleration seismogram respectively. By a reading device (a kind of co-ordinates comparator of simple construction) the amplitudes were read on the enlarged photographs to the fraction of a millimetre. The abscissa (which corresponds to time) was divided on the enlarged photograph into equal lengths of 1/3 mm. This unit division corresponds to 0·0450 sec., assuming the speed of the recording paper to be uniform. The differential coefficient, $\dot{y}$, was obtained as the difference of the adjacent ordinates y_n and y_{n-1} in the actual seismogram, divided by the time difference Δt (0·0450 sec.), that is, $\dot{y}=\frac{y_n-y_{n-1}}{\Delta t}$. The curves obtained by computation are shown in Fig. 4, d and h. As will be seen from the figures, the computed curves closely resemble the actual seismograms.

---

[3] One *Kine* is the unit of velocity on the C.G.S. system, i.e. the velocity of one centimetre per second.

[4] M. ISHIMOTO, "Un sismographe accélérométrique et ses enregistrements," *Bull. Earthq. Res. Inst.*, **9** (1931), 316.

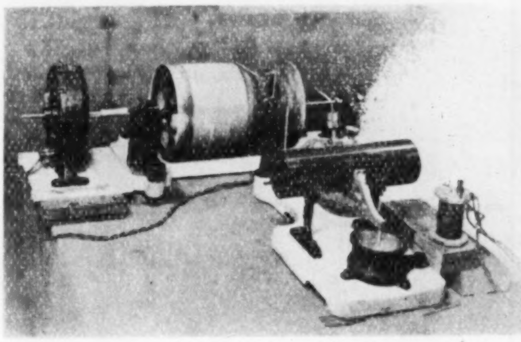

Fig. 3. Velocity seismograph.

We next computed the displacements from the actual velocity seismogram and the velocities from the actual acceleration seismogram. The purpose of the computation was to obtain the integral of the original curves. The numerical integration was done according to Simpson's rule. The abscissa was divided on the enlarged photograph into equal lengths of 1/3 mm., which corresponds to 0·0450 sec. for the velocity seismogram and to 0·0405 sec. for the acceleration seismogram. The ordinate of the required integral Y_n is given by

$$Y_n=\frac{\Delta t}{3}\{(y_0+4y_1+y_2)+(y_2+4y_3+y_4)+\cdots+(y_{n-2}+4y_{n-1}+y_n)\},$$

where y_n is the ordinate of the original curves (n is a multiple of 2) and Δt the length of each equal division of the abscissa. In the case of integrals we must add an integral constant, corresponding to the first ordinate of the integral, but since this is an unknown quantity, the ordinates obtained do not give the absolute value of the integral. In other words, the position of the zero line of the computed curve is undetermined. The displacement curve and velocity curve obtained by this method are shown in Fig. 4, c and g respectively. As shown in the figure, generally speaking, the computed curve and the actual

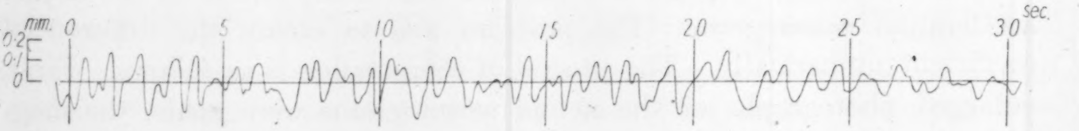

Fig. 4, a. Actual *displacement* seismogram.

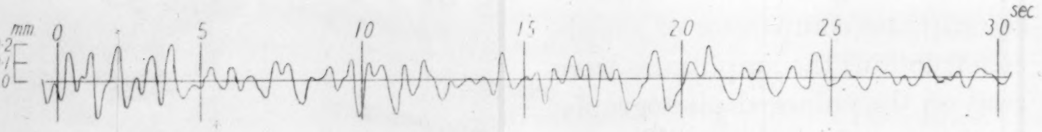

Fig. 4, b. *Displacement* curve computed from the velocity seismogram with ammendment of zero line.

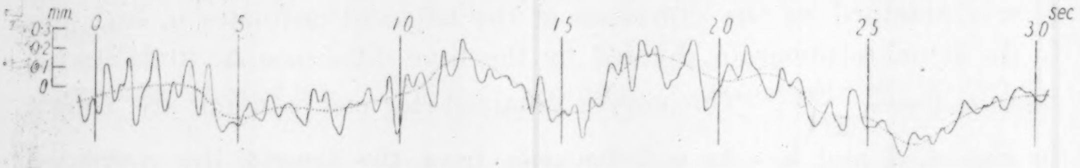

Fig. 4, c. *Displacement* curve computed from the velocity seismogram.

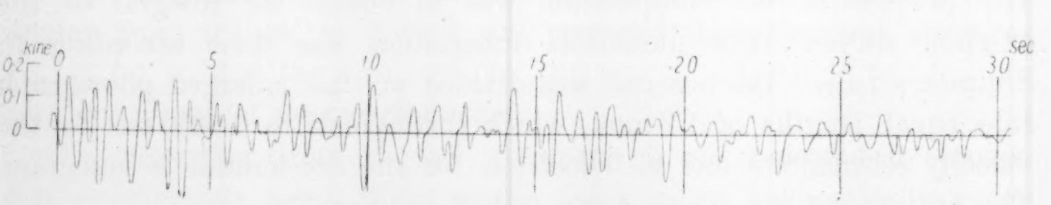

Fig. 4, d. *Velocity* curve computed from the displacement seismogram.

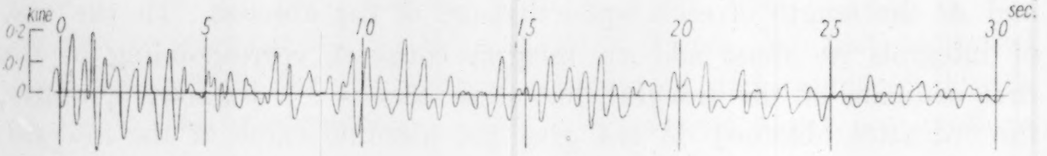

Fig. 4, e. Actual *velocity* seismogram.

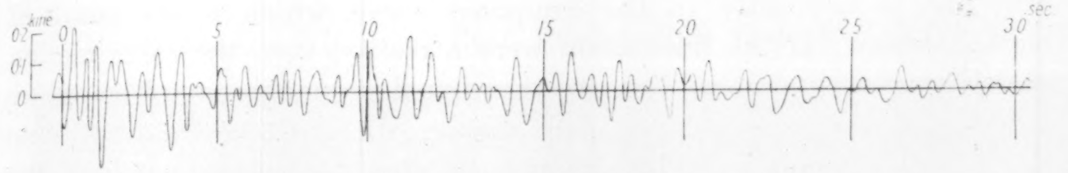

Fig. 4, f. *Velocity* curve computed from the acceleration seismogram with ammendment of zero line.

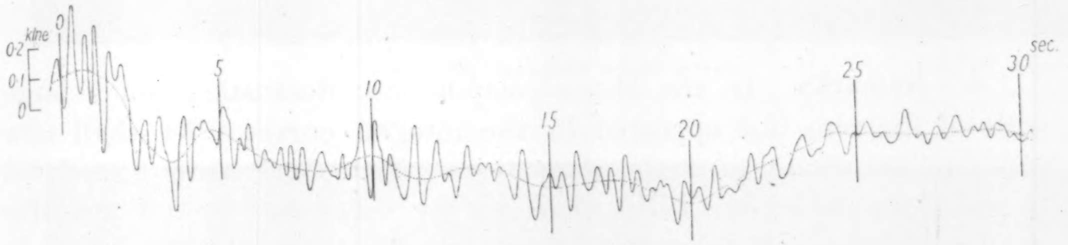

Fig. 4, g. *Velocity* curve computed from the acceleration seismogram.

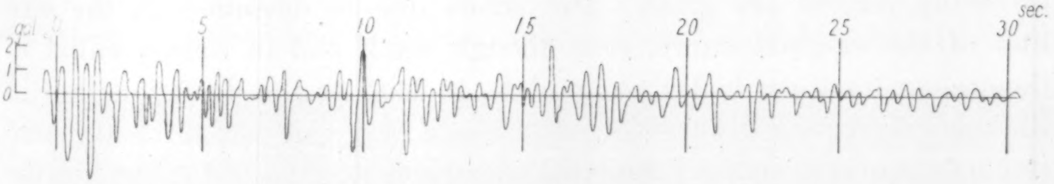

Fig. 4, h. *Acceleration* curve computed from the velocity seismogram.

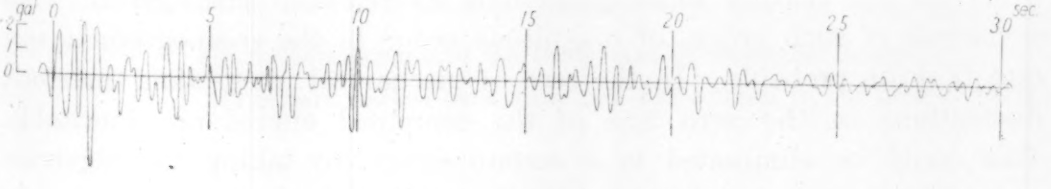

Fig. 4, i. Actual *acceleration* seismogram.

seismogram closely resemble each other, although a fluctuation in the zero line is noticeable in the computed curve, which is the result of certain errors. If the fluctuation were a reality, then the same motion should appear more or less in the actual seismograms. The errors responsible for such fluctuation in the zero line will be examined into later. At any rate, in order to eliminate this fluctuation, we took the algebraic means of ten ordinates of the curve, and plotting this on the diagram, drew a smooth curve through these points (shown by dotted line in the figures). We thus assumed the line to be the zero line of the curve and ammended the curve, as shown in Fig. b and f. The curves ammended in such manner come to look very like the actual seismograms.

4. Remarks. In the above computation, fluctuations on a large scale of the zero line appeared in the integral curves. We shall now examine the cause of such fluctuations. The chief errors introduced in our computation are believed to be the followings: (1) Errors due to irregularities in the speed of the recording paper. (2) Errors in reading the ordinate of the original curve. (3) Errors due to slight deviations in the zero line of the original curve. In the case of numerical integration, since the ordinate of the integral is determined by summation of the ordinates of the original curve, the errors due to (1) and (2) are not so serious, althongh the possibility of errors due to (3) being serious are great. The errors due to deviation in the zero line of the original curve, even though small and in consequential in themselves, may gradually accumulate, so long as the deviations are in the same direction. These errors cause a large deviation in the zero line of the new curve. But the deviation in the zero line of the original curve changes its sense, accidentally, thus resulting in fluctuations in the zero line of the new curve as seen in the figures. By computing the differential coefficient of the fluctuating zero line (dotted line in the figures), the deviations in the zero line of the original curve is estimated to be of the order less than 0·005 kine and 0·03 gal respectively for the velocity seismogram and acceleration seismogram. That deviations of such orders of magnitude occur in the seismogram in our case is quite probable. In the case of mechanical integration, therefore, fluctuations in the zero line of the computed curves are inevitable. This could be eliminated to a certain extent by taking the algebraic mean of a certain number of ordinates of the new curve as has already been done. At all events, it may be said that the close resemblance between the actual seismograms and the computed curves confirm the accuracy of each seismogram.

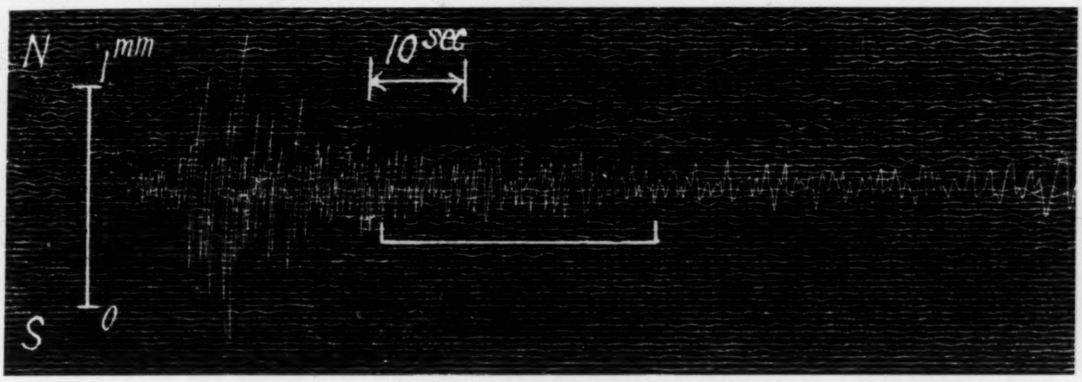

a) Displacement seismogram. (*Full size*)

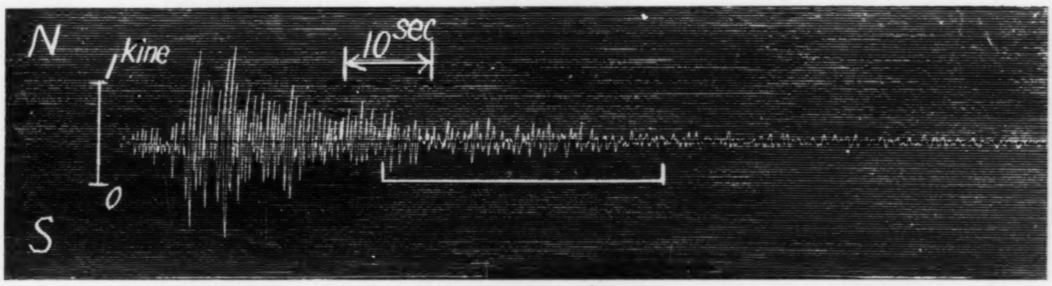

b) Velocity seismogram. (*Full size*)

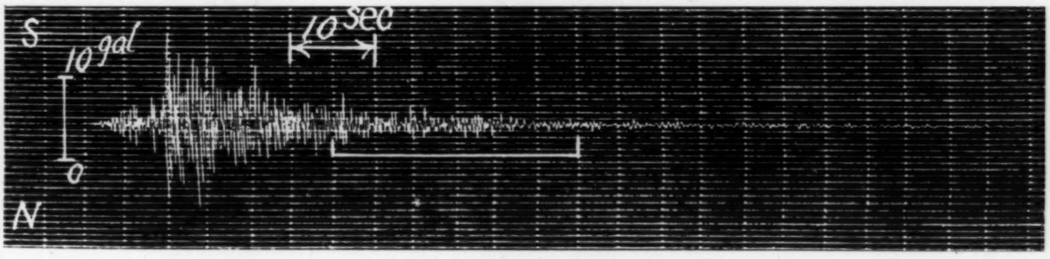

c) Acceleration seismogram. (*Full size*)

Fig. 5. Seismograms of the earthquake of September 1, 1934.
(The part marked by a white line was adopted in our present study.)

In conclusion, the author desires to express his cordial thanks to Professor M. Ishimoto for his kind advices and criticisms, and also to the Council of the Foundation for the Promotion of Scientific and Industrial Research in Japan (Gakuzyutu Sinkôkwai Foundation), who defrayed a part of the cost of the instruments constructed.

---

10. 地震動の變位，速度及加速度の比較

地震研究所 萩原尊禮

前論文に於て筆者は速度地震計の製作に就て述べたが，此の地震計と從來の變位地震計及石本加速度地震計とを並置することに依り，地震動の變位，速度及加速度の3要素を機械的に記錄せしめることが可能となつたわけである．此の結果是等3種の地震計を本研究所地下室の同一床上に取付けて昭和9年8月末より觀測を開始した．

我々が地震計に關する理論的の取扱を爲す場合や，振動臺等に依り實驗を行ふ場合には便宜上地動を數學的に表現し得るもの(例へば單弦運動)と假定する．然し實際の地動は遙かに複雜したものであるので，實際上地震記象がどの程度迄忠實に眞の地動を與へて居るかを吟味することは興味あることであらう．本論文に於ては此の目的に添ふ一つの方法として變位記象及速度記象より夫々數値計算に依り速度及加速度を算出し之を速度記象及加速度記象と比較し，又速度記象及加速度記象より夫々變位及速度を算出し之を變位記象及速度記象と比較した．此の結果何れの場合も計算に依り得た曲線と夫れに相當する實際の記象とは良く一致し，地震記象は正確に地震動を與へて居ることが確められた．

11. *Microseisms of Four Seconds Period observed with Horizontal Seismographs.*

By Fuyuhiko KISHINOUYE,

Seismological Institute.

(Read Oct. 16, 1934.—Received Dec. 20, 1934.)

1. The microseisms at Hongô in Tôkyô, were classified by F. Omori[1] into three types, q, Q_1 and Q_2 according to periods of oscillations. The characteristics of these types were stated by Dr. T. Matuzawa[2] as follows: period and mode of q-type are 2∼3 sec. and regular, those of Q_1-type about 4 sec. and fairly regular, and those of Q_2-type are 6∼9 sec. and irregular. The connexion between microseisms and meteorological conditions has been investigated in many researches to explain how these oscillations are caused.

To obtain a further knowledge of the microseisms the present writer studied the amplitude and the period of Q_1-type oscillations with a harmonic analyser, and then the phase relation of microseisms observed at several places in a small area.

Harmonic analysis of microseisms.

2. A portion of the record of microseisms at about 17 h. on March 14, 1934 (see Fig. 1) obtained with N–S component of an Imamura Portable Seismograph was studied by a Noguchi Harmonic Analyser[3]. The time interval of the analysed portion was 56·3 sec. In theory the figure of the analysed curve must be repeated equally in other intervals. In this analysis the above condition would be nearly satisfied, for the interval was at the middle portion of the total duration of the microseismic oscillations which continued almost stationary for several hours. The portion of the seismogram was enlarged photographically 10·8 times on a sheet of paper to fit for the use of the analyser. The static magnification of the seismograph was 50, so the final magnification of the record became 540 and the interval was 754 mm. long on the paper. The curve in Fig. 2 shows the record on a reduced scale of the actual.

---

[1] F. OMORI, *Bull. Imp. Earthq. Inv. Comm.*, **3** (1909), 1∼35.

[2] T. MATUZAWA, *Journ. Fac. Sci. Imp. Univ. Tokyo.*, [ii], **2** (1927), 205∼263.

[3] K. NOGUCHI, *Journ. Soc. Mech. Eng.*, **27** (1924), 975∼984.

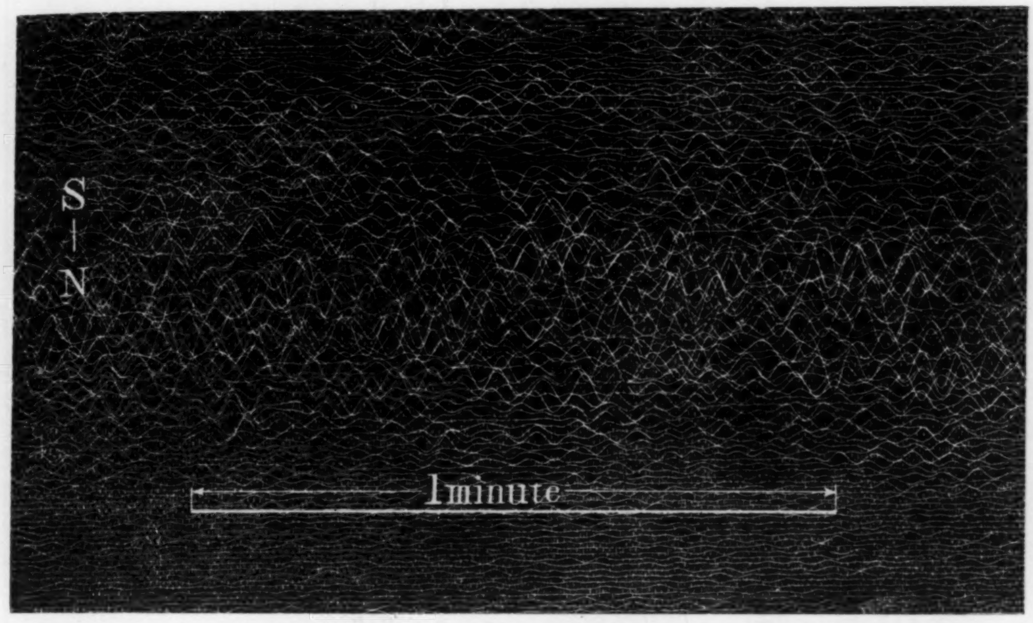

(*Full size the actual.*)

Fig. 1. Portion of record of microseisms. March 14, 1934. Imamura Portable Seismograph. (The recording drum was driven at a speed of one revolution ten minutes.)

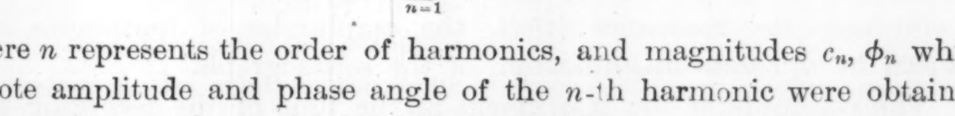

Fig. 2. Analysed portion of record of microseisms. March 14, 1934.

The record was expressed as a function of time t in the form

$$f(t)=c_0+\sum_{n=1}^{\infty} c_n \sin(nt+\phi_n),$$

where n represents the order of harmonics, and magnitudes c_n, ϕ_n which denote amplitude and phase angle of the n-th harmonic were obtained. The results are shown in the following table.

Table I. Constants of Harmonics.

T_n: the period of the oscillation of the n-th order in seconds.

n	0	1	2	3	4	5	6
T_n	—	56·3	28·2	18·7	14·1	11·2	9·38
c_n	5·74	2·95	1·30	1·99	0·98	1·89	0·42
ϕ_n	—	113° 20′	80° 10′	134° 30′	126° 00′	55° 10′	335° 00′

(*to be continued.*)

Table I. (*continued.*)

7	8	9	10	11	12	13
8·05	7·04	6·26	5·63	5·11	4·69	4·33
1·59	0·69	2·92	7·68	9·81	26·30	36·21
76° 50′	347° 30′	149° 40′	39° 25′	39° 50′	23° 00′	78° 40′

14	15	16	17	18	19	20
4·02	3·76	3·52	3·31	3·13	2·96	2·82
30·09	33·63	11·25	10·70	10·54	3·79	0·84
284° 10′	249° 40′	268° 35′	355° 20′	65° 00′	131° 50′	113° 50′

21	22	23	....	30
2·68	2·56	2·44	....	1·88
1·72	2·35	0·99	....	0·74
206° 05′	61° 00′	308° 00′	....	238° 50′

The cases of $n>24$ are skipped in the results, but the case of $n=30$ was measured for the causion's sake.

3. The first maximum of the amplitude c_n lay at $n=15$ and the second $n=13$, corresponding to 3·8 and 4·3 sec. of the periods of oscillations respectively. The harmonic constants of lower orders might be affected by taking the interval of the analysis erroneously. So the writer will discuss hereafter about the harmonics of the order higher than 10. Furthermore the effects of the free period of seismograph or the resonance effect upon the results must be considered, for the period was similar to the periods of the oscillations discussed here. In order to eliminate the resonance effect, the amplitudes of harmonics were reduced by dynamic magnification of the seismograph.

The constants of the instrument at the time of the recording were as follows: the mass of the pendulum-bob $M=7$ kg., the static magnification $V=50$, the period $T_0=6{\cdot}0$ sec., and the damping ratio $v=1{\cdot}26$. The above amplitudes as measured from the record were converted into harmonic earth movements A_n by the well-known formula,

$$A_n=\frac{c_n}{\mathfrak{V}},$$

where $\mathfrak{V}$ denotes the dynamic magnification of the seismograph, or

$$\mathfrak{V}=\frac{V}{\sqrt{\{1-(T_n/T_0)^2\}^2+4\dfrac{0{\cdot}538\,(\log_{10}v)^2}{1+0{\cdot}538\,(\log_{10}v)^2}(T_n/T_0)^2}},$$

and T_n the period of oscillation of the n-th harmonic.

The relationship between the corrected amplitudes and the periods is shown in Fig. 3.

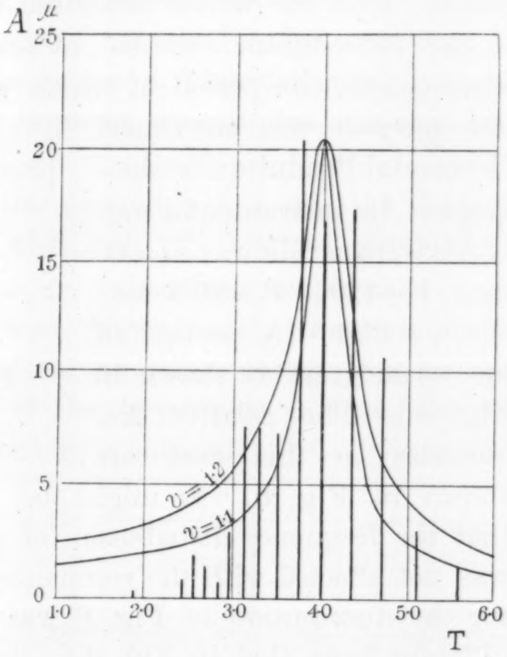

Fig. 3. Amplitudes of harmonics.

Frequency-distributions of periods of microseisms.

4. The most investigators have determined the period of microseisms by frequency-distribution of different periods. So the writer also measured the number of observations of periods on the record shown in Fig. 1, and determined the period of microseisms to compare it with that which has been obtained from the same record by the harmonic analysis. The number of observations of different periods counted in a short interval may be affected with the length of periods, in other words the number of observations of longer periods are less than those of shorter periods in a definite interval. Then to reduce the effects of period, the frequencies were corrected by the following formula,

$$f_n = f'_n \frac{T_n}{T},$$

where T denotes the period of a harmonic of which number of observations was regarded as a standard frequency, f_n the relative frequency of the n-th harmonic to the standard period, and f'_n, T_n frequency and period of the n-th harmonic. The distribution of the corrected frequencies is shown in Fig. 4. The diagram resembles to that in Fig. 3. Therefore the period of microseisms may be obtained by either harmonic analysis or frequency-distribution of periods. Yet there was a doubt about the frequencies

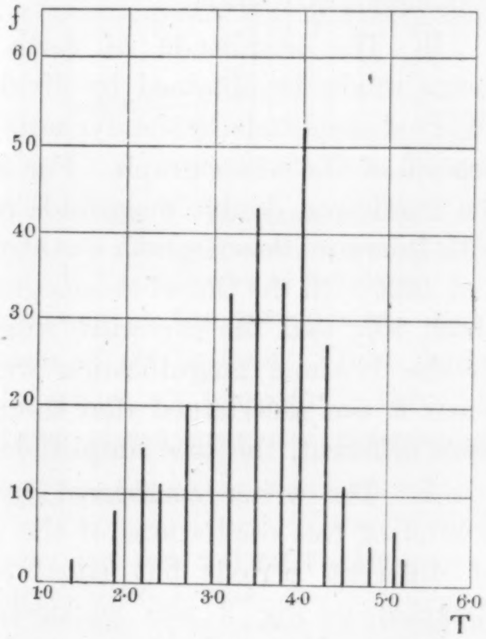

Fig. 4. Frequency-distribution of periods. Imamura Portable Seismograph.

that those would be affected with the resonance effect of the seismograph. Then the writer measured the frequency-distribution of periods on the seismogram recorded at the same time with a different type of seismograph, the period of which was longer. The instrument used for that purpose was an Omori Horizontal Pendulum Seismograph. Its instrumental constants were as follows: $M=60$ kg., $V=120$, $T_0=20{\cdot}3$ sec., and $v=1{\cdot}76$ (A portion of the seismogram is shown in Fig. 5.) The relative frequencies in this case are shown in Fig. 6. It might be proved that the frequency-distribution of periods was not affected with the resonance effect, for the distribution in Fig. 6 was not so different from that in Fig. 4.

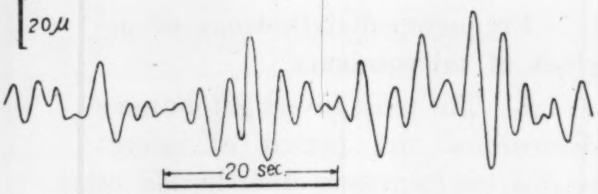

Fig. 5. Portion of record of microseisms. March 14, 1934. Omori Horizontal Pendulum Seismograph.

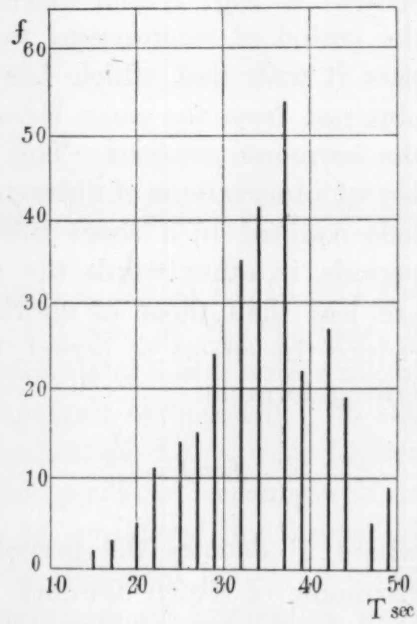

Fig. 6. Frequency-distribution of periods. Omori Horizontal Pendulum Seismograph.

5. The peak of the diagrams in Figs. 3, 4 and 5 obtained by three different methods coincided at the period of about 4 sec. But periods longer than 4 sec. are predominant in the case of the harmonic analysis, and contrary in the case of the frequency-distribution.

6. The amplitude of earth movements might be obtained by dividing the observed amplitude by the dynamic magnification of the seismograph. For instance the maximum double magnitude recorded with Imamura Seismograph was about 160μ and that with the Omori Seismograph was about 80μ, and the corrected magnitudes by the dynamic magnification were equal in both cases at about 80μ. Then it was ascertained that though the constants of the seismographs were different, the true amplitude might be obtained by the reduction.

7. The writer considered hypothetically that the microseisms are a kind of free oscillations of the ground caused by many disturbances of different periods but equal amplitudes, and the amplitude-period diagram in Fig. 3 was considered to suggest a resonance effect of the self-oscillation of the ground. Though the assumption of equal amplitude be not true, it might be not irrational to consider that microseisms are caused by a number of disturbances as F. Omori[4] and Dr. T. Matuzawa[5] have stated. The idea of the experiment carried out by Professors T. Terada and U. Nakaya[6] would be also similar to the above hypothesis, for in their experiment a physical pendulum was subjected to irregular succession of impacts, magnitudes of which were nearly equal.

Assuming the free period of the ground was 4 sec., the damping ratio v which fits the diagram was obtained. The values obtained lay between 1·07 and 1·22, so to make the calculation simple take $v=1{\cdot}1$ and 1·2, and the resonance curves were drawn on the diagram in Fig. 3. The relaxation times correspond to the above values of v are 48·3 and 25·3 sec. respectively. Then if the hypothesis is true, the free oscillations of the ground will die out in a minute.

8. The microseisms in Fig. 2 are like beats of two harmonic oscillations. Assuming beats, periods and maximum double amplitudes of the component oscillations were calculated. The obtained values were $T_1=3{\cdot}8$, $T_2=4{\cdot}3$ in sec., $2A_1$ (max.) $=16{\cdot}6\mu$ and $2A_2$(max.) $=14{\cdot}6\mu$ and the damping ratios equal in both cases as $v=1{\cdot}1$. The combined amplitudes of the two oscillations as shown in Fig. 7.

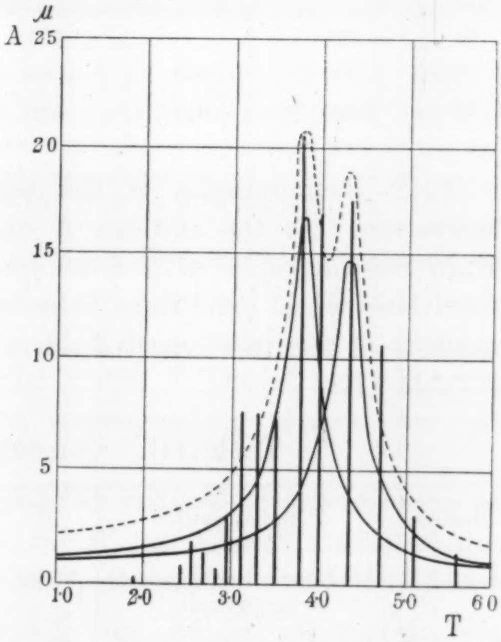

Fig. 7. Resonance curves. Dotted line shows sum of amplitudes in full lines.

Identification of phases of microseisms at several places.

9. F. Omori compared records of microseisms observed at Hongô and Hitotubasi in Tôkyô, about 4 km. distant with each other, and studied the phase relation of microseisms at the two places. But he could not identify corresponding phases of oscillations. From January to March in 1927, Mr. Nasu[8] and the writer set temporarily three horizontal pendulum seismographs at three places near the Seismological

---

[4] F. Omori, *Bull. Imp. Earthq. Inv. Comm.*, **5** (1911), 137.

[5] T. Matuzawa, *loc. cit.*, 263.

[6] T. Terada and U. Nakaya, *Bull. Earthq. Res. Inst.*, **5** (1928), 93~110.

[7] F. Omori, *Bull. Imp. Earthq. Inv. Comm.*, **3** (1909), 119~117.

[8] Mr. N. Nasu measured velocities of seismic waves caused by falling heavy masses from records at the four stations. N. Nasu, *Disin* (*Earthquake*), **1** (1929), 355~364, and *Jap. Journ. Astron. Geophys. Abstracts.*, **11** (1934), 48~49.

Institute of the University to study the phase relation of microseisms at different places. The positions of the temporary stations are shown in Fig. 8. The station A was in the compound of the First Higher School, B in the Seismological Institute, and C and D in the compound of the Hospital of the University. All these stations are on tertiary loam, and the distances between these stations are shown in the following table.

Table II. Distances between Stations. (m.)

	A	B	C
B	520	—	920
C	920	430	—
D	1090	610	520

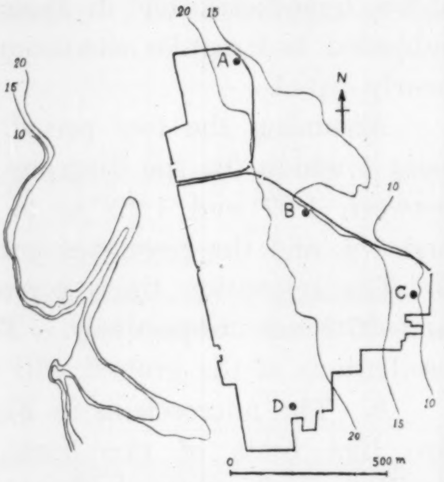

Fig. 8. Positions of stations.

Four seismographs of the same type were not available for the observation. At the stations A and B the Imamura Horizontal Pendulum Seismographs of N-S component were set, and at C and D the Omori Horizontal Pendulum Seismographs of the same component. The constants of the two types of seismograph were nearly similar as shown in Table III.

Table III. Constants of Seismographs.

Station	Instrument	M	V	T_0	v	Speed of drum
A and B	Imamura horiz. pend. seismograph	35 kg.	120	12·0 s.	2·4	60 mm./min.
C and D	Omori horiz. pend. seismograph	40	120	20·0	1·8	25

The time marks were put on the seismograms simultaneously at every minutes with electric current of a circuit which was closed by a chronometer being used in the Institute.

The records of microseisms were in tangle as shown in Fig. 1, and it was very hard to find corresponding minute marks on records. So the comparison of records of four stations was drawn only in several cases. The corresponding phases of microseisms with period about 4 sec. could be identified at the four stations as shown in Fig. 9. The ratios of mean amplitudes for 1 min. at the stations A, B, C and D reduced by static magnification were 1 : 1·3 : 1·4 : 1·3. But there is no similarity among the records of microseisms with period shorter than

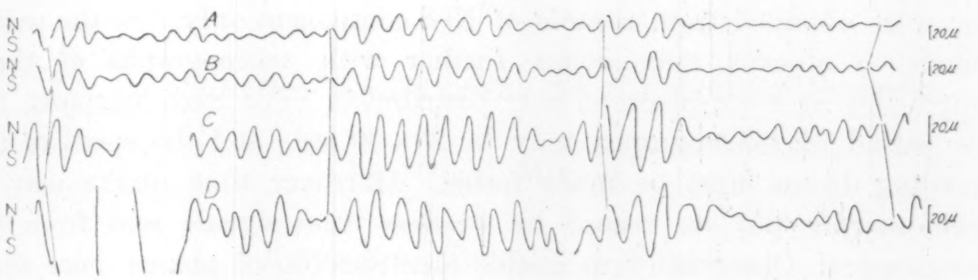

Fig. 9. Comparison of records of microseisms Q_1-type, Feb. 26–27, 1927. Thin lines indicate minute-marks at the same time. The records C and D are enlarged about twice to render time scale comparable.

4 sec. written at the four places for several minutes before the earthquake occurred at 18 h. 05 m. on Feb. 25, 1927 (Fig. 10).

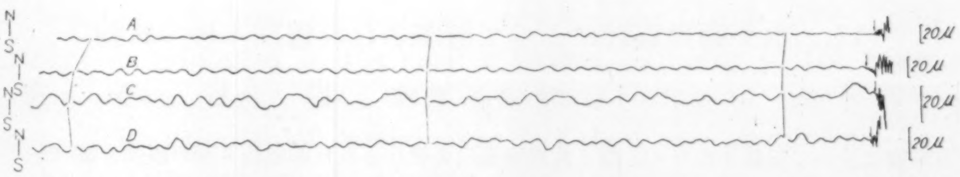

Fig 10. Comparison of records of microseisms of q-type. Arrows indicate the arrival time of the earthquake, $18^h\ 05^m\ 17{\cdot}9^s$ on Feb. 25, 1927.

10. After several weeks the three seismographs were removed to other places. Two of them were set at about 1500 m. S. of the Institute on northern and southern banks of a deep canal called Otyanomidu, and another was set at Hitotubasi where F. Omori had observed microseisms as mentioned before. But corresponding phases were not identified in this case.

11. The writer also in 1927 compared records of microseisms at two places in Kamakura about 50 km. S.S.W. of Tôkyô[9]. One of the two stations was on the ground of tertiary the other of alluvium, and the distance between them was about 1800 m. In this case also corresponding phases were not identified and it was found that periods of microseisms at the two places were different: at the former 4·0 and 2·1 sec. and at the latter about 3·4 sec.

Conclusion.

12. According to the above results, the writer considers that microseisms at Hongô with period about 4 sec. are a kind of free oscillations of a land-block which bounded by vertical planes of discontinuity. And the variation of amplitude like beats may be due to oscillations of different periods of the block in two modes.

But the observations are not sufficient to yield definite results, for

---

9) The result of the observation is not yet published.

they were obtained from records of N–S component only. So the writer intends to observe microseisms further with seismographs of three components at more places closely distributed. For such purposes the free period of seismographs may be 20∼30 sec., and the speed of the recording drums must be made faster. Moreover time marks may be more sharply put on record by wireless time signals sent from the Astronomical Observatory to enable identification of phases more accurate. Lastly the writer wishes that similar observations are carried out at many places, and furnish an explanation of the microseisms.

---

11. 水平動地震計によつて觀測された週期4秒の脈動

地震學教室 岸上冬彦

東京本鄕に於いて記錄された Q_1 型と大森博士に名付けられた週期約4秒の脈動を調べた.

第一に今村式簡單微動計の南北動の記象の一部（第2圖）を野口式調和分析器によつて分析した. その結果, 振動週期 3·8秒と 4·3秒に當るものの振幅が大きかつた(第3圖). 今迄には脈動の週期は, 色々の週期の觀測される回數の頻度分布から求められてゐたので, 比較の爲その方法を同じ記象紙について用ひた(第4圖). 此の地震計の週期は約6秒で脈動の週期が4秒であるから記象に共鳴の影響が入つてゐる恐れがあるので, 此の心配が理論上ない樣に週期の長い大森式地震計の記象で前の測定と殆ど同時刻の部分をとつて頻度分布を調べた(第6圖). 其の結果でも週期約4秒の所に頻度の極大が現はれた. 要するに方法を變へても得られた週期は等しかつた.

振幅と週期の關係を示す圖は共鳴曲線に似てゐるので, 地面が一つの4秒週期の振動體と假定し外から一樣な振幅で色々な週期の振動が與へられて地面が自己振動を起したものとしてその減衰率を求めて見た. その値は 1·1∼1·2 位になつた.

第二に昭和2年に第一高等學校の運動場の北隅（第8圖のA), 大學病院の小兒科の裏（C）と外來患者診療所の南側（D)との3個所に3個の120倍の水平振子地震計を臨時に据え, 地震學教室（B）にある同樣の器械と合計4個所に同一の時計から1分毎に合圖を送つて脈動の位相の比較觀測をした. 約4秒週期の脈動では同位相の振動が見出せた(第9圖)が, 短い週期のものでは判らなかつた(第10圖). 次にお茶の水の南北兩岸と一つ橋とに地震計を移して教室と記象の比較をしたが, 此の場合には位相の對應は出來なかつた.

以上の事實から初めの4個所は1個の地塊の上にあつて, 4秒週期の脈動はその地塊が自己振動を起すことによつて生ずると考へた.

以上は南北動のみの觀測の結果であるが, 今後東西動と上下動も含めた十分な觀測をして見たい. 終りに將來の脈動觀測に關する二三の計畫を記した.

12. *A Statistical Study of the Itô Earthquake Swarms.*

by Naomi MIYABE,

Earthquake Research Institute.

(Read Oct. 17, 1934.—Received Dec. 20, 1934.)

1. In 1930, a number of earthquakes were felt in regions around the Sagami Bay, the epicentres of which were found to be in the neighbourhood of Itô. During the period between February 14 and April 10 the number of these earthquakes reached to about 3700. They are regarded as belonging to the earlier swarm. In May of the same year, another swarm broke out; their epicentres being in nearly the same region. The number of earthquakes felt then was about 500.

As to these earthquake swarms, Prof. Imamura and his collaborators, and Mr. K. Sagisaka of the Central Meteorological Observatory have already pointed out that, in the beginning of the period of the earlier swarm,[1] earthquakes frequently occur at ebb tide. A number of authors have also argued[2] that the tidal loads, tide generating forces, atmospheric pressure and its gradients are more or less correlated with earthquake frequency. These factors are of course important as secondary causes[3] of earthquakes.

The writer, in this paper, discusses the simple and multiple correlations between the fluctuations in daily frequencies of the Ito earthquake swarms and the tidal range, atmospheric pressure and their derivatives with regard to time and space.

2. In studying the correlations between fluctuations in the daily earthquake frequencies and secondary causes, it may be necessary to eliminate the effect of the primary cause. As this however is almost impossible, since we have little knowledge of the primary cause, the fluctuations in the present investigation are calculated on simple assumptions, though it is impossible to know whether such assumptions are appropriate or not.

---

[1] A. IMAMURA and others, *Disin*, **2** (1930), (in Japanese).
K. SAGISAKA, *Kensin-Zihô*, **5** (1930), 131～153, (in Japanese).

[2] F. OMORI, *Rep. Imp. Earthq. Inv. Comm.*, No. 68A (1910), 21～29.
K. HONDA, *Proc. Phys.-Math. Soc. Tokyo*, [ii], **2** (1903～1906), 63～73.
T. TERADA, *Journ. Met. Soc.*, **28** (1909), 1, (in Japanese).
S. T. NAKAMURA, *Jap. Jaurn. Astr. Geophys.*, **3** (1925), 115; **4** (1926), 139.
S. YAMAGUTI, *Bull. Earthq. Res. Inst.*, **8** (1930), 393.
D.M.Y. SOMMERVILL, *M.N.R.A.S., Geophys. Suppl.*, **3** (1932), 1.

[3] In our ignorance of the mechanism of earthquakes, it may be needless to speak of "secondary" and "primary" causes. I use the term "secondary cause," following general usage, meaning the external factors governing the occurrence of earthquakes.

Firstly, the fluctuations in the daily earthquake frequencies are calculated as deviations in the daily frequencies from the mean values, that is,

$$N-\overline{N}.$$

This assumption indicates that the effect of the primary cause is constant throughout the active period of the earthquake swarms.

A glance at the distribution of the daily earthquake frequencies with respect to time shows the seismic activity to have gradually increased to a certain maximum after which it died out. This suggests that the distribution of frequencies may be expressed like a probability curve. Secondly, therefore, we calculate the fluctuations

$$N-N_c,$$

where N is the actual frequency of the earthquakes and N_c is given in the from

$$N_c=N_0e^{-h2(x-x_m)^2},$$

where x is the number of days counted from February 14 for the earlier swarm and from May 1 for the later swarm.

Constants N_0, h^2, x_m in the above expression have been determined by the method of least squares to be

$$N_0=160,\ h^2=0{\cdot}0065,\ x_m=24$$

for the earlier swarm, and

$$N_0=70,\ h^2=0{\cdot}06,\ x_m=12$$

for the later swarm. Deviations in the actual daily earthquake frequencies from those calculated $N-N_c$ and are given in Table I.

Table Ia. N and $N-N_c$. for earlier swarm.

Date	N	$N-N_c$	Date	N	$N-N_c$
Feb. 14, 1930	8	3	Feb. 17, 1930	12	9
15	6	5	18	22	18
16	1	−1	19	6	1

(to be continued.)

Table Ia. (*continued.*)

Date	N	$N-N_c$	Date	N	$N-N_c$
Feb. 20, 1930	47	40	March 17, 1930	112	−31
21	77	67	18	67	−66
22	88	76	19	82	−37
23	40	24	20	46	−63
24	60	40	21	54	−44
25	21	−5	22	109	22
26	12	−20	23	44	−31
27	4	−35	24	114	49
28	40	−6	25	99	44
March 1	138	83	26	93	47
2	40	−25	27	9	−30
3	143	68	28	1	−31
4	100	13	29	133	107
5	74	−22	30	102	82
6	144	35	31	79	63
7	117	−2	April 1	48	36
8	151	8	2	6	−4
9	209	66	3	2	−5
10	98	−53	4	72	67
11	162	4	5	3	−1
12	147	−16	6	2	−1
13	115	−52	7	62	60
14	112	−53	8	2	1
15	55	−103	9	23	23
16	51	−100	10	5	5

Table Ib. N and $N-N_c$ for later swarm.

Date	N	$N-N_c$	Date	N	$N-N_c$
May 1, 1930	1	1	9	101	59
2	2	2	10	43	−13
3	5	4	11	17	−49
4	4	2	12	17	−53
5	3	−2	13	26	−40
6	6	−3	14	51	−5
7	4	−13	15	49	7
8	47	19	16	15	−13

(*to be continued.*)

Table Ib. (*continued.*)

Date	N	$N-N_c$	Date	N	$N-N_c$
May 17, 1930	44	27	May 25, 1930	3	3
18	46	37	26	8	8
19	9	4	27	1	1
20	1	−1	28	2	2
21	1	0	29	0	0
22	25	25	30	0	0
23	4	4	31	4	4
24	3	3			

Needless to say, several other assumptions may be possible besides those mentioned above for eliminating the fluctuations in seismic activity due to the primary cause during certain decades.

3. In the present study, the coefficients have been calculated of the correlations of the fluctuations in earthquake frequencies with the following elements:

(i) Tidal range. The amplitudes of daily variations in the sea level, that is, the tidal range, vary with a period of about 15 days. The data employed in the present study are not the actual tidal range, but those calculated on the assumption that the tidal range varies from spring to nip with a period of 15 days in such a manner as may be expressed by a sinusoidal function of time (number of days).

The values of the tidal ranges employed in the present study are referred to the data of spring and nip ranges at Misaki,[4] the fluctuations of which are shown in Table II together with those of the other elements.

The values of spring and nip ranges at Misaki are approximately equal to those at Itô, the region where the earthquake swarms under consideration occurred.

(ii) Rate of change in the tidal range. The rate of change in the tidal range, that is, the differences in tidal ranges on successive days may be correlated with the fluctuation in the daily earthquake frequencies.

(iii) It is to be regretted that there are no data covering atmospheric pressure at Itô. In the circumstance, the values of the atmospheric pressures, P, as observed at Numadu, at 6 a.m. every day, are used.[5] Numadu is the nearest station to the region of the earthquake swarms. As will be referred to later, earthquakes seem to be more strongly correlated with the pressure gradients than with mere pressure.

---

[4] The data from *Bull. Hydr. Depart., Imp. Jap. Navy*, **7** (1399).

[5] The data from *weather charts*.

There may however be no essential difference between pressure and pressure gradients, so long as they are taken as factors for correlation with fluctuations in the daily earthquake frequencies, as there may be some characteristic features in the mode of distribution of the atmospheric pressure.

(iv) Rate of change in atmospheric pressure, $\frac{\partial P}{\partial t}$. There may be several cases in which earthquake occurrence may be affected by certain dynamical properties of the atmospheric pressure. The writer therefore took as one of the elements the differences in atmospheric pressures on successive days.

(v) Atmospheric pressures gradients. As already discussed by Prof. Terada,[6] earthquake occurrence may be affected to some extent by the pressure gradients in the region where the earthquakes under consideration occurred. The writer therefore calculated the gradients of atmospheric pressure $\frac{\partial P}{\partial x}$ and $\frac{\partial P}{\partial y}$ by combining the data observed at Kôhu and Yokohama with those of Numadu. As the distance between Kôhu and Numadu and that between Yokohama and Numadu are approximately equal, and as moreover the lines connecting these two sets of stations are approximately perpendicular to each other (see Fig. 1),

(pressure at Yokohama)—(pressure at Numadu)

are regarded as $\frac{\partial P}{\partial x}$, and

(pressure at Kôhu)—(pressure at Numadu)

are regarded as $\frac{\partial P}{\partial y}$.

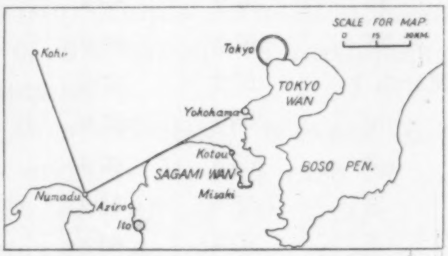

Fig. 1. Map showing the localities of stations.

(vi) Rate of pressure gradients. As referred to in (iv) as for pressure, the variation in pressure gradients may sometimes be taken into consideration as one of the elements that are related in some way or other to the occurrence of earthquakes.

The numerical values of atmopheric pressures observed at Numadu, Yokohama and Kôhu are given in Table II.

The modes of variation of these elements are compared with those of the fluctuations in the daily earthquakes frequencies in Fig. 2.

---

[6] T. Terada, *loc. cit.*, 2).

Table IIa. Atmospheric pressures at Numadu, Yokohama and Kôhu during the period of former swarm.

Date	Numadu	Yokohama	Kôhu	Date	Numadu	Yokohama	Kôhu
Feb. 14, 1930	767·4^{mm}	767·2^{mm}	769·9^{mm}	March 14	53·5^{mm}	52·4^{mm}	54·1^{mm}
15	68·1	68·7	69·9	15	57·7	57·3	58·2
16	65·4	66·1	66·1	16	56·8	57·1	58·6
17	59·8	60·2	61·7	17	62·9	63·0	64·4
18	68·9	69·3	71·2	18	59·0	59·2	61·0
19	69·2	69·7	69·8	19	60·6	60·7	61·2
20	64·3	64·4	65·5	20	61·7	62·8	63·1
21	69·2	69·5	70·3	21	63·2	63·5	65·4
22	67·1	67·4	68·5	22	36·3	67·3	67·9
23	66·5	67·0	67·4	23	66·0	66·8	68·5
24	56·0	55·7	56·2	24	68·3	68·4	70·0
25	53·9	54·2	54·4	25	66·3	67·5	67·2
26	59·5	59·5	60·6	26	67·4	67·3	68·1
27	58·2	58·8	58·9	27	70·4	71·3	70·7
28	67·8	69·0	68·3	28	68·1	67·9	68·2
March 1	67·2	67·3	68·4	29	56·4	55·3	57·1
2	65·7	65·9	66·9	30	59·0	60·0	60·1
3	63·5	63·9	64·4	31	65·3	66·2	66·4
4	55·6	56·2	57·1	April 1	—	—	—
5	65·3	66·3	66·3	2	—	—	—
6	66·2	68·2	68·1	3	59·1	59·4	60·8
7	75·0	75·8	74·9	4	64·0	64·7	66·0
8	67·5	68·8	70·6	5	64·3	64·8	65·7
9	62·5	62·7	63·7	6	63·6	64·4	64·8
10	62·7	63·0	64·3	7	61·6	61·0	61·8
11	67·1	67·8	69·6	8	61·2	62·2	62·5
12	72·8	73·5	75·1	9	55·3	55·2	55·9
13	66·1	66·8	67·5	10	61·7	62·1	61·8

Table IIb. Atmospheric pressures at Numadu, Yokohama and Kôhu during the period of the later swarm.

Date	Numadu	Yokohama	Kôhu	Date	Numadu	Yokohama	Kôhu
May 1	766·2^{mm}	767·0^{mm}	766·6^{mm}	May 4	65·7^{mm}	66·0^{mm}	67·5^{mm}
2	65·5	66·5	66·9	5	63·5	63·4	63·6
3	60·0	60·1	61·0	6	54·6	55·6	54·1

(to be continued.)

Table IIb. (*continued.*)

Date	Numadu	Yokohama	Kôhu	Date	Numadu	Yokohama	Kôhu
May 7	57·7^{mm}	57·6^{mm}	58·9^{mm}	May 20	50·2^{mm}	48·9^{mm}	51·9^{mm}
8	65·4	65·0	66·6	21	56·2	57·0	56·5
9	62·2	61·3	63·7	22	56·5	55·7	56·9
10	50·5	50·0	51·2	23	54·3	53·8	55·4
11	57·5	58·1	58·2	24	62·3	62.8	62·8
12	59·9	60·9	60·8	25	61·9	62·2	62·7
13	59·9	61·0	60·2	26	64·9	65·0	66·0
14	64·8	65·7	65·5	27	64·8	65·4	65·7
15	68·2	67·7	68·7	28	57·3	58·3	59·6
16	65·6	65·5	66·5	29	57·3	57·8	58·3
17	59·5	59·9	61·0	30	58·9	58·5	59·4
18	64·6	65·5	65·5	31	59·7	59·4	61·8
19	66·2	66·1	67·3				

4. For each separate earthquake swarm, simple correlation coefficients are first calculated for both cases of fluctuations in earthquakes frequencies calculated on different assumptions.

The simple correlation coefficients thus calculated between each of the two cases of fluctuations, $N-N_c$ and $N-\overline{N}$, and each of the fluctuations of the elements, R, $\frac{\partial R}{\partial t}$, P, $\frac{\partial P}{\partial t}$, $\frac{\partial P}{\partial x}$, $\frac{\partial P}{\partial y}$, $\frac{\partial}{\partial t}\frac{\partial P}{\partial x}$, $\frac{\partial}{\partial t}\frac{\partial P}{\partial y}$ are given in Table III.

Table III. Simple correlation coefficients
for former swarm.

	R	$\frac{\partial R}{\partial t}$	P	$\frac{\partial P}{\partial t}$	$\frac{\partial P}{\partial x}$	$\frac{\partial P}{\partial y}$	$\frac{\partial}{\partial t}\frac{\partial P}{\partial x}$	$\frac{\partial}{\partial t}\frac{\partial P}{\partial y}$
$N-N_c$	−0·27	0·04	0·15	0·10	−0·02	−0·03	0·17	−0·15
$N-\overline{N}$	−0·43	0·34	0·33	0·22	0·28	0·67	0·41	−0·05

Of the correlation coefficients given in the foregoing table, that between $N-N_c$ and $R-\overline{R}$ is the strongest in the case of fluctuations $N-N_c$. The other coefficients, except for those between $N-N_c$ and $(P-\overline{P})$, $\left(\frac{\partial}{\partial t}\frac{\partial P}{\partial x}-\overline{\frac{\partial}{\partial x}\frac{\partial P}{\partial x}}\right)$, $\left(\frac{\partial}{\partial t}\frac{\partial P}{\partial y}-\overline{\frac{\partial}{\partial t}\frac{\partial P}{\partial y}}\right)$, which are of the order of 0·15 or so, are very small compared with those just mentioned.

As to the correlation coefficients between $N-\overline{N}$ and the other elements, we notice that the numerical values of the coefficients are generally greater than those in the case of the correlation of $N-N_c$

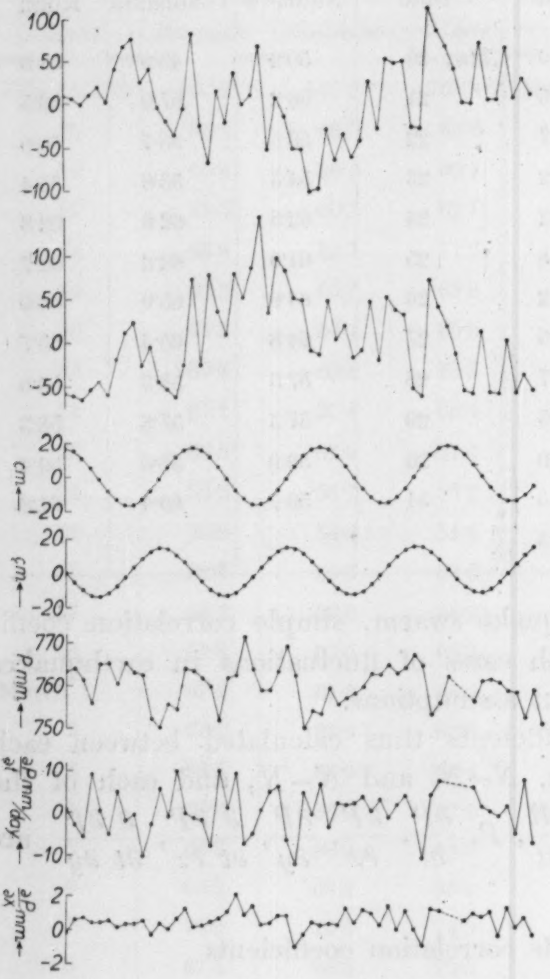

Fig. 2a. Variation in frequency of earthquakes and other elements, *R*, *P*, etc., during the period Feb. 14~Apr. 10, 1930.

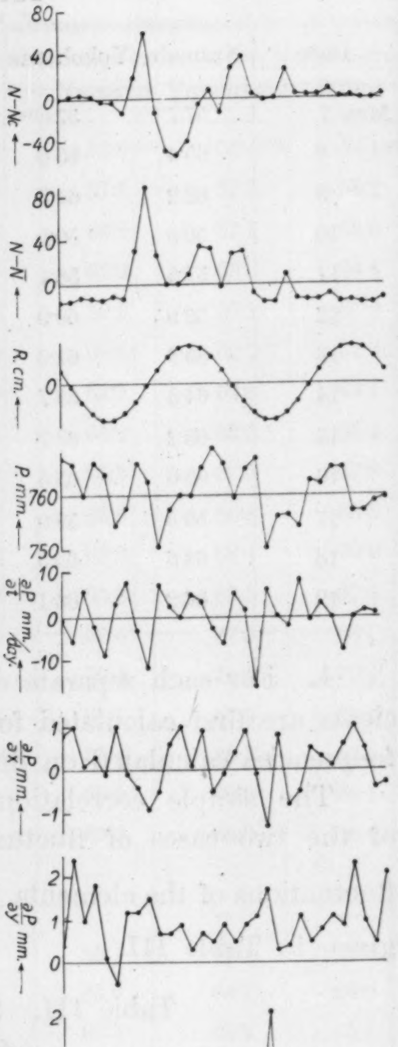

Fig. 2b. Variation in frequency of earthquakes and other elements, *R*, *P*, etc., during the period May 1~May 30, 1930.

with the other elements. Although the correlation coefficient between $N-\overline{N}$ and $\left(\frac{\partial P}{\partial y}-\overline{\frac{\partial P}{\partial y}}\right)$ in particular is exceedingly large, the coefficients between $N-\overline{N}$ and $\left(\frac{\partial}{\partial t}\frac{\partial P}{\partial y}-\overline{\frac{\partial}{\partial t}\frac{\partial P}{\partial y}}\right)$ are very small.

In calculating the coefficients of multiple correlations between $N-N_c$ or $N-\overline{N}$ and a certain set of elements R, P, etc., elements having smaller correlation coefficients with $N-N_c$ or $N-\overline{N}$ are disregarded, that is in the case of $N-N_c$, the multiple correlation coefficients are calculated with regard to sets of elements ; (i) R, P, $\frac{\partial}{\partial t}\frac{\partial P}{\partial t}$, $\frac{\partial}{\partial t}\frac{\partial P}{\partial y}$, (ii) R, P, $\frac{\partial}{\partial t}\frac{\partial P}{\partial x}$, and (iii) R, P, respectively, while in the case of $N-\overline{N}$, the multiple correlation coefficients are calculated with regard to sets of elements ; (i) R, $\frac{\partial R}{\partial t}$, P, $\frac{\partial P}{\partial x}$, $\frac{\partial P}{\partial y}$, $\frac{\partial}{\partial t}\frac{\partial P}{\partial x}$, and (ii) R, $\frac{\partial P}{\partial y}$, $\frac{\partial}{\partial t}\frac{\partial P}{\partial x}$. The multiple correlation coefficients thus calculated are given in Table IV, from which it will be seen that the multiple correlation is stronger in the case of $N-\overline{N}$, to the set elements R, $\frac{\partial P}{\partial y}$, $\frac{\partial}{\partial t}\frac{\partial P}{\partial x}$, while, in the case of $N-N_c$, to the set of elements R, P.

Table IV. Multiple correlation coefficients
for former swarm.

Case	Multiple correlation coefficient
I i) $N-N_c$: R, P, $\frac{\partial}{\partial t}\frac{\partial P}{\partial x}$, $\frac{\partial}{\partial t}\frac{\partial P}{\partial y}$	0·18
ii) 〃 : R, P,	0·26
iii) 〃 : R, P, $\frac{\partial}{\partial t}\frac{\partial P}{\partial x}$	0·06
II i) $N-\overline{N}$: R, $\frac{\partial P}{\partial y}$, $\frac{\partial}{\partial t}\frac{\partial R}{\partial x}$	0·66
ii) 〃 : R, $\frac{\partial R}{\partial t}$, P, $\frac{\partial P}{\partial x}$, $\frac{\partial P}{\partial y}$, $\frac{\partial}{\partial t}\frac{\partial P}{\partial x}$	0·07

As to the May swarm of earthquakes, the simple and multiple correlation coefficients are calculated quite similarly. In this case however the factor $\frac{\partial R}{\partial t}$ is disregarded. The numerical values of the coefficients of simple and multiple correlations are given in Tables V and VI respectively.

Table V. Simple correlation coefficients for later swarm.

	R	P	$\frac{\partial P}{\partial t}$	$\frac{\partial P}{\partial x}$	$\frac{\partial P}{\partial y}$	$\frac{\partial}{\partial t}\frac{\partial P}{\partial x}$	$\frac{\partial}{\partial t}\frac{\partial P}{\partial y}$
$N-N_c$	−0·37	0·07	−0·30	−0·30	0·13	−0·05	0·004
$N-N$	0·08	0·02	0·13	−0·28	0·02	0·04	−0·06

Table VI. Multiple correlation coefficients
for later swarm.

Case	Multiple Correlation Coefficient
I i) $N-N_c$: $R, \frac{\partial P}{\partial t}, \frac{\partial P}{\partial x}, \frac{\partial P}{\partial y}$	0·32
ii) 〃 : $R, \frac{\partial P}{\partial t}, \frac{\partial P}{\partial x}$	0·30
II $N-\overline{N}$: $\frac{\partial P}{\partial t}, \frac{\partial P}{\partial x}$	0·31

In these cases, the multiple correlation coefficients are nearly the same in each case; having an approximate value of 0·3.

5. Since, as just stated, $N-N_c$ or $N-\overline{N}$ is correlated with the elements or sets of elements R, P and their derivatives, any value of $N-N_c$ or $N-\overline{N}$ may be expressed as a function of the corresponding values of the elements, that is, we can form an equation of a regression plane, expressed as

$$(N-N_c) \text{ or } (N-\overline{N})=b_{12}(R-\overline{R})+b_{13}\left(\frac{\partial R}{\partial t}-\overline{\frac{\partial R}{\partial t}}\right)$$
$$+b_{14}(P-\overline{P})+\dots+b_{19}\left(\frac{\partial}{\partial t}\frac{\partial P}{\partial y}-\overline{\frac{\partial}{\partial t}\frac{\partial P}{\partial y}}\right).$$

The factors $b_{12}, b_{13}, \dots b_{19}$ in the above equation can be determined in terms of simple correlation coefficients r_{1p} by using the relation

$$b_{1p}=-\frac{\Delta_{1p}}{\Delta_{11}}\frac{\sigma_1}{\sigma_p}, \quad (p=2, 3 \dots 9)$$

where Δ_{11} and Δ_{1p} are minor determinants of Δ[7] and σ_1, σ_p are standard deviations. The suffixes 1, 2, ...9 of b, r, Δ, and σ designate $N-N_c$ or $N-\overline{N}$ and the elements $(R-\overline{R})$, $\left(\frac{\partial R}{\partial t}-\overline{\frac{\partial R}{\partial t}}\right)$, etc., respectively.

The equations of regression planes thus determined for the cases in which the multiple correlation coefficients are greater than 0·1 are

(A) Earlier Swarm (Feb. 14—Apr. 10, 1930)

I. i) $N-N_c$: $R, P, \frac{\partial}{\partial t}\frac{\partial P}{\partial x}, \frac{\partial}{\partial t}\frac{\partial P}{\partial y}$;

$$N-N_c=-1{\cdot}2(R-\overline{R})+0{\cdot}6(P-\overline{P})$$

---

[7] The determinant Δ is given in the form

$$\Delta=\begin{vmatrix} r_{11} & r_{12} & \dots & r_{19} \\ r_{21} & r_{22} & \dots & r_{29} \\ \vdots & & & \\ r_{91} & \dots & \dots & r_{99} \end{vmatrix}, \quad \begin{matrix} r_{12}=r_{21},\ r_{23}=r_{32},\ \dots, \\ r_{11}=r_{22}=r_{33}=\dots r_{99}=1. \end{matrix}$$

$$+4.7\left(\frac{\partial}{\partial t}\frac{\partial P}{\partial x}-\overline{\frac{\partial}{\partial t}\frac{\partial P}{\partial x}}\right)-6{\cdot}6\left(\frac{\partial}{\partial t}\frac{\partial P}{\partial y}-\overline{\frac{\partial}{\partial t}\frac{\partial P}{\partial y}}\right).$$

ii) $N-N_c$: $R,\ P$;

$$N-N_c=-1{\cdot}0(R-\overline{R})+2{\cdot}1(P-\overline{P}).$$

II. $N-\overline{N}$: $R,\ \dfrac{\partial P}{\partial y},\ \dfrac{\partial}{\partial t}\dfrac{\partial P}{\partial x}$;

$$N-\overline{N}=-0{\cdot}6(R-\overline{R})$$
$$+16{\cdot}5\left(\frac{\partial P}{\partial y}-\overline{\frac{\partial P}{\partial y}}\right)+12{\cdot}3\left(\frac{\partial}{\partial t}\frac{\partial P}{\partial x}-\overline{\frac{\partial}{\partial t}\frac{\partial P}{\partial x}}\right)$$

(B) Later Swarm (May 1—May 31, 1930)

I. i) $N-N_c$: $R,\ \dfrac{\partial P}{\partial t},\ \dfrac{\partial P}{\partial x},\ \dfrac{\partial P}{\partial y}$;

$$N-N_c=-0{\cdot}5(R-\overline{R})$$
$$-0{\cdot}1\left(\frac{\partial P}{\partial t}-\overline{\frac{\partial P}{\partial t}}\right)-1{\cdot}0\left(\frac{\partial P}{\partial t}-\overline{\frac{\partial P}{\partial x}}\right)+2{\cdot}8\left(\frac{\partial P}{\partial y}-\overline{\frac{\partial P}{\partial y}}\right).$$

ii) $N-N_c$: $R,\ \dfrac{\partial P}{\partial t},\ \dfrac{\partial P}{\partial x}$;

$$N-N_c=-0{\cdot}5(R-\overline{R})-1{\cdot}1\left(\frac{\partial P}{\partial t}-\overline{\frac{\partial P}{\partial t}}\right)-6{\cdot}4\left(\frac{\partial P}{\partial x}-\overline{\frac{\partial P}{\partial x}}\right).$$

II. $N-\overline{N}$: $\dfrac{\partial P}{\partial t},\ \dfrac{\partial P}{\partial x}$;

$$N-\overline{N}=-1{\cdot}1\left(\frac{\partial P}{\partial t}-\overline{\frac{\partial P}{\partial t}}\right)+4{\cdot}9\left(\frac{\partial P}{\partial x}-\overline{\frac{\partial P}{\partial x}}\right).$$

With these equations we can calculate the theoretical values of $N-N_c$ or $N-\overline{N}$ by substituting the given values of $(R-\overline{R})$, $\left(\dfrac{\partial R}{\partial t}-\overline{\dfrac{\partial R}{\partial t}}\right)$, $(P-\overline{P})$, $\left(\dfrac{\partial P}{\partial t}-\overline{\dfrac{\partial P}{\partial t}}\right)$, $\left(\dfrac{\partial P}{\partial x}-\overline{\dfrac{\partial P}{\partial x}}\right)$ etc.

The theoretical values of $N-N_c$ or $N-\overline{N}$, calculated by the equations of regression planes given above, and the deviations in the actual values of $N-N_c$ or $N-\overline{N}$ from those theoretically calculated are shown in Table VII.

Table VIIa. $(N-N_c)_{\text{obs.}}-(N-N_c)_{\text{cal.}}$ and $(N-\overline{N})_{\text{obs.}}-(N-\overline{N})_{\text{cal.}}$ for various cases of former swarm.

Case / Date	I, i)	I, ii)	II	Case / Date	I, i)	I, ii)	II
Feb. 14	19	19	−79	Feb. 16	22	9	−46
15	14	14	−62	17	16	25	−61

(to be continued.)

Table VIIa. *(continued.)*

Case / Date	I, i)	I, ii)	II	Case / Date	I, i)	I, ii)	II
Feb. 18	2	8	−64	March 16	−76	−66	−12
19	− 6	−17	−50	17	− 8	−11	49
20	23	28	−29	18	−45	−42	− 4
21	47	42	3	19	−41	−23	27
22	58	55	7	20	−53	−58	−14
23	7	7	−19	21	−51	−49	−42
24	35	50	− 2	22	2	6	31
25	6	17	−30	23	−41	−49	−44
26	−15	− 3	−56	24	−17	26	17
27	−21	−10	−54	25	−16	28	47
28	22	8	7	26	29	33	17
March 1	102	95	16	27	−32	−43	−27
2	− 9	−11	−19	28	−23	−32	−32
3	−50	−54	87	29	120	+136	56
4	20	38	28	30	108	110	58
5	−21	−25	23	31	—	—	—
6	17	24	78	Apr. 1	—	—	—
7	− 5	−37	59	2	—	—	—
8	−21	−13	58	3	5	13	−74
9	51	55	132	4	63	67	− 5
10	−63	−62	13	5	−14	6	−75
11	− 9	− 9	10	6	−13	−12	−55
12	−28	−34	62	7	43	51	−16
13	−43	−49	71	8	−15	− 7	−62
14	−36	−19	66	9	7	30	−47
15	−74	−73	2	10	4	3	−35

Table VIIb. $(N-N_c)_{\mathrm{obs.}}-(N-N_c)_{\mathrm{cal.}}$ and $(N-\overline{N})_{\mathrm{obs.}}-(N-\overline{N})_{\mathrm{cal.}}$ for various cases of later swarms

Case / Date	I, i)	I, ii)	II	Case / Date	I, i)	I, ii)	II
May 1	− 6	− 6	−12	May 6	−15	− 2	−11
2	− 2	0	− 5	7	−19	− 9	−23
3	1	− 6	−19	8	14	7	30
4	− 6	− 6	−10	9	56	39	95
5	− 8	−21	− 6	10	− 9	− 7	15

(to be continued.)

Table VIIb. (*continued.*)

Case / Date	I, i)	I, ii)	II	Case / Date	I, i)	I, ii)	II
May 11	−41	−38	− 1	May 21	− 3	− 2	−14
12	−43	−40	4	22	22	12	5
13	−28	−26	3	23	3	8	−25
14	5	12	33	24	8	8	−12
15	0	6	31	25	10	13	−17
16	−10	−18	3	26	16	16	−10
17	29	34	22	27	10	4	− 6
18	34	39	30	28	8	15	−11
19	− 4	−22	8	29	7	10	−18
20	−11	−12	30	30	4	0	−21

6. The deviations in actual values of $N-N_c$ or $N-\bar{N}$ from the calculated values given in Table VII are plotted in Fig. 3.

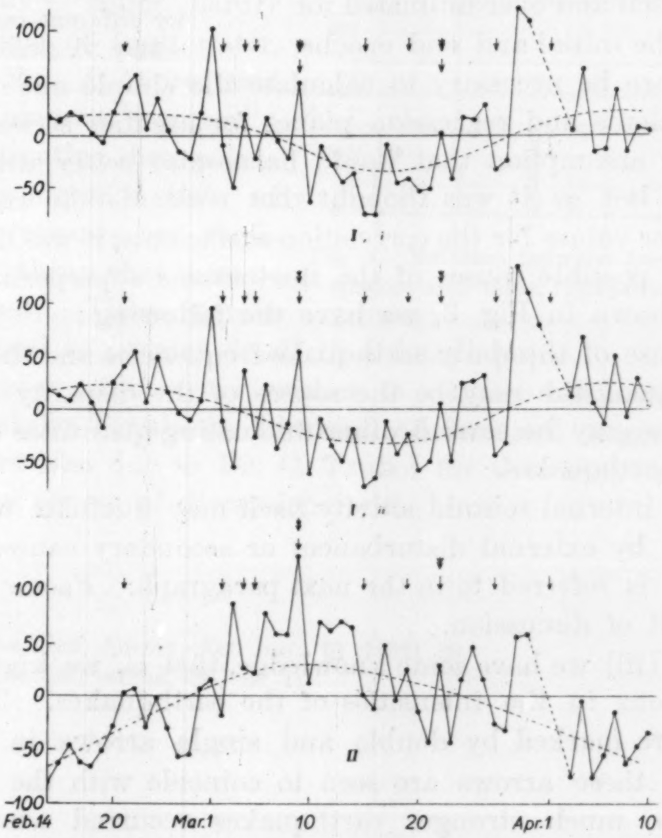

Fig. 3a. Differences between observed and calculated frequencies of earthquakes for different cases. (Feb. 14∼Apr. 10, 1930).

In the curves shown in Fig. 3, we notice general trends as denoted by the dotted lines, superposed by fluctuations having considerable amplitudes.

From the general trends of the curves in Fig. 3, it may be suggested that the assumption on which we have calculated the effects of the primary cause were not satisfactory, that is, $N_{\mathrm{cal.}}$ does not fit in well with the general mode of the variation of actual N. To be more concise, N_c is over-estimated for the values of the middle epoch and under-estimated for the values of adjacent epochs during the period of activity of the earthquakes swarms, while $\overline{N}$ is under-estimated for the values of the middle epoch and over-estimated for the values of the initial and end epochs. It may therefore be necessary to calculate the simple and multiple correlation coefficients and regression planes for another series of N_c based on some other assumption that would harmonize better with the actual values of N, but as it was thought that recalculation would not give better or greater values for the correlation coefficients, it was not attempted.

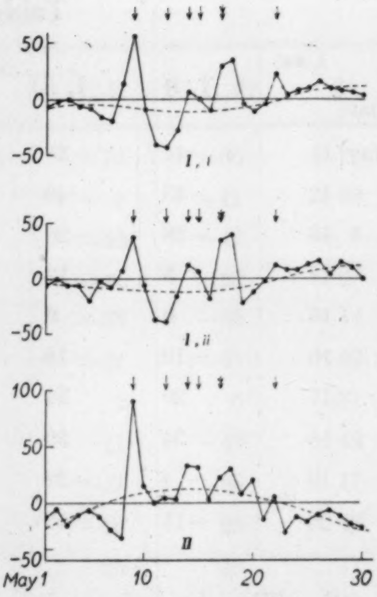

Fig. 3b. Differences between observed and calculated frequencies of earthquakes for different cases. (May 1 ~May 30, 1930).

As to the possible causes of the fluctuations superposing the deviations curves shown in Fig. 3, we have the following:

(i) The use of the daily earthquake frequencies and the fluctuations in the other quantities may be the source of the disparity.

(ii) There may be several other fluctuating quantities that correlate with that of earthquakes.

(iii) The internal seismic activity itself may fluctuate without being affected either by external disturbances or secondary causes.

Factor (i) is referred to in the next paragraph. Factor (ii) however does not admit of discussion.

Of factor (iii) we have some knowledge, that is, we know that there were fluctuations in the intensities of the earthquakes. The stronger earthquakes are marked by double and single arrows in Fig. 3. In several cases, these arrows are seen to coincide with the peaks of the curves, that is, much stronger earthquakes occurred when the actual earthquake frequencies were greater than those estimated from external or secondary causes. This fact does not contradict our experience that strong earthquakes are generally accompanied by a number of smaller shocks. There may besides be another cause for the fluctuation in seismic activity, such as that discussed by Prof. Terada[8] in connection with fluctuations in frequencies of the fall of camelia flowers (Camelia Japonica).

7. As a probable source of disparity between the calculated and the actual valus of $N-N_c$ or $N-\overline{N}$, as just pointed out, may be mentioned the improper selection of data of the factors that were regarded as correlated with the fluctuations in the daily earthquakes frequencies.

In the present study, for instance, the fluctuations in tidal range were used as data of the tidal forces that may be related to the fluctuations in earthquake frequency. This seems to be an example of improperly selected data, for earthquake frequency was proved to be more closely correlated with the heights of the sea level, that is to say, earthquakes occurred most frequently at the time of low water, they being hardly felt at the time of high water, as shown in Fig. 4. reproduced from Prof. Imamura's paper.[9]

For investigating these points however more detailed data of atmospheric pressures are required, the very thing that is wanting at present. These points will be discussed in greater detail in a future paper.

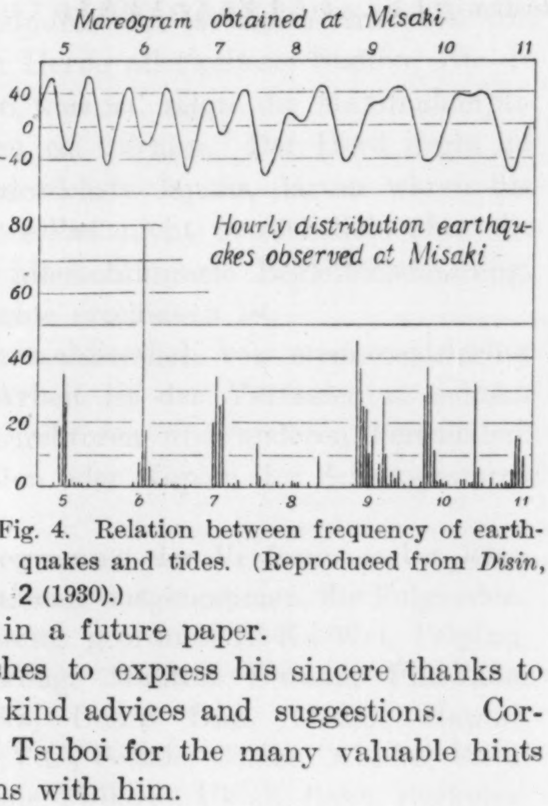

Fig. 4. Relation between frequency of earthquakes and tides. (Reproduced from *Disin*, 2 (1930).)

In conclusion, the writer wishes to express his sincere thanks to Professor Torahiko Terada for his kind advices and suggestions. Cordial thanks are also due to Dr. C. Tsuboi for the many valuable hints received in the course of discussions with him.

---

[8] T. **Terada**, *Bull. Earthq. Res. Inst.*, 10 (1932), 29.

[9] A. **Imamura** and others, *loc., cit.* 1).

12. 伊東地震群に關する統計

地震研究所 宮部直巳

昭和 5 年に頻發した伊東附近の地震は，2 月 14 日乃至 4 月 10 日と 5 月 1 日乃至 5 月 31 日の 2 群に分けることが出來，その地震頻數が，潮汐と密接な關係のあることが，從來指摘されてゐる．又，別の地震群について，氣壓の頻度などと相關々係のあることが知られてゐる．

筆者は，潮汐や氣壓やそれ等の導來函數と伊東地震群の日々の頻數との間の單並びに重相關々係を調べ，地震の頻數が，それ等の要素を變數とする一次函數で表はされるとした場合の係數を統計的に定めた． この式から豫期される頻數と實際の頻數とを比較してみると，尙多少の剩餘がある．是等の剩餘は，data の取り方の不適當なことから生ずるものと，地震活動それ自身の消長に fluctuation のあることから生ずるものとが含まれてゐると考へられる．

13. Seismometrische Untersuchungen des Erdbebens vom 2. März 1933.

I. Bestimmung des Herdes.

Von Takeo MATUZAWA,

Institut für Erdbebenforschung.

(Vorgelegt 18. Dez. 1934.—Eingegangen 20. Dez. 1934.)

1. Vom seismometrischen Standpunkt aus ist dieses Erdbeben von ausserordentlicher Grösse. Die vom Herde allerweiteste Station, Rio de Janeiro, die nämlich ungefähr 162°·6 weit ist, zeigte die Maximalamplitude der wahren Bodenbewegung zu ca. 0·5 mm. Der Herd liegte im Pazifik ziemlich weit von der Nordostküste Japans, darum waren die Schäden durch Bodenerschüttelung selbst nicht beträchtlich, aber die grossen Tunami-Wellen waren die allerschlimmste Begleiterscheinung, über welche schon eine Menge Berichte erschienen ist.

Im vorliegenden wird darum ausschliesslich von seismometrischer Sache die Rede sein. In dieser Arbeit ist der Verfasser zu seinem herzlichen Dank verpflichtet den Direktoren und anderen Personalen, die ihn sehr freundlich mit Originalen oder Kopien der Seismogramme versehen haben.

Die 134 Stationen, deren Seismogramme der Verfasser selbst lesen konnte, sind, manche Japanische Stationen ausgenommen, die Folgenden, nämlich in der Reihe von Entfernung geordnet, Zi-Ka-Wei, Peiping, Nangking, Guam, Baguino, Hongkong, Manila, Butuan, Phu-Lien, Amboina, Alipore, Honolulu, Sitka, Dehra Dun, Medan, Hawaii, Agra, Batavia, Hyderabad, Victoria V.C., Seattle, Colaba, Abisko, Suva, Kodaikanal, Colombo, Samoa, Spokane, Pulkovo, Ukiah, Baku, Berkeley, Mt. Hamilton, Upsala, Bozeman, Tinemaha, Riverview, Santa Barbara Cal., Haiwee, Adelaide, Pasadena, Mt. Wilson, Riverside, Perth, Yalta, La Jolla, Reykjavik, Melbourne, Lund, Lwów, Kopenhagen, Denver, Ivigtut, Hamburg, Helgoland, Leipzig, Budapest, Göttingen, Plauen, Edingburgh, Wien, Eger, Ksara, Beograd, De Bilt, Sofia, Taunus, Stonyhurst, München, Heidelberg, Zagreb, Bidston, Stuttgart, Uccle, Karlsruhe, Strasbourg, Oxford, Kew, Wellington, Zürich, Venezia, Chur, Padova, Sibenik, Parc-St-Maur, Neuchâtel, Chicago, Firenze, Florissant, St. Louis, Helwan, Chiavari, Benevento, Ann Arbor, Ottawa, Shawinigan Falls, Sevenfalls, Toronto, Cincinnati, Pittsburg, Technology, Harvard, Barcelona, Carloforte, Halifax, Guadarajara, Fordham, Georgetown, Manzanillo, Charlottesvilles, Ebro, Columbia, Toledo, Alger-Bouzaréah, Tacubaya, Santa Barbara in Mexico, Cartuja, Veracruz, San Fernando (Cadiz), Oaxaca, Merida, Angra do Heroismo (Açores), Port-au-Prince, San Juan, Balboa, Johannesburg, Huancayo, Capetown, La Paz, Montezuma, Sucre, Santiago, La Plata, und Rio de Janeiro.

Fig. 1 zeigt die Verteilung dieser Stationen, wo der Herd als Mittelpunkt gelegt wird.

Diese Verteilung hat die Untersuchung der sowohl radialen als auch azimutalen Verhältnisse der Wellenfortpflanzung möglich gemacht.

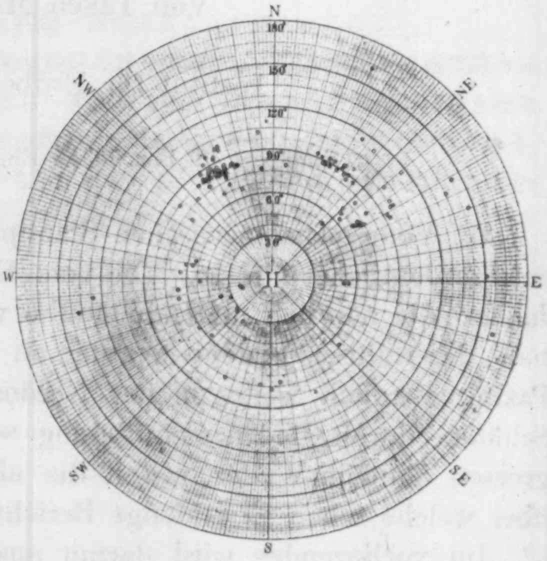

Fig. 1. Verteilung der Stationen, den Herd als Mittelpunkt. Der Radiusvektor zeigt die Herdentfernung.

2. Wie man in Fig. 9 im ersten Heft der vierteljährigen Mitteilung dieses Institutes[1] für 1933 leicht sehen kann, ist die Zusammensetzung der kurzperiodischen Wellen ausserordentlich kompliziert. Langperiodische Seismographen zeigten im Gegenteil vom Anfang an sehr langsame grosse Bewegungen, wie in Fig. 7 und Fig. 8 in demselben Heft. Die wahre Bodenverschiebung, die mit diesen Seismogrammen durch gliedweise Integration der Pendelgleichung berechnet wird, ist wie folgt. (Tabelle I.)

Tabelle I.

t sec.	0	2	4	6	8	10	12	14	16	18	20	22	24
A_N' mm.	0	−0·07	−0·27	−0·6	−1·6	−1·67	−1·87	−2·0	−2·87	−4·26	−5·67	−6·6	−5·9
A_E' mm.	0	−0·14	−0·38	−1·6	−4·3	−6·8	−8·6	−10.2	−13·1	−16·7	−20·3	−20·9	−19·5

t sec.	26	28	30	32	34	36	38	40	42	44	46	48	50
A_N' mm.	−5·6	−4·0	−2·0	+0·5	+0·47	+3·1	+7·6	+8·5	+10·4	+8·5	+9·1	+15·9	+17·3
A_E' mm.	−14·7	−11·0	−5·67	−1·67	+2·53	+8·9	+17·3	+22·2	+18·5	+16·4	+12·9	+12·6	+15·0

In Fig. 2 sieht man horizontale Bewegung des Bodenteilchens, die durch Zusammensetzung dieser Komponenten konstruiert worden ist.

---

[1] *Seismomet. Rep., Earthq. Res. Inst.*, 1933, Part I.

Die Bewegungsrichtung liegt ungefähr in E 35° N–W 35° S, d.h. in der Richtung vom Herd zu Station. Diese langsame Bewegung zeigt also die Charakteristik der P-Wellen, was schon auch in anderen Fällen manchmal bestätigt worden ist.

Im Herdgebiet solches Grossbebens wie dieses muss ganze Menge Bewegungen entstehen. Aber von der seismometrischen Betrachtung soll die langperiodische Bewegung vom grösseren Herdgebiet stammen als die kurzperiodische riffelartige Bewegung. Der Mittelpunkt des Entstehungsortes jeder Gruppe der Wellen soll nicht immer miteinander übereinstimmen. Der Entstehungsort der Bodenbewegung kann theoretisch nicht ein Punkt sein. Aber man kann im allgemeinen wenigstens praktisch einen Punkt bestimmen, den man als Entstehungspunkt der Wellen ansehen kann, wenn die Wellen genug vom Ferne, verglichen mit der Wellenlänge, beobachtet werden.

Der Herd in dieser Arbeit bedeutet solchen Punkt für P-wellen, die genug langperiodisch waren, um die ganze Welt zu erschütteln.

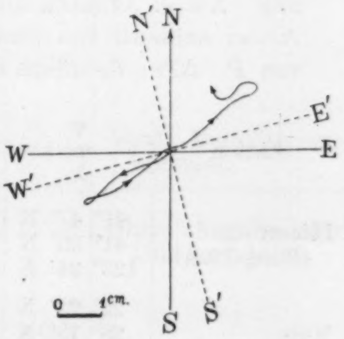

Fig. 2. (N'S')(E'W'), Orientierung der Instrumente.

3. Von Japanischen Beobachtungen hatten H. Honda und M. Takehana[2] den Herd in $\varphi=39^\circ{\cdot}1$ N, $\lambda=144^\circ{\cdot}7$ E gelegt. Erstens wurde ein vom Verfasser versuchsweise gelegter Punkt $\varphi=39^\circ{\cdot}27$ N, $\lambda=144^\circ{\cdot}87$ E als Herd vorausgesetzt, dann wurde Herdentfernung jeder Station berechnet. Bei der Rechnung wurde die geozentrische Breite benutzt. Die beobachtete Zeit ($2^h\,31^m$ als Koordinatenanfang) wurde mit der Macelwane Tabelle[3] vom 1933 verglichen, die Residuen wurden berechnet, und Gleichungen von folgender Form wurden gebildet,

$$\Delta T = T_0 + \frac{\partial T}{\partial \varphi}\delta\varphi + \frac{\partial T}{\partial \lambda}\delta\lambda.$$

Dann kann man mit der Methode der kleinsten Quadrat T_0, $\delta\varphi$ und $\delta\lambda$ bestimmen. Bei diesem Verfahren wurden Stationen von 15° bis 90° Entfernung benutzt, um teils die kurzperiodischen Riffeln teils die Schattenwellen des Erdkerns auszuschalten.

Die endgültige Lage des Herdes ergibt sich zu

$\varphi=39^\circ{\cdot}15\pm0^\circ{\cdot}08$ N m.F. geographische Breite,

$\lambda=144^\circ{\cdot}40\pm0^\circ{\cdot}07$ E m.F.,

$T_0=1^s\pm0^s{\cdot}3$ m.F.,

---

[2] H. Honda u. M. Takehana, *Kensin-Zihô* (Erdbebenberichte), **7** (1933), 87~104.

[3] "A Preliminary Table of Observed Travel Times of Earthquake Wave for Distances between 10° and 180° Applicable only to Normal Earthquakes," November, 1933.

m.F. der einzelnen Beobachtung, $m_r = 2{\cdot}92$ Sek.

Der Anfang der Zeit $17^h\,31^m\,01^s \pm 0^s{\cdot}3$ bedeutet natürlich nicht die Herdzeit dieses Bebens. Die Bemerkung, die zu dem Herdpunkt gegeben worden ist, muss auch zu der Zeitkoordinate gültig sein. Sie kann nur mit Beobachtung am Herd selbst bestimmt werden, was hier nicht der Fall ist. Uberdies ist die Oberflächenstruktur in der Nähe vom Herd in diesem Falle uns ganz unbekannt. Dieser Herdpunkt liegt im Pazifik von ungefähr 8000 m. Tiefe.

Also ist dieser Wert von Zeit-anfang von Bedeutung nur durch Vergleich mit der Macelwane Tabelle.

Das ganze Verfahren ist in Tabelle II zusammengestellt.

Tabelle II.

φ: geographische Breite. φ': geozentrische Breite. λ: Länge. θ: Herdentfernung. Λ_{H-S}: Azimuth vom Herd nach Station (von Süden in Uhrzeiger-richtung). Λ_{S-H}: Azimuth von Station nach dem Herd. T_P: Zeit des ersten Einsatzes von P. ΔT_P: T_P minus die Macelwane Laufzeit.

Station	φ φ' λ	θ	Λ_{H-S} Λ_{S-H}	T_P	ΔT_P	Bemerkung
Hôten (Feng-Tien)	41° 47′ N 41° 36′ N 123° 24′ E	16°·09	105° 37′ 271° 24′	$34^m\ 49^s$	+1·2	Vom Berichte genommen.
Nase	28° 23′ N 28° 13′ N 129° 30′ E	16°·30	54° 10′ 225° 34′	34 50·9	+0·9	Wie oben.
Dairen (Ta-Lien)	38° 54′ N 38° 43′ N 121° 38′ E	17°·58	95° 11′ 278° 27′	35 6·2	+0·2	Wie oben.
Zi-Ka-Wei	31° 11′·5N 31° 1′·5N 121° 26′ E	20°·25	74° 15′ 240° 35′	35 35	− 2	
Peiping	40° 4′ N 39° 53′ N 116° 6′ E	21°·69	101° 14′ 277° 9′	35 46 35 51	−1·9	$35^m\ 46^s$ ist ganz kleiner kurzperiodischer Einsatz.
Nanking	32° 03′ N 31° 53′ N 118° 47′ E	21°·87	78° 56′ 243° 42′	35 49 35 53·5	−1·2	35 49 wie oben.
Isigaki-Zima	24° 20′ N 24° 11′ N 124° 10′ E	22°·53	55° 40′ 224° 39′	35 59·1	−2·0	Vom Berichte genommen.
Taihoku	25° 02′ N 24° 53′ N 121° 31′ E	23°·80	61° 06′ 228° 31′	36 12·5	+2·7	Wie oben.
Taityû	24° 09′ N 24° 00′·5N 120° 41′ E	25°·10	60° 46′ 227° 52′	36 35·8	+9·8	Wie oben.
Taitô	22° 45′ N 22° 33′ N 121° 09′ E	25°·58	57° 45° 225° 20°	36 26	−5·8	Wie oben.

(Fortsetzung folgt.)

Tabelle II. (*Fortsetzung.*)

Station	φ φ' λ	θ	Λ_{H-S} Λ_{S-H}	T_P	ΔT_P	Bemerkung
Guam	13° 24′ N 13° 19′ N 144° 38′ E	25°·65	0° 16′ 180° 13′	36^{m} 59^{s}·7	+27	Von der Rechnung ausgenommen.
Hôko-tô	23° 32′ N 23° 24′ N 119° 33′ E	26°·12	61° 19′ 227° 54′	36 35	−2·2	Vom Berichte genommen.
Kôsyun	22° 00′ N 21° 52′ N 120° 45′ E	26°·38	57° 09′ 224° 38′	36 37·5	+2·3	Wie oben.
Baguino	16° 25′ N 16° 19′ N 120° 36′ E	30°·67	49° 41′ 217° 59′			Ohne Angabe der Uhr-korrektion.
Hongkong	22° 18′ N 22° 10′ N 114° 10′ E	30°·66	66° 04′ 229° 54′	37 18·0	−1·6	
Manila	14° 35′ N 14° 29′·5N 120° 59′ E	31°·91	47° 01′ 215° 49′	37 28·5	−2·5	
Palau	7° 20′ N 7° 17′ N 134° 29′ E	32°·89	19° 05′ 194° 50′	37 35·4	−4·4	Vom Berichte genommen.
Butuan	8° 56′ N 8° 52′·5N 125° 32′ E	34°·46	34° 51′ 206° 36′			Ohne Angabe der Uhr-korrektion.
Phu-Lien	20° 48′ N 20° 40′·5N 106° 38′ E	37°·05	71° 53′ 232° 03′	38 13	+0·5	
Amboina	3° 42′ S 3° 40′·5S 128° 10′ E	45°·16	23° 44′ 198° 14′	39 16	−1·6	
Alipore	22° 32′ N 22° 24′ N 88° 20′ E	50°·03	88° 13′ 237° 03′	40 14	+2·0	Von der Rechnung ausgenommen.
Honolulu	21° 18′ N 21° 10′ N 157° 49′·3W	52°·25	272° 39′ 123° 53′·5	40 12·5	+2·0	
Sitka	57° 03′ N 56° 53′ N 135° 20′·1W	53°·30	222° 17′ 106° 44′	40 16	−1·0	
Medan	3° 35′ N 3° 33′·5N 98° 41′ E	54°·02	61° 23′ 223° 09′	40 26	+3·8	
Dehra Dun	30° 19′ N 30° 09′ N 78° 03′ E	54°·05	102° 26′ 241° 08′	40 21	−1·5	
Hawaii	19° 26′ N 19° 19′ N 155° 16′ W	55°·27	272° 53′ 124° 47′	40 33	+2·0	
Agra	27° 10′ N 27° 0′·5N 78° 05′ E	55°·58	99° 05′ 235° 21′	40 31	−2·0	

(*Fortsetzung folgt.*)

Tabelle II. (*Fortsetzung.*)

Station	φ φ' λ	θ	Λ_{H-S} Λ_{S-H}	T_P	ΔT_P	Bemerkung
Batavia	6° 11′ S 6° 8′·5S 106° 50′ E	56°·86	46° 44′ 214° 38′·5	40^m 43^s·5	+0·9	
Hyderabad	17° 26′ N 17° 19′·5N 78° 27′ E	60°·57	89° 08′ 234° 24′	41 35	+28	Von der Rechnung ausgenommen.
Gonzales Ht. Victoria B.C.	48° 25′ N 48° 13′·5N 123° 19′ W	63°·46	228° 14′ 119° 32′	41 29·5	+3·5	
Seattle	47° 39′ N 47° 28′ N 122° 18′·5W	64°·40	228° 36′ 120° 27′	41 37	+5·0	
Colaba	18° 54′ N 18° 46′ N 72° 49′ E	64°·11	94° 12′ 234° 51′	41 37	+6·0	
Suva	18° 09′ S 18° 02′ S 178° 26′ E	65°·26	324° 36′ 151° 47′	41·3		
Abisko	68° 21° N 68° 13° N 18° 49° E	65°·35	160° 48′·5 223° 37′	41 42	+3·5	
Kodaikanal	10° 14′ N 10° 10′ N 77° 28′ E	65°·66	83° 36′ 231° 24′·6	41 43·5	+3·0	
Colombo	6° 54′ N 6° 52′ N 79° 52′ E	65°·90	79° 09′ 229° 59′	41 44	+6·0	
Apia (Samoa)	13° 48′ S 13° 43′ S 171° 46′ W	66°·77	313° 20′ 144° 28′	41 54	+6·0	
Spokane	47° 44′ N 47° 32′·5N 117° 21′ W	67°·13	226° 35′ 123° 16′	41 50	0·0	
Pulkovo	59° 46′ N 59° 36′ N 30° 19′ E	67°·50	150° 15′ 229° 44′	41 53	0·0	
Ukiah	39° 08′ N 38° 57′ N 123° 13′ W	68°·36	236° 55′ 123° 14′	42 00	+1·6	
Baku	40° 23′ N 40° 11′ N 49° 54′ E	68°·86	125° 36′ 235° 44′	42 06	+4·4	
Berkeley	37° 52′ N 37° 41′ N 122° 16′ W	69°·69	237° 37′ 124° 06′	42 06	−1·0	
Mt. Hamilton	37° 20′ N 37° 09′ N 121° 39′ W	70°·39	237° 47′ 124° 32′	42 10	−1·9	
Bozeman	45° 41′ N 45° 29′ N 111° 02′ W	72°·04	225° 40′·9 127° 23′·2	42 20·1	−1·0	

(*Fortsetzung folgt.*)

Tabelle II. (*Fortsetzung.*)

Station	φ φ' λ	θ	Λ_{H-S} Λ_{S-H}	T_P	ΔT_P	Bemerkung
Upsala	59° 51′ N 59° 41′ N 17° 38′ E	72°·02	155° 6′·5 220° 27′	42^{m} $19^{s}{\cdot}3$	−1·7	
Tinemaha	37° 05′·7N 36° 54′·7N 118° 15′·5W	72°·73	236° 26′·5 126° 00′	42 21·3 42 25·8	+0·5	42 21·3 ist kleiner kurzperiodischer Einsatz.
Riverview	33° 50′ S 33° 39′ S 151° 10′ E	72°·90	354° 32′ 174° 55′	42 27	0·0	
Santa Barbara in Cal.	34° 26′·5N 34° 16′ N 119° 42′·9W	73°·34	239° 25′ 126° 2′·5	42 29·4	0·0	
Haiwee	36° 08′·2N 35° 59′·2N 117° 57′·9W	73°·48	237° 03′ 126° 22′	42 29·4	−0·6	
Adelaide	34° 56′ S 34° 45′ S 138° 35′ E	73°·91	5° 20′·5 185° 03′	42 27·5	−5·5	
Pasadena	34° 08′·9N 33° 58′·2N 118° 10′·3W	74°·54	238° 52′·5 126° 45′	42 30·8 42 36	−0·4	42 30·8 ist kleiner kurzperiodischer Einsatz.
M. Wilson	34° 13′·5N 34° 03′ N 118° 03′·4W	74°·57	238° 45′ 126° 47′	42 32·5 42 36·5	−0·2	42 32·5 wie oben.
Riverside	33° 59′·6N 33° 49′ N 117° 22′·5W	75°·16	238° 35′·5 126° 07′	42 35·2 42 39·2	−0·8	42 35·2 wie oben.
Bergen	60° 24′ N 60° 14′ N 5° 18′ E	75°·17		42 39	−1·0	Vom Stationsberichte genommen.
La Jolla	32° 51′·8N 32° 41′ N 117° 15′·2W	75°·94	239° 29′ 127° 25′	42 44·3	−0·7	
Perth	31° 57′ S 31° 47′ S 115° 50′ E	75°·54	25° 06′ 202° 46′	42 45	+2·5	
Yalta	44° 30′ N 44° 18′·5N 34° 10′ E	75°·64	136° 21′ 228° 29′	42 42	−1·0	
Reykjavik	64° 09′ N 64° 00′ N 21° 57′ W	76°·45	174° 06′ 190° 30′	42 50	+3·0	
Melbourne	37° 50′ S 37° 39′ S 144° 58′ E	76°·62	359° 55′ 179° 55′	42 58	+9	
Lund	55° 42′ N 55° 31′ N 13° 11′ E	76°·75	154° 16′ 216° 32′	42 50	+0·5	
Lwów	49° 50′ N 49° 39′ N 24° 01′ E	76°·96	145° 20′·5 223° 02′·8	42 57·6	+6·6	

(*Fortsetzung folgt.*)

Tabelle II. (*Fortsetzung.*)

Station	φ φ' λ	θ	Λ_{H-S} Λ_{S-H}	T_P		ΔT_P	Bemerkung
Kopenhagen	55° 41′ N 55° 30′ N 12° 27′ E	77°·02	154° 41′ 214° 57′	42^{m}	50^{s}·8	−0·2	
Denver	39° 40′·5N 39° 29′·5N 104° 57′ W	79°·25	227° 29′ 132° 51′	43	1·8	−1·3	
Ivigtut	61° 12′ N 61° 02′ N 48° 11′ W	79°·48	186° 23′ 169° 43′·5	43	3·5	−1·5	
Hamburg	53° 33′·5N 53° 22′·5N 9° 59′ E	79°·58	154° 39′ 213° 56′	43	5·2	−0·6	
Helgoland	54° 11′ N 54° 00′ N 7° 53′ E	79°·74	156° 03′ 212° 29′	43	6·3	−0·1	
Leipzig	51° 20′ N 51° 09′ N 12° 24′ E	80°·53	152° 08′ 215° 24′	43	11	0·0	
Budapest	47° 29′ N 47° 17′·5N 19° 04′ E	80°·90	146° 10′ 219° 36′	43	20·5	+7·5	
Göttingen	51° 33′ N 51° 22′ N 9° 58′ E	81°·24	153° 26′ 213° 49′	43	12·7	−2·3	
Edinburgh	55° 56′ N 55° 45′ N 3° 11′ W	81°·31	162° 32′ 204° 30′	43	16	+0·9	
Wien	48° 15′ N 48° 3′·5N 16° 22′ E	81°·45	148° 05′ 217° 52′	43	11 16	0·0	43 11 ist kleiner kurzperiodischer Einsatz.
Eger	50° 05′ N 49° 53′ N 12° 23′ E	81°·56	151° 18′·5 215° 21′	43	15·7	−0·9	
Ksara	33° 49′ N 33° 39′ N 35° 53′ E	81°·70	127° 27′ 227° 43′	43	19	+2·0	
Beograd	44° 49′ N 44° 37′·5N 20° 27′ E	82°·31	143° 48′ 220° 08′·5	43	17 20	−0·1	43 17 ist kleiner kurzperiodischer Einsatz.
De Bilt	52° 06′ N 51° 55′ N 5° 11′ E	82°·38	156° 21′ 210° 23′	43	21	+0·2	
Sofia	42° 42′ N 42° 31′ N 23° 20′ E	82°·51	140° 42′ 221° 50′	43	20	−1·0	
Taunus	50° 13′ N 50° 02′ N 8° 27′ E	82°·89	153° 35′ 212° 33′·5	43	23·5	+0·5	
Stonyhurst	53° 51′ N 53° 40′ N 2° 28′ W	83°·02	161° 12′ 204° 58′	43	21·5	−2·5	

(*Fortsetzung folgt.*)

Tabelle II. (*Fortsetzung.*)

Station	φ φ' λ	θ	Λ_{H-S} Λ_{S-H}	T_P	ΔT_P	Bemerkung
München	48° 09′ N 47° 57′·5N 11° 36′·5E	83°·44	150° 41′ 214° 35′·5	$43^{m}\ 25^{s}{\cdot}6$	−0·4	
Heidelberg	49° 24′ N 49° 13′ N 8° 43′ E	83°·47	152° 55′ 212° 46′	43 24	−2·0	
Zagreb	45° 49′ N 45° 37′·5N 15° 59′ E	83°·51	146° 54′ 217° 21′	43 29·2	+3·1	
Bidston	53° 24′ N 53° 13′ N 3° 04′ W	83°·58	161° 20′·5 204° 30′	43 23	−3·8	
Stuttgart	48° 46′ N 48° 35′ N 9° 12′ E	83°·75	144° 19′ 212° 59′	43 6·0 43 28	+0·5	43 6·0 ist langsame Bewegung. Nur in horizontalen Komponenten des Galizin Pendels.
Uccle	50° 48′ N 50° 37′ N 4° 22′ E	83°·76	156° 08′ 209° 43′	43 27	−0·6	
Karlsruhe	49° 01′ N 48° 49′ N 8° 25′ E	83°·91	152° 52′ 212° 32′	43 30	+1·9	
Strasbourg	48° 35′ N 48° 23′·5N 7° 46′ E	84°·52	153° 5′·5 211° 59′	43 32	+0·8	
Oxford Engl.	51° 46′ N 51° 35′ N 1° 15′ W	84°·57	159° 43′ 205° 42′	43 33	+1·3	
Kew	51° 28′ N 51° 17′ N 0° 19′ W	84°·59	159° 03′ 206° 22′	43 31	−0·9	
Wellington	41° 17′ S 41° 5′·5S 174° 46′ E	84°·75	337° 50′ 157° 08′	43 32	−0·5	
Zürich	47° 22′ N 47° 11′ N 8° 35′ E	84°·90	151° 58′·5 212° 29′	43 32 43 35	−1	43 32 ist kleine kurzperiodische Bewegung.
Venezia	45° 26′ N 45° 14′·5N 12° 20′ E	85°·37	148° 45′ 214° 56′	43 39	+3·3	
Chur	46° 51′ N 46° 39′·5N 9° 32′ E	85°·44	151° 17′·5 212° 56′	43 31·5 43 35·5	+0·5	43 31·5 wie in Zürich.
Padova	45° 24′ N 45° 12′·5N 11° 52′ E	85°·59	148° 59′·5 214° 37′	43 40·7	+3·8	
Šibenik	43° 03′ N 42° 51′·5N 15° 54′ E	85°·75	145° 16′ 217° 08′	43 59	+21	Von der Rechnung ausgenommen.
Parc St. Maur	48° 48′·6N 48° 37′ N 2° 29′·6E	86°·10	156° 8′·5 208° 25′·5	43 39·2	+0·2	

(*Fortstzung folgt.*)

Tabelle II. (*Fortsetzung.*)

Station	φ φ' λ	θ	Λ_{H-S} Λ_{S-H}	T_P	ΔT_P	Bemerkung
Neuchâtel	47° 00′ N 46° 48′·5N 6° 57′ E	86°·14	152° 43′ 211° 21′	43^m 39^s	−0·4	
Chicago	41 47′ N 41° 36′ N 87° 37′ W	86°·64	216° 21′·8 142° 00′	43 40	−2·0	
Firenze	43° 47′ N 43° 35′·5N 11° 15′ E	87°·17	148° 26′·5 214° 09′	43 45·5	+1·5	
Helwan	29° 51′ N 29° 41′ N 31° 20′ E	87°·23	127° 08′ 225° 25′·5	43 48	+3·0	
Chiavari	44° 19′ N 44° 08′ N 9° 29′ E	87′·43	149° 15′ 213° 35′	43 45	−1·0	
Florissant	38° 48′ N 38 37′ N 90° 22′ W	87°·65	219° 52′·5 140° 26′	43 45·5	−1·5	
St. Louis	38° 38′·3N 38° 27′ N 90° 14′ W	87°·84	219° 54′ 140° 31′·5	43 42	−6·0	
Benevento	41° 08′ N 40° 57′ N 14° 48′ E	87°·78	144° 40′ 216° 29′			Ohne Angabe der Uhrkorrektion.
Ann Arbor	42° 17′ N 42° 06′ N 83° 44′ W	87°·96	213° 51′ 144° 22′	43 46	−2·6	
Ottawa	45° 23′·6N 45° 12′ N 75° 43′ W	88°·47	207° 12′ 149° 44′	43 50	−1·0	
Shawinigan Falls	46° 33′ N 46° 21′ N 72° 46′ W	88°·47	204° 50′·5 151° 46′	43 48·5	−2·5	
Sevenfalls	47° 07′ N 46° 56′ N 70° 49′ W	88°·57	203° 24′·5 153° 08′	43 49·0	0·0	
Toronto	43° 40′ N 43 29′ N 79° 24′·6W	88°·58	210° 21′ 147° 16′	43 52·4	+0·6	
Pittsburg	40° 27′ N 40° 15′·5N 79° 57′ W	91°·07	212° 26′ 146° 56′	44 06	+2·0	
Cincinnati	39° 09′ N 38° 58′ N 84° 30′ W	90°·17	216° 03′ 144° 01′	44 02	+2·3	
Technology	44° 47′ N 44 35′·5N 67° 21′ W	91°·61	202° 14′·5 155° 37′	44 08	+1·0	
Carloforte	39° 08′ N 38° 57′ N 8° 19′ E	92°·26	147° 44′ 212° 12′	44 10	< +3·0	Beginn, bischen früher als 44 10. Nicht genau bestimmbar wegen der Störung durch Zeitmarkierung.

(*Fortsetzung folgt.*)

Tabelle II. (*Fortsetzung.*)

Station	φ φ' λ	θ	Λ_{H-S} Λ_{S-H}	T_P	ΔT_P	Bemerkung
Harvard	42° 30′ N 42° 19′ N 71° 34′ W	92°·45	205° 58′·5 152° 37′	44^{m} 12^{s}	+1·0	
Halifax	44° 38′ N 44° 26′ N 63° 36′ W	92°·88	199° 50·5′ 158° 19·5′	44 15	+2	
Guadarajara	20° 41′ N 20° 33′·5N 103° 50′ W	92°·90	240° 44′ 133° 47′	44 36	+23	
Barcelona	41° 26′ N 41° 15′ N 2° 8′ E	92°·66	152° 58′ 207° 59′	44 11·3	−0·7	
Fordham	40° 52′ N 40° 41′ N 73° 53′ W	93°·07	208° 17′ 150° 59′	44 14	0·0	
Georgetown	38° 54′ N 38° 43′ N 77° 04′ W	93°·56	211° 29′ 148° 42′	44 15	−1·0	
Manzanillo	19° 03′ N 18° 56′ N 104° 20′ W	93°·68	242° 14′ 133° 33′	44 00	−16	Vom Berichte genommen.
Charlottesvilles	38° 02′ N 37° 51′ N 78° 31′ W	93°·71	212° 49′ 147° 49′	44 14·3	−2·7	
Ebro	40° 49′ N 40° 38′ N 0° 30′ E	93°·81	153° 47′ 206° 52′	44 17	0·0	
Columbia	34° 00′ N 33° 49′.5N 81° 02′ W	95°·69	216° 43′ 146° 03′	44 24·6	−1·4	
Toledo	39° 52′ N 39° 41′ N 4° 02′ W	96°·17	156° 31′ 203° 42′	44 25·5	−3·2	
Alger-Bouzaréah	36° 48′ N 36° 37′ N 3° 02′ E	96°·40	150° 09′ 208° 46′	44 29	−1·0	
Tacubaya	19° 24′ N 19° 17′ N 99° 12′ W	96°·90	238° 35′ 135° 32′	44 34·2	+2·2	
Santa Barbara	19° 18′ N 19° 11′ N 98° 54′ W	97°·17	238° 27′ 135° 39′			Beginn unklar.
Cartuja	37° 12′ N 37° 01′ N 3° 36′ W	98°·26	155° 02′ 204° 13′	44 37·5	−1·5	
Veracruz	19° 12′ N 19° 05′ N 96° 08′ W	99°·05	236° 37′ 136° 48′			Beginn unklar.
Oaxaca	17° 01′ N 16° 54′ N 96° 46′ W	100°·20	238° 35′ 136° 18′			Beginn unklar.

(*Fortsetzung folgt.*)

Tabelle II. (*Fortsetzung.*)

Station	φ φ' λ	θ	Λ_{H-S} Λ_{S-H}	T_P	ΔT_P	Bemerkung
San Fernando (Cadiz)	36° 28′ N 36° 17′ N 6° 12′ W	99°·97	156° 45′ 202° 20′	$44^m\ 45^s$	−2·0	
Merida	20° 57′ N 20° 49′ N 89° 37′ W	101°·81	230° 47′ 140° 02′			Beginn unklar.
Angra do Heroismo (Açores)	38° 39′ N 38° 28′ N 27° 14′ W	102°·18	173° 41′ 186° 16′			Beginn unklar.
Port-au-Prince (Haiti)	18° 33′ N 18° 26′·5N 72° 20′ W	113°·15	218° 22′ 149° 33′			Beginn unklar.
San Juan	18° 23′ N 18° 16′ N 66° 07′ W	116°·11	212° 46′ 153° 48′	46 05·1	+4·0	
Balboa (Panama)	8° 58′ N 8° 54′·5N 79° 33′ W	117°·18	230° 38′ 142° 42′			Beginn unklar.
Johannesburg	26° 11′ S 26° 02′ S 28° 04′ E	125°·76	83° 52′ 239° 05′			Erst P_1' ist bemerkbar.
Huancayo	12° 03′ S 11° 58′ S 75° 20′ W	135°·75	245° 51′ 134° 35′	47 43	+8·0	
Capetown	33° 57′·5S 33° 47′ S 18° 27′·5E	136°·81	79° 26′ 246° 52′	50 25	+1·0	Dieses Beginn entspricht P_1'.
La Paz	16° 30′ S 16° 22′ S 67° 08′ W	143°·81	241° 02′ 135° 03′·5	48 16 50 29	+4·0 −6·0	50 29 entspricht P_1'.
Montezuma	22° 37′ S 22° 29′ S 68° 50′ W	147°·36	249° 48′·5 128° 05′			Ohne Angabe der Uhrkorrektion.
Sucre	19° 03′ S 18° 56′ S 65° 16′ W	147°·46	240° 57′ 134° 09′·5	50 46	+6	P_1'.
Santiago	33° 27′ S 33° 16′·5S 70° 42′ W	151°·37	269° 08′ 111° 49′	50 47	+1·0	P_1'.
La Plata	34° 55′ S 34° 44′ S 57° 56′ W	161°·66	283° 47′ 113° 32′	51 00	+3·0	P_1'.
Rio de Janeiro	22° 54′ S 22° 46′ S 43° 13′ W	162°·59	205° 10′ 159° 03′·5	51 00	+2·0	P_1'.

Bei der ΔT Bildung wurde einmal die Abweichung der Bahnlänge im Erdellipsoid von der in der Erdkugel in Betracht gezogen. Aber bei dieser Genauigkeit der einzelnen Beobachtung konnte das Resultat nicht merklich verbessert werden. Für diesen Zweck sollte der mittlere Fehler der Einzelbeobachtung wenigstens unter 2 Sekunden sein. Darum ist dieser Faktor ausser acht gelassen. ΔT verteilt sich ziemlich gleichmässig für alle Entfernungen und Azimuthe. Wir können also die Herdtiefe als normal ansehen.

Nur zwischen 60° und 70° zeichnen sich Plus-werte von ΔT systhematisch aus. Macelwane Kurve knickt ziemlich deutlich an 59° und an 69°, und für dieses Interval ist sie ungefähr geradlinig. Wenigstens für diesen Fall eignen sich besser für beobachtete Material die folgende Werte (Tabelle III).

Tabelle III.

θ	59°	60°	61°	62°	63°	64°	65°	66°	67°	68°	69°
Dieser Fall	$9^{m}\ 56^{s}$	$10^{m}\ 03^{s}$	$10^{m}\ 11^{s}$	$10^{m}\ 18^{s}$	$10^{m}\ 25^{s}$	$10^{m}\ 32^{s}$	$10^{m}\ 38^{s}$	$10^{m}\ 45^{s}$	$10^{m}\ 51^{s}$	$10^{m}\ 57^{s}$	$11^{m}\ 02^{s}$
Macelwane Kurve	$9^{m}\ 56^{s}$	02^{s}	09^{s}	15^{s}	22^{s}	29^{s}	35^{s}	42^{s}	49^{s}	55^{s}	02^{s}

Einige für kurzperiodische Bewegung empfindliche Seismographen in Amerika und Europa registrierten ganz kleine kurzperiodische Wellen um etwa 4 Sekunden früher als ausgeprägte *P*-Wellen, z.B. in Tinemaha, Pasadena, Mt. Wilson, Riverside, Wien, Beograd, Zürich, und Chur, wie in Pl. IV, Fig. 3 a, b, c, gezeigt sind. Über diese Welle wird spätere Mitteilung erwartet.

Stuttgarter Galitzin Horizontal-Pendel registrierten langsame kleine Bewegung um 22 Sekunden früher als gewöhnliche *P*-Wellen, wie in Pl. V. Fig. 4 a, b, gezeigt ist.

Die Bewegungsrichtung ist ganz anders als die vom Herd zu Station, d.h. sie zeigt nicht die Eigenschaft der Dilatationswelle. Das Vertikalpendel zeigt fast keine Spur davon. Andere Europäische Stationen zeigten auch keine Spuren solcher Bewegung. Diese Tatsachen lassen uns vermuten, dass diese Stuttgarter Bewegung eine vom Erdbeben unabhängige zufällige Störung sein sollte.

4. Merkwürdigerweise haben wir in diesem Falle sehr deutliche *P*-Wellen im Schattengebiet des Erdkerns bis zu 143°·81 Herdentfernung, d.h. bis La Paz, beobachten können. Stationen von über etwa 90° Herdentfernung schienen schon zum Schattengebiet des Erdkerns zu gehören. Also fast alle spanische Stationen und manche Stationen im Ostteile Amerikas kommen schon in die Reihe. Innerhalb etwa 100° Herdentfernung, wenn auch im Schattengebiet, ist die Beobachtung von *P* gewöhnlich nicht schwer. Aber darüber hinaus wird deren Beobachtung immer schwerer. Ausser Gutenbergs[4] erster Bemerkung darüber

---

[4] B. Gutenberg, Handb. d. Geophys., 4-1 (1929), 174.

hatten J. B. Macelwane[5] und G. Krumbach[6] deutliche Beobachtung davon bis zu 18500 Km. beim Beben vom 26. Juni 1924 bestätigt und C. G. Dahm[7] beim Hawkes Bay Beben vom 2. Feb. 1931 bis zu 140°.

Hier sind Beobachtungen in San Juan (116°·11), in Huancayo (135°·75) und in La Paz (143°·81) als Beispiel gezeigt. Pl. VI., Fig. 5 a, b, Pl. VII., Fig. 6 und Fig. 7.

Die Laufzeit der Schattenwellen wird durch die folgende Formel ziemlich gut charakterisiert, nämlich

$$\frac{\partial T}{\partial \theta} = 4{\cdot}7 \text{ Sek./Grad.}$$

Oder $$T = 13^{\mathrm{m}}\, 46^{\mathrm{s}} + 4{\cdot}7\, (\theta - 100°).$$

5. Vom Standpunkt der geometrischen Optik für Erdbebenwellen sollten die Kern-Wellen P' ausser der Brennzone fehlen. Im jetzigen Falle entspricht die Station, La Paz, ungefähr dem Brennpunkt. Wirklich tritt die entsprechende Welle in La Paz ganz merkwürdig auf. (Fig. 7) Innerhalb derselben Entfernung hat man in Capetown, Huancayo (Fig. 6), Johannesburg, und wahrscheinlich in San Juan (Fig. 5 a, b) sie beobachten können.

Eingehendere Betrachtung über die Schatten- und Kern-Wellen wird in anderer Stelle stattfinden.

6. Den in dieser Arbeit berechneten Herd annehmend, sind japanische Laufzeiten untersucht worden. Ausser einigen Beobachtungen in Kwantô und Mizusawa Beobachtung, sind die Angaben im Berichte von H. Honda und M. Takehana[8] benutzt worden.

Herdentfernung innerhalb 6° ist mit der folgenden Formel berechnet.

$$\theta^2 = (\delta\varphi')^2 + \{\delta\lambda \cos(\varphi_0' + \varphi')\}^2,$$

wo φ_0', geozentrische Breite vom Herd; φ', geozentrische Breite von Station; $\delta\varphi' = \varphi_0' - \varphi'$; $\delta\lambda$, Längendifferenz zwischen Herd und Station.

Dann ist Laufzeitformel in Reihenentwickelung von Herdentfernung untersucht. Bei der Rechnung wird die Methode der kleinsten Quadrat benutzt. Die Rechenverfahren lauten wie folgt.

Unter Voraussetzung von Quadratformel ergibt sich,

$$T = 31^{\mathrm{m}} + (2^{\mathrm{s}}{\cdot}02 \pm 2{\cdot}0) + (14{\cdot}56 \pm 0{\cdot}57)\,\theta - (0{\cdot}0299 \pm 0{\cdot}03)\,\theta^2,$$

und der m.F. der einzelbeobachtung ist $\pm 3^{\mathrm{s}}{\cdot}47$.

Unter Voraussetzung von kubischer Formel ergibt sich

$$T = 31^{\mathrm{m}} + (1^{\mathrm{s}}{\cdot}6 \pm 0{\cdot}5) + (14{\cdot}55 \pm 0{\cdot}35)\,\theta - (0{\cdot}0022 \pm 0{\cdot}0015)\,\theta^3,$$

---

[5] J. B. MACELWANE, *Gerl. Beitr. z. Geophys.*, **28** (1930), 165～198.

[6] G. KRUMBACH, *Veröff. d. Reichsanstalt f. Erdbebenforschung, Jena*, Heft 16a (1934), 5.

[7] C. G. DAHM, *Bull. Seism. Soc., Amer.*, **23** (1933), 139～157.

[8] H. HONDA und M. TAKEHANA, *l.c.*

und der m.F. der einzelbeobachtung ist $\pm 3^s{\cdot}51$.

Der m.F. der Einzelbeobachtung ergibt sich kleiner bei der Quadratformel als bei der kubischen Formel. Aber die Koeffizienten jedes Gliedes sind viel schärfer bestimmt bei der kubischen Formel als bei der Quadratformel. Das stimmt qualitativ mit dem Jeffreys'schen Verfahren[9] überein, aber die Zahlenwerte der Koeffizienten sind etwas anders. Der Koeffizient 14·55 Sek./Grad entspricht zu 7·65 Km./Sek., welcher etwas grösser ist als meine frühere Bestimmung 7.50 Km./Sek.

Für weitere Untersuchung wird bis auf weiteres diese kubische Formel benutzt. Diese Formel ist mit Beobachtungen innerhalb 15° Herdentfernung bestimmt worden. Trotzdem ganz merkwürdigerweise stimmt sie sehr gut mit der Macelwane Laufzeit bis zu ungefähr 21°. Weiter hinaus biegt die Kurve schneller gegen die θ Achse als die von der Formel berechneten Werte, aber die Biegung scheint stetig stattzufinden. Die ganze Kurve ist in Fig. 8 gezeigt.

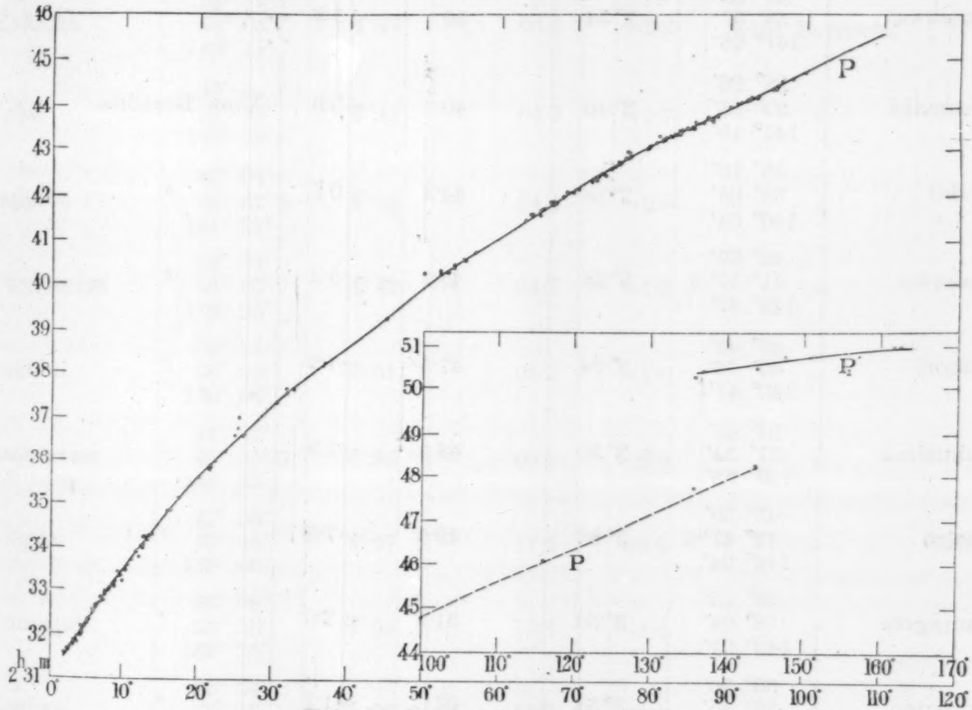

Fig. 8. Laufzeitkurve von P.

Die Biegung der Kurve ist ziemlich stark bis zu ungefähr 32°, dann ist sie beinah geradlinig nur mit weniger Biegung nach der θ Achse.

Die Vermutung von P. Byerly[10] und von I. Lehmann[11], dass die

---

[9] $T=T_0+14{\cdot}30\,\theta-2{\cdot}00\left(\frac{\theta}{10}\right)^3$. *M. N. R. A. S., Geophys. Suppl.*, 2 (1931), 399~407.

[10] P. Byerly, *Bull. Seism. Soc., Amer.*, 24 (1934), 81~99.

[11] I. Lehmann, Transmission Times for Seismic Waves for Epicentral Distances around 20°, Köbenhavn, (1934), 3~45.

Kurve spitzenartig knicken sollte, scheint bei der Genauigkeit dieser Beobachtung nicht einwandfrei bestätigt zu werden.

Das Beobachtungsmaterial ist in Tabelle IV angestellt.

Tabelle IV.

$$\Delta T = T_{\text{beob.}} - (31^{\text{m}} + 1^{\text{s}}{\cdot}6 + 14{\cdot}55\,\theta - 0{\cdot}0022\,\theta^3).$$

Station	φ φ' λ	θ	T_P	ΔT	Bemerkung
Miyako	39° 38′ 39° 27′ 141° 59′	1°·94	$31^{\text{m}}\ 35^{\text{s}}$	+5·2	Vom Berichte.
Morioka	39° 42′ 39° 31′ 141° 10′	2°·56	38·9	+0·1	″
Mizusawa	39° 08′ 38° 57′ 141° 08′	2°·54	40	+1·5	
Isinomaki	38° 26′ 39° 15′ 141° 19′	2°·40	40·3	+3·8	Vom Berichte.
Sendai	38′ 16′ 38° 05′ 140° 54′	2°·88	44·2	+0·7	″
Urakawa	42° 09′ 41° 57′·5 142° 47′	3°·23	45·2	−3·3	″
Aomori	40° 49′ 40° 38′ 140° 47′	3°·24	47·5	−1·2	″
Hukusima	37° 45′ 37° 34′ 140° 28′	3°·39	48·9	−1·9	″
Kusiro	42° 59′ 42° 47′·5 144° 24′	3°·82	49·6	−7·5	″
Yamagata	38° 15′ 38° 04′ 140° 21′	3°·30	51·5	+2·0	″
Onahama	36° 56′ 36° 45′ 140° 54′	3°·54	51·5	−1·1	″
Akita	39° 43′ 39° 32′ 140° 06′	3°·38	51·5	+0·8	″
Aidu	37° 34′ 37° 23′ 140° 07′	3°·78	57	+0·5	″
Nemuro	43° 20′ 43° 08′.5 145° 35′	4°·26	57·5	−5·9	″

(Fortsetzung folgt.)

Tabelle IV. (*Fortsetzung.*)

Station	φ φ' λ	θ	T_P		ΔT	Bemerkung
Obihiro	42° 55′ 42° 43′·5 143° 12′	3°·88	31^m	$58^s{\cdot}5$	+0·5	Vom Berichte.
Muroran	42° 20′ 42° 09′ 140° 58′	4°·09		58·7	−2·2	〃
Hakodate	41° 47′ 41° 36′ 140° 43′	3°·86		58·7	+1·0	〃
Mito	36° 23′ 36° 12′ 140° 28′	4°·16	32	00	−1·9	〃
Tukuba	36° 09′ 35° 58′ 140° 09′	4°·52		00·5	−6·7	Vom Seism. Rep. Earthq. Res. Inst. (1933) Part 1.
Kakioka	36° 14′ 36° 03′ 140° 11′	4°·44		03·8	−2·2	Vom Berichte.
Tyôsi	35° 44′ 35° 33′ 140° 52′	4°·42		04·0	−1·7	〃
Sapporo	43° 04′ 42° 52′·5 141° 21′	4°·53		04·4	−2·9	〃
Utunomiya	36° 34′ 36° 23′ 139° 53′	4°·42		04·7	−1·0	〃
Tukuba	36° 13′ 36° 02′ 140° 06′	4°·51		05·4	−1·6	〃
Asahigawa	43° 47′ 43° 35′·5 142° 22′	4°·86		09·2	−2·9	〃
Niigata	37° 56′ 37° 45′ 139° 03′	4°·37		11·2	+6·2	〃
Kumagai	36° 09′ 35° 58′ 139° 23′	4°·98		12·4	−1·4	〃
Maebasi	36° 24′ 36° 13′ 139° 04′	5 ·06		13·0	−1·9	〃
Tôkyô	35° 41′ 35° 30′ 139° 46′	5°·07		14·0	−1·1	〃
Hongô (Tôkyô)	35° 43′ 35° 32′ 139° 46′	5°·03		14·1	−0·4	〃
Mitaka	35° 40′ 35° 29′ 139° 32′·5	5°·22		14·7	+0·2	Vom Seism. Rep. Earthq. Res. Inst. (1933) Part 1.

(*Fortsetzung folgt.*)

Tabelle IV. (*Fortsetzung.*)

Station	φ φ' λ	θ	T_P	ΔT	Bemerkung
Kiyosumi	35° 09′ 34° 58′ 140° 11′	5°·25	32^{m} 19^{s}·7	+4·9	Vom Seism. Rep. Earthq. Res. Inst. (1933) Part 1.
Kamakura	35° 18′ 35° 07′ 139° 32′	5°·48	21·9	+1·0	〃
Yokohama	35° 26′ 35° 15′ 139° 39′	5°·41	19·9	−0·1	Vom Berichte.
Takada	37° 06′ 36° 55′ 138° 15′	5°·27	20·8	+2·8	〃
Tomisaki	34° 55′ 34° 44′ 139° 50′	5°·60	21·7	−1·0	〃
Oiwake	36° 20′ 36° 09′ 138° 33′	5°·43	22·2	+2·0	〃
Nagano	36° 40′ 36° 29′ 138° 12′	5°·50	22·7	+1·5	〃
Gotenba		(5°·66)	23·1		Vom Berichte Ohne angabe der Koordinaten. θ von Karte berechnet.
Kôhu	35 38′ 35° 27′ 138° 34′	5°·83	24·7	−1·3	Vom Berichte.
Hunatu	35° 30′ 35° 19′ 138° 46′	5°·79	25·0	−0·4	〃
Itô		5°·89	27·1		Vom Berichte. Ohne Angabe der Koordinaten. θ von Karte berechnet.
Misima	35° 07′ 34° 56′ 138° 57′	6°·02	28·9	+0·2	Vom Berichte.
Numadu	35° 06′ 34° 55′ 138° 51′	6°·05	29·4	+0·3	〃
Wazima	37° 23′ 37° 12′ 136° 54′	6°·20	30·2	−1·1	〃
Toyama	36° 41′ 36° 30′ 137° 12′	6°·25	33·2	+1·2	〃
Matumoto	36° 14′ 36° 03′ 137° 58′	5°·93	34·5	+7·1	〃
Iida	35° 31′ 35° 20′ 137° 50′	6°·43	36·5	+1·9	〃

(*Fortsetzung folgt.*)

Tabelle IV. (*Fortsetzung.*)

Station	φ φ' λ	θ	T_P	ΔT	Bemerkung
Takayama	36° 09′ 35° 58′ 137° 15′	6°·47	32^{m} $38^{\mathrm{s}}{\cdot}9$	+3·7	Vom Berichte.
Husiki	36° 47′ 36° 36′ 137° 03′	6°·32	39·4	+6·3	〃
Omaezaki	34° 36′ 34° 25′ 138° 13′	6°·78	41·2	+1·6	〃
Hatizyô	33° 06′ 32° 55′·5 139° 50′	7°·18	45·0	−0·3	〃
Ootomari	46° 39′ 46° 27′·5 142° 46′	7°·48	45·6	−3·9	〃
Gihu	35° 24′ 35° 13′ 136° 46′	7°·22	47·2	+1·3	〃
Ibukiyama	35° 25′ 35° 14′ 136° 24′	7°·45	48·7	−0·4	〃
Hamamatu	34° 42′ 34° 32′ 137° 43′	7°·02	49·4	+6·4	〃
Nagoya	35° 10′ 34° 59′ 136° 58′	7°·22	49·9	+4·0	〃
Kameyama	34° 51′ 34° 40′ 136° 28′	7°·73	54·0	+1·0	〃
Hikone	35° 16′ 35° 05′ 136° 15′	7°·63	56·0	+4·4	〃
Tu	34° 44′ 34° 33′ 136° 31′	7°·77	58	+4·3	〃
Miyadu	35° 32′ 35° 21′ 135° 12′	8°·22	59·0	−1·0	〃
Kyôto	35° 10′ 34° 59′ 135° 44′	8°·05	59·0	+1·5	〃
Oosaka	34° 39′ 34° 28′ 135° 32′	8°·47	33 02·6	−1·0	〃
Toyooka	35° 32′ 35° 21′ 134° 49′	8°·49	03·1	−0·7	〃
Yagi	34° 31′ 34° 20′ 135° 48′	8°·37	03·1	+1·0	〃

(*Fortsetzung folgt.*)

Tabelle IV. (*Fortsetzung.*)

Station	φ φ' λ	θ	T_P	ΔT	Bemerkung
Siomisaki	33° 27′ 33° 16′ 135° 46′	9°·07	$33^{\mathrm{m}}\ 03^{\mathrm{s}}{\cdot}7$	−7·3	Vom Berichte.
Oosaka Sidai			05·9		Ohne Angabe der Koordinaten. Vom Berichte.
Kôbe	34° 41′ 34° 30′ 135° 11′	8°·68	06·3	−0·2	Vom Berichte.
Wakayama	34° 14′ 34° 03′ 135° 10′	8°·95	07·4	−2·0	〃
Sumoto	34° 21′ 34° 10′ 134° 53′	9°·07	11	−1·0	〃
Sikka	49° 14′ 49° 03′ 143° 07′	10°·00	12		〃
Sakai	35° 33′ 35° 22′ 133° 14′	9°·63	18·4	−1·3	〃
Tadôtu	34° 17′ 34° 06′ 133° 46′	9°·88	19·7	−3·6	〃
Okayama	34° 40′ 34° 29′ 133° 56′	9°·45	24·7	+7·5	〃
Kôti	33° 33′ 33° 12′ 133° 32′	10°·57	26·7	−6·1	〃
Muroto	33° 15′ 33° 04′ 134° 11′	10°·21	27·3	−0·6	〃
Niihama	33° 57′ 33° 46′ 133° 15′	10°·42	29·3	−1·4	〃
Matuyama	33° 50′ 33° 38′·5 132° 45′	10°·84	34·5	−2·0	〃
Hamada	34° 54′ 34° 43′ 132° 04′	10°·77	36·3	−0·7	〃
Hirosima	34° 23′ 34° 12′ 132° 27′	10°·75	36·6	+1·3	〃
Simidu	32° 47′ 32° 36′·5 132° 58′	11°·29	42·2	−0·5	〃
Titizima	27° 05′ 26° 56′ 142° 11′	12°·28	46·5	−9·7	〃

(*Fortsetzung folgt.*)

Tabelle IV. (*Fortsetzung.*)

Station	φ φ' λ	θ	T_P	ΔT	Bemerkung
Ooita	33° 14′ 33° 03′ 131° 37′	11°·95	33^{m} 54^{s}·1	+2·3	Vom Berichte.
Simonoseki	33° 57′ 33° 46′ 130° 56′	12°·05	55·2	+2·1	〃
Hukuoka Sidai			56·6		Vom Berichte. Ohne Koordinaten-Angabe.
Miyazaki	31° 55′ 31° 45′ 131° 26′	12°·83	59·1	−4·5	Vom Berichte.
Kumamoto	32° 49′ 32° 38′·5 130° 42′	12°·82	34 00·2	−3.3	〃
Husan	35° 06′ 34° 55′ 129° 02′	12°·93	02·5	−2·4	〃
Hukuoka	33° 35′ 33° 24′ 130° 25′	12°·60	02·8	+2·3	〃
Taikyû	35° 52′ 35° 41′ 128° 36′	12°·98	05·8	+0·1	〃
Nagasaki	32° 44′ 32° 33′·5 129° 52′	13°·45	10·9	−1·1	〃
Ituhara	34° 12′ 34° 01′ 129° 17′	13°·48	12·9	+0·6	〃
Unzendake	32° 44′ 32° 33′·5 130° 15′	13°·17	14·8	+6·6	〃
Saga	33° 15′ 33° 03′·5 130° 18′	12°·87	15·7	+11·5	〃
Keizyô	37° 34′ 37° 23′ 126° 58′	13°·78	16·6	+0·3	〃
Kagosima	31° 34′ 31° 24′ 130° 33′	13°·65	17·3	+2·7	〃
Zinsen	37° 29′ 37° 18′ 126° 38′	14°·05	19·2	−0·7	〃

7. Die ΔT Werte sind in Fig. 9 eingetragen worden.

Obgleich die Werte meistens innerhalb des mittleren Fehlers der einzelnen Beobachtung seien, doch ist die geographische Verteilung des Residuums merkwürdigerweise systematisch. Diese Erscheinung wurde zu erst von S. Kunitomi vermutet, dann in anderer Deutung von H.

Honda[12] ziemlich sicher bestätigt, und nachdem ist sie von anderen Autoren immer wieder diskutiert und bestätigt worden. Hier gibt es nun auch ein Beispiel. Von kleinen Abweichungen abgesehen, stimmt die Verteilung der Anomalie mit den von K. Iida und K. Kanbara[13] untersuchten Fällen überein. Trotz dem grossen mittleren Fehler kōnnen wir diese verteilung des Laufzeitresiduums nicht als zufälligen Beobachtungsfehler sondern als wahre Anomalie ansehen. Wenn man dieser allgemeinen Erscheinung Rechnung tragen sollte, könnte man kleineren mittleren Fehler bekommen.

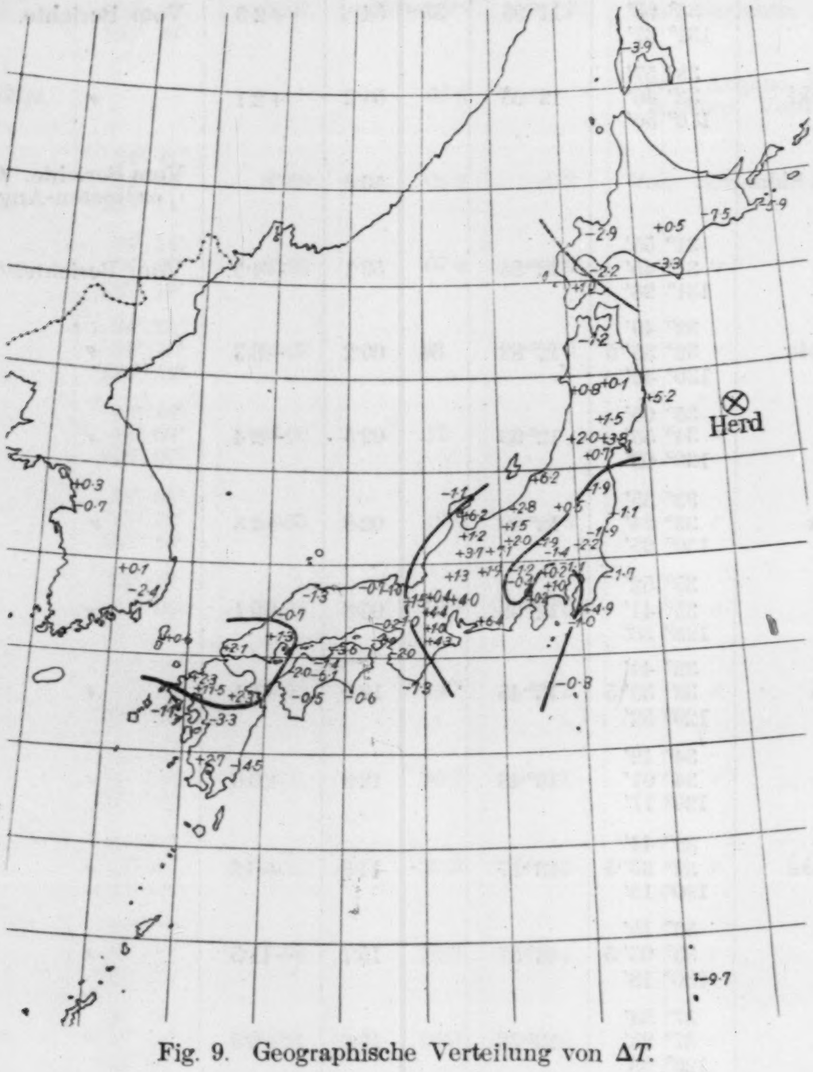
-3.9
-2.9
+0.5
-7.5
-5.9
-2.2
-3.3
-1.2
+0.8
+0.1
+5.2
+1.5
+2.0
+3.8
+0.7
Herd
+6.2
-1.1
+6.2
+2.8
+0.5
-1.9
-1.1
+1.5
+1.2
+2.0
-1.9
-2.2
+3.7
+7.1
-1.4
+1.3
-1.2
-0.2
-1.7
+1.0
+4.9
-1.0
-1.3
-0.7
+1.5
+0.4
+4.0
+4.4
+1.0
+4.3
+6.4
-0.2
-2.0
-0.5
-0.6
-1.3
-0.8
+0.3
-0.7
+0.1
-2.4
-3.3
+2.7
-4.5
-9.7

Fig. 9. Geographische Verteilung von ΔT.

---

[12] H. HONDA, *Kensin-Zihô*, 5 (1932), 111~115.

[13] K. IIDA und K. KANBARA, *Disin*, 6 (1934), 301~317.

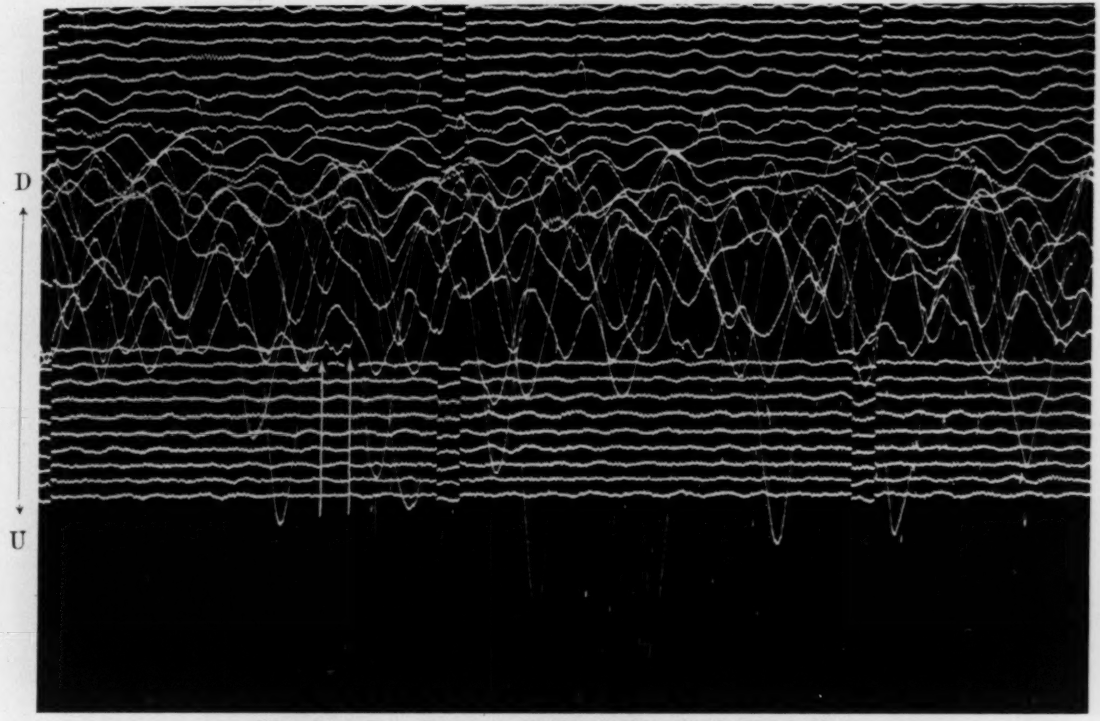

Fig. 3a. Pasadena ($\theta=74.^\circ 54$), Vertikal (Benioff).
$T_0=0.^s5$, $T_1=1.^s5$. Auf 4/5 verkleinert aus Original.

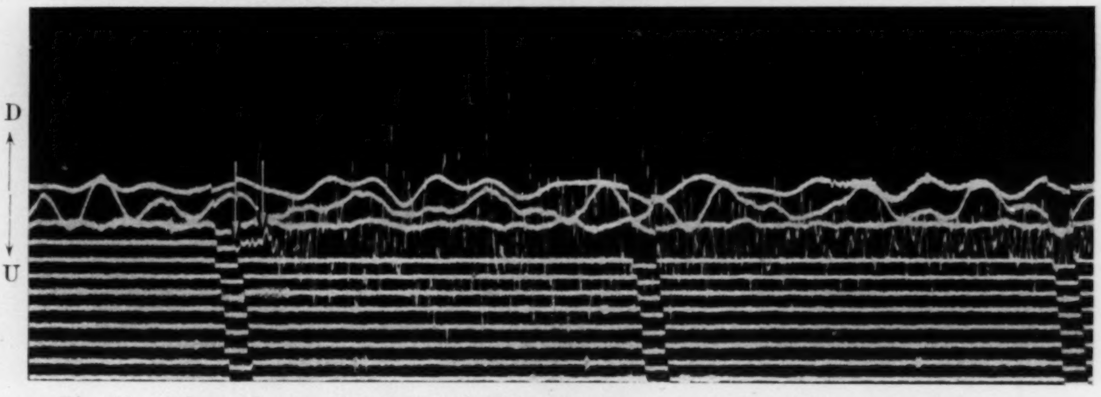

Fig. 3b. Riverside ($\theta=75.^\circ16$), Benioff Vertikal. Auf 4/5 verkleinert aus Original.
$T_0=0.^s5$, $T_1=0.^s2$, $\varepsilon\approx$kritisch.

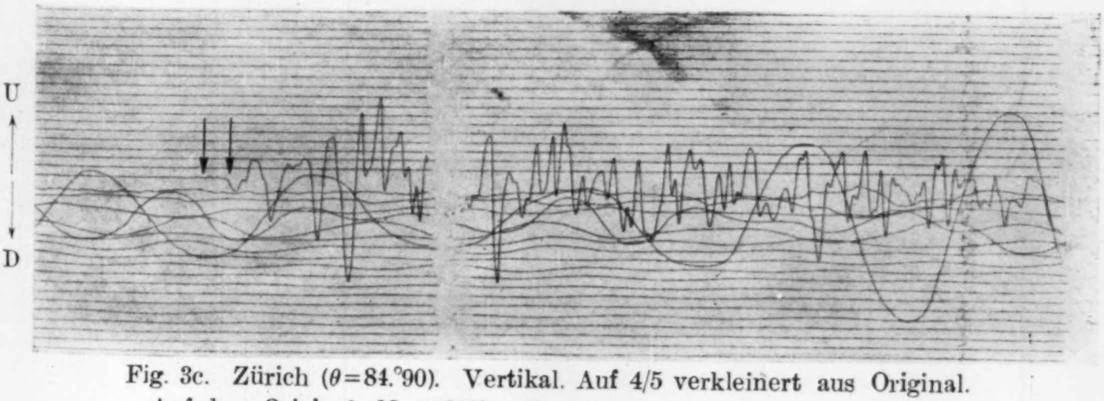

Fig. 3c. Zürich ($\theta=84.^\circ90$). Vertikal. Auf 4/5 verkleinert aus Original.
Auf dem Original, $M=20800$kg, $T_0=1.^s2$, $\varepsilon=2{\cdot}1$, $r=0{\cdot}1$ mm, $V=1600$

（震研彙報 第十三號 圖版 松澤）

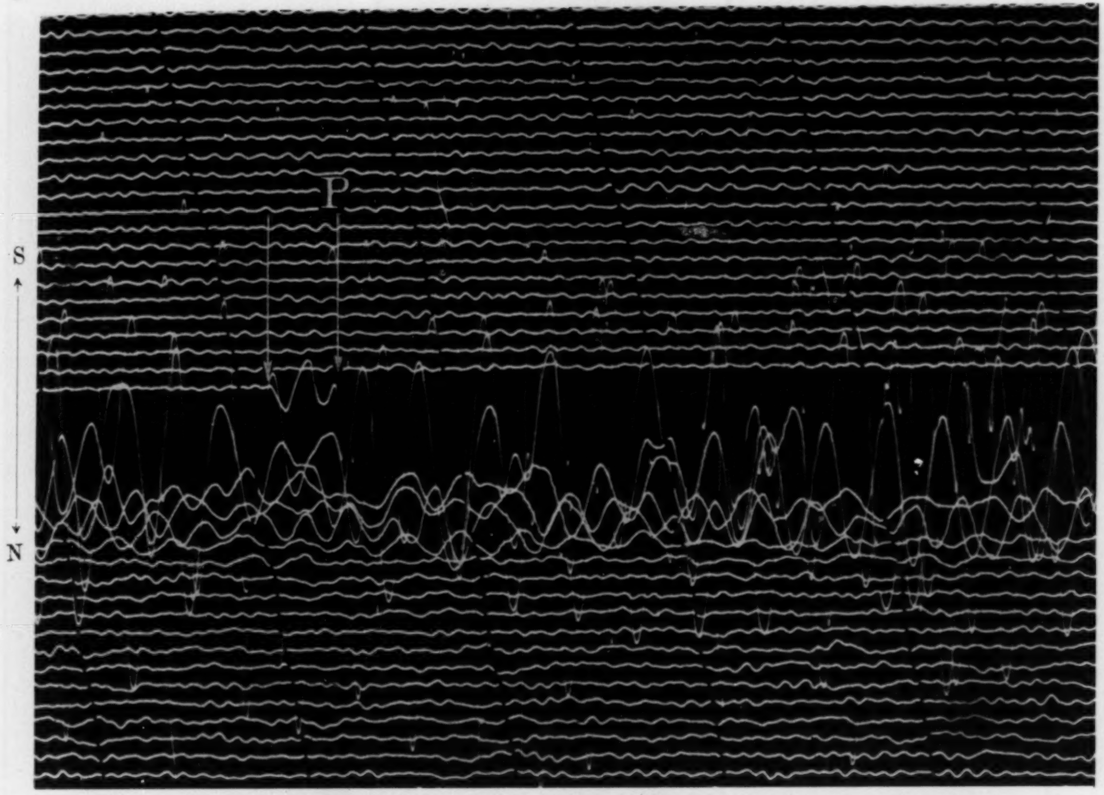

Fig. 4a. Stuttgart ($\theta=83.^\circ 75$). Galitzin NS. Auf 4/5 verkleinert aus Original. Auf dem Original, $T_1=12.^s0$, $T=12.^s1$, $\mu^2=-0{\cdot}10$, $k=112$, $A=100$ cm, $l=11{\cdot}2$ cm.

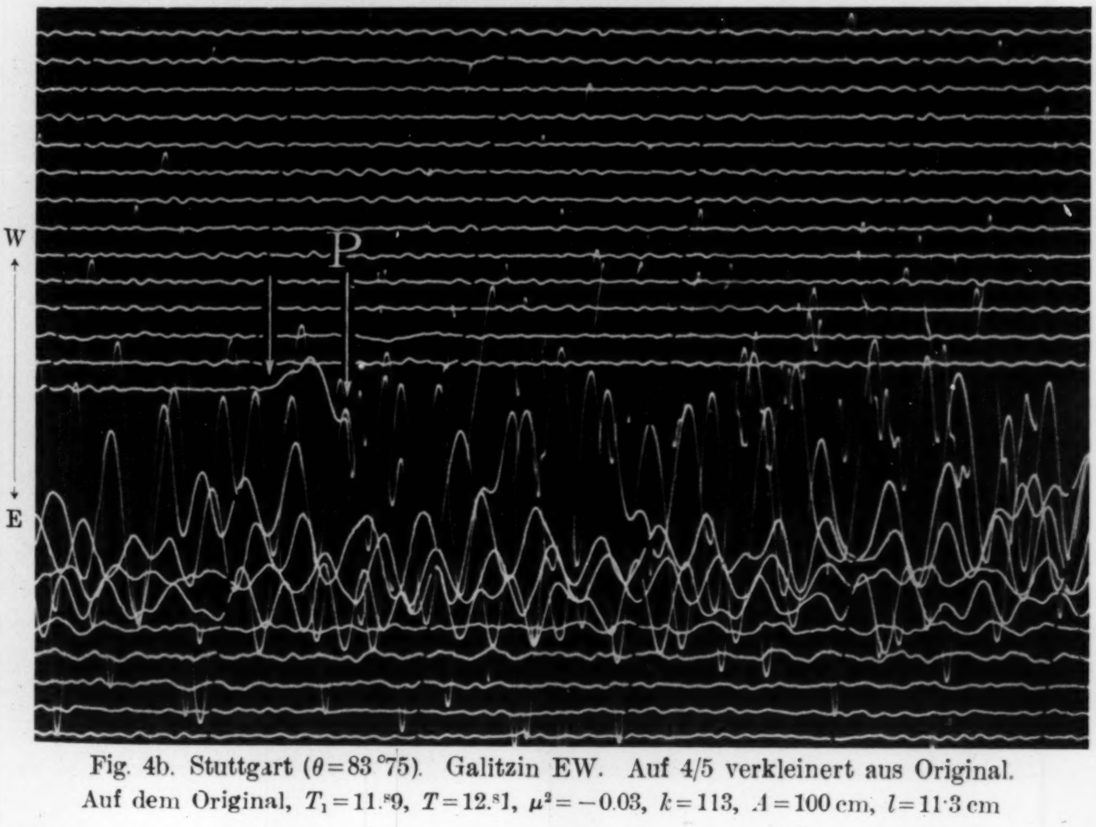

Fig. 4b. Stuttgart ($\theta=83^\circ 75$). Galitzin EW. Auf 4/5 verkleinert aus Original. Auf dem Original, $T_1=11.^s9$, $T=12.^s1$, $\mu^2=-0.03$, $k=113$, $A=100$ cm, $l=11{\cdot}3$ cm

（震研彙報 第十三號 圖版 松澤）

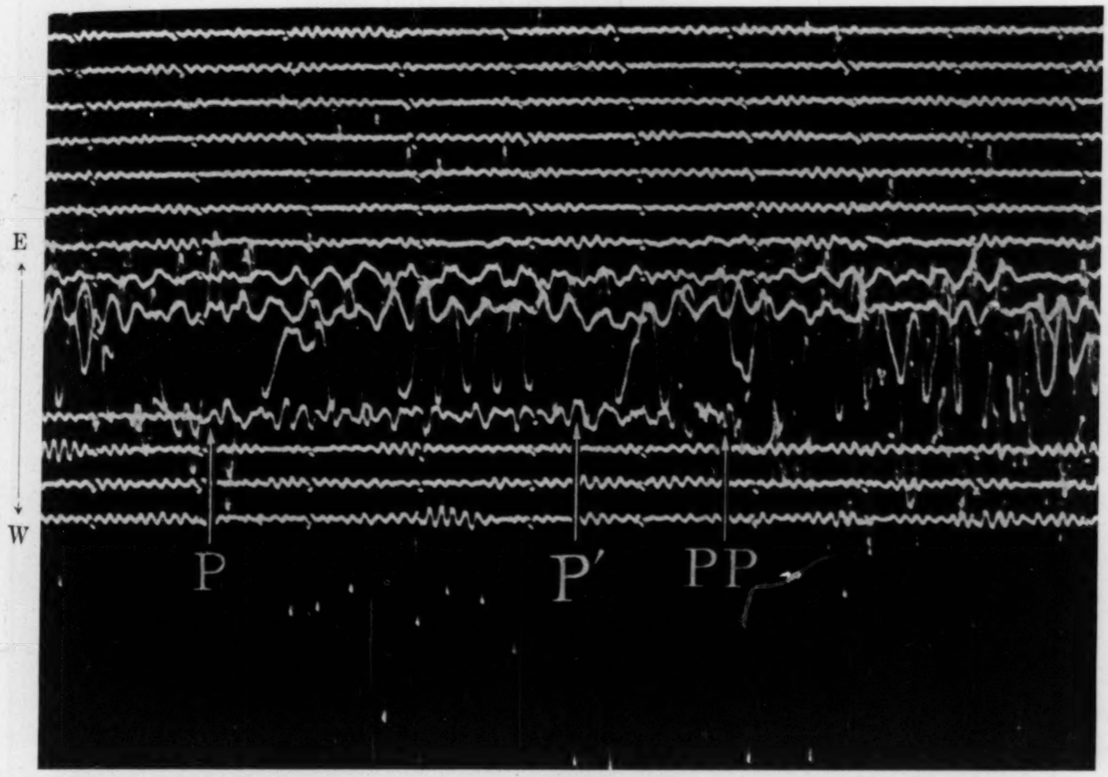

Fig. 5a. San Juan ($\theta=116°.11$). Wenner EW ($T=12$ s). Auf 4/5 verkleinert aus Original.

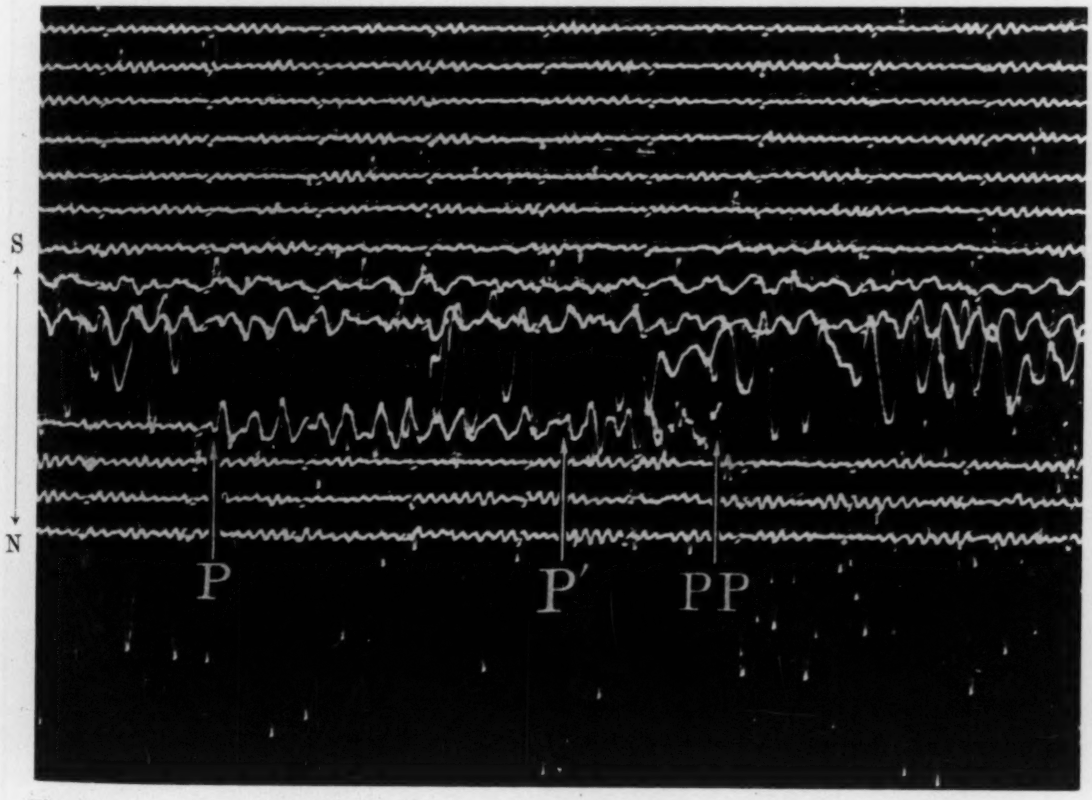

Fig. 5b. San Juan ($\theta=116.°11$). Wenner NS. ($T=12$ s). Auf 4/5 verkleinert aus Original.

（震研彙報 第十三號 圖版 松澤）

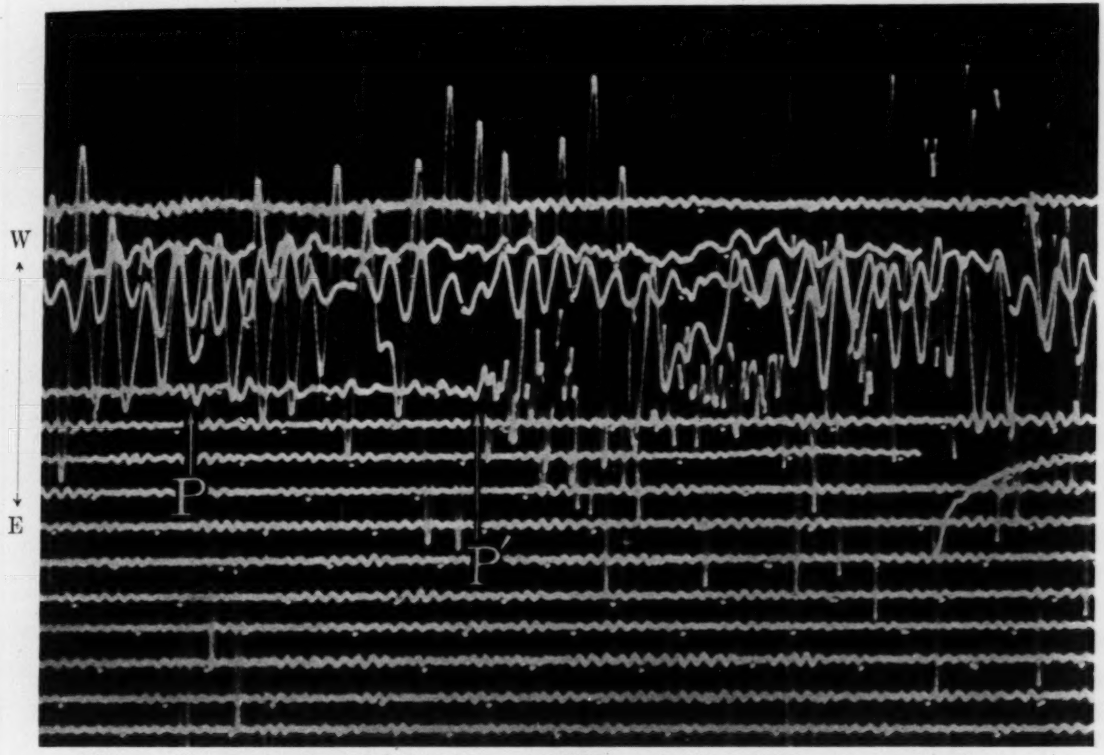

Fig. 6. Huancayo ($\theta=135.^\circ75$), Wenner EW. Auf 4/5 verkleinert aus Original. Auf dem Original, $T_0=11^s$. $V=1400$, $\varepsilon=20:1$.

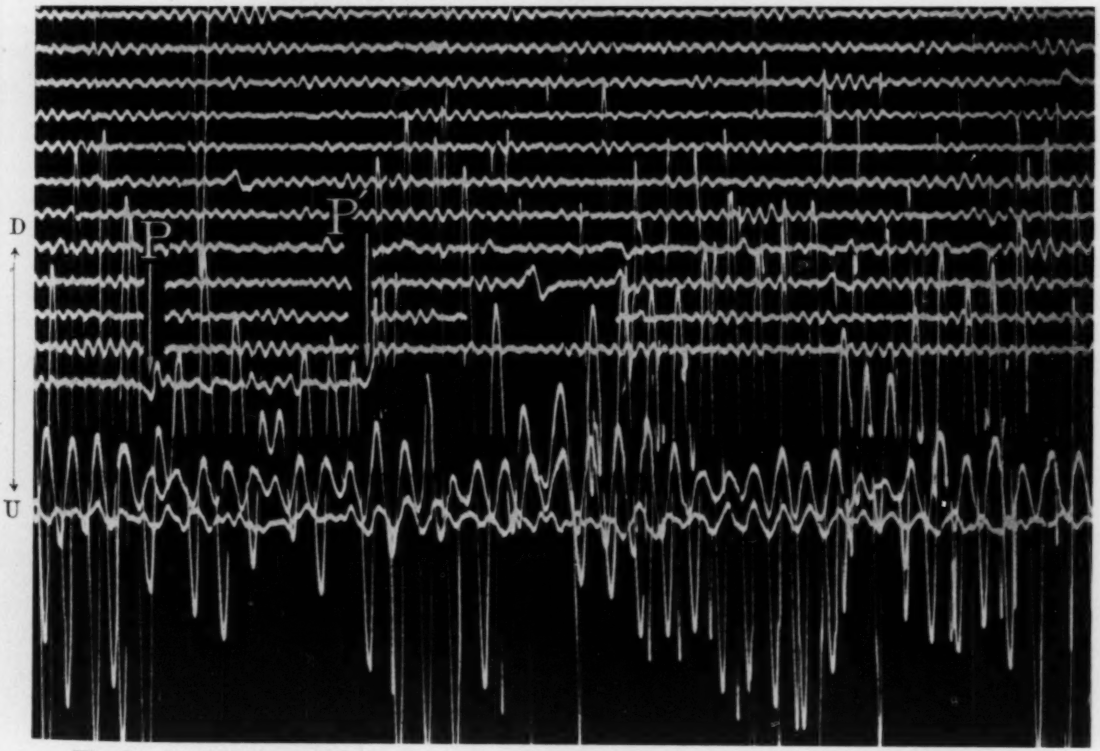

Fig. 7. La Paz ($\theta=143.^\circ81$). Galitzin Vertikal. Auf 4/5 verkleinert aus Original. Auf dem Original, $T_{\rm gal}=11.^s76$, $T_{\rm pend.}=9.^s93$, $\mu^2=-0{\cdot}09$, $k=130{\cdot}6$, $\log l=\bar{3}{\cdot}458$.

（震研彙報 第十三號 圖版 松澤）

13. 昭和8年3月3日の地震

(其の1) 震央

地震研究所 松 澤 武 雄

此の地震は器械觀測から觀ると，震央距離162°.6程離れたRio de Janeireで最大振幅約0·5 mm.程の大きい地震であつた．此の様に大きな地震では，近い所の觀測許りでなく，遠い所の觀測の研究も必要であるから，世界の色々な觀測所の觀測を借りて調べてみた．幸ひ134の觀測所から原圖又は其の寫しを送つてくれた．

(1) P波の觀測から1933年に出たMacelwaneの表に從つて震央を定めると，次の様になる．

$$\varphi=39^\circ{\cdot}15\pm0{\cdot}08\,\mathrm{N},\qquad \lambda=144^\circ{\cdot}40\pm0{\cdot}07\,\mathrm{E},$$

$$O=1933年3月3日2時31分\ 0{\cdot}1\pm0{\cdot}3秒.$$

一つ一つの觀測の平均誤差は $\pm2{\cdot}92$秒であるが，此の O はMacelwaneの表にあわせた場合の時間のはじまりで，震原に於ける發震の時刻と云ふ意味ではない．

(2) 核の蔭に於ける P 波は，震央距離143°.81のLa Paz迄明瞭に觀測された．走時の性質は大體次の様になる．

$$\frac{\partial T}{\partial\theta}=4{\cdot}7.$$

P' 波の焦點の內側に於けるものも，116°.11のSan Juan迄認められた．

(3) 此處にきめた震央を假定して，日本の觀測から走時を定めると次式がよく適合する．

$$T=31^{\mathrm{m}}+(1^{\mathrm{s}}{\cdot}6\pm0{\cdot}5)+(14{\cdot}55\pm0{\cdot}35)\theta-(0{\cdot}0022\pm0{\cdot}0015)\theta^3.$$

各々の觀測の平均誤差は $3^{\mathrm{s}}{\cdot}51$ で，此の式は14°迄の材料できめたものであるが，21°迄よく適合する．走時は21°, 32°の邊で增しかたが大いに變はるが，ByerlyやLehmannの云ふ様な折れる事はない様に思はれる．

(4) 實際の觀測と此の式の値との差をつくると，場所に對する分布は常にあらはれる様な，組織だつたものになる．

14. *Experiments on Artificial Earthquakes.*

By Win INOUYE and Hayabusa KIMURA,

Earthquake Research Insitute.

(Read Nov. 20, 1934.—Received Dec. 20, 1934.)

1. Since the elegant study made by Professor T. Shida, the observations of the initial motions of an earthquake became very significant among observations of many phenomena accompanied by an earthquake to inform us the mechanism of the earthquake. Afterwards, the studies of this problem were much improved by many investigators from both the theoretical and observational sides. Among the investigations the study made on the problem by Professor K. Sezawa[1] and the study based on observed data made recently by Professor M. Ishimoto[2] are specially mentioning. By these investiagtions the mechanisms of many earthquakes were quite cleared up.

Now, the experimental observations of the shakings of the ground caused by artificial sources, for example, the explosion of the dynamite and the fall of a weight on the surface of the ground, were fully made by Professor J. Milne[3]. He stated about the initial motions of these artificial earthquakes as follows.

Near to an origin the first motion is outwards. At a distance from an origin the first motion may be inwards. As to whether it will be inwards or outwards is probably partly dependent on the intensity of the initial disturbance and on the distance of the observing station from the origin.

It seems to us that at a distance from an origin the first outwards motion might be extinguished by the absorption of the soil on the way to the recording station and the second inwards motion which is usually greater than the first motion might be observed as the initial motion.

Afterwards, Professor F. Omori and Professor A. Imamura[4] observed the shocks caused by dynamite explosions in the military exercise ground at Akabane, near Tôkyô. They found that the direction of the initial displacement of an earth particle at the surface in these earthquakes were outwards from or inwards to the origin according to the origins of explosions were at or some depths below the surface of the ground respectively.

---

[1] K. SEZAWA, *Bull. Earthq. Res. Inst.*, 2 (1927), 13∼28.

[2] M. ISHIMOTO, *Bull. Earthq. Res. Inst.*, 10 (1932), 449∼471.

[3] J. MILNE, *Trans. Seis. Soc. of Japan*, 8 (1885), 1∼82.

[4] F. OMORI and A. IMAMURA. *Pub. E. I. C.*, 21 (1905), 67.

2. The authors are now carrying out the experiments on artificial earthquakes in the yard of the branch station of the Earthquake Research Institute at Komaba, Tôkyô. We are mainly studying the initial motions of the shocks caused by the explosions of the explosives enclosed in pipes both ends open or closed at one end, and by the fall of a heavy weight on the surface of the ground or into the pits digged at several depths in the ground.

This note is the preliminary report of the latter.

For example, the arrangements of an experiment are shown in Fig. 1. The recording instruments are horizontal pendulums, the each heavy bob is a cylinder weighing about 300 gr. and the each magnification is about twelve times.

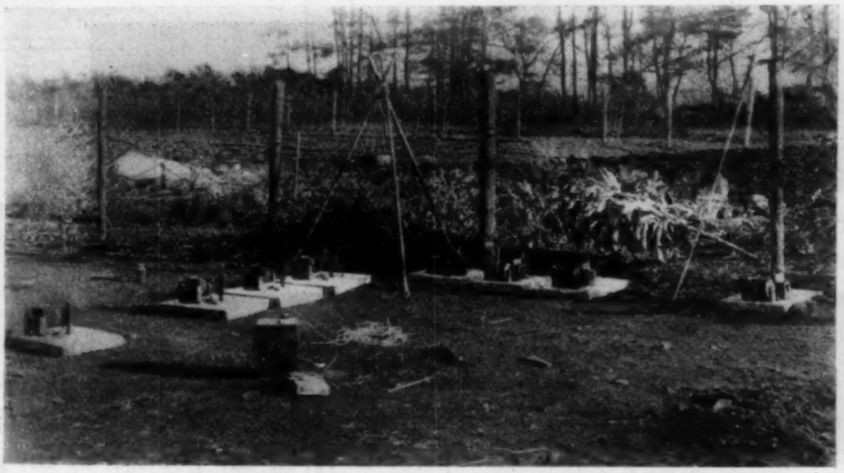

Fig. 1.

The each pendulum has a proper period of about 0·11 sec. and has no damper.

The weight is a iron cylinder weighing about 15 kg. and the diameter is about 19 cm. The amount of the fall of the weight is always about 70 cm.

The pits were digged at 30 cm., 50 cm., 75 cm. and 100 cm. in the ground as narrow as possible to be sufficient for the fall of the weight.

The recording apparatus were mounted at 50 cm., 100 cm., 150 cm., 200 cm. and 250 cm. apart from the origin.

Some of the records obtained by these experiments are shown in Figs. 2 and 3, and the results of observations of the initial motions are plotted in Fig. 4. In the figure the absissa represents the epicentral distance and the ordinate represents the amount of the initial displacement as recorded. It will be seen in the figure, the initial motions were "push" when the weight had fallen to the surface of the ground. Moreover, in this case, the amounts of initial displacements diminished proportionally to the inverse square of the distance from an origin. When the weight had fallen into a pit sufficiently deep, the initial motions near to the origin were "pull" and at a distance from an origin they were "push". By the way, the periods of waves in these earthquakes mostly are about 0·025 sec.

3. It seems to us that there are two possible explanations for the phenomena above stated.

a. The first one is as follows. Near to the origin the ground depressed and at a distance from the origin it bulges out by the impact of the fall of a weight, so that the initial motion is inwards or outwards according to the distance of the observing station from the origin.

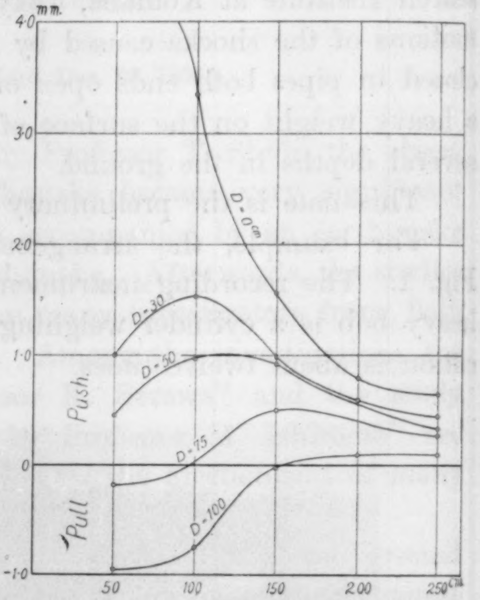

Fig. 4. The relation between the amount of initial motion and the epicentral distance.
D is the depth of the pit.

b. The second and more probable explanation is as follows. The impact of the fall of a weight may be taken as a doublet force without moment. The dilatational wave spreads out downwards and the condensational wave spreads out upwards from the portion of the ground impacted by the fall of the weight. The nodal plain lies horizontally under the base of the weight. If the velocity of propagation of elastic waves in the ground instead of being constant throughout the medium increases according to the depth, the nodal plain is bent up to the surface of the ground at some distance from the origin, so that the initial motion is "pull" or "push" according to the distance is near to or apart from the origin.

The epicentral distance where the nodal surface bent up to the surface of the ground may be given by the following equation:

$$\Delta=\int_0^H \frac{v\,dh}{\sqrt{\left(\frac{v_0}{\alpha}\right)^2-v^2}},$$

where v is the velocity of the elastic wave at any point, v_0 is that at

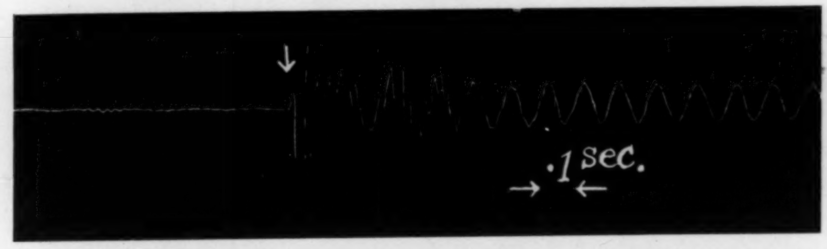

$\Delta = 50$ cm. (Push) *(Full size the actual)*

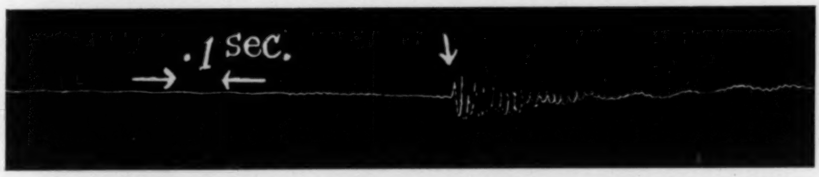

$\Delta = 100$ cm. (Push) *(Full size the actual)*

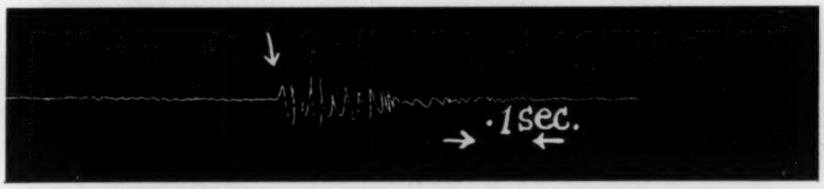

$\Delta = 150$ cm. (Push) *(Full size the actual)*

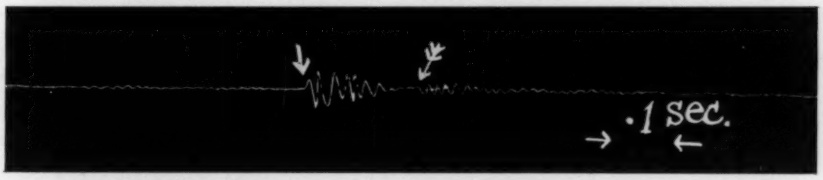

$\Delta = 200$ cm. (Push) *(Full size the actual)*

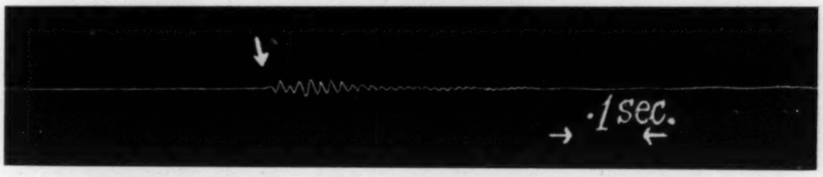

$\Delta = 250$ cm. (Push) *(Full size the actual)*

Fig. 2. The shakings of the ground caused by a fall of a weight into a pit of 30 cm in depth.

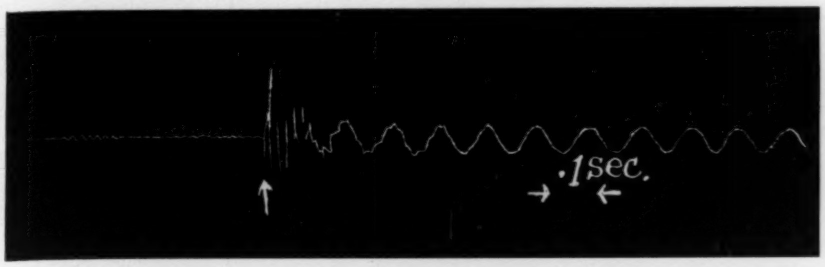

$\Delta = 50$ cm. (Pull) *(Full size the actual)*

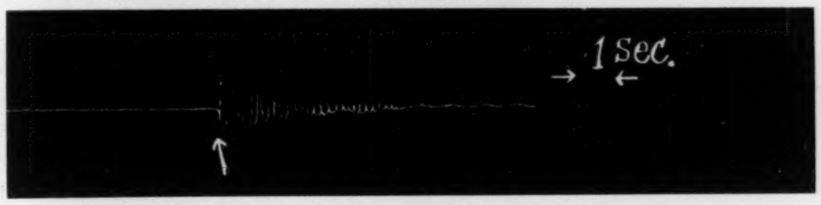

$\Delta = 100$ cm. (Pull) *(Full size the actual)*

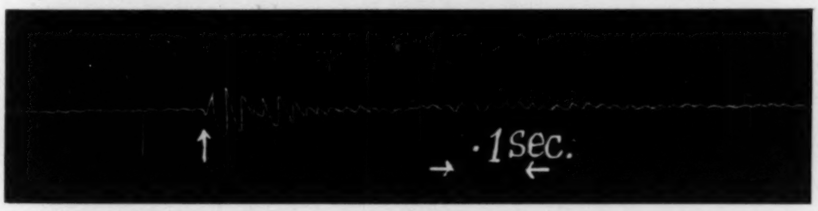

$\Delta = 150$ cm. (Pull) *(Full size the actual)*

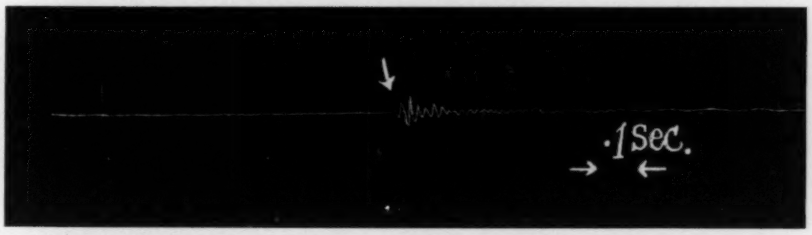

$\Delta = 200$ cm. (Push) *(Full size the actual)*

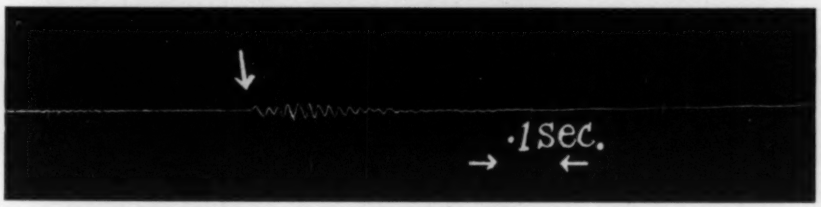

$\Delta = 250$ cm. (Push) *(Full size the actual)*

Fig. 3. The shakings of the ground caused by a fall of a weight into a pit of 100 cm in depth.

the surface of the ground, α is the emergency angle of the nodal surface and H is the depth of the pit.

Now, we assume that the wave velocity increases linearly as the depth increases.

$$v = v_0 + ch.$$

Then,

$$\Delta = \int_{v_0}^{V} \frac{v\,dv}{\sqrt{\left(\frac{v_0}{\alpha}\right)^2 - v^2}} = \frac{v_0}{c}\sqrt{\frac{1}{\alpha^2} - 1},$$

where V is the wave velocity at the depth of the pit.

Next, $$H = \frac{v_0}{c}\left(\frac{1}{\alpha} - 1\right).$$

Eliminating α from these two equations, we obtain

$$c = \frac{2Hv_0}{\Delta^2 - H^2}.$$

Generally, we will obtain different value for the constant c for each experiment changing the depth of the pit, and we can reduce the elastic condition in the earth. In the case of our experiment, when the depth of the pit is 75 cm. the value of $c = 6{\cdot}05\ v_0$, and when the depth of the pit is 100 cm. the value of $c = 1{\cdot}6\ v_0$. This fact suggests that near the surface of the ground the wave velocity diminishes suddenly as the depth decreases.

4. The experiments above stated may serve as examples to depression earthquakes or volcanic earthquakes accompanied by the eruptions of a volcano. In the latter case, the reaction of the eruption may be equivalent to the impact of the fall of a weight into a pit.

---

14. 人工地震の實驗

地震研究所 { 井上宇胤
木村隼

著者等は火藥の破裂, 重錘の落下等に依る人工地震の際の初動の研究をしてゐるが, 此處には重錘を地上並に地中の穴の中に落した際に生ずる地動の初動の觀測結果を報告してある. 此れは陷落地震及び噴火に伴ふ地震の研究並に地下の構造を知る上に幾分役立つものと思ふ.

15. *Experiments on the Visco-elastic Properties of Pitch-like Materials.* (*I*)*

By Kumizi IIDA.

(Read Oct. 16 and Nov. 20, 1934.—Received Dec. 20, 1934.)

Introduction.

As is generally noticed in natural phenomena, to forces long applied, the materials composing the earth's crust exhibit the properties of viscous liquids, and behaving as elastic solids when they are subjected to sudden forces for a short period of time. The former property will be noticed in sedimentary rocks once deposited at the bottom of the sea, but which have since been subjected to folding and in the chronic deformations of the earth's crust as revealed by levellings, and the latter is seen in the propagation of seismic waves.

It will thus be seen that the materials forming the earth's crust possess two different properties, according to the length of time that they are subjected to forces; differences in pressure and temperature being, of course, powerful factors in producing these changes. The author undertook the experiments here described with a view to looking at the matter that is connected with the above described two properties. As a matter of expediency, the experiments were made with such readily accessible substances as commercial black pitch, paraffin, water-glass, and sandstone. The experiments on these substances have in the past been made in order to obtain one of their elastic and viscous properties. The present experiments are different from the past on the point that the author distinguishes clearly the elastic from the viscous properties of a substance.

The physical properties of rocks have been studied by H. Nagaoka[1] (1900), S. Kusakabe[2] (1903), and F. D. Adams and E. G. Coker[3] (1906), so that their elastic properties are now understood. The nature of rocks being so different to that of common metals, no perfectly elastic rock has yet been found, so that Hooke's law does not seem to hold even for very small forces. Water-glass[4] and "Miduame",[5] the Japanese rice jelly, are substances typical of a viscous liquid, the coefficient of viscosity of which was measured by Stokes's method at various temperatures.

---

* Communicated by M. Ishimoto.

[1] H. NAGAOKA, *Pub. Imp. Earthq. Inv. Comm.*, 4 (1900), 47~67; *Phil. Mag.*, 50 (1900), 53.

[2] S. KUSAKABE, *Publ. Imp. Earthq. Inv. Comm.*, 14 (1903) 1~73; 17 (1904), 1~48, etc.

[3] F. D. ADAMS and E. G. COKER., *Carnegie Inst., Washington Publ.*, 46 (1906).

Of pitch-like substances, such as pitch, paraffin, etc., there have been many investigations. All these studies concern their viscosity and seldom their elasticity. The rigidity as well as the viscosity of colloidal solutions have, however, been determined by some investigators. The first investigator to determine it was Th. Schwedoff,[6] who in 1889, examined a single gelatin sol, the method used being that with the concentric cylinder apparatus, as will be described later. He found that the modulus of rigidity in a sol of 0·5 per cent gelatin was 0·535 c. g. s. Later, E. Hatschek and R. S. Jane[7], in 1926, also made detailed investigations by the method just mentioned and found the modulus of rigidity for a sol of 0·3 per cent benzopurpurin at a temperature of 14° C to be 0·75 c. g. s. They later determined the coefficient of viscosity using the Maxwell relation.[8] The apparent viscosity of many colloidal solutions exhibited anomalies in the order of the centipoise when determined by ordinary methods.

The various methods which have been proposed for measuring the internal friction of solids, such as pitch are the following:

B. Weinberg[9] used the method of spiral form torsion or flow in an inclined channel under the action of gravity and obtained $2{\cdot}0\times10^{8}$ at 15°C or $1{\cdot}9\sim2{\cdot}0\times10^{7}$ for the internal friction. V. Obermayer,[10] by the shearing of a paralleropiped and compression of a cylindrical disc, obtained $1{\cdot}0\times10^{8}$ at 15°C and $2{\cdot}7\times10^{8}$ at 12°C respectively. Trouton[11] obtained $1{\cdot}1\times10^{10}$ by the method of longitudinal extension of a cylinder. The shearing of two adjacent parallelopipeds and tearing of asphalt gave Dudeckij[12] $8{\cdot}1\sim8{\cdot}8\times10^{10}$ at 15°C, while Segel,[13] by the axial shearing of a cylindrical layer of sealing wax, obtained $1{\cdot}1\times10^{10}$ at 19°C.

According to the experimental results of F. T. Trouton and E. S. Andrews,[14] pitch behaves differently from that of an ideally or purely viscous body. They measured the viscosity of pitch at constant temperature by clamping cylinders of it at both ends, one of which was kept fixed while a constant torque was applied to the other. They found also the elastic viscous recovery, but did not give the value of the elastic moduli. They obtained $1{\cdot}3\times10^{10}$ at 15°C for the coefficient of viscosity of pitch. The most complete investigation, as far as temperature range is concerned, was that by Pockettino[15] in 1914 on ordinary black pitch. He determined not only the viscosity coefficient, but also the Young's modulus and the Thomson and Tait coefficient of elastic restitution. Three different methods such as the concentric cylinder method, Stokes', and the capillary tube method, were used in three ranges of temperature, from 9°C to 50°C, 34°~80°C, and above 80°C, respectively, the results of which fall accurately on a smooth curve, the value of the viscosity coefficient being from $2{\cdot}35\times10^{10}$ at 9°C to $1{\cdot}19\times10^{2}$ at 99·9°C. In elasticity, by comparing the vibrations of tubes filled with pitch at different temperatures, he found the modulus falls from 720 at 9·8°C, to 330 at 32·3°C, to 64 at 44·3°C, and to 0 at 51·8°C. The coefficient of elastic restitution falls continuously, at first slowly, then more and more rapidly, from 0·92 at 10°C to 0·44 at 28·1°C, to 0·12 at 31°C and to 0·0 at 32°C. Between 32°C and 75°C, pitch is plastic, neither a proper solid nor a liquid.

---

[4] Prof. M. Ishimoto has measured the coefficient of viscosity of water-glass at various temperatures and its values are almost the same of the author's results.

[5] N. Miyabe, *Bull. Earthq. Res. Inst.*, **12** (1934), 199.

[6] Th. Schwedoff, *J. de Physique*, **8** (1889), 341.

[7] E. Hatschek and R. S. Jane, *Koll. Zeitsch.*, **39** (1926), 300.

[8] J. C. Maxwell, *Phil. Mag.*, **35** (1868), 133.

[9] B. Weinberg, *Proc. Ind. Assoc. Cult. Sci.*, **9** (1926), 215; *Ind. J. Phys.*, **1** (1926~1927), 279.

[10] V. Obermayer, *Sitzber. Wien. Akad.*, **75** (1877), 665.

[11] Trouton, *Proc. Roy. Soc. Lond.*, **77** (1900), 426.

[12] V. D. Dudeckij, *J. R. Ph. S.*, **45** (1913), 499.

[13] Segel, *Phys. Zts.*, **4** (1903), 493.

[14] F. T. Trouton and E. S. Andrews, *Proc. Phys. Soc. Lond.*, **19** (1909), 47.

The viscosity of typical pitches has been recently measured by A. B. Manning[16] (1933), using three different methods to cover the range 30°~110°C. All the coal-tar pitches tested behaved as a truly viscous liquid according to his results. Experiments made with bitumen, that is, petroleum pitch, showed properties differing from those of colloids, such as gelatine, rubber, etc. Bitumen therefore appears to have the structure of a gel just described.

Some investigators[17] studied the effect of pressure on the viscosity of pitch-like substances and found that it increased with pressure.

Since, as shown by the studies of certain investigators, the substances just mentioned possess two different properties, elasticity and viscosity, the author desired to know their physical properties, and to distinguish clearly the elastic from the viscous properties of a substance the present experiments therefore were carried out at certain constant temperature and its effect on their properties was taken into consideration, but not the pressure effect.

---

15) A. Pockettino, *Nuovo Cimento*, **8** (1914), 77.

16) *Nature Dec.*, **30** (1933), 1009.

17) For example, W. C. Röntgen, *Wied. Ann.*, **45** (1892), 98; C. Barus, *Phil. Mag.*, **29** (1890), 337

Part I. The Statical Method of Experiments.

1. Theory. We shall first examine the substance by means of the most readily available method—that with the concentric cylinder apparatus.

The upper end of the wire from which an inner cylinder is suspended, is twisted through a constant angle φ; if the substance is merely a viscous liquid, the cylinder rotates with the wire with decreasing velocity until it has moved through the angle φ, i. e. until no torsion is left in the wire. If, however, the substance possesses rigidity, the cylinder does not do so, but only rotates through an angle $\omega(<\varphi)$, and maintains this position for a short time, the elastic deformation of the substance balancing the torque of the wire, which is $k(\varphi-\omega)=k\delta\theta$, k, the torsional moment of the wire per unit angle. It will be noticed that the substance is subjected to a force that is proportional to the rotating angle of the wire.

If the substance is perfectly elastic, the cylinder does not follow the wire, but rotates through an angle θ at the same time that the wire is twisted, and maintains this position for a long time, i. e. θ remains constant.

When the force therefore is proportional to the rotating angle of the wire imparted to the substance, the angular deformation that results must correspond with the property of the substance. This may be held to apply also to the torsional experiment of the cylindrical bar, which, will be dealt with in the next section. It therefore follows that it will be possible to know the property that a substance possesses if we know its angular deformation.

2. The First Experiment. In view of the simple theory mentioned in the preceding section, experiments were carried out statically in order to see whether or not such substances as pitch, paraffin, and a sandstone from Yamaguti, a village in Nagasaki prefecture show viscous property when they are subjected to forces that are proportional to the rotating angle of the wire, for a prolonged period.

(*a*) *The Apparatus.* The apparatus is shown in Fig. 1. The specimen to be tested was prepared in the form of a cylindrical bar by casting the substance in a mould except the sandstone which was cut. The dimensions of the specimens are shown in Table I. The squared end of the specimen (T), was firmly clamped in a vertical position at its two ends to two similar brass parts (A_1), (A_2). A_2 is fixed to the solid frame, A_1 is connected to the steel wire (W), the lower end of which is twisted by the twister lever (R) attached to the wire. The amount of torsion caused in the specimen due to the twisted wire was measured by optically recording the deflection of two lens mirrors (M_1) (M_2), one attached to the rod which moves with the twister lever (R) which is clamped to the lowor end of the wire to enable observation of the fixed image, and the other attached to the pivot to which a magnet (C) is connected in order to magnify the angular deformation of the specimen, assuming that it rotates uniformly. The angular deformation of the specimen was photographically recorded on the drum, 1 meter away from the mirrors.

(*b*) *Observation*. In order to see the angular deformation of the specimen owing to forces that are proportional to the rotating angle of the wire for a prolonged period, the lower end of the wire was twisted at first through a constant angle φ by the twister lever, and

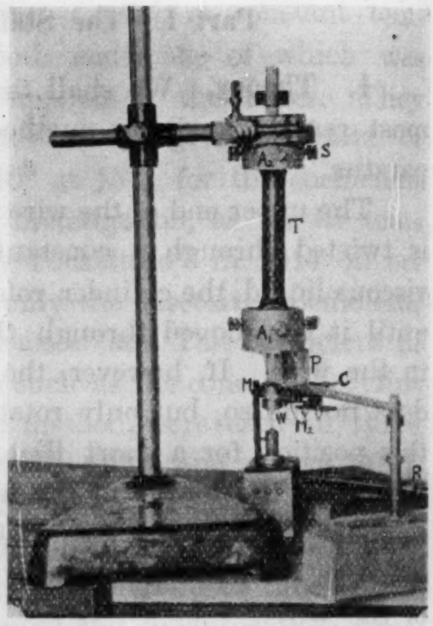

Fig. 1. Twisting apparatus.

T specimen, S screw, A_1, A_2 clamps, W steel wire, M_1, M_2 lens mirrors, P rectangular prism, C magnet, R twister lever.

Table I. Modulus of Rigidity and Apparent Viscosity of Pitch, Paraffin, and Sandstone.

Substance (dimension)	No.	Temp. (°C)	n (c. g. s.)	ε (c. g. s.)
Pitch	1	19·0	$7{\cdot}69\times10^{6}$	$1{\cdot}02\times10^{12}$
(Diameter $=3{\cdot}66^{\mathrm{cm}}$	2	19·7	3·71 〃	1·12 〃
Length $=10{\cdot}5^{\mathrm{cm}}$)	3	20·5	1·07 〃	$7{\cdot}70\times10^{11}$
	4	20·9	0·90 〃	7·50 〃
Paraffin	1	18·8	$7{\cdot}58\times10^{7}$	$9{\cdot}70\times10^{12}$
	2	20·3	4·37 〃	8·40 〃
(Diameter $=3{\cdot}66^{\mathrm{cm}}$	3	20·8	3·26 〃	3·85 〃
Length $=10{\cdot}5^{\mathrm{cm}}$)	4	22·6	$7{\cdot}34\times10^{6}$	2·88 〃
	5	22·8	5·61 〃	2·21 〃
Sandstone	1	21·0	$2{\cdot}46\times10^{9}$	$1{\cdot}85\times10^{14}$
	2	21·9	2·38 〃	1·57 〃
(Diameter $=1{\cdot}5^{\mathrm{cm}}$	3	22·1	2·34 〃	1·56 〃
Length $=10{\cdot}0^{\mathrm{cm}}$)	4	22·5	2·31 〃	1·55 〃

Substance	Water-glass	Pitch	Paraffin	Sandstone
Density	1·69	1·16	0·87	2·51

then allowed to remain in that state for a week. A week's record was thus obtained. The experiment was made in the basement of the Earthquake Research Institute in order to eliminate temperature variation as far as possible. Though it was difficult to keep the temperature constant for a long time, its variation during one week, the duration of the experiment, did not exceed 0·5°C. Since the rigidity of the wire was determined by observing the period of a torsional pendulum, the torsional couple c could be calculated by the formula $c=\frac{\pi r^4 n}{2l}\varphi$, where n is the modulus of rigidity of the wire, and l and r the length and radius of the wire respectively.

3. Results. Some examples of relaxation curves (the curves of the angular deformation) of twisted cylinders are shown in Fig. 6, and some

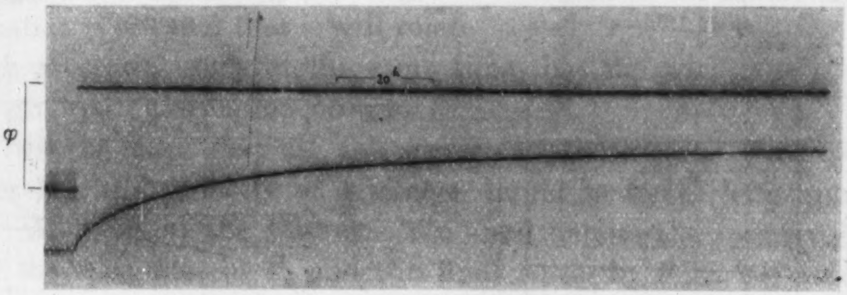

Fig. 2. Record of twisted pitch cylinder (No. 3).

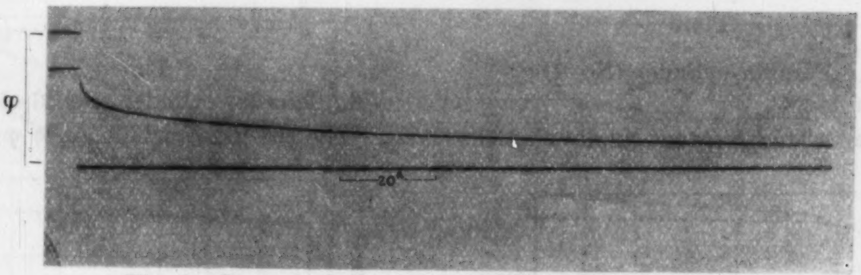

Fig. 3. Record of twisted paraffin cylinder (No. 2).

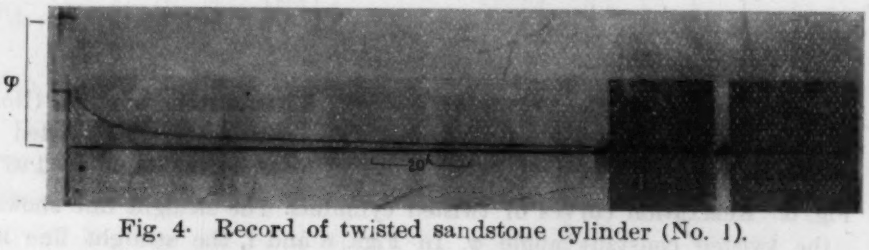

Fig. 4. Record of twisted sandstone cylinder (No. 1).

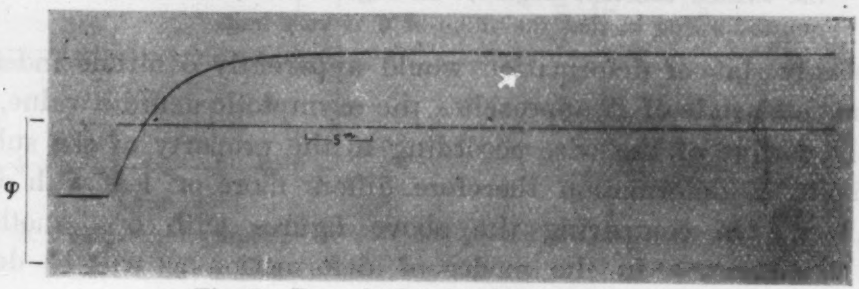

Fig. 5. Record of twisted water-glass.

of their actual records obtained by the apparatus are shown in Figs. 2~5.

When the torque is first applied there is a rapid flow or movement that gradually subsides and eventually reaches a steady state.

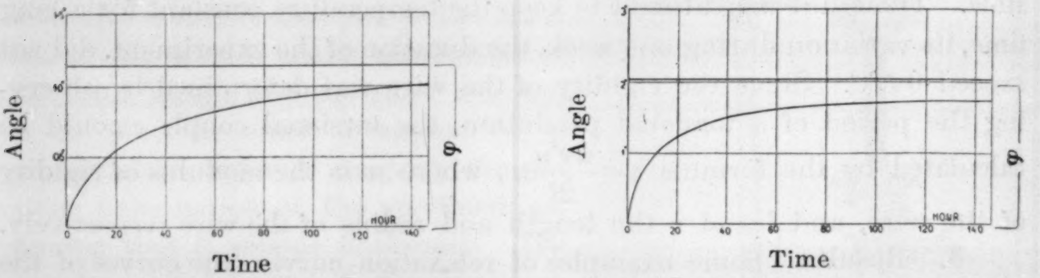

a. Pitch cylinder (No. 1) at 19·0°C. The twisted constant angle $\varphi = 1.15°$.

b. Pitch cylinder (No. 4) at 20·9°C. The twisted constant angle $\varphi = 2·04°$.

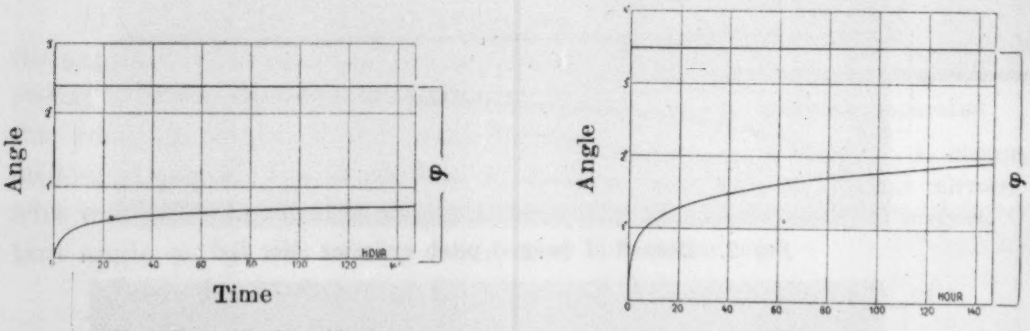

c. Paraffin cylinder (No. 1) at 18.8°C. The twisted constant angle $\varphi = 2·39°$

d. Paraffin cylinder (No. 2) at 20·3°C. The twisted constant angle $\varphi = 3·51°$.

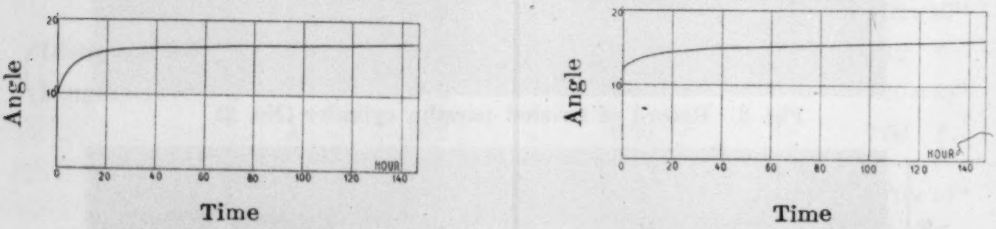

e. Sandstone cylinder (No. 1) at 21·0°C. The twisted constant angle $\varphi = 1·44°$

f. Sandstone cylinder (No. 4) at 22·5°C. The twisted constant angle $\varphi = 1·95°$

Fig. 6. Relaxation curves of twisted cylinders. The straight line shows the twisted constant angle φ. In Figs. e and f, the straight line is omitted owing to that the value of φ is very large.

This steady state of deformation would apparently continue indefinitely, but the final state of it approaches the asymptotic definite value, balancing the torque of the wire according to the property of the substance. The mode of deformation therefore differs more or less with different substances. On comparing the above figures with one another, we notice a difference in the modes of deformation as will be described later in detail.

In order to enable comparison with these figures, the deformation of water-glass is shown in Fig. 7. This curve was obtained by means of the concentric cylinder apparatus. Water-glass is so viscous that, in the final state, the inner cylinder follows the quartz fibre, that is, no torsion is left in the quartz fibre. In this, it is like pitch, but not paraffin and sandstone, so that pitch is more viscous than paraffin, while sandstone is the most elastic. When the torque is applied to sandstone the initial stage of angular deformation is so rapid that it will rotate through a certain angle at the same time that the wire is twisted, after which gradual deformation occurs.

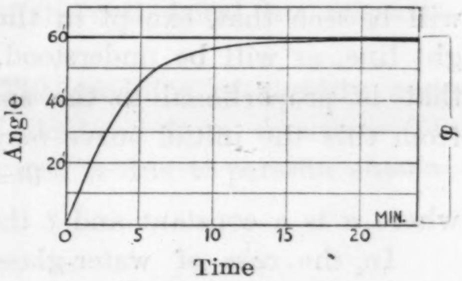

Fig. 7. Relaxation curve of twisted water-glass. The straight line shows the twisted constant angle $\varphi=59'$

It will be seen that all the specimens that were tested possessed more or less the property of a viscous liquid to forces long applied.

4. Analysis of the Curves. We shall denote the angular deformation of the specimen by θ, and the final value by $\theta_{t=\infty}$. We first tried to see whether or not the angular deformation decreases exponentially

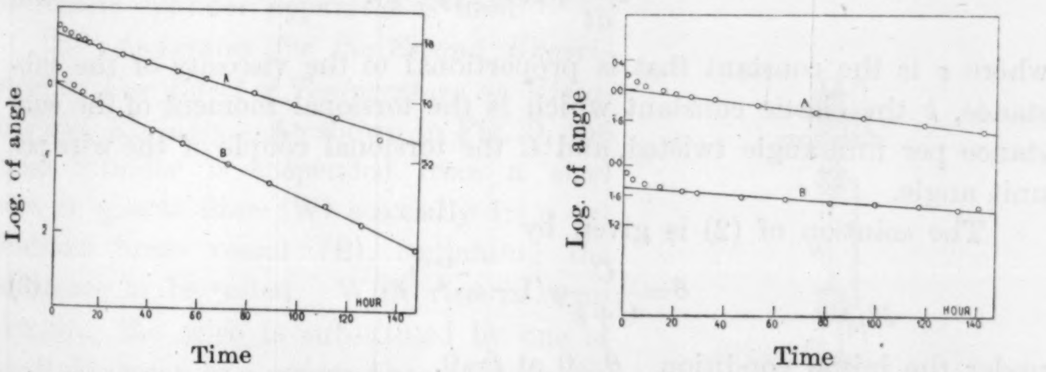

a. Pitch cylinder. A No. 2, B No. 4. b. Paraffin cylinder. A No. 2, B No. 1.

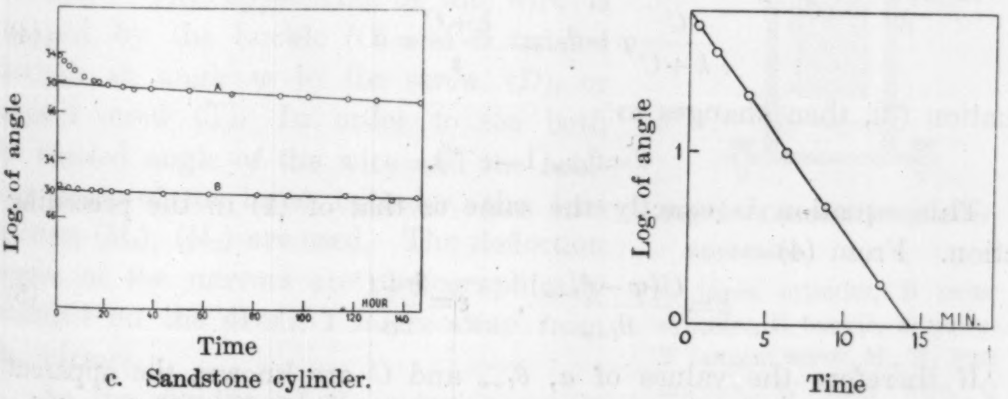

c. Sandstone cylinder.
A No. 1, B No. 4

d. Water-glass

Fig. 8. Curves of time and the log. of angle are almost a straight line.

with time. For this purpose the logarithm of θ was plotted as ordinate and the time as abscissa, an example of which is shown in Fig. 8. It will be seen that, except in the initial stage, all the points lie on a straight line, as will be understood, it seems, by considering that part of k that is proportional to the speed of deformation. We may conclude from this the initial curve may be expressed by

$$\theta=\theta_{t=\infty}(1-e^{-at}), \tag{1}$$

where a is a constant and t the time.

In the case of water-glass, $\theta_{t=\infty}$ equals φ, because no torsion is left in the quartz fibre, but $\theta_{t=\infty}$ does not equal the φ of parrafin, sandstone, and pitch, whose difference between $\theta_{t=\infty}$ and φ is very small. We therefore see that these substances possess rigidity as well as viscosity.

5. Mathematics. Assuming that the resistance of the viscosity of the substance is proportional to the velocity of the deformation, we have in this torsional system to deal with the equation of motion. Its elastic force is proportional to the angular deformation, while the external force is proportional to the rotating angle of the wire. We therefore have the equation

$$\varepsilon\frac{d\theta}{dt}+k\theta=C(\varphi-\theta), \tag{2}$$

where ε is the constant that is proportional to the viscosity of the substance, k the elastic constant which is the torsional moment of the substance per unit angle twisted, and C the torsional couple of the wire per unit angle.

The solution of (2) is given by

$$\theta=\frac{C}{C+k}\varphi(1-e^{-\frac{k+C}{\varepsilon}t}) \tag{3}$$

under the initial condition $\theta=0$ at $t=0$.

If now we put

$$\frac{C}{k+C}\varphi=\theta_{t=\infty}, \quad \frac{k+C}{\varepsilon}=a \tag{4}$$

equation (3), then changes to

$$\theta=\theta_{t=\infty}(1-e^{-at}).$$

This equation is exactly the same as that of (1) in the preceding section. From (4)

$$k=\frac{C(\varphi-\theta_{t=\infty})}{\theta_{t=\infty}}, \quad \varepsilon=\frac{k+C}{a}. \tag{5}$$

If therefore the values of a, $\theta_{t=\infty}$ and C are known, the apparent rigidity and viscosity will easily be found. Further the modulus of rigidity of a cylindrical bar, n, is calculated by the formula

$$n=\frac{2lk}{\pi r^4}, \tag{6}$$

where l and r are the length and radius of the cylindrical bar, respectively.

6. Calculation of the Coefficients. The modulus of rigidity and the apparent viscosity coefficient can be calculated from equations (5) and (6). For example the calculation of ε and n due to paraffin shown in Fig. 6. are as follows.

On paraffin (No. 1) at 18·8°C

$$\varphi=1{\cdot}39^\circ,\quad \theta_{t=\infty}=1{\cdot}000^\circ,\quad C=5{\cdot}72\times10^6,\quad l=10{\cdot}5^{\mathrm{cm}},\quad r=1{\cdot}83^{\mathrm{cm}},$$

$$k=5{\cdot}72\times10^6\times\frac{1{\cdot}39}{1{\cdot}00}=7{\cdot}95\times10^6,\ n=\frac{2l}{\pi r^4}k=9{\cdot}54\times7{\cdot}95\times10^6$$

$$=7{\cdot}58\times10^7\quad a=0{\cdot}00499,\ \varepsilon=\frac{k+C}{a}=\frac{13{\cdot}67\times10^6}{0{\cdot}00499}=9{\cdot}70\times10^{12}.$$

The values obtained by these calculations are shown in Table 1.

7. The Second Experiment. As is generally known, since temperature greatly affects viscosity and rigidity, it is important to see what these effects are. If the temperature rises the cylinder cannot be used, since the cylinder will melt at the high temperature, in which case the concentric cylinder apparatus is used.

(a) *Apparatus for the Second Experiment to show Effect of Temperature on Viscosity and Rigidity.* As shown in Fig. 9, the brass cylinder is suspended from a steel wire or quartz fibre (W) coaxially in a cylindrical brass vessel (B), containing the substance to be tested. With rise in temperature, the wire is substituted by one of small diameter or a quartz fibre of diameter 0·41 mm. The upper end of the wire is clamped by the buckle (C) and is twisted through an angle φ by the screw (D), or tangent screw (T). In order to see both the twisted angle of the wire and the rotating angle of the inner cylinder, the lens mirrors (M_1), (M_2) are used. The deflection angles of the mirrors are photographically recorded on the drum, 1 metre away from the mirrors.

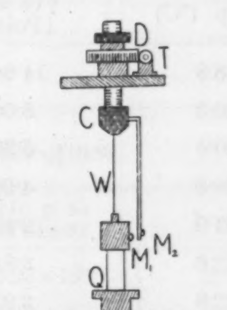

Fig. 9. Concentric cylinder apparatus.

A inner cylinder, B outer cylinder, C buckle, D screw, T tangent screw, M_1, M_2 lens mirrors, W steel wire, Q quartz cylinder, a=1·2 cm., b=1·9cm. h=6 cm.

As the rigidity of the wire or quartz fibre depends on temperature the cylindrical quartz bar (Q) is used to eliminate such effects. In order to regulate the temperature so that it shall remain constant during an experiment, the regulator is connected to the electric utensils, by which the water is heated. Into the water the outer cylinder is submerged, the water being stirred by the stirrer connected to the motor. The temperature was adjusted to be constant within the limits of 0·2°~0·5°C. The torsional couple of the wire and quartz fibre were determined by the vibrational method.

(*b*) *Results.* We have treated this experimental results in the same way as shown in section 3. Since in the case of the concentric cylinder apparatus, the moment due to viscous resistance, M, equals $\frac{4\pi h a^2 b^2}{b^2-a^2}\eta\dot{\theta}$, the constant that is proportional to the viscosity of the substance, ε, equals $\frac{4\pi\eta h a^2 b^2}{b^2-a^2}$, where a and b are respectively the radii of the inner and outer clylinder, h the effective height of the inner cylinder, η the coefficient of viscosity, whence

$$\eta=\frac{1}{4\pi h}\,\frac{b^2-a^2}{a^2b^2}\,\varepsilon.$$

By means of this equation the viscosity coefficient η can be cal-

Table II. Viscosity Coefficient and Apparent Rigidity of Paraffin.

Temp. (°C)	η (c. g. s.) (Poises)	Log η	k (c. g. s.)	Log k
18·8	$14{\cdot}86\times10^{11}$	12·17	$7{\cdot}95\times10^{6}$	6·90
20·3	8·00 ″	11·90	4·58 ″	6.66
20·5	5·35 ″	11·73	3·44 ″	6.54
20·8	4·99 ″	11·70	3·42 ″	6·53
21·6	2·43 ″	11·54	1·76 ″	6·25
22·6	$3{\cdot}84\times10^{10}$	10·58	$7{\cdot}69\times10^{5}$	5·89
22·8	2·93 ″	10·47	5·88 ″	5·77
29·0	$1{\cdot}22\times10^{8}$	8·09	$2{\cdot}81\times10^{4}$	4·52
32·0	$1{\cdot}81\times10^{7}$	7·26	1·52 ″	4·18
34·0	1·10 ″	7·04	$3{\cdot}88\times10^{3}$	3·59
37·1	$2{\cdot}18\times10^{6}$	6·34	2·98 ″	3·47
40·3	$9{\cdot}89\times10^{5}$	6·00	$3{\cdot}72\times10^{2}$	2·57
42·0	6·29 ″	5·80	2·51 ″	2·40
44·5	5·32 ″	5·73	1·59 ″	2·20
46·0	1·66 ″	5·22	1·26 ″	2·10
48·0	1·47 ″	5·17	—	—
50·0	0·42	$\bar{1}{\cdot}62$	—	—
51·8	0·30	$\bar{1}{\cdot}48$	—	—
52·5	0·24	$\bar{1}{\cdot}38$	—	—

Table III. Viscosity Coffiecient and Apparent Rigidity of Pitch.

Temp. (°C)	η (c. g. s) (Poises)	Log η	k (c. g. s)	Log k
19·0	7·57 × 10^{11}	11·88	1·48 × 10^{6}	6·17
19·7	3·92 〃	11·59	1·14 〃	6·06
20·5	3·14 〃	11·50	9·87 × 10^{5}	5·99
20·9	3·10 〃	11·49	9·42 〃	5·97
22·0	2·04 〃	11·31	4·13 〃	5·62
22·4	1·37 〃	11·14	4·12 〃	5·61
30·0	2·08 × 10^{10}	10·32	5·13 × 10^{4}	4·71
34·0	1·29 〃	10·11	2·56 〃	4·41
37·1	1·52 × 10^{9}	9·18	1·59 〃	4.20
44·0	1·69 × 10^{8}	8·23	6·37 × 10^{3}	3·80
48·0	5·31 × 10^{7}	7·73	5·05 〃	3·70
55·1	8·55 × 10^{6}	6·93	3·01 〃	3·48
60·2	2·62 〃	6·42	2·02 〃	3·31
65·0	1·78 〃	6·25	1·63 〃	3.21
70·0	5·72 × 10^{5}	5·76	1·13 〃	3·05
76·5	1·52 〃	5·18	7·73 × 10^{2}	2·89
83·0	4·08 × 10^{4}	4·61	—	—
87·0	2·49 〃	4·40	—	—
90·5	1·66 〃	4·22	—	—
95·1	1·04 〃	4·02	—	—

Table IV. Viscosity Coefficient of Water-glass.

Temp. (°C)	η (c. g. s) (Poises)	Log η	Temp. (°C)	η (c. g. s) (Poises)	Log η
14·3	6·05 × 10^{3}	3·78	32·6	0·23 × 10^{3}	2·37
17·0	3·48 〃	3·54	33·3	0·20 〃	2·31
19·0	2·47 〃	3·39	36·3	0·14 〃	2·16
19·7	2·21 〃	3·34	38·3	0·12 〃	2·07
23·4	1·19 〃	3·08	40·2	0·94 × 10^{1}	1·97
27·3	0·66 × 10^{2}	2·82	40·8	0·87 〃	1·94
27·5	0·56 〃	2·75	42·5	0·75 〃	1·87
28·1	0·50 〃	2·70	44·0	0·61 〃	1·78
31·2	0·34 〃	2·53	47·3	0·44 〃	1·64
31·8	0·30 〃	2·47	48·9	0·37 〃	1·57
32·3	0·25 〃	2·39	50·4	0·33 〃	1·52

culated. The values of the viscosity coefficient and the apparent modulus of rigidity for various temperatures are shown in Tables II–IV

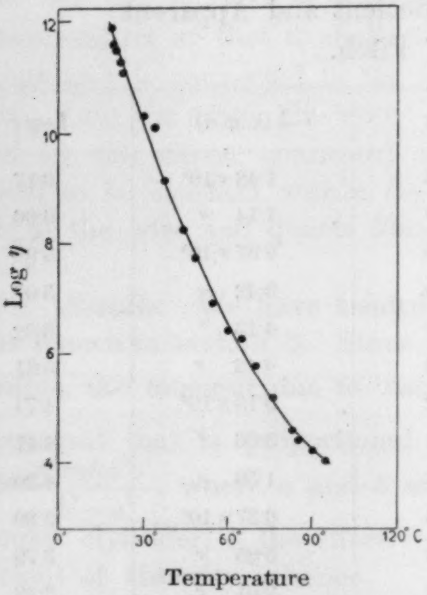

Fig. 10. Curve of temperature and the log. of viscosity coefficient of pitch.

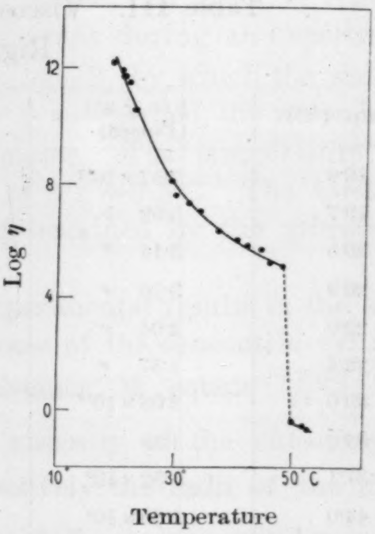

Fig 11. Curve of temperature and the log. of viscosity coefficient of Paraffin.

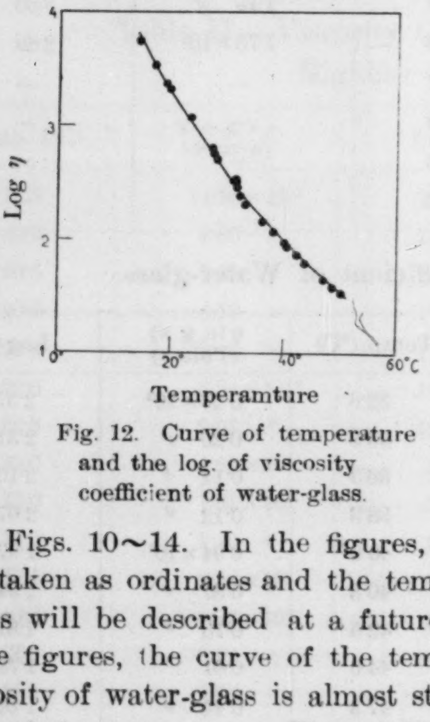

Fig. 12. Curve of temperature and the log. of viscosity coefficient of water-glass.

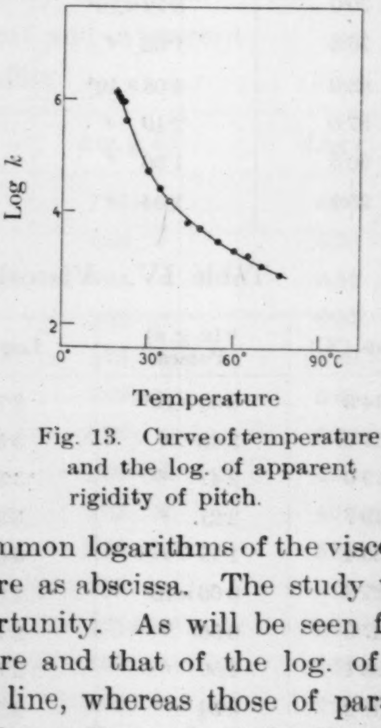

Fig. 13. Curve of temperature and the log. of apparent rigidity of pitch.

and Figs. 10～14. In the figures, the common logarithms of the viscosity are taken as ordinates and the temperature as abscissa. The study with rocks will be described at a future opportunity. As will be seen from these figures, the curve of the temperature and that of the log. of the viscosity of water-glass is almost straight line, whereas those of paraffin and pitch are not so. The rigidities of paraffin and pitch disappear when the temperature reaches values of about 49°C for paraffin and about 80°C for pitch, at which temperatures they change from the solid to the liquid state. It can be noticed that the viscosity of paraffin discontinuously decreases when its melting point is arrived at, whereas no such phenomenon is observed for pitch. When in the course of cooling, the temperature reaches 50·5°C, the solid part of the paraffin that resembles cotton is suspended in the liquid part, but which as soon as the temperature descends below 50°C, solidifies throughout and becomes hard. From this fact, it is ascertained that paraffin is a mixture of substances having various melting points, and so is pitch, although it differs from paraffin in certain respects.

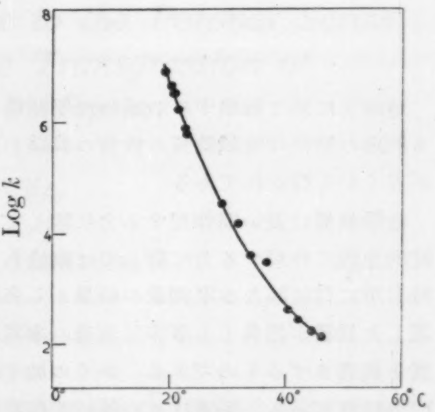

Temperature.

Fig. 14. Curve of temperature and the log. of apparent rigidity of paraffin.

8. Summary and Conclusion to Part I.

1) In the present experiments, the elastic and plastic behaviors of substances such as water-glass, pitch, paraffin, and sandstone were investigated.

2) The angular deformation of these substances caused by a torque that is proportional to the rotating angle of the wire can be expressed by the equation

$$\theta = \frac{c}{c+k}\varphi\left(1-e^{-\frac{k+c}{\varepsilon}t}\right),$$

where the symbols in the equation have the same meaning as before. By means of this equation, the viscous and elastic characteristics of the substances can separately be known.

3) Both the modulus of rigidity and the viscosity coefficient of the substances decrease with the increasing temperature, the former vanishing at the melting points. The viscosity of paraffin discontinuously decreases when its melting point is arrived at, whereas no such phenomenon is observed for pitch.

4) That these substances show dual properties of viscosity and elasticity may well be explained by assuming that the structure of these substances is somewhat similar to that of sponge, the cavity of elastic skeleton of which is filled with viscous liquid.

5) If the material of the earth's crust is assumed to have similar mechanical properties as the materials investigated in this paper, no sensible stress accumulation will take place in it and the folding of mountains and other kindred phenomena may be explained without difficulty.

In conclusion, the present writer wishes to express his best thanks to Professor Mishio Ishimoto under whose kind guidance and encouragement the present work has been carried out and to Professor Torahiko Terada, Drs. Chûji Tsuboi and Ryûtarô Takahasi for their kind advices.

15. 物質の粘彈性性質に關する實驗 (I)

飯田汲事

地球上に於て觀察する地球物理學關係の現象の中，地殼變動に關する問題及び地震波傳播に關する問題の解決は地殼物質の性質の論議が根本問題となる．從つてこの地殼物質の性質に關する研究が古くから行はれてゐる．

地殼物質は長い間作用する力に對しては粘性ある液體のやうな性質を示すのみならず，短い間比較的急激に作用する力に對しては剛性ある固體のやうな性質を示す事は一般に認められてゐる．近時日本に行はれた水準測量の結果から各地に漫性運動が行はれてゐる事や，嘗ては平坦に海底に沈澱した物質が褶曲する事等は前者の事實を裏書きするものであり，地震波傳播等の現象は後者の事實を裏書きするものである．かくの如く地殼物質には，力の作用時間の長短によつて全く異つた二つの性質がある．筆者はこの種の問題を，手近にて容易に得られるピツチ，パラフィン，砂岩，水ガラス等を用ひて實驗する事によつて確めやうと思ひ，靜力的及動力的の二方法によつて物體の捻れによる變化狀態を實驗してみたのである．以上擧げた物質に關する研究も古くから澤山あるが，何れもその粘性か彈性かの何れかの性質についてのみしか論ぜられてゐない．筆者はこの二性質を同時に考慮して研究したのである．先づ第1報として靜力的に求め得られた主な結果を擧げて見れば次の如くである．

(1) ピツチ，パラフィン，砂岩等は長時間作用する力に對しては粘性高き液體の性質が有力に現れ剛性ある固體のやうな性質が比較的とぼしい．ピツチは最も粘性液體の性質に富み，砂岩は最も剛性ある固體の性質に富んでゐる．

(2) これらの物體に廻轉角に比例する歪力を加へた場合，それによつて生ずる廻轉變形角は

$$\theta=\frac{c}{c+k}\varphi\left(1-e^{-\frac{k+c}{\varepsilon}t}\right)$$

なる式によつて表す事が出來る．

この式から物質の粘性及彈性性質が別々に求め得られる．

(3) 是等の物體の剛性率及び粘性係數は溫度の上昇と共に減少し，剛性率は溶融點に達すれば消失する．又パラフィンの粘性係數には固體狀態と液體狀態とで非常な差があるが，ピツチには斯の如き現象が見られない．

(4) これらの物質は以上のやうな粘性及び彈性の二性質を有する事から，これらの物質は海綿構造をなしてゐて，その骨格は彈性體からなり，その間隙は粘性液體で充されてゐると考へる事によつてそれらの性質が容易に說明される．

(5) 地殼物質がこれらの物質と同じ性質を有するならば，歪力の蓄積もあまりに顯著でなく，從つて山脈の褶曲及び其他の同樣な現象が容易に說明し得られる．

動力的方法によつて求められた結果に關しては次の機會に報告する筈である．

16. *The Stratigraphic Relation of the Lower Kadonosawa and the Yotuyaku Series of Iwate to the Poronai Series in Hokkaidô, and the Marine Transgression of the Early Miocene, in Japan.*

By Yanosuke OTUKA,

Earthquake Research Institute.

(Recieved Dec. 20, 1934.)

In this paper the writer wishes to amend some defective expressions of his correlation table of some Japanese Neogene (1934) in his paper[1].

Since 1932, the writer who has been studying the stratigraphy of the northern corner of Iwate prefecture, has schemed the following stratigraphic succession, in descending order :—Suenomatuyama series, Upper Kadonosawa series, Lower Kadonosawa series and the Yotuyaku rseies. The Lower Kadonosawa series contain the following fossils: *Solemya tokunagai* Yokoyama, *Nuculana confusa kongiensis* Otuka, *Arca ninohensis* Otuka, *Ostrea gravitesta* Yokoyama, *Chlamys akitana* Yokoyama, *Taras ferruginata* (Makiyama), *Clementia subdiaphana yazawaensis* Otuka, *Paphia siratoriensis* Otuka, *Dosinia japonica nomurai* Outka, *Dosinia nagaii* Otuka, *Sanguinolaria* (*Soletellina*) *minoensis* (Yokoyama), *Batillaria yamanarii* Makiyama, *Batillaria tateiwai* Makiyama, *Proclava ishiiana* (Yokoyama), *Surculites yokoyamai* Otuka, *Ancistrolepis yudaensis* Otuka, *Conus tokunagai* Otuka, *Ringicula ninohensis* Otuka, etc. Besides these fossils, S. Shimizu has collected *Desmostylus japonicus* Tokunaga et Iwasaki, *Vicarya callosa* Jenkins, which are characteristic species of the Japanese Middle or Lower Miocene. Of these, *Batillaria tateiwai* Makiyama *Batillaria yamanarii* Makiyama, and *Ostrea gravitesta* Yokoyama are characteristic of the Heirokudô formation[2], which is now believed to be Middle or Lower Miocene[3], it was, although, formerly supposed to be Oligocene or Eocene.

From its similar fossils, this formation is contemporaneous with the Neogene Tertiary of Tuyama basin.[4] Recently H. Yabe and S. Mabuti found a *Miogypsina-Operculina* limestone from Neogene near Tuyama basin. On the other hand, some fossils from the Lower Kadonosawa series e. g. *Sanguinolaria* (*Soletellina*) *minoensis* Yokoyama, *Proclava ishiiana* (Yokoyama) are of the Neogene Tertiary of Tukiyosi and Togari[6] in Mino, from which formations many Middle or Lower Miocene Mammals are reported.

---

[1] Y. OTUKA, "Tertiary Structures of the Northwestern End of the Kitakami Mountainland, Iwate Prefecture, Japan," *Bull. Earthq. Res. Inst.*, **12** (1934), 566~638.

[2] I. TATEIWA, *Geol. Atlas Chosen*, **4** (1925).
J. MAKIYAMA, *Mem. Coll. Sci., Kyoto Imp. Univ.*, [*B*], **2** (1926).

[3] T. TAKEYAMA, *Jap. Jour. Geol. Geogr.*, **10** (1933), 139 and 140.

[4] T. TAKEYAMA, *op. cit.* (1933).

[5] H. YABE and S. MABUTI, *Jour. Geol. Soc. Tokyo*, **41** (1934), (in Japanese).

The writer therefore considers that these fossil bearing beds are contemporaneous with the so-called Lower Miocene of Yatuo, Toyama prefecture[7], from which *Vicarya verneuilli* d'Archiac, *Miogypsina ozawai* Hanzawa, and *Operculina complanata* Defrance have been reported, and the *Miogypisina* and *Operculina* horizon of the western half of Northeast Japan, the latter of which S. Hanzawa[8] thinks Langhian or Burdigalian. (The writer thinks this *Miogypsina-Operculina* horizon Middle or Lower Miocene.)

These Miocene beds are usually underlain by coal-bearing or fossil plant bearing beds or characterized by clear unconformity, e. g., the unconformity below the Tuyama Miocene[9], the coal-bearing Ryûdô formation below the Heirokudo formation[10], the Nakamura group and Hiramaki group below the Tukiyosi and Togari groups,[11] the Yotuyaku series below the Lower Kadonosawa series[12], the Oguni plant beds in Yamagata prefecture[13], the Kannonzawa plant beds in Niigata prefecture[14], the fossil plant bearing beds below the Daisima beds in Oga peninsula, etc.

Our knowledge of the stratigraphy of the Isikari coal-field of Hokkaidô, Japan, has greatly advanced owing to the studies of H. Yabe, Oinouye, Imai, Murata, Tagami, and others. H. Yabe and H. Imai[15] have worked out the following stratigraphic succession :—The Kawabata series (upper); the Poronai series, which is of considerable thickness; and consists of black shale, with intercalated thin marl layers and marl nodules, is glauconitic and sandy at the base. The thickness of the basal sandy part varies greatly in places. The characteristic fossils of this series are: *Bulimia* spp. *Venericardia compressa* Yokoyama, *Nucula poronaica* Yokoyama, *Nucula* (*Acila*) *picturata* Yokoyama, *Nuculana* sp. *Tapes ezoensis* Yokoyama, *Turritella wadana* Yokoyama, etc., and the Isikari coal bearing series.

---

[6] H. **YABE**, *Spec. Publ. Bernice P. Bishop Museum*, 7 (1921), 789~790.

[7] S. **IMAMURA**, *Jour. Geol. Soc. Tokyo*, 39 (1932), 310~312, (in Japanese).
S. **HANZAWA**, *Jour. Geol. Soc. Tokyo*, 39 (1932), 723~724 (in Japanese).

[8] H. **YABE**, *Jap. Jour. Geol. Gegr.*, 5 (1926), 95~105.
S. **HANZAWA**, *op. cit.* (1932).

[9] T. **TAKEYAMA**, *Chikyû*, 14 (1930), 91~101, (in Japanese).

[10] I. **TATEIWA**, *op. cit.* (1925); F. **YAMANARI**, *Geol. Atlas Chosen*, 3 (1925).

[11] **YABE**, *op. cit.* (1921).

[12] Y. **OTUKA**, *op. cit.* (1934).

[13] H. **MORITA**, *Jap. Jour. Geol. Geogr.*, 9 (1931), 1~8.

[14] S. **ENDÔ**, "Cainozoic Fossil Plant in Japan," *Iwanami Kôza* (1931), 16, (in Japanese).

[15] H. **YABE**, *op. cit.* (1921), 777~780.

Since then Murata[16] distinguished a transitional intermediate formation, called the Momidiyama intermediate beds, between the Kawabata and the Poronai series. Imai[17], endorsing Murata's opinion, formed an intermediate formation on the upper part of his Poronai series. The Momidiyama intermediate beds, which are of shallow sea origin, consist of (1) black shale bed (*Nucula mirabilis* bed), (2) green conglomerate bed (*Ostrea* and *Glycymeris* bed), (3) dark-grayish shale (*Buccinum* and *Venericardia* bed), (4) green sand and shale bed containing fossil plant remains (*Nucula* and *Venericardia* bed). The *Ostrea* contained in (2) green conglomeate is *Ostrea gravitesta* Yokoyama, a Japanese Middle or Lower Miocene fossil mollusca. On the Kawabata beds lie the Oiwake marine sandy shale beds containing *Lucina* sp., *Solemya* sp. *Pleurotoma* sp., and *Chrysodomus* sp.

From the foregoing, the writer recognizes the transgression of the Poronai period, regression of the Momidiyama and early Kawabata periods, and the transgression of the late Kawabata and Oiwake periods, as has been done by Murata[18].

Recently, Usami, a bachelor of Tokyo Imp. Univ., studied the Uryu-Porosin (Poroni) coal field, north of the Isikari coal field Hokkaidô, and observed the following stratigraphic succession, in descending order:—Ebisima beds, Tôgesita beds, Rurumoppe beds, Sisennosawa beds, Siratori beds, Porosin coal bearing beds, Poronai beds, and Cretaceous formation. The Poronai beds in this coal field contain the following fossils:—*Bulimina* spp., *Venericardia compressa* Yokoyama, *Nucula* (*Acila*) *picturata* Yokoyama, *Nucula poronaica* Yokoyama, *Turritella wadana* Yokoyama, *Yoldia tokunagai* Yokoyama, *Callianassa muratai* Nagao, and are believed to be contemporaneous deposits of the typical Poronai series.

As described by the late G. Koisi[19], the Porosin (or Poroni) beds are coal bearing complex. They are alternations of dark, greensih, coarse-grained sandstone and thin shale beds, the lower part of which contains *Comptoniphyllum japonicum* Nathorst, *Taxodium distichum miocenicum* Heer, etc., which are species of Japanese Middle Tertiary fossil plants. The upper parts of these beds contain *Dosinia nagaii*

---

[16] S. Murata, *Jour. Geol. Soc. Tokyo*, **30** (1923), (in Japanese).

[17] H. Imai, *Jour. Geogr. Japan*, **36** (1922), 145, (in Japanese).

[18] S. Murata, *Hokkaidô Sekitan Kôgyo-Kai Kaihô*, (1932), (in Japanese).

[19] G. Koisi, *Nippon Kogyokaisi*, (1931~1932), (in Japanese).

Geologic Province	Neogene Pacific coast SW. Japan			Setouti			Kwantô & Zyôban	
Locality	Miyasaki prefecture	Wakayama prefecture	Siduoka prefecture	Okayama prefecture	Gihu prefecture	Toyama prefecture	Tiba prefecture	Zyoban coal field
Formation of Early Kadonosawa trans gression	Aburatu series	Tanabe and Miyai series ?	Oigawa series	Tuyama Miocene	Tukiyosi groups / Togari groups	Yatuo series { *Operculins* *Miogypsina* beds.	Sakuma groups	Yunagaya series
Transitional formation (regression)					Hiramaki and Nakamura group	Plant beds.		
Formation of Poronai transgression								Siramizu series

Geologic Province	Tyosen (Corean).		Central Hokkaidô-		West half of Neogene Northeast Japan.				
Locality	North Tyosen	South Tyosen	Isikari coat-field	Uryû-Porosin coal-field	West Hokkaidô	Iwate prefecture	Akita prefecture	Akita-Yamagata prefecture	Niigata prefecture
Formation of Early Kadonosawa trans gression	Heirokudô formation	Low. Enniti formation	Kawabata series	Tôgesita b. Rurumoppe b. Upper } Porosin beds	Lower Kunnui Group.	Lower Kadono sawa series	Nisikurosawa & Daisima beds.	Takasegama beds	*O pereulina* *Miogypsina* horizon.
Transitional formation (regression)	Ryûdô formation	Tyôki formation ?	Momidiyama intermediate beds	Lower } Porosin beds		Yotuyaku series	Plant beds		Kannonzawa plant bed.
Formation of Poronai transgression			Poronai series	Poronai beds					

Otuka, *Dosinia japonica nomurai* Otuka, *Paphia siratoriensis* Otuka, etc., which are fossil mollusca characteristic of the lower Kadonosawa series described above. Along the upper course of the Porosin (or Poroni)-Tatibetu river these Porosin (or Poroni) beds are overlain by the Sisennosawa beds, and along the Rurumoppe river by the Rurumoppe beds. Usami thinks that his Tôgesita beds, overlain by the Sisennosawa beds or Rurumoppe beds, may be contemporaneous with the Kawabata series.

As stated above, the fossil shells from the upper part of the Porosin beds are the same as the fossils from the Lower Kadonosawa series. It may be added that the rocks of the Lower Kadonosawa series and the Yotuyaku series resemble those of the Porosin (or Poroni) beds, hence the Porosin (or Poroni) beds, at least its lower part, may be contemporaneous with the Yotuyaku series. In view of the foregoing statements, the writer is forced to reconsider the stratigraphic horizon of the Poronai series in Hokkaidô.

Judging from the stratigraphic succession, the writer agrees with Murata[20] in the view that the Porosin beds, (at least, the lower part of the Porosin beds)are contemporaneous with the Momidiyama intermediate beds.

This stratigraphic relation is shown in the succession of the underlying Poronai and the overlying Momidiyama beds near Momidiyama or Porosin (or Poroni) beds in the Porosin (or Poroni) coal field.

The writer concludes that the geologic age of the Yotuyaku may be lower Miocene or upper Oligocene, so that the geologic age of the Poronai series is older than the Yotuyaku series. Evidences of transgression of the Early Kadonosawa Period following the regression of Yotuyaku Period are observable in Northern Tyosen (Korean), Honsyû, and Hokkaidô. The following is a list of the deposits which represent these transgression and regression of Miocene period.

---

16. 岩手縣北部新第三系下部門ノ澤統と四ツ役統との北海道幌内統に對する層位學的關係及び日本中新世前半の海進

地震研究所 大塚彌之助

著者はこの論文に於て，先に發表した處の下部門ノ澤統と四つ役統との幌内統に對する層位關係を稍々詳しく定め，前二統を村田理學士の川端層と紅葉山中間層とに對比せんとす．而して紅葉山中間と川端層とに對比せらるゝ北海道石狩炭田の北部なる幌新夾炭層とその上位の諸層とより下部門ノ澤統に持有なる貝化石を含むことをこゝに報告し，上記の對比の一資料にせんとす．

日本中新世前半には幌內統によつて代表せらるゝ海進と，門ノ澤統によつて代表せらる海進とが存在せしものゝ如し．

---

[20] S. Murata, *op. cit.*, (1932).

17. *The Oti Graben in Southern Noto Peninsula, Japan.*

(*Part I*)

By Yanosuke OTUKA,

Earthquake Research Institute.

(Read March 20, 1934.—Received Dec. 20, 1934.)

1. Introduction.
2. Topography.
    - a. The bottom of the Oti graben.
    - b. The northwest part of the Oti graben.
    - c. The southeast part of the Oti graben.
    - d. The other localities.
3. Coastal terraces along the east coast of Noto peninsula.
    - a. Tumuki terrace.
    - b. Hiradoko terrace.
    - c. Matunami terrace.
    - d. Conclusion.
4. Stratigraphy of the environs of the Oti graben.
    - a. The southeast part of the Oti graben.
    - b. The southeast wall of the Oti graben.
    - c. The northwest part of the Oti graben.
    - d. Conclusion.
5. Geologic structure of the environs of the Oti graben.
6. Tectonic history of the Oti graben.
7. Conclusion.
8. Description of fossils.

1. Introduction.

The Noto peninsula, a flat low-reliefed land projecting into the Japan Sea from North Central Japan, consists of andesite, Neogene Tertiary, and Pleistocene terrace deposits on the basal granite and gneiss. At the isthmus of this peninsula, a low depressed land, in which the south bay of Nanao (七尾) and the Oti (邑知) lagoon are situated, runs about N 60°E, and cut the structural connection between the peninsula and the Japanese mainland. This low depressed land has been called by Prof. T. Ogawa[1], the "Oti tectonic valley."

In this paper, the writer studies the stratigraphy of southern Noto and discusses the geotectonic development of this depressed lowland. This study will make it possible to form an idea of the geotectonic development of the Sado island and Yamato submarine bank, both of which lie in the Japan sea, parallel to the Japanese island arc, under the assumption that these island and submarine bank have geologic structural characteristic similar to those of the Noto peninsula.

---

[1] T. OGAWA, *Expl. Text. Geol. Map, Japan*, "Wajima" sheet, 1:200,000, (1908).

As to the topography and geology of southern Noto, many investigators, such as the late N. Yamasaki[2], T. Ogawa, T. Tsujimura[3], J. Makiyama[4] and K. Mochizuki[5] have published the results of their studies, while M. Yokoyama has published his palaeontological results. But in these studies no tectonic characteristics and its history have been discussed thoroughly.

On Sept. 21st, 1933, a destructive earthquake[7] occurred near Nanao, its origin being determined as in the southern part of South Nanao Bay, which makes it necessary to study the geologic structure of this region from the standpoint of seismological geology.

2. Topography.

For convenience the writer divides this region into four parts, namely, (a) the bottom of the Oti graben, (b) the northwest part of the graben, (c) the southeast part of the Oti graben, and (d) other localities.

a. The bottom of the Oti graben. As shown in Fig. 1, the southeast part of a topographic line connecting Zike-Itinomiya (氏家一宮) in Hagui (羽咋)-gori, through Tizi (千路), Notobe (能登部), Yosikawa (良川), Sirouma (白馬) with the town of Nanao, shows very contrasting topographic features to its northwest part. That is, the southeast part of this topographic line is a very flat lowland, while the opposite side of this line is a very steep dissected slope.

And again, the two side of a topographic line connecting Siho (子浦) through Suginoya, Iiyama (飯山), Takabatake (高畠), Kotake (小竹), with Sano (佐野) in Higasiminato-mura (東湊村), shows also a contrasted topography as remarked above. On this line, its southeast side is a very steep slope, while the opposite side is a low flat surface, which is the same plain as that on the southeast side of the former topographic line.

The bottom of the Oti graben is the area between these two topographic lines. These two topographic lines are almost parallel to each

---

2) N. Yamasaki, *Jour. Geol. Soc., Tokyo*, (1908), (in Japanese).

3) T. Tsujimura, Nippon-Tikeisi (Geomorphology of Japan), (1932), (in Japanese).

4) J. Makiyama, *Chikyû*, **14** (1930), (in Japanese).

5) K. Mochizuki, *Geogr., Rev. Japan*, **4** (1928); *Jour. Geol., Tokyo*, **39** (1932); *Geography, Japan*, **2** (1934), (in Japanese).

6) M. Yokoyama, *Jour. Geol. Soc., Tokyo*, **33** (1926); *Imp. Geol. Surv. Japan, Rep.* No. 101 (1928); No. 104 (1929).

7) T. Suzuki, *Bull. Earthq. Res. Inst.*, **12** (1934), 44, (in Japanese).

other, and outside of them are very steep slopes like fault scarps, as just stated. Japanese writers, therefore, called this flat elongated depressed lowland, the "Oti graben" or "Oti tectonic valley". Fig. 1 is a map of this region, shaded or hatchured for every twenty meters height, and on which these two topographic boundary lines are clearly shown. EF and GH in Fig. 1, which are transverse profiles of this depressed lowland, show these topographic boundaries in elevation.

The contour lines of the graben bottom, those in the southwest part, are very simple, occupied by the Oti lagoon, whence this graben derives its name. This southwestern part of the bottom of Oti graben is an Alluvial plain, the southwestern end of which is fringed by sand dunes 30～40 m. above the level of the Japan sea. This sand dune, which continues to the southwest shore of the Japan sea falls in height near the southwest end of the Oti graben, as shown in Fig. 1. That is the 20～40 m. (hatchured) areas in the part of Oti graben decreases relatively to the other part of the sand dune.

While the northeastern half of the bottom of the Oti graben does not show so simple contour lines as those of the southwestern half of the bottom of the graben, it is dissected by many small valleys. This topographic irregularity suggests that the southwestern half of the bottom is relatively lower in height than the northwestern half of the bottom. To verify this suggestion, the writer has projected topographic profiles of the bottom of the graben as shown in Fig. 1, AB, CD. By these two figures the asymmetric reliefs of the graben bottom is clearly brought out. The graben bottom gradually decreases in height toward the southwest, but toward the northeast it rises, although it is dissected near the town of Nanao. On the land surface of the dissected northeastern part of the graben bottom are basal rocks, while Alluvial deposits now fill the dissected valley. The town of Nanao occupies the lowland that was newly formed in the dissected valley in the northeastern part of the graben bottom.

Prof. T. Tsujimura[8] has called attention to the poor development of fanglomeratic deposits derived from the walls of the graben on the southwestern half of the bottom, and explained it by the relative subsidence of the southwestern half of the graben bottom.

The southern bay of Nanao is believed to be a continuation of the graben bottom, but the bottom surface of the bay does not represent the true characteristics of the graben bottom. The island of Onna(-zima) (女島), O(-sima) (雄島), Tera(-sima) (寺島), Karasu(-zima) (烏島), etc., which are elevated reliefs of the graben bottom consist of Tertiary rocks.

---

[8] T. TSUJIMURA, *op. cit.* (1932).

The topographic boundary line, running from Kooda (向田) in Notozima (能登島) to the east of Sanami (佐波) in nearly SSW direction, is considered the northeastern extension of the northwest side of the graben bottom, while the topographic boundary line running from Entunagi (縁繋) to Sobogaura (祖母ケ浦) in Notozima, is supposed to be the northeastern extension of the southeast boundary line of the graben bottom.

The Tokuda terrace, so called in this paper, is a flat surfaced terrace in the graben bottom about 30～40 m. above sea-level, developed near Tokuda (徳田). Going southwestward, this terrace lying northwest of the railway between Tokuda and Nanao station, is covered with Ninomiya (二宮) Alluvial fan, and disappears in the southwest part of its fan.

b. The northwest part of the Oti graben. The northwest part of the Oti graben is divided into three terraces and an Alluvial plain, the plain being the lowest in height. The second lowest is the Tumuki terrace, 35～30 m. above sea-level, which develops at the back of Tumuki (津向) village, northwest of the town of Nanao. The terrace next above the Takasina terrace or hill, about 80～50 m. above sea-level, is a dissected low relief hill developed in Takasina-mura (高階村) and its environs. The topographic characteristics of Takasina hill resemble those of Tama hill near Tôkyô, namely the writer's Dl terrace.

The drainage system of the Takasina hill is very asymmetric, the main divide being near the southeastern margin of this hill extending from Tumuki through Kuramayama (鞍馬山) to Sirouma and Hidume (廿三日). This partial existence of the divide suggests that the valley heads of the drainage system in this hilly country was cut by the topographic boundary line of the Oti graben, which is represented by a straight valley between the graben bottom and Takasina hill.

The highest terrace is about 200 m. above sea-level. It is here called the Akakura mountainland. This mountainland is in the west of Takasina hill, bordered by a meridional topographic boundary. The Akakura mountainland, which is a dissected mountainland of andesite, of which Mt. Akakura (赤藏) is the highest mountain. The topographic boundary of the Akakura mountainland and Takasina hill runs from Taduruhama (田鶴濱) in Wakura-mati (和倉町) to Haruki (春木) and Kurozihukazawa (黒氏深澤) in Toya-mura (鳥屋村). This topographic boundary is not represented in the Oti graben bottom. Fig. 2 shows a sketch of this topographic boundary as seen from the southeast corner of the graben bottom near Kosidi.

As already stated the boundary line between this mountainland and the graben bottom is a steep slope. K. Mochizuki[9] called this

---

[9] K. Mochizuki, *op. cit.* (1934).

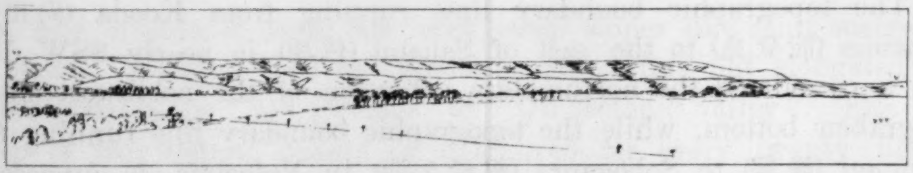

Fig. 2. Schematic sketch of the topographic boundary of the northwest part of the Oti graben seen from southeast corner of the Oti graben bottom near Takebe (武部). vv=Akakura mountainland, v=Takasina hill, vvv=Oti graben bottom.

steep topography the Bizyôsan (眉丈山) fault scarp. The back slope of Bizyosan fault scarp is a dissected low relief surface.

c. The southeast part of the Oti graben. Since the mountainland southwest of the Oti graben is higher than the northwest part of the Oti graben, the height of the fault scarp is greater than in the one northwest. On the ridge of the mountainland many peaks with heights of 460～390 m. are aligned in a N 60°E in direction, the mountainland gradually dropping in height toward the west shore of the bay of Toyama.

The Sekidosan (石動山) fault scarp of Mochizuki[10] is the northwest scarp of this mountainland and the southeast steep slope of the graben. Fig. 7 shows the Sekidosan fault scarp seen from the east shore of the southern bay of Nanao. The Northeastern extension of this fault scarp gradually becomes indistinct and finally disappears near Kogutiseto (小口瀬戸). The writer expected a northeastern extension of the fault scarp on the topographic boundary between Entunagi and Sobogaura in Notozima but here geologic evidences are against this expectation, as will be explained later.

A topographic boundary, a branch of the Sekidosan fault scarp at Yati (谷地) in Higasiminato-mura runs in a N 45°E direction to Oonoki (大野木) on the west shore of the bay of Toyama. The west side of this topographic boundary line is a dissected terrace, less than 110 m. above sea-level, while the east side of this boundary line is a relatively high mountainland, about 300～250 m. above sea-level. This topographic boundary line is clearly shown in Fig. 1, and Fig. 3.

Fig. 3 is a distribution map of these topographic divisions. The Tumuki terrace in this province, about 50 m. above sea-level, broadly develops near Mimuro (三室) and Kadosima (鹿渡島) on the peninsula between the south bay of Nanao and bay of Toyama.

The mountainland which is the back slope of the Sekidôsan fault scarp has relatively low relief surface, which gradually drops in height toward the bay of Toyama, as seen in the summit level in Fig. 4. As Mt. Sekidôsan abruptly rises about 100 m. above this low relief sur-

---

[10] K. MOCHIZUKI, *op. cit.* (1934).

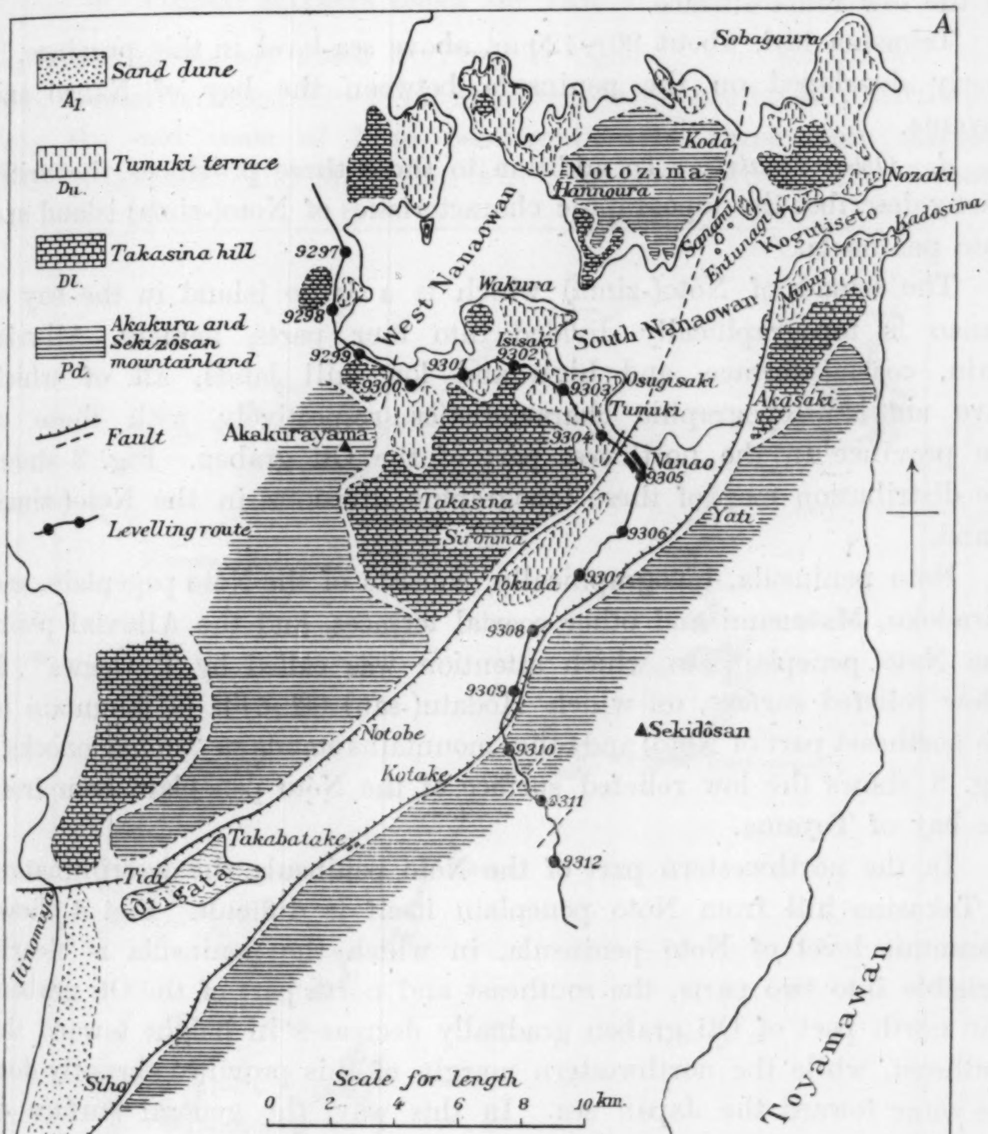
A
Sand dune
Al.
Tumuki terrace
Du.
Takasina hill
Dl.
Akakura and Sekizôsan mountainland
Pd.
Fault
Levelling route
Sobagaura
Notozima
Koda
Hannoura
Nozaki
Kadosima
Kogutiseto
Sangami
Enlunagi
West Nanaowan
South Nanaowan
Wakura
Isisaka
Osugisaki
Tumuki
Nanao
Akasaki
Akakurayama
Takasina
Sironma
Tokuda
Yati
Notobe
Kotake
Sekidôsan
Takabatake
Tidi
Otigata
Itinomiya
Siho
Toyamawan
9297
9298
9299
9300
9301
9302
9303
9304
9305
9306
9307
9308
9309
9310
9311
9312
Scale for length
0
2
4
6
8
10 km.
B
Scale for height
+20
+10
0
-10
-20
mm.
1917
1933
1900
1928
34·8

Fig. 3. A. Topographic division near Nanao.
B. Change of heights of the bench marks in the Nanao district.

face, Mochizuki[11] thinks that Mt. Sekidô(san) may be a monadonock on the low relief surface.

Takasina hill, about 90∼120 m. above sea-level in this province, is poorly developed on the peninsula between the bay of Nanao and Toyama.

d. Other locality. In addition to those three provinces, the writer briefly describes the topographic characteristics of Noto(-zima) island and Noto peninsula.

The island of Noto(-zima) which is a large island in the bay of Nanao is topographically divided into four parts, namely, Alluvial plain, coastal terrace, and high and low hill lands, all of which have similar topographic characteristics respectively with those of the province in the northwest part of the Oti graben. Fig. 3 shows the distribution map of these topographic divisions in the Noto(-zima) island.

Noto peninsula, topographically, consists of the Noto peneplain, and Hiradoko, Matunami and other coastal terraces, and the Alluvial plain. The Noto peneplain, to which attention was called by T. Ogawa[12], is a low reliefed surface, on which Hôdatu(-san) (寶立山) (a mountain in the northeast part of Noto) and other mountains stands as "monadonocks." Fig. 8 shows the low reliefed surface of the Noto peneplain seen from the bay of Toyama.

In the northwestern part of the Noto peninsula, the descrimination of Takasina hill from Noto peneplain itself is difficult. Fig. 4 shows a summit level of Noto peninsula, in which the peninsula is clearly divisible into two parts, the southeast and north part of the Oti graben. The north part of Oti graben gradually decreases in height toward the southeast, while the northwestern margin of this province abruptly does the same toward the Japan sea. In this way, the general surface of the summit level of northern Noto peninsula inclines southeastward, while the main divide of Noto peninsula is situated at the southeast margin of northern Noto peninsula. Regarding these topographic characteristics, the present writer is inclined to the opinion that the Noto peninsula flexuously tilted southeastward after the formation of the so-called Noto peneplain surface. The river systems that were formed during the formation of the Noto peneplain remained on the peneplain surface during its deformation, later draining the present deformed peneplain surface which is represented by the summit level of Noto peninsula (Fig. 4).

---

[11] K. MOCHIZUKI, *op. cit.* (1934).

[12] T. OGAWA, *op. cit.* (1909).

3. Coastal terraces along the east of Noto peninsula.

It was previously noted by Prof. T. Ogawa[13] and Mochizuki[14] that many coastal terraces, 30～40 m. above sea-level, are broadly distributed along the east coast of Noto peninsula. The three main terraces, Tumuki, Hiradoko, and Matunami will now be described. Fig. 5 shows the distribution of these terraces in Noto.

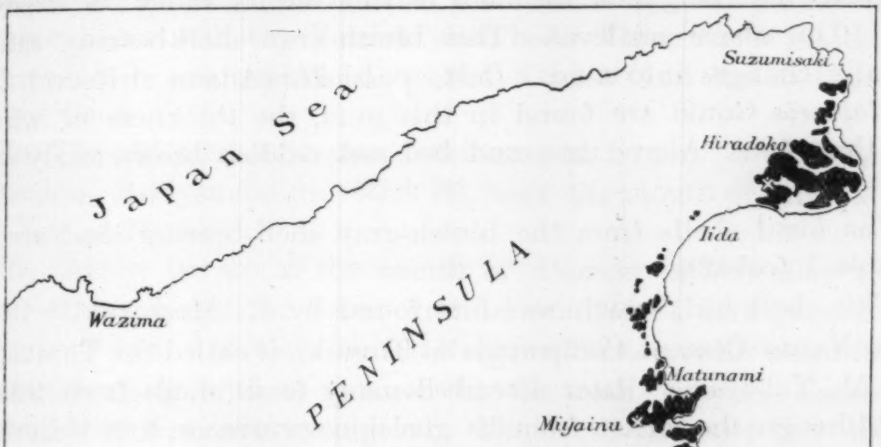
Japan Sea
NOTO PENINSULA
Suzumisaki
Hiradoko
Iida
Wazima
Matunami
Miyairu
Tukumowan
Usetu
Ukawa
Anamidu
Nanaowan
Toyamawan
Notozima
Nanaowan
Tumuki
Nanao
Akasaki
Du terrace
Fossil locality
0 5 10 15 20 km.

Fig. 5. **Distribution map of Du coastal terrace on the east coast of Noto peninsula.**

a. Tumuki terrace. As already stated, Tumuki terrace lies back of

---

13) T. Ogawa, *op. cit.* (1909).

14) K. Mochizuki, *op. cit.* (1932)

Tumuki village, northwest of the town of Nanao. Its height is 30~40 m. above sea-level. The surface of the terrace is flat and consists of erosion surfaces of Tertiary bed rock and deposition surfaces of sand and mud beds underlain by Tertiary bed rock with unconformity. At Osugizaki (大杉崎), the south end of this terrace, there is an exposure of a bluish-gray shell-bearing bed with which a valley of Tertiary bed rock is buried. The height of the floor of this buried valley as exposed is about 10 m. above sea-level. This bluish-gray shell-bearing sand bed gradually changes into mud. *Raeta pulchella* (Adams et Reeve), *Ringicula doliaris* Gould are found in this mud, the thickness of which is more than 4 m. Above this mud bed rest reddish brown sandy surface soils.

The fossil shells from the bluish-gray shell-bearing sand are listed in Table I (col. 2).

This shell bed, which was first found by K. Mochizuki[15] in 1928 in the Nanao Cement Compounds at Tumuki, is called the Tumuki shell bed. M. Yokoyama[16] later described many fossil shells from this bed.

Although the writer from its geologic occurrence, first believed that the Tumuki shell bed has been formed after the formation of the Tumuki terrace, since the shell bed forms the surface of the terrace near Osugizaki as just stated, the inference was error. The Tumuki shell bed may therefore be a pre-Tumuki terrace deposits, and the formation of the surface of Tumuki terrace contemporaneous with or closely related to the formation of the shell bed. That is, the surface of the Tumuki terrace was formed by the abrasion and deposition of the Tumuki shell bed in the dissected valley that was formed during the pre-Tumuki stage. Fig. 9 shows the Tumuki terrace near Osugisaki.

Going south, similar terraces develop near the public park of Nanao and near Tokuda village. The terrace near Tokuda, called Tokuda terrace by the writer, has been described in a previous line. The materials composing Tokuda terrace, which resemble those of Tumuki, is exposed on a cliff south of Hosoguti (細口). The upper part of this exposure is a brown soil that gradually changes into yellow, reddish-brown, or bluish-gray mud. This bluish-gray mud contains ill-preserved fragments of fossil plants, but no marine shells. This mud is underlain by a creamy, grayish sand bed which consists of fine weathered granitic sand. The writer found in it a cast *Batillaria* aff. *fluviatilis* (Potiez et Michaud). This occurrence of marine shell points to an invasion of the sea in the Oti graben bottom during the Tumuki stage. As already stated the Tokuda terrace is geologically and topographically similar to the Tumuki terrace, for which reason the writer is convinced that these two terraces may be contemporaneous with each other.

---

[15] K. MOCHIZUKI, *op. cit.*, (1928).

[16] M. YOKOYAMA, *op. cit.*, (1928).

It may be added that the sand and mud beds forming the Tokuda terrace rest unconformably on the Neogene formation east of Hosoguti and Kokubu (國分).

The coarse grained sand and gravel beds forming the Tumuki terrace surface of Iwaya (岩屋) and Kozima (小島), near Nanao may be contemporaneous with the Tumuki shell bed. These coarse grained sand and gravel beds are underlain by the Kozima and Nanao beds to be described later.

The Tumuki terrace is also distributed in Isizaki (石崎), Sobogaura in Notozima, Sakiyama-mura (崎山村), near the mouth of the south part of the bay of Nanao.

The narrow terrace at the mouth of Akasaki (赤崎) valley in Higasiminato-mura, consists of coarse grained sand and a dark greyish shell-bearing mud bed, underlain by the Neogene Tertiary with unconformity. This shell-bearing mud is exposed on the road between Nanao and Mimuro, about 5 m. above sea-level. The fossil shells of this mud bed are listed in Table I col. 1. A coarse grained granitic sand lies on the shell-bearing mud. The surface of the terrace here is poorly preserved. The writer could not find any stratigraphical relation between these terrace forming beds and the Tumuki terrace.

The Tumuki terrace in Sakiyama-mura is well dissected. The writer failed to find any shell-bearing beds in this province, although he noticed a coarse-grained granitic sand forming the surface of the terrace.

b. Hiradoko terrace. The Hiradoko terrace which was studied by K. Mochizuki[17] is near Iida (飯田), in the northeast part of Noto peninsula. This terrace, 40∼25 m. above sea-level, lies southeast of a line connecting Syôin (正院), east of Iida, and Awadu (粟津) northeast of Syôin. On a cut wall, south of Hiradoko, Mochizuki found a shell-bearing sand mud forming the surface of the Hiradoko terrace. These shell-bearing beds, called the Hiradoko shell bed by K. Mochizuki, is underlain by the Iiduka (飯塚) beds with unconformity. As will be seen from Fg. 10, the exposure on the cut wall near Hiradoko is a depressed relief of Tertiary bed rock, filled with the Hiradoko beds. Fossil shells are found in the upper half of this bed, from which Mochizuki reported 55 species. The fourth column of Table I shows the fossil shells collected here by the writer.

The rock succession of the Hiradoke bed differs slightly from the Tumuki bed in the absence of the upper dark grayish mud. The writer agrees with Mochizuki's opinion, however, that the Hiradoko bed is contemporaneous with the Tumuki bed.

---

[17] K. MOCHIZUKI, *op. cit.*, (1932).

c. Matunami terrace. The coastal region of eastern Noto from Matunami (松波), south of Iida, to Tukumo-wan (九十九灣), is a broad flat terrace, 30～40 m. above sea-level. The width of the terrace sometimes attains to 500～2000 m., the surface being very flat. These topographic characteristics closely resemble those of the Tumuki and Hiradoko terrace, just described. The writer calls this the Matunami terrace. Its width near Akasaki (赤崎) and Miyainu (宮犬) is about 4000 m. On the highway between Usetu (宇出津) and Matunami, a shell bearing mud[18] is exposed at Miyainu, the thickness of which is about 5 m., resting on the Tertiary bed rock with unconformity. This stratigraphical relation clearly resembles that of Hiradoko. The fossil shells collected from these mud beds are listed in column 3 in Table I. The faunal characteristics are very similar to those of Hiradoko.

As previously stated, the coastal terraces along the east shore of Noto peninsula, namely, Hiradoko, Matunami, Tumuki, and Tokuda, are 30～40 m. above sea-level and consist of marine beds. Similar terraces are therefore expected to exist between these terraces. So far as the writer knows, there are many prolongations of the Hiradoko terrace near Ugai (鵜飼) between Matunami and Iida etc. Between Tumuki and Matunami, a narrow belt of the Matunami terrace fringes the seashore from Usetu to Ukawa. These terraces being virtually of the same height, the writer concludes that the east shore of Noto peninsula was uplifted 30～40 m. (or the sea-level lowered 30～40 m.) after the deposition of the Hiradoko and other shell beds. Evidence of this movement is also seen in the Tokuda terrace in the Oti graben. It will thus be seen that the northeast part of the graben developed, physiographically similary to the Tumuki, Matunami, and Hiradoko terraces. Fig. 5 shows the distribution of these terraces along the east shore of Noto peninsula.

d. Conclusion. The geologic age of these shell-bearing terrace deposits deserves careful study. Most of the fossil shells collected from these beds are now living in our seas washed by the warm Kurosio current, some of the warm current species of which now live only in the southern Japan, only a few of such species being found in the lower Pleistocene deposits of Central Japan. The warm current which washes the sea shore on the northwest side of the Japanese islands flows through the Korean straits into the Japan Sea. The occurrence of these warm current fauna in the Pleistocene deposits of this region suggests that the warm current flows into the Japan Sea through the Korean straits.

---

[18] T. OGAWA, *Expl. Text. Geol. Map, Japan*, "Suzumisaki" sheet, 1:200,000, (1907). In this expl. text., T. Ogawa considers these terrace deposits the Youngor Tertiary (dt of Ogawa).

Table I. (1 = Akasaki ; 2 = Tumuki ; 3 = Matunami ; 4 = Hiradoko).

	1	2	3	4
Emarginula crassicostata Sowerby	—	—	—	3
Diodora sieboldii (Reeve)	—	—	1	—
Patelloida saccharina (Linné)*	—	—	1	—
Patelloida conulus (Dunker)	—	—	3	8
Euchelus foveolatus (A. Adams)	—	—	—	5
Solariella aff. *angulata* (Tokunaga)	—	—	—	2
Tegula (*Chlorostoma*) *rustica* (Gmelin)*	—	1	—	—
Skenea nipponica ? Yokoyama	2	—	—	—
Turbo coronatus coreensis Récluz*	3	5	1	—
Astraea (*Calcar*) *haematraga* (Menke)*	—	—	13	3
Iravadia annulata (Dunker)	—	—	3	3
Cingula (*Pseudosetia*) *paludinoides* (Yokoyama)	—	—	—	5
Amphithalamus sp.	—	—	—	2
Alvania concinna A. Adams	—	2	8	—
Rissoina (*Phosinella*) *media* Schwartz*	—	—	1	—
Rissoina (*Rissoina*) *laevicostulata* Pilsbry*	3	40	2	13
Rissoina (*Zebinella*) *yendoi* Yokoyama	—	—	3	—
Pseudoliotia micans (A. Adams)*	—	—	2	—
Turritella fascialis Menke	—	—	20	5
Lemintina imbricata (Dunker)*	2	2	1	—
Siliquaria cumingii (Mörch)*	—	—	—	1
Batillaria multiformis (Lischke)*	—	1	—	—
Obtortio septentrionalis (Tokunaga)	10	40	—	—
Obtortio orientalis (Yokoyama)	2	20	40	30
Obtortio perpupoides (Yokoyama)	3	6	1	40
Scaliola bella A. Adams	—	2	2	16
Diala varia A. Adams	—	2	20	1
Bittium perpusillum Tryon*	5	30	60	6
Bittium numamuranum Yokoyama	—	—	40	30
Cerithium (*Proclava*) *kochi* (Philippi)*	1	4	—	3
Gourmya (*Contumax*) *sordidula* (Gould)	6	37	—	—
Gourmya (*Contumax*) *kobelti* (Dunker)*	1	1	35	—
Triphora (*Inella*) *tricincta* (Dunker)*	—	1	1	1
Triphora sp.	—	2	12	6
Epitonium (*Turbiniscala*) sp.	—	—	2	—
Strombiformis (*Leiostraca*) *shibana* (Yokoyama)	—	—	—	3
Chrysallida (*Miralda*) *gemma* (A. Adams)	—	—	—	5

(*to be continued.*)

Table I. (*continued.*)

	1	2	3	4
Chrysallida (*Babella*) *caelata* (A. Adams)	—	—	—	4
Chrysallida (*Pyrgulina*) *densecostulata* (Garrett)	—	1	11	1
Menestho sp.	—	—	1	—
Menestho lectissimoides (Yokoyama)	—	—	1	—
Odostomia limpida Dall et Bartsch	—	—	1	11
Syrnola cinctella ? A. Adams	—	1	—	—
Cingulina triarata Pilsbry*	—	—	—	1
Turbonilla imbana Yokoyama	—	—	11	—
Turbonilla hiradokoensis Otuka n. sp.	—	—	—	1
Turbonilla sp.	—	1	—	—
Turbonilla (*Strioturbonilla*) *nihona* Otuka n. sp.	—	1	1	3
Turbonilla (*Pyrgiscus*) *matunamiensis* Otuka n. sp.	—	—	1	—
Turbonilla (*Pyrgiscus*) sp.	—	1	—	—
Turbonilla (*Mormula*) sp.	—	—	1	—
Strombus (*Labiostrombus*) *japonicus* Reeve*	—	3	4	42
Polinices didyma (Bolten)*	—	1	—	—
Polinices sagamiensis Pilsbry*	—	—	—	3
Natica concinna Dunker	—	3	—	5
Sinum (*Eunaticina*) *papillum* (Gmelin)*	—	—	—	1
Erato callosa (Adams et Reeve)*	—	—	—	2
Erronea japonica (Schilder)	—	—	5	—
Bursa (*Gyrineum*) *natator* ("Bolten" Röding)	—	—	3	—
Trophon (*Bedeva ?*) *birileffi* Lischke*	—	5	7	3
Thais (*Mancinella*) *bronni* (Dunker)*	1	7	1	1
Pyrene (*Mitrella*) *varians* (Dunker)*	—	5	30	5
Pyrene (*Zafra*) *pumila* (Dunker)*	2	2	5	2
Siphonalia cassideriæformis ornata A. Ad.	—	—	—	2
Engina menkeana (Dunker)*	—	—	—	2
Nassarius (*Hinia*) *festivus* (Powys)*	—	3	—	1
Nassarius (*Tritonella*) *japonicus* (A. Adams)*	—	1	20	—
Nassarius (*Alectrion*) *balteatus* (Lischke)*	—	—	—	1
Nassarius (*Zeuxis*) *caelatus* (A. Adams)	—	—	1	—
Nassarius (*Niotha*) *gemmulatus* (Lamarck)*	—	—	—	2
Nassarius (*Niotha*) *livescens* (Philippi)*	—	12	59	—
Fusinus perplexus (A. Adams)*	—	1	—	—
Oliva mustelina Lamarck*	—	—	—	1
Mitra sp.	—	—	—	1

(*to be continued.*)

Table I. (*continued.*)

	1	2	3	4
Cancellaria (*Narona*) *spengleriana* Deshayes*	2	—	—	1
Clavatula consimilis (Smith)	—	1	—	—
Brachytoma jeffreysii (Smith)*	—	—	2	—
Asthenotoma nivea (Philippi)*	—	—	—	1
Mangelia (*Bela*) sp.	—	—	1	—
Mangelia (*Bela*) sp.	—	—	—	5
Peudorhaphitoma naganumensis Otuka n. sp.	—	—	—	2
Philbertia leuckarti (Dunker)*	—	—	—	1
Asperdaphne subzonata (Smith)	—	1	—	—
Terebra (*Punctoterebra*) *lischkeana* Dunker*	—	—	—	1
Pupa strigosa (Gould)*	—	2	—	2
Ringicula (*Ringiculina*) *doliaris* Gould	—	3	9	1
Ringicula (*Ringiculina*) *yokoyamai* Takeyama	3	—	4	3
Acteocina exilis (Dunker)	—	—	—	15
Retusa minima Yamakawa	—	1	9	20
Rhizorus artiaperta (Yamakawa)	—	2	—	2
Cylichna yamakawai Yokoyama	2	3	—	1
Philine japonica Lischke*	—	—	—	1
Dentalium (*Dentalium*) *hexagonum* Gould*	—	5	20	12
Dentalium (*Antalis*) *motidukii* Otuka n. sp.	—	—	—	1
Siphonodentalium (*Pulsellum*) *ozawai* Yokoyama	—	—	—	1
Nucula sp.	—	—	—	1
Limopsis multistriata (Forskål)*	—	—	—	29
Navicula ocellata (Reeve)*	—	4	24	10
Navicula boucardi (Jousseaume)*	—	—	1	—
Barbatia obtusoides (Nyst)*	—	10	—	—
Barbatia stearnsi (Pilsbry)*	—	—	1	40
Barbatia symmetrica (Reeve)*	3	—	20	40
Barbatia divaricata (Sowerby)	—	—	—	40
Barbatia decussata (Sowerby)	—	2	29	—
Arca subcrenata Lischke*	—	—	1	—
Arca inflata Reeve*	—	3	—	—
Bathyarca uwaensis (Yokoyama)	—	—	—	1
Trichomusculus divaricatus (Philippi)	—	—	7	5
Ostrea denselamellosa Lischke*	—	—	1	—
Ostrea gigas Thunberg*	—	4	—	—
Plicatula horrida Dunker	—	—	—	10

(*to be continued.*)

Table I. (*continued.*)

	1	2	3	4
Chlamys irregularis (Sowerby)*	—	—	—	3
Chlamys nipponensis Kuroda*	2	4	—	1
Pecten laqueatus Sowerby*	—	1	4	20
Spondylus cruentus Lischke*	—	4	4	—
Lima lischkei Lamy	—	—	15	30
Lima basilanica Adams et Reeve*	—	1	—	3
Crassatellites nanus (Adams et Reeve)	—	—	—	4
Beguina japonica (Pilsbry)*	—	1	—	—
Cardita cumingiana Dunker*	—	2	14	10
Basterotia gouldii (A. Adams)	—	—	—	4
Lucina (Myrtea) acutilineata Conrad	—	—	—	20
Lucina contraria Dunker	—	7	—	—
Pillucina pisidium (Dunker)	2	6	15	—
Anodontia bialata (Pilsbry)	—	10	1	—
Codakia divergens (Philippi)	—	1	9	1
Taras lunaris (Yokoyama)	—	—	—	4
Kellya notoensis Yokoyama	—	1	—	—
Scintilla nipponica Yokoyama	—	—	1	—
Jousseaumiella crassa (Yokoyama)	—	—	—	1
Mysella oblongata (Yokoyama)	—	—	—	1
Chama aspersa Reeve*	1	4	40	20
Cardium (Fulvia) muticum Reeve*	1	1	1	2
Cardium (Fulvia) hungerfordi Sowerby	—	—	—	15
Cardium (Trachycardium) ebaranum Yokoyama	—	—	1	2
Gafrarium divaricatum (Gmelin)*	4	6	—	—
Gafrarium (Circe) scriptum stutzeri (Donovan)*	4	15	—	—
Pitar pellucida Lamarck	4	8	1	2
Callista pacifica (Dillwyn)*	—	—	1	20
Chamaeformis meretrix (Linné)*	—	—	—	30?
Dosinia japonica Reeve*	1	2	—	—
Protothaca jedoensis (Lischke)*	—	4	7	—
Paphia euglypta (Philippi)*	—	—	—	4
Paphia undulata (Born)*	—	—	12	—
Petricola japonica Dunker	2	2	—	—
Raeta pulcheila Adams et Reeve	—	2	—	—
Lutraria arcuata Reeve	—	—	—	7
Macoma tokyoensis Makiyama	—	2	2	—

(*to be continued.*)

Table I. (*continued.*)

	1	2	3	4
Macoma truncata Jonas	—	—	3	—
Tellina (Merisca) diaphana Deshayes	—	—	—	1
Tellina (Angulus) iridella v. Martens*	—	—	—	2
Tellina miyatensis Yokoyama	—	—	6	7
Tellina sp.	—	—	—	1
Sanguinolaria (Nuttallia) olivacea (Jay)*	—	1	—	—
Theora (Endopleura) lubrica Gould	—	2	—	—
Solen sp.	—	—	—	2
Aloidis venusta (Gould)	—	—	2	1
Aloidis substriata (Yokoyama)	—	—	—	4
Cryptomya busoensis Yokoyama	—	1	—	—
Mya arenaria japonica Jay*	2	4	—	—
Barnea fragilis (Sowerby)*	1	2	—	—
Barnea dilatata (Souleyet)	—	—	3	2
Pholadidea penita tokyoensis (Yokoyama)	—	2	—	—

According to K. Kikuchi[19], the recent faunal characteristics of the bay of Toyama are of the Kurosio type. Living species in the bay of Toyama and on the coast of Hukui prefecture[20] are marked * in Table I.

On the other hand, during early Pleistocene, probably the writer's dl stage[21], continental mammals, e. g., *Stegodon orientalis* Owen[22], *Elephas namadicus naumanni* Makiyama, *Elephas trogontheri* Pohlig[23], lived in the Japanese island, so that the must have been connected with Asiatic continent during late Pliocene or early Pleistocene. If these mammals had migrated from the Asiatic continent through the landbridge of Korea during early Pleistocene or late Pliocene, the geologic age of the Tumuki, Miyainu and Hiradoko shell beds must be post early Pleistocene or post late Pliocene, since believed that the warm current flows through the Korean strait into the Japan sea. The condition in which these shell beds are deposited on the Tertiary bed rock is similar to the case of the Dl beds on the Pacific coast, e. g., the

---

19) K. Kikuchi, Catal. Mar. Shells Bay of Toyama, (1931).

20) T. Kuroda, Catal. Mar. Shells Hukui Pref., (1933).

21) Y. Otuka, "Dai Si-ki," *Iwanami Kôza* (1931) (in Japanese); *Proc. Pan-Pacific Sci, Congr., Canada* (1933), 1589~1592.

22) H. Matsumoto, *Sci. Rep. Tôhôku Imp. Univ., Geology*, **10** (1926).

23) J. Makiyama, *Jap. Jour. Geol. Geogr.*, **3** (1924); *Mem. Coll. Sci. Kyoto Imp. Univ.*, [*B*], 1 (1924).

Sakisima[24] beds, the Atumi shell beds[25] and the Huruya shell bed[26].

The extent of dissection of the Hiradoko terrace agrees with that of the Du terrace along the Pacific side. Fig. 6a, b show the extent to which dissection has proceeded in the Hiradoko terrace and in the Simosa terrace as calculated by Tayama's method.[27] This similarity in dissection in these two remote terraces may justify the writer in concluding that these two terraces underwent similar dissection since their surface was uplifted.

The east coast of Noto peninsula is now very irregular in outline. Nanao bay, Usetu harbour, Tukumo-wan, and Anamidu-wan are drowned valley topographies. Seeing that these drowned valleys dissect the surface of Hiradoko, Tumuki and Matunami terrace and Alluvial plains are formed in all the valley head of these drowned valleys, the early Alluvial or later Diluvial subsidence, a predominant feature of Japanese islands[28], is seen in this province also.

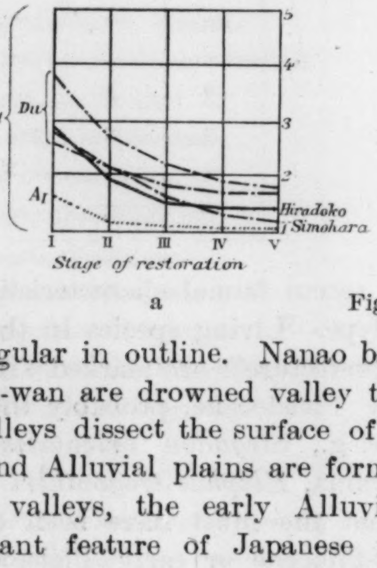

a

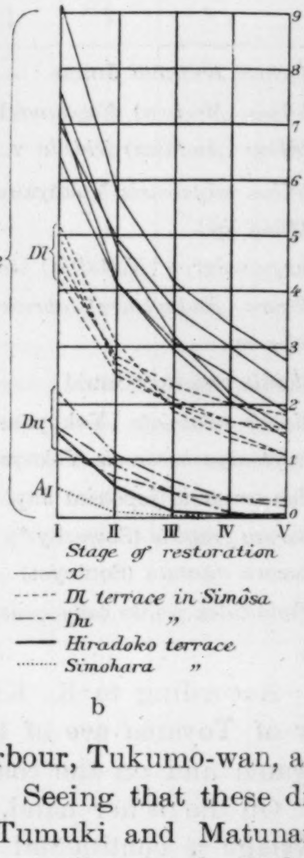

b

Fig. 6

It will be seen from the foregoing that the surface of the Hiradoko, Tumuki, and Matunami terraces may be the Du of the writer, and the shell beds of Tumuki, Miyainu, and Hiradoko either duI or dlII. The Tumuki shell bed originally believed by the writer from its faunal characteristics and its geologic occurrences, to be "aI" (early Holocene), or "duII" (latest Pleistocene), seems to be an error. Warm current fauna is a common characteristic of "dlII" (lower Pleistocene shell beds) on the Pacific coast of southwestern Japan, as pointed out by

---

[24] Y. OTUKA, *Geogr. Rev. Jap.*, 4 (1928) (in Japanese); OIMIKADO, *Chikyû*, 19 (1933), (in Japanese).

[25] OIMIKADO, *Chikyû*, 20 (1933), (in Japanese).

[26] J. MAKIYAMA, *Chikyû*, 12 (1929), (in Japanese).

[27] R. TAYAMA, *Sci. Rep. Saito-hoonkai*, 9 (1930), (in Japanese).

[28] Y. OTUKA, *Proc. Imp. Acad., Japan*, 10 (1934).

Kuroda[29], Matsushita[30], Oimikado[31], and Makiyama[32]. The occurrence of a warm fauna therefore does not affect the conclusion that the Hiradoko, Tumuki, and the Matunami shell beds were deposited during the earlier half of the Pleistocene. The age of these shell-bearing deposits of Noto have, however, to be discussed with great care, particularly as any conclusions with respect to the age of these shell-bearing deposits will be closely related to interpretations regarding the Pleistocene crustal movement of the Japanese island. That is, if the Pleistocene shell-bearing beds on the Pacific and Japan Sea side were contemporaneous with each other, the Japanese islands would be moved by similar crustal movement as one block; whereas if these beds were different in age, the Japanese island would be moved by differential crustal movements on Pacific and Japan sea sides. (to be continued).

---

17. 能登半島南部邑知地溝 (1)

地震研究所 大塚彌之助

この論文は能登半島の南部をN60°Eの方向に横ぎる邑知地溝の地質構造發達史の一部の研究である. 全章を8項に分ち地形・層序・地質構造の順に説明し, 最後の章はこの研究の一資料となつた貝化石類の記載に充てた.

緒論に於ては, この地方を研究された先輩諸兄の論文を擧げてゐる.

地形の項は邑知地溝の地溝底・兩側山地の地形區分に終始し, 最後に能登半島の切峯面に就いて言及した.

能登半島東岸の海岸段丘の項に於いては, 能登半島東岸の海岸段丘を記載し, 各段丘層の性質を述べ, 徳田・津向・松波・平床各段丘の形成の時代を論じてゐる. 種々考察の結果は平床その他各段丘面の形成された時代は從來考察された如く洪積世末期又は沖積世初期と考へるには層位學上・地形學上稍々説明困難な點がある. これらの段丘面は恐らく洪積世中期又は後半の形成にかゝるものらしく, 段丘層は從來考察された如く鮮新世末期と考へるには, 今日の處, 古生物學上矛盾がある.

層位・構造その他に關しては第2に之を譲つた.

---

[29] S. Nakamura and T. Kuroda, *Chikyû*, 1 (1925), (in Japanese).

[30] S. Matsushita. *Chikyû*, 18 (1932), (in Japanese).

[31] Oimikado, *op. cit.*, (1933).

[32] Makiyama, *op. cit.*, (1924, 1929).

（食研彙報　第十三號　圖版　大塚）

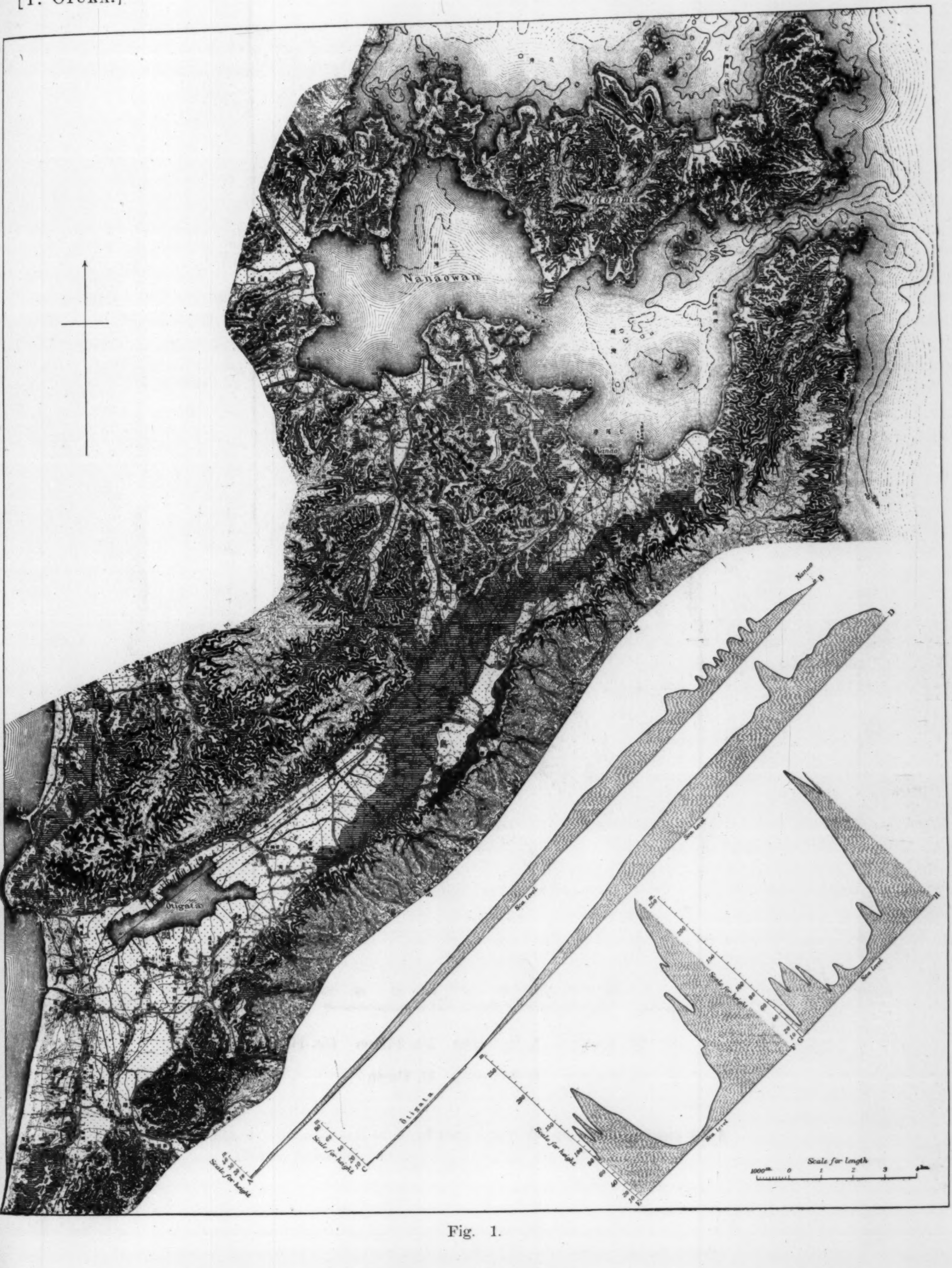
Notozima
Nanaowan
Nanao
Otigata
A
B
C
D
E
F
G
H
Sea level
Scale for height
Scale for length
1000m 0 1 2 3 4km

Fig. 1.

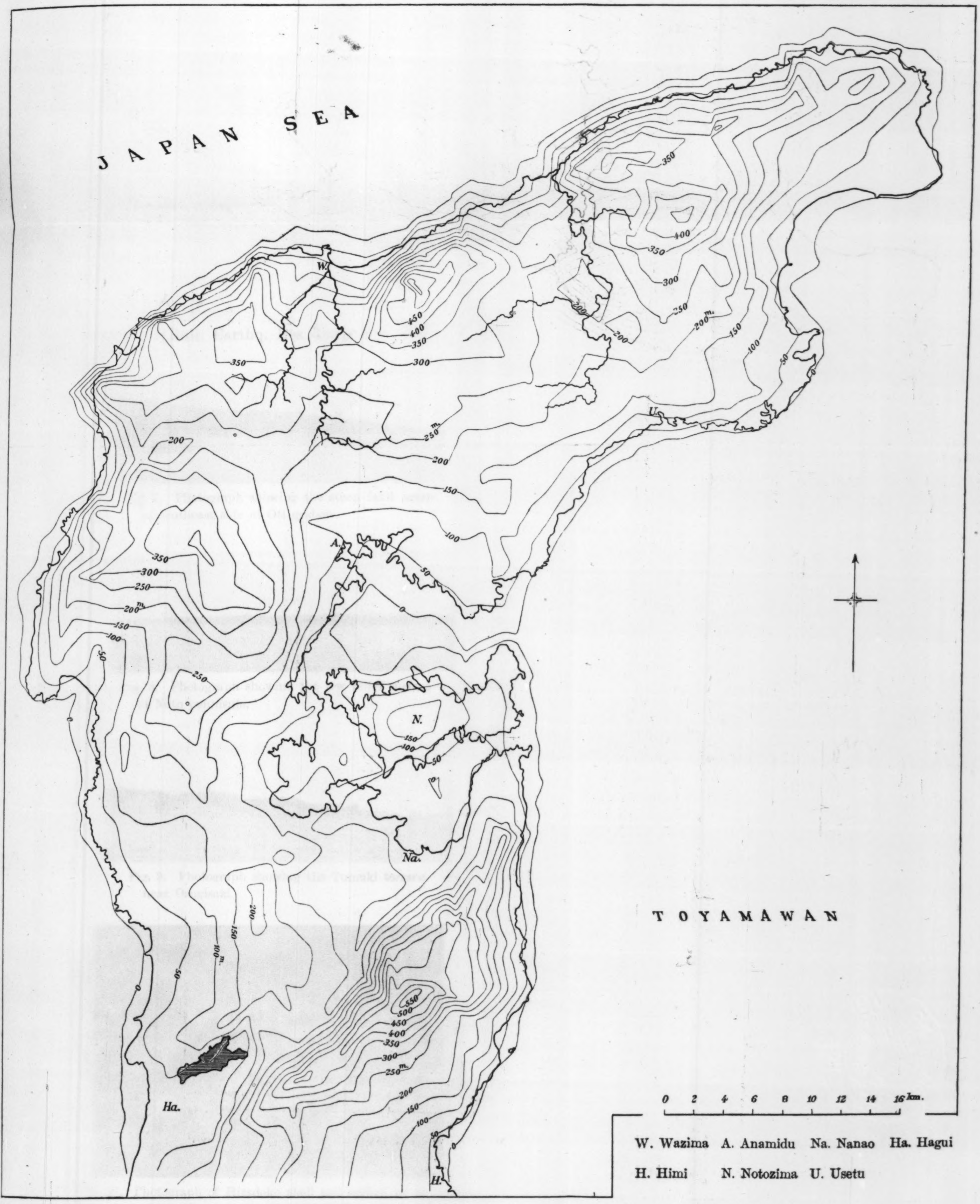
JAPAN SEA
TOYAMAWAN
W.
A.
N.
Na.
Ha.
H.
U.
550
500
450
400
350
300
250 m.
200 m.
150
100 m.
50
0
0 2 4 6 8 10 12 14 16 km.
W. Wazima
A. Anamidu
Na. Nanao
Ha. Hagui
H. Himi
N. Notozima
U. Usetu

Fig. 4. Summit-level of Noto peninsula. (Contour line is referred to the highest points in the 2 km². nets.)
This summit-level has been drawn by K. Yasumuro.

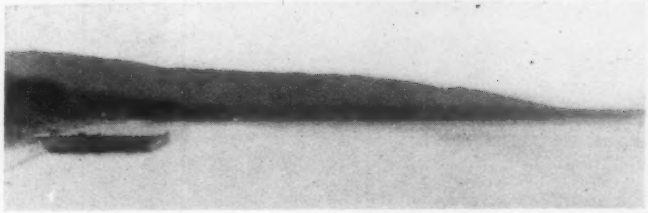

Fig. 7. Photograph showing the steep fault scarp of southeast side of Oti graben.

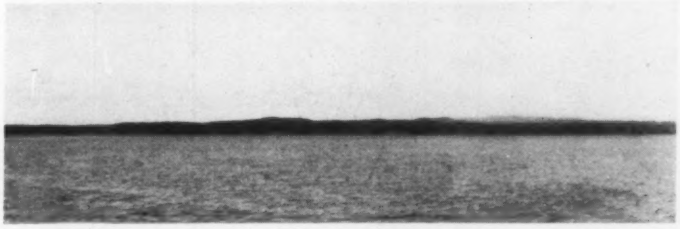

Fig. 8. Photograph showing the low relief surface of Noto peninsula.

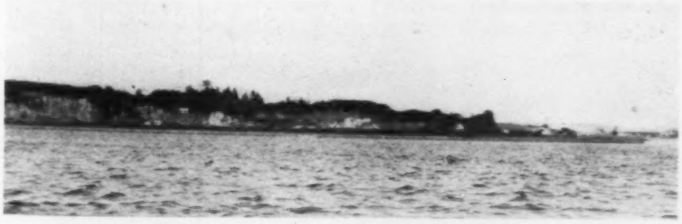

Fig. 9. Photograph showing the Tumuki terrace near Osugisaki.

（震研彙報 第十三號 圖版 大塚）

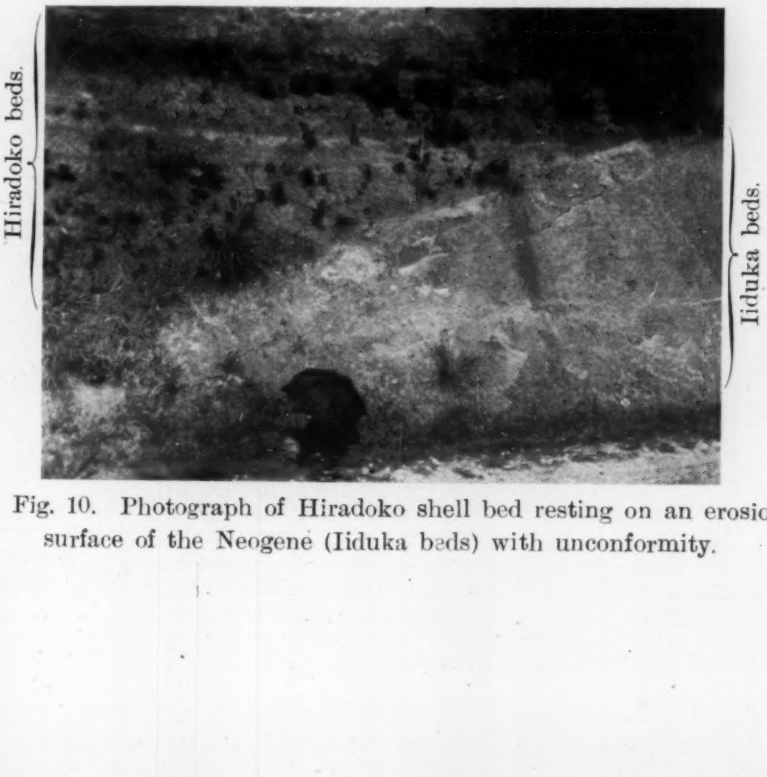

Fig. 10. Photograph of Hiradoko shell bed resting on an erosion surface of the Neogene (Iiduka beds) with unconformity.

18. *Discontinuity in the Dispersion Curves of Rayleigh Waves.*[1]

By Katsutada **SEZAWA** and Kiyoshi **KANAI**,

Earthquake Research Institute.

(Read Dec. 18, 1934.——Received March 20, 1935.)

Some years ago, one of us in dealing with the problem[2] of the dispersion of Rayleigh waves transmitted along the surface of a stratified body, obtained the corresponding dispersion curves of waves of a few cases, such as in which the ratios of the rigidity of the stratum to that of the subjacent medium are 1/2, 1/3, 1/4, 1/5, the densities of both media being the same and the Poisson's condition of elastic constants being satisfied. The equation necessary for obtaining the velocity of transmission was expressed by a determinant of the form:

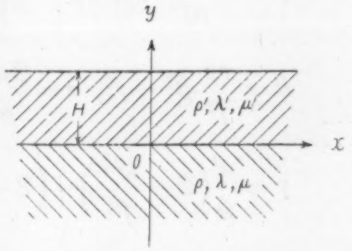

Fig. 1.

$$\begin{vmatrix} -\frac{(f^2-s'^2)}{k'^2}Y_2, & 2\frac{\mu'}{\mu}\frac{ifs'}{k'^2}Y_1, & 0, & -2\frac{\mu'}{\mu}\frac{ifs'}{k'^2}, & 0, & \frac{s'f}{k'^2} \\ -\frac{(f^2-s'^2)}{k'^2}Y_1, & -2\frac{\mu'}{\mu}\frac{ifs'}{k'^2}Y_2, & \frac{\mu'}{\mu}\frac{(f^2-s'^2)}{k'^2}, & 0, & \frac{if^2}{k'^2}, & 0 \\ 2\frac{ifr'}{h'^2}X_1, & \left(2\frac{\mu'}{\mu}\frac{r'^2}{h'^2}-\frac{\lambda'}{\mu}\right)X_2, & -\frac{\mu'}{\mu}\frac{2ifr'}{h'^2}, & 0, & \frac{r'f}{h'^2}, & 0 \\ 2\frac{ifr'}{h'^2}X_2, & \left(2\frac{\mu'}{\mu}\frac{r'^2}{h'^2}-\frac{\lambda'}{\mu}\right)X_1, & 0, & \left(\frac{\lambda'}{\mu}-2\frac{\mu'}{\mu}\frac{r'^2}{h'^2}\right), & 0, & -\frac{if^2}{h'^2} \\ 0, & 0, & -\frac{(f^2+s^2)}{k^2}, & 2\frac{ifs}{k^2}, & -\frac{if^2}{k^2}, & -\frac{sf}{k^2} \\ 0, & 0, & -\frac{2ifr}{h^2}, & \left(2\frac{r^2}{h^2}-\frac{\lambda}{\mu}\right), & -\frac{rf}{h^2}, & \frac{if^2}{h^2} \end{vmatrix} = 0, \quad (1)$$

where $X_1 = \cosh r'H$, $X_2 = \sinh r'H$, $Y_1 = \cos s'H$, $Y_2 = \sin s'H$.

---

[1] Preliminary report published in the *Proc. Imp. Acad.*, **11** (1935), 13.

[2] K. **SEZAWA**, *Bull. Earthq. Res. Inst.*, **3** (1937), 1.

Our recent investigation shows that this reduces to

$$\begin{aligned}\frac{4r's'}{f^2}\left(2-\frac{k'^2}{f^2}\right)\eta-\frac{r's'}{f^2}\left\{4\vartheta+\left(2-\frac{k'^2}{f^2}\right)^2\zeta\right\}\cosh r'H\cos s'H\\ +\frac{r'}{f}\varphi\left\{\frac{4rs'^2}{f^3}+\frac{s}{f}\left(2-\frac{k'^2}{f^2}\right)^2\right\}\cosh r'H\sin s'H\\ +\frac{s'}{f}\varphi\left\{-\frac{4sr'^2}{f^3}+\frac{r}{f}\left(2-\frac{k'^2}{f^2}\right)^2\right\}\sinh r'H\cos s'H\\ +\left\{-\frac{4r'^2s'^2}{f^4}\zeta+\left(2-\frac{k'^2}{f^2}\right)^2\vartheta\right\}\sinh r'H\sin s'H=0,\end{aligned}\tag{2}$$

where

$$\left.\begin{aligned}&\varphi=\frac{\mu'k^2k'^2}{\mu f^4},\quad \zeta=\frac{4rs}{f^2}\left(\frac{\mu'}{\mu}-1\right)^2-\alpha^2,\quad \eta=\frac{2rs}{f^2}\left(\frac{\mu'}{\mu}-1\right)\beta-\alpha\gamma,\\ &\vartheta=\frac{rs}{f^2}\beta^2-\gamma^2,\ \alpha=\frac{2\mu'}{\mu}-\left(2-\frac{k^2}{f^2}\right),\quad \beta=\frac{\mu'}{\mu}\left(2-\frac{k'^2}{f^2}\right)-2,\\ &\gamma=\frac{\mu'}{\mu}\left(2-\frac{k'^2}{f^2}\right)-\left(2-\frac{k^2}{f^2}\right),\\ &r^2=f^2-h^2,\quad s^2=f^2-k^2,\quad r'^2=f^2-h'^2,\quad s'^2=k'^2-f^2,\\ &h^2=\rho p^2/(\lambda+2\mu),\ h'^2=\rho'p^2/(\lambda'+2\mu'),\ k^2=\rho p^2/\mu,\ k'^2=\rho'p^2/\mu',\end{aligned}\right\}\tag{3}$$

in which H is the thickness of the stratum, $2\pi/f$ the wave length, ρ, λ, μ, ρ', λ', μ' the densities and elastic constants of the stratum and the subjacent medium respectively. By means of equation (2) we determined the dispersion curves of Rayleigh waves in a body having such small ratios of rigidities as 1/20 and $1/\infty$. We further reexamined the case in which the ratio is 1/5, the results of which are given in Table I and plotted in Figs. 2, 3, 4.

Table I. ($\rho=\rho'$, $\lambda=\mu$, $\lambda'=\mu'$.)

$\mu/\mu'=5$		$\mu/\mu'=20$				$\mu/\mu'=\infty$			
Part CO′D		Part AOB		Part CO′D		Part AOB		Part COD	
$\frac{2\pi}{fH}$	$\frac{p}{f}\sqrt{\frac{\rho}{\mu'}}$	$\frac{2\pi}{fH}$	$\frac{p}{f}\sqrt{\frac{\rho}{\mu'}}$	$\frac{2\pi}{fH}$	$\frac{p}{f}\sqrt{\frac{\rho}{\mu'}}$	$\frac{2\pi}{fH}$	$\frac{p}{f}\sqrt{\frac{\rho}{\mu'}}$	$\frac{2\pi}{fH}$	$\frac{p}{f}\sqrt{\frac{\rho}{\mu'}}$
2·36	1·645	3·227	1·4142	2·664	1·732	1·000	0·9325	2·525	1·732
3·32	1·732	4·170	1·732	3·88	1·871	1·333	0·958	3·880	1·898
4·060	1·816	4·60	1·871	4·72	2·000	2·000	1·078	4·000	1·914
4·432	1·871	5·14	2·000	5·544	2·236	2·657	1·260	4·619	2·000

(to be continued.)

Table I. (*continued.*)

$\mu/\mu'=5$		$\mu/\mu'=20$				$\mu/\mu'=\infty$			
Part CO′D		Part AOB		Part CO′D		Part AOB		Part COD	
$\frac{2\pi}{fH}$	$\frac{p}{f}\sqrt{\frac{\rho}{\mu'}}$	$\frac{2\pi}{fH}$	$\frac{p}{f}\sqrt{\frac{\rho}{\mu'}}$	$\frac{2\pi}{fH}$	$\frac{p}{f}\sqrt{\frac{\rho}{\mu'}}$	$\frac{2\pi}{fH}$	$\frac{p}{f}\sqrt{\frac{\rho}{\mu'}}$	$\frac{2\pi}{fH}$	$\frac{p}{f}\sqrt{\frac{\rho}{\mu'}}$
5·219	2·000	6·70	2·236	6·192	2·449	3·200	1·446	5·333	2·300
6·637	2·236	11·73	3·000	7·40	2·828	4·000	1·751	8·000	3·45
		15·97	3·464	8·00	3·000	4·619	2·000	28·25	12·25
Part AOB from prev. paper.		20·85	3·715	12·30	3·873	6·097	2·236		
		29·224	3·873	13·65	4·062	7·289	2·449		
		116·0	4·062	16·70	4·472	10·02	3·000		
						20·85	5·477		
						48·50	12·250		

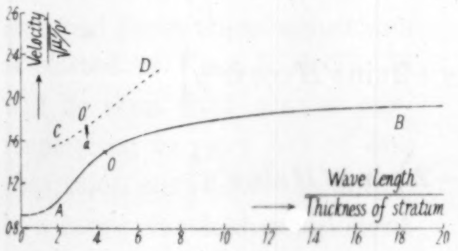

Fig. 2. $\frac{\mu'}{\mu}=\frac{1}{5}$, $\frac{\rho'}{\rho}=1$.

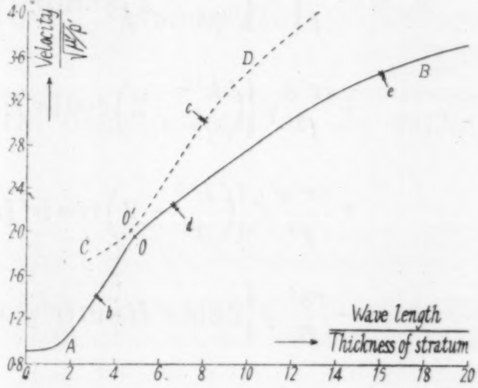

Fig. 3. $\frac{\mu'}{\mu}=\frac{1}{20}$, $\frac{\rho'}{\rho}=1$.

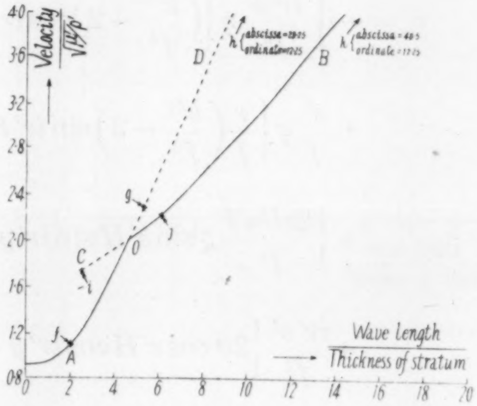

Fig. 4. $\frac{\mu'}{\mu}=\frac{1}{\infty}$, $\frac{\rho'}{\rho}=1$.

It was our belief until recently that only one dispersion curve, excepting those of waves having many horizontal nodal planes in the stratum, is possible in each case of a given ratio of rigidities, but our present calculation shows that there are two dispersion curves of different wave types, even when the ratio is 1/5. The curve AB in Fig. 2 is what we obtained in the previous study, whereas CD is another dispersion curve newly found as the result of a closer examination of the subject. As the ratio decreases, the two curves AB and CD approach each other and tend to bend at O and O′ respectively, while, if the ratio is 1/20, the two curves assume the forms indicated in Fig. 3, fairly sharp discontinuities of inclination appearing at O and O′ in the respective curves. Finally, if the ratio becomes 1/∞, part AO of curve AB joins part O′D of curve CD, while on the other hand another part OB of curve AB joins another part CO′ of curve CD, so that both the newly formed curves, AOD and COB, are now continuous as shown in Fig. 4.

Next, with a view to knowing, whether or not any discontinuity in wave types exists at points O and O′ of the dispersion curves, we examined the expressions for displacement[3]; its horizontal and vertical components within the stratum and in the subjacent medium being written by

$$
\begin{aligned}
u'_y = -\frac{s'}{f}\Big[& -\left(\frac{k'^2}{f^2}-2\right)\eta \sin ir'(H-y) - \frac{2ir's'}{f^2}\eta \sin s'(H-y) \\
& + \frac{ir's}{f^2}\varphi\left\{\left(\frac{k'^2}{f^2}-2\right)\cos ir'H \cos s'y + 2\cos s'H \cos ir'y\right\} \\
& + \frac{ir's'}{f^2}\zeta\left\{\left(\frac{k'^2}{f^2}-2\right)\cos ir'H \sin s'y + 2\sin s'H \cos ir'y\right\} \\
& - \frac{rs'}{f^2}\varphi\left\{2\sin s'H \sin ir'y + \left(\frac{k'^2}{f^2}-2\right)\sin ir'H \sin s'y\right\} \\
& + \vartheta\left\{\left(\frac{k'^2}{f^2}-2\right)\sin ir'H \cos s'y + 2\cos s'H \sin ir'y\right\}\Big], \\
v'_y = -i\Big[& \frac{ir's'}{f^2}\eta\left\{\left(\frac{k'^2}{f^2}-2\right)\cos ir'(H-y) - 2\cos s'(H-y)\right\} \\
& + \frac{s'}{f}\varphi\left\{\frac{r}{f}\left(\frac{k'^2}{f^2}-2\right)\sin ir'H \cos s'y + \frac{2r'^2 s}{f^3}\cos s'H \sin ir'y\right\} \\
& + \left\{\frac{2r'^2 s'^2}{f^4}\zeta \sin s'H \sin ir'y + \left(\frac{k'^2}{f^2}-2\right)\vartheta \sin ir'H \sin s'y\right\} \\
& + \frac{ir's'}{f^2}\left\{2\vartheta \cos s'H \cos ir'y - \left(\frac{k'^2}{f^2}-2\right)\zeta \cos ir'H \cos s'y\right\} \\
& - \frac{ir'}{f}\varphi\left\{\frac{2rs'^2}{f^3}\sin s'H \cos ir'y - \frac{s}{f}\left(\frac{k'^2}{f^2}-2\right)\cos ir'H \sin s'y\right\}\Big], \quad (4)
\end{aligned}
$$

---

3) K. SEZAWA and K. KANAI, *Bull. Earthq. Res. Inst.*. **12** (1934), 641.

$$\left.\begin{aligned} u&=\frac{i\mu' s' k'^2}{\mu f^3}\left[Pe^{ry}+\frac{s}{f}Qe^{sy}\right],\\ v&=-\frac{\mu' s' k'^2}{\mu f^3}\left[\frac{r}{f}Pe^{ry}+Qe^{sy}\right], \end{aligned}\right\} \qquad (5)$$

where

$$\left.\begin{aligned} P=&\frac{2sr'}{f^2}\beta\cos s'H+\frac{2r's'}{f^2}\alpha\sin s'H\\ &-\frac{2sr'}{f^2}\left(2-\frac{k'^2}{f^2}\right)\left(\frac{\mu'}{\mu}-1\right)\cosh r'H+\left(2-\frac{k'^2}{f^2}\right)\gamma\sinh r'H,\\ Q=&-\frac{2r'}{f}\gamma\cos s'H-4\frac{rr's'}{f^3}\left(\frac{\mu'}{\mu}-1\right)\sin s'H\\ &+\frac{r'}{f}\left(2-\frac{k'^2}{f^2}\right)\alpha\cosh r'H-\frac{r}{f}\left(2-\frac{k'^2}{f^2}\right)\beta\sinh r'H. \end{aligned}\right\} \qquad (6)$$

The ratio of horizontal and vertical displacements at the surface obtained from these equations is plotted in Figs. 5, 6, 7. It will be seen that waves corresponding to part AO of one dispersion curve have generally a large vertical component of surface displacement, whereas those of part OB of the same dispersion curve have a large horizontal component. The orbital motion of waves cor-

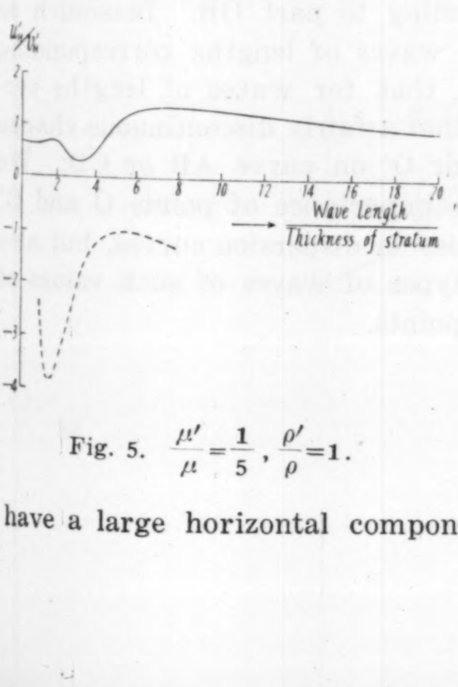

Fig. 5. $\frac{\mu'}{\mu}=\frac{1}{5}$, $\frac{\rho'}{\rho}=1$.

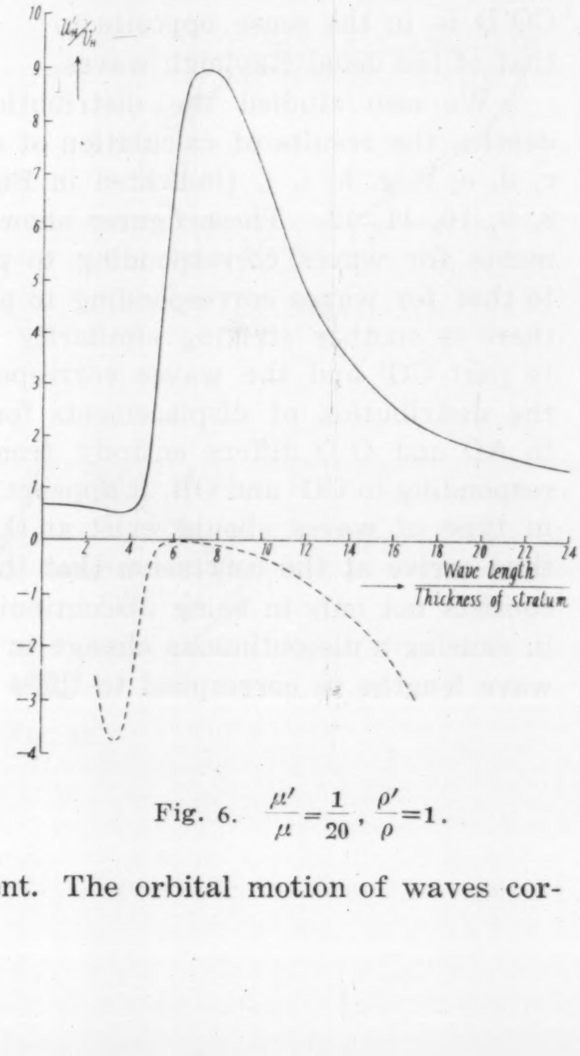

Fig. 6. $\frac{\mu'}{\mu}=\frac{1}{20}$, $\frac{\rho'}{\rho}=1$.

responding to AOB is in the same sense as those of the usual Rayleigh waves transmitted on the surface of a semi-infinite body. As regards waves corresponding to curve CO′D, particularly when the ratio of the rigidities of both media is finite, say 5 or 20, although hardly any discontinuous change in the ratio of horizontal to vertical displacements could be found at the point O′, the curve indicates that the ratio becomes stationary at the same point; in other words, the ratio does not change for a small variation of wave length in the immediate vicinity of that point. It is notable, however, that the orbital motion of waves corresponding to CO′D is in the sense opposite to that of the usual Rayleigh waves.

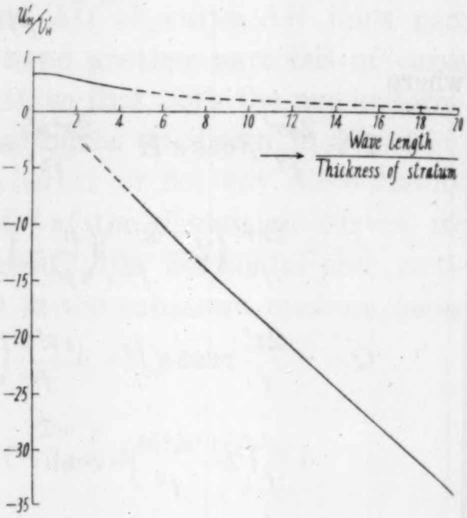

Fig. 7. $\frac{\mu'}{\mu}=\frac{1}{\infty}$, $\frac{\rho'}{\rho}=1$.

We also studied the distribution of displacements at different depths, the results of calculation of cases corresponding to points a, b, c, d, e, f, g, h, i, j, (indicated in Figs. 2, 3, 4) being shown in Figs. 8, 9, 10, 11, 12. These figures show that the distribution of displacements for waves corresponding to part AO is approximately similar to that for waves corresponding to part O′D, while on the other hand there is another striking similarity between the waves corresponding to part CO′ and the waves corresponding to part OB. Inasmuch as the distribution of displacements for waves of lengths corresponding to AO and O′D differs entirely from that for waves of lengths corresponding to CO′ and OB, it appears that a fairly discontinuous change in type of waves should exist at O or O′ on curve AB or CD. We thus arrive at the conclusion that the importance of points O and O′ consists not only in being discontinuities in dispersion curves, but also in causing a discontinuous change in types of waves of such values of wave lengths as correspond to those points.

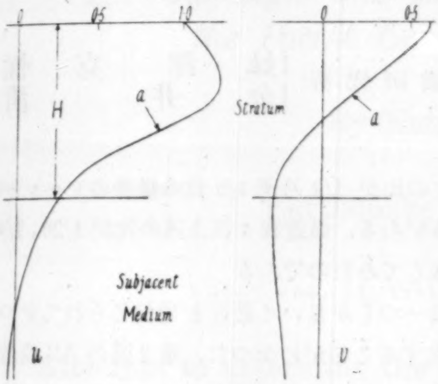

Fig. 8.

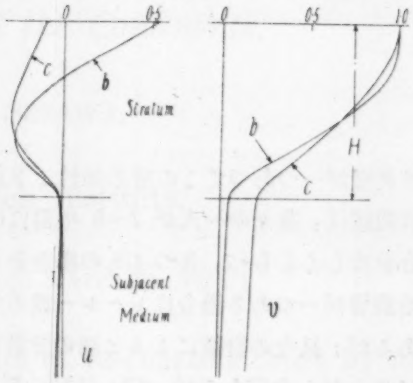

Fig. 9.

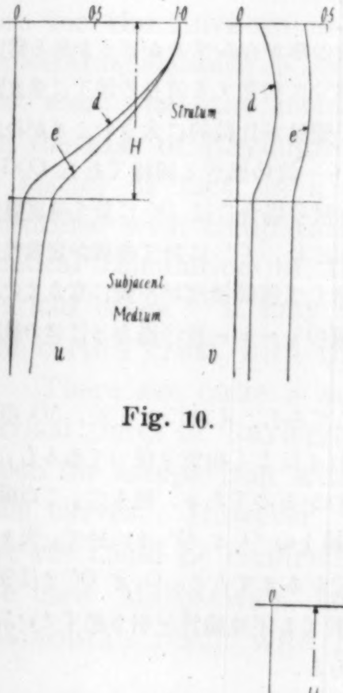

Fig. 10.

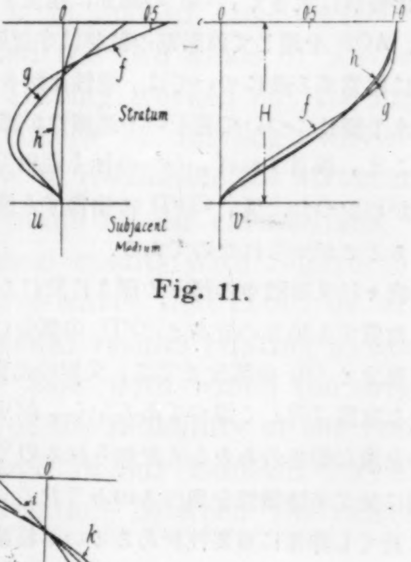

Fig. 11.

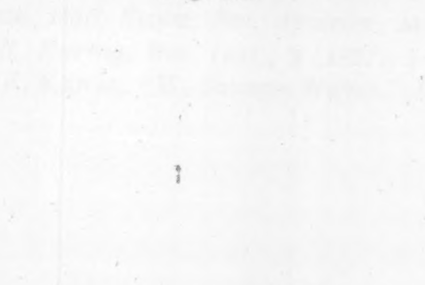

Fig. 12.

18. レーレー波の分散曲線に於ける不連續性

地震研究所 妹澤克惟
金井清

地表層が一つあつてこの層の彈性と下層の彈性との比が 1/2 乃至 1/5 位の場合のレーレー波の分散問題は，我々の一人が 7～8 年前に研究した事がある．最近我々は上述の比が 1/20, 1/∞ の場合を委しくしらべ，且つ 1/5 の場合をも再び吟味してみたのである．

地表層が一つある場合にレーレー波の分散曲線は一つしかないと最近まで信じられてをつたのであるが，只今の計算によると別の分散曲線の存在することがわかつた．第2圖の AB 曲線は以前に出したものであるが，CD は玆に新しく見出された別の分散曲線を示す．彈性の比が增加すると AB と CD とは接近して行き，彈性比が 1/20 になると第3圖の如くなり，且つ O と O′ とに各曲線の傾斜の不連續點が生ずるやうになる．彈性比が 1/∞ になると AB 曲線の AO の部分と CD 曲線の O′D とが結びつき，又 CD 曲線の CO′ と AB 曲線の OB とが連なり，結局第4圖に示すやうに新しく作られた AOD 曲線と COB 曲線とが夫々連續性の曲線となるのである．

次に上述の O 及 O′ に於て波型についても何か不連續的の事が存在するかどうか知る爲に振動變位の式を出してそれをしらべてみたのである．AO の部分に相當する波長の波では垂直變位が比較的に大きく，OB の部分に相當する波長の波では水平變位が比較的に大きいことがわかつた．AOB を通じて波動點の軌跡は半無限體を傳播するレーレー波の場合と同樣である．CO′D 曲線に相當する波については，彈性比が 5 とか 20 のやうに有限の場合には O′ に於て垂直變位又は水平變位について著しい不連續性が認められなかつたけれども，O′ に於て曲線が定常性を持つこと，換言すれば，O′ の極く近所で少しの波長變化に對して波動速度が不變になるといふことがわかつた．又，CO′D に相當する波動の表面變位は普通のレーレー波の場合とは逆の軌跡をとることが知られたのである．

我々は又固體中の種々の深さに於ける變位の分布を研究してみた．それによると，AO の部分に相當する場合の分布と O′D の部分に相當する場合のそれとはよく相似を保つてゐるし，CO′ の部分と OB の部分とでは，又別の相似が存在することがわかるのである．然るに，この兩種の分布狀態は著しく違つてゐるから，AOB 曲線と CO′D 曲線上の O と O′ とに於て，夫々分布の急激な變化のあることが知られるのである．果してそうであるとすると，O と O′ とは分散曲線に於て不連續性を與へるのみでなく，變位の分布狀態に於ても不連續性を引き起すといふ意味に於ても非常に重要性があるといふ結論に到達したわけである．

19. *Rayleigh- and Love-waves transmitted through the Pacific Ocean and the Continents.*

By Katsutada SEZAWA,

Earthquake Research Institute.

(Read Jan. 15, 1935.—Received March 20, 1935.)

Attempts to determine the structure of the earth's crust by means of the arrival time of surface waves have been made by a number of investigators, namely, Gutenberg,[1] Jeffreys,[2] Stoneley,[3] Matuzawa,[4] Byerly,[5] Carder,[6] etc. But, the surface waves studied by them for that purpose were chiefly of the Love-type, the reason for which is probably the fact that the dispersion curves that are easily obtained are for the Love-waves and not for Rayleigh-waves. Provided the epicentral distance is not small, say not less than 20 degree, it does not seem that the identification of the initial phase is more difficult in the case of Rayleigh-waves than it is in that of Love-waves. As a matter of fact, in a case of this kind the two kinds of waves are identified with comparative clearness. Having worked out the mathematical calculation of the dispersion curves of Rayleigh-waves for various cases,[7][8] it may be in order now to reexamine the structure of the earth's crust with the aid of the results of our calculations.

There are quite a number of observed results with regard to the arrival times of Rayleigh-waves and Love-waves that could be drawn upon for comparison with our mathematical results relating to dispersion curves. However, because of the ease with which the original records could be confirmed and in view of the reliability of the results, we used Matuzawa's data[9] that appeared in our Bulletin for 1929. Matuzawa's result with respect to the relation between the velocities of transmission and the periods of oscillation of the respective initial phases of L-waves and M-waves will be found reproduced in Figs. 1, 2. Since it is possible for different kinds of surface waves[10] to exist even in the case of Rayleigh-waves and it seems that the usual surface waves, generally speaking, correspond to that kind having maximum group velocities, the enveloping curves drawn in these figures seem to give the approximate values of the velocities of transmission of the usual surface waves.

---

[1] B. GUTENBERG, *Z. f. Geophys.*, **1** (1925), 100~106; *Phys. Z.*, **27** (1926), 111~114; *Proc. 5th Pac. Sci. Congr., Canada*, **3** (1934), 2511~2521.

[2] H. JEFFREYS, *M. N. R. A. S., Geophys. Suppl.*, **1** (1925), 282~292.

[3] R. STONELEY, *M. N. R. A. S., Geophys. Suppl.*, **1** (1928), 527~532.

[4] 9) T. MATUZAWA, *Bull. Earthq. Res. Inst.*, **6** (1929), 213~229.

[5] P. BYERLY, *Gerl. Beitr. z. Geophys.*, **26** (1930), 27~33.

[6] DEANS S. CARDER, *Bull. Seism. Soc. America*, **24** (1934), 231.

[7] K. SEZAWA, *Bull. Earthq. Res. Inst.*, **3** (1927), 1~18.

[8] K. SEZAWA and K. KANAI, "M_2 Seismic Waves," *Proc. Imp. Acad.*, **11** (1935), 96~98.

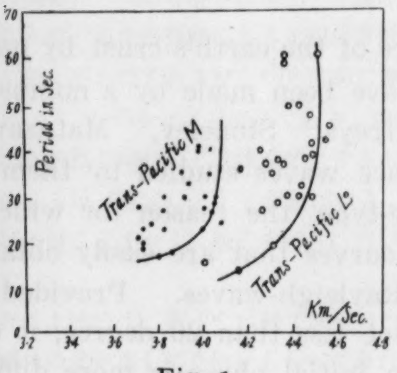

Fig. 1.

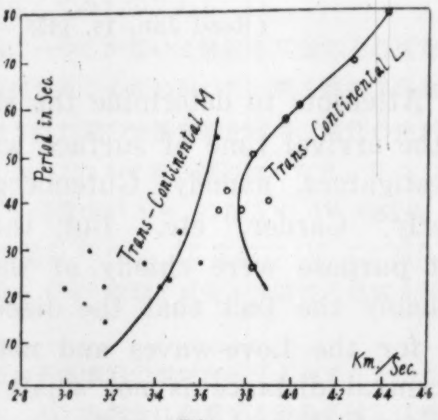

Fig. 2.

After a prolonged study of the subject it is our conclusion that it is urgently necessary to obtain, mathematically, the dispersion curves of Rayleigh-waves as well as those of Love-waves that are transmitted through stratified bodies in such cases of (i) $\rho=\rho'$, $\lambda=\mu$, $\lambda'=\mu'$, $\mu/\mu'=2$, (ii) $\rho/\rho'=1{\cdot}14$, $\lambda=\mu$, $\lambda'=\mu'$, $\mu/\mu'=1{\cdot}65$, where ρ', λ', μ', ρ, λ, μ are the densities and elastic constants of the stratum and the subjacent medium respectively. The dispersion curves of Rayleigh-waves of case (i) was obtained some time ago,[11] that of case (ii) has been elabolated by Mr. Kanai,[12] while the dispersion curves of Love-waves were constructed with very little difficulty. All these curves are shown in Figs. 3, 4, 5, 6. The values for the group velocities were obtained in the usual way.

A careful comparison of the enveloping curves in Figs. 1, 2 with the curves indicating the group and phase velocities in Figs. 3, 4, 5, 6, shows that the four cases of surface waves, namely, trans-Pacific and trans-Continental Rayleigh-waves as well as Love-waves, approximately agree with the present four mathematical results. It should, however, be borne in mind that the curves giving the phase velocities in Figs. 3, 4, 5, 6 were necessary not only for calculating the group velocities,

---

10) 12) K. SEZAWA and K. KANAI, *loc. cit.*
11) K. SEZAWA, *loc. cit.*

but also for deriving the lengths of the actual waves from the periods of oscillation as well as from the velocities of transmission. It will thus be seen that it is possible to find eventually the proper thickness of the stratum as estimated from every feature of dispersion corresponding to the trans-Pacific Rayleigh-waves, trans-Pacific Love-waves, trans-Continental Rayleigh-waves, and the trans-Continental Love-waves. From the nature of the trans-Pacific Rayleigh-waves we get $H=9$ km, $\rho=\rho'$, $\lambda=\mu$, $\lambda'=\mu'$, $\sqrt{\mu'/\rho'}=3{\cdot}2$ km/sec, $\sqrt{\mu/\rho}=4{\cdot}5$ km/sec; from that of the trans-Pacific Love-waves we obtain $H=5$ km, $\rho=\rho'$, $\sqrt{\mu'/\rho'}=3{\cdot}2$ km/sec, $\sqrt{\mu/\rho}=4{\cdot}5$ km/sec; from that of the trans-Continental Rayleigh-waves we find $H=12$ km, $1{\cdot}14\rho'=\rho$, $\lambda=\mu$, $\lambda'=\mu'$, $\sqrt{\mu'/\rho'}=3{\cdot}1$ km/sec, $\sqrt{\mu/\rho}=3{\cdot}7$ km/sec; while from that of the trans-Continental Love-waves we have $H=40$ km, $1{\cdot}14\rho'=\rho$, $\sqrt{\mu/\rho'}=3{\cdot}7$ km/sec, $\sqrt{\mu/\rho}=4{\cdot}5$ km/sec.

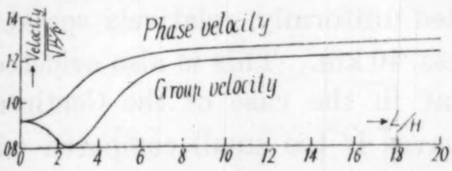

Fig. 3. Rayleigh waves. $\rho=\rho'$, $\mu/\mu'=2$.

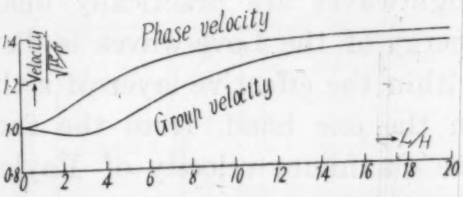

Fig. 4. Love waves. $\rho=\rho'$, $\mu/\mu'=2$.

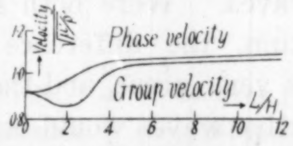

Fig. 5. Rayleigh waves.
$\rho/\rho'=1{\cdot}14$, $\mu/\mu'=1{\cdot}65$.

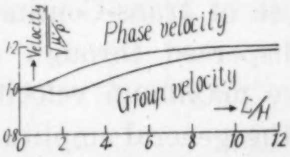

Fig. 6. Love waves.
$\rho/\rho'=1{\cdot}14$, $\mu/\mu'=1{\cdot}65$.

The thickness of the sub-Pacific stratum estimated from Rayleigh-waves does not differ much from that estimated from Love-waves, so that we may be justified in taking the mean value $H=(9+5)/2=7$ km on the assumption that the bottom of the Pacific Ocean consists of a crust of a single surface stratum. The fact, that the maximum velocity of Rayleigh-waves is less than that of Love-waves by about 10%, seems to support this conception.

The thickness of the surface stratum of the Continental crust estimated from Rayleigh-waves is exceedingly small compared with that estimated from Love-waves. Since the energy of the Rayleigh-waves accumulates with considerable intensity quite close to the surface whereas that of the Love-waves is distributed in a sinusoidal form within the stratum,[13] it is probable that the two kinds of waves are dispersed through different strata. Thus, the Continent may be assumed to consist of a double surface strata, the thicknesses of the upper one and the next being 12 km and 28 km respectively. Rayleigh-waves are practically unaffected by the lower layer, while the energy of the Love-waves is distributed uniformly, relatively speaking, within the effective layer of a thickness 40 km. This is also evidenced, on the one hand, from the fact, that in the case of the Continents the maximum velocity of Rayleigh-waves is too small compared with that of Love-waves, and, on the other, from the fact that the amplitudes of trans-Continental Love-waves are extremely small compared with those of trans-Continental Rayleigh-waves. Were both kinds of waves dispersed through a common stratum, the difference in the respective maximum velocities would not be very great, and the difference in the general amplitudes of the respective waves would be of such order as indicated in the trans-Pacific surface waves. Now, the conclusion we have reached from our investigation with the aid of the nature of Rayleigh-waves as well as that of Love-waves is as follows.

The sub-Pacific basin is stratified with a basaltic layer about 7 km thick with a density of 3·0; the transverse waves there being transmitted with a velocity of 3·2 km/sec. The subjacent medium, through which the transverse waves are transmitted with a velocity of 4·5 km/sec, consists of a dunite of probably varying densities, though slight, ranging from 3·0 at the top to 3·5 at a depth of 30 km from the bottom of the basaltic layer. It seems that at such a depth the medium is completely ultrabasic and of density 3·5, although the velocity of transmission of transverse waves differs very little from 4·5 km/sec, being the same as in dunite.

The Eurasian Continent has two superficial layers. The uppermost stratum, which is about 12 km thick, is granitic, of density 2·7, the velocity of the transverse waves being 3·1 km/sec. The second layer, which has a thickness of 28 km seems to be composed of a gabbro of density 3·1, the velocity of transverse waves through this medium being approximately 3·7 km/sec. The third layer, in which the velocity of the transverse waves is 4·5 km/sec, may be an ultrabasic rock of density 3·5.

Figs. 7, 8 are diagrammatic sketches showing the distribution of the proper velocities of transverse waves as well as the densities in the superficial structure of the earth. From Fig. 8 it will be seen that at a depth of 40 km from the level of the Continental surface the masses are practically in isostatic equilibrium. The problem of distribution of density, however, is not important in the present problem; it merely confirms that the estimated distribution of materials as deduced from the nature of wave transmission does not differ very greatly even from the distribution of the density proper to each material.

---

[13] K. SEZAWA and K. KANAI, "Periods and Amplitudes of Oscillations in L- and M-phases," *Bull. Earthq. Res. Inst.*, **13** (1935), 18~38.

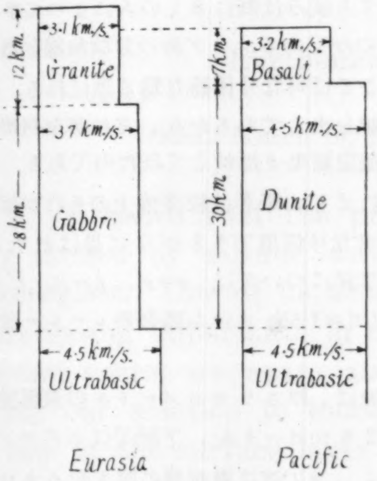
12 km.
3·1 km./s.
Granite
37 km./s.
28 km.
Gabbro
4·5 km./s.
Ultrabasic
Eurasia
7 km.
3·2 km./s.
Basalt
4·5 km./s.
30 km.
Dunite
4·5 km./s.
Ultrabasic
Pacific

Fig. 7. Velocity of transverse waves.

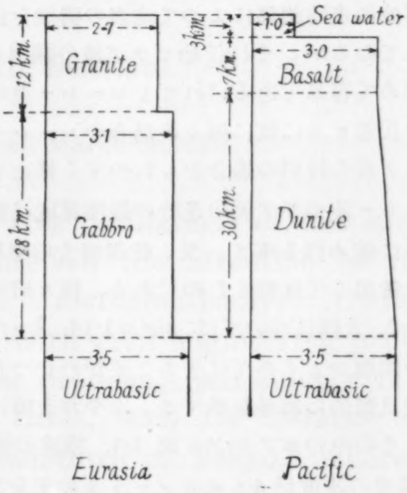
12 km.
2·7
Granite
3·1
28 km.
Gabbro
3·5
Ultrabasic
Eurasia
3 km.
1·0
Sea water
7 km.
3·0
Basalt
30 km.
Dunite
3·5
Ultrabasic
Pacific

Fig. 8. Density.

The result of the present theorising seems to support the views of both Jeffreys and Stoneley for Eurasia and that of Gutenberg for the Pacific Ocean. It should however be borne in mind that the stratification here postulated is merely an effective one. The actual distribution of these materials would be rather of a gradually varying type.

In conclusion I wish to express my thanks to Mr. K. Kanai for his valuable assistance in the present work.

19. 太平洋及大陸を通過するレーレー波及ラブ波

地震研究所 妹澤克惟

表面波の走時關係によつて地表の構造を決定しやうとする試みは既に多くの人によつて手をつけられてゐるが，それは殆どラブ波の關係を用ひたもののみである．ラブ波の分散曲線を出すことは極めて容易であるけれどもレーレー波のそれを出すことは可なり困難な爲と思はれる．筆者は金井氏等と共に既に種々の場合のレーレー波の分散曲線を出してあるから，それ等を利用し，且つラブ波の特別の場合をもたやすく算定して，實際の測定結果と比較してみたのである．

レーレー波やラブ波の走時の觀測算定は無數にあるけれども，筆者は松澤博士のそれが原記錄を容易に確め得る事と，又，松澤博士の整理したものは可なり信用できるやうに思はれたのでそれを借用して比較したのである．種々研究の結果，太平洋については $\rho=\rho'$, $\lambda=\mu$, $\lambda'=\mu'$, $\mu/\mu'=2$, 大陸については $\rho/\rho'=1{\cdot}14$, $\lambda=\mu$, $\lambda'=\mu'$, $\mu/\mu'=1{\cdot}65$ といふ場合のレーレー波とラブ波の問題がよくあてはまることがわかつたのである．

一層具體的の結果を示すと，太平洋を傳はるレーレー波は，厚さ 9 キロメートルの表面層があつて，その中のポアッソン比 1/4, 橫波の速度が每秒 3·2 キロメートル，下層ではポアッソン比 1/4, 橫波の速度が 4·5 キロメートルの所を通過すればよく，ラブ波は表面層の厚さが 5 キロメートルで他は同樣な狀態の所を通過すればよいことが知られた．次に，歐亞大陸を通過するレーレー波は，表面層の厚さ 12 キロメートル，ポアッソン比 1/4, その中での橫波の速度は每秒 3·1 キロメートル，下層では每秒 3·7 キロメートル，ポアッソン比 1/4, 表面層と下層との密度比を 1/1·14 とすればよく，又ラブ波については表面層の厚さ 40 キロメートル，その中での橫波の速度 3·7 キロメートル，下層中での橫波の速度 4·5 キロメートルとすればよいことがわかつたのである．

太平洋ではレーレー波から出した表面層の厚さとラブ波から出したそれの厚さとの平均卽ち 7 キロメートルを取つてもよいと思はれる．それは太平洋を通る兩波の最高速度の比が 10 パーセント位の差があり，共通の一つの層として大して誤がないからである．

大陸の表面層の厚さについては，レーレー波のそれから出したのとラブ波のそれから出したのとは著しく違つてゐるから，兩波は別々の層を通して傳播したとしてもよいのである．實際，レーレー波の勢力は地表の極く附近にのみ集つてゐるものであるし，ラブ波の勢力は或る効果的の層があればその層全體に勢力が分布してゐることが理論的にわかつてゐる．然るに大陸を通過するラブ波の振幅はそのレーレー波のそれに比して著しく小さいことがわかつてゐるし，又ラブ波の最高速度はレーレー波の最高速度に比して著しく高いから，どうしても前述の理論通りに別々の層を傳はつたとする方が都合がよいのである．從て歐亞大陸では表面に厚さ 12 キロメートルの層があり，次に厚さ 28 キロメートルの層があることになるのである．

かくの如くして彈性の分布狀態を圖示すると第 7 圖の如くなるのである．そのやうな岩石狀態の密度の分布を念の爲に圖示してみると第 8 圖の如くなり，イソスタシーも大體に於て保たれ得ることが確められるのである．

この結果は歐亞大陸については偶然にも Jeffreys や Stoneley の結果とよく一致し，太平洋については Gutenberg の結果と餘り違はぬことが知られるのである．

20. *Decay Constants of Seismic Vibrations of a Surface Layer.*

By Katsutada SEZAWA and Kiyoshi KANAI,

Earthquake Research Institute.

(Read March 19, 1935.—Received March 20, 1935.)

1. It seems that the problem of free oscillations of the surface layer excited by seismic waves has received the attention of many seismologists. One of us also discussed it mathematically.[1] Owing to its increasing importance in connection with civil engineering problem in recent years, we again attacked this problem, particularly in extending our solution to more extreme cases, such for instance as in the case of the surface layer in the down-town of Tôkyô,[2] where the elastic constants of the surface layer might probably be but a very small fraction of those of the subjacent medium.

2. In the first place, the problem of forced vibrations will be discussed. Even though the density and the elasticity of the stratum differ extremely, not unlimitedly in mathematical meaning, from those of the substance beneath it, it is probable for the vibrational energy to flow from one medium to the other, so that it is not satisfactory, in dealing with the vibrations of the stratum, to assume that the stratum is an isolated body, whether the problem under consideration is related with free vibrations or with forced ones; in other words, the stratum alone cannot be regarded as a conservative system, but the vibrations in that stratum should be considered as taking place in a dissipative system. The usual way of assuming all the sources of damping to be included in such terms in differential equations of motion that specify the damping forces, namely, viscous fluid damping, solid friction damping, etc., is not correct, at any rate in the present or similar problem. It is rather important to take simultaneous equations of coupled or of effectively coupled vibrations of the stratum as well as the neighbouring media, the terms corresponding to the damping in the original differential equations of motion being not much significant. Thus, for instance, a single equation for the vibrations of a stratum of the type:

---

[1] K. SEZAWA, *Bull. Earthq. Res. Inst.*, **8** (1930), 1~11.

[2] T. SAITA, *Bull. Earthq. Res. Inst.*, **12** (1934), 517~526.

$$\dot{U}+p\ddot{U}+qU=0, \tag{1}$$

which might be used in some cases, should be replaced by

$$\ddot{U}+qU=0, \qquad \ddot{U}_1+q_1U_1=0, \tag{2}$$

where the suffix signifies the vibrations of the subjacent medium. If the subjacent medium has an infinite extension, the vibrations of the stratum take naturally a decaying type. This is due to the energy dissipated outwards through the neighbouring medium, the problem being now of wave propagation and not of pure stationary vibration with energy condensed in a conservative system. It follows that the most convenient way of dealing the present problem is to attack the forced vibrations in the first place and to use the resulting solutions in the determination of the nature of free vibrations.

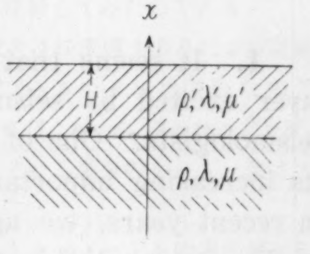

Fig. 1.

3. Let the axis of x be drawn vertically upwards from the lower boundary of a layer of thickness H and let u, ρ, λ, μ, u', ρ', λ', μ' be the displacements, densitities, and elastic constants of the subjacent medium and the stratum respectively. In the case of dilatational waves, the equations of motion of the two media are expressed by

$$\rho\frac{\partial^2 u}{\partial t^2}=(\lambda+2\mu)\frac{\partial^2 u}{\partial x^2}, \qquad \rho'\frac{\partial^2 u'}{\partial t^2}=(\lambda'+2\mu')\frac{\partial^2 u'}{\partial x^2}. \tag{3}$$

In the case of distortional waves, it is necessary to replace $\lambda+2\mu$ by μ and $\lambda'+2\mu'$ by μ'. If the incident waves in the lower medium be of the type:

$$u_1=e^{ih(V_1t-x)}, \tag{4}$$

where $2\pi/h$ is the wave length and V_1 the velocity of transmission, the resulting displacements of the subjacent medium and the stratum are expressed by

$$\left.\begin{aligned} u=u_1+u_2&=e^{ih(V_1t-x)}+Ae^{ih(V_1t+x)}, \\ u'&=Be^{ih'(V_2t-x)}+Ce^{ih'(V_2t+x)}, \end{aligned}\right\} \tag{5}$$

where $2\pi/h'$ is the wave length in the stratum and V_2 the velocity of transmission in that stratum. The boundary conditions at $x=0$ are

$$u=u', \qquad (\lambda+2\mu)\frac{\partial u}{\partial x}=(\lambda'+2\mu')\frac{\partial u'}{\partial x}; \tag{6}$$

while that at the free surface, $x=H$, is

$$\partial u'/\partial x = 0\,, \tag{7}$$

so that from (5), (6), (7) we get

$$\left.\begin{aligned} A &= \frac{(1-\alpha)+(1+\alpha)e^{-2i\beta hH}}{(1+\alpha)+(1-\alpha)e^{-2i\beta hH}}\,, \\ B &= \frac{2}{(1+\alpha)+(1-\alpha)e^{-2i\beta hH}}\,, \\ C &= \frac{2e^{-2i\beta hH}}{(1+\alpha)+(1-\alpha)e^{-2i\beta hH}}\,, \end{aligned}\right\} \tag{8}$$

where $\alpha = \sqrt{\dfrac{\rho'(\lambda'+2\mu')}{\rho(\lambda+2\mu)}}$, $\beta = \sqrt{\dfrac{\rho'(\lambda+2\mu)}{\rho(\lambda'+2\mu')}}$. In the case of distortional waves $\lambda+2\mu$ is replaced by μ and $\lambda'+2\mu'$ by μ'.

If we take the real parts only of all the complex equations, the displacement due to incident waves in the subjacent medium, the displacement due to the vibrations at the free surface of the stratum, and that at the lower boundary of the same stratum become as follows:

$$\left.\begin{aligned} u_1 &= \cos h(V_1 t - x), \\ u'_H &= \frac{2}{\sqrt{\cos^2\beta hH + \alpha^2 \sin^2\beta hH}} \cos\!\left(h'V_2 t - \tan^{-1}\frac{\alpha \sin\beta hH}{\cos\beta hH}\right), \\ u_0 &= \frac{2\cos\beta hH}{\sqrt{\cos^2\beta hH + \alpha^2 \sin^2\beta hH}} \cos\!\left(hV_1 t - \tan^{-1}\frac{\alpha \sin\beta hH}{\cos\beta hH}\right). \end{aligned}\right\} \tag{9}$$

Periodic incident waves naturally cause stationary vibrations of the stratum. We selected five cases, namely $\mu'/\mu = 1/4$, $1/16$, $1/64$, 4, 16, besides the conditions $\rho=\rho'$, $\lambda=\mu$, $\lambda'=\mu'$, and calculated the resulting amplitudes of vibrations at the free surface, $x=H$, and at the boundary $x=0$, for different values of wave length, the result being shown in Figs. 2, 3, 4, 5, 6. In these figures, $V_1 T$ is the length of the incident waves in the lower medium, the amplitudes of the same incident waves being unity. From these figures it will be seen that, if the elasticity of the material composing the stratum is less than that of the one underneath it, the amplitudes of vibration at the surface become relatively large at such periods as are synchronous successively with the natural periods of the stratum. But, owing to the loss of energy that is dissipated from the lower boundary of the stratum, the amplitudes are not strikingly large even in the case $\mu'/\mu = 1/64$, the surface value in this case being merely eight times that at the lower boundary. The vibrations resemble therefore the case in which the material forming the stratu has its own damping resistance. The amplitudes of the lower boundary change with differences in wave length, their maxima being twice the amplitudes of incident waves, which is obvious from the nature of the problem. It seems strange that at periods of synchronous vibrations the lower boundary should become quiescent. This however is merely the result of the fact that the lower boundary becomes a nodal plane of stationary vibrations. When the rigidity of the stratum is higher than that of the subjacent medium, the amplitudes at the surface in synchronous vibrations become rather less than the maximum amplitudes at the same surface. Although this shows that the natural periods themselves have little meaning in connection with the nature of excitation of vibrations, the elastic constants of the stratum relative to those of the subjacent medium seem to play an important part in the problem.

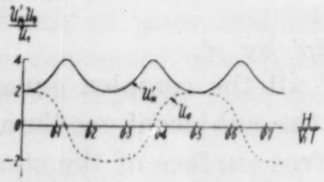

Fig. 2. $\mu'/\mu=1/4$.

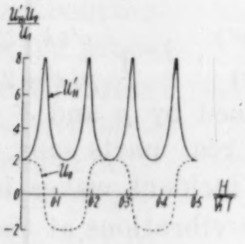

Fig. 3. $\mu'/\mu=1/16$.

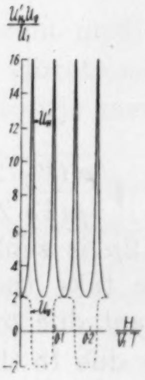

Fig. 4. $\mu'/\mu=1/64$.

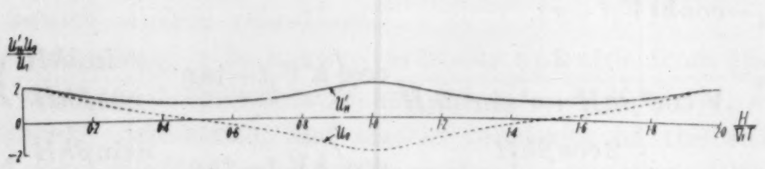

Fig. 5. $\mu'/\mu=4$.

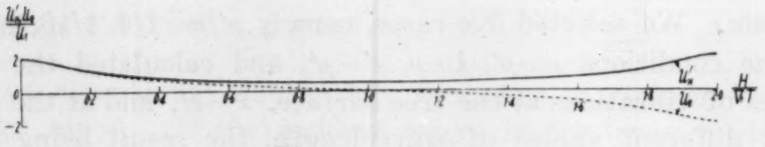

Fig. 6. $\mu'/\mu=16$.

If the incident waves be of irregular type and their displacement be expessed by an infinite series:

$$u_1=\sum_n f_n \cos h_n(V_1 t-x+\varepsilon_n), \tag{10}$$

the resulting amplitudes of vibrations at the free surface, $x=H$, and at the boundary, $x=0$, are of the forms:

$$\left.\begin{aligned} u_H&=\sum_n \frac{2f_n}{\sqrt{\cos^2\beta h_n H+a^2\sin^2\beta h_n H}}\cos\left(h'_n V_2 t-\tan^{-1}\frac{a\sin\beta h_n H}{\cos\beta h_n H}+h_n\epsilon_n\right),\\ u_0&=\sum_n \frac{2f_n\cos\beta h_n H}{\sqrt{\cos^2\beta h_n H+a^2\sin^2\beta h_n H}}\cos\left(h_n V_1 t-\tan^{-1}\frac{a\sin\beta h_n H}{\cos\beta h_n H}+h_n\epsilon_n\right),\end{aligned}\right\}\quad(11)$$

provided $h'_n V_2=h_n V_1$. It appears from these equations that the amplitudes of those components of displacement of such frequencies as are synchronous with the natural ones of the stratum are relatively preponderant in the same displacement, owing to the comparative smallness of the denominator of each term corresponding to those components in the series under consideration, the feature of selective resonance, thus, manifesting itself to some extent.

4. In order to find the nature of free vibrations of the stratum, generalization of solution (5) by means of Fourier's double integrals was resorted to. If the primary incident waves of the type:

$$u_1=F\left(\frac{V_1 t-x}{c}\right), \tag{12}$$

are incident in the subjacent medium, the resulting free vibrations at the free surface as well as at the lower boundary of the stratum are expressed by[3]

$$\begin{aligned} u'_H=&2\sum_{m=0}^{\infty}(-1)^m\frac{(1-a)^m}{(1+a)^{m+1}}F\left(\frac{\beta(V_2 t-2mH)}{c}\right)\\ &+2\sum_{m=0}^{\infty}(-1)^m\frac{(1-a)^m}{(1+a)^{m+1}}F\left(\frac{\beta(V_2 t-\overline{2m+1}H)}{c}\right), \end{aligned}\tag{13}$$

$$\begin{aligned} u_0=&e^{-\left(\frac{V_1 t}{c}\right)^2}+\sum_{m=0}^{\infty}(-1)^m\left(\frac{1-a}{1+a}\right)^{m+1}F\left(\frac{V_1 t-2m\beta H}{c}\right)\\ &+\sum_{m=0}^{\infty}(-1)^m\left(\frac{1-a}{1+a}\right)^{m}F\left(\frac{V_1 t-\overline{2m+1}\beta H}{c}\right). \end{aligned}\tag{14}$$

It is possible for us to take these expressions as indicating a particular form of natural vibrations of the stratum on account of the reason that there is little disturbance excepting the initial incident waves. Whatever the type of wave form of the initial disturbance may be, the decaying nature of vibrations is always the same. The ratio of vibration amplitudes of successive similar phases is constant and expressed by

$$\left(\frac{1-a}{1+a}\right)^2,\quad\text{or}\quad\frac{1-a}{1+a}, \tag{15}$$

with period $4H/V_2$ or $2H/V_2$ according as $a<1$ or $a>1$. The vibrations are therefore of a purely exponential type;

---

[3] K. SEZAWA, *loc. cit.*

$$e^{-kt}, \tag{16}$$

the coefficient of damping being

$$k=\frac{V_2}{2H}\log_e\left|\frac{1+\alpha}{1-\alpha}\right| \tag{17}$$

in all cases. We took the case

$$F\left(\frac{V_1 t-x}{c}\right)=e^{-\frac{(V_1 t-x)^2}{c^2}}, \tag{18}$$

and calculated from (13) and (14) the displacements at the surface and at the lower boundary of the stratum of twelve cases shown in the following table ($\rho=\rho'$ $\lambda=\mu$, $\lambda'=\mu'$);

μ'/μ	1/4	1/16	4	16
H/c	1/5, 1, 5	1/10, 1/2, 5/2	4/5, 4, 20	8/5, 8, 40

The result of the calculation is shown diagrammatically in Figs. 7 ~18. The greater the difference in the elastic constants of the two media, the more slowly decay the vibrations of the stratum, which may be also verified from (15) or (16). Thus, if $\rho=\rho'$ $\lambda=\mu$, $\lambda'=\mu'$, $\mu'=\mu/4$ or $\mu'=4\mu$, we have $(1-\alpha)/(1+\alpha)=1/3$, whereas if $\rho=\rho'$, $\lambda=\mu$, $\lambda'=\mu'$, $\mu'=\mu/16$ or $\mu'=16\mu$, we get $(1-\alpha)/(1+\alpha)=3/5$. Similarly, if $\mu'=\mu/64$, $\mu'=64\mu$, we get $(1-\alpha)/(1+\alpha)=7/9$. It is a remarkable fact that the coefficient of damping of that case in which the ratio of rigidities is specified, is the same as that of the case in which the ratio of the rigidities is the reciprocal of the former one.

5. Although we have no intention at present of comparing our mathematical result with actual experimental data, we know, according to Saita's observation of earthquake movements of the ground at Marunouti,[4] Tokyo, that in a fairly large number of cases relatively large accelerations at the surface are generally three or four times those in the subjacent medium just beneath the stratum under consideration. If we were to assume that the large acceleration at the surface is merely excited at synchronous periods and the large one at the lower boundary of the stratum at other periods not in synchronism, it would follow that, the densities being the same, the elastic constants of the subjacent medium would approximately be from nine to sixteen times those of the surface stratum. This requires that the velocity of bodily waves through the subjacent medium shall be from three to four times those through the surface stratum. It seems therefore that the velocities of trasmission of some bodily waves through these media are probably 200 m/sec and 600∼800 m/sec respectively. Another fact which came out from Saita's analysis of his data that at some special periods the ratio of the amplitude at the surface to that at the lower boundary of the stratum is so large as nine or ten,5) is not difficult in its interpretation. It is very simply accounted for by our mathematical criterion that at the precisely synchronous periods the horizontal plane just beneath the superficial stratum becomes a nodal surface of stationary vibrations. The ratio therefore should become rather infinity in an idealised case. Since it seems no observations have yet been made in regard to the velocity of transmission of seismic waves through the ground in the vicinity of Marunouti, we do not doubt that our result could be confirmed more closely as soon as such observations have been made.

---

[4] T. SAITA, *loc. cit.*

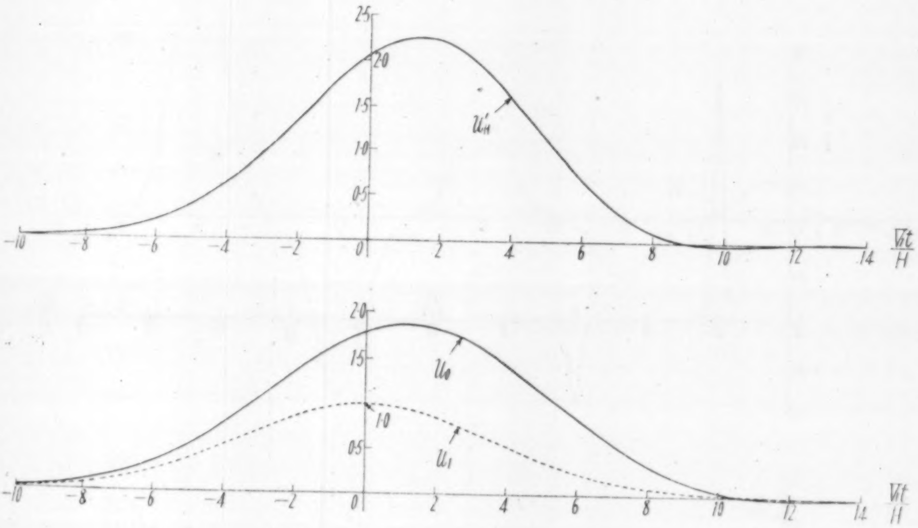

Fig. 7. $\mu'/\mu=1/4$, $H/c=1/5$.

---

5) T. Saita, *loc. cit.*

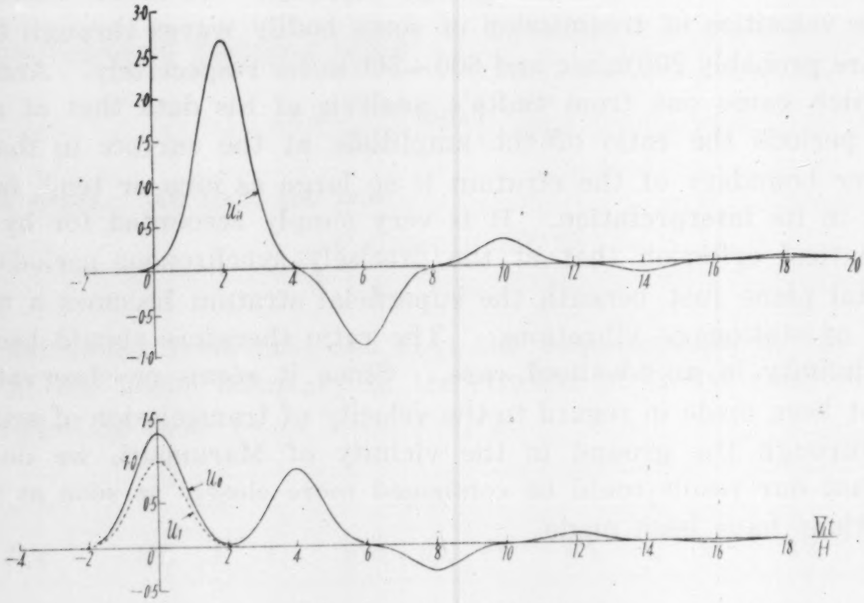

Fig. 8. $\mu'/\mu=1/4$, $H/c=1$.

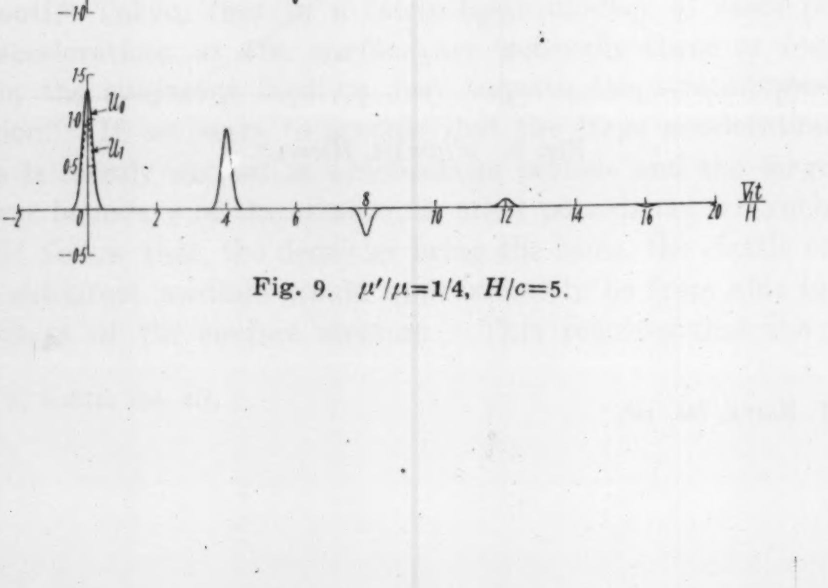

Fig. 9. $\mu'/\mu=1/4$, $H/c=5$.

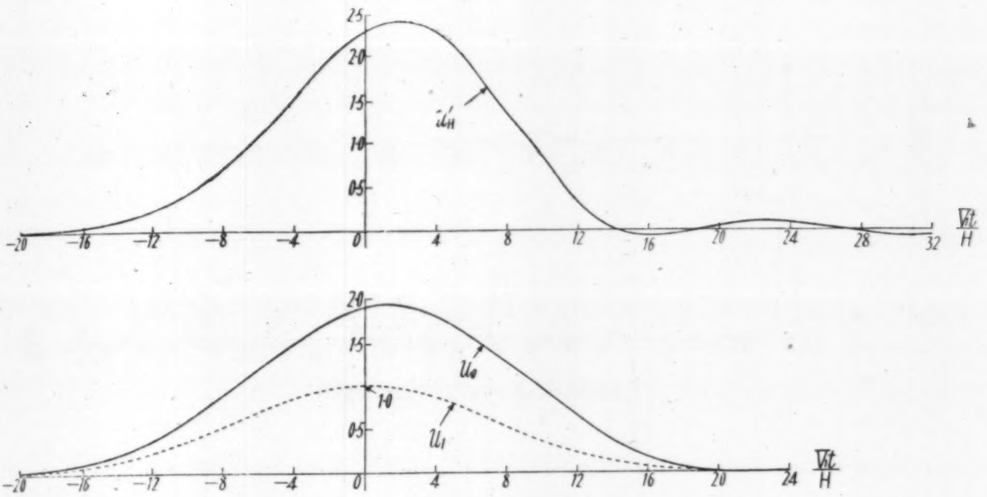

Fig. 10. $\mu'/\mu=1/16$, $H/c=1/10$.

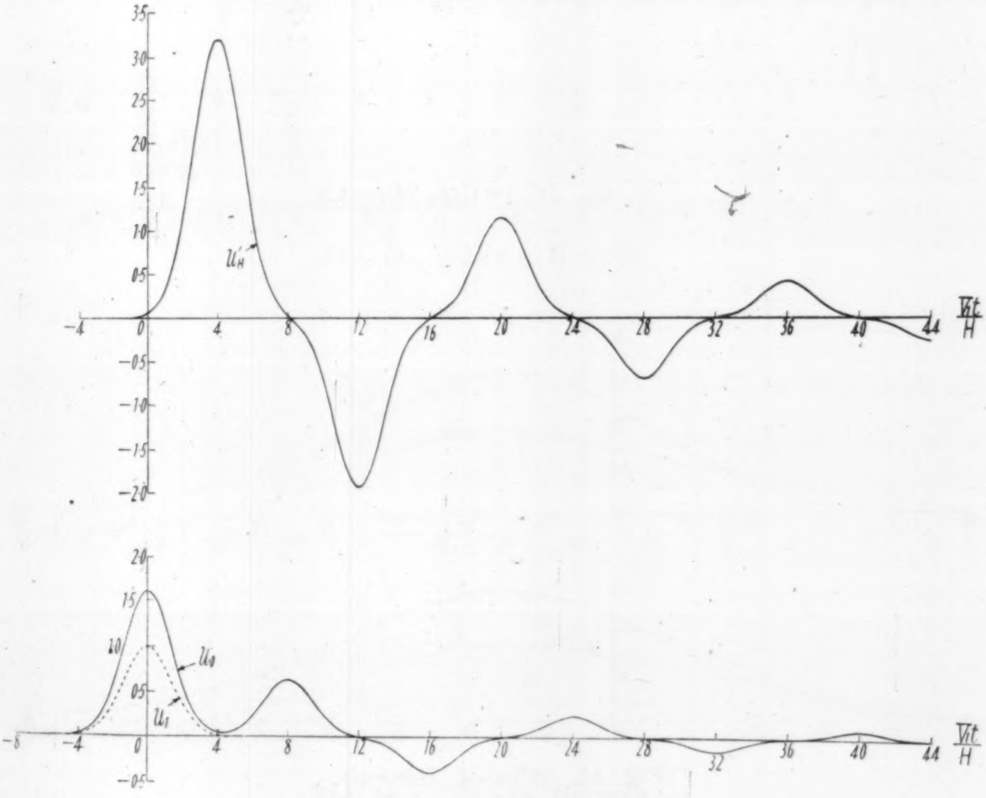

Fig. 11. $\mu'/\mu=1/16$, $H/c=1/2$.

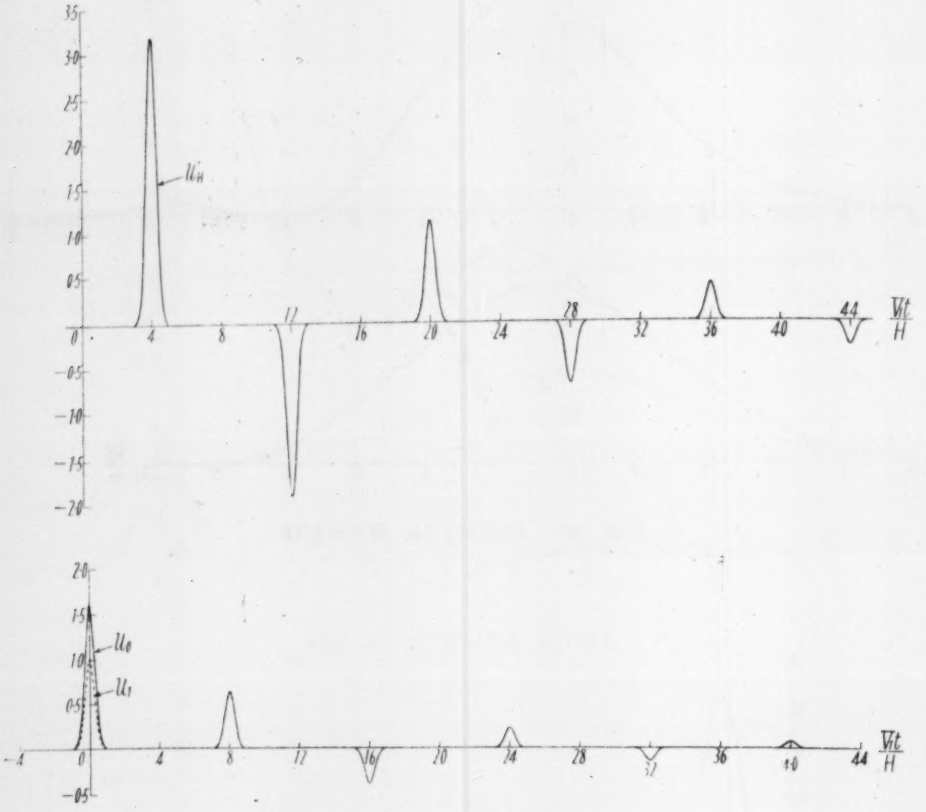

Fig. 12. $\mu'/\mu=1/16$, $H/c=5/2$.

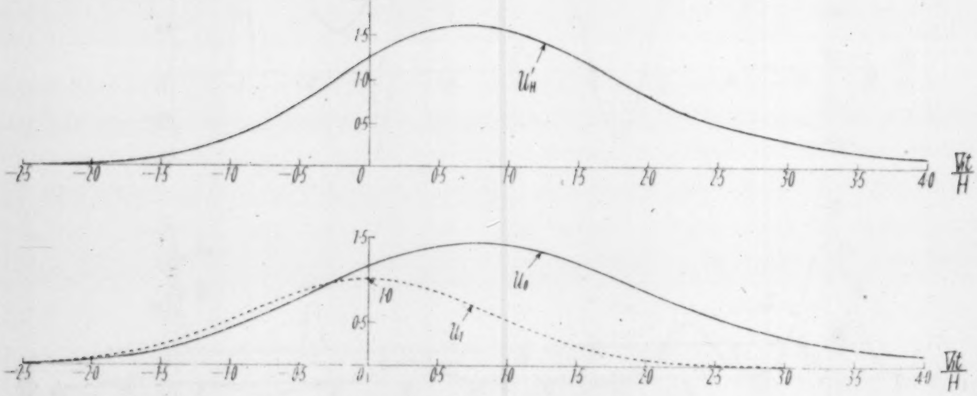

Fig. 13. $\mu'/\mu=4$, $H/c=4/5$.

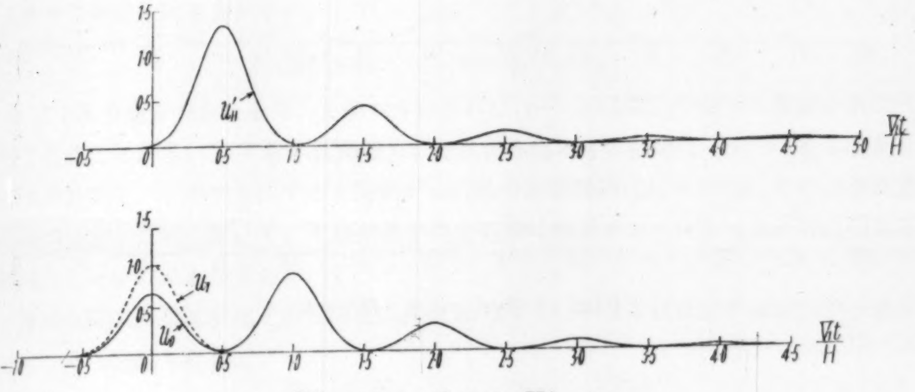

Fig. 14. $\mu'/\mu=4$, $H/c=4$.

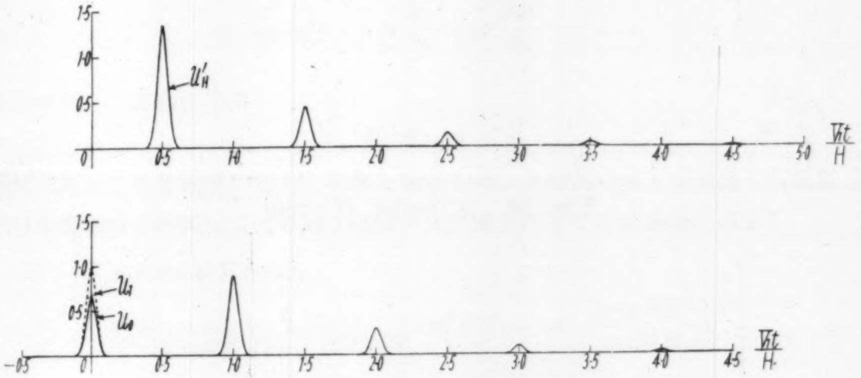

Fig. 15. $\mu'/\mu=4$, $H/c=20$.

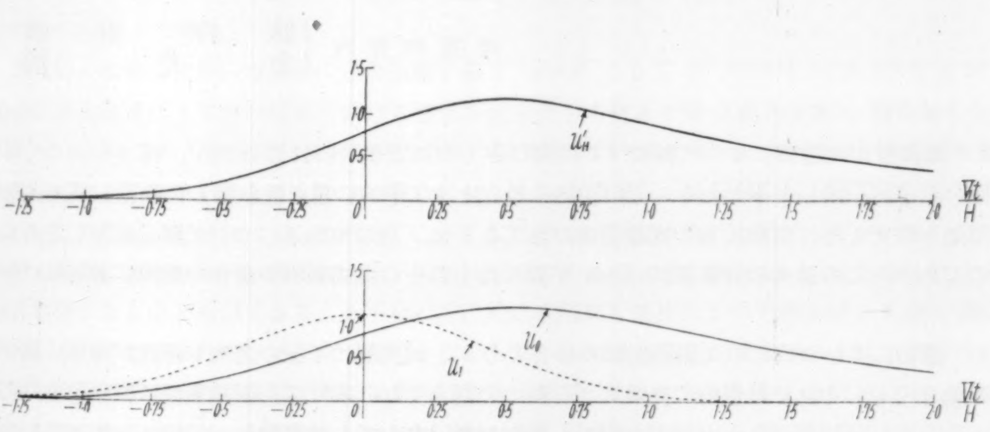

Fig. 16. $\mu'/\mu=16$, $H/c=8/5$.

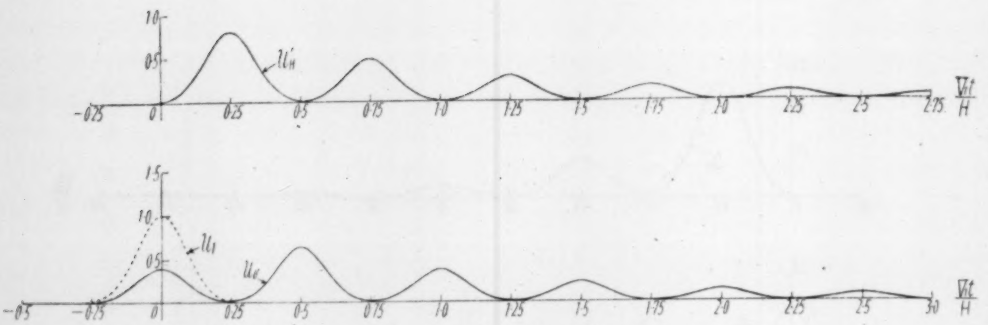

Fig. 17. $\mu'/\mu=16$, $H/c=8$.

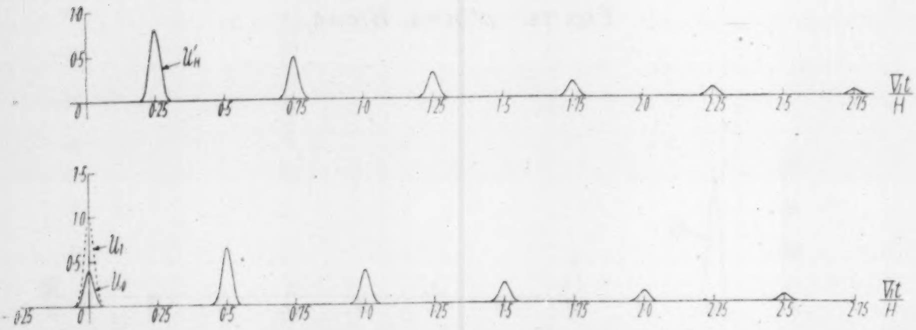

Fig. 18. $\mu'/\mu=16$, $H/c=40$.

20. 地表層の震動減衰恒数

地震研究所 {妹澤克惟
金井清

1. 地表層が地震動によつて振動する問題は多くの地震學者の注意をひき，我々もかつて同じ問題を數學的に論じた事がある．この問題は最近土木工學的に重要性を增したので，我々は再び同問題を研究し特に齊田氏等の實驗結果の出てゐる丸ノ內の地盤等について解法を押し進めてみたのである．この論文の計算法は 5~6 年前に出した一つの地表層の場合の應用に過ぎないのである．

2. 最初に手をつけたのは强制振動の場合である．地表層と下層の密度や彈性が極端に違つてゐる場合でも，それが數學的に無限大と有限との割合でない限りは，兩媒質間に振動勢力の流れがある．それ故振動が自由振動であつても强制振動であつても地表層を一つのコンサバテイヴの組織として力學を取扱ふのは間違つてをり，隣合せの媒體を取つて其聯成組織を考へ，地表層から考へればディスシペーティヴの組織としてその力學を取扱ふべきである．從つて，或場合に取られるかも知れぬやうに，地表層の振動方程式を

$$\ddot{U}+p\dot{U}+qU=0 \tag{1}$$

とする代りに次式を取る方がよい．

$$\ddot{U}+qU=0\,, \qquad \ddot{U}_1+q_1U_1=0\,, \tag{2}$$

玆に 1 は下層の場合の式を示す．このやうにすれば $p\dot{U}$ 又は類似の種々の減衰の項は大して重要でなくなることが多い．下層へ振動勢力が流れ出る爲のその結果は $p\dot{U}$ のある場合と同様になることがわかる．このやうにすると問題が一般的の波動問題になるから，その力學性質上から振動の强制振動を最初に解いて，その結果を自由振動に應用するといふ一見不可思議な方法が非常に便利なことがわかるのである．

3. 簡單の爲に，横波が地下から垂直に入射して厚さ H なる地表層の强制振動を起す場合を考へると，その振動方程式は

$$\rho\frac{\partial^2u}{\partial t^2}=\mu\frac{\partial^2u}{\partial x^2}\,, \qquad \rho'\frac{\partial^2u}{\partial t^2}=\mu'\frac{\partial^2u'}{\partial x^2} \tag{3}$$

となる．玆に u, ρ, μ, u' ρ', μ' は下層と地表層の變位，密度，彈性率である．上層と下層との境界では

$$u=u', \qquad \mu\frac{\partial u}{\partial x}=\mu'\frac{\partial u'}{\partial x} \tag{4}$$

といふ條件があり，地表面では

$$\partial u'/\partial x=0 \tag{5}$$

といふ關係のあることを考慮して (3) の解を求めると，入射波の形と地表面の振動形及び上下層の境に於ける振動形との間には次の如き關係の式が成立つことが理論的にわかる．

$$\left.\begin{aligned} u_1&=\cos h(V_1t-x),\\ u'_H&=\frac{2}{\sqrt{\cos^2\beta hH+\alpha^2\sin^2\beta hH}}\cos\left(h'V_2t-\tan^{-1}\frac{\alpha\sin\beta hH}{\cos\beta hH}\right),\\ u_0&=\frac{2\cos\beta hH}{\sqrt{\cos^2\beta hH+\alpha^2\sin^2\beta hH}}\cos\left(hV_1t-\tan^{-1}\frac{\alpha\sin\beta hH}{\cos\beta hH}\right), \end{aligned}\right\} \tag{6}$$

玆に V_1. V_2, $2\pi/h$, $2\pi/h'$ は夫々下層及び表面層中での速度及び波長である．又 $\alpha=\sqrt{\rho'\mu'/\rho\mu}$, $\beta=\sqrt{\rho'\mu/\rho\mu'}$ である．

週期的入射波は自然に地表層に定常振動を起す．$\rho=\rho'$ として $\mu'/\mu=1/4, 1/16, 1/64, 4, 16$ の場合の地表面及び上下層の境面に於ける震動振幅を出して見ると第 2 圖乃至第 6 圖の如くなる．V_1T は下層中での入射波の波長を示す．之等の圖又は第 (6) 式からわかるやうに，地表層を作る物質の彈性が下層のそれよりも小さいときには，入射波の週期が地表層の固有週期と一致する場合に地表の振幅が比較的に大きくなる．しかし振動勢力が下層へ逃げる爲に $\mu'/\mu=1/64$ 位の場合でも非常に大きいといふ程ではなく，振幅は下層のそれの 8 倍に過ぎない．地表層それ自身に減衰摩擦があるのと相似てゐる．上下層の境に於ける振幅も波長によつて違ふが，其最大値は入射波のそれの 2 倍であることは申すまでもない．又，入射波の週期が地表層のそれと同時性になるときに上下層の境面の振幅が零になるのは一見不思議であるけれども，これは單にそこが節平面となつたのに過ぎないのである．上層が下層よりも高彈性になると，同時性のときの地表の振幅が普通の場合よりも小さくなる．從て，固有振動週期それ自身が振動を勵振する上に意味があるのでなく，彈性の比較的分布がこの問題に重要なる役割を演ずるものであることがわかるのである．

次に，入射波が不規則的なものであつてその變位が次式：

$$u_1=\sum_n f_n \cos h_n(V_1t-x+\varepsilon_n) \tag{7}$$

で表される場合には，地表面と上下層の境面に於ける振動變位は

$$\left.\begin{aligned} u'_H&=\sum_n \frac{2f_n}{\sqrt{\cos^2\beta h_n H+\alpha^2\sin^2\beta h_n H}}\cos\left(h'_n V_2t-\tan^{-1}\frac{\alpha\sin\beta h_n H}{\cos\beta h_n H}+h_n\varepsilon_n\right),\\ u_0&=\sum_n \frac{2f_n\cos\beta h_n H}{\sqrt{\cos^2\beta h_n H+\alpha^2\sin^2\beta h_n H}}\cos\left(h_n V_1t-\tan^{-1}\frac{\alpha\sin\beta h_n H}{\cos\beta h_n H}+h_n\varepsilon_n\right)\end{aligned}\right\} \tag{8}$$

を以て示される．茲に $h'_n V_2=h_n V_1$ である．これ等の式から地表層の固有週期に當る週期の週期的振動が割合によく現れ得るものであることがわかる．卽ちそれ等の週期で上述の式の分母が比較的に小さくなるからであつて，この意味に於て所謂，撰擇共振の傾向は充分あるのである．但し振幅については旣述の條件に從ふべきは勿論である．

4. 茲に於て初めて自由振動の問題に入る．その爲には (6) 式をフーリエ積分で一般化すればよいのである．入射波を

$$u_1=F\left(\frac{V_1t-x}{c}\right) \tag{9}$$

とすれば，地表面と上下層の境面での振動形が次の形を取る．

$$\begin{aligned} u'_H=&2\sum_{m=0}^{\infty}(-1)^m\frac{(1-\alpha)^m}{(1+\alpha)^{m+1}}F\left(\frac{\beta(V_2t-2mH)}{c}\right)\\ &+2\sum_{m=0}^{\infty}(-1)^m\frac{(1-\alpha)^m}{(1+\alpha)^{m+1}}F\left(\frac{\beta(V_2t-\overline{2m+1}H)}{c}\right), \end{aligned} \tag{10}$$

$$\begin{aligned} u_0=&e^{-\left(\frac{V_1t}{c}\right)^2}+\sum_{m=0}^{\infty}(-1)^m\left(\frac{1-\alpha}{1+\alpha}\right)^{m+1}F\left(\frac{V_1t-2m\beta H}{c}\right)\\ &+\sum_{m=0}^{\infty}(-1)^m\left(\frac{1-\alpha}{1+\alpha}\right)^m F\left(\frac{V_1t-\overline{2m+1}\beta H}{c}\right). \end{aligned} \tag{11}$$

初入射波以外には何等の外力が働かないから之等の式は自由振動の或形と見て差支がない．初入射波が如何なる形であらうとも，振動の減衰狀態は常に同じものである．振動の同位相が次々に來るのは $\alpha<1$ 又は $\alpha>1$ に從て，夫々 $4H/V_2$, $2H/V_2$ なる週期を以てする．而して之等の順次の同位相に於ける振幅比は $\alpha<1$ 又は $\alpha>1$ に從て

$$\left(\frac{1-\alpha}{1+\alpha}\right)^2 \quad 又は \quad \frac{1-\alpha}{1+\alpha} \tag{12}$$

で示される．從て振動の減衰は次式の如く完全に自然函數形であり，普通の速度に比例する摩擦のある場合の振動と何等の變りがないのである．卽ち

$$e^{-kt}. \tag{13}$$

只今の場合の減衰係數 k は α が 1 より大なるか小なるかに拘らず

$$k=\frac{V_2}{2H}\log_e\left|\frac{1+\alpha}{1-\alpha}\right| \tag{14}$$

で表される．(9)，(10) から或 F 及び種々の μ'/μ, H/c の場合の地表面及び上下層境面の振動形を圖示すれば第 7〜18 圖の如くなる．兩層の彈性が異なれば異なる程減衰が遲くなることは，之等の圖からも又は (12) 或は (14) 式からもわかる．尙，μ'/μ の値と μ/μ' の値とが等しいやうな可逆の關係があれば，減衰係數が等しくなるのは注意すべきことであると思ふ．

5. 只今の所我々の數理的結果を實際の測定結果と強ひて比較しやうとは思はないけれども，しかし齋田氏の丸ノ内の實驗結果があつたので，それを一見して見た所が，地表の振幅の大きくなつてゐる所と地下の振幅の大きい所とを比較すると，地表のそれは大體に於て地下のそれの 3 倍乃至 4 倍位であることがわかつた．若し，地表の大振幅は同時性の場合に現れた變位とし，地下の大振幅は他の週期の場合の變位であるとすれば，密度が一定のとき，地表層の彈性が地下のそれの 1/9 乃至 1/16 位であることがわかる．その爲には地表層中での固體波の速度は下層中でのその速度の 1/3 乃至 1/4 位であることを必要とする． 從て各層を通しての或固體波の速度は 200 メートル毎秒及び 600〜800 メートル毎秒位と想像される．齋田氏がその實驗結果を分析して出した所の，或週期に於て地上の振幅が地下のそれの 9 倍にも 10 倍にもなるのは，同時性の所で上下層の境面が節平面になるといふことで說明ができる．理想的にいへばこの振幅比は無限大でよい位である．丸ノ内附近を通過する地震固體波の速度觀測が未だないけれども，それが行れた曉にはこの論文の結果は一層よく確められるであらうと思はれる．

21. *Seiche in the Tôkyô Bay Caused by the Land Upheaval on the Occasion of the Great Earthquake of September 1, 1923.**

By Takeo SUZUKI,

Seismological Institute.

(Read Jan. 15, 1935.—Received March 20, 1935.)

1. Introduction. "The Reports of the Imperial Earthquake Investigation Committee No. 100" contains various investigations and valuable data concerning the great earthquake of September 1, 1923. At the end of the second part of this number, No. 100 B, there are published mareograms from various stations in Japan in which the tunami waves due to this earthquake have been recorded. It is a well known fact that a remarkable upheaval or subsidence as well as horizontal displacement of the earth-crust have been produced in the Kwantô District at the time of the earthquake. But it has not yet been studied, in what interval of time such a kind of crustal deformation as this may happen. Professor M. Ishimoto has reached the thought that a certain information concerning the transient movement of land upheaval may be obtained by means of analysis of the mareogram observed at Yokosuka which is considered to have recorded implicitly the process of land upheaval and he has suggested to the writer the study of it. Following his suggestion the writer has studied the mareograms observed at stations around the Tôkyô Bay and attempted to elucidate the observed fact in connection with the deformation of the earth-crust.

2. Reduction of mareograms observed at Yokosuka and Tiba. Immediately after the earthquake, the tunami of more than several metres high visited the coast around the Sagami Bay. The propagation of this tunami waves has been already investigated by Professor T. Terada [1] and S. Yamaguti and K. Suda [2]. Professor T. Terada has remarked with valuable suggestions for future study that an oscillation of period of about one hour has mostly been predominated as a whole in the mareograms recorded at various stations along the Pacific coast of Japan and at those along the Japan Sea coast, on the other hand in the mareogram at Yokosuka alone an oscillation of period of about two hours has remarkably been predominated. The records at Yokosuka

---

* Communicated by T. Matuzawa.

[1] T. TERADA and S. YAMAGUTI, *Rep. Imp. Earthq. Inv. Comm.*, **100-B** (1925) 113~120, (in Japanese).

[2] K. SUDA, *Mem. Imp. Mar. Obs.*, **1** (1924), 173~181.

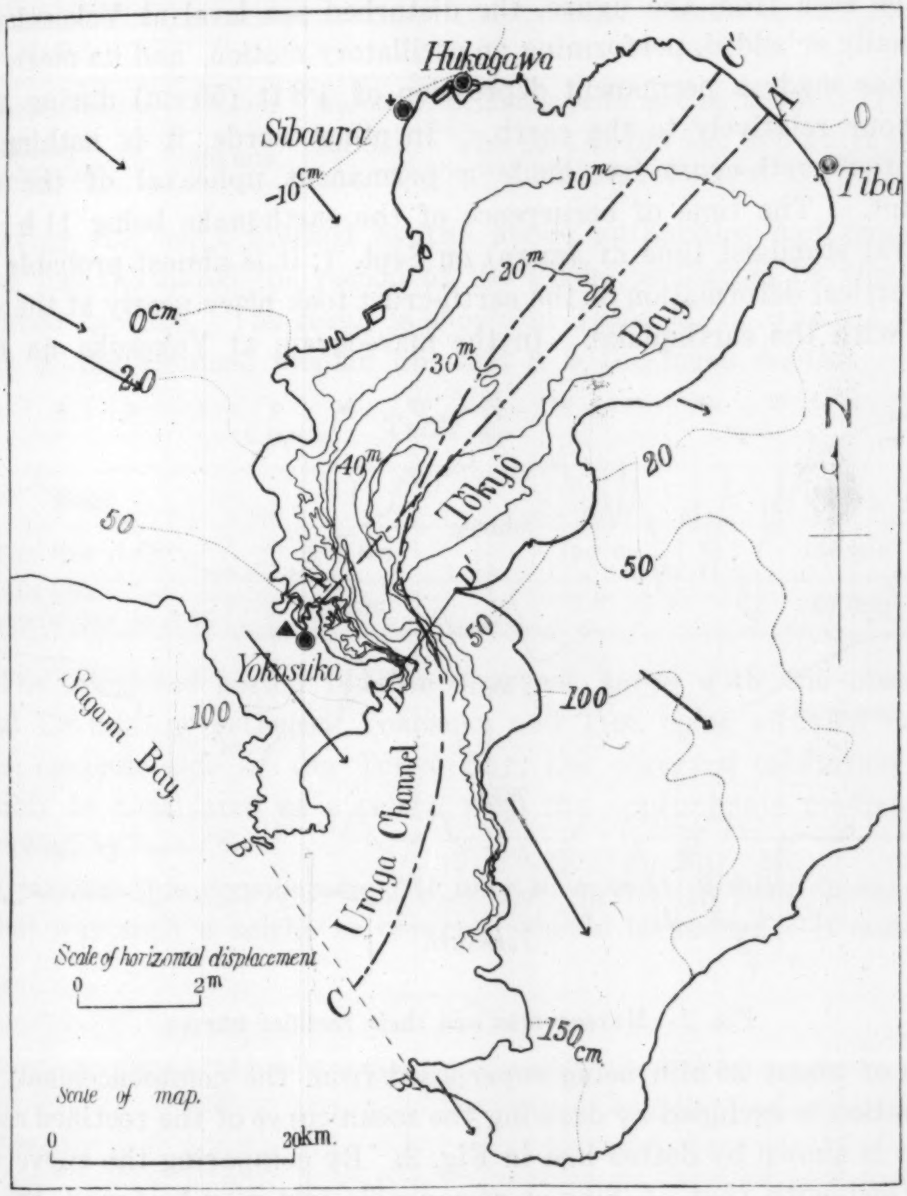
Hukagawa
Sibaura
-10cm
10m
C'
A'
0
Tiba
20m
Bay
0cm
20
30m
20
40m
Tôkyô
N
50
50
D'
50
Yokosuka
100
100
D
Sagami Bay
Uraga Channel
B'
C
B
150cm
Scale of horizontal displacement
0
2m
Scale of map.
0
20km.

Fig. 1. Distribution of vertical deformation and horizontal displacement which are respectively shown by dotted lines and by an arrow.
●: mareographic station,
▲: triangulation point (amount of upheaval=59 cm).

and Tiba are reproduced from the report above mentioned and shown in Fig. 2 and those at Sibaura and Hukagawa in Fig. 3. At first, an attention should be paid to the mareograms at Yokosuka and Tiba. In order to eliminate the tidal fluctuations, the predicted tide curves are constructed in an interval from 8 h on Sept. 1 to 3 h on Sept. 2

by using the tide table which is published by the Hydrographic Department of Japanese Navy, the result being shown in Fig. 2. The rectified curves are also shown in the lower two curves in Fig. 2. As will be seen from the figure, the disturbed sea level at Yokosuka has gradually subsided, performing an oscillatory motion, and its mean position has made a permanent depression of 1·8 ft (55 cm) during about one hour relatively to the earth. In other words, it is nothing but that the earth-crust has made a permanent upheaval of the same amount. The time of occurrence of the earthquake being 11 h 58 m (central standard time of Japan) on Sept. 1, it is almost probable that the vertical deformation of the earth-crust took place nearly at the same time with the earthquake. In the mareogram at Yokosuka an oscillation of about 25 min being superposed from the commencement, this fluctuation is excluded by drawing the mean curve of the rectified record which is shown by dotted line in Fig. 2. By comparing the curve thus smoothed with that of Tiba, a remarkable fact may be found, that is, the sea level at both places changes in general with nearly the same period and at nearly opposite phase. The mean value of observed periods is 126 min at Yokosuka and 125 min at Tiba. Searching for the proper oscillation of the Tôkyô Bay with nearly the same period as that obtained above, the following two oscillations which were investigated by Professor K. Honda[3] and others, may exist, that is, the

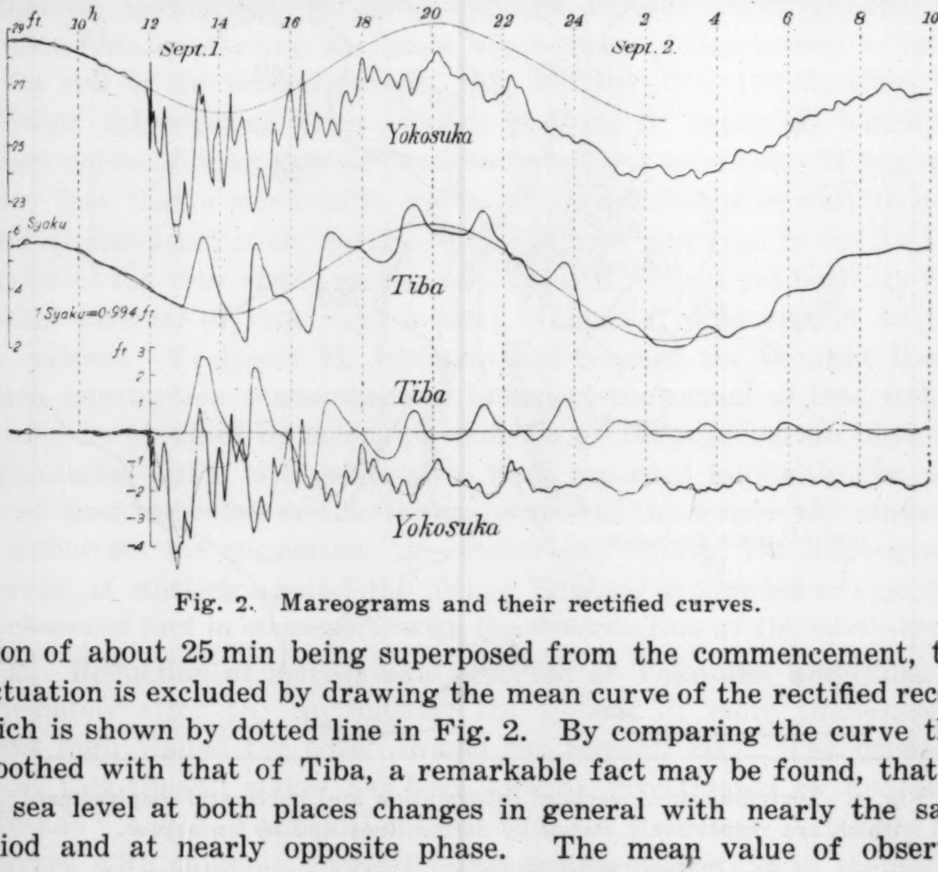

Fig. 2. Mareograms and their rectified curves.

---

[3] K. HONDA, T. TERADA, Y. YOSHIDA and D. ISHITANI, *Pub. Earthq. Inv. Comm.*, **26** (1908).

seiche and the secondary undulation, as is shown in Table I.

Table I.

Mode	$T_{\text{cal.}}$	
Seiche oscillation	158 min	uninodal oscillation with median line AA' (Fig. 1)
Secondary undulation	222 min	oscillation with node at BB' and loop at the end of the bay with median line CC' (Fig. 1)

Following the same method as the above authorities had made, the writer has calculated the period of the seiche oscillation by the chart published in 1925. The result is shown in Table II, in which l is the length of the assumed median line and $\bar{h}$ is the mean depth.

Table II.

Mode	l	$\bar{h}$	$T=2l/\sqrt{g\bar{h}}$
Median line AA'	53·8 km	15·7 m	144 min
Median line perpendicular to AA'	22 km	"	60 min

The calculated period 144 min does not agree with the observed period 126 min, nevertheless Yokosuka and Tiba being situated nearly on the opposite side of the Tôkyô Bay, the observed oscillation may probably be considered as a seiche with the approximate median line AA' (Fig. 1).

Granting this consideration, it may be a next problem to examine in what way such a seiche as observed should be excited. It seems to the writer that this seiche has been caused by the vertical deformation of the earth-crust.

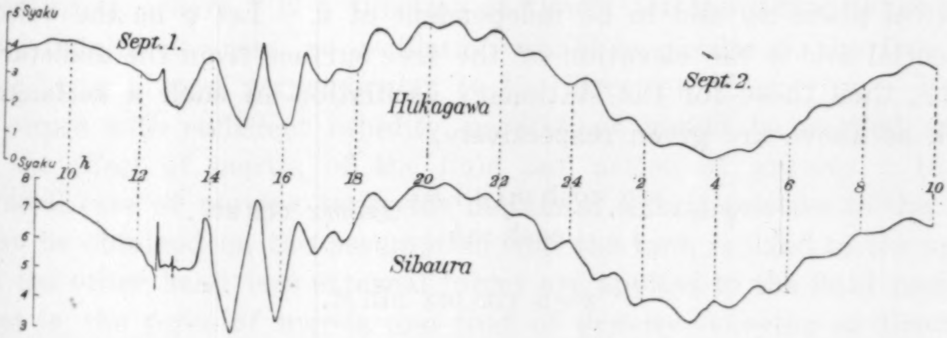

Fig. 3.

On the occasion of this earthquake, a remarkable crustal deformation took place in all over the Kwantô District. The region upheaved or subsided as well as the horizontal displacement of the earth-crust have been precisely determined by means of precise levelling and triangulation carried out by the Land Survey Department[4]. The general aspect of crustal deformation in the neighbourhood of Tôkyô Bay can be seen from Fig. 1. In the southern part of the Tôkyô Bay the land upheaved, but from here to the north the amount of upheaval gradually diminishing no vertical deformation was found in the vicinity of Tiba. Contrarily in the neighbourhood of Tôkyô the land subsided about 10 cm. The amount of upheaval (59 cm) at the triangulation point which is the nearest one to the mareographic station at Yokosuka agrees nearly with that observed from mareogram as already described. Now the general mode of the land upheaval in this region should be considered to be the tilt-movement of the earth-crust, such that the southern end of Tôkyô Bay is raised up and its northern end fixed. On the assumption that the seiche here discussed is due to the tilt-movement of the earth-crust, the writer will study this point.

3. Seiche due to tilt-movement of the earth crust. Notwithstanding that the shape of the Tôkyô Bay is somewhat irregular and the depth distribution is not also uniform as seen from Fig. 1, the part of the Tôkyô Bay closed at DD' may be considered in the first approximation to be a rectangular basin of uniform depth. In the rectangular basin of length l and depth h, take the origin of the coordinates at one end of it, x-axis in the direction of the length and y-axis vertically upwards as is shown in Fig. 4. The motion of the fluid is assumed to take place only in the vertical plane xy and to be independent of z. Let φ be the velocity potential and η the elevation of the free surface from the undisturbed state; then those for the stationary oscillation in such a rectangular tank as above are given respectively,

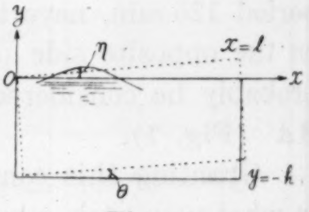

Fig. 4.

$$\varphi = -\frac{ag}{s} \cdot \frac{\cosh m(y+h)}{\cosh mh} \cos mx \cos st \,, \tag{1}$$

$$\eta = a \cos mx \sin st. \tag{2}$$

Symbols in these expressions represent the following quantities;

a: the amplitude of the oscillation,

$\frac{s}{m} = \sqrt{\frac{g \tanh mh}{m}}$: the velocity of the surface wave,

---

[4] Land Survey Department, *Bull. Imp. Earthq. Inv. Comm.*, **11** (1930), 125.

g: acceleration due to gravity,

$\frac{2\pi}{m}$ = wave length, and $\frac{2\pi}{s}$ = period of the motion,

where

$$ml = k\pi\ , \qquad k = 1,\ 2,\ 3, \cdots\cdots$$

Now it is the normal mode of oscillation what is here discussed and then putting

$$\phi_k = a_k \sin st,$$

φ and η are generally represented by the following forms:

$$\varphi = -\sum_k \frac{g}{s^2} \cdot \frac{\cosh m\,(y+h)}{\cosh mh} \cos mx\ \dot{\phi}_k, \tag{3}$$

$$\eta = \sum_k \cos \frac{k\pi x}{l}\ \phi_k\,, \tag{4}$$

where ϕ_k is the normal coordinate.
Let ρ be the density of the fluid, then the kinetic and potential energies in a unit column take the following forms respectively,

$$K.E.:\quad T = \frac{1}{2}\rho \int_{-h}^{0}\int_{0}^{l} \left\{\left(\frac{\partial\varphi}{\partial x}\right)^2 + \left(\frac{\partial\varphi}{\partial y}\right)^2\right\} dx\,dy = \frac{\rho l}{4}\sum_k \frac{1}{m \tanh mh}\dot{\phi}_k^2, \tag{5}$$

$$P.E.:\quad V = \frac{1}{2}g\rho \int_0^l \eta^2 dx = \frac{1}{4}.g\rho l \sum_k \phi_k^2\ . \tag{6}$$

Now let us suppose that this rectangular tank is subjected to a tilting of a small angle θ about a horizontal axis through the origin of coordinates, where θ is a function of time[5]. If the tilting takes place with infinite slowness, no oscillation would be produced, the free surface being always perpendicular to the direction of gravity. But if it occurs with sufficient rapidity, oscillations would be excited owing to the effect of inertia of the fluid and action of gravity. In the general case of moving tank, the motion of a fluid relative to the tank may be obtained on the assumption that the tank is fixed to the space, on the other hand two external forces are applied to the fluid particle, that is, the force of inertia and that of gravity, varying in direction. The x– and y–component of the translation of a fluid particle at a point (x, y) due to tilting are respectively $-y\theta$ and $x\theta$. Consequently the components of inertia force are respectively $y\ddot{\theta}$ and $-x\ddot{\theta}$. The force due to the change of direction of gravity as a result of tilting is $-g\theta$

---

[5] Similar problem has been discussed by G. E. PUVLENKO: *Phil. Mag.*, [vii], **15** (1933), 360~374.

parallel to the x-axis. Let X and Y be respectively the x– and y–component of the external force acting upon a unit mass of water, then

$$X = y\ddot{\theta} - g\theta, \tag{7}$$

$$Y = -x\ddot{\theta}. \tag{8}$$

If ξ and ζ denote the horizontal and vertical displacement of water particle at a point (x, y), then

$$\xi = -\sum_k \frac{mg}{s^2} \cdot \frac{\cosh m\,(y+h)}{\cosh mh} \sin mx \cdot \phi_k\,, \tag{9}$$

$$\zeta = \sum_k \frac{mg}{s^2} \cdot \frac{\sinh m\,(y+h)}{\cosh mh} \cos mx \cdot \phi_k. \tag{10}$$

Let dW be the total work done on the water mass in the interval dt, then

$$\begin{aligned} dW &= \int \rho\, dx\, dy\, X d\xi + \int \rho\, dx\, dy\, Y\, d\zeta \\ &= -\rho \sum_k \frac{mg}{s^2} d\phi_k \int_{-h}^{0} \int_{0}^{l} (y\ddot{\theta} - g\theta) \frac{\cosh m\,(y+h)}{\cosh mh} \sin mx\, dx\, dy \\ &\qquad -\rho \sum_k \frac{mg}{s^2} \ddot{\theta}\, d\phi_k \int_{-h}^{0} \int_{0}^{l} x\, \frac{\sinh m\,(y+h)}{\cosh mh} \cos mx\, dx\, dy \\ &= \rho\, \ddot{\theta} \sum_k \frac{2g}{s^2} \cdot \frac{\cosh mh - 1}{\cosh mh} \left(\frac{2}{m^2} \right) d\phi_k + 2\rho g\theta \sum_k \frac{1}{m^2}\, d\phi_k, \end{aligned} \tag{11}$$

where

$$k = 1,\ 3,\ 5, \cdots\cdots.$$

This work done must be equal to the increase of total energy of the fluid in the same interval dt, consequently

$$\frac{d\,(T+V)}{dt}\, dt = dW. \tag{12}$$

Substituting (5) and (6), an equation which determines ϕ_k will be obtained, that is,

$$\ddot{\phi}_k + s^2\phi_k - \frac{8\,l}{k^2\pi^2} \cdot \frac{\cosh mh - 1}{\cosh mh} \ddot{\theta} - \frac{4s^2 l}{k^2\pi^2}\, \theta = 0. \tag{13}$$

As seen from (11), the work done for the normal coordinate with even number of k vanishes, in other words the corresponding generalized force also vanishes. Consequently the mode of oscillation which has the same phase at both ends of the basin cannot be excited by the tilt-movement above considered. In the above discussion any dissipation of energy has not been taken into account. Hence let us assume for simplicity's sake a dissipative force which is proportional to the velocity of water particle, that is, $\dot{\xi}$ or $\dot{\zeta}$ may exist. Then the equation (13) becomes

$$\ddot{\phi}_k+2\epsilon\dot{\phi}_k+s^2\phi_k-\frac{8l}{k^2\pi^2}\cdot\frac{\cosh mh-1}{\cosh mh}\ddot{\theta}-\frac{4s^2l}{k^2\pi^2}\theta=0\,, \tag{14}$$

where ϵ is a constant which specifies the degree of dissipation.

4. Discussions.

1). At first it is assumed that the tilting of the earth-crust is given in the following expression,

$$\theta=\theta_0\,(1-e^{-\lambda t}), \tag{15}$$

where λ is taken as a parameter. The length of the bay being l, $l\theta_0$ denotes the amount of upheaval at $x=l$ which is the same thing to that of Yokosuka in the present problem. Putting $l\theta_0=H$, the general solution of (14) corresponding to (15) will be given

$$\phi_k=e^{-\epsilon t}(A_k\cos\gamma t+B_k\sin\gamma t)-\frac{8H}{k^2\pi^2}\cdot\frac{\cosh mh-1}{\cosh mh}\cdot\frac{\lambda^2e^{-\lambda t}}{s^2+\lambda^2-2\epsilon\lambda}$$
$$+\frac{4H}{k^2\pi^2}\left(1-\frac{s^2e^{-\lambda t}}{s^2+\lambda^2-2\epsilon\lambda}\right), \tag{16}$$

where A_k and B_k are integration constants to be determined by the initial conditions and $\gamma=\sqrt{s^2-\epsilon^2}$. Thus from (4)

$$\eta=\sum_{k=1,3,5,\cdots}\cos\frac{k\pi x}{l}\phi_k\,. \tag{17}$$

Initial conditions may be written in the following forms:

$$(\eta)_{t=0}=0, \tag{18}$$

$$(\dot{\eta})_{t=0}=\sum_k\cos\frac{k\pi x}{l}(\dot{\phi}_k)_{t=0}\,. \tag{19}$$

Using (17) and (18), A_k is determined, such that

$$A_k=\frac{8H}{k^2\pi^2}\cdot\frac{\cosh mh-1}{\cosh mh}\cdot\frac{\lambda^2}{s^2+\lambda^2-2\epsilon\lambda}-\frac{4H}{k^2\pi^2}\cdot\frac{\lambda^2-2\epsilon\lambda}{s^2+\lambda^2-2\epsilon\lambda}\,. \tag{20}$$

$(\dot{\phi}_k)_{t=0}$ in (19) is obtained by integrating (14) with respect to t in a very small interval of time from 0 to τ, τ being assumed to tend to zero in a limit, thus

$$(\dot{\phi}_k)_{t=0}=\frac{8H}{k^2\pi^2}\cdot\frac{\cosh mh-1}{\cosh mh}\cdot\lambda\,.$$

From (17) and (19),

$$B_k=\frac{1}{\gamma}\left(\frac{8H}{k^2\pi^2}\cdot\frac{\cosh mh-1}{\cosh mh}\cdot\frac{\lambda s^2-\epsilon\lambda^2}{s^2+\lambda^2-2\epsilon\lambda}-\frac{4H}{k^2\pi^2}\cdot\frac{\epsilon(\lambda^2-2\epsilon\lambda)+s^2\lambda}{s^2+\lambda^2-2\epsilon\lambda}\right). \tag{21}$$

Now as will be seen from Fig. 1 or Table II, the depth of the Tôkyô Bay is very small compared with its length; consequently cosh mh in this case does not much differ from unity as is shown in Table III.

Table III.

k	1	3	5	7
cosh mh	1·00000042	1·0000038	1·0000106	1·00002

Hence in the expression of A_k and B_k, the term containing $\cosh mh-1$ may be readily neglected. Thus

$$\phi_k=e^{-\varepsilon t}\left\{-\frac{4H}{k^2\pi^2}\cdot\frac{\lambda^2-2\varepsilon\lambda}{s^2+\lambda^2-2\varepsilon\lambda}\cos\gamma t-\frac{1}{\gamma}\,\frac{4H}{k^2\pi^2}\cdot\frac{\varepsilon(\lambda^2-2\varepsilon\lambda)+s^2\lambda}{s^2+\lambda^2-2\varepsilon\lambda}\sin\gamma t\right\}$$
$$+\frac{4H}{k^2\pi^2}\left(1-\frac{s^2e^{-\lambda t}}{s^2+\lambda^2-2\varepsilon\lambda}\right). \tag{22}$$

It is the expressions at both ends of the bay that is desired, therefore

$$\eta_{x=0}=-\eta_{x=l}=\sum_{k=1,3,5,\cdots}\phi_k\,. \tag{23}$$

Putting $\frac{\lambda}{s}=u$ and $\frac{\varepsilon}{s}=h$,

$$\eta_{x=0}=\frac{H}{2}-\frac{4H}{\pi^2}\sum_{k=1,3,5,\cdots}\frac{1}{k^2}\left\{\frac{ue^{-\varepsilon t}\cos(\gamma t-\varDelta)}{\sqrt{1-h^2}\sqrt{u^2-2hu+1}}+\frac{e^{-\lambda t}}{u^2-2hu+1}\right\}, \tag{24}$$

where

$$\cos\varDelta=\frac{(u-2h)\sqrt{1-h^2}}{\sqrt{u^2-2hu+1}}\,,\qquad \sin\varDelta=\frac{h(u-2h)+1}{\sqrt{u^2-2hu+1}}\,.$$

In Fig. 5 the curves 1, 2, 3, and 4 represent the assumed transient movement of the land which are expressed in the form of (15). Corresponding to these curves, the oscillation of water surface at both ends of the bay is calculated by (24). In numerical calculation the following quantities are used.

$H=l\theta_0=1{\cdot}8$ ft: observed at Yokosuka.

$T_1=126$ min: the period of the gravest mode of oscillation which is not theoretical value but the observed one.

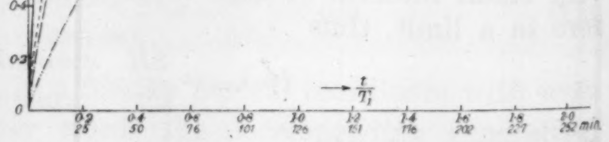

Fig. 5. Assumed curves showing the transient state of the tilt-movement of earth-crust.

Damping ratio$=1{\cdot}14$, which is tentatively obtained from the observed mareogram.

In order to compare the calculated curves with the observed one, the results of calculation are shown in Fig. 6 together with the observed curves. The numbers attached to each curve represent the respective correspondence to those in Fig. 5. The expression of η given by (24) is valid in the case of closed basin. As a result of land upheaval the mean sea level in the Tôkyô Bay has made an elevation of $H/2$, whereas outside the bay the change of sea level may be neglected. But the Tôkyô Bay communicates with the outer sea by the Uraga Channel, so that in order to keep the same level the water in the bay must flow out through the mouth until the elevated sea level may coincide with its former one. Let z denote the difference of the height of water level near the mouth, the velocity of flow being assumed to be nearly equal to $\sqrt{2gz}$, then the fall of the mean sea level in the bay dz' in the interval dt will be given by

$$A_1\sqrt{2gz}\,dt = A_0\,dz' ,$$

where

A_1: area of the vertical section at the mouth,

A_0: area of the free surface of the bay.

If the mouth of the Tôkyô Bay is tentatively taken at DD' (Fig. 1), then A_1/A_0 becomes 0·000206. It is a set of curves corrected by such a rough method as above that are shown in Fig. 6. At a glance,

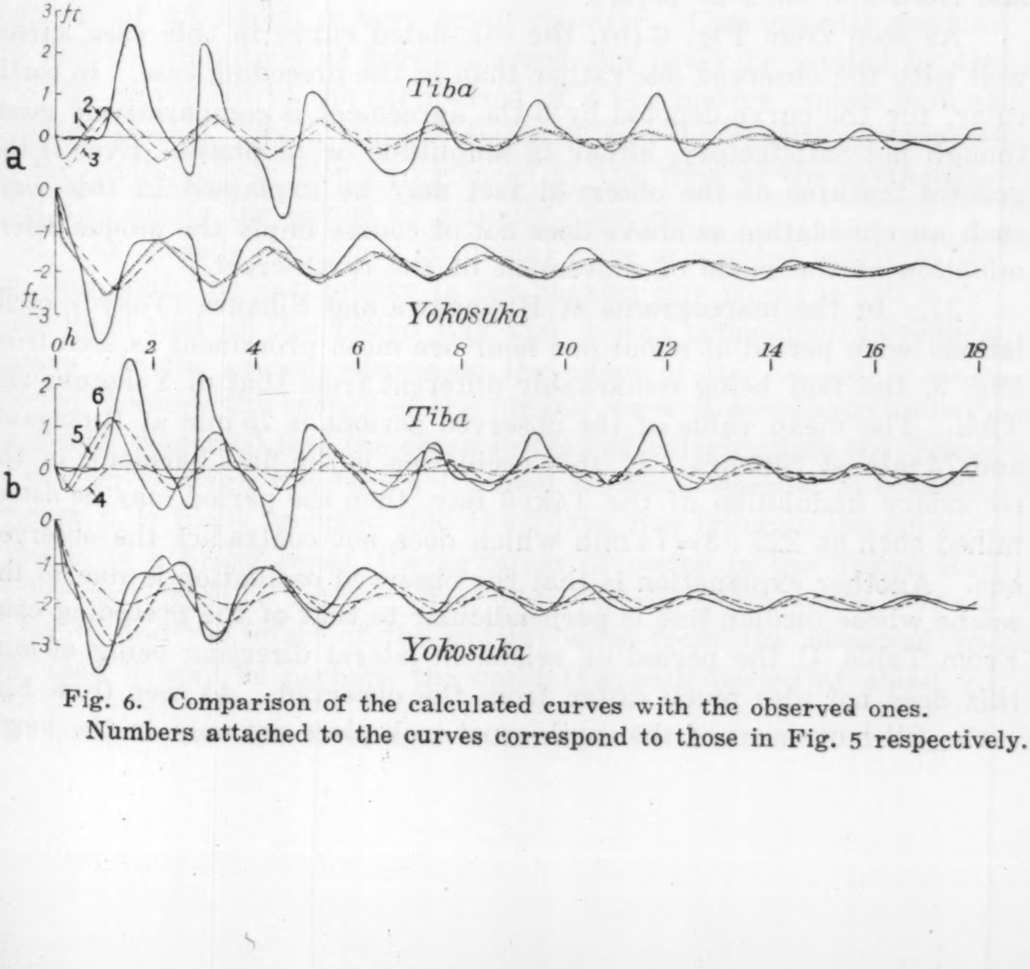

Fig. 6. Comparison of the calculated curves with the observed ones. Numbers attached to the curves correspond to those in Fig. 5 respectively.

the calculated curves denoted by 1, 2, 3, and 4 do not well agree with the observed one. Consequently with such a mode of land upheaval as given by (15), even if the earth-crust tilts suddenly (Case 1), the amplitude of calculated curve does not yet reach that of actually observed one.

2). In the next place, the case in which the tilting of the earth-crust exceeds once the amount of the permanent value and then asymptotically tends to it, shall be examined. In this case θ will be given for example in the form

$$\theta=\theta_0\left[1+(at-1)\,e^{-\lambda t}\right], \tag{25}$$

which has two parameters a and λ. For this case, similarly as before

$$\eta_{x=0}=\frac{H}{2}-\frac{4H}{\pi^2}\sum_{k=1,3,5,\cdots}\frac{1}{k^2}\left[e^{-\varepsilon t}\left(\frac{u\cos(\gamma t-\varDelta)}{\sqrt{1-h^2}\sqrt{u^2-2hu+1}}\right.\right.$$

$$\left.\left.-\frac{\frac{a}{s}\cos(\gamma t-\delta)}{\sqrt{1-h^2}(1-2hu+u^2)}\right)+\frac{(1-at)e^{-\lambda t}}{1-2hu+u^2}+\frac{2\frac{a}{s}(h-u)e^{-\lambda t}}{(1-2hu+u^2)^2}\right], \tag{26}$$

where

$$\cos\delta=\frac{2\sqrt{1-h^2}(h-u)}{u^2-2hu+1}, \qquad \sin\delta=\frac{(u-h)^2-(1-h^2)}{u^2-2hu+1},$$

and $\cos\varDelta$ and $\sin\varDelta$ as before.

As seen from Fig. 6 (b), the calculated curve in this case agrees well with the observed one rather than in the preceding case. In particular, for the curve denoted by 6 the agreement is comparatively good, though not satisfactory, either in amplitude or in phase. Even if the general features of the observed fact may be explained in this way, such an elucidation as above does not of course imply the unique determination of the mode of movement of the earth-crust.

3). In the mareograms at Hukagawa and Sibaura (Tôkyô), oscillations with period of about one hour are most prominent as seen from Fig. 3, the fact being remarkably different from that of Yokosuka and Tiba. The mean value of the observed periods is 75 min at Hukagawa and 74 min at Sibaura. If this oscillation is the first harmonic of the secondary undulation of the Tôkyô Bay, then the period may be determined such as 222÷3=74 min which does not contradict the observed one. Another explanation is that the observed oscillation is due to the seiche whose median line is perpendicular to that of the preceding case. From Table II the period of seiche in lateral direction being 60 min, this does not also much differ from the observed. As seen from Fig. 1 the tilt-movement of the earth-crust took place not only in the longitudinal direction of the bay but also in the lateral direction, it may be presumably considered that the oscillation observed at Tôkyô might be the seiche which was excited by the lateral component of earth-tilting. But, further discussion may be difficult owing to the scantiness of data.

4). The horizontal displacement of the earth-crust in the neighbourhood of the Tôkyô Bay is shown in Fig. 1. with an arrow. It must be necessarily examined in what order of magnitude the seiche may be excited by a horizontal movement of earth-crust, provided that such a movement takes place during a comparatively short interval of time. If a tank is moved by a horizontal acceleration $\ddot{x}$, then the unit mass of water in the tank may suffer an inertia force of $-\ddot{x}$. When the horizontal displacement is expressed by

$$x = x_0(1 - e^{-\lambda t}) , \tag{27}$$

then the elevation of water surface at one end

$$\eta_{x=0} = 4x_0 \sum_{k=1,3,5,\cdots} \frac{\tanh mh}{k\pi} \left\{ \frac{ue^{-\varepsilon t}\cos(rt-\tau)}{\sqrt{1-h^2}\sqrt{u^2-2hu+1}} - \frac{u^2 e^{-\lambda t}}{1-2hu+u^2} \right\} , \tag{28}$$

where

$$\cos\tau = \frac{u\sqrt{1-h^2}}{\sqrt{u^2-2hu+1}} , \qquad \sin\tau = \frac{1-hu}{\sqrt{u^2-2hu+1}} .$$

In a shallow sea such as the Tôkyô Bay tanh mh⁶⁾ is in an order of magnitude of h/l which is very small quantity. Consequently a seiche with such an amplitude as here observed can never be excited by the horizontal movement of the earth-crust of a few metres, unless it is an oscillatory motion. By a similar reason it may be readily understood that the earthquake-motion experienced at the time of the earthquake cannot also excite the seiche as actually observed.

5). As already mentioned, a tunami wave originated nearly at the same time with the earthquake in the Sagami Bay whose depth is far greater than that of the Tôkyô Bay and it was propagated to remote distances. In the present discussion the effect of this tunami is quite neglected, because the energy of the tunami wave is considered to have been mostly dispersed into the ocean instead of entering into the Tôkyô Bay passing through the Uraga Channel which is narrow in breadth. Moreover it is likely accepted that the Tôkyô Bay lying on the epicentral region in a broad sense, the agitation of water in the Tôkyô Bay is rather considered as a direct effect of terrestrial disturbances. If we will try to find the effect of the tunami wave from the observed records, then it may be perhaps the oscillation with period of about 25

---

6) In this expression h is the depth of the bay.

min which was observed at Yokosuka alone (Fig. 2) among four mareograms around the Tôkyô Bay. The calculated period of the secondary undulation of the small bay at Yokosuka does not exceed 13 min at most and thus the observed oscillation may not be the secondary undulation. Now from these discussions as mentioned above it follows that the observed seiche is favourably elucidated on the assumption that it was excited by the tilt-movement of the earth-crust. According to this consideration the earth-crust has upheaved at least in the neighbourhood of the Tôkyô Bay with such a type of mode as discussed in (*2*).

5. Concluding remarks. On the occasion of the great earthquake of Sept. 1, 1923, a remarkable seiche took place in the Tôkyô Bay almost simultaneously with the earthquake. This phenomenon was ascertained by comparing the mareograms observed at Yokosuka and Tiba which are situated nearly opposite each other facing the bay. On the assumption that the vertical deformation of the earth-crust was accompanied by such a seiche as observed, it has been made to estimate the transient movement of crustal deformation. The observed fact is apparently rather favourably explained, if the land upheaved once beyond the amount of permanent upheaval and then settled down to it during about one hour and a half, instead of gradual upheaval. If such a way of elucidation is correct, then the Tôkyô Bay, considered as a fluid pendulum, has played an important rôle in informing us concerning the mode of occurrence of land upheaval.

In conclusion the writer wishes to express his sincere thanks to Professor M. Ishimoto under whose suggestion the present study has been made. Further the writer wishes also to express his best thanks to Professor T. Matuzawa for his kindness in giving valuable advices and in revising the original manuscript.

21. 大正12年9月1日の地震の際土地隆起に伴つて生じた東京灣の靜振

地震學敎室　**鈴木武夫**

大正12年9月1日の地震の際相模灣に起つたと思はれる津浪を記錄した驗潮記錄が震災豫防調査會報告第100號乙の卷末に掲載せられてある．東京灣內の記錄の內橫須賀と千葉との記錄を比較して見ると第2圖にて見られる樣に兩者は共に約2時間程度の週期にて振動して居り而も略位相が逆になつて居ることが見出される．平均週期は橫須賀が126分，千葉が125分である．橫須賀と千葉とは東京灣に面して略相對する位置に在るからこの方向の靜振が生じたとすれば差支へない．東京灣を深さ一樣の矩形の湖と見做して理論上の靜振の週期を求むれば144分となる．これは上記の値より少しく大であるが驗潮儀に記錄されたものは靜振と見做せるであらう．この靜振が土地の隆起運動に伴つて生じたと考へて隆起が如何樣であつたならば實測された程度の靜振が起り得たかを調べた．それによれば地殼は一度永久の隆起量卽ち水準測量で求められたものを越して隆起し過ぎ然る後にそれに落ち著いたとする方が說明し易い．而も大體この隆起運動は1時間半位の間に行はれたとすれば都合がよい．勿論これで隆起の仕方が決定せられた譯ではない．

地震動や數米程度の地殼の水平移動によつては實測された程度の振幅を持つ靜振の生じ得ないことを示し又津浪の影響に就いても考慮した．東京の深川，芝浦に於ける驗潮記錄には主として週期約1時間の振動が卓越して居るがこれについても吟味した．

22. *Notes on the Block Structure of the Earth's Crust.*

By Naomi MIYABE,

Earthquake Research Institute.

(Read Jan. 15, 1935.—Received March 20, 1935.)

1. In previous paper[1], the writer tried to show from analyses of the vertical displacements of triangulation points distributed in the Kwantô district, that the earth's crust could be regarded as consisting of a number of crustal blocks. From analyses of the vertical displacements of bench-marks, similar blocks were found also in a number of other districts as well[2], the boundaries of which approximately coincided with faults and other tectonic lines determined by geologists, as was the case in the Kwantô district.

The horizontal dimensions of these crustal blocks in the Tango and other districts were found to be roughly 10 km, while those of the Kubiki block, the tilting movements of which were first pointed out by the late Professor N. Yamasaki, is approximately 50 km[3]. It will however be noticed after closer investigation of its movements that the Kubiki block is apparently composed of several smaller blocks, each having horizontal dimensions of about 10 km.

The horizontal dimensions of the crustal blocks in the Kwantô district are also about 10 km. It may also be worthy of notice that the distribution of the mean vertical displacements of each block reveals the existence of larger ones containing several primary blocks[4], the horizontal dimensions of which are from about 40 to 50 km, as may be estimated from Fig. 1.

In connection with the block structure of the earth's crust in the Kwantô district, it may be noticed that it consists of horizontal layers, as shown by Dr. T. Matuzawa, who has determined it seismologically.

---

[1] N. MIYABE, *Bull. Earthq. Res. Inst.*, **9** (1931), 256; **9** (1931), 409; **11** (1933), 639.

[2] C. TSUBOI, *Bull. Earthq. Res. Inst.*, **7** (1929), 103; *Jap. Journ. Astr. Geophys.*, **6** (1933), 95.

[3] N. YAMASAKI, *Proc. Imp. Acad.*, **4** (1928), 60.

[4] By primary block is meant those having horizontal dimensions of about 10 km, after usage in the preceding paper, *loc. cit.* 1).

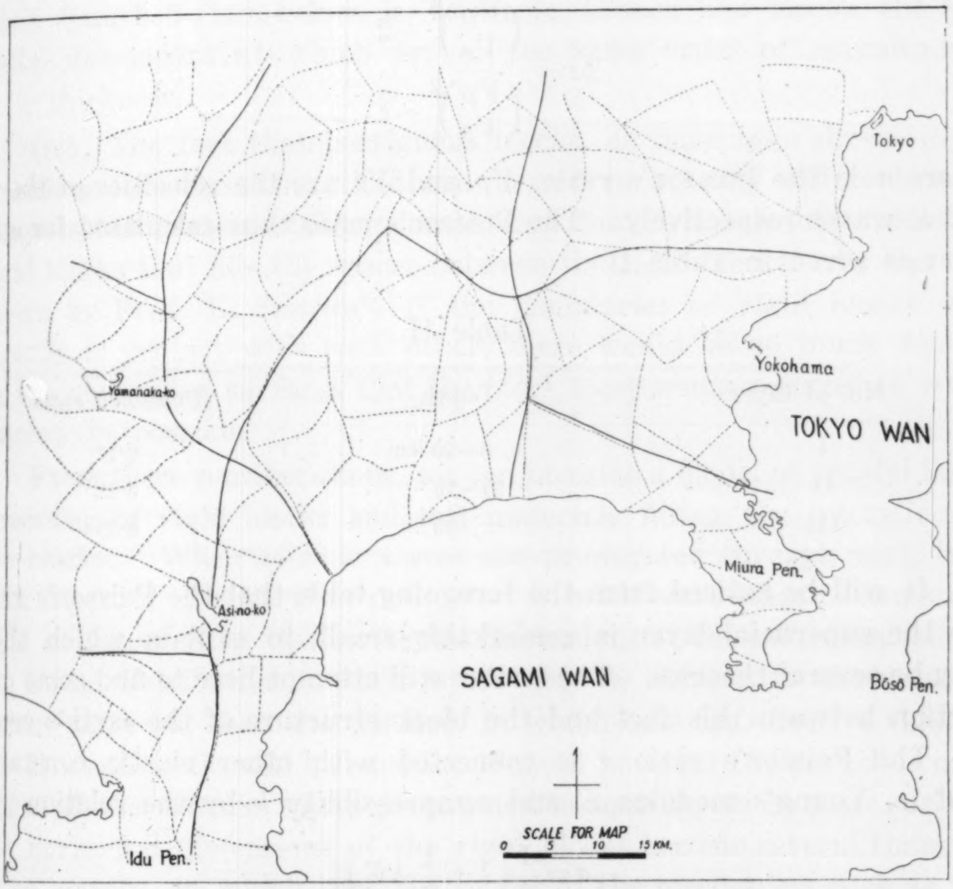
Tokyo
Yokohama
TOKYO WAN
Yamanaka-ko
Asino-ko
Miura Pen.
SAGAMI WAN
Bôsô Pen.
Idu Pen.
SCALE FOR MAP
0 5 10 15 KM.

Fig. 1. Block structure in the Kwantô district.
(Full lines denote estimated boundaries of larger blocks.)

2. According to Dr. Matuzawa[5], the earth's crust in the Kwantô district is composed of three different layers, in each of which the velocities of propagation of the P– and S–waves are different. The depths of these layers and the velocities of the P– and S–waves as determined by Matuzawa for each layer are shown in Table I.

Table I.

No. of layer	Depth	V_P	V_S
I	0∼20 km	5·0 km/sec	3·15 km/sec
II	20∼50	6·1	3·7
III	>50	7·5	4·45

From these data, we can calculate the values of the Poisson's ratio for the respective layers by using the relation

---

[5] T. Matuzawa, *Bull. Earthq. Res. Inst.*, **6** (1929), 117.

$$2\sigma=\frac{\left(\frac{Vp}{Vs}\right)^2-2}{\left(\frac{Vp}{Vs}\right)^2-1},$$

where σ is the Poisson's ratio, Vp and Vs are the velocities of the P- and S-waves respectively. The Poisson's ratio thus calculated for each layer is given in Table II.

Table II.

No. of layer	Depth	Poisson's ratio
I	0~20 km	0·17
II	20~50	0·21
III	>50	0·23

It will be noticed from the foregoing table that the Poisson's ratio for the superficial layer is remarkably small, to explain which there may be several theories. The writer will attempt here to find some connection between this fact and the block structure of the earth's crust.

The Poisson's ratio σ is connected with other elastic constants, that is, Young's modulus E and compressiblity k by the relation

$$\sigma=\frac{1}{2}\left(1+\frac{1}{3}kE\right).$$

The values of σ therefore become smaller as kE become larger. For ordinary homogeneous isotropic materials, the values of k and E are generally of the order of 10^{-12} and 10^{12} respectively.

We could picture to our minds a certain model, the values of elastic constants of which are nearly those of the crustal layers obtained from data of velocities of seismic waves. Such a model would represent the block structure of the earth's crust.

3. We have some hints useful in forming an idea of block structure, such as the following:

(i) As has been shown experimentally by W. A. Zisman[6], the values of Poisson's ratio of several rocks of porous structure are generally much smaller than those of the substance composing the rocks.

(ii) The approximate horizontal dimensions of the blocks, as already shown, are 10 km and 40 km corresponding to the thicknesses of the upper layers, namely 20 km and 50 km.

(iii) As has been shown by Prof. T. Terada[7], a layer of powder, when disturbed from below, is, as a rule, broken into blocks, the horizontal dimensions of which are of the same order of magnitude as their thickness.

---

[6] W. A. ZISMAN, *Proc. Nat. Acad. Sci., U. S. A.*, **19** (1933), 653.

[7] T. TERADA and T. WATANABE, *Proc. Imp. Acad.*, **10** (1934), 143.

(iv) The fact that contiguous blocks, as have been shown in the preceding investigations, tilted and moved in entirely different ways, suggests the presence of some substance that is much softer than the rigid blocks that fills the spaces between the rigid blocks. As has been shown by Prof. K. Sezawa[8], if the boundaries of rigid blocks were directly in contact with each other, there would be so much friction on the contacting surfaces that the block movements referred to would scarcely be possible.

From these considerations, we can imagine a model of crustal layers consisting of rigid blocks and soft materials filling the interstices of the blocks. When seismic waves are propagated through such layer with a period of several seconds, that is, with wave length comparable with or larger than the horizontal dimensions of the individual blocks, the stress distribution in such layers may be similar to those in the porous material, that was yielded, in which case the effective value of the Poisson's ratio will be smaller. Should however the period of oscillation of the seismic waves propagated in such layers be 1 sec. or less, the horizontal dimensions of the rigid blocks become several times the wave lengths, in which case the model of the mechanism such as just described becomes unsuitable for showing that the Poission's ratio becomes smaller.

4. We shall next consider a model similar to that mentioned above, that is, the crustal layer consisting of rigid and soft substances arranged alternately in horizontal direction, as shown in Fig. 2. In the model shown in this figure, the densities, elastic constants, and the horizontal dimensions of the rigid and soft substances are ρ_1, λ_1, μ_1, L_1 and ρ_2, λ_2, μ_2, L_2, respectively. We then assume the following for the sake of simplicity:

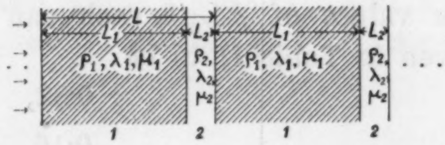

Fig. 2. Schematical configuration of the block structure. The arrows show the direction of propagation of seismic waves.

(i) The seismic waves propagated in the layers are plane waves and the wave front is perpendicular to the direction of propagation.

(ii) The boundaries of blocks of both the rigid and soft substances are also perpendicular to the direction of propagation of the waves.

---

[8] K. SEZAWA, *Bull. Earthq. Res. Inst.*, 10 (1932), 1.

(iii) The horizontal dimensions L_1 and L_2 of the alternate rigid and soft substances are constant, so that we may take the mean velocity of the substaces L_1+L_2 as that of the layers.

(iv) The velocities of propagation of the seismic waves in the two different substances are determined separately by the elastic constants of the substances composing the respective layers.

With these assumptions, we get the following calculations:

$$\frac{L}{Vp_m}=\frac{L_1}{Vp_1}+\frac{L_2}{Vp_2}=\frac{L}{Vp_1}\left\{1-\frac{L_2}{L}\left(1-\frac{Vp_1}{Vp_2}\right)\right\},$$

$$\frac{L}{Vs_m}=\frac{L_1}{Vs_1}+\frac{L_2}{Vs_2}=\frac{L}{Vs_1}\left\{1-\frac{L_2}{L}\left(1-\frac{Vs_1}{Vs_2}\right)\right\}^{9)},$$

where $L=L_1+L_2$, Vp_1, Vp_2 are velocities of the P–waves and Vs_1, Vs_2 those of the S–waves in substances 1 and 2 respectively, while Vp_m and Vs_m are the mean velocities of the P– and S–waves. The effective value of Poisson's ratio in such layers will then be

$$\sigma\doteqdot\sigma_0\left\{1-\frac{L_2}{L}\sqrt{\frac{\mu_1\rho_2}{\mu_2\rho_1}}\left(\frac{\sqrt{3\mu_2}-\sqrt{\lambda_2+2\mu_2}}{\sqrt{\lambda_2+2\mu_2}}\right)\right\},$$

where σ_0 is the Poisson's ratio of the rigid substance which has been taken as 1/4 or 0·25.

Since, as in an actual case, when σ is less than 1/4, λ_2 is less than μ_2 and the numerical values of λ_2, μ_2 may be taken at orders of magnitude smaller than λ_1, μ_1[10], the coefficient of L_2/L becomes larger than unity. Writing the equation in the simpler form,

$$\sigma\doteqdot\sigma_0(1-\beta\, L_2/L),$$

the values of $\beta\, L_2/L$ each can be calculated from the actual values given in Table II to be

0·32, for layer I,
0·16, for layer II.

If then we assume $L_2/L=1/10$ for layer I, we have $\beta=3{\cdot}2$ and $L_2/L=0{\cdot}5/10$ for layer II. The assumed value of 1/10 for layer I and the

---

[9] A similar idea regarding the existence of larger blocks was proposed by Prof. S. Ono, based on the fact that the "Laufzeit" curves are regarded as consisting of segments of curves.

Cf. S. Ono: *Kensin-Zihô.*, **5** (1925), 51, 111, and 221, (in Japanese).

[10] A substance filling the interstices between the rigid blocks, we can imagine, for instance, such substance as compose superficial mud or gravel layers, the elastic constants of which are of the order of 10^{10}, as measured by Mr. Haeno and others.

Cf. S. HAENO, I. MIKAWA, T. HAGIWARA and R. YOSIYAMA, *Disin*, **4** (1932), 465, (in Japanese).

calculated value of $L_2/L = 0{\cdot}5/10$ for layer II are of the same order of magnitude in the matter of errors in determining the approximate extent of the blocks from the data of vertical displacements of triangulation points and bench-marks. Hence, even were there regions of soft rocks as supposed in the above mentioned model, the data of vertical displacements will give us no inkling of their existence.

If therefore there is any likelihood that the assumption just referred to is a first approximation, the idea of block structure for the earth's crust may be plausible, and even if the solution were not unique, it will at any rate be one way of explaining the smallness of σ in the upper layer as deduced from the propagational velocity of seismic waves.

---

22. 地殼の地塊的構造に就て

地震研究所　宮部直巳

三角點又は水準點の垂直變動から推定される地塊の大いさは，10 km 程度のものと 40～50 km 程度のものが比較的著しく目立つてみえる．關東地方では，之に相應して，地表から 20 km 及 50 km の厚さの水平層が，地震波の研究から知られ．尙，其等の層のポアソン比を地震波の傳播速度から求めると 0·17，0·21 等普通に認められてゐる 0·25 よりは著しく小さいものを得る．

地殼が多くの地塊より成り，其等の地塊がかなり自由な運動をなし得る事實などを考慮しつゝ，嘗つて，小野敎授が，地震波の走時曲線が多くの曲線の segments から成るといふ事實に基いて考へられた地塊構造の考へを小區域にまで延長して，ポアソン比の見掛け上小さくなる事と地塊構造とを關聯させて考へてみた．

23. *Deformation of the Earth's Crust in the Iwate and Miyagi prefectures.*

By Naomi MIYABE,

Earthquake Research Institute.

(Read Jan. 15, 1935.—Received March 20, 1935.)

1. In order to study the deformation of the earth's crust in the regions believed to have been considerably disturbed by the Sanriku earthquake of March 3, 1933, with which the great tunami was associated, the horizontal displacements of triangulation points in the prefectures of Iwate and Miyagi and the vertical displacements of the bench-marks along the level lines Tokyo-Miyako, Kamaisi-Kurosawaziri-Akita and Isinomaki-Ayukawa were measured the results of which were recently published[1].

This paper is an attempt to study modes of deformation of the earth's crust by means of the data of horizontal and vertical displacements of triangulation points and bench-marks just referred to.

2. The triangulation points in the region under consideration, the horizontal displacements of which were measured, are 10 primary triangulation points and 26 secondary triangulation points, the latter being mostly near the Pacific coast.

The horizontal displacements of the primary triangulation points occurred in the time interval of these 39~33 years, or from 1890~1900 to 1933, which differs from that in which the displacements of the secondary triangulation points occurred, that is, 36~24 years, or from 1897~1909 to 1933.

The horizontal deformation, Δ etc., are therefore calculated with reference to the primary triangulation points, being separated from those calculated with reference to the secondary triangulation points.

The quantities that represent the horizontal deformation of the earth's crust are

$$\Delta=\frac{\partial u}{\partial x}+\frac{\partial v}{\partial y},$$

---

[1] Rikuti-Sokuryôbu (Military Land Survey), "*Report of Revision of Triangulation and Levellings in the Sanriku Districts*", (Tokyo, 1934).

$$2\zeta=\frac{\partial v}{\partial x}-\frac{\partial u}{\partial y},$$

$$2S=\frac{\partial v}{\partial x}+\frac{\partial u}{\partial y},$$

$$\gamma_{\substack{1\\2}}=\left(\frac{\partial u}{\partial x}+\frac{\partial v}{\partial y}\right)\pm\sqrt{\left(\frac{\partial v}{\partial x}+\frac{\partial u}{\partial y}\right)^2+\left(\frac{\partial u}{\partial x}-\frac{\partial v}{\partial y}\right)^2}\,,$$

$$\tan\theta_1=\frac{\gamma_1-2\dfrac{\partial u}{\partial x}}{\dfrac{\partial v}{\partial x}+\dfrac{\partial u}{\partial y}},$$

$$S_m=\frac{1}{2}(\gamma_1-\gamma_2),$$

where u, v are x- and y-components of horizontal displacement, and Δ, ζ, S, γ_1, γ_2, S_m are divergence, rotation, shear, principal axes of strain, and maximum shear respectively.

These quantities are calculated as before[2] on the assumption that in the area limited by a triangle, the three vertices of which are the triangulation points, the deformation is uniform and continuous. Since, in the present case, no conspicuous faults appeared in association with the earthquake, this assumption might be justified to a certain degree; whereas, as in the case of the Kwantô and the Tango earthquakes, etc.[3], in which discontinuous movements along the faults were observed, the assumption might not be admissible.

The geographical distribution of the triangulation points and the level lines in the region under consideration are shown in Fig. 1. The triangulation points forming triangles and the amounts of the horizontal deformations are given in Tables I a, I b.

In the amounts of the horizontal deformations given in Tables I a, I b, we notice that:

(i) The horizontal deformations calculated for the triangles formed by primary triangulation points are generally smaller than those formed by the secondary triangulation points.

(ii) The horizontal deformation in the region are generally smaller than those in other regions where the earth's crust was disturbed by acute movements associated with destructive earthquakes. This point is discussed later.

---

[2] T. Terada and N. Miyabe, *Bull. Earthq. Res. Inst.*, **7** (1929), 223.

[3] C. Tsuboi, *Jap. Journ. Astr. Geophys.*, **9** (1933), 95.

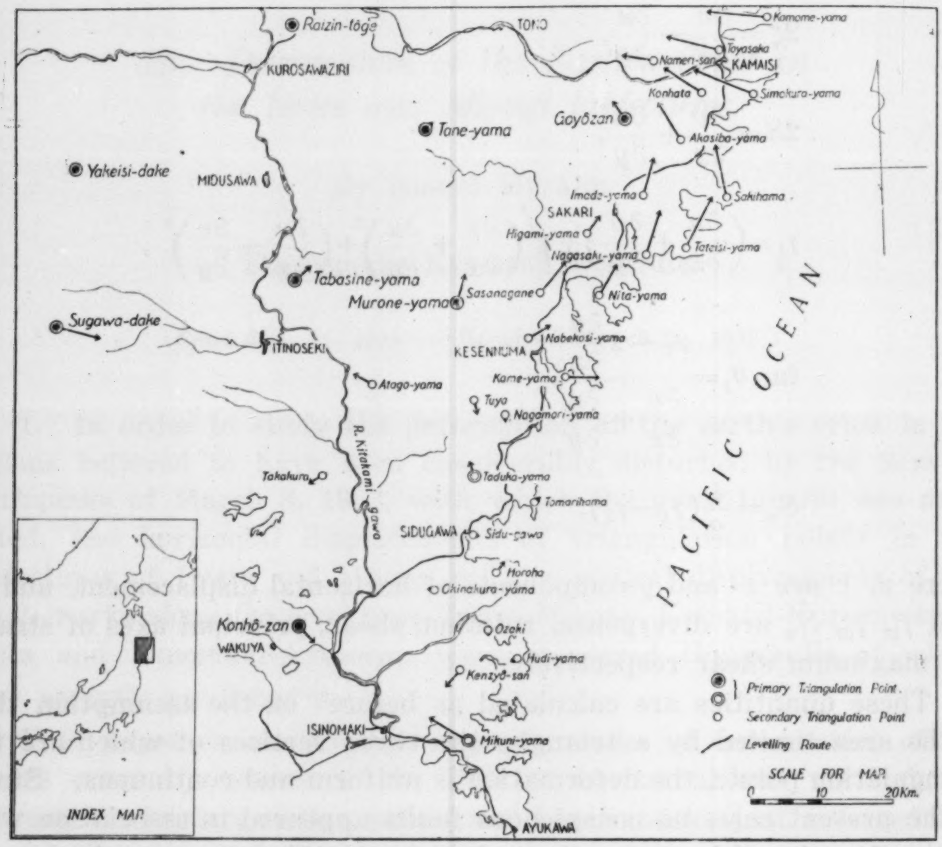
Raizin-tôge
TONO
Kamome-yama
Toyasaka
Nameri-san
KAMAISI
Konhata
Simokura-yama
KUROSAWAZIRI
Goyôzan
Tane-yama
Akosiba-yama
Yakeisi-dake
MIDUSAWA
Imadz-yama
Sakihama
SAKARI
Higami-yama
Nagasaku-yama
Toteisi-yama
Tabasine-yama
Sasanagane
Murone-yama
Nita-yama
Sugawa-dake
ITINOSEKI
KESENNUMA
Nabekosi-yama
Atogo-yama
Kame-yama
Tuya
Nagamori-yama
R. Kitakami gawa
Takakura
Taduka-yama
Tomarihama
SIDUGAWA
Sidu-gawa
PACIFIC OCEAN
Horoha
Chinakura-yama
Konhô-zan
WAKUYA
Ozaki
Hudi-yama
Kenzyô-san
ISINOMAKI
Mikuni-yama
AYUKAWA
INDEX MAP
Primary Triangulation Point
Secondary Triangulation Point
Levelling Route
SCALE FOR MAP
0 10 20Km.

Fig. 1. Distribution of triangulation points and level lines. (Arrows show the horizontal displacements of the triangulation points.)

Table I a.

Δ etc. of triangles formed by primary triangulation points, given in 10^{-5}

Triangulation points	Δ	2ζ	S_m	γ_1	γ_2	θ_1
Tadukayama, Konhôzan, Mikuniyama,	−1.41	0·39	2·12	0·72	−3·53	57°07′
Tabasineyama, Sugawadake, Konhôzan,	−0.15	0·49	1·19	1·04	−1·33	75°21′
Tadukayama, Sugawadake, Konhôzan,	−0.12	0·51	1·22	1·10	−1·33	59°31′
Tadukayama, Tabasineyama, Konhôzan,	−0.13	0·55	1·20	1·06	−1·33	14°01′
Tabasineyama, Tadukayama, Sugawadake,	−0.16	0·64	1·06	0·90	−1·22	77°51′
Muroneyama, Tadukayama, Tabosineyama,	0.18	0·22	1·09	1·28	−0·91	62°55′
Goyôzan, Tadukayama, Muroneyama,	−0.62	−0·89	1·32	0·37	−2·27	−81°42′
Taneyama, Muroneyama, Tabasineyama,	−0.98	0·29	0·57	−0·41	−1·55	25°11′
Tabasineyama, Yakeisidake, Sugawadake,	0.01	1·94	1·09	1·10	−1·08	−65°01′

(to be continued.)

Table I a. (*continued.*)

Triangulation Points	Δ	2ζ	S_m	γ_1	γ_2	θ_1
Goyôzan, Taneyama, Muroneyama,	−1.57	0·64	0·45	−1·12	−2·03	78°00′
Raizintôge, Tabasineyama, Yakeisidake,	−0.18	−0·73	0·76	0·57	−0·94	−88°41′
Raizintôge, Taneyama, Tabasineyama,	−0.27	0·29	0·51	0·24	0·77	−26°26′
Raizintôge, Goyôzan, Taneyama,	−0.32	0·74	0·22	−0·10	−0·54	−66°11′

Table I b.

Δ etc. of triangles formd by secondary triangulation points, given in 10^{-5}

Triangulation Points	Δ	2ζ	S_m	γ_1	γ_2	θ_1
Kenzyôzan, Mikuniyama, Hudiyama,	−2.36	−0·14	5·01	2·64	−7·37	22°44′
Konhô-zan, Mikuniyama, Kenzyôzan,	2.83	−0·70	4·65	7·48	−1·82	72°43′
Okinakura-yama, Konhôzan, Kenzyôzan,	0.34	0·14	2·27	2·60	−1·93	81°41′
Tadukayama, Okinakurayama, Sidukawa,	4.34	−1·67	3·56	7·90	0·79	−35°48′
Tadukayama, Sidukawa, Tomarihama,	2.02	0·67	1·21	3·23	0·82	−69°34′
Takakura, Konhôzan, Okinakurayama,	−0.50	1·57	0·83	0·33	−1·33	−81°08′
Nagamoriyama, Tomarihama, Kameyama,	3.09	2·24	1·92	5·01	1·17	21°54′
Tuya, Tadukayama, Nagamoriyama,	−2.48	−0·18	1·88	−0·61	−4·36	9°09′
Ozaki, Kenzyôzan, Hudiyama,	1.51	−0·44	2·61	4·12	−1·10	48°00′
Okinakurayama, Kenzyôzan, Ozaki,	1.09	−1·70	0·77	1·86	0·33	−68°30′
Horoha, Ozaki, Hudiyama,	1.16	0·48	2·58	3·74	−1·42	58°23′
Horoha, Okinakurayama, Ozaki,	2.57	−0·13	1·24	3·81	1·33	46°09′
Sidukawa, Okinakurayama, Horoha,	0·31	1·10	2·86	3·17	−2·55	14°12′
Tomarihama, Sidukawa, Horoha,	−0.70	1·69	1·74	1·07	−2·44	13°23′
Sasanagane, Nabekosiyama, Nitayama,	1.14	−0·62	2·74	3·88	−1·61	79°40′
Muroneyama, Atagoyama, Tuya,	3.47	−1·42	0·99	4·46	2·48	−76°37′
Muroneyama, Nabekosiyama, Sasanagane,	3·06	−0·37	0·81	3·87	2·24	28°43′
Nitayama, Nabekosiyama, Kameyama,	2.34	1·29	1·79	4·13	0·55	−73°10′
Nabekosiyama, Tuya, Kameyama,	3.86	0·03	0·47	4·33	3·39	68°12′
Takakura, Okinakurayama, Tadukayama,	0.74	0·85	0·89	1·64	−0·15	42°26′
Muroneyama, Tuya, Nabekosiyama,	3.54	−0·38	1·19	4·73	2·35	75°33′

(*to be continued.*)

Table I b. (*continued.*)

Triangulation Points	Δ	2ζ	S_m	γ_1	γ_2	θ_1
Atagoyama, Takakura, Tadukayama,	1.07	1·43	0·49	1·56	0·58	60°11′
Atagoyama, Takakura, Tuya,	−0.84	−2·13	3·64	2·80	4·49	−11°09′
Tuya, Nagamoriyama, Kameyama,	0.36	−2·36	4·60	4·96	−4·24	32°40′
Nagamoriyama, Tadukayama, Tomarihama,	−0.41	−1·28	2·69	2·28	−3·10	−19°45′
Goyôzan, Imadeyama, Akasibayama,	−2.43	3·11	1·08	−1·35	−3·51	−44°26′
Imadeyama, Nagasakiyama, Tateisiyama,	0.84	1·26	2·32	3·16	−1·48	7°21′
Goyôzan, Muroneyama, Higamiyama,	1.32	1·34	2·10	3·41	−0·78	−34°15′
Sitakurayama, Akasibayama, Sakihama,	−2.60	2·04	1·70	−0·90	− 4·30	−47°39′
Akasibayama, Imadeyama, Sakihama,	−2.19	2·91	1·36	−0·83	− 3·55	−64°48′
Imadeyama, Higamiyama, Nagasakiyama,	−0.85	2·38	1·79	0·94	− 2·64	35°43′
Imadeyama, Tateisiyama, Sakihama,	−2.27	3·49	1·84	−0·43	− 4·11	−58°19′
Higamiyama, Nitayama, Nagasakiyama,	−1.65	2·42	2·17	0·52	− 3·82	−38°27′
Higamiyama, Sasanagane. Nitayama,	−1.88	0 44	0·59	−1·29	− 2·47	−30°58′
Higamigama, Muroneyama, Sasanagane,	0.08	2·50	3·40	3·48	− 3·32	−20°07′
Goyôzan, Higamiyama, Imadeyama,	−0.47	3·49	1·00	0·53	− 1·46	16°14′
Namerisan, Toyasaka, Konhata,	−3.27	2·10	0·56	−2·72	− 3·83	47°28′
Namerisan, Goyôzan, Konhata,	−3.08	1·87	0·49	−2·59	− 3·56	− 6°20′
Konhata, Goyôzan, Akasibayama,	0.30	1·47	2·20	2·49	− 1·90	−87°01′
Konhata, Akasibayama, Sitakurayama,	−6.57	−0·45	4·09	−2·49	−10·66	−12°38′
Toyasaka, Konhata, Sitakurayama,	−3.58	1·18	0·84	−2·74	4·42	−61°34′
Kamomeyama, Toyasaka, Sitakurayama,	−2.33	0·28	0·80	−1·53	− 3·13	9°59′
Kamomeyama, Toyasaka, Konhata,	−3.23	1·43	1·09	−2·14	− 4·32	−34°55′

3. The geographical distribution of Δ, 2ζ, S_m, γ_1, γ_2, calculated by means of the horizontal displacements of the primary triangulation points are shown in Figs. 2∼5, while those by means of the data of the secondary triangulation points are shown in Figs. 6∼9.

In the modes of horizontal deformation in this region suggested by the geographical distribution of Δ, etc. (see Figs. 2∼9), we notice the following points:

(i) Although the divergences Δ's in the triangles formed by the primary triangulation points are on the whole negative, in those formed by the secondary triangulation points, the signs are positive in several regions and negative in others. In the latter, we can distinguish regions in which the signs of Δ alternate, being positive

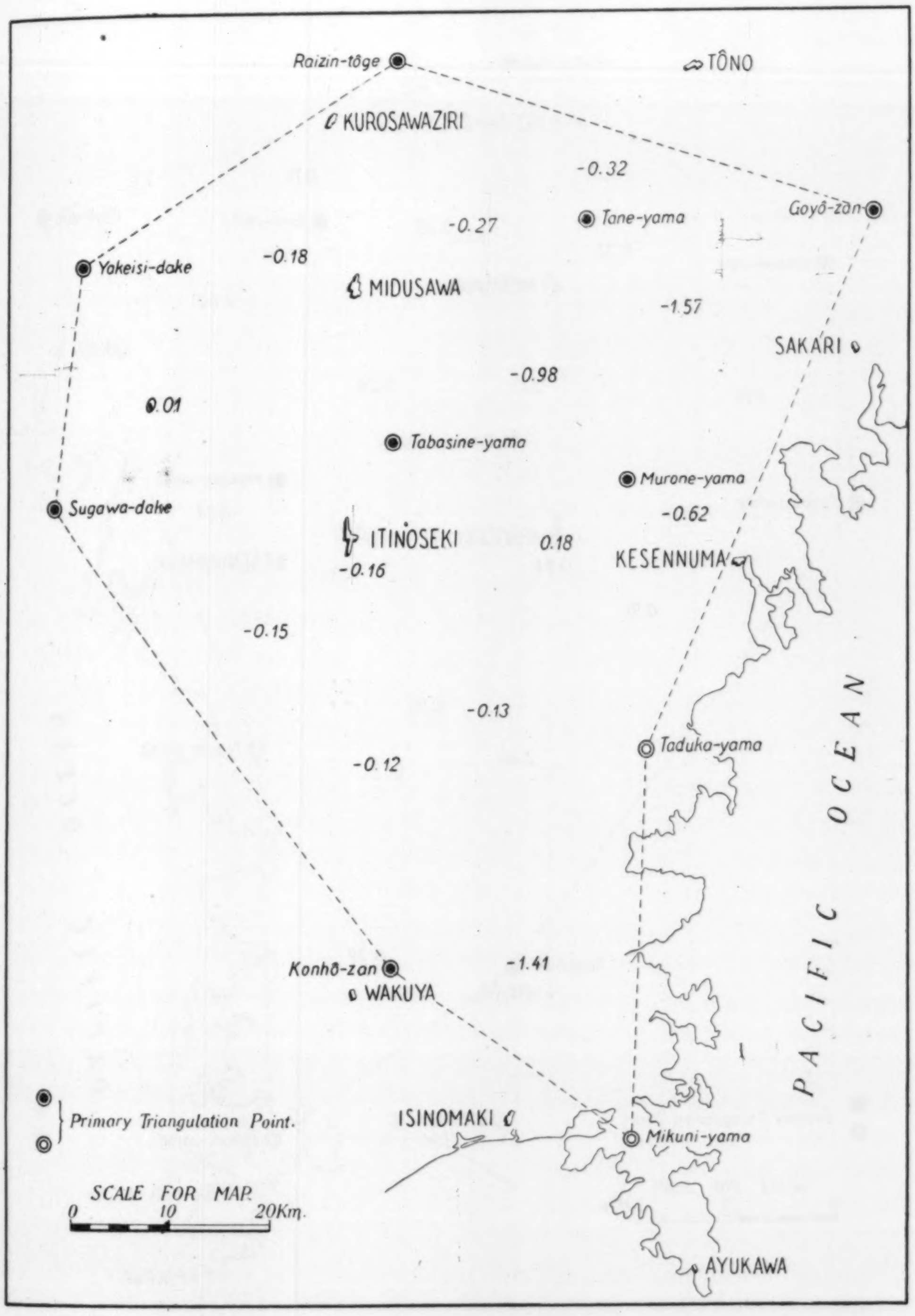
Raizin-tôge
TÔNO
KUROSAWAZIRI
-0.32
Tane-yama
Goyô-zan
-0.27
-0.18
Yakeisi-dake
MIDUSAWA
-1.57
SAKARI
-0.98
0.01
Tabasine-yama
Murone-yama
Sugawa-dake
-0.62
ITINOSEKI
0.18
KESENNUMA
-0.16
-0.15
-0.13
Taduka-yama
-0.12
PACIFIC OCEAN
Konhô-zan
-1.41
WAKUYA
Primary Triangulation Point.
ISINOMAKI
Mikuni-yama
SCALE FOR MAP.
0
10
20Km.
AYUKAWA

Fig. 2. Distribution of Δ of triangles formed by primary triangulation points. (Numerical figures designate amounts of Δ in 10^{-5}).

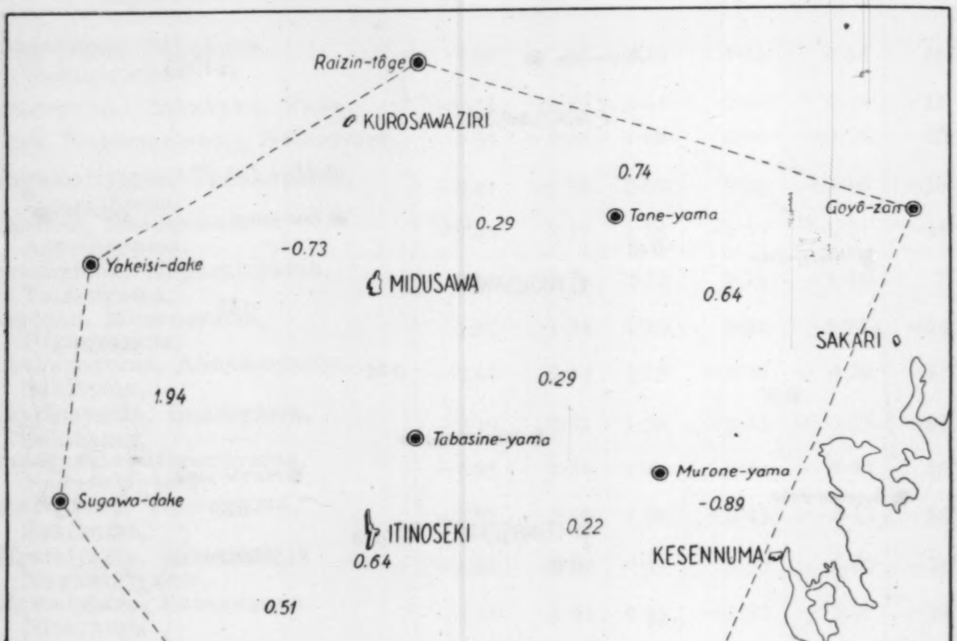
Raizin-tôge
KUROSAWAZIRI
0.74
Goyô-zan
0.29
Tane-yama
-0.73
Yakeisi-dake
MIDUSAWA
0.64
SAKARI
0.29
1.94
Tabasine-yama
Murone-yama
-0.89
Sugawa-dake
ITINOSEKI
0.22
KESENNUMA
0.64
0.51
0.55
Taduka-yama
0.49
PACIFIC OCEAN
0.39
Konhô-zan
WAKUYA
Primary Triangulation Point.
ISINOMAKI
Mikuni-yama
SCALE FOR MAP.
0 10 20Km.
AYUKAWA

Fig. 3. Distribution of 2ζ of triangles formed by primary triangulation points. (Numerical figures designate amounts of 2ζ in 10^{-5}).

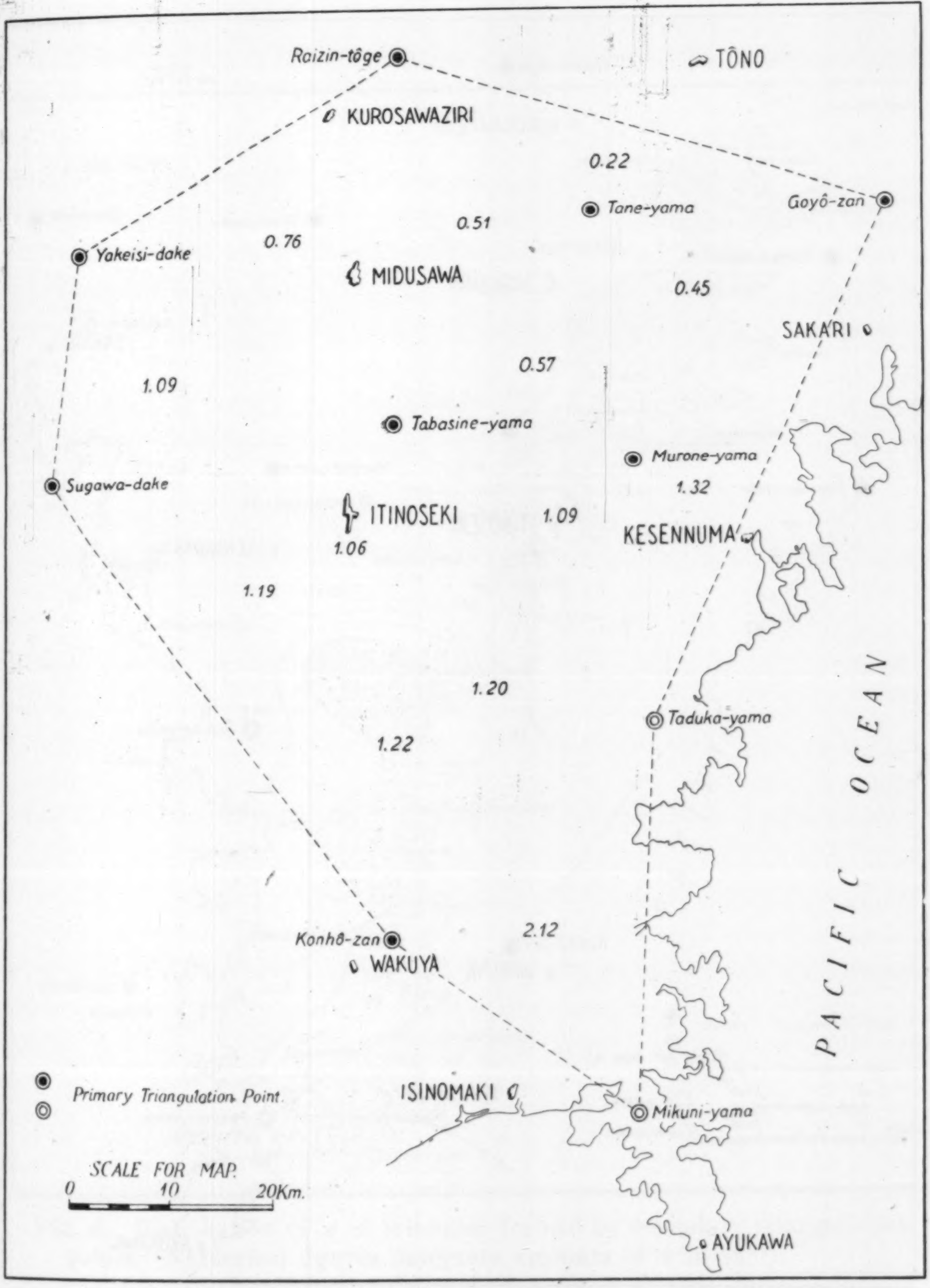
Raizin-tôge
TÔNO
KUROSAWAZIRI
0.22
Tane-yama
Goyô-zan
0.51
Yakeisi-dake
0.76
MIDUSAWA
0.45
SAKARI
0.57
1.09
Tabasine-yama
Murone-yama
1.32
Sugawa-dake
ITINOSEKI
1.09
KESENNUMA
1.06
1.19
1.20
Taduka-yama
1.22
PACIFIC OCEAN
2.12
Konhô-zan
WAKUYA
Primary Triangulation Point
ISINOMAKI
Mikuni-yama
SCALE FOR MAP
0
10
20Km.
AYUKAWA

Fig. 4. Distribution of S_m of triangles formed by primary triangulation points. (Numerical figures designate amounts of S_m in 10^{-5}).

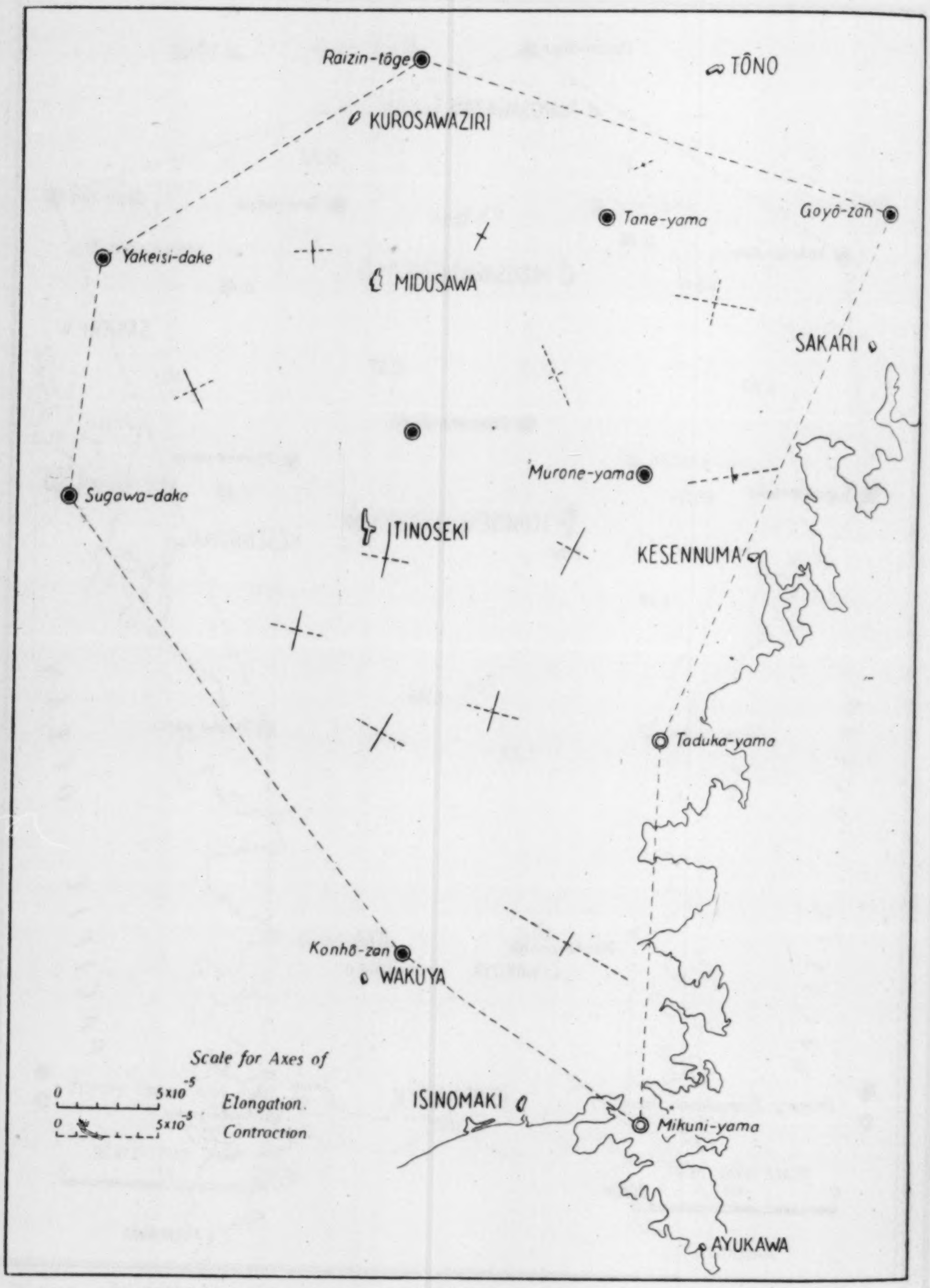
Raizin-tôge
TÔNO
KUROSAWAZIRI
Tane-yama
Goyô-zan
Yakeisi-dake
MIDUSAWA
SAKARI
Murone-yama
Sugawa-dake
TINOSEKI
KESENNUMA
Taduka-yama
Konhô-zan
WAKUYA
Scale for Axes of
0
5×10^{-5}
Elongation.
0
5×10^{-5}
Contraction
ISINOMAKI
Mikuni-yama
AYUKAWA

Fig. 5. Distribution of principal axes of strain in triangles formed by primary triangulation points.

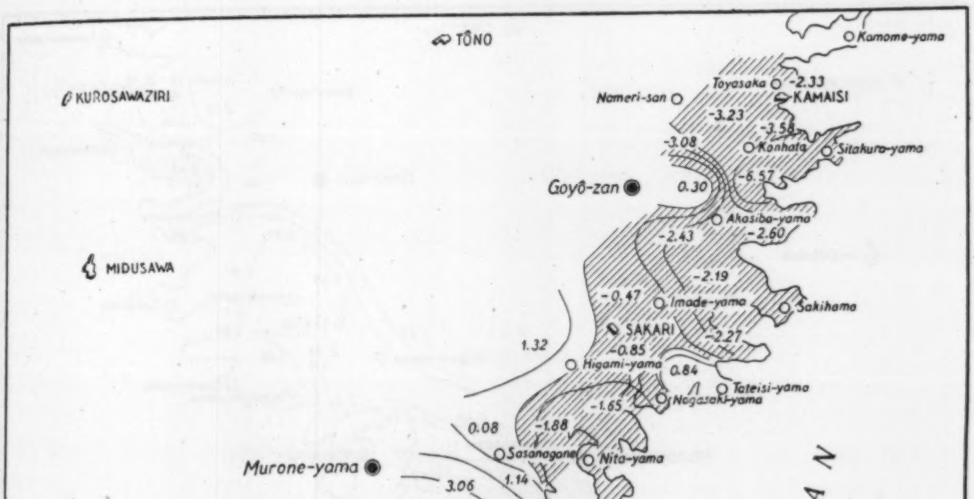
TÔNO
Kamome-yama
KUROSAWAZIRI
Toyasaka
-2.33
Nameri-san
KAMAISI
-3.23
-3.58
-3.08
Konhata
Sitakura-yama
Goyô-zan
0.30
-6.57
Akasiba-yama
-2.43
-2.60
MIDUSAWA
-2.19
-0.47
Imade-yama
Sakihama
SAKARI
-2.27
1.32
-0.85
Higami-yama
0.84
Tateisi-yama
Nagasaki-yama
-1.65
-1.88
0.08
Sasanagane
Nita-yama
Murone-yama
3.06
1.14
ITINOSEKI
Nabekosi-yama
2.34
3.54
KESENNUMA
3.47
3.86
Atago-yama
Kame-yama
Tuya
0.36
Nagamori-yama
-0.84
-2.48
3.09
1.07
-0.41
Takakura
Taduka-yama
2.02
Tomarihama
0.74
4.34
Sidugawa
-0.70
0.31
-0.50
Horoha
Okinakura
2.57
1.16
Konhô-zan
0.34
Ozaki
1.09
WAKUYA
1.51
Hudi-yama
Kenzyo-san
2.83
-2.36
ISINOMAKI
Mikuni-yama
PACIFIC OCEAN
Primary Triangulation Point.
Scondary Triangulation Point.
SCALE FOR MAP.
0
10
20Km.

Fig. 6. Distribution of Δ of triangles formed by secondary triangulation points. (Numerical figures designate amounts of Δ in 10^{-5}).

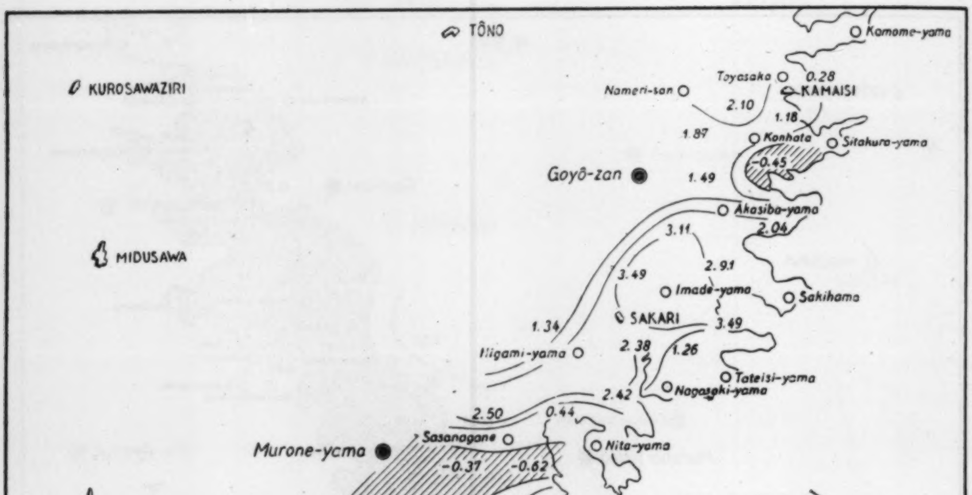
TÔNO
Kamome-yama
KUROSAWAZIRI
Toyasaka
0.28
Nameri-san
KAMAISI
2.10
1.18
1.87
Konhata
Sitakura-yama
-0.45
Goyô-zan
1.49
Akasiba-yama
2.04
3.11
MIDUSAWA
2.9.1
3.49
Imade-yama
Sakihama
SAKARI
3.49
1.34
2.38
1.26
Iigami-yama
Tateisi-yama
2.42
Nagasaki-yama
2.50
0.44
Sasanagane
Murone-yama
Nita-yama
-0.37
-0.62
ITINOSEKI
Nabekosi-yama
1.29
-0.38
KESENNUMA
-1.42
0.30
Atago-yama
Kame-yama
Tuya
-2.36
Nagamori-yama
-2.13
-0.18
2.24
1.43
-1.28
Takakura
Taduka-yama
0.67
Tomarihama
0.85
-1.67
Sidugawa
1.69
1.57
1.10
Horoha
Okinakura-yama
-0.13
Konhô-zan
0.48
0.14
-1.70
Ozaki
WAKUYA
-0.44
Hudi-yama
Kenzyo-san
-0.70
-0.14
ISINOMAKI
Mikuni-yama
PACIFIC OCEAN
Primary Triangulation Point
Secondary Triangulation Point
SCALE FOR MAP.
0
10
20Km

Fig. 7. Distribution of 2ζ of triangles formed by secondary triangulation points. (Numerical figures designate amounts of 2ζ in 10^{-5}).

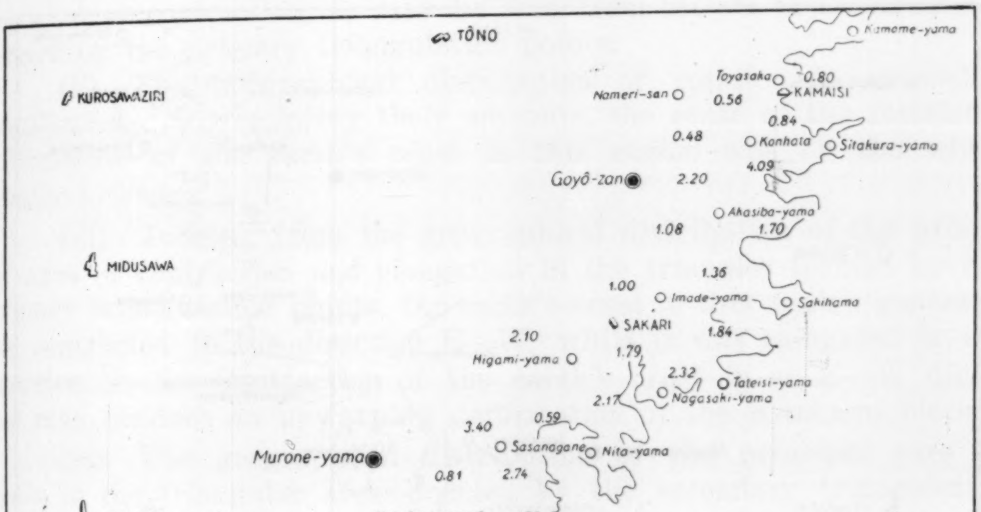
TÔNO
Kamame-yama
KUROSAWAZIRI
Toyasaka
0.80
Nameri-san
0.56
KAMAISI
0.84
0.48
Konhata
Sitakura-yama
4.09
Goyô-zan
2.20
Akasiba-yama
1.08
1.70
MIDUSAWA
1.36
1.00
Imade-yama
Sakihama
SAKARI
2.10
1.84
Higami-yama
1.79
2.32
Tateisi-yama
2.17
Nagasaki-yama
0.59
3.40
Sasanagane
Nita-yama
Murone-yama
0.81
2.74
ITINOSEKI
Nabekosi-yama
1.79
1.19
KESENNUMA
0.99
0.47
Atago-yama
Kame-yama
Tuya
4.60
3.64
Nagamori-yama
1.88
1.92
0.49
2.69
Takakura
Taduka-yama
1.21
Tomari-hama
0.89
3.56
Sidugawa
1.74
0.83
2.86
Horoha
Okinakura-yama
1.24
PACIFIC OCEAN
Konhô-zan
2.27
2.58
0.77
Ozaki
WAKUYA
2.61
Hudi-yama
Kenzyo-san
4.65
5.01
● ◎ } Primary Triangulation Point.
○ Secondary Triangulation Point.
SCALE FOR MAP.
0
10
20Km.
ISINOMAKI
Mikuni-yama

Fig. 8. Distribution of S_m of triangles formed by secondary triangulation points. (Numerical figures designate amounts of S_m in 10^{-5}).

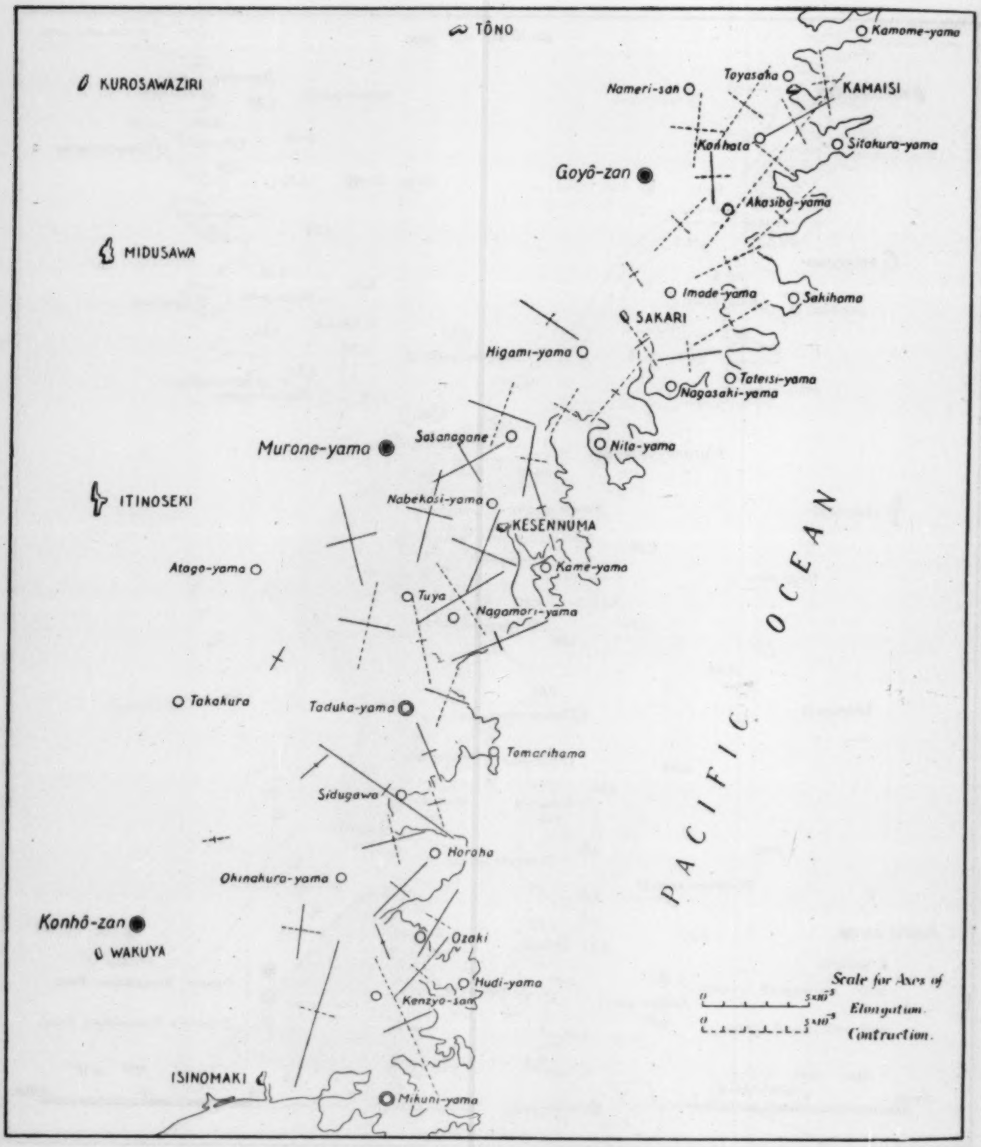
TÔNO
Kamome-yama
KUROSAWAZIRI
Toyasaka
Nameri-san
KAMAISI
Konhata
Sitakura-yama
Goyô-zan
Akasiba-yama
MIDUSAWA
Imade-yama
Sakihama
SAKARI
Higami-yama
Tateisi-yama
Nagasaki-yama
Sasanagone
Murone-yama
Nita-yama
Nabekosi-yama
ITINOSEKI
KESENNUMA
Kame-yama
Atago-yama
Tuya
Nagamori-yama
PACIFIC OCEAN
Takakura
Taduka-yama
Tomarihama
Sidugawa
Horaha
Okinakura-yama
Konhô-zan
WAKUYA
Ozaki
Hudi-yama
Kenzyo-san
Scale for Axes of
0
5×10^{-5}
Elongation.
0
5×10^{-5}
Contraction.
ISINOMAKI
Mikuni-yama

Fig. 9. Distribution of principal axes of strains of triangles formed by secondary triangulation points.

in one and negative in the next. As the triangles formed by the secondary triangulation points are generally smaller than those formed by the primary ones, it may suggest that the mode of deformation was, in detail, more complicated and conspicuous, although it was on the whole a contraction, as may be seen from the Δ's in the triangles formed by the primary triangulation points.

(ii) The geographical distribution of rotation is somewhat complicated. Disregarding their amounts, the sense of the rotational deformation of the earth's crust in this region was on the whole counterclockwise.

(iii) Judging from the geographical distribution of the principal axes of contraction and elongation in the triangles formed by the primary triangulation points, the earth's crust in this region generally had contracted in the direction E—W, while it was elongated in the direction N—S. Contraction of the earth's crust in an E—W direction may conduce an upwarping deformation of the Kitakami block.

(iv) The geographical distribution of the principal axes of strain in the triangular areas formed by the secondary triangulation points is much more irregular than in those formed by the primary triangulation points, as in the case of distribution of Δ, just referred to. We notice however that the region in which the axes of contraction and in which the axes of elongation are greater are distributed alternately along the Pacific coast, corresponding to the distribution of regions of positive and negative divergence.

It may be stated here, as has been pointed out by Dr. Tsuboi[4], that the derived amounts of crustal deformation are only relative, seeing that the points of origin (Yakeisi-dake and Raizin-tôge) were assumed not to have been displaced, so that in the event that they had been displaced, all the measured displacements would be relatively affected according to their distance from the points of origin.

4. The vertical displacements of bench-marks along the level lines shown in Fig. 1 are those that occurred during the 30 years or more interval since the previous survey. The dates of the surveys along the different sections of the level lines are given in Table II.

Table II. Dates of Levelling Surveys.

Section	Previous survey	Recent survey
Isinomaki-Ayukawa	June~July, 1900	May~June, 1933
Isinomaki-Kamaisi	Aug.~Dec., 1900	May~Aug., 1933
Kamaisi-Miyako	Apr.~June, 1901	June~Aug., 1933
Kamaisi-Kurosawaziri	Sept.~Nov., 1900	Aug.~Nov., 1933

---

[4] C. Tsuboi, *Jap. Journ. Astr. Geophys., loc. cit.*

The results of the rerunning of level lines are shown in Figs. 10~12[5]. In these curves showing the vertical displacements of the earth's crust, we notice that (1) the vertical displacements are generally negative, that is, the earth's crust sank relative to the standard datum during the interval between the old and new surveys. To go into details, the depression is more marked in the north near Kamaisi than in the south near Sidukawa. The vertical displacements along the line that crosses the Kitakami mountain range, from Kamaisi to Kurosawaziri, show upwarp, which however is not readily apparent owing to considerable fluctuations in the heights of the upwarp. (2) As will be seen from Figs. 10~12, the vertical displacements along the

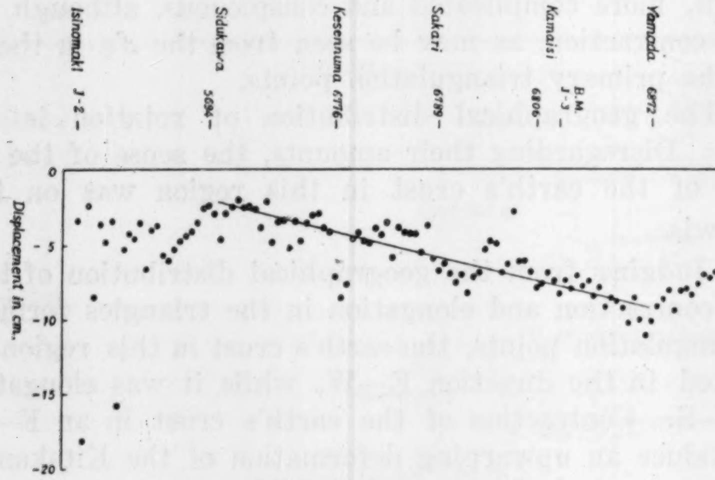

Fig. 10. Vertical displacements of bench-marks along the line Isinomaki-Miyako.

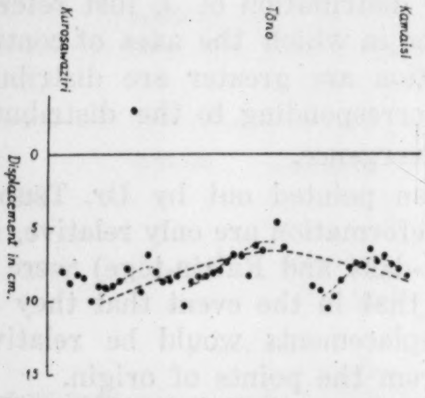

Fig. 11. Vertical displacements of bench-marks along the line Kurosawaziri-Kamaisi.

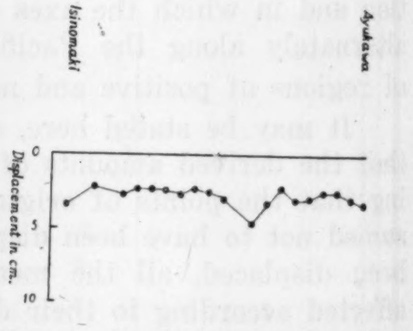

Fig. 12. Vertical displacements of bench-marks along the line Isinomaki-Ayukawa.

---

[5] Reproduced from the *Report of the Military Land Survey, loc. cit.*

level lines fluctuate, these fluctutations being supposed to be due to irregularities in the trends of the lines, and to tiltings and other movements of the smaller crustal blocks.

The maximum amplitude of the fluctuation due to irregularities in the trends of the level lines may be

$$w' = \phi x,^{6)}$$

where ϕ is the angle of general tilting and x the maximum deviation in the position of a bench-mark from the general trend of the level line. Assuming $\phi = 10^{-6}$ and $x = 10$ km, we have for the maximum fluctuation

$$w' = \phi x = 10^{-6} \times 10^{6}\ \mathrm{cm} = 1\ \mathrm{cm},$$

which is of an order of magnitude comparable with the actual amplitude of fluctuation in the vertical displacements.

5. As the level lines pass through regions in which are triangular areas with secondary triangulation points as vertices, the mean vertical displacements of the bench-marks distributed in the triangular areas are compared with the Δ's of the triangles in which the bench-marks are distributed. In Fig. 13, the values of the Δ's of

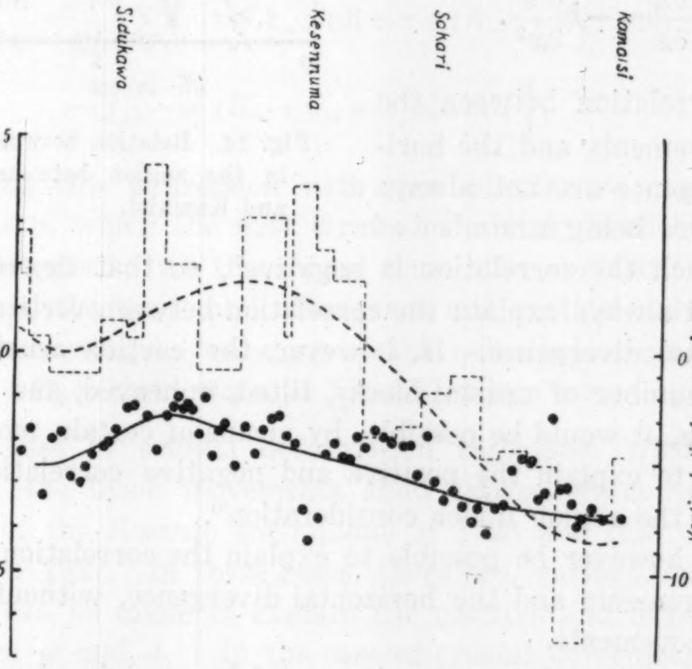

Fig. 13. Horizontal divergence and vertical displacements along the line Isinomaki-Kamaisi. (Segments of dotts the horizontal divergences, along sections of level lines in a triangular areas, the general tendency of which is denoted by a curve of dotted line.)

---

6) Cf. N. MIYABE, *Bull. Earthq. Res. Inst.*, **10** (1933), 278.

the triangular areas are shown by segments of dotted lines, the horizontal extents of these segments being corresponding to the lengths of the level lines in respective triangles. The vertical displacements of the bench-marks are also plotted in the same figure. Although these two curves are approximately parallel to each other in their general trends, there is a region in which the correlation between these two quantities are negative. The general positive correlation between w and $\varDelta$ is also shown in Fig. 14, in which the $\varDelta$'s are plotted against the $\overline{w}$'s of the corresponding triangular areas.

The positive correlation just mentioned may, in some cases, be explained by a flexural deformation of the earth's crust, as shown by Prof. Terada[7]. In this case we have, for the relation between horizontal divergence and w,

$$\varDelta = \frac{\partial u}{\partial x} = -h\frac{\partial^2 w}{\partial x^2}\,.$$

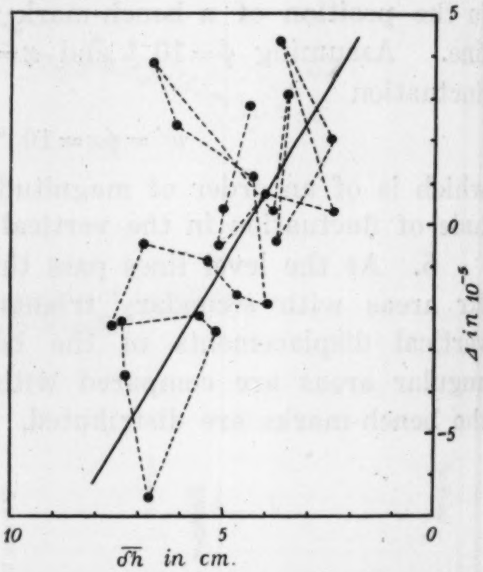

Fig. 14. Relation between $\varDelta$ and $\overline{\delta h}$ in the region between Isinomaki and Kamaisi.

The correlation between the vertical movements and the horizontal divergence are not always positive, there being a number of cases in which the correlation is negative[8], so that flexural deformation does not always explain the correlation between vertical movement and horizontal divergence. If, however, the earth's crust were composed of a number of crustal blocks, tilted, upheaved, and depressed in various ways, it would be possible, by means of certain modes of block movements, to explain the positive and negative correlations between w and $\varDelta$ in the region under consideration[9].

It may however be possible to explain the correlation between the vertical movements and the horizontal divergence, without considering the block movements.

When a surface layer of uniform thickness, lying horizontally between two rigid blocks, is subjected to pressure from below, as shown in Fig. 15, the horizontal and vertical displacements, u and v, at a point on the surface, are given by Prof. Sezawa[10] in the following forms: λ, the Lamé constant of the layer, being assumed to be infinite,

---

[7] T. Terada, *Proc. Imp. Acad.*, **6** (1930), 53.

[8] N. Miyabe, *Bull. Earthq. Res. Inst.*, **9** (1931), 1.

[9] C. Tsuboi, *Jap. Journ. Astr. Geophys.*, *loc. cit.*

$$2\mu u=\sum_{m}\{A_m(-mx\sinh mx)-D_m m\cosh mx\}$$

$$-\sum_{m}\{B'_{m'}+C'_{m'}m'\}\cos m'x, \qquad (1)$$

and

$$2\mu v=\sum_{m'}(-D'_{m'}m')\sin m'x, \qquad (2)$$

where

$$m=\frac{(2n+1)\pi}{a},$$

$$m'=\frac{n'\pi}{b},$$

a=thickness of the surface layer,
b=horizontal extent of the surface layer,

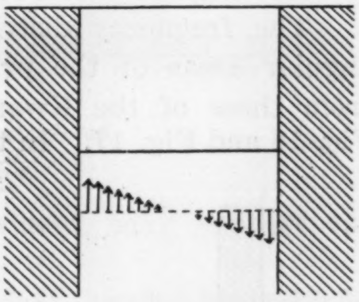

Fig. 15.
(Arrows show pressure from below.)

and A_m, D_m, $B'_{m'}$, $C'_{m'}$, $D'_{m'}$ are constants determined by boundary conditions. The value of Δ, in this case, is therefore given by

$$\Delta=\frac{\partial u}{\partial x}=\frac{1}{2\mu}\Big[\sum_{m}\{-m[A_m\sinh mx+(A_m x+D_m)\cosh mx]\}$$

$$-\sum_{m'}\{-m'(B'_{m'}+C'_{m'}m')\}\sin m'x\Big]. \qquad (3)$$

On comparing this expression with that of (2), we can say that in certain cases in which the first term of the right-hand side of (3) is negligible compared with the second term, the correlation between Δ and v, that is, the horizontal divergence and vertical movements, will be positive according to the signs of the principal terms of the series $\sum_{m'}\{-m'(B'_{m'}+C'_{m'}m')\}\sin m'x$ and $\sum_{m'}(-D'_{m'}m')\sin m'x$.

In the case of crustal deformation associated with destructive earthquakes, the block movements show themselves conspicuously, as in the case of the Kwantô earthquake of 1923 and that of the Tango earthquake of 1927. In these cases, therefore, various modes of block movements can be taken to explain the positive and negative correlations between w aud Δ. In the case of crustal deformation in Iwate and Miyagi prefectures, the deformation may be regarded rather as chronic, as will be discussed in the next paragraph. In these cases, therefore, both the block movements and the crustal deformation shown by Sezawa's calculation may be considered to be probable explanations of the correlation between w and Δ.

---

[10] K. SEZAWA and G. NISHIMURA, *Bull. Earthq. Res. Inst.*, 8 (1930), 13.

6. As already stated, the order of magnitude of the horizontal divergence in the region under consideration is smaller than in those of other regions disturbed by destructive earthquakes.

The frequency distribution of horizontal divergences in the triangular areas of the primary triangulation points is quite different from those of the Kwantô district, as will be seen upon comparing Fig. 16 and Fig. 17. In the case of the Kwantô district, the frequency maximum occurrs at a greater value of Δ. The same thing will also be observed upon comparing the frequency distribution of horizontal divergence in the triangular areas of the secondary triangulation points of this region (Fig. 18) with that of the horizontal divergence within the blocks in the Kwantô district, shown in Fig. 19[11].

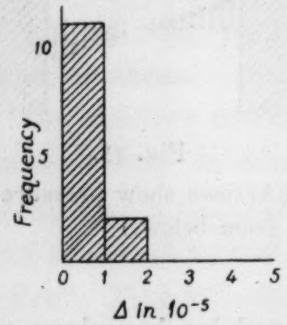

Fig. 16. Frequency distribution of Δ's of triangles formed by primary triangulation points in regions of prefectures of Iwate and Miyagi.

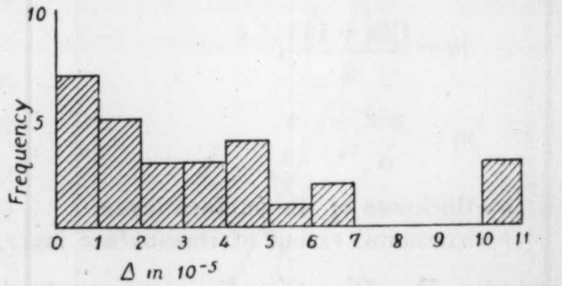

Fig. 17. Frequency distribution of Δ's of trianles formed by primary triangulation points in the Kwantô district.

These facts may suggest that the earth's crust in this regions was not greatly disturbed by the destructive earthquake of March 3, 1933. The fact noticed in the preceding paragraph that, in cases of fluctuations in vertical displacements of bench-marks along

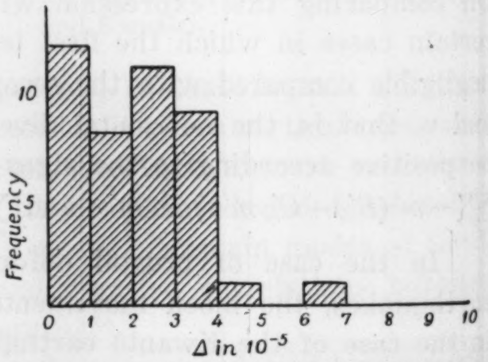

Fig. 18. Frequency distribution of Δ's of triangles formed by secondary triangulation points in the regions of of prefectures of Iwate and Miyagi.

---

11) The approximate extent of the crustal blocks in the Kwantô district is comparable with that of the triangular area of the secondary triangulation points in the Sanriku district, which explain the reason for our comparing the frequency distribution of the magnitudes of their horizontal divergences.

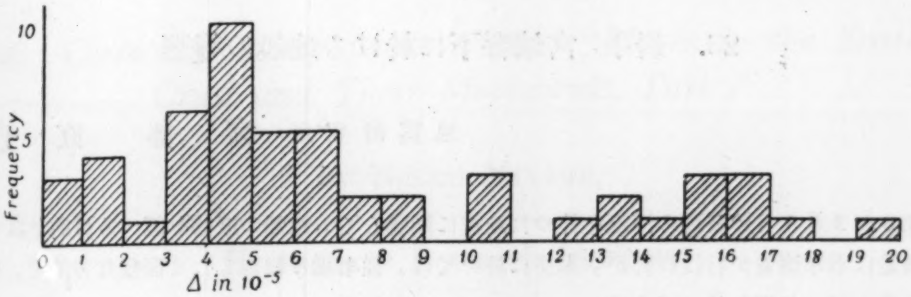

Fig. 19. Frequency distribution of Δ's of crustal blocks in the Kwantô district.

the level lines, block movements are less evident, may support the suggestion just mentioned.

Although block movements were less evident, crustal blocks exist none the less. As we have shown[12], in the quiescent stage following a considerable period of time after a destructive earthquake, or in regions where the earth's crust has not been disturbed by a destructive earthquake during the time interval between successive levelling surveys, as in the case of the Kwantô and the Tôkaidô districts, block movements are less evident, although carefull investigation confirmed the presence of crustal blocks.

7. Summary. In the present paper, the horizontal deformation of the earth's crust in Iwate and Miyagi prefectures are calculated by means of the data of horizontal displacements of the triangulation points distributed in the region under consideration. The geographical distribution or modes of the horizontal deformation are discussed in relation to the vertical movements measured along the level lines.

After comparing the frequency distribution of horizontal divergences in this region with that of the Kwantô district, it is suggested the earth's crust in this region was not disturbed much by the earthquake of March 3, 1933.

In conclusion, the writer wishes to express his sincere thanks to Professor Torahiko Terada for his valuable suggestions. His thanks are due also to Mr. S. Inomata for his assistance in calculating the horizontal deformations and in preparing the figures for this paper.

---

[12] N. MIYABE, *Bull. Earthq. Res. Inst.*, **11** (1933), 639.

23. 岩手，宮城縣下に於ける地殼の變形

地震研究所 宮部直巳

昭和8年3月3日の三陸の津浪を伴つた地震に關聯して，地殼の變動を調べる目的を以て，三角測量並に水準測量が行はれたが，本文に於いては，從來屢々報告したと同様な方法で，その結果の解析を行つた事を述べてある．

今，解析の結果として得られたものゝ中で一つの重要なことは，この地域に於ける地殼の變形の程度が，關東地方などと比較して小なることである．例へば divergence について見ても，その frequency maximum が三陸では $0\sim2{\cdot}3\times10^{-5}$ のところどころにあるのに，關東地方のは $4\sim5\times10^{-5}$ 乃至は 10×10^{-5} のところにある．

又，垂直變動について見ても，地塊運動があまり明瞭でない．

是等の事實は，この地方の地殼が地震ではあまり影響を受けなかつたのではないかとの考を示唆する．

24. *Correction to my paper entitled "Blocks in the Earth's Crust and Their Movements, Part I".*

By Naomi MIYABE,

Earthquake Research Institute.

(Received March 20, 1935.)

In discussing the order of magnitude of the correction term due to topographical slope that should be added to the calculated gradients of the vertical displacements, $\partial h/s$, in the paper entitled "Blocks in the Earth's Crust and their Movements (Part I)", the following approximate relation upon which the discussions are based was introduced:

$$\tan\phi \doteqdot \frac{\partial h}{s}\,.$$

Although it does not materially affect the conclusion deduced in the paper referred to, it has since occurred to me that, in the discussion on the order of magnitude of the correction term due to topographical slope, the same might have been treated more rigorously than has been done.

From Fig. 1 in the paper, we have

$$\tan\phi = \tan(\varphi' - \varphi)$$

$$= \frac{\tan\varphi' - \tan\varphi}{1 + \tan\varphi' \tan\varphi}\,,$$

where

$$\tan\varphi' = \frac{B'C'}{AC'} = \frac{h+\partial h}{s-\partial s}\,,$$

$$\tan\varphi = \frac{h}{s}\,,$$

$$AC = s\,,$$

and

$$AC' = AC - CC' = s - \partial s.$$

We then have

$$\mathrm{trn}\,\varphi' - \tan\varphi = \frac{h+\partial h}{s-\partial s} - \frac{h}{s} = \frac{s\partial h + h\partial s}{s(s-\partial s)}\,,$$

and

$$1 + \tan\varphi' \tan\varphi = \frac{s(s-\partial s) + h(h+\partial h)}{s(s-\partial s)}\,.$$

---

1) M. MIYABE, *Bull. Earthq. Res. Inst.*, **9** (1931), 256.

$$
\begin{aligned}
\therefore\qquad \tan\phi &= \frac{s\delta h + h\delta s}{ss + hh - s\delta s + h\delta h} \\
&= \frac{\delta s}{s}\left\{1+\left(\frac{h}{s}\right)^2 - \frac{\delta s}{s} + \left(\frac{h}{s}\right)\frac{\delta h}{s}\right\}^{-1} \\
&\quad + \frac{\delta sh}{ss}\left\{1+\left(\frac{h}{s}\right)^2 - \frac{\delta s}{s} + \left(\frac{h}{s}\right)\frac{\delta h}{s}\right\}^{-1} \\
&= \frac{\delta h}{s}\left\{1+\tan^2\varphi - \frac{\delta s}{s} + \frac{\delta h}{s}\cdot\tan\varphi\right\}^{-1} \\
&\quad + \frac{\delta s}{s}\tan\varphi\left\{1+\tan^2\varphi - \frac{\delta s}{s} + \frac{\delta h}{s}\cdot\tan\varphi\right\}^{-1}.
\end{aligned}
$$

The principal terms of correction due to topographical slope are therefore $-\left(\frac{\delta h}{s}\right)\tan^2\varphi$, $-\left(\frac{\delta h}{s}\right)^2\tan\varphi$, and $\frac{\delta s}{s}\tan\varphi$. Since the magnitude of $\frac{\delta s}{s}$ is of the same order as, or less than, that of $\frac{\delta h}{s}$, that is, $10^{-4}\sim 10^{-5}$, and seeing that in most actual cases $\tan\varphi$ is generally less than unity, that is, $\varphi \ll \frac{\pi}{4}$, the correction terms due to topographical slope may well be neglected, so that by putting

$$\tan\phi = \frac{\delta h}{s},$$

we shall not far from the truth.

24. "地塊さその運動"第1報の訂正

地震研究所　宮　部　直　巳

"地塊さその運動" 第１報中，傾斜のある場所での垂直變動の gradient に對するその傾斜の影響を論ずる場合に，初めから

$$\tan\phi \doteqdot \frac{\delta h}{s}$$

さ置いてしまつたが，これは次の樣に論じた方が正しく，前の考へ方には誤りがあるやうであるからこゝに訂正しておく．

卽ち，原論文の第１圖から

$$
\begin{aligned}
\tan\phi &= \tan(\varphi' - \varphi) \\
&= \frac{\tan\varphi' - \tan\varphi}{1+\tan\varphi'\tan\varphi}.
\end{aligned}
$$

そこで
$$\tan\varphi'=\frac{h+\delta h}{s-\delta s}\,, \qquad \tan\varphi=\frac{h}{s}$$

であるから，これを入れて結局

$$\tan\phi=\frac{\delta h}{s}\left\{1+\tan^2\varphi-\frac{\delta s}{s}+\frac{\delta h}{s}\tan\varphi\right\}^{-1}$$
$$+\frac{\delta s}{s}\tan\varphi\left\{1+\tan^2\varphi-\frac{\delta s}{s}+\frac{\delta h}{s}\tan\varphi\right\}^{-1}$$

となり，實際の場合の樣に φ が非常に小なる場合には $\tan\phi=\frac{\delta h}{s}$ と置いて差支ないことは前の結果と變りがない．

---

25. 博多灣沿岸水準高低測量*

九州帝國大學
農學部
鈴木清太郎
長澤武雄
中原孫吉

（昭和10年3月19日發表——昭和10年3月20日受理）

著者[1] の一人は嘗て博多灣沿岸の一部の海の中道の地變に就いて調査するところがあつた．その沿岸の浸蝕及增地より土地の沈降隆起を想像せしめたのであつたが，此を直接證明するには明治23年より31年にかけての陸地測量部の高低測量を更に繰返して行ふにあり，猶絕對水準高を知るには測量すべき地域の最寄の海岸に於て平均海面高を知る必要があつた．卽ち此の調査は2部から成立つわけで第1は博多灣の1年間の海面高の調査で第2は水準儀による高低測量である．

I．平均海面高の調査

福岡港內北港町の一地點（北緯 33°35′52″，東經 130°22′53″）に設置せる內務省下關土木出張所博多港修築事務所の自記檢潮器の記錄を同所の好意により借覽し潮位を1時間每に測定しその平均を計算したのが次の數字である．但し基準點は明治25年陸地測量部により東京灣中等潮位を福岡市箕子町水準點（標石番號 3193）に移行せる水準高を 1·0 m とせるを選擇したものである．

第 I 表

年次及期間	潮位 (m)
1931年10月1日～1932年3月31日	1·2295
1932年4月1日～1933年3月31日	1·2298
1933年4月1日～1934年3月11日	1·2154
平均	1·2245

1年間の潮位の變化は第1圖に示す通りで平均8月と2月との潮位差は 36 cm である．然し1年間の平均は極差 14 mm に止まつていて大差はない．此の年次の自記記

---

* 石本所員紹介

[1] 鈴木清太郎 科學 4 (1934)，66 及び 112.

錄より古きものは不幸にして調査することが出來なかつた.

然し幸にも大正6年（1917）の平均海面の調査が前記出張所に於て行はれてをりその數値1·22 m を示してゐる. 猶昭和4年（1929）の水路部によつて實測されたものは平均海面 1·39 m となつてゐる. 但し此の潮位觀測は昭和4年4月から同年8月まで春夏の季節に遂行されたのである. 然るに第1圖に示すように博多灣に於て潮位は春夏が秋冬よりも一般に高いから此の約半年間の平均海面は全1箇年間の平均値に比して高いに相違ない. 故に吾等の値と比較することは當を得ないと信ずる. 故に比較は主として內務省のものを用ふることにしたのである.

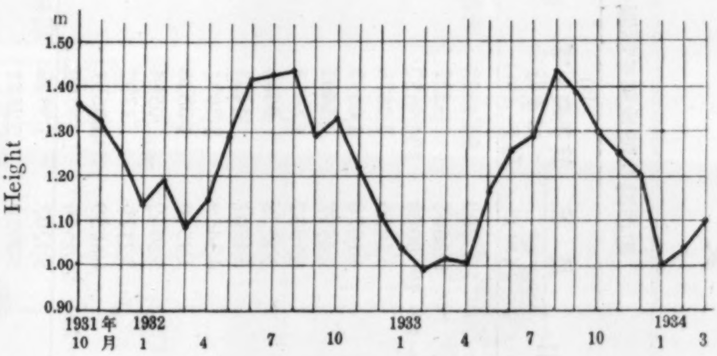

第1圖　博多灣潮位月變化

陸地測量部の實測は明治23年より31年にかけて行はれてゐるが此の時に海面高の實測がないから前記箕子町の水準點の零點と此の時の海面高の差は不明である.

然るに 1917 年の內務省下關土木出張所調査のと 1931 年より 1934 年に至る3箇年間の吾等の調査とを比較し cm までに止めて置けばその差は零である. 而して潮位に大なる變化があつたとは考へられぬから 15～16 年間に水準點の隆起も沈降もなかつたと思考するのが妥當である. 此の最近 16 箇年間に潮位に變化がないのであるから若し更に遡つて 10 年間に大なる地變がなかつたとすればその間に潮位差，從つて箕子町水準點の高さに變化があつたとは考へられない. 尤も明治 31 年（1898）8月10日に福岡縣糸島郡に地震があつた. 福岡測候所の報告によると最大水平動は 24 mm，最大上下動は 7 mm である. 震源地には地割及5坪位の陷落地があつた以外に顯著な斷層は發見されなかつたようである.

猶後節に說くように今回の博多灣沿岸高低測量に於て箕子町の水準點を中心として其の周圍の水準點3箇所の水準高と陸地測量部の水準高との差は殆ど一定でありその差の變化は 7 mm 以內であつて蓋然誤差に近い. 之によつて考ふると過去 30 有餘年間に潮位差，從つて水準高の變化が博多灣內福岡港附近に於て起つたとは考へ難い.

第 II 表

標石所在地					昭和9年測量				明治時代陸地測量部測量の				(A)—(B)	備考
番號又は地名	郡市	町村	大字	字	(A) 高さ (m)	蓋然誤差	月	日	眞高 (m)	(B) 箕子町を零させる時の高さ (m)	年	月		
濱崎山	糸島郡	今津村		濱崎山	94 5660	001	9	18～19	97 4900	94 4522	明治31		1138	△
3·199	〃	今宿村	谷	横町	3535	002	8	9	3 3605	3227	25	9	0308	B. M. の頭磨滅せり
殘島	早良郡	殘島村		殘島	192 1030	019	10	9～19	195 0000	191 9622	30		1408	
3·197	〃	山門村	下山門	生の松原	3 0890	003	8	10	6 1056	3 0678	25	9	0212	B. M. の頭磨滅甚し
3·196	福岡市	——	姪濱町	宮の前	8935	003	8	10	4 1070	1 0692	〃	〃	**1757**	
3·195	〃	——	庄	潟	**5785**	003	8	11	2 4897	**5481**	〃	〃	**0304**	
3·194	〃	——	西町	——	1 8670	001	8	12	4 9032	1 8654	〃	〃	0016	
3·193	〃	——	箕子町	——	0000	000	8	19	3 0378	0000	〃	〃	0000	
1·816	〃	——	橋口町	——	4380	003	8	20	3 4801	4423	23	7	**0043**	
1·815	〃	——	千代町	——	1 3120	004	8	21	4 3469	1 3091	〃	〃	0029	B. M. の頭磨滅せり
1·814	粕屋郡	箱崎町	箱崎	新開	**1 0760**	004	7	4	1 9540	**1 0838**	〃	6	0078	
1·813	〃	多々良村	多々良	西邊田	0610	003	7	5	3 0942	0564	〃	〃	0046	
1·812	〃	〃	松崎	前松原	1810	007	7	6	3 2170	1792	〃	〃	0018	
1·811	〃	香椎村	濱男	鎧坂	3 5910	001	7	7	6 6059	3 5681	〃	〃	0229	
長崎	〃	〃	〃	長崎	23 9890	004	7	8～11	26 9500	23 9122	29		0768	
1·810	〃	和白村	上和白	池尻	2 0050	004	7	8	5 0307	1 9929	昭和 7	10	0121	昭和7年に改埋せり
1·809	〃	〃	下和白	後口	2 2435	004	7	8	5 2919	2 2541	〃	〃	**0106**	
四十ケ浦	〃	〃		四十ケ浦	66 2120	001	9 12	25 3	69 1400	66 1022	明治30		1098	〃
1·808	〃	新宮村	上府	上府濱	4 3235	003	7	10	7 3430	4 3052	昭和 7		0183	
奈多	〃	和白村	——	奈多	18 8445	004	7	26～28	22 0800	19 0422	明治30		**1977**	昭和7年に改埋せり
高濱	〃	志賀島村	——	高濱	11 5060	008	7 12	29～30 1～2	14 4900	11 4522	〃		0538	
志賀島	〃	〃	——	志賀島	173 6755		7 8 11	31 4～6 29～30	176 2900	173 2522	〃		4233	

* 昭和9年測量の高さは箕子町 B. M. の高さを基準さし零させり. △ B. M. は Bench Mark の略.

註 標石番號の所に地名あるは三角點を示し番號あるは水準點なり.

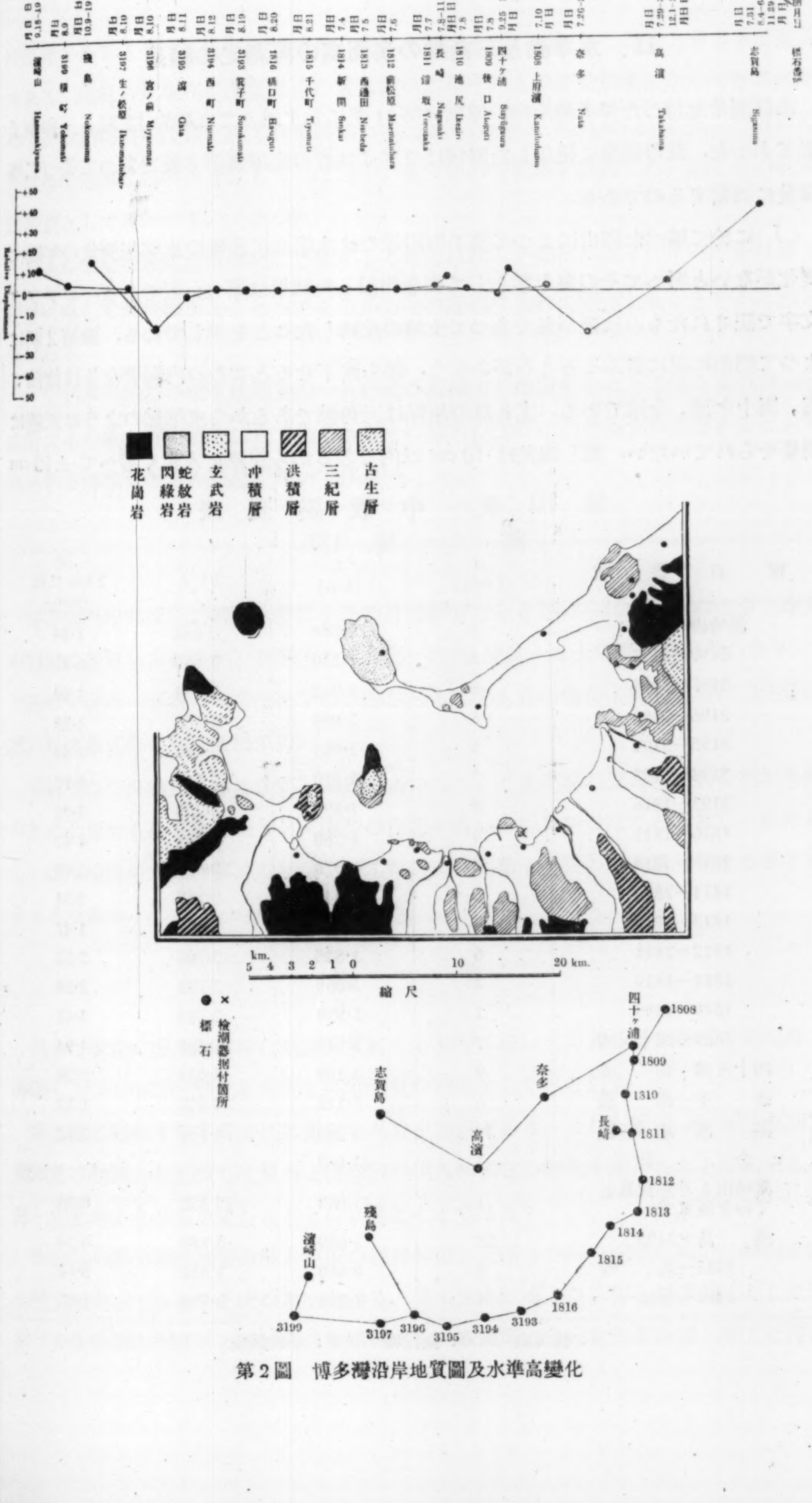
觀測月日
標石番號
濱崎山 Hamasakiyama 9.18-19 月日
3199 横町 Yokomati 8.9 月日
殘島 Nokonosima 10.9-19 月日
3197 生ノ松原 Ikinomatubara 8.10 月日
3196 宮ノ前 Miyanomae 8.10 月日
3195 潟 Gata 8.11 月日
3194 西町 Nisimati 8.12 月日
3193 箕子町 Sunokomati 8.19 月日
1816 橋口町 Hasiguti 8.20 月日
1815 千代町 Tiyomati 8.21 月日
1814 新開 Sinkai 7.4 月日
1813 西邊田 Nisibeda 7.5 月日
1812 前松原 Maematubara 7.6 月日
1811 鐙坂 Yorozaka 7.7 月日
長崎 Nagasaki 7.8-11 月日
1810 池尻 Ikesiri 7.8 月日
1809 後口 Atoguti 7.8 月日
四十ケ浦 Sayûgaura 9.25 月日 12.3 月日
1808 上府濱 Kamifuhama 7.10 月日
奈多 Nata 7.26-28 月日
高濱 Takahama 7.29-30 月日 12.1-2 月日
志賀島 Sigasima 7.31 8.4-6 11.29-30 月日
Relative Displacement
+50 +40 +30 +20 +10 0 -10 -20 -30 -40 -50
花崗岩
閃緑岩
蛇紋岩
玄武岩
沖積層
洪積層
三紀層
古生層
km. 5 4 3 2 1 0 10 20 km.
縮尺
● 標石
× 檢潮器据付箇所
四十ケ浦 1808
1809
1310
長崎 1811
1812
1813
1814
1815
1816
3193
3194
3195
3196
3197
3199
濱崎山
殘島
志賀島
高濱
奈多

第2圖 博多灣沿岸地質圖及水準高變化

II．水準點及三角點の海面高の再測定の結果

高低測量を行つた博多灣沿岸の地點は第 II 表に示す通りで水準點 15 點，三角點 7 點であつた．此の測量に使用した器械はツアイス社の水準儀第 2 號であつて先づ二等測量に該當するのである．

（I）に於て述べた理由によつて箕子町附近では水準高に前後の水準高測量の年間に變化がないと考へてその差を零として表を作製した結果は第 II 表である．ゴチック文字で記されたものは差が負であつて土地の沈降したことを示してゐる．猶第 2 圖によつて明かに眼に訴ふるところがあらう．卽ち沈下せるところの內顯著なるは姪濱，潟，四十ヶ浦，今津である．尤も此の地點は三角點であるから水準點のように正確に測量せられていない．然し誤差は 10 cm 以內であるから誤差を大きく考へて ±10 cm

第 III 表　中數誤差表

標石番號	d (mm)	L (km)	$2\sqrt{L}$	M 1 km に付 (mm)
濱崎山—3199	3	2·088	2·884	1·04
3199—3197	3	3·350	3·660	0·82
3197—3196	5	1·940	2·784	1·80
3196—3195	5	2·050	2·864	1·75
3195—3194	5	1·940	2·784	1·80
3194—3193	2	1·670	2·584	0·77
3193—1816	0	1·890	2·750	0·00
1816—1815	4	1·980	2·814	1·42
1815—1814	8	1·970	2·676	3·00
1814—1813	6	1·840	2·712	2·21
1813—1812	4	1·850	2·720	1·47
1812—1811	6	1·825	2·702	2·22
1811—1810	1	1·950	2·792	3·58
1810—1809	1	1·920	2·768	3·61
1809—四十ヶ浦	7	0·510	1·428	4·90
四十ヶ浦—奈多	9	4·100	4·054	2·20
奈多—高濱	6	5·110	4·522	1·33
高濱—志賀島	18	5·260	4·586	3·92
合計	1	43·063		
濱崎山より志賀島までのを通算す	1	43·063	13·122	0·08
殘島—3196	28	3·609	3·800	0·74
1811—長崎	6	0·680	1·650	3·64
1809—1808	4	1·870	3·736	1·07

d: 往復差　L: 全行程　M: 中數誤差

の誤差があるとしても志加島及殘島，今津方面は土地が隆起してゐると考ふるが妥當である．殘島の水準高の測量はその最も近い對岸小戸との高低測量によつてなされたのであるが特別の注意を以て日を異にして三度も行つた．志賀島の三角點の吾等の得た値は陸地測量部のと比較して 42·55 cm も少いので實測を繰返した．而しその結果は依然として同一のものであつた．

以上の土地の隆起は地學的に意義があると思はれるが姪濱の沈下はその一帶は第三紀層に屬して炭抗のあるところであるからその原因はそれに關連したことであるかと思はれる．

一方奈多三角點の沈下は著著の一人が他の根據より推定せることではあるが猶一面に於てその地一帶脆弱な砂丘であるからその標石の沈降は深き地學的意義あることでないかも知れぬと云ふ懸念がないではない．

III. 結　論

博多灣沿岸の福岡港附近一帶は土地の昇降顯著なるを認められぬがその西岸（姪濱の特別の事情あるを除き）及灣內の二大島—志賀・殘島—は土地隆起の模樣があり，又海の中道の一部奈多一帶は沈下の形跡がある．尤も此の場合は只1箇所の三角點に就いてであるから確言は出來ぬ．

只遺憾なのは興味ある地點が三角點であつたり，又水準點の標石は已むを得ぬ事情のため改埋せられてあつたり，又潮位の自記の古いのがなかつたことである．故に正しい之等地點の土地の昇降の結論を得んためには猶數十年後の再高低測量を必要とすることである．

附　言

以上の報告は博多灣沿岸の高低測量による地變に就いてであるが今新古の陸地圖，海圖によつて平面的變化を考究し高低測量の補足をしやうと思ふ．

第3圖は昭和9年7月4日に撮影した空中寫眞である．これと明治 30 年陸地測量部測量の地圖とを比較して見ると海岸線の出入に相當の變化を認めることが出來る．然し定量的にその差を定むることは容易なことではない．

今海の中道の最狹地帶白濱と中道の頸部和白，三苫との間の區域に就いて新古面積の變化を强いて求めると次の數字を得る．尤も玄海に面した沿岸と博多灣に面した沿岸とでは變遷に相違があるから之を區別するため鐵道より北方を玄海側，南方を博多

灣側と名付け各面積を測るに，

第 III 表

	玄海側 (km²)	博多灣側 (km²)
参謀本部による測量	3·776	2·908
寫眞測量	3·636	2·649
差引	0·140	0·259

何れも近年に於て土地が減少してゐる．博多灣側の方が多く浸蝕されてゐるのは豫想外である．と云ふわけは或る部分は成程玄海側より甚しい浸蝕を受けてゐるが或る部分は土地が增してゐるからである．只海岸線の引き方が二地圖に於て同一でないから以上の數字の信用程度は非常に稀薄であると附言して後の研究者の再試を待つものである．

此の研究は日本學術振興會の補助に依つて出來たものであり，空中寫眞は太刀洗飛行第四聯隊の援助を受け潮位記錄は內務省下關土木出張所の好意によつて調査することが出來た．謹んで感謝の意を表する次第である．猶高低測量は農學士渡邊治人君及黑瀨良照，吉村一男兩君の力を借りてなし得たことが多かつた，厚く御禮を申上ぐる．

---

25. *The Revision of Precise Levelling along the Coast of the Hakata Bay.*

By Seitarô SUZUKI, Takeo NAGAZAWA and Magokiti NAKAHARA,

Faculty of Agriculture, Kyûshû Imperial University.

Three years ago, a diver discovered some parts of sea-bottom with tree stumps embeded about 300 m off the coast from Mitoma to Nata, near the city of Hukuoka. One of the authors estimated the age of the catastrophe not older than about 620 years, supposing that the regressing rate of the coastal line caused by erosion in the past was as much 0·64 m per year as at the present time.

Some traces of subsidence along the coast were noticeable, so the present revision of levelling along the coast of the Hakata Bay, including the district in question, was attempted with the object to compare with that done by the party of the military land survey 1892~1897. The places levelled were 15, including both bench marks and triangulation points, and the result is shown in Table II and Fig. 2 together with that of the first survey. At the same time, the tide-gauge records new and old were examined and it was ascertained that the height of B. M. No. 3193 at Sunokomati near the Hukuoka Harbour where the tide-gauge was installed has not

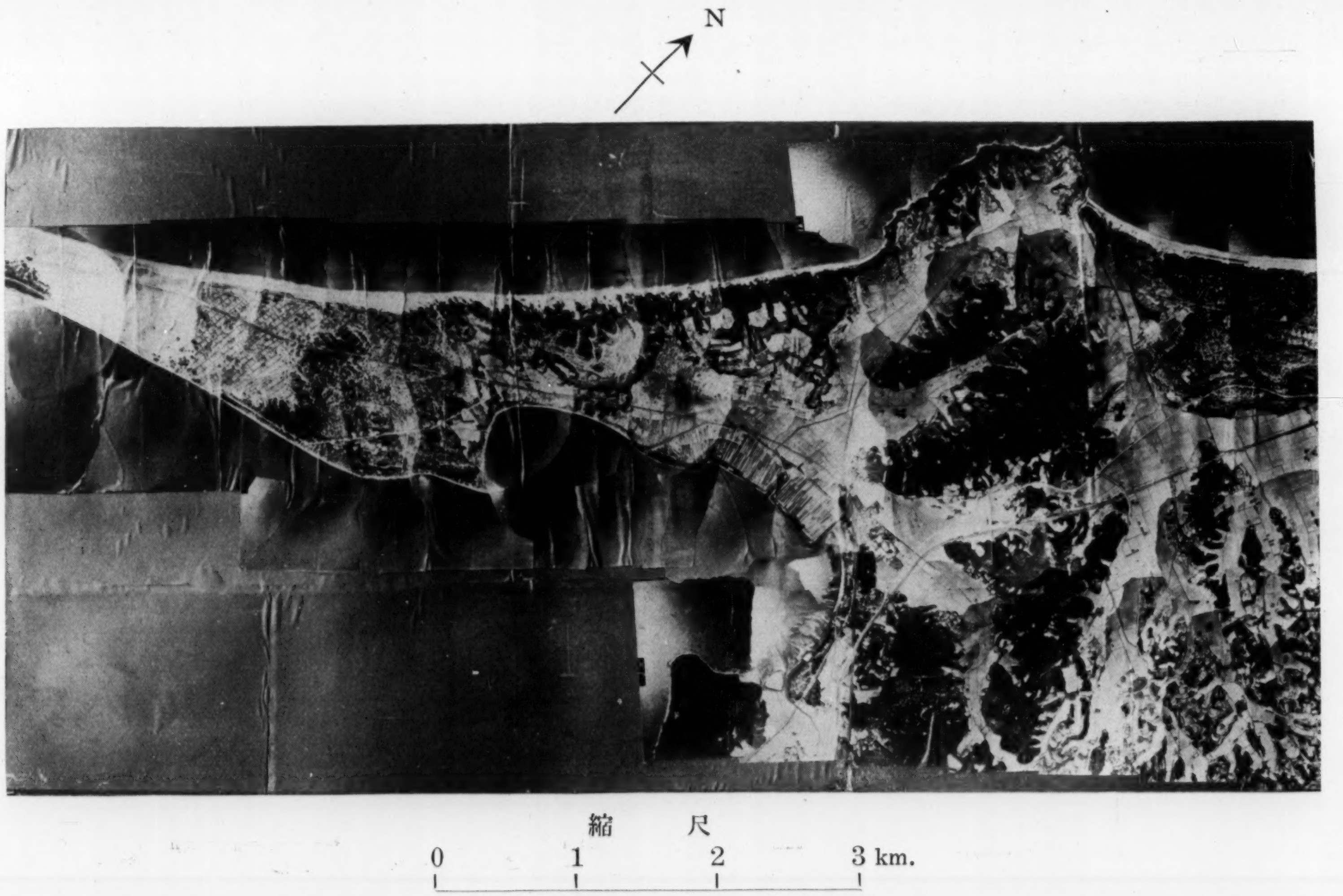

第３圖　空中寫眞による海の中道（撮影月日：昭和９年７月４日午後１時，撮影者：太刀洗飛行第４聯隊藤井少尉）

undergone any serious change during the last 16 years, 1917 to 1933, the height difference being less than 1 cm.

Therefore, B. M. No. 3139 was selected as a datum line and the relative vertical displacements of bench marks and triangulation points during about the last 37 years were calculated.

From this, it can be concluded that the western coastal parts of the Hakata Bay have been remarkably elevated, while some north-western parts a little subsided, the middle, however, not suffered any serious change.

26. 淺間火山中央火口丘の相對的上昇と火口底の昇降變化

地震研究所　水上　武

（昭和9年12月18日發表——昭和10年3月20日受理）

1. 緒　言

淺間火山は我が歴史時代に於て，屢々大噴火を繰返し，而も現今尚ほ，時を隔て屢々爆發を行ひ，或る時は火山灰を散布し，或る時は爆音を廣範圍に傳へる事に依り，本邦の數多の活火山中最も活動性に富む火山の一に數へられる．記錄に依つて認められる過去の噴火の中，1783年の天明大噴火は，最も猛烈な活動にして，150年後の今日尚，山腹或は山麓に見られる熔岩流，輕石の堆積に依り，その火山活動の大規模なりしを知る事が出來る．

淺間山に關する地球物理學方面の研究として，先づ第一に故大森博士[1] の研究を擧げねばならぬ．博士は 1911 年より 1920 年に至る約 10 年間の火山活動期に於ける種々の火山現象の觀測に努力されたが，他方火山彈，火山灰の飛行及び散布に關し，或は爆音の傳播に關して研究された．就中火口の西南，湯の平に地震計を設置して，長期間に亘つて，地震觀測を繼續され，その結果より數多の貴重な研究を發表されて居る．其の後，山本博士[2] は，重力偏差計を使用して，火山附近の重力異常に就いて研究された．

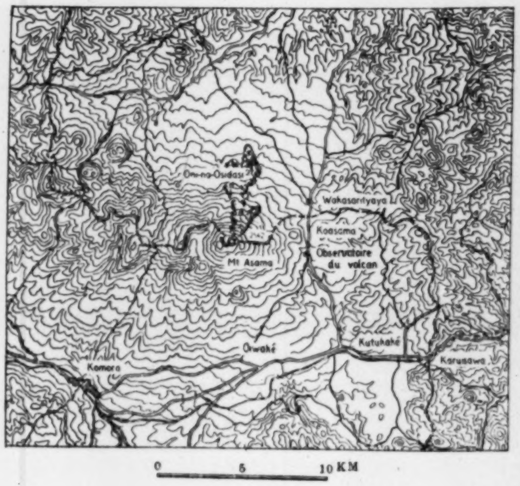
Oni-no-Osidasi
Wakasaritiyaya
Koasama
Observatoire du volcan
Mt Asama
Oiwaké
Kutukaké
Karuisawa
Komoro
0
5
10 KM

第1圖　淺間火山附近の地形圖
(Fig. 1.　La mappe proche du volcan d'Asama.)

---

[1] F. Omori, *Bull. Imp, Earthq Inv, Comm.*, **6** (1912—1914); **7** (1914—1919).

[2] 山本一清　測地學委員會報告　**7** (1921).

尙，最近凡そ 20 年間の爆發に就いての調査研究は八木3)，中條4)，石川5)，福富6)，梶間7) の諸氏及びその他多くの人々に依つて爲されて居る．又最近の研究として，高橋理學士8) は，1932 年以來淺間山の西南麓小諸に，シリカ傾斜計を設置し，地表傾斜の觀測中であるが，1932 年の爆發に際し地表傾斜と爆發の前と後とに於ては，著しき傾斜變化のある事を指摘された．

2. 火口底の昇降變化

淺間火口の深さは，1886 年 H. S. Palmer が始めて測定して以來今日迄凡そ 30 回の測定がある．然しながら，此等の測定と次の測定との期間が，火口の如き急激な變動が繰返される所に對しては，餘りに長過ぎるのであるが，その上，此等の測定は，多數の人々に依つて行はれた爲め，同一地點の深さを示すものではない．從つて此等の結果より直ちに火口底昇降に就て詳細な議論を進める事は出來ない．卽ち，火口の深さは，火口壁上より火口底に至る垂直距離を指すのであるが，東側火口壁と北壁火口壁との高さは，80 m も相違し，而も火口底は勿論平坦ではない．從つて，測定値が正しいとしても，測定地點に依つて 100 m 以上も異なる深さを與へるのである．然しながら，以上の深さの測定を吟味して見ると，1886 年より今日に至る 40 年間に，100 m 以上に達する昇降變化が數回行はれた事は大體認める事が出來るのである．

尙，第2圖は 1910 年 10 月 7 日，火口の南側より，火口內を撮したものであり，第3圖及び第 4~5 圖は，1934 年 10 月 14 日及び 11 月 4 日，同じく南側より火口內を撮つたものである．卽ち 23 年間の時代を異にする此等の寫眞から，火口を比較して見ても，一見して著しい相違が認められるのであるが，特に注意される事は，現在の火口は 1910 年 10 月に比して，その深さを增した事である．後に述べる如く，1934 年 11 月に於ける深さは，南側火口壁より凡そ 180 m なるに對し，1912 年故山崎博士9) は 80 m と測定されて居る．從つてこの山崎博士の測定地點が北側の最低火口壁を選ばれたとしても，現火口底は 1912 年 10 月に比して，70~80 m の上昇を示して居る事になる．

以上に依り，火口底が著しい昇降運動を爲す事は明かであるが，この變化の詳細を

---

3) 八木貞助　地學雜誌　**41** (1929), 193, 744; **42** (1930), 95, 181; **45** (1933), 478, 552, 599.

4) 中條正勝　地學雜誌　**41** (1929); 744, **42** (1930), 95.

5) 石川高見　驗震時報　**4** (1931), 161.
Geoph. Mag., **6** (1932), 193.

6) 福富孝治　地震　**1** (1929), 808, 852; **2** (1930), 64.

7) 梶間百樹　驗震時報　**3** (1929), 400; **4** (1631), 145.

8) 高橋龍太郞　地震研究所彙報　**11** (1933), 1.

9) 山崎直方　震災豫防調査會報告　**73** (1910), 17.

知る爲め，1934 年 7 月より 10 月に至る 4 ケ月に亘り深度測定を行つた．測定方法はウイルトの經緯儀を用ひ，三角測量に依つた．卽ち第 6 圖に示す如く，南側火口緣の比較的平旦な地點に，80 m の基線 AB を採り，AB の長さは布卷尺にて，7 月以來數回測定し，布卷尺の精度の範圍內で充分正確に測定した．又火口底の視準點としては，火口底熔岩の略々中央に在る赫熱熔岩露出部の中央に近き熔岩の一點を用ひた（第 4~5 圖を見よ）．この赫熱熔岩露出部は 1934 年 7 月に於ては東西約 7 m，南北約 10 m の略々楕圓形をなして居たが 11 月に於てはその直經約 1 m 擴大した．斯して視準點に選べる C 點附近は火口底の略々中央なるを以て火口底昇降運動の最も著しい部分と考へられる．

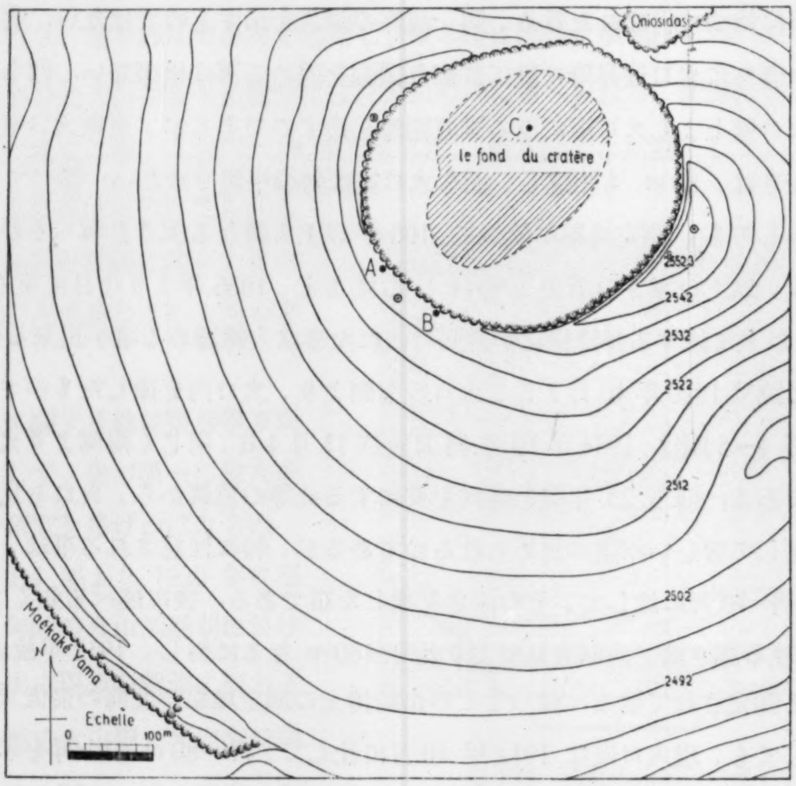
Oniosidasi
C
le fond du cratère
A
B
2552.3
2542
2532
2522
2512
2502
2492
Maekaké Yama
N
Echelle
0
100m

第 6 圖　火口附近の地形圖（昭和 9 年 10 月測量）
◉；昭和 9 年 11 月設置された一等水準點を示す．

Fig. 6. Carte topographique autour du cratère (faite à octobre 1934).

尙，測定は第 6~7 圖に示せる，A，B に於て視準點 C に對する垂直角 θ_1，θ_2，及び水平角 φ_1，φ_2 並びに三角點 A，B の高低差を測つた．卽ち第 7 圖に於ける三角形 A C′B′ 及び A′C″ B とは全く等しき故に，以上，θ_1，θ_2，φ_1 及び φ_2 の測角を行へば A，B，と C との水平距離，並びに垂直距離が求められる．

第 7 圖 に 於 て

A, C の水平距離

$$AC' = A'C'' = AB' \sin\varphi_1 \operatorname{cosec}(\varphi_1 + \varphi_2),$$

B, C の水平距離

$$BC'' = B'C' = AB' \sin\varphi_2 \operatorname{cosec}(\varphi_1 + \varphi_2),$$

A, C の垂直距離

$$C'C = AB' \sin\varphi_1 \operatorname{cosec}(\varphi_1 + \varphi_2) \tan\theta_1,$$

B, C の垂直距離

$$CC'' = AB' \sin\varphi_2 \operatorname{cosec}(\varphi_1 + \varphi_2) \tan\theta_2,$$

$$AB' = A'B = 80 \text{ m}.$$

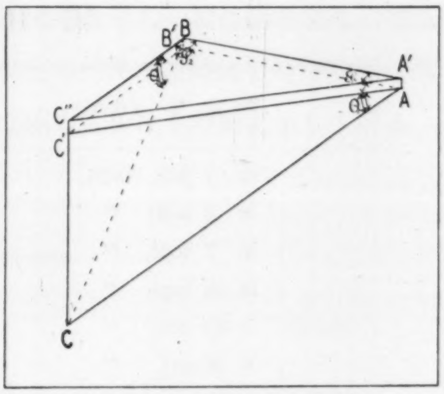

第 7 圖

Fig. 7.

次に 10 月 13 日の測量に依る測定値の例を示す事にする.

第 I 表 (Tableau I)

θ_1	θ_2	φ_1	φ_2
38° 21′ 30″	38° 14′ 20″	83° 29′ 50″	77° 1′ 15″
38° 22′ 48″	38° 13′ 55″	83° 30′ 05″	77° 0′ 03″
38° 20′ 30″	38° 14′ 13″	83° 29′ 20″	76° 59′ 35″
38° 22′ 18″	38° 13′ 50″	83° 30′ 10″	76° 58′ 50″
38° 22′ 54″	38° 14′ 32″	83° 30′ 03″	77° 3′ 20″
moyen 38° 22′ 00″	38° 14′ 10″	83° 29′ 59″	77° 0′ 52″

この結果から

$$AC' = 233{\cdot}697 \text{ m},$$

$$BC'' = 238{\cdot}287 \text{ m},$$

$CC' = 185{\cdot}00$ m となる.

この最後の値に經緯儀の三脚臺の高さ（1·30 m）の補正をすると結局 實際の A と C との垂直距離は 183·70 m となり，B と C との垂直距離は 185·51 m となる. この差 1·81 m は直接 A，B の高低測量に依る値と一致した.

毎週 1 回の測定の內，噴煙多量その他の障碍に依り結局，各觀測に於て，誤差 30 cm 以內の測定値は次に示すものである.

第 II 表 (Tableau II)

測定日 (date)	A と C との垂直距離 (distance verticale entre A et C)
le 7 juil. 1934	160·00 m
le 8 août 〃	162·83 〃
le 7 sept. 〃	183·84 〃
le 28 sept. 〃	184·53 〃
le 13 oct. 〃	183·70 〃
le 26 oct. 〃	179·88 〃

第 II 表に示す如く，火口底は7月より 9 月下旬に至る迄に 25 m の沈降を示し，10月に於て約 5 m の上昇を示した.

然るに，他方，火山は 1932 年の爆發以來，顯著な爆發 1 回も無く，且つ火山觀測所に於ては 1934 年を通じて，火山附近に震央を有する地震として，僅に 1 回の微震を觀測したに過ぎない. 斯の如き火山の不活動の時期に，上記の如き火口内熔岩の著しい昇降變化の見られた事は注目すべき事實である.

次に，1934 年以來，觀測された二，三の火山現象に關して述べる事にする.

火口底熔岩の割目又は火口壁より常に亞硫酸瓦斯及び水蒸氣を主成分とする噴煙を放出して居るが，この噴煙は間斷なく一様に噴出するのではなく，一定の時間的間隔をおいて噴出して居る. 7 月，8 月，9 月に於ては，この間隔は凡そ 5 分で，各回の噴煙量も略々一定と認められたが 10 月初め頃より噴出間隔の大となると共に，噴出量にも變化を認められるに至つたが，11 月になつて噴煙間隔が凡そ 60 分になつた. 而も各回の噴出の勢力も次第に増大し，時には，火山礫を吹き上げるに至つた.

第 III 表 (Tableau III)

測定日 (date)	火口底昇降變化 (Changement de la profondeur du fond de cratère) Δh	測定間隔 (l'intervalle de chaque jalonnement) Δt	昇降速度 $\left(\frac{\Delta h}{\Delta t}\right)$	噴煙間隔 (l'intervalle de fumée poussée de lave dans le cratère)
le 7 juil. 1934				5 min.
	− 2·8 m	32 jours	− 8·7cm/jour	
le 8 août. 〃				5 〃
	−21·0 〃	30 〃	− 70·0 〃	
le 7 sept. 〃				5 〃
	− 0·7 〃	21 〃	− 3·3 〃	
le 28 sept. 〃				20 〃
	+ 0·8 〃	15 〃	+ 5·3 〃	
le 13 oct. 〃				25 〃
	+ 4·8 〃	13 〃	+ 3·7 〃	
le 26 oct. 〃				60 〃

(+) は 上昇 (élévation), (−) は沈降 (dépression) を示す.

第 III 表にこの噴出間隔並びに第 II 表に示せる火口底の深さの相繼ぐ深度變化

(dh)，相繼ぐ測定の間隔，及び火口底昇降運動の速度を表示し，更に第8圖に，噴煙間隔と昇降速度とを圖示した．これを見ると，火口底の沈降する時は，噴煙間隔は何等變化を示さざるに，上昇速度が大になると噴煙間隔の大になる傾向を示して居る．

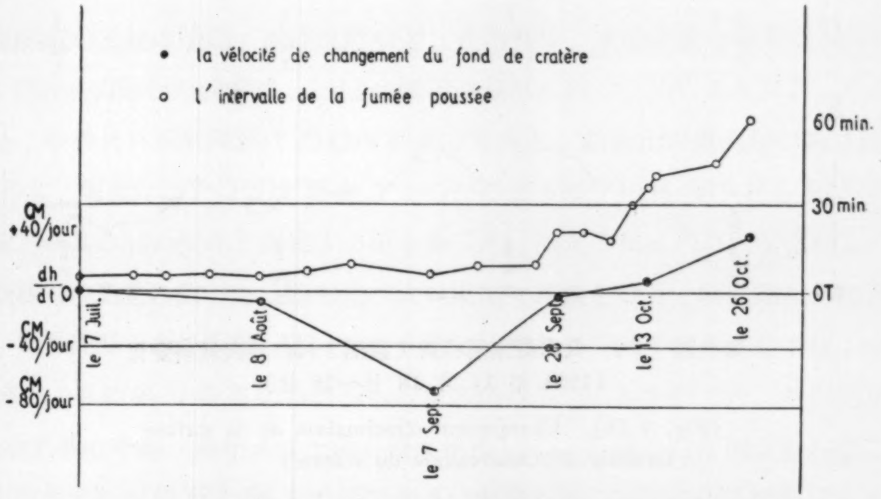

第8圖 火口底昇降速度と火口內熔岩面より噴出する噴煙の間隔

(Fig. 8. Vélocité de changement du fond de cratère et l'intervalle de la fumée poussée du cratère.)

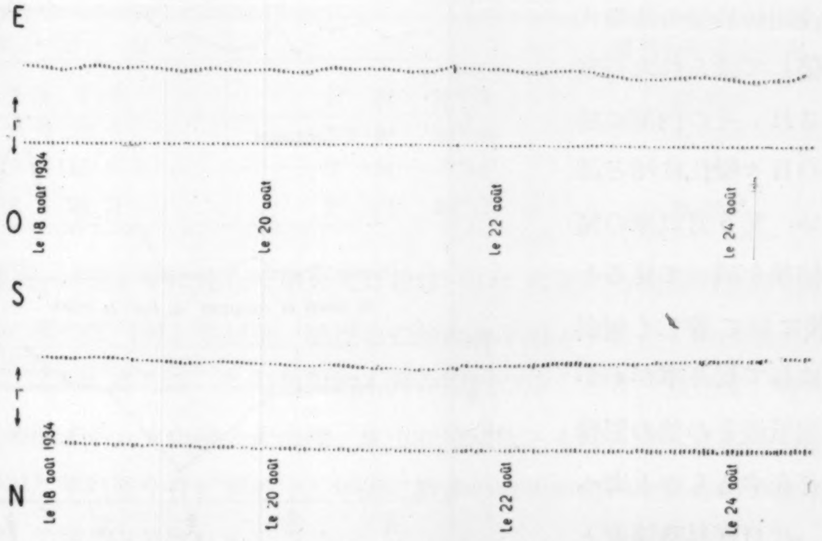

第9圖（イ） 火山觀測所に於て觀測された地表傾斜變化
（1934 年 8 月 18 日～24 日）

(Fig. 9 (a). Changement d'inclinaison de la surface terrestre observée à l'Observatoire du volcan.)

第9圖（イ）及び（ロ）は夫々8月18日より25日に至る，及び11月18日より25日

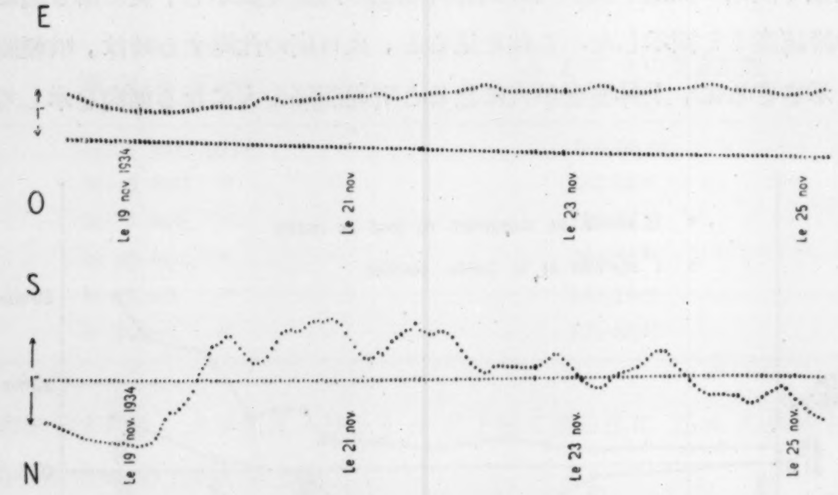

第 9 圖（ロ） 火山觀測所に於て觀測された地表傾斜變化
（1934 年 11 月 18 日～25 日）

（Fig. 9 (b). Changement d'inclinaison de la surface terrestre à l'Observatoire du volcan.）

に至る火山觀測所に於て觀測された傾斜計記象である．前者に於ては地表傾斜は殆ど認められないが後者では可成り傾斜變化を示して居る．傾斜計は小淺間熔岩卽ち集塊火山岩を穿鑿して造られた石室中に設置され，その內部に於ては溫度の日々變化は殆ど認められない．又 5 月以來の傾斜觀測の結果を調べて見ると 10 月以後に於て著しく傾斜變化が現はれて居る事がわかつた．勿論氣溫その他の影響も多少は存在するものと考へられるが，火口底昇降速度との間には，可成り平行の關係の存するもの丶如くである．傾斜變化に關しては，小諸に於ける觀測からも略々同樣な事が認められた．

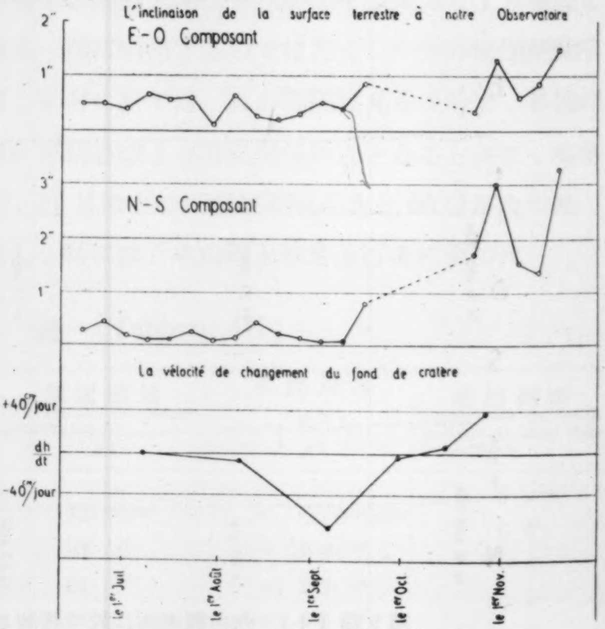

第 10 圖 地表傾斜變化さ火口底昇降速度

（Fig. 10. L'inclinaison de la surface terrestre et la vélocité de changement de la profondeur du cratère.）

以上此等の現象に就ての說明は，今後の種々な觀測を俟つて然る後に明らかになるであう．從つてこゝでは單に事實を述べる事に止める事にする．

3. 中央火口丘の相對的上昇

活火山附近の土地の隆起，或は沈降の著しき事實は，水準測量の結果明らかにされて居る．淺間火山附近の測量は，1912年陸地測量部に依つて施行されたが，その結果に依ると，中央火口丘最高點は 2542m の高さを有し，前掛山の最高點の高さは 2521m であつて，兩者の高さの差は 21m であつた．然るに，1934 年9月，10月に4回の測量を行ひ其の間の變化を測定する事を企てた．測量方法は火口底深度測定に於ける と同様三角測量に依つた．卽ち先づ火口東側に基線を取り，兩最高以外に數點を採つて，兩最高點の水平距離 722·19m を測定し得たので其の後の測定では，中央火口丘最高點より前掛山最高點の標石への垂直角の測定のみを行つた．その結果を第IV表に示す事にする．表中 θ は上述の垂直角にして，最後の行は測量器の臺の補正を施した兩最高點の標石の高さの差である．勿論空氣の屈折に依る誤差はあるが，兩地點は 1000m に足らない距離であり，cm の桁を問題にしないので考慮する必要を認めない．

第 IV 表 (Tableau IV)

測　定　日	θ	兩標石の高さの差
9月 7日	2° 31′ 28″·0	31·20 m
9月 28日	2° 31′ 38″·0	31·26 ″
10月 13日	2° 31′ 9″·6	31·22 ″
10月 26日	2° 31′ 46″·2	31·30 ″

測量の結果，1912 年に比して中央火口丘は 10m に達する相對的上昇を示して居るのである．從つて 1912 年以來，前掛山の標高を不動とすると，現淺間山の最高點の標高は 2252·3m になる．この相對的上昇の原因の少くとも一部分は，噴火に依つて火口丘に堆積する，火山彈，火山礫，火山灰等に依るものと考へる事は至當であらう．而も 1912 年以後今日に至る 22 年間に數多の噴火が起つて居るので堆積物も可成多量に達して居ると思はれる．

尙，前に示した，第6圖は 1934 年 10 月より 11 月に至る期間に施行した平板測量に依る地形圖であつて，この測量に於ても，中央火口丘は約 10m の相對的上昇を爲した事が認められ．圖中等高線は中央火口丘の最高點の標高を 2552·3m として，5m 每に等高線を引いてある．

中央火口丘の相對的上昇に關して，嘗つて八木貞助氏10)に依つて論ぜられた事を一言斷つて置きたい．

4. 1934年11月13日の小爆發

10月以後に於て，火口底の上昇，噴煙の異常，並びに地表傾斜の增大等に依り，多少火山の活動を示すに至つた．11月9日及び10日，火口に於て觀測せる所に依ると，噴煙の量は極めて少く，その噴出の間隔約60分で，噴出に際して猛烈なる音響を伴ひ，時々に直經10～20cmの火山礫が約50m眞上に噴き上げられるのを見た．今火山礫が放出されて後は空氣抵抗を考へず重力のみが働くとすればその初速度は毎秒約50mとなる．一般に，1932年等に於ける淺間の爆發に際して放出される火山彈は毎秒200～400mの初速度を有すると計算されて居るから，この場合は大爆發の際に於けるものに比べて1/4～1/8程度の初速度である．

尙又，火山觀測所に於て，9月頃迄何等鳴動が聞かれなかつたが，10月以後に於て，時々火口方向より鳴動が聞かれた．

11月初め頃より，噴煙の量，時には多く，時には少く，不規則であつたが，11月12日正午頃多量の噴煙放出して居たが午後3時頃より褐色濃厚なる噴煙が，極めて少量噴出するのみとなつた．然るに，翌13日午前8時13分山麓地方に達する音響を發して爆發し，同時に黑煙を噴出したが，その時多少の火山灰が火口附近に散布した樣である．この小爆發に依り，火口の略々中央を南北に張られてあつた直徑3mmのワイヤー・ロープは切斷された．

然るに爆發時並びにその前後を通じて，火山觀測所に於て，地震或は微動は觀測されなかつた．又1934年6月以來，火口を距る東方約6000mの地點に湧出する千ヶ瀧溫泉の溫度は，32·2°で數ヶ月に亘つて觀測したが．變化は，0·2°C以內で，この爆發前後に於ても何等の變化を認められなかつた．

兎に角，1932年以來全く平穩なりし淺間火山も漸く活動の兆を示すに至つた．

5. 結　　語

1934年7月より10月迄の4ヶ月に亘つて，三角測量に依り火口底昇降運動を測定した結果，20m以上に達する昇降が認められた．昇降速度と，火山觀測所，並びに小諸に於て觀測された傾斜變化との間に，多少の關係の存在する事を認めた．

現中央火口丘と前掛山の最高點の標高差は1934年10月及び11月の數回の測定の

---

10)　八木貞助：地學雜誌 **45** (1933), 537.

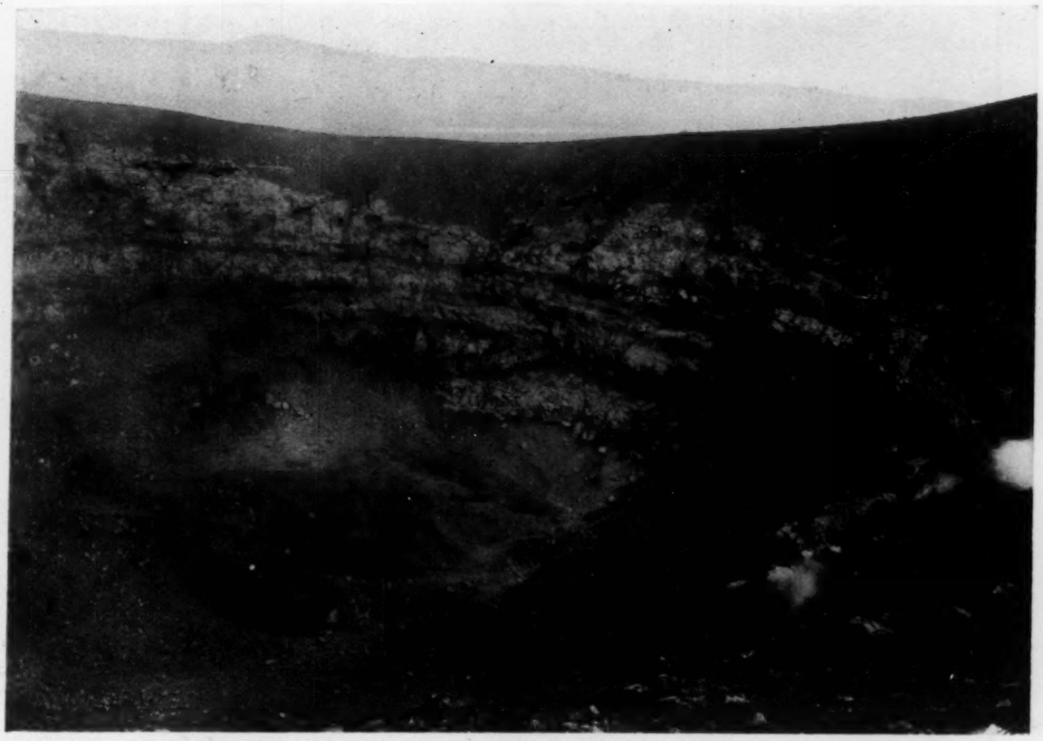

第2圖　明治43年10月7日，南東壁より北方に向つて火口内を撮れるもの(大森博士撮影).

(Fig. 2. La photographie du cratère du 7 octobre 1910, prise par le Prof. Omori.)

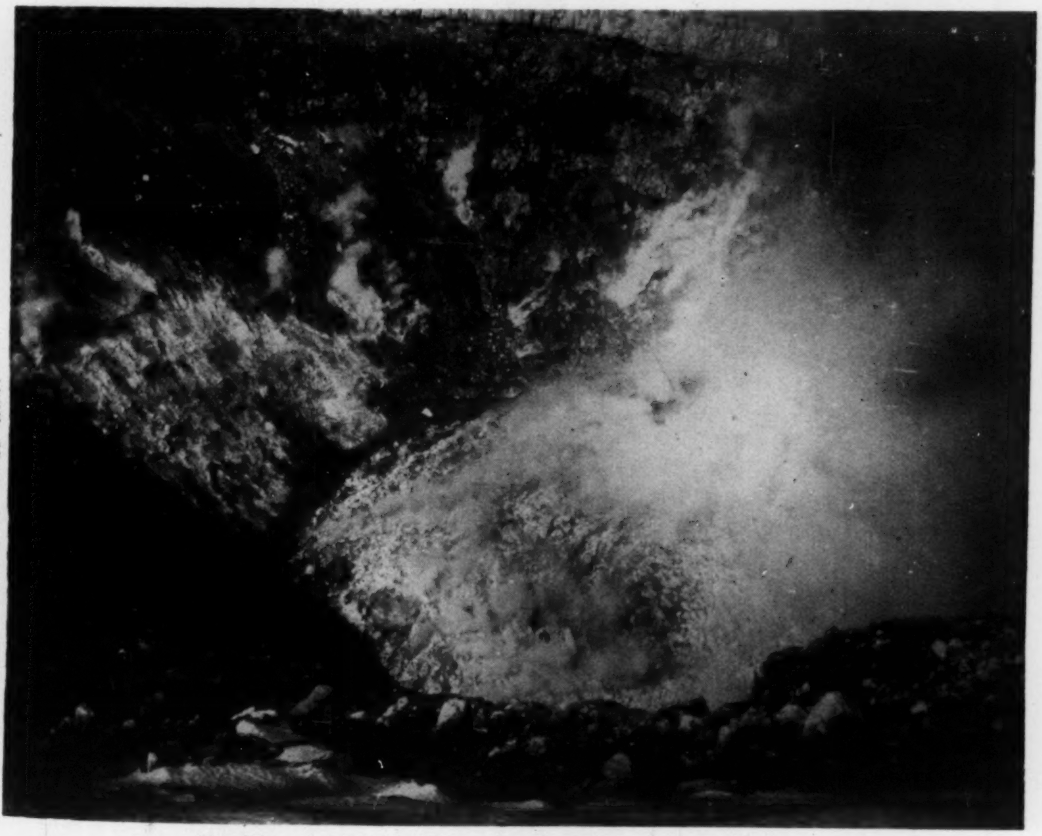

第3圖　昭和9年10月14日，火口壁上西南より寫す.

(Fig. 3. La photographie du fond de cratère prise au 14 octobre 1934.)

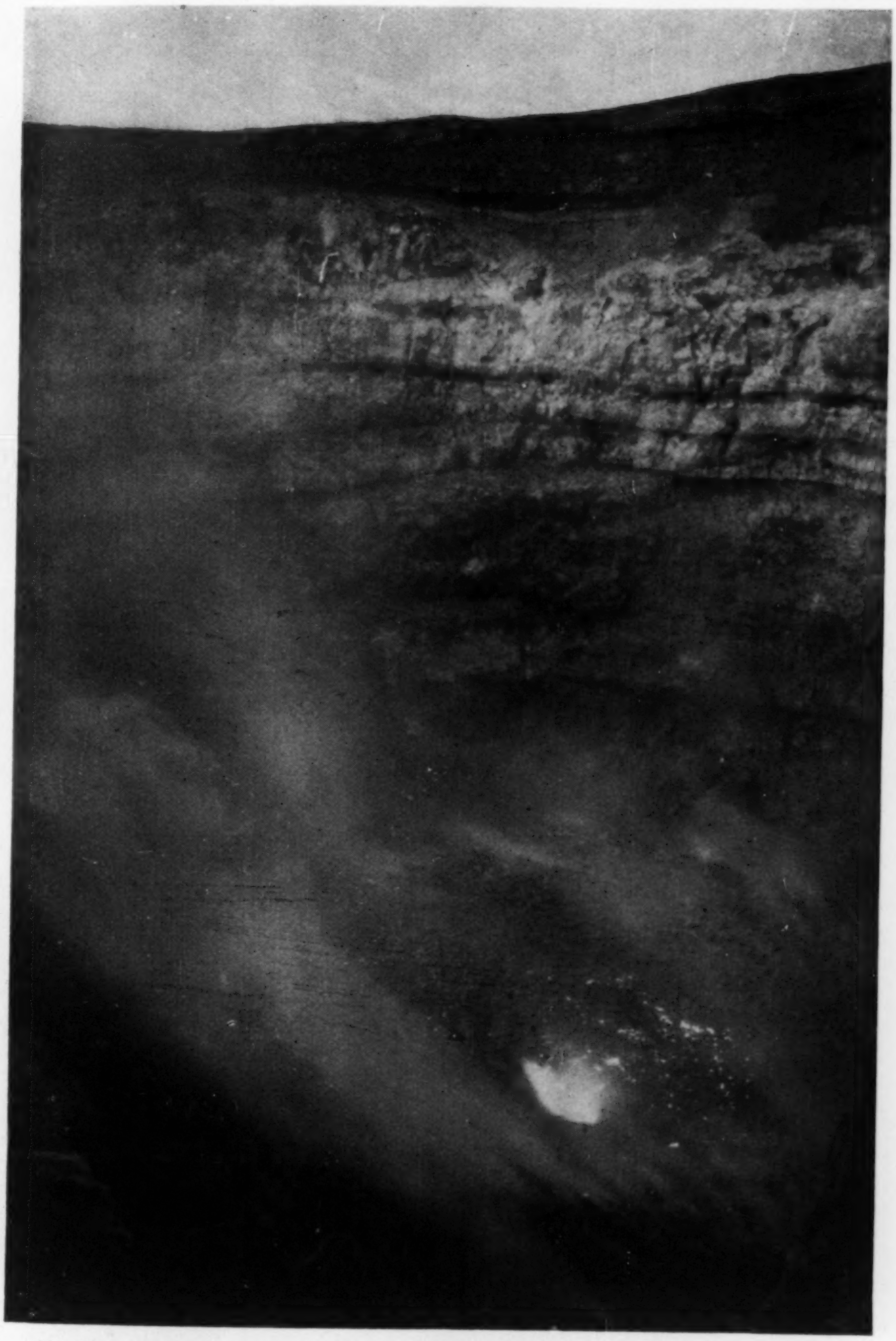

第4圖　昭和9年11月4日午後5時，南方より北方に向つて撮れるもの．火口底略中央白色に見へるは赫熱熔岩の露出せる部分にして火口の深度測定の視準點とせり．

(Fig. 4. La photographie du cratère prise au 4 novembre 1934.)

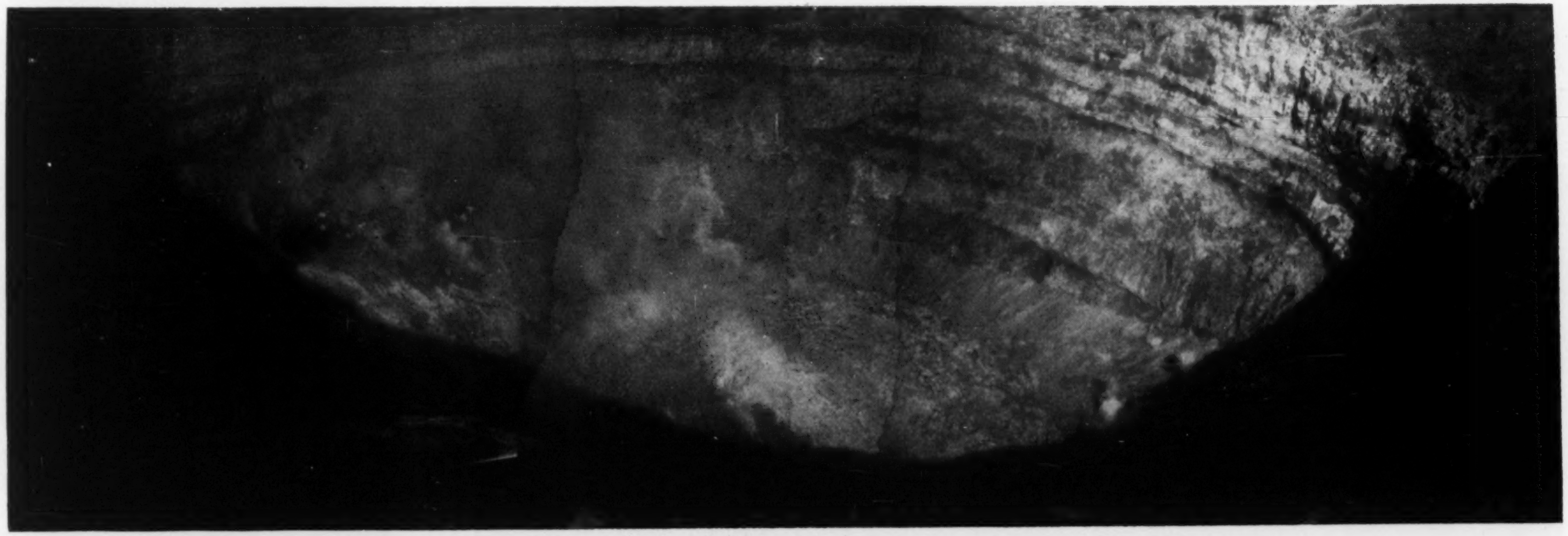

第5圖 昭和9年11月4日午後1時，南方火口壁上より火口內を撮れるもの．火口底の略中央黒色に見へる部分は赫熱熔岩の露出せる部分．

(Fig. 5. La photographie du fond de cratère prise au 4 novembre 1934.)

結果 31·3 m であつて，1912 年の標高差に比して，中央火口丘は 10·3 m の相對的上昇を示して居る事が認められた.

筆を擱くに當り，種々御示教を賜つた石本教授に深く感謝の意を表すると共に火口附近の平板測量の御援助に與つた岩下圓氏に深謝の意を表する次第である.

---

26. *Changements relatifs de l'hauteur du cône central du volcan d'Asama et la profondeur de lave dans son cratère*

par Takeshi MINAKAMI,

Institut de Recherches sur les Tremblements de terre.

1. D'après les résulats du nivellement de précision, appliqué aux certaines régiones du Japon, nous constatons que la croûte terretre déforme dans la composante verticale, c'est-à-dire, elle s'agit quelquefois l'exhaussement quelquefois la dépression. En'outre, il est aussi evident que le changemant topographique de ce genre apparaît remarquablement à l'ocassion d'une éruption volcanique surtout au pied de volcan.

2. Quant au volcan d'Asama, d'après des données imformées depuis 1886, nous pouvons constater, que la lave dans le cratère s'a enfoncé ou s'a élèvé plus que 100 mètres. De plus, nous pouvons constater, d'après les photographies montrées aux Fig. 2, 3, 4 et 5, que il a eu les changements remarquables de la profondeur du cratère.

Nous avons exécuté le jalonnement pour savoir le changemant de la profonfondeur du cratère précisement. Nous avons adopté la méthode de triangulation. (voir Fig. 6 et 7)

D'après les résultats de ce jalonnement, nous pouvons constater que la lave au fund du cratère s'a enfoncé progressivement depuis juillet jusqu' á septembre, mais partir de la première decade d'octobre, elle a comemencé s'élever.

D'ailleurs, il nous semble qu'il y a certaine relation entre la vélocité du changement de la profondeur du cratère et l'inclinaison de la surface terrestre observée à l'Observatoire de volcan (au pied d'Est de volcan).

3. Les résultats du jalonnement de 1912 s'a manifesté que l'hauteur du cône central de ce volcan a été 2542 m au-dessus du niveau de la mer, et celle du sommet de Maékaké-Yama, cône central ancien, a montré 2521 m.

Depuis juillet 1934, nous avons quelquefois exécuté le jalonnement pour élucider le changement relatif entre ces deux sommets du cône central et de Maékaké-Yama. D'après ces résultats, nous avons constaté que le cône central s'a manifesté l'exhaussement relatif de 10 mètres en comparant à l'hauteur de 1912.

27. *Seismometrische Untersuchungen des Erdbebens vom 2. März 1933.*

II. Analyse der in Californien beobachteten Oberflächenwellen.

Von Takeo MATUZAWA,

Institut für Erdbebenforschung.

(Vorgelegt 19. Feb. 1935.—Eingegangen 20. März, 1935.)

1. Elastizitätstheoretisch sind die Oberflächenwellen bisher ziemlich eingehend untersucht worden. Im Gegenteil sind Untersuchungen der beobachteten Erscheinung ganz mangelhaft, es sei denn dass es manche statistische Untersuchungen über Perioden und Fortpflanzungsgeschwindigkeit gibt.

Gelegentlich des oben genannten Japanbebens lieferten uns Stationen in Californien ihre schöne Aufzeichnungen, womit wir viele Eigenschaften der Oberflächenwellen experimentell ziemlich genau feststellen können haben. Fig. 1 zeigt die Verteilung der Stationen.

Dafür möchte ich hier nochmals Herrn H. O. Wood in Pasadena und Herrn Dr. P. Byerly danken.

2. Die Seismogramme der oben genannten Stationen zeigten meistens ganz schöne sinusartig andauernde Wellenzüge, die als Oberflächenwellen angedeutet werden können. (Fig. 2a, 2b, 2c.)

Instrumente für horizontale Komponente sind für alle Stationen von gleicher Konstruktion und zwar Wood-Anderson'sche kurzperiodische Seismographen mit Konstanten $V=2800$, $T=0{\cdot}8$ Sek. und $h=0{\cdot}8$. Vertikale Komponente ist vom Benioff'schen Instrument[1] mit Moll-micro-galvanometer gezeichnet.

Der erste deutliche Einsatz des Wellenzuges ist z. B. in der N–S Komponente der Pasadena Aufzeichnung (kurz vor der 0 Marke in Fig. 2b.) klar ersichtlich. Die entsprechende Phase in Santa Barbara, Mt. Hamilton, und Berkeley liegt ausserhalb der Figur. Die durchschnittliche Fortpflanzungsgeschwindigkeit, nämlich die Herdentfernung (74°·54) dividiert durch die Laufzeit (31 m 50 s ca.), ergibt sich zu ca. 4·4 Km/Sek. Die Periode dieser Phase ist ungefähr 19 Sek. Das entspricht der Dispersionskurve meiner früheren Arbeit.[2]

---

[1] H. BENIOFF, *Bull. Seism. Soc. Amer.*, **22** (1932), 155~169.
Vergrösserung ist ungefähr 2 mal A-Kerve in Fig. 8 derselben Mitteilung.

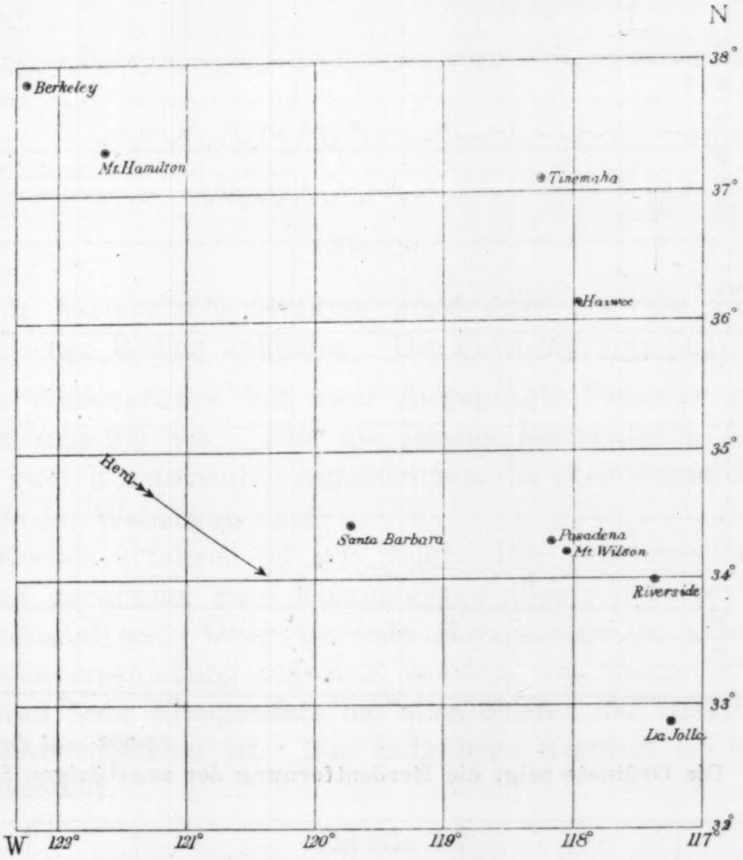

Fig. 1. Der Pfeil fliegt in der Richtung vom Herd nach aussen.

Ca. 3 Min. nach dem ersten Einsatz ist wieder ein ungefähr 2 Minuten gleichmässig andauernder Wellenzug auffällig eingetreten. Die Fortpflanzung dieses Wellenzuges ist in Fig. 2a, 2b, ganz deutlich ersichtlich. Einzelne Phase in der Gruppe ist auch ziemlich sicher identifizierbar von Station zu Station, und zwar Phasenverschiebung ist auch klar. Doch kann man bemerken, dass das Aussehen der Wellenform sich von Station zu Station allmählich ändert. Die E–W Komponente in Pasadena und Riverside (Fig. 2a) z. B. zeigt deutliche Veränderung der Wellenform. Nämlich, in Riverside ist die langperiodische Bewegung ganz ausgeprägter eingetreten als die kurzperiodische, indem in Pasadena das Gegenteil vorkommt. Die Kurve für Riverside erinnert uns an manche Gezeitenkurven mit halbtägigen und eintägigen Wellen. Im folgenden ist eben so wie bei der Gezeitenkurve die harmonische Analyse der Kurven von Santa Barbara, Pasadena, Mt. Wilson und La Jolla versucht.

---

2) T. Matuzawa, *Bull. Earthq, Res. Inst.*, **6** (1929), 223.

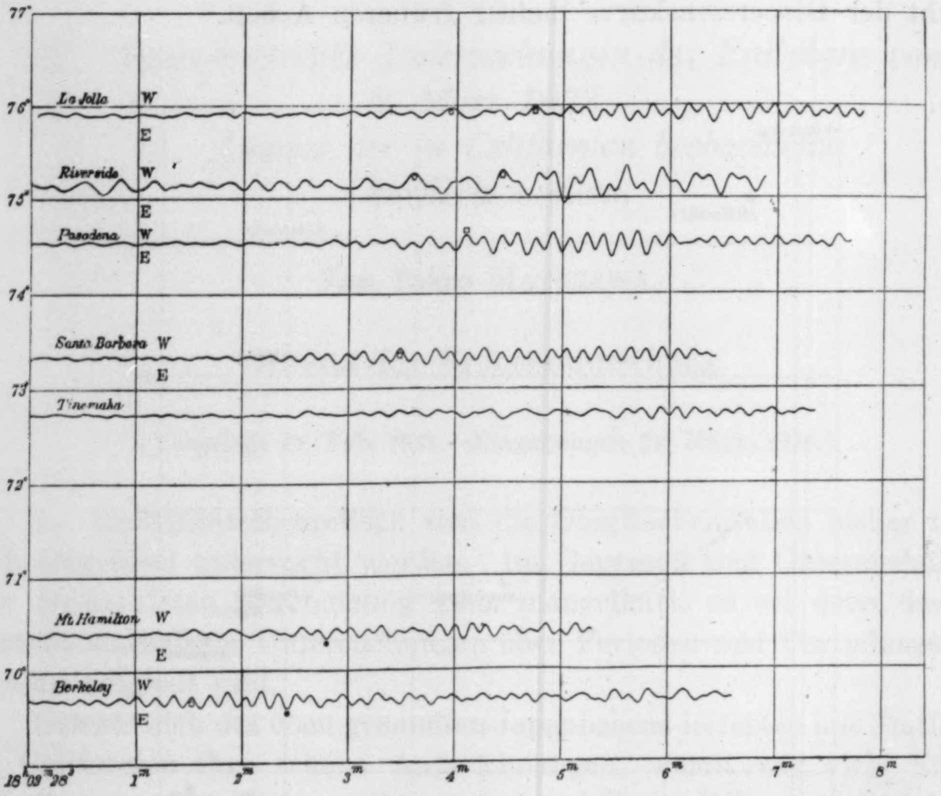

(0·208 mal Original)

Fig. 2a. Die Ordinate zeigt die Herdentfernung der zugehörigen Stationen.

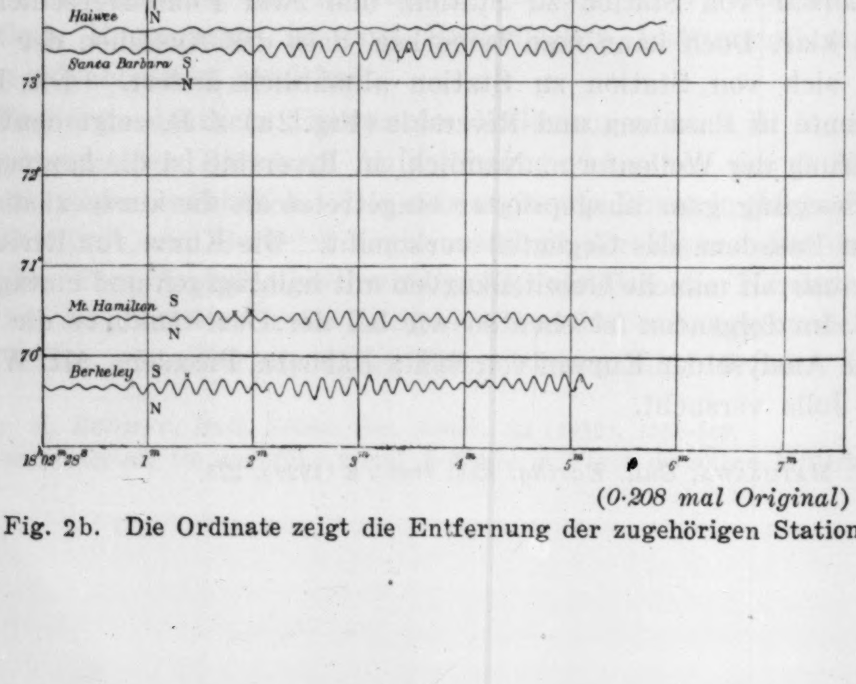

(0·208 mal Original)

Fig. 2b. Die Ordinate zeigt die Entfernung der zugehörigen Stationen.

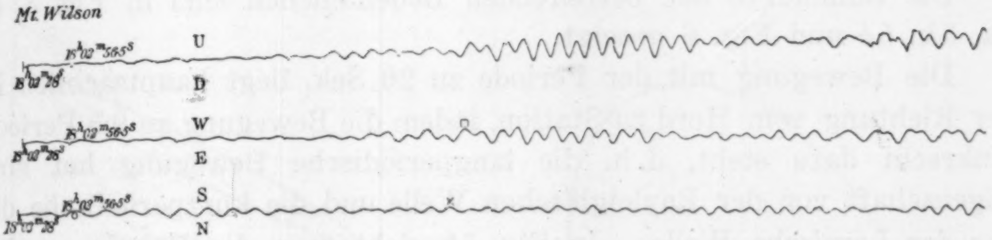

(0·208 mal Original)

Fig. 2c.

3. Für harmonische Analyse muss man erst die Perioden der Bestandteile der Wellen auffinden. Die Periodogrammanalyse der oben erwähnten Wellengruppe hat zwei ausgeprägte Perioden gezeigt, d. s. ca. 20 Sek. und 9·5 Sek. Für die jetzige harmonische Analyse sind nur diese zwei Komponenten angenommen, die aber wesentliche Hauptbestandteile im Wellenzug sind.

Das Rechenverfahren ist wie folgt. Die gegebene Kurve wurde in die oben genannten zwei Komponenten abgetrennt eben so wie bei der Gezeitenanalyse. Dann ist jede Komponente je einzelt auf die wahre Bodenverschiebung reduziert worden, was theoretisch einwandfrei ist, weil jede Komponente bei allen Stufen der Reduktion algebraisch zusammensetzbar ist. Das endgültige Resultat ist in Tabelle I zusammengestellt.

Tabelle I.

$$X=A_1\cos\frac{2\pi}{T}t+B_1\sin\frac{2\pi}{T}t\,,\quad Y=A_2\cos\frac{2\pi}{T}t+B_2\sin\frac{2\pi}{T}t\,,$$

wo X, Y, Koodinaten des Bodenteilchens in Bezug auf die Hauptachsen der elliptischen Bahnkurve.

Station	Komponente	$\sqrt{A_1^2+B_1^2}$	$\sqrt{A_2^2+B_2^2}$	Richtung der grossen Achse	A_1	B_1	A_2	B_2
		mm	mm		mm	mm	mm	mm
Santa Barbara	I(20 s)	0·239	0·066	N 48°40′ W	0·229	−0·067	−0·0008	−0·0672
	II(9·5 s)	0·239	0·0099	N 36°30′ E	−0·0594	−0·232	−0·0097	+0·0025
Pasadena	I	0·359	0·143	N 51°55′ W	−0·351	−0·079	−0·0015	+0·014
	II	0·129	0·274	N 40°30′ E	−0·095	−0·088	−0·188	+0·199
Mt. Wilson	I	0·233	0·0228	N 63°30′ W	−0·203	−0·114	−0·0112	+0·228
	Vertikal		0·29	27°55′ vom Vertikal			+0·220	−0·189
	II	0·129	0·024	N 76°55′ E	−0·0963	−0·085	−0·0161	+0·0178
	Vertikal		0·108	50°35′ vom Vertikal			+0·104	+0·0306
La Jolla	I	0·435	0·0129	N 59°40′ W	+0·050	−0·433	+0·0129	+0·001
	II	0·181	0·045	N 64°30′ E	−0·093	−0·155	+0·039	−0·024

Die Bahnkurve der betreffenden Bodenteilchen sind in Fig. 3, 4, 5a, 5b, 5c und Fig. 6 gezeigt.

Die Bewegung mit der Periode zu 20 Sek. liegt hauptsächlich in der Richtung vom Herd zu Station, indem die Bewegung zu 9·5 Periode senkrecht dazu steht, d. h. die langperiodische Bewegung hat eine Eigenschaft von der Rayleigh'schen Welle und die kurzperiodische die von der Love'sche Welle. In Fig. 5b sieht man die Bahnkurve für die langperiodische Bewegung in der vertikalebene durch die grosse Achse auf Mt. Wilson. Obgleich die grosse Achse bischen vom Vertikal geneigt ist, zeigt die Bewegung hier auch eine wesentliche Eigenschaft der Rayleigh'schen Welle, nämlich, Bodenteilchen bewegt sich im Wellengipfel nach dem Herd und im Wellental vom Herd. Die durchschnittliche Fortpflanzungsgeschwindigkeit ist ungefähr 4·0 Km/Sek, die wieder der transpazifische M-Wellen meiner früheren Arbeit[3] entspricht. Fig. 5c zeigt die Bahnkurve der kurzperiodischen Bewegung in der Vertikalebene durch die grosse Achse. Die Neigung der grossen Achse ist ca. 39° 25′, nämlich, die Grössenordnung der Vertikalbewegung ist ungefähr dasselbe wie bei der Horizontalbewegung. Die Love' sche Welle in horizontal geschichtetem Mittel muss theoretisch keine Vertikalbewegung zeigen. In Wirklichkeit ist aber die Krustenstruktur im oberen Teil der Erde nicht nur senkrecht geschichtet son-

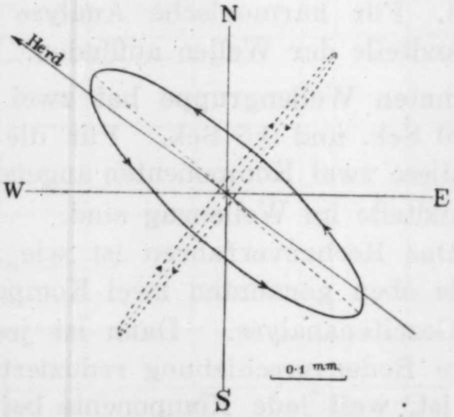

Fig. 3. Ausgezogene Kurve ist die Bahnkurve mit der Periode zu 20 Sek. Gestrichene Kurve ist die Bahnkurve mit der Periode zu 9·5 Sek. Santa Barbara.

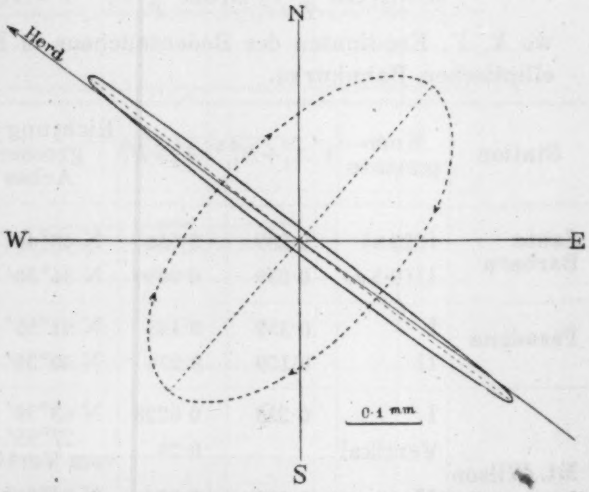

Fig. 4. Ausgezogene Kurve ist die Bahnkurve mit der Periode zu 20 Sek. Gestrichene Kurve ist die Bahnkurve mit der Periode zu 9·5 Sek. Pasadena.

---

[3] T. MATUZAWA, *l. c.*

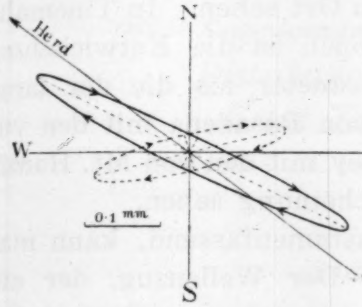

Fig. 5a. Ausgezogene Kurve ist die Bahnkurve mit der Periode zu 20 Sek. Gestrichene Kurve ist die Bahnkurve mit der Periode zu 9·5 Sek.
Mt. Wilson.

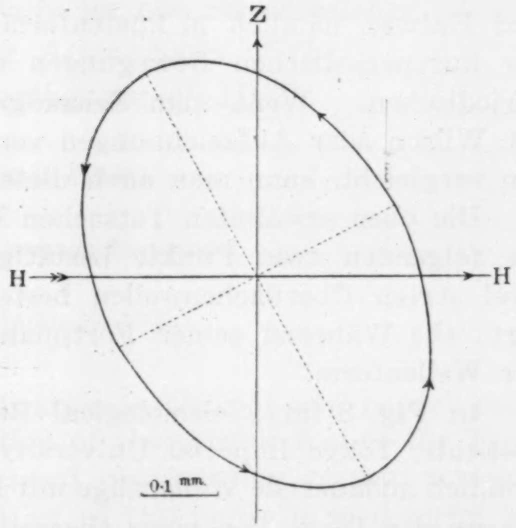

Fig. 5b. Bahnkurve mit der Periode zu 20 Sek. in der Vertikalebene durch die grosse Achse. Der Pfeil H → H fliegt vom Herd nach aussen.
Mt. Wilson.

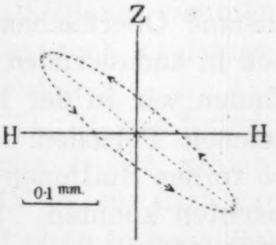

Fig. 5c. Bahnkurve mit der Periode zu 9·5 Sek. in der Vertikalebene durch die grosse Achse.
Mit. Wilson.

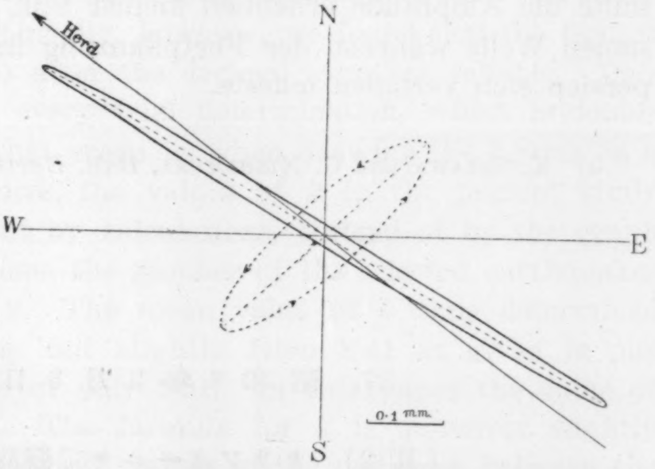

Fig. 6. Ausgezogene Kurve ist die Bahnkurve mit der Periode zu 20 Sek. Gestrichene Kurve ist die Bahnkurve mit der Periode zu 9·5 Sek.
La Jolla.

dern auch horizontal mosaikartig. Darum kann resonanzartige Erscheinung in einem gewissenen Teil der Erde stattfinden, was schon experimentell manchmal beobachtet worden ist. Wenn ein Zug der Love'sche Welle in solchen resonanzfähigen Teil eintritt, dann muss der Wellencharakter einigermassen verändert werden und Vertikalkomponente kann auch entstehen.

Wir sehen in den Figuren der Bahnkurve, dass die Amplitude sich von Station zu Station ziemlich ändert. In Fig. 2a, 2b kann man auch Deformation der Wellenform von Ort zu Ort sehen. In Tinemaha und Haiwee, nämlich in küstenfernen Stationen ist die Entwickelung der kurzperiodischen Bewegungen untergeordneter als die der langperiodischen. Wenn man Seismogramme von Pasadena mit den von Mt. Wilson oder Aufzeichnungen von Berkeley mit den von Mt. Hamilton vergleicht, kann man auch dieselbe Erscheinung sehen.

Die oben erwähnten Tatsachen kurz zusammenfassend, kann man die folgenden zwei Punkte bestätigen; (a) Der Wellenzug, der aus zwei Arten Oberflächenwellen besteht, pflanzt sich von Ort zu Ort fort; (b) Während seiner Fortpflanzung unterliegt er Deformationen der Wellenform.

In Fig. 8 im „Seismological Report of the Earthquake Research Institute, Tokyo Imperial University 1933 Part 1" sehen wir manche ziemlich andauernde Wellenzüge mit Perioden ca. 20 Sek. und ca. 10 Sek. Wegen der Dispersion muss theoretisch eine einsame Oberflächenwelle im Herdgebiet während ihrer Fortpflanzung auch in andauernden Wellenzug übergehen.[4] Aber im jetzigen Falle finden wir in der Herdnahe auch ausgeprägte Wellenzüge mit dergleichen Perioden. Das mag sicher der Hauptgrund sein, dass Wir in so fernen Stationen auch schön andauernde ausgeprägte Wellenzüge beobachten konnten. Sonst sollte die Amplitude erheblich kleiner sein, weil die Energie einer einsamen Welle während der Fortpflanzung im ganzen Intervall der Dispersion sich verteilen müsste.

---

[4] K. SEZAWA und G. NISHIMURA, *Bull. Earthq. Res. Inst.*, **8** (1930), 330～335.

---

27. 昭和8年3月3日の地震

(其2) カリフオーニヤで觀測された表面波

地震研究所 松澤武雄

カリフオーニヤの諸觀測所の地震記象に於ては，表面波に相當する部分に於て見事に續いた簡單な振動の群が現れた．表面波の現はれ始めに近い一つの群について解析を試みた．波群は變形を受けながら傳はつてゐる．波が震央から傳つたものだとすると太平洋の底に對する分散曲線の上にのる．

28. *Supplementary Study on the Stereometrical Distribution of the After-shocks of the Great Tango Earthquake of 1927.*

By Nobuji NASU,

Earthquake Research Institute.

(Received March 20, 1935.)

Introduction. Since the publication in 1929 of our paper[1] relating to the stereometrical distribution of the seismic foci of the Tango after-shocks, data have been obtained necessitating certain revisions and additional comments. The object of this paper is to describe and discuss such revisions and additional facts so as to bring the paper up to date,

(1) It was found that the values of k, the constant factor in the formula $D=kt$, which were determined graphically and listed in TABLE IV of our first paper should have been extended to the second decimal place to be sufficient for determining the seismic focus. In working out the value of k graphically, however, we found that the figures from the second (inclusive) after the decimal were not reliable, This value differ slightly with every trial determination, which is doubtless on account of errors that creep in when drawing the figures on a map. In these circumstances, the values of k in the present study were determined throughout by calculations, instead of by the graph method. In these calculations the number of the selected earthquakes was increased from 8 to 9. The mean value of k thus determined came out as 8·40, differing but slightly from 8·41 as given in our former paper: a difference of only 0·01. In this paper the value of k has been taken as 8·40. The formula for k is moreover slightly corrected by inserting the correct values of the distances between the seismological stations as well as the coordinates of the stations. For convenience, the table containing the determined k is specified in this paper by the same serial numbers as those in the former report, which is TABLE IV in this paper. And since there is no means by which

---

[1] N. NASU, "A Stereometrical Study of the After-shocks of the Great Tango Earthquake with Special Reference to the Mechanism of their Occurrence", *Journ. Facult. Sc.*, [ii], **3** (1929), 29.

[2] *Journ. Facult. Sc., loc. cit.* p. 38, Table v.

we can ascertain the durations of the preliminary tremors at stations that are not included in our network of observations, it is not possible to say that the values of k given in the next table (TABLE V)[2] in the previous paper are correct. For this reason, TABLE V is not included in this paper.

(2) In the present study, the seismic foci were accurately determined from observations made at either three of four stations. There being about 30 foci in our previous study that cannot be regarded as being accurate, these are excluded from the present paper.

(3) The errors in the position of the seismic foci are now calculated to a sufficient extent to enable discussion of the arrangement of the seismically weak zones or fault planes from which the after-shocks originated. In the APPENDIX[3] will be found the calculations of the errors mentioned.

(4) In the diagrams (Figs. 24~33) in our previous paper, showing the vertical distribution of the seismic foci are drawn too many lines on which the foci of shocks are shown to be grouped, included in which are, however, several lines whose distance from the next line does not exceed 2 or 3 km. The actual existence of such planes as indicated by these lines becomes doubtful, were the errors in the seismic foci due to errors in observation taken into consideration. But, on the other hand, however, there is no reason to regard the whole of our previous results as being in error on this account. It must be understood therefore that the lines, or planes, which were determined by projecting the seismic foci to certain vertical plane were merely drawn in certain directions because they were the only directions in which it was possible to draw them from our studies of the disposition of the seismic foci In the present study, an attempt has been made to determine only such conspicuous seismically weak zones as are most likely to exist in reality (Figs. 25~56). Possible errors in the position of the seismic foci are now also taken into consideration. The number of the weak zones, or fault planes, thus determined are less than that determined in our previous study.

(5) Another improvement is that the classification of the seismic foci according to the times in which the earthquakes occurred receives more attention in this paper than it did in the previous one, with the result that the migration of the seismically active centre with time can be illustrated more conveniently than it was possible before.

Lastly, it must be borne in mind that the new treatment of the

---

3) This APPENDIX is published in the *Jap. Journ. Astr. Geophys.*, **12** (1935).

subject in no way affects the general results that were obtained in the case of our previous study.

Determination of k *in the formula for the computation of focal distance by means of the duration of preliminary tremors.*

It is assumed that the four stations, Maiduru, Kinosaki, Kôbe-mura, Taiza, lie on a horizontal plane, $Z=0$. Let the X and Y axes be horizontal, see Figs. 8, and the origin of coordinates be taken at any of the stations, say, Maiduru. Let the X axis be taken on the straight line joining Maiduru and Kinosaki; assuming the northwest as its positive sense. Let the Y axis be taken perpendicular to the former axis with the northeast as its positive sense. Let the coordinates of the four stations be $(0, 0, 0)$, $(x_1, 0, 0)$, $(x_2, y_2, 0)$ and $(x_3, y_3, 0)$, respectively.

Assuming now that the focus lies at a point whose coördinates are (X, Y, Z), we get the following relations for the focal distances of the four stations;

$$D_0=\sqrt{X^2+Y^2+Z^2}=kt_0,$$

$$D_1=\sqrt{(X-x_1)^2+Y^2+Z^2}=kt_1,$$

$$D_2=\sqrt{(X-x_2)^2+(Y-y_2)_2+Z_2}=kt_2,$$

$$D_3=\sqrt{(X-x_3)^2+(Y-y_3)^2+Z^2}=kt_3,$$

where D_0, D_1, D_2, D_3 are the focal distances of the four stations, and t_0, t_1, t_2 and t_3 are the durations of the preliminary tremors at the respective stations.

Solving the simultaneous equations in X, Y, Z and k, we have four expressions, of which the one for the constant factor k is

$$k=\sqrt{\frac{(x_3y_2-x_2y_3)\,d_1^2-(d_3^2y_2-d_2^2y_3)\,d_1}{(x_3y_2-x_2y_3)\tau_1+(y_3\tau_2-y_2\tau_3)\,d_1}},$$

where d_1, d_2, d_3 are the respective distances from Maiduru, of Kinosaki, Kôbe-mura and Taiza; and $\tau_1=t_0^2-t_1^2$, $\tau_2=t_0^2-t_2^2$, $\tau_3=t_0^2-t_3^2$. For

---

4) The numerical values here adopted were determined in the topographical maps of Miyadu and Tottori, scale 1/200,000. Some of the numerical values slightly differ from those which were used in our previous paper, and which are now corrected.

our network of stations, the following numerical values[4] are required in the reduction of the expression for k.

$$d_1=50{\cdot}4\text{ km.}\quad x_1=50{\cdot}4\text{ km.}$$

$$d_2=27{\cdot}0\text{ km.}\quad x_2=25{\cdot}8\text{ km.}\quad y_2=\ 7{\cdot}9\text{ km.}$$

$$d_3=38{\cdot}3\text{ km.}\quad x_3=31{\cdot}9\text{ km.}\quad y_3=21{\cdot}2\text{ km.}$$

Inserting the above given values, the expression for k becomes

$$k=\sqrt{\frac{554355{\cdot}2}{375{\cdot}4t_0^2+295{\cdot}0t_1^2-1068{\cdot}5t_2^2+398{\cdot}2t_3^2}}\,,$$

During a period of about six months after the installation of the second network of stations, there were nine after-shocks for which the seismic foci, as well as the above-mentioned factor could be determined.

By using the formula we calculated the values of k to the second decimal place; the accuracy being sufficient for our present purpose. The values of k are shown in Table IV.

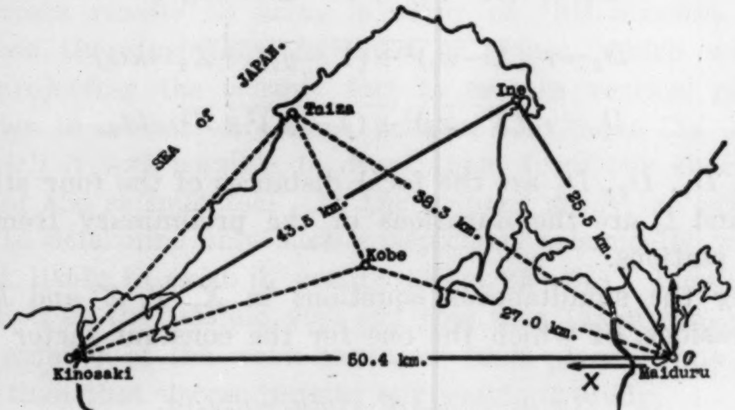

Fig. 8. Networks of the Seismological Stations.

—— the first network.

.... the second network.

The values of k obtained in the Tango after-shocks came out as 8·40 in its mean value.

Table IV. Durations of the Preliminary Tremors, Values of k and Focal Depths of the Earthquakes.

Time of earthquake occurrence.				Duration of the preliminary tremors.				Factor k	Focal depth
				Maiduru	Kinosaki	Kôbe	Taiza		
Month	Day	h	m	sec.	sec.	sec.	sec.		km.
I	30,	5	01	2·5	3·6	1·4	3·0	8·51	6·0
I	30,	18	41	5·1	2·8	2·3	1·7	8·55	12·2
II	12,	21	27	5·0	3·0	2·2	1·6	8·38	12·0
II	14,	20	48	4·0	2·8	1·7	2·8	8·15	11·2
II	18,	18	49	5·0	2·6	2·3	2·4	8·31	14·8
II	19,	5	27	3·3	3·3	1·2	2·0	8·68	10·3
II	29,	10	38	3·2	3·6	2·0	3·3	8·47	13·8
III	1,	22	34	5·5	2·0	2·7	2·9	8·28	13·9
VI	16,	12	06	3·0	3·5	0·9	2·2	8·30	6·7

Distribution of the epicentres of the Tango after-shocks.

During our observations, lasting about $1\frac{1}{2}$ years, the after-shocks recorded at least at one of our stations totaled 1307, and we were able to determine accurately the seismic foci of 446 shocks. Although, in our previous paper,[5] 482 determined foci were reported, among them were about 30 foci that we believe are not so accurate, owing to lack of sufficient observations at one of the stations forming the necessary three. The positions of these foci were determined from the durations of the preliminary tremor and the directions of initial motion at the remaining two stations. In this paper, such foci are excluded. There were several more earthquakes in which the duration of the preliminary tremor at one station exceeded 8·0 sec., so that the positions of the seismic origins determined were not so accurate as those of earthquakes with shorter durations of preliminary tremors. In this paper, therefore these earthquakes are also excluded. There are also a few after-shocks that are excluded or newly added for other reasons.

The positions of the seismic foci were determined mainly graphically, using maps of scales 1/200,000 and 1/400,000. The distances of stations composing the networks are shown in Fig. 8. The horizontal axes of coordinates were taken in the directions as shown in the same figure, while the positions of the seismic origins were expressed by coordinates X, Y, Z; the Z axis being taken downward in its positive sense.

---

[5] N. Nasu, "A Stereometrical Study of the After-shocks of the Great Tango Earthquake with Special Reference to the Mechanism of their Occurrence", *Journ. Facult. Sc.*, [ii], **3** (1929), 29.

The seismic foci of 446 shocks were determined by seismic triangulation, of which 9 were observed from four stations. In these 9 latter earthquakes, the foci were determined by using the values of k, specially determined for each earthquake and not by mean value, $k=8{\cdot}4$.

A few words are necessary regarding the case $Z=0$. When $Z=0$, the three circles drawn with each station as centre generally intersect at a point. Sometimes the arcs thus described merely enclose a circular-arc-triangle. When this circular-arc-triangle could be obtained we assumed that the epicentre lay at the approximate centre of this triangle, and determined the coordinates of this centre. Another cases of $Z=0$, although very rare, is that in which the circles do not intersect, in which case the position of the seismic foci were determined in the following mannner: Assuming the observed values of the preliminary tremor to be smaller than the actual by a certain amount of error, we made corrections for the radii of the circles. The time error was assumed to be 0·1 sec. If the circles having these corrected radii enclosed a circular-arc-triangle, the position of the seismic focus could be determined, otherwise it was impossible.

We must next bear in mind the accuracy in the graphical determination of the seismic focus. The values of X, Y, Z given in Table VI having been determined graphically they, naturally, contain certain errors that crept in when drawing the figures on the maps. The errors in the coordinates, however, were in most cases within about ±0·2 km. when a map of scale 1/200,000 was used, and within about ±0·4 km. in the case of a map of scale 1/400,000; these amounts of errors correspond to 1 mm. on the respective maps, and are the probable error from this source. Thus, the fractions of a kilometer in the values of X, Y, Z in Table VI are not accurate within the errors mentioned, which however do not affect our present study. As a matter of fact, fractions of a kilometer in the coordinates of the seismic focus are not worth troubling about.

Distributions of the epicentres of the after-shocks are shown in Figs. 9∼15.

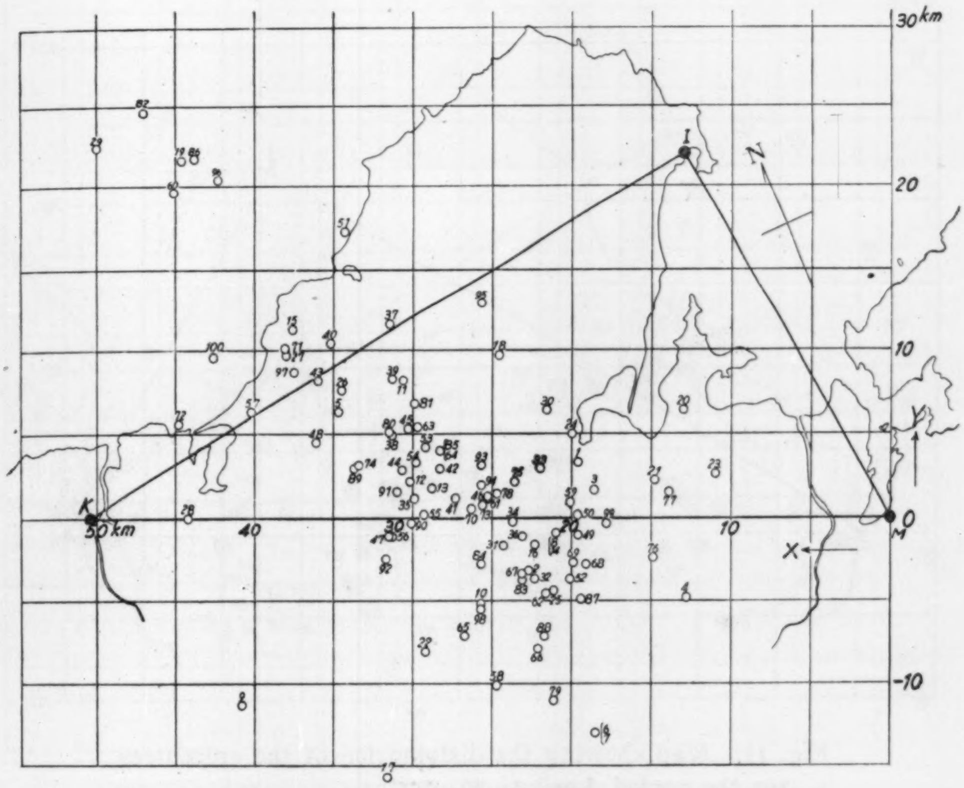
30km
20
10
0
-10
50km
40
30
20
10
I
K
M
O
N
X
Y

Fig. 9. Map showing the distribution of the epicentres for the period March 12~17, 1927.

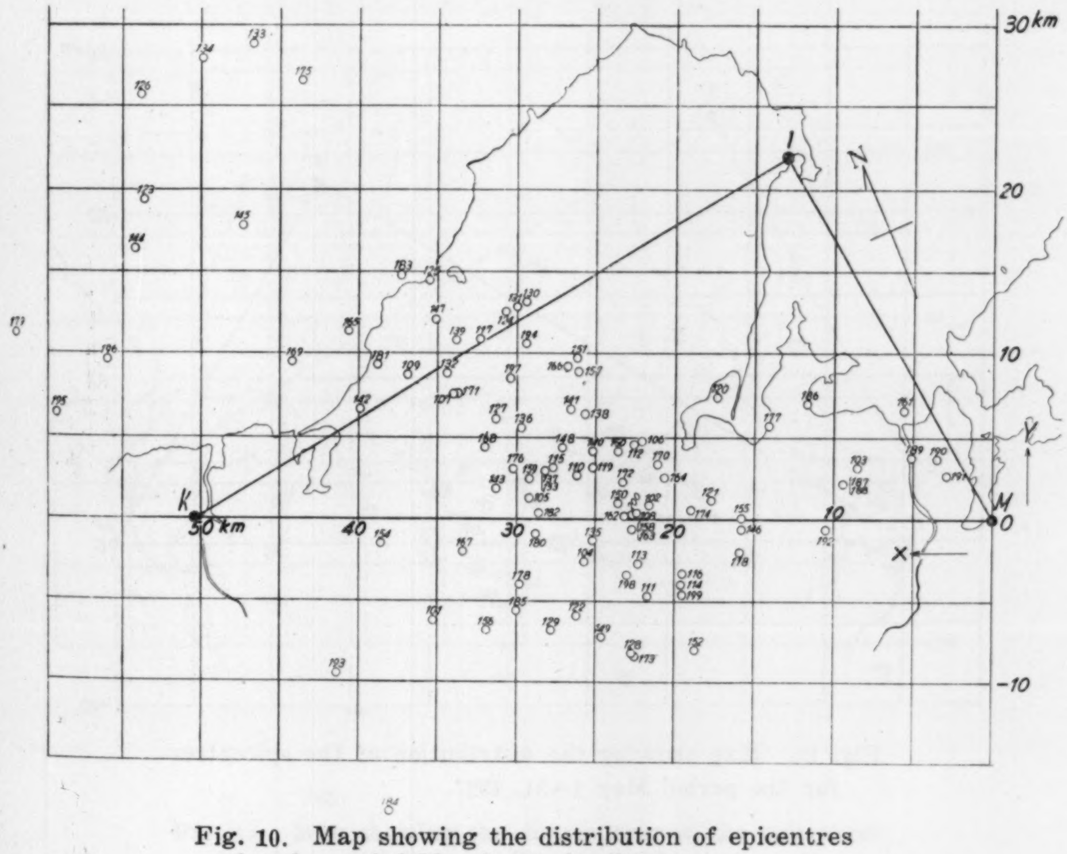
30km
20
10
0
-10
50km
40
30
20
10
I
K
M
O
N
X
Y

Fig. 10. Map showing the distribution of epicentres for the period March 17~April 1, 1927.

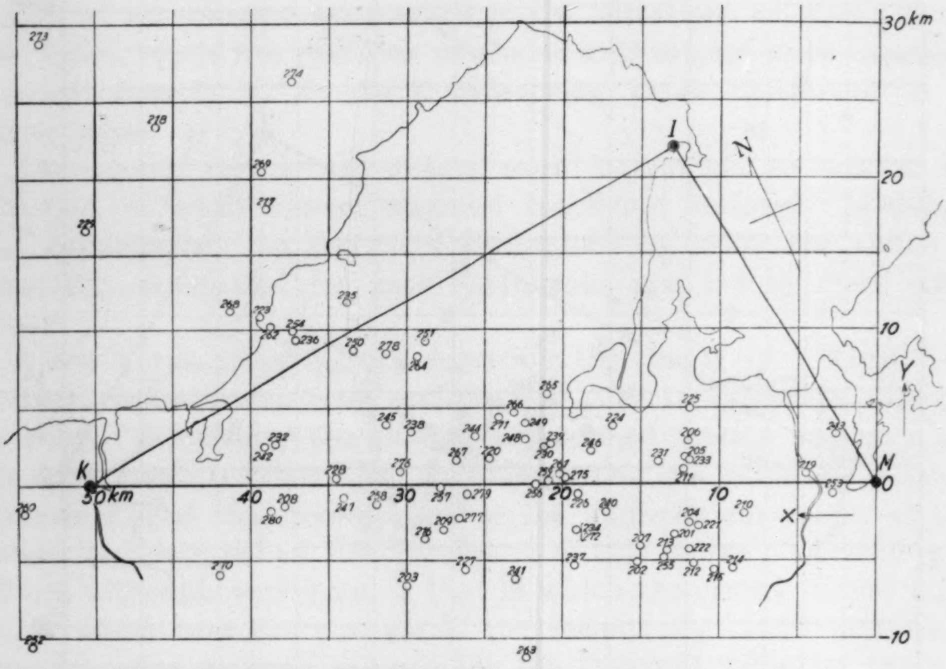
30km
I
N
20
10
Y
K
50km
40
30
20
10
M
0
X
-10

Fig. 11. Map showing the distribution of the epicentres for the period April 1~30, 1927.

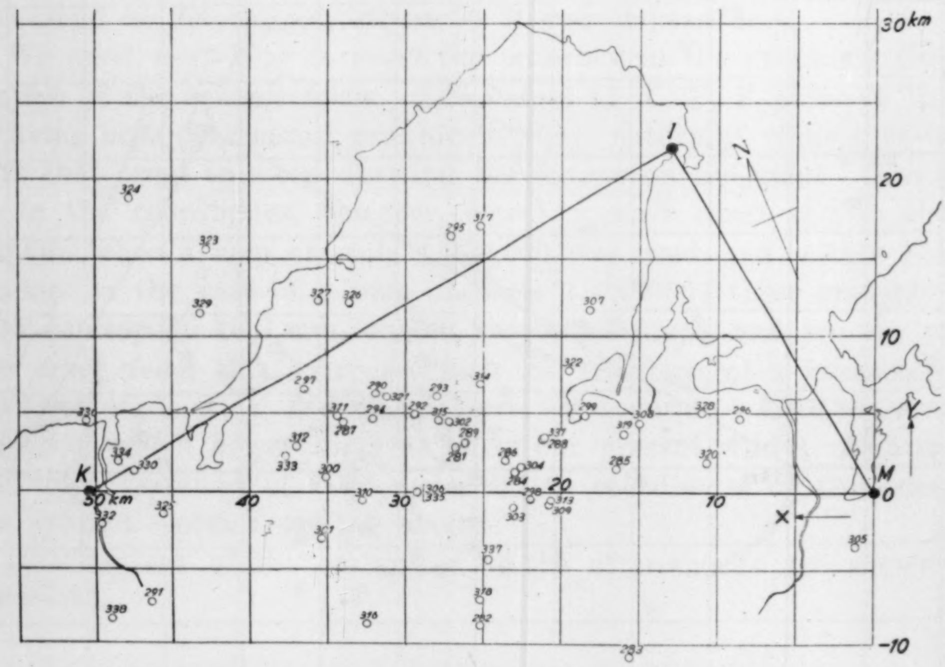
30km
I
N
20
10
Y
K
50km
40
30
20
10
M
0
X
-10

Fig. 12. Map showing the distribution of the epicentres for the period May 1~31, 1927.

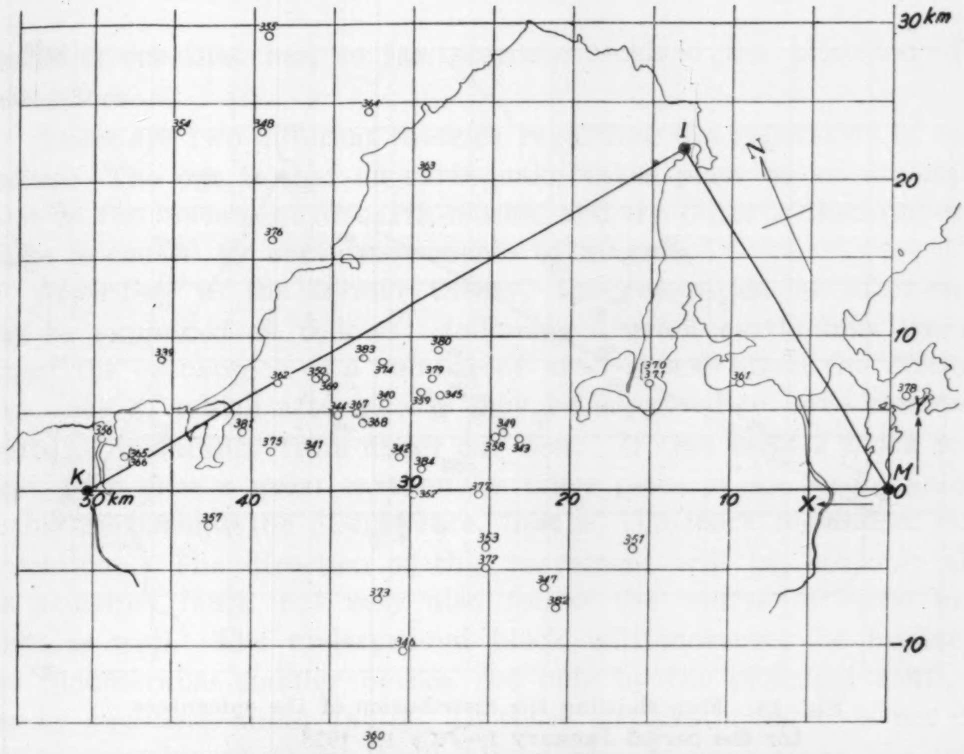
30km
20
10
0
-10
I
N
K
M
Y
X
50 km
40
30
20
10
355
364
354
348
363
376
339
383
380
350
374
379
362
369
340
345
339
344
367
368
370
371
361
378
349
381
375
341
342
358
343
384
356
365
366
377
352
357
353
351
372
347
373
382
346
360

Fig. 13. Map showing the distribution of the epicentres for the period June 1~August 31, 1927.

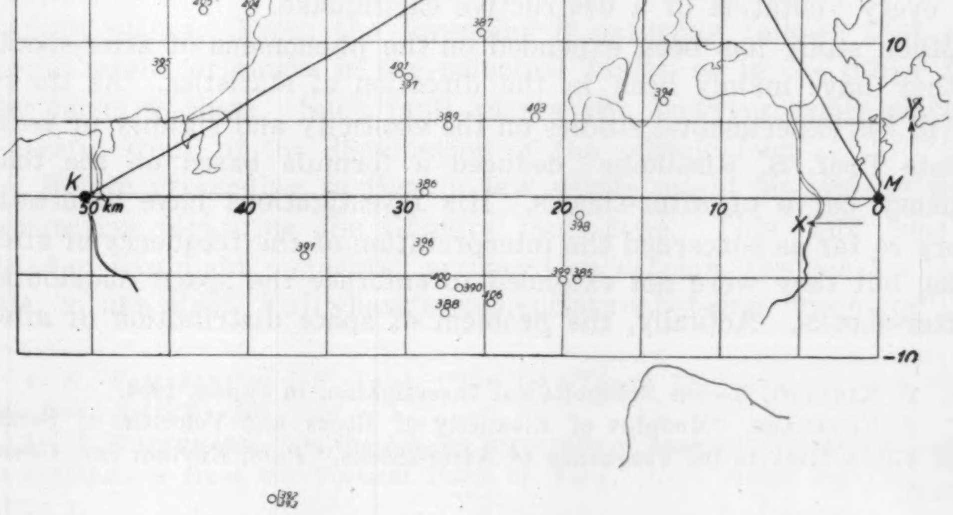
30km
20
10
0
-10
I
N
K
M
Y
X
50 km
40
30
20
10
407
402
405
404
387
395
401
397
394
403
389
386
398
391
396
399
385
400
390
406
388
392
393

Fig. 14. Map showing the distribution of the epicentres for the period Sept. 1~Dec. 31. 1927.

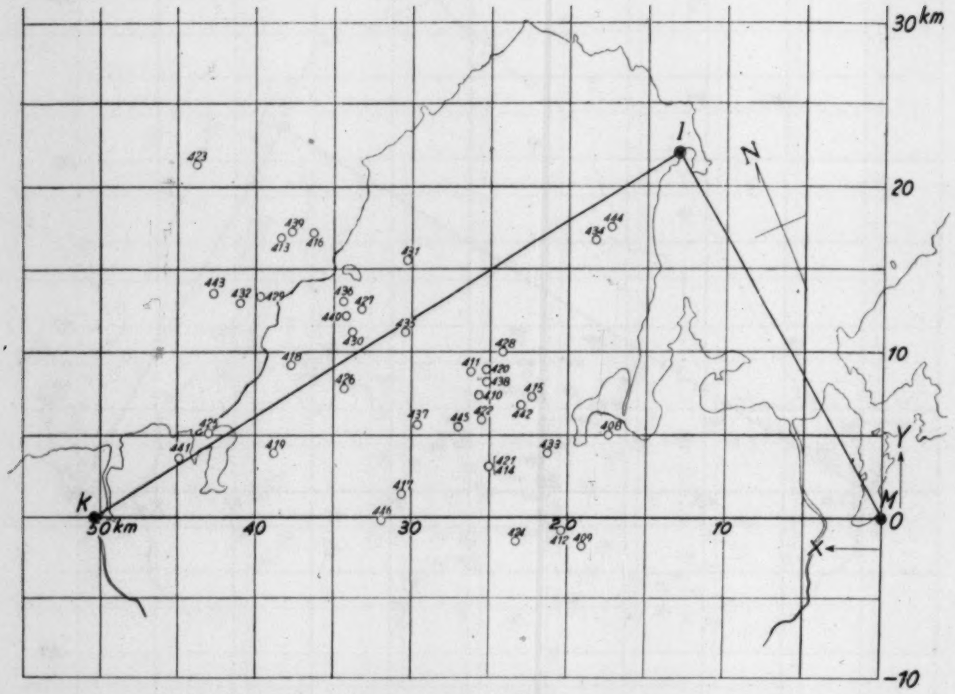
30km
20
10
0
-10
50km
40
30
20
10
K
I
M
N
X
Y
423
439
413
416
431
434
444
443
432
429
436
427
440
435
430
418
426
428
411
420
438
410
415
442
422
445
437
408
425
441
419
433
421
414
417
446
424
412
409

Fig. 15. Map showing the distribution of the epicentres for the period January 1~July 15, 1928.

Distribution of the after-shocks in a vertical plane: stereometrical distribution of the seismic foci of the after-shocks.

A perusal of the history of seismological research in this country will show that instrumental records of after-shocks were first obtained in the case of the great Mino-Owari earthquake of 1891.⁶⁾ Thenceforward, observations of after-shocks became an established feature with every visitation of a destructive earthquake.

Much study has been expended on the phenomena of after-shocks, but they have mainly been in the direction of statistics. As the results of his experimental studies on the elasticity and rigidity of rocks, the late Prof. S. Kusakabe⁷⁾ deduced a formula based on the time-frequency curve of after-shocks. His investigations have been satisfactory so far as concerned the interpretation of the frequency of after-shocks, but they were not extended to embrace the space distribution of after-shocks. Actually, the problem of space distribution of after-

---

6) D. KIKUCHI, Recent Seismological Investigation in Japan, 1904.

7) S. KUSAKABE, "Modulus of Elasticity of Rocks and Velocities of Seismic Waves with a Hint to the Frequency of After-shocks." *Publ. Earthq. Inv. Comm.*, 17 (1904).

shocks is one that has, so far, scarcely received the attention of investigators.

There are two different theories regarding the generation of earthquakes. The one is that an earthquake takes place as an accompaniment to the movement of earth-blocks, and the other is that the earthquake is caused by acute movements of magma.

According to the former theory, the generation of after-shocks may be explained as follows: following a great earthquake we may expect the occurrence of a number of after-shocks about the disturbed area, each of which after-shocks may be supposed to have removed a source of instability from under our feet. If this were a block movement, then once a great earthquake takes place as an accompaniment to this movement, the disturbance, that is, the block movement ought to continue. The direction of this movement will be, not only along the principal fault, but may also follow the course of some minor faults as well. The underground block will moreover be broken up into innumerable smaller blocks, not only by the principal fault, but also by countless minor faults. In these circumstances, it is not difficult to conceive of these small blocks also moving along the minor faults. With every energetic movement of such blocks, earthquakes are bound to occur at their bounding surface.

According to the second theory, while the first big earthquake is generated by certain acute movements of magma, the after-shocks are due to its residual or renewed movement about the originally disturbed area.

Though these two theories differ as to the generation mechanism of earthquakes, on one point they agree, and that is that the earthquakes are liable to originate in weak zones in the earth's crust, such as fault planes. From the foregoing it naturally follows that after-shocks might originate in the principal faults, or in the minor faults contiguous to them. Such fault planes are, however easily traced by a careful study of the distribution of the seismic foci.

Before proceeding further, a few words might be said by way of explanation regarding the Gômura fault zone. This fault zone consisted of five main segments[8] arranged *en échelon*, the *échelon* in this case, to use Prof. Fujiwhara's nomenclature,[9] being "negative"; that

---

[8] N. YAMASAKI and F. TADA, "The Oku-Tango Earthquake," *Bull. Earthq. Res. Inst.*, **4** (1928), 159.

[9] S. FUJIWHARA, "On the *èchelon* Structure of Japanese Volcanic Ranges and its Significance from the Vortical Point of View," *Gerl. Beitr. zur Geophys.*, **16** (1927), 1.

is to say, each segment ran in the second and fourth quadrants when the abscissa was taken coincident with the main trend of the fault zone. This condition manifested itself in the southern part of the Gômura fault zone, but not in the northern. As a probable explanation of this singularity, Prof. Imamura[10] drew attention to the possible difference in the stress distribution between the northern and southern blocks lying west of the Gômura fault, adding, that if such was the case, the stress in the northern block might have been applied in a direction almost perpendicular to the fault, and in the southern part in a direction parallel with the fault.

Here it may not be irrelevant to make a little digression and refer to the experiments made some time ago by Prof. Fujiwhara[11] with the purpose of studying the precise manner of crack-formation. Forces were applied to models made of various substances, and the results showed that with substance feebly resistant to tensional forces, parallel cracks developed obliquely to the line of shear; whereas with substances feebly resistive to bending forces, a group of carcks formed athwart the tensional force. Subjection of the models to uniform tension or compression resulted in the developement one after another of two kinds of cracks, quite regardless of the substance tested, viz., tension cracks and compression cracks. As to these two modes of cracking, those of secondary formation always lay in a direction symmetrical to the primary cracks. To illustrate, if the primary cracks were at an angle of 45°, as would be the case with an isotropic, homogeneous substance, then the secondary cracks developed perpendicularly to the primary cracks. From this it may be inferred that there were many other faults near the principal ones that came into existence with the present earthquake.

The following will illustrate the methods adopted by the writer in studying the positions of seismic foci. As will be evident from the distribution of the fault lines (Fig. 24), the land mass in the Tango seismic area may be divided into a number of small blocks with the faults as the boundaries of their upper surfaces. Though the actual blocks in nature are not regular geometrical figures, we could roughly divide the Tango seismic area into four large blocks as shown in Fig. 24. The boundaries of these blocks are nearly parallel to the predominant faults, such as the Gômura fault, for example. We shall then project the seismic foci in each block on certain vertical planes. For example, we shall take a crustal block No. III, which is bounded by the Gômura fault on the east and by a line nearly parallel to the Yamada fault (the X' axis in Fig. 24) on the south, and project all the foci in this block on a vertical plane normal to the Gômura fault zone, arranging the foci of the shocks according to the times of their occurrence. In our former studies[12] of disposition of the seismic foci of the Tango after-shocks, the foci were classified into the following three classes:

---

[10] A. IMAMURA, "On the Destructive Tango Earthquake on March 7, 1927," *Bull. Earthq. Res. Inst.*, **4** (1928), 179.

[11] S. FUJIWHARA, "Torsional Form on the Earth Surface and the Great Earthquake of Sagami Bay," *Kisyô Syûsi*, [ii], **2~1** (1924).

(1) The foci of the first class, such as those of shocks that occurred early, that is, during a period of about 50 days following the great earthquake, and marked in the diagrams by dots.

(2) The foci of the second class, such as those of shocks that occurred in the next period, that is, during the period from the end of April to the end of August of 1927, and marked by crosses.

(3) The foci of the third class, such as those of shocks that occurred during a period of about eleven months from the beginning of September, 1927, to the end of July the next year, and marked by asterisks.

Upon classifying the foci in this way it was found that they showed quite different positions according to the times of occurrence of the respective earthquakes. But since then it was found convenient in studying the disposition of the foci to arrange them in more classes than the three just mentioned. By doing so, the change in positions of seismically active centres with time could be more clearly shown than could be done heretofore. Thus, in the present study, the foci were divided into several classes according to the times in which the earthquakes occurred, and for each class of foci the distributions of the seismic foci shown in different diagrams. From these diagrams the migrations of the seismically active centres could be clearly studied.

Needless to say, the foci belonging in one class must be sufficiently numerous to enable us to correctly determine the mean position of the seismically active centre. For this reason, at least ten foci belonging in one class were taken.

It will be noticed that some of the foci projected in the above-stated manner may be grouped together into a number of systems of finite lines (foci lying on the same line being generally of the shocks that occurred successively), that are usually nearly parallel to each other. Here it must be remembered that the lines and planes referred to in this paper are not the lines and planes as understood in geometry. They are merely imaginary lines or planes in which the seismic foci lie, hence may not be straight, but assume any irregular form. Thus, as a matter of expediency the lines or planes deduced in the present study are indicated in the diagram by means of smooth curves or straight lines on which the foci are supposed to lie. It must further be understood that the lines as determined from the disposition of the foci show only the mean position of the seismically active zones or planes.

---

[12] N. Nasu, "A Stereometrical Study of the After-shocks of the Great Tango Earthquake," *Journ. Facult Sc.*, [ii], **3** (1929), 29.

In taking the plane of projection parallel to the Gômura fault (the plane in this case being perpendicular to the former plane of projection) a new result is obtained again for the foci in the same block. Thus, in our studies the planes of projection were taken such that the one plane is parallel to the major geomorphologic faults and the other perpendicular to the same faults.

As the errors in the position of the seismic focus become fairly large if the focal depth were to exceed 25 km., particularly the errors in the horizontal directions, foci of such shocks as were deeper than 25 km. were excluded from our present studies.

We shall now consider the block that lies west of the Gômura fault zone.

Block No. III.

The surface of this block is bounded by those two conspicuous faults, the Cômura fault on the east and by the Yamada fault on the south. We studied not only seismic foci with their epicentres within the surface of this block, but also took into consideration foci in contiguous blocks, that is, the foci lying in a region designated as III in Fig. 24 were all studied.

(A) We shall first describe the shocks that occurred west of the Gômura fault zone. Most of the after-shocks that occurred during period March 12∼15 (5∼10 days after the great earthquake) had their origins west of the Gômura fault. The distribution of the epicentres of these shocks is shown in Fig. 25. In the case of 65 earthquakes, the seismic foci could be determined for this period, 39 of which were situated west of the Gômura fault or its extension as shown in the same figure. A notable fact is that these foci were in a zone running parallel to the Gômura fault; a zone of about $2\frac{1}{2}$ km. width. This zone is shown by the hatching area in Fig. 25. From this fact it will easily be seen that were weak zones or fault planes at certain depth, where particularly most of the after-shocks originated during the few days succeeding the great earthquake. For the purpose of determining the depth of this weak zone, we shall project all the foci shown in Fig. 25 on a vertical plane parallel to the X' axis; the plane being nearly parallel to the trend of the Yamada fault. Let X' be the distance of the epicentres from the Y′ axis, which is assumed to be the mean trend of the Gômura fault: X' being positive southwestward and negative northeastward.

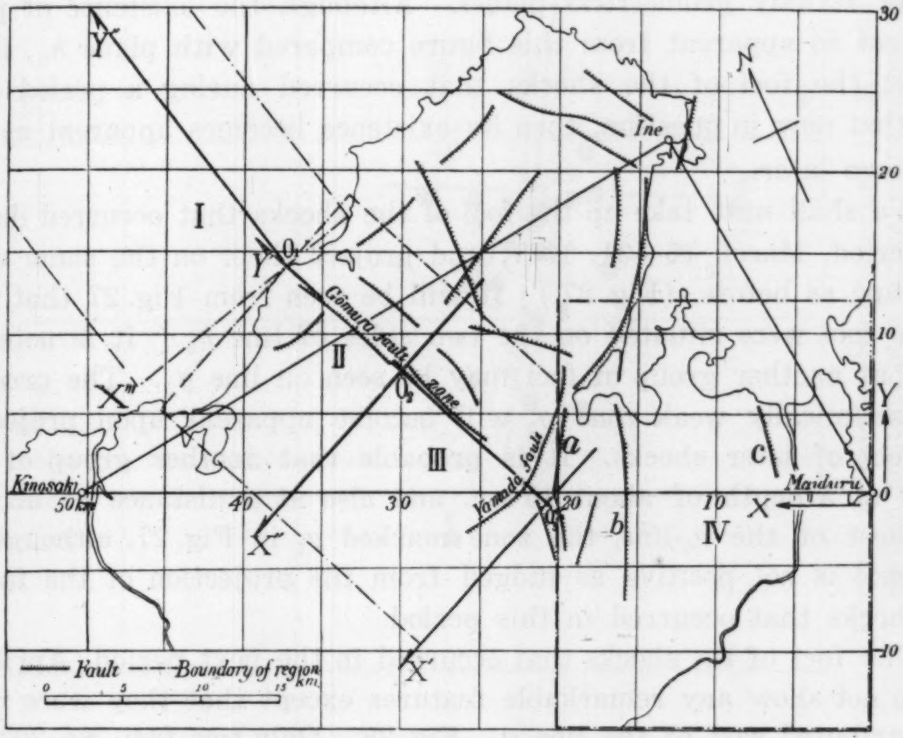

Fig. 24. Map showing the major geomorphologic faults in the Tango district and boundaries of regions which were taken for projections of seismic foci.

The values of X' of the epicentres of the after-shocks which are shown in Fig. 25 are given in Table VII.

Taking the values of X' as abscissa and the focal depth, Z, in Table VII as ordinate, the position of the foci in Fig. 25 are shown in Fig. 26, in which the black circles are the foci in region III and the white circles the foci lying outside of it.

It was found that the seismically weak zones in region III lay at a depth of about 15 km. As may be seen from Fig. 26, while the after-shocks in region III originated from depths of 13·5 km and 22·5 km, most of them were from depths exceeding 15 km, they being confined to a region bordered by the four lines, $Z=15$ km, $Z=20$ km,

$X'=0$ km, $X'=5$ km. It was also found that the earthquakes originated in the planes marked g_0 and h_0, although, as explained these planes are not strictly geometrical planes. Although the existence of plane g_0 is not so apparent from this figure compared with plane h_0, if we project the foci of the shocks that occurred during a period later than that now in question, then its existence becomes apparent as will be shown later.

We shall next take up the foci of the shocks that occurred during the period, March 15~31, 1927, and project them on the same vertical plane as before. (Fig. 27.) It will be seen from Fig. 27 that most of the foci were situated on the two sides of line h_0. It is noteworthy that another group of foci may be seen on line g_2. The presence of a seismically weak zone g_2 will become apparent upon projecting the foci of later shocks. It is probable that another group of foci exists at a depth of about 15 km. and also at a distance of about 5 km. west of the g_0-line, the zone marked g_1 in Fig. 27, although its existence is not positive as judged from the projection of the foci of the shocks that occurred in this period.

The foci of the shocks that occurred in the next period, April 1~30, do not show any remarkable features except that they were mostly distributed east of the line g_2, Fig. 28. Only two foci, No. 203 and No. 208, were situated west of the same line.

The foci of the after-shocks in May, 1927, may be grouped along two lines, h_1 and g_0, as shown in Fig. 29. Line h_1 shows the upper boundary of the seismically active region nearly parallel to line h_0, as already shown in Fig. 27. The position of line h_1, however is somewhat shallower than line h_0. It shows that the seismic activity migrated upward during this period. Of the foci that lie near line h_1, foci No. 300 and No. 310, may be grouped in line g_2 in Fig. 27, and the foci Nos. 337, 335 and 306 grouped in line g_1 in the same diagram. It is undeniable that the seismic activity was mainly confined to line g_0, which is seen to be in the same position as already determined in Fig. 26.

During the next period of three months, from June to August, 1927, the shocks were particularly active in a weak zone indicated by g_1. The distribution of the foci for this period is shown in Fig. 30. As to the distribution in this figure, no foci of shocks could be found on west side of line g_1.

Lastly, we shall take the foci of the shocks that occurred during the eleven months, from September 1927, to the middle of July 1928, and project them in the same manner as we have already done. We

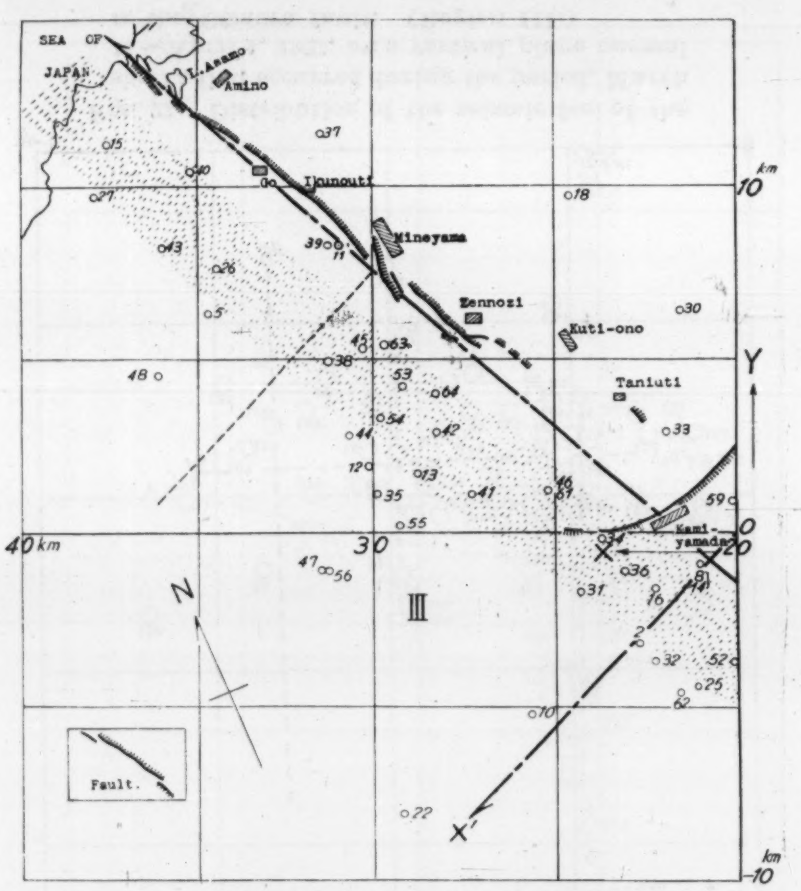
SEA OF JAPAN
L. Asamo
Amino
Go
Iduneuti
Mineyama
Zennozi
Kuti-ono
Taniuti
Kami-yamada
Y
Y'
X
X'
N
III
Fault.
10 km
0
-10 km
40 km
30
20

Fig. 25. Distribution of the epicentres of the after-shocks that occurred near the Gômura fault during a few days following the great earthquake of March 7, 1927.

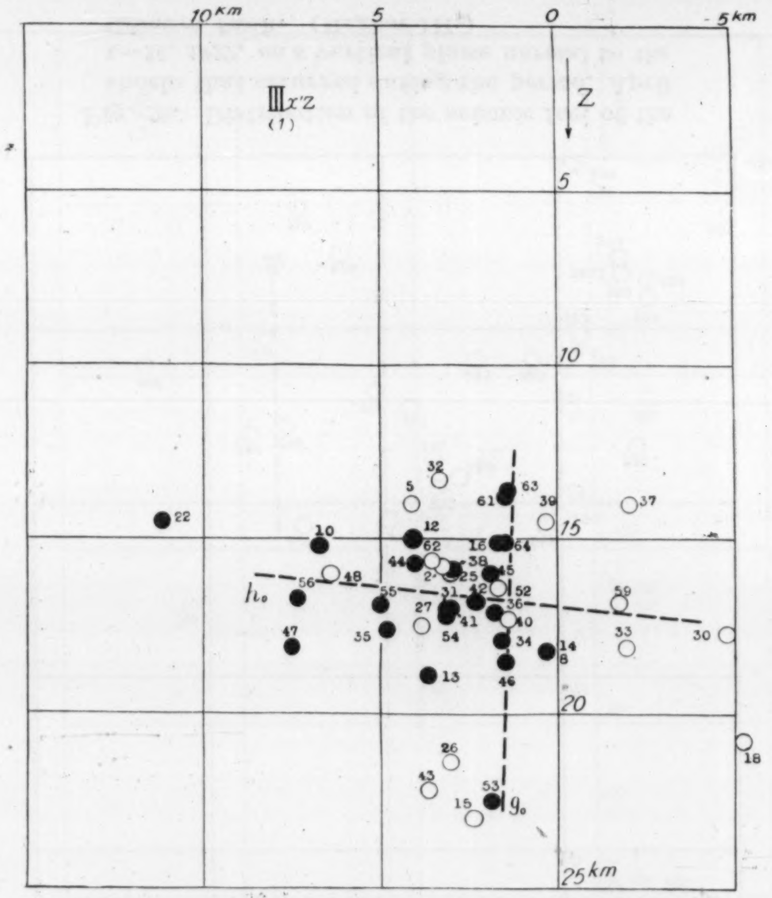

Fig. 26. Seismic foci lying in regions II, III, and environ projected on a vertical plane normal to the Gômura fault. (Distribution for the period, March 12~15, 1927.)
(Black circles are the seismic foci lying west of the Gômura fault and in region III.)

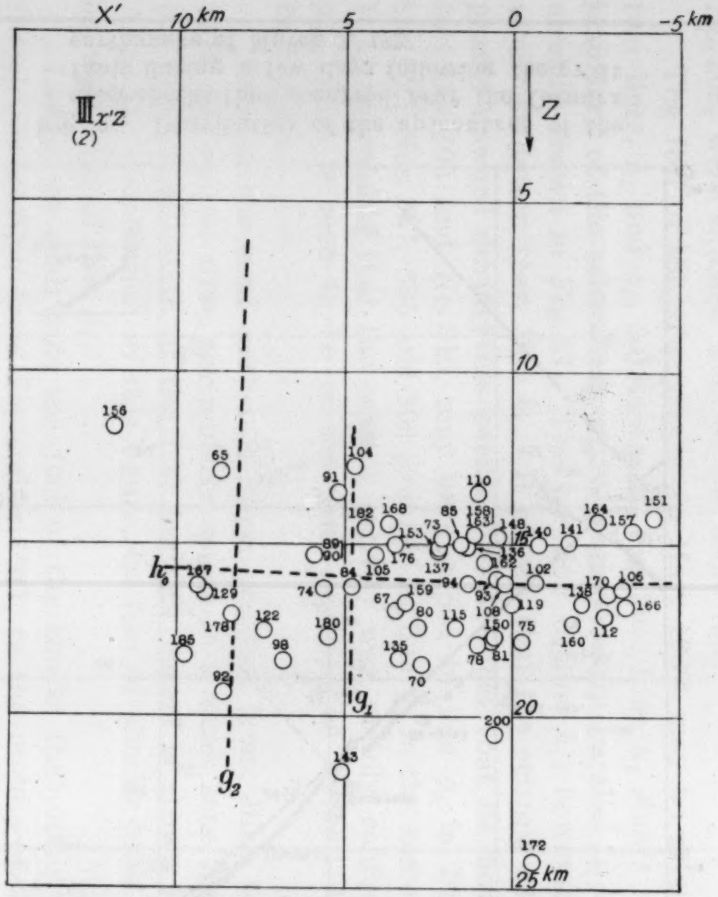

Fig. 27. Distribution of the seismic foci of the shocks that occurred during the period, March 15 ~ April 1, 1927, on a vertical plane normal to the Gômura fault. (Region III.)

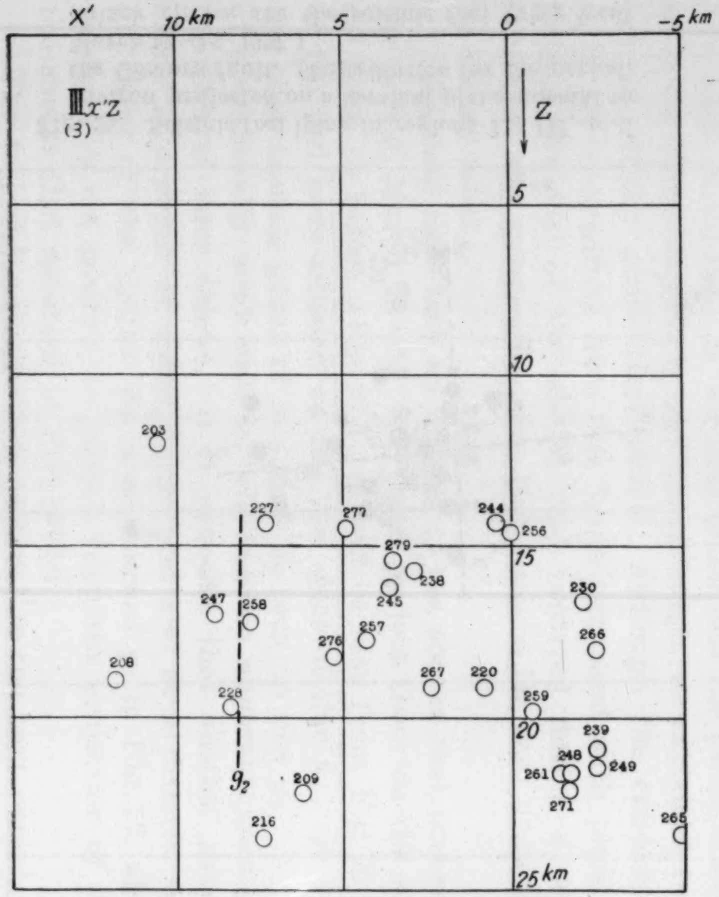

Fig. 28. Distribution of the seismic foci of the shocks that occurred during the period, April 1~30, 1927, on a vertical plane normal to the Gômura fault. (Region III.)

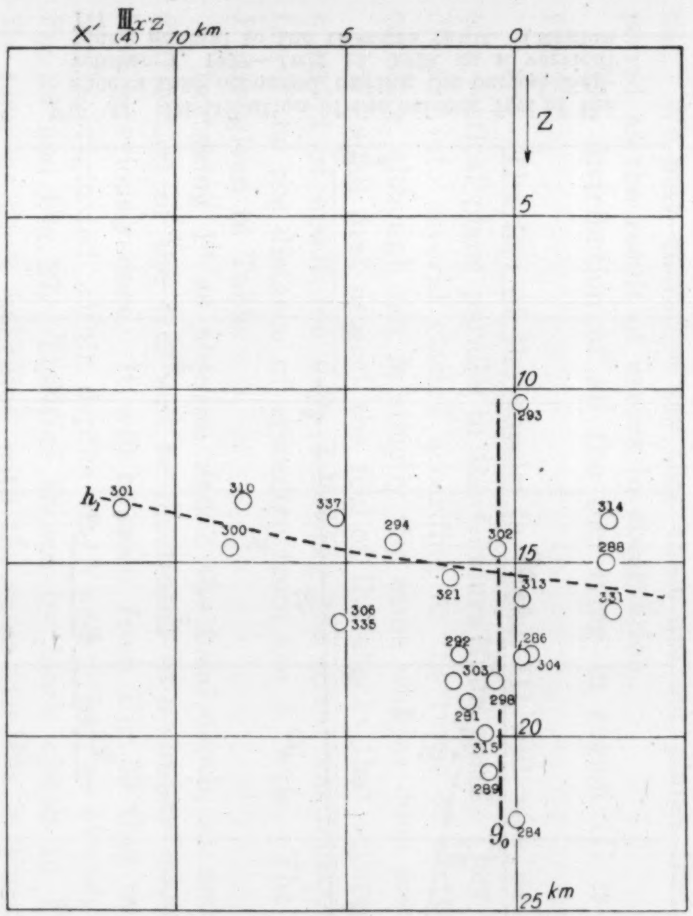

Fig. 29. Distribution of the seismic foci of the shocks that occurred in May, 1927, on a vertical plane normal to the Gômura fault. (Region III.)

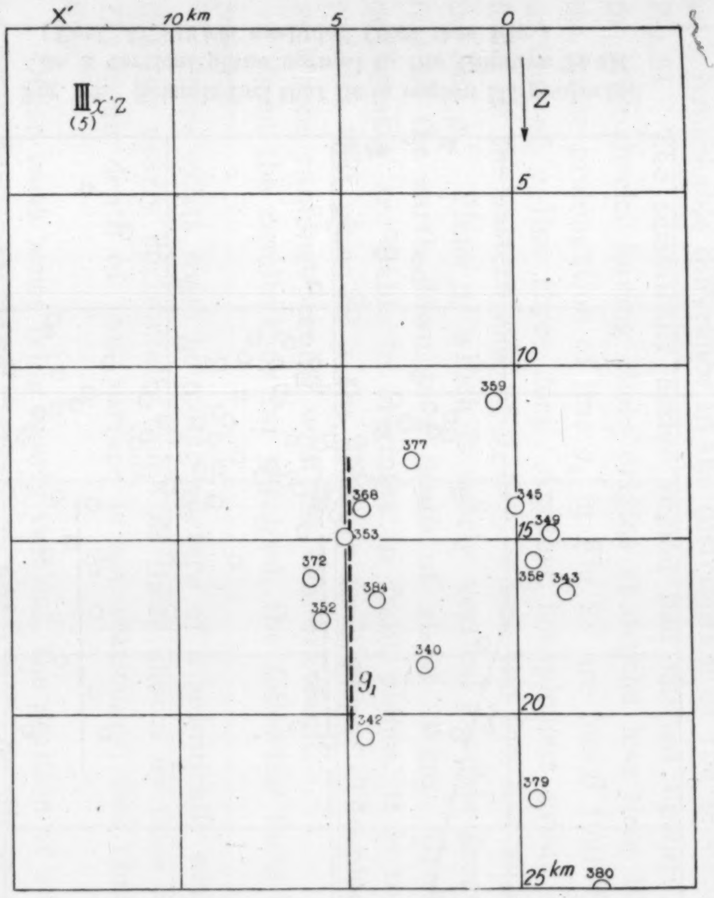

Fig. 30. Distribution of the seismic foci of the shocks that occurred during the period June 1 ~ August 31, 1927, in a vertical plane normal to the Gômura fault. (Region III.)

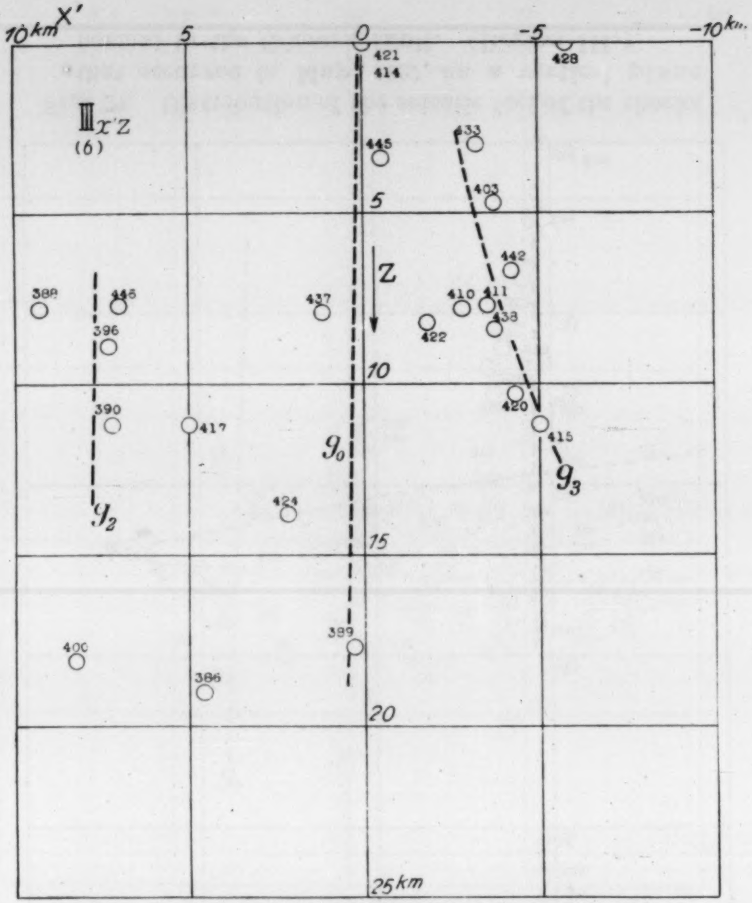

Fig. 31. Distribution of the seismic foci of the shocks that occurred during the period, September 1, 1927∼July 15, 1928, in a vertical plane normal to the Gômura fault. (Region III.)

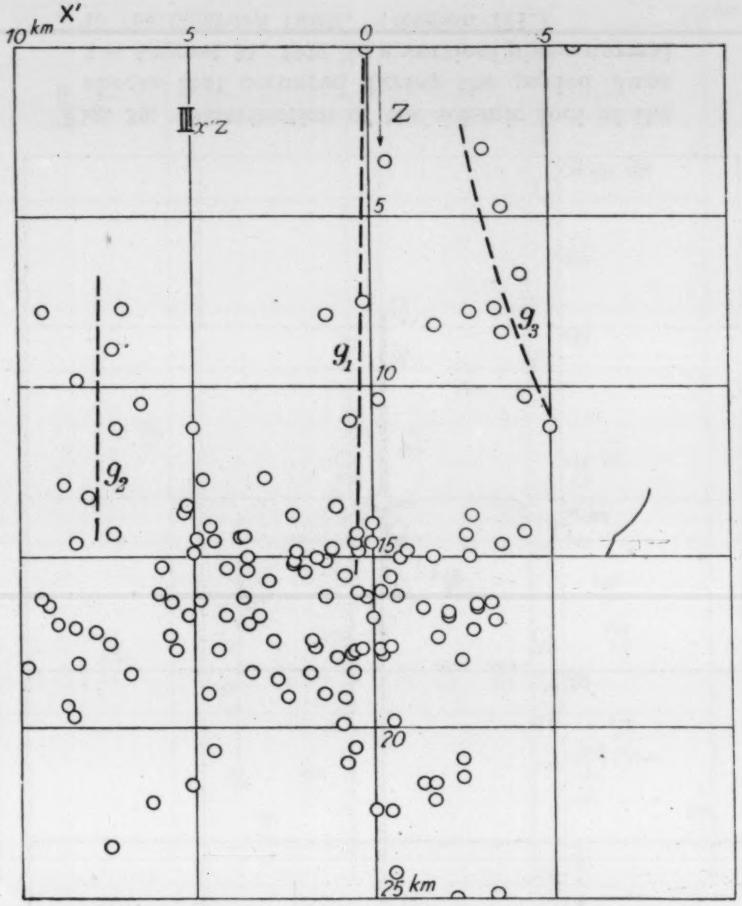

Fig. 32. Seismic foci that lie in region III projected on a vertical plane normal to the Gômura fault. (Foci, $X'>10$ km excluded from this Fig.)

see a remarkable difference in the distribution of the seismic foci, see Fig. 31. The seismically active region had shifted upward, most of the after-shocks having their origins at depths less than 10 km. On the upper prolongation of line g_2 in Fig. 28 are found four foci, while on that of g_0-line three foci. Another conspicuous group of foci is found on the eastern side of g_0-line, where the foci are aligned along the line g_3. Plane g_0 which is nearly vertical extends from the surface of the earth down to a depth of about 15 km. Granting that earthquakes are liable to originate in fault planes, it is then highly probable that plane g_0 is the Gômura fault plane. The plane g_2 is a weak zone running parallel with the Gômura fault.

From the results thus far obtained, the following facts have been revealed:

There exists some bounding surface of a seismically active region that lies nearly horizontally, such as those shown by lines h_0 and h_1. The mean depth of this surface is not stationary, but changes with time.

Other weak zones lying nearly vertical, the position of which could be determined, are those marked g_0 and g_2. The distance between these two planes is about 8 km. Here, we must add that, as shown by calculations, the mean errors in the position of a seismic focus with a depth of about 10 km will not exceed 3 km in horizontal direction. We may therefore say that these are not planes that have appeared as the result of errors in observation.

The distribution of all the foci lying in region III is shown in Fig. 32.

(B) The foci of the shocks in region III will now be projected on a vertical plane parallel to the Gômura fault zone. They were also divided into several classes according to the times of earthquake occurrence, although not in strictly the same way as done previously.

We shall first project the foci of the shocks that occurred during a period of about ten days following the great earthquake, Fig. 33. Let Y' be the distance of epicentre from the X' axis. The values of Y' are given in Table.

In taking Y' as abscissa and Z the focal depth, as ordinate, the distribution of the foci will be illustrated in a similar manner as we have previously done. It will be seen from Fig. 33 that most of the shocks originated within depths of 15 and 20 km, as already shown in Fig. 26 and Fig. 27. The foci shown by black circles in Fig. 33 are the same as those indicated with the same symbols in Fig. 26. They do not show any regular distribution.

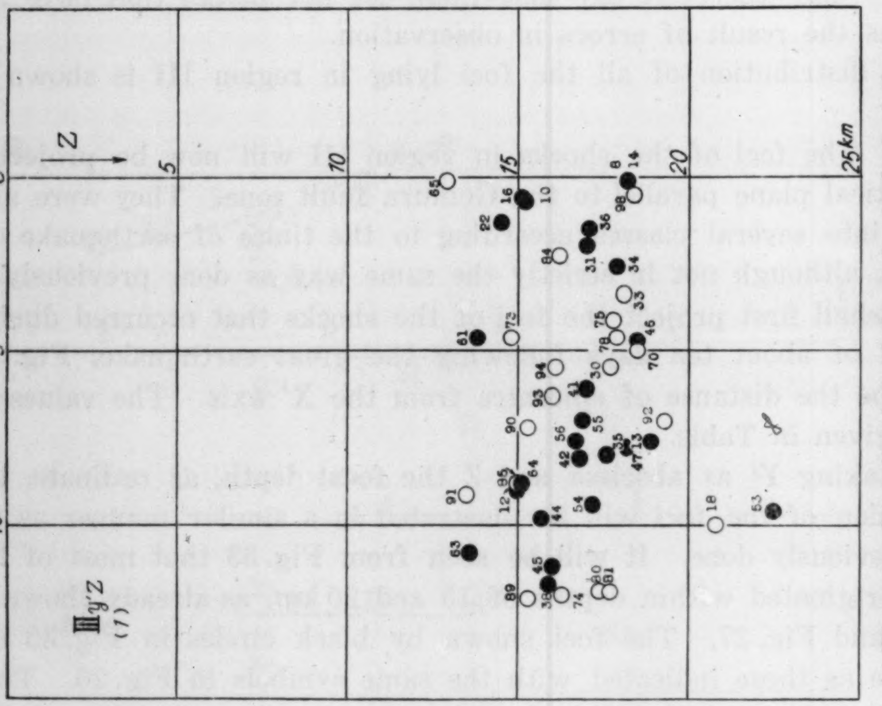

Fig. 33. Distribution of the seismic foci of the shocks that occurred during the period March, 12~17, 1927, on a vertical plane parallel to the Gōmura fault. (Region III.)

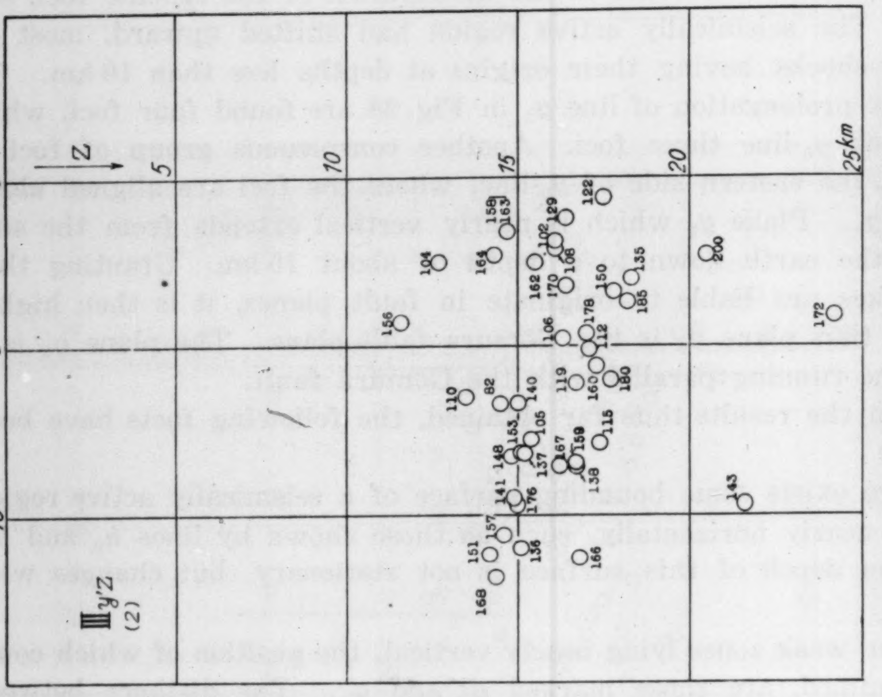

Fig. 34. Distribution of the seismic foci of the shocks that occurred during the period, March 17 ~ April 1, 1927, on a vertical plane parallel to the Gōmura fault. (Region III.)

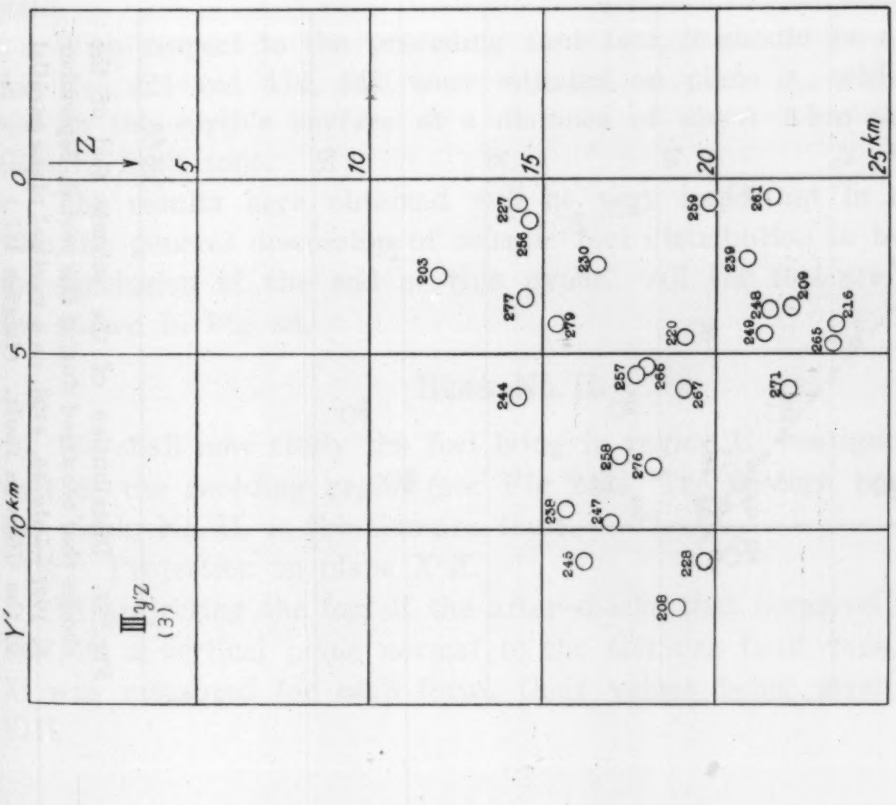

Fig. 35. Distribution of the seismic foci of the shocks that occurred during the period, April 1~30, 1927, on a vertical plane parallel to the Gômura fault. (Region III.)

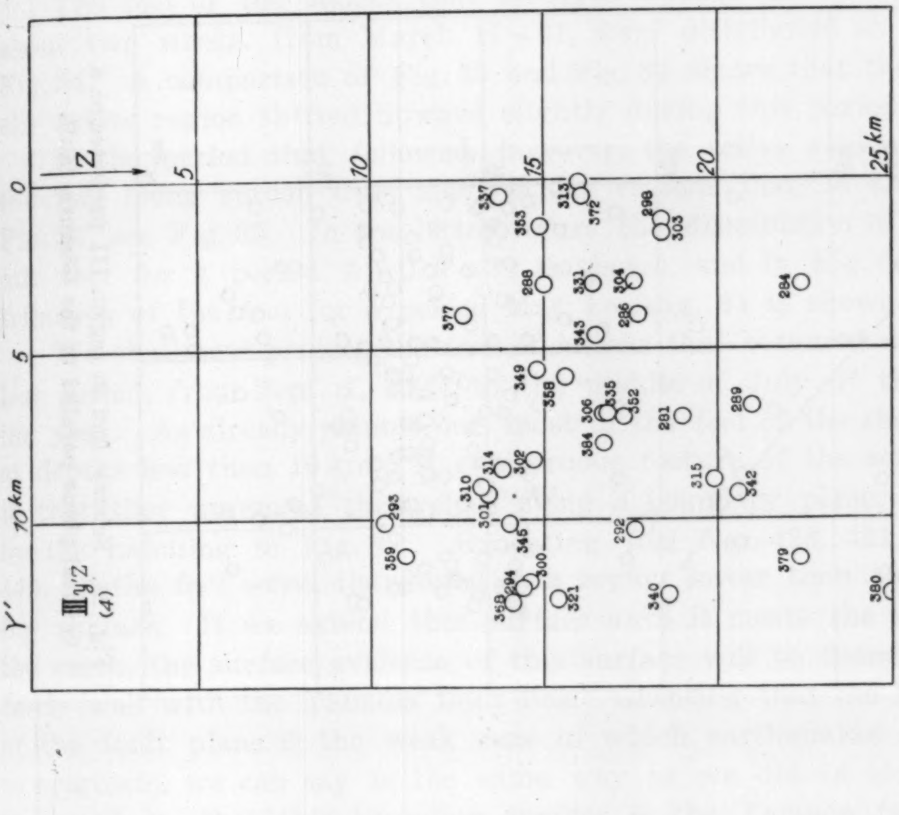

Fig. 36. Distribution of the seismic foci of the shocks that occurred during the period, May 1~August 31, 1927, on a vertical plane parallel to the Gômura fault. (Region III.)

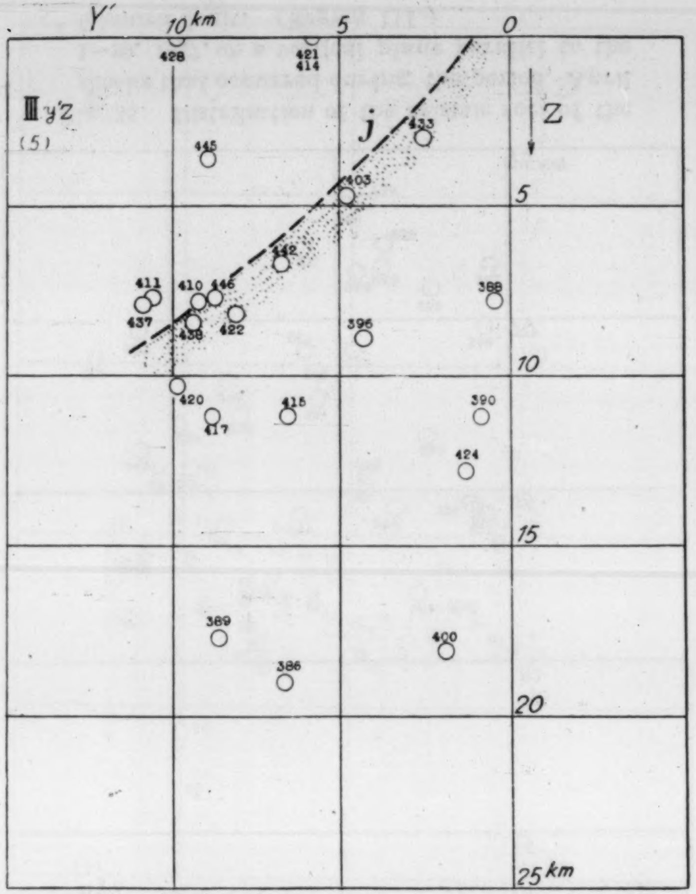

Fig. 37. Distribution of the seismic foci of the shocks that occurred during the period, September 1, 1927~July 15, 1928, on a vertical plane parallel to the Gômura fault. (Region III.)

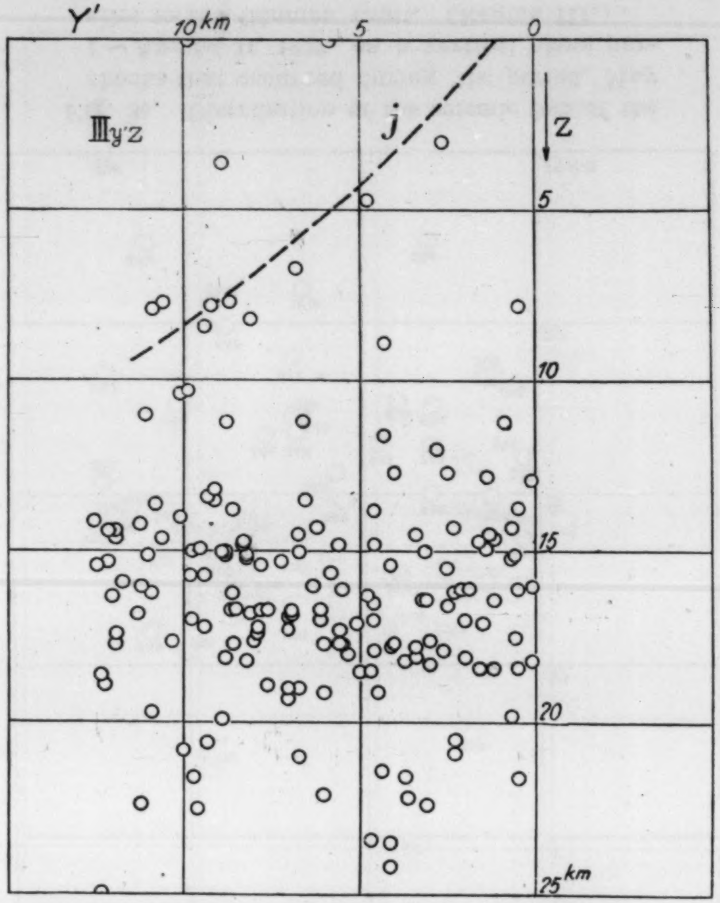

Fig. 38. Seismic foci in region III projected on a vertical plane parallel to the Gômura fault.

The foci of the shocks that occurred during the next period of about two weeks, from March 17∼31, were distributed as shown in Fig. 34. A comparison of Fig. 33 and Fig. 34 shows that the seismically active region shifted upward slightly during this period.

In the period that followed, however, the active region changed, the foci being spread over much wider regions than in the case of Fig. 34, see Fig. 35. In the latter figure the distribution of the seismic foci for a period April 1∼30 is shown, and in Fig. 36 the distribution of the foci for a period May 1∼Aug. 31 is shown.

We shall next project the foci of shocks that occurred during the last period, from Sept. 1, 1927, to the middle of July of the following year. As already pointed out, most of the foci of the shocks were at depths less than 10 km. A conspicuous feature of the seismic foci is that they arranged themselves along a boundary plane, as shown by the hatching in Fig. 37. Excepting foci Nos. 428, 421, 414 and 445, all the foci were distributed in a region lower than this bounding surface. If we extend this surface until it meets the surface of the earth, the surface evidence of this surface will be found to agree fairly well with the Yamada fault line. Granting that the fault zone or the fault plane is the weak zone in which earthquakes are liable to originate, we can say in the same way as we did in the case of the g_0-plane, that this bounding surface is the Yamada fault plane itself.

With respect to the preceding four foci, it should be added that foci Nos. 421 and 414, 445, were situated on plane g_0, while No. 428 was on the earth's surface at a distance of about 6 km east of the Gômura fault zone.

The results here obtained will be very important in connection with the general discussion of seismic foci distribution to be made in the conclusion at the end of this paper. All the foci are projected and shown in Fig. 38.

Block No. II.

We shall now study the foci lying in region II, contiguous northwest of the receding region (see Fig. 24). The eastern boundary of this block, No. II, is the Gômura fault.

(A) Projection on plane $X'Z$.

In projecting the foci of the after-shocks that occurred in March, 1927, on a vertical plane normal to the Gômura fault zone, distance, X' was measured for each focus, their values being given in Table VIII.

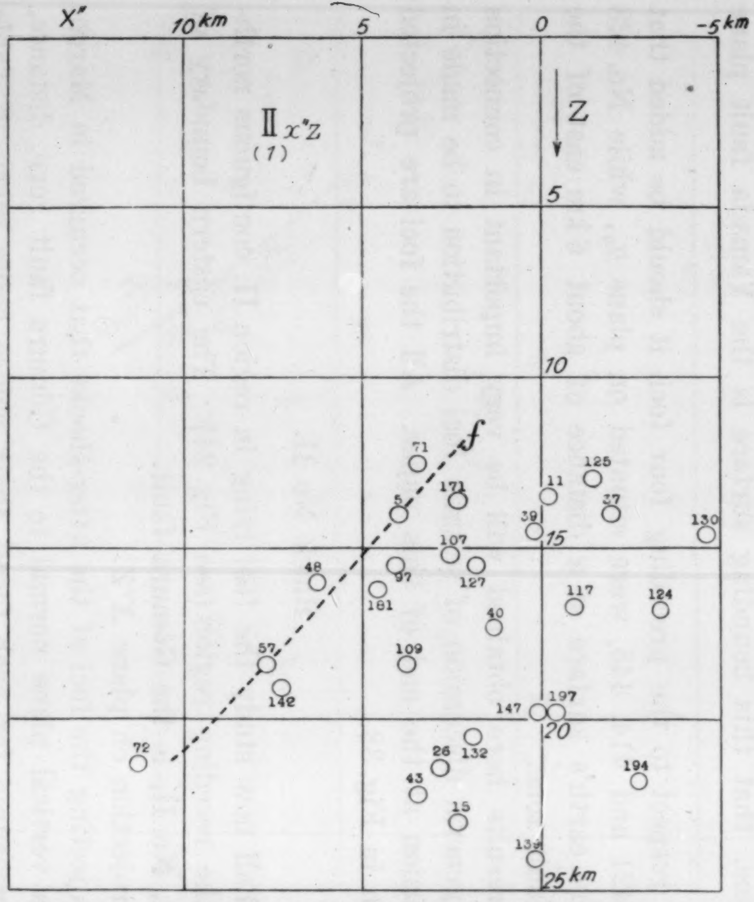

Fig. 39. Distribution of the seismic foci of the shocks that occurred during the period March 12～31, 1927, on a vertical plane normal to the Gômura fault. (Region II.)

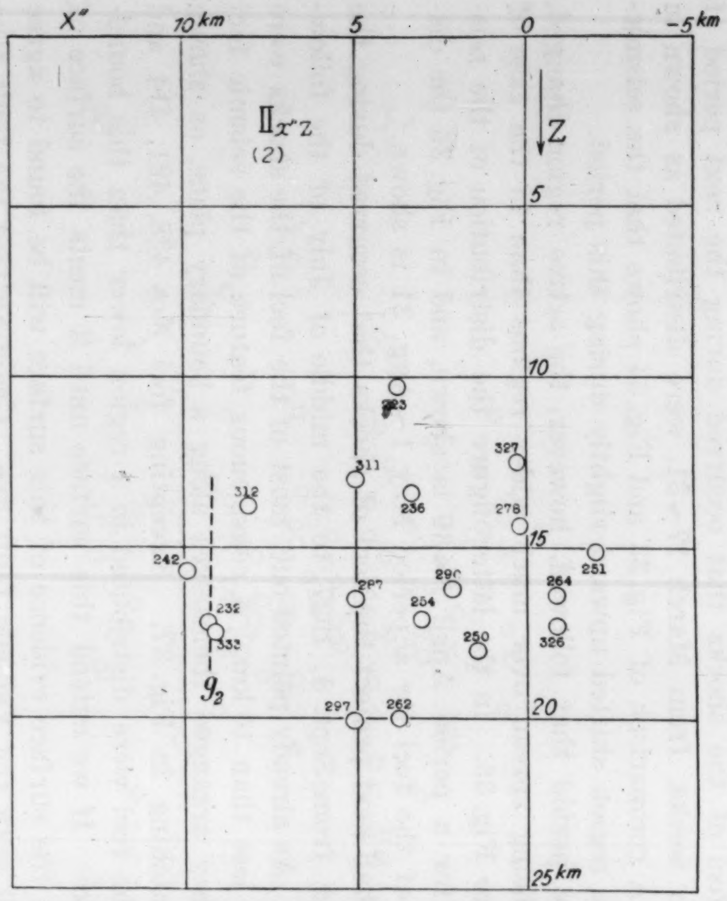

Fig. 40. Distribution of the seismic foci of the shocks that occurred during the period April 1～May 31, 1927, on a vertical plane normal to the Gômura fault. (Region II.)

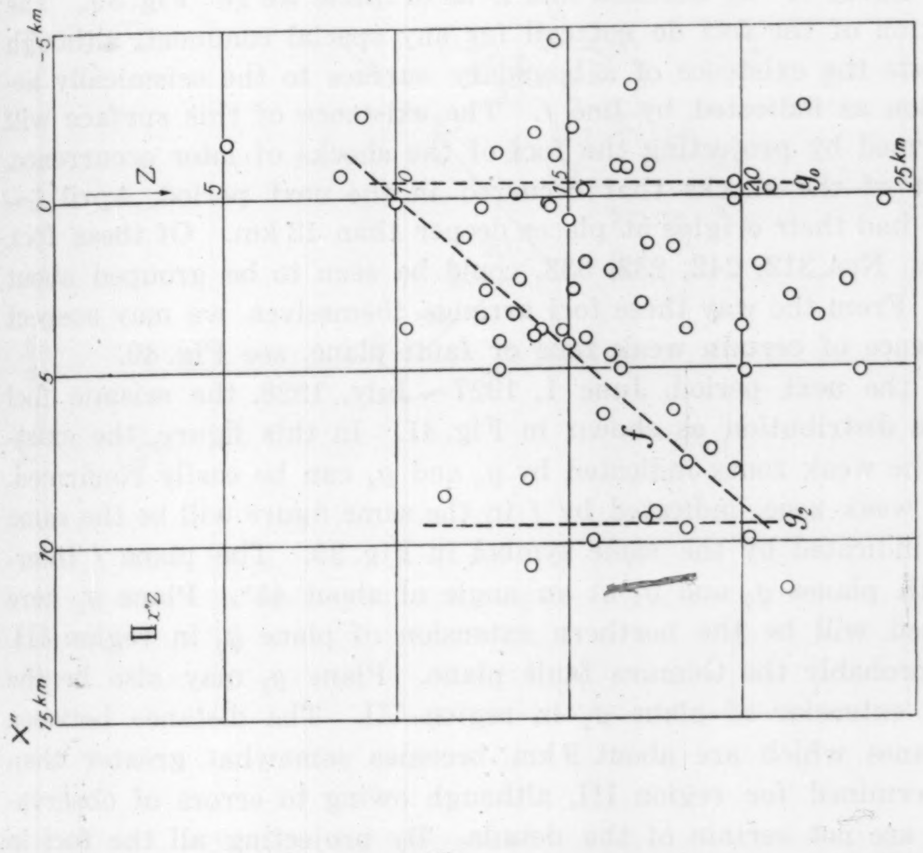

Fig. 42. Seismic foci in region II projected on a vertical plane normal to the Gômura fault.

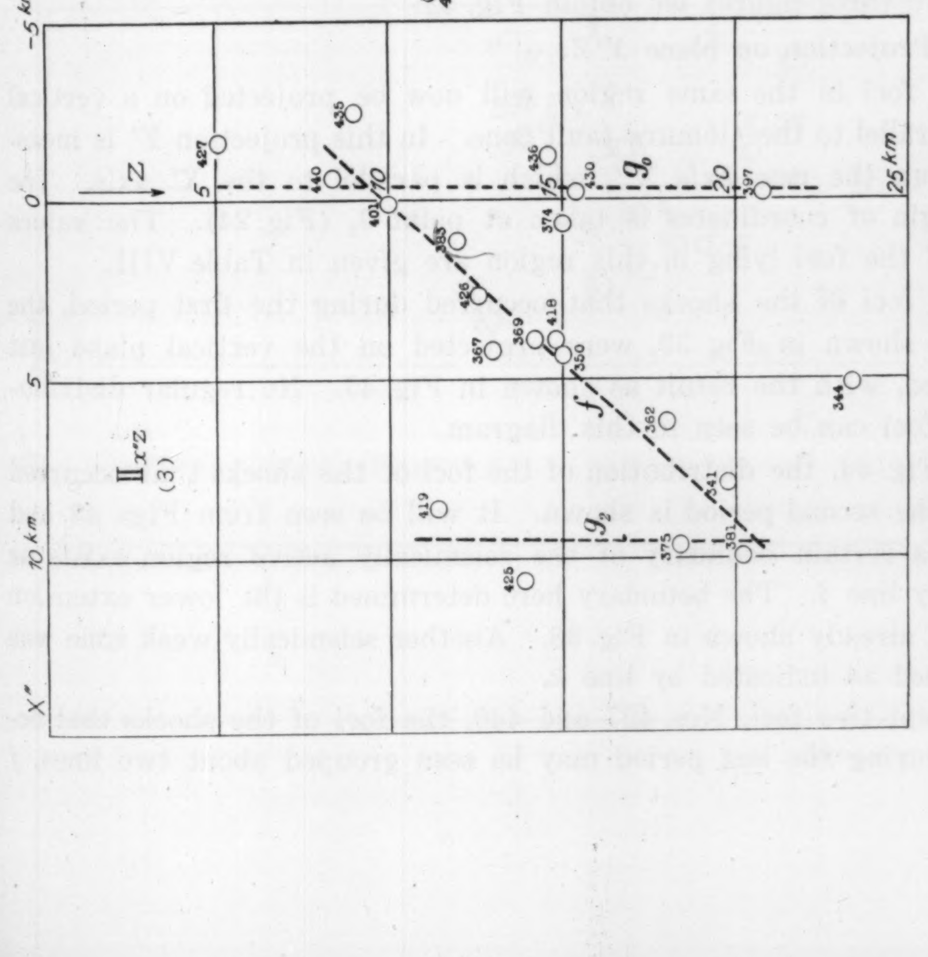

Fig. 41. Distribution of the seismic foci of the shocks that occurred during the period June 1, 1927 ~ July 15, 1928, on a vertical plane normal to the Gômura fault. (Region II.)

By taking X' as abscissa and Z as ordinate we get Fig. 39. The distribution of the foci do not call for any special comment, although it suggests the existence of a boundary surface to the seismically active region as indicated by line f. The existence of this surface will be confirmed by projecting the foci of the shocks of later occurrence.

Most of the shocks that occurred in the next period, April 1～May 31, had their origins at places deeper than 13 km. Of these foci, four, viz., Nos. 312, 242, 232, 333, could be seen to be grouped about line g_2. From the way these foci arrange themselves, we may suspect the presence of certain weak zone or fault plane, see Fig. 40.

For the next period, June 1, 1927～July, 1928, the seismic foci showed a distribution as shown in Fig. 41. In this figure, the existence of the weak zones indicated by g_0 and g_2 can be easily confirmed. Another weak zone, indicated by f in the same figure will be the same surface indicated by the same symbol in Fig. 39. The plane f intersects with planes g_0 and g_2 at an angle of about 45°. Plane g_0 here determined will be the northern extension of plane g_0 in region III. This is probably the Gômura fault plane. Plane g_2 may also be the northern extension of plane g_2 in region III. The distance between these planes which are about 9 km, becomes somewhat greater than that determined for region III, although owing to errors of observation, we are not certain of the details. By projecting all the foci in the above three figures we obtain Fig. 42.

(B) Projection on plane $Y'Z$.

The foci in the same region will now be projected on a vertical plane parallel to the Gômura fault zone. In this projection Y' is measured from the new axis X'', which is parallel to the X' axis. The new origin of coordinates is taken at point 0_2 (Fig. 24). The values of Y' of the foci lying in this region are given in Table VIII.

The foci of the shocks that occurred during the first period, the same as shown in Fig. 39, were projected on the vertical plane just mentioned, with the result as shown in Fig. 43. No regular distribution of foci can be seen in this diagram.

In Fig. 44, the distribution of the foci of the shocks that occurred during the second period is shown. It will be seen from Figs. 43 and 44 that a certain boundary of the seismically active region exists as shown by line j. The boundary here determined is the lower extension of line j, already shown in Fig. 38. Another seismically weak zone was determined as indicated by line k.

Except two foci, Nos. 427 and 440, the foci of the shocks that occurred during the last period may be seen grouped about two lines, j

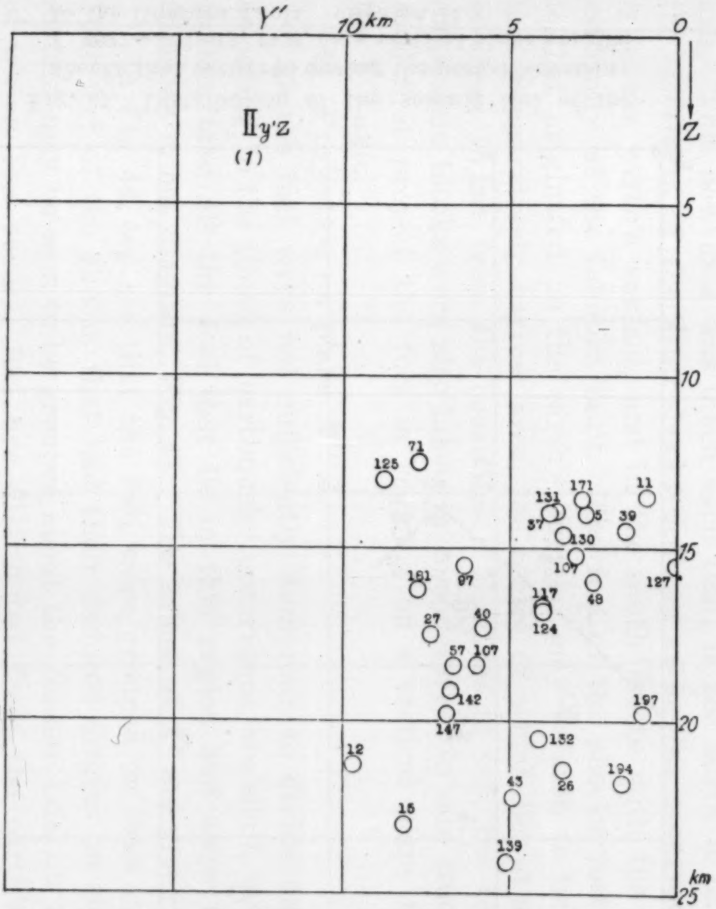

Fig. 43. Distribution of the seismic foci of the that shocks occurred during the period March 12~31, 1927, on a vertical plane parallel to the Gômura fault. (Region II.)

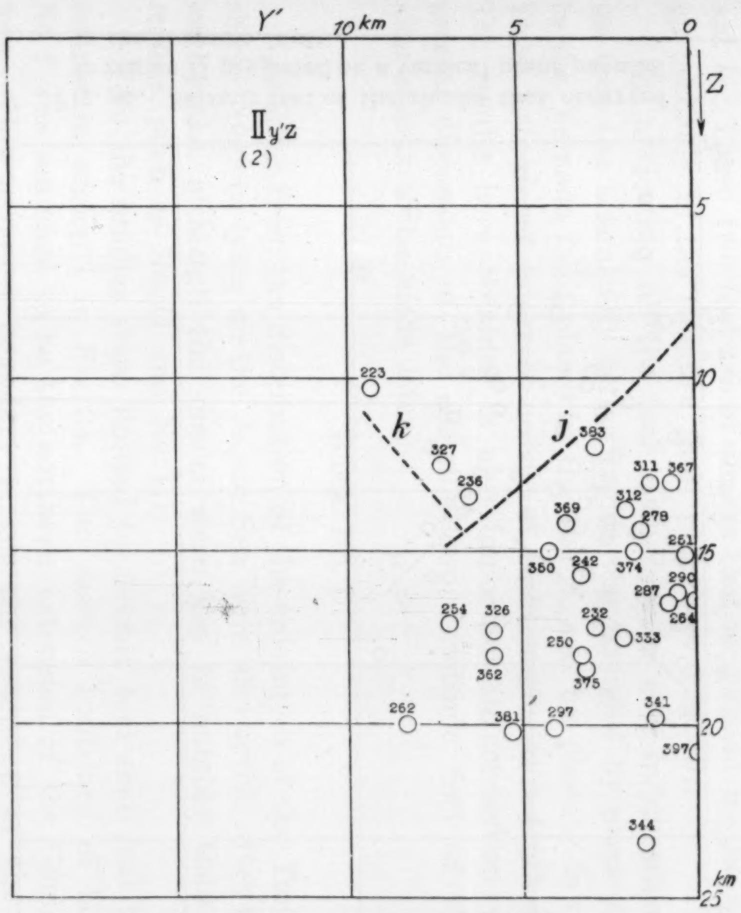

Fig. 44. Distribution of the seismic foci of the shocks that occurred during the period April 1~Oct. 31, 1927, on a vertical plane parallel to the Gômura fault. (Region II.)

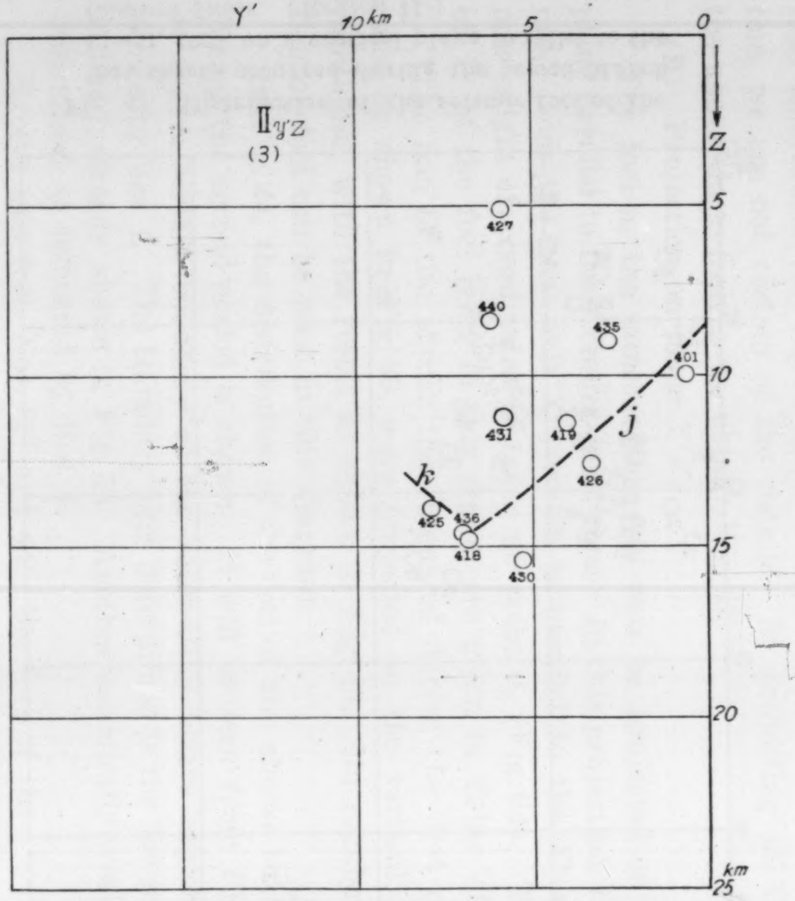

Fig. 45. Distribution of the seismic foci of the shocks that occurred during the period November 1, 1927~July 15, 1928, on a vertical plane parallel to the Gômura fault. (Region II.)

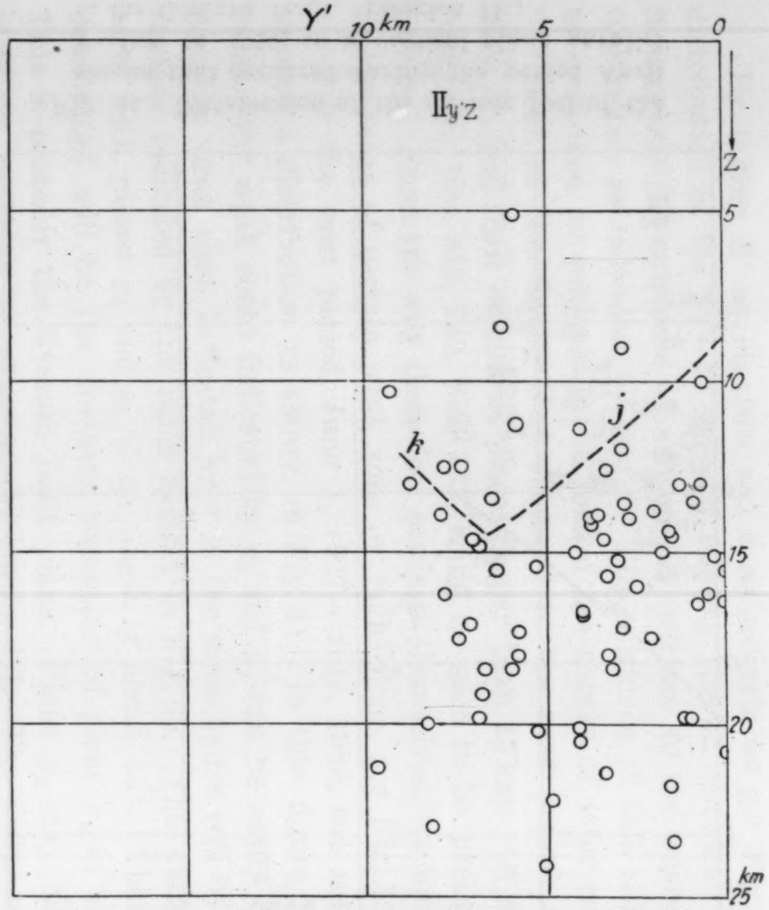

Fig. 46. Seismic foci of the shocks that occurred in region II projected on a vertical plane parallel to the Gômura fault.

and k. These two foci are of shocks that originated in the weak zone g_0, probably in the Gômura fault plane (see Fig. 45).

By projecting all the foci in the region now in question, we can see that the seismically active region was bounded by plane j (perhaps by the Yamada fault plane) in the south, and by plane k in the north. These two planes intersect nearly at right angles at a depth of 15 km. The results here obtained is also important in connection with the general discussion of the distribution of seismic foci of the Tango after-shocks to be made later.

Block No. I.

Judging from the distribution of the epicentres of the Tango after-shocks, regions lying on the Japan Sea were also active after the great earthquake, although the shocks were less in number than in other regions, such as No. II and No. III.

Here the studies were limited to seismic foci that had their epicentres in region I in Fig. 24. The eastern boundary of land block No. I was assumed to be the northern extension of the Gômura fault zone. This assumed boundary is not the extension of the Y′ axis, which shows the mean trend of the Gômura fault zone as found on the actual land surface. It makes an angle of about 10° with the Y′ axis. This new axis was taken such that, in the north it passes near the epicentres of the after-shocks deduced as having occurred virtually on the earth's surface, and in the south meets with the northern extremity of the Gômura fault. The foci of the shocks just referred to that originated on the earth's surface may be seen to be grouped in a comparatively narrow area, the centre of which lies at a distance of about 15 km from the coast line. Needless to say, the foci in the contiguous blocks were also taken in consideration in our studies. We shall first project the foci in region I on a vertical plane normal to the Y″ axis.

(A) Projection on plane $X'''Z$.

As the foci were not sufficiently numerous to divide into classes according to the times of earthquake occurrence, we shall, in this projection, take all the foci that lie in this region and show their distribution in one diagram, Fig. 47. The values of X' are given in Table.

In Fig. 44, we see that the foci were grouped on lines g_0 and g_1. Four foci of the shocks that had their deduced origins on the earth's surface may be seen to be grouped about the former line, on two sides of which line several foci are distributed from the earth's surface to depths greater than 10 km. The plane g_0 in Fig. 47 may be the northern extension of the Gômura fault plane.

Another weak zone is indicated by line g_1 in the same diagram, on both sides of which line several foci may be seen to be grouped. The existence of this weak zone has already been commented on in connection with region III, in which latter region its existence was less certain than in region I.

Another weak zone from which after-shocks originated is that indicated by line g_2. This zone is probably the northern extension of the weak zone, g_2, which was already found in region II and III. But in view of the small number of foci its actual existence is uncertain.

(B) Projection on plane $Y''Z$.

The foci in region I will now be projected on a vertical plane parallel to the Y″ axis. The values of Y'' are given in Table IX.

The results are shown in Fig. 48. A noteworthy fact is that the foci, with only a few exceptions, are in a region lying north of (left in diagram) and below the curve indicated by l. The boundary dips south. Assuming certain errors in the position of the seismic foci we make some corrections in the position of the foci that lies on curve l, when the boundary can then be indicated somewhat schematically by a new curve l'. There are only four foci lying on the upper, or southern side (right-hand side Fig. 48), namely, Nos. 423, 269 and 376, 443. Of these foci Nos. 423 and 376 are situated on line g_0, see Fig. 47, while No. 269 was on the earth's surface, east of line g_0, see also Fig. 47. Only one focus, No. 443, lies west of plane g_0 and on the upper side of curve l. It would lie on line g_1 if it were projected on a vertical plane normal to the Y″ axis, see Fig. 47. On the other hand, the focus just mentioned seems to lie on the upper prolongation of line k which was already shown in Fig. 46; the details will be given later.

The results so far obtained are also important in connection with the general discussion to follow on the distribution of the seismic foci.

Block No. IV.

In our previous paper,[13] four land blocks were taken on the southeastern side of the Yamada fault line, and the distributions of the seismic foci lying in these blocks were shown in different diagrams. The projection of the foci, however, on a vertical plane normal to the faults trending from NE to SW (faults a, b and c in Fig. 24) showed similar results for the foci lying in each block. In the present study, therefore, a wider region, for projection as indicated by IV in Fig. 24

---

[13] N. NASU, *loc. cit.*

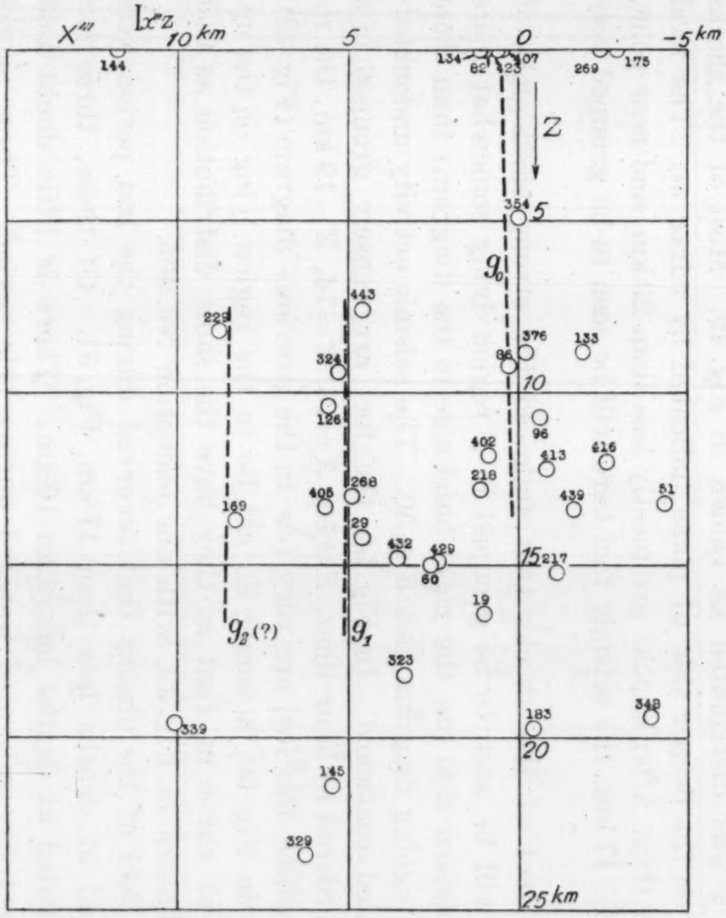

Fig. 47. Distribution of the seismic foci lying in region I on a vertical plane normal to the Y″ axis in Fig. 24.

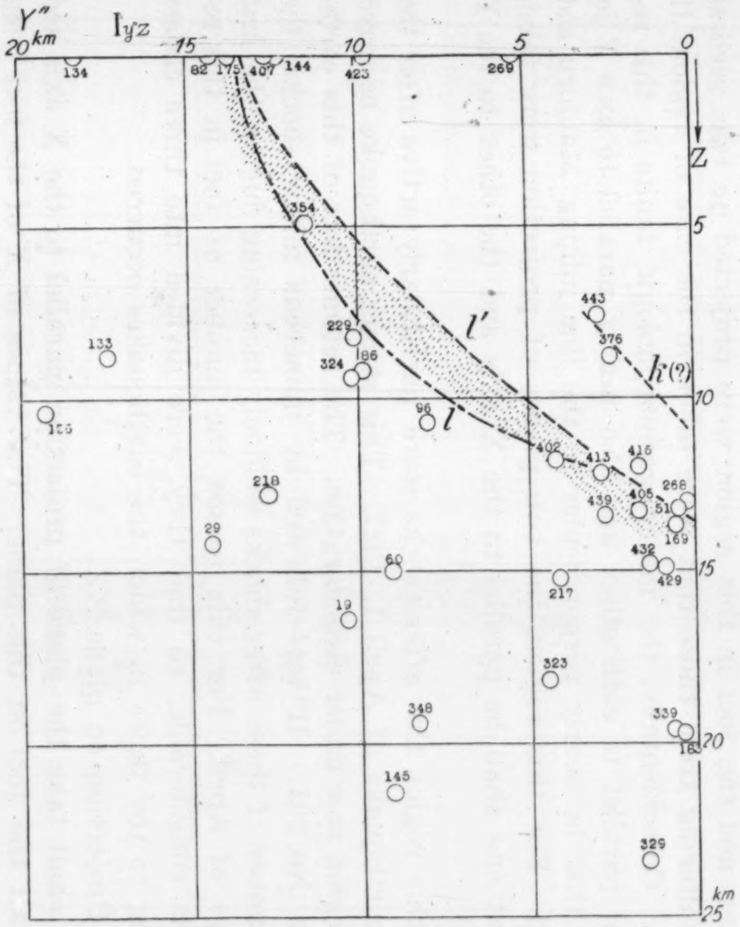

Fig. 48. Distribution of the seismic foci lying in region I projected on a vertical plane parallel to the Y″ axis in Fig. 24.

was taken and the foci in this region were projected on two vertical planes differing from those that were taken in the case of regions II and III. Coincidentally, the major geomorphologic faults in this region run parallel to each other and also nearly parallel to axis Y in Fig. 24, that is, nearly perpendicular to the line joining Maiduru and Kinosaki. For this region, the two planes of projection were taken such that one shall be parallel to the X axis and the other to the Y axis.

In this region the after-shocks were particularly active after the strong earthquake of April 1, 1927. This strong earthquake occurred in the region now under consideration. The seismic foci of this earthquake is No. 201. It was followed by numerous minor shocks, the daily number of these after-shocks suddenly increasing during the first few days of April. For this reason the number of foci in this region was considerable, so that they were divided into three classes according to the times in which the earthquakes occurred.

(A) Projection on plane XZ.

We shall take the plane of projection parallel to the X axis and project all the foci on this plane. The values of X of the foci lying in this region are given in Table X.

The foci of the shocks that occurred before the strong earthquake of April 1 was distributed as shown in Fig. 49. Most of the shocks occurred on the deeper side of plane indicated by curve m. The focal depths of these after-shocks are mostly less than 20 km. and near point, $X=19$, $Z=17$ km, the seismic foci here will be seen to be grouped very thickly.

The foci of the shocks that followed the strong earthquake of April 1 will be seen to be grouped in a region lying somewhat more on the eastern side (on the right-hand side in the diagram) than those in the foregoing diagram, see Fig. 50. The seismic activity undoubtedly migrated eastward. In Fig. 50, the foci are densely grouped in a region bordered by four lines, $Z=10$, $X=15$, $Z=14$, $Z=19$ km, the region in which the foci are very few in the previous diagram (Fig. 49). The foci in Fig. 50, however do not lie in the region lying on the upper side of curve m, that is, they have the same distribution as that already shown in Fig. 49, with one exception No. 305.

The foci of the shocks that occurred during the last period were distributed at depths less than 17 km, Fig. 51. Of these, three foci were situated at depths less than 10 km. There is little doubt that seismic activity migrated upward during this period. Three shocks occurred at depths less than 10 km, that is, in a region lying on the

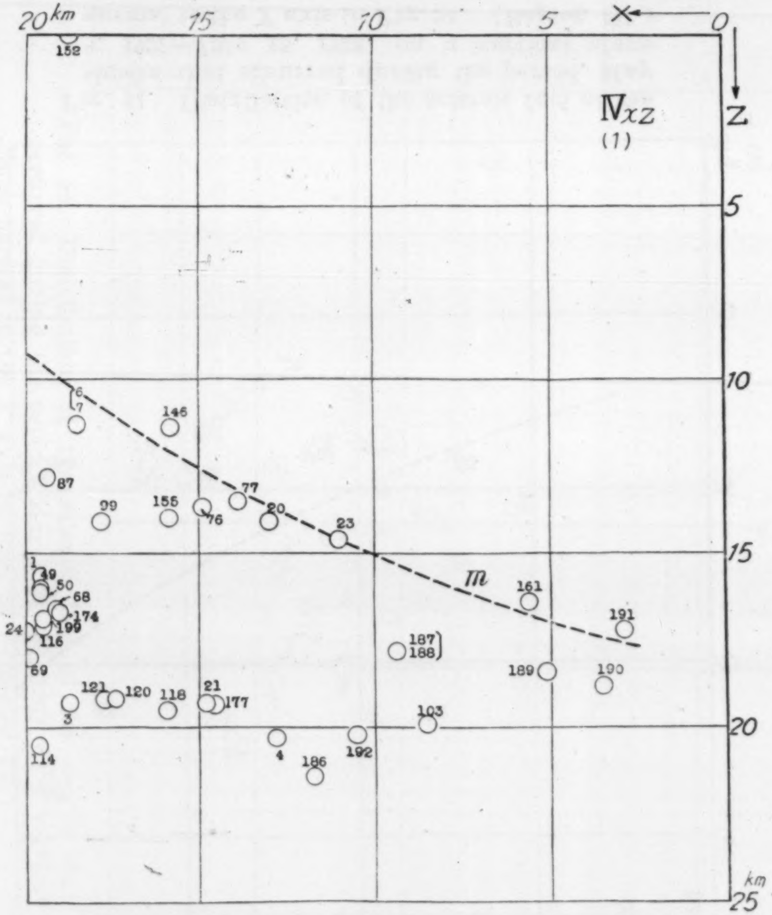

Fig. 49. Distribution of the seismic foci of the shocks that occurred during the period, March 12~31, 1927, on a vertical plane normal to the Y axis in Fig. 24. (Region IV.)

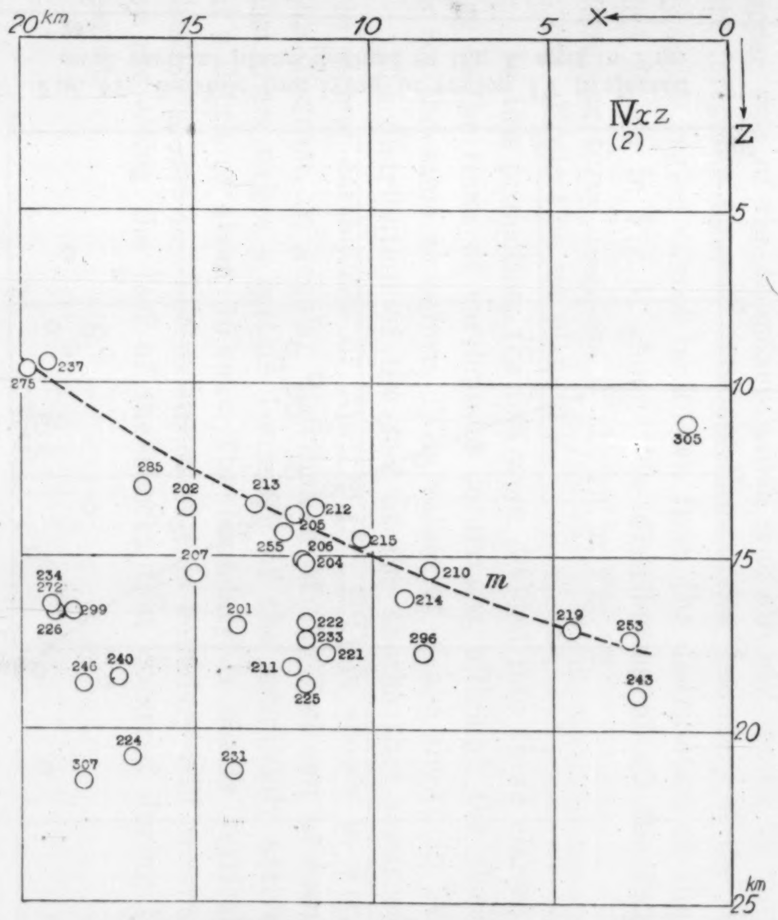

Fig. 50. Distribution of the seismic foci of the shocks that occurred during the period, April 1~May 9, 1927, on a vertical plane normal to the Y axis in Fig. 24. (Region IV.)

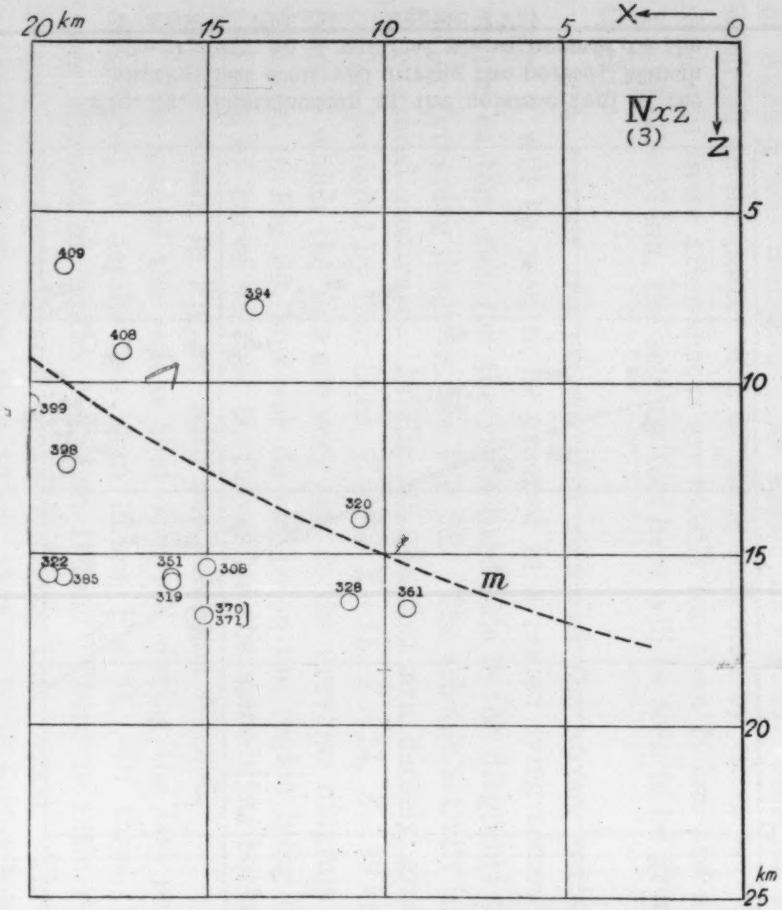

Fig. 51. Distribution of the seismic foci of the shocks that occurred during the period, May 9, 1927~July 15, 1928, on a vertical plane normal to the Y axis in Fig. 24. (Region IV.)

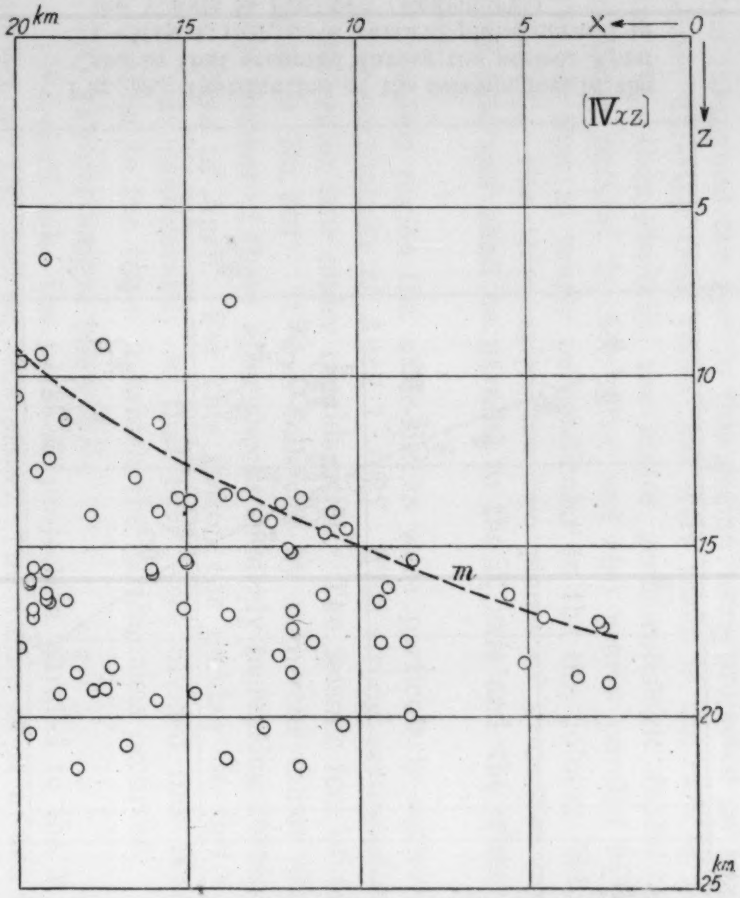

Fig. 52. Seismic foci lying in region IV projected on a vertical plane normal to the Y axis in Fig. 24.

upper side of the boundary which was already shown by curve *m* in the foregoing figures. The existence of the boundary of the seismically active region cannot be known from the distribution of the seismic foci shown in Fig. 51 alone. The distribution of all the foci in the foregoing three diagrams is shown in Fig. 52.

(B) Projection on plane *YZ*.

In this projection, the foci were divided into three classes according to the times of earthquake occurrence, although the classification is not the same as before. The values of *Y* are shown in Table X.

The distribution of the foci of the shocks that occurred before the strong earthquake of April 1 (No. 201) is shown in Fig, 53. In this diagram, no regular distribution of the foci can be seen, except that there exists a certain boundary of the seismically active region at a depth of about 15 km. The boundary is nearly vertical, as indicated by line *p*. The existence of this boundary will become evident by projecting the foci of the shocks that occurred during the next period.

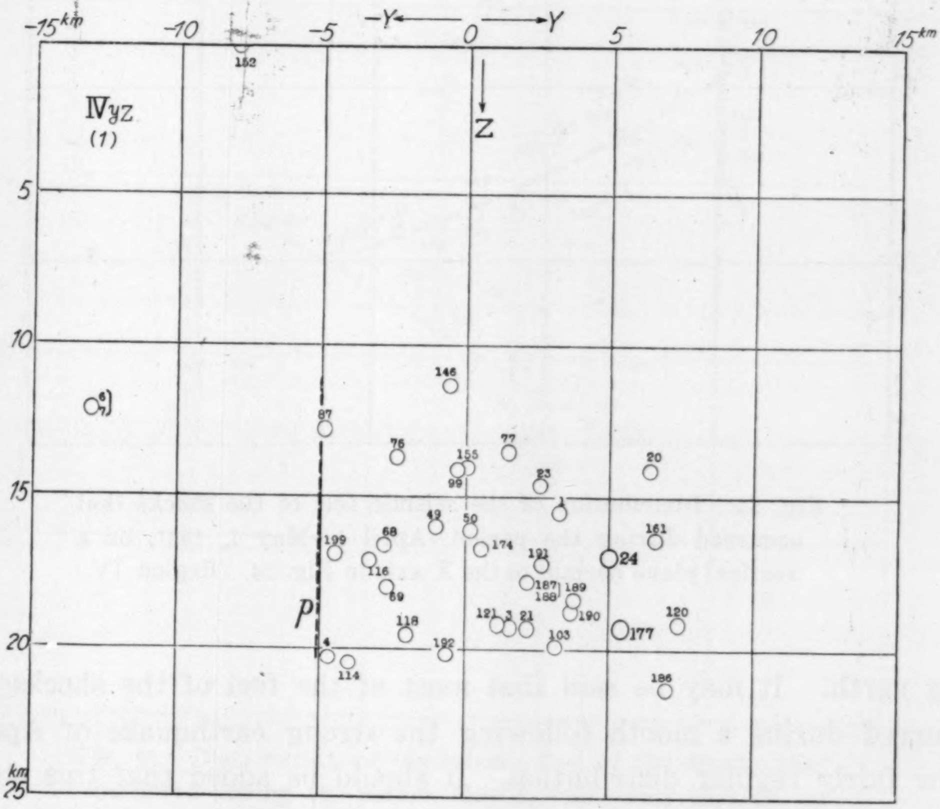

Fig. 53. Distribution of the seismic foci of the shocks that occurred during the period, March 12~31, 1927, on a vertical plane normal to the *X* axis in Fig. 24. (Region IV.)

The foci of the shocks that occurred during the next period, April 1∼May 30, may be grouped on both sides of two lines p and q_1, Fig. 54. Line p indicates the southern boundary of the seismically active region just mentioned. Line q_1 indicates another weak zone dipping north. It may be said that most of the foci of the shocks that occurred during a month following the strong earthquake of April 1 show fairly regular distribution. It should be added that this strong earthquake originated near the intersection of the two planes indicated by lines p and q_1.

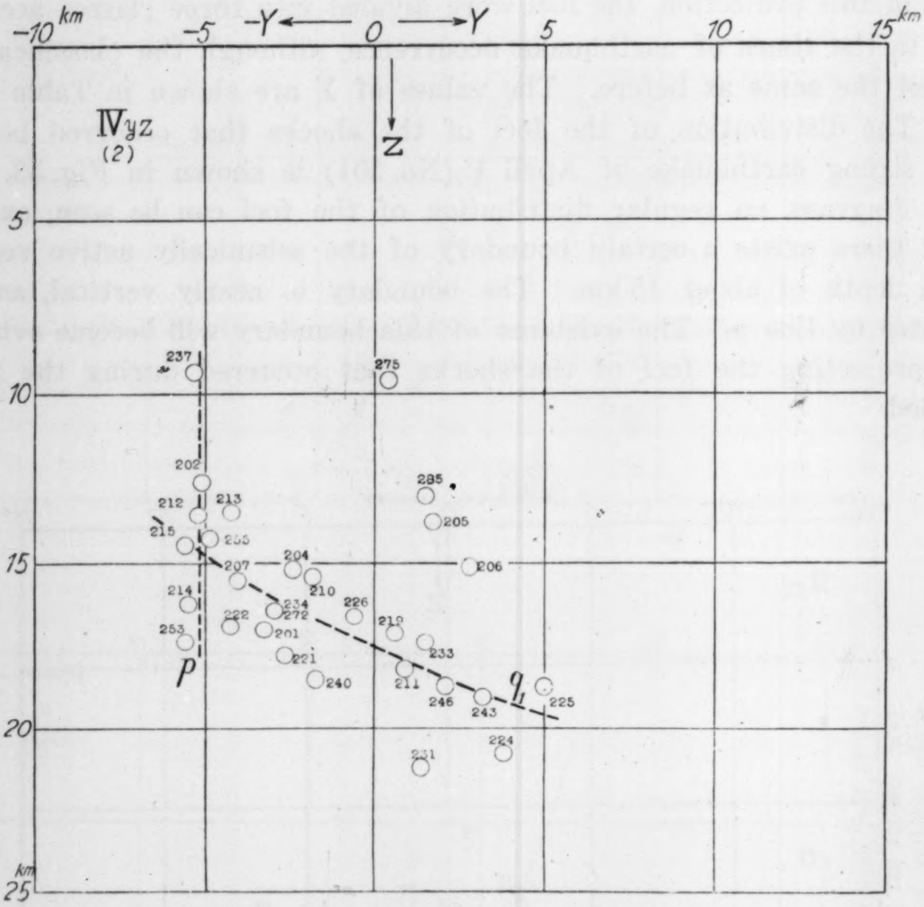

Fig. 54. Distribution of the seismic foci of the shocks that occurred during the period, April 1∼May 1, 1927, on a vertical plane normal to the X axis in Fig. 24. (Region IV.)

The foci of the shocks that occurred during the last period, from

June, 1927, to the middle of July, 1928, show a distribution as shown in Fig. 55. The distribution of the foci makes it clear that the seismic activity migrated upward during this period. Although most of the foci may be seen to be grouped about line q_2, which is nearly parallel to line q_1, in Fig. 54, the former line lies in a shallower region than the latter. The boundary, p, may also be seen in this diagram. The foci Nos. 409, 408, 394, 378 are of shocks that originated in other weak zones, but the details are unknown. The distribution of all the foci that lie in this region is shown in Fig. 56.

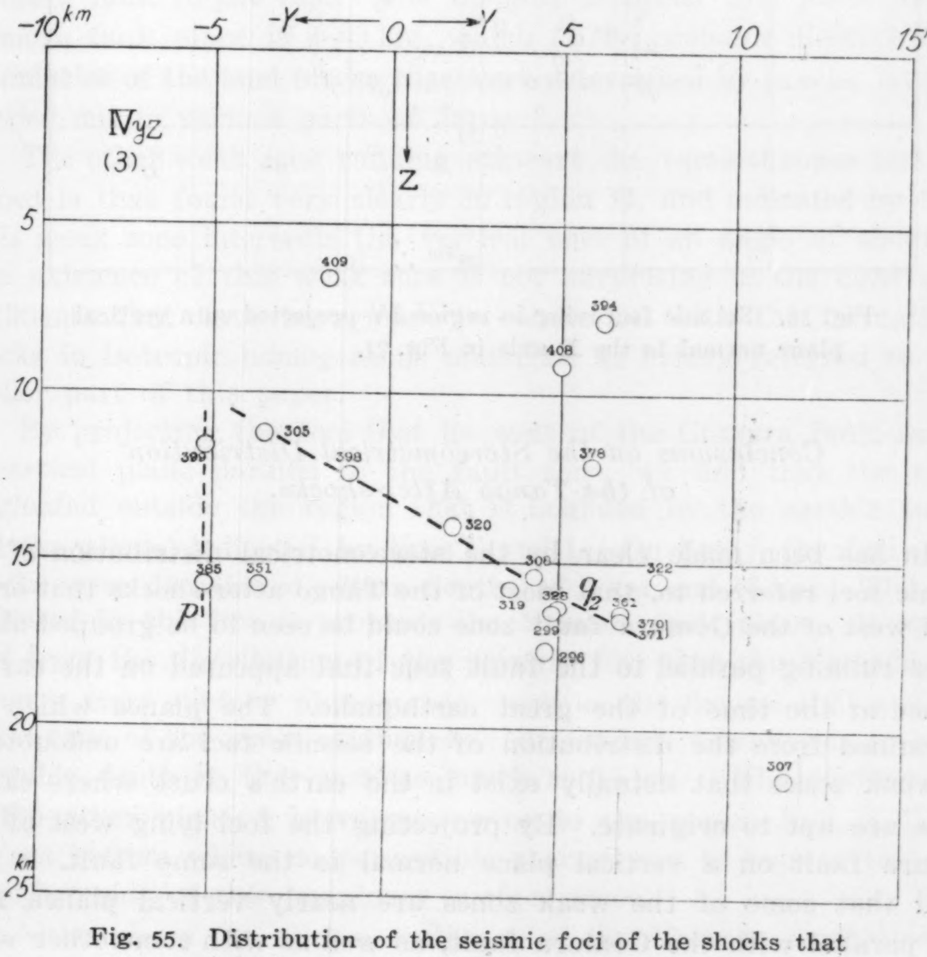

Fig. 55. Distribution of the seismic foci of the shocks that occurred during the period, May 1, 1927~July 15, 1928, on a vertical plane normal to the X axis in Fig. 24.

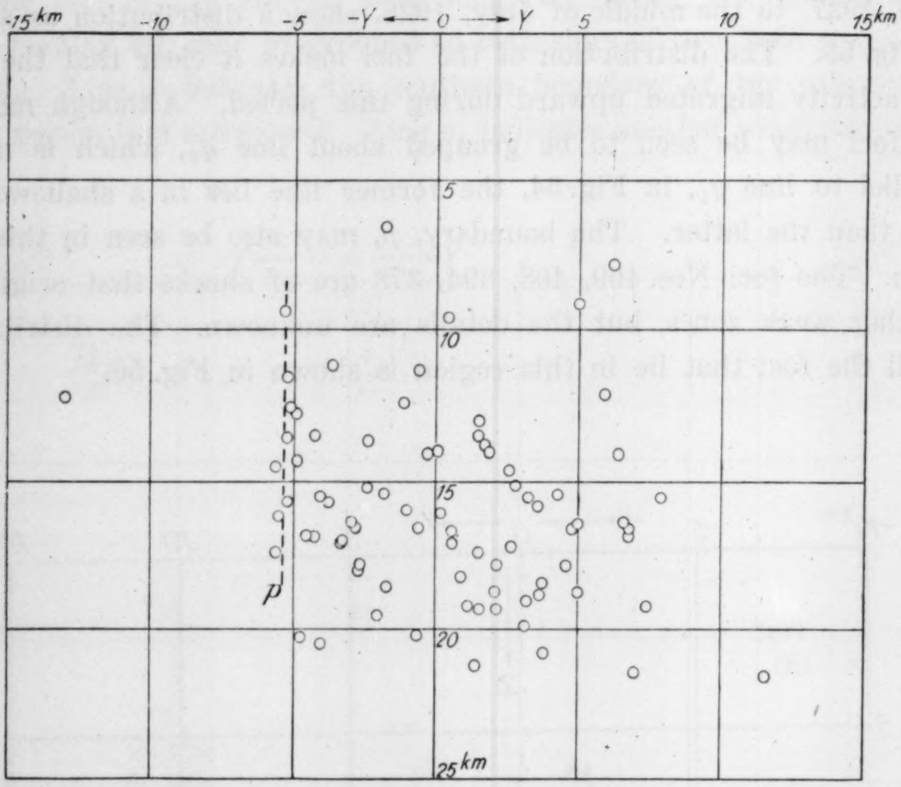

Fig. 56. Seismic foci lying in region IV projected on a vertical plane normal to the X axis in Fig. 24.

Conclusions on the Stereometrical Distribution of the Tango After-shocks.

In has been made clear by the stereometrical distribution of the seismic foci referred to, that most of the Tango after-shocks that originated west of the Gômura fault zone could be seen to be grouped about planes running parallel to the fault zone that appeared on the earth's surface at the time of the great earthquake. The planes which are determined from the distribution of the seismic foci are undoubtedly the weak zones that actually exist in the earth's crust where earthquake are apt to originate. By projecting the foci lying west of the Gômura fault on a vertical plane normal to the same fault, it was found that some of the weak zones are nearly vertical planes, running parallel with the Gômura fault, as well as with some other weak zones lying nearly horizontally. The arrangement of these weak zones can clearly be seen particularly in regions II and III. One of these vertical planes ought to be that whose surface trace was that of the Gômura fault zone as observed on the ground. This plane is indicated in the foregoing studies by line g_0. Judging from the distribution of the seismic foci on this line it is possible to say that along this weak zone the earthquakes originated from the earth's surface to a depth greater than 10 km, and further that this zone runs through the earth's crust that forms the land as well as through the earth's crust that lies under the Japan Sea.

Another conspicuous weak zone, which is also vertical and parallel to the Gômura fault zone, is that indicated by line g_2. In this weak zone, earthquakes originated at fairly shallow depths (less than 10 km) during the later half of the period of our observations, although they did not occur on the earth's surface. This plane may be the western boundary surface of the land blocks bordered by the Gômura fault in the east. The distance between this plane and the Gômura fault plane is 8∼9 km, which is the probable distance of the boundaries of the land blocks that were determined by precise levellings carried out in various parts of Japan.

The other weak zone running athwart the vertical zones just mentioned is that found very clearly in region II, and indicated by line f. This weak zone intersects the vertical ones at an angle of about 45°. The existence of this weak zone is not surprising in the light of experiments that have been made in connection with the formation of cracks in isotropic homogeneous materials as briefly referred to in an earlier part of this paper.

By projecting the foci that lie west of the Gômura fault zone on a vertical plane parallel to the fault zone, we find that the shocks originated outside the region that is bounded by the earth's surface and the planes indicated by lines j and l. On line j, the foci of the shocks were distributed within depths of 3 km and 15 km. The plane indicated by this line is probably the Yamada fault plane. It may be said from the distribution of the seismic foci that the Yamada fault is not a mere surface phenomenon, such as the flexure that appeared at the time of the great earthquake, but extends downwards to a considerable depth–in this case as much as 15 km. The surface trace of the other plane, l, is vague, owing to the reason that it lies on the sea bottom where no perceptible changes can be seen in the chart on either side of this imaginary surface trace.

Although in the region southeast of the Yamada fault line, the seismic foci did not show any remarkable features connected with their distribution, yet by projecting the foci in this region on a vertical plane normal to the major geomorphologic faults lying there (faults a, b, c in Fig. 24) it was found that the origins of the shocks were mainly confined to a region lying below curve m. It is possible that there exists certain boundary surface of the seismically active region which could be indicated by curve m.

By projecting the foci in the same region on a vertical plane parallel to the major faults just mentioned, the southern boundary of the seismically active region can fairly accurately be determined. This boundary is indicated by line p. Further, in taking only the foci of the shocks that occurred during the two months following the strong earthquake of April 1, we can obtain a fairly regular distribution of the seismic foci such that the foci may be seen to be grouped about two lines, p and q_1.

We shall next attempt a brief explanation of the migration of seismic activity along certain weak zones. In our study, the earthquake foci were divided into several classes according to the times of earthquake occurrence, and the distributions of the foci shown for each of these classes. The results obtained show that seismic foci belonging in a certain class may group themselves about certain lines. According to the class of foci projected, the lines assume different positions. For example, in region III, the foci of the shocks that occurred during the 8 days that followed the great earthquake could be seen to be grouped about lines g_0 and h_0, while, the foci of the shocks that occurred in the next period could be seen to be grouped about lines g_0 and h_1. As will be seen from Figs. 26, 27, 29, line h_4 lies in a region somewhat shallower than line h_0 — a fact suggesting that the seismically active region migrated upward. The upper boundaries of the active region indicated by these lines are nearly parallel to each other and lie nearly horizontally. The same may be found in the case of lines q_1 and q_2 which were determined from the distribution of the seismic foci lying in region IV. Another noteworthy fact is that, in region II, the shocks that occurred during the later half of our observations had their origins in shallow places and their foci may be seen to be grouped about lines j and k, while in region III the shocks were particularly active in shallow places and their foci aligned themselves along lines g_3. From the facts so far referred to, it is undeniable that the seismic activity migrated upward during the later half of our observations.

It must be added that the horizontal boundaries of the seismically active region just mentioned change their position upward with time, so that in order to determine this horizontal boundray it is best first to divide the foci into several classes according to the times of earthquake occurrence, and then project each class of foci in a separate diagrams by itself. To project all the foci, regardless of the times of earthquake occurrence, would sometimes end in failure to obtain desired results.

Extended studies of the stereometrical distribution of the seismic foci of the Tango after-shocks enable us to visualise the form and the movement of the land block that played such an important part in the great Tango earthquake. In the following paragraphs an attempt will be made to describe the results of investigation thus obtained.

By projecting on the vertical plane that passes through the surface traces of the Gômura fault, all the seismic foci of after-shocks that occurred within a distance of about 10 km to the west of this fault zone, it was found that in the triangle enclosed by the three lines corresponding to, (1) the projection of the earth's surface, (2) the plane that is probably that of the Yamada fault, and (3) the plane designated *l* or *l'*, no after-shocks at all, except one, wereexper ienced there since the beginning of the observations that were begun immediately after the great earthquake, up to the end of July, 1928, the following year. We may state with confidence, then, that the triangle corresponds to the cross-section of certain blocks that lie on the western side of the Gômura fault zone, where they are cut by a vertical plane parallel to the fault itself.

Strictly speaking, the lower part of the same block has somewhat complicated form. The block now in question is bounded in the north not only by plane *l*, but also by plane *k*. The latter plane was deduced from the distribution of the seismic foci lying in region II. If we take plane *k* in consideration and visualise the cross-section of the block, then the results become as shown in Fig. 57.

In the lower part of the block just mentioned where planes *j*, *k* and *l* meet, several foci of shocks that occurred in the later half of our period of observations are fairly densely distributed. Most of the foci of these shocks may be seen to be grouped about lines *j*, *k*, *l*. From this it may be said that the seismic activity migrated in both directions, one upward along plane *j* and the other along planes *k* and *l*, although the activity mostly migrated along the first plane, that is the Yamada fault.

It should be added that the foci lying inside the region corresponding to the cross-section of the foregoing land block when projected on a vertical plane parallel to the Gômura fault zone are of shocks that originated in the Gômura fault plane, or of the shocks that originated in the contiguous block lying east of the fault plane just mentioned. The solitary focus that lies in the triangle, the cross-section just referred to, is No. 443, that of the shock that occurred on June 20, 1928. It lies on line g_1 when projected on a vertical plane normal to the Gômura fault line (Fig. 47). The upper part of the weak zone indicated by line g_1, which might extend upward and inside the land block just mentioned, suggests that some changes in the form of the land block took place in its lower part about 15 months afterward the great earthquake.

On taking the plane of projection normal to the Gômura fault, it will readily be noticed that land mass lying outside of the land block, the vertical section of which was deduced in the foregoing, may be cut up into several small blocks by planes parallel to the Gômura fault plane. In the land mass lying north of the block just mentioned and in the Japan Sea, are three planes which are indicated by projections marked g_0, g_1, g_2, see Fig. 47; and in that lying on the southern side of plane *j*, the Yamada fault plane, by the same notations are also indicated three planes. But, the existence of plane g_2 is not certain in the former land mass, as also g_1 in the latter land mass. Though the arrangement of the seismically weak zones differs somewhat, there is no question that these weak zones are the boundary of the land blocks that are nearly parallel to the Gômura fault plane.

We shall now visualize the form and the movement of the land block that played such an important part in the recent great earthquake: that is, the block west of the Gômura fault.

Firstly, the block has the form of a triangular prism with one of its side on the earth's surface and its base on, or parallel to the Gômura fault plane.

Secondly, the mechanism as a result of which the present destructive earthquake occurred may be visualised somewhat as follows: Initially, the equilibrium that had obtained in the Tango block was disturbed along the old fault plane, resulting in the new Gômura fault, causing the land block on the western side of this fault to be detached from the surrounding body along the weak zones represented by the Yamada fault plane and the plane marked *l*. The wedge-shaped block thus formed was then elevated and shifted towards the south. The formative process of this block may be regarded in the light of a very ordinary and natural process, akin to that in which a thick wall-like material is cracked by a shearing force, although in our case the force might act nearly parallel to the walls.

As to how much the block was bodily displaced we have no means of knowing, since the block is not a perfect rigid body, although its mean bodily displacement can be deduced from the results of the pre-

and post-earthquake triangulations carried out in the seismic district. Prof. Imamura and F. Kishinouye[14] recalculated the displacements of the geodetic points, the primary and secondary points, lying on the surface of the land block just referred to, reducing each displacement parallel to the Gômura fault zone. The results showed that the triangulation-marks lying on the eastern side of the Gômura fault were displaced towards the north, while those of the western side of the same fault had shifted towards the south, and that the amounts of these displacements diminished with increasing distance from the fault zone. The displacements at Simooka, Isanagosan, and Nyôo, deduced from the observations of 1884∼1888 and August 1927, are shown in the table that follows. These triangulation-marks lie on the surface of the wedge-shaped block in question.

(x), (y)	Simooka	Isanagosan	Nyôo
Distance from the fault (x)	−0·7 km	−4·7 km	−7·0 km
Displacement parallel to the fault (y)	−127 cm	−48 cm	−87 cm

where −x=towards W; −y=towards S.

It the deformation of the land block be admitted as having been caused by its movement, then the mean displacement of this block can be calculated by taking the mean value of y from the foregoing table. The mean displacement thus obtained is −87 cm, that is, 87 cm towards S., or exactly towards SSE.

It is of no less interest to study the vertical movement at the time of the great earthquake of the land block under consideration. From the results of precise levellings, changes in the heights of the land surface are known to be as shown in Fig. 58. This Fig. is taken from the report of the levellings that were carried out by the Military Land Survey.[15] In the map in Fig. 58 the regions that rose up at the time of the great earthquake are shown with hatching, contours for every 20 cm

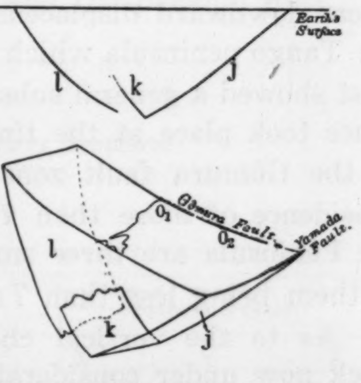

Fig. 57. The wedge-shaped land block that are deduced from the stereometrical distribution of the seismic foci of the Tango after-shocks. (Upper = cross-section, Lower = side view of the land block.)

---

[14] A. Imamura and F. Kishinouye, "On the Horizontal Shift of Dislocation accompanied by the Recent Destructive Earthquakes in the Kwantô District and in Tango Province," *Bul'. Earthq. Res. Inst.*, **5** (1928), 35.

[15] *Report of the Military Land Survey*, (November 1930).

upward displacement being drawn with full-lines and those for every

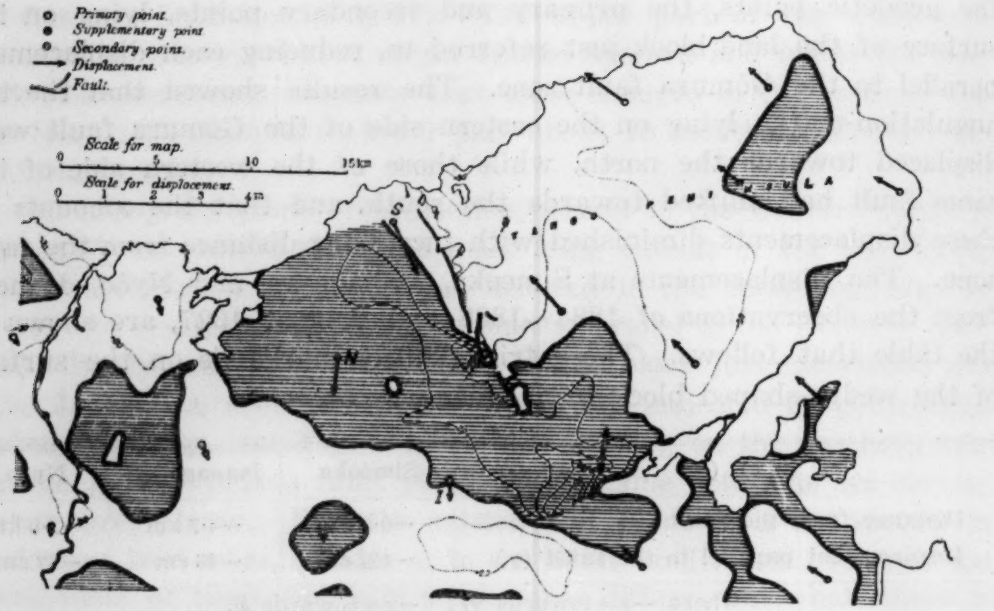

Fig. 58. Map showing the displacements of the triangulation-marks and the changes in level in the Tango district.
(S=Simooka, N=Nyôo, I=Isanagosan.)

20 cm downward displacement in dotted lines. In Fig. 58 we see that the Tango peninsula which was displaced as a whole towards the northwest showed a general subsidence of about 20 cm. Most of this subsidence took place at the time of the great earthquake. The region east of the Gômura fault zone, and adjacent to it, showed a remarkable subsidence of more than 70 cm. Near the northeastern extremity of the Peninsula are three small upheaved areas, the extents of upheaval in them being less than 7 cm.

As to the vertical changes in the surface of the wedge-shaped block now under consideration, we may say that most parts of its surface showed upheaval. We see in Fig. 58, that a fairly large elevated area lies west of the Gômura fault adjacent to it. The width of this area (here by width is meant distance from the fault just mentioned) gradually lessens in the southern part. The extent of upheaval showed increase with decreasing distance from the Gômura fault zone. The region that is enclosed within the full-line contour, indicating a 20 cm upheaval, lies lengthwise, parallel with the Gômura fault. In the region lying north of the Yamada fault, and adjacent to it, the upheaval was particularly great–about 80 cm, which may be due to the fact that the edge of the land block curled up when it forcibly pressed against the land mass contiguous to it.

Ignoring the local minor changes in level which must have actually occurred at the time of the great earthquake on the block surface, this large area that actually upheaved agrees in form and position with the surface of the wedge-shaped block as deduced by the stereometrical projection of the seismic foci of the Tango after-shocks.

In conclusion, the writer desires to express his sense of indebtedness to Prof. K. Suyehiro, the Director of the Earthquake Research Institute, and Professor A. Imamura in particular, under whose able and experienced guidance the present studies were made. Grateful acknowledgements are due to Messrs. K. Wakimoto, Y. Takahasi, Y. Wada, N. Arai, U. Masui, S. Sakamoto, S. Kodama, N. Hayasida and R. Yosioka, whose assistance in the arduous labour of actual seismic observations were of inestimable value.

Table VI.

(A)

Durations of the Preliminary Tremors and the Seismic Foci.

Notations;

D. P. T.=Duration of the preliminary tremors.
t_0=D. P. T. at Maiduru.
t_1=D. P. T. at Kinosaki.
t_2=D. P. T. at Ine.

Time of Occurrence.				D. P. T.			No.	Seismic Focus.		
				t_0	t_1	t_2		X	Y	Z
Month	Day	h	m	sec.	sec.	sec.		km.	km.	km.
III	12,	15	28	3·0	4·1	3·0	1	19·6	3·3	15·5
(1927)			42	3·3	3·8	3·7	2	22·7	− 3·2	15·8
		17	51	3·2	4·4	3·4	3	18·7	1·6	19·3
		18	21	2·9	5·1	4·0	4	12·8	− 4·8	20·3
			41	4·5	2·6	3·6	5	34·7	6·3	14·0
		20	03	3·0	4·3	4·4	6	18·5	−13·0	11·2
			04	3·0	4·3	4·4	7	18·5	−13·0	11·2
			35	3·3	4·1	3·6	8	21·0	− 0·9	18·2
		21	43	5·2	2·2	5·3	9	40·8	−11·3	11·3
	13,	6	30	3·6	3·5	4·0	10	25·7	− 5·2	15·2

(to be continued.)

Table VI. (*continued.*)

Time of Occurrence.				D. P. T.			No.	Seismic Focus.		
				t_0	t_1	t_2		X	Y	Z
Month	Day	h	m	Sec.	Sec.	Sec.		km.	km.	km.
		7	44	4·1	3·0	3·1	11	30·6	8·2	13·5
			53	4·0	3·0	3·6	12	30·2	2·1	15·0
			55	4·1	3·4	3·8	13	28·8	1·7	18·9
		8	28	3·3	4·1	3·6	14	21·0	− 0·9	18·2
		10	20	5·4	3·4	4·2	15	37·6	11·2	23·0
		11	09	3·2	3.8	3·5	16	22·3	− 1·6	15·1
			25	4·3	3·1	5·1	17	31·6	−15·9	8·3
			40	4·0	4·1	3·2	18	24·6	9·7	20·8
		12	47	6·2	3·3	4·2	19	44·6	21·6	16·4
			52	2·4	4·8	2·5	20	13·0	6·4	14·1
		13	02	2·9	4·8	3·3	21	14·8	2·2	19·3
			37	4·0	3·2	4·4	22	29·2	− 8·1	14·5
			42	2·2	5·0	2·9	23	11·0	2·6	14·6
		15	26	3·2	4·2	3·0	24	20·0	5·0	17·2
			34	3·2	4·0	3·8	25	21·1	− 4·4	16·0
		18	20	4·9	3·3	4·0	26	34·5	7·6	21·4
			32	5·1	2·8	3·9	27	38·0	9·7	17·5
		20	23	6·4	3·7	5·8	28	44·2	0·0	30·8
			34	6·7	3·1	4·7	29	50·0	22·4	14·2
		23	27	3·4	4·1	3·0	30	21·6	6·4	17·7
	14,	0	47	3·5	3·7	3·7	31	24·3	− 1·7	17·0
		1	58	3·1	3·7	3·6	32	22·3	− 3·7	13·3
		2	06	3·4	4·0	3·3	33	22·0	2·9	18·1
			14	3·5	3·8	3·6	34	23·7	− 0·2	17·9
		3	53	4·1	3·2	3·8	35	29·9	1·1	17·6
			57	3·4	3·8	3·6	36	23·1	− 1·1	17·1
		5	37	4·3	3·1	3·0	37	31·5	11·5	14·0
			39	4·2	3·0	3·5	38	31·3	4·9	15·9
		6	46	4·2	3·0	3·2	39	31·3	8·3	14·5
			58	4·8	3·0	3·6	40	35·2	10·4	17·3
	14,	7	51	3·8	3·4	3·6	41	27·3	1·1	17·0
			53	3·9	3·3	3·5	42	28·3	2·9	16·8
		10	44	5·1	3·3	4·1	43	36·0	8·2	22·2
		11	20	4·1	3·0	3·6	44	30·7	2·8	15·7
		12	49	4·1	3·1	3·4	45	30·3	5·3	16·0
		13	21	3·7	3·7	3·6	46	25·2	1·2	18·5
		14	02	4·3	3·1	4·2	47	31·5	− 1·1	18·1
			16	4·7	2·6	3·9	48	36·1	4·5	16·0
		18	42	3·0	4·1	3·4	49	19·6	− 1·0	16·0
		19	13	3·0	4·1	3·3	50	19·6	0·2	16·1
			33	4·8	3·2	3·0	51	34·3	17·2	13·2
			54	3·1	4·1	3·7	52	20·1	− 3·7	16·4
		20	12	4·4	3·7	3·9	53	29·2	4·2	22·5
		22	13	4·1	3·2	3·6	54	29·8	3·3	17·2
	15,	3	08	4·0	3·2	3·8	55	29·3	0·2	16·9
		4	28	4·2	3·2	4·0	56	31·3	− 1·1	16·7
			34	5·3	2·6	4·3	57	40·2	6·3	18·4
		7	08	3·6	3·7	4·4	58	24·7	−10·1	14·7
		10	23	3·1	4·1	3·3	59	20·1	0·9	16·8
		12	05	6·1	3·0	4·2	60	45·1	19·6	15·0

(*to be continued.*)

Table IV. (*continued.*)

Time of Occurrence.				D. P. T.			No.	Seismic Focus.		
				t_0	t_1	t_2		X	Y	Z
Month	Day	h	m	sec.	sec.	sec.		km.	km.	km.
		13	40	3·4	3·4	3·3	61	25·2	1·2	13·8
			46	3·2	3·9	3·8	62	21·6	−4·6	15·6
		14	24	3·9	3·0	3·2	63	29·7	5·4	13·6
		16	12	3·8	3·2	3·3	64	28·3	4·0	15·1
			20	3·6	3·3	4·1	65	26·7	−7·1	12·9
			20	3·4	4·0	4·2	66	22·1	−7·9	16·7
			39	3·4	3·8	3·8	67	23·1	−3·4	16·9
			44	3·0	4·2	3·6	68	19·1	−2·8	16·6
			55	3·2	4·2	3·7	69	19·9	−2·7	18·0
		20	34	3·8	3·6	3·7	70	96·3	0·5	18·5
		21	20	4·9	2·4	3·6	71	38·1	10·1	12·5
		23	32	5·9	2·7	4·9	72	44·8	5·6	21·3
	16,	3	22	3·5	3·4	3·4	73	25·7	0·7	14·8
		6	36	4·4	2·8	3·8	74	33·4	3·1	16·3
		9	31	3·5	3·8	3·4	75	23·6	2·1	17·8
		10	51	2·4	4·5	3·3	76	14·9	−2·4	13·7
		11	05	2·3	4·6	2·9	77	13·9	1·5	13·5
			21	3·6	3·7	3·5	78	24·7	1·4	17·9
		12	01	3·2	4·0	4·3	79	21·1	−11·0	12·9
			31	4·3	3·1	3·6	80	31·5	5·1	17·4
	16,	13	39	4·2	3·3	3·4	81	29·9	6·8	17·7
		16	04	6·3	2·9	4·0	82	47·0	24·6	0·0
			51	3·6	4·0	4·0	83	25·1	−3·7	19·5
		17	05	3·6	3·5	3·8	84	25·7	−2·8	16·2
			12	3·8	3·2	3·3	85	28·3	4·0	13·0
			55	5·9	2·9	3·8	86	43·8	21·7	9·2
		23	55	2·8	4·0	3·6	87	19·4	−4·9	12·8
	17,	1	29	3·1	3·8	3·9	88	21·7	−7·1	12·9
		2	05	4·4	2·7	3·8	89	33·7	2·9	15·3
			52	4·0	3·0	3·8	90	30·1	−0·3	15·3
		3	27	4·0	2·8	3·6	91	31·0	1·5	13·5
		4	15	4·4	3·2	4·3	92	31·7	−2·5	19·3
		5	53	3·6	3·5	3·3	93	25·7	3·1	16·0
		6	18	3·6	3·5	3·4	94	25·7	1·9	16·1
			51	6·3	6·7	5·6	95	25·7	12·8	44·4
		7	40	5·7	2·9	3·7	96	42·3	20·4	10·7
			40	4·9	2·6	5·0	97	37·5	8·7	15·5
		14	14	3·8	3·7	4·2	98	25·7	−5·5	18·4
			39	2·7	4·2	3·2	99	17·8	−0·3	14·1
		17	21	6·7	4·5	5·7	100	42·6	9·6	35·8
			23	5·3	3·7	5·3	101	35·3	−6·2	26·8
			52	3·2	3·9	3·3	102	21·6	0·9	16·1
		21	45	2·6	5·5	3·3	103	8·5	3·2	19·9
		22	40	3·4	3·3	3·6	104	25·7	−2·6	12·7
		23	41	3·9	3·1	3·6	105	29·2	1·3	15·3
	18,	0	08	3·3	3·9	3·0	106	22·1	4·8	16·3
		2	42	4·5	2·8	3·5	107	34·0	7·6	15·2
		3	06	3·3	3·8	3·4	108	22·7	0·3	16·1
			44	5·0	2·9	3·9	109	26·9	8·7	18·4
			50	3·5	3·3	3·2	110	26·2	2·7	13·5

(*to be continued.*)

Table IV. *(continued.)*

Time of Occurrence.				D. P. T.			No.	Seismic Focus.		
				t_0	t_1	t_2		X	Y	Z
Month	Day	h	m	sec.	sec.	sec.		km.	km.	km.
		4	52	3·1	3·8	3·7	111	21·7	− 4·7	13·8
		6	16	3·4	3·9	3·1	112	22·6	4·6	17·1
		9	29	3·1	3·7	3·5	113	22·3	− 2·7	13·4
		13	35	3·4	4·7	4·0	114	19·6	− 4·0	20·5
		14	40	3·9	3·4	3·5	115	27·8	3·2	17·4
		21	47	3·1	4·2	3·7	116	19·5	− 3·3	17·1
		23	45	4·5	3·2	3·3	117	32·3	10·9	16·7
	19,	4	35	3·0	4·7	3·7	119	15·9	− 2·0	19·5
		5	17	3·6	3·6	3·3	118	25·2	3·2	16·7
		6	28	3·2	4·6	2·9	120	17·4	7·4	19·2
	19,	8	10	3·1	4·5	3·4	121	17·7	1·2	19·2
		12	51	3·8	3·6	4·2	122	26·2	− 5·9	17·5
		15	50	7·4	3·8	5·7	123	53·6	19·4	25·6
		19	00	4·4	3·4	3·1	124	30·7	12·6	16·8
			54	4·8	2·9	3·2	125	35·5	14·5	13·0
			55	7·2	3·3	5·0	126	53·8	25·7	10·4
	20,	2	36	4·2	3·0	3·4	127	31·3	6·1	15·5
		3	20	3·3	3·8	4·1	128	22·7	− 8·2	14·0
		9	52	3·9	3·4	4·3	129	27·8	− 6·8	16·4
		10	54	4·2	3·4	2·8	130	29·4	13·2	14·6
			54	4·2	3·3	2·8	131	30·0	12·9	13·9
		11	27	4·9	3·3	3·8	132	34·4	8·8	20·5
		13	45	6·6	3·6	4·2	133	46·7	28·9	8·8
		14	12	6·8	3·3	4·4	134	49·9	28·0	0·0
		15	03	3·7	3·7	3·8	135	25·2	− 1·3	18·3
		22	45	4·0	3·1	3·3	136	29·7	5·6	15·1
			45	3·8	3·2	3·4	137	28·2	3·0	15·2
			47	3·7	3·6	3·1	138	25·7	6·4	16·7
	21,	0	11	5·1	3·7	4·0	139	33·8	10·8	24·1
		2	54	3·5	3·5	3·1	140	25·2	4·2	15·0
		11	49	3·7	3·4	3·0	141	26·6	6·7	14·9
		22	21	5·3	2·7	4·3	142	39·9	6·7	19·1
	22,	0	46	4·5	3·4	4·1	143	31·3	1·9	21·6
		2	17	6·7	2·0	4·9	144	54·2	16·4	0·0
		3	16	6·5	3·3	4·8	145	47·3	17·8	21·4
		5	16	2·3	4·3	3·0	146	15·8	− 0·6	11·4
		6	54	5·0	3·3	3·7	147	35·1	12·1	19·8
		12	57	3·7	3·3	3·2	148	27·1	4·4	14·8
		15	18	3·6	3·7	4·2	149	24·6	− 7·2	16·3
		16	58	3·5	3·8	3·5	150	23·6	1·0	17·8
		20	55	3·7	3·5	2·7	151	26·2	9·7	14·2
	23,	1	29	2·3	3·8	3·7	152	18·7	− 8·0	0·0
		4	48	3·8	3·2	3·4	153	28·2	3·0	15·2
		5	55	5·3	3·0	4·9	154	38·6	− 1·5	22·5
		18	52	2·5	4·4	3·1	155	15·8	0·1	14·0
		21	58	4·1	2·7	4·3	156	31·9	− 6·8	11·6
		22	50	3·7	3·5	2·8	157	26·1	8·9	14·6
	24,	1	56	3·2	3·7	3·4	158	22·7	− 0·6	14·7
		6	40	4·0	3·2	3·6	159	29·2	2·5	16·7
		8	41	3·5	3·8	3·2	160	23·6	4·2	17·3

(to be continued.)

Table IV. (*continued.*)

Time of Occurrence.				D. P. T.			No.	Seismic Focus.		
				t_0	t_1	t_2		X	Y	Z
Month	Day	h	m	sec.	sec.	sec.		km.	km.	km.
	24,	8	56	2·2	5·7	2·8	161	5·6	6·6	16·4
		10	18	3·3	3·7	3·4	162	23·2	0·2	15·5
			33	3·2	3·7	3·4	163	22·7	−0·6	14·7
		17	39	3·0	3·9	3·5	164	20·7	2·6	14·3
	25,	0	34	5·5	2·9	4·2	165	40·6	11·4	19·3
		4	14	3·9	3·6	3·0	166	26·8	9·2	16·8
		9	17	4·4	2·8	4·2	167	33·4	−2·0	16·2
		13	36	4·2	2·8	3·5	168	32·0	4·4	14·4
		14	16	5·6	2·1	4·3	169	44·2	9·5	13·7
		17	40	3·2	4·0	3·1	170	21·1	3·4	16·4
		19	13	4·4	2·7	3·4	171	33·7	7·6	13·6
			48	4·0	4·3	3·9	172	23·3	2·3	24·2
		23	33	3·5	4·0	4·3	173	22·5	−8·4	17·2
	26,	7	56	3·0	4·2	3·0	174	19·0	0·6	16·7
	27,	1	21	6·1	3·2	3·6	175	43·6	26·6	0·0
		3	21	4·0	3·0	3·5	176	30·2	3·1	15·0
		4	03	2·9	4·9	3·0	177	14·1	5·7	19·3
		19	54	4·1	3·2	4·2	178	29·8	−4·0	17·0
	28,	8	53	7·5	2·0	6·0	179	62·2	11·2	6·0
	29,	0	52	4·0	3·3	3·9	180	28·8	−0·9	17·7
		5	06	5·1	2·6	3·9	181	38·8	9·3	16·2
		22	02	3·8	3·1	3·6	182	28·6	0·4	14·5
	30,	2	18	5·3	3·3	3·8	183	37·3	14·8	19·7
		4	23	5·1	2·8	5·7	184	38·0	−18·1	8·7
		10	23	4·2	3·3	4·4	185	30·0	−5·6	18·2
		22	30	3·0	5·3	3·1	186	11·7	7·0	21·4
			39	2·4	5·3	3·2	187	9·4	2·2	17·8
			39	2·4	5·3	3·2	188	9·4	2·2	17·8
			41	2·3	5·8	3·2	189	5·1	3·8	18·4
			57	2·3	6·0	3·3	190	3·5	3·7	18·8
		23	18	2·1	6·0	3·3	191	2·9	2·7	17·2
	31,	0	53	2·7	5·3	3·6	192	10·5	−0·6	20·2
		3	35	5·3	2·3	5·3	193	41·4	−9·5	14·3
		9	09	4·5	3·8	3·5	194	29·4	10·6	21·8
			13	7·5	2·8	6·3	195	59·4	6·4	21·0
		11	44	7·7	4·0	6·5	196	56·0	9·6	32·0
		12	14	4·4	3·5	3·5	197	30·4	8·5	19·8
		19	13	3·4	3·8	3·8	198	23·0	−3·4	16·8
IV	1,	2	56	3·1	4·2	3·8	199	19·5	−4·6	16·9
		4	40	3·6	4·1	3·7	200	22·4	0·4	20·5
	1,	6	07	2·6	4·8	3·6	201	13·8	−3·2	17·0
		9	49	2·5	4·5	3·6	202	15·2	−5·1	13·6
		11	42	3·9	2·9	4·2	203	30·0	−6·6	12·0
		14	49	2·3	4·9	3·4	204	11·9	−2·4	15·2
		16	26	2·2	4·8	2·9	205	12·2	1·7	13·8
		18	23	2·3	4·9	2·9	206	12·0	2·8	15·1
		19	24	2·6	4·6	3·0	207	15·0	−4·0	15·5
		20	28	5·0	2·7	4·6	208	37·8	−1·3	18·9
	2,	6	28	4·2	3·8	4·3	209	27·6	−2·9	22·2
		10	29	2·1	5·3	3·4	210	8·4	−1·8	15·4

(*to be continued.*)

Table IV. (*continued.*)

Time of Occurrence.				D. P. T.			No.	Seismic Focus.		
				t₀	t₁	t₂		X	Y	Z
Month	Day	h	m	sec.	sec.	sec.		km.	km.	km.
		11	35	2·6	5·0	3·3	211	12·3	0·9	18·2
		23	18	2·2	4·9	3·6	212	11·6	− 5·2	13·6
	3,	0	05	2·3	4·7	3·5	213	13·3	− 4·3	13·5
		1	34	2·3	5·3	3·8	214	9·1	− 5·5	16·2
		2	07	2·2	5·1	3·7	215	10·3	− 5·6	14·5
	7,	4	47	4·4	3·8	4·5	216	28·8	− 3·5	23·5
		5	37	5·4	3·1	3·6	217	39·0	18·0	15·2
	8,	13	26	6·3	3·2	4·2	218	46·1	23·4	12·8
		17	42	2·1	5·8	3·4	219	4·5	0·6	17·1
	11,	18	54	3·7	3·8	3·6	220	24·7	1·6	19·1
	12,	4	19	2·5	5·1	3·6	221	11·3	− 2·6	17·8
		5	06	2·5	5·0	3·7	222	11·9	− 4·2	16·9
		9	33	5·0	2·2	3·6	223	39·4	10·9	10·3
		21	58	3·2	4·7	3·3	224	16·8	3·8	20·8
		22	19	2·7	5·1	3·0	225	11·9	5·0	18·7
			57	3·0	4·2	3·4	226	19·0	− 0·6	16·6
	13,	0	28	3·6	3·4	4·0	227	26·2	− 5·6	14·3
		7	06	4·7	3·0	4·3	228	34·5	0·4	19·7
		17	55	6·4	2·2	4·6	229	50·6	16·6	8·2
		21	00	3·2	4·0	3·2	230	21·2	2·4	16·6
			52	3·0	5·0	3·5	231	13·9	1·4	21·2
	14,	1	17	5·0	2·5	4·3	232	38·4	2·6	17·2
		2	43	2·5	5·0	3·2	233	11·9	1·5	17·4
		5	57	3·0	4·2	3·6	234	19·1	− 2·9	16·4
		12	36	5·3	4·0	4·2	235	33·8	11·9	26·9
		21	20	4·8	2·5	3·6	236	37·1	9·4	13·4
	15,	1	59	2·6	3·9	3·5	237	19·2	− 5·3	9·4
		2	44	4·0	3·1	3·5	238	29·7	3·4	15·7
		3	51	3·5	4·3	3·5	239	20·8	2·6	20·9
		4	04	3·0	4·5	3·6	240	17·2	− 1·7	18·5
	15,	4	56	3·6	4·0	4·2	241	23·0	− 6·2	18·9
		10	49	5·0	2·3	4·3	242	39·1	2·4	15·7
		14	36	2·3	6·1	3·4	243	2·6	3·2	19·0
	16,	4	52	3·5	3·4	3·2	244	25·6	3·1	14·3
		20	57	4·2	3·0	3·6	245	31·3	3·9	16·2
		21	08	3·1	4·4	3·3	246	18·2	2·1	18·7
		22	34	4·5	2·8	4·2	247	34·0	− 0·8	17·0
	17,	15	23	3·7	4·2	3·6	248	22·4	2·9	21·6
			44	3·7	4·2	3·5	249	22·4	4·0	21·4
	18,	9	39	4·6	3·1	3·6	250	33·4	8·6	18·0
		18	03	4·0	3·3	3·0	251	28·8	9·2	15·1
		20	24	7·1	3·5	7·0	252	54·2	−10·6	27·5
	20,	5	49	2·1	6·0	3·6	253	2·8	− 0·6	17·4
	21,	4	50	5·0	2·8	3·8	254	37·3	9·9	17·1
		5	32	2·4	4·7	3·6	255	13·5	− 4·8	14·3
		11	23	3·1	3·8	3·3	256	21·7	0·0	14·6
		16	43	3·9	3·4	3·8	257	27·8	− 0·2	17·7
	22,	12	31	4·3	3·0	4·1	258	31·9	− 1·2	17·2
		22	35	3·4	4·2	3·6	259	20·9	0·2	19·8
		23	32	7·2	3·2	6·5	260	54·6	− 1·8	22·8

(*to be continued.*)

Table VI. (*continued.*)

Time of Occurrence.				D. P. T.			No.	Seismic Focus.		
				t_0	t_1	t_2		X	Y	Z
Month	Day	h	m	sec.	sec.	sec.		km.	km.	km.
	23.	0	40	3·5	4·4	3·7	261	20·2	0·6	21·6
	24,	15	45	5·3	3·0	4·1	262	38·7	10·2	20·0
	25,	19	27	3·1	3·7	4·2	263	22·3	−11·3	7·8
		22	08	4·1	3·3	3·2	264	29·3	8·2	16·4
	26,	4	36	3·8	4·5	3·5	265	21·0	5·9	23·4
		22	10	3·5	3·9	3·2	266	23·1	1·7	18·0
		23	38	3·9	3·6	3·7	267	26·8	1·5	19·1
			38	5·3	2·3	3·9	268	41·3	11·3	13·0
	27,	2	03	5·3	2·7	3·1	269	39·3	20·5	0·0
		8	07	6·3	4·0	6·1	270	42·0	− 5·9	32·2
			19	3·9	4·1	3·6	271	24·1	4·4	22·1
	28,	2	04	3·0	4·2	3·6	272	19·1	− 2·9	16·4
		8	37	7·5	4·0	5·3	273	53·6	28·8	17·6
		16	26	5·5	3·6	3·1	274	37·4	26·3	8·2
		18	04	2·6	3·8	2·9	275	19·8	0·4	9·6
	29,	9	03	4·2	3·2	3·9	276	30·4	0·8	18·2
			21	3·6	3·3	3·7	277	26·6	− 2·1	14·5
	30,	7	51	4·2	3·0	3·2	278	31·3	8·4	14·4
		12	18	3·6	3·4	3·6	279	26·1	− 0·6	15·4
		13	30	5·2	2·8	4·8	280	38·7	− 1·6	20·5
V	1,	0	28	3·9	3·6	3·6	281	26·8	2·8	19·0
		2	46	3·1	3·1	4·0	282	25·2	− 8·8	0·0
		3	26	4·6	5·9	5·6	283	15·6	−10·8	33·9
		8	48	3·8	4·2	3·8	284	23·0	1·3	22·4
		20	09	2·5	4·3	2·9	285	16·5	1·5	13·0
	2,	21	06	3·5	3·8	3·4	286	23·6	2·0	17·7
	3,	11	48	4·5	2·8	3·8	287	34·0	4·4	16·5
	4,	9	01	3·1	3·9	3·0	288	21·2	3·3	15·0
		10	57	4·0	3·8	3·7	289	26·2	3·1	21·0
	5,	6	13	4·3	3·0	3·5	290	31·9	6·3	16·2
		7	04	5·7	1·6	5·4	291	46·4	− 7·2	10·7
	6,	6	33	4·1	3·3	3·5	292	29·4	4·9	17·6
		17	19	3·6	3·0	2·9	293	28·0	5·6	10·4
	7,	8	13	4·2	2·8	4·5	294	32·1	4·6	14·4
			54	4·8	4·5	3·5	295	27·1	16·4	25·3
		9	00	2·4	5·4	3·0	296	8·6	4·6	17·8
		19	28	5·0	3·0	4·1	297	36·5	6·6	20·1
			39	3·4	4·0	3·6	298	22·0	− 0·5	18·4
		21	15	3·0	4·3	2·9	299	18·5	4·8	16·6
	8,	6	02	4·5	2·5	4·0	300	35·1	1·0	14·6
		9	07	4·5	2·4	4·3	301	35·4	− 3·1	13·4
		11	44	3·7	3·3	3·2	302	27·2	4·4	14·7
		12	44	3·5	3·9	3·7	303	23·1	− 1·1	18·4
		17	06	3·4	3·9	3·4	304	22·6	1·6	17·6
	9,	3	13	1·4	6·0	3·6	305	1·2	− 3·6	11·2
		5	39	4·0	3·2	3·8	306	29·3	0·0	16·8
		7	33	3·6	4·8	2·9	307	18·2	11·6	21·5
		15	55	2·6	4·6	2·8	308	15·0	4·3	15·4
		21	01	3·5	4·3	3·8	309	20·8	− 0·9	20·9
	10,	1	05	4·2	2·6	3·9	310	32·8	− 0·6	13·2

(*to be continued.*)

Table IV. (*continued.*)

Time of Occurrence.				D. P. T.			No.	Seismic Focus.		
				t₀	t₁	t₂		X	Y	Z
Month	Day	h	m	sec.	sec.	sec.		km.	km.	km.
			33	4·4	2·5	3·6	311	34·4	4·8	13·0
			35	4·7	2·3	4·0	312	37·0	2·9	13·8
	11,	2	30	3·1	4·0	3·4	313	20·7	− 0·6	16·0
	12,	19	50	3·5	3·5	2·8	314	25·2	7·0	13·8
	13,	17	43	4·1	3·6	3·6	315	27·9	4·5	19·9
	14,	0	01	4·2	2·7	4·5	316	32·5	− 8·7	11·0
		19	24	5·0	5·0	3·8	317	25·2	17·0	29·3
	16,	3	29	3·2	3·2	3·8	318	25·2	− 7·0	6·6
		11	25	2·7	4·5	2·9	319	16·0	3·6	15·8
		22	57	2·1	5·0	2·9	320	10·7	1·9	14·0
	17,	21	42	4·2	3·0	3·4	321	31·2	6·1	15·4
		23	52	3·1	4·2	2·6	322	19·5	7·9	15·5
	20,	16	51	5·8	3·0	4·2	323	42·8	15·6	18·2
			52	6·2	2·5	4·3	324	47·8	18·8	9·4
		19	21	5·8	2·2	5·2	325	45·6	− 1·5	17·9
	23,	1	36	4·7	3·2	3·4	326	33·6	12·1	17·3
			55	4·7	2·7	3·3	327	35·6	12·2	12·5
		22	18	2·4	5·1	2·8	328	11·0	5·0	16·4
	24,	21	08	6·0	3·2	4·7	329	43·2	15·4	23·4
		23	01	6·0	2·1	5·2	330	47·5	1·4	17·4
	25,	3	27	3·2	4·1	3·1	331	21·1	3·4	16·4
	27,	6	34	6·0	1·1	5·3	332	49·6	− 2·2	9·0
		11	15	3·9	3·4	3·6	333	37·7	2·3	17·5
		17	35	5·9	1·3	5·0	334	48·5	2·0	10·6
	28,	1	41	4·0	3·2	3·8	335	29·3	0·0	16·8
	29,	1	30	6·1	1·1	5·0	336	50·6	4·5	8·0
			30	3·4	3·5	3·8	337	24·7	− 4·4	13·7
		4	32	5·1	1·1	5·6	338	49·0	− 8·4	3·6
VI	6,	9	12	6·0	2·6	4·8	339	45·7	8·5	19·6
		10	45	4·4	3·2	3·7	340	31·7	5·5	18·6
	7,	3	12	4·9	2·6	4·3	341	36·2	2·5	19·8
	8,	12	51	4·4	3·4	4·0	342	30·6	2·2	20·6
	9,	7	58	3·4	3·8	3·2	343	23·2	3·3	16·5
	11,	3	35	5·0	3·4	4·3	344	34·6	4·8	23·4
	13,	4	03	3·8	3·2	3·1	345	28·2	6·0	14·0
	14,	2	46	4·2	3·2	4·7	346	30·4	−10·3	14·7
	15,	3	06	2·8	3·6	3·6	347	21·5	− 6·2	7·2
		8	28	5·9	3·8	3·9	348	39·5	23·2	19·4
	17,	18	30	3·4	3·6	3·1	349	24·2	3·7	14·8
	18,	7	02	4·7	2·6	3·7	350	36·0	7·2	15·0
	19,	18	33	2·7	4·5	3·6	351	16·0	− 3·7	15·7
		21	24	4·1	3·2	3·9	352	29·8	− 0·3	17·3
	22,	10	33	3·5	3·5	3·9	353	25·2	− 3·6	14·9
	24,	19	42	6·0	2·9	3·8	354	44·6	23·2	4·9
	25,	20	19	5·8	3·7	3·2	355	39·1	29·3	0·0
VII	2,	0	27	6·4	3·0	5·7	356	49·5	3·4	25·0
	4,	4	42	5·4	2·1	4·9	357	42·7	− 2·3	15·8
	5,	23	50	3·5	3·6	3·2	358	24·7	3·4	15·6
	6,	3	05	3·8	2·9	3·0	359	29·4	6·2	11·0
		6	41	4·5	3·2	5·3	360	32·3	−16·4	10·8

(*to be continued.*)

Table VI. (*continued.*)

Time of Occurrence.				D. P. T.			No.	Seismic Focus.		
				t_0	t_1	t_2		X	Y	Z
Month	Day	h	m	sec.	sec.	sec.		km.	km.	km.
	7,	5	24	2·4	5·3	2·7	361	9·4	6·8	16·6
			34	5·1	2·7	4·1	362	38·4	6·9	18·0
	11,	22	37	5·0	4·4	3·3	363	29·2	20·5	22·4
	13,	1	02	5·5	4·4	3·5	364	32·8	24·4	21·8
	16,	12	28	6·9	3·9	6·2	365	48·0	2·3	32·8
	20,	7	20	6·9	3·9	6·2	366	48·0	2·3	32·8
	21,	0	57	4·3	2·6	3·5	367	33·4	4·9	13·0
		12	37	4·3	2·7	3·6	368	33·0	4·3	14·1
	23,	7	08	4·6	2·6	3·6	369	35·4	7·2	14·2
	24,	9	23	2·8	4·7	2·7	370	15·1	6·8	16·8
		12	24	2·8	4·7	2·7	371	15·1	6·8	16·8
		13	55	3·6	3·6	4·0	372	25·2	− 4·9	16·1
VIII	4,	7	38	4·2	2·8	4·4	373	32·0	− 7·0	13·0
	5,	11	44	4·3	3·0	3·3	374	31·8	8·3	15·0
		21	40	5·1	2·6	4·4	375	38·8	2·6	18·4
	6,	13	31	5·1	2·6	3·3	376	38·8	16·3	8·8
	7,	0	20	3·4	3·3	3·4	377	25·7	− 0·3	12·7
		19	39	1·6	6·3	2·9	378	−1·0	5·9	12·1
	10,	0	33	4·4	3·8	3·7	379	28·7	7·1	22·4
		10	31	4·6	4·1	3·8	380	28·3	9·1	25·0
	19,	12	45	5·4	2·7	4·6	381	40·6	3·8	20·2
		23	02	3·0	3·9	3·9	382	20·8	− 7·6	12·2
	23,	19	02	4·3	2·7	3·2	383	33·0	8·6	12·0
	30,	23	03	4·0	3·2	3·7	384	29·3	1·4	16·7
IX	17,	4	04	3·0	4·2	3·8	385	19·1	− 5·2	15·7
	18,	7	17	4·1	3·4	3·9	386	28·8	0·3	19·0
	23,	2	17	4·4	4·4	3·6	387	25·2	10·6	25·2
		5	11	3·5	3·0	4·0	388	27·5	− 7·4	7·8
			12	3·9	3·5	3·4	389	27·3	4·7	17·7
			18	3·5	3·2	3·9	390	26·6	− 5·8	11·2
		21	54	5·0	3·0	4·8	391	36·4	− 3·6	20·8
	25,	5	59	5·0	2·7	5·8	392	37·8	−19·6	0·0
		6	09	5·0	2·7	5·8	393	37·8	−19·6	0·0
	27,	8	38	2·0	4·5	2·1	394	13·7	6·2	7·8
X	3,	8	29	6·3	3·3	5·2	395	45·5	8·2	26·0
	14.	12	37	3·6	2·8	3·7	396	28·8	− 3·3	8·9
	22,	3	57	4·4	3·6	3·6	397	29·8	7·7	20·8
	24,	7	57	2·7	4·0	3·2	398	19·0	− 1·1	12·4
	29,	7	46	2·8	3·9	3·6	399	20·0	− 5·2	11·6
XI	10,	11	47	4·0	3·5	4·3	400	27·8	− 5·6	18·1
	12,	0	02	3·9	2·8	2·9	401	30·4	7·9	10·0
	16,	20	29	5·4	2·7	3·6	402	40·6	16·9	11·8
	22,	15	31	2·7	3·5	2·3	403	21·8	5·2	4·7
	26,	20	10	5·3	2·7	3·9	404	39·8	11·9	16·3

Table VI.

(B)

Durations of the Preliminary Tremors and the Seismic Foci.

Notations;

D. P. T.=Duration of the preliminary tremors.
t_0=D. P. T. at Maiduru.
t_1=D. P. T. at Kinosaki.
t_2=D. P. T. at Kobe-mura.
t_3=D. P. T. at Taiza.

Time of Occurrence.				D. P. T.				No.	Seismic Focus.		
				t_0	t_1	t_2	t_3		X	Y	Z
Month	Day	h	m	sec.	sec.	sec.	sec.		km.	km.	km.
XII	28,	12	35	5·5	2·3	2·6		405	42·8	12·0	13·3
	29,	20	42	3·6	3·7	2·6		406	24·6	− 6·8	16·3
	30,	13	52	6·1	2·9	3·0		407	45·6	23·7	0·0
I	4,	1	34	2·4	4·1	1·5		408	17·4	5·0	9·1
	10,	12	32	2·4	3·8	1·6		409	19·1	− 1·8	6·6
	25,	7	10	3·3	3·2	0·9		410	25·7	7·4	7·8
		20	21	3·4	3·2	0·9		411	26·2	8·8	7·7
	30,	5	01	2·5	3·6	1·4	3·0	412	20·4	− 0·8	6·0
		18	14	5·1	2·8	2·3	1·7	413	38·4	16·8	12·2
II	6,	9	21	3·0		0·5	2·3	414	25·0	3·1	0·0
	8,	23	40	3·1		1·4	2·4	415	22·3	7·3	11·2
	12,	21	27	5·0	3·0	2·2	1·6	416	36·3	17·1	12·0
	14,	20	48	4·0	2·8	1·7	2·8	417	30·6	1·4	11·2
	18,	18	49	5·0	2·6	2·3	2·4	418	37·7	9·2	14·8
			49		2·0	2·1	2·6	419	38·8	3·9	11·4
	19,	5	27	3·3	3·3	1·2	2·0	420	25·2	8·9	10·3
	20,	3	45	3·0		0·5	2·3	421	25·0	3·1	0·0
	23,	7	30		3·2	1·0	2·2	422	25·5	5·9	8·2
	26,	7	33		2·6	2·7	1·4	423	43·8	21·3	0·0
	29,	10	38	3·0	3·6	2·0	3·3	424	23·3	− 1·5	13·8
III	1,	22	34	5·5	2·0	2·7	2·9	425	43·0	5·1	13·9
	4,	22	54		2·6	1·8	2·2	426	34·3	7·8	12·6
	5,	17	59		2·6	1·2	1·2	427	33·2	12·6	5·1
	23,	12	43	3·0	3·2		1·5	428	24·2	10·0	0·0
		18	01		2·7	2·5	2·2	429	39·7	13·4	14·9
	27,	8	06		3·0	2·1	2·2	430	33·8	11·2	15·4
		23	10		3·3	1·7	1·5	431	30·3	15·5	11·2
IV	6,	1	49	5·4	2·6		2·3	432	41·0	13·0	14·8
	9,	9	01	2·6	3·5	0·8		433	21·3	3·9	3·0
	22,	3	20	3·0		1·5	1·8	434	18·3	16·7	5·0
V	5,	6	41	4·0	2·9		1·6	435	30·4	11·2	9·0
			41	4·7	3·0		2·0	436	34·4	13·1	14·6
	28,	3	15		2·9	1·1	1·6	437	29·6	5·6	7·9
	29,	0	04	3·3		1·0	2·0	438	25·2	8·2	8·4
VI	1,	8	34		3·0	2·4	1·8	439	37·7	17·2	13·4

(to be continued.)

Table VI. (B) (*continued.*)

Time of Occurrence.				D. P. T.				No.	Seismic Focus.		
				t_0	t_1	t_2	t_3		X	Y	Z
Month	Day	h	m	sec.	sec.	sec.	sec.		km.	km.	km.
	7,	6	31		2·6	1·5	1·5	440	34·2	12·2	8·4
	9,	23	52	5·5	1·5		2·9	441	44·9	3·6	10·8
	16,	12	06	3·0	3·5	0·9	2·2	442	23·0	6·8	6·7
	20,	17	26	5·4		2·3	1·8	443	42·7	13·6	7·6
			29	3·2		2·0	2·2	444	17·3	17·5	10·9
VII	9,	0	19	3·3		0·5	2·0	445	27·0	5·5	3·4
	14,	15	01	3·9		1·5	2·7	446	31·9	− 0·2	7·7

Table VII. Seismic Foci in Region III.

No. of Earthq.	X′	No. of Fig.	Y′	No. of Fig.	Focal Depth.
	km.		km.		km.
8	0·3	26	0·1	33	18·3
10	6·7		0·7		15·2
12	4·1		8·9		15·0
13	3·6		7·6		18·9
14	0·3		0·1		18·1
16	1·7		0·6		15·1
18	− 5·3		10·0		20·8
22	11·2		1·3		14·5
30	− 4·8		5·5		17·7
31	3·1		2·0		17·0
33	− 1·9		3·4		18·1
34	1·6		2·6		17·9
35	4·8		8·0		17·6
36	1·8		1·5		17·1
38	2·9		11·7		15·9
41	3·0		6·1		17·0
42	2·3		8·1		16·8
44	4·0		9·8		15·7
45	1·9		11·2		16·0
46	1·5		4·7		18·5
47	7·5		7·8		18·1
53	1·9		9·6		22·5
54	3·1		9·4		17·2
55	5·0		7·0		16·9
56	7·3		7·6		16·7
61	1·5		4·6		13·8
63	1·4		10·8		13·6
64	1·5		8·8		15·1
65	8·7	27	0·1		12·9
70	2·7		5·0		18·5
73	2·1		4·6		14·8
74	5·6		12·0		16·3
75	− 0·3		4·1		17·8
78	1·0		4·4		17·9
80	2·8		11·9		17·4

(*to be continued.*)

Table VII. *(continued.)*

No. of Earthq.	X′	No. of Fig.	Y′	No. of Fig.	Focal Depth.
	km.		km.		km.
81	0·5		11·9		17·7
84	4·8		2·3		16·2
85	1·5		8·8		15·0
89	5·9		12·1		15·3
90	5·9		7·2	33	15·3
91	5·2		9·1		13·5
92	8·6		7·0		19·3
93	0·4		6·3		16·0
94	1·3		5·5		16·1
98	6·8		0·5		18·4
102	− 0·7		1·9		16·1
104	4·7		2·5		12·7
105	4·1		7·8		15·3
106	− 3·3		4·8		16·3
108	0·2		2·1		16·1
110	1·0		6·5		13·5
112	− 2·8		5·1		17·1
115	1·7		7·9		17·4
119	0·0		6·1		16·7
122	7·4		0·6		17·5
129	9·2		1·2		16·4
135	3·3		3·0		18·3
136	1·3	27	11·0		15·1
137	2·2		8·2		15·2
138	− 2·1		8·6		16·7
140	− 0·8		6·7		15·0
141	− 1·7		9·5		14·9
143	5·1		9·7	34	21·6
148	0·4		8·3		14·8
150	0·6		3·4		17·8
151	− 4·2		11·2		14·2
153	2·2		8·2		15·1
156	11·9		4·3		11·6
157	− 3·6		10·6		14·6
158	1·1		1·6		14·7
159	3·2		8·5		16·7
160	− 1·8		5·6		17·3
162	0·8		2·5		15·5
163	1·1		1·6		14·7
164	− 2·6		2·3		14·3
166	− 3·4		11·3		16·8
167	9·4		8·6		16·2
168	3·7		11·9		14·4
170	− 2·9		3·2		16·4
172	− 0·6		4·1		24·2
176	3·5		9·7		15·0
178	8·4		4·6		17·0
180	5·5		6·0		17·7
182	4·4		6·7		14·5
185	9·8		3·7		18·2

(to be continued.)

Table VII. (*continued.*)

No. of Earthq.	X′	No. of Fig.	Y′	No. of Fig.	Focal Depth.
	km.		km.		km.
200	0·5		2·3		20·5
203	10·6	28	2·8	35	12·0
208	11·9		12·2		18·9
209	6·2		3·6		22·2
216	7·4		4·1		23·5
220	0·9		4·5		19·1
227	7·3		0·7		14·3
228	8·4		10·9		19·7
230	− 2·1		2·5		16·6
238	2·9		9·4		15·7
239	− 2·5		2·3		20·9
244	0·4		6·2		14·3
245	3·6		10·9		16·2
247	8·9		9·8		17·0
248	− 1·7		3·7		21·6
249	− 2·5		4·4		21·4
256	0·0		1·2		14·6
257	4·3		5·6		17·7
258	7·8		7·9		17·2
259	− 0·6		0·7		19·8
261	− 1·4		0·5		21·6
265	− 4·9		4·7		23·4
266	− 2·5		5·4		18·0
267	2·4		6·0		19·1
271	− 1·7		6·0		22·1
276	5·3		8·2		18·2
277	4·9		3·4		14·5
279	3·5		4·1		15·4
281	1·4	29	7·0	36	19·0
284	0·0		3·1		22·4
286	− 0·2		4·0		17·7
288	− 2·7		3·1		15·0
289	0·8		6·7		21·0
292	1·6		10·3		17·6
293	− 0·3		10·1		10·4
294	3·6		12·1		14·4
298	0·6		1·2		18·4
300	8·3		11·9		14·6
301	11·6		9·3		13·4
302	0·5		8·3		14·7
303	1·8		1·6		18·4
304	− 0·5		3·0		17·6
306	5·2		6·9		16·8
310	8·0		9·1		13·2
313	− 0·2		0·1		16·0
314	− 2·8		8·6		13·8
315	0·9		8·9		19·9
321	1·9		12·4		15·4
331	− 2·9		3·1		16·4
335	5·2		6·9		16·8

(*to be continued.*)

Table VII. (*continued.*)

No. of Earthq.	X′	No. of Fig.	Y′	No. of Fig.	Focal Depth.
	km.		km.		km.
337	5·3		0·5	36	13·7
340	2·7	30	12·3		18·6
342	4·5		9·3		20·6
343	−1·4		4·6		16·5
345	0·0		10·1		14·0
349	−1·0		5·6		14·8
352	5·7		7·0		17·3
353	5·0		1·4		14·9
358	−0·5		5·8		15·6
359	0·6		11·1		11·0
368	4·5		12·5		14·1
372	6·0		0·5		16·1
377	3·0		4·0		12·7
379	−0·5		11·2		22·4
380	−2·3		12·3		25·0
384	4·1		7·8		16·7
386	4·6	31	6·7	37	19·0
388	9·4		0·5		7·8
389	0·3		8·6		17·7
390	7·2		0·9		11·2
396	7·3		4·2		8·9
400	8·3		2·0		18·1
403	−3·8		4·8		4·7
410	−2·8		9·2		7·8
411	−3·5		10·6		7·7
414	0·0		5·8		0·0
415	−5·0		6·6		11·2
417	5·0		8·8		11·2
420	−4·3		9·9		10·3
421	0·0		5·8		0·0
422	−1·8		8·1		8·2
424	2·2		1·4		13·8
428	−5·8		9·9		0·0
433	−3·2		3·6		3·0
437	1·2		10·9		7·9
438	−3·7		9·4		8·4
442	−4·2		6·8		6·7
445	−0·5		8·9		3·4
446	7·0		8·7		7·7

Table VIII. Seismic Foci in Region II.

No. of Earthq.	X″	No. of Fig.	Y′	No. of Fig.	Focal Depth.
	km.		km.		km.
5	4·0	39	2·7	43	14·0
11	−0·2		0·9		13·5
15	2·4		8·2		23·0
26	2·9		3·4		21·4
27	3·7		7·4		17·5

(*to be continued.*)

Table VIII. (*continued.*)

No. of Earthq.	X″	No. of Fig.	Y′	No. of Fig.	Focal Depth.
	km.		km.		km.
37	1·9	39	3·8	43	14·0
39	0·2		1·5		14·5
40	1·4		5·8		17·3
43	3·5		4·9		22·2
48	6·3		2·5		16·0
57	7·7		6·7		18·4
71	3·5		7·8		12·5
72	11·3		9·7		21·3
97	4·1		6·4		15·5
107	2·6		3·0		15·2
109	3·8		6·0		18·4
117	−0·9		4·0		16·7
124	−3·3		4·0		16·8
125	−1·4		8·8		13·0
127	1·9		0·0		15·5
130	−4·6		3·4		14·6
131	−3·9		3·6		13·9
132	2·0		4·1		20·5
139	0·2		5·1		24·1
142	7·3		6·8		19·1
147	0·1		6·9		19·8
171	0·4		2·8		13·6
181	4·6		7·8		16·2
194	−2·7		1·6		21·8
197	−0·4		1·0		19·8
223	3·8	40	9·3	44	10·3
232	9·3		2·9		17·2
236	3·4		6·5		13·4
242	9·9		3·3		15·7
250	1·5		3·3		18·0
251	−2·0		0·3		15·1
254	3·1		7·1		17·1
262	3·8		8·3		20·0
264	−0·9		0·0		16·4
278	0·2		1·6		14·4
287	5·0		0·8		16·5
290	2·2		0·5		16·2
297	5·1		4·1		20·1
311	5·0		1·3		13·0
312	8·1		2·0		13·8
326	−0·9		5·8		17·3
327	0·3		7·3		12·5
333	9·1		2·1		17·5
341	7·9	41	1·2		19·8
344	5·1		1·5		23·4
350	4·3		4·2		15·0
362	6·2		5·8		18·0
367	4·2		0·7		13·0
369	3·9		3·7		14·2
374	0·7		1·8		15·0

(*to be continued.*)

Table VIII. *(continued.)*

No. of Earthq.	X″	No. of Fig.	Y′	No. of Fig.	Focal Depth.
	km.		km.		km.
375	9·6	41	3·2		18·4
381	9·9		5·3		20·2
383	1·2		2·9		12·0
397	−0·2		0·0		20·8
401	0·1		0·6	45	10·0
418	3·9		6·8		14·8
419	8·6		4·0		11·4
425	10·6		7·9		13·9
426	2·7		3·3		12·6
427	−1·6		5·8		5·1
430	−0·2		5·3		15·4
431	−5·7		5·6		11·2
435	−2·4		2·8		9·0
436	−1·2		7·0		14·6
440	−0·6		6·2		8·4

Table IX. Seismic Foci in Region I.

No. of Earthq.	X‴	No. of Fig.	Y″	No. of Fig.	Focal Depth.
	km.		km.		km.
19	1·0	47	10·4	48	16·4
29	4·6		14·4		14·2
51	−4·3		0·5		13·2
60	2·6		9·1		15·0
82	1·0		14·3		0·0
86	0·3		9·9		9·2
96	−0·6		8·0		10·7
123	9·4		14·2		25·6
126	5·6		19·3		10·4
133	−1·9		17·4		8·8
134	1·1		18·3		0·0
144	11·8		12·3		0·0
145	5·5		9·1		21·4
169	8·3		0·6		13·7
175	−2·9		13·7		0·0
183	−0·4		0·4		19·7
217	−1·1		4·1		15·2
218	1·1		12·7		12·8
229	8·8		10·1		8·2
268	4·9		0·2		13·0
269	−2·4		5·3		0·0
323	3·4		4·5		18·2
324	5·3		10·2		0·4
329	6·3		1·5		23·4
339	10·1		0·7		19·6
348	−3·9		8·4		19·4
354	0·0		11·6		4·9
376	−0·2		2·5		8·8
402	0·9		4·2		11·8
405	5·7		1·7		13·3

(to be continued.)

Table IX. (*continued.*)

No. of Earthq.	X‴	No. of Fig.	Y″	No. of Fig.	Focal Depth.
	km.		km.		km.
407	0·5	47	12·6	48	0·0
413	−0·8		2·8		12·2
416	−2·6		1·7		12·0
423	0·6		9·7		0·0
429	2·4		0·9		14·9
432	3·6		1·4		15·8
439	−1·6		2·7		13·4
443	4·6		2·9		7·6

Table X. Seismic Foci in Region IV.

No. of Earthq.	X	No. of Fig.	Y	No. of Fig.	Focal Depth.
	km.		km.		km.
1	19·6	49	3·3	53	15·5
3	18·7		1·6		19·3
4	12·8		− 4·8		20·3
6	18·5		−13·0		11·2
7	18·5		−13·0		11·2
20	13·0		6·4		14·1
21	14·8		2·2		19·3
23	11·0		2·6		14·6
24	20·0		5·0		17·2
49	19·6		− 1·0		16·0
50	19·6		0·2		16·1
68	19·1		− 2·8		16·6
69	19·9		− 2·7		18·0
76	14·9		− 2·4		13·7
77	13·9		1·5		13·5
87	19·4		− 4·9		12·8
99	17·8		− 0·3		14·1
103	8·5		3·2		19·9
114	19·6		− 4·0		20·5
116	19·5		− 3·3		17·1
118	15·9		− 2·0		19·5
120	17·4		7·4		19·2
121	17·7		1·2		19·2
146	15·8		− 0·6		11·4
152	18·7		− 8·0		0·0
155	15·8		0·1		14·0
161	5·6		6·6		16·4
174	19·0		0·6		16·7
177	14·1		5·7		19·3
186	11·7		7·0		21·4
187	9·4		2·2		17·8
188	9·4		2·2		17·8
189	5·1		3·8		18·4
190	3·5		3·7		18·8
191	2·9		2·7		17·2

(*to be continued.*)

Table X. (*continued.*)

No. of Earthq.	X	No. of Fig.	Y	No. of Fig.	Focal Depth.
	km.		km.		km.
192	10·5	49	−0·6	54	20·2
199	19·5		−4·6		16·9
201	13·8	50	−3·2	54	17·0
202	15·2		−5·1		13·6
204	11·9		−2·4		15·2
205	12·2		1·7		13·8
206	12·0		2·8		15·1
207	15·0		−4·0		15·5
210	8·4		−1·8		15·4
211	12·3		0·9		18·2
212	11·6		−5·2		13·6
213	13·3		−4·3		13·5
214	9·1		−5·5		16·2
215	10·3		−5·6		14·5
219	4·5		0·6		17·1
221	11·3		−2·6		17·8
222	11·9		−4·2		16·9
224	16·8		3·8		20·8
225	11·9		5·0		18·7
226	19·0		−0·6		16·6
231	13·9		1·4		21·2
233	11·9		1·5		17·4
234	19·1		−2·9		16·4
237	19·2		−5·3		9·4
240	17·2		−1·7		18·5
243	2·6		3·2		19·0
246	18·2		2·1		18·7
253	2·8		−0·6		17·4
255	13·5		−4·8		14·3
272	19·1		−2·9		16·4
275	19·8		0·4		9·6
285	16·5		1·5		13·0
296	8·6		4·6	55	17·8
299	18·5		4·8		16·6
305	1·2		−3·6		11·2
307	18·2		11·6		21·5
308	15·0	51	4·3		15·4
319	16·0		3·6		15·8
320	10·7		1·9		14·0
322	19·5		7·9		15·5
328	11·0		5·0		16·4
351	16·0		−3·7		15·7
361	9·4		6·8		16·6
370	15·1		6·8		16·8
371	15·1		6·8		16·8
385	19·1		−5·2		15·7
394	13·7		6·2		7·8
398	19·0		−1·1		12·4
399	20·0		−5·2		11·6
408	17·4		5·0		9·1
409	19·1		−1·8		6·6

28. 昭和2年丹後大地震の餘震の震原立體分布に關する研究補遺

地震研究所 那須信治

丹後地震の餘震觀測報告（東京帝國大學理學部紀要，[ii]，**3**（1929），29〜129 及び地震研究所彙報 **6**（1929），245 及び **7**（1929），133 に記載）が出版された後震原の立體分布に就いて補足及び訂正を要する箇所があることを認め此論文には主として此等の點が取扱はれてゐる．卽ち主なる補足訂正の點は次の通りである．

（1） 距離係數 k を計算により小數第2位まで求めた．但し前回の報告中8の地震に就いて k を求めたものをこゝでは9の地震に就いて求めた．此の計算の結果平均 $k=8{\cdot}40$ となり，前回の $k=8{\cdot}41$ とは僅かに 0·01 の差があることを見出した．本論文中の震原位置決定には 8·40 の値が採用されてある．又前に發表した表（理學部紀要 [ii]，**3**（1929），38，Table V；震研彙報 **6**（1929），257，Table III）は筆者が實地に測定せざる觀測資料を含み尙ほ不合理と思はれる點もあるので此表は除外することにした．

（2） 前報告中の震原の中約 30 箇は不確實と思はれるので，此論文中では此等の震原を除外した．

（3） 震原位置の誤差は地震の起る弱線の配列を論ずるに十分な程度に精密に計算したが，此處では計算を記載することを省略し必要に應じてその結果のみを引用した．

（4） 前に發表した報告中の震原立體分布圖の中で震原の乘る線を餘りに多數引き過ぎた傾向があつたが，震原位置の誤差を考へるときは實在性が疑はれるやうなものがあつたので本論文中には最も實在し得ると考へられたものゝみを指摘した．

（5） 地震の活動中心の移動を適確に示すために地震を發震日時の順によつて區分したがその區分を前回に報告した時よりは細密に行つて結果は槪して良好の樣に思はれた．

其他細部に亘る訂正補足は尙ほ數箇條あるが全般を貫く大綱に到つては前回の報告中に述べたものと大差はない．

29. *Recent Seismic Activities in the Idu Peninsula.* (*Part 2.*)

By Nobuji NASU,

Earthquake Research Institute.

(Read. March 19, 1935.—Received March 20, 1935.)

The earthquakes that shook so often the Idu district during the period from Feb. 1930 to January 1931, have already been described in an earlier report,[1] in which also were mentioned the distributions of the seismic foci of the Itô earthquake-swarm and the after-shocks of the Idu destructive earthquake of Nov. 26, 1930.

Since then, the method of determining the seismic foci has been improved to such an extent that it is possible now to obtain more accurate results than heretofore of the stereometrical distribution of the seismic foci. I shall now describe the new result of the improved method as applied to Itô earthquakes.

Strong Earthquake of March 22, 1930. Although this Itô earthquake brought no causalities in its train, the particular shock that occurred at 17 h 50 m, March 22 (Japanese standard time) was the strongest of the large number that originated under the Itô Bay. In this paper the distribution of the seismic foci of the shocks that occurred during a few days before and after this strong earthquake will receive special attention in our study of the change in the position of the seismically active centre that probably took place after this strong earthquake.

Network of Seismological Stations. During the few days that preceded the strong earthquake just mentioned, observations were carried out by the network of five stations, namely, Kawana, Itô, Usami, Aziro and Hasima (Fig. 1).

These stations were chosen for the network as they would cover the seismically active centre that lay under Itô Bay. Although Usami was discontinued immediately after the strong earthquake of March 22, the network consisting of the remaining four stations covered most of the seismic foci of the shocks that occurred afterwards.

---

[1] N. NASU, F. KISHINOUE and T. KODAIRA, "Recent Seismic Activities in the Idu Peninsula. (Part 1.)", *Bull. Earthq. Res. Inst.*, **9** (1931), 22~35.

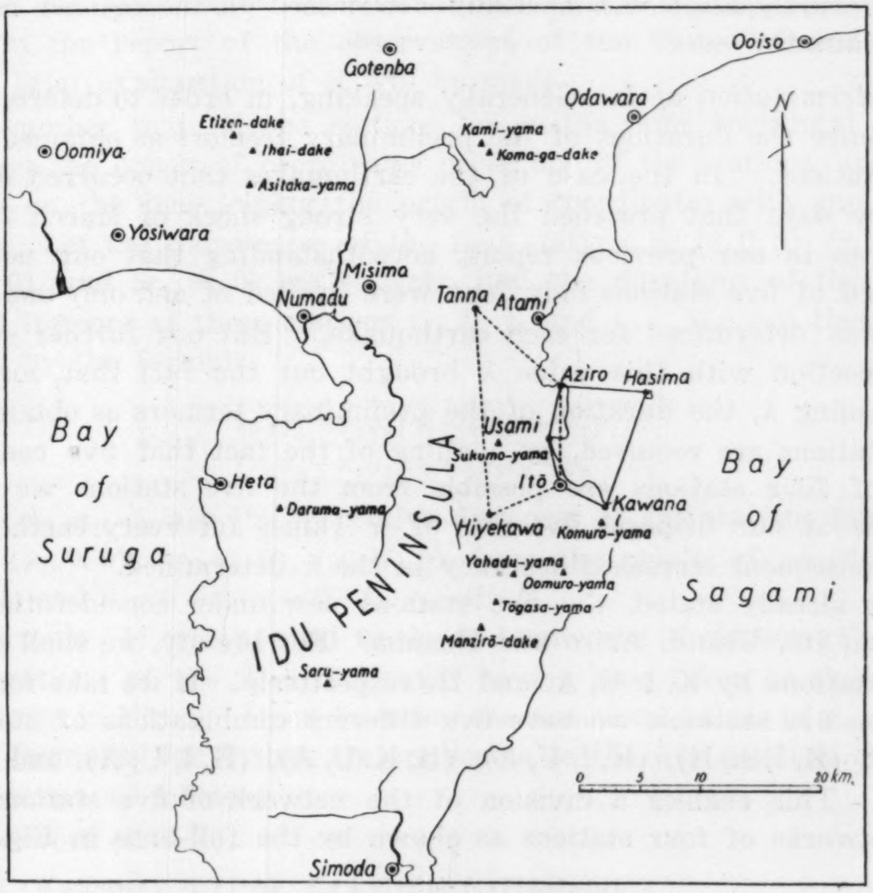
Ooiso
Gotenba
Odawara
N
Etizen-dake
Kami-yama
Oomiya
Ihei-dake
Koma-ga-dake
Asitaka-yama
Yosiwara
Misima
Tanna
Atami
Numadu
Aziro
Hasima
Bay of Suruga
Usami
Sukumo-yama
Itô
Heta
Daruma-yama
Kawana
Hiyekawa
Komuro-yama
Bay of Sagami
Yahadu-yama
Oomuro-yama
Tôgasa-yama
IDU PENINSULA
Manzirô-dake
Saru-yama
0 5 10 20 km.
Simoda

Fig. 1. Map showing the networks of seismological stations.
—— network for the Itô earthquakes.
.... network for the Idu after-shocks.

Method of determining the Seismic Foci. Owing to its being the most convenient method for determining the seismic foci of shocks that occurred in shollow places, the graphical method was used for the Itô earthquakes.

Formula for computing the Focal Distance by means of the Duration of the Preliminary Tremors. As has been stated elsewhere,[2] the constant factor k in the formnla, $D=kt$, which shows the relation between the duration of the preliminary tremors (t) and the focal distance (D), must first be determined, because k varies with the locality in which the earthquake occurs. The value of k that would apply to the Itô earthquakes was specially determined in the manner now to be explained.

---

[2] N. Nasu, "Observations of the Tango after-shocks." *Bull. Earthq. Res. Inst.*, **6** (1929), 24 ~332; **7** (1929), 133~152.

N. Nasu, "A Stereometrical Study of the Aftershocks of the Great Tango Earthquake, etc." *Journ. Fac. Sc.*, [ii], **3** (1929), 29~129.

Determination of k. Generally speaking, in order to determine k, we require the durations of the preliminary tremors as obtained from four stations. In the case of the earthquakes that occurred during the few days that preceded the very strong shock of March 22, referred to in our previous report, notwithstanding that our network consisted of five stations only four were availed of and only one value of k was determined for each earthquake. But our further studies in connection with this value k brought out the fact that, since in determining k, the duration of the preliminary termors as obtained at four stations are required, by availing of the fact that five combinations of four stations are possible from the five stations we have, there is at our disposal five sets of k values for every earthquake, with consequent increased accuracy in the k determined.

As already stated, the five stations now under consideration are Kawana, Itô, Usami, Aziro and Hasima. For brevity, we shall denote these stations by K, I, U, A, and H, respectively. If we take four out of these five stations, we have five different combinations of stations, namely, (K, I, A, H), (K, I, U, A), (H, K, U, A), (H, I, U, A), and (K, I, U, H). This enables a division of the network of five stations into five networks of four stations as shown by the full-lines in Fig. 2.

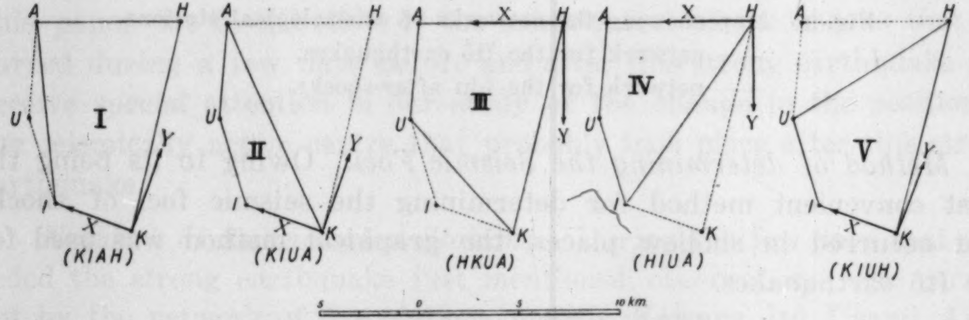

Fig. 2. Networks of four stations.

Since the value of k can be determined by means of the whole networks of four stations just mentioned, we get five different values of k for one earthquake.

It is worth while to examine within what limits the value of k can be determined in the way just mentioned. The answer to this question will undoubtedly be an excellent datum of reference in connection with future observations of local earthquake.

As the general method of determining k by means of the durations of the preliminary termors at four stations has already been given in the report of the observations of the Tango after-shocks,[1] only a brief explanation of it will be made.

Assuming that all the stations lie on the same horizontal plane, $Z=0$, let the origin of coordinates be at one of the stations, and the X axis on the line joining the origin of coordinates with any other station. Let the coordinates of the four stations be $(0, 0, 0)$, $(x_1, 0, 0)$, $(x_2, y_2, 0)$, and $(x_3, y_3, 0)$ respectively, and the durations of the preliminary tremors at these stations t_0, t_1, t_2 and t_3. We can then evaluate k by the formula

$$k=\sqrt{\frac{(x_3y_2-x_2y_3)d_1^2-(d_3^2y_2-d_2^2y_3)d_1}{(x_3y_2-x_2y_3)\tau_1+(y_3\tau_2-y_2\tau_3)d_1}}\,, \tag{1}$$

where d_1, d_2, d_3 are the respective distances of the stations lying at points $(x_1, 0, 0)$, $(x_2, y_2, 0)$, $(x_3, y_3, 0)$ from the origin of coordinates, $(0, 0, 0)$, and $\tau_1=t_1^2-t_0^2$, $\tau_2=t_2^2-t_0^2$, $\tau_3=t_3^2-t_0^2$.

Formula (1) was applied to the five networks of stations (Fig. 2); the directions of the X and Y axes having been taken as shown by the arrows in Fig. 2. Upon inserting the numerical values of x, y, and d, the formulas for k that are applicable to the five network of stations become as follows:

(I) Network (KIAH).

t_0(Kawana), t_1(Itô), t_2(Aziro), t_3(Hasima).

$$\begin{cases} d_1=\text{distance between Kawana and Itô}=4{\cdot}0\text{ km.} \\ d_2=\text{distance between Kawana and Aziro}=11{\cdot}2\text{ km.} \\ d_3=\text{distance between Kawana and Hasima}=10{\cdot}4\text{ km.} \end{cases}$$

$$\begin{cases} x_1=d_1=4{\cdot}0\text{ km. (Coordinates of Itô.)} \\ x_2=7{\cdot}64\text{ km, } y_2=7{\cdot}90\text{ km. (Coordinates of Aziro.)} \\ x_3=1{\cdot}20\text{ km, } y_3=10{\cdot}33\text{ km. (Coordinates of Hasima.)} \end{cases}$$

$$k=\sqrt{\frac{604{\cdot}6816}{62{\cdot}82\,t_0^2-72{\cdot}54\,t_1^2+41{\cdot}32\,t_2^2-31{\cdot}60\,t_3^2}}\,. \tag{1, I}$$

(II) Network (KIUA).

t_0(Kawana), t_1(Itô), t_2(Usami), t_3(Aziro).

$$\begin{cases} d_1=\text{distance between Kawana and Itô}=4{\cdot}0\text{ km.} \\ d_2=\text{distance between Kawana and Usami}=7{\cdot}6\text{ km.} \\ d_3=\text{distance between Kawana and Aziro}=11{\cdot}2\text{ km.} \end{cases}$$

$$\begin{cases} x_1=d_1=4{\cdot}0\text{ km. (Coordinates of Itô.)} \\ x_2=6{\cdot}75\text{ km, } y_2=3{\cdot}50\text{ km. (Coordinates of Usami.)} \\ x_3=7{\cdot}94\text{ km, } y_3=7{\cdot}90\text{ km. (Coordinates of Aziro.)} \end{cases}$$

$$k=\sqrt{\frac{339\cdot504}{-7\cdot94\,t_0^2+25\cdot54\,t_1^2-31\cdot60\,t_2^2+14\cdot00\,t_3^2}}\,. \qquad (1,\text{II})$$

(III) Network (HKUA).

t_0(Hasima), t_1(Aziro), t_2(Kawana), t_3(Usami).

$$\begin{cases} d_1=\text{distance between Hasima and Aziro}=7\cdot1\text{ km.}\\ d_2=\text{distance between Hasima and Kawana}=10\cdot4\text{ km.}\\ d_3=\text{distance between Hasima and Usami}=8\cdot8\text{ km.}\end{cases}$$

$$\begin{cases} x_1=d_1=7\cdot1\text{ km. (Coordinates of Aziro.)}\\ x_2=2\cdot5\text{ km},\ y_2=10\cdot09\text{ km. (Coordinates of Kawana.)}\\ x_3=7\cdot56\text{ km},\ y_3=4\cdot50\text{ km. (Coordinates of Usami.)}\end{cases}$$

$$k=\sqrt{\frac{1186\cdot1703}{-25\cdot34\,t_0^2+65\cdot03\,t_1^2+31\cdot95\,t_2^2-71.64\,t_3^2}}\,. \qquad (1,\text{III})$$

(IV) Network (HIUA).

t_0(Hasima), t_1(Aziro), t_2(Itô), t_3(Usami).

$$\begin{cases} d_1=\text{distance between Hasima and Aziro}=7\cdot1\text{ km.}\\ d_2=\text{distance between Hasima and Itô}=10\cdot7\text{ km.}\\ d_3=\text{distance between Hasima and Usami}=8\cdot8\text{ km.}\end{cases}$$

$$\begin{cases} x_1=d_1=7\cdot1\text{ km.}\\ x_2=6\cdot23\text{ km},\ y_2=8\cdot70\text{ km. (Coordinates of Itô.)}\\ x_3=7\cdot56\text{ km},\ y_3=4\cdot50\text{ km. (Coordinates of Usami.)}\end{cases}$$

$$k=\sqrt{\frac{776\cdot8089}{-7\cdot92\,t_0^2+37\cdot74\,t_1^2+31\cdot95\,t_2^2-61\cdot77\,t_3^2}}\,. \qquad (1,\text{IV})$$

(V) Network (KIUH).

t_0(Kawana), t_1(Itô), t_2(Usami), t_3(Hasima).

$$\begin{cases} d_1=\text{distance between Kawana and Itô}=4\cdot0\text{ km.}\\ d_2=\text{distance between Kawana and Usami}=7\cdot6\text{ km.}\\ d_3=\text{distance between Kawana and Hasima}=11\cdot2\text{ km.}\end{cases}$$

$$\begin{cases} x_1=d_1=4\cdot0\text{ km. (Coordinates of Itô.)}\\ x_2=6\cdot75\text{ km},\ y_2=3\cdot50\text{ km. (Coordinates of Usami.)}\\ x_3=1\cdot20\text{ km},\ y_3=10\cdot33\text{ km. (Coordinates of Hasima.)}\end{cases}$$

$$k=\sqrt{\frac{176\cdot0368}{-38\cdot21\,t_0^2+65\cdot53\,t_1^2+41\cdot32\,t_2^2+14\cdot00\,t_3^2}}\,. \qquad (1,\text{V})$$

A few words should be added here in regard to the nature of the Itô earthquake-swarms, the seismic activity of which, beginning generally with a slight earthquake, is followed almost without intermission during the next few hours by a countless number of shocks. During this time we actually see the tremors being continuously recorded on the seismograms. These continuous tremors often hindered accurate determination of the duration of the preliminary tremors. In the circumstances, notwithstanding the countless number of shocks recorded by instruments, in only a small per cent of them could we accurately determine the duration of the preliminary tremors. There were, however, 38 earthquakes during the few days both before and after the strong earthquake of March 22, in which accurate determination of the duration of the preliminary tremors was possible. The durations at five stations were determined in 10 of these 38 earthquakes, while for the remaining 28 earthquakes the durations were determined at four stations.

Table I shows the values of *k* and the networks of stations (Fig. 2) that were used in determining *k*.

Table I. Durations of the Preliminary Tremors and *k*.

No.	Time of occurrence	Duration of the preliminary tremors.					Net-work	*k*
		Kawana	Itô	Aziro	Hasima	Usami		
		sec.	sec.	sec.	sec.	sec.		km./sec.
1	III 17, $18^{h}45^{m}$		1·45	2·00	1·85	1·60	IV	4·859
2	18, 2 11		1·50	1·95	1·85	1·55	〃	4·413
3	2 20		1·70	2·00	1·75	1·75	〃	5·100
4	2 46		1·55	2·05	1·95	1·70	〃	5·391
5	7 45		1·50	2·10	2·05	1·70	〃	5·412
6	19. 7 29		1·55	1·90	1·85	1·60	〃	5·290
7	7 34		1·55	1·90	1·85	1·60	〃	5·290
8	7 45		1·55	2·00	1·85	1·65	〃	4·893
9	8 00		1·55	1·90	1·85	1·55	〃	4·552
10	10 16	1·75	1·80	2·00	1·80	1·80	I	4·736
							II	5·308
							III	5·207
							IV	5·204
							V	5·095
11	17 12	1·60	1·60	1·90	1·80	1·60	I	5·255
							II	4·806
							III	4·820
							IV	4·763
							V	4·300
12	20, 10 30	1·55	1·70	2·30	2·10	1·90	I	5·430
							II	4·803
							III	4·851
							IV	4·776
							V	4·163
13	11 03	1·50	1·80	2·30	1·80		I	5·182

(to be continued.)

Table I. *(continued.)*

No.	Time of occurrence	Duration of the preliminary tremors.					Net-work	*k*
		Kawana	Itô	Aziro	Hasima	Usami		
	h m	sec.	sec.	sec.	sec.	sec.		km./sec.
14	16 45	1·60	1·60	1·90	1·80	1·60	I	5·255
							II	4·806
							III	4·820
							IV	4·763
							V	4·300
15	22 21	1·50	1·60	2·10	1·80	1·70	I	4·128
							II	4·351
							III	4·130
							IV	4·198
							V	4·773
16	21, 5 33	1·30	1·50	2·15	1·80	1·70	I	4·312
							II	4·413
							III	4·257
							IV	4·292
							V	4·470
17	8 40	1·50	1·50	2·20	2·20	1·70	I	4·901
							II	4·601
							III	4·564
							IV	3·531
							V	4·235
18	22 48	1·50	1·60	1·90	1·60	1·60	I	5·029
							II	4·448
							III	4·508
							IV	4·428
							V	3·902
19	23 24	1·60	1·60	2·20	2·10	1·75	I	4·113
							II	4·601
							III	4·259
							IV	4·387
							V	5·854
20	23 34	1·40		2·10	1·80	1·70	III	4·437
21	22, 16 20	1·40	1·40	1·80	1·70	1·40	I	5·072
							II	4·353
							III	4·470
							IV	4·356

(to be continued.)

Table I. (*continued.*)

No.	Time of occurrence	Duration of the preliminary tremors.					Net-work	k
		Kawana	Itô	Aziro	Hasima	Usami		
	h m	sec.	sec.	sec.	sec.	sec.		km./sec.
21							V	3·677
22	22, 17 02	1·10	1·10	1·70	1·60	1·20	I	4·754
							II	4·571
							III	4·501
							IV	4·492
							V	4·328
23	17 03	1·30	1·40	1·70		1·40	II	4·732
24	18 30	1·50	1·55	1·80		1·55	II	5·123
25	23, 3 02	1·60	1·50	1·90		1·50	II	4·525
26	3 46	1·20	1·45	1·80		1·50	II	4·533
27	12 20	1·30	1·50	1·90		1·60	II	4·980
28	13 00	1·30	1·50	1·75		1·50	II	4·634
29	13 08	1·20	1·45	1·80		1·50	II	4·533
30	29, 3 50	1·30	1·50	2·00	1·65		I	5·219
31	4 04	1·55	1·70	1·80	1·65		I	4·969
32	4 07	1·40	1·45	1·80	1·60		I	5·063
33	5 10	1·30	1·40	1·80	1·60		I	5·970
34	30, 0 06	1·00	1·20	2·00	1·80		I	5·333
35	5 40	1·30	1·50	2·00	1·65		I	5·219
36	31, 11 14	1·35	1·40	1·90	1·75		I	4·948
37	IV 1, 12 17	1·30	1·40	2·20	1·90		I	4·338
38	23 04	1·35	1·50	1·90	1·85		I	5·128

It will be seen from this Table that k varies considerably with the particular network selected for its determination. In the 10 earthquakes in which the observations were made at five stations, k becomes 5·85 at maximum and 3·53 at minimum, while the differences between the values of k determined for each earthquake range between 0·21 and 1·74. All the values of k in Table I lie between 5·90 and 3·53.

An attempt was made to ascertain the relation between the focal depth and the values of k, but without success; no clear relation between these quantities could be found. It seems in order to state that there is no perceptible change in k within the limits of the focal depths now under consideration, and that the mean of the 85 values of k in Table I is applicable to the seismic triangulation of the Itô earthquakes now in question.

Seismic Triangulation of the Itô Earthquakes. As the mean of the 85 values of k shown in Table I came out as 4·70, we used the formula

$$D=4{\cdot}70\,t \tag{2}$$

for computing the focal distance.

In the case of a network of five stations there are ten different combinations of three stations, while in that of four stations there are four combinations. Thus, in the 10 earthquakes that were observed at five stations, 10 different positions of the seismic foci could be determined for each earthquake, and four different positions of the seismic foci for each of the earthquakes that were observed at four stations.

In determining the seismic foci, maps of scale 1/100,000 were used, on which the positions of the seismic foci are shown by the coordinates X', Y', Z; X', Y' being the coordinates of the epicentre and Z the focal depth. The directions of the X' and Y' axes are shown in Fig. 3. The coordinates of the seismic foci determined by the seismic triangulation are shown in Table II. (Triangles: *1*=KIU, *2*=KIA, *3*=KIH, *4*=KUA, *5*=KUH, *6*=KAH, *7*=IUA, *8*=IUH, *9*=IAH, *10*=UAH).

Table II. Seismic Foci of the Itô Earthquakes.

No.	Time of occurrence	Net-work	Seismic focus.			
			X'	Y'	Z	Mean X' Y' Z
			km.	km.	km.	km.
1	III 17, $18^h 45^m$	*7*	1·0	3·8	4·8	
		8	1·4	3·5	5·3	1·43
		10	1·7	3·6	5·5	3·60
		9	1·6	3·5	5·3	5·22
2	18, 2 11	*7*	2·7	3·4	6·1	
		8	2·2	3·8	5·7	2·20
		10	1·9	3·6	5·4	3·63
		9	2·0	3·7	5·6	5·70
3	2 20	*7*	0·1	5·4	4·4	
		8	1·1	4·5	5·8	1·05
		10	1·6	4·9	6·2	4·85
		9	1·4	4·6	5·9	5·58
4	2 46	*7*	0·1	4·4	4·2	
		8	1·4	3·3	5·9	1·38
		10	2·1	3·9	6·4	3·75
		9	1·9	3·5	6·0	5·63
5	7 45	*7*	0·1	3·9	4·3	
		8	1·5	2·8	6·0	1·45
		10	2·2	3·3	6·5	3·23
		9	2·0	2·9	6·1	5·73

(to be continued.)

Table II. (*continued.*)

No.	Time of occurrence	Network	Seismic focus.			
			X'	Y'	Z	Mean X' Y' Z
	h m		km.	km.	km.	km.
6	19, 7 29	*7*	0·8	4·9	4·3	
		8	2·0	3·9	5·8	1·95
		10	2·6	4·4	6·2	4·30
		9	2·4	4·0	5·9	5·50
7	7 34	*7*	0·8	4·9	4·3	
		8	2·0	3·9	5·8	1·95
		10	2·6	4·4	6·2	4·30
		9	2·4	4·0	5·9	5·50
8	7 45	*7*	0·8	4·3	4·8	
		8	1·5	3·8	5·7	1·45
		10	1·8	4·0	5·9	3·98
		9	1·7	3·8	5·7	5·53
9	8 00	*7*	2·5	4·0	5·9	
		8	2·4	4·1	5·8	2·45
		10	2·4	4·1	5·8	4·08
		9	2·5	4·1	5·8	5·83
10	10 16	*1*	1·6	4·7	6·6	
		2	1·6	5·1	6·3	
		3	1·6	4·9	6·4	
		4	1·2	5·5	6·0	
		5	1·5	4·9	6·4	
		6	1·9	4·9	6·4	
		7	0·4	5·7	5·1	
		8	1·4	4·9	6·4	1·51
		9	1·9	5·0	6·5	5·09
		10	2·0	5·3	6·7	6·28
11	19, 17 12	*1*	2·0	4·3	5·8	
		2	2·0	4·5	5·7	
		3	2·0	4·3	5·9	
		4	2·0	4·6	5·7	
		5	2·1	4·3	5·8	
		6	2·2	4·3	5·8	
		7	1·7	4·7	5·4	
		8	2·0	4·3	5·9	2·05
		9	2·2	4·4	5·9	4·42
		10	2·3	4·5	6·0	5·79
12	20, 10 30	*1*	0·6	3·1	6·5	
		2	0·7	3·2	6·5	
		3	0·7	3·0	6·6	
		4	0·6	3·3	6·4	
		5	0·8	3·0	6·6	
		6	1·0	3·0	6·6	
		7	0·3	3·4	6·2	
		8	1·0	3·1	6·7	0·74
		9	1·0	3·1	6·7	3·14
		10	1·0	3·2	6·8	6·56
13	11 03	*2*	−0·7	4·4	5·5	
		3	−0·6	4·3	5·6	−0·58
		6	−0·5	4·3	5·6	4·33
		9	−0·5	4·3	5·7	5·79

(*to be continued.*)

Table II. (*continued.*)

No.	Time of occurrence	Net-work	Seismic focus.			
			X'	Y'	Z	Mean X' Y' Z
	h m		km.	km.	km.	km.
14	20, 16 45	*1*	2·0	4·3	5·8	
		2	2·0	4·5	5·7	
		3	2·0	4·3	5·9	
		4	2·0	4·6	5·7	
		5	2·1	4·3	5·8	
		6	2·2	4·3	5·8	
		7	1·7	4·7	5·4	
		8	2·0	4·3	5·9	2·05
		9	2·2	4·4	5·9	4·42
		10	2·3	4·5	6·0	5·79
15	22 21	*1*	1·2	4·1	5·7	
		2	1·2	3·8	5·9	
		3	1·1	4·1	5·7	
		4	1·4	3·5	6·0	
		5	1·1	4·1	5·6	
		6	0·9	4·1	5·7	
		7	2·1	3·3	6·5	
		8	1·1	4·1	5·6	1·16
		9	0·8	4·0	5·5	3·88
		10	0·7	3·7	5·2	5·70
16	21, 5 33	*1*	0·5	3·6	5·0	
		2	0·4	3·5	5·0	
		3	0·4	3·6	4·9	
		4	0·6	3·2	5·1	
		5	0·5	3·5	5·0	
		6	0·4	3·5	5·0	
		7	1·1	3·1	5·7	
		8	0·5	3·6	4·9	0·50
		9	0·3	3·5	4·9	3·44
		10	0·3	3·3	4·7	5·02
17	8 40	*1*	2·0	2·3	6·3	
		2	2·0	2·3	6·3	
		3	2·0	2·2	6·4	
		4	2·1	2·3	6·4	
		5	2·1	2·2	6·4	
		6	2·1	2·2	6·3	
		7	2·3	2·2	6·5	
		8	2·2	2·3	6·4	2·09
		9	2·1	2·3	6·4	2·25
		10	2·1	2·3	6·3	6·30
19	22 48	*1*	1·1	5·1	4·8	
		2	1·1	4·9	4·9	
		3	1·1	4·8	5·1	
		4	1·3	4·8	5·0	
		5	1·3	4·8	5·0	
		6	1·3	4·8	5·0	
		7	1·8	4·6	5·5	
		8	1·4	4·8	5·1	1·30
		9	1·3	4·8	5·1	4·81
		10	1·3	4·7	5·0	5·05

(*to be continued.*)

Table II. (*continued.*)

No.	Time of occurrence	Network	Seismic focus.			
			X'	Y'	Z	Mean X' Y' Z
			km.	km.	km.	km.
19	$23^{h}\ 24^{m}$	*1*	2·0	2·8	6·7	
		2	2·0	2·8	6·7	
		3	2·0	2·8	6·7	
		4	2·0	2·7	6·7	
		5	1·9	3·0	6·6	
		6	1·7	3·1	6·7	
		7	2·0	2·7	6·7	
		8	1·8	2·9	6·6	1·86
		9	1·6	2·9	6·5	2·85
		10	1·6	2·8	6·4	6·63
20	23 34	*4*	0·9	3·6	5·4	
		5	0·8	3·8	5·3	0·78
		10	0·7	3·7	5·2	3·73
		6	0·7	3·8	5·3	5·30
21	22, 16 20	*1*	2·0	4·4	4·4	
		2	2·0	4·1	4·7	
		3	2·0	4·0	4·8	
		4	2·3	3·9	4·8	
		5	2·2	4·0	4·8	
		6	2·2	4·0	4·8	
		7	3·0	3·7	5·4	
		8	2·4	4·1	4·9	2·23
		9	2·1	4·1	4·8	4·02
		10	2·1	3·9	4·6	4·80
22	17 02	*1*	2·0	3·6	3·1	
		2	2·0	3·6	3·2	
		3	2·0	3·6	3·2	
		4	2·1	3·5	3·2	
		5	2·1	3·6	3·1	
		6	2·0	3·6	3·2	
		7	2·4	3·4	3·5	
		8	2·1	3·6	3·2	2·07
		9	2·0	3·6	3·1	3·56
		10	2·0	3·5	3·0	3·18
23	17 03	*1*	1·3	5·0	2·3	
		2	1·3	5·0	3·3	1·25
		4	1·2	5·1	3·2	5·05
		7	1·2	5·1	3·0	2·95
24	18 30	*1*	1·6	4·7	5·0	
		2	1·6	5·0	4·7	1·33
		4	1·4	5·3	4·5	5·10
		7	0·7	5·4	3·5	4·43
25	23, 3 02	*1*	2·8	3·7	5·9	
		2	2·9	3·6	5·9	3·03
		4	3·0	3·4	6·0	3·50
		7	3·4	3·3	6·2	6·00
26	3 46	*1*	0·2	5·4	1·7	
		2	0·2	5·3	2·0	0·40
		4	0·4	5·1	2·5	5·20
		7	0·8	5·0	3·4	2·40

(*to be continued.*)

Table II. (*continued.*)

No.	Time of occurrence	Net-work	Seismic focus. X′	Y′	Z	Mean X′ Y′ Z
	h m		km.	km.	km.	km.
27	12 20	*1*	0·4	4·7	3·8	
		2	0·4	4·8	3·7	0·28
		4	0·4	4·9	3·6	4·85
		7	−0·1	5·0	2·7	3·45
28	13 00	*1*	0·5	5·6	2·3	
		2	0·4	5·5	2·6	0·58
		4	0·6	5·5	2·6	5·50
		7	0·8	5·4	3·1	2·65
29	13 08	*1*	0·5	5·6	2·3	
		2	0·4	5·5	2·6	0·58
		4	0·6	5·5	2·6	5·50
		7	0·8	5·4	3·1	2·65
30	29, 3 50	*2*	0·8	4·2	4·7	
		3	0·7	4·1	4·5	0·60
		6	0·4	4·1	4·5	4·17
		9	0·5	4·3	4·3	4·50
31	4 04	*2*	0·7	6·1	4·0	
		3	0·7	4·8	5·5	1·50
		6	2·2	4·6	5·2	5·20
		9	2·4	5·3	5·8	5·13
32	4 07	*2*	1·6	4·6	4·5	
		3	1·6	4·4	4·6	1·70
		6	1·8	4·4	4·6	4·47
		9	1·8	4·5	4·6	4·58
33	5 10	*2*	1·3	4·5	3·9	
		3	1·3	4·2	4·3	1·53
		6	1·7	4·1	4·2	4·28
		9	1·8	4·3	4·4	4·20
34	30, 0 06	*2*	0·8	3·0	3·5	
		3	0·8	2·7	3·7	0·93
		6	1·0	2·7	3·7	2·80
		9	1·1	2·8	3·9	3·70
35	5 40	*2*	0·5	4·3	4·4	
		3	0·5	4·1	4·5	0·60
		6	0·7	4·1	4·5	4·18
		9	0·7	4·2	4·6	4·50
36	31, 11 14	*2*	1·7	3·8	4·8	
		3	1·6	3·7	4·9	1·70
		6	1·7	3·7	4·9	3·75
		9	1·8	3·8	4·9	4·88
37	IV 1, 12 17	*2*	1·3	2·3	5·5	
		3	1·3	3·0	5·2	0·83
		6	0·4	3·1	5·2	2·80
		9	0·3	2·8	4·7	5·15
38.	23 04	*2*	0·9	4·6	4·3	
		3	0·9	3·4	5·2	1·60
		6	2·2	3·3	5·0	3·78
		9	2·4	3·8	5·6	5·03

An examination of this Table shows that, even in the same earthquake, the positions of the seismic foci differ slightly from each other according to the triangle chosen in determining the seismic foci. The maximum difference in one direction component according to this Table is 1·9 km, whereas in most earthquakes the difference in the coordinates of the seismic foci does not exceed 1·0 km.

We determined the positions of the seismic foci at points, the coordinates of which have mean values X′, Y′, and Z as determined for each earthquake.

Stereometrical Distribution of the Seismic Foci. The distribution of the epicentres is shown in Fig. 3. In this Figure all the epicentres are seen grouped within a comparatively small area (6 km²). The centre of this area lies about 4 km north of Kawana.

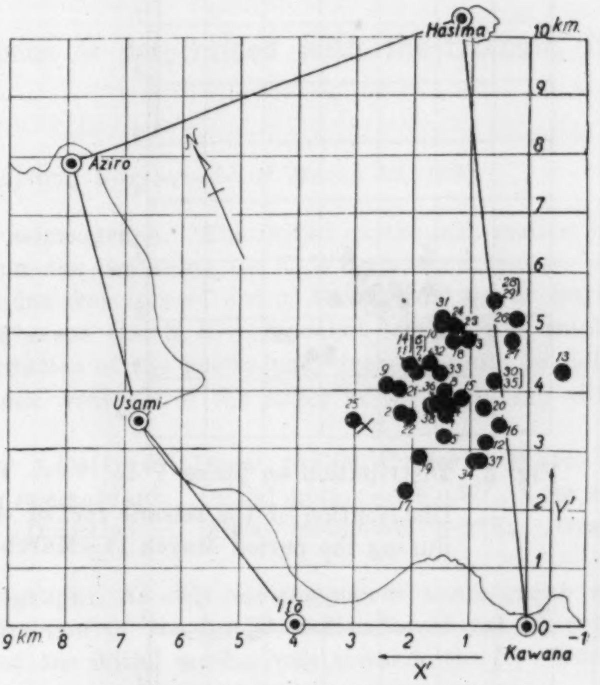

Fig. 3. Distribution of the epicentres of the Itô earthquakes for the period March 19~March 31, 1930.

Upon projecting all the foci on two vertical planes, one parallel to the Y′ axis and the other to the X′ axis, we get Figs.

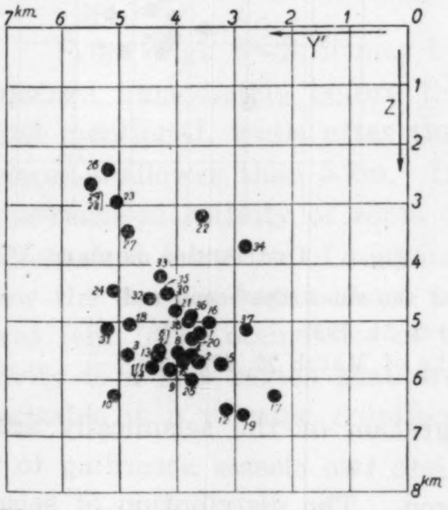

Fig. 4. Distribution of seismic foci on the Y′ Z plane.

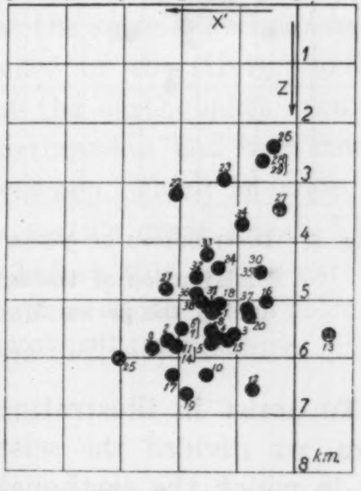

Fig. 5. Distribution of seismic foci on the X′ Z plane.

4 and 5. Roughly speaking, the seismic foci of the Itô earthquakes that occurred during the period now in question may be seen to be grouped on both side of a line dipping SW.

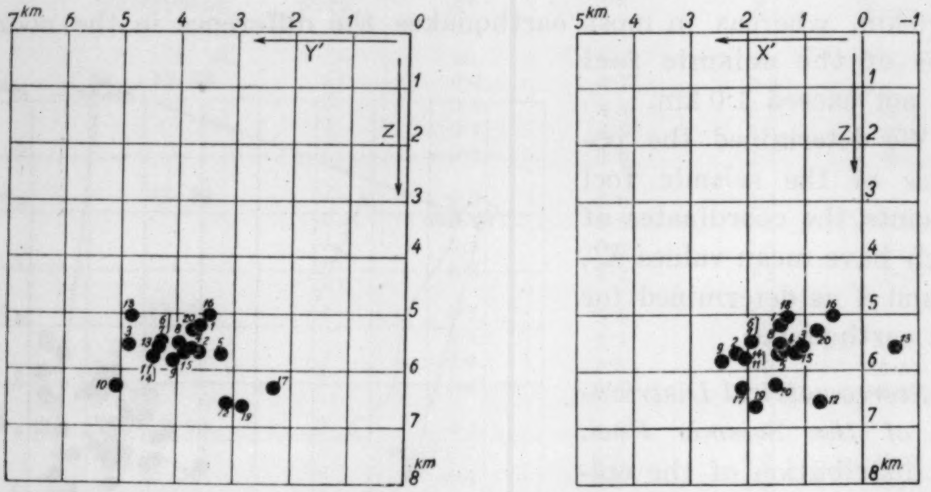

Fig. 6. Distribution on plane Y′Z. Fig. 7. Distribution on plane X′Z.

Distribution of the seismic foci of the shocks that occurred during the period March 19∼March 22, 1930.

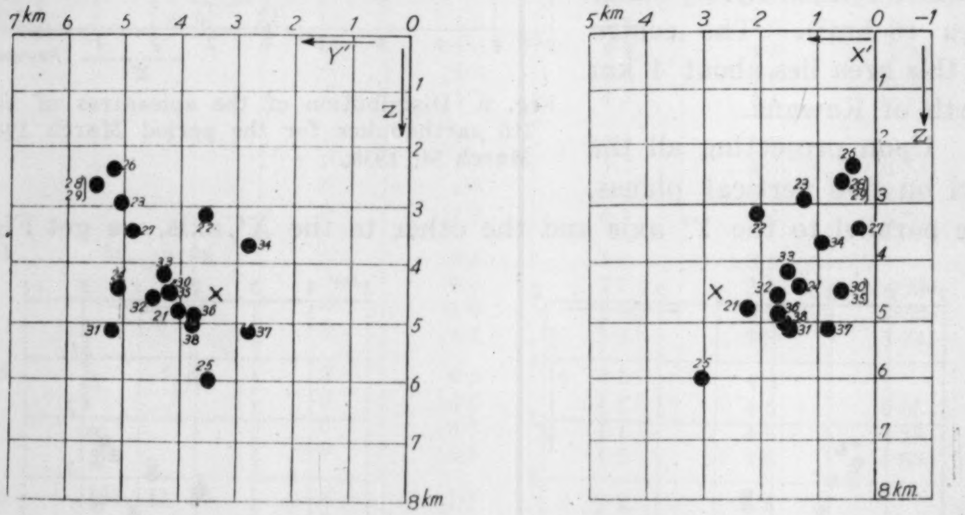

Fig. 8. Distribution on plane *Y′ Z*. Fig. 9. Distribution on plane *X′ Z*.

Distribution of the seismic foci of the shock that occurred during the period March 22∼March 31, 1930. (Cross: the strong earthquake of March 22, 17h 50m.)

To assist in illustrating the migration of the seismically active centre, we divided the seismic foci into two classes according to the time in which the earthquakes occurred. The distribution of seismic foci Nos. 1∼20 on the plane *Y′ Z* and *X′ Z* are shown in Figs. 6 and

7, respectively. Although the seismic foci shown in Figs. 6 and 7 are distributed at depths greater than 5 km, upon projecting the foci of the shocks that occurred afterward, we see that all these seismic foci are distributed at depths less than 5·5 km (Figs. 8 and 9). The seismic focus of the strong earthquake of March 22 is indicated by crosses in the latter figures.

The position of this focus is determined with the triangle, Itô-Hasima-Aziro.

Observations of the Strong Earthquake of March 22, 1930.

Itô: Two horizontal components seismograph. The initial earthquake motion was roughly towards West. From the beginning the E. W. component motion was so large that the writing index was thrown out of the smoked paper during the preliminary tremors, whereas the N. S. component motion was smaller than the former and the duration of the preliminary tremors could be determined. But the writing index went out of the paper at the beginning of the main phase.

Initial motion=1,700 μ S, 3,400(?)μ W. Durat. prelim. tremor=1·25 sec.

Aziro: Two horizontal comonents seismograph. Initial motion=360 μ W′., 3,600 μ S′. (N′=N 34°W, E′=N 56°E) Direction of initial motion=S 28·3°E. Durat. prelim. termor=1·80 sec.

Hasima: N. S. component seismograph. As only one component seismograph was installed there, the exact direction of the initial motion could not be determined, but the component of the initial motion was towards the N. Durat. prelim. tremor=1·80 sec.

Usami: E. S. component seismograph. Initial motion was towards the W. Writing index went out of the paper about 0·5 sec. after the beginning.

Kawana: N. S. component seismograph. The writing index was thrown out towards S by the very first motion.

Seismic focus: $X'=2{\cdot}8$ km, $Y'=3{\cdot}4$ km, $Z=4{\cdot}5$ km.

From Figs. 6∼9, it may be said that the seismic activity migrated upward immediately before the occurrence of the strong earthquake just mentioned, while after that most of the earthquakes occurred at places shallower than 5 km. If these earthquakes had been caused by the renewed activity of some dormant volcano, which is indeed likely, an upward intrusion of magma into the earth's crust about 5 km below the surface began about two hours before this strong earthquake was felt. The occurrence of this earthquake shifted the volcanic activity to a new region shallower than the old; a procedure quite imaginable in a volcanic eruption.

29. 伊豆半島に於ける最近の地震活動に就いて(第2報)

地震研究所 那須信治

昭和5年2月より翌年1月に至る間の伊豆半島に發生したる群生地震の震原の立體分布に就いては，第1報として地震研究所彙報第9號に概要を述べて置いた．其後震原決定の方法を改良し伊東地震の震原分布を再調査しその結果を本論文に書いたのである．

震原決定の方法は地震3點觀測の方法であるが距離係數 k は5箇の內より4箇宛の觀測點を組合せ得る場合には1の地震に就いて5通り求め得る．觀測點が4箇の場合には唯1の k の價を決定し得ることは周知の事柄である．かく一つの地震に就いて求められた k の價には觀測網の選び方により多少差異あることを認めた． 85の k の價の平均は 4·70 となり，これを用ひて3點觀測を行つた．

5箇の觀測點のある場合には3點宛を組合せることにより10通りの震原位置を1の地震に就いて求めることが出來，4箇の場合には4通りの震原位置を求めることが出來る．この樣にして求めたる幾通りかの震原位置を示す坐標 X', Y', Z の平均値を取つてその震原としその分布を圖示した．

3月22日の强震に約2時間先立つて地震活動中心は5粁より淺い所に移り，更にこの强震によつて活動中心が全く淺い所に移動したことが判明し，通常火山の噴火の經過に於いて想像し得る如き活動中心の上方移動を認めることが出來た．

30. *The Great Indian Earthquake of January 15, 1934.*

By Nobuji Nasu,

Earthquake Research Institute.

(Read Sept. 18, 1934.—Received March 20, 1935.)

Having been deputed by the Earthquake Research Institute to proceed to India for the purpose of studying phenomena connected with the great North Bihar earthquake of January 15, 1934, I left Kôbe on April 25, and arrived at Calcutta on May 20. During the ensuing 50 days I travelled through Western Bengal and the United Provinces, where the damage caused by the present earthquake was very serious. In the earlier half of this paper I shall briefly deal with the various phenomena connected with the earthquake and the havoc wrought thereby. Although several opinions have so far appeared in publications regarding the cause of this earthquake, I shall add a few words on the subject in the latter half of this paper. Another subject that calls for careful consideration at this time is the protection of buildings in India from future earthquakes. I shall however deal with the nature of the seismic impulses as observed on the ground and the measurements of the vibrations of buildings, since these are valuable data on which to base our designs for earthquake-proof buildings.

The earthquake that caused such terrible havoc in the northern parts of Bihar and Nepal Valley occurred at about 2 h 13 m p. m. (Indian standard time) on January 15, 1934. The area in which the shocks were acute and great damage to life and property was caused extended from Motihari in Champaran on the west to Purnea on the east — a distance of nearly 200 miles, and from the frontiers of Nepal on the north to Monghyr on the south — a distance of 80 miles. Beyond this, a much wider area, in which the damage was less, extended east into Bengal and Assam and west into the United Provinces. It was felt in the Peninsula as far at least as Bezwada and Bombay. Pilgrims in Khatmandu reported that shocks were felt at Lhasa.

Intensity In the areas most seriously affected by this earthquake the intensity of the shock has been estimated to be VI (*violent*) by the intensity scale in use in Japan or to intensity X by Mercalli's modification of the Rossi-Forel scale.

Three areas are covered by isoseist X (Mercalli), the largest of which runs through North Bihar from Sitamarhi to Madhubani, form-

---

1) According to Dr. A. L. Coulson's preliminary examination of seismograms, the time of occurrence by Davison's table came out as 14h 13m 22s(Indian Standard Time).

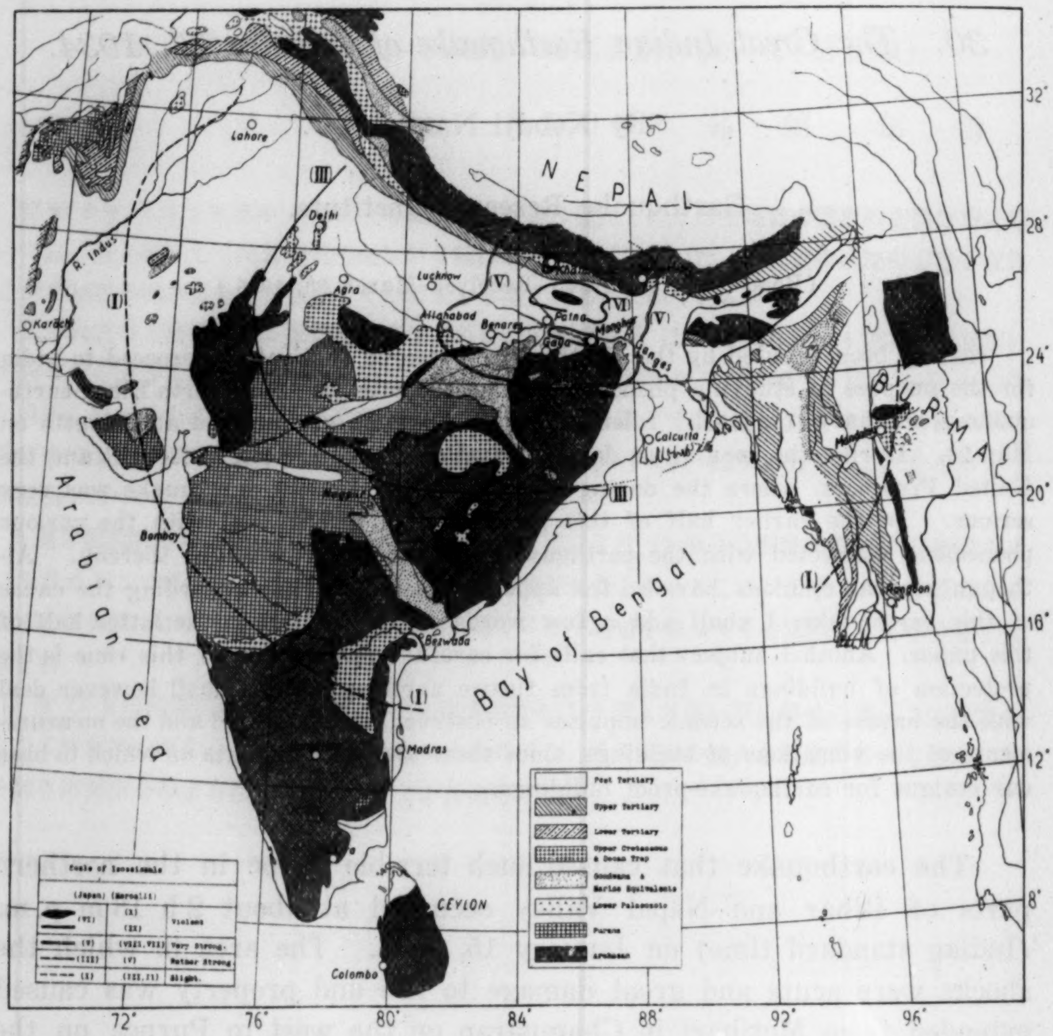
32°
28°
24°
20°
16°
12°
8°
72°
76°
80°
84°
88°
92°
96°
NEPAL
BURMA
Arabian Sea
Bay of Bengal
Lahore
Delhi
Karachi
R. Indus
Agra
Lucknow
Allahabad
Benares
Patna
Monghyr
Gaya
Ganges
Calcutta
Nagpur
Bombay
Bezwada
Madras
CEYLON
Colombo
Mandalay
Rangoon
Scale of Isoseismals
(Japan) (Mercalli)
(VI) (X) (IX) Violent
(V) (VIII, VII) Very Strong.
(III) (V) Rather Strong.
(I) (III, II) Slight.
Post Tertiary
Upper Tertiary
Lower Tertiary
Upper Cretaceous & Decan Trap
Gondwana & Marine Equivalents
Lower Palaeozoic
Purana
Archaean

Fig. 1.

ing the main part of the "slump belt",[2] while the remaining two, though small in area, are in the Nepal (Khatmandu) Valley, and at Monghyr. The acceleration of the earthquake motion in these areas as deduced from overturned objects was probably about 3,000 mm/sec^2.

In three other areas the intensity of the shocks was also *violent*, being IX on the Mercalli scale. The largest affected area, approximately 10,000 sq. miles, lies in North Bihar and along the Terai and southern ranges of Nepal. Although in these areas, as well as in those covered by isoseist X, sand vents and ground fissures were observed, they were rare or absent in the lesser areas covered by isoseist IX just mentioned.

---

[2] The term used for regions in which the ground sank through wide-spread fissuring in "The Preliminary Report on the North Bihar Earthquake of the 15th January" by Dr. J. A. Dunn, J. B. Auden, and A. M. N. Ghosh. I am greatly indebted to this report for much of the description of the effects of the earthquake etc., that I have given in this paper.

The earthquake was so severe that even in Calcutta, 400 miles from the epicentre, the walls and facings of several houses were cracked. The tower of St Paul's Cathedral fell to the ground. At Darjeering, the Government House collapsed and many private houses were badly damaged.

The areas covered by isoseists X and IX are shown in Fig. 1 and that in which the earthquake was felt is also shown in the same figure.

Earthquake Phenomena and Destruction.

Earthquake Motion. Judging from reports received from various sections of the devastated area, the shock was most violent for a period of from 2 to 5 seconds. The largest part of the damage occurred early in the principal portion of the earthquake motion, which was so strong that people had difficulty in standing and were forced either to sit or lie on the ground. The period of the earthquake might have been short, say less than 1 or 1½ seconds, as reported from Sitamarhi. There is the possibilty however that vibrations of much quicker period than this were superposed on waves of periods of about one second. It was the latter vibrations that was responsible for the destruction of brick buildings of comparatively small height, the natural oscillation periods of these vibrations being supposed to be a small fractions of a second.

According to reports of Dr. Dunn and others, surface waves or undulations were observed by many people, the waves being propagated with comparatively small velocity, probably of the order of 2~8 miles per minute on soft ground. These waves, which do not radiate from the epicentre, are generated locally by ground vibration. As to the direction in which these waves were propagated, unfortunately uniformity is lacking in the observations reported.

The most noteworthy phenomenon in connection with this great earthquake is the sand and water vents that appeared throughout the central belt of the earthquake area. So much sand and water had spouted out of the earth that it seemed at one time as if large parts of the richest land in North Bihar had turned into permanent a desert. These fears were however dispelled when a survey carried out by the Government showed that though the damage was on a serious scale, it was by no means so disastrous as was at first apprehended. Of the 4,000 sq. miles covered by these sand deposits to serious extent, in only 300 sq. miles is the deposit thicker than 1 ft, the areas in which the deposit exceeded a thickness of two feet being very small indeed.

Dr. K. S. Caldwell of Patna College made a careful study of the manner in which these sand vents were formed. In his interesting report[3] he classifies the various types of sand deposits as follows:

(1) Wide open fissures. The surface opening that appeared near Simraha was 3~5 ft wide and about 3 ft deep.

(2) At places where the outpouring pressure was not so great the water bearing sand was forced up through small fissures that did not reach the ground surface. These burst out through small isolated craters of sand varying from 1 ft to 3 or 4 ft in diameter. These craters are not the tops of turbular openings going down many feet into the earth.

(3) In the case of wells, deep tanks, or embankments, other conditions arose. Since wells give direct access from the water bearing sand to the ground surface, the water and sand gushed through these ready-made openings often to a height (*according to eye-witnesses*) of 15 ft or more. From such openings the sand is deposited in the form of a flat cone about 100 yards in diameter and varying in thickness from about 1 ft near the centre (sometimes more) to 6 inches at a distance of 15 to 20 yards and gradually thinning out to the edge.

(4) Another type of sand deposit is the basin-like hollow, about 5 ft in diameter and one ft or two ft deep. Hollows of this type were found at places where there had formerly been wells. The site of an old well, now filled in and lying under cultivated land, but whose existence was revealed only through the sand that had gushed out through it, assumes the form just described.

(5) The tanks are mostly 10~15 ft deep, but as the bottom is within a few feet of the water-bearing sand, in regions of high outpouring pressure the sand had found its earliest means of escape into the tank itself. On all occasions when it was reported that the bottoms of such tanks had risen it was found that the bottom, originally mud, was now sand.

(6) Where the road level of an embanked road had sunk as the result of local effects, large quantities of sand were thrown up at the sides, often filling the nullahs.

(7) The sand and water, which must have found an easy way out into the river beds, poured into it from under the surrounding land. Examples of these are also given in the report of Dr. Dunn previously cited. The Balan river on the border of the Darbhanga and Bhagalpur districts became dry for a few seconds as the result of temporary upheaval of the river bed, the water of the Ganges at Luckee Serai receding from mid-stream and sand gushing out from the exposed bed.

All evidences indicate that the sand which appeared on the ground surface came from within 20~30 ft of the ground level, and not 300 or 400 ft as has been frequently reported. It might be added here that the water-bearing sand in the neibourhood of Muzaffarpur-Sitamarhi road, where the sand deposits were most typical, is about 20 feet below the ground surface.

As to the distribution of these cracks, through which such vast quantities of sand had been thrown out, the following facts are reported:

---

[3] Notes on Sand Deposits by Dr. K. S. Caldwell (Mar. 17, 1934).

The cracks were often double, with short branches, but the general effect was an avenue of sand about 50 yards wide and stretching across the country in an unbroken length for a mile. One walking across the country at right angles to one of these sand avenues would meet with others at a distance of 400∼500 yards running roughly in a parallel direction.

These sand avenues were like the crests of waves several hundreds yards apart. (See Figs. 2∼5).

Survey of levels During the earthquake the ground rose and sank in a most alarming manner and it was found that many of the rivers had silted up, while some had ceased to flow. Alterations in levels, even on a small scale, are a very serious matter in an alluvial country like North Bihar, where they are likely to cause the rivers to change their courses. After the great earthquake the Geological Survey of India made a check of the levels, the results being given in a paper issued by the Government of Bihar and Orissa on June 10, 1934. The reports contains a good deal of information concerning levelling of country where lines of levels had not been run before. This part of the material will require detailed study by the drainage engineers. There are however two main lines that were surveyed before the earthquake, so that it is possible to gain a general idea as to how the levels have changed.

The longest of these lines is that which runs from Bagaha in the extreme north-

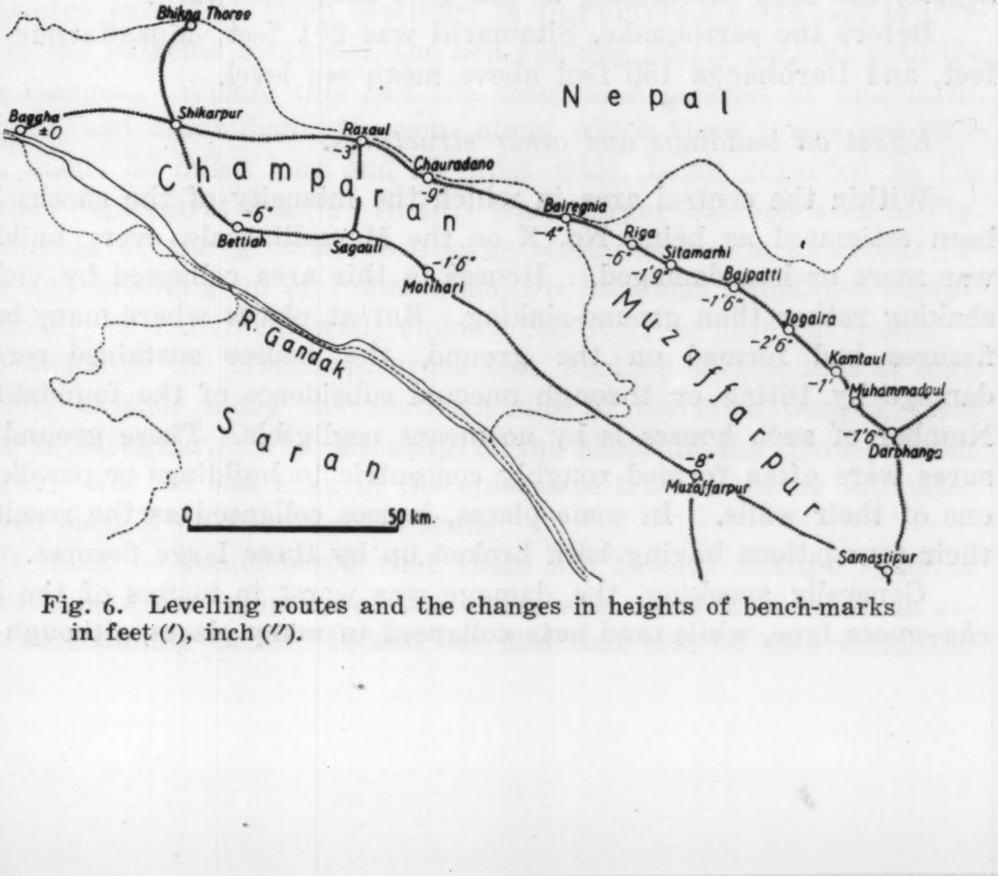
Bhikna Thoree
Nepal
Baggha
±0
Shikarpur
Raxaul
-3'
Champaran
Chauradano
-9"
Bairegnia
-4"
-6"
Bettiah
Sagauli
-1'6"
Motihari
Riga
-6"
Sitamarhi
-1'9"
Bajpatti
-1'6"
Jogaira
-2'6"
Kamtaul
-1'
Muhammadpul
-1'6"
Darbhanga
R. Gandak
Saran
Muzaffarpur
-8"
Muzaffarpur
0
50 km.
Samastipur

Fig. 6. Levelling routes and the changes in heights of bench-marks in feet (′), inch (″).

west of the Champaran district, through Sitamarhi, to Darbhanga, parallel with the railway line. The height of the bench mark at Bagaha was assumed unchanged both before and after the great earthquake. Starting from the west there is no appreciable change as far as Ramnagar. From Ramnagar to Chauradano the levels sank slightly, the depression at Raxaul, for example, being as much as 3 inches, while at Chauradano it was 9 inches; the amount of depression increasing towards the east, but nowhere so much as a foot. Bairegnia sank 4 inches and Riga 6 inches, Sitamarhi railway station 1 foot 9 inches and Bajpatti 1 foot 6 inches. At Jogaira station the drop is 2 feet 6 inches and at Kamtaul 1 foot, while at Darbhanga station the level dropped 1½ feet. East of Darbhanga the falls in level are about one foot.

Another line with which comparisons are possible is that running from Bagaha, through Bettiah and Motihari, to Muzaffarpur. Bettiah sank 6 inches and Motihari 1½ feet. The bench mark at Muzaffarpur showed a subsidence of 8 inches

The measurements that have been quoted are those of what are known as *interred bench marks* or standard bench marks. A large number of bench marks are on railway bridge abutments or on masonry buildings. These showed much greater drops than the interred bench marks, but it is probable that the latter are a truer index to changes in the general level of the country, seeing that a number of heavy buildings have sunk into the surrounding soil, so that lowering of bench marks of fixed to such structures does not necessarily imply sinking of the general surface level.

If the changes along the level lines just mentioned are typical of changes over the surrounding country, it is likely that the present great earthquake caused general sinking of level to a considerable degree, the drop increaseing as one goes south-eastward.

Before the earthquake, Sitamarhi was 201 feet, Muzaffarpur 175 feet, and Darbhanga 155 feet above mean sea level.

Effect on buildings and other structures.

Within the central area in which the intensity of the shocks had been estimated as being No. X on the Mercalli scale, every building was more or less damaged. Houses in this area collapsed by violent shaking rather than ground-sinking. But at places where many large fissures had formed on the ground, the houses sustained serious damage by tilting or through unequal subsidence of the foundations. Number of such houses is by no means negligible. These ground fissures were often formed roughly concentric to buildings or parallel to one of their walls. In some places, houses collapsed as the result of their foundations having been broken up by these large fissures.

Generally speaking, the damage was worst in houses of the *kutcha-pucca* type, while mud huts collapsed in many places, although the substantially built and light *pucca* building escaped with only slight damage. Bamboo huts were nowhere damaged.

Railway lines and bridges.

The railways lines over a wide area were severely buckled, the rails being thrown to either side by as much as 3 or 4 feet, while railway embankments sank in many places. The sufferers were the Bengal and North Western, the East Indian, and the Eastern Bengal Railways. Along the B. and N.-W. Railway, the worst damage, which was in the Tirhut section, was found in buildings and bridges which had cracked to almost complete destruction, the severest damage to bridges occurring in their lower parts, both above and below water. Not one bridge in Tirhut remains undamaged. Fortunately, loss of life along this line was very small. On the E. I. Railway, the causalities from the earthquake were very serious at Jamalpur, where more than a hundred houses in the railway colony collapsed. The damage on the E. B. Railway was confined to tracks, bridges, and culverts on the sections between Purnea and Jogbani and between Murliganj and Behariganj. Most of the seriously damaged bridges were of the brick-arch type.

The Devastated Towns.

The earthquake damage was particularly serious within the belt of country extending from Motihari in the extreme northwest to Purnea in the extreme southeast, the belt running nearly parallel with the river Ganges. Within this belt the shock was severest at Sitamarhi, Bajpatti, and Madhubani, the zone along which these towns are situated, about 50 miles long and 20 miles wide, being regarded as the so-called "epicentral tract". In this tract (larger hatched area in Fig. 7), sinking of the ground, on a large scale resulted in numerous fissures and breaking up of foundations, the buildings sometimes subsiding bodily, or individual walls sinking relatively to adjacent walls.

Outside of the Motihari-Purnea belt, another narrow zone of high intensity extends along the southern side of the river Ganges, from Patna to Monghyr. The intensity of the shock in the down-town of Monghyr was no less than in the epicentral tract, it being estimated to have been X on the Mercalli scale.

It must be remembered that there are several isolated spots or regions where the intensity of the shock was much lower than in regions surrounding them. Indeed, we find that side by side with, and

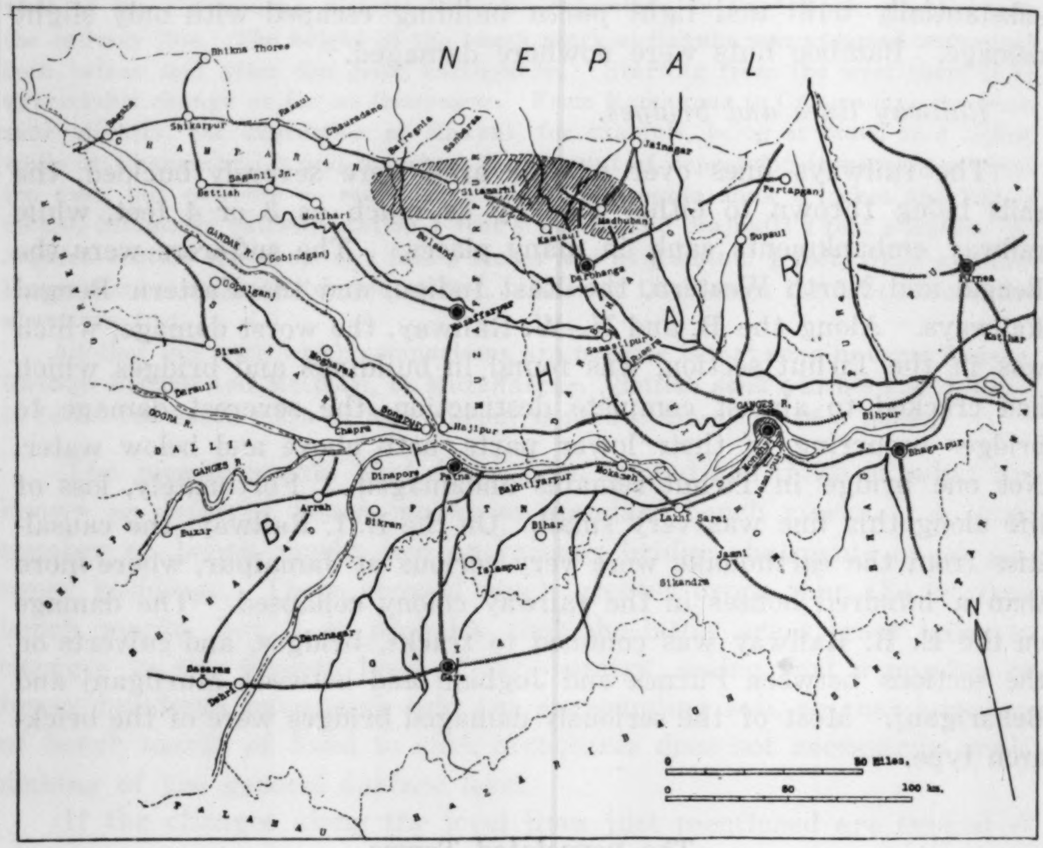
N E P A L
B I H A R
Bhikna Thore
Bagaha
Shikarpur
Raxaul
Chauradano
Bairagnia
Sonbarsa
Sitamarhi
Jainagar
Pertapganj
Madhubani
Kamtaul
Supaul
Purnea
Katihar
Bettiah
Sagauli Jn.
Motihari
Belsand
Darbhanga
Samastipur
Rusera
GANDAK R.
Gobindganj
Gopalganj
Muzaffarpur
Siwan
Bagharak
Darauli
Sonepur
Hajipur
Chapra
GOGRA R.
BALLIA
GANGES R.
Dinapore
Patna
Bakhtiyarpur
Mokameh
Monghyr
Jamalpur
Bihpur
Bhagalpur
Arrah
Bikram
Bihar
Lakhi Sarai
Jamui
Buxar
Islampur
Sikandra
Daudnagar
Sasaram
Dehri
Gaya
CHAMPARAN
SARAN
MUZAFFARPUR
DARBHANGA
MONGHYR
BHAGALPUR
PURNEA
PATNA
GAYA
SHAHABAD
GHAZIPUR
GORAKHPUR
PALAMAU
HAZARIBAGH
SANTAL
0 50 Miles.
0 50 100 km.
N

Fig. 7. Map of Bihar.

close to zones of great destruction, are regions along which the intensity was so much less that buildings and bridges escaped damage, while sand vents and fissures were almost absent. For convenience the damage caused to towns lying north of the Ganges will be described, next that to towns south of the same river, and lastly the damage to Nepal.

North of the Ganges.

Bettiah. The earthquake causalities in this town were not great; not more than at Motihari. Although the surrounding country showed ground cracks and fissures, the town itself showed none. The hospital was ruined and the Catholic Church and Bettiah Raj's buildings were all badly damaged. I understand however that twenty per cent of the damaged houses can be repaired. The well water was not fouled so badly as at Muzaffarpur and other places.

Sitamarhi. In Sitamarhi, a town of 10,000 inhabitants in the Muzaffarpur district, nearly every building came down in the earthquake, no house of whatever type escaped tilting or sinking into the ground. This type of damage was best seen in heavy brick buildings. Sand ejection reached maximum intensity here, filling houses, streets, and drains. Large fissures were formed all over the town. Bridges, roads, and railway tracks were either badly damaged or totally destroyed. In places the road sank six to eight feet.

Purnea. It is said that the earthquake here lasted fully three minutes. All the large buildings were seriously affected. The Civil Court, the largest building, was seriously damaged by fissures that formed across the foundation, the building subsiding as much as 2 feet. Many private dwellings, particularly two-storied structures, were destroyed; 50 per cent of the *pucca* buildings were so badly damaged that they will have to be rebuilt. Roads became undulating through local ground sinking, while the wells either dried or silted up. Water spouted out from fissures in many places.

Rajnagar. Rajnagar was badly damaged by fissures and sand vents, many one-storied houses in this town having suffered from these causes. Nearly all the *kutcha* buildings collapsed, while the majority of the *kutcha-pucca* buildings either came down or subsided. In places the sand deposits are from 2 to 3 feet deep.

Madhubani. About 70 per cent of the buildings either totally or partially collapsed. The damage done to buildings was aggravated by ground fissures splitting the walls and foundations. The famous temple of *Hari Sabha*, however, stands uninjured. Sand and water vents were common sights in the surrounding localities.

Motihari. Here faulting, fissuring, and sand ejection occurred on a very large scale. The principal street of the town had altogether changed in appearance. The picturesque town on the bank of the lake of the same name is now a sorrowful picture. Owing to subsidence along the margin of the lake, the houses have taken a strong list towards the lake. The beds of the Gondak and Sikrahna rivers are reported to have risen owing to deposits of sand, while almost all the water channels in the Motihari sub-divison have been filled up with sand.

Muzaffarpur. Although the greater part of the town of Muzaffarpur, north of the railway station, suffered very badly, the damage south of the station is less extensive. In the last mentioned part of the town, the buildings were damaged by sinking and cracking of the ground. Most of the one-storied *pucca* buildings, such as the English Church, the Deputy Inspector-general's residence, and the Circuit House, however, withstood the earthquake, while most Government buildings north of the railway station, such as the Civil Court, the Collectorate, the Commissioner's Court, were badly damaged. Most of the wells at Muzaffarpur were choked up with sand, while the water in the tanks became shallower as their beds were sanded.

Darbhanga. It is stated that damage here on the whole is less than at Muzaffarpur, the destruction of buildings being not so general, although the heart of the town has been completely ruined. The Darbhanga Raj's buildings and the Nargaona Palace have suffered the most. The Post Office buildings, Northbrook School, and Darbhanga Medical School have also been badly damaged. The earthquake caused the worst havoc at the Katki Bazaar, which is densely packed with two-storied *kutcha-pucca* buildings.

Samastipur. In this town, the maximum destruction is confined to the bazaar area, where a number of two-storied *kutcha-pucca* buildings partially collapsed and others were seriously damaged. On both sides of the railway line, sand was ejected from fissures and the buildings of the sugar factory badly damaged, by shock as well as by ground fissures.

South of the Ganges.

Monghyr. Monghyr is a large, flourishing town situated on the right bank of the Ganges. This town is known to the outside world as containing an old fort and, in its environs a hot spring called Sitakund, the objective of Hindu pilgrims. In this town, the Chawk Bazaar fared the worst; the death-roll at this place alone being according to reports (on Jan. 22) about 500. On both sides of the narrow lanes stood a large number of two or three-storied buildings, in which, unfortunately, an unusually large number of people had congregated on this day from the neighbouring villages for shopping in connection with the "Id" festival. As Monday, Jan. 15, happened to be "Amabasya", the Hidus were looking forward to a bathe in the Ganges, while the Muslims were out shopping in connection with the "Id" festival, so that when the houses began to come down Hindus and Muslims were alike crushed to death.

Monghyr is built on both alluvium and archaean rocks. As is usual, houses built on hard rocks suffered less damage than those built on alluvium. The fort wall collapsed in many places, but the buildings inside it (on archaean rocks) escaped destruction with only slight damage. The main damage to *pucca* buildings occurred on the alluvium along the edge of the high ground.

Patna. Here buildings along the river front suffered most. In the bazaar, many buildings collapsed, especially the tall *kutcha-pucca* buildings. The High Court and the Government Houses showed huge cracks in a number of places.

Gaya. At Gaya the damage was considerable, houses in the localities known as Upperdih and Gayawalbigha suffering the most. The great temple *Bishnupada* and other famous Hindu temples escaped damage. Many buildings in the town were cracked, while here and there were porches down. Ground fissures appeared at several places in the river Falgoo (ordinarily a dry sand bed) whence gushed out water and sand in considerable quantities. The famous temple at Budha Gaya sustained no damage.

Towns in Nepal.

All the three important towns of Khatmandu, Bhatgaon, and Patan were severely shaken and almost all the houses either demolished or damaged. The intensity of the shocks at Khatmandu has been estimated to be X on the Mercalli scale. Large cracks appeared on the maidan and several of the roads in Khatmandu. Amid the havoc caused at Khatmandu, however, the temple of Pasupatinath, the Guardian Deity of Nepal, still stands intact, entirely undamaged.

Contrary to what was first feared, no fire accompanied the earthquake, which is extremely fortunate, seeing that wood enters so largely in the construction of houses here.

Cause of the Earthquake.

It is generally accepted that the present Indian earthquake is due to compressional movement or to the push of the Himalayan mass up the faults. It would seem nearer the truth to say that certain sudden change in bulk occurred in the mass underlying the Himalayan mountain range, which would have the effect of displacing the top crust, thus setting up strains that could be relieved only by bending or fracture of the earth's crust causing the jerky movements of the Great Boundary Fault, the immense reversed fault extending along the southern foot of the Himalayas.

The distribution of Indian earthquakes shows that most of the shocks occur in bulging parts of the Himalayan mountain range. On the other hand, according to a map showing the distribution of gravity anomalies,[4] these parts cover an area where the gravity anomalies showed negative values, that is, a region of underload as the result of abnormally low densities in the earth's crust. This underload may perhaps be accounted for by the low density of the alluvium of the Ganges Valley. The alluvium covers, with unknown thickness, a trough or crustal depression that underlies the Ganges valleys.

The depressed condition of the earth's crust in this region is believed to have existed from time immemorial, which with every great earthquake sinks deeper. The lines of level that were run after the present earthquake show that the region most affected had subsided at the time of the earthquake from a few inches to as much as 2½ feet. In 1833, Bihar suffered a similar violent earthquake, when considerable areas were flooded as the result probably of subsidence of the ground caused by the earthquake.

Nature of the Earthquake Motion.

We shall next consider the nature of the earthquake motion on the ground. Damage to houses seems to be caused by earthquake waves of short periods. The greatest damage occurs when the natural oscillation period of the building itself synchronises with the period of the earthquake waves.

According to observations[5] made in Tôkyō and Yokohama, the period of earthquake motion at certain places always had certain definite values, especially in the case of earthquake motions consisting of short-period vibrations, such as those with periods of less than 1 sec. The periods differed with the position where the observations was made— a fact which suggests that the uppermost soil layer is probably an oscillating body capable of executing vibrations of its own period should earthquake waves of similar period come along. Observations[6] covering ten stations in Tôkyô and Yokohama showed that the natural oscillation periods of the ground differed with place. At Hongo and Marunouti, for example, where the former lies on diluvium that forms the up-town and the latter on alluvium down-town, the largest period at Hongo was 0·3 sec, while at Marunouti it was 0·7 sec. The distance between these two points was only 3·0 km. Generally speaking, on diluvium ground, such as Hongo, Aoyama, etc., the natural period of the ground was comparatively short, the mean value being 0·3 sec, whereas on soft alluvium ground, such as Marunouti and Hukagawa, etc., the period was much longer, with a mean value of 0·4~0·7 sec. An interesting fact[7] noticed at the time of the last Tôkyô earthquake of 1923 is that wooden buildings were affected more by this earthquake down-town than up-town, whereas of heavy construction, such as brick warehouses (go-downs), suffered more serious damage up-towns than down-town. It should be added here that the ordinary Japanese wooden two-storied dwelling houses have periods of natural oscillation of 0·3~0·7 sec., while in the case of low brick buildings they are 0·1~0·4 sec. What has just been stated can therefore be explained by synchronisation of the building with the ground vibration.

---

[4] Published by the Geological Survery of India.

[5] M. Ishimoto, "Observations accélérométriques des secousses sismiques dans les villes de Tôkyô et Yokohama", *Bull. Earthq. Res. Inst.*, **12** (1934), 234.

[6] M. Ishimoto, *ditto.*

Careful studies of earthquake motion revealed that most of the short period waves that were superposed on those of large period were restricted to the superficial soil, rapidly diminishing in amplitude with depth. On comparing the magnitudes of these waves observed on the ground with those under ground, it was found that even a places 10 m below the surface, the amplitude of earthquake motion was far less than that on the ground.[8] Although, the diminishing rate of amplitude varies with the period of the motion, the mean ratio of the amplitudes above and below the surface was 2·5 : 1, the period of oscillation ranging between 0·2 and 0·4 sec. We may thus conclude that the violent motion of the ground which affects houses and other structures are mostly secondary waves produced in the superficial layer.

It has been a common experience that earthquake damage is localised in a certain area or along a certain line. In the present Indian earthquake, damage was most marked over a belt of country some 10 to 20 miles in width extending from Motihari to Purnea. Another zone of high seismic intensity, but slightly less than the former, ran from Muzaffarpur to Darbhanga. Zones of particularly weak formation seem to lie along these regions. This linear distribution of earthquake damage is often due to the existence of zones of particularly soft and weak formation and not to the fact that the seismic origin is of line-form.

In the strong Saitama (Japan) earthquake of 1931, the interesting fact was observed that the damage caused by this earthquake was in the main restricted to a narrow region along the Tone River, whereas the centre of this earthquake as accurately determined by observations was found to lie in the hilly region of Titibu, showing that the earthquake centre and the centre of the affected region do not necessarily lie close to each other. A distance of about 20 km separated the two centres.

As to the most seismic area in India, there is no doubt that the Indo-Gangetic plain and the Assam hills have the strongest claims to this honour. If an earthquake were to originate in the Great Boundary Fault forming the foot hills of the Nepal Himalaya, it is obvious that the greatest damage will occur on the vast Gangetic plain, which unfortunately, is the most densely populated part of India.

---

7) T. SAITA,

8) W. INOUYE, "Comparison of Earth Shakings Above-ground and Underground", *Bull. Earthq. Res. Inst.*, **12** (1934), 712.

Buildings in India.

With respect to buildings in India, especially those in the northern part of the country, the following points with respect construction ought to be taken into consideration in future in order to eliminate such weaknesses in construction as have been demonstrated by the present earthquake.

(1) Use only good quality mortar and bricks: the mortar should have approximately the same strength with respect to compression and tension as the blocks which it binds. The bricks must be of regular shape and laid in a regular uniform manner.

(2) The building must be monolithic, or as near so as possible.

(3) In *kutcha-pucca* buildings, which form a considerable proportion of the town buildings, there should be no loose beams or joists in the upper floors and roofs; the falling of such loose material being a potential danger to life.

(4) The present strength of the walls must be increased: the most suitable form of wall for circumventing the effect of earthquake shocks being those of trapezoidal cross-section or of parabolic cross-section with the vertex downwards as shown in Fig. 8. As to brick buildings, of which the walls are of parabolic cross-section, the following account of experience gained from the Tôkyô earthquake of 1923 might be of interest. In this earthquake, the earthquake-proof brick building of the Seismological Observatory in the compound of the Tôkyô Imperial University sustained no damage, not a fissure having appeared on its walls. On the other hand, a brick column inside this

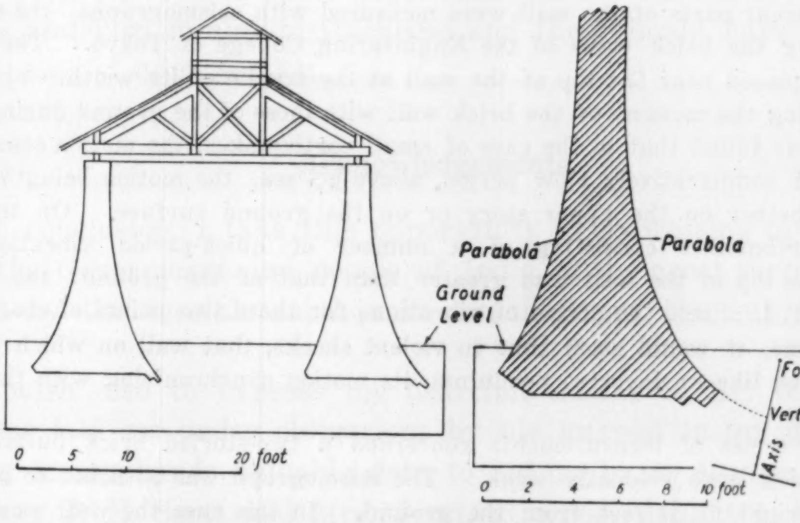

Fig. 8. Walls of parabolic cross-section.

observatory, about 15 feet high and 3 × 3 feet in cross-section, was fractured, and its upper part twisted at an angle of not less than 30°.

The walls of this brick building were of parabolic section with the vertices downwards, 18 ft high, 8 ft thick at the ground level, and 2·3 ft thick at the top. A tiled roof with skylight rested loosely on the walls; an entrance of about 8·5 ft ×11 ft being the only opening in them.

The walls of parabolic cross-section gave uniform strength throughout the height. The cement and mortar that were used in its construction had beed carefully tested beforehand. This building was designed to withstand any shock that is likely to occur in Tôkyô, as also to serve as a standard with which to compare the effects of shocks on brick buildings of the ordinary type. Walls of this type are recommended for *pucca* buildings, as well as for the *kutcha-pucca* building. I believe that even a *kutcha* building, provided it has walls of parabolic or trapezoidal section, will serve to reduce damage and loss of life during an earthquake to the minimum.

We shall add here the results of studies on the behaviour during an earthquake of ordinary brick walls as they used to be constructed in Japan, which form excellent data for reference in connection with future constructions.

Since damages to brick buildings by an earthquake are usually the result of fracturing of their walls in consequence of the violent horizontal shaking, vibra tions of different parts of the wall were measured with seismographs, the example selected being the brick walls of the Engineering College of Tokyo. The instruments were placed near the top of the wall at the middle of its width.

Comparing the motions of the brick wall with those of the ground during earthquakes, it was found that in the case of small earthquakes, the motion consisted of vibrations of comparatively slow period, above 0·5 sec, the motion being virtually the same whether on the upper story or on the ground surface. On the other hand, in earthquakes consisting of a number of quick-period vibrations, the motion at the top of the wall was greater than that of the ground; the average ratio being 2:1. Since the period of vibrations for these two points of observation, were the same, it would seem that in violent shocks, that wall on which the roof rests, behaves like an inverted pendulum, its motion synchronizing with the earthquake motion.

Another series of measurements concerned a two-storied brick building, the walls of which were evidently weak. The seismograph was attached to a 53 feet wall at a height of 31 feet from the ground. In this case the wall was shaken considerably by earthquakes, both the duration and the amplitude of motion being nearly three times those of the ground. The period of natural oscillation of the wall practically constant with a mean value of 0·33 sec., which shows that in an earthquake a weak wall behaves exactly like an elastic spring and executes vibrations of its own period, whatever the period and amplitude of the ground motion.

Another example was a three-storied brick building, which though well designed, stood on the lower ground of Tôkyô. It was found that the motion in the 3rd story did not differ from that in the basement, showing that this brick building behaved as a single mass during an earthquake.

The foregoing examples show that the movements of a brick building during an earthquake differ widely with the quality of the structure.

Lastly, a few remarks will be made regarding the means of minimizing earthquake damage. Obviously the most effective way in which this can be done is to construct the buildings as near earthquake-proof as possible. Although there is little doubt that the reinforced concrete building with iron frame-work easily ranks first in the various kinds of earthquake-proof buildings, owing to the question of cost, to build such structures is not always practicable. During my tour of inspection in connection with the present Indian earthquake, I was strongly impressed with the suitability of the *kutcha-pucca* and *kutcha* style of buildings for India, especially in the districts devasted by the recent earthquake. The unfortunate part of it however is the inability of the average Indian householder to afford to use high grade building materials. Under these circumstances, it is then most important to build a safe structure at no greater cost than one of the old weak type. With special attention to design, it may be possible to build such houses with materials not very much higher in quality than those now in use. For one thing, the heights of *kutcha-pucca* buildings could be restricted to one story, while their walls should not be less than a standard minimum thickness and they should have a parabolic or trapezoidal cross-section.

Acknowledgements.

In conclusion, I take this opportunity of expressing my sympathy with the Government and people of India in the great sorrow and loss caused by the terrible earthquake which forms the subject of this paper.

I wish also to express my heartfelt thanks to Mr. W. E. Brett, who has laid me under obligations by his interest in my mission and placing in my hands valuable data to aid me in my studies. To Commissioner J. E. Scott and Mrs. Scott, at whose delightful home I was privileged to be guest during my stay in Muzaffarpur, I cannot sufficiently express my gratitude for their many personal courtesies which rendered my stay in India so pleasant and enjoyable. I wish sincerely to thank Commissioner Scott, besides, for his innumerable courtesies extended me in his official capacity towards enabling me to prosecute my investigations.

30. 昭和9年1月15日の印度大地震に就いて

地震研究所　那須信治

本論文には印度大地震の踏査報告に加へて本邦最近の地震學より此の地震を見て思ひ浮んだ事を記載した．殊に今同の地震の原因に就いては世上に信じられてゐるヒマラヤ南麓の大斷層の活動とのみ簡單に斷定し得られざることを附記した．

又被害分布と震原の遠近は必ずしも正しき關係を有せず，土地の振動性能に著しく支配されることを示し今同の地震に於ける，モンギール市及びネパールの都市の如く甚だ飛び離れた地點に被害のあつたことも要するにその土地の振動性能に左右された結果であるとし．これ等の地點の眞下に夫々震原を假定するの不自然なることを述べた．

各地の被害狀況は概略をのべるに止めて置いた．

本文の後半に於ては印度に多く用ひられてゐる煉瓦及び煉瓦・泥併用建築物の缺點をのぞくに有効と考へられる事柄を箇條書としてのべ，印度の一般家庭の現狀より到底良質高價の建築材料を使用し得ざる事を認め現在の材料をそのまゝ用ひて，より耐震力ある家屋を建てるために壁の構造には梯形或は抛物線の斷面を有するものを推賞しておいた．尙ほ煉瓦造りは印度に於ては到底放棄することの出來ない建物であるから，これ等の建物が地震の際如何なる振動をするかを本邦に於てなされた實測の結果を擧げ今後の復興建築の參考に供したい希望を有してゐる．

尙ほ今同の地震に於て現はれた土砂の噴出，水準變化等も最も信ずべき資料を引用して記述しておいた．

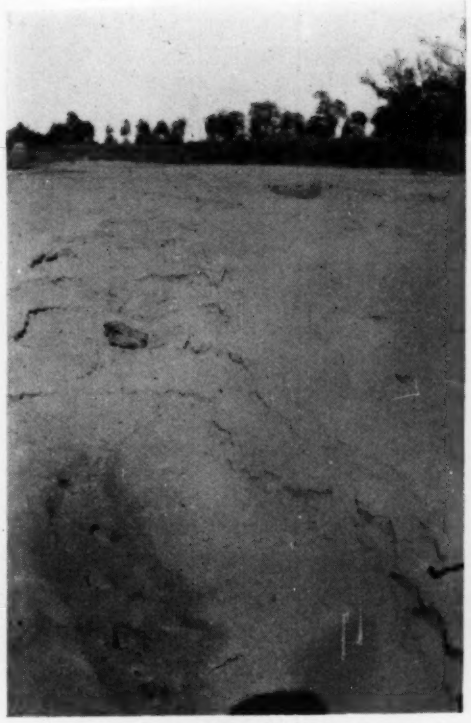

Fig. 2. Sand-deposits and fissures.

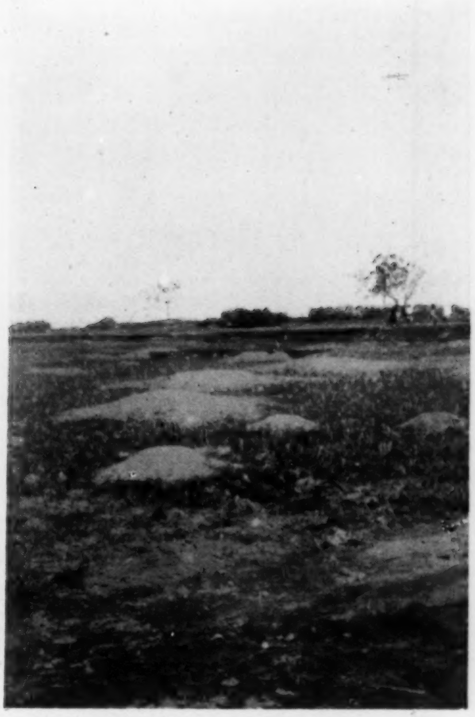

Fig. 3. Craters of ejected sand.

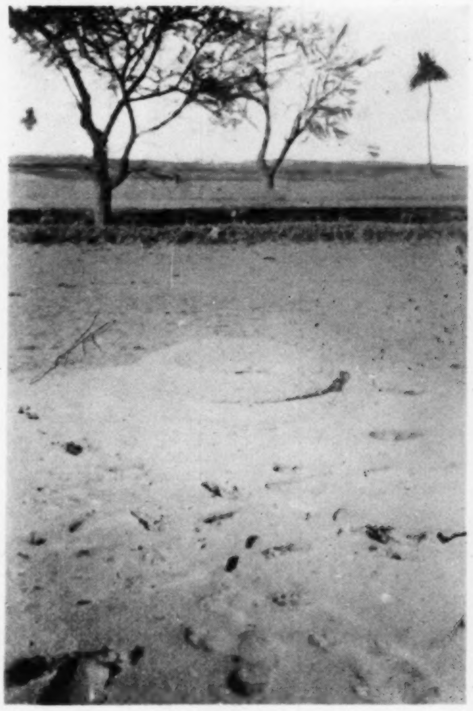

Fig. 4. Craters of ejected sand.

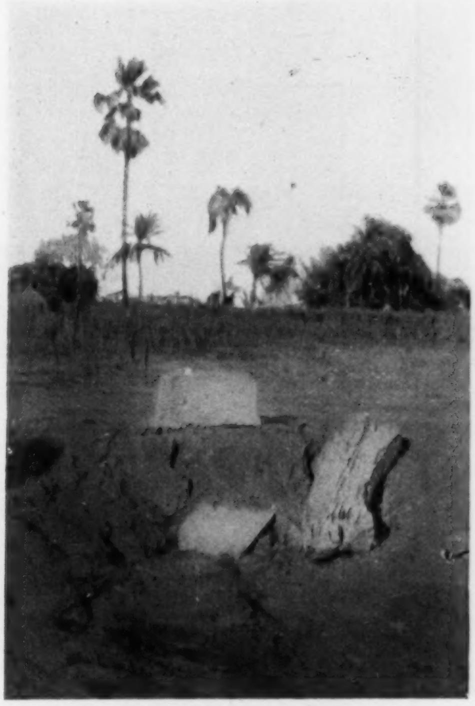

Fig. 5. Two old baked curved tiles and part of wooden cutting edge (Jamo) of the long forgotten well deposited on the surface by the outrash of sand.

(Reproduced from photographs taken by Dr. K. S. Caldwell.)

（震研彙報 第十三號 圖版 那須）

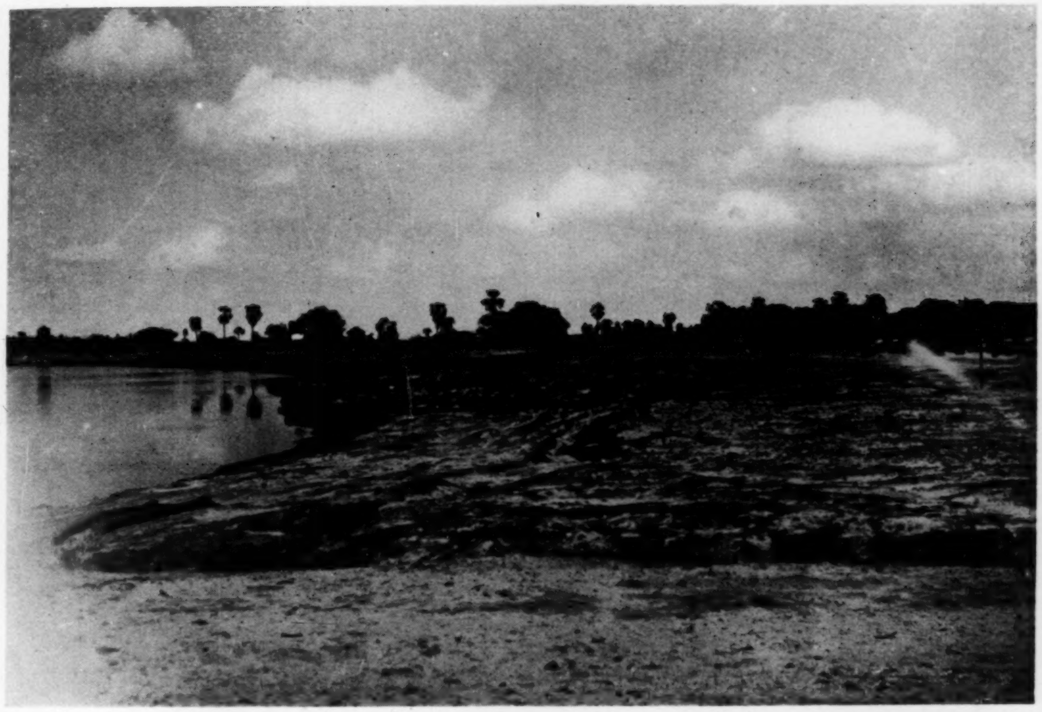

Fig. 9. *N. Nasu, Photo.*

Fig. 10. *N. Nasu, Photo.*

Fissures in the river banks near Muzaffarpur.

{

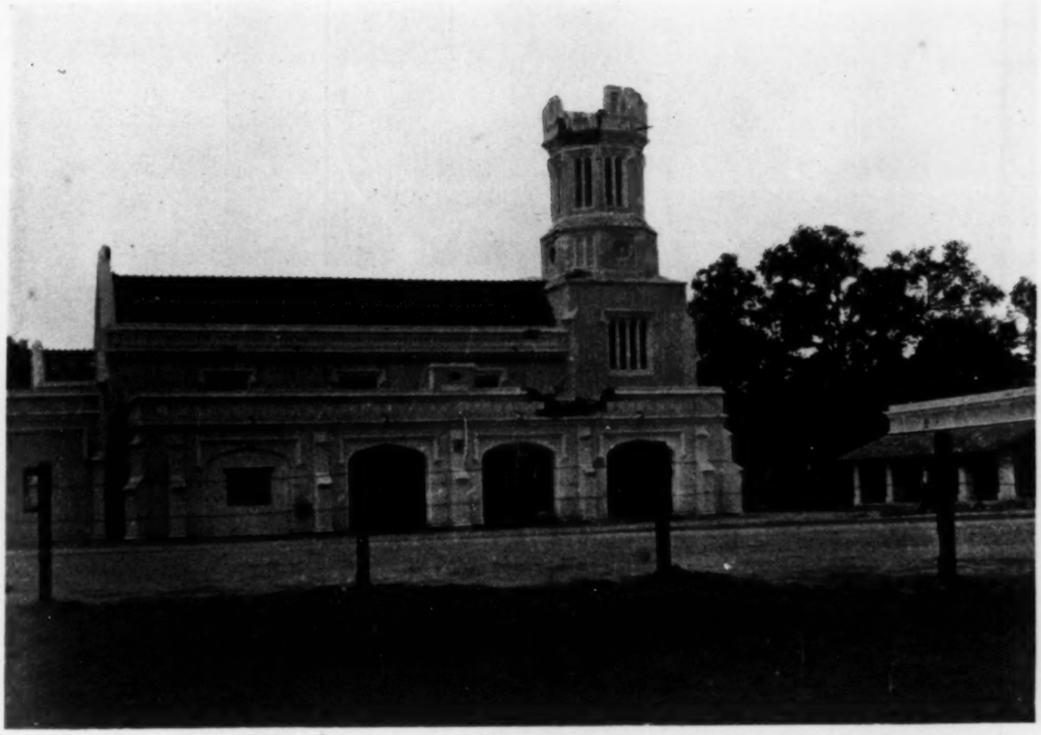

Fig. 11. An office building in Patna. *N. Nasu, Photo.*

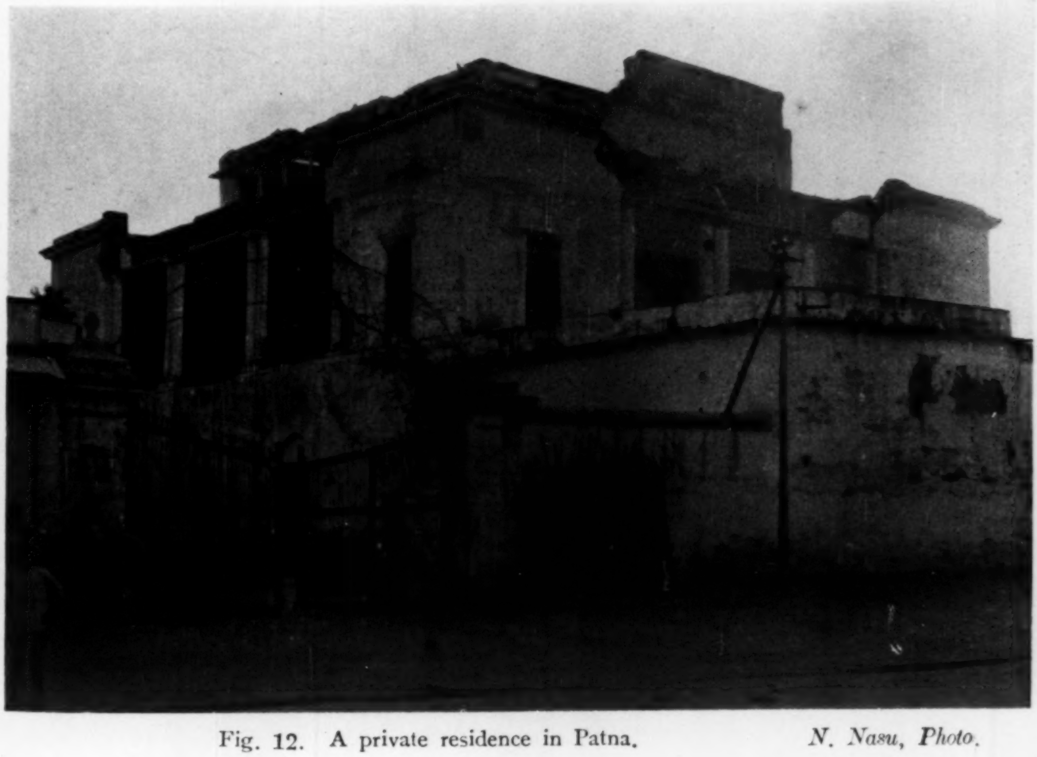

Fig. 12. A private residence in Patna. *N. Nasu, Photo.*

Examples of houses that had their upper parts were broken off by the earthquake.

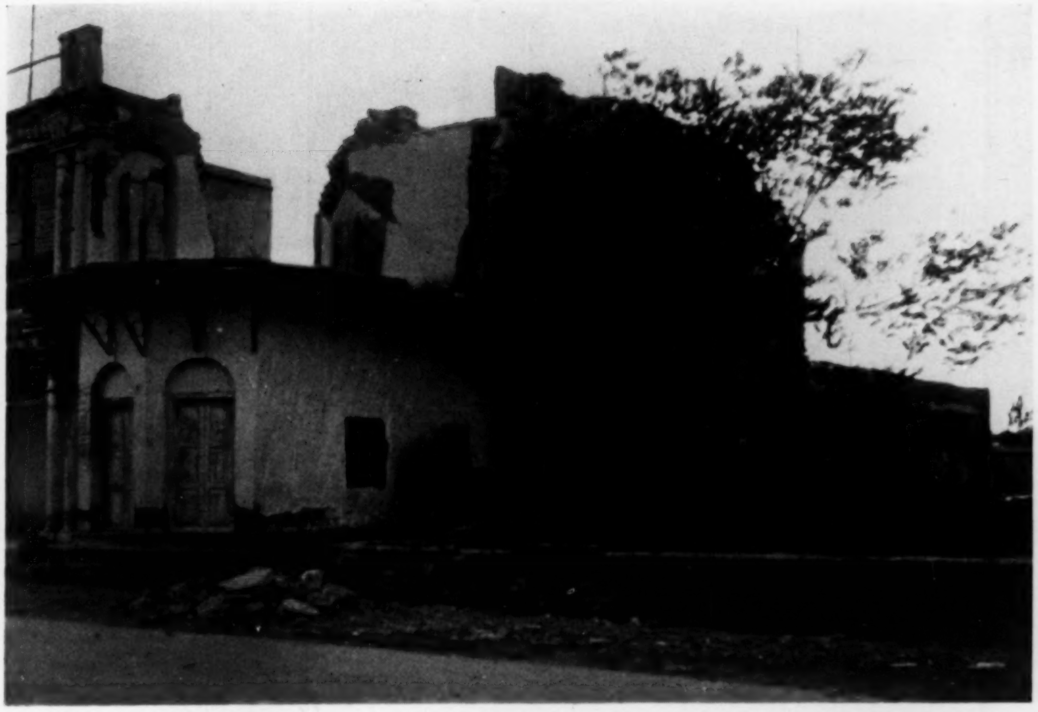

Fig. 13. Aprivate residence in Patna. *N. Nasu, Photo.*

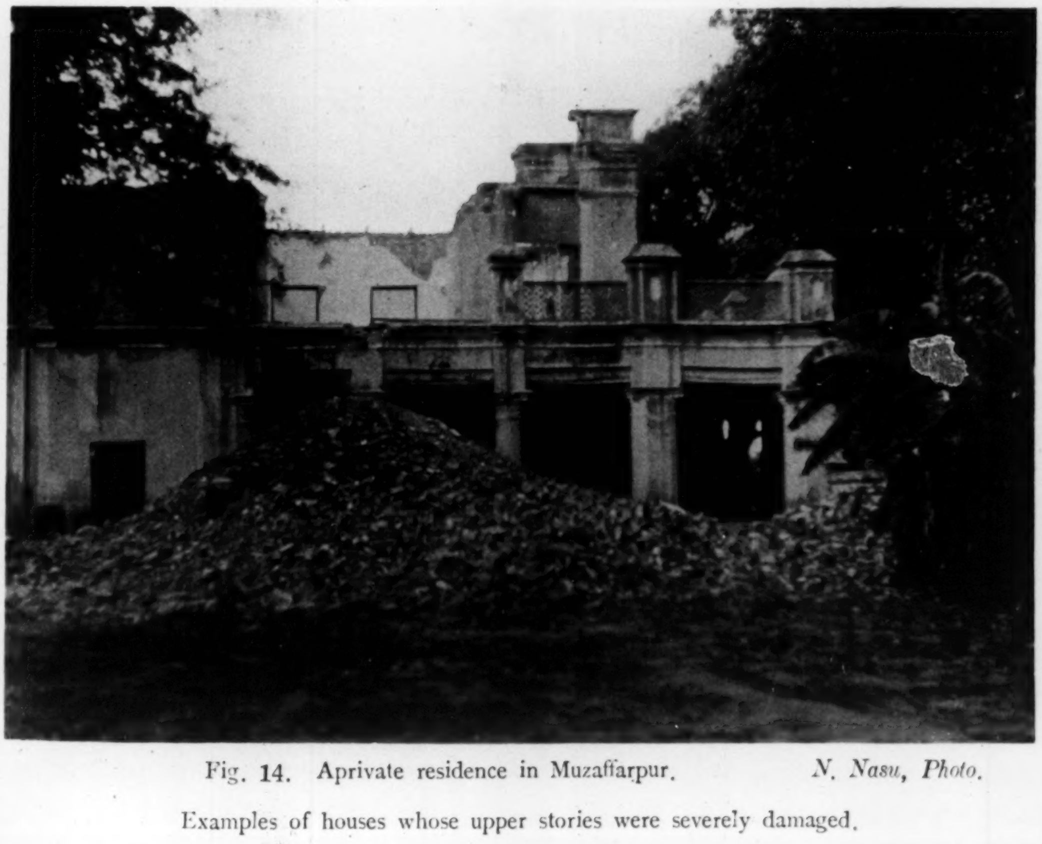

Fig. 14. Aprivate residence in Muzaffarpur. *N. Nasu, Photo.*

Examples of houses whose upper stories were severely damaged.

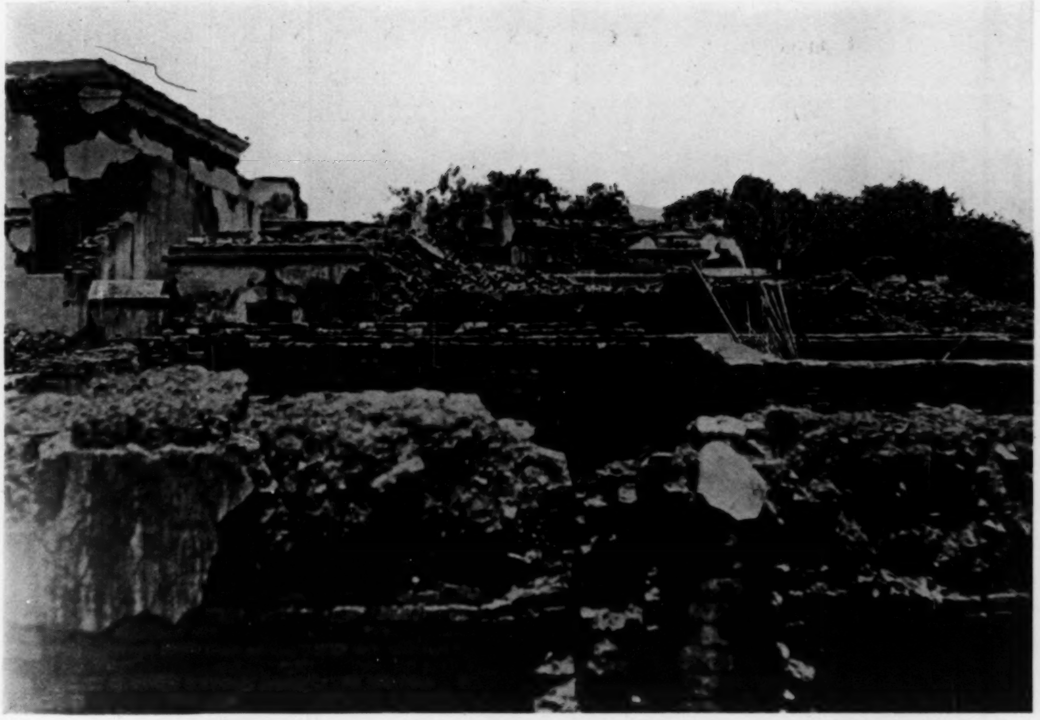

N. Nasu, Photo.

Fig. 15. Two-storied houses completely ruined near the Monghyr Raj's Palace.

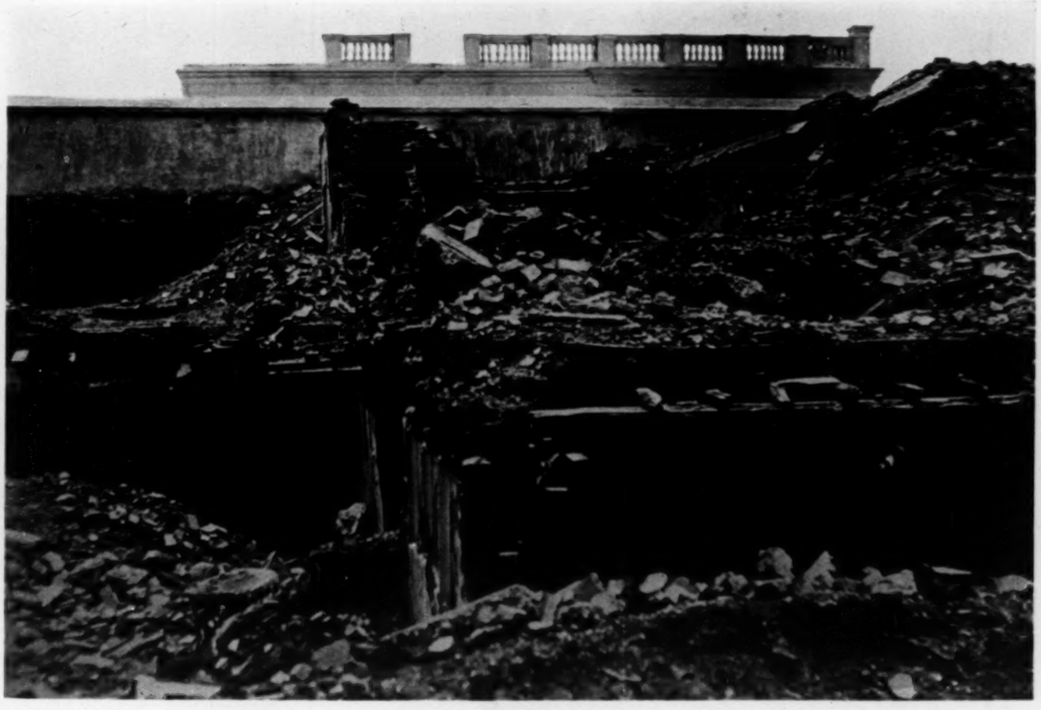

Fig. 16. ditto. *N. Nasu, Photo.*

（震研彙報 第十三號 圖版 那須）

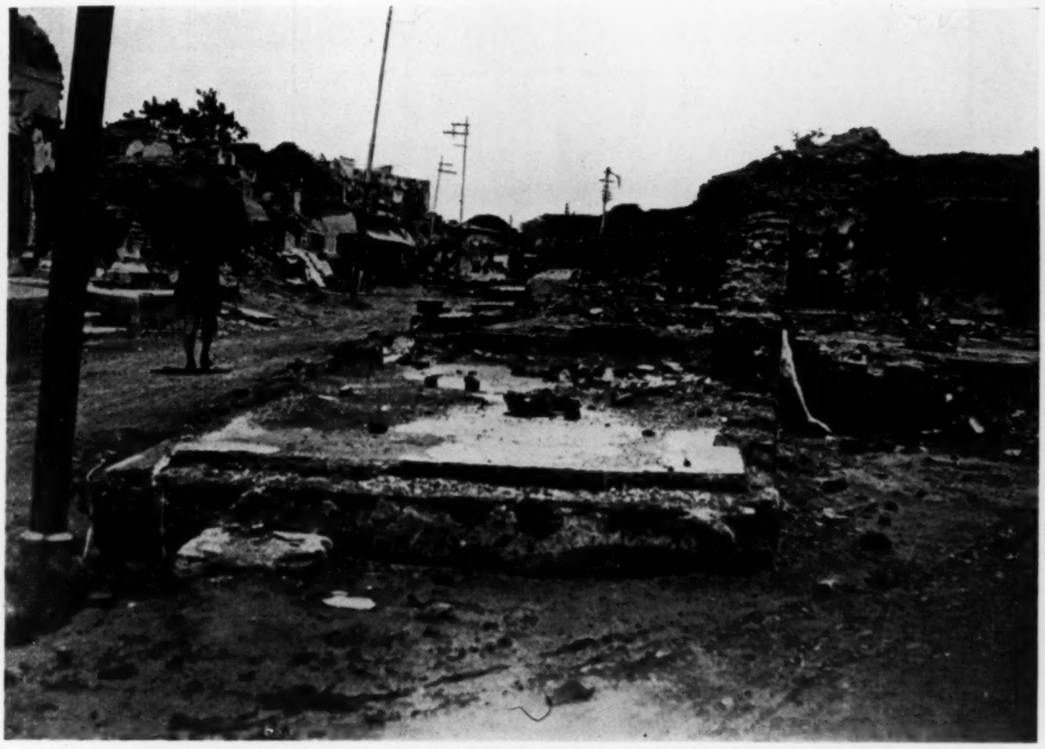

Fig. 17. Ruined town of Monghyr. *N. Nasu, Photo.*

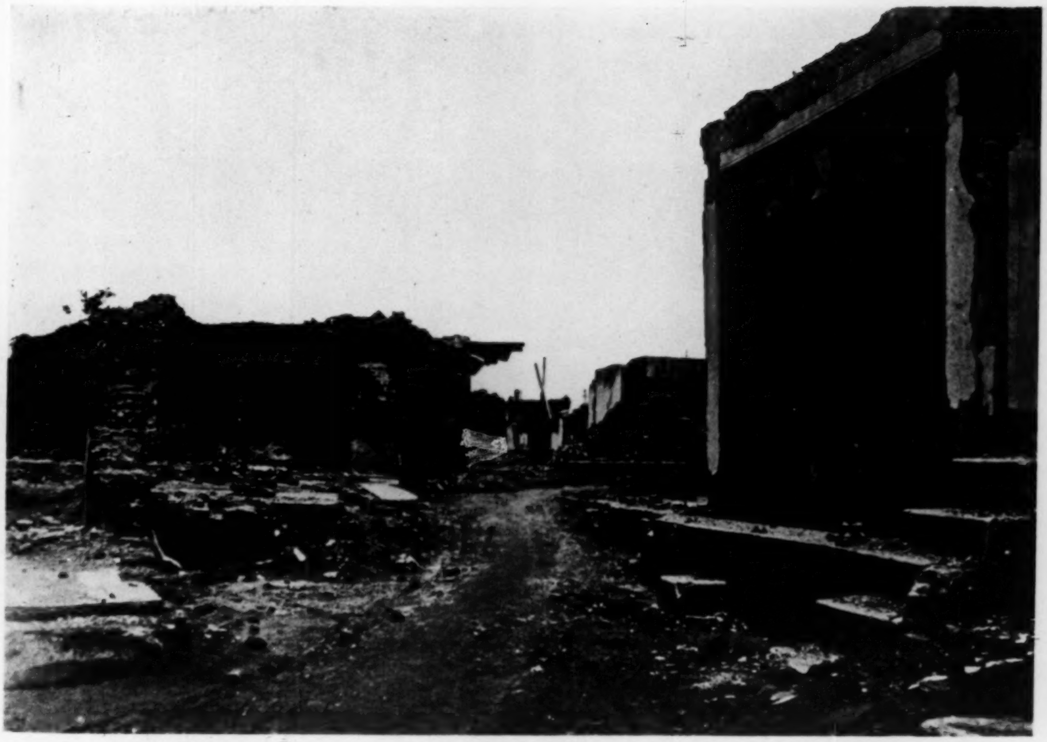

Fig. 18. ditto. *N. Nasu, Photo.*

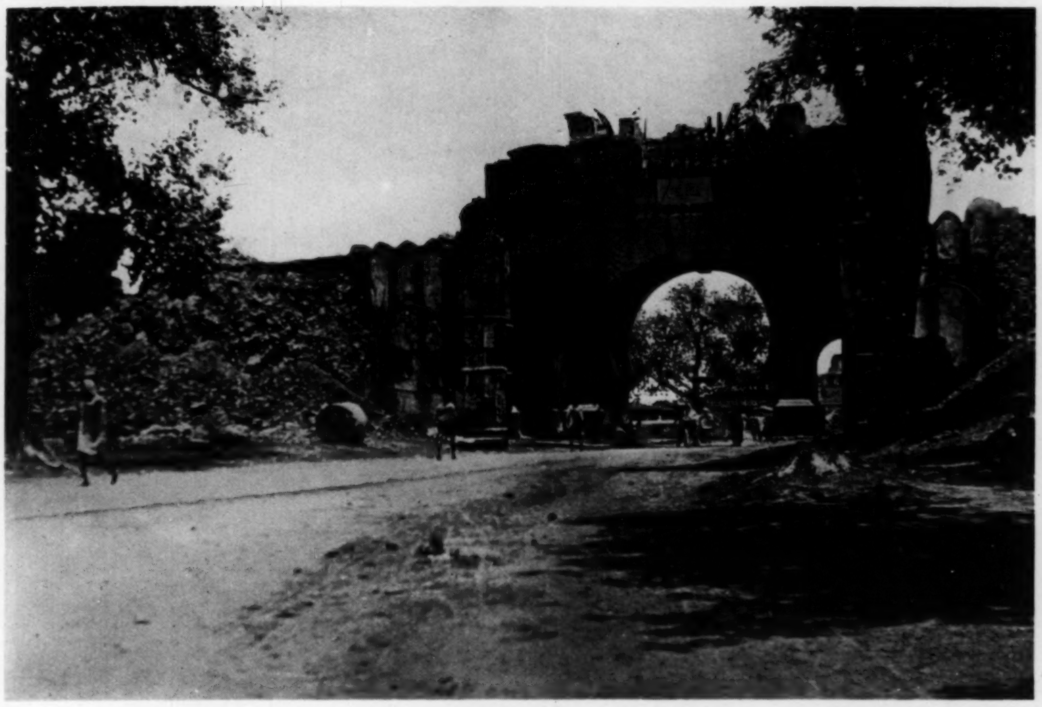

Fig. 19. Gate of Fort Monghyr damaged by the earthquake. *N. Nasu, Photo.*

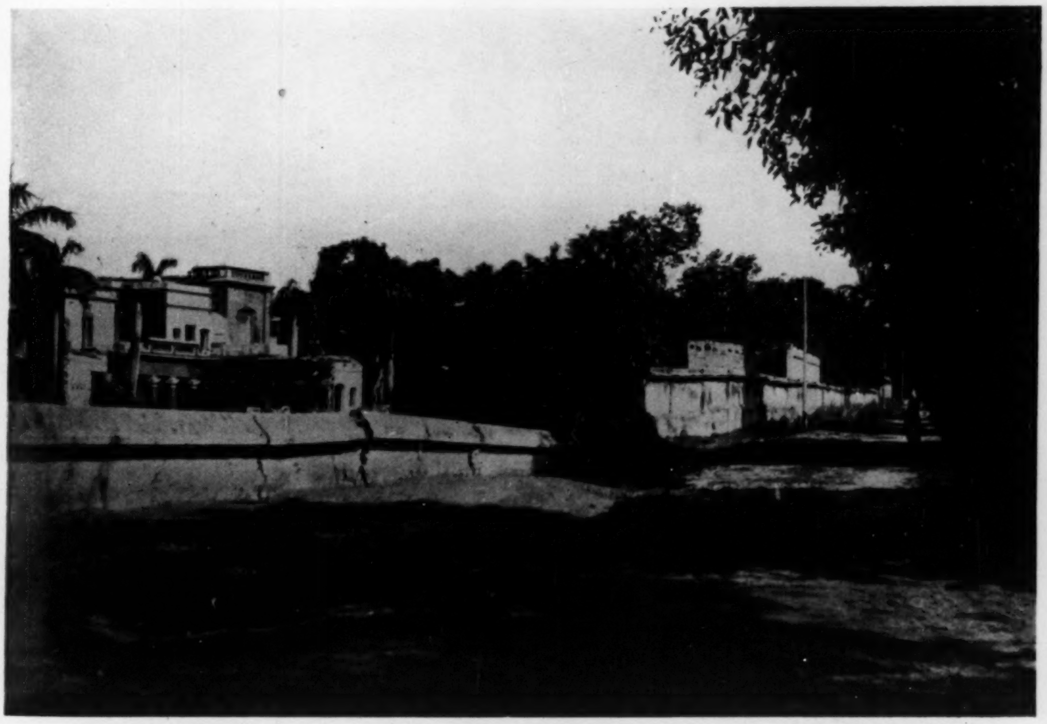

N. Nasu, Photo.

Fig. 20. Sand, ejected from fissures (centre), covered the surface of the road. The ground along fissures subsided.

（震研彙報 第十三號 圖版 那須）

31. *Experiments on the Visco-elastic Properties of Pitch-like Materials. (II).*

By Kumizi IIDA.

(Read Nov. 20, 1934.—Received March 20, 1935.)

Introduction.

In the preceding paper,[1] we described and discussed the results of experiments on the visco-elastic properties of substances, such as pitch, paraffin, sandstone, and water-glass by statical methods of experiments. In discussing the results of these experiments with reference to the geophysical phenomena, namely, the folding of mountains, the chronic deformations of the earth's crust, and the propagation of seismic waves, it was considered desirable to carry out further experiments by dynamical methods to be described here.

When these substances were subjected to forces for a long period of time, though from appearances they seem to be elastic solids, they behaved mostly like a liquid of high viscosity. However we do not know as yet how these substances will behave when subjected to sudden forces for only a short period of time. In the present experiments, therefore, we imparted sudden forces for only a short period of time to these substances in order to ascertain whether or not they behave like an elastic solid. By means of the same method we examined the properties of an artificial visco-elastic substance, as will be shown later. A comparison of the properties of substances such as pitch, paraffin, and sandstone, with those of an artificial visco-elastic substance, is given later in connection with the structure of these substances.

S. Kusakabe[2] obtained his moduli of the elasticity of rocks by kinetic measurements as well as by statical measurements as also the relation between the kinetic and the static moduli. The elastic properties of rocks therefore are now understood, but their viscous properties in their solid states seem to be unknown as yet. The author intends to study the visco-elastic properties of rocks, the present experiment being the first step in that direction.

---

[1] K. IIDA, *Bull. Earthq. Res. Inst.*, **13** (1935), 198~212.

[2] S. KUSAKABE, *Publ. Imp. Earthq. Inv. Comm.*, **22** (1906~1908), 27~49. *Proc. Phys.-Math. Soc., Japan*, **2** (1903~1905), 197~206, 341~352.

Part II. The Dynamical Methods of Experiment.

Experiment I. The Relation between the Moduli of Rigidity and the Magnitude of the Torsional Couple.

1. Methods of Experiment. The apparatus constructed is as show in Fig. 1, its principal part being almost the same as that shown in Fig. 1, in the preceding paper,[3] the main difference being the contrivance for the twisting motion. In order to impart torque to the specimen to be tested, the following device was adopted. The moving coil C, to which the clamp A_2 is connected for clamping the specimen T, rotates freely between the poles P of an electromagnet that is magnetized by the coil K. By means of the key connected to the circuit of the moving coil C, an electric current is made to flow through it for a certain length of time. The intensity of the current is read off from the ammeter A. The motion of the image produced by deflection of the lens mirror M is photographically recorded on a rapidly rotating drum on which a bromide paper is wound, and which is placed about one meter distant from the lens mirror M. The elastic property of the specimen is ascertained from this record. Another lens mirror M_A is attached to a small piece of soft iron that rotates through a small angle around one of its ends. When a current flows through the coil of the small magnet, the coil of which is connected to the circuit of the moving coil C, the small piece of iron is pulled to another small magnet. The deflection of the mirror M_A is photographically recordedwith that of mirror M, the length of time during which the current flowed being known.

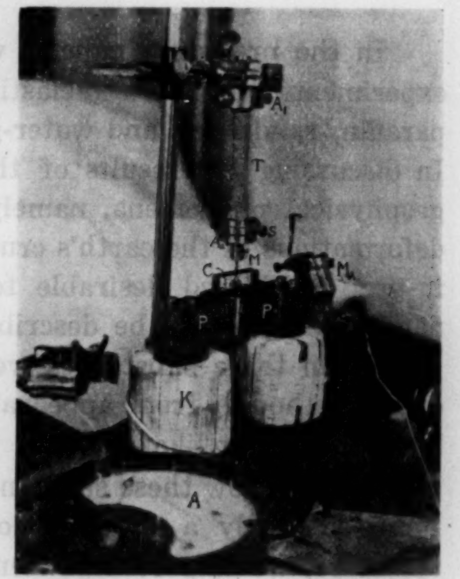

Fig. 1. Twisting apparatus. T, specimen; A_1, A_2, clamps; S, screw; M, lens mirror; C, moving coil; M_A, lens mirror; P, pole of magnet; K, solenoid coil; A, ammeter.

When a current is passed through the moving coil C in the magnetic field, a torsional couple is imparted to the lower end of the specimen

---

[3] K. IIDA, *loc. cit.* It is quoted in proper places.

T, and this twists the specimen. In order to find the magnitude of this couple, instead of the specimen, a steel wire of known rigidity is clamped, and its twisted angle observed. The torsional couples were calculated from this angle by using the formula $C=\frac{\pi r^4 n\varphi}{2l}$, where C is the torsional couple, n the modulus of rigidity, l the length, r the radius, φ the angle of the twisted wire; the last-named angle, which is caused by the electric current, being observed by means of a telescope and scale.

The calibration of the torsional couple is carried out for the following two cases:

1). When the current passing through the moving coil is kept constant, the intensity of the magnetic field is changed.

2). When the intensity of the magnetic field is kept constant, the current passing through the moving coil is changed.

Next, instead of the steel wire, the specimen is clamped. The specimen, which at first is motionless, is twisted as soon as the current is passed through the moving coil C in the magnetic field. If the specimen possesses any elastic property at all, it will return to its initial position by virtue of its elasticity as soon as the circuit connecting to the moving coil C or the solenoid K is opened, so that by observing the elastic recovery of the specimen, we know whether or not it behaves like an elastic solid when subjected to sudden forces for only a short period of time. The temperature is kept constant during the experiment.

2. Results of the Experiments. The actual records obtained by the apparatus are shown in Figs. 2∼4. From the phenomenon of elastic recovery of the specimens shown by these records, we know that these substances possess the property of elastic solids. The same experiment was repeated with water-glass, the coefficient of its viscosity η, which is of the order of $10\sim10^3$ poises at 15°∼50°C, with the lower end of the moving coil C connected to the inner cylinder of the concentric cylinder apparatus, but no phenomenon of elastic recovery could be seen (Fig. 6), whereas upon adding to it very small pieces of black rubber the phenomenon of elastic recovery became plainly evident (Fig. 5). From this fact we may conclude that even the suspension of an elastic substance in the viscous liquid will impart elasticity to a visco-elastic substance when sudden forces are applied for a short period of time. The interest of this investigation lies in the fact that a large number of colloidal solutions have been proved to behave in a manner closely resembling that just described.

The moduli of rigidity n of pitch, paraffin, and sandstone can be calculated from the well-known formula $n=\dfrac{2lC}{\pi r^4 \varphi}$ by measuring the amount of torsion given the specimen by applying a torsional couple, the symbols having the same meaning as before.

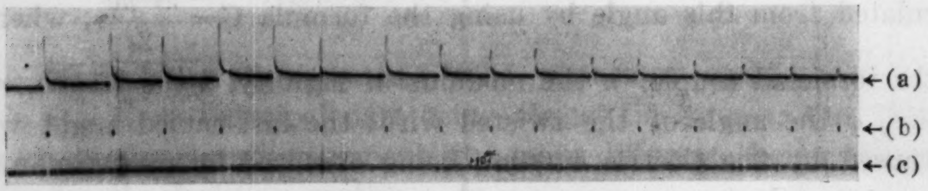

Fig. 2. Record of twisted paraffin cylinder.

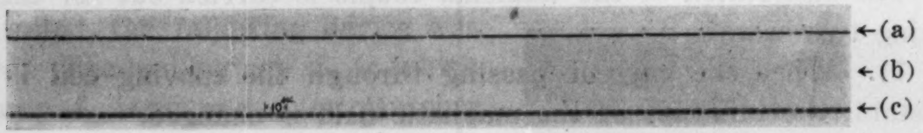

Fig. 3. Record of twisted pitch cylinder.

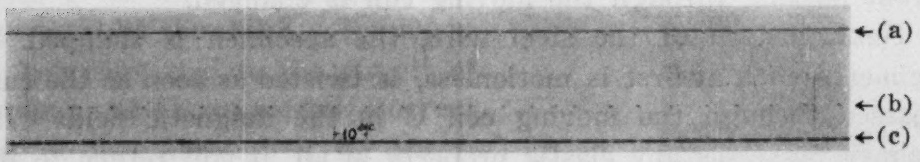

Fig. 4. Record of twisted sandstone cylinder.

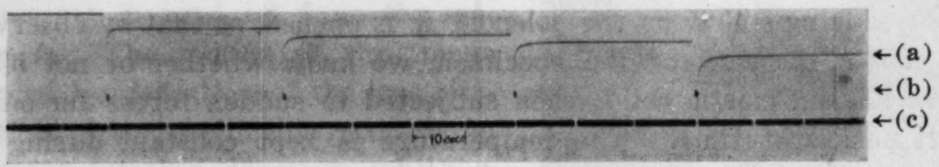

Fig. 5. Record of twisted mixture of rubber and water-glass.

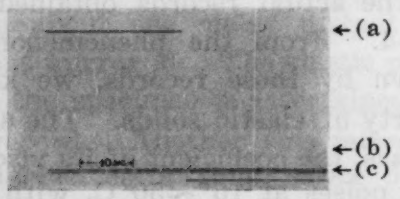

Fig. 6. Record of twisted water-glass.

(a): Angular deformation.
(b): Length of time during which the current flowed.
(c): Time mark.

The curves showing the relation between the moduli of rigidity of the substances thus obtained and the magnitude of the couple are shown in Figs. 7~9 and Tables I~III. In these figures the modulus of rigidity of the substances is taken as ordinate and the magnitude of the couple as abscissa. In this case the length of time for which the couple was applied was one second. From these figures it will be

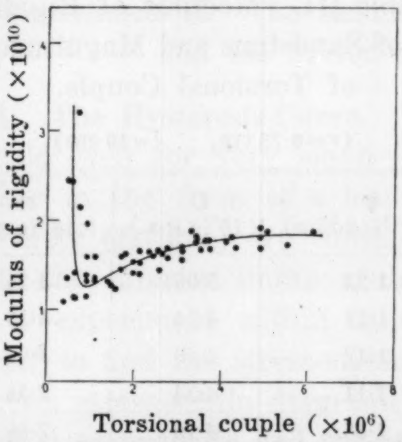

Fig. 7. Relation between the modulus of rigidity of pitch and the torsional couple (temp. 24·8°C).

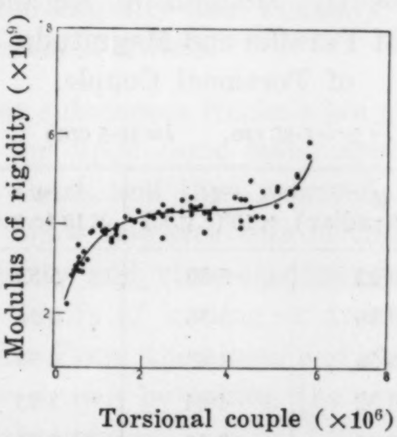

Fig. 8. Relation between the modulus of rigidity of paraffin and the torsional couple (temp. 24·5°C).

seen that at first the moduli of rigedity n of pitch and sandstone, diminishes slightly with decrease in the torsional couple C, the minimum being at a certain value of the couple C. When the torsional couple decreases beyond this certain value of C, $1{\cdot}0 \times 10^6$ in c. g. s. unit, the moduli of their rigidity increase rapidly. The modulus of rigidity of paraffin, however, does not increase within this small range of the couple.

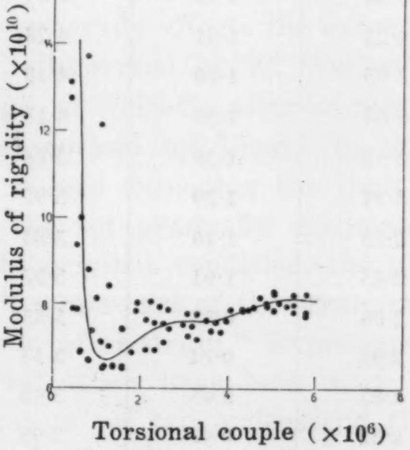

Fig. 9. Relation between the modulus of rigidity of sandstone and the torsional couple (temp. 24·5°C).

Table I. Modulus of Rigidity of Pitch and Magnitude of Torsional Couple.

(Diameter of pitch cylinder, $2r = 2{\cdot}13$ cm. Length of pitch cylinder, $l = 10{\cdot}5$ cm.)

φ $\times 10^{-3}$(radian)	C $\times 10^6$(c. g. s.)	n $\times 10^{10}$(c. g. s.)	φ $\times 10^{-3}$(radian)	C $\times 10^6$(c. g. s.)	n $\times 10^{10}$(c. g. s.)
1·70	6·13	1·88	0·73	2·13	1·52
1·40	5·06	1·88	0·67	2·13	1·66
1·21	4·10	1·77	0·61	2·13	1·82
1·03	3·63	1·78	0·55	1·91	1·81
0·97	3·42	1·83	0·36	1·49	2·15
0·91	3·31	1·89	0·24	0·92	1·97
0·85	2·77	1·69	0·12	0·74	3·21
0·79	2·55	1·68			

Table II. Modulus of Rigidity of Paraffin and Magnitude of Torsional Couple.

($2r=1{\cdot}83$ cm, $l=10{\cdot}5$ cm)

φ $\times10^{-3}$(radian)	C $\times10^{6}$(c.g.s.)	n $\times10^{9}$(c.g.s.)
10·02	5·80	5·52
10·80	5·36	4·74
8·56	4·47	4·98
10·32	4·24	3·93
8·19	3·10	3·61
7·89	2·89	3·49
6·31	2·45	3·70
5·65	2·55	4·30
5·22	1·99	3·64
4·25	1·91	4·28
3·95	1·70	4·10
3·64	1·59	4·17
3·52	1·39	3·78
3·34	1·39	3·97
2·73	1·10	3·84
2·43	1·01	3·97
2·06	0·83	3·83
2·00	0·74	3·53
1·82	0·65	3·40
1·52	0·47	2·95

Table III. Modulus of Rigidity of Sandstone and Magnitude of Torsional Couple.

($r=0{\cdot}75$ cm, $l=10$ cm)

φ $\times10^{-3}$(radian)	C $\times10^{6}$(c.g.s.)	n $\times10^{10}$(c.g.s.)
1·23	5·06	8·26
1·17	4·74	8·15
1·17	4·60	7·92
1·11	4·34	7·86
1·05	4·10	7·86
1·05	3·98	7·62
0·99	3·74	7·57
0·93	3·52	7·62
0·86	3·31	7·76
0·80	3·10	7·78
0·72	2·89	8·05
0·68	2·66	7·88
0·62	2·45	7·94
0·56	2·24	8·04
0·56	2·13	7·64
0·49	1·91	7·84
0·43	1·59	7·44
0·37	1·29	7·02
0·31	1·10	7·14
0·25	1·01	8·15
0·25	0·83	6·67
0·19	0·65	6·87
0·12	0·56	9·39
0·06	0·38	12·73

The same phenomenon, however, may be seen within a smaller couple range than this. According to professor T. Terada, this phenomenon is similar to that of "Thixotropie"[4] ("Die isotherme umkerbare Sol-Gel-Umwandlung") in colloids.

---

[4] **Freundlich**, „*Kolloid-Chemie*" Bd. II, 615.
This work explains "Thixotropie" as follows; „Diese bei konstanter Temperatur verlaufende Sol-Gel-Umwandlung wird als Thixotropie bezeichnet; Sol und Gel, die ein solches Verhalten zeigen, nennt man thixotrop. Der durch Schutteln bewirkte krasse Ubergang von Gel zu Sol ist nur ein gut gekennzeichneter Grenzfall der Thixotropie."

Experiment II. The Relation between Rigidity and Viscosity and the Period of the Repeated Twists.

1. The Hysteresis Curve. With most substances Hooke's law does not hold even for very small stresses; for upon force being applied, whether in the form of a load or as a twist, and then removed, the after-effect (fatigue) are considerable. Since however this is chiefly due to the inferior limits of both elasticity and visco-elasticity,[5] we need to experiment within only narrow limits of loading or twisting in order to find the stress-strain relation. From the stress and strain produced, stress-strain diagrams could be drawn by taking the strain developed as ordinate and the stress as abscissa.

We shall now consider the mechanism involved, a subject that has occupied the attention of many investigators in the past. The length of time that a substance has been subjected to considerable load generally affects the strain caused, and the length of time that a strained substance has been freed from load also generally affects the extent of the elastic recovery. The latter effect, discovered by W. Weber[6] in 1835, is called "Elastische Nachwirkung" or "elastic after-working". The former effect appears to have been noticed by Vicat,[7] in 1834. After a substance has been strained by a load exceeding the limit of perfect elasticity and is then set free, the set gradually diminishes. Since the substance never returns to its original condition, the ultimate deformation is the "permanent set", while part of the strain that gradually disappears is called the "elastic after-strain." Experiments on the gradual flow of solids under great stress have been made by H. Tresca.[8] According to these investigators we can understand that the hysteresis curve is the result of the elastic after-working.

All hysteresis phenomena show that the condition of the substance at any instant depends on its previous states as well as on the external conditions (forces, temperature, etc.) that obtain at that instant. Hysteresis, which always implies irreversibility in the sequence of the states through which a substance passes, is generally traceable to the molecular structure of matter, with the result that theories of molecular action have been invoked to account for the viscosity and elastic after-working by various investigators, for example, J. C. Maxwell,[9] 1890; J. G. Butcher,[10] 1877; O. E. Meyer,[11] 1874. L. Boltzman,[12] 1878, showed that the ultimate condition to which a substance, subjected to constant stress for a very long period of time, must be reduced is plastic flow, which phenomenon, he discussed mathematically with Maxwell. He traced this phenomenon to plasticity and called it "hereditary hysteresis".

---

[5] T. H. C. THOMPSON, "On the Theory of Visco-elasticity". *Phil. Trans. Roy. Soc., London.* [A], **231** (1933), 360.

[6] W. WEBER, *Ann. Phys. Chem.*, (1835) and (1841).
A. E. H. LOVE, *"A Treatise on the Mathematical Theory of Elasticity"*, 4th ed., 116.

[7] VICAT, *ibid*,

[8] H. TRESCA, *ibid.*

Hysteresis is a phenomenon that operates even within the limit of perfect elasticity. The earliest account of this phenomenon is in a paper by Ewing,[13] describing experiments with a steel wire. He showed that the effect in question, which he called "hysteresis", is more marked when the loading and unloading are rapid than when they are slow, but that it is also sensible when they are performed very slowly, so that there appears to be such a thing as "statical hysteresis". According to the studies of B. Hopkinson and G. T. Williams,[14] it appears that with very rapid alternations of stress the observable amount of hysteresis is less than in the case of statical hysteresis. A certain amount of energy seems to be dessipated in putting a specimen through a cycle of stress changes. Ewing poined out the bearing this conclusion has on Wöhler's experiments[15] relating to repeated loading and alternating stress. The subject, however, is still obscure.

Statical hysteresis was the special phenomenon noticed by Ewing, because, as has been already observed, elastic after-working, plasticity, and viscosity are also properties indicating hysteresis. The same may also be said of the property Lord Kelvin[16] calls *fatigue*.

The results of Adams and Coker,[17] and Zisman[18] show clearly that there is an increase in resistance of rock to deformation from repeated loading and unloading of forces. P. W. Bridgman[19] observed a linear hysteresis, the stress-strain diagram of which is a closed reproducible curve.

S. Kusakabe,[20] 1903, studied the torsional hysteresis of rocks and discussed mathematically the hysteresis curves. The hysteresis curves obtained by his experiments were generally complicated shapes, but when the specimens were twisted about cyclically within definite limits of couple, the twist curves were nearly closed ones of simple and regular forms. T. Taniguti and M. Imai,[21] 1934, subjected concrete blocks to repeated compression and obtained hysteresis curves. Their experimental method is similar to Kusakabe's.

---

[9] J. C. Maxwell, *Scientific Papers*, **2** (1890).

[10] J. G. Butcher, *Proc. Math. Soc., London*, **8** (1877).

[11] O. E. Meyer, *J. F. Math.*, **78** (1874).

[12] L. Boltzman, *Ann. Phys. Chem.*, **7** (1878).

[13] J. A. Ewing, *Brit. Assoc. Rep.*, (1859), 502.

[14] B. Hopkinson and G. T. Williams, *Proc. Roy. Soc., London*, **87** (1912), 502.

[15] A. Wöhler, ,,*Ueber Festigkeits versuche mit Eisen und Stahl*,“ *Berlin*, (1870).

[16] Lord Kelvin, *Math. and Phys. Papers*, **3** (1890), 22.

[17] F. D. Adams and E. G. Coker, *Carnegie Inst., Washington Publ.*, **46** (1906).

[18] W. A. Zisman, *Proc. Nat. Acad. Sci.*, **7** (1933), 653.

[19] P. W. Bridgman, *Am. J. Sci.*, **7** (1924), 81 (rocks), *ibid.*, **10** (1925), 359 (tachylite).

[20] S. Kusakabe, *Publ. Imp. Earthq. Inv. Comm.*, **14** (1903), 1~73.

Upon going through the two last-named studies, it will be seen that these investigators experimented with the idea that the substances tested possess elasticity only, with the result that the length of time the substances were subjected to load seems to have been left out of consideration. Since these substances possess viscosity also, experiments with then should have been made under continuous stress with relation to time, i. e., change of stress should be shown in the form of simple harmonic motion. And since experiments with these substances differ from those relating to magnetic induction, and as their deformation under stress depends greatly on the length of time involved, experiments should take into consideration the change in stress with regard to time.

Judging from the numerous studies that have so far been made on the subject of hysteresis, there are at least two causes that result in these curves, the one being the elastic after-effect, i. e., the plastic flow of the materials, and the other the elastic hysteresis or statical hysteresis, the phenomenon of which last is exhibited by elastic substances.

In the present experiments, the author studied the phenomenon of hysteresis due to elastic after-effect, carefully noting the length of time that the substance was subjected to stress.

2. Experiments in Hysteresis. *The Method of Experiment.* When we repeatedly twist the substance to be tested, the strain produced will differ according to the length of time during which the twisting has been repeated, although the torsional couple is constant. We therefore twist the specimens repeatedly by applying torsional couples of various periods, and thus obtain a relation between the stress and the strain of such substances as pitch, paraffin, and sandstone. The curve showing the relation between the stress and the strain is the hysteresis curve.

The apparatus used was the same as that shown in Fig. 1, although we used, besides, a sensible galvanometer. The change in the electric current — the change in stress — is known from the deflection of the mirror attached to the galvanometer.

---

[21] T. Taniguti and M. Imai, "Hysteresis of Concrete and Reinforced Concrete (Part I)", *Bull. Tokyo Univ. Engin.*, **3** (1934), 587.

Since a relation between stress and strain is required in order to obtain the hysteresis curve, we arranged that the axis of rotation of the moving coil C, which is exactly the same as that described in Experiment I, section 1, shall be perpendicular to that of the galvanometer G. This arrangement is shown in Fig. 10. A lens mirror is attached to the lower end of the specimen that is to be tested by being twisted by the rotation of the moving coil C. A plane mirror is attached to the galvanometer G. The ray of light from a slit, which at first falls on the lens mirror, is reflected to a plane mirror, from which it is re-reflected, the image of the slit being formed about one meter distant from the lens mirror. The image of the slit thus formed is photographically recorded on bromide paper. This record is the hysteresis curve desired. In the record, the stress (torsional couple) is taken as ordinate and the strain (angular deformation caused) as abscissa.

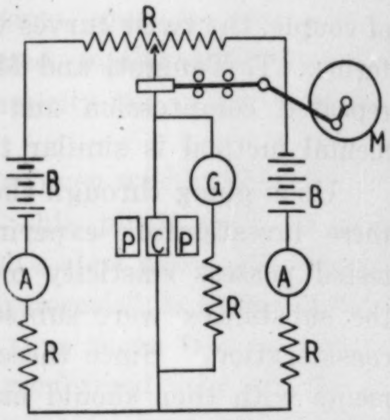

Fig. 10. Arrangement of apparatus for obtaining the hysteresis curve.

A, ammeter; B, battery; G, galvanometer; C, moving coil; M, brass plate rotated by motor; P, pole of magnet; R, resistance.

The galvanometer circuit being connected to that of the moving coil C, any change in stress is given by the deflection of the plane mirror that is attached to the galvanometer.

By the movement of the piston attached to the plate M that moves with the motor, the electric resistance R is enabled to change into one of sine-form, with the result that the curve of the torsional couple imparted to the lower end of the specimen alters to one of sine-form since the change in the torsional couple is proportional to that of the current passing through the moving coil C. For this reason the specimen is twisted repeatedly. The time variation in the electric current is shown in Fig. 11. The resistence R connected to the ammeter A is of 200 ohms. The electromotive force of the two B batteries are each 100 volts. The resistance R, which varies as a simple harmonic as the result of the piston attached to the plate M, is 200 ohms.

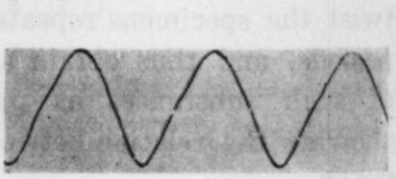

Fig. 11. Variation in magnitude of torsional couple of sine-form.

3. Results of the Experiment. Examples of successive forms of hysteresis curves obtained by repeated twists are shown in Figs. 12~14. Some actual photographs are shown in Figs. 15~17. In the photographs, the stress (torsional couple) is taken as ordinate and the strain (angular deformation of the specimen) produced as abscissa. As shown in Table IV, the length of time for which the twistings were repeated ranges from a few seconds to about 12 minutes.

It will be seen that although such substances as pitch, paraffin, and sandstone, were twisted two or three times, all their hysteresis curves, which are ellipses, close regularly. These curves are almost alike, but with increase in the period of the repeated twists, the major

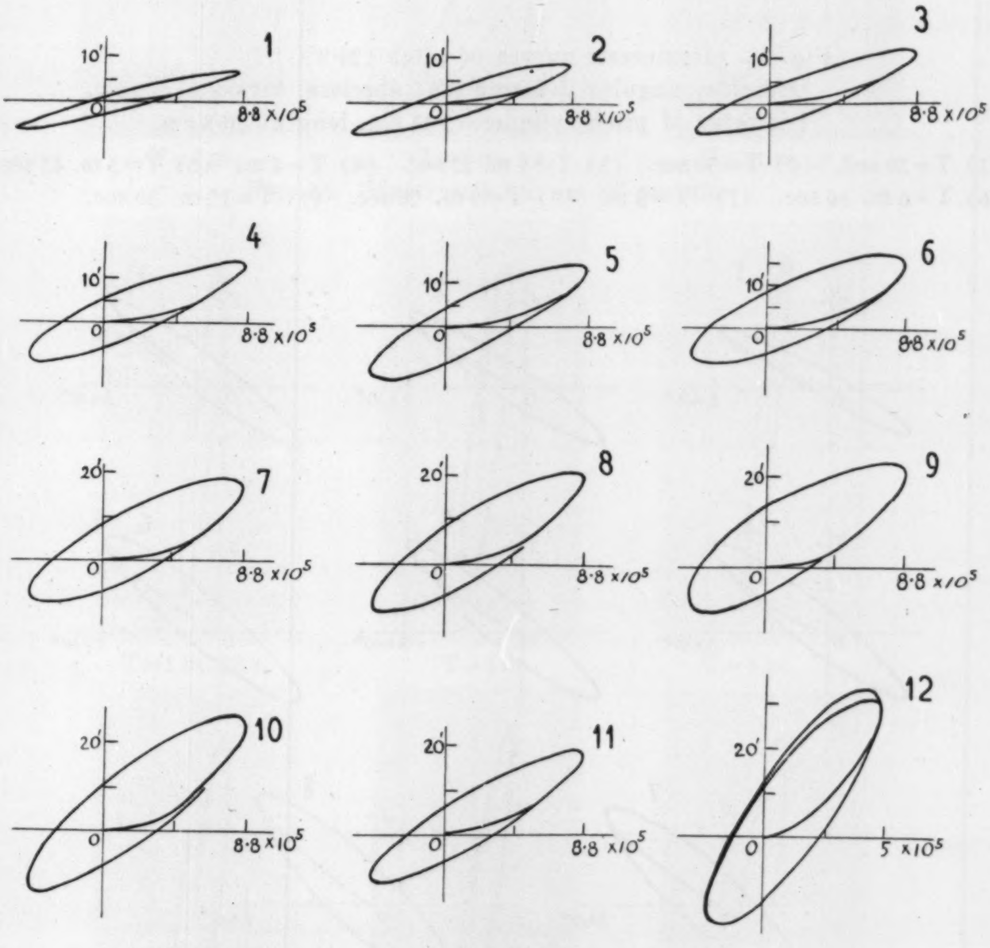

Fig. 12. Hysteresis curves of paraffin (24·8°C).
Ordinate, angular deformation; abscissa, torsional couple.
Diameter of paraffin cylinder=2·13 cm, length=10·5 cm.
(1) Period T=9 sec. (2) T=44 sec. (3) T=1 m. 23 sec. (4) T=3 m.
(5) T=4 m. (6) T=5 m. 35 sec. (7) T=6 m. 50 sec. (8) T=8 m. 5 sec.
(8) T=9 m. 20 sec. (10) T=11 m. 25 sec. (11) T=2 m. 55 sec.
(12) T=1 m. 23 sec. (Diameter of cylinder=1·83 cm).

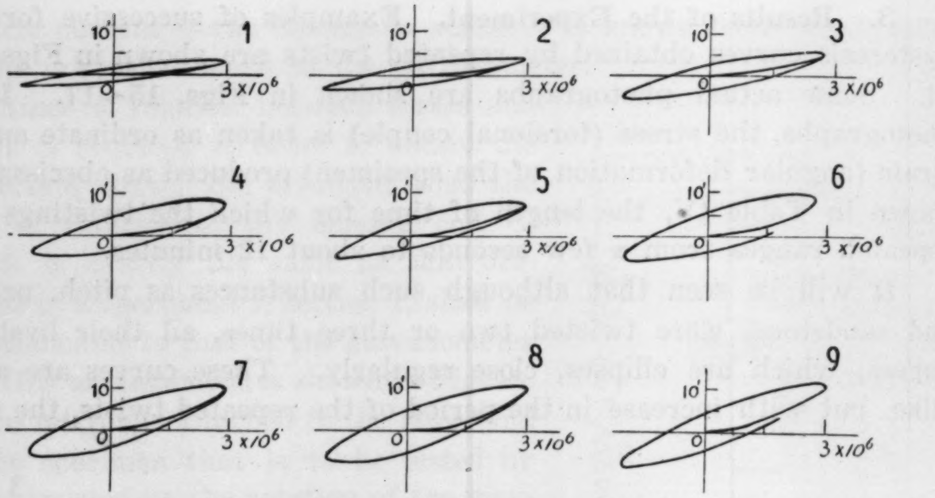

Fig. 13. Hysteresis curves of pitch (24·8°C).
Ordinate, angular deformation; abscissa, torsional couple.
Diameter of pitch cylinder=2·13 cm, length=10·5 cm.

(1) T=30 sec. (2) T=50 sec. (3) T=1 m. 23 sec. (4) T=4 m. (5) T=5 m. 45 sec. (6) T=6 m. 50 sec. (7) T=8 m. (8) T=9 m. 20 sec. (9) T=12 m. 30 sec.

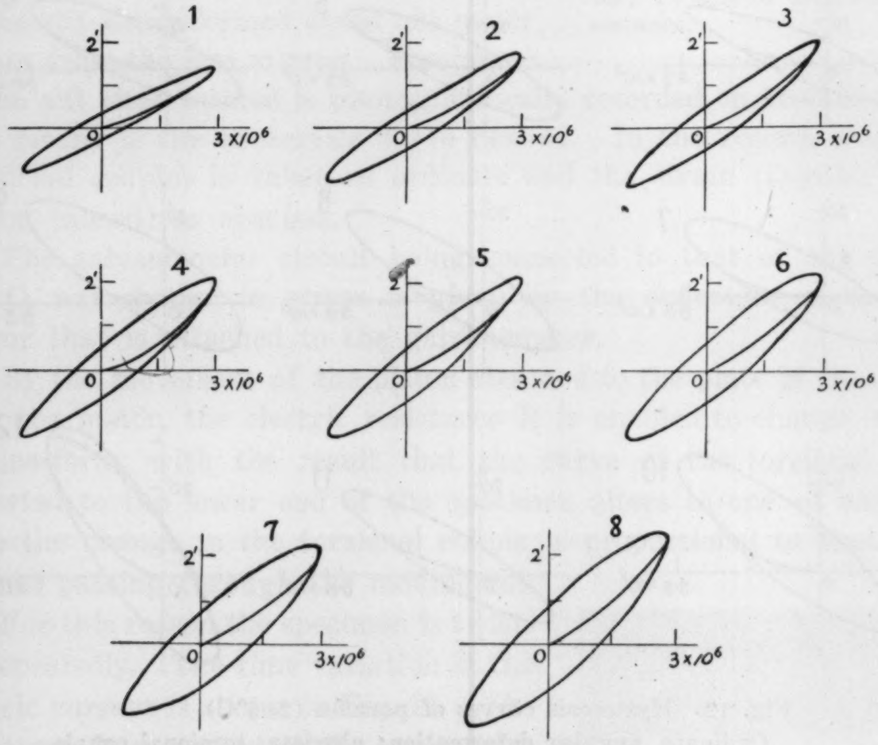

Fig. 14. Hysteresis curves of sandstone (25°C).
Ordinate, angular deformation; abscissa, torsional couple.
Diameter of sandstone cylinder=1·5 cm, length=10·0 cm.

(1) T=1 m. 23 sec. (2) T=2 m. 10 sec. (3) T=2 m. 48 sec. (4) T=4 m. 10 sec. (5) T=5 m. 20 sec. (6) T=6 m. 50 sec. (7) T=8 m. 35 sec. (8) T=11 m. 45 sec.

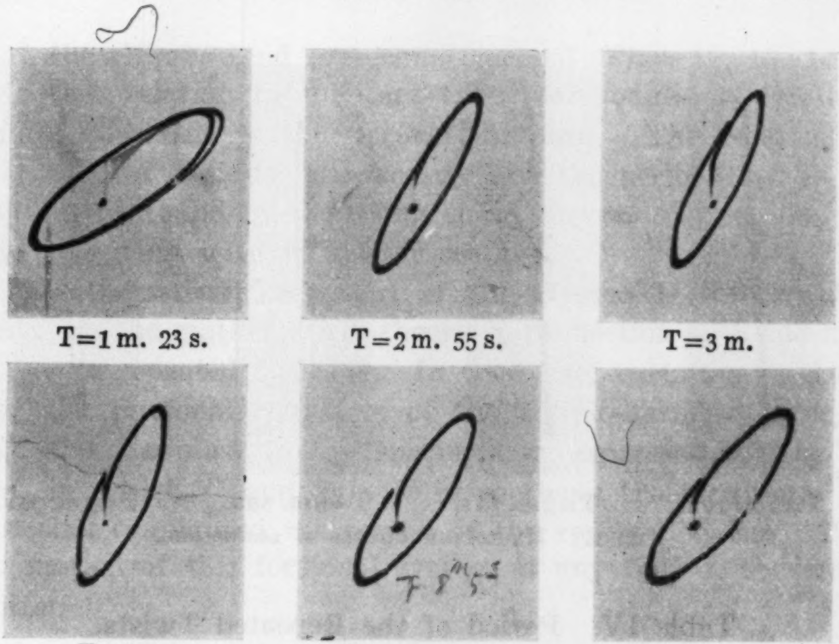

T=1 m. 23 s. T=2 m. 55 s. T=3 m.

T=4 m. T=8 m. 5 s. T=11 m. 25 s.

Fig. 15. Hysteresis curves of paraffin.

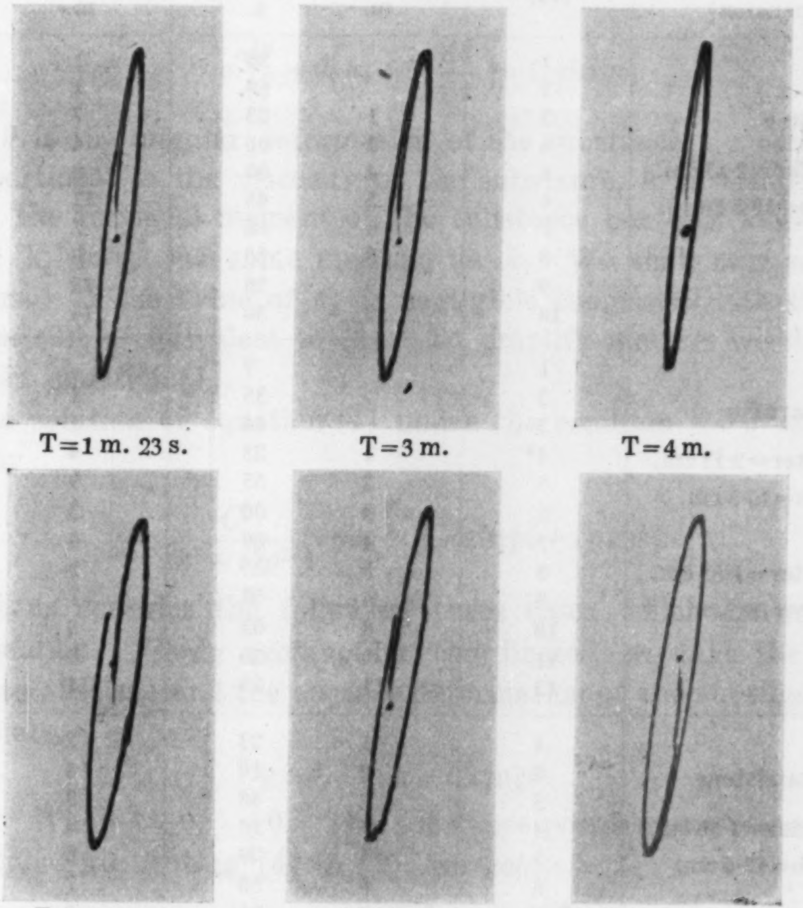

T=1 m. 23 s. T=3 m. T=4 m.

T=6 m. 50 s. T=8 m. T=9 m. 20 s.

Fig. 16. Hysteresis curves of pitch.

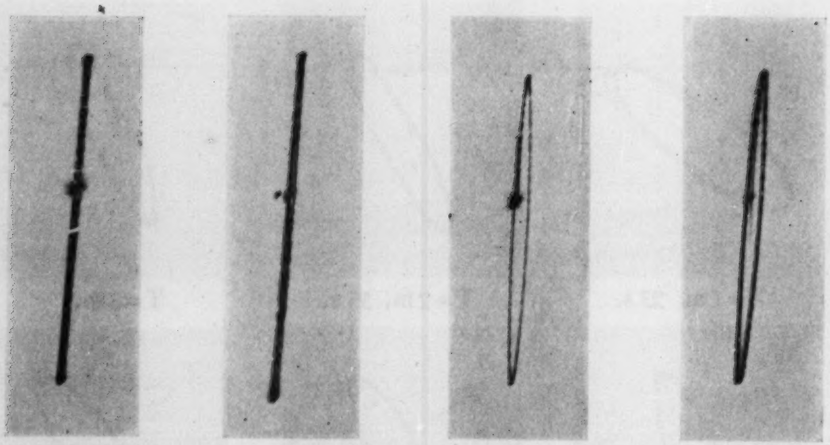

T=2m. 10s. T=2m. 48s. T=6m. 50s. T=8m. 35s.

Fig. 17. Hysteresis curves of sandstone.

Table IV. Period of the Repeated Twists.

Substance (dimension)	No.	Period		Total time	
		m.	s.	m.	s.
	1		30	1	20
	2		50	1	30
Pitch	3	1	23	7	05
	4	3	00	6	11
Diameter=2·13 cm.	5	4	00	8	34
Length=10·5 cm.	6	5	45	11	38
	7	6	50	7	20
	8	8	00	8	40
	9	9	20	12	02
	10	12	30	14	00
	1		9		20
Paraffin	2		35	1	20
	3		44	1	30
Diameter=2·13 cm.	4*	1	23	4	25
Length=10·5 cm.	5	2	55	9	06
	6	3	00	3	30
	7	4	00	4	30
*Diameter=1·83 cm.	8	5	35	5	56
Length=10·5 cm.	9	6	50	7	15
	10	8	05	8	19
	11	9	20	9	54
	12	11	25	11	55
	1	1	23	2	00
Sandstone	2	2	10	4	24
	3	2	48	3	17
Diameter=1·50 cm.	4	4	10	4	10
Length=10·0 cm.	5	5	20	6	12
	6	6	50	7	33
	7	8	35	9	10
	8	11	45	12	26

axes of the ellipses tend to become vertical (Figs. 12, 13, 14.). This has a direct relation to the fact that the moduli of rigidity of the substances diminish as the period lengthens. The relation between their moduli of rigidity or viscosity and the periods of the repeated twists may be found by analysing these curves. These analytical results will be dealt with in a later section.

4. Mathematical Treatment of the Hysteresis Curve. We shall now take up the mathematical theory in connection with the hysteresis curve due to repeated twisting. In this case, variation in the magnitude of the torsional couple is of the simple-harmonic type, so that external force applied to the specimen is expressed by the form of $C \sin pt$, in which C and $2\pi/p$ is respectively the maximum value of the torsional couple and the period of the repeated twists. The equation of motion of this torsional system at any time t, therefore, may be written

$$\epsilon \frac{d\theta}{dt} + k\theta = C \sin pt, \tag{1}$$

or

$$\epsilon \frac{d\theta}{dt} + \theta\left(k_1 + k_2 \frac{d\theta}{dt}\right) = C \sin pt, \tag{2}$$

where θ is the angular deformation of the substance, ϵ a constant that is proportional to the viscosity of the substance, k an elastic constant that is the torsional moment of the substance per unit angle twisted. k_1 and k_2 have the same meaning as k. We shall now solve these equations. If the value of k_2 is negligible compared with that of k_1, equation (2) is equivalent to (1). To simplify matters we shall therefore take equation (1).

The solution of equation (1) under the conditon $\theta = 0$ at $t = 0$ is given by

$$\theta = \frac{C}{k^2 + \epsilon^2 p^2}\left\{\epsilon p e^{-\frac{k}{\epsilon}t} + k \sin pt - \epsilon p \cos pt\right\}. \tag{3}$$

Let us consider the following three cases which can arise from this equation. Using rectangular coordinates, we take the torsional couple as abscissa and the angular deformation of the substance caused as ordinate, i. e.,

$$y = \theta, \qquad x = C \sin pt. \tag{4}$$

(1) When $k \neq 0$, $\epsilon = 0$. The substance possesses no viscosity; only elasticity. Substituting (4) in (3), we get

$$y = \frac{1}{k} x. \tag{5}$$

This equation represents *a straight line through the origin.*

(2) When $k=0$, $\varepsilon \neq 0$. The substance possesses no elasticity; only viscosity. Substituting (4) in (3), we get the equation

$$y=\frac{1}{\varepsilon p}\left\{C-\sqrt{C^2-x^2}\right\},$$

or

$$\frac{x^2}{C^2}+\frac{\left(y-\dfrac{C}{\varepsilon p}\right)^2}{\left(\dfrac{C}{\varepsilon p}\right)^2}=1. \tag{6}$$

This equation represents *an ellipse whose center is at the point* $\left(0, \dfrac{C}{\varepsilon p}\right)$.

(3) When $k \neq 0$, $\varepsilon \neq 0$. The substance possesses both elasticity and viscosity. Substituting (4) in (3) as before, we get

$$y=\frac{1}{k^2+\varepsilon^2p^2}\left\{C\varepsilon p e^{-\frac{k}{\varepsilon}t}+kx-\varepsilon p\sqrt{C^2-x^2}\right\}, \tag{7}$$

in which $e^{-\frac{k}{\varepsilon}t}$ tends to become zero for large values of t.

Hence, after a long period of time, equation (7) is reduced to the general form

$$(k^2+\varepsilon^2p^2)x^2-2k(k^2+\varepsilon^2p^2)xy+(k^2+\varepsilon^2p^2)^2y^2-\varepsilon^2p^2C^2=0. \tag{8}$$

If we put

$$\left.\begin{array}{ll} k^2+\varepsilon^2p^2=a, & -k(k^2+\varepsilon^2p^2)=h \\ (k^2+\varepsilon^2p^2)^2=b, & -\varepsilon^2p^2C^2=C' \end{array}\right\} \tag{9}$$

equation (7) becomes

$$ax^2+2hxy+by^2+C'=0. \tag{10}$$

We shall now determine the curve represented by equation (10), for which purpose the following calculation is necessary:

$$\Delta\equiv\begin{vmatrix} a & h & 0 \\ h & b & 0 \\ 0 & 0 & C' \end{vmatrix}=C'(ab-h^2)=C'a^2p^2\varepsilon^2. \tag{11}$$

Since C' is negative, $a\Delta$ is negative, and $ab-h^2$ is positive. Equation (10) represents, therefore, *an ellipse whose center is at the coordinate origin.*

In order to obtain a simple form of equation (10), we transfer the rectangular axes (x, y) to (X, Y) making an angle θ' with the old. The relations between the old and the new axes are given by

$$\left.\begin{aligned} x&=X\cos\theta'-Y\sin\theta' \\ y&=X\sin\theta'+Y\cos\theta' \end{aligned}\right\}. \tag{12}$$

Substituting (12) in (10) as well as the relation

$$\tan 2\theta' = \frac{2h}{a-b}, \tag{13}$$

equation (10) is reduced to the simple form

$$a'X^2+b'Y^2+C'=0,$$

or

$$\frac{X^2}{-\dfrac{C'}{a'}}+\frac{Y^2}{-\dfrac{C'}{b'}}=1, \tag{14}$$

where a' and b' are the roots of the equation

$$z^2-(a+b)z+(ab-h^2)=0, \tag{15}$$

in which we have to take h, a', and b' such that $a'-b'$ is positive or negative according as h is positive or negative. Hence, by determining the values of a', b', and C', the values of the two constants (k and ϵ) can be obtained.

Again, since equation (13) is given by

$$\begin{aligned} \tan 2\theta' &= \frac{2h}{a-b} \\ &= \frac{2k}{k^2+\epsilon^2p^2-1}, \end{aligned} \tag{16}$$

we can see that θ' becomes large when the values of ϵp and k are small, and also that the major axis of the ellipse tends to become vertical as the period of the twists increases. Consequently the rigidity of the substance diminishes as the period of the twists is increased when θ' is large.

As a matter of fact k depends also on the velocity of the angular deformation of the substance, so that the term k_2 in equation (2) cannot be neglected. The following two cases refered to in the preceding section may, however, be explained without difficulty by the mathematical treatment just given.

(1) The hysteresis curve is an ellipse.

(2) The major axis of the ellipse tends to become vertical as the period of the twist is increased.

The fact that both equation (1) and (2) clearly show how these hysteresis curves are formed will serve as a clue in problems connected with the structure of matter.

5. Analytical Results of the Experiment. Since equation (10) represents an ellipse, as just stated, we use this equation for determining the properties of the substances from their hysteresis curves given in section 3.

We measure the length of the major and minor axis of each curve and the angle θ' showing the inclination of the major axis of the ellipse, and insert these values in equations (9), (14), (15) and (16). We can thus find the values of the two constants, k and ϵ. Using the well-known relation, $n=\dfrac{2lk}{\pi r^4}$, we determine the moduli of rigidity n of the substances. As the area A of the hysteresis curve represents the loss of internal energy of the substance, we measure it with a planimeter. Area A being a measure of the viscosity of the substance, it is possible to determine the relation the change of viscosity has to the period T of the repeated twists. We obtain then the following three relations:

(*a*). *Relation Between n and T.* From the data just obtained, a diagram is constructed on which the values of n are taken as ordinates and the corresponding values of T as abscissae. Figs. 18∼20 are diagrams

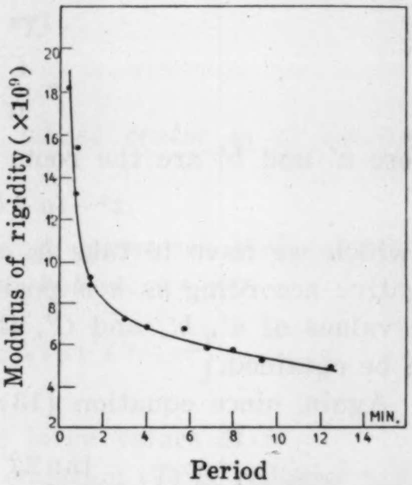

Fig. 18. Relation between the modulus of rigidity of pitch and the period of the repeated twists.

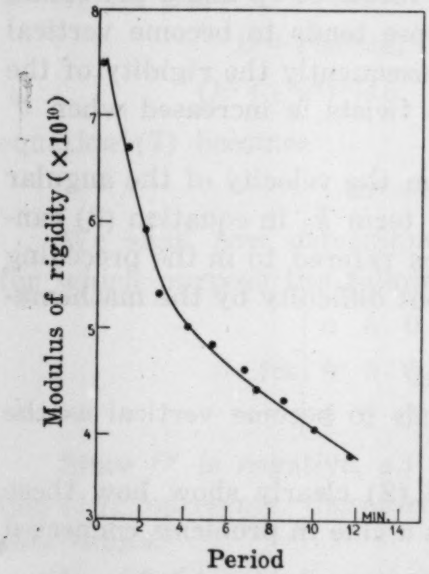

Fig. 19. Relation between the modulus of rigidity of sandstone and the period of the repeated twists.

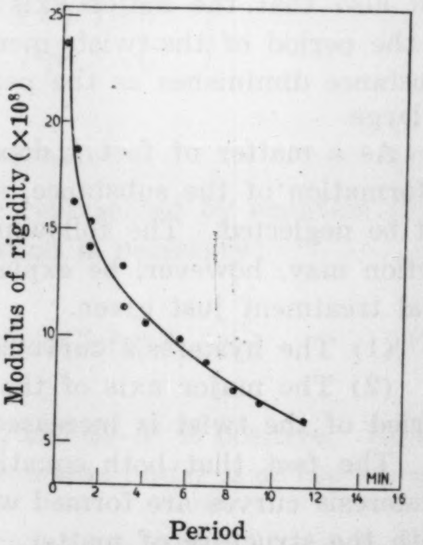

Fig. 20. Relation between the modulus of rigidity of paraffin and the period of the repeated twists.

showing these relations. The values of n are shown in Table V. From these figures we can see that the moduli of rigidity of all these substances decrease with increase in the period of the repeated twists, though the manner in which they decrease differs according to the particular substance.

(*b*). *Relation Between the Apparent Viscosity and the Period T.* We take the period T of the repeated twists as abscissa and the apparent viscosity as ordinate. The relations between the two thus obtained are shown in Figs. 21∼23 and Table V. It will be seen that the apparent viscosity of all these substances increases somewhat rapidly with the increasing period T.

(*c*). *Relation Between Loss of Internal Energy and Angular Deformation θ of the Substance.* We take the loss of internal energy (the area of the hysteresis curve) of the sub-

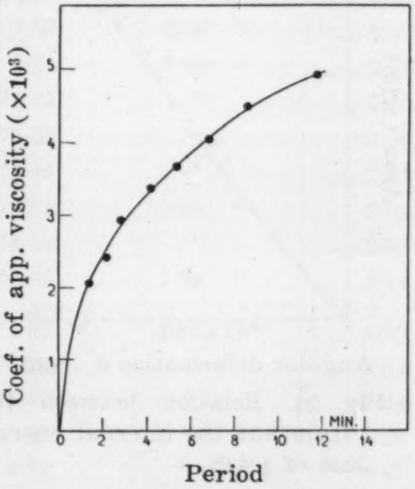

Fig. 21. Relation between the coefficient of apparent viscosity of sandstone and the period of the repeated twists.

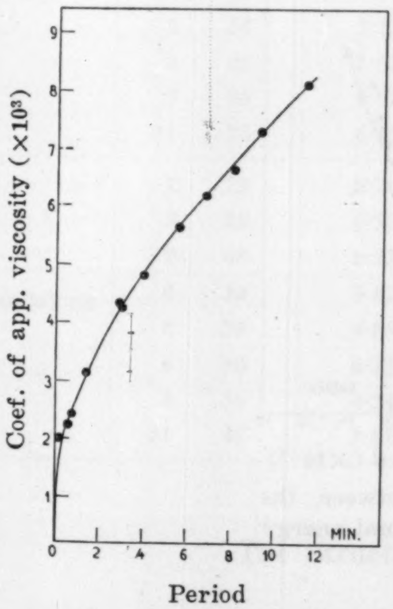

Fig. 22. Relation between the coefficient of apparent viscosity of paraffin and the period of the repeated twists.

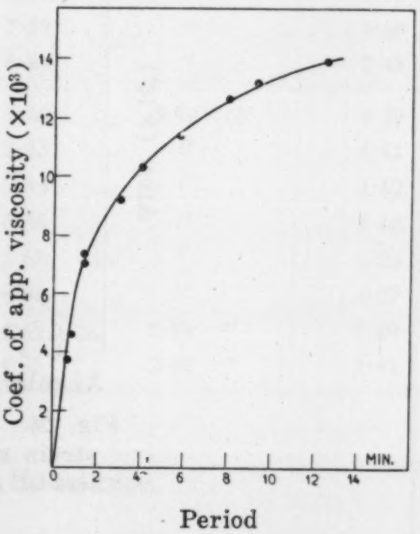

Fig. 23. Relation between the coefficient of apparent viscosity of pitch and the period of the repeated twists.

stance as ordinate and the angular deformation as abscissa, as shown in Figs. 24~26. From these figures it will be seen that in the case of pitch and paraffin, loss of their internal energies increases linearly with their increasing angular deformations (strain), while in the case of sandstone these changes seem to take place somewhat rapidly.

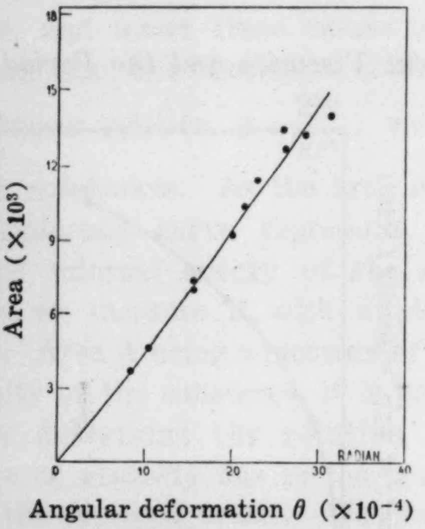

Fig. 24. Relation between the strain and the internal energy loss of pitch.

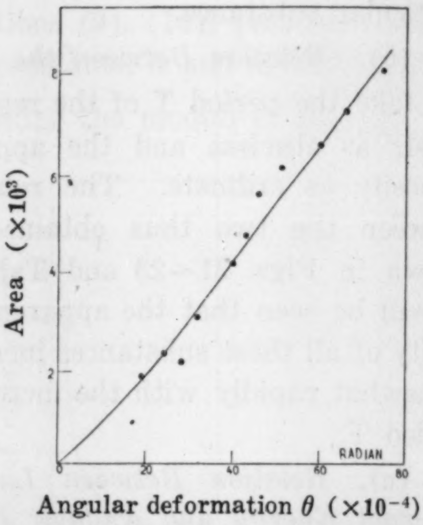

Fig. 25. Relation between the strain and the internal energy loss of paraffin.

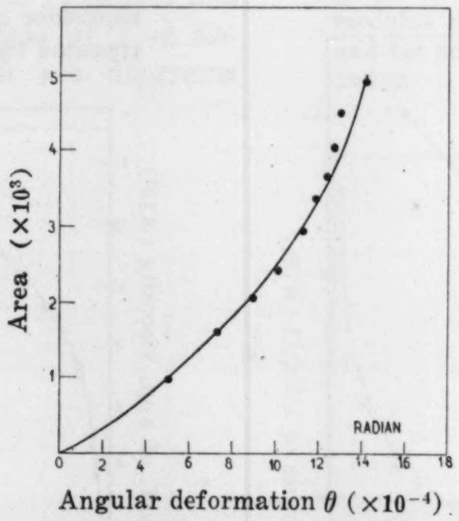

Fig. 26. Relation between the strain and the internal energy loss of sandstone.

Table V. Modulus of Rigidity and Apparent Viscosity of Pitch, Paraffin, and Sandstone.

Substance	Period m.	s.	n (c. g. s.)	ε (c. g. s.) $\times 10^3$	Couple (max.) (c. g. s.)	θ (max.) radian $\times 10^{-3}$
Pitch		40	$18{\cdot}24\times10^9$	3·68	$2{\cdot}98\times10^6$	0·85
		50	15·43 ″	4·60	″	1·05
	1	23	8·88 ″	7·37	2·68 ″	1·57
	3	00	7·22 ″	9·21	2·80 ″	2·01
	4	00	6·81 ″	10·32	″	2·15
	5	45	6·76 ″	11·42	″	2·30
	6	50	5·82 ″	13·45	″	2·59
	8	00	5·72 ″	12·71	2·89 ″	2·62
	9	20	5·24 ″	13·26	″	2·85
	12	30	4·94 ″	14·00	2·98 ″	3·14
Paraffin		9	$2{\cdot}37\times10^9$	1·82	$4{\cdot}87\times10^5$	1·92
		35	1·87 ″	2·11	″	2·82
		44	1·62 ″	2·30	″	2·44
	1	23	1·42 ″	3·07	″	3·20
	2	55	1·31 ″	4·32	″	5·47
	3	00	1·13 ″	4·22	″	4·01
	4	00	1·06 ″	4·80	″	4·30
	5	35	$9{\cdot}92\times10^8$	5·66	″	4·59
	6	50	8·83 ″	6·23	″	5·15
	8	05	7·53 ″	6·71	″	6·02
	9	20	6·91 ″	7·39	″	6·60
	11	25	6·13 ″	8·25	″	7·45
Sandstone	1	23	$6{\cdot}70\times10^{10}$	2·06	$2{\cdot}98\times10^6$	0·89
	2	10	5·92 ″	2·43	″	1·01
	2	48	5·33 ″	2·94	″	1·12
	4	10	5·07 ″	3·38	″	1·18
	5	20	4·85 ″	3·68	″	1·23
	6	50	4·73 ″	4·05	″	1·27
	8	35	4·34 ″	4·49	2·80 ″	1·30
	11	45	3·81 ″	4·93	2·68 ″	1·41

The Structure of the Substance.

As already described in the preceding paper and in this one, substances, such as pitch, paraffin, and sandstone, behave as if they were a liquid of high viscosity or as an elastic solid according to the length of time that they have been subjected to forces. There seems to be little doubt that these substances are formed of matter possessing elasticity and another of viscosity. They may be regarded as mixtures of elastic and viscous matter. Our experiments show that when these substances are subjected to forces long applied, the viscous constituent alone is affected and exhibits the property of viscosity, whereas when they are subjected to forces of sudden short duration, the elastic component alone reacts to the force applied and exhibits elastic properties. In the former case, the substance behaves as if it had no elastic component and in the latter as if it had no viscous constituent. For example, according to the experiment with the mixture described in section 2, Experiment I, a mixture of elastic and viscous substances, such as small pieces of rubber and water-glass, behaves as if it were an elastic substance (rubber) when it is subjected to sudden forces for a short period of time. To forces long applied, the mixture behaves of course as if it were a viscous liquid (water-glass).

That these substances show dual properties of viscosity and elasticity may well be explained by imagining the following two alternative models of their structure. The one assumes that the structure of these substances is somewhat similar to that of a sponge, the cavities of the elastic skeleton of which are filled with viscous liquid, as already stated in the preceding paper, while the other is that the structure of these substances is similar to that in which an elastic substance is suspended in a viscous liquid.

The former conception is useful in explaining the properties of pitch, paraffin, and sandstone; for these substances, when subjected to forces for a long period of time, exhibit the properties of an elastic solid as well as those of a viscous liquid, while the latter is useful in explaining the properties of certain kinds of pitch, since they exhibit merely the properties of a viscous liquid when subjected to forces for a long period of time. Substances having both structures exhibit of course the properties of an elastic solid when subjected to sudden forces for only a short period of time.

If the material composing the earth's crust were assumed to have mechanical properties similar to substances having the structures just described, the earth's crust would behave like a liquid of high viscosity when subjected to forces for a long period of time and like an elastic solid when subjected to sudden forces for only a short period of time, so that mountain folding, chronic deformations of the earth's crust, and propagation of seismic waves could be explained without difficulty.

Summary and Conclusion to Part II.

(1). In the foregoing experiments, the elastic behaviour of substances, such as pitch, paraffin, and sandstone were investigated.

(2). The moduli of rigidity of substances ascertained by the dynamical method are larger than those obtained by the statical method. The moduli of rigidity of substances obtained by the dynamical method alter with variation in the magnitude of the torsional couple.

(3). The stress-strain curve of these substances for repeated twists is an ellipse, the shape of which however varies according to the period of the repeated twists; the longer the period of the repeated twists, the more the major axis of the ellipse tends to become vertical.

(4). The stress-strain curve may be expressed by solving the equation

$$\epsilon\frac{d\theta}{dt}+k\theta=C\sin pt,$$

where the symbols in the equation have the same meaning as before. By means of this equation, the viscous and the elastic characteristics of substances can be known separately.

(5). The moduli of rigidity of these substances decrease with increase in the period of the repeated twists, while their viscosity increases with increase in the period of the repeated twists. The elastic after-effect and the hysteresis are very marked.

(6). That these substances show dual properties of viscosity and elasticity may well be explained by imagining the following two alternative models of their structure; the one being that the structure of these substances is somewhat similar to that of a sponge, the cavities of the elastic skeleton of which are filled with a viscous liquid, as already described in the preceding paper and the other being that the structure of these substances is similar to that in which an elastic substance is suspended in a viscous liquid.

(7). If the material composing the earth's crust were assumed to have properties similar to the substances investigated in this paper, the folding of mountains, the chronic deformations of the earth's crust, and the propagation of seismic waves could be easily explained.

In conclusion, the writer wishes to express his sincere thanks to Professor Mishio Ishimoto, under whose kind guidance and encouragement the present work was carried out, and to Professor Torahiko Terada, and to Drs. Chûji Tsuboi and Ryûtarô Takahasi for their valuable advices.

31. 物質の粘彈性性質に關する實驗(II)

飯田汲事

靜力學的方法の實驗によつて得られた，ピッチ，パラフィン，砂岩等の物質の粘彈性性質に關しては，既に第1報として此の彙報の前號に報告してある．その實驗の結果を地球物理學的現象に應用する場合，山脈の褶曲及びこれに關聯した地殼の漫性變動等は容易に說明し得られるが，これらの物質が短時間の間比較的急激に作用する力に對して如何なる性質を示すかに關する實驗的調查の結果でなければ，地震波傳播等の急激な力の作用によつて起る現象の說明には不十分である．こゝに述べた實驗はこの方面の自然現象を對照として行はれたものであると共に，物質の粘性及び彈性の二性質を考慮に入れて物質の履歷現象を研究したのである．

物質の履歷現象に關する研究の中最も重要と考へられる事は，凡そ物質は粘性及び彈性の二性質を有する故物體に歪力が加へられた場合には，歪力の時間的變化に左右される事が顯著である．從つてこの歪力の時間に對する變化を定義して研究さるべき事である．

實驗に關して得られた主な結果を擧げると次の如くである．

(1) ピッチ，パラフィン，砂岩等の物質は短時間急激に作用する力に對しては，剛性ある固體の性質のみが有力に認められる．

これらの物質の剛性率は振力の函數として變化し，ある振力の範圍內ではその剛性率には左程の變化がないが，振力がある値より小さくなると急激に增加する．これらの物質の剛性率は靜力學的に得られたものに比してその値が比較的大きく求められる．又これらの物質はコロイドの性質に似た所が多い．

(2) これらの物質の履歷曲線は殆んど楕圓形をなしてゐて，加へられた正弦的に變化する振力の周期が比較的小であると楕圓の長軸は小なる傾斜をなし，周期が長くなると楕圓の長軸が直立してくる．この事は物質の彈性がその加へられる振力の周期の長短によつて著しく變化し，周期の短い場合には比較的大きな彈性を有するものである．又粘性は之に反し周期が長くなるにつれて增加する傾向がある．

これらの物質の履歷曲線は次の方程式をとく事によつて容易に得られる．

$$\varepsilon\frac{d\theta}{dt}+k\theta=C\sin pt\,.$$

この式から粘性及び彈性の二性質が別々に求められる．

(3) 物質の構造は，前號に述べた如く海綿構造の外に，粘性物質の中に彈性體が浮游してゐるやうな "suspension" の構造も考へられる．地殼がこれらの物質と同じ性質を有する物質から成立してゐるならば，緩漫に變化する力に對しては全く粘性液體の如く流動して褶曲現象を示すに反し，地震波の如き急激な力の作用の下に生じた波動に對しては全く彈性體として地震波をも傳播せしめ得らるのである．

岩石の性質に關しては次の機會に述べる考へである．

32. 西南日本中央構造線と長崎三角地域とに關する二三の考察

地震研究所　大塚彌之助

(昭和10年3月19日發表――昭和10年3月20日受理)

糸魚川—靜岡地質構造線の西南側である西南日本は中央構造線（Median Dislocation Line）によつて，內帶と外帶とに分れてゐる．中央構造線は略々諏訪湖から高遠を經て，天龍川の流域浦川町に達し，更に西方へ向つて，三河豐川，伊勢櫛田川，紀伊紀ノ川，阿波吉野川の谷を經て松山に至る大斷層帶である．この一部は更に松山から九州臼杵・八代に至り，臼杵—八代地質構造線となり，他の一つは北九州伊萬里方面へ分岐して松山—伊萬里地質構造線と呼ばれてゐる．これらの松山—伊萬里地質構造線と臼杵—八代地質構造線との間に挾まれた楔狀の地域は嘗て Richthofen，矢部長克博士によつて呼ばれた長崎三角地域である[1]．

最近數年間にこの西南日本中央構造線附近の地質學的知識は著しく進んだ．そしてその中生代以前の地殼運動に關しては小林貞一理學士の詳細なる研究が公にされる筈であから，こゝには殆ど論じない積であるが，筆者はこれらの中央構造線，長崎三角地域に關する從來の考へが，最近の地質學的事實によつて如何に證明され，如何に考へ直されなければならぬかに就いて考究し，それによつて中央構造線，長崎三角地域に關する諸概念を稍々詳しく知り得たので公にする事とした．

中央構造線とその周圍に發達する地質系統

中央構造線の周圍に發達する主なる地質系統は上位の方から述べると，冲積統及び洪積統の他に，設樂第三系，石槌山第三系，天草島に發達する始新統・曉新統及び白堊系，和泉砂岩層，秩父古生層上部層，御荷鉾系，三波川系又は結晶片岩系等である．

これらの地質系統の內，三河の設樂第三系[2] は中央構造線の活動の時代を限定する

---

[1] 矢部長克　東北帝國大學理科報告(地質學)，4 (1915)；現代の科學 6 (1918)；地質學雜誌 32 (1926)，201.

[2] 石川成章　地質學雜誌 6，7，8.
納富重雄　七萬分之一，設樂圖幅及び說明書.
K. Mochizuki, *Geology of Ebi District, Mikawa*, (1927), *MS.*
H. Yamanouchi, *Geology of Uragawa District, Tôtômi*, (1927), *MS.*
望月・山內兩氏は *Thyasira bisecta* Conrad, *Chlamys swiftii* Arnold, *Voluta megaspira*? Sowerby, *Nuculana* sp., *Tellina* sp., *Turritella* sp. 等をこの第三系から報じてゐる.

上に重要な地質系統であるが，その古生物學上の資料は極めて乏しい．且つこの分布は納富技師の調査によれば中央構造線を不整合に被覆してゐるやうに見える．筆者が長篠附近で観察した處によると第1圖の如くになり，中央構造線の斷層帶に設樂第三系が斷層で接してゐる．

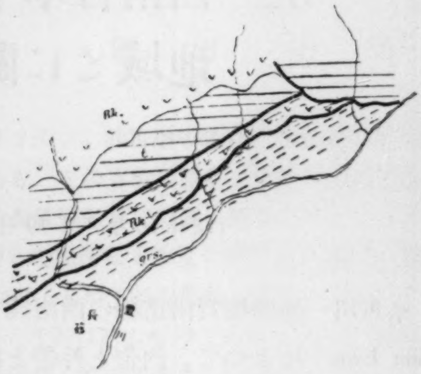

第 1 圖

(Fig. 1. Geologic map near Nagasino, Mikawa. *t* = Tertiary (Sidara); *RK*= Ryoke gneiss; *grs* = Crystalline schist.

石槌山第三系³⁾ は四國の石槌山を構成する地質系統で，安山岩類と交互し，結晶片岩系である三波川系の上に不整合に横はり，主として中央構造線の南側を占めてゐる．砂岩・礫岩・頁岩又は泥岩からなり，層位は殆ど水平か又は緩い波浪狀を示してゐる．海棲化石は殆ど知られないで，植物化石が數種知られてゐて，Nathorst 氏は中新世とした．植物化石中の或る者は紀伊の宮井炭田層中に含れるものと共通してゐる．

筆者は上述の植物化石から時代を確實に決定することは尙早と思ふが，この地層が中部新第三系以上のものでもなく，中部古第三系以下のものでもないことは確實と考へられる．故に石槌山第三系を中部第三系と考へることは安全な考へ方であらう．

佐藤戈止技師によると，この石槌山第三系は鐵道横河原線田窪驛の南部丘陵地の頂上に於て，上部白堊系を不整合に被うてゐる如く報告されてゐるが，佐藤技師はこの上部白堊系を不整合に被うてゐる石槌山第三系と言ふものに就いては多少疑問を抱いておられるやうである．

石槌山第三系は明に中央構造線及びそれに平行した斷層系で截らてゐて，而もその斷層系は低角度の逆斷層の形式である．

1934，坪井誠太郎博士・松澤理學士指導の下に行はれた東京帝大地質學教室の研究の結果によれば，次に述べる和泉砂岩層と石槌山第三系に伴ふ安山岩に類似する安山岩と結晶片岩との斷層角礫を含む極めて低角度の逆斷層系も見出された．

---

3) NATHORST, Palaeontologische Abhandlungen, IV-3.

佐藤戈止　七萬五千分之一，久萬圖幅及び說明書（1929）；松山圖幅及び說明書（1932).

T. MATUMOTO, *Geology of the Kawakami District, Prov. Iyo* (1935), *MS*; NATHORST 氏報告の植物化石は次の如くである；*Carpiniphyllum* sp., *Araliphyllum naumanni* Nathorst, *Phyllites* sp.

佐藤技師報告の植物化石は次の如くである；*Araliphyllum naumanni* Nathorst, *Juglans acuminata* A. Braun., *Tilia* sp.

松本氏報告の植物化石は次の如くである. *Flabellaria* sp. *Smilax china* L. *Salix* sp. *α*, *Salix* sp. *β*, *Salix* cfr. *membranaceus* Hr., *Juglans?* sp., *Carpinus Laxiformis Castanea gottschei* N. *Zelkova* sp., *Zeidora* sp., *Sorbus Lesquerceuxii* Nathorst, *Cornus* cf. *sanguinea* L. *Clematis sibiriakoffi* Nathorst, *Acer* sp., *Liquidamber* sp., *Ficus* sp., *Phyllites* sp., *Phyllites* (*Fagera*) sp.

和泉砂岩層[4]は江原博士の詳しい研究がある．和泉砂岩層は上部白堊系 Senon 階を代表する白堊系であることが知られ，中央構造線の北側を占め，佐藤戈止技師の研究によつて，略々中央構造線に平行した皺曲軸を有する斷層皺曲構造の存在することが確められた．この斷層皺曲構造は，上に述べた東大地質學教室の研究によつても上記の様な複雜な地質構造の存在することが確められた．

江原博士は四國東部や和泉山脈に於いて和泉砂岩が結晶片岩系との境，即ち中央構造線に近づくに從つて，擾亂の程度を增し，多數の逆斷層によつて塊裂してゐることを述べ，中央構造線が和泉砂岩堆積後に生じた壓縮を示す逆斷層系であることを主張されてゐる．又一方小林理學士によつて，和泉砂岩層が内帶に露出する花崗岩上に不整合に横はることが報告されてゐる．

天草島[5]には九州古第三系の下部である本渡層群と彌勒層群と上部白堊系の姫ノ浦層群と下部白堊系と考へられる御所浦層群とが横はつてゐる．古生物學上本渡層群は大部分始新統と考へることができ，彌勒層群は曉新統と考へられ，姫ノ浦層は上部白堊系と考へられ，和泉砂岩層と對比される．

彌勒層群と姫ノ浦層群との層位關係は不整合と考へられてゐるが，構造上著しい傾斜不整合がない．この著しい構造上の傾斜不整合のないことは長尾博士によつても指摘され納富技師の調査された七萬五千分の一天草圖幅の地質斷面圖によつても知られる通り，始新統も上部白堊系も構造上から見ると整合して，同様な皺曲構造を示してゐるので明である．勿論兩層群の分布が異り，始新統（＋曉新統）が上部白堊系を挾まずに直接に古い岩層に接する地方もあるので，白堊紀から始新世に至る間に侵蝕作用か又は造陸運動的な地殼運動か，又は海退かが存在したことを認めることができるが，激しい造構造運動が兩時代の間にのみ介在したとは思はれない．之は後に述べる皺曲の程度を示す指數でも了解できるやうに，始新統の指數も，上部白堊系の指數も殆ど類似してゐる．

この天草島の上部白堊系は上島では結晶片岩系と之を貫く角閃石・黑雲母花崗岩とを不整合に被覆してゐる．矢部博士は長崎三角地域の論文に於いて上部白堊系を基盤

---

4) 江原眞伍　地球 4（1925），345；地質學雜誌 28（1921），220；日本地質學地理學輯報 7（1929），1；日本地質學地理學輯報 9（1932），187.
矢部長克　東北帝國大學理科報告（地質學）11，1（1927）.
小林貞一　地質學雜誌 38（1931），629—640.
佐伯四郎　地質學雜誌 37（1930），517.
佐藤戈止　七萬五千分之一，松山・久萬兩圖幅及び說明書（1929—1932）.

5) 長尾巧　地質學雜誌 29（1922），41，90；東北帝國大學理科報告（地質學）11，1（1927）.
江原眞伍　地質學雜誌 28（1921），220；地質學雜誌 29（1922）.
納富重雄　七萬五千分之一，天草圖幅說明書.

岩層と解され，古第三系・新第三紀以後の火山岩類を被覆岩層と考へられたが，筆者は前に述べたことから，角閃石・黑雲母花崗岩と白堊系との不整合を重視したい．

秩父古生層上部層・御荷鉾系・三波川系又は結晶片岩系は主として中央構造線の南側に所謂帶狀構造を示してゐて（その內結晶片岩系6) は天草島・長崎縣下等に分布してゐる），一つの基盤岩層であり，その構造も極めて複雜してゐるが，その一般層向は略々東西に近く，地層の傾斜は急で一定してゐない．之等の地質系統の排列は中央構造線に接した部分では一般に中央構造線に近い側に三波川系があり，遠い側に秩父古生層が橫はつてゐる．（この配列が往々中央構造線によつて斜斷されてゐる事實から，小林理學士は，面白い結論を出してゐる．）

上に述べたやうな地質系統が現存の中央構造線の兩側に於いて知られてゐるが，その他に一つ重要なものとして花崗岩の分布の問題がある．即ち前に一寸述べたことがある和泉砂岩又は天草島の上部白堊系に被覆されてゐる花崗岩類の分布である．筆者は便宜上之等の花崗岩類を先白堊紀花崗岩と呼ぶ．

松山市の東北高繩半島基部に於いて，和泉砂岩に變質を與へてゐるところの花崗岩は，坪井誠太郎博士・松澤勳理學士7) 及び東大地質學教室の研究によつて，和泉砂岩堆積以前に貫入したものであることが確められた．故に高繩半島の花崗岩も先白堊紀花崗岩の範疇に屬せしめられることゝなつた．從つて西南日本の中央構造線及び臼杵八代線の以北に接して白堊紀以後の貫入を示す花崗岩類は知られてゐない8)．

然るに西南日本の外帶では和泉砂岩を貫く花崗岩類が地表に露出してゐることが確實となつた．故に，少くとも，中央構造線に接した內帶には和泉砂岩堆積後に貫入した花崗岩はみられず，之に反して，外帶には和泉砂岩層又は上部白堊系に貫入した花崗岩が存在するが白堊紀以前の花崗岩は見られない．

この先白堊紀花崗岩は天草群島御所浦島で下部白堊系と考へられる御所浦層群と花崗岩とが相接して露出してゐるが，納富技師は之に就いて說明書で言及してゐない．この層位學的關係が明にされたら更にこの花崗岩の時代に就いて暗示を受けるものがあらう．今は暫く措く．

上に述べた地質學的事實から次の樣な考察が，中央構造線と長崎三角地域に關して

---

6) 金原信泰 二十萬分之一，人吉圖幅及び說明書（1908）．
大築洋之助 二十萬分之一，平戶圖幅及び說明書（1913）．
大日方順三 二十萬分之一，長崎圖幅及び說明書（1912）．

7) 坪井誠太郎・松澤勳 地質學雜誌 42（1935）．

8) 加藤武夫 地質學雜誌 42（1935）．加藤博士は南部九州の花崗岩類が見立礫岩に變質を與へてゐることを指摘されてゐる．見立礫岩は現在古生物學上の證左はないが，その堆積狀態は上部白堊系より古いとは考へられない．

行はれる.

中央構造線は石槌山第三系堆積と同時又は以後にも活動した

中央構造線が石槌山第三系堆積以後に活動したことに就いては石槌山の第三系が逆斷層で和泉砂岩と接してゐるので問題はない. この事實に就いては佐藤戈止技師の地質圖によつて初めて明にされた如く考へられる. 設樂の第三系の一部でさへも，筆者の觀察によれば活動した疑がある. 併し和泉砂岩の皺曲構造が，この石槌山第三系を切る逆斷層群の成生と同時代に成生されたと解することには異論がある.

筆者はその實否を確めるために先づ和泉砂岩層の皺曲構造の一般走向に直角な方向の地質斷面圖(便宜上四國では佐藤技師の松山・久萬兩圖幅から採つた）を選び，その斷面圖に表はされてゐる和泉砂岩層の長さを皺曲に沿つて測定してFとし，その兩端の水平直線距離をLとして $\frac{F-L}{F}$ の値を求めてみた. それによると松山市附近の和泉砂岩層の $\frac{F-L}{F}$ を測定した結果は

$$0{\cdot}227\sim0{\cdot}357$$

の程度であり（天草島の上部白堊系では 0·190～0·223 位であつた)，同樣にして石槌山第三系に就いて $\frac{F-L}{F}$ を求めてみると0·020～0·010程度になる. 故に和泉砂岩と石槌山第三系とはその皺曲の程度に於いて異る點があり，之等兩者が同時代の地殼運動で形成されたとすることは皺曲の程度では贊成できない. 併し一方筆者が嘗て試みたやうに，古い地塊上の地層が，その古い地塊間の部分で著しく皺曲してゐる事實があるので，石槌山第三系は結晶片岩系の如き古い地塊上に横はつてゐるので，和泉砂岩層より皺曲の程度が小さいとも言へる. 併し天草島附近から長崎方面へかけて，結晶片岩が基盤岩石として發達してゐることが地質圖の上で推定されるので，石槌山第三系の基盤に對する關係と著しく異るとは考へられない. それにも係らず $\frac{F-L}{F}$ が 0·190～0·223 程度の値を示してゐることは單に基盤岩石の狀態の相異によつては說明できないやうに思ふ. 筆者は上述の樣な立場から白堊系堆積以後，即ち和泉砂岩堆積以後，石槌山第三系堆積以前に中央構造線の生成を考へ，石槌山第三系堆積以後に，再び中央構造線が加藤博士の所謂「古傷の再動」を示す運動を行つたものと解したのである. 斯くする事によつて，和泉砂岩の皺曲構造と石槌山第三系の皺曲構造との相異が說明されると思ふ. 上記の如き問題も，松山圖幅に於いて，皺曲する和泉砂岩層を不整合に被ふ略々水平に近い礫岩が石槌山第三系のものであることが確實となれば議論の餘地はない.

石槌山第三系を切る逆斷層系が石槌山第三系の堆積と同時代と言ふ事に就いても議論の餘地があるが，この斷層系の一部が岩脈となつたり，石槌山第三系に相伴する安山岩體で不明瞭となつたり，それらの安山岩が斷層角礫となつたりする點をみると[9]同時生成と考へることができる．

中央構造線の生成は白堊紀末期から始新統堆積以後に及んでゐる

中央構造線の成生は矢部博士によつて上部白堊系鳥屋城統堆積以後九州古第三系堆積以前と言ふ様に考へられてゐた．然るに天草島に發達する彌勒層群・本渡層群の地質構造にはこの中央構造線生成の時代に關して我々に疑を懷かせるものがある．

彌勒層群・本渡層群卽ち古第三系下半の地質系統は中央構造線の一延長である臼杵八代線の走向に略々平行な皺曲軸を持つた皺曲構造を示してゐる．然るに納富氏の天草圖幅地質斷面圖を見ると，上部白堊系も古第三系も略々構造的には整合に皺曲し，その間に何等の區別も見出だされない．

筆者は天草圖幅に於てこの皺曲軸の一般走向に對して，直角の方向の地質斷面圖を作り，古第三系の皺曲の程度を求めてみた．古第三系の $\frac{F-L}{F}$ は0·188～0·110程度で，上部白堊系に就いて測定した値0·190～0·223より稍々小さい値を示してゐる．併しその差異は石槌山第三系と天草島古第三系との皺曲の程度の差より遙に小さいものであつて，殆ど差異がないと言つても差支えない程度のものと考へられる．故に若し四國附近で考察した如く，和泉砂岩層の皺曲構造と中央構造線の生成とが關係あるとすれば，天草島の上部白堊系にも四國と同様な皺曲が認められ，この皺曲が少くとも始新統に於いても認められるから，中央構造線の生成は始新統堆積以後に完成したと言ふ事ができる．．

日本の白堊系と古第三系との境界の露出は天草島・常磐炭田・久慈町附近・北海道中央山地・樺太等に知られてゐるが，少くとも天草島・常磐炭田・久慈町附近では，この境界は造構造運動を代表するやうな地質構造上の不整合を示してゐないで，寧ろ造陸運動的地殼運動による不整合，さもなくば皺曲の程度を指示する量から暗示されるやうに白堊紀から始新世へ跨る造構造的地殼運動の存在を暗示するかの如き層位關係を示してゐるに過ぎない．中央構造線・臼杵八代地質構造線の生成は斯の如く，始新統堆積後迄も繼續したと考へられる．矢部博士は中央構造線の生成を "at the end of Mesozoic age or early in the Caenozoic age" と述べたが，新生代の初期の場合に關する說明は更に赤崎層（彌勒層群）堆積以前と限られた．

---

[9] UEMAE, *Geology of the Kawanaka District, Prov. Iyo*, (1935), *MS.*

白堊紀末と考へられてゐた北米大陸の Laramide 地殼變革も今日では始新世に及んでゐることが一般に認められて來てゐるが，日本に於てもこのやうな事が認められることになつた.

矢部博士は長崎三角地域の論文に於いて臼杵八代線を中央構造線より新期の生成と考へられたが，上述の如く上部白堊系と古第三系の少くとも下部との構造から判斷して，臼杵八代線を中央線より新期の生成と考へなければならぬ理由は見當らない．この點筆者は E. Naumann・原田の說に贊成したい.

中央構造線の前身の有無

中央構造線が上部白堊系堆積以前に存在したか否かと言ふ問題は，中央構造線が上部白堊系堆積以後の生成と考へてゐるのであるから無意味な問題である．併し中央構造線の如き內帶と外帶とを分つ樣な地質境界線が存在したか否かの問題は成立する問題である．之に關して次の如き事實を擧げて，その地質境界線の存在してゐた可能性を示すことゝする.

即ち和泉砂岩が內帶に於いては先白堊紀花崗岩の上に不整合に橫はつてゐるのに對して，外帶では外帶に發達する沈積岩と接してゐる．矢部博士が詳しく論じた如く內帶と外帶との上部白堊系が一つの外洋（open sea）に堆積したことを疑ふ資料は今日でもないやうに見える．故に上記の如き下盤の岩石の相異は上部白堊系堆積前に內帶には先白堊紀花崗岩があり，外帶には主として沈積岩が露出してゐたことを示してゐる．須貝理學士によると外帶に發達する上部白堊系中に片岩礫の存在することが確められてゐるが，この事實は結晶片岩系が上部白堊系堆積以前に地表に露出してゐたと解釋するのに都合がよい．現に天草島では結晶片岩系が白堊系に直接に被はれてゐて，白堊系堆積以前に結晶片岩系が地表に露出してゐたことを示してゐる．先白堊紀花崗岩の分布は現在では中央構造線—臼杵八代地質構造線の北側にあり，外帶には露出してゐない．故に中央構造線及び臼杵—八代地質構造線の存在した位置の北側には先上部白堊紀花崗岩の廣い露出區域があり，南側には先白堊紀（又は先上部白堊紀）沈積岩が露出してゐたことを示してゐる．故に中央構造線及び臼杵八代線と略ぼ類似の位置に兩露出區域の境界線が存在してゐたであらうことは略々確實であり，この推定は先白堊紀花崗岩の露出分布と先白堊紀岩層の露出とに基礎を置いてゐる．故にその當時の內帶と外帶との境界が斷層線によるものであつたか，接觸によるものであつたか，又は不整合式のものであつたかは筆者には斷言できない．併し結晶片岩系・二疉—石炭系等が地表に露出してゐて，一方之等を貫いた先白堊紀花崗岩が地表に露出

してゐたので，單なる不整合を示す陸地と海との境界と言うが如きものでなく，接觸か又は斷層の如き性質のものであつたらう事は推察できる．この性質不明瞭の境界線を先白堊紀中央境界線と呼ぶことにする．內帶にある上部白堊系及び始新統の皺曲構造から，現在相接近して中央構造線の兩側に露出してゐる岩層も先白堊紀中央境界線の存在する時代には遙に相距つて露出してゐたであらうことは疑ふ餘地がない．この先白堊紀中央境界線によつて暗示される外帶・內帶を夫々先白堊紀外帶・先白堊紀內帶と便宜上呼び，現在の中央構造線によつて境される西南日本の內帶・外帶と區別しやうと思ふ．矢部博士以前の構造地質學者の所謂中央線は斯の如き意味に於いて取扱へないものであらうか．

長崎三角地域は少くとも先白堊紀花崗岩の露出以後は先白堊紀外帶の延長と考へることができない

長崎三角地域は結晶片岩系の分布から外帶の一部と考へられてゐたが，前に述べたやうに，和泉砂岩層又は姫ノ浦層群たる上部白堊系の構造が長崎三角地域を外帶に屬せしめることを許さない．又，中央構造線の一部と考へてゐた松山—伊萬里線は九州北部で古第三系に被はれてゐて，この古第三系は松山—伊萬里線によつて擾亂を受けてゐない．然るにこの古第三系の天草に於けるものは，上部白堊系の構造と類似の變形を受けてゐる．故に松山—伊萬里線は中央構造線及び臼杵—八代地質構造線から區別して考へられなければならぬ一段古き意味の地質境界線と思考される．斯の如く，又前項に述べた如く中央構造線の一部である臼杵—八代地質構造線は少くとも上部白堊系に關して，中央構造線と同樣の成生過程を持つてゐると考へなければならない．故に長崎三角區域は，中央構造線及び臼杵—八代地質構造線生成後，それらの北側にあることによつて內帶の一部と考へられるべきであらう．

次に長崎三角地域を先白堊紀花崗岩の分布に就いて考へてみると，之又先白堊紀外帶の特徵と言ふよりも寧ろ先白堊紀內帶としての特徵を具へてゐることは前項記載の通である．

上記の事實から考察すると先白堊紀花崗岩が地表に露出して以後長崎三角地域は先白堊紀外帶の延長とは考へられない．

矢部博士の指摘された如く長崎三角地域に於ける結晶片岩の分布は注目すべきもので，之に注目して考へ得られる外帶の延長は先白堊紀花崗岩が地表に露出する以前に於いてのみ認められるものであり，この當時の內帶・外帶に該當するものは先白堊紀花崗岩が地表に露出される以前のもので，結晶片岩の分布を含んだ古外帶とも言ふべ

きものがあらうが，この時期に於ける古內帶なるものゝ特徴に就いては未だ明なことが言へない狀態にある．松山—伊萬里線はこれらの古內帶・古外帶とも言ふべきものゝ境界を意味するであらうが，古內帶の特徴が明にならない今日，この境界線の有無，性質等に就いて何事も述べられない．（小林理學士はこの時期に於ける西南日本の地史を研究され，斯の如き境界線の存在を疑はれてゐる．筆者もこの點に就いて否定する資料は持つてゐない．）

上記の事を要約すると次の如くになる．

1）西南日本中央構造線は第三紀中頃にも壓縮を示す逆斷層運動があつた．

2）石槌山第三系は上部白堊系及び始新統の褶曲構造に比較して著しく揉めてゐない．$\frac{F-L}{F}$ の値は次の如し．

石槌山第三系	0·020～0·010
始新統（天草）	0·188～0·110
上部白堊系（天草）	0·190～0·223
上部白堊系（四國）	0·227～0·357

3）西南日本中央構造線の生成の時期は上部白堊系堆積以後始新統堆積以後に迄及んでゐる．臼杵—八代地質構造線は中央構造線と略々同樣の生成史を持つてゐる．

4）白堊系堆積以前にも內帶・外帶に區分される如き岩層分布の特徴が存在した．その樣な狀態は遲くとも先白堊紀花崗岩の地表に露出した時代以後存在した．併し中央構造線の生成の時期は上部白堊系堆積後であるから，この時期の內帶・外帶に該當するものは今日のものとは異る．故に之を先白堊紀內帶，先白堊紀外帶と呼ぶ．又之等兩帶の境界を先白堊紀中央境界線と呼ぶ．

5）長崎三角地域は先白堊紀花崗岩が地表に露出されて以來は寧ろ先白堊紀內帶・西南日本內帶の特徴を示してゐる．

6）長崎三角地域は先白堊紀花崗岩が地表に露出する以前には，その結晶片岩系の分布から先白堊紀外帶の延長であつたと考へられやうが，この時期に於ける內帶に該當するものゝ地質學的特徴が詳にされてゐないので，內外兩帶に分たるべき性質を示してゐたか否かが明でない．若しありとすれば之を古外帶・古內帶と呼ぶ積で，松山—伊萬里線なる地質構造線は斯の如き場合の地質境界線と考へられる．

7）西南日本の構造線と構造上の各單位の發展の經路は次の樣に表示（第Ｉ表）されるであらう．

第 I 表

<table>
<tr><td rowspan="3">？白堊紀前中生代</td><td>古內帯？</td><td>松山伊萬里線</td><td colspan="2">古外帯？</td></tr>
<tr><td colspan="4">先白堊紀花崗岩の露出</td></tr>
<tr><td>先白堊紀內帯
（古內帯？＋長崎三角地域の古外帯？）</td><td>先白堊紀中央境界線</td><td colspan="2">先白堊紀外帯</td></tr>
<tr><td>白堊紀</td><td colspan="2">白堊紀岩層の堆積
造陸運動
古第三系の堆積開始</td><td colspan="2">中央構造線及び臼杵八代地質構造線の成生</td></tr>
<tr><td rowspan="2">古第三紀</td><td rowspan="2">西南日本內帯</td><td rowspan="2">中央構造線臼杵八代地質構造線</td><td colspan="2">西南日本外帯</td></tr>
<tr><td>石槌山第三系の堆積及び中央構造線の再活動</td><td>後白堊紀花崗岩の露出</td></tr>
<tr><td>新第三紀</td><td colspan="4">設樂第三系の堆積</td></tr>
</table>

追記 1. 先白堊紀花崗岩の一部は天草島では下部白堊系である御所浦層群と相接して横はり，納富技師も江原博士も之に就いて何等層位學的事實を記してをられない．併し矢部博士も御所浦層の基底に一つの赤色頁岩等を含む赤色岩層の横はることを指摘されてゐるが花崗岩（又は片麻岩）に關する層位學的關係を記してをられない．

小林理學士は手取統・領石統等に花崗岩礫の存在することに注意されて，先白堊紀花崗岩の地表に露出してゐた時代を推定されやうとしてゐる．

先白堊紀花崗岩の地表に露はれた時代は少くとも中生代中頃の事であらうことは，小澤博士の論文によつて post-Palaeozoic であることが明にされてゐるから，誤がないであらう．

追記 2. 西南日本中央構造線と設樂第三系との層位學的關係は更に検討する必要がある．

32. *Median Dislocation Line of Southwest Japan and the Nagasaki "Dreiecke."*

By Yanosuke OTUKA,

Earthquake Research Institute.

In this paper the writer summarizes our recent geologic knowledges with respect to the geotectonics of the Median Dislocation Line of Southwest Japan and the Nagasaki "Dreiecke" of F. v. Richithofen and H. Yabe, and arrives at the following conclusions:

1) The Median Dislocation Line was reactive during Middle Tertiary, and the Upper Cretaceous beds overthrust up the Isiduti Middle Tertiary beds with a low angled reversed fault plane.

2) The extent of folding of the Isiduti Middle Tertiary is smaller than that of the Upper Cretaceous and the Eocene strata along the Median Dislocation Line of Southwest Japan. The $\frac{F-L}{F}$ of these beds is obtained as follows: "F" is the length of a stratum measured along the folded structure in a geologic section. "L" is the horizontal length of the geologic section in which the folded structure of the folded stratum of length "F" is contained.

Formations	$\frac{F-L}{F}$
Isiduti Middle Tertiary	0·020………0·010
Palaeogene of Amakusa	0·188………0·110
Upper Cretaceous (Amakusa)	0·190………0·223
Upper Cretaceous (Sikoku)	0·227………0·357

3) The formation of the Median Dislocation Line of Southwest Japan continued since the deposition of the Cretaceous formations (the Izumi sandstone beds and the Himenoura groups) and during the deposition of the early Palaeogene deposit is in Northern Kyûsyû. This crustal movement, which is compressive, might have been contemporaneous with the Laramide (or Laramie) revolution on the American continent.

4) A geologic boundary of rocks dividing pre-Cretaceous southwestern Japan may have existed near the position of the Median Dislocation Line, after the exposure of the pre-Cretaceous granite on the land surface. The writer calls this divisional line the pre-Cretaceous Median Boundary Line which divides the pre-Cretaceous Inner Zone and the pre-Cretaceous Outer Zone.

5) The Nagasaki "Dreiecke" shows rather the geologic characteristics of the Inner Zone of Southwest Japan after the pre-Cretaceous granite near the Median Dislocation Line was exposed on the Land surface.

6) The Nagasaki "Dreiecke" may be regarded as a continuation of "the Outer Zone of Southwest Japan",* judging by the distribution of the crystalline schists, which occurred, at least,

---

* The writer strictly calls the post-Cretaceous Outer Zone of Southwest Japan "the Outer Zone of Southwest Japan", and if outer and inner divisions were existed in the preceding stage of the exposure of the pre-Cretaceous granite, the writer would call these divisions the Palaeo-Outer and -Inner Zone.

before the pre-Cretaceous granite that had developed near the Median Dislocation Line was exposed on the land surface.

7) Following is the development of the geotectonic units of southwest Japan since pre-Cretaceous age;

<table>
<tr><td rowspan="3">Mesozoic (pre Cret.)</td><td>Palaeo-Inner Zone?</td><td>Matuyama-Imari Line?</td><td colspan="2">Palaeo-Outer Zone?</td></tr>
<tr><td colspan="4">Exposure of pre-Cretaceous Granite.</td></tr>
<tr><td>Pre-Cretaceous Inner Zone. (Palaeo-Inner zone + Palaeo-Outer Zone of Nagasaki "Dreiecke".)</td><td>Pre-Cretaceous Median Boundary Line</td><td colspan="2">Pre-Cretaceons Outer Zone.</td></tr>
<tr><td>Cretaceous</td><td colspan="2">Deposition of Cretaceous</td><td colspan="2" rowspan="3">Formation of the Median Dislocation Line & Usuki-Yatusiro Tec. Line.</td></tr>
<tr><td rowspan="2">Palaeogene</td><td colspan="2">Epeirogenesis.</td></tr>
<tr><td colspan="2">Deposition of Early Palaeogene</td></tr>
<tr><td rowspan="3">Neogene</td><td rowspan="2">Inner Zone of Southwest Japan</td><td rowspan="2">Median Dislocation Line & Usuki-Yatusiro Line</td><td colspan="2">Outer Zone of Southwest Japan.</td></tr>
<tr><td>Deposition of Isiduti Tertiary and removing of the Median Disl. Line.</td><td>Exposure of Post-Cret. Granite.</td></tr>
<tr><td colspan="4">Deposition of Sidara Tertiary</td></tr>
</table>

8) The upper limit of the pre-Cretaceous granite will be more accurately defined upon confirmation of the stratigraphic relations between the Lower Cretaceous, the Gosyonoura groups, and the underlying granite exposed at Gosyonoura in Amakusa Islands.

9) The Neogene history of the Median Dislocation Line will be come evident after mapping the stratigraphic distribution of the Sidara Tertiary, which was once regarded as an overlying formation of the Median Dislocation Line.

33. 室戸岬附近の水準再測成果

最近，陸地測量部により，高知縣安藝町より室戸岬に至る區間の水準線路につき施行せられたる水準再測の結果，別圖に示すが如き地殼の垂直變動ありし事明かにせられたり．昭和4年，今村博士の委託によりて測量せられたる結果の一部と共に，陸地測量部の好意によりて，玆に掲載し，研究上の參考に供す．

上記再測成果に關する要項次の如し．

(i)	第1回測量	明治 29～30 年
	第2回測量	昭和4年9月
	第3回測量	昭和10年2～3月

(ii) 垂直變動量は何れも明治 29 年測量の結果との比較にして，安藝町所在の水準點5165號を不動として算出せられたるものなり．

昭和 10 年 5 月　　　　地震研究所

33. *Precise Levellings in the Neighbourhood of the Muroto Promontory.*

A distance of about 50 km, from Aki-mati to the end of the Muroto promontory, in the Kôti prefecture, was recently levelled by the Military Land Survey, the level line in question being shown in the map of annexed figure.

In the figure, the vertical displacements of the bench-marks along the level line, shown in the map, obtained as the result of the recent revision of precise levelling are shown together with those measured in 1929 at the request of Prof. Imamura, the latter being shown by dots.

The dates of the field works are as follows:

1st survey	1896~7;
2nd survey	Sept., 1929;
3rd survey	Feb.~March, 1935.

The vertical displacements deduced and shown in the figure are referred to B. M. 5165, situated in Aki-mati, the height of which is regarded as unchanged during the periods of the successive surveys mentioned above.

May 1935.

Earthquake Research Institute.

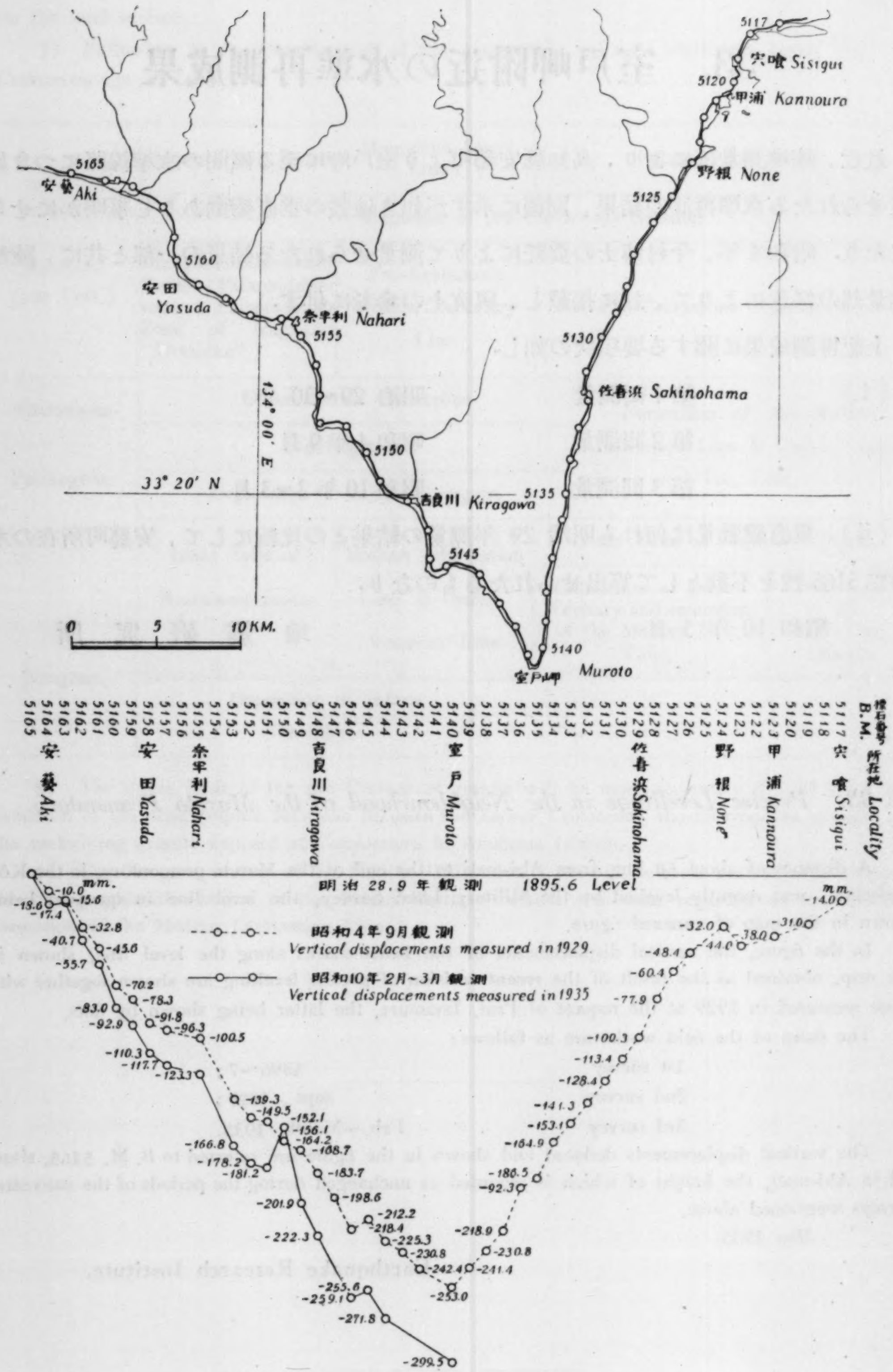
5117
宍喰 Sisigui
5120
甲浦 Kannoura
野根 None
5125
5130
佐喜浜 Sakinohama
5135
5140
室戸岬 Muroto
5145
吉良川 Kiragawa
5150
5155
奈半利 Nahari
安田 Yasuda
5160
5165
安藝 Aki
134° 00' E
33° 20' N
0 5 10 KM.
標石番號 B.M.
所在地 Locality
5117 宍喰 Sisigui
5118
5119
5120
5121
5122
5123 甲浦 Kannoura
5124 野根 None
5125
5126
5127
5128
5129 佐喜浜 Sakinohama
5130
5131
5132
5133
5134
5135
5136
5137
5138
5139
5140 室戸 Muroto
5141
5142
5143
5144
5145
5146
5147
5148 吉良川 Kiragawa
5149
5150
5151
5152
5153
5154
5155 奈半利 Nahari
5156
5157
5158 安田 Yasuda
5159
5160
5161
5162
5163
5164 安藝 Aki
5165
明治 28.9 年觀測 1895.6 Level
mm.
昭和4年9月觀測
Vertical displacements measured in 1929.
昭和10年2月~3月觀測
Vertical displacements measured in 1935
-10.0
-15.6
-18.6
-17.4
-32.8
-40.7
-45.6
-55.7
-70.2
-78.3
-83.0
-91.8
-92.9
-96.3
-100.5
-110.3
-117.7
-123.3
-139.3
-149.5
-152.1
-156.1
-164.2
-166.8
-168.7
-178.2
-181.2
-183.7
-198.6
-201.9
-212.2
-218.4
-222.3
-225.3
-230.8
-242.4
-253.0
-255.6
-259.1
-271.8
-299.5
-14.0
-31.0
-38.0
-32.0
-44.0
-48.4
-60.4
-77.9
-100.3
-113.4
-128.4
-141.3
-153.1
-164.9
-186.5
-92.3
-218.9
-230.8
-241.4

航空研究所
圖書
昭和10. 9. 23

34. The M_2 Seismic Waves.[1]

By Katsutada SEZAWA and Kiyoshi KANAI,
Earthquake Research Institute.

(Read Feb. 19, 1935.—Received June 20, 1935.)

The equation of dispersion curves of Rayleigh waves transmitted through a stratified body,[2] namely

$$\begin{aligned}&\frac{4r's'}{f^2}\left(2-\frac{k'^2}{f^2}\right)\eta-\frac{r's'}{f^2}\left\{4\vartheta+\left(2-\frac{k'^2}{f^2}\right)^2\zeta\right\}\cosh r'H\cos s'H\\&\quad+\frac{r'}{f}\varphi\left\{\frac{4rs'^2}{f^3}+\frac{s}{f}\left(2-\frac{k'^2}{f^2}\right)^2\right\}\cosh r'H\sin s'H\\&+\frac{s'}{f}\varphi\left\{-\frac{4sr'^2}{f^3}+\frac{r}{f}\left(2-\frac{k'^2}{f^2}\right)^2\right\}\sinh r'H\cos s'H\\&\quad+\left\{-\frac{4r'^2s'^2}{f^4}\zeta+\left(2-\frac{k'^2}{f^2}\right)^2\vartheta\right\}\sinh r'H\sin s'H=0,\end{aligned}\tag{1}$$

where

$$\left.\begin{aligned}&\varphi=\frac{\mu'k^2k'^2}{\mu f^4},\quad \zeta=\frac{4rs}{f^2}\left(\frac{\mu'}{\mu}-1\right)^2-\alpha^2,\quad \eta=\frac{2rs}{f^2}\left(\frac{\mu'}{\mu}-1\right)\beta-\alpha\gamma,\\&\vartheta=\frac{rs}{f^2}\beta^2-\gamma^2,\quad \alpha=\frac{2\mu'}{\mu}-\left(2-\frac{k^2}{f^2}\right),\quad \beta=\frac{\mu'}{\mu}\left(2-\frac{k'^2}{f^2}\right)-2,\\&\gamma=\frac{\mu'}{\mu}\left(2-\frac{k'^2}{f^2}\right)-\left(2-\frac{k^2}{f^2}\right),\\&r^2=f^2-h^2,\quad s^2=f^2-k^2,\quad r'^2=f^2-h'^2,\quad s'^2=k'^2-f^2,\\&h^2=\rho p^2/(\lambda+2\mu),\quad h'^2=\rho'p^2/(\lambda'+2\mu'),\quad k^2=\rho p^2/\mu,\quad k'^2=\rho'p^2/\mu',\end{aligned}\right\}\tag{2}$$

in which H is the thickness of the stratum, $2\pi/f$ the wave length, ρ, λ, μ, ρ', λ', μ' the densities and elastic constants of the stratum and the subjacent medium respectively, throws considerable light on the nature of seismic waves as well as on the structure of the earth crust. The M_2 seismic waves that we have newly found from this equation and the application of these waves to the determination of the superficial structure of the earth may be of some interest.

---

[1] Preliminary report published in the *Proc. Imp. Acad.*, **11** (1935), 96.

[2] K. SEZAWA and K. KANAI, "Discontinuity in the Dispersion Curves of Rayleigh Waves," *Bull. Earthq. Res. Inst.*, **13** (1935), 245~250.

After a prolonged study of papers by Matuzawa[3] and a number of other writers we came to the conclusion[4] that it is urgently necessary to obtain, mathematically, the dispersion curves of Rayleigh waves that are transmitted through stratified bodies in such cases as (i) $\rho'/\rho=1{\cdot}14$, $\mu'/\mu=1{\cdot}65$, $\lambda=\mu$, $\lambda'=\mu'$, (ii) $\rho'/\rho=1$, $\mu'/\mu=2$, $\lambda=\mu$, $\lambda'=\mu'$, the former case and the latter approximately corresponding to the stratifications of the Eurasian Continent and the Pacific Ocean respectively. Thus, by means of equation (1) we determined the dispersion curves of Rayleigh waves in bodies whose densities and elastic constants are specified by (i) and (ii), the result being shown in Table I and plotted in Figs. 1, 2.

Table I. $(\lambda=\mu,\ \lambda'=\mu')$

$\rho'/\rho=1{\cdot}14$, $\mu'/\mu=1{\cdot}65$				$\rho'/\rho=1$, $\mu'/\mu=2$			
1 st phase		2 nd phase		1 st phase		2 nd phase	
$\frac{2\pi}{fH}$	$\frac{p}{f}\sqrt{\frac{\rho}{\mu}}$	$\frac{2\pi}{fH}$	$\frac{p}{f}\sqrt{\frac{\rho}{\mu}}$	$\frac{2\pi}{fH}$	$\frac{p}{f}\sqrt{\frac{\rho}{\mu}}$	$\frac{2\pi}{fH}$	$\frac{p}{f}\sqrt{\frac{\rho}{\mu}}$
1·285	0·9325	0·5075	1·049	2·082	1·000	1·030	1·225
1·620	0·949	0·951	1·149	8·910	1·225	1·319	1·296
2·460	1·000	1·162	1·174	225·0	1·296	1·460	1·319
3·920	1·049	1·513	1·196			1·892	1·364
64·7	1·082			Other values from prev. paper[5]		2·400	1·400
						2·780	1·414

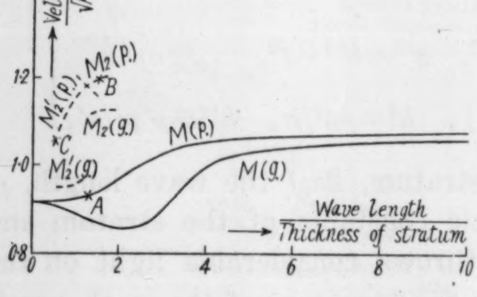

Fig. 1. $\frac{\rho'}{\rho}=1{\cdot}14$, $\frac{\mu'}{\mu}=1{\cdot}65$.

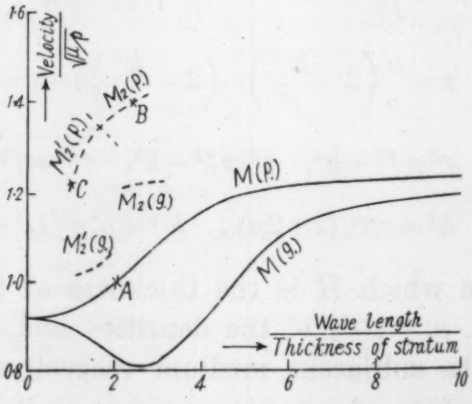

Fig. 2. $\frac{\rho'}{\rho}=1$, $\frac{\mu'}{\mu}=2$.

---

[3] T. MATUZAWA, *Bull. Earthq. Res. Inst.*, **6** (1929), 213~229.

[4] K. SEZAWA, "Rayleigh- and Love-waves transmitted through the Pacific Ocean and the Continents," *Bull. Earthq. Res. Inst.*, **13** (1935), 245~250.

[5] K. SEZAWA, *Bull. Earthq. Res. Inst.*, **3** (1927), 1.

It was found in the course of our previous study[6] that there are two dispersion curves of Rayleigh waves of different types for a stratified body, particularly when the elastic constants of the stratum differ greatly from those of the subjacent medium. Our present result shows that it is still possible for two dispersion curves to exist even in the case in which the difference in the elastic constants as well as that in the densities of the two media are not very marked. The curves in full lines in Figs. 1, 2 give the velocities of transmission for the usual type of Rayleigh waves, while the curves in broken lines give that for another type of the same waves. The two wave types may now be called M waves and M_2 waves respectively.

As will be seen from Figs. 3, 4, which show the distribution of displacements in the body, the nature of M_2 waves differs somewhat from that of waves corresponding to the second dispersion curves found and described in the previous study.[7] The vibrational energy of the present M_2 waves, instead of being accumulated on the free surface, is concentrated mainly in the vicinity of the boundary between the stratum and the subjacent medium, the horizontal component of the displacement at the surface being too small compared with the vertical component. Thus, it is probable that the M_2 waves, if they were to be observed, would not generally give rise to large displacements at the surface, while moreover their horizontal displacement would be exceedingly small.

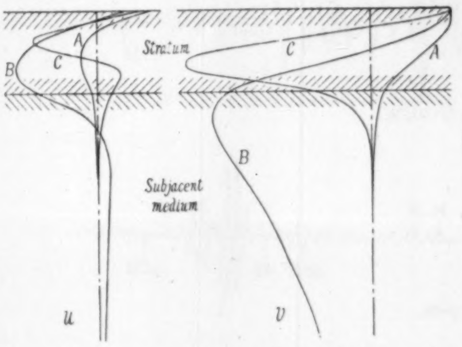

Fig. 3. $\frac{\rho'}{\rho}=1\cdot14$, $\frac{\mu'}{\mu}=1\cdot65$.

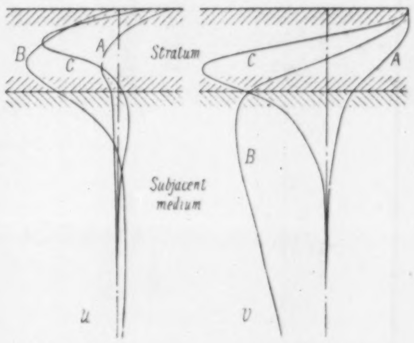

Fig. 4. $\frac{\rho'}{\rho}=1$, $\frac{\mu'}{\mu}=2$.

Careful examination of the dispersion curves for M_2 waves shows that the curve consists of two parts, namely, one for M_2 waves and the other for M_2' waves (if we may so call it), the group velocities of M_2 and M_2' are respectively greater and less than that of the maximum group velocity of M. The distributions of displacements of cases corresponding to points A, B, C (in Figs. 1, 2) which belong respectively to the M, M_2, M_2' waves, were calculated in the same way as that described in the previous paper[8] and diagrammatically shown in Figs. 3, 4. Since the displacement of the waves corresponding to M_2 is distributed relatively uniformly within a certain range of depth in the subjacent layer, while that of M_2' is accumulated rather in the very vicinity of the stratum, it would be a more easy matter to identify the M_2' phase than the M_2 phase from a seismic record, which after all is the result of measurement of motion only on the surface of the earth. It is, however, certain that the periods of oscillation in the M_2 and M_2' phases are relatively short and limited to a certain range, as will be seen from Figs. 1, 2.

---

[6] K. Sezawa and K. Kanai, *loc. cit.* 2).

[7] K. Sezawa and K. Kanai, *ditto.*

In order to confirm the existence of these M_2 and M_2' waves in actual seismic disturbances, we studied the seismic record[9] of the great India Earthquake of January 15, 1934, which was obtained at Tokyo, as shown in Fig. 5. The times of arrival of M_2, M, M_2' are in fairly good accordance with those estimated from Fig. 1; the feature that the oscillations of waves in the M_2 and M_2' phases are of quick type is also clearly recognized. M_2 and M_2' may also be distinguished from each other by the relative amplitudes of their respective oscillations. The identification of M_2 and M_2' was therefore not difficult; not at any rate in the present example.

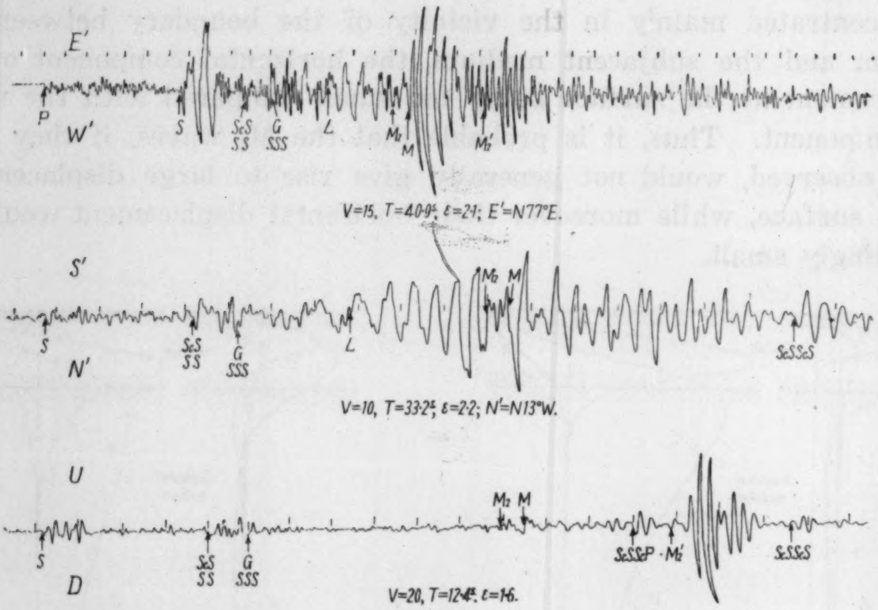

Fig. 5. $\Delta=48°$; India Earthquake, 1934, I 15. Original×1/5.

---

[8] K. SEZAWA and K. KANAI, *loc. cit.* 2).

[9] *Seism. Rep. Earthq. Res. Inst.*, 1934, Pt. 1.

34. M_2 地震波

地震研究所 {妹澤克惟
金井清

彙報第 13 號第 2 冊に於て，地表層がある場合の上下層の彈性が著しく異なる場合の Rayleigh 波に二種類あることを指摘しておいたが，上下層の彈性比がそれ程違はぬ場合にも二種類あるかどうかを吟味して見たのである．しかし，實際の場合に最も近いものを見る爲に，(i) $\rho'/\rho=1{\cdot}14$，$\mu'/\mu=1{\cdot}65$，$\lambda=\mu$，$\lambda'=\mu'$，(ii) $\rho'/\rho=1$，$\mu'/\mu=2$，$\lambda=\mu$，$\lambda'=\mu'$ といふ二つの場合を取つて見た．之等が非常に大切な事は既に我々が研究しておいた所である．この研究の結果，普通の Rayleigh 波以外にも比較的短波長のものに別個の Rayleigh 波が存在し，且つ之は地表層の下面に振動勢力がよく集中してゐることがわかるのである．之を M_2 波と名づけ，地表では上下動の割合に水平動が非常に小さい．その中でも波長によつて群速度が普通の Rayleigh 波の最高群速度よりも速いものと，それよりも遲いものとの二種があり，前者を M_2 波，後者を M_2' 波として見た．而して M_2' 波の方が M_2 波よりも地表の振幅が大きくなる傾向がある．M_2 波は M_2' 波よりも地中深く勢力が分布されてゐるから，振幅も小さくなる譯である．

大陸を通過した遠地地震の例として，昭和 9 年 1 月 15 日の印度地震の東京に於ける觀測結果をしらべて見た所が，M_2，M，M_2' 波ともに存在し，それ等の波は上記の各性質を具備してゐることがわかつた．從つて M_2，M_2' 波は，場合によつて實在し得るものであると思はれるのである．たとひ，M_2，M_2' 波が存在しない場合があつても，それは地震の機構によつたものとしてもよいであらう．

彙報第 13 號第 2 冊中の別の論文で述べたやうに，歐亞大陸の最上層の地表層の厚さは Rayleigh 波の速度から出すことが最もよいのは明かであるが，只今の M_2 波，M 波，M_2' 波のすべてを用ひて恰度 12km（次層は L 波によつて 28km と出る）となる譯であるから，遠地地震の研究は地震なき地方の學者の道樂などといつてゐる譯には行かない．我々の地表下 12km の狀態がこれでわかるとすれば，我々も大いに考へて然るべきであると思ふ．M_2，M_2' 波は勿論の事，この問題に應用できるやうな M 波の場合でさへも七八年前の我々の研究までは何もなかつたのである．尤もそれよりも前にあつた記號だけの方程式位では應用物理學上に殆ど役に立たぬことは勿論である．

35. *Growth and Decay of Seiches in an Epicontinental Sea.*[1]

By Katsutada SEZAWA,

Earthquake Reserch Instieute.

(Read April 16, 1935.—Received June 20, 1935.)

1. The fact that a kind of seiches, which however decays rapidly, appears very often even in an open coast free from the effect of bays or inlets, was discovered by Honda, Terada, Yoshida, and Isitani as the result of a series of observations made at a number of points along the coasts of the Japanese islands.[2] Nomitsu,[3] judging from a recent paper of his, seems to conclude that seiches of that kind are due partly to the free oscillation of water in an epicontinental sea. From the mathematical point of view, the problem whether such seiches that depend on the particular form of sea bottom or other boundary conditions, are likely to persist or not, is rather an important one.[4]

2. We shall first discuss the forced oscillation of the epicontinental sea. Supposing for simplicity that the epicontinental sea and the outer open sea are of uniform depths, their values being ξ', ξ, and we take the axis of x directed outwards with its origin at the common boundary of the two seas under consideration, the elementary solutions for incident and reflected waves in the outer open sea as well as in the epicontinental sea are expressed by

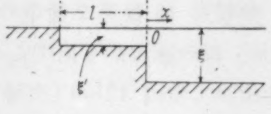

Fig. 1.

---

1) Preliminary report published in the *Proc. Imp. Acad.*, **11** (1935), 177.

2) K. HONDA, T. TERADA, Y, YOSHIDA, and D. ISITANI, *Publ. Earthq. Inv. Comm.*, No. 26 (1908); *Journ. Coll. Sci., Tokyo Imp. Univ.*, **24** (1908).

3) T. NOMITSU's paper read at the General Meeting of Math.-Phys. Soc., Japan, held April 1935, in Oosaka.

4) The paper of M. NAKANO, J. NAKAGAWA, and K. TAKEDA on the experimental study of the accumulation and dissipation of energy of secondary undulations in a bay seems to be more in line than others with the phenomena that I have been studying; *Geophys. Mag.*, **8** (1934), 121∼124.

These authors used Lord Rayleigh's semi-empirical equation in the analysis of dissipation, which however is not a satisfactory one from the point of view of dynamical theory, although it may be helpful in relieving the difficulty of the analysis to some extent.

$$\left.\begin{aligned} u_1 &= -ie^{i(\sigma t+fx)}, & w_1 &= f\xi e^{i(\sigma t+fx)} \\ u_2 &= iAe^{i(\sigma t-fx)}, & w_2 &= f\xi A e^{i(\sigma t-fx)} \\ u_1' &= -iBe^{i(\sigma t+f'x)}, & w_1' &= f'\xi' B e^{i(\sigma t+f'x)} \\ u_2' &= iCe^{i(\sigma t-f'x)}, & w_2' &= f'\xi' C e^{i(\sigma t-f'x)}, \end{aligned}\right\} \qquad (1)$$

where u_1, w_1, u_2, w_2, u_1', w_1', u_2', w_2' are horizontal displacements and surface elevations of the incident and reflected waves in the outer sea and of similar ones in the epicontinental sea respectively, while $2\pi/f$, $2\pi/f'$ are the lengths of the waves in the two seas corresponding to the period $2\pi/\sigma$, so that $\sigma/f=\sqrt{g\xi}$, $\sigma/f'=\sqrt{g\xi'}$. The boundary conditions at $x=0$ may be taken as

$$\xi(u_1+u_2)=\xi'(u_1'+u_2'), \quad w_1+w_2=w_1'+w_2', \qquad (2)$$

while that at the end of the epicontinental sea, $x=-l$, is

$$u_1'+u_2'=0. \qquad (3)$$

Substituting (1) in (2) and (3), we get

$$\left.\begin{aligned} A &= \frac{-(\alpha^2-\alpha)+(\alpha^2+\alpha)e^{-2if'l}}{(\alpha^2+\alpha)-(\alpha^2-\alpha)e^{-2if'l}}, \\ B &= \frac{2}{(\alpha^2+\alpha)-(\alpha^2-\alpha)e^{-2if'l}}, \\ C &= \frac{2e^{-2if'l}}{(\alpha^2+\alpha)-(\alpha^2-\alpha)e^{-2if'l}}, \end{aligned}\right\} \qquad (4)$$

in which $\alpha=\sqrt{\xi'/\xi}=f'\xi'/f\xi$.

Using (1) and (4) and taking the real parts only, we obtain, corresponding to the incident long waves of the stationary type,

$$u_1=\sin f(\sqrt{g\xi}t+x), \quad w_1=f\xi\cos f(\sqrt{g\xi}t+x), \qquad (5)$$

the seiches excited in the epicontinental sea of the form

$$u'=\frac{2\sin f'(x+l)\cos\{f\sqrt{g\xi'}t-\tan^{-1}(\alpha\tan f'l)\}}{\alpha\sqrt{\cos^2 f'l+\alpha^2\sin^2 f'l}}, \qquad \text{(6a)}$$

$$w'=\frac{2f\xi\cos f'(x+l)\cos\{f'\sqrt{g\xi'}t-\tan^{-1}(\alpha\tan f'l)\}}{\sqrt{\cos^2 f'l+\alpha^2\sin^2 f'l}}, \qquad \text{(6b)}$$

where $u'=u_1'+u_2'$, $w'=w_1'+w_2'$, $\alpha=\sqrt{\xi'/\xi}$.

These equations show that the maximum horizontal or vertical displacement of the seiches under resonance condition, $\cos f'l=0$, in the usual sense, is $1/\alpha$ times that of the case in which the incident waves are exceedingly long. This is due to the energy of the seiches having dissipated outward from the common boundary of both seas as waves propagated in the direction opposite to that of the incident waves; otherwise, under resonance conditions, the displacement under consideration would become infinitely large. It is also remarkable that in such resonance condition the vertical displacement at $x=0$ is zero, which is evident from the nature of the problem.

3. In the second place the decaying nature of free seiches will be dealt with. The generalisation of (1) by means of Fourier's integral gives the expressions of incident waves and of the free vibrations of the epicontinental sea as follows:

$$w_1=\frac{1}{2\pi}\int_{-\infty}^{\infty}df\int_{-\infty}^{\infty}\varphi(\tau)e^{if(\sqrt{g\xi}t+x-\tau)}d\tau\,, \tag{7a}$$

$$w'=\frac{\alpha}{\pi}\int_{-\infty}^{\infty}\frac{df}{(\alpha^2+\alpha)-(\alpha^2-\alpha)e^{-if/\alpha}}\int_{-\infty}^{\infty}\varphi(\tau)e^{\frac{if}{\alpha}(\sqrt{g\xi'}t+x-\alpha\tau)}d\tau$$

$$+\frac{\alpha}{\pi}\int_{-\infty}^{\infty}\frac{e^{-2ifl/\alpha}df}{(\alpha^2+\alpha)-(\alpha^2-\alpha)e^{-ifl/\alpha}}\int_{-\infty}^{\infty}\varphi(\tau)e^{\frac{if}{\alpha}(\sqrt{g\xi'}t-x-\alpha\tau)}d\tau\,, \tag{7b}$$

provided $\varphi(x)$, which is the form of the incident waves at $t=0$, is so sharp that it does not much disturb the subsequently excited free oscillation of the epicontinental sea. The above equations generally reduce to

$$w_1=\frac{1}{2\pi}\int_{-\infty}^{\infty}e^{if(\sqrt{g\xi}t+x)}df\int_{-\infty}^{\infty}\varphi(\tau)e^{-if\tau}d\tau\,, \tag{8a}$$

$$w'=\frac{1}{(1+\alpha)\pi}\sum_{m=0}^{\infty}(-1)^m\left(\frac{1-\alpha}{1+\alpha}\right)^m\left\{\int_{-\infty}^{\infty}e^{\frac{if}{\alpha}(\sqrt{g\xi'}t+x-2ml)}df\int_{-\infty}^{\infty}\varphi(\tau)e^{-if\tau}d\tau\right.$$

$$\left.+\int_{-\infty}^{\infty}e^{\frac{if}{\alpha}\{\sqrt{g\xi'}t-x-2(m+1)l\}}df\int_{-\infty}^{\infty}\varphi(\tau)e^{-if\tau}d\tau\right\}. \tag{8b}$$

From these equations it follows that, if the initial impulse involved in the incident waves were of the form

$$w_1=F(\sqrt{g\xi}t+x), \qquad (9)$$

the free seiches excited in the epicontinental sea would be

$$w'=\frac{2}{1+\alpha}\sum_{m=0}^{\infty}(-1)^m\left(\frac{1-\alpha}{1+\alpha}\right)^m\left\{F\left(\frac{\sqrt{g\xi'}\,t+x-2ml}{\alpha}\right)\right.$$
$$\left.+F\left(\frac{\sqrt{g\xi'}\,t-x-2(m+1)l}{\alpha}\right)\right\}. \qquad (10)$$

Such an oscillation is the exponentially damping type with logarithmic decrement

$$\frac{\sqrt{g\xi'}}{2l}\log e\left|\frac{1+\alpha}{1-\alpha}\right|. \qquad (11)$$

The greater the difference in the depths of both the seas, the more slowly do the free seiches decay in the epicontinental sea. Since

$$\log e\left|\frac{1+\alpha}{1-\alpha}\right|=\log e\left|\frac{1+\frac{1}{\alpha}}{1-\frac{1}{\alpha}}\right|,$$

the logarithmic decrement is the same whether $\sqrt{\xi'/\xi}$ is equal to a constant a or equal to the reciprocal $1/a$ of the same constant. In other words, the decrement of the case in which the ratio of depths is specified, is the same as that of the case in which the ratio of the depths is the reciprocal of the former case.

4. Further, equation (7) or (10) may be used in the solution of the growth of the seiches without any alteration in the forms of those equations. By investigating the oscillation indicated by such equations over a range of period in which the disturbance $F(\sqrt{g\xi}t+x)$ is still going on, it is possible to determine the behaviour in the growth of seiches, which is evident from the meaning implied in the equations under consideration.

If the form of the incident waves transmitted in the outer open sea be

$$\left.\begin{aligned} w_1&=\sin f(\sqrt{g\xi}t+x), \qquad &[\sqrt{g\xi}t+x>0]\\ w_1&=0, &[\sqrt{g\xi}t+x<0]\end{aligned}\right\} \qquad (12)$$

we obtain from (10)

$$w'=\frac{2}{1+a}\sum_{w=0}^{\infty}(-1)^m\left(\frac{1-a}{1+a}\right)^m\Big\{F_1(\sqrt{g\xi'}t+x-2ml)$$
$$+F_2(\sqrt{g\xi'}\,t-x-\overline{2m+1}l)\Big\}\,, \tag{13}$$

where

$$F_1(\sqrt{g\xi'}t+x-2ml)=\sin f'(\sqrt{g\xi'}t+x-2ml)\,,$$
$$[\sqrt{g\xi'}t+x-2ml>0] \tag{14a}$$
$$=0\,, \qquad [\sqrt{g\xi'}t+x-2ml<0] \tag{14b}$$
$$F_2(\sqrt{g\xi'}t-x-\overline{2m+1}l)=\sin f'(\sqrt{g\xi'}t-x-\overline{2m+1}l)\,,$$
$$[\sqrt{g\xi'}t-x-\overline{2m+1}l>0] \tag{14c}$$
$$=0\,. \qquad [\sqrt{g\xi'}t-x-\overline{2m+1}l<0] \tag{14d}$$

If $(2n+1)l>\sqrt{g\xi'}t>2nl$, we have

$$w'=\frac{2}{1+a}\Big\{\sum_{m=0}^{n}(-1)^m\left(\frac{1-a}{1+a}\right)^m F_1(\sqrt{g\xi'}t+x-2ml)$$
$$+\sum_{m=0}^{n-1}(-1)^m\left(\frac{1-a}{1+a}\right)^m F_2(\sqrt{g\xi'}t-x-\overline{2m+1}l)$$
$$=\frac{4\cos f'(l+x)}{1+a}\sum_{m=0}^{n-1}(-1)^m\left(\frac{1-a}{1+a}\right)^m\sin f'(\sqrt{g\xi'}t-2ml)$$
$$+\frac{2a_n}{1+a}(-1)^n\left(\frac{1-a}{1+a}\right)^n\sin(\sqrt{g\xi'}t+x-2nl)\,, \tag{15}$$

in which $a_n=1$ or $=0$ according as $\sqrt{g\xi'}t>$ or $<2nl-x$.

If $2(n+1)l>\sqrt{g\xi'}t>(2n+1)l$, we get similarly

$$w'=\frac{4\cos f'(l+x)}{1+a}\sum_{m=0}^{n-1}(-1)^m\left(\frac{1-a}{1+a}\right)^m\sin f'(\sqrt{g\xi'}t-2ml)$$
$$+\frac{2}{1+a}(-1)^n\left(\frac{1-a}{1+a}\right)^n\sin f'(\sqrt{g\xi'}t+x-2nl)$$
$$+\frac{2b_n}{1+a}(-1)^n\left(\frac{1-a}{1+a}\right)^n\sin f'(\sqrt{g\xi'}t-x-\overline{2n+1}l)\,, \tag{16}$$

in which $b_n=1$ or $=0$ according as $\sqrt{g\xi'}t>$ or $<(2n+1)l+(l+x)$.

Now, we are familiar with the expression

$$\frac{1+(-1)^n r^{n+1}\{\cos(n+1)\phi+i\sin(n+1)\phi\}}{1+r(\cos\phi+i\,\mathrm{son}\,\phi)}$$

$$=1-r(\cos\phi+i\sin\phi)+\cdots+(-1)^n r^n(\cos n\phi+i\sin n\phi),$$

so that

$$\sum_{m=0}^{n-1}(-1)^m\left(\frac{1-a}{1+a}\right)^m\cos 2f'lm$$

$$=\frac{1+(-1)^{n-1}\left\{\left(\frac{1-a}{1+a}\right)^{n+1}\cos 2\overline{n-1}f'l+\left(\frac{1-a}{1+a}\right)^n\cos 2nf'l\right\}+\frac{1-a}{1+a}\cos 2f'l}{\left\{1+\frac{1-a}{1+a}\cos 2f'l\right\}^2+\left\{\frac{1-a}{1+a}\sin 2f'l\right\}^2}, \quad (17a)$$

$$\sum_{m=0}^{n-1}(-1)^m\left(\frac{1-a}{1+a}\right)^m\sin 2f'lm$$

$$=\frac{-\frac{1-a}{1+a}\sin 2f'l+(-1)^{n-1}\left\{\left(\frac{1-a}{1+a}\right)^{n+1}\sin 2\overline{n-1}f'l+\left(\frac{1-a}{1+a}\right)^n\sin 2nf'l\right\}}{\left\{1+\frac{1-a}{1+a}\cos 2f'l\right\}^2+\left\{\frac{1-a}{1+a}\sin 2f'l\right\}^2}. \quad (17b)$$

Substituting from these equations in (15) and (16), we obtain

$$w'=\frac{2\cos f'(x+l)}{\sqrt{\cos^2 f'l+a^2\sin^2 f'l}}\Big[\sin\{f'\sqrt{g\xi'}t-\tan^{-1}(a\tan f'l)\}$$

$$+(-1)^{n-1}\left(\frac{1-a}{1+a}\right)^n\sin\{f'\sqrt{g\xi'}t-2f'nl-\tan^{-1}(a\tan f'l)\}\Big]$$

$$+\frac{2A}{1+a}(-1)^n\left(\frac{1-a}{1+a}\right)^n, \quad (18)$$

where (i) $A=a_n\sin f'(\sqrt{g\xi'}t+x-2nl)$, $\begin{cases} a_n=1, & \sqrt{g\xi'}t>2nl-x, \\ a_n=0, & \sqrt{g\xi'}t<2nl-x, \end{cases}$

or (ii) $A=\sin f'(\sqrt{g\xi'}t+x-2nl)$,

$+b_n\sin f'(\sqrt{g\xi'}t-x-2\overline{n+1}l)$, $\begin{cases} b_n=1, & \sqrt{g\xi'}t>(2n+1)l+(l+x), \\ b_n=0, & \sqrt{g\xi'}t<(2n+1)l+(l+x), \end{cases}$

according as (i) $(2n+1)l>\sqrt{g\xi'}t>2nl$, or (ii) $2(n+1)l>\sqrt{g\xi'}t>(2n+1)l$. These oscillations correspond to the incident waves indicated in (12).

Closer examination of the above expressions shows that the seiches grow relatively quickly to the state of stationary oscillation, particularly in the resonance condition, $f'l=\pi/2$. The vertical movement at the end, $x=-l$, begins at the instant $f'\sqrt{g\xi'}t=\pi/2$, and the successive amplitudes at $f'\sqrt{g\xi'}t=\pi,\ 2\pi, \cdots n\pi, \cdots$ are

$$\frac{2}{a}\left\{1-\frac{1-a}{1-a}\right\},\ \frac{2}{a}\left\{1-\left(\frac{1-a}{1+a}\right)^2\right\},\ \cdots\cdot\frac{2}{a}\left\{1-\left(\frac{1-a}{1+a}\right)^n\right\},\ \cdots\cdot \tag{19}$$

respectively. From these expressions it follows that, in the resonance condition, at any rate, the increment of amplitudes of successive oscillations relative to that of the initial one in the case of the growth of seiches is proportional to the amplitudes of successive oscillations in the case of the decay of the seiches. In non-resonance conditions, however, the seiches are not likely to grow at such a rapid rate.

5. With a view to compare the present calculation with actual data, I studied the result obtained by Honda, Terada, etc..[5] The places shown in the following table may be taken as good examples of open coasts.

Place	l (km)	Mean depth (m)		Period=T (min)		Decay const. $=\left(\frac{1-a}{1+a}\right)^2$	
		ξ	ξ'	Calc.	Obs.	Calc.	Obs.
Kanaiwa	30	1000	70	76	59·0	0·34	0·30
Wazima	40	1100	100	85	81·5	0·30	0·40
Kasiwazaki	18	900	90	43	43·3	0·27	0·40
Iwasaki	9	1000	70	23	15·8∼17·3	0·35	0·30
Inubô	34	1500	80	81	66·0	0·81	0·70
Onmaizaki	10	500	55	29	27·7	0·64	0·60
Tei	25	500	60	69	73·9∼77·5	0·62	0·60

I took the longest possible observed periods, excepting however that at Iwasaki, where the observed period is the one with conspicuous amplitudes. The observed decaying constants naturally correspond to the oscillations of these periods.

My sincere thanks are due to Professor Terada for his kind advices during the course of this investigation.

---

[5] K. HONDA, T. TERADA, Y. YOSHIDA, D. ISITANI, *loc. cit.*

35. 陸棚に於けるセイシの成長及老衰

地震研究所 **妹　澤　克　惟**

本多博士，寺田博士其他の方々が昔試みられた研究によれば，灣內は勿論のこと，陸棚と思はれる所にも潮汐の副振動があるやうである．それを數理的に研究して見た所が，陸棚の深さと外海の深さの割合によつて種々の性質のあることがわかつた．

外海に週期的の波動があるときに，陸棚に起るセイシは波動の週期によつて振幅が違ふけれども，共振に當る所の振幅は，極めて長週期の波動の場合の振幅に外海と陸棚の深さの割合の平方根を乘じたものに等しくなり，且つその場合に陸棚の外海と連る所の上下の振幅が零になるものである．之等は波動勢力の外海への逸散を考へて始めて得られる結果である．

次に外海の波動が止つた場合に，陸棚に於けるセイシの老衰狀態は同樣な數理で解き得るが之は勿論勢力の外海への逸散といふことが原因をなすものである．セイシは指數函數的に老衰し，其對數的減率は

$$(\sqrt{g\xi'}/2l)\{\log e(1+\alpha)-\log e(1-\alpha)\}$$

で示される．$\alpha=\sqrt{\xi'/\xi}$ であり，ξ', ξ, l は夫々陸棚，外海の深さ及び陸棚の奧行である．

セイシが外海の波動の爲に成長する機構も數理的に一定の式で表される．但し共振に當るやうな波動では老衰の場合よりも寧ろ速にセイシが成長することがわかるのである．

數理が實際とあふかを見る爲に，本多博士，寺田博士等の觀測結果を借用して灣に無關係な著しい陸棚と思はれる場所の結果と比較して見た所が，セイシの週期は勿論，自由セイシの減衰の割合も可なりよく一致することがわかつたのである．

36. *The Rate of Damping in Seismic Vibrations of a Surface Layer of Varying Density or Elasticity.*

By Katsutada SEZAWA and Kiyoshi KANAI,

Earthquake Research Institute.

(Read June 18, 1935.—Received June 20, 1935.)

1. It is established that the vibrations of a surface layer, whether free or forced, must be of such a damping type as shall depend on the ratio of both density and elastic constants of the layer to those of the subjacent medium.[1] The question may arise as to how the vibrations should be damped in the case of a layer with varying density or elastic constants. Although the way of damping in such a case naturally differs greatly according to the distribution of densities or elastic constants in both the layer and in the subjacent medium, it is nevertheless possible to conclude that the damping is due mainly to the dissipation of vibrational energy into the subjacent medium and very little to other causes of damping, such as internal friction in the ground, etc.. It is therefore obvious that the rate of damping is a certain function of density as well as of the elastic constants, and of no other physical constants.

As already stated in our preceding paper,[2] the method of representing damping by the terms at present used in differential equations of motion, and even by the functions in energy equations specifying damping forces, is not dynamically satisfactory. The semi-empirical form of dissipation function due to Lord Rayleigh[3] appears to have been misused by succeeding mathematicians. It will be plain from the nature of the problem that the dissipation problem of a vibrating body should be attacked by solving the usual simultaneous differential equations of motion for the body under consideration as well as for the neighbouring media through which the energy is dissipated.

2. Let the axis of x be drawn vertically downwards (or upwards) from a certain point 0, and let u, u', ρ, ρ', λ, μ, λ', μ' be the displacements, densities, and elastic constants of the subjacent medium and

---

1), 2) K. SEZAWA and K. KANAI, "Decay Constants of Seismic Vibrations of a Surface Layer", *Bull. Earthq. Res. Inst.*, **13** (1935), 251~264.

[3] Lord RAYLEIGH, *Proc. Math. Soc., London*, [i], **4** (1873), 357~368; *Theory of Sound*, **1**, **2**.

the surface layer respectively, H being the thickness of that layer. In the case of distortional waves transmitted vertically, the equations of motion of the two media are expressed by

$$\rho\frac{\partial^2 u}{\partial t^2}=\mu\frac{\partial^2 u}{\partial x^2}\,, \qquad (1)$$

$$\rho'\frac{\partial^2 u'}{\partial t^2}=\frac{\partial}{\partial x}\left(\mu'\frac{\partial u'}{\partial x}\right). \qquad (2)$$

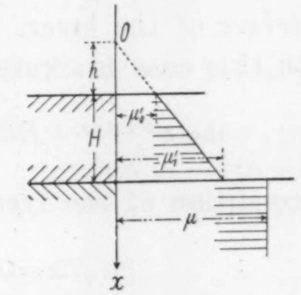

Fig. 1.

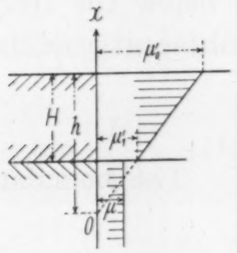

Fig. 2.

In the case of dilatational waves transmitted vertically, it is only necessary to replace μ by $\lambda+2\mu$ and μ' by $\lambda'+2\mu'$, not only in these equations but also in those that will appear hereinafter.

Let us suppose that ρ, μ, ρ' are constants and that μ' varies as

$$\mu'=Ax^n\,, \qquad (3)$$

when equation (2) then transforms to

$$\frac{d^2u'}{dx^2}+\frac{n}{x}\frac{du'}{dx}+\frac{\rho' p^2}{A}\frac{u'}{x^n}=0\,, \qquad (4)$$

provided p is the frequency of vibrations of the disturbance, and the time factor is omitted. The solution of (4) is written

$$u'=x^{\frac{1-n}{2}}\left[CH^{(1)}_{\frac{1-n}{2-n}}\left\{\left(\frac{\rho' p^2}{A}\right)^{\frac{1}{2}}\frac{2}{2-n}x^{1-\frac{n}{2}}\right\}\right.$$

$$\left.+DH^{(2)}_{\frac{1-n}{2-n}}\left\{\left(\frac{\rho' p^2}{A}\right)^{\frac{1}{2}}\frac{2}{2-n}x^{1-\frac{n}{2}}\right\}\right]e^{ipt}\,. \qquad (5)$$

(i) When the elastic constant in the layer increases downwards, the axis of x should be taken also downwards with its origin, 0, at distance h above the free surface, where h is so adjusted that the distribution of elastic constants in the layer is in a specified state. The form of the vibrations in the subjacent medium is found from equation (1), which in the present case is written

$$u=e^{ik(V_1t+x)}+Be^{ik(V_1t-x)}\,, \qquad (6)$$

in which $V_1=\sqrt{\mu/\rho}$, $k=p/V_1$.

(ii) When the elastic constant in the layer increases upwards, the axis of x should be taken also upwards with its origin, 0, at distance h below the free surface of the layer. The form of vibrations in the subjacent medium in this case is expressed by

$$u=e^{ik(V_1t-x)}+Be^{ik(V_1t+x)}. \tag{7}$$

The boundary condition at the free surface $x=h$ is

$$\partial u'/\partial x=0, \tag{8}$$

while the conditions at the lower boundary of the layer, (i) $x=h+H$, (ii) $x=h-H$, are

$$u=u', \quad \mu\frac{\partial u}{\partial x}=\mu'\frac{\partial u'}{\partial x}, \qquad (9),\ (10)$$

in the case of distortional waves. Substituting (5), (6), (7) in (8), (9), (10), we obtain the values of B, C, D.

3. For the case in which the elastic constant in the layer increases linearly downwards with its value Ah at the free surface, we put $n=1$ in (5), and solve (5), (6) so as to satisfy boundary conditions (8), (9), (10). The final solution is expressed by

$$u'=\frac{2}{\sqrt{P^2+Q^2}}\left\{J_0(2k'\sqrt{hx})Y_1(2k'h)-Y_0(2k'\sqrt{hx})J_1(2k'h)\right\}.$$

$$.\cos\left\{pt+k(h+H)-\tan^{-1}\frac{P}{Q}\right\}, \tag{11}$$

in which $k'=p\sqrt{\rho'/Ah}$, and

$$P=\sqrt{\frac{\rho'A(h+H)}{\rho\mu}}\left\{J_1(2k'\sqrt{h(h+H)})Y_1(2k'h)\right.$$

$$\left.-Y_1(2k'\sqrt{h(h+H)})J_1(2k'h)\right\}, \tag{12}$$

$$Q=\{J_0(2k'\sqrt{h(h+H)})Y_1(2k'h)-Y_0(2k'\sqrt{h(h+H)})J_1(2k'h)\}, \tag{13}$$

corresponding to the incident waves

$$u_1=\cos k(V_1t+x). \tag{14}$$

For the case in which the elastic constant in the layer increases linearly upwards with its value Ah at the free surface, we put $n=1$

in (5), and solve (5), (7) so as to satisfy the same boundary conditions, the final solution being

$$u' = \frac{2}{\sqrt{P^2+Q^2}}\left\{-J_0(2k'\sqrt{hx})\,Y_1(2k'h)+Y_0(2k'\sqrt{hx})\,J_1(2k'h)\right\}.$$

$$.\cos\left\{pt-k(h-H)-\tan^{-1}\frac{P}{Q}\right\}, \tag{15}$$

in which $k'=p\sqrt{\rho'/Ah}$, and

$$P=\sqrt{\frac{\rho' A\,(h-H)}{\rho\mu}}\left\{J_1(2k'\sqrt{h\,(h-H)})\,Y_1(2k'h)\right.$$

$$\left.-Y_1(2k'\sqrt{h\,(h-H)})\,J_1(2k'h)\right\}, \tag{16}$$

$$Q=\{J_0(2k'\sqrt{h\,(h-H)})\,Y_1(2k'h)-Y_0(2k'\sqrt{h\,(h-H)})\,J_1(2k'h)\}, \tag{17}$$

corresponding to the incident waves

$$u_1=\cos k(V_1t-x). \tag{18}$$

If the densities or elasticities of the two media were to differ extremely from each other, P would be zero, so that $Q=0$ becomes the frequency equation for the vibrations of the case without dissipation. When the frequency of vibrations becomes relatively large, it is possible to apply asymptotic expansions to the cylindrical functions in (11), (12), (13), (15), (16), (17), so that, under the condition corresponding to resonances at relatively large frequencies, the ratio of the amplitudes at the free surface to those of incident waves becomes

$$2\left(\frac{\rho\mu}{\rho'\mu_1'}\right)^{\frac{1}{2}}\left(\frac{\mu_1'}{\mu_0'}\right)^{\frac{1}{4}}, \tag{19}$$

where $\mu_0'(=Ah)$, $\mu_1'(=A\overline{h+H}$ or $=A\overline{h-H})$, μ are elastic constants at the free as well as the lower surfaces of that layer and in the subjacent medium, whereas ρ', ρ are the respective densities of the two media. Relation (19) arises from the condition, $Q=0$, which should exist at resonance frequencies. Since, again, at frequencies that are relatively large the factor consisting of cylindrical functions in (12) or (16) vanishes periodically with respect to k', P vanishes at such values of k', when the denominator corresponding to the root sign in the expression of u' in (11) or (15) contains only Q, whence it follows that the ratio of amplitudes at the free surface to those of the incident waves assumes the value

$$2\left(\frac{\mu_1'}{\mu_0'}\right)^{\frac{1}{4}}. \tag{20}$$

When $\rho\mu=\rho'\mu_1'$, the ratio of amplitudes at frequencies, relatively large and corresponding to the resonance, becomes

$$2\left(\frac{\mu_1'}{\mu_0'}\right)^{\frac{1}{4}}. \tag{21}$$

It appears therefore from (20) and (21), that, when $\rho\mu=\rho'\mu_1'$, the ratio of the amplitudes of vibrations at the free surface to those of the incident waves tends to take a constant value as shown in (20) and (21). The amplitudes at the lower boundary of the layer change periodically (not sinusoidally periodically) by values twice those of the incident waves. At frequencies corresponding to resonance without dissipation, the amplitudes of vibration at that boundary are necessarily zero.

4. In order to confirm the nature of the vibrations more thoroughly, we selected five cases, namely (i) $\mu_0'/\mu_1'=1/2$, $\mu_1'/\mu=1$; (ii $\mu_0'/\mu_1'=1/16$, $\mu_1'/\mu=1$; (iii) $\mu_0'/\mu_1'=1/16$, $\mu_1'/\mu=1/4$; (iv) $\mu_0'/\mu_1'=16$, $\mu_1'/\mu=1$; and calculated the amplitudes of vibrations at the free surface, u_0', and those at the lower boundary, u_H', of a surface layer for different lengths of incident waves; they are plotted in Figs. 3∼6. In these figures, L_0' is the length of the incident waves in the subjacent layer, the amplitudes of which are assumed to be unity.

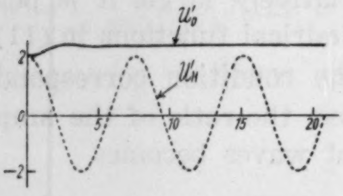

Fig. 3. $\rho'/\rho=1$, $\mu_0'/\mu_1'=1/2$, $\mu_1'/\mu=1$.

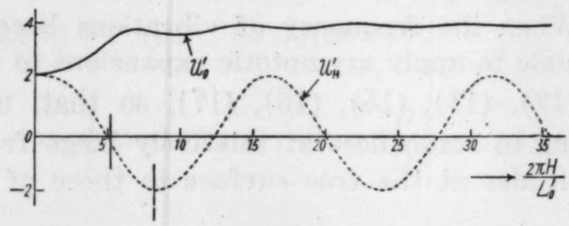

Fig. 4. $\rho'/\rho=1$, $\mu_0'/\mu_1'=1/16$, $\mu_1'/\mu=1$.

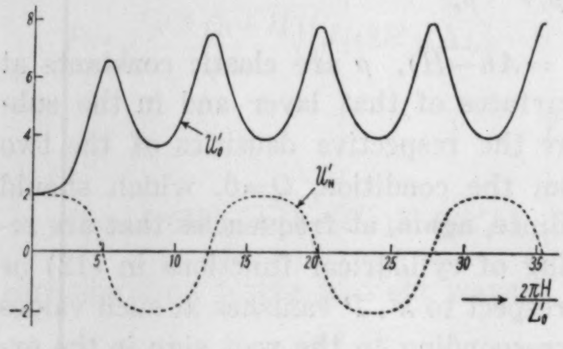

Fig. 5. $\rho'/\rho=1$, $\mu_0'/\mu_1'=1/16$, $\mu_1'/\mu=1/4$.

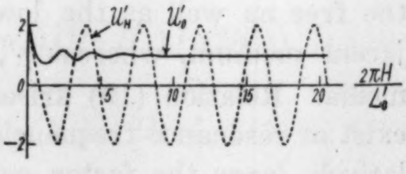

Fig. 6. $\rho'/\rho=1$, $\mu_0'/\mu_1'=16$, $\mu_1'/\mu=1$.

From these figures, one can readily ascertain the nature of the vibrations that we have described in connection with equations (19), (20), (21), $\cdots\cdots$. Should in the case, $\rho\mu=\rho'\mu_1'$, the thickness of the stratum exceed by a few times the length of the incident waves, the amplitudes of vibrations at the free surface will be practically constant for any frequency of vibrations. This shows that the relatively short waves are totally reflected, even when the elastic constant in the layer varies very sharply. Examination of the dynamical theory of the flow of vibrational energy through the layer with respect to the ratio of the amplitudes at the surface to those at the upper boundary of the subjacent medium, also shows that the incident waves are totally reflected.

It is a suitable occasion to add that the action of a seismograph of stiff type like acceleration seismographs resembles the nature of the vibrations of a layer shown in the example (iv). Amplitudes recorded on such seismographs that were set on a soft ground are relatively diminished, particularly in oscillation with periods synchronizing with those of the seismographs. The reverse is the case in similar seismographs set on a rigid ground.

5. In order to find the nature of the free vibrations of the layer, a generalisation of solution (5) by means of Fourier's integral was resorted to under the assumption that the asymptotic expansion is permissible for any wave length. In the case of increasing elasticity with depth, we obtain

$$u'=\frac{1}{\pi}\left(\frac{h+H}{x}\right)^{\frac{n}{4}}\sum_{m=0}^{\infty}(-1)^m\frac{(1-\alpha)^m}{(1+\alpha)^{m+1}}\left[F\left\{\beta\left(V_2t+\psi_2-(2m+1)\psi_1+\frac{h+H}{\beta}\right)\right\}\right.$$
$$\left.+F\left\{\beta\left(V_2t-\psi_2-(2m+1)\psi_1+\frac{h+H}{\beta}\right)\right\}\right], \tag{22}$$

where

$$\left.\begin{aligned}\psi_2&=\frac{2h}{2-n}\left\{\left(\frac{x}{h}\right)^{\frac{2-n}{2}}-1\right\},\quad \psi_1=\frac{2h}{2-n}\left\{\left(\frac{h+H}{h}\right)^{\frac{2-n}{2}}-1\right\},\\ \alpha&=\sqrt{\frac{\rho'A(h+H)^n}{\rho\mu}},\quad \beta=\sqrt{\frac{\rho'\mu}{\rho A h^n}},\quad V_2=\sqrt{\frac{Ax^n}{\rho'}},\end{aligned}\right\} \tag{23}$$

corresponding to incident disturbance

$$u_1=F(V_1t+x). \tag{24}$$

The vibrations are therefore of the exponentially damping type. The ratio of vibration amplitudes of successive similar phases is constant and expressed by

$$\left(\frac{1-\alpha}{1+\alpha}\right)^2. \tag{25}$$

When the elastic constants of both media are continuous at the lower boundary of the layer, we have $\alpha=1$, so that the ratio in (25) is zero and no oscillatory motion is possible, which shows that the waves that come upwards are totally reflected in the neighbourhood of the layer. But this conclusion is based on the assumption that cylindrical functions can be expanded asymptotically for any wave length, which however is not generally valid, so that what we have just stated is only probable for the case of very sharp initial disturbance.

It is possible to get similar expressions for the case in which the elasticity decreases with depth. In the special case, for example, in which the decrement is linear, we have

$$u'=\frac{1}{\pi}\left(\frac{h-H}{x}\right)^{\frac{1}{4}}\sum_{m=0}^{\infty}(-1)^m\frac{(1-\alpha)^m}{(1+\alpha)^{m+1}}\left[F\left\{\beta\left(V_2t-\psi_2+(2m+1)\psi_1-\frac{h-H}{\beta}\right)\right\}\right.$$
$$\left.+F\left\{\beta\left(V_2t+\psi_2+(2m+1)\psi_1-\frac{h-H}{\beta}\right)\right\}\right], \tag{26}$$

where

$$\psi_1=2h\left(\sqrt{\frac{h-H}{h}}-1\right),\quad \psi_2=2h\left(\sqrt{\frac{x}{h}}-1\right),\quad \alpha=\sqrt{\frac{\rho' A(h-H)}{\rho\mu}},$$
$$\beta=\sqrt{\frac{\rho'\mu}{\rho Ah}},\quad V_2=\sqrt{\frac{Ax}{\rho}}, \tag{27}$$

corresponding to incident waves

$$u_1=F(V_1t-x). \tag{28}$$

Since in this case, too, the ratio of amplitudes of successive similar phases is the same as in the preceding one, it is also improbable for the layer to oscillate repeatedly, so long as the elastic constants of both media are continuous at the lower boundary of that layer.

6. An approximate method of solving the problem of damped vibrations of a superficial layer due to dissipation of their energy into the subjacent medium, is to use integral equations. Although this method has already been used by some authors[4] in applying integral equations to the solution of free or forced vibrations of a surface layer lying on an extremely rigid substratum, the case of the decay of seismic vibrations of a surface layer dissipating its energy into the subjacent medium has not received the attention of investigators, probably because of the difficulty in determining the Green's function that fulfills such conditions. We found that this problem can be solved very simply provided the incident waves are of pure periodic type.

---

[4] For instance, T. ITOO, *Journ. Astr. Geophys.*, **12** (1935), 173∼218; The problem as he has worked it out may be attacked in the same way as similar problems are done in the usual textbooks and in a number of professional papers; in his case particularly so, owing to the very simple assumption made with respect to boundary conditions. The usual methods of analytical mathematics would suffice to deal with such problems. However, his attempt to solve the problem of vibrations in a superficial layer subjected to periodic force applied to its lower boundary, by assuming it to be extremely rigid in the case of free vibrations, is opposed to the dynamical point of view.

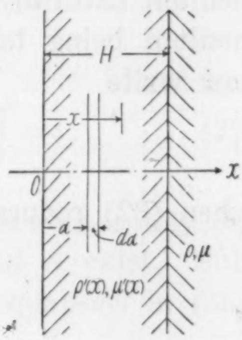

Fig. 7.

Take the axis of x directed downwards with its origin at the free surface of the earth, and let H, $\rho'(x)$, $\mu'(x)$ be the thickness, density, and rigidity of the stratum. Taking into consideration again the special nature of the integral equation, we shall discuss the problem apparently statically. Let the horizontal displacement of the lower boundary of the stratum due to a unit load applied horizontally at any point in the layer be A, its value being finite and different according to the frequency of vibrations, except in the case of zero frequency in which A may take an infinitely large value. The reason why A takes a finite value in vibration problems is very simple. The nodal surface lying just below the common boundary of two media, if the subjacent medium were replaced by the extended part of the upper one, corresponds to the surface supporting the loads in the stratum. The position of the surface under consideration varies as the difference of vibration frequency, and the value of A also differs correspondingly. The horizontal displacement at x due to a unit load applied at $x=a$ in the layer is then such that

$$\left.\begin{aligned} k(x,a) &= \int_x^H \frac{dz}{\mu'(z)} + A, \quad (x>a) \\ k(x,a) &= \int_a^H \frac{dz}{\mu'(z)} + A. \quad (x<a) \end{aligned}\right\} \tag{29}$$

These represent Green's functions for the present problem. In the vibration problem, if the horizontal displacement at $x=a$ be $u'(a)\cos pt$ and the frequency of vibrations be p, then the load due to the inertia force acting on element da at $x=a$, will be

$$p^2\rho'(a)u'(a)\cos pt\, da. \tag{30}$$

The displacement at $x=x$ due to this load is therefore expressed by

$$p^2\rho'(a)u'(a)\cos pt\,da\,k(x,a), \tag{31}$$

so that displacement, $u'(x)\cos pt$, at $x=x$ due to total loads in the layer assumes the form

$$u'(x)=p^2\int_0^H \rho'(a)k(x,a)u'(a)da, \tag{32}$$

the time factor being omitted. The inertia forces in the subjacent medium naturally have no part in the problem; the movement in that medium being taken only in the boundary conditions at $x=H$. We now write

$$\rho'(a)k(x,a)=K(x,a), \tag{33}$$

when (32) reduces to

$$u'(x)=p^2\int_0^H K(x,a)u'(a)da. \tag{34}$$

This is a homogeneous integral equation, $K(x,a)$ being its kernel. The boundary conditions at $x=H$ are such that

$$u'(H)=2\sin(kH+\gamma),^{5)} \tag{35}$$

$$p^2\int_0^H \frac{\partial K(H,a)}{\partial H}u'(a)da=2\left(\frac{\mu}{\mu'}\right)_{x=H}k\cos(kH+\gamma), \tag{36}$$

where μ, $2\pi/k$ are the rigidity and wave length in the subjacent layer, while γ is the phase angle, which may be determined by the conditions of the vibrations. The right-hand sides of (35) and (36) represent the effect of the incident and reflected waves. Now, (35) and (36) are equivalent to the single equation

$$[u'(H)]^2+\left[\frac{p^2}{k}\frac{\mu'}{\mu}\int_0^H \frac{\partial K(H,a)}{\partial H}u'(a)da\right]^2=4. \tag{37}$$

---

5) The form of this expression represents the resulting motion due to incident and reflected waves in the subjacent medium. The importance of γ (as well as of A in Green's function) will now be understood. Many authors seem to have missed the use of γ. Infinitely large amplitudes in vibrations are the result arising from the calculation under such incorrect assumption.

It is necessary to insert a certain quantity similar to γ in all like problems. Even in the problem of microseismic vibrations of a surface layer or in that of seiches in a lake, under periodic pulsation in atmosphere, the insertion of a quantity analogous to γ is important, particularly in the discussion of the oscillations under resonance condition.

For simiplicity in evaluating the integral in (34) satisfying condition (37), we used the trapezoidal rule. We divided the layer into ν equal horizontal slices and put $\beta_0=1/2$, $\beta_1=\cdots=\beta_q=\cdots=\beta_{\nu-1}=1$, $\beta_\nu=1/2$, when (34) is then equivalent to $\nu+1$ simultaneous algebraic equations of the forms

$$\frac{p^2H}{\nu}\sum_{q=0}^{\nu}\beta_q K\left(\frac{sH}{\nu},\ \frac{qH}{\nu}\right)u'\left(\frac{qH}{\nu}\right)=u'\left(\frac{sH}{\nu}\right);\ [s=0,1,2,\cdots,\nu] \tag{38}$$

and (37) is equivalent to

$$[u'(H)]^2+\left[\frac{p^2}{k^2}\frac{\mu'}{\mu}\frac{H}{\nu}\sum_{q=0}^{\nu}\beta_q\frac{\partial K\left(H',\ \frac{qH}{\nu}\right)}{\partial H'}u'\left(\frac{qH}{\nu}\right)\right]^2=4. \tag{39}$$

Eliminating $\nu+1$ values of u' in (38), it is possible to obtain only one value of A, although it may seem that $\nu+1$ values of A exist. Substituting now the value of A thus obtained in $\nu+1$ equations in (38), we get the ratios of

$$u'(0):u'\left(\frac{H}{\nu}\right):\cdots:u'\left(\frac{sH}{\nu}\right):\cdots:u'(H). \tag{40}$$

Substituting these ratios in (39), we obtain the absolute values of

$$u'(0),\quad u'\left(\frac{H}{\nu}\right),\quad \cdots,\quad u'\left(\frac{sH}{\nu}\right),\quad \cdots,\quad u'(H).$$

The solution of more general cases, namely, the case of forces of irregular periods or the one with certain initial conditions, may be easily obtained by the usual familiar methods of analysis.

With a view to compare the result of the present approximate method with that of an accurate one solved by using differential equations, we selected a case such that

$$\rho'(x)=\rho_0',\quad \mu'(x)=\mu_0'\frac{h+x}{h}, \tag{41}$$

when Green's function becomes

$$\left.\begin{aligned} k(x,a)&=\frac{h}{\mu_0'}\log\frac{h+H}{h+x}+A, \quad [x>a] \\ k(x,a)&=\frac{h}{\mu_0'}\log\frac{h+H}{h+a}+A. \quad [x<a] \end{aligned}\right\} \tag{42}$$

Substituting these in (38) and (39) for the two cases (i) $\mu_0'/\mu_1'=1/16$,

$\mu_1'/\mu=1$, $\dfrac{2\pi H}{L'}=k'H=5{\cdot}25(k'h=0{\cdot}35)$, (ii) $\mu_0'/\mu_1'=1/16$, $\mu_1'/\mu=1$, $\dfrac{2\pi H}{L_0'}=k'H=8{\cdot}25(k'h=0{\cdot}55)$, which correspond to the marks shown by the vertical strips in Fig. 4, we calculated the distribution of displacements in the layer. These two examples indicate cases corresponding approximately to (i) $P=0$, and (ii) $Q=0$ respectively in equation (11). The values of A derived from (38) by putting $\nu=4$ are (i) $-2{\cdot}24h^2/\mu_0'H$, (ii) $17{\cdot}5h^2/\mu_0'H$ respectively for the two case under consideration, while the corresponding distributions of displacements obtained from (38), (39) are shown diagrammatically by the full lines in Figs. 7, 8. The accurate values determined by (11) are shown by broken lines in the same figures. The values of A found above were very roughly obtained. It was found that some differences in the values of A are not, in fact, much important in the present calculation of displacement distributions.

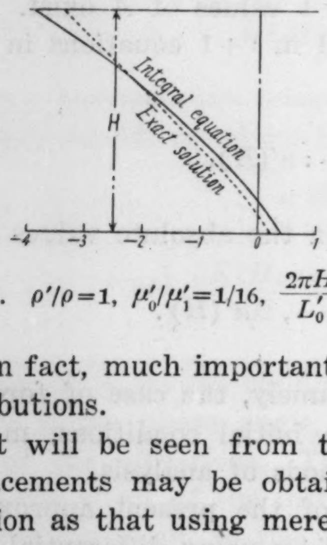

Fig. 8. $\rho'/\rho=1$, $\mu_0'/\mu_1'=1/16$, $\dfrac{2\pi H}{L_0'}=5{\cdot}25$.

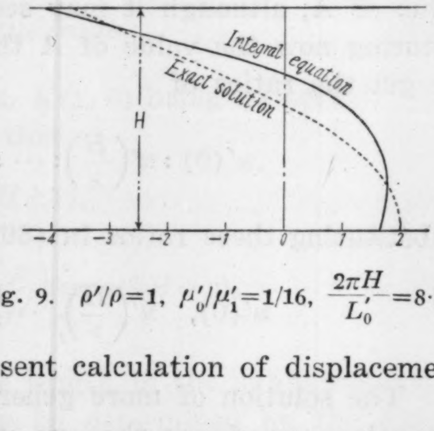

Fig. 9. $\rho'/\rho=1$, $\mu_0'/\mu_1'=1/16$, $\dfrac{2\pi H}{L_0'}=8{\cdot}25$.

It will be seen from the foregoing how the probable values of displacements may be obtained by such a rough method of integral equation as that using merely five trapezoidal ordinates; and also that it is possible to confirm the nature of the dissipation even by the method of integral equations.

36. 不均一彈性又は密度の地表層の震動減衰の割合

地震研究所 {妹澤克惟
金井清

地表層が均一な場合の性質は既に論じてあるが，不均一な場合にも同じやうな性質があるかどうかをしらべて見たところが，場合によつて特殊な性質があることがわかつた．卽ち不均性が可なり著しくても下層との接面のところで連續的になつてをれば，地表層の自由繰返し振動は實際上殆ど起らぬし，又强制振動にしても共振に相當する場合の振幅がそうでない場合と大して變らぬものである．しかしそこに段ができると繰返しの振動が起る．共減衰の係數は兩層の密度及び彈性によつて定まり，内部の摩擦等には關係がなくてもよい．

前記の接面の所で連續的なものでも，低い振動數では共振の所が多少大振幅になるけれども高い振動數では共振の所も共振でない所も振幅に變りがない．而もこの高い振動數の所の振幅の方が低い振動數の所の共振にあたる振幅よりも寧ろ大きいのは變つてゐるといふこともできる．接面の所が不連續な場合には，如何に高い振動數でも夫々の共振の所が大振幅になる．この場合にもやはり低い振動數の場合の共振の大振幅よりも稍々大きい氣味にある．而して之等は大振幅であるとはいへ，彈性と密度の條件によつて或一定値を取ることに變りがない．

地表層の彈性又は密度の値が下層の夫等よりも高い傾向にあるときには，共振にあたる所の振幅が然らざる場合よりも小さくなる．これと同じやうな性質は例へば加速度地震計のやうに剛い地震計の記錄にも現れるやうに思ふ．そのやうな地震計を柔軟な土地の上に置いて測定すると，その地震計の固有週期に近い週期の震動に於ける記錄はその器械の Calibration をやつた場合よりも小なる振幅を與へることになる．逆に地震計の効果的剛度よりも剛い土地の上で用ひると該週期の附近で振幅が寧ろ大きく出る．從て固有週期の極く短い器械で剛い土地の震動を測ると斯る土地では加速度が大きいといふやうな見掛けの結論も出るかも知れぬ．極めて長週期の地震計ではそのやうな憂ひは槪して少いやうに思はれる．同樣な問題は地上の建物についてもいはれるが，別の機會に讓ることにする．

尙，方法を換へて積分方程式の方法を應用して見た．Green の函數の中に變數を置き且つ上層と下層との接面の條件を正確に取ることによつて，勢力が逸散する場合の解が得られるのであつて，そのやうな方法は勢力の逸散が今まで應用數學者の注意を惹かなかつた爲にそれだけ，まだどこにも解いたのが見當らぬやうである．このやうに物理的に必要な注意を拂つて計算すると，可なり近似的に積分方程式を解いても其結果による變位分布は前の正確な場合の變位分布と非常に近いことがわかるのである．但し注意すべきは，この方法は勢力の逸散はあるにしても，入射波が規則正しい週期を持つ場合に限られてゐることである．

37. *On an Elastic Wave Animated by the Potential Energy of Initial Strain.*

By Hirosi KAWASUMI and Ryôiti YOSIYAMA,

Earthquake Research Institute.

(Read May 21, 1935.—Received June 20, 1935.)

One of the writers estimated the energy carried out by seismic waves in case of a few earthquakes and attributed the energy source to the hypocentral regions. Recently Prof. Ishimoto reminded the writers of the possibility of an alternative explanation that the energy may possibly be the released potential energy which has been stored throughout the medium in a strained state. On his advice we have studied the question theoretically and could prove his opinion actually. Although the case we have treated is a very simple case, the result obtained contains something more than expected, so we will describe it in the following.

I. As a nucleus of strain we have adopted the simplest case of "centre of compression or dilatation". We are now concerned with the case in which the initial strain is suddenly released at a limited portion (say $r=a$) by the disappearance of stress prevailing there. We have therefore to study the transient motion from a statical state to another, and we will employ a harmonic wave function and generalise the time factor so as to satisfy the required conditions.

As is well known, relevant wave function corresponding to the characteristic equation

$$\frac{\partial^2\phi}{\partial t^2}=\frac{\lambda+2\mu}{\rho}\nabla^2\phi \qquad (1)$$

is

$$\phi_p=Ar^{-\frac{1}{2}}H^{(1)}_{\frac{1}{2}}(hr)e^{-ipt}+Br^{-\frac{1}{2}}H^{(2)}_{\frac{1}{2}}(hr)e^{ipt}, \qquad (2)$$

where ϕ_p is elementary displacement potential and

$$h^2=\rho p^2/(\lambda+2\mu)=(p/V)^2, \qquad (3)$$

V being the velocity of longitudinal wave. Now put $A=f(p)dp$ and $B=g(p)dp$ and integrate with regard to p from 0 to ∞, the result

$$\phi=\int_0^\infty f(p)r^{-\frac{1}{2}}H_{\frac{1}{2}}^{(1)}(hr)e^{-ipt}dp+\int_0^\infty g(p)r^{-\frac{1}{2}}H_{\frac{1}{2}}^{(2)}(hr)e^{ipt}dp \tag{4}$$

is also a solution of the original equation (1) so long as $f(p)$ and $g(p)$ are independent of t and r. Then the displacement and stress corresponding to (4) are

$$u=\frac{\partial\phi}{\partial r}=-\int_0^\infty f(p)hr^{-\frac{1}{2}}H_{\frac{3}{2}}^{(1)}(hr)e^{-ipt}dp-\int_0^\infty g(p)hr^{-\frac{1}{2}}H_{\frac{3}{2}}^{(2)}(hr)e^{ipt}dp, \tag{5}$$

$$\begin{aligned}\widehat{rr}=\lambda\Delta+2\mu\frac{\partial u}{\partial r}=&\int_0^\infty f(p)\{-(\lambda+2\mu)h^2r^{-\frac{1}{2}}H_{\frac{1}{2}}^{(1)}(hr)+4\mu hr^{-\frac{3}{2}}H_{\frac{3}{2}}^{(1)}(hr)\}e^{-ipt}dp\\&+\int_0^\infty g(p)\{-(\lambda+2\mu)h^2r^{-\frac{1}{2}}H_{\frac{1}{2}}^{(2)}(hr)+4\mu hr^{-\frac{3}{2}}H_{\frac{3}{2}}^{(2)}(hr)\}e^{ipt}dp.\end{aligned} \tag{6}$$

We are now to determine $f(p)$ and $g(p)$ from the condition at the boundary, $r=a$, which is expressed by means of Fourier's double integral theorem

$$\widehat{rr}_{r=a}=\varphi(t)=\frac{1}{2\pi}\int_0^\infty dp\int_{-\infty}^\infty\varphi(\omega)e^{ip(t-\omega)}d\omega+\frac{1}{2\pi}\int_0^\infty dp\int_{-\infty}^\infty\varphi(\omega)e^{-ip(t-\omega)}d\omega. \tag{7}$$

Comparing (6) and (7) we have

$$f(p)=\frac{1}{2\pi\{-(\lambda+2\mu)h^2a^{-\frac{1}{2}}H_{\frac{1}{2}}^{(1)}(ha)+4\mu ha^{-\frac{3}{2}}H_{\frac{3}{2}}^{(1)}(ha)\}}\int_{-\infty}^\infty\varphi(\omega)e^{ip\omega}d\omega, \tag{8}$$

$$g(p)=\frac{1}{2\pi\{-(\lambda+2\mu)h^2a^{-\frac{1}{2}}H_{\frac{1}{2}}^{(2)}(ha)+4\mu ha^{-\frac{3}{2}}H_{\frac{3}{2}}^{(2)}(ha)\}}\int_{-\infty}^\infty\varphi(\omega)e^{-ip\omega}d\omega. \tag{9}$$

Substituting these values into (4), and after a little transformation by means of the relations (3) and $H_{n+\frac{1}{2}}^{(1)}(-z)=(-1)^{n+\frac{1}{2}}H_{n+\frac{1}{2}}^{(2)}(z)$ as well as $\sqrt{\frac{1}{2}\pi z}\,H_{\frac{1}{2}}^{(1)}(z)=ie^{-iz}$ and $\sqrt{\frac{1}{2}\pi z}\,H_{\frac{3}{2}}^{(2)}(z)=\left(-1+\frac{i}{z}\right)e^{-iz}$, we have

$$\phi=\frac{-a}{2\pi\rho r}\int_{-\infty}^\infty\frac{e^{ip\left(t-\frac{r-a}{V}\right)}dp}{(p-\alpha)(p-\beta)}\int_{-\infty}^\infty\varphi(\omega)e^{-ip\omega}d\omega, \tag{10}$$

provided

$$\left.\begin{aligned}\alpha&=i\frac{2\mathfrak{v}^2}{aV}+\frac{2\mathfrak{v}}{a}\sqrt{1-\left(\frac{\mathfrak{v}}{V}\right)^2},\\\beta&=i\frac{2\mathfrak{v}^2}{aV}-\frac{2\mathfrak{v}}{a}\sqrt{1-\left(\frac{\mathfrak{v}}{V}\right)^2},\end{aligned}\right\} \tag{11}$$

and

$$\mathfrak{v}=\sqrt{\frac{\mu}{\rho}}. \tag{12}$$

It is a matter of evaluation of definite integral (10) which we are now concerned.

Our first aim is to solve the case when the stress which has been prevailing is suddenly disappeared. It will be of interest to know the reverse case as well. But it is impossible to solve these cases separately, so we will combine these cases and study the case in which the stress is suddenly generated at $t=0$, and disappears at $t=t_1$ where t_1 is to be taken large sufficiently.

$$\varphi(t)=\begin{cases} 0 & \text{when} \quad t<0, \\ -P_0 & \quad '' \qquad 0<t<t_1, \\ 0 & \quad '' \qquad t_1<t, \end{cases} \tag{13}$$

and

$$\phi=\frac{aP_0}{2\pi\rho r}\int_{-\infty}^{\infty}\frac{e^{ip\tau}dp}{(p-\alpha)(p-\beta)}\int_0^{t_1}e^{-ip\omega}\,d\omega$$

$$=\frac{aP_0}{2\pi i\rho r}\int_{-\infty}^{\infty}\frac{e^{ip\tau}-e^{ip\tau_1}}{p(p-\alpha)(p-\beta)}dp, \tag{14}$$

where $\tau\equiv t-\dfrac{r-a}{V}$ and $\tau_1\equiv\tau-t_1$.

By means of a contour integral along the real axis with a small indentation at the origin and an infinite semi-circle on the upper side of the real axis when τ is positive, or the lower semi-circle when τ is negative, we can easily obtain

$$\int_{-\infty}^{\infty}\frac{e^{ip\tau}dp}{p(p-\alpha)(p-\beta)}=\left\{\begin{array}{ll} 2\pi i\left[\dfrac{1}{2\alpha\beta}+\dfrac{1}{\alpha-\beta}\left(\dfrac{e^{i\alpha\tau}}{\alpha}-\dfrac{e^{i\beta\tau}}{\beta}\right)\right], & \text{when} \quad \tau>0, \\ -\dfrac{\pi i}{\alpha\beta}, & \text{when} \quad \tau<0. \end{array}\right\} \tag{15}$$

And we have

a) when $\tau<0$,

$$\phi=0. \tag{16}$$

b) when $0<\tau<t_1$,

$$\phi=\frac{aP_0}{\rho r}\left[\frac{1}{\alpha\beta}+\frac{e^{i\alpha\tau}}{\alpha(\alpha-\beta)}+\frac{e^{i\beta\tau}}{\beta(\beta-\alpha)}\right]$$

$$=\frac{a^3P_0}{4\mu r}\left[\sqrt{\frac{\lambda+2\mu}{\lambda+\mu}}e^{-\frac{2\mathfrak{v}^2}{aV}\tau}\sin\left\{\frac{2\mathfrak{v}}{a}\sqrt{1-\left(\frac{\mathfrak{v}}{V}\right)^2}\tau+\Delta\right\}-1\right], \qquad (17)$$

where

$$\tan\Delta=\sqrt{\frac{\lambda+2\mu}{\lambda+\mu}}.$$

c) when $0<\tau_1\equiv t-t_1-\dfrac{r-a}{V}$,

$$\phi=\frac{a^3P_0}{4\mu r}\sqrt{\frac{\lambda+2\mu}{\lambda+\mu}}e^{-\frac{2\mathfrak{v}^2}{aV}\tau_1}\left[e^{-\frac{2\mathfrak{v}^2}{aV}t_1}\sin\left\{\frac{2\mathfrak{v}}{a}\sqrt{1-\left(\frac{\mathfrak{v}}{V}\right)^2}\tau+\Delta\right\}\right.$$

$$\left.-\sin\left\{\frac{2\mathfrak{v}}{a}\sqrt{1-\left(\frac{\mathfrak{v}}{V}\right)^2}\tau_1+\Delta\right\}\right]$$

$$\approx-\frac{a^3P_0}{4\mu r}\sqrt{\frac{\lambda+2\mu}{\lambda+\mu}}e^{-\frac{2\mathfrak{v}^2}{aV}\tau_1}\sin\left\{\frac{2\mathfrak{v}}{a}\sqrt{1-\left(\frac{\mathfrak{v}}{V}\right)^2}\tau_1+\Delta\right\}, \qquad (18)$$

if $\dfrac{2\mathfrak{v}^2}{aV}t_1\gg1$.

Thus we see from the above displacement potential ϕ that the disturbance travels with the velocity V at a distance and begins suddenly after a travel time $t=\dfrac{r-a}{V}$. The disturbance consists of a statical part $\dfrac{a^3P_0}{4\mu r}$ and a vibratory part with period $\pi a/\mathfrak{v}\sqrt{1-(\frac{\mathfrak{v}}{V})^2}$ which quickly dies away exponentially with damping ratio $e^{\pi\sqrt{\frac{\mu}{\lambda+\mu}}}$ ($=9{\cdot}22$ when $\lambda=\mu$). And if t_1 is sufficiently large the deformation before arrival of the disturbance which started $r=a$ at $t=t_1$ is practically the statical one, while after the arrival of the latter disturbance ($0<\tau_1$) the statical deformation disappears and only damped harmonic wave remains which at last dies away.

In the representative case b)

$$u=\frac{\partial\phi}{\partial r}=\frac{a^3P_0}{4\mu}\left[\frac{1}{r^2}\left\{1-\frac{1}{\alpha-\beta}\left(\beta e^{i\alpha\tau}-\alpha e^{i\beta\tau}\right)\right\}-\frac{i\alpha\beta}{r}\left(e^{i\alpha\tau}-e^{i\beta\tau}\right)\right]$$

$$=\frac{a^3P_0}{4\mu}\left[\frac{1}{r^2}\left\{1-\sqrt{\frac{\lambda+2\mu}{\lambda+\mu}}e^{-\frac{2\mathfrak{v}^2}{aV}\tau}\sin\left(\frac{2\mathfrak{v}}{a}\sqrt{1-\left(\frac{\mathfrak{v}}{V}\right)^2}\tau+\Delta\right)\right\}\right.$$

$$\left.-\frac{2}{a}\sqrt{\frac{\lambda+\mu}{\mu}}\frac{1}{r}e^{-\frac{2\mathfrak{v}^2}{aV}\tau}\sin\frac{2\mathfrak{v}}{a}\sqrt{1-\left(\frac{\mathfrak{v}}{V}\right)^2}\tau\right]. \qquad (19)$$

$$\dot{u}=\frac{a^3P_0}{4\mu}\frac{i\alpha\beta}{\alpha-\beta}\left[\left(\frac{1}{r^2}+\frac{i\alpha}{Vr}\right)e^{i\alpha\tau}-\left(\frac{1}{r^2}+\frac{i\beta}{Vr}\right)e^{i\beta\tau}\right], \tag{20}$$

$$\widehat{rr}=-\frac{a^3P_0}{r^3}-\frac{a^3P_0}{\alpha-\beta}\left\{\left(\frac{1}{r^3}+\frac{\alpha i}{Vr^2}-\frac{\alpha^2}{4\mathfrak{b}^2r}\right)\beta e^{i\alpha\tau}\right.$$

$$\left.-\left(\frac{1}{r^3}+\frac{\beta^{i}}{Vr^2}-\frac{\beta^2}{4\mathfrak{b}^2r}\right)\alpha e^{i\beta t}\right\}. \tag{21}$$

And the total energy flowing out through a spherical surface at r is

$$E_b=\int_0^{2\pi}d\varphi\int_0^{\pi}\sin\theta d\theta\int_0^{t_1}\{-\widehat{rr}\dot{u}\}r^2d\tau,$$

where t_1 is very large by the assumption and may be replaced by ∞, and

$$E_b=\frac{\pi a^6P_0^2}{\mu r^3}+\frac{\pi a^6P_0^2}{2\mu}\left[\frac{1}{a^3}-\frac{1}{r^3}\right]. \tag{22}$$

The first term in the above equation represents the energy due to the statical deformation and the latter is due to the dynamical part. We can therefore obtain the entities in case c) if we discard the statical part in the equations (19), (20) and (21) and change signs. And the second term in (22) corresponding to the case c)

$$E_c=\frac{\pi a^6P_0^2}{2\mu}\left[\frac{1}{a^3}-\frac{1}{r^3}\right] \tag{23}$$

is zero at $r=a$, and increases with r to the limit $\frac{\pi a^3P_0^2}{2\mu}$.

The statical problem is also obtained by putting $\tau=\infty$ in (17), (19), (20) and (21).

$$\left.\begin{aligned}\phi&=-\frac{a^3P_0}{4\mu r},\\ u&=\frac{a^3P_0}{4\mu r^2},\\ \widehat{rr}&=-\frac{a^3P_0}{r^3}.\end{aligned}\right\} \tag{24}$$

The strain energy function for this case becomes

$$W=\frac{3a^6P_0^2}{8\mu r^6}, \tag{25}$$

and since the potential energy is the volume integral of W, the potential energy stored in the medium from $r=a$ to r is

$$E_p=\int_0^{2\pi} d\varphi\int_0^{\pi} \sin\theta d\theta\int_a^r Wr^2dr=\frac{\pi a^6\mathrm{P}_0^2}{2\mu}\left[\frac{1}{a^3}-\frac{1}{r^3}\right], \tag{26}$$

which is exactly the total energy flux E_c in case c). Thus we could prove that the energy carried out by the elastic wave in case c) is the released potential energy which have been stored in the medium in the strained state.

We cannot therefore overlook the possibility of the above alternative explanation on the origin of seismic energy besides the one emitted from the hypocentral region. But the dependence of E_b and E_c on r is only through the term proportional to $\frac{1}{r^3}$ and they quickly tend to the same limit in both cases. We cannot therefore distinguish between these cases from the observation at large distance from the origin if we do not compare the higher terms in $\frac{1}{r}$ than the accuracy of usual observation can afford. Strictly speaking the energy source in case c) is the whole medium, but from the actual point of view, the most of the energy is confined to comparatively small region near the origin.

It is also to be noted that the displacement is continuous while the velocity of the particle and the stress $\widehat{rr}$ is discontinuous at $\tau=0$ and $\tau_1=0$.

II. Though our first aim has thus been attained, we shall now pay some attention to the appearance of the damped harmonic motion. The period of this wave is dependent on the radius of the boundary sphere a and the velocities of elastic waves. It thus resembles a kind of self-oscillation. The occurrence of this oscillation is due to the singularities in the integrand of the definite integral, and is not merely the result of our assumption of the form $\varphi(t)$. The circumstance bears striking similarity with the forced oscillation of a pendulum. In fact, the forced oscillation of a damped pendulum defined by

$$\ddot{\theta}+2\epsilon\dot{\theta}+n^2\theta=\varphi(t)$$

is easily proved to be

$$\theta=\frac{-1}{2\pi}\int_{-\infty}^{\infty}\frac{e^{ipt}dp}{(p-\alpha)(p-\beta)}\int_{-\infty}^{\infty}\varphi(\omega)e^{-ip\omega}d\omega,$$

which is exactly the same form as (10) provided $\alpha=i\epsilon+\sqrt{n^2-\epsilon^2}$, $\beta=i\epsilon-\sqrt{n^2-\epsilon^2}$. We have ample knowledge on the motion of a pendulum, and we can demonstrate it by experiment. The displacement potential ϕ for a given pressure $\varphi(t)$ at $r=a$ can be inferred from the motion of a pendulum under the same force if t is replaced by $\tau=t-\frac{r-a}{V}$. We shall not therefore enter into detailed discussion of several other examples we have studied, but we cannot help to state some bearing in the interpretation of seismic motions. So far as the writers are aware, elucidation on the occurrence of oscillatory motions in the earthquake motions hitherto proposed are the explanation by the breaking up of the non-periodic initial wave forms by dispersion, or by the self-oscillation of some part of the crust excited by seismic motions, but nothing is known on the mechanism of the alternative explanation by the intrinsic nature caused at a hypocentre notwithstanding prevalently assumed implicitly. We can now add an explanation for it. As we know the occurrence of self-oscillation in the motion of a pendulum at every discontinuity of disturbance, so we are to expect the occurrence of damped harmonic waves in case of an earthquake.

Another point of interest is the proportionality of the period to the radius of the boundary sphere. We are well acquainted with the fact that the period of seismic wave is the longer the larger the earthquake is. One of the writers pointed out that we have to consider a kind of hypocentral region, and the seismic phenomena which take place at the region cannot be inferred from the observation of elastic waves at large distance from the origin. Such a chaos may possibly play some rolls in causing seismic waves by the traction at a boundary surface. Then the well known fact on the length of period of seismic waves can be easily explained.

Finally we state that in case of such simple cases discussed above, the motions at large distance from the origin are

$$u=\mp\frac{a^2P_0}{2\sqrt{\mu(\lambda+\mu)}}\frac{1}{r}\,e^{-\frac{2\mathfrak{v}^2}{aV}\tau}\sin\frac{2\mathfrak{v}}{a}\sqrt{1-\left(\frac{\mathfrak{v}}{V}\right)^2}\,\tau$$

for each case b) and c), and the damping ratio is as large as 9·2 when $\lambda=\mu$, and the motion is hardly different from that of shock type, and the appearance of such a type of motion in actual earthquake makes us feel some interest.

Concluding Remark. We have proved in a simplest case that elastic wave may be animated by the potential energy of initial strain. We have seen also that a kind of damped harmonic wave resembling self-oscillation is excited when stress on a spherical surface is given. Showing the similarity with the motion of a pendulum under a given force we have proposed one of the possible explanations on the vibratory nature of seismic waves. We should expect that similar treatment is applicable in a more general case when stress or displacement of more general form are given on a spherical surface. Indeed we could also see that similar vibratory waves are excited when displacements (excepting a few cases) and stresses of general forms are given on a spherical surface, and the results will be published shortly.

In conclusion the writers wish to express their cordial thanks to Prof. M. Ishimoto for the precious suggestions.

37. 歪の潛勢力によつて起される彈性波

地震研究所 河角 廣
吉山 良一

筆者の１人は 2〜3 の地震の調査に際し地震波によつて運び出される全勢力を推算し，之れを震原域から出たものと考へたが，最近石本敎授は歪の潛勢力も地震波に勢力を供給し得る事を注意せられたので筆者等は共の最も簡單な場合を理論的に計算し，石本敎授の說を實證する事が出來た．

或る球面で突然歪力が消滅する場合に起される彈性波を出して見ると，一種の減衰振動の波で振幅は中心距離に逆比例するもので遠方に於ては靜力學的の變位よりも大きいものであるが，共れによつて運び出される勢力は全く初の歪の潛勢力に等しい事を知つた．逆に歪力が突然加へられる場合も計算し比較して見た．彈性の際限內では，何れの場合にも傳播速度に相違は見られない．

次に振動性の波動の起るのは全く振子の自己振動の起るのと同樣である事を示し，共の週期が球の半徑に比例し彈性波の速度に關係する事から一種の自己振動と見得る事を示し，地震動の性質の１解釋として此の結果が興味ある點を指摘した．更に一般的の場合も同樣に取扱へるがそれは次回に報告する．

---

38. *Pulsatory Oscillations of the Earth's Crust due to Surface[1] Force.**

By Kumizi IIDA.

(Read March 19, 1935.—Received June 20, 1935.)

1. Oscillations of the earth's crust, exceedingly minute, but having no connection with ordinary earthquakes, are matters of constant observation. This subject was first discussed by Milne[2], and later by Omori[3], who classified the pulsations as observed in Tokyo into three types, q, Q_1, and Q_2, according to their periods of oscillations. Since then Prof. T. Matuzawa[4] and Dr. K. Wadati[5] have made detailed studies of these types of pulsations. The Q_1-type has recently been studied by Dr. F. Kishinouye[6].

Although, in the hope of learning the causes of these pulsations, a number of investigators[7] have attempted to trace the connections, if any, between them and meteorological conditions and other agencies that might be at work, the whole subject is still wrapped in mystery. But whatever the primary causes may be, there is no doubt that they are greatly influenced by the geologic and topographic conditions of the regions in which they occur. They seem to be proper oscillations peculiar to the particular locality, combined with forced oscillations as the result of disturbances propagated through the earth's crust. Since this idea was first mooted by F. Omori, problems relating to the proper period of the earth's crust have come to play a very important rôle in seismology, with the result that problems of this kind are being attacked by many investigators[8] from the standpoint of both theory and observation.

---

* Communicated by M. Ishimoto.

[1] For lack of a more suitable word, the writer uses the words *surface force* here to mean forces that operate on the earth's surface, such as winds, etc.,

[2] J. MILNE, *Trans. Seism. Soc., Japan*, **6** (1883); **7** (7884); **11** (1887); **13** (1889); **17** (1893); **18** (1893); **10** (1894).

[3] F. OMORI, *Bull. Earthq. Inv. Comm.*, **1** (1907); **2** (1908); **3** (1909); **5** (1913); **94** (1921), (in Japanese).

[4] T. MATUZAWA, *Journ. Fac. Sci., Tokyo*, [ii], **2** (1927), 205~263.

[5] K. WADATI, *Geophys. Mag.*, **1** (1926~1928), 35.

[6] F. KISHINOUYE, *Bull. Earthq. Res. Inst.*, **13** (1935), 146.

[7] For example, H. SCHÜNEMANN, *Z. f. Geophys.*, **8** (1932), 216.
B. GUTENBERG, „Die Seismishe Bodenunruhe“, (1924), 43.
S. K. BANERJI, *Phil. Trans. Roy. Soc., London*, **229** (1930), 287.

To explain the period of pulsations, E. Wiechert[9] considers the pulsations as stationary waves in the upper layer of the earth's crust, assuming a surface of discontinuity for its bottom. The upper layer of the earth's crust oscillates in such a way that the bottom of that layer forms the nodal plane of the oscillation, the upper surface of the layer being the loop-plane of the said oscillation. He calculated the depth of the layer by means of the formula $D=\frac{1}{4}TV$, where D is the depth of the layer, V the velocity of the transversal wave in the layer, T the period of the pulsation. By a similar treatment, K. Wadati[10] estimated the thickness of the surface layer in Tokyo to be about 1∼2 km.

Prof. H. Nagaoka[11] regards the pulsations as stationary surface tremors of Rayleigh type, assuming the existence of appropriate boundaries. T. Matuzawa[12] thinks these pulsations are coupled oscillations of two oscillating systems. H. Honda[13], who believes these pulsations to be stationary surface tremors of Love type, obtained the mode of oscillation for the Q_2-type, assuming a suitable boundary covering the hypothetical case that the surface layers in Tokyo may be only some ten metres thick. The Q_1-type pulsation seems to be an overtone of that of the Q_2-type.

All these studies just mentioned concern problems of free oscillations of the earth's crust. Recently G. NISHIMURA[14], in discussing the problem of vibrations of a heterogeneous elastic solid due to *surface force*, applied the problem to pulsation. By similar treatment the writer calculated the pulsatory oscillations of the earth's crust due to *surface*

---

[8] K. SUYEHIRO, *Publ. Imp. Acad.*, **4** (1929), 2; *Bull. Earthq. Res. Inst.*, **7** (1930), 467.

M. ISHIMOTO, *Bull. Earthq. Res. Inst.*, **9** (1931), 316; **10** (1932), 171; **17** (1934), 234.

T. SAITA and S. SUZUKI, *Bull. Earthq. Res. Inst.*, **12** (1934), 517.

W. INOUYE, *ibid.*, **12** (1934), 712.

K. SEZAWA, *ibid.*, **8** (1930), 1.

K. SEZAWA and G. NISHIMURA, *ibid.*, **8** (1930), 321.

K. SEZAWA and K. KANAI, *ibid.*, **10** (1932), 1.

[9] E. WIECHERT, *Beiträge zur Geophysik, Ergänzungs Band.*, **2** (1904).

[10] K. WADATI, *loc. cit.*

[11] H. NAGAOKA, *Publ. Earthq. Inv. Comm.*, **22** (1906).

[12] T. MATUZAWA, *loc. cit.*

[13] H. HONDA, *Geophys. Mag.*, **3** (1930), 177.

[14] G. NISHIMURA, *Bull. Earthq. Res. Inst.*, **12** (1934), 403. *Disin*, **5** (1933), 677; **7** (1935), 78, (in Japanese).

force. In the present paper the writer gives a method for calculating the pulsatory oscillations with the aid of integral equations. In discussing the growth of these pulsations and the structure of the earth's crust, there are admittedly many unknown facts, but the pulsations are here treated as shearing vibrations of the upper layer of the earth's crust, it being assumed for simplicity that the medium that lies next below the upper layer is infinitely rigid. The periods of both the free and forced oscillations of the layer (in some simple cases) are calculated and compared with those of pulsations actually observed.

2. Take the x- and y-axis horizontally and the z-axis vertically downwards, the origin being on the surface of the layer (Fig. 1). The equations of motion in the layer are expressed by

$$\left.\begin{aligned} \rho\frac{\partial^2 u}{\partial t^2}+2\epsilon\frac{\partial u}{\partial t}&=\mu\frac{\partial^2 u}{\partial z^2}+\frac{d\mu}{dz}\frac{\partial u}{\partial z}\,, \\ \rho\frac{\partial^2 v}{\partial t^2}+2\epsilon\frac{\partial v}{\partial t}&=\mu\frac{\partial^2 v}{\partial z^2}+\frac{d\mu}{dz}\frac{\partial u}{\partial z}\,, \end{aligned}\right\} \qquad (1)$$

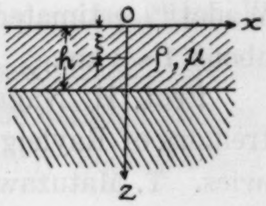

Fig. 1.

where u, v denote displacement components in the x- and y-axis, ϵ the coefficient of damping, μ the rigidity, ρ the density of the layer. Since u is independent of v, the two equations in (1) with respect to u or v can be solved in the same way. We therefore treat only the equation that involves u. In order to obtain the free oscillation of the layer, we must solve the equation

$$\mu\frac{\partial^2 u}{\partial z^2}+\frac{d\mu}{dz}\frac{\partial u}{\partial z}=0\,. \qquad (2)$$

By integrating equation (2) with respect to z, we have

$$\mu\frac{du}{dz}=C\,. \qquad (3)$$

Integrating further, we get

$$u(z)=\int_{(z)}\frac{Cd\xi}{\mu(\xi)}+D\,, \qquad (4)$$

where C and D are the integration constants.

In the present case, we consider the simplest problem in which the medium next below the surface layer is infinitely rigid, so that the boundary conditions are merely denoted by

$$\left.\begin{aligned} &\text{(i)} \qquad z=0\,, \quad \frac{du}{dz}=0\,, \\ &\text{(ii)} \qquad z=h \quad u=0\,, \end{aligned}\right\} \qquad (5)$$

where h is the thickness of the layer.

If we assume that unit force per unit mass at point $z=\xi$, we get

$$\left|\mu\frac{du}{dz}\right|_{\xi+0}^{\xi-0}=1\,,\ \text{or}\ \frac{du}{dz}=-\frac{1}{\mu(\xi)}\,. \tag{6}$$

By means of condition (i) in (5), equation (3) is reduced to $u=\text{const.}$, since $C=0$. By means of (ii) in (5), equation (4) becomes $u=\int_z^h\frac{Cd\xi}{\mu(\xi)}$, whence

$$\left|\frac{du}{dz}\right|_{z=\xi}=C\int_\xi^h\frac{d}{dz}\left(\frac{d\eta}{\mu(\eta)}\right)dz-\frac{1}{\mu(\xi)}=-\frac{C}{\mu(\xi)}\,. \tag{7}$$

Since equation (6) is equivalent to (7), $C=1$.

Thus

$$u=\int_z^h\frac{d\xi}{\mu(\xi)}\,. \tag{8}$$

We assume $G(z,\xi)$ equal $u(z)$ and take it Green's function, which function, of course, satisfies conditions (5). The product of $G(z,\xi)$ and the unit force that is applied at the point $z=\xi$, represents the displacement at that point.

We now introduce a symmetric kernel (Kern) $K(z,s)$

$$\left.\begin{aligned}K(z,s)&=\int_z^h\frac{\rho(\xi)}{\mu(\xi)}\,d\xi, \quad z>s\,,\\ &=\int_s^h\frac{\rho(\xi)}{\mu(\xi)}\,d\xi, \quad z<s\,.\end{aligned}\right\} \tag{9}$$

When the displacement of the layer is given by $\Phi(z,t)=\phi(z)e^{i\lambda t}$, the inertial force produced at point $z=s$ is given by $\rho\lambda^2\phi(s)e^{i\lambda t}ds$. The product of the inertial force and $G(z,\xi)$ equals the displacement produced at point z due to the concentrated mass at $z=\xi$. As there are many concentrated masses at various points between $z=0$ and $z=h$, integration must be made from $z=0$ to $z=h$. We have therefore the displacement $\phi(z)$ given by the homogeneous integral equation

$$\phi(z)=\lambda^2\int_0^h K(z,s)\phi(s)ds. \tag{10}$$

Assuming next that force is concentrated at point $z=\xi$ and that the force per unit mass is $p(\xi)$, the force at the surface of the layer is given by

$$\lim_{\xi\to0}\int_{\xi-\varepsilon_1}^{\xi+\varepsilon_1}p(\xi)d\xi=T, \tag{11}$$

where T is the tangential stress of the wind or other agencies, ε_1 being a very small quantity.

The force at $z=s$ is given by

$$\rho\lambda^2\phi(s)e^{i\lambda t}ds+\rho f(s)e^{i\lambda t}ds+2i\lambda\varepsilon'\rho\phi(s)e^{i\lambda t}ds,$$

assuming that

$$p(\xi)=f(\xi)e^{i\lambda t},\quad \varepsilon'\rho=\varepsilon\,. \tag{12}$$

Then the integral equation governing the forced oscillation of the layer is given by

$$\phi(z)=(\lambda^2+2i\lambda\varepsilon')\int_0^h K(z,s)\phi(s)ds+F(z), \tag{13}$$

where

$$F(z)=\lim_{\xi\to 0}\int_{\xi-\varepsilon_1}^{\xi+\varepsilon_1} p(\xi)K(z,\xi)d\xi=K(z,0)\int_0^{z+0} p(\xi)d\xi \tag{14}$$

$$=K(z,0)T\,.$$

The above equation is a Fredholm's integral equation of the second kind.

Should condition $\int_0^h\int_0^h[K^2(s,z)]^2dzds<1$ be not satisfied, as is generally the case, we must then resort to Schmidt's solution. If we define $\phi_n(z)$ as the normalised principal solutions (normal functions; Eigenfunktionen) of the homogeneous integral equation

$$\phi(z)=\lambda^2\int_0^h K(z,s)\phi(s)ds\,.$$

It is easily proved that

$$\left.\begin{array}{c}\displaystyle\int_0^h[\phi_n(z)]^2dz=1,\quad \int_0^h\phi_n(z)\phi_m(z)dz=0,\\ \displaystyle K(z,s)=\sum_{n=1}^{\infty}\frac{\phi_n(z)\phi_n(s)}{\lambda_n},\end{array}\right\} \tag{15}$$

$$(n=1,\ 2,\cdots\cdots,\quad m=1,\ 2,\cdots\cdots,\quad n\neq m.)$$

where λ_n's are the characteristic numbers (Eigenwerte). We have moreover

$$K^2(z,s)=\int_0^h K(z,\xi)\sum_{n=1}^{\infty}\frac{\phi_n(\xi)\phi_n(s)}{\lambda_n}d\xi$$

$$=\sum_{n=1}^{\infty}\frac{\phi_n(s)}{\lambda_n}\int_0^h K(z,\xi)\phi_n(\xi)d\xi$$

$$=\sum_{n=1}^{\infty}\frac{\phi_n(s)\phi_n(z)}{\lambda_n^2}\,. \tag{16}$$

Now that $K(z,s)$ and $F(z)$ are all continuous, (13) is easily solved. By means of Schmidt's solution, equation (13) can be solved as follows:

$$\phi(z)=F(z)+\sum_{n=1}^{\infty}\frac{\lambda^2+2i\lambda\varepsilon'}{\lambda_n^2-(\lambda^2+2i\lambda\varepsilon')}\phi_n(z)\int_0^h F(z)\phi_n(z)dz. \tag{17}$$

While

$$\frac{\lambda^2+2i\lambda\varepsilon'}{\lambda_n^2-(\lambda^2+2i\varepsilon'\lambda)}=\frac{(\lambda_n^2-\lambda^2)\lambda^2-4\lambda^2\varepsilon'^2+2i\lambda\varepsilon'\lambda_n^2}{(\lambda_n^2-\lambda^2)^2+4\lambda^2\varepsilon'^2},$$

whence equation (17) becomes

$$\phi(z)=F(z)+\sum_{n=1}^{\infty}\frac{(\lambda_n^2-\lambda^2)\lambda^2-4\lambda^2\varepsilon'^2}{(\lambda_n^2-\lambda^2)^2+4\lambda^2\varepsilon'^2}\phi_n(z)\int_0^h F(z)\phi_n(z)dz$$

$$+i\sum_{n=1}^{\infty}\frac{2\varepsilon'\lambda\lambda_n^2\phi_n(z)}{(\lambda_n^2-\lambda^2)^2+4\lambda^2\varepsilon'^2}\int_0^h F(z)\phi_n(z)dz. \tag{18}$$

3. We shall now give some examples in the following cases:

(*1*) *The case in which there is only one surface layer.*

If ρ and μ are all constant, the kernel $K(z,s)$ becomes

$$\left.\begin{aligned}K(z,s)&=\frac{\rho}{\mu}(h-z),\ [z>s],\\&=\frac{\rho}{\mu}(h-s),\ [z<s].\end{aligned}\right\} \tag{19}$$

In this case the "Eigenwerte" and "Eigenfunktionen" of the homogeneous integral equation (10) are given by

$$\left.\begin{aligned}\phi_n(z)&=\sqrt{\frac{2}{h}}\cos\frac{2n-1}{2h}\pi z,\\ \lambda_{2n-1}&=\frac{(2n-1)\pi}{2h}\sqrt{\frac{\mu}{\rho}}.\ n=1,2,\dots\end{aligned}\right\} \tag{20}$$

From these we can calculate the periods and amplitudes of oscillations of the layer. The manner of free oscillation of the layer is shown in Fig. 2.

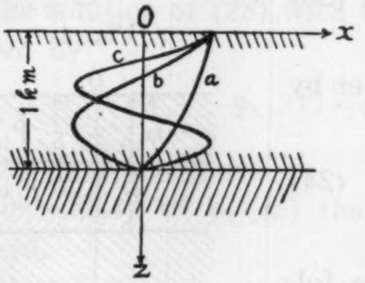

Fig. 2. a, $n=1$; b, $n=2$; c, $n=3$.

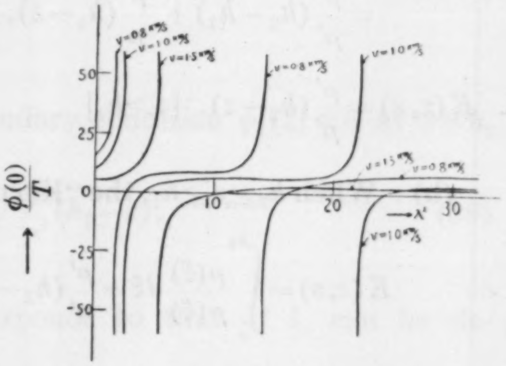

Fig. 3. Relation between $\left[\frac{\phi(z)}{T}\right]_{z=0}$ and λ^2 ($h=1$ km).

Since we obtain in this case

$$\int_0^h F(z)\phi_n(z)dz = T\sqrt{\frac{2}{h}}\,\frac{\rho}{\mu}\int_0^h (h-z)\cos\frac{(2n-1)\pi}{2h}z dz,$$

equation (18) for determining the forced oscillation of the layer becomes

$$\frac{\phi(z)}{T} = \frac{\rho}{\mu}(h-z) + \frac{2\rho}{h\mu}\sum_{n=1}^{\infty}\frac{(\lambda_{2n-1}^2-\lambda^2)\lambda^2-4\lambda^2\varepsilon'^2}{(\lambda_{2n-1}^2-\lambda^2)^2+4\lambda^2\varepsilon'^2}\,\frac{\cos\frac{2n-1}{2h}\pi z}{\frac{(2n-1)^2\pi^2}{4h^2}}$$

$$+\,i\,\frac{2\rho}{h\mu}\sum_{n=1}^{\infty}\frac{2\varepsilon'\lambda\lambda_{2n-1}^2}{(\lambda_{2n-1}^2-\lambda^2)^2+4\lambda^2\varepsilon'^2}\,\frac{\cos\frac{2n-1}{2h}\pi z}{\frac{(2n-1)^2\pi^2}{4h^2}}. \tag{21}$$

The curves of the forced oscillations showing the displacement at $z=0$ for $h=1\text{km}$ when $v\left(\sqrt{\frac{\mu}{\rho}}\right)=0{\cdot}8$ km/sec, 1 km/sec, 1·5 km/sec, $\varepsilon'=0$ are plotted in Fig. 3. When the period of the forced oscillation coincides with that of the free oscillation of the layer, the amplitude of the oscillation at the surface becomes infinitely great (Fig. 3).

(2) *The case of two superficial layers.*

As to the symmetric kernel, we have two cases: (i) $z>s$, (ii) $z<s$. Furter, each case involves the two cases (a) and (b) (Figs. 4, 5).

(i) When $z>s$.

(a) When $h_1 \geqq s \geqq 0$, the "Kern" $K(z,s)$ is given by

$$K(z,s) = \int_z^{h_2}\frac{\rho(\xi)}{\mu(\xi)}d\xi = \int_{h_1}^{h_2}\frac{\rho(\xi)}{\mu(\xi)}d\xi + \int_z^{h_1}\frac{\rho(\xi)}{\mu(\xi)}d\xi$$

$$= \frac{\rho'}{\mu'}(h_2-h_1) + \frac{\rho}{\mu}(h_1-z), \quad [z<h_1] \tag{22}$$

$$K(z,s) = \frac{\rho'}{\mu'}(h_2-z). \quad [z>h_1] \tag{23}$$

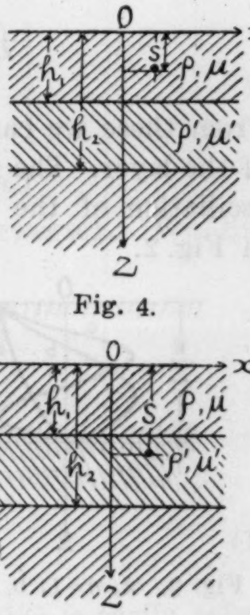

Fig. 4.

(b) When $h_2 \geqq s \geqq h_1$, the "Kern" is given by

$$K(z,s) = \int_z^{h_2}\frac{\rho(\xi)}{\mu(\xi)}d\xi = \frac{\rho'}{\mu'}(h_2-z). \tag{24}$$

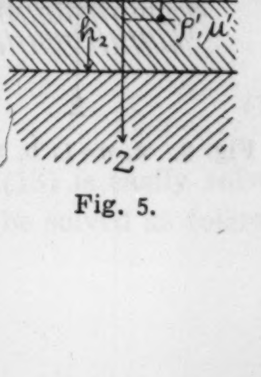

Fig. 5.

(ii) When $z<s$, there are two cases as follows:

(a) When $h_1 \geqq s \geqq 0$, the "Kern" is given by

$$K(z,s)=\int_s^{h_2}\frac{\rho(\xi)}{\mu(\xi)}\,d\xi=\frac{\rho}{\mu}(h_1-s)+\frac{\rho'}{\mu'}(h_2-h_1)\,. \tag{25}$$

(b) When $h_2\geqq s\geqq h_1$, the "Kern" is given by

$$K(z,s)=\int_s^{h_2}\frac{\rho(\xi)}{\mu(\xi)}\,d\xi=\frac{\rho'}{\mu'}(h_2-s). \tag{26}$$

Since the "Kern" in all cases just mentioned are now obtained, we can find the "Eigenwerte" and "Eigenfunktionen" of the integral equation

$$\phi(z)=\lambda^2\int_0^{h_2}K(z,s)\phi(s)ds, \tag{27}$$

governing the free oscillation of the layer in the two cases, such as $h_2\geqq z\geqq h_1$ and $h_1\geqq z\geqq 0$. $\phi_{2,\,n}(z)$ and $\phi_{1,\,n}(z)$ stand for the "Eigenfunktionen" of the former and the latter of the above two cases respectively.

When $h_2\geqq z\geqq h_1$, the homogeneous integral equation

$$\phi(z)=\lambda^2\int_0^{h_2}K(z,s)\phi(s)ds\,,$$

is written

$$\begin{aligned}\phi_2(z)&=\lambda^2\left\{\int_0^{h_1}K(z,s)\,\phi_2(s)ds+\int_{h_1}^{z}K(z,s)\,\phi_2(s)ds+\int_z^{h_2}K(z,s)\phi_2(s)ds\right\}\\&=\lambda^2\left\{\int_0^{h_1}\frac{\rho'}{\mu'}(h_2-z)\phi_2(s)ds+\int_{h_1}^{z}\frac{\rho'}{\mu'}(h_2-z)\phi_2(s)ds+\int_z^{h_2}\frac{\rho'}{\mu'}(h_2-s)\phi_2{}'s)ds\right\}\\&=\lambda^2\frac{\rho'}{\mu'}\left[\int_0^{z}(s-z)\phi_2(s)ds+\int_0^{h_2}(h_2-s)\phi_2(s)ds\right]\\&=\frac{\rho'}{\mu'}\lambda^2\left[\int_0^{z}(s-z)\phi_2(s)ds+\text{const.}\right],\end{aligned} \tag{28}$$

where, constant$=\int_0^{h_2}(h_2-s)\phi(s)ds$.

The solution of (28) with the boundary condition $\phi_2(z)=0$ at $z=h_2$ is given by

$$\phi_{2,\,n}(z)=B\sin\lambda_n\sqrt{\frac{\rho'}{\mu'}}(h_2-z), \tag{29}$$

where B is a constant.

The values of $\phi_{2,\,n}(z)$ that corresponds to that of λ_n can be determined.

When $h_1\geqq z\geqq 0$, we have similarly

$$\phi_1(z)=\lambda^2\int_0^{h_2}K(z,s)\phi_1(s)ds$$

$$=\lambda^2\left[\int_0^z\left\{\frac{\rho'}{\mu'}(h_2-h_1)+\frac{\rho}{\mu}(h_1-z)\right\}\phi_1(s)\,ds+\int_z^{h_1}\left\{\frac{\rho}{\mu}(h_1-s)+\frac{\rho'}{\mu'}(h_2-h_1)\right\}\cdot\phi_1(s)\,ds+\int_{h_1}^{h_2}\frac{\rho'}{\mu'}(h_2-s)\phi_1(s)\,ds\right]$$

$$=\lambda^2\left[\frac{\rho}{\mu}\int_0^z(s-z)\phi_1(s)\,ds+c_1+c_2\right], \tag{30}$$

where

$$c_1=\int_0^{h_1}\left\{\frac{\rho}{\mu}(h_1-s)+\frac{\rho'}{\mu'}(s-h_1)\right\}\phi_1(s)\,ds,$$

$$c_2=\int_0^{h_2}\frac{\rho'}{\mu'}(h_2-s)\phi_1(s)\,ds.$$

The solution of (30) is given by

$$\phi_{1,\,n}(z)=A\cos\lambda_n\sqrt{\frac{\rho}{\mu}}\,z\,, \tag{31}$$

where A is a constant: $A=\lambda^2(c_1+c_2)$.

Next, the boundary conditions are expressed by

$$\left.\begin{aligned}\phi_{1,\,n}(z)&=\phi_{2,\,n}(z),\\ \mu'\frac{\partial\phi_{2,\,n}(z)}{\partial z}&=\mu\frac{\partial\phi_{1,\,n}(z)}{\partial z},\end{aligned}\right\} \tag{32}$$

at $z=h_1$, by $\phi_{2,\,n}(z)=0$ at $z=h_2$, and by $\dfrac{\partial\phi_{1,\,n}(z)}{\partial z}=0$ at $z=0$.

Substituting (29) and (31) in (32), we have

$$A\cos\lambda_n\sqrt{\frac{\rho}{\mu}}\,h_1=B\sin\lambda_n\sqrt{\frac{\rho'}{\mu'}}(h_2-h_1), \tag{33}$$

$$\mu\lambda_n\sqrt{\frac{\rho}{\mu}}\,A\sin\lambda_n\sqrt{\frac{\rho}{\mu}}\,h_1=\mu'\lambda_n\sqrt{\frac{\rho'}{\mu'}}\,B\cos\lambda_n\sqrt{\frac{\rho'}{\mu'}}(h_2-h_1), \tag{34}$$

whence the ratio A/B is expressed by

$$\frac{A}{B}=\frac{\sin\lambda_n\sqrt{\dfrac{\rho'}{\mu'}}(h_2-h_1)}{\cos\lambda_n\sqrt{\dfrac{\rho}{\mu}}\,h_1},\ \text{or}\ \frac{\sqrt{\rho'\mu'}\cos\lambda_n\sqrt{\dfrac{\rho'}{\mu'}}(h_2-h_1)}{\sqrt{\rho\mu}\sin\lambda_n\sqrt{\dfrac{\rho}{\mu}}\,h_1}, \tag{35}$$

and

$$\sqrt{\frac{\rho\mu}{\rho'\mu'}}\tan\lambda_n\sqrt{\frac{\rho}{\mu}}\,h_1\tan\lambda_n\sqrt{\frac{\rho'}{\mu'}}(h_2-h_1)=1\,. \tag{36}$$

By (36) the "Eigenwerte" λ_n for determining the periods of the free oscillation of the layer can be obtained.

Thus, (29) and (31) are readily written

$$\phi_{1,\,n}(z)=B\frac{\sin\lambda_n\sqrt{\dfrac{\rho'}{\mu'}}(h_2-h_1)\,.}{\cos\lambda_n\sqrt{\dfrac{\rho}{\mu}}h_1}\cos\lambda_n\sqrt{\frac{\rho}{\mu}}z\,, \tag{31'}$$

$$\phi_{2,\,n}(z)=B\sin\lambda_n\sqrt{\frac{\rho'}{\mu'}}(h_2-z)\,. \tag{29'}$$

Since $\phi_{1,\,n}(z)$ and $\phi_{2,\,n}(z)$ are the normalized functions, constant B can be determined by the condition

$$\int_0^{h_1}[\phi_{1,\,n}(z)]^2dz+\int_{h_1}^{h_2}[\phi_{2,\,n}(z)]^2dz=1\,. \tag{37}$$

From this condition, we find that

$$\frac{1}{B^2}=\frac{\sin^2\lambda_n\sqrt{\dfrac{\rho'}{\mu'}}(h_2-h_1)}{\cos^2\lambda_n\sqrt{\dfrac{\rho}{\mu}}h_1}\frac{1}{2\lambda_n}\sqrt{\frac{\mu}{\rho}}\left(\lambda_n\sqrt{\frac{\rho}{\mu}}h_1+\frac{1}{2}\sin 2\lambda_n\sqrt{\frac{\rho}{\mu}}h_1\right)$$
$$+\frac{1}{2\lambda_n}\sqrt{\frac{\mu'}{\rho'}}\left(\lambda_n\sqrt{\frac{\rho'}{\mu'}}(h_2-h_1)-\frac{1}{2}\sin 2\lambda_n\sqrt{\frac{\rho'}{\mu'}}(h_2-h_1)\right). \tag{38}$$

Thus, the "Eigenwerte" and "Eigenfunktionen" of the integral equation in the case of two stratified layers can be obtained. An integral equation to determine the forced oscillation of the two stratified layers can be obtained by substituting λ_n, $\phi_{1,\,n}(z)$, and $\phi_{2,\,n}(z)$ in that of (18). Further, in this case, $F(z)$ in (18) is expressed by

$$F(z)=K(z,0)\,T=\left\{\frac{\rho'}{\mu'}(h_2-h_1)+\frac{\rho}{\mu}(h_1-z)\right\}T\,. \tag{39}$$

Thus, we finally get

$$\frac{\phi(z)}{\dfrac{T}{v^2}}=\left\{\frac{m}{m'}(h_2-h_1)+(h_1-z)\right\}+\sum_{n=1}^{\infty}\frac{(\lambda_n^2-\lambda^2)\lambda^2-4\lambda^2\varepsilon'^2}{(\lambda_n^2-\lambda^2)^2+4\lambda^2\varepsilon'^2}\phi_{n'}(z)\,\cdot$$
$$\cdot\int_0^{h_2}\left\{\frac{m}{m'}(h_2-h_1)+(h_1-z)\right\}\phi_{n'}(z)\,dz$$
$$+\,i\sum_{n=1}^{\infty}\frac{2\varepsilon'\lambda\lambda_n^2\phi_{n'}(z)}{(\lambda_n^2-\lambda^2)^2+4\lambda^2\varepsilon'^2}\int_0^{h_2}\left\{\frac{m}{m'}(h_2-h_1)+(h_1-z)\right\}\phi_{n'}(z)\,dz\,, \tag{40}$$

where

$$\left.\begin{aligned}&v=\sqrt{\frac{\mu}{\rho}}\,,\quad m=\frac{\rho'}{\rho}\,,\quad m'=\frac{\mu'}{\mu}\,,\\&\phi_{n'}(z)=\phi_{1,\,n}(z)+\phi_{2,\,n}(z)\,.\end{aligned}\right\} \tag{41}$$

Let us now compute the following simple cases and ascertain the manner of the oscillations.

Example 1. Let the thickness of the first and the second layer be each 1 km and $\rho'=1{\cdot}5\rho$, $\mu'=3\mu$.

From (29′), (31′), (36), (38), we get the values of λ_n, $\phi_{1,n}(z)$ and $\phi_{2,n}(z)$ such that

$$\lambda_1=\frac{64{\cdot}3}{180}v\pi,\quad \phi_{1,1}(z)=1{\cdot}24\cos 64{\cdot}3\,z,\qquad \phi_{2,1}(z)=0{\cdot}75\sin 45{\cdot}65(2-z),$$

$$\lambda_2=\frac{149{\cdot}1}{180}v\pi,\quad \phi_{1,2}(z)=-1{\cdot}08\cos 149{\cdot}3\,z,\qquad \phi_{2,2}(z)=0{\cdot}96\sin 105{\cdot}86(2-z),$$

$$\lambda_3=\frac{265{\cdot}9}{180}v\pi,\quad \phi_{1,3}(z)=1{\cdot}26\cos 265{\cdot}9\,z,\qquad \phi_{2,3}(z)=0{\cdot}58\sin 188{\cdot}79(2-z),$$

$$\lambda_4=\frac{465}{180}v\pi,\quad \phi_{1,4}(z)=1{\cdot}26\cos 465\,z,\qquad \phi_{2,4}(z)=0{\cdot}65\sin 330{\cdot}15(2-z),$$

$$\lambda_5=\frac{591{\cdot}1}{180}v\pi,\quad \phi_{1,5}(z)=-1{\cdot}16\cos 591{\cdot}1\,z,\qquad \phi_{2,5}(z)=0{\cdot}85\sin 419{\cdot}68(2-z).$$

Thus we get the curves of the free oscillations of the layer in this case for $n=1, 2, 3$, and 4 as shown in Fig. 6. Since the periods of the free oscillations are the function of v, we can determine the values of λ_n, that is, T_n for various values of v. The values of T_n are as follows:

v (km/s)	λ_1	λ_2	λ_3	λ_4	T_1 (s)	T_2 (s)	T_3 (s)	T_4 (s)
0·8	0·89	2·08	3·72	6·49	7·04	3·01	1·69	0·67
1·0	1·12	2·60	4·65	8·12	5·62	2·42	1·35	0·78
1·5	1·68	3·90	6·95	12·15	3·74	1·61	0·91	0·52
2·0	2·24	5·20	9·30	16·24	2·80	1·21	0·68	0·39

The manner of free oscillation of the layer in the case of two stratified layers is more complicated than that in the case of one surface layer, especially as the forced oscillations at $z=0$ differ entirely from one another as shown in Fig. 7. As will be seen from Figs. 3

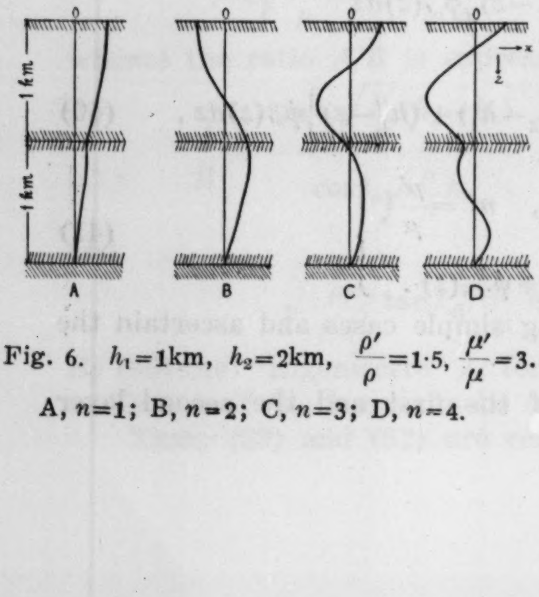

Fig. 6. $h_1=1\text{km}$, $h_2=2\text{km}$, $\frac{\rho'}{\rho}=1{\cdot}5$, $\frac{\mu'}{\mu}=3$.
A, $n=1$; B, $n=2$; C, $n=3$; D, $n=4$.

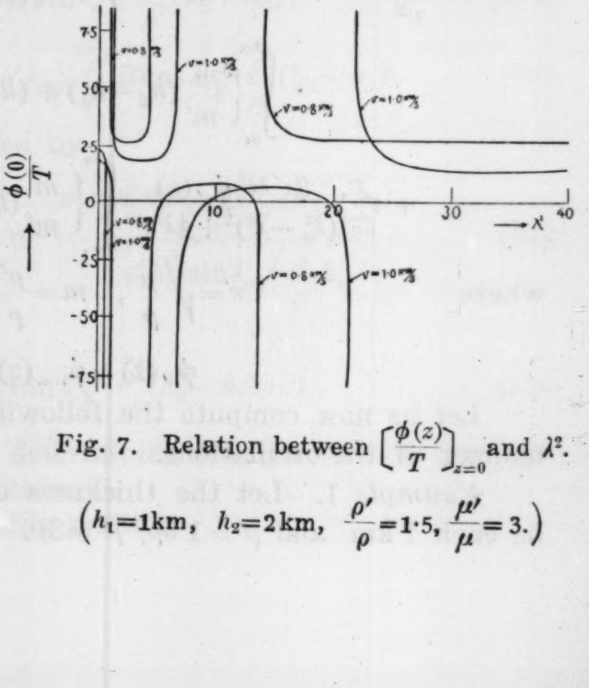

Fig. 7. Relation between $\left[\frac{\phi(z)}{T}\right]_{z=0}$ and λ^2.
$\left(h_1=1\text{km},\ h_2=2\text{km},\ \frac{\rho'}{\rho}=1{\cdot}5, \frac{\mu'}{\mu}=3.\right)$

and 7, in the case of one surface layer the amplitudes of oscillations change from $\phi(z)\rightarrow-\infty$ to $\phi(z)\rightarrow+\infty$, while in the case of two stratified layers, its amplitudes change from $\phi(z)\rightarrow+\infty$ to $\phi(z)\rightarrow+\infty$, or from $\phi(z)\rightarrow-\infty$ to $\phi(z)\rightarrow-\infty$.

Example 2. Let $h_1=0{\cdot}5\,\text{km}$, $h_2=1\,\text{km}$, $\rho=\rho'$, $\mu'=2\mu$. By similar treatment as Example 1, we have

$$\begin{aligned}
\lambda_1&=2{\cdot}02v, & \phi_{1,1}(z)&=1{\cdot}56\cos 116z, & \phi_{2,1}(z)&=1{\cdot}25\sin 81{\cdot}9(1-z),\\
\lambda_2&=5{\cdot}38v, & \phi_{1,2}(z)&=-1{\cdot}44\cos 308z, & \phi_{2,2}(z)&=1{\cdot}37\sin 217{\cdot}5(1-z),\\
\lambda_3&=9{\cdot}22v, & \phi_{1,3}(z)&=1{\cdot}25\cos 529z, & \phi_{2,3}(z)&=1{\cdot}17\sin 372{\cdot}9(1-z),\\
\lambda_4&=12{\cdot}90v, & \phi_{1,4}(z)&=-1{\cdot}16\cos 740z, & \phi_{2,4}(z)&=1{\cdot}16\sin 521{\cdot}8(1-z),\\
\lambda_5&=16{\cdot}38v, & \phi_{1,5}(z)&=1{\cdot}44\cos 939z, & \phi_{2,5}(z)&=1{\cdot}07\sin 662{\cdot}0(1-z).
\end{aligned}$$

The curves showing the free oscillations of the layer for $n=1, 2, 3$, and 4 are shown in Fig. 8, and those of the forced oscillations in Fig. 9. In this case, the periods of the free oscillations are as follows:

v (km/s)	λ_1	λ_2	λ_3	λ_4	T_1 (s)	T_2 (s)	T_3 (s)	T_4 (s)
0·8	1·62	4·30	7·38	10·33	3·87	1·46	0·85	0·61
1·8	2·02	5·38	9·22	12·90	3·10	1·17	0·68	0·49
1·5	3·02	8·06	13·84	19·34	2·08	0·78	0·46	0·33
2·0	4·04	10·76	18·44	25·80	1·56	0·59	0·34	0·24

In this case the values of T_n are smaller than that of the Example 1.

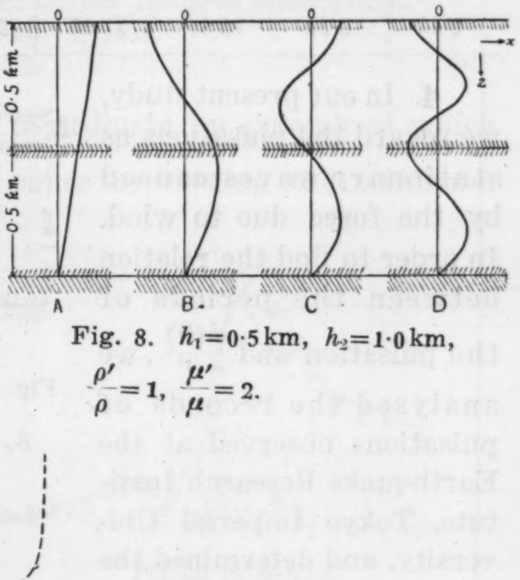

Fig. 8. $h_1=0{\cdot}5\,\text{km}$, $h_2=1{\cdot}0\,\text{km}$, $\dfrac{\rho'}{\rho}=1$, $\dfrac{\mu'}{\mu}=2$.

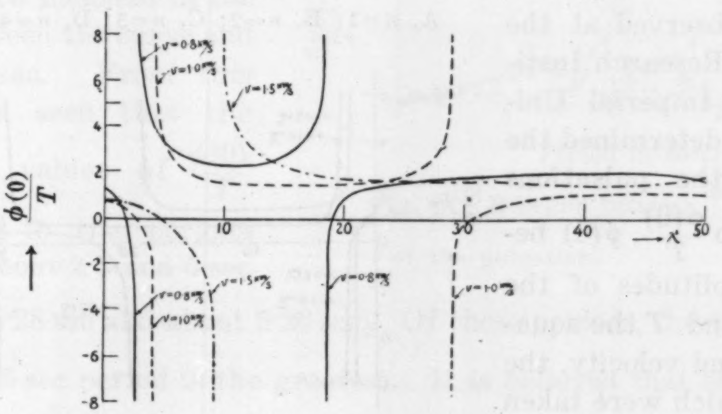

Fig. 9. Relation between $\left[\dfrac{\phi(z)}{T}\right]_{z=0}$ and λ^2.

$\left(h_1=0{\cdot}5\text{km},\ h_2=1\text{km},\ \dfrac{\rho'}{\rho}=1,\ \dfrac{\mu'}{\mu}=2.\right)$

Example 3. Let $h_1=0{\cdot}2\,\text{km}$, $h_2=1{\cdot}2\,\text{km}$, $\rho'=1{\cdot}1\rho$, $\mu'=2{\cdot}2\mu$. As before, we have

$$\lambda_1=1{\cdot}65v,\quad \phi_{1,1}(z)=1{\cdot}25\cos 112z,\quad \phi_{2,1}(z)=1{\cdot}18\sin 79{\cdot}5(1{\cdot}2-z),$$
$$\lambda_2=5{\cdot}45v,\quad \phi_{1,2}(z)=-1{\cdot}70\cos 312{\cdot}5z,\quad \phi_{2,2}(z)=1{\cdot}18\sin 221{\cdot}8(1{\cdot}2-z),$$
$$\lambda_3=8{\cdot}59v,\quad \phi_{1,3}(z)=1{\cdot}50\cos 492{\cdot}5z,\quad \phi_{2,3}(z)=1{\cdot}22\sin 349{\cdot}6(1{\cdot}2-z),$$
$$\lambda_4=12{\cdot}04v,\quad \phi_{1,4}(z)=-1{\cdot}32\cos 690z,\quad \phi_{2,4}(z)=1{\cdot}28\sin 633{\cdot}6(1{\cdot}2-z),$$
$$\lambda_5=15{\cdot}57v,\quad \phi_{1,5}(z)=1{\cdot}30\cos 892{\cdot}5z,\quad \phi_{2,5}(z)=1{\cdot}30\sin 784{\cdot}2(1{\cdot}2-z).$$

The curves showing the free oscillations of the layer for $n=1$, 2, 3, and 4 are plotted in Fig. 10 and those of forced oscillations in Fig. 11. In this case the periods of the free oscillations are as follows:

v (km/s)	λ_1	λ_2	λ_3	λ_4	T_1 (s)	T_2 (s)	T_3 (s)	T_4 (s)
0·8	1·32	4·36	6·87	9·62	4·75	1·44	0·92	0·65
1·0	1·65	5·45	8·59	12·04	3·80	1·15	0·73	0·52
1·5	2·47	8·17	12·88	18·06	2·55	0·77	0·49	0·35
2·0	3·30	10·90	17·15	24·08	1·90	0·62	0·37	0·25

4. In our present study, we regard the plusations as stationary waves caused by the force due to wind. In order to find the relation between the periods of the pulsation and $\frac{\phi(0)}{T}$, we analysed the records of pulsations observed at the Earthquake Research Institute, Tokyo Imperial University, and determined the periods of the pulsations and the ratio $\frac{\phi(0)}{T}$, $\phi(0)$ being the amplitudes of the pulsations, and T the square of the wind velocity, the values of which were taken from the weather-charts of the Central Meteorological Observatory. The instrument used was designed and constructed by Prof. M. Ishimoto, the magnification and the proper

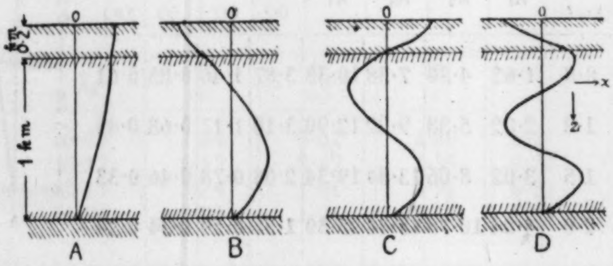

Fig. 10. $h_1=1\,\text{km}$, $h_2=1{\cdot}2\,\text{km}$, $\frac{\rho'}{\rho}=1{\cdot}1$, $\frac{\mu'}{\mu}=2{\cdot}2$.

A, $n=1$; B, $n=2$; C, $n=3$; D, $n=4$.

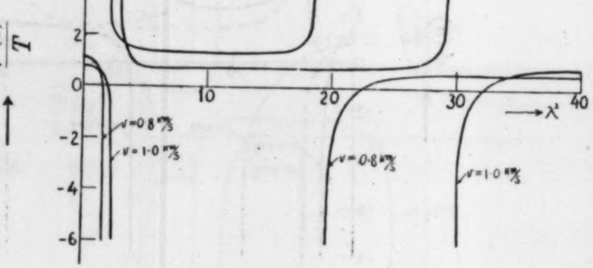

Fig. 11. Relation between $\left[\frac{\phi(z)}{T}\right]_{z=0}$ and λ^2.

$\left(h_1=0{\cdot}2\,\text{km},\ h_2=1{\cdot}2\,\text{km},\ \frac{\rho'}{\rho}=1{\cdot}1,\ \frac{\mu'}{\mu}=2{\cdot}2.\right)$

period of which are 400 and 1·0 sec respectively.

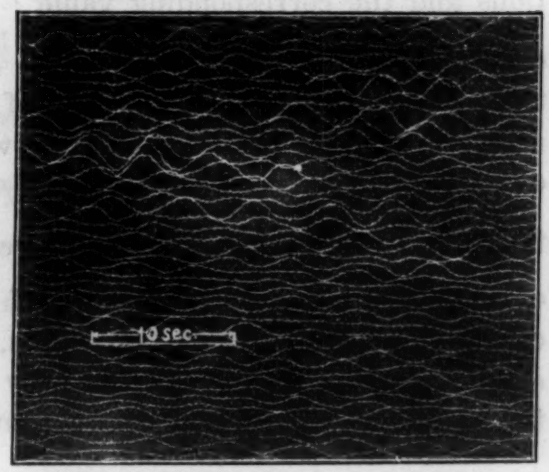

Fig. 12. Portion of actual record obtained by the Ishimoto seismograph. Jan. 1, 1935.

We used the most pronounced records obtained the instrument during the eight months, from August, 1934 to March, 1935. An example is shown in Fig. 12. Since the records represent the acceleration of the pulsatory oscillations of the earth's crust, we compute the displacements from the records by taking the constants of the instrument into consideration and assuming the actual displacement to be of the form of a simple harmonic motion. We take the periods of the pulsations as abscissa and the ratio $\frac{\phi(0)}{T}$ as ordinate, an example of which is shown in Fig. 13. We drew this curve by tracing the maximum values of $\frac{\phi(0)}{T}$ that correspond to a certain value of period by means of such consideration that all the points were included in the space between the curve and the abscissa. From this it will be seen that the maximum values of $\frac{\phi(0)}{T}$ correspond to the periods 0·3, 0·8, about 2·5 and 5 sec (or about 4·28 sec and about 5·20 sec). Of these periods, the value of $\frac{\phi(0)}{T}$ for about 5 sec period is the greatest. It is believed that the state that the value of $\frac{\phi(o)}{T}$ is the greatest is in that of resonance, where resonance means that the amplitude of pulsation becomes very great when the proper period of the layer agrees with the period of the applied forces. The pulsations of about 2·5 and 5 sec here seem to correspond to Omori's q- and Q-type.

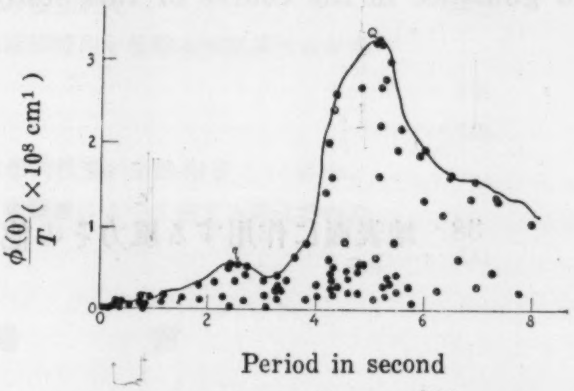

Fig. 13. Relation between $\frac{\phi(0)}{T}$ and period of the pulsation.

When we compare the relation between the periods of the pulsations and the corresponding value $\frac{\phi(0)}{T}$ with that in the case of the examples just mentioned, we shall be able to calculate the constant that is proportional to the square of the wind velocity, and the thickness of the layers besides. As will be seen from the foregoing examples, the larger the thickness of the layers, or the smaller the transverse velocity $\sqrt{\frac{\mu}{\rho}}$ in the layer, the longer is the proper period of their oscillations. Therefore, if the surface layers of the earth's crust were to consist of two layers, the pulsatory oscillations of the earth's crust may be explained by assuming that the thickness of the upper and lower layer are some hundreds of meters and about 1 km respectively, but if the values of $\sqrt{\frac{\mu}{\rho}}$ and $\sqrt{\frac{\mu'}{\rho'}}$ in the layers were smaller than those of the examples, the thickness of these two layers may become smaller than the said values.

In conclusion, the writer desires to express his cordial thanks to Professor Mishio Ishimoto and Dr. R. Takahasi for their kind advices and guidance in the course of this study.

---

38. 地表面に作用する風力その他によつて起される脈動

飯 田 汲 事

この論文は脈動を地表層の歪振動に關係づけて，理論的に地表面の振動問題を取扱つたのである．表面に作用する力によつて起される不均質彈性體の振動問題については，既に西村學士の詳しい計算がある．筆者はこれと同じ問題を積分方程式を用ひて解き，表面層が二つある場合をも求め，二三の簡單な例についてその解法を示した．最後に實際觀測された脈動の周期，振幅，風速との關係を圖示し，これらの圖と計算から得られた値とを比較する事によつて，地表面に働く摩擦力，及び表面層の厚さが夫々求め得られる事を附加しておいた．

39. 不連續面が彈性波の傳播に及ぼす影響(其の6)

(表面層を有する彈性體內の體自由波の生成及び傳播機構. 兩彈性體が境界に於て辷り得る場合)

地震研究所 西村源六郎
金井清

(昭和8年11月21日發表――昭和10年6月20日受理)

內容目次

頁
緒言……519
第1章 表面層を有する半無限固體內を無限長の調和波型縱彈性波が傳播する時の一般解……520
第1節 一般解……520
第2節 地表層の厚さ H, 入射波の波長 L に就て $H/L=0$ なる場合の地表層の振動研究……523
第2章 表面層を有する半無限固體內を衝擊波型縱彈性波が傳播する時の一般解……526
第1節 一般解……526
第2節 兩彈性體の彈性力學的性質が全然相等しい場合, $\theta=30^\circ$ で入射する衝擊波によつて生ずる彈性體內の自由波問題……531

緒言

表面層と其の下にある半無限彈性體との境界に於て，兩彈性體の垂直分應力と垂直分變位とが連續であつて，接面變位及び剪斷分應力が不連續になつてゐる場合の彈性波動問題の研究は，既に初入射波（縱彈性波）が圓函數的な無限長の場合に就て行つた.1) 殊に兩彈性體の密度，彈性係數が全く相等しい場合にも表面層內には重複反射の現象が現はれ，不連續面を境として波動現象に種々の特性のある事を見出した. 尙かゝる場合に於ける地表面に於ける初動の問題に就ては簡單な計算を行つた事がある.2)

---

1) 西村源六郎，金井清　地震研究所彙報 11 (1934), 595.
2) 西村源六郎，金井清　地震研究所彙報 11 (1934), 123.

本論文では第1章に於ては前論文と同じく境界面に於て兩彈性體の相互辷動を許す場合，初入射波が圓函數的な無限長の縦彈性波である場合の研究を再び行ひ，第2章ではフーリエの2重積分公式を利用して第1章の結果を一般化し，衝擊波型の初入射波の場合，兩彈性體內に於ける波動問題を解決した.

第1章　表面層を有する半無限固體內に無限長の調和波型縦彈性波が傳播入射する時の一般解

第1節　一般解

今厚さ H なる表面層，及びその下の媒體の密度，彈性係數を夫々 ρ', λ', μ' 及び ρ, λ, μ と考へる. 直角坐標 (x, y) の原點 0 は兩彈性體の境面上に置き，x 軸はこの不連續面上に，y 軸はこれに直角に採り，上向きを正とする.

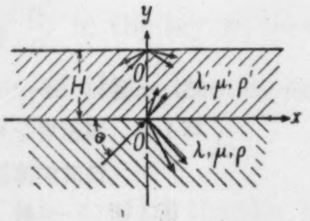

第 1 圖

今 $y<0$ なる媒體に於ける初入射波（縦彈性波）

$$\phi_0 = a e^{i(pt-fx-ry)} \qquad (1)$$

によつて誘起される兩彈性體內の波動問題を解決するのであるが，a は調和波の振動振幅を表はし，f, r に就ては $r^2=\rho p^2/(\lambda+2\mu)-f^2$ なる關係がある. 尙 p に就てはこの入射波の振動週期を T_0 とすれば，$p=2\pi/T_0$ である. (1) なる自由波の入射の爲め地表層及び其の下の媒體中には地表面及び兩彈性體の境界面に於ける彈性力學的條件を滿足する樣な强さを持つ種々の自由波が起されるのであるが，$y<0$ の媒體中には，$y=0$ で反射される縦，横兩彈性波 ϕ_1, ψ_1，地表層內には，$y=0$，$y=H$ なる2面で反射或は屈折する縦，横兩彈性波 $\phi_1', \psi_1', \phi_2', \psi_2'$ を生じ，初入射波と釣合ふのである. 即ち

$$\phi_1 = A'e^{i(pt-fx+ry)}, \qquad \psi_2 = B'e^{i(pt-fx+sy)}, \qquad (2)$$

$$\phi_1' = Ce^{i(pt-fx+r'y)}, \qquad \psi_2' = Ee^{i(pt-fx+s'y)}, \qquad (3)$$

$$\phi_1'' = De^{i(pt-fx-r'y)}, \qquad \psi_2'' = Fe^{i(pt-fx-s'y)}. \qquad (4)$$

勿論これ等調和波は彈性體波動方程式 $\dfrac{\partial^2\phi}{\partial t^2}=\varkappa\nabla^2\phi$，$\dfrac{\partial^2\psi}{\partial t^2}=\varkappa'\nabla^2\psi$ を滿足するものであつて，その强さを決定する A′, B′, C, D, E, F なる6個の常數は境界條件より決定されるものであり，s, r', s' に就ては次の關係あり.

$$s^2=\rho p^2/\mu-f^2, \quad r'^2=\rho' p^2/(\lambda'+2\mu')-f^2, \quad s'^2=\rho' p^2/\mu'-f^2.$$

勿論 ϕ, ϕ_1 の傳播速度は $\{(\lambda+2\mu)/\rho\}^{1/2}$, ψ_1 の傳播速度は $(\mu/\rho)^{1/2}$ である. ϕ_1', ϕ_2' の傳播速度は $\{(\lambda'+2\mu')/\rho'\}^{1/2}$, ψ_1', ψ_2' は $(\mu'/\rho')^{1/2}$ なる傳播速度を有す.

今 x 軸, y 軸方向の變位 u, v を (1), (2), (3), 及び (4) より求める事は容易である. 一般に縱波 ϕ に就ては $u=\dfrac{\partial\phi}{\partial x}$, $v=\dfrac{\partial\phi}{\partial y}$, 横波に就ては, $u=\dfrac{\partial\psi}{\partial y}$, $v=-\dfrac{\partial\psi}{\partial x}$ なる關係で變位は表されるものである. この關係より, (1) に就ては

$$u_0=-if\alpha e^{i(pt-fx-ry)}, \qquad v_0=-ir\alpha e^{i(pt-fx-ry)}, \tag{5}$$

(2) なる ϕ_1, ψ_2 よりは

$$u_1=-ifA'e^{i(pt-fx+ry)}, \qquad v_1=irA'e^{i(pt-fx+ry)}, \tag{6}$$

$$u_2=isB'e^{i(pt-fx+sy)}, \qquad v_2=ifB'e^{i(pt-fx+sy)}, \tag{7}$$

(3) の ϕ_1', ψ_2' よりは

$$u_1'=-ifCe^{i(pt-fx+r'y)}, \qquad v_1'=ir'Ce^{i(pt-fx+r'y)}, \tag{8}$$

$$u_2'=is'Ee^{i(pt-fx+s'y)}, \qquad v_2'=ifEe^{i(pt-fx+s'y)}, \tag{9}$$

(4) の ϕ'', ψ_2'' よりは

$$u_1''=-ifDe^{i(pt-fx-r'y)}, \qquad v_1''=-ir'De^{i(pt-fx-r'y)}, \tag{10}$$

$$u_2''=-is'Fe^{i(pt-fx-s'y)}, \qquad v_2''=ifFe^{i(pt-fx-s'y)}. \tag{11}$$

扨て $y=0$ なる境に於て, 全然剪斷應力が現はれない場合[3] 卽ち辷りを許す場合には,

$$\left.\begin{aligned} &V=V',\ \lambda\left(\frac{\partial U}{\partial x}+\frac{\partial V}{\partial y}\right)+2\mu\frac{\partial V}{\partial y}=\lambda'\left(\frac{\partial U'}{\partial x}+\frac{\partial V'}{\partial y}\right)+2\mu'\frac{\partial V'}{\partial y},\\ &\quad\frac{\partial V}{\partial x}+\frac{\partial U}{\partial y}=0,\quad \frac{\partial V'}{\partial x}+\frac{\partial U'}{\partial y}=0. \end{aligned}\right\} \tag{12}$$

を $y=0$ なる面で滿足し, $y=H$ なる表面に於ては

$$\frac{\partial V'}{\partial x}+\frac{\partial U'}{\partial y}=0,\ \lambda'\left(\frac{\partial U'}{\partial x}+\frac{\partial V'}{\partial y}\right)+2\mu'\frac{\partial V'}{\partial y}=0 \tag{13}$$

を滿足する様に, (5)~(11) の A′, B′, C, D, E, F を調節するのである. (12), (13) に於て

$$\left.\begin{aligned} &U=u_0+u_1+u_2, &&V=v_0+v_1+v_2,\\ &U'=u_1'+u_2'+u_1''+u_2'', &&V'=v_1'+v_2'+v_1''+v_2'' \end{aligned}\right\} \tag{14}$$

---

[3] $y=0$ の面で辷りを許すが, 摩擦抵抗のある場合の計算は次の機會に讓つて置く.

然る時は

$$
\begin{aligned}
\Delta = & -\frac{r}{f}\left(1+\frac{s^2}{f^2}\right)\frac{\mu'}{\mu}\left[-32\frac{r's'}{f^2}\left(1+\frac{s'^2}{f^2}\right)^2\right. \\
& +\left\{\left(1-\frac{s'^2}{f^2}\right)^2+4\frac{r's'}{f^2}\right\}^2\left\{e^{-i(r'+s')H}+e^{i(r'+s')H}\right\} \\
& \left.-\left\{\left(1-\frac{s'^2}{f^2}\right)^2-4\frac{r's'}{f^2}\right\}^2\left\{e^{-i(r'-s')H}+e^{i(r'-s')H}\right\}\right] \\
& -\frac{r'}{f}\left(1+\frac{s'^2}{f^2}\right)\left\{\left(1-\frac{s^2}{f^2}\right)^2+4\frac{rs}{f^2}\right\}\left[\left\{\left(1-\frac{s'^2}{f^2}\right)^2+4\frac{r's'}{f^2}\right\}\left\{e^{-i(r'+s')H}-e^{i(r'+s')H}\right\}\right. \\
& \left.-\left\{\left(1-\frac{s'^2}{f^2}\right)^2-4\frac{r's'}{f^2}\right\}\left\{e^{i(r'-s')H}-e^{i(r'-s')H}\right\}\right]
\end{aligned}
\tag{15}
$$

と置く時，

$$
\begin{aligned}
\frac{\Delta}{\mathfrak{a}}A' = & -\frac{r}{f}\left(1-\frac{s^2}{f^2}\right)\left[-32\frac{r's'}{f^2}\left(1-\frac{s'^2}{f^2}\right)^2\right. \\
& +\left\{\left(1-\frac{s'^2}{f^2}\right)^2+4\frac{r's'}{f^2}\right\}^2\left\{e^{-i(r'+s')H}+e^{i(r'+s')H}\right\} \\
& \left.-\left\{\left(1-\frac{s'^2}{f^2}\right)^2-4\frac{r's'}{f^2}\right\}^2\left\{e^{-i(r'-s')H}+e^{i(r'-s')H}\right\}\right] \\
& +\frac{r'}{f}\left(1+\frac{s'^2}{f^2}\right)\left\{\left(1-\frac{s^2}{f^2}\right)^2-4\frac{rs}{f^2}\right\}\left[\left\{\left(1-\frac{s'^2}{f^2}\right)^2+4\frac{r's'}{f^2}\right\}\left\{e^{-i(r'+s')H}-e^{i(r'+s')H}\right\}\right. \\
& \left.-\left\{\left(1-\frac{s'^2}{f^2}\right)^2-4\frac{r's'}{f^2}\right\}\left\{e^{-i(r'-s')H}-e^{i(r'-s')H}\right\}\right],
\end{aligned}
\tag{16}
$$

$$
\begin{aligned}
\frac{\Delta}{\mathfrak{a}}B' = & 4\frac{r}{f}\left(1-\frac{s^2}{f^2}\right)\frac{r'}{f}\left(1+\frac{s'^2}{f^2}\right)\left[\left\{\left(1-\frac{s'^2}{f^2}\right)^2+4\frac{r's'}{f^2}\right\}\left\{e^{-i(r'+s')H}-e^{i(r'+s')H}\right\}\right. \\
& \left.-\left\{\left(1-\frac{s'^2}{f^2}\right)^2-4\frac{r's'}{f^2}\right\}\left\{e^{-i(r'-s')H}-e^{-i(r'-s')H}\right\}\right],
\end{aligned}
\tag{17}
$$

$$
\begin{aligned}
\frac{\Delta}{\mathfrak{a}}C = & 2\frac{r}{f}\left(1-\frac{s^2}{f^2}\right)\left(1+\frac{s^2}{f^2}\right)\left(1-\frac{s'^2}{f^2}\right)\left[8\frac{r's'}{f^2}-\left\{\left(1-\frac{s'^2}{f^2}\right)^2+4\frac{r's'}{f^2}\right\}e^{-i(r'+s')H}\right. \\
& \left.+\left\{\left(1-\frac{s'^2}{f^2}\right)^2-4\frac{r's'}{f^2}\right\}e^{-i(r'-s')H}\right],
\end{aligned}
\tag{18}
$$

$$\frac{\Delta}{\mathfrak{a}}D=-2\frac{r}{f}\left(1-\frac{s'^2}{f^2}\right)\left(1+\frac{s^2}{f^2}\right)\left(1-\frac{s'^2}{f^2}\right)\left[-8\frac{r's'}{f^2}-\left\{\left(1-\frac{s'^2}{f^2}\right)^2-4\frac{r's'}{f^2}\right\}e^{i(r'-s')H}\right.$$

$$\left.+\left\{\left(1-\frac{s'^2}{f^2}\right)^2+4\frac{r's'}{f^2}\right\}e^{i(r'+s')H}\right],\qquad(19)$$

$$\frac{\Delta}{\mathfrak{a}}E=4\frac{rr'}{f^2}\left(1-\frac{s^2}{f^2}\right)\left(1+\frac{s^2}{f^2}\right)\left[-2\left(1-\frac{s'^2}{f^2}\right)^2+\left\{\left(1-\frac{s'^2}{f^2}\right)^2+4\frac{r's'}{f^2}\right\}e^{-i(r'+s')H}\right.$$

$$\left.+\left\{\left(1-\frac{s'^2}{f^2}\right)^2-4\frac{r's'}{f^2}\right\}e^{i(r'-s')H}\right],\qquad(20)$$

$$\frac{\Delta}{\mathfrak{a}}F=-4\frac{rr'}{f^2}\left(1-\frac{s^2}{f^2}\right)\left(1+\frac{s^2}{f^2}\right)\left[-2\left(1-\frac{s'^2}{f^2}\right)^2+\left\{\left(1-\frac{s'^2}{f^2}\right)^2-4\frac{r's'}{f^2}\right\}e^{-i(r'-s')H}\right.$$

$$\left.+\left\{\left(1-\frac{s'^2}{f^2}\right)^2+4\frac{r's'}{f^2}\right\}e^{i(r'+s')H}\right]\qquad(21)$$

によつて，常數從つて各自由波の强さは決定されるのであるが，これ等は縱橫兩彈性波の傳播速度 $\sqrt{(\lambda+2\mu)/\rho}$ ，$\sqrt{\mu/\rho}$，$\sqrt{(\lambda'+2\mu')/\rho'}$，$\sqrt{\mu'/\rho'}$ 及び，入射角，層の厚さ H，彈性係數，或は入射波の波長の超越函數として表されてゐるのである．(16)～(21) を (6)～(11) に夫々代入する時，初めて，(5) なる調和函數的な入射波による彈性體內の波動問題を解決し得るのである．これ等に關する數値計算的な研究は特殊な場合に就て旣にその一部を報告しておいた[4]．數値計算による詳細の報告は次の時機に讓つて置く．次に地表面の振動問題を解決して置く．

第２節　地表層の厚さ H，入射波の波長 L に就て $H/L=0$ なる場合の地表層の振動研究

第１節の解析結果を實際問題と關係づける場合には地震波の波長は層の厚さに比して非常に長いとするのがよい場合がある．層の厚さ H に比し入射波の波長 L が非常に大きくその極端の場合として $H/L=0$ なる時の波動問題を論じて置く．

扨て $r'H$ 及び $s'H$ は次の關係で與へられるものである．

$$r'H\quad 2\pi\cos\theta\left\{\left(\frac{V_1}{V_1'}\right)^2\sec^2\theta-1\right\}^{1/2}\frac{H}{L},\quad s'H=2\pi\cos\theta\left\{\left(\frac{V_1}{V_2'}\right)^2\mathrm{ses}^2\theta-1\right\}^{1/2}\frac{H}{L}.(22)$$

---

4)　西村源六郎，金井清　地震研究所彙報 11 (1933)，595～631.

但し θ は初入射波の入射角であり，L はこの波の波長，V_1，V_1'，V_2' は夫々縦横兩彈性波の地表層及びその下の媒體内での傳播速度であつて，

$$V_1=\sqrt{\frac{\lambda+2\mu}{\rho}}\,,\quad V_1'=\sqrt{\frac{\lambda'+2\mu'}{\rho}}\,,\quad V_2'=\sqrt{\frac{\mu'}{\rho'}}$$

である．(22) の關係を利用し，$H/L=0$ の時には (15)～(21) より，常數 A', B', C, D, E 及び F は次の樣になる，($H/L=0$ の時はこれ等常數は不定形の極限値として求める必要がある.)

$$\left.\begin{aligned}
&A'=-\frac{\left\{\left(1-\frac{s^2}{f^2}\right)^2-1\frac{rs}{f^2}\right\}}{\left\{\left(1-\frac{s^2}{f^2}\right)^2+4\frac{rs}{f^2}\right\}}\mathfrak{a}\,,\quad B'=-4\frac{\frac{r}{f}\left(1-\frac{s^2}{f^2}\right)}{\left\{\left(1-\frac{s^2}{f^2}\right)^2+4\frac{rs}{f^2}\right\}}\mathfrak{a},\\
&C=-D=\frac{\frac{r}{f}\left(1-\frac{s^2}{f^2}\right)\left(1+\frac{s^2}{f^2}\right)\left(1-\frac{s'^2}{f^2}\right)}{\frac{r'}{f}\left(1+\frac{s'^2}{f^2}\right)\left\{\left(1-\frac{s^2}{f^2}\right)^2+4\frac{rs}{f^2}\right\}}\mathfrak{a}\,,\\
&E=F=-2\frac{\frac{r}{f}\left(1-\frac{s^2}{f^2}\right)\left(1+\frac{s^2}{f^2}\right)}{\left(1+\frac{s'^2}{f^2}\right)\left\{\left(1-\frac{s^2}{f^2}\right)^2+4\frac{rs}{f^2}\right\}}\mathfrak{a}.
\end{aligned}\right\}\quad(23)$$

(23) を (6), (7), (8), (9), (10) 及び (11) に代入する事によつて，地表層の厚さ H に比して (5) なる入射波の波長が無限に長い場合の波動問題は (14) により解決せられる．即ち $\frac{y}{L}\geq\frac{H}{L}$ である事を注意すれば (8), (9), (10), (11) より定狀態になれば地表層には全然水平方向の運動は見られなくなり，次式で與へられる垂直方向の運動のみが起される事が解かる．

$$V'=i\frac{2\pi}{L}\mathfrak{A}\cos\theta\frac{\frac{r}{f}\left(1-\frac{s^2}{f^2}\right)\left(1+\frac{s^2}{f^2}\right)}{\frac{r'}{f}\left(1+\frac{s'^2}{f^2}\right)\left\{\left(1-\frac{s^2}{f^2}\right)^2+4\frac{rs}{f^2}\right\}}$$

$$\cdot\left[\left(1-\frac{s'^2}{f^2}\right)\left\{\left(\frac{V_1}{V_1'}\right)^2\sec^2\theta-1\right\}^{1/2}-4\frac{r'}{f}\right]e^{i(pt-fx)}\,.\qquad(24)$$

尙地表層と下媒體との境では水平方向の運動は不連續であつて，地表層には水平運動はなく（24）で見る如き上下運動のみであるが，下の媒體の $y=0$ の面では次の如き運動が起つてゐるのである．

$$\left.\begin{aligned}
U_{y=0}&=-i\frac{2\pi}{L}\,\mathfrak{a}\cos\theta\left[1-\frac{\left\{\left(1-\dfrac{s^2}{f^2}\right)^2-4\dfrac{rs}{f^2}\right\}}{\left\{\left(1-\dfrac{s^2}{f^2}\right)^2+4\dfrac{rs}{f^2}\right\}}\right.\\
&\qquad\left.+\frac{4\dfrac{r}{f}\left(1-\dfrac{s^2}{f^2}\right)}{\left\{\left(1-\dfrac{s^2}{f^2}\right)^2+4\dfrac{rs}{f^2}\right\}}\left\{\left(\frac{V_1}{V_2}\right)^2\mathrm{ses}^2\theta-1\right\}^{1/2}\right]e^{i(pt-fx)},\\
V_{y=0}&=-i\frac{2\pi}{L}\,\mathfrak{a}\sin\theta\left[1+\frac{\left\{\left(1-\dfrac{s^2}{f^2}\right)^2-4\dfrac{rs}{f^2}\right\}}{\left\{\left(1-\dfrac{s^2}{f^2}\right)^2+4\dfrac{rs}{f^2}\right\}}\right.\\
&\qquad\left.+\frac{4\dfrac{r}{f}\left(1-\dfrac{s^2}{f^2}\right)}{\left\{\left(1-\dfrac{s^2}{f^2}\right)^2+4\dfrac{rs}{f^2}\right\}}\cot\theta\right]e^{i(pt-tr)}
\end{aligned}\right\}\quad(25)$$

（25）より明かな樣に境界面では，$H/L=0$ の場合には分子運動の軌跡は直線的であつて，而もその軌跡の大きさを支配するものは，單に入射波の大きさ $\mathfrak{a}$，入射角 θ，そして，下の媒體の密度，彈性係數 $\left(\text{或は縱橫の兩波の傳播速度}\sqrt{\dfrac{\lambda+2\mu}{\rho}},\ \sqrt{\dfrac{\mu}{\rho}}\right)$ のみであつて，表面層の厚さ，その密度 ρ'，彈性係數 λ'，μ' は全然これには關係しないものであり，且つ入射波の波長 L も無關係である．尙 $H/L=0$ の時には下の媒體內何れの點の運動にも表面層の λ'，μ'，及び ρ' 或は H が關係しない事は（23）に於て A'，B' の式を見れば明かな事であつて，$y=0$ 面で反射されて生ずる縱橫兩彈性波 ϕ_1，ψ_2 の强さを支配するものは（23）の A'，B' のみであつて，地表層の λ'，μ'，ρ' が無關係である事は注意を要す．然るに地表層の運動の振幅は單に λ'，μ'，ρ' のみならず，下の媒體の λ，μ 及び ρ，そして勿論入射波の入射角 θ 及びその强さ $\mathfrak{a}$，波長 L の大きさによつて支配されるものである．

これ等の結果より見て，$H/L=0$ の時には，定狀態では表面層內には橫波の形式をとつて，單に分子の上下運動のみが，下媒體內の縱波の速度 V_1 で水平方向に傳播する事が（24）より見られる．勿論その波長は入射波の波長 L に等しい．尙表面層內の

運動軌跡は直線で垂直方向のみであるが，下の媒體内で $y\geqq L$ の様な深さの所では一般には楕圓運動になり，$y\leqq L$ の様な所卽ち $y=0$ 面に近づくに從つて，軌跡は直線運動となり，$y=0$ 面では（25）より

$$\left\{2-\left(\frac{V_1}{V_2}\right)^2\sec^2\theta\right\}U_{y=0}-2\tan\theta\left\{\left(\frac{V_1}{V_2}\right)^2\sec^2\theta-1\right\}^{1/2}V_{y=0}=0 \tag{26}$$

なる軌跡を畫く事が容易に解かる．尙水平軸 x とこの（26）なる振動軌跡のなす角卽ちこの直線運動の水平軸に對する傾きを α とする時

$$\alpha=\tan^{-1}\frac{2-\left(\dfrac{V_1}{V_2}\right)^2\sin^2\theta}{2\tan\theta\sqrt{\left(\dfrac{V_1}{V_2}\right)^2\sec^2\theta-1}} \tag{27}$$

によつて決定される．

以上によつて $H/L=0$ の時の解析的研究は終へる．$H/L>0$ なる場合には地表層内の運動は可なり複雜で，一般にその運動軌跡は楕圓形をとる樣になり，且つその短軸，長軸の長さが入射角 θ，H/L，V_1，V_2，V_1'，V_2' の超越函數式で表されるのである．既に $V_1=V_1'$，$V_2=V_2'$ の場合に就ては多少その研究結果を圖をもつて示して置いた[5]．

第２章　表面層を有する半無限固體内を衝擊波型縱彈性波が傳播する時の一般解

第１節　一般解

前章第１節で求めた一般解をフーリエの積分公式を利用して，任意の形をした波形が θ なる入射角で $y=0$ なる面に入射する場合の解を求める事とする．この初入射波 ϕ_0 が

$$\phi_0=F(x,y) \tag{28}$$

なる波形を持つてゐるものとすれば，

$$\phi_0=\frac{1}{4\pi^2}\int_{-\infty}^{\infty}e^{i\frac{V_1t}{\cos\theta}f}df\int_{-\infty}^{\infty}dr\int_{-\infty}^{\infty}d\xi\int_{-\infty}^{\infty}F(\xi,\eta)e^{-i(f(x-\xi)+r(y-\eta))}d\eta \tag{29}$$

によつて，入射波は示めされる事は（１）より容易に解かる．從つて第１章の結果を參照して，

---

[5] 西村源六郎，金井清　地震研究所彙報　11（933），595～631.

$$\phi_1=\frac{1}{4\pi^2}\int_{-\infty}^{\infty}e^{i\frac{V_1t}{\cos\theta}f}\frac{A'}{\mathfrak{a}}df\int_{-\infty}^{\infty}dr\int_{-\infty}^{\infty}d\xi\int_{-\infty}^{\infty}F(\xi,\eta)e^{-i\{f(x-\xi)-r(y+\eta)\}}\,d\eta\,, \tag{30}$$

$$\psi_2=\frac{1}{4\pi^2}\int_{-\infty}^{\infty}e^{i\frac{V_1t}{\cos\theta}f}\frac{B'}{\mathfrak{a}}df\int_{-\infty}^{\infty}dr\int_{-\infty}^{\infty}d\xi\int_{-\infty}^{\infty}F(\xi,\eta)e^{-i\left[f(x-\xi)-r\left\{\frac{\sqrt{\left(\frac{V_1}{V_2}\right)^2-\cos^2\theta}}{\sin\theta}y+\eta\right\}\right]}d\eta\,, \tag{31}$$

$$\phi'_1=\frac{1}{4\pi^2}\int_{-\infty}^{\infty}e^{i\frac{V_1t}{\cos\theta}f}\frac{C}{\mathfrak{a}}df\int_{-\infty}^{\infty}dr\int_{-\infty}^{\infty}d\xi\int_{-\infty}^{\infty}F(\xi,\eta)e^{-i\left[f(x-\xi)-r\left\{\frac{\sqrt{\left(\frac{V_1}{V'_1}\right)^2-\cos^2\theta}}{\sin\theta}y+\eta\right\}\right]}d\eta, \tag{32}$$

$$\psi'_2=\frac{1}{4\pi^2}\int_{-\infty}^{\infty}e^{i\frac{V_1t}{\cos\theta}f}\frac{E}{\mathfrak{a}}df\int_{-\infty}^{\infty}dr\int_{-\infty}^{\infty}d\xi\int_{-\infty}^{\infty}F(\xi,\eta)e^{-i\left[f(x-\xi)-r\left\{\frac{\sqrt{\left(\frac{V_1}{V'_2}\right)^2-\cos^2\theta}}{\sin\theta}y+\eta\right\}\right]}d\eta, \tag{33}$$

$$\phi''_1=\frac{1}{4\pi^2}\int_{-\infty}^{\infty}e^{i\frac{V_1t}{\cos\theta}f}\frac{D}{\mathfrak{a}}df\int_{-\infty}^{\infty}dr\int_{-\infty}^{\infty}d\xi\int_{-\infty}^{\infty}F(\xi,\eta)e^{-i\left[f(x-\xi)+r\left\{\frac{\sqrt{\left(\frac{V_1}{V'_1}\right)^2-\cos^2\theta}}{\sin\theta}y-\eta\right\}\right]}d\eta, \tag{34}$$

$$\psi''_2=\frac{1}{4\pi^2}\int_{-\infty}^{\infty}e^{i\frac{V_1t}{\cos\theta}f}\frac{F}{\mathfrak{a}}df\int_{-\infty}^{\infty}dr\int_{-\infty}^{\infty}d\xi\int_{-\infty}^{\infty}F(\xi,\eta)e^{-i\left[f(x-\xi)+r\left\{\frac{\sqrt{\left(\frac{V_1}{V'_2}\right)^2-\cos^2\theta}}{\sin\theta}y-\eta\right\}\right]}d\eta. \tag{35}$$

(30)~(35) に於て，$A'/\mathfrak{a}$，$B'/\mathfrak{a}$，$C/\mathfrak{a}$．$E/\mathfrak{a}$，$D/\mathfrak{a}$ 及び $F/\mathfrak{a}$ は夫々入射角 θ，傳播速度 $\sqrt{\frac{\lambda+2\mu}{\rho}}$，$\sqrt{\frac{\mu}{\rho}}$，$\sqrt{\frac{\lambda+2\mu}{\rho'}}$ 及び $\sqrt{\frac{\mu'}{\rho'}}$ の函數であつて，

$$\left.\begin{aligned}
&a=\tan e,\ b=\left\{\left(\frac{V_1}{V_2}\right)^2\sec^2e-1\right\}^{1/2},\quad a'=\left\{\left(\frac{V_1}{V'_1}\right)^2\sec^2e-1\right\}^{1/2},\\
&b'=\left\{\left(\frac{V_1}{V'_2}\right)^2\sec^2e-1\right\}^{1/2},\ c=\left(\frac{V_1}{V_2}\right)^2\sec^2e,\quad d=2-\left(\frac{V_1}{V_2}\right)^2\sec^2e\,,\\
&c'=\left(\frac{V_1}{V'_2}\right)^2\sec^2e,\quad d'=2-\left(\frac{V_1}{V'_2}\right)^2\sec^2e
\end{aligned}\right\} \tag{36}$$

と置けば，

$$\frac{A'}{\mathfrak{a}}=-\frac{ad}{\Delta}\Big[-32\,a'b'd'^2e^{i(a'+b')fH}+(d'^2+4a'b')^2\{1+e^{i2(a'+b')fH}\}$$
$$-(d'^2-4a'b')^2\{e^{i2b'fH}+e^{i2a'fH}\}\Big]$$

$$+\frac{a'c'(d^2-4ab)}{\Delta}\Big[(d'^2+4a'b')\{1-e^{2i(a'+b')fH}\}$$

$$-(d'^2-4a'b')\{e^{i2b'fH}-e^{i2afH}\}\Big], \tag{37}$$

$$\frac{B'}{\mathfrak{a}}=\frac{4aa'dc'}{\Delta}\Big[(d'^2+4a'b')\{1-e^{i2(a'+b')fH}\}$$

$$-(d'^2-4a'b')\{e^{i2b'fH}-e^{i2a'fH}\}\Big], \tag{38}$$

$$\frac{C}{\mathfrak{a}}=\frac{2acdd'}{\Delta}\Big[-(d'^2+4a'b')8a'b'e^{i(a'+b')fH}$$

$$+(d'^2-4a'b')e^{i2b'fH}\Big], \tag{39}$$

$$\frac{D}{\mathfrak{a}}=-\frac{2acdd'}{\Delta}\Big[-8a'b'e^{i(a'+b')fH}+(d'^2+4a'b')e^{i2(a'+b')fH}$$

$$-(d'^2-4a'b')e^{i2a'fH}\Big], \tag{40}$$

$$\frac{E}{\mathfrak{a}}=\frac{4aa'cd}{\Delta}\Big[(d'^2+4a'b')-2d'^2e^{i(a'+b')fH}$$

$$+(d'^2-4a'b')e^{i2a'fH} \tag{41}$$

$$\frac{F}{\mathfrak{a}}=-\frac{4aa'cd}{\Delta}\Big[(d'^2-4a'b')+(d^2+4a'b')e^{i2(a'+b')fH}$$

$$-2d'^2e^{i(a'+b')fH}\Big], \tag{42}$$

但し

$$\Delta=\alpha+\beta e^{i(a'+b')fH}+\gamma e^{i2(a'+b')fH}+\delta e^{i2a'fH}+\varepsilon e^{i2b'fH} \tag{43}$$

であつて，

$$\left.\begin{aligned}
\alpha&=-ac(d'^2+4a'b')^2\frac{\mu'}{\mu}-a'c'(d^2+4ad)(d'^2+4a'b'),\\
\beta&=32aa'b'cd'^2\frac{\mu'}{\mu},\\
\gamma&=-ac(d'^2+4a'b')^2\frac{\mu'}{\mu}+a'c'(d^2+4ab)(d'^2+4a'b'),\\
\delta&=ac(d'^2-4a'b')^2\frac{\mu'}{\mu}+a'c'(d^2+4ab)(d'^2-4a'b'),\\
\varepsilon&=ac(d'^2-4a'b')^2\frac{\mu'}{\mu}-a'c'(d^2+4ab)(d'^2-4a'b').
\end{aligned}\right\} \tag{44}$$

玆に於て (37)~(44) を見る時，(30)~(35) に於ける f に關する積分に於ては分母分子が f の圓函數より成る超越函數である事が理解される.（分母の形は (43) で與へられてゐる.）從つて，この項を $e^{ia'fH}$, $e^{ib'fH}$ の冪級數に展開するのであるが，この爲めには (43) の逆式である $1/\varDelta$ を展開すれば充分である事がわかる．即ち $1/\varDelta$ を展開すれば，

$$
\begin{aligned}
\frac{1}{\varDelta}&=\left\{\alpha+\beta e^{i(a'+b')fH}+\gamma e^{i2(a'+b')fH}+\delta e^{i2a'fH}+\varepsilon e^{i2b'fH}\right\}^{-1}\\
&=\Biggl[\frac{1}{\alpha}-\left\{\frac{\delta}{\alpha^2}e^{i2a'fH}+\frac{\beta}{\alpha^2}e^{i(a'+b')fH}+\frac{\varepsilon}{\alpha^2}e^{i2b'fH}\right\}\\
&\quad+\Biggl\{\frac{\delta}{\alpha^3}e^{i4a'fH}+2\frac{\beta\delta}{\alpha^3}e^{i(3a'+b')fH}+\left(\frac{\beta^2}{\alpha^3}+2\frac{\delta\varepsilon}{\alpha^3}-\frac{\gamma}{\alpha^3}\right)e^{i2(a'+b')fH}\\
&\qquad+2\frac{\beta\varepsilon}{\alpha^3}e^{i(a'+3b')fH}+\frac{\varepsilon}{\alpha^3}e^{i4b'fH}\Biggr\}\\
&\quad-\Biggl\{\frac{\delta^3}{\alpha^4}e^{i6a'fH}+3\frac{\beta\delta^2}{\alpha^4}e^{i(5a'+b')fH}+\left(3\frac{\beta^2\delta}{\alpha^4}+3\frac{\varepsilon\delta^2}{\alpha^4}-2\frac{\gamma\delta}{\alpha^3}\right)e^{i(4a'+2b')fH}\\
&\qquad+\left(6\frac{\beta\delta\varepsilon}{\alpha^4}+\frac{\beta^3}{\alpha^4}-2\frac{\beta\gamma}{\alpha^3}\right)e^{i3(a'+b')fH}+\left(3\frac{\beta^2\varepsilon}{\alpha^4}+3\frac{\varepsilon^2\delta}{\alpha^4}-2\frac{\gamma\varepsilon}{\alpha^3}\right)e^{i2(a'+2b')fH}\\
&\qquad+3\frac{\beta\varepsilon^2}{\alpha^4}e^{i(a'+5b')fH}+\frac{\varepsilon^3}{\alpha^4}e^{i6b'fH}\Biggr\}\\
&\quad+\Biggl\{\frac{\delta^4}{\alpha^5}e^{i8a'fH}+4\frac{\beta\delta^3}{\alpha^5}e^{i(7a'+b')fH}\\
&\qquad+\left(4\frac{\delta^3\varepsilon}{\alpha^5}+6\frac{\delta^2\beta^2}{\alpha^5}-3\frac{\delta^2\gamma}{\alpha^4}\right)e^{i2(3a'+b')fH}+\left(4\frac{\delta\beta^3}{\alpha^5}+12\frac{\delta^2\beta\varepsilon}{\alpha^5}-6\frac{\gamma\delta\beta}{\alpha^4}\right)e^{i(5a'+3b')fH}\\
&\qquad+\left(12\frac{\varepsilon\beta^2\delta}{\alpha^3}+6\frac{\varepsilon^2\delta^2}{\alpha^5}+\frac{\beta^4}{\alpha^5}+\frac{\gamma^2}{\alpha^3}-3\frac{\beta^2\gamma}{\alpha^4}-6\frac{\gamma\delta\varepsilon}{\alpha^4}\right)e^{i4(\,'+b')fH}\\
&\qquad+\left(4\frac{\varepsilon\beta^3}{\alpha^5}+12\frac{\delta\beta\varepsilon^2}{\alpha^5}-6\frac{\varepsilon\beta\gamma}{\alpha^5}\right)e^{i(3a'+5b')fH}+\left(4\frac{\delta\varepsilon^3}{\alpha^5}+6\frac{\varepsilon^2\beta^2}{\alpha^5}-3\frac{\varepsilon^2\gamma}{\alpha^4}\right)e^{i2(a'+3b')fH}\\
&\qquad+4\frac{\varepsilon^3\beta}{\alpha^5}e^{i(a'+7b')fH}+\frac{\varepsilon^4}{\alpha^5}e^{i8l'fH}\Biggr\}+\cdots\cdots\Biggr].
\end{aligned}
\tag{45}
$$

(45)に於ける級數は初項より第8項目まで採つてあるが，計算の目的によつては今少し項數を增さなければならい事もある．兎に角展開式に於ける各項は夫々力學的の意味を有するものであつて，$F(x, y)$ なる初入射波によつて起される表面層内に於ける數次の反射屈折に關係するものである事は(30)~(35)に(45)を用ひた(37)~(42)を代入すれば解かる．尚かくの如くして求めた展開式は非常に收斂性のよい事は(44)に於ける α の羃が展開式の各項の分母に入つてゐる事より明かであり，尚これは表面層内に於ける自由波の表面及び $y=0$ なる境界面に於ける數次の反射に伴ふてその强さが次第に減少して行く事を示めしてゐるのである．次に(45)を用ひた(37)~(42)の $A'/\mathfrak{a}$, $B'/\mathfrak{a}$, $C/\mathfrak{a}$, $E/\mathfrak{a}$, $D/\mathfrak{a}$ 及び $F/\mathfrak{a}$ を夫々(30)~(35)なる ϕ_1, ψ_2, ϕ_2', ψ_2', ϕ_1'', ψ_2'' に代入すれば，(29)なる波の入射によつて誘起される彈性體内の自由波の問題は解決せられるが，その結果の式は略して置く．一般に彈性體内で反射或は屈折する各自由波の形式は總て

$$F=Q\int_{-\infty}^{\infty} e^{i\left(qH+\frac{V_1t}{\cos\theta}\right)f}\,df\int_{-\infty}^{\infty}dr\int_{-\infty}^{\infty}d\xi\int_{-\infty}^{\infty}F(\xi,\,\eta)\,e^{-i\{f(x-\xi)-r(sy+\eta)\}}\,d\eta \tag{46}$$

の形式となる．位相の違ひを示す q は(45)を用ひた(37)~(42)によつて決定せられてゐる．Q は各自由波の强さに關する常數であつて，これは，入射角 θ, 速度 V_1, V_2, V_1', V_2' の超越函數となつてゐる事は(37)~(42)で明かである．從つて問題は(28)なる ϕ_0 の形即ち $F(x, y)$ を具體的に與へ，(46)なる積分を求める事が出來れば，彈性體中に起る波動現象は完全に解き得る理である．

今例へば

$$F(x, y)=e^{-\frac{(x\cos\theta+y\sin\theta)^2}{c^2}} \tag{47}$$

なる衝擊波型の縱波が入射すると考へる．c は見掛け上の波長に關係したものであり，θ は入射角である．然る時は[6]

$$F=Qe^{-\frac{\{x\cos\theta+sy\sin\theta-qH\cos\theta-V_1t\}^2}{c^2}} \tag{48}$$

となり，これを利用する事によつて問題は完全に解決せられるのである．

---

[6] 妹澤克惟，金井清　地震研究所彙報 **10** (1933), 805.
西村源六郎，金井清　地震研究所彙報 **12** (1934), 292.

第２節　兩彈性體の彈性力學的性質が全然相等しい場合，$\theta=30°$ で入射する衝擊波によつて生ずる彈性體內の自由波問題

さて $\lambda=\lambda'$, $\mu=\mu'$, $\rho=\rho'$, そして $\lambda=\mu$, $\lambda'=\mu'$ なる時，$\theta=30°$ で（47）なる型の波が入射する場合の問題を圖をもつて研究解決する事とする.

（47）はこの場合，

$$F(x,y)=e^{-\frac{\left(\frac{1}{2}\sqrt{3}x+\frac{1}{2}y\right)^2}{c^2}} \tag{49}$$

となる. 從つて

$$\phi=e^{-\frac{\left(\frac{1}{2}\sqrt{3}x+\frac{1}{2}y-V_1t\right)^2}{c^2}}, \tag{50}$$

$$\phi_1=\frac{1}{2}e^{-\frac{\left(\frac{1}{2}\sqrt{3}x-\frac{1}{2}y-V_1t\right)^2}{c^2}}-\frac{1}{2}e^{-\frac{\left(\frac{1}{2}\sqrt{3}x-\frac{1}{2}y-V_1t+\frac{4}{\sqrt{3}}\right)^2}{c^2}}, \tag{51}$$

$$\psi_2=\frac{1}{2\sqrt{3}}e^{-\frac{\left(\frac{1}{2}\sqrt{3}x-\frac{1}{2}y-V_1t\right)^2}{c^2}}+e^{-\frac{\left(x-\sqrt{3}y-V_1t+\frac{4}{\sqrt{3}}H\right)^2}{c^2}}, \tag{52}$$

$$\phi_1'+\phi_1''=\frac{1}{2}\left[-e^{-\frac{\left(x+\frac{1}{\sqrt{3}}y-V_1t+\frac{4}{\sqrt{3}}H\right)^2}{c^2}}+e^{-\frac{\left(x-\frac{1}{\sqrt{3}}y-V_1t\right)^2}{c^2}}\right], \tag{53}$$

$$\psi_2'+\psi_2''=\frac{1}{2\sqrt{3}}\left[e^{-\frac{\left(x+\sqrt{3}y-V_1t+\frac{4}{\sqrt{3}}H\right)^2}{c^2}}+e^{-\frac{\left(x-\sqrt{3}y-V_1t\right)^2}{c^2}}\right] \tag{54}$$

となり，この他には全然波動は彈性體內には生じる事がない. この場合には，(45)を代入した（37）~（42）に於ける無限級數が結局合成の結果次の樣な簡單なものに置き換へられるから，(51)，(52)，(53)，(54)で示めされる夫々の位相波より以外の波卽ち地表面或は $y=0$ なる不連續面での數次反射或は屈折するものは相互に打消し合つて，結局（51）~（54）以外の位相波は現はれない事となる.

$$\frac{A'}{\alpha}=\frac{1}{2}\left\{1-e^{ifH\frac{4}{\sqrt{3}}}\right\},\quad \frac{B'}{\alpha}=\frac{1}{2\sqrt{3}}\left\{1+e^{ifH\frac{4}{\sqrt{3}}}\right\},\quad \frac{C}{\alpha}=-\frac{1}{2}e^{ifH\frac{4}{\sqrt{3}}},$$

$$\frac{D}{\alpha}=\frac{1}{2},\quad \frac{E}{\alpha}=\frac{1}{2\sqrt{3}}e^{ifH\frac{4}{\sqrt{3}}},\quad \frac{F}{\alpha}=\frac{1}{2\sqrt{3}}.$$

玆に於て（14）で示めされる U, V, U', V' を求める時は，

$$\begin{aligned} U=\Bigg[&\frac{-2\left(x-\frac{1}{\sqrt{3}}y-V_1t\right)}{c^2}e^{-\frac{(x-\frac{1}{\sqrt{3}}y-V_1t)^2}{c^2}}-\frac{\left(x+\frac{1}{\sqrt{3}}y-V_1t\right)}{c^2}e^{-\frac{(x+\frac{1}{\sqrt{3}}y-V_1t)^2}{c^2}} \\ &+\frac{\left(x+\frac{1}{\sqrt{3}}y-V_1t+\frac{4}{\sqrt{3}}H\right)}{c^2}e^{-\frac{(x+\frac{1}{\sqrt{3}}y-V_1t+\frac{4}{\sqrt{3}}H)^2}{c^2}}-\frac{(x+\sqrt{3}y-V_1t)}{c^2}e^{-\frac{(x+\sqrt{3}y-V_1t)^2}{c^2}} \\ &-\frac{\left(x+\sqrt{3}y-V_1t+\frac{4}{\sqrt{3}}H\right)}{c^2}e^{-\frac{(x+\sqrt{3}y-V_1t+\frac{4}{\sqrt{3}}H)^2}{c^2}}\Bigg], \end{aligned} \tag{55}$$

$$\begin{aligned} V=\Bigg[&\frac{2}{\sqrt{3}}\frac{\left(x-\frac{1}{\sqrt{3}}y-V_1t\right)}{c^2}e^{-\frac{(x-\frac{1}{\sqrt{3}}y-V_1t)^2}{c^2}}-\frac{1}{\sqrt{3}}\frac{\left(x+\frac{1}{\sqrt{3}}y-V_1t\right)}{c^2}e^{-\frac{(x+\frac{1}{\sqrt{3}}y-V_1t)^2}{c^2}} \\ &+\frac{1}{\sqrt{3}}\frac{\left(x+\frac{1}{\sqrt{3}}y-V_1t+\frac{4}{\sqrt{3}}H\right)}{c^2}e^{-\frac{(x+\frac{1}{\sqrt{3}}y-V_1+\frac{4}{\sqrt{3}}H)^2}{c^2}} \\ &+\frac{1}{\sqrt{3}}\frac{(x+\sqrt{3}y-V_1t)}{c^2}e^{-\frac{(x+\sqrt{3}y-V_1t)^2}{c^2}} \\ &+\frac{1}{\sqrt{3}}\frac{\left(x+\sqrt{3}y-V_1t+\frac{4}{\sqrt{3}}H\right)}{c^2}e^{-\frac{(x+\sqrt{3}y-V_1t+\frac{4}{\sqrt{3}}H)^2}{c^2}}\Bigg], \end{aligned} \tag{56}$$

$$\begin{aligned} U'=\Bigg[&\frac{\left(x+\sqrt{3}y-V_1t+\frac{4}{\sqrt{3}}H\right)}{c^2}e^{-\frac{(x+\frac{1}{\sqrt{3}}y-V_1t+\frac{4}{\sqrt{3}}H)^2}{c^2}} \\ &-\frac{\left(x-\frac{1}{\sqrt{3}}y-V_1t\right)}{c^2}e^{-\frac{(x-\frac{1}{\sqrt{3}}y-V_1t)^2}{c^2}}-\frac{\left(x+\sqrt{3}y-V_1t+\frac{4}{\sqrt{3}}H\right)}{c^2} \\ &\cdot e^{-\frac{(x+\sqrt{3}y-V_1t+\frac{4}{\sqrt{3}}H)^2}{c^2}}+\frac{\left(x-\sqrt{3}y-V_1t\right)}{c^2}e^{-\frac{(x-\sqrt{3}y-V_1t)^2}{c^2}}\Bigg], \end{aligned} \tag{57}$$

$$V'=\frac{1}{\sqrt{3}}\left[\frac{\left(x+\frac{1}{\sqrt{3}}y-V_1t+\frac{4}{\sqrt{3}}H\right)}{c^2}e^{-\frac{(x+\frac{1}{\sqrt{3}}y-V_1t+\frac{4}{\sqrt{3}}H)^2}{c^2}}\right.$$

$$+\frac{\left(x-\frac{1}{\sqrt{3}}y-V_1t\right)}{c^2}e^{-\frac{(x-\frac{1}{\sqrt{3}}y-V_1t)^2}{c^2}}$$

$$+\frac{\left(x+\frac{1}{\sqrt{3}}y-V_1t+\frac{4}{\sqrt{3}}\right)}{c^2}e^{-\frac{(x+\frac{1}{\sqrt{3}}y-V_1t+\frac{4}{\sqrt{3}}H)^2}{c^2}}$$

$$\left.+\frac{(x-\sqrt{3}y-V_1t)}{c^2}\;e^{-\frac{(x-\sqrt{3}y-V_1t)^2}{c^2}}\right]. \tag{58}$$

そしてこれ等の波動を起す爲めの初入射波は

$$\left.\begin{aligned} u_0&=\frac{-2\left(x-\frac{1}{\sqrt{3}}y-V_1t\right)}{c^2}e^{-\frac{(x-\frac{1}{\sqrt{3}}y-V_1t)^2}{c^2}},\\ v_0&=\frac{2}{\sqrt{3}}\frac{\left(x-\frac{1}{\sqrt{3}}y-V_1t\right)}{c^2}e^{-\frac{(x-\frac{1}{\sqrt{3}}y-V_1t)^2}{c^2}}. \end{aligned}\right\} \tag{59}$$

$x=0$, $y=0$ に於ける U, V 及び U', V', そして $x=0$, $y=H/2$ に於ける U', V', $x=0$, $y=H$ に於ける U', V' を夫々 $H/C=0$, $H/C=\frac{1}{3}$, $H/C=1$, $H/C=3$ の場合に就て計算，圖示すると第2a～第5d 圖を得．各圖に於て上圖は，彈性體內各點に於ける水平垂直各方向の變位卽ち U, V 及び U', V' の變化を示し，下圖は各點に於ける運動軌跡を示してゐる．

第2圖 a, b, c, d は $H/C=0$ の場合であるが，表面層には全然水平方向の變位はなく，垂直方向のものだけである．而もその振幅は深さに無關係である．運動の始まる時刻が深さに實際上無關係であつて，$y=0$に初入射波が入射した時より深さの方向には位相の後れなく表面層は一塊となつて，上下運動をするのである，勿論表面層でも水平方向には傳播性のものである事は式を見ても明かである．

第3圖 a, b, c, d は $H/C=\frac{1}{3}$ の場合であるが分子運動は，境界面 $y=0$ に於て

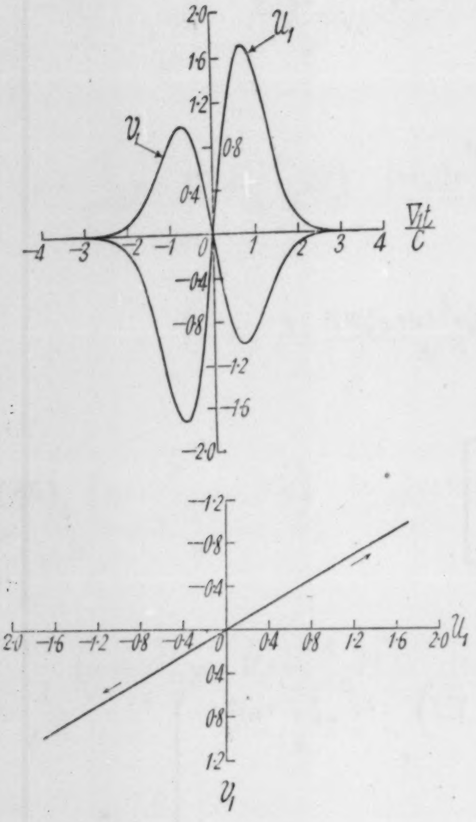

第２圖 a. $\frac{H}{c}=0$，$y=0$.

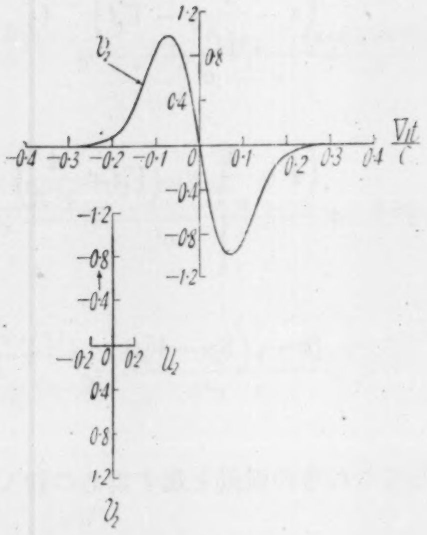

第２圖 c. $\frac{H}{c}=0$，$y=0$.

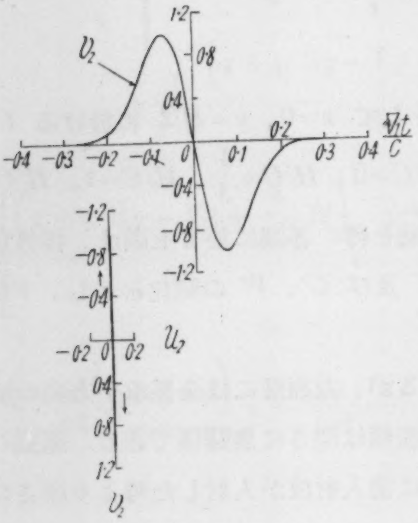

第２圖 b. $\frac{H}{c}=0$，$y=0$.

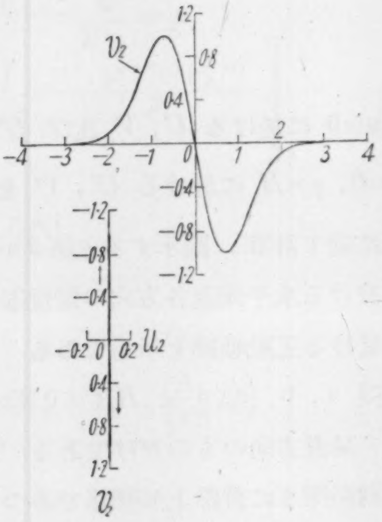

第２圖 d. $\frac{H}{c}=0$，$y=-H$.

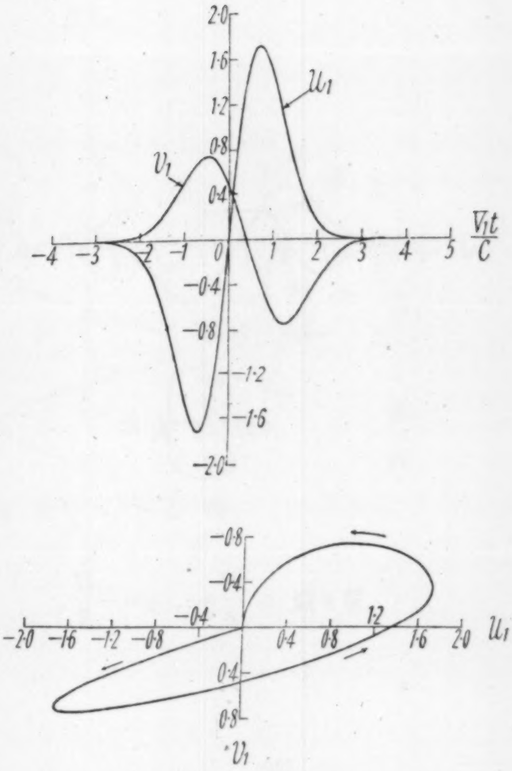

第3圖 a. $\frac{H}{c}=\frac{1}{3}$, $y=0$.

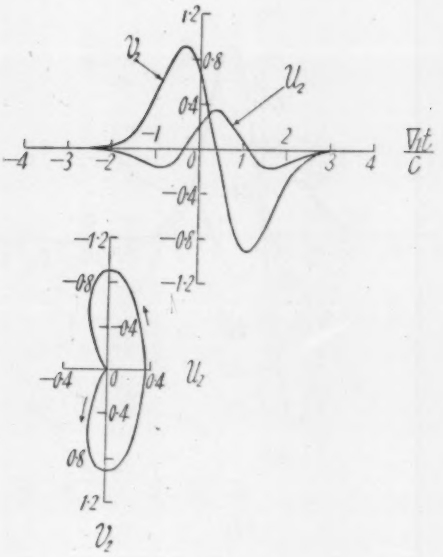

第3圖 c. $\frac{H}{c}=\frac{1}{3}$, $y=-\frac{H}{2}$.

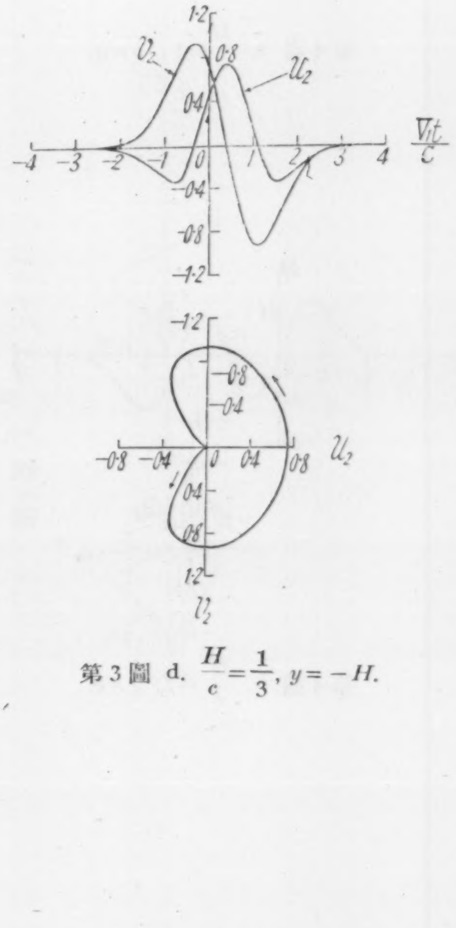

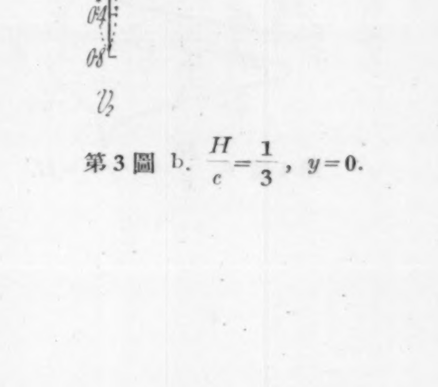

第3圖 b. $\frac{H}{c}=\frac{1}{3}$, $y=0$.

第3圖 d. $\frac{H}{c}=\frac{1}{3}$, $y=-H$.

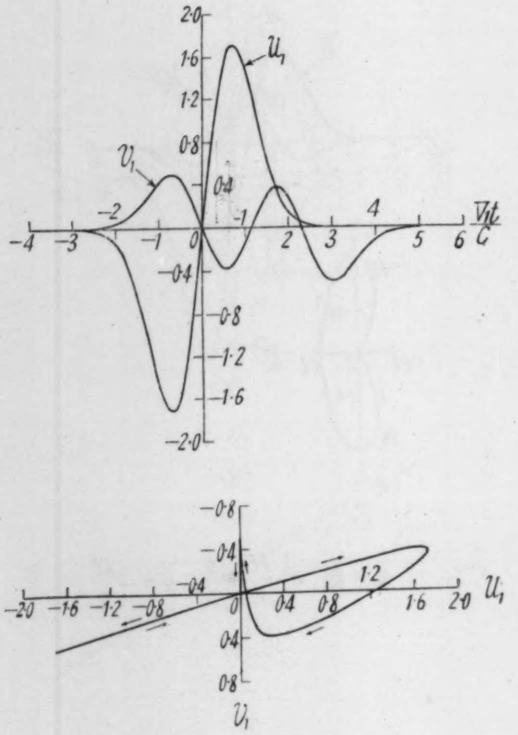

第4圖 a. $\frac{H}{c}=1$, $y=0$.

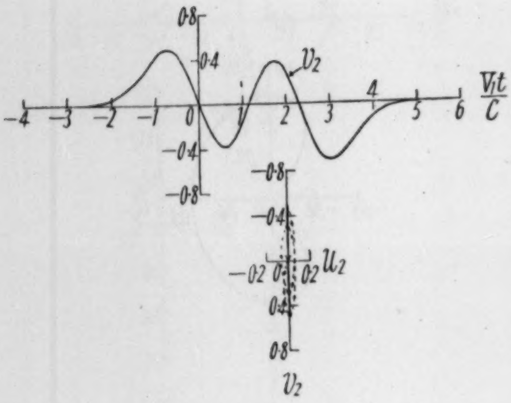

第4圖 b. $\frac{H}{c}=1$, $y=0$.

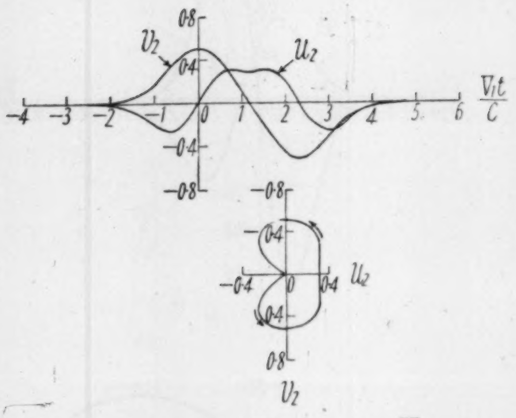

第4圖 c. $\frac{H}{c}=1$, $y=-\frac{H}{2}$.

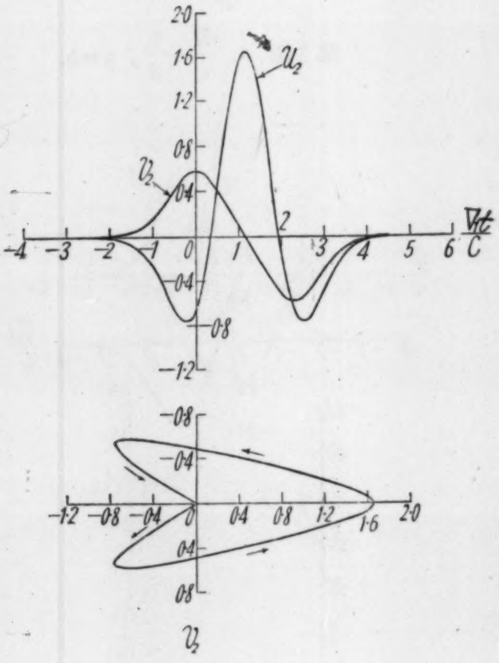

第4圖 d. $\frac{H}{c}=1$, $y=-H$.

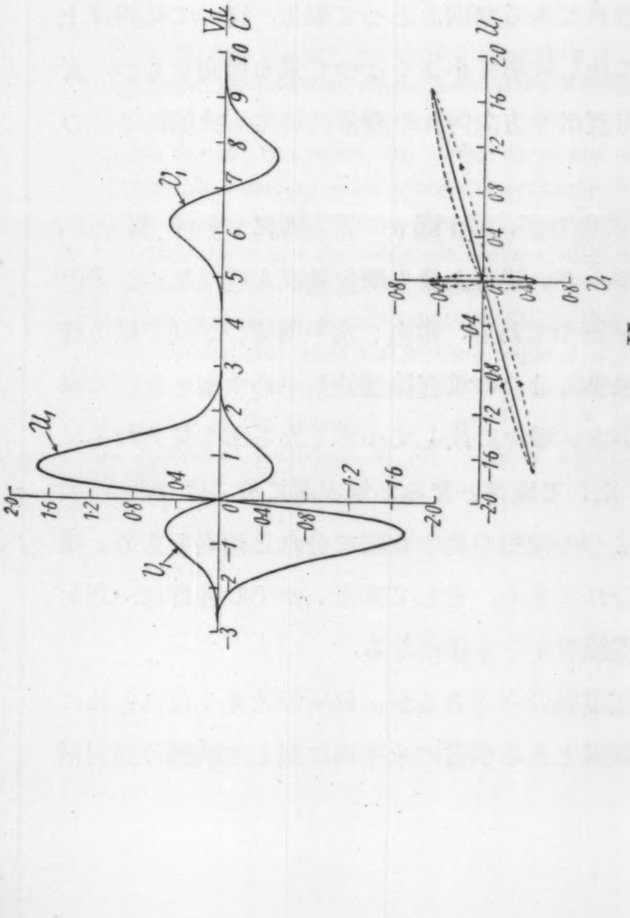

第５圖 a. $\frac{H}{c}=3,\ y=-H.$

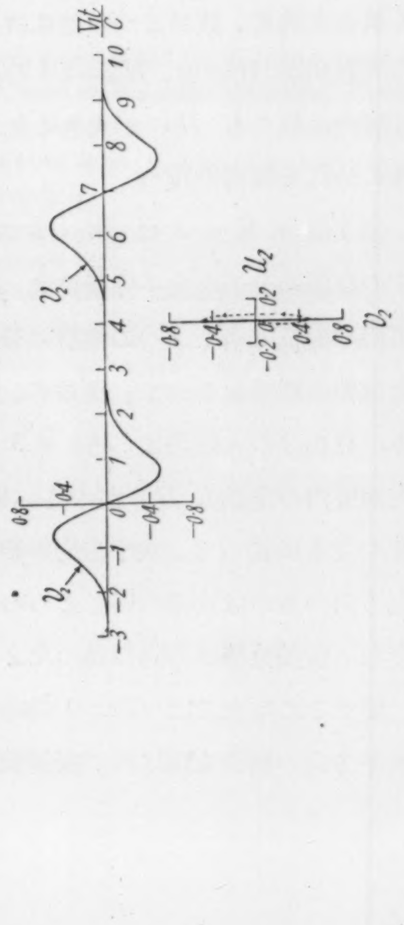

第５圖 b. $\frac{H}{c}=3,\ y=0.$

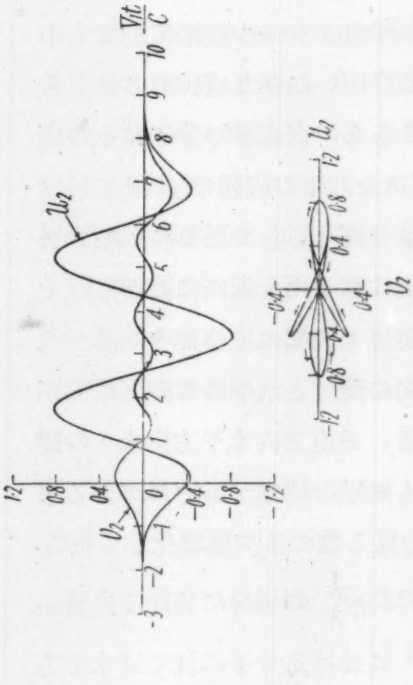

第５圖 c. $\frac{H}{c}=3,\ y=-\frac{H}{c}.$

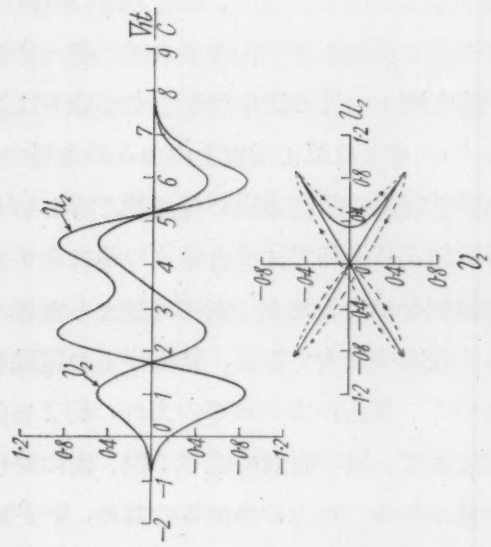

第５圖 d. $\frac{H}{c}=3,\ y=-H.$

も，表面層内に於ても $H/C=0$ の場合と非常に趣きを異にしてゐる事が見られる．$y=0$ に於て，下の媒體は水平方向の變位は $H/C=0$ の場合と殆んど同じ變化をし振幅も等しいのであるが，垂直方向の變位は $H/C=0$ の場合より多少振幅に於ても小さくなり位相も多少後れて來る．從つてその軌跡は $H/C=0$ の樣な直線形とはならず第3圖 a で見る樣な形をとつて分子は運動するのである．表面層の分子はその底 $y=0$ に於ては單に垂直方向のみの運動であつて，これは全然下の媒體の $y=0$ に於ける分子運動の垂直方向の分運動と等しいものである．第3圖 c，d で見る樣に地表層の表面及び内部では垂直變位の他に水平方向の變位も現はれ，而も表面に近づく程その變位量が大となり，表面で最大となる．垂直方向の變位も表面に近い程その量が大きく表面で最大である．見掛け上の運動週期が垂直方向の變位と水平のものとに差があつて，垂直の方が水平の夫れの約2倍位になつてゐる．垂直方向水平方向夫々の變位に就て，層の表面に近づく程，底に於けるものよりも初動の時刻がおくれてゐる事が見られる．以上の事柄等の爲め，分子振動軌跡は圖で見る樣に多少複雜化して來る．

第4圖 a，b，c，d は $H/L=1$ の場合であるが $H/L=\frac{1}{3}$ の場合に於ける性質が益々明かに見られる樣になつて來る．下の媒體の $y=0$ に於ける分子に就ては水平方向の變位はその最大振幅も變動狀況も全く $H/c=0$，$1/3$ の場合と同樣であるが垂直方向の夫れは，全く趣を異にし，最大振幅も $H/c=0$，$1/3$ の場合に比し次第に小さく成ると共に，波が2つの波に次第に分れて來る傾向をとつて來る．從つて見掛け上の入射角が $H/c=0$，$H/c=1/3$ の場合に比し次第に小さくなつて來る傾向をもつ．表面層内に於ても H/c が大きくなる程垂直水平方向何れの變位に於ても次第に2つの群に分れる傾向を持つ．

第5圖 a, b, c, d は $H/c=3$ の場合であるが，第5圖 a で見る樣に，$y=0$ 面では，下の媒體の分子の水平分變位は H/c の小さい場合と量も變化狀況も違はないが垂直方向の變位は全く2つの波群に分れて仕舞つてゐる．垂直，水平兩變位が圖で見る樣な位相の關係をもつて，從つて，運動軌跡も2つの垂直線運動を示めす事となつて來る．見かけの入射角は $H/c=3$ より小さい場合に比して小さくなる事も見られる．表面層内の運動も H/c が小さい場合に比して複雜となるが地表面に於ては H/c が大きくなるに從つて，水平方向の變位は2つの位相の異つた群に分れる傾向をもち，垂直方向のものは位相の同じ2つの群に分れて來る．そして垂直，水平の各群は一對をなし，振動軌跡は方向の異つた2つの直線形をとる樣になる．

要するに地表では $H/c=0$ の時は垂直運動のみであるが，H/c が大きくなると共に水平方向の變位も現はれ，振動軌跡は複雜となるが常に水平面に對して軌跡は面對稱

であつて，２つの異つた直線型軌跡をとる傾向となる．そして初動の方向は $y=0$ 面に入射する初入射波の入射角と同じ角度になるのである．

尙 H/c の値によつて振動狀況が全く異つて來，從つて，適當な H/c の時には彈性體內各點での水平或は垂直方向の變位の時間的變化卽ち見掛けの週期は全く場所によつて異つて來るものである．厚さ H に比して見掛けの波長 c が非常に大きい時にはかゝる現象は見られない．又振幅の一定な無限に長い調和波が入射した時にも矢張り前述の見掛けの週期が場所によつて異る事はない．自由波の傳播によつて各場所により振動週期の相違する事を說明せんと試みるのには，少くとも波長と同じ位數の厚さの層がある事を必要とする．又自由波が圓函數的な無限に續く調和波であつては說明が不可能である．

39. *On the Effect of Discontinuity Surfaces on the Propagation of Elastic Waves.* (*VI*)

By Genrokuro NISHIMURA and Kiyoshi KANAI,

Earthquake Research Institute.

In the first chapter, we studied the nature of free waves propagated in a surface layer and a subjacent semi-infinite elastic body when a dilatational wave of harmonic wave-type of infinite extent is obliquely incident on the common boundary of the two solids. We assume that it is possible for the two solids, the surface layer and the subjacent solid, to slide over each other at the common boundary when a wave is obliquely incident upon it.

In the second chapter we discussed analytically the general properties of vibratory motions of the surface layer and the subjacent medium when a dilatational wave of shock wave-type is obliquely incident on the bottom surface of the surface layer. From numerical calculations, the vibratory motions of certain points of the surface layer and the subjacent solid are shown in the figures for the case when the incident angle θ of the primary wave is 30° and $V_1=V_1'$, $V_2=V_2'$ and $\mu=\mu'$, where V_1, V_2 and μ are the dilatational and the rotational wave velocities and the rigidity of the subjacent solid and V_1', V_2', μ' are those of the surface layer respectively. The dynamical conditions at the common boundary are the same as those assumed in the first chapter.

5

40. 不連續面が彈性波の傳播に及ぼす影響(其の7)

(表面層を有する彈性體内に於ける體自由波の生成及び傳播機構．兩彈性體が密着せる場合)

地震研究所 西村源六郎

(昭和10年6月20日受理)

内容目次

頁
緒 言 …… 540
第1章 無限長の調和波型縱彈性波の入射による表面層を有する半無限固體内の體自由波の生成及び傳播機構 …… 541
第1節 一般解 …… 541
第2節 地表層の厚さ H，入射波の波長 L に就て $H/L=0$ なる場合の地表層の振動問題 …… 547
第2章 衝擊波型縱彈性波の入射による表面層を有する半無限固體内の體自由波の生成及び傳播機構 …… 549

緒 言

此の論文は表面層を有する彈性體内に於ける體自由波の生成，傳播機構を研究したものである．表面層を有する彈性體内に於ける體彈性波の問題に就ては，その境界面に於て兩彈性體が密着した場合の數學的研究が最近妹澤教授，金井清氏1) によつて行はれた．ノットの計算結果を利用して，長谷川助教授2) は5年以前にこの樣な場合の計算，即ち地表面と，境界面に於ける重複反射或は屈折理論を取入れた研究を發表し，驗震學的研究に應用した．著者は金井清氏3) と共に表面層とその下の半無限彈性體とがその境界に於て辷り得る樣な場合に就て，無限長の調和波型或は任意の波形の縱彈性波が入射する時，その彈性體内に生ずる自由波の傳播機構を明かにした．本報告は表面層とその下の媒體との境に於て兩彈性體が密着してゐて，變位の連續性，剪斷及び垂直分應力の連續性をこの境界面で兩彈性體が充す場合の研究を行ひ，第1章

---

1) 妹澤克惟，金井清 地震研究所彙報 **10** (1932), 806; **12** (1934), 269.
2) 長谷川萬吉 *Zs. f. Geophys.*, **6** (1930), 78.
3) 西村源六郎，金井清 地震研究所彙報 **11** (1934), 595; **13** (1935), 519.

では，無限長の調和波型の縦彈性波が入射した時，第２章では，衝撃波型の縦彈性波が入射した時，その彈性體内に於ける波動問題を一般的に研究した．尙第１章では表面層の厚さに較べて入射波の波長が非常に大きい場合も論じた．勿論本計算の特殊な場合に就ては妹澤教授，金井清氏4) の研究が發表されてゐる事は既に述べて置いたが，著者の研究はこの論文に負ふ所非常に大なるものがある．

第１章　無限長の調和波型縦彈性波の入射による表面層を有する半無限彈性體内の體自由波の生成及び傳播機構

第1節　一般解

厚さ H なる表面層の密度，ラーメ彈性係數を夫々 ρ', λ', μ', その下の媒體の夫れ等を ρ, λ, μ とし，この２つの境界面を $y=0$ とする．尙直角坐標の軸の原點は境界面上に置き，x 軸は水平に，y 軸は垂直に下向きを正とする（第１圖參照）．

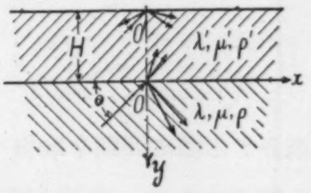

第　1　圖

今 $y\geqq 0$ なる媒體に於ける初入射波を

$$\phi_0=\alpha e^{i(fx-ry-pt)} \tag{1}$$

と置く時，此の ϕ_0 なる自由波に釣合ふ爲めに生ずる表面層及びその下の媒體内の自由波の問題を解決する事とする．(1) に於て，α は初入射波の强さに關係した常數であつて，p はこの調和波の週期に關係したものであり，$r^2=\rho p^2/(\lambda+2\mu)-f^2$ である．さて (1) に釣合ふ爲めには $y\geqq 0$ なる媒體中には

$$\phi=Ae^{i(fx+ry-pt)}, \tag{2}$$

$$\psi=Be^{i(fx+sy-pt)} \tag{3}$$

なる反射波の縱横兩波があり，又表面層内にはこの爲め表面及び底面で反射する波が構成され，これ等を

$$\phi'=Ce^{i(fx-r'y-pt)}+De^{i(fx+r'y-pt)}, \tag{4}$$

$$\psi'=Ee^{i(fx-s'y-pt)}+Fe^{i(fx+s'y-pt)} \tag{5}$$

なる４個の縱橫兩波によつて表はして置く．A, B, C, D, E 及び F は問題の條件より決定されるものであり，又 $s^2=\rho p^2/\mu-f^2$, $r'^2=\rho' p^2/(\lambda'+2\mu')-f^2$ 及び $s'^2=\rho' p^2/\mu'-f^2$ である．(1)〜(5) なる波は勿論波動方程式 $\dfrac{\partial^2\phi}{\partial t^2}=\varkappa\nabla^2\phi$，$\dfrac{\partial^2\psi}{\partial t^2}=\varkappa'\nabla^2\psi$ を滿足するものである．今表面層の水平及び垂直方向の變位を夫々 U', V' とし，下の媒體の夫

---

4) 妹澤克惟，金井清　前出

れ等を U, V とする時，此れ等變位式は容易に (1)〜(5) より誘導する事が出來る．

次に $y=0$ 及び $y=-H$ なる2個の面に於ける彈性力學的の條件を次の樣に置く．$y=0$ に於て，

$$\left.\begin{aligned}&U=U',\ V=V',\\&\lambda\left(\frac{\partial U}{\partial x}+\frac{\partial V}{\partial y}\right)+2\mu\frac{\partial V}{\partial y}=\lambda'\left(\frac{\partial U'}{\partial x}+\frac{\partial V'}{\partial y}\right)+2\mu'\frac{\partial V'}{\partial y},\\&\mu\left(\frac{\partial V}{\partial x}+\frac{\partial U}{\partial y}\right)=\mu'\left(\frac{\partial V'}{\partial x}+\frac{\partial U'}{\partial y}\right).\end{aligned}\right\}\qquad(6)$$

を滿足する樣に，又 $y=-H$ なる表面は自由面であつて $y<-H$ には勢力の傳播がないとすれば，

$$\left.\begin{aligned}&\lambda'\left(\frac{\partial U'}{\partial x}+\frac{\partial V'}{\partial y}\right)+2\mu'\frac{\partial V'}{\partial y}=0,\\&\mu'\left(\frac{\partial V'}{\partial x}+\frac{\partial U'}{\partial y}\right)=0\end{aligned}\right\}\qquad(7)$$

に適合する樣に問題を取扱へば充分である．但し u_0, v_0 は ϕ_0, u_1, v_1 は ϕ, u_2, v_2 は ψ に應ずる水平，垂直の變位，又 u_1', v_1' は ϕ', u_2', v_2' は ψ' による分變位を表はす時，

$$U=u_0+u_1+u_2,\quad V=v_0+v_1+v_2,$$
$$U'=u_1'+u_2',\quad V'=v_1'+v_2'$$

であつて，

$$U=if\mathfrak{a}e^{i(fx-ry-pt)}+ifAe^{i(fx+ry-pt)}+isBe^{i(fx+sy-pt)},\qquad(8)$$

$$V=-ir\mathfrak{a}e^{i(fx-ry-pt)}+irAe^{i(fx+ry-pt)}-ifBe^{i(fx+sy-pt)},\qquad(9)$$

$$U'=ifCe^{i(fx-r'y-pt)}+ifDe^{i(fx+r'y-pt)}+is'Ee^{i(fx-s'y-pt)}+is'Fe^{i(fx+s'y-pt)},\qquad(10)$$

$$V'=-ir'Ce^{i(fx-r'y-pt)}+ir'De^{i(fx+r'y-pt)}-ifEe^{i(fx-s'y-pt)}+ifFe^{i(fx+s'y-pt)}.\qquad(11)$$

兩彈性體がその境界面に於て變位及び垂直分應力，剪斷分應力の連續性と，地表層の表面は自由面で，$y<-H$ には勢力の傳播がないと云ふ條件 (6) 及び (7) を滿足する樣に A, B, C, D, E, F を調節する時は次の結果を得．

$$\left.\begin{aligned}&A=\frac{\Delta_A}{\Delta}\mathfrak{a},\quad B=\frac{\Delta_B}{\Delta}\mathfrak{a},\quad C=\frac{\Delta_C}{\Delta}\mathfrak{a},\\&D=\frac{\Delta_D}{\Delta}\mathfrak{a},\quad E=\frac{\Delta_E}{\Delta}\mathfrak{a},\quad F=\frac{\Delta_F}{\Delta}\mathfrak{a}.\end{aligned}\right\}\qquad(12)$$

但し

$$
\begin{aligned}
\varDelta = 16\frac{r's'}{f^2}\left(1-\frac{s'^2}{f^2}\right)\biggl[& -\mu^2\left\{\left(1-\frac{s^2}{f^2}\right)^2+4\frac{rs}{f^2}\right\}+\mu\mu'\left(1-\frac{s^2}{f^2}+2\frac{rs}{f^2}\right)\left(3-\frac{s'^2}{f^2}\right) \\
& -2\mu'^2\left(1+\frac{rs}{f^2}\right)\left(1-\frac{s'^2}{f^2}\right.\biggr] \\
& +e^{i(r'+s')H}\left\{\left(1-\frac{s'^2}{f^2}\right)^2+4\frac{r's'}{f^2}\right\}\biggl[\mu^2\left(1+\frac{r's'}{f^2}\right)\left\{\left(1-\frac{s^2}{f^2}\right)^2+4\frac{rs}{f^2}\right\} \\
& -\mu\mu'\left\{\left(1+\frac{s^2}{f^2}\right)\left(1+\frac{s'^2}{f^2}\right)\left(\frac{sr'}{f^2}+\frac{rs'}{f^2}\right)+2\left(1-\frac{s^2}{f^2}+2\frac{rs}{f^2}\right)\left(1-\frac{s'^2}{f^2}+2\frac{r's'}{f^2}\right)\right\} \\
& +\mu'^2\left(1+\frac{rs}{f^2}\right)\left\{\left(1-\frac{s'^2}{f^2}\right)^2+4\frac{r's'}{f^2}\right\}\biggr] \\
& +e^{i(r'-s')H}\left\{\left(1-\frac{s'^2}{f^2}\right)^2-4\frac{r's'}{f^2}\right\}\biggl[-\mu^2\left(1-\frac{r's'}{f^2}\right)\left\{\left(1-\frac{s^2}{f^2}\right)^2+4\frac{rs}{f^2}\right\} \\
& +\mu\mu'\left\{\left(1+\frac{s^2}{f^2}\right)\left(1+\frac{s'^2}{f^2}\right)\left(\frac{sr'}{f^2}-\frac{rs'}{f^2}\right)+2\left(1-\frac{s^2}{f^2}+2\frac{rs}{f^2}\right)\left(1-\frac{s'}{f^2}-2\frac{r's'}{f^2}\right)\right\} \\
& -\mu'^2\left(1+\frac{rs}{f^2}\right)\left\{\left(1-\frac{s'^2}{f^2}\right)^2-4\frac{r's'}{f^2}\right\}\biggr] \\
& +e^{-i(r'-s')H}\left\{\left(1-\frac{s'^2}{f^2}\right)^2-4\frac{r's'}{f^2}\right\}\biggl[-\mu^2\left(1-\frac{r's'}{f^2}\right)\left\{\left(1+\frac{s^2}{f^2}\right)^2+4\frac{rs}{f^2}\right\} \\
& +\mu\mu'\left\{2\left(1-\frac{s^2}{f^2}+2\frac{rs}{f^2}\right)\left(1-\frac{s'^2}{f^2}-2\frac{r's'}{f^2}\right)+\left(1+\frac{s^2}{f^2}\right)\left(1+\frac{s'^2}{f^2}\right)\left(\frac{rs'}{f^2}-\frac{r's}{f^2}\right)\right\} \\
& -\mu'^2\left(1+\frac{rs}{f^2}\right)\left\{\left(1-\frac{s'^2}{f^2}\right)^2-4\frac{r's'}{f^2}\right\}\biggr] \\
& +e^{-i(r'+s')H}\left\{\left(1-\frac{s'^2}{f^2}\right)^2+4\frac{r's'}{f^2}\right\}\biggl[\mu^2\left(1+\frac{r's'}{f^2}\right)\left\{\left(1-\frac{s^2}{f^2}\right)^2+4\frac{rs}{f^2}\right\} \\
& +\mu\mu'\left\{\left(1+\frac{s^2}{f^2}\right)\left(1+\frac{s'^2}{f^2}\right)\left(\frac{rs'}{f^2}+\frac{sr'}{f^2}\right)-2\left(1-\frac{s^2}{f^2}+2\frac{rs}{f^2}\right)\left(1-\frac{s'^2}{f^2}+2\frac{r's'}{f^2}\right)\right\} \\
& +\mu'^2\left(1+\frac{rs}{f^2}\right)\left\{\left(1-\frac{s'^2}{f^2}\right)^2+4\frac{r's'}{f^2}\right\}\biggr], \qquad (13)
\end{aligned}
$$

$$
\begin{aligned}
\varDelta_A = 16\frac{r's'}{f^2}\left(1-\frac{s'^2}{f^2}\right)\biggl[& \mu^2\left\{\left(1-\frac{s^2}{f^2}\right)^2-4\frac{rs}{f^2}\right\}-\mu\mu'\left(1-\frac{s^2}{f^2}-2\frac{rs}{f^2}\right)\left(3-\frac{s'^2}{f^2}\right) \\
& +2\mu'^2\left(1-\frac{rs}{f^2}\right)\left(1-\frac{s'^2}{f^2}\right)\biggr]
\end{aligned}
$$

$$
\begin{aligned}
&+e^{i(r'+s')H}\Big\{\Big(1-\frac{s'^2}{f^2}\Big)^2+4\frac{r's'}{f^2}\Big\}\Bigg[-\mu^2\Big(1+\frac{r's'}{f^2}\Big)\Big\{\Big(1-\frac{s^2}{f^2}\Big)^2-4\frac{rs}{f^2}\Big\}\\
&\quad+\mu\mu'\Big\{\Big(1+\frac{s^2}{f^2}\Big)\Big(1+\frac{s'^2}{f^2}\Big)\Big(\frac{r's}{f^2}-\frac{rs'}{f^2}\Big)+2\Big(1-\frac{s^2}{f^2}-2\frac{rs}{f^2}\Big)\Big(1-\frac{s'^2}{f^2}-2\frac{r's'}{f^2}\Big)\Big\}\\
&\quad-\mu'^2\Big(1-\frac{rs}{f^2}\Big)\Big\{\Big(1-\frac{s'}{f^2}\Big)^2+4\frac{r's'}{f^2}\Big\}\Bigg]\\
&+e^{i(r'-s')H}\Big\{\Big(1-\frac{s'^2}{f^2}\Big)^2-4\frac{r's'}{f^2}\Big\}\Bigg[\mu^2\Big(1-\frac{r's'}{f^2}\Big)\Big\{\Big(1-\frac{s^2}{f^2}\Big)^2-4\frac{rs}{f^2}\Big\}\\
&\quad-\mu\mu'\Big\{\Big(1+\frac{s^2}{f^2}\Big)\Big(1+\frac{s'^2}{f^2}\Big)\Big(\frac{sr'}{f^2}+\frac{rs'}{f^2}\Big)+2\Big(1-\frac{s^2}{f^2}-2\frac{rs}{f^2}\Big)\Big(1-\frac{s'^2}{f^2}-2\frac{r's'}{f^2}\Big)\Big\}\\
&\quad+\mu'^2\Big(1-\frac{rs}{f^2}\Big)\Big\{\Big(1-\frac{s'^2}{f^2}\Big)^2-4\frac{r's'}{f^2}\Big\}\Bigg]\\
&+e^{-i(r'+s')H}\Big\{\Big(1-\frac{s'^2}{f^2}\Big)^2+4\frac{r's'}{f^2}\Big\}\Bigg[-\mu^2\Big(1+\frac{r's'}{f^2}\Big)\Big\{\Big(1-\frac{s^2}{f^2}\Big)^2-4\frac{rs}{f^2}\Big\}\\
&\quad+\mu\mu'\Big\{\Big(1+\frac{s^2}{f^2}\Big)\Big(1+\frac{s'^2}{f^2}\Big)\Big(\frac{rs'}{f^2}-\frac{r's}{f^2}\Big)+2\Big(1-\frac{s^2}{f^2}-2\frac{rs}{f^2}\Big)\Big(1-\frac{s'^2}{f^2}-2\frac{r's'}{f^2}\Big)\\
&\quad-\mu'^2\Big(1-\frac{rs}{f^2}\Big)\Big\{\Big(1-\frac{s'^2}{f^2}\Big)^2+4\frac{r's'}{f^2}\Big\}\Bigg]\\
&+e^{-i(r'-s')H}\Big\{\Big(1-\frac{s'^2}{f^2}\Big)^2-4\frac{r's'}{f^2}\Big\}\Bigg[\mu^2\Big(1-\frac{r's'}{f^2}\Big)\Big\{\Big(1-\frac{s^2}{f^2}\Big)^2-4\frac{rs}{f^2}\Big\}\\
&\quad+\mu\mu'\Big\{\Big(1+\frac{s^2}{f^2}\Big)\Big(1+\frac{s'^2}{f^2}\Big)\Big(\frac{r's}{f^2}+\frac{rs'}{f^2}\Big)-2\Big(1-\frac{s^2}{f^2}-2\frac{rs}{f^2}\Big)\Big(1-\frac{s'^2}{f^2}-2\frac{r's'}{f^2}\Big)\Big\}\\
&\quad+\mu'^2\Big(1-\frac{rs}{f^2}\Big)\Big\{\Big(1-\frac{s'^2}{f^2}\Big)^2-4\frac{r's'}{f^2}\Big\}\Bigg],
\end{aligned}
\tag{14}
$$

$$
\begin{aligned}
\varDelta_B=16\frac{rr's'}{f^2}\Big(1-\frac{s'^2}{f^2}\Big)&\Bigg[4\mu^2\Big(1-\frac{s^2}{f^2}\Big)-\mu\mu'\Big(3-\frac{s^2}{f^2}\Big)\Big(3-\frac{s'^2}{f^2}\Big)+4\mu'^2\Big(1-\frac{s'^2}{f^2}\Big)\Bigg]\\
&+e^{i(r'+s')H}2\frac{r}{f}\Big\{\Big(1-\frac{s'^2}{f^2}\Big)^2+4\frac{r's'}{f^2}\Big\}\Bigg[-2\mu^2\Big(1-\frac{s^2}{f^2}\Big)\Big(1+\frac{r's'}{f^2}\Big)\\
&\quad+\mu\mu'\Big(3-\frac{s^2}{f^2}\Big)\Big(1-\frac{s'^2}{f^2}+2\frac{r's'}{f^2}\Big)-\mu'^2\Big\{\Big(1-\frac{s'^2}{f^2}\Big)^2+4\frac{r's'}{f^2}\Big\}\Bigg]
\end{aligned}
$$

$$+e^{i(r'-s')H}2\frac{r}{f^2}\biggl\{\biggl(1-\frac{s'^2}{f^2}\biggr)^2-4\frac{r's'}{f^2}\biggr\}\biggl[2\mu^2\biggl(1-\frac{s^2}{f^2}\biggr)\biggl(1-\frac{r's'}{f^2}\biggr)$$

$$-\mu\mu'\biggl(3-\frac{s^2}{f^2}\biggr)\biggl(1-\frac{s'^2}{f^2}-2\frac{r's'}{f^2}\biggr)+\mu'^2\biggl\{\biggl(1-\frac{s'^2}{f^2}\biggr)^2-4\frac{r's'}{f^2}\biggr\}\biggr]$$

$$+e^{-i(r'+s')H}2\frac{r}{f^2}\biggl\{\biggl(1-\frac{s'^2}{f^2}\biggr)^2+4\frac{r's'}{f^2}\biggr\}\biggl[-2\mu^2\biggl(1-\frac{s^2}{f^2}\biggr)\biggl(1+\frac{r's'}{f^2}\biggr)$$

$$+\mu\mu'\biggl(3-\frac{s^2}{f^2}\biggr)\biggl(1-\frac{s'^2}{f^2}+2\frac{r's'}{f^2}\biggr)-\mu'^2\biggl\{\biggl(1-\frac{s'^2}{f^2}\biggr)^2+4\frac{r's'}{f^2}\biggr)\biggr]$$

$$+e^{-i(r'-s')H}2\frac{r}{f^2}\biggl\{\biggl(1-\frac{s'^2}{f^2}\biggr)^2-4\frac{r's'}{f^2}\biggr\}\biggl[2\mu^2\biggl(1-\frac{s^2}{f^2}\biggr)\biggl(1-\frac{r's'}{f^2}\biggr)$$

$$-\mu\mu'\biggl(3-\frac{s^2}{f^2}\biggr)\biggl(1-\frac{s'^2}{f^2}-\frac{r's'}{f^2}\biggr)+\mu'^2\biggl\{\biggl(1-\frac{s'^2}{f^2}\biggr)^2-4\frac{r's'}{f^2}\biggr], \tag{15}$$

$$\varDelta_C=8\frac{r's'}{f^2}\biggl(1+\frac{s^2}{f^2}\biggr)\biggl(1-\frac{s'^2}{f^2}\biggr)\biggl[-\mu^2\biggl(2\frac{r's}{f^2}-1+\frac{s^2}{f^2}\biggr)+\mu\mu'\biggl(2\frac{r's}{f^2}-1+\frac{s'^2}{f^2}\biggr)\biggr]$$

$$+2e^{-i(r'-s')H}\frac{r}{f}\biggl(1+\frac{s^2}{f^2}\biggr)\biggl\{\biggl(1-\frac{s^2}{f^2}\biggr)^2-4\frac{r's'}{f^2}\biggr\}$$

$$\cdot\biggl[\mu\mu'\biggl\{\frac{s}{f^2}\biggl(1-\frac{s'^2}{f^2}\biggr)+2\frac{s'}{f^2}\biggr\}-\mu^2\biggl\{\frac{s'}{f}\biggl(1-\frac{s^2}{f^2}\biggr)+2\frac{s}{f^2}\biggr\}\biggr]$$

$$+2e^{-i(r'+s')H}\frac{r}{f}\biggl(1+\frac{s^2}{f^2}\biggr)\biggl\{\biggl(1-\frac{s'^2}{f^2}\biggr)^2+4\frac{r's'}{f^2}\biggr\}$$

$$\cdot\biggl[\mu\mu'\biggl\{-\frac{s}{f}\biggl(1-\frac{s'^2}{f^2}\biggr)+2\frac{s'}{f}\biggr\}+\mu^2\biggl\{-\frac{s'}{f^2}\biggl(1-\frac{s^2}{f^2}\biggr)+2\frac{s}{f}\biggr\}\biggr], \tag{16}$$

$$\varDelta_D=8\frac{rs'}{f^2}\biggl(1+\frac{s^2}{f^2}\biggr)\biggl(1-\frac{s'^2}{f^2}\biggr)\biggl[-\mu^2\biggl\{2\frac{r's}{f^2}+1-\frac{s^2}{f^2}\biggr\}+\mu\mu'\biggl\{2\frac{r's}{f^2}+1-\frac{s'^2}{f^2}\biggr\}\biggr]$$

$$+2e^{i(r'+s')H}\frac{r}{f}\biggl(1+\frac{s^2}{f^2}\biggr)\biggl\{\biggl(1-\frac{s'^2}{f^2}\biggr)^2+4\frac{r's'}{f^2}\biggr\}$$

$$\cdot\biggl[-\mu\mu'\biggl\{\frac{s}{f}\biggl(1-\frac{s'^2}{f^2}\biggr)+2\frac{s'}{f}\biggr\}+\mu^2\biggl\{\frac{s'}{f}\biggl(1-\frac{s'^2}{f^2}\biggr)+2\frac{s}{f}\biggr\}\biggr]$$

$$
\begin{aligned}
&+2e^{i(r'-s')H}\frac{r}{f}\left(1+\frac{s^2}{f^2}\right)\left\{\left(1-\frac{s'^2}{f^2}\right)^2-4\frac{r's'}{f^2}\right\}\\
&\cdot\left[\mu\mu'\left\{\frac{s}{f}\left(1-\frac{s'^2}{f^2}\right)-2\frac{s'}{f^2}\right\}+\mu^2\left\{\frac{s'}{f^2}\left(1-\frac{s^2}{f^2}\right)-2\frac{s}{f}\right\}\right], \qquad (17)
\end{aligned}
$$

$$
\begin{aligned}
\varDelta_E=8\frac{rr'}{f^2}\left(1+\frac{s'}{f^2}\right)\left(1-\frac{s'^2}{f^2}\right)&\left[\mu^2\left\{\frac{s'}{f^2}\left(1-\frac{s^2}{f^2}\right)+2\frac{s}{f}\right\}-\mu\mu'\left\{\frac{s}{f}\left(1-\frac{s'^2}{f^2}\right)+2\frac{s'}{f}\right\}\right]\\
&+2e^{-i(r'+s')H}\frac{r}{f}\left(1+\frac{s^2}{f^2}\right)\left\{\left(1+\frac{s'^2}{f^2}\right)^2+4\frac{r's'}{f^2}\right\}\\
&\cdot\left[\mu\mu'\left(1-\frac{s'^2}{f^2}+2\frac{rs'}{f^2}\right)-\mu^2\left(1-\frac{s^2}{f^2}+2\frac{r's}{f^2}\right)\right]\\
&+2e^{i(r'-s')H}\frac{r}{f}\left(1+\frac{s^2}{f^2}\right)\left\{\left(1-\frac{s'^2}{f^2}\right)^2-4\frac{r's'}{f^2}\right\}\\
&\cdot\left[-\mu\mu'\left(1-\frac{s'^2}{f^2}+2\frac{r's}{f^2}\right)+\mu^2\left(1-\frac{s^2}{f^2}-2\frac{r's}{f^2}\right\}\right], \qquad (18)
\end{aligned}
$$

$$
\begin{aligned}
\varDelta_F=8\frac{rr'}{f^2}\left(1+\frac{s'}{f^2}\right)\left(1-\frac{s'^2}{f^2}\right)&\left[\mu^2\left\{\frac{s'}{f^2}\left(1-\frac{s^2}{f^2}\right)-2\frac{s}{f}\right\}+\mu\mu'\left\{\frac{s}{f}\left(1-\frac{s'^2}{f^2}\right)-2\frac{s'}{f^2}\right\}\right]\\
&+2e^{i(r'+s')H}\frac{r}{f}\left(1+\frac{s^2}{f^2}\right)\left\{\left(1-\frac{s'^2}{f^2}\right)^2+4\frac{r's'}{f^2}\right\}\\
&\cdot\left[\mu\mu'\left(1-\frac{s'^2}{f^2}-2\frac{r's}{f^2}\right)-\mu^2\left(1-\frac{s^2}{f^2}-2\frac{r's}{f^2}\right)\right]\\
&+2e^{-i(r'-s')H}\frac{r}{f}\left(1+\frac{s^2}{f^2}\right)\left\{\left(1-\frac{s'^2}{f^2}\right)^2-4\frac{r's'}{f^2}\right\}\\
&\cdot\left[-\mu\mu'\left(1-\frac{s'^2}{f^2}+2\frac{r's}{f^2}\right)+\mu^2\left(1-\frac{s^2}{f^2}+2\frac{r's}{f^2}\right)\right]. \qquad (19)
\end{aligned}
$$

かくして決定した常數 A, B, C, D, E 及び F は (13)~(19) で見る如く，兩彈性體の密度，彈性係數及び入射角 θ の函數となつてゐる．これ等を (8), (9), (10), (11) に代入すれば，本問題を全く解析的に解決し得るのである．妹澤教授[5] は金井清氏と共に入射角が 45° で彈性體がポアソンの條件を滿足し，そして $\dfrac{\mu'}{\mu}=\dfrac{1}{2}$ の場合

---

[5] 妹澤克惟，金井清　前出

を具體的に數計算によつて研究し，地表層の厚さ H と入射波の波長 L との比 H/L を種々與へて地表面の分子運動軌跡を圖的に解決してゐる．

著者は高山威雄氏と共に本計算より得た一般的な結果より具體的の研究を進めてゐるが，これに就ては次の機會に報告する事とする．

第２節　地表層の厚さ H，入射波の波長 L に就て $H/L=0$ なる場合の地表層の振動問題

輓近の地震研究に於ては，地殼の極上層に於ける彈性的不連續面に就て地表層の振動問題を取扱ひ，震災の因つて起る原因はこの地表層に發生する層已有な波動によるものとの說が行はれてゐる．東京市の山ノ手方面の地震動問題に關係して，齊田理學士[6]は鈴木正治氏と共に洪積層を基盤とする深さ 60 ft の沖積層の振動問題を解決したのであるが，かゝる場合の地表層內の波動問題を解決するには實際上として地表層の厚さ H と入射波の波長 L との比 H/L が非常に小さいと考へるのが至當である．從つてこゝではその極端な場合として $H/L=0$ の場合，地表層內に生ずる自由波の問題を解析的に解いて置く．この場合は第１節で求めた結果を用ひて容易に解決が出來る．今

$$V_1=\sqrt{\frac{\lambda+2\mu}{\rho}},\quad V_2=\sqrt{\frac{\mu}{\rho}},\quad V_1'=\sqrt{\frac{\lambda'+2\mu'}{\rho'}},\quad V_2'=\sqrt{\frac{\mu'}{\rho'}}$$

と置き，尙初入射波（1）の入射角を θ とする時，ϑ, ϑ_C, ϑ_D, ϑ_E 及び ϑ_F で夫々次式を代表さす．

$$\begin{aligned}\vartheta=&\left\{\left(\frac{V_1}{V_1'}\right)^2\sec^2\theta-1\right\}^{1/2}\left\{\left(\frac{V_1}{V_2'}\right)^2\sec^2\theta-1\right\}^{1/2}\left(\frac{V_1}{V_2'}\right)^4\sec^4\theta\\&\cdot\left[\left\{2-\left(\frac{V_1}{V_2}\right)^2\sec^2\theta\right\}^2+4\tan\theta\left\{\left(\frac{V_1}{V_2}\right)^2\sec^2\theta-1\right\}^{1/2}\right],\end{aligned}\tag{20}$$

$$\begin{aligned}\vartheta_C=&\tan\theta\left\{\left(\frac{V_1}{V_2'}\right)^2\sec^2\theta-1\right\}^{1/2}\left(\frac{V_1}{V_2}\right)^2\sec^2\theta\\&\cdot\left[4\left\{\left(\frac{V_1}{V_2}\right)^2\sec^2\theta-1\right\}^{1/2}\left\{\left(\frac{V_1}{V_1'}\right)^2\sec^2\theta-1\right\}^{1/2}\left\{\left(\frac{V_1}{V_2'}\right)^2\sec^2\theta-1\right\}\right.\\&\left.+\left\{2-\left(\frac{V_1}{V_2}\right)^2\sec^2\theta\right\}\left\{2-\left(\frac{V_1}{V_2'}\right)^2\sec^2\theta\right\}\left(\frac{V_1}{V_2'}\right)^2\sec_2\theta\right],\end{aligned}\tag{21}$$

$$\vartheta_D=\tan\theta\left(\frac{V_1}{V_2}\right)^2\sec^2\theta\left\{\left(\frac{V_1}{V_2'}\right)^2\sec^2\theta-1\right\}^{1/2}$$

6） 齊田時太郎，鈴木正治　地震研究所彙報 **12**（1934），517.

$$\cdot\left[4\left\{\left(\frac{V_1}{V_2}\right)^2\sec^2\theta-1\right\}^{1/2}\left\{\left(\frac{V_1}{V_1'}\right)^2\sec^2\theta-1\right\}^{1/2}\left\{\left(\frac{V_1}{V_2'}\right)^2\sec^2\theta-1\right\}\right.$$

$$\left.-\left(\frac{V_1}{V_2'}\right)^2\sec^2\theta\left\{2-\left(\frac{V_1}{V_2}\right)^2\sec^2\theta\right\}\left\{2-\left(\frac{V_1}{V_2'}\right)^2\sec^2\theta\right]\right., \tag{22}$$

$$\vartheta_E=-2\tan\theta\left\{\left(\frac{V_1}{V_1'}\right)^2\sec^2\theta-1\right\}^{1/2}\left(\frac{V_1}{V_2}\right)^2\sec^2\theta\left(\frac{V_1}{V_2'}\right)^2\sec^2\theta$$

$$\cdot\left[\left\{\left(\frac{V_1}{V_2'}\right)^2\sec^2\theta-1\right\}^{1/2}\left\{2-\left(\frac{V_1}{V_2}\right)^2\sec^2\theta\right\}\right.$$

$$\left.-\left\{\left(\frac{V_1}{V_2}\right)^2\sec^2\theta-1\right\}^{1/2}\left\{2-\left(\frac{V_1}{V_2'}\right)^2\sec^2\theta\right\}\right], \tag{23}$$

$$\vartheta_F=-2\left(\frac{V_1}{V_2}\right)^2\left(\frac{V_1}{V_2'}\right)^2\tan\theta\,\sec^4\theta\left\{\left(\frac{V_1}{V_1'}\right)^2\sec^2\theta-1\right\}^{1/2}$$

$$\cdot\left[\left\{\left(\frac{V_1}{V_2'}\right)^2\sec^2\theta-1\right\}^{1/2}\left\{2-\left(\frac{V_1}{V_2}\right)^2\sec^2\theta\right\}\right.$$

$$\left.+\left\{\left(\frac{V_1}{V_2}\right)^2\sec^2\theta-1\right\}^{1/2}\left\{2-\left(\frac{V_2}{V_2'}\right)^2\sec^2\theta\right\}\right]. \tag{24}$$

然る時は

$$C=\frac{\vartheta_C}{\vartheta}\mathfrak{a}\,,\qquad D=\frac{\vartheta_D}{\vartheta}\mathfrak{a}\,,\qquad E=\frac{\vartheta_E}{\vartheta}\mathfrak{a}\,,\qquad F=\frac{\vartheta_F}{\vartheta}\mathfrak{a} \tag{25}$$

によつて，これを（10),（11）に代入すれば，地表層内に於ける U', V' を知る事が出來る．定狀態に於ては $y\leq H$ なる事を考へて，

$$\left.\begin{aligned}U'&=\frac{i2\pi}{L}\cos\theta\left[\frac{\vartheta_C+\vartheta_D}{\vartheta}-\left\{\left(\frac{V_1}{V_2'}\right)^2\sec^2\theta-1\right\}^{1/2}\frac{\vartheta_E-\vartheta_F}{\vartheta}\right]e^{i(fx-pt)},\\ V'&=-\frac{i2\pi}{L}\cos\theta\left[\frac{\vartheta_E+\vartheta_F}{\vartheta}+\left\{\left(\frac{V_1}{V_1'}\right)^2\sec^2\theta-1\right\}^{1/2}\frac{\vartheta_C-\vartheta_D}{\vartheta}\right]e^{i(fx-pt)}.\end{aligned}\right\} \tag{26}$$

即ち初入射波の波長 L に比して地表層の厚さ H が非常に小さい時には，定狀態に於ては地表層內には（26）で表される振動を生じ，深さの方向には全然位相の差が見られない運動をなし，地表層內の一點の運動軌跡は１つの直線をなす．そして $H/L>0$ なる場合に於ける樣な楕圓運動軌跡をなす事は決して見られない．分子の直線軌跡の方向卽ち振動方向が水平軸となす角を ψ とすれば，

$$\phi=\tan^{-1}\frac{\left[\left\{\left(\frac{V_1}{V_1'}\right)^2\sec^2\theta-1\right\}^{1/2}\left(\vartheta_D-\vartheta_C\right)-\left(\vartheta_E+\vartheta_F\right)\right]}{\left[\left(\vartheta_C+\vartheta_D\right)-\left\{\left(\frac{V_1}{V_2'}\right)^2\sec^2\theta-1\right\}^{1/2}\left(\vartheta_E-\vartheta_F\right)\right]}$$

によつて與へられる．軌跡の大きさは（26）より求める事が出來る．振動軌跡は（26）より

$$\left[\frac{\vartheta_E+\vartheta_F}{\vartheta}+\left\{\left(\frac{V_1}{V_1'}\right)^2\sec\theta^2-1\right\}^{1/2}\frac{\vartheta_C-\vartheta_D}{\vartheta}\right]U'$$
$$-\left[\frac{\vartheta_C+\vartheta_D}{\vartheta}-\left\{\left(\frac{V_1}{V_1'}\right)\sec^2\theta-1\right\}^{1/2}\frac{\vartheta_E-\vartheta_F}{\vartheta}\right]V'=0 \qquad (27)$$

となり，分子は直線運動をする事が解る．

以上で $H/L=0$ なる場合の解析研究は止めておく．$H/L>0$ の場合に就ては具體的に數計算が出來た時發表する事にする．

第２章　衝撃波型縱彈性波の入射による表面層を有する半無限彈性體内の體自由波の生成及び傳播機構

第１章で求めた一般解をフーリエの積分公式を利用して，任意の形をした波形が θ なる入射角で $y=0$ 面に入射する時，表面層或は下の媒體内に生ずる自由波の問題を一般的に解決して置く．今初入射波 ϕ_0 の波形の分布を

$$\phi_0=F(x,\ y) \qquad (28)$$

とすれば

$$\phi_0=\frac{1}{4\pi^2}\int_{-\infty}^{\infty}e^{-i\frac{V_1t}{\cos\theta}f}df\int_{-\infty}^{\infty}dr\int_{-\infty}^{\infty}d\xi\int_{-\infty}^{\infty}F(\xi,\eta)e^{i\left\{f(x-\xi)-r(y-\eta)\right\}}d\eta \qquad (29)$$

で入射波は示めされる事は（1）より明であり，第１章の結果を利用して，

$$\phi=\frac{1}{4\pi^2}\int_{-\infty}^{\infty}e^{-i\frac{V_1t}{\cos\theta}f}\,\frac{A}{\mathrm{a}}\,df\int_{-\infty}^{\infty}dr\int_{-\infty}^{\infty}d\xi\int_{-\infty}^{\infty}F(\xi,\eta)e^{i\left\{f(x-\xi)+r(y+\eta)\right\}}d\eta\,, \qquad (30)$$

$$\psi=\frac{1}{4\pi^2}\int_{-\infty}^{\infty}e^{-i\frac{V_1t}{\cos\theta}f}\,\frac{B}{\mathrm{a}}\,df\int_{-\infty}^{\infty}dr\int_{-\infty}^{\infty}d\xi\int_{-\infty}^{\infty}F(\xi,\eta)e^{i\left\{f(x-\xi)+r\left(\frac{\sqrt{\left(\frac{V_1}{V_2}\right)^2-\cos^2\theta}}{\sin\theta}y+\eta\right)\right\}}d\eta, \qquad (31)$$

$$\phi'=\frac{1}{4\pi^2}\int_{-\infty}^{\infty}e^{-i\frac{V_1t}{\cos\theta}f}\frac{C}{\mathfrak{a}}df\int_{-\infty}^{\infty}dr\int_{-\infty}^{\infty}d\xi\int_{-\infty}^{\infty}F(\xi,\eta)e^{i\left\{f(x-\xi)-r\left(\frac{\sqrt{\left(\frac{V_1}{V_1'}\right)^2-\cos^2\theta}}{\sin\theta}y+\eta\right)\right\}}d\eta$$

$$+\frac{1}{4\pi^2}\int_{-\infty}^{\infty}e^{-i\frac{V_1t}{\cos\theta}f}\frac{D}{\mathfrak{a}}df\int_{-\infty}^{\infty}dr\int_{-\infty}^{\infty}d\xi\int_{-\infty}^{\infty}F(\xi,\eta)e^{i\left\{f(x-\xi)+r\left(\frac{\sqrt{\left(\frac{V_1}{V_1'}\right)^2-\cos^2\theta}}{\sin\theta}y+\eta\right)\right\}}d\eta, \quad (32)$$

$$\psi'=\frac{1}{4\pi^2}\int_{-\infty}^{\infty}e^{-i\frac{V_1t}{\cos\theta}f}\frac{E}{\mathfrak{a}}df\int_{-\infty}^{\infty}dr\int_{-\infty}^{\infty}d\xi\int_{-\infty}^{\infty}F(\xi,\eta)e^{i\left\{f(x-\xi)-r\left(\frac{\sqrt{\left(\frac{V_1}{V_2'}\right)^2-\cos^2\theta}}{\sin\theta}y-\eta\right)\right\}}d\eta$$

$$+\frac{1}{4\pi^2}\int_{-\infty}^{\infty}e^{-i\frac{V_1t}{\cos\theta}f}\frac{F}{\mathfrak{a}}df\int_{-\infty}^{\infty}dr\int_{-\infty}^{\infty}d\xi\int_{-\infty}^{\infty}F(\xi,\eta)e^{i\left\{f(x-\xi)+r\left(\frac{\sqrt{\left(\frac{V_1}{V_2'}\right)^2-\cos^2\theta}}{\sin\theta}y+\eta\right)\right\}}d\eta. \quad (33)$$

(30)~(33) に於ける $A/\mathfrak{a}$, $B/\mathfrak{a}$, $C/\mathfrak{a}$, $D/\mathfrak{a}$, $E/\mathfrak{a}$, $F/\mathfrak{a}$ に就ては,

$$\left.\begin{aligned}
a&=\tan\theta, & b&=\left\{\left(\frac{V_1}{V_2}\right)^2\sec^2\theta-1\right\}^{1/2},\\
a'&=\left\{\left(\frac{V_1}{V_1'}\right)^2\sec^2\theta-1\right\}^{1/2}, & b'&=\left\{\left(\frac{V_1}{V_2'}\right)^2\sec^2\theta-1\right\}^{1/2},\\
c&=\left(\frac{V_1}{V_2}\right)^2\sec^2\theta, & d&=2-\left(\frac{V_1}{V_2}\right)^2\sec^2\theta,\\
c'&=\left(\frac{V_1}{V_2'}\right)^2\sec^2\theta, & d'&=2-\left(\frac{V_1}{V_2'}\right)^2\sec^2\theta
\end{aligned}\right\} \quad (34)$$

と置き，尙 $\varDelta$ で 次式を代表さす.

$$\varDelta=\alpha+\beta e^{i(a'+b')fH}+\gamma c^{i2(a'+b')fH}+\delta e^{i2a'fH}+\varepsilon e^{i2b'fH}. \quad (35)$$

但し

$$\alpha=(d'^2+4a'b')\begin{bmatrix}\mu'^2(1+ab)(d'^2+4a'b')\\+\mu\mu'\{cc'(ab'+a'b)-2(d+2ab)(d'+2a'b')\}\\+\mu^2(1+a'b')(d^2+4ab)\end{bmatrix},$$

$$\beta=16\,a'b'd'\left[-2\mu'^2(1+ab)d'+\mu\mu'(d+2ab)(3-b')-\mu^2(d^2+4ab)\right],$$

$$\gamma=(d'^2\pm4a'b')\begin{bmatrix}\mu'^2(1+ab)(d'^2+4a'b')\\-\mu\mu'\{cc'(ab'+a'b)+2(d+2ab)(d'+2a'b')\}\\+\mu^2(1+a'b')(d^2+4ab)\end{bmatrix},$$

$$\delta=(d'^2-4a'b')\left[\begin{array}{l}-\mu'^2(1+ab)(d'^2-4a'b')\\ -\mu\mu'\{cc'(ab'-a'b)-2(d+2ab)(d'-2a'b')\}\\ -\mu^2(1-a'b')(d^2+4ab)\end{array}\right],$$

$$\varepsilon=(d'^2-4a'b')\left[\begin{array}{l}-\mu'^2(1+ab)(d'^2-4a'b')\\ +\mu\mu'\{cc'(ab'-a'b)+2(d+2ab)(d'-2a'b')\}\\ -\mu^2(1-a'b')(d^2+4ab)\end{array}\right]. \tag{36}$$

然る時は，

$$\begin{aligned}\frac{A}{\mathfrak{a}}=&\frac{16a'b'd'}{\Delta}e^{i(a'+b')fH}\Big[\mu^2(d^2-4ab)-\mu\mu'(d-2ab)(3-b')+2\mu'^2(1-ab)(d')\Big]\\ &+\frac{(d'^2+4a'b')}{\Delta}e^{i2(a'+b')fH}\left[\begin{array}{l}-\mu^2(1+a'b')(d^2-4ab)\\ +\mu\mu'\{cc'(a'b-ab')+2(d-2ab)(d'-2a'b')\}\\ -\mu'^2(1-ab)(d'^2+4a'b')\end{array}\right]\\ &+\frac{(d'^2-4a'b')}{\Delta}e^{i2a'fH}\left[\begin{array}{l}\mu^2(1-a'b')(d^2-4ab)\\ -\mu\mu'\{cc'(ab'+a'b)+2(d-2ab)(d'-2a'b')\}\\ +\mu'^2(1-ab)\{d'^2-4a'b'\}\end{array}\right]\\ &+\frac{(d'^2+a'b')}{\Delta}\left[\begin{array}{l}-\mu^2(1+a'b')(d^2-4ab)\\ +\mu\mu'\{cc'(ab'-a'b)+2(d-2ab)\{d'-2a'b')\}\\ -\mu'^2(1-ab)(d'^2+4a'b')\end{array}\right]\\ &+\frac{(d'^2-4a'b')}{\Delta}e^{i2b'fH}\left[\begin{array}{l}\mu^2(1-a'b')(d^2-4ab)\\ +\mu\mu'\{cc'(ab'+a'b)-2(d-2ab)(d'-2a'b')\}\\ +\mu'^2(1-ab)(d'^2-4a'b')\end{array}\right],\end{aligned} \tag{37}$$

$$\begin{aligned}\frac{B}{\mathfrak{a}}=&\frac{16aa'b'd'}{\Delta}e^{i(a'+b')fH}\Big[4\mu^2d-\mu\mu'(2+d)(2+d')+4\mu'^2d'\Big]\\ &+\frac{2a(d'^2+4a'b')}{\Delta}e^{i2(a'+b')fH}\left[\begin{array}{l}-2\mu^2d(1+a'b')+\mu\mu'(2+d)(d'+2a'b')\\ -\mu'^2(d'^2+4a'b')\end{array}\right]\\ &+\frac{2a(d'^2-4a'b')}{\Delta}e^{i2a'fH}\left[\begin{array}{l}2\mu^2d(1-a'b')-\mu\mu'(2+d)(d'-2a'b')\\ +\mu'^2(d'^2-4a'b')\end{array}\right]\\ &+\frac{2a(d'^2+4a'b')}{\Delta}\left[\begin{array}{l}-2\mu^2d(1+a'b')+\mu\mu'(2+d)(d'+2a'b')\\ -\mu'^2(d'^2+4a'b')\end{array}\right]\\ &+\frac{2a(d'^2-4a'b')}{\Delta}e^{i2b'fH}\left[\begin{array}{l}2\mu^2d(1-a'b')-\mu\mu'(2+d)(d'-2a'b')\\ +\mu'^2(d'^2-4a'b')\end{array}\right],\end{aligned} \tag{38}$$

$$\frac{C}{\mathrm{a}}=\frac{8ab'cd'}{\varDelta}e^{i(a'+b')fH}\Big[-\mu^2(2a'b-d)+\mu\mu'(2a'b-d')\Big]$$
$$+\frac{2ac(d'^2-4a'b')}{\varDelta}e^{i2b'fH}\Big[\mu\mu'(bd'+2b')-\mu^2(b'd+2b)\Big]$$
$$+\frac{2ac(d'^2+4a'b')}{\varDelta}\Big[\mu\mu'(-bd'+2b')+\mu^2(-b'd+2b)\Big], \tag{39}$$

$$\frac{D}{\mathrm{a}}=\frac{8ab'cd'}{\varDelta}e^{i(a'+b')fH}\Big[-\mu^2(2a'b+d)+\mu\mu'(2a'b+d')\Big]$$
$$+\frac{2ac(d'^2+4a'b')}{\varDelta}e^{i2(a'+b')fH}\Big[-\mu\mu'(bd'+2b')+\mu^2)b'd+2b)\Big]$$
$$+\frac{2ac(d'^2-4a'b')}{\varDelta}e^{i2a'fH}\Big[\mu\mu'(bd'-2b')+\mu^2(b'd-2b)\Big], \tag{40}$$

$$\frac{E}{\mathrm{a}}=\frac{8aa'cd'}{\varDelta}e^{i(a'+b')fH}\Big[\mu^2(b'd+2b)-\mu\mu'(bd'+2b')\Big]$$
$$+\frac{2ac(d'^2+4a'b')}{\varDelta}\Big[\mu\mu'(d'+2a'b)-\mu^2(d+2a'b)\Big]$$
$$+\frac{2ac(d'^2-4a'b')}{\varDelta}e^{i2a'fH}\Big[-\mu\mu'(d-2a'b)+\mu^2(d-2a'b)\Big], \tag{41}$$

$$\frac{F}{\mathrm{a}}=\frac{8aa'cd'}{\varDelta}e^{i(a'+b')fH}\Big[\mu^2(b'd-2b)+\mu\mu'(bd'-2b')\Big]$$
$$+\frac{2ac(d'^2+4a'b')}{\varDelta}e^{i2(a'+b')fH}\Big[\mu\mu'(d'-2a'b)-\mu^2(d-2a'b)\Big]$$
$$+\frac{2ac(d'^2-4a'b')}{\varDelta}e^{i2b'fH}\Big[-\mu\mu'(d'+2a'b)+\mu^2(d+2a'b)\Big]. \tag{42}$$

(30)～(33) に於て，A/a, B/a, C/a, D/a, E/a, F/a は (35), (37), (38), (39), (41), (42) で見る如く，分母，分子に f に關する圓函數を含んだ超越函數である. f に關する積分の爲めこれ等を $e^{ia'fH}$, $e^{ib'fH}$ の冪級數に展開するのであるが，その爲めには，$1/\varDelta$ のみを展開すれば充分であつて，次の如くなる.

$$\frac{1}{\varDelta}=\Big[\frac{1}{\alpha}-\Big\{\frac{\delta}{\alpha^2}e^{i2a'fH}+\frac{\beta}{\alpha^2}e^{i(a'+b)fH}+\frac{\varepsilon}{\alpha^2}e^{i2b'fH}\Big\}+\Big\{\frac{\delta}{\alpha^3}e^{i4a'fH}+2\frac{\beta\delta}{\alpha^3}e^{i(3a'+b')fH}$$
$$+\Big(\frac{\beta}{\alpha^3}+2\frac{\delta\varepsilon}{\alpha^3}-\frac{\gamma}{\alpha^2}\Big)e^{i2(a'+b')fH}+2\frac{\beta\varepsilon}{\alpha^3}e^{i(a'+3b')fH}+\frac{\varepsilon}{\alpha^3}e^{i4b'fH}\Big\}$$

$$
\begin{aligned}
&-\left\{\frac{\delta^3}{\alpha^4}e^{i6a'fH}+3\frac{\beta\delta}{\alpha^4}e^{i(5a'+b')fH}+\left(3\frac{\beta^2\delta}{\alpha^4}+3\frac{\varepsilon\delta^2}{\alpha^4}-2\frac{\gamma\delta}{\alpha^3}\right)e^{i2(2a'+b')fH}\right.\\
&+\left(6\frac{\beta\delta g}{\alpha^4}+\frac{\beta^3}{\alpha^4}-2\frac{\beta\gamma}{\alpha^3}\right)e^{i3(a'+b')fH}+\left(3\frac{\beta^2\varepsilon}{\alpha^4}+3\frac{\varepsilon^2\delta}{\alpha^4}-2\frac{\gamma\varepsilon}{\alpha^3}\right)e^{i2(a'+2b')fH}\\
&\left.+3\frac{\beta\varepsilon^2}{\alpha^4}\varepsilon^{i(a'+5b')fH}+\frac{\varepsilon^3}{\alpha^4}e^{i6b'fH}\right\}+\left\{\frac{\delta^4}{\alpha^5}e^{i8a'fH}+4\frac{\beta\delta^3}{\alpha^5}e^{i(7a+b')fH}\right.\\
&+\left(4\frac{\delta^3\varepsilon}{\alpha^5}+6\frac{\delta^2\beta^2}{\alpha^5}-3\frac{\delta^2\gamma}{\alpha^4}\right)e^{i2(3a'+b')fH}+\left(4\frac{\delta\beta^3}{\alpha^5}+12\frac{\delta^2\beta\varepsilon}{\alpha^5}-6\frac{\gamma\delta\beta}{\alpha^4}\right)e^{i(5a'+3b')fH}\\
&+\left(12\frac{\varepsilon\beta^2\delta}{\alpha^5}+6\frac{\varepsilon^2\delta^2}{\alpha^5}+\frac{\beta^4}{\alpha^5}+\frac{\gamma^2}{\alpha^3}-\frac{3\beta^2\gamma}{\alpha^4}-\frac{6\gamma\delta\varepsilon}{\alpha^4}\right)e^{i4(a'+b')fH}\\
&+\left(\frac{\varepsilon\beta^3}{\alpha^5}+12\frac{\delta\beta\varepsilon^2}{\alpha^5}-6\frac{\varepsilon\beta\gamma}{\alpha^3}\right)e^{i(3a'+5b')fH}+\left(4\frac{\delta\varepsilon^3}{\alpha^5}+6\frac{\varepsilon^2\beta^2}{\alpha^5}-3\frac{\varepsilon^2\gamma}{\alpha^4}\right)e^{i2(a'+3b')fH}\\
&\left.+\frac{\varepsilon^3\beta}{\alpha^5}e^{i(a'+7b')fH}+\frac{\varepsilon^4}{\alpha^5}e^{i8b'fH}\right\}+\cdots\cdots\Big]. \qquad (43)
\end{aligned}
$$

（43）の展開に於ては第８項まで示して置いたが，目的によつては，即ち H/C の大きの關係に從つて，實際上項數を增す必要がある．この（43）を（35）～（42）に代入する時は，A/a, B/a, C/a, D/a, E/a 及び F/a は夫々 $e^{ia'fH}$ 及び $e^{ib'fH}$ の多項式となるのである．從つて，（29）なる初入射波によつて起される彈性體內に生ずる（30),（31),（32),（33）なる自由波は全部

$$F=Q\int_{-\infty}^{\infty}e^{i\left(qH+\frac{V_1t}{\cos\theta}\right)f}df\int_{-\infty}^{\infty}dr\int_{-\infty}^{\infty}d\xi\int_{-\infty}^{\infty}F(\xi,\eta)e^{i\left\{f(x-\xi)-r(wy+\eta)\right\}}d\eta \qquad (44)$$

の型で表はされる事となる．從つて

$$F(x,y)=e^{-\frac{(x\cos\theta-y\sin\theta)^2}{c^2}} \qquad (45)$$

の如く衝撃波型の初入射による彈性體內に生ずる自由波の問題は完全に解決する事が出來るのであつて，q, Q を（35)～(43）の各項に應ずる樣に撰べばよい事となる．この積分法は旣に別の論文[7] で論じておいた．（43）に於ける各項は皆（37),（38),（39),（40),（41),（42）と共に夫々力學的の意味を有し $y=0$ なる兩彈性體の境界面或は $y=H$ なる自由表面に於ける數次の反射或は屈折によつて自由波の强さが減少して行く事を示すものである．具體的な例に就て數計算を行へばこの樣な性質は明かにされるのであるが，次の報告で詳しく論ずる事とする．尙（43）に於て展開

---

[7] 西村源六郎，金井淸　地震硏究所彙報 12 (1934), 292.

式の次數が增すに從つてその項の係數が小さくなる事は，各項の係數の分母 α が分子の $\beta, \gamma, \delta, \varepsilon$ より非常に大きくなる事が具體的の計算に就て明かにされる事を考へれば，解かる事であつて，(48) の展開は數學的の收斂も非常によいものである．

（續く）

---

40. *On the Effect of Discontinuity Surfaces on the Propagation of Elastic Waves. (VII)*

By Genrokuro NISHIMURA,

Earthquake Research Institute.

In the present paper are studied the vibratory motions of a surface layer and a subjacent semi-infinite elastic body when a dilatational wave is obliquely incident on the common boundary where the two solids adhere closely.

In the first chapter, we studied the general properties of free waves propagated in the two solids, namely, in the surface layer and the subjacent solid, when a dilatational wave of harmonic wave-type of infinite extent is obliquely incident on the bottom surface of the surface layer. In the second chapter are explained analytically the general phenomena of wave motion in the two solids when a dilatational wave of shock wave-type is obliquely incident on the common boundary.

---

41. *Supplementary Notes on the Most Suitable Formula for the Japanese Gravity Values.*

By Chûji TSUBOI and Takato FUCHIDA,

Earthquake Research Institute.

(Read June 18, 1935.—Received June 20, 1935.)

In a former paper of his[1], one of the present authors showed by an approximate calculation that the most suitable formula for the Japanese gravity values was

$$\gamma = 977{\cdot}981\ (1 + 0{\cdot}005\,562 \sin^2\varphi)$$

using as data g_0'' at the Japanese gravity stations which are 122 in number. The ellipticity of the geoid corresponding to this gravity formula is 1/322 which is much smaller than the normal value. Although the above calculation was an approximate one, the large departures of the numerical constants in this formula from the corresponding ones in other ordinary formulas cannot be overlooked. This seems to indicate that an abnormal subterranean structure exists in the neighbourhood of Japan noted for the seismic and volcanic activities.

Seeing, however, that there was some incompleteness in the former calculation, the authors intend here to determine the most suitable formula for the Japanese gravity values g_0', not for g_0''. The present calculation, therefore, is based on the Helmert's method of condensation reduction.

The determination of the formula was made by the method of successive approximation. First of all, tentative values were assigned to g_e and β in the formula

$$\gamma = g_e\ (1 + \beta \sin^2\varphi)$$

and from a set of 122 observation equations of the form

$$g_0' - \gamma = \frac{\partial\gamma}{\partial g_e}\Delta g_e + \frac{\partial\gamma}{\partial\beta}\Delta\beta = (1 + \beta\sin^2\varphi)\ \Delta g_e + g_e \sin^2\varphi\Delta\beta,$$

Δg_e and $\Delta\beta$ are determined by the method of least square, the solution being the cerrections to be applied to the constants in the initial tentative formula. Repeating this process until we have $\Delta g_e=0$ and $\Delta\beta=0$, we get the final formula.

---

[1] C. TSUBOI, *Bull. Earthq. Res. Inst.*, **11** (1934), 632.

In the present case, we started from the formula,

$$\gamma=977{\cdot}968\ (1+0{\cdot}005\,640\sin^2\varphi)$$

and obtained

$$\Delta g_e=+0{\cdot}030, \qquad \Delta\beta=-0{\cdot}000\,10.$$

Then as the next approximation, we started from

$$\gamma=977{\cdot}998\ (1+0{\cdot}005\,540\sin^2\varphi)$$

and obtained

$$\Delta g_e=0{\cdot}000, \qquad \Delta\beta=-0{\cdot}000\,002.$$

Thus we get as the final formula

$$\gamma=977{\cdot}998\ (1+0{\cdot}005\,538\sin^2\varphi).$$

The departure of each of the observed g_0' from γ ranges from $+0{\cdot}161$ to $-0{\cdot}111$, the mean without sign being $0{\cdot}035$. This large departure makes the probable error of each of the constants in the formula also large, thus

$$g_e=977{\cdot}998\pm0{\cdot}019, \qquad \beta=0{\cdot}005\,538\pm0{\cdot}000\,053.$$

The reciprocal of the ellipticity of the geoid that corresponds to this gravity formula is $319{\cdot}5\pm5{\cdot}4$.

In Fig. 1 are plotted g_0' at the gravity stations against the corresponding $\sin^2\varphi$. The broken line in the figure which corresponds to the Helmert's formula

$$\gamma=978{\cdot}030\ (1+0{\cdot}005\,302\sin^2\varphi)$$

does not agree well with the gravity values observed in Japan.

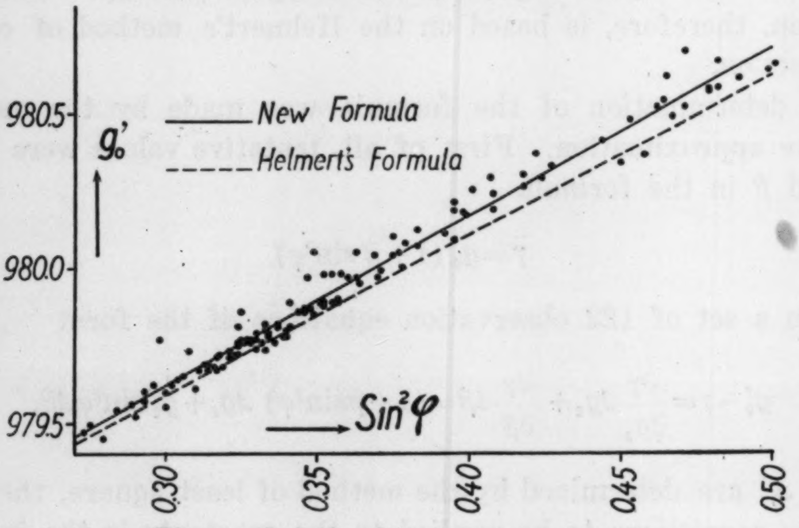

Fig. 1. Relation between g_0' and $\sin^2\varphi$.

Although some further gravity reductions, such as the isostatic or "geological", may considerably reduce the gravity anomalies and the formula based on the gravity values thus reduced may indicate the normal ellipticity of the geoid, it is a noteworthy fact that the ellipticity of the actual geoid in Japan is considerably smaller than the normal one determined from the world wide gravity determination.

41. 日本の重力に最もよく適合する式

地震研究所 坪井忠二
淵田隆門

日本に於ける重力の値 g_0' を材料さし，これに最もよく適合する式を求めて

$$\gamma=977{\cdot}998\,(1+0{\cdot}005\,538\,\sin^2\varphi)$$

を得た．此の式に相當するヂオイドの扁平度の逆數は 319·5±5·4 である．之等の常數が世界の重力の値から定めたものさ著しい差があるのは注意す可き事である．

42. *Recent Changes in Area of the Base Line Rhombus at Mitaka.*

By Chûji TSUBOI,
Earthquake Research Institute.

(Read June 18, 1935.—Received June 20, 1935.)

In the compound of the Tokyo Astronomical Observatory at Mitaka, there is a special set of five geodetic base lines, which are each very nearly 100 m in length and which are so arranged as to form a rhombus consisting of two equilateral triangles NES and NSW with one side NS common to both. (Fig. 1.) This was laid down in 1916 by the Imperial Japanese Geodetic Commission with the object in view to measure the horizontal dilatation or contraction, if any, of the earth's crust near Mitaka. As the writer has already pointed out in previous papers of his,[1] precise measurements of the lengths of these base lines, which have since 1916 been made once a year on the average, showed that the base lines have not remained constant in length, resulting in the increase or decrease of the areas of the two triangles NES and NSW. As the continuation of the previous papers, the results of the length measurements of the base lines that were made twice in 1934 by experts of the Military Land Survey and were placed at the writer's disposal recently will be discussed in the present paper.

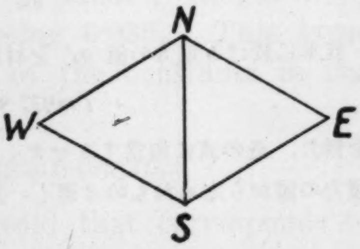

Fig. 1. The base line rhombus.

The lengths of the base lines in February and December of 1934 are as follows:

	NE	ES	NS	SW	NW
	m mm				
Feb. 1934.	100+1·76	100+0·53	100+3·29	100+1·72	100+1·33
Dec. 1934.	100+1·59	100+0·15	100+3·12	100+1·63	100+1·06

Utilising the successive changes in length of the base lines, the specific changes in area of the triangles can be calculated in the following manner.

---

[1] C. TSUBOI, *Proc. Imp. Acad.*, **6** (1930), 367; **7** (1931), 155; *Bull. Earthq. Res. Inst.*, **8** (1930), 384; *Jap. Journ. Astr. Geophys.*, **10** (1933), 93.

The area S of a triangle of which the sides are a, b, and c is given by

$$S=\sqrt{s(s-a)(s-b)(s-c)}\,,$$

where $$s=\frac{1}{2}(a+b+c).$$

We have then

$$\frac{dS}{S}=\frac{1}{2}\left(\frac{ds}{s}+\frac{ds-da}{s-a}+\frac{ds-db}{s-b}+\frac{ds-dc}{s-c}\right).$$

For an equilateral triangle

$$a=b=c,$$

whence $$\frac{dS}{S}=\left(\frac{ds}{s}+\frac{ds}{s-a}\right).$$

As $s=150$ m and $a=b=c=100$ m in the present case, we have

$$\frac{dS}{S}=\frac{ds}{75{,}000}$$

ds being expressed in mm.

The recent changes in area of the triangles thus calculated are as follows:

	⊿NES	⊿NSW
Oct. 1931.		
	$-0{\cdot}22\times10^{-5}$	$-0{\cdot}89\times10^{-5}$
Feb. 1934.		
	$-0{\cdot}48$	$-0{\cdot}35$
Dec. 1934.		

They are all negative and indicate the horizontal contraction of the earth's crust. The continuous observation by R. Takahasi[2] of the length change of the earth's surface crust at Komaba, about 13 km E of Mitaka, also indicates the contraction recently.

The changes in area of the triangles since the first measurement in 1916 are given in Table I and are graphically shown in Fig. 2. It is to be noted that the triangles have undergone specific changes in area of the order of 10^{-5}.

---

2) R. TAKAHASI, *Bull. Earthq. Res. Inst.*, **12** (1934), 760.

Table I. Changes in Area of the Triangles NES and NSW of the Base Line Rhombus in 10^{-5}.

	⊿NES	Integrated	⊿NSW	Integrated
June 1916				
Feb. 1917	−0·04	−0 04	−0·05	−0·05
Oct. 1917	+0·55	+0·51	+0·50	+0·45
Feb. 1918	−0·56	−0·05	−0·36	+0·09
Oct. 1918	−0·06	−0·11	−0·17	−0·08
Dec. 1919	+0·38	+0·27	+0·31	+0·23
Nov. 1920	+0·32	+0·59	+0·34	+0·57
Nov. 1921	+0·05	+0·64	+0·14	+0·71
Nov. 1922	−0·26	+0·38	−0·17	+0·54
Sept. 1923	+2·87	+3·25	+2·97	+3·51
Oct. 1923	−0·46	+2·79	−0·63	+2·88
Jan. 1924	−0·15	+2·64	−0·37	+2·51
Aug. 1924	−0·53	+2·11	−0·16	+2·35
Dec. 1925	+0·55	+2·66	+0·21	+2·56
Dec. 1927	+0·87	+3·53	+1·00	+3·56
March 1929	−0·25	+3·28	−0·14	+3·42
Feb. 1930	−0·41	+2·87	−0·53	+2·89
Oct. 1931	−0·11	+2·76	+0·83	+3·72
Feb. 1934	−0·22	+2·54	−0·89	+2·83
Dec. 1934	−0·48	+2·06	−0·35	+2·48

On the other hand, according to the mareographic observations at Aburatubo which is situated 60 km S of Mitaka and at the top of Miura Peninsula, the height H of a bench-mark here above the mean sea level has undergone secular changes as shown in Fig. 2. Although the height of the annual mean sea level at a coastal station is affected more or less by meteorological conditions over the adjacent sea of the station in the corresponding year, at least some part of the observed change in the level is attributable to the absolute vertical displacement of the earth's crust near the station. The similarity of the two curves showing the changes in H and in

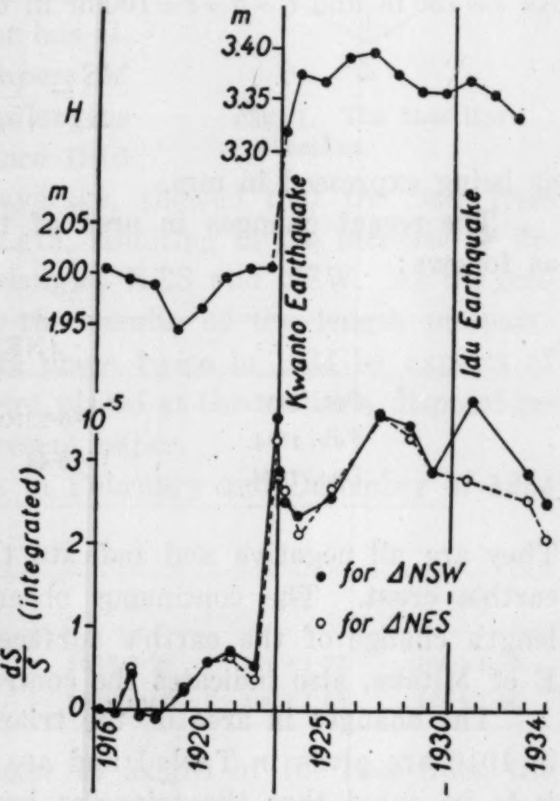

Fig. 2. dS/S ··· Changes in area of the triangles ⊿NES and ⊿NSW.
H ··· Height of the bench-mark at Aburatubo above the annual mean sea level.

area of the triangles is rather striking. The increase or decrease of the areas of the triangles respectively corresponds to the upheaval or depression of the earth's crust at Aburatubo.

It seems thus probable that the change in area of the Mitaka base line rhombus is not of a local character but is some or other manifestation of a larger crust deformation prevailing at least over the southern half of the Kwantô district.

---

42. 三鷹基線菱形の最近の面積變化

地震研究所 坪井忠二

三鷹基線菱形の面積變化に就いては嘗て報告した事があるが，本文では昭和９年２月及び12月に得られた測定結果を材料として，其の後の變化を論じた. 計算の結果によれば面積變化は次の通りである.

	⊿NES	⊿NSW
昭和６年10月	$-0{\cdot}22\times10^{-5}$	$-0{\cdot}89\times10^{-5}$
昭和９年２月	$-0{\cdot}48$	$-0{\cdot}35$
昭和９年12月		

尙面積變化の模様が油壺に於ける水準點の平均海水面上の高さの變化の模様と類似して居るのは著しい事で，これは上述の面積變化が三鷹局部的のものでなく，少くとも關東地方の南半分に起つて居る地殼變動のあらはれである事を暗示する.

43. *Colloids and Seismology.*

By Torahiko **TERADA**,

Earthquake Research Institute.

(Read April 16, 1935.—Received June 20, 1935.)

1. Seismology is a special branch of applied science and owes its essential advancement to the application of our knowledges in almost every department of pure science, i. e., not only of physical, but also of chemical and even of biological sciences. Introduction of any new source of knowledges in the domain of seismology will not fail to shed some new light under which some problems may obtain a further elucidation than might be otherwise possible.

2. Among the fundamental knowledges upon which the investigation of earthquake phenomena are based, the most important are those related to the mechanical properties of materials constituting the different layers of the earth's crust, such as elasticity, plasticity, viscosity, visco-elasticity, etc. In want of exact knowledges about these properties, any reliable theory of seismic phenomena can scarcely be propounded.

3. The materials constituting the earth's crust are mostly colloidal, if we use this word in its widest sense, i. e., in the same sense as we may call any polycrystalline metallic alloy as such. Especially, among the materials constituting alluvial deposits there are many which must be regarded as colloids in the ordinary sense of the word. As regards such a substance, other mechanical properties come into play than are usually taken into consideration in dealing with problems concerning the mechanical behaviour of the surface crust.

4. An example near at hand is the alluvial sedimentation deposited as a river delta. The problems of colloidal sedimentation in such a case was already investigated from many sides. As regards, however, to those very problems which are most closely related to seismology, due attention seems to have not yet been paid. From the seismological point of view, the gradual volume change of the deposited materials subsequents to sedimentation, due to the gradual change in

---

1) For example see Pierre **URBAIN**, "Les science géologiques et la notion d' état colloidal", (1933).

colloidal states of materials, i. e., change in degree of coagulation, swelling, etc., cannot be carelessly put out of consideration, especially in cases when we are to deal with the mode of vertical movements of the earth's crust such as revealed by the results of repeated precise levelling survey. For instance, if there may occur a linear contraction or expansion of only 1/10,000 in a layer of 100 m thickness, it will be observed as a subsidence or upheaval of 10 mm of a bench-mark situated on such a layer, an amount which may easily be detected by means of precise levelling, provided that there exists a point of reference or datum station which is not very far from the above said bench-mark and which is situated upon a substratum not much affected by such a colloidal change of volume.

5. In considering the physical significance of the vertical displacement of bench-mark situated upon a layer consisting of mud, sand and gravels, the following factors must necessarily be considered:

(a) Effect of the change in mode of packing of granular mass, an effect which was fully treated in O. Reynolds's classical investigation.

(b) Effect of electrolytes on the apparent volume of fine sand as was recently investigated by Freundlich and Juliusburger[2] with powdered slate from Solnhofen.

(c) Effect of the change in degree of swelling due to any change in electrolytes content of water circulating in the sedimentary layer.

(d) Effect of volume change connected with the change in content of capillary water due to the capillary force.

6. According to (a), various modes of change in level of the ground surface may be brought about. If a layer of the substratum consisting of granular mass in state of closest packing be violently disturbed by severe shocks of such an intensity as is observed in the epicentral region of destructive earthquake, a sensible dilatation of apparent volume may be produced. The amount of volume change due to this cause is known to be quite sensible, as is demonstrated by sudden drying up of the surface of fine sand layer on a sea shore when trodden upon. Hence, in the case when the thickness of the layer disturbed be of several hundred metres or more as is usual with sedimentary deposit, the total amount of upheaval of the surface may become quite sensible. The upheaval due to this cause may tend afterwards to gradually subside and the subsidence may be accelerated by suitable shocks or vibrations, as may also be demonstrated by laboratory experiment.

---

[2] *Trans. Farady Soc.*, **30** (1934), 333; see also *ibid.*, **31** (1935), 769, in which thixotropic property of "quick sand" is discussed.

In actual cases, therefore, in which a sudden upheaval is observed in the epicentral region of severe earthquake, accompanied with subsequent gradual subsidence, it will be reasonable to inquire whether the above effect may not be involved, at least partly, in the mechanism of the change observed. The following alternative is also conceivable: i. e., the constituent granular matters which were initially in equilibrium in state of closest packing may undergo gradual chemical and physical change and, on account of it, the grains may acquire mechanical and colloidal properties somewhat different from those formerly possessed. This may lead to a deformation in the geometrical shape of grain and consequently to a new mode of closest packing throughout the layer containing these grains. The transition to the new state of packing may be facilitated by seismic shocks or vibrations. It may also be remarked that what is considered above may apply not only to a loose granular mass but to some kinds of rock mass, though in comparatively less degree, if we consider that the subterranean rock layers are run through with numerous joints and fissures.

7. Next, according to (b) and (c), we may consider the following points. Alluvial sedimentations, especially those in the case of the delta of a river discharging into sea, took place in water with a certain concentration of the constituent electrolytes. Afterwards, the upper surface of the sedimentation layer had been exposed to atmosphere. The constant percolation of meteoric precipitation water may have resulted in some change in electrolyte contents of the colloidal matters contained in the layer by a process similar to dialysis, and thence may have led to a change in degree of coagulation and swelling. The latter change may sometimes contribute something to the apparent change in the level of the ground surface, as it is well known that the mechanical stress caused by such a colloidal process may attain enormous amount under favourable circumstances.

8. As regard to the factor (d) above mentioned, we way point out a case in which, the increase of plastered area as well as the development of sewage system in a city, have brought about a considerable lowering of the ground water level. In this case, if the substratum be of such a nature that its apparent volume is sensitive to its content of capillary water, we may expect some sensible change in the height of benchmarks situated on such a ground.[3]. It is well known that some kinds of soil are subjected to very conspicuous contraction

---

[3] Mr. N. Miyabe is at present engaged in the investigation regarding this point and his result will appear in this Bull. in a near future.

by loss of water content.

9. The actual vertical displacement of the surface of the ground revealed by the method of repeated precise levelling may be regarded as the resultant of the displacement of the underlying earth's crust proper due to geotectonic causes plus the elastic and plastic deformation due to some change in surface loading both natural and artificial, and the displacement due to the colloidal volume changes above considered. It is therefore of serious importance to carefully discriminate in what degree the above enumerated colloidal factors are participated in producing the observed change in the heights of bench-marks, especially in the case when the substratum consists of loose alluvial deposits as in the cases of Osaka and some quarters of Tôkyô. Without such a discrimination of complicated causes it is difficult to say anything definitive about the geodynamic process going on in the deeper part of the crust such as is closely connected with the origin of earthquake.

10. In view of the above considerations, the rapid subsidence observed in the course of the last few years in a certain limited area in the city of Tôkyô[4] and also of Osaka[5] may be suspected to be connected at least partly with the causes mentioned above. The areas with the remarkable annual rates of depression are situated on alluvial formations of rather recent origin. Moreover, in the last ten years the plastered areas of streets have been rapidly increasing and in some places a remarkable lowering of underground water level is reported. It is, therefore, premature to conclude from the apparent depression of levelling routes in these areas that the earth's crust proper under these areas are undergoing corresponding rapid deformations and it is too far fetched to anticipate a coming severe earthquake in these regions, before a careful analysis of the observed data into their various components due to the respective causes has been effected.

11. On the other hand, the change in colloidal state is often connected with a change in mechanical stress prevailing in colloidal medium. An example is afforded by enormous pressure exerted by a swelling gel. A change in state of a colloidal alluvial deposit may sometimes give rise to an additional stress upon the surface crust and may eventually play a role as one of the secondary causes of earthquake, in the case when the linear dimension of the area covered with such a layer be comparable with the thickness of the crust in which the potential energy of earthquake is stored up.

---

[4] N. Miyabe, *Proc. Imp. Acad.*, **8** (1932), 417.

[5] A. Imamura, *Proc. Imp. Acad.*, **8** (1932), 378; **11** (1935), 186.

12. Among the other mechanical propoperties of colloids which may be of special interest for seismologists, we may especially mention the *thixotropic* property of some class of colloids. An interesting example was recently studied by Freundlich and Juliusburger in the paper already cited. The present author experimented with a kind of sand called "aosuna (blue sand)" which is an artificial mixture of sand with some organic colloid pigment and commonly used for wall plastering of Japanese houses. A conspicuous stage of thixotropy could be observed, when the sand is made to deposit slowly in water contained in a cylindrical glass vessel. The sand is first thoroughly shook with water and made to deposit. When the sedimentation is ended a slight shock is given to the vessel. The head of the sand column shrinks down by a certain sensible amount. A second shock causes the second shrinkage and so on. When the shocks are thus repeated, a stage is attained when the sand layer is apparently solidified so that by tilting the vessel no flow or deformation of the surface of the sand is observed. By giving, however, a violent shock to the vessel, the solid sand mass is at once transformed into liquid as may be seen from the oscillating motion of its surface. The surface then falls down slightly and again solidified. The thixotropic state may be once more or twice observed by repeating strong shocks. Finally, the whole mass is solidified as far as the present kind of demonstration experiment is concerned.

13. There seems to exist some class of geophysical phenomena which may be rightly explained by taking account of the thixotropic property of earth materials. On the occasion of the Kwantô Earthquake of 1923, a striking case was reported of sudden emergence of buried wooden pillars above the surface of a rice field near the River Sagami. The pillars once formed the piers of an ancient wooden bridge and remained long under the soil, being forgotten even by the inhabitants of the locality. It is probable that the severe shocks of the earthquake, having its epicentre near this locality, momentarily turned the earthy materials surrounding the pillars into a state comparable to a fluid and the wooden pillars were upheaved on account of their own bouyancy, which is large due to the large density of the ambient "fluid".

14. In the case of landslides which are most frequently induced by severe earthquakes this very thixotropic property of earthy substratum may also play some important part, provided that the substratum to be traversed by the "slip-plane" is especially endowed with such property. This consideration will suggest some modification in the usual theory of landslide phenomena.

15. The present note is written with the mere purpose of drawing the attention of seismologists especially those interested with the secular movement of the earth's crust, to those colloidal properties of some crust materials as are here considered, as these properties seem to have not yet been duly taken account of, inspite of their probable importance in connection with many urgent problems of modern seismology.

---

43. コロイドと地震學

地震研究所　寺田寅彦

地震學の基礎として地殼を構成する物質の物理的性質に關する詳細な知識が必要であるが，從來の地震學では地殼を普通の固體と見做し，それの彈性，粘撓性，粘性，粘彈性等を考慮してゐるに過ぎない．多くの場合にはそれで一應十分であらうが，必しもさうでない場合がある．例へば地殼上層が膠狀物質と考へられるもので成立つてゐる場合がさうである．

普通岩石の如きものも廣義に於けるコロイドと見られないこともないが，それよりも，普通沖積層と稱する地層中には普通の意味でコロイドと稱すべきものを含有するものが多い．

從來でもこれ等膠質物の沈積に關する研究は多いが，一旦沈積した後に於けるそれの體積變化に關する膠質物理學的研究は比較的少なく，特に地震學に連關してのさうした研究は甚稀である．然るに近來地震學上から地殼の垂直變動に關する水準測量成果の研究が盛になつて來て，水準線路の昇降から地殼の運動が推定されるやうになつたので，此際に於て膠質的地層の體積がその含水量や電解質含有量の長期變化によつて如何なる程度に變化し得るかを研究し，それを地殼深層までも參與するやうな正當な意味での地殼變動と區別して考へることが必要であると思はれる．

細砂や粘土が水と混合したものは，その水中の電解質含量の多少により著しい體積變化を示すことが知られてゐるので，河口三角洲に堆積した此種の層が水面に露出して後多年降水の滲透を受けて電解質含量を變じ，その爲に起る可逆的或は不可逆的な見掛け上の體積變化を生ずる事も可能である．

又土壤の如きものゝ見掛けの體積は含水量の變化により著しい變化を示すこともよく知られて居る．

此等の變化は數プロセントより時には數十プロセントに達する．假に 100 m の層の厚さが 1% 變れば表面の標高變化は 1 m に達するのである．それで精密水準測量の結果で數粍又は數糎の昇降を論ずる場合にはどうしてもこの因子を度外視することは出來ない．

近年東京の本所，深川，又大阪市の一部が年々著しい沈降を示し，一見地殼の大變動を豫想せしめるものがあるが，此等の地はいづれも比較的新時代の冲積層より成るものであるから上記の如き膠質的變化による體積變化も無視する事が出來ないし，又一方此等地方では最近數年間市街

の舗裝工事並びに下水工事の進捗の結果として地下水の系統に可也著しい變化が起つたであらうと考へられるから，この爲にも表層土壤の體積變化が若干起り得るものと考へなければならない．兎に角此等の諸點を考慮しこれ等に因る水準變化の部分を除去した後でなければ容易に地殼運動等の問題を論ずることは困難であらう．

なほ，膠質の膨潤等により强大な器械的歪力の發生することも知られてゐるから，表面沖積層等の體積變化に伴ふ歪力が地震發生の第二次的誘因として作用する場合もないとは云はれない．

なほ又或種の膠質物に特有な所謂 Thixotropy の現象も地震學と連關して時に考慮を要することがある．例へば地震によつて地下に埋沒してゐた橋脚が浮上がつたりする現象はこれで說明される．又地辷りの場合にもこの性質が重要因子となり得る．

土砂層の見掛けの體積にはレーノルヅの研究した粒子充塡度の影響もあるので，大地震の激動で地盤が擾亂を受けた際この效果で表面が隆起し，その後徐々に落着く場合もあり得るから此點も考慮を要する．又相當深い地層でも多數の裂罅を有する場合には地震の爲に各岩片が平衡位置から移動して見掛けの體積を增す場合があるかも知れない．

此等の諸點を十分考慮に入れた上で地殼變動を論じなければならないので，その爲には將來地震學の範圍內に一般膠質に關する物理化學上の知識を十分に取入れることが望ましいと思はれる．

44. *Relations between Earthquakes and Precipitation, Barometric Pressure, and Temperature.*

By Seiti YAMAGUTI,

Earthquake Research Institute.

(Received June 20, 1935.)

Introduction.

In a previous papers[1], some possible effects of thunderstorm and also of cyclone upon the occurrence of earthquakes were studied. In connection with these problems, the relations between earthquakes and precipitations as well as barometric pressure and temperature, are investigated statistically in the present paper.

This problem was already investigated by Prof. F. Ômori[2], with the result that rather intimate correlation could be found between the earthquakes *observed* at Tôkyô and the precipitations at Niigata and Akita.

More reliable data in these days than in the time of Prof. Ômori for the earthquakes, as well as for the meteorological elements, could be taken from the Abridged Monthly Report of the Central Meteorological Observatory in Japan during the period of just ten years, from June, 1924 to May, 1934.

Method of Investigation.

As for the "felt" earthquakes which occurred in Kwantô District, they were classified into 5 groups according to the locality; these are, Iwaki Oki and Kasima Nada; Tyôsi Oki and Sagami Nada; Kinugawa, Tonegawa and Kasumigaura; Tôkyô and Bôsô Hantô; Sagami (land) and Idu Hantô. They were compared firstly, with the precipitations, the barometric pressure and the temperature on the Japan Sea side, and secondly with those on the Pacific side, and lastly with the differences of the two sides.

The meteorological elements in the Japan Sea side were taken from the data at three stations, Kanazawa, Takata and Niigata, for each season, namely, Spring (March∼May), Summer (June∼Aug.), Autumn (Sept.∼Nov.), Winter (Dec.∼Feb.), and denoted by Q_J, B_J, and T_J for the precipitations, the barometric pressure and the temperature, respectively. Those for the Pacific side were taken from the data at three stations, Tôkyô, Mito and Onahama, and denoted by Q_P, B_P, and T_P, respectively.

---

[1] S. YAMAGUTI, *Bull. Earthq. Res. Inst.*, **12** (1934), 214 and 742.

[2] F. ÔMORI, *Rep. Imp. Earthq. Inv. Comm.*, **68**-1 (1910), 21.

We have calculated the correlation coefficients, of the "felt" earthquakes in respective region above cited in each season, with respect to the corresponding values of Q's, B's and T's, applying the ordinary formula, $r=\dfrac{\sum\Delta x\Delta y}{\sqrt{\sum(\Delta x)^2\sum(\Delta y)^2}}$.

Next, as for the "conspicuous and rather conspicuous" earthquakes, which occurred in Kwantô District, they were classified into two groups, according to their occurrences in land or in marine area, and the correlation coefficients of them with respect to the same meteorological elements as above taken, were calculated similarly as before.

The results are shown in Table I, II and III.

Table I. Correlation Coefficient between the Precipitations, Q (in 100 mm), and the Earthquakes in Kwantô Districts.

Earthquake regions / Season		"Felt" earthquakes					"Conspicuous and rather conspicuous"	
		Iwaki Oki Kasima Nada	Tyôsi Oki Sagami Nada	Kinugawa, Tonegawa Kasumigaura	Tôkyô Bôsô Hantô	Sagami (land) Idu Hantô	Land	Marine
Spring	J	0·16	−0·39	−0·24	0·22	−0·32	−0·25	−0·39
	P	−0·23	**0·43**	0·15	−0·25	−0·33	**−0·54**	0·16
	J−P	0·26	**−0·52**	−0·23	0·30	0·17	0·39	−0·27
Summer	J	0·14	**0·63**	**0·52**	−0·23	−0·06	−0·10	−0·20
	P	**−0·50**	−0·24	0·06	−0·01	0·24	−0·24	−0·04
	J−P	**0·41**	**0·49**	0·17	−0·22	−0·15	0·11	−0·08
Autumn	J	−0·06	−0·03	**0·62**	0·17	**0·78**	0·35	0·30
	P	−0·25	−0·32	0·23	0·21	0·20	0·03	−0·39
	J−P	0·19	0·26	0·07	−0·11	0·10	0·13	**0·47**
Winter	J	−0·07	**−0·57**	−0·06	**−0·73**	−0·36	0·21	**0·61**
	P	−0·38	0·09	0·09	**0·47**	−0·12	−0·16	−0·38
	J−P	0·05	**−0·52**	−0·08	**−0·77**	−0·28	0·23	**0·63**

Table II. Correlation Coefficient between the Barometric pressure, B (in mm. Hg), and the Earthquakes in Kwantô Districts.

Season	Earthquake regions	"Felt" earthquakes					"Conspicuous and rather conspicuous"	
		Iwaik Oki Kasima Nada	Tyôsi Oki Sagami Nada	Kinugawa Tonegawa Kasumigaura	Tôkyô Bôsô Hantô	Sagami (land) Idu Hantô	Land	Marine
Spring	J	0·29	**0·53**	0·01	0·01	−0·07	−0·14	**0·54**
	P	**0·49**	**0·45**	0·01	0·05	−0·05	−0·13	**0·57**
	J − P	**−0·73**	0·13	−0·03	−0·16	−0·05	0·02	−0·20
Summer	J	0·20	0·01	0·05	**0·47**	0·06	**0·42**	0·38
	P	−0·05	−0·11	−0·23	**0·52**	0·16	0·27	0·28
	J − P	0·34	0·16	0·37	−0·01	−0·12	0·18	0·09
Autumn	J	0·21	**0·42**	**−0·40**	0·09	0·13	−0·17	−0·10
	P	0·16	0·36	−0·36	0·20	0·10	−0·12	−0·08
	J − P	0·04	−0·02	0·12	**−0·44**	0·01	−0·09	0·01
Winter	J	0·08	**0·44**	0·05	**0·63**	0·34	−0·25	**−0·51**
	P	−0·02	0·35	0·01	**0·68**	0·32	−0·27	**−0·54**
	J − P	**0·47**	0·23	0·22	**−0·62**	−0·08	−0·13	**0·47**

Table III. Correlation Coefficient between the Temperature (in °C), and the Earthquakes in Kwantô Districts.

Season	Earthquake regions	"Felt" earthquakes					"Conspicuous and rather conspicuous"	
		Iwaki Oki Kasima Nada	Tyôsi Oki Sagami Nada	Kinugawa Tonegawa Kasumigaura	Tôkyô Bôsô Hantô	Sagami (land) Idu Hantô	Land	Marine
Spring	J	0·38	**0·74**	0·07	−0·01	−0·07	**−0·40**	**0·54**
	P	**0·59**	**0·46**	**0·44**	0·09	0·13	0·10	0·34
	P − J	−0·14	0·12	−0·18	0·16	0·01	−0·25	0·18
Summer	J	0·23	**0·47**	0·13	−0·21	**−0·47**	−0·25	0·05
	P	0·21	0·31	0·09	−0·06	**−0·49**	−0·10	0·23
	P − J	0·11	**0·41**	0·09	−0·31	−0·11	−0·31	−0·28
Autumn	J	0·08	**0·46**	**−0·60**	−0·02	**−0·50**	**−0·45**	−0·24
	P	0·15	0·26	**−0·51**	−0·08	**−0·49**	**−0·43**	−0·29
	P − J	−0·31	**0·46**	0·15	0·25	0·28	0·22	0·34
Winter	J	0·11	0·23	0·02	**0·59**	−0·22	−0·35	**−0·73**
	P	0·22	0·34	0·18	**0·50**	−0·38	−0·27	**−0·69**
	P − J	0·34	**0·52**	**0·71**	−0·21	**−0·76**	0·23	0·04

Results and Discussions.

As the period of investigation is only ten years, we can say nothing definite, but we may be able to suggest the following tendency:—

I. For the "felt" earthquakes.

1. The earthquakes in Iwaki Oki and Kasima Nada are liable to occur,
   (*a*) when the precipitation is abundant on the Japan Sea side, and scanty on the Pacific side in summer;
   (*b*) when the barometric pressure and also the temperature are high on the Pacific side, and low on the Japan Sea side in spring. This barometric condition is usually produced when the "high pressure" is prevailing on the Pacific Ocean.
2. The earthquakes in Tyôsi Oki and Sagami Nada are liable to occur,
   (*a*) when the precipitation on the Japan Sea side is comparatively little in winter and in spring; but it is contrary in summer;
   (*b*) when the barometric pressure and the temperature are high on the Japan Sea side in spring. This result is contrary to the case of Iwaki Oki and Kasima Nada.
3. The earthquakes in Kinugawa, Tonegawa and Kasumigaura, are liable to occur,
   (*a*) when the precipitation is abundant on the Japan Sea side in summer and in autumn; this result is similar to the case of Iwaki Oki and Kasima Nada, both regions being situated in the north side of Tonegawa;
   (*b*) when the temperature difference, $(T_P - T_J)$, is great in winter, and also when low temperature prevails on both the sides in autumn.
4. The earthquakes in Tôkyô and Bôsô Hantô are liable to occur,
   (*a*) when the precipitation is comparatively large on the Pacific side, and little in the Japan Sea side in winter; it is similar to the case of Tyôsi Oki and Sagami Nada, both regions being situated on the south side of Tonegawa; the result is contrary to that of Prof. F. Ômori;
   (*b*) when the barometric pressure and also the temperature are high on both sides in winter as well as in summer.
5. The earthquakes in Sagami (land) and Idu Hantô are liable to

occur,

(*a*) when the precipitation on the Japan Sea side is abundant in autumn;

(*b*) when the temperature on the Pacific side is higher than that of the Japan Sea side in winter, and also when the temperature is low on both sides in summer and in autumn.

II. For the "conspicuous and rather conspicuous" earthquakes.

6. The earthquakes in land are liable to occur,

(*a*) when the precipitation on the Pacific side is little in spring;

(*b*) when the barometric pressure is high on the Japan Sea side in summer;

(c) when the temperature is low on both sides in autumn.

7. The earthquakes in marine area are liable to occur,

(*a*) when the precipitation is abundant on the Japan Sea side, and little on the Pacific side, and also the differential precipitation, $(Q_J - Q_P)$, is great in winter; it is similar in autumn; this result corresponds to that of Prof. F. Ômori;

(*b*) when the barometric pressure is low on the Japan Sea side as well as on the Pacific side, and also the barometric pressure difference, $(B_J - B_P)$, is great in winter; this barometric distribution may be produced by a cyclone, frequenting the Pacific Ocean, of which the effect upon the occurrence of earthquakes is already investigated and reported in a previous paper[3]; and when, the barometric pressure is high on both sides in spring;

(c) when the temperature is low on both sides in winter, and it is high on the Japan Sea side in spring. The latter case is similar to the case of the "felt" earthquakes in Tyôsi Oki and Sagami Nada.

8. In general, the "felt" as well as the "conspicuous and rather conspicuous" earthquakes are liable to occur, when the meteorological conditions are abnormal.

9. Large correlation coefficients are generally obtained in winter than in any other seasons, probably due to the fact that the monsoon is most markedly established in winter.

10. The winter precipitations on the Japan Sea side gives the positive correlation coefficient with respect to the "conspicuous and rather conspicuous" earthquakes in Kwantô District, but

---

[3] S. Yamaguti, *loc. cit.*, 1).

it gives negative coefficient with respect to the "felt" earthquakes.

11. The effect of the precipitations on the Japan Sea side upon the occurrence of the earthquakes in Kwantô District is in opposite sense compared with the effect of the precipitation on the Pacific side, and the former is more effective than the latter.

12. To compare the result of the present investigation directly to that of Prof. Ômori, the yearly number, N, of the "conspicuous and rather conspicuous" earthquakes and also the corresponding precipitation, $Q_{J'}$, at Niigata, Yamagata and Akita, were taken, and the correlation coefficients between N and the precipitations at various stations, were calculated similarly as before as shown in Table IV.

Table IV. Correlation Coefficients.

Earthquake regions	Precipitations at various stations.				
	Kanazawa Takata Niigata	Niigata Yamagata Akita	Tôkyô Mito Onahama		
	Q_J	$Q_{J'}$	Q_P	Q_{J-P}	$Q_{J'-P}$
Land	0·06	0·32	−0·15	0·11	0·25
Marine	−0·02	0·21	−0·25	0·20	0·28

The result is not quite conclusive, and only coincides with that of Prof. F. Ômori as regards the sign of correlation. This is due to the fact, that the values of the coefficients vary considerably with the seasons.

Neither the data are sufficient for ensuring the result, so that a definite conclusion regarding the matter must be reserved for a future.

In conclusion, I wish to express my best thanks to Prof. Torahiko Terada under whose supervision the entire work has been carried out and who has given me many useful suggestions throughout the course of my investigation.

44. 地震と雨雪量，氣壓，及氣溫との關係

地震研究所　山口生知

前論文に於て地震に及ぼす雷雨並に低氣壓の影響の可能性に就いて既に研究された．之等の問題と關聯して今同は，地震と雨雪量並びに氣壓及氣溫との關係を統計的に調査して見た．

此問題は以前に大森博士が研究して東京で觀測された地震と新潟及秋田に於ける雨雪量との間には稍々密接な關係あることが報告されて居る．

今日の地震並びに氣象要素に關する材料は，大森博士の時代よりもつと信頼さるべきものと考へられるが故に，大正 13 年 6 月より昭和 9 年 5 月迄滿 10 個年の材料を中央氣象臺發行の氣象要覽より採つて，研究を試みた．

關東地方に起つた「有感覺地震」と，「顯著及稍顯著地震」とを別々に分類して，夫々日本海岸並びに太平洋岸の雨雪量其他の氣象要素との關係を調査して見た．

研究期間が僅かに 10 個年に過ぎないから確かな事は云はれないが，次の傾向あることを暗示することが出來るかと思ふ．

（1） 氣壓並びに氣溫が春太平洋岸に高く，日本海岸に低い時には，磐城沖及び鹿島灘の有感覺地震が起り易い．

（2） 春季日本海岸の氣壓並びに氣溫が高い時には，銚子沖及び相模灘の「有感覺地震」が起り易い．

此の結果は利根川を境として，北方にある磐城沖及び鹿島灘の場合と反對である．

（3） 冬季太平洋岸の溫度が日本海岸の溫度より高くして其差が大なる時に，鬼怒川・利根川霞ケ浦沿岸に「有感覺地震」が起り易い．

（4） 冬季雨雪量が太平洋岸に多くして，日本海岸に少ない時，東京及び房總半島の「有感覺地震」が起り易い．之は大森博士の結果と反對である．

（5） 秋に日本海岸の降雨量が大なる時，相模及び伊豆半島の「有感覺地震」が起り易い．

（6） 冬季及び秋季雨雪量が，日本海岸に多くして太平洋岸に少なく其差が大なる程關東地方の海底に「顯著及び稍顯著地震」が起り易い．之は大森博士の結果と同樣である．

冬季日本海岸並びに太平洋岸共，氣壓が低く然も氣壓差（B_J-B_P）が大なる時にも海底の顯著及び稍顯著地震が起り易い．此の氣壓配置は低氣壓が太平洋上に現はれた時に相當する．

（7） 一般に地震は氣象狀態が變調なる時に起り易い．

（8） 冬季は他の季節より一般に大なる相關係數を與へる．之は恐らく季節風が冬季には最も著しく固定する爲であらう．

（9） 日本海方面に於ける冬季の雨雪量は關東地方の「顯著並びに稍々顯著地震」とは，正の相關係數を與へるが，之に反して「有感覺地震」に對しては負の相關係數を與へて居る．

（10） 關東地方の地震に對する日本海方面の雨雪量の影響は，太平洋岸の雨雪量の影響と反對の結果を與へて居る．而して前者は後者よりも一層影響が大きい．

45. *Geographical Distribution of Hot and Mineral Springs and Deformation of Earth's Crust.*

By Torahiko TERADA and Naomi MIYABE,
Earthquake Research Institute.

(Read Feb. 19, 1935.—Received June 20, 1935.)

In a previous paper,[1] one of the authors pointed out a probable relation which seems to exist between the horizontal divergence $\Delta=\frac{\partial u}{\partial x}+\frac{\partial v}{\partial y}$ of the earth's crust, obtained from the result of repeated triangulations, and the frequency of occurrence of hot and mineral springs in the corresponding district[2]. A discussion was also made to the effect that such a relation might well be expected from some physical consideration. As, on the other hand, there exists a certain correlation between Δ and the vertical displacement of the earth's crust as revealed by repeated precise levellings, except in the districts recently disturbed by severe earthquakes, we may expect that the frequency of occurrence of hot and mineral springs in a district may also show some relation with the secular vertical movements of bench-marks situated in that district. An example of such a relation was shown in the previous paper with regard to the levelling route from Nagaoka to Okitu. In the following, the results of similar investigations made with regard to the other routes (Fig. 1) will be briefly described.

The localities of hot and mineral springs[3] were marked on 1/200000 maps of Land Survey Department, those with the temperature greater and less than 100°F being distinguished by different marks respectively. Taking the levelling route along which the relation now in question is to be investigated, a zone of 20 km breadth was taken on each side of the route parallel to it. From the site of each spring situated within this zone a straight line was drawn which meets the route nearly orthogonally. The point of intersection of this line with the line of route was marked and allotted as belonging to that spring. On the other hand, a diagram (Figs. 2∼9) was drawn of which the abscissa represents the route, taking the distance between successive bench-marks,

---

[1] T. TERADA, *Proc. Imp. Acad.*, **10** (1934), 410.

[2] Literatures regarding this point are given in the previous paper cited.

[3] Data for the geographical distribution of springs were mainly taken from "Nihon-Kôsensi" (日本鑛泉誌), (1886) and R. ISHIZU, "The Mineral Spring of Japan", (1915).

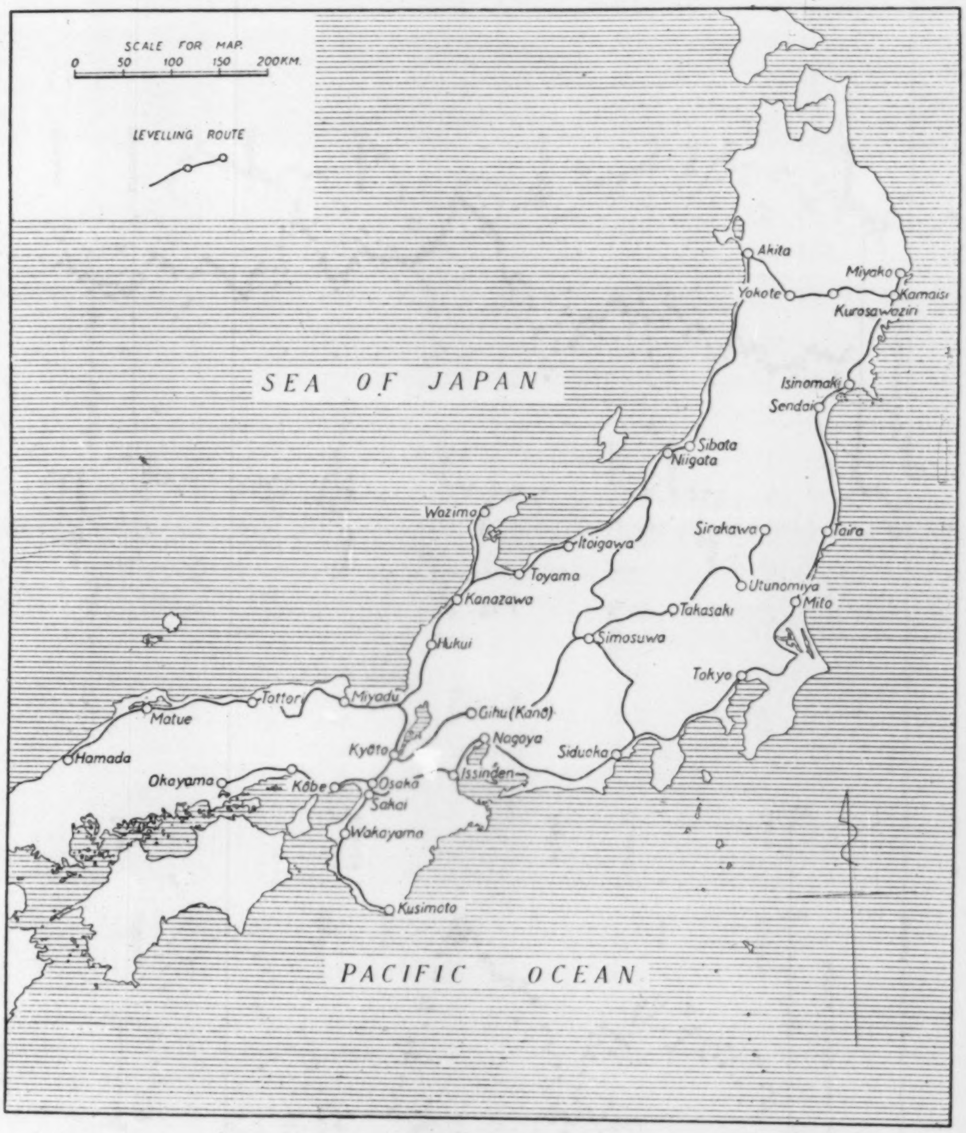
SCALE FOR MAP.
0 50 100 150 200KM.
LEVELLING ROUTE
SEA OF JAPAN
PACIFIC OCEAN
Akita
Miyako
Yokote
Kamaisi
Kurosawaziri
Isinomaki
Sendai
Sibata
Niigata
Wazima
Itoigawa
Toyama
Sirakawa
Taira
Utunomiya
Kanazawa
Takasaki
Mito
Hukui
Simosuwa
Tokyo
Tottori
Miyadu
Matue
Gihu (Kanō)
Nagoya
Kyōto
Siducka
Hamada
Okayama
Kōbe
Osaka
Issinden
Sakai
Wakayama
Kusimoto

Fig. 1. Distribution of levelling routes.

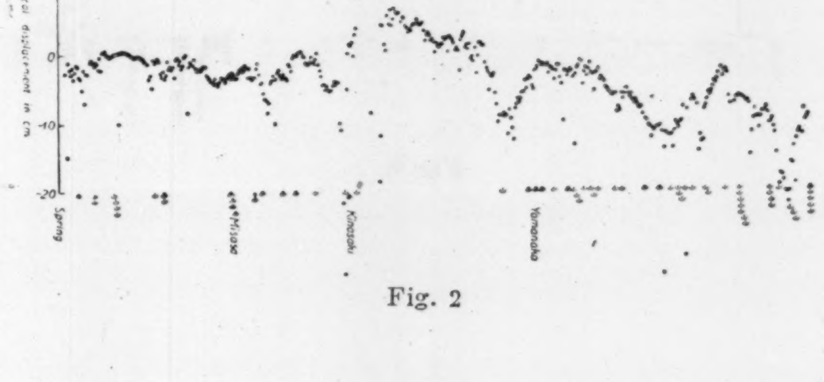

Fig. 2

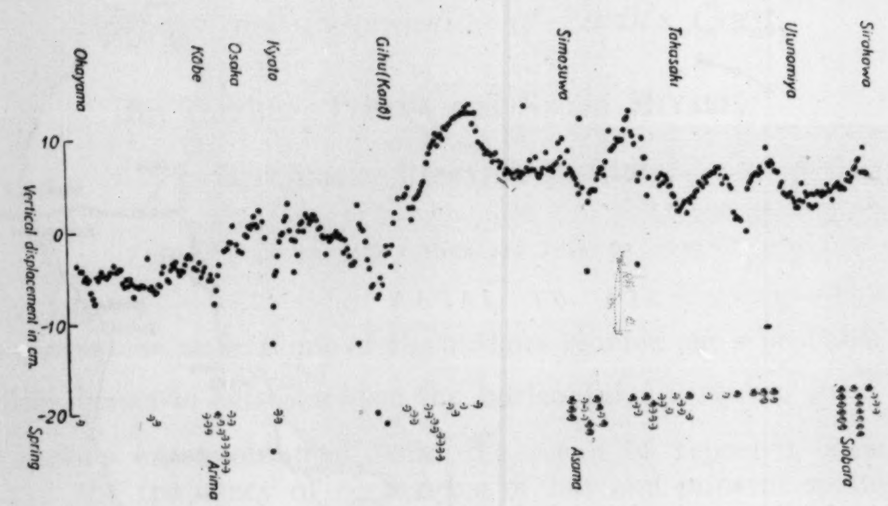
Okayama
Kōbe
Osaka
Kyoto
Gihu(Kanō)
Simosuwa
Takasaki
Utunomiya
Sirakawa
Arima
Asama
Siobara
10
0
-10
-20
Vertical displacement in cm.
Spring

Fig. 3.

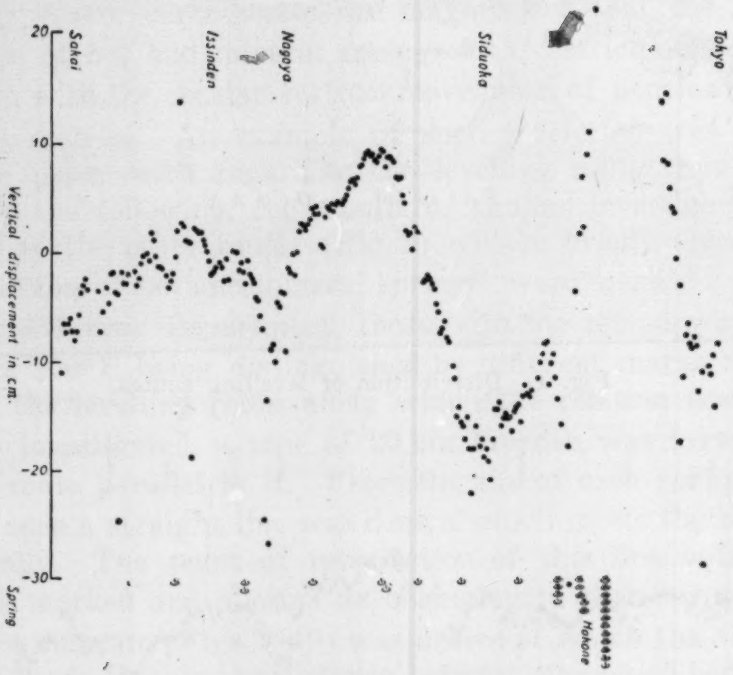
Sakai
Issinden
Nagoya
Siduoka
Tokyo
Hakone
20
10
0
-10
-20
-30
Vertical displacement in cm.
Spring

Fig. 4.

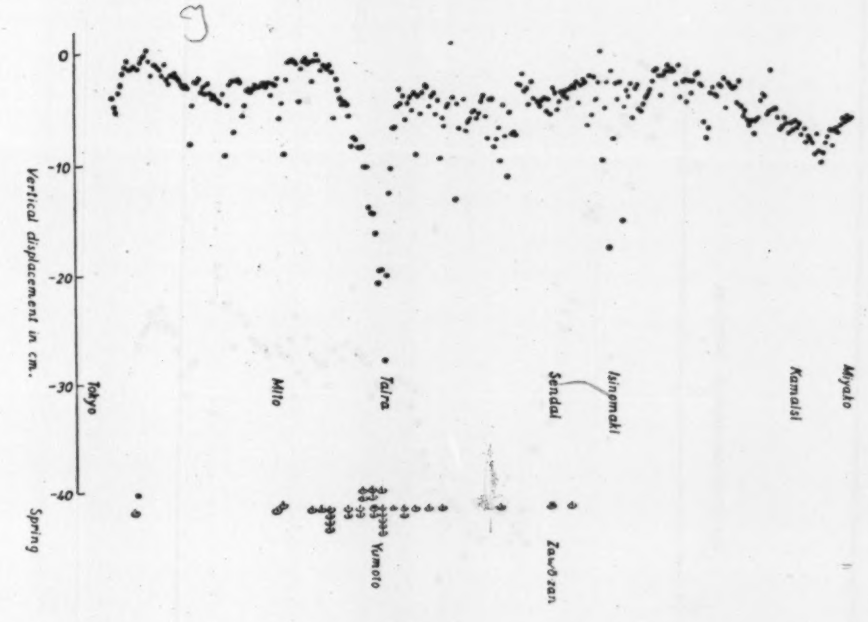
0
-10
-20
-30
-40
Vertical displacement in cm.
Spring
Tokyo
Mito
Taira
Sendai
Isinomaki
Kamaisi
Miyako
Yumoto
Zawô zan

Fig. 5.

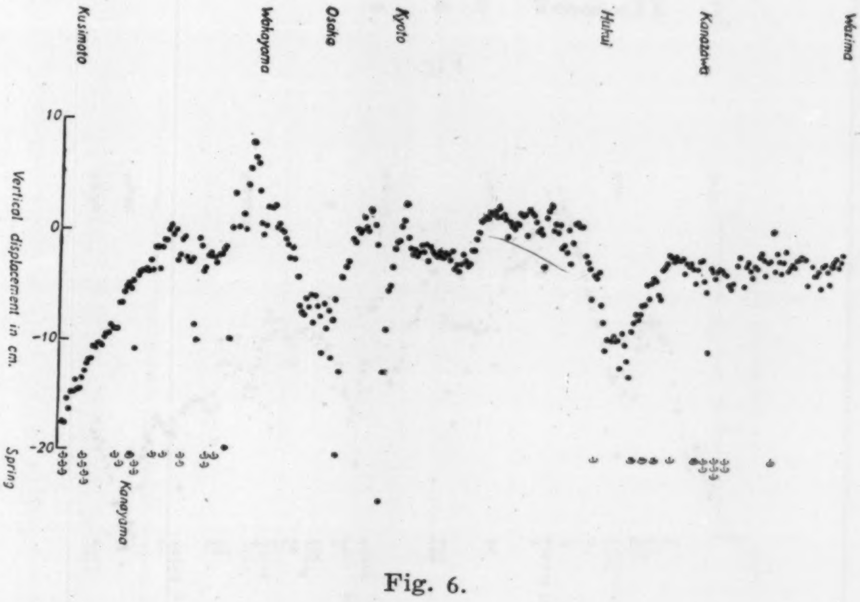
Kusimoto
Wakayama
Osaka
Kyoto
Hukui
Kanazawa
Wazima
10
0
-10
-20
Vertical displacement in cm.
Spring
Kanayama

Fig. 6.

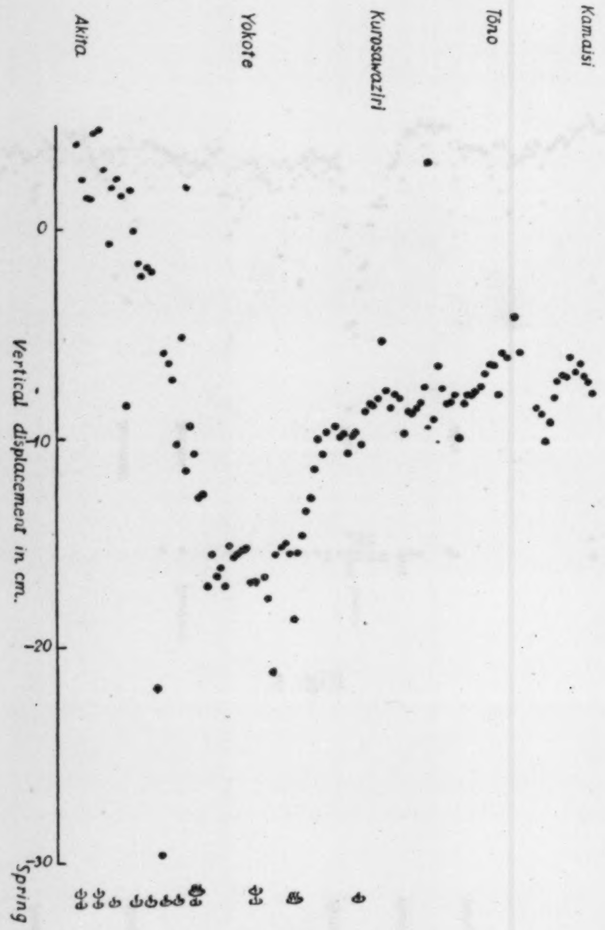
Akita
Yokote
Kurosawaziri
Tōno
Kamaisi
Vertical displacement in cm.
0
-10
-20
-30
Spring

Fig. 7.

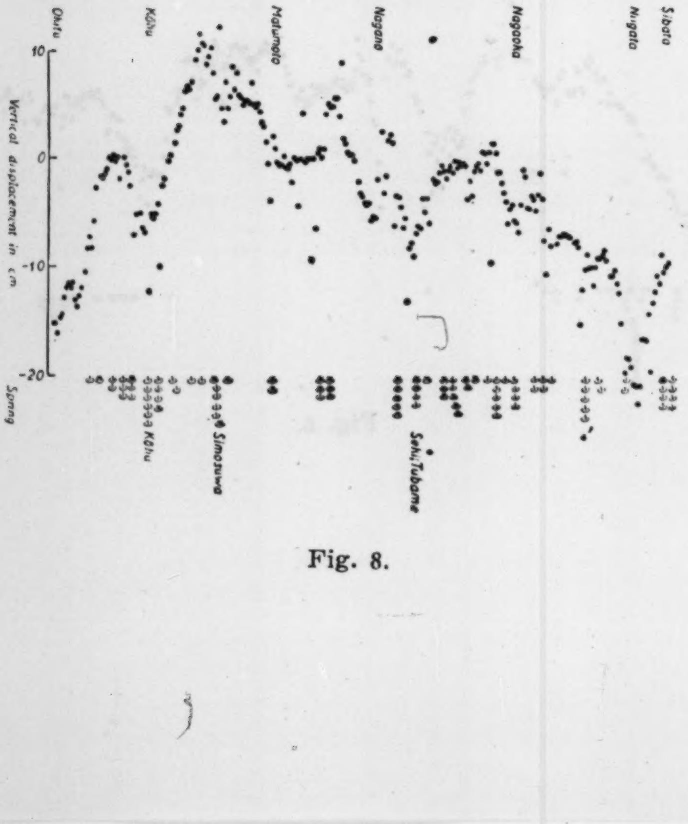
Ohtu
Kōhu
Matumoto
Nagano
Nagaoka
Niigata
Sibata
Vertical displacement in cm
10
0
-10
-20
Spring
Kōhu
Simosuwa
Seki,Tubame

Fig. 8.

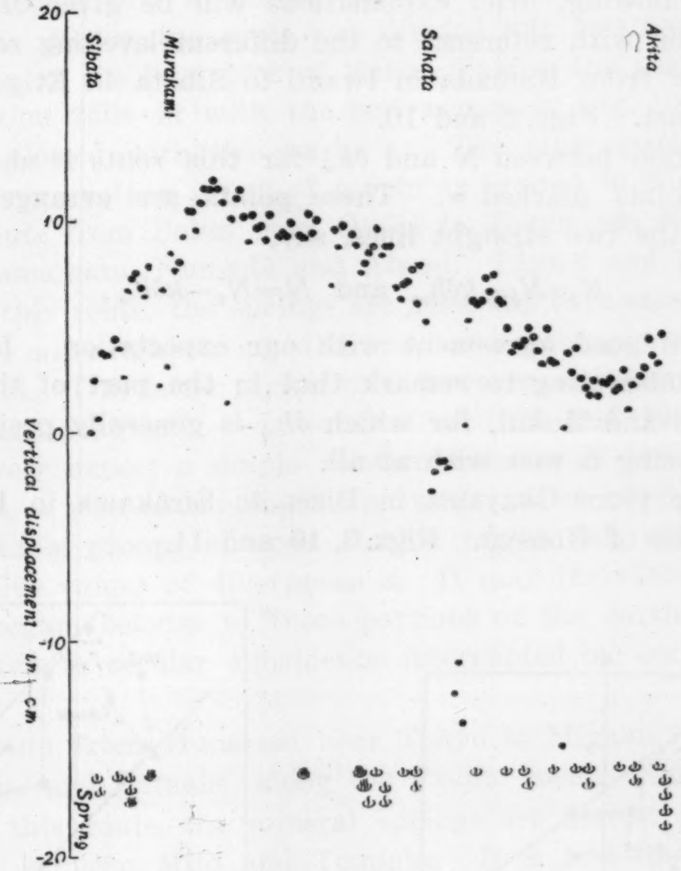

Fig. 9.

supposed all equal, as unit, and the ordinates the vertical displacements of the bench-marks. The positions of the springs on the route, conventionally allotted as in the above described manner, were marked on the axis of abscissa (♨ < 100°F; ♨ > 100°F). Next, the mean vertical displacement $\delta h'_m$ for each segment of the route comprising 25 consecutive bench-marks, i.e., a segment about 50 km in length, was calculated. The number N' of the hot and mineral springs falling in each segment was counted. For the second process of smoothing, the overlapping means δh_m and N over successive three segments were respectively taken.[4] Plotting then N against δh_m for the successive segments, we obtain diagrams as shown in Figs. 10∼17. If there exists a simple relation between the two quantities, the points plotted will show a more or less systematic arrangement according to more or less close correlation.

---

4) In the abstract of this paper given in *Proc. Imp. Acad.*, **11** (1935) 99, the description of this second process of smoothing was dropped.

In the following, brief explanations will be given of the results of investigation with reference to the different levelling routes.

1) Route from Hamada in Iwami to Sibata in Etigo, along the Japan Sea coast. Figs. 2 and 10.

The relation between N and δh_m for this route is shown in Fig. 10 by the points marked ●. These points are arranged within a belt between the two straight lines, say,

$$N = N_0 - k\delta h_m \text{ and } N = N_0' - k\delta h_m .$$

This is in good agreement with our expectation. Referring to Fig. 2, it is interesting to remark that in the part of the route between Miyadu and Hukui, for which δh_m is generally positive, no hot or mineral spring is met with at all.

2) Route from Okayama in Bizen to Sirakawa in Iwaki, along the central line of Honsyû. Figs. 3, 10 and 11.

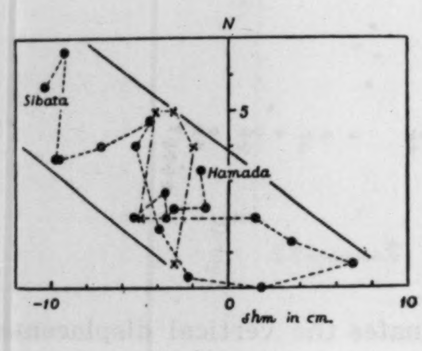

Fig. 10.

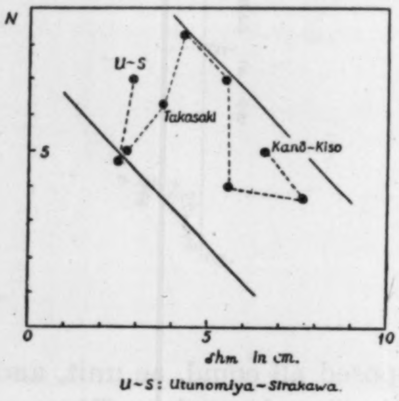

Fig. 11.

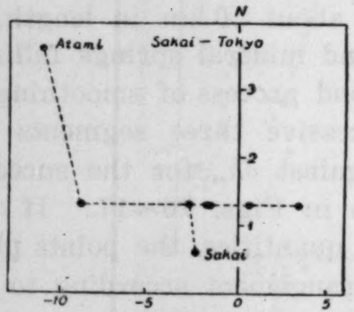

Fig. 12.

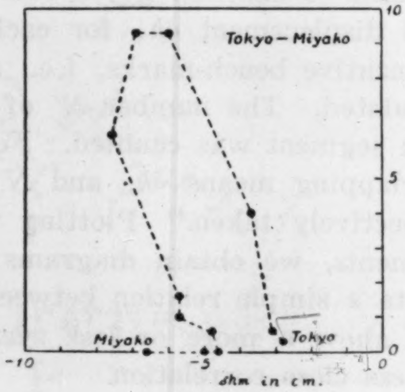

Fig. 13.

The vertical displacement along this route (Fig. 3) shows a remarkable discontinuity in general level near Kanô in the middle part of the route. Hence, the route was divided into two parts respectively extending on the two sides of Kanô. Taking the part W of Kanô, N-∂h_m relation falls in with the belt named in Fig. 10 as shown by the points plotted with the mark ×. The other part, E of Kanô, seems to form another group of points as plotted in Fig. 11.

3) Route from Sakai near Osaka to Tokyo, via Nara, Yokkaiti, Nagoya, Hamamatu, Numadu and Atami. Figs. 4 and 12.

Along this route, the springs are generally rare except in the province of Idu and neighbouring districts, where conspicuous hot springs are abundunt. This latter region was, however, considerably disturbed by the recent destructive earthquakes of 1923 and 1930, so that we could scarcely expect a simple relation between N and ∂h_m. On the other hand, it was shown in the previous paper cited, that some of the remarkable groups of spas of this region fall within the areas with negative values of divergence Δ. It may therefore be suggested that this region belongs to those portions of the earth's crust which are subjected to secular subsidence interrupted by occasional abrupt upheavals.

4) Route from Hunabasi near Tokyo to Miyako in Rikutyû, via Mito, Sendai and Kamaisi, along the Pacific coast. Figs. 5 and 13.

Along this route, the mineral springs are almost concentrated in the region between Mito and Tomioka. It is just this region where a very conspicuous V-shaped depression of the route is observed.[5]

5) Route from Kusimoto in Kii to Wazimazaki in Noto, across the central part of Honsyû. Figs. 6 and 14.

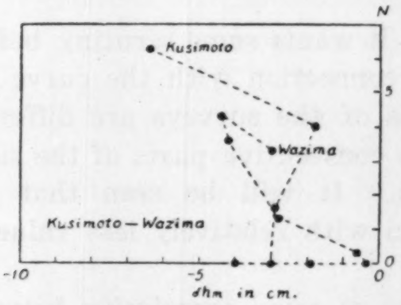

Fig. 14.

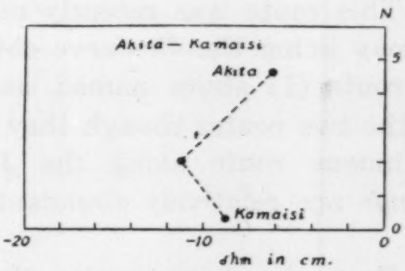

Fig. 15.

Along this route the correlation between N and ∂h_m is not very conspicuous. Still we may observe that most of the hot and mineral springs in this route fall in with the region with $\partial h_m < -20$ mm.

---

[5] T. TERADA and N. MIYABE, *Proc. Imp. Acad.*, **10** (1934), 557; *ibid.*, **11** (1935), 99.

6) Route from Akita, Ugo, on the Japan Sea coast to Kamaisi, Rikutyû, on the Pacific coast, via Yokote, Kurosawaziri and Tôno. Figs. 7 and 15.

Along this route the correlation is not conspicuous, but we may observe that the springs with the temperature higher than 100°F are found all near the minimum of δh-curve (Fig. 7).

7) Route from Okitu, Suruga, on the Pacific coast to Sibata, Etigo on the Japan Sea coast, via Kôhu, Matumoto, Nagano and Niigata. Figs. 8 and 16.

This route which was already dealt with in the previous preliminary report, was revised by means of the same method as used here for the other routes. The result is rather complicated, but we may observe firstly that the general tendency of the negative correlation between N and δh_m may still be traced, except some irregularities, and secondly that very conspicuous swarms of hot springs are mostly met with at or near the minima of δh-curve (Fig. 8).

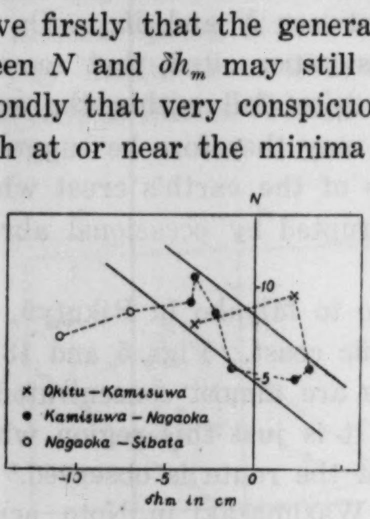

Fig. 16.

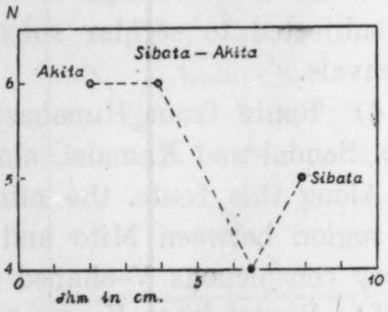

Fig. 17.

8) Route from Sibata in Etigo to Akita in Ugo along the Japan Sea coast. Figs. 9 and 17.

This route was recently revised and it wants some scrutiny before we may bring the δh-curve obtained in connection with the curve for the route (1) above named, as the dates of the surveys are different for the two routes though they form two consecutive parts of the same continuous route along the Japan Sea. It will be seen that the springs are relatively abundant in region with relatively less value of δh.[6]

From the above results, the existence of some correlation between N and δh_m can scarcely be doubted, though the relation is not quite simple. A simple relation can, however, not be expected from the first outset, firstly because we are here comparing N with δh_m instead of

---

[6] The δh-curve along the route from Sibata to Akita is reproduced from the data given in Prof. A. Imamura's paper: A. IMAMURA, *Disin*, **7** (1935), 185.

Δ directly. The displacement δh_m and divergence Δ are not always positively correlated, especially in the regions disturbed by recent earthquakes. Secondly, even the relation between N and Δ cannot be so simple that we may express N as a simple linear function of Δ. It may well be possible that N depends on the mean value of Δ over a very wide region, as well as on the relative value of Δ within a rather narrow locality. Thirdly, the above results may be modified in some measure, if we take the breadth of the zone parallel to the route, which was chosen here as 20 km on either side of the route, as 10 or 30 km, or if we prefer some other method of allotting each spring to a point on the route.

It seems, however, that the new line of investigation here taken up promises to throw some unexpected light on the studies of crust movement if duly pursued with more sufficient data and more elaborate methods. At the present stage, we may suggest already (i) that a segment of the route within which the negative correlation between N and δh_m is very conspicuous is situated on a region which is free from the disturbance due to recent severe earthquakes and (ii) that at a locality which forms a junction between two segments of a route such that the two segments if taken separately show good correlation within themselves, but if taken together show no apparent correlation, we may suspect a real tectonic discontinuity which is active in the present geological age.

It seems highly desirable to investigate the similar relation for the other parts of the worlds.

45. 温泉及鑛泉の分布と地殼運動

地震研究所 {寺田寅彦
宮部直巳

地殼水平移動のダイヴァージエンス Δ が負量を示す地方に溫泉や鑛泉の湧出が多いであらうと期待される理由がある．一方では又この Δ と地殼の垂直運動との間に正相關が屢々認められると云ふ事實がある．それで，實測資料の少ない Δ の代りに資料の豐富な垂直運動の實測値と，水準測量沿線地方の溫泉及鑛泉の分布密度とを比較して見るのも多少の興味がある譯である．この目的で次のやうな方法をとつた．

水準線路の兩側に並行に各 20 km の幅の地帶をとり，その中にある溫泉及鑛泉をこの線路に所屬させた．次に各泉地點から水準路線に大體垂直な線を劃しそれが線路を切る點を其溫泉所屬の點とした．次に水準線を横軸とし各點の垂直運動の量を縱軸とした圖を作り，その横軸の下に溫泉鑛泉の所屬位置を記入した．此圖により垂直運動の正負によつて泉の分布密度がどうちがふかを見ることが出來る．

次には，線路に沿ひ相隣る 25 點の平均垂直運動の量 h'_m とその區間の泉の總數 N' とを計算し，更に此の如き區間を三つづゝ取つて平均した重合平均値 h_m と N とを計算し，この二つを座標軸にとつて相關圖を作つて見た．もし兩者の相關が顯著なれば圖の點は一線上に乘るわけである．

調査の結果は決して簡單ではないが，可成の相關が認められる場合も少くない．殊に長い線路全體としての相關は見えなくても部分的にそれが見られる場合があり，又 h_m の或値が泉の有無の限界を示す場合もある．

問題の相關はあるとしても，その外に色々の原因が共同作用してゐるから，さう簡單な結果が得られないのは當然であるが，それに拘らず，こゝで見られるやうな結果を得たのは，寧ろ最初想像されるやうな物理的關係が可成密接に存する證據とも考へられる．それで更に多くの材料につき又より適當な方法により研究の歩を進めることが出來ればその結果として地殼運動の研究に多少でも新しい光明を與へるやうなものが得られるかも知れないと思はれる．當論文ではこの新しき方向への第一歩として試みに手近な方法をとつて見ただけである．

---

46. *Sinking of the Earth's Crust in Hukagawa, Tokyo, as Deduced from Mareogram Data.*

By Naomi MIYABE,

Earthquake Research Institute.

(Read March 19, 1935.—Received June 20, 1935.)

It has already been, reported that the earth's crust sank considerably in Honzyô and Hukagawa, Tokyo[1]. In order to study the progress of the sinking, a mareograph was installed at Kiba, in Hukagawa, and the heights of the sea level recorded continuously since January 1932 up to the present, so that it is possible to deduce the rate of sinking of the earth's crust at this point from these data. The locality of the mareograph is specially indicated in Fig. 1.

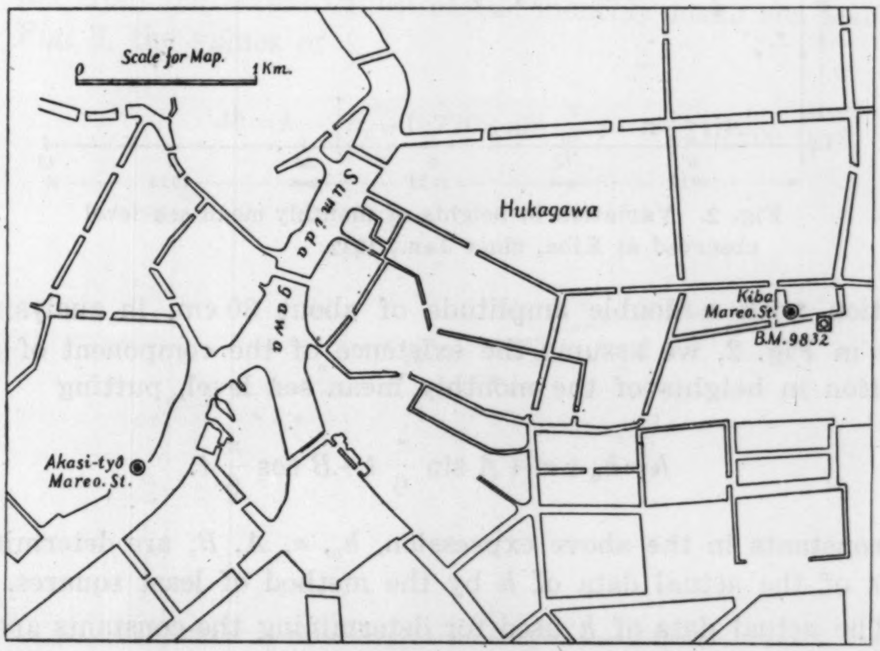

Fig. 1. Localities of mareograph stations.

The mareograph in use, which was constructed by Mr. R. Takahasi[2], a member of our Institute staff, consists of a U-tube containing mercury, one end of which connects with sea water by means of a rubber tube. The movements of the other end of the mercury column following the rise and fall of the sea level, are recorded on the Richard's rotating drum by means of a mechanical lever.

---

[1] N. MIYABE, *Bull. Earthq. Res. Inst.*, **10** (1932), 844~857, etc.

[2] R. TAKAHASI, *ibid.*, **7** (1929), 95~102.

In the present paper, the changes in heights of the monthly mean sea levels as deduced from the mareograms thus obtained are studied.

The monthly mean sea levels, calculated by means of the data of the heights of the sea levels for every hour as read from the mareograms, are shown in Fig. 2. Since, in this figure, we notice an annual variation with a double amplitude of about 30 cm, in analysing the curve in Fig. 2, we assume the existence of the component of annual variation in heights of the monthly mean sea level, putting

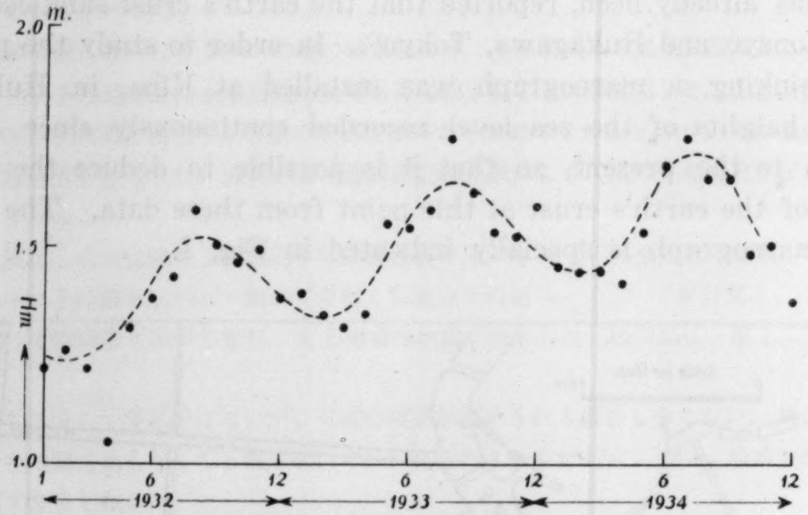

Fig. 2. Variation in heights of monthly mean sea level observed at Kiba, since Jan., 1932.

$$h=h_0+at+A\sin\frac{\pi}{6}t+B\cos\frac{\pi}{6}t.$$

The constants in the above expression, h_0, a, A, B, are determined by means of the actual data of h by the method of least squares.

The actual data of h used for determining the constants are those observed in the period between Jan., 1932 and March, 1933; this being the only interval during which observations were continued without disturbance from mishaps, such as instrumental damage or overflow of mercury due to abnormal rise of sea level owing to strong wind from the SW.

The constants thus determined, taking the origin of the time at

Jan., 1932, are given below with the probable errors:

$$\begin{aligned} h_0 &= 1{\cdot}3042\text{ m} \pm 0{\cdot}0043\text{ m}, \\ a &= 0{\cdot}0102\text{ m} \pm 0{\cdot}0005\text{ m}, \\ A &= -0{\cdot}0708\text{ m} \pm 0{\cdot}0030\text{ m}, \\ B &= -0{\cdot}1210\text{ m} \pm 0{\cdot}0030\text{ m}. \end{aligned}$$

The amplitude of annual variation of the monthly mean sea level is then given by

$$\sqrt{A^2+B^2} = 14{\cdot}02\text{ cm},$$

the double amplitude of which is about 30 cm, as estimated above.

From the rate of rise per month in the monthly mean sea level, we estimate the amount of rise in the monthly mean sea level in 1932 to be 12 cm approximately.

To deduce the rate of rise in heights of monthly mean sea level during the years 1933 and 1934, the term of annual variation calculated by using constants A and B that were determined above, is subtracted from the actual values of the monthly mean sea level. Thus, in Fig. 3, the values of

$$\Delta h = h - \left\{ h_0 - 0{\cdot}7708 \sin \frac{\pi}{6}\, t - 0{\cdot}1210 \cos \frac{\pi}{6}\, t \right\}$$

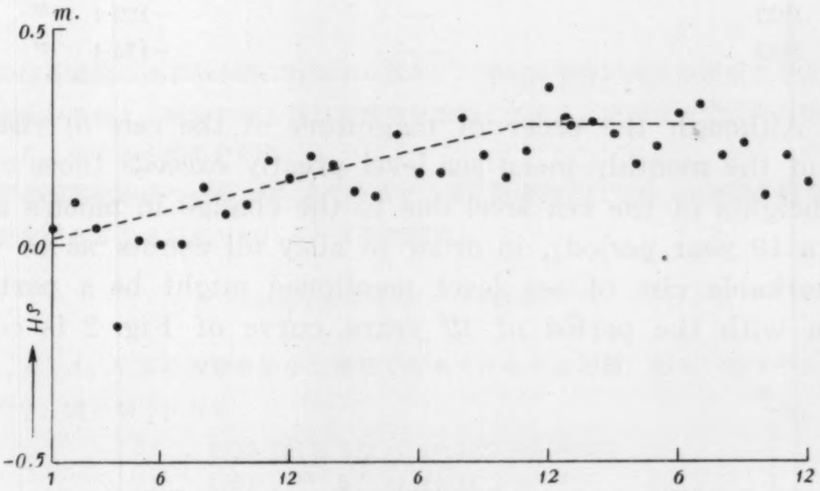

Fig. 3. Secular variation in heights of sea level at Kiba.

are plotted against the time. By means of the data of Δh thus deduced, the values of a were determined as follows:

$$a = 11{\cdot}2\text{ mm per month, for 1933,}$$

$$a = 1{\cdot}8 \sim -1{\cdot}7\text{ mm per month, for 1934.}$$

It is rather striking that the rate of rise in heights of mean sea level was very small or negative in 1934. The fact that the mean sea level depressed considerably since September, 1934, may probably be due to the overflow of considerable amount of mercury from the U-tube of the mareograph at the time of the abnormal rise of sea level associated with the cyclone of September 21, 1934.

The secular rise of the sea level in Hukagawa obtained above may be attributed chiefly to local depression of the earth's crust. The following points may serve to render the above conclusion more plausible:

i) The rate of secular rise of sea level in 1932 and 1933 is approximately equal to the rate of depression of B.M. 9832 situated at Hirai-tyô, Hukagawa, very near the mareograph station as shown in Fig. 1. In Table I, the rates of depression of B.M. 9832 are compared with those where the mareograph is situated, as deduced from mareogram data.

Table I. Rate of sinking.

Period \ Station	B·M·9832	Kiba Mareog. St.
1925~1930	−85·0 mm/year	—— mm/year
1930~1931	−107·1 "	—— "
1929~1932	−90·5 "	—— "
1932	——	−122·4 "
1933	——	−134·4 "

ii) Although the order of magnitude of the rate of rise in the heights of the monthly mean sea level greatly exceeds those of variation in heights of the sea level due to the change in moon's altitudes (nearly a 19 year period), in order to allay all doubts as to whether the remarkable rise of sea level mentioned might be a part of the variation with the period of 19 years, curve of Fig. 2 is compared

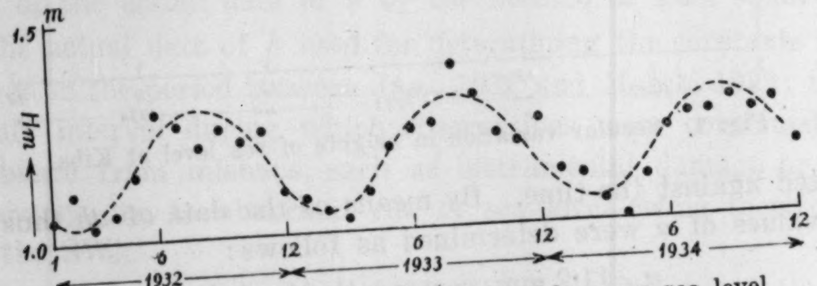

Fig. 4. Variation in heights of monthly mean sea level observed at Akasi-tyô, since Jan., 1932.

with that of Fig. 4, in which latter is given the variation in heights of monthly mean sea level obtained at Akasi-tyô, Kyôbasi, the locality shown in Fig. 1, from which it was proved that the remarkable secular rise of mean sea level as observed in Hukagawa was not noticed in the course of variation in heights of sea level at Akasi-tyô, where relevellings showed that slight crustal depression had also taken place.

As to the cause of such remarkable sinking of the earth's crust in Hukagawa, however, we cannot say anything until more data have accumulated.

As already stated, the sinking of the earth's crust seems to have ceased from the beginning of 1934, as deduced from mareogram data obtained at Kiba, Hukagawa. This cannot however be interpreted to mean that the downward movement of the earth's crust has really ceased, for there is the possibility that during the period in question the mareograph station itself happened to lie on the axis of a tilting movement of the earth's crust.

---

46. 験潮記錄より知られたる深川に於ける地盤の沈降

地震研究所 宮部直巳

深川に於ける地盤の沈下を不斷に計測する爲めに，深川區平井町所在の東京市木場喞筒場内の一隅に驗潮儀を設置し，昭和7年1月以來觀測を繼續してゐる．昨年末までに得た資料を整理してみたところ，次の如き結果を得た．

毎月の平均潮高を時について plot してみると，第2圖の如くになり，年週期の變化の外に，著しき永年變化があることが氣付かれる．月平均潮高を

$$h=h_0+at+A\sin\frac{\pi}{6}t+B\cos\frac{\pi}{6}t$$

として h_0，a，A，B 等の常數を最小二乘法で定めてみると a の値，即ち，毎月の永年變化量は各年度につき，次のやうになる．

1932（昭和7年），$a=10{\cdot}2$ mm/month
1933（〃 8〃），$a=11{\cdot}2$ 〃
1934（〃 9〃），$a=1{\cdot}8\sim-1{\cdot}7$ 〃

これでみると，昭和9年（1934），の變化量が非常に小さい事が知れる．

是等の著しい潮位の上昇は地盤が沈下する結果生ずるものであると思はれる．昭和9年度の沈下量の小さい事の理由はよく分らないが，1點のみに於ける觀測の結果であるから，これが，地盤全體としての沈下又は隆起を示すものであるか否かは遽かに斷定し兼れる所である．

47. 東京横濱市内10個所における地震動加速度觀測 (2)

地震研究所 石本巳四雄

(昭和9年4月16日發表——昭和9年6月20日受理)

1. 緒言

昭和7年，8年における東京横濱市内における地震動觀測結果[1]は已に報告濟のものであるが，本報告は其の續報として昭和9年におけるものである．從つて報告の全貌は前回と其の軌を一にし，異つた事實はない．然し乍ら今回の觀測により一層地震動の性質に對し理解を進め得たと信ずる．

地震動中に卓越する振動周期の各觀測點において同一でない事實は前論文に於て述べた事であるが，前期間中には著しい地震の數少く多くの材料を得る事が出來なかつたに引替へ，昭和9年中には相當數多き地震の出現のあつた關係上，各地域における地震動を一層詳しく調査する事が出來た．

觀測地點は前回と殆ど同樣であるが，東京市内の中深川木場町は廢止し新に目黑區駒場支所が追加された．横濱におけるものは異同はない．觀測器械は前回と同樣であるが，其の中二三は油制振器を空氣制振器に改めた．其の結果として

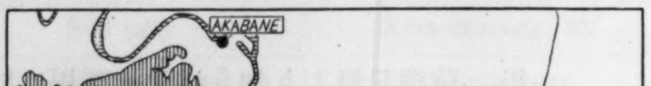
AKABANE
MUKOZIMA
HONGO
KANDA
MARUNOUTI
HUKAGAWA
AOYAMA
KOMABA
0
5 KM

第1圖 東京市内における觀測點位置

---

[1] 石本巳四雄 地震研究所彙報 12 (1934), 234.

氣溫變化による影響から充分免れる事が出來た．なほ何れの器械も屢々半動力的に感度試驗が行はれ，各周期に就て一樣の感度を有する樣に整正した事は勿論である．

昭和7年より昭和9年に至る期間中，東京地方で人體感覺を與へた地震數を表示すると次の如くなる．此等は何れも地震研究所觀測報告によるものである．

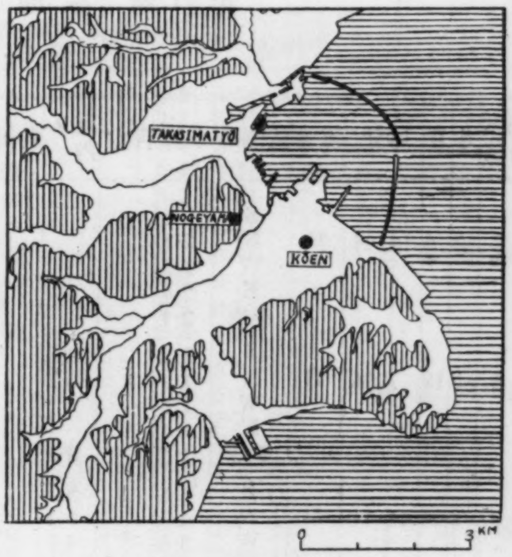

第2圖　横濱市内觀測點位置

第I表　有感地震數

	震度 I	震度 II	震度 III	合計
昭和 7 年	42	16	0	58
8 年	53	9	1	63
9 年	47	15	2	64

但し震央位置により横濱の震度は東京に於けるものと異る場合のあるは當然であつて，例へば東京において震度 I であつても，横濱にては震度 II の如き場合がある．此等は致し方無いが，第 II 表には各地域における地震動最大加速度を掲げて置いたから此れを參照すれば大體の事は判ると思ふ．

2. 最大加速度

各地震に就き各地點における地震動の最大加速度を求めて表となした（第 II 表）．今回は東西南北の成分に就て最大値を求め，其の平均を以て各地の最大加速度となし，此れを平均最大加速度と名付けた．斯かる量が如何なる意味を持つかは知らぬが，兎も角此れが地震動の強さを表はす一つの示數となる事は信じられる．

前回にも述べた事であるが，震源（或ひは震央）距離の小なる地震は山手にて比較的大なる加速度を與へるが，震源距離の大なるものは下町に比較的大なる加速度を與へる，此の事實を確める爲めに東京は本郷におけるものを基準として各地點の加速度を

第II表 各地最大加速度

昭和7年

地震番號	月	日	時分	震度	觀測地	本郷	青山	丸ノ内	神田	深川	向島	赤羽	野毛山	横濱公園	高島町	震央
			h m													
2	2	4	14 44	II	S	2·2										利根川流域
					N	2·1										
					W	1·5										
					E	2·4										
					平均	**2·1**										
5	2	19	7 36	II	S	1·0		0·7								利根川流域
					N	1·7		0·7								
					W	1·7										
					E	1·4										
					平均	**1·5**		**0·7**								
7	2	26	15 12	II	S	5·8		5·3								印幡沼附近
					N	4·3		5·3								
					W	3·6		4·7								
					E	6·8		6·9								
					平均	**5·1**		**5·6**								
10	3	2	4 58	II	S	1·2										荒川沖附近
					N	1·9										
					W	2·1		1·6								
					E	1·5		1·3								
					平均	**1·7**		**1·5**								
19	3	24	7 24	II	S	1·4		3·5								荒川流域
					N	1·0		3·2								
					W	2·2		2·5								
					E	2·2		3·3								
					平均	**1·7**		**3·1**								
20	4	5	4 18	II	S	5·3		7·6								八丈島南東沖
					N	5·1		10·2								
					W	5·0		7·6								
					E	5·7		8·1								
					平均	**5·3**		**8·4**								
21	4	12	3 13	II	S	3·3		3·4								所澤附近
					N	2·9		4·6								
					W	2·1		5·9								
					E	2·9		5·4								
					平均	**2·8**		**4·8**								
23	4	26	12 42	II	S	2·4		4·3								東京灣
					N	2·2		3·4								
					W	2·5		2·8								
					E	3·8		6·1								
					平均	**2·7**		**3·8**								
29	6	16	17 33	II	S	11·6		23·0	12·7			14·8	9·0			小貝川流域
					N	12·0		21·7	12·0			18·2	10·9			
					W	9·0		9·6	9·4			13·8	9·8			
					E	11·4		10·2	8·9			17·1	9·6			
					平均	**11·0**		**16·2**	**10·8**			**16·0**	**9·8**			
30	6	22	9 36	II	S	4·3	6·2	9·9	5·3			5·2	5·0			銚子北方沖
					N	4·1	3·9	11·5	6·0			6·3	5·2			
					W	5·1	3·8	9·4	5·9			8·3	5·1			
					E	5·1	5·0	8·1	7·1			8·3	5·8			
					平均	**4·6**	**4·7**	**9·7**	**6·1**			**7·0**	**5·3**			

（次頁へ續く）

地震番號	月	日	時分	震度	觀測地	本郷	青山	丸ノ内	神田	深川	向島	赤羽	野毛山	横濱公園	高島町	震央
32	7	13	21^h 40^m	II	S	1·9	2·9	1·9	1·6			1·1	4·2			印旛沼附近
					N	1·9	3·8	1·6	1·2			1·1	3·8			
					W	1·1	3·5	2·4	1·2			1·4	5·5			
					E	1·1	2·3	2·4	0·9			1·4	5·1			
					平均	**1·5**	**3·1**	**2·0**	**1·2**			**1·2**	**4·6**			
33	7	14	21 51	II	S	3·3		1·8	1·9				0·9			木更津沖
					N	3·8		1·6	1·6				0·9			
					W	1·9	2·8	2·7	1·4			0·9	0·7			
					E	3·0	4·7	3·3	0·7			0·9	0·7			
					平均	**4·0**	**3·8**	**2·4**	**1·3**			**0·9**	**0·8**			
43	9	19	23 13	II	S	2·4	3·3					1·7	5·2	2·8		富津附近
					N	2·6	2·3					1·0	5·0	3·2		
					W	2·7	2·3					1·7	7·7	3·4		
					E	3·8	2·3					1·3	9·9	3·2		
					平均	**2·9**	**2·5**					**1·4**	**7·2**	**3·2**		
47	10	14	14 36	II	S	2·9	3·9	2·6	3·2		3·0	3·3	4·2	1·5		江戸川流域
					N	3·1	5·5	2·3	3·0		3·4	2·7	4·7	2·2		
					W	2·1	3·3	3·7	2·7			2·9	3·4	1·5		
					E	2·5	3·5	3·5	2·7			2·7	4·6	2·2		
					平均	**2·6**	**4·1**	**3·0**	**2·9**		**3·2**	**2·9**	**4·2**	**1·9**		
56	11	23	17 58	II	S	4·6		5·5	3·8		2·8			3·0	2·4	古河附近
					N	4·8		6·8	3·6		3·4			3·4	3·3	
					W	2·5		4·3	3·5		4·2	2·7		3·2		
					E	2·7		5·6	4·6		5·0	1·8		4·1		
					平均	**3·7**		**5·6**	**3·9**		**3·9**	**2·1**		**3·4**	**2·9**	
57	12	2	2 41	II	S	2·7	4·9	6·4	5·5		6·2		3·5	2·4	1·6	那珂川流域
					N	2·6	5·5	4·9	7·1		6·0		3·8	3·4	1·5	
					W	3·8	4·4	3·7	9·2		9·6		3·2	2·7	2·1	
					E	3·2	4·4	4·3	6·4		8·7		2·2	2·3	1·7	
					平均	**3·1**	**4·8**	**4·8**	**7·1**		**7·6**		**3·2**	**2·7**	**1·7**	

昭和8年

地震番號	月	日	時分	震度	觀測地	本郷	青山	丸ノ内	神田	深川	向島	赤羽	野毛山	横濱公園	高島町	震央
4	2	7	9^h 13^m	II	S	2·6	3·5	1·6	3·5		4·9	7·7	3·4	3·3	1·1	小貝川流域
					N	3·3	4·9	2·3	3·0		4·9	7·7	2·5	3·5	0·9	
					W	3·6	4·4	2·4	3·6		4·4	5·1	2·1	1·7	0·7	
					E	5·5	4·2	2·4	4·5		3·6	9·7	2·1	2·4	0·7	
					平均	**3·7**	**4·3**	**2·1**	**3·7**		**4·5**	**7·6**	**2·5**	**2·7**	**0·9**	
6	2	13	15 51	II	S	2·2	4·9	3·2	4·6	14·1	4·5	5·0	3·2	3·1	2·2	鹿島灘
					N	2·1	4·2	4·1	3·5	18·7	5·1	4·4	2·5	3·1	1·8	
					W	3·3	4·2	4·3	3·6	12·8	2·9	6·7	1·9	2·8	2·2	
					E	2·3	4·5	5·0	3·2	13·2	3·3	4·5	2·3	2·6	1·7	
					平均	**2·5**	**4·5**	**4·2**	**3·7**	**14·7**	**4·0**	**5·2**	**2·5**	**2·9**	**2·0**	
10	3	3	2 32	III	S	18·7	27·3	26·0	33·5	27·7	27·0		22·7		20·7	三陸沖
					N	24·5	29·2	23·5	37·8	32·7	29·2		26·3		16·4	
					W	21·3	36·4	26·6	26·2	44·3	20·4	27·9	21·2		20·7	
					E	25·1	26·5	30·8	23·3	36·6	18·5	33·3	18·7		19·2	
					平均	**22·4**	**29·9**	**26·7**	**30·2**	**35·3**	**21·3**	**30·6**	**22·2**		**19·3**	
15	4	2	18 52	II	S	2·1	2·9	4·8	4·4	14·1	8·4	7·8	3·5	2·0		水戸附近
					N	3·0	4·1	4·3	5·6	13·4	9·7	5·6	3·5	1·8		
					W	3·6	3·3	5·4	3·9	18·3	6·5	5·9	2·7	2·4		
					E	2·5	4·0	5·3	4·6	15·0	11·0	5·9	2·6	2·0		
					平均	**2·8**	**3·6**	**5·0**	**4·6**	**15·2**	**8·9**	**6·3**	**3·1**	**2·1**		

（次頁へ續く）

地震番號	月	日	時分		震度	觀測地	本郷	青山	丸ノ内	神田	深川	向島	赤羽	野毛山	横濱公園	高島町	震央
			h	m													
18	4	5	21	6	II	S	5·2	3·5		2·9	3·6	2·1	2·3	4·9	1·8	1·8	船橋附近
						N	5·1	3·5		1·9	5·0	3·2	1·1	3·5	1·3	1·1	
						W	4·9	3·8		2·1	6·2	2·0	1·8	2·5	1·7	2·2	
						E	4·9	3·5		1·6	4·7	3·0	2·0	3·3	1·9	2·2	
						平均	**5·0**	**3·6**		**2·1**	**4·9**	**2·6**	**1·8**	**3·6**	**1·7**	**1·8**	
28	6	19	6	38	II	S	3·8	8·4	9·6	7·0	12·9	8·6	5·9	6·2	9·5	7·2	金華山沖
						N	3·7	6·8	10·6	6·0	9·8	6·5	6·8	6·2	8·6	7·6	
						W	4·4	6·1	8·0	6·0	9·4	7·5	7·2	7·0	10·8	6·5	
						E	3·9	7·0	8·3	6·9	10·5	7·0	5·9	7·8	13·0	7·8	
						平均	**3·9**	**7·1**	**9·1**	**6·5**	**10·7**	**7·4**	**6·5**	**6·8**	**10·5**	**7·3**	
29	7	6	11	0	II	S	6·4	15·3	10·6	6·9	7·2	23·4	6·6	21·0	8·7	9·2	江戸川河口
						N	5·3	15·6	15·6	5·1	9·1	18·7	8·7	18·9	9·5	7·7	
						W	6·7	13·6	19·5	5·7	18·8	13·3	5·7	21·1		5·6	
						E	5·9	12·3	21·7	5·5	17·3	13·7	4·4	30·6		4·2	
						平均	**6·1**	**14·2**	**16·9**	**5·8**	**13·1**	**17·3**	**6·9**	**22·9**	**9·1**	**6·7**	
38	9	3	1	43	II	S	3·1	5·1	5·1	4·1	3·3	4·1	4·4	3·1		2·0	八丈島南東沖
						N	2·6	4·6	3·4	3·5	2·6	3·7	5·3	2·8		2·3	
						W	1·9	3·1	4·5	1·8	3·8		4·0	3·9		2·2	
						E	1·9	2·4	5·1	3·2	3·8		4·0	3·8		2·2	
						平均	**2·4**	**3·8**	**4·5**	**3·2**	**3·4**	**3·9**	**4·4**	**3·4**		**2·2**	
47	10	9	21	7	II	S	5·8	10·7	9·2	5·5	5·7	15·0	4·0	10·9	9·5	4·9	道志川流域
						N	5·2	13·7	8·5	4·4	5·5	13·3	4·2	13·0	11·0	4·1	
						W	5·4	10·3	9·4	3·9		23·2	2·4	17·0	14·3	3·9	
						E	4·1	12·4	9·1	4·8		16·7	2·2	16·0	14·5	5·2	
						平均	**5·1**	**11·8**	**9·1**	**4·7**	**5·6**	**17·1**	**3·2**	**14·2**	**12·3**	**4·5**	
62	12	8	3	36	II	S	3·2	5·1	6·9	2·5	4·5	4·5	1·7	13·1	6·5	4·4	伊豆北部
						N	2·7	3·1	5·7	2·3	6·0	5·6	2·6	14·0	6·5	4·6	
						W	2·5	3·5	5·1	1·6	5·6	4·2	1·4	15·4	6·3	6·6	
						E	2·5	2·4	5·4	1·6	3·8	2·8	1·8	16·1	5·2	6·2	
						平均	**2·7**	**3·5**	**5·8**	**2·0**	**5·5**	**4·3**	**1·9**	**14·7**	**6·1**	**5·5**	

昭和9年

地震番號	月	日	時分		震度	觀測地	本郷	青山	丸ノ内	神田	向島	赤羽	野毛山	横濱公園	高島町	震央
			h	m												
5	2	1	9	16	II	S	3·3	3·8	8·3	2·1		3·6				相模川河口附近
						N	2·2	3·7	12·2	2·6		2·8				
						W	3·8	3·1	8·2	3·9		3·9				
						E	2·7	3·1	10·4	2·7		4·4				
						平均	**3·0**	**3·4**	**9·8**	**2·8**		**3·7**				
20	4	7	4	10	II	S	7·0	6·2	8·0	8·8	6·8		8·2	4·5	2·7	鹿島灘
						N	7·0	7·4	8·7	9·7	7·2		6·3	4·0	2·2	
						W	6·5	10·4	8·2	7·1	7·4		5·8	4·7	1·6	
						E	5·8	8·7	9·1	8·0	6·2		9·4	4·8	1·3	
						平均	**6·8**	**8·2**	**8·5**	**8·4**	**6·9**		**7·4**	**4·5**	**2·0**	
21	4	11	19	53	II	S	2·3	4·3	3·7	1·8	5·8	5·7	9·9	3·6	3·5	東京灣北東部
						N	2·6	3·1	3·7	2·8	4·7	6·6	8·1	3·8	3·0	
						W	2·1	1·7	4·9	1·8	2·8	4·9	10·0	4·3	2·1	
						E	1·9	2·4	5·6	1·8	2·7	6·0	9·5	4·3	2·1	
						平均	**2·2**	**2·9**	**4·5**	**2·1**	**4·0**	**5·8**	**9·4**	**4·0**	**2·7**	
22	4	15	19	33	II	S	3·3	4·9	6·0	3·4	5·2	3·0	6·2	10·6	7·8	安房南方沖
						N	2·7	3·3	5·0	3·5	3·1	3·7	8·5	10·1	7·1	
						W	2·8	3·0	5·6	4·1	5·0	3·4	5·8	9·8	5·9	
						E	3·0	3·7	6·9	5·3	3·6	2·9	6·9	10·0	7·4	
						平均	**2·9**	**3·7**	**5·9**	**4·1**	**4·2**	**3·3**	**6·9**	**10·1**	**7·1**	

（次頁へ續く）

地震番號	月	日	時分	震度	觀測地	本郷	青山	丸ノ内	神田	向島	赤羽	野毛山	横濱公園	高島町	震央
24	4	27	$7^{h}\ 47^{m}$	II	S	4·0	4·9	6·4		2·3	3·1	9·3	7·6	4·7	安房南方沖
					N	4·0	3·9	8·7		3·7	4·0	10·7	10·8	4·1	
					W	5·0	2·6	6·7	4·8	3·6	3·1	6·9	9·3	4·8	
					E	6·7	3·5	8·7	5·2	4·1	2·3	7·9	5·6	4·8	
					平均	**4·9**	**3·7**	**7·6**	**5·0**	**3·7**	**3·1**	**8·7**	**8·4**	**4·6**	
26	5	9	19 8	II	S	3·5	3·3	4·4	3·1	5·1	8·2	4·7	1·8	1·4	鴻ノ巢附近
					N	3·6	4·1	4·1	3·8	5·1	7·8	4·8	1·8	1·4	
					W	2·7	4·2	2·7	1·8	3·3	9·2	3·1	2·7		
					E	2·8	4·7	5·1	3·2	3·9	9·2	3·6	2·2		
					平均	**3·2**	**4·1**	**4·1**	**3·0**	**4·4**	**8·6**	**4·1**	**2·1**	**1·4**	
28	5	17	20 53	II	S	4·1	20·6	14·7	5·6	8·8	5·0	40·0	9·7	6·5	木更津沖
					N	4·5	17·6	13·0	4·2	7·5	9·8	43·6	9·3	9·0	
					W	3·8	12·8	16·2	4·0	4·3	7·8		13·2	10·4	
					E	4·8	7·0	15·3	3·4	6·0	8·5		13·2	8·6	
					平均	**4·3**	**14·5**	**13·6**	**4·3**	**6·7**	**7·8**	**41·8**	**11·4**	**8·6**	
30	5	31	8 4	II	S	6·8	9·8	12·0	8·1	14·4	14·0	5·3	5·0	4·5	水戸附近
					N	6·0	10·7	14·2	6·6	16·1	8·3	5·1	6·5	2·9	
					W	7·5	9·6	12·3	9·6	10·0	8·7	7·7	5·0	3·5	
					E	7·2	11·3	10·0	6·6	12·5	11·9	10·8	4·7	4·3	
					平均	**7·1**	**10·4**	**12·1**	**7·7**	**13·3**	**10·7**	**7·2**	**5·3**	**3·8**	
32	6	3	16 17	III	S	10·0	11·7	12·4	10·6	54·0	11·4	5·2	4·9	2·0	利根川下流域
					N	7·5	9·8	19·4	12·6	39·0	11·3	4·7	5·4	2·7	
					W	8·2	11·3	27·1	8·5	53·0	8·9	4·1	3·7		
					E	8·0	11·3	17·6	8·5	45·0	9·9	3·9	3·7		
					平均	**8·4**	**11·0**	**19·1**	**10·4**	**47·8**	**10·4**	**4·5**	**4·4**	**2·4**	
36	6	15	14 31	II	S	4·3	3·7	6·7		6·0	6·4	4·2	4·7	2·0	間々田附近
					N	2·7	3·9	5·5	4·4	3·7	5·2	5·7	5·4	2·7	
					W	3·2	3·3	4·6		2·2	7·6	3·6	4·1	2·0	
					E	3·5	4·0	3·6	4·3	2·5	5·4	3·9	5·2	2·0	
					平均	**3·4**	**3·7**	**5·1**	**4·4**	**3·6**	**6·2**	**4·4**	**4·9**	**2·2**	
46	8	3	21 24	III	S	12·2	15·6	31·6	23·7	16·8	13·1	9·2	10·4	7·9	館野附近
					N	9·3	14·6	35·7	23·4	18·7	21·0	9·9	7·6	6·4	
					W	15·0	10·8	24·0	13·4		13·5	14·0		7·2	
					E	11·2	9·8	22·4	12·8		25·2	14·9		7·2	
					平均	**11·9**	**12·7**	**28·4**	**18·4**	**17·8**	**18·2**	**12·0**	**9·0**	**7·2**	
49	9	1	20 17	II	S	10·5	15·2	14·3	9·2	11·6	14·0	9·5	4·9	4·2	水海道附近
					N	8·5	12·8	14·6	9·6	12·8	17·4	9·3	4·0	4·0	
					W	8·0	11·7	13·1	6·9	12·0	13·7	16·2	7·8	4·9	
					E	10·0	10·4	12·6	8·8	11·0	16·0	16·2	7·8	4·7	
					平均	**9·1**	**12·5**	**14·7**	**8·6**	**11·9**	**15·3**	**12·8**	**6·1**	**4·5**	
50	9	17	9 30	II	S	5·5	9·7	7·5	2·9	4·9	5·2	2·9	2·0	1·4	印旛沼
					N	4·0	5·8	8·2	2·5	3·8	3·5	3·1	1·8	1·4	
					W	5·0	3·5	5·4	4·1	4·5	3·1	4·1	4·1	2·6	
					E	3·8	3·1	4·4	5·1	5·4	1·8	4·6	2·2	2·8	
					平均	**4·6**	**5·5**	**6·4**	**3·7**	**4·7**	**3·4**	**3·7**	**2·5**	**2·1**	
51	9	24	13 53	II	S	2·0	2·5	4·4	2·9	2·2	3·3	8·1	10·3	3·4	山口湖附近
					N	2·7	3·1	4·4	2·9	2·2	3·0	8·7	7·5	3·4	
					W	1·9	3·1	5·7	2·4	1·8	2·5	12·0	5·9	4·5	
					E	2·4	2·1	4·0	2·9	2·0	2·3	12·0	4·3	3·3	
					平均	**2·3**	**2·7**	**4·6**	**2·8**	**2·1**	**2·8**	**10·2**	**7·0**	**3·7**	
58	11	27	14 50	I	S	3·3	2·3	4·1			3·1	4·2	3·6	2·5	九十九里濱沖
					N	2·9	2·5	4·4			4·4	3·8	3·3	2·7	
					W	3·0	2·6	5·5		3·8	3·2	3·1	3·3	2·6	
					E	3·0	3·1	4·8		4·2	3·6	3·8	3·5	2·4	
					平均	**3·1**	**2·6**	**4·7**		**4·0**	**3·6**	**3·7**	**3·4**	**2·6**	

（次頁へ續く）

地震番號	月	日	時分	震度	觀測地	本鄕	青山	丸ノ内	神田	向島	赤羽	野毛山	横濱公園	高島町	震央
59	11	28	$0^{h}\ 56^{m}$	II	S	5·2	12·7	8·6	5·3	15·0	18·0	6·8	4·9	2·9	水海道附近
					N	6·0	9·3	7·8	6·4	15·8	16·5	7·4	4·0	2·2	
					W	6·9	10·3	8·6	5·0	11·7	19·4	7·2	5·2	2·6	
					E	8·9	10·4	7·1	5·4	11·0	25·6	8·5	4·1	2·2	
					平均	**6·7**	**10·7**	**8·0**	**5·5**	**13·4**	**20·0**	**7·5**	**4·6**	**2·5**	

比較した．此等は第3圖に示すものであり，横軸には震央距離，縱軸には各地の平均最大加速度と本鄕の平均最大加速度との比を採つた．本鄕と青山とは殆ど常に同樣の最大加速度を與へるが神田におけるものは明瞭に震央距離に關係して消長する事を示して居る．卽ち震央距離 50 m を境として近い場合は本鄕の方が大，遠い場合には神田の方が大となる．

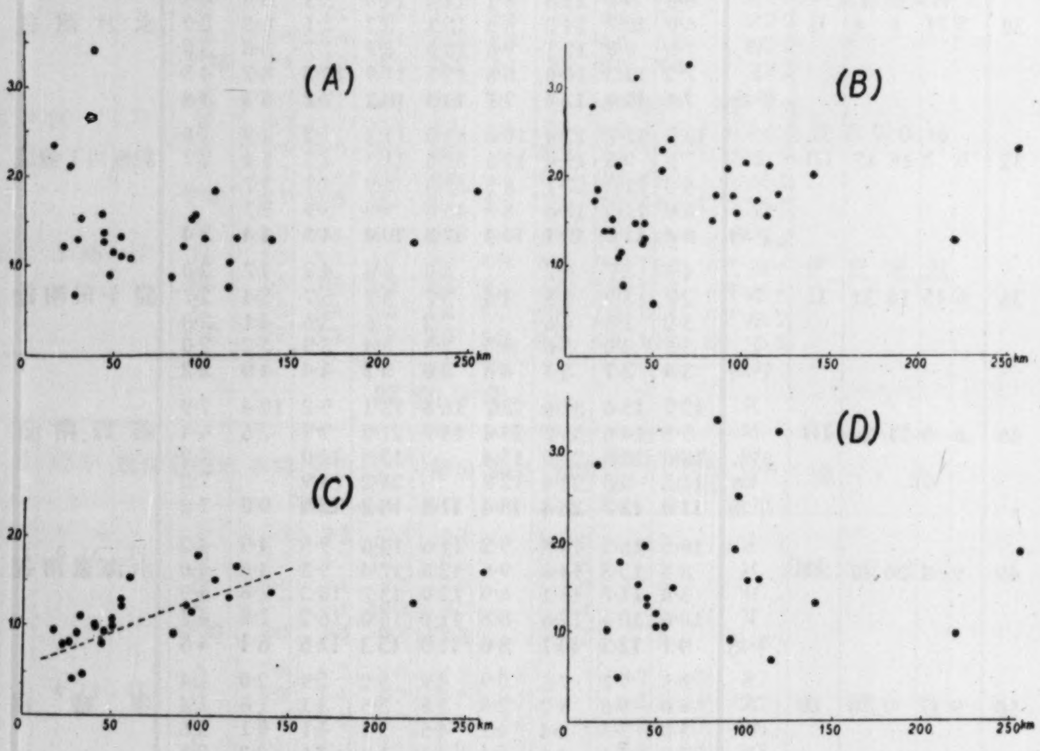

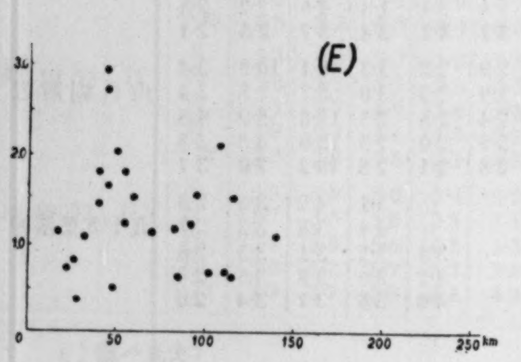

第3圖 東京本鄕を基準とする各地平均最大加速度比

縱軸： 平均最大加速度比
橫軸： 震央距離

(A) 青山，(B) 丸ノ内，(C) 神田，
(D) 向島，(E) 赤羽

横濱においては野毛山を基準として比を求めたが，此の場合には公園，高島町共に著しい關係を示し，震央距離が 100 km 以内ならば野毛山の平均最大加速度は常に大で約2倍以上に達する事も決して珍しくない（第 4 圖）．此等の現象は全く各地盤の良否と密接の關係を有するものであり，震害を論ずる場合に常に影響するものである事を充分注意しなければならない．

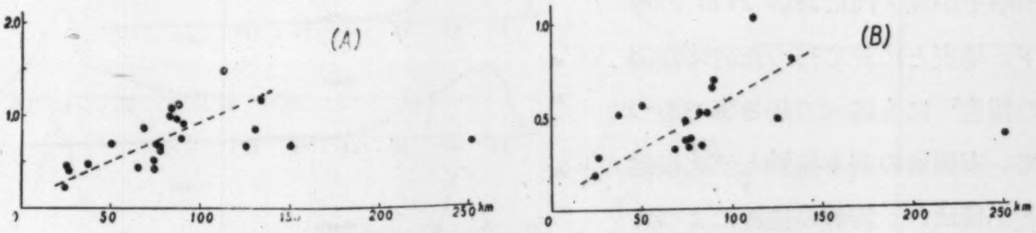

第４圖　横濱野毛山を基準さする各地平均最大加速度比
縱軸：　平均最大加速度比
横軸：　震央距離
(A) 横濱公園，(B) 高島町

3．卓越振動周期

卓越振動周期の決定は前回と同樣各地點に於て得た記象を寫眞により 2·7 倍に引延ばし，各波に印をつけ，順次に 0·1 mm（0·035 秒の時間に當る）迄讀んで差をとり，各 0·1 mm 毎に相當する波數を求め，多少曲線を平坦とする目的上得たる數の相隣る 3 數を平均して結果を出した．

以上の方法を應用した地震は次の５個の地震である．何れも昭和９年中東京附近に發生した加速度の大なる地震である．

	震　央
昭和９年４月７日	鹿　島　灘
５月31日	水戸附近
６月３日	江戸崎附近
８月３日	館　野　附　近
９月１日	水海道附近

以上５個の結果を圖示したものは第５～９圖である．前回に述べたと同樣，震央距離の大小に從つて多少の卓越周期の大小はあるが，山手では一定に近く 0·3 秒附近である．又山手の中にも青山，駒場の如く比較的臺地の奥まつた所にある觀測點では卓越周期は簡單で確率曲線其の儘を示して居る．此れに反し，本鄉の如き臺地の端近く位する觀測點における卓越周期中には下町の震動も混じて居る如くに見える．此の事は已に本鄉と丸ノ内との震動を比較した場合[2]にも注意した事である．

---

[2] 石本巳四雄　地震研究所彙報　10 (1932), 171.

下町に於ける卓越周期の決定は山手における程簡單ではない．即ち曲線の中に2～3の最大値が認められるからである．下町における震動は其の中に高次の倍振動が同時に誘發される結果と信じられる．此の事實は齊田學士が丸ノ内におい24mの地下と地表とに於て行つた同時觀測の報告3)にも述べて居る事であつて，表面層の基本振動と三次振動とが現はれ，震源の遠近によつて現はれ方に相違があると云ふ事であるが，今回の觀測の中，其の卓越周期からも云へる事である．

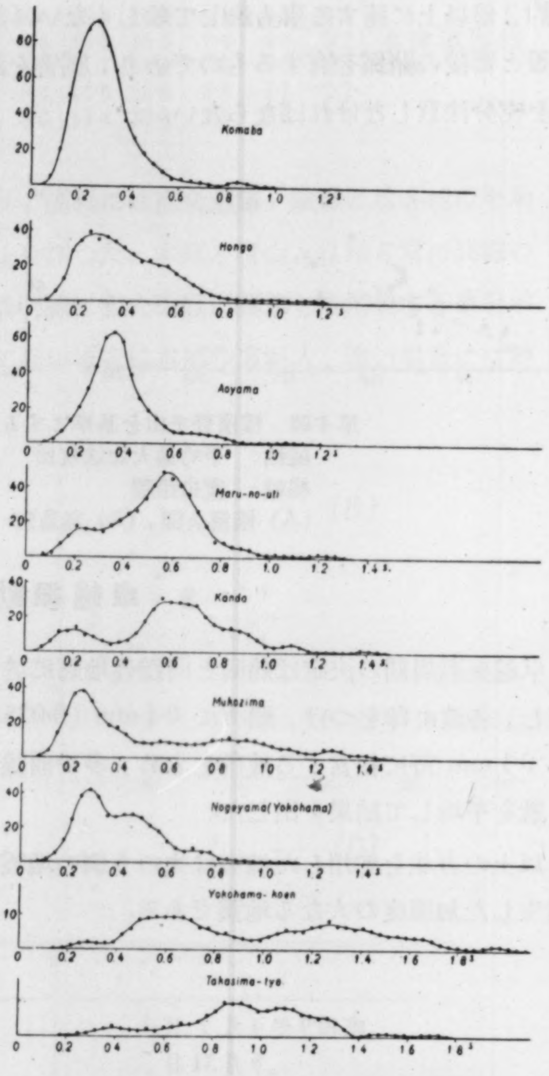

第5圖　昭和9年4月7日鹿島灘地震による東京横濱地方地震動中の卓越周期（縦軸は波數）

第III表は昭和7年より昭和9年に至る頻度曲線から得た極大値を掲げた．山手においては一つの極大であるが，下町においては一般に二つ以上ある．而して其等の周期の比は大體1：3である事が判る．勿論表面層の振動としては5次，7次のものも發生されるのであらうが，三次のものと相接して現はれるため，頻度曲線から決定する事は困難である．又實際此等の振動は表面層の剪斷振動と考へられ，從つて其の振動周期は表面の厚さと其の彈性とに因ると思はれる．即ち表面層の厚さが大である程其の基本振動周期は大となる筈であるが，地震時において何等制限なく大周期の波動が激勵されるや否やは別の問題である．確かに表面層の厚いと考へられる地域の頻度曲線は一樣に平坦になる傾向を有して居る事である．今回の觀測で固有振動周期と認め得た最大のものは横濱公園における1.2秒のものであり，地盤としても相當不良の方に屬する．恐らく此の程度以上の加速度の大なる震動周期は現はれぬものであらう．

---

3)　齊田時太郎　地震研究所彙報　**12** (1934), 517.

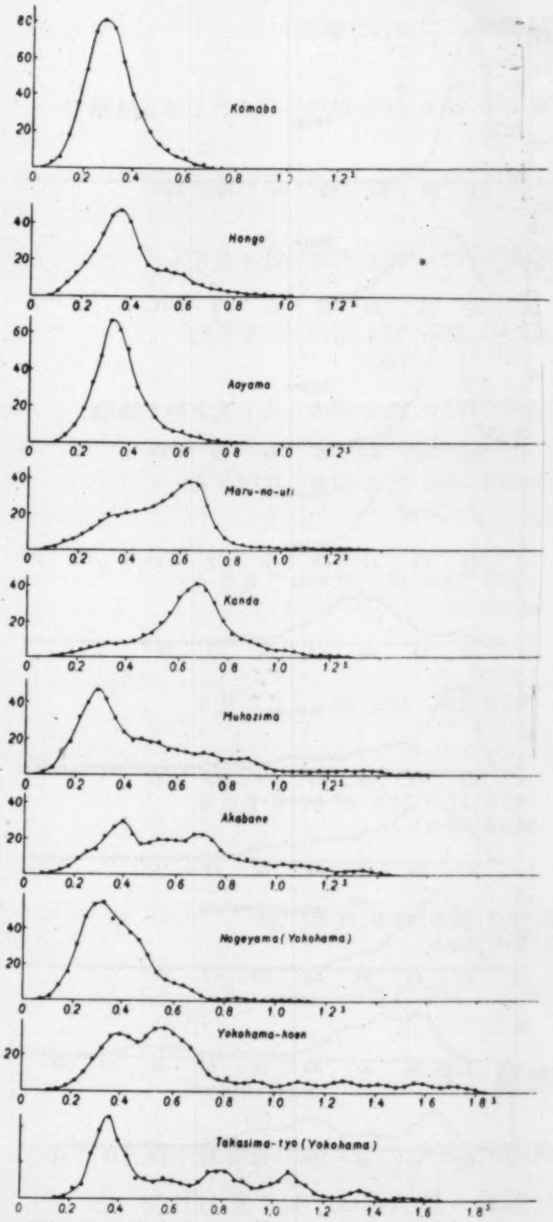

第6圖　昭和9年5月31日水戸附近地震による東京橫濱地方震動中の卓越周期（縱軸は波數）

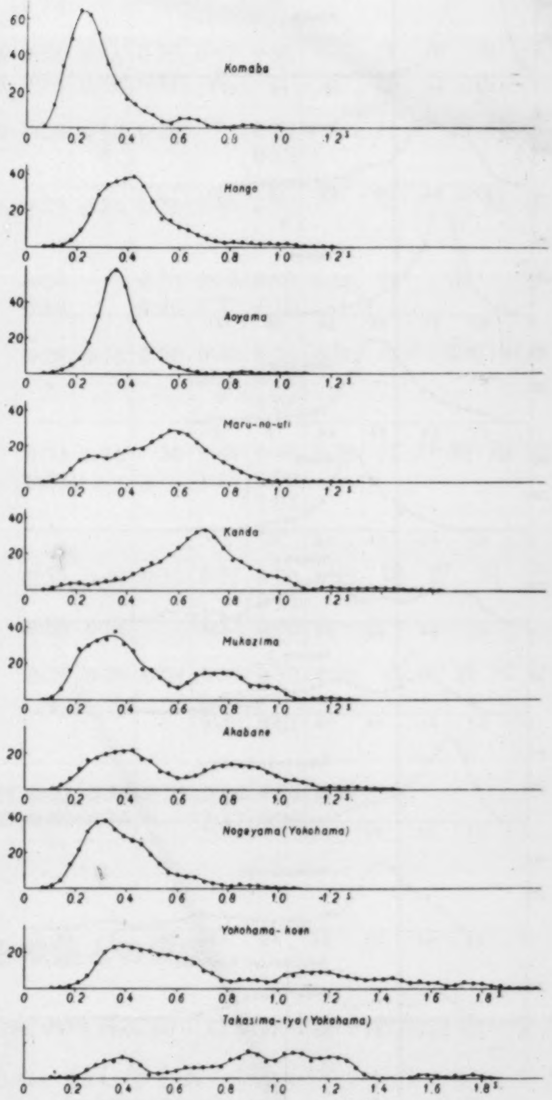

第7圖　昭和9年6月3日江戸崎附近地震による東京橫濱地方震動中の卓越周期（縱軸は波數）

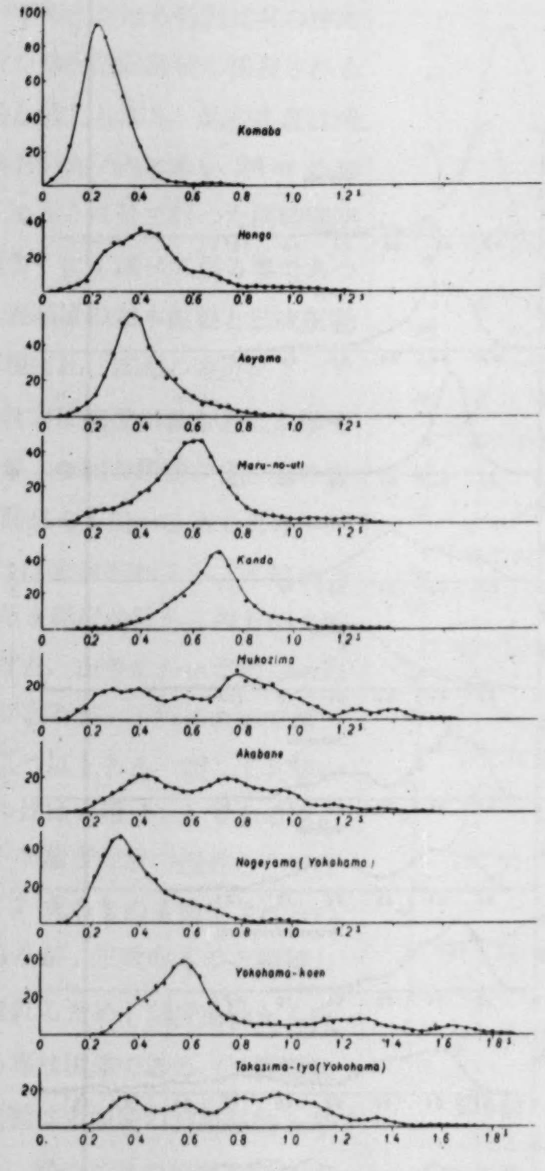

第8圖　昭和9年8月3日館野附近地震による東京横濱地方地震動の卓越周期（縦軸は波數）

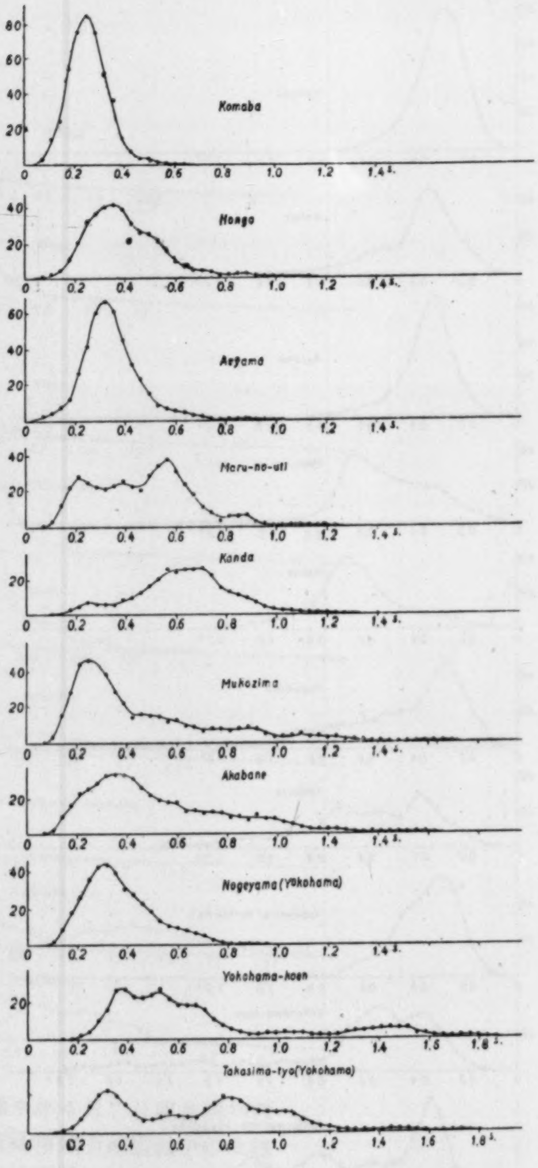

第9圖　昭和9年9月1日水海道附近地震による東京横濱地方地震動の卓越周期（縦軸は波數）

第III表　各地卓越振動周期

	本鄉	青山	丸ノ内	神田	深川	向島	赤羽	野毛山	横濱公園	高島町	駒場	震央
昭和8年3月3日	s 0·34	s 0·35	s 0·68	s 0·21 0·70	s 0·31	s 0·26 0·74	s *	s 0·34	s	s 0·35 *		三陸沖
6月19日	0·41	0·38	0·65	0·72	0·36 0·88	0·26 0·74	0·36 0·80	0·35 0·51	0·57 *	0·85		金華山沖
7月6日	0·23 *	0·29	0·20 *	0·20 *	0·20	0·20	0·20 *	0·25	*	0·20 0·35		江戸川河口
10月9日	0·41	0·27 0·39	0·52		0·36	0·23	0·43	0·25	0·40	0·37		道志川流域
昭和9年4月7日	0·28	0·35	0·58	0·20 0·64		0·24 0·88		0·28 0·46	0·60 1·27	0·90 1·10	0·26	鹿島灘
5月31日	0·35	0·33	0·64	0·68		0·28 *	0·70	0·30	0·40 0·56 *	0·35 0·78 1·06	0·28	水戸（涸沼）附近
6月3日	0·39	0·35	0·59	0·70		0·34 0·85	0·36	·30	0·40 1·16	0·40 0·90 1·07 1·23	0·23	江戸崎附近
8月3日	0·40	0·36	0·61	0·70		0·35 0·80	0·42 0·74	0·31	0·57 1·23	0·35 0·56 0·95	0·22	館野附近
9月1日	0·35	0·32	0·24 0·57	0·24 0·67		0·25 *	0·35	0·31	0·37 0·52 1·48	0·32 0·81	0·25	水海道附近
平均	s 0·37	0·34	0·22 0·60	0·21 0·67	0·31 0·88	0·27 0·80	0·35 0·75	0·35	0·49 1·23	0·36 0·94	0·25	

*……甚だ平坦

4. 震害と地盤との關係

上記の現象から見ると，比較的震央の近い地震に於ては山手の方が加速度が大である．此れは嘗て信じられた事とは逆である．然し乍ら其の振動周期は山手に於て小である結果は木造住宅の如く多少變形しても倒壞しない構造物に對しては害を爲す事は少ない．反之土藏造，煉瓦造のものは大部分最大加速度の値によつて震害を蒙ると考へてよいであらう．從つて震害の問題は建物の構造的相違と地震動の二要素（最大加速度と卓越周期）とを二つ乍ら顧慮する必要がある．

今各地の卓越周期を決定すべき頻度曲線を各地盤の良否に從ひ圖に示すと第 10 圖の如き有様を呈する．震央が比較的近い場合においては加速度の値は卓越周期の小なる所程大となる．恐らく共の周期に逆比例すると考へてよいであらう．地震動は本質

的に斯樣な性質を備へて居るものであるから，各地における卓越周期の存在と其の震動が如何に建物の構造に影響するかを充分研究すべき必要があるのである．木造家屋の振動周期は 0·4~0·6 秒である事から，筑波地方の如き小周期の震動に對しては充分安全性を有するに反し，東京下町の如く 0·6 秒或ひは其れ以上の周期の震動に對しては，比較的小なる加速度であつても損傷を蒙る事が著しい事となり，所謂地盤の悪い所卽ち震害が多く見られると說明出來る．

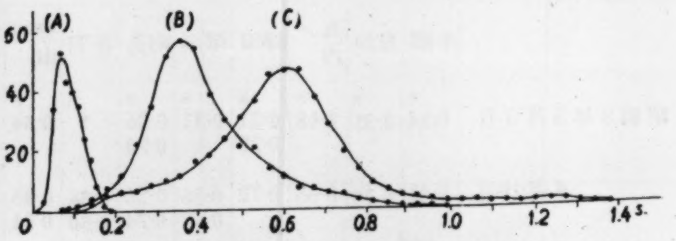

第 10 圖 地盤の良否に從ひ卓越振動周期の異る事を示す（縱軸は波數）
(A) 筑波： 昭和 2 年 6 月 28 日の地震（井上學士による）
(B) 青山： 昭和 9 年 8 月 3 日の地震
(C) 丸ノ內： 同 上

5．水平動各成分における卓越周期の相違

地震動の水平成分は東西，南北の二成分に分つて記錄するのを常とするが，今回の如き加速度地震計觀測に於ても震動全體として孰れも殆ど同形を示す事から，各地域が特別方向にのみ著しく震動すると云ふ事は無いらしい．此れは假令觀測點が丘の緣にある場合（橫濱野毛山の如き）でも差違はない．從つて從來考へられた如き崖上の土地は崖面と直角に多く震動を行ふと云ふ事も多少はあるにしても著しいものではない樣である．

卓越振動周期に就て各成分別々に頻度曲線を造つて見ると一般には大差ないが，所

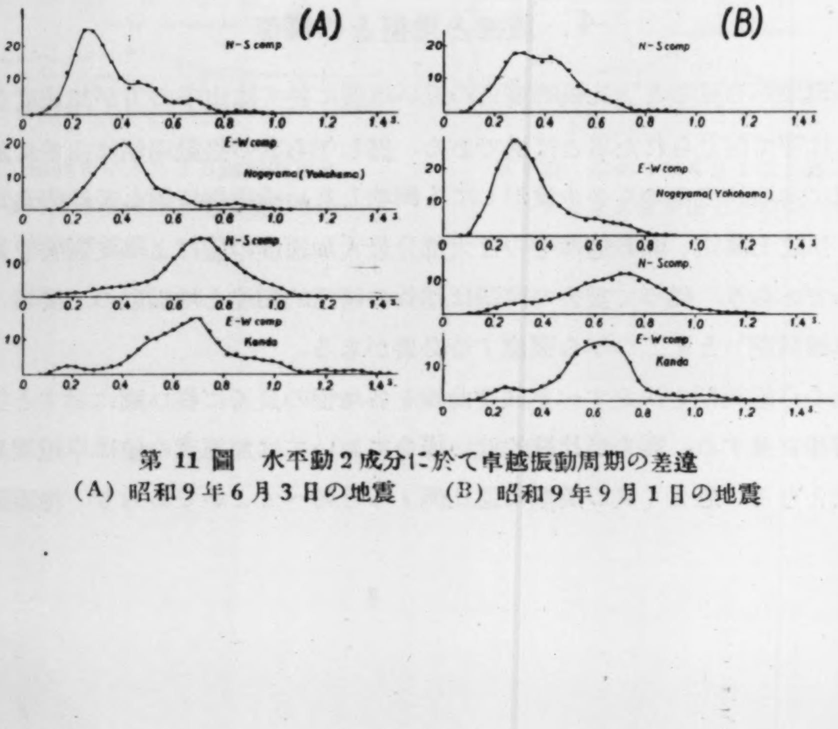

第 11 圖 水平動 2 成分に於て卓越振動周期の差違
(A) 昭和 9 年 6 月 3 日の地震 (B) 昭和 9 年 9 月 1 日の地震

により異る場合がある．第 11 圖は神田及び野毛山におけるものであるが，一成分方向の振動は周期が常に比較的長いと云ふ事も無い樣である．神田においては斯樣の現象は著しくなく，各成分同樣の頻度曲線を示して居る．若し兩成分に於て卓越周期が異ると云ふ事が多分に存する場合には木造家屋の倒壞もある方向に著しい事が大地震の機會に觀察されるであらう．但し物體の顚倒等が一方向に一致する場合の見受けられる事があるが，此れは恐らく其の方向に大なる加速度が存在したと解釋される事が多い樣である．

6. 人工的に誘起される地動と地震動との關係

地震動の中には各地域の表面層の固有振動と考へられるものが大部分である事から，日常人工的にも斯樣の振動が誘發される可能性がある．東京山手における微動を觀測すると，其の振動の卓越周期は常に 0.3 秒である事は已に屢々報告された事であり，此れが地震動の周期とも一致する事から此れは土地の固有のものであると云ふ判定も得られた次第である．日常存する 0.3 秒周期の微動の發生する原因に關しては井上學士[4] の外餘り論ぜられて居ないが，最近本郷の觀測[5] によると其の振幅の消長は毎日殆ど同一の型を繰返すのであつて，日中は大，午前 2～3 時は極めて小となる．又氣象の影響は殆ど無い樣である．從つて此の微動は專ら人工的（主として交通機關）の生ずるものと考へて差支へあるまい．然し乍ら觀測所附近を通過した自動車の振動を檢査して見ると，此れは 0.15 秒程度であり，又附近の煉瓦造を取り壞した時の振動は 0.2 秒の周期が現はれて居る（第 12 圖）．此等の一致しない理由は振動發生場所が近い故かも知れぬ．

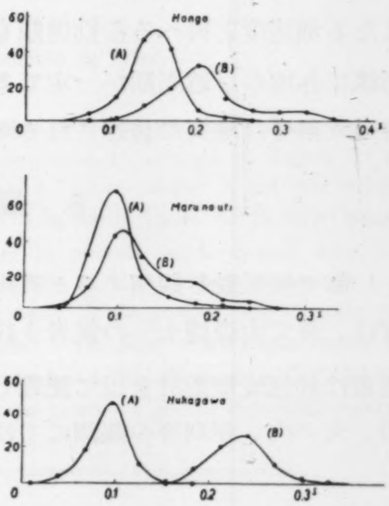

第 12 圖　人工地動中の卓越周期
本郷：（A）自動車によるもの
（B）煉瓦造破壞によるもの
丸ノ内：(A)(B) 日常交通機關によるもの
深川：（A）自動車によるもの
（B）製材所の振動

深川，丸ノ内等においては日常多くの微動が加速度地震計により記錄されて居る．此等の振動の周期頻度曲線を作つて見ると，第 12 圖の如く，此等の卓越周期は何れも該當地域の地震動中に現はれる卓越周期とは一致しない．此の

---

[4] 井上學士は駒場における觀測から，氣象要素と關係を持つと云ふ結果を得た．震研彙報 **12** (1934), 712.

[5] 400 倍の微動計による觀測.

事は恐らく振動を起す源が小面積に限られて居り，表面層全體としての固有振動を誘發せしめるには至らないものと思はれる．山手におけるものゝ一致する理由は恐らく其の基本周期の小なる爲めであらう．

7．最大加度速と卓越周期との關係

卓越周期を問題とする場合，其の加速度の大なるものに就て云はなければならぬのは當然である．前回述べた如く，加速度の大なる振動は少數であり，統計的に周期を決定する事が出來ず，或る方法を採用した．今回の觀測においても前回と同樣，大なる加速度を與へた振動の周期は卓越振動周期と大體一致して居る事は記象を一見しても直ちに判る事である．卽ち周期は殆ど一定であり乍ら振幅（加速度）が種々變化して，最大値にも達して居るのである．此の事實は震災を論ずるに當つても，震動の卓越周期を以て最大加速度の周期として採用して何ら不結果は生じない事となる．

加速度地震計による地震動の觀測が開始されてから未だ大なる地震動に遭遇しないが，昭和6年9月21日の秩父地震の本鄕觀測においては最大加速度として 68 gal を記錄して居る[6]．此の場合の周期も0·3秒附近であつた事からすれば，大地震の場合の大なる加速度を與へる振動周期も各地の卓越振動周期と一致すると見てよいであらう．斯樣に各地の卓越周期が一定である事は，所謂地盤の良否に關係するものであり，震害の大部分は地表に誘起される固有振動に原因すると信じられるのである．

8．震源が接近して起る地震

1 點で地震動を觀測すると震源が接近して居る地震は相似た記象を與へると云ふ事實は，嘗て大森博士[7]の報告された事であり，屢々震源決定に役立つて居る．以上の現象は加速度地震計を以て記錄した記象にも當嵌る事である．卽ち下記の2地震の神田，丸ノ内，赤羽等の觀測にては充分に對照せしめる事が出來る．

	震　央
昭和7年6月16日の地震	館 野 附 近
昭和9年8月3日の地震	

但し所によつて（本鄕の如き）は似ない所もある．此の二つの地震の震源の深さも殆ど同樣であるが，此の二つの地震の附近に震央を有する地震（昭和9年6月3日發生）にて震源稍々淺いものを見ると，此れは似て居ない．

---

[6] 石本巳四雄　地震研究所彙報　10 (1932), 614.

[7] 大森房吉　震災豫防調査會歐文報告　21 (1905), 9.

以上の事實は恐らく初め二つの地震は共の地震波發生の機巧も同型，同方向にあつた事を充分想像する事が出來る．斯様に加速度地震計記象中に現はれる振動は大部分觀測地域の固有性振動であるにも拘らず，充分の類似のある事は，思ふに激勵方法も，表面波擴散樣式も全く同一である結果であらう．

なほ本研究は服部報公會の援助により遂行せられたるもので玆に甚大な謝意を表するものである．又各地觀測に直接當つた諸氏の勞を多とすると共に，地震研究所においては大塚，鈴木の二氏が器械の調整及び記象の整理を擔當して以上の如き結果を得たる事を特に感謝するものである．

---

47. *Observations accélérométriques des secousses sismiques dans les villes de Tôkyô et Yokohama* (2me *rapport*)

par Mishio ISHIMOTO,

Institut de Recherches sur les Tremblements de terre.

Les observations accélérométriques ont été continuées encore pendant 1934 aux mêmes stations dans les deux villes. A cette année nous avons réussi à enregistrer 15 séismes de degrée II et 2 séismes de degrée III. L'accélération maxima correspondée à chaque séisme a été déterminée et montrée dans le tableau II. D'une part elle est superieur á la partie haute de la ville quand la distance épicentrale reste moins que 50 km. D'autre part la période prédominante dans les secousses sismiques est comparativement petite à la partie haute de la ville. Nous constatons que la période prédominante corresponde à celle d'oscillation propre de la couche superficielle du terrain et elle a un rapport serré avec des dommages sismiques. De plus, nous avons essaié de trouver quelque relation entre la période des secousses provoquées artificiellement et la période prédominante dans les secousses sismiques, mais nous n'avons pu constater aucune coïncidence entre eux.

48. On Microseisms of Four Second Period.
(The Second Paper).

By Fuyuhiko KISHINOUYE,

Seismological Institute, Faculty of Science,
Tokyo Imperial University.

(Read May 21, 1935.—Received June 20, 1935.)

1. In a paper in this journal[1] the writer has described some results of observation of microseisms at Hongô in Tôkyô, periods of which are about 4 sec. But in that case records of only N–S component motions were investigated. Then microseisms were studied further by combining three components of the motions.

Seismographs record oscillations with some time-lag which depends upon period and damping of seismographs and period of oscillations. So when resulting motions are obtained by combining components recorded with different types of seismographs, phase differences of the component motions have to be noticed. Then the writer measured constants of many seismographs which were available, and selected following instruments shown in Table I for the investigation because he found that phase differences for microseisms of 4 sec period were least for them.

Table I.

Instrument	Component	M	V	T_0	v	r	δ
Omori horiz. pend. seismograph	E–W	17 kg	15	58·4 s	1·27	0·43	171°
Ditto	N–S	42	20	49·6	1·71	0·15	161
Omori vertical seismograph	U–D	15	20	11·0	1·04	0·20	178

In the above table, M denotes the weight of the pendulum-bob, V the static magnification, T_0 the free period of the seismograph, v the damping ratio, r the coefficient of friction and δ the phase lag for harmonic disturbances with period of 4 sec. The phase difference was somewhat great between N–S and U–D component seismographs and amounted to 17° in angle or about 0·2 sec in time. It was neglected in the combination of components, for it may be not so great as compared with other errors of the observation.

---

[1] F. KISHINOUYE, *Bull. Earthq. Res. Inst.*, **13** (1935), 146～154.

2. Microseisms were large in amplitudes on Jan. 1∼2, 1935. Then simultaneous portions of records of the oscillations obtained with the seismegraphs shown in Table I at about 11 h 30 m on Jan. 1 were taken for the investigation. They were enlarged photographically as large as 1 minute interval of the records became 180 mm. (Minute marks on records of the three seismographs were put on simultaneously with one chronometer.) Amplitudes were read at intervals of 1 mm on the enlarged records, and then divided by dynamic magnifications of the instruments. Fig. 1 shows true earth movements obtained by the above-stated means.

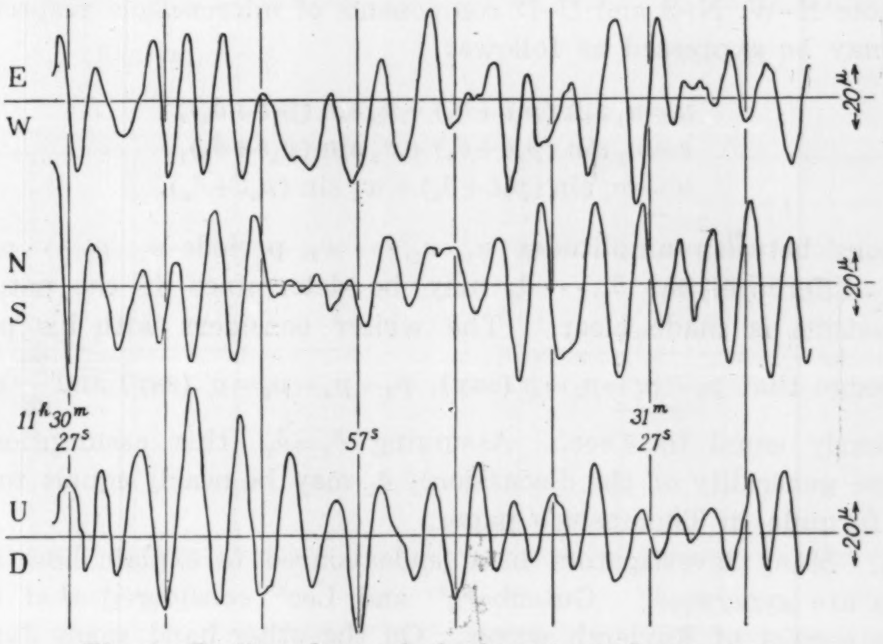

Fig. 1. Portion of record of microseisms. Jan. 1, 1935.

Amplitudes of each component vary like beats of two harmonic motions, and periods of the beats fluctuate between 30 sec and 50 sec. Although periods of the oscillations are nearly equal in each component, phases are different with each component. Azimuths of composed motion of E–W and N–S components and orbits of horizontal motion of an earth particle change incessantly as shown in Fig. 2. This fact has been noticed by Omori[2] and Wadati[3]. The writer moreover combined vertical and horizontal components, and the results are shown in Figs. 3 and 4. These diagrams resemble those in Fig. 2.

---

[2] F. OMORI, *Bull. Earthq. Inv. Comm.*, **5** (1911), 136.

[3] K. WADATI, *Jour. Meteorol. Soc., Japan*, **4** (1926), 83∼86.

3. The orbits of an earth particle were different from those in precessional motion. When amplitudes became small, the azimuth of the motion changed nearly perpendicular to the previous azimuth, and the direction of the rotational motion of the particle also changed opposite to that in the previous azimuth. The change of directions of rotational motion at the least amplitudes may confirm the writer's idea that microseisms of 4 sec period at Hongô are composed of two harmonic oscillations, period and amplitude of them are slightly different, for in theory the amplitude of the resultant motion of such motions varies like beats and the phase changes as much as 180° at the smallest amplitudes as stated by Thompson[4]. Then if u, v, and w denote E–W, N–S and U–D components of microseisms respectively, they may be expressed as follows:

$$\begin{aligned} u&=u_1 \sin (p_1 t+\delta_1)+u_2 \sin (p_1 t+\delta_2), \\ v&=v_1 \sin (p_3 t+\delta_3)+v_2 \sin (p_4 t+\delta_4), \\ w&=w_1 \sin (p_5 t+\delta_5)+w_2 \sin (p_6 t+\delta_6). \end{aligned}$$

Relations between amplitudes $u_1, v_1, \cdots w_2$, periods $p_1, p_2, \cdots p_6$, and phase differences $\delta_1, \delta_2, \cdots \delta_6$ may be determined if the nature of microseisms is made clear. The writer considers with his present knowledge that $p_1=p_3=p_5=p$ (say), $p_2=p_4=p_6=p'$ (say) and $\frac{2\pi}{p}$ and $\frac{2\pi}{p'}$ are nearly equal to 4 sec. Assuming $\delta_1=\delta_3$ (this assumption may not lose generality of the discussion), δ_2 may be nearly equals to $\delta_4+\pi$ by a formula in Thompson's paper.

4. Many investigators have endeavoured to explain how microseisms are generated. Gutenberg[5] and Lee[6] considered that microseisms consist of Rayleigh waves. On the other hand, many Japanese seismologists are of opinion that microseisms are free oscillations of the ground. The above mathematical expressions may denote the motion of particle which is caused by either progressive or stationary waves, and at present there is no data to determine the character of the waves. But according to the results obtained, the writer inclines to consider that microseisms of 4 sec period at Hongô are stationary waves of the ground generated by some origin.

---

4) J. S. THOMPSON, *Phil. Mag.*, **15** (1933), 1~15.

5) B. GUTENBERG, *Bull. Seism. Soc., Amer.*, **21** (1931), 1~24.

6) A. W. LEE, *M. N. R. A. S. Geophys. Suppl.*, **3** (1932), 83~105; *Ditto*, **3** (1934), 238~252 and *Geophys. Mem. Meteorol. Off.*, No. **62** (1934).

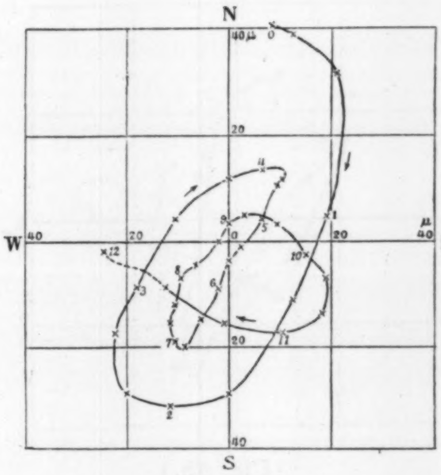

(Fig. 2a.)

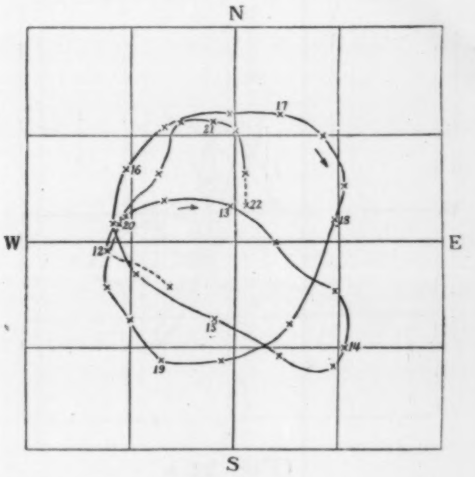

(Fig. 2b.)

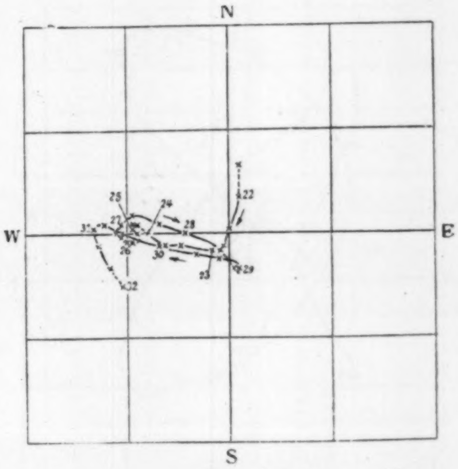

(Fig. 2c.)

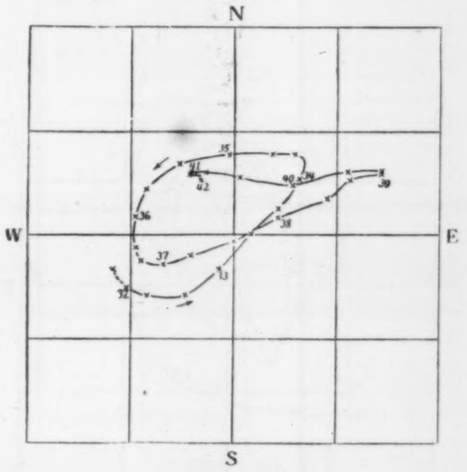

(Fig. 2d.)

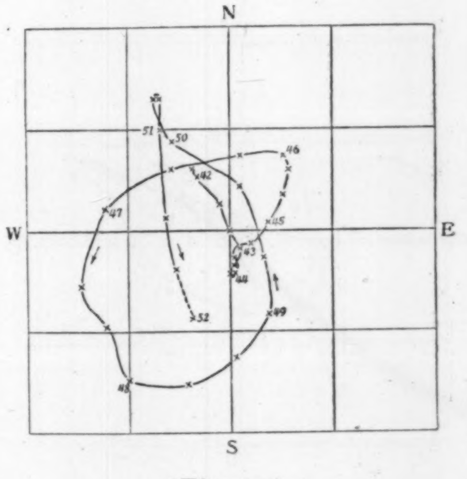

(Fig. 2e.)

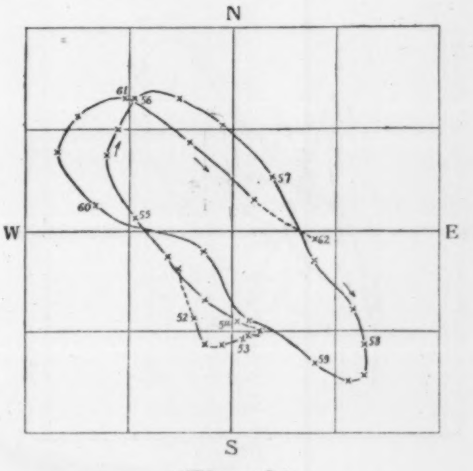

(Fig. 2f.)

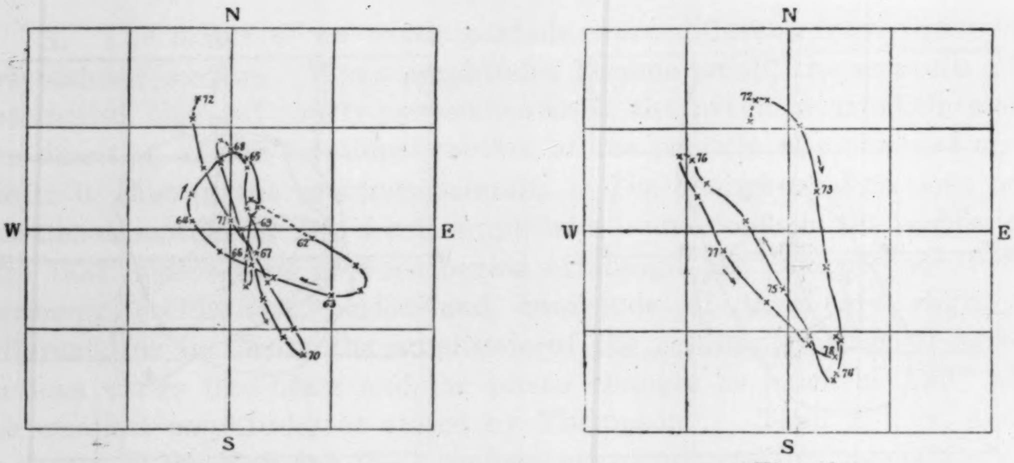

(Fig. 2g.) (Fig. 2h.)

Fig. 2. Ground movement in horizontal plane.
Italic numerals indicate time in second, and arrows direction of motion of an earth particle.

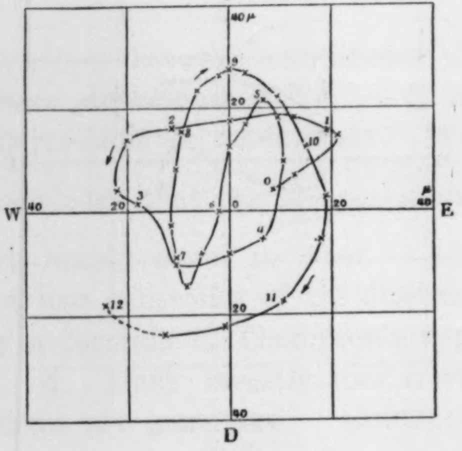

(Fig. 3a.)

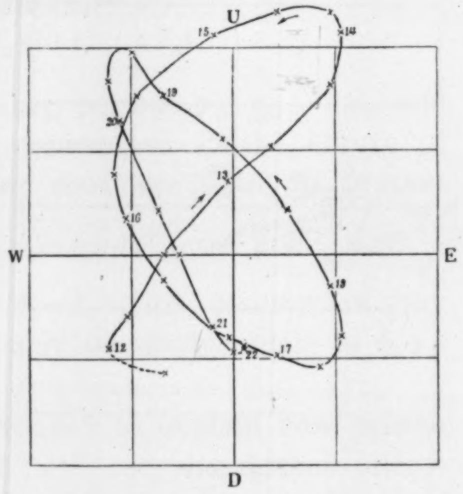

(Fig. 3b.)

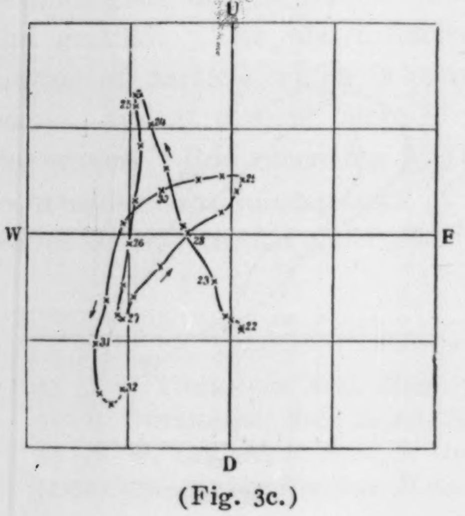

(Fig. 3c.)

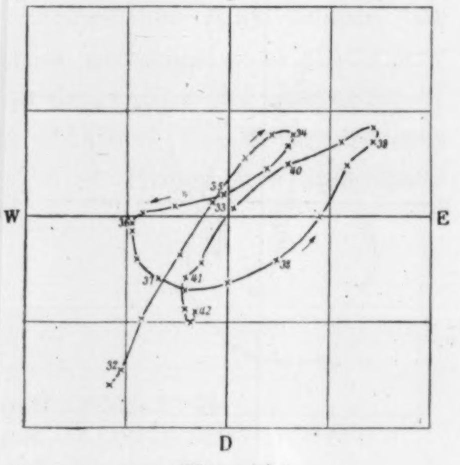

(Fig. 3d.)

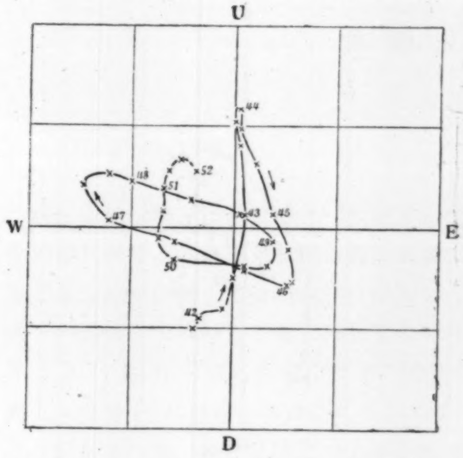

(Fig. 3e.)

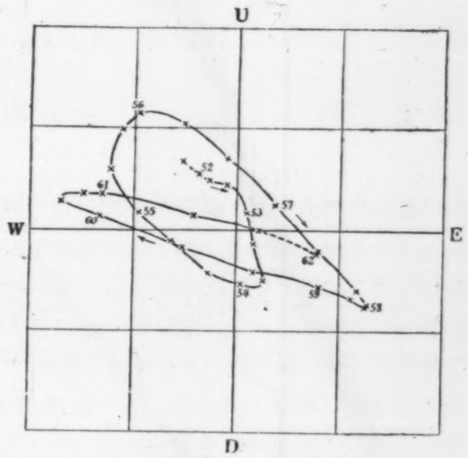

(Fig 3f.)

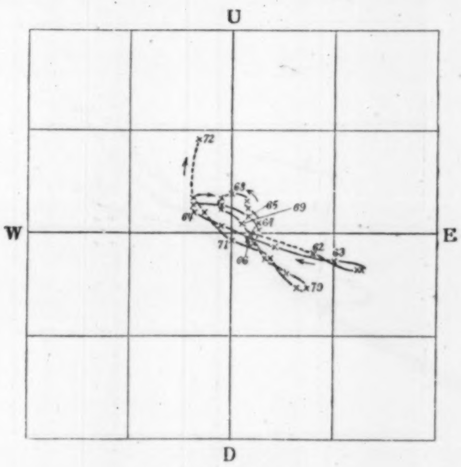

(Fig. 3g.)

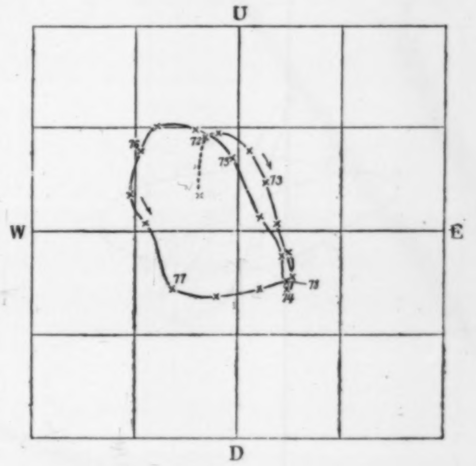

(Fig 3h.)

Fig. 3. Ground movement in meridional plane.

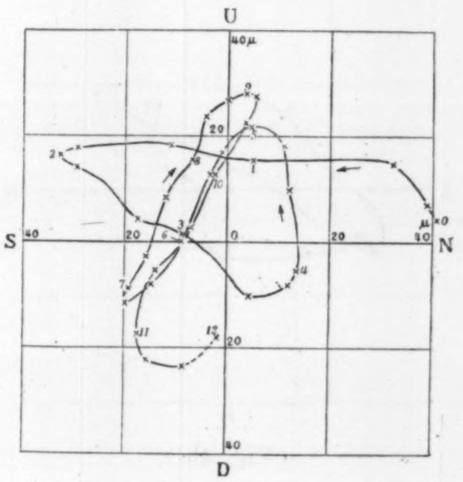

(Fig. 4a.)

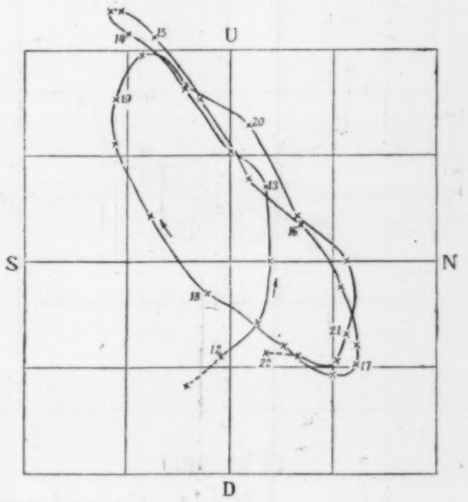

(Fig. 4b.)

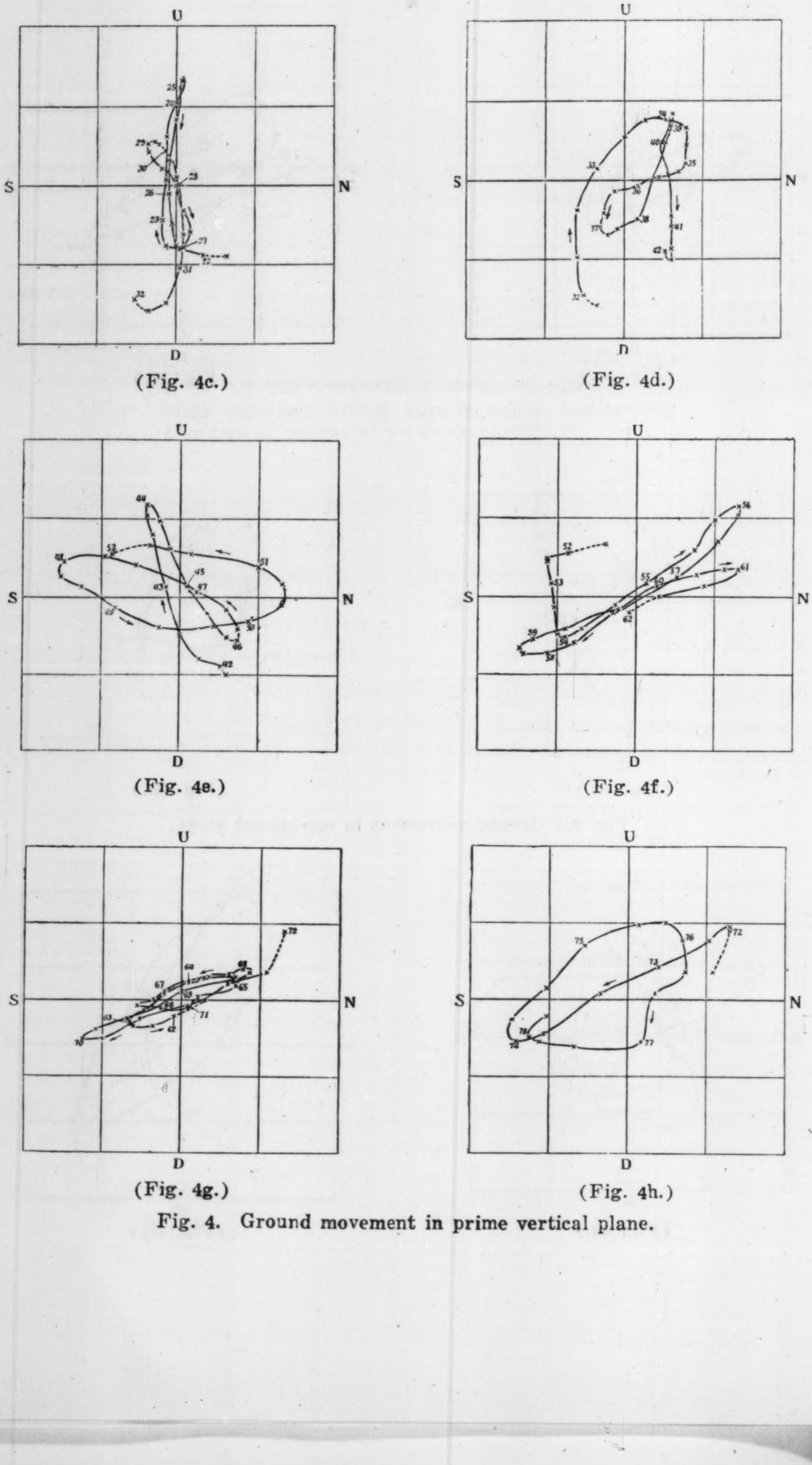

(Fig. 4c.) (Fig. 4d.)

(Fig. 4e.) (Fig. 4f.)

(Fig. 4g.) (Fig. 4h.)

Fig. 4. Ground movement in prime vertical plane.

48. 週期4秒の脈動(其の2)

地震學敎室 岸上冬彦

前に本號 146~154 頁に述べた東京本鄉に於ける週期4秒の脈動の硏究では南北動の記象だけを用ひたので，其の不足を補ふ爲に此處に東西動及び上下動を含めて測つた結果を報告する. 地震記象は地動に對して位相の遲れがあるので先づ其の差の少い地震計を選んだ. 調査に用ひた三成分の器械は大森博士の製られたもので其の常數は第I表に示された通りである. 昭和10年1月1日11時30分頃の振幅の大きい脈動の記象をさつて各成分を組合せた圖を描いた. 水平動は既に大森博士•和達博士の云はれてゐる樣に振動の方位が變化する. 其さ共に廻轉の向も變はるこさが示された. 此こさは二つの週期振幅共に近い値をもつた振動を組合せて出來る唸によく似てゐる. 上下動さ他の成分さ組合せた圖を見ても振動の形の變化が似てゐるので，筆者は前に得た結果も考へに入れて本鄉の週期4秒の脈動は二つの互によく似た振動を組合せたものさ考へ度い.

---

49. *On the Rendaizi Thermal Spring in Southern Idu Peninsula.*

By Takaharu FUKUTOMI and Masakazu NAKADA,
Mitsui Geophysical Observatory.

(Read Mar. 19, 1935.—Received June 20, 1935.)

I. Introduction.

At the time of the strong Idu Earthquake of March 21, 1934, changes occurred in temperature and rate of flow of water in thermal springs distributed in the strongly shaken area, for example, in Rendaizi, Toi, Yugasima etc[1].

Although such changes accompanying great earthquakes have been frequently noticed by many authors[2], the mechanism of occur-

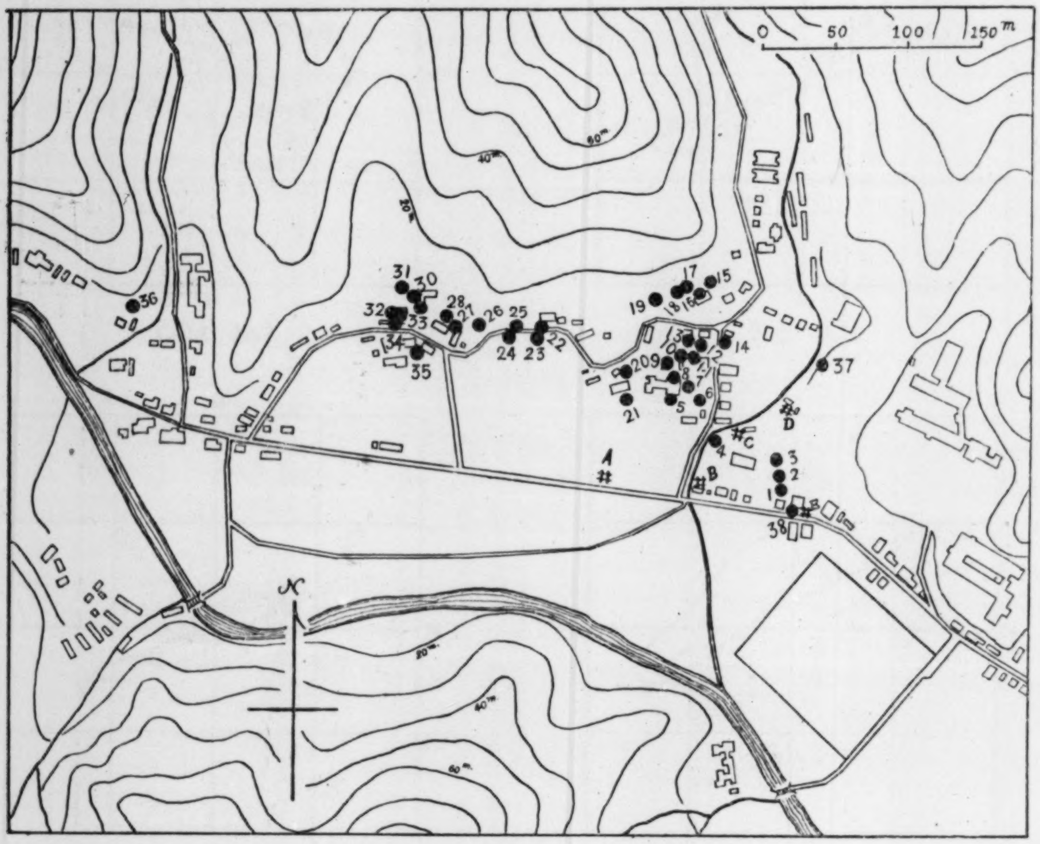
0
50
100
150m
60m
40m
20m
31
30
32
33
34
35
28
27
26
25
24
23
22
19
17
18
16
15
13
14
20
9
8
7
6
5
21
4
C
D
37
A
B
3
2
1
38
36
N
20m
60m
60m

Fig. 1.

---

[1] T. FUKUTOMI, *Bull. Earthq. Res. Inst.*, 12 (1934), 527.

rence of such changes have not been sufficiently elucidated owing to lack of knowledges regarding the physical nature of thermal springs.

The present paper discusses some properties of the Rendaizi thermal spring in southern Idu Peninsula in its normal condition.

The village of Rendaizi is situated at the northern side of a tributary of the River Inôzawa on the small Alluvial plain; a long valley running from W to E and practically surrounded by mountains which are composed of propylite and its tuff and breccia of the lower Tertiary age. There are about 40 thermal springs at present, mostly in the Alluvial plain as shown in Fig. 1.

The writers made observation of temperature and rate of flow of a hot spring (No. 38 in Fig. 1) which belongs to Mr. A. Sawazi to whom our best thanks are due for his courtesy.

II. Temperature of the Rendaizi Thermal Spring.

There are two quite different systems of cold water in Rendaizi, one is underground water which is obtained by normal well, the other is mineral spring which is obtained by artesian well. The latter contains nearly 10 times of Cl amount compared with that of the former and has weak basicity while the former has weak acidity though these two types of water have nearly equal temperature. In the following paragraphs, therefore, "thermal spring" means hot springs as well as tepid ones including the mineral spring in ordinary temperature.

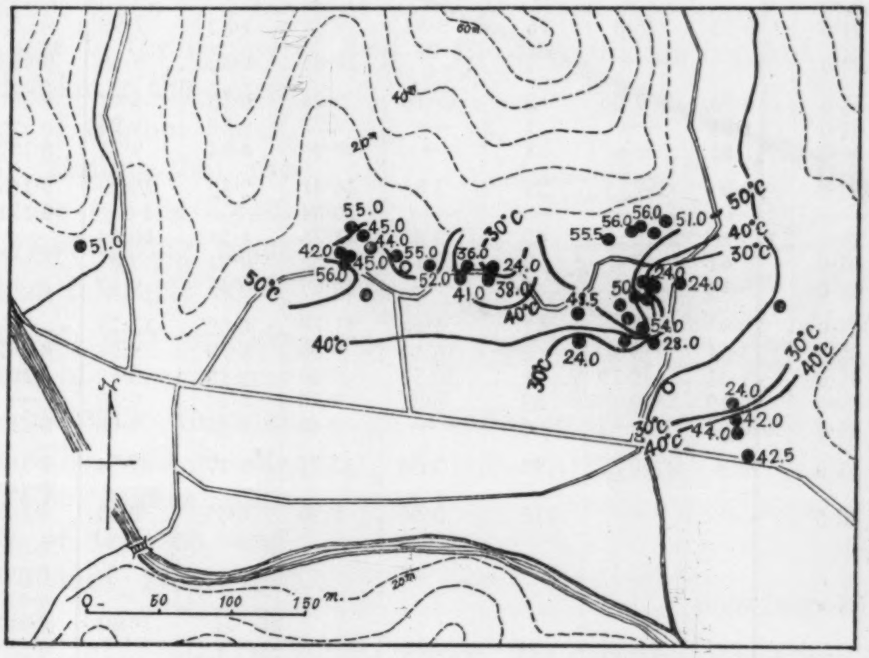

Fig. 2. Distribution of orifice temperature of thermal springs.

---

2) For example, see N. MIYABE, *Disin*, **5** (1933), 21.

Table I.

No.	Orifice temperature of thermal spring.	Rate of flow of hot water.△*	Flow speed. (v)	Depth of the vertical pipe.*	Internal radius of the vertical pipe.*	Height of the orifice above mean sea level.*	Depth of water head below the surface of the ground.*	Height of water head in the vertical pipe above mean sea level.	Some chemical constituents. (化學的性質)	
(番號)	(湧出溫度)	(湧出量)	(湧出速度)	(鑿井の深さ)	(鑿井内徑)	(湧出口海面上高)	(地表下湧出面深)	(湧出面海面上高)	Cl g/l	PH
	°C	l/min.	cm/min.	m	cm	m	m	m		
1	44·0	18·05	396	106	3·81	8·89	0·49	8·40	0·152	8·13
2	42·0	36·2	——	8	——	8·74	9·91	7·83	0·110	8·40
3	24·0	7·2	57	40·2	6·35	8·89	0·49	8·40	——	——
4	——	——	——	——	——	9·34	——	——	——	——
5	——	——	——	2	——	10·34	1·00	9·33	——	——
6	28·0	——	——	——	22·73	9·55	0·64	8·90	——	——
7	54·0	2·35	51·6	39	3·81	9·55	0·39	9·15	0·169	7·39
8	——	——	——	3	——	9·45	0·43	9·05	0·164	7·75
9	——	——	——	3	——	9·63	0·82	8·81	0.127	7·25
10	50·0	0·22	4·8	46	——	10·24	0·61	9·62	——	——
11	——	——	——	——	——	9·87	0·55	9·32	——	——
12	24·0	——	——	2	16·66	10·14	0·79	9·35	0·080	7·10
13	——	——	——	2	——	10·24	0·91	9·33	0·173	7·80
14	24·0	——	——	4	——	10·27	0·89	9·68	——	——
15	51·0	27·10	594	65	3·81	13·20	2·12	11·10	——	——
16	——	——	——	2		11·40	0·79	10·62	——	——
17	56·0	72·3	56·9	55	6·35	13·08	1·82	11·27	0·173	8·28
18	56·0	90·3	71·2	35	6·35	13·63	1·89	11·28	0·173	8·28
19	55·5	144·3	3167	61	3·81	13·47	2 14	11·33	0·173	8·28
20	48·5	3·61	79·2	73	3·81	10·70	0·57	10·33	——	——
21	24·0	0·72	15·8	76	3·81	9·74	1·82	7·92	——	——
22	24·0	——	——	0·9	(78·79 ×73·33)	10·03	0·42	9·60	0·098	7·29
23	38·0	0·90	1·25	3	15·14	9·28	0·30	8·97	——	——
24	41·0	1·81	——	1	——	9·77	0·52	9·24	——	——
25	36·0	1·81	——	1	——	10·06	0·34	9·71	0·132	7·85
26	52·0	9·0	197	29	3·81	14·41	2·12	12·29	0·166	7·50
27	——	——	——	——	——	10·84	——	——	0·171	7·85
28	55·0	126·3	2770	42	3·81	11·76	1·21	10·54	——	——
29	44·0	3·61	7·8	2	12·11	10·55	0·91	9·33	——	——
30	45·0	9·10	——	1	——	10·09	0·45	9·62	——	——
31	55·0	28·9	633	61	3·81	11·78	0·00	11·78	——	——
32	42·0	3·61	5·0	0·9	15·14	9·80	0·79	9·01	0·147	8·15
33	45·0	1·81	2·79	1	14·38	9·80	0·30	9·50	0·163	7·88
34	56·0	94·12	2064	52	3·81	9·80	0·00	9·80	——	——
35	45·0	6·34	——	4	——	9·40	0·30	9·08	0·153	7·90
36	51·0	90·3	4450	91	2·54	13·71	1·17	12·54	0·161	7·84
37	——	——	——	——	——	——	——	——	0·164	8·35
38	42·5°	——	——	110	3·55	8·90	0·49	8·41	0·140	8·02
A	(Normal well)								0·016	6·67
B									0·021	6·80
C									0·018	6·75
D									0·013	6·70
E									0·054	6·75

* Measurement by the Rendaizi Thermal Spring Association.

△ This data is not so accurate.

From the result of observation made by the Rendaizi Thermal Spring Association in July, 1929, map of temperature distribution was drawn as shown in Fig. 2. (See Table I.) The temperature ranges between 57°C in maximum and 25°C in minimum, and it is high at the northern hill-side, decreasing gradually towards the southern plain.

In general, orifice temperature depends on the depth of artesian well; it is high in deep well as shown in Fig. 3.

We examined the relation between orifice temperature and the rate of flow of hot water, and get the result as shown in Fig. 4, that the temperature tends to a constant value for large flow speed. This fact may be due to the escape of heat to the surrounding medium through the conduction in the course of ascent of the hot water. We may assume that the temperature of the Rendaizi thermal spring tends in the deep to nearly 60°C.

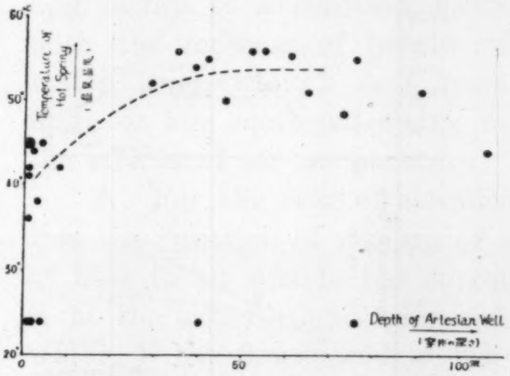

Fig. 3. Relation between orifiice temperature and depth of the artesian well.

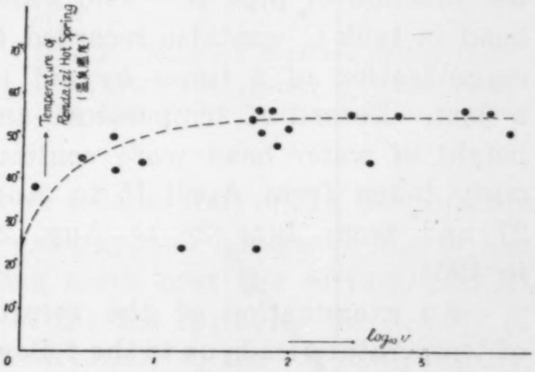

Fig. 4. Relation between orifice temperature and the rate of flow of hot water.

Next, we may mention the result of observations at the Sawazi's thermal spring. The well is situated 8·4 m higher than the level of the sea, and 3·0 km distant from the nearest sea coast. It is about 110 m deep, and its water level is 49 cm below the surface of the ground. Fig. 5 is the elevational sketch map. A

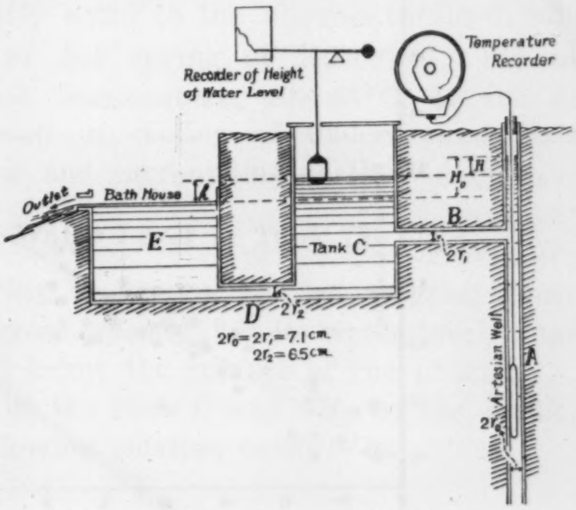

Fig. 5 The elevational sketch map of the Sawazi's hot spring.

is the artesian well, the wall of which consists of stout iron tube 7·1 cm in diameter, and hot water which flows out from A is lead to the tank C by aid of the pipe B, cooled here appropriately and then lead to the bath E by means of the pipe D. Superabundant water overflows from the brim of the bath.

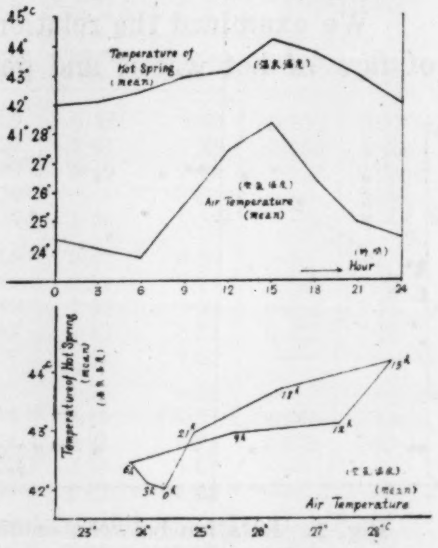

Fig. 6. Relation between the daily change of orifice temperature and that of air temperature.

Temperature was recorded automatically inserting the cylindrical part of the recording thermometer made by Nippon Keiki Seisakusyo in the artesian well about 1 m below the junction of pipe B. The water head in tank C was also recorded in magnification of 2 times by aid of a float. Record of temperature and height of water head were continuously taken from April 15 to Aug. 27 and from June 26 to Aug. 27 in 1934.

An examination of the records of temperature leads us to the following conclusions:–

1. Orifice temperature shows the obvious daily change reaching maximum at about 4 p.m. and minimum at about 1 a.m., the change being correlated with slight lag of phase to the air temperature as shown in Fig. 6, and its double amplitude varies from 1∼3°C. Daily

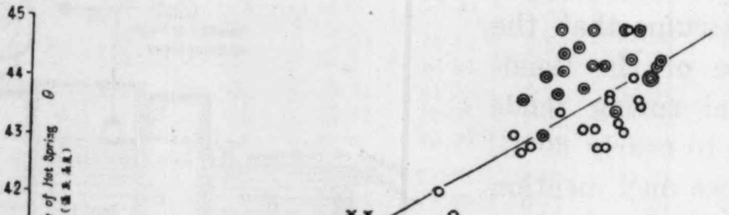

Fig. 7. Relation between the daily mean of orifice temperature and that of air temperature.

mean or monthly mean of temperature of the hot spring has also close relation with the daily mean or monthly mean of air temperature as shown in Fig. 7.

2. Relation between change in water level in the tank C and orifice temperature is shown in Fig. 8. There exists the tendency that the temperature approaches to a constant value with the increase of height of water level, though dots were more or less scattered owing to the effects of air temperature.

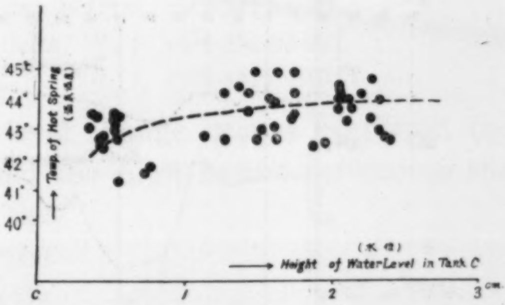

Fig. 8. Relation between orifice temperature and change of water level in tank C.

3. For the sake of simplicity, we assume that orifice temperature θ is the function of cooling of the underground hot water due to loss of heat to air and to the surrounding earth near the surface, and let θ_1 be the underground temperature of the hot spring, ρ the density of water, V the flow speed, c the specific heat, θ_0 the air temperature, S the effective area for heat loss, A the sectional area of the vertical pipe, and K the proportional constant, then we get:–

$$\theta=\frac{\theta_1}{1+\lambda}+\frac{\lambda}{1+\lambda}\theta_0, \text{ where } \lambda\equiv\frac{KS}{AVc\rho}. \tag{1}$$

If we assume that Fig. 7 shows just this relation, we can calculate θ_1 as 51°C. This is nearly equal to the above-mentioned value of underground temperature of hot spring at Rendaizi. We can recognize, therefore, that usual temperature, 40∼43°C, of the hot spring is produced as the result of cooling of underground water owing to the loss of heat to air and surrounding earth.

III. Change of Water Level in Tank C.

The Rendaizi thermal spring in general has not so great power to project the hot water with great velocity, but its water level ranges 40∼200 cm in the vertical well below the surface of the ground.

Between water head $\varDelta h$ in the tank C and $\varDelta H_0$ in the vertical well A in steady state, the following relation exists:–

$$\varDelta h=\frac{\left(\frac{r_1}{r_2}\right)^4}{1+\left(\frac{r_1}{r_2}\right)^4}\varDelta H_0 \text{ or } \varDelta h=0{\cdot}59\,\varDelta H_0. \tag{2}$$

As the difference between the height of pipe B and the water head in the vertical well *A* has much effect to the rate of flow of hot water, the quantity of hot water derived per unit time is irregular for every spring.

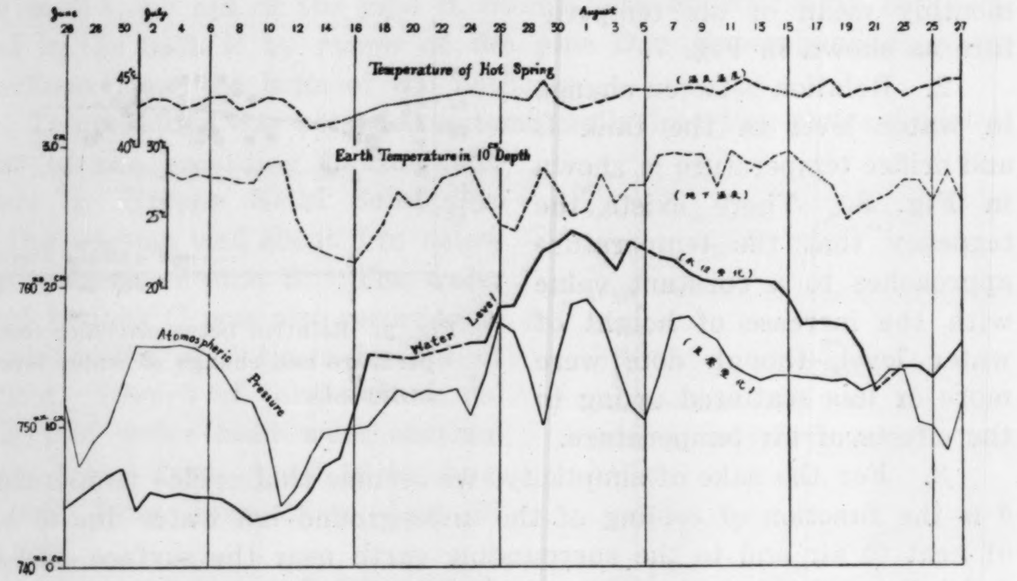

Fig. 9. Relation between the level change in tank C and change in barometric pressure.

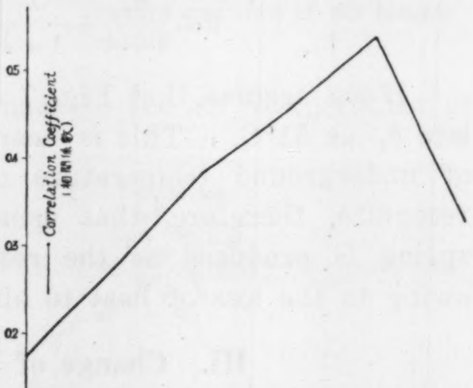

Fig. 10. Correlation factors between the daily mean of level change and that of barometric change.

The following is the result of observations of the change in water level in the tank C:–

1. Though it is not so definite, there exists some relation between the change in water level in the tank C and change in atmospheric pressure recorded there as shown in Fig. 9. Then, the correlation factor r[3] between daily mean of water level x and daily mean of atmospheric pressure y is calculated as shown in the following (Fig. 10).

---

[3] $r = \frac{\Sigma(xy)}{\sqrt{\Sigma(x^2)\Sigma(y^2)}}$.

Level change	—	Baro. change,	2 days after;	$r=0{\cdot}322\pm0{\cdot}094$.[4]
"	—	"	1 day " ;	$r=0{\cdot}535\pm0{\cdot}074$.
"	—	"	the day;	$r=0{\cdot}454\pm0{\cdot}076$.
"	—	"	1 day before;	$r=0{\cdot}381\pm0{\cdot}086$.
"	—	"	2 days " ;	$r=0{\cdot}276\pm0{\cdot}093$.
"	—	"	3 " " ;	$r=0{\cdot}108\pm0{\cdot}102$.

We can see that daily mean of level change occurs nearly in the same phase as barometric change, and the high barometer causes the rising of the level, and the low one the descent of the level. Fig. 11 is the correlation diagram between the daily mean of height of water level in the tank C and the barometric pressure of the day. It may be, then, safely concluded that a certain amount of barometric change in mercury column produces corresponding level change in the vertical well A magnified about 5·6 times.

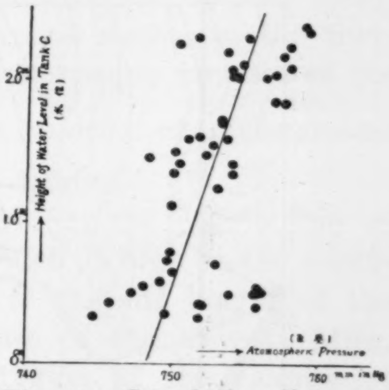

Fig. 11. Correlation diagram between level change in tank C and barometric change on the day.

This is interesting compared with the facts that the level change in the deep artesian well[5] at Tôkyô Imperial University and the rate of flow in a Kamisuwa thermal spring[6] have negative correlation factors with the change in barometric pressure.

2. To examine the effect of rain fall to the change of water level, correlation factor r between the daily mean of the residual change in which the effect of barometric change is taken away and total rain fall during 24 hours from 6 a.m. of the day is also calculated as shown in Fig. 12. We can see that the water level rises abruptly about 3 days after rainfall.

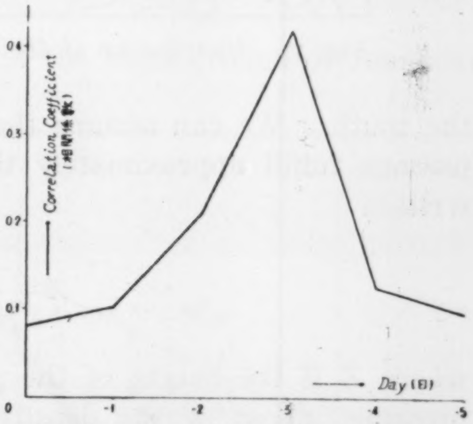

Fig. 12. Correlation factors between the daily mean of level change and daily rain fall.

Effect of the ocean-tide is not noticed, as far as this observation is concerned.

---

4) Probable error.

5) K. Honda, *Publ. Earthq. Inv. Comm.*, **18** (1904), 73.

K. Maeda, *Disin*, **6** (1934), 275.

6) S. Yoshimura and K. Misawa, *Geograph. Rev., Jap.*, **7** (1931), 239

IV. Geographical Distribution of Height of Water Level in Artesian Well.

Next, the geographical distribution of the height of water head in artesian wells above mean sea level in the Rendaizi thermal springs is examined as shown in Fig. 13. It is high in the north and low in the south. We can assume that the thermal spring in underground passage fulfill approximately the Bernoulli's equation, which may be written

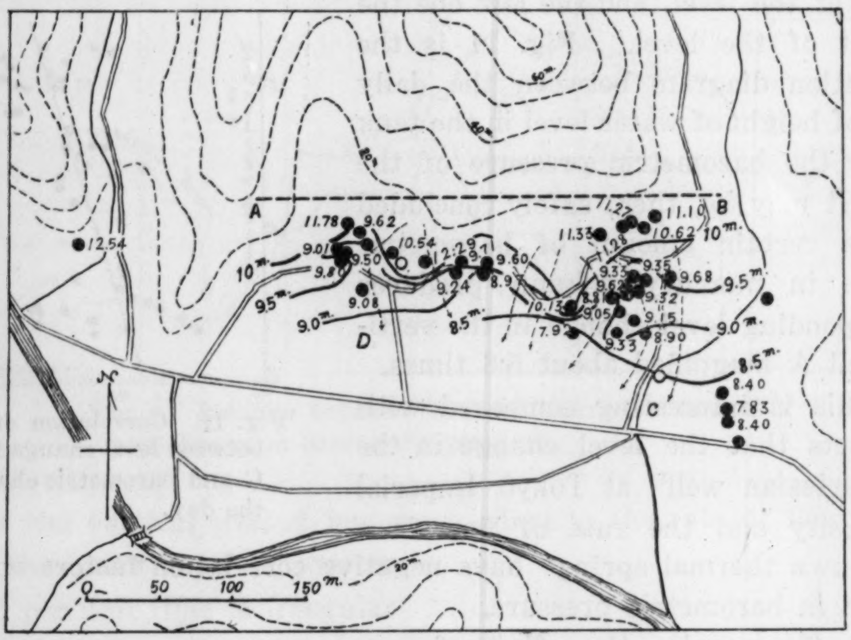
60m
40m
20m
A
B
C
D
12.54
11.78
9.62
9.01
9.80
9.50
10.54
12.29
9.71
9.60
9.24
8.97
9.08
11.33
11.27
11.28
11.10
10.62
9.35
9.33
9.62
9.68
9.32
8.81
10.13
9.05
9.15
9.33
8.90
7.92
8.40
7.83
8.40
10m
9.5m
9.0m
8.5m
N
0 50 100 150m

Fig. 13. Distribution of the height of water head in artesian well.

$$Z+\frac{P}{\gamma}+\frac{C^2}{2g}=H, \tag{3}$$

where Z is the height of the passage above a constant plane, P the pressure, $\gamma=\rho g$, ρ the density of water, C the velocity of stream, g the acceleration of gravity at the earth-surface, H the constant.

In general, if energy loss due to hydraulic resistance exists in the course of ascent of hot water in vein, we get

$$Z+\frac{P}{\gamma}+\frac{C^2}{2g}+h=H, \tag{4}$$

where h is the function of energy loss which will become large with the length of path. Now if we take $A=Z+\frac{P}{\gamma}$ as the height of water level in the artesian well, then

$$A=Z+\frac{P}{\gamma}=H'-\frac{C^2}{2g}-h. \tag{5}$$

Thus we can recognize that the contour line in Fig. 13 as the line of equal $(H'-\frac{C^2}{2g}-h)$, and the orthogonal curve to the contour line will give the horizontal direction of underground stream in the thermal spring, for H' is a constant, h being the increasing function of the path, and $\frac{C^2}{2g}$ the quantity concerned with velocity of underground stream, though the sense of the flow is not definite.

If we take the facts into consideration that the distribution of orifice temperature of the thermal spring which is high in the northward and low in the southward resembles to that of height of the water level, and that in the southern galleries of the Kawazu Mine, which has its galleries under the whole region of the vicinity of Rendaizi, the underground temperature is 13°C, and hot water is not found at all, but in the northern galleries there are 3 or 4 hot springs flowing out and there are also some places where the underground temperature was 41°C at the time of the writers' measurement on March 14, 1935, we can recognize that the heat source of Rendaizi thermal springs is in the northward.

If it is permitted to assume that in the underground of Rendaizi thermal spring there is no change in speed of stream, that is, no change in size of the passage and distribution of the height of water level of hot springs depends on the energy loss in the course of stream, and the path is linearly inclined from north upward to south by angle φ to the surface of the ground, then the height of water level of hot spring A from the mean sea level may be given in the form

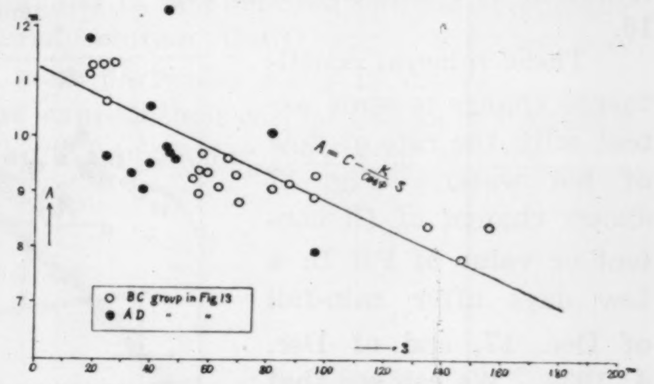

Fig. 14. Hydraulic gradient in the Rendaizi Thermal Spring.

$$A = \text{const.} - \frac{K}{\cos\varphi}\,x, \tag{6}$$

where x is length measured along the line orthogonal to the contour line of the height of water level from an origin, and K is the head of energy loss in the unit length of path.

From the AB line which is taken tentatively in Fig. 13, perpendicular distance to the orifice of hot springs x is measured and the relation between A and x is plotted in Fig. 14. We can see that the relation is approximately linear as shown in equation (6). If we put $\varphi = 11°$, we obtain for the value of K

$$K = 5{\cdot}7 \times 10^{-2}\ \text{C.G.S.}$$

V. Some Chemical Properties.

As already mentioned, water taken from the normal well indicates 6·7～6·8 in PH (weak acidic) and 0·0015% in Cl, while mineral springs show 7·0～8·4 in PH (weak basic) and 0·010～0·017% in Cl. These mineral constituents of the Rendaizi thermal spring measured in Oct. 1934, are shown in Table I. There is a tendency that Cl content increases with the ascent of temperature just like the case of the Simosuwa thermal spring[7] (Fig. 15). Distribution of PH is shown in Fig. 16.

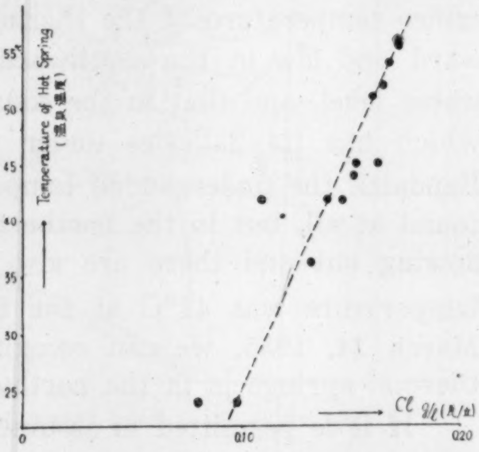

Fig. 15. Relation between Cl content and orifice temperature.

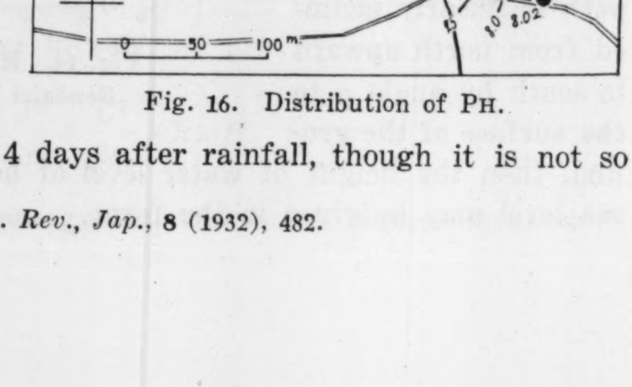

Fig. 16. Distribution of PH.

These mineral constituents change to some extent with the rate of flow of hot water. Fig. 17 shows change of Cl content or value of PH in a few days after rain-fall of Dec. 17, and of Dec. 4, 1934. We can see that there is a tendency that Cl content decreases and value of PH increases 3 or 4 days after rainfall, though it is not so

---

[7] S. YOSHIMURA, *Geograph. Rev., Jap.*, **8** (1932), 482.

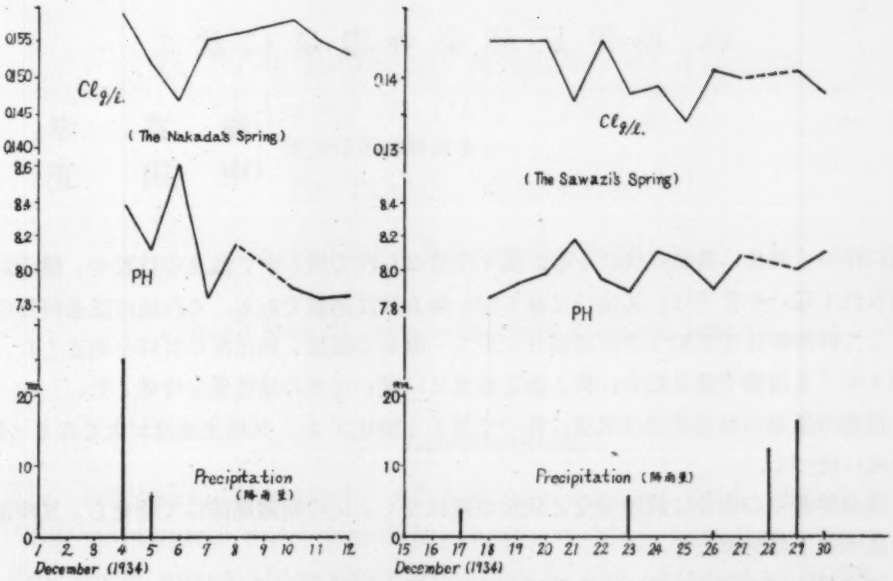

Fig. 17. Change of Cl and value of PH several days after rainfall.

distinct.

If we take into consideration that the rate of flow increases abruptly 3 or 4 days after rain fall, we come to conclusion that Cl content decreases and value of PH increases as the effect of increase in quantity of hot water after rainfall.

This fact suggests us a mechanism in regard to the mixing of the Juvenile water and the Vadose water, that is, the increase of quantity of the Vadose water after rainfall causes the decrease of Cl in amount and the increase of value of PH as the effect of dilution and as the effect of instability of non-buffered solution accompanied by dilution of the buffered solution, $CaCO_3$ etc. But, we may reserve this problem to the more particular study in future.

In conclusion, the writers express their cordial thanks to Professor Takeo Matuzawa and Dr. Chûji Tsuboi for their kind advices.

49. 南伊豆，蓮臺寺溫泉に就て

三井地球物理研究所 福富孝治
中田正一

地震に伴つて溫泉に異狀の現れる事が屢々注意せられて居るが，溫泉の性質や，構造があまりよく知られてない今日では，其依つて來る所を知る事は困難である．それ故に溫泉研究の一つの試みとして靜岡縣賀茂郡稻生澤村蓮臺寺に於て一溫泉の溫度，涌出面の昇降を測定した．此結果と昭和4年7月蓮臺寺溫泉組合に依る測定結果とに就いて次の諸性質を吟味した．

1. 蓮臺寺溫泉の涌出溫度は氣溫に伴つて著しく變化する．又涌出速度が大となると約 60°C の一定値に近づく．

2. 溫泉穿井中の水位は氣壓變化と位相の遲れなく，正の相關關係にて變化し，又降雨後 3～4 日の後水位上昇を來たす．

3. 溫泉涌出面の高さの分布から地下に於ける溫泉流動の水平方向が求められた結果，蓮臺寺に於ては其泉源が北方に在る事が想像される．

4. Cl，PH 等の化學的成分の分布，並びに降雨に依る變化に就いて一言した．

50. *The Explosive Activities of Volcano Asama in 1935. (Part 1.)*

By Takeshi MINAKAMI,

Earthquake Research Institute.

(Read May 21, 1935.—Received June 20, 1935.)

1. Introduction.

The remarkable activity of volcano Asama that began in April 20, 1935, continued until the later part of May the same year.

For some years since the explosions in the autumn of 1932, Asama had been very inactive, with neither eruption of any violence nor earthquakes originating in the volcano. But as reported by the writer in his previous paper, the crater floor, which has been rising since October 1934 as well as the considerable tilting of the earth's surface that had begun in October 1934, was observed at our Observatory, which is situated 5 km away from the crater (Fig. 1). It was in view of these phenomena and the conditions of the vapours emitted

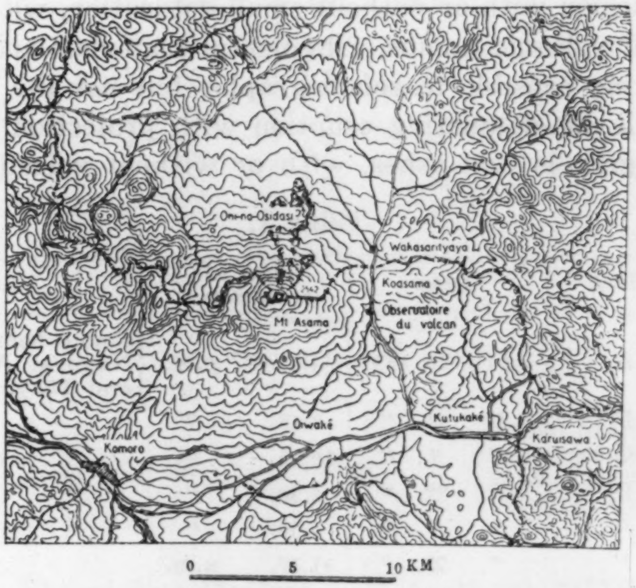
Oni-no-Osidasi
Wakasarityaya
Koasama
2542
Observatoire du volcan
Mt Asama
Owaké
Kutukaké
Karuisawa
Komoro
0
5
10 KM

Fig. 1. Topographic map of volcano Asama and its vicinity.

from the crater, that the writer concluded in the previous paper that the volcano was showing signs of coming activity as early as October 1935. This paper is mainly a description of the sound phenomena and the distribution of volcanic bombs and ashes in the explosion of April 20, 1935. Full details of the explosions that took place after that date, together with the observations made by various means, will be given in following papers.

2. List of Eruptions in April and May 1935.

For convenience of description, the explosions have been divided into the following four stages according to the nature of the outburst.

A; Violent explosion with strong detonation, with projection of numerous volcanic bombs, small fragmental lavas, and ashes; earth-shaking and air vibrations sensible 100 km distant from the volcano.

B; Explosion with strong detonation, with projection of volcanic bombs and ashes, but in less amount than A; earth-shaking and air vibration felt about 50 km distant.

C; Explosion with or without small detonation, with projection of small volcanic bombs, fragmental materials and ashes; earth-shaking sensible to seismographs, but not the air vibration.

D; Small non-detonating eruption with projection of only volcanic gravels and ashes, with or without volcanic tremors.

Table I.

No.	Class	Date	Time of occurrence	Remarks
			h. m. s.	
1	A	April 20, 1935	4.21.02. p.m.	Sound heard in Tôkyô and Nagoya. Ashes fell in Tiba and Tôkyô.
2	D	〃 21, 〃	0.15. 〃	
3	C	〃 〃, 〃	10.25. 〃	
4	D	〃 22, 〃	5.30. 〃	
5	〃	〃 〃, 〃	4.33. 〃	
6	〃	〃 23, 〃	11.37. a.m.	
7	〃	〃 〃, 〃	3.37. p.m.	
8	〃	〃 24, 〃	3.30. a.m.	
9	〃	May 4, 〃	11.15. 〃	
10	B	〃 5, 〃	8.47.05. 〃	Sound heard in Tôkyô.
11	C	〃 〃, 〃	11.18. 〃	
12	D	〃 6, 〃	8.32. 〃	
13	C	〃 〃, 〃	7.50. p.m.	

(*to be continued.*)

Table I. (*continued.*)

No.	Class	Date	Time of occurrence		Remarks
			h. m. s.		
14	C	May 11, 1935	2.22.15.	a.m.	Sound heard in Tôkyô and ashes fell in Tôkyô.
15	B	″ ″, ″	4.06.54.	″	Sound heard in Tôkyô where ashes also fell.
16	″	″ ″, ″	6.26.12.	″	″
17	D	″ ″, ″	8.00.	″	
18	″	″ ″, ″	2.37.38.	p.m.	
19	″	″ ″, ″	4.15.	″	
20	C	″ 14, ″	8.26.	a.m.	
21	A	″ 16, ″	9.15.50.	p.m.	Sound heard in Tôkyô.
22	D	″ 19, ″	8.30.	a.m.	
23	B	″ 20, ″	4.02.08.	″	
24	D	″ ″, ″	8.30.	″	
25	″	″ ″, ″	10.30.	″	
26	″	″ 21, ″	4.13.	p.m.	
27	B	″ 22, ″	11.23.21.	a.m.	Sound heard in Tôkyô.
28	D	″ ″, ″	6.25.	p.m.	
29	″	″ 23, ″	4.25.	a.m.	
30	″	″ ″, ″	11.45.	″	
31	″	″ ″, ″	12.00.	″	
32	C	″ ″, ″	7.11.	″	
33	D	″ 24, ″	10.23.	″	
34	″	″ ″, ″	3.05.	p.m.	
35	″	″ ″, ″	5.21.	″	
36	″	″ ″, ″	8.01.	″	
37	″	″ 25, ″	1.	″	
38	″	″ ″, ″	2.25.	a.m.	
39	″	″ 26, ″	3.20.	″	
40	C	″ ″, ″	2.30.	p.m.	
41	B	″ 28, ″	6.14.49.	″	Sound heard in Tôkyô. A large quantity of ashes fell in the neighbourhood of our Observatory.

3. The violent Explosion of April 20 1935.*

(a) *Deformation of the crater floor caused by this explosion.*

During the period from July to October, 1934, the writer surveyed the crater floor in order to ascertain the rise or fall of the lava in the crater, with the result that although the floor continued to sink from July to September, after the latter part of September it began to rise with a mean daily rate of 20 cm. This elevation of crater floor had amounted to about 50 m just before the explosion. The explosion threw out the massive lava that lay on the crater floor, and which measured 150 m × 150 m × 100 m, in the form of volcanic bombs, volcanic gravels, and volcanic ashes. The lava thus poured out consisted principally of the andesite and pumice-stone that had covered the surface of the crater floor to a thickness of about 1 m, with the result that the total mass of the lava ejected in this explosion, calculated on a mean lava density of 2·0, amounts to

---

* See Fig. 14.

$$4{\cdot}5 \times 10^9\,\mathrm{kg} = 4{\cdot}5 \times 10^6\,\mathrm{tons}.$$

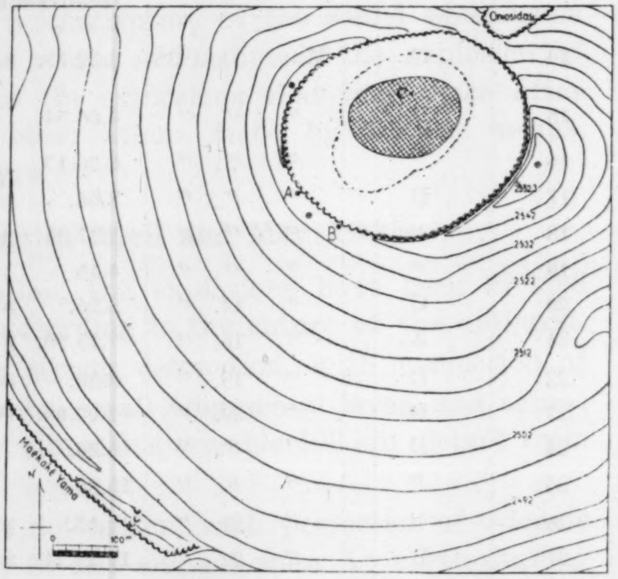

Fig. 2. ▨ ; Crater-bottom scooped out by the explosion.

Fig. 2 is a plan of the lava projected from the crater floor. Fig. 3 shows the rise and fall of point C on the crater floor shown in Fig. 2. Fig. 15 is a photograph of the crater floor taken from the south side on the crater wall in October, 1934. Figs. 16 and 17 are these of the crater floor taken from the same place and in the same direction on six days after the explosions. A mere glance at these photographs is enough to give one an idea of the immense change that occurred in the crater floor. Fig. 17 shows the south slope of the crater floor hollowed out and a part of the floor which was not hollowed out.

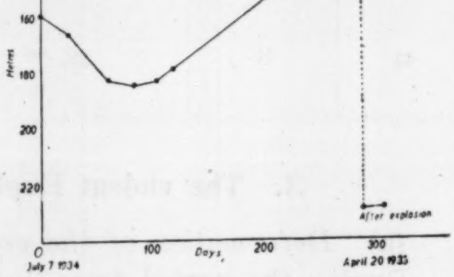

Fig. 3.

(b) *Volcanic bombs, volcanic gravels, and ashes.*

Since as already mentioned, the rocks ejected consisted of andesite and pumiceous rocks that had formed the surface of the crater floor, in the explosions that followed the one forming the subject of this paper, practically no more pumiceous rocks were to be seen. Fragments of that big lava mass of about $4{\cdot}5 \times 10^6$ tons were scattered in all directions in the form of volcanic bombs. These bombs were larger in size and greater in numbers the nearer they were to the crater; the whole surface of the central cone, which is less than 600 m distant from the crater, was covered with new volcanic bombs, of which the largest, 18 m in circumference, fell on the central cone at a distance of about 100 m S. W. of the crater. Assuming the density of this bomb, which consisted of andesite, to be 2·5, the mass is 2×10^5 kg, or 200 tons. Fig. 18 is a photograph of this bomb taken on April 26, 1935, at 6 h a.m., six days after the explosion. This bomb had disintegrated about a week after this photograph was taken. Besides this large one, several smaller bombs larger than 3 m in diameter fell on the central cone. Fig. 19 is a photograph of the holes made by bombs that fell on the snow at Maekaké-Yama, distant about 600 m S. W. of the crater. Generally, the diameter of the holes made on the ground where small fragments of pumiceous lava or volcanic ashes were piled up, are about three to four times those of the volcanic bombs that fell there, while the shape of those holes, regardless of that of the bombs, was always an inverted cone. The cylindrical holes made in the snow are naturally slightly larger in diameter than the bombs themselves. Regardless of size, it is always possible to classify volcanic bombs into two types according to their shape; the one be-

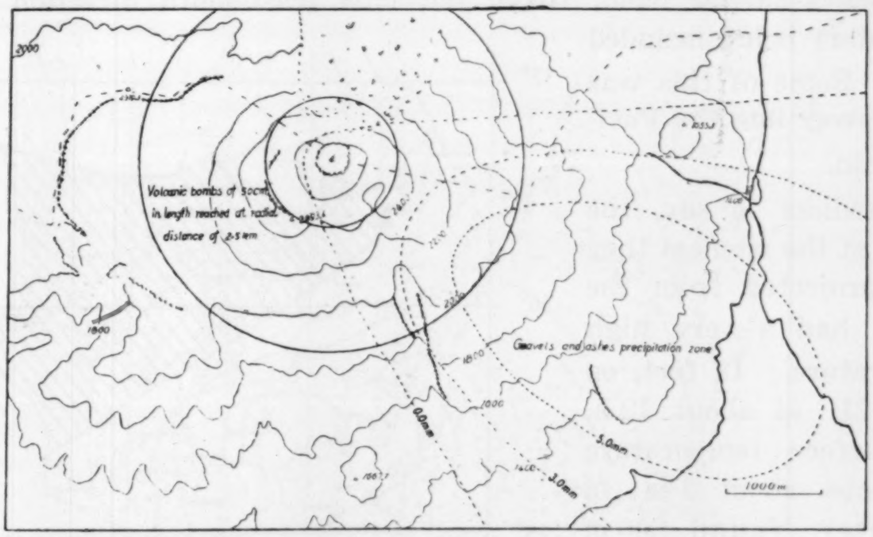
2000
Volcanic bombs of 50cm in length reached at radial distance of 2.5 km
2400
2200
1800
1800
Gravels and ashes precipitation zone
1600
0.0mm
5.0mm
1400
3.0mm
1000m

Fig. 4. Ashes-precipitation scatterd by the explosion on April 20, 1935.

ing either a regular spindle shape or spherical and the other irregular in shape. An example of the former type is shown in Figs. 21～25, and the latter in Figs. 18～26. The cause of these two types of bombs may be due to the particular materials composing the bombs, as also to its softness at the time they were shaped. Bombs of 0·5～1·0 m in diameter travelled to distances within 2500 m from the crater. They are shown in Fig. 4. Small fragmental lava, such as volcanic gravel and ash, being easily transported by wind, travelled to distances more than 2500 m from the crater.

As will be seen from Figs. 4, 5, the gravel and ash precipitation zone was a narrow band, Tôkyô and Tiba (east-south direction from the crater) being included in it. Some of this was blown away into the Pacific Ocean.

Needless to say, the bombs at the moment they were projected from the crater, had a very high temperature. In fact, on April 21, at about 12 h, the surface temperature of bombs about 1 m in diameter, found 800 m east of the crater, was about 400°C, that is 20 hours after the eruption.

Moreover, the surface temperature of the largest bomb in this explosion (bomb shown in Fig. 18) was about 200°C at 6 h a. m. on April 26, six days after the explosion. On the other hand, according to temperature measurements of the lava in the crater floor made by the writer in September and October 1934 by means of an optical pyrometer and thermo-junctions, heated lava had a temperature of about 1000°C. From which it may be concluded that the maximum temperature of bombs at the moment of projection was about 1000°C.

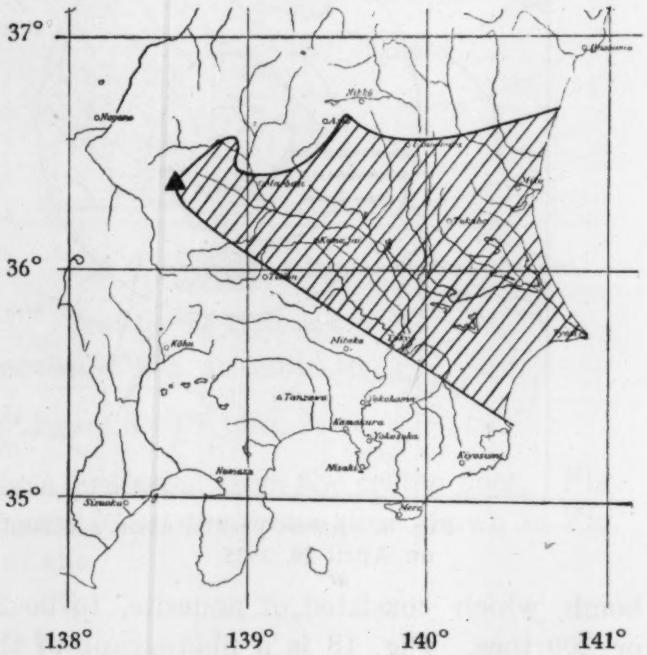

Fig. 5. Ashes-precipitation area.

Consequently, as soon as this explosion occurred, a field fire broke out southward of the volcano, destroying grass and bushes to the extent of an area 1 km square, the spot being shown in Fig. 7. Investigations showed that the fire originated from numerous small bombs that were only about 10∼20 cm in diameter. This field fire, which broke out at 4 h 22 m p. m. on the 20th died out at 11 h p. m.

(c) *The sound of the explosion.*

The sound of the explosion is perhaps the most noteworthy feature of the various volcanic phenomena of Asama. People who happened to be at the foot of the volcano at the time, were astounded while the earthquake caused by the explosion was not violent enough to be felt at the Observatory, the air vibration was so violent that people at the foot of the volcano were made aware of the explosion by the arrival of this sound about 20 seconds after the outburst.

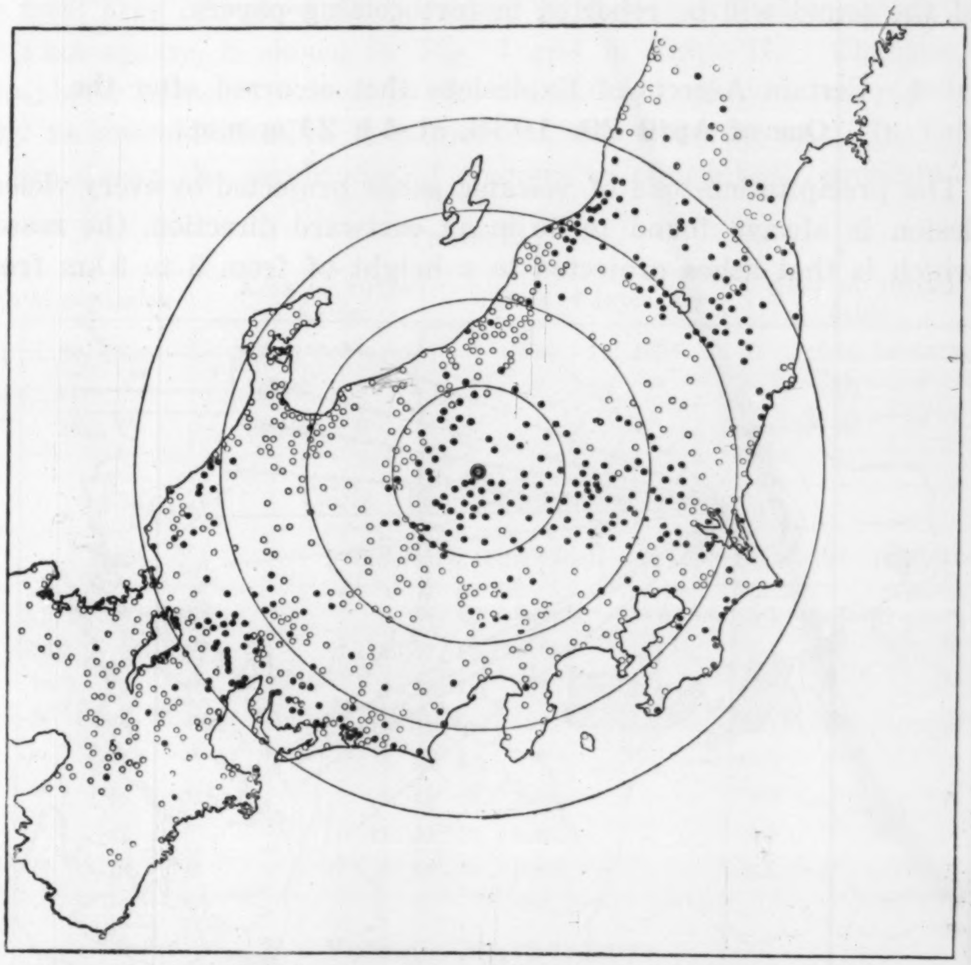

Fig. 6. Sound area ●; sound heard ○; sound not heard.
Radius of circles; 50 km, 100 km, 150 km, 200 km.

At Kutukaké, 10 km ESE of the crater, the air vibration was strong enough to shake houses and shatter window-panes that happened to face the volcano. At Kutukaké also, and at Karuizawa, another foot of the volcano, sliding doors were thrown out of their grooves by the air vibration. For the purpose of ascertaining the sound area, inquiries were sent out to some 2000 primary schools located in the principal islands of Japan. As will be seen from Fig. 6, the sound area may be regarded as being formed of two zones, the inner and the outer. The former extends to a distance of 50 km, North, South, and West, but to a distance of 200 km east of the volcano. The latter consists of two arcs, the inner one with a mean internal radius of 150 km and the outer with the same of 250 km. In the east direction, however, there is no such distinction in the sound area as the inner and outer zones.

The results of our detailed studies concerning the area and velocity of the sound will be reported in forthcoming papers.

4. Certain Aspects of Explosions that occurred after the One of April 20, 1935, at 4 h 21 m p.m..

The precipitation-zone of volcanic ashes projected by every violent explosion is always found to be in an eastward direction, the reason of which is that ashes projected to a height of from 3 to 5 km from

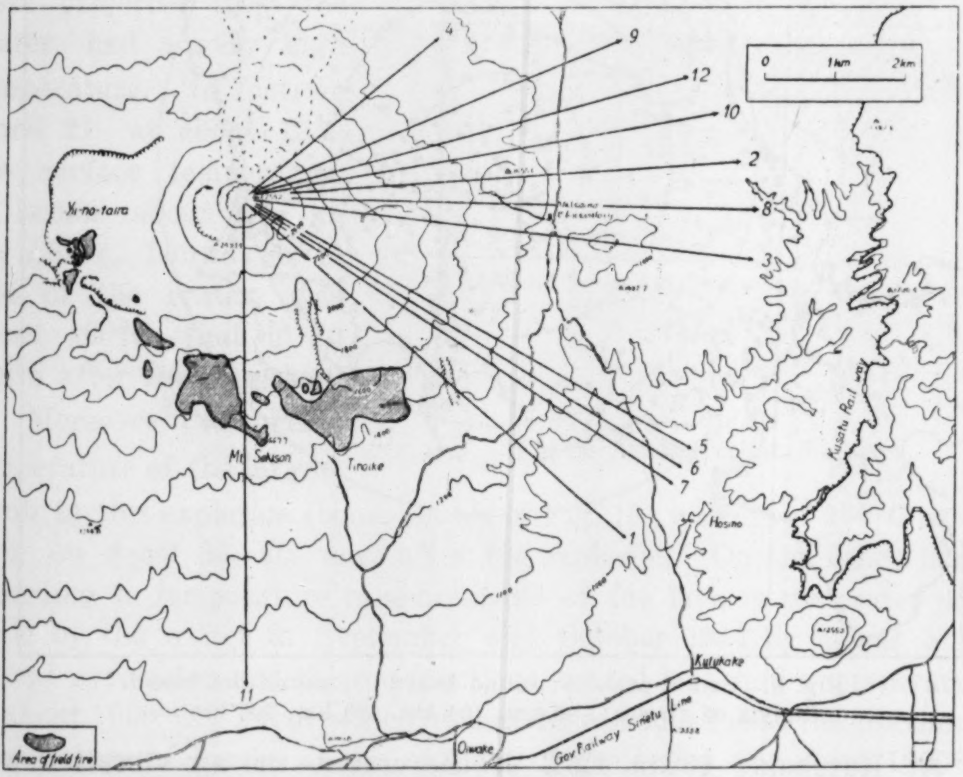
0
1km
2km
4
9
12
10
2
8
3
5
6
7
1
11
Yu-no-taira
Mt. Sekison
Tinoike
Hosino
Kutukake
Oiwake
Gov. Railway Sinetu Line
Kusatu Railway
Area of field fire

Fig. 7. The directions of ashes precipitation scattered by the following explosions.

1, April 20, 4^{h} p.m.
2, ″ 21, 10^{h} p.m.
3, May 5, 8^{h} a.m.
4, ″ 6, 8^{h} a.m.
5, May 11, 2^{h} a.m.
6, ″ 11, 4^{h} a.m.
7, ″ 11, 6^{h} a.m.
8, ″ 16, 9^{h} p.m.
9, May 20, 4^{h} a.m.
10, ″ 22, 11^{h} a.m.
11, ″ 24, 3^{h} p.m.
12, ″ 28, 6^{h} p.m.

the crater, are blown away eastward by the upper wind which always blows in that direction. Fig. 7 shows the directions of the precipitation-zone of the ashes. Of these directions of the precipitation–zone, those toward the north and south were caused by small eruptions, the ashes being blown away by the lower wind, as the result of which in most violent explosions, ashes fell at our Observatory, which is situated east of the volcano. The ashes never fell in a west-direction, even on occasions when they fell at Tôkyô. Komoro at the western foot of the volcano is generally safe from ash-precipitation. Field fires started by volcanic bombs occurred with every violent explosion. The total area of ruined fields caused by violent explosions amounting to 1·3 km square, is shown in Fig. 7 and in Table II. Changes in atmospheric pressure caused by the detonating explosions are registered by an aneroid installed in a room of the Observatory. In Table III, are shown the amplitudes of changes in atmospheric pressure.

Table II.

Date of explosion	Area of ruined fields	Date of explosion	Area of ruined fields
April 20, 1935.	138·35 hectares.	May 22, 1935.	10·00 hectares.
May 11, 〃	10·00 〃	〃 28, 〃	8·00 〃
〃 16, 〃	10·00 〃		Total **177·35** 〃

Table III. Explosions.

Date	Time of occurrence	Change in atm. pressure
	h. m. s.	
April 20, 1935	4. 21. 02. p.m.	6·1 mm./Hg.
May 5, 〃	8. 47. 05. a.m.	3·1 〃
〃 11, 〃	2. 22. 15. 〃	2·1 〃
〃 〃, 〃	4. 06. 54. 〃	1·1 〃
〃 〃, 〃	6. 26. 12. 〃	6·0 〃
〃 16, 〃	9. 15. 50. p.m.	3·0 〃
〃 22, 〃	11. 23. 21. a.m.	2.5 〃
〃 28, 〃	6. 14. 49. p.m.	1.8 〃

5. Volcanic Micro-tremors.

During the year 1934, the seismographs (magnification 100) of our Observatory did not register any volcanic micro-tremors. They were observed for the first time on January 2, 1935, and thereafter. In Table IV are shown the daily numbers of these micro-tremors that were recovered, from which it will be seen that more micro-tremors occurred on days previous to than on the day of the outburst. The total number of micro-tremors for ten days are shown in Fig. 8.

Table IV.

Date	Number of occurrence of micro-tremors	Date	Number of occurrence of micro-tremors	Date	Number ot occurrence of micro-tremors
Dec. 1, 1934	0	Jan. 21, 1935	12	Mar. 12, 1935	9
″ 2, ″	0	″ 22, ″	4	″ 13, ″	3
″ 3, ″	0	″ 23, ″	6	″ 14, ″	5
″ 4, ″	0	″ 24, ″	16	″ 15, ″	7
″ 5, ″	0	″ 25, ″	6	″ 16, ″	11
″ 6, ″	0	″ 26, ″	2	″ 17, ″	17
″ 7, ″	0	″ 27, ″	10	″ 18, ″	5
″ 8, ″	0	″ 28, ″	3	″ 19, ″	4
″ 9, ″	0	″ 29, ″	4	″ 20, ″	4
″ 10, ″	0	″ 30, ″	6	″ 21, ″	4
″ 11, ″	0	″ 31, ″	10	″ 22, ″	5
″ 12, ″	0	Feb. 1. ″	13	″ 23, ″	1
″ 13, ″	0	″ 2, ″	5	″ 24, ″	7
″ 14, ″	0	″ 3, ″	15	″ 25, ″	25
″ 15, ″	0	″ 4, ″	7	″ 26, ″	12
″ 16, ″	0	″ 5, ″	9	″ 27, ″	3
″ 17, ″	0	″ 6, ″	0	″ 28, ″	11
″ 18, ″	0	″ 7, ″	2	″ 29, ″	11
″ 19, ″	0	″ 8, ″	16	″ 30, ″	11
″ 20, ″	0	″ 9, ″	6	″ 31, ″	4
″ 21, ″	0	″ 10, ″	32	Apr. 1, ″	7
″ 22, ″	0	″ 11, ″	6	″ 2, ″	3
″ 23, ″	0	″ 12, ″	5	″ 3, ″	11
″ 24, ″	0	″ 13, ″	5	″ 4, ″	6
″ 25, ″	0	″ 14, ″	12	″ 5, ″	10
″ 26, ″	0	″ 15, ″	24	″ 6, ″	8
″ 27, ″	0	″ 16, ″	9	″ 7, ″	3
″ 28, ″	0	″ 17, ″	6	″ 8, ″	4
″ 29, ″	0	″ 18, ″	5	″ 9, ″	4
″ 30, ″	0	″ 19, ″	6	″ 10, ″	1
Jan. 1, 1935	0	″ 20, ″	5	″ 11, ″	2
″ 2, ″	4	″ 21, ″	9	″ 12, ″	2
″ 3, ″	0	″ 22, ″	6	″ 13, ″	5
″ 4, ″	1	″ 23, ″	32	″ 14, ″	9
″ 5, ″	0	″ 24, ″	13	″ 15, ″	6
″ 6, ″	2	″ 25, ″	7	″ 16, ″	0
″ 7, ″	0	″ 26, ″	15	″ 17, ″	4
″ 8, ″	1	″ 27, ″	8	″ 18, ″	1
″ 9, ″	0	″ 28, ″	13	″ 19, ″	2
″ 10, ″	5	Mar. 1, ″	4	″ 20, ″	2
″ 11, ″	1	″ 2, ″	10	″ 21, ″	0
″ 12, ″	2	″ 3, ″	2	″ 22, ″	5
″ 13, ″	1	″ 4, ″	13	″ 23, ″	1
″ 14, ″	2	″ 5, ″	8	″ 24, ″	3
″ 15, ″	1	″ 6, ″	9	″ 25, ″	2
″ 16, ″	4	″ 7, ″	25	″ 26, ″	10
″ 17, ″	7	″ 8, ″	11	″ 27, ″	8
″ 18, ″	6	″ 9, ″	6	″ 28, ″	2
″ 19, ″	0	″ 10, ″	3	″ 29, ″	10
″ 20, ″	3	″ 11, ″	12	″ 30, ″	13

(to be continued.)

Table IV. (*continued.*)

Date	Number of occurrence of micro-tremors	Date	Number of occurrence of micro-tremors	Date	Number of occurrence of micro-tremors
May 1, 1935	18	May 13, 1935	1	May 25, 1935	14
〃 2, 〃	13	〃 14, 〃	6	〃 26, 〃	16
〃 3, 〃	37	〃 15, 〃	6	〃 27, 〃	56
〃 4, 〃	4	〃 16, 〃	16	〃 28, 〃	29
〃 5, 〃	0	〃 17, 〃	11	〃 29, 〃	15
〃 6, 〃	14	〃 18, 〃	5	〃 30, 〃	8
〃 7, 〃	10	〃 19, 〃	5	〃 31, 〃	9
〃 8, 〃	10	〃 20, 〃	20		
〃 9, 〃	19	〃 21, 〃	18		
〃 10, 〃	2	〃 22, 〃	30		
〃 11, 〃	3	〃 23, 〃	15		
〃 12, 〃	2	〃 24, 〃	8		

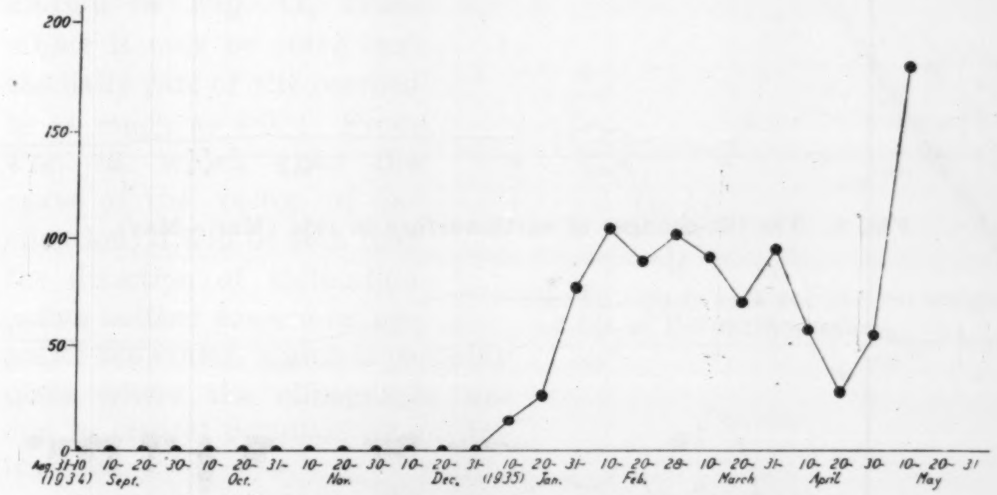

Fig. 8. The number of occurrence of micro-tremors.

6. Tilts of the Earth-surface.

With respects to the relation of volcanic activity to tiltings of the ground, T. A. Jagger[1], from his observations of volcano Kilauea, reported remarkable correlations between the elevation of lava in the crater and the inclinations of the ground. In the case of Asama, Prof. Takahasi[2], at the time of the explosions of 1932, installed a pair of clinographs at Komoro and studied the relation between the explosions and the inclinations of the ground.

In the recent explosions, one of the most outstanding observations made at our Observatory was these inclinations of the ground. Observations of these tilts were continued since 1933 with a pair of clinographs constructed of fused quartz. This apparatus being installed in a cave hollowed out of a massive volcanic rock, atmospheric temperature and humidity in it are sufficiently constant.

---

[1] T. A. JAGGER, *Bull. Seism. Soc., Amer.*, **19** (1929), 38.

[2] R. TAKAHASI, *Bull. Earthq. Res. Inst.*, **11** (1933), 25.

In his previous paper, the writer reported that changes in the inclination of ground had increased since October 1934. Since then until the latter part of February 1935, no conspicuous variations were observed in the range of tilt-change. Since then, however, from the beginning of March 1935, extraordinary variations in inclination began to be observed. Figs. 9, 10, show the tilts of the ground during an inactive period of the volcano (March, 1934∼May, 1934), and in the present active period (March, 1935∼May, 1935). A glance at these two figures will show the remarkable difference in the earth's surface in the two states of the volcano just mentioned. Namely, that the ground began to incline with a daily mean rate of 1·5″ toward the same direction from March to April, 1935. The amount of this inclination eventually reached 50″ with a maximum daily tilt of 2·5″. On April 17, the direction of tilt took a change in the opposite direction, when the ground began to tilt with an extraordinarily daily rate. On April 20, the third day after the foregoing direction of inclination had changed, the severe explosion occurred, when the tilt for that day

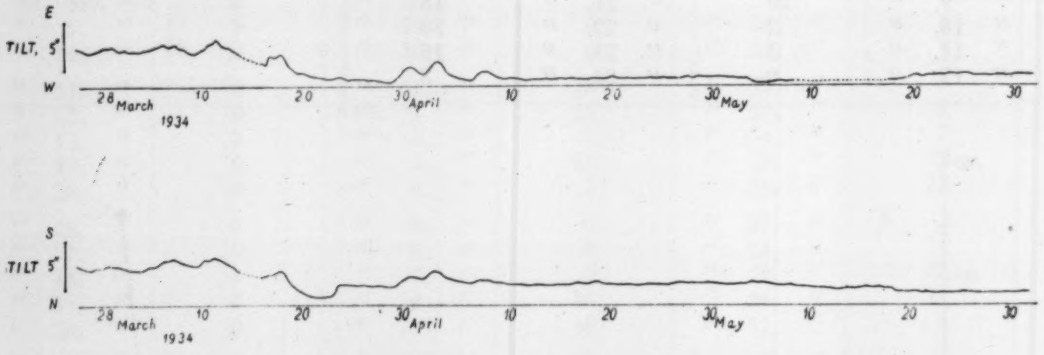

Fig. 9. The tilt-changes of earth-surface in 1934 (Mar.∼May).

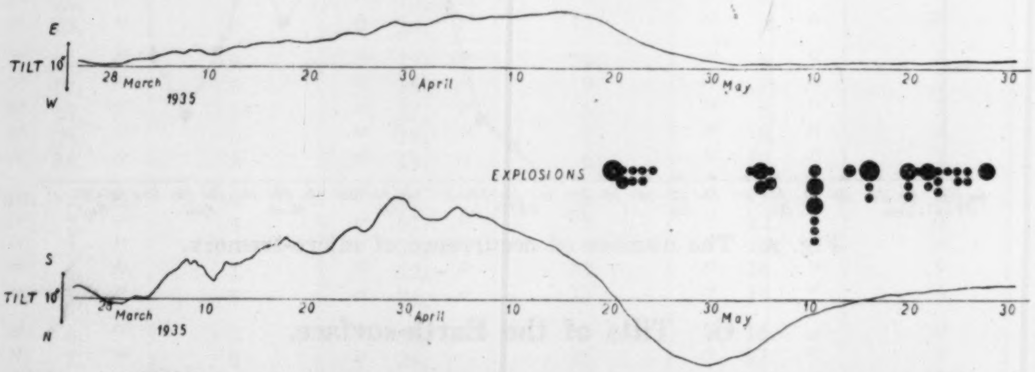

Fig. 10. The tilt-changes of earth-surface in 1935 (Mar.∼May).

reached 2·5″. Unaffected by this explosion, the direction of tilt remained unchanged up to May 2, 1935; the tilt having continued with a mean daily rate of 1·5″. On May 2, the direction of tilt changed again days after which another violent explosion occurred. After that, the daily rate of tilt began to decrease, due in all probability to the fact that the ground gradually began to resume the normal state.

The daily rate of inclination of the ground is shown in Fig. 11, from which it may be noted that the daily rate of tilt reached to as much as 3·0″. From Fig. 12, which gives the curve of the vector of inclination, it will be seen that the direction of inclination points neither toward or opposite the crater, which is probably place where the clinographs are due to crustal peculiarities of the installed.

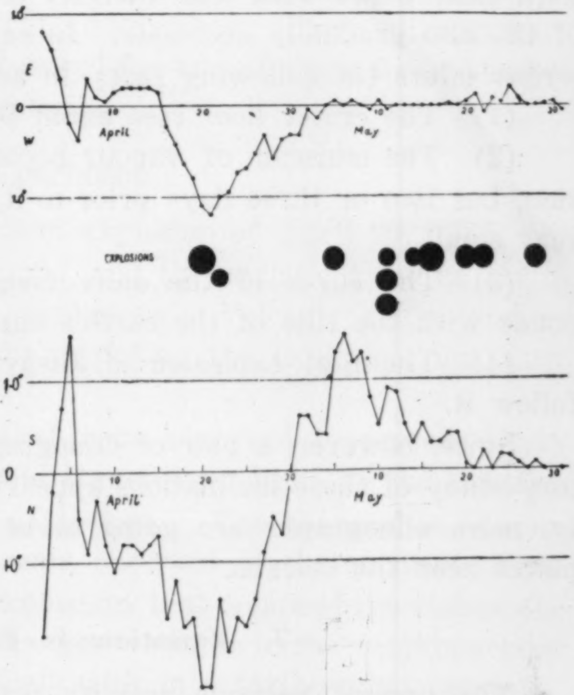

Fig. 11. Daily rate for the variations of tilt of the earth-surface.

It is interesting at all events that the extraordinary tilts of the earth's surface were invariably accompanied by violent explosions, after which the tilts diminished to what they were before the explosion. It may be pointed out in explanation that the pressure of the vapours that provide the energy of explosion acts at the bottom of the crater, but the lava in the crater floor resists it by virtue of its various properties, such as rigidity and viscosity, but with increase of vapour pressure, the resistance of the lava increases with the result that the tilting of the

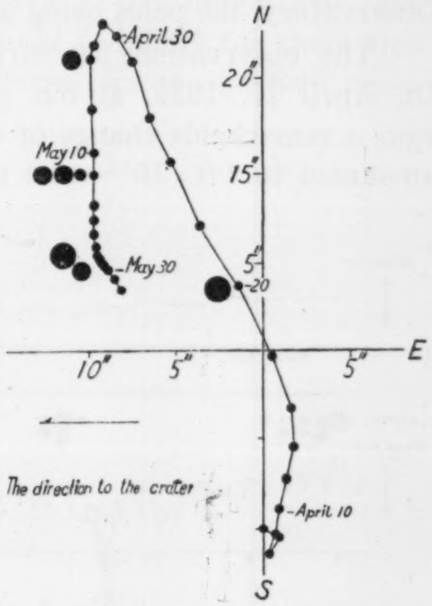

Fig. 12. ●; remarkable explosion.

ground near the crater increases. But once the explosion has occurred, the new thinner lava bed in the crater bottom being unable to withstand the extraordinary pressure of the vapour, the volcano explodes with ease, hence with less intensity of explosion, so that the amount of tilt also gradually decreases. In support of this ideal theory, the writer offers the following facts, in addition to that of tilting.

(1) The crater floor rose about 50 m since October, 1934.

(2) The emission of vapour becomes irregular before the explosion, but two or three days prior to it, the amount of vapour becomes very small.

(3) The curve of the daily frequency of micro-tremors corresponds with the tilts of the earth's surface.

(4) The first explosion is always more violent than those that follow it.

Since, however, a pair of clinographs is insufficient for a satisfactory study of these inclinations appearing at periods of volcanic activity, more clinographs are going to be installed before long at other places near the volcano.

7. Variations in Earth-current.

The present volcanic activity was preceded also by remarkable variations in the earth-currents. To measure them a wire was stretched between two poles fixed in the direction of the volcano from the Observatory, the poles being about 110 m apart and 2 m in the ground.

The observations of earth-currents were begun in October 1934. On April 15, 1935, at 5 h p.m., five days before the violent explosion, a remarkable change of earth-current was observed. This change amounted to $1\cdot0 \times 10^{-3}$ volts per 100 m, while five or six hours before

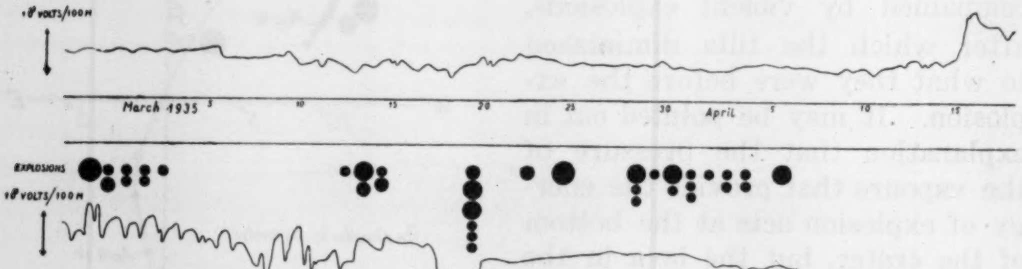

Fig. 13. Variations in earth-current and explosions.

the explosion on April 20, a new variation in earth-current appeared.

As will be seen from Fig. 13, marked changes in earth currents continued to occur until the middle of May. It will be noted that several hours preceding every violent explosion, extraordinary changes in earth-current manifested themselves, which ceased almost entirely as soon as the explosive activity of the volcano diminished. These extraordinary changes in earth-current were observed for several days, for a number of hours before every violent explosion.

8. Conclusion.

This paper describes the violent explosion of April 20, 1935, the changes in the tilting of the ground, and the variations in the earth-currents before and after the explosions. Volcanic micro-tremors occurred during the three months preceding the explosion, but none was observed in 1934.

These volcanic phenomena that were observed to precede every period of explosive activity, should throw some light on the question of the possibility of forecasting explosions. The changes in the intensity of the atmospheric currents observed at the moment of explosions, full details of all the explosions that followed the violent one of April 20, 1935, topographic changes wrought in the neighbourhood of the crater, all these will be dealt with in a forthcoming paper.

In conclusion, the writer wishes to express his cordial thanks to Professor Mishio Ishimoto for his kind advices and suggestions, and also to Mr. Madoka Iwashita and Mr. Teiichi Uchibori for their kind assistance in investigating the sounds of the explosion and field investigations.

50. 1935年の淺間火山の活動（其の1）

地震研究所　水　上　武

1.　1932年以來活動を示さなかつた淺間火山は1935年4月20日午後4時21分突然大爆發した．この爆發後，4月，5月の間に大小爆發數十回に達した．

1934年7月以來，火口底の昇降の測定を行つたが，7月より10月迄に約20 mの沈降を示し，10月終りより上昇を示して居る事は旣に報告した如くであるが，爆發直前には昨年10月より約50 m上昇して居た．

2.　1934年を通じて1回の火山性微動も觀測されなかつたにも拘らず，1935年1月2日以後に於いては，一日に數回又は數十回の微動が現はれた．

シリカ傾斜計に依つて觀測された地表傾斜は昨年10月以來次第に大なる變化を示すに至つたが3~5″程度の變化を繰返すに過ぎなかつた．然るに1935年3月より4月20日迄平均1日に約1·0″の傾斜を同方向に繼續した．卽ち3月20日より4月20日迄に約30″に達する傾斜を示したのである．

地表傾斜は爆發前約2ケ月前より異常の變化を認められたが，最初の爆發後傾斜變化は次第に減少して行つた．

地電流は大爆發5日前の4月15日に大なる變化を示し，以後大爆發前數日又は數時間前に大なる變化の現はれる事が確められた．

3.　なほ4月20日の大爆發の音響調査の結果，內外聽域の明瞭に表れる事がわかつた．この大爆發及びその後の爆發に依つて噴出した火山彈，火山灰の分布，並に火山彈の落下に依つて山腹に起つた野火の被害圖等が記述してある．

4.　爆發地震，空電及び個々の爆發に關する記述は次の機會に報告する考へである．

最後に種々貴重なる御示敎を賜つた石本敎授，高橋助敎授に感謝の意を表すると共に音響調査に御盡力された岩下圓氏並に厳寒零下20°Cの淺間山に在つて觀測を繼續された內堀定市氏に對して深謝の意を表する次第である．なほ又山腹野火の被害面積測量表並に圖は岩村田營林署長有馬農學士の御厚意に依るものなる事を附記して置きたい．

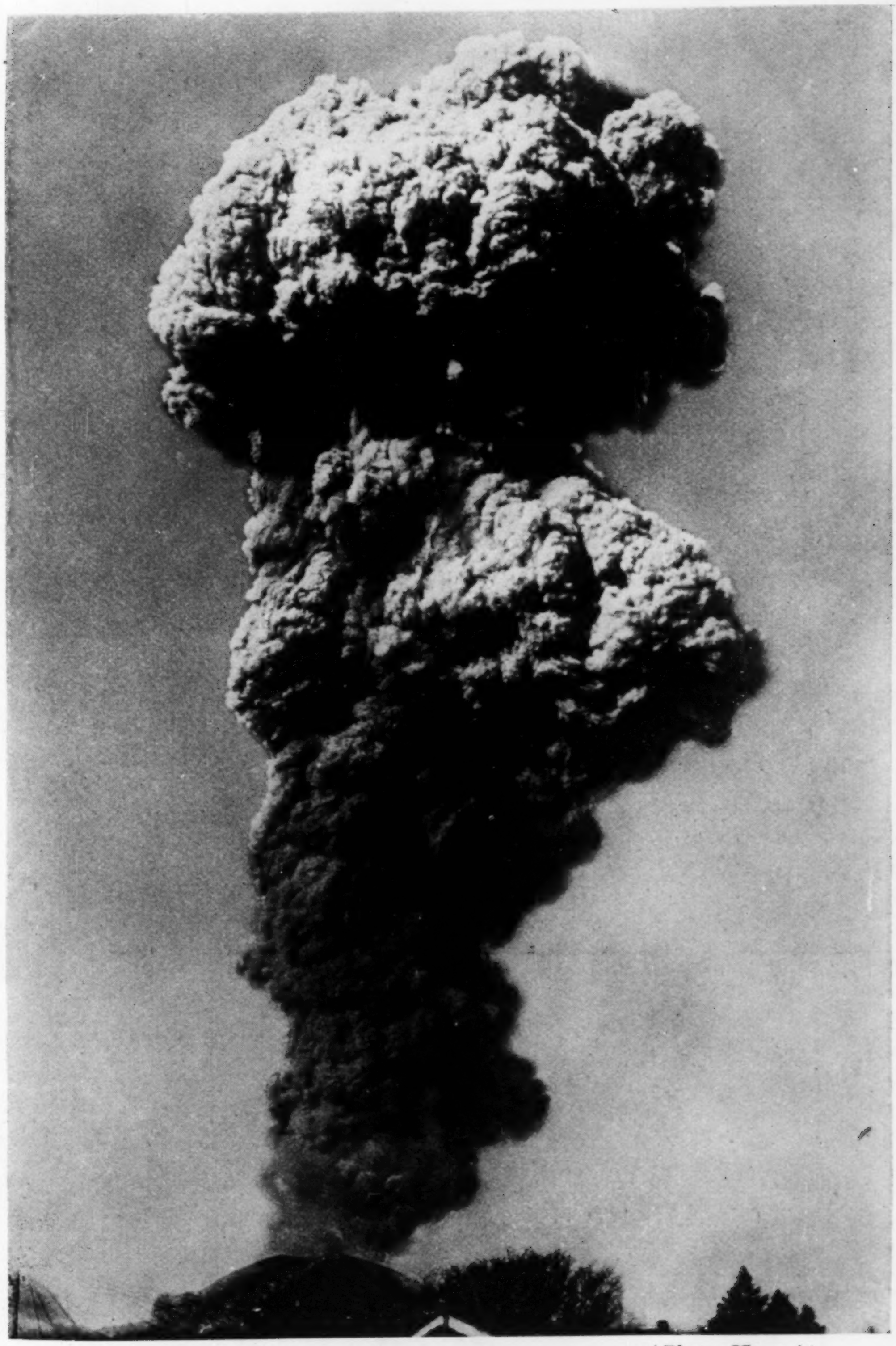

(Photo. Hayami.)

Fig. 14. The violent explosion on April 20, seen from Komoro at the distance of 15 km from the crater.

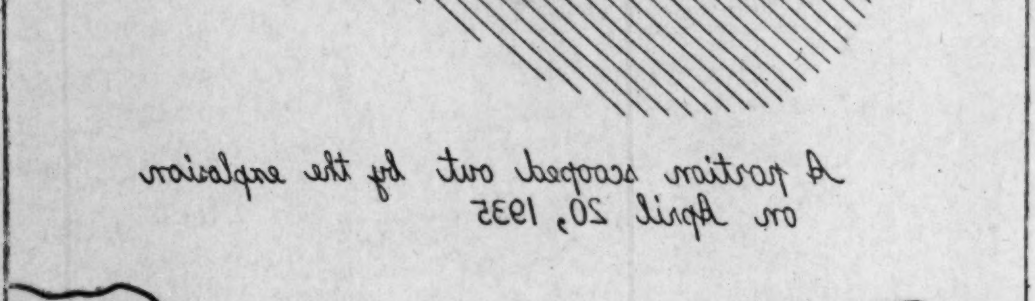
A part of the crater-bottom before the explosion
A portion scooped out by the explosion on April 20, 1935
Crater wall

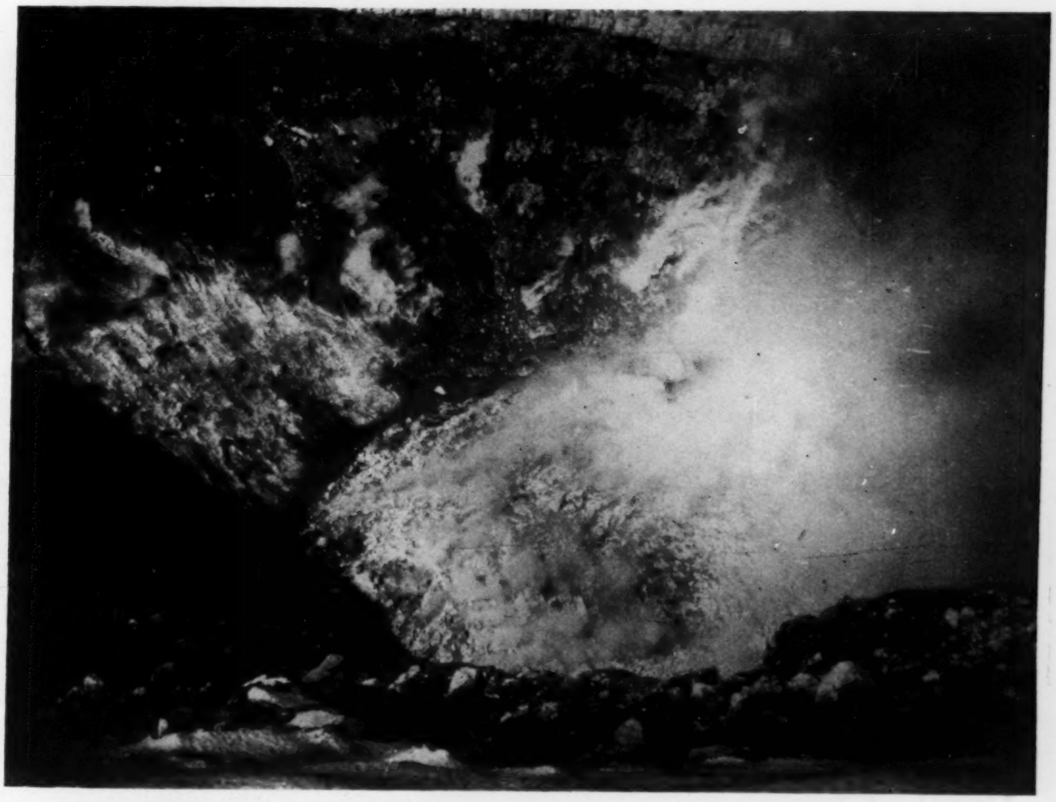

Fig. 15. The crater floor taken from the south-side on the crater wall in October, 1934.

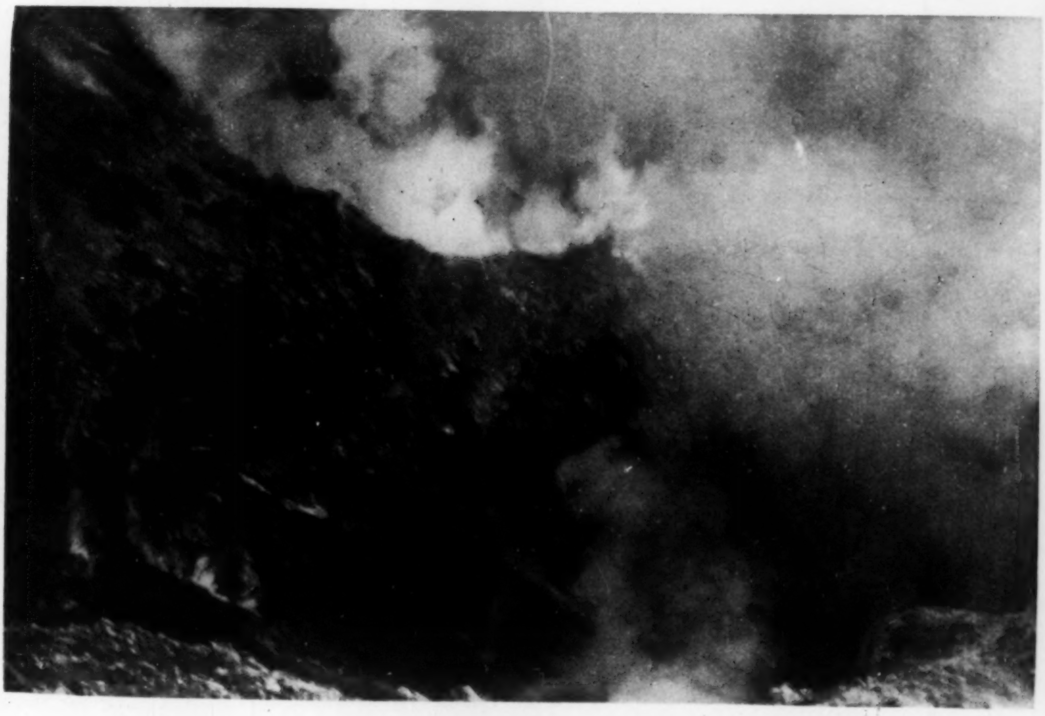

(*Photo. Minakami*, April 26, 1935.)

Fig. 16. The crater bottom seen from the same place and the same direction in Fig. 15.

（震研彙報 第十三號 圖版 水上）

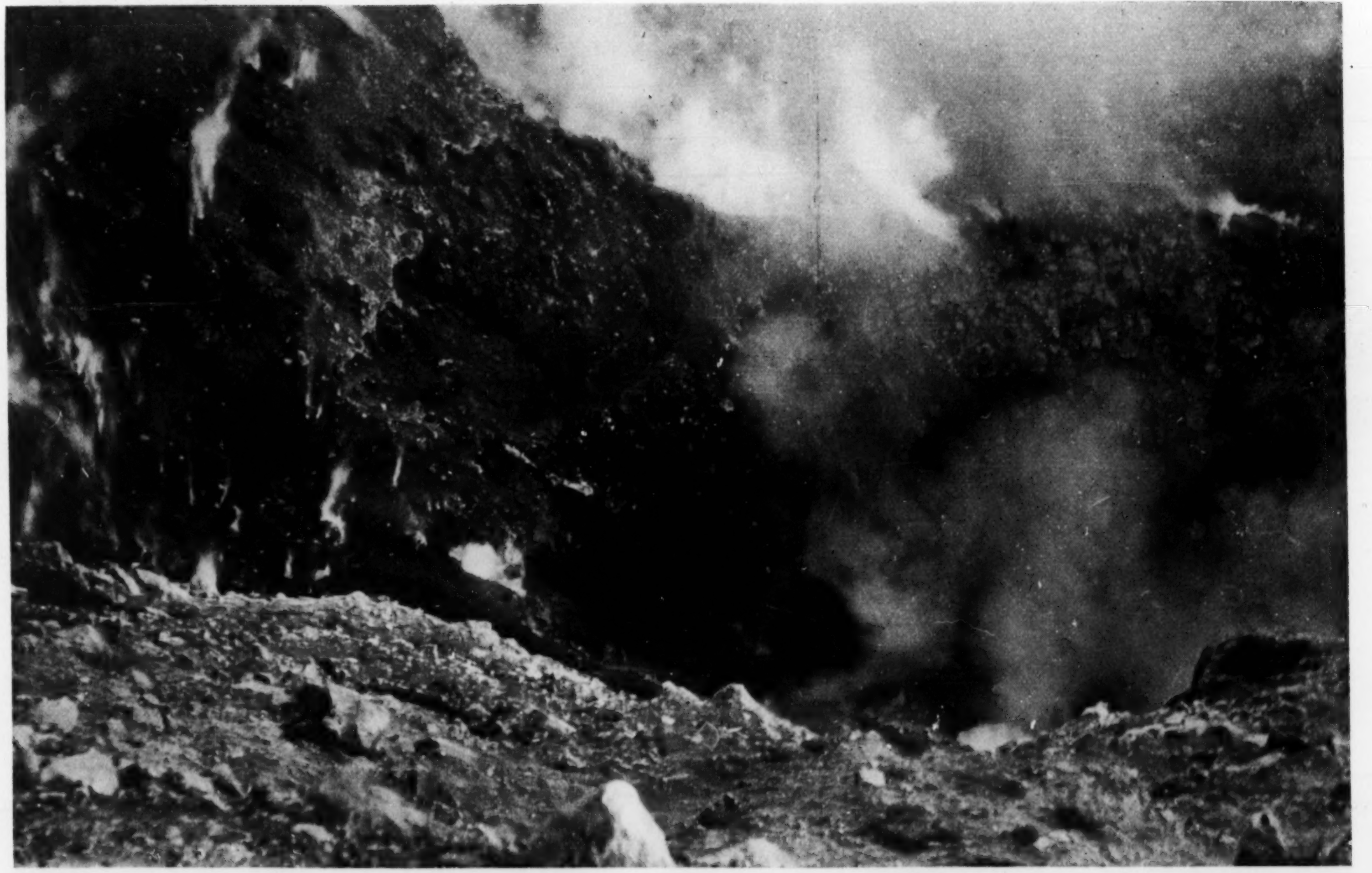

(*Photo. Minakami*, April 26, 1935.)

Fig. 17. The crater bottom seen from south-side on the crater wall.

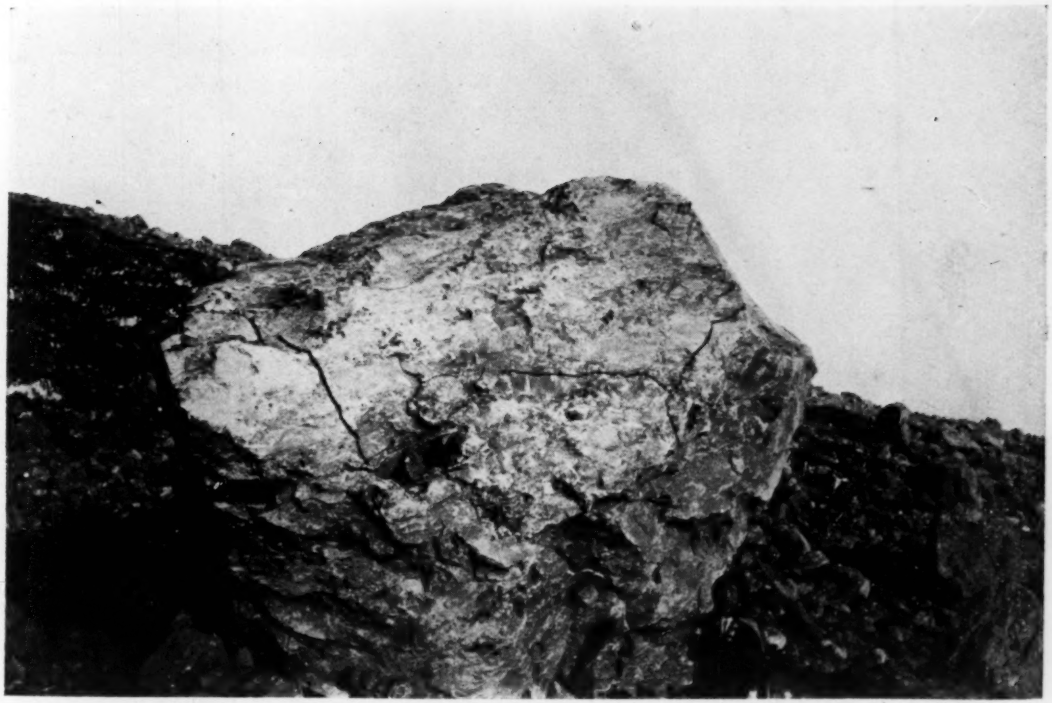

Fig. 18. The largest bomb, about 18 m in circumference, projected to the west-side of central cone by the strong explosion of April 20, 1935.

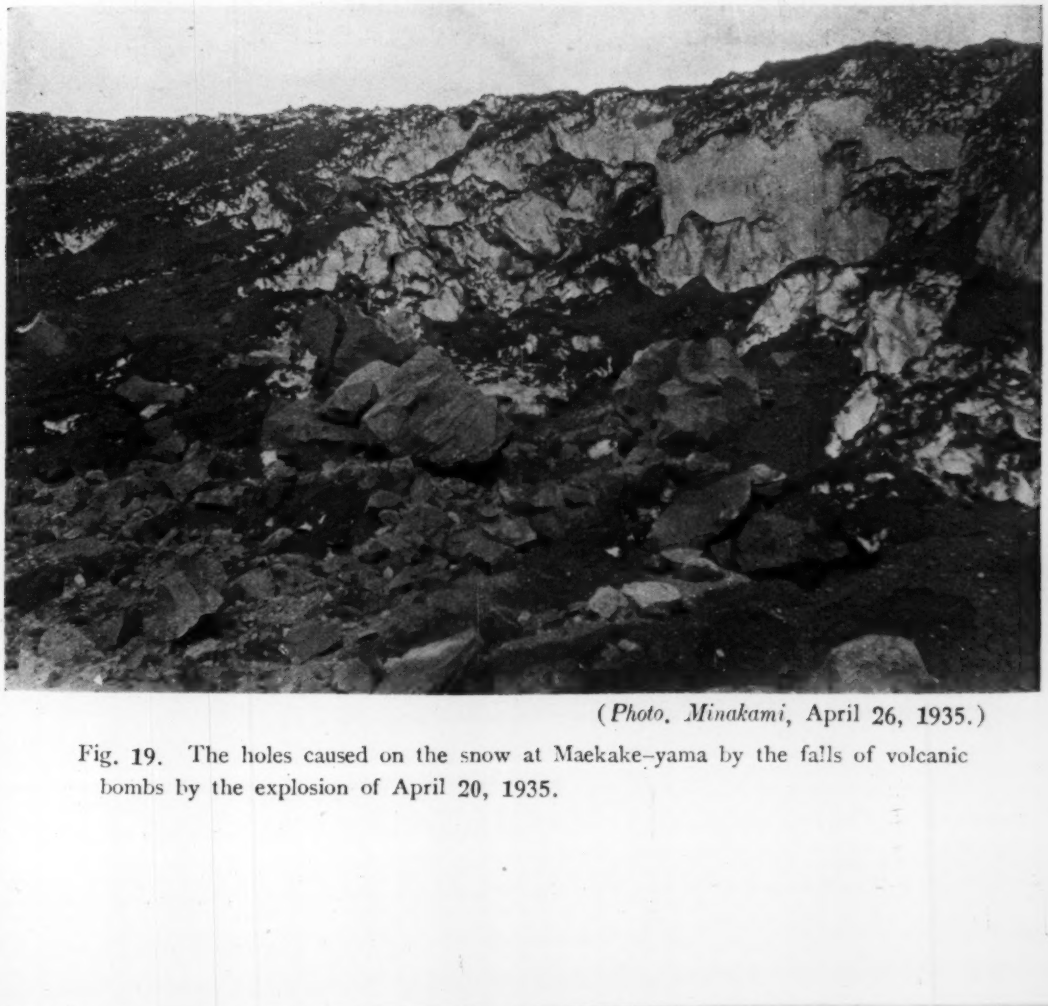

(*Photo. Minakami*, April 26, 1935.)

Fig. 19. The holes caused on the snow at Maekake-yama by the falls of volcanic bombs by the explosion of April 20, 1935.

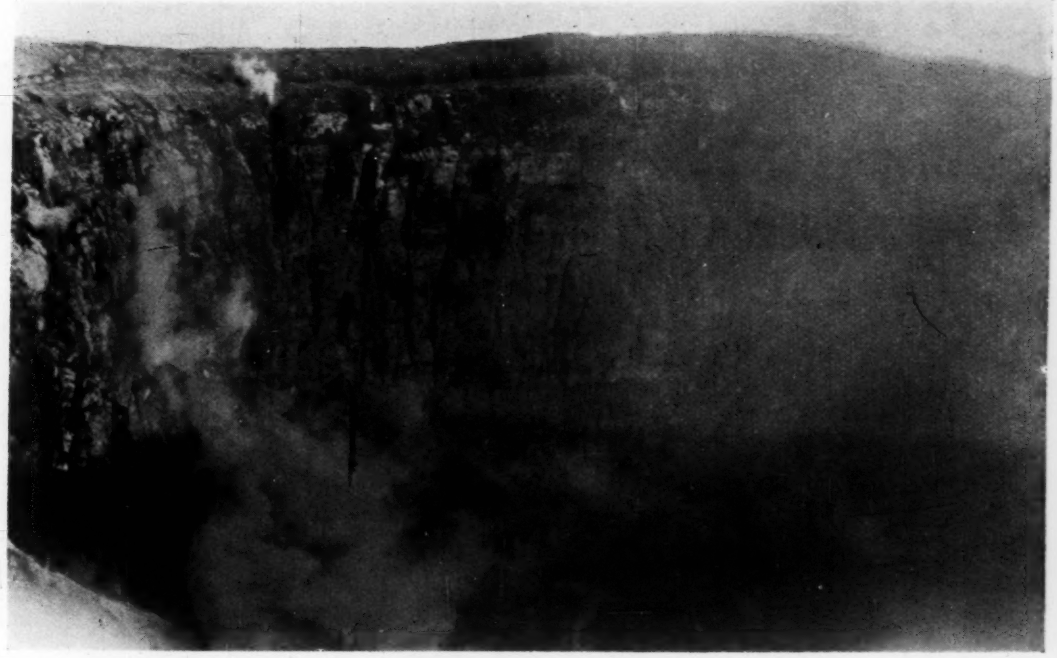

Fig. 20. The west-side of crater wall seen from south-side.

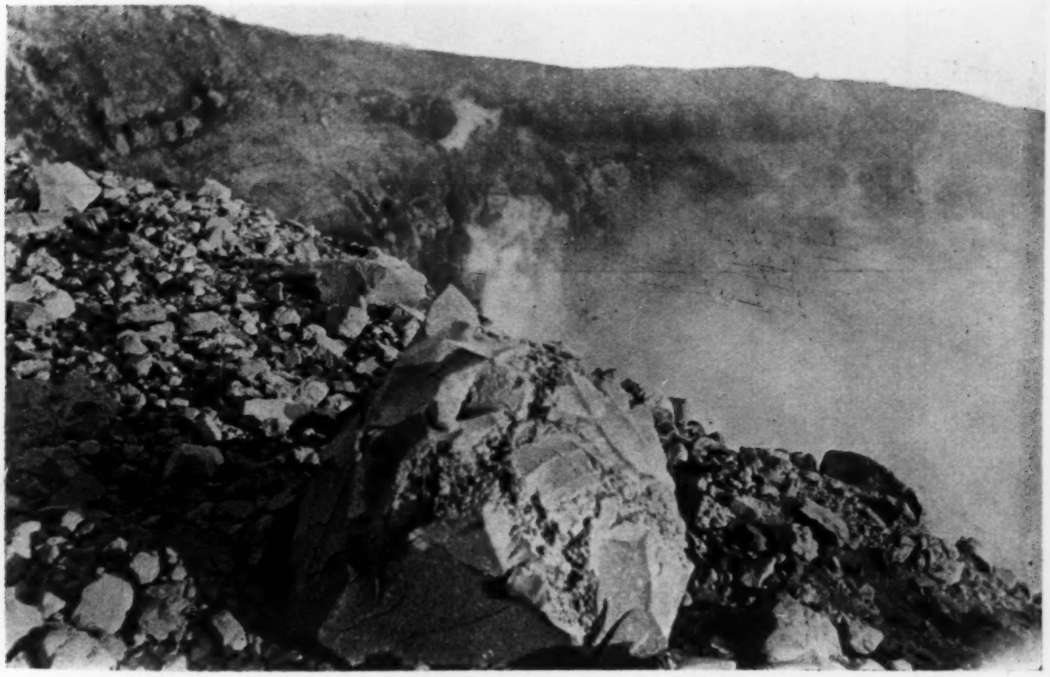

(*Photo. Minakami*, April 26, 1935.)

Fig. 21. A bomb projected on the west-side of crater wall by the explosion of April 20, 1935.

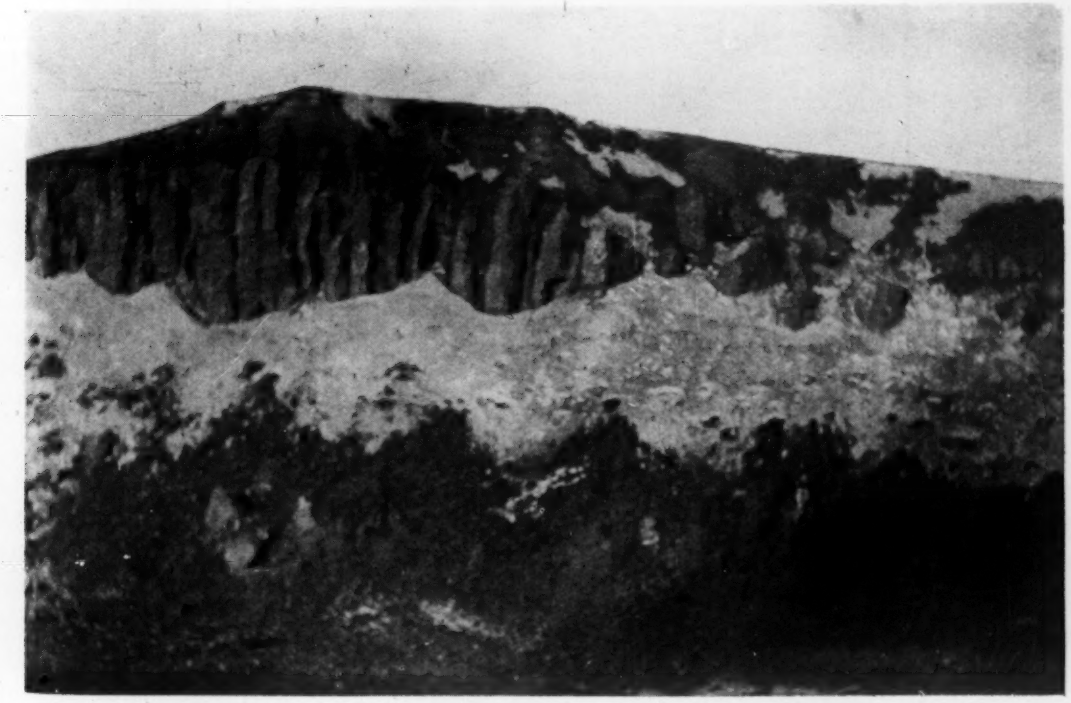

Fig. 22. Maekake-yama seen from the central cone. (April 26, 1935.)

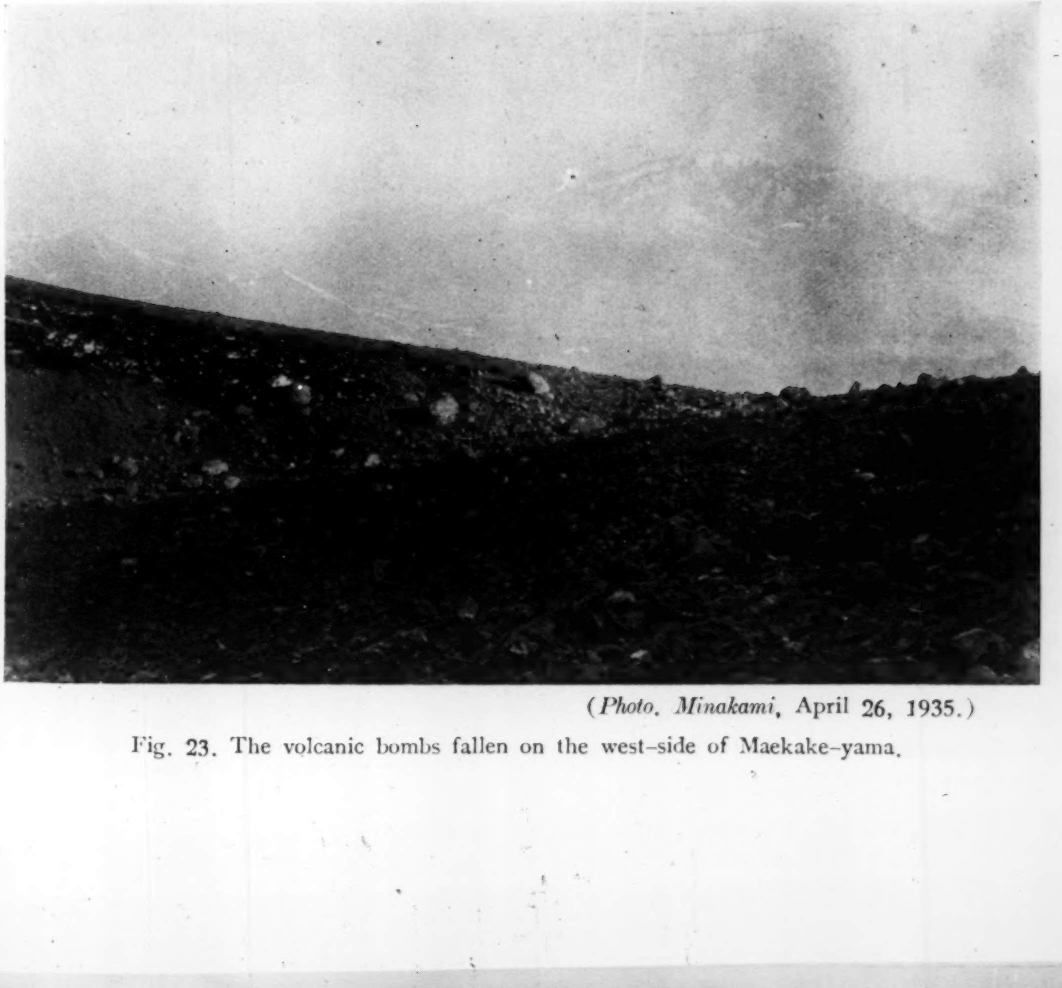

(*Photo. Minakami*, April 26, 1935.)

Fig. 23. The volcanic bombs fallen on the west-side of Maekake-yama.

（震研彙報 第十三號 圖版 水上）

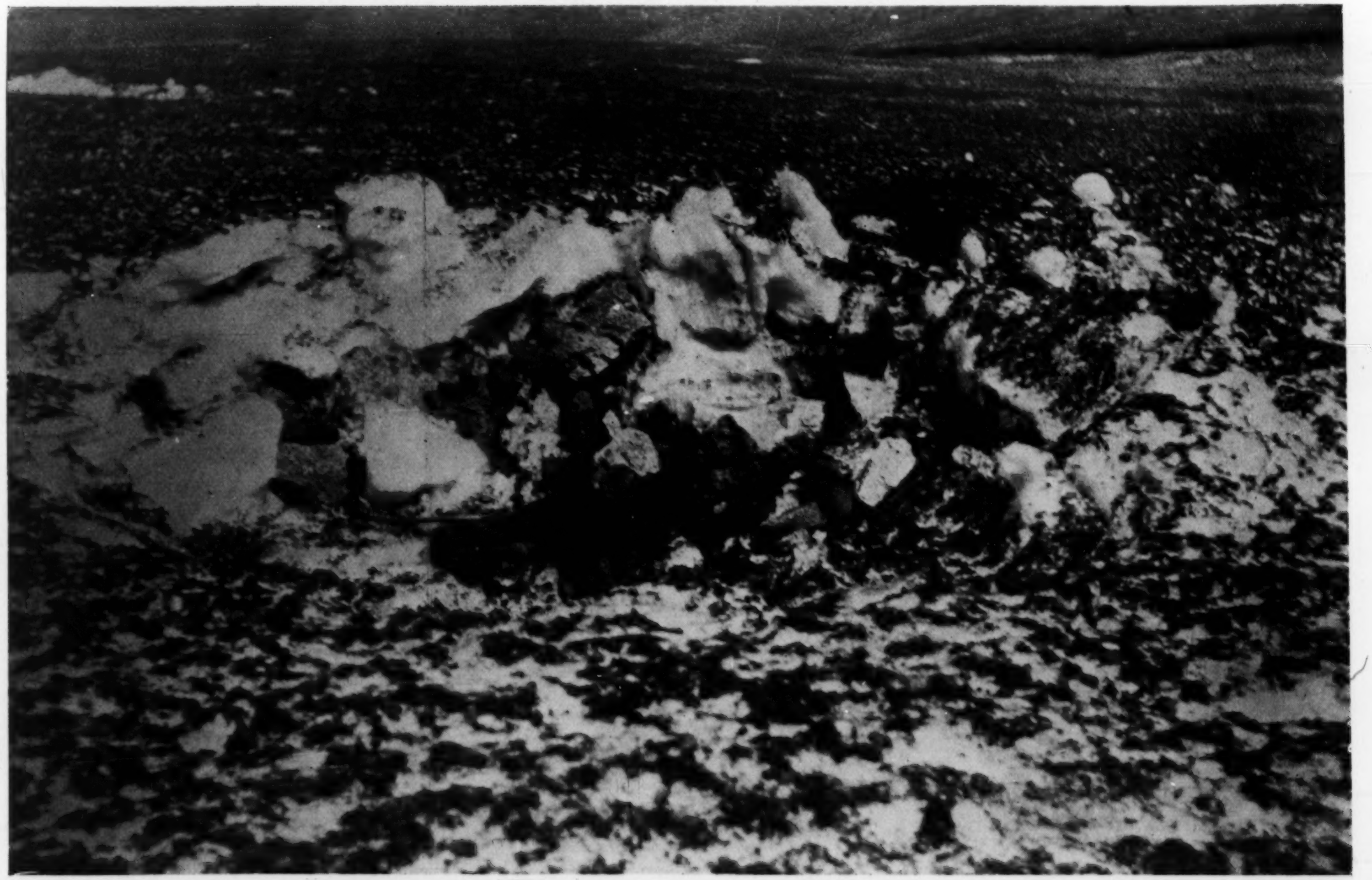

(*Photo. Minakami*, April 21, 1935.)

Fig. 24. A hole caused on the snow by the fall of a bomb, the volcanic ashes on the snow at the distance of 1500 m from the crater.

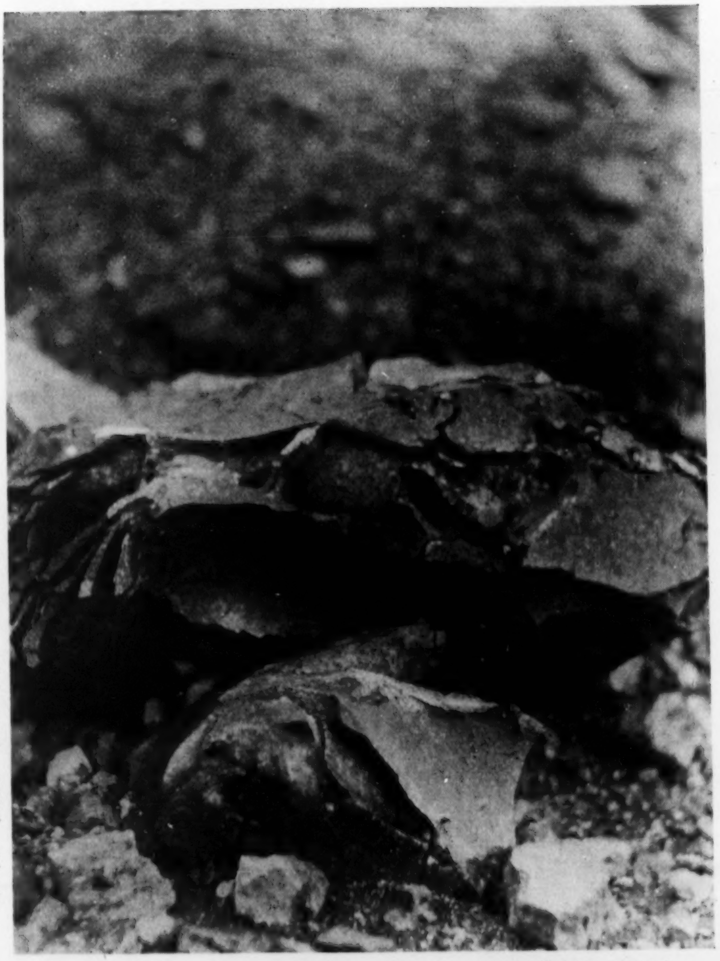

(*Photo. Minakami*, April 21, 1935.)

Fig. 25. A volcanic bomb projected to east at the distance of 1000m by the explosion of April 20, 1935.

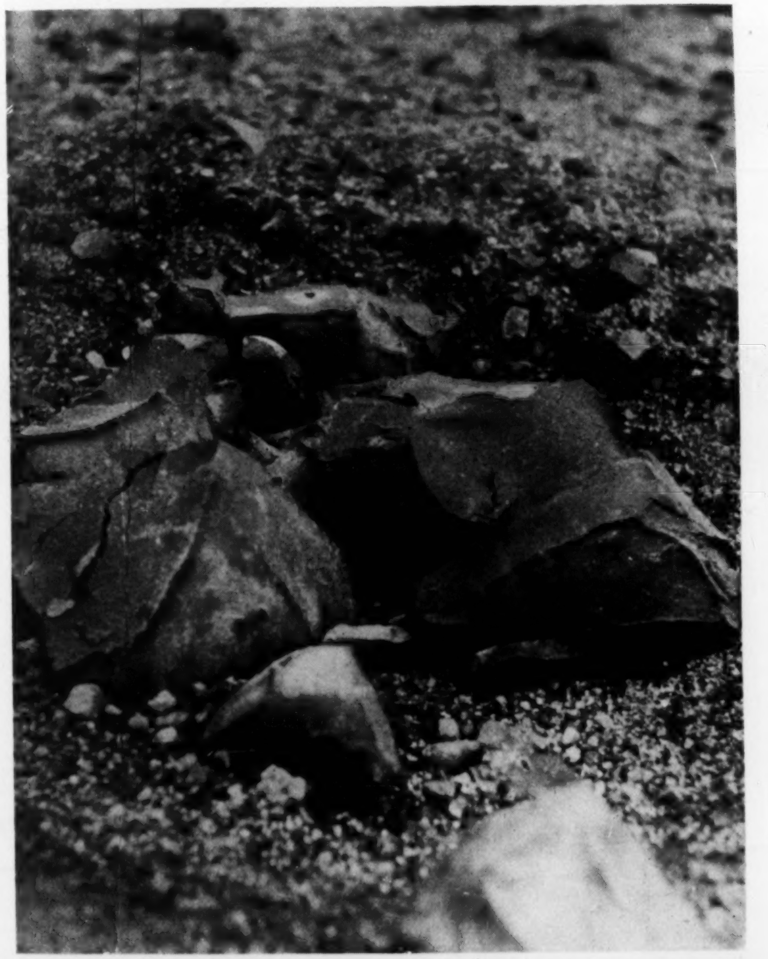

(*Photo. Minakami*, April 21, 1935.)

Fig. 26. A volcanic bomb projected out by the violent explosion of April 20, 1935, at the distance of 2000 m.

（震研彙報 第十三號 圖版 水上）

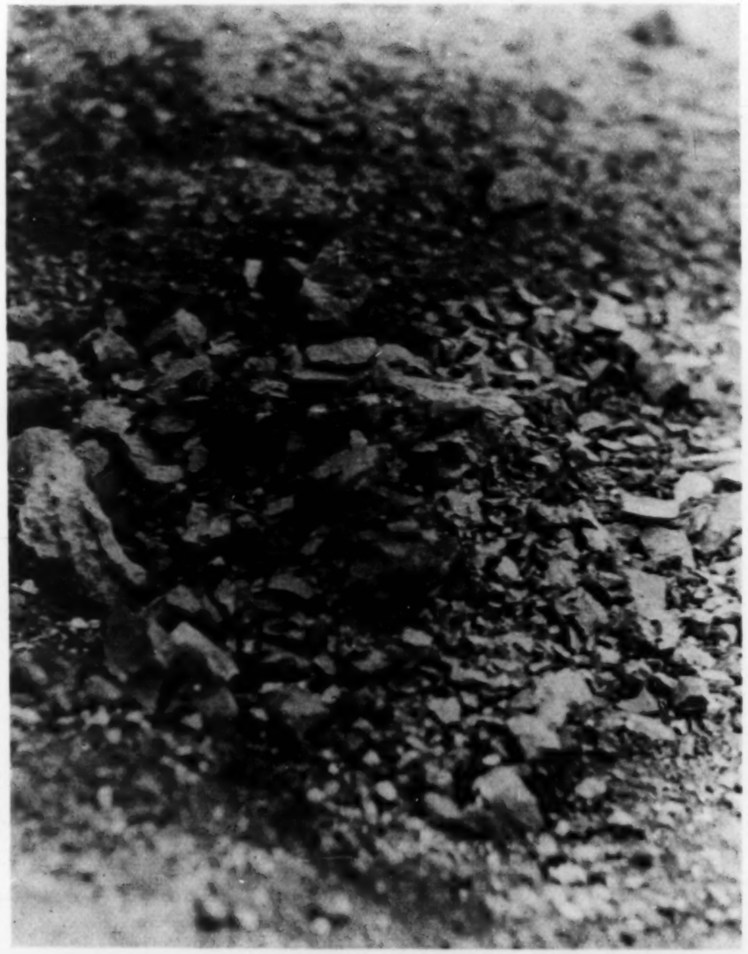

(*Photo. Minakami*, April 21, 1935.)

Fig. 27. The bombs broken into pieces at the distance of about 2 km from the crater.

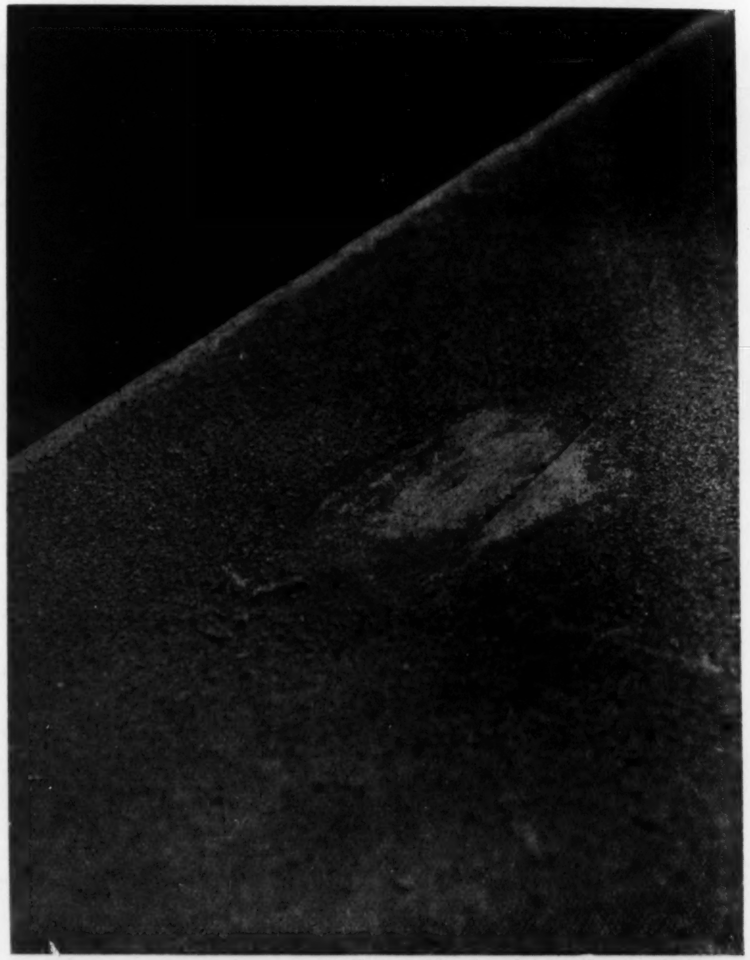

(*Photo. Minakami*, April 21, 1935.)

Fig. 28. The volcanic ashes fallen on a roof of Hosino Onsen at the distance 12 km from the crater, by the explosion of April 20, 1935.

（震研彙報　第十三號　圖版　水上）

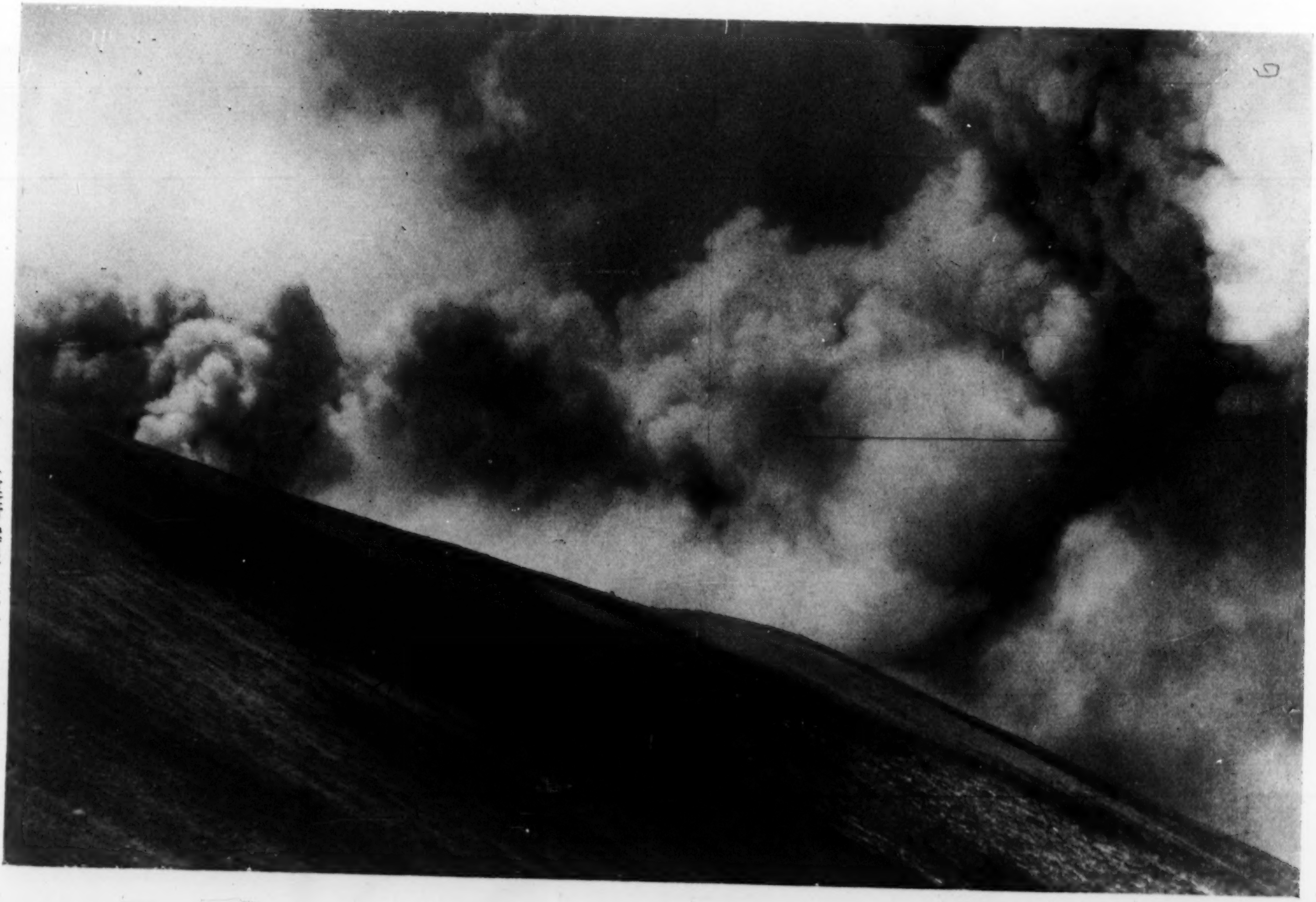

(*Photo, Minakami.*)

Fig. 29. A small explosion of April **21**, **1935**, at about **12**h, seen from east-side at the distance of **700**m from the crater.

（震研彙報 第十三號 圖版 水上）

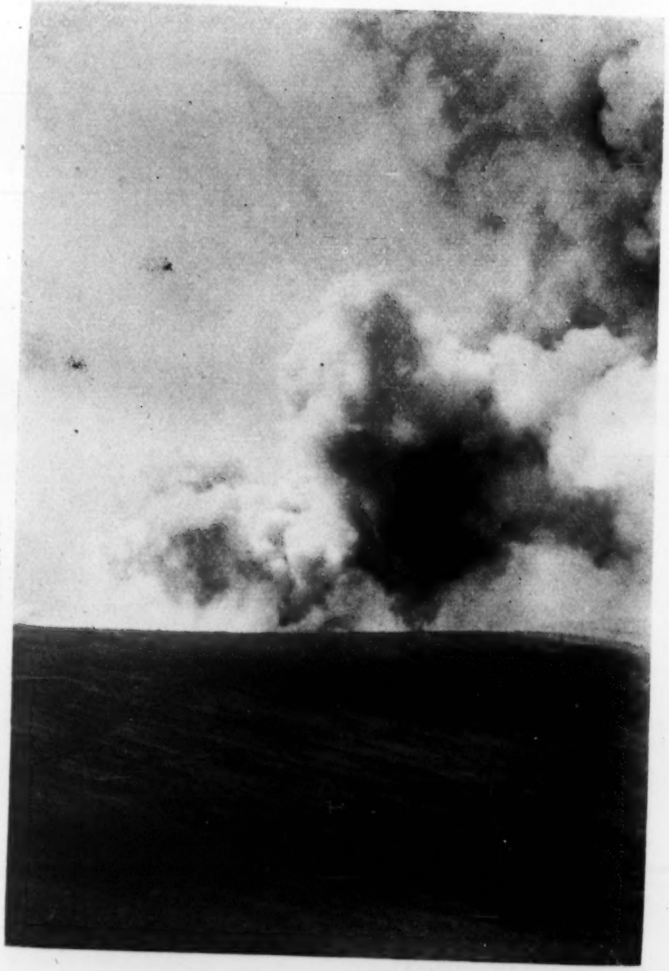

(*Photo, Minakami.*)
Fig. 30. A small explosion of April 21, 1935.

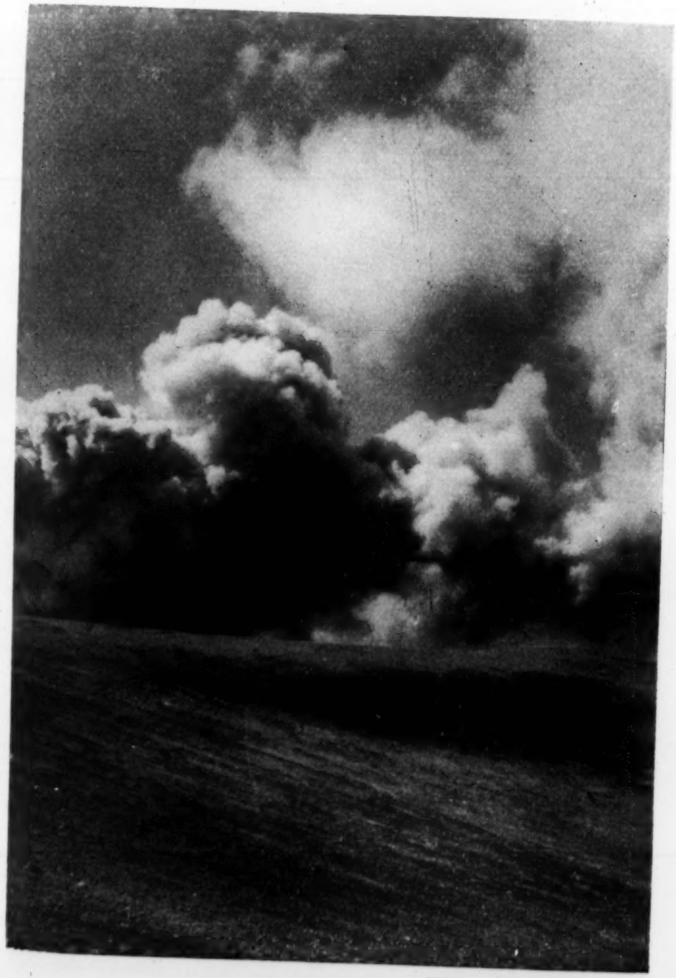

(*Photo, Minakami.*)
Fig. 31. A small explosion of April 21, 1935.

2

9

51. *On Some Lavas of Volcano Huzi (Fuji).*

By Hiromichi TSUYA,

Earthquake Research Institute.

(Read Jan. 15, 1935.—Received June 20, 1935.)

Introduction.

The world-famous dormant volcano Huzi, situated near the shore of Suruga Bay, occupies an area of about 832 sq. km, with its summit 3776 m above sea level, the highest in Japan. It is a regular and beautiful symmetrical cone with gracefully curving slopes diminishing from 34° near the summit to 17° in the middle, on all sides except the southeast, where a prominent shoulder, Hôei-zan, about 1000 m below the summit, gives it a remarkable profile. This projection is part of the wall of a large explosion-crater that opened at the time of the last great explosion of the volcano in 1707. As may be seen on the steep inner slopes of the Hôei-zan explosion-crater or in the Ôsawa valley that deeply cuts the western slope, it is a typically stratified volcano, formed by the accumulation of many successive lava-flows, intercalated with layers of fragmentary materials, bombs, scoriae, lapilli, ashes, etc. The parasitic knobs of the volcano, of which there are more than forty, are either lava or cinder cones.

As is natural with a mountain of such celebrity as Huzi, there is, besides an extensive popular literature of a descriptive character, quite a number of contributions[1] to the geology of the volcano. An examination of some of the earlier works, however, reveals certain conflicts of opinion in the matter of the structure of the volcano, and of the sequence of its lava-flows. As to its petrography, the only available data are those by T. Wada (1882) and by T. Hirabayashi (1899), who described the Huzi rocks as anorthite-basalt and plagioclase-basalt respectively. It was while making a detailed study of the volcanoes of the Idu district, which, adjoining the southeast of Huzi are comprised in the Huzi Volcanic Zone, that the writer became interested in the geology and petrology of Huzi, with the result that within the last few years the writer made several trips to the volcano in accompany with S. Kambara, a civil engineer, who, for the last twenty years has made it a point to utilize his spare time in surveying the sequence of the Huzi lava-flows, devoting special attention to the subject. Since nothing like a complete systematic study, geological as well as petrological, of the volcano has yet been made, the writer offers here as a sort of reconnaissance a short account of the occurrence, together with the microscopical and chemical characters, of six rock specimens from the volcano.

---

[1] WADA, *Trans. Seis. Soc., Japan*, **4** (1882), 31~37.
T. SUZUKI, *Expl. Text Geol. Surv. Map* (1:200000) "Huzi", (in Japanese).
T. HIRABAYASHI, *Rep. Earthq. Inv. Comm.*, **24** (1899), (in Japanese).
H. ISHIWARA, "Geogr. and Geol. of Huzi", (1928), (in Japanese).
T. KATO and K. IHARA, *Guide-Book*, Pan-Pacific Sci. Congr., Tôkyô, (1926).
S. KAMBARA, *Jour. Geogr. Soc., Tokyo*, **47** (1935), 109~123, (in Japanese).

He takes this opportunity of thanking Dr. S. Kambara for his guidance in the field.

Occurrence.

The rocks described in this paper are

1. Lava F_{67-a} (Olivine-bytownite-basalt).
2. Lava F_{67-b} (Two-pyroxene-bearing olivine-bytownite-basalt).
3. Lava F_{67-d} (Augite-bearing olivine-bytownite-basalt).
4. Lava F_{67-e} (Hypersthene-augite-olivine-bytownite-basalt).
5. Aokiga-hara lava (Two-pyroxene-olivine-bytownite-basalt).
6. Hôei-zan scoria (Augite-bearing olivine-bytownite-basalt).

Of these six basalts, numbers $1\sim4$ occur at Makuiwa, about 1580 m above sea level on the S. E. slope and about 2800 m S. E. of Hôei-zan. The exposure here is shown in Fig. 1, where a, b, d, and e correspond to $1\sim4$ respectively.

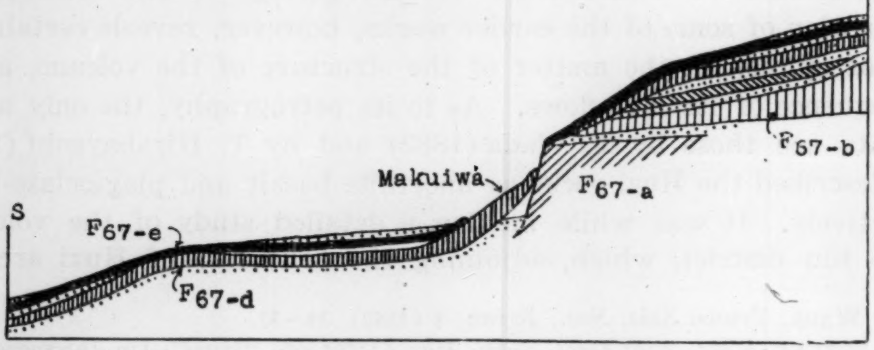

Fig. 1. Diagrammatic section at Makuiwa on the S. E. flank of Huzi. Length of section=300 m approx. Vertical scale much exaggerated.

Lava F_{67-a}, which is the oldest of all the lava-flows exposed at this locality, the base of which however is not exposed, is highly vesicular, ropy in places, with a thickness of more than 10 m. Lavas of this type, which closely resemble Hirabayashi's Misima-Ômiya lava, and which are believed to have poured out at a later period of the extrusion of the latter, are extensively distributed as the lowest exposed lava about the middle height of the southern slope, occupying the valley floors that deeply cut the slope.

Lava F_{67-b}, which is a little later eruption than F_{67-a}, lies on the latter, some pyroclastic beds being sandwitched in between them. Here it occurs as a compact lava-flow, more than 15 m thick, forming an almost perpendicular lava-cliff. Lavas of this type, which are comprised in Hirabayashi's Ôsawa lava, are also widely distributed above the middle height of the southern slope, being exposed as numerous flows alternated by pyroclastic materials, the best exposures of which are met with on the precipitous cliffs of the Ôsawa valley.

Lava F_{67-d}, which occurs as a scoriaceous flow, about 2 m thick, lies on a higher horizon than F_{67-b}. At the locality just mentioned, the lava hangs as a lava-fall over the edge of a precipitous cliff of lava F_{67-a}— a feature likened to that of a hanging curtain. The locality name "Makuiwa" (curtain rock) seems to have originated from that feature. Between the two flows, F_{67-b} and F_{67-d}, is another lava-flow, about 2 m thick, besides pyroclastic materials.

F_{67-e}, which is the youngest exposed lava at Makuiwa, resembles the preceding lava, occurring as a flow, about 2 m thick, and overlying the latter together with some pyroclastic materials.

The Aokiga-hara lava which, in 864 A. D., poured out of the boccas on the N. W. flank, about 2300 m above sea level, and flowed down toward the northwestern foot, is the most conspicuous flow now exposed on the volcano. It covers an area of about 32 sq. km, the greater part of which is thickly forested with conifers. Although the surface of the flow is highly vesicular and broken into blocks that are piled in confused wave-like ridges, its interior is rather compact, retaining many lava-tunnels, -tree-moulds, -caves, etc. Another lava, which probably dates from the same time as the Aokiga-hara lava, is the "Ken-marubi" lava that poured out of the N. W. flank and flowed down northeastward to the vicinity of the town of Yosida.

The Hôei-zan scoria is a lava-fragment that was ejected in 1707, at the time of the great explosive eruption from the S. E. flank of the volcano. The pyroclastic materials, bombs, scoriae, lapilli, ashes, etc., that were ejected from Hôei-zan, a newly opened explosion crater, spread eastward over more than 50 sq. km. The sample of the Hôei-zan scoria here described was collected on the eastern slope of Hôei-zan.

Megascopic Characters.

Lava F_{67-a}. This rock is dark gray and more or less scoriaceous, with, round or oval, vesicles more than 1 mm dia. Plagioclase phenocrysts, which vary in diameter from 2 mm to 1 cm, dominate; while olivine phenocrysts, which is less than 1 mm dia., are rare.

Lava F_{67-b}. This rock is light-gray and non-vesicular. The phenocrysts, which are usually less than 1 mm dia., are plagioclase, olivine, and pyroxene, of which the plagioclase phenocrysts are fairly abundant, although not conspicuous, being scattered through an aphanitic, pale-gray groundmass. The olivine is only sporadically found; rarely two or three individual minerals forming a grouped phenocryst, about 5 mm in diameter. The pyroxene phenocrysts are far less in quantity than the preceding.

Lavas F_{67-d} and F_{67-e}. Megascopically, these two rocks resemble each other. They are dark gray, vesicular, and porphyritic with phenocrysts of plagioclase (1~3 mm), olivine (1 mm), and pyroxene (less than 1 mm dia.).

Aokiga-hara lava. This also closely resembles the preceding rocks. It is slightly vesicular, dark gray to almost black, and studded with prominent, white phenocrysts, 1~2 mm dia., of plagioclase, and also with less conspicuous granules, 0·5~1 mm dia., of olivine and pyroxene.

Hôei-zan scoria. This rock fragment is angular, about 10 cm dia., black, and vesicular with abundant pores (2 mm dia.) uniformly distributed through the rock; only a few plagioclase phenocrysts, rarely over 0·5 mm across, being visible.

Microscopic Characters.

Microscopically, all the six basalts are porphyritic, with phenocrysts

Table I. Modal Compositions (Vol. %) of the Huzi Basalts.

		I	II	III	IV	V	VI
Phenocrysts	Bytownite	21·04	6·71	20·47	23·10	25·15	7·37
	Hypersthene	—	tr.	—	0·21	tr.	—
	Augite	—	tr.	tr.	0·33	0·07	0·02
	Olivine	1·84	2·60	1·60	1·62	2·84	0·87
Groundmass		77·12	90·69	77·93	74·74	71·94	71·74
Total		100·00	100·00	100·00	100·00	100·00	100·00
Vesicles		1·99	—	8·35	9·86	2·29	35·22

I. Lava F_{67-a}, II. Lava F_{67-b}, III. Lava F_{67-d}, IV. Lava F_{67-e},
V. Aokiga-hara lava, VI. Hôei-zan scoria.

of plagioclase and olivine, irrespective of the presence of pyroxene phenocrysts (Figs. 3～8). The phenocrysts are present in variable quantities in all of them; their volume percentages measured micrometrically being shown in Table I, in which the volume percentages of the vesicles in each rocks are also shown.

Phenocrysts.

It will be seen from Table I that the amount of plagioclase phenocrysts is now more than 20% by volume in all the rocks except F_{67-b} and the Hôei-zan scoria, and that the phenocrysts of the mafic minerals (olivine with or without pyroxene) form only a small percentage in these rocks. In F_{67-b}, the phenocrystic plagioclase is hardly distinguishable quantitatively from that mineral in the groundmass, the mineral varying in size gradually from 0·02 mm × 0·1 mm in the groundmass up to 0·5 mm × 1·7 mm in the phenocrysts, for which reason the amount of the mineral in this lava as shown in Table I indicates only approximately those larger than about 0·5 mm dia. In the Hôei-zan scoria, plagioclase occurs lath-shaped microphenocrysts, less than 0·03 mm × 0·5 mm, although a few larger phenocrysts, 0·5 mm average diameter, are found, so that the amount of the mineral has diminished to 7·37%.

The plagioclase phenocrysts, which are euhedral and lath-shaped, are usually twinned. Zonal structure due to chemical difference is usually absent, though rarely a very faint zoning is observed. According to the refractive indices measured with Tsuboi's dispersion method, the phenocrysts are identified as bytownite as shown in Table II.[2] Although the smaller phenocrysts in F_{67-b} and the Hôei-zan scoria are medium bytownite, the larger phenocrysts in these rocks are identified as anorthite $Ab_5\ An_{95}$. The inclusions commonly found in the plagioclase phenocrysts are glass, either colorless or dark-brown. The phenocrysts in lavas F_{67-b}, F_{67-d}, and F_{67-e} have inclusions of pyroxene and magnetite grains, besides the glass base.

Table II. Composition of the Plagioclase and Optical Data of the Mafic Minerals in the Huzi Basalts.

		I	II	III	IV	V	VI
Plagioclase	phenox.	$Ab_{27}An_{73}$	$Ab_5\ An_{95}$ $Ab_{16}An_{84}$	$Ab_{25}An_{75}$	$Ab_{28}An_{72}$	$Ab_{29}An_{71}$	$Ab_5\ An_{95}$ $Ab_{17}An_{83}$
	gr. m.	$Ab_{33}An_{67}$	$Ab_{26}An_{74}$	$Ab_{29}An_{71}$	$Ab_{31}An_{69}$	n.d.	$Ab_{22}An_{78}$

(to be continued.)

---

[2] The plagioclase phenocrysts in numerous Huzi lavas, which are not described in this paper, are also bytownite, nearly $Ab_{25}An_{75}$ by chemical composition.

Table II. (*continued.*)

		I	II	III	IV	V	IV
Hypersthene	n_{1D}	——	1·6987	——	1·6983	1·6983	——
(phenox.)	n_{2D}		1·7077		1·7078	1·7076	
Augite	phenox. n_{1D}	——	1·6967	1·6956	n.d.	1·6979	n.d.
	2V(+)		n.d.	52°	n.d.	n.d.	n.d.
	gr. m. 2V(+)	52°	51° 41°	n.d.	n.d.	n.d.	——
Olivine	α_D	n.d.	1·6794	1·6667	n.d.	n.d.	1·6788
	β_D		1·6985	1·6843			1·7002
(phenox.)	2V(−)	84°	85°	n.d.	84°(?)	86°	84°

I. Lava F_{67-a}, II. Laba F_{67-b}, III. Lava F_{67-d}, IV. Lava F_{67-e},
V. Aokiga-hara lava, VI. Hôei-zan scoria.

Hypersthene phenocrysts, euhedral and 0·3∼1 mm long, are found in F_{67-b}, F_{67-e}, and Aokiga-hara lavas in amounts as shown in Table I. Although the mineral could not be detected in two thin sections of F_{67-b}, a megacryst picked out of the lava was identified by its optical characters as hypersthene. The hypersthene in F_{67-e} is moderately pleochroic (Z—pale green, X or Y—pale brown); its optical plane being parallel to the c-axis. It often has a border of monoclinic pyroxene. The enclosures in it are anhedral olivine grains and euhedral plagioclase prismoids. The hypersthene in the Aokiga-hara lava, which is less pleochroic than the preceding, has enclosures of euhedral plagioclase. In the same lava anhedral hypersthene is rarely enclosed in olivine phenocrysts. The refractive indices measured on cleavage (110) flakes are given in Table II, according to which the approximate chemical composition of the mineral as estimated by the Tomita diagram[3] is $(MgSiO_3)_{67}(FeSiO_3)_{33}$, showing that the difference in the chemical composition of the mineral in the three lavas is small.

Although augite phenocrysts are found in small quantities in all the rocks except lava F_{67-a}, in F_{67-b} and F_{67-d} the mineral occurs as microphenocrysts exhibiting undulatory extinction. In lava F_{67-e}, augite forms euhedral pale-brown phenocrysts, 0·2∼1 mm across, as also in the Aokiga-hara lava. They have enclosures of anhedral olivine. In the Hôei-zan scoria a few pale-brown augite, about 0·3 mm dia., are detected. The refractive indices on the cleavage (110) flakes of the mineral in F_{67-b}, F_{67-d}, and in the Aokiga-hara lavas are given in

---

[3] T. TOMITA, *Jour. Geol. Soc., Tokyo*, **31** (1924), 364, (in Japanese).

Table II. The optic axial angle measured on the crystals in a thin section of F_{67-d} is 52°.

The olivine phenocrysts, which are present in all the six basalts, though in rather small amounts, are euhedral to anhedral, 0·1~1 mm dia., and in thin sections pale yellowish-green or nearly colorless. In the F_{67-b} and the Aokiga-hara lavas the mineral is surrounded by iron-oxide and minute grains of a monoclinic pyroxene, while in lava F_{67-d} it is surrounded only by iron-oxide; and in the remaining rocks by none of these substances. Besides the minute crystals (plagioclase, pyroxene, and magnetite) which are supposed to have crystallized out of the glass enclosures, brown glass is the commonest enclosure in this mineral. The refractive indices and the optic axial angles of the mineral as far as estimated are shown in Table II, according to which the composition of the mineral in the F_{67-b}, F_{67-d}, and Hôei-zan scoria are $Fo_{78}Fa_{22}$, $Fo_{84}Fa_{16}$, and $Fo_{78}Fa_{22}$ respectively.

Groundmass.

The six basalts differ in the crystallinity of the groundmass. The rocks show moreover different crystallinities in their different parts, although generally the groundmass of all the basalts, except F_{67-b}, is hyalocrystalline to dohyaline, consisting of minute plagioclase prismoids, pyroxene and magnetite grains, together with a dark-brown glass base, the proportions of which cannot be measured accurately with the micrometer. Table I shows the percentage of the groundmass calculated by difference. The plagioclase, which is generally less than 0·2 mm long, is either calcic labradorite or sodic bytownite. The pyroxene is usually granular, under 0·1 mm dia. and pale-brown. Although its optical properties could not be accurately determined, it is always of monoclinic variety. The optic axial angle measured on several crystals in a thin section of F_{67-a} was approximately 52°. The groundmass of F_{67-b} is docrystalline to percrystalline, consisting of sodic bytownite (0·05~0·3 mm long), pale-brown monoclinic pyroxene (under 0·1 mm dia.), magnetite granules (0·05 mm dia.), and a little glass. The pyroxene in this groundmass exhibits undulatory extinction. The optic axial angle measured on some crystals of the mineral was 51°, but on others in the same section, 41°. Notwithstanding the high crystallinity of this groundmass, no silica minerals could be detected.

Chemical Characters.

Bulk Composition.

Chemical analysis of the Huzi rock was first made by T. Wada and Korschelt. Another analysis, cited by Wada[4], was made by Luedecke. Although the writer has not seen the original papers, in which these analyses were published, they are not very satisfactory, seeing that Wada had some misgivings in regard to them. A rock specimen collected by Schütt from the wall of the summit crater of the volcano was analyzed by M. Hida under Korschelt's direction. The result of the analysis, Table III, A, which was published by Wada in his paper above referred to, and which showed the basic character of the rock, has since been accepted by many authors, together with those of other Japanese basic volcanic rocks. Recently, S. Kozu[5] published analyses of three rocks (Table III, B, C, D) of the volcano. Of these three rocks analyzed, the basal lava seems to represent one of the older lavas, the term "basal" being used in the same sense as that proposed by H. Ishiwara[6] to cover broadly the older lavas (Hirabayashi's Misima-Ômiya lava, Enkyô lava, etc.) of the volcano. Unfortunately however the locality of the analyzed basal lava is not mentioned by Kozu. Takamarubi is a lava forming a tongue-shaped flow on the N. E. flank of the volcano. The Aokiga-hara lava is the same as that described in this paper.

---

[4] T. Wada, *loc. cit.*

Table III. Old Chemical Analyses of the Huzi Basalts.

	A	B	C	D
SiO_2	49·77	49· 2	49·95	50·57
Al_2O_3	20·57	19·73	18·65	18·67
Fe_2O_3	6·06	4·37	3·70	6·08
FeO	5·11	6·68	8·34	6·15
MgO	5·00	4·07	5·71	5·10
CaO	10·37	10·66	9·82	10·09
Na_2O	1·08	1·38	1·40	1·46
K_2O	0·84	0·78	0·67	0·79
H_2O+	0·73	0·89	0·67	0·70
H_2O-		0·43	0·18	0·20
TiO_2	—	0·21	0·20	0·24
P_2O_5	0·16	0·19	0·22	0·15
MnO	0·20	0·16	0·18	0·14
Total	99·89	99·47	99·69	100·34

A. Summit lava, analyst M. Hida.
B. Basal lava, locality and analyst not stated.
C. Taka-marubi, analyst not stated.
D. Aokiga-hara lava, analyst not stated.

---

[5] S. Kozu, *Bull. Vol. Soc., Japan*, 1 (1933), 13, (in Japanese).

[6] H. Ishiwara, *loc. cit.*

The six basalts now under consideration were chemically analyzed by S. Tanaka of this Institute, with the results shown in Table IV. The table shows that notwithstanding textural and mineralogical variations, no conspicuous difference is found in the bulk compositions of these rocks. The silica percentage is fairly constant, varying from 50·28% in F_{67-a} to 51·30% in the Aokiga-hara lava, and so are also the percentages of the other oxides. In iron-oxides, some variations occur, but the total iron-oxide ($FeO + Fe_2O_3$) is almost the same in all cases.

Table IV. New Chemical Analyses of the
Huzi Basalts, analyst S. Tanaka.

		I	II	III	IV	V	VI	VII
SiO_2		50·28	50·64	50·66	51·05	51·30	51·09	50·84
Al_2O_3		18·30	18·58	18·25	18·35	18·75	17·62	18·31
Fe_2O_3		4·50	3·04	4·78	2·76	1·83	2·64	3·26
FeO		6·89	7·29	5·72	7·72	8·34	8·42	7·40
MgO		3·80	5·58	4·94	4·63	4·80	5·09	4·81
CaO		9·76	10·00	9·98	9·90	9·76	9·68	9·85
Na_2O		2·87	2·64	2·78	2·81	2·55	2·80	2·74
K_2O		0·94	0·61	0·77	0·81	0·71	0·76	0·77
H_2O+		0·20	0·20	0·38	0·40	0·22	0·28	0·28
H_2O-		0·08	0·06	0·13	0·11	0·06	0·06	0·08
TiO_2		1·78	1·15	1·38	1·41	1·43	1·38	1·42
P_2O_5		0·34	0·16	0·25	0·24	0·29	0·26	0·26
MnO		0·20	0·17	0·17	0·18	0·28	0·21	0·20
Total		99·94	100·12	100·19	100·37	100·31	100·29	100·22
Norms								
Q		3·96	1·98	4·14	2·34	2·82	2·04	2·76
Or		5·57	3·34	4·45	5·01	4·45	4·45	4·45
Ab		24·14	22·55	23·59	23·59	21·50	23·59	23·07
An		34·49	36·99	35·05	35·05	37·55	33·38	35·60
Di	$CaSiO_3$	5·11	4·88	5·34	5·23	3·83	5·46	5·26
	$MgSiO_3$	3·01	2·81	3·61	2·81	1·91	2·81	2·91
	$FeSiO_3$	1·85	1·85	1·32	2·24	1·85	2·51	2·11
Hy	$MgSiO_3$	6·42	11·04	8·73	8·73	10·04	9·84	9·03
	$FeSiO_3$	4·62	7·39	3·30	7·65	10·16	8·84	6·86
Mt		6·48	4·40	6·95	3·94	2·55	3·94	4·63
Il		3·34	2·12	2·58	2·73	2·73	2·58	2·73
Ap		0·62	0·31	0·62	0·62	0·62	0·62	0·62

I. Lava F_{67-a}, II. Lava F_{67-b}, III. Lava F_{67-d}, IV. Lava F_{67-e}, V. Aokiga-hara lava, VI. Hôei-zan scoria, VII. Average of the six basalts.

According to the C. I. P. W. quantitative system, they fall under *hessose* (II, 5, 4, 4∼5), with the norms as shown in the same table, which means that the Q/F in them is always smaller than 1/7.

A comparison of Table III and IV shows fairly wide differences in the amounts of some oxids, the amount of Na_2O in Table III being always less than 1·5%, and that in Table IV more than 2·5%; in other words, the normative plagioclase calculated from the old analyses is always less sodic (medium bytownite $Ab_{15}An_{85} \sim Ab_{23}An_{77}$) than that from the new analyses (medium labradorite, see Table V). Thus, although (D) in Table III is the analysis of the same rock as Aokiga-hara lava represented by (V) in Table IV, there is some discrepancy between them; the normative plagioclase of the former ($Ab_{23}An_{77}$) being more calcic than the modal plagioclase phenocrysts ($Ab_{29}An_{71}$) contained in the Aokiga-hara lava, while the normative plagioclase of the latter ($Ab_{36}An_{64}$) is more sodic than this modal one. Moreover, analysis (D), instead of falling under *hessose*, to which the new analysis of the Aokiga-hara lava belongs, does so under *bandose* (II, 4, 4, 4), which means $Q/F > 1/7$. If the two analyses of the Aokiga-hara lava are both correct, these discrepancies are somewhat puzzling, unless we assume that they represent several different facies in the same lava-flow. Since the microscopic characters of the rock specimen represented by analysis (D) have not been published, it is impossible to decide whether or not the specimen differs in microscopic characters from the Aokiga-hara lava described in this paper. In the following discussion, therefore, analysis (V) in Table IV, which seems preferable to the writer, is adopted as correctly representing the chemical composition of the Aokiga-hara lava. Analysis (A) also falls under *bandose*, while (B) and (C) does so under *hessose*.

Table V.

		I	II	III	IV	V	VI
Norm plagioclase		$Ab_{41}An_{59}$	$Ab_{38}An_{62}$	$Ab_{40}An_{60}$	$Ab_{40}An_{60}$	$Ab_{36}An_{64}$	$Ab_{41}An_{59}$
Norm pyroxene	$CaSiO_3$	24	17	22	19	14	18
	$MgSiO_3$	50	57	61	49	49	49
	$FeSiO_3$	26	26	17	32	37	33
$\frac{FeO(+Fe_2O_3)\times 100}{FeO(+Fe_2O_3)+MgO}$		74	64	67	69	68	68

Table V, besides giving the compositions of the normative plagioclase (wt. %) and the normative pyroxene (mol. %), gives also the proportion of the total iron-oxides against magnesia in the six basalts, as calculated from the analyses of Table IV. Although no definite relation can be recognized between the normative plagioclase and the ratio FeO : MgO in the rocks, it is accepted that the amount of $FeSiO_3$ in the normative pyroxene is larger in the younger rocks (IV, V, VI) than in the remaining ones.

Composition of Groundmass.

The approximate chemical compositions of the groundmass of porphyritic rocks will be obtained by subtracting the total amounts of the phenocrystic minerals, whose compositions may be estimated from their optical constants, from the bulk compositions of the rocks. As is clear from Table I, the phenocrysts found in greatest abundance in the Huzi rocks are plagioclase. Although there is usually only a very small amount of mafic phenocrysts in these rocks, olivine predominates over pyroxene, the amounts of which are quite negligible. Table VI gives the results of the subtraction of the plagioclase and olivine phenocrysts from the four rocks–F_{67-a}, F_{67-d}, F_{67-e}, and Aokigahara lavas, all of them containing these phenocrysts. In the table, (I) may depart but little from the actual groundmass composition of the corresponding rock, while the remaining ones represent only approximately the groundmass compositions of the respective rocks, seeing that they contain small amounts of pyroxene phenocrysts that were neglected in the calculation of the groundmass composition. It will be seen at

Table VI. Calculated Groundmass Compositions of the Huzi Basalts.

	I	III	IV	V	X	XI
SiO_2	50·63	51·25	51·57	52·37	51·46	49·70
Al_2O_3	14·87	14·95	14·48	14·51	14·70	14·24
Fe_2O_3	5·81	6·11	3·65	2·51	4·52	3·66
FeO	8·52	6·99	9·88	10·88	9·07	9·96
MgO	4·13	5·41	5·44	5·40	5·10	6·82
CaO	8·54	8·80	8·57	8·11	8·51	9·55
Na_2O	2·85	2·82	2·73	2·52	2·73	2·64
K_2O	1·21	0·98	1·07	0·98	1·06	0·70
H_2O+	0·25	0·49	0·53	0·30	0·39	——
H_2O-	0·10	0·16	0·14	0·08	0·12	——
TiO_2	0·29	1·76	1·86	1·97	1·97	2·23
P_2O_5	0·44	0·31	0·32	0·40	0·34	0·33
MnO	0·25	0·21	0·23	0·38	0·27	0·17

(to be continued.)

Table VI. (*continued.*)

		I	III	IV	V	X	XI
Norms							
Q		6·07	6·37	3·90	5·41	5·35	0·90
Or		7·24	5·57	6·12	5·57	6·12	3·90
Ab		24·12	23·59	23·07	21·50	23·07	22·55
An		24·20	25·59	24·20	25·31	24·76	25·03
Di	$CaSiO_3$	6·27	6·85	6·97	5·19	6·62	8·59
	$MgSiO_3$	3·51	4·52	3·51	2·41	3·61	4·92
	$FeSiO_3$	2·51	1·85	3·30	2·77	2·77	3·30
Hy	$MgSiO_3$	6·73	8·93	10·04	11·04	9·03	12·05
	$FeSiO_3$	5·14	3·43	9·23	12·40	7·39	8·57
Mt		8·33	8·80	5·33	3·70	6·48	5·32
Il		4·40	3·34	3·49	3·79	3·79	4·25
Ap		0·93	0·62	0·62	0·93	0·62	0·62

I. Lava F_{67-a}, III. Lava F_{67-d}, IV. Lava F_{67-e}, V. Aokiga-hara lava, X. Average of the four, XI. Average of 43 plateau basalts, calculated as water free.[7]

any rate that the approximate groundmass composition of Huzi rocks resembles the composition of some plateau basalts (Table VI, XI). Generally speaking, however, the former is more silicic than the plateau basalts from other parts of the world. Compared with the Mull rocks, for example, the groundmass composition of Huzi rocks resembles more the "Non-Porphyritic Central Magma type" than it does the "Plateau Magma type".[8] The rocks of Huzi may be considered to have been derived from a mother liquid more basic than the liquid such as their groundmass would seem to suggest, the relation between these two magmatic liquids being much like that between the two magma types[9] of Mull just mentioned.

Table VII.

		I	III	IV	V	X	XI
Norm plagioclase		$Ab_{50}An_{50}$	$Ab_{48}An_{52}$	$Ab_{49}An_{51}$	$Ab_{46}An_{54}$	$Ab_{48}An_{52}$	$Ab_{48}An_{52}$
Norm pyroxene	$CaSiO_3$	25	25	21	15	22	22
	$MgSiO_3$	48	58	47	46	48	51
	$FeSiO_3$	27	17	32	39	30	27
$\frac{FeO(+Fe_2O_3)\times100}{FeO(+Fe_2O_3)+MgO}$		77	69	71	71	72	66

---

7) R. A. DALY, "Igneous Rocks and the Depths of the Earth", (1933).

8) H. H. THOMAS and E. B. BAILEY, *Mem. Geol. Sur., Scotland*, (1924).

9) N. L. BOWEN, "The Evolution of the Igneous Rocks", Princeton, (1929).

Table VII, besides giving the compositions of the normative plagioclase (wt. %) and the normative pyroxene (mol. %), gives also the proportion of total iron-oxides against magnesia, as calculated from Table VI. It shows that the average groundmass (X) of the rocks of Huzi agrees approximately with the average plateau basalt (XI) in the compositions of both normative plagioclase and pyroxene, except that the former is more ferriferrous than the latter (see Fig. 2).

Comparison of Huzi Basalts with Allied Rocks of the Adjoining Idu District.

In the Idu region, which comprises, in addition to the peninsula of that name, the outlying group of small islands called the Idu Sititô (Seven Idu Islands), are several basaltic volcanoes; Ô-sima, Miyaké-zima, etc., in the Idu Sititô, and the Taga volcano and several parasitic cones of the composite Amagi volcano in the Idu peninsula, all built up of basaltic rocks that erupted either in the Diluvial age or in the Recent. Besides these, there are in the peninsula a number of local lava-flows and intrusive sheets of basaltic nature, ranging in age from Lower Miocene to Pliocene. Upon comparing them with the basalts of Huzi, these basaltic rocks have some characteristic features, microscopical as well as chemical. Without however attempting any detailed discussion of the subject, the writer will now compare the rocks of Huzi with those of the now active Ô-sima volcano as well as of the dormant Miyaké-zima volcano.

S. Tsuboi[10] has offered the view that the basaltic rocks of Ô-sima and Miyaké-zima are genetically related to the rocks of Huzi—a view essentially based on results obtained by means of the optical analysis proposed by him.[11] From the results thus obtained, it is concluded that the porphyritic plagioclase and mafic minerals of the former (Table II) are generally of later stage than these minerals in the latter (Table VIII).

Table VIII.

	I	II
Plagioclase	$Ab_{15}An_{85}$	$Ab_{13}An_{87}$
Hypersthene	n. d.	$n_{1D} = 1{\cdot}6927$ $n_{2D} = 1{\cdot}7000$
Augite	$n_{1D} = 1{\cdot}6865$	$n_{1D} < 1{\cdot}6927$

I. Basaltic bandaite, somma lava of Ô-sima.

II. Miharaite, 1914 lava of the central cone, Mihara-yama, of Ô-sima.

---

[10] S. Tsuboi, *Bull. Earthq. Res. Inst.*, **4** (1928), 131~138.

[11] S. Tsuboi, *ibid.*

A comparison of the rocks of Huzi with the rocks of Ô-sima and Miyaké-zima may be made from the norm contents of these rocks. The normative plagioclase of the former is medium labradorite (Table V), and so is the latter, with the exception of the miharaite, whose normative plagioclase is as calcic as bytownite $Ab_{21}An_{79}$; the normative pyroxene of the former being poorer in $FeSiO_3$ molecule than that of the latter (Fig. 2). The Huzi rocks moreover are distinctly lower in the $FeO(+Fe_2O_3)/MgO$ ratio compared with the rocks of Ô-sima and Miyaké-zima. Another important result from a comparison of the norm contents is that the former is as poor in normative quartz as $Q/F<1/7$, although the latter yields normative quartz to such an extent as $Q/F>1/7$. This fact is partly shown by the actual feature in that none of the Huzi rocks so far observed carry silica mineral such as usually met with in the groundmass of the Ô-sima rocks.[15]

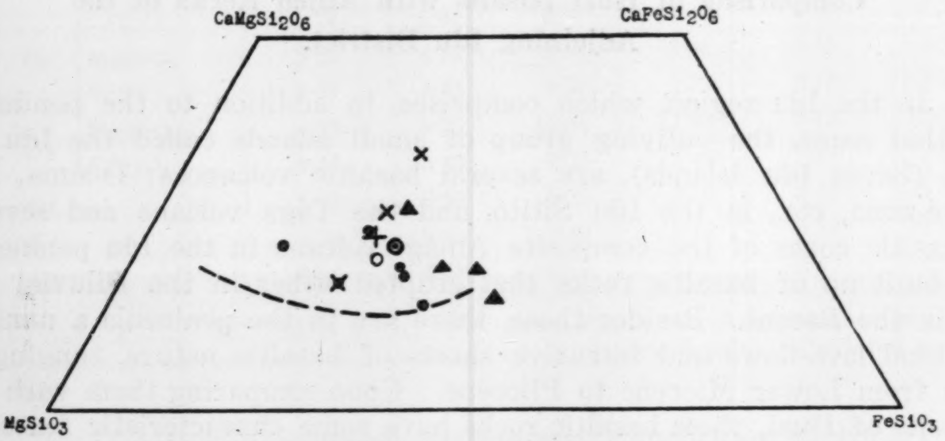

Fig. 2. Compositions of normative pyroxenes in the Huzi basalts and some allied rocks to which reference is made in the text. ● Huzi basalts, ○ Average of the six Huzi basalts, ◉ Average of the groundmass of 4 Huzi basalts, ▲ basaltic rocks of Ô-sima and Miyaké-zima, × "Plateau Magma type" and "Non-Porphyritic Central Magma type" of Mull, + Average of 43 plateau basalts in the world.[12] Broken line represents the two-pyroxene boundary[13] as inferred from pyroxene-andesites and allied rocks in the Idu district.[14]

---

[12] R. DALY, *loc. cit.*

[13] S. TSUBOI, *Jap. Jour. Geol. Geogr.*, **10** (1932), 67~82.

[14] H. TSUYA, *Pan-Pacific Sci. Con., Canada*, (1933), 2394.

[15] H. KUNO, *Bull. Earthq. Res. Inst.*, **11** (1934), 382~390.

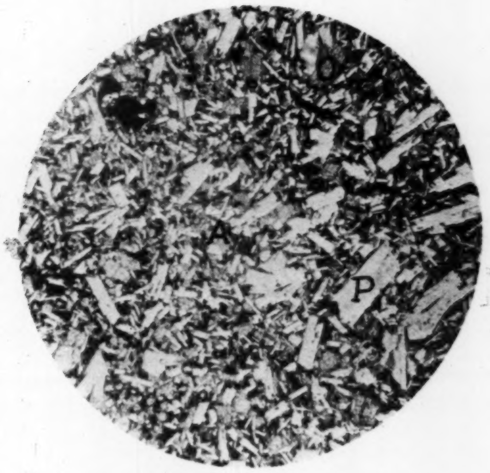

Fig. 3. Groundmass of lava F_{67}–a. A–augite, P–bytownite, O–olivine.

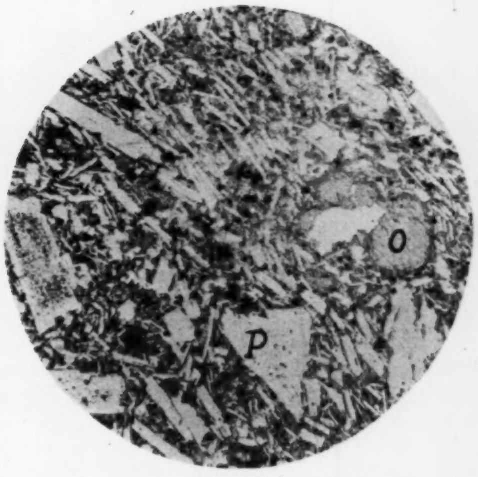

Fig. 4. Lava F_{67}–b. O–olivine, P–bytownite,

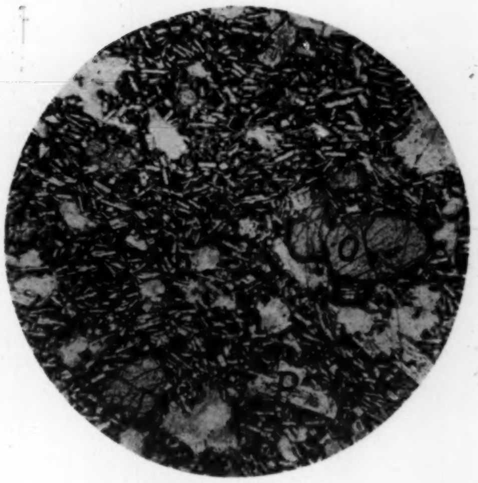

Fig. 5. Lava F_{67}–d. O–olivine, P–bytownite.

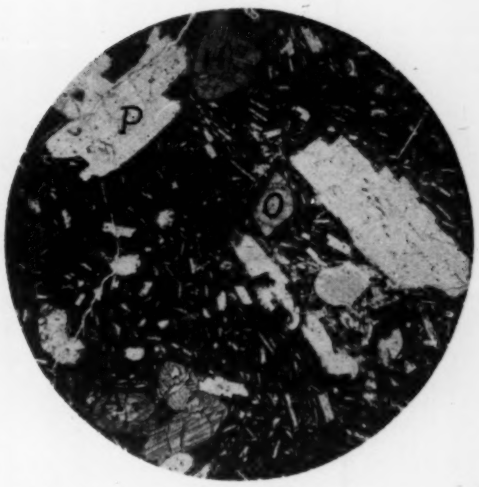

Fig. 6. Lava F_{67}–e. A–augite, H–hypersthene, P–bytownite, O–olivine.

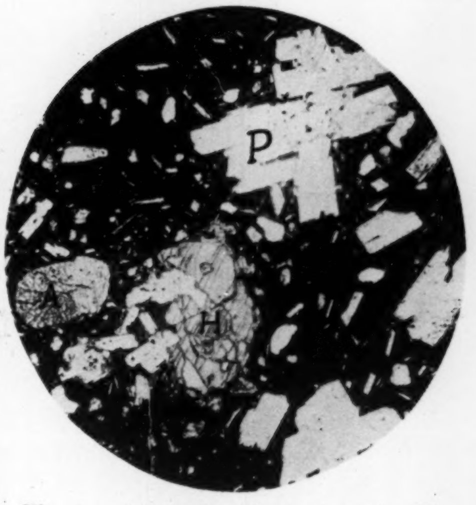

Fig. 7. Aokiga-hara lava. A–augite, H–hypersthene, O–olivine, P–bytownite.

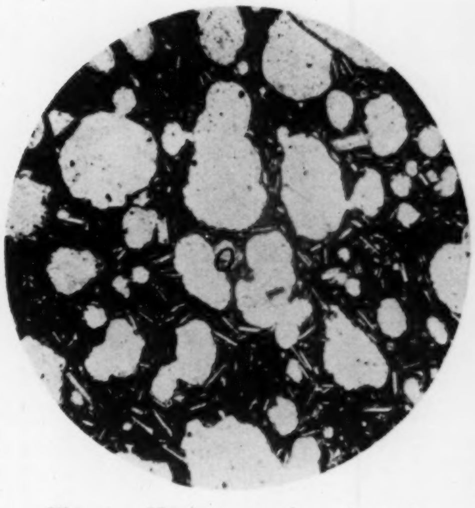

Fig. 8. Hôei-zan scoria. A–augite, O–olivine.

（震研彙報 第十三號 圖版 津屋）

Microphotographs of the Basalts of Huzi (Fuji).
[Magnification in all cases × 15]

51. 富士火山の數種の熔岩に就いて

地震研究所 津屋弘逵

富士火山を構成する熔岩は極めて多數であるが，本文に記載したものは其中次の6種である.

1. 橄欖石・亞灰長石玄武岩（F_{67}-a）
2. 含複輝石―橄欖石・亞灰長石玄武岩（F_{67}-b）
3. 含普通輝石―橄欖石・亞灰長石玄武岩（F_{67}-d）
4. 紫蘇輝石・普通輝石・橄欖石・亞灰長石玄武岩（F_{67}-e）
5. 複輝石・橄欖石・亞灰長石玄武岩（青木原熔岩）
6. 含普通輝石―橄欖石・亞灰長石玄武岩（寶永山岩滓）

以上の中，1乃至4は富士火山の南東腹海拔 1680 m. 附近の幕岩と稱する處に相重なつて露出してゐる. 同處で最も古い熔岩（F_{67}-a）は平林氏の三島・大宮熔岩（震災豫防調査會報告24號，明治 32 年）の1種に似て直徑 1 cm 内外の亞灰長石斑晶を有するものである. 之に次ぐ熔岩（F_{67}-b）は平林氏の大澤熔岩の1種に似て，斑狀構造の著しくない緻密な灰色玄武岩である. 之等は厚さ 10 m 以上の熔岩流をなして露出してゐるが，之等に次ぐ二つの熔岩（F_{67}-d，F_{67}-e）は黑色岩滓質で厚さ 2～3 m の熔岩流をなし，他の同種の二三の熔岩流と相重なり，富士火山の比較的新期の噴出物である. 青木原熔岩は貞觀6年に同火山の北西腹から噴出した熔岩であり，寶永山岩滓は寶永4年寶永爆裂口から拋出された岩滓質熔岩片である. 本文では之等の熔岩に就いて，先づ一般的の顯微鏡的性質を述べ，次に化學分析の結果得られた各熔岩の總化學成分及び此總化學成分と斑晶の化學成分とから推定し得た石基の化學成分に就いて考察し，最後に富士火山熔岩の特性を大島・三宅島等の熔岩の夫と比較論述した.

52. *Arrangement of Micro-Crystals of Calcium Carbonate in Some Fossil Shells,* Glycymeris yessoensis *SOWERBY.*

By Chûji TSUBOI and Morisô HIRATA,

Earthquake Reseasch Institute and
the Institute of Physical and Chemical Research.

(Read May 21, 1935.—Received June 20, 1935.)

It is attempted to study the arrangement of micro-crystals of calcium carbonate in the fossil shells of *Glycymeris yessoensis* SOWERBY by means of X-rays. These fossil shells can be found in Japanese Islands in each of the successive geological formations beginning with Miocene up to the recent. Following seven specimens from different geological formations were examined; (1) Recent, (2) Upper Pleistocence, Susui, Tiba, (3) Lower Pleistocene, Honda, Tiba, (4) Upper Pliocene, Sanukimati, Tiba, (5) Lower Pliocene, Yasuda, Akita, (6) Lower Pliocene, Nagaya, Kanazawa, and (7) Miocene, Kenomaigawa, Hidaka.

Experimental.

It is revealed under microscope that these shells consist of three layers *a*, *b* and *b′* generally, each comprising fine stratifications, as shown in Fig. 1 and the relative thickness of the layers is modified to some extent for different parts of the shell.

A fine beam of X-rays is sent in the direction perpendicular to the specimen cut in the plane perpendicular to the shell surface through its central axis and the diffraction pattern is obtained on the photographic plate placed behind the specimen. The pattern is also obtained in the same way with the specimen cut in the plane parallel to the surface of the shell.

For producing X-rays, a metal tube equipped with copper-anticathode is used. Besides Cu-K radiation, a certain amount of W-L radiation is contained in the X-rays which is due to tungsten sputtered on the anticathode. In the present experiment, however, there is no difficulty in determining whether a certain diffraction ring or spot is due to Cu-K or to W-L.

The degree of dispersion of fibrous arrangement.

It is ascertained from the examination of the X-ray diffraction figures thus obtained that calcium carbonate in the shell of *Glycymeris yessoensis* SOWERBY is in the form of micro-crystals of aragonite and also that they are arranged in fibrous structure, the axis of which being in the direction perpendicular to the stratifications for each layer *a*, *b* or *b′* respectively, while the c-axis of the orthorhombic lattice of aragonite agrees in average with the axis of the fibre. It is to be noticed here that each diffraction spot is elongated along the circular arc with respect to the centre of the diffraction figure as shown in Fig. 11, which is a schematical sketch of the most prominent diffraction pattern due to (021) planes of aragonite lattice. This elongation indicates that a certain amount of fluctuations exists in the orientations of the c-axis of the aragonite lattice in the fossil shells. Thus, the degree of dispersion of these fibrous arrangement, i. e., the range of angle Φ, which the c-axes of aragonite crystals subtend with the axis of fibre (Fig. 12), is estimated for each fossils shells examined and are tabulated in the accompanying table.

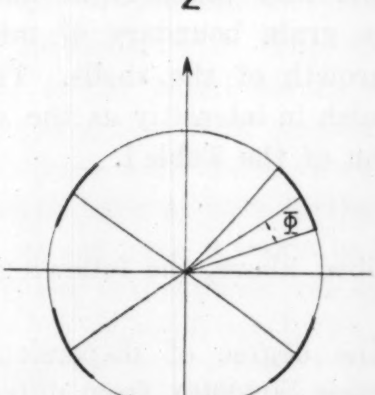

Fig. 11.

Z: Direction of the normal to the stratification.

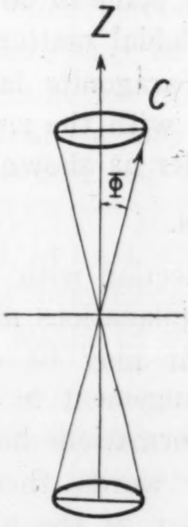

Fig. 12.

Z: Axis of fibrous structure.
C: C-axis of aragonite.

Table I.

Geological epochs and localities	Degree of dispersion of fibrous arrangement, Φ			I. (Middle layer)
	Inner layer	Middle layer	Outer layer	
Recent St. 645.	9°	8·5°		s
Upper pleistocenc Du I, Susui, Tiba.	15	7·5		s
Lower pleistocene Honda, Tiba.	15·8	23		w
Upper pliocene Sanuki, Tiba.	22·5	11·5		ms
Lower pliocene Yasuda, Akita.		13	28°	m
Lower pliocene Nagaya, Kanazawa.		22	31·5	w
Miocene Kenomaigawa, Hidaka.		33	35	w

I: Intensities of the diffractions with smaller angles.
s, strong; m, medium; w, weak.

It is clearly seen that Φ becomes larger as the shell becomes older in geological age. The specimen from Honda which has an extraordinary large value of Φ may be looked upon as exceptional.

The diffraction figure of the shell of Miocene, Hidaka, shows quite different features in comparison with those of other ones (Fig. 9, Fig. 10). A number of discrete Laue-spots are superposed which are due to single crystals of comparatively large dimensions, the largest one of which observed under nicol-microscope being as large as 0·5 mm in diameter. It is also remarkable that some traces of stratifications are kept still distinctly in this Miocene shell (Fig. 3, Fig. 4).

Diffractions with smaller angles.

There are some prominent diffractions with smaller diffraction angles, especially for the middle layer of the shell. They correspond to the molecular periodicity of about 8·4 Å in the direction perpendicular to (021) plane of aragonite crystal, and may probably be due to some biocolloidal matter deposited on the grain boundary of micro-crystals of aragonite in the course of growth of the shells. These diffractions with the smaller angles diminish in intensitiy as the shell becomes older as shown in the last column of the Table I.

Discussion.

In connection with the results described above, the following alternative explanations may be proposed.

First, it may be considered that the degree of dispersion of fibrous arrangement in *Glycymeris yessoensis* SOWERBY from different geological formations had been different in their original living states, or in other words, these fossil shells had not suffered any serious change so far as the arrangement of micro-crystals are concerned in spite of the long geological aging. Dr. Jinzo Tsutsumi[1] examined the arrangements of calcium carbonate for a number of different species of living moluscan shells by means of X-rays and showed that the micro-crystals of calcite or aragonite are in fibrous arrangement, the degree of dispersion of which being a characteristic property for each species. In the present case, therefore, it may not be quite absurd to make such an assumption described above, although without any positive proof.

If we assume next, that the structure of the shells had been the same initially, then the observed changes in the diffraction figures may be looked upon as the effect of aging which the shells had suffered.

---

[1] J. TSUTSUMI: *Memoirs Coll. Sci., Kyoto Imp. Univ.*, [A], **12** (1929), 199.

The shell has not an isotropic structure, but has distinct stratifications as shown above and the elastic properties should, accordingly, be different for different directions. Thus, if the shell with such a structure be put under external stresses, the heterogeneous strain will be developed within it even if the stress be hydrostatical. It is well known that when some polycrystalline metal sheet such as one of alminium is rolled, rearrangements of micro-crystals take place, with the result that a certain axis of the crystal lattice is arranged fibrously in the direction parallel to that of rolling. In the course of aging of fossil shells, nearly the same process of rearrangement of micro-crystals may take place.

There is still another possibility for explaining the rearrangement of micro-crystals in the shells even if any sensible effect of external stress had not existed; namely, if some reagent existing in the boundaries of micro-crystals that is capable of restricting the orientation of each of the micro-crystals to assume the fibrous arrangement, be lost gradually with time, then some disturbances may be expected to occur in the initial fibrous structure. The diminution in intensity of the diffraction with smaller angles described above may be in good accordance with these views. Recrystalizations may also be taken into account, such as seen in the shell of Miocene.

At any rate, it seems to be interesting that, at least with the shells examined in this paper, the age of the geological formations from which they are collected can be roughly estimated by means of some physical method.

The authors express their sincere thanks to Professor T. Terada for his kind suggestions and criticisms on this work, and also to Dr. Y. Otuka who placed the specimens of the fossils examined at our disposals.

52. エゾタマキガヒの化石介殼内に於ける微結晶の配列

地震研究所　坪井忠二
理化學研究所　平田森三

エゾタマキガヒの化石は最近の各地質時代の地層から得られるので，我々は其の介殼の中の微結晶の配列が化石の古さによつて如何に變化するものであるかを X-線によつて調べたのである．調べた標本は

（1）現　　代
（2）上部洪積統（千葉縣酒々井）
（3）下部洪積統（千葉縣響田）
（4）上部鮮新統（千葉縣佐貫）
（5）下部鮮新統（秋田縣安田）
（6）下部鮮新統（石川縣長屋）
（7）中　新　統（北海道慶能舞川）

からのものである．

先づ顯微鏡下で見ると Fig. 1 の樣に介殼は一般に 3 つの層よりなり，その各々にこまかい縞がある事が解る．

用ひた X-線は Cu-K 線であるが，對陰極に着いてゐるタングステンによる W-L 線も少しは混じて居る．然しこれは邪魔にはならない．X-線寫眞は Fig. 5～Fig. 10 に示した通りのもので，これによつて此の介殼の中では各層ともに，霰石の微結晶が集つたものであつて，其の C 軸が前述の縞目に略垂直に揃つて並んでゐる所謂纖維構造をなしてゐる事が解つた．但し寫眞で見られる樣に X-線廻折像は圓弧に沿つて延びて居るが，之は Fig. 12 に示した通り C 軸の方向に Φ だけの不同がある事を示すのである．Fig. 11 の如くにして此の Φ を寫眞から讀み取り表にしたものが Table I である．表で明らかなる樣に Φ の値は古い化石程大きくなつて居る．換言すれば纖維構造の規則正しさが次第に失はれて行くのである．

倘注意すべきは，霰石による廻折像以外に中心點近くに別の廻折像がある事で (Fig. 6)，これは 8·4Å と云ふ大きい間隔を持つた格子面に相當するから恐らく霰石の微結晶の間にある何等かの Biocolloid に由來するものであらう．此の廻折像の强度は古い化石程弱い．

以上の事柄を説明するには色々な方法があらう．第一に今日化石として產するエゾタマキガヒは，それが生きてゐた時から旣に微結晶の配列に於いて現生のものと違つて居たとしても差支ない．第二に斯樣な方向性を持つてゐる介殼が永い間地下に埋れて地壓を受けて居る間に微結晶の配列が變化して來ると云ふ事も考へられる．又第三には微結晶の間に何か Biocolloid があつて，その作用によつて微結晶が纖維構造を保つて居るのが，介殼の死後此の有機物質が次第に分解して仕舞つて微結晶の配列を束縛する事が出來なくなる爲，纖維構造の規則正しさが失はれて行くと考へても差支ない．この考は前述の中心角の小さい廻折像が地質年代と共に强度が弱くなる事ともよく協調する．

説明方法は何れにせよ，少くともエゾタマキガヒではその地質年代の古さが此の樣な物理的方法で，凡そ判定されるのは注意すべき事と思はれるのである．

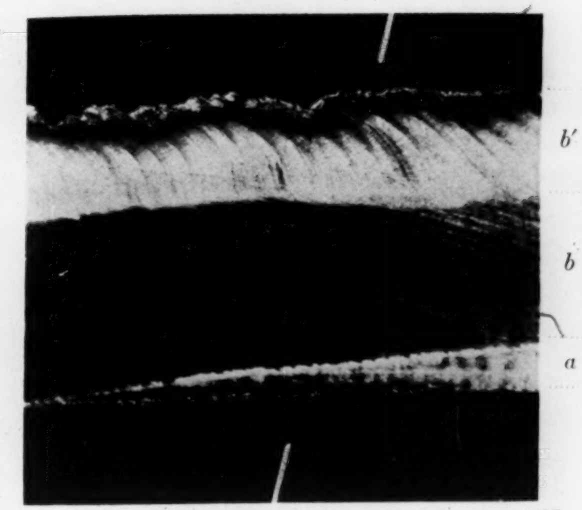

×15

Fig. 1. Structure of the shell of recent. Between crossed nicols.

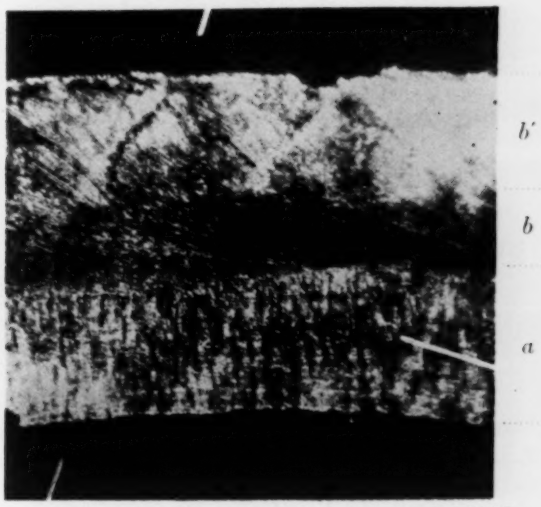

×15

Fig. 2. The shell of lower pliocene. Between crossed nicols.

（震研彙報 第十三號 圖版 坪井・平田）

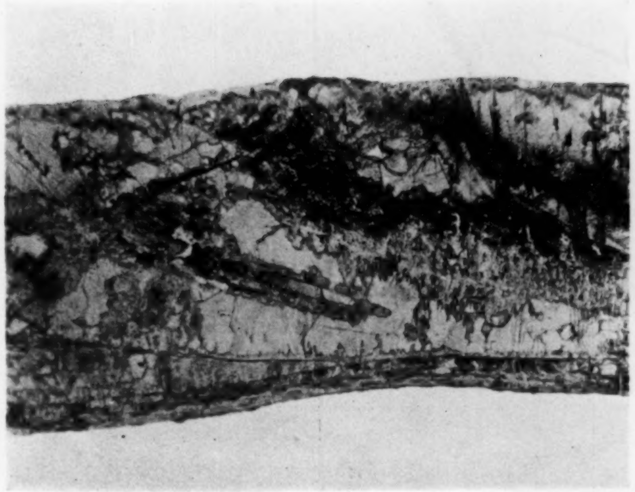

×15

Fig. 3. The shell of miocene.

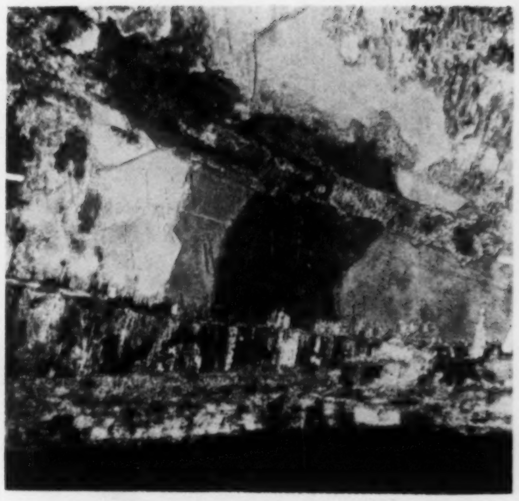

×41

Fig. 4. Single crystals developed in the shell of miocene. Between crossed nicols.

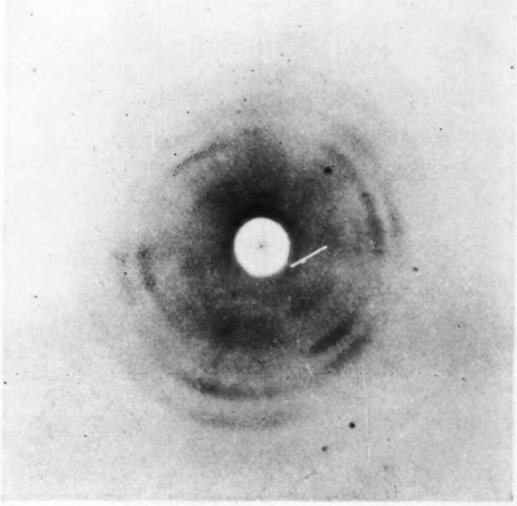

Fig. 5. Specimen 1. Inner layer.

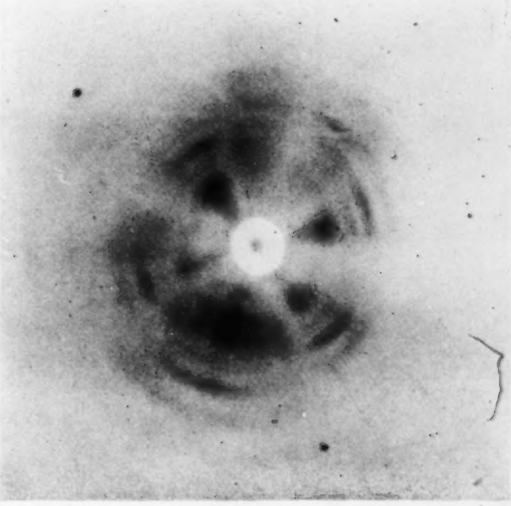

Fig. 6. Specimen 1. Middle layer.

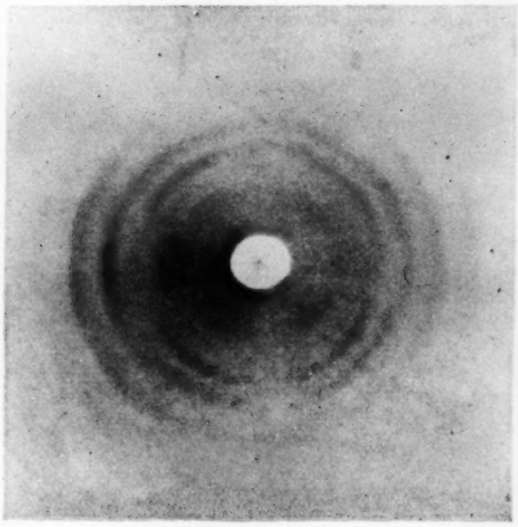

Fig. 7. Specimen 6. Inner layer.

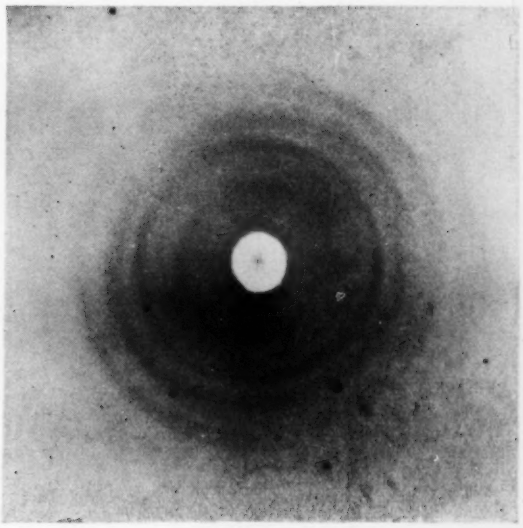

Fig. 8. Specimen 6. Outer layer.

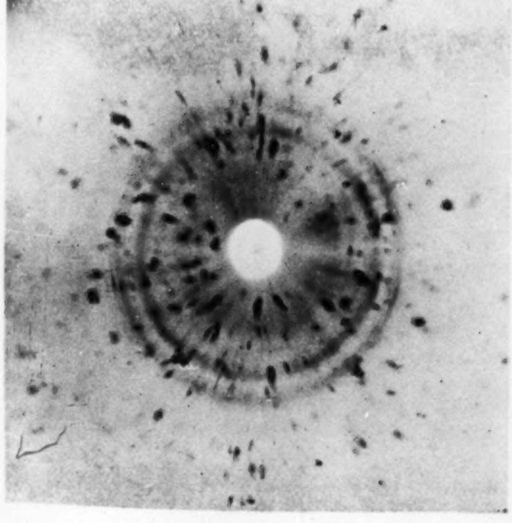

Fig. 9. Specimen 7. Inner layer.

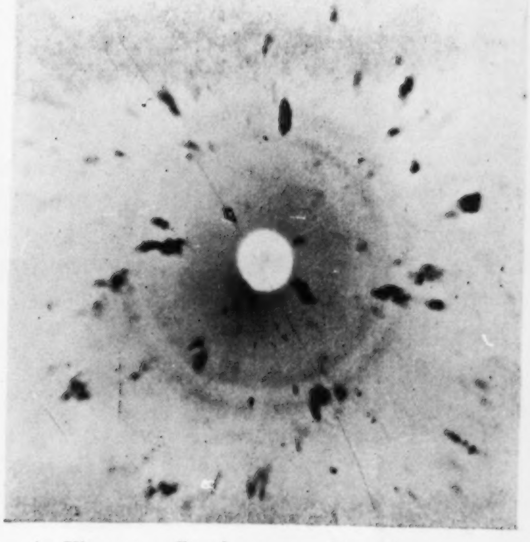

Fig. 10. Specimen 7. Outer layer.

（震研彙報 第十三號 圖版 坪井・平田）

53. *Changes in Rigidity and Internal Friction of Amorphous Silica with Temperature.*[*]

By Kumizi IIDA.

(Read April 16, 1935.—Received June 20, 1935.)

1. Introduction. The changes in the form of seismic waves in the earth's crust and the decay of these waves as the result of internal friction of the materials composing it are familiar matters. These problems, first treated theoretically by Prof. H. Nagaoka,[1] were later studied by Prof. K. Sezawa[2] and other investigators,[3] and the relations of the velocities of seismic waves, to Young's modulus, rigidity, and density of the materials composing the earth's crust were obtained from observations of seismic waves by a number of investigators, whose studies however will not be described here. With the desire to attack such problems as the internal friction and the rigidity and elasticity of materials from the experimental side, the writer carried out the experiments described in this paper.

The form of the materials composing the earth's crust may either be amorphous or complicated crystals. In order to know the properties of such material, amorphous silica was selected as being readily accessible and easily worked. The properties of vitreous silica, its density, rigidity, Young's modulus, etc., have already been ascertained.[4] The modulus of torsional rigidity of quartz fibre was first investigated by Boys,[5] and later by Threlfall,[6] Barnett,[7] Guye and Fréedericksz,[8] and Horton.[9] The most precise measurements of rigidity of vitreous silica are those of F. Horton, who, by means of the method of oscillation of loaded fibre, measured its rigidity between temperatures 20° and

---

[*] Communicated by M. Ishimoto.

[1] H. NAGAOKA, *Proc. Phys.-Math. Soc., Japan*, **3** (1906), 17.

[2] K. SEZAWA, *Bull. Earthq. Res. Inst.*, **3** (1927), 43; *ibid.*, **10** (1932), 19.

[3] For example, B. GUTENBERG, *Phys. z. s.*, **30** (1929), 230.
N. M. HOSARI, *Proc. Roy. Soc.*, **104** (1923), 271.

[4] R. B. SOSMAN, "*The Properties of Silica,*" U. S. A. (1927).

[5] C. V. BOYS, *Phil. Trans. Roy. Soc., London*, **186** (1895), 65.

[6] R. THRELFALL, *Phil. Mag.*, **30** (1890), 99.

[7] S. J. BARNETT, *Phys. Rev.*, **6** (1898), 114.

[8] C. E. GUYE and V. FRÉEDERICKSZ, *Arch. Sci. Phys. Nat.*, **29** (1910), 49

[9] F. HORTON, *Phil. Trans. Roy. Soc., London*, **204** (1905), 407.

1058°C. He also observed the logarithmic decrements of the oscillations of quartz fibre. Similar measurements have also been made by Guye and Morein.[10]

The nature of internal friction in metals has received the attention of a number of workers, such as Honda and Konno,[11] Iokibe and Sakai,[12] Sezawa and Kubo,[13] Ishimoto,[14] Barus,[15] Voigt,[16] Cady,[17] Horton,[18] Higuchi,[19] and Itihara.[20] The values of the coefficients of internal friction (the normal viscosity) of metals obtained by Honda and Konno are of the order of 10^8 in C. G. S. units at room temperature, while those obtained by Sezawa and Kubo are so small as to be of the order of 10^6 in the same units.

The objects of the experiments described here were to gain some knowledge with respect to the geophysical problems just mentioned, to test whether damping is proportional to the velocity of the deformation of the substance, and also whether or not the internal friction of quartz fibre is similar to that of metals.

2. Methods of Experiment. The quartz fibre experimented on were drawn from a bar of quartz, the chemical analysis of which, in bulk composition, was

SiO_2 99·95 wt. %, Al_2O_3 trace,

which shows that the article was fairly pure. Great care was taken in making them in order to get them free of air bubbles and to obtain a true circular cross-section. The dimensions of the tested quartz fibre are shown in Table I. The diameters were measured by a micrometer with an accuracy of 1/100 mm, and their lengths by a calliper of an accu-

Table I. Dimension of Quartz Fibres.

No.	Radius, r. (cm)	Length, l. (cm)
1	$18{\cdot}52\times10^{-3}$	10·15
2	28·05 ″	10·00
3	42·45 ″	11·93
4	51·17 ″	12·36
5	65·40 ″	9·74

---

[10] C. E. GUYE and A. MOREIN, *Arch. Sci. Phys. Nat.*, [v], **2** (1920), 350.

[11] K. HONDA and S. KONNO, *Phil. Mag.*, **42** (1921), 115.

[12] K. IOKIBE and S. SAKAI, *Phil. Mag.*, **42** (1921), 397.

[13] K. SEZAWA and K. KUBO, *Rep. Aeron. Res. Inst., Tokyo,* **7** (1932), 198.

[14] M. ISHIMOTO, *Proc. Phys.-Math. Soc., Japan,* [iii], **1** (1919), 267.

[15] C. BARUS, *Phil. Mag.*, **29** (1890), 337.

[16] W. VOIGT, *Wied. Ann.*, **47** (1892), 671.

[17] W. G. CADY, *Phys. Rev.*, **15** (1920), 146; **19** (1922), 1.

[18] F. HORTON, *Phil. Trans. Roy. Soc., London,* [A], **204** (1905), 1~55.

[19] S. HIGUCHI, *Tech. Rep. Tohoku Imp. Univ.*, **10** (1931), 506.

[20] M. ITIHARA, *Trans. Soc. Mech. Eng.*, **1** (1935).

racy of 1/10 mm.

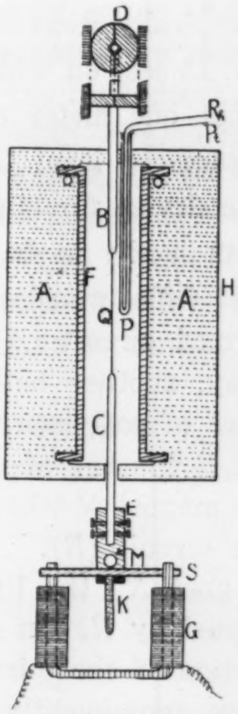

Fig. 1. Sketch of the apparatus.

A, asbestos; B, C, quartz rods; Q, quartz fibre; F, electric furnace; M, lens mirror; E, brass rod; H, tin-plate box; S, soft iron plate; G, electromagnet; P, porcelain tube; K, screw; D, brass clamp, which is divisible into two parts; P_t and R_h are wires of the thermo-couple.

(*a*) *The First Experiments.* The apparatus used is shown in Fig. 1. The quartz fibre *Q* was firmly welded at both its ends to the two quartz rods *B* and *C*, about 8 mm dia. and 20 cm long. The upper end of *B* was firmly wedged in between the two brass clamps *D*, which itself could be firmly clamped by means of other clamps. The lower end of *C* was affixed by means of screws to the brass rod *E*, which, with the soft iron plate *S*, 5·8 cm × 1·4 cm × 0·4 cm, forms the vibrator. To increase the moment of inertia of the vibrator, weights can be attached to the brass rod *E* by means of the screw *K*.

F is an electric furnace, 5 cm internal diameter and 30 cm long, capable of being separated into two parts. Nichrome wires are wound along the longitudinal axis of the inner side of the furnace, which latter is heated by means of an alternating current, 100 volts and 9 amperes, its temperature being measured by means of a thermo-couple consisting of wires of platinum and rhodium. The lower end of the porcelain tube *P* in which these two wires are placed, is situated near the middle of the quartz fibre *Q* to be tested. The temperatures were read off from a millivoltmeter, which was standardised by taking the melting points of such substances as Cu, Ni, Al, Pb, etc., and the boiling point of water. The furnace is placed in a tin-plate box *H*, 35 cm × 17 cm × 17 cm. To prevent heat loss from the furnace, asbestos was packed in the space between the furnace and the box. The temperature, after being raised slowly from that of the room to about 1100°C, was then allowed to cool. The torsional oscillations of the specimen were observed during both rise and fall of the temperature.

The vibrator was set in oscillation by the following device: A momentary current passing through the electromagnet *G*, turns the soft iron plate *S* and sets the specimen in torsional oscillation. The position of the electromagnet was carefully adjusted so as not to cause any lateral vibration of the specimen. The oscillations of the soft iron plate S over the magnet may be the cause of the damping, but since the residual magnetism is very small, its action may be ignored.

A small lens mirror M attached to the brass rod E enables observation of the torsional oscillations. The motion of the mirror is photographically recorded on a rapidly rotating drum (40 cm circumference, rev. 13 sec) on which a bromide paper is wound, and which is placed about one meter distant from the lens mirror M. An electric lamp (motor-car head light) of 10 v. 3·3 amp. serves as the light source. The device for obtaining the period of the oscillations causes the light from a slit to be cut off every 0·5 seconds. A chronometer and a Post Office standard relay was used, and this connected to a battery, formed circuit (A). We made another circuit (B) by means of the relay, another battery, and the solenoidal coil L in Fig. 2. N is a piece of soft iron magnetised by the solenoid L; R the bar of soft steel that is drawn to the magnet N when the current flows through the circuit (B). When R is drawn to the magnet N, the light from slit X is interrupted by R. In the record produced by the motion of the mirror M, many broken points were consequently observed. From the intervals of these points the length of the period of the oscillations was calculated.

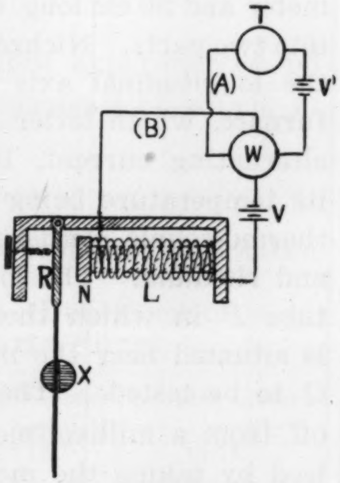

Fig. 2. Arrangement of the timing apparatus.

N, piece of soft iron; L, solenoid coil; R, bar of soft iron; T, chronometer; W, Post Office standard relay; V, battery; X, slit; (A),(B), circuits.

(*b*) *The Second Experiments.* As the result of both internal friction and air resistance, the amplitude of oscillations gradually diminishes. Since we wished to know the internal friction of the specimen, we had to observe the effects of air resistance. To achieve this purpose the second experiment was made with the above described oscillating system enclosed in a bell-jar of thick glass resting tightly on a plane disk. The bell-jar was evacuated by a Gaede rotary pump, by means of which the pressure in the bell-jar was reduced, the lowest value of which was about 1 mm. The pressure is measured with a mercury manometer connected to the bell-jar. The experiments were conducted under different pressures and with different sizes of fibre. We obtained the relation between the logarithmic decrement of the oscillation and the pressure in the bell-jar. Such experiments as those of the bell-jar should, strictly speaking, be made also at temperature ranges of 20°∼1100°C, but to simplify matters they were performed at the room temperature of 20°C. In this way the modulus of rigidity and the coefficient of internal friction were measured.

3. Results of the Experiments. Some examples of actual photographs of torsional oscillations obtained by the apparatus are shown in Fig. 3. It will be seen from these records that the oscillations of this system are of the regular sine wave form with diminishing amplitude. It will also be noticed that since the amplitudes of the oscillations rapidly diminish at high temperature, the logarithmic decrements are great. At over 1000°C the internal friction of the fibre was so great that the oscillations were nearly dead-beat. The internal friction of the fibre is calculated from the logarithmic decrement of the oscillations as follows:

If v be the velocity of a fluid moving in the direction of x, and z an axis perpendicular to x, then the tangential (ordinary) viscosity and the normal viscosity per unit area are given by

$$\left.\begin{aligned} f_t &= \eta\frac{dv}{dz}, \\ f_n &= \xi\frac{dv}{dx}, \end{aligned}\right\} \tag{1}$$

respectively, where η and ξ are the coefficients of tangential and normal viscosity respectively. If resistance be represented by ordinary formula, the equation of motion of this torsional system at any time t is given by

$$I\frac{d^2\theta}{dt^2}+\epsilon\frac{d\theta}{dt}+k\theta=0, \tag{2}$$

where θ is the angle of twist, I the moment of inertia of the attached body, and ϵ, k are two constants depending on the dimensions and the nature of the suspended substance.

If l and r be the length and radius of the specimen respectively, and n its rigidity modulus, we would have the relations[21]

$$k=\frac{\pi n r^4}{2l}, \qquad \epsilon=\frac{\pi\eta r^4}{2l}. \tag{3}$$

The solution of equation (2) is given by

$$\theta=\theta_0 e^{-\frac{\epsilon t}{2I}}\cos\left(\frac{2\pi t}{T}+\alpha\right), \tag{4}$$

---

[21] K. Honda and S. Konno, *loc. cit.*

where θ_0 is the initial amplitude of oscillation, T the period of oscillation, and α a constant.

If λ be the logarithmic decrement of the oscillation, we would have

$$\lambda=\frac{\epsilon T}{4I}=\frac{\pi\eta r^4 T}{8Il},$$

$$\eta=\frac{8Il\lambda}{\pi r^4 T}. \tag{5}$$

Hence, by observing λ and T, η can be determined. For the modulus of torsional rigidity of the specimen, we have

$$n=\frac{8\pi Il}{T^2 r^4}, \tag{6}$$

whence

$$\frac{n}{\eta}=\frac{\pi^2}{T\lambda}. \tag{7}$$

By observing the period of the torsional oscillations the modulus of rigidity n can be calculated if the values of I, l, and r are all constant. The values of n and the observed logarithmic decrement λ, calculated from the observed periods and amplitudes of torsional oscillations at each temperature, are shown in Tables II∼IV, and some examples in Figs. 4∼7. In these figures, n and λ are taken as ordinates and the temperature as abscissa.

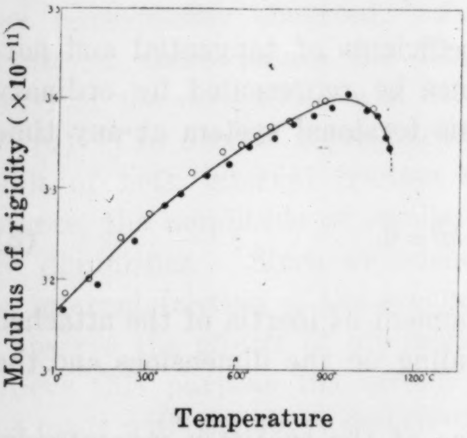

Fig. 4. Curve showing the change in rigidity of amorphous silica fibre with temperature.
Radius of fibre$=18{\cdot}52\times10^{-3}$ cm, length 10·15 cm.
●, heating; ○, cooling.

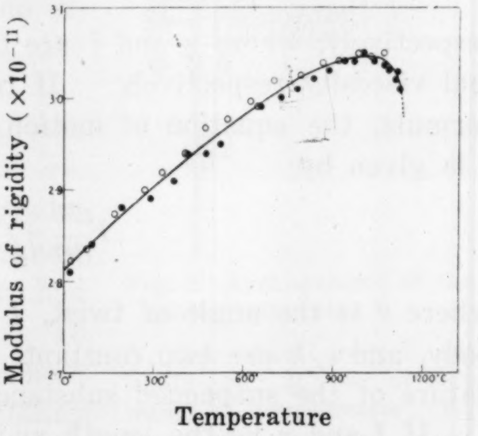

Fig. 5. Curve showing the change in rigidity of amorphous silica fibre with temperature.
Radius of fibre$=65{\cdot}4\times10^{-3}$ cm, length 9·74 cm.
●, heating; ○, cooling.

Since up to a temperature of about 200°C, the rigidity of the fibre increased with temperature as a linear function of it, we may assume

Table II. Modulus of Rigidity and Coefficient of Internal Friction of Amorphous Silica Fibre.

(Radius of the fibre $r=18{\cdot}52\times10^{-3}$ cm, length $l=10{\cdot}15$ cm)

Temp. (°C)	Frequency	Logarithmic decrement $\lambda\times10^3$	Modulus of rigidity n(c. g. s.)$\times10^{-11}$	Coeff. of internal friction η(c. g. s.)$\times10^{-9}$
21·9	1·152	0·60	3·16	4·18
138	1·157	0·72	3·19	4·30
225	1·177	0·68	3·24	4·75
360	1·179	0·69	3·28	4·83
419	1·176	0·75	3·30	5·34
505	1·180	0·78	3·32	5·51
579	1·182	1·10	3·33	7·74
649	1·185	1·56	3·35	10·99
722	1·187	2·62	3·36	18·45
789	1·189	4·50	3·37	31·74
848	1·189	7·13	3·38	50·32
922	1·192	12·77	3·39	90·41
973	1·196	17·94	3·41	127·42
1032	1·192	27·24	3·39	192·89
1073	1·190	39·64	3·37	280·18
1095	1·187	52·04	3·36	366·89
1112	1·185	64·32	3·35	452·72
895	1·194	6·77	3·40	48·01
840	1·196	2·77	3·39	19·65
777	1·193	1·75	3·38	12·34
710	1·192	1·07	3·37	7·60
664	1·193	0·89	3·36	6·32
611	1·190	0·86	3·35	6·10
544	1·185	0·79	3·34	5·54
445	1·183	0·61	3·32	4·29
313	1·170	0·63	3·27	4·37
214	1·167	0·62	3·24	4·33
110	1·159	0·63	3·20	4·58
30	1·155	0·62	3·18	4·30

Table III. Modulus of Rigidity and Coefficient of Internal Friction of Amorphous Silica Fibre.

(Radius of the fibre $r=51.17\times10^{-3}$ cm, length $l=12.36$ cm)

Temp. (°C)	Frequency	Logarithmic decrement $\lambda\times10^3$	Modulus of rigidity n(c. g. s.)$\times10^{-11}$	Coeff. of internal friction η(c. g. s.)$\times10^{-5}$
21	7·625	0·50	2·79	4·72
105	7·620	0·49	2·79	4·61
176	7·691	0·33	2·84	3·19
232	7·733	0·35	2·87	3·39
293	7·765	0·28	2·89	2·66
370	7·769	0·29	2·90	2·76
435	7·800	0·33	2·92	3·23
494	7·800	0·40	2·93	3·89
547	7·826	0·40	2·94	3·90
592	7·826	0·38	2·95	2·92
639	7·846	0·49	2·95	4·75
692	7·857	0·66	2·96	6·41
725	7·875	0·92	2·98	8·97
764	7·882	1·32	2·98	12·91
805	7·888	2·04	2·99	20·00
855	7·889	3·58	3·00	35·09
906	7·894	5·74	3·01	56·24
942	7·924	8·35	3·02	82·11
966	7·940	10·74	3·02	105·77
990	7·954	13·82	3·04	136·41
1009	8·000	16·22	3·03	161·03
1029	7·961	17·38	3·04	171·71
1053	7·950	24·15	3·03	238·25
1075	7·939	29·01	3·02	284·71
1090	7·925	34·26	3·01	336·56
1100	7·927	36·36	3·01	357·67
1116	7·916	42·88	3·00	421·28
1119	7·905	42·66	3·00	418·48
1062	7·960	27·25	3·04	269·18
984	7·960	10·79	3·04	109·07
900	7·944	4·58	3·02	45·15
822	7·920	2·01	3·01	19·76
762	7·900	1·08	2·99	10·59
701	7·881	0·87	2·98	8·55
638	7·860	0·65	2·96	6·33
570	7·840	0·51	2·95	4·39
400	7·794	0·36	2·91	3·50
338	7·800	0·40	2·91	3·95
262	7·769	0·32	2·89	2·10
181	7·739	0·35	2·87	2·44
125	7·714	0·34	2·86	3·22
63	7·690	0·25	2·84	3·00
19	7·625	0·24	2·79	2·33

Table IV. Modulus of Rigidity and Coefficient of Internal Friction of Amorphous Silica Fibre.

($r=65{\cdot}40\times10^{-3}$ cm, $l=9{\cdot}74$ cm)

Temp. (°C)	Frequency	Logarithmic decrement $\lambda\times10^3$	Mod. of rigidity n(c. g. s.)$\times10^{-11}$	Coeff. of internal friction η(c. g. s.)$\times10^{-5}$
20·8	13·833	0·16	2·81	0·82
94	13·900	0·18	2·84	0·89
192	14·000	0·20	2·88	1·03
291	14·000	0·18	2·89	0·93
370	14·081	0·18	2·91	0·95
413	14·130	0·20	2·94	1·05
477	14·133	0·26	2·94	1·37
525	14·176	0·25	2·95	1·28
605	14·095	0·31	2·96	1·62
661	14·266	0·44	2·99	2·29
719	14·307	0·74	3·01	3·89
780	14·316	1·28	3·01	6·70
817	14·350	2·24	3·03	11.76
886	14·363	3·55	3·03	18·66
940	14·355	5·53	3·03	29·05
972	14·378	6·79	3·04	35·73
1004	14·527	8·71	3·06	40·71
1039	14·356	10·53	3·05	55·50
1067	14·372	13·12	3·04	69·01
1082	14·394	15·37	3·04	80·99
1098	14·404	17·59	3·03	92·66
1108	14·392	19·22	3·02	101·31
1117	14·370	22·56	3·01	118·65
1116	14·382	22·18	3·04	116·77
1070	14·413	14·73	3·05	77·70
1025	14·371	9·04	3·05	47·55
984	14·419	5·84	3·06	30·84
920	14·382	3·08	3·04	16·20
845	14·400	1·47	3·04	7·73
772	14·353	0·72	3·03	3·79
707	14·380	0·42	3·02	2·21
653	14·250	0·32	2·99	1·65
626	14·353	0·19	3·00	1·00
544	14·285	0·23	2·98	1·22
471	14·266	0·19	2·97	0·98
410	14·100	0·19	2·94	0·99
327	14·087	0·18	2·93	0·90
270	14·091	0·19	2·92	0·99
167	14·000	0·20	2·88	1·06
81	13·882	0·21	2·83	1·07
21	13·857	0·18	2·82	0·92

that change of rigidity with temperature obeys some such linear law as

$$n_t = n_0(1+\alpha t).$$

It is possible therefore to determine the temperature coefficient α of the modulus, n_0 and n_t being the values of the modulus of the rigidity at 0°C and t°C respectively. From the straight lines drawn in these figures, the values of coefficient α of the modulus are as in the subjoined table.

No.	Radius $r\times10^3$cm	Temp. coeff. α	Mean value of α
1	18·52	0·000109	0·000111
2	28·05	0·000110	
3	42·45	0·000113	
4	51·17	0·000108	
5	65·40	0·000113	

Observer	Value of α
Boys	——
Threlfall	0·000128
Barnett	0·000115
Horton	0·0001235

The mean values of temperature coefficient α between 15°C and 100°C as obtained by other observers have been brought together in the preceding table, from which it will be seen that there are considerable differences in the values of α obtained by different observers. The mean value of α obtained from the present experiments is nearest the result obtained by Barnett. The fibre used by us were much thicker than those used by either Horton or Threlfall.

With rise of temperature the rate of increase gradually diminished, maximum rigidity being attained at about 1000°C. After passing this temperature, rigidity diminished with increase of temperature. The temperature at which the rigidity of the fibre reaches maximum differs slightly with different fibres. Reduction in the diameter of the fibre seems to demand a lower temperature for attaining maximum rigidity. The smaller the diameter of the fibre the larger is their modulus of rigidity. Generally speaking, the modulus of rigidity of the fibres after annealing is larger than that before annealing.

The logarithmic decrement of the torsional oscillations increased with temperature at a rate, which although at first was constant, became much more rapid after about 600°C was reached (Figs. 6, 7). In order to ascertain what part of the observed logarithmic decrement was due to the viscosity of the fibres, another experiment, similar to that just described in the preceding section, was resorted to by using different fibres in the bell-jar. An example of the relation between the logarithmic decrement of the oscillations, without the effect of the air-damping and the pressure in the bell-jar, is shown in Fig. 8. We take the common logarithm of $\sqrt{\lambda_0-\lambda_a}$ and λ_0 as ordinate and the pressure p as

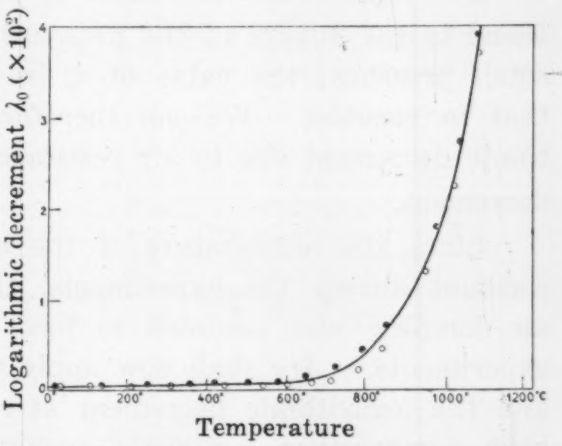

Fig. 6. Relation between observed logarithmic decrement λ_0 of the oscillation and temperature.

The values of λ_0 in the case of cooling are smaller than that in the case of heating.

Radius of the fibre $r=18{\cdot}52\times10^{-3}$ cm.

●, heating; ○, cooling.

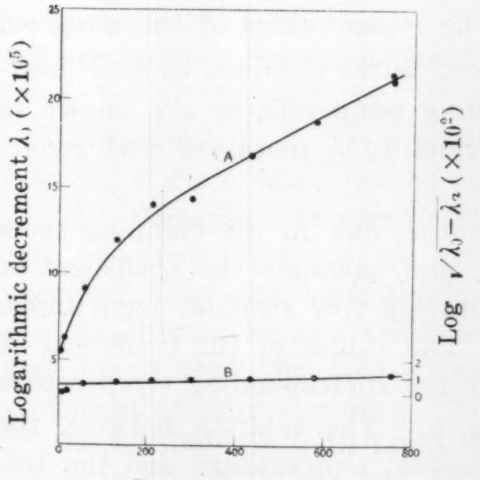

Fig. 8. A. Relation between logarithmic decrement λ_0 and pressure in the bell-jar.

B. Relation between log $\sqrt{\lambda_0-\lambda_a}$ and pressure in the bell-jar.

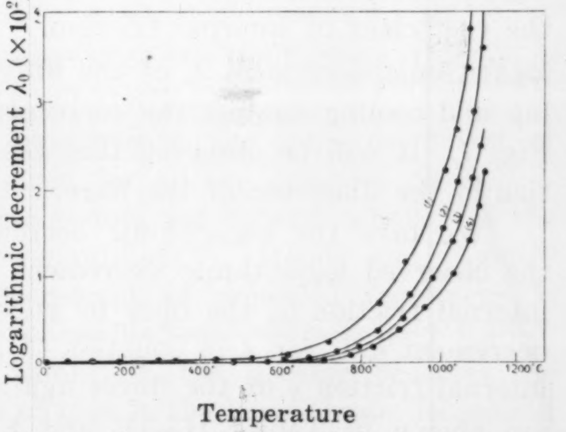

Fig. 7. Curves showing that the logarithmic decrements of the oscillations differ with different fibres at high temperature.

(1) Radius of the fibre $r=18{\cdot}52\times10^{-3}$cm.
(2) $r=42{\cdot}45\times10^{-3}$ cm.
(3) $r=51{\cdot}17\times10^{-3}$ cm.
(4) $r=65{\cdot}40\times10^{-3}$ cm.

abscissa, where λ_0 is the observed logarithmic decrement and λ_a is the logarithmic decrement due to the air-damping.

The logarithmic decrement of the oscillations, $\sqrt{\lambda_0-\lambda_a}$, is proportional to the square of the pressure, p^2, except in the case of very small pressure; the value of λ_0 in the open air being about 4 times that in vacuum. We can therefore deduct the effect of the logarithmic decrement due to air resistance from the observed logarithmic decrement.

Since the temperature of the air surrounding the vibrator was constant during the experiments, the logarithmic decrement due to air-damping was assumed to have the same value throughout the experiments. We shall now apply the relation between the pressure and the logarithmic decrement at room temperature to the case of high temperature. Strictly speaking, this would not be possible, seeing that for the viscosity of the air surrounding the vibrator, the temperattre of which is raised, would increase with temperature. The effect of this increase, however, is probably very small compared with the whole damping effect due to the air, since most of the torsional oscillations would doubtless be caused by the brass rod and the soft iron plate (E and S in Fig. 1). It will also be seen from Tables II~IV that the logarithmic decrement λ_a due to air-damping is itself a small fraction of the actually observed logarithmic decrement λ_0 at high temperature, while from Fig. 6 it is obvious that annealing reduces the coefficient of internal friction. The mean values of the observed logarithmic decrement λ_0 of the different fibres obtained by both heating and cooling against the corresponding temperatures are shown in Fig. 7. It will be observed that the value of λ_0 increases with reduction in the diameter of the fibre.

We take the logarithmic decrement λ_a due to air-damping from the observed logarithmic decrement λ_0 and calculate the coefficient of internal friction of the fibre by substituting this residual logarithmic decrement λ_0-λ_a for λ in equation (5). The values of the coefficient of internal friction η of the fibres against the corresponding temperature are shown in Tables II~IV and Fig. 9. The relation between the coefficient of internal friction η at a certain temperature and the frequency of the oscillating fibres is shown in Fig. 10, in which the frequency is taken as abscissa and the common logarithm of the coefficient of internal friction η as ordinate.

From the last named two figures we can see that the coefficient of internal friction of the fibres differs not only with different fibres, but also with the frequency of the oscillations. At constant temperature, the smaller the diameter of the fibres, the greater their coefficient of internal friction values; and the longer the period of the oscillations, the larger the value of the coefficient of internal friction.

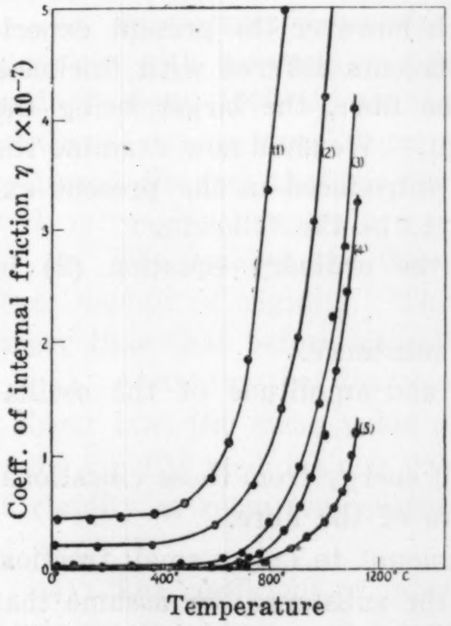

Fig. 9. Curves showing the relation between the coefficients of internal friction and temperature.

(1) Radius of the fibre $r = 18{\cdot}52 \times 10^{-3}$ cm.
(2) $r = 28{\cdot}05 \times 10^{-3}$ cm.
(3) $r = 42.45 \times 10^{-3}$ cm.
(4) $r = 51{\cdot}17 \times 10^{-3}$ cm.
(5) $r = 65{\cdot}40 \times 19^{-3}$ cm.

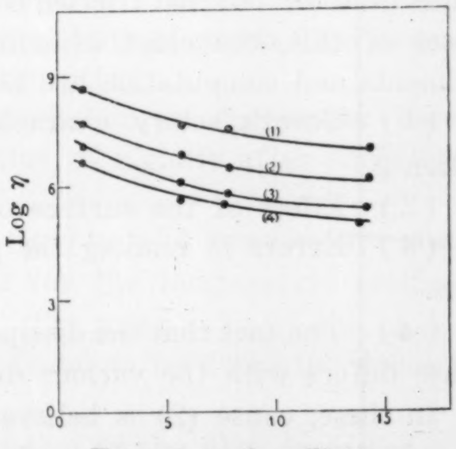

Fig. 10. Relation between log η and the frequency of oscillation at constant temperature θ.

(1) $\theta = 1100°$C.
(2) $\theta = 850°$C.
(3) $\theta = 650°$C.
(4) $\theta = 250°$C.

Consequently, in the present experiments, the same coefficient of internal friction could not be obtained for all the different fibres.

4. Remarks. Internal resistance does not depend wholly on the rate of strain, but also on stress-amplitude.[22] Honda and Konno[23] observed that the logarithmic decrement of annealed specimens is greatly affected by the amplitude of oscillations. Sezawa and Kubo[24] also found that the larger the amplitude, the greater becomes the coefficient of solid viscosity. The change in the logarithmic decrement of the oscillations with temperature was observed by both Horton,[25] Ishimoto,[26] and Iokibe and Sakai.[27] Internal friction therefore does not seem to be constant irrespective of the conditions of oscillation.

---

[22] KIMBALL and LOVELL, *Phys. Rev.*, **30** (1927), 948.
[23] K. HONDA and S. KONNO, *loc. cit.*
[24] K. SEZAWA and K. KUBO, *loc. cit.*
[25] F. HORTON, *Phil. Trans. Roy. Soc., London*, [A], **204** (1905), 1.
[26] M. ISHIMOTO, *loc. cit.*
[27] K. IOKIBE and S. SAKAI, *loc. cit.*

As to the coefficient of internal friction, we think that all quartz fibres should give the same value, which however the present experiments did not. The solid viscosity coefficients differed with thickness of fibre; the smaller the diameter of the fibre, the larger being the values of their internal friction coefficient. We shall now examine the causes of this, the chief of which as introduced in the present experiments and computation are believed to be the following:

(1) Unsatisfactory character of the ordinary equation (2) in section 3.

(2) Effect of the surface of the substance.

(3) Errors in reading the period and amplitude of the oscillations.

(4) The fact that the dissipation of energy from these vibrational bodies differs with the various diameters of the fibre.

In these, cause (2) is believed to amount to only a small fraction. In order to see the surface effect of the substance, we assume that the internal friction is divisible into two parts, the one being proportional to the surface of the fibre and the other to the volume of the fibre, but from calculation we found that the former was very small compared with the latter. This problem therefore will demand much further study. In order to avoid the errors in (3), the records were repeatedly read and their values corrected whenever possible. As to cause (4), although the diameter of the fibre was changed, the moment of inertia of the oscillating system remained constant throughout the experiments, its value being 109·878 in C.G.S. units. The smaller the diameter of the fibres, the longer became the period of the oscillations. During oscillation, a small fraction of energy is lost through the point of suspension outwards, and this energy loss may, in the case of short period oscillation, be more than in the case of long period.

Another form of equation (2) in section 3, namely, an equation involving the normal viscosity coefficient ξ, in place of η, in the damping term, was treated by Honda and Konno[28] and found correct. The effect of tension moreover may be considered. According to Boys,[29] the rigidity of vitreous silica in the form of a fibre is influenced by the tension on the fibre.

Until, therefore, further experiments have been made it is not possible to say which of the foregoing causes is the most important.

---

28) K. HONDA and S. KONNO, *loc. cit.*

29) C. V. BOYS, *loc. cit.*

5. Summary and Conclusion. We may now briefly summarise the results of the present study.

1) In contrast to metals, the modulus of rigidity of quartz fibre increases with increasing temperature, the maximum value being attained at about 1000°C. As the diameter of the fibre is reduced, the maximum temperature seems to be lowered. As to the geophysical problems, the fact that the modulus of rigidity of quartz fibre increases with increasing temperature seems interesting.

2) The smaller the diameter of the fibres, the larger become their moduli of rigidity. The modulus of rigidity after annealing is larger than that before annealing.

3) Assuming that the change in rigidity with temperature obeyed a linear law, the mean value obtained for the temperature coefficient of the rigidity modulus was 0·000111. The mean value of the modulus of rigidity at room temperature was found to be $2{\cdot}93 \times 10^{11}$ dynes per sq. cm.

4) The coefficient of internal friction of the fibre increased with increasing temperature at a rate which, although at first was constant, became much more rapid after about 600°C.

5) The coefficient of internal friction differs with different fibres. The smaller the diameter of the fibre, the larger the coefficient of internal friction, the coefficient of internal friction after annealing being smaller than that before annealing.

6) The coefficient of internal friction of the fibre at room temperature is of the order of 10^5 in C.G.S. units.

In conclusion, the writer wishes to express his sincere thanks to Professor Mishio Ishimoto for his kind guidance and valuable advices throughout the course of these experiments, and to Mr. S. Tanaka for his chemical analysis of the specimens.

53. シリカの剛性率及び固體粘度の溫度による變化

飯田汲事

地震波が地殼內に於て老衰し，又變形すると云ふ事は既によく知られてゐる事實であつて，その理論的方面の研究に於ては，長岡博士を始め妹澤博士その他の人々によつて取扱はれてゐる．地殼物質の剛性，ヤング率，及び密度等に關係せる地震波速度については，地震記象の觀察其の他から多くの人々によつて求められてゐる．これらは何れもその地殼物質の性質が根本問題となつてゐる．筆者は以上の問題に關係せる地殼物質の性質を，實驗的に研究して見たいと考へてその研究に着手したのであつて，その第1報として前號にてピッチ，パラフイン等の性質が岩石に類似せる點を報告した次第である．本論文も地殼物質がこの研究の對照となつてゐる．地殼物質は色々な結晶形のものから成り立つてゐるであらうから，その性質を知るには結晶形構造の性質をも調べなければならぬ．先づ之に至る段階として容易に得られ且細工のたやすい無定形シリカを選びその粘性，剛性の2性質を實驗的に調べて見た．實驗から得られた結果によれば，シリカの剛性率は多くの金屬と異なり約 1000° 迄は徐々に增加する．又粘性は 600° 位から急激に增加する．常溫に於けるシリカの粘性係數は 10^5 (c.g.s.) の程度である．かくの如くシリカの性質を考へると，地殼物質の中には，地殼表層に於けるものよりかへつて大きな剛性率と大きな粘性を持つた物質も，地球の內部に存在する事が可能のやうに思はれる．

7

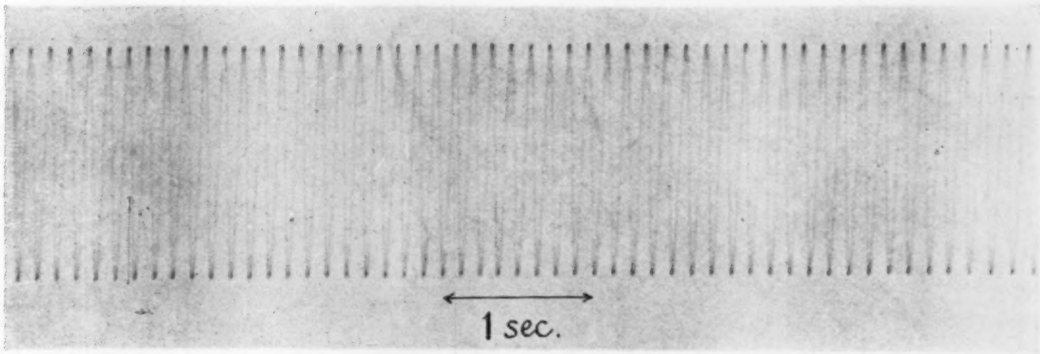

(A) Temp. 232°C (heating).

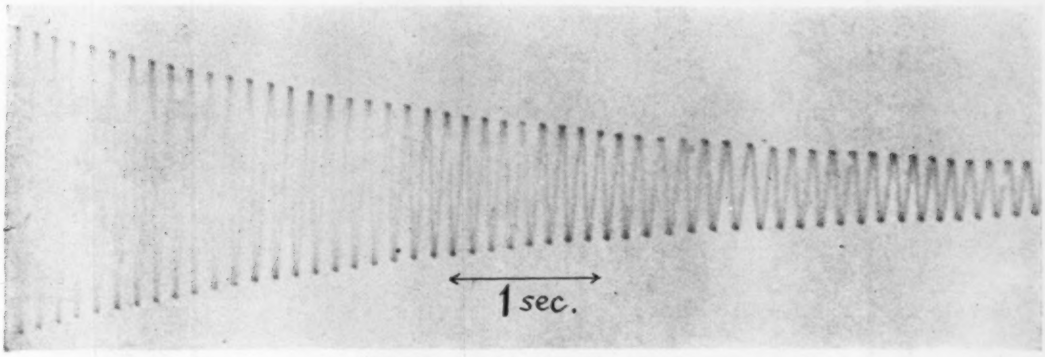

(B) Temp. 1090°C (heating).

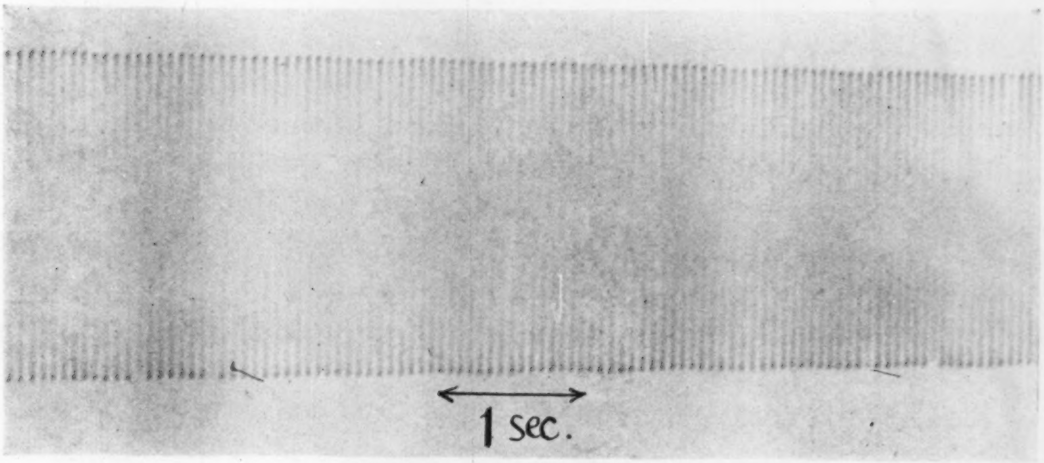

(C) Temp. 845°C (cooling).

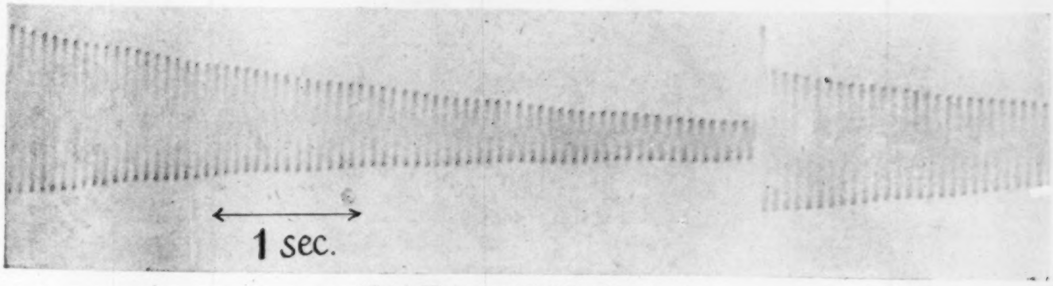

(D) Temp. 1098°C (heating).

Fig. 3. Actual records.

(A) and (B), radius of the fibre $r=51{\cdot}17\times10^{-3}$ cm.
length $l=12{\cdot}36$ cm.
(C) and (D), $r=65{\cdot}40\times10^{-3}$ cm.
$l=9{\cdot}74$ cm.

54. *Decay in the Seismic Vibrations of a Simple or Tall Structure by Dissipation of their Energy into the Ground.*[1]

By Katsutada SEZAWA and Kiyoshi KANAI,

Earthquake Research Institute.

(Read April 16, 1935.—Received June 20, 1935.)

In the absence of some form of damping resistance, almost any structure would suffer serious damage in an earthquake, owing to resonance. The question of air resistance and damping in the material used in the structure as well as in the foundation have been studied by some investigators,[2] but the dissipation of vibrational energy in the form of seismic waves transmitted into the ground, which seems to be the most important part of the problem, has not yet received their attention. Although we stated in a previous paper[3] that the smallness of the amplitudes of a structure in seismic vibrations is due mainly to the radiation or dissipation of vibrational energy into the ground, owing to certain mathematical difficulties, the problem was not followed up until recently when a reinvestigation was made. From the result of our recent calculations with respect to the decaying of seismic vibrations of various structures, the cases of vertical, shearing, and flexural vibrations of a simple as well as of a tall framed structure with floors either rigid or flexible seem to be the problems that we should investigate.

The prevalent belief that, without damping force, the displacements of an oscillating body become infinitely large under resonance conditions, appears to be based on the conception that part of its boundary to which periodic external forces are being applied, cannot be a node of the vibrations in that body. As a matter of fact, the part in question becomes a loop, a node, or an intermediate phase according to the frequency of the vibrations. At the frequency that synchronizes with the natural frequency of the body, the part under consideration becomes a node, with the result that the amplitudes of vibration even under resonance conditions do not exceed a certain limit, which fact will be readily understood if we consider the dissipation of energy. Naturally the same applies to vibrations of a structure subjected to seismic movements of the ground.

---

[1] Preliminary report published in *Proc. Imp. Acad.*, **11** (1935), 174.

[2] The part, "Waves propagated in Beam...," which was appended at the end of the paper "On the Decay of Waves in Visco-Elastic Solid Bodies", *Bull. Earthq. Res. Inst.*, **3** (1927), 50, and similar papers published since then by a number of writers.

[3] § 10 of our paper, "Some New Problems of Forced Vibrations of a Structure", *Bull. Earthq. Res. Inst.*, **12** (1934), 845.

Seismic waves that cause structural damage are sometimes bodily waves and at other times surface waves. The bodily waves are incident to the earth's surface practically normally. The scattered waves that dissipate from the structure into the ground seem to be chiefly bodily waves, including their harmonic waves, associated with surface waves. However, in order to avoid mathematical difficulties, we shall take only the principal terms of scattered waves in the present calculation and ignore the effects from the formation of surface waves.

1. A *Simple structure subjected to incident longitudinal waves.*

The structure is assumed to be a uniform circular cylinder of radius ϵ. Let the incident longitudinal waves with their displacement orientated vertically be

$$u_0 = e^{ih(V_1 t + x)}, \tag{1}$$

where $h^2 = \rho p^2/(\lambda + 2\mu)$, $V_1 = \sqrt{(\lambda + 2\mu)/\rho}$. Assuming then for simplicity that the scattered waves are radiated from a semispherical surface, $r = \epsilon$, shown in Fig. 1, the expressions for the scattered longitudinal and transverse waves become[4)]

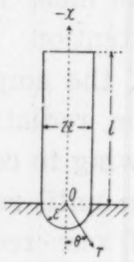

Fig. 1.

$$\Delta = \alpha \cos\theta \frac{e^{i(pt - hr)}}{r}, \tag{2'}$$

$$u_1 = -\frac{\alpha}{h^2}\cos\theta \frac{d}{dr}\frac{e^{i(pt - hr)}}{r}, \quad v_1 = \frac{\alpha}{h^2}\sin\theta \frac{e^{i(pt - hr)}}{r^2}, \tag{2}$$

$$u_2 = -\frac{4\beta}{k^2}\cos\theta \frac{e^{i(pt - kr)}}{r^2}, \quad v_2 = \frac{2\beta}{k^2}\sin\theta \frac{1}{r}\frac{d}{dr}e^{i(pt - kr)}, \tag{3}$$

where u_1, v_1 and u_2, v_2 satisfy the equations of motion for longitudinal and transverse waves respectively, Δ is the dilatation, α, β are

---

4) K. SEZAWA, *Bull. Earthq. Res. Inst.*, **2** (1927), 13~20.

constants determined by boundary conditions, and $h^2=\rho p^2/(\lambda+2\mu)$, $k^2=\rho p^2/\mu$, ρ, λ, μ being the density and elastic constants of the earth.

The reasonable way would be to assume that the waves scatter directly from the bottom end of the structure, $x=0$, but, in order to avoid the mathematical difficulties thus introduced, we assumed the semispherical surface to have the same diameter as that of the structure. Such an assumption does not seriously affect the result of the problem, provided the radius, ε, of the sphere is not large compared with the length of the incident waves. Since from this condition it follows that the spherical surface in question always remains spherical with constant radius, we have at $r=\varepsilon$,

$$-(u_1+u_2)_{max.}=(v_1+v_2)_{max.}, \tag{4}$$

from which we get

$$\frac{\alpha}{\beta}=\frac{2h^2\varepsilon^2\{(4+hk\varepsilon^2)+2i(k-h)\varepsilon\}e^{i(h-k)\varepsilon}}{k^2\varepsilon^2(4+h^2\varepsilon^2)}. \tag{5}$$

The vibratory motion in the structure is expressed by

$$u'=Be^{ih'(V_1't+x)}+Ce^{ih'(V_1't-x)}, \tag{6}$$

where $h'^2=\rho'p^2/E$, $V_1'=\sqrt{E/\rho'}$, ρ', E being density and Young's modulus respectively.

The condition at the upper end of the structure, $x=-l$, is

$$\partial u'/\partial x=0, \tag{7}$$

and the boundary conditions at its lower end are such that the displacements as well as the resultants of vertical stress in the structure are continuous respectively with those in the earth, namely,

$$u'_{x=0}=u_{0\,x=0}+(u_1+u_2)_{r=\varepsilon,\ \theta=0}, \tag{8}$$

$$\begin{aligned}E\pi\varepsilon^2\frac{\partial u'}{\partial x}_{x=0}&=(\lambda+2\mu)\pi\varepsilon^2\frac{\partial u_0}{\partial x}_{x=0}\\&+\int_{\theta=0}^{\frac{\pi}{2}}\int_{\varphi=0}^{2\pi}\left(\lambda\Delta+2\mu\frac{\partial(u_1+u_2)}{\partial r}\right)r^2\cos\theta\sin\theta\,d\theta\,d\varphi_{r=\varepsilon}\\&+\int_{\theta=0}^{\frac{\pi}{2}}\int_{\varphi=0}^{2\pi}\mu\left(\frac{\partial(v_1+v_2)}{\partial r}-\frac{(v_1+v_2)}{r}+\frac{1}{r}\frac{\partial(u_1+u_2)}{\partial\theta}\right)r^2\sin^2\theta\,d\theta\,d\varphi_{r=\varepsilon}.\end{aligned} \tag{9}$$

Substituting (1), (2), (2′), (3), (5), (6) in (7), (8), (9), and neglecting small quantities higher than the second order, and taking the real part only, we get

$$u'=\frac{\left(2+3\frac{\lambda}{\mu}+4\sqrt{\frac{\lambda}{\mu}+2}\right)\cosh h'(l+x)}{\sqrt{\left\{3\sqrt{\frac{\rho'E}{\rho\mu}}\left(\frac{\lambda}{\mu}+2\right)\sin h'l\right\}^2+\left\{4\left(\sqrt{\frac{\lambda}{\mu}+2}-1\right)\cos h'l\right\}^2}}$$

$$\cdot\cos\left\{pt-\tan^{-1}\frac{3\sqrt{\frac{\rho'E}{\rho\mu}}\left(\frac{\lambda}{\mu}+2\right)\sin h'l}{4\left(\sqrt{\frac{\lambda}{\mu}+2}-1\right)\cos h'l}\right\}, \qquad (10)$$

where $h'=p\sqrt{\rho'/E}$, corresponding to the incident waves

$$u_0=\cos(pt+hx). \qquad (1')$$

The left-hand term under the root sign of the denominator of (10) represents the effect of the dissipation of energy scattered as seismic waves. The larger the ratio of E/μ or ρ'/ρ, the larger will be the decrease in the amplitudes of vibration at the periods corresponding to the resonance condition, $\cos h'l=0$, of the case without dissipation of energy. It is also evident that under resonance conditions the displacement at the lower end is always zero. We have calculated the amplitudes

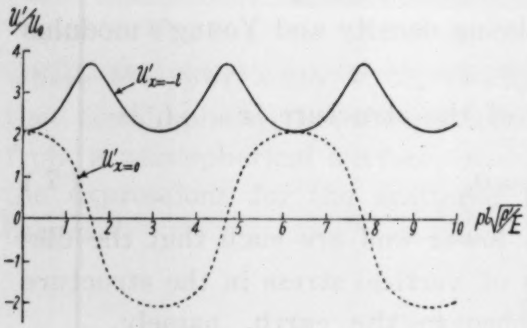

Fig. 2. $\rho'/\rho=1$, $E/\mu=1/10$.

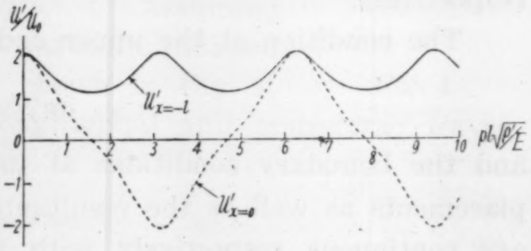

Fig. 3. $\rho'/\rho=1$, $E/\mu=1$.

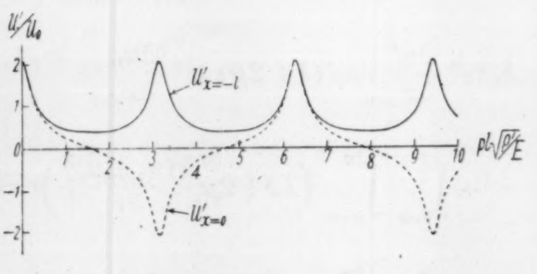

Fig. 4. $\rho'/\rho=1$, $E/\mu=10$.

at $x=-l$ and those at $x=0$ corresponding to various frequencies for the cases, (i) $\rho'/\rho=1$, $\lambda/\mu=1$, $E/\mu=1/10$, (ii) $\rho'/\rho=1$, $\lambda/\mu=1$, $E/\mu=1$, (iii) $\rho'/\rho=1$, $\lambda/\mu=1$, $E/\mu=10$, all of which are shown in Figs. 2, 3, 4.

2. *Free vertical vibrations of a simple structure.*

In order to find the nature of the free vibrations of the structure, we introduce the original complex form of the solution, analogous to u' in (10), namely

$$u'=Be^{ih'(V_1't+x)}+Ce^{ih'(V_1't-x)}, \tag{6'}$$

where

$$B=\frac{R}{P+Qe^{-2ih'l}}\,,\quad C=\frac{Re^{-2ih'l}}{P+Qe^{-2ih'l}}\,, \tag{11}$$

in which

$$\left.\begin{aligned} P&=4\left(\sqrt{\frac{\lambda}{\mu}+2}-1\right)+3\sqrt{\frac{\rho' E}{\rho\mu}\left(\frac{\lambda}{\mu}+2\right)},\\ Q&=4\left(\sqrt{\frac{\lambda}{\mu}+2}-1\right)-3\sqrt{\frac{\rho' E}{\rho\mu}\left(\frac{\lambda}{\mu}+2\right)},\\ R&=10+3\frac{\lambda}{\mu}+4\sqrt{\frac{\lambda}{\mu}+2}\,. \end{aligned}\right\} \tag{12}$$

Generalising (6′) by means of Fourier's integral we get

$$u'=\frac{1}{2\pi}\int_{-\infty}^{\infty}\frac{R\,dh}{P+Qe^{-2ibhl}}\int_{-\infty}^{\infty}f(\sigma)\,e^{ibh\left(V_1't+x+\frac{\sigma}{b}\right)}\,d\sigma$$

$$+\frac{1}{2\pi}\int_{-\infty}^{\infty}\frac{Re^{-2ibhl}dh}{P+Qe^{-2ibhl}}\int_{-\infty}^{\infty}f(\sigma)\,e^{ibh\left(V_1't-x+\frac{\sigma}{b}\right)}\,d\sigma\,. \tag{13}$$

where $h'=bh$, corresponding to the incident disturbance $f(x)$ at $t=0$. Since we know that

$$\frac{1}{P+Qe^{-2ibhl}}=\frac{1}{P}\sum_{m=0}^{\infty}(-1)^m\left(\frac{Q}{P}\right)^m e^{-2imbhl}\,, \tag{14}$$

we have from (13), (14)

$$u' = \frac{1}{2\pi}\left(\frac{R}{P}\right)\sum_{m=0}^{\infty}(-1)^m\left(\frac{Q}{P}\right)^m\left[F\{b(V_1't+x-2ml)\}\right.$$
$$\left. + F\{b(V_1't-x-2\overline{m+1}l)\}\right]. \tag{15}$$

corresponding to the disturbing incident waves in the earth

$$u_0 = F(V_1t+x). \tag{16}$$

The vibrations are thus of a purely exponential type

$$e^{-\varkappa t}, \tag{17}$$

the logarithmic decrement being therefore

$$\varkappa = \frac{V_1'}{2l}\log_e\left|\frac{Q}{P}\right|. \tag{18}$$

The greater the difference in the elastic constants or in the densities of the structure and the earth, the more slowly decay the free vibrations. It is not a matter of importance whether the constants of the earth are greater or less than those of the structure.

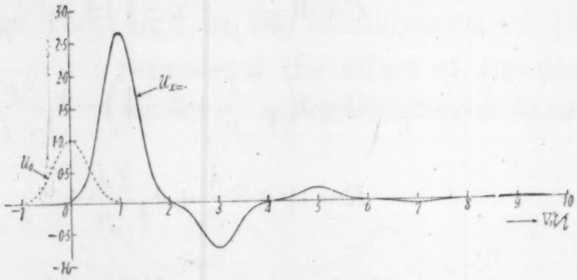

Fig. 5. $\rho'/\rho=1$, $E/\mu=1/10$, $l/c=0{\cdot}365$.

To serve as examples, we took the disturbance

$$F(V_1t+x) = e^{-\frac{(V_1t+x)^2}{c^2}},$$

and calculated the resulting free vibrations of structures corresponding to three cases (i) $\rho'/\rho=1$, $E/\mu=1/10$, $l/c=0{\cdot}365$, (ii) $\rho'/\rho=1$, $E/\mu=1$, $l/c=1{\cdot}155$, (iii) $\rho'/\rho=1$, $E/\mu=10$, $l/c=3{\cdot}651$, the result being plotted in Figs. 5, 6, 7.

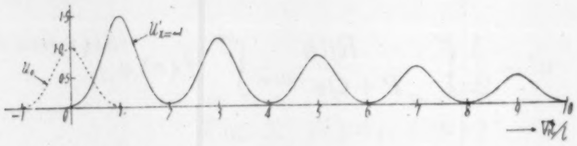

Fig. 6. $\rho'/\rho=1$, $E/\mu=1$, $l/c=1{\cdot}155$.

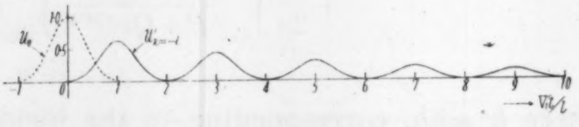

Fig. 7. $\rho'/\rho=1$, $E/\mu=10$, $l/c=3{\cdot}651$.

3. *A tall structure with rigid floors subjected to incident transverse waves.*

It was shown in a previous paper[5] that the motion of a tall building with rigid floors subjected to horizontal oscillation of the ground is analogous to the case of shearing vibrations of a simple structure. We shall discuss the case of an n-storied structure. Let the axis of x be drawn vertically downwards with its origin at the free surface of the earth, and let ρ, λ, μ; $\rho'(=m/al_1)$, $G(=12{\cdot}4Ej^2/l_1^2)$ be the density and the elastic constants of the earth, and the effective density and the effective rigidity of the structure, where E, j, l_1, a are Young's modulus, radius of gyration of section, length and total sum of the sectional areas of the columns between two adjacent floors respectively. Provided the incident transverse waves in the earth are propagated vertically upwards, the boundary conditions are such that there is no effective shearing stress at the upper end of the structure, while the displacement and the shearing stress at its lower end are continuous respectively with those in the earth resulting from incident transverse waves and scattered waves, both longitudinal and transverse. Let the incident waves orientated horizontally be

$$u_0=e^{ik(V_2 +x)}, \tag{19}$$

where $k^2=\rho p^2/\mu$, $V_2=\sqrt{\mu/\rho}$ and the scattered waves be of the forms shown in (2′), (2), (3), the angle θ being now taken as shown in Fig. 8. The relation between α and β is again the same as that in (5). The displacement of the structure is also in horizontal sense and expressed by

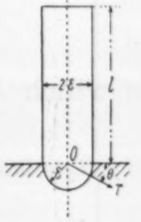

Fig. 8.

$$u'=Be^{ik'(V_2't+x)}+Ce^{ik'(V_2't-x)}, \tag{20}$$

where $k'^2=\rho' p^2/G$, $V_2'=\sqrt{G/\rho'}$. The boundary condition at $x=-l(=-nl_1)$ is

$$\partial u'/\partial x=0, \tag{21}$$

while, at the lower end of that structure, we have the conditions

$$u'_{x=0}=u_{0x=0}+(u_1+u_2)_{r=\varepsilon,\ \theta=0}, \tag{22}$$

$$G\pi\varepsilon^2\frac{\partial u'}{\partial x_{x=0}}=\mu\pi\varepsilon^2\frac{\partial u_0}{\partial x_{x=0}}$$

$$+\int_{\theta=0}^{\pi}\int_{\varphi=0}^{\pi}\mu\left(\frac{\partial(v_1+v_2)}{\partial r}-\frac{(v_1+v_2)}{r}+\frac{1}{r}\frac{\partial(u_1+u_2)}{\partial\theta}\right)r^2\sin^2\theta d\theta\, d\varphi_{r=\varepsilon}$$

---

[5] K. Sezawa and K. Kanai, *Bull. Earthq. Res. Inst.*, **12** (1934), 819.

$$+\int_{\theta=0}^{\pi}\int_{\varphi=0}^{\pi}\left(\lambda\Delta+2\mu\frac{\partial(u_1+u_2)}{\partial r}\right)r^2\sin\theta\cos\theta\,d\theta d\varphi_{r=\varepsilon}\,. \tag{23}$$

In this case, also, for reasons already given, the assumption with respect to the semispherical surface holds. Proceeding as in the previous case we finally get

$$u'=\frac{\left(7\sqrt{\dfrac{\lambda}{\mu}+2}-4\right)\cos k'(l+x)}{\sqrt{\left\{3\sqrt{\dfrac{\rho' G}{\rho\mu}\left(\dfrac{\lambda}{\mu}+2\right)}\sin k'l\right\}^2+\left\{4\left(\sqrt{\dfrac{\lambda}{\mu}+2}-1\right)\cos k'l\right\}^2}}$$

$$\cdot\cos\left\{pt-\tan^{-1}\frac{3\sqrt{\dfrac{\rho' G}{\rho\mu}\left(\dfrac{\lambda}{\mu}+2\right)}\sin k'l}{4\left(\sqrt{\dfrac{\lambda}{\mu}+2}-1\right)\cos k'l}\right\}, \tag{24}$$

in which $k'=p\sqrt{\rho'/G}$, $l=nl_1$, corresponding to the incident waves

$$u_0=\cos(pt+kx). \quad (19')$$

We calculated the amplitudes at $x=-l$ and those at $x=0$ for various frequencies for the cases, (i) $\rho'/\rho=10$, $\lambda/\mu=1$, $G/\mu=1/500$, (ii) $\rho'/\rho=10$, $\lambda/\mu=1$, $G/\mu=0{\cdot}0318$, (iii) $\rho'/\rho=10$, $\lambda/\mu=1$, $G/\mu=1$ and plotted the results in Figs. 9, 10, 11. They show certain features of vibrations similar to those in the previous case. We specially selected a relatively large ρ'/ρ, with a view to finding the amplitude of an actual tall, framed structure.

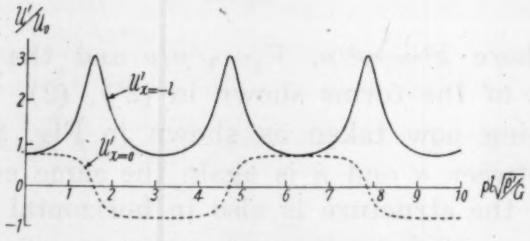

Fig. 9. $\rho'/\rho=10$, $G/\mu=1/500$.

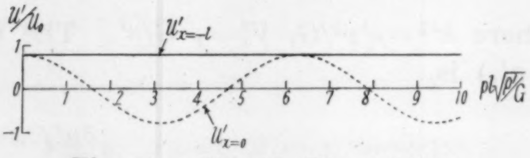

Fig. 10. $\rho'/\rho=10$, $G/\mu=0{\cdot}0318$.

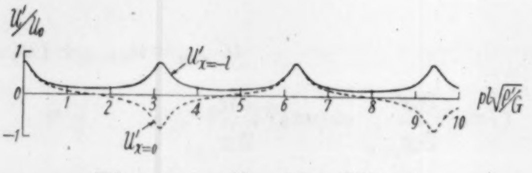

Fig. 11. $\rho'/\rho=10$, $G/\mu=1$.

4. *Free horizontal vibrations of a tall structure with rigid floors.*

With the same mathematics as that used for vertical vibrations, we get the following equation of free vibrations for this case:

$$u' = \frac{1}{2\pi}\frac{R}{P}\sum_{m=0}^{\infty}(-1)^m\left(\frac{Q}{P}\right)^m\Big[F\{b(V_2't+x-2ml)\}$$

$$+F\{b(V_2't-x-\overline{2m+1}\,l)\}\Big], \tag{25}$$

corresponding to the initial disturbance incident to the earth's surface

$$u_0 = F(V_2t+x). \tag{26}$$

$P,\ Q,\ R$ in (25) signify

$$\left.\begin{aligned} P&=4\left(\sqrt{\frac{\lambda}{\mu}+2}-1\right)+3\sqrt{\frac{\rho' G}{\rho\mu}\left(\frac{\lambda}{\mu}+2\right)}, \\ Q&=4\left(\sqrt{\frac{\lambda}{\mu}+2}-1\right)-3\sqrt{\frac{\rho' G}{\rho\mu}\left(\frac{\lambda}{\mu}+2\right)}, \\ R&=7\sqrt{\frac{\lambda}{\mu}+2}\ -4\,. \end{aligned}\right\} \tag{27}$$

It is possible to prove that the logarithmic decrement in this case is expressed by

$$\frac{\sqrt{G/\rho'}}{2l}\log\frac{3\sqrt{(\rho' G/\rho\mu)(\lambda/\mu+2)}+4\left(\sqrt{\dfrac{\lambda}{\mu}+2}-1\right)}{3\sqrt{(\rho' G/\rho\mu)(\lambda/\mu+2)}-4\left(\sqrt{\dfrac{\lambda}{\mu}+2}-1\right)}\,. \tag{28}$$

If the type of the initial disturbance be

$$F(V_2t+x) = e^{-\frac{(V_2t+x)^2}{c^2}},$$

the free vibrations of the structure corresponding to the three cases, (i) $\rho'/\rho = 10$, $\lambda = \mu$, $G/\mu = 1/500$, $l/c = 0.02828$, (ii) $\rho'/\rho = 10$, $\lambda = \mu$, $G'/\mu = 0{\cdot}0318$, $l/c = 0{\cdot}1127$, (iii) $\rho'/\rho = 10$, $\lambda = \mu$, $G'/\mu = 1$, $l/c = 0{\cdot}6324$, assume the forms shown in Figs. 12, 13, 14.

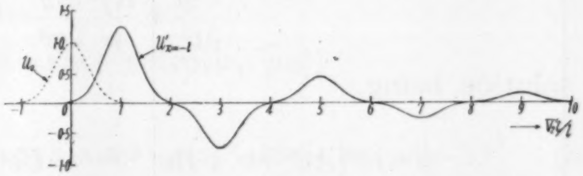

Fig. 12. $\rho'/\rho = 10$, $G/\mu = 1/500$, $l/c = 0{\cdot}02828$.

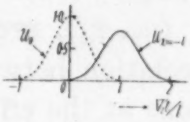

Fig. 13. $\rho'/\rho = 10$, $G/\mu = 0{\cdot}0318$, $l/c = 0{\cdot}1127$.

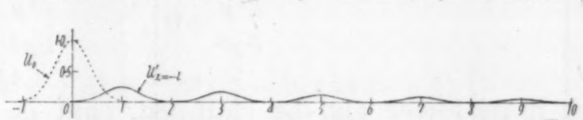

Fig. 14. $\rho'/\rho = 10$, $G/\mu = 1$, $l/c = 0{\cdot}6324$.

5. *The problem of shearing vibrations of a simple structure.*

The problem of horizontal vibrations of a tall structure with rigid floors, studied in the preceding two sections, was nothing more than a modification of the case of a simple structure under horizontal shearing vibrations. The problem in its original form may therefore be at the same time one for the shearing vibrations of a simple structure. Solutions (24), (25), (27) may straightway be converted into solutions of the present case with however the proviso that ρ', G, l are respectively the density, rigidity, and the height of the simple structure under consideration.

6. *A tall structure with flexible floors subjected to incident transverse waves.*

In a previous paper[6] we stated that the motion of a tall building with flexible floors subjected to horizontal movement of the ground is analogous to the transverse vibrations of an elastic rod. We shall discuss an n-storied structure. Referring to Fig. 8, let ρ, λ, μ; $\rho'(=m/al_1)$, j be the density and elastic constants of the earth, the effective density of the structure and the radius of gyration of a section of a column, where m, l_1, a are masses concentrated on every floor, and the length and total sum of the sectional areas of columns between two adjacent floors respectively.

The equation of vibratory motion of the structure is now written

$$\frac{\partial^2 y}{\partial t^2}+\frac{Ej^2}{\rho'}\frac{\partial^4 y}{\partial x^4}=0\,, \tag{29}$$

its solution being

$$y=e^{ipt}[Ae^{i\sqrt{p}cx}+Be^{-i\sqrt{p}cx}+Ce^{\sqrt{p}cx}+De^{-\sqrt{p}cx}]\,, \tag{30}$$

in which $c=(\rho'/Ej^2)^{1/4}$. The forms of incident waves, u_0, and scattered waves, $(u_1,\ v_1)$, $(u_2,\ v_2)$, are respectively the same as those in (19), (2), (3). The relation between α and β is also the same as in (5).

The conditions at the effective upper end, $x=-l\{=(n+1/2)l_1\}$[7] are

$$\frac{\partial^2 y}{\partial x^2}=0\;, \qquad \frac{\partial^3 y}{\partial x^3}=0\;, \tag{31}$$

and, if its lower end be clamped, that is, the structure stands normal

---

6) K. SEZAWA and K. KANAI, *Bull. Earthq. Res. Inst.*, **12** (1934), 818.

7) K. SEZAWA and K. KANAI, *ibid.*.

to the earth's surface at its lower end, we have

$$y_{x=0}=u_{0x=0}+(u_1+u_2)_{r=\epsilon\ x=0}\,, \tag{32}$$

$$\partial y/\partial x_{x=0}=0\,, \tag{33}$$

$$\begin{aligned}-E\pi\epsilon^2 j^2\frac{\partial^3 y}{\partial x^3}_{x=0} &= \mu\pi\epsilon^2\frac{\partial u}{\partial x}_{x=0}\\ &+\int_{\theta=0}^{\pi}\int_{\varphi=0}^{\pi}\mu\left(\frac{\partial(v_1+v_2)}{\partial r}-\frac{(v_1+v_2)}{r}+\frac{1}{r}\frac{\partial(u_1+u_2)}{\partial\theta}\right)r^2\sin^2\theta\,d\theta\,d\varphi_{r=\epsilon}\\ &+\int_{\theta=0}^{\pi}\int_{\varphi=0}^{\pi}\left(\lambda\Delta+2\mu\frac{\partial(u_1+u_2)}{\partial r}\right)r^2\sin\theta\cos\theta\,d\theta\,d\varphi_{r=\epsilon}\,,\end{aligned} \tag{34}$$

the assumption with respect to ϵ being the same as in the preceding case. After a prolonged investigation we obtained

$$\begin{aligned}\left.\begin{matrix}A\\B\end{matrix}\right\}=\frac{4e^{-ik\epsilon}}{\Theta k^2\epsilon^2(h^2\epsilon^2+4)}&\left\{\left[-\frac{4}{3}(k\epsilon-h\epsilon)\left\{2(h^2\epsilon^2+2)+\frac{\lambda}{\mu}h^2\epsilon^2\right\}-k\epsilon(h\epsilon k\epsilon+4)\right]\right.\\ &+i\left[-\frac{4}{3}(k\epsilon-h\epsilon)(h^2\epsilon^2k\epsilon+2h\epsilon+4k\epsilon)+\frac{2}{3}\frac{\lambda}{\mu}h^2\epsilon^2(h\epsilon k\epsilon+4)\right.\\ &\left.\left.+k\epsilon(h^2\epsilon^2k\epsilon+2h\epsilon+2k\epsilon)\right]\right\}\\ &\cdot\left\{\pm(\cos\sqrt{p}cl\sinh\sqrt{p}cl+\sin\sqrt{p}cl\cosh\sqrt{p}cl)\right.\\ &\left.+i(-\cos\sqrt{p}cl\cosh\sqrt{p}cl+\sin\sqrt{p}cl\sinh\sqrt{p}cl-1)\right\},\end{aligned} \tag{35}$$

$$\begin{aligned}\left.\begin{matrix}C\\D\end{matrix}\right\}=\frac{-4e^{-ik\epsilon}}{\Theta k^2\epsilon^2(h^2\epsilon^2+4)}&\left\{\left[\frac{4}{3}(k\epsilon-h\epsilon)(h^2\epsilon^2k\epsilon+2h\epsilon+4k\epsilon)\right.\right.\\ &\left.-\frac{2}{3}\frac{\lambda}{\mu}h^2\epsilon^2(h\epsilon k\epsilon+4)-k\epsilon(h^2\epsilon^2k\epsilon+2h\epsilon+2k\epsilon)\right]\\ &\left.+i\left[-\frac{4}{3}(k\epsilon-h\epsilon)\left\{2(h^2\epsilon^2+2)+\frac{\lambda}{\mu}h^2\epsilon^2\right\}-k\epsilon(h\epsilon k\epsilon+4)\right]\right\}\\ &\cdot\left\{e^{\pm\sqrt{p}cl}(\cos\sqrt{p}cl\pm\sin\sqrt{p}cl)+1\right\},\end{aligned} \tag{36}$$

$$\beta=\frac{-8}{\Theta}\Big[\frac{E}{\mu}\varepsilon j^2p^{3/2}c^3(\cos\sqrt{pcl}\sinh\sqrt{pcl}+\sin\sqrt{pcl}\cosh\sqrt{pcl})$$

$$+ik\varepsilon(\cos\sqrt{pcl}\cosh\sqrt{pcl}+1)\ , \qquad (37)$$

where

$$\Theta=\frac{-16\,e^{-ik\varepsilon}}{k^2\varepsilon^2(h^2\varepsilon^2+4)}\Bigg\{\Big[\frac{2}{3}(\cos\sqrt{pcl}\cosh\sqrt{pcl}+1)\Big\{2(k\varepsilon-h\varepsilon)(h^2\varepsilon^2k\varepsilon$$

$$+2h\varepsilon+4k\varepsilon)-\frac{\lambda}{\mu}h^2\varepsilon^2(h\varepsilon k\varepsilon+4)\Big\}$$

$$+\frac{E}{\mu}\varepsilon j^2p^{3/2}c^3(\cos\sqrt{pcl}\sinh\sqrt{pcl}+\sin\sqrt{pcl}\cosh\sqrt{pcl})(h\varepsilon k\varepsilon+4)\ \Big]$$

$$-i\Big[\frac{4}{3}(\cos\sqrt{pcl}\cosh\sqrt{pcl}+1)(k\varepsilon-h\varepsilon)\Big\{2(h^2\varepsilon^2+2)+\frac{\lambda}{\mu}h^2\varepsilon^2\Big\}$$

$$+\frac{E}{\mu}\varepsilon j^2p^{3/2}c^3(\cos\sqrt{pcl}\sinh\sqrt{pcl}+\sin\sqrt{pcl}\cosh\sqrt{pcl})(h^2\varepsilon^2k\varepsilon$$

$$+2h\varepsilon+2k\varepsilon)\Big]\Bigg\}. \qquad (38)$$

Substituting these values in the original equations, neglecting small quantities higher than the second order, and taking the real part only, we finally get

$$y=\Big\{(\cos\sqrt{pcl}\cosh\sqrt{pcl}+1)(\cosh\sqrt{pcx}+\cos\sqrt{pcx})$$

$$+\sin\sqrt{pcl}\sinh\sqrt{pcl}(\cosh\sqrt{pcx}-\cos\sqrt{pcx})$$

$$+(\cos\sqrt{pcl}\sinh\sqrt{pcl}+\sin\sqrt{pcl}\cosh\sqrt{pcl})(\sinh\sqrt{pcx}-\sin\sqrt{pcx})\Big\}\Phi, \qquad (39)$$

where

$$\Phi=\frac{\left(7\sqrt{\frac{\lambda}{\mu}+2}-4\right)\cos\left(pt-\tan^{-1}\Psi/\chi\right)}{2\sqrt{\Psi^2+\chi^2}}\ ,\quad C=\left(\frac{\rho'}{Ej^2}\right)^{1/4}=\left(\frac{m}{l_1Eaj^2}\right)^{1/4}, \qquad (40),\ (41)$$

in which

$$\Psi=3\sqrt{\frac{\lambda}{\mu}+2}\left(\frac{Ej^2}{\mu kl^3}\right)(\sqrt{p}cl)^3(\cos\sqrt{p}cl\sinh\sqrt{p}cl+\sin\sqrt{p}cl\cosh\sqrt{p}cl), \quad (42)$$

$$\chi=4\left(\sqrt{\frac{\lambda}{\mu}+2}-1\right)(\cos\sqrt{p}cl\cosh\sqrt{p}cl+1), \quad (43)$$

$Ej^2(\sqrt{p}cl)^3/\mu kl^3$ in (42) being equivalent to $\sqrt{E^{1/2}j\rho'^{3/2}p/\mu\rho}$. The displacement (39) corresponds to the incident transverse waves

$$u_0=\cos(yt+kx). \quad (44)$$

It is worth noticing that $\chi=0$ is the frequency equation of vibrations of the structure which is free at its upper end and absolutely clamped at its lower end, while $\Psi=0$ is the frequency equation of vibrations of a free-free bar whose length is twice the height of the structure.

The nature of the problem for the case under resonance conditions is similar to that of the preceding cases, except with the difference that, in the present problem, however small may be the ratio $Ej^2/\mu kl^3$, the amplitudes of vibrations under higher resonance conditions become rather less than those at frequencies out of resonance. This may also be seen from Figs. 15, 16, 17, which show the amplitudes at $x=-l$

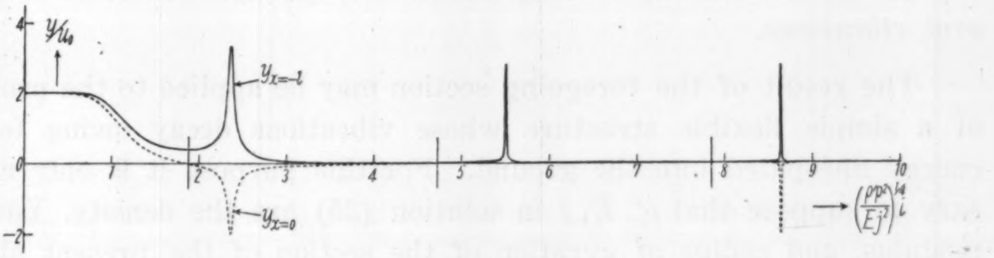

Fig. 15. $\lambda/\mu=14$, $\frac{Ej^2}{\mu kl^3}=16{\cdot}38$.

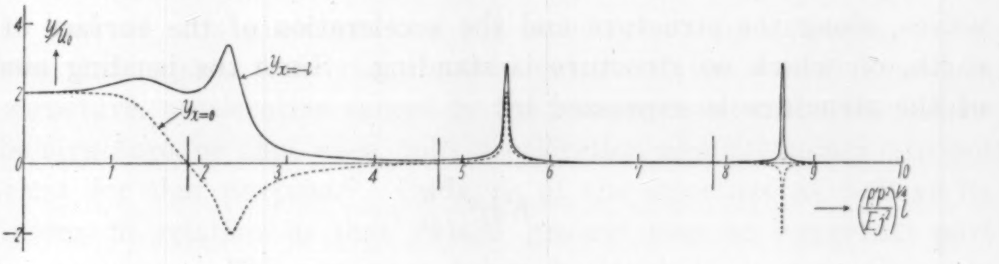

Fig. 16. $\lambda/\mu=14$, $\frac{Ej^2}{\mu kl^3}=3{\cdot}305$.

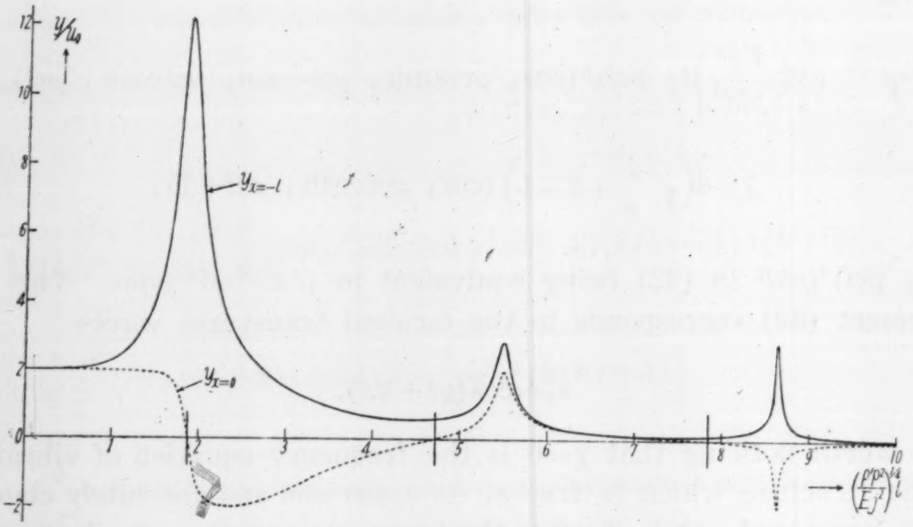

Fig. 17. $\lambda/\mu = 14$, $\dfrac{Ej^2}{\mu k l^3} = 0{\cdot}5464$.

and at $x=0$ of the cases, $Ej^2/\mu kl^3 = 16{\cdot}38$, $3{\cdot}305$, $0{\cdot}5462$, at different $\rho' (= m/al_1)$ corresponding to the incident waves of unit amplitudes transmitted through the earth, in which $\lambda = 14\,\mu$. The short vertical strips represent the frequencies with which the resonance should take place in the usual sense.

7. *Distribution of bending moments of a simple structure in flexural vibrations.*

The result of the foregoing section may be applied to the problem of a simple flexible structure whose vibrations decay owing to the energy dissipated into the ground. For this purpose it is only necessary to suppose that ρ', E, j in solution (35) are the density, Young's modulus, and radius of gyration of the section of the present simple structure.

It is of some interest to investigate the relation between the bending moments distributed, as the result of incident and reflected waves, along the structure and the acceleration of the surface of the earth, on which no structure is standing. Since the bending moment of the structure is expressed by

$$Eaj^2 \frac{d^2 y}{dx^2}, \tag{45}$$

where y is given by equation (39) and the acceleration of the ground surface by

$$\left(2\frac{\partial^2 u}{\partial t^2}\right)_{x=0} . \tag{46}$$

It is possible to make the ratio of these quantities dimensionless by multiplying (46) by $\rho' a l^2$, the ratio thus modified being

$$Eaj^2\frac{\partial^2 y}{\partial x^2}\bigg/\rho' a l^2\left(2\frac{\partial^2 u_0}{\partial t^2}\right). \tag{47}$$

Figs. 18～24 show such values for the cases $(\rho' p^2/Ej^2)^{1/4} l=1$, 1·875, 2·1, 2·365, 3·5, 4·73, 5·498, besides the condition that $Ej^2/\mu k l^3=0{\cdot}5462$ remains constant. These figures tell us that, given the acceleration

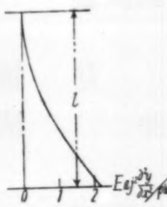

Fig. 18. $\left(\frac{\rho' p^2}{Ej^2}\right)^{\frac{1}{4}} l=1.$

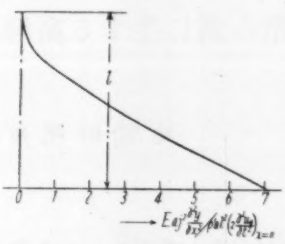

Fig. 19. $\left(\frac{\rho' p^2}{Ej^2}\right)^{\frac{1}{4}} l=1{\cdot}875.$

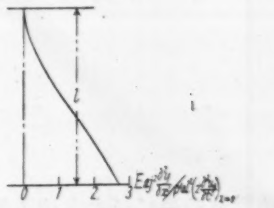

Fig. 20. $\left(\frac{\rho' p^2}{Ej^2}\right)^{\frac{1}{4}} l=2{\cdot}1.$

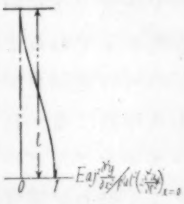

Fig. 21. $\left(\frac{\rho' p^2}{Ej^2}\right)^{\frac{1}{4}} l=2{\cdot}365.$

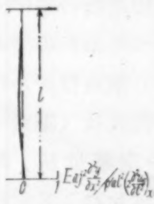

Fig. 22. $\left(\frac{\rho' p^2}{Ej^2}\right)^{\frac{1}{4}} l=3{\cdot}5.$

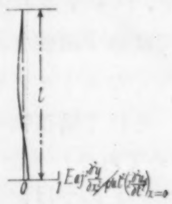

Fig. 23. $\left(\frac{\rho' p^2}{Ej^2}\right)^{\frac{1}{4}} l=4{\cdot}73.$

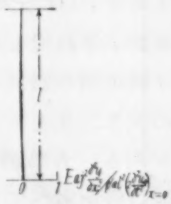

Fig. 24. $\left(\frac{\rho' p^2}{Ej^2}\right)^{\frac{1}{4}} l=5{\cdot}498.$

and frequency of seismic vibrations, the bending moment or bending stress induced at a given part of the structure is determinate. It is evident that, apart from the physical nature of the material used in the structure, acceleration cannot be the only parameter for the failure of the structure, or that even both acceleration and frequency are not sufficient for that purpose.[8] The type of the structure as well as its conditions in relation to that of the ground play an important part in the problem. The ordinates taken horizontally in the curves in

---

[8] K. SEZAWA, *Publ. Bureau Centr. Séism. Int.*, [A], No. 10 (1934), 113.

Figs. 18∼24 indicate how the distribution and magnitudes of bending moments in the structure change with any change in the period, provided however that acceleration in free ground (no structures) is always unity and that the particular type of structure as well as its conditions in relation to that of the ground are specified.

In conclusion we wish to express our thanks to the Council of the Foundation for the Promotion of Scientific and Industrial Research of Japan, with whose aid the progress of the present work was greatly assisted.

---

54. 勢力の地下逸散の爲に生ずる高層構造物の震動減衰

地震研究所 妹澤克惟
金井清

地震波の中にはあらゆる週期の波が存在してゐることは多くの記録を見れば明かである．從て，構造物に何等かの振動減衰性がなければ，如何に强度のある構造物でも共振を起し結局は破壞を免れないであらう．彙報第 12 號で説明したやうに，構造物の破壞は材料の破壞的性質を別問題とすると，(i) 土地の加速度，(ii) 土地の週期，(iii) 構造物の型の三個のもので決定できたのであるが，それでも共振の所では必ず破壞することになつてゐたのである．果してそうであるとすると構造物の設計の基準がなくなることになる．しかし減衰性があれば，共振の所の震動力が一定の大さに止まる譯である．それで構造物の材料の内部抵抗（筆者の一人も七八年前に考へたことがある．力學的に最も初めであつたと記憶する）や空氣抵抗，基礎のプラスチックなどによる減衰性を考へて見ると之等のものではどうしても追付かぬことがわかる．そこで勢力が彈性波として再び地中へ逸散するものとして計算して見ると非常に大きな減衰があり得，且つ如何なる割合に減衰するかといふこともはつきり數量的に算定できるのである．而して之は前揭の三種の性質以外に (iv) 構造物の性質と土地の性質との關係から決定されるのである．構造物と土地との結合狀態や振動の數理等については本文に示してある通りであつて，それ等の Elements はすべて他の多くの實驗結果が基礎となつてゐるから，そこに數學上の勝手な假定などといふものは何もない．寧ろ他の地震現象説明論などで其場あたりの氣分で議論をされるのとは全く譯が違つてゐる．

この論文に於て，單一構造物に上下動や水平動の働く場合や高層構造物に水平動や上下動が働く場合の强制振動及び自由振動が，(i) 種々の週期，(ii) 構造物のないときの土地の種々の加速度，(iii) 種々の構造型，(iv) 土地の性質と構造物の性質との關係によつて數量的に決定できることを示してある．共振に當る强制振動でも其振幅其他が一定のものであるから之等を基準として構造物を設計すればよい譯である．

共振の狀態に於ては構造物又は土地の基礎に當る部分が夫々の振動の節點に近いといふことか

らでも共振に於ても構造物の振幅が大して大きくはないといふことが了解できるであらう．又，構造物の剛度が土地のそれに比して大きければ大きい程，共振のときの振幅が小さくなることは注目に値すると思ふ．而も之等の剛度は夫々の彈性力と密度との積（場合によつては多少複雜な積）に比例してゐるものである．

構造物の固有振動の減衰の恒數も上述のものの一部分で定まり，固體粘性などは問題にならない．

床が撓み易い高層構造物や煙突などの震動については種々面白いことがあるけれども茲には省略し本文中の説明に讓ることにする．

只今の研究によつてこれまで多くの構造學者（又は力學家）の研究した構造物の振動問題，殊に共振の概念は根本的に正しくなかつたといふことはいひ得ると思ふ．

55. *Energy Dissipation in Seismic Vibrations of a Framed Structure.*

By Katsutada SEZAWA and Kiyoshi KANAI,

Earthquake Research Institute.

(Read May 21, 1935.—Received June 20, 1935.)

1. In one[1] of our papers published last year, we determined the distribution of bending moments in the columns of a multi-storied structure under periodic earthquake movements of the ground. Since however the nature of dissipation of vibrational energy was not perfectly understood by us at the time, we discussed the problem in that paper under the assumption that the movement of the lower end or foundation of the structure is the same as that of a free ground surface, that is, one on which no structure is standing. From the results of our foregoing paper[2], it is evident that such an assumption is not permissible unless the effective stiffness or density of the structure differs widely from the rigidity or the density of the ground on which the structure rests. Our present calculation shows that, owing to the dissipation of vibrational energy into the ground, the amplitudes of vibrations of a structure do not exceed a certain limit even under resonance conditions. We also come to a similar conclusion with respect to the bending moments in any member of the structure. This fact appears to answer the question what strength is necessary in the earthquake-proof construction of a structure, that is liable to be subjected to resonating seismic vibrations.

In this paper we investigate three kinds of structures, namely, (i) structures with rigid floors and clamped base, (ii) structures with flexible floors and clamped base, (iii) structures with rigid floors and hinged base. Rigid and flexible floors correspond to the "clamped and supported floors" of the previous paper[3]. By "rigid floor" is meant a floor so rigid as never to bend through horizontal oscillations, as practically obtained in actual buildings; while by "flexible floor" is meant a floor so flexible as to yield to horizontal oscillations, a condition however that hardly obtains in actual construction, excepting in a structure with very long and weakly spanned floors.

---

[1] K. SEZAWA and K. KANAI, "Some New Problems of Forced Vibrations of a Structure", *Bull. Earthq. Res. Inst.*, **12** (1934), 823~853. This paper will hereinafter be referred to as paper (B).

[2] K. SEZAWA and K. KANAI, "Decay in the Seismic Vibrations of a (Simple or Tall) Structure by Dissipation of their Energy into the Ground", *Proc. Imp. Acad.*, **11** (1935), 174; *Bull. Earthq. Res. Inst.*, **13** (1935), 681~697.

[3] K. SEZAWA and K. KANAI, *ibid.*.

As to the number of stories we have treated three cases, namely one-, two-, and three-storied for each of the three types of structure. The waves are assumed to be of the same nature as in the case of a simple structure subjected to horizontal oscillations.

2. *A structure with rigid floors and clamped base.*

Both incident and dissipated waves are assumed to have the same forms as those stated in the preceding paper[4]. The equation of motion of the columns for each floor is the same as that used in last year's paper[5], namely,

$$\frac{\partial^4 y_s}{\partial x_s^4}=0\,, \qquad (1)$$

its solution being

$$y_s=(A_s+B_sx_s+C_sx_s^2+D_sx_s^3)e^{ipt}\,, \qquad (2)$$

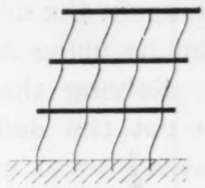

Fig. 1.

where s signifies the case for columns between the $(s-1)$th and the sth floors, x_s is the coordinate of a current point on the same columns measured negatively from their respective lower ends, and y_s is the horizontal deflection of the point x_s. If l_s be the length of the columns under consideration, the boundary conditions for an n-storied structure are

$$x_n=-l_n;\quad \frac{\partial y_n}{\partial x_n}=0\,,\quad E_nI_n\frac{\partial^3 y_n}{\partial x_n^3}+m_n\frac{\partial^2 y_n}{\partial t^2}=0, \qquad (3),\ (4)$$

$$x_s=-l_s\,,\quad x_{s+1}=0;\quad y_s=y_{s+1}\,,\quad \frac{\partial y_s}{\partial x_s}=0\,,\quad \frac{\partial y_{s+1}}{\partial x_{s+1}}=0, \qquad (5),\ (6),\ (7)$$

$$E_{s+1}I_{s+1}\frac{\partial^3 y_{s+1}}{\partial x_{s+1}^3}=E_sI_s\frac{\partial^3 y_s}{\partial x_s^3}+m_s\frac{\partial^2 y_s}{\partial t^2}\,, \qquad (8)$$

$$(s=1, 2, \cdots, n-1.)$$

$$x_1=0;\quad y_{1x_1=0}=u_{0x_1=0}+(u_1+u_2)_{r=\varepsilon,\ \theta=0}\,,\ \frac{\partial y_1}{\partial x_{1x_1=0}}=0, \qquad (9),\ (10)$$

---

[4] Paper (B).

[5] K. SEZAWA and K. KANAI, *loc. cit. ante.* in 2).

$$-E_1\pi\varepsilon^2 j^2 \frac{\partial^3 y_1}{\partial x^3_{1_{x_1=0}}} = \mu\pi\varepsilon^2 \frac{\partial u_0}{\partial x_{1_{x_1=0}}}$$

$$+\int_{\theta=0}^{\pi}\int_{\varphi=0}^{\pi}\mu\left(\frac{\partial(v_1+v_2)}{\partial r}-\frac{(v_1+v_2)}{r}+\frac{1}{r}\frac{\partial(u_1+u_2)}{\partial\theta}\right)r^2\sin^2\theta d\theta d\varphi_{r=\varepsilon}$$

$$+\int_{\theta=0}^{\pi}\int_{\varphi=0}^{\pi}\left(\lambda\Delta+2\mu\frac{\partial(u_1+u_2)}{\partial r}\right)r^2\sin\theta\cos\theta d\theta d\varphi_{r=\varepsilon}, \tag{11}$$

where m_s is the mass concentrated on the sth floor, and l_s, E_s, I_s are the length, Young's modulus, and the sum of the moments of inertia of cross sections of the columns between the $(s-1)$th and the sth floors, l_1, E_1, $I_1(=\pi\varepsilon^2 j^2)$ being the same for the lowest columns. ρ, λ, μ are again the density and elastic constants of the earth, while we shall soon be using $h^2=\rho p^2/(\lambda+2\mu)$ and $k^2=\rho p^2/\mu$.

Solving the problem in the same way as in the previous paper, we get the deflection of the columns, corresponding to the incident waves,

$$u_0=\cos(pt+kx), \tag{12}$$

as follows:

(i) $n=1$,

$$y_1=\frac{\left(7\sqrt{\frac{\lambda}{\mu}+2}-4\right)\left\{(12-\gamma)+3\gamma\left(\frac{x}{l}\right)^2+2\gamma\left(\frac{x}{l}\right)^3\right\}}{4\sqrt{P^2+Q^2}}\cos\left(pt-\tan^{-1}\frac{P}{Q}\right), \tag{13}$$

where

$$P=9\sqrt{\frac{\lambda}{\mu}+2}\left(\frac{Ej^2}{\mu kl^3}\right)\gamma, \quad Q=(12-\gamma)\left(\sqrt{\frac{\lambda}{\mu}+2}-1\right), \tag{14}$$

$$\gamma=\frac{mp^2l^3}{EI}. \tag{15}$$

(ii) $n=2$,

$$y_1=\frac{\left(7\sqrt{\frac{\lambda}{\mu}+2}-4\right)}{4\sqrt{P^2+Q^2}}\left[\left\{(12-\gamma_1)(12-\gamma_2)-12\gamma_2\eta\right\}\right.$$

$$\left.+\left\{12\gamma_2\eta+\gamma_1(12-\gamma_2)\right\}\left\{3\left(\frac{x_1}{l_1}\right)^2+2\left(\frac{x_1}{l_1}\right)^3\right\}\right]\cos\left(pt-\tan^{-1}\frac{P}{Q}\right), \tag{16}$$

$$y_2=\frac{3\left(\sqrt{\frac{\lambda}{\mu}+2}-4\right)}{\sqrt{P^2+Q^2}}\Bigg[(12-\gamma_2)$$

$$+\gamma_2\left\{3\left(\frac{x_2}{l_2}\right)^2+2\left(\frac{x_2}{l_2}\right)^3\right\}\Bigg]\cos\left(pt-\tan^{-1}\frac{P}{Q}\right), \tag{17}$$

where

$$\left.\begin{aligned}P&=9\sqrt{\frac{\lambda}{\mu}+2}\left(\frac{E_1j_1^2}{\mu k l_1^3}\right)\left\{12\gamma_2\eta+\gamma_1(12-\gamma_2)\right\},\\ Q&=\left(\sqrt{\frac{\lambda}{\mu}+2}-1\right)\left\{(12-\gamma_1)(12-\gamma_2)-12\gamma_2\eta\right\},\end{aligned}\right\} \tag{18}$$

$$\gamma_1=\frac{m_1p^2l_1^3}{E_1I_1},\quad \gamma_2=\frac{m_2p^2l_2^3}{E_2I_2},\quad \eta=\frac{E_2I_2l_1^3}{E_1I_1l_2^3}. \tag{19}$$

(iii) $n=3$,

$$y_1=\frac{\left(7\sqrt{\frac{\lambda}{\mu}+2}-4\right)}{4\sqrt{P^2+Q^2}}\Bigg\{\Big[12\zeta\gamma_3\{12\eta+(12-\gamma_1)\}$$

$$-(12-\gamma_3)\{(12-\gamma_1)(12-\gamma_2)-12\eta\gamma_3\}\Big]-\Big[12\zeta\gamma_3(12\eta-\gamma_1)+$$

$$(12-\gamma_3)\{\gamma_1(12-\gamma_2)+12\eta\gamma_2\}\Big]\left\{3\left(\frac{x_1}{l_1}\right)^2+2\left(\frac{x_1}{l_1}\right)^3\right\}\Bigg\}\cos\left(pt-\tan^{-1}\frac{P}{Q}\right), \tag{20}$$

$$y_2=\frac{3\left(7\sqrt{\frac{\lambda}{\mu}+2}-4\right)}{\sqrt{P^2+Q^2}}\Bigg[\{12\zeta\gamma_3-(12-\gamma_2)(12-\gamma_3)\}$$

$$-\{12\zeta\gamma_3+\gamma_2(12-\gamma_3)\}\left\{3\left(\frac{x_2}{l_2}\right)^2+2\left(\frac{x_2}{l_2}\right)^3\right\}\Bigg]\cos\left(pt-\tan^{-1}\frac{P}{Q}\right), \tag{21}$$

$$y_3=\frac{-36\left(7\sqrt{\frac{\lambda}{\mu}+2}-4\right)}{\sqrt{P^2+Q^2}}\Bigg[(12-\gamma_3)$$

$$+\gamma_3\left\{3\left(\frac{x_3}{l_3}\right)^2+2\left(\frac{x_3}{l_3}\right)^3\right\}\Bigg]\cos\left(pt-\tan^{-1}\frac{P}{Q}\right), \tag{22}$$

where

$$\left.\begin{aligned}P&=-9\sqrt{\frac{\lambda}{\mu}+2}\left(\frac{E_1j^2}{\mu k l_1^3}\right)\Big[12\zeta\gamma_3(\gamma_1-12\eta)-(12-\gamma_3)\{\gamma_1(12-\gamma_2)+12\eta\gamma_2\}\Big],\\ Q&=\left(\sqrt{\frac{\lambda}{\mu}+2}-1\right)\Big[12\zeta\gamma_3\{12\eta+(12-\gamma_1)\}\\ &\qquad\qquad-(12-\gamma_3)\{(12-\gamma_1)(12-\gamma_2)-12\eta\gamma_2\}\Big],\end{aligned}\right\} \tag{23}$$

$$\gamma_1=\frac{m_1p^2l_1^3}{E_1I_1},\quad \gamma_2=\frac{m_2p^2l_2^3}{E_2I_2},\quad \gamma_3=\frac{m_3p^2l_3^3}{E_3I_3},\quad \eta=\frac{E_2I_2l_1^3}{E_1I_1l_2^3},\quad \zeta=\frac{E_3I_3l_2^3}{E_2I_2l_3^3}. \tag{24}$$

In the special case $E_1=E_2=\cdots=E$, $I_1=I_2=\cdots=I$, $l_1=l_2=\cdots=l$, $m_1=m_2=\cdots=m$, we have

(i) $n=1$, the same as (13), (14), (15).

(ii) $n=2$,

$$y_1=\frac{\left(7\sqrt{\frac{\lambda}{\mu}+2}-4\right)}{4\sqrt{P^2+Q^2}}\Bigg[(\gamma^2-36\gamma+144) -\gamma(\gamma-24)\left\{3\left(\frac{x_1}{l}\right)^2+2\left(\frac{x_1}{l}\right)^3\right\}\Bigg]\cos\left(pt-\tan^{-1}\frac{P}{Q}\right), \tag{16'}$$

$$y_2=\frac{3\left(7\sqrt{\frac{\lambda}{\mu}+2}-4\right)}{\sqrt{P^2+Q^2}}\Bigg[-(\gamma-12) +\gamma\left\{3\left(\frac{x_2}{l}\right)^2+2\left(\frac{x_2}{l}\right)^3\right\}\Bigg]\cos\left(pt-\tan^{-1}\frac{P}{Q}\right), \tag{17'}$$

where

$$\left.\begin{aligned} P&=9\sqrt{\frac{\lambda}{\mu}+2}\left(\frac{Ej^2}{\mu kl^3}\right)\gamma(24{-}{-}\gamma),\\ Q&=\left(\sqrt{\frac{\lambda}{\mu}+2}-1\right)(\gamma^2-36\gamma+144),\end{aligned}\right\} \tag{18'}$$

$$\gamma=\frac{mp^2l^3}{EI}. \tag{19'}$$

(iii) $n=3$,

$$y_1=\frac{\left(7\sqrt{\frac{\lambda}{\mu}+2}-4\right)}{4\sqrt{P^2+Q^2}}\Bigg[(\gamma^3-60\gamma^2+864\gamma-1728) -\gamma(12-\gamma)(36-\gamma)\left\{3\left(\frac{x_1}{l}\right)^2+2\left(\frac{x_1}{l}\right)^3\right\}\Bigg]\cos\left(pt-\tan^{-1}\frac{P}{Q}\right), \tag{20'}$$

$$y_2=\frac{3\left(7\sqrt{\frac{\lambda}{\mu}+2}-4\right)}{\sqrt{P^2+Q^2}}\Bigg[-(\gamma^2-36\gamma+144) -\gamma(24-\gamma)\left\{3\left(\frac{x_2}{l}\right)^2+2\left(\frac{x_2}{l}\right)^3\right\}\Bigg]\cos\left(pt-\tan^{-1}\frac{P}{Q}\right), \tag{21'}$$

$$y_3=\frac{-36\left(7\sqrt{\dfrac{\lambda}{\mu}+2}-4\right)}{\sqrt{P^2+Q^2}}\left[(12-\gamma)\right.$$

$$\left.+\gamma\left\{3\left(\frac{x_3}{l}\right)^2+2\left(\frac{x_3}{l}\right)^3\right\}\right]\cos\left(pt-\tan^{-1}\frac{P}{Q}\right), \qquad (22')$$

where

$$\left.\begin{aligned} P&=-9\sqrt{\frac{\lambda}{\mu}+2}\left(\frac{Ej^2}{\mu kl^3}\right)\gamma(12-\gamma)(36-\gamma),\\ Q&=\left(\sqrt{\frac{\lambda}{\mu}+2}-1\right)(\gamma^3-60\gamma^2+864\gamma-1728)\,,\end{aligned}\right\} \qquad (23')$$

$$\gamma=\frac{mp^2l^3}{EI}. \qquad (24')$$

The maximum values of the bending moments $E_sI_s\,(d^2y_s/dx_s^2)$ at each end of the columns corresponding to the maximum values of acceleration of the ground on which no structure rests were determined from the above equations for the special case $E_s=E$, $I_s=I$, $l_s=l$, $m_s=m$, $Ej^2/\mu kl^3=0{\cdot}05$, $\lambda/\mu=14$, and for various values of ml^3/EI; they are diagrammatically shown in Figs. 2, 3, 4. Vertical strips in these

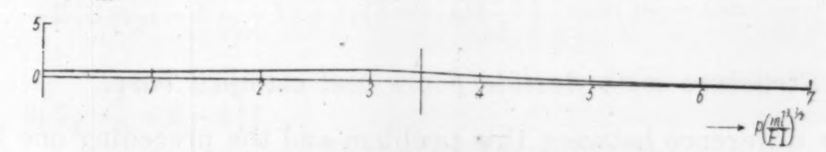

Fig. 2. The case of a singled-storied structure with rigid floor and clamped base.

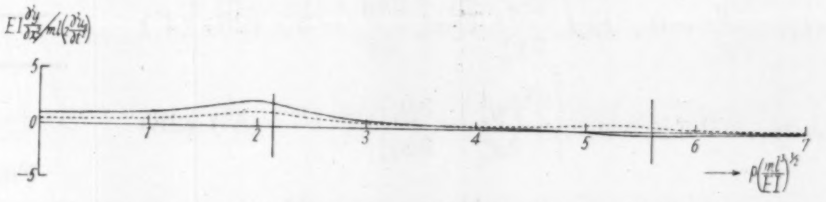

Fig. 3. The case of a two-storied structure with rigid floors and clamped base. Full line: lowest columns. Broken line: second columns.

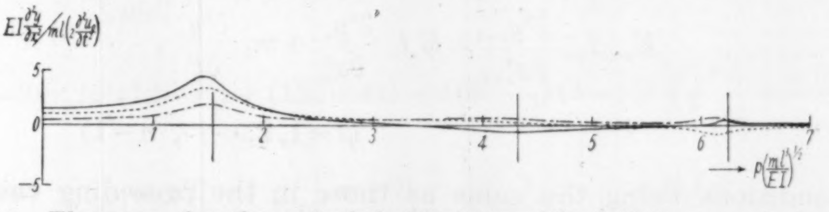

Fig. 4. The case of a three-storied structure with rigid floors and clamped base. Full line: lowest columns. Broken line: second columns. Chain: third columns.

figures represent the cases corresponding to resonance conditions. These figures show that the bending moments of the columns in the structure, even under resonance conditions, are not very large—a fact that will be recognized more clearly on comparing the present result with Figs. 3, 4 of paper (B). When writing paper (B), we had hopes that the infinitely large bending moments under resonance conditions, as shown in Figs. 3, 4, $\cdots$ of that paper, could be reduced to certain finite values by the introduction of some form of damping resistance, which however is now being realized by more rational methods. It is a matter of importance whether $Ej^2/\mu kl^3=0{\cdot}05$ is probable or not in an actual case. We shall take the case of a concrete structure standing on alluvium ground, when it is then possible to assume that $E/\mu=10$, $j^2/l^2=1/1000(l/j=33)$, $1/kl=5(l=5\text{ m.}, 2\pi/k=160\text{ m})$, whence it follows that $Ej^2/\mu kl^3=0{\cdot}05$. We find that the assumed value of $Ej^2/\mu kl^3$ does not differ much from an actual case. It is rather probable that in the usual structures,[6] E/μ may take greater values, in which case the dissipation would be more pronounced than in the one we have calculated.

3. *Structure with flexible floors and clamped base.*

The difference between this problem and the preceding one is merely with respect to floor conditions. Here we have

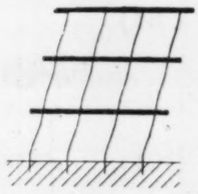

Fig. 5.

$$x_n=-l_n;\ \frac{\partial^2 y_n}{\partial x_n^2}=0,\ E_nI_n\frac{\partial^3 y_n}{\partial x_n^3}+m_n\frac{\partial^2 y_n}{\partial t^2}=0,\quad (25)\ (4')$$

$$x_s=l_s,\ x_{s+1}=0;\ y_s=y_{s+1},\ \frac{\partial y_s}{\partial x_s}=\frac{\partial y_{s+1}}{\partial x_{s+1}},\quad (5')\ (26)$$

$$E_{s+1}I_{s+1}\frac{\partial^2 y_{s+1}}{\partial x_{s+1}^2}=E_sI_s\frac{\partial^2 y_s}{\partial x_s^2},\tag{27}$$

$$E_{s+1}I_{s+1}\frac{\partial^3 y_{s+1}}{\partial x_{s+1}^3}=E_sI_s\frac{\partial^3 y_s}{\partial x_s^3}+m_s\frac{\partial^2 y_s}{\partial t^2},\tag{8'}$$

$$(s=1,2,\cdots,n-1)$$

other conditions being the same as those in the preceding case. The final solutions of the problem corresponding to the incident waves

$$u_0=\cos(pt+kx),\tag{12'}$$

are as follows:

---

[6] K. SEZAWA and K. KANAI's paper which will appear in a forthcoming bulletin of the Institute.

(i) $n=1$,

$$y_1=\frac{\left(7\sqrt{\frac{\lambda}{\mu}+2}-4\right)}{2\sqrt{P^2+Q^2}}\left[2(3-\gamma)+\gamma\left\{3\left(\frac{x}{l}\right)^2+\left(\frac{x}{l}\right)^3\right\}\right]\cos\left(pt-\tan^{-1}\frac{P}{Q}\right), \tag{28}$$

where $$P=9\sqrt{\frac{\lambda}{\mu}+2}\left(\frac{Ej^2}{\mu k l^3}\right)\gamma, \quad Q=4\left(\sqrt{\frac{\lambda}{\mu}+2}-1\right)(3-\gamma), \tag{29}$$

$$\gamma=\frac{mp^2l^3}{EI}. \tag{30}$$

(ii) $n=2$,

$$\begin{aligned}y_1=\frac{\left(7\sqrt{\frac{\lambda}{\mu}+2}-4\right)}{4\sqrt{P^2+Q^2}}&\Big\{[-3\eta\gamma_2\{\xi^2(12-\gamma_1)+12\xi+4\}+4(3-\gamma_1)(3-\gamma_2)]\\&+3\{3\eta\gamma_2(-\xi^2\gamma_1+2\xi+2)+2\gamma_1(3-\gamma_2)\}\left(\frac{x_1}{l_1}\right)^2\\&+2\{3\eta\gamma_2(-\xi^2\gamma_1+1)+\gamma_1(3-\gamma_2)\}\left(\frac{x_1}{l_1}\right)^3\Big\}\cos\left(pt-\tan^{-1}\frac{P}{Q}\right),\end{aligned} \tag{31}$$

$$\begin{aligned}y_2=\frac{3\left(7\sqrt{\frac{\lambda}{\mu}+2}-4\right)}{4\sqrt{P^2+Q^2}}&\Big[-2\{3\xi\eta\gamma_2(2\xi+1)-2(3-\gamma_2)\}\\&-2\xi\{3\eta\gamma_2(2\xi+1)+\gamma_1(3-\gamma_2)\}\left(\frac{x_2}{l_2}\right)\\&+\gamma_2(\xi\gamma_1+2)\left\{3\left(\frac{x_2}{l_2}\right)^2+\left(\frac{x_2}{l_2}\right)^3\right\}\Big]\cos\left(pt-\tan^{-1}\frac{P}{Q}\right),\end{aligned} \tag{32}$$

where

$$\left.\begin{aligned}P&=9\sqrt{\frac{\lambda}{\mu}+2}\left(\frac{E_1j^2}{\mu k l_1^3}\right)\left\{3\eta\gamma_2(-\xi^2\gamma_1+1)+\gamma_1(3-\gamma_2)\right\}\\Q&=\left[-3\eta\gamma_2\{\xi^2(12-\gamma_1)+(12\xi+4)\}+4(3-\gamma_1)(3-\gamma_2)\right]\left(\sqrt{\frac{\lambda}{\mu}+2}-1\right),\end{aligned}\right\} \text{33)}$$

$$\gamma_1=\frac{m_1p^2l_1^3}{E_1I_1}, \quad \gamma_2=\frac{m_2p^2l_2^3}{E_2I_2}, \quad \xi=\frac{l_2}{l_1}, \quad \eta=\frac{E_2I_2l_1^3}{E_1I_1l_2^3}. \tag{34}$$

(iii) $n=3$. The general case omitted.

In the special case, $E_1=E_2=\cdots=E$, $I_1=I_2=\cdots=I$, $l_1=l_2=\cdots=l$, $m_1=m_2=\cdots=m$, we have

(i) $n=1$, the same as (28), (29); (30).

(ii) $n=2$,

$$y_1=\frac{\left(7\sqrt{\frac{\lambda}{\mu}+2}-4\right)}{4\sqrt{P^2+Q^2}}\left[(7\gamma^2-108\gamma+36)-3\gamma(5\gamma-18)\left(\frac{x_1}{l}\right)^2\right.$$
$$\left.-4\gamma(2\gamma-3)\left(\frac{x_1}{l}\right)^3\right]\cos\left(pt-\tan^{-1}\frac{P}{Q}\right), \tag{31'}$$

$$y_2=\frac{3\left(7\sqrt{\frac{\lambda}{\mu}+2}-4\right)}{4\sqrt{P^2+Q^2}}\left[-2(11\gamma-6)+2\gamma(\gamma-12)\left(\frac{x_2}{l}\right)\right.$$
$$\left.+\gamma(\gamma+2)\left\{3\left(\frac{x_2}{l}\right)^2+\left(\frac{x_2}{l}\right)^3\right\}\right]\cos\left(pt-\tan^{-1}\frac{P}{Q}\right), \tag{32'}$$

where

$$\left.\begin{aligned}P&=18\sqrt{\frac{\lambda}{\mu}+2}\left(\frac{Ej^2}{\mu k l^3}\right)(3-2\gamma)\gamma\,,\\ Q&=\left(\sqrt{\frac{\lambda}{\mu}+2}-1\right)(7\gamma^2-108\gamma+36)\,,\end{aligned}\right\} \tag{33'}$$

$$\gamma=\frac{mp^2l^3}{EI}\,. \tag{34'}$$

(iii) $n=3$,

$$y_1=\frac{\left(7\sqrt{\frac{\lambda}{\mu}+2}-4\right)}{2\sqrt{P^2+Q^2}}\left\{2(13\gamma^3-393\gamma^2+1296\gamma-108)\right.$$
$$+3\gamma(-19\gamma^2+294\gamma-216)\left(\frac{x_1}{l}\right)^2$$
$$\left.+\gamma(-31\gamma^2+372\gamma-108)\left(\frac{x_1}{l}\right)^3\right\}\cos\left(pt-\tan^{-1}\frac{P}{Q}\right), \tag{35}$$

$$y_2=\frac{3\left(7\sqrt{\frac{\lambda}{\mu}+2}-4\right)}{2\sqrt{P^2+Q^2}}\left\{4(-23\gamma^2+171\gamma-18)\right.$$
$$+\gamma(7\gamma^2-216\gamma+324)\left(\frac{x_2}{l}\right)+6\gamma(2\gamma^2-13\gamma-18)\left(\frac{x_2}{l}\right)^2$$
$$\left.+\gamma(5\gamma^2+10\gamma-24)\left(\frac{x_2}{l}\right)^3\right\}\cos\left(pt-\tan^{-1}\frac{P}{Q}\right), \tag{36}$$

$$y_3=\frac{3\left(7\sqrt{\frac{\lambda}{\mu}+2}-4\right)}{2\sqrt{P^2+Q^2}}\Bigg[12(3\gamma^2+23\gamma-6)+2\gamma(-\gamma^2-15\gamma+234)\left(\frac{x_3}{l}\right)$$

$$-\gamma(\gamma^2+36\gamma+12)\left\{3\left(\frac{x_3}{l}\right)^2+\left(\frac{x_3}{l}\right)^3\right\}\Bigg]\cos\left(pt-\tan^{-1}\frac{P}{Q}\right), \tag{37}$$

where

$$\left.\begin{aligned} P&=9\sqrt{\frac{\lambda}{\mu}+2}\left(\frac{Ej^2}{\mu kl^3}\right)\gamma(-31\gamma^2+372\gamma-108)\,,\\ Q&=4\left(\sqrt{\frac{\lambda}{\mu}+2}-1\right)(13\gamma^3-393\gamma^2+1296\gamma-108)\,,\end{aligned}\right\} \tag{38}$$

$$\gamma=\frac{mp^2l^3}{EI}. \tag{39}$$

The maximum values of bending moments $E_sI_s(\partial^2y_s/\partial x_s^2)$ at each end of the columns corresponding to the maximum values of acceleration of the ground on which no structure stands were determined from the above equations for the special case $E_s=E$, $I_s=I$, $l_s=l$, $m_s=m$, $Ej^2/\mu kl^3=0{\cdot}05$, $\lambda/\mu=14$, and for various values of ml^3/EI. They are diagrammatically shown in Figs. 6, 7, 8. Although the bending moments of the present case under the first resonance condition are excessively large compared with the one of the previous case, namely the structure with rigid floors, it is still certain that the moments under higher resonance conditions are exceed-

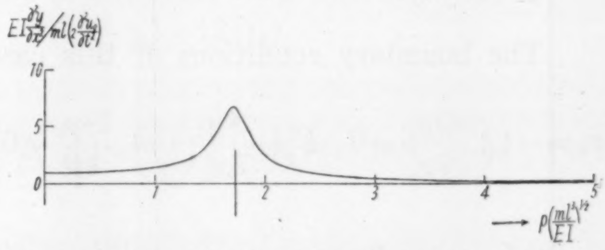

Fig. 6. The case of a singled-storied structure with flexible floor and clamped base.

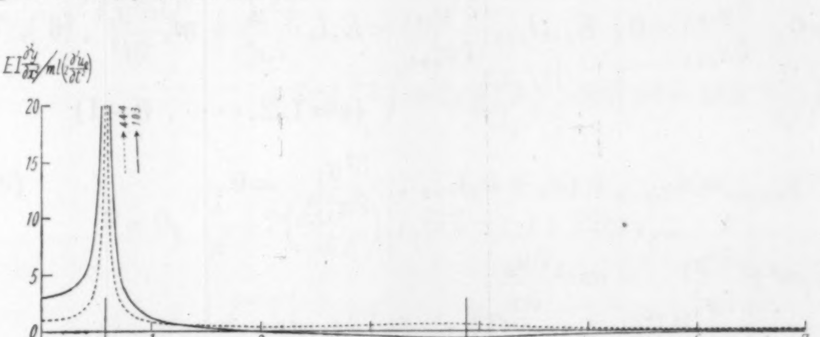

Fig. 7. The case of a two-storied structure with flexible floors and clamped base. Full line: lowest columns. Broken line: second columns.

ingly small. Nevertheless, it will be found, upon comparing our present result with those shown in Figs. 10, 11 of paper (B), that the respective moments under frequencies out of resonance are approximately equal for both this and the last cases, notwithstanding the great difference between them under every resonance condition.

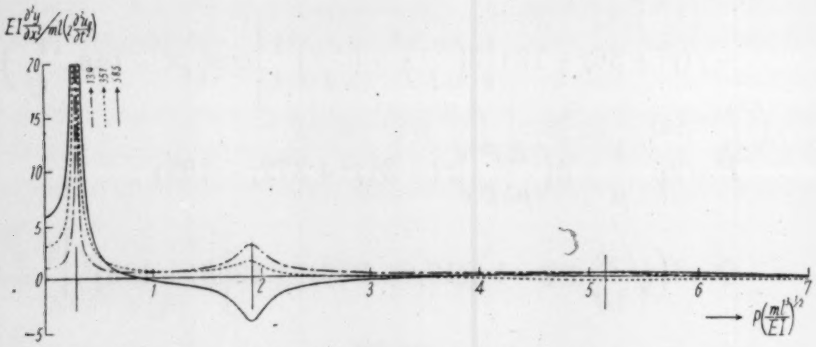

Fig. 8. The case of a three-storied structure with flexible floors and clamped base. Full line: lowest columns. Broken line: second columns. Chain: third columns.

4. *A structure with rigid floors and hinged base.*

The boundary conditions of this case are

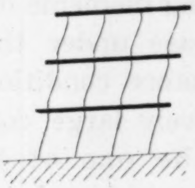

Fig. 9.

$$x_n=-l_n;\quad \frac{\partial y_n}{\partial x_n}=0\,,\quad E_nI_n\frac{\partial^3 y_n}{\partial x_n^3}+m_n\frac{\partial^2 y_n}{\partial t^2}=0\,,\qquad (3')\ (4'')$$

$$x_s=-l_s\,,\ x_{s+1}=0;\ y_s=y_{s+1}\,,\qquad (5'),$$

$$\frac{\partial y_s}{\partial x_s}=0\,,\ \frac{\partial y_{s+1}}{\partial x_{s+1}}=0\,,\ E_{s+1}I_{s+1}\frac{\partial^3 y_{s+1}}{\partial x_{s+1}^3}=E_sI_s\frac{\partial^3 y_s}{\partial x_s^3}+m_s\frac{\partial^2 y_s}{\partial t^2}\,,\ (6'),(7'),(8'')$$

$$(s=1,2,\cdots,n-1)$$

$$x_1=0;\quad y_{1_{x_1=0}}=u_{0_{x_1=0}}+(u_1+u_2)_{r=\varepsilon}\,,\quad \frac{\partial^2 y_1}{\partial x^2_{1_{x_1=0}}}=0\,,\qquad (9'),\ (40)$$

$$-E_1\pi\varepsilon^2 j^2\frac{\partial^3 y_1}{\partial x^3_{1_{x_1=0}}}=\mu\pi\varepsilon^2\frac{\partial u_0}{\partial x}_{x=0}$$

$$+\int_{\theta=0}^{\pi}\int_{\varphi=0}^{\pi}\mu\left(\frac{\partial(v_1+v_2)}{\partial r}-\frac{(v_1+v_2)}{r}+\frac{1}{r}\frac{\partial(u_1+u_2)}{\partial\theta}\right)r^2\sin^2\theta d\theta d\varphi_{r=\varepsilon}$$

$$+\int_{\theta=0}^{\pi}\int_{\varphi=0}^{\pi}\left(\lambda\Delta+2\mu\frac{\partial(u_1+u_2)}{\partial r}\right)r^2\sin\theta\cos\theta d\theta d\varphi_{r=\varepsilon}\,.\qquad (11')$$

The condition for ε is the same as in the preceding cases. The solutions of the problem corresponding to the incident waves

$$u_0 = \cos(pt + kx), \tag{12''}$$

are as follows:

(i) $n=1$,

$$y = \frac{\left(7\sqrt{\frac{\lambda}{\mu}+2}-4\right)}{2\sqrt{P^2+Q^2}}\left\{2(3-\gamma)-3\gamma\left(\frac{x}{l}\right)+\gamma\left(\frac{x}{l}\right)^3\right\}\cos\left(pt-\tan^{-1}\frac{P}{Q}\right), \tag{41}$$

where

$$P = 9\gamma\sqrt{\frac{\lambda}{\mu}+2}\left(\frac{Ej^2}{\mu k l^3}\right), \quad Q = 4(3-\gamma)\left(\sqrt{\frac{\lambda}{\mu}+2}-1\right), \tag{42}$$

$$\gamma = \frac{mp^2l^3}{EI}. \tag{43}$$

(ii) $n=2$,

$$y_1 = \frac{\left(7\sqrt{\frac{\lambda}{\mu}+2}-4\right)}{2\sqrt{P^2+Q^2}}\Big[2\{(3-\gamma_1)(12-\gamma_2)-12\eta\gamma_2\}$$
$$+\{\gamma_1(12-\gamma_2)+12\eta\gamma_2\}\left\{-3\left(\frac{x_1}{l_1}\right)+\left(\frac{x_1}{l_1}\right)^3\right\}\Big]\cos\left(pt-\tan^{-1}\frac{P}{Q}\right), \tag{44}$$

$$y_2 = \frac{3\left(7\sqrt{\frac{\lambda}{\mu}+2}-4\right)}{\sqrt{P^2+Q^2}}\Big\{(12-\gamma_2)$$
$$+3\gamma_2\left(\frac{x_2}{l_2}\right)^2+2\gamma_2\left(\frac{x_2}{l_2}\right)^3\Big\}\cos\left(pt-\tan^{-1}\frac{P}{Q}\right), \tag{45}$$

where

$$\left.\begin{aligned} P &= 9\sqrt{\frac{\lambda}{\mu}+2}\left(\frac{E_1j^2}{\mu k l_1^3}\right)\left\{\gamma_1(12-\gamma_2)+12\eta\gamma_2\right\}, \\ Q &= 4\left(\sqrt{\frac{\lambda}{\mu}+2}-1\right)\left\{(3-\gamma_1)(12-\gamma_2)-12\eta\gamma_2\right\}, \end{aligned}\right\} \tag{46}$$

$$\gamma_1 = \frac{m_1p^2l_1^3}{E_1I_1}, \quad \gamma_2 = \frac{m_2p^2l_2^3}{E_2I_2}, \quad \eta = \frac{E_2I_2l_1^3}{E_1I_1l_2^3}. \tag{47}$$

(iii) $n=3$,

$$y_1=\frac{\left(7\sqrt{\frac{\lambda}{\mu}+2}-4\right)}{2\sqrt{P^2+Q^2}}\Big\{2[(3-\gamma_1)\{12\zeta\gamma_3-(12-\gamma_2)(12-\gamma_3)\}$$

$$+12\eta\{12\zeta\gamma_3+\gamma_2(12-\gamma_3)\}]+[12\eta\{12\zeta\gamma_3+\gamma_2(12-\gamma_3)\}$$

$$-\gamma_1\{12\zeta\gamma_3-(12-\gamma_2)(12-\gamma_3)\}]\Big\{3\left(\frac{x_1}{l_1}\right)-\left(\frac{x_1}{l_1}\right)^3\Big\}\cos\left(pt-\tan^{-1}\frac{P}{Q}\right), \tag{48}$$

$$y_2=\frac{3\left(7\sqrt{\frac{\lambda}{\mu}+2}-4\right)}{\sqrt{P^2+Q^2}}\Big[\{12\zeta\gamma_3-(12-\gamma_2)(12-\gamma_3)\}$$

$$-\{12\zeta\gamma_3+\gamma_2(12-\gamma_3)\}\Big\{3\left(\frac{x_2}{l_2}\right)^2+2\left(\frac{x_2}{l_2}\right)^3\Big\}\Big]\cos\left(pt-\tan^{-1}\frac{P}{Q}\right), \tag{49}$$

$$y_3=\frac{-36\left(7\sqrt{\frac{\lambda}{\mu}+2}-4\right)}{\sqrt{P^2+Q^2}}\Big[(12-\gamma_3)$$

$$+\gamma_3\Big\{3\left(\frac{x_3}{l_3}\right)^2+2\left(\frac{x_3}{l_3}\right)^3\Big\}\Big]\cos\left(pt-\tan^{-1}\frac{P}{Q}\right), \tag{50}$$

where
$$\left.\begin{aligned}P&=9\sqrt{\frac{\lambda}{\mu}+2}\left(\frac{E_1j^2}{\mu kl_1^3}\right)\Big[\gamma_1\{12\zeta\gamma_3-(12-\gamma_2)(12-\gamma_3)\}\\&\qquad\qquad-12\eta\{12\zeta\gamma_3+\gamma_2(12-\gamma_3)\}\Big],\\Q&=4\left(\sqrt{\frac{\lambda}{\mu}+2}-1\right)\Big[(3-\gamma_1)\{12\zeta\gamma_3-(12-\gamma_2)(12-\gamma_3)\}\\&\qquad\qquad+12\eta\{12\zeta\gamma_3+\gamma_2(12-\gamma_3)\}\Big],\end{aligned}\right\} \tag{51}$$

$$\gamma_1=\frac{m_1p^2l_1^3}{E_1I_1},\ \gamma_2=\frac{m_2p^2l_2^3}{E_2I_2},\ \frac{m_3p^2l_3^3}{E_3I_3},\ \xi=\frac{l_2}{l_1},\ \eta=\frac{E_2I_2l_1^3}{E_1I_1l_2^3},\ \zeta=\frac{E_3I_3l_2^3}{E_2I_2l_3^3}. \tag{52}$$

In the special case where $E_1=E_2=\cdots=E$, $I_1=I_2=\cdots=I$, $l_1=l_2=\cdots=l$, $m_1=m_2=\cdots=m$, we get

(i) $n=1$, omitted.

(ii) $n=2$,

$$y_1=\frac{\left(7\sqrt{\frac{\lambda}{\mu}+2}-4\right)}{2\sqrt{P^2+Q^2}}\Big[2(\gamma^2-27\gamma+36)$$

$$+\gamma(\gamma-24)\Big\{3\left(\frac{x_1}{l}\right)-\left(\frac{x_1}{l}\right)^3\Big\}\Big]\cos\left(pt-\tan^{-1}\frac{P}{Q}\right), \tag{44′}$$

$$y_2=\frac{3\left(7\sqrt{\frac{\lambda}{\mu}+2}-4\right)}{\sqrt{P^2+Q^2}}\left[(12-\gamma)\right.$$

$$\left.+\gamma\left\{3\left(\frac{x_2}{l}\right)^2+2\left(\frac{x_2}{l}\right)^3\right\}\right]\cos\left(pt-\tan^{-1}\frac{P}{Q}\right), \qquad (45')$$

where

$$\left.\begin{aligned}P&=9\sqrt{\frac{\lambda}{\mu}+2}\left(\frac{Ej^2}{\mu kl^3}\right)\gamma(24-\gamma)\,,\\ Q&=4\left(\sqrt{\frac{\lambda}{\mu}+2}-1\right)(\gamma^2-27\gamma+36)\,,\end{aligned}\right\} \qquad (46')$$

$$\gamma=\frac{mp^2l^3}{EI}. \qquad (47')$$

(iii) $n=3$,

$$y_1=\frac{\left(7\sqrt{\frac{\lambda}{\mu}+2}-4\right)}{2\sqrt{P^2+Q^2}}\left[2(\gamma^3-51\gamma^2+540\gamma-432)\right.$$

$$\left.+\gamma(12-\gamma)(36-\gamma)\left\{3\left(\frac{x_1}{l}\right)-\left(\frac{x_1}{l}\right)^3\right\}\right]\cos\left(pt-\tan^{-1}\frac{P}{Q}\right), \qquad (48')$$

$$y_2=\frac{3\left(7\sqrt{\frac{\lambda}{\mu}+2}-4\right)}{\sqrt{P^2+Q^2}}\left[-(\gamma^2-36\gamma+144)\right.$$

$$\left.+\gamma(\gamma-24)\left\{3\left(\frac{x_2}{l}\right)^2+2\left(\frac{x_2}{l}\right)^3\right\}\right]\cos\left(pt-\tan^{-1}\frac{P}{Q}\right), \qquad (49')$$

$$y_3=\frac{36\left(7\sqrt{\frac{\lambda}{\mu}+2}-4\right)}{\sqrt{P^2+Q^2}}\left[(\gamma-12)\right.$$

$$\left.-\gamma\left\{3\left(\frac{x_3}{l}\right)^2+2\left(\frac{x_3}{l}\right)^3\right\}\right]\cos\left(pt-\tan^{-1}\frac{P}{Q}\right), \qquad (50')$$

where

$$\left.\begin{aligned}P&=9\sqrt{\frac{\lambda}{\mu}+2}\left(\frac{Ej^2}{\mu kl^3}\right)\gamma(\gamma-12)(36-\gamma)\,,\\ Q&=4\left(\sqrt{\frac{\lambda}{\mu}+2}-1\right)(\gamma^3-51\gamma^2+540\gamma-432)\,,\end{aligned}\right\} \qquad (51')$$

$$\gamma=\frac{mp^2l^3}{EI}. \qquad (52')$$

We have calculated the maximum values of the bending moments $E_sI_s(\partial^2 y/\partial x^2)$ for each end of the columns corresponding to the maximum values of acceleration of the ground free of any structures, for the special case $E_s=E$, $I_s=I$, $l_s=l$, $m_s=m$, $Ej^2/\mu kl^3=0{\cdot}05$, $\lambda/\mu=14$, and for various values of ml^3/EI. They are plotted in Figs. 10, 11, 12. The nature of the problem for frequencies out of resonance is again similar to that without dissipation, but the bending moments of the present case under resonance conditions take certain values between those under the corresponding conditions of the two cases, namely, the one for the structure with rigid floors and the other for the structure with flexible floors, in

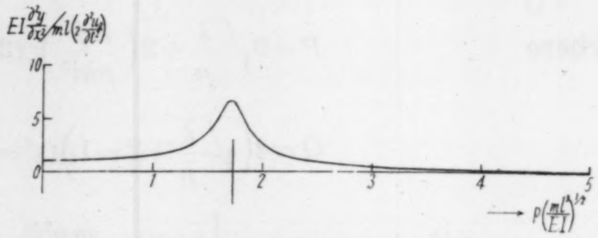

Fig. 10. The case of a singled-storied structure with rigid floor and hinged base.

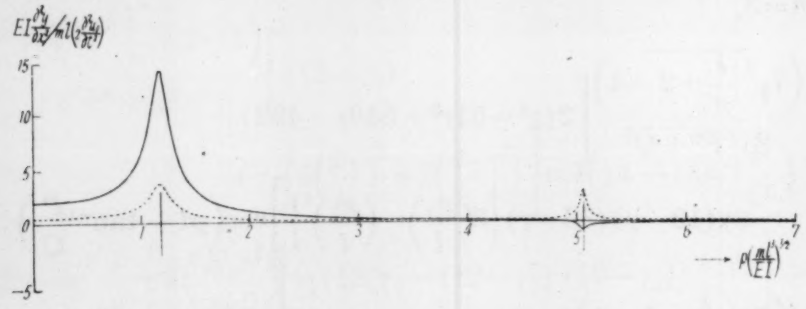

Fig. 11. The case of a two-storied structure with rigid floors and hinged base. Full line: lowest columns. Broken line: second columns.

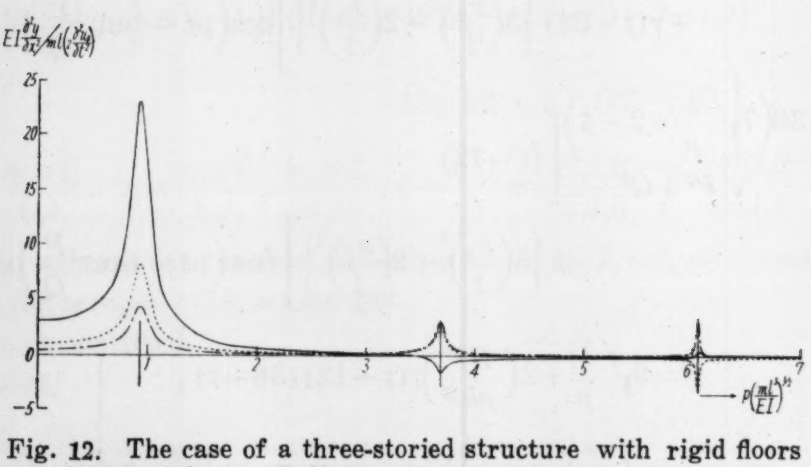

Fig. 12. The case of a three-storied structure with rigid floors and hinged base. Full line: lowest columns. Broken line: second columns. Chain: third columns.

both of which the structures are clamped at the base. Another feature, that can be confirmed from these figures, is that, although the moments at high frequencies are exceedingly small, the greatest one among such moments is not necessarily induced in the lowest columns. This nature, which may also be found even by the examination of preceding cases, appears to answer the question what part of a building would suffer a serious damage during earthquake movements.

5. *Concluding remarks.*

The solutions of the lateral deflection of the respective structures as here elaborated, may be applied to all cases with any value of $Ej^2/\mu kl^3$. The larger the ratio of $Ej^2/\mu kl^3$, the smaller become the amplitudes or bending moments at the periods corresponding to the resonance condition in the usual sense. Since $Ej^2/\mu kl^3$ is the product of E/μ, $(j/l)^2$, $L/2\pi l$, where L is the wave length of the incident waves in the earth, it follows that, the elasticity of the earth being given, the amplitudes or the bending moments under resonance conditions may be made smaller and smaller by increasing the elastic constants or the sectional area of the columns. Curious as it may seem, it is possible to get a similar effect by increasing the mass of the structure. To increase the mass of the structure, keeping the stiffness of columns at a constant value, is dynamically equivalent to increasing the fre- quency of seismic vibrations as revealed from the form of the parameter $p(ml^3/EI)^{1/2}$ that we used in every case. Even under the first resonance condition p may be made smaller in lieu of increa-s ing m, while $L/2\pi l$ becomes accordingly larger. This is analogous to increasing $Ej^2/\mu kl^3$ in the vicinity of the first resonance.

It may be remarked again that, by putting $Ej^2/\mu kl^3=0$ in any of the solutions given in this paper, we would have exactly the same solution as in that of the corresponding case shown in paper (B).

The items determining the feature of seismic vibrations of a structure, besides the nature of materials used in it, are now evident and may be enumerated as: (i) the acceleration of the ground on which no structure rests, (ii) periods of seismic vibrations, (iii) the form of the structure, (iv) the effective stiffness of the structure relative to that of the ground.

The nature of the dissipation of seismic vibrations in actual structures is now being studied, the results of which we hope to be able to publish in a forthcoming publication.[7]

---

[7] *loc. cit. ante.* in 6).

Our present investigation was greatly assisted by aid received, from the Foundation for the Promotion of Scientific and Industrial Research of Japan, to the Council of which we wish to express our sincere thanks.

---

55. 架構構造物の震動に於ける勢力逸散

地震研究所 {妹澤克惟
金井清

彙報第 12 號の論文に於てその中の結果について言及して置いたやうに，共振の所の無限大の振幅は勢力の地下逸散によつて或一定の大さに限定されることが數理的にわかるのである．構造物は一層から三層までのものを夫々について (i) 基礎と床とが夫々固定の狀態のもの，(ii) 基礎が固定され，床が撓み易いもの，(iii) 基礎で鉸脚になり，床が固定のものに分けて考へ，且つ土地に種々の加速度及び週期の地震があるときの振動狀態を研究したものである．之等についても (a) 構造物がないときの土地の加速度，(b) 震動の週期，(c) 構造物の型，(d) 構造物の剛度と土地の剛度との關係，(e) 構造物の材料の性質によつて構造物の震動性はすべて決定できるのである．數量的の結果は本文中に委しく出てゐる．

構造物をできるだけ剛くする方がよいのは，靜力學的の强度の意味や，共振を避けることよりも，寧ろ共振狀態に於ける振幅や柱の屈曲モーメントが小さくなるといふことに於て意味があるのである．又，高次の共振の所程，振幅やモーメントが益々小さくなり，斯る場合の振幅やモーメントは共振を外れた所の振幅やモーメントよりも小さくなることが知られるのである．之等の事實は振動勢力の地下逸散を度外視しては到底得られないのである．

床の撓み方が中位の場合は別に計算をやつて見なければならぬけれども，實際問題としてそのやうな場合は非常に少いから今直ちにその計算をやつて見るには及ばないと考へられる．

尙，柱と土地との結合狀態について，これ迄構造學者がやつたやうに中間位の固定といふ假定などは，振動減衰上には大した意味のないことがわかる．

又，この論文中の結果に於て假りに勢力逸散性を除いて見ると，すべての解は彙報第 12 號に述べたものと夫々一致するのである．

この論文では解の方程式だけは一般にあふやうにやつてあるけれども，數値計算の例としては最も可能的な一二の場合についてのみである．それで今後は實際の建物の寸法について計算を試み，それによつて各建物がたとひ共振を起しても如何なるモーメントしか起り得ないかと云ふ事を推定して置きたい考である．この問題は，逸散のために建物の共振があまり出ないことを意味してゐるから，地震を待つてやり得る實驗の結果もそれ程はつきりした値が出ないことを暗示してゐる．しかし，只今のやうな方法で Prediction をやつて置く事は，其計算の Elements がやはり實驗室で正確に測つた値であるだけそれだけ，信頼して貰つてよいものと思ふ．卽ち，この計算は振動實驗では到底出し得ず而も物理的にも應用的にも大切な問題の解を與へるものである．

56. *Vibrational Causes of the Overturning of Railway Carriages on the Setagawa Bridge in the Typhoon of Sept. 21, 1934.*

By Katsutada SEZAWA,
Earthquake Research Institute.

(Read May 21, 1935.—Received June 20, 1935.)

1. The typhoon which struck the mid-western part of Japan on Sept. 21, 1934, caused considerable damage, among which the overturning of a railroad train on the Setagawa Bridge, crossing River Seta near Lake Biwa, is an example. Although information is scanty with respect to the details of that accident, it seems established that the overturning was due mainly to the strong winds that struck the train as it was crossing the bridge. Even were the origin of the accident of an aerodynamic nature, it is still possible to postulate one aerodynamical static cause and two aerodynamical vibrational causes. One of the vibrational causes is the turbulent wind in more or less periodic motion and the other the stationary strong wind that gives rise to unstable oscillation of the railway carriages. My intention here is to examine the two vibrational causes rather than the dynamical static cause.

2. The periodic turbulent wind will first be discussed. It is well known that when wind currents flow through a rigid obstacle, periodic Kármán vortices[1] or more general periodic turbulences[2] are formed behind or around that obstacle. According to Nagaoka's conclusion,[3] the overturning of the carriages was caused by just such wind action. It seems that the forced oscillation of the carriages was in resonance condition under the periodic wind force. Not many reliable experiments have been made concerning the periodicity of the growth of Kármán vortices behind an obstacle, but the experiment of Crausse and Baubiac[4] seems worth mentioning at this juncture. They found the relation between the velocity of the fluid and the frequency of vortex generation behind a cylindrical obstacle of circular section, using liquid jets of different kinds and measuring it with a hot wire anemometer. In order to make their result applicable to the present wind problem with sufficient similarity of conditions, I transformed the parameters into VT/D aud Reynolds's number VD/ν, where D is the diameter of the cylinder, V the velocity of the fluid, ν the kinematic coefficient of viscosity, and T the period of formation of vortices (or fluctuations in wind force). It is possible to prove that, if the Reynolds's number were the same for different fluid motions, the configuration of the vortices, including general turbulent flow, relative to the obstacle should be arranged always in similar types. The small dots in Fig. 1 were marked from data due to Crausse and Baubiac, using Reynolds's number of logarithmic scale. Data in Reynolds's number greater than 10,000 were not obtained, and I extrapolated the curve passing through these dots to as much of the same number as 10^7, and found that, for $V=20$ m/s, $D=2$ m, $\nu=0{\cdot}130$, T becomes 0·95 s. We shall find later that the period of free oscillation of the rolling type as that of a carriage of wall height 2 m (which is slightly less than actual) is 0·95 s. Even should Reynolds's numbers differ more or less for differently shaped bodies, it is still probable that the overturning under consideration took place under resonance conditions in the periodic vortical or turbulent motion of strong wind. Again, even were the extrapolated curve in Fig. 1 drawn in every other possible way, the resultant deviated period of vortices at the given wind speed would be of the same order as the original one. It is therefore obvious that the cause as explained by Nagaoka's conclusion is the principal one, at any rate for the accident on Setagawa Bridge.

---

[1] TH. v. KÁRMÁN, *Gött. Nachr.* 1911, 509; 1912, 547; *Phys. Z.*. **13** (1912).

[2] H. NAGAOKA, *Proc. Math.-Phys. Soc.*, [iii], **1** (1919).

[3] H. NAGAOKA's paper read at the monthly meeting of the Earthq. Res. Inst., Nov. 20, 1934; unpublished.

[4] E. CRAUSSE et BAUBIAC, *C. R.*, **192** (1931), 1355~57, 1529~31.

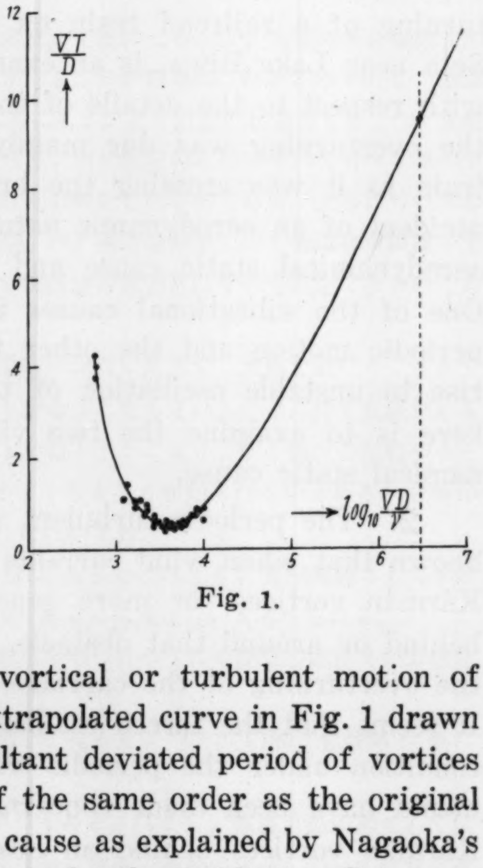

Fig. 1.

3. The unstable oscillations of a carriage due to strong wind will next be dealt with, although it may be rather a secondary cause. It is known that there are frequently downward (or upward) wind currents along a river bank. The vertical component of such a current imparts, particularly, such vibrational energy to a train of cars as to cause horizontal oscillation as well as angular rolling, both of which are generally coupled. The coupled oscillation becomes unstable (oscillatory unstable, but not aperiodic unstable) under certain conditions of the problem. Taking the case of a bogie and referring to Fig. 2, the notations used are as follows:

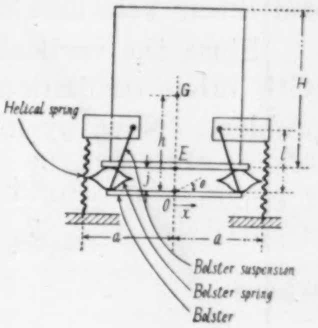

Fig. 2.

$z,\ x,\ \theta$ = vertical, horizontal, and angular displacements of the carriage with respect to O,

G = centre of gravity,

k = mass radius of gyration about G,

h = GO,

j = OE,

$2a$ = distance between helical springs on both sides of the bogie,

M = mass of bogie including bogie truck,

s = elastic resistance of all helical springs, including the effect of all bolster springs, on one side of bogie per unit vertical displacement,

$c_1 s\, \partial/\partial t$ = damping and dissipation resistance of . . . . ,

T/l = elastic resistance of all bolster suspensions on one side of bogie per unit angular displacement of suspension,

$(c_2 T/l)\partial/\partial t$ = damping and dissipation resistance of . . . . ,

l = effective length of bolster suspension,

L = length of bogie car,

H = wall height of bogie car,

c_m = moment coefficient of wind force about O,

c_f = sidewise dragging coefficient of wind force,

ρ = density of air,

V = speed of air current always flowing vertically.

The equations of motion of the carriage with respect to O which is fixed in the car are:

$$M\ddot{z}+2sz+2sc_1\dot{z}=0, \tag{1}$$

$$M\ddot{x}-Mh\ddot{\theta}+\frac{2T}{l}x+\frac{2T}{l}c_2\dot{x}\pm\frac{\partial c_f}{\partial\theta_0}\frac{\rho}{2}V^2LH\theta'=0, \tag{2}$$

$$M(k^2+h^2)\ddot{\theta}-Mh\ddot{x}+2sa^2\theta+2a^2c_1\dot{\theta}\pm\frac{\partial c_m}{\partial\theta_0}\frac{\rho}{2}V^2LH^2\theta'=0, \tag{3}$$

where the upper and lower ones of double signs belong to the respective cases of downward and upward wind currents, θ_0 specifies the rolling angle in the vicinity of $\theta=0$, while θ' is written in place of

$$\theta'=\theta+\frac{H/2+j}{V}\dot{\theta}\pm\frac{1}{V}\dot{x}, \tag{4}$$

the second and third terms in (4) denoting angular displacements of the carriage relative to the wind direction due to the respective angular and linear velocities of the same carriage.

Since the vertical oscillation given by equation (1) is not coupled with other oscillations, equation (1) is not necessary in the present problem. Now, by means of (4), equations (2) and (3) reduce to

$$a_{11}\ddot{\theta}+b_{11}\dot{\theta}+c_{11}\theta+a_{12}\ddot{x}+b_{12}\dot{x}=0, \tag{3'}$$

$$a_{21}\ddot{\theta}+b_{21}\dot{\theta}+c_{21}\theta+a_{22}\ddot{x}+b_{22}\dot{x}+c_{22}x=0, \tag{2'}$$

where

$$a_{11}=M(k^2+h^2), \qquad b_{11}=2sa^2c_1\pm\frac{\partial c_m}{\partial\theta_0}\frac{\rho}{2}LH^2\Big(\frac{H}{2}+j\Big)V,$$

$$c_{11}=2sa^2\pm\frac{\partial c_m}{\partial\theta_0}\frac{\rho}{2}LH^2V^2, \qquad a_{12}=-Mh,$$

$$b_{12}=\frac{\partial c_m}{\partial\theta_0}\frac{\rho}{2}LH^2V, \qquad a_{22}=M, \qquad b_{22}=\frac{2T}{l}c_2+\frac{\partial c_f}{\partial\theta_0}\frac{\rho}{2}LHV,$$

$$c_{22}=\frac{2T}{l}, \qquad a_{21}=-Mh, \qquad b_{21}=\pm\frac{\partial c_f}{\partial\theta_0}\frac{\rho}{2}LH\Big(\frac{H}{2}+j\Big)V,$$

$$c_{21}=\pm\frac{\partial c_f}{\partial\theta_0}\frac{\rho}{2}LHV^2.$$

Putting

$$\left.\begin{aligned}\theta&=c_{11}e^{\lambda_1 t}+c_{12}e^{\lambda_2 t}+c_{13}e^{\lambda_3 t}+c_{14}e^{\lambda_4 t},\\ x&=c_{21}e^{\lambda_1 t}+c_{22}e^{\lambda_2 t}+c_{23}e^{\lambda_3 t}+c_{24}e^{\lambda_4 t},\end{aligned}\right\} \tag{5}$$

and substituting these in (2′), (3′), and eliminating the coefficients of (5), we get the following frequency equation for determining λ_1, λ_2, λ_3, λ_4

$$A_0\lambda^4+A_1\lambda^3+A_2\lambda^2+A_3\lambda+A_4=0, \tag{6}$$

in which

$$\left.\begin{aligned}A_0&=|aa|, \quad A_1=|ab|+|ba|, \quad A_2=|ac|+|ca|+|bb|,\\ A_3&=|bc|+|cb|, \quad A_4=|cc|,\end{aligned}\right\} \tag{7}$$

$|mn|$ signifying that $|mn|=\begin{vmatrix}m_{ii} & n_{ik}\\ m_{ki} & n_{kk}\end{vmatrix}$.

It will be seen from (5) that, if the real parts of all the λ_s are negative, the vibratory motion is stable, while, if the real part of any of the λ_s is positive, the motion is unstable. In the latter case, the amplitudes of vibrations become larger and larger with lapse of time t, regardless of whether the type of vibrations be periodic or aperiodic. This fact is strictly conditioned by Routh's criterion,[5] namely, if

$$A_0>0,\quad A_1>0,\quad A_2>0,\quad A_3>0,\quad A_4>0, \tag{8}$$

$$\Delta=A_1A_2A_3-A_0A_3^2-A_4A_1^2>0, \tag{9}$$

the vibratory motion is stable, while, if

$$\Delta<0 \tag{10}$$

in place of (9), the motion is unstable. At the critical state of stability, $\Delta=0$, the frequency of vibrations (the numbers in radians) is expressed by

$$\sqrt{A_3/A_1}\,. \tag{11}$$

In a special case of coupled oscillations of two degrees of freedom, the type of motion becomes ternary[6] and there is a similar discriminant Δ for stability.

In order to get the critical wind speed to cause unstable oscillation of the railway carriage, some likely numerical values were assumed as follows:

$$M=10^4\text{ kg mass},\quad k=1\text{ m},\quad h=1\text{ m},\quad a=1\text{ m}\quad H=2\text{ m},\quad j=0{\cdot}5\text{ m},$$

$$L=15\text{ m},\quad \rho=1{\cdot}2\text{ kg mass/m}^3,\quad s=5.10^4\text{ kg}=5.10^4.9{\cdot}8\text{ kg m/s}^2,$$

$$T=5.10^3\text{ kg}=5.10^3.9{\cdot}8\text{ kg mass/s}^2,\quad l=0{\cdot}05\text{ m},$$

whence we get

$$a_{11}=2.10^4\text{ kg mass m}^2,\qquad b_{11}=\left\{10^6c_1\pm54\frac{\partial c_m}{\partial\theta_0}V\right\}\text{ kg mass m}^2\text{/s},$$

$$c_{11}=\left\{10^6\pm36\frac{\partial c_m}{\partial\theta_0}V^2\right\}\text{ kg mass m}^2\text{/s}^2,\qquad a_{12}=-10^4\text{ kg mass m},$$

$$b_{12}=36\frac{\partial c_m}{\partial\theta_0}V\text{ kg mass m/s},\qquad a_{22}=10^4\text{ kg mass},$$

$$b_{22}=2.10^6c_2+18\frac{\partial c_f}{\partial\theta_0}V\text{ kg mass/s},\qquad c_{22}=2.10^6\text{ kg mass/s}^2,$$

---

5) E. J. ROUTH, *Advanced Rigid Dynamics* (London, 1905), 221.

6) In the special case that $A_0=0$ or $A_4=0$ in (9), the frequency equation becomes of third degree and the motion is ternary; if $A_4=0$, the discriminant for stability becomes

$$\Delta=A_1A_2-A_0A_3>0,$$

the frequency of vibrations being then $\sqrt{A_2/A_0}$. I applied such a criterion to certain problems a few years ago: K. SEZAWA, *Journ. Aeron. Res. Inst.*, No. 74 (1930), 404~408; No. 87 (1931), 622~626.

$$a_{21}=\pm 21\frac{\partial c_f}{\partial\theta_0}V \text{ kg mass m/s}, \qquad c_{21}=\pm 18\frac{\partial c_f}{\partial\theta_0}V^2 \text{ kg mass m/s}^2,$$

from which we obtain (omitting the names of the scale),

$$A_0=10^8, \quad A_1=\Big[4.10^{10}c_2+10c_1\Big]+\left[\begin{matrix}63\\9\end{matrix}\right\}.10^4\frac{\partial c_f}{\partial\theta_0}\begin{matrix}+90\\-18\end{matrix}\Big\}.10^4\frac{\partial c_m}{\partial\theta_0}\Big]V,$$

$$A_2=\Big[5.10^{10}+2.10^{12}c_1c_2\Big]+\Big[\pm 108.10^6c_2\frac{\partial c_m}{\partial\theta_0}+18.10^6c_1\frac{\partial c_f}{\partial\theta_0}\Big]V$$

$$+\Big[\pm 18.10^4\frac{\partial c_f}{\partial\theta_0}\pm 36.10^4\frac{\partial c_m}{\partial\theta_0}\Big]V^2,$$

$$A_3=\Big[2.10^{12}c_1+2.10^{12}c_2\Big]+\Big[\pm 108.10^6\frac{\partial c_m}{\partial\theta_0}+18.10^6\frac{\partial c_f}{\partial\theta_0}\Big]V\pm 72.10^6c_2\frac{\partial c_m}{\partial\theta_0}V^2,$$

$$A_4=2.10^{12}\pm 72.10^6\frac{\partial c_m}{\partial\theta_0}V^2,$$

the upper or lower one of each double-valued term corresponding to downward or upward current as the case may be. I have calculated from the above quantities the values of discriminants, $\varDelta=A_1A_2A_3-A_0A_3^2-A_4A_1^2$, in five cases, namely,

(a) Downward wind,

$$\frac{\partial c_m}{\partial\theta_0}=-0{\cdot}2, \quad \frac{\partial c_f}{\partial\theta_0}=1, \quad c_1=c_2=10^{-4},$$

(b) Downward wind,

$$\frac{\partial c_m}{\partial\theta_0}=-0{\cdot}2, \quad \frac{\partial c_f}{\partial\theta_0}=1, \quad c_1=c_2=10^{-5},$$

(c) Downward wind,

$$\frac{\partial c_m}{\partial\theta_0}=-0{\cdot}2, \quad \frac{\partial c_f}{\partial\theta_0}=1, \quad c_1=c_2=0,$$

(d) Upward wind,

$$\frac{\partial c_m}{\partial\theta_0}=-0{\cdot}1, \quad \frac{\partial c_f}{\partial\theta_0}=1, \quad c_1=c_2=10^{-4},$$

(e) Upward wind,

$$\frac{\partial c_m}{\partial\theta_0}=-0{\cdot}1, \quad \frac{\partial c_f}{\partial\theta_0}=1, \quad c_1=c_2=0,$$

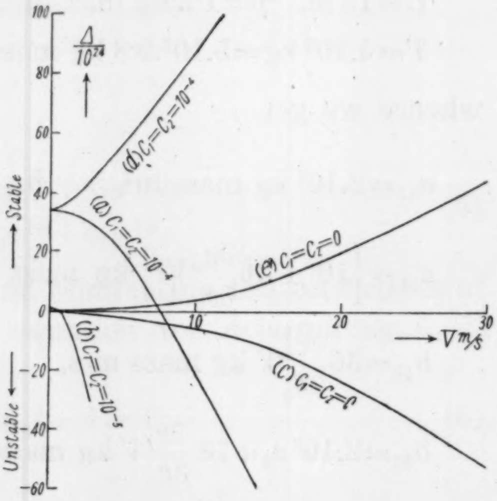

Fig. 3.

the result being plotted in Fig. 3. This figure shows that for downward current, instabilities in cases (a), (b), (c) take place respectively at wind speed $V=7{\cdot}6$ m/s, 0·76 m/s, 0 m/s, while for upward current the vibrations are stable at any wind speed. It should be remarked that, unless damping or dissipation exists in the carriage, its free vibrations are unstable for any small downward wind current.

It is possible to determine accurately the equations of vibratory motion for the case without wind current[7] as well as for the one at critical wind speed, and fairly accurately for those at other wind speeds. In all cases we write

$$\lambda_1,\ \lambda_2,\ \lambda_3,\ \lambda_4 = p \pm iq,\ \ p' \pm iq',$$

and put them in (6). The solutions of the free vibrations corresponding to the three kinds of downward current and under conditions $\partial c_m/\partial\theta_0 = -0{\cdot}2$, $\partial c_f/\partial\theta_0 = 1$, $c_1 = c_2 = 10^{-4}$, are

(i) $V=0$ (stable),

$$x = \alpha e^{-\cdot 0228\,t}\cos(21{\cdot}4\,t+\beta) + \gamma e^{-\cdot 00216\,t}\cos(6{\cdot}65\,t+\delta),$$
$$\theta = \alpha' e^{-\cdot 0228\,t}\cos(21{\cdot}4\,t+\beta') + \gamma' e^{-\cdot 00216\,t}\cos(6{\cdot}65\,t+\delta'),$$

(ii) $V=7{\cdot}6$ m/s (critical),

$$x = \alpha e^{-\cdot 0421\,t}\cos(21{\cdot}2\,t+\beta) + \gamma\cos(6{\cdot}65\,t+\delta),$$
$$\theta = \alpha' e^{-\cdot 0421\,t}\cos(21{\cdot}2\,t+\beta') + \gamma'\cos(6{\cdot}65\,t+\delta'),$$

(iii) $V=10$ m/s (unstable),

$$x = \alpha e^{-\cdot 0466\,t}\cos(21{\cdot}2\,t+\beta) + \gamma e^{\cdot 000686\,t}\cos(6{\cdot}65\,t+\delta),$$
$$\theta = \alpha' e^{-\cdot 0166\,t}\cos(21{\cdot}2\,t+\beta') + \gamma' e^{\cdot 000686\,t}\cos(6{\cdot}65\,t+\delta'),$$

$\alpha, \beta, \alpha', \beta'$ being contants to be determined from initial conditions.

The first term of each solution belongs to principally horizontal oscillation and the second to mainly rolling osillation. The approximate periods of the two osillations are 0·29 s and 0·95 s respectively. The equations also show that, although the period of the carriage is not practically changed, the rolling oscillation will have negative damping beyond the critical speed. It is therefore now obvious that, under unstable conditions, the amplitudes of successive oscillations become larger and larger, the energy of large oscillations being continually supplied from air current.

In conclusion I wish to express my sincere thanks to Professor Nagaoka for his kind advices during the course of this investigation and also to Mr. Kanai for his valuable assistance in preparing this paper.

---

[7] K. SEZAWA, *Rep. Japanese Association for Applied Mechanics*, Tokyo, 1931; *Sindôgaku* (Tokyo, 1932), 357.

56. 瀨田川鐵橋に於ける車輛顚覆の振動的原因

地震研究所 妹澤克惟

昭和９年９月21日の颱風による被害は數々あるが，瀨田川鐵橋に於て鐵道車輛が顚覆したのもその一例である．鐵橋上で而も烈風中での事故であるから，原因を風力に持つて行くべきは當然であるけれども，尙それを空氣力學上の靜力學的原因と空氣力學上の振動的原因とに分けることができる．靜力學的の原因卽ち飛行機の翼を持上るやうな力や壁に風があたるやうな作用も見逃し難いけれども，玆には特に振動的原因のみを考へることにした．

振動的原因には二つのものが考へられ，一つは列車を直角に通過する空氣の流れの中に生ずる週期的擾流である．これは颱風後間もなく長岡博士が其說明に用ひられた原因であつて，筆者はそれを確める爲に，旣にある實驗から Reynolds 數を用ひて比較して見た所が，或風速に於けるその擾流變化の週期が車體の動搖の週期と大體一致することがわかつた．それで車體は共振的の振動によつて顚覆したとして先づ差支ないと思はれる．

次に振動力學上の興味から，空氣の流れの中に週期的の變化のない場合でも高い風速で車體が不安定な動搖をなして顚覆することがないかといふことをしらべて見た．車體に數種のばねがあり，そのばねの位置，車體の重心の位置，風壓のかゝり具合によつて車體の自由振動が種々の型式を取り，或風速に於てはその自由振動が不安定になることがあるのである．而してその不安定は普通の單一振子の不安定などと異なり，もつと高次の方程式から決定できるものであるし，且つそれが不安定となつてからでも週期的振動をなすのであるから，原位相にあることが不安定といふことなどとは大いに異なり，顚覆に最も適當した不安定となるものである．但しこのやうに自由振動をなすものが大振幅になる爲には必ず勢力の供給がなくてはならぬのであるが，現在の場合には風がその勢力を供給するわけである．果してこのやうな原因で車輛が顚覆したとすると擾流中の週期的力が殆どなくても必ずある風速で危險となるから，車體形の少し位の變化ではこの作用を免れることができぬ譯であつて，それよりも寧ろばねや重心の方を適當に變へた方が効果が多いのである．

---

57. 岡山—鳥取, 鳥取—米子, 及び 岡山—米子間水準再測成果

最近，陸地測量部に於いて，岡山一鳥取，鳥取一米子，岡山一米子等各區間の一等水準線路に就き，再測を施行せられたり．その結果，上記の水準線路上に在る各水準點の垂直變動は第1乃至第3圖に，その地理的分布と共に示すが如きものを得たり．是等の結果は，研究資料に供すべく，陸地測量部の好意により此に掲載を許されたるものにして，同部の好意に對しては，深謝の意を表する次第なり．

尙，成果に關する要項は次の如し．

1） 各水準線に於ける測量年次は下表に示す．

區　　間	前　測　量	新　測　量
岡山一鳥取	昭和4年2月～7月	昭和10年1月～3月
鳥取一米子	昭和2年10月～昭和3年5月	昭和10年1月～2月
岡山一米子	明治23年11月～明治24年2月	昭和10年1月～3月

2） 垂直變動量は，岡山に在る水準點交第379號を不動として算出せられたるものとす．

昭和10年6月　　　　地震研究所

---

57. Results of Recent Precise Levellings along the lines Okayama—Tottori, Tottori—Yonago and Okayama—Yonago.

Precise levellings are recently revised by the Military Land Survey, along the lines, Okayama—Tottori, Tottori—Yonago and Okayama—Yonago. The relative vertical displacements of the bench-marks along these level lines obtained by comparing the results of the recent measurements with those of earlier ones are shown in Figs. 1～3, together with maps showing the geographical distribution of the level lines.

The dates of the field works for the different sections are as follows:

Sections	Earlier survey	Recent survey
Okayama-Tottori	Feb.～July, 1929.	Jan.～March, 1935.
Tottori-Yanago	Oct., 1927～May., 1928.	Jan.～Feb, 1935.
Okayama-Konago	Nov., 1890～Feb., 1891.	Jan.～March. 1935.

The vertical displacements deduced and shown in the plates are referred to B. M. J-379, situated at Okayama, the height of which is regarded as unchanged during the period of the successive surveys mentioned above.

June, 1935.

The Earthquake Research Institute.

昭和10年(1935)

[illegible]	所在地	Locality	[illegible]	[illegible]
交379	岡山市	Okayama	2月~Feb 24	
1001	同		21	
1002	横井村		17	
1003	同		20	往復不良改測 一〇.一一.一三
1004	野谷村		19	
1005	同		19	往復不良改測 一〇.一一.一三
1006	牧山村		19	
1007	宇垣村		15	
1008	同		16	
1009	金川町	Kanagawa	16	往復不良改測 一〇.一一.一六
1010	同		17	
1011	同		18	
1012	同		20	往復不良改測 一〇.一一.一〇
1013	竹枝村		21	
1014	同		21	
1015	福渡町	Hukuwatari	23	
1016	同		25	
1017	同		26	
1018	[illegible]目村		28	
1019	[illegible]川村		28	
1020	同		3月~Mar 1	
1021	弓削町	Yuge	2	
1022	誕生寺村		3	
1023	[illegible]村		4	[illegible] 一〇.三.一二
1024	同		4	
1025	同		6	[illegible] 一〇.三.一六
1026	佐良山村		6	往復不良改測 一〇.三.一六
1027	同		8	
1028	同		10	往復不良改測 一〇.三.一八
1029	同		11	往復不良改測 一〇.三.一八
1030	津山市	Tuyama	8	往復不良改測 一〇.三.一
第82			2月~Feb 26	
1031	同		25	
1032	同		27	往復不良改測 一〇.一一.一八
1033	高野村		25	往復不良改測 一〇.一一.一四
1034	同		21	
1035	[illegible]村		17	往復不良改測 一〇.一一.一〇
1036	同		20	往復不良改測 一〇.一一.一〇
1037	[illegible]野村		18	
1038	[illegible]村		19	往復不良改測 一〇.一一.一三
1039	同		1月~Jan 19	
1040	[illegible]田村		19	
1041	[illegible]村		17	[illegible] 一〇.一.一六
1042	同		15	
1043	同		14	
1044	同		13	
1045	同		13	
1046	那岐村		14	
1047	同		18	
1048	同		16	
1049	土師村		16	
1050	同		16	
1051	智頭町	Tizu	15	
1052	同		13	
1053	同		14	
1054	[illegible]村		17	
1055	同		19	
1056	同		20	[illegible] 一〇.一.一八
1057	用瀬町	Yôgase	21	
1058	大[illegible]村		23	
1059	国英村		23	往復不良改測 一〇.一.二七
1060	同		27	
1061	同		26	
1062	河原町	Kawahara	26	
1063	[illegible]田村		31	
1064	同		2月~Feb [illegible]	
1065	同		2	
1066	鳥取市	Tottori	4	
1067	同			往復不良改測 一〇.二.六

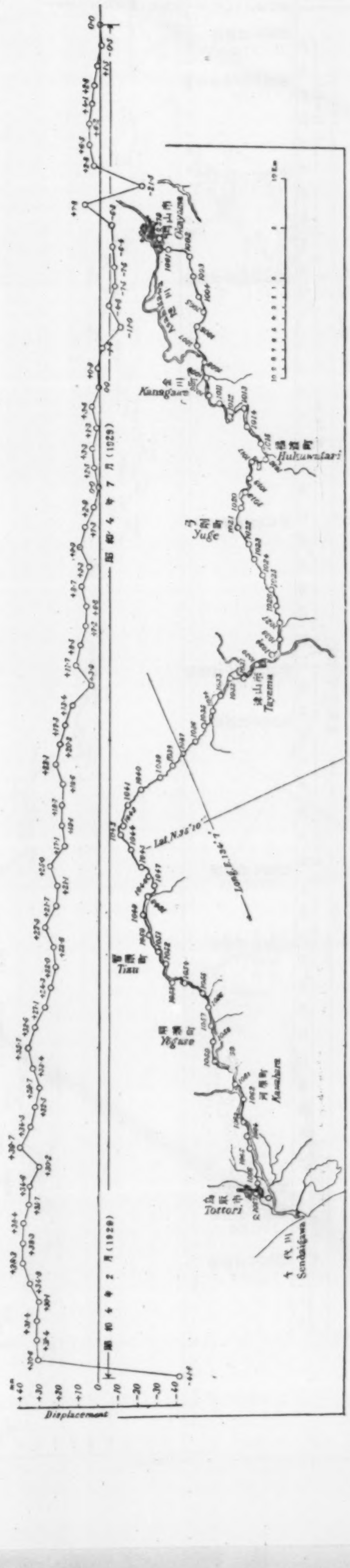

標石番號	所在地	Locality	觀測月日	起點交一〇六七ノ變動量ハ岡山市交三七九ヲ不動トシタル檢測ノ値トス
交1067	鳥取市	Tottori	昭和10年(1935) 2月~Feb 28	位置不良改埋 一〇、二、六
1068	同		29	
1069	千代水村		29	埋沒位置不良改埋 一〇、二、六
1070	湖山村		25	
1071	同		24	
1072	末恒村		24	
1073	同		1月~Jan 29	埋沒濟位置改埋 一〇、一、二八
1074	同		27	
1075	寶木村		24	
1076	瑞穗村		26	
1077	正條村		26	露出位置不良改埋 一〇、一、二六
1078	同		2月~Feb 1	
1079	同		1	
1080	青谷町	Aoya	5	
1081	同		4	
1082	中郷村		3	
1083	青谷町	Aoya	8	
1084	泊村		8	
1085	同		10	
1086	同		12	
1087	宇野村		10	傾斜舊位置改埋 一〇、二、一一
1088	橋津村		1月~Jan 24	
1089	長瀬村		25	
1090	同		22	
1091	日下村		28	
1092	倉吉町	Kurayosi	27	
1093	同		29	埋沒位置不良改埋 一〇、一、二九
1094	社村		31	
1095	灘手村		2月~Feb 5	位置不良改埋 一〇、一、三一
1096	同		2	
1097	大誠村		4	
1098	由良町		10	
1099	社村		8	
1100	逢束村		10	
1101	八橋町	Yabase	9	位置不良改埋 一〇、二、一〇
1102	同		14	
1103	赤崎町	Akasaki	12	
1104	同		14	位置不良改埋 一〇、二、一三
1105	安田村		24	
1106	下中山村		24	
1107	逢阪村		25	
1108	同		27	
1109	光德村		28	
1110	同		29	
1111	御來屋町	Mikuriya	30	
1112	庄內村		31	
1113	所子村		2月~Feb 1	
1114	高麗村		3	位置不良改埋 一〇、二、四
1115	淀江町	Yodoe	4	位置不良改埋 一〇、二、五
1116	同		5	
1117	大和村		8	位置不良改埋 一〇、二、六
1118	日吉津村		9	
1119	車尾村		12	
交1120	米子市	Yonago		

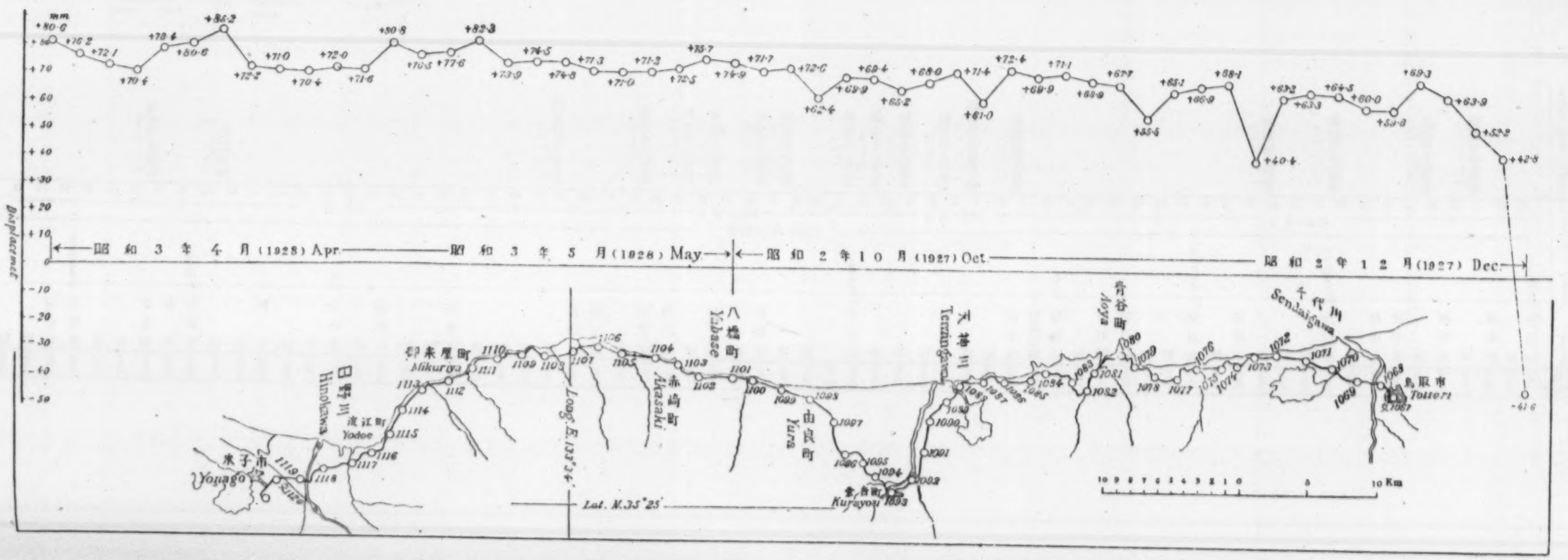

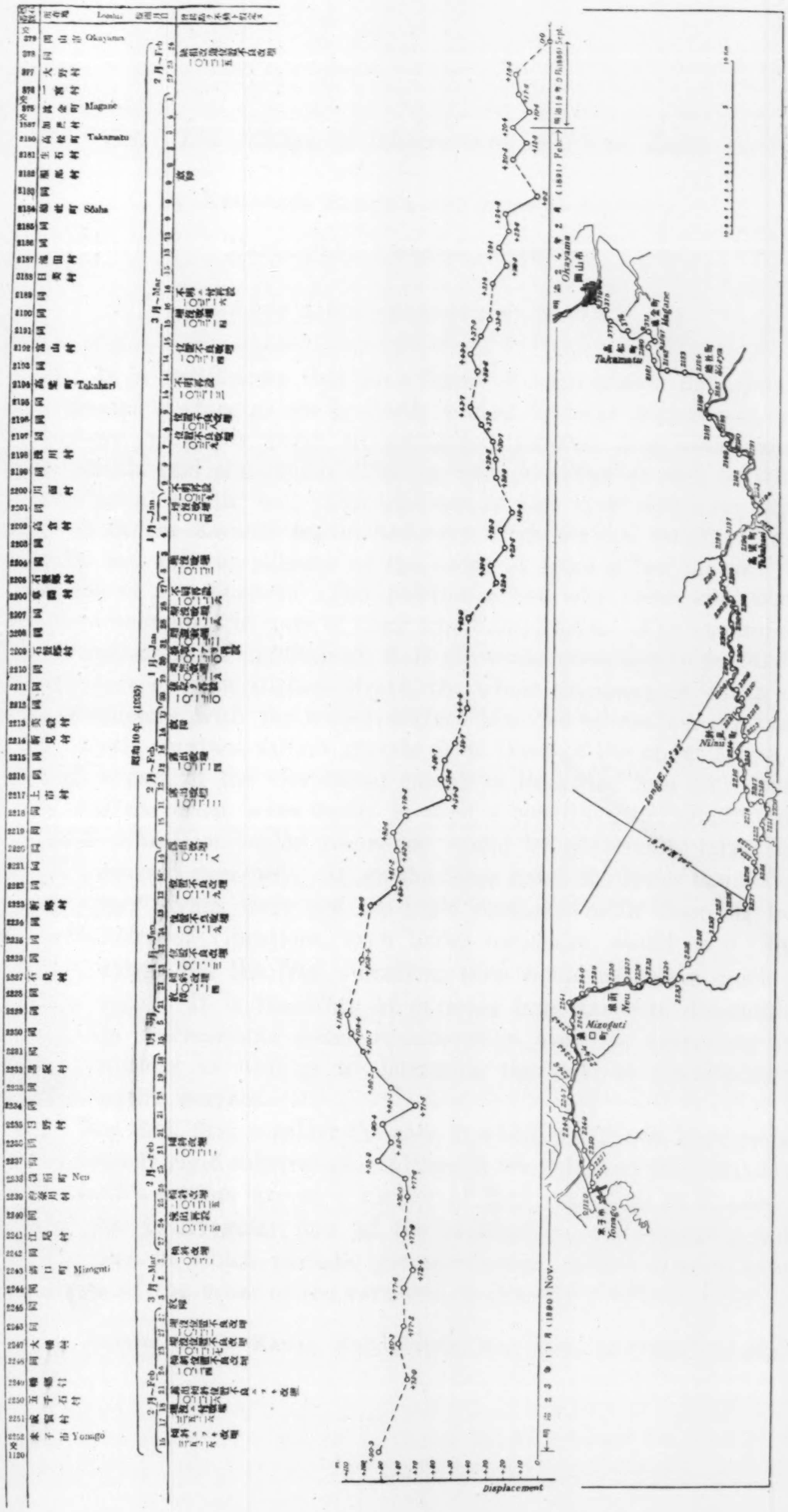
Okayama
Magane
Takamatu
Sôzya
Takahasi
Niimi
Neu
Mizoguti
Yonago
昭和10年 (1935)
Displacement
明治24年2月 (1891) Feb.
明治23年11月 (1890) Nov.
Long. E. 133°30′

58. *The Nature of Microseisms of Local Type.*

By Katsutada SEZAWA and Kiyoshi KANAI,

Earthquake Research Institute.

(Read July 2, 1935.—Received Sept. 20, 1935.)

1. It is well known that such forms of microseismic disturbance on a ground surface as are probably caused by local impulses in the atmosphere, generally point to undamped coupled free oscillations, their periods and amplitudes differing with localities as well as with meteorological conditions. Disturbances of this type that have been observed in the Kwanto region had very often periods ranging from 10 to 30 sec, with amplitudes of the order of from a few microns to a fraction of a milimeter. The question arises why these vibrations should be undamped in spite of their small amplitudes. For undamped free vibrations to be maintained, it is obviously necessary to postulate the existence of some surface strata, the whole thickness of which is a few kilometers, with the lowest surface bounded by another stratum whose elastic constant differs greatly from those of the upper strata,[1] although a part of the vibrational energy is dissipated into air. But, if the surface crust were really in such a condition, the amplitudes of forced vibrations under resonance would be abnormally large, as will be discussed presently. If, on the other hand, the lower boundary of the upper strata were not too rigid compared with these strata, the amplitudes of vibrations, even under resonance, would be within a certain range, but the free vibrations then would assume a quickly damping type. It is therefore of pressing importance to determine whether the microseisms under consideration are free vibrations or forced vibrations as well as to determine the state of stratification near the earth's surface.

2. We shall first consider the case in which a uniform layer rests on an extremely rigid substratum. Although the pulsatory disturbances on the earth's surface are as a matter of fact variations in dynamic pressure due to irregular flow of the atmosphere, for simplicity we take the case in which periodic pressure waves, whose approximate intensity is of the order of the variation in dynamic pressure, impinge on the ground surface. The differential equation determining the pressure change $p_0\partial\xi/\partial x$ in air may then be expressed by

---

[1] K. SEZAWA and K. KANAI, *Bull. Earthq. Res. Inst.*, **13** (1935), 251~264, 484~495.

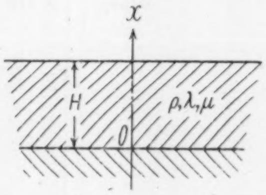

Fig. 1.

$$\frac{\partial^2\xi}{\partial t^2}=c^2\frac{\partial^2\xi}{\partial x^2}, \tag{1}$$

the axis of x being taken vertically upwards from the lower boundary of the layer. Since in this equation it is assumed that the pressure change takes place isothermally, owing to the relatively slow variations in the state of the air, we may put $c^2=p_0/\rho_0$, so that the air pressure varies as $p_0\partial\xi/\partial x$, where p_0, ρ_0, ξ are mean pressures as well as density in atmosphere and displacement of any point in the air in oscillation considered statically. The solution of (1), which is the result of vibration in air with amplitude a, is expressed by

$$\xi=2\imath\sin(fx+\gamma)\cos pt, \tag{2}$$

where $f^2=p^2/c^2=\rho_0p^2/p_0$. The vertical vibration of the surface layer of the earth is obtained from the equation

$$\rho\frac{\partial^2u}{\partial t^2}=(\lambda+2\mu)\frac{\partial^2u}{\partial x^2}, \tag{3}$$

ρ, λ, μ, u being density, elastic constants, and the displacement of the layer respectively. The solution of this equation satisfying the condition at the lower boundary of the layer, $x=0$, is expressed by

$$u=A\sin f'x\cos pt, \tag{4}$$

in which $f'^2=\rho p^2/(\lambda+2\mu)$. The conditions at the upper surface of the layer are

$$u=\xi, \qquad (\lambda+2\mu)\partial u/\partial x=p_0\partial\xi/\partial x. \tag{5), (6}$$

We thus finally get

$$\xi=2a\sin\left[f(x-H)+\tan^{-1}\{\alpha\tan f'H\}\right]\cos pt, \tag{7}$$

$$u=\frac{2a\alpha\sin f'x\cos pt}{\sqrt{\alpha^2\sin^2 f'H+\cos^2 f'H}}, \tag{8}$$

where $\alpha=\sqrt{\rho_0p_0/\rho(\lambda+2\mu)}$. If we put $\rho_0=0{\cdot}00129$, $p_0=76\,.\,13{\cdot}6\,.\,980$, $\rho=2$, $\lambda+2\mu=10^{11}$, we obtain $\alpha=0{\cdot}809\,.\,10^{-4}$. It should be borne in mind however that, under resonance, the common boundary of the two media becomes loops of vibrations for the layer as well as for the air. We have calculated the values of u at the free surface for different values of $f'H$, that is, for different frequencies of the pulsations in air, the result being plotted in Fig. 2.

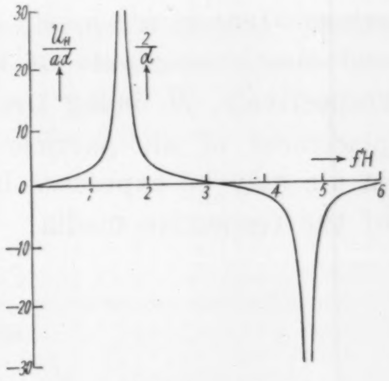

Fig. 2.

Let us take as an example the case, in which the maximum in pressure variation in air is 1/10,000 of the barometric pressure, and which roughly corresponds to a variation in wind velocity of 4·5m/sec, while the period of the same variation $2\pi/p$ is 10 sec. Then, if V be the velocity of sound waves, we have $f=p/V=(2\pi/10)/280.10^2=2{\cdot}24.10^{-5}\,\mathrm{cm}^{-1}$, so that under resonance conditions, $f'H=\pi/2$ (roughly corresponding to $H=1{\cdot}5$ km$\sim$3 km in rocks of superficial nature), we have $2a=(\partial\xi/\partial x)/f=(1/10{,}000)/2{\cdot}24.10^{-5}=4{\cdot}5$ cm, whence the maximum value of $2u$ $(=4a)$ becomes 9 cm. This is obviously much too large to expect in microseisms under such small pulsations in the air pressure, thus rendering improbable the existence of an extremely rigid substratum.

3. In order to ascertain the nature of the free vibrations of the layer, generalization of a solution of types (7) and (8) by means of Fourier's integral was resorted to. The form of the free vibrations of the layer is such that

$$u=2a\sum_{m=0}^{\infty}(-1)^m\frac{(1-\alpha)^m}{(1+\alpha)^{m+1}}\left\{F\left[\beta\left\{Vt+x+H\left(\frac{1}{\beta}-\overline{2m+1}\right)\right\}\right]\right.$$
$$\left.+F\left[\beta\left\{Vt-x+H\left(\frac{1}{\beta}-\overline{2m+1}\right)\right\}\right]\right\}, \qquad (9)$$

where $\beta=f'/f$, corresponds to the initial disturbance

$$\xi_0=F(ct+x)\,, \qquad (10)$$

which is supposed to act on the free surface. Thus, the damping factor is given by

$$(1-\alpha)^2/(1+\alpha)^2\,. \qquad (11)$$

Since α is very small compared with unity, it is possible to expect undamped free vibrations in this case. But since for the reason that, in almost resonance conditions, the amplitudes of forced vibrations become abnormally large, the presence of an extremely rigid substratum under the surface layer is hardly possible.

4. We shall next take the case in which the ratio of the elasticity of the surface layer to that of the subjacent medium is finite, so that it is possible for the vibrational energy in the layer to dissipate not only in air but also in the subjacent medium under consideration. Let u, u', ρ, ρ', λ, μ, λ', μ' be the displacements, densities, and elastic constants of the surface layer and the subjacent medium respectively, H being the thickness of the layer, while ξ is the displacement of air particle such that the change in dynamic pressure in air may be expressed by $p_0 \partial\xi/\partial x$. The solutions for the vibrations of the respective media

$$\xi = ae^{i(pt+fx)} + Ae^{i(pt-fx)}, \tag{12}$$

$$u = Be^{i(pt+f'x)} + Ce^{i(pt-f'x)}, \tag{13}$$

$$u' = De^{i(pt+f''x)}, \tag{14}$$

where $f^2=\rho p^2/p_0$, $f'^2=\rho p^2/(\lambda+2\mu)$, $f''^2=\rho' p^2/(\lambda'+2\mu')$, are to be substituted in the conditions

$$x=0; \qquad u=u', \qquad (\lambda+2\mu)\frac{\partial u}{\partial x}=(\lambda'+2\mu')\frac{\partial u'}{\partial x}, \tag*{(15), (16)}$$

$$x=H; \qquad u=\xi, \qquad (\lambda+2\mu)\frac{\partial u}{\partial x}=p_0\frac{\partial \xi}{\partial x}. \tag*{(17), (18)}$$

The final solutions for ξ, u, u' take the forms

$$\xi = a\cos(pt+fx) + \frac{a\sqrt{\{(\alpha^2\alpha'^2-1)\cos^2 f'H+(\alpha^2-\alpha'^2)\sin^2 f'H\}+\{2\alpha(1-\alpha'^2)\cos f'H\sin f'H\}^2}}{\{(\alpha\alpha'+1)\cos f'H\}^2+\{(\alpha+\alpha')\sin f'H\}^2}$$
$$.\cos\left[pt-fx+2fH+\tan^{-1}\left\{\frac{2\alpha(1-\alpha'^2)\cos f'H\sin f'H}{(\alpha^2\alpha'^2-1)\cos^2 f'H+(\alpha^2-\alpha'^2)\sin^2 f'H}\right\}\right], \tag{19}$$

$$u=\frac{2a\alpha\sqrt{\alpha'^2\cos^2 f'x+\sin^2 f'x}}{\sqrt{\{(\alpha\alpha'+1)\cos f'H\}^2+\{(\alpha+\alpha')\sin f'H\}^2}}$$
$$.\left\{pt+fH-\tan^{-1}\left(\frac{\alpha+\alpha'}{\alpha\alpha'+1}\tan f'H\right)+\tan^{-1}\left(\frac{1}{\alpha'}\tan f'x\right)\right\}, \tag{20}$$

$$u'=\frac{2a\alpha\alpha'}{\sqrt{\{(\alpha\alpha'+1)\cos f'H\}^2+\{(\alpha+\alpha')\sin f'H\}^2}}$$
$$.\left\{pt+f''x+fH-\tan^{-1}\left(\frac{\alpha+\alpha'}{\alpha\alpha'+1}\tan f'H\right)\right\}, \tag{21}$$

where $\alpha=\sqrt{\rho_0 p_0/\rho(\lambda+2\mu)}$, $\alpha'=\sqrt{(\lambda+2\mu)\rho/(\lambda'+2\mu')\rho'}$. We have calculated the surface displacements for two cases, namely (i) $\mu/\mu'=1/4$, (ii) $\mu/\mu'=1/16$, under the conditions that $\rho=\rho'$, $\lambda=\mu$, $\lambda'=\mu'$, the result being plotted in Figs. 3, 4. It will be seen that, owing to the great dissipation of vibrational energy into the subjacent medium, the amplitudes of vibrations at the surface are fairly small, even under resonance conditions.[2] Taking an example similar to that in the preceding section, we put $a=(\partial\xi/\partial x)/f=4{\cdot}5$ cm, so that the maximum value of $u(=2a\alpha C)$, C being the ordinates in Figs. 3, 4, become 14·6 microns and 29 microns for the respective cases of $\mu/\mu'=1/4$ and $\mu/\mu'=1/16$. These are more like the values probably to be expected in an actual microseism. If the period of pulsation in air be 30 sec, we have 44 microns and 60 microns for the amplitudes on the ground surface for the respective cases. The wind speed of 4·5 m/sec and its fluctuation period of 10 to 30 sec are rather underestimates, and we may expect larger amplitudes of microseisms in the case of strong wind, say 20 or 30 m/sec.

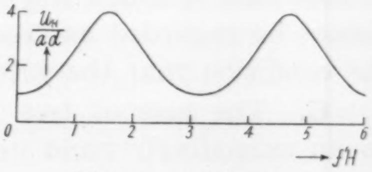

Fig. 3. $\mu/\mu'=1/4$.

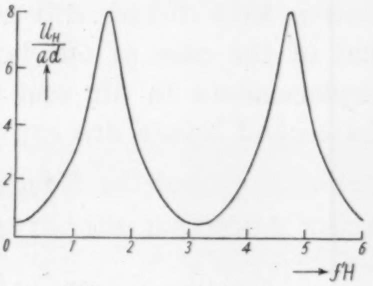

Fig. 4 $\mu/\mu'=1/16$.

5. The forms of damped free vibrations corresponding the above case are obtained as in the preceding problem by using elementary solutions and generalizing such solutions by means of Fourier's integrals, the result being

$$u=2\alpha(1+\alpha')\sum_{m=0}^{\infty}(-1)^m\frac{(1-\alpha)^m(1-\alpha')^m}{(1+\alpha)^{m+1}(1+\alpha')^{m+1}}F\left\{\beta\left(Vt+x+\frac{H}{\beta}-H\overline{2m+1}\right)\right\}$$

$$-2\alpha(1-\alpha')\sum_{m=0}^{\infty}(-1)^m\frac{(1-\alpha)^m(1-\alpha')^m}{(1+\alpha)^{m+1}(1+\alpha')^{m+1}}F\left\{\beta\left(Vt-x+\frac{H}{\beta}-H\overline{2m+1}\right)\right\}, \tag{22}$$

$$u'=4\alpha\alpha'\sum_{m=0}^{\infty}(-1)^m\frac{(1-\alpha)^m(1-\alpha')^m}{(1+\alpha)^{m+1}(1+\alpha')^{m+1}}F\left\{\beta\beta'\left(V't+x+\frac{H}{\beta\beta'}-\frac{H}{\beta'}\overline{2m+1}\right)\right\}, \tag{23}$$

where $\beta=f'/f$, $\beta'=f''/f'$, corresponding to the disturbance

$$\xi_0=F(ct+x). \tag{24}$$

---

[2] The calculated microseismic amplitudes of the ground surface may be made small by introducing viscous resistance in the surface layer when the substratum is exceedingly rigid. However, the value of coefficient of resistance is then too large to be expected from the data of earthquake waves. Furthermore, it is impossible for microseismic amplitudes for any wave length to be equally small under such resistance.

The decay factor

$$\frac{(1-\alpha)^2(1-\alpha')^2}{(1+\alpha)^2(1+\alpha')^2} \tag{25}$$

in this case is much less than unity. This tells us that microseisms cannot be regarded as free vibrations of the surface layer even under the condition that the subjacent medium is not infinitely rigid.

6. The case of two surface layers resting on an exceedingly rigid medium could be solved in a similar way, although the nature of the answer thus found will not differ greatly from that of the case of one layer. The equations of displacements in air and in the first as well as the second layers are expressed by

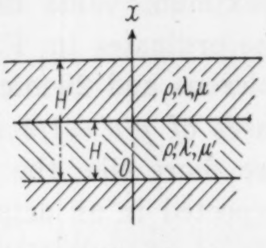

Fig. 5.

$$\xi = ae^{i(pt+fx)} + Ae^{i(pt-fx)}, \tag{26}$$

$$u = Be^{i(pt+f'x)} + Ce^{i(pt-f'x)}, \tag{27}$$

$$u' = De^{i(pt+f''x)} + Ee^{i(pt-f''x)}, \tag{28}$$

in which $f^2=\rho_0 p^2/p_0$, $f'^2=\rho p^2/(\lambda+2\mu)$, $f''^2=\rho' p^2/(\lambda'+2\mu')$, the conditions at the boundaries being

$$x=0; \quad u'=0, \tag{29}$$

$$x=H; \quad u'=u, \qquad (\lambda+2\mu)\frac{\partial u}{\partial x} = (\lambda'+2\mu')\frac{\partial u'}{\partial x}, \tag*{(30), (31)}$$

$$x=H'; \quad u=\xi, \qquad (\lambda+2\mu)\frac{\partial u}{\partial x} = p_0\frac{\partial \xi}{\partial x}. \tag*{(32), (33)}$$

The final solutions become

$$\xi = \frac{2a}{\sqrt{P^2+Q^2}}\cos\left\{f(x-H') - \tan^{-1}\frac{P}{Q}\right\}\cos\left\{pt+fH'+\tan^{-1}\frac{P}{Q}\right\}, \tag{34}$$

$$u = \frac{2a\alpha\sqrt{\alpha'^2\sin^2 f''H + \cos^2 f''H}}{\sqrt{P^2+Q^2}}$$

$$\cdot\cos\left\{f'(x-H) - \tan^{-1}\frac{\cot f''H}{\alpha}\right\}\cos\left\{pt+fH'+\tan^{-1}\frac{P}{Q}\right\}, \tag{35}$$

$$u' = \frac{2a\alpha\alpha'}{\sqrt{P^2+Q^2}}\sin f''x \cos\left\{pt+fH'+\tan^{-1}\frac{P}{Q}\right\}, \tag{36}$$

where

$$\left.\begin{aligned} P &= \cos f'(H'-H)\cos f''H - \alpha'\sin f'(H'-H)\sin f''H, \\ Q &= \alpha\{\sin f'(H'-H)\cos f''H + \alpha'\cos f'(H'-H)\sin f''H. \end{aligned}\right\} \tag{37}$$

Two cases, namely (i) $\mu/\mu'=1/4$, (ii) $\mu/\mu'=1/16$ $(H'=2H)$, other conditions being the same as in the preceding one, were calculated, the results being shown diagrammatically in Figs. 6, 7. In this case too, owing to the fact that the energy is capable of flowing only into air but not into the deep stratum of the earth, the maximum values of the surface displacements become very large. It is nevertheless certain that for some ratios of μ/μ' as well as of H/H', the resonance periods for different types of vibrations approach each other, so that the selective forced vibrations would resemble the coupled free ones, at any rate, in the type of vibrations.

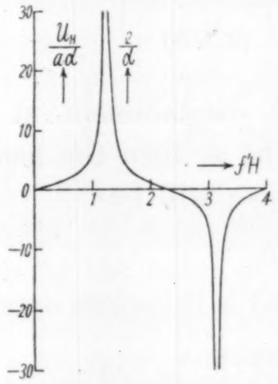

Fig. 6. $\mu/\mu'=1/4$.

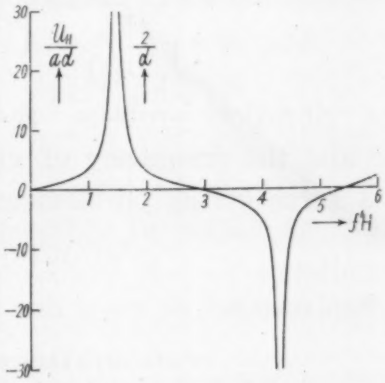

Fig. 7. $\mu/\mu'=1/16$.

7. An approximate method of solving the problem of damped vibrations, due to dissipation of their energy into the air, is by integral equations. The method is similar to that employed in the previous paper.[3] Although the case in which the subjacent medium is infinitely rigid is of no practical importance, as mentioned in Section 2, we shall nevertheless show how integral equations may be applied to such dissipative system.

Take the axis of x directed upwards with its origin at the lower boundary of the surface layer, and let H, $\rho(x)$, $L(x)$ be the thickness, density, and elastic constant of the stratum respectively. Taking into consideration the special nature of the integral equation, we shall discuss the problem as being a static one. Let the reaction of the air at the free surface of the layer due to a unit load within that layer be A, its value being different according as the frequency of vibrations are different. The vertical displacement at x due to a unit load applied at $x=a$ in the layer is then expressed by Green's function such that

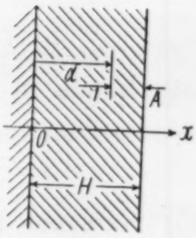

Fig. 8.

---

[3] K. Sezawa and K. Kanai, *Bull. Earthq. Res. Inst.*, **13** (1935), 490.

$$\left.\begin{aligned} k(x, a) &= (1-A)\int_0^x \frac{dz}{L(z)}\,, \qquad (x<a) \\ k(x, a) &= \int_0^\alpha \frac{dz}{L(z)} - A\int_0^x \frac{dz}{L(z)}\,. \qquad (x>a) \end{aligned}\right\} \tag{38}$$

If in the vibration problem, the vertical displacement at $x=\alpha$ be $u(a)\cos pt$ and the frequency of vibrations be p, then the load due to the inertia force acting on element da at $x=a$ will be

$$p^2\rho(a)u(a)\cos pt\, d\alpha\,. \tag{39}$$

The displacement at $x=x$ due to this load is therefore expressed by

$$p^2\rho(a)u(a)\cos pt\, da\, k(x, a)\,, \tag{40}$$

so that displacement $u(x)\cos pt$ at $x=x$ due to the total loads in the layer assumes the form

$$u(x) = p^2\int_0^H \rho(a)k(x, a)u(a)da\,, \tag{41}$$

the time factor being omitted. The movement in air is taken only for boundary conditions at $x=H$. We now write

$$\rho(a)k(x, a) = K(x, a)\,, \tag{42}$$

whence (41) reduces to the homogeneous integral equation

$$u(x) = p^2\int_0^H K(x, a)\, u(a)d\alpha\,, \tag{43}$$

$K(x, a)$ being its kernel. The boundary conditions at $x=H$ are such that

$$u(H) = 2\sin(k'H+\gamma)\,, \tag{44}$$

$$p^2\int_0^H \frac{\partial K(H, a)}{\partial H}u(a)da = \frac{2p_0k'}{L_{x=H}}\cos(k'H+\gamma)\,, \tag{45}$$

where p_0, $2\pi/k'$ are the barometric pressure and wave length of the disturbance in air respectively. Since

$$\left[\frac{\partial K(x, a)}{\partial x}\right]_{x=H} = -\rho(H)\frac{A}{L(H)}\,,$$

(45) reduece to

$$-p^2\int_0^H A\rho(a)u(a) = 2p_0k'\cos(k'H+\gamma)\,. \tag{45$'$}$$

From (44), (45′) we get

$$\Big[u(H)\Big]^2 + \left[\frac{p^2A}{p_0k'}\int_0^H \rho(a)\,u(a)da\right]^2 = 4\,. \tag{46}$$

By the trapezoidal rule for evaluating the integral, (43) and (46) are equivalent to

$$\frac{p^2H}{\nu}\sum_{q=0}^{\nu}\beta_q K\left(\frac{sH}{\nu},\ \frac{qH}{\nu}\right)u\left(\frac{qH}{\nu}\right)=u\left(\frac{sH}{\nu}\right), \tag{43'}$$

$$\Big[u(H)\Big]^2+\frac{p^2A^2H^2}{p_0^2k'^2\nu^2}\left[\sum_{q=0}^{\nu}\beta_q\rho\left(\frac{qH}{\nu}\right)u\left(\frac{qH}{\nu}\right)\right]^2=4\,, \tag{46'}$$

where $\beta_0=1/2$, $\beta_1=\cdot\cdot\cdot\cdot=\beta_q=\cdot\cdot\cdot\cdot=\beta_{\nu-1}=1$, $\beta_\nu=1/2$. Eliminating $\nu+1$ values of u in (43′), it is possible to obtain the value of A. Substituting the value of A thus obtained in $\nu+1$ equations in (46′), we get the ratios

$$u(0):\ u\left(\frac{H}{\nu}\right):\ \cdot\cdot\cdot\cdot:\ u\left(\frac{sH}{\nu}\right):\ \cdot\cdot\cdot\cdot:\ u(H)\,. \tag{47}$$

Substituting these ratios in (46), we obtain the absolute values of

$$u(0)\,,\ u\left(\frac{H}{\nu}\right),\ \cdot\cdot\cdot\cdot,\ u\left(\frac{sH}{\nu}\right),\ \cdot\cdot\cdot\cdot,\ u(H)\,.$$

With a view to comparing the result of the present approximate method with that of an accurate one in Section 2, we selected the case

$$\rho(x)=\rho_0\,,\qquad \mu(x)=\mu_0\,, \tag{48}$$

when the Green's function becomes

$$\left.\begin{aligned} k(x,\,a)&=(1-A)\frac{x}{\mu_0}\,, &&(x<a)\\ k(x,\,a)&=\frac{a-Ax}{\mu_0}\,. &&(x>a)\end{aligned}\right\} \tag{49}$$

After substituting these values in (43′), (46′) for the two cases (i) $f'H=\pi/2$ (resonance condition), (ii) $f'H=1$, we calculated the distribution of displacements in the layer. If we were to take five ordinates, namely, $\nu=4$, A would take the form

$$A=\frac{1-32\phi+320\phi^2-1024\phi^3+512\phi^4}{1-32\phi+320\phi^2-1024\phi^3}\,, \tag{50}$$

where $\phi=4/(f'H)^2$. The result of the calculation is shown diagrammatically by the full lines in Figs. 9, 10; in which the accurate values determined by (8) are shown by broken lines.

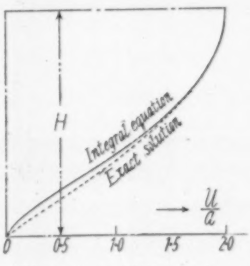

Fig. 9. $f'H=\pi/2$.

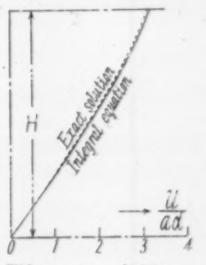

Fig. 10. $f'H=1$.

8. *Concluding Remarks.*

From a comparison of the results obtained in Section 2, 3, 4, 5 it seems now established that microseismic vibrations of local type are mainly formed by selective forced vibrations of the surface layers due to the pulsation in air pressure on the surface of the earth, and also that the rigidities of the underlying strata are not very large compared with those of the upper layers, the ratio of the rigidities for the two being probably in the range $3\sim20$. Under this condition the amplitudes of microseisms range from a few microns to a hundred microns when the variation of 4·5 m/sec in wind velocity takes place with period of the order of 10 to 30 sec. Even in such a state, no free oscillations can be maintained because of the fact that the energy is dissipated relatively rapidly into the subjacent medium. The flow of energy into air, when the underlying media are assumed to be extremely rigid, is too small to participate in the dissipation, in which case the vibratory motion of the surface layers under resonance becomes exceedingly large, say 9 cm in amplitude, even in a very slightly disturbed condition of the atmosphere, say a variation of wind velocity 4·5 m/sec with period 10 sec. It is also impossible to expect large damping due to solid viscosity in meterials. It follows therefore that microseims of local type cannot be free vibrations of the earth's upper layers unless we assume that no resonance conditions would ever arise. It would seem that the regular periodic motion in the microseisms under consideration has its origin only in atmospheric disturbances of such a character as would give rise to easy selective resonance of the surface layers. This implies that the variation of atmospheric condition is due to an aggregate of fairly regular periodic pulsations. Records of air conditions obtained by means of meteorological instruments, and data of vibrations of tall buildings in strong wind seem to confirm this conclusion.

---

58. 局所的脈動の性質

地震研究所 { 妹澤克惟
金井清

局所的脈動（和達博士の命名と思ふ）といはれてゐる種類の脈動はその原因が大體に於てその土地の地表上の大氣の狀態にあるとすることは大して異存がないと思はれる．しかし，その振動の形が殆ど減衰しない聯成振動の形をなす爲に，それが一つか數個の地表層の自由振動であるかのやうに思はれ易いものである．これを明瞭にするために地表層の臺をなしてゐる下層の彈性を地表層のそれに比して適當に大きくした場合と無限に大きな場合の夫々の自由振動と大氣の擾亂のための强制振動とを計算してみたのである．

假りに下層が極端に剛い場合を取つて見ると自由振動としてその振動性を永續させることは可能である．これは空中へ勢力逸散があつても大して影響をもたない．しかし强制振動で選擇共振をやると風速變化 4·5 m 位が 10 秒毎に起つても 9 cm 位の地表振幅が容易に出る． これを少くする爲に粘性抵抗を入れても普通の地震波位で豫期できる位の抵抗値では到底追付かぬし，のみならず，種々の週期の振動の振幅を比較して見るとその根本性が違つてゐることがわかる，それでどうしても下層を非常に剛くして置くことは許されぬことが知られる．

次に下層を地表層よりも適當に剛く，卽ち下層の剛度を地表層のそれの 3 倍乃至 20 倍位にして選擇共振の振幅を見ると，風速變化 4·5 m が 10 秒から 20 秒位の週期で變化しても數microns から數十 microns 位の地表振幅となり，風速變化が 20 m から 30 m にもなるともつと大きな地表振幅となる．之は實際の觀測とよく一致してゐる．しかし同樣な場合の自由振動を見ると，下層への勢力逸散の爲に振動が餘りにもよく減衰するから自由振動でないことは明かである．從て問題はこの場合の共振强制振動に落着くより外仕方がないと思ふ．

このやうにして見ると脈動は大體に於て强制振動であつて，その振幅の大なる規則正しい部分は選擇共振であり，その原因が大氣狀態の擾亂に存在することが知られるであらう．而して脈動の振幅が長く續くのは地表層が長く自由振動をなす爲でなく大氣の擾亂が比較的に規則正しい週期的振動の集りであつてそれが長く續く結果に過ぎないのである．氣象器械による大氣狀態の觀測や，强風中に於ける高層建物の振動結果等からもこの傾向を確め得ると思ふ．

---

59. *Elastic Waves Produced by Applying Statical Force to a Body or by Releasing it from a Body.*

By Katsutada SEZAWA,

Earthquake Research Institute.

(Read Sept. 17, 1935.—Received Sept. 20, 1935.)

1. The idea that, if a boundary force that gave rise to statical strain in an elastic body were released, all the strain energy that was stored in the body would be transmitted outwards in the form of elastic waves, seems to be prevalent among many seismologists. That was also my belief in connection with the explanation of the large energy of seismic waves that were released at the time of the Great Kwanto Earthquake of 1923.1) The same view, apparently held by a number of people, is maintained even by some new writers, such as Kawasumi and Yosiyama.2) A few years ago,3) however, I had reason to change my opinion to the one that, from the dynamical point of view, it is not probable. I now believe that waves should rather be generated from the very boundary where the statical force is released. Although the strain energy stored in the elastic body may be released by the neutralizing action due to the original propagated waves, no extra energy can be formed by resolution of the statical strain energy in the body.

2. To understand the nature of the problem, we shall first discuss the case in which statical force is applied to part of an elastic body that was free from stress or strain before the application of that force. The energy given by the applied force differs with the rapidity or speed with which that force is applied. If the force were applied very slowly, the amount of energy imparted to the body would be exactly the same as that of the statical strain energy to be stored in that body corresponding the steady action of the force when a statical force acts stationarily. If the force were applied with a certain speed, the amount of the energy would exceed the strain energy

---

1) My paper read at Colloq. Meetings in Fac. Eng. as well as in Seism. Inst., Tokyo Imp. Univ., 1924.

2) H. KAWASUMI and R. YOSIYAMA, *Disin*, **7** (1935), 359∼375; *Bull. Earthq. Res. Inst.*, **13** (1935), 496∼503.

3) K. SEZAWA, Section 9, *Rep. Aeron. Res. Inst.*, No. 45 (1928).

under consideration. The greater the speed with which the force is applied, the greater the energy required.

Consider the case in which a force applied to a certain part of the body is slowly increased from zero to its ultimate value F. If the total energy given by the same force be E_0 and the energy statically stored in the body due to a statical force F be E_s, we should have

$$E_0 = E_s. \tag{1}$$

If, on the other hand, the case is one in which the force F is applied with some rapidity, the energy E required is

$$E = E_s + E_w, \tag{2}$$

where E_w is the excess part of the energy. When no energy is dissipated, whether in the form of heat or other inelastic forms, E_w should be the energy that is dissipated as elastic waves. Since dynamical theory shows that when a force F is applied with infinitely great rapidity, the energy E_1 imparted by the same force is

$$E_1 = 2E_s, \tag{3}$$

the wave energy E_{w1} produced in consequence of the exceedingly quick application of the force becoming

$$E_{w1} = E_s. \tag{4}$$

Similarly, it is possible to prove that the amount of energy E done by the applied force acting with a certain finite rapidity and that of energy E_w of the dissipated waves corresponding to the same case are both restricted to the ranges respectively of

$$E_0 < E < E_1, \qquad 0 < E_w < E_{w1}. \qquad (5), (6)$$

3. We shall next deal with the case in which a statical force F that was being applied to a part of an elastic body is released with different degrees of rapidity. Dynamically, the problem is the same as the one in which a negative force F is applied to the body subjected to a permanent statical force F. If the force F were released extremely slowly, the amount of energy due to F that is imparted to the body would be equal to the total energy already stored in the body, whereas, if the force were released with some rapidity, the amount of energy would exceed that of the energy that had been and was being stored statically in the body. Using the same notations, and proceeding in the same way as in the preceding case, we get

$$E_0=E_s\,, \tag{1'}$$

$$E=E_s+E_w\,, \tag{2'}$$

$$E_1=2E_s\,, \qquad E_{w1}=E_s\,, \qquad (3'),\ (4')$$

$$E_0<E<E_1\,, \qquad 0<E_w<E_{w1}\,. \qquad (5'),\ (6')$$

It should be remembered that E_s, E_w in this case represent the released statical strain energy and the energy in the dissipated waves respectively, both due to release of the statical force with a certain degree of rapidity.

It appears from these considerations that, in the release of the statical force, no wave energy can be sent out directly from the region in which the statical strain energy had been and was being stored, but the source of the same energy is, in fact, the energy imparted in the release of the statical force at the origin. In other words, the energy of elastic waves is equal to the excess part of the work in neutralizing the statical strain originally stored in the body.

4. In the two preceding sections the problem was discussed merely in its relation to total energy and its components. The same conception however could be extended to each infinitesimal part of the body. Let the external force for application or release be localized at a certain part of a body with infinite extension in space and elastic waves be radiated outwards from that localized part. Assuming that the part in question is a point, the total energy $E_{r\infty}$ passing through a spherical surface of radius r with its centre at the point of application of the force is expressed by

$$E_{r\infty}=E-E_{sr}\,, \tag{7}$$

where E_{sr} is the statical strain energy that is to be stored within spherical volume of radius r — a natural consequence of the principle of energy shown already and of the assumption that the elastic body is extending to infinity in all directions. $E_{r\infty}$, which contains the energy passing through the spherical surface, consists of two parts, namely, the energy that is radiated outwards in the form of pure elastic waves and the energy that is to be stored in the form of statical strain energy in the body outside the spherical surface. Thus, in the case of very slow application of the force, $E_{r\infty}$ is nothing but the statical strain energy to be stored in the body outside the spherical surface, whereas in the case of exceedingly quick application of the force, $E_{r\infty}$ contains both wave energy E_w and the strain energy, $E_{s0}-E_{sr}$, the value of E_w being exactly half that of the energy E emerging at the origin.

Since the case of releasing the force that had been applied to a part of the body is the same as the one in which a negative force is applied to the body subjected to a permanent statical force, it is possible to prove in the same way that the energy $E_{r\infty}$ in such a case passing through the spherical surface of radius r with its centre at the point of release of the force, is expressed by

$$E_{r\infty}=E-E_{sr}\,, \tag{7'}$$

where E is the energy emerging at the origin and E_{sr} is the statical strain energy which was originally stored in the spherical volume of radius r. The difference in the nature of the problem as the result of differences in the rapidity with which the force is released is the same as that when the force is applied.

5. To prove the foregoing statements we shall take a case somewhat similar to that discussed by Kawasumi and Yosiyama.[4] Statical pressure is applied to or released from (at various speeds) a spherical cavity of radius a inside an elastic body that is extending in all directions to infinity. In the case of application of the pressure to the cavity in question, pressure P in the intermediate stages of the application may be expressed by such forms as

$$\left.\begin{array}{ll} P=0, & (r=a,\quad t<0) \\ P=-P_0e^{-ct}(1-e^{-qt})\,, & (r=a,\quad t>0) \end{array}\right\}^{5)} \tag{8}$$

where P_0 is the intensity of the final pressure and c should be made zero after the evaluation of necessary integrals. For sudden application of the pressure it is necessary to put $q=\infty$, while for very slow application of the same pressure we shall have to put $q\rightarrow 0$. It is possible to get different cases for the rapidity with which the pressure is applied by taking different values of q. The integral expression of a similar problem has already been given by Kawasumi and Yosiyama[6] in the form

---

[4] H. KAWASUMI and R. YOSIYAMA, *loc. cit.* 2).

[5] It should be borne in mind that (8) does not necessarily represent the condition of actual free surface of an elastic body. But, it rather indicates a mere state of a surface within the body. Thus, in the present problem the elastic waves are always transmitted outwards through this surface; no special force is applied or released at this surface.

[6] H. KAWASUMI and R. YOSIYAMA, *loc. cit.* 2); I took similar notations as those used by Kawasumi and Yosiyama for easiness in comparing the results.

$$\phi=\frac{1}{2\pi}\int_0^\infty\frac{\{H^{(1)}_{1/2}(hr)/\sqrt{r}\}e^{-ipt}dp}{\{-(\lambda+2\mu)h^2H^{(1)}_{1/2}(ha)/\sqrt{a}+4\mu hH^{(1)}_{3/2}(ha)/a^{3/2}\}}\int_{-\infty}^{\infty}Pe^{ip\omega}d\omega$$

$$+\frac{\{H^{(2)}_{1/2}(hr)/\sqrt{r}\}e^{ipt}dp}{\{-(\lambda+2\mu)h^2H^{(2)}_{1/2}(ha)/\sqrt{a}+4\mu hH^{(2)}_{3/2}(ha)/a^{3/2}\}}\int_{-\infty}^{\infty}Pe^{-ip\omega}d\omega\,,^{7)} \qquad (9)$$

where ϕ satisfies the wave equation

$$\frac{\partial^2\phi}{\partial t^2}=\frac{\lambda+2\mu}{\rho}\Delta^2\phi\,,$$

the radial displacement and stress being expressed by $u=\partial\phi/\partial r$ and $rr=(\lambda+2\mu)\partial u/\partial r+2\lambda u/r$ respectively. By means of the conditions in (8), (9) reduces to (for $\tau>0$)

$$\phi=\frac{a}{2\pi i\rho r}\left\{\int_{-\infty}^{\infty}\frac{e^{ip\tau}dp}{(p-ic)(p-\alpha)(p-\beta)}-\int_{-\infty}^{\infty}\frac{e^{ip\tau}dp}{(p-iq)(p-\alpha)(p-\beta)}\right\}, \qquad (10)$$

provided $\tau=t-(r-a)/v$, v being $\sqrt{(\lambda+2\mu)/\rho}$. Here, use should be made of $c\to0$. Evaluating this integral by means of a contour integral, we find that, for $\tau>0$,

$$\phi=\frac{aP_0}{\rho r}\left[\left(\frac{1}{\alpha\beta}-\frac{e^{-q\tau}}{Q}\right)+\frac{1}{\alpha-\beta}\left(\frac{1}{\alpha}-\frac{1}{\alpha-iq}\right)e^{i\alpha\tau}-\frac{1}{\alpha-\beta}\left(\frac{1}{\beta}-\frac{1}{\beta-iq}\right)e^{i\beta\tau}\right], \qquad (11)$$

ϕ being zero for $\tau<0$. In the above equation ρ is the density of the solid and

$$\left.\begin{aligned}&\alpha\beta=-4\mu/\rho a^2\,, \qquad \alpha+\beta=4i\mu/\rho av\,,\\ &Q=(\alpha-iq)(\beta-iq)=-\left(\frac{4\mu}{\rho a^2}-\frac{4\mu q}{\rho av}+q^2\right),\end{aligned}\right\} \qquad (12)$$

Q being negative in all cases. The radial displacement and stress, for $\tau>0$, are now expressed by

$$u=\frac{a^3P_0}{4\mu}\left[\frac{1}{r^2}+\frac{\alpha\beta}{Q}\left(\frac{q}{vr}-\frac{1}{r^2}\right)e^{-q\tau}+\frac{\beta q}{(\alpha-\beta)(\alpha-iq)}\left(\frac{\alpha}{vr}-\frac{i}{r^2}\right)e^{i\alpha\tau}\right.$$

$$\left.-\frac{\alpha q}{(\alpha-\beta)(\beta-iq)}\left(\frac{\beta}{vr}-\frac{i}{r^2}\right)e^{i\beta\tau}\right]^{8)}, \qquad (13)$$

---

7) From the point of view of mathematical theory there are a good deal of criteria with respect to the existence of the integral, however it would not be important now to investigate them thoroughly.

8) Somewhat exponential or oscillatory terms in the expression and others are the mere consequence in the treatment of problems of wave propagation in two or three dimensions; it is obvious that this cannot be the origin of the actual oscillatory feature of seismic waves. See H. LAMB, *Proc. Math. Soc., London*, **35** (1903), 141, etc.

$$\widehat{rr} = -\frac{a^3P_0}{r^3} + \frac{a^3P_0\alpha\beta}{Q}\left(\frac{1}{r^3} - \frac{q}{vr^2} + \frac{q^2}{4\mathfrak{a}^2r}\right)e^{-q\tau}$$

$$+\frac{ia^3P_0\beta q}{(\alpha-\beta)(\alpha-iq)}\left(\frac{1}{r^3} + \frac{i\alpha}{vr^2} - \frac{\alpha^2}{4\mathfrak{a}^2r}\right)e^{i\alpha\tau}$$

$$-\frac{ia^3P_0\alpha q}{(\alpha-\beta)(\beta-iq)}\left(\frac{1}{r^3} + \frac{i\beta}{vr^3} - \frac{\beta^2}{4\mathfrak{a}^2r}\right)e^{i\beta\tau}, \tag{14}$$

where $\mathfrak{a}^2 = \mu/\rho$. To obtain the final distribution of u and $\widehat{rr}$, we put $\tau = \infty$ and $q \to 0$ in these equations and get

$$u = \frac{a^3P_0}{4\mu r^2}, \quad \widehat{rr} = -\frac{a^3P_0}{r^3}, \tag{15}$$

regardless of whether q be large or small, excepting however the case when q is exactly zero. These are respectively equal to the displacement and stress due to statical pressure P_0 applied to the spherical cavity.

Now, $\partial u/\partial t$ takes the form

$$\frac{\partial u}{\partial t} = \frac{a^3P_0}{4\mu}\left[\frac{\alpha\beta q}{Q}\left(\frac{1}{r^2} - \frac{q}{vr}\right)e^{-q\tau} + \frac{\alpha\beta q}{(\alpha-\beta)(\alpha-iq)}\left(\frac{1}{r^2} + \frac{i\alpha}{vr}\right)e^{i\alpha\tau}\right.$$

$$\left. - \frac{\alpha\beta q}{(\alpha-\beta)(\beta-iq)}\left(\frac{1}{r^2} + \frac{i\beta}{vr}\right)e^{i\beta\tau}\right], \tag{16}$$

whence the total energy transmitted through the spherical surface of radius r is written

$$E_{r\infty} = 4\pi r^2\int_0^\infty\left(-\widehat{rr}\frac{\partial u}{\partial t}\right)d\tau.^{9)} \tag{17}$$

Substituting (14) and (16) in (17), we finally get

$$E_{r\infty} = \frac{\pi a^9P_0^2}{\mu r^3} + \frac{\pi a^6P_0^2}{2\mu\left(\frac{4\mu}{\rho a^2} - \frac{4\mu q}{\rho av} + q^2\right)^2}\left[-\left(\frac{4\mu}{\rho a^2}\right)^2\left(\frac{1}{r^3} - \frac{2q}{vr^2}\right)\right.$$

$$+\frac{1}{a^3}\left(q^2 + \frac{4\mu q}{\rho av} + \frac{4\mu}{\rho a^2}\right)q^2 - \frac{1}{r^3}\left(q^2 - \frac{8\mu q}{\rho av} + \left(\frac{4\mu}{\rho av}\right)^2\right)q^2$$

$$-\frac{2}{r}\left(\frac{4\mu}{\rho a^2}\right)^2\left(\frac{1}{v^2} + \frac{1}{4\mathfrak{a}^2}\right)q^2 - \frac{8\mu}{\rho a^2r^2v}\left(-\frac{4\mu}{\rho av} + q\right)q^2$$

---

9) H. KAWASUMI and R. YOSIYAMA, *loc. cit.* 2); A. E. H. LOVE, *Mathematical Theory of Elasticity*, 4th ed. (Combridge, 1927), § 61, p. 93.

$$
\begin{aligned}
-\frac{\dfrac{4\mu}{\rho a^2}q}{\left(\dfrac{4\mu}{\rho a^2}+\dfrac{4\mu q}{\rho a v}+q^2\right)}\biggl\{&\frac{\rho}{\mu v}\left[\left(\frac{4\mu}{\rho a^2}\right)^2+\frac{4\mu q^2}{\rho a^2}\right]q^2 \\
&-\frac{2}{r}\left(\frac{1}{r^2}+\frac{1}{4a^2}\right)\left[\left(\frac{4\mu}{\rho a^2}\right)^2+\frac{16\mu^2}{\rho^2 a^3 v}q+\frac{4\mu}{\rho a^2}q^2\right]q \\
&\qquad+\frac{2}{vr^2}\left[\left(\frac{4\mu}{\rho a^2}\right)^2+\frac{32\mu^2}{\rho^2 a^3 v}q+\left(\frac{4\mu}{\rho a v}\right)^2 q^2-q^4\right] \\
&\qquad+\frac{2}{r^3}\left[-\frac{16\mu^2}{\rho^2 a^3 v}+\left(\frac{16\mu^2}{a^2\rho^2 v^2}+\frac{4\mu}{\rho a^2}\right)q+q^3\right]\biggr\}\Biggr]^{[10]}. \qquad (18)
\end{aligned}
$$

In the case where pressure is applied infinitely slowly, we put $q \to 0$, whence

$$E_{r\infty}=\frac{\pi a^6 P_0^2}{2\mu r^3},^{[11]} \qquad (19)$$

its value at $r=a$ being $E_{a\infty}=\dfrac{\pi a^6 P_0^2}{2\mu a^3}$. We know that the strain energy in a unit volume at $r=r$ is[12]

$$
\begin{aligned}
e_{sr}&=\frac{\lambda+2\mu}{2}\left(\frac{\partial u}{\partial r}+\frac{2}{r}\right)^2-\frac{\mu}{2}\left(\frac{4}{r^2}+\frac{8}{r}\frac{\partial u}{\partial r}\right) \\
&=\frac{3a^6 P_0^2}{8\mu r^6}.
\end{aligned}
$$

Thus the total strain energy that is stored inside a spherical volume of radius r as the result of statical pressure P_0 applied to the cavity $r=a$ becomes

$$E_{sr}=4\pi\int_a^r e_{sr}r^2 dr=\frac{\pi a^6 P_0^2}{2\mu}\left(\frac{1}{a^3}-\frac{1}{r^3}\right). \qquad (20)$$

From (19) the difference between the two energies $E_{a\infty}$ and $E_{r\infty}$ is

$$E_{a\infty}-E_{r\infty}=\frac{\pi a^6 P_0^2}{2\mu}\left(\frac{1}{a^3}-\frac{1}{r^3}\right). \qquad (21)$$

Whence

$$E_{sr}=E_{0\infty}-E_{r\infty}. \qquad (22)$$

This means that the energy transmitted through the surface $r=r$ is equal to the difference between the energy applied to the origin and the energy stored statically inside the spherical volume of radius r. The equation (21) also shows that all energy due to the very slow application of the force to the origin is stored as statical strain energy, namely,

---

[10] K. **KANAI** found that this expression can be reduced to a very simple form, which will appear in a near future.

[11] Such energy flows outwards even in the case of release of force in consequence of (9).

[12] A. E. H. **LOVE**, *loc. cit.*, p. 102.

$$E_{a\infty}=E_s\,, \tag{23}$$

E_s being taken throughout the space to infinity.

For the case where pressure is applied suddenly, we put $q=\infty$, whence from (18)

$$E_{r\infty}=\frac{\pi a^6 P_0^2}{2\mu}\left(\frac{1}{a^3}+\frac{1}{r^3}\right), \tag{24}$$

the energy applied at the origin being therefore

$$E_{a\infty}=\frac{\pi a^3 P_0^2}{\mu}\,,$$

This is equivalent to twice the value of $E_{r\infty}$ at $r=\infty$. In this case too we have

$$E_{a\infty}-E_{r\infty}=\frac{\pi a^6 P_0^2}{2\mu}\left(\frac{1}{a^3}-\frac{1}{r^3}\right). \tag{21$'$}$$

The relation

$$E_{sr}=E_{a\infty}-E_{r\infty} \tag{22$'$}$$

also holds. At $r=\infty$ we have

$$E_{r\infty}=E_{\infty\infty}=\frac{\pi a^3 P_0^2}{2\mu}\left(=E_w\right), \tag{25}$$

half the energy applied at the origin being transmitted to infinity in the form of pure elastic waves. The remaining half is stored in the body as statical strain energy.

6. Since the case of release of the statical pressure that had been applied to a spherical cavity is dynamically the same as the one in which a negative pressure is applied to a body subjected to a permanent statical pressure, it is possible to deal with the problem in exactly the same way as in the preceding case.[13] The solution is the same as that in (18). In any case

$$E_{a\infty}-E_{r\infty}=E_{sr} \tag{22$''$}$$

---

[13] The possibility of superposition of tension and compression is obvious in mathematical theory of elasticity in which linear relation between stress and strain exists. Without this conception the mathematics like Fourier's integral cannot be used. The corresponding energy flow is also understood by aid of the idea noticed in 11). The detailed explanation regarding the release of force will appear in a near future.

holds. If the pressure is released very quickly, the energy applied to the origin is equal to twice the value of the statical strain energy or equal to that of the wave energy transmitted to infinity. It is, thus, impossible to evolve wave energy from the strained part of an elastic body even in sudden release of the force at the origin. Half the value of the energy at the origin, however, is consumed in resolving the statical strain, the remaining half alone being transmitted in the form of pure elastic waves to infinity.

In conclusion, I wish to express my indebtedness to Drs. Kawasumi and Yosiyama, whose calculations referred to have greatly assisted me in presenting my theory.

---

59. 靜力學的力を加へ又は除く爲に生ずる彈性波

地震研究所 妹澤克惟

地殼に靜力學的歪を與へつゝあつた力を除去すると，その地殼の中に貯へられてをつた靜力學的歪勢力が彈性波の形となつて遠方へ傳播するであらうといふ考が或地震學者には信じられてゐたやうに思はれる．私自身も大正十二年關東地震の直後そのやうな意見をいだいたこともあるが，七八年前からはそのやうな考方の正しくないことがわかり，もつと正確な見方をもつやうになつた．しかし事柄が割合に簡單な爲に殊更に論文で示さうとも思はなかつたけれども，最近に至りまだ二三人の地震專門家が前のやうな考を堅く取つてその爲に多くの人が誤解に陷ることも無いとも限らぬことを恐れ，啓蒙的意味をもつてこの論文を書いて見たのである．但し念の爲に附加へたいことは，たとひ，地震が靜力學的力の變化によると假定した範圍內でも，この論文で取扱ふやうな場合のみが彈性波を起す機構ではないことである．

委しい考方は本文中にあるから省略するけれども，一例としてある限定された區域に靜力學的の力が加つてをつたとき，その力を取去つた爲に如何なる波動が出るかを考へてみる．一寸考へると，その力を取去つた爲に前述の區域の周圍に貯へられてをつた靜力學的歪がとれてそれが地震波として傳播しそうに見えるけれども，決してそうでなく，原區域に生じた勢力が周圍に波動して，旣に貯へられてをつた歪の勢力を解消する爲に費されつゝ傳播して行くものである．それで原區域の力の除去の速さを極端におそくすると，その勢力が歪の勢力を除去する爲にのみ費されてしまひ，遠方まで純粹の波動として傳はる勢力は全然存在しない．これに反して，その速さを速くすると勢力が少しづゝ餘計にかゝり，極端に速くすると，原勢力は極端に遲い場合の二倍だけ要することがわかる．このことは衝擊問題の常識からもわかると思ふ．卽ちこの場合に純粹の波動勢力はもとからあつた靜力學歪の勢力と同値を取るから，その計算を試みたものでもうつかりするとだまされ易いものである．又，如何に仕事を加へてもその擾亂の速さは必ず彈性波の速度を取ることは當然である．原區域から出た波動（すべての擾亂を含み）が或半徑を通過する

場合その半徑を通して出る全勢力は，原區域で與へた勢力と，原區域からその半徑までの彈性的空間に貯へてをつた靜力學的歪の勢力との差に等しいことが明かである.

このやうな問題は例題について數値を入れた計算を試みても當然同じに出るものである.

上の説明により，原點に加はつた勢力が傳播して半徑とともに減じこそすれ，途中で勢力を集めつゝ波動するやうなことのないのは當然である．再び念の爲に附加へたいことは，こゝに論じた場合は，固體の空間に歪勢力を與へつゝあつたその力を除き去る場合を論じてゐるのであつて互に關係のない歪勢力と力との間のものに觸れて居らぬことである.

靜力學的力を除去するときに外方へ流れる勢力と，同じ大さの靜力學的力を加へる場合に外方へ流れる勢力とが等しい理由は，本文中にも所々に述べてはあるけれども，之を了解できぬ人々にために次の機會の論文で委しくまとめて説明する考である.

---

60. *The Effect of Sharpness of Discontinuities on the Transmission and Reflection of Elastic Waves.*

By Katsutada SEZAWA and Kiyoshi KANAI,

Earthquake Research Institute.

(Read October 15, 1935.—Received Sept. 20, 1935.)

1. The theory of reflection and refraction of waves at discontinuities within an elastic body was first studied by Knott[1] quite a number of years ago, while its more practical side has been developed recently by the investigations of Kawasumi and Suzuki.[2] The assumption made in these investigations regarding the distribution in the nature of the material is that the density or elasticity of the material varies very sharply at the discontinuities under consideration. It appears however that the condition thus assumed could hardly exist in reality, the probability being rather that the distribution of material in the immediate vicinity of the discontinuities in the earth would vary more or less gradually, the amplitudes of transmitted (refracted) and reflected waves through these discontinuities differing somewhat with difference in the lengths of the incident waves.[3]

2. For simplicity, take the case of transverse waves, and let ρ_0, μ_0, ρ_2, μ_2 be the densities and rigidities of the medium in which the primary waves u are incident and those in which the waves u_2 are transmitted. Suppose that at the discontinuity under consideration there is an intermediate layer of thickness H, in which the density and elasticity vary in obedience to a certain law, and let the density, rigidity, and the displacement there be ρ_1, μ_1, u_1 respectively. Let, again,

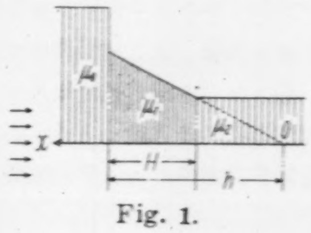

Fig. 1.

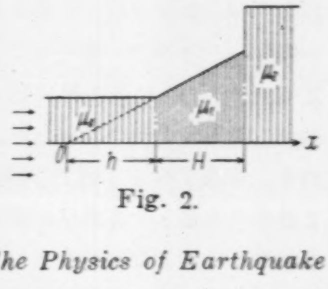

Fig. 2.

---

[1] C. G. KNOTT, *Phil. Mag.*, [v], **45** (1899), 64~97; *The Physics of Earthquake Phenomena* (Oxford, 1908).

[2] H. KAWASUMI and T. SUZUKI, *Disin*, **4** (1932), 277~307.

[3] The nature of gradually varying discontinuity does not much affect the propagation of waves parallel to that discontinuity as in the case of dispersive surface waves, in spite of its great effect on the transmission of bodily waves through that discontinuity.

the densities be the same everywhere, and the rigidity in the intermediate layer vary linearly as

$$\mu_1 = Ax, \tag{1}$$

the axis of x being taken as shown in Figs. 1, 2 and furthermore, there be a certain "step" or abrupt variations in rigidity distribution between that intermediate layer and the medium with higher rigidity, as will be seen in the same figures. Then, we have the equations of vibratory motion in the first as well as in the second media, and also in the intermediate layer as follows:

$$\rho_0 \frac{\partial^2 u_0}{\partial t^2} = \mu_0 \frac{\partial^2 u_0}{\partial x^2}, \qquad \rho_2 \frac{\partial^2 u_2}{\partial t^2} = \mu_2 \frac{\partial^2 u_2}{\partial x^2}, \tag{2), (3}$$

$$\rho_1 \frac{\partial^2 u_1}{\partial t^2} = \frac{\partial}{\partial x}\left(\mu_1 \frac{\partial u_1}{\partial x}\right), \tag{4}$$

where $u_0 = u + u'$, in which u' is the displacement of the reflected waves in the first layer. In the case of dilatational waves it is generally necessary to put $\lambda + 2\mu$ in lieu of μ. The solutions of these equations are

$$u_0 = u + u' = e^{ik(V_1 t \pm x)} + B e^{ik(V_1 t \mp x)}, \tag{5}$$

$$u_1 = \left\{ C H_0^{(1)}\left(2\sqrt{\frac{\rho_1 p^2}{A} x}\right) + D H_0^{(2)}\left(2\sqrt{\frac{\rho_1 p^2}{A} x}\right)\right\} e^{ipt}, \tag{6}$$

$$u_2 = E e^{ik''(V_3 t \pm x)}, \tag{7}$$

corresponding to the incident waves

$$u = e^{ik(V_1 t \pm x)}, \tag{8}$$

where $V_1 = \sqrt{\mu_0/\rho_0}$, $V_3 = \sqrt{\mu_2/\rho_2}$, $kV_1 = k''V_3 = p$. In these equations, the upper or lower term (or sign) of the two expressions (in a vertical row) is taken according as whether or not the first medium is more rigid than the second.

If h be the distance from the origin of x to the boundary plane between the medium (in which the primary waves are incident) and the intermediate layer as shown in Figs. 1, 2, then

$$x = h; \qquad u_0 = u_1, \qquad \left.\begin{matrix} mAh \\ Ah \end{matrix}\right\} \frac{\partial u_0}{\partial x} = Ah \frac{\partial u_1}{\partial x}, \tag{9), (10}$$

$$x = \left\{\begin{matrix} h-H; \\ h+H; \end{matrix}\right. \qquad u_1 = u_2, \qquad \left.\begin{matrix} A(h-H) \\ A(h+H) \end{matrix}\right\} \frac{\partial u_1}{\partial x} = \left.\begin{matrix} A(h-H) \\ mA(h+H) \end{matrix}\right\} \frac{\partial u_2}{\partial x}, \tag{11), (12}$$

where m is the ratio of the rigidity of the medium having the greater elastic constant (between μ_0 and μ_2) to the greatest value of the rigidity (μ_1) of the intermediate layer. Substituting (5), (6), (7) in these boundary conditions, we get

$$u_0=u+u'=\cos k(V_1t\pm x)+\sqrt{\frac{(a+b)^2+(-c+d)^2}{(-a+b)^2+(c+d)^2}}$$

$$.\cos\left(k(V_1t\mp x\pm 2kh)\pm\tan^{-1}\frac{N}{M}\right\}, \qquad (13)$$

$$u_1=\left.\begin{matrix}2\sqrt{m}\\2\end{matrix}\right\}\sqrt{\frac{e^2+f^2}{(-a+b)^2+(c+d)^2}}$$

$$.\cos\left\{k(V_1t\pm h)\pm\tan^{-1}\frac{f(-a+b)-e(c+d)}{e(-a+b)+f(c+d)}\right\}, \qquad (14)$$

$$u_2=\left.\begin{matrix}2\sqrt{m}\\2\end{matrix}\right\}\frac{g}{\sqrt{(-a+b)^2+(c+d)^2}}\cos\left[k\left\{V_1t\pm\left(h-\left.\begin{matrix}\sqrt{m}\\\frac{1}{\sqrt{m}}\end{matrix}\right\}\alpha\alpha'\sqrt{h(h\mp H)}\right.\right.\right.$$

$$\left.\left.\left.+\left.\begin{matrix}\sqrt{m}\\\frac{1}{\sqrt{m}}\end{matrix}\right\}\alpha\alpha'\sqrt{\frac{h}{h\mp H}x}\right)\right\}\mp\tan^{-1}\left(\frac{c+d}{-a+b}\right)\right], \qquad (15)$$

where

$$M=(a+b)(-a+b)+(c+d)(-c+d), \qquad (16)$$

$$N=-(a+b)(c+d)+(-c+d)(-a+b), \qquad (17)$$

$$a=\left.\begin{matrix}1\\\sqrt{m}\end{matrix}\right\}\alpha\alpha'\{-J_1(\phi)Y_0(\psi)+Y_1(\phi)J_0(\psi)\}, \qquad (18)$$

$$b=\left.\begin{matrix}\sqrt{m}\\1\end{matrix}\right\}\{-J_0(\phi)Y_1(\psi)+Y_0(\phi)J_1(\psi)\}, \qquad (19)$$

$$c=\alpha\{-J_1(\phi)Y_1(\psi)+Y_1(\phi)J_1(\psi)\}, \qquad (20)$$

$$d=\alpha'\sqrt{m}\{-J_0(\phi)Y_0(\psi)+Y_0(\phi)J_0(\psi)\}, \qquad (21)$$

$$e=-J_0(\chi)Y_1(\psi)+Y_0(\chi)J_1(\psi), \qquad (22)$$

$$f=\alpha'\{-J_0(\chi)Y_0(\psi)+Y_0(\chi)J_0(\psi)\}, \qquad (23)$$

$$g=-J_0(\psi)Y_1(\psi)+Y_0(\psi)J_1(\psi), \qquad (24)$$

$$\left.\begin{matrix}\phi=\left.\begin{matrix}2\sqrt{m}\\2\end{matrix}\right\}\alpha kh\,,\quad \psi=\left.\begin{matrix}2\sqrt{m}\\2\end{matrix}\right\}\alpha k\sqrt{h(h\mp H)}\,,\quad \chi=\left.\begin{matrix}2\sqrt{m}\\2\end{matrix}\right\}\alpha k\sqrt{hx}\,,\\ \alpha=\sqrt{\rho_1/\rho_0}\,,\qquad \alpha'=\sqrt{\rho_2/\rho_1}\,.\end{matrix}\right\} \qquad (25)$$

Using these expressions, we calculated the displacement u' at $x=h$

and the one which is u_2 at (i) $x=h-H$ or (ii) $x=h+H$, each corresponding to the two different cases of rigidity conditions. The details of the calculated cases are classified into i) $m=1$, $\mu_2/\mu_0=1/2$, ii) $m=1$, $\mu_2/\mu_0=1/16$, iii) $m=1$, $\mu_2/\mu_0=2$, iv) $m=1$, $\mu_2/\mu_0=16$, v) $m=2$, $\mu_2/\mu_0=1/16$, vi) $m=2$, $\mu_2/\mu_0=16$, the results being plotted in Figs. 3∼8. In these figures $L(=2\pi/k)$ is the length of the incident waves.

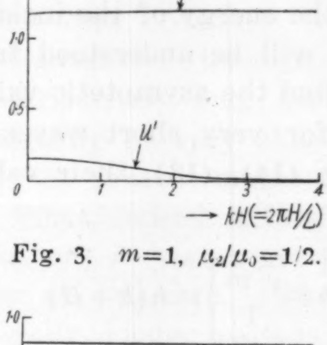

Fig. 3. $m=1$, $\mu_2/\mu_0=1/2$.

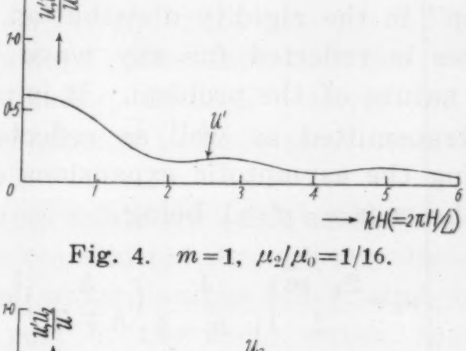

Fig. 4. $m=1$, $\mu_2/\mu_0=1/16$.

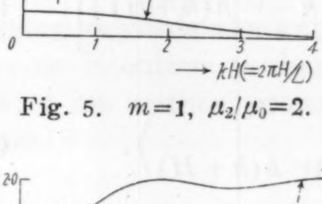

Fig. 5. $m=1$, $\mu_2/\mu_0=2$.

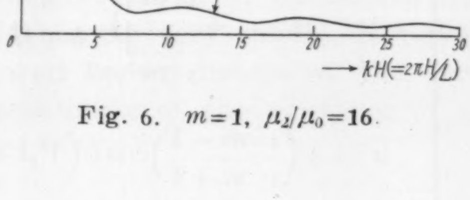

Fig. 6. $m=1$, $\mu_2/\mu_0=16$.

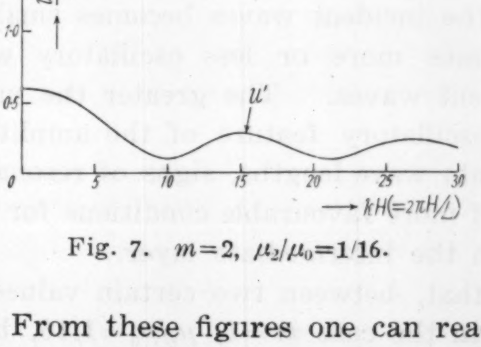

Fig. 7. $m=2$, $\mu_2/\mu_0=1/16$.

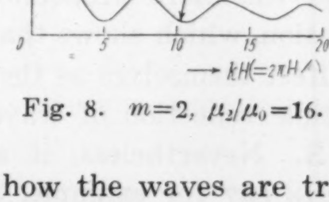

Fig. 8. $m=2$, $\mu_2/\mu_0=16$.

From these figures one can readily see how the waves are transmitted through the discontinuity under consideration. Should the length of the incident waves be very long compared with the thickness of the intermediate layer, namely $kH\rightarrow 0$, the amplitudes of the reflected waves u' and the transmitted waves u_2 relative to those of the incident waves u will assume the same values as obtained by Knott and others in their purely hypothetical cases. However, for shorter waves, the amplitudes of transmitted waves generally take greater values, and those of reflected waves smaller values. If the distribution of rigidities of the intermediate layer were continuous with both the outer media and the length of incident waves were sufficiently small, the amplitudes of the reflected waves would then vanish and those of the transmitted waves tend to assume the asymptotic values, indicating that the whole energy of the incident waves in the first layer is transmitted into the second. When $m=2$, that is when there is a "step" in the rigidity distribution, some of the energy of the incident waves is reflected for any wave length, as will be understood from the nature of the problem. It is possible to find the asymptotic values of transmitted as well as reflected waves for very short waves by taking the asymptotic expansions of u_2, u' in (14), (13), their values in the case $\alpha=\alpha'=1$ being

$$u_2=\left.\begin{matrix}2\sqrt{m}\\2\end{matrix}\right\}\frac{1}{\sqrt{m}+1}\left(\frac{h}{h\mp H}\right)^{\frac{1}{4}}\cos k\left[V_1t\pm h\mp\left.\begin{matrix}\sqrt{m}\\\frac{1}{\sqrt{m}}\end{matrix}\right\}\sqrt{h(h\mp H)}\right.$$

$$\left.\pm\left.\begin{matrix}\sqrt{m}\\\frac{1}{\sqrt{m}}\end{matrix}\right\}\sqrt{\frac{h}{h\mp H}}x-\left.\begin{matrix}2\sqrt{m}\\2\end{matrix}\right\}\left(h-\sqrt{h(h\mp H)}\right)\right], \tag{26}$$

$$u'=\pm\left(\frac{\sqrt{m}-1}{\sqrt{m}+1}\right)\cos k\left(V_1t\mp x+\left\{\begin{matrix}2h\\2h-4\sqrt{h(h+H)}\end{matrix}\right.\right). \tag{27}$$

Although, generally speaking, the amplitudes of transmitted waves through discontinuities increase and those of reflected waves decrease, both according as the length of the incident waves becomes smaller, the variation in amplitudes becomes more or less oscillatory with respect to the length of the incident waves. The greater the value of m, the more pronounced the oscillatory feature of the amplitude variation, which shows that at certain wave lengths, signs of resonance manifest themselves as the result of more favourable conditions for the multiple reflection of waves within the intermediate layer.

3. Nevertheless, it appears that, between two certain values of $2\pi H/L$, say for example, 2 and 5 in the case $m=1$, $\mu_2/\mu_0=1/16$, both amplitudes u_2 and u' tend to assume the most varying values, whence it follows that when the length of the incident waves is from a few times to a certain fraction of the thickness of the layer, the amplitudes of the reflected and transmitted waves assume values that differ greatly according as the lengths of the incident waves differ. This suggests that any attempt to ascertain the nature of the discontinuities within the earth by comparing merely the amplitudes of different phases without any regard to the wave lengths, is not likely to meet with satisfactory results.

The discontinuity that forms the boundary of the earth's core, instead of having a geometrical sharp surface as imagined, is more than likely to be such that the intermediate layer will have a certain effective thickness, like the one assumed in the present investigation. It follows then that the relatively long waves are more easily reflected at the core boundary, whereas the relatively short ones are likely to be transmitted through that boundary. The fact that *ScS* waves have relatively long periods of oscillation, while P' waves are not necessarily of very slow oscillation, appears to have some connection with the present mathematical result.

Since, indeed, in longitudinal waves relatively quick oscillations are prevalent, P' waves are likely to be transmitted through any discontinuity on the core. The transverse waves, on the other hand, have generally longer periods, and the part of the same waves, that is transmitted into the core, would be again partially reflected on the opposite surface of the core, so that the energy of transverse waves arriving towards the antipode would become very small. However, I have no intention to disregard the well known nature of the earth's core; I am rather proposing the possibility of the existence of such a fact.

60. 不連續面の鋭さが彈性波の透過反射に及ぼす影響

地震研究所 妹澤克惟
金井清

彈性體の不連續面で彈性波が反射屈折をなす理論は，はるかに以前 Knott によつて考へられてから絶えず多くの人々の注意をひいて來たけれども，何れの場合にもその不連續面が幾何學的に薄い面であるといふ假定のものになされたから，入射波の波長によつてその反射屈折の性質が變ることはなかつたのである．しかし少し考へて見ると，實際には寧ろ不連續の所が漸變的に變化する場合の方が至當のやうに思はれる．波動が表面波のやうに不連續面に平行に傳播する場合には大して影響がないけれども，この面を横切る場合には大いに影響があるものである．

このやうに横切つて通過する場合の計算を試みてみると種々の性質があり，波長が極めて長い場合には Knott の計算と同樣な結果が出るけれども，波長が短くなると通過する方の波の勢力が著しく大きくなり，反射する波の勢力が非常に小さくなるものである．

地球の核の表面にある不連續面も恐らくはある厚さがあつて，この間で漸次變化してゐるのではなからうか．果してそうであるとすると，地震の縱波は大體に於て短波長のものが多いから，地球の核の表面の所を波の勢力が全部通過して核內從て地球の反對側までへも達するのでないかとも思はれる．又，地震の横波は長波が多いから ScS 波の如き反射波が優勢になるとも考へられる．但しこのやうな長波の場合には通過する波の勢力も相當にあるけれども，反對側の核面で再び反射する部分が多いから，地球の核を通過する横波の勢力が非常に小さくなるといふこともできる．この機構から ScS が大きいといふことゝ，S′ が小さいといふことゝ一脈通じるところがあるやうにも思はれる．以上は大體の傾向を示すだけであつて，核には横波を通過させる剛性が少いといふ事柄を特に打消す譯ではないのである．

61.　偏心物體の廻轉に依つて起された地表面の波に就いて

地震研究所　井上宇胤

(昭和10年9月17日發表—昭和10年9月20日受理)

1. 近年獨逸に於て土質調査委員會[1]が主となつて電氣モートルに依つてエキセントリツク・マツスを廻轉せしめた場合に生ずる地表面の波動に就いて研究し，種々有益な結果を得て居る．但し此の場合に觀測される波は主としてレーレー波であるらしいとの事であつて未だ如何なる波であるか確然たる決定は見ない．此れに類した事は既に本研究所に於て寺田寅彦教授，坪井忠二博士[2]に依つて模型實驗がなされてゐる．其の際には寒天を媒質とし其の中に埋めた眞鍮の棒を電氣モートルに取附けたエキセントリツク・ホイールで動かして振動を生ぜしめ，表面波が生ずる事，寒天を切つて崖を作ると，其の緣で波が反射して，定常波が出來る事，堀を掘つて波長の數分の一の幅や深さの堀によつても，對岸の振幅を著しく減少させる事が出來る事等を觀測されて居る．著者は本研究所駒場支所の周圍の地中を傳はる彈性波の速度特に表面波の速度を決定する目的の爲に，此等に類した實驗を行つたのである．

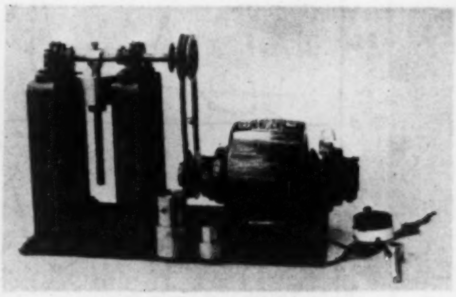

第　1　圖

2. 當支所の庭にエキセントリツク・マツスを電氣モートルに依つて廻轉せしめる裝置を据附け，此のエキセントリツク・マツスを種々取換へて，種々の振動數の振動を得る樣にした．此の裝置は第1圖に示す如きものであつて，一つの鐵板上に取附け其の鐵板を深さ 1·3 m に達する 6 本の杭に固定した長さ 1 m 幅 40 cm の四角に組んだ角材の上下からボールトで締め附けた三組の細長い鐵板にボールトで固定した．此の實驗に使用した電氣モートルは8分の1馬力のものであり，エキセントリツク・マツスは次の表に示す如き程度のものであつた爲に以上の如き裝置にて，エキセントリツク・マツスと地面との結合は充分であつた．

---

[1] R. Köhler, *ZS. f. Geophys.*, (1934), 386; A. Ramspeck, *ZS. f. Geophys.*, (1934), 387.

[2] T. Terada and C. Tsuboi, *Bull. Earthq. Res. Inst.*, **3** (1927), 55.

實驗番號	マ ッ ス	偏心距離	回 轉 數	遠 心 力
No. 1	228 gr	3·0 cm	35·7	$3{\cdot}48\times10^5$ dyne
〃 2	194	6·4	31·3	4·82 〃
〃 3	497	4·2	27·8	6·40 〃
〃 4	706	4·3	25·3	7·67 〃
〃 5	584	5·4	23·3	6·76 〃
〃 6	1006	4·5	21·8	8·47 〃
〃 7	1093	5·0	20·2	8·80 〃

此のエキセントリツク・マツスの廻轉に依つて生じた地表面の振動を，地中に埋めた數十個の小さいコンクリートの臺上を次々と一臺の地震計を移動せしめて觀測した．此の庭の西に接して南北に長さ 27 m，深さ 2·7 m，上部の幅 3·5 m の堀があるが，此の堀と振動源との間の地表面の振動を主として測定した．エキセントリツク・マツスの振動面は堀に直角であり，測定した地動も堀に直角な水平成分，即ち振動源に對してラジアルの水平成分のみである．使用した地震計は逆立振子型の水平動地震計で，重錘の重さ約 1·3 kg，週期 0·3 秒，倍率 200 倍のもので，制振器は無い．電氣モートルの廻轉を始めると，暫くして回轉が一様になるに從つて地震計に記録される振幅も一定になつて來るが，共の様に一定になつた所の振幅を測定した．

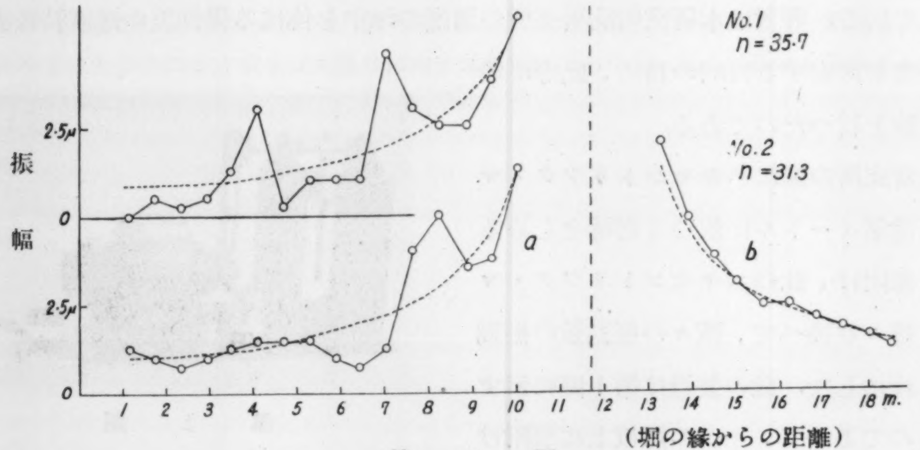

第 2 圖

3· 先ず，堀の無い方の側の振動を測定して見た所第 2 圖中の No. 2 の b に示す如き結果を得た．同圖中の點線は地面の振動の振幅が振動源よりの距離に反比例するものとして計算したものであるが，圖に依つて明かなる如く實際の振動の振幅は振動源よりの距離に反比例して減少して居る．此の事は波の減衰の事もあるが，先ず振動源よりの振動の勢力が平面的に擴がつて行く事を示すものと思はれる．

次に振動源の回轉數を種々に變へた場合の振動源と堀との間の地表面の振動の振幅

を測定した．夫等の結果の夫々一例を第2圖，第3圖，第4圖に圖示してある．圖中に振動源の位置を波線で示してある．

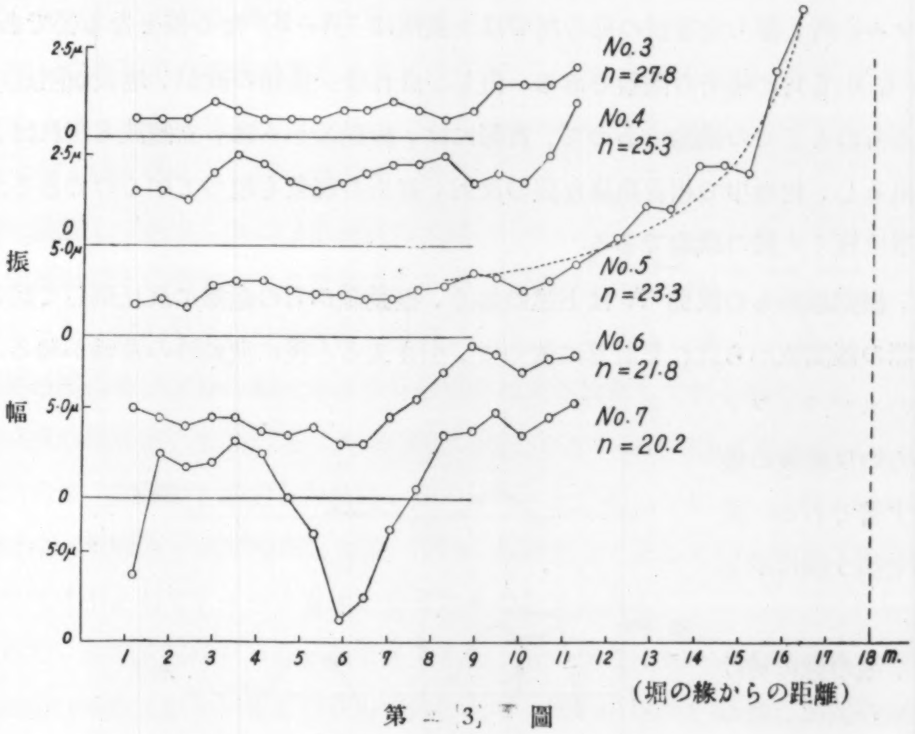

第 3 圖

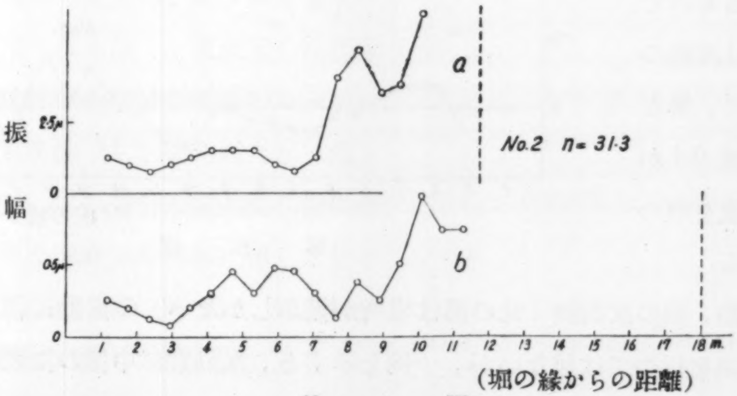

第 4 圖

振動源の回轉數が比較的小なる間は，地表面の振動の振幅が大であつたので，堀の緣と振動源との距離は場所のゆるす限り遠くした．此の距離は約 18 m であつた．此れに反し，振動源の回轉數が比較的大なる場合は小さい地動しか得られなかつた爲に堀と振動源との距離を約 11·7 m に縮少した．此等の圖中の點線は地動の振幅が，振動源よりの距離に反比例して減少するものとして，計算した値であるが，圖に依つて見られる如く，觀測された地動は略々振動源よりの距離に反比例して減少して居る．此の上に堀からの反射に依つて生じた定常波が重なつて居るのが見られる，

振動源からの振動の振幅を A，堀からの反射波の振幅を B とすると，觀測された地動のマキシマムの所，即ち定常波の腹の所では，其の振幅は（A+B）となり，地動のミニマムの所，即ち定常波の節の所では，振幅は（A−B）なる値となる筈である．此の A も B も共に場所の函數である．但し，此れは一種類の波が，地表面附近のみを傳はるものとしての議論であつて，實際には，振動源からは，立體波も出れば，表面波も出るし，尚地中で相當複雜な波の反射，屈折の現象も起つて居るのであるから以上の事は極く大體の議論である．

さて，振動源からの波動 A は上述の如く，振動源からの距離に反比例して居るから，實際の觀測値から此れを計算に依つて，引き去ると後に波動性の曲線が殘る．此の曲線のエンベロツプが堀からの反射波の振幅を示す筈である．其の數例を第5圖に示してある．

さて，堀の緣に於ける B/A の値は，堀の反射能に關するものであるが，此れは波動の振動數に依つて，異なるらしく，大體 0·4 から 1·0 の間の値を取つて居る樣である．

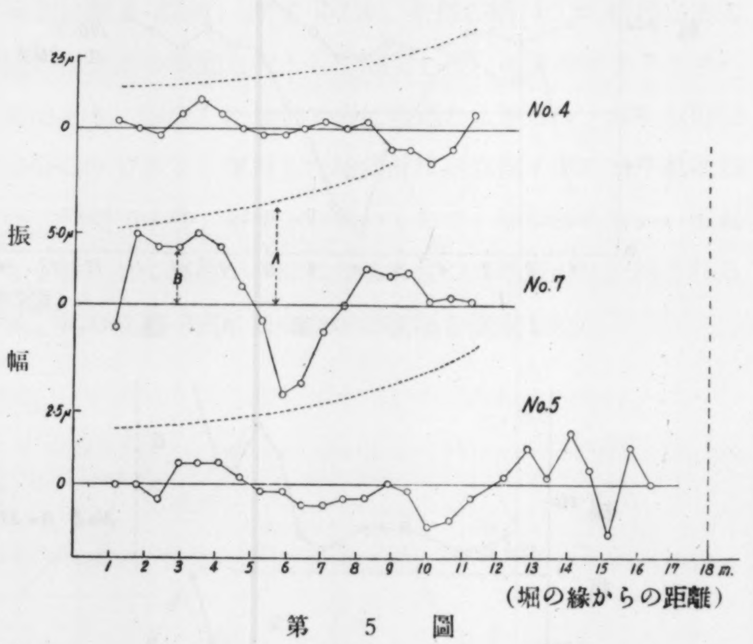

第 5 圖

堀の中の振動，堀の反對側（此の部は場所が僅かしかない）の振動に就いては，未だ充分なる觀測を行つては居ないが，一例を示すと，振動數が中位の振動の場合に，堀の此方側では 3μ 程の振幅があつたのに對し，反對側では，1μ の振幅であり，堀の內部では，地下 0·9 m と 1·8 m の段の所では，約 0·25μ，地下 2·7 m の堀の底に於ては，約 0·12μ の振幅であつた．

さて，振動源からの波動と，堀からの反射波動とで定常波が生じて居るとすると，此の定常波の波長は，振動源からの波動の波長の半分に當る筈であるから，此の定常波の波長を測定して，振動源よりの波の波長を算出する事が出來る．振動源よりの波動の波長と，其の振動數とから求めた波の速度を第6圖に示してある．尚振動源よりの距離に從つて，波動の振動數の變化する事はまづ認められなかつた．又第4圖に示

す如く，實驗 No. 2 の場合には，振動源と堀との距離が 11·7 m であつた a の場合と，其の距離が 18 m であつた b の場合とでは，定常波の波長が異なつた結果を示し，同一の振動數の波動で異なる早さのものがある事を示して居る.

さて第6圖に依ると，波の速度は，波の週期に關係して居り，其の分散曲線の大勢は，妹澤教授[3] の研究せられた層のある場合のレーレー波の早さの分散曲線の中の，表面層の剛性率が下層の剛性率の半分の場合に大略該當して居る樣である.

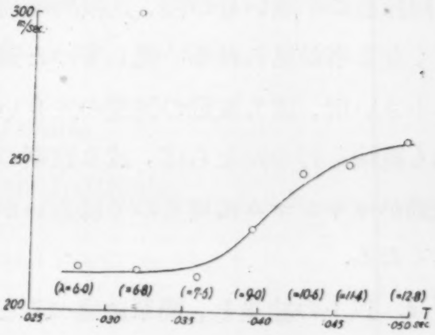

第 6 圖

當支所の地層は，地表から 1 m 程は軟い表土であり，其の下に厚さ約 3 m のローム層がある. 振動源を固定した杭は，此のローム層迄達して居り，且軟い表土中の波の速度は，重錘落下試驗等から大體 100 m 毎秒程度であるらしいので，此處に觀測された波は主として，ローム層中を傳はるものと思はれる.

そこで，此の波動はレーレー波であるとし，層の厚さはローム層の 3 m を採用し，波の週期の極めて短かい場合の波の速度として，200 m 毎秒を採つて波の速度の分散曲線を書き直して見たのが第7圖である.

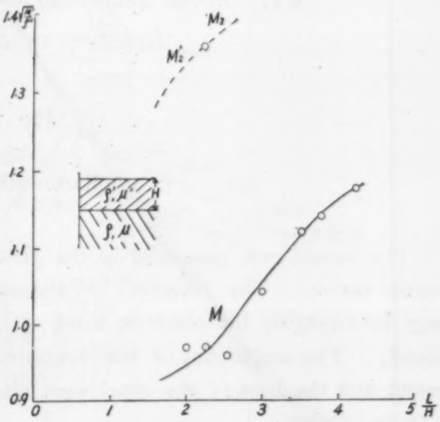

第 7 圖

圖に依つて見られる如く，表面層の剛性率が，下層の剛性率の半分の場合のレーレー波の速度分散曲線 M が得られたが，尙上記の實驗 No. 2 の場合の振動源が堀に近い場合は，此の速度分散曲線に屬して居るが，振動源が堀から遠い場合は，妹澤教授の M_2 波の部に相當して居る樣である. 此れは如何なる理由に依つたのであるか，今の所全く不明であるが，M_2 波は M 波に比較すると地表面の水平成分は，可成り小さいものとなる筈であるが，實際此處に觀測された M_2 波と思はれる波は，波動の振幅が振動源よりの距離に反比例して減少する事を考に入れて比較すると， M 波の場合の4割の大きさしか無い事も偶然の一致とは考へられぬ事である. 尙參考の爲に，各實驗の際のエキセントリツク・マツスの回轉による遠心力と，振動源から 1·7 m の所で觀測されるであらうと思はれる地動の

---

[3] K. SEZAWA and K. KANAI, *Bull. Earthq. Res. Ist.*, **13** (1935), 471.

振幅を計算したものとを，比較の爲圖示すると第8圖の如きものを得た．即ち振動源の回轉數の小さいもの程，比較的地動が大きくなる事が見られる．然しもつと回轉數の小さい所，即ち振動の週期の大きい場合迄も實驗を行つたならば，或る週期の所で地動がマキシマムに成るのではないかと考へてゐる．

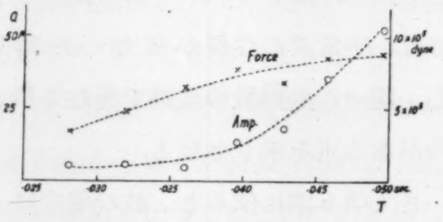

第 8 圖

4. 以上の結果を，簡單に述べると，エキセントリツク・マツスを電氣モートルで廻轉せしめる振動源と堀との間の地表面の地動の水平成分を觀測して見た所，波動の波長の數分の一の深さと幅を持つ堀であるにも拘はらず，堀からの反射波に依つて定常波が生じて居る事が觀測された．此の定常波の波長から波動の速度を測定すると地表附近の剛性波の速度は 約 220 m 毎秒程度，下層を傳はる波の速度は約 300 m 毎秒程度である事を知つた．尙此の場合の表面層は，厚さ約 3 m 程度のローム層であると思はれる．

---

61. Some Experiments on the Waves generated by the Rotation of Some Eccentric Masses.

By Win INOUYE,

Earthquake Research Institute.

The waves were generated in the ground by the rotation of an eccentric mass driven by an electric motor. The frequency of the rotation of this electric motor was changed within some range by changing the eccentric mass. The waves were projected to the canal digged in the ground. The amplitudes of the horizontal component of the vibrations of the surface of the ground and the base of the canal were observed by transporting a horizontal seismometer from one place to another.

The author observed the standing waves existed by the reflections of the waves from the canal, in spite of lesser dimensions of the depth and the breadth of the canal several times than the dimensions of the wave lengths. Moreover, it seems to the author that the observed waves are the surface waves of Rayleigh type.

62. *On the Sinking of the Earth's Crust in the Eastern Part of the City of Tokyo.*

By Naomi MIYABE,

Earthquake Research Institute.

(Read Sept. 17, 1935.—Received Sept. 20, 1935.)

1. As already reported[1)], the surface of the earth's crust in Honzyô, Hukagwa, and neighbourhood, i.e., the eastern part of Tokyo, was found to have subsided considerably during the last ten years or so. The amount of sinking since 1923, was found to be 1·6 m at most. It might therefore be of interest to inquire into various causes that are believed to brought out this subsidence.

Before dealing with the causes of the sinking, the results of the preceding studies will be summarized briefly.

(i) The bench-marks in Tokyo and vicinity that have subsided

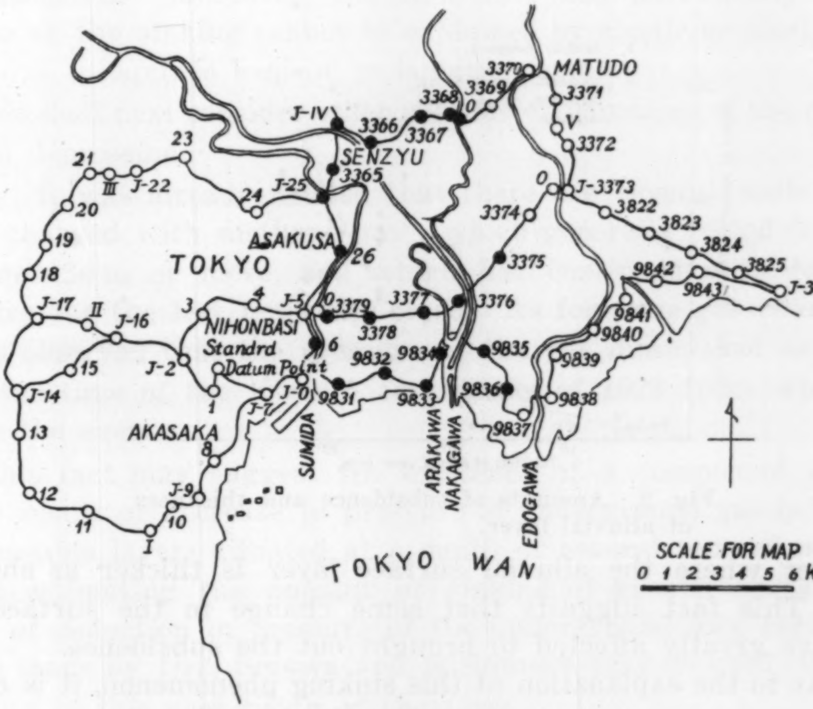
MATUDO
3370
3369
3368
0
3371
V
3372
J-IV
3366
3367
SENZYU
3365
J-25
23
21
III
J-22
24
20
19
18
ASAKUSA
26
TOKYO
0
J-3373
3374
3822
3823
3824
3825
J-3826
3375
9842
9843
J-17
II
J-16
3
4
J-5
0
3379
3377
3376
NIHONBASI
Standrd
Datum Point
3378
9841
9840
6
9832
9834
9835
9839
15
J-2
J-14
1
J-0
J-7
9831
9833
9836
9838
9837
13
AKASAKA
8
SUMIDA
ARAKAWA
NAKAGAWA
EDOGAWA
12
J-9
11
10
I
TOKYO WAN
SCALE FOR MAP
0 1 2 3 4 5 6 km.

Fig. 1. Distribution of bench-marks.
Marks • denote the bench-marks subsided remarkably.

[1)] N. MIYABE, *Bull. Earthq. Res. Inst.*, **10** (1932), 844~857; **13** (1935), 587~591.

remarkably during these ten years are indicated in Fig. 1 by ●, from which it will be noticed that the region of greatest subsidence lies between the Sumidagawa and the Yedogawa, the northern boundary of which approximately coincides with the line connecting Senzyu and Matudo. The northern part of Asakusa, near Senzyu; the neighbourhood of Hama-tyô, Nihonbasi; the Tameike valley, Akasaka; and the zone from Marunouti to Kanda are also zones of subsidence, although the extent to which they have sunk are not so large as in Honzyô and Hukagawa[2].

(ii) From the vertical displacements[3] of bench-marks that are believed to have occurred during the period from Nov. 1929 to Feb. 1932, the earth's crust in Honzyô and Hukagawa which seems to consist of several crustal blocks, tilted and subsided considerably, as has been shown in the preceding paper[4].

(iii) The velocities of sinking of many of the bench-marks situated in this region have accelerated up to the present; several in fact appear to have reached maximum, although the general tendency of the velocity of sinking to increase does not seem to have stopped.

(iv) It is also noticed that, in general, the amounts of subsidence

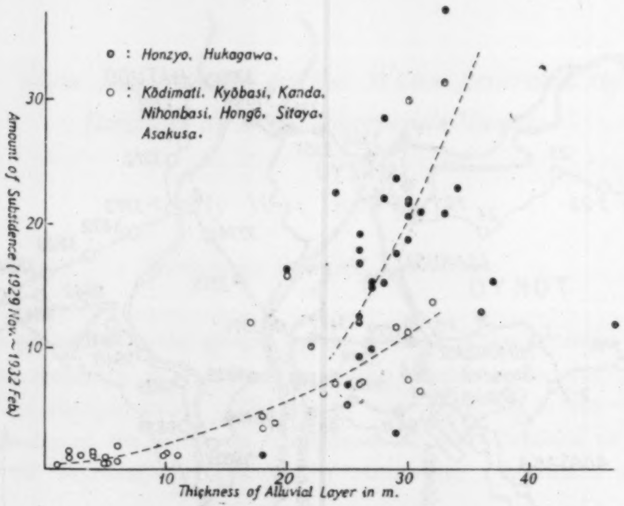

Fig. 2. Amounts of subsidence and thickness of alluvial layer.

are greater where the alluvial surface layer is thicker as shown in Fig. 2. This fact suggests that some change in the surface layer might have greatly affected to brought out the subsidence.

2. As to the explanation of this sinking phenomenon, it is regrett-

---

[2] N. MIYABE, *Proc. Imp. Acad.*, **9** (1933), 588~591.

[3] The data of vertical displacements of bench-marks utilised in this study were obtained by relevellings made by the Tokyo municipality.

[4] N. MIYABE, *loc.cit.* 1).

able that, with no other data in our possession expecting those relating to the deformation of the earth's surface, there is no means of deciding which is the most plausible one among the several possible causes of the subsidence, as will be discussed in the following paragraphs.

Some attribute the sinking merely to settling of the superficial layers of filling earth that was used in the reclamation of this district to a thickness of about 1～3 m. If so, then since the subsidence of the earth's crust in this district amounts to more than 1 m since the time of the Kwantô earthquake of 1923, the layer of filling earth should have compressed to about half its original thickness or it should have disappeared, which seems hardly possible.

A possible cause of sinking was dealt with in the preceding paper[5], wherein we calculated the probable extent of sinking for the case in which the surface layer of the earth's crust is regarded as an elastic substance and also for the case in which it is regarded as sandy material, due to surface load of the filling earth. The result was that the amount of sinking estimated in neither of the two cases was large enough to account for the remarkable extent of sinking that occurred. Moreover, the slow rate and particularly the acceleration of the sinking cannot be explained by elastic or plastic deformation due to surface load of reclamation earth.

We shall next consider other possible explanations of the remarkable crustal depression.

3. It was already noticed that there are several wells in Hukagawa charged with methane gas[6], which generally issued from depths of about 30 m or more, and which has continued with considerable pressure for the last ten years or so. As for some gas-charged wells, it was observed that the pressure of the gas diminished considerably since the time of the Kwantô earthquake of 1923 from what it was before the event.

This fact may suggest the existence of a component of sinking as the result of decrease in pressure of underground gas held between impermeable layers situated at a depth of several tens of metres.

In estimating the amount of sinking of ground surface as the result of reduction in pressure of the underground gas, certain calculations made by Drs. Sezawa and Nishimura may be used, the portion applying to this case being of the form

---

[5] N. MIYABE, *loc. cit.*

[6] N. MIYABE, *Proc. Imp. Acad.*, **7** (1931), 344～347.

$$u = \frac{\Delta p}{\mu}\frac{b}{a}\frac{\vartheta_0}{\vartheta_0'},$$

for maximum displacement in the simplest form of deformation, and in which a, b, are the vertical and horizontal dimensions respectively, μ the rigidity of the disturbed surface layer, and Δp the change in pressure, the layer being assumed to be incompressible and elastic. We consider the case when the value of u for the case when $b \gg a$ or $b \doteqdot 100\,a$ is of the order of 1.

For an actual case, the change in pressure, Δp, of the underground gas may be estimated to be nearly 3/10 of the atmospheric pressure, which is derived from the fact that, before the earthquake, the underground water was discharged by the pressure of the gas to a height of about 12 feet above the ground. By substituting these numerical figures, the extent of ground sinking due to exhaustion of underground gas is estimated to be of the order of 1 mm, when μ is assumed to be of the order of 10^8 c.g.s., the result however is negligible when compared with the actual subsidence.

4. The residents of Honzyô, Hukagawa, Sunamati, etc., that is, in the Kôtô district of Tokyo, have noticed a remarkable drop in the level of the water of the wells.

Although the exact extent to which the water level has sunk cannot be estimated with sufficient accuracy, it seems to be of the order of several metres compared with the level before the earthquake of 1923. Since clay contracts when dried or unhydrated, the surface layer of the earth in this region, which is composed of clay and sand to a depth of about 30 m, might have suffered vertical contraction owing to lowering of the underground water level.

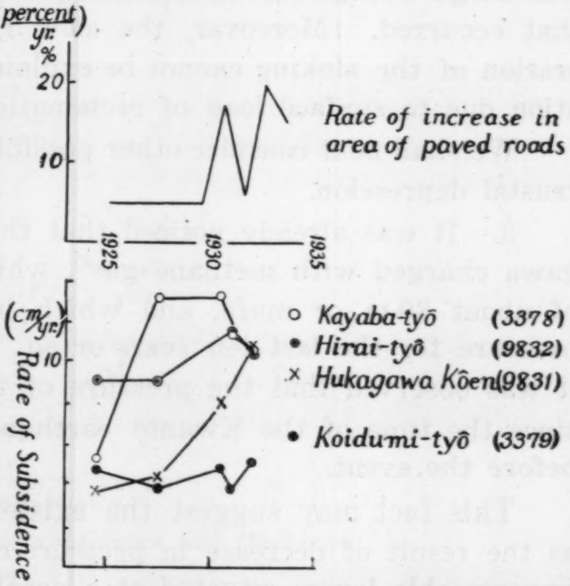

Fig. 3. Change in rates of subsidence and of increase in area of paved roads, in Tokyo.

In our laboratory experiments[8], the contraction in linear dimen-

---

[7] K. SEZAWA and G. NISHIMURA, *Bull. Earthq. Res. Inst.*, **8** (1930), 13.

[8] The method of the experiment very simple, that is, the volume and weight of the mass of clay contained in a meter glass are messured once a day.

sions of a mass of clay when unhydrated amounted to several tens percent as shown in Fig. 5, in which the percent contraction of the clay mass is plotted against the decrease in water contents. If this result could be applied without any modification to explain the actual extent of the crustal subsidence in Honzyô and Hukagawa, the lowering of the underground water level should be of the order of 10 m, which however seems to be too much.

The underground water level will naturally remain at constant depth so long as the supply and the outgo of the water are in equilibrium.

But with disturbance of water supply or increase in water consumption (plus seepage) the level of the underground water would sunk, resulting in another equilibrium level lower than before[9].

The disturbance in water supply would arise from congestion of houses as the result of city planning, the drainage system becoming more regular, and the roads becoming all paved, whereas consumption of the underground water would increase with increased industrial activities.

Hence, as the sinking of the ground surface is in positive correlation with the sinking of the level of the underground water, it may also be expected that the sinking will go on along with increase in the area of paved roads or with decrease in the area of unpaved roads, which may be taken as a measure of the development of the city. In Fig. 3, the changes in rate of vertical displacement of a number of bench-marks, together with changes in the area of paved

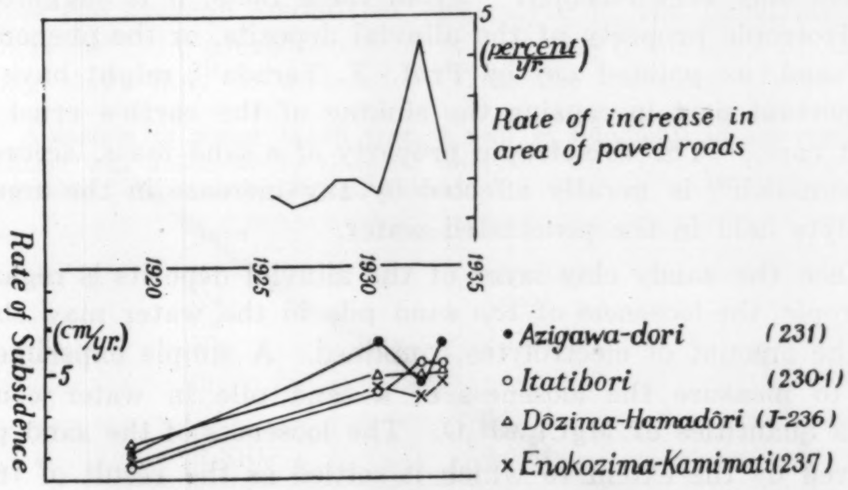

Fig. 4. Change in rates of subsidence and of increase in area of paved roads, in Osaka.

---

9) When consumption increases and the level of the underground water is lowered, the gradient of the level increases. Hence, the supply of underground water will also increase so that the level stays at a lower position of equilibrium.

roads, in Honzyô and Hukagawa are shown. The two curves are fairly parallel to each other.

A similar relation is also shown between vertical earth movements and the areal percentage of unpaved roads in Osaka, as shown in Fig. 4.

5. From geological survey made by the Reconstruction Bureau[10] in which data obtained by borings were used, it was found that the surface layer of the earth's crust in Honzyô, Hukagawa and neighbourhood consists of alluvial deposits to a depth of about 30 m, which is very much thicker than the same layer in the region west of the Sumidagawa, as also that these layers of alluvial deposits are mostly sandy clays or clayey sands.

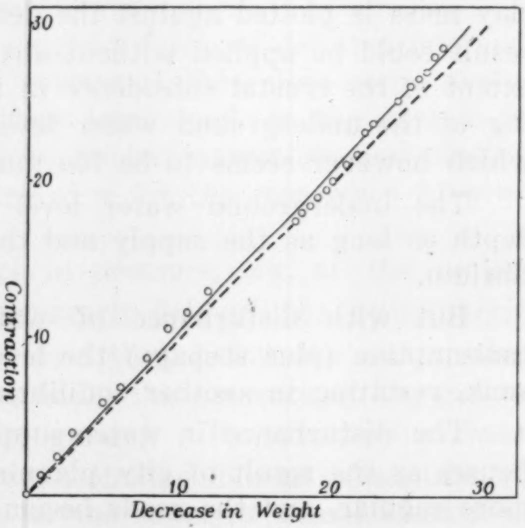

Fig. 5. Contraction of a mass of clay by being unhydrated.

It also came to light that about 380 years ago the shore line in Hukagawa was about 1 km north of, but parallel to, the present shore line, all of which shows that the alluvial layers in this region were deposited only very recently. From these facts, it is suggested that the thixotropic property of the alluvial deposits, or the phenomena of quick sand, as pointed out by Prof. T. Terada[11], might have played an important part in causing the sinking of the earth's crust in the present case. The thixotropic property of a sand mass, according to H. Freundlich[12] is geratly affected by any increase in the amount of electrolyte held in the penetrated water.

Since the sandy clay layer of the alluvial deposits is regarded as thixotropic, the looseness of the sand pile in the water may also vary with the amount of electrolytes contained. A simple experiment was made to measure the looseness of a sand pile in water containing various quantities of $MgCl_2.6H_2O$. The looseness of the sand pile was measured by the extent to which it settled as the result of trains of feeble shocks given to it. The results are shown in Fig. 6, in which the extent of settling are plotted against the concentration of $MgCl_2.6H_2O$

---

10) Reconstruction Bureau, "The Results of Geological Surveys in Tokyo and Yokohama", (Tokyo, 1925), (in Japanese).

11) T. TERADA, *Bull. Earthq. Res. Inst.*, **13** (1935), 562~568.

12) H. FREUNDLICH, *Proc. Faraday Soc.*, **31** (1935), 769~773.

in the penetrated water.

From this figure, we notice that a very small quantity of electrolyte is sfficient to consideraby increase the looseness of the thixotropic sand clays.

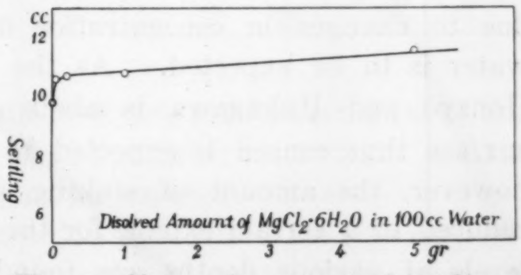

Fig. 6. Change in amount of settling of loosely piled sand mass in electrolytic solution due to concentration.

When the level of an underground water that has been kept in equilibrium with the sea water penetrates the sand layer in the manner shown schematically in Fig. 7, the level of the underground water is lowered by x m, that is to say, the boundary of the sea water AC′B′ in Fig. 7 will be elevated by y m, which is related to x so that

$$y=\frac{\rho_0}{\rho-\rho_0}x,$$

where ρ_0 is the density of plain water, that is, 1, and ρ is the density of sea water, which is slightly greater than 1.

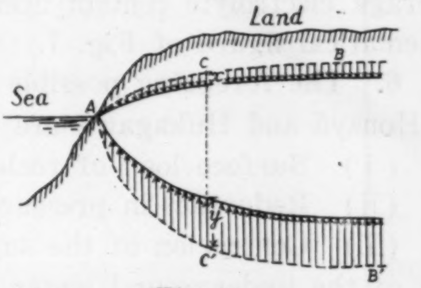

Fig. 7.

Thus the average amount of electrolyte in the penetrated water may increase[13], in consequence of which the thixotropy of the layer of sandy clays may be affected. Thus the lowering of the level of

---

13) A sample of water taken from a well in Sunamati in the region under consideration was subjected to chemical analysis, with results as shown in the following table. Analysis by Mr. S. Tanaka.

Ions	Quantities in 1 litre water
K	0·0945 gr.
Na	1·1656
Ca	0·3594
Mg	0·1969
Cl	2·5262
SO_4	0·0658
HCO_3	0·8917
H_2SiO_3	0·0461
Total	5·5417
Oxygen required	0·0070

The depth of the bottom of the well is 3m and that of the surface of the water 22 cm from the ground surface. The temperature of the water was 17°C, while the open air temperature was 26°C.

The result of this analysis shows that the water of this well contains more ions of Na, Mg, Ca, etc. than those of ordinary underground water, which is regarded as owing to penetration of more sea water.

the underground water is instrumental in settling still further the surface layers.

Judging from the experiment, further settling (a few percent) due to changes in concentration of the electrolyte in the penetrated water is to be expected. As the thickness of the surface layer in Honzyô and Hukagawa is about 30 m, the sinking of the ground surface thus caused is expected to be several tens of cm. Actually, however, the amount of sinking expected from this cause may be reduced to a certain extent, for the reason that the underground water levels at various depths are found to be seperated by impermeable layers, so that the lowering of one of these underground water levels may not always permit the penetration of the sea water, that is, the average electrolyte content does not always increase, as shown in the schematical figure of Fig. 7.

6. The foregoing possible causes of sinking of the earth's crust in Honzyô and Hukagawa are now summarized.

(i) Surface load of reclamation earth.

(ii) Reduction in pressure of the underground gases.

(iii) Contracion of the surface layer of the soil caused by lowering of the underground water level.

(iv) Effects of increase in concentration of electrolytes in the underground water on the thixotropic sand layer, caused by penetration of the sea water.

These are all equally probable explanations of the phenomenon, and yet the extent of sinking that could be attributed to any one of them is insufficient to explain the actual subsidence. It is therefore my opinion that these four causes are operating jointly with the crustal deformation generally going on in much wider areas such, for example, as those recognized as block movements[14] and the general subsidence in the alluvial plains remarked by Dr. C. Tsuboi[15].

In conclusion, the writer wishes to express his sincere thanks to Professor Torahiko Terada for his valuable suggestions given through the present investigation.

---

[14] N. MIYABE, *loc. cit.*

[15] C. TSUBOI, *Jap. Journ. Astr. Geobhys.*, **9** (1933), 95.

62. 江東地域に於ける地盤の沈下

地震研究所 宮部直巳

本所深川等，所謂，江東方面に於いて，地盤の沈下の著しい事は既に知られてゐる所である.

本論文では，その沈下の理由について考へ得べきことを二三擧げてみたのであるが，要するに今日では，その何れの理由が勝つてゐるかを判定する事が困難である.

沈下の量と，表面の冲積層の厚さとの關係を調べてみると，今までのところでは，大體に於いて，冲積層の厚い場所程沈下量が大であるといふやうな傾向も見えるので，表面の冲積層の收縮などゝ言ふことも，無視し得ない沈下の理由の一つであらうと思はれるが，それ許りであるとも言へないやうである.

尙，研究が進められてゐるから，今後の成果に期待するより外はない.

63. *A Model Experiment on the Mechanism of Occurrence of Earthquake.*

By Seiti YAMAGUTI,
Earthquake Research Institute.

(Read June 18, 1935.—Received Sept. 20, 1935.)

Introduction.

In a previous paper[1], we have remarked that, near the epicentres of the "deep" earthquakes, "conspicuous and rather conspicuous" earthquakes rarely occur immediately before or after the respective earthquakes, and that, three conspicuous maxima of frequencies of the latter are found in the regions at about −500, 500 and 1000 in kilometres measured from the maximum of the former.

With regard to these results, Prof. Torahiko Terada suggested, that if a spherical part of the crust at the "deep" earthquake origin lying several hundred kilometres beneath the earth surface, happens to expand or yield by some cause, the maximum shearing stress may occur in a conical surface with semivertical angle of about 45° and the vertex at the centre of sphere, and the fracture may propagate along these directions towards the earth surface.

It was the first aim of the present experiment to verify these suggestions. The second object was to verify the fact already noticed by the author that, very near the thunderstorms and the cyclonic centres, and also near the region of great precipitations, earthquakes very rarely occur at the time of these meteorological occurrence, and a remarkable maximum of frequency of the latter seems to exist about several hundred kilometres apart from the formers[2].

This experiment was carried out during the period of about 15 months from March, 1934 to June, 1935.

Method of Experiment.

Taking a rectangular wooden tank, T_1, whose sides are 20, 30 and 60 cm, and placing in it a spherical caoutchouc-balloon, *B*, of good material, whose initial diameter was 4·0 cm, connected with a very fine flexible caoutchouc-tube (dia =1·5 mm) to a open manometer, *M*, as well as to a cylindrical air chamber, *V* (dia=4·0 cm), as shown in Fig. 1, a large quantity of agar-agar dissolved in warm water was poured into this tank and cooled for one day or two, until it solidified up to the innermost part. The bottom end of *V* is connected with a caoutchouc tube (dia =8 mm), to a water tank, *H*, of which the head is held about 150 cm high, and the water surface in *V* is raised up gradually at the rate of 1 cm/min. The air contained in *V* and *B* is thus compressed and the balloon, *B*, was compelled to expand until

---

[1] S. YAMAGUTI, *Bull. Earthq. Res. Inst.*, **11** (1933), 501~504.

[2] *Bull. Earthq, Res. Inst.*, **12** (1934), 214~221, 742~753; **13** (1935), 569~575.

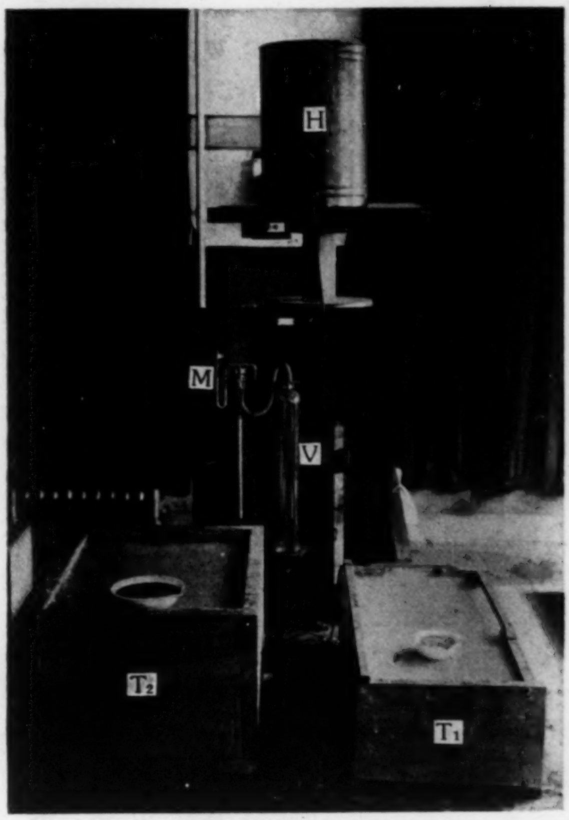

Fig. 1.

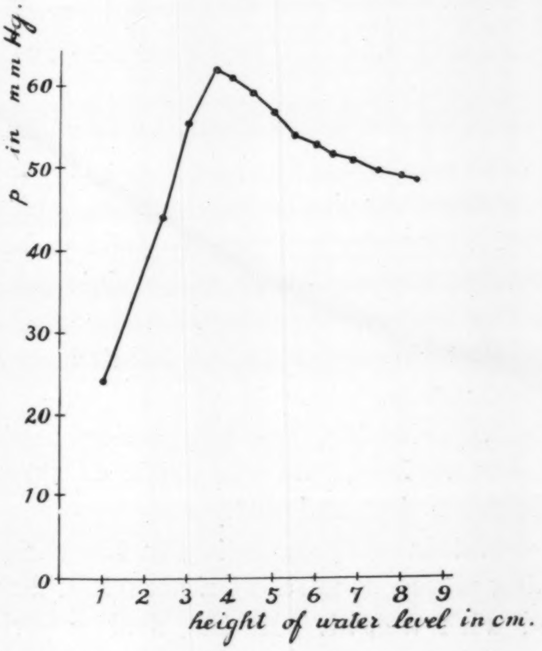

Fig. 2, *a*. Pressure-Water level curve.

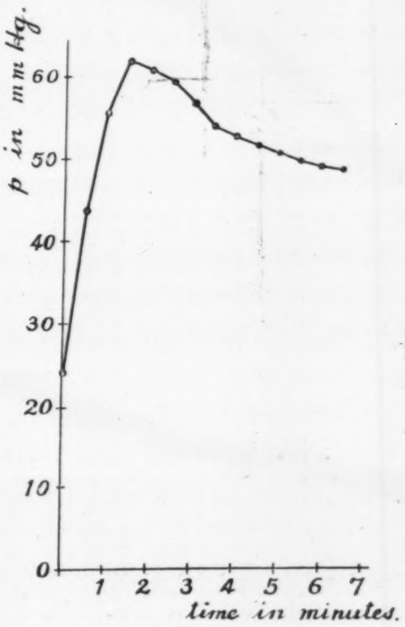

Fig. 2, *b*. Pressure-Time curve.

the crack was produced in agar-agar. The pressure, p, at the beginning of producing crack was read when the mercury meniscus of M begins to fall down while the water level in V is continued to rise up, which relation is shown in Fig. 2, a and b, and in Fig. 3. This photogram of the motion of mercury meniscus was taken by illuminating from upward, on the rolling film, which was rolled by the rate of 1 revolution per 90 seconds.

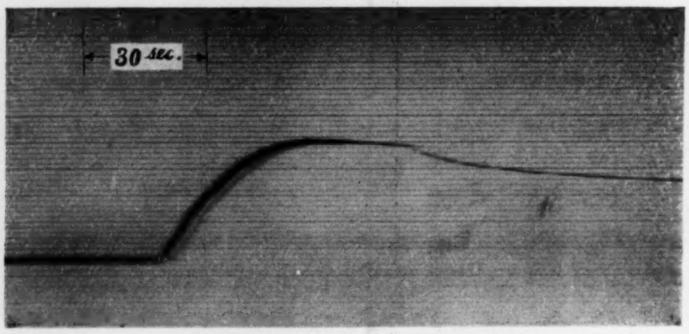

Fig. 3.

The general features of the cracks which were developed on the surface are shown in Figs. 11,a∼11,e. Radial gaping cracks are the tension cracks due to the bulging up of the surface, while the conical cracks shown in Figs. 11,a and 11,b are the shear cracks here interested. The configuration of the shear cracks starting from the bottom and extending to the surface were studied by cutting the agar-agar with a vertical plane through the centre of balloon, and parallel to the longest side, the angle of inclination, θ, of the crack line from vertical, being measured.

The dry sticks of agar-agar used in one experiment, were 60 and 100 in number and 450 and 750 grams in mass for the tanks T_1 and T_2 respectively, the volume of T_2 being $30 \times 40 \times 50$ cubic centimetres.

To see if the crack in question really starts from the bottom but not from the surface by the tension at the surface, a glass plate with the weight of 1 kg, was put over the surface to prevent the surface cracking. It was fully recognized that the shear cracks studied grow from the inner part, very near the balloon.

From the results of about 30 experiments, the suggestion made by Prof. T. Terada, above cited, was verified, and the angle of shear crack, θ, was found to be lying between 40° and 50°.

Next, we tried to study the variation of θ, according to the variation of position of a surface loading which consists of a porcelain dish with hemispherical bottom, loaded with weight. In the first experiment, the depth, e, of the centre of balloon (initial diametre, $D_0=4$

cm), from the surface was fixed at about 9 cm, and a dish, P, with radius of curvature, $\rho=12{\cdot}2$ cm, loaded with weight, $W=2{\cdot}29$ kg (weight of dish included), was put at the various distances, d, or $r=d/e=0\cdots 3{\cdot}7$, from the so-called "epicentre" of a balloon along the centre axis of the tank, T_1. For the tank, T_2, the values of $D_0=5$ cm, $e=12$ cm, $\rho=8{\cdot}2$, and $W=2{\cdot}15$ kg were taken, and the values of r was changed from zero to 2·1. Thus, the values of θ for different r' s, were obtained and plotted against r, as shown in Fig. 4, a and b for the tanks,

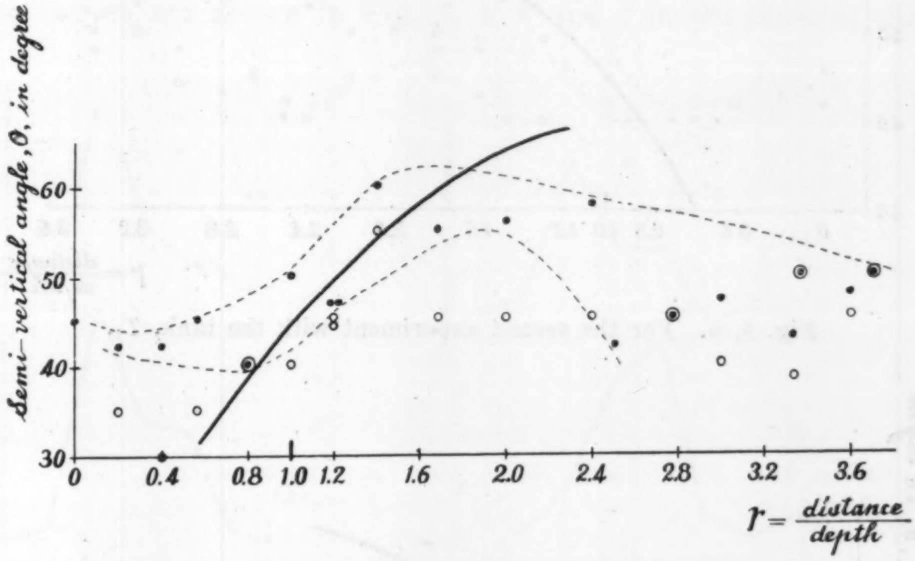

Fig. 4, *a*. For the first experiment with the tank, T_1

T_1 and T_2 respectively, in which the marks ● correspond to the cracks in the same side as the weight, and ○ to those in the opposite side with respect to the balloon.

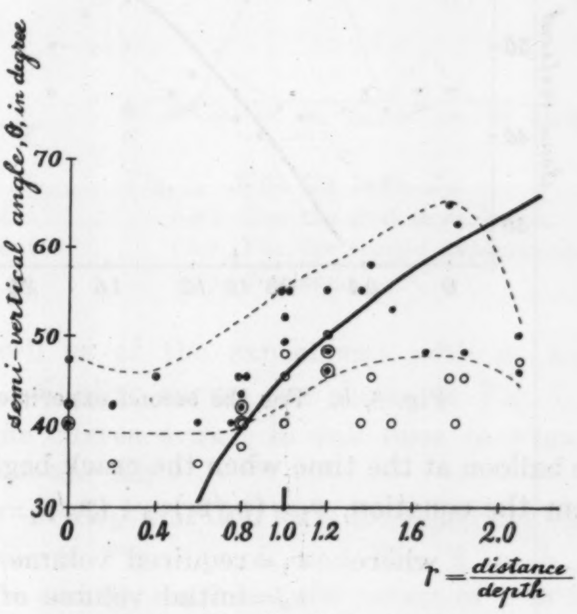

Fig. 4, *b*. For the first experiment with the tank, T_2

In the second experiment, ta make the boundary effect of the tank as small as possible, smaller values of D_0, e, ρ and W were taken; those were $D_0=3{\cdot}0$ cm, $e=7$ cm, $\rho=4{\cdot}5$ cm, and $W=1{\cdot}63$ kg for the tank, T_1, and $D_0=3{\cdot}5$ cm, $e=7$ cm, the crack was produced in agar-agar. The pressure, p, at the beginning of producing crack was read when the mercury meniscus of M begins to fall down while the water level in V is continued to rise up, which relation is shown in Fig. 2, a and b, and in Fig. 3. This photogram of the motion of mercury meniscus was taken by illuminating from upward, on the rolling film, which was rolled by the rate of 1 revolution per 90 seconds.

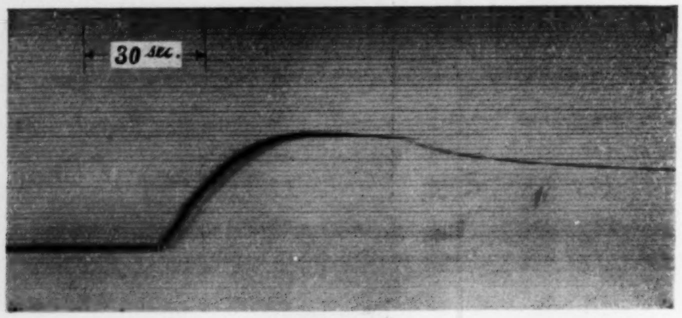

Fig. 3.

The general features of the cracks which were developed on the surface are shown in Figs. 11,a∼11,e. Radial gaping cracks are the tension cracks due to the bulging up of the surface, while the conical cracks shown in Figs. 11,a and 11,b are the shear cracks here interested. The configuration of the shear cracks starting from the bottom and extending to the surface were studied by cutting the agar-agar with a vertical plane through the centre of balloon, and parallel to the longest side, the angle of inclination, θ, of the crack line from vertical, being measured.

The dry sticks of agar-agar used in one experiment, were 60 and 100 in number and 450 and 750 grams in mass for the tanks T_1 and T_2 respectively, the volume of T_2 being $30 \times 40 \times 50$ cubic centimetres.

To see if the crack in question really starts from the bottom but not from the surface by the tension at the surface, a glass plate with the weight of 1 kg, was put over the surface to prevent the surface cracking. It was fully recognized that the shear cracks studied grow from the inner part, very near the balloon.

From the results of about 30 experiments, the suggestion made by Prof. T. Terada, above cited, was verified, and the angle of shear crack, θ, was found to be lying between 40° and 50°.

Next, we tried to study the variation of θ, according to the variation of position of a surface loading which consists of a porcelain dish with hemispherical bottom, loaded with weight. In the first experiment, the depth, e, of the centre of balloon (initial diametre, $D_0=4$

cm), from the surface was fixed at about 9 cm, and a dish, P, with radius of curvature, $\rho=12{\cdot}2$ cm, loaded with weight, $W=2{\cdot}29$ kg (weight of dish included), was put at the various distances, d, or $r=d/e=0\cdots 3{\cdot}7$, from the so-called "epicentre" of a balloon along the centre axis of the tank, T_1. For the tank, T_2, the values of $D_0=5$ cm, $e=12$ cm, $\rho=8{\cdot}2$, and $W=2{\cdot}15$ kg were taken, and the values of r was changed from zero to 2·1. Thus, the values of θ for different r' s, were obtained and plotted against r, as shown in Fig. 4, a and b for the tanks,

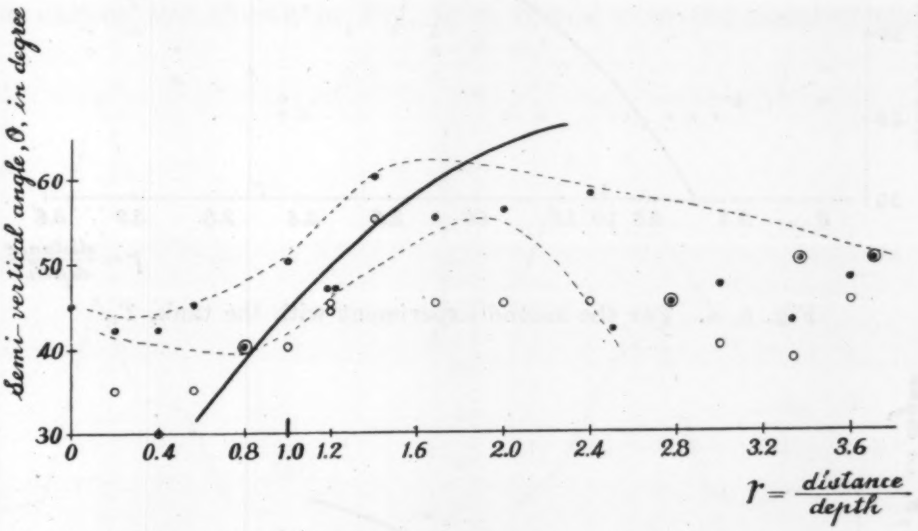

Fig. 4, a. For the first experiment with the tank, T_1

T_1 and T_2 respectively, in which the marks ● correspond to the cracks in the same side as the weight, and ○ to those in the opposite side with respect to the balloon.

In the second experiment, ta make the boundary effect of the tank as small as possible, smaller values of D_0, e, ρ and W were taken; those were $D_0=3{\cdot}0$ cm, $e=7$ cm, $\rho=4{\cdot}5$ cm, and $W=1{\cdot}63$ kg for the tank, T_1, and $D_0=3{\cdot}5$ cm, $e=7$ cm,

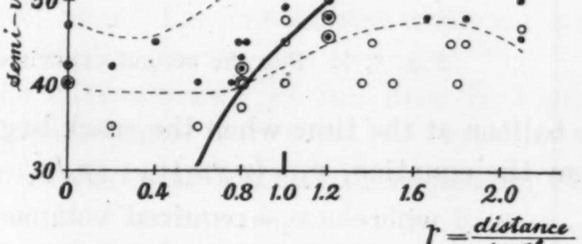

Fig. 4, b. For the first experiment with the tank, T_2

Table I. Table II.

For the tank, T_1						Tor the tank, T_2					
The first experiment			The second experiment			The first experiment			The second experiment		
r	p		r	p		r	p		r	p	
0·0	51	Mean of $p=60{\cdot}0$ for $r\leqq 1{\cdot}0$	0·0	77	Mean of $p=64{\cdot}0$ for $r\leqq 1{\cdot}0$	0·0	50	Mean of $p=53{\cdot}2$ for $r\leqq 1{\cdot}0$	0·0	67·5	Mean of $p=66{\cdot}2$ for $r\leqq 1{\cdot}0$
0·0	68		0·2	58		0·0	54		0·2	54·5	
0·2	58		0·4	58		0·0	68		0·3	61	
0·4	58		0·5	72		0·3	63		0·5	91·5	
0·6	74		0·6	59		0·4	62		0·7	57	
0·8	52		0·7	64		0·8	43		0·7	60·5	
1·0	56		0.9	54		0·8	44		0·7	61	
1·0	62		1·0	79		0·8	49		0·8	61	
1·2	52	Mean of $p=56{\cdot}3$ for $r>1{\cdot}0$	1·1	51·5	Mean of $p=61{\cdot}3$ for $r>1{\cdot}0$	0·9	39		0·8	90·5	
1·2	56		1·1	57·5		0·8	49		0·9	58	
1·4	56		1·1	60·5		1·0	50		1·0	78	
1·7	66		1·2	66		1·0	54		1·2	57·5	Mean of $p=58{\cdot}3$ for $r>1{\cdot}0$
2·0	51		1·2	71		1·0	59		1·2	62·5	
2·4	56		1·2	76		1·0	60·5		1·2	67	
2·5	54		1·3	46		1·2	40	Mean of $p=49{\cdot}7$ for $r>1{\cdot}0$	1·3	55	
3·0	50		1·3	72		1·2	41		1·4	50·5	
3·4	54		1·4	64		1 2	46		1·5	45	
3·4	66		1·4	59·5		1·2	61		1·5	76	
3·6	56		1·5	63		1·4	44		1·7	55·5	
3·6	58		1·5	66		1·4	68		1·7	64	
			1·6	65		1·5	48		1·8	50·5	
			1·6	67		1·7	61		2·0	48	
			1·8	51		1·8	42·5		2·0	61·5	
			1·8	52·5		1.8	48·5		2·0	67	
			1·8	66		1·8	50		2·2	50·5	
			1·8	75		2·0	58		2·2	61·5	
			1·9	54·5		2·1	40		2·2	62	
			2·0	72		2·1	48·5		2·4	47	
			2·0	76					2·5	53·5	
			2·2	58					2·5	58·5	
			2·2	72					2·7	47·5	
			2·4	58					2·7	66	
			2·5	53					2·7	68·5	
			2·7	59					2·8	64	
			2·8	52					2·8	67	
			3·0	54							
			3·2	52							
			3·4	61							

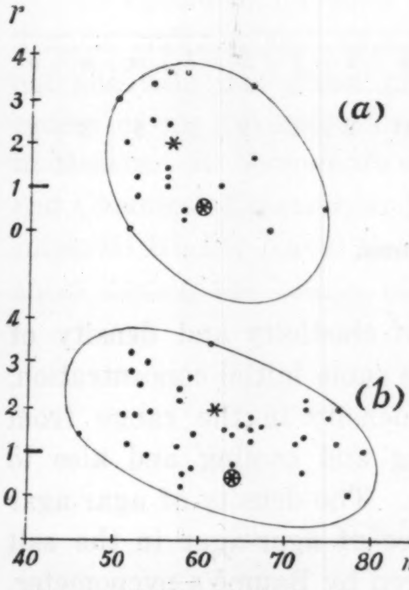

Fig. 8. With the tank, T_1.

(*a*) For the first experiment.

(*b*) For the second experiment.

$*$: Mean for $r>1$

⊛: Mean for $r\leqq 1$

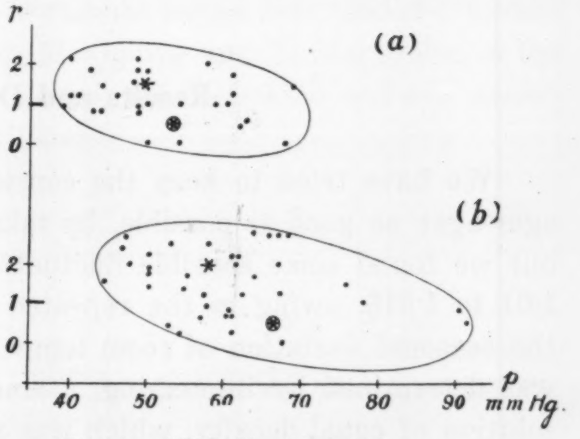

Fig. 9. With the tank, T_2.

(*a*) For the first experiment.

(*b*) For the second experiment.

$*$: Mean for $r>1$

⊛: Mean for $r\leqq 1$

The forms of surface cracks are summarised and classified into 15 kinds approximately as shown in Fig. 10, *a*, *b*, *c*, ……*n* and *o*. The percentages of the occurrences of the different cracks are shown in Table III. The greatest percentage value is shown in the case of *d*, of which the most cracks are inclined by the angles of about 30° and 150°, and some others by the angles of about 60° and 120°, referred to the longitudinal axis of the tank.

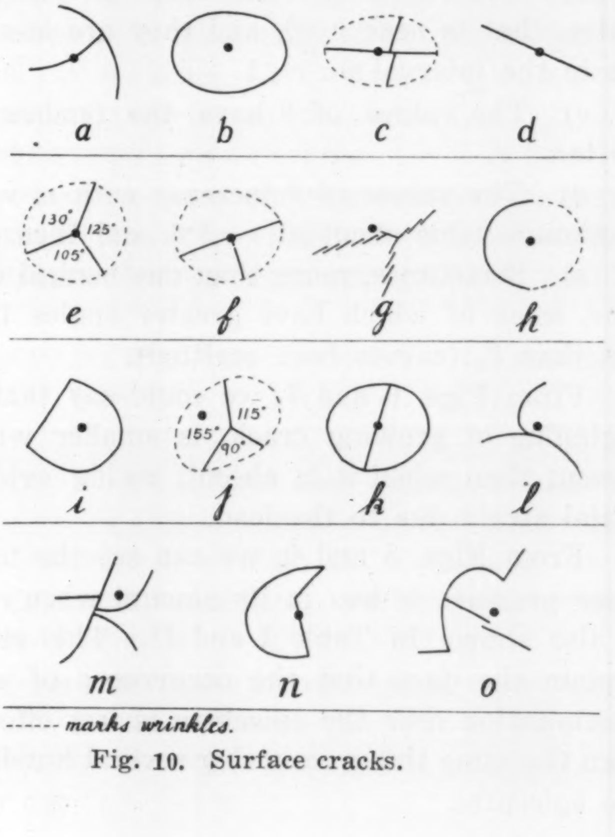

Fig. 10. Surface cracks.

Table III.

Kinds of cracks	*a*	*b*	*c*	*d*	*e*	*f*	*g*	*h*	*i*	*j*	*k*	*l*	*m*	*n*	*o*
Percentages of the occurrences	3	2	3	26	11	9	7	11	2	4	2	7	5	3	5

Results and Discussions.

We have tried to keep the constancy of elasticity and density of agar-agar as good as possible, by taking the same initial concentration, but we found some sensible fluctuation of density in the range from 1·01 to 1·015, owing to the repeated boiling and cooling and also to the seasonal variation of room temperature. The density of agar-agar was determined by immersing, a small piece of agar-agar in the salt solution of equal density, which was measured by Baumé's pycnometer.

From Figs. 4 and 5, we may be able to say the followings:–

a) The values of the angles, θ, i. e. the inclination of shear crack against the vertical are always greater in the same side as the surface load than in the opposite side with respect to the epicentre of the balloon.

b) The values of θ are about 45° when the load is near the epicentre, that is near $r=0$, and they are less than 45°, when the load lies in the interval $0<r<1$.

c) The values of θ have the tendency to approach the curve $\theta_0=\tan^{-1} r$.

d) The values of θ increase with r, when $r>1$, until reaching a maximum value about at $r=1·8$, and then decrease for greater r.

e) Sometimes, more than one conical cracks appear at the same time, some of which have greater angles than $\theta_0=\tan^{-1}r$, and others less than θ_0 (curves here omitted).

From Figs. 6 and 7, we could say that the inner pressure at the beginning of growing crack, is smaller when the surface loading is present than when it is absent, owing evidently to the effect of the initial strain due to the load.

From Figs. 8 and 9, we can see the tendency that the maximum inner pressure is less in its amount when $r>1$, than when $r\leqq1$, which is also shown in Table I and II. This result may, for some extent, explain the fact that the occurrence of a thunderstorm, cyclone or precipitation near the epicentre is less effective in causing earthquake than the same thing occurring several hundred kilometres distant from the epicentre.

In conclusion, I wish to express my best thanks to Prof. Torahiko Terada under whose supervision the entire work has been carried out and who has given me many useful suggestions throughout the course of my investigation. I also wish to express my cordial thanks to Messrs. R. Yamamoto and T. Watanabe in the Institute of Physical and Chemical Research and also to M. Ogawa and T. Maruyama in the Imperial Higher Naval College in Tôkyô, for their kind and able assistances during the course of experiments.

---

63. 地震發生機巧に關する一つの模型實驗

地震研究所 山口生知

前論文に於いて著者は次の事を指摘して置いた．卽ち深層地震の震源近くに於いては，其の直ぐ前後に於いて，顯著及稍顯著地震の起る事が極めて稀にして深層地震帶より測つて約 ±500 km 及 1000 km の地點に，顯著及稍顯著地震の最も起り易い處があると云ふことである．

此の結果に關して寺田寅彥博士は次の如き暗示を與へられた．若しも地下數百 km の深層地震の震源に相當する處に在る地殼の或る球形の部分が何等かの原因に依つて，膨脹或は收縮するならば，此の球の中心に頂點を持ち半頂角 45° なる圓錐面上に於いて最大應力が起り，地殼の破壞は之等の方向に添うて地表に向つて傳はるものと考へられる．と云ふのである．

今回の實驗の第一の目的は，此の暗示を證明せんとすることである．

第二の目的は，著者が旣に注意して置いたところの次の事實を證明する爲めである．卽ち雷雨や低氣壓の近く又は雨雪量の多い地點の近くに於いては，それ等のもの丶發生と同時に地震の起ることが極めて稀であつて，それ等の地點より數百粁隔てた處に地震が發生し易い，と云ふことを證明する爲めである．

實驗の裝置は第1圖に示す通り寒天を入れる角槽は容積が 20×30×60 cm³ なる木製の角槽を用ひ，其の中に良質の丸いゴム球を入れ，熱湯に溶した寒天を注ぎ込みたる後1日或は2日間放擲して自然に凝固させる樣にした．

而してゴム球の一端は細いゴム管で壓力計に連絡し，同時に圓筒形の空氣室の上端に繫がる樣にした．而して空氣室の下端は直徑 8 mm のゴム管を用ひて高所にある水槽 H に連絡し空氣室の下端の水面を徐々に上昇せしめて，角槽の中のゴム球を膨脹させることが出來る樣にしたものである．かくして寒天の內部に於いて割目の發生する時の壓力は，氣筒下部の水面が上り續けて居るにも拘はらず，壓力計內の水銀頭が下り始める時を以つて其の壓力の讀とした．

剪斷力に依る割目の形は風船の中心を通り角槽の長さの方向に平行な鉛直面で，切つて見ると球心を通る鉛直線と約 45° の角度をなし，底から出發して表面まで屆いて居ることが確かめられた．卽ち約 30 回の實驗の結果に依り先に述べた寺田博士の暗示を證明することが出來た．而して此の角度 θ の大いさは 40° から 50° の間にあることが分つた．

次に寒天の表面に半球形の底を有する陶器製の皿を置き其中に錘を乗せたものを角槽の中心線上色々の場所に動かして見た時の，角度θの變化を研究した.

又ゴム風船の眞上より皿の中心までの距離と寒天の表面よりゴム風船の中心までの深さとの比をとり此の比の値rと，割目の發生する時の壓力pとの關係を調べて見た.

之等の結果は次の通りである

1） 剪斷力に依る割目の線が鉛直線と傾く角度θの値は風船の中心に對して表面荷重と同じ側は反對側よりもいつでも大きい.

2） 荷重が風船の眞上にある時はθの値は約45°にして，$0<r<1$の間に於いては45°より小である.

3） θの値は$\theta_0=\tan^{-1}r$なる曲線に近づく傾向を持つて居る.

4） $r>1$なる時は，θの値はrと共に增加し$r=1{\cdot}8$邊で一つの最大値をとりそれより次第に減ずる.

5） 時には圓錐形の割目が二つ以上出來ることがあり一つは$\theta_0=\tan^{-1}r$より大に他はθ_0より小なることが多い.

6） 割目が發生する時の壓力pの値は，表面荷重が有る時は無い時よりも小である之は明らかに荷重に依る最初の歪の影響であると考へられる.

7） 最大內壓pの値は表面荷重の位置に依つて異なり$r>1$なる時は$r\leqq 1$なる時よりも小なる樣な傾向がある.

此の結果は雷や，低氣壓或は雨雪量等が震源近くに起つた時よりも，數百粁距つた遠方に發生した時の方が地震が起り易いと云ふ事實を幾分說明するものと思はれる.

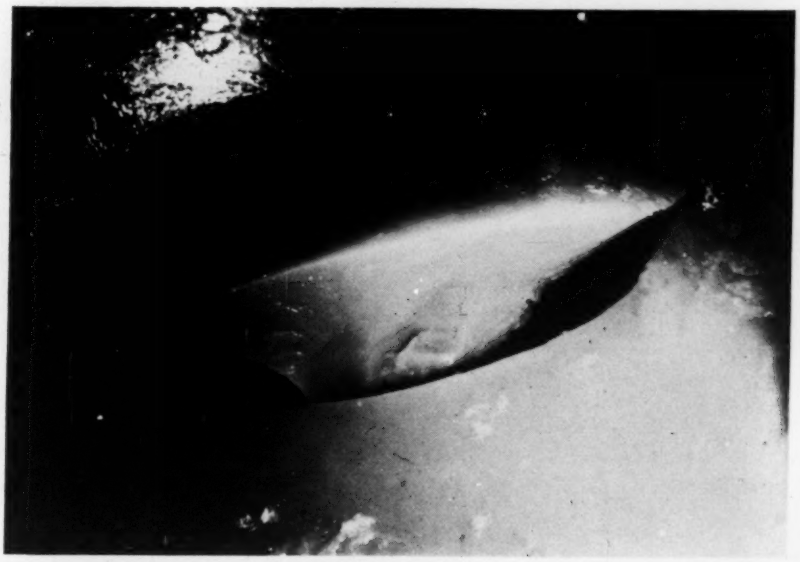

Fig. 11, *a*.

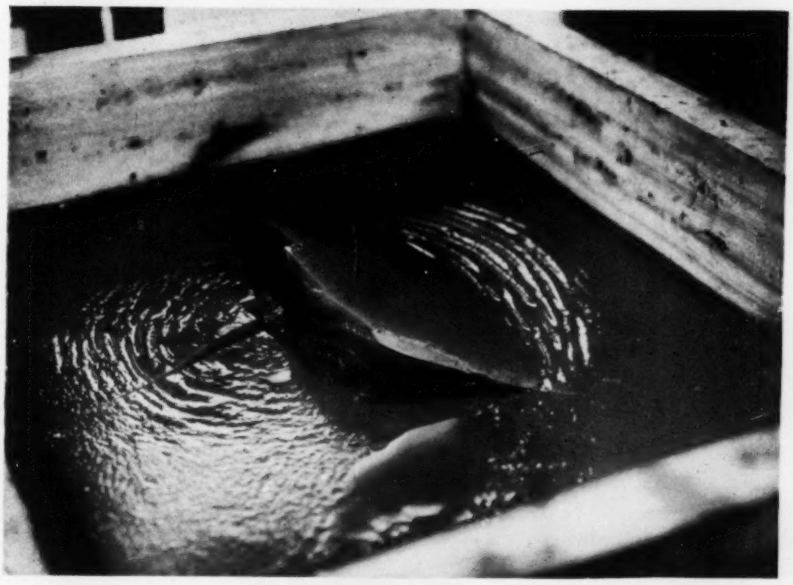

Fig. 11. *b*.

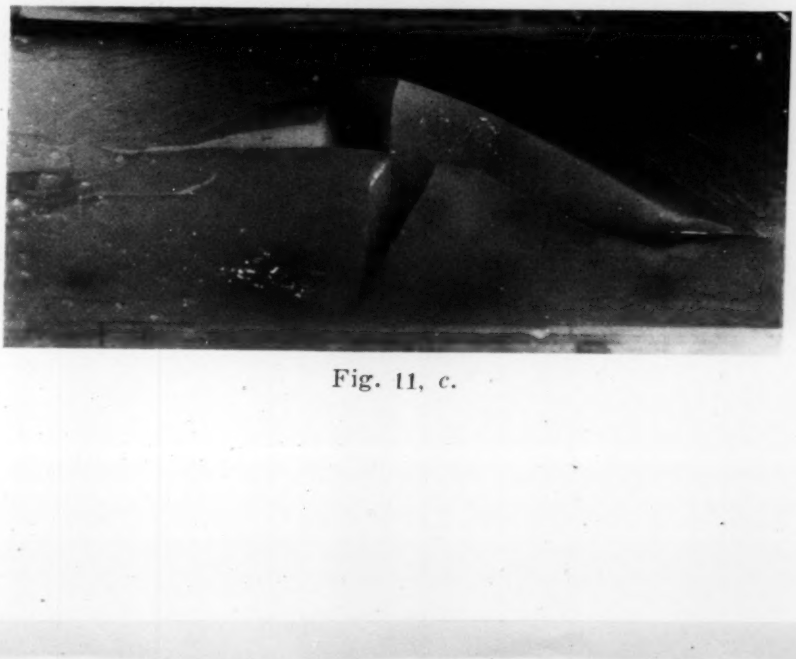

Fig. 11, *c*.

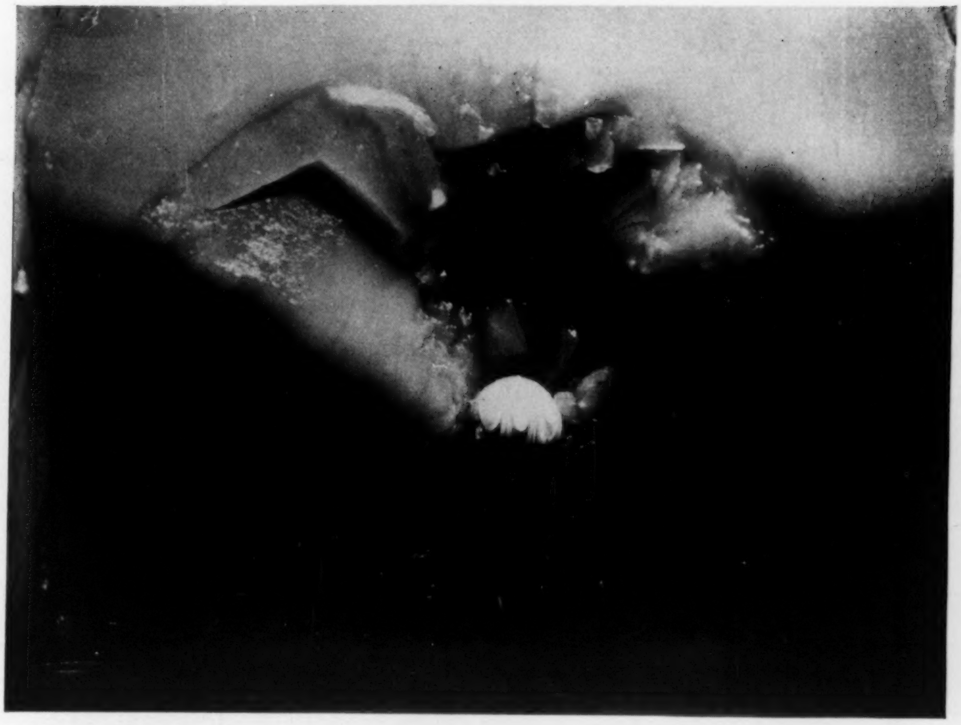

Fig. 11, *d*.

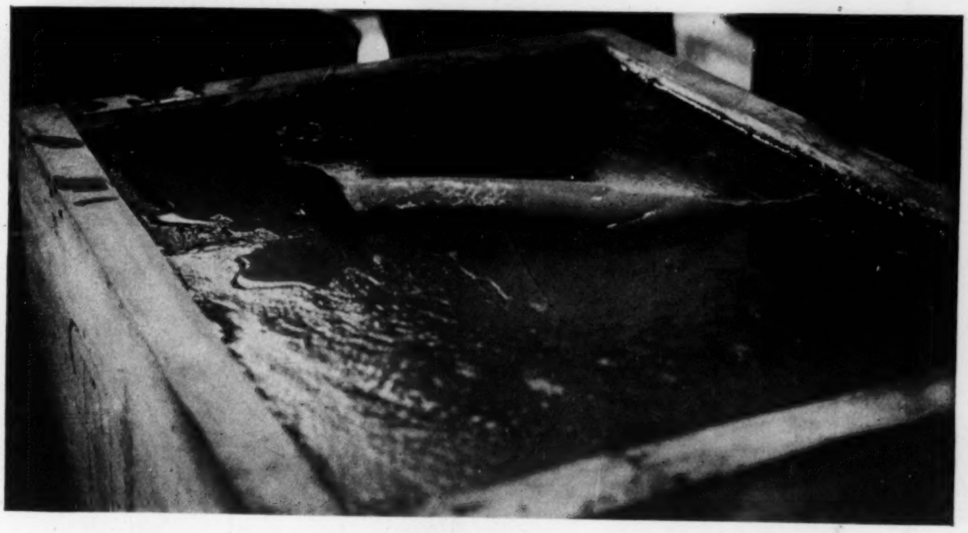

Fig. 11, *e*.

64. *The Air Damper.*

By Takahiro HAGIWARA,

Earthquake Research Institute.

(Read June 18, 1935.—Received Sept. 20, 1935.)

1. The air damper, which consists of a movable piston enclosed in a fixed cylinder, has been long in use for damping the pendulums of seismographs while recently it has been put into use for damping pendulums of short period, such as that of an acceleration seismograph. Hitherto the proportion between the resistance and the velocity of the piston was theoretically deduced under the assumption that the air in the cylinder is incompressible. Actually however the air must be more or less compressed and expanded as the pressure in the cylinder is increased and decreased by the motion of the piston. This paper discusses the effect of the compressibility of the air on the resisting force of the damper.

2. The air damper of a seismograph generally has the form of Fig. 1, *a* and *b*, the section of the piston being either a circle or a rectangle. Since type *b* is equal to two of type *a* joined together, we need consider only type *a*. Generally when an incompressible viscous fluid flows steadily through a tube with different pressures at the two ends of the tube, the outflow of the fluid from one of the ends per unit time is proportional to the pressure difference. This relation also holds when the flow of the fluid is not steady, provided the effect of the inertia of the fluid can be neglected, that is, $p=\alpha\frac{dv}{dt}$, where p is the pressure difference, v the volume of outflow, t the time, and α the constant determined by the viscosity of the fluid and the geometrical size of the tube. When the tube is of simple

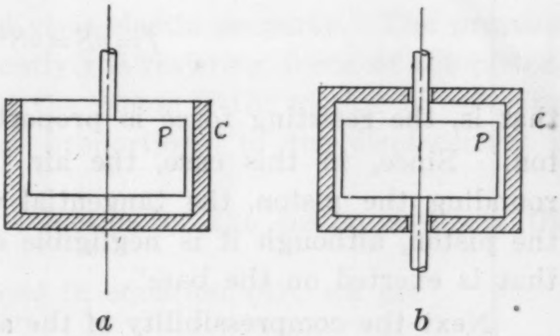

Fig. 1. Two types of the air damper.
P piston, *C* cylinder.

form the value of α can be calculated, some examples of which follow.

(a) Straight pipe of uniform rectangular section, of which one side a is very small compared with the other b. $\alpha=\dfrac{12\,\eta l}{a^3 b}$ (where η is the viscosity coefficient of the fluid, l the length of the pipe.

(b) Straight pipe of uniform circular section. $\alpha=\dfrac{8\eta l}{\pi r^4}$ (where r is the radius).

(c) Straight pipe formed of two co-axial circular cylinders. $\alpha=\dfrac{6\eta l}{\pi e^3 r}$ (where r is the radius of one cylinder, e the difference in radius of the two cylinders and $r \gg e$).

As regards the air damper $\dfrac{dv}{dt}=S\dfrac{d\xi}{dt}$, where S is the sectional area of the piston and ξ the displacement of the piston from the neutral position. The pressure increase of the air in the damper is therefore given by $p=\alpha S\dfrac{d\xi}{dt}$, and the resisting force exerted on the piston

$$f=pS=\alpha S^2\,\frac{d\xi}{dt}\,, \tag{1}$$

that is, the resisting force is proportional to the velocity of the piston. Since, in this case, the air flows through the clearance surrounding the piston, the tangential viscous force acts on the side of the piston, although it is negligible compared with the normal force that is exerted on the base[1].

Next the compressibility of the air will be considered. We denote the pressure and the volume of air contained in the damper at the outset by P_0 and V_0 respectively, P_0 being equal to the pressure of free air. After time t, P_0 and V_0 become P_0+p and V respectively, and the total outflow of air through the clearance amounts to volume V'. If we assume for simplicity that the phenomenon is isothermal, then

---

[1] If, for example, the section of the damper is circular $\alpha=\dfrac{6\eta l}{\pi e^3 r}$ and $S=\pi r^2$, where r is the radius of the piston, e the clearance, l the length of the piston along the axis, and η the viscosity coefficient of air. Hence $f=\dfrac{6\pi\eta l r^3}{e^3}\times\dfrac{d\xi}{dt}$.

The tangential force is given by $f'=\dfrac{6\pi\eta l r^2}{e^2}\times\dfrac{d\xi}{dt}=\dfrac{e}{r}\times f$.

If $r=4$ cm and $e=0{\cdot}1$ mm, $f'\fallingdotseq 0{\cdot}0025\times f$.

$$\left.\begin{aligned} &P_0(V_0-V')=(P_0+p)V,\\ &V_0=Sh,\\ &V=S(h-\xi),\\ &V'=\int_0^t \frac{p}{\alpha}dt, \end{aligned}\right\} \tag{2}$$

where h is the distance between theb ase of the piston and the cylinder, α the constant determined by the viscosity and the geometrical size of the clearance. Hence

$$P_0\left(\xi S-\int_0^t \frac{p}{\alpha}dt\right)=Sph-Sp\xi. \tag{3}$$

Generally p and ξ are very small compared with P and h respectively, so that in the foregoing equation we ignore the product $p\xi$. Rewriting the equation then in the differential form,

$$\frac{dp}{dt}+\frac{P_0}{\alpha Sh}p=\frac{P_0}{h}\frac{d\xi}{dt}\cdot \tag{4}$$

This equation shows the so-called visco-elastic property. The pressure increase in the damper (consequently the resisting force of the piston) is proportional to the velocity of the piston if the motion is comparatively slow, whereas it becomes proportional to the displacement if the motion rapid.

We shall next see when the motion of the piston assumes the sine form. Putting $\frac{d\xi}{dt}=\xi_0\omega\sin\omega t$ in equation (4), we get

$$\frac{dp}{dt}+\frac{P_0}{\alpha Sh}p=\frac{P_0\xi_0\omega}{h}\sin\omega t. \tag{5}$$

The solution of the equation for the stationary state is

$$p=\frac{\xi_0\omega\alpha S\sin\omega t}{1+\left(\frac{\omega\alpha Sh}{P_0}\right)^2}-\frac{\frac{\xi_0P_0}{h}\cos\omega t}{1+\left(\frac{P_0}{\omega\alpha Sh}\right)^2} \tag{6}$$

$$\left.\begin{aligned} \text{or}\quad p &= \frac{\xi_0\omega\alpha SP_0\sin(\omega t-\delta)}{\sqrt{P_0^2+(\omega\alpha Sh)^2}}, \\ \tan\delta &= \frac{\omega\alpha Sh}{P_0}. \end{aligned}\right\} \qquad (7)$$

As will be seen from equation (6), pressure increase p has one term in phase with the velocity of the piston and another out of phase. In equation (7), δ is the phase difference between the resultant force and the velocity of the piston. If ω is very small (that is to say, the period of motion of the piston is large), the second term on the righthand side of equation (6) vanishes and p is exactly in phase with the velocity of the piston. If ω is very large the first term vanishes and p is proportional to the displacement of the piston, in which case the restitutive force of the pendulum increases by the retarding force of the damper and the proper period of the pendulum apparently shortens. We notice, however, that such disturbances can be avoided to a certain extent by making h (the distance between the base of the piston and the cylinder) sufficiently small.

3. We investigated the foregoing theory by an experiment. A sketch of the experimental arrangement is given in Fig. 2. The damper used here is the same as that used in the Ishimoto acceleration seismograph. The section of the piston perpendicular to its axis is circular with a diameter of 8 cm and a length along the axis of 4 cm; the clearance being 0·1 mm. The piston was set in simple harmonic motion by means of a D. C. motor. A manometer (M) was attached to the damper. The tube connecting the cylinder and the manometer is about 5 cm long, with an inside diameter of 0·5mm. The volume of the air contained in the manometer and the tube is negligible compared with that contained in the damper. The manometer consists of a stretched circular rubber membrane with a diameter of 1 cm and a thickness of 0·2 mm. A fine phosphorbronze wire is attached to the centre of the membrane, which is stretched

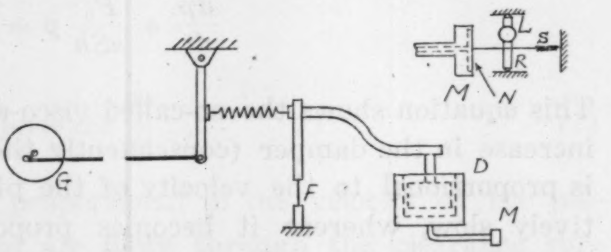

Fig. 2. Sketch of the experimental arrangement.
D damper, *F* flat spring, *G* D. C. motor, *M* manometer, *R* roller, *L* lens mirror, *S* weak herical spring, *N* rubber membrane.

by a weak spring. The wire, contacting with the roller (R), translates the motion of the membrane into a rotation of the mirror about its vertical axis. The displacement of the piston is also translated into a rotation of the plane mirror about its horizontal axis. The ray of light from a point source, which at first falls on the lens mirror, is reflected to the plane mirror and then reflected back again to the photographic plate, on which an image of the point source is formed. In this way we obtained Lissajous' figures on the plate, in which the pressure is taken as abscissa and the displacement of the piston as ordinate. The sensibility of the manometer was calibrated statically with a known pressure. Since the free vibration of the membrane is sufficiently rapid, the sensibility is not affected by the vibration period of the change of pressure as far as this experiment went.

The experiments covered the case where h is 0·55 and 0·20 cm. The vibration period of the piston ranged from 0·1 sec to 1 sec. One of the records obtained are shown in Fig. 3. We calculated the phase differences from the records with respect to various periods and compared them with the values that were calculated by means of equation (7), the results of which are shown in Fig. 4, in which the full lines are the theoretical values and the plottings those obtained by experiment. It will be seen that the two values, theoretical and experimental, are in fair accord.

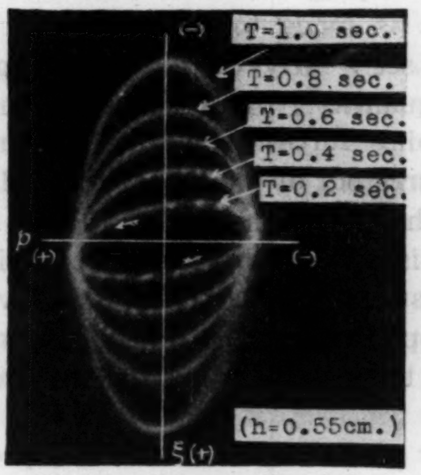

Fig. 3. An example of the records (Lissajous' figures).

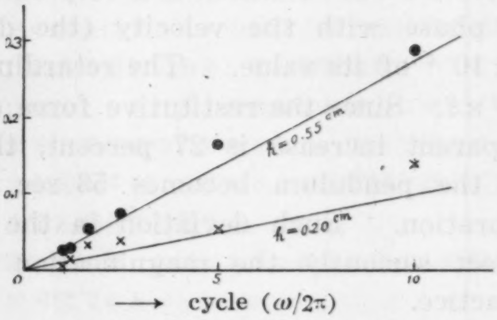

Fig. 4. The full lines are theoretical values, while the plottings are experimental.

4. We shall see how the compressibility of the air in the damper affects the constants of the seismograph in the following two cases.

a) An acceleration seismograph (short period pendulum). An acceleration seismograph with the following conditions is assumed. Mass of pendulum 15 kg; proper period 0·15 sec. Damper of circular section and area 50 cm² (diameter about 8 cm). In this case, the value of α will be required to be 500 to damp the pendulum in the critical state. It is further assumed that the distance between the base of the piston and the cylinder (h) is 0·2 cm and the period of earthquake motion is 0·1 sec. The effects are then calculated by equation (6) and (7). The phase difference between the retarding force of the damper and the velocity of the piston (δ) is 17°30′. The retarding force in phase with the velocity decreases about 1 percent of its value as compared with the case of a very slow motion of the piston. The retarding force out of phase becomes $2{\cdot}3\times10^6\times\xi$, but as the restitutive force of the pendulum itself is $2{\cdot}6\times10^7\times\xi$, there is an apparent increase in this force of about 10 percent.

b) A seismograph with long period. A seismograph with the following conditions is assumed. Mass of pendulum 40 kg; proper period of pendulum 60 sec . As to the damper, $S=50$ cm^2 and $h=$ 2 cm. The value of α for the critical damping state is then 3·36. It is further assumed that the pendulum is made to vibrate owing to earthquake motion with a period of 1 sec . By calculation we get $\tan\delta=2{\cdot}1\times10^{-9}$, which is a very small quantity. The retarding force in phase with the velocity (the damping force) decreases by only 4×10^{-6} of its value. The retarding force out of phase becomes $1{\cdot}1\times10^2\times\xi$. Since the restitutive force of the pendulum is $4{\cdot}0\times10^2\times\xi$, its apparent increase is 27 percent, that is to say, the apparent period of the pendulum becomes 53 sec in stead of 60 sec, for the given vibration. Such deviation in the proper period, however, does not affect seriously the magnification of the seismograph in ordinary practice.

The foregoing two examples show that the effects of compressibility of the air can be avoided to a certain extent by a proper design of the damper.

In conclusion, the present writer wishes to express his thanks to Professor M. Ishimoto for his kind advices and criticisms in the course of these studies.

64. 空氣制振器に就て

地震研究所　萩原　尊禮

1. 空氣制振器は從來比較的長週期の地震計の制振器として使用せられて來たが，最近に於ては加速度地震計の如き短週期の地震計の制振にも利用せられる樣になつた．空氣制振器は一般にピストン型を爲したものであるが，ピストンの速度と之に働く反抗力（制振力）との比例的關係は理論的には空氣の不可壓縮性を假定することに依つて求められる．然し實際にはピストンの運動に從ひ內部の空氣の壓力は增大又は減少せしめられるのであるから，空氣の膨脹壓縮の生ずることは當然である．本文は此の空氣の膨脹壓縮の現象が制振力に對し如何なる影響を持つかを理論的に吟味し，此の結果を實驗に依つて確めたものである．

2. 結果の槪略を次に列擧する．

ピストンに働く反抗力は比較的緩慢な運動に對してはピストンの速度に比例するが，極めて急激な運動に對してはピストンの變位に比例する．

今ピストンが正弦運動を行ふ場合を考へると，反抗力はピストンの速度と同位相のものと，之と 90° だけ相違した位相（卽ちピストンの變位と同位相）のものとに分解出來る．振動週期の大なる場合は異位相の力は同位相の力に比較して小となり，極端に大なる週期に對しては異位相の力は消失し速度と同位相の反抗力のみとなる．此の場合はピストンの反抗力は完全に其の速度に比例するのであつて空氣の不可壓縮性を假定した場合と同じである．然し振動週期が小となるに從つてピストンの速度と同位相の反抗力は次第に減少し，之に反し異位相の反抗力は增大する．極端に小なる振動週期に對しては同位相の力は消失し異位相の力のみとなる．卽ち反抗力はピストンの變位に全く比例し，見かけ上振子の復元力を增大する．之はピストンの間隔を通して空氣の出入することなく空氣の彈性に依り反抗力を生ずる場合に相當する．

空氣の可壓縮性は制振器の反抗力に如上の影響を齎すが，之はピストンの底と壔との距離を適當に小とすることに依り或る程度迄免れることが可能である．

3. 以上の結果は實驗的にも確めることが出來た．

4. 實際問題としては，加速度地震計にあつては現在の如く 0·1 秒程度より大なる週期の地動を目標としてゐる限り上に述べた影響は餘り問題とならないが，之より小なる週期の地動の記錄を必要とする場合は此の影響から免れる樣に制振器を設計することは相當困難であらう．

又長週期地震計にあつては比較的少なる週期の地震に對しては制振器の反抗力に依り見かけ上振子の週期は減少するが，餘りに少なる週期の地震の記錄は長週期地震計の目的とする所では無く，又多少振子週期が見かけ上減少しても地動週期が振子週期に比較して相當小である以上地震計倍率に左程の影響はない．從つて現在より遙かに精密を要する樣な測定でない限り問題にならない．

65. *The Explosive Activities of Volcano Asama in 1935. (Part 2).*

By Takeshi MINAKAMI,

Earthquake Research Institute.

(Read July 2, 1935.—Received Sept. 20, 1935.)

1. Introduction.

In his previous paper, the writer[1] described the explosive activities of volcano Asama in April and May, 1935, and the various volcanic phenomena observed. Volcanic micro-tremors, that is, volcanic micro-earthquakes, occurred during the three months before the violent explosion on April 20, 1935, remarkable inclinations of the earth-surface were observed as early as two months before the explosion, while variations in earth-currents were noticed several days and also four or five hours before the occurrences of the severe explosion.

During April and May the volcano was unusually active, quieting down from the early part of June, but resuming its activities in August with frequent explosions and small eruptions, which however were not so violent as those of April and May. The volcanic micro-tremors felt during June, July were also not so frequent as in April and May, although they increased again in August. In this paper, the writer discuses volcanic micro-tremors, or volcanic micro-earthquakes, the remarkable variations in the vapours emitted from the crater, and the antenna-earth currents that were recorded at the moment of the explosion.

2. List of Eruptions in June, July and August, 1935.

In the foregoing list, the eruptions are divided into four classes according to the nature of the explosion as fully treated in the previous paper. It will be seen that the number of eruptions corresponding to C and D, are 5 and 29. No such violent explosions as correspond to A or B occurred in June, July and August, most of them being very small eruptions without either detonation or large lava throws, but only volcanic gravels or ash.

---

[1] T. MINAKAMI, *Bull. Earthq. Res. Inst.*, **13** (1935), 629.

Table I.

No.	Class	Date	Time of occurrence	Remarks
			h. m. s.	
42	D	May 30, 1935	7, 20 p.m.	
43	C	June 16, 〃	8, 30 〃	Sound heard in Komoro and Iwamurata.
44	D	〃 18, 〃	7, 30 〃	
45	D	〃 19, 〃	4, 57 〃	
46	D	〃 23, 〃	7, 40 〃	
47	D	〃 25, 〃	7, 16 a.m.	
48	D	〃 27, 〃	10 〃	
49	C	July 2, 〃	11, 42, 54 〃	Pumice stone fell at our Observatory.
50	D	〃 4, 〃	5, 35 p.m.	
51	D	〃 9, 〃	6, 25 a.m.	
52	D	〃 25, 〃	10, 50 〃	
53	D	August 2, 〃	2, 10 p.m.	
54	D	〃 2, 〃	2. 29 〃	
55	D	〃 2, 〃	4, 40 〃	
56	C	〃 4, 〃	7, 29, 54 a.m.	Sound heard in Kitakaruizawa.
57	D	〃 5, 〃	10, 40	
58	D	〃 13, 〃	5 p.m.	
59	D	〃 15, 〃	5 a.m.	
60	C	〃 17. 〃	4, 50, 57 p.m.	Gravels and ashes fell at Kutukake.
61	D	〃 18, 〃	7, 50 a.m.	
62	D	〃 18, 〃	4, 55 p.m.	
63	D	〃 19, 〃	1, 20 〃	
64	D	〃 21, 〃	6, 05 a.m.	
65	D	〃 21, 〃	7 〃	
66	D	〃 21, 〃	7, 51 〃	
67	D	〃 21, 〃	4, 50 p.m.	
68	D	〃 22, 〃	1, 25 〃	
69	D	〃 26, 〃	3, 40 〃	
70	C	〃 28, 〃	8, 10, 10 a.m.	Sound heard at Nagano.
71	D	〃 30, 〃	6, 09 〃	
72	D	〃 30, 〃	7, 25 〃	
73	D	〃 30, 〃	7, 46 〃	
74	D	〃 30, 〃	9, 03 〃	
75	D	〃 31, 〃	6 〃	

3. Changes in the Crater and the Central Cone.

The volcanic bombs, gravels, and ashes ejected from the crater accumulated on the central cone and about it. In violent explosions, such as the one on April 20, 1935, the larger part of what falls on the central cone consists of large bombs, while small fragmental lava, such as gravels and ashes, fall at distances from the crater. But in the case of small eruptions, the ejections are mostly volcanic gravels and ashes, which are not thrown to such heights as in that of a violent explosion, with the result that the bulk of them falls on the central cone. The materials that fall on the central cone at the time of an explosion are not only new lava projected from the crater-floor, but also old lava torn off from parts of the crater-wall by the force of the explosion, as the result of which a part of it falls back into the crater. As an example, a part of the crater-wall on the south side, 50 m long and 3∼5 m wide, was broken off by the explosions that occurred on May, 1935. This broken crater-wall corresponds to the crater shown in the photograph (Fig. 21) in the previous paper. Naturally, the amount of volcanic material that piles up during an active period is considerable. In the eruptions which occurred in May, the total quantity of ejecta precipitated on the central cone, consisting of volcanic gravel and ash, showed a thickness of more than 1·5 m. In the following Fig. 1, are shown the depths of these precipitations on the central cone from a margin of the crater on easterly direction. Fig. 10 shows ejecta on the snow and a cavity hollowed out in the snow by a bomb on the eastern side of the central cone at a radial distance of 200 m from the edge of the crater.

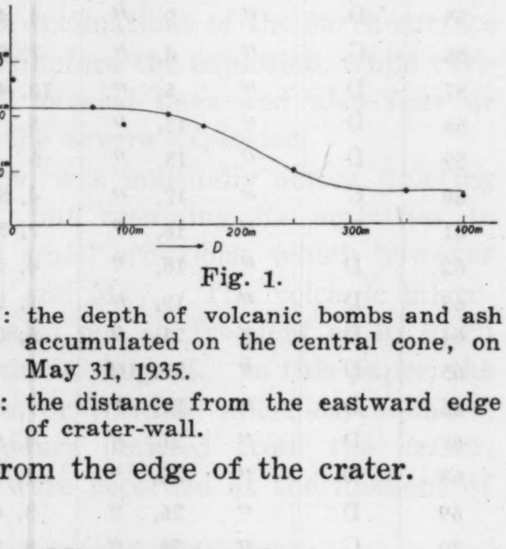

Fig. 1.

H: the depth of volcanic bombs and ash accumulated on the central cone, on May 31, 1935.

D: the distance from the eastward edge of crater-wall.

4. Volcanic Micro-tremors (Micro-earthquakes).

The volcanic-tremors that began to be felt from January 2, 1935, were still going on at the beginning of September, the same year. The daily frequencies of these micro-earthquakes as registered by the seismograph (magnification 100) installed at our Observatory, 5 km distant from the crater, are shown in Table II.

Some of the micro-earthquakes have motions that are almost a regular sine-curve, and having almost constant periods and amplitudes, it is difficult to determine their phases, while others resemble ordinary earthquakes with their various periods and amplitudes. The two kinds of micro-earthquakes are shown in Fig. 8. Notwithstanding the wide

Table II.

Date	Number of occurrence of micro-tremors	Date	Number of occurrence of micro-termors	Date	Number of occurrence of micro-termors
June 1, 1935	4	July 1, 1935	5	August 1, 1935	1
″ 2, ″	6	″ 2, ″	47	″ 2, ″	1
″ 3, ″	5	″ 3, ″	3	″ 3, ″	8
″ 4, ″	0	″ 4, ″	3	″ 4, ″	6
″ 5, ″	5	″ 5, ″	7	″ 5, ″	2
″ 6, ″	3	″ 6, ″	7	″ 6, ″	6
″ 7, ″	1	″ 7, ″	2	″ 7, ″	0
″ 8, ″	1	″ 8, ″	2	″ 8, ″	0
″ 9, ″	1	″ 9, ″	0	″ 9, ″	0
″ 10, ″	1	″ 10, ″	3	″ 10, ″	4
″ 11, ″	1	″ 11, ″	3	″ 11, ″	1
″ 12, ″	0	″ 12, ″	5	″ 12, ″	5
″ 13, ″	0	″ 13, ″	2	″ 13, ″	8
″ 14, ″	3	″ 14, ″	2	″ 14, ″	3
″ 15, ″	3	″ 15, ″	1	″ 15, ″	3
″ 16, ″	2	″ 16, ″	2	″ 16, ″	4
″ 17, ″	0	″ 17, ″	7	″ 17, ″	27
″ 18, ″	0	″ 18, ″	2	″ 18, ″	0
″ 19, ″	0	″ 19, ″	15	″ 19, ″	1
″ 20, ″	1	″ 20, ″	4	″ 20, ″	0
″ 21, ″	1	″ 21, ″	3	″ 21, ″	7
″ 22, ″	6	″ 22, ″	5	″ 22, ″	8
″ 23, ″	1	″ 23, ″	1	″ 23, ″	4
″ 24, ″	0	″ 24, ″	3	″ 24, ″	4
″ 25, ″	0	″ 25, ″	2	″ 25, ″	2
″ 26, ″	1	″ 26, ″	8	″ 26, ″	2
″ 27, ″	5	″ 27, ″	7	″ 27, ″	36
″ 28, ″	0	″ 28, ″	3	″ 28, ″	33
″ 29, ″	3	″ 29, ″	12	″ 29, ″	34
″ 30, ″	0	″ 30, ″	3	″ 30, ″	16
		″ 31, ″	3	″ 31, ″	32

difference in the nature of these two kinds of micro-tremors, this paper will deal only with their relations generally with other phenomena.

The daily occurrence of micro-earthquakes and the occurrence of eruption are shown in Fig. 2. Generally speaking, when micro-earthquakes are frequent, violent explosions are also frequent. As will be seen from Fig. 2, and violent eruptions before May 11, occurred on days of minimum micro-earthquake ocurrence, whereas after that the explosions occurred on days of maximum micro-earthquake occurrence. For the active period of April and May, however, since violent explosions occurred one after another, it is not easy to trace the exact relationship between each eruption and the frequency of micro-earthquakes. To obviate this difficulty, the writer selected three eruptions that occurred with some interval of time between them, namely those of July 2, August 4, and 28. In the case of these explosions, many micro-earthquakes occurred from 20 to 24 hours before the outbursts as well from 1 to 2 hours after them, when the occurrence frequency attains to maximum, after which they suddenly decreased. In Fig. 3, a, b, and c are shown the total number of micro-earthquakes for every two hours

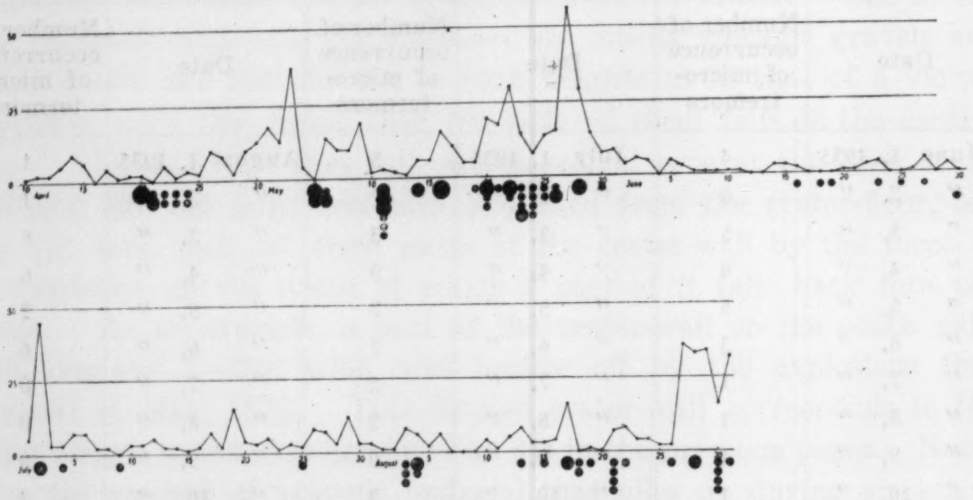

Fig. 2. Daily numbers of occurrence of volcanic micro-earthquake.
● : explosion.

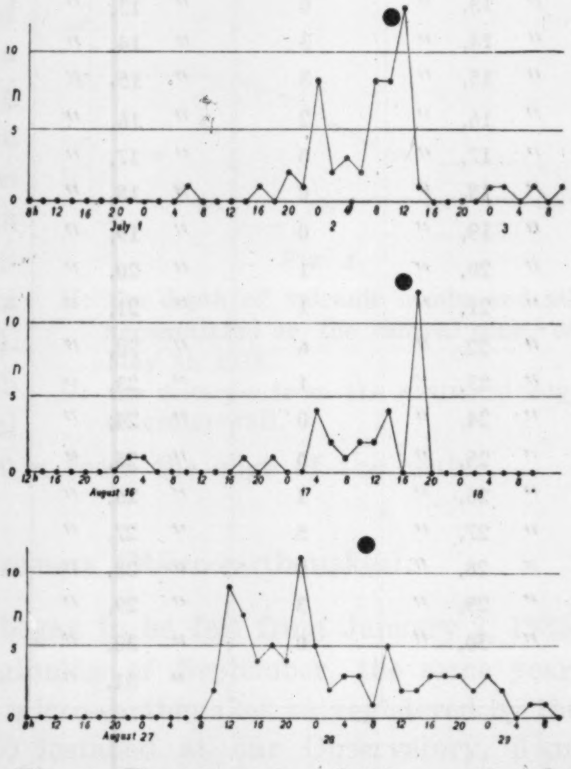

Fig. 3. The occurrence of micro-earthquake and the explosion.
n: numbers of occurrence of micro-earthquakes for every 2 hours.
●: explosion.

before and after the explosion. The forms of the curves in Fig. 3, a and b resemble each other, while that in Fig. 3, c differs somewhat from the other two, because after the explosion of August 28 shown in Fig. 3, c, many small eruptions occurred on August 30, with the result that after the eruption on August 28 micro-earthquakes continued.

The longest duration of these volcanic earthquakes is 25 min and the shortest 3 sec. Table III gives the mean duration of micro-earthquakes and their frequency. Of the total 1808 micro-earthquakes that occurred in this period of activity (Jan. 1935—Aug. 1935), those less than 10 sec in duration amounted to 501. Those whose durations exceeded 60 sec are comparatively few, forming only 19% of the total. In Table IV, and Fig. 4 are shown the mean durations of micro-earth-

Table III.

Date	Total num. of micro-earthq.	Mean duration of micro-earthq.	Date	Total num. of micro-earthq.	Mean duration of micro-earthq.
Jan. 1~ 5	5	65·4$^{\text{sec.}}$	May 1~ 5	83	26·6$^{\text{sec.}}$
6~10	19	67·4	5~10	55	35·6
11~15	3	46·1	11~15	39	40·2
16~20	17	68·6	16~20	57	28·4
21~25	37	43·9	21~25	85	38·3
26~30	33	42·1	26~30	124	26·6
Fev. 31~ 4	50	27·6	June 31~ 4	24	89·0
5~ 9	38	43·4	5~ 9	11	84·1
10~14	56	30·0	10~14	5	44·8
15~19	48	17·2	15~19	5	61·0
20~24	49	51·7	20~24	9	81·0
Mar. 25~ 1	39	24·6	25~29	10	220·8
2~ 6	41	34·8	July 30~ 4	56	50·1
7~11	73	36·5	5~ 9	18	109·6
12~16	37	24·3	10~14	15	80·4
17~21	33	25·3	15~19	27	79·5
22~26	51	41·9	20~24	16	76·8
27~31	33	53·6	25~29	32	125·1
Apr. 1~ 5	39	39·9	Aug. 30~ 3	16	130·3
6~10	21	33·3	4~ 8	14	77·8
11~15	26	55·4	9~13	18	62·6
16~20	23	71·1	14~18	37	40·1
21~25	33	62·1	19~23	20	45·9
26~30	39	29·9	24~28	77	36·0

Table IV.

Duration of micro-earthq.	Numbers of micro-earthq.	Duration of micro-earthq.	Numbers of micro-earthq.
sec. sec.		sec. sec.	
0~ 10	501	200~210	5
10~ 20	248	210~220	4
20~ 30	220	220~230	5
30~ 40	165	230~240	3
40~ 50	145	240~250	6
50~ 60	73	250~260	1
60~ 70	62	260~270	1
70~ 80	52	270~280	0
80~ 90	49	280~290	5
90~100	43	290~300	1
100~110	35	300~310	1
110~120	31	310~320	1
120~130	29	320~330	1
130~140	27	330~340	0
140~150	23	340~350	1
150~160	29	350~360	2
160~170	14	360~370	1
170~180	8	370~380	0
180~190	8	380~390	0
290~200	6	390~400	0

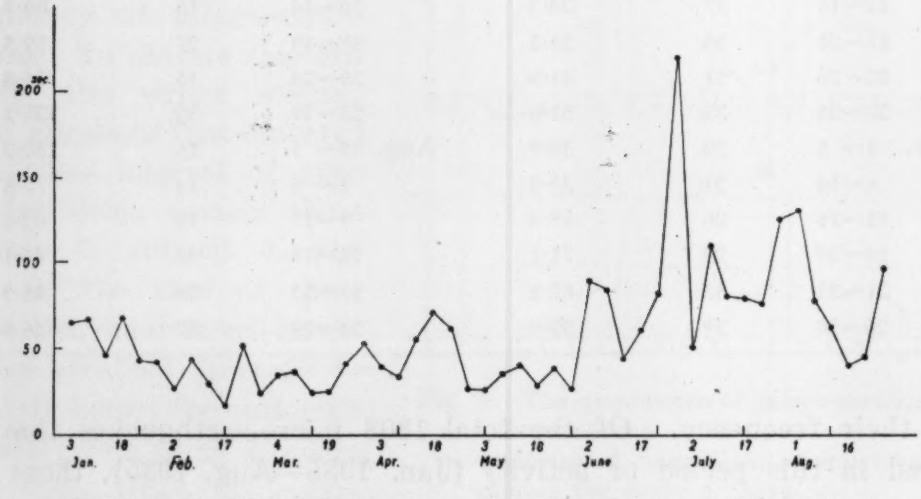

Fig. 4. Variations in the mean duration of micro-earthquakes occurred for every five days.

quakes for every successive five days, together with the number that occurred, from which it will be seen that the durations in July and August are longer than those in April and May. Fig. 5 gives the number that occurred with their average durations for every five days.

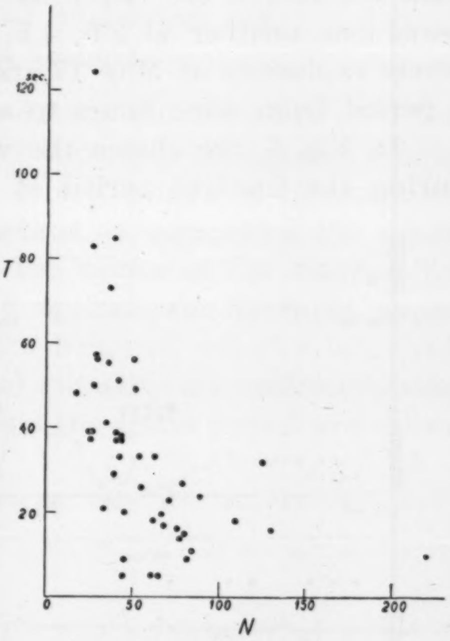

Fig. 5.

T; mean duration of micro-earthquakes for successive five days.
N; numbers of occurrence of micro-earthquakes for successive five days.

5. Variations in the Volume of the Vapour emitted from the Crater.

From the crater-floor or from fissures in the crater-wall, vapours containing principally steam and sulphurous acid gas issue without cessation. During certain inactive periods of the volcano, however, such as those in the years 1933 and 1934, the volume of the vapours emitted is almost constant, excepting after long and heavy rain; when the volume is usually large. At all events, the variations in the volume of vapour from day to day during the active period are so great as to form no comparison with the variations during the inactive period. Moreover in the active season, there are changes not only in the volume of the vapour emitted, but in its quality as well. Usually, a day or some hours preceding a violent eruption, the quantity of vapour becomes so small that from the foot of the volcano we can not find the vapour. Asama volcano showing no vapour issuing from it before an eruption is shown in Fig. 20 a.

The writer in his previous paper[2)], reported that the volume of the vapour became somewhat irregular since October 1934, which however was not very pronounced untill the middle of April, 1935, when on the day before the violent eruption of April 20, 1935, the quantity of vapour suddenly diminished to an extraordinary small volume and continued so until the explosion occurred. During 5 or 6 hours that preceded the explosoin on May 5, 1935, the issue of vapour virtually ceased.

On May 10, 1935, at noon, so much vapours issued from the volcano that the writer was unable to approach the crater. From 3 h

---

2) T. MINAKAMI, *Bull. Earthq. Res. Inst.*, **13** (1935), 318.

p.m., no more vapour issued from the crater. This condition lasted until 2 h a.m. of the following day, when three violent explosions followed one another at 2 h, 4 h, and 6 h in the morning. In the later severe explosions of May 17 and 22 also, emission of vapour ceased for a period from some hours to a day preceding the explosions.

In Fig. 6, are shown the variations in the volume of the vapour during the inactive period of 1934 and during the active period of 1935. The remarkable changes in the vapour volume during the active period, and their relations to the occurrence of explosions are shown in Fig. 6 b.

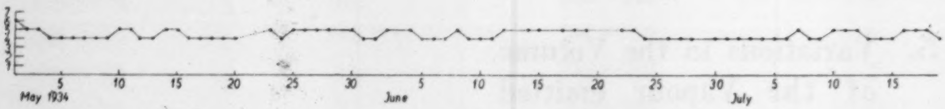

Fig. 6 a.

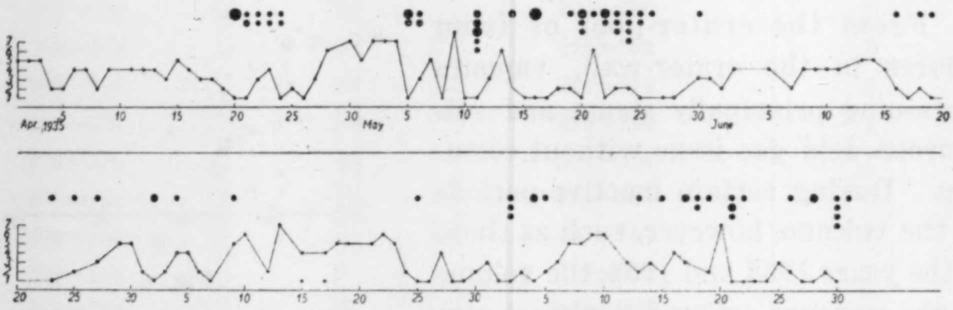

Fig. 6 b.

The quanty of vopour ejected from the crater and the explosions.

V; quanty of vapour, 1; very small, 2; small, 3; a little small,
4; normal, 5; a little much, 6; much, 7; very much.
●; explosion.

Fig. 6 a. The variations of vapour in inactive period (1934).
Fig. 6 b. The variations of vapour in active period (1935).

Fig. 11, a, b, c, show a periodic emissions of vapour that occurred during the active period of May, 1935, a condition that generally continues for from 1 to 2 hours before the vapour ceases to issue.

On the whole, however, there is no definite correlation between the volume and character of the vapours emitted. What is almost a fixed rule however is that during the active period, the volume of the vapour that issues from the crater changes more frequently and at shoter intervales than when the volcano is quiet, together with the phenomena just mentioned of the volume of the vapours diminishing to almost nil a day or some hours preceding an eruption.

Observations moreover force us to the conclusion that the longer the vapourless condition lasts, the more violent will be the explosion that follows.

6. Variations in Terrestrial Magnetism and in the Antenna-earth Currents[3].

There seems to be no doubt that during the activities of a volcano, terrestrial magnetism in its vicinity undergoes changes on a large scale. Since October 1934, observations of declinations of the magnetic needle were continued by the simple method of supporting the needle on a point, and a mirror attached to the center of the magnet, the variations in declination being recorded optically on bromide paper. This magneto-meter is installed in a cave hollowed out of a large volcanic rock, in which the temperature and humidity are sufficiently constant. The variations in declination during the active period are shown in Fig. 7. Although much more rapid changes in terrestrial magnetism, such as those that last for only few secends or minutes, occur at the time of an explosion, rapid variations of this kind cannot be recorded by this magneto-meter.

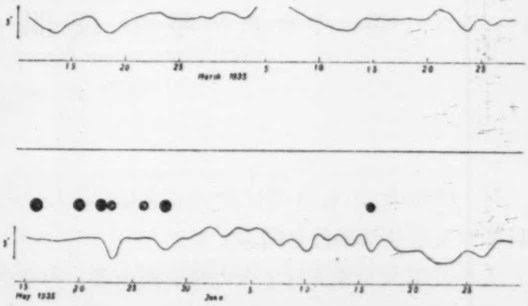

Fig. 7. Variations of magnetic declination. ● : explosion.

The writer learnt from residents at the foot of the volcano that both before and after a violent explosion, radios are quite useless owing to the electric disturbances, which knowledge led him to make observations of antenna-earth currents. The antenna employed for this purpose is 20 m long and stands 5 m above the ground. Observations made it clear that extraordinary antenna-earth currents passed through the earth at the time of the explosions. Records of these antenna-earth currents on May 22, 24, and 26, are reproduced in Fig. 9.

As to the origin of these antenna-earth currents, it may be mentioned that the large quantity of vapour of high temperature that is thrown out by the explosion cools in the upper atmosphere, with consequent electric storms on a very large scale, the volcanic ejecta moreover carry electric charges that collide with one another.

The subject is one that requires much further study. We need to know, for example, the quantity of electric charge possesed by the ejected lava fragments as well as the time-relations between the occurrence of the explosion and the appearance of the antenna-earth currents.

---

[3] Prof. S. Nakamura and Dr. Y. Kato study about the volcanic activities in Japan and the variations in the terrestrial magnetism.

The large quantity of steam emitted by the explosion is condensed in the atmosphere, with the result that however fair the weather before, as soon as the explosion occurs, it rains for from 1 to 2 hours in the vicinity of the crater, and below the steam cloud as it drifts away with the wind. In cold weather, instead of rain, it is snow or hail. Fig. 20 a, b show Asama before and after a violent outburst.

In conclusion, the writer wishes to express his sincere thanks to Professor Mishio Ishimoto for his kind advices and encouragement in the course of these studies.

---

65. 1935年の淺間火山の活動（其の2）

地震研究所 **水上 武**

1. 1935年の4，5月に於いて示した著しい火山活動は6，7月に至つて，やゝ衰へたが，8月に至つて再び活動性を同復した．

大小の噴火で飛び出す火山彈，火山礫，火山灰の中央火口丘に堆積する量は著しく，5月31日の調査では，その堆積量の最も著しい處は，厚さ1米以上に達して居る．その後の噴火で，更にその堆積量を增し，中央火口丘の水準點三個は全くその下に埋沒してしまつた．この事實からも中央火口丘の前掛山に對する相對的上昇を説明する事が出來よう．

2. 火山性微動或は火山に源を有する微小地震が，本年1月の初めから發生した事は，前論文で述べた．1月から8月迄に現はれた此等微小地震に就いて，繼續時間及び發生同數を調べて見た．又7月及び8月に起つた，やゝ大きい爆發に就いて，微小地震の發生と爆發時間との關係を調べて見た結果，爆發20時間前より著しく，微小地震の現はれる事がわかつた．然し，4，5月に起つた爆發との關係に就いては，爆發が相次いで數多起つて居るので，個々の爆發と微動發生同數との精密な時間的關係を見出す事は困難である．

3. 爆發前に噴煙量の著しく少くなる事は土地の人々に依つて言はれて居たので，昨年より1日に數同噴煙量の觀測を行つて居た．その結果，活動期に於いては，噴煙量が著しく變化する事，並に爆發1日前又は4〜5時間前から，爆發に至る迄は噴煙量の著しく少い事が確められた．

4. 簡單な方法で，地磁氣の偏角を昨年10月以來觀測して居たが，3分程度の變化が觀測された．

山麓住民より，爆發前後に，ラジオに雜音が著しく入る爲に，聽取不可能になる事を報告されたので，ラジオ用のアンテナを，その儘使用して，アンテナ・アース・カレントの觀測を行つた．その結果，少くとも爆發後には著しい，カレントの流れる事が判つたが，爆發前に，常に現はれるか，否かは，尙研究の餘地がある．

最後に，常に，貴重な御示敎と激勵とを賜はつた，石本敎授に深謝の意を表すると共に，觀測に或は實地踏查に援助された內堀定市，佐藤邦夫兩氏に感謝の意を表す．

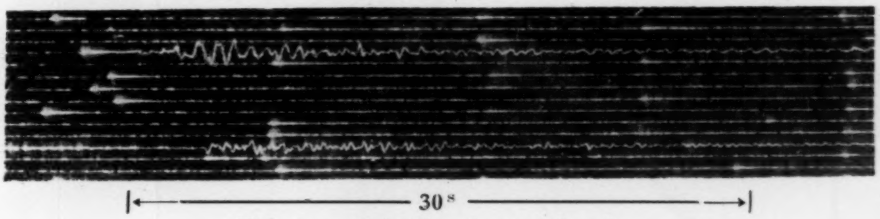

Fig. 8 a. Volcanic micro–earthquake.
(mag. × 120)

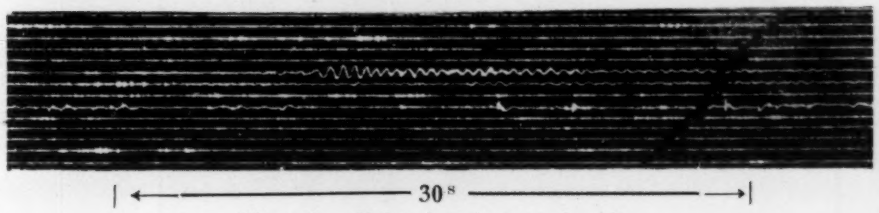

Fig. 8 b. Volcanic micro earthquake.
(mag. × 120)

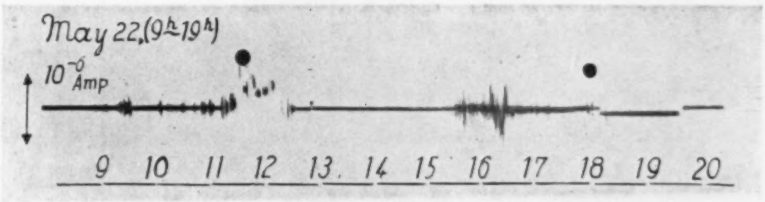

Fig. 9 a. Antenna–earth currents. ● Explosion.

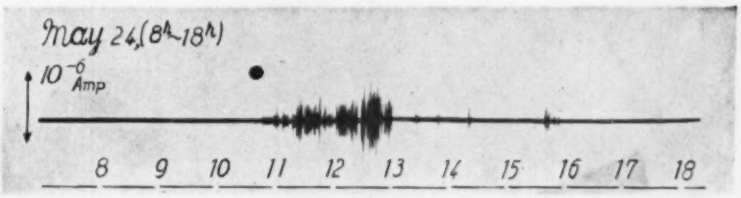

Fig. 9 b. Antenna–earth currents. ● Explosion.

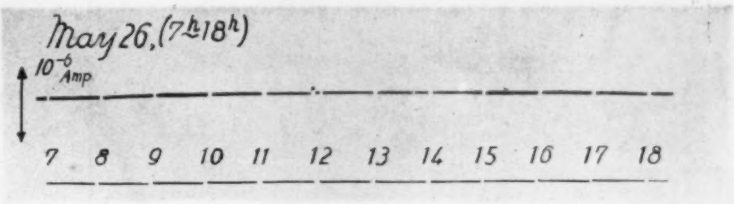

Fig. 9 c. Antenna-earth currents.

（震研彙報 第十三號 圖版 水上）

（震研彙報　第十三號　圖版　水上）

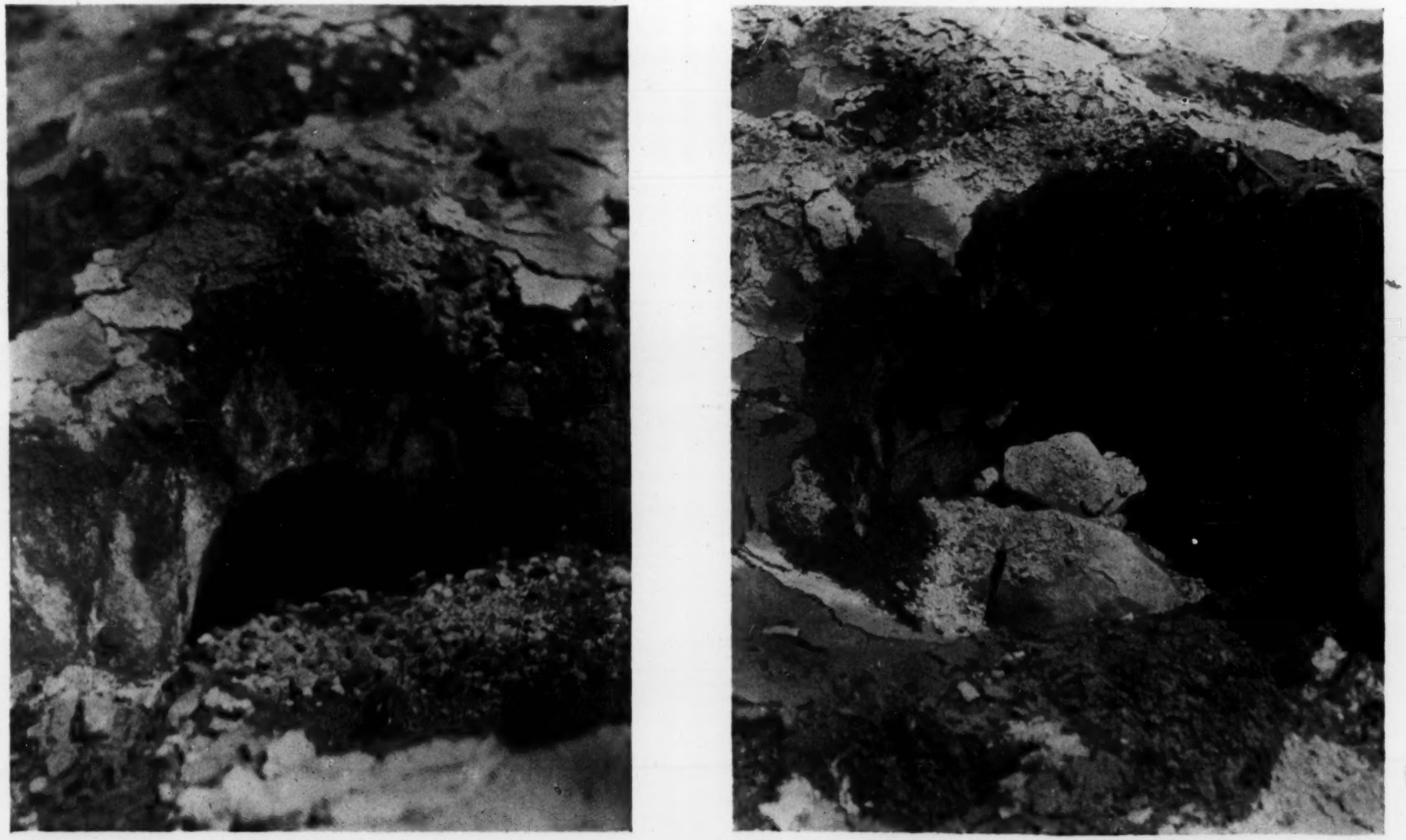

(*Photo. Minakami*, May 31, 1935.)

(a) (b)

Fig. 10. Depression on the snow caused by fall of a bomb. Ash accumulated on the snow.

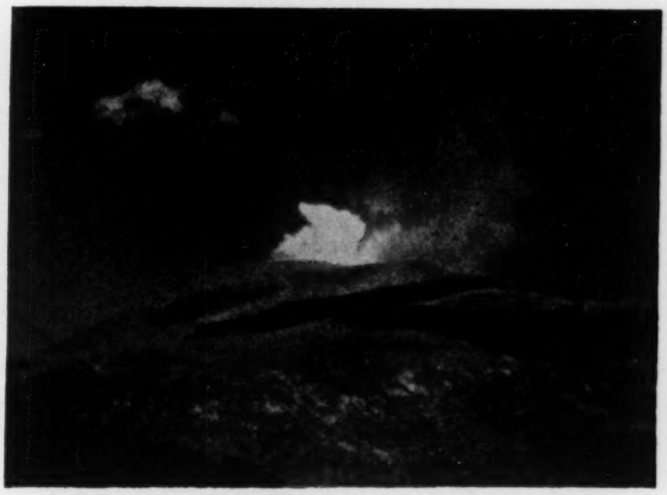

Fig. 11 a.

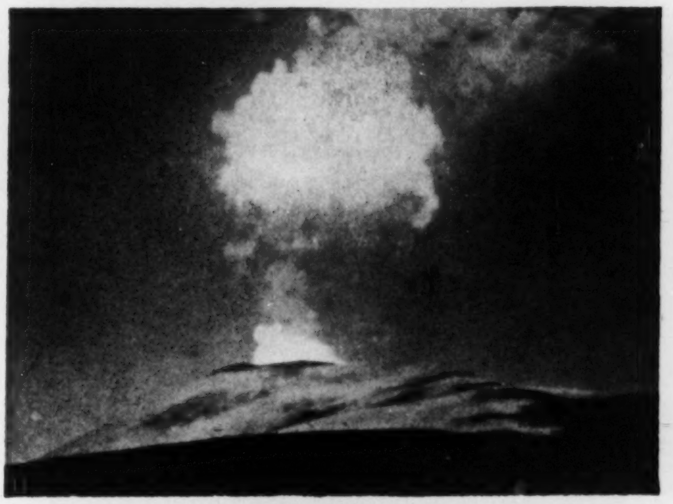

Fig. 11 b.

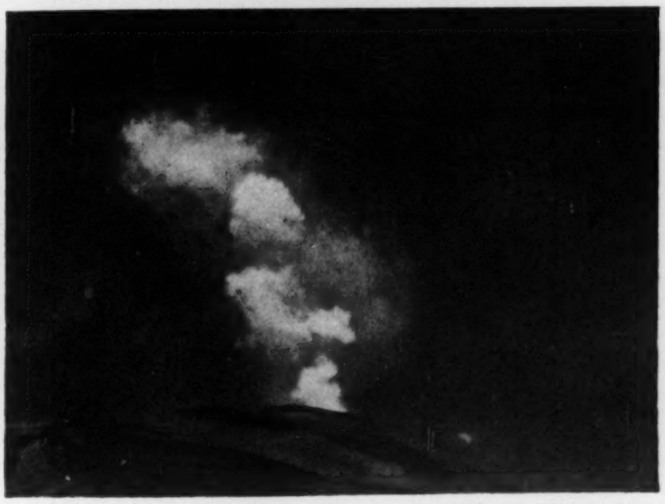

(Photo. Minakami.)

Fig. 11 c.

Fig. 11 a, b, c. Periodic emission of vapour.

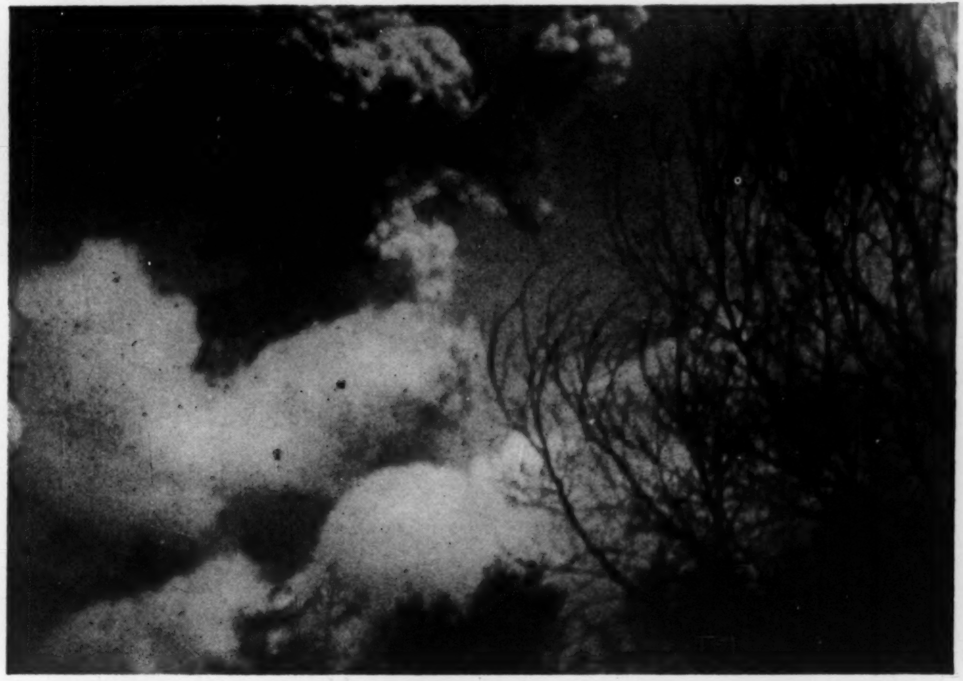

(*Photo. Minakami.*)

Fig. 12. The explosion on May 5 at 9 a. m. as seen from Kutukake.

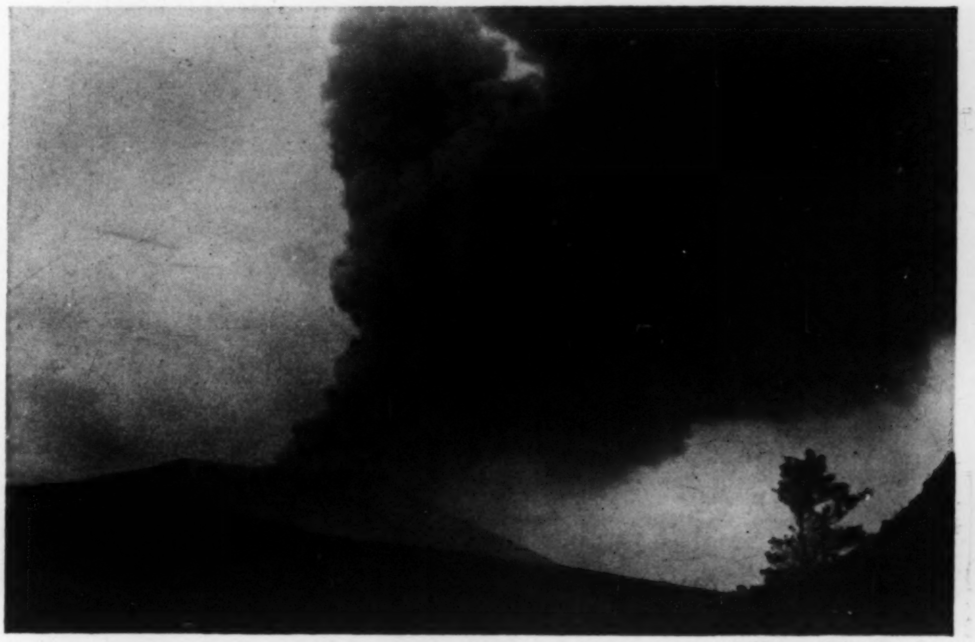

(*Photo. Minakami.*)

Fig. 13. A large emission of vapour on May 5, about 11 a. m.

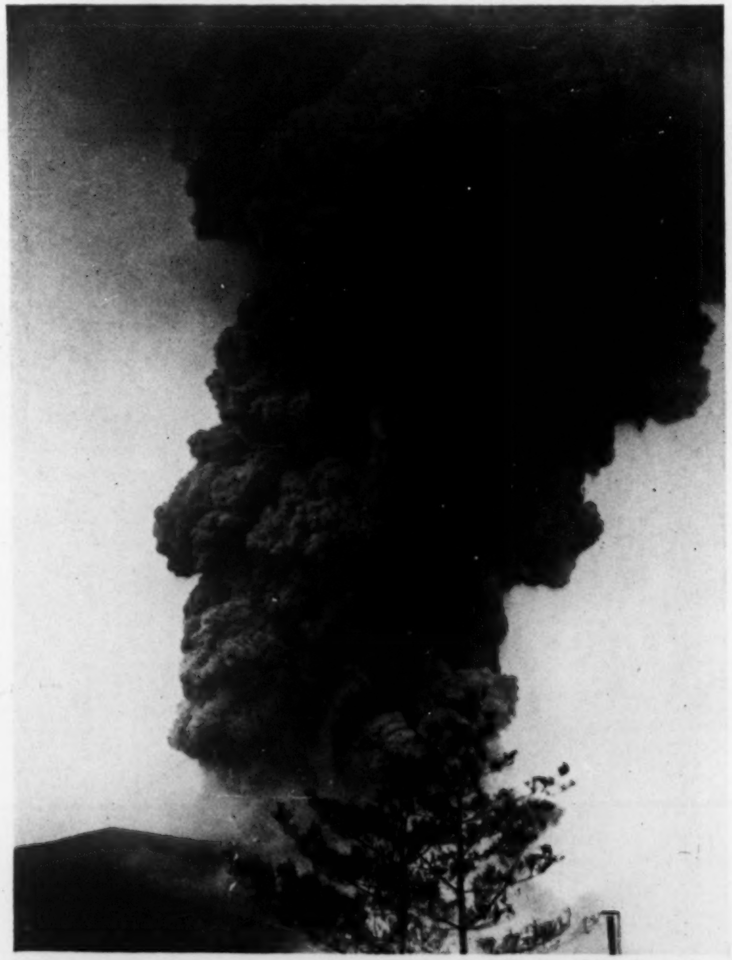

(*Photo. Minakami.*)

Fig. 14. The violent explosion on May 22 as seen from our Observatory.

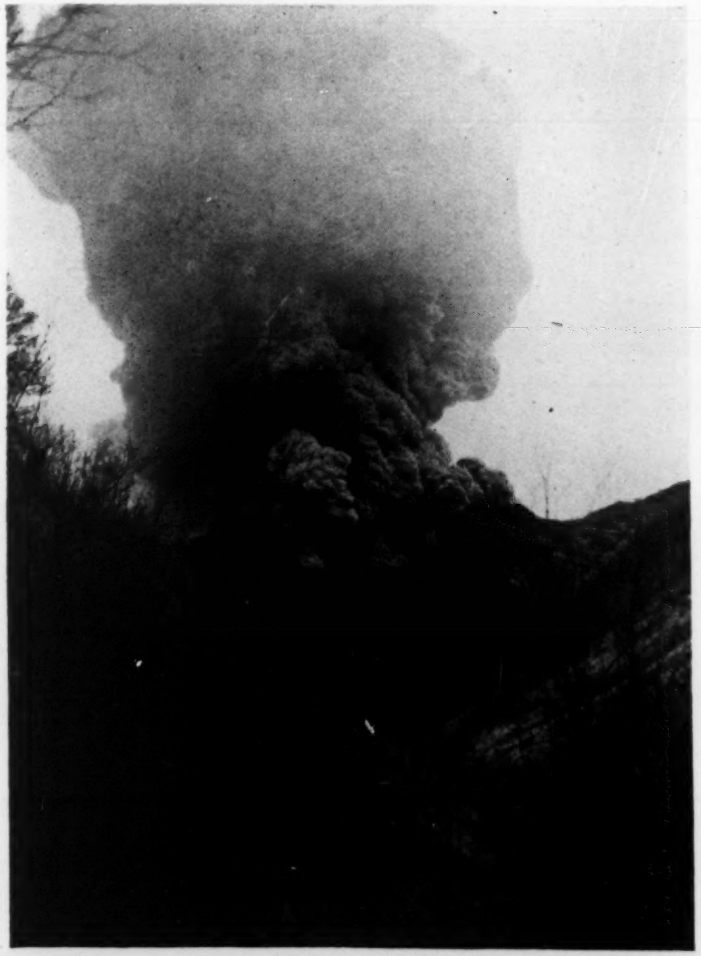

(*Photo. Yomiuri Sinbun.*)

Fig. 15. The violent explosion on May 22 as seen from the west.

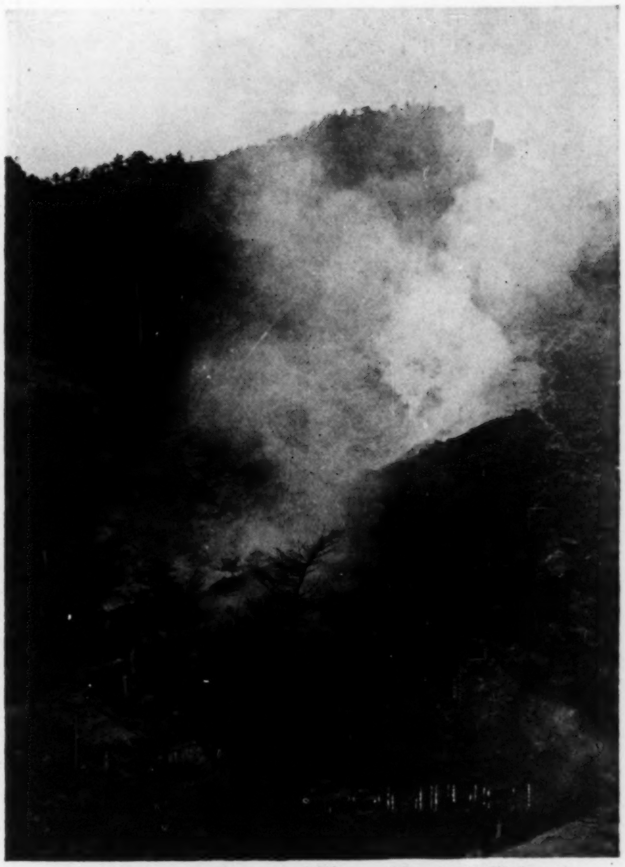

(*Photo. Yomiuri Sinbun.*)

Fig. 16. Field fire extinguished by fall of bombs at the time of the explosion on May 22.

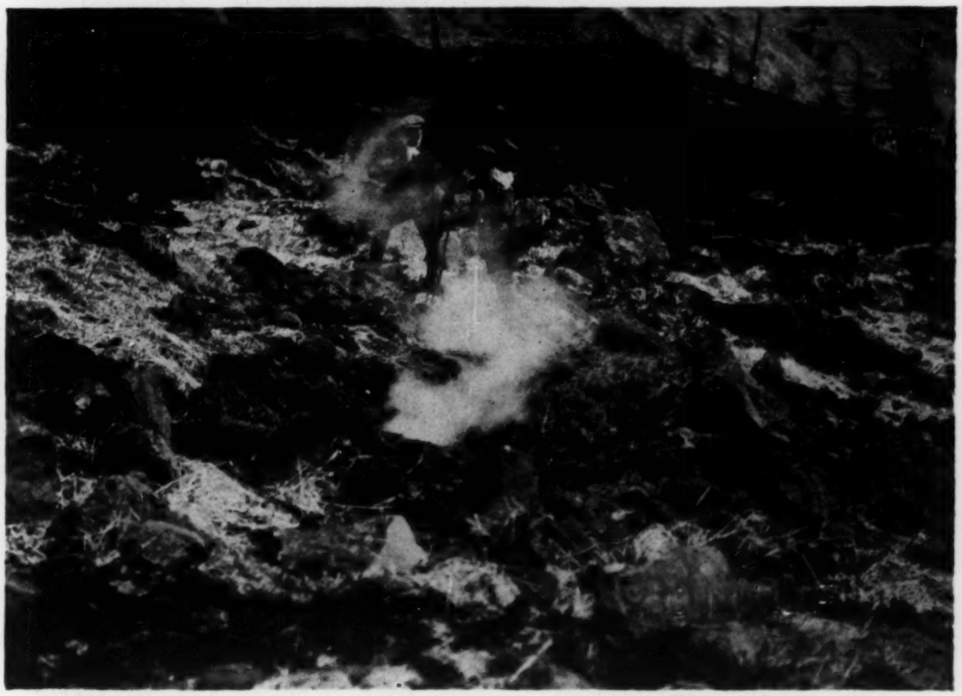

(*Photo. Yomiuri Sinbun.*)

Fig. 17. New bombs ejected by the violent explosion on May 22.

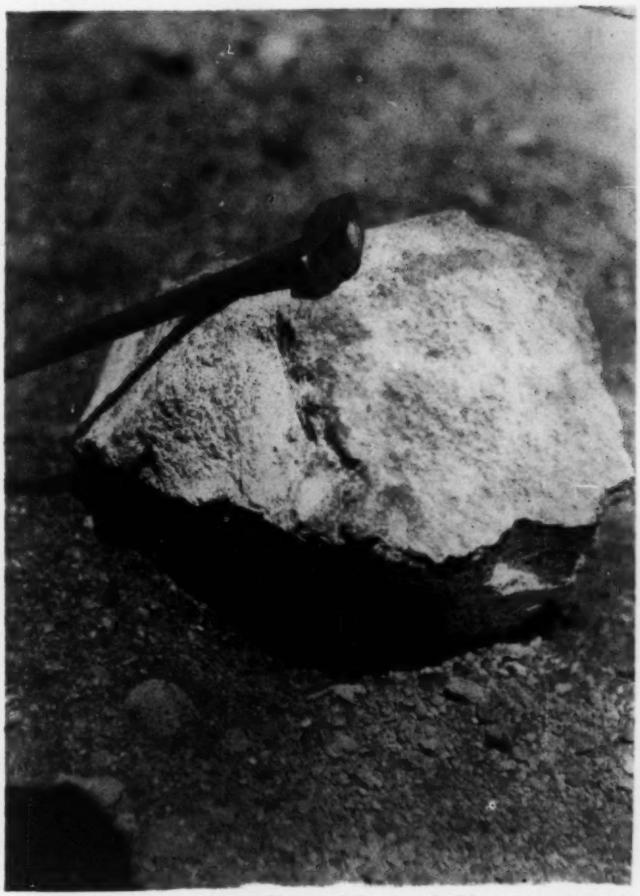

(*Photo. Minakami*, May 31, 1935.)

Fig. 18. A bomb that fell at a distance of 1 km from the crater.

（震研彙報 第十三號 圖版 水上）

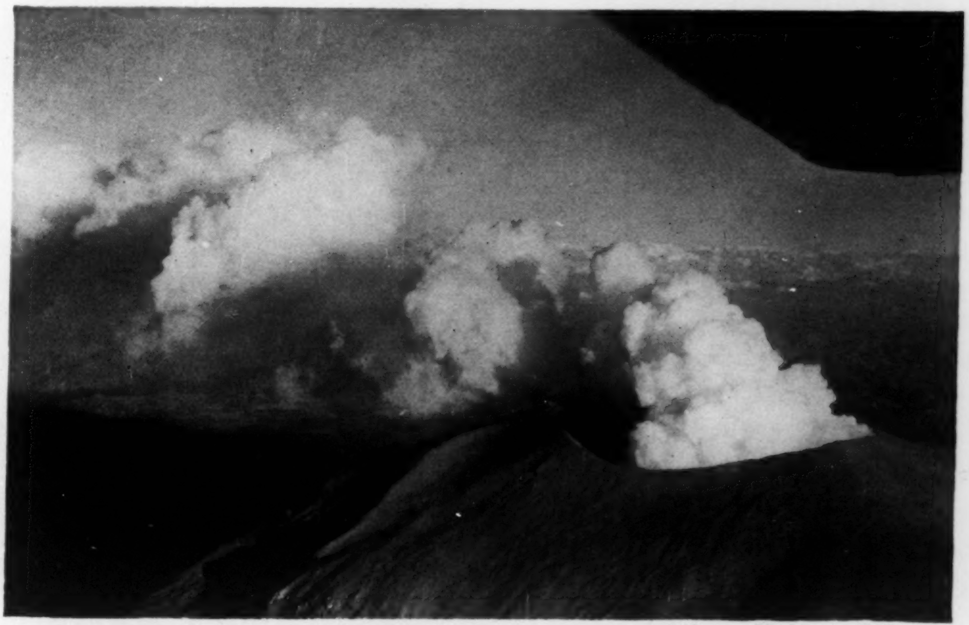

(*Photo. Yomiuri Sinbun.*)

Fig. 19. The crater of volcano Asama as seen from the north-west, at 3 p. m., May 22, 1935.

（震研彙報 第十三號 圖版 水上）

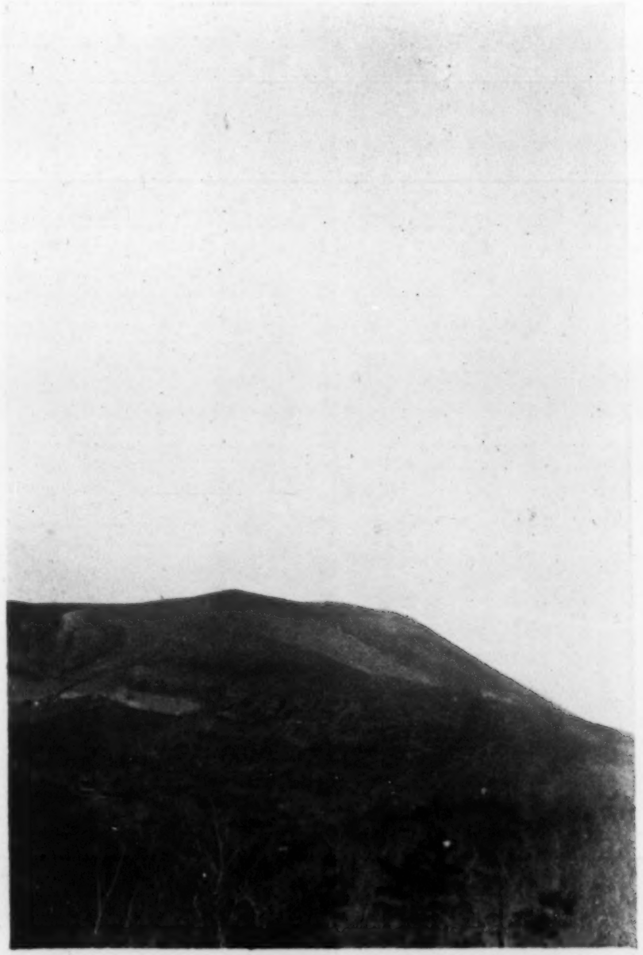

(a)

Fig. 20 a. Asama before a violent explosion.

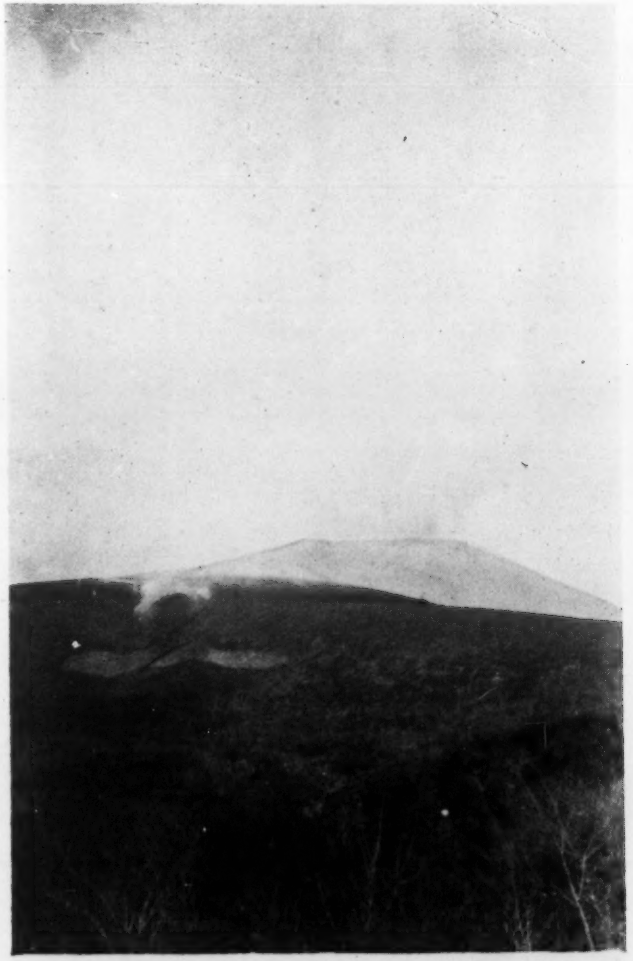

(b) (*Photo, Minakami*)

Fig. 20 b. Asama after a violent explosion. (Snow on the central cone and Maékaké Yama in the background.)

66. 淺間山小爆發の二例に就て

地震研究所 寺田寅彦

（昭和10年9月17日發表 — 昭和10年9月20日受理）

（1） 昭和10年8月4日朝7時半頃淺間山が小爆發をした. 4月以來の顯著な爆發に比べてはミニアチユア的のものであらうが, 偶然その時千ケ瀧グリーンホテルに居合はせてその現象を目撃したから, 色々心付いた點を記錄して參考に供したいと思ふ.

爆發の音は特異なものではあるが一番近い類似の音を求めれば,「はつぱ」卽ちダイナマイトで岩山を崩すときの爆音がそれであらう. 遠くで聞く大砲や近くで聞く瓦斯の爆發などゝは餘程ちがつた音である. 唯一と聲ではなくて, 例へば「ドカン, ドカ, ドカ, ドカーン」とでも形容されるやうな不規則なリズムをもつた爆音であつた. さうしてそれに續いて, 多分反響と思はるゝ「ゴー」といふ餘響が 2~3 秒間聞かれた. その音色は山岳地方に於ける雷鳴の餘響と殆同じものである. 主要爆音の單一でなく數聲に分かれて聞こえたは何かからの反響によるものか, それとも爆發自身がさういふ風に段階を刻んで起つたかを判斷する根據は考へつかないが, 音の音色から考へると, 寧ろ後者であらうと思はれた.

音を聞いてからホテルの屋上の露臺に出て淺間の方を眺めたが山は生憎雲冠を頂いて見へない. 併し上層は靑空であつたから少時待つてゐると, 雲の上緣から稍赤褐色を帶びた灰色のコリフラワー型の噴烟の頭部が現はれ次第に高くなつて行つた. 高く上がるに從つて褐色は消え白味がゝつて來て, 烟塊の膚の粒狀の凸凹が少なくなり, 擾亂運動の減衰が想像された. 仰角 40~50° に達する頃は丁度靈芝などのやうな恰好をした渦環が數葉累積した形になつた. 放電現象に注意したが全く發見することが出來なかつた. 約10分後位から灰が降り初めた. 自分はそれから星野溫泉に下つたが, 同所でも降灰は地面一體を 1~2 mm の厚さに蔽ふ程度に見られた. 8時30分, 卽爆發後約1時間半で旣に降灰は止んだ. 9時頃には最早噴烟の大部分は風に搬び去られて千ケ瀧の上空には見られなかつたが, その代りに蒼白い煙草の煙のやうなものが薄い卷雲のやうになつて風に從つて流れて行くのが見えた. その色と速度から見て卷雲ではなく淺間の噴烟であることは確實である. この薄烟が恐らく火山內部から出る固有の瓦斯狀噴出物であつて, 爆發當初に出る灰砂は勿論として水蒸氣の大部分は火口

內表層の破壞の產物であらうと想像された．もしさうでなければ爆發後の噴烟も水蒸氣を凝縮させて雲狀の噴烟として流れる筈である．兎に角此事實は極めて注意すべきもので今後の問題を提供するものと思はれる．

星野溫泉の池に灰砂の落下するのが丁度小雨が降つてゐるやうに見えたが，降灰の終つた頃氣が付いて見ると池の水が平常とちがつて著しく乳白色を呈してゐた．

降灰中星野溫泉旅館構內で園丁が樹木の手入れをしてゐたが，降灰中も平氣で仕事を續けてゐた．千ケ瀧星野間を往來してゐる人達の中にはしきりに眼をこすつて居るものもあつた．

星野に降つた灰砂を採集して，持合せた双鏡顯微鏡（×20）で覗いて見た．砂粒はいづれも多稜形の岩石破片を心核として，その表面に海綿狀の灰質被覆物を被つてゐる．（附圖寫眞 A 參照）．心核（寫眞 B）には黑色のが多いが眞白いのも交つてゐる．被覆物は杉葉形或は霧氷形に心核表面に集積してゐて，極めて脆く剝落し易い．それでかういう灰砂の標本は試驗管や罎に入れて運搬すれば原形は失はれてしまうのである．特別な方法で採集し保存することが必要であると思はれる．寫眞に示した標本も注意して運搬したに拘らず杉葉狀被覆の尖つた部分が剝落して原形を損してゐるやうである．

如何にして此樣な被覆物が出來たかは今後硏究さるべき興味深き問題であらうと思はれる．併し大體に於て霧氷の沈積に類した過程で生じたであらうといふ事はその形態上の肖似から暗示される．唯如何にして微細な灰粒子が互に膠着しつゝ集積したかといふことに關して色々な物理的化學的，特に膠質化學的問題が殘されてゐることゝ思はれる．さうして多分この問題は或程度迄實驗室內で實驗的に解決さるべきものと思はれる．

以上は現場に於ける觀察の大要であるが，なほ以下に若干補遺的の事項を追記して參考に供したいと思ふ．

噴烟の頭の上昇速度は自分の豫想してゐたよりは緩徐なものであつた．自分の掌の幅と比較して視角と地圖から知られる距離と頭で數へた秒數とのデータから概算した上昇速度は每秒 50～60 m の程度であつた．勿論これは山の頂上數粁昇つた後に於ける速度であるから火口を出たばかりの速度はこれの數倍であつたことゝ想像される．

烟の達した垂直の高さに就ては，生憎當時上層の風向が山から自分の方に向いてゐた爲に目測に不利な狀況であつたが大體の仰角と距離から判斷して約 7～8 km 程度であつたかと思はれる．

前述の如く噴烟柱の外側の層の小凹凸は擾亂渦動の强度を示すものと思はれる．噴出速度が大なれば大なる程渦動の速度も增すと同時に渦環や渦柱の大きさが減じてその數を增すであらうといふ事は他の場合から類推される．この渦動の細かさを統計的數量的に決定することが出來れば有益であらうと思はれるが，その一つの方法として次のやうなことが考へられる．

噴烟柱の寫眞の乾板に就て，噴烟の種々の高さの部分に引いた水平線に沿ふてミクロフオトメーターの自記曲線を求めれば，各部分につき一つの不規則な波狀曲線が得られる譯である．この曲線に就て統計的分析法を適用し，もし卓越した週期があらばその週期を決定することが出來るであらうし，又週期は求め難いとしても地磁氣記曲線から擾亂度を求める方法，例へば小野澄之助氏[1]の方法を利用して一種の統計的數値を決定することも出來るであらう．又大山義年氏[2]が砂粒の混合度を測定するに用ゐた方法をこの場合に適用することも出來やうかと思ふ．勿論寫眞を用ゐる限りその照射度，現像度，乾板の種類によつて結果が區々になるであらうし．又當時の天候や時刻によつても影響されるであらうが，それ等の點を十分に考慮した上で研究を重ねたら，少くも一つの有益な參考資料となるべき結果が得られるのではないかと思はれるので，兎も角も一つのヒントとして玆に附記する．

降灰の特殊な構造の生因に就ても色々のことが考へられる．第一には中核の岩石細粒とそれに附着した灰の微粒との間の相對速度が問題になる．それなしには此の如き附着集積は起らないのである．第二には石と灰，又灰と灰の粒が相觸れたときに兩者を膠着せしめる作用が必要である．こゝに一つの膠質學的な問題がある．この際に水蒸氣或はそれが粒子表面に吸着された薄層の作用が問題になるであらう．第三には粒子の荷電が問題になる．大きな砂粒と微細な灰粒とで反對の荷電をもつといふことも不可能ではない．第四には强烈な短音波が空氣中に浮游する微塵 aerosol を凝集膠着させる作用[3]のあることが知られてゐるので此のやうな效果の可能性も考慮されなければならない．又一方では灰粒表面が高溫の爲に熔融狀態にあるといふ可能性も遽に否定することは出來ない．

要するにこの降灰の特異な構造は極めて多様な研究題目を提供するものであつて，それ等を追究すれば火山噴出の機構に關して意外な知識の端緒を得るかも知れないと思つたので，後日の參考の爲に所見を記しておく次第である．

---

[1] S. Ono, *Annual Rep. C. Met. Obs. Jap.*, “Magn. Obs. f. 1916”; *Jap. Journ. Astr. Geophy.*, **3** (1925), 1.

[2] 大山義年 理化學研究所彙報 **14** (1935), 570.

[3] O. Brandt u. H. Freund, *ZS. f. Phy.*, **94** (1935), 348.

（2） 8月17日午後5時頃にも爆發があつた．此日のは8月4日のよりも或意味で强大であつたかと思はれるが，その音響傳播に關する異常に就て注意すべきものがあると思はれるから，序に所見を記しておき度いと思ふ．

此日の爆發は沓掛千ケ瀧方面からは雲に遮られて見られなかつたのみならず，その音響も極めて微弱にしか聞かれなかつた．當時自分は星野溫泉別館の南向きのベランダで顯微鏡を覗いてゐたが全く音響にも氣波にも氣付かず，屋內にゐた家族も同樣であつた．併し本館にゐた水上武君は氣波らしいものを建具の振動によつて感じたさうである．又星野別莊地の北部の丘上の家では爆發の音を聞き又爆發の最初の音に引續いて岩山の崩れ落ちでもするやうなゴーゴーといふ音がしばらく聞こえたさうである．又グリーンホテルの從業員の多くは爆音にも氣付かずに居たしその後の轟音も知らなかつたさうで，この點8月4日のと著しく趣を異にしてゐる譯である．

一方では又北輕井澤法政大學村で偶然この日の爆發をその最初から目擊した友人松根豊次郎君の談話によると同地で聞かれた爆音は相當强く多數の人の注意を喚起する程度であつたさうである．同地でも爆發當時淺間頂上は低い雲層を被つてゐたが，その層の上に噴烟の上るを發見し間もなく爆音を聞いたさうである．噴烟の頂上の仰角をその當時のこの觀測者の記憶を呼出して貰つて推算した處では矢張 10 km 位のものであつたと思はれる．

烟柱には放電を伴ひ，又巨大な岩塊の投げ上げられるのも二三見えたさうである．

又爆發後間もなく淺間を蔽つてゐた雲帽が消散して山の形がはつきり見えるやうになつたさうで，これは偶然かも知れないが或は噴火の影響かも知れないから今後の注意を要すると思はれる．

舊輕井澤では稍鈍い爆音を聞いた人がある．

兎に角この日の音響の聞こえた程度の分布が，僅に 10 km 以內の範圍で上記の如く區々であるのは注意すべき現象であつて，後日の硏究を待つて明にしなければならない問題を提供するものと思はれる．從來の所謂異常聽域と同種の現象と考へるべきか，或は異種のものと考へるべきかも疑問である．

(A)

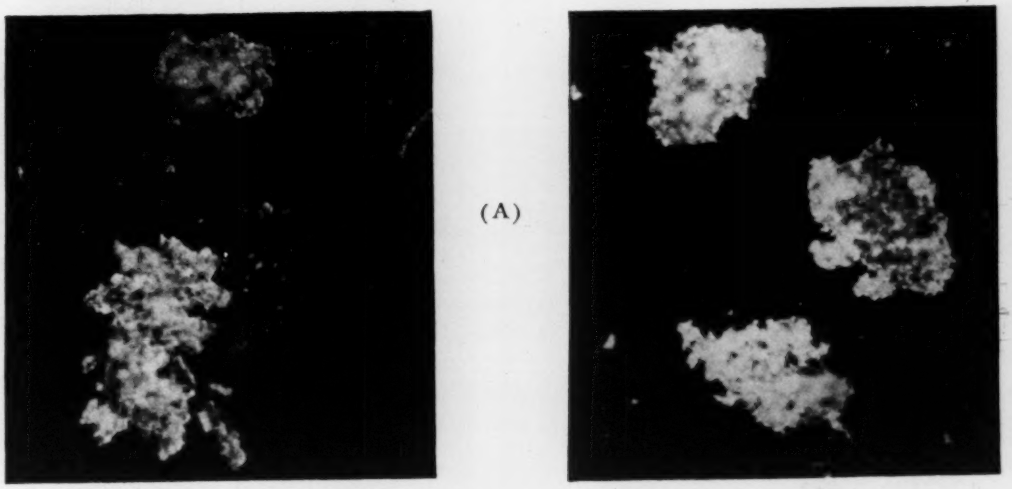

×30 ×30

(B)

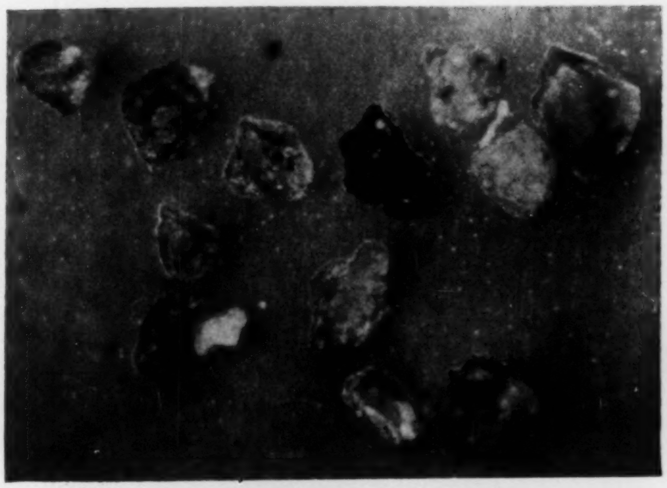

(A) の表面の灰を洗ひ落した心核 ×30

(C)

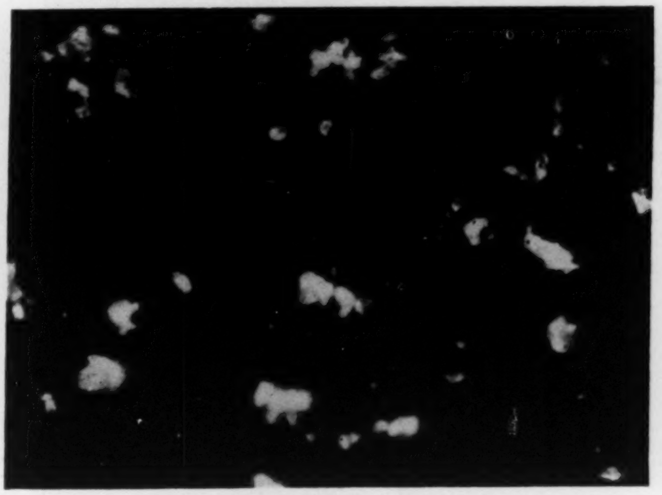

(A) の表面から洗はれた灰粒 ×200

（震研彙報 第十三號 圖版 寺田）

66. *On Two Cases of Minor Eruption of Mt. Asama.*

By Torahiko TERADA,

Earthquake Research Institute.

Two cases of minor eruption of Mt. Asama are described. A sample of ash collected on the occasion of the eruption on Aug. 4, 1935, consists of compact nuclei of rock fragment, a few tenth of mm in diameter, which is covered with a spongy mantle of aggregated fine ash particles. Possible causes of the origin of such a structure are suggested. As for the eruption of Aug. 17, 1935, an abnormal distribution of the intensity of audible sound within a narrow range of 10 km from the crater is described.

---

67. *The Oti Graben in Southern Noto Peninsula, Japan.* (*Part 2*).

By Yanosuke OTUKA.

Earthquake Research Institute.

(Read March 20, 1934—Recieved Sept. 1935.)

4. Stratigraphy of the Environs of the Oti graben.

In this chapter, the stratigraphy of the environs of the Oti graben is described. The writer observed the following stratigraphic succession in this district:–The basal complex, which is the marble bearing gneiss and the granite near Sekidosan (石動山), is intruded by andesite and its derivatives that are overlain by the Neogene Tertiary beds.

For convenience, the writer has divided this district into three parts, namely, the southeastern part, the southeastern wall, and the northwestern part, all of the Oti graben.

The southeastern part consists of the Sekidosan mountainland and the west coast of Toyama bay. Although the stratigraphy of this province has been studied by MOCHIZUKI,[1] YAMANOUCHI,[2] and ESASHI,[3] only the former has so far published his work on the stratigraphic divisions with some brief remarks, the papers of ESASHI and YAMANOUCHI being as yet unpublished. In this paper, the writer, in order to avoid undue profusion of stratigraphic terms, will restrict himself as far as possible to those that have been adopted by previous authours, resorting to new ones only when absolutely necessary. The following stratigraphic succession is observed in this province in descending order:–Alluvial deposits, the Sazanami terrace deposits, the Himi sand beds, the Yabuta silt beds, the Yositaki mud beds, the Domi sand beds and andesites, and the Kosidi granite and gneiss.

The province of the southeast wall of the Oti graben includes the major parts of the southeast wall of the Oti graben, and the Sakiyama peninsula between the South Nanao bay and the bay of Toyama. The stratigraphic succession in this province as observed, in descending order is:–Alluvial deposits, the Akasaki and the Sakiyama terrace deposits, the Nozaki silt beds, the Entunagi mud beds, the Iori sand beds, the Domi conglomerate beds and the andesites, and the Kosidi granite and gneiss, besides which are the talus deposits and fanglomerates derived from the southeast scarp of the graben. The Nozaki and the Entunagi beds are exposed in the eastern half of Noto(-zima) Island.

---

[1] K. MOCHIZUKI, *Geogr. Rev. Japan*, **4**, (1928), (in Japanese).
[2] H. YAMANOUCHI, *Grad. Thet. Geol. Inst., Imp. Univ. Tokyo*, (1928).
[3] S. ESASHI, *Grad. Thet. Geol. Inst., Kyoto. Imp. Univ.*, (1925).

The northwestern part of the Oti graben consists of the Tumuki shell beds, the Kozima sand beds, the Wakura, Akaura, and Nanao beds, the last four of which are Neogene. The basal complex of this province are the andesite mass and its agglomeratic mass and gneiss breccias. The Hanoura (半ノ浦) beds, so-called by T. OGAWA,[4] in Noto (-zima) Island is a deposit contemporaneous with the Nanao beds.

Beside these beds, there are exposed at Hukami (深見), near Taduruhama (田鶴濱), loose sand and silt beds, which may be contemporaneous with MIMURA's[5] Takasina beds. The lastnamed, believed to be younger Neogene, are underlain by the Wakura beds with unconformity near Hukami. Basal andesite masses are exposed at Tadatu (直津) in Nisiminato-mura, Wakura, the Akakura mountainland, and Hosoguti. Gneissic breccias are exposed south of Yosikawa, at the foot of the Bizyosan fault scarp.[6]

Detailed stratigraphy.

a. The southeast part of the Oti graben.

The stratigraphy of the southern part of this province was studied by ESASHI, MOCHIZUKI, and YAMANOUCHI. ESASHI's manuscript, which is preserved in the Kyoto Imperial University, has been referred to in part by Prof. J. MAKIYAMA.[7] MOCHIZUKI's opinion has been published in his papers. YAMANOUCHI's paper, which is in manuscript, and which is now preserved by the Tokyo Imperial University, has been referred to in part by MOCHIZUKI.[8]

MOCHIZUKI,[9] has worked out the following stratigraphic succession of strata in descending order: the Himi, Nadaura, Yositaki, Kumabuti, and Ketagata beds. According to J. MAKIYAMA,[10] ESASHI's stratigraphic succession consists of three series, namely, upper, middle, and lower. The lower, called the Yokawa series, is a thick complex of tuffaceous mudstone and sandstone. The middle, called the Yabuta series, be contemporaneous with the Omma series near the city of Kanazawa (金澤).

---

4) T. OGAWA, *Expt. Text. Geol. Map. Japan* "Wajima" sheet, 1: 200,000, (1908).

5) S. MIMURA, *Grad. Thet. Geol. Inst., Kyoto Imp. Univ.*, (1928).

6) K. MOCHIZUKI, *op. cit.* (1928).

7) J. MAKIYAMA, *Chikyu*, **14** (1930), (in Japanese).

8) K. MOCHIZUKI, *op. cit.* (1928).

9) K. MOCHIZUKI, *op. cit.* (1928).

10) J. MAKIYAMA, *op. cit.* (1930).

The lower part of the Yabuta series is the Yabuta tuffaceous fine sand and silt beds, containing *Thyasira nipponica* YABE and NOMURA, while the upper is the Izumo pumiceous sand with many shallow-sea mollusca. The Yabuta series is concordant with the Yokawa series in the north of Yabuta village, but discordant with the Yokawa, west of the town of Himi (氷見). The fossils from the Yabuta series is a shallow-sea fauna found west of Himi. The upper series is called the Kubo series.

The writer observed the following stratigraphic succession in this province (Table II). Fig. 11 is a geologic map of this district.

Table II.

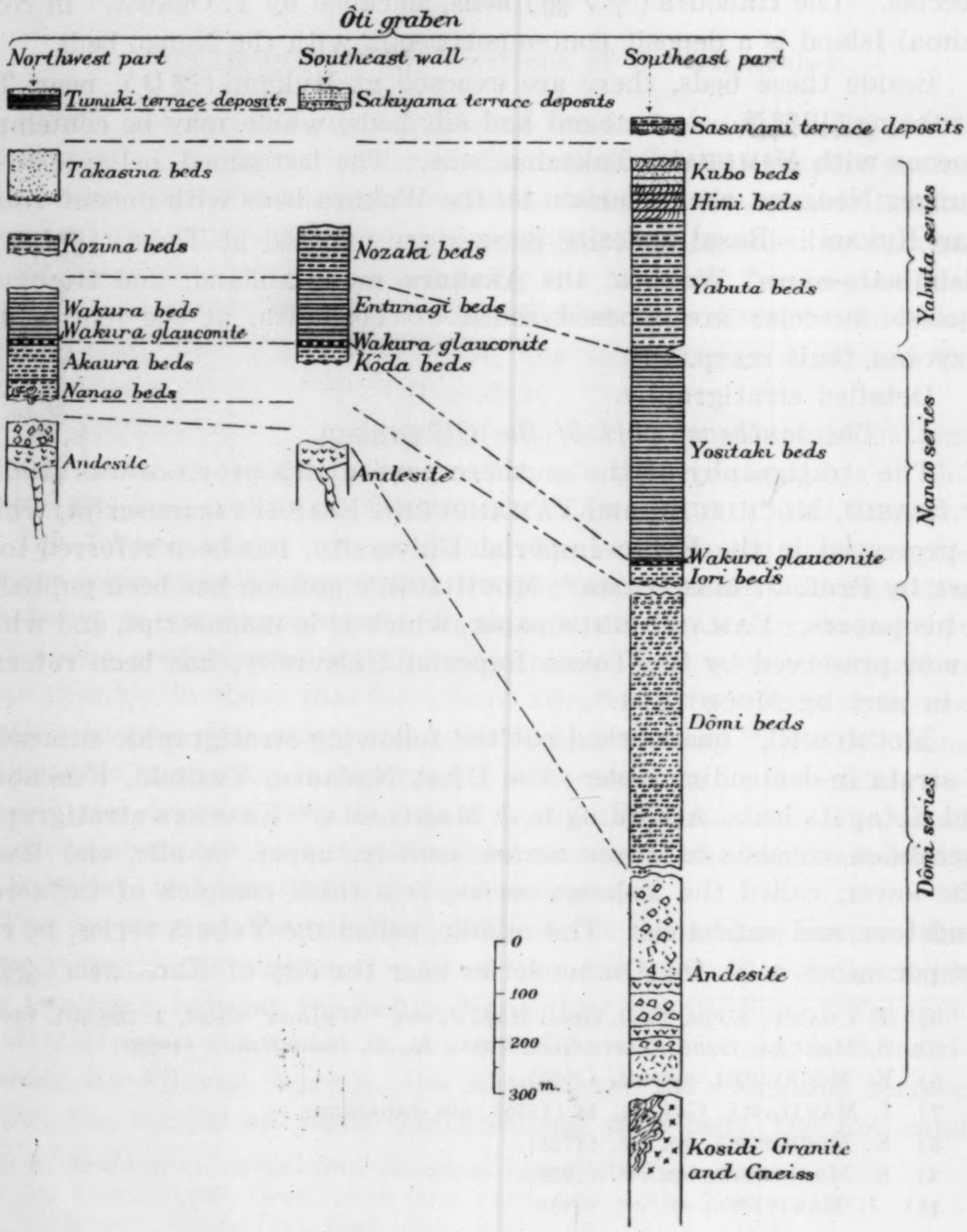
Ōti graben
Northwest part
Southeast wall
Southeast part
Tumuki terrace deposits
Sakiyama terrace deposits
Sasanami terrace deposits
Takasina beds
Kozina beds
Wakura beds
Wakura glauconite
Akaura beds
Nanao beds
Andesite
Nozaki beds
Entunagi beds
Wakura glauconite
Kōda beds
Andesite
Kubo beds
Himi beds
Yabuta beds
Yabuta series
Yositaki beds
Nanao series
Wakura glauconite
Iori beds
Dōmi beds
Dōmi series
Andesite
Kosidi Granite and Gneiss
0
100
200
300 m.

The Sazanami terrace deposits.

Of the many coastal terraces along the west coast of Toyama bay, the writer's Sazanami terrace, about 60~70 m above sea-level, is developed near Sazanami (佐々波) in Kitaoonomi-mura, Isikawa prefecture (Fig. 11). It extends from Musizaki (虫崎), north of Sazanami, to the environs of Hanazono. The material of the terrace deposits, which rest horizontally on Tertiary bed rock, consists mostly of weathered sand and rounded gravels of varying thicknesses, of which the white fine weathered quartzite pebbles which are often mistaken for pumice, are characteristic of these deposits.

Field observations (Sazanami terrace deposits) (Fig. 11, [Plate]).

Between Hanazono and Kurosaki.

Loc. 1. Gravel beds, unconsolidated, rest on dark greyish mudstone beds with unconformity. Gravel beds almost horizontal; varying in thickness, but generally about 4 m.

Loc. 2. Thickness of gravel beds gradually decreases from loc. 1 to loc. 2. Size of gravels small, about 0·5 cm diameter; white pumice like weathered quartzite grains visible in reddish-brown fine sands and gravels. Gravels unconsolidated, resting on bed rocks with unconformity. Surface of terrace accords with depositional surface of gravel beds.

Loc. 3. Kurosaki. No gravel beds here, but reddish-brown soils, in which white quartz grains are visible, are developed. Height of terrace near Kurosaki about 60~70 m, as in loc. 1 and 2.

Between Simosazanami and Musizaki.

Loc. 4. Fine-grained sand and gravel beds about 3 m thick, which rest on bed rock with unconformity, form surface of terrace about 60~70 m above sea-level. These gravels about 1 cm diameter. White pebbles of weathered quartzite found in these beds. Surface of terrace very flat with rice fields on them. Some small mounds, about 2 or 3 m high, scattered on terrace surface.

Loc. 5. On small road descending from surface of terrace to Musizaki (loc. 6), no rocks exposed. Similar terraces formed near Kamisazanami, Musizaki, and Iori on west coast of Toyama bay. The terraces, 60~70 m high, near Oonoki in Kitaoonomi-mura and Yamasaki in Sakiyama-mura may be contemporaneous with the terraces near Sazanami, Hanazono. Sazanami terrace deposits everywhere barren of fossils.

The Himi beds.

The Simazaki beds.

The Simazaki beds may be either ESASHI's Izumo beds or part of the Himi beds of MOCHIZUKI. In this paper, the writer treats the Simazaki beds as a part of the Himi beds. The Simazaki beds are alternations of sand and fine-sand bed, containing many fossil mollusca, bryozoa, and sponges. These beds are exposed on wall of hill scarp behind Simazaki village, in Zyunityo-mura.

Sand beds pumiceous, and sometimes crossbedded; pumice of these beds mostly andestic tuff.

Table III. Fossils from the Himi beds.
(Simazaki) (Otuka, 1935).

Puncturella nobilis (A. ADAMS)
Puncturella hirasei OTUKA n. n.
Umbonium akitanum SUZUKI
Homalopoma amussitata (GOULD)
Tachyrhynchus venustellus (YOKOYAMA)
Antiplanes kamchatica DALL
Navicula boucardi (JOUSSEAUME)
Arca amicula YOKOYAMA
Glycymeris aff. *rotunda* (DUNKER)
Limopsis tokaiensis YOKOYAMA
Pseudamussium intuscostatum (YOKOYAMA)
Chlamys swiftii etchegoini (ANDERSON)
Patinopecten tokyoensis kimurai (YOKOYAMA)
Patinopecten plebejus YOKOYAMA
Anomia sp.
Ostrea sp.
Lima subauriculata MONTAGU
Astarte hakodatensis YOKOYAMA
Astarte alaskensis DALL
Venericardia ferruginosa (A. ADAMS et REEVE)
Venericardia ferruginea (A. ADAMS)
Venericardia nakamurai YOKOYAMA
Corbicula sp.
Lucina acutilineata CONRAD
Cardium sp.
Macoma aff. *tokyoensis* MAKIYAMA
Tellina salmonea (CARPENTER)
Aloidis venustus (GOULD)
Myadora fluctuosa GOULD
Thracia transmontana YOKOYAMA
Waldeheimia sp.

The writer's Simazaki fauna, the fauna of Simazaki beds, is a shallow-sea fauna, influenced by cold current.

Table III gives the species collected from the Simazaki sand beds. From this list, the writer concludes that the Simazaki beds are not older than middle Pliocene in age, and not younger than earliest Pleistocene.

Field observations:

Near Simazaki, Zyunityo-mura. (Fig. 12)

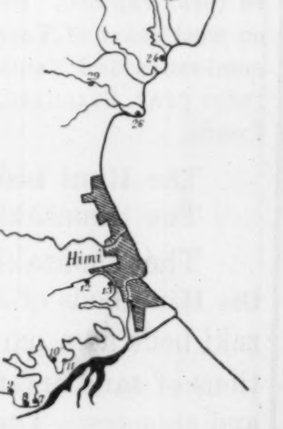

Fig. 12.

Zyunityo. Loc. 7. Alternation of sand and fine sand, strike about N60°E, dip about 3°~5° SW. Fossiliferous, calcareous, coarse grained.

Loc. 8. Fossiliferous sands exposed, on middle part of cliff wall, back of Simazaki village; stratification almost horizontal.

Loc. 9. Alternation of coarse-grained sand and fine sand; strike about N15°~20°E, dip 3° ES; barren of fossils.

Loc. 10, 11, 12. Consolidated coarse-grained sand, calcareous.

Loc. 13. Greyish-blue sand, fossiliferous, differing slightly from typical rocks of Simazaki shell beds.

The Yabuta beds.

ESASHI's Yabuta beds are typically exposed on a hill scarp at Yabuta, Ao village, in Yabuta-mura. A part of MOCHIZUKI's Nadanoura beds are in the Yabuta beds.

These beds may be seen between Ozakai (大境) (in Unami-mura) through the villages of Unami, Yabuta, and Ao. The coasts of these villages are collectively called Nadanoura (灘浦).

The Yabuta beds consist of bluish grey silt beds, the sandy shale of some Japanese authors; the stratification consisting of thick bed, in which calcareous nodules are often contained in the bedding planes. *Thyasira nipponica* YABE et NOMURA is a characteristic and commom species in these beds.

The upper limit of the Yabuta beds is not exposed in this province. According to MOCHIZUKI and ESASHI, the Yabuta beds are overlain by the Himi (Izumo) beds with conformity. The lower limit of the Yabuta beds is underlain by the upper Yositaki beds. According to J. MAKIYAMA,[10] Yabuta beds are underlain by the Yokawa (the writer's Yositaki) series with erosional unconformity southeast of the town of Himi. MOCHIZUKI has reported the following fossil mollusca from the Yabuta beds (Table IV).

Table IV. Fossils from the Yabuta beds
(After MOCHIZUKI)

Nuculana pernuloides (ADAMS) (DUNKER)
Nuculana ramsayi (SMITH)
Nuculana sp.
Yoldia japonica PILSBRY
Thyasira nipponica YABE et NOMURA
Lucina acutilineata CONRAD
Petricola aequistriata SOWERBY
Tellina (Arcopagia) siamensis ? MARTENS
Zirfaea subconstricta (YOKOYAMA)
Dentalium sp.
Natica janthostoma DESHAYES

Field observations: (Fig. 11, 12.)

Ozakai (in Unami-mura, Himi-gori, Toyama pref.)

Loc. 14. Conformable stratigraphic relation exposed on sea cliff. Yabuta beds distinguished from uuderlying Yositaki beds by color of weathered surfaces of these two formations.

Loc. 15. Boundary of Yositaki and Yabuta beds. The latter strike about N40° ~45°E; dip about 5° SE.

Loc. 16. Exposures of Yabuta beds numerous in Ozakai.

Loc. 17. Strike about N40°E, dip 10° ES. Silt beds; fossiliferous.

Loc. 18. Strike and dip more or less disturbed; northern part of this locality N80°E: 15°SE; but southern N35°W: 5°NE. Fossiliferous coarse grained sandstone.

Loc. 19. Strike N55°E, dip 10°SE; Strike and dip south of loc. 19 take general trend N35°E.

Loc. 20. Yabuta beds exposed.

Loc, 21. Upper Yositaki beds exposed.

Unami

Loc. 22. Yabuta beds exposed on sea cliff; more or less sandy, strike N35°E, dip 7°SE; Good exposures.

Loc. 23. Yabuta beds extend to summit of this mountain spur.

Yabuta

Loc. 24. Type locality of Yabuta beds.

Loc. 25. Boundary of Yabuta and Yositaki beds exposed here.

Loc. 26. Yubuta beds exposed.

The Yositaki mud beds.

The Yositaki beds, so named by MOCHIZUKI, are black mud beds exposed near Yositaki village. These beds are overlain by the Yabuta beds with conformity in the northern part of this province but with unconformity in the southwestern part. In this paper ESASHI's Yokawa series, and parts of MOCHIZUKI's Nadanoura and Yositaki beds are included in the Yositaki mud beds.

The present writer has subdivided the Yositaki beds into three parts, namely, the upper Yositaki, the Nakada pumice bed, and the lower Yositaki.

The upper Yositaki beds, which are overlain by the Yabuta, are typically exposed at Sugata in Nakada-mura. The weathered surface of these beds, which consists of dark greyish or black mud, are coloured with some brown or yellow substance. These beds are barely distinguishable from the lower Yositaki beds. Their stratification, although indistinct, is massive. The upper Yositaki beds are barren of fossils except certain very small white objects, as figured in fig. 218, Pl. LVII.

The Nakada tuffaceous beds, which are overlain by the upper Yositaki, are typically exposed on the northeast shore of Nakada (loc. 27), in Mera-mura (village). They are well exposed everywhere in Nakada, but scarcely so in the other localities, with the result that the distribution of these tuffaceous beds had to be determined with only a few field observations. The pumice of the Nakada tuffaceous beds in the type locality, which are about 2 cm in diameter, came from andesite tuff.

In the Sugata valley the writer failed to find any exposures of these beds, while in the Yabuta valley (loc. 28), he found a sand bed directly overlain by the Nakada tuffaceous beds of the type locality. Nakada tuffaceous beds are exposed at the eastern end of a reservoir, west of Ao (loc. 29) (about 600 m northwest of a bench mark at Ao). The size of the pumice here exceeds 1 cm in diameter.

From the few observations made of the Nakata tuffaceous sand, and by the relations of these exposures, it was found that the Nakada tuffaceous beds generally strike N30°E, and intercalate with the Yositaki beds, as shown in Fig. 11.

The lower Yositaki beds. As was done by MOCHIZUKI, the writer has selected for type locality the lower Yositaki beds on the dark greyish mud exposed at Yositaki, in Ao-mura.

The rocks of these beds, which closely resemble to those of the upper bed, rarely contain marly nodules. The lower Yositaki beds near Nakanami show platy joints, which IIZUKA[11] calls Nakanami black platy shale. The lower Yositaki beds near Tonohama are often cracked into fine blocks of about 3 cm diameter. IIZUKA calls this facies of the lower Yositaki, the Tonohama black shale.

The lower Yositaki beds contain thin tuffaceous beds, its lower limit being underlain by the Iori sand beds (loc. 30). The lower Yositaki beds gradually change their facies to sandy near the boundary of the Iori beds and the lower Yositaki beds.

Aphrocallistes sponge, and other fossils were collected from this boundary.

Generally, the lower Yositaki beds are barren of fossils, although they contain minute white objects about 3 mm. long, as shown in Fig. 218, Pl. LVII.

The distribution of the lower Yositaki beds is as shown in fig. 11. As will be seen from this map, the distribution of the lower Yositaki beds extends from Iori in Kitaoonomi-mura through Musizaki, Sazanami, and Hanazono, to Yositaki in Yatusiro-mura, generally with strike N 15°∼20°E, and dip 5°∼2°E in the northern part and strike N 45°E, dip 10°∼20°SE in the southern.

The Iori beds.

The type locality of the Iori beds is the sandstone exposed near Iori in Kitaoonomi-mura, Isikawa prefecture. The Iori sandstone beds, which are greyish blue, alternates with sandstone both calcareous and non calcareous. The weathered surfaces of these rocks are tinged brown.

---

[11] IIZUKA, "Nippon Tisitukosansi", Imp. Geol. Surv. Japan (1932), 148.

The Iori beds at the type locality gradually merge into the overlying Yositaki beds with conformity, up to a thickness of a meters. This stratigraphic relationship is easily observed on the shore of southern Iori (loc. 30). The thickness of the Iori beds varies considerably. Fossils are rare in these beds.

The following fossils were collected from the sea-shore of Iori:

Aphrocallistes sp.
Chlamys crassivenia YOKOYAMA
Terebratulina quantoensis YOKOYAMA
Terebratella aff. crossei (DAVIDSON)

From the Iori beds exposed at Tobayasi (外林) (loc. 31), in Kitaoonomi-mura, *Chlamys crassivenia* YOKOYAMA was obtained, besides which the following fossils were collected from the shores of Siratori (loc. 32) in Kitaoonomi-mura, and from Kamisazanami in Kitaoonomi-mura: *Terebratulina*? sp., *Terebratulina caput-serpentis* (LINNÉ,) *Chlamys swiftii etchegoini*? (ANDERSON), *Chlamys* sp.

Terebratulina caput-serpentis (LINNÉ) was collected from the Iori sand beds under the bridge of high way at Kamisazanami (loc. 33).

These beds are not developed in the southern part of this province.

Glauconite sandstone bed, which is often developed between the Yositaki and the Iori beds, is exposed at Asao (麻生) and Sazanami in Kitaoonomi-mura, and Kurosaki (黒崎), Oiide (生出) (Fig. 15) in Minamioonomi-mura. As will be described later, similar glauconite sand is exposed between the Wakura mud beds and the upper Nanao (the Akakura sand beds).

Although as already mentioned, the upper limit of these beds is always overlain by the Yositaki beds, either with conformity or unconformity, the lower limit is underlain by the next underlying Domi beds, agglomerates, and andesites.

The Domi beds.

The Domi beds consist of black sandstone, conglomerate, agglomerate breccia, and greyish sandstone, all exposed near Domi (loc. 34) in Kitaoonomi-mura.

These beds will be subdivided according to its rocks when further studies have been made, until when they will be treated as a single formation. MOCHIZUKI's Kumabuti beds may probably be included in the Domi beds. The conglomerate of the Domi beds in the type locality consists of subrounded black pyroxene andesite pebbles of about 5 cm diameter. The sand and fine conglomerate alternations of the Domi beds contain many silicified woods.

The total thickness of the Domi beds, which in the type locality is about 250 m, thins out near Sazanami, whereas near Oguri, Simidudaira, it is about 200 m. On the road (loc. 35) from Suno in Kitaoonomi-mura to the town of Nanao, where the Domi beds contain fossil plants, the writer collected a cone of *Sequoia* aff. *sempervirens* ENDLICHER. As far as the writer knows, this plant fossil is a characteristic species of the Japanese Miocene.

It is notable that the Domi beds exposed south of the line connecting Takebe in Kosidi-mura and Onotomari in Minamioonomi-mura, contain thick yellow tuffaceous sandy beds and a few conglomerates.

Volcanic mass.

Overlain by the foregoing sedimentary rocks, andesite masses are exposed at a number of places, such as at Takebe in Kosidi-mura, Oonotomari in Minamioonomi-mura, Oiide in Minamioonomi-mura. These volcanic masses are exposed north of the line connecting Takebe (武部) and Oonotomari (大泊).

The Siratori volcanic mass.

The Siratori volcanic mass is an andesite mass exposed on the seashore between Siratori and Domi (百海). This pyroxene andesite is distributed only over a small area.

The Kooziyama andesite mass.

The Kooziyama andesite mass, which is exposed on the highway (loc. 36) between Nanao and Iori, south of Kooziyama (柑子山) in Kitaoonomi-mura. As shown in Fig. 16, this andesite mass extruded the yellow tuffaceous rocks, the original position of which cannot be traced near this locality. The andesite, and the agglomeratic conglomerate exposed near Kooziyama overlie the Kooziyama andesite mass with slight unconformity.

The eastern end of this andesite mass is cut by a fault by which the east part is thrown downward.

The Asao agglomerate and andesite mass.

The agglomerate and andesite mass, exposed for some distance near Simidudaira (清水平) and Asao (loc. 37) in upper Simosazanami valley, consist of two pyroxene andesite and augite bearing olivine andesite, their agglomerate, and other pyroclastic material. Its structure is not definitely known. This mass is overlain by the Domi beds with unconformity.

The configuration of the boundary of the unconformity between the Domi beds and the Asao mass is very irregular in its height as shown in Fig. 11. In their external features, the Oiide agglomerate and andesite mass, to be described in the next paragraph, closely resemble this mass. This unconformity is exposed near Suno (須能) in Kitaoonomi-mura.

Field observations (Boundary between Domi beds and Asao agglomerate and andesite mass).

Loc. 38. Alternation of yellowish tuffaceous coarse grained sandstone and agglomerate exposed on the upper part: andesitic agglomerate exposed below the alternation with unconformity.

Loc. 39～40. Weathered andesite.

Loc. 41. Yositaki beds underlain by agglomerate and andesite mass, intercalating brownish-yellow irregulary stratified volcanic material; exposure shown Fig. 14.

Loc. 42. Glauconite sandstone bed exposed.

Loc. 43. Boundary between the Iori and Domi beds and the Yositaki beds exposed.

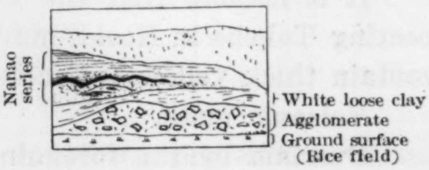

Fig. 14

Loc. 44. Light yellowish tuff here intercalated.

Loc. 45. Alternation of dark brownish sandstone and conglomerate underlain agglomerate with unconformity; at Simidudaira, alternation strikes N45°W and dips NE 10°～18°; agglomerates and light yellowish tuff exposed on a small road between loc. 8 and Asao.

Loc. 47. Domi conglomerate beds exposed.

Loc. 48. Domi beds, closely allied to those at Simidudaira, exposed. These Domi beds overlie agglomerate at valley floor of Sazanami valley on road between Nanao and Suno.

Loc. 49. Similar exposure as that of loc. 78. Southeast wall of this valley consists of volcanic material.

Loc. 51. This exposure consists of more or less soft loose weathered soils supposed to be the Domi beds. No exposures of agglomerate or andesite on road connecting Suno and Nanao.

Loc. 52. Boundary of Domi beds and andesite and agglomerate mass exposed west of Suno. Boundary plane almost horizontal, dipping about 5° eastward.

Loc. 53. Boundary of Domi sandstone and andesite agglomerate seen here.

Loc. 54, 55. Exposure of Yositaki beds and weathered glauconite sandstone beds, the Domi beds, and andestic agglomerate seen here stratified in (descending) order named.

Loc. 56. Iori sandstone exposed, but not the Asao agglomerate and andesite mass.

The Oiide agglomerate and andesite.

The andesite rocks exposed on the upper course of Kumabuti is called the Oiide volcanic mass.

This volcanic mass, which is exposed for a considerable length along the Kumabuti valley, consists of pyroxene andesite and agglomerate, and yellowish tuffite beds, the distribution of which is shown in Fig. 11.

The Minakami green tuffite beds.

The whitish yellow tuffite beds, intercalated with the Oiide agglomerates, gradually changes color to green (loc. 58), resembling the so-called green tuff formation of northeast Japan. This Minakami green tuffite may antedate the upper part of the Oiide agglomerate mass, but its exact stratigraphic relation is not known. Although the present writer distinguishes these green tuffite beds from the Oiide mass here, the two formations are treated as one in the geologic map (Fig. 11).

The Kosidi gneiss.

The Kosidi gneiss, which is exposed on the northeastern slopes of Mt. Sekido(-san), consist of biotite gneiss and marble, its general strike being about N45°W. This rocks was metamorphosed by injection of the Kosidi granite, which is exposed behind Kosidi village.

b. The southeast wall of the Oti graben.

Raised beach of Akasaki.

At the mouth of the Akasaki valley (loc. 61) in Higasiminato-mura, a shell bearing silt bed rests unconformably on Tertiary bed rock in a small area about 10 m high. This silt bed is overlain by a thick brown sand bed. The fossil shells collected from this silt bed are shown in Table I, col. 1 (in Part 1). Judging from these shells and their stratigraphic relations, the bed may be similar to the Tumuki bed, as explained in Part 1.

The Sakiyama terrace deposits.

The so-called Sakiyama terrace bed is a loose coarse grained granitic sand bed, forming a 30～40 m terrace in Sakiyama-mura. This terrace bed, the thickness of which is about 5 m, but varying in places, rests unconformably on Tertiary bed rock.

The writer could find no fossils in this bed, which is well exposed on the sea-cliff at Mimuro (loc. 62) and Unoura (loc. 63) in Sakiyama-mura.

From its attitude and height of terrace, this terrace bed may be contemporaneous with the Tumuki terrace bed.

The Nozaki silt beds.

Besides these surface terrace deposits just described from this province, Neogene formation is exposed in the area from the eastern part of Notozima to Sakiyama peninsula.

The Nozaki beds so called by MOCHIZUKI, is the uppermost of these Neogene formations. The type locality of these beds is Nozaki (野崎) in Higasizima-mura. The Nozaki beds, which consist of bluish grey tuffaceous silt beds, whose dry weathered surface is light grey, end in which marly nodules are often found, are sometimes stratified as shown in Fig. 17 (loc. 64). Among the fossil shells commonly found in these beds are *Thyasira nipponica* YABE and NOMURA, *Turritella fortilirata saishuensis* YOKOYAMA, and *Nuculana onoyamai* OTUKA.

These beds, which are distributed over the southeastern half of Higasizima-mura and the greater part of Sakiyama-mura, extending to Higasiminato-mura, are narrowly exposed near Kozima in Nanao town, MIMURA calls them the Kozima beds. Judging from its rocks, fossils, and stratigraphic position, as has been done by Onoyama,[12] these Nozaki beds may be contemporaneous with the Yabuta beds already described.

Owing to absence of the overlying Neogene beds, the upper limit of the Nozaki beds is unknown. Its lower limit however is underlain by the Entunagi beds, although the boundary between these two beds is not very sharp.

Near Higasiminato and Sakiyama-mura, some white tuffaceous beds of about 1 m thick are interbedded near the boundary of these two formations, which tuffaceous zones enabled the writer to easily distinguish the Nozaki beds from the Entunagi, although in most cases the writer had distinguish the one from the other by its rocks, these tuffaceous beds being often of uncertain formation in other localities.

The fossil localities of the Nozaki beds lie north of Nozaki (loc. 66), Kamiyukawa (loc. 67) in Sakiyama-mura, Nakamura (loc. 68), Kayato (栢戸), Tono (殿), Uwaso (上澤), and Matuo (松尾) (loc. 71), Tobeiyati (藤平谷内) (loc. 86, 87) in Higasiminato-mura.

The following fossil shells were collected by the writer from these localities (Table V).

Table V. Fossils from the Nozaki beds.
(Y. OTUKA, 1935).

Nuculana onoyamai OTUKA
Acila divaricata (HINDS)
Glycymeris yessoensis (SOWERBY)
Arca amicula YOKOYAMA
Chlamys sp.
Lima sp.
Mytilus sp.
Astarte alaskensis DALL
Thyasira nipponica YABE et NOMURA
Lucina acutilineata CONRAD
Turritella fortilirata saishuensis YOKOYAMA
Turritella fortilirata motidukii OTUKA
Epitonium angulatosimile OTUKA
Neptunea uwasoensis (OTUKA)

---

[12] T. ONOYAMA, *op. cit.* (1933).

The Entunagi beds.

The Entunagi beds are massive dark-greyish mud beds, the exposed parts of which, like the Yositaki beds already described, are tinged yellow. The weathered surface of the Entunagi beds is reddish brown. Small white objects (*Sagarites* ? sp.) and *Aphrocallistes* sponge are contained in them, the latter being very common in the basal part of the Yositaki beds. The type locality of the Entunagi beds is Entunagi (縁繋) in Nakanosima-mura. These beds, which are underlain by the Notozima andesite and the Koda beds, may be contemporaneous with the Wakura beds to be described later.

These beds are to be seen most everywhere in Nakanosima-mura, and from Sobogaura in Higasizima-mura, to Akasaki in Higasiminato-mura. Near Akasaki, they contain marly nodules. The islands Karasu (-zima), Tera (-sima), Yome (-sima), and Kosiki (-zima), all in South Nanao bay, consist of Entunagi beds.

Some tuffaceous beds near the upper limit of the Entunagi beds seem to be related to the Nakada tuffaceous zone of the Yositaki beds. These tuffaceous beds may be seen in the grounds of the Yatugasaki Primary School (loc. 72) in Higasizima-mura, in a cliff (loc. 73) near the tunnel between Nozaki and Koda, at a point (loc. 74) 500 m west of Nozaki, in the west and east (loc. 75) of Hidesima (日出島), and in Kadosima (鹿渡島) (loc. 76) in Sakiyama-mura, on the sea shore (loc. 77) of Mimuro, Konogi (此木) (loc. 78) in Higasiminato-mura, in the eastern hill (loc. 79) of Akasaki, and in Tobeiyati (loc. 80), Matuo (loc. 81), U-waso (loc. 82), and Kayato (loc. 34), Nakamura (loc. 84, 85), all in Higasiminato-mura.

Other localities of the Entunagi beds extend from Onogi (大野木), Kitaoonomi-mura, through Himura, Tobayasi, to Matuo in Higasiminato-mura along the Ikakeyama flexure zone, which last will be described later.

The Koda beds.

The Koda beds are ovelain by the Entunagi beds with unconformity, a glauconitic sand bed being intercalated between the two beds. This glauconitic sand bed is exposed on the road (loc. 88) between Koda and Sanami, and in the grounds of a shrine (loc. 89) east of Koda village. South of these exposures, this glauconitic sand bed is indistinct.

The Koda beds, which are closely allied to the Akaura and the Nanao beds in the Northwest province of the Oti graben, in rock characters, and which consist of coarse grained white or light greyish sandstone, are believed to be contemporaneous, stratigraphically, with the Akaura beds.

The Koda beds, narrowly distributed in Higasiminato-mura and Sakiyama-mura, differ slightly in rock features from the type.

Stratigraphically the fossil bearing sandstone (the Iori beds) near Tobayasi, Iori may be contemporaneous with the Koda sandstone.

The Domi beds.

The Domi beds in this province are found on the southeast side of the Oti graben, where they consist of coarse grained conglomerate and alternation of sand and mud bed of variable thickness. Near Kosidi-mura, the components of the gravels in the conglomerate are mainly andesites, granite and gneiss, but on the north, these beds consist mainly of andesites and their agglomerates.

These andesites and their agglomerates and the gneiss and the granite underlain with unconformity by the Domi beds.

The Korosa agglomerate.

The agglomerate exposed near Korosa in Tokuda-mura, and called the Korosa agglomerate, consists of pyroxene andesite, and is overlain by the Domi beds.

The Takebe andesite.

This pyroxene andesite is exposed in the east valley of Takebe, adjoinning Kosidi granite.

The Kosidi granite.

This granite which is exposed in Ninomiya valley, Kosidi-mura, intrudes into the Kosidi biotite gneiss.

The Kosidi biotite gneiss.

The Kosidi biotite gneiss is exposed on the steep southeast slope of the Oti graben, near Ninomiya in Kosidi village, the general trend of the gneissosity being about N 60°E. The marble intercalated in this gneisose rock is worked as raw material for cement.

c. Northwestern part of the Oti graben.

The formations exposed here, besides the Alluvium and the Tumuki and Tokuda terrace deposits, show stratigraphic succession of Neogene as follows, in descending order:–

The Kozima, Wakura, Akaura, and Nanao beds, andesites, and gneiss breccias.

The Kozima beds.

The Kozima beds are the silty sandstone formation exposed on the hill scarp behind Kozima, west of Nanao. They are more or less tuffaceous, and contain many fossil foraminifera, mollusca, etc.

The fossils collected from these beds (loc. 91) are *Turritella fortilirata motidukii* Otuka, *Epitonium angulatosimile* Otuka, *Astarte hakodatensis* Yokoyama, *Cardium* sp., etc., many species of *Polymorphinidae*.

Near Iwaya (岩屋) at Nanao, these beds, which are underlain by the Nanao beds with unconformity are overlain by the gravel beds and coarse grained sand beds of Tumuki. The fossil mollusca, *Epitonium angulatosimile* OTUKA, *Turritella fortilirata motidukii* OTUKA, and *Astarte hakodatensis* YOKOYAMA are common species of Omma series of ONOYAMA, near the city of Kanazawa, from which the writer concludes that these Kozima beds may be contemporaneous with the Omma and Nozaki beds already described.

The Wakura beds.

The Wakura beds are a dark greyish massive mud or silt formation containning many diatoms.

The exposed surface of these beds is tinged yellow, the weathered parts being reddish brown.

T. OGAWA[13] gave it its name owing to its being typically exposed at Wakura, between the Wakura hot spring town and the Wakura railway station.

Isizaki, the northeast part of Isizaki-mura is the precise locality where the Wakura beds are exposed.

These beds are exposed also in the island of Noto (-zima) from Hanoura to Byobuzaki and Suso, and in the western part of Wakura from Tazuruhama to Sirahama and Kasasiho-mura. The Wakura beds exposed in the western half of Notozima are distributed in patches, resting on the Tertiary andesite bed rock with unconformity around this part of the island.

Hakonairie (箱名入江) and Magari (曲) in Nakanosima-mura, Suso-(須曾) (loc. 99)-Hanoura, and Minami (南) (loc. 90) in Nisizima-mura, are the other localities of Wakura beds in Noto (zima). The basal part of the Wakura beds exposed at Tadatu (直津) (loc. 93) and Minami and containing *Aphrocallistes* sp., are limited by a glauconitic sandstone bed, such as is seen in the basal part of the Entunagi (Yositaki) beds. This glauconitic sandstone bed, which is well exposed on a railway cutting south of the Wakura station, the writer calls the Wakura glauconitic sandstone bed.

Field observations on the Wakura glauconitic sandstone bed.

Loc. 90. In the southeastern part of Minami in Nisizima-mura, Is. Noto (-zima), Wakura glauconitic sandstone bed exposed on road between Minami and Magari. The almost horizontal bed contains *Aphrocallistes* sp.

Loc. 94. Takada in Akakura-mura. Glauconitic sandstone bed visible here on highway, but owing to weathered condition, exposure indistinct.

Loc. 95. On railway cutting southeast of Wakura station. Strike, N 40°E: dip 5°NW (type locality.)

---

[13] T. OGAWA, *op. cit.*, (1908).

Loc. 96. On cutting along highway south of Wakura station.

Loc. 97. On road between Akaura and Hunao.

Loc. 98. On cliff southeast of Tadatu (Fig. 11). Wakura glauconitic sandstone bed here underlain by andesite and agglomerate with unconformity, intercalating with thin Akaura sand.

The Nanao beds.

The Akaura beds.

The Nanao beds are subdivided into two formations, the upper, the Akaura and, the lower, the Nanao. The Akaura beds, so named by K. MOCHIZUKI, are the greyish white coarse grained sand beds exposed near lake Akakura. These coarse grained sand consist of granitic sand, with rarely marine fossils. They are underlain by the Nanao beds with conformity, being rarely crossbedded, and are exposed from the southern part of Isizaki in Isizaki-mura to Siratori in Tokuda-mura, where they are underlain by the Takasina andesite and its agglomerate.

In Is. Noto (-zima), these beds are narrowly exposed around the Island at Minami, and Suso-Byobusaki-Hanoura.

The Nanao beds.

The next underlying beds, called Nanao beds by Prof. T. OGAWA[14] are contemporaneous with his Hanoura beds.

Iwaya (loc. 100), west of Nanao and Tumuki (loc. 101), north of Nanao are the type localities of these beds.

The Nanao beds at Iwaya contain many fossil mollusca and brachiopoda, the writer having collected the following species there (Table VI).

Table VI. Fossils from the Nanao beds.
(Y. OTUKA, 1935).

Patinopecten kagamianus (YOKOYAMA)
Chlamys notoensis YOKOYAMA
Chlamys hastatus ingeniosa? YOKOYAMA
Terebratulina septentrionalis COUTHOUY
Terebratulina japonica (SOWERBY)
Magelania lenticularis tenuis HAYASAKA
Coptothyris grayi aomoriensis HAYASAKA
Chlamys crassivenia YOKOYAMA
Pecten sp.
Laqueus rubellus SOWERBY
Isurus hastalis SOWERBY
Carcharodon megalodon (CHARLESWORTH)
Carcharodon sp.
Carcharias cuspidatus (AGASSIZ)

Latter 7 species were not collected by the writer.

---

[14] T. OGAWA, *op. cit.* (1908).

Besides these fossil mollusca and brachiopoda, we find many bryozoa, spines of echinodermata, and foraminifera, but the characteristic species of the Kozima beds that overlie the Nanao beds with unconformity were not found in the Nanao beds here.

Among of the fossils, *Patinopecten kagamianus* YOKOYAMA and *Carcarodon megalodon* CHARLESWORTH are species common to the Middle Neogene of Japan.

According to ONOYAMA, these fossil mollusca resemble to those contained in his Omma series, while *Patinopecten kagamianus* (YOKOYAMA) is a characteristic species of ONOYAMA's Minamikanda series, which are overlain by the Omma series with slight unconformity.

Patinopecten kagamianus (YOKOYAMA) and *Chlamys notoensis* YOKOYAMA occur in the Saoyama series near Sendai, which is considered by H. YABE, to be Tortonian or Sarmatian in age, from which the writer is convinced that the Nanao beds may be contemporaneous deposits with the Minamikanda of ONOYAMA, and probably older than the Omma series. The Wakura beds above the Nanao beds are therefore contemporaneous with the Yositaki and the Entunagi beds, which are overlain by the Nozaki and the Yabuta beds with unconformity, while the Yabuta beds are certainly contemporaneous with the Omma series.

As far as the writer knows, no sedimentary rocks older than the Nanao beds are found in this province, although some volcanic rocks are found below the Nanao beds with unconformity.

The other exposures of the Nanao beds is in Hanoura, in Nisizima-mura, in which they are exposed below the sea-level. The mineral phosphates of this region come from these Nanao beds. Fossil localities of the Nanao series are loc. 100, 102, 103, 104, and 105.

The Takasina andesite and agglomerate.

The Takasina andesite and agglomerate are exposed on the west slope (loc. 106) of the pass between Iwaya, near Nanao, and Hannyano in Takasina-mura, and also west of Tadatu, in Nisiminato-mura.

These andesite beds are overlain by the Wakura and the Nanao beds with unconformity.

The Akakurayama andesite.

The Akakurayama andesite mass is what forms the mountain Akakura (yama). It is exposed at Otu (大津) (loc. 107) inKan agasaki-mura, clearly showing platy joints. It is overlain by the Wakura beds with unconformity at Otu.

---

15) H. YABE, *Rep. Geol. Palaeontol. Inst., Tohoku Imp. Univ.* **12** (1935), 23, (in Japanese).

The Notozima andesite.

The western half of Is. Noto (-zima) consists mainly of this andesite, which is overlain by the Wakura beds and the Koda beds with unconformity. Two pyroxene andesite is exposed at Hanoura.

Breccias of Gneiss.

The steep slope of the northwestern side of the Oti graben consists of gneiss breccias. The writer failed to trace the original gneiss mass whence these breccias came. On the top of this steep slope a coarse grained sandstone beds lie on the breccias, which here may be a basal conglomerate of those coarse grained sandstone beds.

MIMURA,[16] who described the Takasina beds, thought they might be Pliocene. The present writer observed these beds both in Takasinamura and Tazuruhama village, in the latter of which they rest on the Wakura mud beds with unconformity.

d. Conclusion.

Correlation of strata.

In the preceeding chapters the writer has described the stratigraphic succession in these three provinces. In this one he discusses the chronologic relationships of these stratigraphic successions.

Palaeontologically and petrologically, it is not unreasonable to correlate the Nozaki beds in the east of Is. Notozima with the Yabuta beds on the west shore of the bay of Toyama. The Wakura beds can be correlated with the Entunagi beds in Is. Notozima. These two beds consist of the same dark greyish muds. *Aphrocallistes* sp. occurs in the basal part of the Entunagi, the Wakura, and the Yositaki beds. In the basal parts of these, a glauconitic sandstone bed is sometimes exposed. These evidences may justify the correlation of these three beds with one another. The Entunagi beds which as will be described later, are exposed on the Ikakeyama flexuous zone, are underlain by the Iori sandstone near Tobeiyati with conformity. Since the Iori sandstone beds are overlain by the Yositaki with conformity at Iori, the Yositaki beds and the Entunagi beds (or the Wakura beds) are underlain by the same Iori beds with conformity. They must be stratigraphically contemporaneous with each other.

The writer has already described the occurrence of tuffaceous beds between the Entunagi and the Nozaki beds, which become indistinct toward the north. As the tuffaceous bed corresponding to this tuffaceous bed lying between the Entunagi and the Nozaki beds in the southeast, the writer is able to name the Simazaki sand of the Himi beds and the Nakada tuffaceous beds in the southeast province of the Oti graben. As just described, the basal part of the Yositaki beds are exposed at Iori, while the Nakada tuffaceous beds are exposed in the upper half of the Yositaki beds, the Yabuta beds being interbedded between the Simazaki beds and the Yositaki beds. The Simazaki beds are, stratigraphically, the upper horizon of the tuffaceous bed between the Entunagi beds and the Nozaki beds. It being impossible to correlate the Simazaki beds with the upper part of the Entunagi beds from palaeontological grounds, the writer is of opinion that the Nakada tuffaceous beds may be contemporaneous with the tuffaceous beds between Entunagi beds and the Nozaki beds.

---

[16] MIMURA, *Grad. Thetis. Geol. Inst., Kyoto Imp. Univ.*

The fossil mollusca collected from the Simazaki beds listed in Table III, show that the Simazaki beds is not so old as the typical Omma beds near Kanazawa. Of these, a few species are reported only from the upper Pliocene. The Yabuta beds below the Simazaki, which may be the lower half of the Pliocene, is correlated with the Omma series as has been done by ONOYAMA.

The geologic age of the Nanao beds is the most important point for discussion. The fossil mollusca from the Nanao beds may not be the oldest Neogene. The strata containing these fauna in other localities are the Moniwa beds near Sendai, the Omma series near Kanazawa, and the Neogene beds of Simane prefecture.

The molluscan fauna of the Moniwa beds near Sendai studied by H. MATSUMOTO.[17] *Patinopecten kagamianus* (Yokoyama) and *Chlamys notoensis* Yokoyama are the common species of the Nanao and Moniwa beds. A part of the Moniwa beds may be contemporaneous with the Nanao beds.

ONOYAMA, from the palaeontological point of view, correlates the Nanao beds with his Tagawa beds,[18] but the writer is unable to agree with his views. He collected *Chlamys notoensis* (YOKOYAMA) and *Chlamys crassivenia* (YOKOYAMA) from his Tagawa beds, both of which are characteristic of the Nanao beds. His Tagawa (part of Omma) beds however contain no *Patinopecten kagamianus* (YOKOYAMA), which is a characteristic species of ONOYAMA's Minamikanda series below the Omma series. The Nanao moreover is lower than the Omma. The Nanao beds may therefore be contemporaneous with a certain part of his Minamikanda series.

The Neogene Tertiary of Simane perfecture, which is the type locality of *Patinopecten kagamianus* (YOKOYAMA.), TUBOTA[19] divided this Neogene Tertiary, the Sinzi group, into the following subdivisions in descending order: the Huzina, Kimati, Sagusa, Sakura, and the Sandy tuffaceous beds. The upper beds contain *Cultellus izumoensis* YOKOYAMA, *Macoma optiva* (YOKOYAMA) and *Patinopecten kagamianus* (Yokoyama), etc. ONOYAMA correlates these beds with his Minamikanda series, in which the writer is in agreement.

---

[17] H. MATSUMOTO, *Sci. Rep. Tohoku Imp. Univ.* [ii] **13** (1930), 95～105.

[18] T. ONOYAMA, *Chikyu* **19** (1933), 276.

[19] R. TSUBOTA, *Grad. Thetis Geol. Inst., Kyoto Imp. Univ.* (1932).

The Domi beds below the Nanao beds, being volcanic land deposits, contain *Sequoia* sp. (aff. *sempervirens* ENDLICHER) and other silicified woods. According to ENDO,[20] *Sequoia* flourished during the Japanese middle Tertiary. Since the Nanao beds which may be upper or middle Miocene, are younger than the Domi, the last named beds may be middle or lower Miocene.

The Miocene *Miogypsina-Operculina* horizon of Northwest Japan is situated in the lower half of ONOYAMA'S Minamikanda series.

The Wakura, Entunagi, and the Yositaki beds resemble the Kubiki mud series (so-called black shale formation) of the oilfields of Northeast Japan, which contain *Pseudamussium peckahmi* (Gabb),[21] and *Aphrocallistes* sp. The Wakura beds also contain latter fossil. Though these formations are generally barren of fossils, the occurrence of these fossils shows that the formations may be contemporaneous with each other. These formations being believed to be upper Miocene by Japanese geologists, the Nanao beds may be older than the Kubiki mud series, Wakura, and other formations.

From these considerations the Nanao beds may be middle Miocene or upper Miocene. On this-basis the writer makes the general stratigraphic succession near the Oti graben to be as follows:

The Tumuki, Hiradoko, Sakiyama terrace deposits may be Pleistocene, and the writer calls them the Hiradoko series. The Sazanami terrace may belong to another group of Pleistocene deposits or it may be contemporaneous with the Hiradoko series.

The Takasina beds of MIMURA may be upper Pliocene. The Himi beds may be upper or middle Pliocene and occupy the upper horizon of the Yabuta series. The Yabuta, Nozaki, and Kozima beds may be middle or lower Pliocene, and contemporaneous with ONOYAMA'S Omma series. The writer calls these beds the Yabuta series.

The Yositaki, Entunagi, and Wakura mud beds are collectively called the Wakura beds. The Yabuta beds are underlain by the Wakura mud beds with para-unconformity.

The Iori, Koda, Akakura, and Nanao sand beds are grouped under

---

[20] S. ENDÔ, "Japanese Neogene Flora", *Iwanamikoza* (1933), (in Japanese).

[21] T. OSE, *Jour. Geol. Soc., Japan* (1934), (in Japanese).

Nanao sand beds. The Nanao series, which consist of the Wakura mud and Nanao sand beds, may be contemporaneous with the major part of ONOYAMA's Minamikanda series, the upper Miocene or middle Miocene. The Domi series consist of the Domi beds and other andesitic pyroclastic formations resting on the Kosidi granite and gneiss. The geologic age of the Domi series may be lower or middle Miocene. Table VII is a correlation table of some Japanese Neogene.

Table VII. Correlation Table of Some Japanese Neogene
(Y. OTUKA 1935).

<table>
<tr><th>Localities</th><th>Lower half of Pliocene</th><th colspan="3">Miocene</th></tr>
<tr><td rowspan="2">Akita-pref. (By CHITANI)</td><td rowspan="2">Yuri series</td><td colspan="3">Ogasima series</td></tr>
<tr><td>Hunagawa</td><td>Onagawa beds</td><td>Daisima</td></tr>
<tr><td rowspan="2">Niigata-pref. (By OMURA)</td><td rowspan="2">Tyuetu series</td><td colspan="3">Kubiki series</td></tr>
<tr><td>Teradomari</td><td></td><td></td></tr>
<tr><td rowspan="2">Southern Noto (OTUKA)</td><td rowspan="2">Yabuta series</td><td colspan="2">Nanao series</td><td rowspan="2">Domi ser.</td></tr>
<tr><td>Wakura</td><td>Akaura & Nanao</td></tr>
<tr><td>Northern Noto (By MOCHIZUKI)</td><td>absent</td><td>Iiduka beds</td><td>Wakayama beds</td><td>Orido beds</td></tr>
<tr><td>Kanazawa (By ONOYAMA)</td><td>Omma series</td><td colspan="3">Minamikanda series</td></tr>
<tr><td>Idumo (By TSUBOTA)</td><td>absent</td><td colspan="3">Huzina and Kimati beds</td></tr>
<tr><td>Sendai (By YABE)</td><td>?</td><td>?</td><td>Moniwa beds</td><td></td></tr>
</table>

5. The geologic structure of the environs of the Oti graben. (see Fig. 11 and 13).

In this chapter, the writer describes the geologic structure of the environs of the Oti graben. First, we shall consider the crustal movements as inferred from the rocks, the thickness of strata, and the distribution of the geologic formations, and considered second, the structural history of the Oti graben as establisned from the deformation of the strata.

In these provinces, the andesite, the agglomerate, and the tuffite of the Domi series directly rest on the basement complex of the Kosidi granite and gneiss with unconformity. And on these andesite and pyroclastic rocks, the Domi conglomerate and sandstone beds, in which the silicified wood and other fossil plant leaves are contained, are laid. As no intercalating beds are found between the basal complex and the Domi pyroclastic rocks, the andesite of the Domi series would extrude directly on the erosional surface of the basal complex. The thickness of this volcanic formation varies, and it sometimes exceeds 400 m. Since the Domi series contain continental plant leaves and large stems of silicified woods without marine evidences, it would appear that this volcanism occurred on the land surface. Since the Domi conglomerate consists of andesites, basal granite, and gneiss, during the Domi stage, the andesitic volcanism was active in the granite and gneiss mountains, while the rivers dissected these volcanic lands. The relative heights of these volcanoes and mountains exceed 400 m.

During the succeeding stage, the Nanao transgression or Nanao regional subsidence occurred, as the result of which the marine Nanao series were deposited on the Domi series with unconformity. The lower part of the Nanao series consists of coarse grained sand, e. g. the Akaura sand beds, the Nanao sand beds, the Iori sand beds, and the Koda sand beds. These sand beds which are thick near Iori and Nanao, about 150 m thin out toward the south. The black mud beds of the upper Nanao series, e. g., the Wakura, the Entunagi, and the Yositaki beds, are distributed over a wide area, overlapping the underlying sandstone; the thickness of these beds varies. On the west coast of Toyama Bay the thickness of these mud beds increases about 100 m. They may be seen overlapping the sand beds near Is. Noto (-zima) and Sekidosan.

In Noto (-zima) island, the mud beds are directly underlain by the Notozima andesite without the Nanao sand beds. The line of unconformity between the mud and the andesite is closely related to the contour lines of recent topography. The depressed reliefs are occupied by the mud beds, while the upheaved reliefs consist of the underlying andesite (see geologic section EF in Fig. 13), which peculiarity in the geology and topography may be explained as follows: The Nanao series began to deposit on the dissected reliefs of Notozima andesite before the andesite areas were completely denuded, the valleys composed of the soft Nanao series being easily dissected again owing to the different resisting powers of the andesite and the Nanao series.

Consequently during the early Nanao stage, this area was drowned, and irregular outlines of the sea shore and small islands were formed; that is to say the land was subsided relatively to the sea during the early Nanao stage, before the land was denuded.

The mud beds, the upper part of the Nanao series, namely, the

Wakura beds, became broadly exposed on the Suzu-misaki, northern Noto. The writer found these mud beds on the Sekidosan mountainland, 400 m above sea-level (Fig. 11). This extensive distribution of thick beds of pelagic fine muddy beds suggests that the mud beds cover the whole Noto peninsula, at any rate the Sekidosan mountainland. Notwithstanding this wide distribution, the thickness of the mud beds varies considerably which may be explained by the erosion that succeeded the Nanao stage before the deposition of the Yabuta series to be described later.

According to J. MAKIYAMA, the Nanao series are unconformably overlain by the Yabuta series with an erosional surface. Near Nanao, the lower part of the Nanao series are unconformably overlain by the Yabuta series without the upper Nanao series, while the unconformity between the Nanao and the Yabuta seems to be a para-unconformity resembling the unconformity seen between the Kakegawa series and the Tamari series in Siduoka prefecture[22] and also between the Takanabe groups and the Tuma groups in Miyasaki prefecture.[23]

If the Nanao series near Nanao had really denuded away, the writer is opinin that the area near Nanao upheaved relative to the other part, which would be favourable to denudation of the Nanao series before the deposition of the Yabuta series.

It appears to the writer that the Yabuta series were deposited on a relatively flat surface. The thickness of the Yabuta series runs fairly uniform the rocks showing only a small variety, although it is impossible to tell whether or not the Yabuta series completely covered the Sekidosan area during the early Yabuta stage. It may however be true, that the east of Nanao, Sakiyama peninsula, and Noto (-zima) island, and the west coast of Toyama bay, at least, were at one time covered by the Yabuta sea. The Yabuta series consist of pelagic calcareous sands and pelagic species of fossil mollusca, e. g., *Thyasira nipponica* YABE and NOMURA, *Yoldia onoyamai* OTUKA, *Turritella fortilirata saishuensis* YOKOYAMA, *Epitonium angulatosimile* OTUKA etc., whence it may accepted that the sea in which the Yabuta series was deeply deposited covered the broad area of Noto. But during the late Yabuta stage, the sea-bottom gradually shallowed and the sea regressed. The upper Yabuta, the Himi beds, show this regression. The Himi beds consist of coarse-grained sand containing shallow sea and brackish molluscan remains. It was during this stage, that Mt. Sekidosan must have emerged from the sea.

---

[22] J. MAKIYAMA, *Mem. Coll. Sci., Kyoto Imp. Univ.*, [B], 3, 1.

[23] Y. OTUKA, *Geogr. Rev. Japan.*, (1930), 1048~1074, (in Japanese).

Summarising the foregoing, the following crustal movements in this region may be inferred:

(1) Volcanism was active on the erosional surface of granite and gneiss. River erosion predominaed during this stage.

(2) The Domi conglomerate contained silicified woods, land plants, and plant leaves.

(3) Marine transgression (or subsidence of land) of the Nanao stage occurred before river erosion had ended (Miocene). Beginning of the deposition of the lower Nanao series.

(4) Progress of marine transgression (or gradual subsidence of land). Deposition of the upper Nanao series.

(5) Local elevation of the land near the Oti graben bottom.

(6) Deposition of the Yabuta series. (Local denudation of the Nanao series. Gradual subsidence of the land). (Early Pliocene.)

(7) Beginning of the regression (or gradual upheaval of the land).

(8) Deposition of the shallow sea formation near Simazaki.

(9) Upheaval of the land. Beginning of the late Tertiary erosional stage. Formation of the Akakura mountainland and Takasina hill. (Late Pliocene—Early Pleistocene.)

(10) Gradual subsidence of land. Marine erosion of the Sazanami and Tumuki stage.

(11) Upheaval of land. Formation of the Sazanami and Tumuki terrace. (Late Pleistocene.)

(12) Rejuvenation of rivers. Dissection of these terraces begin.

(13) Subsidence of land. Formation of irregular outline of the recent shore line.

In the next paragraph, the writer will study the crustal movement inferred from deformation of the strata, and in doing so classifies the deformation of the geologic formation into faulting and folding.

Faulting.

Owing to lack of good exposures, the faults in this region could not be accurately determined, although no large fault of megatectonical importance was found. In the Domi beds and the beds below them many minor faults and folds were found, which however are the necessary accompaniment of megatectonic deformations.

The followings are the principal faults in these regions:

Ogoti fault.

The Ogoti fault extends from Ogoti, north of Mt. Sekidosan, westward to Takebe. In a small valley south of Takebe, Kosidi-mura, Kasima-gori, Isikawa-pref, Kosidi granite contacts with andesite and its agglomeratate in a vertical fault plane, which strikes about N80°W, or EW, and which, though covered with the Domi conglomerate near Korosa, reappears on the north slope of Mt. Sekidosan at Ogoti. Though the eastern extension of this fault line seems to reach Oonotomari in Minamioonomi-mura, the writer was unable to find any exposure of this fault line there. An exposure, on the shore of Oonotomari, shown some minor faults (strike about N80°E) cutting a conglomerate mixed with breccias of gneiss and andesite (N45°～20°W: NE15°～45°).

This conglomerate exposed near the boundary of basal gneiss and the Domi beds at Hirasawa, Mera-mura, Himi-gori, and on the southeast side of the Oti graben, the gneiss breccias at Oonotomari suggest that the boundary of the basal gneiss is somewhere near the exposure. The Yositaki beds here strikes N60°W, and dip NE30° in a small valley south of Toonohama, the strike of which deviates from the general trend of the Yositaki beds, although the original trend is recovered near Hanazono. At an exposure 2700 m west of the village of Toonohama, the Yositaki beds abruptly disappear and the slope of the mountain steepens, the breccias of basal gneiss being seen on the slope. This exposure of gneiss breccias suggests that the basal gneiss may be exposed near the slope, but this fault line is generally hidden by the overlying strata. The part of the fault line that is exposed near Korosa seems to be covered by the Domi beds. But andesite and agglomerate of the lower Domi series are cut by this fault line, the southeast part of which is upheaved relatively to the opposite side, where basal Kosidi gneiss covered by the Domi beds is exposed. On the opposite side are developped thick andesite and agglomerate. The character of the gravels in the upper part of the Domi series on both side of the fault line differ from each other. On the southwest part of this fault line, this conglomerate consists of gneiss, while on the opposite side the breccias of gneiss gradually decrease in both frequency and size while toward northeast black andesite blocks increase.

Kooziyama fault.

The Kooziyama fault, which is a small normal fault that runs N～S or N15°E from the northeast part of Kooziyama, dips 60° westward and cuts the Iori beds. There is a down-throw on its eastern part. The strike and dip of the strata are N15°E, and 30°～18°E. Another small fault parallel to this Kooziyama fault was observed west of Kooziyama village.

Siratori fault.

The Siratori fault is a small vertical fault running westward from the northern end of Siratori village, in Kitaoonomi-mura. Geologically, the part north of this fault line is the down throw side, while topographically this fault scarp is obsequent. The sandstone of the Iori beds on the north side of the fault is vertically flexed up along this fault plane. The south side of this fault forms a land slide topography, in which a large area of the slope slips gradually toward the sea.

Ikakeyama flexure and fault.

The Ikakeyama flexed zone and fault extend from Oonoki to Tobayasi through Himuro, west of Mt. Ikake. Along this zone, the strata on the west side are flexed up steeply westward, and sometimes vertically faulted.

Observations on the route from Himuro to Tomari.

The Nozaki beds are exposed almost horizontally at Himuro, but near the pass between Himuro and Kamiyukawa, they strike N20°W and dip 10°E.

East of the pass, these beds strike N30°E and dip 30°W, while west of the exposure just mentioned, they strike N35°E, and dip 45°W, and strike N30°E, and dip 70°W. In this way the angle of dip gradually increases as the exposure goes eastward, while on the top of the pass the angle of dip rapidly decreases, the strata being exposed horizontally.

This flexed zone changes into a vertical fault west of Mt. Ikake. The exposure of this fault is seen at a reservoir south of Kayato (Fig. 18), in which locality, the Yabuta series contacts directly with the Domi beds on account of this fault, but not with the Nanao series.

On a small road in the Domi valley from Domi village to Nakamura village, the following exposures were observed. The larger part of the Domi valley consists of Domi beds containing silicified woods. On the western end of the Domi village, black sands and black conglomerates containing silicified woods, are exposed.

Black andesitic sand and gravel beds containing much silicified wood, and which are exposed at the west end of Domi village, dip either horizontally or gently eastward. At the water fall on the valley floor of the Domi, west of Domi, these sand and gravel beds of the Domi series strike N18°W and dip 15°W. An anticline may be seen between these two above mentioned localities. The westerly dip of these strata gradually becomes steep toward the west. The black mud of the upper Nanao series is exposed near the turn in the Domi valley. In the meridional valley of the upper course of the Domi valley, the upper part of the Nanao series strikes from N15°E to N30°E and dip in 40°W. Although on the slope from Sawano to Nakamura, the upper part of the Nanao series and the Yabuta series have the same inclination of strata as the preceeding locality, their dips become somewhat steep, about 45°. On this slope, the writer observed a white tuff zone continued to Matuo.

At the Nanakura village, the westward dip of the Yabuta series becomes quite gentle, then gently dipping eastward about 10°~3° to form a syncline.

A similar structure is seen on the road from Uwaso to Tobayasi; namely, N10°E; E5° at Uwaso (loc. 70); N35°E: NW20° at Uwaso (loc. 83); N30°E: NW36°, east of Uwaso (loc. 82); N32°E: NW45°, east of Uwaso (loc. 85). Thus the dip gradually increases as one goes eastward, the underlying strata appearing in succession. But on the top of the Ikake range, where the Nanao series are exposed, the dip suddenly becomes gentle.

This flexed zone, which extends westward along the highway between Iori and Nanao to Yati and Sano in Higasiminato-mura, unites with the flexure of the east wall of the Oti graben.

Field observations near Matuo:

At the north end of Matuo village may be seen that a white tuff bed strikes N45°W and dips 10°NE.

In the valley, southeast of Matuo village, is exposed the boundary of the Nanao and the Yabuta series. The strata as measured on the underlying Nanao series strikes N60°E and dips in 45°NW.

On the road connecting Matuo village with the Iori and Nanao highway, 150 m distant from the highway, the upper part of the Nanao series strike in N75°E, and dip 30°N.

Near the summit of the highway, sand beds of the Nanao series strike EW, and dip 35°N.

At a point 300 m southeast of the pass, the gravel beds of the Domi series strike N80°E, and dip 25°N.

The Nanao series strike EW, and dip 30°N on the sharp turn of the highway on its west slope; they also strike N85°E, and dip 35°N in the valley of Sano in Higasiminato-mura. At the head of the Sano valley, the Domi conglomerate is exposed.

The overlying Yabuta series which are exposed east of Sano village, strike N 70°~75°E and dip 18°~40°N.

In the southeast valley of Sano, the valley, immediately southeast valley of the highway, the Nanao series are exposed, striking N45°E, and dipping 82°W. The inclination of these strata is very steep. At the exposure 200 m east of the exposure, just mentioned, the strata dip 45°N.

Flexure and fault zone of the southeast wall of the Oti graben.

The steep southeast slope of the Oti graben is topographically visible in Is. Noto (-zima), as described in the chapter under "Topography", but there is no geologic evidence there of this flexure and fault zone. Near Akasaki, in Higasiminato-mura, we find a flexure and a fault, which seem to be parallel to the topographic boundary line.

On the sea shore, south of Akasaki in Higasiminato-mura, the upper Nanao series, which strike in N10°W or NS and dip 18°W, are cut by a normal fault that strikes about N10°~20°W, and steeply dips (about 70°W), while a tuff bed, which is horizontally intercalated near the upper part of the Nanao series is exposed on the west side of this fault, which is a down throw.

In the west down thrown side of this fault, the strata strikes N30°W, and dip 32°W.

In the Akasaki valley, the upper part of the Nanao series, which contains marly nodules, are exposed on the valley floor. It dips westward near the sea shore, while 500 m east of it, the strata dips 5°~3°E, forming a gentle anticline. The Yabuta series appear above the Nanao series 700 m east from the sea shore.

The fault just mentioned, which runs through Kaimonzi toward Tobeiyati, cuts in a vertical plane the Yabuta series north of Kaimonzi village.

Judging from the exposures along the road from the north of Tobeiyati to Nakamura, over a mountain pass, the Yabuta series strike NS and dip 45°W near a shrine at the western foot of the pass, while the angles of dip gently diminish east of the shrine. At the exposure 100 m east of the shrine, the strike is N10°W, and dip 33°W. On the exposure 550 m east of the shrine, the strike is N40°E, and the dip 5°E, forming a gentle anticline. The fault observed at Kaimonzi disappears in this locality. A gentle anticline is seen in the south valley of Kaimonzi.

The Yabuta series strike NS and dip 20°W at the Tamon shrine of Tobeiyati. In the bottom of the Tobeiyati valley, the angles of dip gradually descreases. At a point 900 m east of Tamon shrine, the strike is N25°E, and the dip is 14°E. The axis of the asymmetrical anticline near Kaimonzi is situated 500 m east of the Tamon shrine, the west wing of which anticline is steeper than the east wing. It gradually disappears toward the south, merging into the Ikakeyama flexed zone.

These structures were inferred from the position of the Yabuta and the Nanao series in the Sakiyama peninsula. On the southern part of this area is exposed a flexure on a large scale, forming the geologic southeast wall of the Oti graben.

Two valleys south and north of Siroyama in Yatago-mura show this flexed structure. Traversing this south valley of Siroyama from the northwest, thick talus deposits are spread out in the form of a fan from the mouth of this valley toward the graben bottom. This valley dissects the steep slope of the southeast wall of the Oti graben. At the foot of the wall, the coarse grained sandstone of the Domi series is exposed, its strike being N70°E, and dip 30°N. A little southeast of this exposure, an alternation of reddish-brown coarse and fine sand beds, with strike N60°E, and dip 55°N, are exposed on the valley wall; on the next southeast exposure along this valley the strike and dip of the strata are N70°~75°E and 35°N.

In the bottom of this valley, the alternation of coarse and fine sand beds gradually change to coarse and to alternation of gravel and coarse-grained sand beds. The gravel beds consist largely of subangular blocks of gneiss and granite.

The angle of this structure, which dips 30°W continues under Siroyama, abruptly decreases on the southeastern part of Siroyama, with the result that, in this valley, the faults do not show the graben structure, the evidences of the geologic structure show pointing rather to a flexed structure.

In the north valley of Siroyama, where a similar flexed structure is observable, the strike is N50°E and the dip 60°NW.

Near Kunogi and Notozima in Tokuda village, a similiar structure is exposed namely, the strata has a westward dip at the foot of the southeast wall of the Oti graben, but horizontal at the summit. The anticlinal part between the horizontal beds near the summit and the steeply inclined beds on the graben wall has eroded away exposing the lower part of the Domi series, and sometimes basal granite and gneiss. In the valleys of Eso and Takebe, the andesite rocks of the lower part of the Domi series, are exposed on the anticlinal part.

The Kotoge fault, which is exposed on this southeast wall of the Oti graben near Takebe, does not affect the topography of the southeast wall of the Oti graben.

On the road from Ninomiya through Syakusitoge to Sekidosan, clear outcrops are exposed, showing that the Domi series overlie the basal gneiss with unconformity. The gneissosity generally strikes N 20°E, the dipping gently eastward. (Steep dips rare.) Near Syakusitoge a fault that is exposed, cuts the Domi beds. This fault strikes N10°W, and dips 80°W. Some normal faults parallel to the southeast fault scarp of the Oti graben are exposed on the northwest slope of the pass between Kotake and Himi.

The Domi beds on this slope strike about N40°~50°E, parallel to the general trend of this fault scarp, and dip northwestward 32°, 50°, 40°. But near Kitakihara, a village on the upper part of this slope, the basal gneiss and granite are exposed. On the summit of the pass, the Domi beds reappear horizontally. On the southeast slope of this pass, the Domi beds gently dip southeastward with the overlying formations namely the Domi, the Nanao, and the Yabuta series, appearing in the order named with a gentle dip.

From the foregoing geologic observations, the southeast wall, at any rate, of the Oti graben, is the geologic fault and flexed zone owing to which the graben bottom depressed relatively to the Sekidosan mountainland. The width of the flexed zone is 1·1 km, at its widest part (the thickness of the Domi beds measured on this flexed zone is about 600 m). Since in the southeast part of this flexed zone, the strata gently dips southeastward, the width of these area of gentle dip as measured at right angles to the general trend being from about 2 km at the narrowest and 12 km at the widest, the anticline between the flexed zone of the southeast wall of the Oti graben and the gently dipping part southeast of the flexed zone is not a simple anticline as seen in the simple folding structure, but an asymmetric syncline, where narrow west wing itself is considered to be a boundary zone between the block of the graben bottom and the block forming the southeast part of the Oti graben.

A similar relation is observable in the Ikakeyama flexure. The width of this flexed zone which is only 200∼400 m, sometimes changes into a steep normal fault. The dips of the strata along this flexure zone are about 50°. While the northwest part of this flexure consists of the gently southeasterly dipping Yabuta series. This gently dipping area whose width measured at right angles to the general trend is about 2 km is cut by the Kaimonzi fault, from all of which the Ikakeyama flexed zone may be considered the southeastern boundary line of the block forming the gently dipped area.

These geologic facts lead the writer to believe in the existence of a block whose strata gently dip southeastward and are bounded by a zone of flexure and faulting. As will be discussed later, the geologic facts that the structure of the block gently dips southeastward, while the block is depressed relatively to the southeast side with normal fault and flexed zone, support the conclusion that the blocks which were formed by tension cracks on the backbone of an anticline on a large scale are depressed by gravity relatively to the wings of the anticline.

Fault in the northwest part of the Oti graben.

As described in the chapter on topography, the northwest side of the Oti graben is by its straight discordant boundary line, considered a clear fault topography while the geologic evidences of fault topography in the graben are very rare. Most of the evidences may be concealed by the younger talus deposits. Prof. J. Makiyama, found a fault near Tizi by which the northwest side has been thrown down. Lack of exposed faults cannot, however, nullify the fault scarp topography of the northwest side of the Oti graben. It could easily by assumed that the geologic fault is concealed under the Alluvial or younger deposits. But near Hosoguti, southeast of Kokubu on the northeast part of the Oti graben, the Nanao beds are exposed below the Tokuda terrace deposits in the graben bottom, from which geologic facts the writer is forced to conclude that the northwest margin of the graben bottom is not so greatly displaced relatively to the northwest part of the graben, seeing that topographically the straight valley of Oharaigawa may be considered a fault valley representing the northwest margin of the Oti graben, while the Nanao beds are exposed on both side of the straight valley and are not displaced relatively to each other.

At arie, southeast of Tokuda station, a deep boring was made from the results of which the Nanao beds seem to exend about 200 m below the ground surface of the graben bottom. Judging from the geologic map, the Nanao beds should be exposed on the land surface of Arie, whereas contrary to what we should expect as just stated, boring showed the Nanao sand beds at great depth. A relative depression of the graben bottom is therefore recognizable near Arie. From the lack of geologic evidences in the fault scarp topography of northwest wall of the Oti graben, some authors may deny the existence of a fault. For the lack of geologic evidence there are two possibilities; the one being that no fault exists, the other being that the fault is completely concealed by the younger deposits. In the former case, there is unquestionably no fault, whereas in the latter case, it may or may not be present. The writer therefore presumes the existence of fault from the auxiliary topographic and geologic features that do not contradict its existence, although its exact position, expect that it is on the northwest side of the Oti graben is naturally not determinable. As described in the chapter on topography, the river system on the back slope of the fault scarp like topography northwest of the graben is cut by the straight valleys and fault scarp of the northwest wall of the Oti graben. These head-cut river systems lead the writer to conclude that the northwest wall of the Oti tectonic valley originated from either a fault or a fault scarp.

The geologic structure of the northwest part of the Oti graben gently tilts northwestward, the basal part (gneiss breccias) cropping out at the foot of the fault-scarp-like slope. The Domi beds on the southeast wall are flexed downward and submerged under the bottom of the graben. It is therefore necessary to expect a fault or flexure structure on the northwest side of the graben bottom in order to explain the presence of these submerged formations in the northwest part of the graben.

Akaura flexure.

The Akaura beds, a part of the Nanao series, and distributed from Akaura to Sirouma, gently dip northwestward, and are overlain by the Wakura beds. The Akaura flexure is exposed at Hyakumatu near the Akaura lagoon and the pass (72 m south of Kurama-yama) west of Kozima near Nanao. The general dip of the Akaura beds is gentle and about 2° ~ 3°, while on the flexed zone, the dip becomes steep toward the east, the western side of this zone having upheaved relatively to the opposite side. The northern and southern ends of this flexed zone were not traced. The width of the flexed zone is about 200 m. These displacement characteristics of the flexure differ completely from those of the Ikakeyama flexure.

Noto-zima.

Notozima (island) shows a structure quite independent of the preceeding localities. This island, which consists of two parts, the east and west is divided by the line that connects Koda and Sanami. The eastern side of the line consists of the Yabuta and Nanao series, and the west of andesite and the Nanao series.

The geologic structure of the east part is gentle and monoclinal. The Nanao series, which is underlain by the Notozima andesite, lie at the base of the Tertiary. The Yabuta series overlie the Nanao with conformity. These formations strike about N 20° ~ 30° E, and dip 5° E. This monoclinal structure is disturbed by the Nozaki flexure, which is exposed at Nozaki, the eastern end of the island. On this flexed zone the Nozaki beds of the Yabuta series dip 50° W and strike N 10° E. The northern end of this flexed zone is submerged in Toyama bay, while its southern end disappear near Koguti-seto.

This flexed zone dips steeply westward against the general dip of this area. In its sence of displacement, these characteristics of the flexed zone are similar to those of the Ikakeyama flexure.

The geologic nature of the boundary between the Notozima andesite and the Nanao series may be unconformity, but there is no fault. If any fault exists, it is probably a small scale one. The Nanao series, distributed around the andesite mass, occupies the depressed part of the andesite mass with unconformity. These Nanao series are developed almost horizontally, as may be seen at Magari in Nakanosima-mura, the bay head of Hakonairie, in Minami in Nisizima-mura, and in Hanoura and Suso. Comparing the heights of these almost horizontal Nanao series with that of Koda, the writer could find no difference between them, so that if any faults exist between the Nanao series and Notozima andesite along the line connecting Koda and Sanami, they are most likely on a small scale.

From the topographic map, the southeast wall of the Oti graben seems to extend from Hutaana along the topographic line to Sobogaura in Is. Noto (-zima), but so far as the writer knows, no geologic evidences of the flexure and fault have been found along the line neither in the Nanao nor the Yabuta series.

The northwestern wall of the Oti graben seems to extend to the topographic line of Koda and Sanami, but, as previously said the geologic evidence, if it could be called so, is merely an unconformity which may not be the result of a fault.

Folding.

The folding structure of the geologic formation developed near the Oti graben has already been described.

The eastern area of Sekidosan is a monoclinal structure dipping southeastward about 10°~20°, with a younger formation exposed southeast of the older. The angles of dip gradually decrease toward the Sekidosan ridge, on which the lowest formation, the Domi series, is exposed. The Domi series exposed here are disturbed by minor folds and faults with very irregular strike and dip of strata. But in its larger structural relations, the strata forms an anticline of which on a large scale, the axis is situated along the ridge of Sekidosan. The exposure at Sekidosan, Arigahara, southeast of Kotake; Kitakihara pass; Arayama pass; Korosa; Masugata pass, and the east ridge of Siroyama, show horizontal strata. As both the flexed structure of the southeast wall of the Oti graben and the Ikakeyama flexure affect the Yabuta series, these flexed structures may postdate the formation of the Yabuta series; tnat is the geologic Oti graben was formed after the early Yabuta stage.

The writer ventures to say that, before the formation of its graben structure, the Oti graben area was a broad anticline, the southeastern wing of which is the southeast slope of *S*ekidosan, and the northwestern wing the northwest part of the Oti graben. The anticlinal axis is situated along the graben bottom. After the formation of the anticline, some underground geologic blocks near the anticlinal axis were depressed by gravity, and the overlying strata flexed along the margin of these depressed blocks. Figure 19 shows these structures besides the distribution of the dip angles, from which the distribution of the flexed zone may be clearly seen.

6. Tectonic history of the Oti graben.

Tectonic history of the Oti graben since the deposition of the Domi stage may easily be inferred.

There was a land surface on which the Kosidi granite and gneiss were exposed during pre- or early Miocene. There are no clues pointing to the relative heights of the reliefs of the land surface, which last was laid just before the deposition of the Domi series.

During the early Domi stage, volcanic activities were frequent on this land surface, as may be inferred from all these andesite masses namely, Akakurayama, Notozima, Kooziyama, Asao and Siratori andesites. The andesite exposed so widely in the Noto peninsula are the products of this stage. Relief forming went on extensively during this volcanic stage. Mountains of granite and gneiss and volcanoes were prominent features in this region, all of which in due course were dissected by rivers. The Domi conglomerate was formed during this erosional stage, and so was the Ogoti fault, the southern part of which was upheaved while its north side was depressed, and in which was accumulated the thick Domi conglomerate.

The Domi series, which have a continental character were dissected by river erosion. But the transgression of the Nanao series occurred before river erosion had dissected out these mountains and volcanoes of the Domi stage.

The writer previously said[24] that the volcanic activity was succeeded either by transgression of the sea or subsidence of land. In Noto, a similar relation of volcanic activity to transgression or subsidence is seen in the case of the Domi and the Nanao series. Evidence that deposition began before erosion had completed its work is seen in the Nanao series of Is. Notozima, as previously stated.

The transgression of the Nanao sea which affected a wide area, is believed to be the extension of Miocene marine transgression of *Operculina-Miogypsina* horizon which is distributed over the western half of northeast Japan, western Hokkaido, and in the prefectures of Isikawa, Toyama, Gihu, Siga, Hirosima, Okayama and Simane, and in Tyosen.

Noto, during this stage, was an archipelago. The Nanao stage was succeeded by upheaval of land, characterized by upwarping.

---

[24] Y. OTUKA, *Bull. Earthq. Res. Inst.*, **12**, 3.

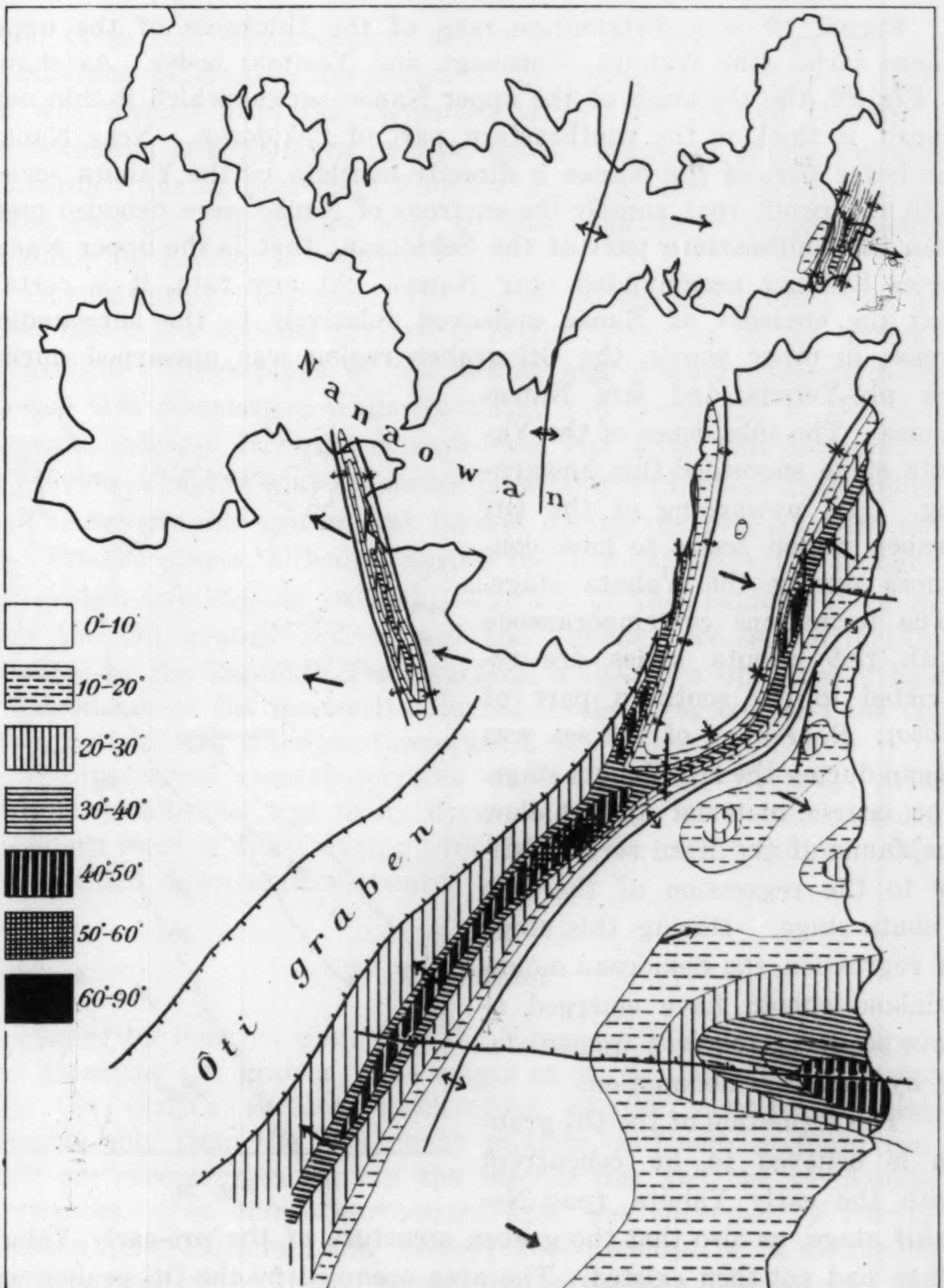
Nanao wan
Oti graben
0°-10°
10°-20°
20°-30°
30°-40°
40°-50°
50°-60°
60°-90°
Anticline
Syncline
Strike

Fig. 19. Distribution map of angles of dip.

Figure 19 is a distribution map of the thickness of the upper Nanao series (the Wakura, Entunagi, and Yositaki beds). As shown in Fig. 20, the thickness of the upper Nanao series, which is thin near Nanao, is thick in the southeastern part of Sekidosan. Near Nanao, the lower part of the Nanao is directly overlain by the Yabuta series, with the result that namely the environs of Nanao were denuded more than the southeastern part of the Sekidosan; that is the upper Nanao series had not accumulated near Nanao. At any rate, it is certain that the environs of Nanao upheaved relatively to the surrounding areas; in other words, the Oti graben region was upwarped during the pre-Yabuta and late Nanao stages. The subsidence of the Yabuta stage succeeded this upwarping. The upwarping of the Oti graben region seems to have continues during the Yabuta stage. (The formations contemporaneous with the Yabuta series are restricted to the southern part of Noto). Regression of the sea was began during the late Yabuta stage. The coarse material and shallow sea fauna of the Himi series testify to the regression of the late Yabuta stage. During this stage of regression, the Sekidosan mountainland should have emerged above sea-level, followed immediately by subaerial denudation.

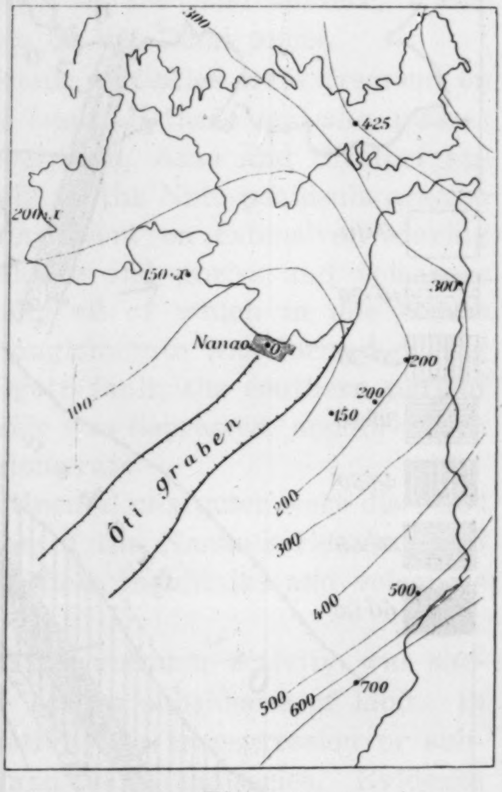

Fig. 20.

The formation of the Oti graben is believed to be concurrent with the early Yabuta (post-Nozaki) stage, as also that the graben structure of the pre-early Yabuta stage had not then existed. The area occupied by the Oti graben was rather upwarped before or during the early Yabuta stage.

The writer therefore believes that the Oti graben structure was formed in the post-early Yabuta stage, namely, post-early Pliocene, while the low reliefed surface of the Sekidosan, Akakura mountainland, were, topographically speaking formed during latest Pliocene. The amount of topographic displacement of the Oti graben is about 200 m, while the geological displacement exceeds 1000 m. The difference between these two displacements shows that the geologic graben was in existence before the formation of the topographic graben, which last was formed after the formation of the low reliefed surface of the Sekidosan and Akakura mountainland. Since the geologic graben was formed during post-early Pliocene and pre-latest Pliocene, the age of the geologic Oti graben may be late Pliocene. Topographically, the following history is inferred.

During latest Pleistocene, the region of the Oti graben was denuded into a low reliefed surface after the formation of the geologic Oti graben. Upwarpings of the Sekido and Akakura mountainland followed this denudation, while the tilting and upwarping of the Noto peninsula, inferred from the summit-level, and which was described in the previous chapter, may be contemporaneous with these upwarpings.

The topographic graben was formed during the post-Akakura and post-Takasina stages, although during the Tumuki stage, the topographic graben had already existed. The sea of the Tumuki stage invaded the Oti graben and formed the Tokuda terrace. After the formation of the Tumuki terrace surface, a 30~40 m upheaval of land (or subsidence of the sea-level) occurred in these regions, and the Oti graben bottom was tilted southwestward.

The upheaved coastal terraces were dissected. Recently, after which they subsided and many drowned valleys were formed along the eastern coast of Noto, during which stage, the graben bottom seems to have tilted down southwestward.

7. Conclusion.

The writer does not think that the Nanao earthquake of 1933 originated from the Oti graben. The origin of the earthquake deep seated below the earth's surface, mechanisms of the earthquake being inferrable only from the earthquake motions, although geologic conditions are necessary to explain the mechanisms and the earthquake disturbances. The Nanao earthquake area was surveyed by Rikutisokuryobu (the Military Land Survey) and discribed by T. SUZUKI.[25] As will be seen from these reports the earthquake disturbances are closely related to the geologic structure. According to the report of Rikutisokuryobu, the bench marks (Nos. 9300, 9301, 9302, 9303, 9304) between Wakura and Nanao all situated near the epicentre of the Nanao earthquake were upheaved, and bench marks on each side of the graben and graben bottom seem to have moved in diffferent ways. (See Fig. 3 B in Part 1.)

According to SUZUKI, the Akaura lagoon sank during the earthquake, while bench mark no. 9302, situated on Tertiary, near the Akaura lagoon rather upheaved, so that the depression of the Akaura lagoon during the earthquake may be explained by the settling of loose Alluvial mud and sand around the lagoon through earthquake motion.

---

[25] T. SUZUKI, *Bull. Earthq. Res. Inst.*, **12**, **1.**

The towns on the loose Alluvial deposits were severely shaken by the earthquake, much more so than those on the bed rock. This difference in the distribution of earthquake damage as related to the geology of the region may be explained by the shock resisting nature of the houses and the character of the earthquake motions, which suffer changes in their passage through loose material.

Additional notes.

It will be seen from the foregoing discussions that the volcanic activities were succeeded by marine transgression during a time so short as the Japanese early Neogene.

That a depressed structure had formed along the back bone of an anticlinel structure was made evident by a study of the Oti graben. This geologic characteristics has been studied by AMPFERER,[26] CLOOS,[27] E. SEIDL.[28] But in the case of the Oti graben, the faults that form along the backbone of an anticline as the result of the tension cracks are replaced by flexure structure. This characteristic of the Oti graben structure may not harmonise with the results of experiments made by other writers. To explain this flexuous structure, it is necessary to consider the pre-existing block structure or the underground block structure below the Neogene beds of Noto.

It is therefore the intention of the writer to try and ascertain by further studies the particular agency or agencies that were responsible for the anticline, and whether or not the flexures described in the foregoing pages are the result of pre-existent block structure.

The writer has expected that this study will make it possible to form an idea of the geotectonic development of the Sado island and Yamato submarine bank, under the assumption that these island and bank have geologic structural characteristic similar to those of the Noto peninsula. It will be expected from the foregoing studies that these island and bank have been formed into the recent isolated topography since the Diluvial age, and that their geology should have been isolated since the later Pliocene. This expectation will partly make sure by the study of geologic structure of Sado island.

---

26) AMPFERER, *Zeischr. Geomorphologie* **1** (1925).

27) CLOOS, *Geol. Rundschau*, **19** (1928).

28) SEIDL, "Bruch und Fliess Formen der Technischen Mechanik, und ihre Anwendung auf Geologie und Bergbau", (1934), 215.

[Y. OTUKA.]

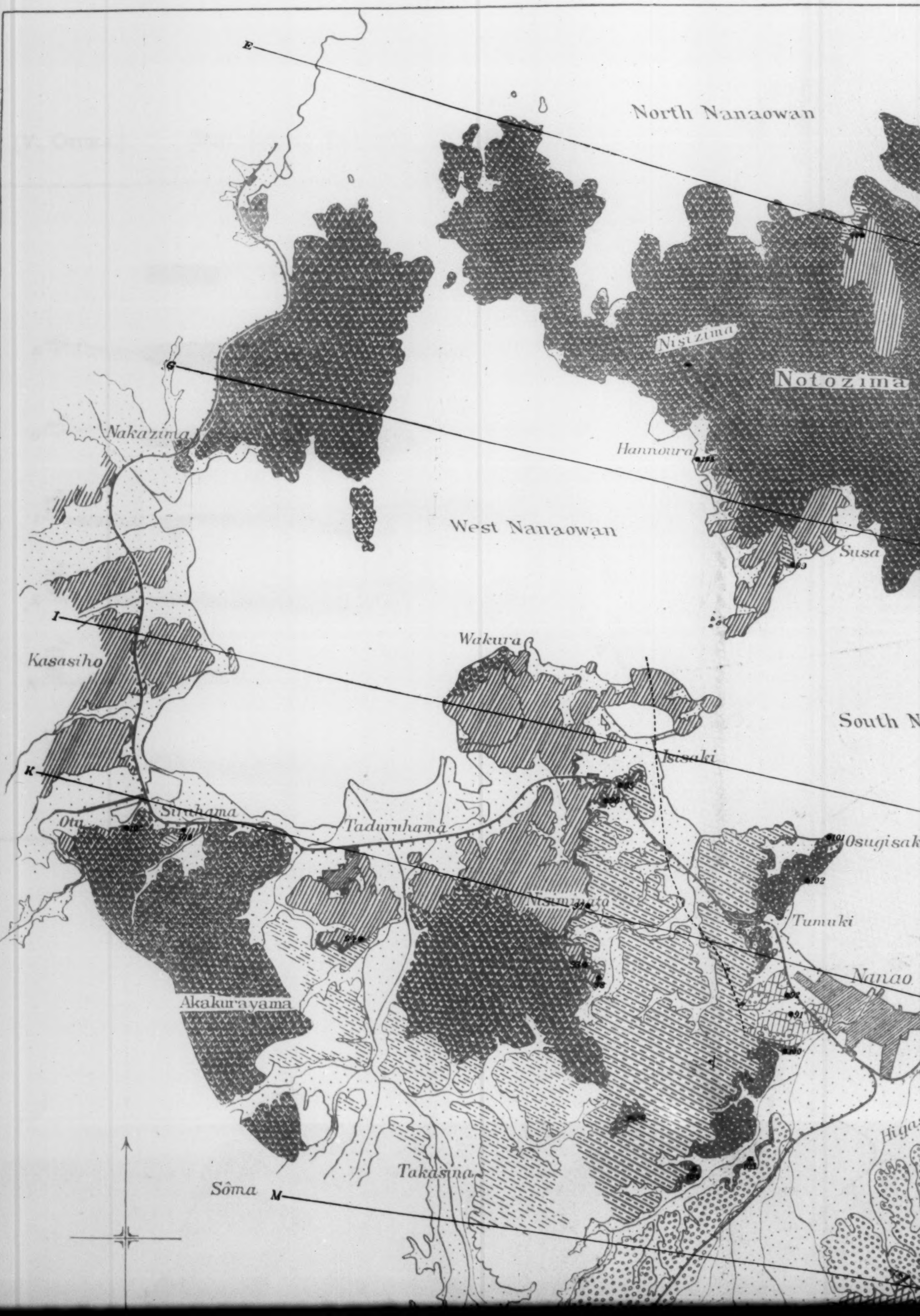
E
North Nanaowan
Nisizima
Notozima
G
Nakazima
Hannoura
West Nanaowan
Susa
I
Wakura
Kasasiho
South N
Isisaki
K
Sirahama
Oti
Taduruhama
Osugisak
Tumuki
Nanao
Akakurayama
Takasina
Sôma
M
Higa

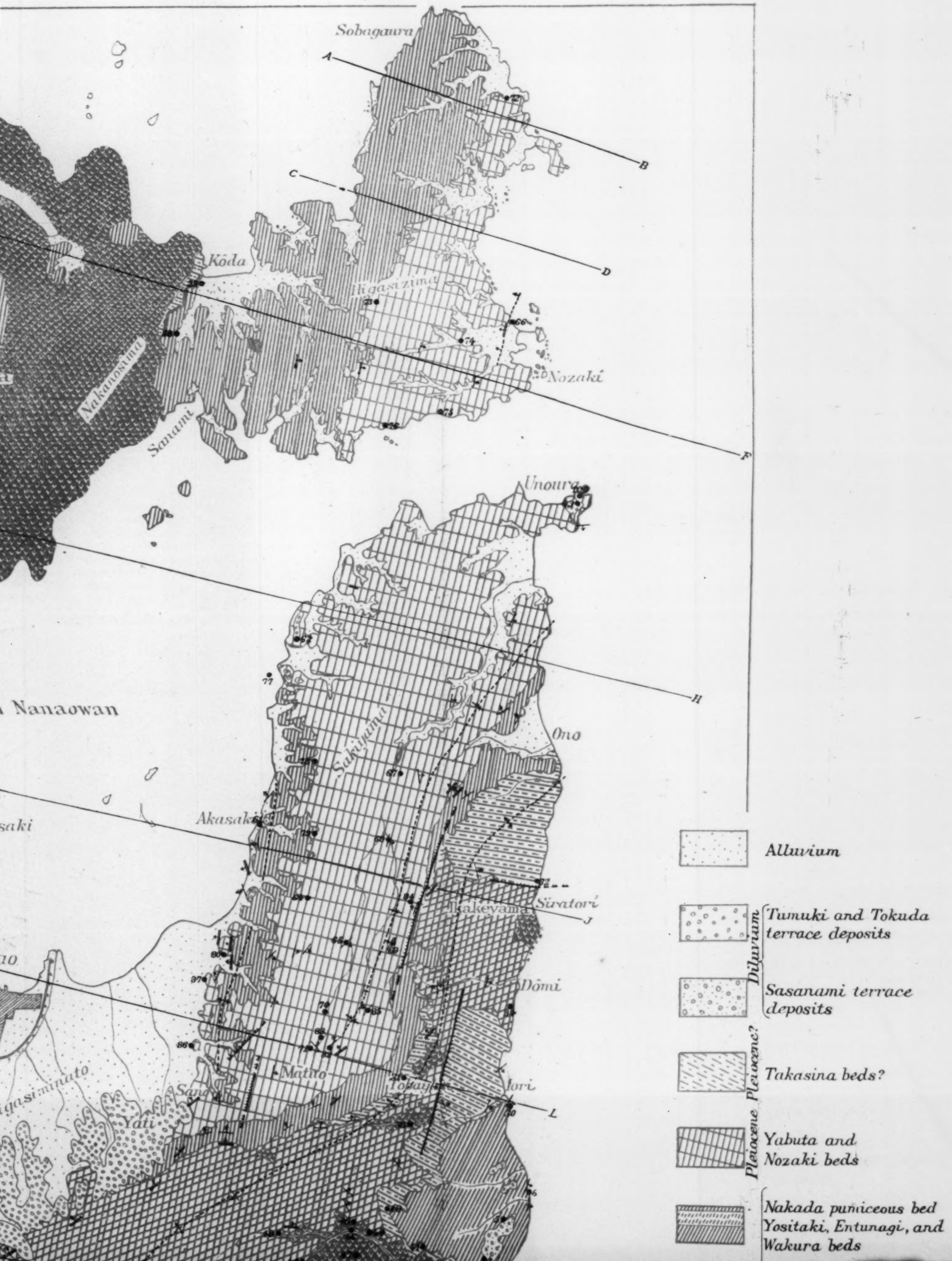
Sobagaura
A
B
C
D
Kôda
Higasizima
Nakanosima
Sanami
Nozaki
F
Unoura
H
Nanaowan
Sakiyama
Ono
Akasaki
Siratori
J
Takeyama
Dômi
Matto
Sano
Tokayu
Iori
L
Yati
Higasiminato
Alluvium
Tumuki and Tokuda terrace deposits
Sasanami terrace deposits
Diluvium
Takasina beds?
Pleiocene?
Yabuta and Nozaki beds
Pleiocene
Nakada pumiceous bed
Yositaki, Entunagi, and Wakura beds

（震研彙報　第十三號　圖版　大塚）

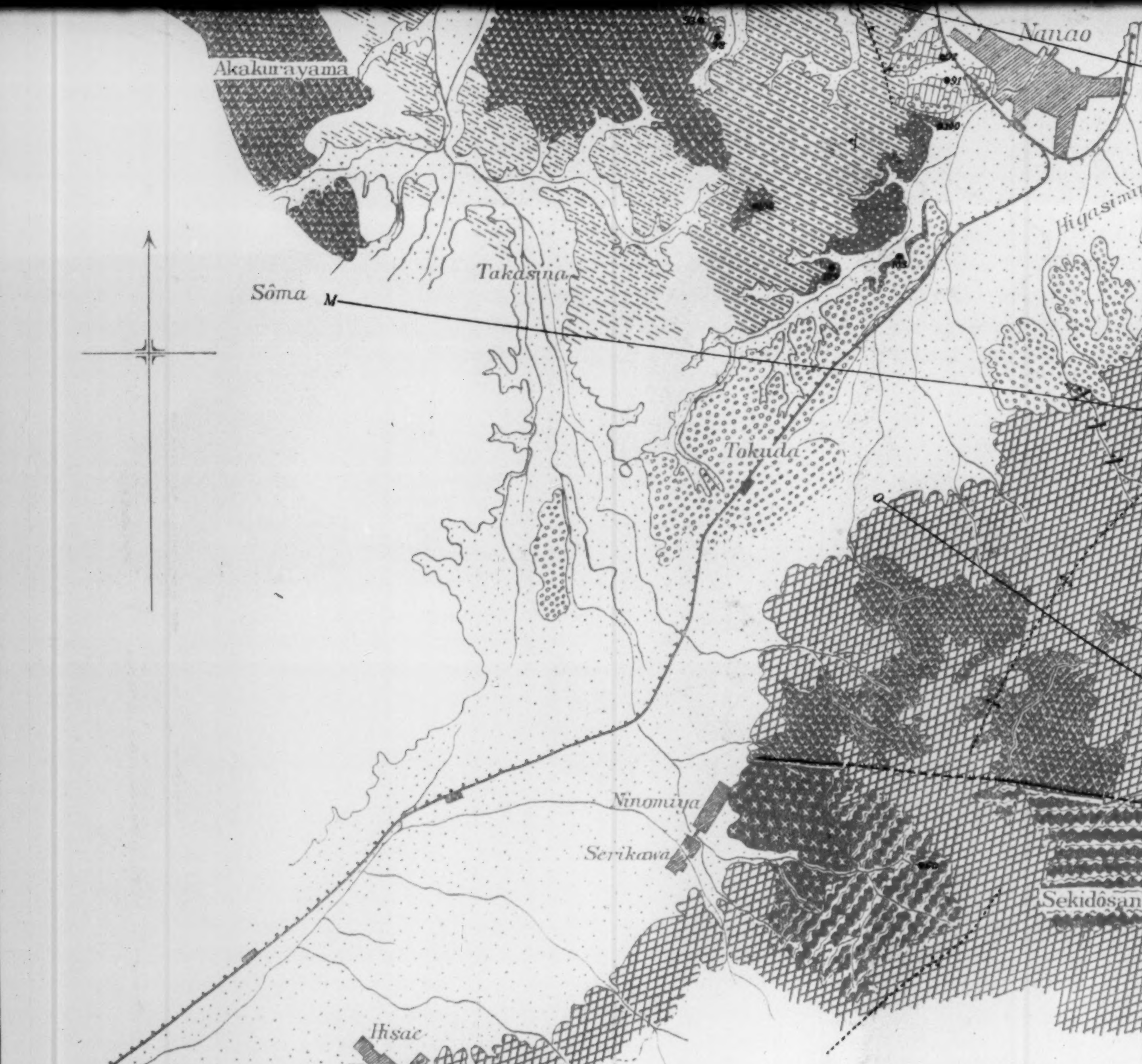
Akakurayama
Nanao
Higasimi
Sôma
M
Takasina
Tokuda
O
Ninomiya
Serikawa
Sekidôsan
Hisae
0
1
2
3
4
5 km.

Fig. 11.
Geological Map of the Env
(by Yanosuke OTUKA

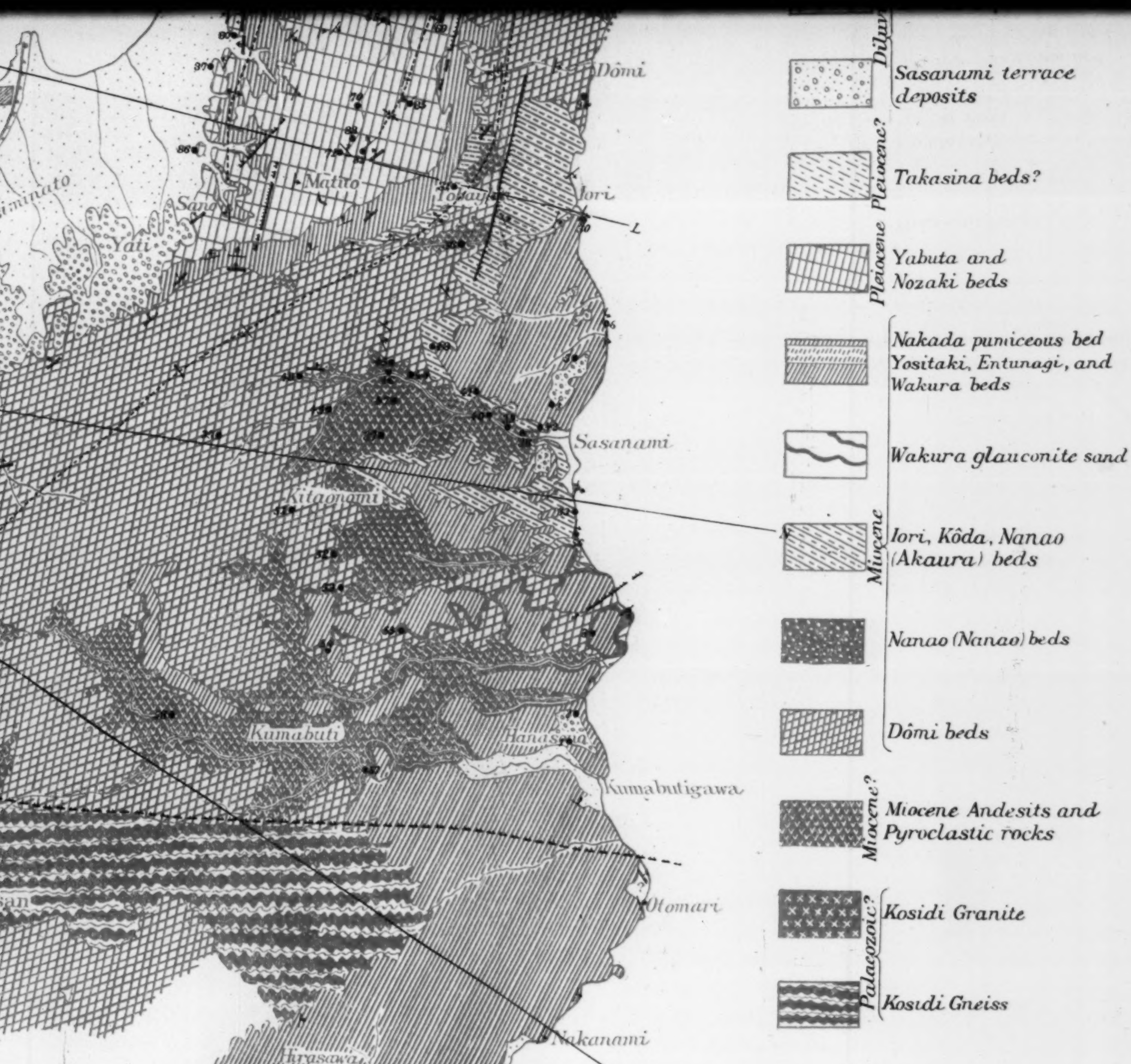
Dômi
Matito
Sano
Yati
Iori
Touyi
L
Sasanami
Kitaonami
N
Kumabuti
Hanasaki
Kumabutigawa
Otomari
Nakanami
Hirasawa
P
Q
Nakada
Sugata
Abusima
Unami
R
Diluv.
Sasanami terrace deposits
Pleiocene?
Takasina beds?
Pleiocene
Yabuta and Nozaki beds
Nakada pumiceous bed
Yositaki, Entunagi, and Wakura beds
Wakura glauconite sand
Miocene
Iori, Kôda, Nanao (Akaura) beds
Nanao (Nanao) beds
Dômi beds
Miocene?
Miocene Andesits and Pyroclastic rocks
Palaeozoic?
Kosidi Granite
Kosidi Gneiss
Fault
Anticline
Syncline
Flexure
0-10° 11-30° 35-50° 51-70° 71-90° Dip and Strike
•51 Localities

.

nvirons of Nanao

KA. 1935).

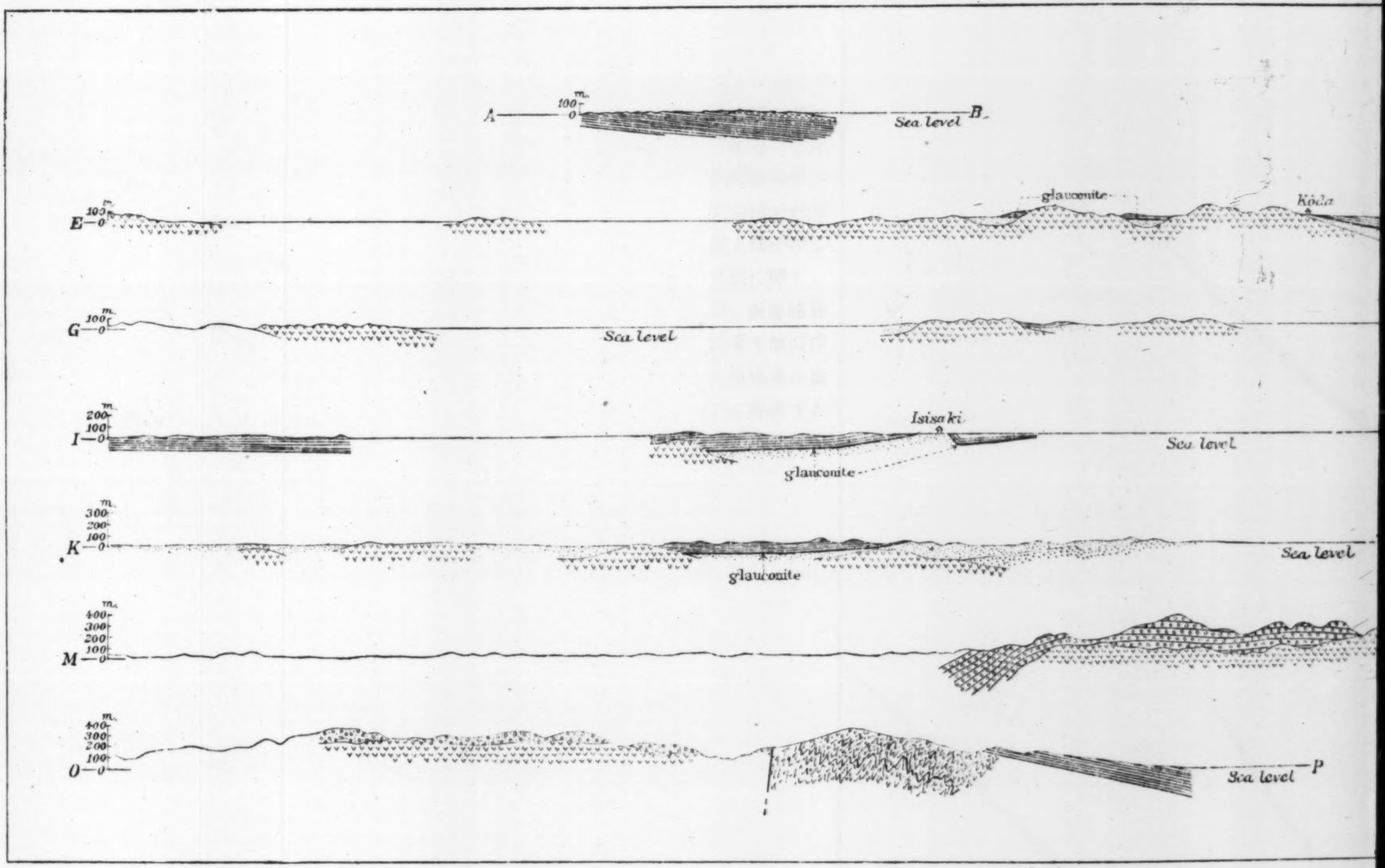
A
100 m.
0
B
Sea level
E
100 m.
0
glauconite
Kōda
G
100 m.
0
Sea level
I
200 m.
100
0
Isisaki
glauconite
Sea level
K
300 m.
200
100
0
glauconite
Sea level
M
400 m.
300
200
100
0
O
400 m.
300
200
100
0
Sea level
P

Fig. 13. Geological profile of the environs of Nanao by Yanosuke OTUK

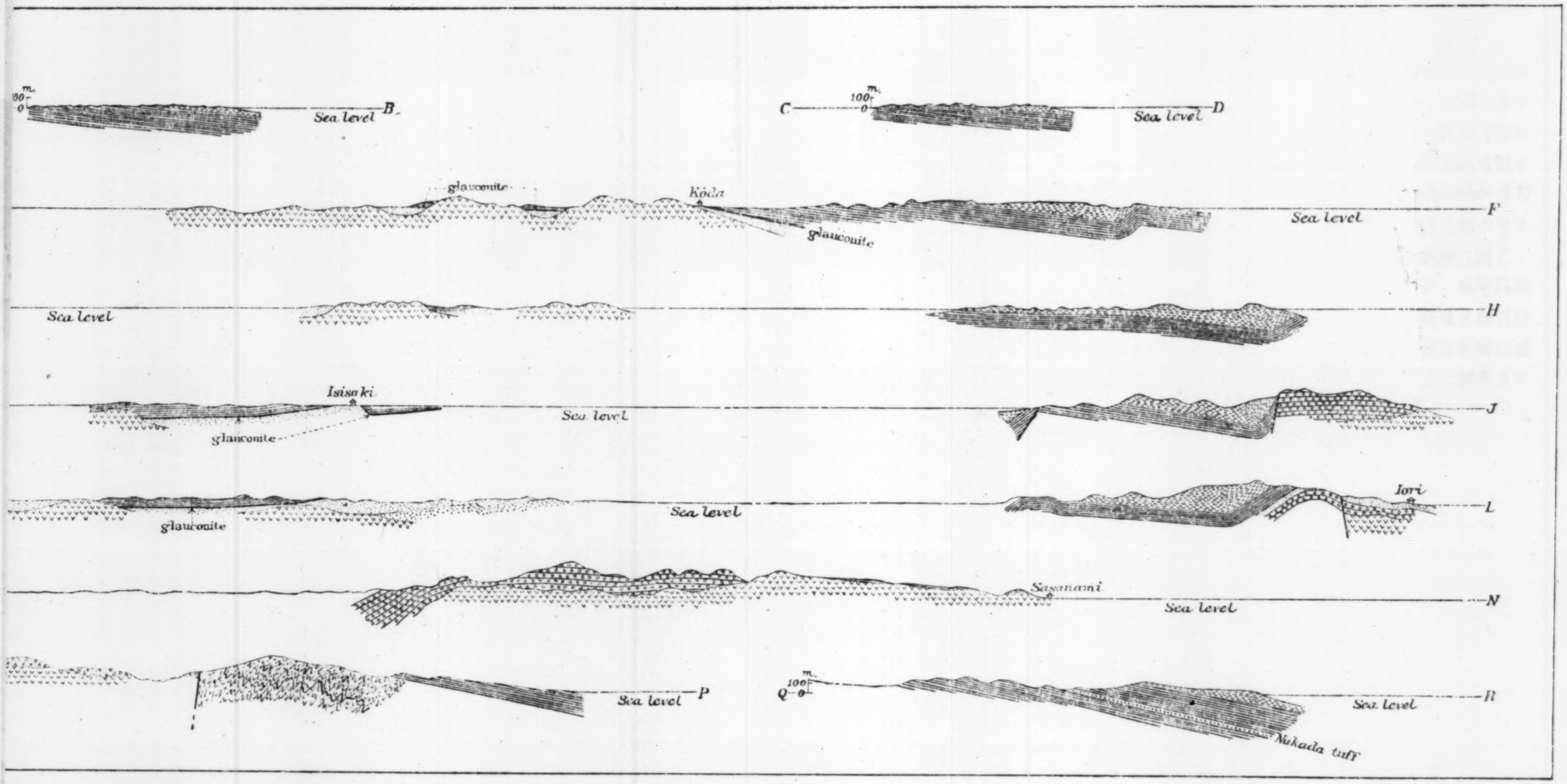
m.
100
0
Sea level
B
C
m.
100
0
Sea level
D
glauconite
Kōda
glauconite
Sea level
F
Sea level
H
Isisaki
glauconite
Sea level
J
glauconite
Sea level
Iori
L
Sasanami
Sea level
N
Sea level
P
m.
100
Q
0
Sea level
R
Nakada tuff

Fig. 13. Geological profile of the environs of Nanao by Yanosuke OTUKA. (1935).

[illegible] of Nasu by Yanosuke OTUKA (1935).

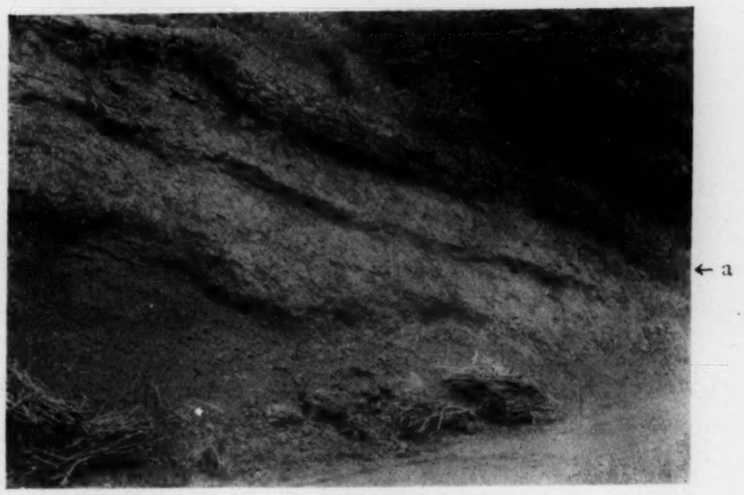

Fig. 15. Exposure of Wakura glauconite sandstone (a) near Oiide.

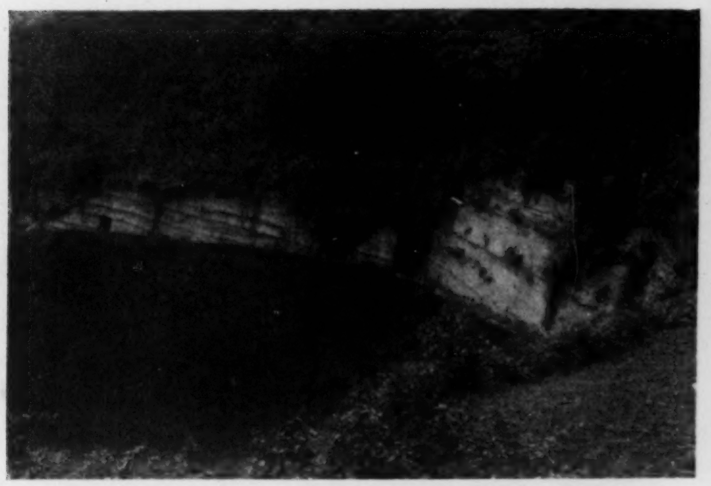

Fig. 17. Alternation of marly beds of Lower Yabuta series near Akasaki.

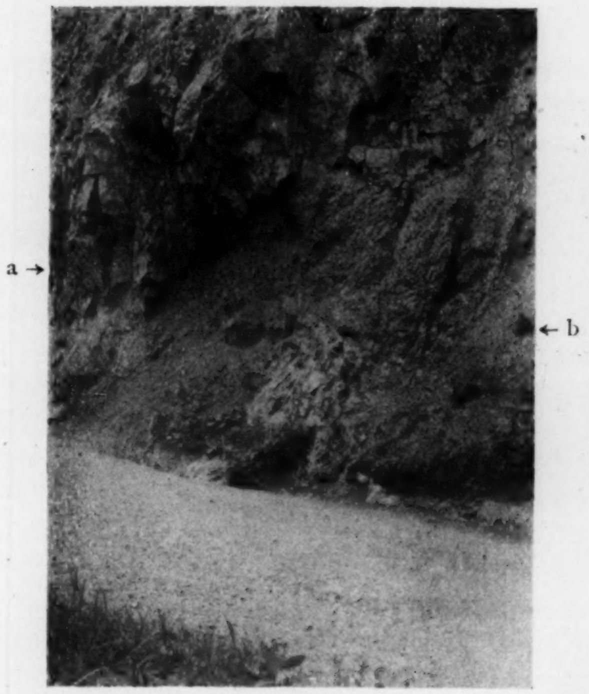

Fig. 16. Exposure of Kooziyama andesite (a) which intruded into yellow tuff (b).

Fig. 18. Exposure of fault of Ikakeyama flexed zone. The Yabuta series are exposed on the left side of this figure, and the Domi series on the right.

（震研彙報 第十三號 圖版 大塚）

能登半島南部邑知地溝 (2)

地震研究所 **大塚彌之助**

この論文に於いては邑知地溝の東北部の層位及び構造に就いて論じた.

著者は先づこの地域を邑知地溝の東南部・邑知地溝の東南側・邑知地溝の西北部に分ち，之等各地域の層序を決定してゐる.（第2表參照）. 七尾統の地質時代は中上部中新統としてゐる.

次に之等各地域の層序を比較對比して，地質構造論を行ふ基礎を作つてゐる.

地質構造の章では，第1に造陸運動的地殼運動を考察してゐる. 著者によれば火山活動は沈降運動を伴ふことを指摘し，百海火山活動期に七尾海進時代が續いてゐることを擧げてゐる.

第2に斷層・皺曲等地層の層位から知られる地殼運動を論じ，邑知地溝に向つて落込む地溝式地質構造の存在を指摘してゐる. 併し注意しておくことはこの地溝式をなす各地塊の境界は斷層でなく主として撓曲構造によつて代表されてゐる事實である. 且つ一般傾斜は地溝の東南では東南方へ，地溝の西北では西北方へ向つてゐることである. この地質構造上の地溝は藪田統堆積中か又はそれより以後に構成せられたものであると. この地溝構造構成以前の邑知地溝地域が地質學上如何なる構造上の特性を持つてゐたかは，興味ある問題であるが，著者は七尾統上部の厚さの分布圖を作り，邑知地溝地域が最も薄くなつてゐるので，之を藪田統堆積以前の削剝に歸し，此の地域に軸を有する曲隆運動の存在を推定してゐる. 著者は之等の地質學的事實が，曲隆構造背部に張力裂罅を生じて，その背部各地塊が重力によつて陷入る諸種の模型實驗の結果と類似性あるを說いてゐる. 各地塊の境界は實驗によれば斷層で代表されるべきであるが，邑知地溝の場合には撓曲構造で境界が代表されてゐるので，この構造上の相異の說明として，地下に潛在する地塊構造を認めやうとしてゐる.

---

68. *The Oti Graben in Southern Noto peninsula, Japan.*
(*Part 3*)

By Yanosuke OTUKA,
Earthquake Research Institute.

(Received Sept. 20, 1935.)

8. Description of fossils.

GASTROPODA.

***Emarginula* LAMARCK, 1801.**

***Emarginula crassicostata* SOWERBY**

Plate LIII, Figures 21 a, b.

1863 *Emarginula crassicostata* SOWERBY, Thesaurus Conchyliorum, **3**, p. 214, Pl. 11, figs. 41, 42.

1934 *Emarginula crassicostata*, HIRASE, A collection of Japanese Shells, Pl. 63, fig. 1.

SOWERBY describes this species as follows:

"Shell oval, somewhat narrowed in front, with close, thick, noduliferous radiating ribs, the interstices clathrate; apex posterior; back arched; cicatrix above the suture carinated, foveolate. Oval, arched; with thick, rather close beaded ribs, the apex very posterior."

Three specimens collected.

Geologic age.—Pleistocene-Recent. Geogr. distr.—Central and western Japan. Occurrence.—Hiradoko (3 specimens), Hypotype No. 2076 in Coll. Earthquake Research Institute (height 3·7 mm.)

***Puncturella* LOWE, 1827.**

***Puncturella nobilis* (A. ADAMS)**

Plate LIII, Figures 23 a, b, c, 23′ a, b.

1866 *Cemoria nobilis* A. ADAMS, Ann. Mag. Nat. Hist. p. 422.

1863 *Cemoria nobilis*, SOWERBY, Thes. Conch., **3**, p. 208, Pl. 245, figs. 6~9.

1922 *Puncturella nobilis*, YOKOYAMA, Jour. Coll. Sci. Tokyo Imp. Uuiv. **44**, 1, p. 116, Pl. 6, fig. 4.

Geol. age.—Pliocene-Recent. Geogr. distr.—Matusima Bay; Mutu Bay; Hokkaido. Occurrence.—Simazaki (Himi Beds. 3 specimens) Hypotype No. 2024, Coll. Earthq. Res. Inst. (height 4·2 mm.)

There are two forms in the writer's collection. The description of slender form (Fig. 23 a, b, c, in Plate LIII) is as follows:

"Shell small, conical; vertex acuminate, vertically minutely coiled; radiating ribs strong, equidistant, with weak secondary radiating rib (sometimes 2 or obsolete) in the interstices; interstices concentrically striated. Number of primary radiating ribs 17 in type specimen.

Measurements.—Height 5 mm, length 6 mm, width 4·8 mm. (with No. 2025, Coll. Earthq. Res. Inst.) Occur.- Simazaki (Himi series).

Sowerby's Fig. 9 of *Puncturella nobilis* in Pl. 245 (SOWERBY's Thesaurus Conch. 3) resembles this form in its outline. This form has a slender and higher shell than the form of Fig. 23′ a, b in Plate LIII."

***Puncturella hirasei* OTUKA n. n.**

Plate LIII, Figures 22 a, b, c.

1934 *Puncturella gigantea*, HIRASE, Coll. Japanese Shells, Pl. 62, fig. 7. (not of SCHEPMAN, 1908.)

Shell moderate, conical; vertex small, acute, vertically minutely coiled; radiating ribs numerous, more than 60, more or less equidistant, sometimes with weak secondary ribs in interstices. Interstices narrow elongated lozenge. Margin crenulated.

Fossil specimen has more or less broader radiating ribs, and narrower interstices than the living specimen.

Geol. age.—Pliocene-Recent. Geogr. distr.—Northern Japan, and Japan Sea. Occur.—Simazaki (Himi beds), Monotype No. 2026, Coll. Earthq. Res. Inst.

Puncturella (*Craniopsis*) *gigantea* SCHEPMAN[29] is closely allied to this new species, but this species is more compressed shell. *Puncturella hirasei* Otuka measures 9·5 mm high; 18·5 mm long diameter; 14·5 mm short diameter.

Puncturella galeata GOULD[30] in another allied shell. But Gould's species is higher shell with rude radiating ribs.

Puncturella major DALL[31] is closely allied to *Puncturella hirasei* Otuka, but the former species has numerous fine ribs.

***Diodora* GRAY, 1821.**

***Diodora sieboldii* (REEVE)**

Plate LIII, Figure 24.

1850 *Fissurella sieboldii* REEVE, Conch. Icon., sp. 102.

1928 *Fissurella sieboldii*, YOKOYAMA, Imp. Geol. Surv. Japan, Rep. 101, p. 124, Pl. 19, fig. 4.

1934 *Diodora sieboldii*, HIRASE, Coll. Japanese Shells. Pl. 62, fig. 5.

Geol. age.—Pleistocene-Recent. Geogr. distr.—Tiba-pref., Sagami Bay, Wakayama pref., Nagasaki pref., Amami-Osima, Hukui pref. Oc-

---

29) SCHEPMAN, Siboga Exped. *Prosobranchiata*, Pt. 1, p. 88, (1908). Pl. 7, fig. 4.

30) GOULD, *Proc. Bost. Soc. Nat. Hist.*, **2** (1846), 159.

31) DALL, *Proc. U. S. Nat. Mus.*, **14**, 186.

currence—Miyainu (1)* (Hypotype No. 2077, Coll. E. R. I. (length 6·5 mm); Tumuki.

Patelloida QUOY and GAIMARD, 1834.

Patelloida saccharina (LINNÉ)

Pl. LIII. Fig. 25.

1758 *Patella saccharina* LINNÉ, Syst. Nat. ed. 10, p. 781.

1934 *Patelloida saccharina*, HIRASE, A collection of Japanese shells, Pl. 56, f. 1.

Geol. age.—Pleistocene-Recent. Geogr. distr.—Tiba pref., Amami-Osima (KURODA), Toyama Bay (KIKUCHI). Occurrence.—Miyainu (1) Hypotype No. 2078, Coll. E. R. I. (length 23·5 mm)

Patelloida conulus (DUNKER)

Pl. LIII, Fig. 26. a, b.

1861 *Patella conulus* DUNKER, Mollusca Japonica, p. 24, Pl. 3, f. 20.

Shell small, conical, slightly convex; aperture nearly elliptical, vertex more or less blunt, smooth, nearly central, but minute; surface ornamented with obsolete radiating ribs (number about 40), decussated with concentric lines of growth; margin entire, polished, thinned; anterior and posterior margin slightly produced; inner surface smooth, with large muscular impression.

Geol. age.—Pleistocene-Recent. Geogr. distr.—Hukui pref., Miyagi pref. Occur.—Miyainu (3) No. 2080; Hiradoko (8) Hypotype No. 2079, Coll. E. R. I. (length 3·8 mm).

Euchelus PHILIPPI, 1847.

Euchelus foveolatus (A. ADAMS)

Pl. LIII. Fig. 27 a, b, c.

1851 *Monodonta foveolata* A. ADAMS, Proc. Zool. Soc. London, p. 176.

SOWERBY describes this species as follows: "Shell small, globose-conic, solid, white, very minutely perforated; spire short; whorls about 4, convex, encircled by strong spiral ribs, the interstices between them deeply, coarsely pitted by the prominence of strong, regular, longitudinal lamellae, continuous over the spirals. The penultimate and next earlier whorls have 3 spirals (the subsutural one sometimes subobsolete), the outer lip inserted upon the fourth; on the last whorl near the aperture there are 7, but sometimes more, by reason of the interpolation of one or two interstitial riblets on the upper surface; two or three submedian ribs are generally more prominent; suture canaliculate; aperture rounded, columella slightly concave, rather wide, flat, not toothed on base, umbilical perforation minute.

No. 1.	height 7·2 mm,	diameter 7 mm (Hypotype).
No. 2.	" 5 mm,	" 5 mm.

---

* Number of collected specimen.

Geogr. distr.—Philippines. Geol. age.—Pleistocene-Recent. Occurrence.—Hiradoko (5), Hypotype No. 2081, Coll. E. R. I.

***Solariella* S. Wood, 1842.**

***Solariella* aff. *angulata* (Tokunaga)**

1906 *Trochus* (*Minolia*) *angulatus* Tokunaga, Jour. Coll. Sci. Imp. Univ. Tokyo, **21**, 2, p. 30, Pl 2, f. 5.

1922 *Solariella angulata*, Yokoyama, Jour. Coll. Sci. Tokyo Imp. Univ. **44**, 1, p. 111, Pl. 5, f. 20.

Specimens from Hiradoko very small. Living specimens collected from Japan Sea and Sagami Bay. Measurements of specimens from Sagami Bay: height 14 mm, diameter 14 mm.

Geologic. age.—Lower Pleistocene-Recent. Geographic distribution. —Sagami Bay, Kisyû Nada, and Hukui pref. Southerm Kwanto (Tiba pref.) Occurrence.—Hiradoko (2) No. 2082, Coll. Earthq. Research Institute. (diameter 1·8 mm)

***Tegula* Lesson, 1832.**

***Tegula* (*Chlorostoma*) *rustica* (Gmelin)**

Pl. LIII. Fig. 28, a, b.

Trochus rustica Chemnitz, Conch. Cab. **5**, p. 89, f. 1645, 1646.

1821—0 *Trochus rustica* Gmelin, Syst. Nat. ed. 13, p. 3572.

1934 *Tegula* (*Chlorostoma*) *rustica*, Hirase, Coll. Jap. Shell, Pl. 67, f. 7.

Geol. age.—Pleistocene-Recent. Geogr. distr.—Honsyu, Sikoku, and Kyusyu. Occurrence. - Tumuki (1) Hypotype No. 2086, Coll. E. R. I., (height 28 mm; diameter 29 mm).

***Umbonium* Link, 1807.**

***Umbonium* (*Suchium*) *akitanum* Suzuki**

Pl. LIV, Fig. 62, 63.

1934 *Umbonium akitanum* Suzuki, Jour. Geol. Soc. Tokyo, **41**, p. 63, f. 1.

Shell depressed-conical; whorls about 5~6, of which first two or three embryonal and smooth, the remainder slightly convex; surface spirally sculptured, the sculpture consisting of many spiral threads whose interspaces are narrower than threads. Number of spiral threads about 10 or 9 on penultimate whorl; upper part of spiral threads *moniliferum* type; base slightly convex with fine spiral lines.

Although this species has a striking resemblance to *Umbonium* (*Suchium*) *moniliferum costatum* (Kiener)[32] in its sculpture, the former has a depressed shell with more weak spiral threads and weak basal spiral lines.

Prof. M. Yokoyama[33] reported this species from the Pliocene formation of the Akita Oil-fields as *Umbonium suchiense*, but *Umbo-*

---

[32] Kiener, *Species General Iconographic Coquilles Vivantes, Roulette*, (1838 ~9) p. 10, Pl. 2, fig. 5.

[33] M. Yokoyama, *Jour. Fac. Sci. Imp. Univ. Tokyo* (2), **1**, 9 (1926), p. 380.

nium suchiense YOKOYAMA[34] has a subsutural tubercle band and many sharp spiral ridges.

Although the specimen from Simazaki is fragmental, the writer is confident that it is the very species noted by K. SUZUKI.

Geol. age.—Pliocene of Northwestern Japan. Occour.—Simazaki (Himi series) Hypotype No. 2028, Coll. E. R. I. (diameter 11·5 mm. Pl. LIV, fig. 52).

Skenea **FLEMING, 1824.**

Skenea nipponica **? YOKOYAMA**

Plate LIV, Figures 93 a, b, c.

1920 *Skenea nipponica* YOKOYAMA, Jour. Coll. Sci. Tokyo Imp. Univ. **39**, art. 6, p. 75, Pl. 5, fig. 1.

1922 *Skenea nipponica*, YOKOYAMA, Jour. Coll. Sci. Tokyo Imp. Univ. **44**, art. 1, p. 81, Pl. 4, fig. 7.

Geol. age.—Lower Pleistocene-Recent. Geogr. distr.—Central Japan. Occur.—Tumuki (2) Hypotype No. 2384, Akasaki (2).

Homalopoma **CARPENTER, 1864.**

Homalopoma amussitata **(GOULD)**

Pl. LIV, Fig. 61.

1861 *Turbo amussitata* GOULD, Proc. Boston Soc. Nat. Hist., **8**, 14.

1820 *Leptothyra amussitata*, YOKOYAMA, Jour. Coll. Sci. Tokyo Imp. Univ., **39**, p. 85, Pl. 5, fig. 21.

Geol. age.—Hokkaido, Sanriku coast, Matusima Bay. Geogr. distr. —Pliocene-recent. Occur.—Simazaki, (Himi series), Hypotype No. 2043, Coll. E. R. I. (diameter 7 mm).

Turbo **LINNÉ, 1758.**

Turbo (Lunella) coronatus coreensis **RÉCLUZ**

1853 *Turbo coreenisis* RÉCLUZ, Jour. de Conch. p. 1245, Pl. 8, f. 2.

1920 *Turbo (Marmorostoma) coreensis*, YOKOYAMA, Jour. Coll. Sci. Tokyo, Imp. Univ., **39**, 6, p. 84~85, Pl. 5, f. 19, 20.

1934 *Turbo (Lunella) coreensis*, HIRASE, Coll. Japanese Shell, Pl. 74, f. 1.

Geol. age.—Pleistocene-Recent. Geogr. distr.—South Tyosen, Honsyu, Sikoku, Kyusyu. Occur.—Tumuki (5) No. 2084; Akasaki (2) No. 2053; Miyainu (1) No. 2085, Coll. E. R. I.

Astraea **(BOLTEN) RÖDING, 1798.**

Astraea (Calcar) haematraga **(MENKE)**

Pl. LIII, Fig. 40, a, b.

1829 *Trochus haematragus* MENKE, Catal. Coll. Malsb. Pyrmonti, p. 18.

1924 *Astralium (Cyclocantha) haematragus*, YOKOYAMA, Jour. Coll. Sci. Tokyo Imp. Univ., **45**, 1, p. 32, Pl. 2, f. 7.

1934 *Astraea (Calcar) haematraga*, HIRASE, Coll. Jap. Shell, Pl. 74, f. 4.

---

[34] M. YOKOYAMA, *Jour. Coll. Sci. Tokyo Imp. Univ.*, **45**, 2 (1923), p. 13, Pl. 2, fig. 1.

Geol. age. — Pleistocene-Recent. Geogr. distr.—Tiba prefecture, Wakayama pref., Kagosima pref., Toyama Bay, Hukui pref. Occur.—Miyainu (13) Hypotype No. 2088 (diameter 18·5 mm); Hiradoko (3) No. 2087.

***Iravadia* BLANFORD, 1867.**

***Iravadia annulata* (DUNKER)**

Pl. LIII, Fig. 34; text fig. (Fig. 220).

1860 *Rissoina annulata* DUNKER, in Malakoz. Bl. **6**, p. 235.

1861 *Rissoina annulata* DUNKER, Moll. Jap. p. 12, Pl. 2, f. 12.

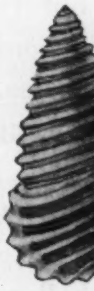

Fig. 220

Shell small, elongate ovate; whorls about 7, first two embryonal and smooth, remainder distinctly spirally keeled; number of keel two or three on upper three whorls, and three or four on last two whorls; interspaces between these keels ornamented with two or three keels; aperture with varice, on which keels are extended; inner surface of aperture smooth; inner lip slightly arcuated. Measurements on Hiradoko specimens are.

	Height	Diameter	Apical angles.	
No. 1.	4·3 mm	2·1 mm	50°~55°	(Hypotype)
No. 2.	4·1 mm	1·8 mm	〃	
No. 3.	4·0 mm	2·0 mm	〃	

Iravadia ornata Blanford[35] resembles this species, but the latter has a higher spire and finer regular keels.

The former species has two broad spiral keels on the penultimate whorl.

Geol. age.—Pleistocene-Recent. Geogr. distr.—Japan (DUNKER), Hukui pref. Occur.—Miyainu (3), No. 2090; Hiradoko (3) Hypotype No. 2089, Coll. E. R. I.

***Cingula* (FLEMING 1828) H. & A. ADAMS 1854.**

***Cingula (Pseudosetia) paludinoides* (YOKOYAMA)**

1927 *Rissoa (Cingula) paludinoides* YOKOYAMA, Jour. Fac. Sci. Imp. Univ. Tokyo, (2), **1**, 10, p. 415, Pl. 46, f. 23.

Geol. age.—Pleistocene-Recent. Geogr. distr.—Tokyo. Occurrence.—Hiradoko (5) No. 2156, Coll. E. R. I.

***Amphithalamus* CARPENTER 1865.**

Amphithalamus yendoi* (YOKOYAMA)

Plate LIV, Figure 86 a, b.

1927 *Rissoina yendoi* YOKOYAMA, Jour. Fac. Sci. Imp. Univ. Tokyo, (2), **1**, 10, p. 415, Pl. 46, f. 27.

1927 *Turbonilla (Careliopsis) filiola* YOKOYAMA, Jour. Fac. Sci. Imp. Univ. Tokyo, (2), 1, 10, pp. 453, 454, Pl. 51, f. 26.

---

[35] Blanford in Küster, Conch Cab., Pl. 15, b. fig. 1.

* *Rissoina (Zebinella) yendoi* YOKOYAMA in Table I, Part I.

This species is closely allied to *Rissoina* (*Amphithalamus*) *alphesiboei* MELVILL.[36] But the latter species has a narrower shell.

Rissoina (*Amphithalamus*) *aristoei* MELVILL[37] is another allied shell, but this species is shorter than the Yokoyama's species.

Turbonilla (*Careliopsis*) *filiola* YOKOYAMA may be identical with this species.

Geol. age.—Pleistocene-?. Occur.—Miyainu (3) Hypotype No. 2094, Coll. Earthq. Res. Inst.

Amphithalamus ? _tumukiensis_ OTUKA n. sp.*

Fig· 221 (text figure.)

Shell small, elongate ovate; nuclear whorls about 2 1/2 well rounded, smooth; spirals of nuclear whorls more or less compressed; post-nuclear whorls about 3 1/2, inflated, well rounded, marked by fine incised, equally spaced spiral grooves, of which about 37 on penultimate whorl, and fine unequally spaced axial incremental lines; suture strongly constricted; periphery of last whorl well rounded. Aperture large, semi-circle, slightly expanded, its margin not attached to preceeding whorls; its basal part broadly canaliculated. Base marked by fine incised grooves and fine axial incremental lines as on preceeding whorls; umbilical chink very narrow.

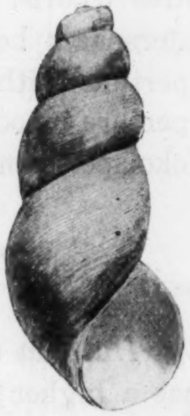

Fig. 221

Measurement: Height 2·8 mm, diameter 1·1 mm.

The present writer could not assign this species to any genus. *Cingula* H. and A. ADAMS, 1854, is a genus with characteritics similar to this species, but *Cingula* has no canaliculate aperture. Genus *Amphithalamus* CARPENTER, 1865, does not represent this species.

Cingula aleutica DALL[38] in an allied form of this new species, but the former has more rounded aperture and more inflated whorls.

Geol. age.—Pleistocene. Geogr. distr.—Tumuki, Isikawa prefecture. Occurence.—Tumuki, Noto (1), Monotype No. 2096, Coll. E. R. I.

Alvania RISSO, 1826.

Alvania concinna A. ADAMS

1861 *Alvania concinna* A. ADAMS, Ann. Mag. Nat. p. 138.

---

[36] MELVILL, *Proc. Mal. Soc.* **10**, (1912~3), p. 244, Pl. 11, fig. 5 (5 mm high, 2 mm diameter.)

[37] MELVILL, *Proc. Mal. Soc.* **10**, (1912~3), p. 245, Pl. 11, fig. 6. (3·5 mm high, 1 mm diameter.)

[38] DALL, *Proc. U. S. Nat. Mus.*, **9**, 307 (1886), Pl. 3, fig. 11.

* *Amphithalamus* sp. in Table I, Part I.

1924 *Rissoa* (*Alvania*) *concinna*, YOKOYAMA, Jour. Coll. Sci. Tokyo Imp. Univ. **45**, 1, p. 25, Pl. 5, f. 11.

1928 *Rissoa* (*Alvania*) *sadoensis* YOKOYAMA, Jour. Fac. Sci. Imp. Univ. Tokyo, (2), **1**, 8, p. 272, Pl. 33, f. 12.

Shell small, ovate conic, imperforate, solid; whorls about 6, of which 2 or 2 1/2 embryonal and smooth, remainder convex, longitudinally costate and spirally striated; longitudinal costae strong on upper whorls, but obsolete on later whorls. Costae rounded, slightly oblique, somewhat curved with concave side towards front, about 16 on upper whorl and about 12 or 11 on penultimate whorl, close together, distinct near lower suture. Periphery rounded; base abruptly narrowed, with about 10 spiral threads; aperture oval, pointed behind, sharply rounded in front, with periostome obsoleted behind inner margin of aperture.

Geol. age.—Pliocene-Recent. Geogr. distr.—Northern and western Japan (Matusima Bay, Hukui prefecture, and Tusima.) Occ.—Miyainu (8) No. 2092; Tumuki (2) No. 2091, Collection of the Earthquake Research Institute.

According to KURODA, there are many intermediate forms between *Alvania concinna* A. ADAMS and *Alvania sadoensis* YOKOYAMA. He thinks that these two species are one and the same, although *Alvania concinna* A. ADAMS has 2 or 2 1/2 nuclear whorls, whereas *Alvania sadoensis* YOKOYAMA has only 2 or 1 1/2, Although the longitudinal costae of the former is obsolete on the last whorl, the latter has a strong costae on it.

Rissoina D'ORBIGNY, 1840.

Rissoina (*Phosinella*) *media* SCHWARTZ

1860 *Rissoina media* SCHWARTZ, Fam. Rissoiden, p. 92, fig 56.

1924 *Rissoina* (*Phosinella*) *cancellata*, YOKOYAMA, Jour. Coll. Sci. Tokyo Imp. Univ., **45**, 1, p. 26. Pl. 5, fig. 10.

Tryon gives the following descripetton of this species:

"Solid, white or yellowish, semipellucid, shining, with 18~20 longitudinal crossed by spiral ridges. Whorls 8, subconvex, with distinct but narrow suture, the base with a funiculum of three spiral riblets, lip sinuous, produced below, varix crenulated."

Geol. age.—Pleistocene-Recent. Geogr. distr.—Hukui prefecture, Ceylon, Java, Nicobar Is. Occurrence.—Miyainu (1) No. 2092, Collection of the Earthq. Res. Inst.

Rissoina (*Rissoina*) *laevicostulata* PILSBRY

Plate LIII, Fig. 29, a, b.

1904 *Rissoina* (*Rissolina*) *laevicostulata* PILSBRY, Proc. Acad. Nat. Sci. Philadelhia, **56**, p. 27, Pl. 5, fig. 54, 54 a.

PILSBRY described this species in detail as follows:

"Shell narrowly ovate acuminate, regularly tapering from the last whorl, white, with a red-brown bluish on the back of the last whorl, moderately solid. Sculpture of about 20 rounded, obliquely longitudinal slightly sinuous ribs about as wide as the intervals, both ribs and intervals smooth. Whorls about 8, moderately convex, the last with a very strong, heavy varix behind the outer lip, and with a convex siphonal fasciole at the base, bounded above by a groove and regularly plicate, the ribs passing over it. Aperture semioval, the outer lip thick and sinuous, columella margin but slightly concave. A shallow but distinct channel at its base in the basal margin."

This form is related to *Rissoina costulata* (DUNKER)[39], but differs from it in its more numerous ribs. *Rissoina plicatula* (GOULD)[40], an unfigured species, also seems to be related to it.

Geol. age.—Pleistocene-Recent. Geogr. distr.—Sagami Bay, Hukui prefecture. Occurrence.—Tumuki (40) No. 2321; Miyainu (2), Hypotype No. 2322; Hiradoko (13) No. 2323; Akasaki (3) No. 2324.

Pseudoliotia TATE, 1898.

Pseudoliotia micans (A. ADAMS)

1850 *Cyclostrema micans* A. ADAMS, Proc. Zool. Soc. London, p. 43.
1861 *Cyclostrema pulchellum* DUNKER, Moll. Jap. p. 20, Pl. 3, fig. 5.

The following description of this species is by M. YOKOYAMA:

"Shell very small, thick, subglassy, shining, depressed. Whorls about four, rapidly growing, first two nuclear, smooth and rounded; third (penultimate) shouldered, with the surface between the shoulder and the upper suture somewhat sunken, below very steep or almost vertical and flattish, longitudinally ribbed, with ribs about sixteen in number, elevated though rounded on top, separated by broader interstices which are finely longitudinally striate. Body-whorl double shouldered with the upper shoulder weaker, angulate at periphery, the angle being elevated with top rounded, so that the surface above the angle is somewhat concave; ribs about twenty in number with interstices striate as on the preceeding whorl. Shoulders and angle tubercular at the points of intersection with the ribs. Base three-angled, the angles becoming weaker as they go downward, the third one surrounding the large and deep imblicus within which there is still a weaker one. These angles are all crossed by longitudinal ribs, with the crossing points tubercular. Aperture subcircular with a thickened continuous peristome."

Geol. age.—Pliocene ?-Pleistocene-Recent. Geogr. distr.—Central and western Japan. Occurrence.—Miyainu (2) No. 2097, Collection of the Earthquake Research Institute.

---

[39] DUNKER, *Moll. Jap.* (1861). p. 12, Pl. 2, fig. 11.
[40] GOULD, *Proc. Boston. Soc. N. H.* 7, (1861), p. 401.

***Tachyrhynchus* MÖRCH, 1868.**

***Tachyrhynchus venustellus* (YOKOYAMA)**

1927 *Bittium venustellnm* YOKOYAMA, Jour. Fac. Sci. Imp. Univ. Tokyo, (2), **2**, 4, p. 175, Pl. 47, fig. 7.

Geol. age.—Pliocene. Occ.—Simazaki (Himi series), No. 2045, Coll. E. R. I.

***Tachyrhynchus* ? sp.**

Pl. LIV, Fig. 87.

Occur.—Simazaki (Himi series).

***Turritella* LAMARCK, 1799.**

***Turritella fascialis* MENKE**

Pl. LIII, Fig. 51.

1828 *Turritella fascialis* C. T. MENKE, Syn. Teth. Moll., 83.
1849 *Turritella fascialis*, REEVE, Conch. Icon., **13**, Pl. 10, fig. 47.
1886 *Turritella fascialis*, TRYON,s Man. Conch., **8**, p. 197, Pl. 59, fig. 36, 37.
1634 *Turritella fascialis*, HIRASE, Col. Jap. Shells, Pl, 86, fig. 2.

Shell small, high-turreted; whorls numerous, nearly flat, spirally sculptured, slightly angulated little above suture on apical part. Ribs normally more than 10 on later whorl, one of which is suprasutural, being usually not prominent. Of the two upper, one middle and one lower rib stronger than others. These strong ribs finely noded, but weaker ones smooth; below lower strong ribs, three fine ribs present. Between lower and middle strong ribs two or three fine ribs present; and between upper two strong and middle, one or two fine ones present. Interspaces between these ribs smooth or longitudinally striated with fine growth lines; nuclear whorls about 2, smooth; following 2 whorls ornamented with one strong rib.

This species is closely allied to *Turritella fortililrata nipponica* YOKOYAMA[41], but the latter has a larger shell, and equally arranged ribs.

Geol. age.—Pleistocene-Recent. Geogr. distr.—Nagasaki pref., Kisyu-nada, Sagami Bay, Hukui pref. Occurrence.—Miyainu (20), Hypotype No. 2098 (length 11·5 mm and 10·5 mm); Hiradoko (5) No. 2099.

***Turritella fortilirata saishuensis* YOKOYAMA**

1923 *Turritella saishuensis* YAKOYAMA, Jour. Coll. Sci. Tokyo Imp. Univ., **44**, 7, Pl. **1**, fig. 2.

1934 *Turritella fortilirata saishuensis*, OTUKA, Bull. Earthq. Res. Inst. Tokyo Imp. Univ., **12**, 3, p. 622, Pl. 51, fig. 103.

Geol. age.—Middle neogene-Pliocene. Geogr. distr.—Saisyuto (Plio-

---

41) M. YOKOYAMA, *Jour. Coll. Sci. Tokyo Imp. Univ.* **39**. 6 (1920), pp. 71~72, 7, Pl. 4, figs. 16~19.

cene), Isikawa pref. (Pliocene). Occur.—Hukazawa (Nozaki beds).

***Turritella fortilirata motidukii* OTUKA**

Pl. LIV, Fig. 53.

1935 *Turritella fortilirata motidukii* OTUKA, Jour. Geol. Soc. Japan, **42**, 503, p. 508.

MOCHIZUKI collected from Nozaki beds a new form of *Turritella fortilirata* Sowerby, habing only three distinct spiral threads, without intersticial lines. Fig. 53 in Pl. LIV show this new form of *Turritella fortilirata*. The present writer has named this new form *Turritella fortilirata motidukii* OTUKA (Jour. Geol. Soc. Jap. **42**, 503, p. 508.)

Occur.—Kozima and Tobeiyati.

***Lemintina* RISSO, 1826.**

***Lemintina imbricata* (DUNKER)**

1860 *Vermetus imbricatus* DUNKER, Malakoz. Bl. p. 204.

1861 *Vermetus imbricatus*, DUNKER, Moll. Jap. p. 17, Pl. 2, fig. 18.

1920 *Thylacodes medusae*, YOKOYAMA, Jour. Coll. Sci. Tokyo Imp. Univ., **39**, p. 61, Pl. 4, fig. 7.

1930 *Thylacodes imbricatus*, YAMAKAWA, Kairui-zuhu, Pl. 8, fig. 1.

Geol. age.—Pleistocene-Recent. Geogr. distr.—Miyagi-pref , Kyusyu, Hukui-pref., Toyama bay. Occur.—Tumuki (2) No. 2109; Miyainu (1) No. 2110; Akasaki (2) Coll. E. R. I.

***Siliquaria* LAMARCK, 1799.**

***Siliquaria cumingii* (MÖRCH)**

Pl. LIII, Fig. 49.

1860 *Tenagodus* (*Siliquarius*) *cumingii*, MÖRCH, Proc. Zool. Soc., p. 404.

1934 *Siliquaria cumingii*, HIRASE, Coll. Jap. Shell, Pl. 85, fig. 12.

Geol. age.—Pleistocene-Recent. Geogr. distr.—Sagami Bay, Kyusyu, Amami-osima. Kisyu-nada, Hukui-pref. Toyama-Bay. Occurrence. Hiradoko (1), Hypotype No. 2111, Coll. E. R. I.

***Batillaria* BENSON, 1842.**

***Batillaria multiformis* (LISCHKE)**

Pl. LIV. Fig. 79.

1862 *Lampania multiformis* LISCHKE, Jap. Meeresconch., **1**, p. 74, Pl. 7, fig. 1~10.

1920 *Potamides* (*Batillaria*) *multiformis*, YOKOYAMA, Jour. Coll. Sci. Tokyo, Imp. Univ., **39**, 6, p. 69, Pl. 4, fig. 9.

1934 *Batillaria multiformis*, HIRASE, Coll. Jap. Shells, Pl. 84, fig. 15.

Geol. age.—Pleistocene-Recent. Geogr. distr.—Honsyu, Kyusyu. Ryukiu, Taiwan. Occur.—Tumuki (1), Hypotype No. 2112, Coll. E. R. I.

***Obtortio* HEDLEY, 1899.**

***Obtortio septentrionalis* (TOKUNAGA)**

1906 *Rissoa septentrionalis* TOKUNAGA, Jour, Coll. Sci. Tokyo Imp. Univ. **21**, 2, p. 26, Pl. 1, fig. 55.

1922 *Fenella septentrionalis*, YOKOYAMA, Jour. Coll. Sci. Tokyo Imp. Univ., **44**, 1, p. 80, Pl. 4, fig. 5, 6.

Geol. age.—Upper Pliocene-Pleistocene-Recent. Geogr. distr.—Tokyo bay. Oc.—Tumuki (40), No. 2119; Akasaki (10) C. E. R. I.

***Obtortio orientalis* (YOKOYAMA)**

Pl. LIV, Fig. 91 a, b.

1920 *Fenella orientalis* YOKOYAMA, Jour. Coll. Sci. Tokyo Imp. Univ., **39**, 6, p. 74, Pl. 4, fig. 12.

Geol. age.—Pleistocene-Recent. Geogr. distr.—Tokyo bay. Occurrence.—Tumuki (20), No. 2113; Miyainu (40), Hypotype No. 2114; Hiradoko (30) No. 2115; Akasaki (2), Coll. Earthq. Res. Inst.

***Obtortio perpupoides* (YOKOYAMA)**

Pl. LIII, Fig. 31.

1927 *Fenella perpupoides* YOKOYAMA, Jour. Fac. Sci. Imp. Univ., **39**, 6, p. 74, Pl. 4, fig. 12.

Geol. age.—Pleistocene-Recent. Geogr. dist.—Tokyo bay. Occur. —Tumuki (6), No. 2118; Miyainu (1), No. 2117; Hiradoko (40), Hypotype No. 2116; Akasaki (3), Coll. E. R. I.

***Scaliola* A. ADAMS, 1860.**

***Scaliola bella* A. ADAMS**

1860 *Scaliola bella* A. ADAMS, Ann. Mag. Nat. Hist., p. 120.

1887 *Scaliola bella*, TRYON, Man. Conch., **9**, p. 85, Pl. 17, fig. 39.

1932 "*Rissoa*" (?) sp., OTUKA, Venus., **3**, 2, pp. 110~111. fig. 2, c.

Shell small, turreted, umbilicated, white. Whorls about $7\sim8\,^{1}/_{2}$, rounded, simple, argillaceous. Later whorls free; suture greatly impressed; aperture circular; periostome continuous; margin acute. Measurements based on specimens from Hiradoko are:

Height. 3·5 mm; Diameter. 1·3 mm (No. 2120, Coll. E. R. I).

Geol. age.—Lower Pleistocene (Gobantyo shell beds, Tokyo city)-Recent. Geogr. distr.—Japan Sea. Occure.—Tumuki (2), No. 2121; Miyainu (2) No. 2120; Hiradoko (16), No. 2123, Coll. E. R. I.

"*Rissoa* ?" sp. from Lower Pleistocene of Gobantyô, in Kôzimati-ku, Tokyo, agrees with this species.

***Diala* A. ADAMS, 1861.**

***Diala varia* A. ADAMS**

Pl. LIV, Fig. 80.

1861 *Diala varia* ADAMS, Ann. Mag. Nat. Hist., p. 243.

1924 *Litiopa* (*Diala*) *semistriata*, YOKOYAMA, Jour. Coll. Sci. Tokyo Imp. Univ., **45**, 1, p. 25, Pl. 1, fig. 20.

Geol. age.—Pleistocene-Recent. Geogr. distr.—Western Japan. Occurrence.—Tumuki (2), Hypotype No. 2122; Miyainu (20) No. 2124; Hiradoko (1), No. 2125, Coll. E. R. I.

***Bttium* GRAY, 1847.**

***Bittium numamuranum* YOKOYAMA**

1924 *Bittium numamuranum* YOKOYAMA, Jour. Coll. Sci. Tokyo Imp. Univ., **45**, p. 20, Pl. 1, fig. 13.

1924 *Cerithiopsis hilaris* YOKOYAMA, Jour. Coll. Sci. Tokyo Imp. Univ., **45**, p. 21, Pl. 1, fig. 8.

This species resemble *Bittium perpusillum* of YOKOYAMA[42], but *Bittium perpusillum* TRYON[42] has a narrower and longer shell than the latter species.

Cerithiopsis hilaris YOKOYAMA may be a young specimen of this species.

Geol. age.—Pleistocene-Recent. Geogr. distr.—Awa and Toyama. Occurrence.—Miyainu (40) No. 2127; Hiradoko (30) No. 2126.

Bittium satomii **(YOKOYAMA)***

1924 *Cerithiopsis satomii* YOKOYAMA, Jour. Coll. Sci. Tokyo Imp. Univ., **45**, p. 22, Pl. 1, fig. 23.

This species may be identical with *Bittium perpusillum* TRYON (=*Cerithium pusillum* DUNKER, 1860)[43].

Geol. age.—Pleistocene-Recent. Geogr. distr.—Hukui pref. Occurrence.—Tumuki (30) No. 2130; Miyainu (60) No. 2129; Hiradoko (6) No. 2128; Akasaki (5) Coll. E. R. I.

Cerithium **BRUGUIÈRE, 1789.**

Cerithium (Proclava) kochi **(PHILIPPI)**

Plate LIV, Fig. 78.

1875 *Cerithium kochi* PHILIPPI, Abbild. u. Beschr. **3**, *Cerithium*, p. 2 (14), Pl. 1, fig. 3.

1922 *Cerithium (Clava) kochi*, YOKOYAMA, Jour. Coll. Sci. Tokyo Imp. Univ., **44**, 1, p. 71, Pl. 3, fig. 13.

1934 *Cerithium kochi*, HIRASE, Coll. Jap. Shells, Pl. 83. fig. 5.

Geol. age.—Pleistocene-Recent. Geogr. distr.—Mutu Bay, Japan Sea, Toyama Bay, Tokyo Bay, Kisyu-nada, Kyusyu. Oc.—Tumuki (4), Hypotype, No. 2132; Hiradoko (3) No. 2131; Akasaki, Coll. E. R. I.

Gourmya **FISCHER, 1884.**

Gourmya (Contumax) sordidula **(GOULD)**

Plate LIII, Figs. 41 a, b.

1849 *Cerithium sordidulum* GOULD, Proc. Boston Soc. Nat. Hist., **3**, p. 119.

Shell elongate, acuminate, many whorled, slightly convex in lower half. Whorls about 11, of which nuclear 2 or 3, smooth, later whorl longitudinally plicate and spirally threaded; point of intersection of plicae and threads more or less tubercular. Spiral sculpture consists of three especially large threads and many fine ones on ultimate and penultimate whorl. Between suture and upper large one are two spiral threads and between upper and middle large threads, two or three fine ones present; distance between midlle and lowest ones somewhat large, in which three fine spiral threads visible; below lowest large one, three or four fine spiral threads visible; below these spiral threads is a finely tuberculated spiral thread sunk into the succeeding whorl in upper whorls.

---

[42] YOKOYAMA, *Jour. Coll. Sci. Tokyo Imp. Univ.*, **39**, 6 (1920), p. 67, Pl. 4, fig. 13.

[43] TRYON, *Man. Conch.* **9**, p. 145, Pl. 30, fig. 17. {(=*Cerithium pusillum* DUNKER) *Moll. Jap.* (1860), p. **11**, Pl. 2, fig. 6 (Not of GOULD.)}.

* *Bittium perpusillum* TRYON in Table I, Part I.

Number of longitudinal costae about 19–16 on ultimate whorl and 17–13 on penultimate whorl. Basal sculpture consists of 8–7 beaded spiral threads, of which two especially large; between these basal beaded spiral threads are intercalaetd one or two fine spiral threads. Later whorls have swollen varices at intervals of about half whorl. Aperture ovate, with sinus above it defined by cord on inner lip; outer lip strengthened by varix, sulcate within, there being usually pair of lirae between termination of two spiral threads of exterior; inner lip coated with rather thick callous deposit, which is thickend at upper and lower part; channel short and oblique.

Geol. age.—Pleistocene-Recent. Geol. distr.—Hukui prefectire, Mie prefecture. Oc.—Akasaki (6); Tumuki (37) Hypotype No. 2133, Coll. E. R. I.

***Gourmya* (*Contumax*) *kobelti* (DUNKER)**

Plate LIII, Fig. 42.

1877 *Cerithium kobelti* DUNKER, in malakoz. Bl., **24**, p. 67.

1920 *Cerithium kobelti*, YOKOYAMA, Jour. Coll. Sci. Tokyo Imp. Univ., **39**, 6, p. 66, Pl. 4, fig. 10.

1934 *Cerithium kobelti*, HIRASE, Coll. Jap. Shells, Pl. 83, fig. 11.

Geol. age.—Pliocene-Recent. Geogr. distr.—Tiba pref., Kisyu-nada, Kyusyu, Toyama Bay, Hukui pref. Occurrence.—Tumuki (5) Hypotype, No. 2134; Miyainu (35) No. 2135; Akasaki (1) Coll. E. R. I.

***Triphora* BLAINVILLE, 1828.**

***Triphora* (*Inella*) *tricincta* (DUNKER)**

1860 *Triforis cingulata* DUNKER in malakoz. Bl. **6**, p. 236.

1862 *Triforis cingulata*, DUNKER, Moll. Jap. p. 10, Pl. 2, fig. 1.

1882 *Triforis tricincta* DUNKER, Index Moll. Jap. p. 109.

Geol. age.—Pleistocene-Recent. Geogr. distr.—Japan. Occurrence. —Miyainu (1) No. 2142; Hiradoko (1) No. 2136; Tumuki (1).

Triphora aff. purpurata* (PILSBRY)

Plate LIII, Fig. 33.

1895 *Triforis purpuratus* PILSBRY Cat. Mar. Moll Jap. p. 58.

Geol. age.—Pleistocene-Recent? Geogr. distr.—Noto, Sagami? Occurrence.—Tumuki (2) No. 2138; Hiradoko (6) No. 2139; Miyainu, (12) Hypotype No. 2137, Coll. E. R. I.

---

* *Triphora* sp. in Table I, Part I.

Epitonium **(BOLTEN) RÖDING, 1798.**

Epitonium (Turbiniscala) **sp.**

This species is closely allied to *Epitonium* (*Turbiniscala*) *angustum* (DUNKER)[44], but is much smaller (about 4 mm high), and has wider apical angles.

Occurrence.—Miyainu (2) No. 2140, Coll. E. R. I.

Epitonium (Boreoscala) angulatosimile **OTUKA**

Pl. LIII, Fig. 45, 46, 47, 48.

1931 *Epitonium* (*Boreoscala*) *simile*, KURODA, Geol. Middle Sinano, part 4. p. 77~78, Pl. 10, fig. 82.

1935 *Epitonium* (*Boreoscala*) *angulatosimile* OTUKA, Jour. Geol. Soc. Jap. **42**, p. 509, p. 492, fig. 3, d, e, f.

Shell imperforate, thick, rather solid, elongate, conical; whorls convex, contiguous, not disjointed, ornamented with strong distinct longitudinal ribs which number about 14—12, slightly curved posterior, occasionally varicose. Spiral ridges indistinct, flattened, closely set, about 5 on ultimate whorl. Suture fairly deep, obscured by longitudinal ribs. Mouth ovate, somewhat angulate above. Outer lip strengthened by last rib; Produced anterior inner lip thickened at base. Basal ridge more or less well defined and angulate.

This shell is closely allied to *Epitonium* (*Boreoscala*) *simile* (SOWERBY)[45] from the British Pliocene, but the latter has a more rounded shell. Basal ridge of the former shell is more angulate than that of the latter.

Epitonium (*Boreoscala*) *groenlandicum* (CHEMNITZ)[46] is another allied species, but ours has a more slender shell and more rounded whorl.

The measurements of *Epitonium* (*Boreoscala*) *angulatosimile* OTUKA are as follows:

No. of sp.	Length	Diameter	
No. 1. (Fig. 46)	25 mm	17 mm	(Holotype: No. 1924.)
No. 2. (Fig. 48)	43 mm	15 mm	(Paratype: No. 2141.)
No. 3. (Fig. 47)	30 mm	12·5 mm	(Paratype: No. 2141.)
No. 4. (Fig. 45)	29 mm	15·5 mm	(No. 1925.)

Geol. age.—Middle Neogene. (Sinano and Kaga). Occur.—Tobeiyati (type locality) in Higasiminato-mura, (Nozaki beds); Kozima (Kozima beds).

Strombiformis **DACOSTA, 1778.**

Strombiformis (Leiostraca) shibana **(YOKOYAMA)**

Pl. LIV, Fig. 71, 70.

1927 *Eulima* (*Leiostraca*) *shibana* YOKOYAMA, Jour. Fac. Sci. Imp. Univ. Tokyo, (2), **1**, 10, p. 418, Pl. 47, fig. 8.

---

44) DUNKER, *Moll. Jap.* (1861), p. 13, Pl. 1., fig. 24.

45 SOWERBY, *Min. Conch.* **1**, P. 49, Pl. 16, fig. 1, 2.

46) CHEMNITZ, *Conch. Cab.*, **11**, (1795), p. 155, Pl. 195 a, figs. 1878~79.

Geol. age.—Pleistocene-Recent ? Geogr. distr.—Tokyo. Occurrence.—Hiradoko (3) Hypotype No. 4143, Coll. E. R. I.

Chrysallida CARPENTER, 1857.

Chrysallida (*Miralda*) *gemma* A. ADAMS

Plate LIV, Fig. 84.

1861 *Parthenia gemma* A. ADAMS, Ann. Mag. Nat Hist. **8**, p. 302.

1906 *Odostomia* (*Miralda*) *gemma*, DALL et BARTSCH, Proc. U. S. Nat. Mus., **30**, p. 356~7, Pl. 22, fig. 1.

Shell small, glassy, imperforate, ovately conical; spire moderately elevated, composed of nuclear whorl deeply and obliquely immersed in first of succeeding turns, four or five whorls regularly separated by clear suture; surface of whorl ornamented with three spiral ridges, and many longitudinal ribs, two upper spiral ridges of which are granulose at intersected part of spiral ridges and axial ribs. Intersticials between middle and lower ridges and sutural line ornamented with fine longitudinal striae. Base with two spiral nontuberculose ridges. Aperture lozenge, with thin callus deposits; columella arcuate, with one columellar fold.

Colour white. The following are measurements of the specimens from Hiradoko.

	Length	Diameter	
No. 1	2·5 mm	1·3 mm	(Hypotype)

Geol. age.—Pleistocene-Recent. Geogr. distr.—Japan.

Occur.—Hiradoko (5) Hypotype, No. 2144, Coll. E. R. I.

Chrysallida (*Babella*) *caelata* (A. ADAMS)

Plate LIV, Fig. 85.

1863 *Parthenia caelata* A. ADAMS, Jour. Linne. Soc. London, **7**, p. 4.

1906 *Turbonilla* (*Babella*) *caelatior* DALL et BARTSCH, Proc. U. S. N. Mus. **30**, p. 347, Pl. 17, fig, 9.

Shell small, subglassy, ovately conical, imperforate. Spire elevated; whorls composed of one smooth embryonal and 5 (normal) or 4 excavated whorls; embryonal whorl 3, vertically elevated and about one-third immersed in first of them; excavated whorls ornamented with regular obliquely arranged vertical ribs which abruptly terminate near clearly defined suture line. Number of vertical ribs about 23 on last whorl, and about 24 on penultimate whorl in this specimen. Supra and sub sutural spiral threads well defined by suture line. Aperture rhombic, with one columnar fold, base with one subsutural thread and fine longitudinal growth lines. Colour white.

No. of sp.	Length	Diameter
(1)	3 mm	1·4 mm
(2)	2·75 mm	1·3 mm
(3)	2·5 mm	1·2 mm
(4)	2·5 mm	1·2 mm

Geol. age.—Pleistocene-Recent. Geogr. distr.—Japan, Tokyo Bay. Occurrence.—Hiradoko (4), Hypotype, No. 2145, Coll. E. R. I.

This species is closely allied to *Pyrgulina bartschi* DAUTZENBERG et FISCHER[47], but the latter has four whorls and many spiral basal sculpture. Although the longitudinal ribs in the former species terminate with tubercle at both ends, those of the latter do so with one more tubercle in the middle.

***Pyrgulina* A. ADAMS, 1863.**

***Pyrgulina densecostulata* (GARRETT)**

Plate LIV, Figure 96.

1906 *Odostomia* (*Pyrgulina*) *densecostulata* GARRETT, DALL et BARTSCH, Proc. U. S. Nat. Mus. 30, p. 350, Pl. III, fig. 4.

Shell small, elongately ovately conical; spire elevated. Whorl composed of 1 smooth embryonal and 4 or 5 sculptured whorls; embryonal whorl smooth, deeply depressed in the succeeding whorls; whorls sculptured with many longitudinal costae and spiral threads. Costellae number about 24 on ultimate whorl, and about 22 on penultimate whorl; spiral threads number about 8, obsolete on longitudinal costellae. Periphery rounded; base convex, provided with longitudinal costellae and spiral threads as on whorls. Aperture semi-oval, sharper end being behind; inner margin of aperture has one fold.

	Length	Diameter (Specimen from Miyainu)
(1)	3·3 mm	1·25 mm
(2)	4·3 mm	1·7 mm

Geol. age.—Pleistocene-Recent. Geogr. distr.—Central Japan, Tokyo bay. Occurrence.—Tumuki (1) No. 2158; Miyainu (11) No. 2151; Hiradoko (1) No. 2152, Coll. E. R. I.

This shell resembles *Turbonilla* (*Pyrgiscus*) *candidissimus* DALL et BARTSCH[48] but the latter, besides having a more elongate conical shell, is more compressed at body whorl.

***Menestho* MÖLLER, 1842.**

***Menestho* sp.**

Plate LIV, Figure 98.

This species is closely allied to *Odostomia* (*Evalea*) *sulcata* A. ADAMS[49], but the latter species has a shorter shell.

Odostomia (*Evalea*) *lirata* A. ADAMS[50] is another allied species. But this species has a shell with more weak shoulder than the species from

---

47) DAUTZENBERG et FISCHER, *Jour. d. Conch.*, 54, (1906), p. 191, Pl. 7, fig. 1.

48) DALL et BARTSCH, *Proc. U. S. Nat. Mus.* 30, 1452, p. 342~3, Pl. 17. fig. 3. {(=Dunkeria candida A. ADAMS, *Ann. Mag. Nat. Hist.*, 8, (1861), p. 301.}

49) A. ADAMS, *Ann. Mag. Nat. Hist.* (1860), p. 418.

50) A. ADAMS, *Ann. Mag. Nat. Hist.* (1860), p. 418.

Miyainu.

Occurrence.—Miyainu (1) Hypotype, No. 2148, Coll. E. R. I.

Menestho lectissimoides **(YOKOYAMA)**

1927 *Odostomia* (*Odetta*) *lectissimoides* YOKOYAMA, Jour. Fac. Sci. Imp. Univ. Tokyo, (2), **1**, 10, p. 421, Pl. 47, fig. 12.

Geol. age.—Pleistocene. Geogr. distr.—Noto, Musasi. Oc.—Miyainu.

Odostomia **FLEMING, 1813.**

Odostomia limpida **DALL et BARTSCH**

Plate LIV. Figure 59.

1906 *Odostomia* (*Odostomia*) *limpida* DALL et BARTSCH, Proc. U. S. Nat. Mus. **30**, p. 364, Pl. 26, fig. 7.

Geol. age.—Pleistocene-Recent. Geogr. distr.—Central and western Japan. Occurrence.—Miyainu (1) Hypotype, No. 3154; Hiradoko (11), No. 2155, Coll. E. R. I.

Cingulina **A. ADAMS, 1860.**

Cingulina triarata **PILSBRY**

Plate LIV, Figure 100.

1904 *Turbonilla* (*Cingulina*) *triarata* PILSBRY, Proc. Acad. Nat. Sci. Philadelphia, **56**, p. 31, Pl. 5, fig. 48.

1922 *Turbonilla* (*Cingulina*) *triarata*, YOKOYAMA, Jour. Coll. Sci. Tokyo Imp. Univ., **44**, p. 31, Pl. 5, fig. 14.

Geol. age.—Pleistocene-Recent. Geogr. distribution.—Noto, Hizen, Nagasaki, Sagami. Occurrence.—Hiradoko (1) Hypotype, No. 2157, Coll. E. R. I.

Turbonilla **RISSO, 1826.**

Turbonilla **aff.** ***imbana*** **YOKOYAMA**

Plate LIV, Figures 56, 57, 58, 59.

1922 *Turbonilla* (*Chemnitzia*) *imbana* YOKOYAMA, Jour. Coll. Sci. Tokyo Imp. Univ., **44**, 1, p. 101, Pl. 4, fig. 35.

Geol. age.—Pleistocene.

Occurrence.—Miyainu (11) Hypotype, No. 2158.

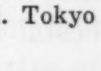

Fig. 222.

Turbonilla **(*Strioturbonilla*)** ***nihona*** **OTUKA n. sp.**

Fig. 222, 223. (text-figure; Fig. 222 shows apical part.)

Shell small, slender, white; nuclear whorls helicoid immerged into one third or half into post-nuclear whorl, well rounded, having their axis at right angles to axis of post-nuclear turns; post-nuclear whorls smooth, rather high between sutures, moderately rounded, marked by axial ribs, which are about as wide as spaces seperating them, and extend strongly to very summit of whorl where they render the well-marked sutures

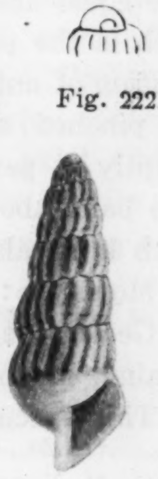

Fig. 223. *Turbonilla nihona* OTUKA

crenulate. About 16 of these ribs on first, 12 on second, 16 on penultimate and ultimate. Depressed intercostal spaces terminate abruptly at periphery. Spiral markings consist of two equall and equally spaced spiral cords in intercostal spaces between sutures near periphery; base smooth.

The holotype has 6 post-nuclear whorls and measures 3 mm long, 1·3 mm diam. This species is closely allied to *Turbonilla* (*Strioturbonilla*) *sagamiensis* YOKOYAMA[51] in its sculpture, but smaller than the latter, which is 8 mm long and has a distinct suture.

Turbonilla infantula DALL et BARTSCH[52] is another allied species, but without spiral cords.

Occurrence.—Tumuki (1) Homoeotype, No. 2161; Miyainu (1) Homoeotype No. 2160; Hiradoko Holotype and Hypotype No. 2159.

Outer lip of hypotype slightly broken.

Turbonilla (*Pyrgiscus*) *matunamiensis* OTUKA n. sp.

Fig. 224. (text-figure).

Shell elongate conic and slender. Nuclear whorls 2, helicoid, deeply immersed in first post-nuclear turn, above which appear only half of nuclear whorls; lastnamed well rounded, having their axis about right angles to axis of post nuclear turn; post nuclear whorls smooth, moderately shouldered at summit; later one slightly exserted at summit, marked by strong, slightly sinuous, protoractive axial ribs, of which 12 occur upon first, 15 on second, 16 on third, 18∼20 on penultimate and ultimate turn. Intercostal spaces about as wide as ribs, marked by three equal and equally spaced spiral cords, first of which is the periphery and third at posterior termination of anterior third between the sutures. Suture pinched; depressed intercostal spaces terminate abruptly at periphery; base very short, well rounded, marked by broad plain band about 5 unequal and unequally spaced strong incised lines, which intervals narrow regularly toward columella.

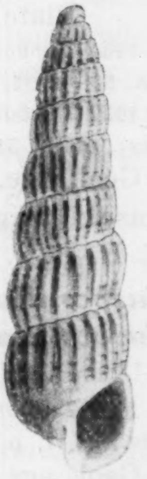

Fig. 224. *Pyrgiscus matunamiensis* OTUKA

Monotype: Length 4·1 mm, diameter 1 mm.

Geologic age.—Pleistocene. Geogr. distr.—Noto. Occurrence.—Miyainu, Monotype, No. 2162. Coll. E. R. I.

This specimen is closely allied to the preceeding species, but the former has a longer shell and basal sculpture.

---

[51] M. YOKOYAMA, *Jour. Coll. Sci. Tokyo Imp. Univ.*, **44**, 1, (1922). p. 104. Pl. 5, fig. 12.

[52] DALL et BARTSCH, *Proc. U. S. Nat. Mus.* **30**, (1906), p. 338, Pl. 20, fig. 2.

Turbonilla (*Pyrgiscus*) *pequensis* DALL et BARTSCH[53] is another allied species, which however has less number of straighter axial ribs than this new species.

The monotype of this species has 8 post-nuclear whorls and 2 nuclear whorls. On the last whorl of this type specimen, two more spiral cords are feebly marked in the posterior part of the intercostal spaces.

***Turbonilla* sp.**

Although this species is closely allied to *Turbonilla* (*Chemnitzia*) *edoensis* YOKOYAMA[54], it is smaller than the latter, being about 2·9 mm long.

Occurrence: Tumuki (1) No. 2163, Coll. E. R. I.

***Turbonilla* (*Pyrggiscus*) sp.**

This species is closelly allied to *Turbonilla* (*Pyrgiscus*) *lara* DALL et BARTSCH[55] from California, but the former has 11 spiral threads on the penultimate whorl.

Occurrence.—Tumuki (1) No. 2164 Coll. E. R. I.

***Turbonilla* (*Mormula*) sp.**

Turbonilla (*Mormula*) *ambusta* DALL et BARTSCH[56] is an allied species, but *Turbonilla* (*Mormula*) *ambusta* differs entirely from *Turbonilla* (*Mormula*) sp. from Miyainu, in its sculpture.

Occurrence.—Miyainu (1), No. 2165, Coll. E. R. I.

***Turbonilla hiradokoensis* OTUKA n sp.**

Plate LIV, Figures 90 a, b.

Shell moderate size, very elongate conic, milk white. Nuclear whorls 2 ¹/₂, large, well rounded, abour one fourth immersed in first post-nuclear whorl, having axis at right angles to axis of later whorls. Number of axial ribs 18 on first post-nuclear, 15 on second, 16 on third, 23~24 on penultimate, 22 on ultimate whorl. Post-nuclear whorls decidedly rounded, slighty shouldered and somewhat constricted at periphery, marked by very strong lamellar oblique axial ribs and deeply impressed intercostal apices about twice as wide as ribs; ribs not fused at summit but terminate strongly at cusps, rendering outline of summit wavy; they fuse at periphery and there suddenly terminate the deep intercostal spaces. Base smooth, with fine incremental lines.

---

[53] DALL et BARTSCH, *Smith. Inst. U. S. Nat. Mus. Bull.*, **68**, (1909), p. 79, Pl. 7, figs. 5, 5 a.

[54] M. YOKOYAMA, *Jour. Fac. Sci. Imp. Univ. Tokyo*, (2), **1**, (1927), p. 424, Pl. 47, fig. 24.

[55] DALL et BARTSCH, *Smith. Inst. U. S. National Mus. Bull.*, **68**, (1909), p. 107, Pl. 10, figs. 6, 6 a, 6 b.

[56] DALL et BARTSCH, *Smith. Inst. U. S. National Mus. Bull.*, **68**, (1909), pp. 115~6, Pl. 11, fig. 13.

This shell is closely allied to *Turbonilla scrobiculata* YOKOYAMA[57] in its sculpture. But the former species is decidedly small. YOKOYAMA measured 11 mm in the height of the latter species. Height of new species is about 5·5 mm.

Occur.—Hiradoko (1) Monotype, No. 2167, C. E. R. I.

***Syrnola* A. ADAMS, 1860.**

***Syrnola cinctella*? A. ADAMS**

1860 *Syrnola cinctella* A. ADAMS, Ann. Mag. Nat. Hist. **6**, p. 333.

Geol. age.—Pleistocene-Recent. Geogr. distr.—Korean str., Noto. Occurrence.—Tumuki (1), No. 2166, Coll. E. R. I.

***Strombus* LINNÉ, 1758.**

***Strombus* (*Labiostrombus*) *japonicus* REEVE**

Pl. LIV, Fig. 99.

1851 *Strombus japonicus* REEVE, Conch. Icon., fig. 42.

1922 *Strombus japonicus*, YOKOYAMA, Jour. Coll. Sci. Tokyo Imp. Univ., **44**, 1, p. 70, Pl. 3, fig. 12.

Geol. age.—Pleistocene-Recent. Geogr. distr.—Tiba pref., Kisyu-nada, Kyusyu, Hukui pref. Occurrence.—Tumuki (3), No. 2170; Miyainu (4) No. 2169; Hiradoko (42), Hypotype No. 2168, Coll. E. R. I.

***Polynices* MONTFORT, 1810.**

***Polynices didyma* (BOLTEN)**

1798 *Albula didyma* BOLTEN, Mus. Bolten. (2), p. 20.

1920 *Polinices* (*Neverita*) *ampla* PHILIPPI of YOKOYAMA, Jour. Coll. Sci. Tokyo Imp. Univ., **39**, 6, p. 77~78, Pl. 5, fig. 6.

Geol. age.—Miocene ?-Recent. Geogr. distr.—Hokkaidô, Honsyu, Sikoku, Kyûsyû. Tyôsen. Occurrence.—Tumuki (1), No. 2171, Coll. E. R. I.

***Polynices sagamiensis* PILSBRY**

Pl. LIII, Fig. 36.

1904 *Polinices sagamiensis* PILSBRY, Proc. Acad. Nat. Sci. Philadelphia, **56**, p. 23, Pl. 4, fig. 37, 37 a.

This species is readily distinguished from *Polynices draparnaudii* RÉCLUZ, *Polynices effusa* SWAINSON, *Polynices powisianus* RÉCLUZ, *Polynices cumingianus* RÉCLUZ, by the large size of the umbilical lobe and the strong cord around the umbilical crescent.

Geol. age.—Pliocene-Recent. Geogr. distribution.—Sagami Bay, Kisyû-nada, Toyama Bay, Hukui pref. Occurrence.—Hiradoko (3), Hypotype, No. 2172, Coll. E. R. I.

---

57) M. YOKOYAMA, *Jour. Coll. Sci. Tokyo Imp. Univ.*, **44**, 1, (1922), p. 102, Pl. 4, fig. 38.

Natica SCOPOLI, 1777.

Natica concinna DUNKER

Pl. LIII, Fig. 32.

1860 *Natica concinna* DUNKER in malakoz. Bl. p. 232.

1934 *Natica concinna*, HIRASE, Coll. Jap. Shells, Pl. 90, fig. 6.

Shell globose, solid, moderately small; suture well marked, subdepressed, angled about 130° between shell surface of ultimate and penultimate whorl at suture. Number of whorls about $4\,{}^1/_2{\sim}5$, Surface ornamented with microscopical spiral lines and fine oblique growth lines; aperture semicircular; inner lip slightly arcuated; parietal callus small, funnicle running spirally up apertural wall; weak but definite ridge defines outer margin of umbilicus.

Measurements of these specimens from Miyainu are:

	Length	Diameter.
No. 1. (Hypotype)	15 mm	14·2 mm
No. 2.	14 mm	12·5 mm
No. 3.	12·5 mm	11·5 mm

This shell is closely allied to *Natica janthostoma* DESHAYES[58], but the latter has a larger funnicle and narrower umbilicus, and on spiral ridge defining the outer margin of the umbilicus area.

Geol. age.—Pleistocene-Recent. Geogr. distr.—Northern and western Japan. Occurrence.—Tumuki (3), No. 2175; Hiradoko (3) No. 2184; Miyainu (5) Hypotype No. 2173.

Sinum (BOLTEN) RÖDING, 1798.

Sinum (*Eunaticina*) *papillum* (GMELIN)

Plate LIV, Figure 64.

1791~2 *Nerita papilla* GMELIN, Syst. Nat. **ed. 13**, p. 3675.

1922 *Sigaretus* (*Eunaticina*) *papilla*, YOKOYAMA, Jour. Coll. Sci. Tokyo Imp. Univ., **44**, 1, p. 84, Pl. 5, fig. 8.

Specimen from Hiradoko has a shell with more or less depressed spire and finer spiral threads than the type species.

Geol. age.—Pleistocene-Recent. Geogr. distr.—Mutu Bay, Matusima Bay, Tokyo Bay, Wakayama pref., Hukui pref., Toyama Bay. Occur.- Hiradoko. Hypotype. No. 2176, Coll. Earthq. Res. Inst.

Earato RISSO, 1826.

Erato callosa (ADAMS et REEVE)

Plate LIV, On the right of Figure 69.

1850 *Erato callosa* ADAMS et REEVE, Zool Voy. Samarang, p. 25, Pl. 10, fig. 32.

1922 *Erato callosa*, YOKOYAMA, Jour. Coll. Sci Tokyo Imp. Univ., **44**, 1, p. 69, Pl. 3, fig. 11.

Geol. age.—Pliocene-Recent. Geogr. distr.—Amami-oosimi, Kyusyu, Sikoku, Tiba pref., Toyama Bay. Occur.—Hiradoko, (2), Hypotype

---

[58] DESHAYES, *Revue Zool.*, p. 361.

No. 2177, Coll. E. R. I.

***Erronea* TROSCHEL, 1863.**

***Erronea japonica* (SCHILDER)**

Plate LIV, Figures 52 a, b.

1870 *Cypraea macula* SOWERBY, Thes. Conch., **4**, p. 96, Pl. 323, fig. 380~381.

1924 *Cypraea candida*, YOKOYAMA, Jour. Coll. Sci. Tokyo Imp. Univ., **44**, 7, p. 18, Pl. 2, fig 1.

1931 *Cypraea japonica* SCHILDER, Beitr. Kenntn. *Cypraeacea*, **4**, 12~14 (Zool, Anz. **96**, 65.)

Geol. age.—Pleistocene-Recent. Geogr. distr.—Central and Western Japan. Occur.—Miyainu, Hypotype No. 2178, Coll. Earthq. Res. Inst.

***Bursa* (BOLTEN) RÖDING, 1798.**

***Bursa* (*Gyrineum*) *natatoria* ("BOLTEN" RÖDING)**

Plate LIII. Figures 50 a, b.

1798 *Tritonium natator* "BOLTEN" RÖDING, Mus. Boltenianum Cat. Cimeliorum, p. 127, sp. 1636.

1780 *Buccina bufonia compressa* CHEMNITZ (ex. parte), Conch. Cab., **4**, p. 78, Pl. 128, fig. 1229, 1230 (tantum).

1852 *Apollon olivator* MEUSCHEN in MÖRCH, Catal. Yoldi, 1, p. 106.

1906 *Bursa natatrix*, DAUTZENBERG et FISCHER, Jour. d. Conch., p. 158.

Geol. age.—Pleistocene-Recent. Geogr. distr.—Southern and western Japan. Occur.—Miyainu (3), Hypotype, No. 2179.

***Trophon* MONTFORT, 1810.**

***Trophon* (*Bedeva*) *birileffi* LISCHKE**

Plate LIII, Figures 30 a, b.

1871 *Trophon birileffi* LISCHKE, malakoz. Bl. **18**, p. 39.

1871 *Trophon birileffi*, LISCHKE, Jap. Meeres Conch., **2**, p. 32.

1922 *Trophon pachyraphe*, YOKOYAMA, Jour. Coll. Sci. Tokyo Imp. Univ., **44**, 1, p. 63, Pl. 3, fig. 1.

Geol. age.—Pliocene-Recent. Geogr. distr.—Kyusyu, Hukui pref., Kisyu-nada, Tokyo bay. Occur.—Tumuki (5) No. 2180; Miyainu (7) Hypotype No. 2181 (15 mm high); Hiradoko (3) No. 2182.

***Thais* (BOLTEN) RÖDING, 1798.**

***Thais* (*Mancinella*) *bronni* (DUNKER)**

Pl. LIV, Fig. 77.

1860 *Purpura bronni* DUNKER, in malakoz. Bl. **2**, p. 235.

1861 *Purpura bronni*, DUNKER, Moll. Jap. p. 5, Pl. **1**, fig. 23.

1934 *Thais* (*Mancinella*) *bronni*, HIRASE, Coll. Jap. Shells, Pl. **110**, fig. 4.

Geol. age—Pliocene-Recent. Geogr. distr.—Akita pref., Toyama Bay, Hukui pref., Kyusyu, Kisyu-nada, Tiba pref., Miyagi pref. Occur. —Tumuki (7), No. 2183; Miyainu (1), No. 2185; Hiradoko (3) Hypotype No. 2184; Akasaki (1) Coll. E. R. I.

***Pyrene* (BOLTEN) RÖDING, 1798.**

***Pyrene* (*Mitrella*) *varians* (DUNKER)**

Plate LIV, Figure 82 a, b.

1860 *Amycla varians* DUNKER in malakoz. Bl. **6**, p. 231.

1861 *Amycla varians*, DUNKER, Moll. Jap. p. 6, Pl. **1**, fig. 17.

1920 *Columbella* (*Mitrella*) *dunkeri*, YOKOYAMA, Jour, Coll. Sci. Tokyo Imp. Univ., **39**, 6, p. 59, Pl. 3, fig. 15

1934 *Pyrene* (*Mitrella*) *varians*, HIRASE, Coll. Jap. Shells, Pl. 107, fig. 7.

Geol. age.—Pliocene-Recent. Geogr. distr.—Mutu-Bay, Toyama Bay, Matusima Bay, Kisyu nada, Kyusyu. Occur.—Tumuki (5) Hypotype, No. 2187; Miyainu (30) No. 2186; Hiradoko (5) No. 2188, Coll. E. R. I.

***Pyrene* (*Zafra*) *pumila* (DUNKER)**

Plate LIV, Figure 76 a, b.

1860 *Columbella pumila* DUNKER, in malakoz. Bl. **6**, p. 224.

1861 *Columbella pumila*, DUNKER, Moll. Jap., p. 6, Pl. **1**, fig. 4.

1927 *Columbella* (*Atilia*) *pumila*, YOKOYAMA, Jour. Fac. Sci. Imp. Univ. Tokyo, (2), **1**, 10, p. 412, Pl. 46, fig. 10.

1934 *Pyrene* (*Anachis*) *pumila*, HIRASE, Coll. Jap. Shells, Pl. **107**. fig. 13.

Geol. age.—Pleistocene-Recent. Geogr. distr.—Amami-osima, Kyusyu, Kisyu-nada, Tokyo-Bay, Matusima Bay, Hukui pref., Toyama Bay. Occurrence.—Tumuki (2) Hypotype No. 2189; Miyainu (5) No. 2190; Hiradoko (2) No. 2191; Akasaki (2) Coll. E. R. I.

***Neptunea* (BOLTEN) RÖDING, 1798.**

***Neptunea uwasoensis* (OTUKA)**

Plate LIV, Figure 75.

1935 *Chrysodomus nwasoensis* OTUKA, Jour. Geol. Soc. Japan, **42**, 503, p. 510. fig. 3 g. (on p. 492.)

Shell of moderate size, heavy and solid; whorls more than 4 (type specimen is missed its apex), which surface are divided into upper and lower by a strong spiral keel; angles between upper and lower surface about 125°; on the upper surface of penultimate and ultimate whorls, 2 strong spiral ribs and fine interstcial grooves (about 5~6 in interspace between spiral ribs and keel on ultimate whorl) are visible. On lower surface, 3 strong spiral ribs and some intersticial grooves visible. Base ornamented with about 11 strong spiral and 8 oblique ribs, between which a weak secondary spiral thread presents. Sometimes, tertiary finer one is visible between these spiral ribs and threads.

Height about 57·5 mm; diameter 33·5 mm.

Geol. age.—Lower Pliocene. Occur.—Uwaso (Yabuta beds.) (monotype, No. 1915, C. E. R. I.)

This new species is closely allied to *Neptunea* (*Neptunea*) *andersoni hawleyi* (CARSON)⁵⁹⁾, but the former has a shell with more pro-

---

59) CARSON, *Bull. Soc. Calif. Acad. Sci.*, **25**, pt. 2 (1926), p. 55, Pl. 2, fig. 3.

duced shoulder and with more and finer intersticial grooves.

Neptunea (*Neptunea*) *antiqua despecta* (LINNEAUS)[60] is another allied species. But the new species has strong spiral ribs on the shell surface.

Neptunea (*Neptunea*) *lirata* (MARTYN)[61] has a shell with small number of spiral ribs.

Siphonalia A. ADAMS, 1863.

Siphonalia sp.

2 fragments of a species of *Siphonalia* were collected at Hiradoko (Rg. No. 2192).

They seems to be fragments of *Siphonalia cassidariaeformis ornata* A. ADAMS.

Engina Gray, 1839.

Engina menkeana (DUNKER)

1860 *Cantharus* (*Pollia*) *menkeanus* DUNKER in malakoz. Bl 6, p. 222.
1861 *Cantharus menkeanus*, DUNKER, Moll. Jap., p. 7, Pl. 1, fig. 7.

Geol. age.—Pleistocene-Recent. Geogr. distr.—Central western Japan. Occurrence.— Hiradoko (2), No. 2193, Coll. E. R. I.

Nassarius FRORIEP, 1806.

Nassarius (Hinia) festivus (POWYS)

Pl. LIII, Fig. 39 a, b.

1832 *Nassa festiva* POWYS, Proc. Zool. Soc., p. 95.
1861 *Nassa lirata* DUNKER, Moll. Jap., p. 7, Pl. 1, fig. 22.
1934 *Nassarius festivus*, HIRASE, Coll. Jap. Shells, p. 106, fig. 10.

Geol. age.—Pliocene-Pleistocene-Recent. Geogr. distr.—Tiba pref., Kyusyu. Mutu Bay, Toyama Bay. Occur.—Tumuki (2), No. 2203 ; Miyainu (3) Hypotype No. 2194 ; Hiradoko (?), No. 2195, Coll. E. R. I.

Nassarius (Tritonella) japonicus (A. ADAMS)

Pl. LIII, Fig. 37.

1851 *Nassa japonica* A. ADAMS, Proc. Zool. Soc., p. 110.
1934 *Nassarius japonicus*, HIRASE, Coll. Jap. Shells, Pl. 106, fig. 12.

Geol. age.—Pliocene-Pleistocene-Recent. Geogr. distr—Matusima Bay, Tokyo Bay, Sagami Bay, Toyama Bay, Kyusyu. Occur.—Tumuki (1) Hypotype, No. 2196 ; Miyainu (20) No. 2197.

Nassarius (Alectrion) balteatus (LISCHKE)

Pl. LIII. Fig. 35 a, b.

1868 *Nassa balteata* LISCHKE, Jap. Meeres Conch., 1, p. 16, Pl. 5, fig. 10, 11.
1934 *Nassarius balteatus*, HIRASE, Coll. Jap. Shells, Pl. 106, fig. 4.

Shell ovate, conic ; moderately thick with slightly convex spire ;

---

[60] GRANT and GALE, *Mem. San Diego Soc. N. H.* 1, 1, p. 653, Pl. 28, fig. 10.

[61] T. MARTYN, *Figures of Nondescript. Shells*, 2, (1784), table 2, Pl. 43.

yellowish brown with fine reddish brown spiral lines and irregular transverse patterns. Whorls 7∼6 $^1/_2$, moderately inflated, sperated by depressed suture, apical two being protoconch, conic smooth, polished, the succeeding 2 $^1/_2$∼3 being cancellately sculptured by somewhat coarse, oblique axial ribs and 4∼5 spiral grooves; interspace between the upper two grooves of which is tuberculated, sculpture then gradually fading away and becoming almost smooth toward last whorl, except however the very faint undulations with fine growth striae and obscure spiral striations; last whorl occupying about two-thirds whole length; base with 4 spiral sulci; aperture ovate, purplish brown inside; outer lip somewhat sinuated, edge obtuse, with notch below; inside thickened with 12 feeble horizontal short ridges; outer margin varixed, ascends a little at suture; inner lip arcuate, parietal wall not defined by callous deposits, with feeble toooth and shallowly channeled posteriorly; columella wall slightly concave, laminately calloused; callus with 4 folds; fasciole feebly sculptured with 4 grooves; channel very short, wide.

This species is closely allied to *Nassarius glans* LINNÉ[62], but the latter has a more acute spire, while the inner side of the aperture is smoother.

Nassarius (*Zeuxis*) *tateyamensis* KURODA[63] has a more elongated, well defined form, and thin callous deposits on the inner side of the aperture without any conspicuous coloration.

Geol. age.—Pleistocene-Recent. Geogr. distribution.—Sagami Bay, Kisyu-nada, Tosa Bay, Setouti, Hukui pref., Toyama Bay. Occur.—Hiradoko (1) Hypotype, No. 2198, Coll. E. R. I.

Nassarius (Zeuxis) caelatus (A. ADAMS)

Pl. LIII, Fig. 44.

1851 *Nassa caelata* A. ADAMS, Proc. Zool. Soc., p. 79.

1920 *Nassa livescens*, YOKOYAMA, Jour. Coll. Sci. Tokyo Imp. Univ., **39**, 6, p. 58, Pl. 3, fig. 18.

1929 *Nassarius* (*Zeuxis*) *caelatus*, T. FUJITA, Venus, **1**, 3, p. 91.

1934 *Nassarius caelatus*, HIRASE, Coll. Jap. Shells, Pl. 106, fig. 5.

Geol age.—Pliocene-Pleistocene-Recent. Geogr. distr.—Tiba pref., Sagami Bay, Kisyu nada, Kyusyu, Hukui pref., Toyama Bay. Occur. —Miyainu (1), Hypotype No. 2199, Coll. E. R. I.

Nassarius (Niotha) gemmulatus (LAMARCK)

Pl. LIII, Fig. 43 a, b.

1822 *Buccinum gemmulatum* LAMARCK, Anim. sans. vert. **10**, p. 169.

1928 *Nassa* (*Niotha*) *gemmulata*, YOKOYAMA, Imp. Geol. Serv. Japan, Rep. No. 101, p. 40, Pl. 2, fig. 7.

---

[62] LINNÉ, *Syst. Nat. ed* 12, p. 1200.

[63] T. KURODA, *Venus*, **1**, 3.

1934 *Nassarius gemmulatus*, HIRASE. Coll. Jap. Shells, Pl. 106, fig. 9.

Geol. age.—Pliocene-Pleistocene-Recent. Geogr. distr—Tokyo Bay, Sagami Bay, Kisyu-nada, Kyusyu, Hukui pref., Toyama pref., Amami-osima. Occur.—Hiradoko (2) Hypotype No. 2200.

***Nassarius* (*Niotha*) *livescens* (PHILIPPI)**

Pl. LIII, Fig. 28, Pl. LIV, Fig. 74.

1848 *Buccinum livescens* PHILIPPI, Zeitschrift für. Mal. p. 135.

1934 *Nassarius livescens*, HIRASE, Coll. Jap. Shells, Pl. 106, fig. 8.

Geol. age.—Pleistocene-Recent. Geogr. distr.—Kyusyu, Tosa Bay, Setouti, Kisyu-nada, Sagami Bay, Mutu Bay, Toyama Bay, Hukui perf., China, Java, Philippines. Occur.—Matunami (59), Hypotype No. 2201; Tumuki (12), Hypotype No. 2202.

***Fusinus* RAFINESQUE, 1815,**

***Fusinus perplexus* (A. ADAMS)**

Pl. LIV, Fig. 81.

1864 *Fusum perplexum* A. ADAMS, Jour. Linne. Soc., 7, p. 106.

1907 *Fusus perplexus*, HIRASE, Conchological Magazine, Japan, 1, 9, Pl. 15, fig. 105.

1927 *Fusus nodoso-plicatus*, YOKOYAMA, Jour. Fac. Sci. Imp. Univ. Tokyo, (2), 1, Pl. 46, fig. 14.

Geol. age.—Pleistocene-Recent. Geogr. distr.—Mutu-Bay, Toyama Bay, Tiba pref., Sagami Bay, Kisyu nada, Kyusyu, Setouti, Hukui pref. Occur.—Tumuki (1) Hypotype No. 2204.

***Oliva* BRUGUIÈRE, 1789 (MARTYN 1789).**

***Oliva mustelina* LAMARCK**

Pl. LIV, Fig. 60.

1844 *Oliva mustelina* LAMARCK, Anim. sans vert. ed. 2. **10**, p. 616.

1927 *Oliva mustelina*, MAKIYAMA, Men. Coll. Sci. Kyoto Imp. Univ., B, **3**, 1, p. 79, Pl. 3, fig. 14, 15.

Geol. age.—Pliocene-Pleistocene-Recent. Geogr. distr.—Toyama Bay, Hukui pref., Kyusyu, Sagami Bay, Sikoku. Occur.—Hiradoko (1) No. 2205.

***Mitra* LAMARCK, 1799.**

***Mitra* sp.**

A fragment of *Mitra* sp. No. 2206 was collected from Hiradoko.

***Cancellaria* LAMARCK, 1799.**

***Cancellaria* (*Narona*) *spengleriana* DESHAYES**

1843 *Cancellaria spengleriana* DESHAYES, Anim. sans vert. **9**, p. 415.

1920 *Cancellaria spengleriana*, YOKOYAMA, Jour. Coll. Sci. Tokyo Imp. Univ., **39**, 6, p. 44, Pl. 2, fig. 3, 2.

Geol. age.—Miocene-Pliocene-Pleistocene-Recent. Geogr. distr.—Honsyu, Sikoku, Kyusyu. Occur.—Hiradoko (1) No. 2207; Akasaki.

***Clavatula* LAMARCK, 1801.**

***Clavatula consimilis* (SMITH)**

Pl. LIV, 103 a, b, c.

1879 *Pleurotoma consimilis* SMITH, Proc. Zool. Soc. London, p. 188, Pl. 19, fig. 11.
1934 *Clavatula consimilis* HIRASE, Coll. Jap. Shells, Pl. 115, fig. 5.

Geol. age.—Pleistocene-Recent. Geogr. distr.—Tokyo Bay, Matusima Bay, Hukui pref. Occur.—Tumuki (1), Hypotype No. 2208.

Antiplanes DALL, 1902.

Antiplanes kamchatica DALL

1919 *Antiplanes kamchatica* DALL, Proc. U. S. Nat. Mus., **56**, p. 33, Pl. 10, fig. 1.
1921 *Antiplanes kamchatica*, DALL, Bull. U. S. Nat. Mus., 112, p. 71.
1934 *Antiplanes kamchatica*, HIRASE, Coll. Jap. Shells, Pl. 115, fig. 11.

Geol. age.—Pliocene-Recent. Geogr. distr.—Bering Sea, Japan Sea, Kaga (Pliocene). Occur.—Simazaki (No. 2021).

Brachytoma SWAINSON, 1840.

Brachytoma jeffreysii SMITH

1875 *Drillia jeffreysii* SMITH, Ann. Mag. Nat Hist., p. 417.
1920 *Pleurotoma (Drillia) principalis*, YOKOYAMA, Jour. Coll. Sci. Tokyo Imp. Univ., **39**, 6, p. 36, Pl. 1, fig. 20.

Geol. age.—Pliocene-Pleistocene-Recent. Geogr. distr.—Tokyo Bay, Sagami Bay, Setouti, Wakayama pref., Matusima Bay. Occur.—Miyainu (2) No. 2206, Coll. E. R. I.

Asthenotoma HARRIS et BURROWS, 1891.

Asthenotoma yokoyamai notoensis OTUKA n. subsp.*

Plate LIV, Figure 101.

Shell rather small, turriculate; spire moderately high; whorls more than 10, regularly increasing, surface nearly flat, spirally sculptured. Embryonal whorls broken. Sculpture of post-nuclear whorls consist of spiral ribs. Penultimate whorl ornamented with 3 equally interspaced strong equall spiral ribs on lower half, 1 strong rib near suture, and 3 weak threads between upper strong rib and lower strong ribs. Subsutural area a weak spiral thread visible. Spiral sculptures of body whorl similar to penultimate. But in type specimen a weak thread appears in interspace between upper two of 3 lower strong spiral ribs. Base slightly contracted ornamented with 6 equally interspaced equall ribs and few oblique ribs.

Geologic age.—Pleistocene. Occur.—Hiradoko, Monotype No. 2207, (height 17·2 mm)

This species closely allied to *Asthenotoma yokoyamai* MAKIYAMA[64] in its sculpture. *Asthenotoma yokoyamai* MAKIYAMA has eight whorls and has weak spiral thread in interspace between upper 2 of 3 lower strong spiral ribs on the body whorl.

---

[64] J. MAKIYAMA, *Mem. Coll. Sci. Kyoto Imp. Univ.* (*B*), **3**, **1**, (1927), p. 95~96.

* *Asthenotoma nivea* (PHILIPPI) in Table I.

The present writer obtained another *Asthenotoma* from Sagami Bay, which is called *Asthenotoma komakimonos* OTUKA n. sp. (Fig. 225, text fig.) Following description is based on three specimens from Sagami Bay.

"Shell rather small, turriculate; dark brown in color; spire moderately high; whorls about 12, regularly increasing, surface nearly flat, spirally sculptured. Embryonal whorls about 3, first 2 of which smooth, third longitudinally plicated. Sculpture of post-nuclear whorls consist of spiral ribs. Penultimate whorl ornamented with 3 equally interspaced equall strong spiral ribs on the lower half, 3 weak and 1 strong on upper half of whorl, and 1 weak on subsutural area above 1 strong rib. Lowest strong rib sometimes sprasutural. One preceeding whorl of penultimate upper most one of 3 weaks disappears. Spiral sculptures of body whorl similar to penultimate. Base slightly contracted ornamented with 5 equally interspaced equall ribs and few oblique ribs."

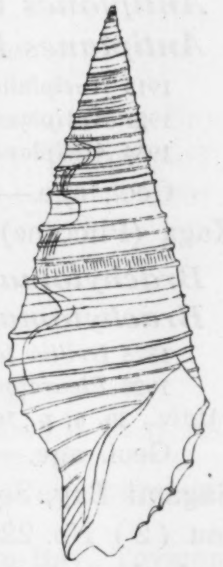

Fig. 225. *Asthenotoma komakimonos* n. sp.

Geol. age.—Recent. Occur.—Sagami Bay 13 m deep. Holotype and Cotype. No. 2499. (height 15 mm, diameter 5·4 mm; height 14.8 mm, diameter 4·7 mm)

Asthenotoma komakimonos OTUKA has 3 spiral weak threads between upper strong rib and lower strong ribs, but *Asthenotoma yokoyamai notoensis* OTUKA has 2 threads.

Asthenotoma makimonos (JOUSSEAUME)[65)] is closely allied to the species written above. But the former species is large and differs from the latter three species in its surface ornamentations.

Asthenotoma pouloensis (JOUSSEAUME)[66)] from Malacca is another allied shell, but this species has a large and broad shell.

***Mangelia* RISSO, 1826.**

Mangelia makiyamai* OTUKA n. sp.

Plate LIV, Figure 94 a, b, 95.

Shell very small; spire terraced, lower half conic. Sculpture consists of slightly curved obliquely longitudinal ribs, 9∼10 on last whorl, the last one behind, near lip. These are crossed by spaced spiral groo-

---

65) F. JOUSSEAUME, *Bull. Soc. Zool. France,* (1883), p. 198, Pl. 10, Fig. 4.

66) F. JOUSSEAUME, *Bull. Soc. Zool. France,* 1883), p. 199.

* *Mangelia* (*Bella*) sp. in Table I, Part I,

ves, 3～4 on penultimate whorl. Whorls about 6 1/2 (in type specimen). Nuclear whorls 2 1/2, smooth, convex. Post-nuclear whorls weakly shouldered with spiral ridge near upper third of whorl, flattened, sloping above shoulder, slightly contracting below it; last whorl similarly angular, convex below shoulder, contracted below middle. Outer lip thin, with moderately deep rounded annal fasciole between suture and shoulder margin. Inner side of aperture smooth. Length 4·6 mm, diameter 2·0 mm.

Occurrence.—Hiradoko (5) (Holotype and Cotype, No. 2330); Matunami (4) (No. 2329).

This species is closely allied to *Mangelia kamakurana* PILSBRY[67] 1904, but has less number of longitudinal ribs. The spiral sculpture of the former is simple, while the latter species has primary and secondary fine threads and more angulated shoulder. All the specimens of the former examined by the writer have thin outer lip: Pilsbry's species has thick outer lip.

Cythara tabatensis (TOKUNAGA)[68] is another allied species, but has a shell without spiral sculpture.

***Philbertia* MONTEROSATO, 1884.**

Philbertia tincta* (REEVE)

Plate LIV, Figures 83 a, b.

1846 *Pleurotoma tincta* REEVE, Conch. Icon., **1**, Pl. 38, fig. 347.

1904 *Clathurella centrosa* PILSBRY, Proc. Acad. Nat. Sci. Philadelphia, **56**, p. 12, Pl. 1, figs. 7, 7 a, 7 b.

1922 *Pseudodaphnella tincta*, HEDLEY, Rec. Australian Museum, **13**, 6.

Shell fusiform-turrete greyish white; rather thick. Nuclear whorl 2 1/2, first of which rounded convex, second ornamented with fine oblique axial lines; post-nuclear whorl about 4 (in specimen from Hiradoko shell bed) slightly angulated at upper fourth of whorl. Sculpture of many slightly oblique, longitudinal ribs, narrower than their concave interspaces, and about 11 to 10 in number on last whorl; last rib much larger, forming stout lip-varix. These ribs crossed by almost equally spaced equal spiral threads, about 4 on penultimate whorl, second of which is on shoulder. The first spiral thread on space above shoulder slightly weaker than others. First and second post-nuclear whorls sculptured with two septal threads; last whorl bears thick varix behind outer lip, which is thick. Aperture with two more weak

---

67) PILSBRY, *Proc. Acad. Nat. Sci. Phiradelphia*, **56** (1904), p. 10, Pl. 2, figs. 11, 11 a. (as *Mangilia.*)

68) S. TOKUNAGA, *Jour. Coll. Sci. Tokyo Imp. Univ.*, **21**, 2 (1906), p. 15, Pl. 1, fig. 27. (as *Pleurotoma.*)

* *Philbertia leuckarti* (DUNKER) in Table I., Part I.

teeth within outer lip, upper one large; annal sinus deep and rounded at end of space above shoulder. Lower part of base ornamented with oblique 3～5 beaded cords. Length 4·5 mm.

Geologic age.—Pleistocene-Recent. Geogr. distr.—Ogasawara, Mutu Bay (Nomura), Tokyo Bay, Noto. Occurrence.—Tumuki (1) No. 2331; Hiradoko (5) No. 2333, Coll. Earthq. Res. Inst.

This species is closely allied to *Philbertia leuckarti* (DUNKER)[69]. But according to Dunker's description, the latter species is 7 mm long while the former species is less than 5 mm.

***Asperdaphne* HEDLEY, 1922.**

***Asperdaphne subzonata* (SMITH)**

Plate LIV, Figure 104 a, b.

1927 *Daphnella subzonata* SMITH, Proc. Zool. Soc. London, p. 197, Pl. 19, fig. 27.

Shell fusiform, rather solid. Suture distinct, contracted. Nuclear whorls broken; post-nuclear whorls about 1 $^1/_2$ sculptured with almost equally spaced fine unequal spiral cords and strong longitudinal ribs, except ultimate and penultimate whorl. On first post-nuclear whorl 9 longitudinal ribs, spiral cords obsolete; on second post-nuclear whorl 11 to 12 longitudinal ribs, spiral cords 2 or 3; on third post-nuclear whorl, 12～13 longitudinal ribs and 3 primary spiral cords between which weak secondary cords appear; on fourth, 14～15 longitudinals, 3 strong primary spirals and 4 secondary spiral cords, and 8 weak tertiary spiral cords; on sixth, 18～19 longitudinals, 4 primary spirals, 4 secondary spirals, more than eight tertiary spirals, and many fine quarternary spiral cords. On penultimate whorl, longitudinal ribs suddenly becomes weak and ornamented with weak longitudinal furrows, but spiral sculpture continues as preceeding whorls. On penultimate whorl, 4 primaries, more than 6 secondaries, more than 11 tertiaries, more than 20 quarteries, and sometimes more finer cords observable. Ultimate wohrl long, more than half shell length, ornamented with longitudinal inclemental lines and spiral sculptures. Base contracted below, with many unequal spiral cords as on whorls. Aperture semi-oval, inner margin of which smooth, concave. Outer lip thick, but beveled to an edge, obliquely and deeply excised above to form annal sinus. Canal short and rather shallow.

Geologic age.—Pleistocene-Recent. Geogr. distr.—North of Kyusyu (Pilsbry). Occurrence.—Hiradoko (1) No. 2334, Coll. E. R. I.

***Pseudorhaphitoma* BÖTTGER, 1895.**

***Pseudorhaphitoma naganumaensis* OTUKA n. sp.**

Plate LIV, Figure 102 a, b.

---

[69] DUNKER, *Moll. Jap.* (1861), p. 2, Pl. 1, fig. 1.

Shell small, fusiform, with rather high spire, solid, strong. Nuclear whorls 3, first two of which convex rounded, smooth, third ornamented with about 17 to 14 oblique longitudinal furrows; post-nuclear whorls about 5, slightly angulated, ornamented with coarse spiral riblets and many lines of very fine tubercles and 8 round longitudinal riblets which continue through every whorl. First post-nuclear whorl in type specimen, coarse spiral ribs about 3, middle of which most prominent on angle, upper of which relatively weak. Three lines of fine tubercles between succeeding suture line and lowest coarse riblet, also between middle and lowest. Two or three lines of fine tubercles visible between uppermost and middle coarse riblet; between uppermost coarse riblet and preceeding suture, 4 or 5 lines of fine tubercles visible. Second post-nuclear whorl sculptured with three coarse spiral riblets, between which and sutures, 4 to 6 lines of fine tubrcles present respectively. On third post-nuclear ones, three coarse riblets and 6 to 10 lines of fine tubercles present. Size of these fine tubercles about 45 on a line of 1 mm length. Ultimate whorl long, half shell length ornamented with three spiral riblets and lines of fine tubercles as in preceeding whorls. Base ornamented with almost equally spaced 5 to 6 spiral riblets, in interspaces of which are many lines of fine tubercles. Aperture narrow, both lips slightly arcuate; blunt at ends; inner lip smooth; inner margin of outer lip with teeth. Annal sinus above teeth broad, round, but deep; varix curves slightly backward near annal. Canal short.

	Length	Diameter
No. 1	7·6 mm	2·7 mm (Holotype, No. 855, Matusima Bay, Living).
No. 2	5·9 mm	2·3 mm (No. 2333, Hiradoko, Pleistocene).
No. 3	7·2 mm	2·8 mm (No. 552. Naganuma, Pliocene).

This species is closely allied to *Pseudorhaphitoma fairbankii* (NEVILL)[70] from the Indian Ocean, but the latter species has less number of longitudinal riblets and many teeth on the inner margin of the outer lip. The latter species is about 6 mm long.

Pseudorhaphitoma bipyramidata HEDLEY[71] is another allied species to this new species. But the former has seven longitudinal riblets.

Geol. age.—Pliocene-Recent. Geogr. distr.—Cnetral Japan. Occur. Matusima bay in Miyagi pref. Holotype, No. 855; Hiradoko, No. 2333; Naganuma in Kanagawa pref. No. 552.

***Pseudorhaphitoma*? sp.**

Plate LIV, Figures 97 a, b.

Occurrence.—Hiradoko (1) No. 2382.

---

[70] *Jour. Asiat.Soc. Bengal*; TRYON's, *Man. Conch.* Pl. 22, fig. 48.

***Terebra* BRUGUIÈRE, 1789.**

***Terebra* (*Punctoterebra*) *lischkeana* DUNKER**

1882 *Terebra lischkeana* DUNKER, in malakoz. Bl. **24**, p. 74.
1882 *Terebra lischkeana*, DUNKER, Index, Moll. p. 71, Pl. 5, figs. 13~16.
1920 *Terebra lischkeana*, YOKOYAMA, Jour. Coll. Sci. Tokyo Imp. Univ., **39**, 6, p. 31, Pl. 1, fig. 10.

Geol. age.—Pliocene-Recent. Geogr. distr.—Sagami Bay, Setouti, Kyusyu, Hukui pref., Toyama Bay. Occur.—Hiradoko (2) No. 2336, Coll. E. R. I.

***Ringicula* DESHAYES, 1838.**

***Ringicula* (*Ringiculella*) *doliaris* GOULD**

Plate LIV, Figures 65.

1860 *Ringicula doliaris* GOULD, Proc. Boston Soc. Nat. Hist. **7**, p. 324.
1935 *Ringicula* (*Ringiculella*) *doliaris*, TAKEYAMA, Venus, **5** (2, 3,) 80, Pl. 5, fig. 17, 18.

Geol. age.—Pleistocene-Recent. Occurrence.—Tumuki No. 2337; Hiradoko No. 2339, Coll. E. R. I.

***Ringicula* (*Ringiculella*) aff. *yokoyamai* TAKEYAMA**

1922 *Ringicula musashinoensis*, YOKOYAMA, Jour. Coll. Sci. Tokyo Imp. Univ., **44**, 1. p. 30, fig. 16, 17. (not of YOKOYAMA, 1920).
1935 *Ringicula* (*Ringiculina*) *yokoyamai* TAKEYAMA, Venus, **5**, 2~3, pp. 74~78, Pl. 5, fig. 19, 20; Pl. 6, fig. 21~25.

Geol. age.—Pleistocene. Occurrence.—Miyainu (4), Hiradoko (3) No. 2339, Coll. E. R. I.

***Solidula* FISCHER von WALDHEIM, 1807.**

Solidula strigosa* (GOULD)

Plate LIV, Figures 54.

1859 *Buccinulus strigosus* GOULD, Proc. Bost. Soc. Nat. Hist., 7, p. 141.
1922 *Solidula strigosa*, YOKOYAMA, Jour. Coll. Sci. Tokyo Imp. Univ., **44**, p. 22, Pl. 1, fig. 1.

Geol. age.—Pleistocene-Recent. Geogr. distr.—Tokyo bay, Setouti, Noto. Occurrence.—Tumuki (2) Hiradoko (2) Coll. E. R. I.

***Acteocina* GRAY, 1847.**

***Acteocina exilis* (DUNKER)**

Plate LIV, Figures 56 a, b.

1860 *Tornatina exilis* DUNKER, in malakoz. Bl. **6**, p. 222.
1861 *Tornatina exilis*, DUNKER, Moll. Jap. p. 25, Pl. 2, fig. 14.
1922 *Tornatina exilis*, YOKOYAMA, Jour. Coll. Sci. Tokyo Imp. Univ., p. 24, Pl. 1, fig. 4.

Geol. age.—Pliocene-Recent. Geogr. distr.—Japan. Occur.—Hiradoko (15) No. 2342, Coll. E. R. I.

***Retusa* BROWN, 1827.**

---

71) HEDLEY, *Records of Australian Museum*, **13**, 6 (1922), p. 308, 309, Pl. 51, fig. 132.

* *Pupa strigosa* (GOULD) in Table I, Part I.

***Retusa minima* YAMAKAWA**

Plate LIV, Fig. 55.

1911 *Retusa minima* YAMAKAWA, Jour. Geol. Soc. Tokyo, **18**, 212, p. 47, Pl. 11, fig. 21~24.

1922 *Retusa truncata* YOKOYAMA, Jour. Coll. Sci. Tokyo Imp. Univ., **44**, 1, p. 25, Pl. 1, fig. 7.

Geol. age.—Pleistocene. Occur.—Tumuki (1) No. 2341 ; Hiradoko (44) No. 2340 ; Miyainu (9), Coll, E. R. I.

***Rhizorus* MONTFORT, 1810.**

***Rhizorus artiaperta* (YAMAKAWA)**

Plate LIV, Figures 57, 58.

1911 *Volvula artiaperta* YAMAKAWA, Jour. Geol. Soc. Tokyo, **18**, p. 50, Pl. 11, fig. 33~36.

1927 *Volvula artiaperta* YOKOYAMA, Jour. Fac. Sci. Imp. Univ., Tokyo, (2), 1, 10, p. 407, Pl. 46, fig. 4.

Geol. age.—Pliocene?-Pleistocene-Recent. Geogr. distr.—? Occur. —Tumuki (1) No. 2344; Hiradoko (2) No. 2343, Coll. E. R. I.

***Cylichna* LOVEN, 1846.**

***Chlichna yamakawai* YOKOYAMA**

1911 *Bullinella striata* YAMAKAWA, Jour. Geol. Soc. Tokyo, **38**, 5, p. 51, Pl. 11, fig. 37~38.

1920 *Cylichna yamakawai* YOKOYAMA, Jour. Coll. Sci. Tokyo Imp. Univ., **39**, 6, p. 29, Pl. 1, fig. 7.

Geol. age.—Pliocene-Pleistocene. Geogr. distr.—? Occurrence.—Tumuki (3) No. 2346; Hiradoko (1) No. 2345; Akasaki (2).

***Philine* ASCANIUS, 1772.**

***Philine japonica* LISCHKE.**

1872 *Philine japonica* LISCHKE, Malakoz. Bl. **19**, p. 105.

1874 *Philine japonica*, LISCHKE, Jap. Meeresconch., **3**, p. 77, Pl. 5, fig. 13, 14.

1927 *Philine japonica*, YOKOYAMA, Jour. Fac. Sci. Imp. Univ. Tokyo, (2), **1**, 10, p. 408, Pl. 46, fig. 5.

Geol. age.—Pleistocene-Recent. Geogr. distr.—Central Japan. Occur.—Hiradoko (1).

SCAPHOPODA

***Dentalium* LINNÉ, 1758.**

***Dentalium* (*Dentalium*) *hexagonum* GOULD**

Plate LIV, Fig. 88.

1859 *Dentalium hexagonum* GOULD, Proc. Bost. Soc. N. H. **7**, p. 166.

1860 *Dentalium sexcostatum* SOWERBY, Thes. Conch, **3**, p. 103, Pl. 223.

1931 *Dentalium hexagonum*, HIRASE, Jour. Conch. **19**, 5, p. 133~134, Pl. 3, fig. 2.

Geol. age.—Pliocene-Recent. Geogr. distr.—Tokyo Bay, Noto, Hiradoko. Nagasaki. Occurrence.—Tumuki (5) No. 2398; Miyainu (20) No. 2399; Hiradoko (12) No. 2400.

***Dentalium* (*Antalis*) *motidukii* OTUKA n. sp.**

Plate LIV, Figure 89.

The writer has only one complete specimen from Hiradoko bed. This speciemen is smaller than *Dentalium pretiosum*[72] SOWERBY described by Hirase. It is opaque white, ivory like with some light buff rings. Sculptures like *weinkauffi*, but longitudinal threads are fine; primary threads number about 10 at the apical part, and the tertiary threads about 40 in the middle part of the shell length. The apical part very weakly notched on the convex side. The length of the shell is about 16 mm. The diameter of apical part 0·5 mm; the aperture is 2·0 mm in diameter.

Occurrence.—Hiradoko (1) No. 2400, Monotype.

Dentalium (*Antalis*) *weinkauff* DUNKER[73] is a large shell.

Dentalium (*Antalis*) *buccinulum* GOULD[74] is closely allied to this new species, but the former has no distinct about 30 longitudinal sculptures on the apical one third of the shell length.

Dentalium (*Antalis*) *pretiosum* SOWERBY is an allied species, but this species has a long shell with a short apical notch and numerous fine longitudinal threads.

Dentalium (*Antalis*) *rhabdotum* PILSBRY[75] has some rude longitudinal sculptures on the whole shell surface.

Dentalium (*Antalis*) *marukawai* OTUKA[76] has a long fine shell with a deep apical notch.

***Siphonodentalium* M. SARS, 1859.**

***Siphonodentalium* (*Pulsellum*) *ozawai* YOKOYAMA**

1928 *Siphonodentalium* (*Pulsellum*) *ozawai* YOKOYAMA, Jour. Fac. Sci. Imp. Univ. Tokyo, (2), **1**, Pt. 8, p. 239, Pl. 3, 4, fig. **11**.

1931 *Siphonodentalium* (*Pulsellum*) *ozawai*, HIRASE, Jour. Conch., **19**, p. 140, Pl. 3, fig. 12.

Geol. age.—Pliocene-Recent. Geogr. distr.—Toyama Bay (KIKUCHI, and HIRASE). Occurrence.—Hiradoko (1) No. 2401.

PELECYPODA

***Nucula* LAMARCK, 1799.**

***Nucula* sp.**

A small *Nucula* (*Nucula*) was collected.

Occurrence.—Hiradoko No. 2384, Coll. E. R. I.

***Acila* H. and A. ADAMS, 1858.**

***Acila divaricata* (HINDS)**

---

[72] SOWERBY, *Thesaurus Conch.*, **3**, (1866),

[73] GOULD, *Proc. Bost. Soc. Nat. Hist.*, **7**, p. 141, (1859).

[74] DUNKER, *Malak.* Bl. **24**, (1877), p. 68.

[75] PILSBRY, *Proc. Acad. Nat. Sci. Philadelphia*, (1905), p. 116, Pl. 5, figs. 45, 46, 47.

[76] OTUKA, *Venus*, **4**, 3, pp. 159~161, figs. a~f.

1843 *Nucula divaricata* HINDS, Proc. Zool. Soc. London, p. 97.
1850 *Nucula mirabilis* ADAMS et REEVE, Samarang, Moll., p. 75, Pl. 21, fig. 8.
1934 *Nucula divaricata*, H. G. SCHENCK, Bull. Mus. Royal. Hist. Nat. Belgique, **10**, 20, pp. 41~2.

Geol. age.—Miocene-Recent. Geogr. distr.—Hokkaido, Honsyu, Hukui pref., Toyama pref. Occur.—Kayato (Nozaki beds).

Nuculana LINK, 1907.

Nuculana onoyamai OTUKA

Plate LV, Figures 105, 106.

1935 *Nuculana onoyamai* OTUKA, Jour. Geol. Soc. Japan, **42**, 503, pp. 507~8, fig. 3 b, c (p. 492).

Shell small, thick, solid, equivalve, inequilateral; the posterior side longer, rostrated with a slight curve; the anterior end rounded; surface sculptured with fine concentric lines and three weak and a prominent ridge, which divides a postero-dorsal depressed area, from beak to postero-ventral margin. The postero-dorsal surface ornamented with concentric sculpture and a weak ridge from beak to postero-ventral margin. A weak ridge (or a weak groove) runs from beak to antero-ventral margin. Apex small, but obtuse. Teeth v-shaped; horizontal ridge on inner side of posterior end is prominent.

	Length	height	thickness
No. 1.	23 mm	13 mm	5 mm (with one valve)(Holotype)
No. 2.	18 mm	11 mm	3 mm (with one valve)(Cotype)

This new species is closely allied to *Nuculana* sp. 1[77], from Japan sea in its sculpture. But fossil species are slightly larger, and thicker than the latter sp. Concentric sculpture in fossil species is slightly weaker than the latter species. Horizontal ridge on inner side of posterior end and radiating anterior ridge (or a groove) are obsolete in the Japan sea species.

This new species is closely allied to *Nuculana pernula* MÜLLER[78] from Arctic Ocean, but the former has a less prominent beak and longer shell than the latter.

Nuculana conceptionis (DALL)[79] resembles to this new species, but the former species has longer shell.

Occurrence.—Kamiyukawa (Yabuta series) No. 2528, C. E. R. I.

Limopsis SACCO, 1827.

Limopsis multistriata (FORSKÅL)

Plate LV, Figures 113 a, b.

1775 *Arca multistriata* FORSKÅL, Descr. Anim. Itin. Orient, p. 123.
1843 *Pectunculus cancellata* REEVE, Proc. Zool. Soc. London.

---

77) Y. OTUKA, *Bull. Earthq. Res. Inst.* **13**, (1934), 3, p. 608, Pl. 74, figs. 12, 13.

78) MÜLLER, *Beschaft. Ges. Naturf. Freunde zu Berlin*, **44**, 55, (1977).

79) DALL, *The Nautilus*, **10** (1896), 1, p. 2.

1862 *Limopsis woodwardii* A. ADAMS, Proc. Zool. Soc., 1862, p. 231.

1922 *Limopsis woodwardii*, YOKOYAMA, Jour. Coll. Sci. Imp. Univ., **44**, 1, p. 192 ~193, Pl. 17, fig. 5.

1930 *Limopsis multistriata*, KURODA, "Venus" **1**, 6, App. p. 17., sp. 59. fig. 26.

Geol. age.—Pliocene-Recent. Geogr. distr.—Taiwan, Yakusima, Noto, Awa. Occurrence.—Hiradoko (29) No. 2402, Col. E. R. I.

***Limopsis tokaiensis* YOKOYAMA**

1910 *Limopsis tokaiensis*, YOKOYAMA, Jour. Geol. Soc. Tokyo, **17**, 205, p. 1, Pl. 9, figs. 1~3, 5, 6.

Geol. age.—Pliocene-Recent. Geogr. distr.—Central Japan, Kyusyu (Hyuga). Occurrence.—Zyunityô, Simazaki, nr. Himi. No. 2035, Coll. E. R. I.

***Glycymeris* DACOSTA, 1778.**

***Glycymeris rotunda* (DUNKER)**

1882 *Pectunculus rotundus* DUNKER, Index. Moll. Jap., p. 236, Pl. 16, figs. 9, 10.

1920 *Pectunculus nipponicus* YOYOYAMA, Jour. Coll. Sci. Imp. Univ. Tokyo, **39**, p. 168, Pl. 18, figs. 3~6, 7.

1922 *Pectunculus yamakawai* YOKOYAMA, Jour. Coll. Sci. Imp. Univ. Tokyo, **44**, p. 190, Pl. 16, figs. 4, 5.

Geol. age.—Pliocene-Recent. Geogr. distr.—Tokyo bay (Dunker), Wakasa (Hirano), Kii, Nagasaki, Tosa, Iyo (Hirase, Kaneko), Tazima (Yagura), Hyuga (Yokoyama). Occurrence.—Zyunityo No. 2045, Coll. E. R. I.

***Navicula* BLAINVILLE, 1825.**

***Navicula ocellata* (REEVE)**

Plate LV, Figures 109, 110.

1844 *Arca ocellata* REEVE, Conch. Icon., sp. 102.

1904 *Arca ocellata*, PILSBRY, Proc. Acad. Nat. Sci. Philadelphia, **56**, p. 560, Pl, 4, fig. 21.

This shell very resembles to *Navicula boucardi* (JOUSSEAUME)[80] in its outline, but the former has smooth ligament area scored by only a few, usually imperfect ligament grooves. The teeth in the former species are finer than the latter.

Geol. age.—Pleistocene-Recent. Geogr. distr.—Awa, Kii, Hizen. Occurrence.—Tumuki (4) No. 2386; Miyainu (24) No. 2385; Hiradoko (10) No. 2403, Coll. E. R. I.

***Navicula boucardi* (JOUSSEAUME)**

(1894 *Arca boucardi* JOUSSEAUME, The Humming Bird, 4, p. 41).

1904 *Arca kobeltiana* PILSBRY, Proc. Acad. Nat. Sci. Philadelphia, **56**, p. 559, Pl. 40, figs. 16~19.

1906 *Arca rectangularis* TOKUNAGA, Jour. Coll. Sci. Imp. Univ. Tokyo, **21**, 2, p. 61, Pl. 3, fig. 23 a~c.

Geol. age.—Miocene-Recent. Geogr. distr.—Hokkaido, Mutu bay,

---

[80] JOUSSEAUME, *The Humming Bird*, 4, p. 41. (1894).

Tokyo bay ?, Noto, Setouti, Tanegasima. Occurrence.—Miyainu (1) No. 2396; Simazaki, Zyunityo, No. 2019, Coll. E. R. I.

***Barbatia* GRAY, 1847.**

***Barbatia obtusoides* (NYST)**

Plate LVII, Figures. 198, 197.

1848 *Arca obtusoides* NYST, Mem. Acad. Belgique, **22**, (1847), p. 50.

1844 *Arca obtusa* REEVE, Conch. Icon., sp. 77 (Non (Philippi) de Koninck, 1842).

1869 *Arca decurvata* LISCHKE, Jap. Meeres Conch., **1**, p. 148.

1928 *Arca decurvata* YAKOYAMA, Rep. Imp. Geol. Surv. Jap., No. 101, p. 128, Pl. 20, fig. 4.

Geol. age.—Pleistocene-Recent. Geogr. distr.—Miyagi pref. Tiba pref., Wakayama pref., Ryukyu, Taiwan. Occur.—Tumuki (10) No. 2389, Coll. E. R. I.

***Barbatia stearnsi* (PILSBRY)**

1895 *Arca stearnsi* PILSBRY, Cat. Mar. Mol. Jap., p. 148, Pl. 3, fig. 8~10.

1920 *Arca stearnsi*, YOKOYAMA, Jour. Coll. Sci. Tokyo Imp. Univ., **39**, 6, p. 165, Pl. 16, fig. 9.

Geol. age.—Pliocene-Recent. Geogr. distr.—Tokyo bay, Toyama Bay, Wakayama pref., Kyusyu, Setouti, Amami-Osima. Occurrence.—Miyainu (1) No. 2388; Hiradoko (40) No. 2408, Coll. E. R. I.

***Barbatia symmetrica* (REEVE)**

Plate LV, Figures 107 a, b.

1844 *Arca symmetrica* REEVE, Conch. Icon, sp. 117, fig. 120 (not fig. 117).

Yokoyama's *Arca symmetrica* (Jour. Coll. Sci. Imp. Univ. Tokyo **39**, p. 166, Pl. 17, Fig. 7, 8.) may be a distinct species. S. NOMURA[81] has distinguished this species from *Barbatia symmetrica* (REEVE), and has proposed a specific name *Barbatia yokoyamai* for YOKOYAMA's species (Pl. LV, Figs. 108, 113.)

Geol. age.—Pliocene-Recent. Geogr. distr.—Kii, Hizen, Toyama, Tokyo. Occurrence.—Miyainu (33) No. 2391; Hiradoko (80) No. 2409; Akasaki (3), Coll. E. R. I.

Barbatia reticulata* (GMELIN)

Plate LV, Figures 111 a, b.

(1791~2 *Arca reticulata* GMELIN, Syst. Nat., et. **13**, p. 3311.)

1833 *Byssoarca divaricata* SOWERBY, Proc. Zool. Soc. London, p. 22.

1930 *Barbatia reticulata*, KURODA, Venus, **1**, 6, App. p. 25, fig. 34.

1923 *Arca* (*Barbatia*) *domingensis*, YOKOYAMA, Jour. Coll. Sci. Tokyo Imp. Univ., **45**, 1, p. 60, Pl. 5, fig. 6 (not of LAMARCK).

Geol. age.—Pleistocene-Recent. Geogr. distr.—Toyama, Kadusa, Kii, Hizen, Amami. Occurrence.—Hiradoko (40) No. 2410.

---

[81] NOMURA, *Sci. Rep. Tohoku Imp. Univ.*, (2), **16**, 1, (1933), p. 41, Pl. **1**, fig. 3 a~d.

* *Barbatia divaricata* (SOWERBY) in Table I, Part I.

Barbatia decussata **(SOWERBY)**

Plate LV, Figures 118.

1833 *Byssoarca decussata* SOWERBY, Proc. Zool. Soc. London, p. 22.

1924 *Arca (Barbatia) decussata*, YOKOYAMA, Jour. Coll. Sci. Tokyo, Imp. Univ. **45**, p. 59.

Geol. age.—Pleistocene-Recent. Geogr. distr.—Awa Sagami, Kii, Tosa, Kyusyu, Ryukyu, Taiwan. Occurrence.—Tumuki (2) No. 2387; Miyainu (29) No. 2390, Coll. E. R. I.

Arca **LINNÉ, 1758.**

Arca subcrenata **LISCHKE**

1869 *Arca subcrenata* LISCHKE, Malakoz. Bl., **16**, p. 107.

1869 *Arca subcrenata*, LISCHKE, Jap. Meeres Conch., **1**, p. 146, Pl. 9, fig. 1~3.

Geol. age.—Pliocene-Recent. Geogr. distr.—Miyagi pref., Tokyo bay, Sikoku, Kyusyu, Setouti, Toyama, Ryukyu. Occur.—Miyainu (1) No. 2394, Coll. E. R. I.

Arca inflata **REEVE**

1844 *Arca inflata* REEVE, Conch. Icon., sp. 30.

1859~67 *Arca broughtoni* SCHRENCK, Reis, Amurl., Zool., Moll. p. 578, Pl. 24. fig. 1~3.

1906 *Arca tenuis* TOKUNAGA, Jour. Coll. Sci. Tokyo Imp. Univ., **21**, 2, p. 58, Pl. 4, fig. 12, b.

Geol. age.—Pliocene-Recent. Geogr. distr.—Hakodate, Mutu bay, Noto, Tokyo bay, Kyusyu. Occurrence.—Tumuki (5) (No. 3395).

Arca amicula **YOKOYAMA**

1925 *Arca amicula* YOKOYAMA, Jour. Fac. Sci. Imp. Univ. Tokyo, (2), **1**, p. 19, Pl. 7, fig. 2~4.

1934 *Arca amicula*, OTUKA, Bull. Earthq. Res. Inst., **2**, 3, p. 609, Pl. 47, fig. 20.

Geol. age.—Miocene-Pliocene. Geogr. distr.—Sinano, Iwate pref. Akita pref. Isikawa pref. Occurrence.—Kayato (Nozaki beds), Simazaki No. 2029.

Bathyarca **KOBELT, 1891.**

"*Bathyarca*" *uwaensis* (YOKOYAMA)

Plate LV, Figures 114, 115.

1928 *Arca uwaensis* YOKOYAMA, Jour. Fac. Sci. Imp. Univ. Tokyo, (2), **2**, p. 349, Pl. 67, figs. 13, 14.

1928 *Bathyarca uwaensis*, KURODA, Venus, **2**, **1**, App. p. 33.

Geol. age.—Pliocene-Recent. Geogr. distr.—Musasi, Hyuga. Occurrence.—Hiradoko (1). No. 2392, Coll. E. R. I.

Some living specimens of this species were collected from Hyuganada by Soyomaru.

Trichomusculus **IREDALE, 1924.**

Trichomusculus divaricatus **(PHILIPPI)**

Plate LV, Figures 116, 117.

1847 *Modiola divaricata* PHILIPPI, Zeitschr. f. Malak. p. 115.
1851 *Modiola divaricata*, PHILIPPI, Abbild. u. Beschr. **3**, p. 21, Pl. 2, fig. 8.
1933 *Trichomusculus divaricatus*, KURODA, Venus, **4**, 1, App. p. 136, sp. 415.

Geol. age.—Pleistocene-Recent. Geogr. distr.—Noto, Kii, Kadusa, Nagasaki, Amami Osima. Occur.—Miyainu (7) No. 2419; Hiradoko (5) No. 2420.

Anomia **(LINNÉ) MÜLLER, 1776.**

Anomia **sp.**

Occur.—Zyunityo, Simazaki. No. 2041, Coll. E. R. I.

Ostrea **LINNÉ, 1758.**

Ostrea denselamellosa **LISCHKE**

1869 *Ostrea denselamellosa* LISCHKE, Malakoz. Bl. **16**, p. 109.
1869 *Ostrea denselamellosa*, LISCHKE, Jap. Meeres Conch., **1**, p. 177, Pl. 13, fig. a, b. Pl. 15, fig. 1.

Geol. age.—Pliocene-Recent. Geogr. distr.—Hokkaido, Honsyu, Sikoku, Kyusyu. Occur.—Miyainu (5) No. 2421, Coll. E. R. I.

Ostrea gigas **THUNBERG**

(1793 *Ostrea gigas* THUNBERG, K. Vet. Ac. Nya. Handl. **4**, p. 140.)
1895 *Ostrea gigas*, PILSBRY, Cat. Mar. Moll. Jap. p. **145**.
1920 *Ostrea gigas*, YOKOYAMA, Jour. Coll. Sci. Tokyo Imp. Univ., **3**. 6, p. 162, Pl. 15, fig. 1~4, Pl. 17, fig. 2 (only).

Geol. age.—Miocene-Pliocene-Pleistocene-Recent. Geogr. distr.—Hokkaido, Honsyu, Sikoku. Kyusyu, Amami Osima. Occur.—Tumuki (4) No. 2422, Coll. E. R. I.

Ostrea **sp.**

Occur.—Simazaki No. 2042, Coll. E. R. I.

Plicatula **LAMARCK, 1801.**

Plicatula horrida **DUNKER**

1882 *Plicatula horrida* DUNKER, Index Moll. Jap. p. 247, Pl. **11**, figs. 6, 7.
1882 *Plicatula irregularis* DUNKER, Index Moll. Jap., p. 261, Pl. **11**, fig. 5.
1924 *Plicatula irregularis*, YOYOYAMA, Jour. Coll. Sci. Tokyo, Imp. Univ., **45**, 1, p. 55, Pl. **4**, figs. 5, 6.
1931 *Plicatula horrida*, KURODA, Venus, **3**, **1**, App. p. 79.

Geol. age.—Pleistocene-Recent. Geogr. distr.—Saga pref., Wakayama pref., Tiba pref. Occur.—Hiradoko (10) No. 2423, C. E. R. I.

Pseudamussium **H. and A. ADAMS, 1858.**

Pseudamussium intuscostatum **(YOKOYAMA)**

1920 *Pecten intuscostatus* YOKOYAMA, Jour. Coll. Sci. Imp. Univ. Tokyo, **39**. 6, p. 156, Pl. 13, figs. 9, 10.
1922 *Pecten tenuicostulatus* YOKOYAMA, Jour. Coll. Sci. Imp. Unvi. Tokyo, **44**, 1, p. 184, Pl. 17, fig. 15.
1931 *Pseudamussium intuscostatum*, KURODA, Venus, **3**, 1, App. p. 80, sp. 250.

Geol. age.—Pliocene-Recent. Geogr. distr.—East coast of Honsyu, Kii, Noto. Occur.—Simazaki, Zyunityo No. 2018.

Chlamys **(BOLTEN) RÖDING, 1718.**

Chlamys irregularis **(SOWERBY)**

1842 *Pecten irregularis* SOWERBY, Thes. Conch., 1, p. 69, Pl. 13, figs. 51, 52.

Geol. Age.—Pliocene-Recent. Geogr. distr.--Nagasaki, Tusima, Bay of Toyama, Tiba pref. Mutu. Occur.—Hiradoko (3), No. 2424, Coll. E. R. I.

Chlamys swiftii etchegoini **(ANDERSON)**

Plate LV, Figure 140.

1905 *Pecten etchegoini* ANDERSON, Proc. Calif. Acad. Sci., (3), **2**, p. 198, Pl. 18, fig. 92, 93.

1934 *Pallium swiftii etchegoini*, OTUKA, Bull, Earthq. Res. Inst. **12**, pt. 3, p. 613.

Geol. age.—Pliocene-Miocene. Geogr. distr.—West coast of America, Northeast Japan. Occur.—Simazaki, No. 2020; Siratori No. 1914, Coll. E. R. I.

Chlamys hastatus **aff.** ***ingeniosa*** **YOKOYAMA**

1929 *Chlamys hastatus ingeniosa* YOKOYAMA, Imp. Geol. Surv. Rep. No. 104, p. 5, Pl. 6, fig. 2.

1934 *Chlamys hastatus* aff. *ingeniosa*, OTUKA Bull. Earthq. Res. Inst. **12**, p. 611, 611, Pl. 47, fig. 25.

Geol. age.—Miocene?-Lower Pliocene? Oocur.—Iwaya(Nanao beds) No. 1137 ? Coll. E. R. I.

Chlamys crassivenia **(YOKOYAMA)**

Plate LV, Figures 137, 139, 141.

1929 *Pecten* (*Chlamys*) *crassivenia* YOKOYAMA, Imp. Geol. Surv. Rep. No. 104, p. 6, Pl. 6, fig. 1.

Type specimen lacks both ears. MOCHIZUKI sends to the writer some specimens with ears. Fig. 137, 139, 141 in Plate LV show these specimens.

Geol. age.—Miocene-Lower Pliocene. Geogr. distr.—Isikawa pref.; Iwate pref.; Toyama pref. Occur.—Iori (Iori beds) No. 1904, 1905, 1906; Tobayasi No. 1912, 1913, Coll. E. R. I.

Chlamys notoensis **(YOKOYAMA)**

1929 *Pecten notoensis* YOKOYAMA, Imp. Geol. Surv. Japan, Rep. No. 104, p. 4, Pl. 3, Pl. 4, Pl. 5, figs. 1, 2.

1930 *Pecten natoriensis* MATSUMOTO, Sci. Rep. Tohoku Imp. Univ., (2), **13**, 3, p. 104, Pl. 40, figs. 10, 11.

1930 *Pecten natoriensis subovalis* MATSUMOTO, Sci. Rep. Tohoku Imp. Univ., (2), **13**, 3, p. 105, Pl. 40, fig. 12.

1930 *Pecten natoriensis inequilateralis* MATSUMOTO, Sci. Rep. Tohoku Imp. Univ., (2), **13**, 3, p. 105, Pl. 40, figs. 13, 14.

Geol. age.—Pliocene (ONOYAMA)-Miocene. Geogr. distr. – Pliocene (Toyama pref.); Natori in Ugo (Miocene); Isikawa pref. (Miocene); Enniti, South Tyosen (Miocene by KANEHARA). Occur.—Iwaya near Nanao (Nanao beds).

Chlamys nipponensis **KURODA**

1861 *Pecten laetus* GOULD, Proc. Boston Soc. N. H., **8**, p. 39, (Not of *Pecten laetus* Gould, Proc. Bost. Soc. N. H., **3**, p. 345, 1850, a new Zealand species).

1920 *Pecten laetus*, YOKOYAMA, Jour. Coll. Sci. Tokyo Imp. Univ., **39**, 6, p. 152, Pl. 14, figs. 1, 2.

1932 *Chlamys farreri nipponensis* KURODA, Venus, 3, 2, App. p. 91.

Geol. age.—Pliocene-Recent. Geogr. distr.—Hokkaido, Honsyu, Sikoku, Kyusyu. Occur.—Tumuki (4) No. 2425; Hiradoko (1) No. 2426; Akasaki (2) (No. 2052); Simazaki, Zyunityo (Himi bed) No. 2033, Coll. E. R. I.

***Chlamys* sp.**

Plate LV, Figure 143.

This shell is a shell of *Chlamys islandicus* MÜLLER type. It has a large shell (about 150 mm in height) with many bifurcated ribs which are 3 in 10 mm width at the ventral margin. These ribs are crossed by fine concentrical grows lines. Interstices of these bifurcated ribs are narrower than the rib.

Only one fragmental specimen was collected.

Occurrence.—Tobeiyati in Higasiminato-mura (Nozaki beds) (No. 1923).

***Pecten* MÜLLER, 1776.**

***Pecten laqueatus* SOWERBY**

1842 *Pecten laqueatus* SOWERBY, Thesaurus Conch., **1**, p. 46, Pl. 15, fig. 101.

1844 *Pecten antonii* PHILIPPI, Abbild. u. Beschr. **1**, p. 99, Pl. 1, fig. 1.

1922 *Pecten excavatus*, YOKOYAMA, Jour. Coll. Sci. Tokyo Imp. Univ., **44**, 1, p. 183, Pl. 15, fig. 6, 7. (not of ANTON)

Geol. age.—Pliocene-Recent. Geogr. distr.—Hokkaido, Honsyu, Sikoku, Kyusyu. Occurr.—Tumuki (1) No. 2433; Miyainu (4) No. 2434; Hiradoko (20) No. 2435.

***Patinopecten* DALL, 1898.**

***Patinopecten tokyoensis kimurai* (YOKOYAMA)**

Plate LVII, Figure 212.

1925 *Pecten kimurai* YOKOYAMA, Jour. Coll. Sci. Imp. Univ. Tokyo, **45**, 5, p. 27, Pl. 4, figs. 1~6; Pl. 2, fig. 4.

1934 *Patinopecten tokyoensis kimurai*, OTUKA, Bull. Earthq. Res. Inst., **12**, pt. 3, p. 613.

Geol. age. - Middle Neogene-Pliocene. Geogr. distr.—Hukusima pref., Isikawa pref., Iwate pref., Hokkaido. Occurrence.—Simazaki, Himi (Himi beds) No. 2030, Coll. E. R. I.

***Patinopecten plebejus* (YOKOYAMA)**

1926 *Pecten plebejus* YOKOYAMA, Jour. Fac. Sci. Imp. Univ. Tokyo, (2), **1**, pt. 8, p. 305, p. 305, p. 136, figs. 1, 2.

1931 *Pecten* sp., K. Mochizuki, Isikawaken Tennenkinenbutu Hokoku, **7**, Pl. 34, fig. 2, Pl. 35, fig. 3.

Geol. age.—Pliocene. Geogr. distr.—Sado, Noto, Iwaki ?. Occur.

—Simazaki, Himi (Himi beds) No. 2037, Coll. E. R. I.

Patinopecten kagamianus (YOKOYAMA)

Plate LV, Figures 128, 134.

1923 *Pecten kagamianus* YOKOYAMA. Jap. Jour. Geol. Geogr. **2**, p. 2, Pl. 11, fig. 1.

1926 *Pecten permirus* YOKOYAMA, Jour. Geol. Soc. Tokyo, **33**, p. 9, Pl. 2.

1929 *Pecten (Patinopecten?) kogamianus*, YOKOYAMA, Imp. Geol. Surv. Japan, Rep. 104, pp. 2~4, Pl. 1, Pl. 2.

1930 *Patinopecten plicicostulatus* MATSUMOTO, Sci. Rep. Tohoku Imp. Univ. Sendai, (2), **13**, 3, pp. 105, 106, Pl. 40, fig. 15.

Geol. age.—Upper Miocene. Geogr. distr.—Miyagi pref., Simane ref., Isikawa pref., (in Miocene). Occur.—Iwaya, Kokubu (Nanao beds) (No. 1138).

Spondylus LINNÉ, 1758.

Spondylus cruentus LISCHKE

Plate LV, Figure 129.

1868 *Spondylus cruentus* LISCHKE, malakoz. Blätt. **15**, p. 221.

1869 *Spondylus cruentus*, LISCHKE, Jap. Meeres Conch, **1**, p. 172, Pl. 12, fig. 1 ~5.

1922 *Spondylus cruentus*, YOKOYAMA, Jour. Coll. Sci. Tokyo Imp. Univ., **44**, 1, p. 179, Pl. 14, fig. 24.

Geol. age.—Pliocene-Recent. Geogr. distr.—Tiba pref., Toyama pref., Sikoku, Kyusyu. Occur.—Tumuki (4) No. 2437; Miyainu (4) No. 2436, C. E. R. I.

Lima CUVIER, 1798.

Lima lischkei LAMY

Plate LV, Figure 132, 133.

1877 *Lima japonica* DUNKER, malakoz. Bl., **2**, p. 70 (Not of A. ADAMS).

1885 *Lima dunkeri* SMITH, Challenger Report, Lamellibranchia, p. 291 (Not of HAGENOW, 1642).

1924 *Lima dunkeri*, YOKOYAMA, Jour. Coll. Sci. Tokyo Imp. Univ., **45**, 1, p. 45. Pl. 5, fig. 19.

1930 *Lima lischkei* Lamy, Jour. d. Conch., **74**, 3, p. 196.

1932 *Lima lischkei*, KURODA, Venus, 3, 4, App. p. 115.

Geol. age.—Pliocene? (Katase beds)-Pleistocene-Recent. Geogr. distr.—Sagami bay, Toyama bay, Wakayama pref., Sikoku. Occur.—Miyainu (15) No. 2438; Hiradoko (30) No. 2439, Col. E. R. I.

Lima basilanica ADAMS et REEVE

Plate LV, Figures 131, 130.

1843 *Lima angulata* SOWERBY, Thesaurus Conch. **1**, p. 86, Pl. 22, fig. 39, 40.

1850 *Lima basilanica* ADAMS et REEVE, Zool. "Samarang", Moll., p. 75, Pl. 21, fig. 6.

1850 *Lima orientalis* ADAMS et REEVE, Zool. "Samarang", Moll. p. 75, Pl. 21, fig. 7.

1906 *Lima hakodatensis* TOKUNAGA, Jour. Coll. Sci. Tokyo Imp. Univ., **21**, 2, p. 64, Pl. 3, fig. 27 (a, b.)

1932 *Lima basilanica*, KURODA, Venus, **3**, App. p. 114, fig. 131.

Geol. age.—Pliocene-Recent. Geogr. distr.—Matusima bay; Noto; Tokyo bay; Wakayama pref.; Sikoku; Kyusyu; Taiwan. Occur.—Tumuki (8) No. 2440; Hiradoko (3) Coll. E. R. I.

***Limatula* S. V. WOOD, 1839.**

***Limatula subauriculata* (MONTAGU)**

Plate LV, Figures 121, 122.

1808 *Pecten subauriculatus* MONTAGU, Test. Brit. Suppl. p. 63, Pl. 26, fig. 2.

1843 *Lima subauriculata* SOWERBY, Thesaurus Conch, **1**, p. 84, Pl. 22.

1920 *Lima subauriculata*, YOKOYAMA, Jour. Coll. Sci. Imp. Univ. Tokyo, **39**, 6, p. 150, Pl. 12., fig. 10.

Geol. age.—Pliocene-Recent.Geogr. distr.—Northern Pacific, Atlantic, Karahuto. Occur.—Simazaki, (Himi beds) No. 2017, Coll. Earthq. Res. I.

***Crassatellites* KRUEGER, 1823.**

***Crassatellites nanus* (ADAMS et REEVE)**

Plate LVI, Figures 146, 147.

1850 *Crassatella nana* ADAMS et REEVE, Zoology of the Voyage of H. M. Samarang, Mollusca, p. 81~2, Pl. 23, fig. 2.

Geol. age. - Pleistocene-Recent. Geogr. distr.—Central and western Japan. Occur.—Hiradoko (4) No. 2505, Coll. Earthq. Res. Inst.

***Trapezium* MEGERLE von MÜHLFELD 1811.**[82]

Trapezium japonica* PILSBRY

Plate LVII, Figures 202, 203.

1905 *Trapezium japonicum* PILSBRY, Proc. Acad. Nat. Sci. Philadelphia, p. 119, Pl. 5, figs. 34, 35, 36.

1922 *Trapezium nipponicum* YOKOYAMA, Jour, Coll. Sci. Tokyo Imp. Univ., **44**, 1, p. 167, Pl. 13, fig. 17.

1922 *Traaezium liratum*, YOKOYAMA. Jour. Coll. Sci. Tokyo Imp. Univ., **44**, 1, p. 168, Pl. 13, fig. 16.

Geol. age.—Pleistocene-Recent. Geogr. distr.—Tokyo bay, Setouti, Sikoku, Matusima bay. Occurrence.—Tumuki(1) No. 2441, Coll. Earthq. Res. Inst.

***Astarte* SOWERBY, 1816.**

***Astarte hakodatensis* YOKOYAMA**

Plate LVI, Figures 148, 149, 150.

1920 *Astarte hakodatensis* YOKOYAMA, Jour. Coll. Sci. Tokyo Imp. Univ., **39**, 6, p. 140, Pl. 11, figs. 5, 6.

1922 *Astarte hakodatensis*, YOKOYAMA, Jour. Coll. Sci. Tokyo Imp. Univ., **44**, 1, p. 164.

1926 *Astarte hakodatensis*, YOKOYAMA, Jour. Fac. Sci. Imp. Univ. Tokyo, (2), **1**, 8, p. 299.

1933 *Astarte hakodatensis*, SASAKI, Suisan Kenkyu Iho, **3**, p. 16, sp. 59.

Geol. age.—Pliocene-Recent. Geogr. distr.—Hokkaido (Living);

---

[82] *Trapezium*, Mus. Calonn., 1798=Nom. Nud.

* *Beguina japonica* (PILSBRY) in Table I, Part I.

Lower and Upper Musasino formation. Sado (Pliocene), Isikawa pref. (Pliocene). Occur.—Simazaki (Himi beds) No. 2027, Coll. Earthq. Res. Inst.

Astarte alaskensis **DALL**

Plate LVII, Figure 195.

1903 *Astarte alaskensis* DALL, Proc. U. S. Mus., **26**, 944, Pl. 63, fig. 2.

1924 *Astarte alaskensis* OLDROYD, Stanford University Publ. Geol. Sci. **1**, 1, p. 106, Pl. 13, fig. 20.

1926 *Astarte sulcata*, YOKOYAMA, Jour. Fac. Sci. Tokyo Imp. Univ., (2), **1**, 8, p. 298, Pl. 37, figs. 9, 10. (not of DACOSTA).

1933 *Astarte undata*, SASAKI, Suisankenkyuiho, **3**, p. 16, sp. 58, Pl. 2, fig. 14. (not of GOULD)

Geol. age.—Pliocene-Recent. Geogr. distr.—Northern Pacific. Occur.—Simazaki, (Himi beds) No. 2023.

Cardita **BRUGUIÈRE, 1792.**

Cardita cumingiana **DUNKER**

Plate LVI, Figures 157 a, b.

1860 *Cardita cumingiana* DUNKER, Malakoz. Bl. **6**, p. 223.

1861 *Cardita cumingiana*, DUNKER, Moll. Jap., p. 29, Pl. 3, fig. 18.

1920 *Cardita cumingiana*, YOKOYAMA, Jour. Coll. Sci. Tokyo Imp. Univ., **39**, 6, p. 137, Pl. 10, fig. 16; Pl. 11, fig. 1.

Geol. age.—Pliocene ?-Recent. Geogr. distr.—Mutu bay, Matusima bay, Toyama bay, Tokyo bay, Wakayama pref., Kyusyu, Amami Osima. Occur.—Tumuki (2) No. 2443; Miyainu (14) No. 2444; Hiradoko (20) No. 2445, Coll. Earthq. Res. Inst.

Venericardia **LAMARCK, 1801.**

Venericardia ferruginosa **(ADAMS et REEVE)**

Plate LVII, Figures. 210, 211.

1850 *Cardita ferruginosa* ADAMS et REEVE, Zoology Voy. H. M. S. Samarang, sp. 78, Pl. 21, fig. 21.

1920 *Venericardia cipangoana* YOKOYAMA, Jour. Coll. Sci. Tokyo Imp. Univ., **44**, 139, Pl. 11, figs. 3, 4.

1934 *Venericardia ferruginosa*, OTUKA, Bull. Earthq. Res. Inst., **12**, 3. p. 614.

Geol. age.—Miocene-Recent. Geogr. distr.—Honsyu, Japan sea, Northern Japan. Occur.-Simazaki No. 2031, Coll. Earthq. Res. Inst.

Venericardia ferruginea **(A. ADAMS)**

Plate LVI, Figures 174 a, b.

1888 *Cardita ferruginea* ADAMS, Syst. Conchylien Cabinet, Martini and Chemnitz, *Cardita*, p. 17, Pl. 6, fig. 11.

1920 *Venericardia ferruginea*, YOKOYAMA, Jour. Coll. Sci. Tokyo Imp. Univ., **44**, 137, Pl. 11, fig. 2.

1934 *Venericardia ferruginea*, OTUKA, Bull. Earthq. Res. Inst., **12**, 3, p. 614.

Geol. age.—Miocene-Recent. Geogr. distr.—Northern Japan. and Central Japan. Occur.—Simazaki (Himi beds) No. 2032, Coll. Earthq. Res. Inst.

Venericardia nakamurai YOKOYAMA

1923 *Venericardia nakamurai* YOKOYAMA, Jour. Coll. Sci. Tokyo Imp. Univ., **44**, 7, pp. 5, 6, Pl. 1, fig. 9.

1926 *Venericardia nakamurai*, YOKOYOMA, Jour. Fac. Sci. Imp. Univ. Tokyo, (2), **1**, 8, p. 298, Pl. 36, fig. 3.

1627 *Venericardia nakamurai*, YOKOYAMA. Jour. Fac. Sci. Imp. Univ. Tokyo, (2), **2**, 4, p. 169.

This species may be identical with *Venericardia prolongata* CARPENTER, 1864.[83] The Japanese species has more vertical muscular impression than the American species.

Geol. age.—Pliocene. Geogr. distr.—Saisyu-to, Isikawa pref., Sado island. Occur.—Simazaki (Himi beds) No. 2016.

Corbicula MEGERLE von MÜHLFELD, 1811.

Corbicula sp.

Plate LVII, Figure 196.

Occur.—Simazaki (Himi beds) No. 2034.

Basterotia C. MAYER, 1859.

Basterotia gouldii (A. ADAMS)

Plate LV, Figs. 125, 126, 127, 128.

1864 *Eucharis gouldii* A. ADAMS, Ann. Mag. Nat. Hist., p. 309.

1920 *Basterotia gouldii*, YOKOYAMA, Jour. Coll. Sci. Imp. Univ. Tokyo, **39**, 6, p. 108, Pl. 7, fig. 7.

Geol. age.—Pleistocene-Recent. Geogr. distr.—Sagami bay; Setouti: Kyusyu. Occur.—Hiradoko (4), No. 2446, Coll. Earthq. Res. Inst.

Thyasira (LEACH) LAMARCK, 1818.

Thyasira nipponica YABE et NOMURA

Plate LVII, Figure 194.

1925 *Thyasira bisecta nipponica* YABE et NOMURA, Sci. Rep. Tohoku Imp. Univ., (2), **7**, **4**, p. 48, Pl. 24, fig. 2 (a, b), 3 a, b.

1925 *Thyasira bisecta*, YOKOYAMA, p. 14 (not of CONRAD).

1931 *Thyasira nipponica*, KURODA, Gology of Middle Sinano, Fossil Shells, pp. 48~49, Pl. 5, fig. 28.

Geol. age.—Oligocene-Recent. Geogr. distr.—Japan Sea; Sagami-bay; Northern Japan. Occur.—Kayato, Nozaki, Yabuta beds.

Thyasira yabei KURODA

1931 *Thyasira yabei* KURODA, Geology of Middle Sinano, Fossil Shells, pp. 49~50.

Geol. age.—Miocene ?-Recent. Geogr. distr.—Northern Japan; Japan sea. Occur.—Nozaki (Yabuta series.) No. 2447, Coll. E. R. I.

Taras RISSO, 1826.

Taras lunaris (YOKOYAMA)

Plate LVI, Figs. 167 a, b, 175, 176.

1927 *Diplodonta lunaris* YOKOYAMA, Jour. Fac. Sci. Imp. Univ. Tokyo, (2), **1**, 10, p. 433, Pl. 50, figs. 5, 6.

---

83) CARPENTER, *Suppl. Rep. Brit. Assoc.*, (1864), pp. 236 and 642.

Geol. age.—Pleistocene. Geogr. distr.—Isikawa pref., Southern Kwanto. Occur.—Hiradoko (4) No. 2448, Coll. Earthq. Res. Inst.

***Lucina* BRUGUIÈRE, 1797.**

***Lucina (Lucinoma) acutilineata* CONRAD.**

1849 *Lucina acutilineata* T. A. CONRAD, U. S. Exped., x, Geol., p. 725.

1850 *Lucina annulata* EEEVE, Conch. Icon., **6**, *Lucina*, sp. 17, Pl. 4, fig. 17.

1920 *Lucina borealis*, YOKOYAMA, Jour. Coll. Sci. Tokyo Imp. Univ., **39**, 6, p. 133, Pl. 10, fig. 6.

1934 *Lucina acutilineata*, OTUKA, Bull. Earthq. Res. Inst., **13**, 3, p. 614.

Geol. age.—Oligocene-Recent. Geogr. distr.—Northern Pacific. Occur.—Hiradoko (20) No. 2449, Coll. Earthq. Res. Inst.

***Pillucina* PILSBRY, 1920.**

***Pillucina pisidium* (DUNKER)**

Plate LVII, Figures 200 a, b.

1860 *Lucina pisidium* DUNKER, Malakoz. Bl. p. 227.

1861 *Lucina pisidium*, DUNKER, Moll. Jap., p. 28, Pl. 3, fig. 9.

1920 *Lucina pisidium*, YOKOYAMA, Jour. Coll. Sci. Tokyo Imp. Univ., **39**, 9, pp. 132~133, Pl. 10, fig. 6.

Geol. age. -Pliocene-Recent. Geogr. distr.—Hokkaido; Matusima bay; Amami Osima. Occur. -Tumuki (6) No. 2450; Miyainu (15) No. 2451; Akasaki (2), Coll. E. R. I.

"*Lucina*" *contraria* DUNKER

Plate LVII, Figure 190, 191.

1882 *Lucina contraria* DUNKER, Index. Moll. Mar. Jap., p. 215, Pl. 13, figs. 12, 13, 14.

1920 *Lucina contraria* YOKOYAMA, Jour. Coll. Sci. Tokyo Imp. Univ., **39**, 6, p. 134, Pl. 10, fig. 8.

Geol. age.—Miocene-Recent. Geogr. distr.—Central Japan. Occur. —Tumuki (7), No. 2452, Coll. Earthq. Res. Inst.

***Anodontia* LINK, 1807.**

***Anodontia bialata* (PILSBRY)**

Plate LVI, Figures 153, 154.

1895 *Loripes bialata* PILSBRY, Cat. Mar. Mol. Jap. p. 133—4, Pl. 3, figs. 13, 14.

1927 *Loripes philippiana*, YOKOYAMA, Jour. Fac. Sci. Imp. Univ. Tokyo, (2), 1, p. 434, Pl. 50, figs. 1, 2. (not of REEVE)

Geol. age.—Pleistocene-Recent. Geogr. distr.—Setouti, Noto, Tokyo bay, Mutu bay. Occur.—Tumuki (10) No. 2453; Miyainu (1) No. 2454; Akasaki (2) No. 2056, Coll. E. R. I.

***Codakia* SCOPOLI, 1777.**

***Codakia divergens* (PHILIPPI)**

Plate LVI, Figures 177, 178.

1851 *Lucina divergens* PHILIPPI, Abbild. Beschr. **3**, p. 103, *Lucina* Pl. 2, fig. 4.

1923 *Codakia bella delicatula*, YOKOYAMA, Jour. Coll. Sci. Tokyo Imp. Univ., **44**, p. 50, Pl. 3, fig. 8.

Geol. age. — Pleistocene-Recent. Geogr. distr. Kyusyu, Sikoku, Honsyu. Occur. – Tumuki(1) No. 2456; Miyainu(9) No. 2457; Hiradoko (1) No. 2473, Coll. E. R. I.

***Kellya* TURTON, 1822. (=*Kellia*)**

***Kellya notoensis* YOKOYAMA**

Plate LVI, Fig. 163; LVII, Fig. 195.

1928 *Kellya notoensis* YOKOYAMA, Imp. Geol. Surv. Japan, **101**, p. 127, Pl. 19, fig. 13.

Geol. age.—Pleistocene. Geogr. distr.—Tumuki (Pleistocene). Occur. - Tumuki (1) No. 2458, Coll. Earthq. Res. Inst.

***Scintilla* DESHAYES, 1855.**

***Scintilla nipponica* YOKOYAMA**

Plate LVI, Figure 182 a, b.

1924 *Scintilla nipponica* YOKOYAMA, Jour. Coll. Sci. Tokyo Imp. Univ., **45**, 1, Pl. 4, fig. 1.

Geol. age.—Early Holocene. Geogr. distr. - Awa (Coral bed). Occur. - Miyainu (1) No. 2463, Coll. Earthq. Res. Inst.

***Jousseaumiella* BOURNE, 1907.**

"*Jousseaumiella*" *crassa* (YOKOYAMA)

Plate LVII, Figures 207, 208.

1927 *Montacuta? crassa*, YOKOYAMA, Jour. Fac. Sci. Imp. Univ. Tokyo, (2), p. 433, Pl. 49, figs. 4, 5.

Geol. age.—Pleistocene. Geogr. distr.—Tokyo in Pleistocene deposits. Occur.—Hiradoko (1), No. 2464, Coll. Earthq. Res. Inst.

***Mysella* ANGAS, 1877. (=*Rochefortia* VELAIN 1878).**

***Mysella oblongata* (YOKOYAMA)**

Plate LVII, Figures 213, 214.

1922 *Montacuta oblongata* YOKOYAMA, Jour. Coll. Sci. Tokyo Imp. Univ., **44**, 1, p. 157, Pl. 13, figs. 9, 10.

Geol. age.—Pleistocene. Geogr. distr.—Tokyo in Pleistocene deposit. Occur.—Hiradoko (1), No. 2465, Coll. Earthq. Res. Inst.

***Chama* (LINNÉ, 1758) BRUGUIÈRE, 1789.**

***Chama aspersa* REEVE**

Plate LV, Figures 119, 120, 123, 124.

1846 *Chama aspersa* REEVE, Conch. Icon., **4**, *Chama* sp. 24.
1934 *Chama kikuzaru* HIRASE, *Coll. Japanese Shells*, Pl. 26,

Geol. age.—Pliocene-Recent. Geogr. distr.—Toyama bay, Hukui pref., Sagami bay, Kii, Sikoku. Occur.—Akasaki (1) No. 2061; Tumuki (4) No. 2466; Miyainu (40) No. 2467; Hiradoko (20) No. 2468, Coll. Earthq. Res. Inst.

***Papyridea* SWAINSON, 1840.**

***Papyridea(Fulvia) muticum* (REEVE)**

Plate LVI, Figures 160, 165.

1844 *Cardium muticum* REEVE, Conch. Icon. *Cardium*, Pl. 6, fig. 32.

Geol. age.—Miocene ?-Recent. Geogr. distr.—Hakodate, Mutu bay, Noto, Matusima, Tokyo, Nagasaki, Setouti. Occur.—Tumuki (1) No. 2469; Miyainu (1) No. 2470; Hiradoko (2) No. 2471; Akasaki (1) No. 2057, Coll. E. R. I.

***Papyridea* (*Fulvia*) *hungerfordi* (SOWERBY)**

Plate LVI, Figures 155, 156, 164, 166.

1901 *Cardium hungerfordi* SOWERBY, Jour. of Malacology, 8, p. 103.

1904 *Cardium* (*Leiocardium*) *hungerfordi*, PILSBLY, Proc. Acad. Nat- Sci. Philadelphia, 56, p. 555~556, Pl. 41, fig. 17.

Geol. age.—Pleistocene-Recent. Geogr. distr.—Sagami bay, Tokyo bay, Toyama bay, Hiradoko. Occur.—Hiradoko (15) No. 2472, Coll. E. R. I.

***Cardium* LINNÉ, 1758.**

***Cardium* sp. (*shinjiense* ? YOKOYAMA)**

Occur.—Simazaki, (Himi beds) No. 2038, Coll. Earthq. Res. Inst..

***Corculum* (BOLTEN) RÖDING, 1798.**

***Corculum* (*Fragum*) *ebaranum* YOKOYAMA**

Plate LVI, Figures 170, 171.

1927 *Cardium ebaranum*, YOKOYAMA, Jour. Fac. Sci. Imp. Univ. Tokyo, (2), 1, 10, p. 430~1, Pl. 48, fig. 15.

Geol. age.—Pleistocene. Geogr. distr.—Tokyo. Occur.—Miyainu (1) No. 2475; Hiradoko (2) No. 2476.

***Gafrarium* (BOLTEN) RÖDING, 1798.**

***Grafrarium divaricatum* (GMELIN)**

Plate LVI, Figure 179.

Venus divaricatus CHEMNITZ, Conch. Cab. 6, p. 317, Pl. 30, fig. 316.

1869 *Cytherea divaricata* GMELIN, in PFEIFFER's Syst. Conch. Cab. MARITINI CHEMN., p. 44, Pl. 16, fig. 8.

1928 *Circe divaricata*, YOKOYAMA, Imp. Geol. Surv. Rep., 101, p. 127, Pl. 20, fig. 1,

Geol. age.—Pleistocene-Recent. Geogr. distr.—Ise, Sikoku, Kyusyu, Hukui, Toyama, Tokyo. Occur.—Tumuki (6) No. 2474; Akasaki (4) No. 2047, Coll. Earthq. Res. Inst.

***Gafrarium* (*Circe*) *scriptum stutzeri* (DONOVAN)**

Plate LVI, Figure 180.

1825 *Venus stutzeri* DONOVAN, Naturalist's Repository, 3, Pl. 78.

1921 *Venus stutzeri*, PILSBRY, The Nautilus, 34, 4.

Circe, scripta personata DESHAYES may be synonym with this sp.

Geol. age.—Pleistocene-Recent. Geogr. distr.—Central and western Japan. Occur.—Akasaki(4) No. 2047; Tumuki(15) No. 2475, C. E. R. I.

***Saxidomus* CONRAD, 1837.**

***Saxidomus purpuratus* (SOWERBY)**

1855 *Tapes purpuratus* SOWERBY, Thes. Conch. 2, p. 692, Pl. 150, figs. 124, 125.

Geol. age.—Pleistocene-Recent. Geogr. distr.—Hakodate, Mutu bay, Matusima bay, Tokyo bay, Setouti. Occur.—Akasaki No. 2050.

***Pitar* RÖMER, 1857.**

Pitar lineolata* SOWERBY.

Plate LVI, Figures 158, 159.

1855 *Cytherea lineolata* SOWERBY, Thesaurus Conch., **2**, p. 786, sp. 124, Pl. 168, figs. 214, 215.

1924 *Meretrix* (*Callista*) *limatula*, YOKOYAMA, Jour. Coll. Sci. Imp. Univ. Tokyo, **44**, 7, p. 43, Pl. 2, fig. 21, (Not of SOWERBY).

Zigzag pattern is feebly preserved on the surface of these fossil specimens.

Geol. age.—Pleistocene-Recent. Geogr. distr.—Ryukyu, Amami Osima. Occurence.—Tumuki (8) No. 2477; Miyainu (1) No. 2478; Hiradoko (1) No. 2479; Akasaki (4), Coll. E. R. I.

***Callista* (POLI, 1791) MÖRCH, 1853.**

***Callista pacifica* (DILLWYN)**

Plate LVI, Figure 181.

1817 *Venus pacifica* DILLWYN, Cat. Rec. Shells **1**, p. 175.

1855 *Cytherea sinensis*, SOWERBY, Thes. Conch., **2**, p. 624, Pl. 131, figs. 78, 80.

1864 *Cytherea chinensis*, PFEIFFER, Syst. Conch. Cab. Mart, Chemn., **11**, pt. 1, p. 31, Pl. 11, fig. 2.

1920 *Meretrix* (*Callista*) *chinensis*, YOKOYAMA, Jour. Coll. Sci. Imp. Univ. Tokyo, **39**, 6, p. 120, Pl. 8, figs. 9, 10.

Geol. age.—Cretaceous-Pliocene-Recent. Geogr. distr.—Central and western Japan, China. Occur.—Miyainu (1) No. 2488; Hiradoko (20) No. 2489, C. E. R. I.

***Meretrix* LAMARCK, 1799.**

Meretrix meretrix* (LINNÉ)*

1758 *Venus meretrix*, LINNÉ, Syst. Nat. ed. 10, p. 686.

1927 *Meretrix gordonis* YOKOYAMA, Jour. Fac. Sci. Tokyo Imp. Univ., Sec. (2), **1**, p. 429, Pl. 48, figs. 13, 14.

Geol. age.—Pliocene-Recent. Geogr. distr.—Hokkaido, Honsyu, Sikoku, Kyusyu. Occur.—Hiradoko (30) No. 2490, Coll. Earthq. Res. Inst.

***Dosinia* SCOPOLI, 1777.**

***Dosinia japonica* REEVE**

1850 *Artemis japonica* REEVE, Conch. Icon., *Artemis*, Pl. 3, fig. 17.

1920 *Dosinia troscheli*, YOKOYAMA, Jour. Coll. Sci. Tokyo Imp. Univ., **39**, 6, p. 119, Pl. 8, figs. 5, 6. (Not of LISCHKE).

Geol. age.—Pliocene-Recent. Geogr. distr.—Central and western Japan. Occur.—Akasaki (1) No. 2049; Tukuki (2) No. 2491, Coll. Earthq. Res. Inst..

***Protothaca* DALL, 1902.**

---

* *Pitar pellucida* LAMARCK in Table I, Part I.

** *Chamaeformis meretrix* LINNÈ in Table I, Part I.

Protothaca jedoensis **(LISCHKE)**

1874 *Venus jedoensis* LISCHKE, Jap. Meeres Conch., 3, p. 84, Pl. 7, figs. 1~9.

1920 *Venus jedoensis*, YOKOYAMA, Jour. Coll. Sci. Tokyo Imp. Univ., 39, 6, p. 120, Pl. 8, figs. 9, 10.

Geol. age.—Pliocene-Recent. Geogr. distr.—Hokkaido, Honsyu, Sikoku, Kyusyu. Occur.—Akasaki, (2) No. 2046; Tumuki (15) No. 2492; Miyainu (7) No. 2493, Coll. Earthq. Res. Inst.

Paphia **(BOLTEN) RÖDING, 1798.**

Paphia euglypta **(PHILIPPI)**

Plate LVI, Figures 172, 173.

1847 *Venus euglyptus*, PHILIPPI, Zeitschr. f. Malak., p. 89.

1934 *Paphia (Paphia) euglypta*, HIRASE, Coll. Japanese Shell. Pl. 38, fig. 5.

Geol. age.—Pliocene-Recent. Geogr. distr.—Central western Japan, Kyusyu. Occur.—Hiradoko (4) No. 2494, C. E. R. I.

Paphia **sp.**

A fragmental specimen was collected from Hukazawa.

Occur.: Hukazawa (Nozaki bed).

Paphia (Paratapes) undulata **(BORN)**

Plate LVI, Figures 168, 169.

~ *Venus undulata* BORN, Mus. Caes. Mind. p. 67.

1934 *Paphia (Paratapes) undulata*, HIRASE, Coll. Jap. Shell. Pl. 39, fig. 5.

1928 *Tapes undulatus*, YOKOYAMA, Imp. Geol. Surv. Japan, Rep., 101, p. 82, Pl. 8, fig. 2.

Geol. age.—Pliocene-Recent. Geogr. distr.—Southern Japan, Central and western Japan. Occur.—Miyainu (12) No. 2495, C. E. R. I.

Petricola **LAMARCK, 1801.**

Petricola japonica **DUNKER**

Plate LVII, Figures 188, 189.

1882 *Petricola japonica* DUNKER, Index. moll. p. 209, Pl. 9, figs. 4, 5, 6.

1928 *Petricola japonica*, YOKOYAMA, Imp. Geol. Surv. Rep. 101, Pl. 14, figs. 14, 15.

1934 *Petricola japonica*, KURODA, Venus, 4, 6, p. 386.

Geol. age.—Pleistocene-Recent. Geogr. distr.—Kyusyu, Honsyu. Occur.—Tumuki (2) No. 2496; Akasaki (2), Coll. E. R. I.

Raeta **GRAY, 1853.**

Raeta pulchella **(ADAMS et REEVE)**

1848 *Poromya pulchella* ADAMS et REEVE, Zoology Voy. Samarang. Moll., p. 83, Pl. 23, fig. 1.

1854 *Mactra rostralis*, DESHAYES, Proc. Zool. Soc., p. 69.

1927 *Raeta pulchella*, MAKIYAMA, Mem. Coll. Sci. Kyoto Imp. Univ.. B, 3, 1, p. 54.

Geol. age.—Pliocene-Recent. Geogr. distr.—Tokyo bay, Setouti, Saga pref. Occur.—Tumuki (2).

Lutraria **LAMARCK, 1799.**

***Lutraria arcuata* REEVE**

1854 *Lutraria arcuata* REEVE, Conch. Icon. **8**, *Lutraria*, sp. 6.

Geol. age.—Pliocene-Recent. Geogr. distr.—Hizen, Amami Osima, Wakayama pref. Occur.—Hiradoko (7) No. 2503, Coll. Earthq. Res. Inst.

***Sanguinolaria* LAMARCK, 1799.**

***Sanguinolaria* (*Nuttallia*) *olivacea* (JAY)**

1856 *Psammobia olivacea* JAY, Rep. M. C. PERRY, U. S. N. Jap. Exp., p. 292, Pl. 1, figs. 8, 9.

1922 *Soletellina olivacea*, YOKOYAMA, Jour. Coll. Sci. Tokyo Imp. Univ., **39**, 6, p. 138, Pl. 7, fig. 11, Pl. 9, fig. 17.

Geol. age.—Pleistocene-Recent. Geogr. distr.—Tisima, Hokkaido, Honsyu, Sikoku, Kyusyu. Occur.—Tumuki (1) No. 2504, C. E. R. I.

***Theora* H. *and* A. ADAMS, 1856.**

***Theora lubrica* GOULD**

1861 *Theora lubrica* GOULD, Proc. Bost. Soc. Nat. Hist. **8**, 14.

1882 *Theora lubrica*, DUNKER, Index. Moll. Mar. Jap., p. 181, Pl. 7, figs. 20~22.

1927 *Theora lubrica*, YOKOYAMA, Jour. Fac. Sci. Imp. Univ. Toko, (2), **1**, 10, p. 429, Pl. 48, figs. 11, 12.

Geol. age.—Pliocene-Recent. Goegr. distr.—Hakodate (Stimpson), Tokyo bay, Setouti, Saga pref. Occur.—Tumuki (2), Miyainu (1), No. 2523, Coll. E. R. I.

***Macoma* LEACH, 1819.**

***Macome* (*Pseudometis*) *praerupta* SALISBURY**

Plate LVI, Figures 161, 162.

1843 *Tellina truncata* JONAS, in PHILIPPI, Abbild. u. Beschr., **1**, p. 71, *Tellina*, Pl. 1, fig. 2. (Not of LINNÉ, 1767).[34]

1934 *Macoma* (*Psammacoma*) *truncata*, HIRASE, Coll. Jap. Shell, Pl. 45, fig. 5.

1934 *Macoma* (*Pseudometis*) *praerapta* SALSUBRY, Proc. Malac. Soc. **21**, 2, p. 90.

Geol. age.—Pleistocene-Recent. Geogr. distr.—Kii, Sikoku, Tokyo bay. Occur.—Miyainu (3) No. 2500, Coll. Earthq. Res. Inst.

***Macoma tokyoensis* MAKIYAMA**

1920 *Macoma dissimilis*, YOKOYAMA, Jour. Coll. Sci. Imp. Univ. Tokyo, **39**, 6, p. 116~117, Pl. 7, figs. 19, 20. (oot of MARTENS.)

1927 *Macoma tokyoensis* MAKIYAMA, Mem. Coll. Sci. Kyoto Imp. Univ., (B), **1**, 50.

1934 *Macoma tokyoensis*, OINOMIKADO, Venus., **4**, 6, p. 355, figs. 1, 2, 3.

Geol. age.—Miocene ?-Pliocene-Recent. Geogr. distr.—Northern-Central Japan. Occur.—Tumuki (2) No. 2501; Miyainu (2) No. 2502; Simazaki ? (3) No. 2039, Coll. E. R I.

***Macoma* (*Psammacoma*) *awajiensis* SOWERBY**

Plate LVII, Figures 192, 193.

1914 *Macoma awajiensis* SOWERBY, Ann. Mag. Nat. Hist. (8), **14**, p. 38, Pl. 2, fig. 11.

---

84) *Macoma truncata* LINNÉ (=*Macoma pulchella* LAMARCK)

Shell white, thin, transversely elongated, inequivalves and inequilateral; surface sculptured with fine concentric striae. Posterior margin obtusely truncated. Posterior area defined by a blant keel from beak to postero ventral margin. Posterior area sculptured with fine concentric striae. Beak situated posterior two fifth of dorsal margin. Posterior dorsal margin slightly concave, anterior dorsal margin slightly arched or straight. Anterior margin broadly rounded. Radial striations visible from beak to ventral margin with magnifieing lens. Ventral margin slightly arched. Cardinal teeth small, two on each valve, diverged. Lateral teeth absent.

Fossil specimens from Miyainu measures 10·5 mm long and 3·5 mm thick with one valve.

Geol. age.—Pleistocene-Recent. Geogr. distr.—Awazi, Simidu harbour. Occur.—Miyainu (2) No. 2508; Hiradoko No. 2509, C. E. R. I.

***Merisca* DALL, 1900.**

***Merisca diaphana* DESHAYES**

Plate LVI, Figures 151, 152.

1854 *Tellina diaphana* DESHAYES, Proc. Zool. Soc. London, p. 364, No. 216.

1871 *Tellina diaphana*, RÖMER, Conch. Cab. MARTINI CHEMNITZ, **10**, 4, p. 47, Pl. 13, figs. 7, 8, 9.

Geol. age.—Pleistocene-Recent. Geogr. distr.—Central and western Japan. Occur.—Hiradoko (1) No. 2507.

***Angulus* MEGERLE von MÜHLFELD, 1811.**

***Angulus (Fabulina) iridella* (v. MARTENS)**

1865 *Tellina iridella* v. MARTENS, Ann. Mag. Nat. Hist., p. 431.

1924 *Tellina iridella*, YOKOYAMA, Jour. Coll. Sci. Tokyo Imp. Univ., **45**, 1, p. 41, Pl. 5, fig. 23.

Geol. age.—Pleistocene-Recent. Geogr. distr.—Tokyo bay, Sagami bay, Setouti, Hukui pref. Occur.—Hiradoko (2) No. 2506, Coll. Earthq. Res. Inst.

Angulus (Fabulina) miyatensis* (YOKOYAMA)

1020 *Tellina miyatensis* YOKOYAMA, Jour. Coll. Sci. Tokyo, Imp. Univ., **39**, 6, p. 115, Pl. 7, fig. 18.

Geol. age.—Pleistocene-Recent. Geogr. distr.—Sagami bay, Southern Kwanto. Occur.—Hiradoko (7) No. 2534, Coll. Earthq. Res. Inst.

***Angulus (Peronidia) salmonea* (CARPENTER)**

1894 *Maera salmonea* CARPENTER, Brit. Assn. Adv. Sci. Rep. for 1863, p. 639.

1930 *Tellina (Moerella) salmonea*, ARNOLD, Mem. Calif. Acad. Sci., **3**, p. 157, Pl. 13, fig. 7.

1924 *Tellina (Moerella) salmonea*, OLDROYD, Univ. Washington Publ. Puget Sound Biol. Station, **4**, p. 51, Pl. 41, fig. 3 a, b.

1934 *Tellina (Peronidia) salmonea*, OINOMIKADO, Chikyu, **22**, 4, p. 37~39, text fig.

---

* *Tellina miyatensis* YOKOYAMA in Table I, Part I.

Geol. age.—Miocene-Recent. Geogr. distr.—Northern Japan. Northern America., Is. Sado, Tiba pref. Occur.—Simazaki (Himi beds) No. 2036.

***Arcopagia* BROWN, 1827.**

Arcopagia* (*Pinguitellina*)[85] *kurodai* OTUKA n. sp.

Plate LVI, Figures 185, 186, 187.

Shell small, elliptical, moderate in thickness, almost equilateral; surface sculptured with fine concentric lamina and few deep incremental lines; Ventral margin broadly arcuated; postero- and antero-dorsal margin slightly arcuated forming angles (about 130°) at beak; anterior and posterior margins narrowly rounded. Posterior surface slightly flexed. Beak small. Cardinal teeth two, small, diverged; lateral teeth prominent, one on postero and other on antero dorsal margin. Parial sinus large and deep (text fig. 226.).

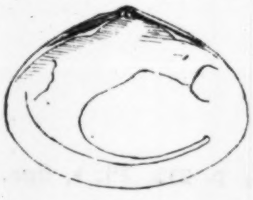

Fig. 226. *Arcopagia* (*Pinguitellina*) *kurodai* OTUKA n. sp.

Height (from beak to ventral) 8 mm; length (from postero-margin to antero-margin) 9·7 mm; thickness 2·1 mm (with one valve).

This species is closely allied to *Arcopagia* (*Pinguitellina*) *nux* Hanley,[86] but the latter species has a more inequilateral shell with more flexed posterior margin.

Occur. - Miyainu, Monotype, No. 2579, Coll. E. R. I.

***Solen* LINNÉ, 1758.**

***Solen* sp.**

Occurrence - Hiradoko (2), No. 2511, Coll. E. R. I.

***Aloidis* MEGERLE von MÜHLFELD, 1811.**

***Aloidis venustus* (GOULD)**

1861 *Corbula venusta* GOULD, Proc. Boston Soc. Nat. Hist., **8**, 14.

1920 *Corbula venusta*, YOKOYAMA, Jour. Coll. Sci. Tokyo Imp. Univ., **39**, 6, p. 107, Pl. 7, figs. 4~6.

Geol. age. Pliocene-Recent. Geogr. distr.—Hukui pref., Tokyo bay, Toyama bay, Matusima bay, Mutu bay, Hakodate. Occur.—Hiradoko (2), No. 2512; Miyainu (2) No. 2513; Simazaki (15) No. 2022, Coll. Earthq. Res. Inst.

***Aloidis substriatus* (YOKOYAMA)**

Plate LVII, Figures 204, 205, 206.

1922 *Corbula substriata* YOKOYAMA, Jour. Coll. Sci. Tokyo Imp. Univ., **44**, 1, p. 125, Pl. 7, fig. 3.

---

[85] *Rec. Australian Museum*, **16**, **1**, p. 76. Pl. 5, figs. 6~8.

[86] HANLEY, *Proc. Zool. Soc.*, 1844; Thes. Conch., *Tellina*, fig. 33.

* *Tellina* sp. in Table I, Part I.

Geol. age. - Pleistocene. Geogr. distr. - Southern Kwanto. Occur. - Hiradoko (4) No. 2514, Coll. E. R. I.

***Cryptomya* CONRAD, 1848.**

***Cryptomya busoensis* YOKOYAMA**

1922 *Cryptomya busoensis* YOKOYAMA, Jour. Coll. Sci. Tokyo Imp. Univ., **44**, 1, p. 126, Pl. 7, figs. 1, 2.

1934 *Cryptomya busoensis*, OTUKA, Bull. Earthq. Res. Inst., **12**, 3, p. 620, Pl. 48, fig. 52.

Geol. age.—Miocene-Recent. Geogr. distr.—Tokyo bay (Otuka); Matusima bay (Nomura); Mutu bay (Nomura); Noto. Occur. - Tumuki (1) No. 2518, Coll. Earthq. Res. Inst.

***Mya* LINNÉ, 1758.**

***Mya arenaria* LINNÉ**

1758 *Mya arenaria*, LINNÉ, Syst. Nat. Ed. 10, p. 670.

1856 *Mya japonica*, JAY, in PERRY's Jap. Exp. Rep. Shell, p. 232, Pl. 1, figs. 7, 10.

Geol. age. - Pleiocene-Recent. Geogr. distr.—Hokkaido, Mutu bay, Matusima bay, Tokyo bay, Setouti, Toyama bay. Occur.—Tumuki (4) No. 2519; Akasaki (2) No. 2051, Coll. Earthq. Res. Inst.

***Barnea* (LEACH) RISSO, 1826.**

Barnea japonica* (YOKOYAMA)

1920 *Pholadomya japonica* YOKOYAMA, Jour. Coll. Sci. Tokyo Imp. Univ., **39**, 6, p. 106, Pl. 6, figs. 30, 31.

1934 *Barnea dilatata*, HIRASE, Coll. Jap. Shell., Pl. 54, fig. 2. (not of SOULEYET)

Geol. age. Pleistocene-Recent. Geogr. distr.—Central Japan. Occur.—Miyainu.

Barnea dilatata (SOULEYET)[87] (=*Pholas latissima* SOWERBY)[88] is closely allied to this species, but the former species is more equilteral shell than *Barnea japonica* (YOKOYAMA).

***Barnea fragilis* (SOWERBY)**

Plate LVII, Figure 201.

1849 *Pholas fragilis* SOWERBY, Thes. Conch., 2, p. 488, Pl. 108, figs. 92, 93.

1922 *Pholas fragilis*, YOKOYAMA, Jour. Coll. Sci. Tokyo, Imp. Univ., **39**, 6, p. 104, Pl. 6, fig. 29.

Geol. age.—Pliocene-Recent. Geogr. distr.—Hokkaido, Honsyu, Sikoku, Kyusyu. Occur.—Tumuki (2) No. 2520, Coll. Earthq. Res. Inst.

***Martesia* (LEACH) BLAINVILLE, 1825.**

Martesia striata* (LINNÉ)*

Plate LVII, Figures 183, 184.

---

[87] SOULEYET, *Rev. Zool. Soc. Cuvier.* p. 176.

[88] SOWERBY, *Proc. Zool. Soc. London,* (1849), p. 162; PHLIIPPI, *Abbild. Beschr.* 3. p. 127, Pl. 2, figs. 1.

* *Barnea dilatata* (SOULEYET) in Table I, Part I.

** *Pholadidea penita tokyoensis* (YOKOYAMA) in Table I, Part I.

Plate LIII.

Plate LIII.

Fig. 21. *Emarginula crassicostata* SOWERBY.
Fig. 22. *Puncturella hirasei* OTUKA, n. n.
Fig. 23. *Puncturella nobilis* (A. ADAMS).
Fig. 23. *Puncturella nobilis* (A. ADAMS).
Fig. 24. *Diodora sieboldii* (REEVE).
Fig. 25. *Patelloida saccharina* (LINNÉ).
Fig. 26. *Patelloida conulus* (DUNKER).
Fig. 27. *Euchelus foveolatus* (A. ADAMS).
Fig. 28. *Tegula (Chlorostoma) rustica* (GMELIN).
Fig. 29. *Rissoina (Rissoina) laevicostulata* PILSBRY.
Fig. 30. *Trophon (Bedeva) birileffi* LISCHKE.
Fig. 31. *Obtortio perpupoides* (YOKOYAMA).
Fig. 32. *Natica concinna* DUNKER.
Fig. 33. *Triphora* aff. *purpurata* (PILSBRY).
Fig. 34. *Iravadia annulata* (DUNKER).
Fig. 35. *Nassarius (Alectrion) balteatus* (LISCHKE).
Fig. 36. *Polinices sagamiensis* PILSBRY.
Fig. 37. *Nassarius (Tritonella) japonicus* (A. ADAMS).
Fig. 38. *Nassarius (Niotha) livescens* (PHILIPPI).
Fig. 39. *Nassarius (Hinia) festivus* (POWYS).
Fig. 40. *Astraea (Calcar) haematraga* (MENKE).
Fig. 41. *Gourmya (Contumax) sordidula* (GOULD).
Fig. 42. *Gourmya (Contumax) kobelti* (DUNKER).
Fig. 43. *Nassarius (Niotha) gemmulatus* (LAMARCK).
Fig. 44. *Nassarius (Zeuxis) caelatus* (A. ADAMS).
Fig. 45. *Epitonium (Boreoscala) angulatosimile* OTUKA.
Fig. 46. *Epitonium (Boreoscala) angulatosimile* OTUKA.
Fig. 47. *Epitonium (Bcreoscala) angulatosimile* OTUKA.
Fig. 48. *Epitonium (Boreorcala) angulatosimile* OTUKA.
Fig. 49. *Siliquaria cumingii* (MÖRCH).
Fig. 50. *Bursa (Gyrineum) natatoria* ("BOLTEN" RÖDING).
Fig. 51. *Turritella fascialis* MENKE.

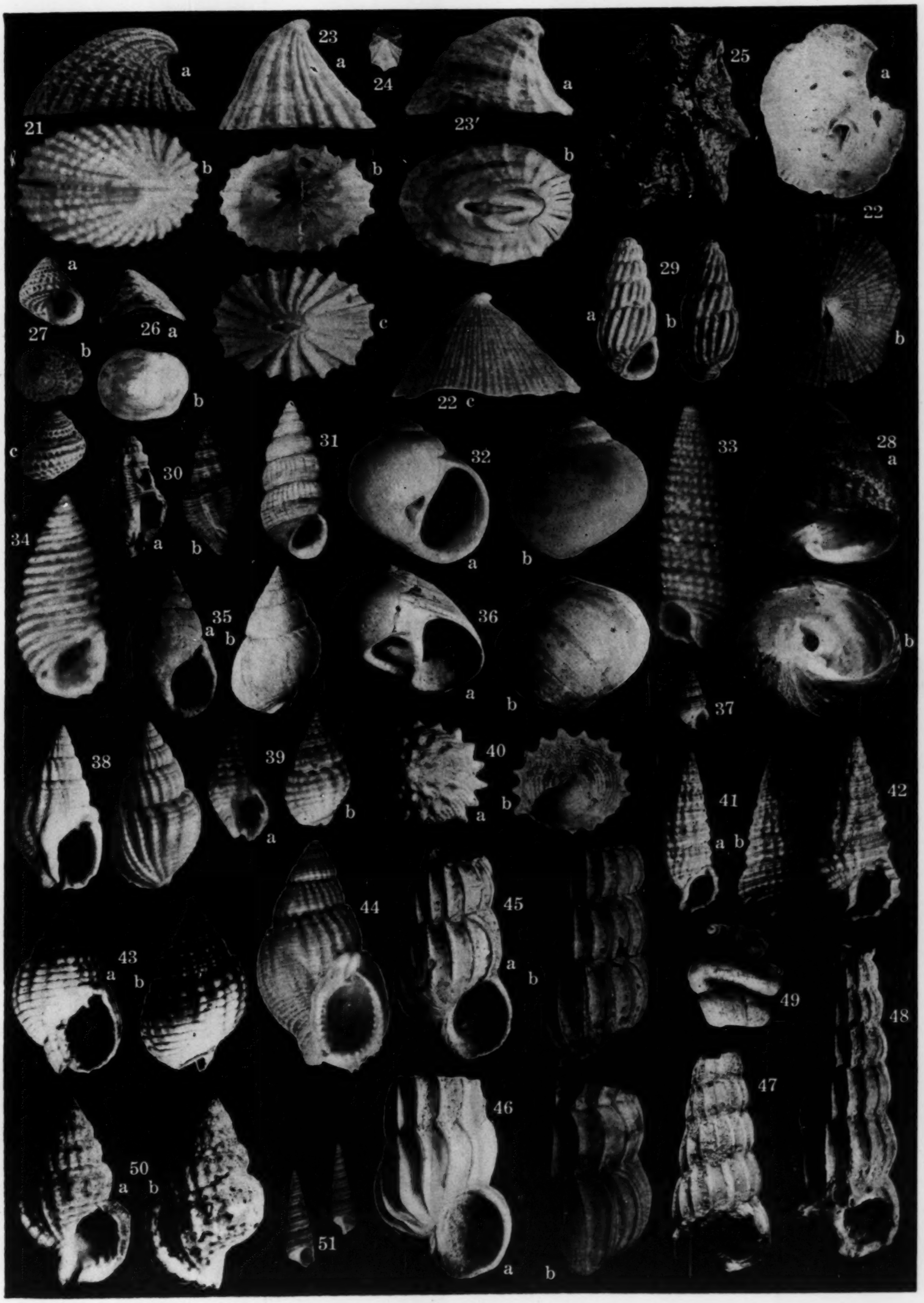
21 a
21 b
23 a
24
23' a
23' b
25
22 a
22
22 b
22 c
23 b
27 a
27 b
27 c
26 a
26 b
23 c
29 a
29 b
31
32 a
32 b
33
28 a
28 b
30 a
30 b
34
35 a
35 b
36 a
36 b
37
38
39 a
39 b
40 a
40 b
41 a
41 b
42
43 a
43 b
44
45 a
45 b
49
48
47
46 a
46 b
50 a
50 b
51

Figs. 21~51.

（震研彙報 第十三號 圖版 大塚）

Plate LIV.

Plate LIV.

Fig. 52 *Erronea japonica* (SCHILDER).
Fig. 53. *Turritella fortilirata motidukii* OTUKA. n. sbsp.
Fig. 54. *Solidula strigosa* (GOULD).
Fig. 55. *Retusa minima* YAMAKAWA.
Fig. 56. *Acteocina exilis* (DUNKER).
Fig. 57. *Rhizorus artiaperta* (YAMAKAWA).
Fig. 58. *Rhizorus artiaperta* (YAMAKAWA).
Fig. 59. *Odostomia limpida* DALL et BARTSCH.
Fig. 60. *Oliva mustelina* LAMARCK.
Fig. 61. *Homalopoma amussitata* (GOULD).
Fig. 62. *Umbonium* (*Suchium*) *akitanum* SUZUKI.
Fig. 63. *Umbonium* (*Suchium*) *akitanum* SUZUKI.
Fig. 64. *Sinum* (*Eunaticina*) *papillum* (GMELIN).
Fig. 65. *Ringicula doliaris* (GOULD).
Fig. 66. *Turbonilla* aff. *imbana* YOKOYAMA.
Fig. 67. *Turbonilla* aff. *imbana* YOKOYAMA.
Fig. 68. *Turbonilla* aff. *imbana* YOKOYAMA.
Fig. 69. *Turbonilla* aff. *imbana* YOKOYAMA.
Fig. 70. *Strombiformis* (*Leiostraca*) *shibana* (YOKOYAMA).
Fig. 71. *Strombiformis* (*Leiostraca*) *shibana* (YOKOYAMA).
Fig. 72. Gen. sp. unknown.
Fig. 73. Gen. sp. unknown.
Fig. 74. *Nassarius* (*Niotha*) *livescens* (PHILIPPI).
Fig. 75. *Neptunea uwasoensis* (OTUKA).
Fig. 76. *Pyrene* (*Zafra*) *pumila* (DUNKER).
Fig. 77. *Thais bronni* (DUNKER).
Fig. 78. *Cerithium* (*Proclava*) *kochi* (PHILIPPI).
Fig. 79. *Batillaria multiformis* (LISCHKE).
Fig. 80. *Diala varia* A. ADAMS.
Fig. 81. *Fusinus perplexus* (A. ADAMS).
Fig. 82. *Pyrene* (*Mitrella*) *varians* (DUNKER).
Fig. 83. *Philbertia tincta* (REEVE).
Fig. 84. *Chrysallida* (*Miralda*) *gemma* (A. ADAMS).
Fig. 85. *Chrysallida* (*Babella*) *caelata* (A. ADAMS).
Fig. 86. *Amphithalamus yendoi* (YOKOYAMA).
Fig. 87. *Tachyrhynchus* ? sp.
Fig. 88. *Dentalium* (*Dentalium*) *hexagonum* GOULD.
Fig. 89. *Dentalium motidukii* OTUKA. n. sp.
Fig. 90. *Turbonilla hiradokoensis* OTUKA, n. sp.
Fig. 91. *Obtortio orientalis* (YOKOYAMA).
Fig. 92. *Ringicula* sp.
Fig. 93. *Skenea nipponica* ? YOKOYAMA.
Fig. 94. *Mangelia makiyamai* OTUKA. n. sp.
Fig. 95. *Mangelia makiyamai* OTUKA. n. sp.
Fig. 96. *Pyrgulina densecostulata* (GARRETT).
Fig. 97. *Pseudorhaphitoma* sp.
Fig. 98. *Menestho* sp.
Fig. 99. *Strombus* (*Labiostrombus*) *japonicus* REEVE.
Fig. 100. *Cingulina triarata* PILSBRY.
Fig. 101. *Asthenotoma yokoyamai notoensis* OTUKA, n. subsp.
Fig. 102. *Pseudorhaphitoma naganumaensis* OTUKA. n. sp.
Fig. 103. *Clavatula consimilis* (SMITH).
Fig. 105. *Asperdaphne subzonata* (SMITH).

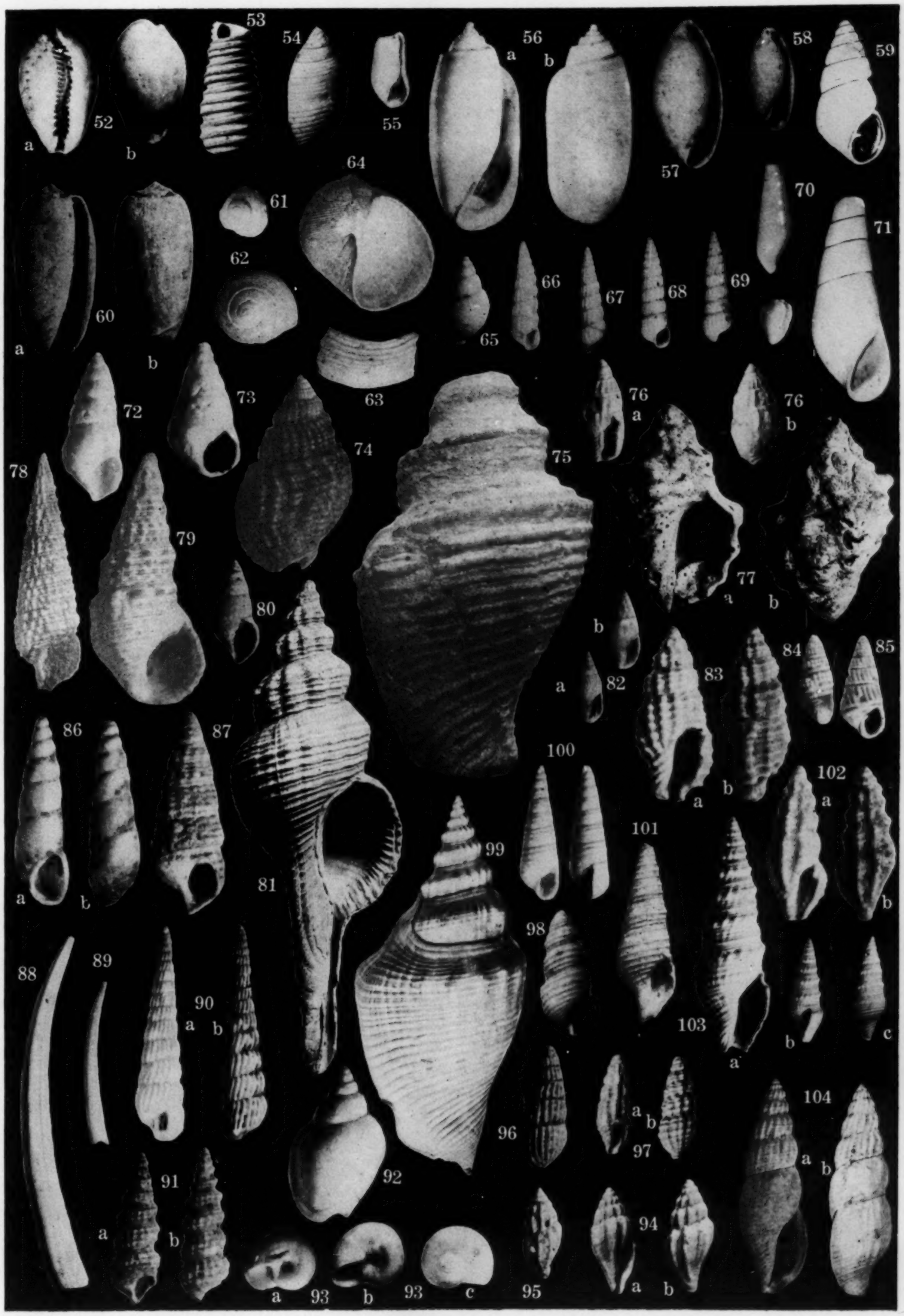
52 a b
53
54
55
56 a b
57
58
59
60 a b
61
62
63
64
65
66
67
68
69
70
71
72
73
74
75
76 a b
77 a b
78
79
80
81
82 a b
83 a b
84
85
86 a b
87
88
89
90 a b
91 a b
92
93 a b c
94 a b
95
96
97 a b
98
99
100
101
102 a b
103 a b c
104 a b

（震研彙報 第十三號 圖版 大塚）

Figs. 52～104.

Plate LV.

Plate LV.

Fig. 105. *Nuculana onoyamai* OTUKA.
Fig. 106. *Nuculana onoyamai* OTUKA.
Fig. 107. *Barbatia symmetrica* (REEVE).
Fig. 108. *Barbatia yokoyamai* (NOMURA).
Fig. 109. *Navicula ocellata* (REEVE).
Fig. 110. *Navicula ocellata* (REEVE).
Fig. 111. *Barbatia reticulata* (GMELIN).
Fig. 112. *Barbatia yokoyamai* NOMURA.
Fig. 113. *Limopsis multistriata* (FORSKÅL).
Fig. 114. *"Bathyarca" uwaensis* (YOKOYAMA).
Fig. 115. *"Bathyarca" uwaensis* (YOKOYAMA).
Fig. 116. *Trichomusculus divaricatus* (PHILIPPI).
Fig. 117. *Trichomusculus divaricatus* (PHILIPPI).
Fig. 118. *Barbatia decussata* (SOWERBY).
Fig. 119. *Chama aspersa* REEVE.
Fig. 120. *Chama aspersa* REEVE.
Fig. 121. *Limatula subauriculata* (MONTAGU).
Fig. 122. *Limatula subauriculata* (MONTAGU).
Fig. 123. *Chama aspersa* REEVE.
Fig. 124. *Chama aspersa* REEVE.
Fig. 125. *Basterotia gouldii* (A. ADAMS).
Fig. 126. *Basterotia gouldii* (A. ADAMS).
Fig. 127. *Basterotia gouldii* (A. ADAMS).
Fig. 128. *Basterotia gouldii* (A. ADAMS).
Fig. 129. *Spondylus cruentus* LISCHKE.
Fig. 130. *Lima basilanica* ADAMS et REEVE.
Fig. 131. *Lima basilanica* ADAMS et REEVE.
Fig. 132. *Lima lischkei* LAMY.
Fig. 133. *Lima lischkei* LAMY.
Fig. 134. *Barbatia* sp.
Fig. 135. *Barbatia* sp.
Fig. 136. *Chlamys* sp. From Nanao bed.
Fig. 137. *Chlamys crassivenia* YOKOYAMA.
Fig. 138. *Patinopecten kagamianus* (YOKOYAMA).
Fig. 139. *Chlamys crassivenia* YOKOYAMA.
Fig. 140. *Chlamys swiftii etchegoini* (ANDERSON).
Fig. 141. *Chlamys crassivenia* YOKOYAMA.
Fig. 142. *Chlamys* sp. From Nanao beds.
Fig. 143. *Chlamys* sp. From Nozaki beds.
Fig. 144. *Patinopecten kagamianus* YOKOYAMA.
Fig. 145. *Propeamussium transnipponica* MOCHIZUKI MS.

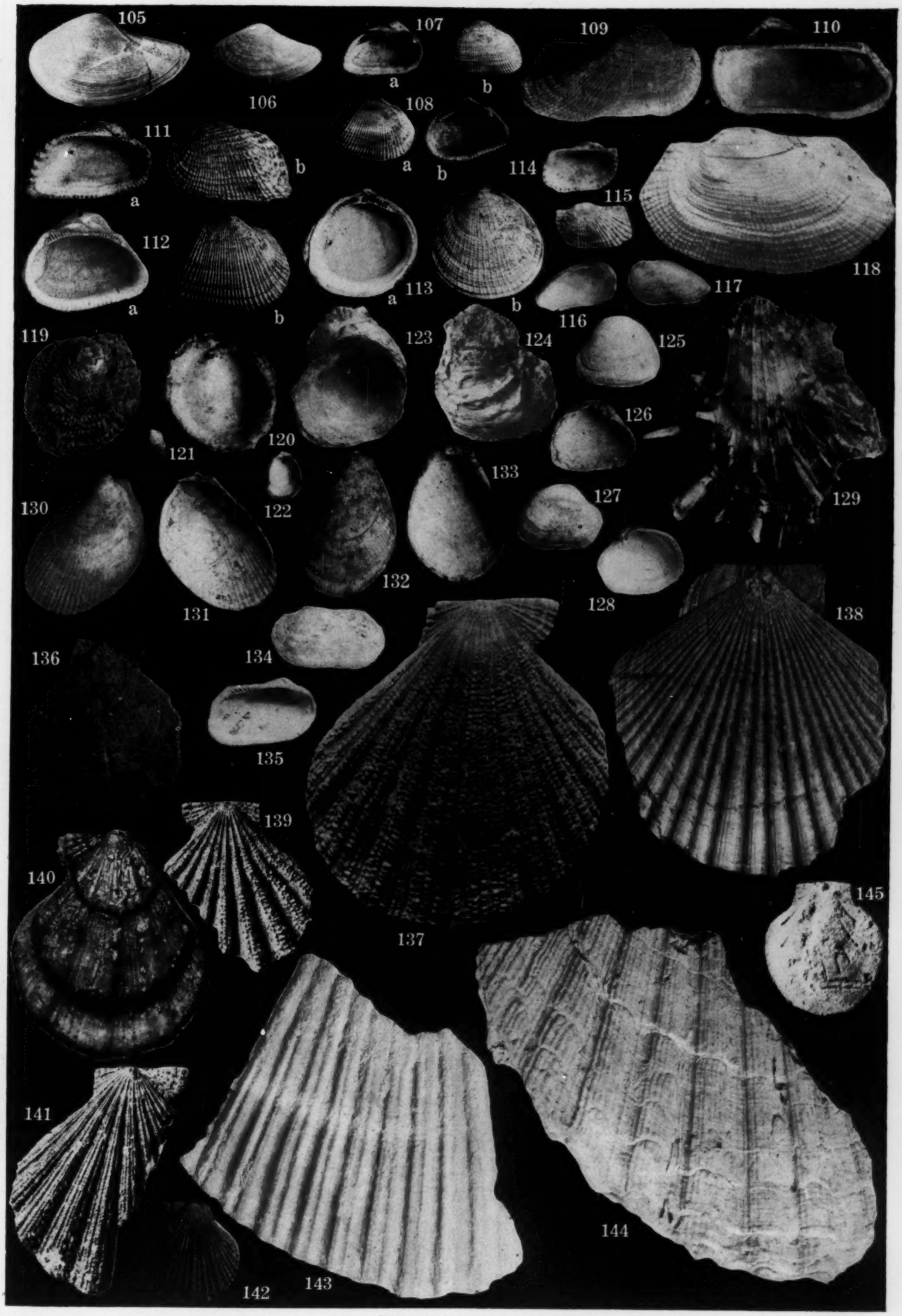
105
106
107
a
b
108
a
b
109
110
111
a
b
112
a
b
113
a
b
114
115
116
117
118
119
120
121
122
123
124
125
126
127
128
129
130
131
132
133
134
135
136
137
138
139
140
141
142
143
144
145

Figs. 105～145.

（震研彙報 第十三號 圖版 大塚）

Plate LVI.

Plate LVI.

Fig. 146. *Crassatellites nanus* (ADAMS et REEVE).
Fig. 147. *Crassatellites nanus* (ADAMS et REEVE).
Fig. 148. *Astarte hakodatensis* YOKOYAMA.
Fig. 149. *Astarte hakodatensis* YOKOYAMA.
Fig. 150. *Astarte hakodatensis* YOKOYAMA.
Fig. 151. *Merisca diaphana* (DESHAYES).
Fig. 152. *Merisca diaphana* (DESHAYES).
Fig. 153. *Anodontia bialata* (PILSBRY).
Fig. 154. *Anodontia bialata* (PILSBRY).
Fig. 155. *Papyridea (Fulvia) hungerfordi* (SOWERBY).
Fig. 156. *Papyridea (Fulvia) hungerfordi* (SOWERBY).
Fig. 157. *Cardita cumingiana* DUNKER.
Fig. 158. *Pitar lineolata* (SOWERBY).
Fig. 159. *Pitarc lineolata* (SOWERBY).
Fig. 160. *Papyridea (Fulvia) muticum* (REEVE).
Fig. 161. *Macoma (Pseudometis) praerupta* SALISBURY.
Fig. 162. *Macoma (Pseudometis) praerupta* SALISBURY.
Fig. 163. *Kellya notoensis* YOKOYAMA.
Fig. 164. *Papyridea (Fulvia) hungerfordi* (SOWERBY).
Fig. 165. *Papyridea (Fulvia) muticum* (REEVE).
Fig. 166. *Papyridea (Fulvia) hungerfordi* (SOWERBY).
Fig. 167. *Taras lunaris* (YOKOYAMA).
Fig. 168. *Paphia (Paratapes) undulata* (BORN).
Fig. 169. *Paphia (Paratapes) undulata* (BORN).
Fig. 170. *Corculum (Fragum) ebaranum* (YOKOYAMA).
Fig. 171. *Corculum (Fragum) ebaranum* (YOKOYAMA).
Fig. 172. *Paphia euglypta* (PHILIPPI).
Fig. 173. *Paphia euglypta* (PHILIPPI).
Fig. 174. *Venericardia ferruginea* (A. ADAMS).
Fig. 175. *Taras lunaris* (YOKOYAMA).
Fig. 176. *Taras lunaris* (YOKOYAMA).
Fig. 177. *Codakia divergens* (PHILIPPI).
Fig. 178. *Codakia divergens* (PHILIPPI).
Fig. 179. *Gafrarium divaricatum* (GMELIN).
Fig. 180. *Gafrarium (Circe) scriptum stutzeri* (DONOVAN).
Fig. 181. *Callista pacifica* (DILLWYN).
Fig. 182. *Scintilla nipponica* YOKOYAMA.

（震研彙報 第十三號 圖版 大塚）

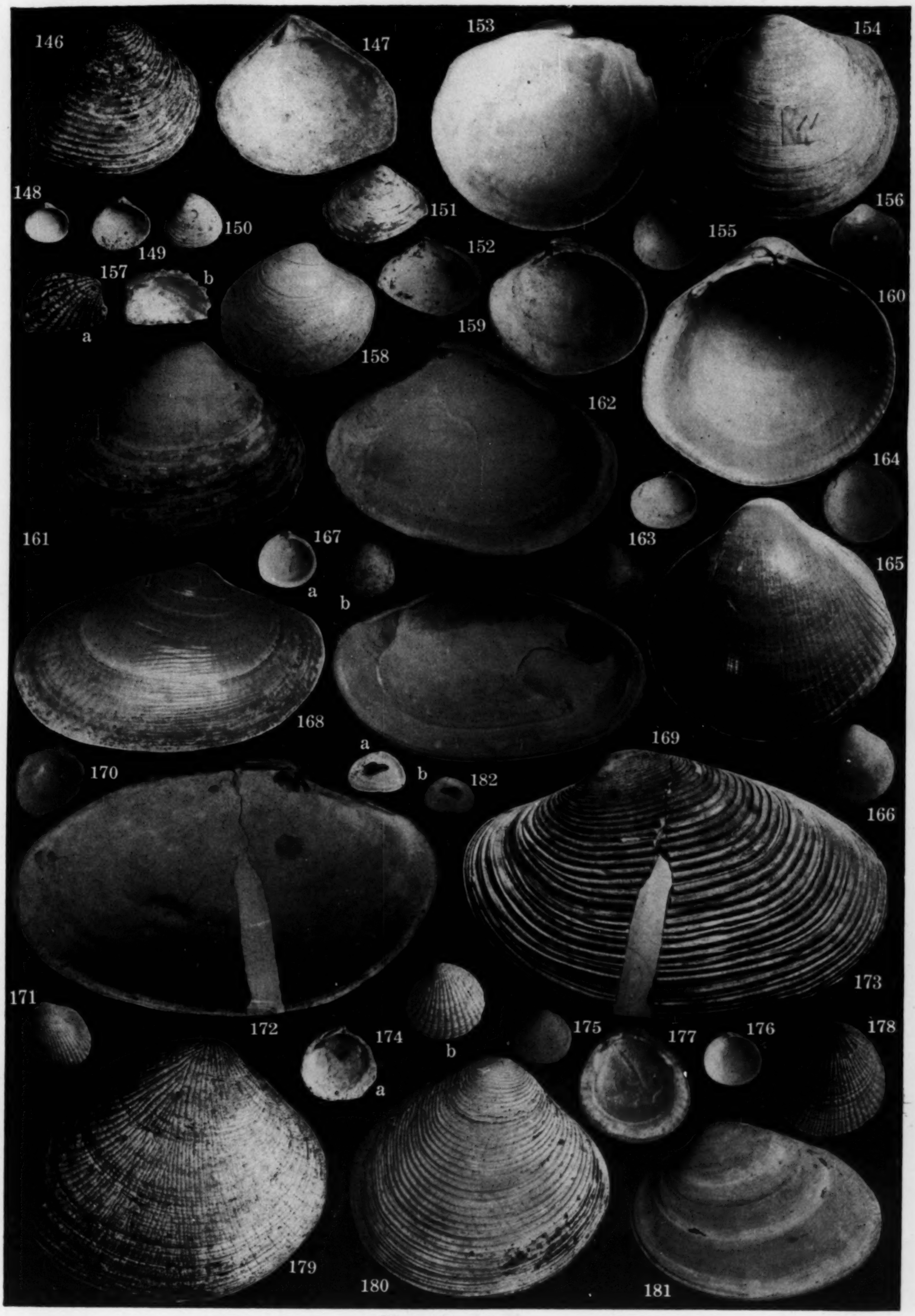
146
147
153
154
148
151
149
150
156
155
152
157
b
a
158
159
160
162
164
163
161
167
a
b
165
168
169
170
a
b
182
166
173
171
172
174
b
a
175
177
176
178
179
180
181

Figs. 146～182.

Plate LVII.

Plate LVII.

Fig. 183. *Martesia striata* (LINNÉ).
Fig. 184. *Martesia striata* (LINNÉ).
Fig. 185. *Arcopagia (Pinguitellina) kurodai* OTUKA n. sp.
Fig. 186. *Arcopagia (Pinguitellina) kurodai* OTUKA n. sp.
Fig. 187. *Arcopagia (Pinguitellina) kurodai* OTUKA n. sp.
Fig. 188. *Petricola japonica* DUNKER.
Fig. 189. *Petricola japonica* DUNKER.
Fig. 190. *"Lucina" contraria* DUNKER.
Fig. 191. *"Lucina" contraria* DUNKER.
Fig. 192. *Macoma (Psamacoma) awajiensis* SOWERBY.
Fig. 193. *Macoma (Psamacoma) awajiensis* SOWERBY.
Fig. 194. *Thyasira nipponica* YABE et NOMURA.
Fig. 195. *Astarte alaskensis* DALL.
Fig. 196. *Corbicula* sp.
Fig. 197. *Barbatia obtusoides* (NYST).
Fig. 198. *Barbatia obtusoides* (NYST).
Fig. 199. *Kellya notoensis* YOKOYAMA.
Fig. 200. *Pillucina pisidium* DUNKER.
Fig. 201. *Barnea fragilis* (SOWERBY).
Fig. 202. *Trapezium japonicum* PILSBRY.
Fig. 203. *Trapezium japonicum* PILSBRY.
Fig. 204. *Aloidis substriatus* (YOKOYAMA).
Fig. 205. *Aloidis substriatus* (YOKOYAMA).
Fig. 206. *Aloidis substriatus* (YOKOYAMA).
Fig. 207. *"Jousseaumiella" crassa* (YOKOYAMA).
Fig. 208. *"Jousseaumiella" crassa* (YOKOYAMA).
Fig. 209. *Myadora fluctuosa* (GOULD).
Fig. 210. *Venericardia ferruginosa* (ADAMS et REEVE).
Fig. 211. *Venericardia ferruginosa* (ADAMS et REEVE).
Fig. 212. *Patinopecten tokyoensis kimurai* (YOKOYAMA).
Fig. 213. *Mysella oblongata* (YOKOYAMA).
Fig. 214. *Mysella oblongata* (YOKOYAMA).
Fig. 215. *Aphrocallistes* sp.
Fig. 216. *Aphrocallistes* sp.
Fig. 217. *Aphrocallistes* sp.
Fig. 218. *Sagarites* ? sp. (White materials contained in Yositaki beds).
Fig. 219. *Oulastraea crispata* (LAMARCK) from Tumuki bed.

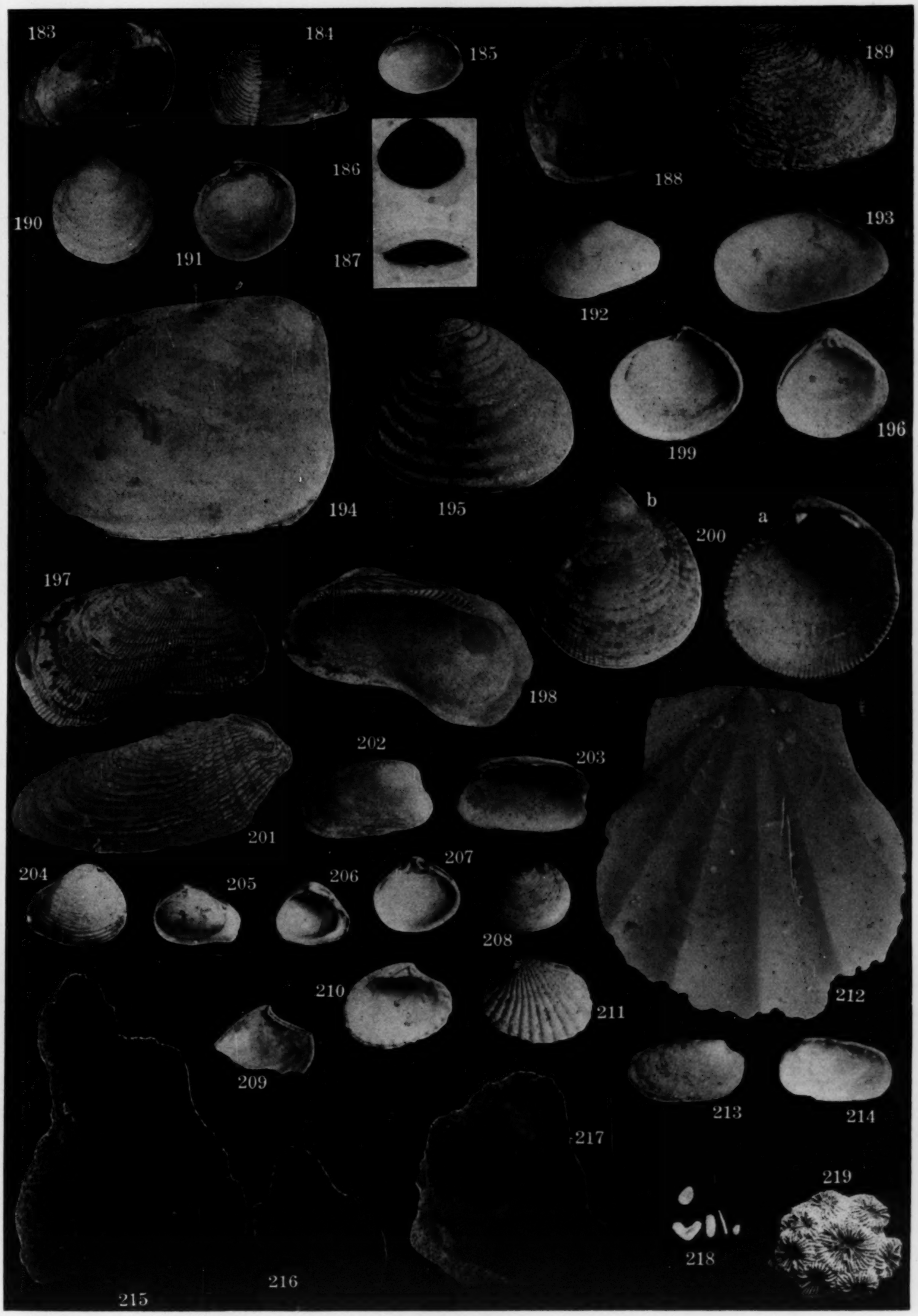
183
184
185
189
186
187
188
190
191
193
192
194
195
199
196
b
200
a
197
198
202
203
201
212
204
205
206
207
208
210
211
209
213
214
217
219
218
215
216

Figs. 183～219.

（震研彙報 第十三號 圖版 大塚）

1758 *Pholas striata* LINNÉ, Syst. Nat. ed. 10, p. 669.

1906 *Martesia striata*, TOKUNAGA, Jour. Coll. Sci. Tokyo Imp. Univ., **21**, 2, p. 35, Pl. 2, fig. 18.

1927 *Martesia striata tokyoensis*, YOKOYAMA, Jour. Fac. Sci. Imp. Univ. Tokyo, (2), **1**, 10, p. 428, Pl. 48, figs. 2, 3.

Geol. age.—Pleistocene-Recent. Occur.—Tumuki (2) No. 2521, Coll. Earthq. Res. Inst.

Myadora GRAY, 1840.

Myadora fluctuosa (GOULD)

Plate LVII, Figure 209.

1860 *Myadora fluctuosa* GOULD, Bost. Soc. Nat. Hist., **8**.

1990 *Myadora fluctuosa*, SMITH, Proc. Zool. Soc. London, p. 583.

1922 *Myadora fluctuosa*, YOKOYAMA, Jour. Coll. Sci. Tokyo, Imp. Univ., **44**, 1, pp. 170~171, Pl. 14, figs. 6, 7.

Geol. age.—Pliocene-Recent. Geogr. distr.—China, Kagosima, Tokyo bay. Occur.—Simazaki (Himi beds) (1) No. 2040, C. E. R. I.

Thracia (LEACH) BLAINVILLE, 1824.

Thracia transmontana (YOKOYAMA)

1922 *Thracia transmontona* YOKOYAMA, Jour. Coll. Sci. Tokyo, Imp. Univ., **44**, 1, p. 172, Pl. 14, figs. 13, 14.

Geol. age.—Pliocene-Recent. Geogr. distr.—Tokyo bay, Southern Kwanto, Noto. Occur.—Simazaki (3) No. 2015, Coll. Earthq. Res. Inst.

---

68. 能登半島南部邑知地溝（3）

地震研究所 大塚彌之助

この論文は前に發表した（1），（2）の化石種の鑑定・記載の記録に當てた．之は前2論文の基礎をなすものである．從來この項は費用の點から主とし省略され勝ちなものであつたが，基礎資料を公にしない結果，構造地質學の進歩を妨げる場合が多いので公にすることとした．

新種10種の記載，從來使用されてゐた同義語の整理もしてあり，屬名は京大黑田氏・Thiele氏・Grant & Gale兩氏のものを參考した．前論文中に使用せる種名中この論文（3）に於いて改良せられたものも數種あり，之は*を附して注意してある．

Index of Species.

Acila divaricata (HINDS)··········880
Acila H. and A. ADAMS, 1898··········880
Acila mirabilis (ADAMS et REEVE) ···881
Acteocina exilis (DUNKER)··········878
Acteocina GRAY, 1847 ··········878
Albula didyma BOLTEN··········866
Aloidis MEGERLE von MÜHLFELD, 1811··········899
Aloidis substriatus (YOKOYAMA) ······899
Aloidis venustus (GOULD)··········899
Alvania concinna (A. ADAM)··········852
Alvania RISSO, 1826 ··········852
Alvania sadoensis (YOKOYAMA)··········852
Amphithalamus alphesiboei MELVILL··852
Amphithalamus aristaci MELVILL······852
Amphithalamus CARPENTER, 1865 ····851
Amphithalamus tumukiensis OTUKA n. sp.··········852
Amphithalamus yendoi (YOKOYAMA)··851
Amycla varians DUNKER··········869
Angulus (Fabulina) iridella (v. MARTENS)··········897
Angulus (Fabulina) miyatensis (YOKOYAMA) ··········897
Angulus MEGERLE von MÜHLFELD, 1811··········897
Angulus (Peronidia) salmonea (CARPENTER) ··········897
Anodontia bialata (PILSBRY) ··········892
Anodontia LINK, 1808 ··········892
Anomia (LINNÉ), MÜLLER, 1776 ······885
Anomia sp. ··········885
Antiplanes DALL, 1902 ··········873
Antiplanes kamchatica DALL··········873
Apollon olivater MEUSCHEN ··········868
Arca amiculà YOKOYAMA··········884
Arca (Barbatia) decussata SOWERBY··884
Arca (Barbatia) domingensis, YOKOYAMA ··········883
Arca boucardi JOUSSEAUME··········882
Arca broughtoni SCHRENCK··········884
Arca decurvata LISCHKE ·····883
Arca inflata REEVE··········884
Arca kobeltiana PILSBRY ··········882
Arca LINNÉ, 1758 ··········884
Arca multistriata FORSKÅL· ·········· ·881
Arca ocellata REEVE ·········· ······882
Arca obtusa REEVE··········883
Arca obtusoides NYST ··········883
Arca rectangularis TOKUNAGA ······882
Arca reticulata GMELIN ··········883
Arca stearnsi PILSBRY ··········883
Arca subcrenata LISCHKE ··········884
Arca symmetrica REEVE ··········883
Arca tenuis TOKUNAGA··········884
Arca uwaensis YOKOYAMA ··········884
Arcopagia BROWN, 1827 ··········899
Arcopagia nux HANLEY··········899
Arcopagia (Pinguitellina) kurodai OTUKA n. sp.··········899
Arcopagia (Pinguitellina) nux (HANLEY) ··········899
Asperdaphne HEDLEY, 1922··········876
Asperdaphne subzonata (SMITH) ······876
Astarte alaskensis DALL ··········890
Astarte hakodatensis YOKOYAMA ······889
Astarte SOWERBY, 1816 ··········889
Astarte sulcata, YOKOYAMA ··········890
Astarte undata, SASAKI ··········890
Asthenotoma Harris et BURROWS, 1891··········873
Asthenotoma komakimonos OTUKA n. sp.··········874
Asthenotoma makimonos (JOUSSEUME) 874
Asthenotoma pouloensis (JOUSSEUME) 874
Asthenotoma yokoyamai MAKIYAMA 873
Asthenotoma yokoyamai notoensis OTUKA n. sp.··········873
Astraea (BOLTEN) RÖDING, 1798 ······850
Astraea (Calcar) haematraga (MENKE) ··········850
Astrarium (Cyclocantha) haematraga MENKE ··········850
Barbatia decussata (SOWERBY)··········881
Barbatia GRAY, 1847 ··········883
Barbatia obtusoides (NYST) ··········883
Barbatia reticulàta (GMELIN) ··········883
Barbatia stearnsi (PILSBRY) ··········883
Barbatia symmetrica (REEVE) ··········883
Barbatia yokoyamai NOMURA ··········883
Barnea dilatata (SOULEYET) ··········900
Barnea fragilis (SOWERBY)··········900

Barnea japonica (Yokoyama) ········900
Barnea (Leach) Risso, 1826 ············900
Basterotia C. Mayer, 1859 ··· ··········891
Basterotia gouldi (A. Adams) ·········891
Bathyarca Kobelt, 1891 ··················884
Bathyarca uwaensis (Yokoyama) ···884
Batillaria Benson, 1842 ··················856
Batillaria multiformis (Lischke)······856
Bittium Gray, 1847 ·························857
Bittium numamuranum Yokoyama···857
Bittium perpusilum Tryon ···············858
Bittium satomii (Yokoyama)············858
Bittium venustellum Yokoyama ······855
Brachytoma jeffreysii Smith············873
Brachytoma Swainson, 1840 ·········873
Buccinulus strigosus Gould ········ ···878
Buccinum gemmulatum Lamarck······871
Bullinella striata Yamakawa ······ ··879
Bursa (Bolten) Röding, 1798 ·········868
Bursa (*Gyrineum*) *natatoria* (Bolten "Röding") ················· ···868
Bursa natrix, Dautzenberg et Fischer ·····································868
Byssoarca decussata Sowerby ·········884
Byssoarca divaricata Sowerby· ········883
Callista pacifica (Dillwyn) ············895
Callista (Poli 1791) Mörch, 1853······895
Cancellaria Lamarck ·····················872
Cancellaria (*Narona*) *spengleriana* Deshayes ···································872
Cantharus menkenana Dunker ······870
Cantharus (*Pollia*) *menkeana* Dunker ·······································870
Cardita Bruguière, 1792 ···················890
Cardita cumingiana Dunker············890
Cardita ferruginea A. Adams ·········890
Cardita ferruginosa Adams et Reeve ··890
Cardium hungerfordi Sowerby·········894
Cardium (*Leiocardium*) *hungerfordi* Sowerby ···································894
Cardium Linné, 1758·························894
Cardium muticum Reeve ··················894
Cardium sp. ·································894
Cemoria nobilis A. Adams ···············846
Cerithiopsis hilaris Yokoyama·········858
Cerithiopsis satomii Yokoyama·········858
Cerithium Bruguière, 1789··············858
Cerithium kobelti Dunker ················859
Cerithium kochi Philippi··················858
Cerithium (*Proclava*) *kochi* (Philippi)··· ·································858
Cerithium pusillum Dunker ············858
Chama aspersa Reeve ······················893
Chama kikuzaru Hirase ····················893
Chama (Linné) Bruguière, 1789······893
Chlamys (Bolten) Röding, 1798······885
Chlamys crassivenia Yokoyama ·····886
Chlamys farreri nipponensis Kuroda ·· 887
Chlamys hastatus aff. *ingeniosa* Yokoyama ·····································886
Chlamys irregularis (Sowerby) ······886
Chlamys islandicus Müller ············887
Chlamys nipponensis Kuroda············886
Chlamys notoensis (Yokoyama)·········886
Chlamys sp. ···································887
Chlamys swiftii etchegoini (Anderson)···································886
Chrysallida (*Babella*) *caelata* (A. Adams)·····································861
Chrysallida Carpenter, 1857············861
Chrysallida (*Miralda*) *gemma* A. Adams···861
Chrysodomus uwasoensis Otuka ······869
Cingula aleutica Dall ······················852
Cingula (*Pseudosetia*) *paludinoides* (Yokoyama) ································851
Cingula (Fleming) H. A. Adams, 1854···851
Cingulina A. Adams, 1860 ················863
Cingulina triarata Pilsbry···············863
Circe divaricata Gmelin ·················894
Circe scripta personata Deshayes ···894
Clathurella centrosa Pilsbry············875
Clavatula Lamarck, 1801···················872
Clavatula consimilis (Smith)············872
Codakia bella delicatula Pilsbry ······892
Codakia Scopoli, 1777 ······················892
Codakia divergens (Philippi) ·········892
Columbella (*Mitrella*) *dunkeri*, Yokoyama ·································869
Columbella pumila Dunker···············869
Corbicula Megerle von Mühlfeld, 1811···891
Corbicula sp. ··································891
Corbula substriata Yokoyama ·········899
Corbula venusta Gould···················899
Corculum (Bolten) Röding, 1798 ···894
Corculum (*Fragum*) *ebaranum* Yokoyama ·····································894
Crassatella nana Adams et Reeve······889
Crassatellites Krueger, 1825 ············889

Crassatellites nanus (ADAMS et REEVE) ·········889
Cryptomya busoensis YOKOYAMA ······900
Cryptomya CONRAD, 1848·········900
Cyclostrema micans ADAMS·········854
Cyclostrema pulchellum DUNKER ······854
Cylichna LOVEN, 1846 ·········879
Cylichna yamakawai YOKOYAMA ······879
Cypraea candida, YOKOYAMA·········868
Cypraea japonica SCHILDER ·········868
Cypraea macula SOWERBY ·········868
Cythara tabatensis (TOKUNAGA) ······875
Cytherea chinensis CHEMNITZ ·········895
Cytherea lineolata SOWERBY ·········895
Cytherea divaricata GMELIN ·········894
Daphnella subzonata SMITH ·········876
Dentalium (Antalis) buccinulum GOULD ·········880
Dentalium (Antalis) motidukii OTUKA n. sp. ·········879
Dentalium (Antalis) marukawai OTUKA ·········880
Dentalium (Antalis) pretiosum SOWERBY ·········880
Dentalium (Antalis) rhabdotum PILSBRY·········880
Dentalium (Antalis) weinkauffi DUNKER ·········880
Dentalium (Dentalium) hexagonum GOULD ·········879
Dentalium LINNÉ, 1758·········879
Dentalium pretiosum SOWERBY ·········880
Dentalium sexcostatum SOWERBY·········879
Diala A. ADAMS, 1861 ·········857
Diala varia A. ADAMS ·········857
Diodora GRAY, 1821 ·········847
Diodora sieboldii (REEVE)·········847
Diplodonta lunaris YOKOYAMA ·········891
Dosinia japonica REEVE·········895
Dosinia SCOPOLI, 1777 ·········895
Drillia jeffreysii SMITH ·········873
Emarginula crassicostata SOWERBY···846
Emarginula LAMARCK ·········846
Engina GRAY, 1859·········870
Engina menkeana (DUNKER)·········870
Epitonium (BOLTEN) RÖDING, 1798···860
Epitonium (Boreoscala) angulatosimile OTUKA·········860
Epitonium (Boreoscala) groenlandicum (CHEMNITZ) ·········860
Epitonium (Boreoscala) simile (SOWERBY) ·········860
Epitonium simile (SOWERBY) ·········860
Epitonium (Turbiniscala) angustum (DUNKER)·········860
Epitonium (Turbiniscala) sp.·········360
Erato callosa (ADAMS et REEVE) ······867
Erato RISSO, 1826 ·········867
Erronea japonica (SCHILDER)·········868
Erronea TROSCHEL, 1863 ·········868
Eucharis gouldii A. ADAMS ·········891
Euchelus foveolatus (A. ADAMS)······848
Euchelus PHILIPPI, 1847 ·········848
Eulima (Leiostraca) shibana YOKOYAMA ·········860
Fenella orientalis YOKOYAMA·········857
Fenella perpupoides YOKOYAMA·········857
Fenella septentrionalis (TOKUNAGA)···856
Fissurella sieboldii REEVE·········847
Fusinus perplexus (A. ADAMS)·········872
Fusinus RAFINESQUE, 1815 ·········872
Fusum perplexum A. ADAMS·········872
Fusus perplexus (A. ADAMS)·········872
Fusus nodosoplicatus, YOKOYAMA······872
Gafrarium (BOLTEN) RÖDING, 1798···894
Gafrarium (Circe) scriptum stutzeri (DONOVAN)·········894
Gafrarium divaricatum (GMELIN) ···894
Glycymeris DACOSTA, 1778·········882
Glycymeris nipponicus (YOKOYAMA)···882
Glycymeris rotunda (DUNKER) ·········882
Gourmya (Contumax) kobelti (DUNKER) ·········859
Gourmya (Contumax) sordidula (GOULD) ·········858
Gourmya FISCHER, 1884 ·········858
Homalopoma amussitata (GOULD)······850
Homalopoma CARPENTER, 1864·········850
Iravadia annulata (DUNKER)·········851
Iravadia BLANFORD, 1867·········851
Iravadia ornata BLANFORD ·········851
Jousseaumiella BOURNE, 1907 ·········893
Jousseaumiella crassa (YOKOYAMA)···893
Kellya notoensis YOKOYAMA ·········892
Kellya TURTON, 1822 ·········892
Lampania multiformis LISCHKE ····· 856
Leda conceptionis DALL·········881
Lemintina imbricata (DUNKER)·········856
Lemintina RISSO, 1826 ·········856
Leptothyra amussitata (GOULD)·········850
Lima angulata ADAMS et REEVE ······888
Lima basilanica ADAMS et REEVE······888

Lima Cuvier, 1798 ······ 888
Lima dunkeri Smith ······ 888
Lima hakodatensis (Tokunaga) ······ 888
Lima lischkei Lamy ······ 888
Lima japonica Dunker ······ 888
Lima orientalis Adams et Reeve ······ 888
Limatula subauriculata (Montagu) ······ 889
Limatula S. V. Wood, 1838 ······ 889
Limopsis multistriata (Forskal) ······ 881
Limopsis Sacco, 1827 ······ 881
Limopsis tokaiensis Yokoyama ······ 881
Limopsis woodwardii A. Adams ······ 882
Litiopa (*Diala*) *semistriata*, Yokoyama ······ 857
Loripes bialata Pilsbry ······ 892
Loripes philippiana, Yokoyama ······ 892
Lucina acutilineata T. A. Conrad ······ 892
Lucina annulata Reeve ······ 892
Lncina borealis, Yokoyama ······ 892
Lucina Bruguière, 1797 ······ 892
"*Lucina*" *contraria* Dunker ······ 892
Lucina divergens Philippi ······ 892
Lucina (*Lucinoma*) *acutilineata* Conrad ······ 892
Luciua pisidium Dunker ······ 892
Lutraria arcuata Reeve ······ 897
Lutralia Lamarck, 1799 ······ 896
Macoma dissimilis, Yokoyama ······ 897
Macoma Leach, 1819 ······ 897
Macoma (*Psammacoma*) *awajiensis* Sowerby ······ 897
Macoma (*Psammacoma*) *truncata* (Jonas) ······ 897
Macoma (*Pseudometis*) *praerupta* Salisbury ······ 897
Macoma tokyoensis Makiyama ······ 897
Mactra rostralis Deshayes ······ 896
Maera salmonea Carpenter ······ 898
Mangelia kamakurana Pilsbry ······ 875
Mangelia makiyamai Otuka n. sp. ······ 874
Mangelia Risso, 1826 ······ 874
Martesia (Leach) Blainbille, 1825 ······ 900
Martesia striata (Linné) ······ 900
Martesia striata tokyoensis Yokoyama ······ 901
Menestho lectissimoides (Yokoyama) 863
Menestho Möller, 1842 ······ 862
Menestho sp. ······ 862
Meretrix (*Callista*) *chinensis*, Yokoyama ······ 895
Meretrix gordonis Yokoyama ······ 895
Meretrix Lamarck, 1799 ······ 895
Meretrix (*Callista*) *limatula*, Yokoyama ······ 895
Meretrix meretrix (Linné) ······ 895
Merisca Dall, 1900 ······ 898
Merisca diaphana (Deshayes) ······ 898
Mitra Lamarck, 1799 ······ 872
Mitra sp. ······ 872
Modiola divaricata Philippi ······ 885
Montacuta ? crassa Yokoyama ······ 893
Montacuta oblongata Yokoyama ······ 893
Monodonta foveolata A. Adams ······ 848
Mya arenaria Linné ······ 900
Mya japonica A. Adams ······ 900
Mya Linné, 1758 ······ 900
Myadora fluctuosa (Gould) ······ 901
Myadora Gray, 1840 ······ 901
Mysella Angas, 1877 ······ 893
Mysella oblongata (Yokoyama) ······ 893
Nassa balteata Lischke ······ 870
Nassa caelata A. Adams ······ 871
Nassa festiva Powys ······ 870
Nassa japonica A. Adams ······ 870
Nassa lirata Powys ······ 870
Nassa livescens Philippi ······ 872
Nassa livescens, Yokoyama ······ 871
Nassa (*Niotha*) *gemmulata* Lamarck 871
Nassarius (*Alectrion*) *balteatus* (Lischke) ······ 870
Nassarius festivus (Powys) ······ 870
Nassarius Froriep, 1806 ······ 870
Nassarius glans (Linné) ······ 871
Nassarius (*Hinia*) *festivus* (Powys) ······ 870
Nassarius japonicus (A. Adams) ······ 870
Nassarius (*Niotha*) *gemmulatus* (Lamarck) ······ 871
Nassarius (*Niotha*) *livescens* (Philippi) ······ 872
Nassarius tateyamensis Kuroda ······ 871
Nassarius (*Tritonella*) *japonicus* (A. Adams) ······ 870
Nassarius (*Zeuxis*) *caelatus* (A. Adams) ······ 871
Natica concinna Dunker ······ 867
Natica janthostoma Deshayes ······ 867
Natica Scopoli, 1777 ······ 867
Navicula Blainville, 1825 ······ 882
Navicula boucardi (Jousseaume) ······ 882
Navicula ocellata (Reeve) ······ 882
Neptunea (Bolten) Röding, 1798 ······ 869
Neptunea (*Neptunea*) *andersoni hawleyi* (Carson) ······ 869

Neptunea (Neptunea) antiqua despecta (LINNÉ) ············870
Neptunea (Neptunea) lirata (MARTYN) ············870
Neptunea uwasoensis (OTUKA) ············869
Nerita papilla GMELIN ············867
Nucula LAMARCK, 1799 ············880
Nucula sp. ············880
Nuculana conceptionis DALL ············881
Nuculana LINK, 1807 ············881
Nuculana onoyamai OTUKA ············881
Nuculana pernula MÜLLER ············881
Nuculana sp. 1. ············881
Obtortio HEDLEY, 1899 ············856
Obtortio orientalis (YOKOYAMA) ············857
Obtortio perpupoides (YOKOYAMA) ···857
Obtortio septentrionalis (TOKUNAGA) 856
Odostomia (Evalea) lirata A. ADAMS ············862
Odostomia (Evalea) sulcata A. ADAMS ············862
Odostomia FLEMING, 1813 ············863
Odostomia limpida DALL et BARTSCH 863
Odostomia (Miralda) gemma (A. ADAMS) ············862
Odostomia (Odetta) lectissimoides YOKOYAMA ············863
Odostomia (Pyrgulina) densecostulata GARRETT ············862
Oliva BRUGUIÈRE, 1789 ············872
Oliva musterina LAMARCK ············872
Ostrea denselamellosa LISCHKE ············885
Ostrea gigas THUNBEBG ············885
Ostrea LINNÉ, 1758 ············885
Ostrea sp. ············885
Pallium swiftii etchegoini, OTUKA ···886
Paphia (BOLTEN) RÖDING, 1798 ············896
Paphia euglypta (PHILIPPI) ············896
Paphia (Paratapes) undulata (BORN) ············896
Papyridea (Fulvia) hungerfordi (SOWERBY) ············884
Papyridea (Fulvia) muticum (REEVE) ············893
Papyridea SWAINSON, 1840 ············893
Parthenia caelata A. ADAMS ············861
Parthenia gemma A. ADAMS ············861
Patella conulus DUNKER ············848
Patella saccharina LINNÉ ············848
Patelloida conulus (DUNKER) ············848
Patelloida QUOY and GAIMARD, 1834···848
Patelloida saccharina (LINNÉ) ············848
Patinopecten DALL, 1898 ············887
Patinopecten kagamianus (YOKOYAMA)888
Patinopecten permirus YOKOYAMA ···888
Patinopecten plebejus (YOKOYAMA)···887
Patinopecten plicicostulatus MATSUMOTO ············888
Patinopecten tokyoensis kimurai (YOKOYAMA) ············887
Pecten crassivenia YOKOYAMA ············886
Pecten etchegoini ANDERSON ············886
Pecten excavatus, YOKOYAMA ············887
Pecten intuscostatus YOKOYAMA ············885
Pecten irregularis SOWERBY ············886
Pecten kagamianus (YOKOYAMA) ············888
Pecten laetus GOULD ············887
Pecten laqueatus SOWERBY ············887
Pecten MÜLLER, 1776 ············887
Pecten natriensis inequilateralis MATSUMOTO ············886
Pecten natriensis MATSUMOTO ············886
Pecten natriensis subovalis MATSUMOTO ············886
Pecten notoensis YOKOYAMA ············886
Pecten permirus YOKOYAMA ············888
Pecten plebejus YOKOYAMA ············887
Pecten tenuicostulatus YOKOYAMA ···885
Pectunculus rotundus DUNKER ············882
Pectunculus cancellata REEVE ············881
Pectunculus nipponicus YOKOYAMA ···882
Pectunculus yamakawai YOKOYAMA···882
Petricola japonica DUNKER ············896
Petricola LAMARCK, 1801 ············896
Philbertia leuckarti (DUNKER) ············876
Philbertia MONTEROSATO, 1884 ············875
Philbertia tincta REEVE ············875
Philine ASCANIUS, 1772 ············879
Philine japonica LISCHKE ············879
Pholodomya japonica YOKOYAMA ············900
Pholas fragilis SOWERBY ············900
Pholas latissima SOWERBY ············900
Pholas striata LINNÉ ············901
Pillucina PILSBRY, 1921 ············892
Pillucina pisidium (DUNKER) ············892
Pitar lineolata SOWERBY ············895
Pitar RÖMER, 1857 ············895
Plicatula horrida DUNKER ············885
Plicatula irregularis DUNKER ············885
Plicatula LAMARCK, 1801 ············885
Pleurotoma consimilis SMITH ············873
Pleurotoma (Drillia) principalis PILSBRY ············873
Pleurotoma tincta REEVE ············875
Polinices cumingianus RÉCLUZ ············866

Polinices didyma (BOLTEN) 866
Polinices draparnaudii RÉCLUZ 866
Polinices effusa SWAINSON 866
Polinices MONTFORT, 1810 866
Polinices (Neverita) ampla PHILIPPI 866
Polinices powisianus RÉCLUZ 866
Polinices sagamiensis PILSBRY 866
Poromya pulchella ADAMS et REEVE 896
Potamides (Batillaria) multiformis LISCHKE 856
Protothaca DALL, 1902 895
Protothaca jedoensis (LISCHKE) 896
Psammobia olivacea JAY 897
Pseudamussium H. and A. ADAMS 1858 885
Pseudamussium intuscostatum (YOKOYAMA) 885
Pseudoliotia TATE, 1898 854
Pseudoliotia micans (A. ADAMS) 854
Pseudorhaphitoma bipyramidata HEDLEY 877
Pseudorhaphitoma BÖTTGER 876
Pseudorhaphitoma fairbankii (NEVILL) 877
Pseudorhaphitoma naganumensis OTUKA 876
Pseudorhaphitoma ? sp. 877
Puncturella (Craniopsis) gigantea SCHEPMAN 847
Puncturella galeata GOULD 847
Puncturella gigantea SCHEPMAN 847
Puncturella hirasei OTUKA 847
Puncturella LOWE 846
Puncturella major DALL 847
Puncturella nobilis (A. ADAMS) 846
Pupa strigosa (GOULD) 878
Purpura bronni DUNKER 868
Pyrene (BOLTEN) RÖDING, 1798 868
Pyrene (Mitrella) varians (DUNKER) 868
Pyrene (Zafra) pumila (DUNKER) 869
Pyrgulina A. ADAMS 862
Pyrgulina bartschi DAUTZENBERG et FISCHER 862
Pyrgulina densecostulata (GARRETT) 862
Raeta GRAY, 1853 896
Raeta pulchella (ADAMS et REEVE) 896
Retusa BROWN, 1827 878
Retusa minima YAMAKAWA 879
Retusa truncata YAMAKAWA 879
Rhizorus artiaperta (YAMAKAWA) 879
Rhizorus MONTFORT, 1810 879
Ringicula DESHAYES, 1838 878
Ringicula dorialis GOULD 878
Ringicula musashinoensis YOKOYAMA 878
Ringicula (Ringiculella) doliaris GOULD 878
Ringicula yokoyamai TAKEYAMA 878
Rissoa (Alvania) concinna A. ADAMS 853
Rissoa (Alvania) sadoensis YOKOYAMA 853
Rissoa (Cingula) paludinoides YOKOYAMA 851
Rissoa septentrionalis TOKUNAGA 856
Rissoa ? sp. OTUKA 857
Rissoina (Amphithalamus) alphesiboei MELVILL 852
Rissoina (Amphithalamus) aristoei MELVILL 852
Rissoina annulata DUNKER 851
Rissoina costulata (DUNKER) 854
Rissoina D' ORBIGNY, 1840 853
Rissoina media SCHWARTZ 853
Rissoina (Phosinella) media SCHWARTZ 853
Rissoina (Phosinella) cancellata, YOKOYAMA 853
Rissoina plicatula (GOULD) 854
Rissoina (Rissoina) laevicostulata (PILSBRY) 853
Rissoina (Rissolina) laevicostulata PILSBRY 853
Rissoina yendoi YOKOYAMA 851
Sanguinolaria LAMARCK, 1799 897
Sanguinolaria (Nuttallia) olivacea (JAY) 897
Saxidomus CONRAD, 1837 894
Saxidomus purpuratus (SOWERBY) 894
Scaliola A. ADAMS, 1860 857
Scaliola bella A. ADAMS 857
Scintilla DESHAYES, 1855 893
Scintilla nipponica YOKOYAMA 893
Sigaretus (Eunaticina) papilla GMELIN 867
Siliquaria cumingii (MÖRCH) 856
Siliquaria LAMARCK, 1799 856
Sinum (BOLTEN) RÖDING, 1798 867
Sinum (Eunaticina) papillum (GMELIN) 867
Siphonalia A. ADAMS, 1863 870
Siphonalia sp. 870
Siphonodentalium M. SARS, 1859 880

Siphonodentalium (*Pulsellum*) *ozawai* YOKOYAMA ······880
Skenea FLEMING, 1824 ······850
Skenea nipponica ? YOKOYAMA ······850
Solariella aff. *angulata* (TOKUNAGA) 849
Solariella S. WOOD, 1842 ······849
Solen LINNÉ, 1758 ······899
Solen sp. ······899
Soletellina olivacea (JAY) ······897
Solidula FISCHER von WALDEHEIM, 1807 ······878
Solidula strigosa (GOULD) ······878
Spondylus cruentus LISCHKE ······888
Spondylus LINNÉ, 1758 ······888
Strombiformis DACOSTA, 1778 ······860
Strombiformis (*Leiostraca*) *shibana* (YOKOYAMA) ······860
Strombus japonicus REEVE ······866
Strombus (*Labiostrombus*) *japonicus* REEVE ······866
Strombus LINNÉ, 1753 ······866
Syrnola A. ADAMS, 1860 ······866
Syrnola cinctella ? A. ADAMS ······866
Tachyrhynchus MÖRCH, 1868 ······855
Tachyrhynchus venustellus (YOKOYAMA) ······855
Tapes purpuratus SOWERBY ······894
Tapes undulata (BORN) ······896
Taras lunaris YOKOYAMA ······891
Taras RISSO, 1826 ······891
Tegula (*Chlorostoma*) *rustica* (GMELIN) ······849
Tegula LESSON, 1832 ······849
Tellina diaphana DESHAYES ······898
Tellina iridella v. MARTENS ······898
Tellina miyatensis YOKOYAMA ······898
Tellina salmonea (CARPENTER) ······898
Tellina truncata JONAS ······897
Tenagodus (*Siliquarius*) *cumingii* MÖRCH ······856
Terebra BRUGUIÈRE, 1789 ······878
Terebra (*Punctoterebra*) *lischkeana* DUNKER ······878
Thais (BOLTEN) RÖDING, 1798 ······868
Thais (*Mancinella*) *bronni* (DUNKER) ······868
Theora H. and A. ADAMS, 1856 ······897
Theora lubrica GOULD ······897
Thracia (LEACH) BLAINVILLE, 1824 ······901
Thracia transmontana (YOKOYAMA) 901
Thyasira bisecta CONRAD ······891
Thyasira bisecta nipponica YABE et NOMURA ······891
Thyasira nipponica YABE et NOMURA 891
Thyasira (LEACH) LAMARCK, 1818 ······891
Thyasira yabei KURODA ······891
Thylacodes imbricatus, YAMAKAWA ······856
Thylacodes medusae, YOKOYAMA ······856
Tornatina exilis DUNKER ······878
Trapezium japonica PILSBRY ······889
Trapezium liratum YOKOYAMA ······889
Trapezium MEGERLE von MÜHLFELD, 1811 ······889
Trapezium nipponicum YOKOYAMA ······889
Trichomusculus divaricatus (PHILIPPI) ······884
Trichomusculus IREDALE, 1924 ······884
Triforis cingulatus DUNKER ······859
Triforis tricincta DUNKER ······859
Triphora BLAINVILLE, 1828 ······859
Triphora aff. *purpurata* (PILSBRY) ······859
Triphora (*Inella*) *tricincta* (DUNKER) 859
Tritonium natorium "BOLTEN" RÖDING ······868
Trochus haematraga MENKE ······850
Trochus (*Minolia*) *angulatus* TOKUNAGA ······849
Trochus rustica CHEMNITZ ······849
Trochus rustica GMELIN ······849
Trophon (*Bedeva*) *birileffi* LISCHKE ······868
Trophon birileffi LISCHKE ······868
Trophon MONTFORT, 1810 ······868
Trophon pachyraphe, YOKOYAMA ······868
Turbo amussitata GOULD ······850
Turbo coreensis RÉCLUZ ······850
Turbo LINNÉ, 1758 ······850
Turbo (*Lunella*) *coronatus coreensis* RÉCLUZ ······850
Turbo (*Marmorostoma*) *coreensis* RÉCLUZ ······850
Turbonilla aff. *imbana* YOKOYAMA ······863
Turbonilla hiradokoensis OTUKA n. sp. ······865
Turbonilla infantula DALL et BARTSCH ······864
Turbonilla RISSO, 1826 ······863
Turbonilla scrobiculata YOKOYAMA ······866
Turbonilla sp. ······865
Turbonilla (*Babella*) *caelatior* DALL et BARTSCH ······861
Turbonilla (*Careliopsis*) *filiola* YOKOYAMA ······851

Turbonilla (Chemnitzia) edoensis YOKOYAMA ··· 865
Turbonilla (Chemnitzia) imbana YOKOYAMA ··· 863
Turbonilla (Cingulina) triarata PILSBRY ··· 863
Turbonilla (Mormula) ambusta DALL et BARTSCH ··· 865
Turbonilla (Mormula) sp. ··· 865
Turbonilla (Pyrgiscus) candidissimus DALL et BARTSCH ··· 862
Turbonilla (Pyrgiscus) lara DALL et BARTSCH ··· 865
Turbonilla (Pyrgiscus) matunamiensis OTUKA ··· 864
Turbonilla (Pyrgiscus) pequensis DALL et BARTSCH ··· 865
Turbonilla (Pyrgiscus) sp. ··· 864
Turbonilla (Strioturbonilla) nihona OTUKA n. sp. ··· 863
Turbonilla (Strioturbonilla) sagamiensis YOKOYAMA ··· 864
Turritella fascialis MENKE ··· 855
Turritella fortilirata motidukii OTUKA ··· 856
Turritella fortilirata nipponica YOKOYAMA ··· 855
Turritella fortilirata saishuensis YOKOYAMA ··· 855
Turritella fortilirata SOWERBY ··· 856
Turritella **LAMARCK, 1799** ··· 855
Umbonium (Suchium) akitanum SUZUKI ··· 849
Umbonium (Suchium) moniliferum costatum (KIENER) ··· 849
Umbonium LINK, 1807 ··· 849
Umbonium suchiense YOKOYAMA ··· 849
Venericardia cipangoana YOKOYAMA 890
Venericardia ferruginea (A. ADAMS) 890
Venericardia ferruginosa (ADAMS et REEVE) ··· 890
Venericardia **LAMARCK, 1801** ··· 890
Venericardia nakamurai YOKOYAMA 891
Venericardia prolongata CARPENTER 891
Venus divaricatus CHEMNITZ ··· 894
Venus jedoensis LISCHKE ··· 896
Venus euglyptus PHILIPPI ··· 896
Venus meretrix LINNÉ ··· 895
Venus pacificus DILLWYN ··· 895
Venus stutzeri DONOVAN ··· 894
Vermetus imbricatus DUNKER ··· 856
Volvula artiaperta YAMAKAWA ··· 879

69. *On the Omogo Acidic Rocks.*

By Hiromichi TSUYA,

Earthquake Research Institute.

(Read July 2, 1935.—Received Sept. 20, 1935.)

Introduction.

In the northwestern part of Éhimé prefecture, Sikoku, and its south (outer zone) in that part of the so-called Median Dislocation Line of southwest Japan, which runs nearly equatorially from the central part of the Main Island, through Sikoku, to Kyûsyû, is a somewhat continuous belt, about 10 km wide, of Tertiary formation (sedimentary and volcanic) that stretches westward for about 30 km from Mt. Isiduti, on the boundary between Éhimé and Kôti prefectures, to the town of Kuma and beyond. The Omogo acidic rocks, the subject of this paper, occupy the southern side of Mt. Isiduti, in an irregular area extending in direction about 5 km N-S and 8 km E-W. They are intrusive into the Tertiary formation and comprise at least three well-defined rock-types—small central masses of porphyritic granodiorite and fine-grained (aplitic) granite, surrounded by an outer quartz-porphyry mass of a greatly varied character.

It is of interest in this connection to recall M. Sawatari's account[1] of the Kumano acidic rocks in the southern part of Wakayama prefecture, Kii, seeing that in the occurrence of both effusive and plutonic rock facies, and in the fact that they belong to the post-Miocene series of eruptives of the district, they resemble the mass now to be discussed.

Attention should also be drawn to the presence of granitic rocks (granite and granite-porphyry) in the Sobosan district at the boundary between Ôita and Miyazaki prefectures, Kyûsyû, besides the fact that, according to T. Kato[2], they are intrusives (stocks and dikes) not only into the Upper Palaeozoic and Upper Cretaceous formations, but also into the earlier members (quartz-porphyry, lithoidite, vitrophyre andesite, and porphyrite) of the Early Tertiary volcanics in the district which, besides the earlier members, include as later ones another series of liparite and dacite.

---

[1] M. SAWATARI, *Jour. Geol. Soc., Tokyo*, **40** (1933), 25, (in Japanese).

[2] T, KATO, *Bull. Vol. Soc., Japan*, **2** (1933), 1, (in Japanese).

Furthermore, the granitic rocks of the Uwazima district in the southwestern part of Éhimé prefecture are also known as younger intrusives into the Cretaceous formation of the district[3]. In this connection it is remarkable that S. Tsuboi and I. Matsuzawa[4] failed to recognize any intrusive relation between the Izumi sandstone series (Upper Cretaceous) and the granites of the Takanawa peninsula (inner zone of S.W. Japan) in Éhimé prefecture, the possibility of which had formerly been entertained by many geologists. They found that the metamorphosed rocks with which the granites are in contact in an intrusive relation, are not the Izumi sandstone series, but an older, probably Palaeozoic, formation unconformably overlain by that series. From this fact they concluded that the granites of the Takanawa peninsula are older than the Upper Cretaceous, adding that these granites differ entirely, geologically, from the granitic rocks of the Uwazima district just mentioned.

Thus in the outer zone of southwest Japan we find at least four localities (Omogo, Uwazima, Kuma, and Sobosan) of younger granitic rocks of rather small extent, without however any laccomorphic or bathomorphic normal granites, which in the inner zone are extensively distributed, and which here intruded at least twice during the Mesozoic (pre-Jurassic and post-Jurassic or more probably post-Lower-Cretaceous).

No detailed geologic work on the Omogo acidic rocks nor any microscopical descriptions of them have so far been published, although the mass has been known to include a number of distinguishable rock-types[5]. In 1934, the writer had an opportunity of observing the mass and of examining its rocks. Although unfortunately his field observations could not be extended to cover more than a restricted area along the river Omogo that runs through the mass, what results that were obtained are described in the following pages.

Geological Remarks.

Before describing the petrography a short account of the general geological succession will be given of the Tertiary and the volcanic belt that stretches from Mt. Isiduti to the Kuma district.

---

[3] S. YEHARA, *Jap. Jour. Geol. Geogr.*, **7** (1929), 18.

[4] S. TSUBOI and I. MATSUZAWA, *Jour. Geol. Soc., Tokyo*, **41** (1934), 741, (in Japanese).

[5] T. OGAWA, Expl. Text Geol. Map (1: 200,000), "Kôti", Imp. Geol. Sur., (1931).

According to H. Sato[6], author of the Imperial Geological Survey map (1: 75,000) "Kuma" and "Matuyama", in which the western half of the belt just mentioned is included, the Tertiary (probably Miocene) formation of the Kuma district consists of a series, about 200 m thick, of liparitic white tuff, shale, and fossil-plant-bearing sandstone, and of a basal conglomerate bed, about 300 m thick, resting directly on the crystalline schists that are extensively developed on the southern side of the Median Dislocation Line in Sikoku. The volcanic rocks found there are liparite, rhombic-pyroxene-andesite, sanukite, biotite-andesite, trachytoid andesite, and flow-breccia, which have successively intruded into or erupted over the Tertiary and other older formations. Of these, rhombic-pyroxene-andesite, which occurs as lava-flows, has the widest distribution, forming a well-marked mountain range that runs along the central line of the belt just mentioned, from Mt. Katuraga-mori (1224 m), west of the Kuma basin, through Mt. Saragaminé (1271 m), to Mt. Isizumi (1456 m) in the middle part of the belt. Lying outside of Sato's geologic maps, the eastern half of the belt has been reserved for further detailed survey. It is believed that the rhombic-pyroxene-andesite extends continuously further east from the last-mentioned mountain to Mt. Isiduti (1981 m) at the eastern end of the belt, seeing that the area colored as "propylite" in the old Geological Survey maps (200,000) "Matuyama" and "Kôti" is exactly the same in the Kuma district as that occupied by Sato's rhombic-pyroxene-andesite, which extends further east to Mt. Isiduti. The areas on either side of the central range, composed of rhombic-pyroxene-andesite, are relatively low-lying ground consisting mainly of Tertiary formation and small masses of the afore-mentioned volcanic rocks, while the areas that embrace this Tertiary and volcanic belt are extensive tracts of older formations, namely, the Izumi sandstone series on the north and the crystalline schist system on the west, south, and east.

The point of vantage for examining the Omogo acidic rocks is the floor of the upper course of the river Omogo, which has cut a gorge "Omogo-kei" through the southern side of Mt. Isiduti. On walking up the river bank for a distance of about 9 km from Totihara at the end of the drive-way from the town of Kuma to Mt. Isiduti, we arrive at Kam'mon (barrier), where the valley-walls narrow so much as to virtually bar further progress. Here a black massive rock occurs in contact with the crystalline schists that are exposed all the

---

6) H. SATO, Expl. Text Geol. Map (1: 75,000), "Kuma", Imp. Geol. Sur., (1929); *ibid.*, "Matuyama", (1931).

way from Totihara. Microscopically, this rock is an altered tuff containing angular fragments of partially calcitized and albitized plagioclase and a little quartz, scattered through a more or less recrystallized matrix, without any fresh mafic minerals except magnetite, apatite, pyrite, and chloritized biotite (?). T. Ogawa[7] regarded the tuff as a member of the Omogo acidic rocks, the area of which in his geologic map is colored as liparite. It is however suggested that it be marked as a Tertiary tuff, which may be correlated with that in the Isiduti-yama Tertiary formation, and explained that it has been affected thermally by the intrusion of the Omogo acidic rocks. The high angle contact of the crystalline schist with the tuff at Kam'mon is consequently inferred as representing a fault between them.

Proceeding north for about 2·5 km along the valley from Kam'mon to Toraga-taki, at a water-fall situated almost in the center of the area of the Omogo acidic rocks, we can see successively outcrops of dark quartz-porphyry in contact with the tuff just mentioned, porphyritic granodiorite, finer-grained (aplitic) granite of lighter color at Kaméhara, and grayish quartz-porphyry at Kumabuti and Toraga-taki. According to Ogawa, the Omogo acidic rocks (his liparite) pass into "propylite" on the summit of Mt. Isiduti, and that the two are different parts of one and the same stock-like intrusive into the Isiduti-yama Tertiary formation that surrounds the mass almost everywhere excepting the southern margin of the mass, along which however occurs the questionable tuff we encountered at Kam'mon. If he is correct, the former then seems to be the lower part of a Tertiary volcanic focus that has been denuded of its superstructure, seeing that, according to Sato, the mountainous district of Kuma is composed of extensive lava-flows (locally associated with agglomerate) of the rhombic-pyroxene-andesite which is believed to be identical with the "propylite", forming a continuous ridge extending from Mt. Isiduti to the district in question. Although however we have as yet no evidence to oppose the assumption that the Omogo acidic rocks and the "propylite" on the summit of Mt. Isiduti form a continuous mass, the assumption does not seen altogether warranted, the whole subject needing further study before finality can be attained. Granted for argument's sake that the "propylite" by itself does form a separate mass, yet the Omogo acidic rocks may be regarded en block as a shallow-seated intrusive into the Tertiary and older formations, although little can be said as yet of its space-form in relation to the country rocks nor of the distribution of the distinctive rock-types of which it is composed.

---

[7] T. **Ogawa**, *loc. cit.*

Petrographic Description.

(1) *Porphyritic augite-bearing hornblende-biotite-granodiorite* (Fig. 2).

The coarsest member of the Omogo acidic rocks is a porphyritic hornblende-biotite-granodiorite of medium texture exposed for a distance of a few hundred meters halfway between Kam'mon and Kaméhara. Megascopically, it somewhat resembles the porphyritic hornblende-biotite-granite of the Takanawa peninsula, consisting as it does of plagioclase, orthoclase, quartz, biotite, and hornblende. Of the feldspars, which although usually white, are sometimes tinged yellow, plagioclase exhibits polysynthetic twin-lamellae. Dark-green or almost black hornblende and black biotite with golden-yellow tint are disseminated in the feldspathic white ground.

Microscopically, the rock is seriate porphyroid in fabric. The constituent minerals measured micrometrically are shown in Table I.

Table I.
Mineralogical Composition of the Porphyritic Hornblende-biotite-granodiorite of Omogo (Vol %).

Quartz	19·89
Orthoclase	22·33
Plagioclase	47·20
Biotite	5·97
Hornblende	3·97
Augite	0·18
Magnetite	0·46
Apatite	tr.
Total	100·00

Plagioclase, which is the most conspicuous mineral in the rock, occurs in euhedral to subhedral crystals, up to 1 cm long, tending to stand out with a slight porphyritic habit. These are usually twinned according to the albite, Carlsbad, and pericline laws. The majority of them consist of two chemically different zones, more calcic core and less calcic shell. The core part, which again exhibits a faint zoning, is andesine $Ab_{56}An_{44}$, according to the refractive indices ($n_{1D}=1·5502$, $n_{2D}=1·5562$) measured by the dispersion method on its cleavage flakes (010 or 001). Its optic axial angle (2V) measured on the universal stage varies from (+) 78° to (+) 85°. The shell part, which according to its optic axial angle 2V= (–) 82°, was identified as calcic oligoclase $Ab_{70}An_{30}$, approx. It is remarkable that, besides including magnetite grains and apatite needles, the plagioclase has enclosures of augite, which is only rarely found as isolated crystals in the rock. The augite enclosures are euhedral to anhedral, 0·01～0·1 mm dia., and pale green. It is sometimes rimmed by or partially altered to a brown biotite. The optic axial angle of the augite is large, with $c \wedge Z = 50°$, approx. Minute magnetite grains are included in the mineral.

Potash-feldspar, which fails to develop idiomorphic boundaries, occurs usually in anhedral crystals, up to 1 mm dia., although its crystallographic faces are sometimes observed when the mineral is in contact with quartz. It is usually completely clouded with fine, dust. Neither twin nor microperthitic intergrowth with plagioclase is discernible. $X \wedge a$ (basal cleavage trace) $= 9°$, optic axial angle $2V = (-)$ 74°. The potash-feldspar was therefore identified as ordinary orthoclase, which however does not show myrmekitic development in contact with the plagioclase, although the latter crystals are often embayed irregularly by the former. Enclosures in the orthoclase are plagioclase, biotite, hornblende, magnetite, and apatite.

In many ways quartz occurs like the orthoclase, it being usually anhedral, up to 1 mm dia., and sometimes filling the interstices of the remaining minerals, Besides the very fine dust, the enclosures are the same as those in the orthoclase. Quartz is usually intergrown in a mosaic manner with the orthoclase, while in some cases, the former protrudes as a wedge into or encloses the latter, though the reverse relation is also observed. There is no micrographic intergrowth of these minerals.

Biotite, which is euhedral against both orthoclase and quartz, but anhedral against plagioclase, is up to 0·5 mm dia. and strongly pleochroic with *X*—yellow, *Y*—dark greenish brown, *Z*—dark greenish brown. It is of meroxene type with the optical plane parallel to (010). Optic axial angle $2E = 24°50'$. $\beta_D = \gamma_D = 1·6600$. $2V = (-)14°50'$, as calculated from the apparent optic angle $2E$ by assuming $\beta_D = 1·6600$. The mineral has inclusions of plagioclase, apatite, magnetite, and zircon. This last mineral is surrounded by a pleochroic halo. Although the biotite is usually fresh, epidote rarely occurs along its cleavage plane.

Hornblende, 0·5～1·0 mm dia., is euhedral to subhedral and moderately pleochroic with *X*—yellowish green, *Y*—green, *Z*—deep green. The mineral is optically negative with $2V = 82°$; $Z \wedge c = 19°$. The twinning is as usual. The refractive indices measured on the cleavage flakes (110) by the dispersion method are $n_{1D} = 1·6616$, $n_{2D} = 1·6778$. The inclusions are plagioclase, magnetite, and apatite. Much of the hornblende is inverting to biotite along its margin or along the cleavages. It is frequently decolored, when it is then fibrous in texture.

Monoclinic pyroxene, except when present as small enclosures in the plagioclase crystals, occurs sparingly as isolated crystals, up to 0·5 mm dia. It is a pale green augite with $Z \wedge c' = 50°$. No pleochroism is discernible. The mineral is altered marginally to green hornblende and at the extreme periphery to biotite. Sometimes it forms only small cores surrounded by a broad rim of the hornblende.

Accessory minerals, always smaller than 0·2 mm dia., occur as inclusions in the principal minerals just enumerated.

(2) *Fine-grained biotite-granite* (Fig. 3).

Fine-grained granite, the finest-grained rock-type thus far found in the Omogo acidic rocks, is exposed at Kaméhara, forming a vertical cliff, a few hundred meters high, on one side of the river Omogo. Megascopically, it is almost equigranular, consisting of plagioclase, orthoclase, quartz, and biotite, although a few porphyritic plagioclase crystals and biotite clots are observed. It is almost white, with minute flakes of dark green or almost black biotite disseminated in the whitish ground, which consists of feldspar and quartz.

Microscopically, the rock is seriate homoid in fabric, consisting of plagioclase, orthoclase, quartz, and biotite, besides accessory minerals, in decreasing order of magnitude. There is a marked decrease in grain-size as compared with that of the porphyritic granodiorite just mentioned, a decrease of mafic minerals, with an increase of orthoclase and a more sodic plagioclase as the dominant feldspars.

Plagioclase occurs in two well-defined types. A few porphyritic plagioclase occur as euhedral crystals, 2∼5 mm dia., twinned according to the albite and pericline laws. These crystals, which are a very faintly zoned andesine $Ab_{52}An_{48}$, with $n_{1D} = 1·5530$ and $n_{2D} = 1·5581$, are sometimes internally sericitized. The commoner but smaller plagioclase occurs as euhedral to subhedral crystals, 0·2∼0·5 mm dia., twinned according to the albite and Carlsbad laws. These crystals are faintly zoned, their composition ranging from medium oligoclase to albite, with $Z \wedge (010) = 90°$ in the core and $Z \wedge (010) = 73°$ in a section nearly perpendicular to X. With the exception of a few apatite needles and dust material, the plagioclase is usually devoid of inclusions.

Orthoclase occurs as anhedral crystals up to 1 mm dia., twinned according to the Carlsbad law. Microperthitic intergrowth with plagioclase is discernible. The refractive indices measured on the cleavage flakes (001 or 010) by the dispersion method are $n_{1D} = 1·5224$,

$n_{2D}=1{\cdot}5233$. The mineral contains inclusions of plagioclase, biotite, and a few apatite, besides dust material.

Quartz is quite abundant in irregular grains, 0·1∼0·5 mm dia., enclosing the same minerals as do the orthoclase.

Biotite occurs as euhedral flakes, 0·2 mm dia., many of which are bleached and altered to chlorite and often associated with epidote and magnetite, The freshest biotite flake found so far is pleochroic. X—pale-greenish, Y or Z—dark greenish brown, with $\gamma_D=1{\cdot}6545$. Besides enclosing apatite needles, the mineral contains inclusions of zircon surrounded by pleochroic halos.

(3) *Augite-hypersthene-biotite-quartz-porphyry* (Figs. 4 and 5).

Lying immediately south of the porphyritic granodiorite and north of the fine-grained granite just mentioned are several porphyritic rocks of peculiarly varied characters, both megascopically and microscopically, strongly suggesting a mixture of liparitic magma and foreign andesitic material, and which may therefore be best grouped as quartz-porphyry or liparite.

As we approach Simo-Kumabuti, less than 1 km north of Kaméhara, the fine-grained granite gives place to a porphyritic rock characterized by diverse megascopic characters as well as by patchy distribution of black xenolithic material. One part of the rock, consisting of feldspar, quartz, and biotite, is very similar to the fine-grained granite exposed at Kaméhara, although the former is more porphyritic and contains numerous black patches that are not found in the latter.

Another part of the rock, composed of feldspar, quartz, biotite, and pyroxene, is light-gray, strongly porphyritic, but devoid of black patches. This light-gray, porphyritic rock is continuously exposed from the last-mentioned locality to Toraga-taki, the northern extremity of the writer's field investigation of the intrusive mass.

In the south between Kaméhara and Kam'mon, and immediately south of the porphyritic granodiorite locality, is exposed a porphyritic rock that is similar in mineral composition to the light-gray porphyritic rock from Simo-Kumabuti and Toraga-taki, but which is more porphyritic and darker than the latter, while parts of it are so dark that locally it becomes a dark-gray andesitic rock with phenocrystic plagioclase and pyroxene.

The microscopic characters of the porphyritic rocks differ with divergences in their megascopic characters. The granitic part of the rock from Simo-Kumabuti, which consists of plagioclase (porphyritic andesine and smaller oligoclase-albite), quartz, and greenish brown biotite, together with accessory magnetite, apatite, and secondary epidote, is similar in many of its microscopic characters to the equivalent rock of Kaméhara. The black patch or dark xenolithic material with which the granitic part is mixed in confusion at Simo-Kumabuti, contains phenocrysts of plagioclase (andesine) in a granular groundmass. Many of the phenocrysts, 0·2∼0·5 mm dia., show crushed ends, although they are sometimes either rounded or indented by inlets of the groundmass, which latter is a minute aggregate of sodic plagioclase laths (less than 0·1 mm long), interstitial potash-feldspar and quartz grains (0·01∼0·05 mm dia.), and biotite flakes (0·01∼0·02 mm long). Besides being disseminated in the groundmass, the biotite occurs as glomeroporphyritic aggregates associated with plagioclase and magnetite. Both phenocrysts and groundmass are occasionally traversed by microscopic veinlets consisting of biotite flakes, granular quartz and potash-feldspar. The black patches are therefore regarded as xenoliths derived from a porphyritic volcanic rock which, after being caught in the intruding mass, were affected thermally as well as chemically by the host-material.

The light-gray porphyritic rock from Simokuma-buti and Toragataki shows, microscopically, phenocrysts of plagioclase, potash-feldspar, quartz, hypersthene, augite, and biotite in a granular biotite-quartz-feldspar groundmass, besides accessory magnetite, apatite, and secondary epidote. Many of the phenocrysts are crushed, presenting either a jagged, rounded, or embayed outline with inlets of the groundmass. Plagioclase, 0·5∼1 mm dia., which is a slightly zoned andesine ($2V = (+)\ 77° \sim 86°$) with inclusions of apatite needles, magnetite grains, and rounded crystals of pyroxene, is sometimes surrounded by a very thin rim of potash-feldspar, or is merged into the granular quartz-feldspar aggregate of the groundmass with no sharp boundary between them. Phenocrystic potash-feldspar, which is subordinate in quantity to the plagioclase, is a transversely cracked sanidine, 0·5∼1 mm dia., with a small optic angle, twinned according to the Carlsbad law. The mineral carries inclusions of plagioclase. Quartz, 0·5 mm dia., angular to rounded, is traversed with irregular cracks, along which the groundmass material penetrates. Except dust material, no inclusion is discernible. Hypersthene, 0·2∼1 mm long, is rather weakly pleochroic with X—pale yellow, Y—pale yellowish brown, Z—pale green or nearly colorless. $2V = (-)54° \sim 58°$. n_{1D}(in 110)$>1·7136$. Augite, 0·2∼0·5 mm dia., is pale brown with $2V = 52°$, approx. Both hypersthene and augite are frequently surrounded by or penetrated along their cleavages by biotite flakes (0·01∼0·5 mm dia., brown,

$\beta_D \doteqdot \gamma_D = 1{\cdot}6600$). The pyroxenes carry inclusions of magnetite, plagioclase and apatite. Besides occurring in and around the pyroxenes, the biotite are scattered as isolated flakes, 0·02~0·3 mm long, through the rock. One of these biotite flakes, of deep reddish brown color, showed $\beta_D \doteqdot \gamma_D = 1{\cdot}6718$. The groundmass, through which the above-mentioned phenocrystic minerals are dispersed, is a granular aggregate composed of quartz and potash-feldspar, less than 0·02 mm dia., besides a few plagioclase laths, biotite flakes, and accessory minerals.

A porphyritic rock from near Kam'mon consisting of phenocrysts of andesine, sanidine, quartz, hypersthene, augite, and biotite, together with a microcryptocrystalline groundmass, resembles the preceding rock,

Table II. Microscopic Characters of the Omogo Acidic Rocks.

	(1)	(2)	(3)		
			a	b	c
Quartz	+	+	+	△	△ ×
Potash-feldspar	2V(−)=74°	$n_{1D} = 1{\cdot}5224$ $n_{2D} = 1{\cdot}5233$	+	×	△ (sanidine) ×
Biotite	$\gamma_D = 1{\cdot}6600$ 2V(−)=14°50′	$\gamma_D = 1{\cdot}6545$	+	× □	△ ($\gamma_D = 1{\cdot}6718$) × □ ($\gamma_D = 1{\cdot}6600$)
Albite, Oligoclase	2V(−)=82° $Ab_{70}An_{30}$~?	$Ab_{85}An_{15}$~Ab_{100} Z∧(010)=90~73° in Sec. ⊥X	+	×?	×?
Hornblende	$n_{1D} = 1{\cdot}6616$ $n_{1D} = 1{\cdot}6778$ 2V(−)=82° Z∧c=19°	—	—	—	—
Andesine	$n_{1D} = 1{\cdot}5502$ $n_{2D} = 1{\cdot}5562$ $Ab_{56}An_{44}$ (2V(+)=78~85°)	$n_{1D} = 1{\cdot}5530$ $n_{2D} = 1{\cdot}5581$ $Ab_{52}An_{48}$	+	△	△
Hypersthene	—	—	—	±	△ ($n_{1D} = 1{\cdot}7136$) (2V=54~58°)
Augite	2V=large Z∧c=50°	—	—	±	△ (2V=52°)

(+ present, − absent, △ present as phenocrysts, × present in groundmass, □ present as reaction-rim at the periphery of pyroxene)

(1) Porphyritic granodiorite.
(2) Fine-grained granite.
(3) Quartz-porphyry {a fine-grained granitic. b, c >andesitic.

which however differs from the latter in that the phenocrystic pyroxene is often altered along the cleavages or around the periphery to chlorite and calcite associated with magnetite, while the groundmass exhibits very feeble flow-lines in delicate shades of color (eutaxitic structure). This rock contains microscopic angular xenoliths of pyroxene-andesite composed of phenocrystic augite and plagioclase (andesine) and a hyalopilitic groundmass.

Chemical Composition.

The three distinctive types of the Omogo acidic rocks were chemically analyzed by S. Tanaka, analyst of this Institute, with results as given in Table III, together with their norms, normative plagioclase, and ratio of iron-oxide to magnesia.

Table III. Chemical Composition of Omogo Acidic Rocks; analyst S. Tanaka.

	1	2	3		1	2	3
SiO_2	73·70	65·68	64·02	Q	30·33	19·64	16·70
Al_2O_3	14·14	15·54	16·33	Or	27·85	22·82	20·04
Fe_2O_3	0·10	0·42	0·44	Ab	31·36	27·26	28·31
FeO	1·76	3·91	4·72	An	4·73	16·41	18·91
MgO	0·28	1·88	2·32	C	1·22	——	0·20
CaO	0·95	3·59	4·00	Py* $CaSiO_3$	——	0·23	——
Na_2O	3·73	3·20	3·35	Py* $MgSiO_3$	0·70	4·72	5·82
K_2O	4·67	3·86	3·39	Py* $FeSiO_3$	2·77	5·54	7·12
H_2O+	0·65	0·91	0·40	Mt	0·23	0·70	0·70
H_2O-	0·17	0·13	0·11	Il	0·30	1·52	1·52
TiO_2	0·15	0·76	0·82	Ap	tr.	0·31	0·31
P_2O_5	tr.	0·13	0·21	Normative plagioclase	$Ab_{87}An_{13}$	$Ab_{62}An_{38}$	$Ab_{60}An_{40}$
MnO	0·03	0·08	0·10	$\frac{FeO+Fe_2O_3}{MgO}$	6·60	2·28	2·20
Total	109·33	100·09	100·13				

* Normative pyroxene (Di+Hy).

1. Fine-grained biotite-granite.
2. Porphyritic augite-bearing hornblende-biotite-granodiorite.
3. Augite-hypersthene-biotite-quartz-porphyry.

Of the three rock-types, the most acidic fine-grained biotite-granite has a chemical composition representing normal granite or liparite, thus lending support to the view that contamination of andesitic material was slightest in this rock, a view that has already been expressed on mineralogical grounds. There is therefore the possibility that the fine-grained biotite-granite may represent the normal magma of the Omogo acid intrusive, from which the various rock-types were derived by means of incorporation of andesitic material.

Table IV.

	A	B	C	D
SiO_2	72·17	71·60	65·70	72·25
Al_2O_3	14·11	14·30	16·23	14·04
Fe_2O_3	0·25	0·20	0·50	0·38
FeO	2·10	2·38	4·06	2·32
MgO	0·50	0·48	1·33	0·67
CaO	1·34	2·10	4·24	2·13
Na_2O	3·33	3·46	3·45	3·43
K_2O	4·58	3·93	2·42	3·17
$H_2O +$	0·87	0·51	0·54	0·64
$H_2O -$	0·22	0·20	0·23	0·21
TiO_2	0·32	0·25	0·66	0·35
P_2O_5	0·14	0·05	0·12	0·22
MnO	0·03	0·05	0·09	0·19
Total	99·96	99·51	99·57	100·00

A. Biotite-granite-porphyry[8], Nati, Wakayama Pref., S. Tanaka, anal.
B. Hornblende-biotite-granite. Takahama, Ehimé Pref., S. Tanaka, anal.
C. Porphyritic hornblende-biotite-granodiorite. Kikuma, Ehime Pref., S. Tanaka, anal.
D. Average of 94 Japanese granites[9].

Compared with normal Japanese granite, as for example the hornblende-biotite-granite of the Takanawa peninsula (Table IV, B), or with the average of 94 Japanese granites (Table IV, D), the fine-grained biotite-granite is lower in iron, magnesia, and lime but higher in silica and alkalis. Although it resembles the analysis of the biotite-granite-porphyry in the Kumano acidic rocks (Table IV, A), it is slightly poorer in iron and lime, but richer in silica than the latter.

The porphyritic augite-bearing hornblende-biotite-granodiorite resembles in chemical composition the augite-hypersthene-biotite-quartz-porphyry, notwithstanding the marked contrast of their microscopical characters. They are much poorer in silica and alkalis, but notably richer in iron, magnesia, and lime than the fine-grained biotite-granite. The FeO: MaO ratio in the former is much smaller than that in the latter. Compared with normal granodiorite, as for example the hornblende-biotite-granodiorite of the Takanawa peninsula (Table IV, C), the granodiorite of Omogo is distinctly higher in potash.

Normatively, the fine-grained biotite-granite is richer in quartz, orthoclase, and albite, but poorer in anorthite and pyroxene than the other two rock-types. The normative plagioclase of the former is sodic oligoclase, while that of the latter is intermediate andesine. As these variations in the norm composition of the three rock-types are directly related to variations in their mode, it may be said that the porphyritic augite-bearing hornblende-biotite-granodiorite and augite-hypersthene-biotite-quartz-porphyry represent material that resulted from contamination of andesitic xenoliths and xenocrysts (pyroxene and basic plagioclase) in an acid magma that might not have differed so greatly in chemical composition from the fine-grained biotite-granite.

---

[8] M. SAWATARI, *loc. cit.*

[9] J. SUZUKI and T. NEMOTO, *Jour. Fac. Sci.*, Hokkaido Imp. Univ., **3** (1935), 1.

Summary and Conclusions.

The Omogo acidic rocks on the south side of Mt. Isiduti in Éhimé prefecture, Sikoku, occur as shallow-seated intrusive into the so-called Isiduti-yama Tertiary, probably Miocene, of that district, which is composed of conglomerate, sandstone, shale, and tuff, besides various volcanic rocks including liparite, pyroxene-andesite, mica-andesite, etc.

The intrusive mass comprises several rock-types which may be dealt with petrographically under three headings:— (1) fine-grained biotite-granite composed practically of sodic plagioclase, orthoclase, quartz, and biotite; (2) porphyritic augite-bearing hornblende-biotite-granodiorite, consisting practically of plagioclase, orthoclase, quartz, biotite, hornblende, and augite, and constituting a subordinate portion of the mass; and (3) augite-hypersthene-biotite-quartz-porphyry, rich in phenocrystic plagioclase and pyroxene, besides a few phenocrysts of sanidine, biotite, and quartz.

These petrographic types suggest that although crystallization-differentiation of neither acidic nor basic magma can alone account for their origin, contamination of a pre-existing pyroxene-andesite with an acid (granitic or liparitic) magma is partly at least responsible for their genesis, the main reasons for this suggestion being as follows:—

(1) Microscopic xenoliths of pyroxene-andesite are found in the quartz-porphyry near Kam'mon.

(2) The fine-grained biotite-granite from Simo-Kumabuti carries black patches suggestive of xenoliths derived from a pre-existing porphyritic volcanic rock, the latter being traversed by microscopic veinlets of the former.

(3) The quartz-porphyry carries crushed crystals of andesine and

pyroxenes, which may be regarded as xenccrysts derived from xenoliths akin to the pyroxene-andesite xenoliths in the same rock. The porphyritic granodiorite contains porphyritic crystals of andesine and augite similar to those in the quartz-porphyry.

(4) Neither the quartz-porphyry nor the fine-grained biotite-granite carry hornblende, although they must have undergone more rapid consolidation than the hornblende-bearing granodiorite, seeing that, besides the xenocrysts, the quartz-porphyry is strongly porphyritic with phenocrysts of quartz, potash-feldspar, sodic plagioclase, and biotite, and that the granite is finer-grained than the granodiorite.

(5) The quartz-porphyry differs but little in chemical composition from the granodiorite, although they exhibit great differences in texture of mineral association.

(6) The fine-grained biotite-granite, which has few indication of xenocrysts, except a few xenocrystic andesine, is much more acidic in chemical composition than the quartz-porphyry and the granodiorite.

The main phenomena observed in the Omogo acidic rocks may be reasonably explained by assuming that an acid magma, originally saturated with quartz, potash-feldspar, sodic plagioclase, and biotite, intruded into a subsurface pyroxene-andesite mass after the manner of "piecemeal stoping", and that the former reacted with the xenoliths derived from the latter in different ways according to the different rates of cooling within it during the time that its emplacement and crystallization were going on. The marginal parts of the intruding mass cooled so rapidly that hybrid quartz-porphyry resulted, in which the xenocrystic pyroxenes were converted

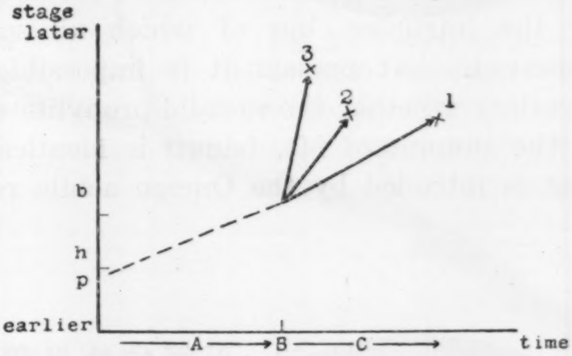

Fig. 1. Diagram showing the genetical relationship of the three principal types of the Omogo acidic rocks.

1. Porphyritic augite-bearing hornblende-biotite-granodiorite.
2. Fine-grained biotite-granite.
3. Hypersthene-augite-biotite-quartz-porphyry.

Ordinate: Stage in the cooling history of the intruding mass as represented by the mafic minerals. p—pyroxene stage, h—hornblende stage, b—biotite-stage.

Abscissa: Time elapsed during the cooling history of the intruding mass. A—deep-seated parent magma period, B—time of intrusion and of incorporation of xenoliths, C—shallow-seated intrusive period.

marginally or along cleavages into biotite. At the central part, where it cooled more slowly than the margin, the most acidic biotite-granite resulted with minimum incorporation of xenoliths. The granodiorite may be regarded as representing a product from the inner part of the intruding mass, where, notwithstanding that the mass was incorporated with the xenoliths to the same extent as in the margins, its coolig was so slow that reaction between the magma and the xenoliths was favorable for producing the coarsest-grained granodiorite. The hornblende crystals in the granodiorite, which are not inherent in the intruding mass, may be regarded as a product derived from the pyroxene xenocrysts through favorable reaction between these xenocrysts and the intruding mass saturated with biotite.

Although the space-form of the Omogo acidic rocks is still a matter for further detailed field survey, it is suggested tentatively that it may be a relatively small laccolithic intrusive into a pre-existing pyroxene-andesite mass that once formed part of the area now occupied by the intrusive, but of which all superficial traces may have disappeared. At present it is impossible to state with any degree of certainty whether the so-calld propylite (or rhombic-pyroxene-andesite) at the summit of Mt. Isiduti is identical with that pyroxene-andesite that is intruded by the Omogo acidic rocks.

---

69. 面河酸性岩類に就いて

地震研究所 津屋弘達

愛媛縣さ高知縣さの境に位する石鎚山の南側の景勝地である面河溪には二十萬分の一地質圖“高知”及び同說明書に流紋岩さして記載されてゐる酸性岩體が露出してゐる. 此火山岩體は同地方の結晶片岩系及び石鎚山第三紀層を貫き，肉眼的並びに顯微鏡的に次の三岩型に大別される.

1. 斑狀含單斜輝石-角閃石·黑雲母花崗閃綠岩
2. 細粒質黑雲母花崗岩
3. 單斜輝石·斜方輝石·黑雲母·石英粗面岩

本文では之等の岩石の岩石學的性質を記載し，其成因を論じ，地下深處の岩漿溜より黑雲母に飽和せる流紋岩質の熔岩が第三紀層中に迸入し，同層中の一員たる輝石安山岩を捕獲し，相互に相反應し，迸入體の各部分が冷却速度及び捕獲岩片の量を異にせる結果，上記の各岩型を生じたるものなるこさを結論した.

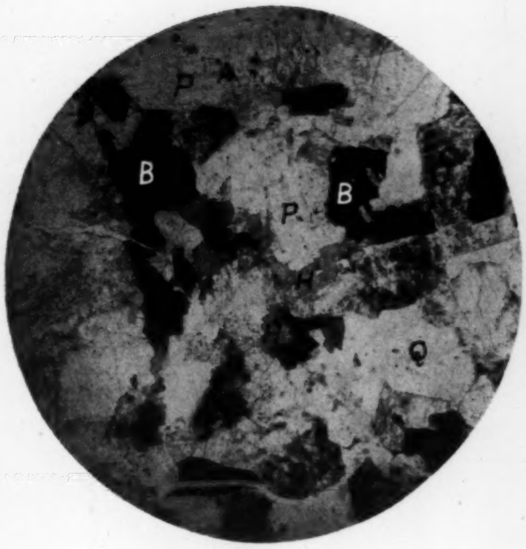

Fig. 2. Porphyritic granodiorite.
A···augite, B···biotite, H···hornblende, O···orthoclase, P···andesine, Q···quartz.
×15.

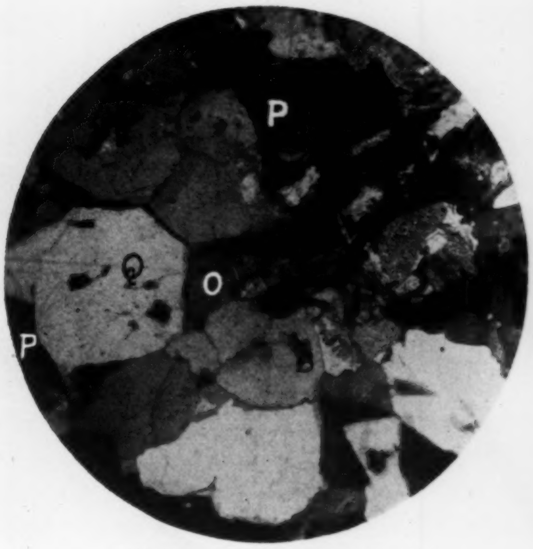

Fig. 3. Fine-grained granite.
B···biotite, O···orthoclase, P···albite-oligoclase, Q···quartz.
×33.

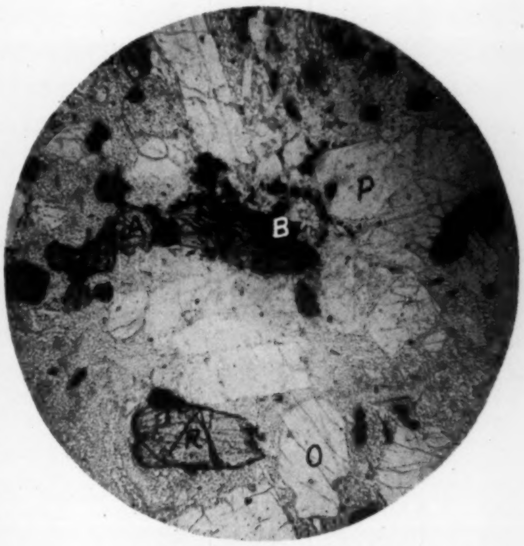

Fig. 4. Quartz-porphyry.
A···augite, B···biotite, O···sanidine, P···andesine, R···hypersthene. ×15.

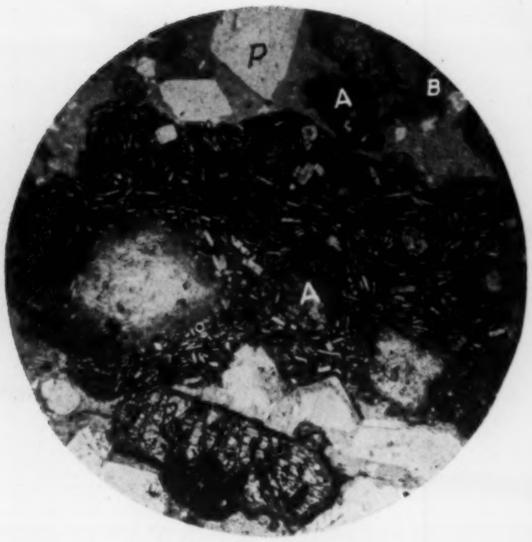

Fig. 5. Ditto, with inclusion of pyroxene-andesite. ×15.

Microphotographs of the Omogo Acidic Rocks.

（震研彙報 第十三號 圖版 津屋）

70. *Energy Dissipation in Seismic Vibrations of Actual Buildings.*

By Katsutada SEZAWA and Kiyoshi KANAI,

Earthquake Research Institute.

(Read Sept. 17, 1935.-Received Sept. 20, 1935.)

1. In the previous paper[1] we studied the nature of decay in the seismic vibrations of a framed structure by their energy dissipating into the ground. The problems discussed in that paper were connected with the vibrations of certain hypothetical buildings, whose structural conditions differed little from those of an actual building. Through the courtesy of the Mitsubishi Co. we were enabled to study the same problem with respect to actual modern style buildings owned by the said Company. For the problem discussed in the present paper, we selected three buildings of different stories, namely, three-, four-, and five-storied reinforced concrete structures, all three in Marunouti, a business quarter in the downtown of Tokyo. The three-storied building, numbered Middle 13th House (Naka-13gô-kan), was built in April 1915; the four-storied one, numbered No. 6 of Middle 12th Lot of Houses (Naka-12gô-kan 6gô), was constructed in April 1920; while the five-storied building, called the Annexe of the East 7th House (Higasi-7gô-kan Bekkan), was completed in August 1929. The first and second are let for business offices and the last for a restaurant (Marunouti-kaikan).

Because of the fact that the basements of all three buildings are of very strong construction and that their heights are much less than those of the other floors, we made our calculations on the assumption that, the effect of neglecting the basement floors being corrected in some way, the ground floors were directly connected to the earth's surface. Since moreover the beams, etc., forming the members of the floors, are of sufficiently rigid construction, we shall treat the problem as one of a structure with rigid floors and clamped base.[2] The method of calculation was shown in the preceding paper.[3] Seeing that we have not yet found a theoretical expression for the case of a four-, a five-, or more generally, an n-storied structure, it behooves us to calculate them before proceeding further.

---

[1] K. SEZAWA and K. KANAI, "Energy Dissipation in Seismic Vibrations of a Framed Structure," *Bull. Earthq. Res. Inst.*, **13** (1935), 698~714.

[2] In next occasion we shall discuss the problem as one of a structure with flexible floors, although such a condition is hardly realized.

[3] K. SEZAWA and K. KANAI, *ibid.* 1).

2. *Theoretical solution for an n-storied structure with rigid floors and clamped base.*

The solution of the vibratory motion of columns between $(s-1)$th and sth floors is

$$y_s=(A_s+B_sx_s+C_sx_s^2+D_sx_s^3)e^{ipt}, \tag{1}$$

where x_s is the coordinate of a point of the same columns measured negatively from their respective lower ends, y_s the horizontal deflection of point x_s, while A_s, B_s, C_s, D_s are constants to be determined by boundary conditions. Let l_s, E_s, I_s be the length, Young's modulus, and the sum of the moments of inertia of cross sections of all the columns between the $(s-1)$th and the sth floors. Then the boundary conditions shown in the preceding paper,[4] namely,

$$x_n=-l_n;\quad \frac{\partial y_n}{\partial x_n}=0,\quad E_nI_n\frac{\partial^3 y_n}{\partial x_n^3}+m_n\frac{\partial^2 y_n}{\partial t^2}=0, \tag{2), (3}$$

$$x_s=-l_s,\quad x_{s+1}=0;\quad y_s=y_{s+1},\quad \frac{\partial y_s}{\partial x_s}=0,\quad \frac{\partial y_{s+1}}{\partial x_{s+1}}=0, \tag{4), (5), (6}$$

$$E_{s+1}I_{s+1}\frac{\partial^3 y_{s+1}}{\partial x_{s+1}^3}=E_sI_s\frac{\partial^3 y_s}{\partial x_s^3}+m_s\frac{\partial^2 y_s}{\partial t^2}, \tag{7}$$

$$(s=1,\ 2,\cdots\cdots,\ n-1)$$

$$x_1=0;\quad y_{1_{x_1=0}}=u_{0_{x_1=0}}+u_{r=\varepsilon,\ \theta=0},\quad \frac{\partial y_1}{\partial x_{1_{x_1=0}}}=0, \tag{8), (9}$$

$$\begin{aligned}-E_1\pi\varepsilon^2j^2\frac{\partial^3 y_1}{\partial x^3_{1_{x_1=0}}}&=\mu\pi\varepsilon^2\frac{\partial u_0}{\partial x_{1_{x_1=0}}}\\&+\int_{\theta=0}^{\pi}\int_{\varphi=0}^{\pi}\mu\Big(\frac{\partial v}{\partial r}-\frac{v}{r}+\frac{1}{r}\frac{\partial u}{\partial\theta}\Big)r^2\sin^2\theta d\theta d\varphi_{r=\varepsilon}\\&+\int_{\theta=0}^{\pi}\int_{\varphi=0}^{\pi}\Big(\lambda\Delta+2\mu\frac{\partial u}{\partial r}\Big)r^2\sin\theta\cos\theta d\theta d\varphi_{r=\varepsilon},\end{aligned} \tag{10}$$

---

[4] K. SEZAWA and K. KANAI, *loc. cit.* 1).

where $\varDelta$, u, v are such that

$$\left.\begin{aligned} \varDelta &= \alpha\cos\theta\,\frac{e^{i(pt-hr)}}{r}, \quad \frac{\alpha}{\beta}=\frac{i(k-h)}{2k^2\varepsilon}\,e^{i(h-k)\varepsilon}, \\ u &= -\frac{\alpha}{h^2}\cos\theta\,\frac{d}{dr}\,\frac{e^{i(pt-hr)}}{r}-\frac{4\beta}{k^2}\cos\theta\,\frac{e^{i(pt-kr)}}{r^2}, \\ v &= \frac{\alpha}{h^2}\sin\theta\,\frac{e^{i(pt-hr)}}{r^2}+\frac{2\beta}{k^2}\sin\theta\,\frac{e^{i(pt-kr)}}{r^2}, \end{aligned}\right\} \tag{11}$$

corresponding to the transverse waves

$$u_0=e^{i(pt+kx)}, \tag{12}$$

in which $h^2=\rho p^2/(\lambda+2\mu)$, $k^2=\rho p^2/\mu$, incident vertically on the ground surface.

The final solutions are

$$P'\beta=2.\text{const.}, \quad Q'\beta=8i(k-h)\varepsilon.\text{const.}, \tag{13}$$

$$A_1+P'\beta=1, \quad \frac{18E_1\varepsilon j_1^2}{\mu}D_1+Q'\beta=-3i\varepsilon k, \tag*{(14), (15)}$$

$$B_s=0, \quad C_s=\frac{3}{2}l_sD_s, \quad (s=1,\ 2,\cdots\cdots,\ n) \tag*{(16), (17)}$$

$$A_s=\frac{1}{2}(2A_{s-1}+l_{s-1}^3D_{s-1}), \quad (s=2,\ 3,\cdots\cdots,\ n) \tag{18}$$

$$D_s=\frac{E_{s-1}I_{s-1}}{12E_sI_sl_{s-1}^3}\{-2\gamma_{s-1}A_{s-1}+(12-\gamma_{s-1})l_{s-1}^3D_{s-1}\}, \qquad (s=2,\ 3,\cdots\cdots,\ n) \tag{19}$$

$$A_n=\frac{12-\gamma_n}{2\gamma_n}l_n^3D_n, \tag{20}$$

where $\gamma_s=m_sp^2l_s^3/E_sI_s$ and m_s is the mass concentrated on the sth floor. Eliminating $P'\beta$, $Q'\beta$ between these solutions, it is possible to determine the values of all the constants A_s, B_s, C_s, D_s. In the special case, $n=4$ and $E_1=E_2=E_3=E_4$, $I_1=I_2=I_3=I_4$, $l_1=l_2=l_3=l_4$, $m_1=m_2=m_3=m_4$, the curvatures in the columns in the respective floors are expressed by

$$\frac{d^2y_1}{dx_1^2}\left(\frac{l^2}{2\gamma}\right)=\frac{6}{\sqrt{\mathfrak{A}^2+\mathfrak{B}^2}}(24-\gamma)\left\{24(6-\gamma)+(12-\gamma)^2\right\} \cdot\left\{1+2\left(\frac{x_1}{l}\right)\right\}\cos\left(pt-\tan^{-1}\frac{\mathfrak{B}}{\mathfrak{A}}\right), \tag{21}$$

$$\frac{d^2y_2}{dx_2^2}\left(\frac{l^2}{2\gamma}\right)=\frac{6.12}{\sqrt{\mathfrak{A}^2+\mathfrak{B}^2}}(12-\gamma)(36-\gamma)$$
$$\cdot\left\{1+2\left(\frac{x_2}{l}\right)\right\}\cos\left(pt-\tan^{-1}\frac{\mathfrak{B}}{\mathfrak{A}}\right), \tag{22}$$

$$\frac{d^2y_3}{dx_3^2}\left(\frac{l^2}{2\gamma}\right)=\frac{6.12^2}{\sqrt{\mathfrak{A}^2+\mathfrak{B}^2}}(24-\gamma)\left\{1+2\left(\frac{x_3}{l}\right)\right\}\cos\left(pt-\tan^{-1}\frac{\mathfrak{B}}{\mathfrak{A}}\right), \tag{23}$$

$$\frac{d^2y_4}{dx_4^2}\left(\frac{l^2}{2\gamma}\right)=\frac{6.12^3}{\sqrt{\mathfrak{A}^2+\mathfrak{B}^2}}\left\{1+2\left(\frac{x_4}{l}\right)\right\}\cos\left(pt-\tan^{-1}\frac{\mathfrak{B}}{\mathfrak{A}}\right), \tag{24}$$

where

$$\left.\begin{aligned}\mathfrak{A}&=-12\gamma(24-\gamma)^2+\{-12\gamma+(12-\gamma^2)\}^2,\\ \mathfrak{B}&=\frac{12}{a}\sqrt{\frac{EIm}{l^3\rho\mu}}\sqrt{\gamma}(24-\gamma)\{24(6-\gamma)+(12-\gamma)^2\},\end{aligned}\right\} \tag{25}$$

in which ρ, μ are the density and the rigidity of the earth, and a is the total area of the cross sections of the columns on each floor.

In the special case, $n=5$ and $E_1=E_2=\cdots\cdots=E_5=E$, $I_1=I_2=\cdots\cdots=I_5=I$, $l_1=l_2=\cdots\cdots=l_5=l$, $m_1=m_2=\cdots\cdots=m_5=m$, we get similarly

$$\frac{d^2y_1}{dx_1^2}\left(\frac{l^2}{2\gamma}\right)=\frac{6}{\sqrt{\mathfrak{A}^2+\mathfrak{B}^2}}\{(12-\gamma)^2-12\gamma\}\{(12-\gamma)(48-\gamma)+144\}$$
$$\cdot\left\{1+2\left(\frac{x_1}{l}\right)\right\}\cos\left(pt-\tan^{-1}\frac{\mathfrak{B}}{\mathfrak{A}}\right), \tag{26}$$

$$\frac{d^2y_2}{dx_2^2}\left(\frac{l^2}{2\gamma}\right)=\frac{6.12}{\sqrt{\mathfrak{A}^2+\mathfrak{B}^2}}(24-\gamma)\{(12-\gamma)(24-\gamma)-12\gamma\}$$
$$\cdot\left\{1+2\left(\frac{x_2}{l}\right)\right\}\cos\left(pt-\tan^{-1}\frac{\mathfrak{B}}{\mathfrak{A}}\right), \tag{27}$$

$$\frac{d^2y_3}{dx_3^2}\left(\frac{l^2}{2\gamma}\right)=\frac{6.12^2}{\sqrt{\mathfrak{A}^2+\mathfrak{B}^2}}(12-\gamma)(36-\gamma)\left\{1+2\left(\frac{x_3}{l}\right)\right\}\cos\left(pt-\tan^{-1}\frac{\mathfrak{B}}{\mathfrak{A}}\right), \tag{28}$$

$$\frac{d^2y_4}{dx_4^2}\left(\frac{l^2}{2\gamma}\right)=\frac{6.12^3}{\sqrt{\mathfrak{A}^2+\mathfrak{B}^2}}(24-\gamma)\left\{1+2\left(\frac{x_4}{l}\right)\right\}\cos\left(pt-\tan^{-1}\frac{\mathfrak{B}}{\mathfrak{A}}\right), \tag{29}$$

$$\frac{d^2y_5}{dx_5^2}\left(\frac{l^2}{2\gamma}\right)=\frac{6.12^4}{\sqrt{\mathfrak{A}^2+\mathfrak{B}^2}}\left\{1+2\left(\frac{x_5}{l}\right)\right\}\cos\left(pt-\tan^{-1}\frac{\mathfrak{B}}{\mathfrak{A}}\right), \tag{30}$$

where

$$\left.\begin{aligned}\mathfrak{A}&=12\gamma(12-\gamma)(24-\gamma)(36-\gamma)\\ &\quad-\{(12-\gamma)^2-12\gamma\}[(12-\gamma)\{(12-\gamma)^2-24\gamma\}-144\gamma],\\ \mathfrak{B}&=\frac{12}{a}\sqrt{\frac{EIm}{l^3\rho\mu}}\sqrt{\gamma}\{(12-\gamma)^2-12\gamma\}\{(12-\gamma)(48-\gamma)+144\}.\end{aligned}\right\} \tag{31}$$

In both cases, the form of the incident waves is

$$u_0 = \cos(pt + kx), \tag{32}$$

so that the displacement of the ground surface on which no structure rests, is

$$u_0 = 2\cos pt. \tag{32'}$$

The special case, $n=3$, was dealt with in the preceding paper.[5]

3. *Middle* 13*th House* (Naka-13gô-kan).

The general plan of all the floors being virtually the same, we have given a sketch of only the first floor (the next above the ground floor) as an example. The construction details of the columns, beams, floors, walls, etc., were all carefully examined and noted, although they will be omitted here, owing to the great labour that will be involved in arranging them in convenient form. As to the elaborate numerical calculations that had to be made in determining the section moduli as well as the distribution of mass, particularly in the treatment of such elements as consist of composite materials of steel and concrete,[6] we shall not give any details of them on account of the difficulty of tabulating the results in any simple form. Nevertheless, the parts of such columns and walls as were taken in obtaining the section moduli are shown by thick lines in the sketch, Fig. 1, while the total areas and moments of inertia of cross sections of the columns in every floor as well as the total mass concentrated on every floor (the mass of the columns and walls are concentrated on the floor next above them), etc., are shown in the following table.

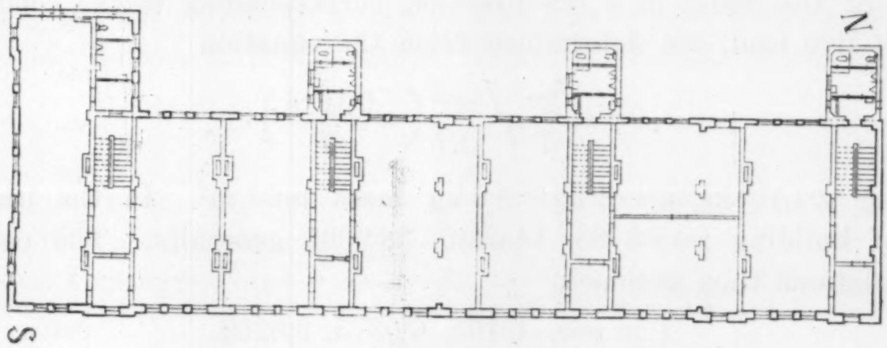

Fig. 1. Naka-13gô-kan, First floor. Scale 1/500.

---

[5] K. SEZAWA and K. KANAI, *loc. cit.* 1).

[6] *The Architectural Engineering Pocket Book* (Tokyo, 1933) was the authority which we mostly used.

Table I. Middle 13th House (Naka-13gô-kan).

Floor			Ground	1st	2nd	Roof	Mean
Height of floor below		l (m)	2·58	3·82	3·52	3·52	3·62+·32
Area of vertical members		a (m^2)	33·83	31·34	31·34	22·66	28·45
Mt. inertia of vertical members		I (m^4)	11·23	2·54	2·54	2·54	2·54
Beams	volume	(m^3)	46·75	46·19	46·75	47·02	
	weight	(kg)	$1{\cdot}123.10^5$	$1{\cdot}109.10^5$	$1{\cdot}123.10^5$	$1{\cdot}129.10^5$	
Floors	volume	(m^3)	72·54	72·54	72·54	72·54	
	weight	(kg)	$1{\cdot}741.10^5$	$1{\cdot}741.10^5$	$1{\cdot}741.10^5$	$1{\cdot}741.10^5$	
Columns	volume	(m^3)	18·85	27·97	25·35	25·32	
	weight	(kg)	$0{\cdot}453.10^5$	$0{\cdot}672.10^5$	$0{\cdot}608.10^5$	$0{\cdot}608.10^5$	
Walls	volume	(m^3)	87·3	110·5	101·75	71·27	
	weight	(kg)	$2{\cdot}095.10^5$	$2{\cdot}653.10^5$	$2{\cdot}442.10^5$	$1{\cdot}711.10^5$	
Total weight		m (kg)	$5{\cdot}412.10^5$	$6{\cdot}106.10^5$	$5{\cdot}845.10^5$	$5{\cdot}120.10^5$	$5{\cdot}69.10^5$
Area of floor		(m^2)		600	600	600	600

To arrive at the mean height of the floors, we added 1/3 of the part of the basement height above the ground level to the actual mean 'tween-floor height from the ground to the 2nd floors. In the foregoing table it is assumed that there is no live load on any floor.

When, as in the present case, it is possible to assume that $I_1=I_2=I_3(=I)$, $m_1=m_2=m_3(=m)$, $l_1=l_2=l_3(=l)$ the periods of the free oscillations of the house in a NS-direction, corresponding to the condition without live load, are determined from the equation

$$\sqrt{\gamma}=\frac{2\pi}{T}\sqrt{\frac{ml^3}{EI}}\left(=\frac{0{\cdot}1618}{T}\right),$$

E being $2{\cdot}1.10^9\ \mathrm{kg/m^2}=2{\cdot}1.10^9.9{\cdot}8$ kg mass $\mathrm{m/s^2/m^2}$. In the present type of building $\gamma=2{\cdot}3765$, $18{\cdot}6630$, $38{\cdot}9605$ generally. The periods of oscillations thus become

$$T \text{ in sec}=0{\cdot}105,\ 0{\cdot}0375,\ 0{\cdot}0260.$$

As already pointed out, the floors as well as the base in the present calculation are supposed to be clamped. In order to obtain the periods of oscillations when there is a live load of intensity 370 kg/m^2 on each floor (including the roof for convenience of calculation—which is allowing somewhat unduly), we find that the periods of oscillation in NS-direction take the form

$$\sqrt{\gamma}=\frac{2\pi}{T}\sqrt{\frac{ml^3}{EI}}\left(=\frac{0{\cdot}1818}{T}\right),$$

where the value of γ is the same as that without live load. The periods then become

$$T \text{ in sec} = 0{\cdot}118,\ 0{\cdot}0420,\ 0{\cdot}0291.$$

Now, if we take $\rho = 2.10^3$ kg mass/m^3, $\mu = 8.10^7$ kg mass/ms^2 (corresponding to $\sqrt{\mu/\rho} = 200$ m/s), the values of $Ej^2/\mu k l^3$ for the two conditions, with and without live load, are

$$\frac{Ej^2}{\mu k l^3} = \frac{1}{a}\sqrt{\frac{mEI}{l^3 \rho\mu}}\,\frac{1}{\sqrt{\gamma}} = \frac{1{\cdot}939}{\sqrt{\gamma}},\quad \frac{2{\cdot}18}{\sqrt{\gamma}}$$

respectively. The maximum values of the bending moments $M = E_s I_s . (d^2 y_s/dx_s^2)$ at each end of the columns corresponding to the maximum values of the acceleration of the ground (on which no structure rests) and in which $\lambda = 14\mu$ were determined from the equation shown in the preceding paper[7]; the two cases, with and without live load, are diagrammatically shown in Figs. 2, 3. The vertical strips in these figures represent cases corresponding to resonance conditions in the case without dissipation. These figures show that the bending moments of the columns, even under resonance conditions, are not very marked and are rather less than the one at zero frequency, provided the values of the acceleration at any period are the same. It follows therefore that the practical method of considering the effect of seismic vibrations on a structure, that is, assuming the inertia force to be a statical

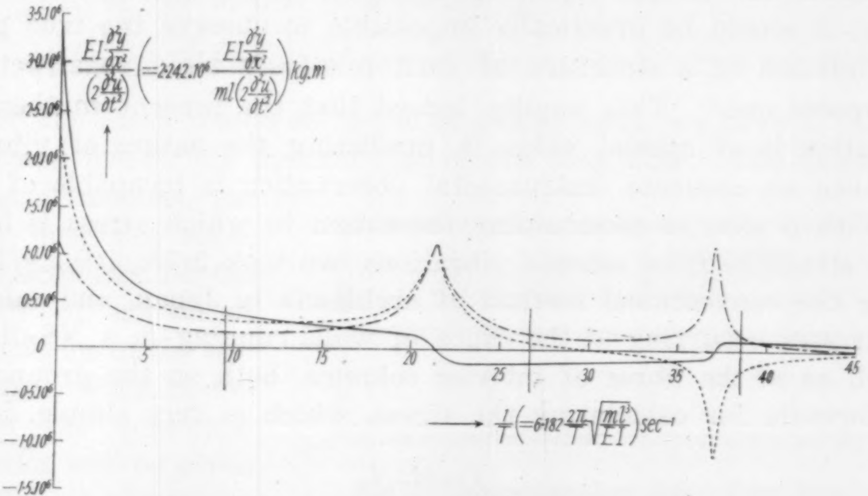

Fig. 2. Naka-13gô-kan. NS-movement (without live load). Full, broken, and chain lines represent moments in columns of ground, first, and second floors respectively.

---

[7] K. SEZAWA and K. KANAI, *loc. cit.* 1).

force, appears to be a relatively safe one provided the intensity of the acceleration are the same at any period.

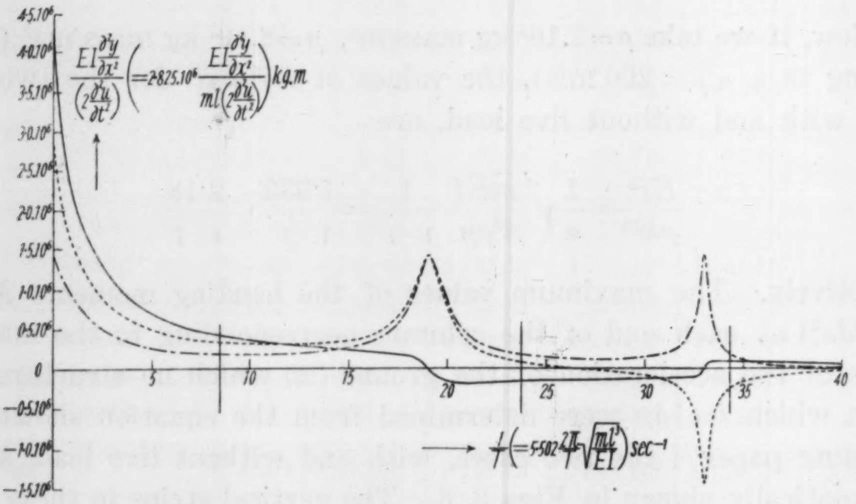

Fig. 3. Naka-13gô-kan. NS-movement (with live load). Full, broken, and chain lines represent moments in columns of ground, first and second floors respectively.

It may now be remarked that, owing to the great dissipation of the vibrational energy, especially near where there are resonance conditions, it would be practically impossible to observe the true periods of vibrations of a structure of such relatively rigid construction as the present one.[8] This implies indeed that the present mathematical calculation is of special value in predicting the nature of vibrations that even an accurate instrumental observation is incapable of doing.

With a view to ascertaining the extent to which stress is induced in the structure from seismic vibrations, we took $2(\partial^2 u/\partial t^2)=g/10$, following the conventional method of architects in Japan, and calculated the stresses occurring at the edges of walls running in a NS-direction as well as at the fibres of interior columns, both on the ground floor. The formula for calculating the stress, which is very simple, is

$$f=Mz/I,$$

where M and I are the total bending moments and total moments of inertia of the columns on a given floor, while f is the fibre stress induced at a distance z from the neutral axis of every structural member. The results for the case without live load are

---

[8] When the floor is assumed flexible, relatively high peaks manifest themselves at the points corresponding to the resonance in the bending moment curves in Figs. 2, 3.

maximum stress in wall $=10{\cdot}6$ kg/cm^2,
maximum stress in column $=2{\cdot}03$ kg/cm^2;⁹⁾

while the results for the case with live load are

maximum stress in wall $=13{\cdot}4$ kg/cm^2,
maximum stress in column $=2{\cdot}56$ kg/cm^2.

These values closely approximate that allowable as the working strength of a reinforced concrete structure in tension. In order to compare these stresses with the normal stresses in vertical structural members due to the vertical stationary load of the building, we obtained the following numerical values:

For the case without live load

normal stress in the vertical members in the ground floor $=5{\cdot}96$ kg/cm^2,
ditto on the first floor $=3{\cdot}83$ kg/cm^2,
ditto on the second floor $=2{\cdot}56$ kg/cm^2.

For the case with live load

normal stress in the vertical members on the ground floor $=7{\cdot}505$ kg/cm^2,
ditto on the first floor $=4{\cdot}85$ kg/cm^2,
ditto on the second floor $=3{\cdot}285$ kg/cm^2.

4. *No. 6 of Middle 12th Lot of Houses* (Naka-12gô-kan 6gô).

For the same reason as in the preceding case, we have in this one also shown merely the general plan of the first floor. The thick lines in Fig. 4 indicate the vertical members taken in the calculation for the moments of inertia of cross sections of the columns, etc. While no details of the numerical calculation will be given here, the total areas as well as the moments of inertia of the columns, and the total mass concentrated on every floor, etc., are shown in Table II.

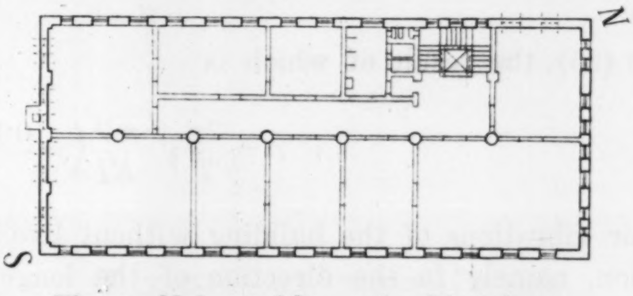

Fig. 4. Naka-12gô-kan 6gô. First floor. Scale 1/500.

---

9) When the walls receive damages in earthquake shocks and become incapable of being strength members, stresses in columns due to the same moments assume very large values.

Table II. No. 6 of Middle 12th Lot of Houses (Naka-12gô-kan 6gô).

Floor			1st	2nd	3rd	Roof	Mean
Height of floor below		l (m)	3·48	3·48	3·48	4·09	3·632+·383
Area of vertical members		a (m^2)	18·99	17·72	16·96	16·22	17·47
Mt. inertia of vertical members (NS-movement)		I (m^4)	1·777	1·701	1·681	1·662	1·705
Mt. inertia of vertical members (EW-movement)		I (m^4)	1·185	1·148	1·130	1·110	1·143
Beams	volume	(m^3)	27·6	28·37	28·37	27·77	
	weight	(kg)	$0{\cdot}663.10^5$	$0{\cdot}6807.10^5$	$0{\cdot}6807.10^5$	$0{\cdot}6663.10^5$	
Floors	volume	(m^3)	41·5	41·2	41·2	40·93	
	weight	(kg)	$0{\cdot}9968.10^5$	$0{\cdot}99.10^5$	$0{\cdot}99.10^5$	$0{\cdot}9825.10^5$	
Columns	volume	(m^3)	27·6	21·82	17·82	18·3	
	weight	(kg)	$0{\cdot}663.10^5$	$0{\cdot}5246.10^5$	$0{\cdot}428.10^5$	$0{\cdot}4395.10^5$	
Walls	volume	(m^3)	31·4	34·75	37·67	45·08	
	weight	(kg)	$0{\cdot}754.10^5$	$0{\cdot}8347.10^5$	$0{\cdot}905.10^5$	$1{\cdot}082.10^5$	
Total mass		m (kg)	$3{\cdot}0768.10^5$	$3{\cdot}030.10^5$	$3{\cdot}0037.10^5$	$3{\cdot}1703.10^5$	$3{\cdot}07.10^5$
Area of floor		(m^2)	424·5	424·5	424·5	424·5	

To obtain the mean height of the floors, we added 1/4 of the part of the basement floor above the ground level to the actual mean height of the floors from the ground to the third floors. All weights in this table are exclusive of any live load. In this case too it is possible to put $I_1=I_2=I_3=I_4(=I)$, $l_1=l_2=l_3=l_4(=l)$, $m_1=m_2=m_3=m_4(=m)$, when the periods of free vibrations corresponding to the condition without live load are determined by

$$\mathfrak{A}=0$$

in (25), the result of which is

$$\sqrt{\gamma}=\frac{2\pi}{T}\sqrt{\frac{ml^3}{EI}}\left(=\frac{0{\cdot}1496}{T}\right)$$

for vibrations of the building without live load moving in a NS-direction, namely in the direction of the longer side of the building, E being $2{\cdot}1.10^9$ kg/m^2$=2{\cdot}1.10^9.9{\cdot}8$ kg mass m/s^2/m^2. Again, we know $\gamma=$ 1·4475, 12, 28·166, 42·386 generally. The periods thus become

$$T \text{ in sec}=0{\cdot}124,\ 0{\cdot}0432,\ 0{\cdot}0282,\ 0{\cdot}230.$$

For vibrations of the building without live load again, but moving in an EW-direction, namely, in direction perpendicular to the longer side of the building, we have

$$\sqrt{\gamma}=\frac{2\pi}{T}\sqrt{\frac{ml^3}{EI}}\left(=\frac{0{\cdot}1828}{T}\right),$$

whence

$$T \text{ in sec}=0{\cdot}152,\ 0{\cdot}0527,\ 0{\cdot}0344,\ 0{\cdot}0281.$$

The periods of vibrations for the case with live load 370 kg/m^2 on every floor (including the roof for safety) and in a NS-direction, are determined from the equation

$$\sqrt{\gamma}=\frac{2\pi}{T}\sqrt{\frac{ml^3}{EI}}\left(=\frac{0{\cdot}176}{T}\right),$$

which gives

$$T \text{ in sec}=0{\cdot}146,\ 0{\cdot}0508,\ 0{\cdot}0332,\ 0{\cdot}0270.$$

Using the same values of ρ, μ, the values of $\frac{Ej^2}{\mu k l^3}$, namely $\frac{1}{a}\sqrt{\frac{mEI}{l^3\rho\mu}}\frac{1}{\sqrt{\gamma}}$, corresponding to the three cases become: (i) $\frac{1}{a}\sqrt{\frac{mEI}{l^3\rho\mu}}\frac{1}{\sqrt{\gamma}}=\frac{1{\cdot}85}{\sqrt{\gamma}}$ for the case without live load and moving in NS-direction, (ii) $\frac{1}{a}\sqrt{\frac{mEI}{l^3\rho\mu}}\frac{1}{\sqrt{\gamma}}=\frac{1{\cdot}514}{\sqrt{\gamma}}$ for the case without live load and moving in EW-direction, (iii) $\frac{1}{a}\sqrt{\frac{mEI}{l^3\rho\mu}}\frac{1}{\sqrt{\gamma}}=\frac{2{\cdot}175}{\sqrt{\gamma}}$ for the case with live load and moving in NS-direction. Figs. 5, 6, 7 represent the cases respectively corresponding to (i), (ii), (iii). The vertical strips

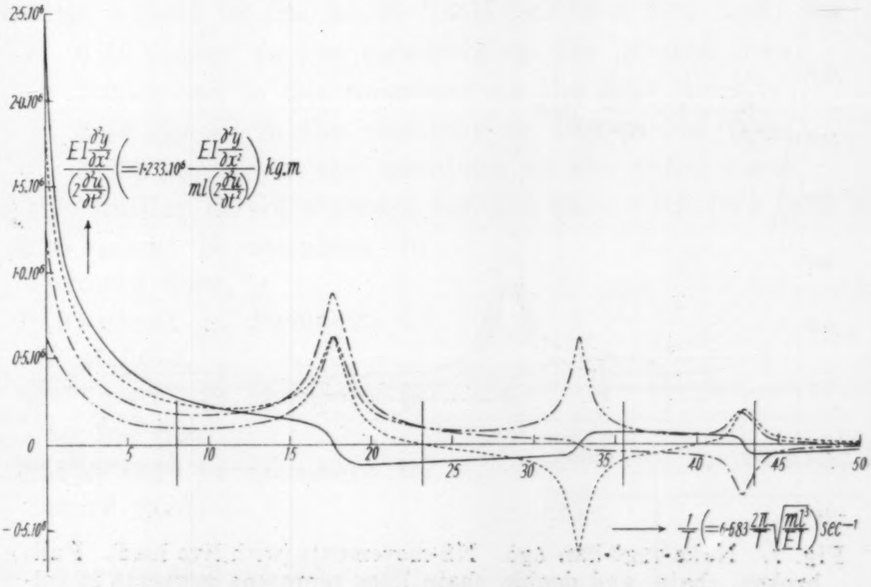

Fig. 5. Naka-12gô-kan 6gô. NS-movements (without live load). Full, broken, chain, and double chain lines represent moments in columns of ground, first, second, and third floors respectively.

indicate the cases corresponding to resonance conditions. It will also be seen that the bending moments at zero frequency would be the greatest, were the acceleration the same at any frequency.

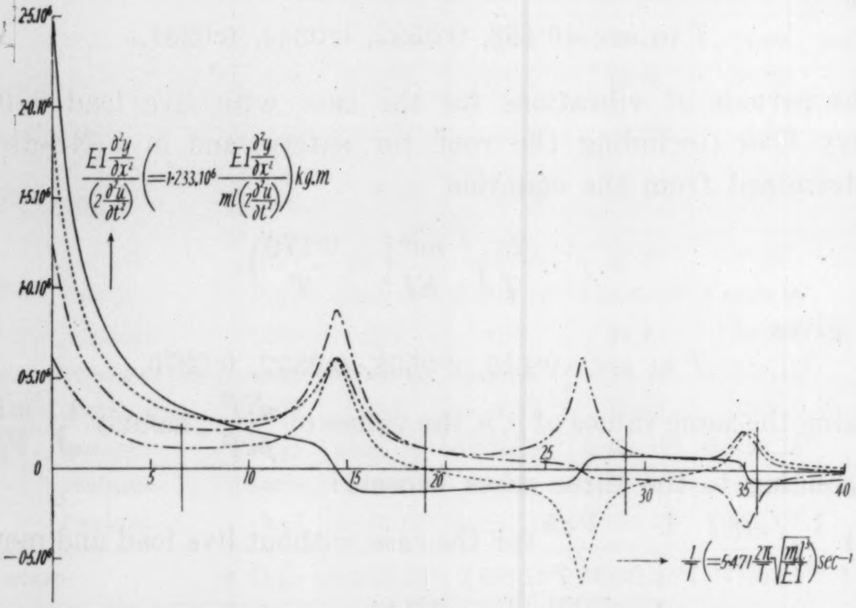

Fig. 6. Naka-12gô-kan 6gô. EW-movements (without live load). Full, broken, chain, and double chain lines represent moments in columns of ground, first, second, and third floors respectively.

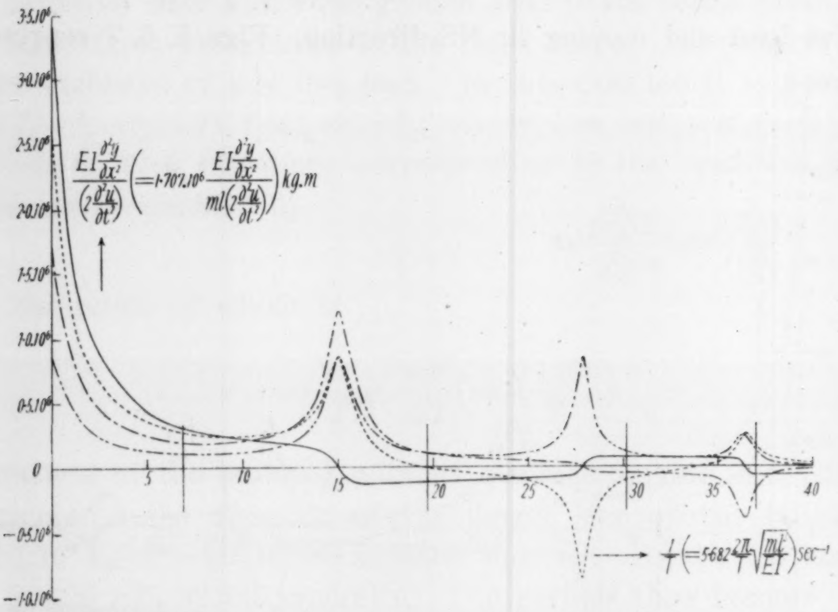

Fig. 7. Naka-12gô-kan 6gô. NS-movements (with live load). Full, broken, chain, and double chain lines represent moments in columns of ground, first, second, and third floors respectively.

In order to obtain the order of the stresses induced in the columns and walls in seismic vibrations, we use the conventional formula $2(\partial^2 u/\partial t^2)=g/10$ and introduce the equation

$$f=Mz/I,$$

and remembering that the structure is of reinforced concrete, we get the following results:

(i) fibre stress in the exterior columns attached to the walls running in NS-direction$=3{\cdot}73$ kg/cm^2,

(ii) fibre stress in the walls running in NS-direction$=8{\cdot}34$ kg/cm^2,

(iii) fibre stress in the interior round columns$=4{\cdot}71$ kg/cm^2,

for the case without live load and moving in NS-direction; while for the case of vibrations in EW-direction under no live load, we have

(i) fibre stress in the exterior columns attached to the walls running in EW-direction$=5{\cdot}56$ kg/cm^2,

(ii) fibre stress in the walls running in EW-direction$=12{\cdot}43$ kg/cm^2,

(iii) fibre stress in the interior round columns$=7{\cdot}04$ kg/cm^2.

Finally, for the case with live load and moving in NS-direction, we have

(i) fibre stress in the exterior columns attached to the walls running in NS-direction$=5{\cdot}16$ kg/cm^2,

(ii) fibre stress in the walls running in NS-direction$=11{\cdot}54$ kg/cm^2,

(iii) fibre stress in the interior round columns$=6{\cdot}53$ kg/cm^2.

All these results concern the members on the ground floor.

The direct stresses caused by the steady action of the vertical load due to the weight of the house itself (without live load) are

6·46 kg/cm^2 in the members on the ground floor,
5·2 kg/cm^2 in the members on the first floor,
3·64 kg/cm^2 in the members on the second floor,
1·953 kg/cm^2 in the members on the third floor;

while the similar direct stresses for the case with live load are

8·95 kg/cm^2 in members in ground floor,
7·19 kg/cm^2 in members in first floor,
5·03 kg/cm^2 in members in second floor.
2·68 kg/cm^2 in members in third floor.

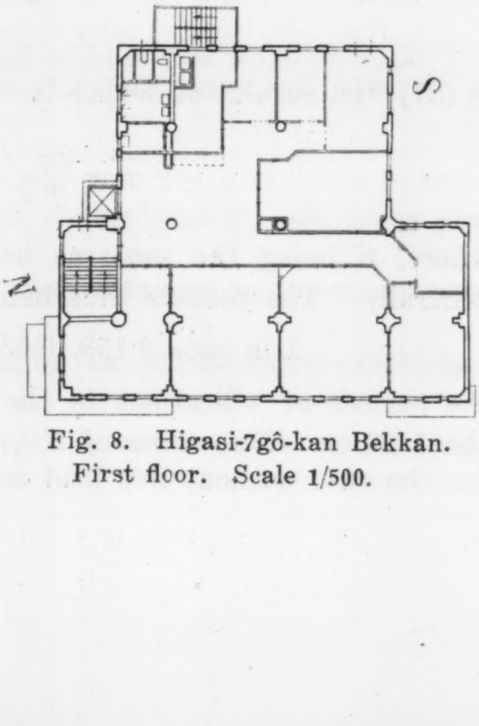

Fig. 8. Higasi-7gô-kan Bekkan. First floor. Scale 1/500.

5. *Annexe of East 7th House* (Higasi-7gô-kan Bekkan).

The general plan of the first floor is shown in Fig. 8, the thick lines indicating the vertical members taken in the calculation of the moments of inertia of cross sections of the columns. The principal calculated items are shown in Table III.

Table III. Annexe of East 7th House (Higasi-7gô-kan Bekkan).

Floor		1st	2nd	3rd	4th	Roof	Mean
Height of floor below	l (m)	3·64	3·36	3·36	3·36	3·64	3·46+0·18
Area of vertical members	a (m^2)	29·51	21·06	20·19	13·19	12·81	20·9
Mt. inertia of vertical members (NS-movement)	I (m^4)	1·570	1·274	1·232	1·005	0·963	1·208
Beams	volume (m^3)	17·22	17·13	18·06	10·11	7·09	
	weight (kg)	0·4135.10^5	0·4113.10^5	0·4335.10^5	0·2427.10^5	0·1702.10^5	
Floors	volume (m^3)	54·7	54·7	54·7	36·6	33·57	
	weight (kg)	1·313.10^5	1·313.10^5	1·313.10^5	0·879.10^5	0·807.10^5	
Columns	volume (m^3)	42·25	37·48	32·7	15·51	13·05	
	weight (kg)	1·014.10^5	0·9.10^5	0·785.10^5	0·3723.10^5	0·3127.10^5	
Walls	volume (m^3)	65·03	33·35	35·16	28·86	33·55	
	weight (kg)	1·562.10^5	0·8007.10^5	0·844.10^5	0·6938.10^5	0·806.10^5	
Total mass	m (kg)	4·3025.10^5	3·425.10^5	3·3755.10^5	2·1878.10^5	2·0959.10^5	3·078.10^5

To obtain the mean height of the floors we added 1/5 of the part of the basement height above the ground level to the actual mean of the 'tween-floor height from the ground to the fourth floors. Again, it appears possible in the present case to put $I_1=I_2=I_3=I_4=I_5(=I)$, $m_1=m_2=m_3=m_4=m_5(=m)$, $l_1=l_2=l_3=l_4=l_5(=l)$. The periods of vibrations corresponding to the case without live load and moving in NS-direction can be obtained by putting

$$\mathfrak{A}=0$$

in (31), the results of which is

$$\sqrt{\gamma}=\frac{2\pi}{T}\sqrt{\frac{ml^3}{EI}}\left(=\frac{0{\cdot}1537}{T}\right),$$

where, E being the same as before, $\gamma=0{\cdot}973,\ 8{\cdot}30,\ 20{\cdot}3,\ 33{\cdot}95,\ 44{\cdot}2$ generally. The periods thus become

$$T \text{ in sec}=0{\cdot}158,\ 0{\cdot}0532,\ 0{\cdot}341,\ 0{\cdot}0264,\ 0{\cdot}0232,$$

the periods of vibrations in the case with live load being higher by about 20 %. The values of $Ej^2/\mu kl^3$ for the movement in NS-direction for the case without live load is

$$\frac{Ej^2}{\mu k l^3}=\frac{1}{a}\sqrt{\frac{mEI}{l^3\rho\mu}}\frac{1}{\sqrt{\gamma}}=\frac{1\cdot 506}{\sqrt{\gamma}}\,.$$

The maximum values of the bending moments $M=E_s I_s(\partial^2 y_s/\partial x_s^2)$ at each end of the columns, corresponding to the maximum values of acceleration of the ground (on which no structure is standing) was determined from (26)~(31). In this case too the values of ρ, μ were assumed as in preceding cases. The result is shown in Fig. 9, indicating that the moments at zero frequency of vibrations assume the greatest values.

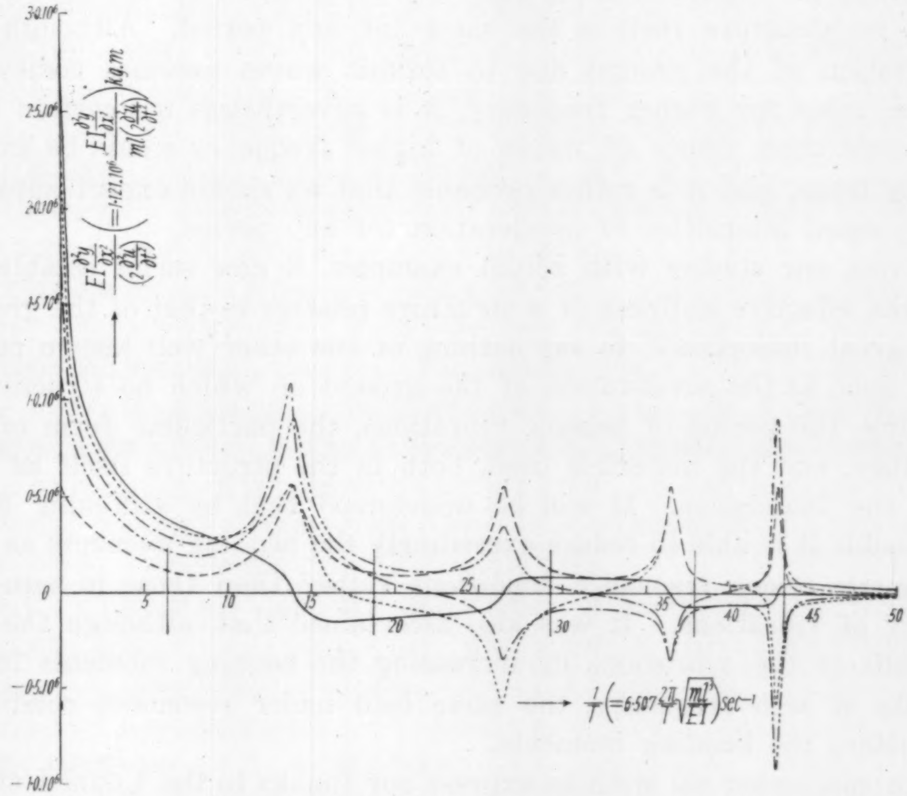

Fig. 9. Higasi-7gô-kan Bekkan. NS-movements (without live load). Full, broken, chain, double chain, and stripped lines represent moments in columns of ground, first, second, third, and fourth floors respectively.

To ascertain the stress induced in the columns and walls in seismic vibrations, we put $2(\partial^2 u/\partial t^2)=g/10$, conventionally, and using the relation $f=Mz/I$ we get:

(i) fibre stress in the exterior columns attached to the walls running in NS-direction = 9·85 kg/cm²,

(ii) fibre stress in the walls running in NS-direction = 28·13 kg/cm²,[10]

---

[10] Fibre stress in this case is fairly large; this is too large to be allowed in bending stress in reinforced concrete structure.

(iii) fibre stress in the interior columns $=7{\cdot}911\ \mathrm{kg/cm^2}$,

all of which are on the ground floor.

The direct stresses due to vertical dead load induced in the vertical members on the ground, first, second, third, and fourth floors are $5{\cdot}21\ \mathrm{kg/cm^2}$, $5{\cdot}26\ \mathrm{kg/cm^2}$, $3{\cdot}79\ \mathrm{kg/cm^2}$, $3{\cdot}24\ \mathrm{kg/cm^2}$, $1{\cdot}635\ \mathrm{kg/cm^2}$ respectively.

6. We now arrive at the conclusion that the bending moments or stresses under resonance conditions are rather less than those at zero frequency, the condition being that the acceleration of the ground on which no structure rests is the same for any period. Although the acceleration of the ground due to seismic waves assumes somewhat greater value for higher frequency, it is nevertheless not certain that the acceleration values of waves of higher frequency would be exceptionally large, and it is rather probable that we should expect approximately equal intensities of acceleration for any period.

From our studies with actual examples, it now seems established that the effective stiffness of a structure relative to that of the ground is of great importance, to say nothing of the other well known conditions, such as the acceleration of the ground on which no structure is standing, the period of seismic vibrations, the particular form of the structure, and the materials used, both in the structure itself as well as in the foundation. It will be understood that by stiffening floors as possible it is able to reduce exceedingly the bending moments as well as stresses under resonance conditions rather than those in zero frequency of vibrations. It was also ascertained that, although the live load affects the vibrations by increasing the bending moments in the vicinity of zero frequency, the same load under resonance conditions diminishes the bending moments.

In conclusion we wish to express our thanks to the Council of the Foundation for the Promotion of Scientific and Industrial Research of Japan, with whose aid the work was greatly assisted, and also to the members of the Mitsubishi Co., through whose courtesy we obtained access to much valuable data for the present investigation.

70. 三菱仲13號館，仲12號館6號，東7號館別館の震動に於ける勢力逸散性

地震研究所 妹澤克惟
金井清

前の論文に於て述べたところの震動勢力の地下逸散によつて建物が著しく耐震的になるといふ理論を實際の建物に應用して或地震動に於ける耐震性を確めて見たのである．之等の3階，4階，5階建は何れも鐵筋コンクリート作りで地下室を有してゐるけれども，之等の地階は非常に強い構造であり且つ有效部分の高さが低いために適當な方法で取除いて考へた．又，各床はその構造からわかるやうに決して屈曲しない剛いものであると假定して計算を試みた．屈曲すると考へることは寧ろ面白くないけれども念のために次の機會によく確める積りである．

若し建物がないときの地表の加速度を一定とするならば，建物の何れの場合にもその共振週期(逸散のないときの)に於て柱の屈曲モーメントが他の週期のときよりも寧ろ小さくなるのである．而して週期の極めて長いときのモーメントが最も大きくなり，土地の加速度がどの週期でも同じならば，震動力を靜力學的に取ることが最も安全であるといふ結論に達したのである．

我國の建築計算家が假定してゐるやうに土地の加速度を $g/10$ として見ると之等の建物はコンクリートの許し得る最高張力近くまでの屈曲應力を取ることもある．殊に東7號館別館の壁は相當の應力にも達するけれども柱の方はまだ充分安全である．之等は何れも零の frequency の場合であつてそれよりも速い震動では應力がはるかに小さくなり，共振の所は殆ど心配がない程度のものである．實際問題として無限大の週期で上のやうに大きな加速度を取ることはないから，結局何れの場合にも建物が耐震的であることがわかるのである．

何れにしても振動勢力の一部分が地下へ逸散する爲に，建物の共振の機會が少くなるのであつて之は非常に好都合のことといはればならぬ．實際，木造家屋位でやつと常識程度の共振があるのであつて，この研究に用ひたやうな建物にそのやうに大きな共振のないことは誰にも想像がつくであらうが，只今の逸散の研究によつて一層明瞭になつた譯である．但し只今研究した建物に於て特に逸散性が強いことは，その構造の性質からもよくうなづかれる．この逸散といふことはその力學的の分析が我々の研究まで誰も氣がつかなかつたやうであるから，振動力學上からでも一寸のみ込みにくいかも知れぬけれども，それが大切なことは之迄しばしば論じた通りである．

この研究によつて建物の破壞に大切な事は，建物の型，地震動の加速度，その週期，建物及び基礎の材料的性質の外に，建物と土地との比較的剛度といふことが重要なものであることがわかる．この性質の爲に建物の積載荷重はのろい振動には有害であるけれども共振附近では寧ろ有益なものであることが知られる．

この計算では各階に相當する振動の數學的理論の研究以外に鐵筋コンクリート材の種々の複雜な計算に多大の勞力を費したものであることを附加へて置く．結論として，一般に床をできるだけ剛くすることは，これまで考へてゐたやうにのろい震動に於けるモーメントや應力を少くすることよりも共振狀態に於ける夫等を著しく少くすることに非常に效力があり，この意味に於て剛い建物が特に耐震的であるといふことがわかるのである．

71. 靜岡强震に就て

地震研究所 {那須信治
保田柱二}

（昭和10年9月20日受理）

昭和10年7月11日午後5時25分靜岡市附近に發した地震は大正6年5月18日午前4時7分靜岡縣下を襲つた强震以來のものにて靜岡淸水兩市に可なりの損害を與へた．共有感覺區域は中央氣象臺の發表によれば，本州中部地方，關東地方，近畿地方等の大部分及び中國地方，東北地方等の一部分に迄及んでゐる．東京にては稍緩漫なる震動を感じ，弱震（弱き方）程度のものであつた．東京本鄉に於ける石本式加速度計による最大加速度は，南北成分にて5·30ガル（週期0·36秒），東西成分にて4·17ガル（週期0·28秒），垂直成分にて2·00ガル（週期0·31秒）である．

地震計觀測

關東地方に起る地震研究の目的を以て，本所にては關東地方に於て適當な地點を撰び地震計を据へ付け，東京帝國大學理學部地震學教室と協力して觀測に從事して居る．次に東京及此等地點に於て本地震を觀測せる結果を掲ぐ．

第Ⅰ表　觀測地點の位置，地震計の種類及常數

觀測所	位置		種類	成分	重錘の目方	倍率	自己振動の週期	制振率
	東徑	北緯						
	度 分 秒	度 分 秒			瓩		秒	
東京	139 45 59	35 42 40	今村式簡單微動計	東西	7	50	7	1·5
				南北	7	50	7	1·5
			大森式地動計	東西	17	15	63·1	4·5
			〃　〃	南北	42	20	52·6	3·0
			〃　〃	上下	10	20	12·4	1·6
駒場	139 41 01	35 39 18	今村那須式簡單微動計	東西	7	50	5·0	1·55
				南北	7	50	4·5	1·42
				上下	7	18	2·5	1·27
三鷹	139 32 32	35 40 21	那須式地震計	北東，南西	15	80	1·3	2·6
				北西，南東	15	80	1·4	6·0
			大森式微動計	東西	60	4·8	36	1·18
			〃　〃	南北	60	4·8	36	1·18

（次頁へ續く）

第 I 表

観測所	位置 東徑	 北緯	種類	成分	重錘の目方	倍率	自己振動の週期	制振率
	度 分 秒	度 分 秒						
筑波	140 06 36	36 12 39	萩原式携帶地震計	東西	6 瓩	39	3·85 秒	3·1
				南北	6	43	4·07	6·9
鎌倉	139 32 39	35 18 32	今村式簡單微動計	東西	7	50	7	1·5
				南北	7	50	7	1·5
			今村式地震計	上下	4	10	10	2·0
			今村式强震計	東西	2	2	10	2·0
				南北	2	2	10	2·0
				上下	0·45	2	5	2·0
清澄	140 09 02	35 09 22	今村那須式簡單微動計	東西	7	50	7	1·6
				南北	7	50	7	1·9
				上下	7	28	7	1·2
秩父	139 04 54	35 58 56	今村式簡單微動計	東西	7	50	6	1·8
				南北	7	50	6	1·8
小山	138 53 59	35 21 20	今村式簡單微動計	東西	7	25	6	1·6
				南北	7	25	6	1·6
吉原	138 41 07	35 09 35	大森式簡單微動計	東西	12	25	4	1·5
				南北	12	25	4	1·5
			今村式强震計	東西	2	2	10	2·0
				南北	2	2	10	2·0
				上下	0·45	2	5	2·0
淺間	138 34 21	36 24 08	那須式地震計	東西	15	100	3	4·0
				南北	15	100	3	4·0

吉原に於ける地震計の位置 N=N30°E　淺間に於ける地震計の位置 N=N33°E

第 II 表 静岡强震觀測表

觀測所	發震時	繼續時間 初期微動	 總	最大動(全振幅) 南北動 大さ	 週期	 東西動 大さ	 週期	初動 大さ	 方向	震度
	時 分 秒	秒	分	粍	秒	粍	秒	ミクロン		
東京	17 25 11·6	18·2	40	4·200	3·10	2·50	2·50	13S 30W	S65°·5W	II
駒場	17 25 09·9	17·2	13	(針外る)		(針外る)		18S 40W 300D	S65°·5W	II
三鷹	17 25 09·0	16·0	25	4·700	4·53	4·030	3·33	3·5S 7W	S63°W	II

(次頁へ續く)

觀測所	發震時	繼續時間		最大動(全振幅)				初動		震度
		初期微動	總	南北動		東西動		大さ	方向	
				大さ	週期	大さ	週期			
	時 分 秒	秒	分	粍	秒	粍	秒	ミクロン		
筑波	17 25 18·3	24·5?	13							0
鎌倉	17 25 06·9	13·0	15	10·000	5·3	1·750	1·66	24S 56W 225D	S66°·8W	III
清澄	17 25 13·2	19·4	20	2·686	4·13	2·440	4·51	2S 11W 50D	S79°·5W	0
秩父		15·6	16	1·760	3·07	1·740	3·07	245S 172W	S36°W	II
小山		9·0		(針外る)		(針外る)		298S 825W	S70°·5W	III
吉原		4·5	22	13·200	1·08	29·300	1·08	120N 460W	N76°W	IV
淺間	17 25 13·0	19·0								
須崎	17 25 00·0	8·6	25	3·2+		5·2+		541S 534E	S46°E	III

須崎に於ける觀測の結果は，三井地球物理研究所員福富理學士の好意に依つて得たものである．

震央 上記各地に於ける初期微動繼續時間は可なり能く計測し得たるを以て，之を用ひて大森公式 x 粁 $= ky$ 秒（x は震原距離，y は初期微動繼續時間，k は係數）によつて震原及び深さを求めて見た．吉原，小山，須崎等震央に近き所に於ては $k=7{\cdot}42$ とし，其他の所にては $k=8$ とした．此結果によつて見れば第 1 圖に示す如く震央の位置として約東經 138°26·2′，北緯 34°59·4′ を得，約 15 粁の深さとなる．

震災地踏査

筆者の一人は靜岡清水兩市の被害調査の爲め本所の神永幸三，杉山友紀兩名と共に翌 12 日午前 10 時 30 分東京驛發の列車にて西下，同午後 1 時 30 分靜岡驛着，被害の最も甚しかりし部分の調査を迅速に行つた．

（一） 震災分布の概況 今回地震被害は靜岡清水の兩市に局限され，他の地方には著しき被害なき模様なり．安倍川の左岸地區草薙山々地に至る方面及び靜岡清水間鐵道線の兩側に被害の主なるものが分布されて居る．

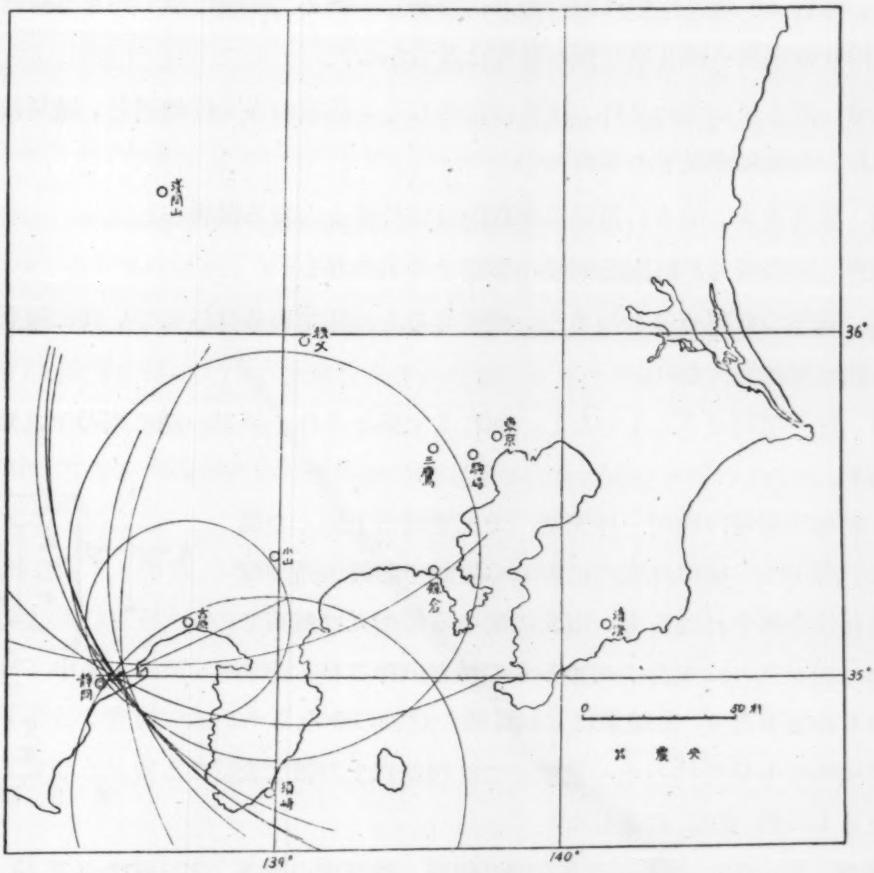
浅間山
秩父
東京
三鷹
駒場
小山
鎌倉
大宮
静岡
清澄
須崎
36°
35°
139°
140°
0
50 粁
× 震央

第　1　圖

（二） 各地の被害狀況

清水市 被害統計 死 1，傷 55，半壞 111 戶，全壞 55 戶.

東海道線を西下し，列車が清水市の北々東約 2 粁袖師村にさしかゝるや，家屋被害らしきものを初めて見る，其以東には屋根瓦の落下せしもの皆無，煉瓦積煙突或は土管積煙突等の倒壞せるものなし.

清水市の北端江尻町に至りて初めて家屋の傾斜，屋根瓦の落下，壁の落剝等外觀に現はるゝ著しき被害を見る．家屋傾斜の被害は可なりありて農家 470 戶の內50戶に達すと云ふ，全壞程度のものもあつた.

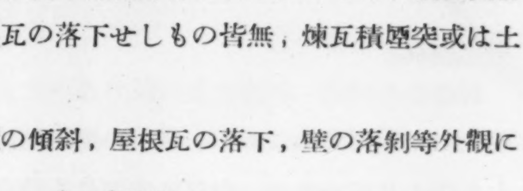
清水港岸壁
荷物
1.8米
海面
陥没浸水

第　2　圖

清水市街は家屋の傾斜，倒壞，隨所にあるも静岡市に比すれば被害の程度小なり．海岸近くの倉庫は概ね土臺を外れ，東へ 10 糎程の移動をなす．岸壁の崩壞は既に新聞紙上に報ぜられ居る通り，長さ約

300 米，幅約 60 米の岸壁は前のめりに傾斜し，第2，24圖に示す如き有様となつてゐる．岸壁倉庫第一號及第二號の被害は甚しかつた．

元追分 清水市の西約2粁，被害は稍甚しく，農家の多くは傾斜し，隨所に納屋の倒壞あり，半壞程度以上のもの多し．

草薙 被害僅少，清水行電鐵草薙驛附近は外見上大なる被害なし．

櫻井戸 電鐵櫻井戸驛附近家屋の傾斜せるもの多し．

古庄 家屋の傾斜せるもの多く，倒壞せるもの相當ある見込にて，殊に運動場前驛に至る間家屋被害大なり．

曲金 各戸傾斜せざるものなし．何れも土臺を外れ，殆ど一樣に東乃至北東の向きに移動す．

縣立農事試驗場は納屋一棟倒壞，煉瓦煙突頂上近くの部分折れて落下す．家屋は東西に著しく振動せし故東西兩側の屋根瓦は全部ずれたるも，南北に面せる屋根瓦は無事であつた．窓ガラスは東西に面せるもの殆ど破碎され，南北向きのもの無事なり．此現象は當試驗場の建物のみならず，一般民家にても見受けらる．當地にては傾斜以上の被害を受けたるもの約 50% に達した．

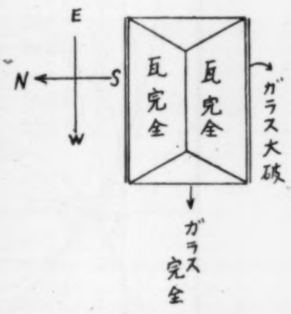

第 3 圖

靜岡市 舊市街にては家屋內の壁の龜裂，煉瓦塀の倒壞，不安定なる墓石，石燈籠の倒れたもの隨所にあり，家屋被害の目立つたものは木骨コンクリート造商店である．厚さ 1~2 糎のモルタールの外裝は龜裂剝落し，木骨を現はせるもの至る所にあり．木造家屋の傾斜せるものも相當あるが其程度は輕少である．市內の土藏は殆んど其棟瓦破損し，壁も落ちて居る．墓石は約半數倒れ，瀨戸物屋の損害も相當著し．

縣廳舍の被害 縣廳は舊城趾外濠內にあり，赤煉瓦の建物にて龜裂多數にあり，屋上の煙突は將に轉落せんとして辛ふじて止まり，內部各室何れも致命的龜裂を生じた．此建物は明治20年頃の建築に係り，昭和5年11月26日北伊豆地震後補强されたもので，近く他に移轉の豫定なりしと云ふ．縣廳前の城の石垣は長さ約 15 米の間崩壞して外濠に落ち，又縣廳正門の門柱の頭部破壞轉落す，此等は何れも强震の際に起れるものにあらずして夜半（1 時半頃）に起つたもので，恐らく强震の爲めに受けたる損傷が餘震に依て全く破壞されたるものなるべし．

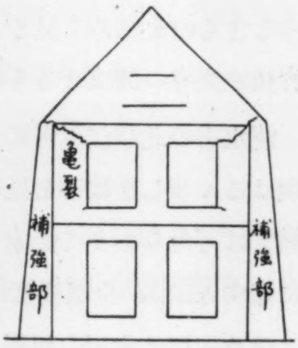

第 4 圖

舊市街より大谷に至る間は今回の地震にて最も著しき被害を受けた.

小鹿　建物は全部使用に堪へざる程度に破壊され，死者1名，傷者 12 名を出し，大谷に次いで死傷者多し．一重積煉瓦壁倒れ，幼女1名壓死す．此部落から堀之內に至る間，並に大谷に至る間盛上げ道路龜裂至る所にあり.

宮川　家屋は使用不可能なる程度に被害を受く.

大谷　全戶倒壞に等しき迄に破損し，二階建の家屋挫折して一階建の如き觀を呈せるもの多く，今回の災害の中心地である．警戒嚴重で震災後數日間公用者以外は部落內通行を嚴重に禁止した．此部落は主に農家にて217戶あり，死者4名，傷者 35 名を算し，火災1戶を出した.

高松　大谷の西隣高松も大谷同樣の被害あり，主に農家で全戶232あり，死者1名，傷者2名を出した.

敷地，宮下，西島　何れも家屋破損の程度大にして使用不能なるもの大多數なるも，倒壞せしものはなかつた.

濱村，中島，石田，中田各部落も前者と同樣の程度である．東大谷は大谷高松に比し被害著しく輕微である.

被害分布と地質との關係　静岡市東南の平地には上述の如く著しき被害あるも，所

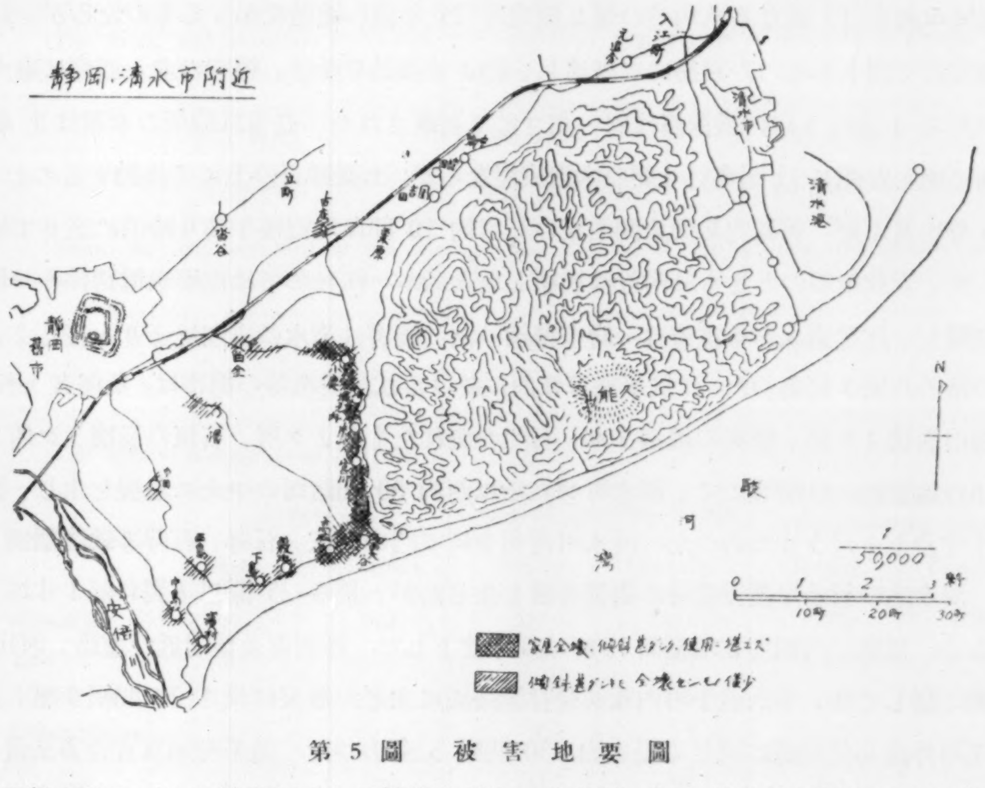
静岡・清水市附近
静岡舊市
古庄
草薙
曲金
安倍川
入江町
清水市
清水港
久能
駿河
湾
N
1/50,000
0 1 2 3 粁
10町 20町 30町
家屋全壊、傾斜甚ダシク、使用ニ堪エズ
傾斜甚ダシキモ全壊セシモノ僅少

第5圖　被害地要圖

謂草薙山地にては比較的輕少なる被害を見た．安倍川下流々域は沖積層なる事は常識

にて判斷し得ることであるが草薙山地（久能山々地と云ふ方判然なり）には洪積層發達し，また第三紀層のところもある，而して今回の地震被害が安倍川下流々域の東椽に近き所に主に現はれたるは興味ある現象にて，地質の境界線に於て，被害の異常なる分布を示した好例であると云ひ得る．

餘震　今回の地震の餘震は 11 日夕刻から翌 12 日朝迄，靜岡にて有感覺のもの僅に 1 回，無感覺のもの數回ありたるに過ぎず．

大正 6 年 5 月 18 日の靜岡地震　此地震は今回のものと同様靜岡清水地方に可なりの被害を與へた．故大森博士は文部省震災豫防調査會報告第 88 號乙にて可なり詳述されて居る．之によると發震時は午前 4 時 7 分，震原は北緯 35 度 7 分，東經 138 度 2 分，靜岡市の北 65 度西，約 9 里の距離にある大井天龍兩河上流間の古生層山地に當る．靜岡清水燒津方面に強く感じ，井水の増減があつた．靜岡市兩替町の某商店の防火煉瓦壁は高さ 23 尺，幅 7 間，厚さ煉瓦一枚のものなるが，地上高さ 8 尺の邊より崩壊して，隣家の屋根を打ち抜き，爲めに死者 2 名，傷者 1 名を生じた．呉服町四丁目の某商店は安政元年 11 月の震災後特に意を用ひて建築せるものにて，些しの震害なかりしも，其屋上の高き煉瓦は崩落した．其他屋壁の裂罅，石碑石燈籠等の轉倒あり，停車場附近鷹匠町邊は土地柔軟の場所なるを以て震害多かつた．停車場附近山口製餡所の高さ 13 間なる八角形の煉瓦煙突は 25 年前の建造にかゝるものなるが，此の地震にて頂上から 17 尺邊にて破壊し，約 2 寸移動を受け，煙突の北々西側に取り付けたる 4 分の 1 吋の鐵線條は同一高さにて切斷された．農事試驗所の本館は北 40 度西に面した間口 11 間奥行 4 間の木造家屋なるが，土臺腰石の上にて移動すること 1 寸 3 分に及んだ．舊城內兵營東側內濠の石垣約 10 間は地震後午前 9 時頃に至りて崩壊した，安政地震のときも此附近は崩壊したと云ふ．江尻にては電燈線電話線各一個所切斷し，江尻清水とも電燈は一時全部消へた．震害は清水の方江尻よりも甚しく，庇の落ちた家 3 軒あつた．江尻警察署管內に於ける江尻清水等の損害は，負傷者 5 名，石塀の崩壊 4 ヶ所，煙突の破損 5 本，石門の倒れたもの 2 ヶ所，石垣の崩壊 3 ヶ所，道路の龜裂約 180 間等にて，清水町羽衣橋以西約 80 間路面の中央に龜裂を生じ，裂口 5 寸乃至 1 尺 5 寸であつた．清水町實相寺にて門の石柱，石塀，石碑等破壊顚倒した．清水港の繋船岸護岸堤防に龜裂多數を生じたが，長さ 25 間以下裂口幅 1 寸以下である．繋船岸內側埋立地盤面 15 坪は 5 寸沈下した．靜岡市及び附近の道路，河川，港灣に關しては，市內追手町內濠兵營往還路面に生じた龜裂は長さ 70 間幅 5 厘，西草深町外濠兵營往還に同じく長さ約 350 間幅 5 分あつた．追手町知事官舍裏法留石垣は南側及北側方面 2 ヶ所龜裂し外部に押出された．鐵道に關しては江尻草薙間 113

哩 61 鎖附近にて土留石垣玉石空積面積 2 坪崩壊した．静岡驛にては貨物上家の柱繼手 6 本破損し，給水柱の下部鐵管破壊し，石炭臺の煉瓦石立柱の多數は裂罅を生じ若しくは切斷された．此地震の餘震も今回の静岡強震と同様に甚だ小數であつた．

今回の地震被害地踏査の迅速に行はれたるは全く當研究所の神永幸三，杉山友紀兩君の敏速なる活動に依るといへども，静岡縣廳に奉職中の今村博士令息文雄氏が各地の正確なる情報と踏査上の諸便宜を我々に與へられたことに大いに依ると信ず．玆に厚く謝意を表す．

---

71. *The Siduoka Earthquake of July 11, 1935.*

By Nobuji Nasu and Chuji Yasuda,

Earthquake Research Institute.

On July **11, 1935** at 5h 25m p.m. the Pacific coast of the central Japan was visited by a strong earthquake. The shock was felt by persons as far as in the Tohoku districts in the north-east, in the Tyugoku in the west. The seismic damage caused by this earthquake however was limited in a comparatively small region covering the cities of Siduoka and Simidu.

The shock was moderate in Tokyo; the maximum accelerations as observed at Hongo by the Ishimoto acceleration seismographs are as follows:

N.S.-comp.	E.W.-comp.	Vertical comp.
5·30 gal	4·17 gal	2·00 gal

From the data obtained at ten seismological stations of our Institute, the seismic origin of this earthquake has been determined as below.

λ	φ	Depth.
138°26·2′ E	34°59·4′ N	15 km

The seismic damage is as follows:

Locality	Person		Collapsed Dwelling houses		Collapsed Non-dwelling houses	
	Died	Wounded	Totally	Partially	Totally	Partially
Siduoka	8	218	237	1412	372	1042
Udo	0	8	73	151	47	97
Simidu	1	68	53	263	28	103
Other places	0	5	0	4	4	5
(sum)	9	299	363	1830	451	1247

The most afflicted towns are Ooya and Takamatu (about 5 km SE of Siduoka city), where most of the houses rendered inhabitable, Figs. 13～20.

After-shocks were very few; During 12 hours following the strong earthquake only one sensible after-shocks and a few insensible shocks were experienced at Siduoka.

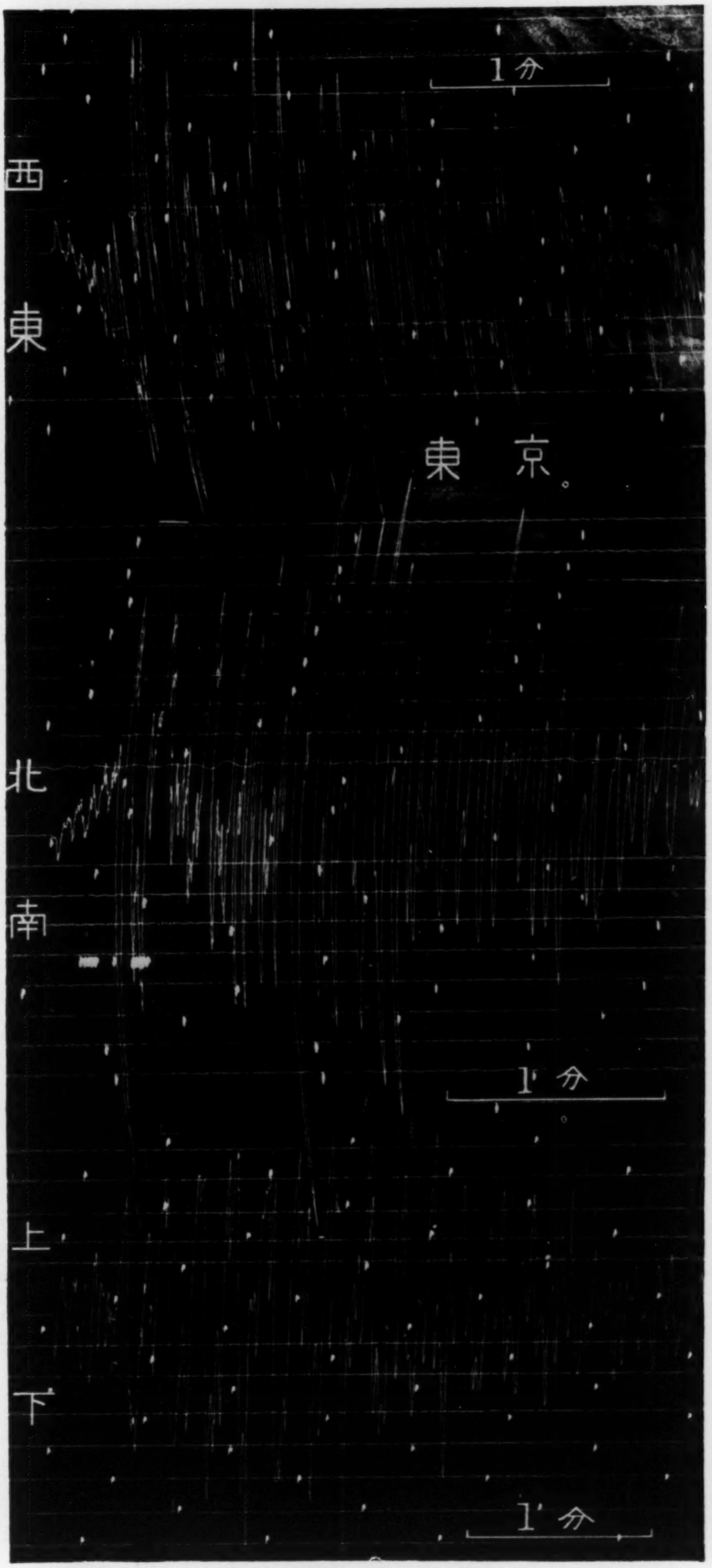

（震研彙報 第十三號 圖版 那須・保田）

第6圖 東京（本郷）觀測記象（第I表參照）(原記象大)

(震研彙報 第十三號 圖版 那須・保田)

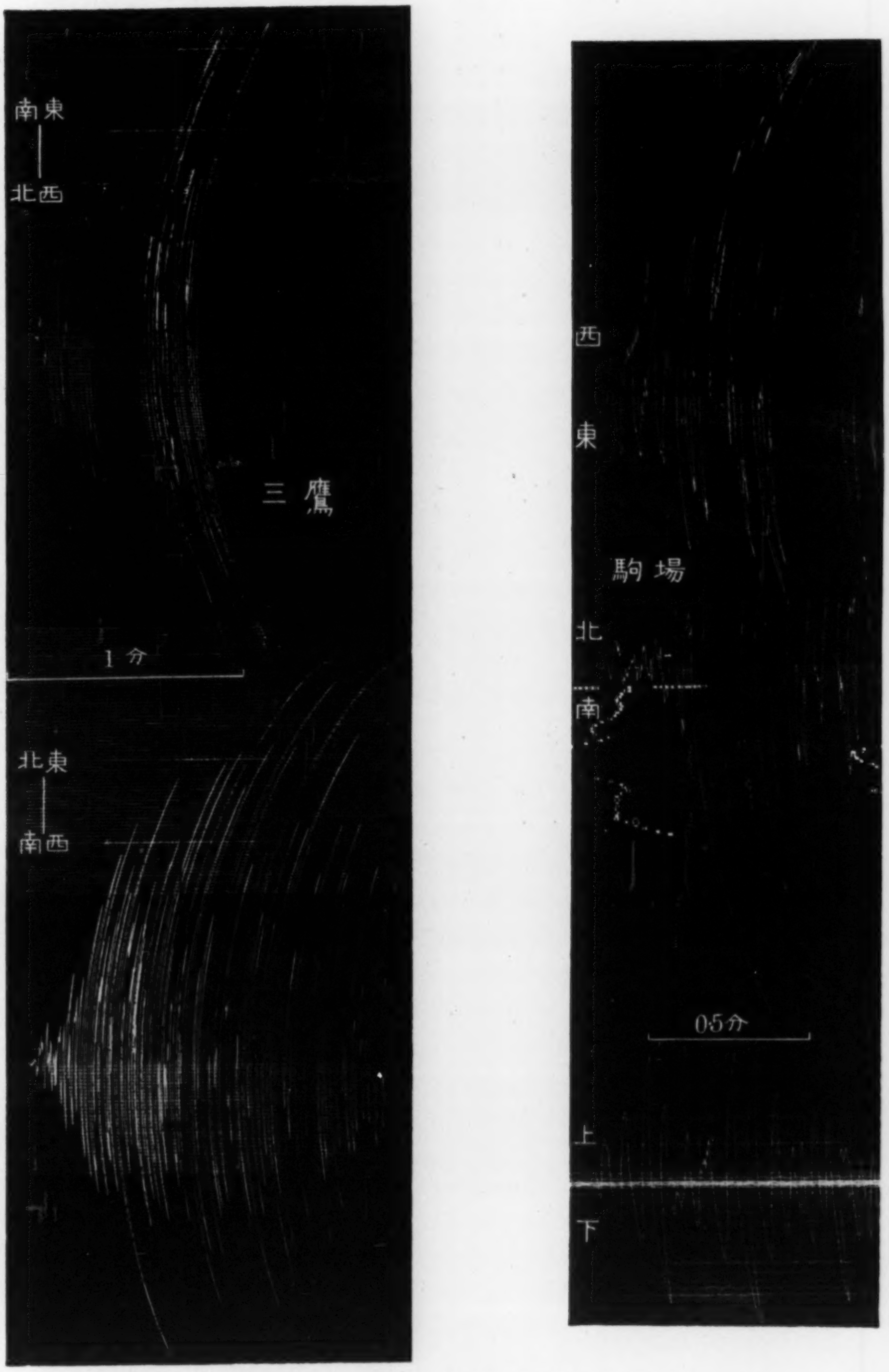

第7圖 三鷹，駒場觀測記象（第I表參照）（原記象の 1/2）

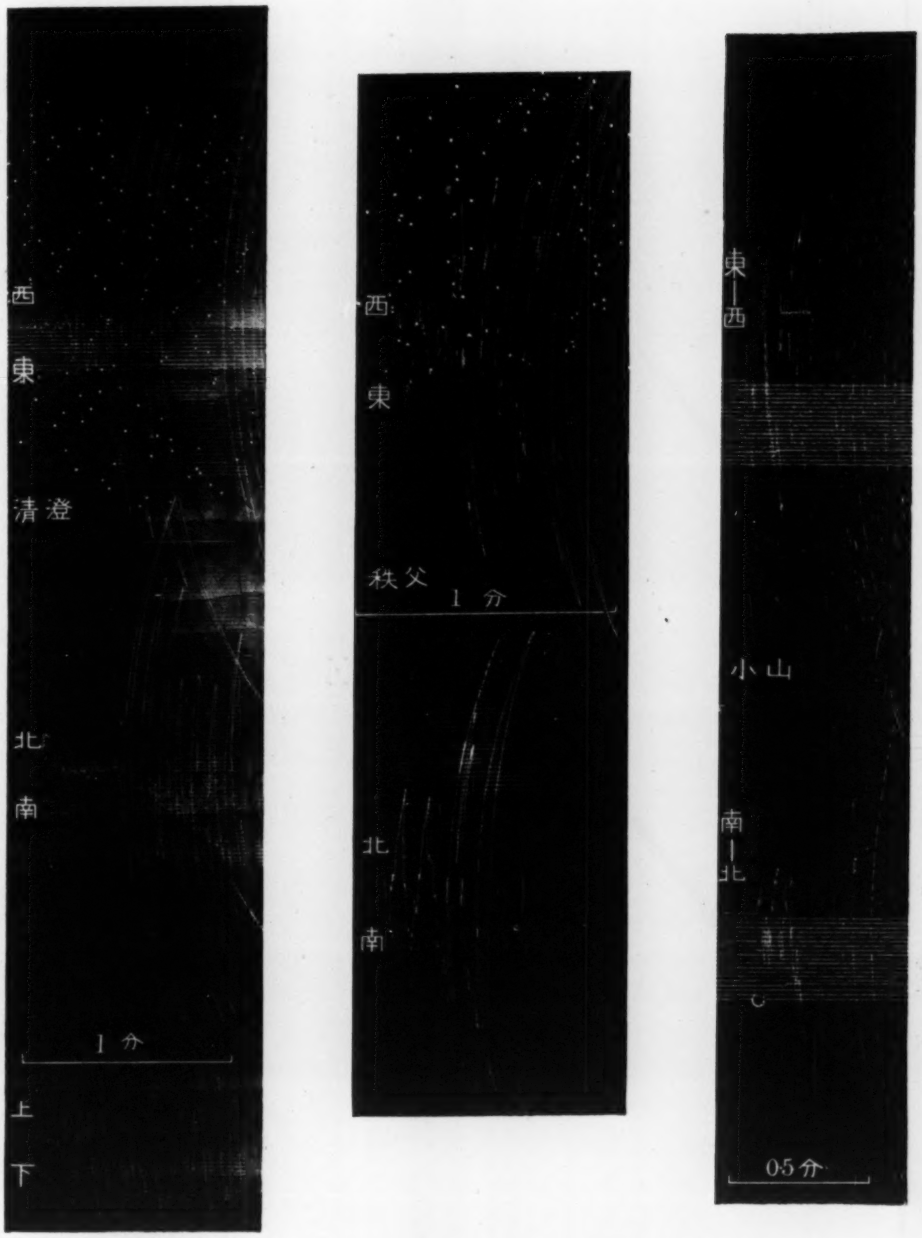

第8圖 清澄，秩父及小山觀測記象（第I表參照）（原記象の 1/2）

7

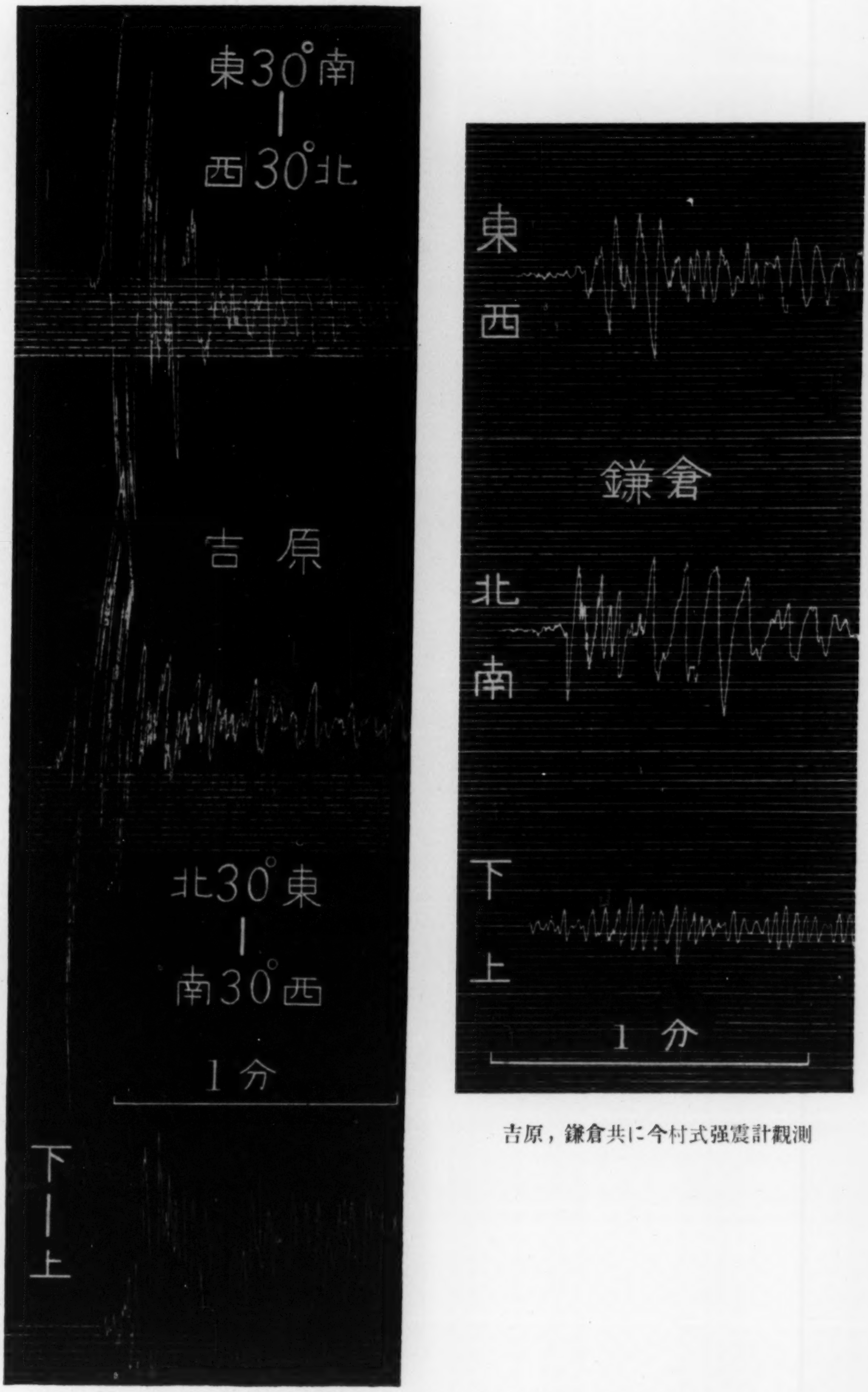

吉原，鎌倉共に今村式强震計觀測

第9圖　吉原，鎌倉觀測記象（第I表參照）（原記象大）

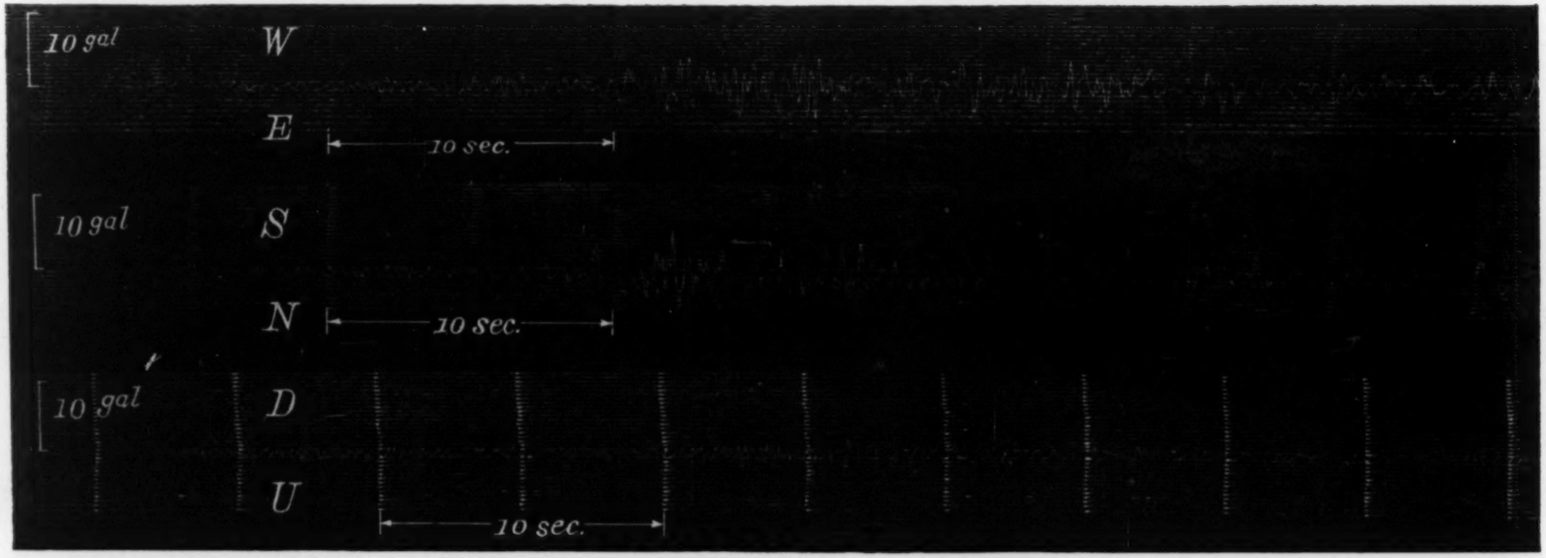

第10圖 石本式加速度地震計記象，東京本郷觀測

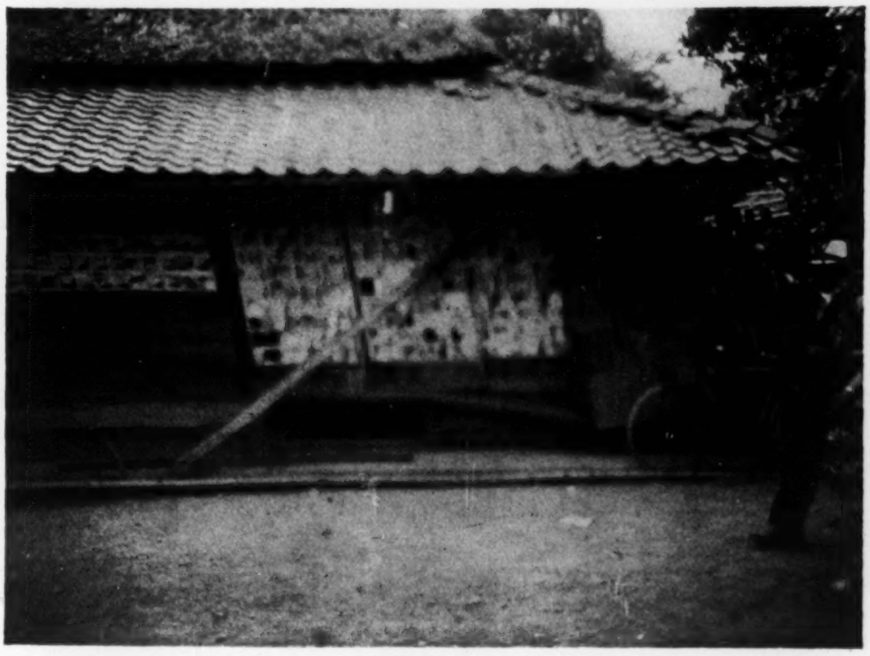

（昭和 10. 7. 12. 撮影）

第 11 圖　靜岡市高松に於ける家屋傾斜の有樣
Takamatu (Siduoka)

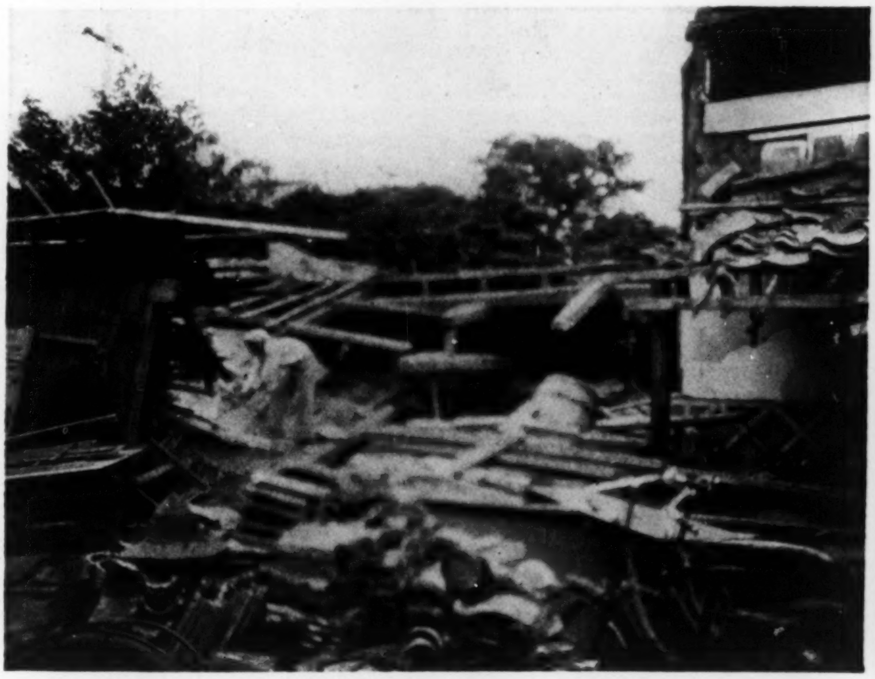

（昭和 10. 7. 12. 撮影）

第 12 圖　靜岡市高松に於ける土藏倒壞
Takamatu (Siduoka)

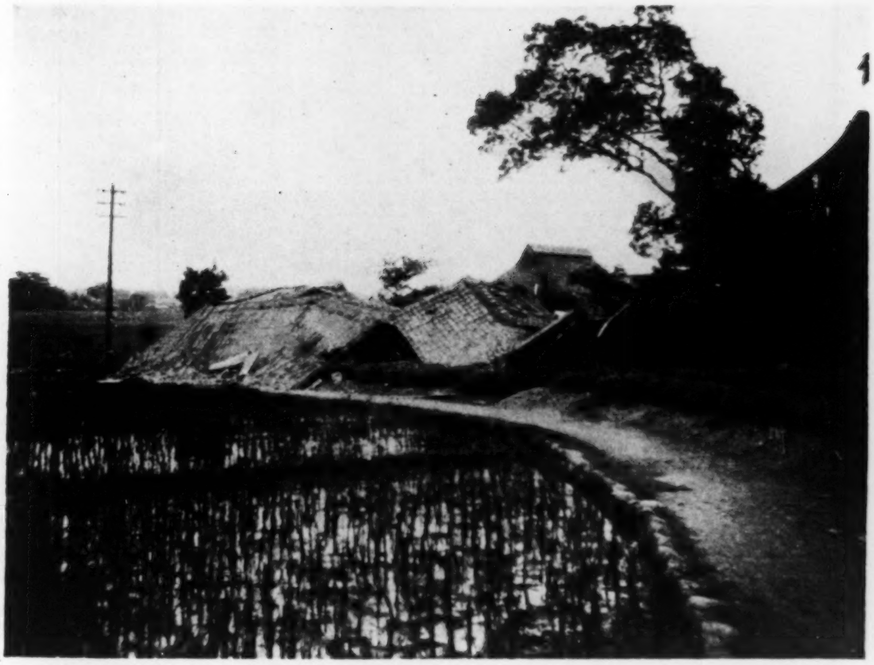

(昭和 10. 7. 12. 撮影)

第 13 圖 靜岡市小鹿家屋の倒壞
Kozika (Siduoka)

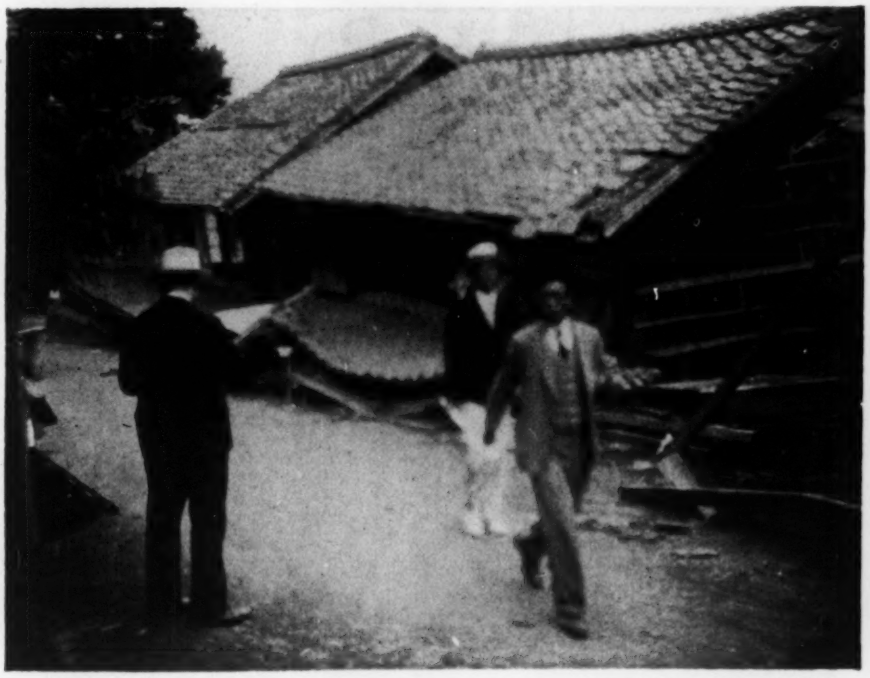

(昭和 10. 7. 12. 撮影)

第 14 圖 靜岡市大谷. 二階建家屋の被害
Ooya (Siduoka)

(震研彙報 第十三號 圖版 那須・保田)

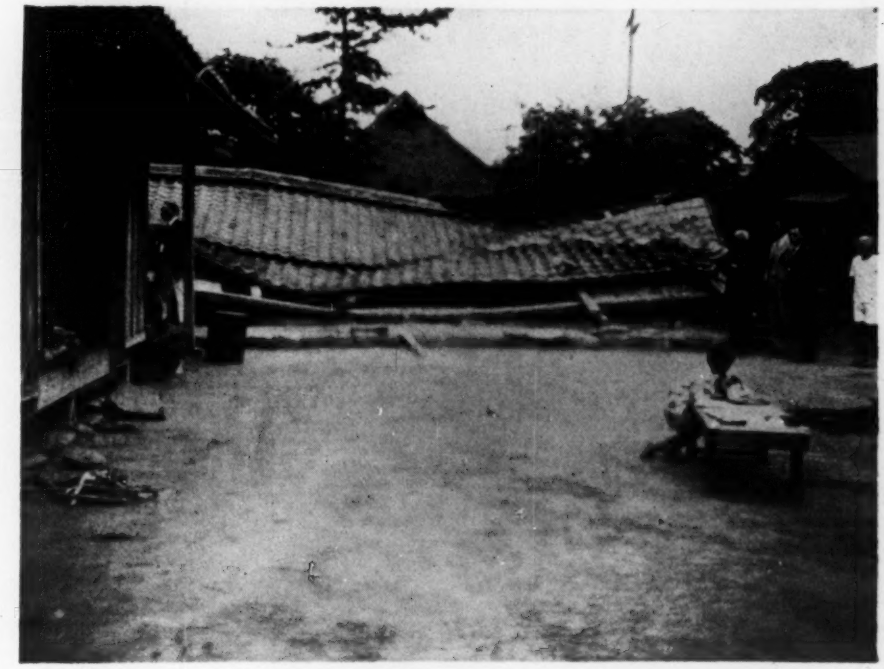

(昭和 10. 7. 12. 撮影)

第 15 圖 靜岡市大谷. 平屋建納屋の倒壞

Ooya (Siduoka)

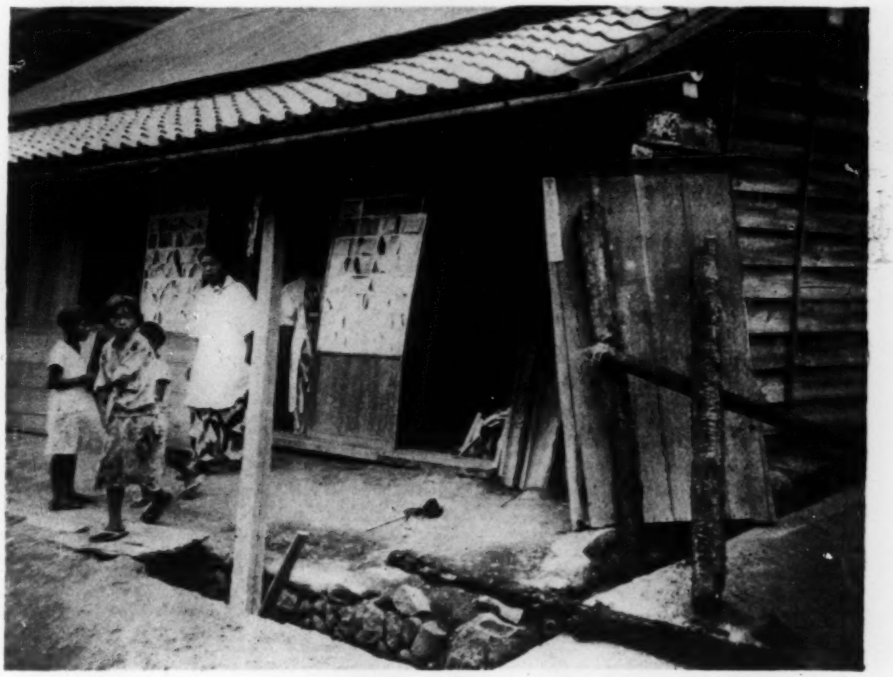

(昭和 10. 7. 12. 撮影)

第 16 圖 靜岡市大谷. 家屋の傾斜

Ooya (Siduoka)

（震研彙報 第十三號 圖版 那須・保田）

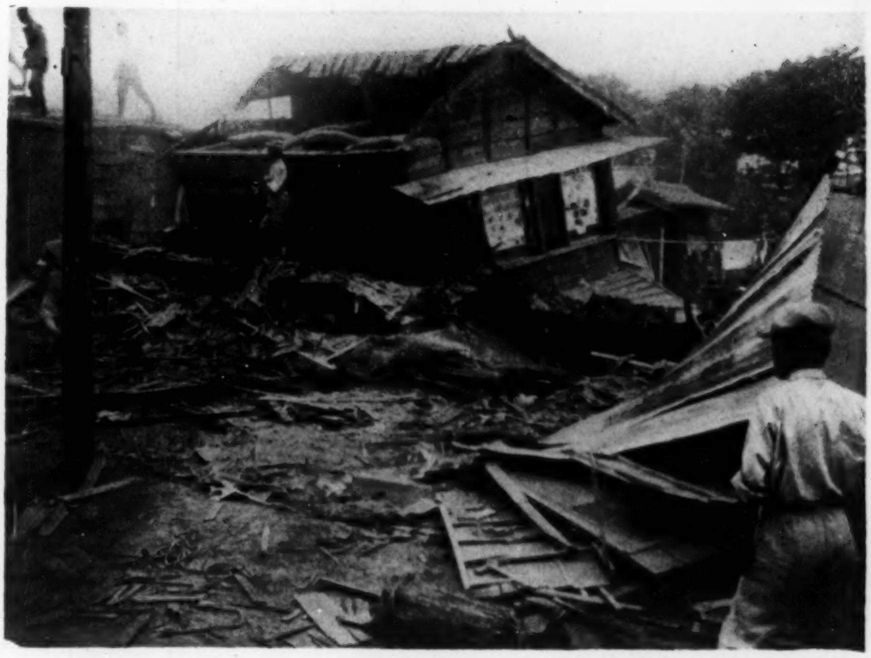

(昭和 10. 7. 12. 撮影)

第 17 圖 靜岡市大谷. 二階建家屋の被害

Ooya (Siduoke)

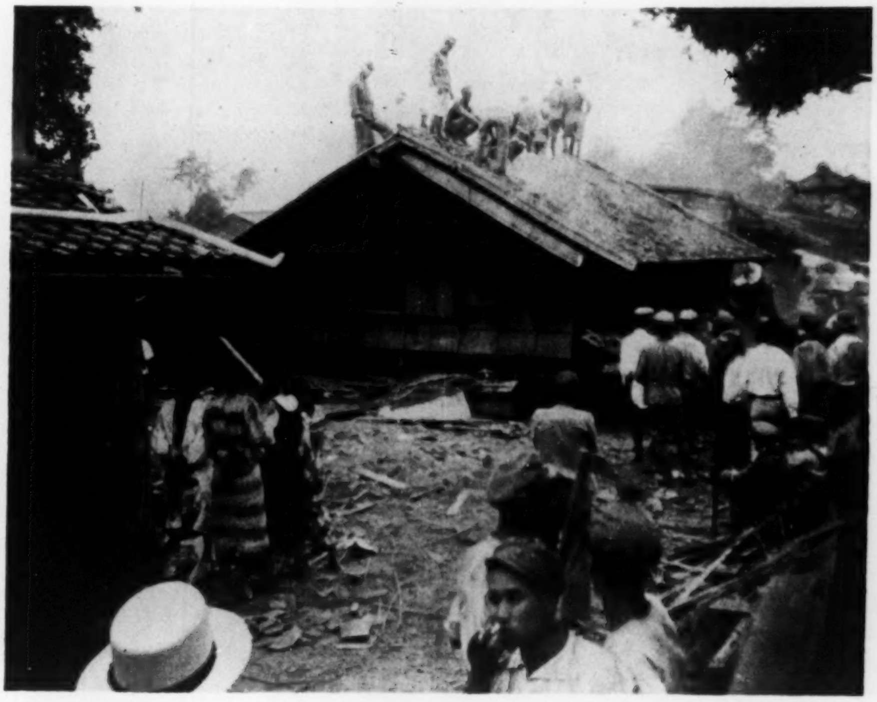

(昭和 10. 7. 12. 撮影)

第 18 圖 靜岡市大谷. 二階建家屋の被害

Ooya (Siduoka)

(震研彙報 第十三號 圖版 那須・保田)

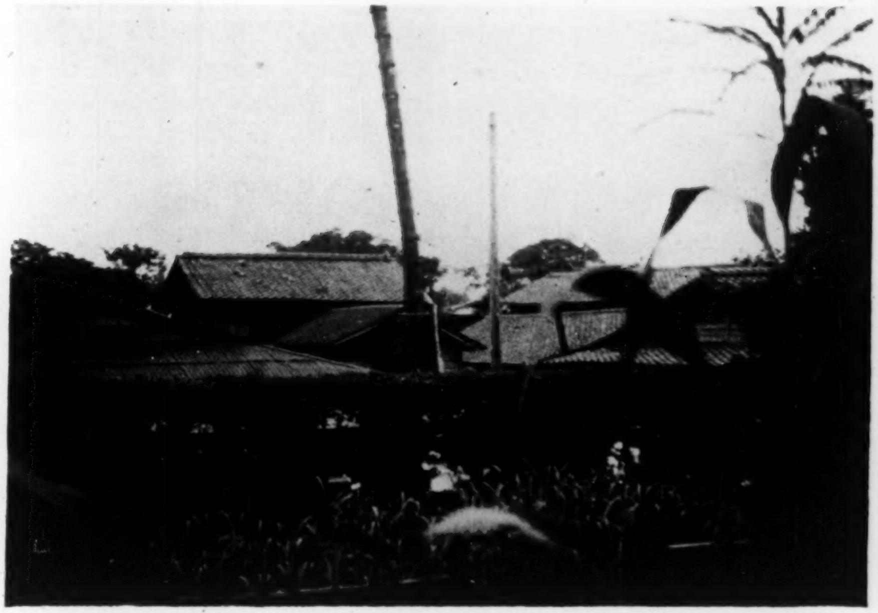

（昭和 10. 7. 12. 撮影）

第 19 圖　東大谷に於ける土管積煙突彎曲せしも倒壞せず

Ooya (Siduoka)

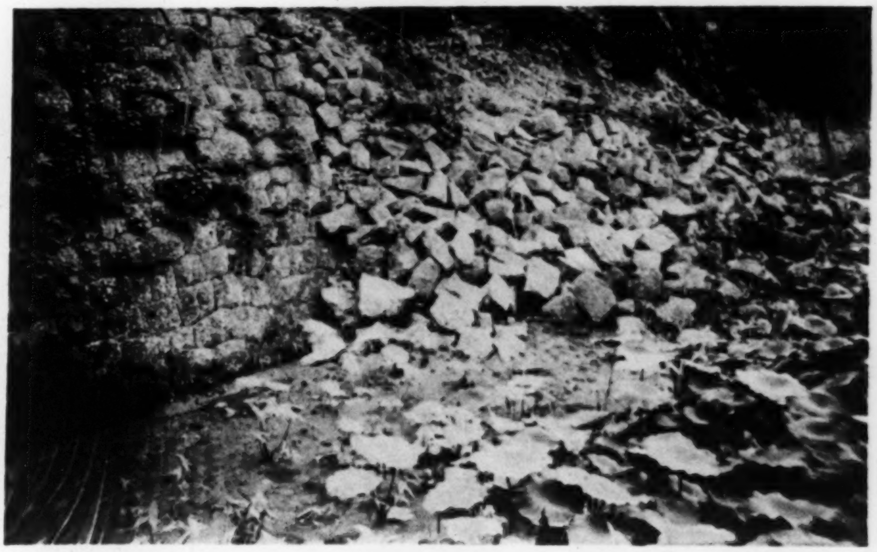

（昭和 10. 7. 12. 撮影）

第 20 圖　靜岡縣廳前壕の石崖崩壞

Siduoka city

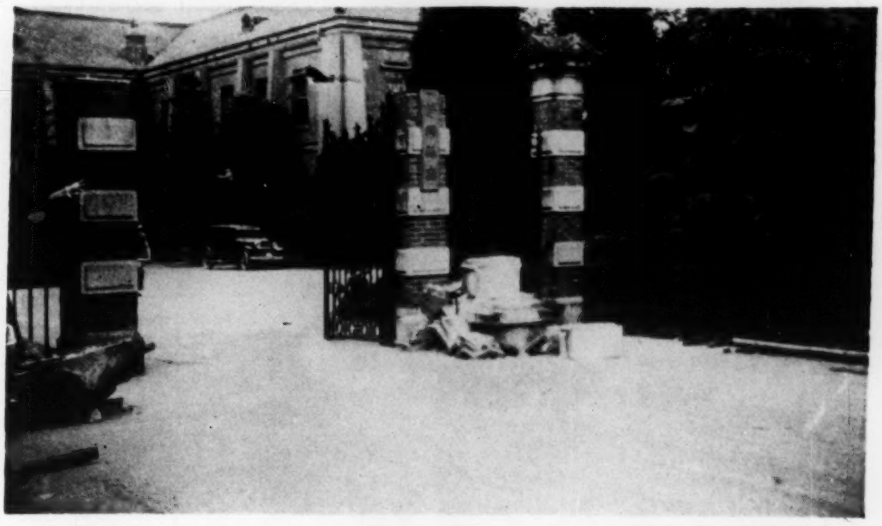

（昭和 10. 7. 12. 撮影）

第 21 圖　靜岡縣廳正門の柱上部振り落さる

Siduoka city

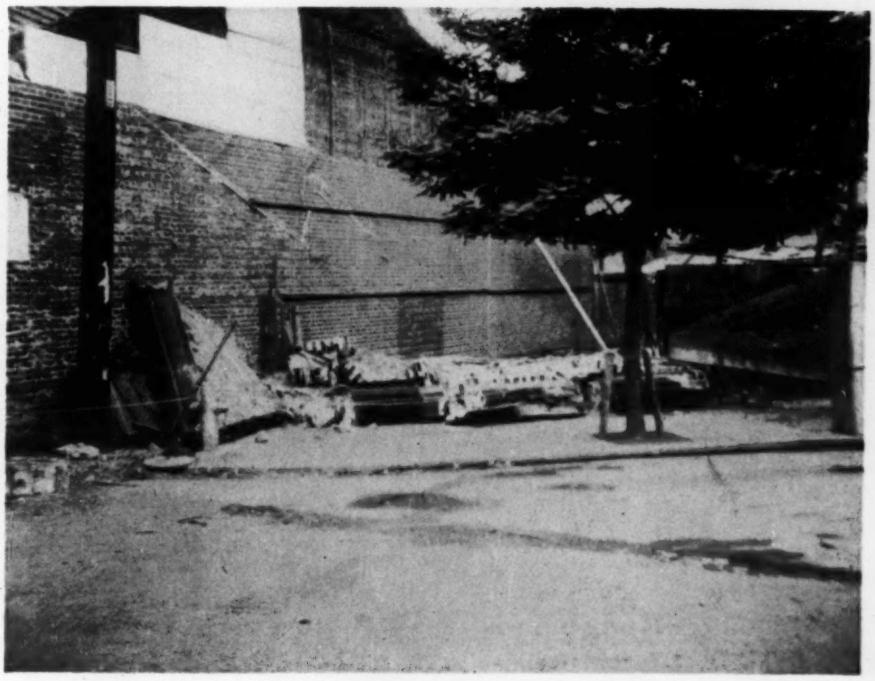

（昭和 10. 7. 12. 撮影）

第 22 圖　靜岡市內某所煉瓦壁の上部崩壞

Siduoka city

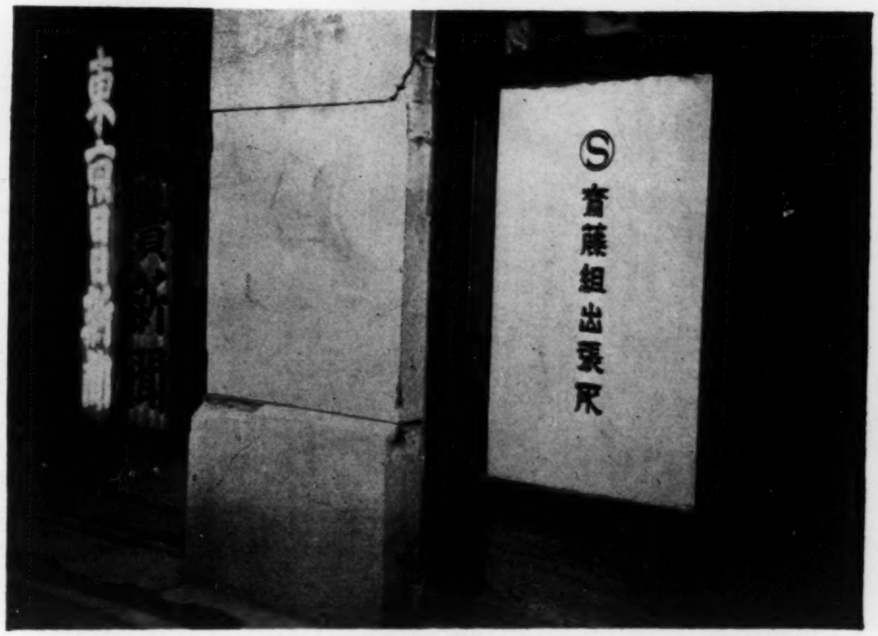

(昭和 10. 7. 12. 撮影)

第 23 圖 靜岡市内某所．商店造り建物の外装モルタール龜裂

Siduoka city

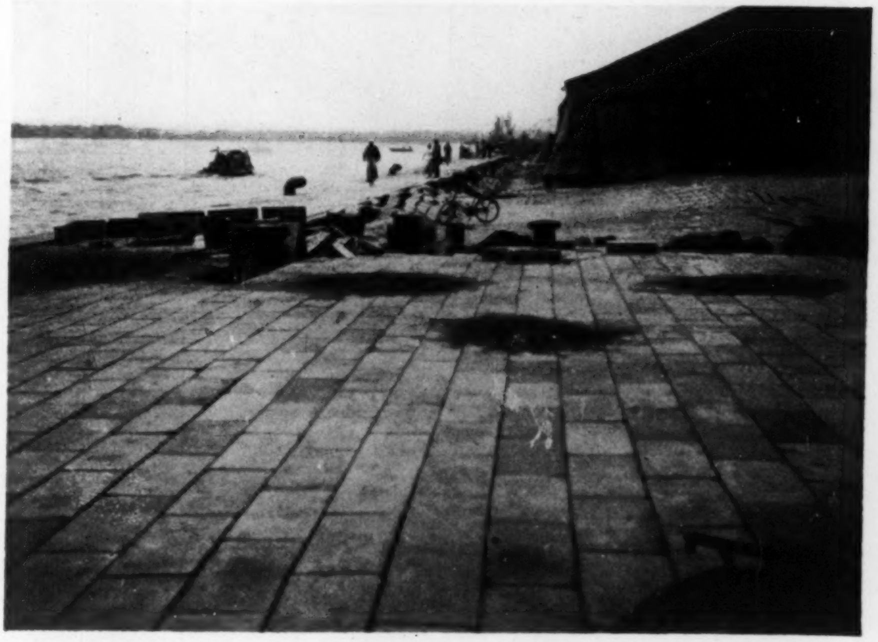

(昭和 10. 7. 12 撮影)

第 24 圖 清水港岸壁の被害

Simidu city

72. 昭和10年7月11日の靜岡地震に就て

地震研究所　萩原尊禮

（昭和10年9月17日發表——昭和10年9月20日受理）

緒言

昭和10年7月11日17時25分頃靜岡縣靜岡市附近に勃發した地震は靜岡，清水兩市及び其の隣接諸町村に於て著しく震害を蒙れる箇所を生じ，倒壞住家總計360餘戶，死者9名を出した．筆者は地震後鈴木正治氏と共力して該地方の3箇所に加速度地震計を設置し餘震の觀測に具へた傍，被害地の實地踏查を行つた．尙，1箇所に於ては地電流變化の觀測をも合せ行つた．

今回の地震は破壞的地震としては決して大規模のものではなく，極めて限られた地域に大なる災害を齎したものであつて，被害甚大を傳へられた靜岡市（最近舊靜岡市に隣接町村を合併せるもの）と雖も家屋の倒壞を出したのは其の南東部に限られ，所謂舊靜岡市にあつては構造物に左程の損傷はなく，殊に其の北部に於ては被害らしきものを認め難い程度であつた．他面，地震動の有感覺區域も破壞的地震としては其の面積は甚だ狹小であつて，震央から凡そ 300 km 以內の區域に止つた．此の如き現象は震源の淺所に存したことゝ地震の規模の小であつたことゝに依つて說明し得られるのであらう．今若し地震の柄と云ふ言葉が許されるとしたならば，被害區域並に地震動有感覺區域の面積より見て今回の地震の柄は去る昭和6年9月21日の西埼玉地震と略々同程度である樣に思はれるのである．

震央

保田柱二氏は東京本鄉，駒場，三鷹，清澄，秩父，吉原，下田（三井地球物理研究所）等に於ける初期微動繼續時間より震央を有度山北西麓（震源の深さ約 15 km）に求められた1)．固より震央附近の觀測材料を欠く關係上其の正確さに於ては劣るものがあるが，各觀測點の材料が互に矛盾しないことより見て可成りの信用を置くを得べく，震央は大體に於て此の附近にあつたものと見て差支へないであらう．之は後に述

1） 那須，保田兩氏の報文參照（本號734頁）．

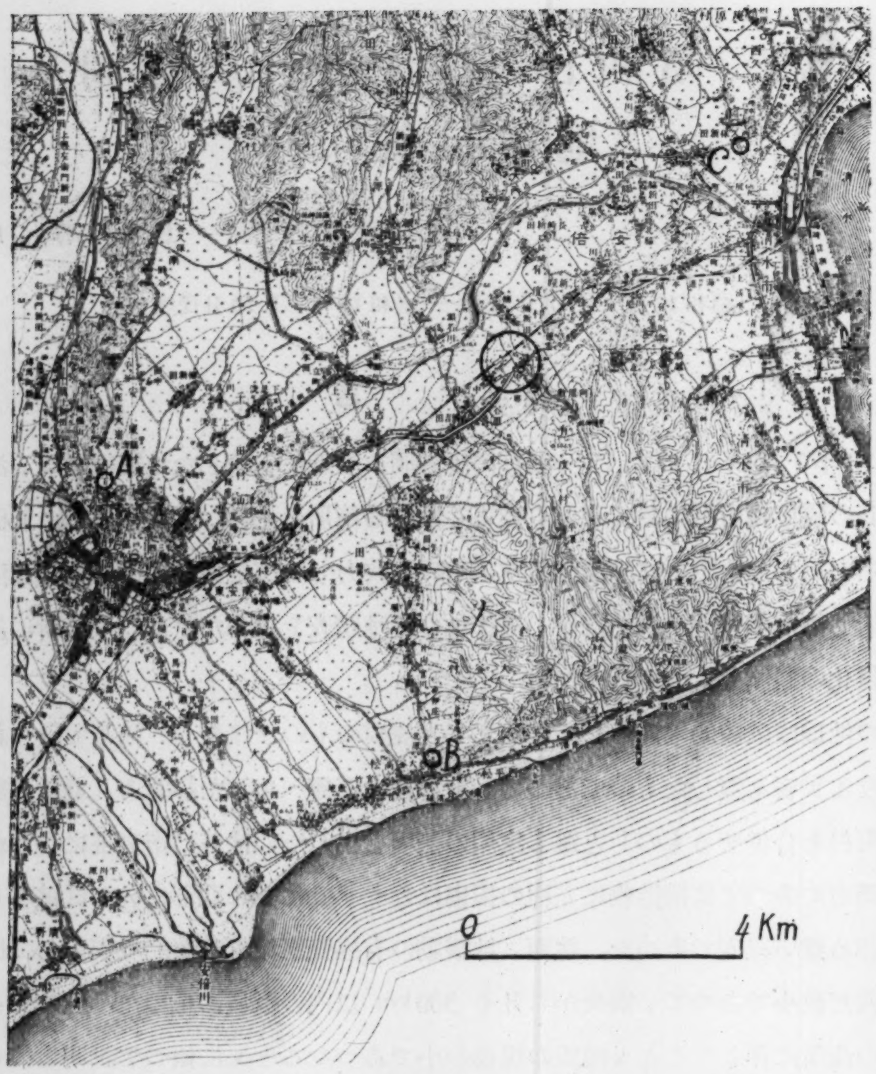

第2圖 ○ 餘震の震央，A 靜岡高等學校，B 大谷小學校，C 庵原中學校

べる近地觀測に依り求められた餘震の震央位置と略々一致して居る. 今回の地震で實際に被害の大であつたのは寧ろ此處に決定せられた震央より隔つた地域であるが，我々の所謂震源は最初に地震波を發生せる場所であるから多大の勢力を有する地震波を發生せる箇所は必ずしも震源と同一であることを要さないし，又地表に於ける地震動は其の土地の地盤の硬軟に依つて甚だしく影響せられるものであるから，震央必ずしも被害最大の地域と一致する必要はない. 之に關しては尙被害分布の項に於て詳論する.

餘　　震

今回の地震の餘震の回數は極めて少く7月12日1時22分，及7月17日4時29分の2回に有感覺地震を發生したに過ぎず，其の後約2ヶ月に至る今日まで有感覺の餘

震は發生してゐない．筆者等は餘震觀測の目的を以て靜岡市東大谷大谷小學校，靜岡市大岩靜岡高等學校，淸水市大手町庵原中學校（第1圖參照）の3點に水平成分加速度地震計を設置し，大谷小學校に於ては7月13日12時より，靜岡高校に於ては7月15日12時より，庵原中學校に於ては7月17日15時より夫々觀測を開始した．餘震は8月26日迄に7回觀測せられた．次表に示す通りである．

觀測せられた餘震[2)]

日　時	靜岡高等學校			大谷小學校			庵原中學校		
	初期微動繼續時間	最大加速度	主要動の週期	初期微動繼續時間	最大加速度	主要動の週期	初期微動繼續時間	最大加速度	主要動の週期
月 日 時 分	秒	ガル	秒	秒	ガル	秒	秒	ガル	秒
7 17 4 29	3·7	2·7	0·16	3·9	7·5	0·3			
7 25 8 30	不　明			不　明					
7 30 5 04	3·1	0·7		3·1	1·0				
7 30 10 17	3·0	1·4	0·13	3·1	1·4	0·15	2·9	2·4	0·10
8 3 9 07	1·4	1·0							
8 5 23 51	3·4	1·0	0·14	3·3	1·0	0·10	3·3	0·5	
8 7 23 06	3·4	0·5		3·3	0·8		3·2	0·5	

尙，大谷小學校に於ては7月15日14時より7月20日15時迄加速度地震計の他に微動計（倍率 100，東西成分）に依る觀測を行つたが加速度地震計に記錄せられた地震以外には地震動の記錄は認められなかつた．

餘震の震央

上に揭げた餘震觀測の結果を見るに3觀測點の初期微動繼續時間は略々相等しく3秒に近い値を示してゐる．從つて震央は3觀測點を結ぶ三角形の略々外心に相當する地點卽ち有度村草薙近傍に存することが知られる．初期微動繼續時間より震源距離を算定する所謂大森公式（$\varDelta=kT$，此處に $\varDelta$ は震源距離，k は常數，T は初期微動繼時間）の常數 k の値は現在の場合は約6を採用するのが至當と思はれる[3)]．今假に k の値を6と採ると震源の深さは 15~20 km の程度となる．上の表の中只一つ靜岡高校に於ける觀測中に初期微動繼續時間 1·4 秒と云ふ極めて短かいものがあり，之に相當する地震動は他の2點に於ける記象には全く現れて居ない．然し靜岡高校に於ける記象に現れたものは小いながら立派に地震動の形態を備へたものであつて，P相S相共に明瞭に讀取り得るのであるから，或は靜岡市北部の淺所にも小地震の發生があつた

2） 主要動の週期は主要動10振動に對する平均である．

3） 那須博士は吉原附近の地震の近地觀測に際し k の値として6を得て居られる．現在の場合は諸種の條件が之に良く類似して居るのである．

のではないかと思はれるのである.

過去の地震

静岡地方は安政1年11月4日の所謂安政大地震には著しい災害を受けたが，大正6年5月18日には局部的地震に依り多少の被害を蒙つて居る．大正6年の地震に依る被害は今回のものよりは遙かに輕少であるが，靜岡市，清水市（當時の江尻町）に於て煉瓦塀，煙突の破壞，住家の壁の損傷あり其の被害分布狀況は今回のものに甚だ類似してゐる．震央は東京及京都の初動方向に各測候所に於て計測せられた初期微動繼續時間を斟酌して濱松の北10里天龍川の稍々上流に求められてゐる[4]．當時の東京に於ける初期微動繼續時間は24秒であり今回の地震に於ては18秒であつたことより其の震央は今回のものより西方に距つた地點に存したことは明白である．然も震害の比較的大であつた地域が今回と類似せることは注目すべきである，尙此の地震は今回の場合と同じく餘震が殆ど伴はなかつたことが報告せられてゐる．此の地方はこの他昭和5年11月26日の北伊豆地震に際し多少の損傷を受けたが，平時は地震活動の甚だ少い地域で平素地震を感ずることは稀であつた．

被害分布

靜岡，清水兩市の中間に半徑約 3 km の主として洪積層礫岩よりなる小山塊があるが，今便宜上之を有度山塊と名附けて置く．今回の地震の災害區域は一言にして云へば此の山塊の南東側を除く緣周一帶と山塊北部の巴川流域の沖積層地帶である．就中，山塊の西側に於て栗原，聖一色より大谷，高松に至る直線狀に列つた諸部落，山塊の北東側に於ける上原，有東坂，船越等及巴川流域に於ける瀬名川，楠，長崎新田，澁川（巴川通り）等が特に災害の顯著であつた所である．次に各部落に就き實地踏査の結果を列擧する．

有度山西緣

高松　住家の倒壞13，半壞94を出し大谷と共に今回の地震で最も多く倒壞家屋を出した所である．倒壞住家數は大谷より少いが，半潰住家の數は大谷より遙かに多い．約 30 cm 東方へ移動せる家屋があつた．北方 300 m 隔つた所にある高松神社の鳥居（南面して立つ）は損傷を受けずに立つてゐた．

大谷　倒壞住家27，半潰住家46で，西大谷に於ては2階家1戸が倒壞のため火災

4）氣象集誌（大正6年），268.
震災豫防調査會報告，88-B（1919），56.

を起し燒失してゐる．東大谷に於ける一商家の土藏は，壁は損傷を受けたが倒壞には至らなかつた．又東大谷東部にある煉瓦造倉庫は龜裂は甚だしかつたが之も倒壞はしなかつた．住家にて30 cm 東方へ移動せるものがあつた．高松，大谷は海岸に平行に流れる大谷川に沿つた町であるが，此の川の海岸寄りの側に於ては被害は目立つて少く倒壞住家は1戸もない．高松，大谷は此の如く多數の倒壞家屋を出したが，其の分布を調査して見るに倒壞家屋は一樣に分布せられてゐるのではなく幾箇所かの部分に集中して居るのが見られる．第2圖は高松，大谷の倒壞住家の分布をスケツチせるものである．東大谷大正寺に於ては寺院前の石燈籠（所謂春日燈籠であつて，胴體は圓壔狀のものである．以後特に斷らない限り石燈體は皆胴體の圓壔狀のものゝみを取扱つて居る）2箇何れも東20° 北に倒れた．寺院横手の小石燈籠は1箇は東20° 北に，1箇は西20° 北へ倒れた．無緣塚は北20° 東の方向へ崩れた．

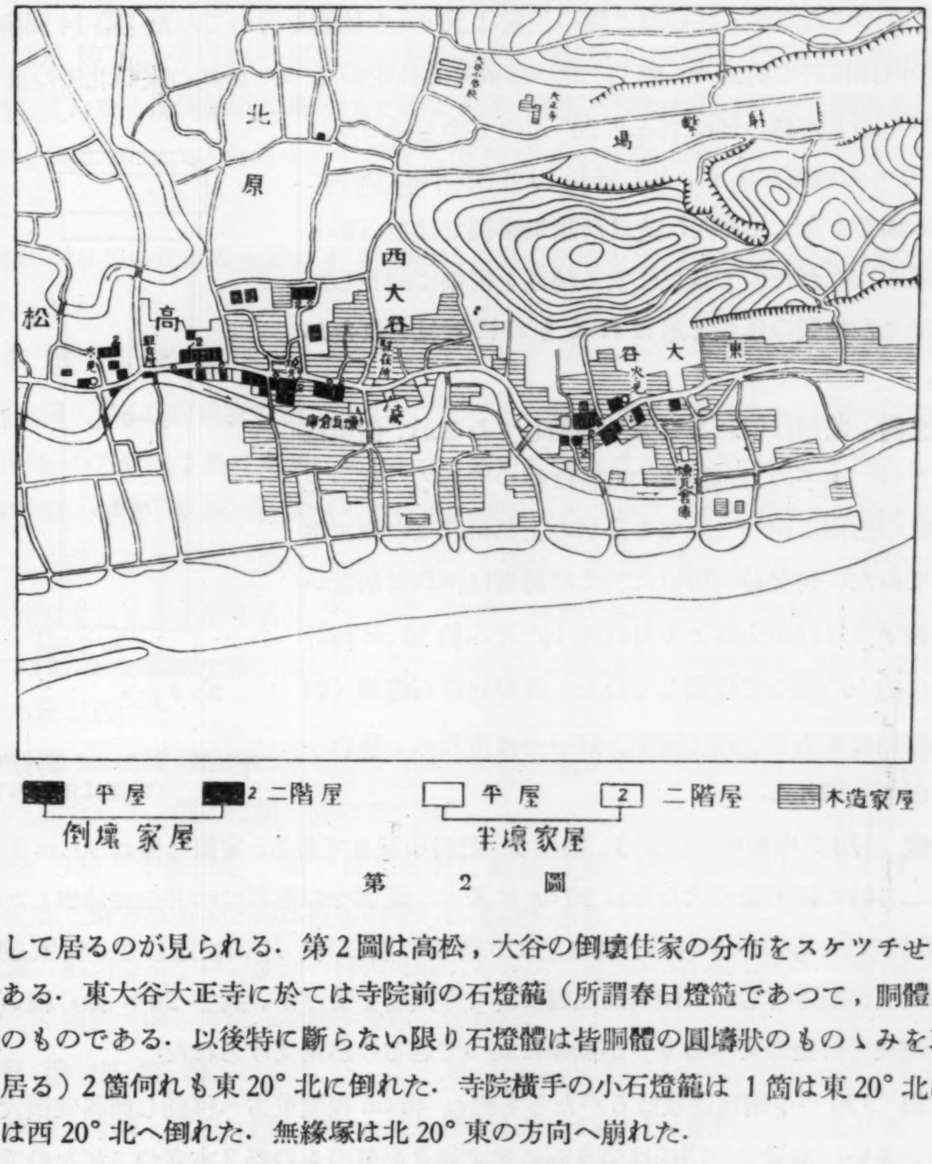
大谷小學校
大正寺
射撃場
北原
西大谷
駐在所
高松
火見
煉瓦倉庫
土藏
東大谷
火見
煉瓦倉庫
平屋
2 二階屋
倒壞家屋
平屋
2 二階屋
半壞家屋
木造家屋

第2圖

伊庄　家屋は倒壞なく數糎東20° 北へ移動したが破損は少い．

宮川　20° 位傾斜せる住家はあつたが倒壞家屋はない．山神社の鳥居は倒れてゐない．

片山　家屋は何れも東20° 北へ30 cm 程度の移動を行つて居るが13戸中1戸の倒壞住家もなく，僅かに納屋1戸倒壞せるのみであつた．極端な例では30 cm 以上の移動をなして居るに拘らず，障子紙も破れず建附も狂つて居ない家があつた（第13圖参照）．直徑約30 cm，高さ5 m，針金の支へある煉瓦管の煙突が倒壞せずに立つてゐるのが見られた．又外徑40 cm，長さ60 cm のコンクリート管を16箇聯ぎ四隅に1inch のアングルを當てゝ締付けてある茶工場煙突（高さ10 m，針金の支へあり）は何等損傷なく立つてゐたが，其の直ぐ傍の住家は30 cm の移動を行つてゐた（第14圖参照）．道路の西側に於て約50 cm 東15° 北へ移動せる住家があつたが其の家の北側の裏手より床下を通り南側の畑に至る北20° 東の方向を持つた長さ約10 m の地裂があり，其の延長10 m 程の間は畑中に多數の龜裂を生じてゐた．之は所謂地裂線ではないかとの疑惑が持たれたので延長に當る地點を精細に調査したが結局この地裂の延長と思はれるものは發見されなかつた．

堀之内　家屋は何れも東方へ移動してゐるが，倒壞住家はない．山手の方が比較的被害は輕少である．第一王子神社の西南に向つて立てる鳥居の上部が北東の側に落下してゐた．伊勢神明神社に於ては鳥居は倒れて居ないが，御手洗は柱が土臺より外れ西10° 北へ約50 cm 時計廻りに約10° 廻つて移動してゐた．拜殿前の石燈籠（胴體の斷面は正方形，西に面す）は一つは東側へ，他の一つは南側に倒れた．

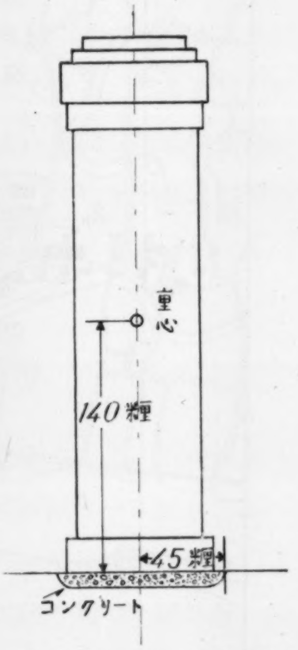

第3圖　顚倒せる煉瓦門柱
（斷面は正方形）

小鹿　170戸中倒壞は住家3，納屋5，肥料小屋9である．家屋は概ね30 cm 東方へ移動し，特に移動量の大なるは50 cm に及ぶ．龍雲寺の墓石は殆ど全部轉倒したが，東側に倒れたものが多い．小鹿は之より南部の堀の內，片山に比して一般家屋の傾斜，破損が頗る著しい．煙突は此處に於ても損傷を受けず，高さ20 m 餘の細い煉瓦管の煙突（針金の支へあり）が無事に立つて居るのが見受けられた．

池田　130戸中倒壞住家は6戸なるも概ね40 cm 程度東方へ移動し傾斜破損大なるものが多い．本覺寺の門柱は第3圖に示す如き形狀のものが2本立つて居たのであるが，北側のものは顚倒し南側のものは其の儘殘つて居た（第18圖参照）．本堂前の石燈籠2箇は一つは東45° 北へ，他の一つは東36° 北へ倒れ，本堂横手の石經は東60°

北へ倒れた．又墓地内の石籠燈2箇は東35° 北と東46° 北の方向へ倒れた．墓石は概して北東側へ倒れて居た．本堂は損傷極めて少く移動も無く壁も餘り破損してゐない．池田神社は鳥居，御手洗共に東側に倒れたが拜殿は破損少く移動も無く，拜殿前の石燈籠は屋根が東側に落ちてゐた．畑守稻荷は約 50 m の高地にあるが參道の鳥居は上部が東側に落ち拜殿前の石燈籠4箇は東方へ倒れ，拜殿も可成りの損傷を受けて居た．

聖一色　71戸中住家の倒壊は1戸であるが，池田同様傾斜破損の著しい家屋が多い．家屋は概ね 30～40 cm 東方へ移動を行つてゐる．圓福寺の墓石は大半東側へ倒れ，本堂は東10° 北へ約15 cm 移動し，本堂前手の茅葺の堂（2間× 2·5間）は東へ 40 cm 移動してゐた．淺間神社の鳥居は上部は東側へ落ち石燈籠は東10° 南に倒れた．直徑40 cm，高さ10 m，針金の支へある煉瓦煙突が2本損傷なく並立してゐるのが見られた．

栗原　60戸中住家の全壊は4，約半數は相當の損害を蒙つてゐる．家屋移動は 30cm 程度である．

有度山北縁

國吉田　114戸中住家の倒壊は1戸であるが殆ど全部家屋が 30 cm 位東へ移動した．廣野神社の石燈籠2箇は東側に倒れたが，東方に向いて立つ鳥居は倒れて居なかつた．

中吉田，谷田　是等の部落は有度山塊の傾面にあり栗原，國吉田よりは稍々高地である．此處に至ると家屋被害は著しく減少し倒壊，半倒壊等は無く軒先 2～3 寸の傾斜が被害大なる部に屬する程度である．家屋の移動も顯著でなく，柱が土臺石から離れた家はない．壁も上塗のないものは殆ど破損して居ない．中吉田に2戸大破損を受けた土藏があつた．

中之郷　に於ても被害は小であつて家屋の約半數が東へ移動したが 2～3 cm に足らない程度であり，壁の破損も極めて少ない．

草薙　150戸中倒壊なく30戸位が東方に數糎移動した．山手の方が特に被害が少い．之より東方に至ると再び被害の著しい地域がある．

上原　倒壊家屋2戸，家屋の移動は著しくない（東方へ 10 cm 程度）が東部に於ては著しく傾斜大破して居る家屋が集中してゐた．

有度山東縁

有東坂，今泉　家屋は概ね 20 cm 東へ移動し稍々時計式に廻轉せるものが多く，何れも著しく破損を受けて居る．有東坂庚申堂（茅葺3間×3間，建物は西20° 南へ向きて建つ）は東へ 9 cm 移動し時計と同じ向きに僅か廻轉して居た．

船越　倒壊に等しき住家1戸のみにて他は倒壊を免れたが，何れの家屋も傾斜破損

は著しい．家屋の移動量は比較的大で東へ30cm程度である．此處の家屋も時計式に少しく廻轉して居るのが見られた．一新築瓦家（建坪25坪）は東50°南へ25cm移動し時計式に約5°の廻轉をして居た．

南矢部 倒壞家屋無く被害は極めて少い．家屋の移動は東へ10cm程度である．

北矢部 家屋移動は目立たず稀に2～3cm移動せるものがある程度であるが，家屋の損傷は南矢部より稍々多い．

南矢部より南部に至れば破害は頓に減少する．

駒越 破損せる家屋無く障子紙も破れてゐない程度である．

駒越より東方三保方面は更に被害少く，

折戸 に於ては稀に壁の上塗の破損ある程度であり，

宮方 に於ては全く被害無く三穗神社のあぶなげな石燈籠も倒れては居なかつた．

有度山南緣

增 駒越と同様障子紙の破れも無い程度である．

蛇塚 障子紙の破れが目に着いたが家屋の破損はない．

根古屋，安居，古宿，青澤 何れも障子紙の破れが多少見られる程度で壁の損傷も少い．

中平松 障子紙の破れが目立ち，部落の西方に於ては東へ數糎の家屋移動があつた．大谷川の河口附近を境として之より西方に至ると急激に被害を增し，

西平松 に於ては相當の破損家屋あり，更に西に進めば今回最も多數の倒壞家屋を出した大谷，高松に達するのである．

有度山塊上の部落

向屋敷，馬走，平澤 何れも被害は輕微である．平澤に於ては家屋の移動全く無く，障子紙僅かに破れ，瓦の少しく落下した家がある程度である．

有度山塊北方の平地（主として邑川流域）

古庄 86戸中住家の倒壞17，半壞50餘戸，家屋は30～35cm東方へ移動して居る．淡島神社の石燈籠は2箇の中1箇は東へ，1箇は西へ倒れた．

長沼 倒壞住家9，半壞39戸を出し古庄と同程度の震害を蒙つて居る．

上土 倒壞家屋は無いが傾斜家屋は多い．有度山塊山緣に於ては家屋は例外なく東方へ移動して居たが，上土に於て稍々南寄り西方へ10cm程度の移動を行つて居るものが多く，家屋の傾斜も西方へ向いて居る．

上土本田 東禪寺の墓石は東又は西に倒れた．

川合 住家は壁が落ち僅かに傾いた程度で屋根瓦の被害は殆どない．玄祐寺の山門

は西へ倒壞し，本堂前の小堂は西へ傾いた．住職の語る所に依れば墓石の轉倒方面は一定してゐなかつたと云ふ．

瀬名川 100戸中倒壞家屋は無いが著しく破損せる20餘戸があつた．街道の北側は著しく破損が少い．

楠，楠新田 85戸中倒壞住家は無く約30戸が軒先2～3寸傾斜した．新田の方が幾分被害著しく6軒大傾斜せる家屋がある．家屋移動は東へ10cm程度である．

長崎，長崎新田 倒壞家屋は無く家屋移動は東南へ約10cmである．

七ツ新田 54戸中大破せるもの30戸あり，家屋の移動は東へ15cm程度である．

吉川（キツカハ） 住家は倒壞無く東へ15cm移動した．

澁川 巴川堤防通りの家屋は10餘軒倒壞した．家屋の移動量は堤防附近にて10cm餘であつた．

巴川の北側の山緣に於ける部落は何れも被害は殆ど無いと云つても良く，例へば

南沼上 に於ては少數の家の瓦が夫々2～3枚落ちた程度で，大部分の家は壁障子の破損も無く，

瀬名 に於ては一般に瓦，壁の損傷無く漆喰壁が少しく落ち建附が2～3分狂つたに過ぎないのである．

有度山塊西方の平地

宮竹 倒壞家屋無く，家屋の移動は25cm程度で東25° 北に向ふ．家屋の破損は高松に比較して著しく少い．風祭社の南面して立つ鳥居は倒れた．此の神社附近にある一住家の高さ2mの鐵筋コンクリートの塀（略々南北に沿ふ）は未だ工事中にてコンクリートを打つてから尙日が淺く見受けられたが破損を免れて居た．

敷地 家屋の移動は10cm以内で破損は少い．

大島 家屋移動は約10cmである．

西島 90戸中全壞に等しきもの1戸あり，家屋の移動は東20° 北へ5cm程度のものが多い．

濱村，中島 家屋移動は明瞭でない．濱村海岸の大濱公園の25m プールは少しも破損を受けなかつた．

安部川東岸の堤防 は西島，中島部落附近に於て堤防上の路に堤防に平行な小龜裂があつた．

石田，中田，中 有度山西方の平地中では比較的家屋の損傷の多い所である．障子紙の破れ著しく，2～3寸傾ける家多く，家屋の移動は東へ10cm以内である．但し倒壞家屋はない．

中原 南部の部落に比し家屋の破損少く，大抵の家は建附が少しく狂つた程度である.

馬淵，稻川，有東 は共に家屋の損傷少く，傾いた家屋も稀である. 此の邊の家屋は移動は認められない.

八幡 稻川と大差なく稀に傾斜した家屋がある程度である.

小黑 稀に東北へ 2〜3 cm 移動せる家屋はあるが破損は少い.

尙此の外に靜岡，淸水兩市の市街地及び淸水港に於ける震害に就いて記述すべきであるが，之は齊田氏の詳細な調査があるので同氏の報文に委ね，此處では只靜岡市の北部賤機山の附近に至れば全く家屋の損傷の無いことを記して置く.

地震動の推定並に木造家屋被害に關する考察

今回の被害の狀況を見るに特に著しく我々の注意を惹くところのものは構造物が揃つて同一方向に移動又は轉倒したことである. その方向は災害顯著な區域にあつては概して共通に東方である. 斯くの如く多くの構造物が同一方向に規則正しく移動又は顚倒することは主要動の最初に極めて大きい加速度が存在したことを意味してゐる. 此の地方の住民の談に依れば，最初に強い上下動を感じたが暫くにして大搖れが來て身體が投げ出される如く感じたと云ふ. 顚倒した石燈籠を見ても其れが一氣に顚倒したことが明白であつて，崩れ落ちる樣に破壞した形跡は無く（第11圖及第20圖參照)，寫眞に見られる如く顚倒した石燈籠の各部は顚倒の方向に直線的に配列されて居る. 尤も構造物の同一方向への移動に關しては，主要動の最初に於ける大なる加速度に依つて一氣に移動せしめられたと考へる以外に，振動性の地震動に依り何回かに亙つて移動したと考へることが出來ぬでもない. 即ち地動の水平加速度に依り構造物重心に之を水平移動せしめんとする力が働き，之が底面の摩擦に打勝つ時は構造物の移動が生ずるのであるが，此の時地動に下方向の加速度が同時に存在する時は見かけ上其の構造物の重さを減少せしめ，底面の摩擦を減少し，比較的小なる水平加速度に依り構造物を移動せしめることが出來，反對に上方向の加速度が同時に存在する時は見かけ上の重さの増加に依り底面の摩擦を増加し水平の移動は比較的困難となる. 故に地盤の水平方向の振動と上下方向の振動とが同一週期を持ち其の位相が相對的に變化しない時，即ち或る特定の方向 A に水平加速度が向ふ時に限り上方向の加速度が生じ，水平加速度が之と反對の方向へ向ふ時は下方の加速度が生ずる樣な現象が起れば，特定なる方向 A の向きにのみ移動が可能となる. 然し地盤の振動は特種の表面波の場合を除いては上下振動と水平振動とは夫々獨立した自由度に於ける振動であるか

ら，前述の様な條件を滿す確率は極めて小でなければならない．從つて今回の如く有度山塊緣周の地域全般に亙つて斯くの如き現象が共通に起つたとは考へ難いのである．斯の如く複雜な現象を强いて考へることなく最も簡潔に主要動の初めに當り優れて大なる加速度の存在したことに依つて一氣に構造物の移動も起り，顚倒も生じたと考へるのが至當であらう．

今回の木造家屋の移動量は大なるものは40 cm 餘に及んだのであるが，之を一氣に移動したと考へる時は地動は相當に大なる加速度を持つたばかりでなく，變位も亦少くも40 cm 餘に達したことが推察出來るのである．轉倒物體中最も規模の大なるものは池田本覺寺の煉瓦門柱であつた．此の立面圖は第3圖に示してあるが，此の水平斷面は正方形である．土面上に僅か 5 cm の厚さにコンクリートを敷き其の上に煉瓦を積上げて角柱を形成したものであつて　土面への附着力は省略出來るから角柱の轉倒と見做して差支へないのである．此の門柱は2本西方へ向つて立つて居たが北側のものが東へ顚倒し，西側のものは顚倒を免れた（第18圖參照）．地震當時此の附近に偶然居合せた一農夫5) の語るところに依れば大搖れが來た時門柱が一氣に倒れるのを目擊したと云ふ．此の門柱の重心迄の高さは 140 cm，底面の幅は 90 cm であるから，今假に水平加速度のみに依り顚倒せしめられたとすると少くも300ガルの加速度が算出せられる．而して顚倒に際して重心は底面の幅の半分 45 cm を移動せねばならぬから地動の變位も亦少くとも 45 cm あつたことゝなる．然も一方の門柱は顚倒を免れたことから地動は此の角柱を顚倒せしめ得る條件の略々限界にあつたと見るべく，大體に於て此の附近の最大加速度は300ガル，最大變位は45 cm と見做して差支へないであらう（勿論，玆に論ずる變位は永久的變位を意味するものではない．地震主要動の初頭に於ける變位のみを論じて居るのである）．又此の角柱の重心を靜止の位置から不安定の位置迄持來す期間中300ガル程度の加速度が繼續しなければならないのであるから，加速度は瞬間的のものではないことが察知出來る．今地盤が一定の加速度 α を以て水平に動き，時間 T の後に變位 d を行つたとすると

$$\int_0^T dt' \int_0^{t'} \alpha\, dt = d,$$

---

5) 池田町寺尾柳甫氏　同氏は地震當時本覺寺北側の茶畑に居たが，突然東の方で底力のある地唸りがしたのではつと思ふ間も無く搖れ始め，畑から道（門柱北約3間）まで飛出した時一番大きく搖れた．其の時門柱は恰も大きい力で突倒したかの樣に一度に倒れた．二つ共同じ樣になつたと思つたが一方のみ殘つて居たのは後で氣附いたと云ふ．

初期の條件として速度も變位も零であるとすれば

$$\frac{1}{2}aT^2=d.$$

今 $a=300$ ガル，$d=45$ cm とすると $T=0·55$ 秒となる．300 ガルより大なる加速度が存在したと假定すれば，T の値は之より小となるが石碑，石鳥居の如き基礎に比較的强固に附着せるものゝ倒壞折損が無かつたことから推して之より大なる加速度が存在したとは考へられない．又下方の加速度が同時に存在した場合を考へると，上に得た 300 ガルの値は多少小となる．今水平加速度と同程度の下向きの加速度が存在したと假定すると，水平加速度は少くとも 230 ガルとなるが，主要動に斯の如き大なる上下方向の加速度が存在したかどうかは疑問である．要するに池田附近に於ては主要動の初めに孤立的に大なる加速度を持つた地震動が存在し 300 ガル程度の加速度が約 0·5 秒繼續したと云ふことが出來る．他の家屋移動の大なる地域も大體に於て之と類似して居ると云へよう．

次に比較のため振動性の地動が幾何の變位を持つかを計算して見るに，A を加速度振幅，D を變位振幅，T を週期とすると，

$$A=\frac{4\pi^2D}{T^2}$$

であるから，今 $A=300$ ガルとすると $T=0·1$ 秒，0·3 秒，1·0 秒に對し夫々 $D=0·08$ cm，0·68 cm，7·6 cm となり，振動性の地震動に於ては最大加速度 300 ガルの場合は普通考へられる地動の週期に對して數十糎の變位振幅を持つことは出來ないことが判る．又餘り大なる週期を持つた振動性の地震動の存在しなかつたことは煙突の如き細長い構造物が倒壞を免れたことから推察出來る．故に今回の如く數十糎の變位を持つた地震は土地表層に於ける固有振動ではなく，震源より地震波として到達したものゝ中に其の要素が含まれて居たと考へられる．

次に考ふべきは，此の大なる加速度と變位を持つた地動は木造家屋を移動し，角柱を轉倒せしめたが，木造家屋の破壞に關しては如何なる働きを爲したであらうかと云ふことである．今回の被害地を通覽するに家屋移動の大なる處必ずしも家屋破損の大なる處ではなかつた．其の最も良き例は片山である，此の部落に於ては家屋は 40 cm 程度の移動を行ひ乍ら其の受けたる破損は極めて少い．之に反して家屋の移動量少くして反つて破損家屋の多くを出した處がある．巴川流域の部落は之に屬する．又片山と小鹿とを比較するに兩部落の距離は極めて近く家屋の移動量も略々相匹敵するのであるが，家屋の破損に於いては兩者に著しい差異がある．片山に於ては倒壞，半

壞の家屋無く破損程度は極めて輕微であるが，小鹿に於ては3戸の倒壞家屋を生じ，倒壞を免れた家屋と雖も何れも甚しく破損を蒙つて居るのである．之に依つて見るに家屋の移動を生ぜしめたところの地動は家屋の破壞そのものには餘り大なる役割を演じなかつたと云へる．然らば家屋の破損を大ならしめ，或は之を倒壞せしめたものは前述の大なる加速度と變位を持つた弧立的の地動に續く振動性の地震動ではなかつたであらうか．

土地の表面層に固有の振動の存在し，之に依り構造物の震害が左右せられることは既知の事實[6] であるが，今家屋を移動せしめた地動が家屋破損に餘り與らなかつたとなると土地の固有振動に依つて家屋の破損の大小が決定されたと見るのが至當であらう．

木造家屋は比較的小なる變位振幅を以て振動する時は完全な彈性體と見做し得るが，同時に大なる變形を許し得る性質を具へて居るから，之を破壞に迄持來すには相當大なる變形を與へる必要がある．故に地動の加速度は如何に大であつても其の變位振幅が大でない限り之を破壞せしめることは困難である．然し木造家屋自身一種の振動體である以上，其れの振動週期に近き週期を持つ地震動が存在する時は共鳴現象に依り之を大なる變位振幅を以て振動せしめ破損或は倒壞せしめるに充分な變形を生ずることが出來る．此の見地より土地表層の固有振動週期が重要性を持つことが察知出來るのである．比較的大なる加速度を有する地震動は一般に小は 0·1 秒程度より大は1秒程度であることが知られて居るが，斯の如き週期の地震動に於ては加速度振幅は大であつても其の變位振幅は比較的小であることは前に例示せる通りである．從つて木造家屋が强制的に振動せしめられて居る限りは地動の加速度が如何に大であつても大なる災害を生じ得ないのであつて，之を大破し倒壞せしめるためには共鳴振動に依り大なる變位振幅を生ぜしめることを要する．而して木造家屋の振動週期たる大約 0·5 秒に近き週期の固有振動を有する土地は軟弱なる冲積層地域に限られ，火成岩並に古き水成岩より成る地域に於ける固有振動の週期は之より短く，小なるものは 0·1 秒或は其れ以下となるのである．

餘震觀測に於ける加速度記象を見るに靜岡高校に於ては主要動中に 0·15 秒程度の週期の地動が見られ，大谷小學校に於ては 0·15 秒と 0·3 秒の週期が認められ，清水庵原中學校に於ては 0·1 秒の週期が見られた．7月17日の微震に際しては大谷小學校に於ては靜岡高校に於けるより遙かに大なる加速度を示し 0·3 秒の週期の地震動が明瞭に現れた．

6） 例へば，石本巳四雄　地震研究所彙報　**13** (1935)，592.

静岡地方の地質圖を見るに北方の山地は中生層及玄武岩の硬質なる岩石より成つて居る. 賤機山には玄武岩の露出があり，此の東方の山地は中生層に屬し，有度山塊は主として洪積層礫岩より成つて居る. 有度山北西の平野中の小丘，谷津山・八幡山は第三紀頁岩に屬する. 之に依つて見るに此の地方は平地の冲積地域を除いて山地は地盤は强固である. 静岡高校，庵原中學に於ける地震動週期の短いことは此の種の硬質の岩石上にあるためであつて此の附近に被害は殆ど無い. 大谷小學校は有度山の山縁にあり地震動週期は 0·3 秒を示す. 平野の冲積地帯に於ては恐らく之より大なる週期の地震動が現れたであらう.

今家屋破損の大であつた地方の地質を見るに，巴川流域に於ては軟弱な冲積層が相當發達して居ると見られるから土地表層の固有振動の週期も比較的大で木造家屋に大くの災害を與へたのであらう. 又有度山西方の平野中の比較的木造家屋の破損の大であつた石田附近も冲積層が比較的發達し軟弱な地盤を形成してゐると見れば良い. 次に有度山塊山縁の部落中特に被害の大であつた部落——小鹿，池田，聖一色等，並に大原，有東坂，船越等——に於ては夫々附近に幾つかの沼が存在して居ることが氣付かれる.（1/25000 の地圖を見れば明白である.）上記の部落が特に被害の大であつたことは過去に於て此の區域が沼池であつた關係上軟弱な地盤を形成して居る様に思はれる. 尚，大谷高松の被害に就て一考する必要がある. 是等の部落は震央より比較的隔つた地に存在するに拘らず其の木造家屋被害は今回の災害地を通じて最も甚しく地震直後には震央は大谷附近であるとさへ傳へられた. 大谷，高松の附近の地形を見て誰しも氣付くことは大谷川の存在である. 此の小河川は高松附近より海岸に平行に走り西平松の西部に於て海に注いでゐるが，此の河川に沿つた高松，大谷の部落が上述の如き被害を受けたのである. 然し大谷川は河川としては甚だ小なるものに屬し其の河幅は僅か 10 m，地表より河底迄の深さは約 3 m である. 斯くの如き小河川の存在其のものが其の附近の地震動に直接影響を齎したとは考へ難い. 其は此の河川に沿つた部落と雖も海岸寄りの側にあるものは比較的被害が輕微であることから見ても明かである. 此の小河川に沿つた地域の被害が大であつたことは，此の附近に過去に於て大なる河川が存在し今日は大谷川は其の名殘り川として存在するとすれば，附近に冲積層の發達して居ることが説明出來るであらう.

地變及海水異常

今回の地震に於ては地震動に依つて生じた畑，路面等の龜裂及斷崖の崩落は諸所に存在したが，所謂斷層，地裂線等地震動以外の力の作用に依り生じたと斷定出來る地

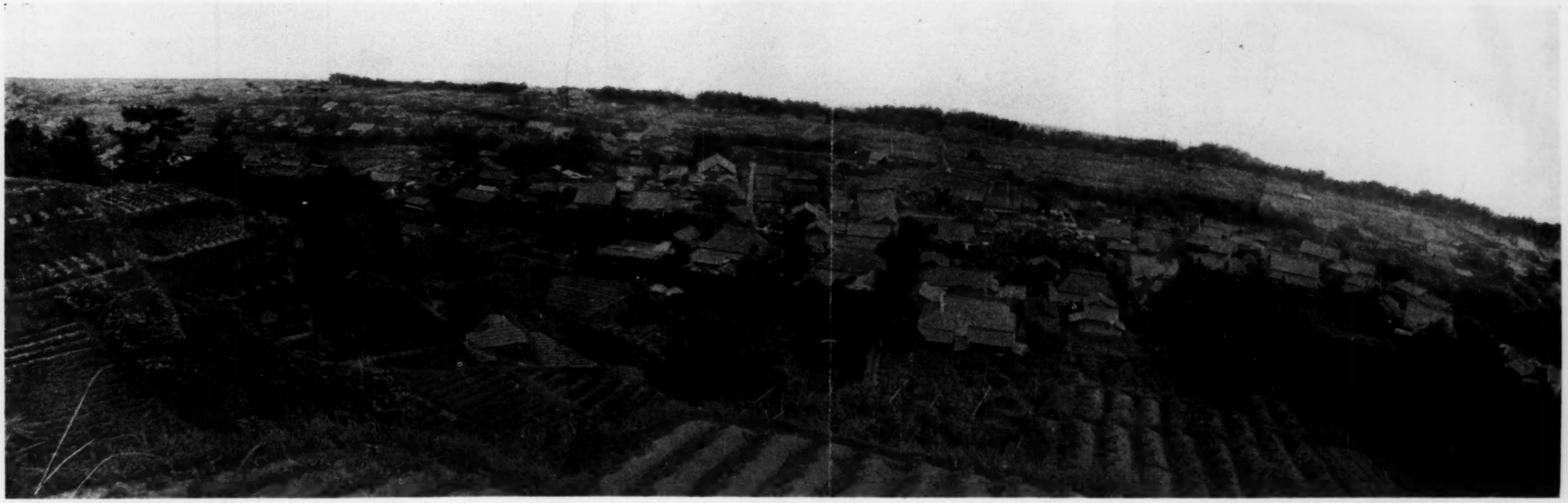

第4圖　東大谷全望

×印は倒壞家屋多き所

第5圖　東大谷

第6圖　西大谷，住家の倒壞失燒

第7圖 西大谷

（震研彙報 第十三號 圖版 萩原）

第8圖 西大谷

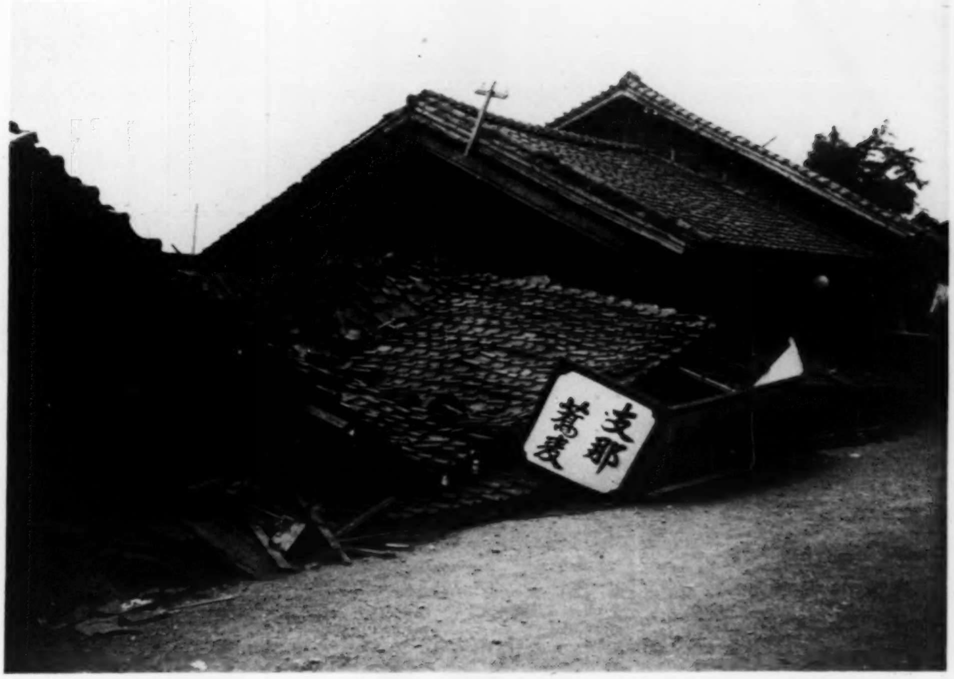

第 9 圖　高　　松

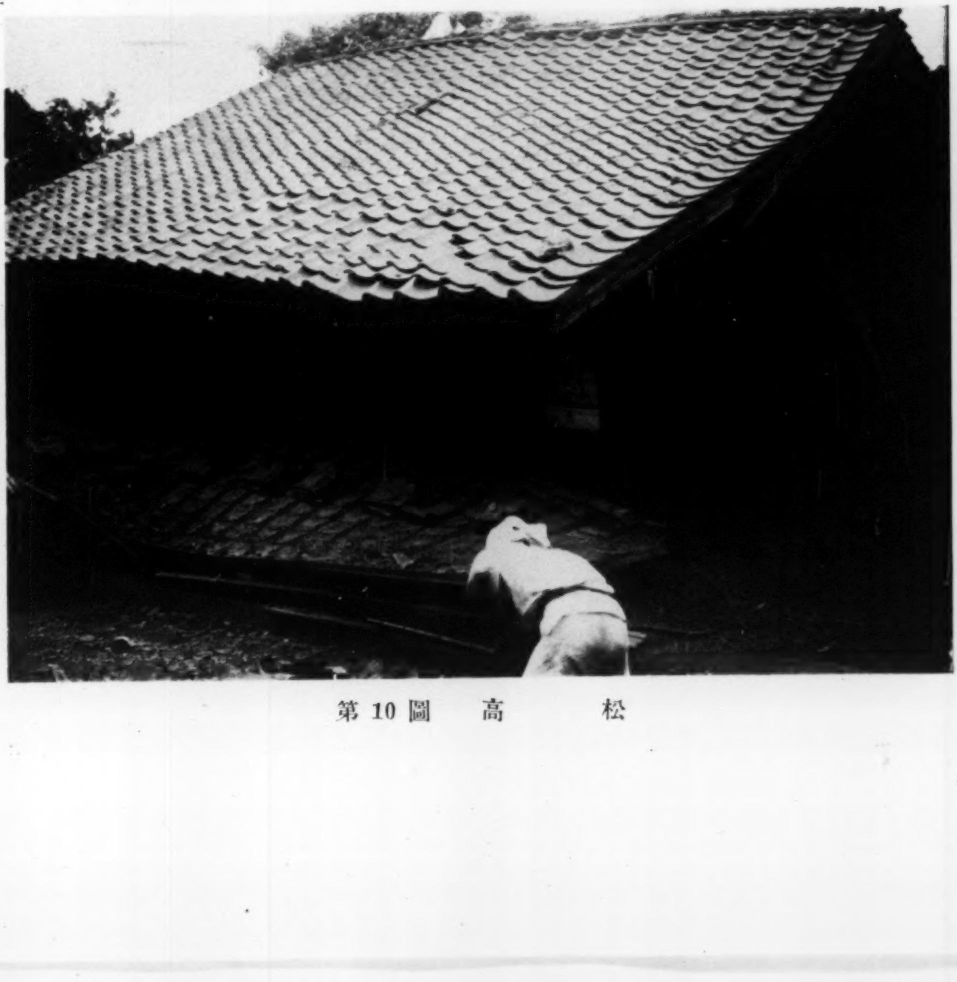

第 10 圖　高　　松

（震研彙報 第十三號 圖版 萩原）

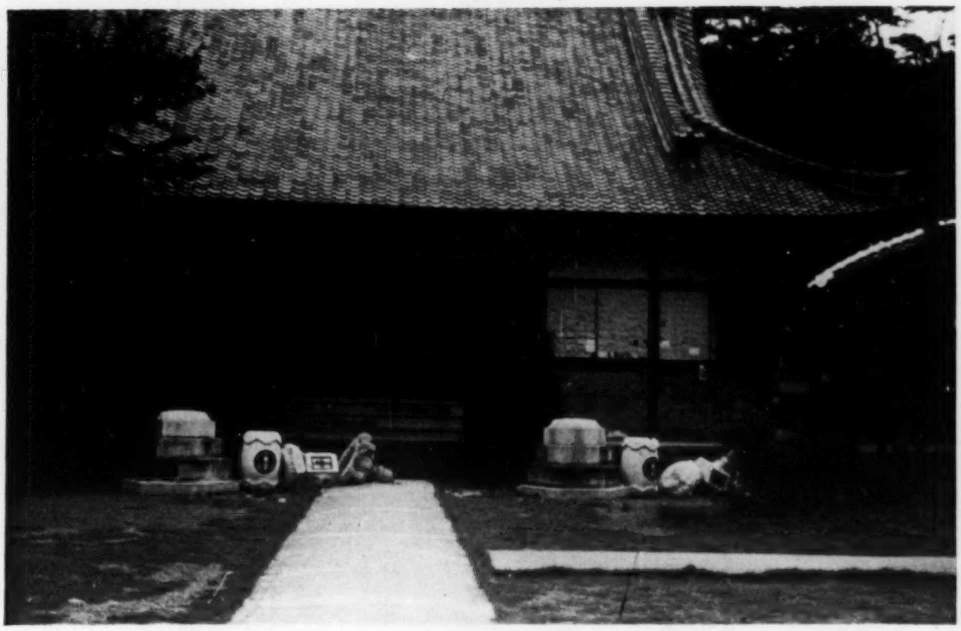

第11圖　東大谷，大正寺の轉倒石燈籠

第12圖　片山附近の地質(洪積層礫岩)

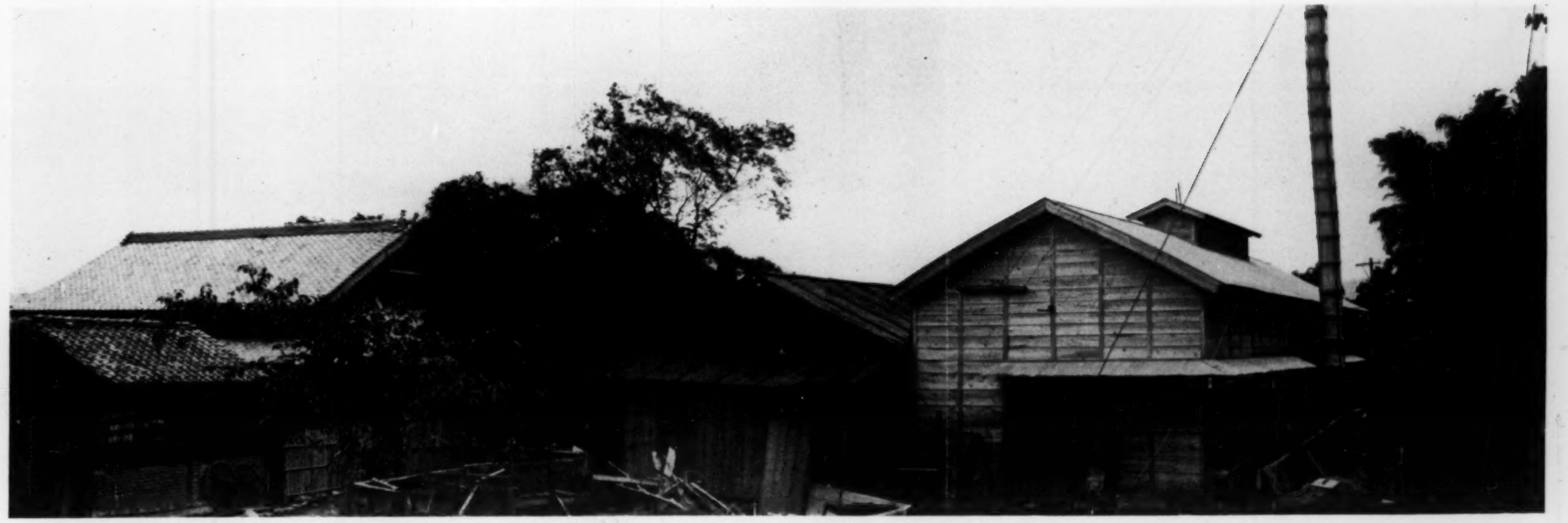

第 14 圖　片山，寫眞左手の家屋は約 30cm 移動せるも煙突には被害無し

（震研彙報 第十三號 圖版 萩原）

第 13 圖　宮川，家屋の移動
（約 30 糎移動せるも障子紙も破れす建附も狂はない）

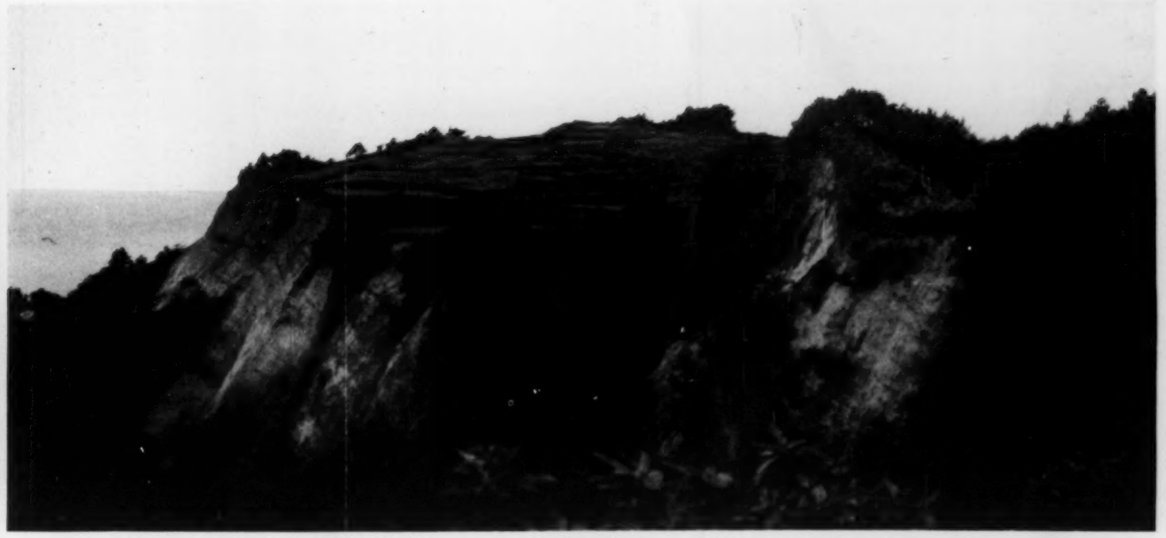

第 21 圖　有度山斷崖の崩落（古宿北方）

第15圖　堀之内，地震時沼中に噴水せる跡

第16圖　小　鹿

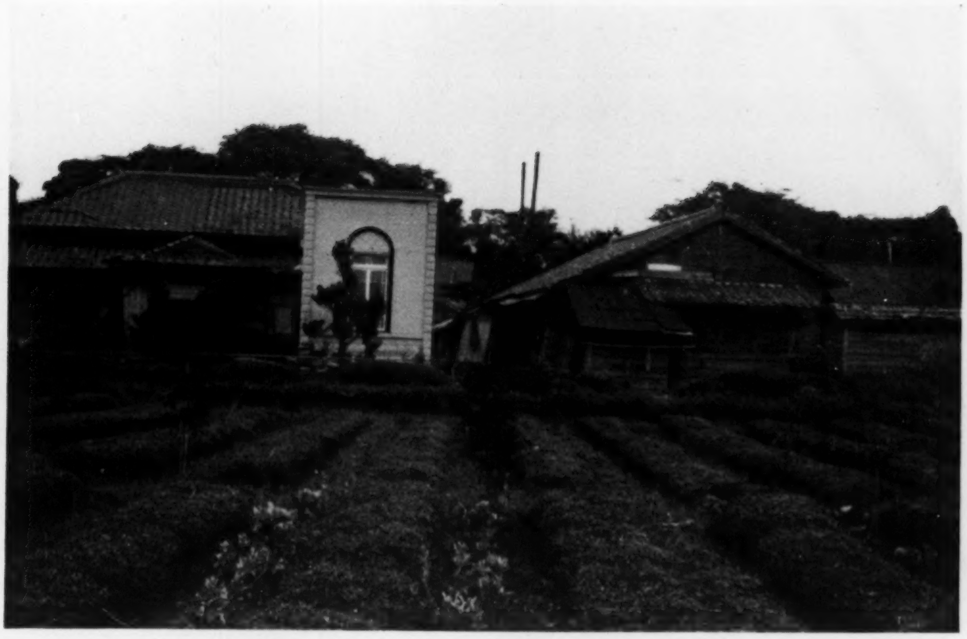

第 17 圖　小鹿，家屋は大破せるも煙突は破損せず

第 18 圖　池田，本覺寺煉瓦門柱の轉倒

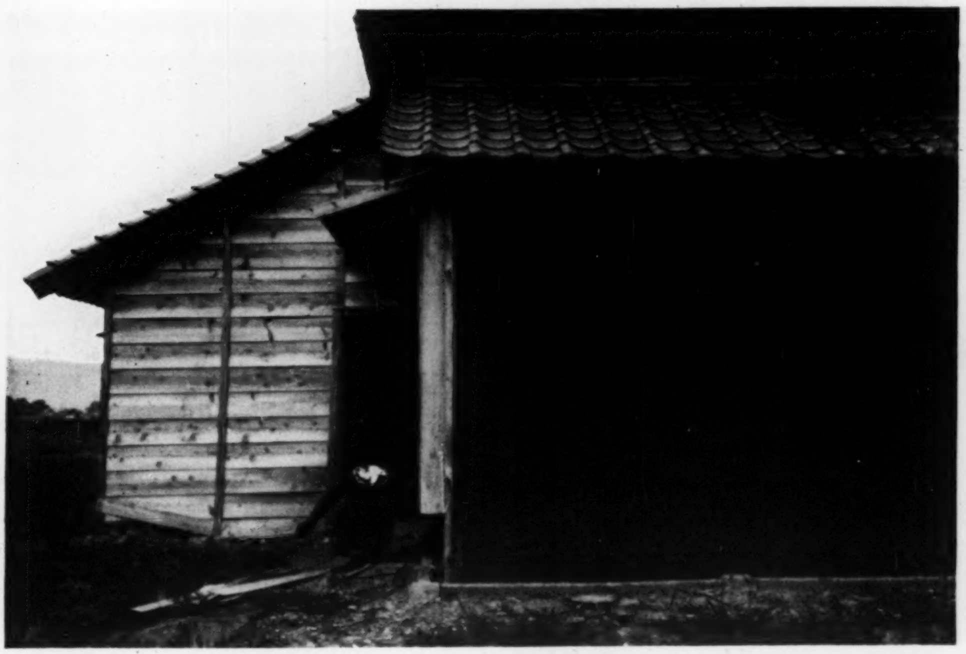

第 19 圖　船越，家屋の移動(25 cm)

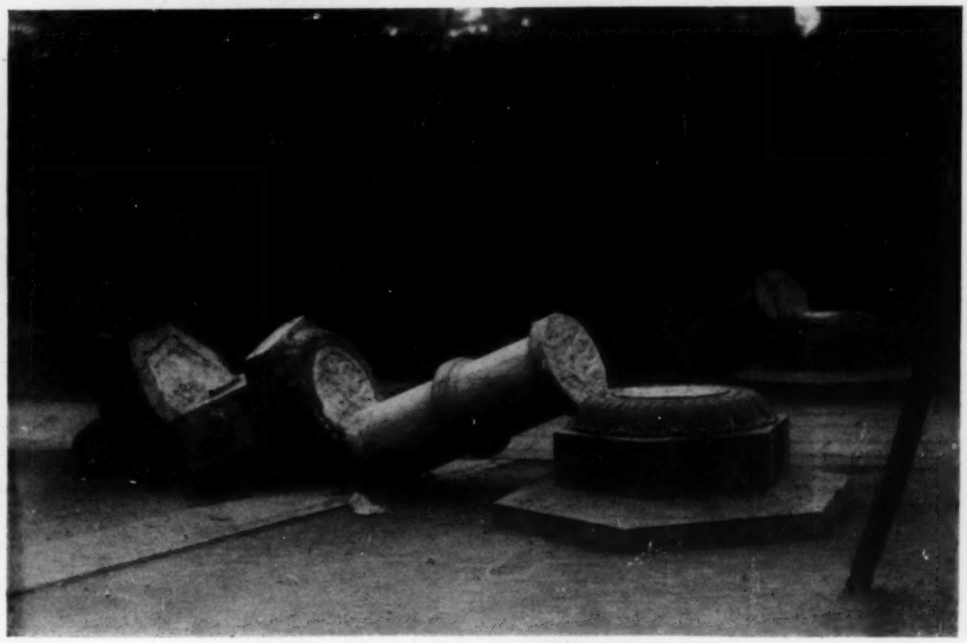

第 20 圖　靜岡市紺屋町，小梳神社の石燈籠の轉倒

變は肉眼的觀察に依つては發見出來なかつた.

有度山の南部は急峻な斷崖となり海に望んで居るが此の斷崖は上部に於て約2～3間の奥行が失はれる程度の崩落が久能山東方を除いて隨所に起つた.

海水の異常に關しては安倍川河口より三保に至る間の海岸に於ける住民に之を質問したが何人も之を認たものはなかつた.

地電流變化の觀測

地電流變化の觀測は大谷小學校に於て行はれた. 電極は小學校校庭の3隅に埋められ電極間の距離は東西85 m, 南北70 mである. 記錄裝置は電流計のフレを光學的に記錄せしめるもので, 電流回路に直列に5萬オームの抵抗を挿入した. 感度は東西方向のものは記錄紙上1 mmが1·2ミリボルトに, 南北方向のものは1 mmが1·5ミリボルトに相當し, 記錄紙の進行速度は1日に就き4 cmである.

觀測は7月13日19時より約1箇月間行はれたが, 此の期間には特異な地電壓變化は起らなかつた.

終りに臨み, 種々激勵の言葉を賜つた石本教授, 並に地震計設置に際し甚大なる援助を與へられた靜岡高等學校金原教授に對し深く感謝の意を表する次第である. 尙, 地震觀測に關し便宜を與へられた靜岡高等學校, 庵原中學校, 及び大谷尋常高等小學校の職員の方々に對して厚く御禮申上げる.

---

72. *The Sizuoka Earthquake of July 11, 1935.*

By Takahiro HAGIWARA,

Earthquake Research Institute.

A strong earthquake occurred in the neighbourhood of Sizuoka city at 17 h 25 m, July 11, 1935. Although damage was confined to a comparatively small area, 360 dwelling houses were demolished and 9 persons killed. The epicentre was determined to be $\lambda = 138°26'$ and $\varphi = 34° \ 59'$. The largest damage occurred in regions surrounding the Udo mountain block and in the basin of the Tomoegawa River. Only two aftershocks were felt in this region, the epicentres of which were found to lie in the north foot of the Udo mountain block by means of the network of the seismological stations temporarily erected after the earthquake.

73. 昭和10年7月11日靜岡地震震害調査報告*

靜岡高等學校 {金原壽郎
竹村千幹

（昭和10年9月17日發表——昭和10年9月20日受理）

序

昭和10年7月11日午後5時25分頃靜岡地方を襲つた强震による被害區域は東は清水市の東方庵原川に始り，西は安倍川の西方小坂川に至る靜岡清水兩市を含む平野であつて，特に有度山塊の西緣，北緣，及び巴川下流に於て激甚を極めた箇所が多い．

地震發生と共に靜岡縣及び靜岡，清水兩市當局を初めとして，近接町村に於ては多數の人員を被害地に特派して應急の處置を講ずると同時に，被害の狀況を主として經濟的見地より詳細に調査され，その結果も已に公表されたものが多々ある模樣である．

筆者等も地震の直後被害地を直接に踏査し，主として地震動の狀況を知る上に參考となるべき諸種の材料を出來るだけ蒐集して見たので，是を纒めて玆に報告することゝした．地震研究所，中央氣象臺等よりも幾多の專門家が出張せられて各種の踏査を行はれた模樣であるから，中にはその報告と重複する點も少くないであらうが，本報告が讀者諸賢に何等かの御參考となることが出來れば望外の幸である．

靜岡市は近年その隣接町村を合併して地域極めて廣大なものとなり，それと同時に土地名の改稱せられたものも決して尠くないが，本報告に於ては便宜上舊名を使用し，參謀本部の地圖に從つて記述を進めることゝした．

（1） 家屋の被害程度とその分布

家屋の被害は各方面に於て最も詳細に調査された事項であつて，此れに關する詳細な數字については縣廳，市役所に於て作製した表もあるのであるが，その中で全壞，半壞或は大破等の定義が明でないために，調査員の如何によつて，その區別に多少の相違を生じたであらうことは已むを得ない事柄である．

扨吾々の調査では，被害を數量的に表はすことは到底困難であつて，且又調査の目

---

* 寺田所員紹介

的から云つても左程必要なことではないと思はれるので，各部落を單位として考へ，先づ此を一巡して視察の上，各部落の狀態を比較對照して被害の甚だしいものより此を7階級に分類してあらはして見た．従つて各階級の示す被害の程度を適確に云ひあらはすことは出來ないが，大體次の如き程度のものである．

（1） 全壞家屋がかなりあつて，他は概ね半壞或は大破．

（2） 概ね半壞で，被害の少いものでも大破の程度が多い．

（3） 半壞がかなりあつて，大破のものが多い．

（4） 半壞も時々あるが，大體大破乃至壁の落下した程度のものが多い．

（5） 壁の落下したものもかなりあるが，家屋がやゝ損傷を受け，壁に龜裂の入つたものが多い．

（6） 棚の上の物體は落下し，壁にはやゝ龜裂が入つて居るものが多い．

（7） 被害としてはない．柱時計は止つた家も止らない家もある．

猶上記の中で，

（i） 全壞とは，完全に倒壞したものは勿論であるが，一旦取壞しの上，建て直さなければならないものをも含めて居る．

（ii） 半壞とは，必ずしも建て直しを必要とはしないが，家屋が傾き，柱が折れなどして，支柱を用ひて危く支へられては居るが，全體的に大修理を施さなければ今後倒壞のおそれあるものを指す．

（iii） 大破とは家屋に歪を生じ，壁土は落下して，局部的には大修理を必要とするが，倒壞のおそれがあるとまでは考へられないものを云ふことにした．

以上各部落を單位として評價したが，靜岡市及び清水市は地域が廣大であるから，此を便宜上數區に分けて考へることゝして，略圖上に被害階級を分布したものが第1圖である．猶此等の部落の中には，戸數の極めて多いところと少いところとがあつて，特に有度山上の日本平の如きは僅かに4戸を數えるに過ぎないがすべて同等に取扱つて見た．

一つの部落の中でも家屋の構造，土地の關係によつて被害狀況の甚しく異ることがある．全壞家屋の附近に被害輕微の家屋を見出すことが往々あつて，その相違が如何なる原因に基くか判明しない場合が多いが，大體に於て次の傾向を認めることが出來やう．

（i） 多くの家屋が連續して一列に並んで居る時は，兩端に位するものゝ被害は大きい．

（ii） 川緣にある家屋は被害が大きい．この傾向は幅1間程の小川に於ても認め

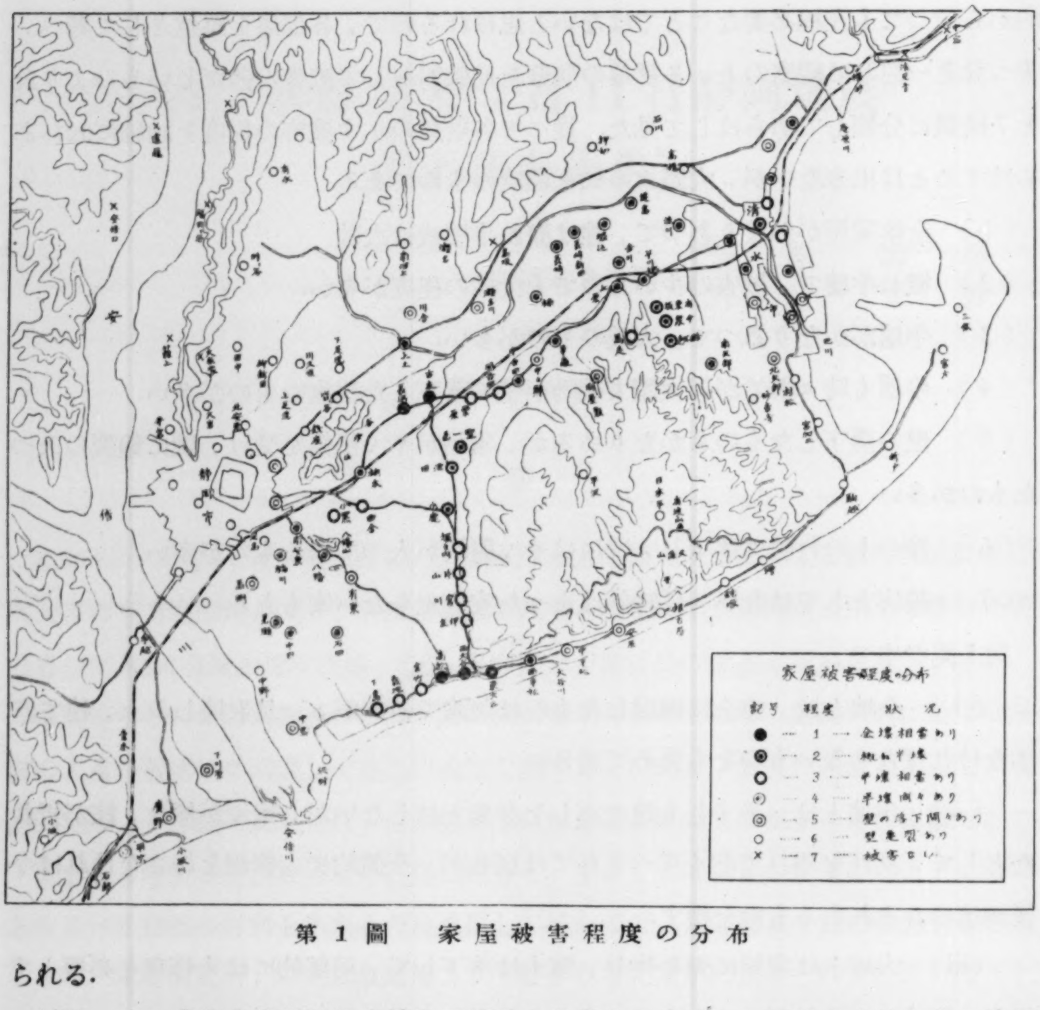
家屋被害程度の分布
記号 程度 状況
● … 1 … 全壊相當あり
◉ … 2 … 概ね半壊
○ … 3 … 半壊相當あり
⊙ … 4 … 半壊間々あり
◎ … 5 … 壁の落下間々あり
○ … 6 … 壁龜裂あり
× … 7 … 被害ない

第１圖　家屋被害程度の分布

られる．

（iii）やゝ高き土地が田地と境して居るやうなところで，この境の土地にある家屋の被害は大きい．

此を要するに，土地或は家屋の連續が急に中斷されて居るやうな場合に，この境界線附近にあるものゝ被害は大きいと云ふことが云へるやうである．

扨第１圖は各部落を全體的に見てこの被害等級をあらはしたものであるから，最悪の條件の下にある場合には例へば，階級４の土地にも全壞家屋の間々あることは勿論である．その著しい例は有度山の最北端にある上原部落である．この部落の東端には半壞家屋十數戶あつて，完全倒壞の家屋さへあるのである．上原は有度山の裾にあつて稍々小高き土地であり，北は低地となつて田畑である．この土地を國道東海道が通じて居るが，その東端に於ては國道の北側が急に低地となり，剩さへその南方には，殆んど此と接して，狐ケ崎遊園地內に東西約 100 m にも及ぶ池がある．被害の甚だしいのはこの池の北側であつて，局部的地形が地震には最惡の場所となつて居るためであらうと思はれるのである．上原全體としての平均の被害は左程大きなものではない．

かやうな實例は隨所に存在するのであるが，一々此を記載することは止め，翻つて第1圖の示す各地の被害狀況をその地形と共に記載して見やう.

(A) 有度山西緣の部落（聖(ヒジリ)一色(シキ)より伊庄に至る間）

北は聖一色より南は伊庄に至る間の家屋は概ね獨立家屋であつて，所謂田舍家と云ふべきものが多く，構造上に大差は認められない. 先づ聖一色を一巡して見ると大方の家屋は半壞の程度で，家は傾き，柱は外れ，然かも家屋全體が土臺石より數十糎も移動し，甚だしきは 50 cm にも上つて居つて，間々全壞家屋が見受けられると云ふ狀態で，一般に危く全壞を免れたと見られるものが多く，如何にこの土地の地震動の激しかつたかを想像するに充分である.

此れより南方の池田，小鹿は殆んど同じ狀態であるが，堀之內以南へ進むに從つて部落は次第に山手寄りとなり，それと共に被害も次第に減少して居る. 堀之內，片山，宮川の各部落の西部は小鹿等と同じく平地であるが，東部は小高き山地となつて居つて，此の山地にある部分の被害は意外に少いのである. 此れによつて見れば，此等の部落が比較的被害の少いのは山手寄りにあると云ふ地盤關係で說明するのが妥當のやうに考へられる.

更に南方，伊庄，北原と進めば，被害も次第に減少するが，大谷に至つて再び激震區域に遭遇することゝなるのである.

(B) 南方海岸沿ひの部落（濱村より三保に至る間）

西部の中島，濱村の被害は圖の如く比較的輕微なものであつて，この東方にある大濱公園には殆んど被害が見當らないが，海岸線に平行な道路によつて東へ進み，下島に至れば被害は急激に增加する. 下島の南方には東に流れる小川があつて，その支流の一つは下島の西端を南に流れて居る. 此の川を境として，此を東に渡れば被害は不連續的に增加し，それより東行するに從つて次第に激しくなり，大谷に至つて最も激甚を極めて居る. 下島，敷地，宮竹では部落の北端が主としてひどく，南方道路沿ひの部分は此れより甚だしく輕い. 大谷川を渡つて高松に行けば，道に面する家屋の被害は極めて甚だしいが，北部は却つて減少して居る傾向がある. 更に西大谷に於ては道路と大谷川との間に挾まれた區域の被害は最も甚だしく，概ね全壞と云ふことが出來るが，此れより北方及び大谷川南方においては全壞家屋は稀である.

扨，小鹿方面より南下する縣道との交叉點を境として，道は東大谷の部落に進むのであるが，この交叉點附近には，被害の至つて輕微な部分がある. 此の地點は有度山の一端が著しく接近した部分であつて，伊庄，北原等と同樣な地形にあつたことが幸したものと考へられるのである.

此れより道は大谷川と共に東南に向ひ，有度山よりやゝ遠ざかるにつれて，再び被害激甚區域に遭遇するのであつて，道路沿ひの南北共に倒壞家屋夥しく，西大谷と共に今回の地震による震害の最も甚だしかつ區域となつて居る．然るに道が北東に進んで山沿ひとなり，大谷川をやゝ離れるに及んで顯著に減少し始め，此れより東の西平松，中平松，古宿と進むにつれて益々輕微となり，東照宮に名高き根古屋に行けば殆んど無被害の狀態に近い．この間僅々１里足らずにして，最激震區域より殆んど無被害區域となり，根古屋以東蛇塚，駒越を經て，三保松原に至る間は大體根古屋と同等である．

以上を總括して考へて見れば，要するに震害は主として大谷川及びその西方を流れる川の附近であつて，下島以西，高松北部，更に石田，有東に被害が少く，又大谷以東が極めて顯著に減少して居る點より考へて，大谷，高松の被害が甚だしかつたのは全く地盤によるもので，若し聖一色，小鹿等と地盤に於て相違がなかつたならば被害に於ても大差がなかつたのではあるまいかと想像せられるのである．

（Ｃ） 東海道沿線の部落（靜岡淸水兩市間）

靜岡市內に於ても東部谷津山の附近に於てはかなりの被害が認められるが，此れより舊東海道に沿つて東に進み，曲金に至れば被害は極めて顯著となり，半壞，大破が至るところに見受けられるのであが，更に東に向つて長沼，古庄に行けば最も激甚を極めて居る．

靜岡淸水兩市間には東海道の他，靜淸國道と呼ばれる國道が近年開通されたのであるが，長沼，古庄は此等兩國道の交叉點に當つて居る．今古庄の震害について云へば，その北部に於ては比較的少く，家屋に多少の損傷を與へた程度であるに反し，兩國道沿ひの部分が主として被害を蒙り，特に古庄より栗原に通ずる東海道沿ひの部分は大方全壞の狀態に近い．又長沼に於ても，靜淸國道沿ひ，特にその南方が甚だしいが，此も國道の近傍であつて更に南方鐵道線路に近き方には被害が少い．

川の存在のために，その附近の被害の增加することは各所に認められる所であるが，古庄，長沼に於ては道路の存在のためにこの事があつたかの如き觀を呈して居る．扨，此れより東，栗原，國吉田，中之鄕と進むに連れ，道は次第に山手に入つて有度山塊の裾野を進むことゝなるが，それと共に被害は減り，中之鄕に至れば益々減少の傾向を示し，草薙を經て前述の上原を通り，平川地に至る間は大同小異の狀態で淸水市に至るのである．

（Ｄ） 有度山塊東北緣の部落（平川地，妙音寺間）

平川地より南に分れ，名刹龍華寺に至る路に沿ふて進めば，この地方の被害の意想

外に大なることに驚くであらう．有東坂，今泉は家屋の構造，被害の狀態が聖一色を彷髴せしめるものがあり，船越に於ては特に西部の山に近き方が甚だしいが，東部の平地に於ては此れより餘程輕くなつて居るのである．この事實は堀之內，片山に於けるものとは全然正反對であつて興味ある問題の一つであると考へられる．

有度山の地形は西部とは著しく異り，西部を假りに遠淺の海に譬へれば，この地方は岸壁とも云ふべき形をなして居る．これが第一に考へられる著しい相違である．又今回の地震には，後に述べるやうに，その地震動の方向に極めて特徵があつて，恐らくは S- 波の最初に著しく大きな西向きの加速度があつて震害の多くはこのために一度に起つたものではないかと考へられるのであるが，この地動の特性も亦或は何等かの關係を持つて居るのかも知れないと思はれるのである．

有東坂より西に向ひ山越えに馬走に行くことが出來る．馬走の被害も亦かなり激しい．馬走は東，西，南と山に圍まれた土地ではあるが，北は平川地より田圃續きで低い土地であることを思ひ合はせれば，一見山中の部落の如くであつて實は入江となつて居るので，有東坂其の他と同様に考へらるべき區城である．

扨て船越より山傳ひに南下して南矢部に行けば被害は大いに減少し更に妙音寺に至れば極めて少い．

この邊は地形上から見れば船越附近と大して區別なく，强いて云へば有度山の形狀がやゝ平坦となつて居ると云へる程度であるが被害がかやうに減少して居るのは最早地震勢力の中心より遠ざかつたためではないだらうか．この東方の海岸線，卽ち清水市を見ても，巴川河口を境としてそれ以南には大した被害はないのである．

（E） 清水市內

被害の大きい區域に今一つ清水市がある．清水市は清水港に臨み東部には埋立地多く然かも市內を縱走する巴川がある．この影響のためか市內に於ける被害は相當に大きく，且つ局部的にその狀況が異り甚だ複雜であるが，大體に於て巴川以東に被害の大きいところが多く，鐵道線路以北に於ては巴川に近き志茂町，傳馬町が最も甚だしく，以南に於ては，島崎及び入船町附近が最も甚しい様である．更に巴川以西に於ては北より，入江町，上清水，下清水と並び此の地方は云はゞ山手に當り被害は比較的少いのである．

靜清國道は入江町に入つて二手に分れ，その中一つは一旦南下し上清水，下清水の中間を東に進んで波止場に向つて居るが，この國道の附近には被害の比較的大きい部分が點在して居る．これを直ちに國道の存在のためとは云へないこと勿論であるが，上述の古庄，長沼の被害と合せ考へれば，そこに何等かの因果關係を想像したくなる

のである．

猶，澁川で，部落の北端巴川の北岸にある瓦工場は軒を連ねて完全に倒壞したが，此等は勿論非住家であつて，家屋の構造上倒壞し易きものと考へられ，特にこの部分のみに地震動の大きかつたものとは考へられない．

（F）有度山中

有度山中には家屋至つて少く，小部落として僅に平澤及び向屋敷を數え得るのみである．向屋敷にはかなりの被害があるが平澤及び日本平には殆ど被害なしと云ふことが出來る．その他山上の山小屋の如きも何等の變化を示して居らない．

要するに，向屋敷の如く比較的低地にある部分は被害があつても山上には何等の被害なしと云ひ得るので有度山塊の地盤のよいことを示すものであらう．

（G）その他の部落

以上で有度山の緣邊及び清水市についての記載を終つたが，被害の比較的大きい地方として，谷津山南方の曲金及び小黑を擧げなければならない．圖上，古庄，長沼，曲金，小黑，八幡，稻川，見瀨と並んだ一つの曲線を考へると此が比較的被害の大きい區域を示すやうでもあるが，此等の部落と聖一色及び大谷との中間は大體田畑であつて，その間に有東部落一つ存在するだけである．有東は八幡に比すればその被害は確に小いが，此を以て上記の曲線が一つの連續した被害區域と考へることが出來るか否かは疑問である．

その他の地方に於ては特に記載すべきことなく，有度山塊より遠ざかり北部山岳に近づくと共に被害が減少して居つて，安倍川の存在は被害狀況の分布に何等の特異性を與へて居らない．

（2）土地の被害

家屋の被害と土地の被害とは又別であつて家屋被害の大きいところ必ずしも土地の被害が大きいのではない．今此を各種に分類して記載して見やう．

（A）山上の被害

山中の被害踏査は極めて困難であつて，到底是を詳細に知ることが出來ない．豫め被害のあることを傳へ聞き，その土地を實見するより他に方法がないので踏査洩れとなつた部分のあることは止むを得ないことである．

扨，有度山中最も被害の甚しいのは，日本平南方の崖崩れである．有度山はその西部より北部にかけては，なだらかな斜面をなし，その頂上に近きところに景勝地日本平を有するのであるが，その南方は數十丈の斷崖絶壁となつて久能山を隔てゝ駿河灣に向

つて居る. 崖崩れの甚しいのはこの斷崖であつて, 日本平に立つて南方を見渡せば, 山と云はず崖と云はず, すべて崩れないところはなく, 文字通り赤裸々の狀態と化してしまつた. 一見地震動の甚しかつたことを思はせるものがあるが, その地質地形から考へて, 崖崩れの起るのは當然であり, 斷崖となつて居ることが已に崖崩れを起し易い證據であるとも云へるのであるが, 前條にも述べた通り土地の不連續になつた地點であるから, 此も亦被害を助長する一つの原因になつて居るのかも知れないのである.

此の崖崩れも日本平及びその西部地方に多く, 東部は比較的減少し, 蛇塚の北方に於ては殆んど見受けられない.

久能山地方における名物苺畑はこの南方, 海に面したところにあつて, その石垣のすべり落ちたものが殆んど大部分であるが, 此も同じく主として久能山以西に甚しく, 蛇塚に至れば何等の被害がない.

かやうに崖と云ひ石垣と云ひ, 大體同じ條件のものゝ被害が東部に於て減少して居ることは確に地震勢力の小さかつたことを物語つて居ると云へやう.

畑の被害の大きいところは, 西南端の大谷及び伊庄部落東方の山地であつて大谷小學校裏など最も甚だしいやうである. 有度山の地形はこの邊に於て多くの襞を形成して居つて, 西北部の如く傾斜の緩かな土地と異り, 畑は山腹の急斜面に階段的に出來て居るもので, 云はば被害を受け易い狀態になつて居る. この階段が崩れ, 地割れを生じたものであるから, 此を西北部と同列に考へることは出來ないのである.

扨, 地震動は有度山西方の緩かな斜面上に於てもかなり激烈なものがあつたやうで, 當時聖一色東方の山上にあつた農夫等の語るところによれば, 地面は下から湧き上つて來る如く, 到底直立することが出來ず, 皆地上に伏して難を避けたと云ふことであつた. 此の地方には畑の被害も相當にあるやうに聞いたので, 實地踏査に出掛けた譯である.

先づ, 聖一色より山中の部落平澤に至る小徑に沿ふて東に進めば, 山は緩かな斜面になつて居るが, その沿道を注意して見ても, 畑の被害は勿論, 龜裂一つさへ見當らない. この斜面を登り詰めたところは概ね茶畑であつて, 此れより東は急坂となつて平澤部落に下ることが出來る. 被害のあつたのはこの頂上の附近であると聞いて居つたが, 不幸にして吾々は此れを發見することが出來なかつた. 何分見渡す限り平坦な茶畑であるから, 見通しの利かないために發見出來なかつたことゝ思はれる. 唯この土地で特に東側が斷崖となつて居る部分には小規模の龜裂が時々見受けられるので, 恐らく問題の被害もこの地形と關聯して居るものではないかと思はれる. 地震動がかなり大きなものであつたらしいと考へられる一方に於て, 土地被害が一般に見當らない

のは寧ろ意外である．猶この土地の附近にあつた山小屋には何等の異常も認められないのである．

次に有度山の東北端，有東坂と馬走の間に横る馬の背の如き南北の尾根がある．この尾根に沿つて南北に走る長さ 100 m にも及ぶ龜裂があると土地の人々が語つて居つたが，この地點は踏査して見なかつた．

有度山以外では八幡山中に小規模の崖崩れがある．特に東北端には南北に十數米の龜裂があつて，その東部は西部に比して最大 10 cm 程の沈下を示して居る．但しこの地點は，東，北，西共に斷崖となつて居るところである．

この他，谷津山，有東山，賤機山には此れと云ふ被害は見當らなかつた．

(B) 道路の龜裂

道路の龜裂として比較的大きいものは小鹿大谷間道路の大谷に近いところ，及び八幡高松間道路の有東高松間にあるものなどであるが，此等の道路は共に略南北に走つて居つて，然かもその兩側は田圃となつて低くなつて居るのであるから，一種の崖崩れの性質をもつて居る．

川べり或は堀に接した道路に龜裂を生じ易いことは地形上寧ろ當然のことゝ考へられるが，靜岡市内の如く被害の少い地點でもその外濠に沿つた道路には龜裂を生じた箇所がある．

この他極めて小規模の龜裂は各所に點在して居つて，中には果して今回の地震のために生じたものか否かが明瞭でないものもあるが，龜裂の方向について氣の付いたことは；

(i) 道路を横切るものは少く，且つ

(ii) 大體南北に走る龜裂が多い

と云ふことである．從つて南北に通ずる道路に多いと云ふ事にもなる．但し川べりの如く特殊の地形にあるものは例外であること勿論である．

被害の殆んどない靜岡市西部，賤機山西方の道路にも時々南北方向の小龜裂があつた．

又靜淸國道谷津山南方に於て，鋪裝道路面を横切る龜裂があつた．國道はこの邊東北に向つて居るので龜裂は東南に向つて居る．然しこの龜裂は道路面だけであつて更に東南に伸びて居る樣子は見えなかつた．

龜裂の方向に現れた一つの傾向は，次に述べる地震動の主なる振動方向が東一西乃至東北一西南であることゝ考へ合はせれば，そこに密接な關係があることを思はせるものがある．

(C) 清水港岸壁

土地の被害として最も經濟的に打撃を蒙つたものは清水港岸壁である．巴川河口より北へ約 300m（?）程の間は岸壁を形成する部分とその後方の土地とは相對的に變位をなして東西に分れ，その間に陷沒地帶を生じて茲に海水の侵入したところもある．岸壁自身もやゝ東に變位し，然も東に傾いて居ることは認められるが，單にこれだけとしては，あまりに陷沒地帶が大きすぎるやうである．

岸壁の如く土地の不連續になつたところは已に被害の大きいことが豫想せられる上に不幸にも岸壁が南北に造られてあつたことが特に今回の震害を大きくした原因であつたらう．清水港には岸壁が多いが特にこの部分に大被害があつたと云ふのは單に巴川河口に當るためのみであつたらうか．

(D) 其の他

その他の地方にも小規模の龜裂，崖崩れなどあるが吾々の踏査した範圍では何れもその地形上當然と考へられるもののみで，特殊の意味をもつと思はれるやうなものはなく，斷層と云ふやうなものは全然見當らなかつた．

(3) 家屋の振動

以上は主として地震動の强さと關係ある事項であるが，次に地震動の振動方向に關係するものとして第一に家屋の振動狀態についての調査結果を記して見やう．

(A) 家屋の傾き

今回の地震に極めて顯著な一つの事項は家屋の倒れ或は傾きの方向が殆んど一定して居ると云ふことである．然しながらこの事實は主として有度山以西に於て見られるものであつて，清水市内の如きでは必ずしもそうではないやうに思はれるので，傾きの方向に關する分布狀態を部落別に調査して見た．

ところが或部落に於ては極めて整然と殆んどすべての家屋が東側に傾いて居る．此は主として有度山以西に於て被害の甚しい土地に現はれた現象であるが，又他の部落では種々の方向に傾いたものがあつて，何れともその方向の決定し難いところもあるのである．此れは主として被害の比較的輕い部落に現はれた現象であるが，清水市は被害程度の分布が極めて複雜であるやうにその傾きの方向も場所によつて非常に異つて居る．

扨，或る部落に於て傾きの方向が極めて顯著に一定して居るやうな場合でも，それが激震區域に屬して居らない時には，その中に少數の例外があつて全く異つた方向を取つて居るのである．此れはその家屋の構造にもよるのであらうが，又一つにはその

特殊の條件に基くものであらう．如何なる條件がかやうな特異例を生ぜしめたかについては，全く不明の場合が尠くないが，東西方向の傾きについては次の如き傾向のあることは，かなり明瞭に認められるのである．

（i） 川或は低地の際に建つ家屋は川或は低地の方に傾き，

（ii） 家屋が連續して建つて居る時には，その兩端のものは夫々外方に傾く．

但し（ii）の場合には內方に倒れることは困難であらうが，多少の傾きは何れにも自由であると考へられる樣な場合にもこの傾向がある．

かやうな特殊の狀態にあるものを除いても，部落の一部は東に傾き，他の部分は南に傾くやうな場合があつて，全體として此れを決定しかねるやうな時には，此れを東及び南の二つの方向あるものとした．

かやうにして傾きの方向を矢印にて示し，此れを略圖の上に分布したものが第2圖である（第2圖以下は土地名を記入してないが，第1圖を參照していたゞきたい．）．二つの方向はあるが，その中の一方が劣勢であると思はれる時には此れを小さい矢印で示してある．猶玆に用ひた傾きと云ふ言葉は明瞭な傾きの他，僅かの歪をも含ませてあるから，被害の小い部落にも及んで居るのである．

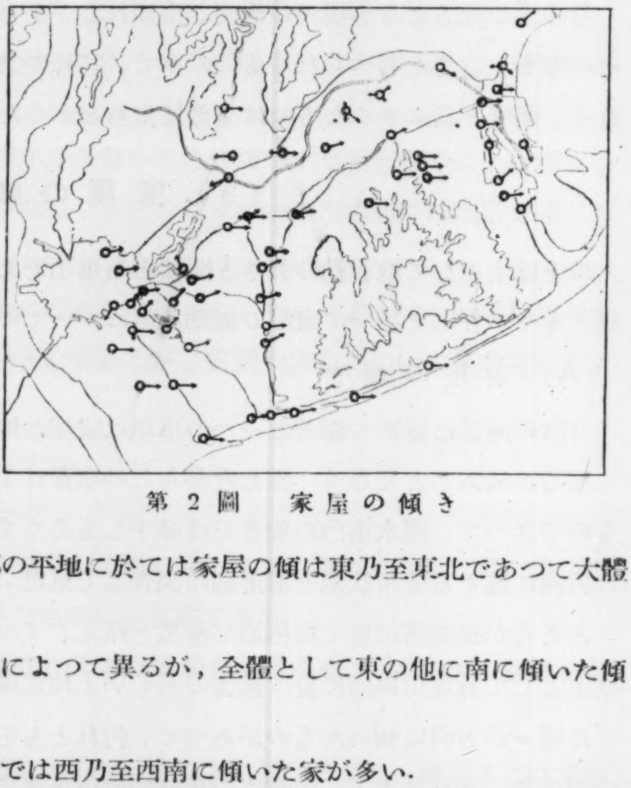

第 2 圖　家屋の傾き

此の分布圖について見れば，

（i） 有度山緣邊並にその西部の平地に於ては家屋の傾は東乃至東北であつて大體皆一樣である．

（ii） 清水市の附近では各區域によつて異るが，全體として東の他に南に傾いた傾向がある．

（iii） 巴川上流にある上土附近では西乃至西南に傾いた家が多い．

以上（i）に揭げた區域に於ける傾きの方向が非常に一致して居るのは，S-波の初めに餘程特殊の非對稱的なものがあつたためであらうが，（iii）の區域が此と反對の方向を持つて居るのは如何なるためであらうか．然かもこの區域の被害は決して輕微なものでなく，上土には倒壞家屋さへも存在して居るのである．それと同時に，清水市地方がやゝ南がゝつて居ることは有度山の西方には見られないことであつて，此も

注目に價する事柄であらう.

（B） 家屋の辷り

家屋の傾きには多少共辷りを伴つて居る. 辷りは簡單な平行移動でなく廻轉をも含んで居る. そのために移動の大きさを簡單に知ることは困難である. 又同一地點で 30 cm 以上も辷つた家屋の隣りに殆んど辷りを認め得ないものがあると云ふ狀態で, 此の點被害程度よりも更にその差異が甚しい. 辷りの大きさは, その土地の地形以外に家屋の構造そのものによることゝ思はれるが, この間に直ちに見分けられるやうな關係は發見出來なかつた. 例へば瓦屋根と藁葺屋根とによる相違と云ふやうなものは判然としないのである.

扨, 辷りの大體の程度を定めて再び此れを圖上に分布するために, 各部落を次の標準によつて分類して見た.

（1） 中には 40 cm 以上も辷つた家屋もあるが 20 cm 位辷つた家は普通である.
（2） 中には 20 cm 以上も辷つた家屋もあるが 10 cm 位辷つた家は普通である.
（3） 中には 10 cm 以上も辷つた家屋もあるが 5 cm 位辷つた家は普通である.
（4） 多少すべつて居る.

此れを第2圖と同樣にあらはしたものが第3圖である. 此れによつて見ても判るやうに, 辷りの方向は大體傾きと同じであつて, 三つの區域に分けられるのであるが, 被害程度との關係については記すべきことがある. 今大谷地方と堀之内西部とを比較

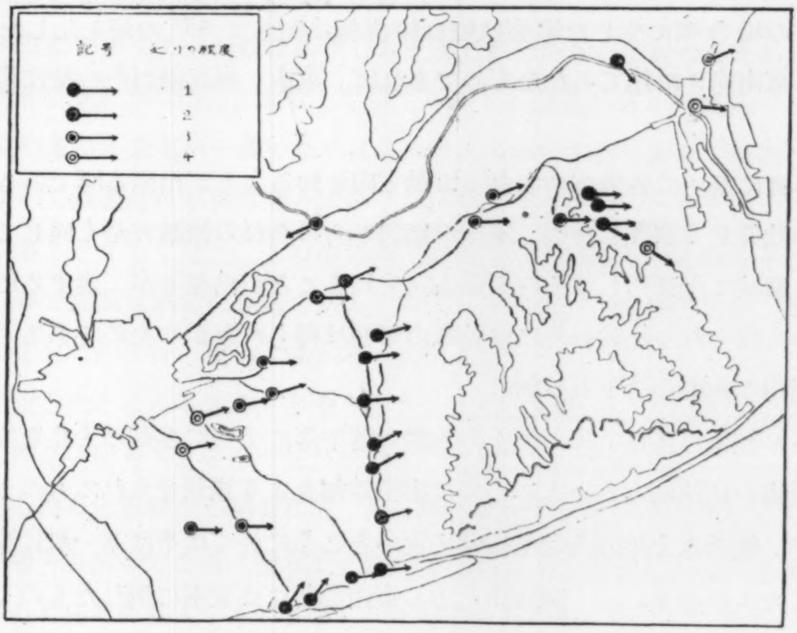

第3圖 家屋の辷り

して見ればその被害にはかなりの相違が認められるが，辷りの大きさから見れば大した差異はないのである．

然も堀之內，片山附近で判明したことは辷つた家屋は却つて被害の少いと云ふことである．筆者の實見した家屋の如きは 30 cm 以上も辷りを生じたに關らず，障子の破れさへ殆んど見えず，聞くところによれば棚上の物體さへも落下しなかつたと云ふ話であるが，その附近には辷りが比較的小さくて半壞の家屋が存在して居るのである．この事實は家屋の建築上注目すべき事柄であらう．下島，宮竹なども堀之內，片山等と似通つた狀態にある．

猶この辷りは一般に次第に移動して行つたと云ふやうな形跡はなく，飛び移つたと考へられるものが多いので，上下動の加速度はかなり大きなものであつたやうに見えるのである．

（C） 戶障子の破損，壁の龜裂

家屋傾斜の方向が極めて整然として居るやうに，障子の破損，壁の龜裂の狀態にも整一的の傾向は顯著に顯れて居る．

例へば有度山西方に於て家屋傾斜が東になつて居るところでは，障子，壁の面が東西面內にあるものは著しく損傷を受けて居るが，此れと直角な面內にあるものは，非常に被害が少い．（全壞半壞家屋の如きは勿論別である．）

而してこの場合壁に生じた龜裂は概ね鉛直線に對して 45° の傾をなした直線である．家屋が東南向きに建てられたものであれば，東南，東北兩面內の壁は共に損害を受けて居る．

以上の事實に基いて各地方の主なる振動方向を知ることが出來る譯であるから，筆者等はその狀態をも調査したが，家屋の傾斜から得られる結論と全く同じである．唯被害輕微な區域に迄應用してその振動方向を知ることが出來るが，要するに上記の傾き，辷りから得られる結論以外には特殊の事柄は得られなかつたのである．

（D） 屋內の物體の落下及び倒れ

震害の更に輕微な區域では，棚上の物體の落下等によつて振動の大略を知るより他はない．被害の比較的大きいところでは家屋の傾きより豫想せられるものと同一の結果であるが，輕微な土地卽ち北部山岳に近いところに於てはやはり一般に東側に倒れ或は落下したものが多いが，賤機山北方の東西部落には東南に倒れたものゝ多いことが事實である．

（4） 石燈籠及び墓石の轉倒

家屋の形狀は複雜であるから，前條に述べた事項より地震動の正確な方向を推察す

ることが出來ない．此れを知るために地上の溜水の溢れ方を調べる事も考へたのであるが，何分此れは實例も少く且つ痕跡が明でないために不適當であるから，直接土地に接し最も對稱的で且つ比較的不安定な石燈籠の轉倒方向を知るために全力を注いだのである．玆に石燈籠と云ふのは所謂春日燈籠及び殆んど此れと同樣の形をしたものを指して云ふので雪見燈籠の如きは除外して考へた．

猶，墓石の中には頂を半球形とした圓壔形（嚴格には上部の半徑の方が大きい）のものもあるので，その形が對稱であると云ふことから此れも參考にして見た．

扨，靜岡市內及びその南方隣接部落には大邸宅が多く，幸にも燈籠を有する家が多いので充分にその方向を調べることが出來たが，その他に於ては神社佛閣を除いては數多く存在しないので，筆者等が全力を注いだにも關らず，その成績をあまり擧げることの出來なかつたのはまことに遺憾であつた．

石燈籠も家屋と同じく，方向の一定して居る所と然らざるところとがあつて，地震動のあまり激しくなかつた土地に於ては，同一の神社內にも種々の方向に倒れたものがある．その理由の判明しないものも多いが，調査を進めるに連れて最初の中は"若しや"と思ひ，終りには"又か"と思はれるやうになつた關係がある．

（i） 池の周りにある燈籠は池の方に倒れ，
（ii） 坂道にあるものは坂下の方に倒れる

と云ふのが此れであつて，此れは必ずしも土臺石が已に傾いて居つたためといふのではない．家屋の傾き方の場合と比較して見てもそこに關係があり相に思へるのである．

石燈籠そのものゝ分布が一樣でなく且その數も少いのであるから，轉倒方向分布圖を作るに當つて到底此れを部落別とすることが出來ないから，已むを得ずその所在地別に記入することゝして見た．この中靜岡市及びその近傍は比較的數も多く方向も一定して居るので此等は適當に纏めて記入したが，その他の土地に於ては，所在地について夫々決定して行つた．從つて僅かに一基より判定した所もあり，數基よりその平均として判定したところもある．かやうなところは此れを一つの矢印で方向を示したが，判定し得ない場合もあるので此れは數本の矢印を用ひて現した．この中特に或る方向が信用し得ると思はれる場合には，此れを比較的大なる矢印で示してあることは家屋傾斜の場合と同樣である．猶明瞭に特殊の事情ありと思はれるものは是を省き，更に丸型墓石も參考に記入することゝして出來上つたものが第4圖である．

家屋の傾きより豫想せられる結果以外には何等特別のことはないのであるが，北方の山岳に近い方面では，その方向があまり一定して居ないのである．恐らく此等の地方では石燈籠は一擊によつて倒れたのでないためであらう．

次に有度山西方の部落の中，大谷，小鹿，下島方面は激震區域であつて，その方向の一致して居るべきは家屋の傾きより見ても寧ろ當然のやうに思へるので，此れを除き，靜岡舊市及びその隣接南方部落内にあるもの全部を數へ，これを轉倒方位について如何に分布して居るかを調べて見ると第5圖を得るのであるが，此れによつて一つには燈籠を轉倒せしめた原因の加速度が各地によつて殆んど同一であつたことが判ると共に又一つには石燈籠の轉倒が如何に地震動に忠實であつたかも判る譯である.

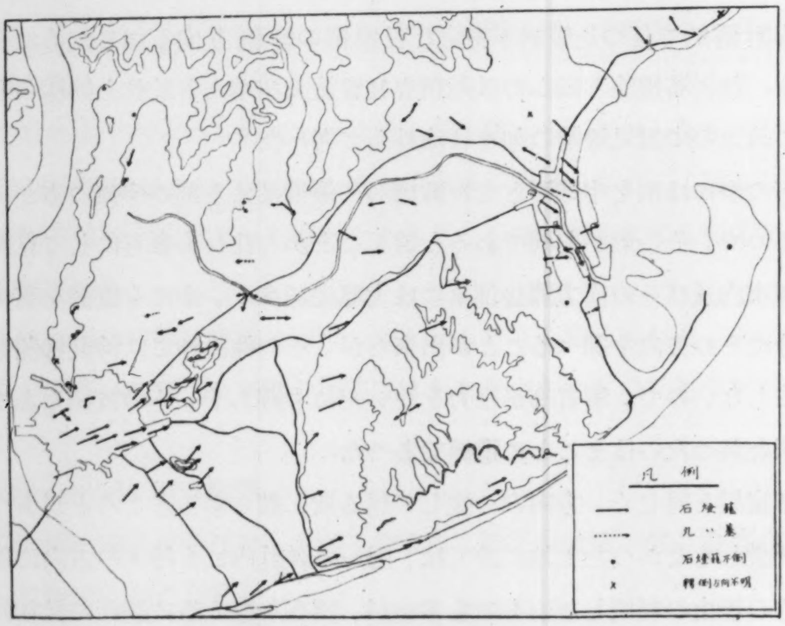

第4圖　石燈籠の轉倒方向

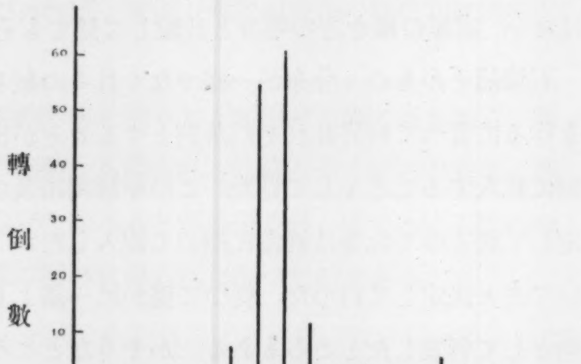

第5圖　靜岡舊市街及び隣接南方部落に於ける石燈籠の轉倒

猶，古庄，平澤及び清水市内のある神社に於て拜殿に向ふ道の左右にあつた二つの燈籠が殆んど一直線をなして皆夫々道の外側に倒れて居るのに遭遇した（第4圖參照）が，然しその理由については全く不明である.

最後に普通の墓石であるが，小鹿の本覺寺の如きは激震區域でその墓石數百個は殆んどすべて倒れてしまつたのであるが，その方向は大體として東向きの傾向があると思はれる程度であつて嚴格には判定し難い．この事は又大谷の大正寺その他の寺院内

墓地に於ても同樣である．恐らく墓石は次第に土臺石上を辷つて最後に落下すると云ふ經路を取つたものであらう．

又墓石は廻轉したものが多い．その方向は一つの墓地內に於ても一般には色々であつて，唯何れかの廻轉が他のものよりその數に於て多少勝つて居ると云ふ程度であるが，谷津山の北側にある陸軍墓地內のものゝ廻轉が全部反時計方向であつたのは甚だ興味ある現象の一つである．

附　　記

以上で地震動の强さ並に方向の各地による分布狀態に關する記載を大體終つたのであるが，猶一言附け加へるべき事柄がある．今震害狀態の分布圖を一瞥すれば直ちに考へられることは，被害の比較的顯著な區域と云ふのは，大谷及び谷津山を大體中心として畫いた2本の NE—SW 直線間に挾まれた部分であると云ふことであつて，この中北方に想像した直線と云ふのは大體北部山岳の裾を連ねた直線に近いものであるが，南方に考へた直線と云ふのは大谷と清水市南部とを結んだものであつて，此の線より以南は被害が急激に減少して居ると云ふのは爭へない事實である．

かやうに東北—西南の直線を想像しながら被害分布を考へて見ると，何かそこには關係らしいものが見えないではないのである．

小鹿より北東に進めば，畑の被害極めて甚だしいと云はれた地點があり，山中の被害地向屋敷，馬走を通り，龜裂ありと云はれた尾根を通つて激震地有東坂に至り，更に此れを延長すれば清水市內における最被害地，志茂町に到達する．

前述の古庄，曲金，八幡，稻川，馬淵と結んだ直線も大體この方向を取つて居るのである．その他にもこの直線上に强ひて持ち來らすことの出來るものもないではない．

次に被害は有度山の周圍に於て大きいが山上にはないと云ふことが出來る．この事から見れば有度山北方の東海道沿線部落の被害はむしろ意想外に大きいのであつて，不幸此等の諸部落が聖一色等と同樣な平地にあつたものとすれば，その被害の程度も想像に餘りあるものがあつたらう．唯その北方にある楠新田，長崎等の諸部落の被害が比較的少いのは北部山岳にも近いと云ふことから說明がつきそうにも思へるのである．

(5) 井戶水の變化

靜岡地方では地下水の湧出が盛であつて掘拔井戶を利用する家庭が非常に多い．從つてその水壓に變化を生ずる時は直ちに此れを知ることが出來るのである．

地震直後にあらはれた顯著な現象の一つはこの水壓の增減である．筆者の自宅は第1圖北安東附近にあるのであるが，地震直後にはかなりの增水を見たが少時にして止り，それより後は急に水壓約 15 cm の減水を示し，約1ケ月の後に至つて始めて舊狀に復することが出來たのである．とろこが，中には地震直後より引き續き增水を示したところも存在する．減水と云へども一時的には增加したものが多いやうであるが，この一時的增加はしばらく措き，その增減を調べて見ると明に增加した區域，明に減少した區域の他に，增加と減少とがあつて何れとも判定し難いところもあるのである．

井戸の深さが調査出來なかつたので，この間何等の結論も得られないのであるが，その分布は第6圖によつてあらはされる．

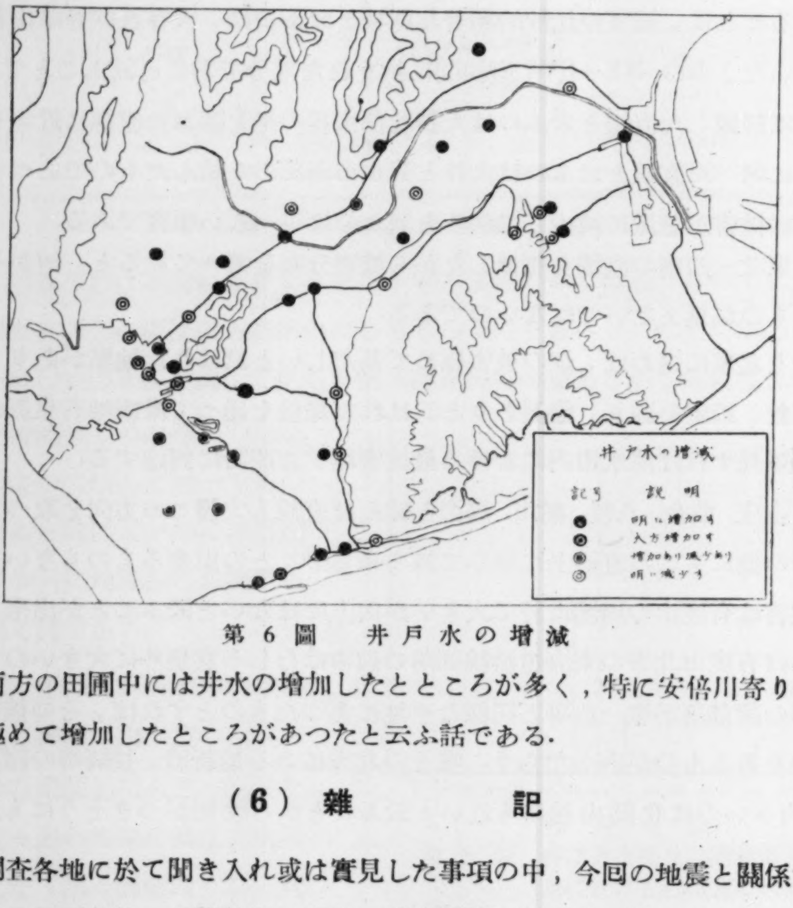

第6圖　井戸水の增減

有度山西方の田圃中には井水の增加したとところが多く，特に安倍川寄りには直後少時の間極めて增加したところがあつたと云ふ話である．

(6)　雜　　記

最後に調査各地に於て聞き入れ或は實見した事項の中，今回の地震と關係すると考へられるもの二三を拾つて斷片的に記し，讀者諸賢の御參考に供しやう．

(A)　大正12年9月1日關東地震との比較

今回の地震は，北方山岳寄りの方面に於ては，その强さは關東地震の時と大差がない模樣である．從つて柱時計の如きも，ある方向に向いて掛けられたものは停止した

が，此れと直角に向いて居るものは止らなかつたと云ふところがある．所が關東地震の時止つた時計は今回は止らなくて却つてその時止らなかつたものが今回止つたと云ふことを時々聞き，更に壁の小龜裂にも此れと同様なことのあるのを耳にした．此れによつて見れば主なる振動の方向が兩者に於て互に直角になつて居つたと考へられるのである．

（B） 地鳴り

有東坂，今泉等に於て地鳴りの様子を聞いて見ると殆んど口を揃へて次の如く語つて居る．最初西南の山中に飛行機或は自動車の音の如きものが聞えたと思つて居る中に激震に襲はれたと云ふのである．

又聖一色東方の山中の畑に居つたと云ふ者の話でも，先づ小鹿方面より音がやつてきて，地震動が此れに續いたと云つて居る．

何れも略西南の方面から最初に音の傳つたことを意味するやうで，玆にも再び SW—EN 方向が登場してくるのは面白い．

（C） 小鹿の池

小鹿より堀之內に至る道路の東には東西に並んで二つの池があつて，その中東側のものはやゝ小くて此れを女池と呼んで居るやうであるが，この池は東西約半町南北約1丁餘りのものであるが，その中央部が地震のため急に隆起して池中島を作つたと云はれ，當地方の評判になつて居るので實見して見たが，元來この池は水深 2～3 尺の淺いもので池中には至るところ芦が生えて居るのであつて，その中央南寄りの部分にある芦は約1畝歩ばかりが泥土と共に浮き上り，そのため芦は倒れて一見島を作つたかのやうな狀態となつて居る．然し果して池底が隆起したものか，或は芦の一團が根こそぎ浮き上つたものか定かでないが，此れが地震のためとすれば何れにしてもこの地方の地震動の如何に激しかつたかを想像するに充分である．

（D） 大谷川の鰻

地震以前7～8時間卽ち午前10時頃より大谷川及びその支流を多くの小魚（主として鰻の子供）が群をなして下つて行つたと云ふ事で，時恰も干蘭盆の直前に當り，殺生を禁ずる風習があるために此れを捕へることの出來ないのを甚だ殘念に思つて居たところ，計らずも激震に見舞はれたと云ふことであつて，かやうな現象は未だ曾て無かつたと云ふのがこの邊の噂であつて，事實らしく，興味あることゝ思はれる．

（E） その他

その他にも地震前に井戸水が濁つたとか，鮒が暴れたとかの噂もあるが，何れも信を措くに當らない．又地震當夜靜岡より見て大谷方面に極めて盛んな稻光のあつたこ

とは事實であるが，これは發光現象と見られるものでなく，單なる稲光が偶然にも多かつたと見るべきであらう．

最後に海には何等の異狀を呈さなかつたと云ふのが眞實であると思はれる．

稿を終るに臨み，吾々の調査に援助を惜まれなかつた藤安，伏見，春原，市川，松永，鹽島の諸君に謝意を表したい．特に靜岡市内西部及び用宗方面の調査には伏見，春原兩君に負ふところの少くないことを附記して置かう．

猶本調査は寺田先生の發案に基いて行つたものである．

73. *Reports on the Siduoka earthquake of July 11, 1935.*

By Tosirô KINBARA and Timoto TAKEMURA,

Siduoka High School.

The present report contains following articles, in which are described what we have observed at the time of the Siduoka earthquake of July 11, 1935:

(1) Geographical distribution and modes of damages of houses.
(2) Cracks on the ground and landslides.
(3) Modes of vibrations of houses which may be suggested from data of their horizontal displacements.
(4) Modes of upsets of *Isidôrô* (Sacred lantern made of stone) and *Hakaisi* (monument stone).
(5) Some changes in underground water level.
(6) Miscellaneous phenomena.

Some discussions are also made, from physical point of view, regarding the subjects in the respective articles referred to above.

74. 昭和10年7月11日 靜岡地震に就て

地震研究所　齊田時太郎

（昭和10年9月17日發表－昭和10年9月20日受理）

内容

本文は震災地及其附近を一週間に亙り踏査し見聞せる事項の中，各地に於ける地震動の人身感覺，燈籠の顚倒方向の局部的差異，被害分布の地形地質的解說，家屋移動と地質並に建築年齢との關係，及大正9年5月18日靜岡地震との比較等を述べてある．

1．人身感覺　靜岡市の南西方面より北東方面に向ふ順序にて述べる．**相良町**，**川崎町**，**島田町**にては上下動を殆感ぜずドンと云ふ音を聞くと間もなく水平の緩やかな震動を感じた．音も聞きし者と聞かざる者とあり，其方向は北或は東北であつた．**燒津町**，**藤枝町**，**岡部町**に於ても大體以上の如くであるが，上下動の感じは稍優る如くであつた．**藁科川の中流**の八幡に於ても上下動を著しく感ぜず音は東或は東南に聞きしと云つた．**安倍川の中流**俵澤，平野に於ても殆上下動を知らず，音を東或は南の方向に聞くと間もなく緩やかな水平動を感じた．**靜岡市**，**清水市**の各部落に於ては何れも强き上下動を感じ，音もこれと同時であつたが其方向は何れよりとも明かに云ひ得ざるやうである，**清水港内**にて當時釣をなせる人の言によれば人體が一尺も舟と共に突き上げられたかの如くであつたとのことである．**興津町**，**由比町**に於ては上下動もかなり强く感じたものゝ如く，音は聞いたと云ふもあり聞かなかつたと云ふ者もあつた．聞いた者は其方向を何れも三保方面卽ち南又は南々西と指した．

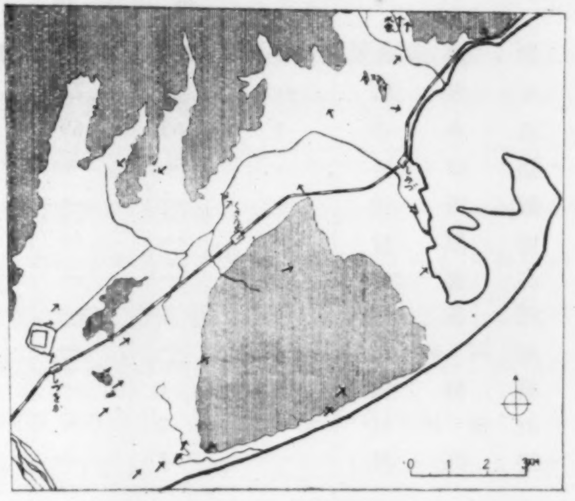

第1圖　石燈籠顚倒方向

2．石燈籠の顚倒方向　震害狀況調査の傍，二萬五千分の一地形圖に神祠の符號を付けた所を尋ねて，石燈籠の顚倒方向を調べた結果は別葉第1圖の如くである，圖中矢の方向が其顚倒方向で，○とせるは

顚倒せざるものである．これによると，巴川右岸の地區にては，略顚倒方向一致し東北乃至東北東の方向にあるも，其上流左岸の瀨名淺畑沼附近のものは，これと反對方向を示してゐる．清水市と庵原村との中間の地區に於ては，北乃至北北西の方向で巴川右岸の地區と略直角をなしてゐる．住家の震害最甚なる有度丘陵の西緣部と，谷津山八幡山有東山をつらねる線との間の地區の家屋（主として平家建）の傾斜及移動方向と，石燈籠の顚倒方向とは良く一致することが認められる．二階建（例東洋モスリン工場內の住家）の二三は，以上とは反對の方向をとつてゐるものを見たが，平家と二階建とでは地震動に對する震動性能を異にする故，當然のことで寧ろ筆者にとつては，興味あることであつた．震災地の小學校の數校に於て，戰利品の魚雷を設置してあつた．先年北伊豆地震に際して，江間小學校のものが滑動して，地動の變位を記錄したことがあつたので，今回も注意をして調べたところ震度最も甚だしかりし，靜岡市農事試驗場北方の西豊田小學校のものは滑動せる樣子を示さなかつたが，この小學校に隣接する神社の社務所は數種の滑動をなしてゐた．こゝより震度輕微なる麻機小學校，千代田小學校，瀨名小學校，飯田村小學校のものは，當然異狀なかつた．この項を終るにあたり，直徑約1米の機雷が鉛直軸のまはりに，上より見て時計式に約20度回轉せるを，庵原川中流の部落にて見たことを添へておく（寫眞參照）．要するに今回の地震による，物體の顚倒方向は實に整然としてゐる．

3. 被害の概略　靜岡縣廳の調査によれば次表の通りである．

第I表

市町村名	人		世帶		家屋（棟數）			
	死	傷	全潰	半潰	全潰住家	全潰非住家	半潰住家	半潰非住家
靜岡市	8	218	297	1548	237	372	1412	1042
有度村	—	8	73	151	73	47	151	97
清水市	1	68	69	313	53	28	263	103
袖師村	—	—	—	1	—	—	1	—
飯田村	—	—	—	—	—	2	—	2
庵原村	—	—	—	—	—	1	—	—
高部村	—	—	—	1	—	1	1	—
西奈村	—	1	—	5	—	—	2	1
兩河內村	—	—	—	1	—	—	—	1
廣幡村	—	1	—	—	—	—	—	—
東益津村	—	2	—	—	—	—	—	—
岡部町	—	1	—	—	—	—	—	—
計	9	299	439	2020	363	451	1830	1246

なほ住家，非住家，商品，山林，耕地，道路，橋梁，河港灣，縣有建物備品，學校建物設備品，神社，寺院等の損害を見積るときは 820 萬圓餘となる由である．

次に各地の被害狀況の概略を述べる．大井川下流の冲積層平野の**島田町**，**藤枝町**，**燒津町**等に於ては，被害らしきものを見ず．藤枝町より岡部町に至る間の**廣幡附近**には住家の障子紙の破損せるを二三見るも，**岡部町**に至れば何等被害なく宇津ノ谷峠を經て，**丸子**に至る時は障子紙の破損せるを見る．安倍川右岸の**用宗**，**長田村**には，障子紙の破れしもの及び土壁に小龜裂を生ぜしものあり，安倍川の支流藁科川流域の部落は何等被害なく安倍川の本流の各部落も同樣被害はなかつたが，**舊靜岡市**には煉瓦或は石造の塀の中，南北に設置されたものゝ多數は，略東側に倒潰してゐた．縣廳前の石崖も南北に長く造られたる所の一部が，何れも東或は西の方向に崩潰してゐた．製茶工場の多數ある安西の石造倉庫で被害のあつたものを見なかつた．大岩附近に二三の土壁に龜裂を生ぜし住家を見し他舊靜岡市の北部並北西部には，被害らしきものが無かつた，時計も止らず棚のものも落ちなかつた所があるやうである．城内追手町の不二高等女學校の塔の煉瓦壁に龜裂を生じてゐた．住家の被害としては靜岡驛の北部の鷹匠町，傳馬町，譽田町，院內町，晉羽町等にて屋根瓦の墜落せるところ，土壁に大小の龜裂を生ぜしものも多く見られた．驛の南側の旭町，森下町附近は構造薄弱に見らるゝ家屋の多いため，相當傾斜をなせるものがあつた．東若松町，小黑，曲金附近は一軒として滿足なるものなき程度にて，被害甚大なるを感じた．倒潰に等しきもの，全體として滑動せるもの，大傾斜をなせるもの等其數少からざるものであつた．この附近にある東洋モスリン工場の一部が倒潰し，三光紡績工場の無筋コンクリート造のボイラー室，其他に大損害を與へたのは今回の家屋震害として注目すべきものであつた．八幡山，有東山附近の部落を見るに山脚に近きは被害としては，障子紙の破損に止る程度のものもあるが，遠くはなれて東方の水田中の部落曲金に至るほど，被害甚だしかつた．長沼，古庄何れも被害甚だしく國吉田，池田に至れば更に其の災度を高め，數十糎の大移動をなせるものを認めた．更に有度山丘陵の西緣部の部落を南下すれば小鹿は池田に劣らぬ狀況にて駐在所の大破せるが目に留つた．大谷村の片山，宮川は幾分輕微となり伊庄は更に被害輕少なる如く考へられた．しかしこれ等の輕少なる被害地に於ても，家屋は相當滑動し柱の枘を折り，或は差鴨居と柱との仕口にて，柱の折損せるもの等一見氣付かぬ震害を受けたものがあつた．西大谷，高松は今回の震害にて，最も全潰率の大なる地區であるが，其地域の極めて狹小なることが注目される．高松より海岸に沿ひ砂丘上を西すればするほど著しく被害は輕少となる．安倍川の左岸の中野附近に於ても同樣である．大谷より有度山丘陵の南緣を東進する

と同様に被害は著しく減少し障子紙の破損すら無きほどである．静岡市の北部の麻機方面は被害全く無きも谷津山の北側の沓之谷，千代田，上土，川合等には大傾斜をなせるものを見た．**瀬名**の部落は被害なきも，巴川を渡り有度山丘陵の北縁の各部落は，何れも屋根瓦の脱落土壁の龜裂，軸部の損傷，或は十數糎の移動をなせる等，相當の被害を表はしてゐるが池田，國吉田等に比すれば著しく輕きものであるが，**澁川有東坂**，**今泉**は多數の全潰家屋を出した．こゝは池田，國吉田，大谷，高松の次位にある被害顯著な部落といふべきであらう．**飯田村**，**庵原村**，**高部村**各部落には多少の被害ありしも，土壁の損傷などが主なるものゝ如く見られた．**袖師村**も上記の諸村と同程度といふべきであらう．**清水市**に於ては巴川流域で，被害の著しいのが注目される．清水驛附近の土藏造の土壁の剝落し，市内一般民家の屋根瓦の一部は脱落し，間内の壁には龜裂を生ぜる等，輕微ながらも何れの住家も，震害を受けてゐたやうである．港町電車終點に在る三階建の住家が，倒潰せんばかりに大傾斜をなせるに，其附近の石造倉庫の殆全部は，震害を受けてゐなかつた．築港岸壁の被害は，今回の震害中損害見積額の第一位を占むるものであらう．先年の北伊豆地震にて，被害を受けしことあり，當時補强改修せるに，今回其の補强に止め改修せざる部分が，破壞せられたのである．岸壁の一部は上部にて 5 米，底部にて 4 米近くの變位を 250 米餘に亙りてなせるため，裏込の砂土は大沈下をなし，その上に建てられたる鐵骨倉庫の柱は，基礎の支持を失ひ遂に倒潰するに至つた．**村松**，**宮加三**，**駒越**，**三保**等は被害らしきものを見ず．駒越より海岸に沿ひ西すれば，**增**，**蛇塚**，**根古屋**等の部落に至るが，何れも被害は輕微にて二三障子紙の破損，屋根瓦の移動など見受けられた．久能山東照宮の石段は想像以上に被害なく，二三の石の移動が認めらるゝ位で，被害なしといふべきである．石燈籠は殆倒潰し，神社の被害は認められなかつたが，登口の右側の門が東方へ傾斜してゐたが，この門は相當に古いものであつた．

極めて簡略であるが以上を以て被害地の狀況の說述を終り，尙靜岡，清水兩市及有度村に於ける死傷者，住家，非住家の被害狀況調を，町字別になせるを次に示さう．これによれば地盤の相異等により震動の性質の異なることが知られる．

第 II 表　靜岡市死傷者調

町名	死者	傷者	計	町名	死者	傷者	計
兩替町一	—	1	1	鷹匠町三	—	4	4
〃　二	—	1	1	東鷹匠町	—	6	6
紺屋町	2	1	3	傳馬町	—	2	2
鷹匠町二	—	2	2	響田町	—	1	1

町名	死者	傷者	計	町名	死者	傷者	計
鑄物師町	—	1	1	下石町二	—	1	1
院内町	—	3	3	寺町三	—	2	2
下横田町	—	1	1	新通二	—	1	1
榮町二	—	1	1	〃三	—	1	1
東町	—	1	1	安倍川町	—	2	2
相生町一	—	1	1	福住町	—	2	2
音羽町	—	6	6	青木町	—	1	1
春日町	—	4	4	川邊三友町	—	2	2
南町一	—	3	3	駒形通二	—	1	1
〃二	—	1	1	〃六	—	2	2
〃三	—	1	1	天王寺町二	—	1	1
〃四	—	1	1	彌勒二	—	2	2
旭町	—	1	1	中原	—	1	1
森下町一	—	2	2	西脇	—	1	1
〃二	—	1	1	下島	—	1	1
〃三	—	3	3	高松	1	6	7
八幡本町一	—	1	1	石田	—	1	1
〃二	—	1	1	稻川一	—	1	1
〃三	—	2	2	〃二	—	1	1
〃四	—	1	1	〃三	—	2	2
〃六	—	1	1	馬淵本町	—	8	8
〃七	—	3	3	中田	—	3	3
〃八	—	1	1	見瀨	—	1	1
小黑一	—	1	1	末廣町	—	1	1
東若松町一	—	2	2	神明町	—	1	1
〃二	—	1	1	北番町	—	1	1
〃三	—	1	1	柳町	—	1	1
豊原町	—	2	2	水落一	—	1	1
曲金一	—	1	1	〃二	—	1	1
〃四	—	1	1	〃三	—	2	2
〃五	—	1	1	東草深二	—	1	1
長沼	—	2	2	西草深	—	1	1
古庄	—	4	4	宮崎町	—	1	1
栗原	—	1	1	富士見町	—	1	1
國吉田	—	3	3	安西五	—	2	2
聖一色	—	1	1	材木町	—	1	1
池田	—	3	3	東大谷	1	16	17
小鹿	2	4	6	西大谷	2	13	15
新富町一	—	1	1	沓之谷	—	3	3
〃二	—	2	2	錢座	—	2	2
上新富町	—	1	1	上土	—	1	1
七間町三	—	1	1	川合	—	2	2

町名	死者	傷者	計	町名	死者	傷者	計
用宗	—	1	1	青木	—	1	1
石部	—	2	2	合計	8	191	199

第 III 表 有度村重輕傷者調（但死者なし）

字別	重傷	輕傷	計	字別	重傷	輕傷	計
吉川	—	2	2	草薙	—	—	—
七ツ新屋	—	—	—	上原	1	1	2
長崎新田	—	—	—	馬走	—	—	—
長崎	—	—	—	有東坂今泉	1	1	2
楠	—	1	1	澁川	1	—	1
楠新田	1	—	1	北脇	—	1	1
中之郷	1	—	1	北脇新田	—	—	—
中吉田	—	—	—	堀込	—	—	—
谷田平澤	—	—	—	合計	5	6	11

第 IV 表 清水市死傷者調

區域別	死亡	重傷	輕傷	計
辻	—	7	12	19
江尻	—	5	17	22
入江	—	9	5	14
清水	1	10	21	32
不二見	—	—	5	5
三保	—	—	—	—
合計	1	31	60	92

第 V 表 靜岡市住家半潰以上の被害調

町名	全燒全潰	半潰	總數	被害率	全潰率
鷹匠町一		2	300	0·6	
傳馬		1	332	0·3	
院内		1	136	0·7	
日出		2	147	1·3	
中田		5	198	2·5	
中野		1	21	0·5	
下島	1	6	69	11·6	1·4
敷地	6	45	114	50·9	5·2

町名	全燒全潰	半潰	總數	被害率	全潰率
宮竹	3	36	79	53·1	3·8
高松	35	55	110	**100·0**	**31·8**
宮川片山	1	35	73	47·9	
西大谷	28	50	119	**100·0**	**24·3**
東大谷	17	56	137	65·6	12·4
西平松		24	138	17·3	
中平松	1	2	64	6·2	1·5
古宿		1	60	1·6	
安居		1	82	1·3	
根古屋		1	96	1·0	
稻川二		4	444	0·9	
南町一		2	216	0·9	
南町二		6	219	2·7	
旭町		9	76	11·8	
森下一		14	118	11·1	
〃　二		12	322	3·7	
〃　三		13	148	8·7	
東森下		1	62	1·6	
八幡本七	1		68	2·8	1·4
有東		8	91	8·8	
小黑一	1		51	3·9	2·0
〃　二	1	5	55	12·8	1·8
〃　三	4	2	56	17·8	7·1
〃　四		3			
東若松一		11	62	17·7	
〃　二		19	67	28·4	
〃　三		16	61	26·2	
豊原		53	111	47·7	
曲金一	4	11	107	17·7	3·7
〃　二		9	51	17·6	
〃　三	1	16	66	27·2	1.5
〃　四		10	52	19·2	
〃　五	1	26	26	**100·0**	**4·0**
小鹿	6	85	171	56·8	3·5
池田	20	87	134	**94·7**	**14·9**
聖一色	5	58	73	**93·1**	**6·8**
國吉田	10	52	62	**100·0**	**16·1**
栗原	5	40	60	**83·3**	**8·3**
古庄	5	44	90	60·0	5·5
長沼	9	39	224	25·4	4.1
東柚木		5	89	5·6	
沓之谷		17	408	4·1	

町名	全燒全潰	半潰	總數	被害率	全潰率
錢座		1	174	0	
千代田		3	155	1·9	
上土		6	115	5·2	
川合		10	195	5·1	
合計	167	1021			

この表にある被害率は全潰數を2倍して半潰數に加へたるものゝ百分率である，有度村及清水市に於ける被害率もこれと同樣である.

第 VI 表　有度村家屋被害調（但非家屋を含む）

字別	總棟數	全潰	半潰	大破	小破	被害率
吉川	332		3	130	199	0·9
七ツ新屋	158		22	63	73	13·9
長崎新田	98			40	58	0
長崎	202			80	121	0
楠	96	1	2	46	47	4·1
楠新田	155	1	14	92	48	10·3
中之郷	244		1	96	147	0·4
中吉田	189		5	70	114	2·7
谷田平澤	169		4	63	102	2·4
草薙	449		6	173	270	1·3
上原	259	2	7	116	134	4·5
馬走	194	2	13	94	85	8·7
有東坂今泉	419	33	68	193	125	**31·9**
濵川	387	20	13	225	129	**23·5**
北脇	110			44	66	0
北脇新田	101	1		40	61	0
堀込	65			26	39	0

第 VII 表　清水市住家被害調

區域別	總數	全潰	半潰	破損	被害率
辻	1673	29	33	735	5·4
江尻	1949	28	109	1748	8·5
入江	1934	31	72	1086	6·8
清水	2572	5	115	1902	4·8
不二見	2251	5	28	1239	1·7
三保	1004	0	0	0	0

4. 被害分布の地質地形による考察　第2圖は第 V, VI, VII 表に示せる被害率を，地形略圖へ記入せるもので，これによると被害區域は安倍川河口より，靜岡驛，谷津山北麓を經て巴川右岸，袖師村，有度山東麓を含む楕圓形の地區にて，共長軸の方向が，共區城内の家屋の移動方向並石燈籠の顚倒方向と一致する．80％以上の被害率を有する地域は，谷津山，八幡山，有東山と有度山麓との間の沖積層平野で，長徑 3500 m 短徑 1500 m 位の楕圓にて示される範圍と，大谷川が砂丘を一回轉して切斷する，海岸に平行なる 500 m 位の極めて小區域とで，他はこれ等に比して著しく被害輕微であるが，有度村の有東坂今泉，澁川が稍顯著な被害を示してゐる．これを地形上より見れば，安倍川流域の中野，中島濱村附近，有度山丘陵上及有度山南麓が最も被害少く，これについで砂丘上の下島，及谷津山と八幡山との間の地域及巴川流域の一部が，稍被害を増し，有度山西麓に於て最も著しき被害を示す．これを地盤上より見れば，安倍川流域の砂利層の厚き所及有度山體の上が最も被害少く砂利及び砂よりなり，砂丘上は稍被害を増す．沖積層にありては，層の厚さによるらしく考へられる．例へば靜岡市清水公園前の井戸受負業者志保澤清氏の語るところによれば，谷津山，八幡山の間に於ては 50 尺位にてこれ等の山の基盤に突きあたるが，八幡山の東側の東洋モスリン工場にては 120 尺位にて基盤に突きあたる．而して共地質は粘土砂の互層よりなつてゐる．地震當時同工場内には直徑9尺の井戸を堀りつゝあり，共各層の厚さを地表より逐次書き下せば，次の如くである．

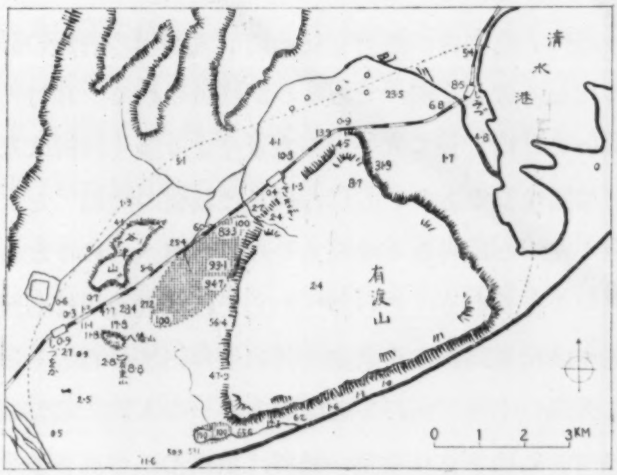

第2圖　家屋被害分布

埋土	2.0 尺,	粘土	5.0,	砂	2.5,	粘土	3.5,
砂利	3.5 尺,	砂	5.0,	粘土	4.0,	砂利	6.8,
粘土	4.0 尺,	砂利	4.0,	粘土	4.0,		

地表より 13 尺下りしとき，草木の腐蝕せるもの多數表はる．なほ同氏の語るところによれば高松大谷は地表より 50 尺～60 尺は粘土質砂で，共下部は砂利である．靜岡驛構内にては 120 尺，馬場町，安西方面にては，100 尺位までは全く砂利のみの層よりなるさうである．これによつて考へると，今回最も被害甚大なりし曲金，池田，

國吉田は極めて厚い軟弱なる地盤よりなつてゐるらしい．有度山麓にて浸蝕谷の堅固なる地盤上にあると考へられる，伊庄及片山，宮川の或部分が著しく被害が輕微であり，これに反して谷を浸蝕して造られた土砂の堆積上に建てた部落は，被害顯著であるのは當然と考へられる．

高松，西大谷の被害を見るに，大谷川の右岸の砂丘上にある部落の震害は，其左岸に比して著しく輕少であるのが注目される．宮竹と東大谷との間の地盤が其東西より低いことは，嘗て大谷川の水量今より多く河幅大なるもので，高松大谷は其時造られた堆積地盤であり，右岸の砂丘は地盤の隆起1) と，海流との作用で造られた地盤で，全く左岸とは異なる地質よりなると考へられるならば，今回の被害の著しき差異は當然のことである．この考へからすれば大谷川は名殘川と稱すべきである．左岸地區の宅地は殆道路側は1米或は其以上の高さの石垣を以て造られてゐることは，其の東方及西方の宅地が何れも道路面と同一の天然の地盤面にあることゝ異り，且つ道路と大谷川とにはさまれた狹い地所は川に沿ふて高さ數米の護岸工事を施してあるなど，何れも今回の被害を大ならしめたことになつてゐると考へられる．例ば久能街道が高松にて東へ直角に方向を變へるところは，川と道路との距離は數米であり，此所へ建てられた住家が何れも大破或は倒潰してゐる．周圍に石垣を築いて宅地とせるものは，有度山麓の部落に多く見られるが，地震動にてこれ等が崩壞して，建物に二次的に被害を増したと認められるものが多いやうであつた．

高松，大谷の地域と曲金，國吉田に亙る廣大なる地域の震害を對比すると，第V表にて見らるゝ通り著しき相異がある．高松，大谷にては全潰家屋が卓越し，曲金，國吉田にては半潰家屋が卓越してゐる．被害率を第V表に付記せる如く定義すれば，二者何れも同等の被害であるが，其内容は全く反對である．同一地盤で同程度の家屋の震害を考へるとすれば，全潰率にて其震度は略推定されるが，今回の如く沖積粘土砂層の平地と，砂丘と山麓との接する局部的に異なる地盤のところでは，震動の性質が全く異なると考へられることは，石本教授の東京橫濱に於ける地震動の觀測2) で明かなことであるが，この事實を今回の地震動の性質は物體の顚倒方向の整一であることより推定すれば，破壞作用を有する震動時間は極めて短時間であつたらうと想像されることゝ合せて考へると，この二地域に於ける震動の性質は曲金，國吉田に於て加速度は高松より小さく，周期は大きいと考へられる．

1）槇山次郎「久能山さ三保松原」地理教材さしての地形圖　第1輯，164頁．

2）石本巳四雄「東京橫濱市內10個所における地震動加速度觀測（1)」地震研究所彙報 **11**（1934），234～248．

即ち震動の性質が高松，大谷にては衝擊的であるが，曲金，國吉田にては緩やかなるものであつたらうと考へられる．從つて家屋の被害は高松大谷にては小破，大破，半潰，全潰といふ順序で，相當の時間を經て進まず，一瞬にして構造の强弱より何れにか決定されたのに，曲金，國吉田にありては相當の時間を要して被害が進展したと考へられる．震害を地盤の相異即ち地震動の性質の相異と關係せしめて研究することに興味を持つ筆者にとりては，今回の地震にて良き資料を與へられた．

これを要するに今回の地震による，家屋災害の中心は池田，聖一色附近にあり，高松，大谷は地形地質關係により現はれた局部的の被害と考へる．

5. 家屋の滑動　被害概況を說述せる際，旣にのべたる如く有度山丘陵の西麓に於て數十糎，北麓に於て10糎程度の住家の滑動を見たが，小祠にありては清水市の北方飯田村，庵原村に於ても見られたが，其の滑動量は數糎程度であつた．旣往の震災に於て建物の滑動は屢々認められ，共滑動量は被害率大なる地域に於て多く，構造より見れば軸部の堅固なるものは薄弱なるものより多く，軸部同樣ならば屋根の重量の小なるものほど多く滑動することは疑のなき事實と考へる，即ち構造物の振動周期の小なるものほど滑動し易いといふことである．しかし關東大震に於て，片瀨龍口寺五重塔が2尺近くも滑動したことがあるから，構造物の振動周期としては，最も大なるものと考へられる五重塔に於ても，地震動の極めて大なるときは滑動する．今回の被害に於ても亦以上の性質が明かに現はれてゐる，特に筆者の興味を感ぜしは飯田村の一小丘陵上の八坂神社と稱する建物の例である．水屋は極めて簡單な構造であつたが，堀立柱の地面に接するところが幾分腐蝕し，之を動かして共固有振動周期を調べたところ，約1秒前後であつたが，地震では倒潰を免れてゐた．尙二基の石燈籠は何れも倒潰してゐた．拜殿と神殿は何れも瓦葺の略同等の大さであつたが，拜殿には筋違を少し施してあり，神殿には之がなかつた．地震で筋違のある拜殿は 10 糎近く滑動せるも，神殿の方は滑動しなかつた．

西大谷高松に於て瓦葺平家建の略同樣な形態を有するもの，50 棟餘について其の滑動變位を筆者の測定せる結果を次に示さう．

第 VIII 表　住家滑動量調

地名	戸主氏名	滑動量 cm	建物の年齢	柱の大さ cm	備考
西平松	海野久作	0	30	13	
	長島仙太郎	33	20	13	欅の柱數本あり

地名	戸主氏名	滑動量 cm	建物の年齢	柱の大さ cm	備考
東大谷（大谷川左岸）	齋藤虎雄	18	100	13	
	神谷伊平	10	100	13	仕口弛むもの丶如し
	神谷善男	0	11	13	
	小林竹次郎	14	50	14	
	鈴木源左衛門	2	90	12	安政元年 11 月の地震にあふ
	風間長五郎	0	50	14	
	杉山勝吉	0	40	12	中二階
	望月源作	6	1	13～15	柱折損
	神谷傳吉	25	8	13	柱折損
	望月彦右衛門	5	12	12·5	
	大村傳作	0	60	13	
	神谷清一	1	50	16	
	大村藤次郎	0	50	14	6 年前修理
	八木源吉	10	50	15·5	大正 8 年修理，修理せる部が滑動す
	大村吉松	10	60	14	
	岩崎儀三郎	31	22	16	欅の柱を用ふ柱折損
	深澤乙吉	30	30	13～15	欅の柱を用ふ柱折損
	大村清吉	22	7	16	欅の柱を用ふ
高松（大谷川左岸）	岩崎重吉	0	40	13·5	
	永島健一	55	18	14	柱折損
	天野金作	47	6	13	柱折損
	天野亀吉	12	25	12	
	漆畑彌太郎	15	43	12	柱折損
	岩崎榮作	5	50	12	
	岩崎綱次郎	0	50	14	大傾斜す
	天野亮一	50	15	14	大黒柱其他欅柱あり
	岩崎鐵太郎	6	80	11	欅柱を用ふ
	漆畑清十	10	80	14·5	
宮竹	井口鍊	0	40	10·5	
高松（大谷川右岸）	岩崎兼吉	10	50	13	10 數年前移築せるもの
	漆畑周一	10	15	12	
	稲葉治作	8	200	14·5	德川初期の建築さ云ふ
	稲葉興助	8	50	12	
	岩崎庄平	30	7	14·5	欅柱を用ふ柱柄損傷
	望月大吉	0	40	13	今年春移築
	八木周平	0	50	13	
	望月角藏	0	100	14	
	久保田常藏	0	6	14	

地名	戸主氏名	滑動量 cm	建物の年齢	柱の大さ cm	備考
西大谷（大谷川右岸）	大村金作	0	15	13	
	大村秀作	18	4	13	
	深澤熊次郎	6	10	13	
	大村淺吉	33	5	13	大黒柱あり柱，枘損傷
	八木義三郎	20	50	12	増改築す
	岩崎勇作	0	60	12	
	岩崎源作	0	50	11	13 年前移築
	神谷佐平	0	40	12·5	
	櫻井市藏	3	80	13·5	
	山田平吉	3	45	14·5	
	望月國男	0	7	12	

この表にて40年以上を經過せるものゝ，年數は精確なことは判明せず，先代からの云ひ傳へによるものが多い．第3圖はこれ等の平均をとりて作れるもので，今回の地震にて最も滑動量の多きは，15 年乃至 18 年を經過せるもの，殆滑動せざるは 40 年位のものと云ふ數値を得た．100 年以上を經るものは，寧ろ滑動し易き傾向を示す．これは長年月に亙り存在するほどのものは相當堅固であるか，或は改修をなせる等の關係によるものと考へられる．

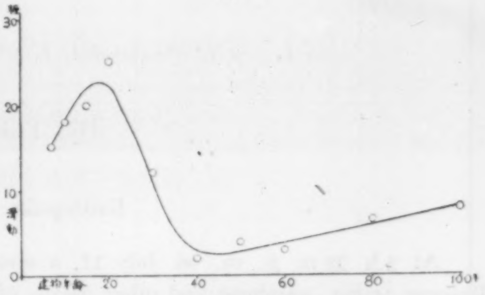

第 3 圖　住家滑動と建築年齢との關係

6. 地變　今回の地震にて地質構造に關係ありと考へらるゝ地變は氣付かれなかつた．有度山丘陵の崖崩れを初として，道路，築堤の龜裂沈下等は被害の著しきところは勿論，其他靜岡沖積層平野の各地に多數現はれた．麻機に於て水田が長さ 50 m 幅 10 m 餘傾斜陷沒してゐると考へらるゝを見たが，其傾斜の走向は略南北と東西であつた．鐵道線路の震害を鐵道職員の語るところによれば，靜岡，袖師間に築堤の沈下は數個所に現はれたが，只一個所草薙，靜岡間の後久川橋梁附近にて，築堤若干隆起せりと云ふ．沈下は常なるも隆起は筆者に異樣に感ぜられた．

7. 海水の變化　大谷海岸にて地震の前後海水は極めて平靜であつたさうであるが，清水港にて釣舟にありし人は地震後著しく波立ちしと語つた．

8. 大正 6 年 5 月 18 日靜岡地震[3] による被害との比較　この地震の震源は

---

3) 震災豫防調査會報告　第 88 號乙.

靜岡市より北 65 度西へ約 9 里を距たる大井，天龍兩河上流間の古生層山地にあつたが，靜岡，清水，燒津附近に於て強く感じ，靜岡市内にて煉瓦塀の倒落，煙突の破壊あり，農事試驗所の本館は 1 寸 3 分も移動するなど相當の被害があり，就中停車場附近鷹匠町邊は震害著しかつた．江尻清水にては電燈線，電話線の切斷するもあり，石塀，煙突の破損は數個所に生じた．當時と今日とで兩市の狀況は著しく異るも，今回震害の多かりしところは震源を異にする場合にも，同樣に震源地となることを示し，震害は地表層の性質と共上の構造物との性質とで大體定まり，震源の位置及び發表機構によるものでないと云ふ例を示すものと考へられる．

74. *The Shizuoka Earthquake of July 11th, 1935.*

By Tokitaro SAITA,

Earthquake Research Institute.

At 5 h 25 m p. m. on July 11, a severe earthquake occurred in Shizuoka and its vicinity. Railway traffic, telephone and other means of communications were temporarily suspended, while many houses were demolished and a number of fissures reported. There were also men who were pinned under collapsed building and killed. The writer of this paper remarked the local difference of the overturning direction of stone-lanterns and investigated the damages to building in geological attitude. He pointed out too the amount of the sliding of buildings according to earthquake vibration varied with the age of buildings.

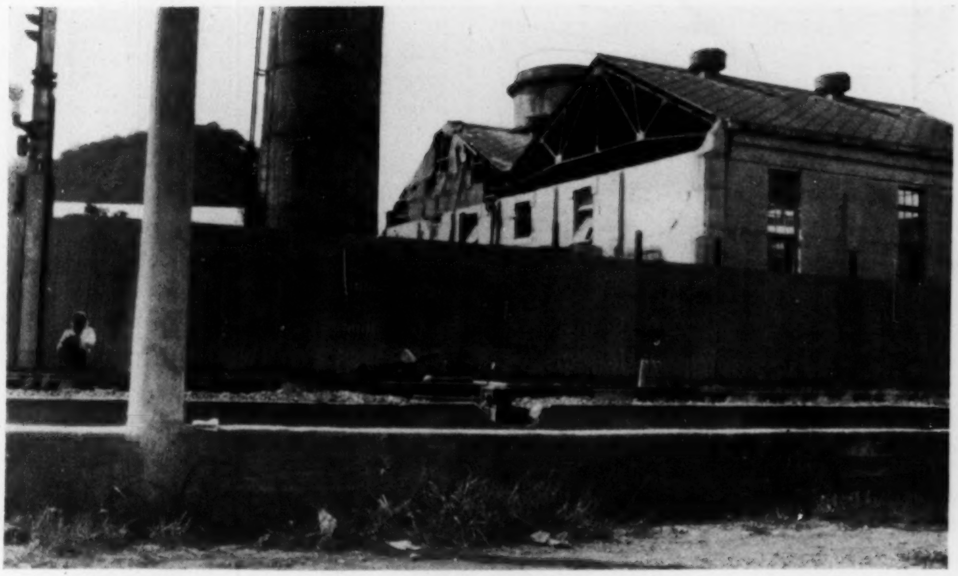

第4圖　靜岡市長沼三光紡績工場

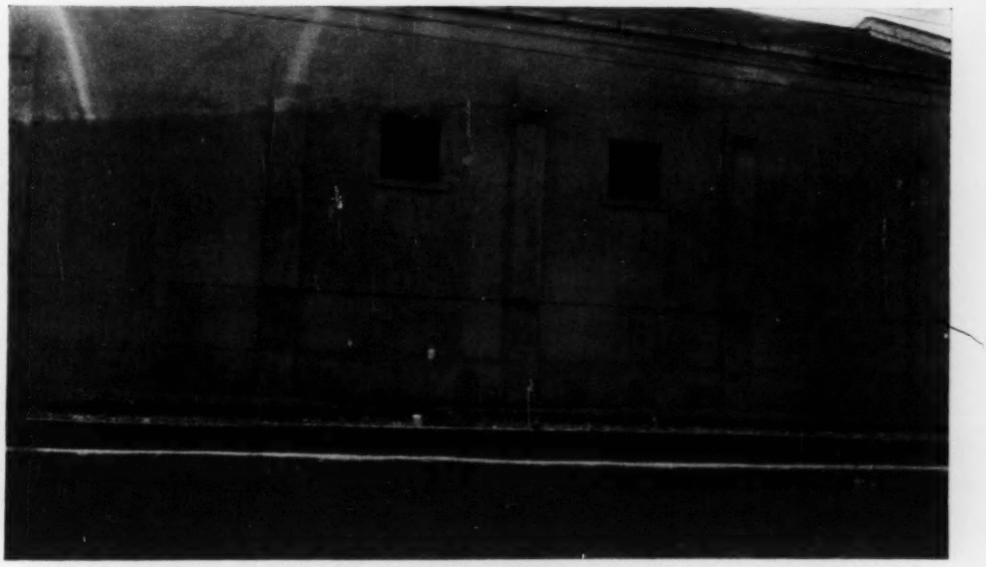

第5圖　同上壁體の滑動

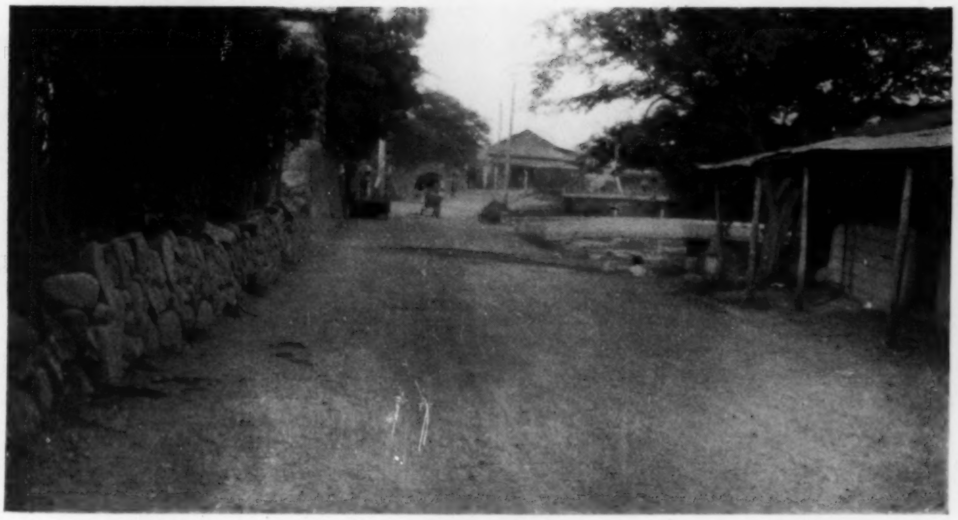

第6圖　靜岡市西大谷宅地々形

（震研彙報　第十三號　圖版　齊田）

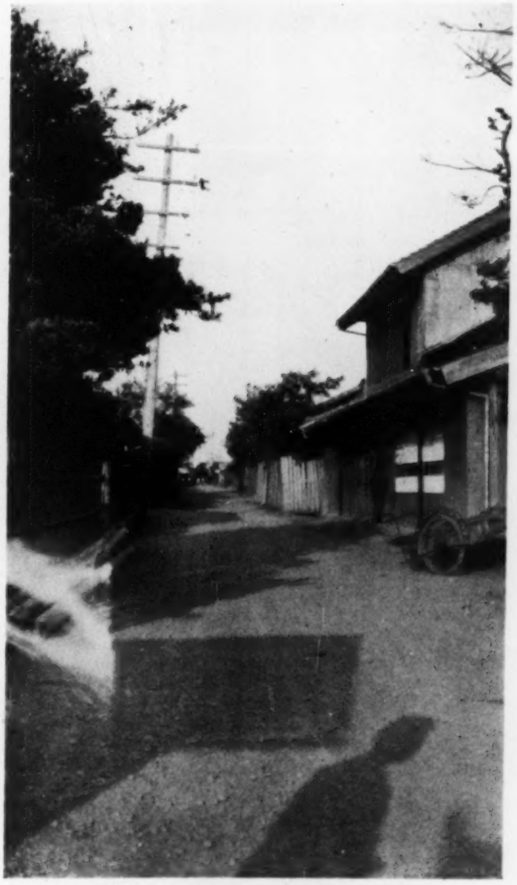

第7圖　靜岡市西平松宅地々形

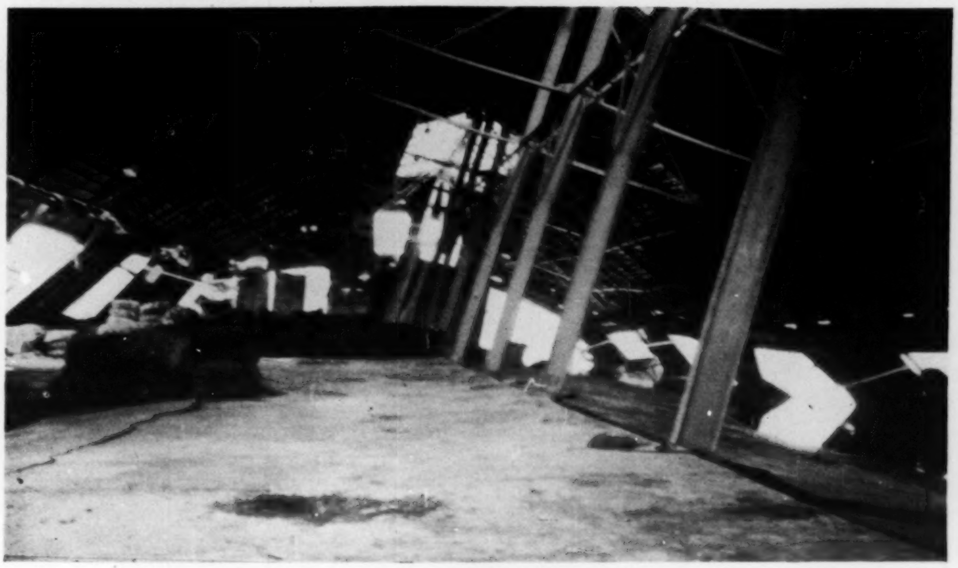

第8圖　清水市兩岸壁倉庫

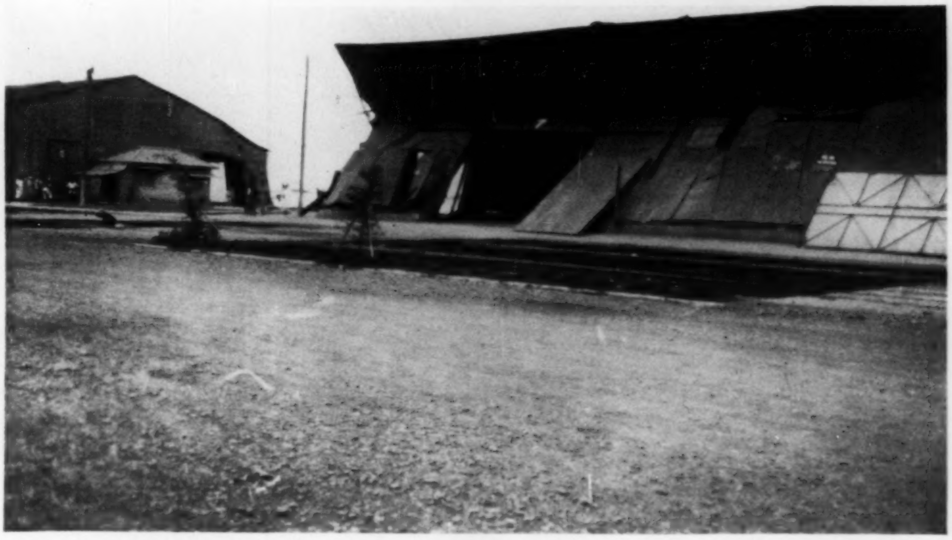

第9圖　同　上

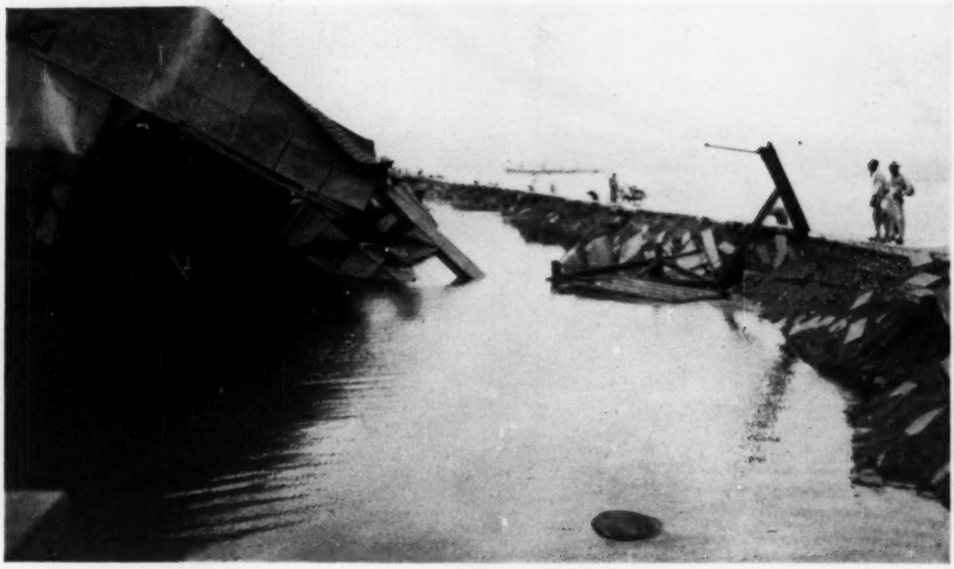

第10圖 清水市兩岸壁倉庫

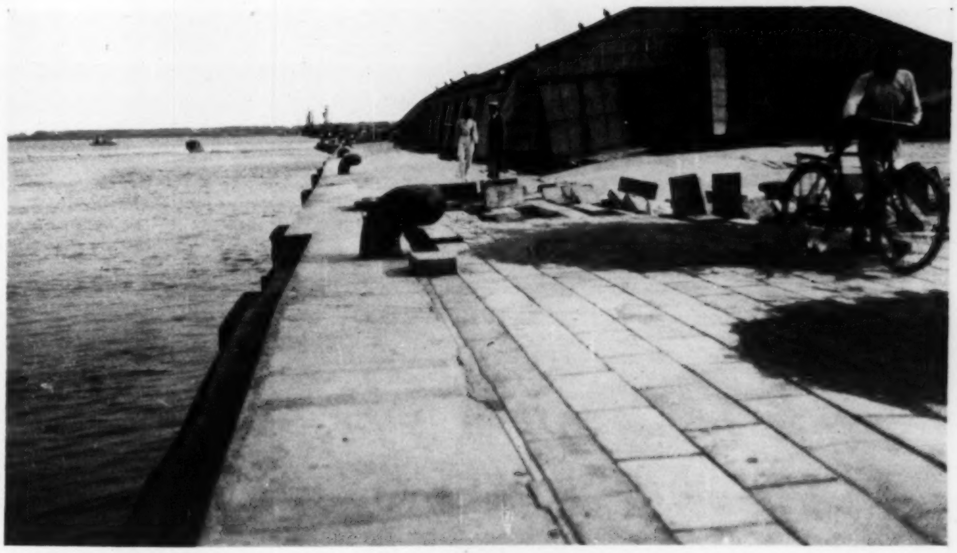

第11圖 同 上

（震研彙報 第十三號 圖版 齊田）

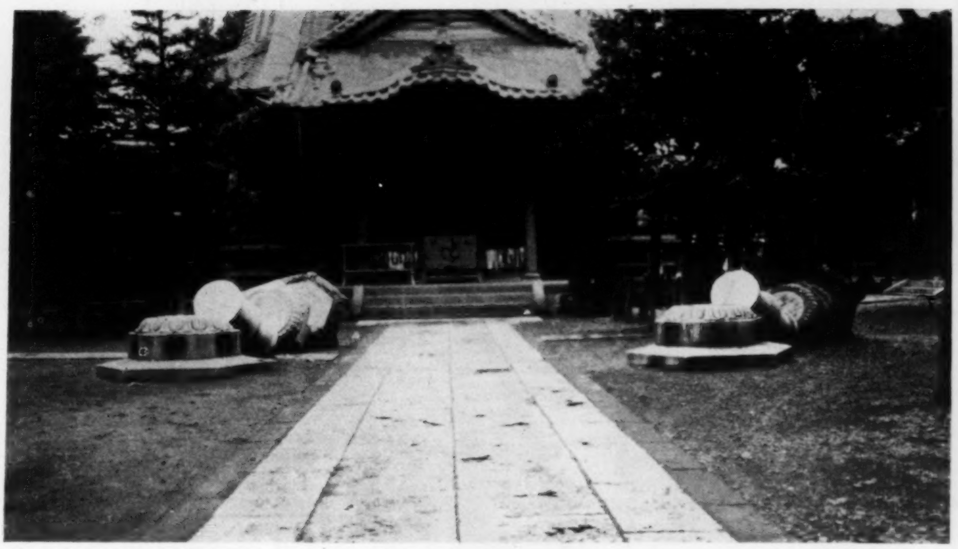

第 12 圖 靜岡驛前小梳神社

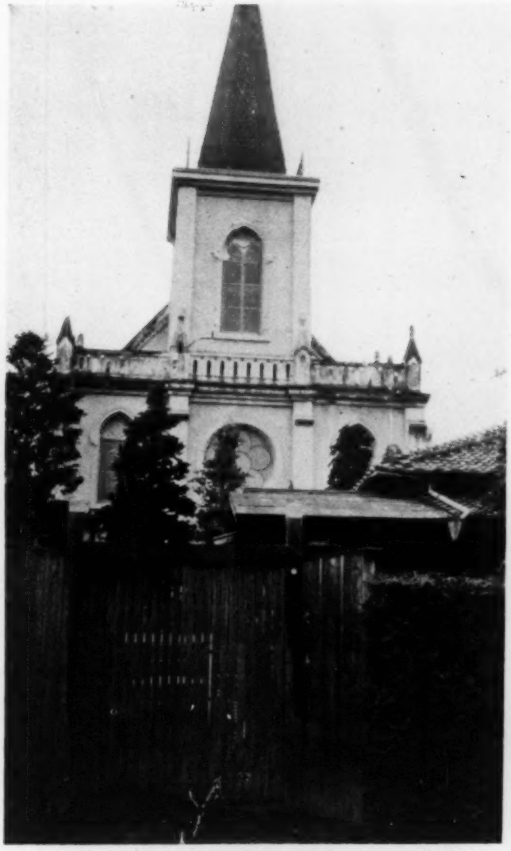

第 13 圖 靜岡市城内不二高等女學校
塔屋に亀裂を生ず

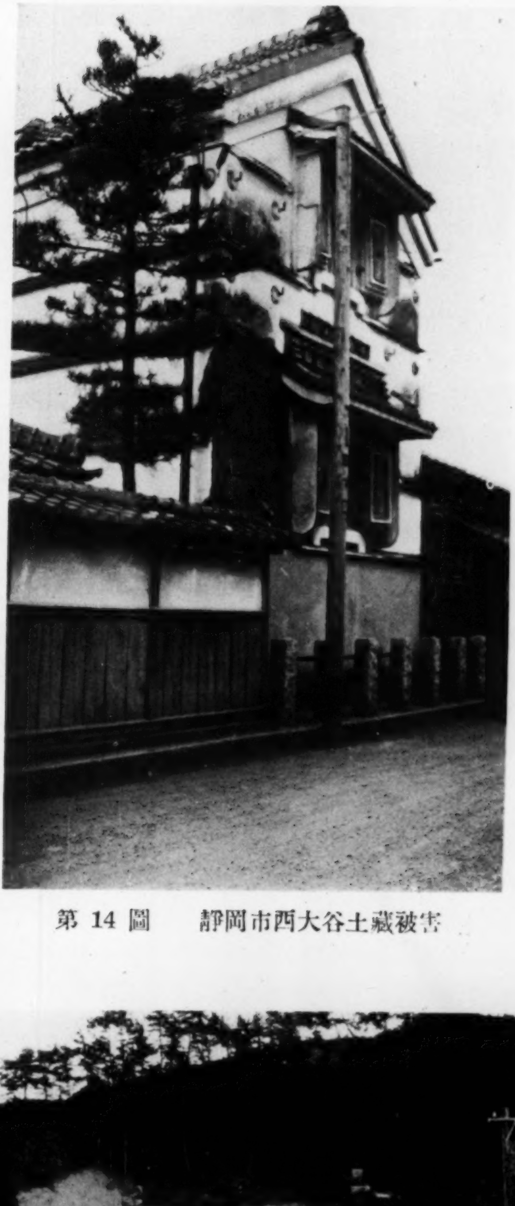

第 14 圖　靜岡市西大谷土藏被害

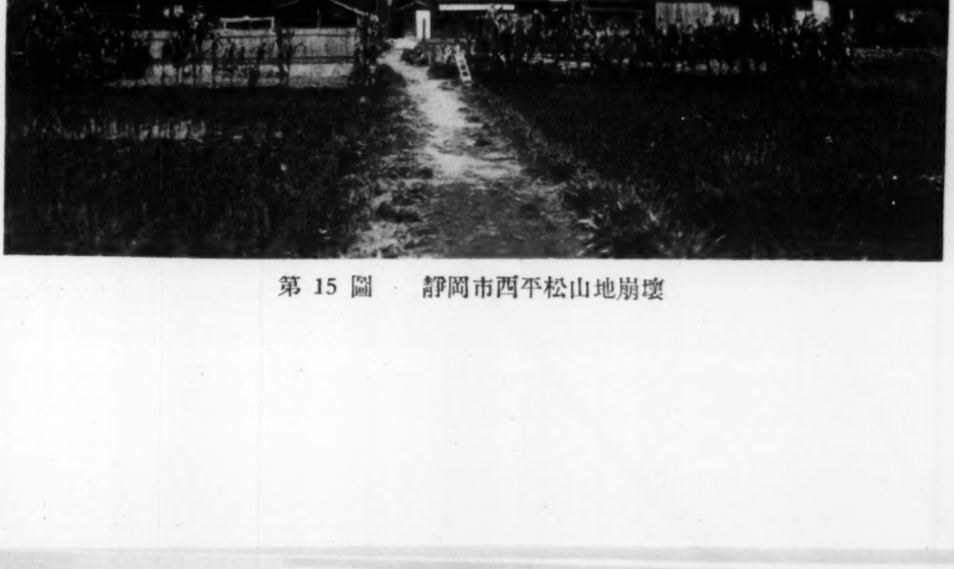

第 15 圖　靜岡市西平松山地崩壞

（震研彙報 第十三號 圖版 齊田）

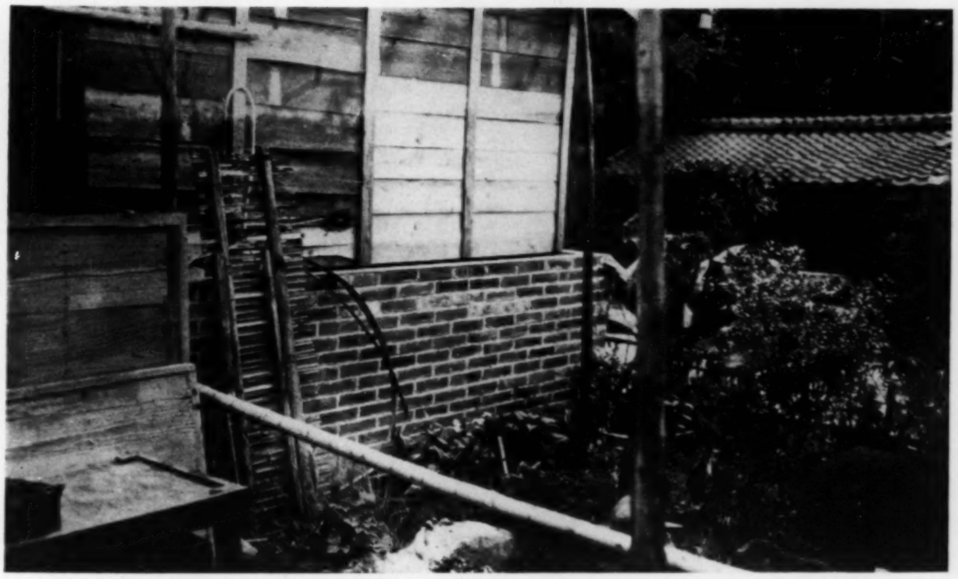

第 16 圖　靜岡市高松倉庫滑動

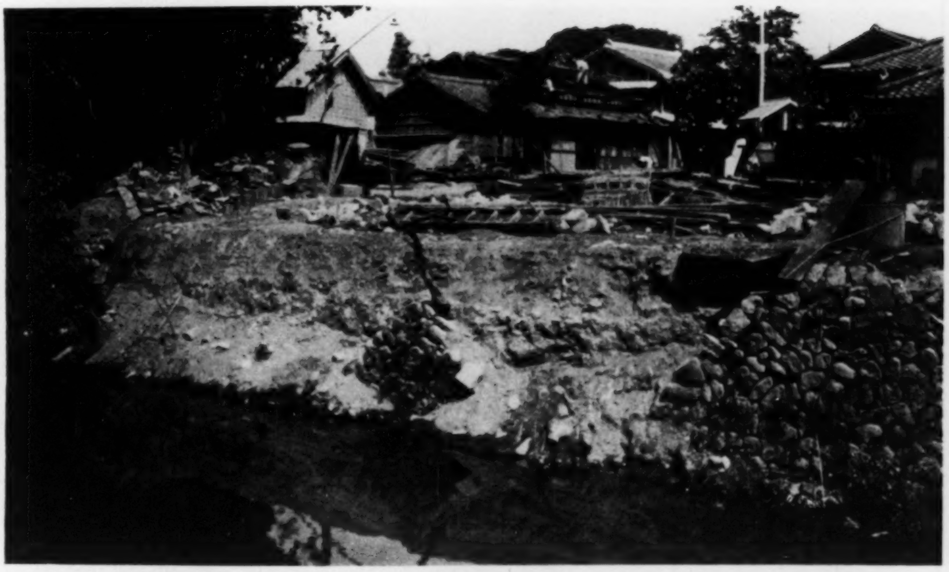

第 17 圖　靜岡市高松大谷川護岸工崩壞し家屋も亦全潰す
（寫眞は既に片附けを終了せるさころを示す）

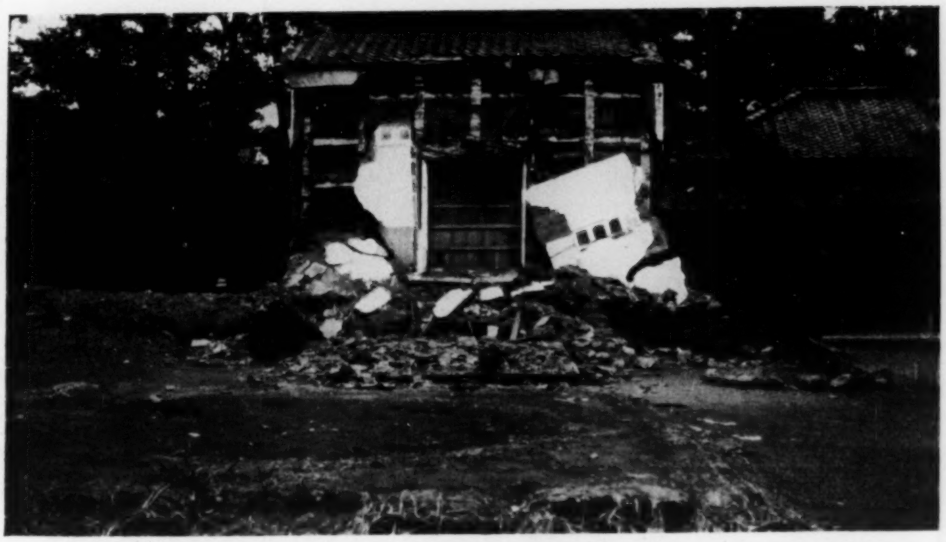

第18圖　有度村草薙神社土藏

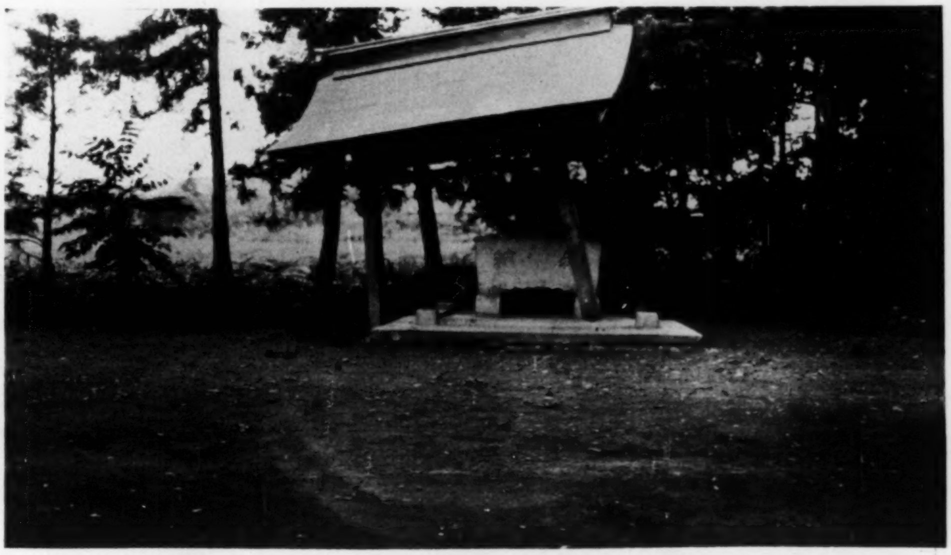

第19圖　靜岡市小鹿神社水屋

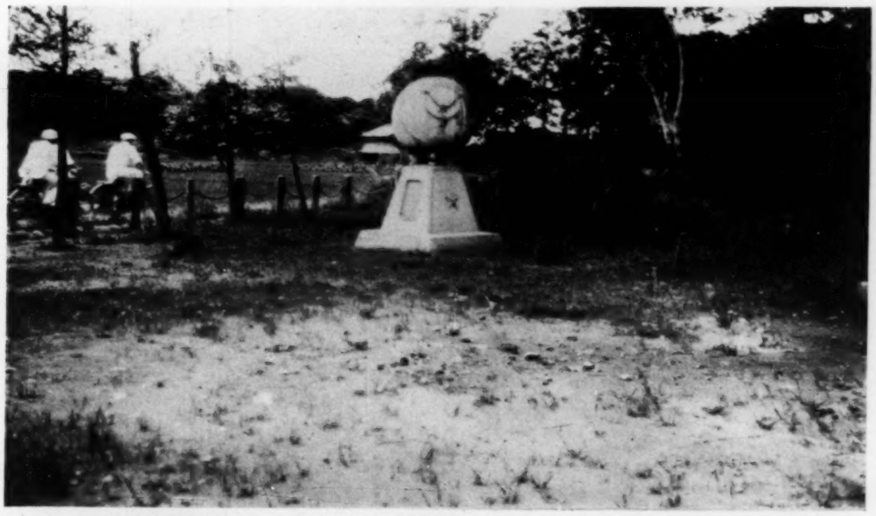

第 20 圖　庵原村，鉛直軸のまはりに廻轉せる水雷

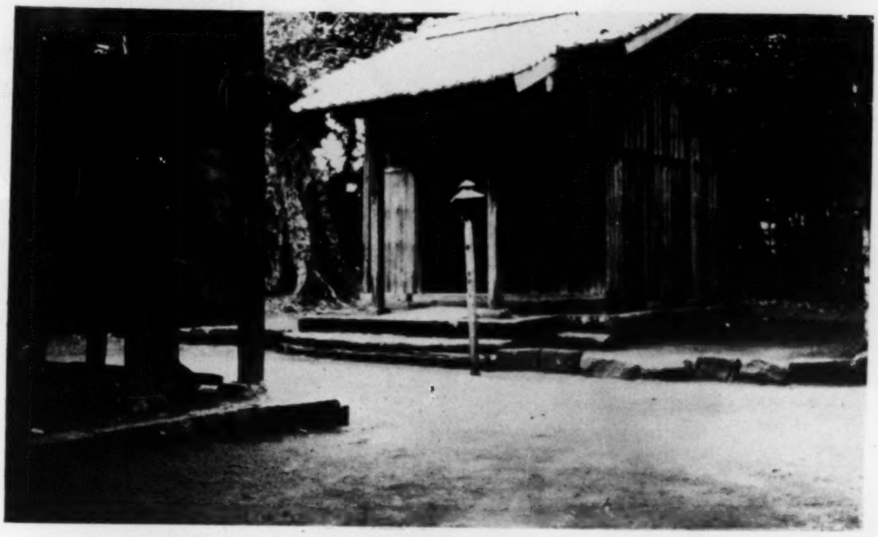

第 21 圖　飯田村八坂神社（右は神殿，左は拜殿）筋違を施せる拜殿のみ滑動

（震研彙報　第十三號　圖版　齊田）

第 22 圖　同　　上

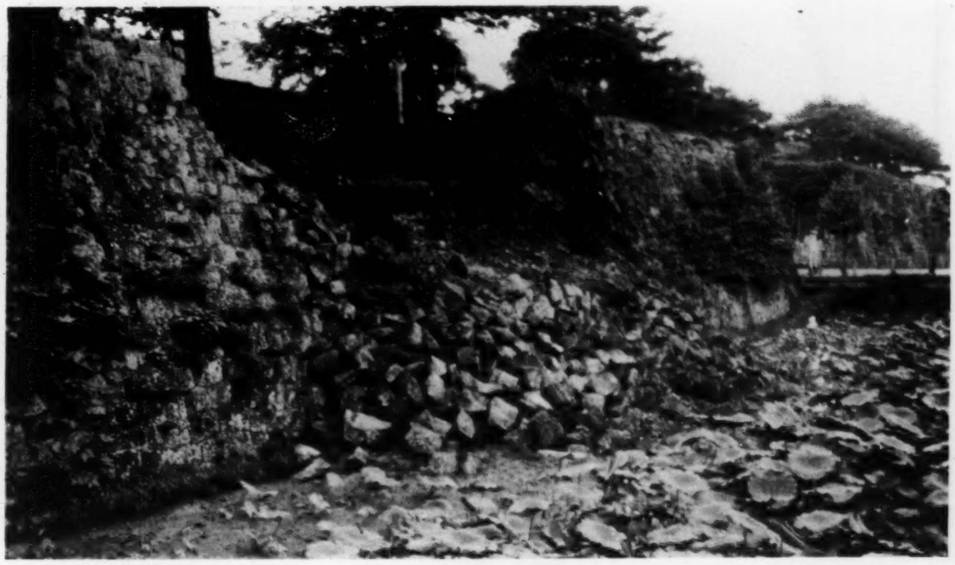

第 23 圖　靜岡縣廳石垣の崩壞

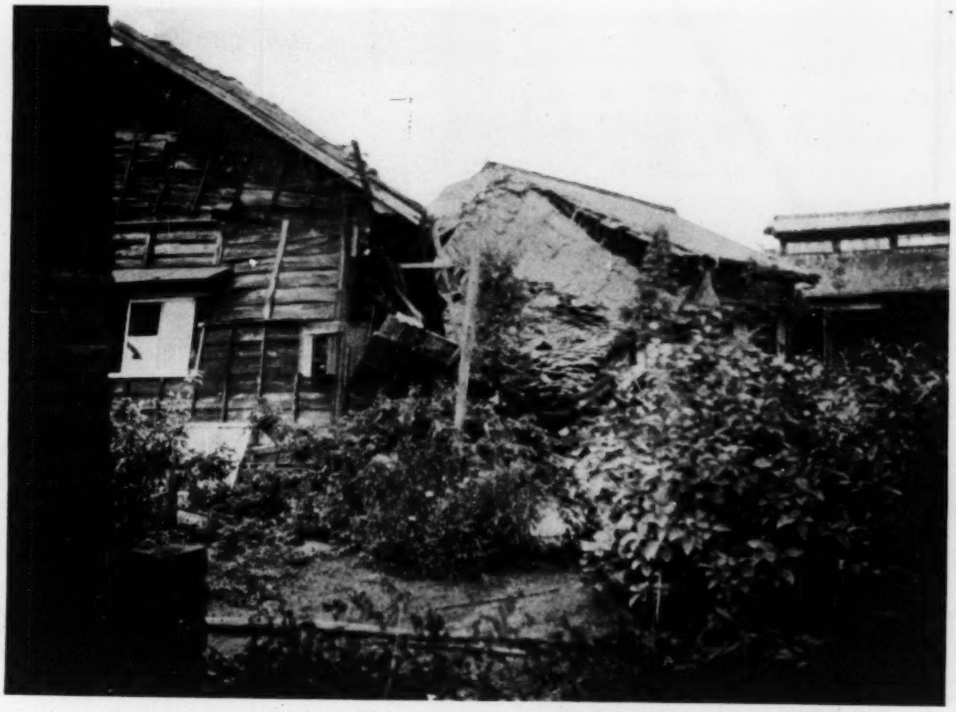

（那須・神永・杉山三氏の撮影）

第 24 圖　靜岡市曲金農事試驗場

（震研彙報 第十三號 圖版 齊田）

75. *Damages to the Quay Walls of Simizu Harbour due to the Earthquake on July 11, 1935, and the Seismic Stability of the Quay Walls.*

By Haruo MATUO,

Research Office of Public Works,
Department of Home Affairs.

(Read Sept. 17, 1935.—Received Sept. 20, 1935.)

The quay walls which are situated along the coast of City of Simuzu had severe damages to a part of them by the earthquake on July 11, 1935. The damages are here briefly described. The earth pressure exerted by the back filling earth during the earthquake is calculated under some assumptions and the stability of the quay walls is checked here.

Simizu Harbour

The work of the harbour construction with the total cost of ¥ 8,630,000 was commenced in 1921 and is expected to complete by Mar. 1936. The kind of quay walls included in the work is as shown in Table I.

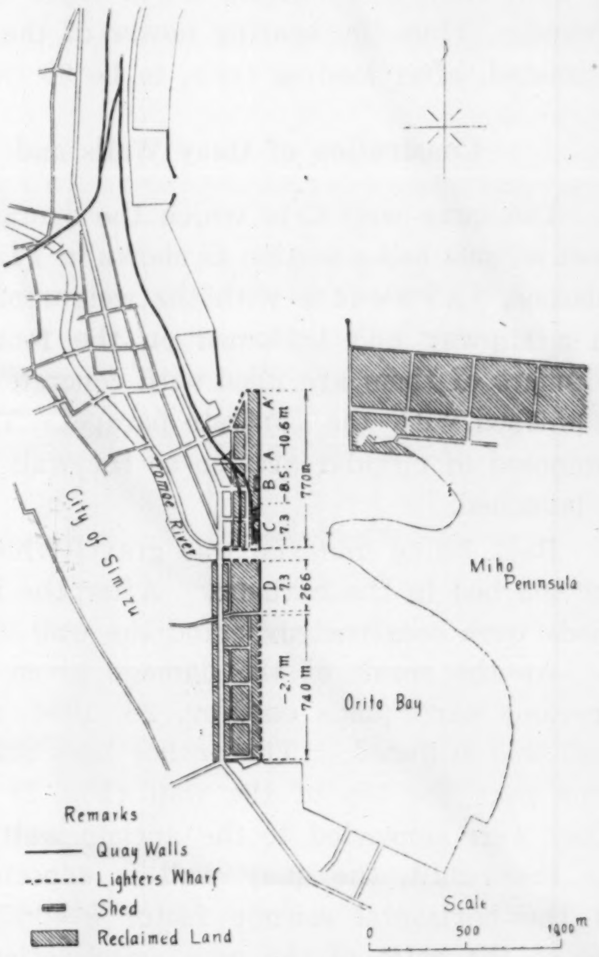
City of Simizu
Tomoe River
A'
A
B
C
D
-10.6m
-8.5
-7.3
-7.3
-2.7m
770m
266
740m
Miho Peninsula
Orito Bay
Remarks
Quay Walls
Lighters Wharf
Shed
Reclaimed Land
Scale
0
500
1000m

Fig. 1. Plan of Simizu Harbour.

These quay walls are situated near the mouth of the Tomoe River and nearly parallel to the original coast line some 200 m distant from it and the original depth of water at the site was some 2 m. The ground of the site is mainly

Table I.

		Water depth below L. W. L.	Length of the quay wall
Deep water quay wall	A′	10·6 m	149·3 m
〃	A	10·6	211·7
〃	B	8·5	183·4
〃	C	7·3	225·3
〃	D	7·3	265·8
Lighter wharf		2·7	739·7

composed of clay mixed with sand and gravel to the depth of 50 m or more. The foundation of the gravity type quay wall was formed by excavation and putting 3·5 m layer of gravel on the excavated ground. Thus the bearing power of the foundation on the gravel is estimated, after loading tests, to be 30 t/m^2.

Constrution of Quay Walls and Damages to Them.

The quay wall C to which the damages by the earthquake were most serious had a section as shown in Fig. 2. The reinforced concrete caissons, $7 \times 7{\cdot}9 \times 14$ m with the weight of 425 tons were constructed on a slipway and bottomed on the foundation. After the hollow cylinders of them are filled with concrete and gravel, the top of them is finished with the concrete parapet. The wall of the caisson was composed of circular arcs so as the wall may act as arches when it is launched.

Back filling material was gravel which was obtained by dredging the sea bed in the harbour. After the back filling was finished, the sheds were constructed behind the wall on pile foundation.

As the result of the damage given to the quay wall B by the previous earthquake on Nov. 26, 1930, remaining part of the quay wall was stiffened. The anchor bars attached to the caisson at that time near the top of the wall (Fig. 2) were of 4 rails of 30 kg/m. They were connected to the anchor wall some 26 m. from the quay. As the result, the quay wall is expected to resist the earthquake of the horizontal seismic factor $k=0{\cdot}15$. Here the seismic factor means the ratio of the max. acceleration of earthquake to that of gravity. By recent earthquake on July 11, 1935, whose horizontal seismic factor is estimated 0·25, the quay wall C was shifted forward as shown with the shaded line in Fig. 2. The length of the quay wall was 225 m and the max. amount horizontally shifted was 5·7 m,

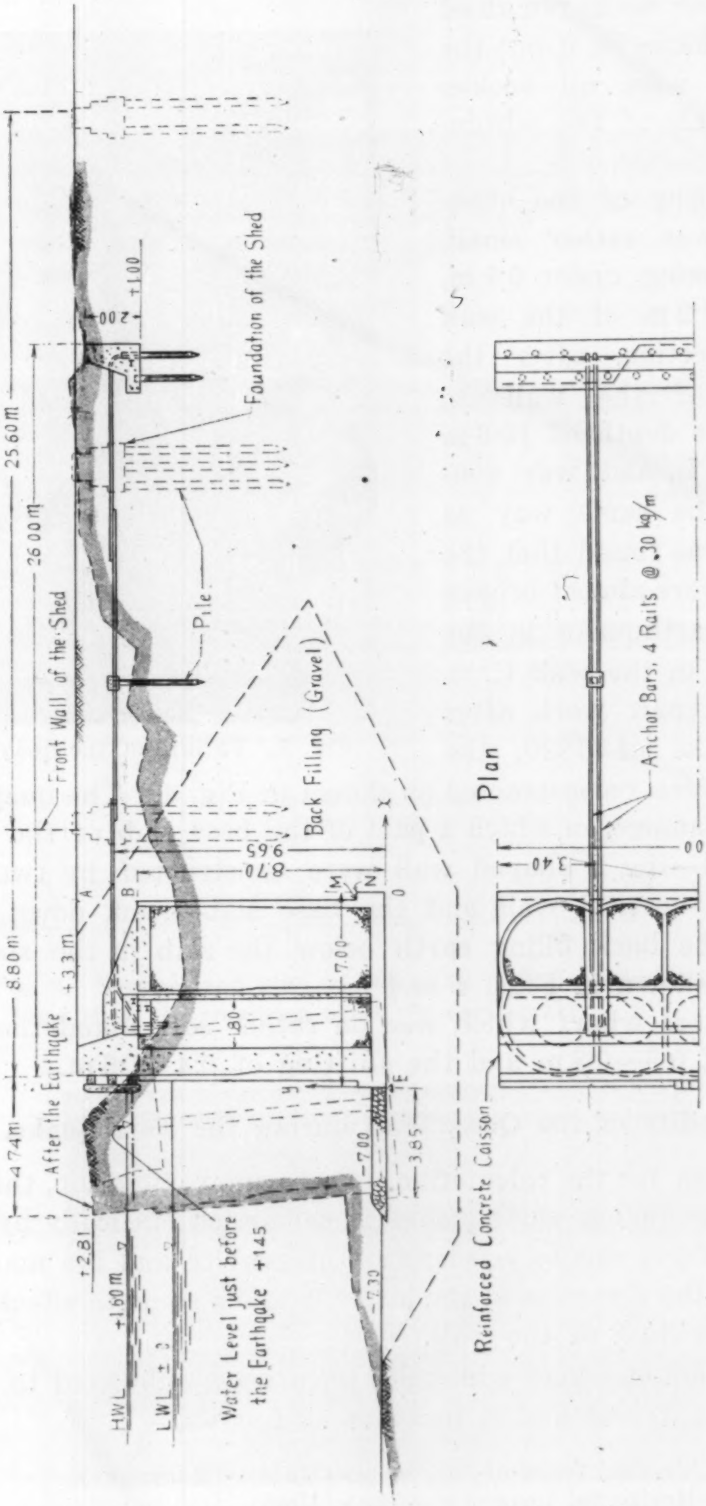
Section
Plan
Front Wall of the Shed
Pile
Foundation of the Shed
Back Filling (Gravel)
After the Earthqake
Water Level just before the Earthqake +1.45
HWL
LWL ± 0
Reinforced Concrete Caisson
Anchor Bars, 4 Rails @ 30 kg/m
25.60 m
26.00 m
8.80 m
4.74 m
+3.3 m
+1.00
2.00
9.65
8.70
7.00
1.80
-7.00
-7.30
3.85
+2.81
+1.60 m
14.00
3.40
A
B
M
N
O
X
Y
E

Fig. 2. Section and plan of the quay wall C. Shaded broken lines show the condition after failure.

and as the result the shed collapsed as in Fig. 3.

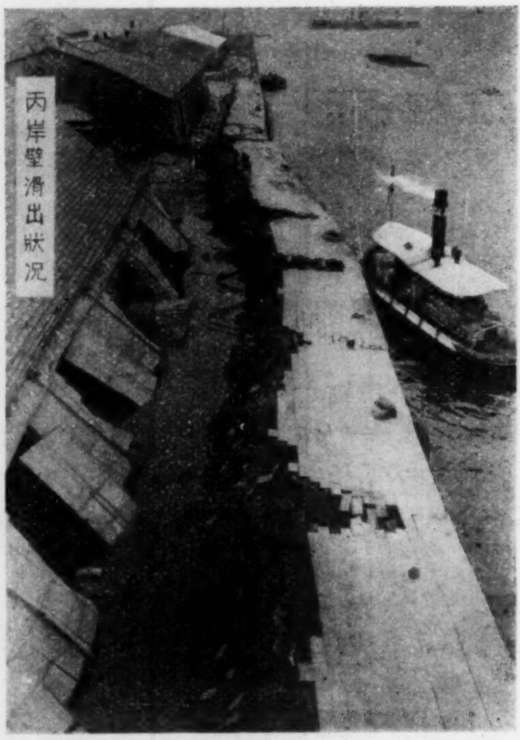

Fig. 3. Failure of the quay wall C.

The anchor walls remained still with no harm on it but the anchor bars were all broken off at the joints of two adjoining rails.

The shifting of the other quay walls was rather small, the amount being under 0·1 m, except 0·5∼1·2 m of the wall D. By inspection, after the earthquake, of the wall A, which has the depth of 10·6 m below L. W. L. and was constructed in the same way as the wall C, was found that the anchor bars were almost broken off by the earthquake in the same way as in the wall C.

By the repair work after the earthquake of 1930, the quay wall B were reconstructed as shown in Fig. 4. The quay suffered rather trifle damage, in which a part of the base slab of the L shaped bulkhead wall—the L shaped wall were constructed by two separate pieces of the vertical wall and the base slab—sunk down with the mound and the back filling earth below the slab in the shed flowed out there as shown in Figs. 4 and 5.

The lighters wharf which was on rather soft foundation suffered the setting of 0·5∼0·8 m and the shifting of 0·4∼1·6 m.

Stability of the Quay Wall during the Earthquake.

Assumption for the calculation. As an approximation, the stability of quay walls during earthquakes is calculated statically by applying the resultant force due to acceleration of gravity and the max. seismic acceleration—the direction of the latter is taken so as to effect the most dangerous condition of the wall.

The relation of forces which act on a mass subjected to buoyancy is somewhat different and it becomes as follows,

Vertical force ·················· $g\times$(Mass)—(Buoyancy).
Horizontal force ··· ········ $kg\times$(Mass).

Seismic Earth Pressure. The seismic earth pressure above the

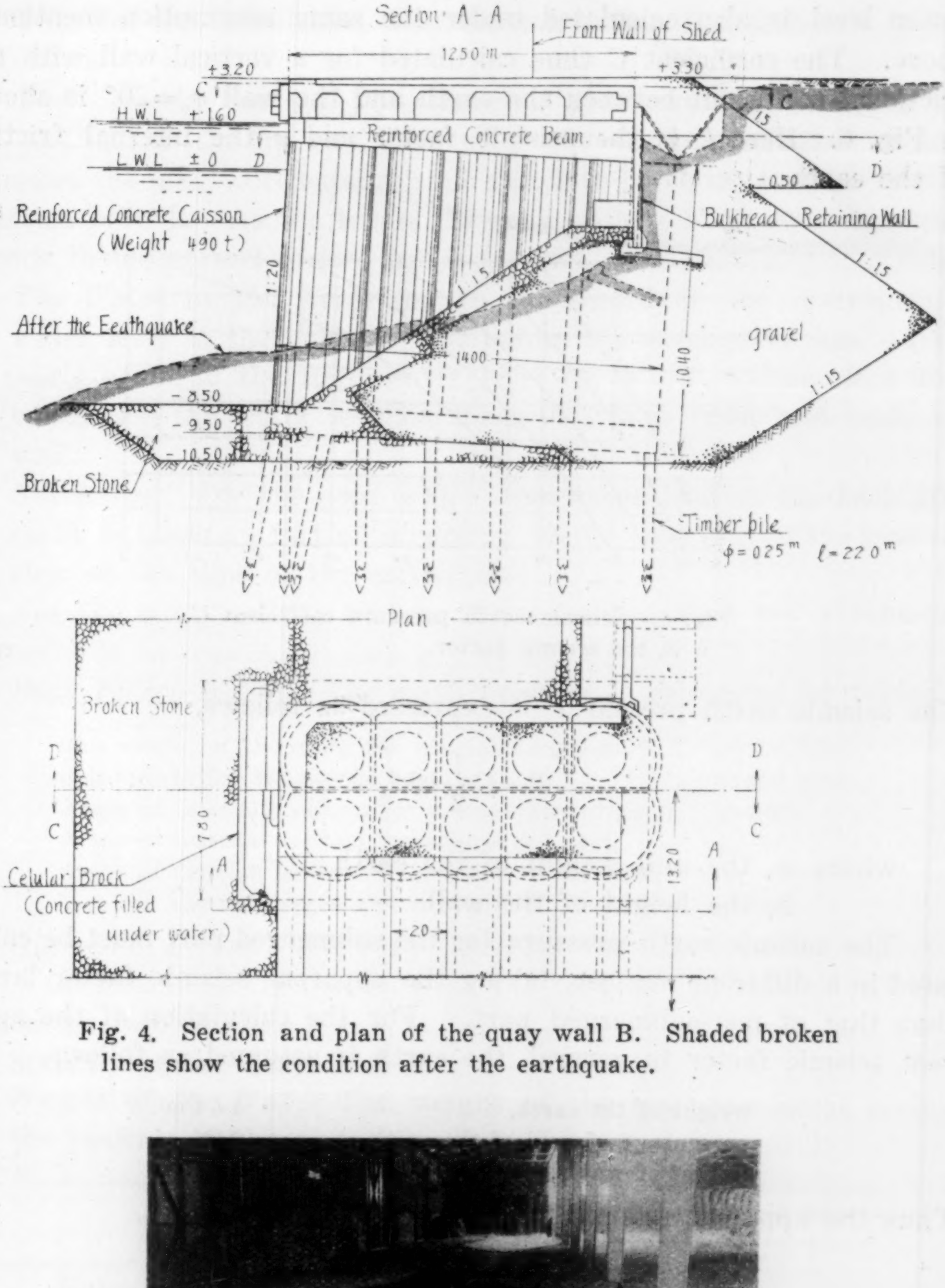
Section A - A
Front Wall of Shed
12.50 m
+3.20
+3.30
C
H.W.L. +1.60
L.W.L. ±0
D
Reinforced Concrete Beam.
1:5
C
D
-0.50
Reinforced Concrete Caisson
(Weight 490 t)
Bulkhead
Retaining Wall
1:20
1:1.5
1:1.5
After the Eathquake
14.00
gravel
10.40
1:1.5
-8.50
-9.50
-10.50
Broken Stone
Timber pile
φ=0.25m l=22.0m
Plan
Broken Stone
D
C
D
C
7.50
A
13.20
A
Celular Brock
(Concrete filled
under water)
20

Fig. 4. Section and plan of the quay wall B. Shaded broken lines show the condition after the earthquake.

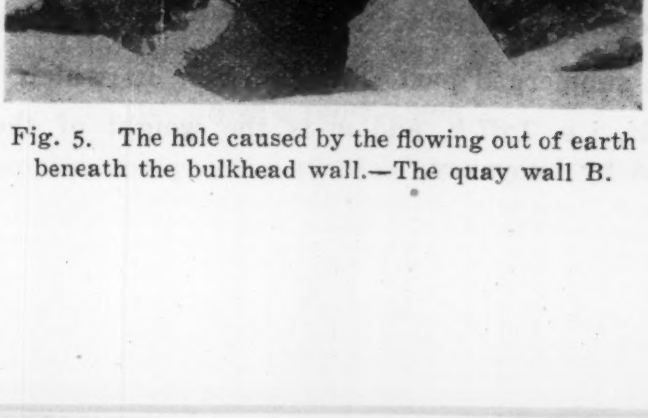

Fig. 5. The hole caused by the flowing out of earth beneath the bulkhead wall.—The quay wall B.

water level is also calculated under the same assumption mentioned above. The coefficient C thus calculated for a vertical wall with the frictional coefficient between the earth and the wall $\varphi_0=20°$ is shown in Fig. 6. Here k is the seismic factor and φ the internal friction of the earth.

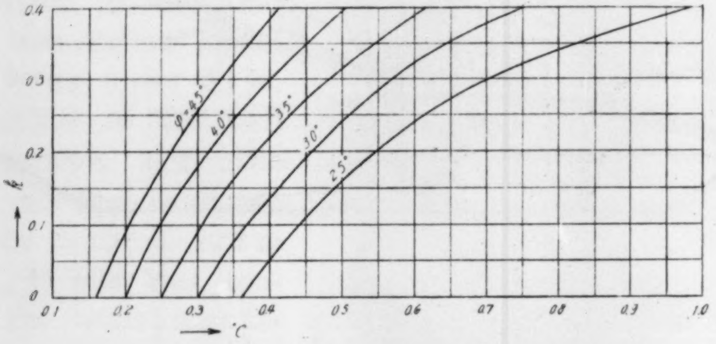

Fig. 6. Seismic earth pressure coefficient C.
k is the seismic factor.

The seismic earth pressur P is expressed as follows,

$$P=C\frac{1}{2}wh^2,$$

where w, the unit weight of the earth
h, the height of the wall.

The seismic earth pressure for the submerged part must be calculated in a different manner, taking the apparent seismic factor larger than that of non-submerged part. For the calculation of the apparent seismic factor in general, the earth is assumed as follows,

weight of the earth,	1·6 t/m^3,
percentage of void of the earth,	36%,
weight of water,	1·0 t/m^3.

Thus the apparent seismic factor k' becomes as follows,

$$k'=\frac{1{\cdot}6\,k}{(1{\cdot}6+0{\cdot}36)-1}=1{\cdot}67\,k,$$

where k is the seismic factor for the non-submerged part. In the above equation the numerator expresses the horizontal force acting on a unit volume of the earth while the denominator the vertical force. Thus for the submerged part $P=C\,\frac{1}{2}\,wh^2$, in which C is the coefficient for k', i. e. $1{\cdot}67\,k$, and w is the weight of the earth under water effected by buoyancy.

Data for the Calculation. For the calculation the data are taken as follows,

The Seismic Factor. By observing grave stones fell down by the earthquake in the city, just after the earthquake, the author estimates the max. horizontal seismic factor to be about $k=0{\cdot}25$ in the direction N 70°E. As the line of the quay walls is N–S, the component seismic factor normal to the line is $k=0{\cdot}23$.

The Water Level. According to the record of the mareograph the water level in the harbour just before the earthquake was $+1{\cdot}45$ m, nearly equal to the high water level of O. S. T. Therefore for the calculation the water level is taken $+1{\cdot}45$ m front and back of the wall.

Surcharge. For the quay wall C surcharge load on the back filling earth is taken $q=1{\cdot}0\,\mathrm{t/m^2}$ according to the condition of the load in the shed at the time of the earthquake.

For the quay wall A, $q=0$ as there was no shed nor surcharge there.

Back Filling Earth. The earth pressure is calculated by taking,

unit weight of the earth for non-submerged part,	$w=1{\cdot}6\ \mathrm{t/m^3}$,
unit weight for submerged part,	$w=1{\cdot}0\ \mathrm{t/m^3}$,
Angle of internal friction for non-submerged part,	$\varphi=35°$,
Angle of internal friction for submerged part,	$\varphi=30°$,
Angle of friction between the earth and the wall, both for non-submerged and submerged,	$\varphi_0=20°$.

Allowable Stress. Pressure intensity for the foundation $p=30\ \mathrm{t/m^2}$. Coefficient of friction between the base of the caisson and the foundation $f=0{\cdot}45$.

Stability of the Quay Wall C.

Weight of the Wall. The weight of the wall per linear meter and the position of the centroids are as follows,

	Weight (t)	Position of the centroid (m)	
		x	y
Without buoyancy	140·7	3·47	5·16
With buoyancy	83·5	3·38	5·66

x, y axes are taken as shown in Fig. 2.

Horizontal Force to the Wall. With the earthquake of the seismic factor 0·23, horizontal force W_h to the wall is

$$W_h=0{\cdot}23\times 140{\cdot}7=32{\cdot}3\ t.$$

Height of the application point $y=5{\cdot}16$ m.

Earth Pressure. Dividing the total height into two parts above and below the water level and with the coefficicient C from the diagram of Fig. 6, the earth pressure is calculated as follows,

Divisions	w (t/m³)	φ	h (m)	C	$q+wh$ (t/m²)	p (t/m²)	P	y (m)
					(A) 1·00	0·43		
AB	1·6	35°	1·85	0·42	(B) 3·96	1·65 1·94	1·91	9·68
BC	1·0	30°	8·95	0·49[1] 0·73[2]	(C) —	8·46[3]	46·50	3·50
							$\sum P=48\cdot41$	$y=3\cdot75$

1). Coefficient of earth pressure when $\varphi=30°$, $k=0\cdot230$,

2). Coefficient of earth pressure when $\varphi=30°$, $k'=0\cdot384$,

3). $8\cdot95\times1\times0\cdot73+1\cdot94=8\cdot46$.

Resultant (1). Assuming the anchor bars do not work at all. (Fig. 7 (a))

Resultant of forces at the base	$R=126\cdot7\ t.$
Vertical component of R	$N=100\cdot1\ t.$
Horizontal component of R	$H=\ 77\cdot8\ t.$
The ratio $f=\dfrac{H}{N}=\tan\theta=0\cdot78$;	$\theta=37°50'$.

Moment of forces about C (Fig. 7)

$$M_c=83\cdot5(7\cdot00-3\cdot38-0\cdot30)+32\cdot3\times5\cdot16+48\cdot4\times3\cdot75\times\cos20°=614\cdot0\ t\ m.$$

Eccentricity of R from the centre of the base

$$e=\frac{M_c}{N}-\left(\frac{b}{2}-0\cdot3\right)=2\cdot94\ \text{m},$$

$$b'=3\left(\frac{b}{2}-e\right)=1\cdot68\ \text{m},$$

Max. pressure intensity $P_{max}=\dfrac{2N}{b'}=119\cdot0\ \text{t/m}^2$.

Resultant (2). Assuming the anchor bars work fully. (Fig. 7 (b)) The force Q on the anchor bar per linear meter of the wall is calculated as follows,

$$Q=\frac{M_c-M_c'}{h'}$$

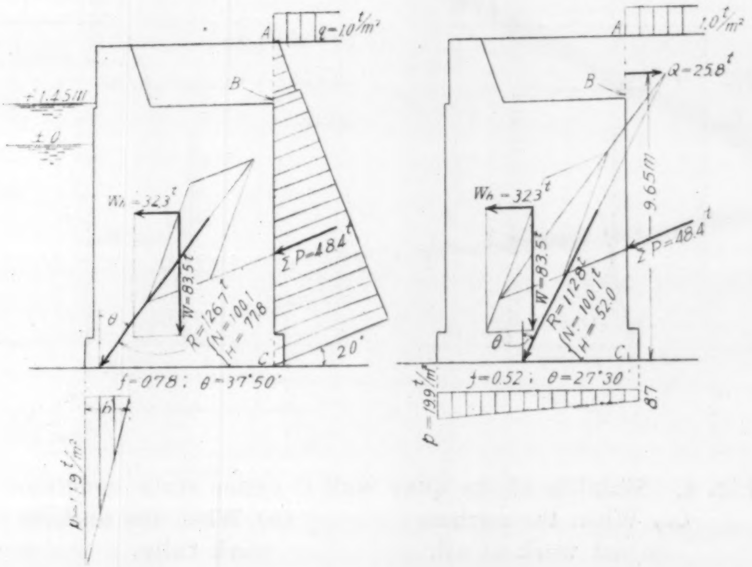
A
q=1.0 t/m²
B
+1.45 m
±0
Wh=32.3 t
W=83.5 t
ΣP=48.4 t
R=126.7 t
N=100.1
H=77.8
θ
C
20°
f=0.78 ; θ=37°50′
b
p=11.9 t/m²
A
1.0 t/m²
B
Q=25.8 t
9.65 m
Wh=32.3 t
W=83.5 t
ΣP=48.4 t
R=112.8 t
N=100.1 t
H=52.0
θ
C
f=0.52 ; θ=27°30′
p=19.9 t/m²
8.7

Fig. 7. Stability of the quay wall *C* under the earthquake of $k=0{\cdot}23$.

(a) When the anchors do not work at all. (b) When the anchors work fully.

where M_c' the moment of forces about C under static condition while M_c the value mentioned above; h' height of the anchor bar from C.

We find the forces as follows,

$$Q=25{\cdot}8\ t. \qquad R=112{\cdot}8\ t. \qquad N=100{\cdot}1\ t.$$

$$H=77{\cdot}8-25{\cdot}8=52{\cdot}0\ t. \qquad f=0{\cdot}52.$$

$$\theta=27^\circ 30'. \qquad M_c=365{\cdot}6\ \text{tm}.$$

$$e=0{\cdot}456\ \text{m}. \qquad p=\frac{N}{b}\left(1\pm\frac{6e}{b}\right)=\begin{cases}19{\cdot}9\ \text{t/m}^2\\ 8{\cdot}7\ \text{t/m}^2.\end{cases}$$

From Q we find the unit combined tensile stress σ of the anchor bar at its max. $\sigma=10{\cdot}5\ \text{t/cm}^2$.

For comparison the stability of the same wall in static condition is shown in Fig. 8, in which (a) is when anchor bars work not at all and (b) when they work fully to the extent that the pressure distribution on the base become uniform. The values M_c' above mentioned corresponds to the case (a).

The Cause of Failure Estimated. The resultants of (1) and (2) are two extreme cases and it seems probable that the condition just before the failure is intermediate between them. As the resultant (2) is calculated under the assumption that the wall when static the anchor bars do not work and that the amount of forces increased by the

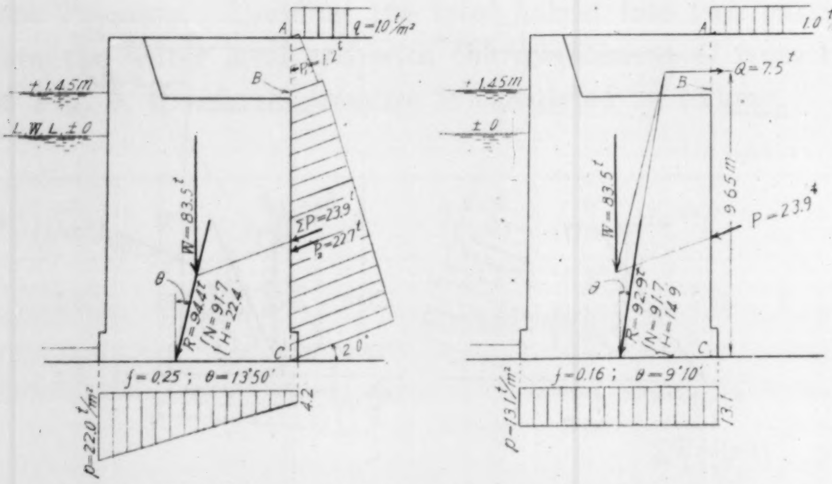

Fig. 8. Stability of the quay wall *C* under static condition.
(a) When the anchors do not work at all.
(b) When the anchors work fully.

seismic force is supported by the anchor bars and the horizontal force on the base, we would conclude that the condition of forces just before the damage is rather akin to (2) than (1).

Under the condition (2), $f=0{\cdot}52$ and $\sigma=10{\cdot}5$ t/cm² are both larger than the allowable stresses, among which f is expected less than the ultimate sliding coefficients — though the allowable coefficient is 0·45 — while σ is far larger than the ultimate tensile stress 6·0 t/m² of the rail steel. Therefore the breaking of the rail is supposed to be the first failure. After the breaking of the rail the distribution of forces is supposed became akin to (1) and caused the shifting and tilting.

Stability of the Quay Wall A. With the same assumption the stability of the quay wall A which has almost the same section as *C* — though the dimension is different — is shown in Fig. 9 (a) and (b). For the case Fig. 9 (b) $\sigma=13{\cdot}0$ t/cm² far larger than the allowable stress, and $f=0{\cdot}50$ a little larger than the allowable value. Though the shifting of the wall was small — about 0·1 m — but by inspection after the earthquake it was found that almost all the anchor bars were broken off. The cause of little damage of the quay walls is not as yet fully accounted for, as well as the little damage on the quay wall D which has just the same section as C. Little difference of prudence for the execution seems to be an important factor for it.

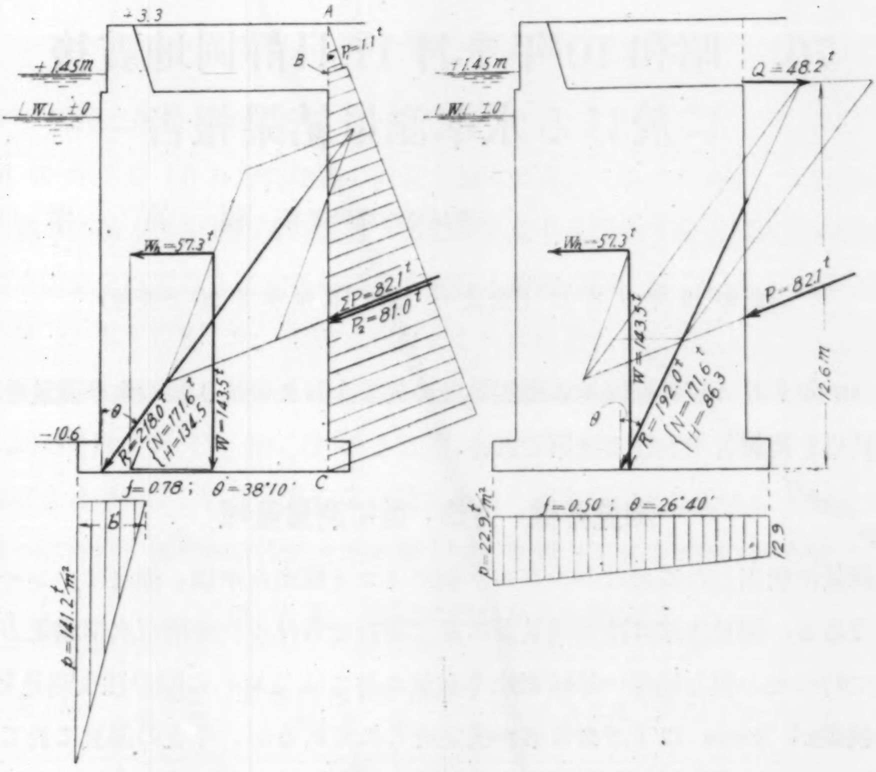
+3.3
A
$P_1=1.1^t$
B
+1.45m
L.W.L. ±0
$W_h=57.3^t$
$\Sigma P=82.1^t$
$P_2=81.0^t$
θ
−10.6
$R=218.0^t$
$N=171.6^t$
$H=134.5$
$W=143.5^t$
$f=0.78$; $\theta=38°10'$
C
b
$p=141.2\ t/m^2$
+1.45m
L.W.L. ±0
$Q=48.2^t$
$W_h=57.3^t$
$P=82.1^t$
$W=143.5^t$
θ
$R=192.0^t$
$N=171.6^t$
$H=86.3$
12.6m
$f=0.50$; $\theta=26°40'$
$p=22.9\ t/m^2$
12.9

Fig. 9. Stability of the quay wall A under the earthqauke of $k=0{\cdot}23$.

(a) When the anchors do not work at all.

(b) When the anchors work fully.

---

75. 清水港岸壁の震害と之に對する安定計算

内務省土木試驗所　**松尾春雄**

昭和 10 年 7 月 11 日の靜岡清水地方の地震に依る清水港岸壁の震害の狀況及之等岸壁に對し地震時安定計算を試みた結果を述べる．

76.　昭和10年7月11日靜岡地震後に於ける水準測量結果報告

三井地球物理研究所　福富孝治

（昭和10年9月17日發表――昭和10年9月20日受理）

昭和10年7月11日靜岡地震後震災地に於て今日までに3回の水準測量を施行した。此結果を御報告申上げる次第である.

測量器械，方法，並に測量區域

水準測量に使用した器械はバンベルグ製ウイルド精密水準儀，標尺はインバール製のものである．測量方法は陸地測量部に於て施行せられる一等精密水準測量方法[1]に準據して行つた．但し通常一等精密水準測量に於ては2kmの間の往復測量を行ひ，共閉塞誤差が3mm以下である事が規定せられて居るが，今度の測量に於ては極めて近間隔に次節に述べるが如き臨時水準點を設けた事と，出來るだけ多くの材料を得る爲めに片道の測量に止めた關係上共誤差の大きさの知られなかつたのは殘念であつたが，今度の測量の信用度に就いては第4回測量の際に論ずる考である．共點は諒とせられたい.

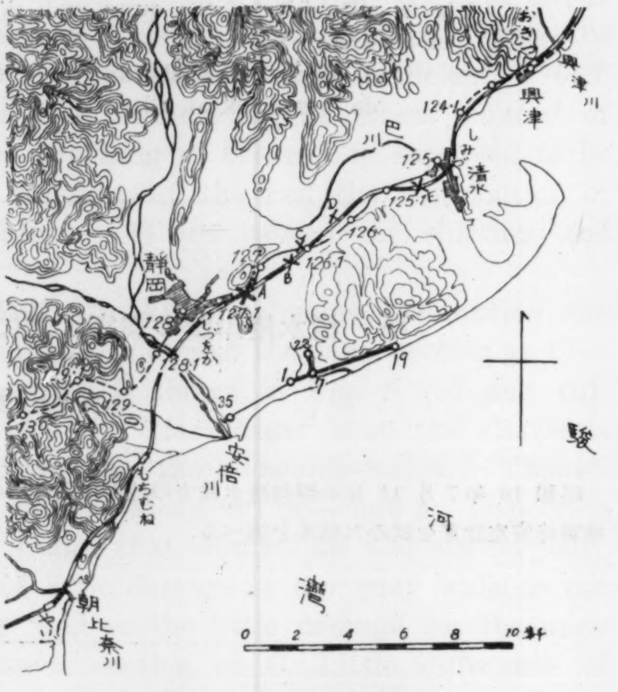
おきつ
興津川
興津
124·1
巴川
しみづ
125
清水
125·1
E
D
C
126
B
126·1
127
A
靜岡
127·1
128
しづをか
128·1
129
130
35
1
22
7
19
安倍川
もちむね
朝比奈川
やいづ
駿
河
灣
0
2
4
6
8
10粁

第1圖　靜岡附近水準線路

測量區域は第1圖に示す通り久能山下より阿倍川堤防に到る海岸に沿つた水準線路と，舊東海道に沿ひ靜岡市長田手越に在る陸地測量部一等水準點128·1より靜岡縣庵原郡袖師村に在る一等水準點124·1に到る16km間の水準線路との二つである.

1）大前憲三郎氏著　陸地測量學.

測量結果

A）海岸に沿ふ水準線路

昭和 10 年7月 11 日靜岡地震の際最も被害の甚大であつた高松，大谷附近の地變を知る爲め高松より少し西方の宮竹，風祭神社より久能山下根古屋に到る間に 19 點の臨時水準點を設置し，又大谷の街より大谷小學校の間に第 20 號より第 22 號の 3 點，合計 22 點を設置した．臨時水準點としては自然岩石の突出部又は土木構造物の中，局部運動を爲さない様なものを選んで其突出部にエナメルにて印を附して用ひた．

第1回測量は7月 15，16，17 の3日間，第2回測量は7月 25，26 日の2日間，第3回は8月 31 日，9月2日の2日間である．第3回測量の際には今村先生の御希望に依つて宮竹，風祭神社臨時水準點第1號より西方阿倍川堤防に到る間に 11 點の

第 I 表　海岸に沿ひたる水準線路

所在地	水準點番號	昭和10年7月15日標高	昭和 10 年7月 15，16. 17 日乃至7月25, 26 日間變化	昭和 10 年7月 25，26 日乃至8月 31 日9月2日間の變化
		m.	mm.	mm.
靜岡市　宮竹	1	−2·4087	+1·1	−4·0
〃　高松	2	−5·0897	+4·1	−4·2
〃　〃	3	−4·8497	+4·3	−2·8
〃　〃	4	−5·0426	+6·3	−3·0
〃　〃	5	−4·4984	+7·6	−2·8
〃　西大谷	6	−4·0689	+6·3	−3·8
〃　〃	7	−5·9019	+5·0	−1·4
〃　西大谷	20	−1·3399	+4·4	−1·6
〃　北原	21	+1·3271	+3·8	−2·7
〃　〃	22	+0·4710	+1·9	−4·8
〃　東大谷	8	−6.1950	+5·5	−1·6
〃　〃	9	−6·1865	+4·5	−0·8
久能村　西平松	10	−5·6858	+2·6	+0·5
〃　〃	11	−4·7821	+3·5	+2·5
〃　中平松	12	−5·3241	+3·1	+1·3
〃　〃	13	−3·9100	+1·3	+4·3
〃　青澤	14	−3·1950	+2·6	+2·1
〃　〃	15	−2·8678	+5·7	——
〃　古宿	16	−3·8084	+4·7	−1·9
〃　安居	17	−4·5903	+3·9	−2·7
〃　〃	18	−3·1366	+2·9	−3·1
〃　根古屋	19	0*	0#	0#

* 標高は 19 號點を 0 と假定す．　# 變化は 19 號點を不動と假定す．

臨時水準點を設けて測量を行つた. 久能山下根古屋第 19 號點の標高を 0 及垂直變化量を不動と見做した場合の結果は第I表に示す如くであつて，第1回と第2回の期間中に於ける高低差（II—I）並に第3回と第2回の期間中に於ける高低差(III—II) を圖示すれば第 2 圖の如くである.

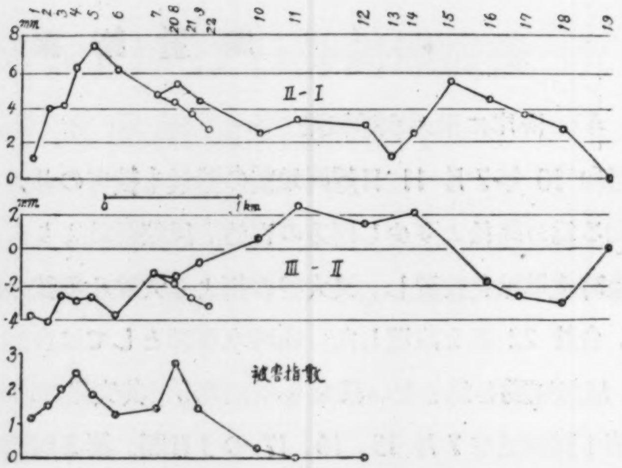

第 2 圖

(II—I) は 第1回測量 (7 月 15, 16 日, 1935)—第2回測量 (7 月 25, 26 日, 1935) 間約 10 日間の各水準點垂直變化量.

(III—II) は 第2回測量 (7 月 25, 26 日, 1935)—第3回測量 (8月 31 日, 9 月 2 日, 1935) 間約 37 日間の各水準點垂直變化量.

$$\text{被害指數} = \frac{3\times(\text{全潰住家數})+2\times(\text{半潰住家數})+1(\text{輕損住家數})}{(\text{全住家數})}$$

B)　舊東海道に沿つた水準線路

舊東海道に沿つた水準線路については，7 月 27 日，28 日の兩日靜岡市院內町 127·1 水準點より，長沼，栗原水準點を經て有度村草薙 126 水準點に到る 6 km の間の水準測量を第1回として行つた. 然して各水準點間には約 500 m 毎に臨時水準點を設

第 II 表　舊東海道に沿ひたる水準線路

所　在　地		標石番號	昭和6年9月改正標高	明治33年乃至昭和6年變化	昭和6年9月乃至昭和10年9月5, 8日間變化	昭和10年7月27, 28日乃至昭和10年9月5, 8日間變化
			m	mm.	mm.	mm.
靜　岡　市	長田手越	128·1	17·6174	+30·4	+17·7	——
〃	梅屋町	128	21·3237	+18·6	+14·0	——
〃	院內町	127·1	16·8713	0#	0#	0#
〃	曲　金	1				+1·5
〃	柚ノ木	2				+2·9
〃	長　沼	3				+1·1 (?)
〃	長　沼	127	11·8026*	+38·8	+17·3	+2·3
〃	長　沼	4				+2·6
〃	古　庄	5				+3·3
〃	〃	6				+4·5
〃	栗　原	126·1	13 4536*	+66·3	+14·4	+3·1
安部郡 有度村	國吉田	7				−0·2
〃	中之郷	8				−1·2
〃	草　薙	9				−5·1
〃	草　薙	126	23·7911	+66·9	− 1·3	−7·1
〃	平川地	125·1	14·8774	+73·1	+12·4	——
清　水　市	江尻町	125	3·8410	+51·7	−12·3	——

* は昭和6年9月水準點改埋測.　# 院內町水準點を不動とす.

置した．次いで凡そ 41 日の後9月5日より8日迄の間に於て靜岡市長田手越 128 1 水準點より清水市 125 水準點に到る間の第2回水準測量を行つた．共結果は第 II 表及第3圖に示す通りである．

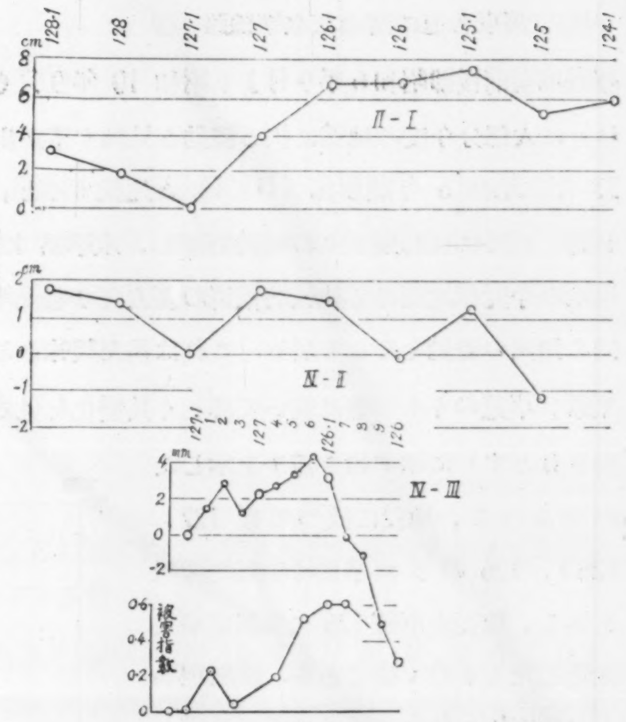

第 3 圖

(II–I) は明治 33 年 6 月及至 10 月—昭和 6 年 9 月間垂直變化量．

(IV–II) は昭和 6 年 9 月—昭和 10 年 9 月 5～8 日間垂直變化量．

(IV–III) は昭和 10 年 7 月 27，28 日—昭和 10 年 9 月 5～8 日間垂直變化量．

$$\text{被害指數}=\frac{2\times(\text{全潰住家數})+1\times(\text{半潰住家數})}{(\text{全住家數})}$$

論　　議

A） 海岸に沿つた水準線路

靜岡地震後に於ける沿線の變動は第2圖に示す如く極めて複雜である．先づ（II—I）の地震直後 10 日間に於ける變化を見るに高松，東大谷附近並に青澤，古宿附近が數粍の相對的隆起を行つて居る．今道路に沿つて見られた家の被害を全潰，半潰，輕損，無被害の 4 階級に區分してその各々の數を a，b，c，d とすれば $\frac{3a+2b+c}{a+b+c+d}$ は共被害の程度を表す一指數と見る事が出來る故に，これを作ると第2圖を得た．これを上述の測量結果と比較して見るに高松，大谷附近の垂直變化の變異點附近に於て被害が著しく大であつた事は興味ある事である．次に（III—II）37 日間の變動を見るにこれは略々（II—I）と逆向の運動を示して居る．特に高松第5號水準點より中平松第 14 號點に到る間は略々剛體的運動をなし，（II—I）に於ては N 7° E の方向へ $5{\cdot}4\times10^{-6}$ C.G.S. の傾斜運動を行つたに反し，（III—II）に於ては N 46° W の方向へ $5{\cdot}3\times10^{-6}$ C.G.S. の傾斜運動をなした．卽ちこの部分は一邊の長さ約 2 km の小地塊をなす事が解つた．又全體としての垂直變動は（II—I）卽地震直後の 10 日間の變動の範圍は，最大約 7 mm であつたのに，共後 37 日間に於ける垂直變動は最大約 7 mm であつて卽 10 日間に對しては約 2 mm に衰へたのであつて，地震後變動が漸次靜止の狀態に近づきつゝあるを示すのであらう．

B） 舊東海道に沿つた水準線路

靜岡地震前後卽昭和6年9月より昭和10年9月6日の約4年間に於ける變化（IV—II）は大部分今度の地震に依る變動と見做す事が出來るであらうが，之を地震前明治33年—昭和6年間變化（II—I）と比較すると，全體としては後者が東上りの變動を爲したるに反し東下りの變動をなし，水準點127～125·1卽長沼，栗原，草薙，平川地の今度の地震にて比較的被害の甚大なりし土地の4水準點を除く外は略々後者と同じ傾向の變動をなして居る．これは甚だ興味ある事と思はれる．今院内町，長沼，栗原，草薙の4水準點に就いて詳しく其變化を見るならば第4圖（院內町水準點の變動を0とす）に示す如き樣子を示したのであつて，地震に依つては127，126·1，126の3水準點は相對的隆起を示し，地震後草薙126水準點は漸次沈降したるものゝ樣である．萩原理學士の研究²⁾に依れば靜岡地震の餘震の震央は何れも草薙附近であつた事も此の地變と何等かの關係があるのかも知れない．尙此部分の地震後に於ける臨時水準點の垂直變動は第3圖に示される通りであるが，圖中臨時水準點第2號附近は谷津山龜裂，靜岡電氣鐵道線路の被害，靜淸國道，國鐵東海道線等に約200mの間に涉つて損傷のあつた所であり，又臨時水準點6～7號附近に於ては鐵道線路の異狀，靜岡電氣鐵道高架道に半米の沈下等あり，國道にも可成りの損傷ある所があつて，垂直變化量が之等の附近にて急な變異をなして居る事も，又今村博士³⁾が第1線，第2線として引かれた構造線と略々一致した場所である事も興味ある事である．第3圖最下は靜岡市役所の調査に依る住家被害表から被害を示す一方法として

$$\frac{2\times(\text{全潰住家數})+1\times(\text{半潰住家數})}{(\text{全住家數})}$$

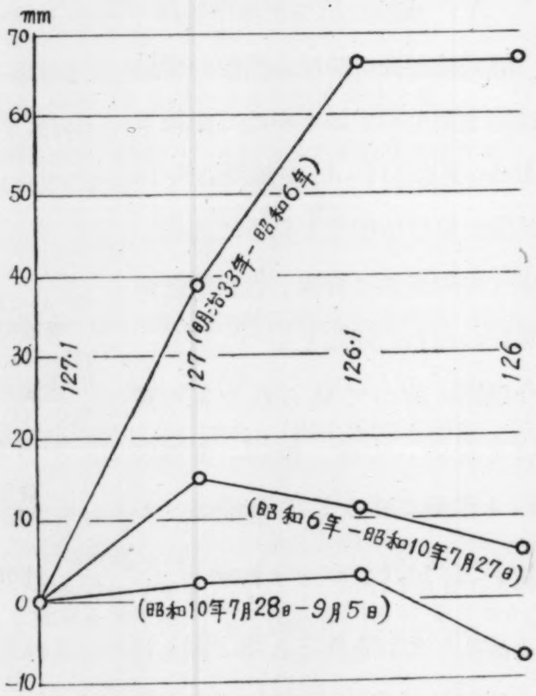

第4圖 院內町，長沼，栗原，草薙水準點の地震前後に於ける變動.

2） 萩原尊禮 地震研究所彙報 13 (1935), 951.

3） 今村明恒 地震 7 (1935), 951.

を水準線路に沿つて求め圖示したものであつて水準變化の變異點附近に於て被害の大なる事を示して居る.

終りに臨み此調査，研究に當り，御助言，御援助を賜つた寺田先生、今村先生，坪井忠二先生，宮部技師，陸地測量部の守屋技師，武藤技師に厚く御禮申上げる．又測量に關しては標尺の借用を許され，又種々御援助を賜つた陸地測量部に對して深謝の意を表する次第である.

追　加

昭和 10 年 10 月 15 日～10 月 21 日の間に於て，第4回目の靜岡地方の水準測量を行つた．其結果を此處に追加補足する次第である.

第5圖及第 III 表は海岸に沿つた水準線路の昭和 10 年8月 31 日，9 月 2 日より 10 月 15～17 日に至る約 46 日間に於る垂直變動量（IV～III）を示し，第6圖及第 IV 表は舊東海道に沿つた水準線路の昭和 10 年9月 5～8 日より 10 月 18～21 日に至る約 43 日間に於る垂直變動量（V～IV）を示して居る.

第 III 表　海岸に沿ひたる水準線路に於る垂直變動（IV～III）

所在地		水準點番號	昭和 10 年 10 月 15 日標高	昭和 10 年8月 31 日9月2日乃至10 月 15，16，17 日間の變化
			m.	mm.
久能村	青澤	14	+1·7634	−3·3
〃	中平松	12	−0·3652	−2·8
〃	西平松	11	+0·1785	−2.6
〃	〃	10	−0·7252	+0·2
靜岡市	東大谷	9	−1·2243	+1·2
〃	北原	22	+5·5618	+3·9
〃	〃	21	+6·4211	+3·0
〃	西大谷	20	+3.7554	+2·7
〃	〃	7	−0·8067	+1·9
〃	〃	6	+1·0247	+1·3
〃	高松	5	+0·5960	−0·2
〃	〃	4	+0·0510	+0·4
〃	〃	3	+0·2420	+0·4
〃	〃	2	0*	0#
〃	宮竹	25	+1.4834	−1·1
〃	〃	26	+2.2854	−0·4
〃	敷地	28	+2.8595	−0·8

第 III 表

所在地		水準點番號	昭和 10 年 10 月 15 日 標高	昭和 10 年 8 月 31 日 9 月 2 日及至 10 月 15, 16, 17 日間の變化
			m.	mm.
靜岡市	敷地	29	+2·2278	−1·8
〃	下島	30	−0·4776	−1·9
〃	〃	31	−2·5547	−1·0
〃	西島	32	−2·5284	−3·5
〃	〃	33	−2·1520	−3·6
〃	中島	34	−1·4332	−5·5
〃	〃	35	−1·0408	−3·5

*　標高は 2 號點を 0 と假定す.　　#　變化は 2 號點を不動と假定す.

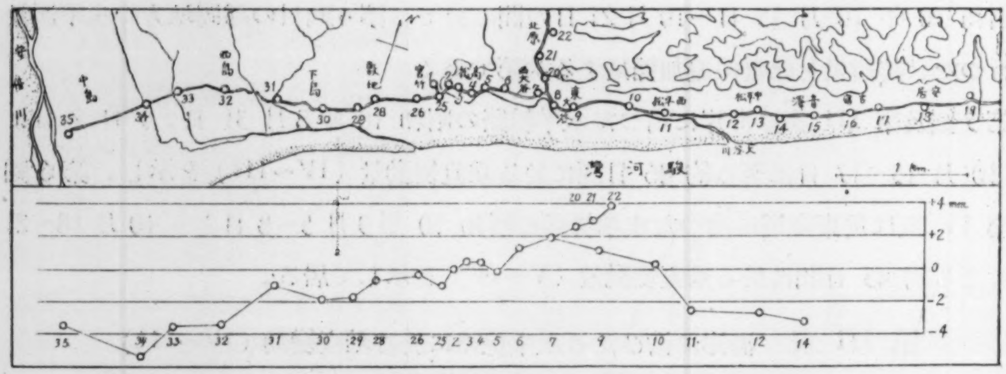

安倍川
中島
西島
下島
敷地
宮竹
駿河灣
1 km.
35
34
33
32
31
30
29
28
26
25
2
3
4
5
6
7
8
9
10
11
12
13
14
15
16
17
18
19
20
21
22
+4 mm.
+2
0
−2
−4

第 5 圖　海岸に沿つた水準點と其垂直變動 (IV～III) (但し 2 號點を不動と假定す.)

第 IV 表　舊東海道に沿ひたる水準線路に於る垂直變動 (V～IV)

所在地		標石番號	昭和 10 年 10 月標高	昭和 10 年 9 月 5, 8 日乃至 10 月 18, 21 日間變化
			m.	mm.
靜岡市	院內町	127·1	0*	0#
	曲金	1	− 1·7023	−1·4
	柚木	2	− 3.1307	−6·0
	長沼	3	− 4.7838	−3·4
	長沼	127	− 5·0551	−3·7
	長沼	4	− 7·7075	+1·0
	古庄	5	− 7·2901	+7.2
	古庄	6	− 7·3988	+7·7
	栗原	126·1	− 3·3965	+6·8
有度村	國吉田	7	+ 8·3088	+6·4
	中之鄉	8	+14·8474	+4·9
	草薙	9	+ 6.3549	+3.3
	草薙	126	+ 6·9208	+2·3
	草薙	10	+ 7·3367	+1·5

第 IV 表

所在地		標石番號	昭和 10 年 10 月標高	昭和 10 年 9 月 5，8 日及至 10 月 18，21 日間變化
			m.	mm.
有度村	草薙	11	+ 9·0933	+2·8
	草薙	12	+ 8·3465	+1·8
	上原	13	+ 1·7721	+4·0
	平川地	125·1	− 1·9809	+0·6
清水市	元追分	14	−11·3815	+2·5
	入江町	15	−10·6294	+6·2
	江尻町	125	−13·0333	+9·3

*　標高は 127·1 水準點を 0 と假定す.　　♯　變化は 127·1 水準點を不動と假定す.

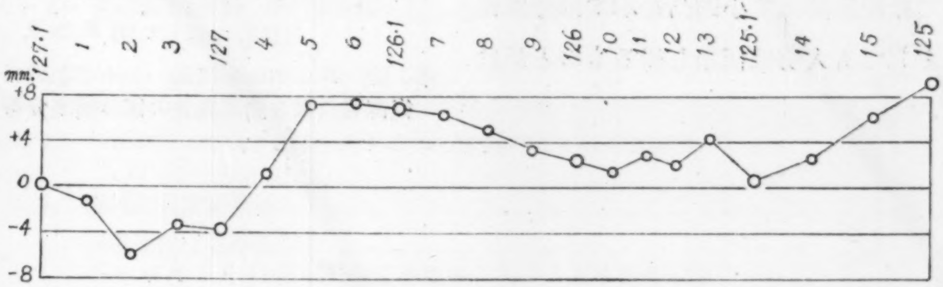

第 6 圖　舊東海道に沿つた水準點の垂直變動（V～IV）（但し 127·1 水準點を不動と假定す）

前の測量と比較する爲め，今海岸に沿つた水準線路中 2-7-14 の水準點に就て見るに，此期間に於る垂直變動（IV～III）の範圍は約 46 日間に約 5 5 mm であつて卽ち 10 日間には約 1·2 mm となり，地震直後の 10 日間卽ち（II～I）の値約 7 mm，其後 8 月頃の 10 日間（III～II）の値約 2 mm に對して小さく，變動が漸次靜止しつゝある事を示して居る.

又海岸線 25 號水準點より 35 號水準點に至る延長線に就て見るに此間には阿倍川寄りの水準點は漸次沈降を行つたものの如く，5-2-25-35 の水準點を含む地盤は略々一つの地塊をなし，西方へ傾動をなした様に見える. この地塊と本文に述べた 5～14 の水準點を含む地塊との境界附近に於て地震の被害が最も激烈であつた事は注目に値ひする.

最後に上記水準測量の精度に就て一言し度い. 今度は單なる片道の測量を行つたに過ぎないので，その精度に就て論ずる事は出來ないが，筆者が昭和 9 年 8 月南伊豆，柿崎半島に於て同じ器械，同じ方法で行つた往復測量結果に就いて述べる. 其際に於ける往復測量に依る閉塞誤差は略々 2 km の水準點間に就て

（嵐留—道路分岐點）間往復　　+0 8 mm，
（柿崎—道路分岐點）間往復　　−3·3 mm，

であつたが，今度の測量に於ても略々同程度の誤差と考へて差支へあるまいと思ふ．又短距離の臨時水準點間に於る測量の誤差に就ての大體を知る爲に凡そ100m間隔の多くの2水準點間の往復測量の閉塞誤差の値の頻度曲線を作つたのに第7圖を得た．

卽ち 100m 位の間隔にて作られた臨時水準點間の測定誤差は多くは ±1mm 以下である事が解る．從て上記の垂直變動の圖に於ては短距離にて小凹凸を示す部分は怪しいとしても大勢は信用し得るものと思はれる．

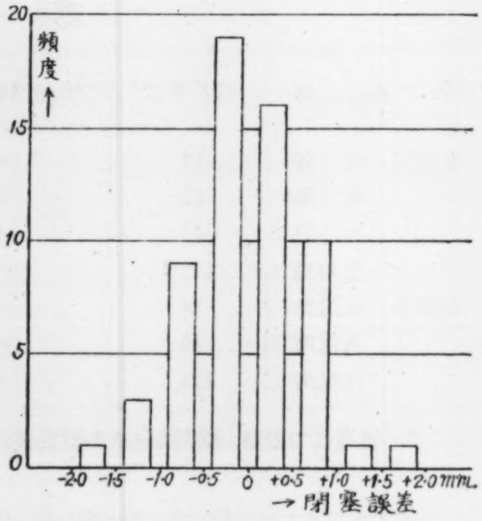

第7圖 凡そ100米間隔の2水準點群の往復測量に依る閉塞誤差の値の頻度分布

---

76. *On the Result of Precise Levellings in the Strongly Shaken Area of the Siduoka Earthquake of July 11th, 1935.*

By Takaharu FUKUTOMI,

Mitsui Geophysical Observatory.

After the destructive Siduoka earthquake of July 11th, 1935, in strongly shaken area a precise levelling along a route of old Tôkaidô extending from Tegosi, Siduoka, to Sodesi near Ôkitu, and that along a route extending from Kunôsan-sita to the eastern bank of the river Abe along Suruga Bay were carried out in four times.

The relative vertical displacements of the bench marks along these level lines obtained by comparing the results of the recent measurements with those of earlier ones are shown in Table I—IV and in Figs. 2∼6. The writer made some discussions for the results.

——所　報——

○談話會記事

第107回地震研究所談話會

1. 西武藏野の地下水と地質構造と聚落	今村學郎 矢島仁吉
1. 偏心廻轉體に依つて起された地表面の波に就て	井上宇胤
1. 日本島外側に於ける地震活動の消長	坪井忠二
1. 靜力學的力を加へ又は除く爲に生ずる固體の彈性波	妹澤克惟
1. 三菱仲13號館，仲12號館6號，東7號館別館の震動に於ける勢力逸散性	妹澤克惟 金井清
1. 江東地域の地盤沈下に關する考察	宮部直巳
1. ヘルグロッツ・ウォーヘルトの式の擴張並に其の一證明法	河角廣 本間正作
1. 淺間山爆發實見記	寺田寅彦
1. 靜岡地震被害調査報告	金原壽郎
1. 昭和10年7月11日靜岡地方地震後に於ける水準測量結果報告（第1報）	福富孝治
1. 地震に伴ひたる南伊豆蓮臺寺溫泉の異狀（豫報）	福富孝治
1. 昭和10年7月11日靜岡地震に就て	萩原尊禮
1. 清水港の岸壁の震害に就て	松尾春雄
1. 昭和10年7月11日靜岡地震調査報告	齊田時太郎

第108回地震研究所談話會

1. 千葉市附近の地下水と地質構造と震害	吉村信吉 山本莊毅
1. 靜力學的力を加へ又は除く爲に生ずる固體の彈性波のわかり易い説明	妹澤克惟
1. 不連續面の鋭さが彈性波の透過反射に及ぼす影響	妹澤克惟 金井清
1. 三菱仲7號館別館，仲8號館別館，仲13號館の種々の狀態に於ける震動勢力の逸散性	妹澤克惟 金井清
1. 淺間火山の一等水準測量の結果	高橋龍太郎
1. 小淺間山外一點の鉛直線偏倚	高橋龍太郎

第 13 號 索 引

頁

淵田隆門；坪井忠二・淵田隆門　参照
福富孝治（76）昭和10年7月11日静岡地震後に於ける水準測量結果報告（邦文）……1010
福富孝治・中田正一（49）南伊豆蓮臺寺溫泉に就て（英文）…… 616
萩原尊禮（10）地震動の變位，速度及加速度の比較（英文）…… 138
萩原尊禮（64）空氣制振器に就て（英文）…… 783
萩原尊禮（72）昭和10年7月11日の静岡地震に就て（邦文）…… 951
平田森三；坪井忠二・平田森三　参照
飯田汲事（15）物質の粘彈性性質に關する實驗（I）（英文）…… 198
飯田汲事（31）物質の粘彈性性質に關する實驗（II）（英文）…… 433
飯田汲事（38）地表面に作用される風力その他によつて起される脈動（英文）… 504
飯田汲事（53）シリカの剛性率及び固體粘度の溫度による變化（英文）…… 665
今村學郞（6）地殼運動の分類（英文）…… 80
井上宇胤（61）偏心物體の廻轉に依つて起された地表面の波に就いて（邦文）… 757
井上宇胤・木村隼（14）人工地震の實驗（英文）…… 194
石本巳四雄（9）地震動の表面層內に於ける擴散（佛文）…… 130
石本巳四雄（47）東京横濱市內10個所における地震動加速度觀測（2）（邦文）… 592
金井清・西村源六郞；西村源六郞・金井清　参照
金井清・妹澤克惟；妹澤克惟・金井清　参照
川畑幸夫（5）日本に適合する回轉楕圓體の近似的計算（英文）…… 54
河角廣・吉山良一（37）歪の潜勢力によつて起される彈性波（英文）…… 496
木村隼；井上宇胤・木村隼　参照
金原壽郞・竹村千幹（73）昭和10年7月11日静岡地震震害調査報告（邦文）… 966
岸上冬彥（11）水平動地震計によつて觀測された週期4秒の脈動（英文）…… 145
岸上冬彥（48）週期4秒の脈動（其の2）（英文）…… 608
松尾春雄（75）清水港岸壁の震害と之に對する安定計算（英文）…… 999
松澤武雄（3）地球の核の蔭に於ける波（獨文）…… 39
松澤武雄（13）昭和8年3月3日の地震（其1）震央（獨文）…… 171

松澤武雄　（27）昭和8年3月3日の地震（其2）カリフォーニアで觀測された表面波（獨文）…… 328
水上　武　（8）地殼の上層內に震源を有する地震の初動分布と不連續層の厚さ（佛文）…… 114
水上　武　（26）淺間火山中央火口丘の相對的上昇と火口底の昇降變化（邦文）… 318
水上　武　（50）1935年の淺間火山の活動（其の1）（英文）…… 629
水上　武　（65）1935年の淺間火山の活動（其の2）（英文）…… 790
宮部直巳　（7）山崩れの研究（英文）…… 85
宮部直巳　（12）伊東地震群に關する統計（英文）…… 155
宮部直巳　（22）地殼の地塊的構造に就て（英文）…… 280
宮部直巳　（23）岩手，宮城縣下に於ける地殼の變形（英文）…… 286
宮部直巳　（24）“地塊とその運動”第1報の訂正（英文）…… 307
宮部直巳　（46）驗潮記錄より知られたる深川に於ける地盤の沈降（英文）…… 587
宮部直巳　（62）江東地域に於ける地盤の沈下（英文）…… 763
宮部直巳・寺田寅彥；寺田寅彥・宮部直巳　參照
長澤武雄；鈴木清太郎・長澤武雄・中原孫吉　參照
中田正一；福富孝治・中田正一　參照
中原孫吉；鈴木清太郎・長澤武雄・中原孫吉　參照
那須信治　（28）昭和2年丹後大地震の餘震の震原立體分布に關する研究補遺（英文）…… 335
那須信治　（29）伊豆半島に於ける最近の地震活動に就いて（第2報）（英文）… 400
那須信治　（30）昭和9年1月15日の印度大地震に就いて（英文）…… 417
那須信治・保田桂二　（71）靜岡强震に就て（邦文）…… 942
西村源六郎　（40）不連續面が彈性波の傳播に及ぼす影響（其の7）（邦文）…… 540
西村源六郎・金井清　（39）不連續面が彈性波の傳播に及ぼす影響（其の6）（邦文）…… 519
西村源六郎・高山威雄・金井清　（4）灣口に於ける水位變化に伴ふ灣內海水の運動（其の2）（邦文）…… 46
大塚彌之助　（16）岩手縣北部新第三系下部門の澤統と四ツ役統との北海道幌內統に對する層位學的關係及び日本中新世前半の海進（英文）…… 213
大塚彌之助　（17）能登半島南部邑知地溝（I）（英文）…… 218

大塚彌之助　（67）能登半島南部邑知地溝（II）（英文）…… 806

大塚彌之助　（68）能登半島南部邑知地溝（III）（英文）…… 846

大塚彌之助　（32）西南日本中央構造線と長崎三角地域とに關する二三の考察（邦文）…… 457

齊田時太郎　（74）昭和10年7月11日靜岡地震に就て（邦文）…… 985

妹澤克惟　（1）深さのある震源から發生するラブ波（英文）…… 1

妹澤克惟　（19）太平洋及大陸を通過するレーレー波及ラブ波（英文）…… 245

妹澤克惟　（35）陸棚に於けるセイシの成長及老衰（英文）…… 476

妹澤克惟　（56）瀬田川鐵橋に於ける車輛顚覆の振動的原因（英文）…… 715

妹澤克惟　（59）靜力學的力を加へ又は除く爲に生ずる彈性波（英文）…… 740

妹澤克惟・金井清　（2）L位相M位相の振動週期及振幅（英文）…… 18

妹澤克惟・金井清　（18）レーレー波の分散曲線に於ける不連續性（英文）…… 237

妹澤克惟・金井清　（20）地表層の震動減衰恒數（英文）…… 251

妹澤克惟・金井清　（34）M_2 地震波（英文）…… 471

妹澤克惟・金井清　（36）不均一彈性又は密度の地表層の震動減衰の割合（英文）…… 484

妹澤克惟・金井清　（54）勢力の地下逸散の爲に生ずる高層構造物の震動減衰（英文）…… 681

妹澤克惟・金井清　（55）架構構造物の震動に於ける勢力逸散（英文）…… 698

妹澤克惟・金井清　（58）局所的脈動の性質（英文）…… 729

妹澤克惟・金井清　（60）不連續面の鋭さが彈性波の透過反射に及ぼす影響（英文）…… 750

妹澤克惟・金井清　（70）三菱仲13號舘，仲12號舘6號，東7號舘別舘の震動に於ける勢力逸散性（英文）…… 925

鈴木武夫　（21）大正12年9月1日の地震の際土地隆起に伴つて生じた東京灣の靜振（英文）…… 266

鈴木清太郎・長澤武雄・中原孫吉　（25）博多灣沿岸水準高低測量（邦文）…… 310

高山威雄；西村源六郎・高山威雄　參照

竹村千幹；金原壽郎・竹村千幹　參照

寺田寅彦　（43）コロイドと地震學（英文）…… 562

寺田寅彦　（66）淺間山小爆發の二例に就て（邦文）…… 801

寺田寅彦・宮部直巳　（45）溫泉及鑛泉の分布と地殼運動（英文）…… 576

坪井忠二　（42）三鷹基線菱形の最近の面積變化（英文）……………………………… 558

坪井忠二・平田森三　（52）エゾタマキガヒの化石介殼內に於ける微結晶の配列（英文）…………………………………………………………………………… 660

坪井忠二・淵田隆門　（41）日本の重力に最もよく適合する式（英文）…………… 555

津屋弘逵　（51）富士火山の熔岩に就いて（英文）…………………………………… 645

津屋弘逵　（69）面河酸性岩類に就いて（英文）……………………………………… 910

山口生知　（44）地震と雨雪量，氣壓，及氣溫との關係（英文）………………… 569

山口生知　（63）地震發生機巧に關する一つの模型實驗（英文）………………… 772

保田柱二；那須信治・保田柱二　参照

吉山良一；河角廣・吉山良一　参照

（33）室戸岬附近の水準再測成果（邦文）………………………………………… 469

（57）岡山—鳥取，鳥取—米子，及び岡山—米子間水準再測成果（邦文）……… 723

Index to Vol. XIII.

Page

FUCHIDA, T., *See* TSUBOI, C. and FUCHIDA, T.

FUKUTOMI, T. (76) On the Result of Precise Levellings in the Strongly Shaken Area of the Siduoka Earthquake of July. 11th, 1935. (in Japanese) ……… 1010

FUKUTOMI, T. and NAKADA, M. (49) On the Rendaizi Thermal Spring in Southern Idu Peninsula. (in English) ……… 616

HAGIWARA, T. (10) A Comparison of the Displacement, the Velocity, and the Acceleration Seismograms. (in English) ……… 138

HAGIWARA, T. (64) The Air Damper. (in English) ……… 783

HAGIWARA, T. (72) The Sizuoka Earthquake of July 11, 1935. (in Japanese) ……… 951

HIRATA, M., *See* TSUBOI, C. and HIRATA, M.

IIDA, K. (15) Experiments on the Visco-elastic Properties of Pitch-like Materials. (I). (in English) ……… 198

IIDA, K. (31) Experiments on the Visco-elastic Properties of Pitch-like Materials. (II). (in English) ……… 433

IIDA, K. (38) Pulsatory Oscillations of the Earth's Crust due to Surface Force. (in English) ……… 504

IIDA, K. (53) Changes in Rigidity and Internal Friction of Amorphous Silica with Temperature. (in English) ……… 665

IMAMURA, G. (6) Classification of Crustal Movements. (in English) ……… 80

INOUYE, W. (61) Some Experiments on the Waves generated by the Rotation of Some Eccentric Masses. (in Japanese) ……… 757

INOUYE, W. and KIMURA, H. (14) Experiments on Artificial Earthquakes. (in English) ……… 194

ISHIMOTO, M. (9) La diffusion des secousses sismiques dans la couche superficielle du terrain. (en français) ……… 130

ISHIMOTO, M. (47) Observations accélérométriques des secousses sismiques dans les villes de Tôkyô et Yokohama (2me rapport).

(en Japonais) ………… 592

KANAI, K. and NISHIMURA, G., *See* NISHIMURA, G. and KANAI, K.

KANAI, K. and SEZAWA, K., *See* SEZAWA, K. and KANAI, K.

KAWABATA, Y. (5) Approximate Determination of the Spheroid most nearly Representing the Surface of Japan. (in English) … 54

KAWASUMI, H. and YOSIYAMA, R. (37) On an Elastic Wave Animated by the Potential Energy of Initial Strain. (in English) … 496

KIMURA, H., *See* INOUYE, W. and KIMURA, H.

KINBARA, T. and TAKEMURA, T. (73) Reports on the Siduoka Earthquake of July 11, 1935. (in Japanese) ………… 966

KISHINOUYE, F. (11) Microseisms of Four Second Period observed with Horizontal Seismographs. (in English) ………… 146

KISHINOUYE, F. (48) On Microseisms of Four Second Period. (The Second Paper). (in English) ………… 608

MATUO, H. (75) Damages to the Quay Walls of Simizu Harbour due to the Earthquake on July 11, 1935, and the Seismic Stability of the Quay Walls. (in English) ………… 999

MATUZAWA, T. (3) Über Schattenwellen und Kernwellen. (in deutsch) ………… 39

MATUZAWA, T. (13) Seismometrische Untersuchungen des Erdbens vom 2. März 1933. (I) Bestimmung des Herdes. (in deutsch) ………… 171

MATUZAWA, T. (27) Seismometrische Untersuchungen des Erdbebens vom 2. März 1933. (II) Analyse der in Californien beobachteten Oberflächenwellen. (in deutsch) ………… 328

MINAKAMI, T. (8) Distribution des mouvements initiaux d'un séisme dont le foyer se trouve dans la couche superficielle et détermination de l'épaisseur de cette couche. (en français) …… 114

MINAKAMI, T. (26) Changements relatifs de l'hauteur du cône central du volcan d'Asama et la profondeur de lave dans son cratére. (en Japonais) ………… 318

MINAKAMI, T. (50) The Explosive Activities of Volcano Asama in 1935. (Part 1). (in English) ………… 629

MINAKAMI, T. (65) The Explosive Activities of Volcano Asama in 1935. (Part 2). (in English) 790

MIYABE, N. (7) A Study of Landslides. (in English) 85

MIYABE, N. (12) A Statistical Study of the Itô Earthquake Swarms. (in English) 155

MIYABE, N. (22) Notes on the Block Structure of the Earth's Crust. (in English) 280

MIYABE, N. (23) Deformation of the Earth's Crust in the Iwate and Miyagi prefectures. (in English) 286

MIYABE, N. (24) Correction to my paper entitled "Blocks in the Earth's Crust and Their Movements, Part I". (in English) 307

MIYABE, N. (46) Sinking of the Earth's Crust in Fukagawa, Tokyo, as Deduced from Mareogram Data. (in English) 587

MIYABE, N. (62) On the Sinking of the Earth's Crust in the Eastern Part of the City of Tokyo. (in English) 763

MIYABE, N. and TERADA, T., *See* TERADA, T. and MIYABE, N.

NAGAZAWA, T., *See* SUZUKI, S., NAGAZAWA, T. and NAKAHARA, M.

NASU, N. (28) Supplementary Study on the Stereometrical Distribution of the After-shocks of the Great Tango Earthquake of 1927. (in English) 335

NASU, N. (29) Recent Seismic Activities in the Idu Peninsula. (Part 2). (in English) 400

NASU, N. (30) The Great Indian Earthquake of January 15, 1934. (in English) 417

NASU, N. and YASUDA, C. (71) The Siduoka Earthquake of July 11, 1935. (in Japanese) 942

NISHIMURA, G. (40) On the Effect of Discontinuity Surfaces on the Propagation of Elastic Waves. (VII). (in Japanese) 540

NISHIMURA, G. and KANAI, K. (39) On the Effect of Discontinuity Surfaces on the Propagation of Elastic Waves. (VI). (in Japanese) 519

NISHIMURA, G., TAKAYAMA, T. and KANAI, K. (4) On the Long Waves in a Bay of Variable Section Generated by the Changes in the Elevation at the Mouth of It. (in Japanese) ……………… 46

OTUKA, Y. (16) The Stratigraphic Relation of the Lower Kadonosawa and the Yotuyaku Series of Iwate to the Poronai Series in Hokkaidô and the Marine Transgression of the Early Miocene, in Japan. (in English) ……………… 213

OTUKA, Y. (17) The Oti Graben in Southern Noto Peninsula, Japan. (Part I). (in English) ……………… 218

OTUKA, Y. (67) The Oti Graben in Southern Noto Peninsula, Japan. (Part 2). (in English) ……………… 806

OTUKA, Y. (68) The Oti Graben in Southern Noto Peninsula, Japan. (Part 3). (in English) ……………… 846

OTUKA, Y. (32) Median Dislocation Line of Southwest Japan and the Nagasaki "Dreiecke". (in Japanese) ……………… 457

SAITA, T. (74) The Shizuoka Earthquake of July 11th, 1935. (in Japanese) ……………… 985

SEZAWA, K. (1) Love-waves Generated from a Source of a certain Depth. (in English) ……………… 1

SEZAWA, K. (19) Rayleigh- and Love-waves transmitted through the Pacific Ocean and the Continents. (in English) ……………… 245

SEZAW, K. (35) Growth and Decay of Seiches in an Epicontinental Sea. (in English) ……………… 476

SEZAWA, K. (56) Vibrational Causes of the Overturning of Railway Carriages on the Setagawa Bridge in the Typhoon of Sept. 21, 1934. (in English) ……………… 715

SEZAWA, K. (59) Elastic Waves Produced by Applying Statical Force to a Body or by Releasing it from a Body. (in English) ……………… 740

SEZAWA, K. and KANAI, K. (2) Periods and Amplitudes of Oscillation in L- and M-phases. (in English) ……………… 18

SEZAWA, K. and KANAI, K. (18) Discontinuity in the Dispersion Curves of Rayleigh Waves. (in English) ……………… 237

SEZAWA, K. and KANAI, K. (20) Decay Constants of Seismic Vibrations of a Surface Layer. (in English) ……………… 251

SEZAWA, K. and KANAI, K. (34) The M_2 Seismic Waves. (in English) 471

SEZAWA, K. and KANAI, K. (36) The Rate of Damping in Seismic Vibrations of a Surface Layer of Varying Density of Elasticity. (in English) 484

SEZAWA, K. and KANAI, K. (54) Decay in the Seismic Vibrations of a Simple or Tall Structure by Dissipation of their Energy into the Ground. (in English) 681

SEZAWA, K. and KANAI, K. (55) Energy Dissipation in Seismic Vibrations of a Framed Structure. (in English) 698

SEZAWA, K. and KANAI, K. (58) The Nature of Microseisms of Local Type. (in English) 729

SEZAWA, K. and KANAI, K. (60) The Effect of Sharpness of Discontinuities on the Transmission and Reflection of Elastic Waves. (in English) 750

SEZAWA, K. and KANAI, K. (70) Energy Dissipation in Seismic Vibrations of Actual Buildings. (in English) 925

SUZUKI, T. (21) Seiche in the Tôkyô Bay Caused by the Land Upheaval on the Occasion of the Great Earthquake of September 1, 1923. (in English) 266

SUZUKI, S., NAGAZAWA, T. and NAKAHARA, M. (25) The Revision of Precise Levelling along the Coast of the Hakata Bay. (in Japanese) 310

TAKAYAMA, T., *See* NISHIMURA, G. and TAKAYAMA, T.

TAKEMURA, T., *See* KINBARA, T. and TAKEMURA, T.

TERADA, T. (43) Colloids and Seismology. (in English) 562

TERADA, T. (66) On Two Cases of Minor Eruption of Mt. Asama. (in Japanese) 801

TERADA, T. and MIYABE, N. (45) Geographical Distribution of Hot and Mineral Springs and Deformation of Earth's Crust. (in English) 576

TSUBOI, C. (42) Recent Changes in Area of the Base Line Rhombus at Mitaka. (in English) 558

TSUBOI, C. and HIRATA, M. (52) Arrangement of Micro-Crystals of Calcium Carbonate in Some Fossil Shells, *Glycymeris yessoensis* SOWERBY. (in English) 660

TSUBOI, C. and FUCHIDA, T. (41) Supplementary Notes on the Most Suitable Formula for the Japanese Gravity Values. (in English) 555

TSUYA,H. (51) On Some Lavas of Volcano Huzi (Fuji). (in English) 645

TSUYA, H. (69) On the Omogo Acidic Rocks. (in English) 910

YAMAGUTI, S. (44) Relations between the Earthquakes and Precipitation, Barometric Pressure, and Temperature. (in English) 569

YAMAGUTI, S. (63) A Model Experiment on the Mechanism of Occurrence of Earthquake. (in English) 772

YASUDA, C., *See* NASU, N. and YASUDA, C.

YOSIYAMA, R., *See* KAWASUMI, H. and YOSIYAMA, R.

(33) Precise Levellings in the Neighbourhood of the Muroto Promontory. (in Japanese) 469

(57) Results of Recent Precise Levellings along the Lines Okayama—Tottori, Tottori—Yonago and Okayama—Yonago. (in Japanese) 723

4